frontiers
RESEARCH TOPICS

SPIKE-TIMING-DEPENDENT PLASTICITY: A COMPREHENSIVE OVERVIEW

Hosted by
Henry Markram, Wulfram Gerstner and
Per Jesper Sjöström

frontiers in COMPUTATIONAL NEUROSCIENCE
frontiers in SYNAPTIC NEUROSCIENCE

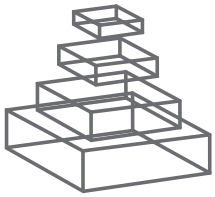

frontiers

Cover image provided by Ibbl sarl, Lausanne CH

ISSN 1664-8714
ISBN 978-2-88919-043-0
DOI 10.3389/978-2-88919-043-0

ABOUT FRONTIERS

Frontiers is more than just an open-access publisher of scholarly articles: it is a pioneering approach to the world of academia, radically improving the way scholarly research is managed. The grand vision of Frontiers is a world where all people have an equal opportunity to seek, share and generate knowledge. Frontiers provides immediate and permanent online open access to all its publications, but this alone is not enough to realize our grand goals.

FRONTIERS JOURNAL SERIES

The Frontiers Journal Series is a multi-tier and interdisciplinary set of open-access, online journals, promising a paradigm shift from the current review, selection and dissemination processes in academic publishing.
All Frontiers journals are driven by researchers for researchers; therefore, they constitute a service to the scholarly community. At the same time, the Frontiers Journal Series operates on a revolutionary invention, the tiered publishing system, initially addressing specific communities of scholars, and gradually climbing up to broader public understanding, thus serving the interests of the lay society, too.

DEDICATION TO QUALITY

Each Frontiers article is a landmark of the highest quality, thanks to genuinely collaborative interactions between authors and review editors, who include some of the world's best academicians. Research must be certified by peers before entering a stream of knowledge that may eventually reach the public - and shape society; therefore, Frontiers only applies the most rigorous and unbiased reviews.
Frontiers revolutionizes research publishing by freely delivering the most outstanding research, evaluated with no bias from both the academic and social point of view.
By applying the most advanced information technologies, Frontiers is catapulting scholarly publishing into a new generation.

WHAT ARE FRONTIERS RESEARCH TOPICS?

Frontiers Research Topics are very popular trademarks of the Frontiers Journals Series: they are collections of at least ten articles, all centered on a particular subject. With their unique mix of varied contributions from Original Research to Review Articles, Frontiers Research Topics unify the most influential researchers, the latest key findings and historical advances in a hot research area!
Find out more on how to host your own Frontiers Research Topic or contribute to one as an author by contacting the Frontiers Editorial Office: researchtopics@frontiersin.org

SPIKE-TIMING-DEPENDENT PLASTICITY: A COMPREHENSIVE OVERVIEW

Hosted By
Henry Markram, Ecole Polytechnique Fédérale de Lausanne, Switzerland
Wulfram Gerstner, Ecole Polytechnique Fédérale de Lausanne, Switzerland
Per Jesper Sjöström, The Research Institute of the McGill University Health Centre, Canada

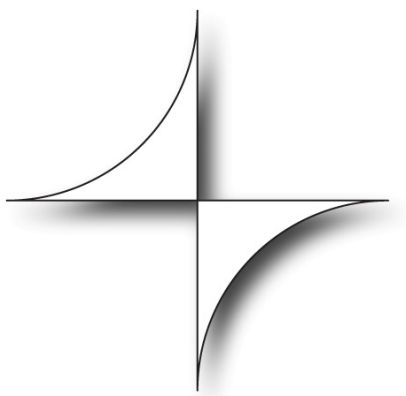

Hebb proposed that neurons that fire together, also wire together, which has provided the necessary logical context for understanding the role of synaptic strengthening in information storage in the brain. However, Hebb did not discuss in depth how synapses might be weakened. It was many years later that the active decrease of synaptic strength was introduced, by the discovery of long-term depression as elicited by low frequency stimulation of afferent inputs. In 1994, it was found that the precise relative timing of pre and postsynaptic spikes determined not only the magnitude, but also the sign of synaptic plasticity, a phenomenon that later became known as Spike-Timing-Dependent Plasticity, or STDP. Therefore, neurons that fire together may not necessarily wire together, depending on the precise timing of the spiking activity.

In the subsequent fifteen years, STDP has been found in multiple brain regions and in many different species, including humans. The size and shape of the temporal windows for which positive and negative synaptic strength changes are elicited may vary with brain region and synapse type, but the core principle of STDP has remained unchanged.

During the same fifteen-year-long time period, a large number of theoretical studies have also been conducted. Classical theories of unsupervised learning and Hebbian synaptic plasticity have almost invariably been formulated in terms of firing rates, but theoreticians have for a long time been considering what the timing requirements of synaptic plasticity are. The intriguing theoretical problem of time in Hebbian learning led to first models of STDP that

paralleled and even preceded the actual discovery of STDP. In the past few years, the simple picture of additive STDP models has been expanded upon, and several nonlinear aspects and biophysical details have been added. Theoretical predictions of the functional consequences of STDP in simple or large neuronal networks have appeared. STDP algorithms have thus become a mainstream learning algorithm for modelling neural networks.

Here, we have brought together key experimental and theoretical research on STDP. These papers review these trends and provide a forum for recent advances in the theory and experiments of STDP.

Table of Contents

frontiers in
SYNAPTIC NEUROSCIENCE

EDITORIAL
published: 12 July 2012
doi: 10.3389/fnsyn.2012.00002

Spike-timing-dependent plasticity: a comprehensive overview

H. Markram[1], W. Gerstner[2] and P. J. Sjöström[3]*

[1] *Brain Mind Institute Life Science, Ecole Polytechnique Federale de Lausanne, Lausanne, Switzerland*
[2] *Ecole Polytechnique Federale de Lausanne, Lausanne, Switzerland*
[3] *Department of Neurology and Neurosurgery, Centre for Research in Neuroscience, The Research Institute of the McGill University Health Centre, Montreal, QC, Canada*
**Correspondence: jesper.sjostrom@mcgill.ca*

Edited by:
Mary B. Kennedy, Caltech, USA

Reviewed by:
Mary B. Kennedy, Caltech, USA

WHY TIMING MATTERS

A neuron embedded in a neuronal network is bombarded with thousands of inputs every minute. But which ones are important? Which information should the neuron listen to and pass along to downstream neurons?

During brain development and during learning, this is a formidable problem that the vast majority of neurons in the brain have to solve – how to correctly choose and fine-tune the inputs from one's neighbors without any other information than that which is received from these neighbors themselves. Some of these neighbors provide good information while others do not. Who to trust? How can you determine who to pay attention to?

Many decades ago, the Canadian neuropsychologist Hebb (1949), the Polish neurophysiologist Konorski (1948), as well as the Spanish anatomist Ramón y Cajal (1894) all had similar ideas that could potentially help explain how neurons wire up. The basic idea was essentially that – in the words of the present-day neuroscientist Shatz (1992) – "*cells that fire together, wire together.*" In other words, if things keep happening more or less simultaneously, you may assume that there is a common cause for the firing. More importantly, if one of the cell is active systematically just slightly before another, the firing of the first one might have a causal link to the firing of the second one and this causal link could be remembered by increasing the wiring of connections, a notion we call synaptic plasticity. In short, timing matters because it may indicate causality.

Even though Hebb did propose an ordering of firing in his "phase sequences" (Hebb, 1949), the view that coincident activity in connected neurons is what matters in plasticity practically dominated modern neuroscience research well into the mid 1990s. Although some few studies had indeed been carried out prior to this (e.g., Levy and Steward, 1983), neuroscientists typically did not consider the precise timing of inputs in their synaptic plasticity experiments. But this changed rapidly when a flurry of studies were published in the mid 1990s. Theoreticians realized just how important temporal order was for conveying and storing information in neuronal circuits, and to hook them up correctly. And experimenters realized that they had almost completely ignored this one factor – time – in their experiments, while they at the same time saw how the synaptic connections of the brain had mechanisms in place that clearly should make them acutely sensitive to timing. Thus the field of Spike-Timing-Dependent Plasticity – or STDP – was born, via the first key studies of Henry Markram (Markram and Sakmann, 1995; Markram et al., 1997) and Gerstner et al. (1996).

With STDP, a neuron embedded in a neuronal network can determine which neighboring neurons are worth listening to by potentiating those inputs that predict its own spiking activity. However, the neuron in question pays less attention to those neighboring neurons that fail to do this. In other words, the neuron pays less attention to neighbors speaking gibberish. The net result is that our sample neuron can integrate inputs with predictive power and transform this is into a meaningful predictive output, even though the meaning itself is not strictly known by the neuron. In STDP we thus have a very simple and elegant algorithm for appropriately hooking up neurons in the brain. Little wonder that there has been so much excitement surrounding the discovery of STDP.

THE STDP RESEARCH TOPIC: A BRIEF INTRODUCTION

This Frontiers Research Topic eBook has been divided into eight sections, of which six contain reviews and two comprise original research articles. The first section is called *The Conceptual Development of STDP*, and deals with the history leading up to the discovery of STDP. Markram et al. (2011) outlines the history of timing in plasticity, beginning with Aristotle some 2000 years ago. Sjöström and Gerstner (2010) next define and briefly outline the STDP concept. Because the history of anything is necessarily subjective, this section also includes personal accounts, published as Opinion pieces. Contributors include the Nobel prize winner Cooper (2010), who famously helped outline the Bienenstock–Cooper–Munro theory of metaplasticity (Bienenstock et al., 1982); the electrophysiologist Levy (2010), who arguably carried out some of the very first timing-dependence experiments in plasticity (Levy and Steward, 1983); and the theoretician Gerstner (2010), who in a theoretical study (Gerstner et al., 1996) independently predicted and anticipated Henry Markram's report of STDP (Markram and Sakmann, 1995; Markram et al., 1997).

In the second section, *The Biological Relevance of STDP* is discussed. Lisman and Spruston (2010) are first out and argue that STDP is limited plasticity paradigm that cannot unify the field of plasticity, because its biological relevance is overrated. This is an important criticism – which the authors have made before (Lisman and Spruston, 2005) – that researchers in the STDP field should take to heart and try to address. Schulz (2010) develops this point, making the case that plasticity in the intact brain is likely to be much more complicated than in simple *in vitro* experiments. In a more specific argument, Shouval et al. (2010) suggest that STDP is in reality a result of something more fundamental, which they propose is intracellular calcium signals. In addition, they argue in

favor of mechanism-driven modeling, rather than theory driven by phenomenology. Fregnac et al. (2010) make the case that there is limited evidence supporting an actual functional role of STDP in the intact brain, an important point that should be compared to those of Schulz (2010) and of Lisman and Spruston (2010). By comparing two different induction protocols, they conclude that classical STDP might be limited to the critical period *in vivo*. Finally, Buchanan and Mellor (Buchanan et al., 2010) focus on STDP in the hippocampus, showing that for this brain region the experimental literature seems to be particularly fraught with disagreement. But there is common ground, which is defined by post-synaptic calcium transients, thus echoing the point made by Shouval et al. (2010).

Section three deals with *Mechanisms: Inducing, Expressing, and Controlling STDP*. Seguing from the previous section, Graupner and Brunel (2010) begin by providing an overview of biophysical models of synaptic plasticity, including those based on calcium and those based on signaling cascades, with a special emphasis on bistable synapses. Following on this, Froemke et al. (2010b) explore how STDP depends on where the synapse is located in the dendritic arbor, and what the functional consequences of this location dependence might be (for a related article here-in, see Clopath and Gerstner, 2010). Turning next to the pre-synaptic side and how it governs STDP, Rodriguez-Moreno et al. (2010) overview recent findings on the role of pre-synaptically located NMDA receptors in timing-dependent long-term depression (cf. Duguid and Sjöström, 2006). But pre or post-synaptic mechanisms cannot suffice – as Pawlak et al. (2010) show in the ensuing paper, STDP must be somehow controlled by a third factor, which is likely a neuromodulatory gate. Finally, Froemke et al. (2010a) discuss the consequences of temporally non-linear spike-pair interactions in STDP. They show that factors such as spike triplets and rate also determine plasticity, although differently in neocortex compared to hippocampus.

This brings us to the next set of questions: Does STDP always look the same? In fact, has STDP been found at all synapse types? In section four, these and other questions are addressed as we learn about *The Diverse Phenomenology of STDP*. Shulz and Jacob (2010) compare STDP in different species and brain regions, in particular *in vivo*, and find that variability depends not only on synapse type, but also on network state and neuromodulation, thus arguing for the need for more research. Müller-Dahlhaus et al. (2010) report on STDP-like changes in the human brain as evidenced by transcranial magnetic stimulation. Richards et al. (2010) subsequently report on *in vivo* STDP in the optic tectum of the tadpole, *Xenopuslaevis*, where some of the first evidence for the existence of STDP was found. So far, we have focused on the plasticity of excitation, but it is important not to neglect the plasticity of inhibitory circuits, as is pointed out in the review by Lamsa et al. (2010). After this, Roberts and Leen (2010) discuss the role of anti-Hebbian STDP in computational features such as predictive sensory cancelation and novelty detection in the electrosensory system of the weakly electric fish. Next, Fino and Venance (2010) overview the state of the striatal STDP field, where some conflicting results have been reported. The authors argue that these discrepancies are due to diversity in synaptic learning rules across different cell types, but probably also to experimental conditions. Finally, Larsen et al. (2010) review STDP in the sensory neocortex, arguing that the properties of STDP change over development, to achieve optimal tuning of neurons as conditions change with maturation. To conclude, STDP exists in humans, tadpole, and electric fish alike, but it may vary with the specific cell and synapse type as well as with developmental stage.

Timing is not everything, however, and in section five, titled *STDP and Beyond*, we learn about other forms of plasticity and how they interact with timing-dependent learning rules. Watt and Desai (2010) discuss how homeostatic plasticity is necessary for a neuron to keep its cool as the world changes, for example as inputs connect up during development. Such homeostatic plasticity may act on synapses or on the excitability of the cell itself. Debanne and Poo (2010) go beyond the synapse to the plasticity of intrinsic excitability of the pre or the post-synaptic cell, overviewing how this is linked to the induction of STDP, as well as what its spatial extent is.

In section six, entitled *STDP: Consequences in Health and Disease*, the impact of STDP on circuits is discussed. Butts and Kanold (2010) make the interesting argument that – because early activity patterns typically do not possess the fast correlation structures that STDP is sensitive to, but mature activity patterns do – STDP may first be masked, only to emerge later in development and be present in the mature brain (for a different view, see Fregnac et al., 2010). Next up is Gilson et al. (2010), who explore STDP in recurrent neuronal networks. Although several theoretical studies have explored the role of STDP in individual cells, Gilson et al. (2010) discuss the consequences of STDP in the circuit, with a focus on weight dynamics and the evolution of different network structures. Finally, Meredith and Mansvelder (2010) overview STDP in neurodevelopmental learning disorders, using the Fragile X syndrome as a starting point. They propose that studying STDP in a disease context may provide an opportunity to link cognition and learning rules.

The two last sections consist of original research articles grouped into theoretical and experimental studies. Due to lack of space, we regrettably cannot introduce these contributions individually here.

CONCLUDING REMARKS

There is no doubt that STDP is a novel plasticity paradigm of great interest that holds particular promise for biological and computational relevance. STDP has in fact dramatically reshaped the field of synaptic plasticity over the past decade or so. But this is not to say that STDP has been a panacea for all problems neuroscientific. Clearly cells that fire together wire together, there is no doubt about that, so the coming of STDP has not rendered the classical literature obsolete by any means. Also, the advent of STDP has raised many questions. Can we really be sure that STDP actually happens in the intact brain? Most studies have been carried out in a dish, after all, so we should not assume that these artificial activity patterns imposed on the tissue in the dish are necessarily relevant. If STDP does exist, does it exist in all animal species? After all, if STDP is inherently important for brain functioning, it should have been relatively preserved by evolution. And should there not be a way of turning STDP on and off? It does not seem to be the case that we constantly learn and rewire our brains to every stimulus we encounter; our brains are quite selective filters when it comes to information storage. If the STDP paradigm shift is to be more than a revolution in a dish, a much-improved understanding of this phenomenon is desperately and urgently needed. This Frontiers

Research Topic eBook on STDP has aimed to help achieve precisely this, by comprehensively overviewing what is known, outlining what is not known, highlighting controversy, and pointing out where we need to direct our research efforts next. This research is important, because it is about how your brain works.

REFERENCES

Bienenstock, E. L., Cooper, L. N., and Munro, P. W. (1982). Theory for the development of neuron selectivity: orientation specificity and binocular interaction in visual cortex. *J. Neurosci.* 2, 32–48.

Buchanan, K., Elgar, D., Blackman, A., Tudor Jones, A., and Sjöström, P. (2010). Differential expression of presynaptic NMDA receptors in neocortex. *FENS Abstr.* 5, 014.2.

Butts, D. A., and Kanold, P. O. (2010). The applicability of spike time dependent plasticity to development. *Front. Synaptic Neurosci.* 2:30. doi: 10.3389/fnsyn.2010.00030

Clopath, C., and Gerstner, W. (2010). Voltage and spike timing interact in STDP – a unified model. *Front. Synaptic Neurosci.* 2:25. doi: 10.3389/fnsyn.2010.00025

Cooper, L. N. (2010). STDP: spiking, timing, rates and beyond. *Front. Synaptic Neurosci.* 2:14. doi: 10.3389/fnsyn.2010.00014

Debanne, D., and Poo, M. M. (2010). Spike-timing dependent plasticity beyond synapse – pre- and post-synaptic plasticity of intrinsic neuronal excitability. *Front. Synaptic Neurosci.* 2:21. doi: 10.3389/fnsyn.2010.00021

Duguid, I., and Sjöström, P. J. (2006). Novel presynaptic mechanisms for coincidence detection in synaptic plasticity. *Curr. Opin. Neurobiol.* 16, 312–322.

Fino, E., and Venance, L. (2010). Spike-timing dependent plasticity in the striatum. *Front. Synaptic Neurosci.* 2:6. doi: 10.3389/fnsyn.2010.00006

Fregnac, Y., Pananceau, M., Rene, A., Huguet, N., Marre, O., Levy, M., and Shulz, D. E. (2010). A re-examination of Hebbian-covariance rules and spike timing-dependent plasticity in cat visual cortex in vivo. *Front. Synaptic Neurosci.* 2:147. doi: 10.3389/fnsyn.2010.00147

Froemke, R. C., Debanne, D., and Bi, G.-Q. (2010a). Temporal modulation of spike-timing-dependent plasticity. *Front. Synaptic Neurosci.* 2:19. doi: 10.3389/fnsyn.2010.00019

Froemke, R. C., Letzkus, J. J., Kampa, B. M., Hang, G. B., and Stuart, G. J. (2010b). Dendritic synapse location and neocortical spike-timing-dependent plasticity. *Front. Synaptic Neurosci.* 2:29. doi: 10.3389/fnsyn.2010.00029

Gerstner, W. (2010). From Hebb rules to spike-timing-dependent plasticity: a personal account. *Front. Synaptic Neurosci.* 2:151. doi: 10.3389/fnsyn.2010.00151

Gerstner, W., Kempter, R., van Hemmen, J. L., and Wagner, H. (1996). A neuronal learning rule for sub-millisecond temporal coding. *Nature* 383, 76–81.

Gilson, M., Burkitt, A., and Van Hemmen, L. J. (2010). STDP in recurrent neuronal networks. *Front. Comput. Neurosci.* 4:23. doi: 10.3389/fncom.2010.00023.

Graupner, M., and Brunel, N. (2010). Mechanisms of induction and maintenance of spike-timing dependent plasticity in biophysical synapse models. *Front. Comput. Neurosci.* 4:23. doi: 10.3389/fncom.2010.00023.

Hebb, D. O. (1949). *The Organization of Behavior*. New York: Wiley.

Konorski, J. (1948). *Conditioned Reflexes and Neuron Organization*. Cambridge: Cambridge University Press.

Lamsa, K. P., Kullmann, D. M., and Woodin, M. A. (2010). Spike-timing dependent plasticity in inhibitory circuits. *Front. Synaptic Neurosci.* 2:8. doi: 10.3389/fnsyn.2010.00008

Larsen, R. S., Rao, D., Manis, P. B., and Philpot, B. D. (2010). STDP in the developing sensory neocortex. *Front. Synaptic Neurosci.* 2:9. doi: 10.3389/fnsyn.2010.00009

Levy, W. B. (2010). Discovering associative long-term synaptic modification and timing dependence of plasticity – a very brief and personal history. *Front. Synaptic Neurosci.* 2:149. doi: 10.3389/fnsyn.2010.00149

Levy, W. B., and Steward, O. (1983). Temporal contiguity requirements for long-term associative potentiation/depression in the hippocampus. *Neuroscience* 8, 791–797.

Lisman, J., and Spruston, N. (2005). Postsynaptic depolarization requirements for LTP and LTD: a critique of spike timing-dependent plasticity. *Nat. Neurosci.* 8, 839–841.

Lisman, J., and Spruston, N. (2010). Questions about STDP as a general model of synaptic plasticity. *Front. Synaptic Neurosci.* 2:140. doi: 10.3389/fnsyn.2010.00140

Markram, H., Gerstner, W., and Sjöström, P. J. (2011). A history of spike-timing-dependent plasticity. *Front. Synaptic Neurosci.* 3:4. doi: 10.3389/fnsyn.2011.00004

Markram, H., Lübke, J., Frotscher, M., and Sakmann, B. (1997). Regulation of synaptic efficacy by coincidence of postsynaptic APs and EPSPs. *Science* 275, 213–215.

Markram, H., and Sakmann, B. (1995). Action potentials propogating back into dendrites triggers changes in efficacy of single-axon synapses between layer V pyramidal cells. *Soc. Neurosci. Abstr.* 21, 2007.

Meredith, R. M., and Mansvelder, H. D. (2010). STDP and mental retardation: dysregulation of dendritic excitability in fragile X syndrome. *Front. Synaptic Neurosci.* 2:10. doi: 10.3389/fnsyn.2010.00010

Müller-Dahlhaus, F., Ziemann, U., and Classen, J. (2010). Plasticity resembling spike-timing dependent synaptic plasticity: the evidence in human cortex. *Front. Synaptic Neurosci.* 2:34. doi: 10.3389/fnsyn.2010.00034

Pawlak, V., Wickens, J. R., Kirkwood, A., and Kerr, J. N. D. (2010). Timing is not everything: neuromodulation opens the STDP gate. *Front. Synaptic Neurosci.* 2:146. doi: 10.3389/fnsyn.2010.00146

Ramón y Cajal, S. (1894). The Croonian lecture: la fine structure des centres nerveux. *Proc. R. Soc. Lond. B Biol. Sci.* 4, 444–468.

Richards, B. A., Aizenman, C. D., and Akerman, C. J. (2010). In vivo spike-timing-dependent plasticity in the optic tectum of *Xenopus laevis*. *Front. Synaptic Neurosci.* 2:7. doi: 10.3389/fnsyn.2010.00007

Roberts, P. D., and Leen, T. K. (2010). Anti-hebbian spike-timing-dependent plasticity and adaptive sensory processing. *Front. Comput. Neurosci.* 4:156. doi: 10.3389/fncom.2010.00156

Rodriguez-Moreno, A., Banerjee, A., and Paulsen, O. (2010). Presynaptic NMDA receptors and spike timing-dependent long-term depression at cortical synapses. *Front. Synaptic Neurosci.* 2:18. doi: 10.3389/fnsyn.2010.00018

Schulz, J. M. (2010). Synaptic plasticity in vivo: more than just spike-timing? *Front. Synaptic Neurosci.* 2:150. doi: 10.3389/fnsyn.2010.00150

Shatz, C. J. (1992). The developing brain. *Sci. Am.* 267, 60–67.

Shouval, H. Z., Wang, S. S.-H., and Wittenberg, G. M. (2010). Spike timing dependent plasticity: a consequence of more fundamental learning rules. *Front. Comput. Neurosci.* 4:19. doi: 10.3389/fncom.2010.00019

Shulz, D. E., and Jacob, V. (2010). Spike timing dependent plasticity in the intact brain: counteracting spurious spike coincidences. *Front. Synaptic Neurosci.* 2:137. doi: 10.3389/fnsyn.2010.00137

Sjöström, P. J., and Gerstner, W. (2010). Spike-timing dependent plasticity. *Scholarpedia J.* 5, 1362.

Watt, A. J., and Desai, N. S. (2010). Homeostatic plasticity and STDP: keeping a neuron's cool in a fluctuating world. *Front. Synaptic Neurosci.* 2:5. doi: 10.3389/fnsyn.2010.00005

Received: 12 June 2012; Accepted: 21 Jun 2012; published online: 12 July 2012.
Citation: Markram H, Gerstner W and Sjöström PJ (2012) Spike-timing-dependent plasticity: a comprehensive overview. Front. Syn. Neurosci. ***4****:2. doi: 10.3389/fnsyn.2012.00002*

frontiers in
SYNAPTIC NEUROSCIENCE

REVIEW ARTICLE
published: 29 August 2011
doi: 10.3389/fnsyn.2011.00004

A history of spike-timing-dependent plasticity

***Henry Markram*[1]*, *Wulfram Gerstner*[1] *and Per Jesper Sjöström*[2,3]**

[1] *Brain Mind Institute, Ecole Polytechnique Fédérale de Lausanne, Lausanne, Switzerland*
[2] *Department of Neuroscience, Physiology and Pharmacology, University College London, London, UK*
[3] *Department of Neurology and Neurosurgery, Centre for Research in Neuroscience, The Research Institute of the McGill University Health Centre, Montreal General Hospital, Montreal, QC, Canada*

Edited by:
Mary B. Kennedy, Caltech, USA

Reviewed by:
Kei Cho, University of Bristol, UK
Takeshi Sakaba, Max Planck Institute for Biophysical Chemistry, Germany
Yves Frégnac, CNRS UNIC, France
Larry Abbott, Columbia University, USA

***Correspondence:**
Henry Markram, Brain Mind Institute, Ecole Polytechnique Fédérale de Lausanne, CH-1015 Lausanne, Switzerland.
e-mail: henry.markram@epfl.ch

How learning and memory is achieved in the brain is a central question in neuroscience. Key to today's research into information storage in the brain is the concept of synaptic plasticity, a notion that has been heavily influenced by Hebb's (1949) postulate. Hebb conjectured that repeatedly and persistently co-active cells should increase connective strength among populations of interconnected neurons as a means of storing a memory trace, also known as an engram. Hebb certainly was not the first to make such a conjecture, as we show in this history. Nevertheless, literally thousands of studies into the classical frequency-dependent paradigm of cellular learning rules were directly inspired by the Hebbian postulate. But in more recent years, a novel concept in cellular learning has emerged, where temporal order instead of frequency is emphasized. This new learning paradigm – known as spike-timing-dependent plasticity (STDP) – has rapidly gained tremendous interest, perhaps because of its combination of elegant simplicity, biological plausibility, and computational power. But what are the roots of today's STDP concept? Here, we discuss several centuries of diverse thinking, beginning with philosophers such as Aristotle, Locke, and Ribot, traversing, e.g., Lugaro's *plasticità* and Rosenblatt's perceptron, and culminating with the discovery of STDP. We highlight interactions between theoretical and experimental fields, showing how discoveries sometimes occurred in parallel, seemingly without much knowledge of the other field, and sometimes via concrete back-and-forth communication. We point out where the future directions may lie, which includes interneuron STDP, the functional impact of STDP, its mechanisms and its neuromodulatory regulation, and the linking of STDP to the developmental formation and continuous plasticity of neuronal networks.

Keywords: synaptic plasticity, spike-timing-dependent plasticity, bidirectional plasticity, long term depression, long term plasticity, history, learning, memory

TIMING IS EVERYTHING

Already in antiquity, philosophers such as Aristotle observed the need for repeating sequences of activation in order to link mental representations (reviewed in Fregnac, 2002). In *De Memoria Et Reminiscentia*, Aristotle argued "*Acts of recollection, as they occur in experience, are due to the fact that one movement has by nature another that succeeds it in regular order*" (cited in Hartley, 1749; James, 1890). This is an intuitively appealing way of describing recollection, but it also implies causative chains of events. How can the mind establish causal relationships between events in the outside world? Indeed, it instinctively seems correct and very human to assume that the repeated and persistent temporal ordering of events A and B actually means that event A somehow *causes* event B. In fact, this mode of thinking is so human that concluding that B is caused by A in this scenario may make others accuse us of the logical fallacy of false cause, also known as *post hoc ergo propter hoc*.

Even so, this way of establishing causal and acausal relationships between events in the outside world seems to be key to how individual synaptic connections in the brain operate: typically, synapses are increased in strength if presynaptic spikes repeatedly occur before postsynaptic spikes within a few tens of milliseconds or less, whereas the opposite temporal order elicits synaptic weakening, a concept known as spike-timing-dependent plasticity (STDP; **Figures 1A,B**). It is as if synapses in the brain are rewarded via strengthening if its activity consistently predicts the postsynaptic activity, while repeated failure at predicting the postsynaptic cell's activity – "postdiction" – results in punishment via synaptic weakening. As shall be discussed in more detail later, there are however many different types of STDP (Caporale and Dan, 2008; Sjöström et al., 2008). In this historical overview, we aim to briefly trace the historical background leading up to the STDP cellular learning paradigm in modern neuroscience research.

THE ROOTS OF PLASTICITY

Aristotle first introduced in his treatise *De Anima* the notion of the mind as a *tabula rasa*, or a blank slate, an idea that in the eleventh century was further developed by the Islamic philosopher Avicenna (also known as *ibn-Sina*), who argued that the mind was a blank slate at birth that was later developed through education. This idea was in stark contrast to that of Plato, Aristotle's teacher, who argued in, e.g., *Phaedo* that the human mind was created in the heavens, pre-formed and ready, and was then sent to Earth to join the body. Philosophers have thus long argued as to whether we primarily are a product of nature or of nurture.

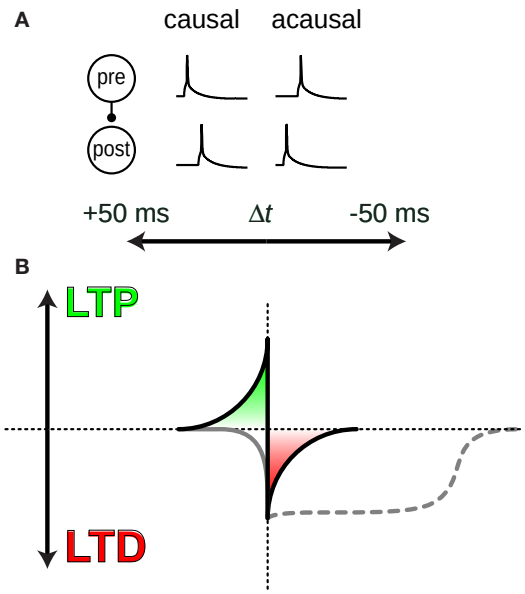

FIGURE 1 | Defining Spike-Timing-Dependent Plasticity (A) A presynaptic cell connected to a postsynaptic cell repeatedly spiking just before the latter is in part causing it to spike, while the opposite order is acausal. (B) In typical STDP, causal activity results in long-term potentiation (LTP), while acausal activity elicits long-term depression (LTD; Markram et al., 1997b; Bi and Poo, 1998; Zhang et al., 1998). At some cortical synapses, the temporal window for LTD (dashed gray line) is extended (Feldman, 2000; Sjöström et al., 2001). These temporal windows are often also activity dependent, with LTP being absent at low-frequency (gray continuous line, Markram et al., 1997b; Sjöström et al., 2001), and postsynaptic bursting relaxing the LTD timing requirements to hundreds of milliseconds (Debanne et al., 1994; Sjöström et al., 2003).

In modern times, the clean-slate view of the brain is normally accredited to the seventeenth century English philosopher, John Locke. Locke (1689) proposed that we are born without any preconceptions or innate ideas and that experience completely molds the brain, thus nurture determines who we are. This notion is central to Locke's empiricism, which emphasizes the individual's ability to author his or her own destiny. The *tabula rasa* view on learning in the brain had a powerful effect on subsequent philosophers and psychologists, and became generally accepted in psychology by the mid nineteenth century. It for example features in Sigmund Freud's psychoanalysis, and is in fact still today a major paradigm in many respects.

The seventeenth and eighteenth century philosophers, such as Thomas Hobbes, David Hume, Étienne de Condillac, and David Hartley, drove the shift to empiricism by claiming a physical basis for behavior, learning, and memory. An important related question that these philosophers were trying to answer was how habits come about. These questions lead to a series of fundamental postulates of associative learning, contiguity, synchronization, and succession of events. Hartley, for example, wrote "*Any sensations A, B, C etc., by being associated with one another a sufficient Number of Times, get such a power over the corresponding Ideas, a, b, c, etc., that any one of the sensations A, when impressed alone shall be able to excite in the Mind, b, c, etc., the ideas of the rest.*" (Hartley, 1749).

By the mid nineteenth century, philosophers, psychologists, and early physiologists, neurosurgeons, and the first neuroscientists started seeking the mechanisms that form the physiological bases of learning and memory and locked on to the notion that associating information is the ultimate law governing brain function. Philosophers during this time even expressed their surprise at how the "ancient ones" could have thought otherwise. The influential French philosopher Théodule Ribot writes, "*It is remarkable that this discovery was made so late. Nothing is simpler, apparently, than to notice that this law of association is the truly fundamental, irreducible phenomenon of our mental life; that it is at the bottom of all our acts; that it permits of no exception; that neither dream, revery, mystic ecstasy, nor the most abstract reasoning can exist without it; that its suppression would be equivalent to that of thought itself. Nevertheless no ancient author understood it, for one cannot seriously maintain that a few scattered lines in Aristotle and the Stoics constitute a theory and clear view of the subject. It is to Hobbes, Hume, and Hartley that we must attribute the origin of these studies on the connection of our ideas. The discovery of the ultimate law of our psychologic acts has this, then, in common with many other discoveries: it came late and seems so simple that it may justly astonish us.*" (Ribot, 1870). The Scottish Philosopher, Alexander Bain writes, "*Actions, sensations, and States of Feeling, occurring together or in succession, tend to grow together, or cohere, in such a way that, when any one of them is afterwards presented to the mind, the others are apt to be brought up in idea.*" (Bain, 1855).

The idea that changes at *junctions between neurons* might account for learning and memory by changing the way information flows in the brain was already speculated in the later half of the nineteenth century. The earliest references that explicitly pins down the *junctions between cells* as the physical element that must change to enable learning and memory, even before the existence of synapses was known, is probably that of Bain; "*For every act of memory, every exercise of bodily aptitude, every habit, recollection, train of ideas, there is a specific grouping or coordination of sensations and movements, by virtue of specific growth in cell junctions.*" (Bain, 1873).

William James (**Figure 2**), a leading American psychologist, driven by the belief that truth was relative and shaped by the learned usefulness of events, lay down the foundations for many years of speculations on the specific causal conditions that would strengthen these *junctions*. "*The psychological law of association of objects thought of through their previous contiguity in thought or experience would thus be an effect, within the mind, of the physical fact that nerve-currents propagate themselves easiest through those tracts of conduction which have been already most in use. . .the phenomenon of habit in living beings are due to the plasticity of the organic materials of which their bodies are composed. . .And it is too the infinitely attenuated currents that pour in through these latter channels (*sensory nerve roots*) that the hemispherical cortex shows itself to be so peculiarly susceptible. The currents, once in, must find a way out. In getting out they leave traces in the paths they take. . .So nothing is easier than to imagine how, when a current once traversed a path, it should traverse it more readily still the second time.*" (James, 1890).

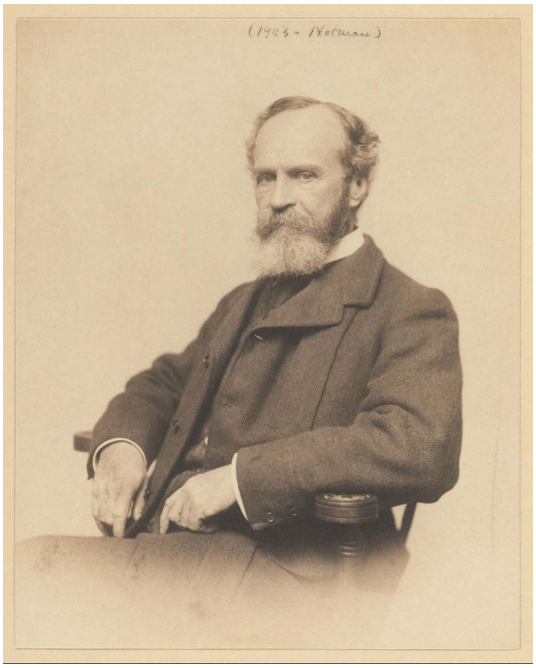

FIGURE 2 | William James Source: Houghton Library, Harvard University, Call number pfMS Am 1092 (1185) #83, with permission.

James considered repetition, intensity, and competition key determinants of associations. "*The amount of activity at any given point in the brain-cortex is the sum of tendencies of all other points to discharge into it, such tendencies being proportionate (1) to the number of times the excitement of each other point may have accompanied that of the point in question; (2) to the intensity of such excitement; and (3) to the absence of any rival point of functionality disconnected with the first point, into which the discharges might be diverted.*" James also postulated a neural mechanism of associative learning, "*After discrimination, association!. . .a stimulus which would be inadequate by itself to excite a nerve centre to effective discharge may, by acting with one or more other stimuli (equally ineffectual by themselves alone) bring the discharge about. . .Let us then assume as the basis of all our subsequent reasoning this law: When two elementary brain-processes have been active together or in immediate succession, one of them, on reoccurring, tends to propagate its excitement into the other.*" (James, 1890). This associative learning rule is strikingly similar to that proposed by Donald Hebb about half a century later (see below).

One may be tempted to think that early philosophers and psychologists considered timing of events only vaguely, but in fact a remarkable number of psychophysical studies were conducted in the nineteenth century in an attempt to define the temporal unit of perception and the temporal unit of associations of perceptions. Measurements varied from 750 ms down to as little as 2 ms for the units of perception and as little as 50 ms for associations of events (see James, 1890). The sequential timing and succession of events was considered critical in these early theories of mind and in particular learning and memory. James writes, "*Time-determinations apart,. . .objects once experienced together tend to become associated in the imagination, so that when any one of them is thought of, the others are likely to be thought of also, in the same order of sequence or coexistence as before. This statement was named the law of mental association by contiguity.*" Shadworth Hodgson, an English philosopher and close colleague of James, writes, "*Memory aims at filling the gap with an image which has at some particular time filled it before, reasoning with one which bears certain time-and space-relations to the images before and after.*" (James, 1890).

The later half of the nineteenth century was also the period when the experimental foundations for classical conditioning where being laid down. Ivan Pavlov's 12 years of experiments on conditioned salivation and digestion in his dog were published in 1897. The principle was laid down that there are pre-set physiological reactions (salivation) that can be triggered by an unconditioned stimulus (smell of food) and that any arbitrary neutral stimulus (e.g., the color of one's shirt) can be converted into a conditioned stimulus if presented at the same time as the unconditioned stimulus. Temporal ordering on a timescale of seconds was essential (Pavlov, 1897).

The foundations for the electrical properties of the brain and the discovery of the action potential were laid down in the latter part of the nineteenth century. Building on the work of the Italians Luigi Galvani and Allesandro Volta in the 1790s, Matteucci (1838) showed that living organisms generate electricity, thus giving rise to the concept of bioelectricity – the electric fish was of course a great help in this scientific revolution (Sances et al., 1980). Following on from this work, the German physician Emil du Bois Reymond, with the theoretical help of Hermann von Helmholtz, went on to develop methods of extracellular electrical recording and stimulation, which he used to discover the action potential in 1848 (du Bois Reymond, 1848). His work essentially founded experimental neuroscience in general and electrophysiology in particular. By the late 1890s neurosurgeons, neurologists, and neurophysiologist were using these new electrophysiological methods to study changes in the flow of electrical potentials in the nervous system by stimulating and recording from nerve tracts. Julius Bernstein, a student of du Bois Reymond and Helmholtz succeeded in 1868 to record the time course of action potentials with sub millisecond resolution (Bernstein, 1868; reviewed in Schuetze, 1983) and later in his life developed the theory of the equilibrium membrane potential of neurons generated by separation of ionic charges by the cell membrane (Bernstein, 1902).

Perhaps the most important work during this time was by the early Oxford neuroscientists Sir Victor Horsley and Francis Gotch in the 1890s (Gotch and Horsley, 1891). Horsley and Gotch used *in vivo* extracellular field recording and stimulation to identify the locus of epileptic seizures in humans. They were among the early explorers of functional specialization and lateralization of the brain some 50 years before Penfield's systematic study of the homunculus (Penfield and Boldrey, 1937). In relation to synaptic plasticity, they stimulated the cerebral cortex and recorded in the spinal cord and sciatic nerve of cats and monkeys while also monitoring changes in muscle contraction. "*. . .the dura mater was exposed at the level of the motor area of the lower limb; the spinal cord*

was then exposed at the level of about the 7th dorsal vertebra; raised in air and connected to the non-polarized electrodes. . .These results indicate (1) that the rise in the (potential) *difference is occasioned not merely by direct application of the stimulating agent to the cord, but as a consequence of the presence of a series of excitatory processes, whether these are produced by nerve impulses entering below by afferent channels, or from above by cortical efferent ones. . ..(2) They also show that the rise is least in the case of the excitatory cord changes evoked by cortical stimulation, in which case the limit of rise is not only small, but soon attained, . . . when the columns of the cord itself are excited, the rise is greater, . . . It would thus appear that one of the main features in the rise is the extent to which the nerve structure of the cord are thrown into activity. . .*" (Gotch and Horsley, 1891). Their records on woodcuts actually show initial facilitation followed by depression of the evoked local field potentials.

The German neuroanatomist von Waldeyer-Hartz (1891) among others lay down the neuron doctrine – the idea that the brain is a system composed of separate neurons. At the same time, the documentation of neuronal composition of the brain began with the work of the Spanish physician-turned-neuroanatomist Santiago Ramón y Cajal (**Figure 3**) and the Italian pathologist Camillo Golgi. Ramón y Cajal (1894) had also proposed that long-term memories do not need new neurons, but rather the *growth of new connections* between existing neurons. The *junction between neurons* only became known as a "*synapse*" at the turn of the century after Sir Charles Sherrington declared that the "*tip of a twig of the arborescence is not continuous, but merely in contact with the substance of the dendrite or cell-body on which it impinges*" and that "*Such a special connection of one nerve cell with another might be called a 'synapsis'* " (Sherrington, 1897, 1909).

Yet Sherrington did not speculate on the possible relation between synaptic plasticity and learning. Tanzi (1893), an Italian neuropsychiatrist put forward the very first hypothesis that associative memories and practice-dependent motor skills may depend on a localized facilitation of transmission of *already existing connections* some 4 years before Sherrington coined the term "synapsis." Tanzi and his disciple Ernesto Lugaro clearly admired Ramón y Cajal and his ideas of the nervous system as an aggregate of neurons separated by small distances. Influenced by Ramón y Cajal's ideas of *neurotropism*, they hypothesized that nervous excitation must encounter some difficulty in crossing this space between neurons and that repetitive activity of the neuronal path (such as during learning of a specific task) would lead to hypertrophy of the neurons and thus facilitate easier crossing of the space between them (Tanzi, 1893). Lugaro (1898, 1906, 1909) expanded on this view, combining it with his new insight on chemical neurotransmission which attempts to explain how nerves find their targets via gradients of diffusible messengers. He also argued that coincident activity drives modifications of connections between neurons and used familiar and modern-sounding terminology such as "The plasticity of the nervous elements" ("La plasticità degli elementi nervosi cerebrali") and "plastic activity of neurons" ("attività plastica dei neuroni"). Lugaro was thus the first to coin the term *plasticity* to synaptic modification (Lugaro, 1898, 1906, 1909).

FIGURE 3 | Santiago Ramón y Cajal Source: Wikimedia Commons, public domain.

By the end of the nineteenth century, it was widely believed that information flow must change in the brain for learning and memory to occur, that synapses control the flow of information, that they are the neural substrate of learning and memory, and that learning requires repeated and persistent activation without competing inputs, and that it is the temporal organization of events that determines the strength of associations – the glue to build memories.

PLASTICITY IN THE EARLY TWENTIETH CENTURY

The first half of the twentieth century witnessed a number of landmark studies that had a great influence on our views of chemical synapses, neurotransmitters, neuronal processing, direction of information flow in neurons, learning, memory, and behavior. First, the notion of chemical synapses became well defined, building on the nineteenth century work of Claude Bernard, by contributions from many great scientists such as Langley, Elliot,

Dale, Loewi, Feldberg, and Brown (for a review, see Bennett, 2000). Chemical synapses were more attractive for learning and memory processes than electrical synapses because they impose a sense of direction to the flow of information in the brain. The actual direction however was a topic of rather intense debate until the 1930s. Ramón y Cajal (1911) was preoccupied with the direction of flow of information between neurons, which he emphasized using artistic arrows in his many drawings, although Cajal's arrows sometimes pointed in the wrong direction.

While these neural principles were laid down, Karl Lashley was literally trying to cut out memories from the brain. His failure to find "the engram" led to the important conclusion that memory – and brain function in general – depends on "*mass functioning of many neurons.*" (Lashley, 1929). In the 1930s, the Canadian neurosurgeon Wilder Penfield – who was greatly inspired by Sherrington – developed the Montréal procedure for treating patients with intractable epilepsy by destroying pathological tissue. By locally stimulating the brain of awake patients to ascertain the origin of the seizure, he could excise the epileptogenic area while at the same time preserving healthy brain tissue. This technique also permitted the creation of maps of the sensory and motor cortices of the brain, known as the cortical homunculus, a view that counter balanced Locke's *tabula rasa* vision of the brain. Penfield thus contributed greatly to our understanding of localization and lateralization in the brain (Penfield and Boldrey, 1937). This was also around the time that John Watson, the founder of behaviorism, proposed that negative associations could just as easily replace positive ones, through his famous but ethically questionable experiments on *Little Albert*. With this young boy, he demonstrated that a previously rewarding conditioning stimulus (playing with a white rat) could easily become negatively associated (by a loud noise). Watson thus went to the extreme end of the nature-versus-nurture argument and claimed that the environment can create any personality (Watson and Rayner, 1920). Experiments such as the one on *Little Albert* reinforced the notion that the brain begins as a clean-slate – a *tabula rasa* – on which experience shapes the individual. The clean-slate hypothesis is central to synaptic plasticity as it implies that the connectivity and strength of synaptic connections are entirely shaped by experience. In other words, circuits have full freedom to reconfigure and existing synapses are unrestricted with respect to change following experience.

Later, Burrhus Skinner argued that classical conditioning was not sufficient to explain all habits, traits, and tendencies, and instead developed operant conditioning. This denotes the formation of an association with an event that is accidentally found to have a positive behavioral outcome, similar to what is today commonly known as trial-and-error learning (Skinner, 1938).

By the 1930s, it had become clear that information flowed from presynaptic axons to postsynaptic dendrites, that all inputs were integrated at the soma, and that – once the threshold for action potential generation was reached – the information propagated along the axon of the postsynaptic cell. Sir John Eccles, a student of Sherrington's, was perhaps the first to speculate that once an action potential is generated and propagates down the axon, it would also be momentarily reflected back into the dendrites (Eccles and Sherrington, 1931).

The work of Rafael Lorente de Nó, a student of Cajal's, however put forward the winning notion of the time that "*The only possibility for... [a neuron]... using all the impulses seems to be, first, that each synapse sets only a subliminal (chemical or other) change able of summation and, second, that the conduction through the synapses is not followed by a refractory period. The subliminal changes are summated first in the dendrites then the surrounding of the axon. When the change reaches threshold value, an explosive discharge through the axon takes place. . .The axon... enters in a refractory state, but the cell body and dendrites do not do so, they continue receiving and adding subliminal changes until the threshold value is reached again and the axon has recovered....*" (Lorente de Nó, 1934). Lorente de Nó also went on to develop the early concepts of neural network function with the concepts of recurrent chains of neurons in which activity would reverberate persistently without leaving. His work influenced his Chinese student Feng (1941) to produce some of the early twentieth century records of synaptic facilitation, which also sparked the early neural network theories by cybernetician Warren McCulloch and logician Walter Pitts (McCullogh and Pitts, 1943). It was these early recurrent network ideas that created the notion of "infinite loops within loops" – once information enters a neural system it may persistently reverberate and not easily leave.

The next leap in synaptic plasticity was made in the discoveries of synaptic changes that lasted for several minutes after the tetanic stimulus was over. Post-tetanic potentiation seemed to have been discovered in the early part of the twentieth century by the American neurophysiologist and behaviorist, Ralf Gerard (1930). Other important early works in the 1940s included those of Lloyd (1949) and Larrabee and Bronk (1947). "*It is our purpose to describe certain observations which reveal long-lasting effects of nervous activity that increase the stimulating action of nerve impulses at a synapse. The transient effects of an electric stimulus and the brief duration of a nerve impulse have emphasized the role of rapidly occurring events in the nervous system. On the other hand, physiological and psychological observations reveal many phenomena, which must be due to long persistent effects of nerve impulses within the central nervous system. Among these are the after-effects which continue for many minutes following a visual stimulus. . ., the sensory effects of intense mechanical vibrations which may continue for days, and the process of learning. These are among the obscure and challenging problems of neurology. It is probable that such phenomena are due to long-lasting changes in the properties of neurones and of synapses caused by previous activity.*" (Larrabee and Bronk, 1947).

Inspired by Pavlov's work, Gerard also restated a long-held understanding from empiricist psychology that "*in the course of establishing a conditioned reflex, a particular afferent system comes to exercise control over an efferent one upon which it normally has no action. In neurological terms, this means that two brain centers become able to interact physiologically as a consequence of having been repeatedly set into action together. . .On the other hand, it has long been known (Ralf Gerard, 1930), though often overlooked, that a few seconds tetanus may leave, even in nerve, considerable after-potentials which actually increase in magnitude during three or four minutes and endure for over fifteen.*" (Gerard, 1949). Gerard (1949) realized the importance of these "after-effects" of an action potential for learning, memory and behavior. He noted, "*What occurs*

at a given synapse can be highly variable. . .It is not over when an impulse flashes across a synapse and onto its destination. It leaves behind ripples in the state of the system. The fate of a later impulse can thus be at least a little influenced by the past history of the neurones involves, by what happened before – and when. So we begin to get some increased freedom in accounting for behavior." (Gerard, 1949).

By the end of the first half of the twentieth century, the pieces were in place for an early unification of ideas and a comprehensive theory of learning and memory based on synaptic plasticity. Long-lasting changes in synaptic efficacy were widely speculated upon, speculations that were fuelled by these early discoveries of short-term plasticity and post-tetanic potentiation.

HEBBIAN PLASTICITY AND ASSEMBLIES

The Canadian neuropsychologist Donald Hebb (**Figure 4**) – who was a student of Wilder Penfield as well as of Karl Lashley – made considerable headway at developing the concept of the distributed location of memory. In his book "*The Organization of Behavior*," Hebb brought together many of the earlier ideas and findings on plasticity and learning and memory in a tremendously influential formal postulate of the neural mechanisms of learning and memory (Hebb, 1949), although Hebb himself later claimed that he "was not proposing anything new" (Berlucchi and Buchtel, 2009). Memories could be stored if the connections that repeatedly drive activity in a cell become strengthened because this would couple specific groups of neurons together and explain how neurons could be molded together in an assembly as a function of past experience. "*Let us assume that the persistence or repetition of a reverberatory activity (or "trace") tends to induce lasting cellular changes that add to its stability.[. . .] When an axon of cell A is near enough to excite a cell B and repeatedly or persistently takes part in firing it, some growth process or metabolic change takes place in one or both cells such that A's efficiency, as one of the cells firing B, is increased.*" (Hebb, 1949). Even though Hebb explicitly stated that "*The general idea is an old one, that any two cells or systems of cells that are repeatedly active at the same time will tend to become "associated," so that activity in one facilitates activity in the other*" (Hebb, 1949), strengthening of connections between co-active cells has become known as *Hebbian plasticity* and the resulting groups of cells joined together through this form of plasticity even today go under the moniker of *Hebbian assemblies* (**Figure 5**).

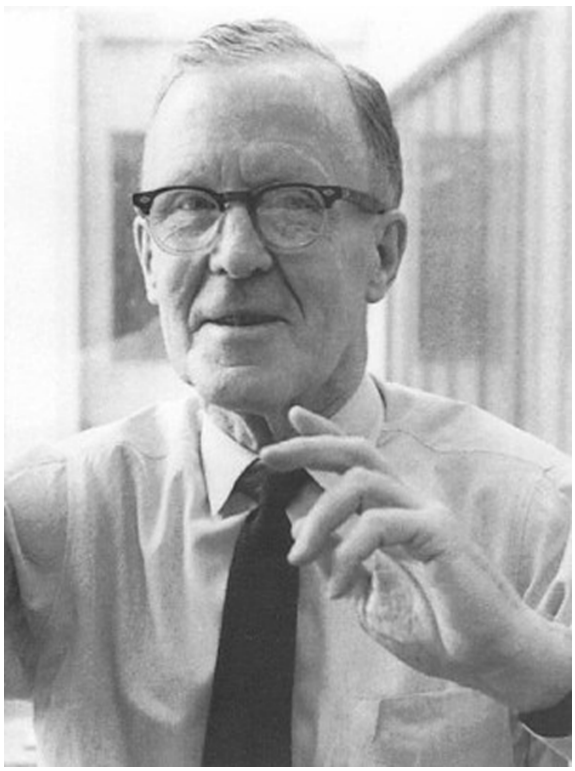

FIGURE 4 | Donald Hebb.

Hebb considered these assemblies as representing percepts and the basis of thought. Key to this notion is the need for closed-loop circuits and re-entrant paths in the brain, thus leading to reverberating activity being held for some period of time by the circuit. In this view, this reverberating activity represents the environmental event that triggered it, and these re-entrant closed-loop circuits are wired up in the first place by the very processes of perceptual learning that Hebb proposed in his famed postulate. But it is key that this system can also be intrinsically excited in the brain in the absence of the sensory stimulus that originally helped organize it. As Hebb put it, "*You need not have an elephant present to think about elephants*" (Hebb, 1972). Hebb also went further to propose that assemblies are linked in chains to create a phase sequence, which he considered the neural basis of the thought process, via chains of percepts. The notion of phase sequences is perhaps not entirely clear, but one key element seems to be the idea that the same cells and assemblies can partake in several different percepts depending on which cells and assemblies are co-active as well as on which fired before and which fire after. Different phase sequences may thus represent different thought processes, and the same cells may be part of different thought processes via different phase sequences. What is clear is that a temporal ordering of activity in cells is central to the phase sequence in Hebbian assemblies (Hebb, 1949, 1972).

The idea that memories were held in cell assemblies was actually proposed before Hebb. For example, Joseph Edgar DeCamp stated

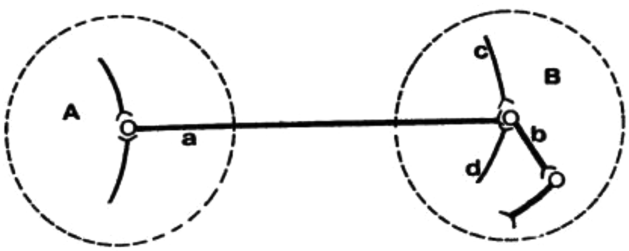

FIGURE 5 | An illustration of the Hebbian postulate and a small assembly of cells. Here, presynaptic cell a, along with afferents c and d, repeatedly and persistently drive the postsynaptic cell b, thus leading to a long-term increase in the connective strength between cells a and b (reprinted with permission from Hebb, 1972).

that "*From the neurological standpoint, in the learning of a series of syllables, we may assume that a certain group of synapses, nerve-cells, nerve paths, centres, etc., are involved. Immediately after the learning process that after-discharge continues for a short time, tending to set the associations between the just learned syllables.*" (DeCamp, 1915). Hebb's comprehensive unification of the many previous ideas was particularly important, because it laid the foundation for subsequent generations to build upon.

One year before Hebb published his 1949 book, the Polish neurophysiologist Konorski (1948) had already published remarkably similar ideas on synaptic plasticity and its relation to learning. In his book, Konorski aimed to show that morphological changes in neuronal synaptic connections are the substrate of learning (Zielinski, 2006). In other words, he argued against the view that the formation of new connections was important, and instead emphasized the role of changes in already existing pathways that were for some reason not already in use. Coincident activation of neuronal centers should lead to the formation of actual excitatory pathways between them, based on pre-existing potential connections, argued Konorski. But Konorski also conceived of a key role for inhibition in such processes: When the receiving neuronal center became less active after activation of the transmitting center, inhibitory connections are enabled. Either way, Konorski explicitly pointed out the role of repetition and repetition intervals in these processes. Interestingly, Konorski also proposed the existence of what we now jokingly refer to as grandmother cells, although he termed them "gnostic units," thus predicting the existence of e.g., neurons that respond to particular faces (Quiroga et al., 2005).

Although Jerzy Konorski's ideas sprung from those of Ivan Pavlov, they were not entirely in agreement. This posed a problem in the Communist East – Pavlov was religiously held in high esteem both in the Soviet Union and in Poland. Konorski thus found himself as well as his work being suppressed for political reasons. For more than a decade after and around the publication of his book, he became relatively isolated from the West, and the impact of his work was probably not as great in the West as it should have been. Researchers such as Hebb, Adrian, and Eccles, however, in all likelihood fully appreciated the importance of his proposals at a very early stage (Zielinski, 2006). Today, some researchers prefer to speak of Hebb–Konorski plasticity (e.g., Lamprecht and LeDoux, 2004), although the concept of Hebbian plasticity is clearly in wider use.

In the early 1990s, Carla Shatz (1992) summarized the Hebbian postulate as "*cells that fire together wire together*" to inputs in the visual system that strengthen together if they are active at the same time as the postsynaptic cell, thus leading to ocular dominance column formation in early development due to retinal waves. This Hebbian slogan caught on and is now in wide colloquial use in the field. It is important to note, however, that if interpreted superficially, this slogan does not reflect all of what Hebb meant, because, strictly speaking, Hebb's rule is directional: cell A helps fire cell B. In addition, provided that they are persistently co-active, Hebb suggested the possible formation of assemblies of any neurons, even previously unconnected ones: "*When one cell repeatedly assists in firing another, the axon of the first cell develops synaptic knobs (or enlarges them if they already exist). . .*" (Hebb, 1949). How a neuron assists the firing of target neuron that it is not connected was supposedly via the activation of other neurons that were connected to that neuron.

Nevertheless, in synaptically coupled assemblies of neurons, future stimulation of even a few of the members of the group would tend to reactivate the entire assembly of neurons, thus recreating the activity state that represented past experience and recalling a memory of the past event. The Hebbian principle was not only catchy because of its clear-cut and experimentally testable formulation; it also rendered synaptic plasticity immediately and intuitively meaningful by positioning it in the context of neuronal assemblies. Hebb's postulate was also particularly powerful because it gave a possible neural explanation to two notions held by early philosophers and psychologists: that information enters the brain and reverberates, thus leaving persistent traces; and that information flow in the brain must change for learning and memory to occur (Hebb, 1949).

The Hebbian principle is fundamentally a causal selection principle based on rewarding synapses for successfully driving a postsynaptic neuron. It was therefore also a natural neural mechanism for association of simultaneous and sequential perceptual events, speculated for over a century (see above). Between 1950 and 1967, Hebb's ideas spurred a plethora of studies by Shimbel, Brindley, Eccels, Ito, and Szentagothai, to mention but a few, who attempted to explain how synaptic plasticity could account for Pavlov and Watson's classical conditioning as well as for Skinner's operant conditioning.

In 1964, Eric Kandel and Ladislav Tauc showed that pairing an EPSP with a conditioning stimulus in the giant marine snail *Aplysia* caused a long-lasting facilitation of the EPSP (Kandel and Tauc, 1964). More importantly, Kandel's work strongly linked synaptic plasticity with behavioral associative learning of the gill withdrawal reflex in *Aplysia.* Because the presumed link between synaptic plasticity and information storage in the mammalian brain has not yet been established (Stevens, 1998; Sjöström et al., 2008), the importance of Kandel's (2001) research on learning in *Aplysia* is difficult to overstate. Presently, the molecular, biophysical and cellular mechanisms that underlie behavioral learning in *Aplysia* are known in great detail. Although this form of plasticity is not Hebbian, the firm evidence for a role of synaptic plasticity in learning in the marine snail – literally ranging all the way from molecules to memory – thus forms a solid foundation for on-going plasticity and memory research in mammals, where the role of synaptic plasticity in memory storage remains to be formally proven (Stevens, 1998). It should be pointed out, however that in mammals tremendous progress has been made in linking fear conditioning to synaptic plasticity in the amygdala (Maren and Fanselow, 1996; Rodrigues et al., 2004; Maren, 2005).

Approximately two decades after Hebb published his postulate, Terje Lømo (**Figure 6**) presented his work from Per Andersen's laboratory at a conference of the Scandinavian Physiological Society, showing that high-frequency electrical stimulation in the dentate gyrus of the rabbit hippocampus elicited responses that kept growing (Lømo, 1964; Bliss and Lømo, 1970, 1973). Tim Bliss joined the Andersen group in 1968 and showed together with Lømo that the condition for persistent growth of response amplitude was the

FIGURE 6 | Tim Bliss, Per Andersen, Terje Lømo.

high-frequency stimulation itself (Lømo, 1964; Bliss and Lømo, 1970, 1973). While tetanic stimulation was already used for about 100 years, Bliss and Lømo's study was the first to demonstrate that the effects could last much longer than short-term facilitation or post-tetanic potentiation. These findings lent experimental support to Hebb's hypothesis that synapses are strengthened if they are involved in successfully driving a cell, since sufficiently strong high-frequency stimulation of afferent fibers could reasonably be assumed to drive activity in postsynaptic cells.

STRENGTHENING AND WEAKENING IN THEORY

Hebb's learning rule did not provide for an active mechanism to weaken synapses – he proposed that synapses would weaken if they were unused and that "*less strongly established memories would* gradually *disappear unless reinforced*" through a slow "*synaptic decay.*" (Hebb, 1949). His book spurred intense debate in the theoretical community whether memory can be stored in cell assemblies. In 1956, a group in IBM research labs including Rochester, Holland, Haibt, and Duda tested the formation of Hebbian cell assemblies in a simulation on one of the biggest computers at the time. They realized that a standard Hebb rule does not work and proposed a variant of Hebbian learning that essentially amounts to a co-variance learning rule, combined with an additional feature of weight normalization so that during learning the total sum of all synaptic weights onto the same postsynaptic neuron remains constant, a feature used later in many studies of cortical map formation and unsupervised learning. In their paper they review the ideas of Hebbian learning and stated: "*It is evident that the mechanism that Hebb postulated would tend to cause recollections. The question of whether or not the postulate is sufficient is, in a sense, the main topic of this paper. If no additional rule were made, the Hebb postulate would cause synapse values to rise without bound. Therefore, an additional rule was established: The sum of the synapse values should remain constant. This meant that, if a synapse was used by one neuron to help cause another to fire, the synapse would grow. On the other hand, if a synapse was not used effectively, it would degenerate and become even less effective, because active synapses would grow and then, to obey the rule about a constant sum of magnitudes, all synapses would be reduced slightly, so the inactive synapses would decrease.*" (Rochester et al., 1956). This study thus postulated the existence of heterosynaptic weakening via a competitive mechanism, based on two important insights: the co-variance learning rule in combination with overall weight normalization. In order to measure whether a synapse was effective in driving the postsynaptic neuron, the authors introduced local variables $x - \bar{x}$ where x is the presynaptic activity and $\bar{x}$ its average, and analogously $y - \bar{y}$ for postsynaptic activity. The co-variance rule was implemented by calculating $\frac{(x-\bar{x})(y-\bar{y})}{\mathrm{std}(x-\bar{x})\mathrm{std}(y-\bar{y})}$ where std is the standard deviation (Rochester et al., 1956).

An early lasting mathematical formulation inspired by Hebb and his followers, was made by Frank Rosenblatt at Cornell University in his famous notion of the brain as a perceptron learning machine. Rosenblatt, influenced by many aspects of the brain's plasticity and the early reports on the trillions of synapses in the human brain, was the first to introduce the concept of the "bivalent system" to "reward and punish" synaptic connections by making them stronger or weaker. He proposed a multi-layer perceptron where neurons in the middle layer, called A-units, received fixed random connections from the input layer. The projections from the A-units to the output were plastic. The output layer had a winner-takes-all connectivity, so that only one output was active at a time. He proposed a learning rule that would apply to all synapses from a given A-unit that had a connection to the active output. Hence, this rule was not Hebbian, as it would also apply to another connection from the same A-unit to an inactive output. His first rule distinguishes between two cases: active A-units with a projection to the active output and inactive A-units with a projection to the active output. In the main part of the paper, he studies unsupervised learning, but toward the end of the paper he continues: "*In all of the systems analyzed up to this point, the increments of value gained by an active A-unit, as a result of reinforcement or experience, have always been positive, in the sense that an active unit has always gained in its power to activate the responses to which it is connected. In the gamma-system, it is true that some units lose value, but these are always the inactive units, the active ones gaining in proportion to their rate of activity. In a bivalent system, two types of reinforcement are possible (positive and negative), and an active unit may either gain or lose in value, depending on the momentary state of affairs in the system. If the positive and negative reinforcement can be controlled by the application of external stimuli, they become essentially equivalent to "reward" and "punishment," and can be used in this sense by the experimenter. Under these conditions, a perceptron appears to be capable of trial-and-error learning.*" (Rosenblatt, 1958).

Strengthening and weakening synaptic connections by the degree of their causality became a topic of debate in the mid 1960s. Some predicted that cerebellar parallel fiber inputs should strengthen when activated simultaneously with climbing fibers, whereas others argued that they should weaken: Brindley (1964), Marr (1969), and Grossberg (1969) voted in favor of potentiation, while Albus (1971) argued for depression. Although Marr (1971) erroneously favored potentiation, he was one of the first mathematicians to nevertheless claim that he could use Hebb's rules to explain how the neocortex, cerebellum, and hippocampus operate.

A few years later, Gunter Stent tried to explain the loss of connections suggested by Hubel and Wiesel's monocular deprivation experiments (Hubel and Wiesel, 1965; Wiesel and Hubel, 1965), by postulating the inverse to Hebbian learning (Stent, 1973). Stent proposed that "*When the presynaptic axon of cell A repeatedly and persistently fails to excite the postsynaptic cell B while cell B is firing under the influence of other presynaptic axons, metabolic change takes place in one or both cells such that A's efficiency, as one of the cells firing B, is decreased.*" Stent also proposed a learning rule for inhibitory connections, whereby the failure of an inhibitory input to silence the postsynaptic cell would elicit weakening of that input, thus working in synergy with Hebbian excitatory inputs. This formulation is in fact precisely what Konorski conjectured regarding inhibitory plasticity more than two decades earlier (see above), except that Stent formulated his inhibitory learning rule the other way around. Von der Malsburg (1973) also implemented bidirectional plasticity, but indirectly by normalizing the changes induced by long-term potentiation (LTP). The concepts of Stent and von der Malsburg revived the nineteenth century views that intensity and competition was an important consideration in the decision to change a synapse.

In an attempt to explain ocular dominance column development and eye suture experiments carried out in the 1970s, Elie Bienenstock, Leon Cooper, and Paul Munro, unified the earlier key discoveries and developed a mathematical model whereby low-frequency activity of the postsynaptic neuron during presynaptic stimulation would lead to long-term depression (LTD) while high-frequency activity would lead to LTP with a variable frequency threshold marking the transition between the two. The model became known as the BCM learning rule (Bienenstock et al., 1982; also see Cooper, 2010). This was a landmark in the history of the theory of plasticity not only because of the computational power of the model, but also because it gave convincing theoretical arguments for the existence of a new form of plasticity: homosynaptic LTD. In this form of plasticity, synapses are depressed not because they are inactive during a competing input, nor because they are co-active with the wrong input, as in the cerebellum. Rather, in classical homosynaptic LTD, it is a specific frequency requirement that determines plasticity. Temporal order however plays little or no role. In addition, the BCM rule introduces key concepts in cellular learning rules, such as competition among inputs and metaplasticity. Metaplasticity – which denotes "the plasticity of plasticity" (Abraham and Bear, 1996) – ensures both a degree of stability in neurons and competition.

DENDRITES AND PLASTICITY

The period shortly after the publication of Hebb's book was also an important time for synaptic and dendritic integration and neuronal computation. Sir John Eccles, another luminary student of Sherrington's, carried out extensive studies on short-term plasticity until the 1960s (see Eccles et al., 1941; Eccles, 1946, 1964). Eccles (1964) felt that "*[u]nder natural conditions synapses are activated by trains of impulses that may be of relatively high frequency...It is therefore imperative to study the operation of synapses during repetitive activation.*" Sir Bernard Katz (**Figure 7**), a student of Eccles, took the study of short-term plasticity in a statistical direction to better understand its mechanisms (Del Castillo and Katz, 1954), which gave rise to the quantal hypothesis of neurotransmitter release. The quantal hypothesis became important for later synaptic plasticity studies because it provided a means to dissect the pre versus postsynaptic mechanism underlying synaptic plasticity.

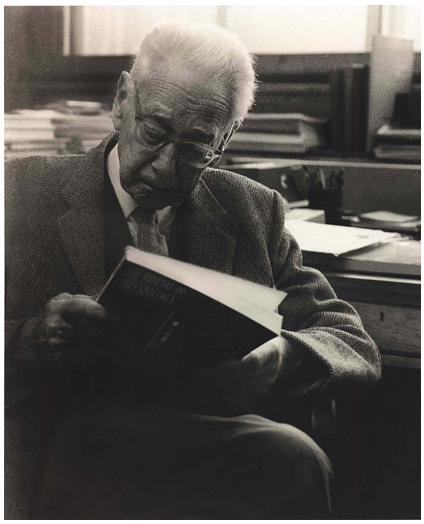

FIGURE 7 | Sir Bernard Katz.

Though a visionary of the dynamics of synaptic transmission, Eccles discarded the notion that dendrites are relevant for the integration of synaptic input (Eccles, 1960). A student of Eccles, Wilfred Rall disagreed and developed – in spite of many years of disagreement with Eccles – a comprehensive mathematical theory of how synaptic potentials are summated in the dendrites of a neuron, thereby giving rise to its axonal spiking output (Rall, 1955, 1957, 1959, 1960, 1962). The field of synaptic integration and dendritic computation had thus finally begun. Surprisingly, this field was to develop quite separately from the field of synaptic plasticity for many years, even though Rall and Rinzel (1971) did propose early on that changing spine neck resistance could alter synaptic weight. Similarly, Bliss and Lømo (1973) argued that alterations in spine structure could underlie LTP through the reduction of spine resistance. The idea that the back-propagating action potential has a role as an arbiter of causality in synaptic plasticity, however, required many more years to emerge (see below).

CLASSICAL LTP AND LTD

The excitement arising from the discovery of hippocampal plasticity triggered a veritable avalanche of studies. Douglas and Goddard (1975) showed that repeated high-frequency bursts were more effective in inducing LTP than a single long tetanic train. This was an important landmark in the history of synaptic plasticity, not only because repeated brief bursts became a popular protocol to induce LTP, but also because it demonstrated the importance of repeated and persistent *periods* of stimulation to induce LTP, which was predicted in the nineteenth century and elaborated by Hebb. Douglas and Goddard also named the phenomenon LTP at

the suggestion of Per Andersen (Douglas and Goddard, 1975). A flood of experimental and theoretical studies followed in a race to test different aspects of Hebb's postulate and to tease apart the underlying cellular, synaptic, and network mechanisms (Malenka, 2003). Much of this race was dominated by disputes over the pre or postsynaptic locus of the change, only to be settled by the fact that synapses can change in many ways, either pre or postsynaptically, or both (for a review, see Malenka and Nicoll, 1999).

Bruce McNaughton made the next landmark discovery that supported Hebb's associative principle, when he experimentally tested James' "law of association" and Hebb's associative learning postulate. He showed that two weakly activated pathways, which would not succeed on their own to induce LTP after tetanic stimulation, could indeed cooperate to induce LTP in both their connections (McNaughton et al., 1978; McNaughton, 2003). This was central to Hebb's hypothesis for associative memories where components of a memory can reinforce other components and even other related memories. This was a landmark study because it revealed a neural substrate for classical conditioning that had already become the bedrock of psychology. The same year, Baranyi and Feher (1978) found that pairing EPSPs recorded intracellularly with antidromic action potentials could trigger conditioned facilitation. They concluded that discharge of the postsynaptic action potential alone, without necessarily being triggered by synaptic input was important in the induction of the potentiation (Baranyi and Feher, 1978).

Gary Lynch and colleagues discovered LTD in the hippocampus around this time. They found that, while tetanic stimulation induced LTP of the activated pathway, the inactive pathway underwent LTD (Lynch et al., 1977). Moreover homosynaptic LTD was found to occur at the activated pathway provided that the activation frequency was low (Dunwiddie and Lynch, 1978). In psychological terms, this phenomenon may be seen as a neural correlate for passive extinction of memories, but is also reminiscent of James' view that there should be no competition among pathways that carry different information.

William Levy and Oswald Steward soon after explored the effect on a weak pathway (contralateral entorhinal to dentate pathway) in the hippocampus that was not capable of LTP on its own, but only when combined with a strong pathway (ipsilateral). They also found LTD in the inactive pathway following potentiation of another pathway (as found by Lynch), but additionally found that the potentiated weak pathway could be depotentiated if tetanized on its own afterward (Levy and Steward, 1979) – a phenomenon that has since become known as "depotentiation." Thus any future activity of the weak pathway without the conditioned stimulus would lead to depotentiation. The subsequent year, it was discovered that low-frequency stimulation of a potentiated pathway also induced depotentiation (Barrionuevo et al., 1980), thus emphasizing the extinction of a newly associated pathway that is weakly active or weakly synchronous with the conditioning pathway.

In contrast to what Brindley (1964), Marr (1969), and Grossberg (1969) postulated in the late 1960s (see above), Ito et al. (1982) found heterosynaptic LTD of the parallel fibers in the cerebellum caused when the climbing fibers where simultaneously activated. In this form of LTD, the synapses were active at the time that a conditioning stimulus was being applied, the inverse of Hebbian associative LTP as shown by McNaughton. This inverse of LTP was elegantly consistent with the growing notion that the parallel fibers carry an error, which must decrease during learning and was thus also consistent with notions of classical conditioning. It should be noted, however, that this form of plasticity is neither Hebbian nor classical STDP.

In 1988, Yves Frégnac et al reported a cellular analog of visual cortex plasticity *in vivo* (Frégnac et al., 1988). They found that by repeated pairing of visual stimulation with direct positive or negative iontophoretic stimulation of a cortical neuron, they could often restructure the functional preference of the cell in question in a manner consistent with Hebb's postulate. The experimenter could thus alter a cell's receptive field in a form of supervised learning paradigm, interestingly even in the mature brain. This study also provided some of the first results consistent with the existence of homosynaptic LTD in neocortex.

The discovery of homosynaptic LTD has been reported in many studies (e.g., Dunwiddie and Lynch, 1978; Bramham and Srebro, 1987; Frégnac et al., 1988), but is typically attributed to two studies, one by Serena Dudek and Mark Bear and the other by Rosel Mulkey and Robert Malenka, both conducted in the hippocampus (Dudek and Bear, 1992; Mulkey and Malenka, 1992). These teams used long periods of precisely timed low-frequency stimulation to achieve depression, an approach that is perhaps biologically implausible (see e.g., Perrett et al., 2001). Nevertheless, this particular induction protocol became a major LTD paradigm for years to come and is still in use, probably because it is quite reliable. In general, the problem of extracellular stimulation would haunt the search for true homosynaptic plasticity for some time, since extracellular stimulation potentially activates heterogeneous inputs and possibly even neuromodulatory fibers (see Bear, 1999).

The early 1980s was also the time when the molecular substrate for associative plasticity was discovered in the unique properties of the NMDA receptor. This remarkable receptor only opens to allow a calcium influx after the presynaptic terminal has released glutamate and the postsynaptic membrane has been depolarized (Collingridge et al., 1983; Harris et al., 1984; Wigström and Gustafsson, 1984; Slater et al., 1985) but not with either condition alone – an elegant molecular coincidence detector.

THEORETICAL ASSOCIATIONS

The German engineer Karl Steinbuch showed in (Steinbuch et al., 1965) that a Hebbian learning rule is useful for forming associations between inputs and outputs, a scenario that was later termed a hetero-associative memory. In his model system, learning happens at the "synaptic" connection points between a set of parallel input wires (transporting a binary coded pattern of input features representing the stimulus) and output wires (the pattern index of "meaning") running orthogonally to the inputs. The learning rule he uses is motivated by conditioned reflexes between stimulus and response and is essentially Hebbian in nature. At the crossing point between an input line j carrying a binary signal x_j and an output line i with binary signal y_i, the synapse measures the correlation, $c_{ij} = y_i(2x_j - 1)$, between pre and postsynaptic signals. The correlation c_{ij} takes a value of $+1$ if both input and outputs are

active; it is −1 if the input is inactive, but the output active; and zero if the output is inactive. The correlation is summed over T time steps, and the connection is increased if the result passes a threshold. The up and down regulation of the correlation signal during the summation time in combination with the threshold process assures that spurious correlations do not lead to a change of the synapse, but only consistent associations between inputs and outputs. As an electrical engineer, Karl Steinbuch even proposed a possible implementation of such a Hebbian rule by a physical system built from contact points between silver and silver bromide – and thereby constructed the first associative learning memory system, essentially a correlation memory system. In 1965, Steinbuch was granted a patent for his concept learning machine (Steinbuch et al., 1965), which states:

"*An electrical circuit arrangement is provided in which combinations of input information signals . . . are assigned to corresponding output meanings. Input and output leads are arranged in a matrix of column wires and row wires. A device at each crossing point or intersection of a column wire and a row wire is arranged to be altered to change its condition by means of currents flowing simultaneously in both these wires. The marking of a row wire by a current flowing therein however can only effect the change of condition of such a device upon repeated current signals being applied to its associated column wire while current is still flowing in the row wire. This repeated action with respect to intersections of the matrix is referred to hereinafter as the learning phase.*"

The work of Steinbuch inspired Teuvo Kohonen, who cites Steinbuch in his article on correlation matrix memories (Kohonen, 1972). In his paper, which appeared at the same time as a similar study by Anderson (1972), Kohonen gives an elegant mathematical analysis of the properties of such a matrix memory system. Despite the abstract mathematical formulation, the biological inspiration of these studies is clear in both papers.

Other early models of associative memories around this time, such as that by Willshaw et al. (1969) formulated how a network of neurons could learn to associate a particular activity pattern involving a subset of neurons with one out of many other types of patterns. This would require a learning rule where synapses change during coincident activity in connected pairs of neurons, much like what Hebb suggested.

Also, in 1973, Leon Cooper proposed that, "*for such modifications to occur, there must be a means of communication between the cell body and the dendrite ends in order that the information be available at the appropriate connections; this information must move in a direction opposite to the flow of electrical signals.*" (Cooper, 1973). While Cooper did not emphasize that the back-propagating action potential could carry this information back into the dendrites to all the synapses, he did realize that all the synapses had to somehow be informed about the cell's spiking output (cf. Cooper, 2010).

In all models of hetero-associative memories, the stimulus A is associated with a later response or output Y, but no temporal order is explicitly defined, and temporal asymmetry is thus absent from. Similarly, the Hopfield model for auto-associative memory and pattern completion, where memory items were regarded as static objects (Hopfield, 1982) and the BCM model (Bienenstock et al., 1982) also simplified spike-timing out of the equations. In the Hopfield model, time plays a key role during the retrieval of a stored pattern, since it takes several time steps until the memory pattern is completed and fully retrieved, but time is of no importance during learning. In the BCM formulation, the average firing rate of any synaptic pathway and that of the postsynaptic neuron was important. In neither of these models, however, did the learning rule need precise relative timing of spiking of pre and postsynaptic neurons to trigger LTP or LTD.

TIMING REQUIREMENTS OF LEARNING IN MODELS

As discussed earlier, timing in the sequence and association of events have been considered vital for over a century. How neurons could orchestrate their timing was also extensively considered. For example, Gerard (1949) wrote: "*Another form of interaction is manifested in the synchronized electrical beating of large numbers of neurones. This is widely manifest in neural masses - from the synchronized discharges of the uniformly illuminated retina (Adrian and Matthews, 1928), or the like impulse trains set up from the two respiratory centers and recorded in the phrenic nerves (Gasser and Newcomer, 1921), to the regular alpha rhythm of the human occipital cortex, and the equivalent regular beat of the isolated frog olfactory bulb (Libet and Gerard, 1939). How is this interaction achieved?*" If observations such as these – which hint at neuronal synchrony – are taken at face value, at least two important questions arise. The first one concerns the timescale of neuronal events such as synchrony, coincidence, and causality. In fact, the precision of timing for effective synaptic plasticity perplexed David Marr in the early 1970s. He proposed that the coincidence between the parallel and climbing fiber inputs must be "*about the same time.*" He further clarified this approximate phrasing by saying: "*At about the same time¨ is an intentionally inexact phrase: the period of sensitivity needs to be something like 50-100 msec*" (Marr, 1969), which was around the same interval that the early psychologists proposed.

In 1977, Terry Sejnowski developed the first mathematical model for bidirectional associative synaptic modification driven by the proportion of coincident and anti-coincident spiking activity as part of a proposed competition between the timing of inputs. He called it the "*time-dependent non-linear model*" and proposed that "*. . .the change in synaptic strength is proportional to the covariance between discharges of the parallel and climbing fiber: then the synapses increases in strength when the discharges are positively correlated, decreases in strength when the discharges are negatively correlated, and maintains a constant average strength when the discharges are uncorrelated.*" (Sejnowski, 1977b). Sejnowski went beyond the typically loose phrasing of synchronous activity to precise coincidences of single spikes by proposing that the "*coincidence window for strengthening is 2ms (comparable to the time course of an action potential). . .*" *and about 20 ms for "single anti-coincidences*" (Sejnowski, 1977a,b). However, Sejnowski simplified and reduced the precision of this statement by embedding these temporally precise events as discharge rates in the average membrane potential of his co-variance model. Nevertheless, this model marked the beginning of a movement of theory away from behavioral time scales to those of spiking neurons as a mechanism to judge whether pathways should potentiate or depress.

The second question concerns the organization of sequences of neuronal events in time. Despite the fact that all classical and operant conditioning experiments have an important temporal component, since the response happens after the stimulus, theories like the Rescorla–Wagner theory of conditioning (Rescorla and Wagner, 1972) do not include timing in their mathematical formulae. The reason for this is somewhat unclear. One possible explanation is that timing issues were considered so obvious that it was not necessary to overload the mathematical formalism and, if necessary, the reader would be able to add timing in his or her mind. Similarly, the hetero-associative memories of Steinbuch, Willshaw, Anderson, Kohonen, and others, did not focus on the relative timing of input and output. Regardless, one important distinction between the classical condition and these associative memory models should be pointed out: the timescale on which the former operates is in seconds rather than milliseconds.

In 1976, the German researcher Gerd Willwacher published an article where he considered an extension from instantaneous – or time-less – associations to those with a temporal dimension. He expands on his ideas of Hebbian learning: "*If two neurons are activated at the same time, mutual symmetric links are formed as synaptic connections between them. The intensity of the connection is proportional to the duration and intensity of the synchronous activity. The symmetric connection implies the function of parallel association. In the case of temporally shifted activity of the two units, asymmetric connections will be formed. The asymmetric connections result in a sequential association.*" (Willwacher, 1976).

In 1984, Valentino Braitenberg popularized the concept of asymmetric learning rules in his book "Vehicles" (Braitenberg, 1984), as he introduced the rectifying "Ergotrix" wire to enable his animal-like vehicles to distinguish causal from non-causal relationships. The Hopfield model of the early 80s inspired a large number of physicists to enter the field of theoretical neuroscience. One of the intriguing questions at that time was whether the Hopfield model could be generalized so that it could replay sequences of patterns rather than only static patterns. Similar to the insights of Willwacher, researchers realized that the key was to have asymmetric connections: if in a spatio-temporal sequence neuron j has to fire before i, the connection should be directed from j to i. Andreas Herz and Leo van Hemmen showed that such asymmetric connections could arise naturally, if timing issues and transmission delays are taken correctly into account during Hebbian learning. They also considered generalizations of Hebbian learning, where synchrony was defined not necessarily between the momentary activity of pre- and postsynaptic neurons, but between the postsynaptic spike and a low-pass filtered form of the presynaptic activity (Herz et al., 1988). Neurons in these Hopfield-like networks were binary and did not have any refractory period or intrinsic neuronal dynamics, so that in this approach toward sequence learning in associative memories (Sompolinsky and Kanter, 1986; Herz et al., 1988; Kleinfeld and Sompolinsky, 1988), the time scale was not well defined. Whilst the learning rule lead to asymmetric connections that reflected temporal order, it was formulated in discrete steps of time that could represent anything, from 1 ms to 1 s. Activity of a formal artificial model neuron could thus be interpreted as an episode of high firing rate as well as a single spike – the unit of time was the duration of one memory item.

Until the end of the 1980s, it was common to consider average rates and membrane potentials as measures of activity. In the early 1990s, Misha Tsodyks, Wulfram Gerstner, and others translated associative memory models from firing rates to spiking neurons, both for stationary patterns (Amit and Tsodyks, 1991; Gerstner and van Hemmen, 1992) and for sequences of patterns (Gerstner et al., 1993). In 1993, Gerstner and colleagues proposed that potentiation of synaptic strength can only be triggered if a postsynaptic spike coincides with the EPSP caused by incoming synaptic input and theorized that crucial information for plasticity, necessary for the learning of spatio-temporal spike patterns, would be missed if the usual averaging of firing rates or postsynaptic membrane potentials were considered (Gerstner et al., 1993). This coincidence window was assumed to be in the range of 1 ms. In these models, the time scale of co-activation of pre- and postsynaptic neurons was rationalized by the need for a hypothetical back-propagating spike that had to provide an unknown signal, which had to coincide with neurotransmitter release to elicit potentiation. The model showed only the importance of the causal order of timing of presynaptic activity before the postsynaptic spike in driving potentiation and did not deal with temporally precise conditions for depression.

DEFINING COINCIDENCE IN EXPERIMENTS: IT IS ABOUT TIME

Although the learning of associations clearly requires the introduction of the concept of time, since associations should take place only for events that are coincident in time, surprisingly few early experimental studies directly examined the role of timing in plasticity. In many reports, it was thus not clear what "coincidence" referred to. Was it a matter of minutes, second, milliseconds?

McNaughton et al. (1978) were probably the first to experimentally explore the importance of timing of the postsynaptic spike relative to the input timing in plasticity as part of the "logic" conditions for the association of events. They pointed out that "*the discharge of the postsynaptic cell plays a pivotal role in Hebb's initial postulate. . .*" and attempted various methods to block the discharge of postsynaptic neurons during the tetanic stimulation by activating recurrent inhibition 20–50 ms before the tetanic stimulation. At that time, the only way to confirm that the postsynaptic neurons were not spiking was to examine the population spike and they found that the associative LTP was unaffected when there was no detectable population spike during the conditioning tetanus. They reported that, "*the timing of the postsynaptic discharge with respect to the high-frequency input is not important over, at least, a 25 msec interval.*" (McNaughton et al., 1978). In 1981, Baranyi and Feher, published a follow-up study to their 1978 paper showing thatto induce LTP, the timing requires for EPSPs and a burst of spikes was 100 ms (Baranyi and Feher, 1981). However, the order of EPSPs and spikes in the pairing was not important, so no temporal asymmetry akin to that of classical STDP was found.

In 1983, Levy and Steward examined the timing constraints for associative plasticity by triggering a train of stimuli in one pathway before or after a train of stimuli in another pathway (Levy and Steward, 1983) They found a clear temporal asymmetry such that weak-before-strong activation evoked LTP in the weak, whereas strong-before-weak stimulation resulted in LTD in the weak input.

They did not however explore the specific relative timing of single spikes. They concluded, "*that perfect temporal contiguity is not a requirement of this prototypical elemental memory unit.*" Like Cooper, Levy, and Steward also concluded that the associative signal is "*in the postsynaptic cell or some portion thereof. Regardless of whether the critical signal is cell discharge, as Hebb reasoned, or simply a massive local dendritic depolarization. . . these processes eventually 'feed back' to regulate individual synapses...*" (Levy and Steward, 1983).

A few years later, Gustafsson and Wigström (1986) too investigated the timing requirements of hippocampal plasticity using either two inputs or one input paired with postsynaptic current injection (Gustafsson et al., 1987). Interestingly, they studied the role of pairing with individual volleys (Wigström et al., 1985), in a manner very similar to some of the early STDP studies (e.g., Bi and Poo, 1998; Zhang et al., 1998; Feldman, 2000). Gustafsson and Wigström, however, did not report the temporal asymmetry of hippocampal plasticity that Levy and Steward reported and that is so characteristic of classical STDP (Caporale and Dan, 2008; Sjöström et al., 2008). But others have reproduced this variability of the timing requirements in hippocampal plasticity (e.g., Kelso et al., 1986; Wittenberg and Wang, 2006; Buchanan and Mellor, 2007), although its precise reasons remain unknown (for a review, see Buchanan and Mellor, 2010). Perhaps some important experimental parameter is yet unaccounted for.

After Masao Ito discovered parallel fiber LTD, Ekerot and Kano (1985) tested Marr's timing predictions more explicitly, but found similar levels of LTD when the parallel fiber input arrived anywhere between 20 ms before and 150 ms after the climbing fiber input. They concluded that the precise relative timing was not critical for associative plasticity, as Marr had proposed (see Ito, 1989). In 1989, Stanton and Sejnowski reported a similar experiment to that of Levy and Steward, but in a different part of the hippocampus (Stanton and Sejnowski, 1989). They too found bidirectional LTP and LTD depending on the timing of weak and strong trains of stimulation, and they also observed LTD due to weak-after-strong input activation. This study suggested that LTD could be induced by simultaneous hyperpolarization of the postsynaptic neuron, suggesting that membrane potential can gate plasticity and that this may in fact underlie the timing rule. Although the findings of Stanton and Sejnowski have been called into question, with some studies reporting contradictory results (Kerr and Abraham, 1993; Paulsen et al., 1993), their study drove the research on timing in plasticity forward.

The year following Stanton and Sejnowski's paper, Wolf Singer and colleagues reported that the level of hyperpolarization and depolarization determines whether LTP or LTD will result in the same pathway after the same tetanic conditioning (Artola et al., 1990). This study brought the focus of plasticity research further onto the postsynaptic neuron, because the key signal was dependent on the level of depolarization of the neuron, and not necessarily produced by any synaptic input in particular.

In 1994, Dominique Debanne and colleagues took the Singer study a step further and showed that the timing of a 250-ms-long depolarization relative to incoming inputs could determine whether LTD or LTP would result (Debanne et al., 1994). This added to the Singer study because now depolarization could act in the same way as hyperpolarization if it occurred before the input. In other words, it was the level of depolarization and hyperpolarization evoked in any way – even artificially – that determined the direction of synaptic plasticity.

These aforementioned studies thus introduced and parameterized the role of time in synaptic plasticity. Time is thus key not only to STDP, but also to classical rate and depolarization-dependent forms of plasticity. But timing is also key to for example ocular dominance column formation in the developing brain, as summarized colloquially in the early 1990s by Carla Shatz with "*fire out of sync, lose your link*" to depict how asynchronous activity in early development retinal waves results in visual system inputs weakening if they are consistently not able to drive the postsynaptic cell (personal communication, Carla Shatz, 1992). The notion of a critical role of timing in brain plasticity was thus bubbling for years and decades in the field before being directly discovered.

THE BACK-PROPAGATING SPIKE AND STDP

Lorente de Nó's notion of the direction of information flow influenced interpretations of neuronal and synaptic processing until the 1990s. Eccles (1961) hypothesized that the spike can propagate in both directions, while Cooper (1973) and Levy and Steward (1983) hypothesized that some signal must propagate back to the synapses to prepare synapses for plasticity. Gerstner et al. (1993) also hypothesized that individual pre–post spike times contain more information for plasticity than average rates, so that the precise timing of a postsynaptic action potential needs to be communicated to the synapse.

It was the landmark discovery by Greg Stuart, in Bert Sakmann's laboratory – using dual patch-clamp recordings from the soma and dendrites of the same neuron – that changed this field. This experiment unequivocally demonstrated that the action potential actively propagates back into the dendrites (Stuart and Sakmann, 1994). Henry Markram, also in Sakmann's laboratory at the time, showed that single subthreshold synaptic potentials could trigger a low level of calcium influx (Markram and Sakmann, 1994) and that a single action potential left behind a much larger, 100 ms-long wake of calcium as it propagated back into the dendrite (Markram et al., 1995). Markram was also developed the technique of paired patch-clamp recordings of isolating monosynaptic connections between pyramidal neurons in the neocortex and he questioned how this wake of calcium triggered by the back-propagating action potential would impact synaptic input (see below).

Up until this stage, LTP and LTD had almost been exclusively studied using extracellular electrical shocks of input fibers to neurons. With this experimental paradigm, it is difficult to avoid heterosynaptic and polysynaptic effects even by attempting to stimulate a single afferent pathway. It is also difficult to avoid stimulating neuromodulatory afferents, which are known to exert profound effects on neurons, synaptic transmission, and synaptic plasticity. With this technique precise timing of activity in pre and postsynaptic neurons is not known. Up until this time, 60 years after Hebb, there was also still no direct demonstration that the synaptic connections between two neurons could change.

In 1991, Roberto Malinow reported the first such evidence. In a heroic study, he isolated four monosynaptically connected CA3–CA1 pyramidal pairs in the acute hippocampal slice. He

then evoked LTP in these connections by simultaneously eliciting bursts of spikes in the pre and the postsynaptic neuron (Malinow, 1991). This was the first study that can be said to be truly homosynaptic and that most closely tested Hebb's (1949) prediction that strengthening would occur "*[w]hen an axon of cell A is near enough to excite a cell B and repeatedly or persistently takes part in firing it.*"

In 1995, at the Annual Society for Neuroscience Meeting, Henry Markram reported the first experimental study on the importance of precise relative timing of spikes emitted by the pre and postsynaptic neurons at monosynaptic connections between pairs of neurons in the neocortex (Markram and Sakmann, 1995). A watershed marked by relative timing of single spikes on a timescale of a few tens of milliseconds – as opposed to relative timing of competing inputs, general depolarization or trains of stimuli – determined the direction and amplitude of the synaptic change (Markram et al., 1997b). The back-propagating spike could be seen as representing the integrated sum of all synaptic inputs and is therefore an ideal associative signal between all individual synaptic inputs coming in along the dendrite. The postsynaptic spike was generated by direct current injection and therefore these changes are also not heterosynaptic. The postsynaptic spike alone could act as an associative signal consistent with previous findings that merely polarizing the membrane during synaptic input can trigger synaptic plasticity. This study revealed LTP for causal pre-before-postsynaptics pike timings with 10 ms temporal displacement, while LTD was elicited by acausal pre-after-postsynaptic spike timings, even though both conditions were elicited at the same frequency. In other words, cells that fire together do not always wire together, because timing matters too. Larger timing differences of 100 ms, however, did not evoke any plasticity. This phenomenon was later named STDP (Song et al., 2000). These experiments also showed that blockade of postsynaptic spiking abolished the LTP, as did NMDA receptor antagonism. There was furthermore a tendency for synaptic depression if the presynaptic spike failed to evoke a postsynaptic spike, reminiscent of what Stent proposed for excitatory inputs (see above and Stent, 1973).

In 1996, two theoretical studies on STDP were published. Gerstner et al. (1996) extended their earlier idea of spike-based Hebbian potentiation to spike-based causal potentiation and non-causal depression, although still with a 1-ms time window to explain how the receptive fields in the barn owl auditory system could develop with such exquisite temporal precision. This paper was formulated at the level of spikes and contained a drawing of a theoretical STDP function without knowledge of the results of Markram et al. (1997b). Larry Abbott and Ken Blum also published a timing-dependent model of plasticity that year and applied it to a hippocampal model to explain rodent navigation experiments (Abbott and Blum, 1996; Blum and Abbott, 1996). The model was formulated as a rate model, with an asymmetric Hebbian rule for causal potentiation under the pre-before-post condition on a time scale of a few hundred milliseconds. In the Blum and Abbott (1996) study, depression for pre-after-post timings was furthermore mentioned as a possibility. Although formulated in terms of rates, it is straightforward to reinterpret the Blum and Abbott study in an STDP framework.

Henry Markram and Misha Tsodyks developed a now widely used test stimulus for synapses going beyond the single shock to test synaptic transmission to a train of presynaptic action potentials that could reveal the short-term plasticity of the connection and reported that Hebbian pairing does not necessarily change the synaptic efficacy of synapses, but also their short-term dynamics. This revived the earlier Eccles work on the importance of high-frequency stimulation in testing transmission in synaptic pathways and added a new facet to long-term plasticity – that short-term plasticity can change in the long-term, a notion they called redistribution of synaptic efficacy, or RSE (Markram and Tsodyks, 1996b). Tsodyks and Markram also developed a model of dynamic synaptic transmission that demonstrates how simply changing various synaptic parameters alters synaptic transmission and introduced the notion that the probability of release, synaptic depression and facilitation determine the coding of the transmitted signal (Tsodyks and Markram, 1997; Tsodyks et al., 1998). At the same time, Larry Abbott and Sacha Nelson reported similar findings, using a different phenomenological model that did not directly link short-term plasticity parameters to synaptic properties such as vesicle depletion or probability of release (Abbott et al., 1997; Varela et al., 1997).

The STDP study by Markram and colleagues was published in 1997 (Markram et al., 1997b), back-to-back with a report by Magee and Johnston (1997), in which dendritic recordings were used to show that LTP is more readily induced when the action potential propagates back into the dendrites than when it is not, thus acting as an associative signal.

In 1997, Curtis Bell and colleagues reported the timing requirements of synaptic plasticity in the cerebellar-like electric lobe of the mormyrid electric fish. This study followed up on findings going back more than a decade earlier (Bell, 1981). Bell et al. (1997) used a stimulus protocol similar to that which Stanton and Sejnowski used in the hippocampus, with extracellular stimulation of two independent parallel fiber inputs paired with depolarization of a single inhibitory Purkinje-like neuron. They revealed causally induced LTD and non-causally induced LTP by displacing the relative timing of the stimulated inputs from −600 ms across to +600 ms with respect to the depolarization of the postsynaptic neuron. In these experiments, the coincidence window was inverted, falling anti-symmetrically around 60 ms on either side of exact coincidence, with an additional non-associative potentiation component. This was a landmark finding, showing that dramatically different forms of STDP exist (Caporale and Dan, 2008; Sjöström et al., 2008). It should furthermore be noted that this form of STDP is nothing like the classical form of parallel fiber plasticity reported by Ito in the cerebellum (Ito et al., 1982). Not only does Bell's STDP have different induction requirements and is partially non-associative (Bell et al., 1997), it also has a use-dependent form of depression (Han et al., 2000).

In 1998, Debanne et al. (1998) found that individual spike-pairings evoked STDP at connections between synaptically coupled neurons in hippocampal slice cultures. This was an extension to their 1994 study of temporal asymmetry with respect to postsynaptic depolarization (Debanne et al., 1994), inspired by Stent's conjecture (Stent, 1973) and by prior work with Yves Frégnac (Debanne et al., 1995). As for the neocortex, they found potentiation for causal, pre-before-post spike-pairings, while the opposite temporal order resulted in LTD. In addition however, they also

discovered a striking asymmetry in the width of the causal and acausal temporal windows such that the LTD window was considerably larger than that of LTP (Debanne et al., 1998). This type of imbalance in timing-dependent LTP and LTD was later reproduced in neocortical layer-2/3 by Feldman (2000) and layer-5 by Sjöström et al. (2001). In theoretical models, Kempter et al. (1999a) as well as Sen Song and Larry Abbott (Song et al., 2000) showed that this type of imbalance may help preserve stability, while the total width of the STDP function determines the correlation time scale in synaptic plasticity (Kempter et al., 1999a; Song and Abbott, 2001).

In 1998, Guo-qiang Bi, Li Zhang, and Mu-ming Poo (Bi and Poo, 1998; Zhang et al., 1998) examined the causal STDP window in great detail by mapping out the synaptic changes for a large number of timings covering essentially the entire coincidence window. For example, using paired recordings in dissociated neuronal cultures, Bi and Poo found a roughly 40-ms-long coincidence window, with an astoundingly rapid 1-ms transition between LTP and LTD for near-perfect coincidence between pre and postsynaptic cell activity. This sudden transition between LTP and LTD is in biological terms essentially instantaneous and thereby quite surprising, but was later reproduced in neocortex (Celikel et al., 2004) and is now considered one of several hallmark features of STDP.

WHERE IS STDP RESEARCH AT NOW?

Several more recent studies of STDP have focused on parameterizing STDP with respect to factors such as rate, higher-order spiking motifs, or dendritic location (for a review, see Froemke et al., 2010a). For example, Robert Froemke and Yang Dan reported in 2002 that the first spike pairing in a train of triplet or quadruplet spike-pairings determines whether LTP or LTD ensues in layer-2/3 pyramidal cells (Froemke and Dan, 2002). Similar although not entirely identical findings were reported in hippocampal cell culture by Guo-qiang Bi's team (Wang et al., 2005). On the other hand, Sjöström et al. (2001) found that STDP is quite non-linear with frequency, so that LTD is promoted at low-frequency, while LTP is evoked at high-frequency regardless of temporal order (also see Markram et al., 1997b; Froemke et al., 2006). These findings thus link the older classical rate-dependent LTP literature with the newer STDP studies, by showing that rate and timing-dependent forms of plasticity co-exist at the same synapse type (Nelson et al., 2002).

Froemke et al. (2005) later also found that STDP depends on synaptic location in the dendritic arbor of layer-2/3 pyramidal cells, with more LTD farther from the soma. In 2006, a similar but more extreme case was reported by Sjöström and Häusser (2006) in neocortical layer-5 pyramidal cells, in which plasticity induced by high-frequency pairing at distal inputs is either Hebbian or non-Hebbian depending on the depolarization state of the dendrite. The same year, Letzkus et al. (2006) reported a striking reversal of the timing requirements for STDP along the apical dendrite of layer-5 pyramidal cells. These location-dependent forms of STDP have been extensively reviewed more recently (Sjöström et al., 2008; Froemke et al., 2010b).

Importantly, parameterizations such as these have been key to the development of well-tuned computer models of cellular learning rules, whether these models are phenomenological or mechanistic in nature, and whether they are formulated within timing or rate-dependent learning rule paradigms (Shouval et al., 2002; Clopath et al., 2010; Rackham et al., 2010; Mihalas, 2011). Parameterizations of the non-linear voltage and frequency dependence of STDP (Markram et al., 1997b; Sjöström et al., 2001; Froemke et al., 2006), for example, has led to the Claudia Clopath model which accounts for a large number of experimental results from slice experiments (also see Clopath and Gerstner, 2010) while making the crucial prediction that network connectivity motifs may be a reflection of the neural code (Clopath et al., 2010).

Most STDP studies have been carried out *in vitro*, in the acute slice (e.g., Markram et al., 1997b; Sjöström et al., 2001; Froemke and Dan, 2002) or using cultured neurons (Debanne et al., 1994; Bi and Poo, 1998). Studying cellular learning rules *in vitro* has many advantages, by providing excellent experimental control. But *in vitro* preparations are obviously also fraught with complications and alternative interpretations due to the simplifications and artifacts introduced by the preparation itself. The acute brain slice, for example, is entirely devoid of natural neuromodulation, and many connections are severed during dissection. Showing evidence for STDP *in vivo*, in the intact brain, is thus of utmost importance. Already in 1998, Mu-ming Poo and colleagues showed that STDP exists *in vivo*, using the retinotectal preparation of the *Xenopus* tadpole (Zhang et al., 1998). Evidence in support of STDP *in vivo* was subsequently also demonstrated in rodents, cats, and even in humans, chiefly in a set of studies by the groups of Yang Dan (Yao and Dan, 2001; Yao et al., 2004; Meliza and Dan, 2006), Joseph Classen (Stefan et al., 2000; Müller-Dahlhaus et al., 2010), Tobias Bonhoeffer (Schuett et al., 2001), Dan Feldman (Feldman, 2000; Allen et al., 2003; Celikel et al., 2004; Jacob et al., 2007), and Dan Shulz (Jacob et al., 2007; Shulz and Jacob, 2010). It should be noted, however, that many of these studies find results *consistent* with STDP, but in principle some of the same effects could also result from circuit phenomena in combination with co-variance learning rules.

Studies from Martin Heisenberg's and Gilles Laurent's laboratories also provide intriguing evidence for the existence of STDP *in vivo* in insects, such as the fruit fly *Drosophila melanogaster* (Tanimoto et al., 2004) and the locust *Schistocerca americana* (Cassenaer and Laurent, 2007). Here, this temporally sensitive form of plasticity appears to be key to olfactory learning and information transfer. Although some controversy remains regarding the general relevance of STDP as a cellular learning paradigm (Lisman and Spruston, 2005), this preservation of timing sensitivity in cellular learning across millions of years of evolution would seem to suggest that STDP is not just relevant but actually rather important (Lisman and Spruston, 2010; Shulz and Jacob, 2010). Precisely how important and for what remains to be elucidated, which leaves us neuroscientists with some very exciting future directions.

CONCLUSIONS AND FUTURE DIRECTIONS

In this article, we covered the development of some of the ideas on learning, memory, and plasticity that led up to the discovery of STDP and further studies that revealed more intricate features of STDP and that demonstrated the ubiquity of this phenomenon. We overviewed philosophical, psychological, theoretical, and experimental developments, and we have seen how these interact

and also how they often develop in relative isolation of each other. This (partial) history of timing in synaptic plasticity research takes us all the way back to Aristotle, beginning with the *tabula rasa* concept, through William James's notion of the temporal needs for associative memories, passing via Hebb's neural postulate for synaptic modifications, to the present. Since we have taken big strides through the centuries, we have necessarily had to leave out many important concepts that surely contributed to the evolution of these ideas. The *Frontiers in Synaptic Neuroscience* Special Topic on STDP provides us with a snapshot of the present-day state of research as well as a glimpse into the future. When combined with this history, one can perhaps better speculate on future directions. A number of core issues are worth pointing out.

Clearly not all forms of plasticity depend on the back-propagating action potential (Sjöström et al., 2008), but STDP in its classical form does provide a unique neural mechanism for the determination of causality and non-causality on the millisecond timescale. This timing-centric view of plasticity is not meant to imply that spike rate is irrelevant. Roughly synchronized bursts of activity in connected neurons also lead to potentiation regardless of the precise millisecond timing (Sjöström et al., 2001; Froemke et al., 2006; Butts et al., 2007). At high frequencies, synaptic plasticity is thus determined by rate rather than by timing, which potentially explains earlier conclusions drawn by McNaughton, Ito, Levy, Gustafsson, and others about the lack of timing dependence on the millisecond timescale. Synaptic plasticity is also most sensitive to timing within a spiking frequency window (Sjöström et al., 2001), suggesting that the relative spike-timing in connected neurons only mediates bidirectional weight changes in this mid-range of spiking frequencies. Rate-dependent models may therefore accurately describe synaptic plasticity for when firing rates are in a larger dynamic range, while the STDP model may more precisely describe synaptic plasticity induced across mid-range frequencies when spiking activity is furthermore temporally relatively precise (Sjöström et al., 2001). Indeed, recent modeling studies highlight how the dual timing and rate dependence of plasticity adds tremendous flexibility and computational power to the brain during the development of cortical circuits (Clopath and Gerstner, 2010; Clopath et al., 2010; Gilson et al., 2010).

The determinants of synaptic plasticity are however more complex than that. As detailed in this review, subthreshold depolarization can also determine the amplitude and sign of synaptic plasticity (Artola et al., 1990). Clearly, strong depolarization elicits more spikes and potentially stronger potentiation, but abolishing spikes does not necessarily prevent such strong depolarization-induced plasticity (Golding et al., 2002; Remy and Spruston, 2007; Hardie and Spruston, 2009). This suggests that strong depolarization is sufficient to evoke a similar amount of plasticity as a few spikes. On the other hand, slight depolarization that is not enough to trigger spiking tends to initiate depression if combined with synaptic input (Markram et al., 1997b; Sjöström et al., 2001, 2004; Sjöström and Häusser, 2006). Furthermore, the temporal asymmetry as well as the mechanistic underpinnings of spike-timing-dependent LTD (Sjöström et al., 2003) are indistinguishable from LTD triggered by pairing presynaptic input with subthreshold depolarization (Sjöström et al., 2004). The depression triggered by subthreshold depolarization during synaptic input may be analogous to the effects of low-frequency stimulation and is therefore consistent with earlier findings of low-frequency stimulation as a protocol to induce LTD and is also consistent with the BCM rate model (Clopath and Gerstner, 2010; Clopath et al., 2010; Cooper, 2010). The depression of synapses that participate in attempts to drive a neuron to spiking, but reaching only subthreshold levels is also consistent with the Stentian notion of punishment for failure (Stent, 1973). In the causal, Hebbian model for increasing synaptic transmission (i.e., pre driving post), synapses can therefore be punished for a failed attempt at driving a neuron or for a late arrival of the input – both cases representing a wasted synaptic effort – but these synaptic failures are pardoned when activity rates are high.

The profile of the STDP window can take on different degrees of asymmetry and can even be inverted such that post-after-pre leads to depression rather than strengthening (Abbott and Nelson, 2000; Caporale and Dan, 2008). As outlined above, such an inverted STDP window was first found for inputs onto inhibitory Purkinje-cell-like neurons in the mormyrid electric fish (Bell et al., 1997), and has since also been found, for example, at excitatory synapses onto inhibitory cells of the neocortex (Holmgren and Zilberter, 2001). In the electric fish, this form of STDP is thought to stabilize the membrane potential of the postsynaptic neuron by effectively canceling predictable variations in the input (Roberts and Bell, 2000). It is worth noting, however, that not all inhibitory cell types possess identical plasticity learning rules (Kullmann and Lamsa, 2007; Lamsa et al., 2010). A key question that thus remains open is: Why is it that a number of STDP learning rules are specific to certain types of synaptic connections?

Another key area for future experimental studies is the relationship between STDP and short-term plasticity. STDP and rate-dependent models have largely assumed that only the strength of synapses changes. But as pointed out above, Markram and Tsodyks demonstrated in 1996 that if the change is in the release probability then it is not a straightforward strengthening of the synapse (Markram and Tsodyks, 1996b). An increased probability of release due to LTP will enhance low but not high-frequency transmission, simply because synapses also depress faster. The converse decrease in release probability after LTD induction also produces less short-term depression or even facilitation (Sjöström et al., 2003). On the other hand, an increased rate of recovery from depression enhances only high-frequency transmission, while synaptic facilitation enhances transmission in mid-range frequencies (Markram et al., 1998). The conditions that would lead to a uniform strengthening of synapses across all frequencies may in fact be quite limited: increased postsynaptic receptor numbers, or increased numbers of synaptic contacts per connection, and similar. LTP studies have traditionally tried to pin down a single plasticity expression mechanism, but it has become clear that there are a plethora of such mechanisms (Malenka and Bear, 2004). It has also been easier to develop computer algorithms that deal with only changes in synaptic weights rather than with more complicated alterations in synaptic dynamics, which means there have been only a few studies relating STDP to short-term plasticity (for examples, see Senn et al., 2001; Carvalho and Buonomano, 2011). In reality, however, it is most likely that synapses can change in

many different ways and that many of these ways lead to changes in the dynamics of synaptic transmission and not in a uniform change of efficacy across a high-frequency train of pulses. Changing synaptic dynamics generally changes the temporal sensitivity of synapses: an open question is how this temporal sensitivity relates to timing requirements in synaptic plasticity. Altering synaptic weights is a direct change in gain, while altering synaptic dynamics modifies a neuron's sensitivity to the temporal coherence of its inputs (Markram and Tsodyks, 1996a; Abbott et al., 1997). How this change in temporal sensitivity reorganizes activity patterns in a recurrent local circuit with STDP remains entirely unknown.

An analogous problem exists with the structural plasticity of circuits. Learning algorithms use synaptic plasticity rules derived from already existing synapses to reorganize the connectivity within a group of neurons. Such models assume that it is valid to apply synaptic plasticity rules to reconfigure connectivity as well – i.e., to microcircuit plasticity. For example, wiring and rewiring of a neural circuit appears to face strikingly different problems that STDP might not sufficiently address, such as how axons and dendrites communicate when no synapse is present in order to decide whether to form a synapse. It is also not at all clear how a multi-synaptic connection can be switched on and off. Le Be and Markram (2006) provided the first direct demonstration of induced rewiring of a functional circuit in the neocortex, that is, the appearance and disappearance of multi-synaptic connections, which requires hours of general stimulation. It is however clear that glutamate release is a key determinant in synapse formation (Engert and Bonhoeffer, 1999; Kwon and Sabatini, 2011). Regardless, additional studies are therefore required to further investigate what Le Be and Markram termed long-term microcircuit plasticity, or LTMP, and to examine its links to other forms of plasticity, such as STDP.

As shown by the teams of Jason Kerr, Alfredo Kirkwood, and Guo-qiang Bi, STDP is also under powerful neuromodulatory control (Seol et al., 2007; Pawlak and Kerr, 2008; Zhang et al., 2009; Pawlak et al., 2010). These findings are crucially important, since it is quite unclear how STDP can do anything useful at all if it is not possible to somehow gate or modulate it. Indeed, blocking neuromodulation severely impairs virtually all known forms of learning and memory (Bear and Singer, 1986; Hasselmo, 1995; Kilgard and Merzenich, 1998; Li et al., 2006; Gelinas and Nguyen, 2007; Hasselmo and Sarter, 2011), and abnormalities in neuromodulation are implicated in virtually every known psychiatric disease (Toda and Abi-Dargham, 2007; Sara, 2009). A loss of neuromodulation is also implicated in neurodegenerative disease (Aleman and Torres-Aleman, 2009). From a clinical perspective, the role of neuromodulation in synaptic plasticity is arguably one of the most crucial issues to be resolved. Yet, the vast majority of experiments are conducted under conditions where the degree of neuromodulation is unknown or non-existent. A link between synaptic plasticity and the memory functions of neuromodulators emerged from the finding that acetylcholine modulates NMDA receptor activity (Markram and Segal, 1990). It is also worth noting that the neuromodulation of STDP potentially extends beyond the "big five" – acetylcholine, noradrenaline, serotonin, dopamine, and histamine – to neuropeptides, hormones, and immunological agents. Much more work is therefore needed to understand the functional role and mechanisms of neuromodulatory control in unsupervised learning rules such as STDP, for which neuromodulation may provide global supervision or, at the very least, a degree of regulation.

Future studies will also need to clarify the relationship between synaptic learning rules and homeostatic plasticity (Turrigiano et al., 1998; Turrigiano and Nelson, 2000, 2004). It is important to note that Hebbian plasticity algorithms are intrinsically unstable: persistent correlated firing in connected neurons results in synaptic strengthening, which in turn brings about increased levels of correlated firing, thus resulting in a form of positive feedback that can cause synapses to grow uncontrollably (Watt and Desai, 2010). Although certain forms of STDP keep the firing rate of the postsynaptic neuron in a stable regime (Kempter et al., 1999a,b, 2001; Song et al., 2000; van Rossum et al., 2000), at least below a critical frequency (Tsodyks, 2002), this intrinsic stabilization feature may not be quick enough to keep track of rapidly increasing rates in a highly connected network. Here is where homeostatic plasticity – discovered by Gina Turrigiano and colleagues in the mid 1990s (Turrigiano et al., 1994, 1998) – may provide negative feedback to keep postsynaptic activity within reasonable bounds. This form of plasticity may thus play a vital role in ensuring that synaptic plasticity rules do not drive synaptic weights into a range where the neuron cannot be driven to fire at all, or becomes excessively sensitive to any input (Toyoizumi et al., 2005, 2007a; Clopath and Gerstner, 2010; Clopath et al., 2010). Building models without homeostatic plasticity typically requires artificial compensatory assumptions such as global weight normalization, but even with homeostatic rate normalization, individual synapses may need to be additionally bounded. Finding links between STDP and the BCM learning rules seems key to future progress in our understanding of the relationship between intrinsically unstable synaptic plasticity and stability-promoting mechanisms such as synaptic scaling (Turrigiano et al., 1998; Turrigiano and Nelson, 2000; Izhikevich and Desai, 2003; Watt and Desai, 2010). It also is key that the link between homeostatic plasticity and long-term microcircuit plasticity is elucidated (Le Be and Markram, 2006).

Additionally, understanding the relationship between synaptic and homeostatic plasticity will likely require taking neuroenergetics into account since energy supply from mitochondria ultimately is what determines the membrane potential, restricts firing rates, speed of repolarization, synaptic plasticity, etc. Energetics may therefore provide interesting links between the BCM rule, STDP, and homeostasis (Toyoizumi et al., 2007b; Clopath and Gerstner, 2010; Clopath et al., 2010; Cooper, 2010; Watt and Desai, 2010).

Future studies will need to cast light on the network topology of Hebbian assemblies, that is how neurons of an assembly interconnect, a problem that presumably will at least in part require a graph theoretical approach (Bullmore and Sporns, 2009). One important question is whether topologies are determined by experience only, or by pre-defined experience-independent mechanisms. This lies at the heart of the nature-versus-nurture debate. Subsequent to the publication of Hebb's postulate, theorists pointed out that these assemblies would not be very useful for storing multiple memories if synapses saturate (e.g., Fusi, 2002), since – with neurons strongly coupled via saturated synapses – assemblies would homogenize such that all produce similar outputs, which is not an ideal memory

storage system. Theorists such as Rochester, Rosenblatt, Sejnowski, and Stent therefore proposed that synaptic depression must also be exist, to allow for more optimal information storage (see above). Paradoxically, Hebb's proposal alone does not produce useful Hebbian assemblies – as LTP alone is not sufficient, there was a need for an extension to bidirectional plasticity. Yet, there is plenty of

suggestive evidence for functional assemblies in terms of the patterned activity of neurons (Dudai, 1989; Abeles, 1991; Kandel, 2006; Byrne, 2008). In fact, we also know from paired recordings that synaptic connectivity often clusters, showing higher reciprocal coupling than expected from random uniform distributions (Markram et al., 1997a; Song et al., 2005; Perin et al., 2011). It also seems quite plausible that high-order motifs in clusters of local cells – a more intricate topology of connectivity (Song et al., 2005; Perin et al., 2011) – can be inferred from synaptic plasticity learning rules in combination with the history of activity of the neurons in question (Clopath and Gerstner, 2010; Clopath et al., 2010). Indeed, a recent study shows that, in mouse visual cortex, pyramidal neurons with similar feature selectivity are significantly more frequently interconnected, yet functionally dissimilar neurons are still connected at considerable albeit lower rates (Ko et al., 2011). This functional bias of cell connectivity is in basic agreement with a Hebbian-like learning rule such as frequency-dependent STDP (Markram et al., 1997b; Sjöström et al., 2001; Froemke et al., 2006) acting during the development of visual cortex neuronal receptive fields, with firing of sufficiently high-frequency to enable overrepresentation of reciprocal connections (Song et al., 2005; Clopath et al., 2010; Perin et al., 2011).

Structural assemblies imposed by topographic connectivity can furthermore be shaped by the region in which the neurons reside (Yoshimura and Callaway, 2005; Yoshimura et al., 2005; Kampa et al., 2006), their afferents and efferents (Le Be et al., 2007; Brown and Hestrin, 2009a,b) – many of which display cell–cell specific connectivity patterns (Markram et al., 1997a; Stepanyants et al., 2004; Song et al., 2005) – as well as by ontogenetic relationship among cells (Yu et al., 2009). How STDP and other forms of plasticity operate on top of these potential constraints remains to be shown. To reconcile activity dependent plasticity and its role in molding assemblies with pre-specified connectivity will depend on the nature of the configuration of connectivity and synaptic weight distributions that results within synaptically coupled assemblies. The nature of this connectivity may finally resolve the nature-versus-nurture debate that set the path for synaptic plasticity research and that has persistently remained unresolved for more than 2000 years. We suspect future research may show that the nature-versus-nurture debate is largely due to a false dichotomy (Traynor and Singleton, 2010). These two forces are in all likelihood inextricably linked in shaping the brain during development and therefore also in forming the self. Precisely how remains unknown, but we place our bets on timing-dependent plasticity being involved one way or the other.

ACKNOWLEDGMENTS

We thank Yves Frégnac, Carla Shatz, Alanna Watt, Rui P. Costa, Kate Buchanan, and Alex Moreau for help and useful discussions and Melissa Cochrane editorial help on locating references and providing editorial comments. We thank John Lisman for the photos of Bliss, Andersen, and Lømo, and of Bernard Katz. This work was funded by the The Blue Brain Project (Henry Markram), and the EU FACETS and EU BrainScales Project (Wulfram Gerstner and Henry Markram), the UK Medical Research Council Career Development Award G0700188 (Per Jesper Sjöström), FP7 grant #243914 "Brain-i-Nets" (Per Jesper Sjöström and Wulfram Gerstner).

REFERENCES

Abbott, L. F., and Blum, K. I. (1996). Functional significance of long-term potentiation for sequence learning and prediction. *Cereb. Cortex* 6, 406–416.

Abbott, L. F., and Nelson, S. B. (2000). Synaptic plasticity: taming the beast. *Nat. Neurosci.* 3(Suppl.), 1178–1183.

Abbott, L. F., Varela, J. A., Sen, K., and Nelson, S. B. (1997). Synaptic depression and cortical gain control. *Science* 275, 220–224.

Abeles, M. (1991). *Corticonics: Neural Circuits of the Cerebral Cortex*. Cambridge: Cambridge University Press.

Abraham, W. C., and Bear, M. F. (1996). Metaplasticity: the plasticity of synaptic plasticity. *Trends Neurosci.* 19, 126–130.

Adrian, E. D., and Matthews, R. (1928). The action of light on the eye: part III. The interaction of retinal neurones. *J. Physiol.* 65, 273–298.

Albus, J. S. (1971). A theory of cerebellar function. *Math. Biosci.* 10, 25–61.

Aleman, A., and Torres-Aleman, I. (2009). Circulating insulin-like growth factor I and cognitive function: neuromodulation throughout the lifespan. *Prog. Neurobiol.* 89, 256–265.

Allen, C. B., Celikel, T., and Feldman, D. E. (2003). Long-term depression induced by sensory deprivation during cortical map plasticity in vivo. *Nat. Neurosci.* 6, 291–299.

Amit, D. J., and Tsodyks, M. V. (1991). Quantitative study of attractor neural network retrieving at low spike rates: I. Substrate-spikes, rates and neuronal gain. *Network* 2, 259.

Anderson, J. A. (1972). A simple neural network generating an interactive memory. *Math. Biosci.* 14, 197–220.

Artola, A., Brocher, S., and Singer, W. (1990). Different voltage-dependent thresholds for inducing long-term depression and long-term potentiation in slices of rat visual cortex. *Nature* 347, 69–72.

Bain, A. (1855). *The Senses and the Intellect*, 1st Edn. London: John W. Parker and Son.

Bain, A. (1873). *Mind and Body. The Theories of Their Relation*. New York: D. Appleton & Company.

Baranyi, A., and Feher, O. (1978). Conditioned changes of synaptic transmission in the motor cortex of the cat. *Exp. Brain Res.* 33, 283–298.

Baranyi, A., and Feher, O. (1981). Intracellular studies on cortical synaptic plasticity. Conditioning effect of antidromic activation on test-EPSPs. *Exp. Brain Res.* 41, 124–134.

Barrionuevo, G., Schottler, F., and Lynch, G. (1980). The effects of repetitive low frequency stimulation on control and "potentiated" synaptic responses in the hippocampus. *Life Sci.* 27, 2385–2391.

Bear, M. F. (1999). Homosynaptic long-term depression: a mechanism for memory? *Proc. Natl. Acad. Sci. U.S.A.* 96, 9457–9458.

Bear, M. F., and Singer, W. (1986). Modulation of visual cortical plasticity by acetylcholine and noradrenaline. *Nature* 320, 172–176.

Bell, C. C. (1981). An efference copy which is modified by reafferent input. *Science* 214, 450–453.

Bell, C. C., Han, V. Z., Sugawara, Y., and Grant, K. (1997). Synaptic plasticity in a cerebellum-like structure depends on temporal order. *Nature* 387, 278–281.

Bennett, M. R. (2000). The concept of transmitter receptors: 100 years on. *Neuropharmacology* 39, 523–546.

Berlucchi, G., and Buchtel, H. A. (2009). Neuronal plasticity: historical roots and evolution of meaning. *Exp. Brain Res.* 192, 307–319.

Bernstein, J. (1868). Ueber den zeitlichen Verlauf der negative Schwankung des Nervenstroms. *Pflugers Arch.* 1, 173–207.

Bernstein, J. (1902). Untersuchungen zur Thermodynamik der bioelektrischen Strome. *Pflugers Arch. ges. Physiol.* 92, 521–562.

Bi, G. Q., and Poo, M. M. (1998). Synaptic modifications in cultured hippocampal neurons: dependence on spike timing, synaptic strength, and postsynaptic cell type. *J. Neurosci.* 18, 10464–10472.

Bienenstock, E. L., Cooper, L. N., and Munro, P. W. (1982). Theory for the development of neuron selectivity: orientation specificity and binocular interaction in visual cortex. *J. Neurosci.* 2, 32–48.

Bliss, T. V., and Lømo, T. (1970). Plasticity in a monosynaptic cortical pathway. *J. Physiol. (Lond.)* 207, 61P.

Bliss, T. V., and Lømo, T. (1973). Long-lasting potentiation of synaptic transmission in the dentate area of the anaesthetized rabbit following stimulation of the perforant path. *J. Physiol.* 232, 331–356.

Blum, K. I., and Abbott, L. F. (1996). A model of spatial map formation in

the hippocampus of the rat. *Neural. Comput.* 8, 85–93.

Braitenberg, V. (1984). *Rules and Regularities. In Vehicles, Experiments in Synthetic Psychology.* Cambridge, MA: The MIT Press, 55–61.

Bramham, C. R., and Srebro, B. (1987). Induction of long-term depression and potentiation by low- and high-frequency stimulation in the dentate area of the anesthetized rat: magnitude, time course and EEG. *Brain Res.* 405, 100–107.

Brindley, G. S. (1964). The use made by the cerebellum of the information that it receives from sense organs. *I.B.R.O. Bull.* 3, 80.

Brown, S. P., and Hestrin, S. (2009a). Cell-type identity: a key to unlocking the function of neocortical circuits. *Curr. Opin. Neurobiol.* 19, 415–421.

Brown, S. P., and Hestrin, S. (2009b). Intracortical circuits of pyramidal neurons reflect their long-range axonal targets. *Nature* 457, 1133–1136.

Buchanan, K. A., and Mellor, J. R. (2007). The development of synaptic plasticity induction rules and the requirement for postsynaptic spikes in rat hippocampal CA1 pyramidal neurones. *J. Physiol. (Lond.)* 585, 429–445.

Buchanan, K. A., and Mellor, J. R. (2010). The activity requirements for spike timing-dependent plasticity in the hippocampus. *Front. Synaptic Neurosci.* 2:11. doi: 10.3389/fnsyn.2010.00011

Bullmore, E., and Sporns, O. (2009). Complex brain networks: graph theoretical analysis of structural and functional systems. *Nat. Rev. Neurosci.* 10, 186–198.

Butts, D. A., Kanold, P. O., and Shatz, C. J. (2007). A burst-based "Hebbian" learning rule at retinogeniculate synapses links retinal waves to activity-dependent refinement. *PLoS Biol.* 5, e61. doi: 10.1371/journal.pbio.0050061

Byrne, J. H. (2008). *Learning and Memory: A Comprehensive Reference.* London: Academic Press.

Caporale, N., and Dan, Y. (2008). Spike timing-dependent plasticity: a Hebbian learning rule. *Annu. Rev. Neurosci.* 31, 25–46.

Carla Shatz, J. (1992). The developing brain. *Sci. Am.* 267, 60–67.

Carvalho, T. P., and Buonomano, D. (2011). A novel learning rule for long-term plasticity of short-term synaptic plasticity enhances temporal processing. *Front. Integr. Neurosci.* 5:20. doi: 10.3389/fnint.2011.00020

Cassenaer, S., and Laurent, G. (2007). Hebbian STDP in mushroom bodies facilitates the synchronous flow of olfactory information in locusts. *Nature* 448, 709–713.

Celikel, T., Szostak, V. A., and Feldman, D. E. (2004). Modulation of spike timing by sensory deprivation during induction of cortical map plasticity. *Nat. Neurosci.* 7, 534–541.

Clopath, C., Busing, L., Vasilaki, E., and Gerstner, W. (2010). Connectivity reflects coding: a model of voltage-based STDP with homeostasis. *Nat. Neurosci.* 13, 344–352.

Clopath, C., and Gerstner, W. (2010). Voltage and spike timing interact in STDP – a unified model. *Front. Synaptic Neurosci.* 2: 25. doi: 10.3389/fnsyn.2010.00025

Collingridge, G. L., Kehl, S. J., and McLennan, H. (1983). Excitatory amino acids in synaptic transmission in the Schaffer collateral-commissural pathway of the rat hippocampus. *J. Physiol. (Lond.)* 334, 33–46.

Cooper, L. N. (1973). "A possible organization of learning and memory," in *Proceedings of the Nobel Symposium on Collective Properties of Physical Systems*, eds B. Lundqvist, S. Lundqvist, and V. Runnstrom-Reio (Aspen Garden: Nobel), 252–264.

Cooper, L. N. (2010). STDP: spiking, timing, rates and beyond. *Front. Synaptic Neurosci.* 2:11. doi: 10.3389/fnsyn.2010.00014

Debanne, D., Gahwiler, B. H., and Thompson, S. M. (1994). Asynchronous pre- and postsynaptic activity induces associative long-term depression in area CA1 of the rat hippocampus in vitro. *Proc. Natl. Acad. Sci U.S.A.* 91, 1148–1152.

Debanne, D., Gähwiler, B. H., and Thompson, S. M. (1998). Long-term synaptic plasticity between pairs of individual CA3 pyramidal cells in rat hippocampal slice cultures. *J. Physiol.* 507, 237–247.

Debanne, D., Shulz, D. E., and Fregnac, Y. (1995). Temporal constraints in associative synaptic plasticity in hippocampus and neocortex. *Can. J. Physiol. Pharmacol.* 73, 1295–1311.

DeCamp, J. E. (1915). A Study of retroactive inhibition. *Psychol. Monogr.* 19.

Del Castillo, J., and Katz, B. (1954). Statistical factors involved in neuromuscular facilitation and depression. *J. Physiol. (Lond.)* 124, 574–585.

Douglas, R. M., and Goddard, G. V. (1975). Long-term potentiation of the perforant path-granule cell synapse in the rat hippocampus. *Brain Res.* 86, 205–215.

du Bois Reymond, E. (1848). *Untersuchungen über thierische Elektrizitkät.* Berlin: Reimer.

Dudai, Y. (1989). *The Neurobiology of Memory*. Oxford: Oxford University Press.

Dudek, S. M., and Bear, M. F. (1992). Homosynaptic long-term depression in area CA1 of hippocampus and effects of N-methyl-D-aspartate receptor blockade. *Proc. Natl. Acad. Sci. U.S.A.* 89, 4363–4367.

Dunwiddie, T., and Lynch, G. (1978). Long-term potentiation and depression of synaptic responses in the rat hippocampus: localization and frequency dependency. *J. Physiol. (Lond.)* 276, 353–367.

Eccles, J. C. (1946). Synaptic potentials of motor neurones. *J. Neurophysiol.* 9, 89–120.

Eccles, J. C. (1960). *The Properties of the Dendrites, Structure and Function of the Cerebral Cortex.* New York: American Elsevier.

Eccles, J. C. (1961). The mechanism of synaptic transmission. *Ergeb. Physiol.* 51, 299–430.

Eccles, J. C. (1964). *The Physiology of Synapses.* New York: Academic Press.

Eccles, J. C., Katz, B., and Kuffler, S. W. (1941). Nature of the "endplate potential" in curarized muscle. *J. Neurophysiol.* 4, 362–387.

Eccles, J. C., and Sherrington, C. (1931). Studies on the Flexor Reflex. IV. After-Discharge. *Proc. R. Soc. Lond. B Biol. Sci.* 107, 586–596.

Ekerot, C. F., and Kano, M. (1985). Long-term depression of parallel fibre synapses following stimulation of climbing fibres. *Brain Res.* 342, 357–360.

Engert, F., and Bonhoeffer, T. (1999). Dendritic spine changes associated with hippocampal long-term synaptic plasticity. *Nature* 399, 66–70.

Feldman, D. E. (2000). Timing-based LTP and LTD at vertical inputs to layer II/III pyramidal cells in rat barrel cortex. *Neuron* 27, 45–56.

Feng, T. P. (1941). Studies on the neuromuscular junction. XXVI. The changes of the end-plate potential during and after prolonged stimulation. *Chin. J. Physiol.* 16, 301–372.

Fregnac, Y. (2002). "Hebbian synapses," in *The Handbook of Brain Theory and Neural Networks*, ed. M.A. Arbib (Cambridge, MA: The MIT Press), 515–521.

Frégnac, Y., Shulz, D., Thorpe, S., and Bienenstock, E. (1988). A cellular analogue of visual cortical plasticity. *Nature* 333, 367–370.

Froemke, R. C., and Dan, Y. (2002). Spike-timing-dependent synaptic modification induced by natural spike trains. *Nature* 416, 433–438.

Froemke, R. C., Debanne, D., and Bi, G.-Q. (2010a). Temporal modulation of spike-timing-dependent plasticity. *Front. Synaptic Neurosci.* 2:19. doi: 10.3389/fnsyn.2010.00019

Froemke, R. C., Letzkus, J. J., Kampa, B. M., Hang, G. B., and Stuart, G. J. (2010b). Dendritic synapse location and neocortical spike-timing-dependent plasticity. *Front. Synaptic Neurosci.* 2:29. doi: 10.3389/fnsyn.2010.00029

Froemke, R. C., Poo, M., and Dan, Y. (2005). Spike-timing-dependent plasticity depends on dendritic location. *Nature* 434, 221–225.

Froemke, R. C., Tsay, I. A., Raad, M., Long, J. D., and Dan, Y. (2006). Contribution of individual spikes in burst-induced long-term synaptic modification. *J. Neurophysiol.* 95, 1620–1629.

Fusi, S. (2002). Hebbian spike-driven synaptic plasticity for learning patterns of mean firing rates. *Biol. Cybern.* 87, 459–470.

Gasser, H. S., and Newcomer, H. S. (1921). Physiological action currents in the phrenic nerve. An application of the thermionic vacuum tube to nerve physiology. *Am. J. Physiol.* 57, 1–26.

Gelinas, J. N., and Nguyen, P. V. (2007). Neuromodulation of hippocampal synaptic plasticity, learning and memory by noradrenaline. *Cent. Nerv. Syst. Agents Med. Chem.* 7, 17–33.

Gerard, R. W. (1949). Physiology and psychiatry. *Am. J. Psychiatry* 106, 161–173.

Gerstner, W., Kempter, R., van Hemmen, J. L., and Wagner, H. (1996). A neuronal learning rule for sub-millisecond temporal coding. *Nature* 383, 76–81.

Gerstner, W., Ritz, R., and van Hemmen, J. L. (1993). Why spikes? Hebbian learning and retrieval of time-resolved excitation patterns. *Biol. Cybern.* 69, 503–515.

Gerstner, W., and van Hemmen, J. L. (1992). Universality in neural networks: the importance of the "mean firing rate." *Biol. Cybern.* 67, 195–205.

Gilson, M., Burkitt, A., and Van Hemmen, L. J. (2010). STDP in recurrent neuronal networks. *Front. Comput. Neurosci.* 4:23. doi: 10.3389/fncom.2010.00023

Golding, N. L., Staff, N. P., and Spruston, N. (2002). Dendritic spikes as a mechanism for cooperative long-term potentiation. *Nature* 418, 326–331.

Gotch, F., and Horsley, V. (1891). Croonian lecture: on the mammalian nervous system; its functions

and their localisation determined by an electrical method. *Philos. Trans. R. Soc. Lond., B, Biol. Sci.* 182, 267–526.

Grossberg, S. (1969). On the production and release of chemical transmitters and related topics in cellular control. *J. Theor. Biol.* 22, 325–364.

Gustafsson, B., and Wigström, H. (1986). Hippocampal long-lasting potentiation produced by pairing single volleys and brief conditioning tetani evoked in separate afferents. *J. Neurosci.* 6, 1575–1582.

Gustafsson, B., Wigström, H., Abraham, W. C., and Huang, Y. Y. (1987). Long-term potentiation in the hippocampus using depolarizing current pulses as the conditioning stimulus to single volley synaptic potentials. *J. Neurosci.* 7, 774–780.

Han, V. Z., Grant, K., and Bell, C. C. (2000). Reversible associative depression and nonassociative potentiation at a parallel fiber synapse. *Neuron* 27, 611–622.

Hardie, J., and Spruston, N. (2009). Synaptic depolarization is more effective than back-propagating action potentials during induction of associative long-term potentiation in hippocampal pyramidal neurons. *J. Neurosci.* 29, 3233–3241.

Harris, E. W., Ganong, A. H., and Cotman, C. W. (1984). Long-term potentiation in the hippocampus involves activation of N-methyl-D-aspartate receptors. *Brain Res.* 323, 132–137.

Hartley, D. (1749). *Observations on Man, His Frame, His Duty, and His Expectations.* London: Cambridge University Press.

Hasselmo, M. E. (1995). Neuromodulation and cortical function: modeling the physiological basis of behavior. *Behav. Brain Res.* 67, 1–27.

Hasselmo, M. E., and Sarter, M. (2011). Modes and models of forebrain cholinergic neuromodulation of cognition. *Neuropsychopharmacology* 36, 52–73.

Hebb, D. O. (1949). *The Organisation of Behavior*. New York: Wiley.

Hebb, D. O. (1972). *A Textbook of Psychology.* Montréal: W. B. Saunders Co.

Herz, A. V. M., Sulzer, B., Kühnvan, R., and van Hemmen, J. L. (1988). The Hebb rule: representation of static and dynamic objects in neural nets. *Europhys. Lett.* 7, 663–669.

Holmgren, C. D., and Zilberter, Y. (2001). Coincident spiking activity induces long-term changes in inhibition of neocortical pyramidal cells. *J. Neurosci.* 21, 8270–8277.

Hopfield, J. J. (1982). Neural networks and physical systems with emergent collective computational abilities. *Proc. Natl. Acad. Sci. U.S.A.* 79, 2554–2558.

Hubel, D. H., and Wiesel, T. N. (1965). Binocular interaction in striate cortex of kittens reared with artificial squint. *J. Neurophysiol.* 28, 1041–1059.

Ito, M. (1989). Long-term depression. *Annu. Rev. Neurosci.* 12, 85–102.

Ito, M., Sakurai, M., and Tongroach, P. (1982). Climbing fibre induced depression of both mossy fibre responsiveness and glutamate sensitivity of cerebellar Purkinje cells. *J. Physiol. (Lond.)* 324, 113–134.

Izhikevich, E. M., and Desai, N. S. (2003). Relating STDP to BCM. *Neural. Comput.* 15, 1511–1523.

Jacob, V., Brasier, D. J., Erchova, I., Feldman, D., and Shulz, D. E. (2007). Spike timing-dependent synaptic depression in the in vivo barrel cortex of the rat. *J. Neurosci.* 27, 1271–1284.

James, W. (1890). *The Principles of Psychology.* New York: Henry Holt and Company.

Kampa, B. M., Letzkus, J. J., and Stuart, G. J. (2006). Cortical feedforward networks for binding different streams of sensory information. *Nat. Neurosci.* 9, 1472–1473.

Kandel, E. R. (2001). The molecular biology of memory storage: a dialog between genes and synapses. *Biosci. Rep.* 21, 565–611.

Kandel, E. R. (2006). *In Search of Memory: The Emergence of a New Science of Mind*, 1st Edn. New York: W. W. Norton & Company.

Kandel, E. R., and Tauc, L. (1964). Mechanism of prolonged heterosynaptic facilitation. *Nature* 202, 145–147.

Kelso, S. R., Ganong, A. H., and Brown, T. H. (1986). Hebbian synapses in hippocampus. *Proc. Natl. Acad. Sci. U.S.A.* 83, 5326–5330.

Kempter, R., Gerstner, W., and van Hemmen, J. L. (1999a). Hebbian learning and spiking neurons. *Phys. Rev. E* 59, 4498–4514.

Kempter, R., Gerstner, W., and van Hemmen, J. L. (1999b). "Spike-based compared to rate-based Hebbian learning," in *Advances in neural information processing systems*, eds M.S. Kearns, S.A. Solla, and D.A. Cohn (Cambridge, MA: MIT Press), 125–131.

Kempter, R., Gerstner, W., and van Hemmen, J. L. (2001). Intrinsic stabilization of output rates by spike-based Hebbian learning. *Neural Comput.* 13, 2709–2741.

Kerr, D. S., and Abraham, W. C. (1993). Comparison of associative and non-associative conditioning procedures in the induction of LTD in CA1 of the hippocampus. *Synapse* 14, 305–313.

Kilgard, M. P., and Merzenich, M. M. (1998). Cortical map reorganization enabled by nucleus basalis activity. *Science* 279, 1714–1718.

Kleinfeld, D., and Sompolinsky, H. (1988). Associative neural network model for the generation of temporal patterns. Theory and application to central pattern generators. *Biophys. J.* 54, 1039–1051.

Ko, H., Hofer, S. B., Pichler, B., Buchanan, K. A., Sjöström, P. J., and Mrsic-Flogel, T. D. (2011). Functional specificity of local synaptic connections in neocortical networks. *Nature* 473, 87–91.

Kohonen, T. (1972). Correlation matrix memories. *IEEE Trans. Comput.* C-21, 353–359.

Konorski, J. (1948). *Conditioned Reflexes and Neuron Organization.* Cambridge: Cambridge University Press.

Kullmann, D. M., and Lamsa, K. P. (2007). Long-term synaptic plasticity in hippocampal interneurons. *Nat. Rev. Neurosci.* 8, 687–699.

Kwon, H. B., and Sabatini, B. L. (2011). Glutamate induces de novo growth of functional spines in developing cortex. *Nature* 474, 100–104.

Lamprecht, R., and LeDoux, J. (2004). Structural plasticity and memory. *Nat. Rev. Neurosci.* 5, 45–54.

Lamsa, K. P., Kullmann, D. M., and Woodin, M. A. (2010). Spike-timing dependent plasticity in inhibitory circuits. *Front. Synaptic Neurosci.* 2:8. doi: 10.3389/fnsyn.2010.00008

Larrabee, M. G., and Bronk, D. W. (1947). Prolonged facilitation of synaptic excitation in sympathetic ganglia. *J. Neurophysiol.* 10, 139–154.

Lashley, K. S. (1929). *Brain Mechanisms and Intelligence. A Quantitative Study of Injuries to the Brain.* Chicago: University of Chicago Press.

Le Be, J. V., and Markram, H. (2006). Spontaneous and evoked synaptic rewiring in the neonatal neocortex. *Proc. Natl. Acad. Sci. U.S.A.* 103, 13214–13219.

Le Be, J. V., Silberberg, G., Wang, Y., and Markram, H. (2007). Morphological, electrophysiological, and synaptic properties of corticocallosal pyramidal cells in the neonatal rat neocortex. *Cereb. Cortex* 17, 2204–2213.

Letzkus, J. J., Kampa, B. M., and Stuart, G. J. (2006). Learning rules for spike timing-dependent plasticity depend on dendritic synapse location. *J. Neurosci.* 26, 10420–10429.

Levy, W. B., and Steward, O. (1979). Synapses as associative memory elements in the hippocampal formation. *Brain Res.* 175, 233–245.

Levy, W. B., and Steward, O. (1983). Temporal contiguity requirements for long-term associative potentiation/depression in the hippocampus. *Neuroscience* 8, 791–797.

Li, S.-C., Brehmer, Y., Shing, Y. L., Werkle-Bergner, M., and Lindenberger, U. (2006). Neuromodulation of associative and organizational plasticity across the life span: empirical evidence and neurocomputational modeling. *Neurosci. Biobehav. Rev.* 30, 775–790.

Libet, B., and Gerard, R. W. (1939). Control of the potential rhythm of the isolated frog brain. *J. Neurophysiol.* 2, 153–169.

Lisman, J., and Spruston, N. (2005). Postsynaptic depolarization requirements for LTP and LTD: a critique of spike timing-dependent plasticity. *Nat. Neurosci.* 8, 839–841.

Lisman, J., and Spruston, N. (2010). Questions about STDP as a general model of synaptic plasticity. *Front. Synaptic Neurosci.* 2:140. doi: 10.3389/fnsyn.2010.00140

Lloyd, D. P. (1949). Post-tetanic potentiation of response in monosynaptic reflex pathways of the spinal cord. *J. Gen. Physiol.* 33, 147–170.

Locke, J. (1689). *An Essay Concerning Human Understanding*, 38th Edn. London: William Tegg.

Lømo, T. (1964). Frequency potentiation of excitatory synaptic activity in the dentate area of the hippocampal formation. *Acta Physiol. Scand.* 68, 128.

Lorente de Nó, R. (1934). Studies on the structure of the cerebral cortex. II. Continuation of the study of the ammonic system. *J. Psychol. Neurol.* 46, 113–177.

Lugaro, E. (1898). Le resistenze nell'evoluzione della vita. *Rivista moderna di cultura* 1, 29–60.

Lugaro, E. (1906). *I problemi odierni della psichiatria.* Milano: Sandron.

Lugaro, E. (1909). *Modern Problems in Psychiatry.* (Translated by D. Orr and R. G. Rows). Manchester: The University Press.

Lynch, G. S., Dunwiddie, T., and Gribkoff, V. (1977). Heterosynaptic depression: a postsynaptic correlate of long-term potentiation. *Nature* 266, 737–739.

Magee, J. C., and Johnston, D. (1997). A synaptically controlled, associative signal for Hebbian plasticity in hippocampal neurons. *Science* 275, 209–213.

Malenka, R. C. (2003). The long-term potential of LTP. *Nat. Rev.* 4, 923–926.

Malenka, R. C., and Bear, M. F. (2004). LTP and LTD: an embarrassment of riches. *Neuron* 44, 5–21.

Malenka, R. C., and Nicoll, R. A. (1999). Long-term potentiation – a decade of progress? *Science* 285, 1870–1874.

Malinow, R. (1991). Transmission between pairs of hippocampal slice neurons: quantal levels, oscillations, and LTP. *Science* 252, 722–724.

Maren, S. (2005). Synaptic mechanisms of associative memory in the amygdala. *Neuron* 47, 783–786.

Maren, S., and Fanselow, M. S. (1996). The amygdala and fear conditioning: has the nut been cracked? *Neuron* 16, 237–240.

Markram, H., Gupta, A., Uziel, A., Wang, Y., and Tsodyks, M. (1998). Information processing with frequency-dependent synaptic connections. *Neurobiol. Learn. Mem.* 70, 101–112.

Markram, H., Helm, P. J., and Sakmann, B. (1995). Dendritic calcium transients evoked by single back-propagating action potentials in rat neocortical pyramidal neurons. *J. Physiol. (Lond.)* 485, 1–20.

Markram, H., Lubke, J., Frotscher, M., Roth, A., and Sakmann, B. (1997a). Physiology and anatomy of synaptic connections between thick tufted pyramidal neurones in the developing rat neocortex. *J. Physiol. (Lond.)* 500, 409–440.

Markram, H., Lübke, J., Frotscher, M., and Sakmann, B. (1997b). Regulation of synaptic efficacy by coincidence of postsynaptic APs and EPSPs. *Science* 275, 213–215.

Markram, H., and Sakmann, B. (1994). Calcium transients in dendrites of neocortical neurons evoked by single subthreshold excitatory postsynaptic potentials via low-voltage-activated calcium channels. *Proc. Natl. Acad. Sci. U.S.A.* 91, 5207–5211.

Markram, H., and Sakmann, B. (1995). Action potentials propogating back into dendrites triggers changes in efficacy of single-axon synapses between layer V pyramidal cells. *Soc. Neurosci. Abstr.* 21, 2007.

Markram, H., and Segal, M. (1990). Acetylcholine potentiates responses to N-methyl-d-aspartate in the rat hippocampus. *Neurosci. Lett.* 113, 62–65.

Markram, H., and Tsodyks, M. (1996a). Redistribution of synaptic efficacy between neocortical pyramidal neurons. *Nature* 382, 807–810.

Markram, H., and Tsodyks, M. (1996b). Redistribution of synaptic efficacy: a mechanism to generate infinite synaptic input diversity from a homogeneous population of neurons without changing absolute synaptic efficacies. *J. Physiol. Paris* 90, 229–232.

Marr, D. (1969). A theory of cerebellar cortex. *J. Physiol. (Lond.)* 202, 437–470.

Marr, D. (1971). Simple memory: a theory for archicortex. *Philos. Trans. R. Soc. Lond., B, Biol. Sci.* 262, 23–81.

Matteucci, C. (1838). Sur le courant électrique ou propre de la grénouille. *Bibl. Univ. Genève* 15, 157–168.

McCullogh, W. S., and Pitts, W. H. (1943). A logical calculus of the ideas immanent in nervous activity. *Bull. Math. Biophys.* 5, 115–113.

McNaughton, B. L. (2003). Long-term potentiation, cooperativity and Hebb's cell assemblies: a personal history. *Philos. Trans. R. Soc. Lond., B, Biol. Sci.* 358, 629–634.

McNaughton, B. L., Douglas, R. M., and Goddard, G. V. (1978). Synaptic enhancement in fascia dentata: cooperativity among coactive afferents. *Brain Res.* 157, 277–293.

Meliza, C. D., and Dan, Y. (2006). Receptive-field modification in rat visual cortex induced by paired visual stimulation and single-cell spiking. *Neuron* 49, 183–189.

Mihalas, S. (2011). Calcium messenger heterogeneity: a possible signal for spike-timing-dependent plasticity. *Front. Comput. Neurosci.* 4:158. doi: 10.3389/fncom.2010.00158

Mulkey, R. M., and Malenka, R. C. (1992). Mechanisms underlying induction of homosynaptic long-term depression in area CA1 of the hippocampus. *Neuron* 9, 967–975.

Müller-Dahlhaus, F., Ziemann, U., and Classen, J. (2010). Plasticity resembling spike-timing dependent synaptic plasticity: the evidence in human cortex. *Front. Synaptic Neurosci.* 2:34. doi: 10.3389/fnsyn.2010.00034

Nelson, S. B., Sjöström, P. J., and Turrigiano, G. G. (2002). Rate and timing in cortical synaptic plasticity. *Philos. Trans. R. Soc. Lond., B, Biol. Sci.* 357, 1851–1857.

Paulsen, O., Li, Y. G., Hvalby, O., Anderson, P., and Bliss, T. V. (1993). Failure to induce long-term depression by an anti-correlation procedure in area CA1 of the rat hippocampal slice. *Eur. J. Neurosci.* 5, 1241–1246.

Pavlov, I. P. (1897). *The Work of the Digestive Glands English Translation by W. H. Thompson, London, 1902.* (London: Griffin).

Pawlak, V., and Kerr, J. N. (2008). Dopamine receptor activation is required for corticostriatal spike-timing-dependent plasticity. *J. Neurosci.* 28, 2435–2446.

Pawlak, V., Wickens, J. R., Kirkwood, A., and Kerr, J. N. D. (2010). Timing is not everything: neuromodulation opens the STDP gate. *Front. Synaptic Neurosci.* 2, 146. doi: 10.3389/fnsyn.2010.00146

Penfield, W., and Boldrey, E. (1937). Somatic motor and sensory representation in the cerebral cortex of man as studied by electrical stimulation. *Brain Res.* 60, 389–443.

Perin, R., Berger, T. K., and Markram, H. (2011). A synaptic organizing principle for cortical neuronal groups. *Proc. Natl. Acad. Sci. U.S.A.* 108, 5419–5424.

Perrett, S. P., Dudek, S. M., Eagleman, D., Montague, P. R., and Friedlander, M. J. (2001). LTD induction in adult visual cortex: role of stimulus timing and inhibition. *J. Neurosci.* 21, 2308–2319.

Quiroga, R. Q., Reddy, L., Kreiman, G., Koch, C., and Fried, I. (2005). Invariant visual representation by single neurons in the human brain. *Nature* 435, 1102–1107.

Rackham, O., Tsaneva-Atanasova, K., Ganesh, A., and Mellor, J. (2010). A Ca2+-based computational model for NDMA receptor-dependent synaptic plasticity at individual post-synaptic spines in the hippocampus. *Front. Synaptic Neurosci.* 2, 31. doi: 10.3389/fnsyn.2010.00031

Ralf Gerard, W. (1930). Delayed action potentials in nerve. *Am. J. Physiol.* 93, 337–341.

Rall, W. (1955). A statistical theory of monosynaptic input-output relations. *J. Cell. Physiol.* 46, 373–411.

Rall, W. (1957). Membrane time constant of motoneurons. *Science* 126, 454.

Rall, W. (1959). Branching dendritic trees and motoneuron membrane resistivity. *Exp. Neurol.* 1, 491–527.

Rall, W. (1960). Membrane potential transients and membrane time constant of motoneurons. *Exp. Neurol.* 2, 503–532.

Rall, W. (1962). Electrophysiology of a dendritic neuron model. *Biophys. J.* 2, 145–167.

Rall, W., and Rinzel, J. (1971). Dendritic spine function and synaptic attenuation calculations. *Prog. Abstr. Soc. Neurosci. First Ann. Mtg.* 64.

Ramón y Cajal, S. (1894). The Croonian Lecture: La Fine Structure Des Centres Nerveux. *Proc. R. Soc. Lond., B, Biol. Sci.* 4, 444–468.

Ramón y Cajal, S. (1911). *Histologie du Système Nerveux de l'Homme et des Vertebrés*, Vol. 2. Paris: Malone.

Remy, S., and Spruston, N. (2007). Dendritic Spikes induce single-burst long-term potentiation. *Proc. Natl. Acad. Sci. U.S.A.* 104, 17192–17197.

Rescorla, R. A., and Wagner, A. R. (1972). "A theory of Pavlovian conditioning: variations in the effectiveness of reinforcement and nonreinforcement," in *Classical Conditioning II: Current Research and Theory*, eds A. H. Black and W. F. Prokasy (New York: Appleton Century Crofts), 64–99.

Ribot, T. (1870). *La Psychologie Anglaise Contemporaine.* Paris: Librairie philosophique de Ladrange.

Roberts, P. D., and Bell, C. C. (2000). Computational consequences of temporally asymmetric learning rules: II. Sensory image cancellation. *J. Comput. Neurosci.* 9, 67–83.

Rochester, N., Holland, J., Haibt, L., and Duda, W. (1956). Tests on a cell assembly theory of the action of the brain, using a large digital computer. *IRE Trans. Inf. Theory* 2, 80–93.

Rodrigues, S. M., Schafe, G. E., and LeDoux, J. E. (2004). Molecular mechanisms underlying emotional learning and memory in the lateral amygdala. *Neuron* 44, 75–91.

Rosenblatt, F. (1958). The perceptron: a probabilistic model for information storage and organization in the brain. *Psychol. Rev.* 65, 386–408.

Sances, A., Myklebust, J., Larson, S. J., and Cusick, J. F. (1980). The evoked potential and early studies of bioelectricity. *J. Clin. Eng.* 5.

Sara, S. J. (2009). The locus coeruleus and noradrenergic modulation of cognition. *Nat. Rev.* 10, 211–223.

Schuett, S., Bonhoeffer, T., and Hubener, M. (2001). Pairing-induced changes of orientation maps in cat visual cortex. *Neuron* 32, 325–337.

Schuetze, S. M. (1983). The discovery of the action potential. *Trends Neurosci.* 6, 164–168.

Sejnowski, T. J. (1977a). Statistical constraints on synaptic plasticity. *J. Theor. Biol.* 69, 385–389.

Sejnowski, T. J. (1977b). Storing covariance with nonlinearly interacting neurons. *J. Math. Biol.* 4, 303–321.

Senn, W., Markram, H., and Tsodyks, M. (2001). An algorithm for modifying neurotransmitter release probability based on pre- and postsynaptic spike timing. *Neural. Comput.* 13, 35–67.

Seol, G. H., Ziburkus, J., Huang, S., Song, L., Kim, I. T., Takamiya, K., Huganir, R. L., Lee, H. K., and Kirkwood, A. (2007). Neuromodulators control the polarity of spike-timing-dependent synaptic plasticity. *Neuron* 55, 919–929.

Sherrington, C. S. (1897). "The central nervous system," in *A Textbook of Physiology*, 7th Edn, ed. M. Foster (London: Macmillan), 3, 929.

Sherrington, C. S. (1909). On plastic tonus and proprioceptive reflexes. *Q. J. Exp. Physiol.* 2, 109–156.

Shouval, H. Z., Bear, M. F., and Cooper, L. N. (2002). A unified model of NMDA receptor-dependent bidirectional synaptic plasticity. *Proc. Natl. Acad. Sci. U.S.A.* 99, 10831–10836.

Shulz, D. E., and Jacob, V. (2010). Spike timing dependent plasticity in the intact brain: counteracting spurious spike coincidences. *Front. Synaptic Neurosci.* 2, 137. doi: 10.3389/fnsyn.2010.00137

Sjöström, P. J., and Häusser, M. (2006). A cooperative switch determines the sign of synaptic plasticity in distal dendrites of neocortical pyramidal neurons. *Neuron* 51, 227–238.

Sjöström, P. J., Rancz, E. A., Roth, A., and Hausser, M. (2008). Dendritic excitability and synaptic plasticity. *Physiol. Rev.* 88, 769–840.

Sjöström, P. J., Turrigiano, G. G., and Nelson, S. B. (2001). Rate, timing, and cooperativity jointly determine cortical synaptic plasticity. *Neuron* 32, 1149–1164.

Sjöström, P. J., Turrigiano, G. G., and Nelson, S. B. (2003). Neocortical LTD via coincident activation of presynaptic NMDA and cannabinoid receptors. *Neuron* 39, 641–654.

Sjöström, P. J., Turrigiano, G. G., and Nelson, S. B. (2004). Endocannabinoid-dependent neocortical layer-5 LTD in the absence of postsynaptic spiking. *J. Neurophysiol.* 92, 3338–3343.

Skinner, B. F. (1938). *The Behavior or Organisms: An Experimental Analysis.* New York: Appleton-Century-Crofts.

Slater, N. T., Stelzer, A., and Galvan, M. (1985). Kindling-like stimulus patterns induce epileptiform discharges in the guinea pig in vitro hippocampus. *Neurosci. Lett.* 60, 25–31.

Sompolinsky, H., and Kanter, I. I. (1986). Temporal association in asymmetric neural networks. *Phys. Rev. Lett.* 57, 2861–2864.

Song, S., and Abbott, L. F. (2001). Cortical development and remapping through spike timing-dependent plasticity. *Neuron* 32, 339–350.

Song, S., Miller, K. D., and Abbott, L. F. (2000). Competitive Hebbian learning through spike-timing-dependent synaptic plasticity. *Nat. Neurosci.* 3, 919–926.

Song, S., Sjöström, P. J., Reigl, M., Nelson, S., and Chklovskii, D. B. (2005). Highly nonrandom features of synaptic connectivity in local cortical circuits. *PLoS Biol.* 3, e68. doi: 10.1371/journal.pbio.0030068

Stanton, P. K., and Sejnowski, T. J. (1989). Associative long-term depression in the hippocampus induced by hebbian covariance. *Nature* 339, 215–218.

Stefan, K., Kunesch, E., Cohen, L. G., Benecke, R., and Classen, J. (2000). Induction of plasticity in the human motor cortex by paired associative stimulation. *Brain* 123, 572–584.

Steinbuch, K., Jaenicke, W., and Reiner, H. (1965). *Learning Matrix.* C.I.P. Office. Available at: http://brevets-patents.ic.gc.ca/opic-cipo/cpd/eng/patent/717227/summary.html

Stent, G. S. (1973). A physiological mechanism for Hebb's postulate of learning. *Proc. Natl. Acad. Sci. U.S.A.* 70, 997–1001.

Stepanyants, A., Tamas, G., and Chklovskii, D. B. (2004). Class-specific features of neuronal wiring. *Neuron* 43, 251–259.

Stevens, C. F. (1998). A million dollar question: does LTP=memory? *Neuron* 20, 1–2.

Stuart, G. J., and Sakmann, B. (1994). Active propagation of somatic action potentials into neocortical pyramidal cell dendrites. *Nature* 367, 69–72.

Tanimoto, H., Heisenberg, M., and Gerber, B. (2004). Experimental psychology: event timing turns punishment to reward. *Nature* 430, 983.

Tanzi, E. (1893). I fatti e le induzioni dell'odierna istologia del sistema nervoso. *Riv Sper Fren Med Leg* 19, 419–472.

Toda, M., and Abi-Dargham, A. (2007). Dopamine hypothesis of schizophrenia: making sense of it all. *Curr. Psychiatry Rep.* 9, 329–336.

Toyoizumi, T., Pfister, J.-P., Aihara, K., and Gerstner, W. (2005). Generalized Bienenstock–Cooper–Munro rule for spiking neurons that maximizes information transmission. *Proc. Natl. Acad. Sci. U.S.A.* 102, 5239–5244.

Toyoizumi, T., Pfister, J.-P., Aihara, K., and Gerstner, W. (2007a). Optimality model of unsupervised spike-timing-dependent plasticity: synaptic memory and weight distribution. *Neural. Comput.* 19, 639–671.

Toyoizumi, T., Pfister, J. P., Aihara, K., and Gerstner, W. (2007b). Optimality model of unsupervised spike-timing-dependent plasticity: synaptic memory and weight distribution. *Neural. Comput.* 19, 639–671.

Traynor, B. J., and Singleton, A. B. (2010). Nature versus nurture: death of a dogma, and the road ahead. *Neuron* 68, 196–200.

Tsodyks, M. (2002). Spike-timing-dependent synaptic plasticity - the long road towards understanding neuronal mechanisms of learning and memory. *Trends Neurosci.* 25, 599–600.

Tsodyks, M., Pawelzik, K., and Markram, H. (1998). Neural networks with dynamic synapses. *Neural. Comput.* 10, 821–835.

Tsodyks, M. V., and Markram, H. (1997). The neural code between neocortical pyramidal neurons depends on neurotransmitter release probability. *Proc. Natl. Acad. Sci. U.S.A.* 94, 719–723.

Turrigiano, G., Abbott, L. F., and Marder, E. (1994). Activity-dependent changes in the intrinsic properties of cultured neurons. *Science* 264, 974–977.

Turrigiano, G. G., Leslie, K. R., Desai, N. S., Rutherford, L. C., and Nelson, S. B. (1998). Activity-dependent scaling of quantal amplitude in neocortical neurons. *Nature* 391, 892–896.

Turrigiano, G. G., and Nelson, S. B. (2000). Hebb and homeostasis in neuronal plasticity. *Curr. Opin. Neurobiol.* 10, 358–364.

Turrigiano, G. G., and Nelson, S. B. (2004). Homeostatic plasticity in the developing nervous system. *Nat. Rev. Neurosci.* 5, 97–107.

van Rossum, M. C. W., Bi, G. Q., and Turrigiano, G. G. (2000). Stable Hebbian learning from spike timing-dependent plasticity. *J. Neurosci.* 20, 8812–8821.

Varela, J. A., Sen, K., Gibson, J., Fost, J., Abbott, L. F., and Nelson, S. B. (1997). A quantitative description of short-term plasticity at excitatory synapses in layer 2/3 of rat primary visual cortex. *J. Neurosci.* 17, 7926–7940.

von der Malsburg, C. (1973). Self-organization of orientation sensitive cells in the striate cortex. *Kybernetik.* 14, 85–100.

von Waldeyer-Hartz, H. (1891). Ueber einige neuere Forschungen im Gebiete der Anatomie des Centralnervensystems. *Dtsch. Med. Wochenschr.* 17, 1352–1356.

Wang, H. X., Gerkin, R. C., Nauen, D. W., and Bi, G. Q. (2005). Coactivation and timing-dependent integration of synaptic potentiation and depression. *Nat. Neurosci.* 8, 187–193.

Watson, J. B., and Rayner, R. (1920). Conditioned emotional reactions. *J. Exp. Psychol.* 3, 1–14.

Watt, A. J., and Desai, N. S. (2010). Homeostatic plasticity and STDP: keeping a neuron's cool in a fluctuating world. *Front. Synaptic Neurosci.* 2:5. doi: 10.3389/fnsyn.2010.00005

Wiesel, T. N., and Hubel, D. H. (1965). Comparison of the effects of unilateral and bilateral eye closure on cortical unit responses in kittens. *J. Neurophysiol.* 28, 1029–1040.

Wigström, H., and Gustafsson, B. (1984). A possible correlate of the postsynaptic condition for long-lasting potentiation in the guinea pig hippocampus in vitro. *Neurosci. Lett.* 44, 327–332.

Wigström, H., Gustafsson, B., and Huang, Y. Y. (1985). A synaptic potential following single volleys in the hippocampal CA1 region possibly involved in the induction of long-lasting potentiation. *Acta Physiol. Scand.* 124, 475–478.

Willshaw, D. J., Buneman, O. P., and Longuet-Higgins, H. C. (1969). Non-holographic associative memory. *Nature* 222, 960–962.

Willwacher, G. (1976). Fiihigkeiten eines assoziativen Speichersystems im. *Vergleich zu Gehirnfunktionen. Biol. Cybernetics* 24, 181–198.

Wittenberg, G. M., and Wang, S. S. -H. (2006). Malleability of spike-timing-dependent plasticity at the CA3-CA1 synapse. *J. Neurosci.* 26, 6610–6617.

Yao, H., and Dan, Y. (2001). Stimulus timing-dependent plasticity in cortical processing of orientation. *Neuron* 32, 315–323.

Yao, H., Shen, Y., and Dan, Y. (2004). Intracortical mechanism of stimulus-timing-dependent plasticity in visual cortical orientation tuning. *Proc. Natl. Acad. Sci. U.S.A.* 101, 5081–5086.

Yoshimura, Y., and Callaway, E. M. (2005). Fine-scale specificity of cortical networks depends on inhibitory cell type and connectivity. *Nat. Neurosci.* 8, 1552–1559.

Yoshimura, Y., Dantzker, J. L., and Dan, Y. (2005). Excitatory cortical neurons form fine-scale functional networks. *Nature* 433, 868–873.

Yu, Y. C., Bultje, R. S., Wang, X., and Shi, S. H. (2009). Specific synapses develop preferentially among sister excitatory neurons in the neocortex. *Nature* 458, 501–504.

Zhang, J. C., Lau, P. M., and Bi, G. Q. (2009). Gain in sensitivity and loss in temporal contrast of STDP by dopaminergic modulation at hippocampal synapses. *Proc. Natl. Acad. Sci. U.S.A.* 106, 13028–13033.

Zhang, L. I., Tao, H. W., Holt, C. E., Harris, W. A., and Poo, M. (1998). A critical window for cooperation and competition among developing retinotectal synapses. *Nature* 395, 37–44.

Zielinski, K. (2006). Jerzy Konorski on brain associations. *Acta Neurobiol. Exp. (Wars)* 66, 75–84; discussion 85–90, 95–77.

Conflict of Interest Statement: The authors declare that the research was conducted in the absence of any commercial or financial relationships that could be construed as a potential conflict of interest.

Received: 20 February 2011; paper pending published: 19 April 2011; accepted: 25 July 2011; published online: 29 August 2011.

*Citation: Markram H, Gerstner W and Sjöström PJ (2011) A history of spike-timing-dependent plasticity. Front. Syn. Neurosci. **3**:4. doi: 10.3389/fnsyn.2011.00004*

Spike-timing dependent plasticity†

Jesper Sjöström[1] and Wulfram Gerstner[2]

[1] *McGill University, Montreal, QC, Canada*
[2] *School of Computer and Communication Sciences, School of Life Sciences, Brain Mind Institute, Ecole Polytechnique Fédérale de Lausanne, Lausanne, Switzerland*

Spike-timing dependent plasticity (STDP) is a temporally asymmetric form of Hebbian learning induced by tight temporal correlations between the spikes of pre- and postsynaptic neurons. As with other forms of synaptic plasticity, it is widely believed that it underlies learning and information storage in the brain, as well as the development and refinement of neuronal circuits during brain development (e.g., Dan and Poo, 2004; Sjöström et al., 2008). With STDP, repeated presynaptic spike arrival a few milliseconds before postsynaptic action potentials leads in many synapse types to long-term potentiation (LTP) of the synapses, whereas repeated spike arrival after postsynaptic spikes leads to long-term depression (LTD) of the same synapse. The change of the synapse plotted as a function of the relative timing of pre- and postsynaptic action potentials is called the STDP function or learning window and varies between synapse types. The rapid change of the STDP function with the relative timing of spikes suggests the possibility of temporal coding schemes on a millisecond time scale.

EXPERIMENTAL STDP PROTOCOL

In a typical spike-timing dependent plasticity (STDP) protocol (Markram and Sakmann, 1995; Markram et al., 1997; Bi and Poo, 1998; Sjöström et al., 2001), a synapse is activated by stimulating a presynaptic neuron (or presynaptic pathway) shortly before or shortly after making the postsynaptic neuron fire by injection of a short current pulse. The pairing is repeated for 50–100 times at a fixed frequency (for example 10 Hz). The weight of the synapse is measured as the amplitude (or initial slope) of the postsynaptic potential. The change of the synaptic weight is plotted as a function of the relative timing between presynaptic spike arrival and postsynaptic firing, see **Figure 1**. The resulting plot is the STDP function or learning window. It is worth noting that different synapse types can have quite different forms of STDP function (Abbott and Nelson, 2000; Bi and Poo, 2001). Compared to many other synaptic plasticity induction protocols, STDP is especially attractive since it is believed to be biologically plausible. In the intact brain, action potentials are often quite precisely timed to stimuli in the outside world, although this is not true for all brain regions and cell types. Nevertheless, STDP is very likely to be induced under such circumstances and many studies provide strong evidence that this is indeed the case (Zhang et al., 1998; Allen et al., 2003; Meliza and Dan, 2006; Jacob et al., 2007).

BASIC STDP MODEL

The weight change Δw_j of a synapse from a presynaptic neuron j depends on the relative timing between presynaptic spike arrivals and postsynaptic spikes. Let us name the presynaptic spike arrival times at synapse j by t_j^f where $f = 1,2,3,...$ counts the presynaptic spikes. Similarly, t^n with $n = 1,2,3,...$ labels the firing times of the postsynaptic neuron. The total weight change Δw_j induced by a stimulation protocol with pairs of pre- and postsynaptic spikes is then (Gerstner et al., 1996; Kempter et al., 1999)

$$\Delta w_j = \sum_{j=1}^{N}\sum_{n=1}^{N} W\left(t_i^n - t_j^f\right) \tag{1}$$

where $W(x)$ denotes one of the STDP functions (also called learning window) illustrated in **Figure 1**.

A popular choice for the STDP function $W(x)$

$$W(x) = A_+ \exp\left(-x/\tau_+\right) \quad \text{for } x > 0 \tag{2}$$

$$W(x) = -A_- \exp\left(x/\tau_-\right) \quad \text{for } x > 0 \tag{3}$$

which has been used in fits to experimental data (Zhang et al., 1998) and models (e.g., Song et al., 2000). The parameters A_+ and A_- may depend on the current value of the synaptic weight w_j. The time constants are on the order of $\tau_+ = 10$ ms and $\tau_- = 10$ ms.

VARIANTS OF STDP MODELS

ONLINE IMPLEMENTATION OF STDP MODELS

Spike-timing dependent plasticity with an STDP function as in Eq. 2 can be implemented in an online update rule using the following assumptions. Each presynaptic spike arrival leaves a trace $x_j(t)$ which is updated by an amount $a_+(x)$ at the moment of spike arrival and decays exponentially in the absence of spikes:

$$\tau_+ \frac{dx_j}{dt} = -x + a_+(x)\sum_j \delta\left(t - t_j^f\right) \tag{4}$$

The biophysical nature of the variable x need not to be specified, but potential candidates are the amount of glutamate bound to postsynaptic receptors; or the fraction of NMDA receptors in the open state. Similarly, each postsynaptic spike leaves a trace y

$$\tau_- \frac{dy}{dt} = -y + a_-(x)\sum_n \delta\left(t - t^n\right) \tag{5}$$

†Reproduced from Scholarpedia, 5(2):1362. doi:10.4249/scholarpedia.1362,

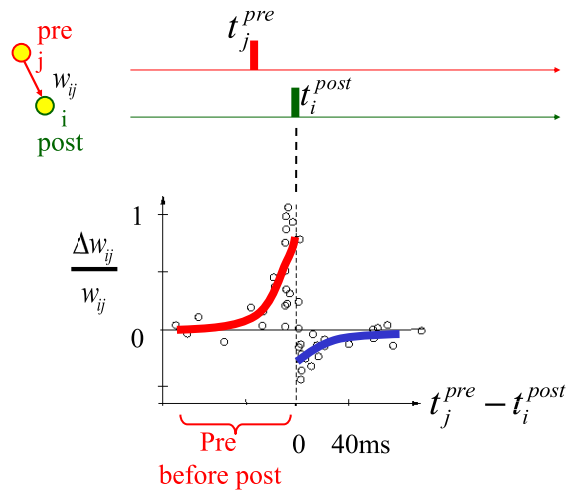

FIGURE 1 | Spike-timing dependent plasticity (schematic): the STDP function shows the change of synaptic connections as a function of the relative timing of pre- and postsynaptic spikes after 60 spike pairings. Schematically redrawn after Bi and Poo (1998).

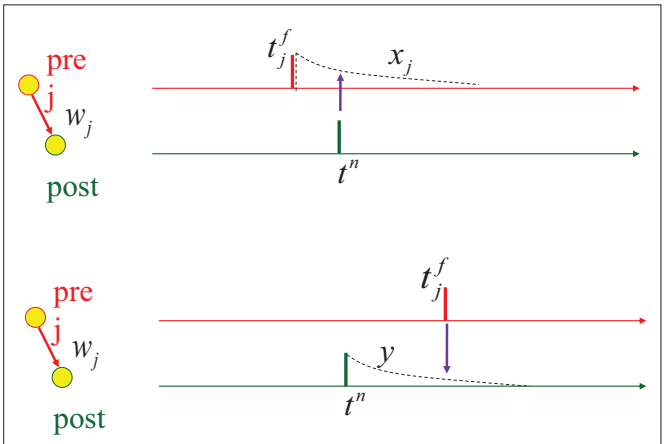

FIGURE 2 | Spike-timing dependent plasticity can be implemented by local variables. Top: A presynaptic spike leaves a trace $x_j(t)$ which is read out (arrow) at the moment of the postsynaptic spike. The weight change is proportional to that value $x_j(t_n)$ Bottom: A postsynaptic spike leaves a trace $y(t)$ which is read out (arrow) at the moment of a presynaptic spike.

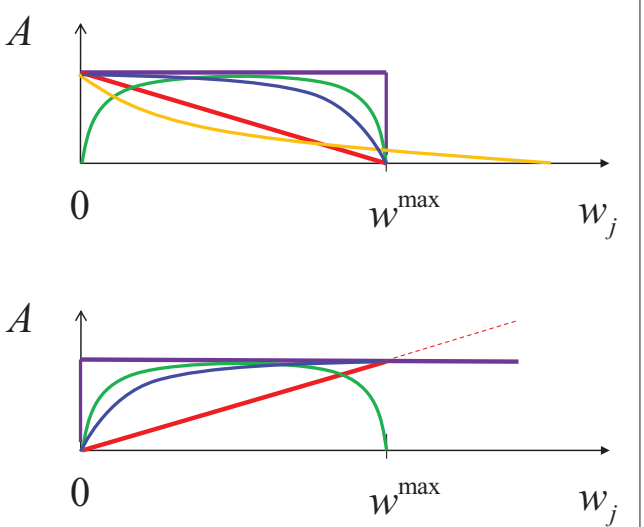

FIGURE 3 | Top: Potentiation remains bounded if the parameter $A_+(w_j)$ has hard bounds (magenta), linear soft bounds (red), a non-linear soft-bound at w^{max} (blue), or two-sided non-linear soft bounds (green). With the yellow weight dependence, potentiation is the smaller the larger the weight, but does not have a fixed upper bound. Bottom: Analogously, depression is stopped at zero weights choosing some bounds for $A_-(w_j)$.

which increases by an amount $a_-(y)$ at the moment of postsynaptic spikes. This trace could possibly be interpreted as the voltage at the synapse caused by a backpropagating action potential; or by calcium entry due to a backpropagating action potential. The weight change is then

$$\frac{dw_j}{dt} = A_+(w_j)x(t)\sum_n \delta(t-t^n) - A_-(w_j)y(t)\sum_f \delta(t-t_j^f) \qquad (6)$$

Thus, the weight is increased at the moment of postsynaptic firing by an amount that depends on the value of the trace x left by the presynaptic spike. Similarly, the weight is depressed at the moment of presynaptic spikes by an amount proportional to the trace y left by previous postsynaptic spikes. Integration of Eq. 5 yields Eq. 2. For an illustration see **Figure 2.**

WEIGHT DEPENDENCE: HARD BOUNDS AND SOFT BOUNDS

For biological reasons, it is desirable to keep the synaptic weights in a range $w^{min} < w_j < w^{max}$. This can be achieved by an appropriate choice of the functions $A_+(w_j)$ and $A_-(w_j)$. For the sake of simplicity, the lower bound is set in most models to zero, $w^{min} = 0$. A choice

$$A_+(w_j) = (w^{max} - w_j)\eta_+ \quad \text{and} \quad A_-(w_j) = w_j\eta_-$$

with positive constants η_+ and η_- is called soft bounds or multiplicative weight dependence. The choice

$$A_+(w_j) = \Theta(w^{max} - w_j)\eta_+ \quad \text{and} \quad A_-(w_j) = \Theta(-w_j)\eta_-$$

is called hard bounds, see **Figure 3**. Here $\Theta(x)$ denotes the Heaviside step function. In practice, hard bounds mean that an update rule with fixed parameters η_+ and η_- is used until the bounds are reached (Gerstner et al., 1996; Kempter et al., 1999; Roberts and Bell, 2000; Song et al., 2000). Soft bounds mean that, for large weights, synaptic depression dominates over potentiation (Kistler and van Hemmen, 2000; van Rossum et al., 2000; Rubin et al., 2001). It is possible to interpolate between the two cases (Gütig et al., 2003).

TEMPORAL ALL-TO-ALL VERSUS NEAREST-NEIGHBOR SPIKE INTERACTION

If the sum in Eq. 2 goes over all presynaptic spike arrivals and all postsynaptic spikes, then all spike pairs contribute equally. This case has been called all-to-all spike interaction (**Figure 4**). It is also possible to restrict the interactions so that only nearest spikes

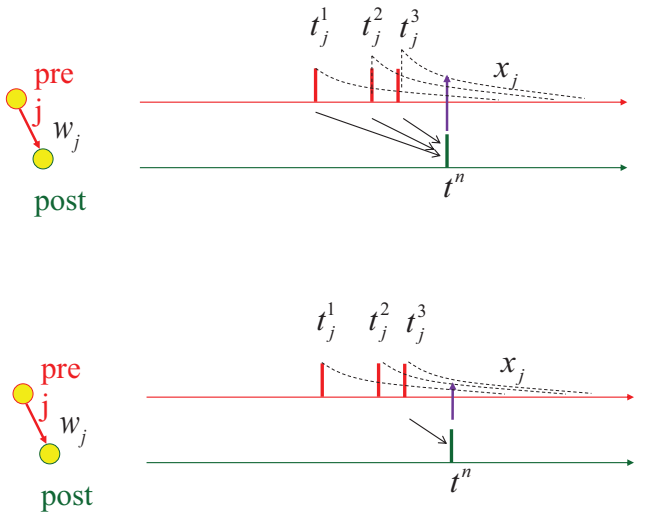

FIGURE 4 | Top: All three presynaptic spikes interact (black arrows) with a later postsynaptic spike (all-to-all interaction). This can be implemented by a trace $x_j(t)$ which accumulates. Bottom: Only the most recent presynaptic spike interacts (black arrow) with a later postsynaptic spike (nearest-neighbor interaction). This can be implemented by a trace $x_j(t)$ which starts after each presynaptic spike at the same value.

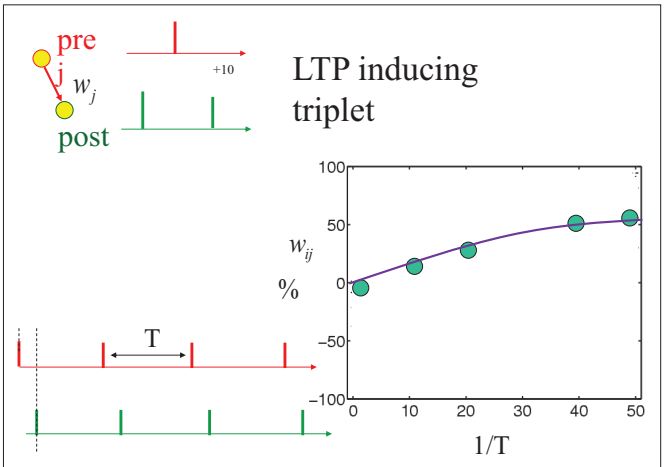

FIGURE 5 | Top: In a triplet model, the elementary building block of LTP is not a pair, but a combination of 1 pre and 2 postsynaptic spikes. Bottom: Frequency dependence of LTP. The same number of pre-post pairings at 10 ms is repeated at different intervals T. On the right, the amount of LTP is given as a function of the repetition frequency 1/T, redrawn after Sjöström et al. (2001).

interact. In the mechanistic update rule of Eq. 5, nearest-neighbor interaction can be implemented as follows. The potentiation at the moment of the postsynaptic spike should depend only on the time since the most recent presynaptic spike. To achieve this, suppose that the trace variable x is increased at the moment of presynaptic spikes by an amount $a_+(x) = 1 - x_-$ where x_- denotes the value of the variable x just before the update. In other words, the update of x is not cumulative but goes always to a fixed value of one, so that the influence of previous spikes is canceled; see Morrison et al. (2007) for a review.

TRIPLET RULE OF STDP

Pair-wise interaction between spikes as in Eq. 1 would predict that 60 repetitions of pre-post pairings (say, presynaptic spikes 10 ms before postsynaptic ones) give the same result independent of whether the pairing is repeated at 1 or 5 Hz. At frequencies above 25 Hz, a pair-wise interaction model would predict a reduced potentiation, since in addition to the pre–post pair at 10 ms virtual post–pre pairs at 30 ms are created – that should lead to depression. However, in experiments the opposite is observed (Senn et al., 2001; Sjöström et al., 2001). The frequency dependence of STDP experiments can be accounted for if one assumes that the basic building block of potentiation during STDP experiments is not a pair-wise interaction as assumed in Eq. 1, but a triplet interaction between two postsynaptic spikes and one presynaptic spike (see **Figure 5**). Such a triplet interaction can be implemented in the mechanistic model if one works with two postsynaptic traces y_1 and y_2 with two different time constants, rather than a single trace (Pfister and Gerstner, 2006). Such a model is also compatible with explicit triplet experiments (Wang et al., 2005) while a pair-based model is not.

HOMEOSTATIC TERMS

In addition to the pair-based and triplet-based STDP effects mentioned above, one can also consider STDP models where an isolated postsynaptic or presynaptic spike induces a small change of the synaptic weight, even if not paired with another spike. These terms can be used in models to yield a homeostatic control of the total input into the postsynaptic neuron (Kempter et al., 1999; van Rossum et al., 2000).

Another possibility to implement homeostasis into STDP models is by making the parameter A_- in Eq. 2 depend on the mean firing rate calculated as a running average over a time scale of seconds (Pfister and Gerstner, 2006).

VOLTAGE DEPENDENCE

Experiments and models of STDP suggest that synaptic weight changes are caused by the tight temporal correlations between pre- and postsynaptic spikes. However, other experimental protocols where presynaptic spikes are paired with a fixed depolarization of the postsynaptic neuron (e.g., under voltage clamp) show that postsynaptic spikes are not necessary to induce long-term potentiation (LTP) and depression of the synapse (Artola et al., 1990; Ngezahayo et al., 2000; Sjöström et al., 2004). Moreover, the voltage of the postsynaptic neuron just before generation of action potentials influences the direction of change of the synapse, even if the spike-timing is held fixed (Sjöström et al., 2001), suggesting that postsynaptic voltage is more fundamental than spike-timing. Indeed, a model of synaptic plasticity that postulates pairing between presynaptic spike arrival and postsynaptic voltage contains STDP models as a special case (Brader et al., 2007; Clopath et al., 2010).

BIOPHYSICAL MODELS

Since signaling chains involved in the induction of long-term potentation and depression are partially unknown, most models of STDP are phenomenological models. However, some models

attempt to identify variables such as the traces x and y in the above mechanistic model with specific biophysical quantities. A few examples:

- Senn–Markram–Tsodyks model. The model shares features with the mechanistic triplet model above and identifies some of the variables with internal states of the NMDA receptor and unspecified second messengers (Senn et al., 1997, 2001).
- Karmarkar–Buonomano model. The model emphasizes the fact that the pathways for upregulation and downregulation are independent and give interpretations of internal variables in terms of NMDA receptor, calcium, and backpropagating action potentials (Karmarkar and Buonomano, 2002).
- Shouval model. The model of Shouval starts from the hypothesis that the intracellular calcium concentration in the vicinity of the synapse controls the up- and downregulation of synaptic weights (Shouval et al., 2002).
- Rubin et al. model. The model gives a detailed account of some of the signaling steps translating the calcium time course into synaptic weight changes (Rubin et al., 2005).
- Lisman model. The model focuses on the autophosphorylation of CaMKII as a critical step for memory formation (Lisman and Zhabotinsky, 2001; Lisman, 2003). The calcium based model can be simplified and shows STDP (Graupner and Brunel, 2007).

RELATION OF STDP TO OTHER LEARNING RULES

STDP AND HEBBIAN LEARNING RULES

Spike-timing dependent plasticity can be seen as a spike-based formulation of a Hebbian learning rule. Hebb formulated that a synapse should be strengthened if a presynaptic neuron "repeatedly or persistently takes part in firing" the postsynaptic one (Hebb, 1949). This formulation suggests a potential causal relation between the firing of the two neurons. Causality requires that the presynaptic neuron fires slightly before the postsynaptic one. Indeed, in standard STDP experiments on synapses onto pyramidal neurons, potentiation of the synapse occurs for pre-before-post timing, in agreement with Hebb's postulate. Hebb did not, however, postulate the existence of synaptic weakening (Hebb, 1949). The existence of a temporal window for weakening of connective strength in the typical STDP learning rule is in a sense an extension to the Hebbian postulate.

The existence of synaptic weakening, however, was postulated long before the discovery of STDP. Stent (1973) argued already that the input from a presynaptic cell that is consistently not co-active with the postsynaptic cell should be weakened. One important distinction as compared to STDP is that the Stentian extension to Hebb's postulate does not emphasize temporal contrast, only persistent lack of coincidence (Stent, 1973), and it is therefore more akin to heterosynaptic long-term depression (LTD) than to STDP (Sjöström et al., 2008). Standard STDP, on the other hand, possesses a characteristic temporal asymmetry (**Figure 1**; Abbott and Nelson, 2000; Caporale and Dan, 2008; Sjöström et al., 2008).

STDP VERSUS RATE-BASED LEARNING RULES

Under the assumption of stationary Poisson statistics for the firing times of pre- and postsynaptic neurons, the most relevant aspect of the STPD function is its integral and an STDP model can be mapped to an equivalent rate-based learning rule (Kempter et al., 1999). Under the assumption of independence between pre- and postsynaptic firing, the total weight change is $\Delta w_{ij} = \alpha f_i(t) f_j(t)$ where $f_j(t)$ and $f_i(t)$ denote the firing rate of pre- and postsynaptic neurons averaged over some time T and $\alpha = \int W(s)ds$ is the integral over the learning window. If the integral is positive, STDP is identical to standard rate-based Hebbian learning. For negative integral, as often used in modeling, STDP corresponds to an anti-Hebbian rate rule.

However, the assumption of independence of pre- and postsynaptic firing is obviously wrong since it neglects the causal correlations generated by the interaction of the two neurons. A more precise mapping to rate models can be achieved if the postsynaptic neuron is described as an inhomogeneous Poisson Process with a rate $f_i(t) = \gamma \Sigma_j \Sigma_f \in (t - t_j^f)$ where t_j^f denotes the spike times of a presynaptic neuron j generated by a Poisson process of rate $f_j(t)$ and $\in(s)$ for $s > 0$ describes the time course of a postsynpatic potential. The total weight change in a period T is then $\Delta w_{ij} = \alpha f_i(t) f_j(t) + \beta f_j(t)$ where $\beta = \gamma \int_0^\infty \in(s) W(s) ds$ is the integral over the "causal" part of the learning window, i.e., over all times with "pre-before-post" relation (Kempter et al., 1999). For standard STDP models $\beta > 0$, i.e., presynaptic spike arrival leads on average to a positive change of the synapse, because it is likely to cause postsynaptic firing. This is then often combined with a negative integral over the STDP function $\alpha < 0$ so that random pairings of pre- and postsynaptic firings leads to a decrease of the synapse (Gerstner et al., 1996; Song et al., 2000). The functional consequences of such a choice are discussed below (see Rate normalization).

STDP AND BIENENSTOCK–COOPER–MUNRO RULE

Spike-timing dependent plasticity can also be related to a non-linear rate model where the weight change depends linearly on the presynaptic rate, but non-linearly on the postsynaptic rate (Bienenstock et al., 1982). This can be achieved in two different ways. The first possibility is to implement standard STDP with nearest-neighbor instead of all-to-all coupling (see above). This leads to a non-linearity consistent with the Bienenstock–Cooper–Munro (BCM) rule (Izhikevich and Desai, 2003). The second possibility is to use a triplet STDP rule (see above) instead of the standard pair-based rule (**Figure 6**). If potentiation requires a triplet of two postsynaptic spike and one presynaptic spike (with post–pre–post or pre–post–post firings in temporal proximity) while depression is modeled by the interaction of a post–pre-pair, then the equivalent rate model under a Poisson firing assumption as above is $\Delta w_{ij} = a_+ [f_i]^2 f_j - a_- f_i f_j = \phi(f_i - \vartheta) f_j$ where ϑ describes the minimal postsynaptic frequency for potentiation and ϕ is a quadratic function (Pfister and Gerstner, 2006). If the amount a_- of depression increases with the mean postsynaptic frequency, then the threshold shifts with the mean postsynaptic rate. In this case the triplet rule of STDP becomes identical to the BCM rule (Bienenstock et al., 1982).

FUNCTIONAL CONSEQUENCES

As described above, STDP models can be related to rate models under the assumption of Poisson firing of both pre- and postsynaptic neurons. Hence STDP rules inherit functional consequences known for rate models. In particular, the relation of synaptic learning to principal component analysis; to receptive field development; to clustering and map formation does not change fundamentally

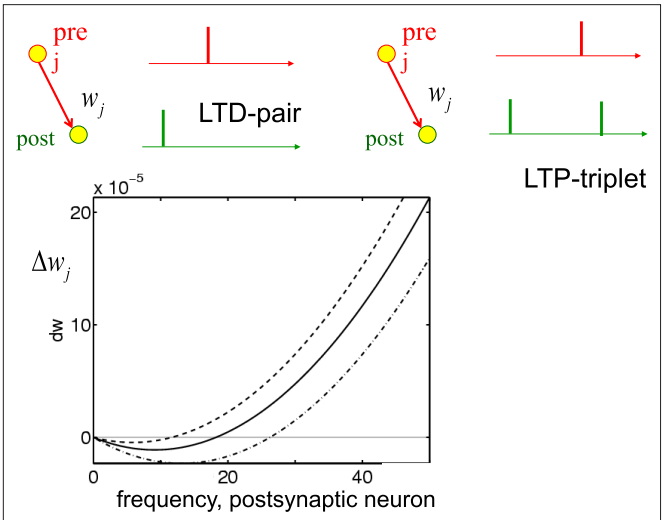

FIGURE 6 | A STDP rule (top) where post–pre pairs cause LTD and post–pre–post triplets cause LTP generates for Poisson input a frequency dependence of weight changes as in the BCM model (bottom).

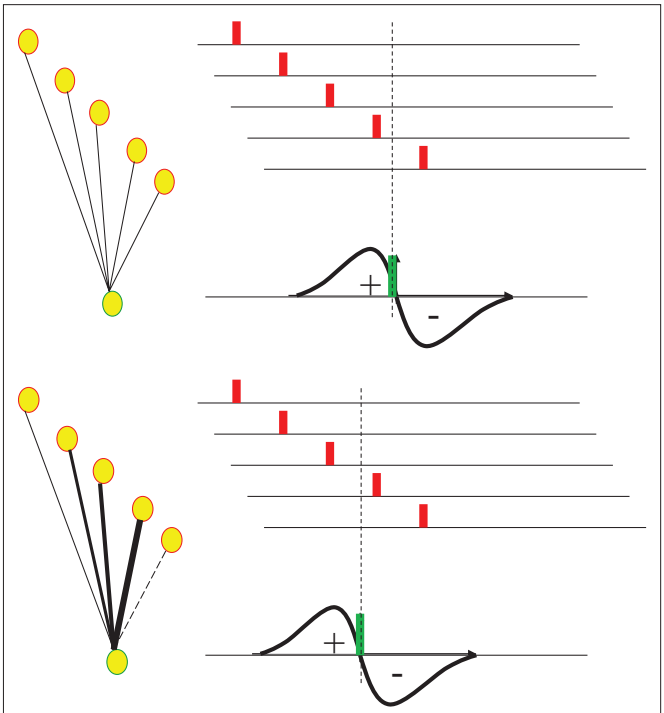

FIGURE 7 |Top: Presynaptic neurons are firing one after the other and cause the postsynaptic neuron to fire a single action potential (green vertical bar). The STDP function will strengthen those synapses that have been activated just before the postsynaptic spike. Bottom: If the stimulation pattern repeats the new synaptic weights make the postsynaptic neuron fire earlier.

if one switches from rate-based to spike-based models (Kempter et al., 1999; Song and Abbott, 2001). In the rest of this section we focus on aspects that are specific to STDP and go beyond known features of rate-based learning.

SPIKE–SPIKE CORRELATIONS

The postsynaptic depolarization caused by spike arrival at an excitatory synapse makes the postsynaptic neuron more likely to fire. In all spiking neuron models (including Poisson models driven by presynaptic input) this leads to a correlation of the spikes of pre- and postsynaptic neurons on the timescale of milliseconds. These spike–spike correlations contribute to learning in STDP models (Kempter et al., 1999), but are completely neglected in standard rate models of learning. See the section "STDP versus rate-based learning rules."

REDUCED LATENCY

Suppose a postsynaptic neuron is connected to N presynaptic neurons that fire one after another in a sequence 1-2-3-…-N over several milliseconds; see **Figure 7**. Suppose that the synaptic input makes the postsynaptic neuron fire between the firings of presynaptic neurons N-1 and N. As a result of STDP the connection from neuron N to the postsynaptic neuron is weakened (because of the post-before-pre timing) whereas the connections from neurons N-1, N-2, N-3… to the postsynaptic neuron are reinforced (because of appropriate pre-before-post firing). After several repetitions of the same stimulus, the postsynaptic neuron fires earlier, i.e., with reduced latency, because of the stronger input. Hence the timing of the postsynaptic spike shifts forward in time (Mehta et al., 2000; Song et al., 2000).

TEMPORAL CODING

Since STDP is sensitive to spike-timing on the millisecond rate, it can be used in temporal coding paradigms. Examples include tuning of synaptic connections in a model of sound source localization in the auditory pathway (Gerstner et al., 1996); learning of spatio-temporal spike patterns in a model of associative memory (Gerstner et al., 1993); suppression of predictable signals in a model of the electrosensory system of electric fish (Roberts and Bell, 2000); learning time-order codes (Guyonneau et al., 2005); amongst others.

RATE NORMALIZATION

Rate-based Hebbian learning is intrinsically unstable: synaptic inputs that drive the neuron to a high firing rate will be strengthened further. On one hand, such an instability is necessary to make the neuron detect, and become sensitive, to weak correlations in the input. On the other hand, this leads not only to a growth of individual synapses, but also to an explosion of the firing rate of the postsynaptic neuron. In practice, in rate-based learning the growth of synapses and firing rates is controlled by (i) introducing upper and lower bounds for individual weights and (ii) renormalization of the weights of each time step or each episode. Renormalization can alternatively be implemented online by a rate-dependent decay term of the weights (Oja, 1982). Surprisingly, STDP models with an appropriate set of parameters do not need such an explicit normalization step (Kempter et al., 1999, 2001; Song et al., 2000).

As discussed above in section "STDP versus Rate-based learning rules," the equivalent rate model of a standard STDP rule is $\Delta w_{ij} = \alpha f_i(t) f_j(t) + \beta f_j(t)$. For a choice of parameter where the integral over the STDP function is negative ($\alpha < 0$) and pre-before-post firings lead to potentiation ($\beta > 0$), the firing rate of the postsynaptic

neuron has a stable fixed point, while the learning rule is sensitive to the temporal correlations between pre- and postsynaptic neurons (Kempter et al., 2001).

EXPERIMENTAL RESULTS AND OPEN QUESTIONS

DIVERSITY OF STDP

Spike-timing dependent plasticity varies tremendously across synapse types and brain regions (Abbott and Nelson, 2000). Even so, it is worth recollecting that the temporal asymmetry of classical STDP is also remarkably well preserved and is found in species as different as rat, frog, locust, zebra finch, cat, and probably also humans (reviewed in Caporale and Dan, 2008; Sjöström et al., 2008). In mammals, STDP has also been uncovered in multiple brain regions, such as prefrontal, entorhinal, somatosensory, and visual cortices, hippocampus, striatum, the cochlear nucleus, and the amygdala (cf. Caporale and Dan, 2008; Sjöström et al., 2008). The activity requirements that govern STDP at many of these different synapses, however, is variable. For example, the width of the temporal windows for LTD and LTP appear to be roughly equal at hippocampal excitatory synapses (Bi and Poo, 1998; Zhang et al., 1998; Nishiyama et al., 2000), whereas the LTD timing window is considerably wider than that of LTP at several neocortical synapses (Feldman, 2000; Sjöström et al., 2001).

For some synapses, the STDP timing window is inverted as compared to the classical form of STDP, so that pre-before-post timings result in LTD whereas the opposite temporal order results in LTP. This is the case at, e.g., inhibitory connections onto neocortical L2/3 pyramidal neurons (Holmgren and Zilberter, 2001), at corticostriatal synapses (Fino et al., 2005) as well as in the electrosensory lobe of the mormyrid electric fish (Bell et al., 1997). The timing requirements for STDP at connections between spiny stellate cells in rat somatosensory cortex are yet again different: Here, synapses undergo LTD seemingly regardless of temporal order (Egger et al., 1999). In neocortical layer-5 pyramidal neurons, the timing requirements also depend critically on synapse location in the dendritic tree: Whereas proximal inputs undergo classical STDP, distal synapses are subject to a "temporally inverted" STDP rule (Letzkus et al., 2006). These same inputs also undergo non-Hebbian LTD or Hebbian LTP depending on the state of depolarization of the apical dendrite (Sjöström and Häusser, 2006).

The activity requirements of STDP may thus vary considerably not only across brain regions and synapse types, but also within a cell, in different dendritic compartments. One open question is what this variability is good for. Since it is well-established that synaptic plasticity underpins neural circuit development (Katz and Shatz, 1996), this implies that the STDP rules engaged during development determine circuit functionality in the mature brain. In other words, this variability of STDP is most likely not coincidental.

BIOPHYSICAL AND BIOCHEMICAL MECHANISMS

Both LTP and LTD depend on intracellular calcium transients: LTP is triggered by brief and strong postsynaptic calcium events, whereas LTD is induced by smaller, more prolonged calcium elevations, a concept known as the calcium hypothesis in synaptic plasticity (Sjöström et al., 2008). This calcium dependence of plasticity is critically dependent on the activation of postsynaptic NMDA receptors residing in the spine: These NMDA receptors detect the coincidence of glutamate release due to the presynaptic spike and depolarization due to the postsynaptic spike, resulting in a supralinear rise in postsynaptic calcium during LTP (Yuste and Denk, 1995; Koester and Sakmann, 1998; Schiller et al., 1998). The calcium hypothesis, however, is probably an oversimplification, since additional sources of calcium such as voltage-dependent calcium channels (Magee and Johnston, 1997; Bi and Poo, 1998) and other signaling mechanisms such as metabotropic glutamate receptors (Nevian and Sakmann, 2006) also contribute to STDP.

Downstream to the calcium influx is calmodulin, which may provide a watershed readout mechanism (DeMaria et al., 2001) to distinguish between LTP and LTD-promoting calcium signals (Sjöström and Nelson, 2002; Sjöström et al., 2008). Eventually, the enzyme calcium/calmodulin-dependent kinase II, or CaMKII, is affected by the calcium transient. This enzyme has been hypothesized to encode synaptic weight through gradations in the fraction of active subunits (Lisman, 1985, 1989; Lisman and Zhabotinsky, 2001; Lisman et al., 2002).

Although there is a relative consensus regarding the mechanisms underlying potentiation, it is less clear-cut with depression. In one view, sublinear calcium summation triggers LTD (Koester and Sakmann, 1998), perhaps because postsynaptic NMDA receptors are suppressed during STDP timings inducing LTD (Froemke et al., 2005). It is, however, becoming increasingly clear that the presynaptic terminal too actively participates in the induction of STDP. In particular, presynaptically located NMDA receptors trigger timing dependent LTD (Sjöström et al., 2003; Rodriguez-Moreno and Paulsen, 2008). The calcium hypothesis is thus clearly flawed and more work is required to elucidate the biophysical and biochemical mechanisms that underpin STDP.

ROLE OF BACKPROPAGATING ACTION POTENTIALS

The NMDA-receptor-based spine coincidence detector described above requires that an action potential backpropagating from the initiation zone near the axon hillock into the dendritic tree makes it all the way to the synapse. If, however, a synapse is so distal from the soma that backpropagating action potentials fail and propagate passively, then it may not sufficiently depolarize NMDA receptors in the spine to allow opening and calcium influx (Golding et al., 2002; Sjöström and Häusser, 2006). The prevalence of such failures of action potential backpropagation depend on the biophysical properties and morphology of the dendritic arbor, on sub and suprathreshold activity patterns, as well as on neuromodulatory state (Sjöström et al., 2008). For example, dendritic depolarization may boost otherwise failing backpropagating action potentials, thus promoting LTP of suitably timed synaptic inputs in the distal dendritic tree (Sjöström and Häusser, 2006). This is not to say that backpropagating action potentials are necessarily critical for NMDA-receptor-based LTP; local dendritic spikes may entirely replace them, at least under some circumstances (Golding et al., 2002). STDP, however, is by definition dependent on relatively global action potentials in the postsynaptic cell.

VOLTAGE DEPENDENCE AND COOPERATIVITY IN STDP

Classically, NMDA-receptor-based synaptic plasticity is closely connected to the degree of activation of the postsynaptic cell: Moderate depolarization only partially opens NMDA receptors, resulting in

relatively low calcium levels and in LTD, whereas strong depolarization results in more massive calcium responses and in LTP (Artola et al., 1990; also see above). In keeping with this, pairing presynaptic spikes with subthreshold postsynaptic depolarization results in timing dependent depression (Markram et al., 1997; Sjöström et al., 2004).

Another hallmark feature of classical LTP is cooperativity; the notion that high-frequency stimulation of a weak pathway results in LTP only if in synchrony with a stronger pathway (McNaughton et al., 1978). Some have argued that this requirement for cooperativity among inputs to reach the threshold for LTP is a reflection of a need to reach the postsynaptic spike threshold. If this line of reasoning were true, then STDP should not exhibit a cooperativity requirement, since there is by definition always postsynaptic spiking. It turns out, however, that neocortical STDP does require a sufficient number of inputs to be co-activated in order to elicit LTP, even in the presence of postsynaptic spiking (Sjöström et al., 2001). It has been demonstrated that this cooperativity requirement in STDP arises due to a voltage dependence, so that large depolarizations (e.g., due to a large number of synchronous inputs) enable potentiation, whereas small ones fail to do so (Sjöström et al., 2001). This voltage dependence is at least in part due to the fact that action potentials backpropagate decrementally into the dendritic tree unless they are boosted by a relatively depolarized dendritic state (Sjöström and Häusser, 2006). In other words, in STDP, the backpropagating action potential may require help to make it to the synapse, especially for synapses far from the soma, otherwise it cannot sufficiently depolarize the spine coincidence detector to trigger potentiation.

Although it is relatively well-established that STDP is voltage-dependent and that backpropagating action potentials are crucial, it is unclear to what extent other voltage-dependent mechanisms contribute. For example, calcium influx directly mediated by voltage-dependent calcium channels may contribute. Another open question is if a form of STDP exists for local dendritic spikes, i.e., in the absence of postsynaptic spiking output (cf. Golding et al., 2002).

INDUCTION VERSUS EXPRESSION OF LONG-TERM POTENTIATION

By and large, STDP refers to an experimental plasticity induction protocol. It may thus be tempting to conclude that the controversial question of how synaptic plasticity is expressed – in particular the so-called pre versus post debate in LTP (Malenka and Nicoll, 1999) – is not relevant to STDP models. Such a conclusion, however, may be hasty.

Although it has been disputed on good grounds (e.g., Bolshakov and Siegelbaum, 1994), the canonical view remains that LTP at Schaeffer collateral inputs to CA1 pyramidal cells is postsynaptically expressed (Malenka and Nicoll, 1999). In this view, potentiation is a simple synaptic gain control that underlies information storage in the brain.

With presynaptic LTP, however, the situation is considerably more complex, because presynaptic LTP does not only change the synaptic gain, it also affects information transfer across the synapse. At excitatory connections of neocortical layer-5, LTP is apparently expressed through an upregulation of the probability of release, thus resulting in an increase of short-term depression, a concept known as Redistribution of Synaptic Efficacy (RSE; Markram and Tsodyks, 1996). Consistent with this finding, the induction of timing dependent depression at layer-5 synapses in visual cortex results in a long-term down regulation of short-term depression through an apparent decrease of the probability of release (Sjöström et al., 2003), which is in effect anti-RSE.

Since short-term depression effectively differentiates rates on a given input with respect to time, this may lead to brief onset and offset bursts of activity in the postsynaptic cell as input rates change (Abbott et al., 1997). A cell with short-term depressing inputs thus becomes an efficient coherence detector (Markram and Tsodyks, 1996; Abbott et al., 1997). By extension, the presence of RSE at its synaptic inputs may thus make a neuron more sensitive to input coherence (Markram and Tsodyks, 1996), while anti-RSE (Sjöström et al., 2003) may do the opposite.

The up or down regulation of short-term depression in a network of connected neurons would presumably alter the statistics of spike-timing dramatically. Given the acute sensitivity of STDP to spike-timing, it thus follows that a network with STDP triggering RSE may result in complex loops between STDP and network activity. The ensuing dynamics of activity are likely to be quite different from those in a network where STDP does not trigger RSE. To our knowledge, this possibility and its functional consequences for network coding has not yet been explored, neither theoretically nor experimentally. In fact, most models introduce the synaptic weight as formal parameter that corresponds to the amplitude of the EPSP or the maximum conductance during synaptic transmission. However, if one combines an STDP model with a model of short-term plasticity with several parameters, the term "synaptic weight" is not precise enough, since long-term plasticity may affect the parameters of short-term plasticity differentially. The basic question of what we mean by synaptic weight thus remains to be addressed properly.

MAINTENANCE OF LONG-TERM POTENTIATION

The focus of STDP as an experimental paradigm (and therefore of this article) is the induction of plasticity by suitable protocols. The question of how the changes induced by synaptic plasticity are maintained over a period of hours, weeks, or even years as expected for long-term memory is the topic of Maintenance of synaptic plasticity.

INFLUENCE OF NEUROMODULATORS

Spike-timing dependent plasticity depends on the presence or absence of neuromodulators such as dopamine (Pawlak and Kerr, 2008; Zhang et al., 2009). These studies suggest that neuromodulators are more than simple switches that turn plasticity on or off. Neuromodulation cannot be considered as a simple multiplicative factor. Rather the presence of neuromodulators changes the temporal profile of STDP (Pawlak and Kerr, 2008; Zhang et al., 2009).

The modulation of STDP by a third factor such as dopamine has potentially interesting functional consequences that turn STDP from unsupervised learning into a reward-based learning paradigm (Pfister et al., 2006; Farries and Fairhall, 2007; Florian, 2007; Izhikevich, 2007; Legenstein et al., 2008).

DISCRETE OR CONTINUOUS SYNAPSES

Most models describe the synaptic weight as a continuous variable, although it is quite conceivable that weights are coded in discrete jumps. In fact, certain benefits would arise from such discrete

synaptic weights. For example, bistability of individual synapses would help to assure the long-term stability of synapses over weeks or years in the presence of molecular turnover (Lisman, 1985). While this is a strong argument in favor of discrete synapses it does not preclude that, on a shorter time scale, synaptic weights undergo continuous synaptic depression or facilitation which would be overlaid on the discrete long-term dynamics.

Since in the typical STDP experiment, results are averaged across several synapses, the question of whether single synapses respond to plasticity protocols with discrete or continuous changes cannot readily be answered. There are at least two studies suggesting that synaptic weights onto CA1 pyramidal neurons in the hippocampus are altered in discrete steps (Petersen et al., 1998; O'Connor et al., 2005). Other studies, however, appear to be in disagreement with this view. For example, recent glutamate uncaging experiments suggest that weights change continuously (Tanaka et al., 2008).

Finally, even if weights are discrete, it is difficult to provide conclusive experimental evidence showing stepwise changes in plasticity. The stochastic nature of neurotransmitter release, for example, hampers such experiments, by adding noise to the point that stepwise changes might be masked, although glutamate uncaging would help address this problem. Furthermore, the situation might be complex, and plasticity may for example be discrete postsynaptically and continuous presynaptically. Last but not least, synapses are at different distances from the soma and their corresponding postsynaptic potentials are therefore subjected to different amounts of dendritic filtering as they propagate toward the soma. Since most connections in the brain are made up of more than one synaptic contact, which are made onto different dendritic compartments at different electrotonic distances from the soma, the net result is that any discrete steps that might exist would be exceedingly difficult to find conclusive evidence for experimentally. Even if weights were discrete, synaptic weight distributions would seem continuous and discrete plasticity would appear continuous.

Whether synapses typically are discrete or continuous thus remains an open but very intriguing question.

HISTORY OF STDP

The first experiments with precisely timed pre- and postsynaptic spikes at a millisecond temporal resolution were performed by Markram and Sakmann (1995), Markram et al. (1997) soon followed by others (Bell et al., 1997; Bi and Poo, 1998; Debanne et al., 1998; Zhang et al., 1998). While the first publications on true STDP experiments came out in the mid-1990s temporal requirements for the coincidence of pre- and postsynaptic activity had already been investigated in 1983 in experiments by Levy and Stuart (1983) albeit with a lower temporal resolution using bursts of spikes rather than individual action potentials. These early experiments can be understood as temporally asymmetric Hebbian learning under a rate coding hypothesis, but also as precursors of modern STDP experiments.

The first model using an STDP function with potentiation and depression at a millisecond resolution was published in 1996 (Gerstner et al., 1996). Modelers and theoreticians interested in Hebbian learning have been interested in temporally asymmetric forms of Hebbian learning in the context of sequence learning with pre-before-post LTP for spike patterns (Gerstner et al., 1993) and asymmetric LTP/LTD for behavioral sequences (Abbott and Blum, 1996) and even earlier, already in the mid 1980s, in the context of associative memories (Sompolinsky and Kanter, 1986; Herz et al., 1988; Kleinfeld and Sompolinksy, 1988). In standard attractor networks of memory, the learning rule includes terms of the Hebbian form $f_i(t)f_j(t)$ where $f_j(t)$ and $f_i(t)$ denote the firing rate of pre- and postsynaptic neurons in the rate pattern present at time step t. In order to learn sequences of patterns (or non-stationary attractors) the learning rule should contain terms of the form $f_i(t)f_j(t-1)$, i.e., a form of temporally asymmetric Hebbian learning that correlates the firing rate of the postsynaptic neuron i at time t with that of a presynaptic neuron j during the time step $t-1$ (Sompolinsky and Kanter, 1986; Herz et al., 1988; Kleinfeld and Sompolinksy, 1988). In 1993, Gerstner and van Hemmen started to translate ideas from sequence learning in discrete-time rate models to the case of spiking neurons in continuous time and formulated a learning rule where presynaptic spikes arrival a few milliseconds before postsynaptic firing leads to a potentiation of synapses (Gerstner et al., 1993). Depression of synapses was unspecific and not part of the spike-timing dependent learning rule. For purely theoretical reasons Gerstner and colleagues postulated in a paper submitted to Nature in 1995 that presynaptic spike arrival before postsynaptic firing should lead to potentiation whereas the reverse timing should lead to depression. Referees of that paper asked whether there was any experimental support for this speculation. In the mean time Markram et al. published an abstract in the Society of Neuroscience meeting of 1995, which was then cited by Gerstner et al. so as to convince the referees and the theory paper was published in Nature in 1996 (Gerstner et al., 1996). To our knowledge, this is the first paper that plotted synaptic plasticity as a function of the relative timing of individual pre- and postsynaptic action potentials. The work of Markram that came out in 1995 at the Society of Neuroscience meeting as an abstract (Markram and Sakmann, 1995) and in 1997 as a full article (Markram et al., 1997) was in fact conducted in 1992–1993 while Henry Markram was a postdoctoral fellow in the laboratory of Bert Sakmann.

REFERENCES

Abbott, L. F., and Blum, K. I. (1996). Functional significance of long-term potentiation for sequence learning and prediction. *Cereb. Cortex* 6, 406–416.

Abbott, L. F., and Nelson, S. B. (2000). Synaptic plasticity: taming the beast. *Nat. Neurosci.* 3, 1178–1183.

Abbott, L. F., Varela, J. A., Sen, K., and Nelson, S. B. (1997). Synaptic depression and cortical gain control. *Science* 275, 220–224.

Allen, C. B., Celikel, T., and Feldman, D. E. (2003). Long-term depression induced by sensory deprivation during cortical map plasticity in vivo. *Nat. Neurosci.* 6, 291–299.

Artola, A., Bröcher, S., and Singer, W. (1990). Different voltage-dependent thresholds for inducing long-term depression and long-term potentiation in slices of rat visual cortex. *Nature* 347, 69–72.

Bell, C. C., Han, V. Z., Sugawara, Y., and Grant, K. (1997). Synaptic plasticity in a cerebellum-like structure depends on temporal order. *Nature* 387, 278–281.

Bi, G., and Poo, M. (2001). Synaptic modification of correlated activity: Hebb's postulate revisited. *Annu. Rev. Neurosci.* 24, 139–166.

Bi, G. Q., and Poo, M. M. (1998). Synaptic modifications in cultured hippocampal neurons: dependence on spike timing, synaptic strength, and postsynaptic cell type. *J. Neurosci.* 18, 10464–10472.

Bienenstock, E. L., Cooper, L. N., and Munro, P. W. (1982). Theory for the development of neuron selectivity: orientation specificity and binocular interaction in visual cortex. *J. Neurosci.* 2, 32–48.

Brader, J., Senn, W., and Fusi, S. (2007). Learning real-world stimuli in a neural network with spike-driven synaptic dynamics. *Neural Comput.* 19, 2881–2912.

Caporale, N., and Dan, Y. (2008). Spike timing-dependent plasticity: a Hebbian learning rule. *Annu. Rev. Neurosci.* 31, 25–46.

Clopath, C., Buesing, L., Vasilaki, E., and Gerstner, W. (2010). Connectivity reflects coding: a model of voltage-based spike-timing-dependant-plasticity with homeostasis. *Nat. Neurosci.* 13, 344–352.

Debanne, D., Gähwiler, B. H., and Thompson, S. M. (1998). Long-term synaptic plasticity between pairs of individual CA3 pyramidal cells in rat hippocampal slice cultures. *J. Physiol.* 507, 237–247.

DeMaria, C. D., Soong, T. W., Alseikhan, B. A., Alvania, R. S., and Yue, D. T. (2001). Calmodulin bifurcates the local Ca2+ signal that modulates P/Q-type Ca2+ channels. *Nature* 411, 484–489.

Egger, V., Feldmeyer, D., and Sakmann, B. (1999). Coincidence detection and changes of synaptic efficacy in spiny stellate neurons in rat barrel cortex. *Nat. Neurosci.* 2, 1098–1105.

Farries, M. A., and Fairhall, A. L. (2007). Reinforcement learning with modulated spike timing-dependent synaptic plasticity. *J. Neurophysiol.* 98, 3648–3665.

Feldman, D. E. (2000). Timing-based LTP and LTD at vertical inputs to layer II/III pyramidal cells in rat barrel cortex. *Neuron* 27, 45–56.

Fino, E., Glowinski, J., and Venance, L. (2005). Bidirectional activity-dependent plasticity at corticostriatal synapses. *J. Neurosci.* 25, 11279–11287.

Florian, R. V. (2007). Reinforcement learning through modulation of spike-timing-dependent synaptic plasticity. *Neural Comput.* 19, 1468–1502.

Froemke, R., Poo, M., and Dan, Y. (2005). Spike-timing-dependent synaptic plasticity depends on dendritic location. *Nature* 434, 221–225.

Gerstner, W., Kempter, R., van Hemmen, J. L., and Wagner, H. (1996). A neuronal learning rule for sub-millisecond temporal coding. *Nature* 386, 76–78.

Gerstner, W., Ritz, R., and van Hemmen, J. L. (1993). Why spikes? Hebbian learning and retrieval of time-resolved excitation patterns. *Biol. Cybern.* 69, 503–515.

Golding, N. L., Staff, N. P., and Spruston, N. (2002). Dendritic spikes as a mechanism for cooperative long-term potentiation. *Nature* 418, 326–331.

Graupner, M., and Brunel, N. (2007). STDP in a bistable synapse model based on CaMKII and associated signaling pathways. *PLoS Comput. Biol.* 3, e221. doi: 10.1371/journal.pcbi.0030221

Gütig, R., Aharonov, R., Rotter, S., and Sompolinsky, H. (2003). Learning input correlations through nonlinear nonlinear temporally asymmetric Hebbian plasticity. *J. Neurosci.* 23, 3697–3714.

Guyonneau, R., VanRullen, R., and Thorpe, S. J. (2005). Neurons tune to the earliest spikes through STDP. *Neural Comput.* 17, 859–879.

Hebb, D. O. (1949). *The Organization of Behavior; A Neuropsychological Theory.* New York: Wiley.

Herz, A. V. M., Sulzer, B., Kühn, R., and van Hemmen, J. L. (1988). The Hebb rule: representation of static and dynamic objects in neural nets. *Europhys. Lett.* 7, 663–669.

Holmgren, C. D., and Zilberter, Y. (2001). Coincident spiking activity induces long-term changes in inhibition of neocortical pyramidal cells. *J. Neurosci.* 21, 8270–8277.

Izhikevich, E. (2007). Solving the distal reward problem through linkage of STDP and dopamine signaling. *Cereb. Cortex* 17, 2443–2452.

Izhikevich, E., and Desai, N. (2003). Relating STDP to BCM. *Neural Comput.* 15, 1511–1523.

Jacob, V., Brasier, D. J., Erchova, I., Feldman, D., and Shulz, D. E. (2007). Spike timing-dependent synaptic depression in the in vivo barrel cortex of the rat. *J. Neurosci.* 27, 1271–1284.

Karmarkar, U., and Buonomano, D. V. (2002). A model of spike-timing dependent plasticity: one or two coincidence detectors? *J. Neurophysiol.* 88, 507–513.

Katz, L. C., and Shatz, C. J. (1996). Synaptic activity and the construction of cortical circuits. *Science* 274, 1133–1138.

Kempter, R., Gerstner, W., and van Hemmen, J. L. (1999). Hebbian learning and spiking neurons. *Phys. Rev. E* 59, 4498–4514.

Kempter, R., Gerstner, W., and van Hemmen, J. L. (2001). Intrinsic stabilization of output rates by spike-based Hebbian learning. *Neural Comput.* 13, 2709–2741.

Kistler, W. M., and van Hemmen, J. L. (2000). Modeling synaptic plasticity in conjunction with the timing of pre- and postsynaptic action potentials. *Neural Comput.* 12, 385–405.

Kleinfeld, D., and Sompolinksy, K. (1988). Associative neural network model for the generation of temporal patterns. Theory and application to central pattern generators. *Biophys. J.* 54, 1039–1051.

Koester, H. J., and Sakmann, B. (1998). Calcium dynamics in single spines during coincident pre- and postsynaptic activity depend on relative timing of back-propagating action potentials and subthreshold excitatory postsynaptic potentials. *Proc. Natl. Acad. Sci. U.S.A.* 95, 9596–9601.

Legenstein, R., Pecevski, D., and Maass, W. (2008). A learning theory for reward-modulated spike-timing-dependent plasticity with application to biofeedback. *PLoS Comput. Biol.* 4, e1000180. doi: 10.1371/journal.pcbi.1000180

Letzkus, J. J., Kampa, B. M., and Stuart, G. J. (2006). Learning rules for spike timing-dependent plasticity depend on dendritic synapse location. *J. Neurosci.* 26, 10420–10429.

Levy, W. B., and Steward, O. (1983). Temporal contiguity requirements for long-term associative potentiation/depression in the hippocampus. *Neuroscience* 8, 791–797.

Lisman, J. (. (1989)). A mechanism for the Hebb and the anti-Hebb processes underlying learning and memory. *Proc. Natl. Acad. Sci. U.S.A.* 86, 9574–9578.

Lisman, J. (2003). Long-term potentiation: outstanding questions and attempted synthesis. *Philos. Trans. R. Soc. Lond. B Biol. Sci.* 358, 829–842.

Lisman, J., Schulman, H., and Cline, H. (2002). The molecular basis of CamKII function in synaptic and behavioural memory. *Nat. Rev. Neurosci.* 3, 175–190.

Lisman, J., and Zhabotinsky, A. (2001). A model of synaptic memory: A CaMKII/PP1 switch that potentiates transmission by organizing an AMPA receptor anchoring assembly. *Neuron* 31, 191–201.

Lisman, J. E. (1985). A mechanism for memory storage insensitive to molecular turnover: a bistable autophosphorylating kinase. *Proc. Natl. Acad. Sci. U.S.A.* 82, 3055–3057.

Magee, J. C., and Johnston, D. (1997). A synaptically controlled, associative signal for Hebbian plasticity in hippocampal neurons. *Science* 275, 209–213.

Malenka, R. C., and Nicoll, R. A. (1999). Long-term potentiation–a decade of progress? *Science* 285, 1870–1874.

Markram, H., Lubke, J., Frotscher, M., and Sakmann, B. (1997). Regulation of synaptic efficacy by coincidence of postsynaptic APs and EPSPs. *Science* 275, 213–215.

Markram, H., and Sakmann, B. (1995). Action potentials propagating back into dendrites trigger changes in efficacy. *Soc. Neurosci. Abs.* 21.2.

Markram, H., and Tsodyks, M. (1996). Redistribution of synaptic efficacy between neocortical pyramidal neurons. *Nature* 382, 807–810.

McNaughton, B. L., Douglas, R. M., and Goddard, G. V. (1978). Synaptic enhancement in fascia dentata: cooperativity among coactive afferents. *Brain Res.* 157, 277–293.

Mehta, M. R., Quirk, M., and Wilson, M. (2000). Experience-dependent asymmetric shape of hippocampal receptive fields. *Neuron* 25, 707–715.

Meliza, C. D., and Dan, Y. (2006). Receptive-field modification in rat visual cortex induced by paired visual stimulation and single-cell spiking. *Neuron* 49, 183–189.

Morrison, A., Aertsen, A., and Diesmann, M. (2007). Spike-timing-dependent plasticity in balanced random networks. *Neural Comput.* 19, 1437–1467.

Nevian, T., and Sakmann, B. (2006). Spine Ca2+ signaling in spike-timing-dependent plasticity. *J. Neurosci.* 26, 11001–11013.

Ngezahayo, A., Schachner, M., and Artola, A. (2000). Synaptic activity modulates the induction of bidirectional synaptic changes in adult mouse hippocampus. *J. Neurosci.* 20, 2451–2458.

Nishiyama, M., Hong, K., Mikoshiba, K., Poo, M. M., and Kato, K. (2000). Calcium stores regulate the polarity and input specificity of synaptic modification. *Nature* 408, 584–588.

O'Connor, D., Wittenberg, G., and Wang, S. H. (2005). Graded bidirectional synaptic plasticity is composed of switch-like unitary events. *Proc. Natl. Acad. Sci. U.S.A.* 102, 9679–9684.

Oja, E. (1982). A simplified neuron model as a principal component analyzer. *J. Math. Biol.* 15, 267–273.

Pawlak, V., and Kerr, J. N. D. (2008). Dopamine receptor activation is required for corticostriatal spike-timing-dependent plasticity. *J. Neurosci.* 28, 2435–2446.

Petersen, C., Malenka, R., Nicoll, R., and Hopfield, J. (1998). All-or-none potentiation of ca3-ca1 synapses. *Proc. Natl. Acad. Sci. U.S.A.* 95, 4732–4737.

Pfister, J. P., and Gerstner, W. (2006). Triplets of spikes in a model of spike timing-dependent plasticity. *J. Neurosci.* 26, 9673–9682.

Pfister, J. P., Toyoizumi, T., Barber, D., and Gerstner, W. (2006). Optimal spike-timing dependent plasticity for precise action potential firing in supervised learning. *Neural Comput.* 18, 1309–1339.

Roberts, P. D., and Bell, C. C. (2000). Computational consequences of temporally asymmetric learning rules: II. Sensory image cancellation. *J. Comput. Neurosci.* 9, 67–83.

Rodriguez-Moreno, A., and Paulsen, O. (2008). Spike timing-dependent long-term depression requires presynaptic NMDA receptors. *Nat. Neurosci.* 11, 744–745.

Rubin, J., Gerkin, R., Bi, G., and Chow, C. (2005). Calcium time course as a signal for spike-timing-dependent plasticity. *J. Neurophysiol.* 93, 2600–2613.

Rubin, J., Lee, D. D., and Sompolinsky, H. (2001). Equilibrium properties of temporally asymmetric Hebbian plasticity. *Phys. Rev. Lett.* 86, 364–367.

Schiller, J., Schiller, Y., and Clapham, D. E. (1998). NMDA receptors amplify calcium influx into dendritic spines during associative pre- and post-synaptic activation. *Nat. Neurosci.* 1, 114–118.

Senn, W., Markram, H., and Tsodyks, M. (2001). An algorithm for modifying neurotransmitter release probability based on pre- and post-synaptic spike timing. *Neural Comput.* 13, 35–67.

Senn, W., Tsodyks, M., and Markram, H. (1997). "An algorithm for synaptic modification based on exact timing of pre- and post-synaptic action potentials," in *Artificial Neural Networks – ICANN'97*, eds W. Gerstner, A. Germond, M. Hasler, and J.-D. Nicoud (Heidelberg: Springer), 121–126.

Shouval, H. Z., Bear, M. F., and Cooper, L. N. (2002). A unified theory of NMDA receptor-dependent bidirectional synaptic plasticity. *Proc. Natl. Acad. Sci. U.S.A.* 99, 10831–10836.

Sjöström, P. J., and Häusser, M. (2006). A cooperative switch determines the sign of synaptic plasticity in distal dendrites of neocortical pyramidal neurons. *Neuron* 51, 227–238.

Sjöström, P. J., and Nelson, S. B. (2002). Spike timing, calcium signals and synaptic plasticity. *Curr. Opin. Neurobiol.* 12, 305–314.

Sjöström, P. J., Rancz, E. A., Roth, A., and Häusser, M. (2008). Dendritic excitability and synaptic plasticity. *Physiol. Rev.* 88, 769–840.

Sjöström, P. J., Turrigiano, G. G., and Nelson, S. B. (2001). Rate, timing, and cooperativity jointly determine cortical synaptic plasticity. *Neuron* 32, 1149–1164.

Sjöström, P. J., Turrigiano, G. G., and Nelson, S. B. (2003). Neocortical LTD via coincident activation of presynaptic NMDA and cannabinoid receptors. *Neuron* 39, 641–654.

Sjöström, P. J., Turrigiano, G. G., and Nelson, S. B. (2004). Endocannabinoid-dependent neocortical layer-5 LTD in the absence of postsynaptic spiking. *J. Neurophysiol.* 92, 3338–3343.

Sompolinsky, H., and Kanter, I. (1986). Temporal association in asymmetric neural networks. *Phys. Rev. Lett.* 57, 2861–2864.

Song, S., and Abbott, L. F. (2001). Cortical development and remapping through spike timing-dependent plasticity. *Neuron* 32, 339–350.

Song, S., Miller, K. D., and Abbott, L. F. (2000). Competitive Hebbian learning through spike-timing-dependent synaptic plasticity. *Nat. Neurosci.* 3, 919–926.

Stent, G. S. (1973). A physiological mechanism for Hebb's postulate of learning. *Proc. Natl. Acad. Sci.* 70, 997–1001.

Tanaka, J., Horiike, Y., Matsuzaki, M., Miyazaki, T., Ellis-Davies, G. C., and Kasai, H. (2008). Protein synthesis and neurotrophin-dependent structural plasticity of single dendritic spines. *Science* 319, 1683–1687.

van Rossum, M. C. W., Bi, G. Q., and Turrigiano, G. G. (2000). Stable Hebbian learning from spike timing-dependent plasticity. *J. Neurosci.* 20, 8812–8821.

Wang, H. X., Gerkin, R. C., Nauen, D. W., and Bi, G. Q. (2005). Coactivation and timing-dependent integration of synaptic potentiation and depression. *Nat. Neurosci.* 8, 187–193.

Yuste, R., and Denk, W. (1995). Dendritic spines as basic functional units of neuronal integration. *Nature* 375, 682–684.

Zhang, J. C., Lau, P. M., and Bi, G. Q. (2009). Gain in sensitivity and loss in temporal contrast of stdp by dopaminergic modulation at hippocampal synapses. *Proc. Natl. Acad. Sci. U.S.A.* 106, 13028–13033.

Zhang, L. I., Tao, H. W., Holt, C. E., Harris, W. A., and Poo, M.-M. (1998). A critical window for cooperation and competition among developing retinotectal synapses. *Nature* 395, 37–44.

SCHOLARPEDIA REFERENCES

- LeDoux, J. E. (2008). Amygdala. *Scholarpedia* 3, 2698.
- Milnor, J. W. (2006). Attractor. *Scholarpedia* 1, 1815.
- Eliasmith, C. (2007). Attractor network. *Scholarpedia* 2, 1380.
- Redgrave, P. (2007). Basal ganglia. *Scholarpedia* 2, 1825.
- Blais, B. S., and Cooper, L. (2008). BCM theory. *Scholarpedia* 3, 1570.
- Braitenberg, V. (2007). Brain. *Scholarpedia* 2, 2918.
- Izhikevich, E. M. (2006). Bursting. *Scholarpedia* 1, 1300.
- Meiss, J. (2007). Dynamical systems. *Scholarpedia* 2, 1629.
- Shouval, H. Z. (2009). Maintenance of synaptic plasticity. *Scholarpedia* 4, 1606.
- Eichenbaum, H. (2008). Memory. *Scholarpedia* 3, 1747.
- Shouval, H. Z. (2007). Models of synaptic plasticity. *Scholarpedia* 2, 1605.
- Llinas, R. (2008). Neuron. *Scholarpedia* 3, 1490.
- Purves, D. (2009). Neuroscience. *Scholarpedia* 4, 7204.
- Spruston, N. (2009). Pyramidal neuron. *Scholarpedia* 4, 6130.
- Alonso, J.-M., and Chen, Y. (2009). Receptive field. *Scholarpedia* 4, 5393.
- Holmes, P., and Shea-Brown, E.-T. (2006). Stability. *Scholarpedia* 1, 1838.
- Pikovsky, A., and Rosenblum, M. (2007). Synchronization. *Scholarpedia* 2, 1459.
- Moore, J. W. (2007). Voltage clamp. *Scholarpedia* 2, 3060.

RECOMMENDED READING

Bi, G., and Poo, M. (2001). Synaptic modification of correlated activity: Hebb's postulate revisited. *Annu. Rev. Neurosci.* 24, 139–166.

Dan, Y., and Poo, M.-M. (2004). Spike timing-dependent plasticity of neural circuits. *Neuron* 44, 23–30.

Sjöström, P. J., Rancz, E. A., Roth, A., and Häusser, M. (2008). Dendritic excitability and synaptic plasticity. *Physiol. Rev.* 88, 769–840.

SEE ALSO THE SCHOLARPEDIA ARTICLES ON

Learning, Models of synaptic plasticity, Long-term depression, Long-term potentiation, Memory, Neuron, Synapse, Synaptic plasticity, Maintenance of synaptic plasticity

Sponsored by: Eugene M. Izhikevich, Editor-in-Chief of Scholarpedia, the peer-reviewed open-access encyclopedia

Reviewed by: Anonymous

Accepted on: 2010-02-10 22:28:22 GMT

Retrieved from http://www.scholarpedia.org/w/index.php?title=Spike-timing_dependent_plasticity&oldid=91801

Categories:

- Synapse
- Computational Neuroscience
- Spiking Networks
- Neural Networks
- Neuroscience
- Computational intelligence

frontiers in
SYNAPTIC NEUROSCIENCE

OPINION ARTICLE
published: 07 June 2010
doi: 10.3389/fnsyn.2010.00014

STDP: spiking, timing, rates and beyond

Leon N Cooper*

Department of Physics, Institute for Brain and Neural Systems, Brown University, Providence, RI, USA
**Correspondence: inc@brown.edu*

Our view of the world has changed dramatically since it was realized in the early 1970s that networks of neurons can form mappings that are associative, content addressable and relatively invulnerable to the loss of individual neurons or synapses – thus potential candidates for memory storage in the animal brain (Anderson et al., 1972). But how, we asked ourselves, could such mappings be constructed in networks of neurons? That is, how could the values of vast numbers of synapses be adjusted to obtain a mapping that corresponds to an appropriate memory?

One possibility was that synaptic modification followed the famous Hebbian rule: "When an axon in cell A is near enough to excite cell B and repeatedly and persistently takes part in firing it, some growth process or metabolic change takes place in one or both cells such that A's efficiency in firing B is increased" (Hebb, 1949). Or, "Neurons that fire together wire together." In restricted circumstances this gave a mapping with some of the properties of memory.

But, though Hebb had proposed this idea in 1949, it had hardly become fashionable in the biological community. I recall giving talks on this subject, being greeted with condescending smiles and, perhaps, a pat on the head from established neurophysiologists: "You're very clever young man, but what shred of evidence do you have that synapses modify?" I remember, in particular, an extended conversation with a famous neuroscientist in the late 70s: "We have no evidence whatsoever for Hebbian modification in the ugly little sea snail that I am studying," he would say. (The evidence has since been obtained, Lin and Glanzman, 1994.) I remember, in exasperation, suggesting "Well perhaps that's the difference between an ugly little sea snail and a good looking tenured professor at a major university."

It was evident, of course, that Hebbian modification could be only part of the story, since synapses would grow in strength without bound. Thus one early question was: How would such modification be stabilized? Another question was: How is the required information made available at the synaptic junction? The input rate is locally available. The integrated cell response to the inputs from all of the cell's dendrites is not. Thus, in order for the information required for Hebbian modification to be available locally, I conjectured that it must be propagated backwards (by depolarization or spiking in the direction opposite to the usual information flow) from the cell body to each of the synapses, see **Figure 1** (Cooper, 1973).

Although such conjectures seemed attractive, there was, in fact, little or no evidence for synaptic modification of any kind at that time. The primary question thus became: Can we find any evidence for synaptic modification? If so, what is its form? Further, what is its cellular and molecular basis – thus the cellular and molecular basis for learning and memory storage?

One way to attack these questions lay in the experimental observation that many cortical neurons are selective. Selectivity is relatively common in the nervous system. Hubel and Wiesel (1962, 1970) observed edge detectors in area 17 (V1) of visual cortex of kittens. By the mid 1970s there had already been years of experimentation in visual cortex that had led to two (sometimes controversial) conclusions: In animals with "normal" visual experience, visual cortical neurons are selective and binocular; further, these properties depend on the visual experience of the animal (Blakemore and Cooper, 1970; Hirsch and Spinelli, 1971; Pettigrew and Freeman, 1973; Imbert and Buisseret, 1975).

Thus it seemed that the input–output relations of these neurons could be altered by visual experience – a possible indication of synaptic modification that might be testable experimentally. Could these experience dependent changes in the input–output properties of neurons be attributed to synaptic modification? If so what kind of modification could explain what was seen?

Early models were rate based (von der Malsburg, 1973; Nass and Cooper, 1975; Perez et al., 1975; Cooper et al., 1979). In particular the BCM theory (Bienenstock et al., 1982), created to stabilize Hebbian modification and give the desired neuron selectivity, has diverse consequences that have been shown to be in agreement with observation (Cooper et al., 2004). Essential postulates of BCM are the existence the LTD and LTP regions as well as the sliding modification threshold. These are very simple mathematical requirements but demand rather complicated cell properties. Are they there?

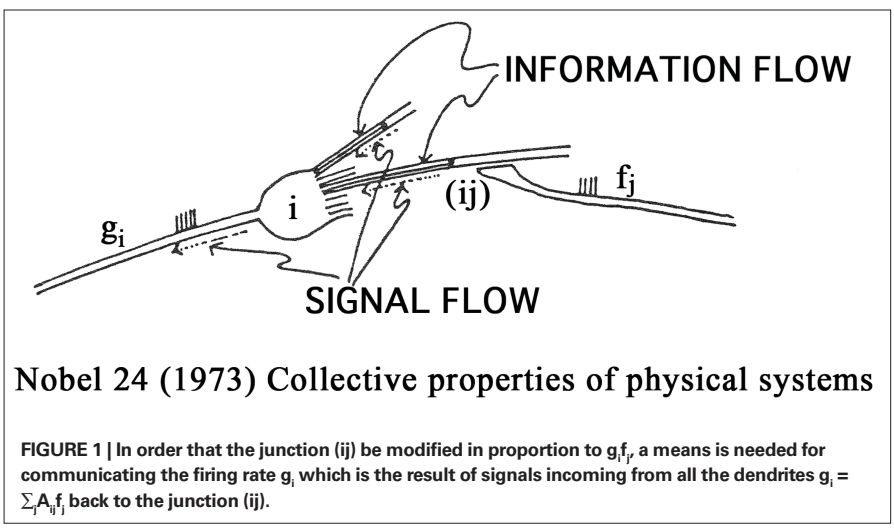

FIGURE 1 | In order that the junction (ij) be modified in proportion to $g_i f_j$, a means is needed for communicating the firing rate g_i which is the result of signals incoming from all the dendrites $g_i = \sum_j A_{ij} f_j$ back to the junction (ij).

Do neurons really possess these properties? While there was experimental evidence for LTP (Bliss and Lømo, 1973), there was little indication that LTD existed in neocortex or Hippocampus. Such questions were the inspiration for the experiments that led to the first observation of LTD and the sliding modification threshold (Dudek and Bear, 1992; Kirkwood et al., 1996).

The existence of the back propagating action potential was established with the work of (Amitai et al., 1993; Kim and Connors, 1993 and Stuart and Sakmann, 1994); it was further shown that this was required for LTP (Magee and Johnson, 1997). Earlier work (Levy and Steward, 1983) had suggested that timing of the various synaptic inputs played a crucial role in LTD and LTP. But the discovery of STDP gave striking confirmation not only of the existence of the back propagating action potential but of its important role in synaptic modification (Markram et al., 1997; Bi and Poo, 1998). As is attested in many articles in this volume the details of synaptic modification depend exquisitely on the timing of the pre-and postsynaptic spikes.

Among the outstanding questions that confront us at the moment is how to obtain STDP synaptic modification as well as BCM type rate-based theories from more fundamental considerations. Attempts in this direction have been made in several ways: One can try to go from STDP spike models to rate-based models such as BCM. In particular, Gerstner and others have made attempts in this direction (Izhikevich and Desai, 2003; Pfister and Gerstner, 2006). In this approach one is confronted with timing problems. For high frequency inputs, for example, which are the pre and which are the postsynaptic spikes? Other attempts to relate spikes to rates as well as to make connections to BCM have been made (Abarbanel et al., 2002; Appleby and Elliott, 2005; Blais et al., 2009).

Another approach is to attempt from fundamental biophysical models to obtain both STDP as well as BCM rate-based models (Castellani et al., 2001; Shouval et al., 2002a,b). In addition to STDP and presynaptic frequency dependent synaptic plasticity, pairing (voltage clamped) induced synaptic plasticity has been observed. Is there is a single underlying mechanism that can account for different methods of inducing synaptic plasticity?

It had been proposed that a moderate elevation of calcium above baseline produces LTD while a larger elevation produces LTP. (Lynch et al., 1983; Geiger and Singer, 1986; Bear et al., 1987; Lisman, 1989). A calcium control hypothesis that can be derived from lower-level molecular models has been shown to be capable of accounting for the plasticity induced using the various induction mechanisms mentioned above (Shouval et al., 2002b). It required an additional assumption that the back propagating action potential have a wide component. Experimental results suggest that in some dendrites back propagating action potentials are wider than in soma (Magee and Johnson, 1997).

The wide component of the back propagating action potential is also capable of explaining the seeming a-causal behavior of the post–pre spike sequence. The pre-post sequence in which the back propagating action potential is presumably initiated at least in part by the pre spike gives the expected LTP. However in the post–pre sequence the post spike might be thought to be produced by spikes arriving at other inputs that should not modify the post–pre site. This would occur if we imagine that the post-signal is accompanied by stochastic pre-signals that initiate both LTD and LTP, giving, on average, no change in the synapse.

It has been suggested that the cellular and molecular basis for LTD and LTP involve changes in the number of postsynaptic AMPA receptors as well as phosphorylation and dephosphorylation of specific gluR1 sites on the AMPA receptors (Nayak et al., 1998; Carroll et al., 1999; Shi et al., 1999; Hayashi et al., 2000; Lee et al., 2000). One possibility for the molecular basis of the sliding modification threshold might be variations of the NR2A/2B ratios since changing the NR2A/2B ratio changes the amounts of current that flow through the NMDA receptors. Experience dependent variations of these ratios that have been observed experimentally (Quinlan et al., 1999; Cho and Bear, 2010). It has also been suggested that the h current may play a role as a basis for the sliding modification threshold (Narayanan et al., 2005).

We thus have a variety of candidates for the cellular and molecular basis for synaptic modification. Among the major remaining questions is to put all of this together in a consistent theory that yields both STDP and rate-based results that is in agreement with observation. And then, of course, this has to be put into networks of neurons to show how we can arrive at brain function, from receptive field formation, learning and memory to mental states including consciousness.

My guess is that we will leave our students a few problems to keep them busy.

REFERENCES

Abarbanel, H., Huerta, R., and Rabinovich, M. I. (2002). Dynamical model of long-term synaptic plasticity. *Proc. Natl. Acad. Sci. U.S.A.* 99, 10132–10137.

Amitai, Y., Friedman, A., Connors, B. W., and Gutnick, M. J. (1993). Regenerative activity in apical dendrites of pyramidal cells in neocortex. *Cereb. Cortex* 3, 26–38.

Anderson, J., Cooper, L. N., Nass, M., Freiberger, W., and Grenender, W. (1972). Some properties of a neural model for memory. AAAS Symposium.

Appleby, P. A., and Elliott, T. (2005). Synaptic and Temporal Ensemble Interpretation of Spike-Timing-Dependent Plasticity. *Neural. Comput.* 17, 2316–2336.

Bear, M. F., Cooper, L. N., and Ebner, F. F. (1987). A physiological basis for a theory of synapse modification. *Science* 237, 42–48.

Bi, G. Q., and, Poo, M. M. (1998). Synaptic modifications in cultured hippocampal neurons: dependence on spike timing, synaptic strength, and postsynaptic cell type. *J. Neurosci.* 18, 10464–10472.

Bienenstock, E. L., Cooper, L. N., and Munro, P. W. (1982). Theory for the development of neuron selectivity: orientation specificity and binocular interaction in visual cortex. *J. Neurosci.* 2, 32–48.

Blais, B. S., Cooper, L. N., and Shouval, H. Z. (2009). Effect of correlated lateral geniculate nucleus firing rates on predictions for monocular eye closure versus monocular retinal inactivation. *Phys. Rev. E Stat. Nonlin. Soft Matter Phys.* 80, 061915-1-9. (see appendix).

Blakemore, C., and Cooper, G. F. (1970). Development of the brain depends on visual environment. *Nature* 228, 477–478.

Bliss, T. V. P., and Lømo, T. (1973). Long-lasting potentiation of synaptic transmission in the dentate area of the anaesthetized rabbit following stimulation of the perforant path. *J. Physiol.* 232, 331–356.

Carroll, R. C., Beattie, E. C., Xia, H., Lüscher, C., Altschuler, Y., Nicoll, R. A., Malenka, R. C., and von Zastrow, M. (1999). Dynamin-dependent endocytosis of ionotropic glutamate receptors. *Proc. Natl. Acad. Sci. U.S.A.* 96, 14112–14117.

Castellani, G. C., Quinlan, E. M., Cooper, L. N., and Shouval, H. Z. (2001). A biophysical model of bidirectional synaptic plasticity: dependence on AMPA and NMDA receptors. *Proc. Natl. Acad. Sci. U.S.A.* 98, 12772–12777.

Cho, K. K. A., and Bear, M. F. (2010). Promoting neurological recovery of function via metaplasticity. *Future Neurobiol.* 5, 21–26.

Cooper, L. N. (1973). "A possible organization of animal memory and learning," in *Nobel Symposium on Collective Properties of Physical Systems*, eds B. Lundquist and S. Lundquist (New York: Academic Press), 252–264.

Cooper, L. N., Intrator, N., Blais, B. S., and Shouval, H. Z. (2004). *Theory of Cortical Plasticity*. Singapore: World Scientific Publishing.

Cooper, L. N., Liberman, F., and Oja, E. (1979). A theory for the acquisition and loss of neuron specificity in visual cortex. *Biol. Cybern.* 33, 9–28.

Dudek, S. M., and Bear, M. F. (1992). Homosynaptic long-term depression in area CA1 of hippocampus and effects of *N*-methyl-D-aspartate receptor blockade. *Proc. Natl. Acad. Sci. U.S.A.* 89, 4363–4367.

Geiger, H., and Singer, W. (1986). A possible role of calcium currents in developmental plasticity. *Exp. Brain Res. Ser.* 14, 256–270.

Hayashi, Y., Shi, S. H., Esteban, J. A., Piccini, A., Poncer, J. C., and Malinow, R. (2000). Driving AMPA receptors into synapses by LTP and CaMKII: requirement for GluR1 and PDZ domain interaction. *Science* 287, 2262.

Hebb, D. O. (1949). *The Organization of Behavior*. New York: Wiley.

Hirsch, H. V. B., and Spinelli, D. N. (1971). Modification of the distribution of receptive field orientation in cats by selective visual exposure during development. *Exp. Brain Res.* 12, 509–527.

Hubel, D. H., and Wiesel, T. N. (1962). Receptive fields, binocular interaction and functional architecture in the cat's visual cortex. *J. Physiol. (Lond.)* 160, 106–154.

Hubel, D. H., and Wiesel, T. N. (1970). The period of susceptibility to the physiological effects of unilateral eye closure in kittens. *J. Physiol. (Lond.)* 206, 419–436.

Imbert, M., and Buisseret, P. (1975). Receptive field characteristics and plastic properties of visual cortical cells in kittens reared with or without visual experience. *Exp. Brain Res.* 22, 2–36.

Izhikevich, E., and Desai, N. (2003). Relating STDP to BCM. *Neural Comput.* 15, 1511–1523.

Kim, H. G., and Connors, B. W. (1993). Apical dendrites of the neocortex: correlation between sodium-, and calcium-dependent spiking, and pyramidal cell morphology. *J. Neurosci.* 13, 5301–5311.

Kirkwood, A., Rioult, M. G., and Bear, M. F. (1996). Experience-dependent modification of synaptic plasticity in visual cortex. *Nature* 381, 526–528.

Lee, H. K., Barbarosie, M., Kameyama, K., Bear, M. F., and Huganir, R. (2000). Regulation of distinct AMPA receptor phosphorylation sites during bidirectional synaptic plasticity. *Nature* 405, 955–959.

Levy, W. B., and Steward, O. (1983). Temporal contiguity requirements for long-term associative potentiation/depression in the hippocampus. *Neuroscience* 8, 791–797.

Lin, X. Y., and Glanzman, D. L. (1994). Long-term potentiation of Aplysia sensorimotor synapses in cell culture: regulation by postsynaptic voltage. *Proc. Biol. Sci.* 255, 113–118.

Lisman, J. A. (1989). A mechanism for the Hebb and the anti-Hebb processes underlying learning and memory. *Proc. Natl. Acad. Sci. U.S.A.* 86, 9574–9578.

Lynch, G., Larson, J., Kelso, S., Barrionuevo, G., and Schottler, F. (1983). Intracellular injections of EGTA block induction of hippocampal long-term potentiation. *Nature* 305, 719–721.

Magee, J., and Johnson, D. (1997). A synaptically controlled, associative signal for Hebbian plasticity in hippocampal neurons. *Science* 275, 209–213.

Markram, H., Lubke, J., Frotscher, M., and Sakmann, B. (1997). Regulation of synaptic efficacy by coincidence of postsynaptic APs and EPSPs. *Science* 275, 213–215.

Narayanan, R., Brager, D. H., Fan, Y., and Johnston, D. (2005). I_h as a candidate mechanism for sliding the BCM modification threshold. *Soc. Neurosci. Abstr.* 737.5.

Nass, M., and Cooper, L. N. (1975). A theory for the development of feature detecting cells in visual cortex. *Biol. Cybern.* 19, 1.

Nayak, A., Zastrow, D., Lickteig, R., Zahniser, N., and Browning, M. (1998). Maintenance of late-phase LTP is accompanied by PKA-dependent increase in AMPA receptor synthesis. *Nature* 394, 680–683.

Perez, R., Glass, L., and Shlaer, R. J. (1975). Development of specificity in the cat visual cortex. *J. Math. Biol.* 1, 275–288.

Pettigrew, J. D., and Freeman, R. D. (1973). Visual experience without lines: Effects on developing cortical neurons. *Science* 182, 599–601.

Pfister, J. P., and Gerstner, W. (2006). Triplets of spikes in a model of spike timing-dependent plasticity. *J. Neurosci.* 26, 9673–9682.

Quinlan, E. M., Philpot, B. D., Huganir, R. L., and Bear, M. F. (1999). Rapid, experience-dependent expression of synaptic NMDA receptors in visual cortex in vivo. *Nat. Neurosci.* 2, 352–357.

Shi, S. H., Hayashi, Y., Petralia, R. S., Zaman, S. H., Wenthold, R. J., Svoboda, K., and Malinow, R. (1999). Rapid spine delivery and redistribution of AMPA receptors after synaptic NMDA receptor activation. *Science* 284, 1811.

Shouval, H. Z., Bear, M. F., and Cooper, L. N. (2002a). A unified model of NMDA receptor-dependent bidirectional synaptic plasticity. *Proc. Natl. Acad. Sci. U.S.A.* 99, 10831–10836.

Shouval, H. Z., Castellani, G. C., Blais, B. S., Yeung, L. C., and Cooper, L. N. (2002b). Converging evidence for a simplified biophysical model of synaptic plasticity. *Biol. Cybern.* 87, 383–391.

Stuart, G., and Sakmann, B. (1994). Active propagation of somatic action potentials into neocortical pyramidal cell dendrites. *Nature* 367, 69–72.

von der Malsburg, C. (1973). Self-organization of orientation sensitive cells in the striate cortex. *Kybernetik* 14, 85–100.

Received: 23 March 2010; accepted: 19 May 2010; published online: 07 June 2010.

Citation: Cooper LN (2010) STDP: spiking, timing, rates and beyond Front. Syn. Neurosci. ***2****:14. doi: 10.3389/fnsyn.2010.00014*

frontiers in
SYNAPTIC NEUROSCIENCE

OPINION ARTICLE
published: 02 December 2010
doi: 10.3389/fnsyn.2010.00149

Discovering associative long-term synaptic modification and timing dependence of plasticity – a very brief and personal history

William B Levy*[1,2]

[1] *Department of Neurosurgery, University of Virginia, Charlottesville, VA, USA*
[2] *Department of Psychology, University of Virginia, Charlottesville, VA, USA*
**Correspondence: wlevy@informedsimplifications.com*

My long-term career goal was, and is, to construct credible quantitative theories of the biological basis of cognitive function. My approach is severely reductive which was a problem early on. We knew nothing about associative synaptic modification, the heart and soul of such cognitive theories. So motivated, I went to Virginia to work with my good friend Oswald Steward. In particular, I wanted to improve upon the observations of McNaughton (1977). His primary result was a demonstration of the intensity-dependence of long-term potentiation (LTP; a result that Bliss et al., 1973 looked for and somehow missed).

Before arriving in Virginia, I knew a two-stimulating-electrode experiment (using provably independent and non-overlapping inputs) was necessary to produce an unequivocal demonstration of associative LTP. Unfortunately, I had no specific idea of how to do the experiment. When Ossie explained his discovery of the crossed entorhinal cortex to dentate gyrus pathway and showed me the baseline physiology ongoing in his lab, I seized on the opportunity presented by two independent monosynaptic pathways suitable for associative studies. A small number of layer II cells project monosynaptically to the ipsilateral and contralateral dentate gyrus. Using a one stimulating electrode in the left dentate gyrus and a second stimulating electrode in the right dentate gyrus yielded the necessary independent monosynaptic excitatory pathways converging on the same postsynaptic neurons. Although we began with just the intention of studying LTP, we quickly discovered a postsynaptic-dependent, synaptic long-term depression. This discovery was essentially unavoidable due to all the controls built into studying the bilateral path on both sides of the brain and studying the effect of brief high frequency stimulation of just one entorhinal cortex while recording from both the left and right dentate gyri. In essence, we were running two experiments at once, one by recording from the left dentate gyrus and one by recording from the right dentate gyrus. As we were finishing up the manuscript for this work (Levy and Steward, 1983), I began thinking about the next study, and these thoughts must have been influenced by my earlier training.

As background, there were my undergraduate studies in psychology and an awareness that stimuli used for conditioning worked best if they preceded a shock in negative reinforcement or a reactivated pressable lever for positive reinforcement. I also knew the Pavlovian paradigms (see discussion in Levy and Steward, 1983) and was aware of associative timing experiments in this behavioral context.

Once again, by recording on both sides of the brain while performing an associative timing experiment, we automatically examined a pre-then-post as well as a post-then-pre activity paradigm. That is, if the left stimulating electrode was active before the right stimulating electrode, then recording from the left dentate gyrus was a depression paradigm while recording from the right dentate gyrus was a potentiation paradigm. Thus the spike-timing effect was discovered. The published experiments themselves were completed before the end of 1980 and were reported at a wonderful little gathering in 1981 at Brown University (hosted by Leon Cooper and eventually published in 1985; Levy, 1985).

Shortly after our publication, in which postsynaptic cell firing in the dentate gyrus was controlled by each ipsilateral pathway, Gustafsson et al. (1987) published a timing study in CA1. They used intracellular control of postsynaptic excitation. However, their temporal resolution was lower than our work. With later studies came higher temporal resolution (Bi and Poo, 1998). Our later work showed that the accuracy of timing was better than 20 ms and – by using large, multiple TTX injections – that we really were in complete control of the EC inputs (Lopez et al., 1990). Another pretty set of studies by Ossie's student Geoff White show that STDP could be localized within a dendritic region (White et al., 1988, 1990). Later in the decade, Holmes and Levy (1990) worked out the biophysics of the potentiation portion of the spike timing rule.

My major experimental regret is the drug experiments that I shunned early on (but see Desmond et al., 1991). My undergraduate and graduate experience with neuropharmacology left me with skepticism concerning drug specificity, and I was mistaken not to accept and use the rapidly developing glutamate receptor pharmacology of the early 1980s. Nevertheless, the two original Levy and Steward (1979, 1983) studies were enough to embark on my goal of quantitative modeling with half of the STDP playing a major role in later theoretical work (Levy and Desmond, 1985; Levy, 1989; Levy et al., 1990).

REFERENCES

Bi, G. Q., and Poo, M. M. (1998). Synaptic modification in cultured hippocampal neurons: dependence on spike timing, synaptic strength, and postsynaptic cell type. *J. Neurosci.* 18, 10464–10472.

Bliss, T. V. P., and Lømo, T. (1973). Long-lasting potentiation of synaptic transmission in the dentate area of the anaesthetized rabbit following stimulation of the perforant path. *J. Physiol.* 232, 331–356.

Desmond, N. L., Colbert, C. M., Zhang, D. X., and Levy, W. B. (1991). NMDA receptor antagonists block the induction of long-term depression in the hippocampal dentate gyrus of the anesthetized rat. *Brain Res.* 552, 93–98.

Gustafsson, B., Wigström, H., Abraham, W. C., and Huang, Y.-Y. (1987). Long-term potentiation in the hippocampus using depolarizing current pulses as the conditioning stimulus to single volley synaptic potentials. *J. Neurosci.* 7, 774–780.

Holmes, W. R., and Levy, W. B. (1990). Insights into associative long-term potentiation from computational

models of NMDA receptor-mediated calcium influx and intracellular calcium concentration changes. *J. Neurophysiol.* 63, 1148–1168.

Levy, W. B. (1985). "Associative changes at the synapse: LTP in the hippocampus," in *Synaptic Modification, Neuron Selectivity and Nervous System Organization*, eds W. B Levy, J. Anderson, and S. Lehmkuhle (Hillsdale, NJ: Lawrence Erlbaum Assoc., Inc.), 5–33.

Levy, W. B. (1989). "A computational approach to hippocampal function," in *Computational Models of Learning in Simple Neural Systems*, eds R. D. Hawkins and G. H. Bower (New York: Academic Press), 243–305.

Levy, W. B., Colbert, C. M., and Desmond, N. L. (1990). "Elemental adaptive processes of neurons and synapses: a statistical/computational perspective," in: *Neuroscience and Connectionist Models*, eds M. A. Gluck and D. E. Rumelhart (Hillsdale, NJ: Lawrence Erlbaum Assoc., Inc.), 187–235.

Levy, W. B., and Desmond, N. L. (1985). "The rules of elemental synaptic plasticity," in *Synaptic Modification, Neuron Selectivity and Nervous System Organization*, eds W. B Levy, J. Anderson, and S. Lehmkuhle (Hillsdale, NJ: Lawrence Erlbaum Assoc., Inc.), 105–121.

Levy, W. B., and Steward, O. (1979). Synapses as associative memory elements in the hippocampal formation. *Brain Res.* 175, 233–245.

Levy, W. B., and Steward, O. (1983). Temporal contiguity requirements for long-term associative potentiation/depression in the hippocampus. *Neuroscience* 8, 791–797.

Lopez, H. S., Burger, B., Dickstein, R., Desmond, N. L., and Levy, W. B. (1990). Associative synaptic potentiation and depression: quantification of dissociable modifications in the hippocampal dentate gyrus favors a particular class of synaptic modification equations. *Synapse* 5, 33–47.

McNaughton, B. L. (1977). Dissociation of short-and long-lasting modification of synaptic efficacy at the terminals of the perforant path. *Seventh Annual Meeting of the Society for Neuroscience*, Anaheim, CA, Abstract.

White, G., Levy, W. B., and Steward, O. (1988). Evidence that associative interactions between synapses during the induction of long-term potentiation occur within local dendritic domains. *Proc. Natl. Acad. Sci. U.S.A.* 85, 2368–2372.

White, G., Levy, W. B., and Steward, O. (1990). Spatial overlap between populations of synapses determines the extent of their associative interaction during the induction of long term potentiation and depression. *J. Neurophysiol.* 64, 1186–1198.

Received: 07 September 2010; accepted: 05 November 2010; published online: 02 December 2010.

*Citation: Levy WB (2010) Discovering associative long-term synaptic modification and timing dependence of plasticity – a very brief and personal history. Front. Syn. Neurosci. **2**:149. doi: 10.3389/fnsyn.2010.00149*

frontiers in
SYNAPTIC NEUROSCIENCE

OPINION ARTICLE
published: 09 December 2010
doi: 10.3389/fnsyn.2010.00151

From Hebb rules to spike-timing-dependent plasticity: a personal account

Wulfram Gerstner*

Laboratory of Computational Neuroscience, Brain Mind Institute, École Polytechnique Fédérale de Lausanne, Lausanne, Switzerland
**Correspondence: wulfram.gerstner@epfl.ch*

For my master thesis in physics, I spent my days in an experimental lab working with electronics, liquid nitrogen, vacuum pumps, and tiny semiconductor lasers. It seemed every day another component of the set-up would fail–I felt utterly misplaced. But then a friend told me about an a fascinating new field in physics that linked statistical physics to brain science. It was an exciting period: the papers by Hopfield (Hopfield, 1982) and their mathematical analysis (Amit et al., 1985) were all new, and the Kohonen self-organizing map (Kohonen, 1984) was analyzed by physicists next door (Ritter and Schulten, 1988). In 1988, I decided to change field and apply my theoretical modeling skills to neuroscience.

I learned the tricks of mathematical analysis of Hopfield networks during an internship with Leo van Hemmen at the university of Munich early in 1989, which filled the time before I started a one-year stay as a visiting scholar at Berkeley in the lab of Bill Bialek. The hot topic in Munich (Herz et al., 1989) as well as in some other labs (Kleinfeld, 1986; Sompolinsky and Kanter, 1986) was an extension of the Hopfield model so as to store memories not in the form of stationary attractors, but as sequences of activity patterns (Herz et al., 1989). The networks were constructed with binary neurons that are either "on" or "off" and evolved in discrete time. Andreas Herz, who was then a student of Leo van Hemmen's, discovered that, when signal transmission delays are correctly taken into account, both static and dynamic memories can be stored by the same Hebb rule (Herz et al., 1989). But what puzzled me at that time was the assumption of discrete time: Is it 1 ms per memory pattern or 2 ms, why not 20 or 0.5 ms? What sets this time scale?

When I moved to Berkeley in the summer of 1989, I was strongly impressed by the ideas of spike-based coding (Bialek et al., 1991), a topic of intense discussions in the Bialek lab at that time. My personal goal became to translate Hopfield models into spiking networks where the intrinsic neuronal time scale would be clearly defined (Gerstner, 1991; Gerstner and van Hemmen, 1992). After my return to Munich, I wondered whether my spiking networks would be able to learn spatio-temporal spike patterns. In analogy to earlier work on sequence learning (Herz et al., 1991), I realized that this would only be possible if I used a Hebbian learning rule which reflects the causality principle implicit in Hebb's formulation: the timing must be such that synapses that contribute to firing the postsynaptic neuron are maximally strengthened. Hence long-term potentiation (LTP) must be maximal if the spike arrives at the synapse 1 or 2 ms *before* the postsynaptic spike so as to compensate for the rise time of the excitatory postsynaptic potential (Gerstner et al., 1993). The timing conditions were summarized in a figure, reprinted here as **Figure 1**. I also realized that I needed to postulate a back propagating action potential, so as to inform the synapse about the timing of postsynaptic spikes. For the sake of a little anecdote: one referee did not like such a naive postulate and asked me to mention explicitly that such a back propagating spike had never been found – so that's what I wrote in the 1993 paper (Gerstner et al., 1993). Interestingly, 20 years earlier Leon Cooper had also seen the need to transmit information to the site of the synapse, but formulated his idea in a rate-coding picture (Cooper, 1973).

In the 1993 paper, I assumed some unspecified chemical process that would set the "window of coincidences" for the causal pre-before-post situation. I postulated a coincidence window for asymmetric Hebbian learning with millisecond resolution, in order for the network to learn on this time scale. In the summer of 1994, Hermann Wagner, a barn owl expert, joined the Technical University of Munich for a sabbatical. He told us about the astonishing capacity of the owl's auditory system to resolve time on the sub-millisecond scale, which is necessary to locate prey in complete darkness. Different neurons in the auditory nucleus in charge of detecting coincidences between spikes arriving from the left and right ears have different receptive fields in the temporal domain – for the theoreticians in the group of Leo van Hemmen a wonderful challenge.

Von der Malsburg, Kohonen, Bienenstock and colleagues as well as many others (von der Malsburg, 1973; Willshaw and von der Malsburg, 1976; Bienenstock et al., 1982; Kohonen, 1984) had shown in the 1970s and 1980s that the development of spatial receptive fields can be described by models based on Hebbian learning, but how could learning be possible for spiking neurons that have to learn features in the temporal domain? That was the topic of many discussions in the lab, in particular with Richard Kempter, a bright PhD student. From my previous experience with referees, it was clear that I could not simply postulate a Hebbian coincidence window of learning with a resolution of 10 μs to solve the task of learning temporal structures at that time scale – time constants in the auditory nuclei are faster than in visual cortex, but probably do not go below 1 ms.

After several nights of intense thinking, I suggested one morning to Richard that we should somehow exploit competition between good and bad timings, similar to spatial competition in networks with center excitation and surround inhibition, but translated to the problem of learning in the temporal domain. We therefore postulated what we called a Hebbian learning window with two regimes: good timings (i.e., presynaptic spikes arriving just before a postsynaptic firing event) should lead to a potentiation of the synapses, while bad timings (presynaptic spikes arriving after a postsynaptic spike) should lead to depression. Richard implemented the idea in a simulation and it worked

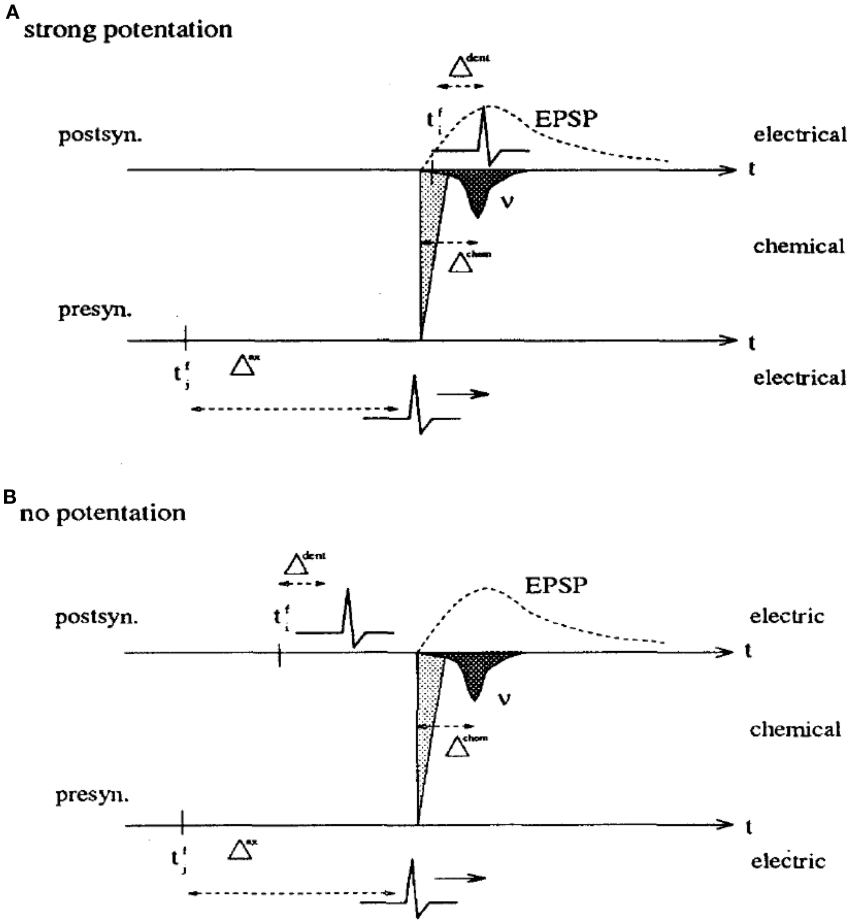

FIGURE 1 | A copy of Figure 3 in Gerstner et al. (1993) with caption: Hebbian learning at the synapse. The presynaptic neuron j fires at time t_j^f and the postsynaptic neuron i at t_i^f. It takes a time Δ^{ax} and Δ^{dent}, respectively, before the signal arrives at the synapse. At the presynaptic terminal neurotransmitter is released (shaded) and evokes an EPSP (dashed) at the postsynaptic neuron. In **(A)** the dendritic spike arrives slightly after the neurotransmitter release and matches the time window defined by some chemical processes, so the synaptic efficacy is enhanced. In **(B)** the postsynaptic neuron fired too early and no strengthening of the synapse occurs.

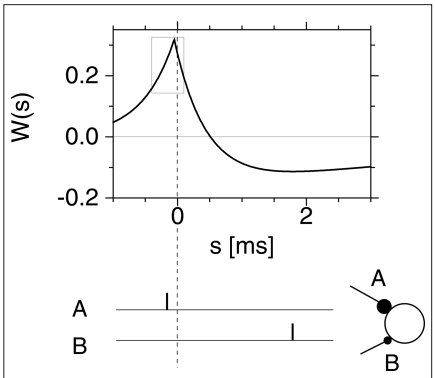

FIGURE 2 | A copy of Figure 2d in Gerstner et al. (1996), with caption: "The postsynaptic firing occurs at time $s = 0$ (vertical dashed line). Learning is most efficient if presynaptic spikes arrive shortly before the postsynaptic neuron starts firing as in synapse A. Another synapse B which fires after the postsynaptic spike is weakened."

beautifully. The graph of our hypothetical Spike-Timing-Dependent Plasticity (STDP) function as published in 1996 is included here as **Figure 2**.

We submitted our results in May 1995 to the 8th Neural Information Processing Conference (NIPS8) where we presented them in December that year (Kempter et al., 1996). The writing of the full paper started in the summer of 1995, before I left for a short postdoctoral period at Brandeis, where I stayed from September to December 1995. By the time we finally submitted the paper in February 1996, an abstract of Henry Markram and Bert Sakmann had been published in the Society of Neuroscience meeting from November 1995, which we cited in the final version of our manuscript, together with the paper of Debanne et al. (1994) for synaptic depression, so as to convince the referees that our assumptions were not entirely outrageous. For some reason, we missed to cite the paper of Levy and Stewart (Levy and Stewart, 1983).

While at Brandeis, I also learned that Larry Abbott and Kenny Blum had been working on ideas of asymmetric Hebbian learning in the context of hippocampal circuits involved in a navigation problem (Abbott and Blum, 1996). The Abbott-Blum paper from 1996 is formulated in a rate-coding picture and implements asymmetric Hebbian learning with a time window for LTP for pre-before-post (and the possibility of LTD for reverse timing) in the range of a few hundred milliseconds or a few seconds, but the formalism can easily be reinterpreted as STDP. When I joined Brandeis in 1995, the paper was already submitted and Kenny Blum had left, but Larry Abbott and myself continued this line of work together (Gerstner and Abbott, 1997).

REFERENCES

Abbott, L. F., and Blum, K. I. (1996). Functional significance of long-term potentiation for sequence learning and prediction. *Cereb. Cortex* 6, 406–416.

Amit, D. J., Gutfreund, H., and Sompolinsky, H. (1985). Spin–glass models of neural networks. *Phys. Rev. A* 32, 1007–1032.

Bialek, W., Rieke, F., de Ruyter van Stevenick, R. R., and Warland, D. (1991). Reading a neural code. *Science* 252, 1854–1857.

Bienenstock, E. L., Cooper, L. N., and Munroe, P. W. (1982). Theory of the development of neuron selectivity: orientation specificity and binocular interaction in visual cortex. *J. Neurosci.* 2, 32–48.

Cooper, L. N. (1973) "A possible organization of animal memory and learning," in *Nobel Symposium on Collective Properties of Physical Systems*, eds B. Lundquist and S. Lundquist (New York: Academic Press), 252–264.

Debanne, D., Gähwiler, B. H., and Thompson, S. M. (1994). Asynchronous pre- and postsynaptic activity induces associative long-term depression in area CA1 of the rat Hippocampus in vitro. *Proc. Natl. Acad. Sci. U.S.A.* 91, 1148–1152.

Gerstner, W. (1991) "Associative memory in a network of "biological" neurons," in *Advances in Neural Information Processing Systems 3*, Conference in Denver 1990, eds R. P. Lippmann, J. E. Moody, and D. S. Touretzky (San Mateo, CA: Morgan Kaufmann Publishers), 84–90.

Gerstner, W., and Abbott, L. F. (1997). Learning navigational maps through potentiation and modulation of hippocampal place cells. *J. Comput. Neurosci.* 4, 79–94.

Gerstner, W., Kempter, R., van Hemmen, J. L., and Wagner, H. (1996). A neuronal learning rule for sub-millisecond temporal coding. *Nature* 383, 76–78.

Gerstner, W., Ritz, R., and van Hemmen, J. L. (1993). Why spikes? Hebbian learning and retrieval of time–resolved excitation patterns. *Biol. Cybern.* 69, 503–515.

Gerstner, W., and van Hemmen, J. L. (1992). Associative memory in a network of "spiking" neurons. *Network* 3, 139–164.

Herz, A. V. M., Li, Z., and van Hemmen, J. L. (1991). Statistical mechanics of temporal association in neural networks with transmission delays. *Phys. Rev. Lett.* 66, 1370–1373.

Herz, A. V. M., Sulzer, B., Kühn, R., and van Hemmen, J. L. (1989). Hebbian learning reconsidered: representation of static and dynamic objects in associative neural nets. *Biol. Cybern.* 60, 457–467.

Hopfield, J. J. (1982). Neural networks and physical systems with emergent collective computational abilities. *Proc. Natl. Acad. Sci. U.S.A.* 79, 2554–2558.

Kempter, R., Gerstner, W., van Hemmen, J. L., and Wagner, H. (1996). "Temporal coding in the sub-millisecond range: model of barn owl auditory pathway," in *Advances in Neural Information Processing Systems 8*, conference in Denver 1995, (Cambridge: MIT Press), 124–130.

Kleinfeld, D. (1986). Sequential state generation by model neural networks. *Proc. Natl. Acad. Sci. U.S.A.* 83, 9469–9473.

Kohonen, T. (1984). *Self-Organization and Associative Memory*. Berlin, Heidelberg, New York: Springer-Verlag.

Levy, W. B., and Stewart, D. (1983). Temporal contiguity requirements for long-term associative potentiation/depression in hippocampus. *Neuroscience* 8, 791–797.

Ritter, H., and Schulten, K. (1988). Convergency properties of kohonen's topology conserving maps: fluctuations, stability and dimension selection. *Biol. Cybern.* 60, 59–71.

Sompolinsky, H., and Kanter, I. (1986). Temporal association in asymmetric neural networks. *Phys. Rev. Lett.* 57, 2861–2864.

von der Malsburg, C. (1973). Self-organization of orientation selective cells in the striate cortex. *Kybernetik* 14, 85–100.

Willshaw, D. J., and von der Malsburg, C. (1976). How patterned neuronal connections can be set up by self-organization. *Proc. R. Soc. Lond., B, Biol. Sci.* 194, 431–445.

Received: 19 May 2010; accepted: 11 November 2010; published online: 09 December 2010.

*Citation: Gerstner W (2010) From Hebb rules to spike-timing-dependent plasticity: a personal account. Front. Syn. Neurosci. **2**:151. doi: 10.3389/fnsyn.2010.00151*

frontiers in
SYNAPTIC NEUROSCIENCE

PERSPECTIVE ARTICLE
published: 04 October 2010
doi: 10.3389/fnsyn.2010.00140

INTRODUCTION BY CHIEF EDITOR MARY B. KENNEDY

The Editors of the Special Issue on "Spike-Timing Dependent Plasticity," Jesper Sjöström and Henry Markram, asked John Lisman and Nelson Spruston to summarize and elaborate on their 2005 commentary (Lisman, J., and Spruston, N. (2005). Postsynaptic depolarization requirements for LTP and LTD: a critique of spike timing-dependent plasticity. Nat Neurosci 8, 839-841) in light of more recent research. Their manuscript sparked a good deal of discussion in the interactive review forum. Lisman and Spruston responded to the many issues and questions raised by reviewers and the result is a useful and informative exposition of their reservations about the concept of Spike-Timing Dependent Synaptic Plasticity (STDP). Jesper Sjöström agreed to write a reply supporting the utility of the concept. We think the two points of view, not entirely mutually exclusive, provide a healthy debate for the field and we hope readers enjoy it!

Questions about STDP as a general model of synaptic plasticity

John Lisman[1]* and Nelson Spruston[2]

[1] *Department of Biology and Volen Center for Complex Systems, Brandeis University, Waltham, MA, USA*
[2] *Department of Neurobiology and Physiology, Northwestern University, Evanston, IL, USA*

Edited by:
Henry Markram, Ecole Polytechnique Fédérale de Lausanne, Switzerland

Reviewed by:
Niraj S. Desai, The Neurosciences Institute, USA
Dominique Debanne, Aix-Marseille, France
Wulfram Gerstner, Ecole Polytechnique Fédérale de Lausanne, Switzerland
Guo-Qiang Bi, University of Pittsburgh, USA
Per Jesper Sjöström, University College London, UK
Jan M. Schulz, University of Bern, Switzerland

****Correspondence:***
John Lisman, Department of Biology and Volen Center for Complex Systems, Brandeis University, Waltham, MA, USA.
e-mail: lisman@brandeis.edu

According to spike-timing-dependent plasticity (STDP), the timing of the Na^+ spike relative to the EPSP determines whether LTP or LTD will occur. Here, we review our reservations about STDP. Most investigations of this process have been done under conditions in which the spike is evoked by postsynaptic current injection. Under more realistic conditions, in which the spike is evoked by the EPSP, the results do not generally support STDP. For instance, low-frequency stimulation of a group of synapses can cause LTD, not the LTP predicted by the pre-before-post sequence in STDP; this is true regardless of whether or not the EPSP is large enough to produce a Na^+ spike. With stronger or more frequent stimulation, LTP can be induced by the same pre-before-post timing, but in this case block of Na^+ spikes does not necessarily prevent LTP induction. Thus, Na^+ spikes may facilitate LTP and/or LTD under some conditions, but they are not necessary, a finding consistent with their small size relative to the EPSP in many parts of pyramidal cell dendrites. The nature of the dendritic depolarizing events that control bidirectional plasticity is of central importance to understanding neural function. There are several candidates, including backpropagating action potentials, but also dendritic Ca^{2+} spikes, the AMPA receptor-mediated EPSP, and NMDA receptor-mediated EPSPs or spikes. These often appear to be more important than the Na^+ spike in providing the depolarization necessary for plasticity. We thus feel that it is premature to accept STDP-like processes as the major determinant of LTP/LTD.

Keywords: Ca spike, Na spike, NMDA, LTP, LTD

It is well established that depolarization of the postsynaptic neuron can promote LTP by allowing the activation of NMDA receptors. Furthermore, smaller depolarizations may be necessary for the induction of LTD. Given this role of postsynaptic voltage in plasticity, it is important to establish how such depolarization is generated. According to the literal interpretation of Hebb's postulate, postsynaptic action potentials produce the required depolarization. This idea has been made plausible by the finding (Stuart and Sakmann, 1994) that action potentials backpropagate from the soma into the dendrite and can thus affect the synapses there.

The field of STDP developed after the observation that the timing of backpropagating Na^+ spikes relative to the EPSP can determine the sign of synaptic plasticity (reviewed in Caporale and Dan, 2008). It is thus now widely assumed that such spikes are critical in the synaptic plasticity process; indeed, this assumption is the basis of numerous theoretical models. However, there are serious reasons to doubt whether spike timing is a major determinant of synaptic plasticity. Almost all experiments demonstrating STDP have been done under conditions in which the experimenter induces the postsynaptic spike by current injection. If STDP is an important phenomenon, it must also apply when the spike is evoked naturally by the EPSP. In a previous review, we presented a critique of STDP, questioning whether it occurs under such natural conditions (Lisman and Spruston, 2005). We thank the editors of this volume for inviting us to summarize this critique here. In the interest of brevity, we express our concerns about STDP in a series of short questions/answers. Readers wanting additional information should consult our previous review.

1. Question: *Is a Na^+* spike necessary for synaptically induced LTP? Answer: *Eliminating the spike often has no effect* (Golding et al., 2002; Remy and Spruston, 2007; Hardie and Spruston, 2009).
2. Question: *Does the lack of a requirement for the Na^+* spike make sense? Answer: *Yes, because dendritic recordings show that back-propagating action potentials are always brief and often small (especially in distal dendrites) compared to other forms of dendritic depolarization* (Stuart et al., 1997).
3. Question: *Are Na^+* spikes necessary for synaptically induced LTD? Answer: *Not in general. LTD can be induced following low-frequency stimulation with or without spikes* (Dudek and Bear, 1992; Sjöström et al., 2001; Staubli and Ji, 1996; Wittenberg and Wang, 2006). *Na^+* spikes tend to enhance LTD, despite the fact that according to STDP the pre-before-post timing predicts LTP.
4. Question: *Perhaps the spike is unimportant during synaptically induced LTP/LTD, but doesn't the spike do the job in STDP protocols (when the spike is induced by current injection)?* Answer: *The repetition rates typically used are so high that other types of dendritic events such as Ca^{2+}* spikes may be inadvertently induced by summation of EPSPs, complicating the interpretation. If lower repetition rates are used, single spikes no longer induce LTP/LTD unless larger EPSPs are used, suggesting the importance of additional sources of depolarization (Sjöström et al., 2001).
5. Question: *Theoretical work has shown that the causal role of the presynaptic spike in generating the EPSP, which then generates the postsynaptic spike, is an elegant principle; should this concept be revised?* Answer: *Yes, there are cases in which the EPSP evokes a spike, but the result is LTD, not LTP (see question 3) and there are cases when the spike is not necessary for LTP (see question 1). Thus, spike timing is probably not the best approach to modeling synaptic plasticity (see below).*
6. Question: *Theoretical work has shown that the timing relation of presynaptic and postsynaptic events can produce important computations; should this be given up?* Answer: *No. Timing will inevitably be important because of the properties of the NMDA receptor (depolarization before glutamate binding doesn't open the channel, whereas the reverse order does). When we learn what the critical depolarizing event is (or are), timing will certainly be important.*
7. Question: *If the backpropagating spike is not the critical factor for synaptic plasticity, what is?* Answer: *The AMPA-mediated EPSP, NMDA receptor-mediated plateau potentials, and dendritically initiated Ca^{2+}* spikes are plausible candidates (Gordon et al., 2006; Kampa et al., 2007).
8. Question: *Isn't STDP elegant because of its computational consequences?* Answer: *No, it isn't as elegant as it may seem because information can't be read out (by EPSP-evoked spikes) without modifying stored information. If there is a higher threshold for plasticity (e.g., bursts or calcium spikes), it becomes possible to read out information using single spikes without modifying stored information.*
9. Question: *How is the critical source of the postsynaptic depolarization required for plasticity going to be determined?* Answer: *It's a hard problem. Some of the most advanced methods (paired recording and glutamate uncaging) will not suffice because they don't stimulate inhibition. Given the likely role of voltage-dependent conductances (including NMDA receptors), the occurrence and duration of depolarizing events will depend strongly on inhibition, which must therefore be part of the overall story* (Davies et al., 1991; Remondes and Schuman, 2002).

We are encouraged by a recent model that explains a wide range of experimental observations using an approach that does not focus on the backpropagating action potential as the sole source of dendritic depolarization (Clopath et al., 2010). Using a combination of factors related to the pre and postsynaptic membrane potentials (see also Spruston and Cang, 2010), the model explains the dependence of LTP/LTD on stimulus frequency, postsynaptic bursting, and the synaptic depolarization. Future implementations of the model could seek to explain the dependence of synaptic plasticity on specific biophysical events, such as dendritic spikes and inhibition, in compartmental models of neurons with elaborate dendritic trees endowed with a variety of conductances. It will also be of interest to see whether this class of model can also explain why the phase of synaptic stimulation during theta frequency oscillations can determine whether LTP or LTD is induced (Huerta and Lisman, 1995; Hyman et al., 2003; Kwag and Paulsen, 2009).

REFERENCES

Caporale, N., and Dan, Y. (2008). Spike timing-dependent plasticity: a Hebbian learning rule. *Annu. Rev. Neurosci.* 31, 25–46.

Clopath, C., Büsing, L., Vasilaki, E., and Gerstner, W. (2010). Connectivity reflects coding: a model of voltage-based STDP with homeostasis. *Nat. Neurosci.* 13, 344–352.

Davies, C. H., Starkey, S. J., Pozza, M. F., and Collingridge, G. L. (1991). GABA autoreceptors regulate the induction of LTP. *Nature* 349, 609–611.

Dudek, S. M., and Bear, M. F. (1992). Homosynaptic long-term depression in area CA1 of hippocampus and effects of *N*-methyl-D-aspartate receptor blockade. *Proc. Natl. Acad. Sci. U.S.A.* 89, 4363–4367.

Golding, N. L., Staff, N. P., and Spruston, N. (2002). Dendritic spikes as a mechanism for cooperative long-term potentiation. *Nature* 418, 326–331.

Gordon, U., Polsky, A., and Schiller, J. (2006). Plasticity compartments in basal dendrites of neocortical pyramidal neurons. *J. Neurosci.* 26, 12717–12726.

Hardie, J., and Spruston, N. (2009). Synaptic depolarization is more effective than back-propagating action potentials during induction of associative long-term potentiation in hippocampal pyramidal neurons. *J. Neurosci.* 29, 3233–3241.

Huerta, P. T., and Lisman, J. E. (1995). Bidirectional synaptic plasticity induced by a single burst during cholinergic theta oscillation in CA1 in vitro. *Neuron* 15, 1053–1063.

Hyman, J. M., Wyble, B. P., Goyal, V., Rossi, C. A., and Hasselmo, M. E. (2003). Stimulation in hippocampal region CA1 in behaving rats yields long-term potentiation when delivered to the peak of theta and long-term depression when delivered to the trough. *J. Neurosci.* 23, 11725–11731.

Kampa, B. M., Letzkus, J. J., and Stuart, G. J. (2007). Dendritic mechanisms controlling spike-timing-dependent synaptic plasticity. *Trends Neurosci.* 30, 456–463.

Kwag, J., and Paulsen, O. (2009). The timing of external input controls the sign of plasticity at local synapses. *Nat. Neurosci.* 12, 1219–1221.

Lisman, J., and Spruston, N. (2005). Postsynaptic depolarization requirements for LTP and LTD: a critique of spike timing-dependent plasticity. *Nat. Neurosci.* 8, 839–841.

Remondes, M., and Schuman, E. M. (2002). Direct cortical input modulates plasticity and spiking in CA1 pyramidal neurons. *Nature* 416, 736–740.

Remy, S., and Spruston, N. (2007). Dendritic spikes induce single-burst long-term potentiation. *Proc. Natl. Acad. Sci. U.S.A.* 104, 17192–17197.

Sjöström, P. J., Turrigiano, G. G., and Nelson, S. B. (2001). Rate, timing, and cooperativity jointly determine cortical synaptic plasticity. *Neuron* 32, 1149–1164.

Spruston, N., and Cang, J. (2010). Timing isn't everything. *Nat. Neurosci.* 13, 277–279.

Staubli, U. V., and Ji, Z. X. (1996). The induction of homo- vs. heterosynaptic LTD in area CA1 of hippocampal slices from adult rats. *Brain Res.* 714, 169–176.

Stuart, G. J., and Sakmann, B. (1994). Active propagation of somatic action potentials into neocortical pyramidal cell dendrites. *Nature* 367, 69–72.

Stuart, G. J., Spruston, N., Sakmann, B., and Häusser, M. (1997). Action potential initiation and backpropagation in neurons of the mammalian CNS. *Trends Neurosci.* 20, 125–131.

Wittenberg, G. M., and Wang, S. S.-H. (2006). Malleability of spike-timing-dependent plasticity at the CA3-CA1 synapse. *J. Neurosci.* 26, 6610–6617.

Conflict of Interest Statement: The authors declare that the research was conducted in the absence of any commercial or financial relationships that could be construed as a potential conflict of interest.

Received: 02 April 2010; paper pending published: 23 April 2010; accepted: 13 August 2010; published online: 04 October 2010.

Citation: Lisman J and Spruston N (2010) Questions about STDP as a general model of synaptic plasticity. Front. Syn. Neurosci. 2:140. doi: 10.3389/fnsyn.2010.00140

LISMAN AND SPRUSTON RESPONSE TO REVIEWERS

We thank the reviewers for their comments, most of which were understanding of our skeptical position. However, several reviewers strongly disagreed with us. We suggest that these disagreements have to do with the definition of STDP. In the widely used Neuroscience text by Purves et al. (2008), an entire page is devoted to STDP. A simple definition is given: LTD is triggered when the postsynaptic spike occurs in a time window before the presynaptic spike and LTP is triggered by a postsynaptic spike that occurs in a time window after the presynaptic spike. It is stated that the spike provides the depolarization that allows Ca^{2+} entry through the NMDA channel to trigger synaptic plasticity.

All science involves simplifications. We feel that STDP, as defined above, constitutes a dangerous oversimplification. Many theoretical papers have utilized the form of STDP defined above to understand how synaptic plasticity explains brain function. The conclusions of these papers must be regarded with skepticism because the simplified view of plasticity incorporated into this definition of STDP is quite far from the truth. It ignores the fact that both LTP and LTD can occur without postsynaptic spikes and that spikes that obey the pre–post timing rule – predicted to result in LTP – can produce LTD instead (in the hippocampus). Finally, spikes don't even reach many synapses, whereas other processes strongly depolarize those synapses. None of these observations are taken into consideration by the textbook definition of STDP. One reviewer believed that we don't think that spikes and timing are important in plasticity. To the contrary, we believe they are a part of the story, along with many other factors. So far, no simple formulation has resulted that would provide non-experts or theorists with a clear understanding of the voltage processes that determine whether LTP or LTD will occur. This is not embarrassing; there are many others memory processes that are not well understood. The neuroscience community needs to understand that synaptic plasticity is still not well understood and that the elegant rules of STDP do not capture enough of the truth to be applied as a general model of synaptic plasticity in naturally active neural circuits.

Several reviewers made good points about our concern that experimentally induced postsynaptic spikes might not be sufficient to induce plasticity. One of our concerns was that the backpropagating action potentials, at high frequency or in combination with synaptic input, could trigger a Ca^{2+} spike (Larkum et al., 1999) and that this Ca^{2+} spike is what is critical for LTP induction (Kampa et al., 2006). One reviewer made the valid point that the biophysical mechanism does not matter for the essential concept: thus even if the backpropagating Na^{+} spike works by triggering another type of electrical event, it still remains true that the Na^{+} spike has a causal role.

For STDP to be considered valid *in vivo*, it must at a minimum be demonstrated to occur in experiments where the spike occurs realistically (i.e., by the action of the EPSP) rather than by injection of current into the postsynaptic cell. We referred to experiments showing that spikes evoked by the EPSP are not necessary for LTP, contrary to STDP. Three reviewers objected to this challenge to STDP. One objected, citing Magee and Johnston (1997). However, that paper is not relevant because spikes were induced by somatic current injection rather than synaptically. Another rightly pointed to a paper that used low repetition rates (0.3 Hz) to induce LTP (Campanac and Debanne, 2008). However, the factors that cause very similar protocols to induce LTD in other studies (Wittenberg and Wang, 2006) need to be identified. Finally, a reviewer claimed that Zhang et al. (1998) proved the importance of spikes produced by the EPSP. This paper is indeed one of the few papers that measured spikes evoked by the EPSP (in tectal cells of *Xenopus*). The authors posed the critical question of whether spikes are necessary for LTP. To investigate this, they gave synaptic stimulation while voltage clamping the cell to −70 mV and found that LTP could not be induced. However, because all forms of synaptically induced depolarization (AMPA-mediated EPSPs, Ca^{2+} spikes, NMDA spikes) will be reduced under voltage-clamp, this experiment cannot be used to demonstrate the specific role of the Na^{+} spike. It is quite possible that when more experiments are done, it will turn out that Na^{+} spikes are indeed critical in these cells (contrary to what was found in the hippocampus). However, a field must not go beyond the data. The existing data argues only that Na^{+} spikes can influence various forms of LTP and LTD; simple rules regarding the timing of presynaptic and postsynaptic spikes do not explain enough of the experimental data to be regarded as a good model of plasticity in naturally active neural circuits. Thus, the textbook definition of STDP should be viewed with skepticism and more robust models of synaptic plasticity should be pursued. One review article referred to this notion as "beyond classical STDP" (Kampa et al., 2007). We agree that we need to move beyond classical STDP, but wonder if a different moniker will better represent the dependence of LTP and LTD on factors other than just timing.

REFERENCES

Campanac, E., and Debanne, D. (2008). Spike timing-dependent plasticity: a learning rule for dendritic integration in rat CA1 pyramidal neurons. *J. Physiol.* 586, 779–793.

Kampa, B. M., Letzkus, J. J., and Stuart, G. J. (2006). Requirement of dendritic calcium spikes for induction of spike-timing-dependent synaptic plasticity. *J. Physiol.* 574, 283–290.

Kampa, B. M., Letzkus, J. J., and Stuart, G. J. (2007). Dendritic mechanisms controlling spike-timing-dependent synaptic plasticity. *Trends Neurosci.* 30, 456–463.

Larkum, M. E., Zhu, J. J., and Sakmann, B. (1999). A new cellular mechanism for coupling inputs arriving at different cortical layers. *Nature* 398, 338–341.

Magee, J. C., and Johnston, D. (1997). A synaptically controlled, associative signal for Hebbian plasticity in hippocampal neurons. *Science* 275, 209–213.

Purves, D., Augustine, G. J., Fitzpatrick, D., Hall, W. C., LaMantia, A., McNamara, J. O., and White, L. E. (2008). *Neuroscience*, 4th Edn. Sunderland, MA: Sinauer Associates, Inc.

Wittenberg, G. M., and Wang, S. S.-H. (2006). Malleability of spike-timing-dependent plasticity at the CA3-CA1 synapse. *J. Neurosci.* 26, 6610–6617.

Zhang, L. I., Tao, H. W., Holt, C. E., Harris, W. A., and Poo, M. (1998). A critical window for cooperation and competition among developing retinotectal synapses. *Nature* 395, 37–44.

Of mice and men: why investigate timing in plasticity?

Per Jesper Sjöström

Department of Neuroscience, Physiology and Pharmacology, University College London, London, UK

But little Mouse, you are not alone,
In proving foresight may be vain:
The best laid schemes of mice and men
Go often askew,
And leave us nothing but grief and pain,
For promised joy!

Robert Burns, 1785

In their critique of STDP, Lisman and Spruston highlight several points regarding STDP that they feel are problematic. The majority of these points center around the postsynaptic Na^+ spike and its role in synaptic plasticity. They argue that the postsynaptic Na^+ spike is not necessary in plasticity, which might seem to reduce the importance and generality of the STDP concept. For example, they point out that you can induce LTP in the hippocampus without somatic Na^+ spikes; dendritic spikes are sufficient (Golding et al., 2002). Also, when Na^+ spikes are "evoked naturally" via incoming EPSPs, LTD instead of LTP is induced (Wittenberg and Wang, 2006), even though your typical STDP experimental paradigm would result in LTP under similar conditions (cf. Magee and Johnston, 1997). Lisman and Spruston also argue that the standard textbook definition of STDP is unclear, which in all fairness it probably is.

It is tempting to debate each individual point, because for each paper supporting a point (e.g., Wittenberg and Wang, 2006), one can find another in disagreement (e.g., Campanac and Debanne, 2008). This, however, would not seem interesting or worthwhile. Besides, Lisman and Spruston do highlight in their critique some general and bigger-picture shortcomings in the STDP field that need to be addressed. For example, the focus on the role of the somatic action potential in STDP could mean that researchers are heading down the wrong path, since plasticity can also depend on the timing of local dendritic spikes (cf. Froemke et al., 2010b). Also, the existence of classical STDP can be questioned on experimental grounds, at least in the hippocampus (Buchanan and Mellor, 2010). Finally, STDP might be secondary or perhaps even epiphenomenal to other, more fundamental learning rules (Shouval et al., 2010).

So, instead of belaboring the details of the postsynaptic Na^+ spikes and its role in plasticity (which I have belabored elsewhere, cf. Sjöström et al., 2008), I wish to emphasize the striking and ubiquitous timing dependence of synaptic plasticity that has been borne out of the STDP experimental paradigm. Indeed, changes in temporal differences as small as a millisecond can switch the sign of plasticity from LTD to LTP or vice versa (Froemke et al., 2010a). Intriguingly, this acute sensitivity of plasticity to temporal order appears to exist across species as diverse as *Xenopus laevis* (Richards et al., 2010; Tsui et al., 2010), rodents (Froemke et al., 2010a), and humans (Müller-Dahlhaus et al., 2010; Silva et al., 2010). This preservation of STDP across the 340 millions years of evolution that have passed since the mammalian amniote ancestors diverged from the amphibian reptiliomorph counterparts would seem to support the idea that it is important.

And yet, even though the phenomenology of this acute timing-dependence in plasticity has been preserved, the mechanisms that underlie it can vary tremendously at different synapse types in the same mammalian brain. Seemingly identical forms of timing-dependent LTD, for example, rely on presynaptic NMDA receptors at some central synapse types but not at others (Rodriguez-Moreno et al., 2010). Could STDP have been invented by nature several times, through convergent evolution? Finally, the timing requirements of plasticity are often cell specific, with different cell types of the same brain region exhibiting specialized forms of STDP (Fino and Venance, 2010), of which inhibitory cells are a particularly striking case (Lamsa et al., 2010).

To conclude, since STDP exists – in many forms and at many synapse types, remarkably well preserved in its classical form in species as diverse as mice and men – we scientists are compelled to investigate it. We are driven to ask: why are these temporally sensitive learning rules so ubiquitous in the central nervous system, why so diverse, yet so specific, and why *so preserved?* Although evoking the postsynaptic Na^+ spike via direct current injection may be less than entirely natural, it seems to me a reasonable starting point and an experimental scheme as good as any for the investigation of temporal sensitivity. Nevertheless, as Robert Burns observed over 200 years ago, proving foresight may be vain, and the best laid schemes go often askew. We thus need to keep in mind that our present interpretations may be overly influenced by fleeting fads and ephemeral fashions in science, and may well turn out to be only partially correct or even entirely erroneous in the future. Ultimately, this is what Lisman and Spruston's critique should remind us of (Lisman and Spruston, 2005), and herein lies its strength. Indeed, maybe STDP as a model of plasticity can be improved upon?

REFERENCES

Buchanan, K. A., and Mellor, J. R. (2010). The activity requirements for spike timing-dependent plasticity in the hippocampus. *Front. Syn. Neurosci.* 2:11. doi: 10.3389/fnsyn.2010.00011.

Campanac, E., and Debanne, D. (2008). Spike timing-dependent plasticity: a learning rule for dendritic integration in rat CA1 pyramidal neurons. *J. Physiol.* 586, 779–793.

Fino, E., and Venance, L. (2010). Spike-timing dependent plasticity in the striatum. *Front. Syn. Neurosci.* 2:6. doi: 10.3389/fnsyn.2010.00006.

Froemke, R. C., Debanne, D., and Bi, G.-Q. (2010a). Temporal modulation of spike-timing-dependent plasticity. *Front. Syn. Neurosci.* 2:19. doi: 10.3389/fnsyn.2010.00019.

Froemke, R. C., Letzkus, J. J., Kampa, B. M., Hang, G. B., and Stuart, G. J. (2010b). Dendritic synapse location and neocortical spike-timing-dependent plasticity. *Front. Syn. Neurosci.* 2:29. doi: 10.3389/fnsyn.2010.00029.

Golding, N. L., Staff, N. P., and Spruston, N. (2002). Dendritic spikes as a mechanism for cooperative long-term potentiation. *Nature* 418, 326–331.

Lamsa, K. P., Kullmann, D. M., and Woodin, M.A. (2010). Spike-timing dependent plasticity in inhibitory circuits. *Front. Syn. Neurosci.* 2:8. doi: 10.3389/fnsyn.2010.00008.

Lisman, J., and Spruston, N. (2005). Postsynaptic depolarization requirements for LTP and LTD: a critique of spike timing-dependent plasticity. *Nat. Neurosci.* 8, 839–841.

Magee, J. C., and Johnston, D. (1997). A synaptically controlled, associative signal for Hebbian plasticity in hippocampal neurons. *Science* 275, 209–213.

Müller-Dahlhaus, F., Ziemann, U., and Classen, J. (2010). Plasticity resembling spike-timing dependent synaptic plasticity: the evidence in human cortex. *Front. Syn. Neurosci.* 2:34. doi:10.3389/fnsyn.2010.00034.

Richards, B. A., Aizenman, C. D., and Akerman, C. J. (2010). In vivo spike-timing-dependent plasticity in the optic tectum of *Xenopus laevis*. *Front. Syn. Neurosci.* 2:7. doi: 10.3389/fnsyn.2010.00007.

Rodriguez-Moreno, A., Banerjee, A., and Paulsen, O. (2010). Presynaptic NMDA receptors and spike timing-dependent long-term depression at cortical synapses. *Front. Syn. Neurosci.* 2:18. doi: 10.3389/fnsyn.2010.00018.

Shouval, H. Z., Wang, S. S.-H., and Wittenberg, G. M. (2010). Spike timing dependent plasticity: a consequence of more fundamental learning rules. *Front. Comput. Neurosci.* 4:19. doi: 10.3389/fncom.2010.00019.

Silva, G. T., Verhoog, M. B., Goriounova, N. A., Loebel, A., Hjorth, J., Baayen, J. C., de Kock, C. P. J., and Mansvelder, H. D. (2010). Human synapses show a wide temporal window for spike-timing-dependent plasticity. *Front. Syn. Neurosci.* 2:12. doi: 10.3389/fnsyn.2010.00012.

Sjöström, P. J., Rancz, E. A., Roth, A., and Häusser, M. (2008). Dendritic excitability and synaptic plasticity. *Physiol. Rev.* 88, 769–840.

Tsui, J., Schwartz, N., and Ruthazer, E. S. (2010). A developmental sensitive period for spike timing-dependent plasticity in the retinotectal projection. *Front. Syn. Neurosci.* 2:13. doi: 10.3389/fnsyn.2010.00013.

Wittenberg, G. M., and Wang, S. S.-H. (2006). Malleability of spike-timing-dependent plasticity at the CA3-CA1 synapse. *J. Neurosci.* 26, 6610–6617.

frontiers in
SYNAPTIC NEUROSCIENCE

GENERAL COMMENTARY
published: 22 November 2010
doi: 10.3389/fnsyn.2010.00150

Synaptic plasticity *in vivo*: more than just spike-timing?

Jan M. Schulz*

Department of Physiology, University of Bern, Bern, Switzerland
**Correspondence: schulz@pyl.unibe.ch*

A commentary on

Questions about STDP as a general model of synaptic plasticity.
by Lisman, J., and Spruston, N. (2010). Front. Syn. Neurosci. 2:140. doi: 10.3389/fnsyn.2010.00140.

In their recent Perspective Article, Lisman and Spruston (2010) succinctly describe the crucial shortcomings of spike-timing-dependent plasticity (STDP) to serve as a unifying principle of synaptic plasticity. In particular, it is convincingly argued that postsynaptic depolarization rather than a somatic action potential (AP) is necessary and sufficient for the explanation of most results that have usually been interpreted within the STDP framework. I would like to add that we know even less about the importance of single backpropagating APs for synaptic plasticity *in vivo*.

Direct evidence for STDP *in vivo* is limited and suffers from the fact that the used protocols significantly deviate, more often than not, from the traditional pairing of single pre- and postsynaptic spikes (Shulz and Jacob, 2010). Thus, many studies use long-lasting large-amplitude postsynaptic potentials (PSP), and pairing usually involves multiple postsynaptic spikes or high repetition rates. Our own experience from cortico-striatal synaptic plasticity experiments indicates that classic STDP may be less effective *in vivo* than commonly expected (Schulz et al., 2010). A limited number of pairings (60 times) of cortical PSPs with a single current-induced postsynaptic AP at a slow rate (every 5 s) resulted in smaller and much more variable synaptic plastic changes than in previous *in vitro* studies that used comparable protocols (Pawlak and Kerr, 2008; Fino et al., 2010; Schulz et al., 2010). On the other hand, we did find that regular somatic AP discharge during the pre-post pairings was necessary for any synaptic potentiation and that the direction of induced plasticity was crucially dependent on the relative timing of the synaptic inputs to the somatic AP on a millisecond-timescale (Schulz et al., 2010). This is strikingly different from previous *in vitro* studies that suggested that even large current-induced subthreshold depolarizations are sufficient to induce synaptic changes at the cortico-striatal synapse over a wider range of timing intervals (Fino et al., 2009). These results demonstrate that one has to be very careful with extrapolating from *in vitro* results to the *in vivo* situation. Several factors have to be taken into account.

First, most *in vitro* studies on STDP use cell cultures or acute slices from young animals, where neural circuits are naturally more plastic than in the adult brain (e.g., Meredith et al., 2003). While results obtained from such preparation are important for our understanding of developmental processes, their relevance to our concepts of learning is less clear.

Second, the network state *in vitro* is fundamentally different from the *in vivo* situation. In acute slices in particular, background synaptic activity is almost absent. Pairing of unitary PSPs with single postsynaptic APs is usually insufficient to induce STDP under these conditions (Markram et al., 1997; Kampa et al., 2006). Only if large PSPs and/or bursts of postsynaptic APs are evoked, that induce a dendritic calcium spike, STDP will be observed. These observations directly support Lisman and Spruston when they argue that active dendritic mechanisms of depolarization like NMDA and Ca^{2+} spikes may be more relevant for synaptic plasticity than backpropagating APs. *In vivo*, however, most telencephalic neurons are in a high-conductance state (Rudolph et al., 2005). In this state, the input resistance is dramatically decreased in soma and dendrites. At the same time, active dendritic mechanisms may become more readily available due to the depolarized membrane potential. Therefore, it is not trivial to predict how this state will affect STDP. In the only study so far, that simulated the high-conductance state with the dynamic clamp technique *in vitro* (Delgado and Desai, 2008), classic STDP became a lot less effective and the timing window was greatly reduced.

Third, natural inhibition is often pharmacologically blocked in *in vitro* studies on STDP. Yet, inhibition powerfully regulates STDP: in the hippocampus, STD-potentiation cannot be induced using single postsynaptic spikes during the pairing in slices from young adult mice; however, STD-potentiation can be re-established by either using postsynaptic spike bursts or by blocking GABA-mediated inhibition (Meredith et al., 2003). In the striatum, blocking GABA-mediated inhibition results in the reversal of the STDP-timing rule in slices from juvenile rats (Fino et al., 2010). We think that the reversed timing rule of the narrower STDP-window that we observed in the adult striatum *in vivo* may also be a result of lateral inhibitory mechanisms (Schulz et al., 2010).

A fourth factor is neuromodulation. Neuromodulators like dopamine could regulate when strong postsynaptic depolarization is capable of changing the weight of active synapses and when not (Pawlak and Kerr, 2008; Schulz et al., 2010). This could be a result of the modulation of intrinsic properties and synaptic transmission; at the same time, neuromodulators can also directly interact with the biochemical pathways that mediate synaptic plastic changes (Valjent et al., 2005). Neuromodulatory regulation could be an elegant solution to prevent regular read-out of stored information, in the form of somatic spiking, from altering the stored information. In contrast, Lisman and Spruston's suggestion that dendritic spikes could regulate synaptic plasticity without being affected by regular read-out seems improbable, since dendritic spikes are also very likely to be an essential part of the read-out process of information stored in distal synapses (Rudolph et al., 2005; Larkum et al., 2009).

In summary, it seems probable that synaptic plasticity in the intact brain is governed by rules that are much more complex than the traditional interpretation of STDP. In my opinion, it should be of concern to all those who model animal learning that,

in general, studies using less physiological conditions appear to be more successful at reproducing classic STDP. Instead, the defining postsynaptic event may vary between simple postsynaptic depolarization, local dendritic spike, single back-propagating APs and AP bursts, depending on neuron type, developmental stage and network state. As pointed out by Lisman and Spruston, the precise timing between pre- and postsynaptic events will remain of crucial importance. However, it becomes increasingly evident that the outcome will not only depend on these but also of converging inhibitory and neuromodulatory inputs.

REFERENCES

Delgado, J. Y., and Desai, N. S. (2008). In vivo-like conductances limit spike-timing dependent plasticity. *Soc. Neurosci. Abstr.* 39, 40–43.

Fino, E., Deniau, J.-M., and Venance, L. (2009). Brief subthreshold events can act as Hebbian signals for long-term plasticity. *PLoS ONE* 4, e6557. doi: 10.1371/journal.pone.0006557.

Fino, E., Paille, V., Cui, Y. H., Morera-Herreras, T., Deniau, J. M., and Venance, L. (2010). Distinct coincidence detectors govern the corticostriatal spike timing-dependent plasticity. *J. Physiol. (Lond.)* 588, 3045–3062.

Kampa, B. M., Letzkus, J. J., and Stuart, G. J. (2006). Requirement of dendritic calcium spikes for induction of spike-timing-dependent synaptic plasticity. *J. Physiol.-Lond.* 574, 283–290.

Larkum, M. E., Nevian, T., Sandler, M., Polsky, A., and Schiller, J. (2009). Synaptic integration in tuft dendrites of layer 5 pyramidal neurons: a new unifying principle. *Science* 325, 756–760.

Lisman, J., and Spruston, N. (2010). Questions about STDP as a general model of synaptic plasticity. *Front. Syn. Neurosci.* 2:5. doi: 10.3389/fnsyn.2010.00140.

Markram, H., Lubke, J., Frotscher, M., and Sakmann, B. (1997). Regulation of synaptic efficacy by coincidence of postsynaptic APs and EPSPs. *Science* 275, 213–215.

Meredith, R. M., Floyer-Lea, A. M., and Paulsen, O. (2003). Maturation of long-term potentiation induction rules in rodent hippocampus: role of GABAergic inhibition. *J. Neurosci.* 23, 11142–11146.

Pawlak, V., and Kerr, J. N. D. (2008). Dopamine receptor activation is required for corticostriatal spike-timing-dependent plasticity. *J. Neurosci.* 28, 2435–2446.

Rudolph, M., Pelletier, J. G., Pare, D., and Destexhe, A. (2005). Characterization of synaptic conductances and integrative properties during electrically induced EEG-activated states in neocortical neurons in vivo. *J. Neurophysiol.* 94, 2805–2821.

Schulz, J. M., Redgrave, P., and Reynolds, J. N. J. (2010). Cortico-striatal spike-timing dependent plasticity after activation of subcortical pathways. *Front. Syn. Neurosci.* 2:23. doi: 10.3389/fnsyn.2010.00023.

Shulz, D. E., and Jacob, V. (2010). Spike timing dependent plasticity in the intact brain: counteracting spurious spike coincidences. *Front. Syn. Neurosci.* 2:137. doi: 10.3389/fnsyn.2010.00137.

Valjent, E., Pascoli, V., Svenningsson, P., Paul, S., Enslen, H., Corvol, J. C., Stipanovich, A., Caboche, J., Lombroso, P. J., Nairn, A. C., Greengard, P., Herve, D., and Girault, J. A. (2005). Regulation of a protein phosphatase cascade allows convergent dopamine and glutamate signals to activate ERK in the striatum. *Proc. Natl. Acad. Sci. U.S.A.* 102, 491–496.

Received: 08 October 2010; accepted: 09 November 2010; published online: 22 November 2010.

*Citation: Schulz JM (2010) Synaptic plasticity in vivo: more than just spike-timing? Front. Syn. Neurosci. **2**:150. doi: 10.3389/fnsyn.2010.00150*

frontiers in
COMPUTATIONAL NEUROSCIENCE

REVIEW ARTICLE
published: 01 July 2010
doi: 10.3389/fncom.2010.00019

Spike timing dependent plasticity: a consequence of more fundamental learning rules

Harel Z. Shouval[1]*, Samuel S.-H. Wang[2] and Gayle M. Wittenberg[3]

[1] *Department of Neurobiology and Anatomy, The University of Texas Medical School at Houston, Houston, TX, USA*
[2] *Department of Molecular Biology and Princeton Neuroscience Institute, Princeton University, Princeton, NJ, USA*
[3] *Medical Informatics, Siemens Corporate Research, Princeton, NJ, USA*

Edited by:
Per Jesper Sjöström, University College London, UK

Reviewed by:
Wulfram Gerstner, Ecole Polytechnique Fédérale de Lausanne, Switzerland
Nicolas Brunel, Centre National de la Recherche Scientifique, France

***Correspondence:**
Harel Z. Shouval, Department of Neurobiology and Anatomy, The University of Texas Medical School at Houston, 6431 Fannin St., Houston, TX 77303, USA.
e-mail: harel.shouval@uth.tmc.edu

Spike timing dependent plasticity (STDP) is a phenomenon in which the precise timing of spikes affects the sign and magnitude of changes in synaptic strength. STDP is often interpreted as the comprehensive learning rule for a synapse – the "first law" of synaptic plasticity. This interpretation is made explicit in theoretical models in which the total plasticity produced by complex spike patterns results from a superposition of the effects of all spike pairs. Although such models are appealing for their simplicity, they can fail dramatically. For example, the measured single-spike learning rule between hippocampal CA3 and CA1 pyramidal neurons does not predict the existence of long-term potentiation one of the best-known forms of synaptic plasticity. Layers of complexity have been added to the basic STDP model to repair predictive failures, but they have been outstripped by experimental data. We propose an alternate first law: neural activity triggers changes in key biochemical intermediates, which act as a more direct trigger of plasticity mechanisms. One particularly successful model uses intracellular calcium as the intermediate and can account for many observed properties of bidirectional plasticity. In this formulation, STDP is not itself the basis for explaining other forms of plasticity, but is instead a consequence of changes in the biochemical intermediate, calcium. Eventually a mechanism-based framework for learning rules should include other messengers, discrete change at individual synapses, spread of plasticity among neighboring synapses, and priming of hidden processes that change a synapse's susceptibility to future change. Mechanism-based models provide a rich framework for the computational representation of synaptic plasticity.

Keywords: STDP, synaptic plasticity, mechanistic models, calcium, learning rules, long-term depression, long-term potentiation

It is amateurs who have one big bright beautiful idea that they can never abandon. Professionals know that they have to produce theory after theory before they are likely to hit the jackpot. -Francis Crick.

The term "spike timing dependent plasticity" (STDP) refers to the observation that the precise timing of spikes significantly affects the sign and magnitude of synaptic plasticity (Bell et al., 1997; Markram et al., 1997; Bi and Poo, 1998). For example, at connections between mammalian pyramidal neurons (Markram et al., 1997; Bi and Poo, 1998; Feldman, 2000; Nishiyama et al., 2000; Sjöström et al., 2001; Wittenberg and Wang, 2006) a presynaptic spike preceding a postsynaptic spike within a narrow time window leads to long-term potentiation (LTP); if the order is reversed, long-term depression (LTD) results. In a common experimental paradigm, presynaptic and postsynaptic spike pairs are evoked repeatedly with a fixed time interval, Δt. This pairing is repeated at low frequency and the resulting change in synaptic response size is measured. Repeating this experiment for many values of Δt gives the timing-dependence of plasticity. Such an STDP curve is assumed to be useful for predicting the plasticity that results when Δt is variable, e.g., for arbitrary trains of presynaptic and postsynaptic spikes that occur under less controlled conditions. In this way the STDP curve is interpreted as a learning rule that defines how a particular type of synapse participates in information storage and ultimately brain circuit function.

Certainly the discovery of STDP represented a major advance over previous means of inducing synaptic plasticity, which relied on less controlled stimulation such as the delivery of strong (tetanic) stimuli to entire presynaptic axon tracts. In contrast, the minimal nature of STDP protocols carried with it two hopes: that the activity patterns used were more realistic, and that the various properties of synaptic plasticity could eventually be accounted for by knowing the timing of all the spikes. This is realized in theoretical models by assuming that cumulative plasticity is predicted by a simple superposition of spike pairs that repeatedly sample the STDP curve ("linear STDP") (Gerstner et al., 1996; Kempter et al., 1999; Abbott and Nelson, 2000; Song et al., 2000; van Rossum et al., 2000; Gütig et al., 2003; Izhikevich and Desai, 2003). In this sense STDP has been considered as a possible *first law of synaptic plasticity*.

This appealingly simple viewpoint neglects the actual mechanisms that change synaptic strength. Synaptic plasticity is induced by a variety of receptor-generated second messengers, which in turn activate kinases, phosphatases, and other downstream targets. A first-law view of STDP largely disregard these molecular

and cellular mechanisms in favor of the view that the essential character of synaptic plasticity can be separated from messy biological details.

In this article we review the considerable experimental evidence that real learning rules occupy a parameter space of high dimensionality that is not easily reduced or even approximated using spike pairs alone. Such parameters as stimulation frequency or even the total number of presynaptic and postsynaptic spikes have a large influence on the sign and magnitude of net plasticity. In addition, major nonlinearities arise from the history of spike activity on timescales longer than the width of the STDP curve as well as the location and spatial pattern of synaptic activity on and across neurons. Finally, on time scales of tens of minutes and shorter, single synapses undergo plasticity in what appears to be a sudden and all-or-none manner.

Can these and other nonlinearities be tamed without losing the conceptual appeal of a rule-based approach? We suggest that this complexity is naturally captured by models of synaptic plasticity that are based on cellular mechanisms. Consideration of signaling machinery allows the creation of a model that can be driven by any activity pattern to mimic a variety of experimental induction protocols, as well as natural activity patterns that occur in living animals. We focus in particular on one messenger, calcium, that can potentially account for much of the complexity seen in several commonly studied forms of synaptic plasticity.

A BRIEF HISTORY OF PLASTICITY

The hypothesis that memory formation may correspond to changes in the connections between neurons dates back to Konorski, (1948), Hebb, (1949) and other work reviewed in Squire, (1987). In a striking early formulation, Hebb cited the functional notion of causality by postulating that a presynaptic neuron that repeatedly drives a postsynaptic neuron to fire should eventually cause the presynaptic neuron to become more efficient in driving the postsynaptic neuron. For this to occur, the presynaptic neuron would presumably fire immediately before the postsynaptic neuron. Hebb's rule has profoundly influenced neuroscience and machine learning.

The discovery of long-term potentiation in the perforant path input to the dentate gyrus of the hippocampus (Bliss and Gardner-Medwin, 1973; Bliss and Lømo, 1973) provided the first experimental evidence for synaptic plasticity. Now the most widely used experimental model is a nearby type of synapse between pyramidal neurons of hippocampal areas CA3 and CA1. High-frequency tetanic stimulation of CA3 axons, which drive postsynaptic CA1 neurons to fire, leads to long-term potentiation (LTP), an increase in the synaptic response in CA1 to single stimuli (**Figure 1A**).

Subsequently Hebb's postulate was extended to encompass LTD as a necessary converse of LTP (Stent, 1973; Sejnowski, 1977). Based on observations of the development and plasticity of visual cortex (Wiesel and Hubel, 1963), Bienenstock, Cooper, and Munro (BCM) theorized (Bienenstock et al., 1982) and several groups (Dudek and Bear, 1992; Mulkey and Malenka, 1992) demonstrated experimentally that if a presynaptic neuron drives a postsynaptic neuron only weakly, LTD of the active synapses (homosynaptic LTD) would occur. These results are consistent with the bidirectional "BCM rule" in which the direction and magnitude of plasticity depends on a postsynaptic activity variable (**Figure 1A**).

Empirical search revealed that LTP was robustly induced with 1-s-long stimuli (high-frequency tetanus, 100 Hz), while LTD required 15 min of stimulation (low-frequency, 1 Hz; **Figure 1A**). Pairing low-frequency presynaptic stimulation with postsynaptic depolarization (to 0 mV for LTP, to −30 mV for LTD) was also found to elicit these phenomena robustly in voltage-clamp experiments (**Figure 1B**), suggesting that the strength of postsynaptic activation determines the sign of plasticity (Artola et al., 1990; Ngezahayo et al., 2000). These protocols were not physiologically realistic, but they did enable detailed studies of molecular mechanisms of inducing, expressing and maintaining synaptic plasticity. Another thread of research was the exploration of naturalistic-seeming patterns of neural activity. It was found that a necessary part of LTP induction at CA3–CA1 synapses was bursts of stimulation at intervals corresponding approximately to the theta frequency (**Figure 1C**; Rose and Dunwiddie, 1986; Larson and Lynch, 1988), which occurs *in vivo* in the hippocampus during active behavior and REM sleep. However, in neither thread of work was spiking in the postsynaptic neuron controlled or measured (though see Levy and Steward, 1983).

At the time, computational neuroscience was oriented toward connectionist-inspired learning models in which a neuron's activity was described by a continuously varying firing rate (Wilson and Cowan, 1973; Sejnowski, 1977; Bienenstock et al., 1982; Oja, 1982; Hopfield, 1984; Rumelhart and McClelland, 1987) with very little work considering the timing of discrete spikes. Currently much of the attention has shifted to computational models with spiking neurons in which spike timing might actually carry information, or where computations are too quick for obtaining good rate estimates (Hopfield, 1995; Amit and Brunel, 1997; Gerstner and Kistler, 2002). This shift to spiking models has intensified considerably following the demonstration of STDP (**Figure 1D**). Spike timing-dependence has since become a foundation on which both theorists and experimentalists seek to build a general understanding of synaptic change, learning, and memory recall.

STDP AS THE "FIRST LAW" OF SYNAPTIC PLASTICITY?

The discovery of diverse forms of timing-dependent plasticity at different synapses generated excitement because it appeared that such learning rules reflected different information processing and storage needs depending on the particular neural circuit (**Figure 2A**). These timing-dependent rules are sometimes interpreted as kernels, timing-dependent functions that can predict other properties of synaptic plasticity simply by a superposition of the effects of all pre/post spike pairs. A large body of theoretical work now models plasticity in such a manner (Kempter et al., 1999; Song et al., 2000; van Rossum et al., 2000; Rao and Sejnowski, 2001; Gütig et al., 2003; Izhikevich and Desai, 2003; Cassenaer and Laurent, 2007; Fiete et al., 2010). In this simplifying approach STDP is viewed as the "first law" of synaptic plasticity.

A first-law use of plasticity curves induced by pairs of spikes requires one to assume a strong form of linearity. Timing-dependent learning curves as shown in **Figure 1D** are typically measured by giving of order 100 pairs of spikes. Computational models assume that one pair of spikes evokes of order 1/100th the amount of plasticity seen in the curve (**Figure 2A**). The result of all induction

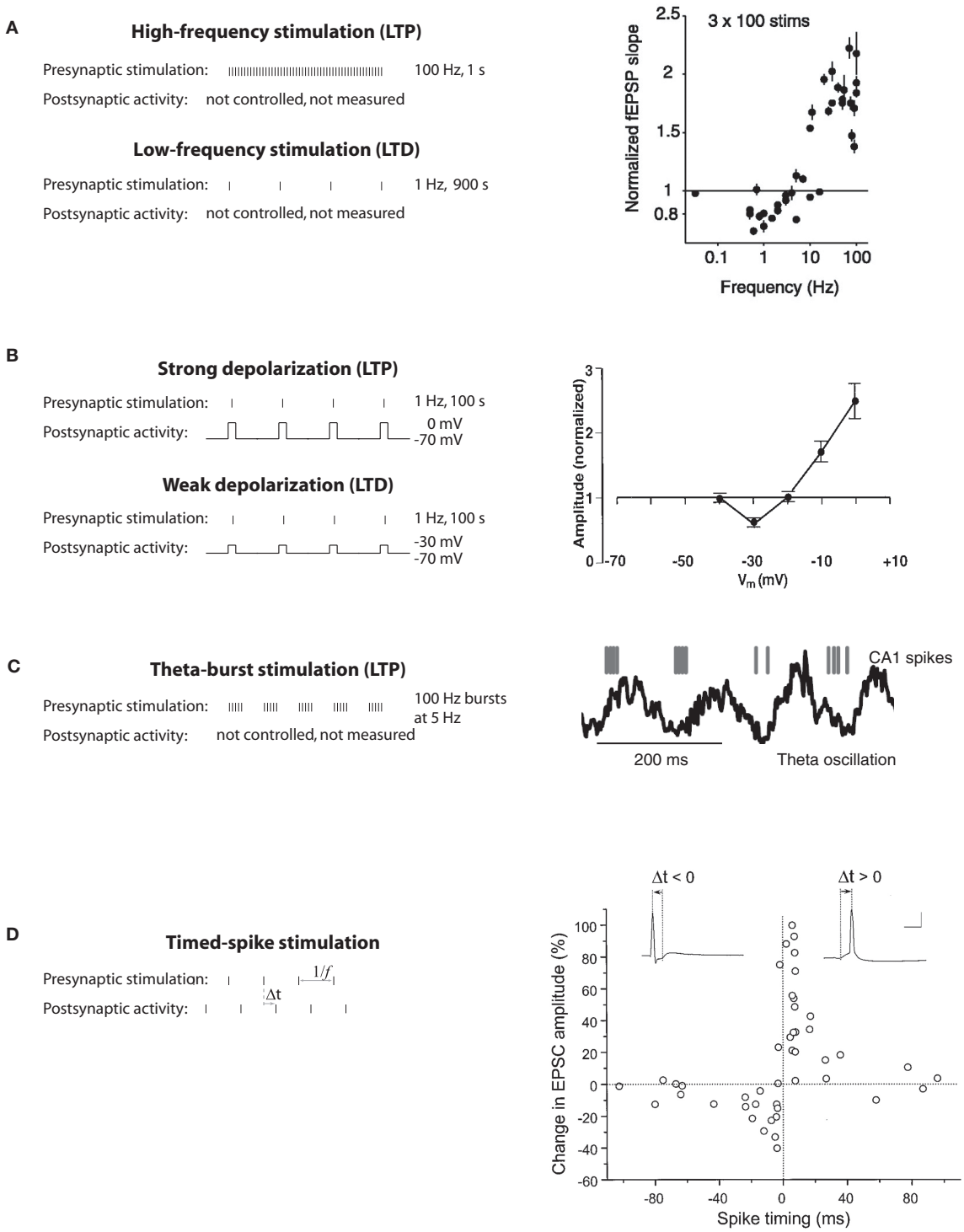

FIGURE 1 | Classical induction protocols for synaptic plasticity. (A) Changing the stimulation frequency of robust extracellular stimulation affects the sign and magnitude of synaptic plasticity. Left: high-frequency stimulation results in LTP whereas low-frequency stimulation produces LTD. Right: frequency vs. plasticity curve (from O'Connor et al., 2005a). **(B)** Low-frequency stimulation paired with voltage clamping of the postsynaptic cell can also result in LTP or LTD depending on the postsynaptic voltage. Left: moderate depolarization produces LTD where as large depolarization produces LTP. Right: depolarization vs. plasticity curve (from Ngezahayo et al., 2000). **(C)** Theta-burst stimulation tries to mimic more naturalistic conditions. In the hippocampus of awake behaving animals there is a strong theta-frequency oscillation (right). Left: In a theta-burst induction protocol, short high-frequency bursts are delivered each 200 ms, or at a frequency of 5 Hz, within the theta range (from Hirase et al., 1999). **(D)** STDP protocols are induced by precisely stimulating the presynaptic afferents at a specific time (Δt) before or after a postsynaptic spike. Right: The precise Δt determines the sign and magnitude of synaptic plasticity (from Bi and Poo, 1998).

protocols, including pre-STDP-era experiments, is then calculated by summing the impact of all spike pairs produced during induction (**Figure 2B**, red line segments).

Such an approach has been successfully applied to certain systems such as barrel cortex (for instance see Feldman, 2000; Allen et al., 2003; Feldman and Brecht, 2005). To account for further complexity, from this starting point an ever more intricate series of computational models has grown.

ALL PAIRS ARE EQUAL

The simplest and most common assumption is that all spike pairs count equally (Kempter et al., 1999; Song et al., 2000). Each spike pair has a given Δt associated with it, the time between the presynaptic and postsynaptic spike in the pair (**Figure 2B**, top). Using the kernel for that synapse, each Δt translates into a change in synaptic weight (Δw), and the total synaptic weight change is simply the linear sum of all the changes. Mathematically, this is done by convolving the STDP kernel with the cross-correlation function between the presynaptic and postsynaptic neuron.

NEAREST NEIGHBOR TAKES ALL

An alternative to counting all spike pairs in two complex trains is to count only plasticity arising from neighboring spike pairs (Izhikevich and Desai, 2003) (**Figure 2B**, bottom). This rule requires a definition of neighbor pairs, for instance counting the nearest postsynaptic spike to each presynaptic spike (**Figure 2B**, green lines). Alternatively, one could start from each postsynaptic spike, leading to a different set of spike pairs. A generalization of

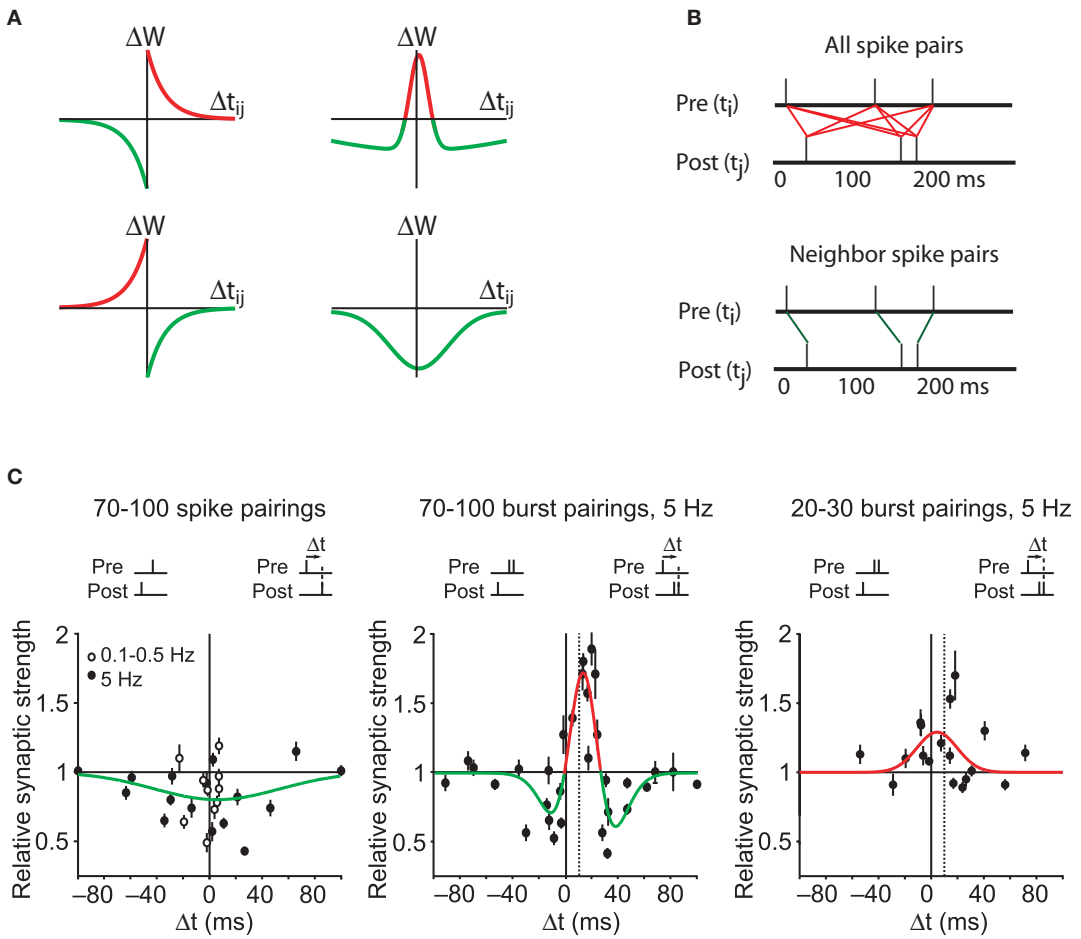

FIGURE 2 | Spike timing dependent plasticity as the *first law of synaptic plasticity*. **(A)** Measurements of synaptic plasticity for protocols in which presynaptic and postsynaptic action potentials are repeatedly separated in time by an interval Δt_{ij} are made to construct an STDP "kernel" (see STDP as the "first law" of synaptic plasticity? for definition) for a given synapse type. Kernel shapes have been taken to be synapse-specific representations of learning rules (for review see Abbott and Nelson, 2000; Wittenberg and Wang, 2006). **(B)** Illustration of two common methods for using STDP kernels to predict plasticity from an epoch of neural activity. Left: contributions to plasticity from all pairwise combinations of presynaptic and postsynaptic spikes are included. Right: Only nearest neighbor spike pairs are included. **(C)** Experiments have demonstrated that very different kernels can be measured at a single synapse. Left: At the CA3–CA1 synapse pairing single presynaptic and postsynaptic action potentials leads to an LTD-only rule. Based on the linear STDP model illustrated in **(A,B)**, no spike pattern would ever result in LTP. Middle: By adding a second postsynaptic action potential, LTP can be induced. This is not predicted by linear STDP. Dashed vertical line corresponds to the time of the first postsynaptic action potential. Right: By decreasing the number of pairings to 20–30, the depression window disappears and an LTP-only kernel is measured. From such a kernel, the existence of LTD would not be predicted. Data from Wittenberg and Wang (2006).

"nearest neighbor takes all" is "nearest neighbor takes more," in which a discount function is used to weight near spike pairs more heavily than distant spike pairs (Froemke and Dan, 2002). Such a spike suppression model adds some physiological plausibility, and additional degrees of freedom for fitting, and consequently an improved fit to data.

ADDITIVE VS. MULTIPLICATIVE PLASTICITY

Another move toward realism is the replacement of additive plasticity with a multiplicative rule (van Rossum et al., 2000; Gütig et al., 2003). LTP and LTD are known to saturate. In an additive model spike pairs contribute until an upper or lower bound is reached. In a multiplicative model the magnitude of change depends on the current synaptic weight, with diminishing contributions as synaptic weight approaches the upper or lower limit. This provides a smoother form of saturation.

EVIDENCE AGAINST STDP AS A FIRST LAW

A variety of ways in which experiments can deviate from a kernel-style approach can be seen in an applet http://nba.uth.tmc.edu/homepage/shouval/applets/v1/applet02.htm that explores the ensuing predictions. This applet allows the reader to choose a kernel as well as frequency and other parameters. In addition, a rich body of experimental work, starting before the discovery of STDP and continuing after it, can be used to test kernel-based superposition models for inconsistencies.

LOW-FREQUENCY STIMULATION INDUCES CAUSAL LTD

The first quandary, recognized almost immediately, is the need to explain why low-frequency stimulation of CA3 presynaptic axons results in CA3–CA1 LTD. An STDP kernel with equal-duration timing windows for potentiation and depression suggests two scenarios, neither of which predicts LTD: (1) Presynaptic stimulation drives postsynaptic firing, in which case the timing is in the causal direction and should result in LTP. (2) The presynaptic stimulation does not drive postsynaptic firing, which should result in no plasticity.

In one suggested repair to the model, it was noted that if the postsynaptic neuron fired spontaneously and randomly, and the STDP depression window was larger in area than the potentiation window, LTD would result (Kempter et al., 1999; Song et al., 2000). However, this hypothesis is directly falsified by recordings of the postsynaptic neuron during low-frequency (1 Hz) stimulation of CA3–CA1 synapses in the classical protocol (Dudek and Bear, 1992; Mulkey and Malenka, 1992). Under this condition, all evoked postsynaptic action potentials occurred within 25 ms after presynaptic stimulation yet resulted in LTD (Wittenberg and Wang, 2006). In fact, pairing single presynaptic and postsynaptic action potentials led to an LTD-only STDP kernel (Pike et al., 1999; Wittenberg and Wang, 2006; **Figure 2C**, left). Such a kernel can never generate LTP by superposition[1]. Considering that much of what is known about LTP arises from studies of CA3–CA1 synapses, this finding presents a major roadblock to the general applicability of STDP as a first law.

[1]http://nba.uth.tmc.edu/homepage/shouval/applets/v1/applet02.htm

HIGH-FREQUENCY STIMULATION INDUCES ANTI-CAUSAL LTP

Similarly, starting from an entirely negative STDP kernel, increasing the presynaptic frequency cannot convert LTD to LTP. This problem dates back to the first observations of STDP. Markram et al. (1997) showed in neocortical synapses that causal pairings with $\Delta t = 10$ ms led to LTP-only when pairing was done at frequencies above 10 Hz. Conversely, Sjöström et al. (2001) additionally showed that at high enough frequencies the timing-dependent rule becomes LTP-only, i.e., both positive and negative timings produce LTP. Thus plasticity for a particular timing can adopt positive or negative sign depending on pairing frequency.

NONLINEAR INTERACTIONS AMONG POSTSYNAPTIC ACTION POTENTIALS

At CA3–CA1 synapses, several additional mechanisms have been observed to convert causal timing-dependent LTD to causal timing-dependent LTP at CA3–CA1 synapses. The first of these is a firing burst (Pike et al., 1999) or even a pair of spikes (Wittenberg and Wang, 2006) in the postsynaptic neuron, both of which lead to LTP where single spikes lead to LTD. Thus the contribution to plasticity of postsynaptic spikes is affected quite strongly by their arrival in bursts.

NONLINEARITIES IN PLASTICITY ACCUMULATION

Plasticity also accumulates in a nonlinear fashion with respect to the number of pairings (Dudek and Bear, 1992; Yang et al., 1999; Mizuno et al., 2001). At CA3–CA1 synapses, under conditions that allow LTP – pairing presynaptic action potentials with postsynaptic bursts – an LTP-only rule emerges after 10 pairings, but a bidirectional rule requires 100 pairings (Wittenberg and Wang, 2006). Thus plasticity must accumulate as a nonlinear function of the number of stimuli, with depression accumulating more slowly than potentiation.

INFLUENCE OF ACTIVITY ON LONGER TIMESCALES

Finally, neural activity can influence later plasticity for seconds and minutes significantly longer than the STDP window. It has long been understood that neural activity that does not trigger measurable plasticity may have a profound influence on the effects of subsequent neural activity on in synapse strength. A classic example is priming. Rose and Dunwiddie (1986) demonstrated that LTP could be induced with as few as four stimuli to the CA3 pathway, so long as the stimuli were preceded 170 ms earlier by a single priming stimulus. A single burst of five stimuli at 100 Hz without the priming pulse failed to generate plasticity. None of the variations of STDP models described above can explain this primed-burst potentiation. Other work supports the interpretation that activity on this longer timescale is a requirement for LTP (Larson and Lynch, 1988).

In summary, the concept of STDP as the first law of synaptic plasticity is inconsistent with a large body of prior and subsequent existing work. Many parameters other than spike timing have a great enough influence on synaptic plasticity as to generate timing-dependent rules that are either LTD-only or LTP-only, even at the same synapse (**Figure 2C**).

ATTEMPTS TO RESCUE LINEAR STDP

Although linear superposition of STDP kernels fails, it has still been used as a starting point for making corrections or arguments. Such corrections have met with limited success.

Spike suppression models (Froemke and Dan, 2002; Froemke et al., 2006) were constructed to account for the failure of linear superposition of spike pairs to account for spike triplets and quadruplets in experiments in visual cortex. Although this model does improve fits to data in neocortical slices, it cannot account for the qualitative failures we have described. In particular, if low-frequency pairings lead to a depression-only rule (Markram et al., 1997; Sjöström et al., 2001; Wittenberg and Wang, 2006), the spike suppression model does not explain the emergence of LTP when the pairing frequency is increased or when bursts of postsynaptic spikes are used.

In the case of hippocampal cultures (Wang et al., 2005), results measured using spike triplets have led to a further correction to the linear STDP model. The spike suppression model accounts for the fact that a pre-post-pre spike sequence produces LTP, but not the fact that a post-pre-post sequence can do the same. The patch to the model is an additional rule in which LTP wins over LTD if LTP is triggered first. The generalization of this rule to more complex spike patterns with multiple presynaptic and postsynaptic spikes, resulting in interleaved LTP and LTD epochs, is unclear. A related, more rigorous approach includes higher-order multispike kernels (Pfister and Gerstner, 2006), which by virtue of having more parameters can account for more of the variance in a data set. The multispike kernel method has been separately applied to hippocampal culture data (Wang et al., 2005) and to some neocortical data (Sjöström et al., 2001) but has not been applied, to our knowledge, to triplet and quadruplet data in visual cortical slices (Froemke and Dan, 2002) or to data from hippocampal slices (Nishiyama et al., 2000; Wittenberg and Wang, 2006). This approach requires a new fit for every system, and constitutes a descriptive approach for summarizing the findings at a particular synapse. Also, several problems – nonlinear accumulation and long-timescale effects such as priming – remain unexplained. More rules could undoubtedly be created.

At this point, the initial appeal of the STDP concept has started to dim. The intricacy of the approach is starting to resemble the tax code of a developed country. Does another framework exist in which rules for plasticity arise more naturally?

THE MECHANISTIC ALTERNATIVE: A BIOCHEMICAL MESSENGER-BASED MODEL

Here we present an approach based on known biochemical intermediates in the induction of plasticity. In this approach, a mechanistic model is constructed by converting known biological mechanisms to assumptions that are formulated mathematically. These assumptions constitute a model that can be simulated or analyzed under different conditions. The model is constrained by matching the output of the model to experimental results.

As an example we present the calcium-dependent plasticity model (CaDP) of (Shouval et al., 2002). The CaDP model can explain several observed experimental nonlinearities and can be easily modified by adding components that may account for further experimental observations. Such a model can also be used to simulate various slice plasticity protocols (Shouval et al., 2002; Cai et al., 2007) and receptive field plasticity *in vivo* (Yeung et al., 2004; Yu et al., 2008). Here we focus on STDP-style experiments that are hard to explain by linear superposition models.

The CaDP model is based on three key assumptions.

(1) Calcium elevation in spines determines the sign, magnitude and rate of synaptic plasticity. A moderate elevation in calcium results in LTD whereas a large elevation in calcium levels results in long-term potentiation (LTP) (**Figure 3A**, left). We also assume that the rate of plasticity is a monotonically increasing function of calcium, η (**Figure 3A**, middle).
The calcium assumption is based on experimental evidence (Cummings et al., 1996; Yang et al., 1999) and has been previously suggested in models of calcium-dependent kinase-phosphatase systems in postsynaptic spines (Lisman, 1989). Mathematically it is described by the equation:

$$\frac{dw_i}{dt} = \eta([\mathrm{Ca}]_i)\left(\Omega([\mathrm{Ca}]_i) - \lambda w_i\right)$$

where w_i is the synaptic efficacy of synapse i, $[Ca]_i$ is the calcium concentration at synapse i, and λ is a decay time constant. The functions Ω and η (Shouval et al., 2002) determine the sign and rate of synaptic plasticity and are depicted in **Figure 3A**. Ω is a function of calcium concentration and is defined by two thresholds θ_d and θ_p (**Figure 3A**) that control the sign and magnitude of synaptic plasticity.

(2) The source of calcium is influx through NMDA receptors which pass calcium and are gated by both glutamate and voltage. NMDA receptors can therefore report the coincidence of presynaptically released glutamate and postsynaptic depolarization by allowing calcium into a dendritic spine. NMDA receptors are relatively slow-gating receptors, with time constants in the range of 50–200 ms, a scale comparable to time windows for timing-dependent plasticity.

(3) Back-propagating action potentials (BPAP) in the postsynaptic neuron leave a lingering post-action potential current in the dendrite. The BPAP is the source of depolarization. The assumption of a lingering tail is necessary in order to explain a time window for LTD when the postsynaptic spike precedes the presynaptic spike.

The results of this model depend on a variety of parameter assumptions. Although we will focus on accounting for CA3–CA1 plasticity rules, parameters can be adjusted to account for plasticity properties at other synapses.

TWO TIMING WINDOWS FOR LTD

In **Figure 3B** we show induction of STDP with the CaDP model. The functions for Ω, η, and the voltage response of the back-propagating action potential are depicted in **Figure 3A**, and the NMDA receptor conductance for calcium ions (G_{NMDA}) is set at an appropriate value. These assumptions produce a three-peaked learning rule (**Figure 3B**): post-pre LTD, pre-post LTP, and pre-post LTD at larger values of Δt. This second LTD window is seen at some synapses (Nishiyama et al., 2000; Woodin et al., 2003; Wittenberg and Wang, 2006) whereas it is absent or less prominent in neocortical synapses examined to date.

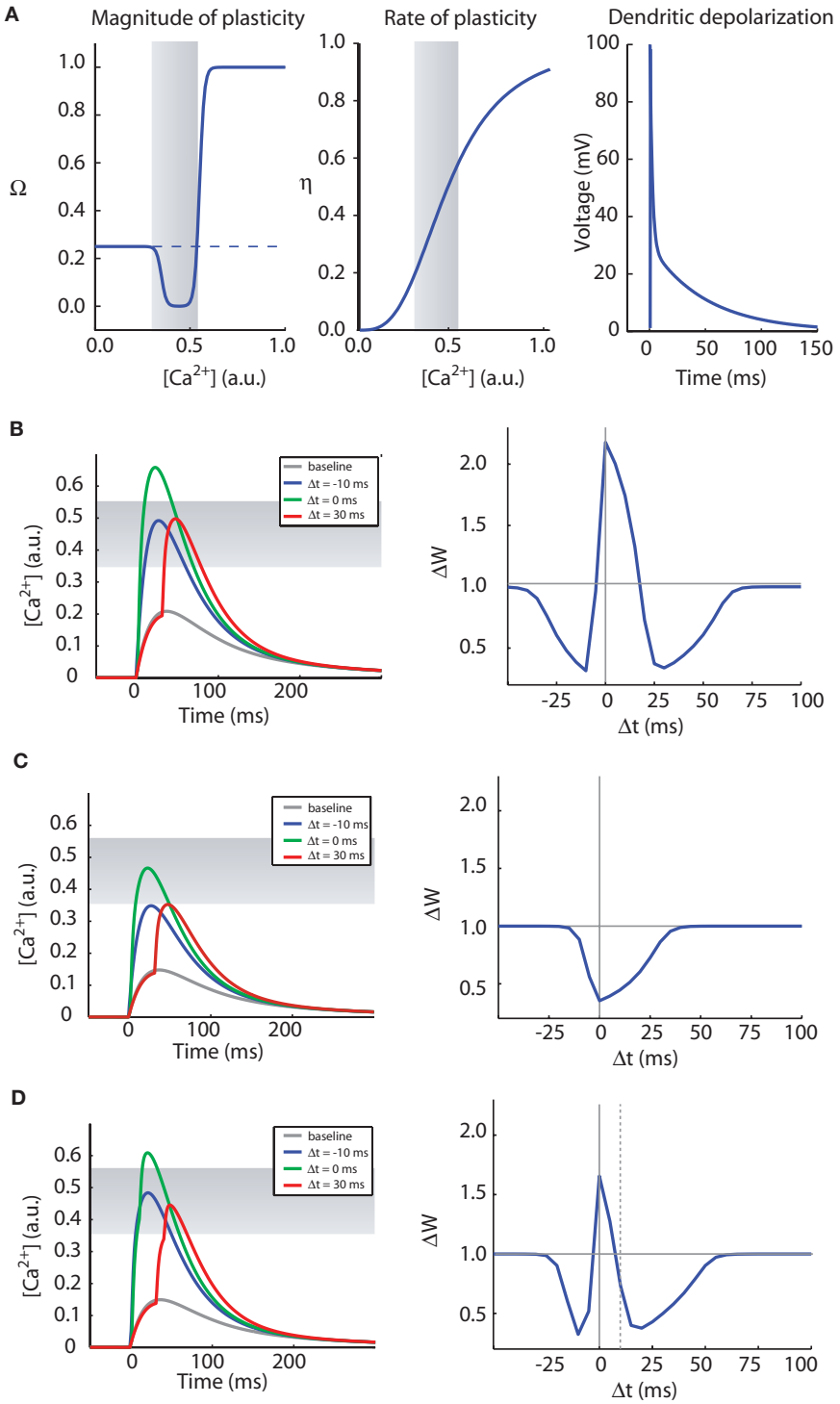

FIGURE 3 | The CaDP model can account for various forms of spike timing dependent plasticity. (A) The key functions controlling the CaDP model. Left: The Ω function controls the sign and magnitude of calcium-dependent synaptic plasticity, the gray shading marks the LTD region. Center: the η function controls the calcium-dependent rate of plasticity. Right: the shape of the back-propagating action potential with its long tail current. **(B)** The results of an STDP induction protocol, simulating the CaDP model with G_{NMDA} = 1/420 (μM/mV). Left: the calcium transients for baseline, Δt = –10 ms, 0 ms and 30 ms. Here the LTD threshold is θ_d = 0.35 and the LTP threshold is θ_p = 0.55. The LTD region is indicated by the gray shading. Right: the complete STDP curve, which exhibits, post-pre LTD, pre-post LTP and also pre-post LTD. **(C)** The same as **(B)** but with G_{NMDA} = 1/600 (μM/mV). Here all values of Δt produce LTD. **(D)** The same as **(C)** but with two postsynaptic spikes. The timing of the two postsynaptic spikes is indicated by the vertical lines, and the time between the two post spikes is 10 ms. Here we get a complete STDP curve with one LTP window and two LTD windows.

If the NMDA conductance is reduced by 30%, single postsynaptic spikes no longer produce LTP at low pairing frequencies (**Figure 3C**). Now if a burst of two postsynaptic spikes or more is paired with each presynaptic spike, a three-peaked timing-dependent plasticity curve again results (**Figure 3D**). This rule resembles the triphasic rule that is possible at CA3–CA1 synapses (Nishiyama et al., 2000; Wittenberg and Wang, 2006). This is illustrated in the CaDP applet available at: http://nba.uth.tmc.edu/homepage/shouval/applets/v1/applet01.htm. Other proposed mechanistic models also generate a second LTD window (Kitajima and Hara, 2000; Abarbanel et al., 2002; Karmarkar et al., 2002).

Yet neocortical synapses have multiple mechanisms for LTD including metabotropic glutamate receptor or cannabinoid receptor-dependent signaling (van Rossum et al., 2000; Sjöström et al., 2003; Bender et al., 2006) but lack a prominent second LTD window. Biochemical veto mechanisms have been proposed that can overrule the second LTD window in neocortical synapses (Rubin et al., 2005) but allow it to be expressed at CA3–CA1 synapses. A difference could also be based on biological heterogeneity, for instance the relative abundance of calcium release in CA1 neurons compared with neocortical pyramidal neurons (Nakamura et al., 2000). Finally, stochastic properties of synaptic transmission in conjunction with the CaDP model may significantly reduce the magnitude of the second LTD window (Shouval and Kalantzis, 2005).

FREQUENCY-DEPENDENCE OF LTP INDUCTION BY POSTSYNAPTIC SPIKES AND BURSTS

In neocortical synapses, LTP results from single postsynaptic spikes at high pairing frequencies, but not at low pairing frequencies (Markram et al., 1997; Sjöström et al., 2001). At high enough frequencies LTD is eliminated entirely. This frequency-dependence is qualitatively consistent with results at CA3–CA1 synapses (Wittenberg and Wang, 2006). Such a transition from bidirectionality to all-LTP falls naturally from the function Ω.

In this simple example we have not included the effects of short-term synaptic dynamics (Tsodyks et al., 1998). In models, short-term facilitation and depression can alter the frequency-dependence of plasticity (Cai et al., 2007) and may account for properties of the plasticity induced by multi-spike protocols (Froemke and Dan, 2002; Wang et al., 2005).

FUTURE DIRECTIONS: MOVING TOWARDS A COMPREHENSIVE LEARNING RULE

Models that are based on biophysical mechanisms show promise in capturing the fullness of real learning rules. The simple CaDP model described here can account for a number of key aspects of the observed malleability of STDP. In this final section we survey some salient experimental observations that suggest ways in which the CaDP model could be amended and improved. Incorporation of additional mechanism-based rules can move modeling efficiently toward a more complete representation of synaptic learning rules. The point of view of modeling biophysical mechanisms goes beyond calcium: in synapses where other second messengers drive plasticity (Huang et al., 1994; Salin et al., 1996), calcium is not the appropriate target for modeling. Finally, although parsimony argues against adding all the mechanisms described at once, one or more mechanisms could be incorporated for a particular need.

Additional mechanisms that may influence learning rules fall into three broad categories: (a) *additional properties of calcium signaling and other messengers*, which may influence the dependence of plasticity on *temporal activity* on time scales of seconds; (b) dendritic excitation and other *locally spreading signals*, which may influence the dependence of plasticity on the *spatial location and pattern* of synaptic input; and (c) additional properties of plasticity such as *saturable, binary, and irreversible changes in synaptic strength*, which may contribute to *very long time scale rules*, such as metaplasticity. We describe some of these mechanisms and their consequences.

CALCIUM AND OTHER MESSENGERS

Additional sources of calcium may shape timing-dependence

Although the existing CaDP model assumes that calcium rises only from NMDA receptor opening, calcium may be elevated by calcium-permeable AMPA receptors, voltage-gated calcium channels, and calcium release from internal stores (Higley and Sabatini, 2008). Each of these sources is known to contribute to the induction of synaptic plasticity, and may shape the rule. For example, calcium entry through AMPA receptors would be relatively timing-independent and therefore broaden timing windows for plasticity. At cerebellar parallel fiber-Purkinje cell synapses timing-dependence of LTD (Wang et al., 2000a; Safo and Regehr, 2008) may arise from the properties of calcium release driven by the second messenger IP_3 (Sarkisov and Wang, 2008).

Calcium buffering and release suggest longer timescale rules

Synaptic plasticity is regulated by activity on time scales longer than the width of measured STDP kernels. In this regard it is interesting to note that calcium signals are buffered and therefore attenuated by intracellular binding molecules. Some of these molecules are proteins such as calbindin and parvalbumin, which have binding kinetics on the order of 0.1–1 s and saturate at moderate levels of calcium. They are found in hippocampal CA1 pyramidal neurons, cerebellar Purkinje neurons, and many interneurons. A high-frequency pairing requirement for LTP could arise from saturation of buffer proteins. Accumulated calcium also could trigger further calcium release, again leading to a dependence on long time scales. For example, in primed-burst LTP, in which LTP induction depends on activity at the 5 Hz theta frequency at the CA3–CA1 synapse (Rose and Dunwiddie, 1986; Larson and Lynch, 1988; Wittenberg and Wang, 2006) calcium accumulated during the priming activity might saturate buffers or enhance calcium-induced calcium release during the subsequent burst (Schiegg et al., 1995).

Intermediate messengers beyond calcium

Measured calcium dynamics alone are insufficient to account for the direction of synaptic plasticity in the basal dendrites of layer 2/3 pyramidal neurons of the somatosensory cortex (Schultz, 2002; Nevian and Sakmann, 2006). This finding suggests that fluorescence measurements may not capture the key variables that predict plasticity, such as fine spatial and temporal calcium dynamics, or because messengers apart from calcium play a significant role. Indeed, calcium entry through voltage-gated channels may

be needed for plasticity in the absence of a measurable calcium signal (Yasuda et al., 2003). Additionally, some signal transduction pathways activated during plasticity might depend on other messengers such as cAMP (Huang et al., 1994; Salin et al., 1996) and endocannabinoids (Safo and Regehr, 2008).

Spike timing dependent plasticity is also modulated by neuromodulatory neurotransmitters. Recently Seol et al. (2007) have shown that in slices of visual cortex, β-adrenergic receptors are necessary for inducing spike timing dependent LTP and muscarinic (M1) receptors are essential for inducing LTD, results that are consistent with *in vivo* observations. Neuromodulation may translate behavioral state into a capacity for change: for instance, dopamine may act as a reward signal to drive reinforcement learning (Schultz, 2002). Dopamine is capable of subsecond dynamics (Gonon, 1997) providing a substrate for rapid regulation of learning rules (Pawlak and Kerr, 2008). Such effects may be modeled by including messenger molecules such as cyclic AMP, or perhaps simply the neurotransmitters themselves. Recent observations have shown that in cultured synapses, dopamine acting through D1 receptors can convert an antisymmetric STDP rule to a potentiation-only rule with broad timing-dependence that spans both sides of the zero timing condition (Zhang et al., 2009). Such a phenomenon is consistent with enhancements in dendritic excitability, NMDA receptor function, or other calcium signaling or detection machinery.

LOCALLY SPREADING SIGNALS

Dendritic excitability suggests dependence on local spatial and temporal activity patterns

In spike pair-generated plasticity, the sign and amount of change is known to depend on the dendritic location of the synapse (Froemke et al., 2005). Thus even in a simple case, dendrites are electrically inhomogeneous. In addition, dendrites show a rich range of excitable properties (Sjöström et al., 2008). Dendritic spikes are commonly evoked by sufficiently dense excitation to activate voltage-gated channels (Miyakawa et al., 1992; Wang et al., 2000a) (Larkum and Nevian, 2008; Sjöström et al., 2008) or NMDA receptors themselves (Schiller and Schiller, 2001; Major et al., 2008). Consequently, plasticity can be evoked via local dendritic spikes independent of somatic firing (Hartell, 1996; Golding et al., 2002).

Such observations can naturally be incorporated into CaDP models as upstream steps that regulate the amount of calcium entry. This requires modeling of active dendritic conductances, or identification of rules that map cellular activity to patterns of change in dendritic voltage. Such models should be able to account for the properties of plasticity driven by dendritic spikes (Larkum and Nevian, 2008; Sjöström et al., 2008). Dendritic excitation may also account for locally spreading heterosynaptic LTP and LTD, in which synaptic activity can cause plasticity at near (Johnston et al., 2003) by synapses (Engert and Bonhoeffer, 1997; Wang et al., 2000b).

Spreading signals and local priming in dendrites

Signaling molecules may spread from active to inactive synapses. Svoboda and colleagues (Yasuda et al., 2006; Harvey and Svoboda, 2007; Zhong et al., 2009) have demonstrated that activity at one synapse on a CA1 neuron can increase the sensitivity of that synapse to further change without inducing plasticity. This effect lasts approximately 10 min and requires the phosphorylation of Ras, a calcium-dependent G protein that regulates MAP kinase. They also demonstrated that the priming effect can spread about 10 μ, thereby sensitizing neighboring spines to an induction stimulus that would otherwise not lead to plasticity.

Such spreading signals are not limited to synaptic plasticity, nor are they always local. An old phenomenon somewhat unappreciated in models is the fact that the induction of plasticity is typically accompanied by changes in the excitability of the postsynaptic neuron. It has also been shown that activity can lead to local changes in dendritic excitability on a scale of microns (Johnston et al., 2003; Sjöström et al., 2008) comprising a form of information storage (Narayanan and Johnston, 2007).

These complexities suggest that molecular mechanisms of plasticity may account for priming on a location and proximity-dependent basis. In one attractive hypothesis, co-activation of nearby inputs on an excitable dendrite could serve to drive plasticity in a group of synapses. In this scenario, functionally related inputs could become clustered if the plasticity signal drives LTP (Mehta, 2004; Larkum and Nevian, 2008). Conversely, LTD driven by large calcium signals, which occurs at parallel fiber-Purkinje cell synapses, might lead to repulsion of related inputs from one another and thus sparse mapping on the dendritic arbor.

SATURABLE, BINARY, AND IRREVERSIBLE CHANGES IN SYNAPTIC STRENGTH

Binary and saturable synapses

The CaDP model described here produces graded synaptic weights. However, the induction of plasticity appears experimentally to be sudden and discrete, and possibly even a two-state system of binary strength (Petersen et al., 1998; O'Connor et al., 2005b). Several models have taken the observations of discrete plasticity states into account (Abarbanel et al., 2005; Graupner and Brunel, 2007; Clopath et al., 2008). Possible substrates for discrete states include CaMKII autophosphorylation (Lisman and Zhabotinsky, 2001) and other maintenance mechanisms are also likely to form discrete states (Aslam et al., 2009). Such binary changes have been observed on time scales of tens of minutes; on longer time scales, the levels of such states could change. For instance, the "high" state could be defined by the number of slots for AMPA receptor insertion (McCormack et al., 2006), which could change via metaplastic and homeostatic mechanisms (Rioult-Pedotti et al., 2007).

Metaplasticity

Stepwise, saturable change in synaptic strength has two consequences. First, the saturation of plasticity suggests that even for a fixed rule for mapping calcium to plasticity, the measured learning rule will depend on the initial synaptic strength. This can account for the finding that after saturation of LTD, a potentiation-only learning rule results, and vice versa, a simple form of change in a learning rule over time, or metaplasticity (O'Connor et al., 2005a). Second, when the number of active synapses is small, as occurs between pairs of neurons, the amount and sign of plasticity can vary considerably based on counting statistics alone. Saturable change at individual terminals could even account for the observation that a

given amplitude of calcium transient can evoke either LTP or LTD (Nevian and Sakmann, 2006) without revoking assumption (1) of the CaDP model.

For both Hebbian rate-based learning rules and linear STDP-based rules, runaway synaptic plasticity can occur (Bienenstock et al., 1982; Oja, 1982). The problem is not solved by imposing upper and lower bounds on synaptic weights, since synaptic weights can still saturate, leading to nonselective cells that respond equally to many input patterns. This problem of linear STDP models is associated with causality, which tends to result in presynaptic neurons firing slightly before postsynaptic neurons, and thus producing LTP. Therefore, synaptic saturation observed in linear STDP can be addressed by using an STDP kernel with slightly more LTD than LTP (Kempter et al., 1999; Song et al., 2000).

Mechanistic models, which try to account for system level phenomena, like rate-based models, require stabilization mechanisms (Yeung et al., 2004; Yu et al., 2008; Clopath et al., 2010). It has been suggested that synaptic scaling (Turrigiano et al., 1998) might result in overall homeostatic change that reduces change in total synaptic strength on a neuron, which can prevent runaway plasticity.

Such stabilization mechanisms seem related to metaplasticity observed experimentally (Abraham and Bear, 1996). Metaplasticity is at times used as a catch-all term for changes in learning rule. It is feasible that metaplasticity and synaptic scaling (Yeung et al., 2004) may arise naturally from cellular mechanisms that have a stabilizing influence. Synaptic plasticity models should therefore incorporate biophysical implementations of stabilization mechanisms for comparison to experiment.

Irreversible locking-in of plasticity

Experimentally, LTP is not the same on all time scales. For example, the late phase of LTP (L-LTP) has elements of consolidation, lasting for hours or longer, and requires protein synthesis and stronger activation than most LTP induction protocols (Frey et al., 1993). On shorter time scales, a related phenomenon, is the irreversibility of LTP under stimulation conditions more intense than the minimum needed to induce potentiation (Stäubli and Chun, 1996; O'Connor et al., 2005a). Such a "lock-in" (O'Connor et al., 2005a) concept has been modeled using deeper levels of plasticity (Stäubli and Chun, 1996; Fusi et al., 2005; O'Connor et al., 2005b). This approach has not yet been combined with spike timing-dependent models of learning.

EPILOGUE

This review has focused on bringing a directed dose of mechanistic complexity to theoretical models, moving beyond the initial notion that STDP is essentially a first law of synaptic plasticity. We advocate the use of simple biophysical models of plasticity that can be constrained both by the realism of their mechanistic assumptions and by comparison with experiment.

Although the high dimensionality of the parameter space governing synaptic plasticity appears daunting (**Figure 4**), new approaches may be helpful. At present, sampling this parameter space typically requires monitoring the electrophysiological response of one postsynaptic cell for up to an hour. Simultaneous patching of multiple neurons can increase the number of experiments which can be performed in parallel, but this approach is not scalable. However, technologies such as patterned and spatially resolved uncaging (Civillico et al., 2010) and optogenetic manipulation of identified neuron types (Gradinaru et al., 2007) enable many connections to be probed on a high-throughput basis. These experimental directions promise to provide quantities of data necessary to constrain models better. As progress in these areas continues, the ability to sample the parameter space will improve.

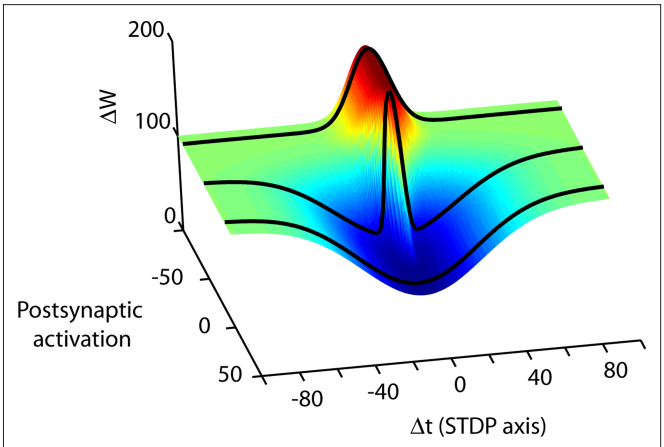

FIGURE 4 | Spike timing is merely one dimension in the high-dimensional synaptic learning rule. A conceptual illustration of a learning rule in three dimensions is shown. Depending on the choice of activity parameters other than spike timing, many different STDP rules can be measured at a synapse (from Wittenberg and Wang, 2006). The second axis represents the transition from parameters that more strongly activate depression (D-rule) to parameters that more strongly activate potentiation (P-rule). By choosing parameters that activate only a single rule, the spike timing-dependence of LTP and LTD can be measured separately. At the CA3–CA1 synapse, potentiation is initiated by as few as 20 causal pairings of presynaptic action potentials with postsynaptic bursts repeated at 5 Hz or higher. Depression does not require high-frequency stimulation or postsynaptic bursts but requires more pairings than LTP. Stimulus conditions that satisfy the temporal requirements for both the potentiation rule and the depression rule lead to a bidirectional spike-timing-dependent plasticity curve. In neocortex one can shift along the P–D axis by changing the pairing frequency (Sjöström et al., 2001), or by neuromodulator concentration (Seol et al., 2007).

Biophysically oriented models of plasticity may also eventually be useful in network models in order to predict the properties of circuit structure. For example, standard STDP models favor the elimination of reciprocal connections between cortical neurons because any given timing would lead to LTP in one direction and LTD in the other direction. This is contradicted by the fact that early experiments (Markram et al., 1997) were done at reciprocally connected pairs, as well as the well-known phenomenon that distant neocortical areas are often reciprocally connected (Felleman and Van Essen, 1991). Of interest is recent work (Clopath et al., 2010) presenting a phenomenological model of plasticity that includes additional aspects of plasticity such as frequency-dependence, and that allows both unidirectional and bidirectional connections to develop. Additional rules such as these come easily from mechanistic considerations, suggesting that a biophysical approach can eventually help account for circuit-level phenomena.

Ultimately we should strive to create biophysically based system levels model of neuronal circuits. Such models will enable us to connect the molecular and cellular level basis of plasticity to

its consequences on the circuit and system levels, and to test the models both on the basis of their underlying low-level assumptions as well as on their higher-level predictions. The space of models and activity parameters to explore can be reduced considerably by sampling activity patterns likely to occur in a behaving animal, and advances in recording methods promise to provide continuing new sources of data. In this regard a valuable source of insight into any synapse's function is the experimental literature on multiple levels: *in vivo* activity patterns, plasticity, and behavior.

An open question is whether, over the natural stimuli of a synapse in a given region, final plasticity rules will be so high-dimensional that very complex, essentially descriptive rules will be needed for realistic modeling. We take the optimistic view that "real rules", which are nevertheless relatively simple, can be found, and that this is more easily accomplished using a biophysical approach. Although the linear STDP models do not account for most of the experimental results, much of the original appeal of this approach lay in the possibility that it could be used in higher-level models. A key future question is whether a biophysically based approach can contribute a simple description sufficient to help model working neural circuits. Such an approach may also aid the eventual understanding of the role of spike timing – and many other factors – in determining the principles by which neural circuits learn.

ACKNOWLEDGMENTS

Harel Z. Shouval was supported by a grant from the NIH (2P01-NS038310). Samuel S.-H. Wang was supported by a grant from the NIH (1R01-NS045193) and is a W. M. Keck Distinguished Young Scholar in Medical Research. We thank Mark S. Goldman for his comments on the manuscript and Michael J. Byrne for the Java applets.

REFERENCES

Abarbanel, H. D., Huerta, R., and Rabinovich, M. I. (2002). Dynamical model of long-term synaptic plasticity. *Proc. Natl. Acad. Sci. U.S.A.* 99, 10132–10137.

Abarbanel, H. D., Talathi, S. S., Gibb, L., and Rabinovich, M. I. L. (2005). Synaptic plasticity with discrete state synapses. *Phys. Rev. E Stat. Nonlin. Soft Matter Phys.* 72, 031914.

Abbott, L. F., and Nelson, S. B. (2000). Synaptic plasticity: taming the beast. *Nat. Neurosci.* 3(Suppl.), 1178–1183.

Abraham, W. C., and Bear, M. F. (1996). Metaplasticity: the plasticity of synaptic plasticity. *Trends Neurosci.* 19, 126–130.

Allen, C. B., Celikel, T., and Feldman, D. E. (2003). Long-term depression induced by sensory deprivation during cortical map plasticity *in vivo*. *Nat. Neurosci.* 6, 291–299.

Amit, D. J., and Brunel, N. (1997). Model of global spontaneous activity and local structured activity during delay periods in the cerebral cortex. *Cereb. Cortex* 7, 237–252.

Artola, A., Brocher, S., and Singer, W. (1990). Different voltage-dependent thresholds for inducing long-term depression and long-term potentiation in slices of rat visual cortex. *Nature* 347, 69–72.

Aslam, N., Kubota, Y., Wells, D., and Shouval, H. Z. (2009). Translational switch for long-term maintenance of synaptic plasticity. *Mol. Syst. Biol.* 5, 284.

Bell, C. C., Han, V. Z., Sugawara, Y., and Grant, K. (1997). Synaptic plasticity in a cerebellum-like structure depends on temporal order. *Nature* 387, 278–281.

Bender, V. A., Bender, K. J., Brasier, D. J., and Feldman, D. E. (2006). Two coincidence detectors for spike timing-dependent plasticity in somatosensory cortex. *J. Neurosci.* 26, 4166–4177.

Bi, G. Q., and Poo, M. M. (1998). Synaptic modifications in cultured hippocampal neurons: dependence on spike timing, synaptic strength, and postsynaptic cell type. *J. Neurosci.* 18, 10464–10472.

Bienenstock, E. L., Cooper, L. N., and Munro, P. W. (1982). Theory for the development of neuron selectivity: orientation specificity and binocular interaction in visual cortex. *J. Neurosci.* 2, 32–48.

Bliss, T. V. P., and Gardner-Medwin, A. R. (1973). Long-lasting potentiation of synaptic transmission in the dentate area of the unanaestetized rabbit following stimulation of the perforant path. *J. Physiol.* 232, 357–374.

Bliss, T. V. P., and Lømo, T. (1973). Long-lasting potentiation of synaptic transmission in the dentate area of the anaesthetized rabbit following stimulation of the perforant path. *J. Physiol.* 232, 331–356.

Cai, Y., Gavornik, J. P., Cooper, L. N., Yeung, L. C., and Shouval, H. Z. (2007). Effect of stochastic synaptic and dendritic dynamics on synaptic plasticity in visual cortex and hippocampus. *J. Neurophysiol.* 97, 375–386.

Cassenaer, S., and Laurent, G. (2007). Hebbian STDP in mushroom bodies facilitates the synchronous flow of olfactory information in locusts. *Nature* 448, 709–713.

Civillico, E. F., Rickgauer, J. P., and Wang, S. S.-H. (2010). "Targeting and excitation of photoactivatable molecules: design considerations for neurophysiology experiments," in *Photoactivatable Molecules for Biology,* eds J. J. Chambers and R. H. Kramer (New York: Humana Press), (in press).

Clopath, C., Busing, L., Vasilaki, E., and Gerstner, W. (2010). Connectivity reflects coding: a model of voltage-based STDP with homeostasis. *Nat. Neurosci.* 13, 344–352.

Clopath, C., Ziegler, L., Vasilaki, E., Busing, L., and Gerstner, W. (2008). Tag-trigger-consolidation: a model of early and late long-term-potentiation and depression. *PLoS Comput. Biol.* 4, e1000248. doi:10.1371/journal.pcbi.1000248.

Cummings, J. A., Mulkey, R. M., Nicoll, R. A., and Malenka, R. C. (1996). Ca2+ signaling requirements for long-term depression in the hippocampus. *Neuron* 16, 825–833.

Dudek, S. M., and Bear, M. F. (1992). Homosynaptic long-term depression in area CA1 of hippocampus and effects of N-methyl-D-aspartate receptor blockade. *Proc. Natl. Acad. Sci. U.S.A.* 89, 4363–4367.

Engert, F., and Bonhoeffer, T. (1997). Synapse specificity of long-term potentiation breaks down at short distances. *Nature* 388, 279–284.

Feldman, D. E. (2000). Timing-based LTP and LTD at vertical inputs to layer II/III pyramidal cells in rat barrel cortex. *Neuron* 27, 45–56.

Feldman, D. E., and Brecht, M. (2005). Map plasticity in somatosensory cortex. *Science* 310, 810–815.

Felleman, D. J., and Van Essen, D. C. (1991). Distributed hierarchical processing in the primate cerebral cortex. *Cereb. Cortex* 1, 1–47.

Fiete, I. R., Senn, W., Wang, C. Z. H., and Hahnloser, R. H. R. (2010). Spike-time-dependent plasticity and heterosynaptic competition organize networks to produce long scale-free sequences of neural activity. *Neuron* 65, 563–576.

Frey, U., Huang, Y. Y., and Kandel, E. R. (1993). Effects of cAMP simulate a late stage of LTP in hippocampal CA1 neurons. *Science* 260, 1661–1664.

Froemke, R. C., and Dan, Y. (2002). Spike-timing-dependent synaptic modification induced by natural spike trains. *Nature* 416, 433–438.

Froemke, R. C., Poo, M. M., and Dan, Y. (2005). Spike-timing-dependent synaptic plasticity depends on dendritic location. *Nature* 434, 221–225.

Froemke, R. C., Tsay, I. A., Raad, M., Long, J. D., and Dan, Y. (2006). Contribution of individual spikes in burst-induced long-term synaptic modification. *J. Neurophysiol.* 95, 1620–1629.

Fusi, S., Drew, P. J., and Abbott, L. F. (2005). Cascade models of synaptically stored memories. *Neuron* 45, 599–611.

Gerstner, W., Kempter, R., van Hemmen, J. L., and Wagner, H. (1996). A neuronal learning rule for sub-millisecond temporal coding. *Nature* 383, 76–81.

Gerstner, W., and Kistler, W. M. (2002). *Spiking Neuron Models: Single Neurons, Populations, Plasticity*. Cambridge: Cambridge University Press.

Golding, N. L., Staff, N. P., and Spruston, N. (2002). Dendritic spikes as a mechanism for cooperative long-term potentiation. *Nature* 418, 326–331.

Gonon, F. (1997). Prolonged and extrasynaptic excitatory action of dopamine mediated by D1 receptors in the rat striatum *in vivo*. *J. Neurosci.* 17, 5972–5978.

Gradinaru, V., Thompson, K. R., Zhang, F., Mogri, M., Kay, K., Schneider, M. B., and Deisseroth, K. (2007). Targeting and readout strategies for fast optical neural control *in vitro* and *in vivo*. *J. Neurosci.* 27, 14231–14238.

Graupner, M., and Brunel, N. (2007). STDP in a bistable synapse model based on CaMKII and associated signaling pathways. *PLoS Comput. Biol.* 3, e221. doi:10.1371/journal.pcbi.0030221.

Gütig, R., Aharonov, R., Rotter, S., and Sompolinsky, H. (2003). Learning input correlations through nonlinear temporally asymmetric Hebbian plasticity. *J. Neurosci.* 23, 3697–3714.

Hartell, N. A. (1996). Strong activation of parallel fibers produces localized calcium transients and a form of LTD that spreads to distant synapses. *Neuron* 16, 601–610.

Harvey, C. D., and Svoboda, K. (2007). Locally dynamic synaptic learning rules in pyramidal neuron dendrites. *Nature* 450, 1195–1200.

Hebb, D. O. (1949). *Organization of Behavior*. New York: John Wiley and sons.

Higley, M. J., and Sabatini, B. L. (2008). Calcium signaling in dendrites and spines: practical and functional considerations. *Neuron* 59, 902–913.

Hirase, H., Czurko, A., Csicsvari, J., and Buzsaki, G. (1999). Firing rate and theta-phase coding by hippocampal pyramidal neurons during 'space clamping'. *Eur. J. Neurosci.* 11, 4373–4380.

Hopfield, J. J. (1984). Neurons with graded response have collective computational properties like those of two-state neurons. *Proc. Natl. Acad. Sci. U.S.A.* 81, 3088–3092.

Hopfield, J. J. (1995). Pattern recognition computation using action potential timing for stimulus representation. *Nature* 376, 33–36.

Huang, Y. Y., Li, X. C., and Kandel, E. R. (1994). cAMP contributes to mossy fiber LTP by initiating both a covalently mediated early phase and macromolecular synthesis-dependent late phase. *Cell* 79, 69–79.

Izhikevich, E. M., and Desai, N. S. (2003). Relating STDP to BCM. *Neural. Comput.* 15, 1511–1523.

Johnston, D., Christie, B. R., Frick, A., Gray, R., Hoffman, D. A., Schexnayder, L. K., Watanabe, S., and Yuan, L. L. (2003). Active dendrites, potassium channels and synaptic plasticity. *Philos. Trans. R. Soc. Lond., B, Biol. Sci.* 358, 667–674.

Karmarkar, U. R., Najarian, M. T., and Buonomano, D. V. (2002). Mechanisms and significance of spike-timing dependent plasticity. *Biol. Cybern.* 87, 373–382.

Kempter, R., Gerstner, W., and van Hemmen, L. (1999). Hebbian learning and spiking neurons. *Phys. Rev. E* 59, 4498–4514.

Kitajima, T., and Hara, K. (2000). A generalized Hebbian rule for activity-dependent synaptic modifications. *Neural. Netw.* 13, 445–454.

Konorski, J. (1948). *Conditioned Reflexes and Neuron Organization*. Cambridge: Cambridge University Press.

Larkum, M. E., and Nevian, T. (2008). Synaptic clustering by dendritic signalling mechanisms. *Curr. Opin. Neurobiol.* 18, 321–331.

Larson, J., and Lynch, G. (1988). Role of N-methyl-D-aspartate receptors in the induction of synaptic potentiation by burst stimulation patterned after the hippocampal theta-rhythm. *Brain Res.* 441, 111–118.

Levy, W. B., and Steward, O. (1983). Temporal contiguity requirements for long-term associative potentiation/depression in the hippocampus. *Neuroscience* 8, 791–797.

Lisman, J. (1989). A mechanism for the Hebb and the anti-Hebb processes underlying learning and memory. *Proc. Natl. Acad. Sci. U.S.A.* 86, 9574–9578.

Lisman, J. E., and Zhabotinsky, A. M. (2001). A model of synaptic memory: a CaMKII/PP1 switch that potentiates transmission by organizing an AMPA receptor anchoring assembly. *Neuron* 31, 191–201.

Major, G., Polsky, A., Denk, W., Schiller, J., and Tank, D. W. (2008). Spatiotemporally graded NMDA spike/plateau potentials in basal dendrites of neocortical pyramidal neurons. *J. Neurophysiol.* 99, 2584–2601.

Markram, H., Lubke, J., Frotscher, M., and Sakmann, B. (1997). Regulation of synaptic efficacy by coincidence of postsynaptic APs and EPSPs. *Science* 275, 213–215.

McCormack, S. G., Stornetta, R. L., and Zhu, J. J. (2006). Synaptic AMPA receptor exchange maintains bidirectional plasticity. *Neuron* 50, 75–88.

Mehta, M. R. (2004). Cooperative LTP can map memory sequences on dendritic branches. *Trends Neurosci.* 27, 69–72.

Miyakawa, H., Lev-Ram, V., Lasser-Ross, N., and Ross, W. N. (1992). Calcium transients evoked by climbing fiber and parallel fiber synaptic inputs in guinea pig cerebellar Purkinje neurons. *J. Neurophysiol.* 68, 1178–1189.

Mizuno, T., Kanazawa, I., and Sakurai, M. (2001). Differential induction of LTP and LTD is not determined solely by instantaneous calcium concentration: an essential involvement of a temporal factor. *Eur. J. Neurosci.* 14, 701–708.

Mulkey, R. M., and Malenka, R. C. (1992). Mechanisms underlying induction of homosynaptic long-term depression in area CA1 of the hippocampus. *Neuron* 9, 967–975.

Nakamura, T., Nakamura, K., Lasser-Ross, N., Barbara, J. G., Sandler, V. M., and Ross, W. N. (2000). Inositol 1,4,5-trisphosphate (IP3)-mediated Ca2+ release evoked by metabotropic agonists and backpropagating action potentials in hippocampal CA1 pyramidal neurons. *J. Neurosci.* 20, 8365–8376.

Narayanan, R., and Johnston, D. (2007). Long-term potentiation in rat hippocampal neurons is accompanied by spatially widespread changes in intrinsic oscillatory dynamics and excitability. *Neuron* 56, 1061–1075.

Nevian, T., and Sakmann, B. (2006). Spine Ca2+ signaling in spike-timing-dependent plasticity. *J. Neurosci.* 26, 11001–11013.

Ngezahayo, A., Schachner, M., and Artola, A. (2000). Synaptic activity modulates the induction of bidirectional synaptic changes in adult mouse hippocampus. *J. Neurosci.* 20, 2451–2458.

Nishiyama, M., Hong, K., Mikoshiba, K., Poo, M. M., and Kato, K. (2000). Calcium stores regulate the polarity and input specificity of synaptic modification. *Nature* 408, 584–588.

O'Connor, D. H., Wittenberg, G. M., and Wang, S. S.-H. (2005a). Dissection of bidirectional synaptic plasticity into saturable unidirectional processes. *J. Neurophysiol.* 94, 1565–1573.

O'Connor, D. H., Wittenberg, G. M., and Wang, S. S.-H. (2005b). Graded bidirectional synaptic plasticity is composed of switch-like unitary events. *Proc. Natl. Acad. Sci. U.S.A.* 102, 9679–9684.

Oja, E. (1982). A simplified neuron model as a principal component analyzer. *J. Math. Biol.* 15, 267–273.

Pawlak, V., and Kerr, J. N. (2008). Dopamine receptor activation is required for corticostriatal spike-timing-dependent plasticity. *J. Neurosci.* 28, 2435–2446.

Petersen, C. C., Malenka, R. C., Nicoll, R. A., and Hopfield, J. J. (1998). All-or-none potentiation at CA3-CA1 synapses. *Proc. Natl. Acad. Sci. U.S.A.* 95, 4732–4737.

Pfister, J. P., and Gerstner, W. (2006). Triplets of spikes in a model of spike timing-dependent plasticity. *J. Neurosci.* 26, 9673–9682.

Pike, F. G., Meredith, R. M., Olding, A. W., and Paulsen, O. (1999). Rapid report: postsynaptic bursting is essential for 'Hebbian' induction of associative long-term potentiation at excitatory synapses in rat hippocampus. *J. Physiol.* 518(Pt 2), 571–576.

Rao, R. P., and Sejnowski, T. J. (2001). Spike-timing-dependent Hebbian plasticity as temporal difference learning. *Neural. Comput.* 13, 2221–2237.

Rioult-Pedotti, M. S., Donoghue, J. P., and Dunaevsky, A. (2007). Plasticity of the synaptic modification range. *J. Neurophysiol.* 98, 3688–3695.

Rose, G. M., and Dunwiddie, T. V. (1986). Induction of hippocampal long-term potentiation using physiologically patterned stimulation. *Neurosci. Lett.* 69, 244–248.

Rubin, J. E., Gerkin, R. C., Bi, G. Q., and Chow, C. C. (2005). Calcium time course as a signal for spike-timing-dependent plasticity. *J. Neurophysiol.* 93, 2600–2613.

Rumelhart, D. E., and McClelland, J. E. (1987). *Parallel Distributed Processing, Vol.1 Foundations*. Cambridge, MA: MIT press.

Safo, P., and Regehr, W. G. (2008). Timing dependence of the induction of cerebellar LTD. *Neuropharmacology* 54, 213–218.

Salin, P. A., Malenka, R. C., and Nicoll, R. A. (1996). Cyclic AMP mediates a presynaptic form of LTP at cerebellar parallel fiber synapses. *Neuron* 16, 797–803.

Sarkisov, D. V., and Wang, S. S. -H. (2008). Order-dependent coincidence detection in cerebellar Purkinje neurons at the inositol trisphosphate receptor. *J. Neurosci.* 28, 133–142.

Schiegg, A., Gerstner, W., Ritz, R., and van Hemmen, J. L. (1995). Intracellular Ca2+ stores can account for the time course of LTP induction: a model of Ca2+ dynamics in dendritic spines. *J. Neurophysiol.* 74, 1046–1055.

Schiller, J., and Schiller, Y. (2001). NMDA receptor-mediated dendritic spikes and coincident signal amplification. *Curr. Opin. Neurobiol.* 11, 343–348.

Schultz, W. (2002). Getting formal with dopamine and reward. *Neuron* 36, 241–263.

Sejnowski, T. J. (1977). Storing covariance with nonlinearly interacting neurons. *J. Math. Biol.* 4, 303–321.

Seol, G. H., Ziburkus, J., Huang, S., Song, L., Kim, I. T., Takamiya, K., Huganir, R. L., Lee, H. K., and Kirkwood, A. (2007). Neuromodulators control the polarity of spike-timing-dependent synaptic plasticity. *Neuron* 55, 919–929.

Shouval, H. Z., Bear, M. F., and Cooper, L. N. (2002). A unified model of NMDA receptor-dependent bidirectional synaptic plasticity. *Proc. Natl. Acad. Sci. U.S.A.* 99, 10831–10836.

Shouval, H. Z., and Kalantzis, G. (2005). Stochastic properties of synaptic transmission affect the shape of spike time-dependent plasticity curves. *J. Neurophysiol.* 93, 1069–1073.

Sjöström, P. J., Rancz, E. A., Roth, A., and Häusser, M. (2008). Dendritic excitability and synaptic plasticity. *Physiol. Rev.* 88, 769–840.

Sjöström, P. J., Turrigiano, G. G., and Nelson, S. B. (2001). Rate, timing, and cooperativity jointly determine cortical synaptic plasticity. *Neuron* 32, 1149–1164.

Sjöström, P. J., Turrigiano, G. G., and Nelson, S. B. (2003). Neocortical LTD via coincident activation of presynaptic NMDA and cannabinoid receptors. *Neuron* 39, 641–654.

Song, S., Miller, K. D., and Abbott, L. F. (2000). Competitive Hebbian learning through spike-timing-dependent synaptic plasticity. *Nat. Neurosci.* 3, 919–926.

Squire, L. R. (1987). *Memory and Brain*. New York: Oxford University Press.

Stäubli, U., and Chun, D. (1996). Factors regulating the reversibility of long-term potentiation. *J. Neurosci.* 16, 853–860.

Stent, G. S. (1973). A physiological mechanism for Hebb's postulate of learning. *Proc. Natl. Acad. Sci. U.S.A.* 70, 997–1001.

Tsodyks, M., Pawelzik, K., and Markram, H. (1998). Neural networks with dynamic synapses. *Neural. Comput.* 10, 821–835.

Turrigiano, G. G., Leslie, K. R., Desai, N. S., Rutherford, L. C., and Nelson, S. B. (1998). Activity-dependent scaling of quantal amplitude in neocortical neurons. *Nature* 391, 892–896.

van Rossum, M. C., Bi, G. Q., and Turrigiano, G. G. (2000). Stable Hebbian learning from spike timing-dependent plasticity. *J. Neurosci.* 20, 8812–8821.

Wang, H. X., Gerkin, R. C., Nauen, D. W., and Bi, G. Q. (2005). Coactivation and timing-dependent integration of synaptic potentiation and depression. *Nat. Neurosci.* 8, 187–193.

Wang, S. S.-H., Denk, W., and Häusser, M. (2000a). Coincidence detection in single dendritic spines mediated by calcium release. *Nat. Neurosci.* 3, 1266–1273.

Wang, S. S.-H., Khiroug, L., and Augustine, G. J. (2000b). Quantification of spread of cerebellar long-term depression with chemical two-photon uncaging of glutamate. *Proc. Natl. Acad. Sci. U.S.A.* 97, 8635–8640.

Wiesel, T. N., and Hubel, D. H. (1963). Effects of Visual Deprivation on Morphology and Physiology of Cells in the Cats Lateral Geniculate Body. *J. Neurophysiol.* 26, 978–993.

Wilson, H. R., and Cowan, J. D. (1973). A mathematical theory of the functional dynamics of cortical and thalamic nervous tissue. *Kybernetik* 13, 55–80.

Wittenberg, G. M., and Wang, S. S.-H. (2006). Malleability of spike-timing-dependent plasticity at the CA3-CA1 synapse. *J. Neurosci.* 26, 6610–6617.

Woodin, M. A., Ganguly, K., and Poo, M. M. (2003). Coincident pre- and post-synaptic activity modifies GABAergic synapses by postsynaptic changes in Cl- transporter activity. *Neuron* 39, 807–820.

Yang, S. N., Tang, Y. G., and Zucker, R. S. (1999). Selective induction of LTP and LTD by postsynaptic [Ca2+]i elevation. *J. Neurophysiol.* 81, 781–787.

Yasuda, R., Harvey, C. D., Zhong, H., Sobczyk, A., van Aelst, L., and Svoboda, K. (2006). Supersensitive Ras activation in dendrites and spines revealed by two-photon fluorescence lifetime imaging. *Nat. Neurosci.* 9, 283–291.

Yasuda, R., Sabatini, B. L., and Svoboda, K. (2003). Plasticity of calcium channels in dendritic spines. *Nat. Neurosci.* 6, 948–955.

Yeung, L. C., Shouval, H. Z., Blais, B. S., and Cooper, L. N. (2004). Synaptic homeostasis and input selectivity follow from a calcium-dependent plasticity model. *Proc. Natl. Acad. Sci. U.S.A.* 101, 14943–14948.

Yu, X., Shouval, H. Z., and Knierim, J. J. (2008). A biophysical model of synaptic plasticity and metaplasticity can account for the dynamics of the backward shift of hippocampal place fields. *J. Neurophysiol.* 100, 983–992.

Zhang, J. C., Lau, P. M., and Bi, G. Q. (2009). Gain in sensitivity and loss in temporal contrast of STDP by dopaminergic modulation at hippocampal synapses. *Proc. Natl. Acad. Sci. U.S.A.* 106, 13028–13033.

Zhong, H., Sia, G. M., Sato, T. R., Gray, N. W., Mao, T., Khuchua, Z., Huganir, R. L., and Svoboda, K. (2009). Subcellular dynamics of type II PKA in neurons. *Neuron* 62, 363–374.

Conflict of Interest Statement: The authors declare that the research was conducted in the absence of any commercial or financial relationships that could be construed as a potential conflict of interest.

Received: 07 March 2010; paper pending published: 17 April 2010; accepted: 07 June 2010; published online: 01 July 2010.

Citation: Shouval HZ, Wang SS-H and Wittenberg GM (2010) Spike timing dependent plasticity: a consequence of more fundamental learning rules. Front. Comput. Neurosci. ***4****:19. doi: 10.3389/fncom.2010.00019*

frontiers in
SYNAPTIC NEUROSCIENCE

ORIGINAL RESEARCH ARTICLE
published: 09 December 2010
doi: 10.3389/fnsyn.2010.00147

A re-examination of Hebbian-covariance rules and spike timing-dependent plasticity in cat visual cortex *in vivo*

Yves Frégnac[1]*, Marc Pananceau[1,2], Alice René[1], Nazyed Huguet[1], Olivier Marre[1], Manuel Levy[1] and Daniel E. Shulz[1]

[1] *Centre National de la Recherche Scientifique, Unité de Neuroscience, Information et Complexité, Gif-sur-Yvette, France*
[2] *Université Paris-Sud, Orsay, France*

Edited by:
Henry Markram, Ecole Polytechnique Federale de Lausanne, Switzerland

Reviewed by:
Jochen Triesch, Johann Wolfgang Goethe University, Germany
John Lisman, Brandeis University, USA
Nicolangelo L. Iannella, RIKEN Brain Institute, Japan

***Correspondence:**
Yves Frégnac, Centre National de la Recherche Scientifique, Unité de Neuroscience, Information et Complexité, UPR CNRS 3293, Gif-sur-Yvette F-91198, France.
e-mail: fregnac@unic.cnrs-gif.fr

Spike timing-dependent plasticity (STDP) is considered as an ubiquitous rule for associative plasticity in cortical networks *in vitro*. However, limited supporting evidence for its functional role has been provided *in vivo*. In particular, there are very few studies demonstrating the co-occurrence of synaptic efficiency changes and alteration of sensory responses in adult cortex during Hebbian or STDP protocols. We addressed this issue by reviewing and comparing the functional effects of two types of cellular conditioning in cat visual cortex. The first one, referred to as the "covariance" protocol, obeys a generalized *Hebbian* framework, by imposing, for different stimuli, supervised positive and negative changes in covariance between postsynaptic and presynaptic activity rates. The second protocol, based on intracellular recordings, replicated *in vivo* variants of the *theta-burst* paradigm (TBS), proven successful in inducing long-term potentiation *in vitro*. Since it was shown to impose a precise correlation delay between the electrically activated thalamic input and the TBS-induced postsynaptic spike, this protocol can be seen as a probe of causal ("pre-before-post") STDP. By choosing a thalamic region where the visual field representation was in retinotopic overlap with the intracellularly recorded cortical receptive field as the afferent site for supervised electrical stimulation, this protocol allowed to look for possible correlates between STDP and functional reorganization of the conditioned cortical receptive field. The rate-based "covariance protocol" induced significant and large amplitude changes in receptive field properties, in both kitten and adult V1 cortex. The TBS STDP-like protocol produced in the adult significant changes in the synaptic gain of the electrically activated thalamic pathway, but the statistical significance of the functional correlates was detectable mostly at the population level. Comparison of our observations with the literature leads us to re-examine the experimental status of spike timing-dependent potentiation in adult cortex. We propose the existence of a correlation-based threshold *in vivo*, limiting the expression of STDP-induced changes outside the critical period, and which accounts for the stability of synaptic weights during sensory cortical processing in the absence of attention or reward-gated supervision.

Keywords: Hebb, intracellular, correlation, potentiation, depression, receptive field, V1, adult plasticity

INTRODUCTION

Our understanding of the potential role of associative synaptic plasticity in the malleability of cortical network function during development, perception and learning has up to now been heavily influenced by a single, simple but seminal concept (Hebb, 1949): that the correlational structure of activity patterns between pre- and postsynaptic neurons determines the changes in the transmission efficacy of synaptic connections.

According to Hebb's rule, the change of the weight from a presynaptic neuron to a postsynaptic neuron depends only on the spiking history of the presynaptic cell and postsynaptic neurons, but does not take into account changes at other neurons "unseen" by the active synapse or other contextual signals. In spite of the fact that Hebb's rule only predicts strengthening of synaptic weights, most theoretical algorithms inspired by Hebb include both associative potentiation and normative depression rules (reviews in Brown et al., 1990; Bi and Poo, 2001; Frégnac, 2002; Gerstner and Kistler, 2002; Brown and Milner, 2003). The Hebbian rule has been the basis of several classical rate-based models applied to unsupervised learning (Oja, 1982; Kohonen, 1989) and developmental and functional epigenesis (Von der Malsburg, 1973; Bienenstock et al., 1982) in cortical networks. Its formalism has been further adapted to follow the timing precision of the spiking process itself (Gerstner et al., 1996; Abbott and Nelson, 2000; van Rossum et al., 2000; Gerstner and Kistler, 2002).

Abbreviations: ABS, Artola–Bröcher–Singer plasticity rule; BCM, Bienenstock–Cooper–Munro plasticity rule; LGN, lateral geniculate nucleus; LTD, long-term depression; LTP, long-term potentiation; mPSP, monosynaptic postsynaptic potential; NMDA, *N*-methyl D-aspartate; pPSP, polysynaptic postsynaptic potential; PSTH, post-stimulus time histogram; PSTW, post-stimulus time waveform; RF, receptive field; SDO, sensitivity-direction-orientation polar selectivity analysis; STDP, spike timing-dependent plasticity; S+, positive covariance between pre- and postsynaptic activities; S–, negative covariance between pre- and postsynaptic activities; TBS, theta-burst stimulation; TBS_S+, theta-burst stimulation associated with an intracellular current pulse; V1, primary visual cortex (area 17 in the cat).

Although, Hebbian algorithms were formulated as a two-factor rule based on firing rates rather than spike events, their application to the *in vivo* situation appeared rapidly limited by the presence of on-going activity, hence pre-existing correlations, in the resting state of the network, and by the local nature of the rule, limited to the active synaptic site. In particular, these rules did not take into account other information related to the on-going internal state of the network in which the considered neuron was embedded, or the general stimulus-driven or learning context. The inclusion of an additional control factor can be seen as a form of "meta-plasticity" (plasticity of the induction or expression of plasticity) and allows a permissive graded control of the expression of Hebbian plasticity in primary visual cortex, known to occur during critical periods of development (Bienenstock et al., 1982; Bear et al., 1987). It accounts for the observed gating of cortical plasticity, through the permissive action of noradrenergic and dopaminergic "print now" neuromodulatory signals (Crow, 1968; Kety, 1970) and oculomotor proprioceptive reafference (Frégnac, 1987). It also complies to the synaptic tagging hypothesis, where prior activity at a synapse changes its ulterior susceptibility to undergo synaptic potentiation (Frey and Morris, 1997). Other versions of three-factor rules were later introduced, which attributed a specific gating role to diffusible brain-derived neurotrophic factors in hippocampal long-term potentiation (LTP) and to nitric oxide in cerebellar long-term depression (LTD) (Crepel, 1998). Similar three-term rules have been generalized to incorporate the behavioral context of classical conditioning in a Hebbian framework (Klopf, 1988).

The more advanced variants of Hebb's rule share the same general equation, where the change of synaptic efficacy with respect to time is equal to the product of three variables: one is contextual, and linked to state-dependent control and learning efficiency, and the two remaining terms are linked respectively to presynaptic and postsynaptic activity (reviews in Frégnac and Shulz, 1994; Frégnac, 2002). The so-called "covariance hypothesis" introduced by Sejnowski (1977) and applied in visual cortex by Bienenstock et al. (1982) uses a multiplicative scalar controlling learning efficiency and replaces the pre- and postsynaptic terms by the departure of instantaneous pre- and postsynaptic activities from their (or a non-linear function of their) respective average values over a certain time window. Since the multiplication of the two activity-dependent terms is mathematically equivalent to a covariance product, the rule obeys a "sign rule" and predicts potentiation of synaptic efficacy when pre- and post-activities increase phasically together (positive covariance) and depression when one term increases while the other decreases (negative covariance). The theoretical sophistication of the BCM rule is that it includes a local postsynaptic "floating plasticity threshold," which avoids saturation or cancellation of synaptic weights and results in self-normalization (see Frégnac, 2002 for a more extensive review). Additional processes, such as synaptic scaling and synaptic redistribution have been since proposed to account for a more global homeostasis of the mean network activity irrespectively of distributed associative synaptic changes (Abbott and Nelson, 2000).

The validity of these theoretical learning rules has been investigated experimentally in Hebbian supervised paradigms where the first contextual term is set arbitrarily in the permissive state: irrespectively of the internal state of the preparation, an external supervisor (most of the time, the experimenter!) imposes an artificial correlational state between pre- and postsynaptic neurons. Experiments, including those from our laboratory, show classically that forced coincident activity induces LTP of synaptic efficiency, whereas non-coincident activity either evokes LTD or no change (Kelso et al., 1986; Frégnac et al., 1988; Reiter and Stryker, 1988; Bear et al., 1990; Bear and Malenka, 1994; review in Frégnac, 2002; **Figure 1**). When first described, the observed plasticity curves (change in synaptic efficiency vs post- and presynaptic delay) were found to be symmetric in time, i.e., no strict temporal ordering was required between the onset of pre- and postsynaptic activation. The temporal contiguity requirement of Hebbian potentiation in sensory neocortex, motor cortex and hippocampus was first estimated in the ±50 ms range, both *in vivo* (Baranyi and Feher, 1981) and *in vitro* (Wigström and Gustafsson, 1985; Frégnac et al., 1994a; Harsanyi and Friedlander, 1997); but see Levy and Steward (1983) and Levy (1985).

In the past 15 years, refined work using dual patch recordings *in vitro* in silent networks demonstrated an even tighter temporal contingency rule (10 ms range), termed "spike timing-dependent plasticity" and the decisive importance of the temporal order between the test postsynaptic potentials (PSP) and the back propagating postsynaptic spike in deciding whether potentiation or depression occurs (Markram et al., 1997): if the postsynaptic cell fires an action potential a few milliseconds after the presynaptic cell, in such a way as to reproduce a causal pre → post relation, LTP is induced, whereas the opposite temporal order results in LTD (Debanne et al., 1997; Markram et al., 1997; Feldman, 2000; Bi and Poo, 2001; Sjöström and Nelson, 2002). Synaptic plasticity, however, was further shown to be also determined by additional non-Hebbian factors, such as the number of postsynaptic spikes in a burst (Sjöström et al., 2001; Froemke and Dan, 2002; Froemke et al., 2005b), postsynaptic depolarization (Sjöström et al., 2001, 2004; Sjöström and Häusser, 2006), and neuromodulation (Kasamatsu et al., 1985; Bear and Singer, 1986; Seol et al., 2007; Pawlak and Kerr, 2008). The outcome of the pairing was shown to depend also on the distance of the synapse from the soma (Froemke et al., 2005a; Letzkus et al., 2006; Sjöström and Häusser, 2006), suggesting the further participation of intrinsic conductance distributions in the dendrites and efficiency of backpropagation of the postsynaptic spike. The spatial gradient of synaptic change along the dendrite results in part from the attenuation of the back propagating action potentials during high frequency trains of action potentials. Dendritic depolarization can boost backpropagation of action potentials and switch plasticity between LTD and LTP at distal dendrites (Sjöström and Häusser, 2006). The action potential attenuation can be persistently counteracted by a long-lasting increase in neuronal intrinsic excitability requiring an elevation of the postsynaptic calcium concentration and the activation of CaMKII (Tsubokawa et al., 2000). This last effect may be highly dependent on the on-going level of inhibition as shown in other sensory systems (Van den Burg et al., 2007). Thus, propagation of action potential back to the dendrite depends on the recent activity of the neuron and its long-term modulation may play a role in the subsequent induction of associative synaptic plasticity.

Over the last 20 years, a large variety of afferent stimulation protocols (**Figure 1A**) have been used to control both (directly) presynaptic and (indirectly) postsynaptic states and induce LTP and

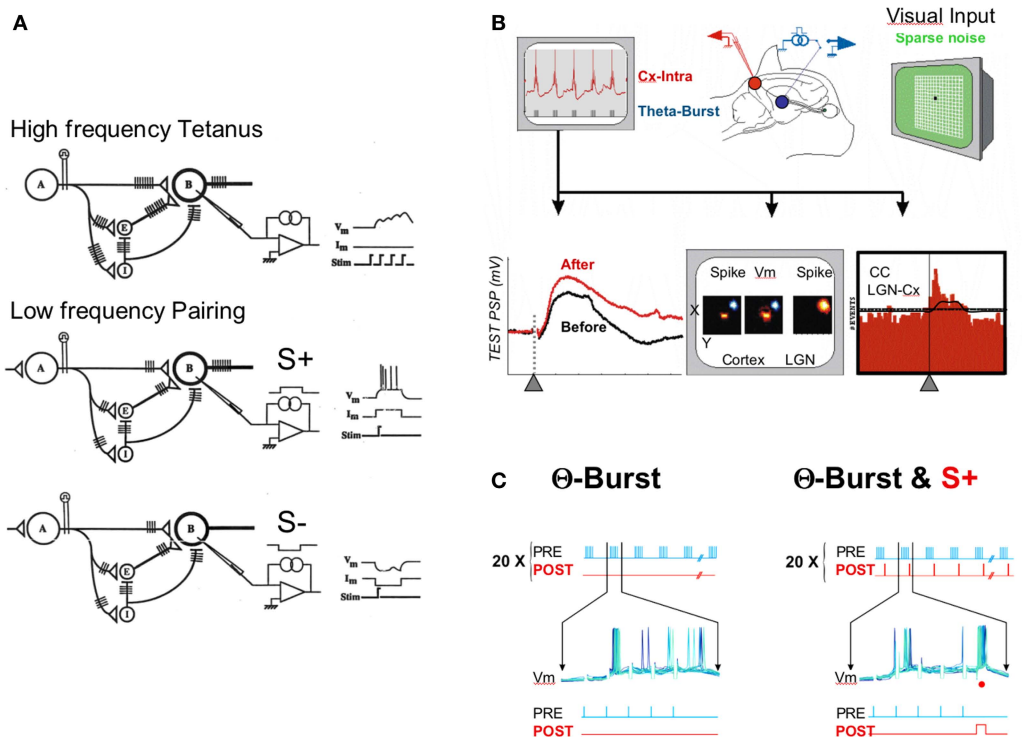

FIGURE 1 | Protocols. (A) Correlation-based protocols. Upper row, high frequency tetanus of afferent pathway activates monosynaptic and polysynaptic excitatory and inhibitory pathways. It is used in LTP protocols to promote the build-up of postsynaptic depolarization and concomitant pre- and postsynaptic firing in target cells. Lower row, differential pairing experiments where the electrical or sensory activation of an afferent pathway is paired with an intracellular depolarizing pulse forcing the target cell to fire (S+). Alternately, another pathway is paired with an intracellular hyperpolarizing pulse resulting in forced synaptic failure (S–). This differential low frequency pairing was used in Frégnac et al. (1988). **(B,C)** Theta-burst protocols. A train of five high frequency pulses repeated at a theta-rhythm is applied in the thalamus (in blue) while recording intracellularly from a potential target cortical cell (in red). The synaptic response to a low frequency (0.2 Hz) thalamic stimulation (lower left inset), the visual receptive field maps (middle) and the cross-correlation histograms between thalamic and cortical spikes (CC, right lower inset) are compared before and after conditioning. In **(C)**, the intracellular membrane potential (Vm) recording during TBS (left panel) is visualized during the burst period. In the TBS_S+ protocol example (right panel), each fifth stimulation pulse in the high frequency burst of the TBS is paired with a depolarizing intracellular pulse (red dot) forcing the cortical cell to spike.

LTD in hippocampal (Dudek and Bear, 1992; Mulkey and Malenka, 1992; Bear and Malenka, 1994; Malenka, 1994) and neocortical slices (Dudek and Bear, 1993; Kirkwood et al., 1993; Kirkwood and Bear, 1994). Unlike in Hebbian supervised paradigms, these protocols did not explicitly require an exogenous control of the postsynaptic discharge pattern. Nevertheless, it is generally admitted that most of their effects can be explained on the basis of the induced correlation between pre- and postsynaptic activities, hence by spike timing-dependent plasticity (STDP) or Hebbian-like processes. Low frequency presynaptic stimulation trains (1 Hz, 900 pulses) induce LTD, whereas presynaptic theta-burst stimulation [a high frequency (100 Hz) burst volley repeated at 5–7 Hz] induces LTP. The efficiency of these protocols in visual cortex has been reported to be age-dependent when the afferent volley originates from the white matter, and to be strongest at the peak of the critical period in kittens (Kirkwood et al., 1993). A different susceptibility period has been found in supragranular layers: NMDA-receptor activation dependent LTP can be still promoted in adult cortex if the strong inhibitory influence originating from layer IV, and normally elicited by thalamic stimulation, is bypassed pharmacologically (Artola and Singer, 1987) or if the afferent volley is applied directly in the superficial layers (Bear et al., 1992; Kirkwood et al., 1995). Age-dependency regulation is less obvious for LTD induction (but see Dudek and Friedlander, 1996), and strong layer variations have been also observed, with a diversity of molecular pathways involved (dominated by NMDA-receptor activation in layer 2–3 and mGluR in layer 6) and an absence of effect in layer 4 (Rao and Daw, 2004).

On the whole, most of the evidence gathered *in vitro* suggests that theta-burst patterned stimulation induces a robust developmental form of LTP of thalamo-cortical synapses, in particular in kitten and young rodent visual cortex. This may account for the functional epigenetic changes occurring during the critical period of ocular dominance and orientation preference (Kirkwood et al., 1996; review in Frégnac and Imbert, 1984). The apparent down-regulation of susceptibility of layer IV to express LTP has been replicated in the somatosensory cortex (Crair and Malenka, 1995), which strengthens the parallel drawn between LTP and the critical period of sensitivity to sensory deprivation (review in Foeller and Feldman, 2004).

In spite of these data and the success of STDP as a phenomenological rule accounting for associative plasticity *in vitro*, limited support for a functional role of LTP has been provided *in vivo*

(see Discussion for a more extensive review). In particular, there is very little experimental data exploring co-evolution of synaptic plasticity and changes in sensory responses during Hebbian or STDP protocols, particularly in adult cortex. An example of such an approach can be found in the work of Heynen, Bear and colleagues, trying to relate monocular deprivation, LTD and LTP to bidirectional modifications of visual acuity (Heynen and Bear, 2001; Iny et al., 2006).

The present paper addresses this issue, by reviewing and comparing two series of attempts to modify synaptic efficacy and functional responses in single neurons recorded in kitten and cat visual cortices:

- The first type of protocol used a *Hebbian framework* to implement, through iontophoretic or intracellular means, supervised positive and negative changes in covariance between postsynaptic and presynaptic activities during the time of recording of the same cell (**Figure 1A**). The main findings of this already published work are summarized here, since they still constitute the largest functional changes reported so far in a single visual cortical neuron (Frégnac et al., 1992, 1988; Shulz and Frégnac, 1992; Debanne et al., 1998; Frégnac and Shulz, 1999): the alternate imposition, for the same cell, of "high" rates of responses for a given input feature and "low" rates for another input leads to long-lasting changes in sensory responsiveness which favors the response for the positively reinforced feature. The reported effects constitute cellular analogs of functional epigenesis and provide the earliest demonstrations of Hebbian-induced changes in adult cortex. In addition to the forms of associative plasticity predicted by the Hebbian rule and its pseudo-Hebbian correlates (Hebb, 1949; Stent, 1973), these experiments confirm some specific predictions of the covariance hypothesis (Bienenstock et al., 1982). In particular, they outline a form of homosynaptic depression, when presynaptic activity is associated with repetitive failure in synaptic transmission (Reiter and Stryker, 1988; Blais et al., 1999), hence a form of plasticity which requires only a subthreshold postsynaptic change (and no spike).
- The second type of protocol, used in a group of new unpublished intracellular experiments, replicates *in vivo* variants of the *theta-burst paradigm*. The rationale of these experiments was twofold: (1) to apply electrical stimulation protocols (theta-burst stimulation, TBS), proven to be successful in inducing LTP *in vitro,* in order to produce a change in the cortical synaptic response to a test thalamic pathway, and (2) to measure the functional consequence of this artificial activity control on target cortical properties, assessed with visual stimuli. With these two purposes in mind, the electrical test stimulus and the high frequency stimulation burst (TBS used for conditioning) were applied in a thalamic region where the visual field representation was in retinotopic proximity or overlapped with the intracellularly recorded cortical receptive field. Since TBS was shown to improve pre-post synaptic correlation in most of the recorded cells without changing their mean activity, the novelty of this protocol was to provide a probe for functional changes caused by causal STDP mechanisms ("pre-before-post") in adult cat cortex *in vivo* (**Figures 1B,C**). In addition, since each theta-burst input is composed by several presynaptic shocks, and thus creates multiple spike delay interactions within a burst, we superimposed, in certain cells, Hebbian supervised pairings added at a fixed intra-burst phase to the theta-burst (**Figure 1C**, right panel). These additional experiments show new evidence *in vivo* of how the supervised reconfiguration of the precise postsynaptic spiking pattern alters in a reversible way the primary effect of high frequency bursts to the cortex.

The Section "Discussion" will compare the various instances of experimental evidence of Hebbian-like or STDP-like correlates of functional plasticity in visual cortex *in vivo* and re-examine the status of spike timing-dependent LTP in adult cortex.

MATERIALS AND METHODS

ANIMAL PREPARATION AND RECORDING TECHNIQUES

Electrophysiological extracellular and intracellular recordings were made in the primary visual cortex of anesthetized and paralyzed kittens and cats, according to the American Physiological Society's Guiding Principles in the Care and Use of Animals. Animals used in these experiments have been bred in the Central CNRS Animal Care facilities at Gif-sur-Yvette. In brief, animals were anesthetized with an intra-muscular injection of alfaxalone/alphadolone (Saffan®, Schering-Plough, 13.5 mg kg^{-1}), a catheter was inserted into the femoral vein for infusion of anesthetic (alfaxalone/alphadolone, flow rate: 2.6 mg kg^{-1} h^{-1}) supplemented with isotonic saline and glucose during the remainder of the experiment. After endotracheal cannulation, the animal was positioned in a stereotaxic Horsley–Clarke frame. Pancuronium bromide (Pavulon®, Organon, flow rate: 0.2 mg kg^{-1} h^{-1}) was added to the perfusion to prevent eye movements. The animal was artificially ventilated at a rate adjusted to maintain end-tidal CO_2 between 3.5 and 4.2%. Body temperature was kept at 38.5° using a feedback-controlled heating pad. EKG and EEG were monitored continuously to control the proper level of anesthesia through-out the experiment. Ocular application of both atropine 1% (Europhta) and phenylephrine clorhydrate 5% (Néosynéphrine®, Europhta) was used to dilate the pupils, block accommodation, and retract the nictitating membranes. Eyes were refracted, fitted with the appropriate corrective lenses and focused on the monitor screen set at 57 cm from the eyes. Small craniotomies (less than 4 mm diameter) were made over the dorso lateral geniculate nucleus (LGN) (see section below) and the primary visual cortex. The stability of recording was improved by cementing (GC Reline, GC America Inc.) the skull to additional fixation bars and a small recording chamber was fixed such as to enclose the cranial openings. After dura incision and electrode placement, the holes were filled with agar, heavy mineral oil, or a silicone grease (Kwick-Cast, World Precision Instrument) to seal the recording chamber and protect the underlying cortex from drying.

LGN recording and stimulation

In all theta-burst experiments, a tungsten microelectrode (2.5–4 MΩ, Frederick Haer) was inserted into the LGN, ipsilateral to the cortical recording site. The electrode tip was positioned in LGN layer A representing the central visual field (stereotaxic Horsley–Clarke coordinates $A = 5–6$; $L = 8–9$; $p = 3–4$) at a depth

of 11–12 mm from the pial surface. The final electrode position was typically adjusted within 100–200 μm from the point at which the first contralateral visual responses where encountered. The LGN multi-unit signal was amplified, filtered (300 Hz–10 kHz) and sampled (at 8 kHz) for further off-line spike discrimination. LGN units were typically characterized by a small monocular receptive field (RF) and their ability to follow high temporal frequency stimulation. The recording LGN electrode was also used as a stimulating electrode through which constant current, negative pulses of 0.2 ms duration were applied at 0.1 Hz (except for theta-burst). The test LGN stimulation intensities ranged from 40 to 360 μA, as required to reliably evoke PSP in the simultaneously intracellularly recorded cortical cell. Short and fixed latency responses following 100 Hz train stimulation were considered as monosynaptic.

Intracellular cortical recordings

Intracellular recordings of cortical cells were obtained using 60–90 MΩ sharp electrodes pulled from 1.5 mm borosilicate glass capillaries (WPI) and filled with 2 M potassium methyl-sulfate (containing 4 mM potassium chloride to avoid tip polarization). The microelectrode was positioned around the retinotopic representation of the area centralis (p = 1.5–2.5; L = 2–4) (Albus, 1975; Tusa et al., 1978), and adjusted when possible to obtain some spatial overlap between the thalamic and the cortical receptive fields. Electrode track penetration started along a latero-medial axis, from the area 17–18 border to the depth of the medial area 17 bank (ranging from 680 to 4150 μm). Intracellular postsynaptic potentials were recorded in current-clamp bridge mode with an Axoclamp-2B amplifier (Axon instruments) and digitized at 8 kHz after adequate low-pass filtering. The EEG was recorded over of the homotopic contralateral cortex of the intracellular recording site. All electrophysiological signals were amplified and filtered in parallel with a CyberAmp 380 (Axon instruments), fed to an A/D interface (DIGIDATA 1200, Axon instruments) port and were further processed using a custom-made analysis program (Elphy™, Sadoc CNRS-UNIC) running on a PC computer.

PLASTICITY PROTOCOLS

Covariance-based

The rationale that was applied to implement the covariance plasticity rule is summarized in **Figure 1A**. Opposite changes were imposed in the temporal correlation between two test sets of synaptic inputs on the one hand, and the output signal of the cell on the other hand. An external supervisor imposed the cell's rate of firing for a given sensory input (usually a "non-preferred" feature) at a "high" level (S+ pairing), and, in alternate trials, blocks the cell's response to another distinct (usually "preferred") input (S− pairing). The control of postsynaptic activity was imposed in two ways: for extracellular pairings (electrodes filled with KCl 3 M, 10–20 MΩ), the recordings were juxtacellular (spikes of several mV and same polarity as intracellular), which allowed the application of small intensity iontophoretic currents (less than ±10 nA) and recording of the cell's activity even during pairing (see also Andrew and Fagan, 1990). For intracellular pairings (electrodes filled with KCH_3SO_4 2 M, 50–100 MΩ), a brief pulse of depolarizing or hyperpolarizing current (less than ±3 nA for 50–200 ms) was applied through the intracellular electrode (KMs, 50–70 MΩ) and synchronized with the stimulus features according to the stimulation protocol.

STDP-based

Theta-burst stimulation was applied through the thalamic stimulation electrode (**Figure 1B**). A TBS train was defined by 10 bursts of 5 pulses at 100 Hz, each burst repeated at a theta frequency (5 Hz). A conditioning sequence was composed of 25 TBS trains, repeated at every 10 s. Stimulus pulse intensity was set to the test level used to trigger the control PSP. In addition to this protocol and for a restricted number of cells, we also imposed supervised postsynaptic firing at a specific temporal phase during each high frequency burst (TBS_S+ in **Figure 1C**). This was achieved by injecting brief (4–6 ms) intracellular current pulses (0.5–1.0 nA), while keeping the temporal relation between the current pulse and the high frequency volley constant. Depending on the pairing, the postsynaptic firing was generally imposed for the first or the fifth presynaptic event of the LGN burst.

ANALYSIS OF ELECTRICALLY EVOKED SYNAPTIC RESPONSES

Measurements of the latency, the initial slope, the time and peak of the maximum response and the integral of the depolarizing component of the PSP relative to the pre-stimulus baseline at each trial were used to quantify synaptic modifications. Fifty to 100 successive thalamo-cortical PSPs triggered at 0.2 Hz by the LGN stimulation were recorded before and after the TBS application and the level of significance of the changes was assessed by using both parametric (Student t-test, $p < 0.001$) and non-parametric tests (Kolmogorov–Smirnov, $p < 0.01$). We also partitioned the integral PSP changes in amplitude range blocks by 20% steps compared to the initial test response.

VISUAL STIMULATION AND ANALYSIS OF RF CHANGES

Once the RF was localized using a semi-automated search with a scalable drifting bar, the ocular dominance and orientation preference of visual responses were qualitatively determined. Stimulation was maintained through the dominant eye for the remaining part of the experiment. The spatio-temporal structures of the cortical (intracellular) and thalamic (multi-unit) receptive fields were mapped with sparse noise [dark (1 cd m^{-2}) and bright (25 cd m^{-2}) pixels, with a mean screen luminance (13 cd m^{-2})]. Depending on the cells and the thalamo-cortical RF arrangement, the chosen size of each pixel ranged from 0.2° to 0.7° (mean: 0.5°) to cover an explored region of 8–20°. ON and OFF durations were usually set at 26.7 or 53.4 ms (corresponding to 4–8 consecutive frames for a 150-Hz refresh rate monitor).

The forward correlations with visual stimulation of the subthreshold (membrane potential) response of the cortical cell and the supra-threshold (action potentials) responses of the simultaneously recorded thalamic and cortical cells were computed for each position and contrast of the stimulus. Post-stimulus time histograms (PSTH) of the visually evoked discharges and the post-stimulus time waveform (PSTW) of the subthreshold responses were then integrated over a 50 ms duration sliding window (in 1 ms steps). X-Y and X-t receptive field maps were then expressed as a Z-score relative to the on-going activity prior to the response onset. The

optimal receptive field map was defined as the map taken at the post-stimulus latency at which a significant response (given by the *Z*-score value compared to pre-stimulus condition, $p < 0.05$) was observed for the largest number of pixel positions. The optimal RF maps taken before and after the TBS application at the same latencies were compared to quantify the functional impact of the thalamo-cortical synaptic plasticity on the RF structure.

Modification of the spatial RF was quantified using a polar analysis carried out on the optimal X-Y maps: the cortical visual response profile was integrated on a radial partition of the RF space in 24 sectors of 15° centered on the initial cortical RF center before TBS (**Figure 8**, left cartoon). The bisector of the first sector was aligned for each cell with the reference axis defined by the alignment of the cortical and thalamic RF centers, such that 0° designated a RF shift toward the LGN-RF center. This polar representation made it possible to apply quantification measures which have been used classically for the study of orientation and direction tuning modifications (Wörgötter and Eysel, 1987). An sensitivity-direction-orientation (SDO) analysis was used to measure the polar and directional selectivity of the change in the sector-based distribution produced by the TBS pairing. This calculus is based on the assumption that the radial distribution of RF changes, pooled over all conditioned cells, can be approximated by an angular (α) cosine function of the form $R(\alpha) = Ao + \Sigma_j [Aj \cos(j\alpha)]$, with the summation index j taking a value of «1» for directional and «2» for orientational tuning, corresponding to a truncated expansion of the Fourier decomposition limited to the first two harmonics. The phase and gain of the first-order and second-order components are measured with a Fast Fourier Transform. The SDO analysis allows the extraction of an index of anisotropy (IA) of the spatial RF change (as the gain of the 1st order component of the decomposition, equivalent to the strength (D) in Wörgötter and Eysel annotation) and the Direction of Anisotropy (Θ), i.e., the most likely direction of the spatial change (as the phase of the 1st order component, equivalent to the preferred direction (PD) in Wörgötter and Eysel annotation): thus IA and Θ give respectively the norm and the angle of a vector representing the average weighted shift in RF anisotropy.

RESULTS

PROTOCOL 1: SUPERVISION OF COVARIANCE BETWEEN PRE- AND POSTSYNAPTIC ACTIVITIES

A classical approach used to demonstrate the functional implication of Hebbian-like mechanisms *in vivo* relies on the study of various forms of visual cortical plasticity induced by manipulations of environmental features, during development and in adulthood (review in Frégnac and Imbert, 1984). The plasticity protocols reviewed here focus on the consequences of Hebbian rules at the individual cell level. Rather than submitting the entire cortical network to an environmental "surgery" of the whole visual field (global clamp of cortex input), cellular analogs of learning restrict the extent to which cortical activity is modulated to the immediate environment of the recorded cell (local perturbation mode). With this approach, the experimenter controls the postsynaptic firing of the recorded cell and imposes a supervision signal which will simulate locally the functional effects of anomalous visual experience during critical periods of development, whereas the majority of the "unseen" units in the network remain unaffected. Two techniques of postsynaptic activity supervision were achieved: (1) by iontophoretic pulses applied through the juxtacellular KCl recording electrode or (2) by current pulses using intracellular techniques (see Materials and Methods). The first method was better suited to control the firing rate whereas the second one imposed precisely the spike timing of the conditioned cells.

In collaboration with Elie Bienenstock, Simon Thorpe, Dominique Debanne and Attila Baranyi, we (Yves Frégnac and Daniel E. Shulz) developed some 25 years ago a series of electrophysiological supervised Hebbian paradigms (Frégnac et al., 1988, 1992, 1994a,b; Shulz and Frégnac, 1992; Shulz et al., 1993; Debanne et al., 1995, 1998; Frégnac and Shulz, 1999). These sets of experiments were devised to quantify the functional impact of supervised control of covariance between pre- and postsynaptic activity and compare the observed effects with the predictions of theoretical models, specifically the so-called BCM rule introduced by Elie Bienenstock and Leon Cooper's group in their seminal paper (Bienenstock et al., 1982).

The differential pairing protocols presented in **Figure 2** have been considered as cellular analogs of functional epigenesis of mammalian V1 since they reproduce functional changes occurring without supervision in freely behaving animals, during development or following early manipulation of the visual environment, for instance an orientation-biased environment (**Figure 2A**), monocular deprivation (**Figure 2B**), optically induced interocular orientation disparity and rearing restricted to a fixed phase and spatial frequency (data not shown; Shulz and Frégnac, 1992). **Figures 2C,D** illustrate the effects of covariance-based pairing protocols on the spatial ON–OFF (or Simple/Complex) organization of visual cortical receptive fields. Surprisingly, at least in the eyes of the reviewers when this work was submitted, the probability of inducing functional changes was reported to be comparable in the kitten during the critical period and in older kittens and adults, suggesting that plasticity might extend well beyond the classical critical period in the presence of an external supervision signal provided by the experimenter, attention or behavioral reward (Frégnac et al., 1988). Since the local supervised learning procedures, applied at the cellular level, imposed an external control of the evoked discharge (through current injection and potassium iontophoresis or field effects), these findings suggest that this type of supervision might bypass systemic homeostatic mechanisms which normally block the expression of plasticity in the mature brain. However, the largest effects were induced in the youngest animals at the peak of the critical period. The major findings are summarized below.

Orientation selectivity plasticity

Early studies on the effects of visual exposure restricted to a fixed orientation (Blakemore and Cooper, 1970; Hirsch and Spinelli, 1970) showed the induction of a significant bias in the cortical representation in favor of the orientation to which kittens had been exposed. Two different interpretations were historically proposed, calling for either selective (the "functional verification" hypothesis) or instructive ("tabula rasa" alternative) mechanisms. However, in view of the inherent limitations of analysis based on the comparison of populations of neurons recorded extracellularly in different animals, no definitive answer could

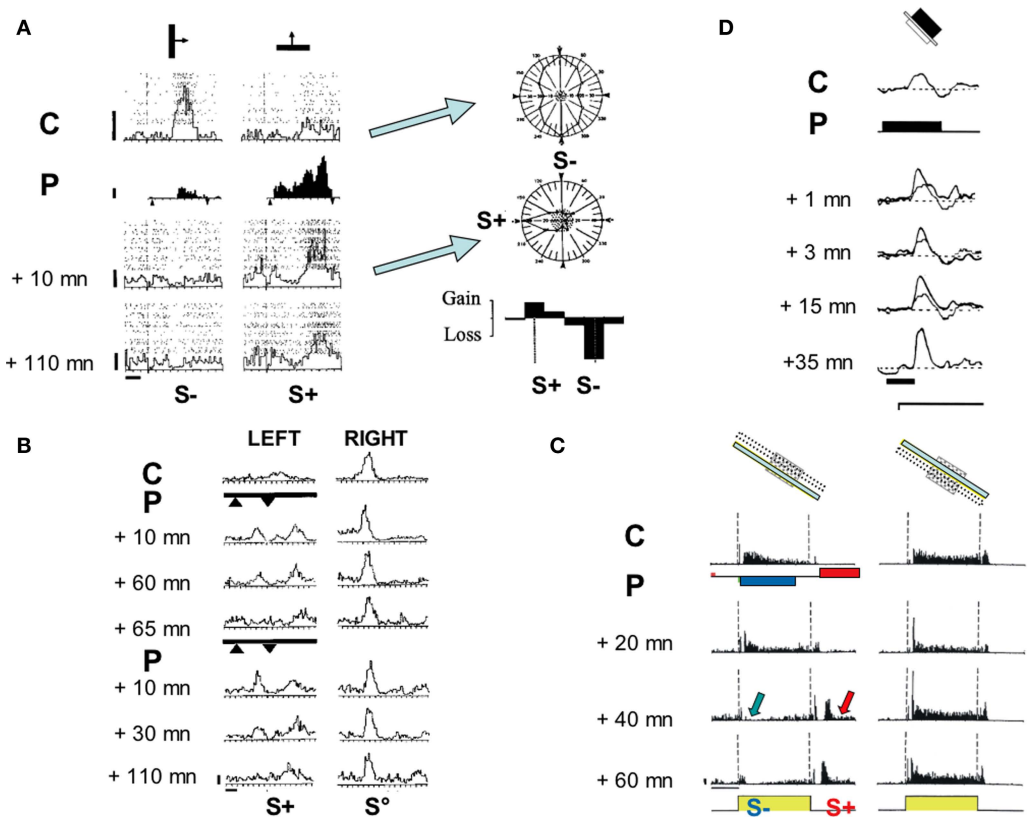

FIGURE 2 | Functional impact of the covariance-based algorithm in kitten V1. (A) Change in orientation preference (adapted from Frégnac et al., 1992): Cell recorded in a visually deprived kitten at the peak of the critical period. *Left panel:* PSTHs represent visual responses to a moving bar for two different orientations (40 runs each). Superimposed dot displays represent spiking responses for each individual trial. Left column, responses for the initially preferred stimulus (vertical orientation). Right, initially non-preferred stimulus (horizontal orientation). From top to bottom, evolution of the relative preference as a function of time, before (C: control), during differential pairing (P) and at two delays following pairing. During pairing (P, filled histograms, 60 associations), a positive current pulse (+3 nA) was applied during the sweep of the horizontal bar across the discharge field (arrowheads, S+), and interleaved with a negative current pulse (–7 nA) when the vertical bar was presented (arrowheads, S–). The visual response became respectively potentiated for the S+ stimulus and depressed for the S– orientation (+10 min). The effects were still present 110 min after pairing. Calibration bars: vertical 5 ap s^{-1}, horizontal 1 s and 1.5°. *Right panel:* Polar orientation tuning curves were established for the same cell before (Control) and after pairing (+10 min). The mean spontaneous activity level is shown by the stippled area. The orientations used during pairing are indicated by S+/S– symbols. The lower graph represents the differences between the normalized tuning curves before and after pairing (folded on a 180° scale) expressed as gains and losses as a function of the orientation of the stimulus (calibration: ±20%). Following pairing, the cell changed its orientation preference by 90°, and became tuned to the positively-reinforced orientation and direction. **(B)** Ocular dominance change (adapted from Shulz and Frégnac, 1992). Cell recorded in a 4.5-week-old normally reared kitten. PSTHs represent visual responses to stimulation of the left (left column) and the right (right column) eyes, before and after two pairings (thick lines). The increase of the visual response to the left eye (+40%), imposed during the first pairing (9 S+ pairings) was retained for 60 min. After extinction (+65 min), this effect was reinstated by a second pairing (imposing a 90% increase in firing during 24 S+ trials), which was retained for 110 min. The response to stimulation through the unpaired (S°) right eye was unchanged. Calibration: vertical 10 ap s^{-1}, horizontal 1 s and 1.5°. **(C)** Change of the ON/OFF balance (adapted from Debanne et al., 1998). Cell recorded in a 6-week-old kitten. PSTHs represent the cell's response to the presentation (ON) and extinction (OFF) of an optimally oriented bar in a fixed position of the RF (cartoon). Before pairing (C, control), a tonic "ON" response and a more transient "OFF" response were observed uniformly across the RF. The pairing procedure (P, data not shown) consisted of 50 associations of a negative current pulse (–3 nA, 2120 ms duration) with the onset of the light bar and a positive current pulse of similar duration (+3.2 nA) following the offset of the same stimulus with a constant delay of 500 ms. A progressive change developed over 40 min after pairing, resulting in a significant depression of the "ON" response ($p < 0.0005$), whereas a late "OFF" response appeared *de novo* in the paired position. The latency of the new response precisely matched the onset delay of the iontophoretic pulse used during pairing. The "ON—OFF" ratio was unchanged in the unpaired position. The modification in the paired position was still present 1 h after the end of the pairing procedure, at which time the neuron was lost. Calibration bars: 1 s; 20 ap s^{-1}. **(D)** Intracellular pairing (adapted from Frégnac et al., 1994b). Simple cell recorded intracellularly *in vivo* in a 10-week-old kitten. Averaged composite potential evoked by the onset of the stimulus in the ON subfield (C: control, 21 trials). During pairing (P, black line) the stimulus onset was paired with a depolarizing pulse (200 ms, 1.2 nA, 30 associations). A significant potentiation of the PSP was induced after pairing (thin line: control PSP, thick lines: after pairing at 1, 3, 15, and 35 min). The unpaired OFF response in the OFF subfield (not shown), the resting membrane potential (–67 mV, dotted lines) and the input resistance (30 MΩ) were unchanged following pairing. Calibration bar: 100 ms.

be given in those early days. Note that the later use of intrinsic imaging (Sengpiel et al., 1999; Tanaka et al., 2006) allows now to conclude that the reorganization of orientation maps was caused indeed by the expansion of domains maximally responding to exposed orientation as well as the strong reduction of responses to unexposed orientations.

We applied our protocol of associative conditioning to demonstrate plasticity of orientation and direction selectivity during the time of recording of single cortical cells (Frégnac et al., 1988, 1992). The response of the recorded neuron was artificially reinforced during the presentation of a given orientation/direction (S+) and suppressed while presenting a different (but fixed) orientation (S–) through the same eye (see **Figure 2A**, left panel). Orientation tuning measurement was used to quantify the generalization of the effects to stimuli other than those used during the conditioning (column of polar plots in **Figure 2A**, right panel). A significant polar asymmetry favoring the S+ preference domain was observed in 30% of conditioned cells, leading to a displacement of the peak of preferred response toward the reinforced orientation/direction.

As a general rule, these changes in tuning selectivity appeared to be linked to the competitive imbalance imposed between the two orientations presented during pairing: independently of their angular separation, a gain in responsiveness was observed around the "positively-reinforced" stimulus, whereas a loss was observed around the "negatively reinforced" one, leading sometimes to the total eradication of the initial visual response. However the amplitude of the orientation shift was related to the initial selectivity of the neuron: the probability of observing large changes in orientation preference (up to 90°) was significantly higher in initially weakly oriented neurons than in already selective ones, suggesting that most changes resulted from up- and down-regulations of pre-existing responses (Frégnac et al., 1988, 1992). This shift in functional preference could reach up to 90° for orientation and corresponded to the *de novo* emergence of a new directional selectivity at the peak of the critical period (see example in **Figure 2A**). Our findings were replicated in kitten (Greuel et al., 1988) and later in adult cat cortex (McLean and Palmer, 1998), using a pharmacological control of postsynaptic activity. The phenomenology of the reported functional changes were supportive of the BCM theory predictions: (1) the largest changes were observed in cells which were the less selective and the most totipotent to stimulus features, and (2) changes were more readily observed in immature than in already specialized cortex, reflecting a dependency of the "floating plasticity threshold" on past experience.

Ocular dominance plasticity

Unilateral eye closure by lid suture performed from the third postnatal week quickly produces a dramatic change in cortical binocularity, i.e., most visual cortical neurons respond exclusively to the open eye (Wiesel and Hubel, 1963). Binocular competitive interaction between visual inputs for dominance of central connections appears to be a major mechanism involved in the effects of monocular deprivation at the cortical level: the closure of one eye produces more drastic changes than binocular closure itself. Following monocular deprivation, cortical cells become dominated or exclusively driven by the open eye, whereas preventing binocular vision by dark rearing does not affect ocular dominance (review in Frégnac and Imbert, 1984). Using moving stimuli, we simulated the effect of imbalance between the two eyes by alternately driving the same cell to a high level (S+) of activity through one eye, and a low level (S–) of firing rate through the other eye, and studying the effects on ocular dominance after 15–80 imposed associations (Shulz and Frégnac, 1992). **Figure 2B** illustrates a case where the spatio-temporal profile of the response to the "reinforced eye" – in addition to its magnitude – was altered: a new peak appeared as the result of an increase in responsiveness and was restricted to the previously unresponsive flank of the receptive field (delineated by filled triangles in **Figure 2B**) where iontophoresis had been applied concurrently with visual stimulation.

Spatial organization of ON–OFF responses

The covariance-based protocol was also adapted to control the plasticity of the spatial ON–OFF organization by inducing changes in the ON–OFF balance selective to the paired location of visual cortical receptive fields (RFs) (Debanne et al., 1998). Covariance supervision was imposed alternately in the same RF position, to boost the evoked response to a "high" level of firing (S+ pairing) for the ON (or OFF) presentation of a light bar, and, in interleaved trials, to reduce the response to the opponent OFF (or ON) feature to a "low" level (S– pairing). These differential pairings were performed iontophoretically during juxtacellular recordings (**Figure 2C**; Debanne et al., 1998) or intracellularly by current injection (**Figure 2D**; Frégnac et al., 1994b; Debanne et al., 1995). In agreement with the covariance hypothesis, they resulted in long-lasting changes of the ON vs OFF balance, favoring the response (ON or OFF) which had been paired with the "high" level of imposed activity.

Modifications consisted mostly of the strengthening and/or weakening of short and long-latency responses (100–800 ms); the amplitude change was on average half of that imposed during pairing. In a few cells, the *de novo* expression of a supra-threshold response was induced for an initially ineffective visual stimulation. Most modifications were observed in the paired position, and restricted to that region of the RF, suggesting that they probably resulted from selective changes in the transmission gain of the synapses which were activated during pairing. In a few cells, a fixed delay pairing procedure was applied, in which the iontophoretic current pulse application lagged behind the presentation or the end of the visual stimulus by a few 100 ms, and some of the conditioned cells retained, for several tens of minutes, a temporal pattern of activity with a phase lag reproducing that imposed during pairing. An example of such an effect is shown in **Figure 2C**, where a long-latency response develops as a recall of the imposed delayed firing. The spatial selectivity of the effect is demonstrated by the fact that the ON–OFF balance remains unchanged in the unpaired position (right column). Our findings of induced changes in the simple/complex profile of visual cortical RFs were also corroborated by a follow-up study using a phase conditioning protocol (McLean and Palmer, 1998), where the authors observed the induction of counter-phased modulated responses to stimuli presented at the spatial phase which initially did not evoke any response (« null» phase).

Most of the changes reviewed so far were produced by extracellular pairing protocols, without access to the subthreshold synaptic events which may be modified by the Hebbian pairing procedure. In these experiments, the iontophoretic pulses used to control the excitability of the conditioned cell recruited potentially two mixed effects: (1) the first one was seen during juxtacellular recordings and corresponded to direct current effects triggering or suppressing the spike initiation (through field effect at the soma); (2) the second

one, evoked mostly during S+ pairings, relied on rapid changes in the extracellular potassium level. A possible side-effect may arise, due to uncontrolled potassium-dependent modification of presynaptic activity and release of neuromodulators. In order to avoid or reduce these side-effects, we made, in collaboration with Attila Baranyi, intracellular recordings (most likely intrasomatic) and used direct current injection to control the postsynaptic state of activation. This allowed a more selective pairing procedure during which the visually triggered PSP was temporally associated with a concomitant depolarizing or hyperpolarizing current pulse injection into the target cell (**Figure 2D**; Frégnac et al., 1994b; Debanne et al., 1995). We could then measure changes of visually evoked subthreshold synaptic potentials directly and thus interpret the observed functional changes in terms of plasticity of synaptic transmission. Similar experiments were attempted *in vitro* in rat and kitten visual cortical slices by Yves Frégnac in collaboration with Michael Friedlander and colleagues (Frégnac et al., 1994a), where the visual input was replaced by the electrical stimulation of the optic radiation or layer II–III axons. In the majority of conditioned cells, both *in vivo* and *in vitro*, the sign of the change (potentiation or depression) of the composite postsynaptic potential was predicted by the sign of the imposed change of the membrane potential during pairing. The effects appeared associative, since they were not observed when the current pulse was applied unrelated to visual stimulation.

The exact cellular mechanisms involved in functional changes remain difficult to unravel *in vivo*, since one cannot separate easily increased excitation from reduced concomitant inhibition. Blocking of inhibition *in vivo* leads to epileptic activity, and most pharmacological dissection methods used *in vitro* are no longer applicable. Data comparison suggest that enhancement in the efficacy of excitatory synaptic transmission is the most likely mechanism for the LTP observed after afferent stimulation of visual pathways both *in vitro* (Artola and Singer, 1987) and *in vivo* (Komatsu et al., 1988). Similarly, in our case, postsynaptic responses during S+ pairing were probably pushed beyond the threshold level at which NMDAR-dependent Ca^{2+} flux is sufficient to induce LTP of active synapses (see Bear, 2003 for a review).

PROTOCOL 2: THETA-BURST

Plasticity of thalamo-cortical and cortico-cortical synapses was explored following a high frequency stimulation (TBS) to sites in the LGN connected synaptically with neurons recorded intracellularly in primary visual cortex area 17. The theta-burst conditioning consists of a short high frequency sequence of five thalamic electrical stimulation pulses (each 10 ms apart) repeated at 5 Hz (every 200 ms). Intracellular recordings were obtained from 49 V1 cells, and in 34 cases, the full protocol (thalamic TBS and visual receptive field mapping) was carried out. Our aim was to assess at the same time the plasticity of the thalamo-cortical connections in response to an electrical (extraneous) thalamic tetanus and its functional consequences on the receptive field organization of the cortical target cells.

Single shocks of the thalamus, repeated at a low frequency (0.2 Hz), were applied before and after TBS to measure changes in the composite synaptic efficiency of the conditioned pathway. Postsynaptic responses to 50–100 stimulus cycles were averaged to provide a baseline control. The low rate of frequency stimulation was chosen to avoid short-term synaptic adaptation (Nelson, 1991) and the stimulation intensity was set below spiking threshold. Monosynaptic (mPSP) components in the composite synaptic responses were characterized by a short latency, very little latency jitter and the ability to follow high frequency stimulation (100 Hz). Polysynaptic (pPSP) components were observed with diverse latencies reflecting possibly the parallel recruitment of different synaptic pathways.

To evaluate the TBS train effect, the analog synaptic response waveforms evoked before and after the TBS application were stripped from spike contamination and averaged. The waveforms were then subtracted to visualize the temporal profile of the overall synaptic change (blue traces in **Figure 3**). The *t*-test comparison ($p < 0.001$) of peak responses and integral values (see Materials and Methods) before and after TBS showed that 44% of monosynaptic EPSPs and 56% of polysynaptic EPSPs were significantly potentiated ($n = 17$), while 39% of monosynaptic EPSPs and 25% of polysynaptic EPSPs were depressed ($n = 11$), while the remaining cases were unchanged. Note that the *in vivo* situation differs greatly from *in vitro* conditions, where it is pharmacologically possible to block inhibitory pathways (through application of GABA antagonists in the bath). Most LTP/LTD *in vitro* studies usually focus on the rising slope of the early monosynaptic event. *In vivo*, the measure of the rising slope is unreliable (since contaminated by concomitant inhibition) and the full waveform underlying spike activity has to be considered. Since the functional effects result from combined modifications of mono and polysynaptic components, we were obliged to use a combination of criteria to assess PSP changes.

Potentiation of the PSP was defined in three ways: as an increase in the peak amplitude, an increase in the integral of the response or as a reduced response latency. Conversely depression was expressed as a reduction of the PSP size and/or a lengthening of its latency. The monosynaptic and polysynaptic components appeared modified in the same proportions. In six conditioned cells, the TBS application did not trigger spikes during the high frequency bursts, resulting either in an absence of change ($n = 3$) or a depression ($n = 3$). In the other cells, where TBS imposed reliable correlation between pre-post firing (see examples in **Figure 4**), significant changes were observed in 90% of cases. Potentiation was more readily observed than depression (61 vs 29%) underlying the role of the postsynaptic discharge in synaptic potentiation induction.

One should note that *in vivo* statistical tests (parametric and non-parametric) readily show significant changes ($p < 0.001$ here). However, these numbers have to be taken with caution since not all data obey normal distributions, and differences in variance were often seen between before and after pairing. Furthermore, numerous sources of variability are not controlled *in vivo*, for instance changes in the EEG reflecting the global state of the preparation, or changes in on-going intracellular activity with possible spontaneous interference of "up" and "down" states, and these may result in non-stationarities (see Discussion). Only half of cells (irrespectively of statistical significance) showed changes less than ±20% in PSP integral value, which attests for a high variance in the *in vivo* preparation. The respective proportions of cases with potentiation and depression beyond 20% reached respectively 26 and 11%.

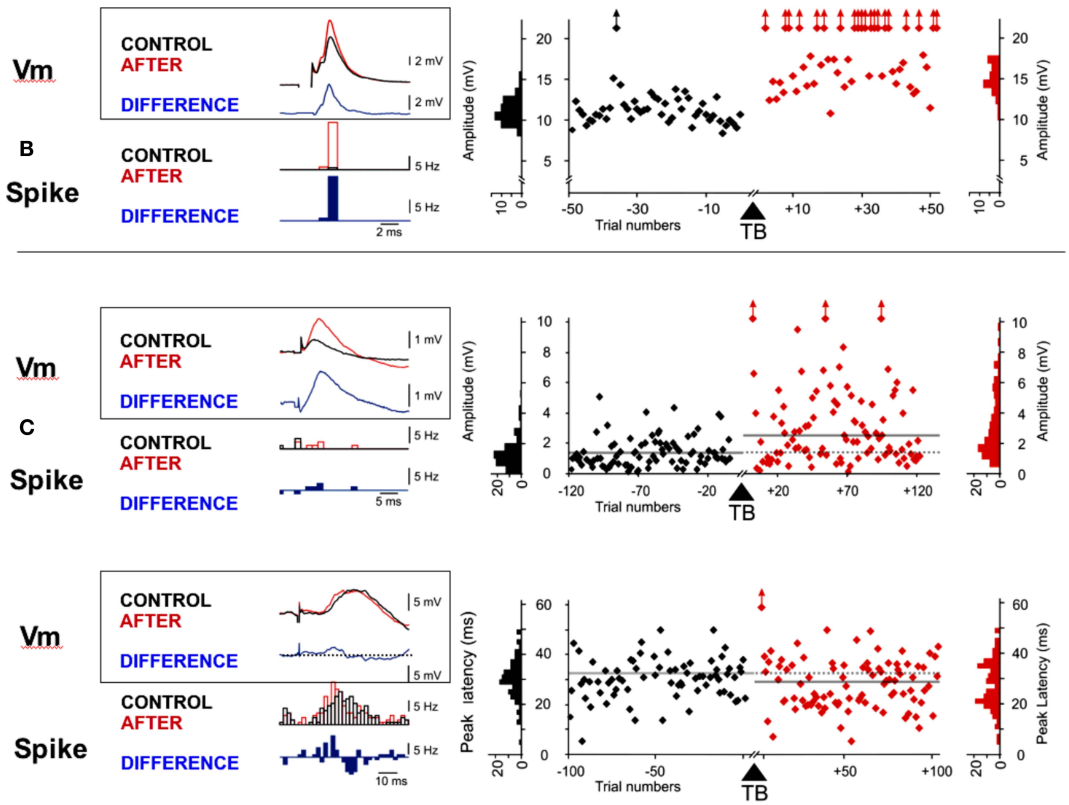

FIGURE 3 | Examples of LTP in adult visual cortex induced by theta-burst. Synaptic changes were observed on both monosynaptic **(A)** and polysynaptic **(B,C)** components of the test PSP by comparing the amplitude **(A,B)** or the latency **(C)** of the PSPs recorded before and after TBS. The left panels show overlaid averaged PSPs (at rest) and PSTHs (with a + 5mV depolarization) obtained before (CONTROL, in black) and after (in red) TBS. The difference ("CONTROL" – "AFTER") waveforms are shown below (in blue). The right panels show the time course of the amplitudes or latencies measured on individual PSPs during the pre- and post-TBS periods. Distributions of the measured values are displayed on each side of the plots. **(A)** Potentiation of the peak amplitude of a monosynaptic response from 11.1 mV (σ = 1.5 mV) to 15 mV (σ = 1.9 mV), $p < 0.001$. **(B)** Potentiation of a composite polysynaptic response, where the peak amplitude increased from 1.4 to 2.7 mV ($p < 0.001$). **(C)** Latency shortening ($p < 0.05$) of the peak response from 30.3 to 27.8 ms. Note the intermittent occurrence of shorter peak latencies (18–20 ms) after TBS.

Figure 3 shows individual examples of the potentiation induced by TBS stimulation in the peak amplitude of a mPSP (**Figure 3A**) and in the amplitude (**Figure 3B**) and the latency of the peak of a pPSP (**Figure 3C**). For the mPSP example, the mean amplitude of the synaptic response increased by 35%, from 11.1 mV (±1.5 mV) to 15.0 mV (±1.9 mV) after theta-burst stimulation of LGN input ($p < 0.001$). **Figure 3B** shows an example in which a pPSP was significantly increased (from 1.4 to 2.7 mV; $p < 0.001$) at the same time that the across-trial variability of responses increased, suggesting that synaptic changes could be partly due to the recruiting of new synaptic contacts that were previously ineffective. Note as a consequence the fact that the same afferent volley stimulation generally led to more spikes riding on the PSP following TBS (when tested before and after TBS at a resting state depolarized by +5 mV). In two of the "potentiated" cells, the detected change was a significant reduction of the onset or peak response latency, without a change in the peak amplitude. The difference between averaged PSPs obtained before and after TBS (blue trace in **Figure 3C**) shows an example of potentiation mainly visible in the rising slope of the composite pPSP. As a consequence, the distribution of spikes triggered by the thalamic afferent volley (tested at a more depolarized state) was displaced toward shorter latencies following TBS (blue histogram in **Figure 3C**).

In order to interpret the expression of synaptic changes as a function of the interaction between pre- and postsynaptic activity, we analyzed the activity patterns imposed during the theta-burst. In many cases, the repetitive application of high frequency bursts during the TBS train resulted in the cumulative build-up of depolarization due to temporal summation of elementary responses to a single thalamic shock. This slow dynamic tendency toward cumulative depolarization was visible in the form of augmenting responses from one burst to the next, over the full train duration. These augmenting-like responses were observed during the 5 Hz TBS in 47% of cases, and resulted in twice as much potentiation (64.3 vs 37.5%) and half as much depression (35.1 vs 50% of cases), when compared to TBS trains where no cumulative recruitment was seen. This suggests that the level of depolarization reached during the high frequency thalamic burst controls the expression of synaptic potentiation, at least partly, as already shown *in vitro* (Sjöström et al., 2001).

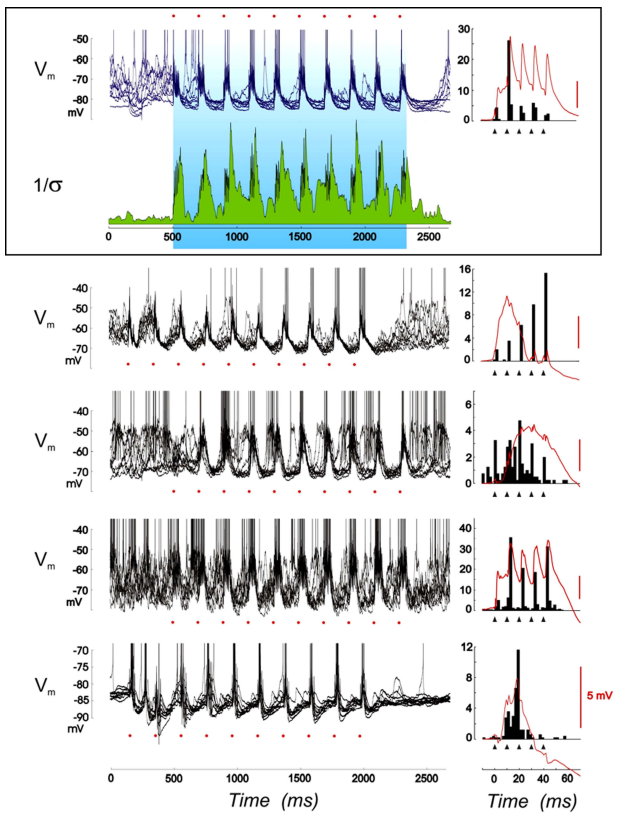

FIGURE 4 | Changes of covariance between pre- and postsynaptic activities imposed during theta-burst. For each of the five cells presented, the voltage traces are synchronized with the onset of each theta-burst train and repetitions are overlaid. The reproducibility of the recorded waveform, shown for the first cell only (inset, second row from the top), is high, especially in-between the high frequency bursts, whose individual onsets are underlined by red dots. The variability reduction in the Vm dynamics is quantified by the inverse of the standard deviation (σ) of the waveforms computed over the 25 TBS repetitions (1/σ index, green plot) and shown with the voltage waveform for one of the cells (top inset). In the right column, the mean voltage waveform (in red) synchronized with each burst onset is shown for the duration of the burst and overlaid with the mean spike pattern imposed by the high frequency volley (black filled histogram). Black filled triangles show the occurrence of individual electrical thalamic shocks.

In contrast to these highly phasic activation periods, between bursts, a clamp of the Vm trajectory was observed resulting in the silencing of postsynaptic activity (see also Kara et al., 2002). This effect is apparent when comparing overlaid voltage traces synchronized with the TBS onset. The second row in **Figure 4** illustrates a drop in variability of the stimulus-locked voltage waveform: the inverse of the standard deviation (1/σ) increases transiently with each burst (due to the forced positive covariance imposed by the brief tetanus) and progressively stabilizes to a high level during the time course of the repolarizing phase separating successive bursts. Consistently from cell to cell, TBS was efficient to drive the postsynaptic firing at a theta-rhythm, with tight positive correlation epochs within each high frequency burst, while suppressing responses to all inputs that may spontaneously occur between bursts. In most cells, the correlation between the thalamic electrical shock (triangles in **Figure 4**, right panel) and TBS-induced postsynaptic spikes was increased within the bursts, resulting in a tight control of spike timing. This observation suggests that TBS is a reliable way *in vivo* to favor STDP-like plasticity processes at positive presynaptic-postsynaptic delays (causal STDP). Note nevertheless that the spontaneous changes in the level of on-going activity at the time the burst is applied may affect the voltage-dependence of the synaptic responses during individual shocks of the TBS pairing, and possibly recruit additional factors controlling the expression of plasticity (Sjöström et al., 2001).

Another interesting observation from the study of postsynaptic activity during TBS is the correlation often observed in potentiated cases between the spike distribution pattern imposed during the TBS and the temporal profile of the synaptic subthreshold modification (**Figure 5A**). **Figure 5B** illustrates the time-course similarity ("isomorphism") between the forced PSTH pattern and the voltage difference curve obtained by subtracting the average PSP before and after TBS. This observation is highly reminiscent of the earlier report during covariance-based protocols that the fine temporal time course of multiple presynaptic/postsynaptic spike interactions imposed during prolonged high frequency firing (S+) sculpts a memory-like recall in the temporal waveform of the induced functional change (i.e., expressed after the pairing). For comparison, the isomorphism found in positive covariance-based protocols with static ON- or OFF-stimuli is illustrated in **Figure 5C** (see Figure 12 in Debanne et al., 1998).

To unambiguously demonstrate the importance of the timing of the postsynaptic action potential generation with respect to the arrival of the presynaptic afferent volley, we decided to submit 11 cells (which were also all tested with a simple TBS protocol) to a hybrid TBS-Hebbian conditioning protocol, where postysnaptic firing was imposed by an external supervisor (the experimenter), in a manner equivalent to S+ pairing) synchronized with the TBS train (imposing the presynaptic pattern). 25 such "TBS_S+" protocols were carried out by selecting one (and only one) of the five thalamic shocks of a given rank in the high frequency burst for a given cell, and injecting a few milliseconds later an intracellular current pulse strong enough (0.5–1.0 nA) to reliably trigger a postsynaptic spike. Delays from 2 to 8 ms were explored in such a way as not to interfere with the following thalamic shock. Thus the postsynaptic Hebbian supervision signal was applied at the same temporal phase for all the bursts applied during the TBS train and precisely time-locked to the presynaptic afferent volley. As shown in the three examples of the average postsynaptic spike pattern imposed during the TBS burst (green PSTHs in **Figure 6**), the addition of such a depolarizing current pulse (red dot) drastically reshaped the timing control of the postsynaptic firing during TBS: it changed spiking probability selectively for the first thalamic shock (cells A, B, and C of **Figure 6**, left), the second thalamic shock (cell B of **Figure 6**, middle), the third thalamic shock (cell C of **Figure 6**, middle) or the fifth thalamic shock (cells B and C of **Figure 6**, right), according to the chosen phase of the intracellular injection pulse.

Figure 6A shows a case in which a large potentiation was induced by pairing conditions in which the postsynaptic supervised spike followed the presynaptic spike by a few milliseconds, a result consistent with *in vitro* STDP. **Figures 6B,C** illustrate two other cases where the application of the intracellular current injection

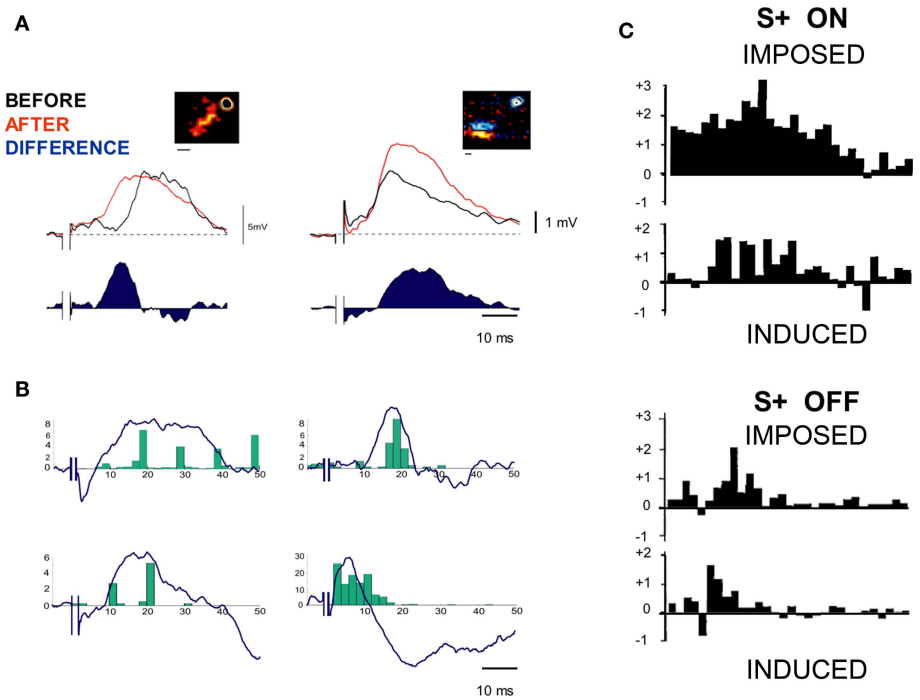

FIGURE 5 | Similarity between recalled and imposed postsynaptic patterns. **(A)** Examples of synaptic changes observed in the case of two cells. Insets represent the respective positions of cortical and thalamic RFs. The difference "AFTER–BEFORE" waveform (blue) shows the time course of the potentiation, corresponding to a shortening of latency (left) or an increase in peak amplitude (right). **(B)** Isomorphism between recalled and imposed postsynaptic patterns during *TBS:* The mean difference curves obtained for four different cells are superimposed with the mean spike pattern imposed during the conditioning bursts. This is done by realigning the trigger event of the control and post-TBS responses with the first thalamic shock in each high frequency burst applied during TBS. Note the similarities between the imposed spike distribution (green) and the temporal profile of the PSP change (blue). **(C)** Isomorphism between recalled and imposed postsynaptic patterns during S+ covariance-based protocols (adapted from Debanne et al., 1998). Upper panel, imposed effects of S+ pairings of ON-responses. The PSTH changes ("DURING pairing" minus "BEFORE pairing"), synchronized with the stimulus onset have been normalized relative to the mean count of each bin estimated by averaging responses before and during pairing. Lower panel, induced effects. In this latter case, the PSTHs represent "AFTER" minus "BEFORE" changes. Note for each condition (top, ON responses, bottom, OFF responses) the similarity in the time course of the activity change pattern (increase for S+ and decrease for S–) locked with the stimulus onset. On average, the amplitude of the induced change is half that of the imposed change.

time-locked to the fifth pulse of the afferent high frequency tetanus led to a significant potentiation, whereas similar supervised pairing time-locked to the intermediate part of the bursts resulted in depression (middle panels in **Figures 6B,C**). From these results, we can draw the conclusion that reshaping the postsynaptic pattern during TBS can transform depression effects into potentiation, or change the balance between excitation and inhibition, and that the multiple interactions that coexist during the high frequency burst are responsible for the observed changes. As already shown *in vitro*, the impact of these multiple pre-post spike interactions in controlling the sign of plasticity may depend on the rank order of the postsynaptic spikes with respect to the presynaptic multiplets (Froemke and Dan, 2002; modeled by Pfister and Gerstner, 2006).

A second aim of our experiments was to search for possible functional consequences of the plasticity induced by the TBS, in particular by looking at reconfiguration of the spatio-temporal structure of the cortical RF. We attempted to detect whether changes in location and/or extent (such as displacement, enlargement or contraction) of the subthreshold cortical RF – toward or away from the thalamic input RF – could be correlated with changes (potentiation or depression) of the synaptic response to the electrical stimulation of the thalamus. In order to do so, the cortical subthreshold RF was mapped before and after TBS by a forward correlation analysis of subthreshold responses evoked during sparse noise stimulation. For each pixel, the visually evoked PSPs were integrated over a 50-ms moving window and the reference optimal map was defined for the delay for which the RF extent was maximum. Comparison of the optimal receptive field maps recorded before and after pairings (for the same delay) was carried out on a pixel-by-pixel basis. The two largest individual cases of RF modification are presented in **Figure 7**. In the first case (**Figure 7A**), a clear increase in the mPSP amplitude was induced after TBS and this synaptic change was correlated with an enlargement of the subthreshold cortical RF. When comparing the optimal X-Y maps of the cortical subthreshold RF measured before (top left in **Figure 7A**) and after (bottom left) TBS, the functional change is visualized as a lateral spread of the cortical responsive zone, which invades part of the region of the visual field in which the LGN input was localized (yellow contour). The second example in **Figure 7B** shows modifications of the composite synaptic response to a test electrical stimulation of the thalamus (left column) and visual RF changes (right column) induced by four successive TBS_S+ pairing protocols in the same cortical cell. In this latter case, spatial stability of the RF was observed when the synaptic response was unchanged

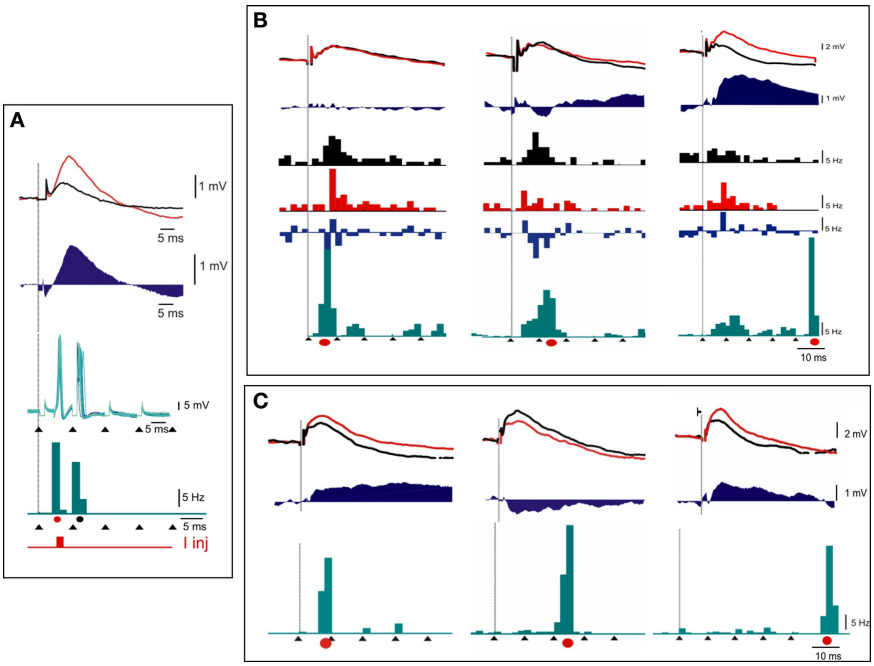

FIGURE 6 | Interaction between theta-burst and supervised Hebbian pairings: case examples. Three examples of the effects of TBS_S+ protocols, where a brief (4 ms) intracellular current pulse is added in phase with the 1st [cells **(A)**, **(B)**, and **(C)**], 2nd or 3rd [cells **(B)** and **(C)**], or 5th (cells **(B)** and **(C)**] electrical shock of the high frequency thalamic burst (black arrow heads). Both averaged PSPs (upper graphs) and PSTHs (lower histograms), recorded in response to a low frequency electrical thalamic shock (vertical line) before and after pairing, are represented with the same color codes [black for CONTROL, red for AFTER conditioning, and blue for difference ("AFTER"–"BEFORE")]. The imposed spike pattern during the burst is represented below, with the same temporal scale in green, and the current pulse occurrence during S+ pairing is indicated by a red dot. Note that in one of the cells **(C)**, the hybrid conditioning results in potentiation when the intracellular current coincides with the first shock, depression when it coincides with the third shock. Potentiation is reinstated when the current pulse coincides with the fifth shock. See text for detailed comments.

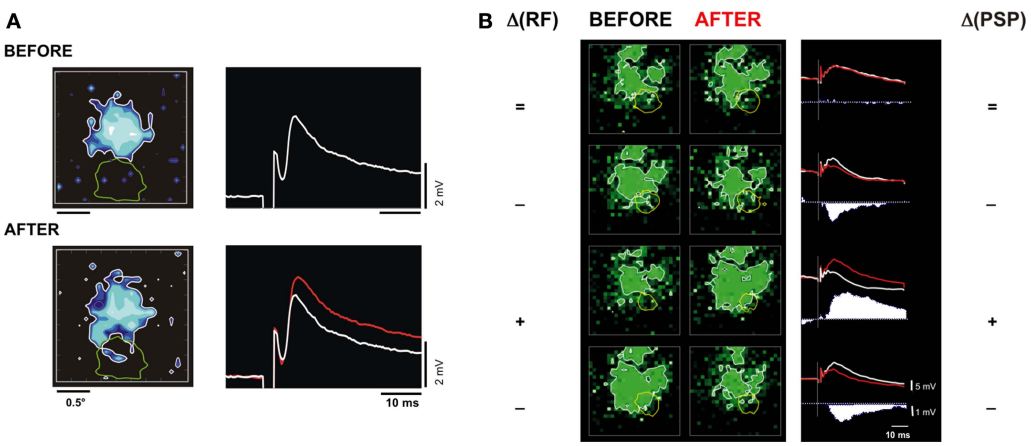

FIGURE 7 | Correlation between synaptic change induced by TBS and the spatial reorganization of the cortical RF. (A) Cell 1. The two rows show respectively the subthreshold RF map of a V1 cell (left inset, in blue) and its mean PSP response to an individual LGN shock (right inset), observed BEFORE (top) and AFTER (bottom) thalamic TBS conditioning. In the right inset, the white and red records are respectively the PSP taken before and after TBS. In the left inset, note in the visual X-Y maps, after TBS, the enlargement of the subthreshold cortical RF in a spatial region in overlap with the LGN discharge field location (green contour). **(B)** Cell 2. Synaptic and spatial RF changes for another V1 cell submitted to successive conditioning protocols in which the high frequency thalamic bursts were paired with an intracellular current injection pulse (TBS_S+). Visual maps (left column) and PSPs (right columns) are displayed in the chronological order from the top to the bottom. The 1st row depicts results obtained after a TBS_S+ (paired with the first pulse of the burst). For the second, third, and the fourth rows, the intracellular pulse was paired respectively with the second, fifth, and fourth pulse of the bursts. After each conditioning, the symbols (on each side of the figure) indicate the signs of the RF extent (left, "+" for expansion, "–" for contraction, "=" for unchanged) and the synaptic response (right side) changes. The difference "AFTER" minus "BEFORE" of the test responses are shown as filled post-stimulus time waveforms. Note that the successive invasion and withdrawal of the cortical RF (green contour) from the visual LGN discharge field (yellow contour) are consistent with the sign of the synaptic changes.

(**Figure 7B**, first row), whereas enlargement or contraction of the cortical subthreshold RF were correlated respectively with TBS-induced synaptic potentiation (**Figure 7B**, third row) or depression (**Figure 7B**, second and fourth rows).

The relative scarcity of these correlated observations at the single cell level (two significant cases only out of 34 – 6%) is certainly constrained by the fact that thalamic and cortical RFs centers were most of the time in spatial offset and the effects too small to reach statistical significance at the single cell level (but see population study below). Another limitation of our protocols is that the duration of intracellular recording did not allow us time to test for possible occlusions (suggestive of shared input) between the electrical stimulation and visually-induced synaptic activation. We could not be sure that the contingent of synaptic responses conditioned by the TBS were part of the afferent thalamo-cortical set recruited during the mapping of visual responses. Because of the time variability of excitability and absolute levels of visual responses (that may explain minute modifications of the receptive field contour), we opted for a population analysis of the effects, presented below, rather than for a cell-by-cell analysis.

To further analyze these results, we quantified the regional changes of the spatial profiles of the optimal X-Y RF maps for each cell (**Figure 8**) and then applied a Fourier analysis of orientation-selective and direction-selective polar plots (the so-called "sensitivity-direction-orientation" SDO analysis in Wörgötter and Eysel, 1987; see Materials and Methods). For this analysis, the center of gravity of the RF was determined before applying TBS application and its displacement was followed thereafter. All changes were plotted in a polar coordinate system, centered around the cortical RF and whose 0° axis was defined by the vector linking the cortical and thalamic RFs. When pooling all the cells of the same class (see below) together and adding the observed anisotropy vectors, the SDO analysis gave us two quantifications of a global trend: an IA and a polar measure of the Directionality (Θ) of the changes observed at the population level. These indices correspond respectively to the norm and the direction of the mean displacement vector of the center of gravity of the cortical RF.

Most remarkably, in spite of their low statistical significance at the single cell level, three coherent changes in visual receptive field organization became apparent at the population level, when the visual changes were grouped and averaged across cells which showed comparable TBS effects. **Figure 8** illustrates, from left to right, the polar distribution of the visual effects pooled separately for three categories of cells, which were found to be "unchanged," "potentiated," or "depressed" by TBS. As shown by the vector sum of the individual cell changes (lower row in **Figure 8**), the center of gravity of the subthreshold cortical RFs of "TBS-potentiated" cells was on average displaced toward the LGN-RF location (Θ = –13°, red vector). In contrast, the same vector sum applied to cases of "TBS-depressed" cells showed a shift away from the thalamic RF location (Θ = –229°, blue vector in **Figure 8**). No significant displacement was found for cells whose test synaptic response was unchanged by TBS (black vector). We conclude that the functional RF reorganization that we observed most likely results from selective potentiation or depression of synaptic responses triggered by visual input in overlap with the presumed RFs of the TBS-conditioned thalamic fibers/cells.

DISCUSSION

This comparative overview of previously published covariance-based studies and our new STDP-like theta-burst pairing experiments shows that, although synaptic changes can be induced *in vivo* during the recording time of single cells in both cases, the former type of protocols generally leads to larger functional effects

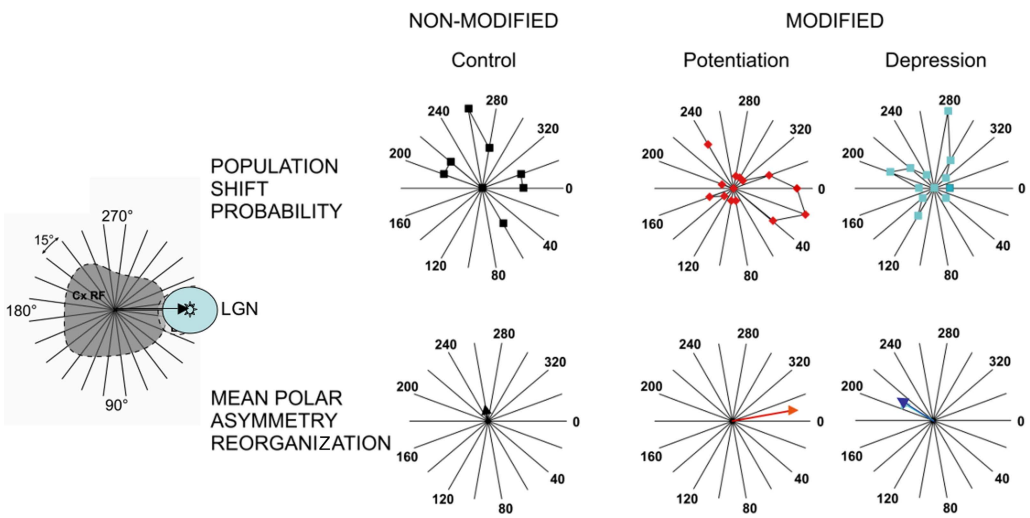

FIGURE 8 | Sensitivity-direction-orientation analysis of the spatial reorganization of RFs induced by TBS: Population study. To quantify the change of the RF shape, a polar SDO analysis was carried out on the visual RF maps obtained before and after TBS (for details, see Materials and Methods and text). Cells have been separated according to the TBS effects on the test synaptic response to a LGN electrical shock in three groups: from left to right, not significantly modified (black), TBS-potentiated (red) or TBS-depressed (blue). Upper panel shows the mean polar plots of RF anisotropy changes, and the lower panel gives the weighted displacement vector (TBS-Non_Modified: IA = 6.6%; DA = 81°; TBS-Potentiated: IA = 31.8%, DA = –13°; TBS-Depressed: IA = 16.3%, DA = 229°). 0° indicates shift of the recorded cortical RF center toward the LGN-RF center, as shown by the arrow in the left cartoon.

at the single cell level than those produced by STDP-based paradigms, at least in the adult cat cortex (see also review in Shulz and Jacob, 2010).

While TBS-induced functional effects that can be unambiguously correlated with the artificial-stimulus induced synaptic change are rather scarce, our experiments demonstrate that such a stimulation protocol can indeed produce significant synaptic changes in thalamo-cortical and cortico-cortical connections in adult V1. Although it is generally thought that plasticity is frozen in the anesthetized and paralyzed animal in the absence of some supervising or behavior-related signal (Hein et al., 1970, 1979; Buisseret et al., 1978; Frégnac, 1987), this finding *per se* may not be so surprising, since the experimenter imposes an extraneous presynaptic regime by stimulating thalamic afferents in a forced manner. Indeed, our intracellular recordings show that theta-burst trains can impose paroxysmic correlation states between thalamic and cortical activities during the time of the conditioning train, which differ strongly from those evoked by a natural sensory drive. **Figure 4** shows several examples of cortical cells, monosynaptically activated from the thalamus, where the covariance between pre- and postsynaptic activities is controlled tightly during the burst itself: a succession of fast pre-post spiking events is observed during the burst (right column), while polysynaptic activity in the cortex is suppressed during the profound hyperpolarizing phase following and separating each burst at a theta frequency (see also Kara et al., 2002). During this silenced period, the cortex is clamped whereas the thalamic fibers still provide an on-going bombardment and the global activity pattern during the full conditioning train shares a strong similarity with alternate S+/S− pairings in supervised covariance-based protocols. In addition, each following tetanic burst may benefit from the waning of presynaptic depression triggered by the after-burst GABAB inhibition, whose duration is generally shorter than the theta-rhythm period (Molyneaux and Hasselmo, 2002).

Taken together, these observations indicate that the dynamic changes imposed in the covariance between pre- and postsynaptic activities may be the key factor in predicting the outcome of any conditioning protocol. This interpretation fits with our data, old and new, and can be related to other pioneer adult learning experiments in the awake behaving animal, whether supervision is imposed externally by the experimenter (Calhusac et al., 1991), or is mediated via self-generated attention related modulatory signals as shown in auditory (Ahissar et al., 1992, 1996) and somatosensory (Wang et al., 1995) cortex. In particular, Ahissar and collaborators elegantly applied cross-correlation techniques to the study of plasticity of "functional connectivity" between pairs of neurons in the auditory cortex in awake monkeys performing a sensory discrimination. The correlation of activity between two neurons was artificially controlled by immediately activating the target cell of the pair (the postsynaptic cell) by the presentation of its preferred auditory stimulus, each time the other cell fired spontaneously. Under these positive covariance conditions, reversible changes in functional coupling could be induced only when the animal was attentive to the tone used to control the activity of the postsynaptic cell. These changes were short-lived, lasting only for a few minutes, but, most remarkably, followed the covariance hypothesis predictions: potentiation of the functional link was induced when the coupling measured by cross-correlation techniques ("effective connectivity" in Aertsen et al., 1989) was increased during the pairing protocol; conversely, depression was observed when coupling was effectively reduced during the Hebbian association period.

Other interesting parallels can be made between the various protocols presented here and specific properties of STDP demonstrated *in vitro*, and may account for shared effects at a mechanistic level. For instance, during paired recordings *in vitro* the STDP efficiency in inducing LTP has been shown to require an extension of the pairing constraints not only to two precisely phase-locked events, but to higher-order patterns such as triplets (of the type "post"-"pre"-"post" or one "pre", two "post" according to Sjöström et al., 2001 and modeled by Pfister and Gerstner, 2006). In our S+ protocols *in vivo*, the covariance change is maintained for durations longer than 50 ms, and pairings with multiple postsynaptic spikes do occur. In our hybrid theta-burst and supervised Hebbian conditioning, potentiation effects are more easily revealed when the spiking is imposed for the last (fifth) stimulation shock during the burst. If one compares this latter situation to the reinforcement of the first thalamic shock in the burst, the pairing pattern is closer to a "post-pre-post" than to the "pre-post-pre" configuration known to be less effective in inducing potentiation (Froemke and Dan, 2002; Pfister and Gerstner, 2006). The forced S+ pairing at the end of the burst also benefits from the cumulative depolarization which builds-up in some cells during the high frequency tetanus (see examples 1, 3, 4 from the top in **Figure 4**). It has been shown that only bursts of action potentials above a critical frequency (100 Hz) induce dendritic spikes (Larkum et al., 1999). Action potential bursts need also to exceed roughly the same critical frequency to induce STDP (Kampa et al., 2006), suggesting a threshold requirement for dendritic spikes, and it is likely that the theta-burst pattern in our protocol attained that frequency. Consequently, the enhanced efficacy of the pairing during the last shock of the burst could be explained by the fact that regenerative Ca^{2+} dependent dendritic potentials are particularly evident in some cells by the end of a burst (see Figure 1 in Larkum et al., 1999). For the negative covariance change, one should also note the similarity between our S− protocols and some variants of STDP protocols used by Sjöström *in vitro,* where depression is observed when a hyperpolarization current is added in-between current-induced spikes during high frequency pairings. The difference still remains that during most STDP and theta-burst protocols, presynaptic and postsynaptic activities are phase-locked for each occurrence of the presynaptic spike, whereas, during covariance-based protocols, presynaptic and postsynaptic activities are controlled in two independent ways (the stimulus feature for presynaptic activity, the current-induced for postsynaptic firing).

Apart from these similarities, the functional impact of the two types of protocols seems to differ, not so much in the sign of the induced changes, but in their respective amplitude and probability of induction. Several explanations are possible for why the rate-based covariance manipulation experiments showed a much larger potential for plasticity *in vivo* than currently reported by theta-burst, Spike Timing-Dependent and Stimulus-Timing-Dependent protocols (Yao and Dan, 2001; Fu et al., 2002). One possible reason is linked to the local supervised vs global unsupervised nature of some of the conditioning protocols. The imposition of a local

perturbation, as engineered by the sole control of the postsynaptic firing of the paired cell in our covariance-based protocols, will induce a regional reorganization in a weakly coupled network. In contrast, a global clamp of cortical input, as imposed by the sequential presentation of distinct features in stimulus-timing-dependent protocols, may have a limited effect at the single cell level: in this latter situation, a large part of the cortical network is conjointly activated by the two sequential stimuli which often cover a large part of the visual field and the recruitment of multiple interactions may cancel the lateral spread of competitive effects. In our S+/S− protocols, the constraints from the rest of the network in stabilizing the columnar preference, hence the conditioned cell's preference, may be weaker, allowing the cell's response to escape locally from the global assembly behavior.

Another possible explanation is that some associativity threshold has to be reached in adult cortex for expressing plasticity, which goes well beyond the pairing of two single events. Although Hebbian-like changes have been observed in the adult auditory cortex when the awake behaving monkey is attentive (Ahissar et al., 1992), these changes are short-lived and do not compare in strength with those we observed in kitten V1 cortex. A similar reasoning may apply to STDP: since the most compelling evidence for a functional role of STDP *in vivo* has been mostly demonstrated during development and in Xenopus (Tao et al., 2001; Mu and Poo, 2006), one may question to what extent plasticity can be reliably revealed by using similar STDP-based protocols *in vivo* in adult mammalian cortex. The only comparable experiment in cat and rat V1 cortex comes from the studies from the group of Yang Dan. In a first series of experiments, Dan's team devised very ingenious visuo-visual pairing protocols where the timing of the presynaptic volley and postsynaptic volleys were indirectly controlled by manipulating the asynchronous timing of presentation of various features of the visual input (orientation, position) (Yao and Dan, 2001; Fu et al., 2002). These differential protocols relied however on the assumption that inputs representing each of the two selected stimulus features (presented sequentially) were separable in terms of presynaptic neuronal population activation, omitting to take into account the reverberant activity produced by each of the stimuli at the postsynaptic level. Furthermore, the interaction of components in the target response was not measured in these studies. A second problematic issue is that most of the functional changes that the group of Yang Dan reported at the single cell level were of moderate amplitude (mean reported value of 2.8°), well below the experimental precision of their RF or tuning curve measures (12–15° step in Yao and Dan's study). In spite of these limitations, the visuo-visual pairing protocols were assessed at the population level, under the additional assumption that the same plasticity rule would apply across cells and high performance bootstrap techniques were used to show a significant effect at the population level. The interpretation we derive from these extracellular stimulus-dependent-plasticity studies is that, in contrast to covariance control protocols, visuo-visual pairings produce almost undetectable changes at the single cell level but significant incremental changes, observable only at the population level.

More direct and sophisticated attempts have been made *in vivo* with intracellular techniques. In rat V1, Meliza and Dan (2006) achieved a "tour de force" experiment, in which the spatio-temporal RF of each neuron was measured under voltage clamp conditions, before and after STDP protocols. To induce modification of the RF, the authors switched the recording to current-clamp configuration, and repetitively paired the visual stimulus at one of the four RF locations (spaced by 11–13°) with a brief intracellular current injection (6–8 ms) that forced postsynaptic spiking. This protocol can be seen as analogous to the STDP induction protocol in rat visual cortical slices (Sjöström et al., 2001; Froemke and Dan, 2002), except that presynaptic activation was caused by visual, rather than electrical, stimulation. Modifications of the visual responses, potentiation and depression were observed within a selectivity window of ~±50 ms, similar to that observed in rat visual cortical slices.

Interpretation of the results obtained for positive delays is less straightforward than for negative delays and can be questioned in two ways: the first issue concerns the spatial selectivity of the effect. Meliza and Dan reported significant response modifications at the unpaired locations, which, when restricted to the potentiation cases in the paired location, were uncorrelated in sign (both potentiation and depression could be seen in the unpaired location, see Figure 4E in Meliza and Dan, 2006 and red inset in **Figure 9**, this paper) and often larger in amplitude than those induced in the paired location. The diversity in hetero-positional effects was found to be linked on whether the pairing was applied at the center or the flank of the RF. From a functional perspective, the location dependence of the RF plasticity they described seemed to favor potentiation of the weak parts of the RF and to facilitate shifts of the RF center to neighboring locations when stimuli at these locations were followed by postsynaptic spiking. Nevertheless, the fact that the amplitude of the hetero-positional effects was often larger than that observed in the paired position and the unusually large width of the stimulus (hence, of the spatial separation bin size between explored positions), raise the issue of the specificity of the spatial selectivity in the reported effects.

Comparison with the STDP literature is further complicated by the fact that, in Meliza and Dan's experiment, the "pre"-"post" pairing interval is defined as the interval between the peak of the visually evoked inward current and the peak of the postsynaptic action potential. This convention differs from the classical definition where the "pre"-"post" interval is defined between the first presynaptic spike or the subthreshold PSP onset, and the somatic postsynaptic spike (see for instance Figures 2D,H in Mu and Poo, 2006). In **Figure 10** we have qualitatively realigned the results of Meliza and Dan, shown in Figure 2E of their original paper, with the classical STDP convention (i.e., removing the average delay from response onset to peak response), and plotted the STDP curve as a function of the "pre"-"post" delay (where the zero time, indicated by the purple dotted *y*-axis, signals the firing time of the first presynaptic spike in the sensory input volley). This realignment has two consequences: (1) the STDP curve obtained by Meliza and Dan would still predict significant depression for negative delays; (2) However, the outcome of the pairing for positive delays would be highly variable on a cell-by-cell basis: for a delay window of 0 to +20 ms, as many cases of depression ($n = 4$) and potentiation ($n = 3$) would be observed. To the difference of Meliza and Dan, we conclude that positive "pre"-"post" delays do not result in systematic potentiation in adult sensory cortex *in vivo*. A similar conclusion was reached in adult rat somatosensory cortex by Shulz and

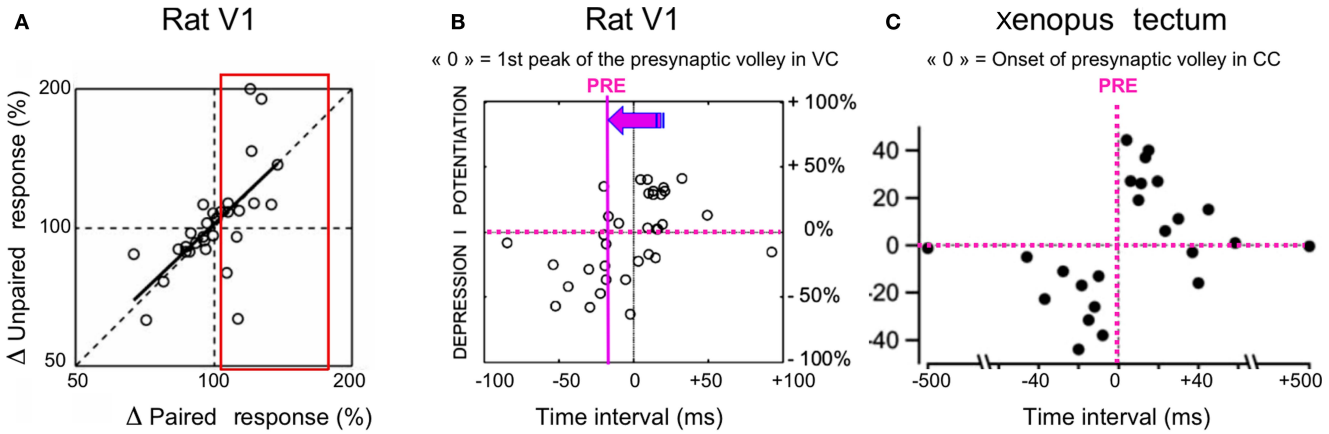

FIGURE 9 | Re-examination of *in vivo* STDP. (A) Rat visual cortex, taken from Figure 4E in Meliza and Dan (2006): change in unpaired RF region vs change in the paired region (log-log scale) following STDP intracellular pairings (see text for details). Each point represents an individual cell. The oblique regression line is a linear fit calculated on all cases (potentiation and depression). The red inset underlines the lack of spatial selectivity for potentiation effects, whose amplitudes are often larger for the unpaired than for the paired positions. **(B)** Rat visual cortex, adapted from Figure 2E in Meliza and Dan (2006): Change in amplitude of visual response at paired location as a function of pairing interval. Each symbol represents one cell. The *x*-axis coordinates of the original plot have been inverted in sign, to make the STDP curve comparable to that shown in **(C)**. "0" represents the occurrence of the peak inward current measured in voltage clamp (VC). The purple *y*-axis, shifted to the left, represents the most likely arrival time of the first presynaptic spike. The position difference between the two-*y* axes corresponds to the mean delay separating the onset from the peak input. **(C)** Xenopus tectum, taken from Figure 2H in Mu and Poo (2006): STDP curve induced by repetitive single-bar stimulation in the developing retino-tectal system of Xenopus. The graph is aligned on the presynaptic volley onset and shows a clear partition of spike timing-dependent depression (negative delays) and potentiation (positive delays) of tectal responses, recorded in current clamp (CC). Each point represents the result from one experiment.

collaborators together with the group of Dan Feldman (Jacob et al., 2007). In summary, these different studies show for the least that STDP-induced potentiation remains difficult to establish *in vivo* in adult cortex, and that associative plasticity remains dominated by selective depression.

This raises the question whether the impact of STDP for inducing incremental strengthening in functional connectivity in adult cortex has been largely over-stated in the literature. This effect, expected from the consensus achieved on the basis of the *in vitro* literature, may in fact be more elusive *in vivo*, especially in the adult cortex (review in Shulz and Jacob, 2010). This difficulty in replication may come from the usual difficulties associated with *in vivo* experiments, which constrain all experimental intracellular studies including ours. A fair statement should be to consider that very few unambiguous single cell cases of LTP have been published so far in adult rodent and cat sensory cortices: in general, the duration of the control periods are too short to exclude non-stationarities and slow trends in synaptic efficacies are visible in the longer post-conditioning periods of some reports. Among uncontrolled factors in the anesthetized preparation, is the role of inhibition: it is seen as a suppressive gate by many, which may interfere with the dendritic spread of back propagating action potentials (Engelmann et al., 2008). Although inhibitory interneurons modulate many neuronal processes, the evidence for plasticity at inhibitory synapses remains scarce. Some studies report strengthening of inhibitory synapses in negative rate covariance regimes (Komatsu and Iwakiri, 1993; Komatsu, 1994, 1996; Holmgren and Zilberter, 2007). Spike timing-dependent plasticity of inhibitory synapses has been also reported (Haas et al., 2006) as well as spike timing-dependent depression of excitatory synapses on fast spiking inhibitory interneurons (Lu et al., 2007). An additional factor that has to be taken into account is the complex interaction between back propagating action potentials and the local excitable properties of the dendritic tree. Dendrites contain voltage-activated channels, but also they can support fast action potential-like events mediated by voltage-activated Na^+ channels, or slower, regenerative events mediated by voltage-activated Ca^{2+} channels (Stuart et al., 1997). Due to intense background synaptic activity *in vivo*, these conductances may have a particular impact on the spread of back propagating action potentials (Sjöström and Hausser, 2006) and eventually help or interfere with STDP induction (van den Burg et al., 2007).

The last conclusion concerns the validity of inferences that one may be tempted to make for the *in vivo* case from consensual plasticity rules only substantiated in *in vitro* conditions in developing networks. Many experimental reports point to the possibility that homeostasis rules may be exacerbated in the slice or organotypic culture preparations (review in Frégnac, 1999; Turrigiano and Nelson, 2000). The possibility for such deafferented networks of undergoing lesion-induced or post-traumatic forms of plasticity to recover an operational range of synaptic efficiency may not be so readily expressed in the intact brain. Nonetheless, deafferentation of cortical regions by peripheral lesions lead to receptive fields reorganization that are more readily explained by STDP than correlation rate-based plasticity rules (Young et al., 2007). The second main difference between the *in vitro* and the *in vivo* cases is the presence *in vivo* of irregular on-going activity. This bombardment ensures a basal level of correlation between spontaneous inputs (linked with the high level of on-going activity in thalamus and the profusion of recurrent intracortical circuits) and cortical cells. During sensory

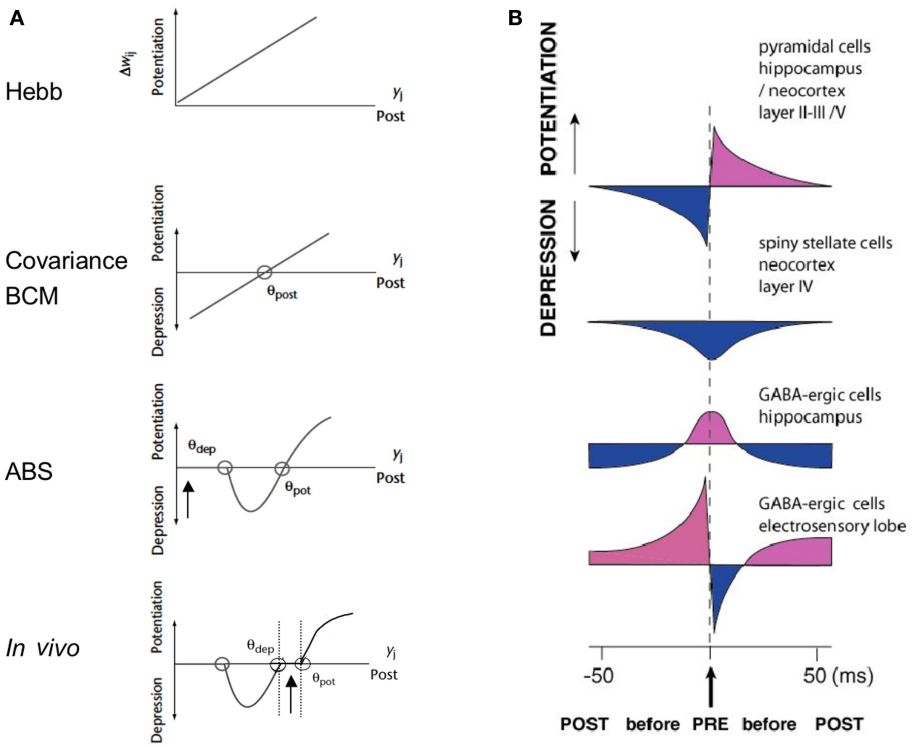

FIGURE 10 | For a diversity of plasticity rules *in vitro* and *in vivo*. (A) Generalized Hebbian forms of plasticity. From top to bottom, Hebb's rule (top) and the most often observed rules of homosynaptic plasticity established *in vitro* and *in vivo* (bottom). Each graph expresses the theoretical relationship between the induced synaptic change (positive ordinates for potentiation, negative for depression) and postsynaptic activity at the time of the association. The slope is proportional to presynaptic activity. The simple Hebbian rule predicts potentiation only. The covariance rule (second from the top) and A-B-S rule (third from the top) predict both depression and potentiation with, respectively, one (Θpost) or two postsynaptic thresholds (Θdep and Θpot in Artola et al., 1990). Bottom: covariance rule observed *in vivo*, where a dead-zone lies near the operating regime (vertical arrow) of the synapse during sensory processing (Frégnac et al., 1988; Frégnac, 1991). **(B)** Diversity of forms of STDP established *in vitro*. The induced synaptic change is expressed as a function of the temporal delay between presynaptic firing (zero time reference) and postsynaptic spike occurrence (adapted from Abbott and Nelson, 2000; Frégnac, 2002). A mirror form of STDP is also observed in inhibitory neurons of the electrosensory lobe of the electric fish (Bell et al., 1997).

activation, positive co-variation between pre- and postsynaptic activities is observed without changing receptive field properties, at least in the anesthetized and paralyzed preparation (review in Frégnac and Imbert, 1984). In view of the relative difficulty of inducing acute functional changes in the intact neocortex, we proposed some 20 years ago the existence of a threshold in the expression of STDP *in vivo* outside the critical period, which accounts for the stability of synaptic weights during normal sensory processing (Frégnac et al., 1988, 1994a; Frégnac, 1991). The observation that synaptic or functional changes can be induced by a supervised control of presynaptic (theta-burst) and postsynaptic (STDP and Hebbian) activities, as shown here, agrees with the view that, in the intact brain, expression of plasticity would require some drastic reconfiguration of covariance or correlation changes between pre-and postsynaptic activities, which goes well beyond evoked changes by natural stimuli. Additional boosting control signals are needed, such as those self-generated by the brain under the form of attention-gated or reward-driven processes during behavioral learning, that push the correlational state detected by the synapse beyond the level reached during normal sensory processing. This "correlation change threshold" hypothesis would thus require that the covariance change between pre- and postysnaptic activities during the associative learning is large enough and is maintained long enough to push away the operational working regime of the synapse from its non-adaptive "read-only" state (bottom graph in **Figure 10A**, taken from Frégnac, 1991; see also Ahissar et al., 1992 for an implementation). It would be only by trespassing the required correlation change threshold(s), that the expression of association-induced functional changes would be validated in adult cortex by reward or behavior.

ACKNOWLEDGMENTS

We thank Drs Kirsty Grant and Andrew Davison for their help in reviewing this manuscript. This work has been supported by the CNRS, the DGA, the Agence Nationale de la Recherche (ANR) and EC contracts Sensemaker (FP5-2001-IST 34712), Facets (FP6-2004-IST-FETPI 15879) and Brain-i-nets (FP7-2009-ICT-FET 243914). All research procedures concerning the experimental animals and their care adhered to the American Physiological Society's Guiding Principles in the Care and Use of Animals, to the French (JO 87-848), the European Council Directive 86/609/EEC and to European Treaties Series 123 and was also approved by the regional ethics committee "Ile-de-France Sud" (Certificate 05-003).

REFERENCES

Abbott, L. F., and Nelson, S. B. (2000). Synaptic plasticity: taming the beast. *Nat. Neurosci.* 3, 1178–1183.

Aertsen, A., Gerstein, G. L., Habib, M. K., and Palm, G. (1989). Dynamics of neuronal firing correlation: modulation of "effective connectivity". *J. Neurophysiol.* 61, 900–917.

Ahissar, E., Haidarliu, S., and Shulz, D. (1996). Possible involvement of neuromodulatory systems in cortical Hebbian-like plasticity. *J. Physiol. (Paris)* 90, 353–360.

Ahissar, E., Vaadia, E., Ahissar, M., Bergman, H., Arieli, A., and Abeles, M. (1992). Dependence of cortical plasticity on correlated activity of single neurons and on behavioral context. *Science* 257, 1412–1415.

Albus, K. (1975). A quantitative study of the projection area of the central and the paracentral visual field in area 17 of the cat: I. The precision of the topography. *Exp. Brain Res.* 24, 159–179.

Andrew, R. D., and Fagan, M. (1990). A technique for controlling the membrane potential of neurons during unit recording. *J. Neurosci. Methods* 33, 55–60.

Artola, A., Bröcher, S., and Singer, W. (1990). Different voltage-dependent thresholds for inducing long-term depression and long-term potentiation in slices of rat visual cortex. *Nature* 347, 69–72.

Artola, A., and Singer, W. (1987). Long-term potentiation and NMDA receptors in rat visual cortex. *Nature* 330, 649–652.

Baranyi, A., and Feher, O. (1981). Synaptic facilitation requires paired activation of convergent pathways in the neocortex. *Nature* 290, 413–415.

Bear, M. F. (2003). Bidirectional synaptic plasticity: from theory to reality. *Philos. Trans. R. Soc. Lond. B* 358, 649–655

Bear, M. F., Cooper, L. N., and Ebner, F. (1987). A physiological basis for a theory of synapse modification. *Science* 237, 42–48.

Bear M. F., Kleinschmidt, A., Gu, Q., and Singer, W. (1990). Disruption of experience-dependent synaptic modifications in striate cortex by infusion of an NMDA receptor antagonist. *J. Neurosci.* 10, 909–925.

Bear, M. F., and Malenka, R. (1994). Synaptic plasticity: LTP and LTD. *Curr. Opin. Neurobiol.* 4, 389–399.

Bear, M. F., Press, W. A., and Connors, B. W. (1992). Long-term potentiation in slices of kitten visual cortex and the effects of NMDA receptor blockade. *J. Neurophysiol.* 67, 841–851.

Bear, M. F., and Singer, W. (1986). Modulation of visual cortical plasticity by acetylcholine and noradrenaline. *Nature* 320, 172–176.

Bell, C., Han, V., Sugawara, Y., and Grant, K. (1997). Synaptic plasticity in a cerebellum-like structure depends on temporal order. *Nat. Neurosci.* 387, 278–281.

Bi, G. Q., and Poo, M. (2001). Synaptic modification by correlated activity: Hebb's postulate revisited. *Annu. Rev. Neurosci.* 24, 139–166.

Bienenstock, E., Cooper, L. N., and Munro, P. (1982). Theory for the development of neuron selectivity: orientation specificity and binocular interaction in visual cortex. *J. Neurosci.* 2, 32–48.

Blais, B. S., Shouval, H. Z., and Cooper, L. N. (1999). The role of presynaptic activity on the ocular dominance shift in monocular deprivation: comparison of homosynaptic and heterosynaptic mechanisms. *Proc. Natl. Acad. Sci. U.S.A.* 96, 1083–1087.

Blakemore, C., and Cooper, G. F. (1970). Development of the brain depends on the visual environment. *Nature* 228, 419–478.

Brown, T. H., Ganong, A. H., Kairiss, E. W., and Keenan, C. L. (1990). Hebbian synapses: biophysical mechanisms and algorithms. *Annu. Rev. Neurosci.* 13, 475–511.

Brown, R. E., and Milner, P. M. (2003). The legacy of Donald O. Hebb: more than the Hebb synapse. *Nat. Rev. Neurosci.* 4, 1013–1019.

Buisseret, P., Gary-Bobo, E., and Imbert, M. (1978). Ocular motility and recovery of orientational properties of visual cortical neurones in dark-reared kittens. *Nature* 272, 816–817.

Calhusac, P. M. B., Rolls, E. T., and Marriott, F. H. C. (1991). Potentiation of neuronal responses to natural visual input paired with postsynaptic activation in the hippocampus of the awake monkey. *Neurosci. Lett.* 124, 39–43.

Crair, M. C., and Malenka, R. C. (1995). A critical period for long-term potentiation at thalamocortical synapses. *Nature* 375, 325–328.

Crepel, F. (1998). Nitric oxide and long-term depression in the cerebellum. *Trends Neurosci.* 21, 63–64.

Crow, T. (1968). Cortical synapses and reinforcement: a hypothesis. *Nature* 219, 736–737.

Debanne, D., Gahwiller, B. H., and Thompson, S. M. (1997). Bidirectional associative plasticity of unitary CA3-CA1 EPSPs in the rat hippocampus in vitro. *J. Neurophysiol.* 77, 2851–2855.

Debanne, D., Shulz, D. E., and Frégnac Y. (1995). Temporal constraints in associative synaptic plasticity in hippocampus and neocortex. *Canad. J. Physiol. Pharmacol.* 73, 1295–1311.

Debanne, D., Shulz D. E., and Frégnac Y. (1998). Activity dependent regulation of on- and off-responses in cat visual cortical receptive fields. *J. Physiol.* 508, 523–548.

Dudek, S. M., and Bear, M. F. (1992). Homosynaptic long-term depression in area CA1 of hippocampus and effects of *N*-methyl-D-aspartate receptor blockade. *Proc. Natl. Acad. Sci. U.S.A.* 89, 4363–4367.

Dudek, S. M., and Bear, M. F. (1993). Bidirectional long-term modification of synaptic effectiveness in the adult and immature hippocampus. *J. Neurosci.* 13, 2910–2918.

Dudek, S. M., and Friedlander, M. J. (1996). Developmental down-regulation of LTD in cortical layer IV and its independence of modulation by inhibition. *Neuron* 16, 1097–1106.

Engelmann, J., van den Burg, E., Bacelo, J., de Ruijters, M., Kuwana, S., Sugawara, Y., and Grant, K. (2008). Dendritic backpropagation and synaptic plasticity in the mormyrid electrosensory lobe. *J. Physiol. (Paris)* 102, 233–245.

Feldman, D. E. (2000). Timing-based LTP and LTD at vertical inputs to layer II/III pyramidal cells in rat barrel cortex. *Neuron* 27, 45–56.

Foeller, E., and Feldman, D. E. (2004). Synaptic basis for developmental plasticity in somatosensory cortex. *Curr. Opin. Neurobiol.* 14, 89–95.

Frégnac, Y. (1987). "Cellular mechanisms of epigenesis in cat visual cortex," in *Imprinting and Cortical Plasticity*, eds J. P. Rauschecker and P. Marler (New York: John Wiley and Sons), 221–266.

Frégnac, Y. (1991). "Computational approaches to network processing and plasticity," in *Long-Term Potentiation*, ed. M. B. J. L. Davis (Cambridge, MA/London: MIT Press), 425–435.

Frégnac, Y. (1999). The tale of two spikes. *Nat. Neurosci.* 2, 299–301.

Frégnac, Y. (2002). "Hebbian synaptic plasticity," in *Handbook of Brain Theory and Neural Networks*, ed. M.A. Arbib (Cambridge: The MIT Press), 515–522.

Frégnac, Y., Burke, J., Smith, D., and Friedlander, M. J. (1994a). Temporal covariance of pre and postsynaptic activity regulates functional connectivity in the visual cortex. *J. Neurophysiol.* 71, 1403–1421.

Frégnac, Y., Debanne, D., Shulz, D. E., and Baranyi, A. (1994b). "Does post synaptic membrane potential regulate functional plasticity in kitten visual cortex?" in *Long-Term Potentiation*, eds. M. Baudry and J. L. Davis (Cambridge: MIT Press), 227–264.

Frégnac, Y., and Imbert, M. (1984). Development of neuronal selectivity in the primary visual cortex of the cat. *Physiol. Rev.* 64, 325–434.

Frégnac, Y., and Shulz, D. E. (1994). "Models of synaptic plasticity and cellular analogs of learning in the developing and adult vertebrate visual cortex," in *Advances in Neural and Behavioral Development*, eds V. Casagrande and P. Shinkman (Norwood, NJ: Neural Ablex Publ.), 149–235.

Frégnac, Y., and Shulz, D. E. (1999). Activity-dependent regulation of receptive field properties of cat area 17 by supervised Hebbian learning. *J. Neurobiol.* 41, 69–82.

Frégnac, Y., Shulz, D. E., Thorpe, S., and Bienenstock, E. (1988). A cellular analogue of visual cortical plasticity. *Nature* 333, 367–370.

Frégnac, Y., Shulz, D. E., Thorpe, S., and Bienenstock, E. (1992). Cellular analogs of visual cortical epigenesis: I. Plasticity of orientation selectivity. *J. Neurosci.* 12, 1280–1300.

Frey, U., and Morris, R. G. (1997). Synaptic tagging and long-term potentiation. *Nature* 385, 533–536.

Froemke, R., and Dan, Y. (2002). Spike-timing-dependent synaptic modification induced by natural spike trains. *Nature* 416, 433–438.

Froemke, R., Poo, M., and Dan, Y. (2005a). Spike-timing-dependent synaptic plasticity depends on dendritic location. *Nature* 434, 221–225.

Froemke, R., Tsay, I., Raad, M., Long, J., and Dan, Y. (2005b). Contribution of individual spikes in burst-induced long-term synaptic modification. *J. Neurophysiol.* 95, 1620–1629.

Fu, Y. X., Djupsund, K., Gao, H., Hayden, B., Shen, K., and Dan, Y. (2002). Temporal specificity in the cortical plasticity of visual space representation. *Science* 296, 1999–2003.

Gerstner, W., Kempter, R., van Hemmen, L., and Wagner, H. (1996). A neuronal learning rule for sub-millisecond temporal coding. *Nature* 383, 76–78.

Gerstner, W., and Kistler, W. M. (2002). *Spiking Neuron Models*. Cambridge: Cambridge University Press.

Greuel, J. M., Luhmann, H. J., and Singer, W. (1988). Pharmacological induction of use-dependent receptive field modifications in the visual cortex. *Science* 242, 74–77.

Haas, J. S., Nowotny, T., and Abarbanel, H. D. I. (2006). Spike-timing-dependent plasticity of inhibitory synapses in the entorhinal cortex. *J. Neurophysiol.* 96, 3305–3313.

Harsanyi, K., and Friedlander, M. J. (1997). Transient synaptic potentiation in the visual cortex. I Cellular mechanisms. *J. Neurophysiol.* 77, 1269–1283.

Hebb, D. O. (1949). *The Organization of Behavior*. New York: John Wiley and Sons, 337.

Hein, A., Held, R., and Gower, E. C. (1970). Development and segmen-

tation of visually-controlled movement by selective exposure during rearing. *J. Comp. Physiol. Psychol.* 73, 181–187.

Hein, A., Vital-Durand, F., Salinger, W., and Diamond, R. (1979). Eye movements initiate visual-motor development in the cat. *Science* 204, 1321–1322.

Heynen, A. J., and Bear, M. F. (2001). Long-term potentiation of thalamocortical transmission in the adult visual cortex in vivo. *J. Neurosci.* 21, 9801–9813.

Hirsch, H. V. B., and Spinelli, D. N. (1970). Visual experience modifies distribution of horizontally and vertically oriented receptive fields in cats. *Science* 168, 865–871.

Holmgren, C. D., and Zilberter, Y. (2007). Coincident spiking activity induces long-term changes in inhibition of neocortical pyramidal cells. *J. Neurosci.* 27, 8270–8277.

Iny, K., Heynen, A. J., Sklar, E., and Bear, M. F. (2006). Bidirectional modifications of visual acuity induced by monocular deprivation in juvenile and adult rats. *J. Neurosci.* 26, 7368–7374.

Jacob, V., Brasier, D. J., Erchova, I., Feldman, D., and Shulz, D. E. (2007). Spike timing-dependent synaptic depression in the in vivo barrel cortex of the rat. *J. Neurosci.* 27, 1271–1284.

Kampa, B. M., Letzkus, J. J., and Stuart, G. J. (2006). Requirement of dendritic calcium spikes for induction of spike-timing-dependent synaptic plasticity. *J. Physiol.* 574, 283–290.

Kara, P., Pezaris, J. S., Yurgenson, S., and Reid, R. C. (2002). The spatial receptive field of thalamic inputs to single cortical simple cells revealed by the interaction of visual and electrical stimulation. *Proc. Natl. Acad. Sci. U.S.A.* 99, 16261–16266.

Kasamatsu, T., Watabe, K., Heggelund, P., and Scholler, E. (1985). Plasticity in cat visual cortex restored by electrical stimulation of the locus coeruleus. *Neurosci. Res.* 2, 365–386.

Kelso, S. R., Ganong, A. H., and Brown, T. H. (1986). Hebbian synapses in hippocampus. *Proc. Natl. Acad. Sci. U.S.A.* 83, 5326–5330.

Kety, S. (1970). "Biogenic amines in the central nervous system: their possible roles in arousal, emotion and learning," in *The Neurosciences: Second Study Program*, ed. F. O. Schmitt (New York: Rockefeller University Press), 324–336.

Kirkwood, A., and Bear, M. F. (1994). Hebbian synapses in visual cortex. *J. Neurosci.* 14, 1634–1645.

Kirkwood, A., Dudek, S. M., Gold, J. T., Aizenman, C. D., and Bear, M. F. (1993). Common forms of synaptic plasticity in the hippocampus and neocortex in vitro. *Science* 260, 1518–1521.

Kirkwood, A, Lee, H. K., and Bear, M. F. (1995). Co-regulation of long-term potentiation and experience-dependent synaptic plasticity in visual cortex by age and experience. *Nature* 375, 328–331.

Kirkwood, A., Rioult, M. C., and Bear, M. F. (1996). Experience-dependent modification of synaptic plasticity in visual cortex. *Nature* 381,526–528.

Klopf, A. H. (1988). "Classical conditioning phenomena predicted by a drive-reinforcement model of neuronal function," in *Neural Models of Plasticity*, eds J. H. Byrne and W. O. Berry (New York: Academic Press), 104–132.

Kohonen, T. (1989). *Self-Organization and Associative Memory*. Berlin: Springer.

Komatsu, Y. (1994). Age-dependent long-term potentiation of inhibitory synaptic transmission in rat visual cortex. *J. Neurosci.* 14, 6488–6499.

Komatsu, Y. (1996). GABAB receptors, monoamine receptors, and postsynaptic inositol trisphosphate-induced Ca2+ release are involved in the induction of long-term potentiation at visual cortical inhibitory synapses. *J. Neurosci.* 16, 6342–6352.

Komatsu, Y., Fujii, K., Maeda, J., Sakaguchi, H., and Toyama, K. (1988). Long-term potentiation of synaptic transmission in kitten visual cortex. *J. Neurophysiol.* 59, 124–141.

Komatsu, Y., and Iwakiri, M. (1993). Long-term modification of inhibitory synaptic transmission in developing visual cortex. *Neuroreport* 4, 907–910.

Larkum, M. E., Kaiser, K. M. M., and Sakmann, B. (1999). Calcium electrogenesis in distal apical dendrites of layer 5 pyramidal cells at a critical frequency of back-propagating action potentials. *Proc. Natl. Acad. Sci. U.S.A.* 96, 14600–14604.

Letzkus, J. J., Kampa, B. M., and Stuart, G. J. (2006). Learning rules for spike timing-dependent plasticity depend on dendritic synapse location. *J. Neurosci.* 26, 10420–10429.

Levy, W. B. (1985). "Associative changes at the synapses: LTP in the hippocampus," in Synaptic *Modification, Neuron Selectivity, and Nervous System Organization*, eds W. B. Levy, J. A. Anderson, and S. Lehmkuhle (Hillsdale, NJ: Erlbaum), 5–34.

Levy, W. B., and Steward, O. (1983). Temporal contiguity requirements for long-term associative potentiation/depression in the hippocampus. *Neuroscience* 8, 791–797.

Lu, J. T., Li, C. Y., Zhao, J. P., Poo, M. M., and Zhang, X. H. (2007). Spike-timing-dependent plasticity of neocortical excitatory synapses on inhibitory interneurons depends on target cell type. *J. Neurosci.* 27, 9711–9720.

Malenka, R. C. (1994). Synaptic plasticity in the hippocampus: LTP and LTD. *Cell* 78, 535–538.

Markram, H., Lübke, J., Frotscher, M., and Sakmann, B. (1997). Regulation of synaptic efficacy by coincidence of postsynaptic APs and EPSPs. *Science* 275, 213–215.

McLean, J., and Palmer, L. A. (1998). Plasticity of neuronal response properties in adult cat striate cortex. *Vis. Neurosci.* 15, 177–196.

Meliza, C. D., and Dan, Y. (2006). Receptive-field modification in rat visual cortex induced by paired visual stimulation and single-cell spiking. *Neuron* 49, 183–189.

Molyneaux, B. J., and Hasselmo, M. B. (2002). GABAB presynaptic inhibition has an in vivo time constant sufficiently rapid to allow modulation at theta frequency. *J. Neurophysiol.* 87, 1196–1205.

Mu, Y., and Poo, M.-M. (2006). Spike timing-dependent LTP/LTD mediates visual experience-dependent plasticity in a developing retinotectal system. *Neuron* 50, 115–125.

Mulkey, R. M., and Malenka, R. C. (1992). Mechanisms underlying induction of homosynaptic long-term depression in area CA1 of the hippocampus. *Neuron* 9, 967–975.

Nelson, S. B. (1991). Temporal interactions in the cat visual system. I. Orientation-selective suppression in the visual cortex. *J. Neurosci.* 11, 344–356.

Oja, E. (1982). A simplified neuron model as a principal component analyzer. *J. Math. Biol.* 15, 267–273.

Pawlak, V., and Kerr, J. N. (2008). Dopamine receptor activation is required for corticostriatal spike-timing-dependent plasticity. *J. Neurosci.* 28, 2435–2446.

Pfister, J. P., and Gerstner, W. (2006). Triplets of spikes in a model of spike timing-dependent plasticity. *J. Neurosci.* 26, 9673–9682.

Rao, Y., and Daw, N. W. (2004). Layer variations of long-term depression in rat visual cortex. *J. Neurophysiol.* 92, 2652–2658.

Reiter, H. O., and Stryker, M. P. (1988). Neural plasticity without postsynaptic action potentials: less-active inputs become dominant when kitten visual cortical cells are pharmacologically inhibited. *Proc. Natl. Acad. Sci. U.S.A.* 85, 3623–3627.

Sejnowski, T. J. (1977). Statistical constraints on synaptic plasticity. *J. Theor. Biol.* 69, 387–389.

Sengpiel, F., Strawinski, P., and Bonhoeffer, T. (1999). Influence of experience on orientation maps in cat visual cortex. *Nat. Neurosci.* 2, 727–732.

Seol, G. H., Ziburkus, J., Huang, S., Song, L., Kim, I. T., Takamiya, K., Huganir, R. L., Lee, H. K., and Kirkwood, A. (2007). Neuromodulators control the polarity of spike-timing-dependent synaptic plasticity. *Neuron* 55, 919–929.

Shulz, D., Debanne, D., and Frégnac, Y. (1993). Cortical convergence of ON- and OFF-pathways, and functional adaptation of receptive field organization in cat area 17. *Prog. Brain Res.* 95, 191–205.

Shulz, D., and Frégnac, Y. (1992). Cellular analogs of visual cortical epigenesis: II. Plasticity of binocular integration. *J. Neurosci.* 12, 1301–1318.

Shulz, D. E., and Jacob, V. (2010). Spike timing dependent plasticity in the intact brain: counteracting spurious spike coincidences. *Front. Neurosci.* 4:137. doi: 10.3389/fnsyn.2010.00137.

Sjöström, P. J., and Häusser, M. (2006). A cooperative switch determines the sign of synaptic plasticity in distal dendrites of neocortical pyramidal neurons. *Neuron* 51, 227–238.

Sjöström, P. J., and Nelson, S. B. (2002). Spike timing, calcium signals and synaptic plasticity. *Curr. Opin. Neurobiol.* 12, 305–314.

Sjöström, P. J., Turrigiano, G. G., and Nelson, S. B. (2001). Rate, timing, and cooperativity jointly determine cortical synaptic plasticity. *Neuron* 32, 1149–1164.

Sjöström, P. J., Turrigiano, G. G., and Nelson, S. B. (2004). Endocannabinoid-dependent neocortical layer-5 LTD in the absence of postsynaptic spiking. *J. Neurophysiol.* 92, 3338–3343.

Stent, G. (1973). A physiological mechanism for Hebb's postulate of learning. *Proc. Natl. Acad. Sci. U.S.A.* 70, 997–1001.

Stuart, G., Spruston, N., Sakmann, B., and Häusser, M. (1997). Action potential initiation and backpropagation in neurons of the mammalian CNS. *Trends Neurosci.* 20, 125–131.

Tanaka, S., Ribot, J., Imamura, K., and Tani, T. (2006). Orientation-restricted continuous visual exposure induces marked reorganization of orientation maps in early life. *Neuroimage* 30, 426–477.

Tao, H. W., Zhang, L. I., Engert, F., and Poo, M. (2001). Emergence of input specificity of lts during development of retinotectal connections in vivo. *Neuron* 31, 569–580.

Tsubokawa, T., Offermanns, S., Simon, M., and Kano, M. (2000). Calcium dependent persistent facilitation of spike backpropagation in the CA1 pyramidal neurons. *J. Neurosci.* 20, 4878–4884.

Turrigiano, G. G., and Nelson, S. B. (2000). Hebb and homeostasis in neuronal plasticity. 10, 358–364.

Tusa, R. J., Palmer, L. A., and Rosenquist, A. C. (1978). The retinotopic

organization of area 17 (striate cortex) in the cat. *J. Comp. Neurol.* 177, 213–236.

Van den Burg, E., Engelmann, J., Bacelo, J., and Grant, K. (2007). Etomidate reduces initiation of backpropagating dend ritic action potentials: implications for sensory processing and synaptic plasticity during anesthesia. *J. Neurophysiol.* 97, 2373–2384.

van Rossum, M. C. W., Bi, Q., and Turrigiano, G. G. (2000). Stable Hebbian learning through spike-timing-dependent plasitcity. *J. Neurosci.* 20, 8812–8821.

Von der Malsburg, C. (1973). Self-organization of orientation sensitive cells in the striate cortex. *Kybernetik* 14, 85–100.

Wang, X., Merzenich, M. M., Sameshima, K., and Jenkins, W. M. (1995). Remodelling of hand representation in adult cortex determined by timing of tactile stimulation. *Nature* 378, 71–75.

Wiesel, T. N., and Hubel, D. H. (1963). Single-cell responses in striate cortex of kittens deprived of vision in one eye. *J. Neurophysiol.* 26, 1003–1017.

Wigström, H., and Gustafsson, B. (1985). On long-lasting potentiation in the hippocampus: a proposed mechanism for its dependence on coincident pre- and postsynaptic activity. *Acta Physiol. Scand.* 123, 519–522.

Wörgötter, F., and Eysel, U. T. (1987). Quantitative determination of orientational and directional components in the response of visual cortical cells to moving stimuli. *Biol. Cybern.* 57, 349–355.

Yao, H., and Dan, Y. (2001). Stimulus timing-dependent plasticity in cortical processing of orientation. *Neuron* 32, 315–323.

Young, J. M., Waleszczyk, W. J., Wang, C., Calford, M. B., Dreher, B., and Obermayer, K. (2007). Cortical reorganization consistent with spike timing- but not correlation-dependent plasticity. *Nat. Neurosci.* 10, 887–895.

Conflict of Interest Statement: The authors declare that the research was conducted in the absence of any commercial or financial relationships that could be construed as a potential conflict of interest.

Received: 19 May 2010; paper pending published: 29 June 2010; accepted: 28 October 2010; published online: 09 December 2010.

*Citation: Frégnac Y, Pananceau M, René A, Huguet N, Marre O, Levy M and Shulz DE (2010) A re-examination of Hebbian-covariance rules and spike timing-dependent plasticity in cat visual cortex in vivo. Front. Syn. Neurosci. **2**:147. doi: 10.3389/fnsyn.2010.00147*

frontiers in
SYNAPTIC NEUROSCIENCE

REVIEW ARTICLE
published: 07 June 2010
doi: 10.3389/fnsyn.2010.00011

The activity requirements for spike timing-dependent plasticity in the hippocampus

Katherine A. Buchanan[1] and Jack R. Mellor[2]*

[1] *Department of Neuroscience, Physiology and Pharmacology, University College London, London, UK*
[2] *Medical Research Council Centre for Synaptic Plasticity, Department of Anatomy, University of Bristol, Bristol, UK*

Edited by:
Per Jesper Sjöström, University College London, UK

Reviewed by:
Wickliffe C. Abraham, University of Otago, New Zealand
Guo-Qiang Bi, University of Pittsburgh, USA
Dominique Debanne, Université de la Méditerranée, France

***Correspondence:**
Jack R. Mellor, Medical Research Council Centre for Synaptic Plasticity, Department of Anatomy, University of Bristol, Bristol BS8 1TD, UK.
e-mail: jack.mellor@bristol.ac.uk

Synaptic plasticity has historically been investigated most intensely in the hippocampus and therefore it is somewhat surprising that the majority of studies on spike timing-dependent plasticity (STDP) have focused not in the hippocampus but on synapses in the cortex. One of the major reasons for this bias is the relative ease in obtaining paired electrophysiological recordings from synaptically coupled neurons in cortical slices, in comparison to hippocampal slices. Another less obvious reason has been the difficulty in achieving reliable STDP in the hippocampal slice preparation and confusion surrounding the conditions required. The original descriptions of STDP in the hippocampus was performed on paired recordings from neurons in dissociated or slice cultures utilizing single pairs of presynaptic and postsynaptic spikes and were subsequently replicated in acute hippocampal slices. Further work in several laboratories using conditions that more closely replicate the situation *in vivo* revealed a requirement for multiple postsynaptic spikes that necessarily complicate the absolute timing rules for STDP. Here we review the hippocampal STDP literature focusing on data from acute hippocampal slice preparations and highlighting apparently contradictory results and the variations in experimental conditions that might account for the discrepancies. We conclude by relating the majority of the available experimental data to a model for STDP induction in the hippocampus based on a critical role for postsynaptic Ca^{2+} dynamics.

Keywords: hippocampus, synaptic plasticity, STDP

The classic asymmetrical spike timing curve between pairs of synaptically connected hippocampal neurons in dissociated culture described by Bi and Poo (1998) or in organotypic slice cultures by Debanne et al. (1998) have become synonymous with the field of spike timing-dependent plasticity (STDP). These data have been reproduced almost ubiquitously to demonstrate the elegance of spike timing plasticity induction. From this seemingly straightforward description the story of STDP in the hippocampus has followed a rather more complicated and tortuous route. Many groups have taken advantage of the stalwart of plasticity research, the Schaffer collateral to CA1 pyramidal cell synapse in the acute hippocampal slice preparation, to further characterize the requirements for STDP induction. At first glance the research that has emerged from this field is confusing with different groups showing different, seemingly contradictory results regarding the exact requirements for STDP induction. Now, as STDP in the hippocampus enters its second decade a clearer picture is starting to form and many of the previous controversies are helping to produce a more unified picture of STDP induction at this classic synapse and in the hippocampus as a whole.

STDP IN THE HIPPOCAMPUS: THE DATA

Since the time of Hebb's postulate many groups have investigated the timing requirements for plasticity induction in the hippocampus (Levy and Steward, 1979; Gustafsson et al., 1987; Stanton and Sejnowski, 1989; Debanne et al., 1994). Using pairs of single presynaptic and postsynaptic action potentials Bi and Poo (1998) and Debanne et al. (1998) were the first to fully characterize the timing window for the induction of what we now term STDP, in the hippocampus. They took advantage of cultured hippocampal preparations which allow pairs of connected cells to be recorded from with relative ease. This allows one to precisely control the spiking of both the presynaptic and the postsynaptic neuron. In a similar fashion, recordings between pairs of mono-synaptically connected pyramidal neurons in cortical slices also demonstrated reliable STDP (Markram et al., 1997; Sjostrom et al., 2001) which raised the possibility that STDP is a general phenomenon for all synapses exhibiting NMDA receptor-dependent synaptic plasticity. Bi and Poo and Debanne et al. demonstrated that the direction and magnitude of synaptic plasticity could be dictated by the precise millisecond timing of single presynaptic and postsynaptic spikes. If presynaptic spikes precede postsynaptic spikes by up to 30 ms (positive spike timing interval) then LTP was induced, whereas if the presynaptic spike occurred after the postsynaptic spike (negative spike timing interval) LTD ensued. The magnitude of LTP and LTD was greatest when the spikes were closest together leading to a switch from maximal LTD to maximal LTP over a narrow time window of only a few milliseconds. This spike timing window offered an extremely elegant model for plasticity induction *in vivo* and has proved popular with groups modeling information storage in the brain (e.g., Song et al., 2000; Drew and Abbott, 2006).

Recordings in dissociated hippocampal cultures have their drawbacks, in particular the divergence of culture conditions from an intact hippocampal network. After the initial description of STDP

in dissociated hippocampal cultures many groups investigated STDP timing curves in hippocampal slices. Paired Recording of connected CA3–CA1 pyramidal cells in acute hippocampal slices is extremely difficult owing to very low connectivity rates so this has been restricted to organotypic cultured slices. These experiments revealed that synchronous pairing of single presynaptic action potentials with postsynaptic bursts of action potentials lead to the induction of LTP whereas LTD could be induced if this stimulation was given asynchronously (Debanne et al., 1996, 1999). The use of organotypic slice culture also has its drawbacks and it is unclear what developmental stage this cultured network represents. As a result many groups have resorted to investigating STDP in the acute hippocampal slice preparation through pairing extracellular Schaffer collateral stimulation with action potential initiation in patched CA1 pyramidal cells.

Nishiyama et al. witnessed the same STDP curve observed by Bi and Poo, when pairing Schaffer collateral stimulation with single post synaptic spikes in hippocampal slices from young adult rats. They also observed an additional LTD window at positive spike timing intervals between 15 and 20 ms. They argue that this additional LTD window may be due to the presence of inhibitory inputs that are lacking in cultured preparations (Nishiyama et al., 2000). Subsequent experiments have shown that the use of Cs^+ ions in the internal electrode solution by Nishiyama et al. fundamentally alters the induction of synaptic plasticity by STDP protocols (Wittenberg and Wang, 2006; Isaac et al., 2009). Indeed, other groups have been unable to induce STDP with single postsynaptic spikes when using K^+ ion based internal electrode solutions. Instead, the pairing of Schaffer collateral stimulation with a burst of postsynaptic action potentials is required for the induction of LTP in acute hippocampal slices (Pike et al., 1999; Watanabe et al., 2002; Meredith et al., 2003; Wittenberg and Wang, 2006; Buchanan and Mellor, 2007; Carlisle et al., 2008). The importance of postsynaptic bursting is also supported by the effectiveness of a variety of burst firing stimulation protocols to induce LTP at this synapse (Debanne et al., 1994, 1998; Frick et al., 2004; Buchanan and Mellor, 2007). The requirement for postsynaptic burst firing appears to have a developmental profile and is critical for plasticity induction in slices from adult animals (Meredith et al., 2003; Buchanan and Mellor, 2007). Meredith et al. were able to induce LTP through pairing EPSPs with single postsynaptic spikes in adult slices if fast GABAergic inhibition was blocked. This suggests the maturation of inhibition may underlie the requirement for postsynaptic bursts, although this result was not replicated in other studies (Pike et al., 1999; Buchanan and Mellor, 2007). None of the aforementioned studies have systematically investigated the timing dependence of presynaptic spikes with postsynaptic burst firing. For this information we must turn to experiments on hippocampal slices taken from immature animals (<P21).

In slices from juvenile animals spike timing induction protocols have produced a variety of results. Pairs of single presynaptic and postsynaptic spikes given at positive spike timing intervals have been found to induce either; no plasticity (Buchanan and Mellor, 2007), LTD (Wittenberg and Wang, 2006; Campanac and Debanne, 2008) or LTP (Meredith et al., 2003; Buchanan and Mellor, 2007; Campanac and Debanne, 2008) dependent on specific experimental conditions. Several groups have described a frequency dependency to the induction of STDP where LTP is only induced when positive spike timing pairs are repeated at 10 Hz or greater and no plasticity or a small amount of LTD is observed when positive spike pairs are repeated at lower frequencies (5 Hz). In these cases the spike pair repetition rate becomes the dominating factor and the resultant plasticity is timing independent (Wittenberg and Wang, 2006; Buchanan and Mellor, 2007). Timing dependence can be reintroduced when single EPSPs are paired with a postsynaptic burst (Wittenberg and Wang, 2006). In contrast, two other studies were able to induce LTP with positive spike timing pairs repeated at lower frequencies (Meredith et al., 2003; Campanac and Debanne, 2008). The reasons for the discrepancies between results from different groups is not immediately apparent although it is of note that only two of the studies (Meredith et al., 2003; Buchanan and Mellor, 2007) made use of a control input pathway to determine the induction of synaptic plasticity. In addition, it has been shown that postsynaptic spiking is relatively less important than EPSP amplitude for the induction of STDP in the immature hippocampus compared to the mature network (Buchanan and Mellor, 2007). This suggests that differences in the EPSP amplitude used during STDP induction could explain observed discrepancies.

In all cases, although the significance of precise spike timing in the induction of synaptic plasticity in the hippocampus is questionable, the plasticity observed is still dependent on the coincidence of presynaptic and postsynaptic activity as EPSPs or postsynaptic action potentials given on their own fail to induce plasticity. Also, a timing window is still observed as spike timing intervals of ±100 ms fail to induce any change in synaptic strength (Meredith et al., 2003; Wittenberg and Wang, 2006; Buchanan and Mellor, 2007; Campanac and Debanne, 2008).

So, the pursuit of the elegant hippocampal spike timing curve described by Bi and Poo seems to have lost its way. In its place we have a variety of spike timing window shapes described by different groups under different experimental conditions (**Figure 1**). But out of this seemingly contradictory mess there seems to be a common underlying theme that is starting to unveil a clearer picture of STDP rules in the hippocampus.

A UNIFYING THEORY TO DESCRIBE STDP IN THE HIPPOCAMPUS

Due to a long history of plasticity research at the Schaffer collateral-CA1 pyramidal cell synapse much is known about the downstream mechanisms that determine the expression of synaptic plasticity. The critical trigger for plasticity is the influx of Ca^{2+} through NMDA receptors where local peak $[Ca^{2+}]$ is crucial in setting levels of CAMKII and PP1 activity (Lisman and Zhabotinsky, 2001) and therefore determining both the magnitude and direction of the resultant plasticity (Bienenstock et al., 1982; Lisman, 1989; Yang et al., 1999). This increase in postsynaptic $[Ca^{2+}]$ is dependent on the level of postsynaptic depolarization to relieve the Mg^{2+} block from NMDA receptors and many of the apparent controversies regarding STDP induction in the hippocampus may be explained in this context. In turn, postsynaptic depolarization will be influenced by a number of factors such as action potential back-propagation, modulation of dendritic membrane potential and excitability, EPSP amplitude, presence of inhibitory synaptic transmission and frequency of stimulation. We shall consider each of these factors in turn.

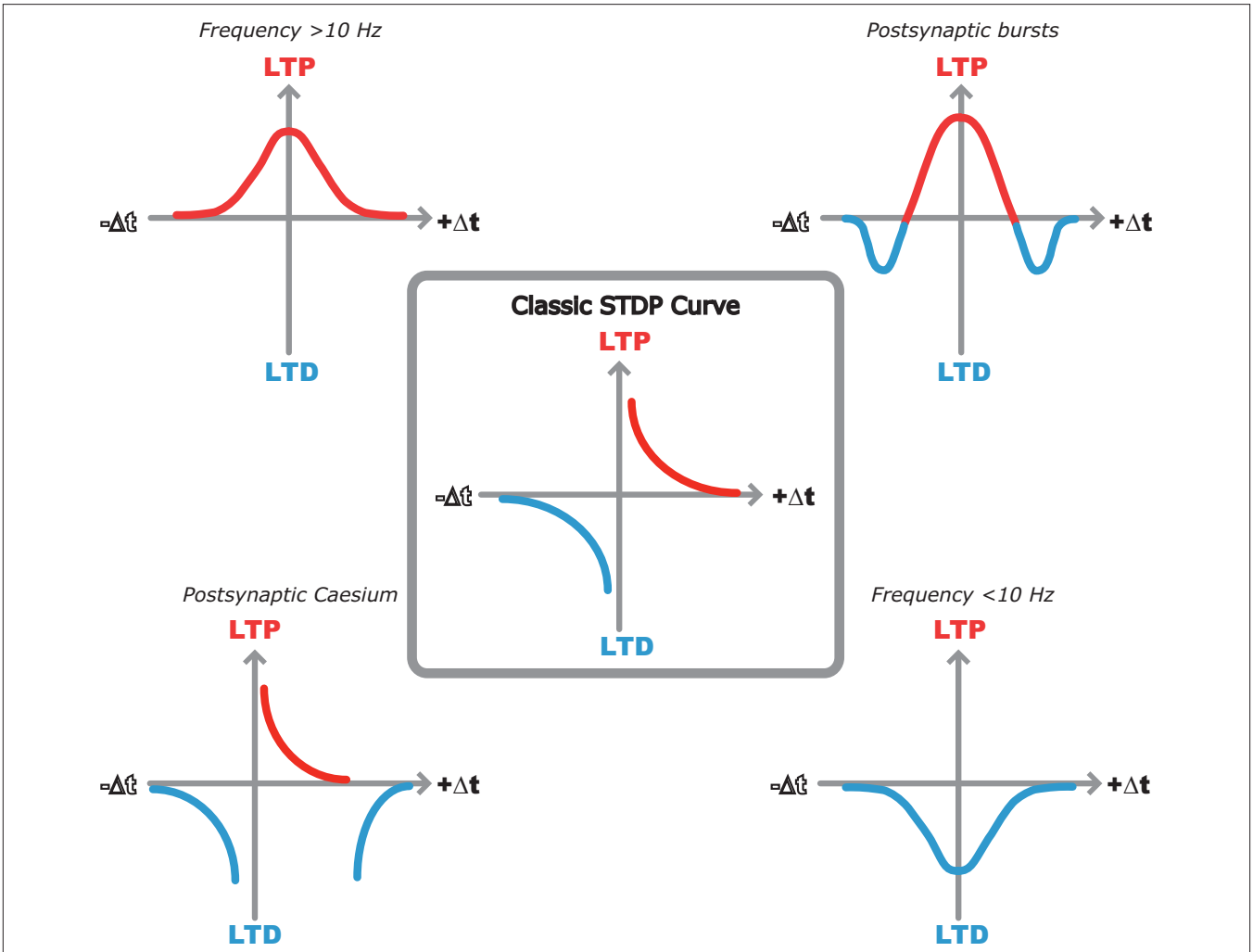

FIGURE 1 | Multiple STDP timing windows in the hippocampus. Center, classic STDP curve originally described by Bi and Poo (1998) in dispersed hippocampal cultures. Top left, LTP only window when spike timing pairs are repeated at 10 Hz or greater in hippocampal slices (Buchanan and Mellor, 2007). Top right, bidirectional STDP window observed when single EPSPs are paired with postsynaptic bursts (Wittenberg and Wang, 2006). Bottom right, LTD only window when spike timing pairs are repeated at less than 10 Hz (Wittenberg and Wang, 2006). Bottom left, classic STDP window with additional LTD window observed with postsynaptic cesium in hippocampal slices (Nishiyama et al., 2000).

Bursts of action potentials produce a larger and more prolonged postsynaptic depolarization and therefore a much greater spine $[Ca^{2+}]$ than single spikes. This results in efficient induction of LTP (Pike et al., 1999; Buchanan and Mellor, 2007; Carlisle et al., 2008) or conversion of LTD to LTP (Wittenberg and Wang, 2006). At longer positive spike timing intervals the postsynaptic burst lags too far behind the EPSP to reach the threshold for LTP. Although calcium levels are still elevated beyond those observed for EPSPs or postsynaptic bursts alone leading to the observation of a second LTD window (**Figure 1**; Wittenberg and Wang, 2006). In the absence of bursts, other mechanisms for enhancing postsynaptic excitability are required to activate NMDARs and induce synaptic plasticity.

Depolarizing the membrane by perfusing Cs^+ into the neuron from the patch pipette will broaden and increase the back-propagation of somatic action potentials (Wittenberg and Wang, 2006) as well as depolarizing the membrane allowing single postsynaptic spikes to induce STDP in adult hippocampal slices. An additional LTD window is observed at longer positive STIs due to the calcium levels dropping below the threshold for LTP but not LTD (Nishiyama et al., 2000; Wittenberg and Wang, 2006). Similarly, enhancing excitability by activation of neuromodulatory receptors, for example muscarinic acetylcholine receptors, reduces spike attenuation (Tsubokawa and Ross, 1997) and facilitates LTP induction (Isaac et al., 2009). This may be particularly critical in the slice preparation where external neuromodulatory inputs are removed. Modulation of other ionic conductances such as the sAHP can also regulate the induction of STDP again illustrating the critical role played by membrane excitability (Fuenzalida et al., 2007).

The magnitude of the EPSP used to induce STDP will contribute to the depolarization seen within the spine and therefore to NMDA receptor activation during STDP induction. This could explain discrepancies between reports since synaptic response

amplitude varies from EPSCs of ~50 pA (Buchanan and Mellor, 2007) to ~50–150 pA (Wittenberg and Wang, 2006) to EPSPs of ~3–5 mV (Meredith et al., 2003; Campanac and Debanne, 2008). Larger EPSPs could produce sufficient depolarization during single pairs of presynaptic and postsynaptic stimulation to induce LTP (Meredith et al., 2003; Campanac and Debanne, 2008). Interestingly, repetitive stimulation of individual suprathreshold EPSPs (EPSPs that are large enough to induce an action potential) induces LTD (Wittenberg and Wang, 2006) which predicts that the same will occur for suprathreshold stimulation during extracellular recording even at low stimulation frequencies. Also the driving of multiple action potentials by bursts of EPSPs induces LTP (Buchanan and Mellor, 2007). Conversely, in dissociated culture conditions EPSC amplitude was found to be inversely correlated with LTP induction although the EPSC amplitude range is much greater (30–2000 pA) than that used in acute slices (Bi and Poo, 1998).

Blockade of $GABA_A$ receptors can also enhance excitability and therefore allow the induction of LTP by single pairs of spikes (Meredith et al., 2003). This could also explain some age dependent effects on STDP induction since the mature GABAergic network in adults may increase the threshold for action potential back-propagation whereas in younger animals a less mature GABAergic network allows single spikes to back-propagate fully. However, there is also evidence that somatically induced action potentials are unable to provide the postsynaptic depolarization required for the induction of LTP in slices from juvenile animals. When somatic action potentials are blocked by focal TTX application LTP can still be induced if the level of presynaptic stimulation is increased. This suggests that dendritically initiated spikes may play a critical role in the induction of LTP in slices from younger animals (Buchanan and Mellor, 2007).

The frequency dependence of STDP in juvenile hippocampal slices can also be explained through differences in the levels of postsynaptic depolarization. Above a frequency of 10 Hz individual action potentials do not repolarize back to the resting membrane potential before the next action potential in the train (Buchanan and Mellor, 2007). This results in a residual level of depolarization throughout the train of spike pairings which may increase postsynaptic depolarization and enhance NMDAR activation. In addition, $[Ca^{2+}]$ will summate at higher frequencies ensuring spike timing pairs reach the threshold for LTP. Below 10 Hz there is little or no residual depolarization and the coincidence of EPSPs and action potentials are only able to produce enough depolarization to reach the threshold for LTD (Sjostrom et al., 2001; Wittenberg and Wang, 2006; Buchanan and Mellor, 2007).

The timing independence of STDP observed by several groups can also be explained through differences in postsynaptic depolarization. At higher frequencies the level of residual depolarization may mean that any degree of near coincidence is capable of increasing the postsynaptic calcium above the threshold for LTP (Buchanan and Mellor, 2007). Also the majority of experiments in hippocampal slices are done in the presence of $GABA_A$ receptor blockers which could prolong the duration of the postsynaptic depolarization caused by both the EPSP and the back-propagating action potential. This could result in a much broader timing window for the induction of plasticity.

A Ca^{2+} hypothesis for the induction of synaptic plasticity by pairs of presynaptic and postsynaptic spikes was first formalized in a model for STDP based on $[Ca^{2+}]$ (Shouval et al., 2002). Since then it has been revised to include the activation of calmodulin and CAMKII (Shouval et al., 2002; Rubin et al., 2005; Graupner and Brunel, 2007; Helias et al., 2008; Urakubo et al., 2008) and in this issue a model is presented specifically designed to model the Ca^{2+} dynamics within the spines of CA1 pyramidal cell dendrites during STDP at Schaffer collateral synapses in the hippocampus (Rackham et al., 2010 under review). This paper illustrates how most of the current data on synaptic plasticity induction can be replicated by such a model and can potentially unify current thinking on STDP in the hippocampus. It will be interesting to see if future experiments measuring spine calcium dynamics during STDP, similar to those performed at cortical synapses (Nevian and Sakmann, 2006), confirm such a Ca^{2+} based model for the induction of synaptic plasticity.

REFERENCES

Bi, G. Q., and Poo, M. M. (1998). Synaptic modifications in cultured hippocampal neurons: dependence on spike timing, synaptic strength, and postsynaptic cell type. *J. Neurosci.* 18, 10464–10472.

Bienenstock, E. L., Cooper, L. N., and Munro, P. W. (1982). Theory for the development of neuron selectivity – orientation specificity and binocular interaction in visual-cortex. *J. Neurosci.* 2, 32–48.

Buchanan, K. A., and Mellor, J. R. (2007). The development of synaptic plasticity induction rules and the requirement for postsynaptic spikes in rat hippocampal CA1 pyramidal neurones. *J. Neurosci.* 585, 429–445.

Campanac, E., and Debanne, D. (2008). Spike timing-dependent plasticity: a learning rule for dendritic integration in rat CA1 pyramidal neurons. *J. Physiol. (Lond.)* 586, 779–793.

Carlisle, H. J., Fink, A. E., Grant, S. G., and O'Dell, T. J. (2008). Opposing effects of PSD-93 and PSD-95 on long-term potentiation and spike timing-dependent plasticity. *J. Physiol. (Lond.)* 586, 5885–5900.

Debanne, D., Gahwiler, B. H., and Thompson, S. M. (1994). Asynchronous pre- and postsynaptic activity induces associative long-term depression in area CA1 of the rat hippocampus *in vitro*. *Proc. Natl. Acad. Sci. U.S.A.* 91, 1148–1152.

Debanne, D., Gahwiler, B. H., and Thompson, S. M. (1996). Cooperative interactions in the induction of long-term potentiation and depression of synaptic excitation between hippocampal CA3–CA1 cell pairs *in vitro*. *Proc. Natl. Acad. Sci. U.S.A.* 93, 11225–11230.

Debanne, D., Gahwiler, B. H., and Thompson, S. M. (1998). Long-term synaptic plasticity between pairs of individual CA3 pyramidal cells in rat hippocampal slice cultures. *J. Physiol. (Lond.)* 507, 237–247.

Debanne, D., Gahwiler, B. H., and Thompson, S. M. (1999). Heterogeneity of synaptic plasticity at unitary CA3-CA1 and CA3-CA3 connections in rat hippocampal slice cultures. *J. Neurosci.* 19, 10664–10671.

Drew, P. J., and Abbott, L. F. (2006). Extending the effects of spike-timing-dependent plasticity to behavioral timescales. *Proc. Natl. Acad. Sci. U.S.A.* 103, 8876–8881.

Frick, A., Magee, J., and Johnston, D. (2004). LTP is accompanied by an enhanced local excitability of pyramidal neuron dendrites. *Nat. Neurosci.* 7, 126–135.

Fuenzalida, M., Fernandez de Sevilla, D., and Buno, W. (2007). Changes of the EPSP waveform regulate the temporal window for spike-timing-dependent plasticity. *J. Neurosci.* 27, 11940–11948.

Graupner, M., and Brunel, N. (2007). STDP in a bistable synapse model based on CaMKII and associated signaling pathways. *PLoS Comput. Biol.* 3, e221. doi: 10.1371/journal.pcbi.0030221.

Gustafsson, B., Wigstrom, H., Abraham, W. C., and Huang, Y. Y. (1987). Long-term potentiation in the hippocampus using depolarizing current pulses as the conditioning stimulus to single volley synaptic potentials. *J. Neurosci.* 7, 774–780.

Helias, M., Rotter, S., Gewaltig, M. O., and Diesmann, M. (2008). Structural plasticity controlled by calcium based correlation detection. *Front. Comput. Neurosci.* 2:7. doi:10.3389/neuro.10.007.2008.

Isaac, J. T., Buchanan, K. A., Muller, R. U., and Mellor, J. R. (2009).

Hippocampal place cell firing patterns can induce long-term synaptic plasticity *in vitro*. *J. Neurosci.* 29, 6840–6850.

Levy, W. B., and Steward, O. (1979). Synapses as associative memory elements in the hippocampal formation. *Brain Res.* 175, 233–245.

Lisman, J. (1989). A Mechanism for the Hebb and the anti-Hebb processes underlying learning and memory. *Proc. Natl. Acad. Sci. U.S.A.* 86, 9574–9578.

Lisman, J. E., and Zhabotinsky, A. M. (2001). A model of synaptic memory: a CaMKII/PP1 switch that potentiates transmission by organizing an AMPA receptor anchoring assembly. *Neuron* 31, 191–201.

Markram, H., Lubke, J., Frotscher, M., and Sakmann, B. (1997). Regulation of synaptic efficacy by coincidence of postsynaptic APs and EPSPs. *Science* 275, 213–215.

Meredith, R. M., Floyer-Lea, A. M., and Paulsen, O. (2003). Maturation of long-term potentiation induction rules in rodent hippocampus: role of GABAergic inhibition. *J. Neurosci.* 23, 11142–11146.

Nevian, T., and Sakmann, B. (2006). Spine Ca2+ signaling in spike-timing-dependent plasticity. *J. Neurosci.* 26, 11001–11013.

Nishiyama, M., Hong, K., Mikoshiba, K., Poo, M., and Kato, K. (2000). Calcium stores regulate the polarity and input specificity of synaptic modification. *Nature* 408, 584–588.

Pike, F. G., Meredith, R. M., Olding, A. W. A., and Paulsen, O. (1999). Postsynaptic bursting is essential for 'Hebbian' induction of associative long-term potentiation at excitatory synapses in rat hippocampus. *J. Physiol. (Lond.)* 518, 571–576.

Rubin, J. E., Gerkin, R. C., Bi, G. Q., and Chow, C. C. (2005). Calcium time course as a signal for spike-timing-dependent plasticity. *J. Neurophysiol.* 93, 2600–2613.

Shouval, H. Z., Bear, M. F., and Cooper, L. N. (2002). A unified model of NMDA receptor-dependent bidirectional synaptic plasticity. *Proc. Natl. Acad. Sci. U.S.A.* 99, 10831–10836.

Sjostrom, P. J., Turrigiano, G. G., and Nelson, S. B. (2001). Rate, timing, and cooperativity jointly determine cortical synaptic plasticity. *Neuron* 32, 1149–1164.

Song, S., Miller, K. D., and Abbott, L. F. (2000). Competitive Hebbian learning through spike-timing-dependent synaptic plasticity. *Nat. Neurosci.* 3, 919–926.

Stanton, P. K., and Sejnowski, T. J. (1989). Associative long-term depression in the hippocampus induced by Hebbian covariance. *Nature* 339, 215–218.

Tsubokawa, H., and Ross, W. N. (1997). Muscarinic modulation of spike backpropagation in the apical dendrites of hippocampal CA1 pyramidal neurons. *J. Neurosci.* 17, 5782–5791.

Urakubo, H., Honda, M., Froemke, R. C., and Kuroda, S. (2008). Requirement of an allosteric kinetics of NMDA receptors for spike timing-dependent plasticity. *J. Neurosci.* 28, 3310–3323.

Watanabe, S., Hoffman, D. A., Migliore, M., and Johnston, D. (2002). Dendritic K+channels contribute to spike-timing dependent long-term potentiation in hippocampal pyramidal neurons. *Proc. Natl. Acad. Sci. U.S.A.* 99, 8366–8371.

Wittenberg, G. M., and Wang, S. S. H. (2006). Malleability of spike-timing-dependent plasticity at the CA3–CA1 synapse. *J. Neurosci.* 26, 6610–6617.

Yang, S. N., Tang, Y. G., and Zucker, R. S. (1999). Selective induction of LTP and LTD by postsynaptic [Ca^{2+}]i elevation. *J. Neurophysiol.* 81, 781–787.

Conflict of Interest Statement: The authors declare that the research was conducted in the absence of any commercial or financial relationships that could be construed as a potential conflict of interest.

Received: 22 January 2010; paper pending published: 15 February 2010; accepted: 17 May 2010; published online: 07 June 2010.

Citation: Buchanan KA and Mellor JR (2010) The activity requirements for spike timing-dependent plasticity in the hippocampus. Front. Syn. Neurosci. ***2****:11. doi: 10.3389/fnsyn.2010.00011*

frontiers in
COMPUTATIONAL NEUROSCIENCE

REVIEW ARTICLE
published: 17 September 2010
doi: 10.3389/fncom.2010.00136

Mechanisms of induction and maintenance of spike-timing dependent plasticity in biophysical synapse models

Michael Graupner[1]* and Nicolas Brunel[2,3]

[1] *Center for Neural Science, New York University, New York City, NY, USA*
[2] *Laboratoire de Neurophysique et Physiologie, Université Paris Descartes, Paris, France*
[3] *Centre National de la Recherche Scientifique, Paris, France*

Edited by:
Wulfram Gerstner, Ecole Polytechnique Fédérale de Lausanne, Switzerland

Reviewed by:
Mark C. W. van Rossum, University of Edinburgh, UK
Lorric Ziegler, Ecole Polytechnique Fédérale de Lausanne, Switzerland

****Correspondence:***
Michael Graupner, Center for Neural Science, New York University, 4 Washington Place, New York, NY 10003-6603, USA.
e-mail: michael.graupner@nyu.edu

We review biophysical models of synaptic plasticity, with a focus on spike-timing dependent plasticity (STDP). The common property of the discussed models is that synaptic changes depend on the dynamics of the intracellular calcium concentration, which itself depends on pre- and postsynaptic activity. We start by discussing simple models in which plasticity changes are based directly on calcium amplitude and dynamics. We then consider models in which dynamic intracellular signaling cascades form the link between the calcium dynamics and the plasticity changes. Both mechanisms of induction of STDP (through the ability of pre/postsynaptic spikes to evoke changes in the state of the synapse) and of maintenance of the evoked changes (through bistability) are discussed.

Keywords: STDP, biophysical models, bistability, induction, maintenance, protein signaling cascade, calcium control hypothesis, CaMKII

INTRODUCTION

Long-term synaptic modifications have long been postulated to occur in response to the simultaneous activation of both pre- and postsynaptic neurons (Hebb, 1949). Recent experimental techniques allow precise control over pre- and postsynaptic spiking activity. Such experiments provide evidence at the single-cell level that coincidence between afferent input with postsynaptic spiking evokes long-term modifications. In general, presynaptic input (onset of the excitatory postsynaptic potential – EPSP) occurring closely before or after a postsynaptic action potential results in maximal synaptic modification, while no plasticity occurs if the temporal difference between both is large.

In the hippocampus (Levy and Steward, 1983; Gustafsson et al., 1987; Magee and Johnston, 1997; Bi and Poo, 1998), the Xenopus tectum (Zhang et al., 1998), the visual cortex (Markram et al., 1997; Sjöström et al., 2001), and the somatosensory cortex (Feldman, 2000) an EPSP occurring prior to the backpropagating action potential (pre–post pairing) evokes long-term potentiation (LTP), and the anti-causal order, i.e., the EPSP occurs after the postsynaptic neuron spiked (post–pre pairing), leads to long-term depression (LTD). Such a temporal order of potentiation and depression occurrence is generally referred to as the "classical" spike-timing dependent plasticity (STDP) rule. Since the early STDP experiments, numerous studies in different brain regions and under varying experimental conditions have revealed a plethora of STDP shapes (see Abbott and Nelson, 2000 for a review). Further studies investigating plasticity results in response to triplets and quadruplets of spikes have highlighted the non-linearity of plasticity results (Bi and Wang, 2002; Froemke and Dan, 2002; Wang et al., 2005). In this review we will mostly focus on biophysical models accounting for the "classical" form of STDP observed in hippocampal and neocortical pyramidal cells as well as in retinotectal connections.

What are the biochemical mechanisms operating at the synapse leading to the observed plasticity outcomes? Enormous experimental effort has been devoted to the identification of the molecular players both mediating and modulating synaptic plasticity (Malenka and Bear, 2004). Tremendous advances have been made in identifying which constituents take part in the induction of LTP for pre–post pairs or LTD for post–pre pairs, for example. The biological mechanisms underlying spike-timing synaptic plasticity have furthermore inspired mathematical models that strive to reproduce aspects of STDP results.

Other less well studied questions are: What is the nature of the synaptic change (continuous or discrete)? What biological machinery stably maintains the evoked synaptic state over time scales of minutes to hours or more? Only a few experimental studies have investigated synaptic changes on putative single synaptic connections. These studies consistently find all-or-none switch like events (Petersen et al., 1998; Bagal et al., 2005; O'Connor et al., 2005b). These experiments suggest that the synapse exists in only two states of high- and low transmission strength respectively, and that transitions between these states can be evoked by specific stimulation protocols.

Synapse models including protein signaling cascades often exhibit bistability due to positive feedback loops in the modeled pathways. In such models, synaptic changes correspond to transitions between two states, and the stable maintenance of synaptic changes is accounted for by bistability (we discuss briefly in section

Abbreviations: EPSP/C, excitatory postsynaptic potential/current; LTP, long-term potentiation; LTD, long-term depression; STDP, spike-timing dependent plasticity; CA, *Cornu Ammonis* area; CaMKII, calcium/calmodulin-dependent protein kinase II; BPAP, backpropagating action potential; VDCC, voltage-dependent calcium channel; NMDA-R, *N*-methyl-D-aspartic acid receptor; mGluR, metabotropic glutamate receptor; AMPA-R, α-amino-3-hydroxyl-5-methyl-4-isoxazole-propionate receptor; CaM, calmodulin; PP1, protein phosphatase 1; PKA, protein kinase A; I1, inhibitor 1; cAMP, cyclic adenosine monophosphate; MAPK, mitogen-activated protein kinase.

"Bi/multistable models based on alternative mechanisms" recent models that have more than two stable states). In the absence of bistability, changes evoked by a given stimulation protocol are expected to decay in time. Therefore, models lacking bistability are not expected to possess long-term memory properties at the level of a single synapse (but see Delord et al., 2007). Alternatively, stable memory retention has been proposed to rely on reinforcing the LTP/LTD of a synapse through network dynamics, thus stabilizing otherwise unstable synapses (Abraham and Robins, 2005; Billings and van Rossum, 2009).

Here, we review "biophysical" models of synaptic plasticity whose aim is to reproduce spike-timing dependent plasticity experiments but also to understand the mechanisms that convert a given firing pattern of pre- and postsynaptic cells into a specific synaptic change. Such approaches are to be distinguished from purely phenomenological models of STDP which directly link the time difference between pre- and postsynaptic spikes to a particular synaptic change (see Morrison et al., 2008 for a review). In particular, we focus on models which try to link the calcium dynamics evoked by pre- and postsynaptic activity to observed plasticity outcomes. We discuss in particular how specific biophysical features give rise to specific components of the STDP outcome. We start from phenomenological models of synaptic plasticity based purely on the dynamics of calcium concentration in dendritic spines (section 'Phenomenological models based on calcium dynamics'). We then turn to models that explicitly describe the protein signaling cascades that have been shown experimentally to be involved in synaptic plasticity, with a special emphasis on calcium/calmodulin-dependent protein kinase II (CaMKII)-based models (section 'Models including biochemical signaling cascades beyond calcium'). We point out that, unlike the more phenomenological models based on calcium only, the detailed models exhibit bistable behavior, which allows them to maintain synaptic changes for (in principle) arbitrary amounts of time. Last, we discuss how such bistable synapse models can account for spike-timing dependent plasticity.

PHENOMENOLOGICAL MODELS BASED ON CALCIUM DYNAMICS

An increase in postsynaptic calcium concentration is a necessary (Lynch et al., 1983; Zucker, 1999; Mizuno et al., 2001; Ismailov et al., 2004; Nevian and Sakmann, 2006) and sufficient (Malenka et al., 1988; Neveu and Zucker, 1996; Yang et al., 1999) signal to induce synaptic changes. We start here by briefly reviewing the experimental evidence supporting this statement. We then turn to discuss phenomenological models reproducing STDP plasticity results based on the calcium concentration dynamics.

CALCIUM IS A KEY SIGNAL FOR PLASTICITY: EXPERIMENTAL DATA

In most synapses, synaptic activation leads to calcium entry in the postsynaptic terminal through *N*-methyl-D-aspartic acid receptor (NMDA-R)-channels (Koester and Sakmann, 1998; Yuste et al., 1999; Kovalchuk et al., 2000). Backpropagating action potentials (BPAPs) produce calcium influx through voltage-dependent calcium channels (VDCCs) (Jaffe et al., 1992; Yuste and Denk, 1995; Majewska et al., 2000; Sabatini and Svoboda, 2000). The induction of LTP at the hippocampal Schaffer collateral – CA1 neuron synapse necessitates activation of NMDA receptors (Collingridge et al., 1983; Bliss and Collingridge, 1993), while basal synaptic transmission and the maintenance of the potentiated state are not affected by NMDA blockade (Morris et al., 1986). The requirement of NMDA activation for LTP induction has also been identified between thick, tufted layer V pyramidal neurons in rat visual cortex (Artola and Singer, 1987; Bear et al., 1992; Markram et al., 1997; Sjöström et al., 2001), in layer IV to layer II/III pyramidal cell synapses in the somatosensory cortex (Castro-Alamancos et al., 1995; Feldman, 2000; Nevian and Sakmann, 2006), and in the lateral geniculate nucleus (Hahm et al., 1991; Mooney et al., 1993).

Long-term potentiation induction evoked by STDP protocols also depends on the large calcium influx through NMDA-Rs in the hippocampus (Magee and Johnston, 1997) and the somatosensory cortex (Nevian and Sakmann, 2006). The induction of spike-timing dependent LTD, however, is mediated by the activation of presynaptic NMDA-Rs (Sjöström et al., 2003; Bender et al., 2006; Nevian and Sakmann, 2006). Nevian and Sakmann (2006) show in the somatosensory cortex that burst-pairing induced LTD is independent of postsynaptic activation of NMDA-Rs, while the postsynaptic calcium influx through VDCCs is necessary for the induction of LTD. On the other hand, VDCC antagonists (nimodipine for L-type channels; or Ni^{2+} for T-type channels) block spike-timing evoked LTP without any effect on baseline EPSPs in hippocampal slices (Magee and Johnston, 1997). In hippocampal cultures, Bi and Poo (1998) report that blocking L-type Ca^{2+} channels (by nimodipine) does not affect LTP induction by pre–post pairings but prevents LTD induction in response to post–pre pairings.

Long-term potentiation and LTD rely on calcium influx through different channels but both require postsynaptic calcium elevations (Lynch et al., 1983; Malenka et al., 1988; Neveu and Zucker, 1996; Yang et al., 1999; Zucker, 1999; Mizuno et al., 2001; Ismailov et al., 2004; Nevian and Sakmann, 2006). One of the main conclusions from those studies is that LTP is triggered by a brief increase of calcium with relatively high magnitude, whereas a prolonged modest rise of calcium reliably induces LTD. Neveu and Zucker (1996) show that the release of caged-calcium by photolysis in hippocampal CA1 pyramidal cells is sufficient to evoke LTP and LTD, and that concurrent presynaptic activity is not required. Nevian and Sakmann (2006) demonstrate that LTP and LTD are equally sensitive to fast (1,2-bis(O-aminophenoxy)ethane-*N,N,N',N'*-tetraacetic acid – BAPTA) and slow (ethylene glycol tetraacetic acid – EGTA) Ca^{2+} buffers loaded in the postsynaptic cell. They conclude that the calcium sensors that trigger the long-lasting synaptic changes respond to the global, volume-averaged increase in intracellular calcium concentration rather than to local calcium concentrations in microdomains. Note that cortical LTD involving the activation of metabotropic glutamate receptors (mGluRs) and retrograde signaling (see below) also requires postsynaptic calcium elevations (Nevian and Sakmann, 2006).

MODELS BASED EXCLUSIVELY ON THE DYNAMICS OF CALCIUM CONCENTRATION

How do synaptic modifications emerge from specific patterns of pre- and postsynaptic spiking? We discuss in this section a first series of biophysical models that have tried to reproduce STDP results from the postsynaptic calcium dynamics induced by pre- and postsynaptic activity. While such models readily account for LTD

induction in response to post–pre pairs and for LTP in response to pre–post pairs, they consistently observe a second LTD window for pre–post pairs with large time differences, Δt, between pre- and postsynaptic spikes.

We start by discussing the properties of postsynaptic calcium transients evoked by spike-pairs with different Δts. An isolated postsynaptic spike generates a short-lasting calcium transient due to opening of VDCCs induced by the depolarization through the BPAP (see $\Delta t = -100$ ms case in **Figure 1A**). Likewise, an isolated presynaptic spike generates a long-lasting calcium transient due to NMDA channel opening (**Figure 1A**). When the presynaptic spike is immediately followed by a postsynaptic spike, the strong depolarization by the BPAP increases drastically the voltage-dependent NMDA-R mediated calcium current due to removal of the magnesium block (Nowak et al., 1984; Jahr and Stevens, 1990; magenta line in **Figure 1A**). This supralinear superposition of the two contributions at positive Δts is particularly apparent in the maximal amplitude and the integral of the calcium transients (**Figure 1B**). Note that the dependence of calcium dynamics on Δt is not fully captured by amplitude or integral alone. In fact, varying Δt changes in a pronounced fashion the amplitude histogram of the calcium transient even in ranges where the maximal amplitude or the integral depend very weakly on Δt (compare for example protocols with $\Delta t = -100$ and -20 ms in **Figure 1C**).

In calcium-based models, the induced synaptic weight change is determined by the time course of the calcium transients triggered by pre- and postsynaptic spikes (Shouval et al., 2002; Cai et al., 2007). The magnitude and sign of the resulting synaptic changes are based on the calcium control hypothesis (**Figure 2A**) which is derived from experimental evidence showing that different calcium levels trigger different forms of synaptic plasticity (Yang et al., 1999; Zucker, 1999; Mizuno et al., 2001; Ismailov et al., 2004; Nevian and Sakmann, 2006). According to this hypothesis, no modification occurs when the calcium level is below a threshold θ_d which is larger than the resting concentration. If calcium resides in an intermediate calcium range, between θ_d and a second threshold $\theta_p > \theta_d$, the synaptic weight is decreased. Finally, if calcium increases above the second threshold, θ_p, the synaptic strength is potentiated (**Figure 2A**).

Models based on the calcium control hypothesis explains to a large extent the spike-timing dependence of plasticity, as shown in **Figure 2**, provided the maximal amplitude of the calcium transient for pre–post pairings at short Δt is larger than the potentiating threshold θ_p. Post–pre pairings evoke calcium transients which linearly superimpose and therefore yield moderate calcium elevations promoting LTD. Pre–post pairings result in supralinear superpositions of the calcium transients which attain high calcium levels required to evoke LTP. If Δt grows larger, the calcium transients pass again through a region of moderate levels inducing LTD (see **Figure 2C**). Note that Shouval et al. (2002) assume the dominant source of calcium influx to be NMDA-Rs (compare **Figures 1A and 2B**). They furthermore model the BPAPs with a slow after-depolarizing tail which increases the range of interaction between the postsynaptic spike and NMDA activation by the presynaptic action potential for $\Delta t < 0$. That interaction range defines the width of the LTD window in their model (compare LTD range in **Figure 2C** without after-depolarizing tail, and the LTD range obtained in Shouval et al. (2002), reproduced in **Figure 2D**).

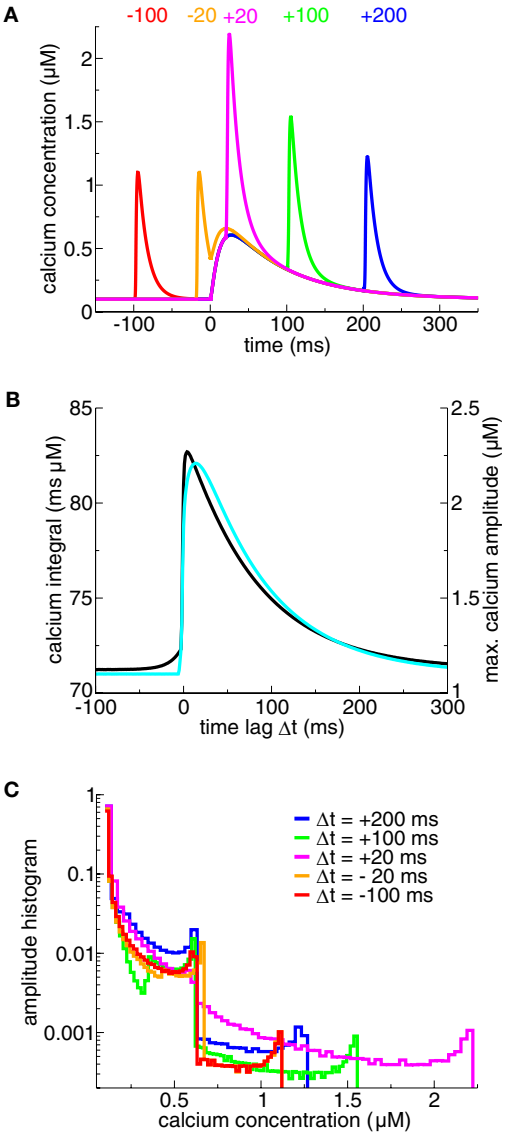

FIGURE 1 | Calcium dynamics in response to spike-pairs for different Δts. **(A)** Calcium transients for five different time differences between pre- and postsynaptic spikes, Δts (marked in the panel in ms). The transients are generated using the model for postsynaptic calcium and postsynaptic membrane potential dynamics presented in Graupner and Brunel (2007). There, the postsynaptic membrane potential is modeled using the Hodgkin–Huxley formalism in a single compartment. In the model, calcium influx is mediated by VDCCs (high-voltage activated L-type current) and voltage-dependent NMDA-Rs. The presynaptic spike is occurring at $t = 0$ ms. The presynaptically evoked calcium amplitude is 0.5 μM and the postsynaptic Ca^{2+} amplitude is 1 μM (Sabatini et al., 2002). Note that the calcium amplitudes are the only parameters that are changed compared to Graupner and Brunel (2007). **(B)** Maximal calcium amplitude (cyan line, right-hand y axis) and integral of the calcium transient (black line, left-hand y axis) as a function of Δt. **(C)** Calcium amplitude distributions of calcium transients evoked by spike-pairs for five different Δts. The five calcium transients shown in **(A)** give rise to the amplitude distributions shown in the same color. The histograms are calculated by binning the calcium concentration (bins size ΔCa = 0.02 μM for $\Delta t = -100, -20, +100$ ms, and 0.035 μM for $\Delta t = +20, +200$ ms) and counting the number of data points whose amplitude falls in each bin. The amplitude histograms illustrate the fraction of time spent at a certain calcium level by the calcium trace for a given Δt.

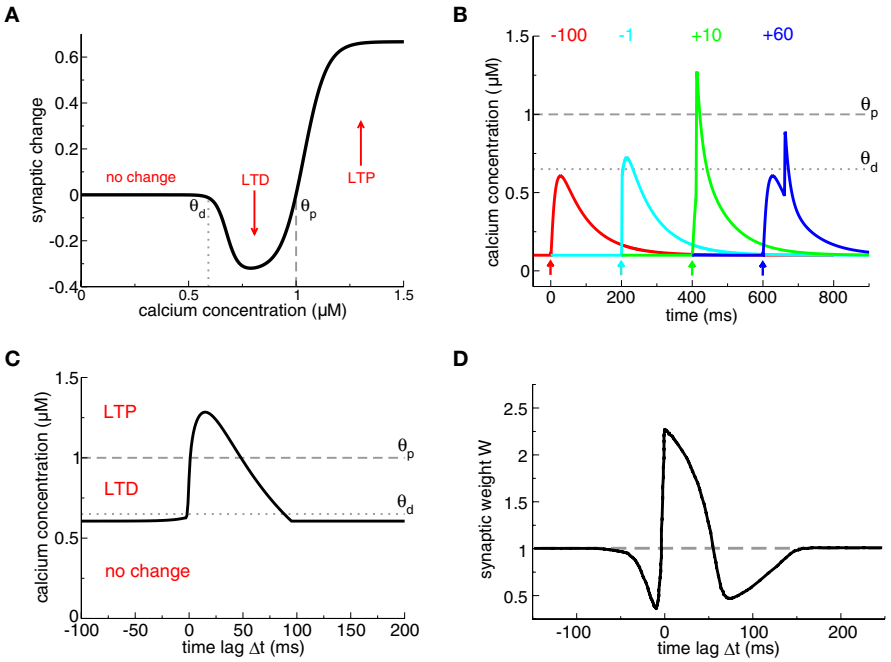

FIGURE 2 | Plasticity results based on calcium control hypothesis. **(A)** Calcium control hypothesis. The calcium control hypothesis implies that low calcium levels do not evoke any changes, intermediate calcium levels (between θ_d and θ_p) depress the synapse (corresponding to an LTD event) and high calcium transients (above θ_p) potentiate the synapse (corresponding to an LTP event). Note that depression and potentiation are not sudden events but occur with a calcium-dependent time constant, such that LTP induction is faster than LTD induction (see Shouval et al., 2002 for more details). **(B)** Calcium transients evoked by spike-pairs and mediated exclusively by NMDA-Rs. In this plot, we use the model of Graupner and Brunel (2007), except that calcium influx occurs through NMDA-Rs only, i.e., there is no Ca^{2+} current mediated by VDCCs, as in Shouval et al. (2002). Otherwise, we use the same parameters as in **Figure 1**, i.e., the presynaptically evoked Ca^{2+} amplitude is 0.5 μM. Calcium transients are shown for four different Δts (values given in the panel in ms). The timing of the presynaptic spike is indicated by an arrow for each particular Δt. The thresholds θ_d (dotted line) and θ_p (dashed line) from the calcium control hypothesis (see **A**) are chosen appropriately, that is, large Δt transients do not cross any threshold, short negative Δt transients cross θ_d, and short positive Δt transients cross θ_p. **(C)** Maximal calcium amplitude as a function of Δt, plotted together with the thresholds θ_d (dotted line) and θ_p (dashed line). **(D)** Plasticity outcomes in response to spike-pairs. Spike-pairs with short positive Δts evoke LTP. Spike-pairs with short negative and with large positive Δts lead to LTD. Figure reproduced from Shouval et al. (2002). Note the large extent of the LTD range for short negative Δts as compared to **(C)**. The difference is due to the slow after-depolarizing tail of the BPAP used in Shouval et al. (2002). See text for more details.

Most STDP spike-pair experiments however have not found a "second LTD window" at large positive Δt (but see Nishiyama et al., 2000; Wittenberg and Wang, 2006). Shouval and Kalantzis (2005) show that stochastic properties of synaptic transmission can markedly reduce the LTD magnitude at positive time lags. The main idea is that the NMDA-mediated calcium transients at large positive Δts show a high level of relative fluctuations (high coefficient of variation) since the effective number of activated NMDA receptors is small. It is shown that a low number of NMDA-Rs (~10) gives rise to a sufficient amount of variability to average out the second LTD window (Shouval and Kalantzis, 2005).

Adding features such as short-term depression, stochastic transmitter release, and BPAP depression/facilitation to calcium-based models allows to reproduce spike-triplet data of hippocampal and visual cortex neurons (Cai et al., 2007). The non-linearity of plasticity results between pre–post–pre and post–pre–post triplets is attributed in this model to the consecutive occurrence of either two presynaptic- or two postsynaptic spikes, respectively. Depending on the recovery dynamics of neurotransmitter release, release probability and the depression/facilitation dynamics of BPAPs, two successive presynaptic spikes (in pre–post–pre triplets) and two successive postsynaptic spikes (in post–pre–post triplets) can generate markedly different calcium dynamics leading to different plasticity results.

The class of models described in this section has been surprisingly successful in reproducing experimental results about spike-timing dependent plasticity, given the simplicity of the models. However, these models leave open the question of the mechanisms that translate a given calcium level into a particular synaptic change.

MODELS BASED ON CALCIUM DYNAMICS AND ABSTRACT READOUT SYSTEMS

We now turn to models that include additional dynamical variables driven by the calcium concentration. These phenomenological variables can be seen as calcium-sensitive "detectors" mediating LTP and LTD (Karmarkar et al., 2002; Abarbanel et al., 2003; Rubin et al., 2005; Badoual et al., 2006). Such phenomenological detectors are assumed to represent biological signaling pathways in an abstract fashion.

Both Karmarkar et al. (2002) and Badoual et al. (2006) account for STDP using distinct but converging dynamical variables modeling calcium- and mGluR (see section 'Models including biochemical signaling cascades beyond calcium')-activated pathways. In Badoual et al. (2006), an "LTP-mediating" enzyme is activated by large calcium transients (see **Figures 3A,B**). In contrast, LTD is evoked by the coincident activation of two enzymes, one activated by calcium and the other briefly activated by the presence of glutamate (see black dashed line in **Figure 3A**), potentially describing a mGluR-mediated signaling cascade. In turn, LTD occurs only when calcium is present at the time of the occurrence of the presynaptic spike, which is the case if the presynaptic spike is preceded by a BPAP (see **Figures 3A,B**). The model also accounts for plasticity results in response to pre–post–pre triplets in the visual cortex (Froemke and Dan, 2002). Karmarkar and Buonomano (2002) implement the calcium- and the mGluR pathway by assuming two functionally distinct calcium pools. In that view, calcium influx through VDCCs modulates the mGluR-mediated pathway leading to LTD induction, while calcium from NMDA-Rs is involved in LTP induction.

Abarbanel et al. (2003) propose a non-linear competition between two calcium-sensitive detectors to evoke LTP/LTD, that is, phosphorylation and dephosphorylation processes which relate to the α-amino-3-hydroxyl-5-methyl-4-isoxazole-propionate receptor (AMPA-R, see section 'Models including biochemical signaling cascades beyond calcium') conductance. The half activation concentrations of the two opposing processes (described by Hill functions) are chosen well above the calcium amplitudes of single pre- or postsynaptic transients (Abarbanel et al., 2003). In consequence and similar to the results of Shouval et al. (2002), plasticity results in response to spike-pair stimulation yield LTD for short negative Δ*t*s, LTP for short positive Δ*t*s, and a further LTD window for large positive Δ*t*s (compare with **Figure 2D**, Abarbanel et al., 2003).

Rubin et al. (2005) propose a "detector" system based on pathways resembling the CaMKII kinase-phosphatase system (see below), implementing three calcium-sensitive detectors ("P", "A", and "V", see **Figure 3C**). In that model, high, short-lasting calcium levels evoke LTP by activating a detector promoting the increase of synaptic weight ("P" in their model, see **Figures 3C,D**).

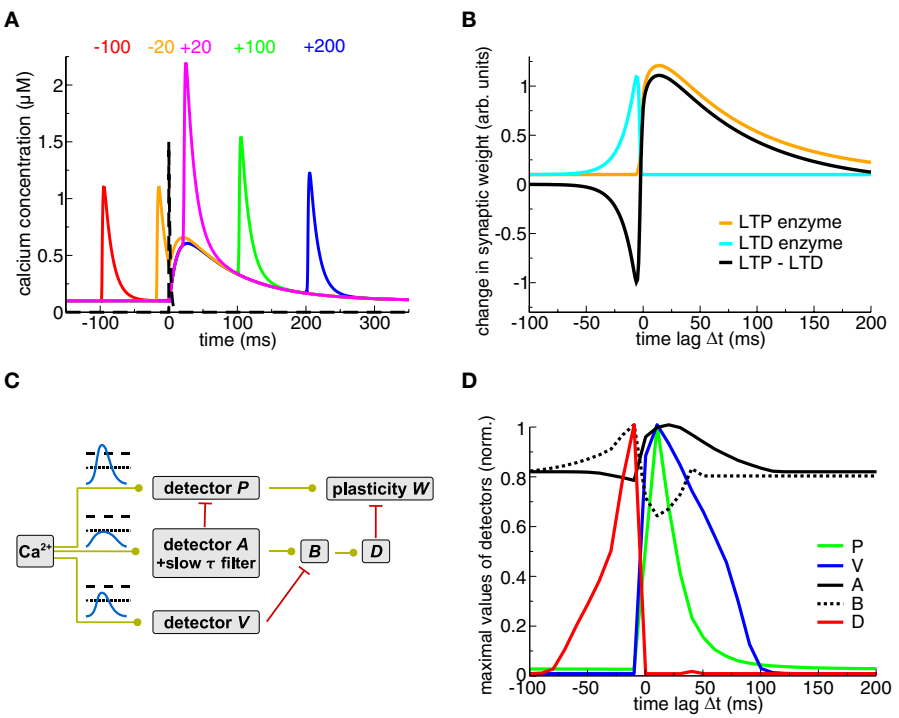

FIGURE 3 | Plasticity results based on phenomenological readout systems. **(A)** Calcium- and glutamate transients evoked by spike-pairs for five different Δ*t*s. The calcium transients are identical to the ones in **Figure 1A.** The presynaptic spike occurs at $t = 0$ ms leading to the release of glutamate in the synaptic cleft (black dashed line, see Badoual et al., 2006 for details). **(B)** Schematic representation of the STDP curve from the biophysical models by Karmarkar et al. (2002) and Badoual et al. (2006). An "LTD enzyme" (cyan line) is activated by glutamate and calcium, e.g., it is represented here to be proportional to the calcium concentration at the occurrence of the presynaptic spike ($t = 0$ ms in panel **A**). An "LTP enzyme" (orange line) is activated by high calcium concentrations, e.g., it is represented here to be proportional to the maximal calcium concentration of spike-pair evoked transients. The total change in synaptic weight (black line) is the difference between both. See Karmarkar et al. (2002) and Badoual et al. (2006) for more details. **(C)** Phenomenological calcium detector system (Rubin et al., 2005). The three different detector systems respond to different calcium signals (illustrated in the panel, see text). The interactions of the detector cascades drive the evolution of the readout variable, the synaptic weight *W*. Green lines with circles denote activation of the target activity, and red lines with bars signify inhibition of the target. Adapted from Rubin et al. (2005). **(D)** Maximal detector levels with respect to Δ*t*. The maximal values of the detector variables (shown in **C**) over a spike-pair cycle is depicted. Note the resemblance of the "D" and "P" activation with the LTP and LTD enzyme activation, respectively, in panel **(B)**. Figure kindly provided by Jonathan Rubin (see Rubin et al., 2005 for more details).

Another detector builds up in response to low and prolonged calcium elevations (agent "A" and in turn "B") evoking LTD above a certain threshold. Importantly, intermediate calcium levels activate a "Veto" agent ("V") with a fast time constant providing fast tracking of the calcium transient. This veto mechanism suppresses the LTD induction pathway (**Figures 3C,D**). The dynamics of the "veto" mechanism prevents in particular the appearance of LTD for large positive Δts in response to spike-pair stimulation (see **Figure 3D** and Gerkin et al., 2010 for an in-depth review of the model).

The models discussed here indicate that synaptic changes combine in a highly non-linear fashion in between spike-pairs and are most likely not a result of piecewise, linear additions of changes evoked by single spike-pairs. Attention should be drawn to the fact that in all the models discussed so far, the time constant of the synaptic variable has to become essentially infinite at resting calcium concentration for the evoked synaptic changes not to decay after the presentation of the stimulation protocol. In the presence of noise and/or finite time constants, such models cannot maintain the evoked synaptic changes in a stable manner. This is in contrast to the models described in the next section, in which bistability leads naturally to maintenance of the evoked synaptic state.

MODELS INCLUDING BIOCHEMICAL SIGNALING CASCADES BEYOND CALCIUM

Several specific biochemical pathways have been shown to be involved in induction and maintenance of long-term synaptic modifications. We briefly list experimental evidence emphasizing the role of the CaMKII kinase-phosphatase system in synaptic plasticity. We also discuss another line of experimental studies suggesting that synaptic changes are binary all-or-none transitions. We then turn to review biochemical models investigating the dynamics of the CaMKII system. We point out that such models generally exhibit bistability suggesting the CaMKII system to be involved in both induction and maintenance of synaptic changes. See Kotaleski and Blackwell (2010) for a more general review of modeling approaches of the molecular mechanisms underlying LTP and LTD.

PROTEIN SIGNALING CASCADES LINKING CALCIUM TRANSIENTS TO SYNAPTIC CHANGES: EXPERIMENTAL DATA

The postsynaptic calcium signal activates a multitude of calcium-responsive signaling cascades that have been identified to mediate or modulate LTP/LTD induction and expression as well as learning and memory (see review by Malenka and Bear, 2004). Here, we review three key pathways mediating long-term changes in hippocampal CA3–CA1 synapses: (i) the CaMKII-dependent cascade, (ii) the cyclic adenosine monophosphate (cAMP)-dependent protein kinase A (PKA) cascade, (iii) and the calcineurin cascade. See **Figure 4** for a schematic depiction of the biochemical pathways. Note that we limit the discussion to the biochemistry involved in spike-timing dependent plasticity at the Schaffer collateral – CA1 neuron synapse. Although synaptic plasticity in other systems rely on different induction pathways and expression mechanisms (e.g., in the cerebellum, Hansel et al., 2006), the CA3–CA1 synapse exhibits characteristics which are shared by other glutamatergic excitatory synapses throughout the mammalian brain, including the cerebral cortex (Kirkwood et al., 1993).

Calcium/calmodulin-dependent protein kinase II

In its basal state, the enzymatic activity of the CaMKII towards target proteins is extremely low. Regulation of intracellular calcium levels allows the neuron to link neural activity with the phosphorylation level of CaMKII. CaMKII activation is governed by calcium/calmodulin (Ca^{2+}/CaM) binding and is prolonged beyond fast-decaying calcium transients by its autophosphorylation (Fink and Meyer, 2002). Autophosphorylation of CaMKII at the autoregulatory domain occurs after calcium/calmodulin binding to two neighboring subunits in the CaMKII holoenzyme ring and enables the enzyme to remain autonomously active after dissociation of calcium/calmodulin (Hanson and Schulman, 1992). See reviews by Hudmon and Schulman (2002) and Griffith (2004) for more details of the regulation of CaMKII activity.

In its activated state, CaMKII is reversibly translocated to a postsynaptic density (PSD)-bound state where it interacts with multiple LTP related partners structurally organizing protein anchoring assemblies (Shen and Meyer, 1999; Hayashi et al., 2000; Fink and Meyer, 2002; Lisman et al., 2002; Colbran, 2004). The direct phosphorylation of the AMPA receptor GluR1 subunit by CaMKII enhances AMPA channel function (Mammen et al., 1997; Derkach et al., 1999), and drives AMPA receptors into synapses (Hayashi et al., 2000; see also review article by Lisman et al., 2002). Mutated mice lacking the ability of CaMKII autophosphorylation exhibit profound deficits in hippocampus-dependent learning and memory and also completely fail to exhibit LTP induction in the hippocampal CA1 subfield under standard stimulation protocols (Giese et al., 1998). Furthermore, LTP induction in the hippocampus via spike-timing stimulation protocols is blocked in the presence of KN-62, a specific blocker of CaMKII which binds to the enzyme and blocks the activation by calcium/calmodulin (Wang et al., 2005).

The role of CaMKII beyond induction of synaptic long-term modifications remains controversial. Enzymatic activity of CaMKII decreases to baseline within ~15 min after LTP induction (Lengyel et al., 2004). This is in agreement with recent findings indicating that autonomous CaMKII activity is not required for LTP maintenance or for memory storage/retrieval *in vivo* (Buard et al., 2010). In contrast, Sanhueza et al. (2007) show that a non-competitive inhibitor of CaMKII can reverse LTP suggesting that a component of synaptic memory maintenance is attributable to CaMKII in CA1 synapses.

Cyclic adenosine monophosphate-dependent protein kinase A

The cAMP-dependent PKA cascade is thought to mediate synapse to nucleus signaling and seems to initiate synthesis of proteins and RNA during the late phase of LTP induction in the hippocampal area CA1 (on time scales > 1 h; Abel et al., 1997; Nguyen and Kandel, 1997). These studies suggest that the early phase of LTP induction and basal synaptic transmission are not affected by cAMP–PKA inactivation. In hippocampus to prefrontal cortex connections however, LTP induction is accompanied by a rapid increase in PKA activity during the early phase (Jay et al., 1998). Also for the CA3–CA1 pathway, LTP induction by high-frequency stimulations can be blocked by inhibiting postsynaptic cAMP–PKA in contrast to the experimental results above (Blitzer et al., 1995, 1998). The requirement of PKA for LTP induction can be overcome

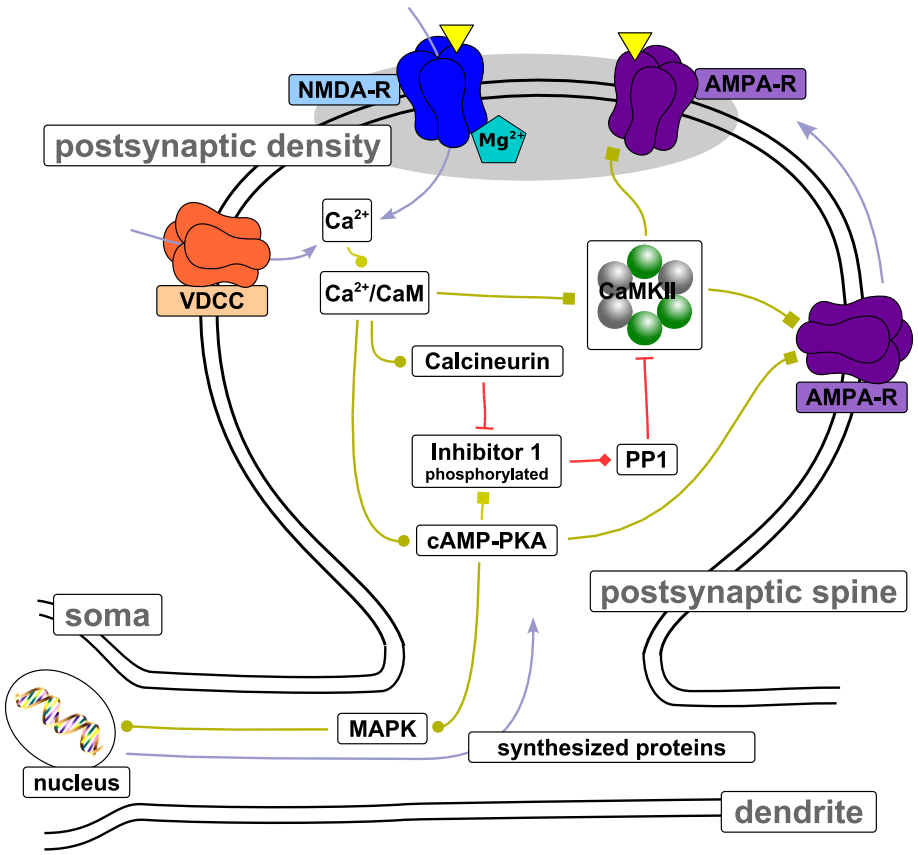

FIGURE 4 | Protein signaling cascades involved in LTP/LTD. The figure shows biochemical pathways that have been identified to be involved in LTP/LTD induction and maintenance at the Schaffer collateral – CA3 neuron synapse. Light blue arrows indicate transport of the corresponding entity. Light green connections indicate stimulation of target activity. Squares at the end of light green connections indicate that the stimulation is due to phosphorylation of the target. Red connections depict inhibition of target activity through dephosphorylation (indicated by a bar at the end of the connection) or binding (indicated by the diamond at the end of the connection). The yellow triangles illustrate neurotransmitter binding to receptors located in the postsynaptic density. Note that the spatial proportions between spine, dendrite, and soma are not preserved. See text for more details.

by direct inhibition of postsynaptic phosphatases (Blitzer et al., 1995), suggesting that PKA gates LTP by blocking/or competing with protein phosphatases (see below).

The calcium-sensitivity of the PKA pathway relies upon calcium/calmodulin-initiated conversion of adenosine triphosphate into cAMP by adenylyl cyclase (Cooper et al., 1995). Elevation of cAMP, in turn, activates the cAMP-dependent PKA (Carr et al., 1992; Glantz et al., 1992). Stimulating this pathway by increasing the adenylyl cyclase activity is shown to induce LTP in hippocampal slices without the requirement for any electrical stimulation, an effect that can be blocked with PKA inhibitors (Frey et al., 1993). Similarly, overexpression of adenylyl cyclase in transgenic mice enhances LTP and learning (Wang, 2004). Though PKA directly phosphorylates the AMPA receptor GluR4 subunit, both PKA activity and CaMKII activity are necessary to incorporate AMPA-Rs into the cell membrane (Esteban et al., 2003).

The signaling cascade continues towards the nucleus through the mitogen-activated protein kinase (MAPK). PKA activates this enzyme after hippocampus-dependent learning in mice. Furthermore, MAPK inhibitors block the maintenance of LTP (Waltereit and Weller, 2003; Sweatt, 2004). This cascade targets the cAMP-responsive element-binding protein (CREB) in the nucleus and therefore governs the expression of LTP/memory effector proteins (Bozon et al., 2003; Chen et al., 2003). These results indicate that this branch of the cAMP-dependent signaling cascade plays a key role during the late phase of LTP most likely accompanied by altered gene expression (Goelet et al., 1986; Alberini et al., 1995).

Calcineurin

Experimental results indicate that the sign of hippocampal synaptic plasticity is regulated by the balance between protein phosphorylation and dephosphorylation mediated by PKA and calcineurin, respectively. Consistent with this idea, overexpression of calcium/calmodulin-dependent calcineurin in the forebrain of transgenic mice is found to impair an intermediate and PKA-dependent phase of LTP, as well as the transition from short- to long-term memory and memory retrieval (Mansuy et al., 1998; Winder et al., 1998). On the other hand, inhibition of calcineurin activity facilitates LTP *in vitro* and *in vivo* in a PKA-dependent manner (Malleret et al., 2001). Consistent with these findings, LTD evoked during STDP stimulation by post–pre spike-pairs is blocked in the presence of calcineurin inhibitors while the same blockade unmasks potentia-

tion for spike-triplets (Wang et al., 2005). Similar results are found for presynaptic stimulation protocols of varying frequencies inducing LTD at low (1 –10 Hz) and LTP at high frequencies (10 –100 Hz) in control conditions (O'Connor et al., 2005a). A kinase inhibitor (inhibiting CaMKII and protein kinase C) blocks LTP and reveals LTD for 1 –100 Hz stimulation protocols. On the other hand, a phosphatase inhibitor (blocking protein phosphatase 1, PP1, and protein phosphatase 2A) prevents LTD for intermediate stimulation frequencies (1 –10 Hz) but leaves LTP induction unchanged at high stimulation frequencies (> 10 Hz; O'Connor et al., 2005a).

The results discussed so far suggest that the kinase and the phosphatase pathways interact at one or several points in the signaling cascade. A possible converging point of the cAMP–PKA and the calcineurin pathways is inhibitor 1 (I1, see **Figure 4**). Evidence for the role of I1 as a point of convergence is: (i) Hippocampal LTD induction involves calcium/calmodulin-dependent calcineurin dephosphorylating I1 (Mulkey et al., 1994), (ii) Synaptic stimulation that induces cAMP-dependent LTP raises the amount of phosphorylated I1 in the CA1 region (Blitzer et al., 1998). This increase is dependent on PKA activity since it is blocked by PKA inhibitors. Phosphorylated I1 is a specific blocker of PP1 (Ingebritsen and Cohen, 1983). Hence, the differential calcium-dependent activation of the calcineurin and the cAMP–PKA pathway is expressed in the phosphorylation level of I1 which in turn inhibits PP1 in its phosphorylated state. During the induction of hippocampal LTD, the inactivation of I1 through dephosphorylation increases PP1 activity (Mulkey et al., 1994). Disruption of PP1 binding to synaptic targeting proteins is reported to block synaptically evoked LTD but does not affect basal synaptic transmission in CA1 pyramidal cells. PP1 has no direct access to synaptic AMPA-Rs, but it is the only phosphatase able to dephosphorylate CaMKII in the PSD (Strack et al., 1997).

Which molecular pathways underlie spike-timing dependent plasticity in other brain areas? LTD seems to involve retrograde signaling to the presynaptic terminal in the visual and the somatosensory cortex (Sjöström et al., 2003; Nevian and Sakmann, 2006). Both postsynaptic calcium elevations mediated by VDCCs as well as the activation of mGluRs are necessary for such LTD induction. An application of a mGluR antagonist results in a complete block of LTD but has no effect on the calcium transients (Nevian and Sakmann, 2006). This block of LTD is attributable to the disruption of the G-protein coupled cascade involving retrograde endocannabinoid signaling (Piomelli, 2003; Sjöström et al., 2003, 2004; Nevian and Sakmann, 2006). Calcium in turn modulates the efficiency of the G-protein coupled phospholipase C-dependent pathway which synthesizes endocannabinoids (Hashimotodani et al., 2005; Maejima et al., 2005). Note that a mGluR- and postsynaptic calcium-dependent form of LTD has also been found at the Schaffer collateral – CA1 synapse (Stanton et al., 1991; Bolshakov and Siegelbaum, 1994; Otani and Connor, 1998). The simultaneous presence of two seemingly independent LTD-inducing pathways, that is, a mGluR- and a PP1-dependent cascade, at Schaffer collateral – CA1 synapses sparks ongoing debates (Lisman, 2009). Some of the controversy might be settled in light of a recent study showing that in contrast to PP1-dependent LTD (Debanne et al., 1996), multiple converging Schaffer collateral inputs are required for the induction of mGluR-dependent LTD in a CA1 pyramidal cell (Fan et al., 2010).

More proteins have been suggested to be related to LTP/LTD, such as protein kinase C, phosphatidylinostiol 3-kinase, tyrosine kinase Src to name just a few of them (see reviews by Bliss and Collingridge, 1993; Malenka and Bear, 2004). Apart for the pathways involving CaMKII and associated proteins, the signal transduction pathways involved in triggering long-term synaptic changes remain elusive with many potential players but few definite answers about specific roles in induction and maintenance mechanisms.

NATURE OF SYNAPTIC CHANGES – EXPERIMENTAL EVIDENCE FOR BISTABLE SYNAPSES IN THE HIPPOCAMPUS

We now turn to experiments which address the nature of synaptic changes and suggest that these changes are switch-like all-or-none transitions, consistent with a bistable system.

In experiments on long-term synaptic modifications, LTP (resp. LTD) refers to a long-lasting increase (resp. decrease) of the EPSP recorded at the soma of the postsynaptic neuron after the stimulation protocol. LTP/LTD protocols typically involve the stimulation of a large number of afferents – the recorded signals and changes in EPSP size stem therefore from an ensemble of synapses and reflect properties of a compound signal. For this reason, most of the plasticity experiments provide no insights into the nature of synaptic changes at the single-synapse level. A few plasticity experiments at the Schaffer collateral – CA1 synapse address the question whether synaptic strength changes occur in an analog or a digital manner (Petersen et al., 1998; O'Connor et al., 2005b). In other words, is the size of the EPSP at the level of a single synapse changing continuously or can it take specific values only (despite the variability due to neurotransmitter release, diffusion, and channel opening)? If the latter is true, can the synapse take two, three, or more states? In the most simple case of two stable states, the synaptic efficacy can be considered a binary variable in the long-term.

Experiments by Petersen et al. (1998) and O'Connor et al. (2005b) address this question using a minimal stimulation technique on Schaffer collateral – CA1 connections, whose aim is to evoke single-synapse responses (Raastad, 1995; Bolshakov and Siegelbaum, 1995; Stevens and Wang, 1995; Isaac et al., 1996). The excitatory postsynaptic current (EPSC) size increases abruptly during the LTP stimulation protocol and decreases abruptly during the LTD protocol (**Figure 5A**, O'Connor et al., 2005b). Applying statistical tests to this change in EPSC size leads the authors to the conclusion that the changes are all-or-none, sudden switch-like events, taking place on the time scale of seconds (O'Connor et al., 2005b). They show furthermore that these events saturate synapses to full potentiation or depression. That means that once a synapse got potentiated it cannot be potentiated a second time, but the potentiation can be reversed by a subsequent LTD induction protocol. Accordingly, a second LTD induction protocol cannot decrease EPSC size further suggesting that the investigated synapse has two stable states, that is, the synapse is binary. Results obtained by Petersen et al. (1998) on potentiation of putative single-synapses reach the same conclusion, but LTD induction has not been considered in this study. Bagal et al. (2005) use glutamate uncaging paired with brief postsynaptic depolarization and report long-lasting potentiation of single dendritic spines in hippocampal CA1 cells. This potentiation shares many features with conventional LTP such as a dependence on NMDA activation and the ability to

be reversed, or depotentiated, in a NMDA-R-dependent manner by low-frequency stimulus trains. Again, potentiation was expressed in a stepwise, all-or-none manner.

These experimental results suggest that synapses can be described as occupying two states of low- or high transmission efficacy (see **Figure 5B**). These states can be termed DOWN and UP states, respectively. In that framework, LTP corresponds to a transition from the DOWN to the UP state, while LTD corresponds to a transition from the UP to the DOWN state. This implies that potentiation or depression observed in experiments involving stimulation of ensembles of synapses are a combination of multiple step-like events of single synapses. LTP (resp. LTD) experiments on such an ensemble start from a mixture of states and can either partially or maximally potentiate (resp. depress) all connections (O'Connor et al., 2005b). Therefore, smooth plasticity curves (such as STDP curves) can be obtained through averaging over multiple synapses of otherwise discrete single synaptic changes (Appleby and Elliott, 2005).

A key mechanism proposed for the expression of LTP involves an increase in the number of functional AMPA-Rs in the plasma membrane (see reviews by Malenka and Nicoll, 1999; Malinow and Malenka, 2002) or the phosphorylation state of AMPA-Rs (Benke et al., 1998; Lee et al., 2000, 2003; see also review by Soderling and Derkach, 2000) or both. Consequently, binary changes would imply that synaptic changes always involve a cluster of AMPA receptors, inserted all at once in the membrane (see scheme in **Figure 5B** and review by Lisman, 2003). Note that the number of AMPA receptors in the PSD of a spine is believed to vary from none for silent synapses to around 50 (Kennedy, 2000).

As a means of information storage, graded synaptic changes (Bienenstock et al., 1982; Oja, 1982) are more susceptible to drift due to biochemical noise (e.g., protein turnover) and ongoing neural activity than all-or-none binary changes (see, e.g., discussion in Petersen et al., 1998). Thus synaptic discreteness might help to make information storage in a neural network robust. However, we should emphasize that the experiments described in this section are limited to time scales on the order of minutes. On longer time scales, step-like changes of synaptic strength might give way to events like altered gene expression that may take a more continuous character.

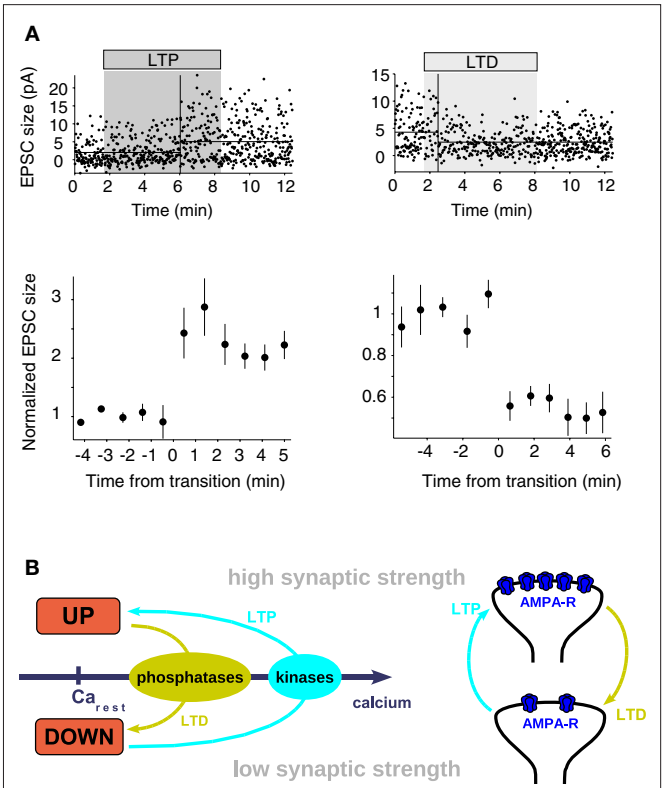

FIGURE 5 | The bistable synapse. (A) Unitary plasticity events take place in single, reversible steps. The depicted synaptic changes are measured in hippocampal CA1 neurons in response to minimal stimulation of the Schaffer collateral pathway. Putative single-synapse responses (EPSCs) recorded before, during (shaded region) and after the LTP (above, left-hand side) and the LTD (above, right-hand side) stimulation protocol are shown as a function of time. To illustrate the immediate step-like transitions 10-response bins are grouped and aligned with respect to the point of transition at $t = 0$ min for the LTP (below, left-hand side) and the LTD (below, right-hand side) event (figure adapted from O'Connor et al., 2005b). **(B)** Scheme of a bistable synapse. A bistable synapse exhibits two stable states – DOWN and UP – at resting calcium levels, i.e., transitions between both states are not possible (or happen with vanishingly low probability) at resting calcium levels. The UP and the DOWN states are characterized by high and low synaptic strength, respectively. Since intracellular calcium elevations are a necessary and sufficient signal to induce LTP and LTD, transitions from the DOWN to the UP state (LTP, cyan arrows) supposedly occur during high amplitude calcium transients, while transitions from the UP to the DOWN state (LTD, light green arrows) occur if the system is exposed to moderate calcium concentrations for a long time (left panel). Low and high calcium transients activate protein phosphatases and protein kinases, respectively, whose activation switch the system between the UP and the DOWN states. The two discrete states are likely expressed by different numbers of functional AMPA receptors in the membrane in the hippocampus (right panel). See text for more details.

BISTABLE MODELS BASED ON THE CaMKII KINASE – PHOSPHATASE SYSTEM

We now turn to review a line of modeling research addressing the issue of maintenance of the evoked synaptic state during the early phase of LTP/LTD. The mathematical studies presented here show that detailed biochemical models of protein networks often exhibit bistability and therefore behave as bistable switches. Positive feedback loops are at the origin of such switches which express in the simplest form two stable states. Those stable states are proposed to maintain evoked synaptic states beyond stimulation protocols.

As outlined above, the expression of plasticity involves multiple molecular players. Molecules, however, have a short lifetime of the order of minutes to days, whereas some memories can be retained for years. Despite the fact that long-term modifications involve structural reorganization, altered gene transcription and new protein synthesis in the late phase (see review by Malenka and Bear, 2004), the question remains how the induced state can be preserved by a machinery involving a limited number of proteins in the presence of protein turnover. Here, we also discuss models which show that bistable switches formed by an ensemble of proteins can recruit newly synthesized proteins to adopt a particular "stored" state and thus retain state information despite molecular turnover.

The problem of synaptic stability is first noted by Crick (1984) who suggests that cooperative interactions among proteins can overcome the problem of molecular turnover for long-term memory. The idea of a molecular switch storing information beyond

protein lifetime is further developed by Lisman (1985). By using known enzymatic reactions, he shows in a simple mathematical model that a kinase can exist in two stable states: a unphosphorylated "off" state and a phosphorylated "on" state. Transitions from "off" to "on" can be induced by another phosphorylating kinase and the evoked state acts autocatalytically to sustain the phosphorylation level and to phosphorylate downstream kinases. Reverse transitions could be induced by phosphatase activity. The first candidate protein proposed to be at the origin for such a switch is the CaMKII. Theoretical studies in the late 1980s show that the complex holoenzyme composed of 12 subunits can exhibit a switch-like behavior due to calcium-independent autophosphorylation even in the presence of phosphatase activity and of protein turnover (Lisman and Goldring, 1988).

We now turn to the description of a specific mathematical model of CaMKII autophosphorylation/dephosphorylation behavior (Zhabotinsky, 2000, see also Okamoto and Ichikawa, 2000 for a closely related model). This model shows that the CaMKII protein can exhibit a bistable phosphorylation behavior in a range of calcium concentrations. It includes crucial biochemical details of calcium-triggered autophosphorylation and dephosphorylation of the CaMKII protein: (i) initial and subsequent phosphorylation steps are calcium–calmodulin dependent; (ii) subsequent phosphorylation steps are facilitated due to the increase in calcium/calmodulin affinity of a phosphorylated subunit and the fact that a phosphorylated subunit stays active as catalyst for the autophosphorylation reaction (see section 'Protein signaling cascades linking calcium transients to synaptic changes: experimental data' and Hudmon and Schulman, 2002); and (iii) the dephosphorylation of CaMKII subunits by PP1 is implemented according to the Michaelis–Menten scheme (Michaelis and Menten, 1913). These features lead to three steady-states of the CaMKII phosphorylation level in a range of calcium concentrations: a stable weakly phosphorylated steady-state (i.e., a DOWN state), a stable highly phosphorylated state (i.e., an UP state) and an intermediate unstable fixed-point (see **Figure 6B**). This unstable steady-state separates the basins of attraction of the two stable steady-states. The range of bistability is shown to potentially include the resting calcium concentration, providing stability of UP and DOWN states at resting conditions.

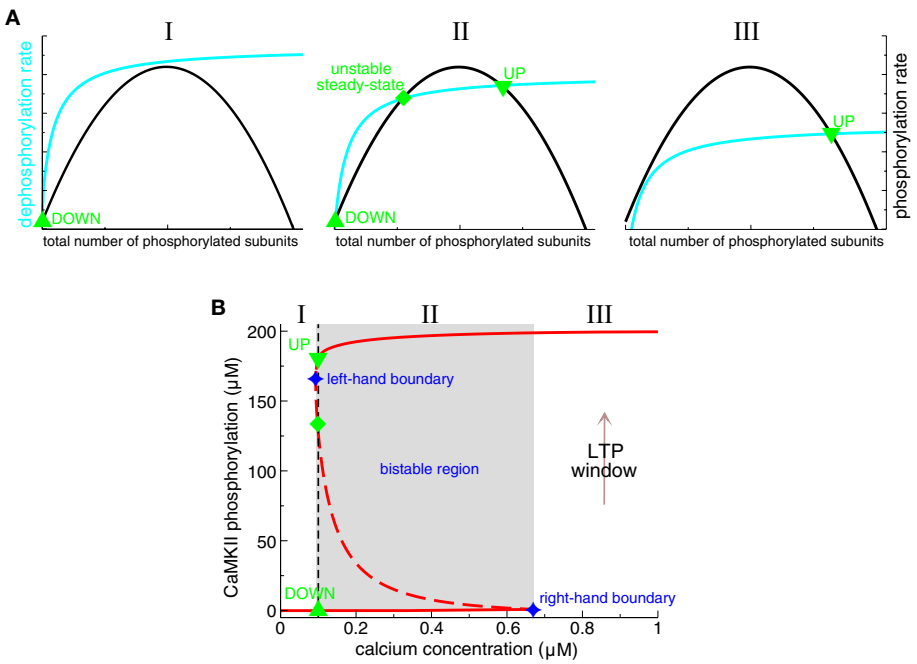

FIGURE 6 | Bistability of the CaMKII phosphorylation level. (A) Total phosphorylation (black lines) and dephosphorylation rates (cyan lines) illustrating the steady-states of the system. The overall phosphorylation and dephosphorylation rates are shown as functions of the total number of phosphorylated subunits of CaMKII holoenzymes. The intersection points of both rates characterize balanced phosphorylation and dephosphorylation and mark the steady-states of the system. Depending on the relative position of both curves, there can be either a single stable steady-state present (I and III), or three steady-states (II). When three steady-states are present, two of them are stable (an "UP" state with a high phosphorylation level, and a "DOWN" state with low phosphorylation level) and the intermediate steady-state is unstable. (I) only the DOWN state is stable when dephosphorylation is strong, and/or phosphorylation is weak (left-hand panel), (II) bistability occurs if phosphorylation and dephosphorylation are balanced (middle panel), (III) the UP state is the only stable state if dephosphorylation is weaker than phosphorylation (right-hand panel). Note that the dephosphorylation rate saturates and the phosphorylation rate vanishes at high total phosphorylation levels. See text for more details. **(B)** Concentration of phosphorylated CaMKII subunits as a function of calcium in detailed biochemical models (Okamoto and Ichikawa, 2000; Zhabotinsky, 2000). In such models, the phosphorylation level of the CaMKII exhibits a bistable behavior. That is, two stable phosphorylation states – a weakly and a highly phosphorylated state – exist in a range of calcium (region II, middle panel in **A**, Ca∈[0.094,0.67] μM, gray area, adapted from Zhabotinsky, 2000). Stable steady-states are depicted by full red lines and unstable fixed points by the dashed line. UP to DOWN transitions occur below the left-hand boundary of this bistable region (region I), and DOWN to UP transition are evoked if the system is exposed during a sufficiently long interval to calcium concentrations higher than the right-hand boundary of the bistable region ("LTP window", region III). In Zhabotinsky (2000) the bistable region includes the calcium resting concentration Ca_0 = 0.1 μM. Reproduced from Zhabotinsky (2000).

What is the mechanism of the bistability in the phosphorylation behavior of CaMKII subunits? This question can be answered by inspecting the total rates of autophosphorylation and dephosphorylation of CaMKII subunits. **Figure 6A** shows schematically how both rates vary as a function of the total number of phosphorylated subunits. The intersection points, the points where the total autophosphorylation rate balances the total dephosphorylation rate, mark the three steady-states of the system (**Figure 6A**, middle panel). The left- and the right-hand steady-states are stable and the middle one is unstable. Two criteria are necessary for these three intersection points to emerge: (i) The total dephosphorylation rate has to saturate at high phosphorylation levels (see cyan lines in **Figure 6A**). Such a saturation naturally occurs if dephosphorylation is described according to the Michaelis–Menten scheme, which is valid if the enzyme (PP1) is present in small amounts compared to the substrate (phosphorylated subunits). (ii) The cooperativity of autophosphorylation is at the origin of the bump-like behavior of the total autophosphorylation rate. Subsequent phosphorylation in the ring is faster than the initial autophosphorylation rate since only a single calcium/calmodulin complex is required as compared to two for the initiation step (Hudmon and Schulman, 2002). Without this facilitation of autophosphorylation, the total rate would stay constant with increasing number of phosphorylated CaMKII subunits and the three intersection points with the dephosphorylation rate could not be realized. In summary, the saturation of the phosphatase activity dephosphorylating CaMKII combined with the cooperativity of the autophosphorylation rate yields the bistability of the CaMKII phosphorylation level.

These mathematical models have a number of limitations. First, they are strictly speaking valid only in the limit of a large number of interacting molecules. Only a relatively small number of CaMKII proteins are however present in a typical PSD – of the order 50 –100 holoenzymes (Harris and Stevens, 1989; Hanson and Schulman, 1992; McNeill and Colbran, 1995; Doi et al., 2005). Furthermore, the average lifetime of a single CaMKII protein is about 30 h independently of its phosphorylation state (Ehlers, 2003). This raises the question of the stability of the CaMKII switch with respect to stochastic fluctuations induced by protein turnover. Miller et al. (2005) investigate this question using the model of Zhabotinsky (2000), and show that the CaMKII switch composed of a realistic number of CaMKII protein is stable for years even in the presence of protein turnover, phosphatase as well as free calcium fluctuations.

Second, the localization of CaMKII is not restricted to the PSD, but translocation and diffusive exchange between the PSD and the cytosol create an ongoing flux (Shen and Meyer, 1999; Shen et al., 2000; Sharma et al., 2006). This raises the question of how these exchanges affect the stability of the CaMKII switch. Hayer and Bhalla (2005) investigate both the stability of the CaMKII switch and the insertion of AMPA receptors in the presence of protein trafficking and turnover. Besides the bistability of the CaMKII phosphorylation level, they identify an independent AMPA receptor switch based on self-recruitment of receptors into the synapse (Ehlers, 2000; Esteban et al., 2003). Depending on whether both switches function completely independently, or tightly coupled determines if three or two stable states exist in such a system, respectively. The average lifetime of such switches depends on the coupling and ranges from 24 h to more than a year (Hayer and Bhalla, 2005). The existence of a second switch besides CaMKII ensuring the maintenance of AMPA receptors in the membrane could be a means to maintain the evoked synaptic state on longer time scales. This is a crucial issue since CaMKII enzymatic activity decreases to baseline within ~15 min after LTP induction (Lengyel et al., 2004; see above).

Finally, several experimental studies have shown that in some cases LTD is not a simple reversal of previously evoked LTP (termed depotentiation) but rather involves separate biochemical mechanisms (Zhuo et al., 1999, see also section 'Protein signaling cascades linking calcium transients to synaptic changes: experimental data'). To account for these experimental results, there should be at least three states available to the synapse: a "basal state", a potentiated state, and a depressed state. Depotentiation would correspond to the transition from potentiated to basal, while LTD would be the transition from basal to depressed. Pi and Lisman (2008) propose a model which accounts for bidirectional changes starting from a basal state of the synapse. They demonstrate that the coupling of a kinase (e.g., CaMKII) and a phosphatase switch (e.g., protein phosphatase 2 A, PP2A) could give rise to tristability of the synapse. Both switches stably maintain the induction of LTP and LTD through respective autocatalytic reactions (compare with Lisman, 1985). The phosphatase switch is proposed to be based on PP2A since LTD induction results in persistent activation of the PP2A (Thiels et al., 1998).

STDP IN CaMKII-BASED BISTABLE MODELS

Using the knowledge about biochemical pathways involved in the induction of synaptic changes and the existence of bistability in such networks, two recent studies have investigated STDP in CaMKII-based models (Graupner and Brunel, 2007; Urakubo et al., 2008). These two studies describe known protein signaling cascades providing the link between the calcium level and the phosphorylation level of the CaMKII protein (see **Figure 4**), whose phosphorylation level exhibits bistability. In addition, Urakubo et al. (2008) describe AMPA receptor trafficking which translates CaMKII bistability into bistable synaptic conductance since AMPA-Rs are clustered in the PSD through phosphorylation by CaMKII.

The calcium control hypothesis (**Figure 2A**) implies no synaptic changes for resting and low calcium levels, LTD at intermediate calcium levels and LTP induction at high calcium elevations. These three functionally different calcium regions translate for a bistable system into the following three criteria: (i) UP and DOWN states should exist at resting and low levels of calcium. This requirement assures the stability of the evoked synaptic state under resting conditions and activity which does not lead to considerable calcium accumulations. (ii) Prolonged, intermediate calcium elevations should move the system from the UP to the DOWN state. Such transitions would take place in the range of calcium levels typically present in response to LTD stimulation protocols. Starting from the DOWN state, no transition should occur. Note that such a "LTD region" does not exist in Zhabotinsky (2000) and Okamoto and Ichikawa (2000) (compare **Figure 6B**). (iii) Repetitive exposures to high calcium levels should move the system from the DOWN to the UP state. Such a transition conforms to a LTP event occurring

in response to fast and high calcium transients ("LTP window" in **Figure 6B**). In contrast, no transition should occur in such conditions if the system resides initially in the UP state.

Realistic calcium transients evoked by spike-pairs with short positive Δ*t*s move the CaMKII system from the weakly to the highly phosphorylated state, that is, LTP occurs corresponding to criterion (iii) above (**Figures 8B,C**) (Graupner and Brunel, 2007; Urakubo et al., 2008). In both models, such high calcium transients boost CaMKII autophosphorylation and inhibit PP1 activity dephosphorylating the CaMKII protein (**Figure 8A**). High calcium concentrations have previously been shown to move the CaMKII system from the DOWN to the UP state (Okamoto and Ichikawa, 2000; Zhabotinsky, 2000, see "LTP window" **Figure 6B**).

In addition, both Graupner and Brunel (2007) and Urakubo et al. (2008) show that the parameters of the protein signaling cascade can be set such that there is a region at intermediate calcium levels within which the CaMKII moves from the UP to the DOWN state (see **Figure 7C**, region II). That region, called "LTD-window", emerges from an elevation in active PP1 which in turn stems from the calcium-dependent activation of the calcineurin pathway (see section 'Protein signaling cascades linking calcium transients to synaptic changes: experimental data and **Figure 7**). Importantly, calcium transients in response to spike-pairs with short negative Δ*t*s are shown to amplify PP1 activity leading to LTD transitions, which corresponds to criterion (ii) above (**Figures 8A,B**) (Graupner and Brunel, 2007).

Both studies show that STDP plasticity results can be accounted for (at least on short time scales, see Obs. 1 in **Figure 8C**) if the balance between calcineurin- and cAMP–PKA activation results in high PP1 activity for post–pre pairs and low PP1 activity together with strong autophosphorylation for pre–post pairs (**Figure 8A**) (Graupner and Brunel, 2007; Urakubo et al., 2008). The studies differ however in the way how that differential response is obtained. Graupner and Brunel (2007) demonstrate that the activation of the calcineurin pathway at intermediate calcium concentrations and of the cAMP–PKA pathway at high calcium concentrations

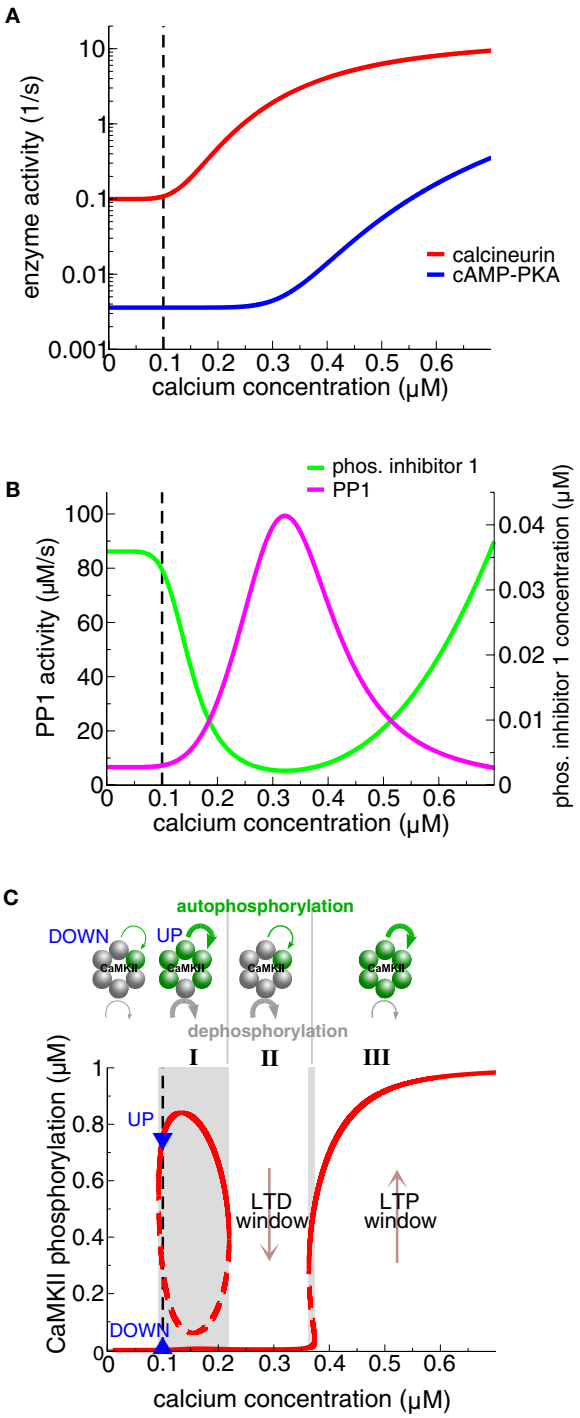

FIGURE 7 | Steady-states of the protein signaling cascade and the CaMKII phosphorylation level exhibiting bistability and an "LTD window". (A) Calcineurin and cAMP–PKA activities as a function of calcium. The model assumes that the calcineurin pathway activates at moderate calcium levels, while the cAMP–PKA pathway activates at high calcium levels. See **Figure 4** for a depiction of the signaling cascades. **(B)** Phosphorylated I1 and PP1 activities as a function of calcium. The activation of the calcineurin pathway at intermediate calcium levels promotes I1 dephosphorylation (green line) and in turn activation of PP1 activity (magenta line). Activation of the cAMP–PKA pathway at high calcium levels promotes I1 phosphorylation and thereby PP1 inhibition. The differential activation of calcineurin vs. cAMP–PKA gives therefore rise to a peak of PP1 activity at intermediate calcium levels. **(C)** Steady-states of the phosphorylated CaMKII subunit concentration and the autophosphorylation – dephosphorylation balance as functions of calcium. The upper row illustrates rings of six functionally coupled subunits of the CaMKII holoenzyme. A gray subunit stands for dephosphorylated and a green one for phosphorylated. The green and the gray curved lines indicate calcium-dependent autophosphorylation and PP1-mediated dephosphorylation, respectively. Their width corresponds to the strength of the respective process in the three different calcium regions (I, II, and III). At low calcium levels, including the calcium resting level (region I), autophosphorylation and dephosphorylation balance each other at two different CaMKII phosphorylation levels, giving rise to bistability at resting calcium (Ca_0 = 0.1 μM, lower panel). The PP1 activity dephosphorylating CaMKII has a peak at intermediate calcium levels (magenta line in panel **B**). As a result, the UP state loses stability, leaving the weakly phosphorylated state as the only stable steady-state in region II ("LTD window"). The PP1 dephosphorylation activity is suppressed and autophosphorylation is strong at high calcium levels ("LTP window", region III). Consequently, the highly phosphorylated state is the only stable state of the CaMKII system in region III. The resting calcium concentration is indicated by the dashed black line in all panels. Figures are adapted from Graupner and Brunel (2007).

is sufficient to obtain the STDP curve (**Figures 7A and 8B**). They show in particular that the stronger cAMP–PKA pathway activation due to higher calcium elevations for large positive Δt protocols acts like a realistic veto preventing LTD transitions to occur in this range (compare **Figures 3C,D**, and Rubin et al., 2005). In contrast, Urakubo et al. (2008) suggest time-difference sensitive allosteric kinetics of the NMDA receptor to be at the origin of STDP results. Based on experimental data, they include the suppression of NMDA-R-mediated currents by calcium/calmodulin binding in their model (Ehlers et al., 1996; Rycroft and Gibb, 2004). In order to achieve a timing-dependent suppression of NMDA-Rs, they assume that calcium/calmodulin suppresses rapidly glutamate-unbound NMDA-Rs but suppresses slowly the glutamate-bound NMDA-R. This allosteric model leads to inhibition of calcium influx for post–pre pairs activating PP1, and boosts calcium influx for pre–post pairs resulting in PKA activation in conjunction with CaMKII autophosphorylation (**Figure 8A**). Urakubo et al. (2008) show furthermore that their allosteric model predicts correctly the direction of synaptic plasticity in response to spike-triplet and -quadruplet stimulation as obtained in the visual cortex (Froemke and Dan, 2002).

The shape of the STDP results in response to spike-pair stimulation in bistable models depends on the initial distribution of synapses across UP and DOWN states. All synapses are initially in the DOWN state and no noise is present in the model by Urakubo et al. (2008). Their long-term plasticity results are therefore discrete showing deterministic DOWN to UP transitions for pre–post pairs with short Δts (**Figure 8C**, Obs. 2). Graupner and Brunel (2007) assume an equal initial occupation of UP and DOWN states, that is, 50% of the synapses are initially in the UP and 50% in the DOWN state. Together with noisy calcium transients, they obtain smooth STDP results reflecting stochastic transitions for pre–post and post–pre pairs with short time differences (**Figure 8B**). Note that O'Connor et al. (2005b) find that 71 ± 11% of Schaffer collateral-CA1 synapses could potentiate or were unable to depress,

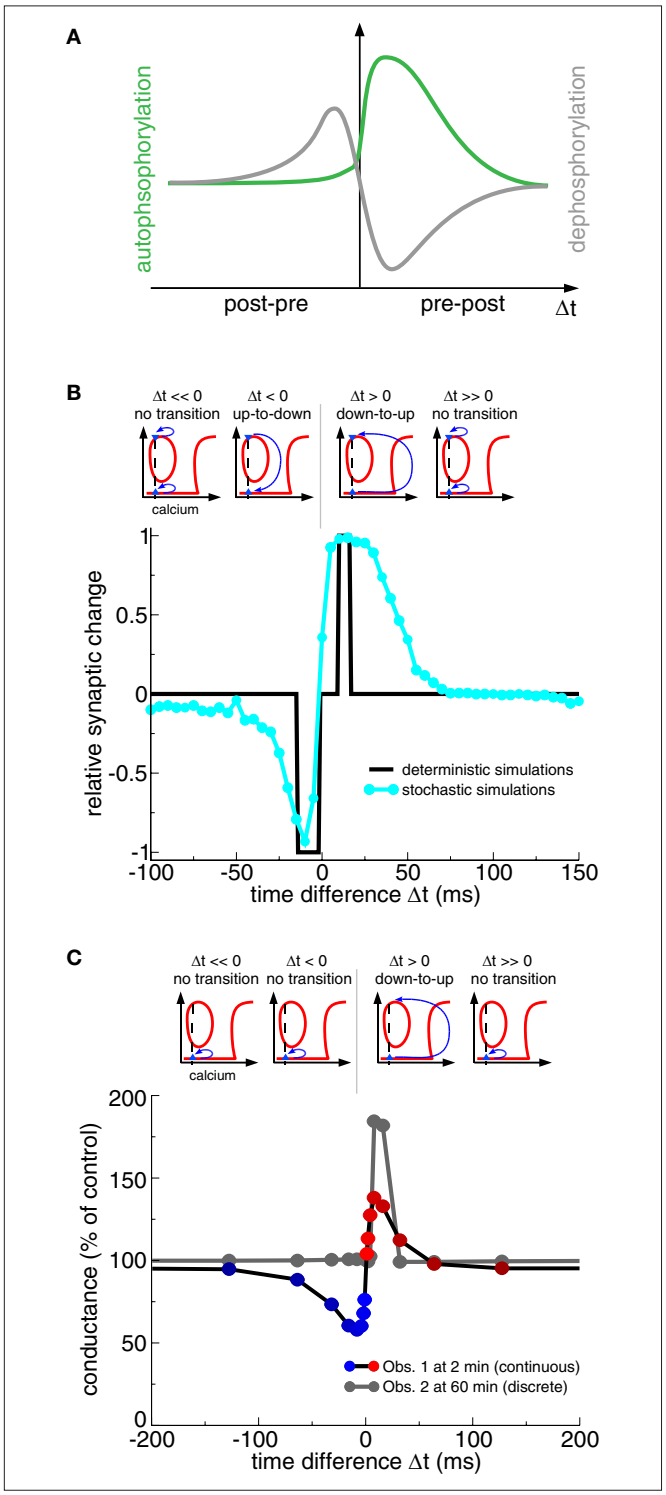

FIGURE 8 | Transition dynamics of the CaMKII phosphorylation level in response to the STDP protocol as a function of Δt. (A) The total level of PP1 activity after the presentation of a pre- and postsynaptic spike-pair as a function of Δt (gray line), and the maximal rate of phosphorylation of a CaMKII subunit for the same protocol (green line). Note the resemblance of the PP1 activity and the phosphorylation rate as a function Δt to the activity of the "LTD" and the "LTP" enzymes in **Figure 3B,** and to the "P" and "D" activation in **Figure 3D**, respectively. Adapted from Graupner and Brunel (2007). **(B)** CaMKII transition behavior in response to the STDP stimulation protocol (Graupner and Brunel, 2007). Bidirectional transitions between the DOWN and the UP states in response to calcium transients evoked by the STDP stimulation protocol are illustrated in the upper row. Up-to-down transitions occur when PP1 activity is high and autophoshorylation reaches moderate levels (see panel **A**) which is the case when $\Delta t < 0$ (lower panel). $\Delta t > 0$ stimulation protocols yield large calcium elevations which strongly activate autophosphorylation and suppress PP1 activity (see panel **A**) evoking down-to-up transitions (lower panel). The CaMKII transition results are summarized in the lower panel for stimulation with deterministic calcium transients (black line) and noisy calcium transients (cyan line). Results adapted from Graupner and Brunel (2007). **(C)** CaMKII transition behavior in response to the STDP stimulation protocol (Urakubo et al., 2008). As in **(B)** transitions between the DOWN and the UP state in response to STDP stimulation are illustrated in the upper row. Note that all CaMKII proteins are initially in the DOWN state (blue triangle). As a result, only down-to-up transitions are observed for short positive Δts, despite the fact that the steady-states of the phosphorylated CaMKII also exhibit a "LTD window" (compare with **Figure 7C**). Spike-timing dependent synaptic conductance changes are shown at 2 min (Obs. 1) and at 60 min (Obs. 2) after the onset of stimulation (lower panel). Synaptic changes show a continuous character right after the deterministic stimulation protocols (Obs. 1), while the changes are discrete on the long run due to bistability (Obs. 2). Results adapted from Urakubo et al. (2008).

and 29 ± 11% of the synapses could depress or were unable to potentiate, suggesting that synapses initially occupy both states but with unequal probabilities.

In summary, the CaMKII system can reproduce experimentally observed transition behavior in response to the STDP spike-pair stimulation protocol. The bistability of the CaMKII kinase – phosphatase system allows furthermore to stably maintain the evoked state.

BI/MULTISTABLE MODELS BASED ON ALTERNATIVE MECHANISMS

The models discussed so far generate bistability through the properties of the CaMKII kinase – phosphatase system. However, other potential mechanisms giving rise to bistability have been described in recent years, and we discuss them shortly in this section. We also mention models with more than two stable states – three in practice. In such models, multistability is generated through coupling of several bistable switches.

The CaMKII kinase – phosphatase system discussed so far is only a part of the extensive protein signaling network at the synapse (Bhalla and Iyengar, 1999). Bhalla and Iyengar (1999) account for the convergence of mGluR- and NMDA-R-activated pathways based on known interactions involving a multiplicity of proteins (such as protein kinase C and MAPK, for example). It is shown that positive feedback loops in such protein networks give rise to bistability. In contrast to the studies outlined in the previous section, the intrinsic activation and the intrinsic enzymatic properties of single proteins are not resolved in Bhalla and Iyengar (1999) (the intersubunit autophosphorylation of CaMKII is not described at length, for example). Instead, two types of signal transmission mechanisms are implemented: (i) protein–protein interactions as well as enzymatic reactions such as protein phosphorylation and dephosphorylation; (ii) and protein degradation or production of intracellular messengers.

Castellani et al. (2009) describe the two step phosphorylation cycle of AMPA receptors using enzymatic Michaelis–Menten equations. Phosphorylation steps occur through PKA and CaMKII activity and both dephosphorylation steps are mediated by PP1, the concentration of which are used as input variables of the system. The non-linearity of the Michaelis–Menten description endows the system with bistability depending on the CaMKII concentration. The receptor exists in the dephosphorylated state only at low CaMKII concentrations; in its phosphorylated state at high CaMKII concentrations; and can exist in both states at intermediate CaMKII levels. Castellani et al. (2009) use furthermore a stochastic formulation of their phosphorylation scheme to investigate the stability of the states at low receptor numbers and in the presence of noise.

Similarly, Delord et al. (2007) propose a one-step phosphorylation cycle of a substrate "*S*" (e.g., synaptic AMPA-Rs). Phosphorylation and dephosphorylation are mediated by kinases and phosphatases, respectively, and their respective rates are calcium-dependent. The maintenance of plastic modifications relies on negligible reaction rates in basal conditions, that is, the de- and phosphorylation rates are on the order of 1/month at resting calcium concentrations. Moreover, Delord et al. (2007) show that information coding and memory maintenance are robust to stochastic fluctuations in their model.

The late phase of LTP involves the synthesis of new proteins (Frey et al., 1988; Kang and Schuman, 1996). Aslam et al. (2009) demonstrate that self-sustained regulation of translation can form a bistable synaptic switch that persistently regulates the onsite synthesis of plasticity-related proteins. In particular, they model the CaMKII – cytoplasmic polyadenylation element-binding protein (CPEB1) molecular loop which stably increases the local CaMKII concentration at the potentiated synapse. Protein–protein interactions are implemented based on standard Michaelis–Menten-type kinetics in that approach.

The phosphorylation of the AMPA receptor by CaMKII enhances synaptic AMPA channel function (Mammen et al., 1997; Derkach et al., 1999; Hayashi et al., 2000). Hayer and Bhalla (2005) show that the combination of a CaMKII- and a AMPA receptor switch can lead to tri- or bistability, depending on whether both switches function completely independently, or tightly coupled, respectively. The independent AMPA receptor switch in that model is based on self-recruitment of receptors into the synapse (see discussion of the Hayer and Bhalla, 2005 model at the end of section 'Bistable models based on the CaMKII kinase – phosphatase system'). Similarly, Pi and Lisman (2008) obtain tristability through coupling of a bistable kinase- and a bistable phosphatase switch (see discussion of Pi and Lisman, 2008 at the end of section 'Bistable models based on the CaMKII kinase – phosphatase system').

Another possibility for bistability to arise is the modulation of trafficking rates due to local clustering of receptors in the synaptic membrane (Shouval, 2005). Contrary to the approaches described above, the stability of synaptic efficacies stems from local interactions between individual receptors within a single synapse in that model. This leads to metastable states that can outlast the lifetime of individual receptors, thus providing a mechanism for long-term maintenance of bidirectional synaptic changes.

Besides the existence of bi- and multistability, the question whether experimental stimulation protocols known to induce LTP/LTD evoke transitions between the stable steady-states has not been tested in these models.

DISCUSSION

We reviewed here biophysical models describing how pre- and postsynaptic activity patterns can translate into changes of synaptic efficacy and how those changes can be maintained persistently. We compared several classes of models that incorporate an increasing amount of biological details. A first class of models are based on calcium dynamics, with the possible addition of "readout" variables that translate information contained in the local calcium transients into experimentally observed plasticity results. Those models account for induction of STDP, but leave open the question of the maintenance of synaptic changes over long time scales. A second class of models include explicitly specific protein signaling cascades present at the synapse. These models typically feature bistability, which allows them to stably maintain evoked synaptic changes over long-time scales. Furthermore, several models belonging to this class have been shown recently to be able to reproduce experimentally observed STDP results.

The studies discussed here share a number of common features. Pathways decreasing synaptic strength (e.g., protein phosphatases) activate at intermediate calcium levels, while pathways increasing synaptic strength (e.g., protein kinases) activate at high calcium levels. This is embodied in the calcium control hypothesis (**Figure 2A**) but it is not sufficient to account for STDP experiments

that do not see a second LTD range at positive Δts (see **Figure 2**). Models with effectively three calcium-triggered pathways ("P", "A", and "V" detectors in Rubin et al., 2005; calcineurin, cAMP–PKA, direct CaMKII phosphorylation pathways in Graupner and Brunel, 2007) or with the inclusion of converging pathways other than calcium (mGluR-mediated pathways in Karmarkar and Buonomano, 2002 and Badoual et al., 2006; allosteric kinetics of NMDA receptors in Urakubo et al., 2008) have been proposed to yield LTD at short negative Δts and LTP at short positive Δts only.

The detailed biophysical models discussed here predict that synapses should have a small number of stable states (two in the simplest case). Whether synapses are bistable or not is a controversial issue. At first sight, it seems difficult to accept the idea of a binary system on the basis of recorded synaptic changes, which show a continuous character in most experiments (Dudek and Bear, 1992; Bi and Poo, 1998; Ngezahayo et al., 2000). However, continuous changes can be reconciled with binary individual synapses, if one takes into account stochasticity inherent in synaptic processes and the fact that stimulation protocols typically comprise ensembles of synapses (Appleby and Elliott, 2005; Graupner and Brunel, 2007). The all-or-none potentiation behavior, which one would expect from a bistable synapse, can therefore only be revealed during stimulation of single synapses (Petersen et al., 1998; Bagal et al., 2005; O'Connor et al., 2005b). Bistability has been observed experimentally in a number of distinct biochemical systems (Degn, 1968; Naparstek et al., 1974; Eschrich et al., 1980; Frenzel et al., 1995). It allows to durably store information in a noisy environment in which a continuous variable would progressively deteriorate due to ongoing perturbations.

One implication of bistability at the level of a single synapse is that LTP is the reversal of LTD and vice versa. Experimentalists have however reported several types of decrease in synaptic strength. LTD (decrease of efficacy from "basal" strength) and depotentiation (decrease of efficacy after potentiation) have been considered to be two distinct processes. Some of the differences between the two can be reconciled in bistable models by considering that a "basal" condition is likely to be a mix of synapses in the UP and the DOWN state. In CA3–CA1 hippocampal synapses, 71% of synapses seem to be initially in the DOWN state, and the remaining 29% in the UP state (O'Connor et al., 2005b). This difference in UP and DOWN state occupations gives in principle rise to a higher probability to evoke LTP than LTD. Furthermore, a LTD protocol will decrease synaptic strength by provoking up-to-down transitions in some synapses that were initially in the UP state. On the other hand, the initial conditions are different in depotentiation protocols because a larger fraction of the synapses are in the UP state. However, some studies indicate that depotentiation and LTD might operate through different molecular mechanisms (Zhuo et al., 1999; Lee et al., 2000; Jouvenceau et al., 2003). More complex models than the ones discussed here would be necessary to account for these experimental data with respect to induction and maintenance of synaptic changes (see discussion of Pi and Lisman, 2008 at the end of section 'Bistable models based on the CaMKII kinase – phosphatase system').

The CaMKII-based models discussed here suggest that the signaling cascades involved in the early phase of LTP/LTD (<60 min) also maintain the evoked synaptic changes on the long run via bistability. Another possibility for stable memory storage could be that the protein synthesis mechanisms recruited during the late phase of LTP/LTD (Krug et al., 1984; Frey et al., 1988) are bistable (see Aslam et al., 2009), while the early mechanisms triggering those changes are not. Such a possibility has been investigated in models of synaptic tagging and capture (Clopath et al., 2008; Barrett et al., 2009). These models account for the synapse-specific capturing of plasticity-related proteins that are synthesized in the cell body and globally available. In both models, the consolidation mechanism involved in the late phase of synaptic plasticity exhibits bistability (or quasi-bistability through very slow time scales in Barrett et al., 2009).

All the models presented here focus on STDP outcomes evoked with spike-pairs. Few of these studies address plasticity results in response to spike-triplets or -quadruplets (Rubin et al., 2005; Badoual et al., 2006; Urakubo et al., 2008), and none of those investigate the rate dependence of STDP results, i.e., how do plasticity results change if the frequency of the spike-pair presentation is varied (see Sjöström et al., 2001; Wittenberg and Wang, 2006). It remains to be shown that the proposed signaling cascades account for experimental plasticity results obtained with all these distinct stimulation protocols. Furthermore, it remains to be elucidated how differences in the underlying biochemical machinery at a synapse give rise to different plasticity results in different brain areas in response to a given stimulation protocol (e.g. compare STDP results obtained in the hippocampus: Magee and Johnston, 1997; Bi and Poo, 1998; the cortex: Markram et al., 1997; Sjöström et al., 2001; or a cerebellum-like structure Bell et al., 1997, for example). Biophysically detailed models can help to obtain insights into such differences by elucidating which component of the models is related to which property of the plasticity outcome. Finally, one future challenge for such synapse models remains to investigate synaptic plasticity in response to naturalistic activity patterns occurring *in vivo*.

All the studies discussed here focus on the direction and amplitude of synaptic changes. To our knowledge, none of the studies has investigated the underlying temporal dynamics of synaptic changes in detail. O'Connor et al. (2005b) report that synaptic changes are sudden switch-like events, taking place on the time scale of seconds. LTP transitions occur on average 1.3 min after the onset of the stimulation protocol and LTD transitions on average after 3.1 min (O'Connor et al., 2005b). In the experiments of Bagal et al. (2005), the step-like potentiation event occurs ≈38 s after the pairing pulse and when it occurs it is expressed in less than 10 s. How can the underlying protein signaling cascades give rise to such temporal dynamics? What defines how many presentations of a certain stimulation pattern are required to evoke a transition? That also relates to the question of how synaptic changes are summed up across individual stimulation patterns? Continuing effort from experimentalists and modelers is required to answer those questions, which relate to the underlying time course of learning in the intact brain.

The models reviewed here account for protein signaling cascades local to one synapse. However, CaMKII, for example, is actively translocated to the PSD upon synaptic activation (Strack et al., 1997; Schulman, 2004; Merrill et al., 2005). Experiments show furthermore that spines are not biochemically isolated compart-

ments but interact with each other in an activity-dependent manner (Harvey et al., 2008). As a result, LTP at individual synapses reduces the threshold for potentiation at neighboring synapses (Harvey and Svoboda, 2007). How competition or positive feedback between synapses can lead to sparse or clustered plasticity models of memory storage on single dendritic branches remains to be addressed in the models outlined here.

We reviewed here biophysical models of single synapses. A challenge for future modeling studies is to insert such synaptic dynamics in networks, in order to understand how they affect network dynamics and how they allow networks to durably store information provided by external inputs. A prerequisite for such an endeavor would be to derive simplified models (i.e., described by the smallest possible number of variables) that keep the main qualitative features of the biophysically detailed models (i.e., bistability, ability to reproduce plasticity outcomes seen in experiment). Work in this direction is in progress (Graupner and Brunel, in preparation).

An interesting question is whether and how the emerging synaptic connectivity patterns in such models will be different from studies implementing phenomenological spike-based learning rules based on spike-pairs or -triplets (reviewed in Morrison et al., 2008). Such investigations should further advance our understanding of the role of synaptic plasticity in shaping the spatio-temporal dynamics of recurrent networks and thereby memory formation.

ACKNOWLEDGMENTS

We would like to thank Wulfram Gerstner for encouraging us to write a review paper. MG was partly supported by grants from the National Institutes of Health (DC005787-01A1), the Deutscher Akademischer Austausch Dienst (DAAD), the Ministère des Affaires étrangères du Gouvernement Français, the Agence Nationale de la Recherche (ANR) Neurosciences, and the Centre National de la Recherche Scientifique (CNRS). NB was supported by ANR grants ANR-05-NEUR-030 and ANR-08-SYSC-005.

REFERENCES

Abarbanel, H. D. I., Gibb, L., Huerta, R., and Rabinovich, M. (2003). Biophysical model of synaptic plasticity dynamics. *Biol. Cybern.* 89, 214–226.

Abbott, L., and Nelson, S. (2000). Synaptic plasticity: taming the beast. *Nat. Neurosci.* 3(Suppl.) 1178–1183.

Abel, T., Nguyen, P. V., Barad, M., Deuel, T. A., Kandel, E. R., and Bourtchouladze, R. (1997). Genetic demonstration of a role for PKA in the late phase of LTP and in hippocampus-based long-term memory. *Cell* 88, 615–626.

Abraham, W. C., and Robins, A. (2005). Memory retention–the synaptic stability versus plasticity dilemma. *Trends Neurosci.* 28, 73–78.

Alberini, C. M., Ghirardi, M., Huang, Y. Y., Nguyen, P. V., and Kandel, E. R. (1995). A molecular switch for the consolidation of long-term memory: cAMP-inducible gene expression. *Ann. N.Y. Acad. Sci.* 758, 261–286.

Appleby, P. A., and Elliott, T. (2005). Synaptic and temporal ensemble interpretation of spike-timing-dependent plasticity. *Neural Comput.* 17, 2316–2336.

Artola, A., and Singer, W. (1987). Long-term potentiation and NMDA receptors in rat visual cortex. *Nature* 330, 649–652.

Aslam, N., Kubota, Y., Wells, D., and Shouval, H. Z. (2009). Translational switch for long-term maintenance of synaptic plasticity. *Mol. Syst. Biol.* 5, 284.

Badoual, M., Zou, Q., Davison, A. P., Rudolph, M., Bal, T., Frégnac, Y., and Destexhe, A. (2006). Biophysical and phenomenological models of multiple spike interactions in spike-timing dependent plasticity. *Int. J. Neural Syst.* 16, 79–97.

Bagal, A. A., Kao, J., P. Y., Tang, C.-M., and Thompson, S. M. (2005). Long-term potentiation of exogenous glutamate responses at single dendritic spines. *Proc. Natl. Acad. Sci. U.S.A.* 102, 14434–14439.

Barrett, A. B., Billings, G. O., R. Morris, G. M., and van Rossum, M. C. W. (2009). State based model of long-term potentiation and synaptic tagging and capture. *PLoS Comput. Biol.* 5:1, e1000259. doi:10.1371/journal.pcbi.1000259.

Bear, M. F., Press, W. A., and Connors, B. W. (1992). Long-term potentiation in slices of kitten visual cortex and the effects of NMDA receptor blockade. *J. Neurophysiol.* 67, 841–851.

Bell, C., Han, V., Sugawara, Y., and Grant, K. (1997). Synaptic plasticity in a cerebellum-like structure depends on temporal order. *Nature* 387, 278–281.

Bender, V. A., Bender, K. J., Brasier, D. J., and Feldman, D. E. (2006). Two coincidence detectors for spike timing-dependent plasticity in somatosensory cortex. *J. Neurosci.* 26, 4166–4177.

Benke, T. A., Lüthi, A., Isaac, J. T., and Collingridge, G. L. (1998). Modulation of AMPA receptor unitary conductance by synaptic activity. *Nature* 393, 793–797.

Bhalla, U., and Iyengar, R. (1999). Emergent properties of networks of biological signaling pathways. *Science* 283, 381–387.

Bi, G., and Poo, M. (1998). Synaptic modifications in cultured hippocampal neurons: dependence on spike timing, synaptic strength, and postsynaptic cell type. *J. Neurosci.* 18, 10464–10472.

Bi, G. Q., and Wang, H. X. (2002). Temporal asymmetry in spike timing-dependent synaptic plasticity. *Physiol. Behav.* 77, 551–555.

Bienenstock, E. L., Cooper, L. N., and Munro, P. W. (1982). Theory for the development of neuron selectivity: orientation specificity and binocular interaction in visual cortex. *J. Neurosci.* 2, 32–48.

Billings, G., and van Rossum, M. C. W. (2009). Memory retention and spike-timing-dependent plasticity. *J. Neurophysiol.* 101, 2775–2788.

Bliss, T., and Collingridge, G. (1993). A synaptic model of memory: long-term potentiation in the hippocampus. *Nature* 361, 31–39.

Blitzer, R. D., Connor, J. H., Brown, G. P., Wong, T., Shenolikar, S., Iyengar, R., and Landau, E. M. (1998). Gating of CaMKII by cAMP-regulated protein phosphatase activity during LTP. *Science* 280, 1940–1942.

Blitzer, R. D., Wong, T., Nouranifar, R., Iyengar, R., and Landau, E. M. (1995). Postsynaptic cAMP pathway gates early LTP in hippocampal CA1 region. *Neuron* 15, 1403–1414.

Bolshakov, V. Y., and Siegelbaum, S. A. (1994). Postsynaptic induction and presynaptic expression of hippocampal long-term depression. *Science* 264, 1148–1152.

Bolshakov, V. Y., and Siegelbaum, S. A. (1995). Regulation of hippocampal transmitter release during development and long-term potentiation. *Science* 269, 1730–1734.

Bozon, B., Kelly, A., Josselyn, S. A., Silva, A. J., Davis, S., and Laroche, S. (2003). MAPK, CREB and Zif268 are all required for the consolidation of recognition memory. *Philos. Trans. R. Soc. Lond. B. Biol. Sci.* 358, 805–814.

Buard, I., Coultrap, S. J., Freund, R. K., Lee, Y.-S., Dell'Acqua, M. L., Silva, A. J., and Bayer, K. U. (2010). CaMKII "autonomy" is required for initiating but not for maintaining neuronal long-term information storage. *J. Neurosci.* 30, 8214–8220.

Cai, Y., Gavornik, J. P., Cooper, L. N., Yeung, L. C., and Shouval, H. Z. (2007). Effect of stochastic synaptic and dendritic dynamics on synaptic plasticity in visual cortex and hippocampus. *J. Neurophysiol.* 97, 375–386.

Carr, D. W., Stofko-Hahn, R. E., Fraser, I. D., Cone, R. D., and Scott, J. D. (1992). Localization of the cAMP-dependent protein kinase to the postsynaptic densities by A-kinase anchoring proteins. Characterization of AKAP 79. *J. Biol. Chem.* 267, 16816–16823.

Castellani, G. C., Bazzani, A., and Cooper, L. N. (2009). Toward a microscopic model of bidirectional synaptic plasticity. *Proc. Natl. Acad. Sci. U.S.A.* 106, 14091–14095.

Castro-Alamancos, M. A., Donoghue, J. P., and Connors, B. W. (1995). Different forms of synaptic plasticity in somatosensory and motor areas of the neocortex. *J. Neurosci.* 15, 5324–5333.

Chen, A., Muzzio, I. A., Malleret, G., Bartsch, D., Verbitsky, M., Pavlidis, P., Yonan, A. L., Vronskaya, S., Grody, M. B., Cepeda, I., Gilliam, T. C., and Kandel, E. R. (2003). Inducible enhancement of memory storage and synaptic plasticity in transgenic mice expressing an inhibitor of ATF4 (CREB-2) and C/EBP proteins. *Neuron* 39, 655–669.

Clopath, C., Ziegler, L., Vasilaki, E., Büsing, L., and Gerstner, W. (2008). Tag-trigger-consolidation: a model of early and late long-term-potentiation and depression. *PLoS Comput. Biol.* 4:12, e1000248. doi:10.1371/journal.pcbi.1000248.

Colbran, R. J. (2004). Targeting of calcium/calmodulin-dependent protein kinase II. *Biochem. J.* 378, 1–16.

Collingridge, G. L., Kehl, S. J., and McLennan, H. (1983). Excitatory amino acids in synaptic transmission in the schaffer collateral-commissural pathway of the rat hippocampus. *J. Physiol.* 334, 33–46.

Cooper, D., Mons, N., and Karpen, J. (1995). Adenylyl cyclases and the interaction between calcium and cAMP signalling. *Nature* 374, 421–424.

Crick, F. (1984). Memory and molecular turnover. *Nature* 312, 101.

Debanne, D., Gähwiler, B. H., and Thompson, S. M. (1996). Cooperative interactions in the induction of long-term potentiation and depression of synaptic excitation between hippocampal CA3-CA1 cell pairs *in vitro*. *Proc. Natl. Acad. Sci. U.S.A.* 93, 11225–11230.

Degn, H. (1968). Bistability caused by substrate inhibition of peroxidase in an open reaction system. *Nature* 217, 1047–1050.

Delord, B., Berry, H., Guigon, E., and Genet, S. (2007). A new principle for information storage in an enzymatic pathway model. *PLoS Comput. Biol.* 3: 6, e124. doi:10.1371/journal.pcbi.0030124.

Derkach, V., Barria, A., and Soderling, T. (1999). Ca^{2+}/calmodulin-kinase II enhances channel conductance of alpha-amino-3-hydroxy-5-methyl-4-isoxazolepropionate type glutamate receptors. *Proc. Natl. Acad. Sci. U.S.A.* 96, 3269–3274.

Doi, T., Kuroda, S., Michikawa, T., and Kawato, M. (2005). Inositol 1,4,5-trisphosphate-dependent Ca^{2+} threshold dynamics detect spike timing in cerebellar purkinje cells. *J. Neurosci.* 25, 950–961.

Dudek, S., and Bear, M. (1992). Homosynaptic long-term depression in area CA1 of hippocampus and effects of N-methyl-D-aspartate receptor blockade. *Proc. Natl. Acad. Sci. U.S.A.* 89, 4363–4367.

Ehlers, M. D. (2000). Reinsertion or degradation of AMPA receptors determined by activity-dependent endocytic sorting. *Neuron* 28, 511–525.

Ehlers, M. D. (2003). Activity level controls postsynaptic composition and signaling via the ubiquitin-proteasome system. *Nat. Neurosci.* 6, 231–242.

Ehlers, M. D., Zhang, S., Bernhadt, J. P., and Huganir, R. L. (1996). Inactivation of NMDA receptors by direct interaction of calmodulin with the NR1 subunit. *Cell* 84, 745–755.

Eschrich, K., Schellenberger, W., and Hofmann, E. (1980). *In vitro* demonstration of alternate stationary states in an open enzyme system containing phosphofructokinase. *Arch. Biochem. Biophys.* 205, 114–121.

Esteban, J. A., Shi, S.-H., Wilson, C., Nuriya, M., Huganir, R. L., and Malinow, R. (2003). PKA phosphorylation of AMPA receptor subunits controls synaptic trafficking underlying plasticity. *Nat. Neurosci.* 6, 136–143.

Fan, W., Ster, J., and Gerber, U. (2010). Activation conditions for the induction of metabotropic glutamate receptor-dependent long-term depression in hippocampal CA1 pyramidal cells. *J. Neurosci.* 30, 1471–1475.

Feldman, D. E. (2000). Timing-based LTP and LTD at vertical inputs to layer II/III pyramidal cells in rat barrel cortex. *Neuron* 27, 45–56.

Fink, C. C., and Meyer, T. (2002). Molecular mechanisms of CaMKII activation in neuronal plasticity. *Curr. Opin. Neurobiol.* 12, 293–299.

Frenzel, J., Schellenberger, W., and Eschrich, K. (1995). Bistability and damped oscillations in the fructose 6-phosphate/fructose 1,6-bisphosphate cycle in cell-free extracts from rat liver. *Biol. Chem. Hoppe Seyler* 376, 17–24.

Frey, U., Huang, Y. Y., and Kandel, E. R. (1993). Effects of cAMP simulate a late stage of LTP in hippocampal CA1 neurons. *Science* 260, 1661–1664.

Frey, U., Krug, M., Reymann, K. G., and Matthies, H. (1988). Anisomycin, an inhibitor of protein synthesis, blocks late phases of LTP phenomena in the hippocampal CA1 region *in vitro*. *Brain Res.* 452, 57–65.

Froemke, R. C., and Dan, Y. (2002). Spike-timing-dependent synaptic modification induced by natural spike trains. *Nature* 416, 433–438.

Gerkin, R. C., Bi, G.-Q., and Rubin, J. E. (2010). *Hippocampal Microcircuits: A Computational Modeler's Resource Book*, Vol. 5. Springer Series in Computational Neuroscience.

Giese, K., Fedorov, N., Filipkowski, R., and Silva, A. (1998). Autophosphorylation at Thr286 of the alpha calcium-calmodulin kinase II in LTP and learning. *Science* 279, 870–873.

Glantz, S. B., Amat, J. A., and Rubin, C. S. (1992). cAMP signaling in neurons: patterns of neuronal expression and intracellular localization for a novel protein, AKAP 150, that anchors the regulatory subunit of cAMP-dependent protein kinase II beta. *Mol. Biol. Cell* 3, 1215–1228.

Goelet, P., Castellucci, V. F., Schacher, S., and Kandel, E. R. (1986). The long and the short of long-term memory–a molecular framework. *Nature* 322, 419–422.

Graupner, M., and Brunel, N. (2007). STDP in a bistable synapse model based on CaMKII and associated signaling pathways. *PLoS Comput. Biol.* 3, 2299–2323. doi:10.1371/journal.pcbi.0030221.

Griffith, L. C. (2004). Regulation of calcium/calmodulin-dependent protein kinase II activation by intramolecular and intermolecular interactions. *J. Neurosci.* 24, 8394–8398.

Gustafsson, B., Wigström, H., Abraham, W. C., and Huang, Y. Y. (1987). Long-term potentiation in the hippocampus using depolarizing current pulses as the conditioning stimulus to single volley synaptic potentials. *J. Neurosci.* 7, 774–780.

Hahm, J. O., Langdon, R. B., and Sur, M. (1991). Disruption of retinogeniculate afferent segregation by antagonists to NMDA receptors. *Nature* 351, 568–570.

Hansel, C., de Jeu, M., Belmeguenai, A., Houtman, S. H., G. Buitendijk, H. S., Andreev, D., C. Zeeuw, I. D., and Elgersma, Y. (2006). alphaCaMKII is essential for cerebellar LTD and motor learning. *Neuron* 51, 835–843.

Hanson, P. I., and Schulman, H. (1992). Neuronal Ca^{2+}/calmodulin-dependent protein kinase. *Annu. Rev. Biochem.* 61, 559–601.

Harris, K. M., and Stevens, J. K. (1989). Dendritic spines of CA1 pyramidal cells in the rat hippocampus: serial electron microscopy with reference to their biophysical characteristics. *J. Neurosci.* 9, 2982–2997.

Harvey, C. D., and Svoboda, K. (2007). Locally dynamic synaptic learning rules in pyramidal neuron dendrites. *Nature* 450, 1195–1200.

Harvey, C. D., Yasuda, R., Zhong, H., and Svoboda, K. (2008). The spread of Ras activity triggered by activation of a single dendritic spine. *Science* 321, 136–140.

Hashimotodani, Y., Ohno-Shosaku, T., Tsubokawa, H., Ogata, H., Emoto, K., Maejima, T., Araishi, K., Shin, H.-S., and Kano, M. (2005). Phospholipase Cbeta serves as a coincidence detector through its Ca^{2+} dependency for triggering retrograde endocannabinoid signal. *Neuron* 45, 257–268.

Hayashi, Y., Shi, S. H., Esteban, J. A., Piccini, A., Poncer, J. C., and Malinow, R. (2000). Driving AMPA receptors into synapses by LTP and CaMKII: requirement for GluR1 and PDZ domain interaction. *Science* 287, 2262–2267.

Hayer, A., and Bhalla, U. S. (2005). Molecular switches at the synapse emerge from receptor and kinase traffic. *PLoS Comput. Biol.* 1:2, 137–154. doi:10.1371/journal.pcbi.0010020.

Hebb, D. (1949). *The Organization of Behavior: A Neurophysychological Theory*. New York: Wiley.

Hudmon, A., and Schulman, H. (2002). Neuronal Ca^{2+}/calmodulin-dependent protein kinase II: The role of structure and autoregulation in cellular function. *Annu. Rev. Biochem.* 71, 473–510.

Ingebritsen, T. S., and Cohen, P. (1983). Protein phosphatases: properties and role in cellular regulation. *Science* 221, 331–338.

Isaac, J. T., Hjelmstad, G. O., Nicoll, R. A., and Malenka, R. C. (1996). Long-term potentiation at single fiber inputs to hippocampal CA1 pyramidal cells. *Proc. Natl. Acad. Sci. U.S.A.* 93, 8710–8715.

Ismailov, I., Kalikulov, D., Inoue, T., and Friedlander, M. J. (2004). The kinetic profile of intracellular calcium predicts long-term potentiation and long-term depression. *J. Neurosci.* 24, 9847–9861.

Jaffe, D. B., Johnston, D., N. Lasser-Ross, Lisman, J. E., Miyakawa, H., and Ross, W. N. (1992). The spread of Na^{+} spikes determines the pattern of dendritic Ca^{2+} entry into hippocampal neurons. *Nature* 357, 244–246.

Jahr, C., and Stevens, C. (1990). A quantitative description of NMDA receptor-channel kinetic behavior. *J. Neurosci.* 10, 1830–1837.

Jay, T., Gurden, H., and Yamaguchi, T. (1998). Rapid increase in PKA activity during long-term potentiation in the hippocampal afferent fibre system to the prefrontal cortex *in vivo*. *Eur. J. Neurosci.* 10, 3302–3306.

Jouvenceau, A., Billard, J.-M., Haditsch, U., Mansuy, I. M., and Dutar, P. (2003). Different phosphatase-dependent mechanisms mediate long-term depression and depotentiation of long-term potentiation in mouse hippocampal CA1 area. *Eur. J. Neurosci.* 18, 1279–1285.

Kang, H., and Schuman, E. M. (1996). A requirement for local protein synthesis in neurotrophin-induced hippocampal synaptic plasticity. *Science* 273, 1402–1406.

Karmarkar, U. R., and Buonomano, D. V. (2002). A model of spike-timing dependent plasticity: one or two coincidence detectors? *J. Neurophysiol.* 88, 507–513.

Karmarkar, U. R., Najarian, M. T., and Buonomano, D. V. (2002). Mechanisms and significance of spike-timing dependent plasticity. *Biol. Cybern.* 87, 373–382.

Kennedy, M. (2000). Signal-processing machines at the postsynaptic density. *Science* 290, 750–754.

Kirkwood, A., Dudek, S. M., Gold, J. T., Aizenman, C. D., and Bear, M. F. (1993). Common forms of synaptic plasticity in the hippocampus and neocortex *in vitro*. *Science* 260, 1518–1521.

Koester, H. J., and Sakmann, B. (1998). Calcium dynamics in single spines during coincident pre- and postsynaptic activity depend on relative timing of back-propagating action potentials and subthreshold excitatory postsynaptic potentials. *Proc. Natl. Acad. Sci. U.S.A.* 95, 9596–9601.

Kotaleski, J. H., and Blackwell, K. T. (2010). Modelling the molecular mechanisms of synaptic plasticity

using systems biology approaches. *Nat. Rev. Neurosci.* 11, 239–251.

Kovalchuk, Y., Eilers, J., Lisman, J., and Konnerth, A. (2000). NMDA receptor-mediated subthreshold Ca^{2+} signals in spines of hippocampal neurons. *J. Neurosci.* 20, 1791–1799.

Krug, M., Lössner, B., and Ott, T. (1984). Anisomycin blocks the late phase of long-term potentiation in the dentate gyrus of freely moving rats. *Brain Res. Bull.* 13, 39–42.

Lee, H., Barbarosie, M., Kameyama, K., Bear, M., and Huganir, R. (2000). Regulation of distinct AMPA receptor phosphorylation sites during bidirectional synaptic plasticity. *Nature* 405, 955–959.

Lee, H.-K., Takamiya, K., Han, J.-S., Man, H., Kim, C.-H., Rumbaugh, G., Yu, S., Ding, L., He, C., Petralia, R. S., Wenthold, R. J., Gallagher, M., and Huganir, R. L. (2003). Phosphorylation of the AMPA receptor GluR1 subunit is required for synaptic plasticity and retention of spatial memory. *Cell* 112, 631–643.

Lengyel, I., Voss, K., Cammarota, M., Bradshaw, K., Brent, V., Murphy, K. P., Giese, S. J., Rostas, J. A., and Bliss, T. V. (2004). Autonomous activity of CaMKII is only transiently increased following the induction of long-term potentiation in the rat hippocampus. *Eur. J. Neurosci.* 20, 3063–3072.

Levy, W. B., and Steward, O. (1983). Temporal contiguity requirements for long-term associative potentiation/depression in the hippocampus. *Neuroscience* 8, 791–797.

Lisman, J. (1985). A mechanism for memory storage insensitive to molecular turnover: a bistable autophosphorylating kinase. *Proc. Natl. Acad. Sci. U.S.A.* 82, 3055–3057.

Lisman, J. (2003). Long-term potentiation: outstanding questions and attempted synthesis. *Philos. Trans. R. Soc. Lond. B. Biol. Sci.* 358, 829–842.

Lisman, J., Schulman, H., and Cline, H. (2002). The molecular basis of CaMKII function in synaptic and behavioural memory. *Nat. Rev. Neurosci.* 3, 175–190.

Lisman, J. E. (2009). The pre/post LTP debate. *Neuron* 63, 281–284.

Lisman, J. E., and Goldring, M. A. (1988). Feasibility of long-term storage of graded information by the Ca^{2+}/calmodulin-dependent protein kinase molecules of the postsynaptic density. *Proc. Natl. Acad. Sci. U.S.A.* 85, 5320–5324.

Lynch, G., Larson, J., Kelso, S., Barrionuevo, G., and Schottler, F. (1983). Intracellular injections of EGTA block induction of hippocampal long-term potentiation. *Nature* 305, 719–721.

Maejima, T., Oka, S., Hashimotodani, Y., T. Ohno-Shosaku, Aiba, A., Wu, D., Waku, K., Sugiura, T., and Kano, M. (2005). Synaptically driven endocannabinoid release requires Ca^{2+}-assisted metabotropic glutamate receptor subtype 1 to phospholipase Cbeta4 signaling cascade in the cerebellum. *J. Neurosci.* 25, 6826–6835.

Magee, J., and Johnston, D. (1997). A synaptically controlled, associative signal for Hebbian plasticity in hippocampal neurons. *Science* 275, 209–213.

Majewska, A., Brown, E., Ross, J., and Yuste, R. (2000). Mechanisms of calcium decay kinetics in hippocampal spines: role of spine calcium pumps and calcium diffusion through the spine neck in biochemical compartmentalization. *J. Neurosci.* 20, 1722–1734.

Malenka, R., and Nicoll, R. (1999). Long-term potentiation–a decade of progress? *Science* 285, 1870–1874.

Malenka, R. C., and Bear, M. F. (2004). LTP and LTD: an embarrassment of riches. *Neuron* 44, 5–21.

Malenka, R. C., Kauer, J. A., Zucker, R. S., and Nicoll, R. A. (1988). Postsynaptic calcium is sufficient for potentiation of hippocampal synaptic transmission. *Science* 242, 81–84.

Malinow, R., and Malenka, R. C. (2002). AMPA receptor trafficking and synaptic plasticity. *Annu. Rev. Neurosci.* 25, 103–126.

Malleret, G., Haditsch, U., Genoux, D., Jones, M., Bliss, T., Vanhoose, A., Weitlauf, C., Kandel, E., Winder, D., and Mansuy, I. (2001). Inducible and reversible enhancement of learning, memory, and long-term potentiation by genetic inhibition of calcineurin. *Cell* 104, 675–686.

Mammen, A. L., Kameyama, K., Roche, K. W., and Huganir, R. L. (1997). Phosphorylation of the alpha-amino-3-hydroxy-5-methylisoxazole4-propionic acid receptor GluR1 subunit by calcium/calmodulin-dependent kinase II. *J. Biol. Chem.* 272, 32528–32533.

Mansuy, I. M., Mayford, M., Jacob, B., Kandel, E. R., and Bach, M. E. (1998). Restricted and regulated overexpression reveals calcineurin as a key component in the transition from short-term to long-term memory. *Cell* 92, 39–49.

Markram, H., Lübke, J., Frotscher, M., and Sakmann, B. (1997). Regulation of synaptic efficacy by coincidence of postsynaptic APs and EPSPs. *Science* 275, 213–215.

McNeill, R. B., and Colbran, R. J. (1995). Interaction of autophosphorylated Ca^{2+}/calmodulin-dependent protein kinase II with neuronal cytoskeletal proteins. characterization of binding to a 190-kDa postsynaptic density protein. *J. Biol. Chem.* 270, 10043–10049.

Merrill, M. A., Chen, Y., Strack, S., and Hell, J. W. (2005). Activity-driven postsynaptic translocation of CaMKII. *Trends Pharmacol. Sci.* 26, 645–653.

Michaelis, L., and Menten, M. (1913). Die Kinetik der Invertinwirkung. *Biochem. Z.* 49, 333–369.

Miller, P., Zhabotinsky, A. M., Lisman, J. E., and Wang, X.-J. (2005). The stability of a stochastic CaMKII switch: dependence on the number of enzyme molecules and protein turnover. *PLoS Biol.* 3:4, e107. doi:10.1371/journal.pbio.0030107.

Mizuno, T., Kanazawa, I., and Sakurai, M. (2001). Differential induction of LTP and LTD is not determined solely by instantaneous calcium concentration: an essential involvement of a temporal factor. *Eur. J. Neurosci.* 14, 701–708.

Mooney, R., Madison, D. V., and Shatz, C. J. (1993). Enhancement of transmission at the developing retinogeniculate synapse. *Neuron* 10, 815–825.

Morris, R. G., Anderson, E., Lynch, G. S., and Baudry, M. (1986). Selective impairment of learning and blockade of long-term potentiation by an N-methyl-D-aspartate receptor antagonist, AP5. *Nature* 319, 774–776.

Morrison, A., Diesmann, M., and Gerstner, W. (2008). Phenomenological models of synaptic plasticity based on spike timing. *Biol. Cybern.* 98, 459–478.

Mulkey, R., Endo, S., Shenolikar, S., and Malenka, R. (1994). Involvement of a calcineurin/inhibitor-1 phosphatase cascade in hippocampal long-term depression. *Nature* 369, 486–488.

Naparstek, A., Romette, J. L., Kernevez, J. P., and Thomas, D. (1974). Memory in enzyme membranes. *Nature* 249, 490–491.

Neveu, D., and Zucker, R. S. (1996). Long-lasting potentiation and depression without presynaptic activity. *J. Neurophysiol.* 75, 2157–2160.

Nevian, T., and Sakmann, B. (2006). Spine Ca^{2+} signaling in spike-timing-dependent plasticity. *J. Neurosci.* 26, 11001–11013.

Ngezahayo, A., Schachner, M., and Artola, A. (2000). Synaptic activity modulates the induction of bidirectional synaptic changes in adult mouse hippocampus. *J. Neurosci.* 20, 2451–2458.

Nguyen, P. V., and Kandel, E. R. (1997). Brief theta-burst stimulation induces a transcription-dependent late phase of LTP requiring cAMP in area CA1 of the mouse hippocampus. *Learn. Mem.* 4, 230–243.

Nishiyama, M., Hong, K., Mikoshiba, K., Poo, M. M., and Kato, K. (2000). Calcium stores regulate the polarity and input specificity of synaptic modification. *Nature* 408, 584–588.

Nowak, L., Bregestovski, P., Ascher, P., Herbet, A., and Prochiantz, A. (1984). Magnesium gates glutamate-activated channels in mouse central neurones. *Nature* 307, 462–465.

O'Connor, D. H., Wittenberg, G. M., and Wang, S. S.-H. (2005a). Dissection of bidirectional synaptic plasticity into saturable unidirectional processes. *J. Neurophysiol.* 94, 1565–1573.

O'Connor, D. H., Wittenberg, G. M., and Wang, S. S.-H. (2005b). Graded bidirectional synaptic plasticity is composed of switch-like unitary events. *Proc. Natl. Acad. Sci. U.S.A.* 102, 9679–9684.

Oja, E. (1982). A simplified neuron model as a principal component analyzer. *J. Math. Biol.* 15, 267–273.

Okamoto, H., and Ichikawa, K. (2000). Switching characteristics of a model for biochemical-reaction networks describing autophosphorylation versus dephosphorylation of Ca^{2+}/calmodulin-dependent protein kinase II. *Biol. Cybern.* 82, 35–47.

Otani, S., and Connor, J. A. (1998). Requirement of rapid Ca^{2+} entry and synaptic activation of metabotropic glutamate receptors for the induction of long-term depression in adult rat hippocampus. *J. Physiol.* 511, 761–770.

Petersen, C., Malenka, R., Nicoll, R., and Hopfield, J. (1998). All-or-none potentiation at CA3-CA1 synapses. *Proc. Natl. Acad. Sci. U.S.A.* 95, 4732–4737.

Pi, H. J., and Lisman, J. E. (2008). Coupled phosphatase and kinase switches produce the tristability required for long-term potentiation and long-term depression. *J. Neurosci.* 28, 13132–13138.

Piomelli, D. (2003). The molecular logic of endocannabinoid signalling. *Nat. Rev. Neurosci.* 4, 873–884.

Raastad, M. (1995). Extracellular activation of unitary excitatory synapses between hippocampal CA3 and CA1 pyramidal cells. *Eur. J. Neurosci.* 7, 1882–1888.

Rubin, J. E., Gerkin, R. C., Bi, G.-Q., and Chow, C. C. (2005). Calcium time course as a signal for spike-timing-dependent plasticity. *J. Neurophysiol.* 93, 2600–2613.

Rycroft, B. K., and Gibb, A. J. (2004). Regulation of single NMDA receptor channel activity by alpha-actinin and calmodulin in rat hippocampal granule cells. *J. Physiol.* 557(Pt 3), 795–808.

Sabatini, B. L., Oertner, T. G., and Svoboda, K. (2002). The life cycle of Ca^{2+} ions in dendritic spines. *Neuron* 33, 439–452.

Sabatini, B. L., and Svoboda, K. (2000). Analysis of calcium channels in single spines using optical fluctuation analysis. *Nature* 408, 589–593.

Sanhueza, M., McIntyre, C. C., and Lisman, J. E. (2007). Reversal of synaptic memory by Ca^{2+} /calmodulin-dependent protein kinase II inhibitor. *J. Neurosci.* 27, 5190–5199.

Schulman, H. (2004). Activity-dependent regulation of calcium/calmodulin-dependent protein kinase II localization. *J. Neurosci.* 24, 8399–8403.

Sharma, K., Fong, D. K., and Craig, A. M. (2006). Postsynaptic protein mobility in dendritic spines: long-term regulation by synaptic NMDA receptor activation. *Mol. Cell. Neurosci.* 31, 702–712.

Shen, K., and Meyer, T. (1999). Dynamic control of CaMKII translocation and localization in hippocampal neurons by NMDA receptor stimulation. *Science* 284, 162–166.

Shen, K., Teruel, M. N., Connor, J. H., Shenolikar, S., and Meyer, T. (2000). Molecular memory by reversible translocation of calcium/calmodulin-dependent protein kinase I. *Nat. Neurosci.* 3, 881–886.

Shouval, H. Z. (2005). Clusters of interacting receptors can stabilize synaptic efficacies. *Proc. Natl. Acad. Sci. U.S.A.* 102, 14440–14445.

Shouval, H. Z., Bear, M. F., and Cooper, L. N. (2002). A unified model of NMDA receptor-dependent bidirectional synaptic plasticity. *Proc. Natl. Acad. Sci. U.S.A.* 99, 10831–10836.

Shouval, H. Z., and Kalantzis, G. (2005). Stochastic properties of synaptic transmission affect the shape of spike time-dependent plasticity curves. *J. Neurophysiol.* 93, 1069–1073.

Sjöström, P. J., Turrigiano, G. G., and Nelson, S. (2001). Rate, timing, and cooperativity jointly determine cortical synaptic plasticity. *Neuron* 32, 1149–1164.

Sjöström, P. J., Turrigiano, G. G., and Nelson, S. B. (2003). Neocortical LTD via coincident activation of presynaptic NMDA and cannabinoid receptors. *Neuron* 39, 641–654.

Sjöström, P. J., Turrigiano, G. G., and Nelson, S. B. (2004). Endocannabinoid-dependent neocortical layer-5 LTD in the absence of postsynaptic spiking. *J. Neurophysiol.* 92, 3338–3343.

Soderling, T. R., and Derkach, V. A. (2000). Postsynaptic protein phosphorylation and LTP. *Trends Neurosci.* 23, 75–80.

Stanton, P. K., Chattarji, S., and Sejnowski, T. J. (1991). 2-amino-3-phosphonopropionic acid, an inhibitor of glutamate-stimulated phosphoinositide turnover, blocks induction of homosynaptic long-term depression, but not potentiation, in rat hippocampus. *Neurosci. Lett.* 127, 61–66.

Stevens, C. F., and Wang, Y. (1995). Facilitation and depression at single central synapses. *Neuron* 14, 795–802.

Strack, S., Choi, S., Lovinger, D. M., and Colbran, R. J. (1997). Translocation of autophosphorylated calcium/calmodulin-dependent protein kinase II to the postsynaptic density. *J. Biol. Chem.* 272, 13467–13470.

Sweatt, J. D. (2004). Mitogen-activated protein kinases in synaptic plasticity and memory. *Curr. Opin. Neurobiol.* 14, 311–317.

Thiels, E., Norman, E. D., Barrionuevo, G., and Klann, E. (1998). Transient and persistent increases in protein phosphatase activity during long-term depression in the adult hippocampus *in vivo*. *Neuroscience* 86, 1023–1029.

Urakubo, H., Honda, M., Froemke, R. C., and Kuroda, S. (2008). Requirement of an allosteric kinetics of NMDA receptors for spike timing-dependent plasticity. *J. Neurosci.* 28, 3310–3323.

Waltereit, R., and Weller, M. (2003). Signaling from cAMP/PKA to MAPK and synaptic plasticity. *Mol. Neurobiol.* 27, 99–106.

Wang, F. (2004). Steering growth cones with a CaMKII/calcineurin switch. *Neuron* 43, 760–762.

Wang, H.-X., Gerkin, R. C., Nauen, D. W., and Bi, G.-Q. (2005). Coactivation and timing-dependent integration of synaptic potentiation and depression. *Nat. Neurosci.* 8, 187–193.

Winder, D., Mansuy, I., Osman, M., Moallem, T., and Kandel, E. (1998). Genetic and pharmacological evidence for a novel, intermediate phase of long-term potentiation suppressed by calcineurin. *Cell* 92, 25–37.

Wittenberg, G. M., and Wang, S. S.-H. (2006). Malleability of spike-timing-dependent plasticity at the CA3-CA1 synapse. *J. Neurosci.* 26, 6610–6617.

Yang, S., Tang, Y., and Zucker, R. (1999). Selective induction of LTP and LTD by postsynaptic $[Ca^{2+}]$i elevation. *J. Neurophysiol.* 81, 781–787.

Yuste, R., and Denk, W. (1995). Dendritic spines as basic functional units of neuronal integration. *Nature* 375, 682–684.

Yuste, R., Majewska, A., Cash, S. S., and Denk, W. (1999). Mechanisms of calcium influx into hippocampal spines: heterogeneity among spines, coincidence detection by NMDA receptors, and optical quantal analysis. *J. Neurosci.* 19, 1976–1987.

Zhabotinsky, A. M. (2000). Bistability in the Ca^{2+}/calmodulin-dependent protein kinase-phosphatase system. *Biophys. J.* 79, 2211–2221.

Zhang, L. I., Tao, H. W., Holt, C. E., Harris, W. A., and Poo, M. (1998). A critical window for cooperation and competition among developing retinotectal synapses. *Nature* 395, 37–44.

Zhuo, M., Zhang, W., Son, H., Mansuy, I., Sobel, R. A., Seidman, J., and Kandel, E. R. (1999). A selective role of calcineurin A-alpha in synaptic depotentiation in hippocampus. *Proc. Natl. Acad. Sci. U.S.A.* 96, 4650–4655.

Zucker, R. S. (1999). Calcium- and activity-dependent synaptic plasticity. *Curr. Opin. Neurobiol.* 9, 305–313.

Conflict of Interest Statement: The authors declare that the research was conducted in the absence of any commercial or financial relationships that could be construed as a potential conflict of interest.

Received: 04 February 2010; paper pending published: 18 May 2010; accepted: 25 August 2010; published online: 17 September 2010.

*Citation: Graupner M and Brunel N (2010) Mechanisms of induction and maintenance of spike-timing dependent plasticity in biophysical synapse models. Front. Comput. Neurosci. **4**:136. doi:10.3389/fncom.2010.00136*

frontiers in
SYNAPTIC NEUROSCIENCE

REVIEW ARTICLE
published: 21 July 2010
doi: 10.3389/fnsyn.2010.00029

Dendritic synapse location and neocortical spike-timing-dependent plasticity

Robert C. Froemke[1]*, Johannes J. Letzkus[2], Björn M. Kampa[3], Giao B. Hang[4,5] and Greg J. Stuart[6]

[1] *Departments of Otolaryngology and Physiology/Neuroscience, Molecular Neurobiology Program, The Helen and Martin Kimmel Center for Biology and Medicine, Skirball Institute of Biomolecular Medicine, New York University School of Medicine, New York, NY, USA*
[2] *Friedrich Miescher Institute for Biomedical Research, Basel, Switzerland*
[3] *Brain Research Institute, University of Zurich, Zurich, Switzerland*
[4] *Howard Hughes Medical Institute, University of California, Berkeley, CA, USA*
[5] *Department of Molecular and Cell Biology, Division of Neurobiology, Helen Wills Neuroscience Institute, University of California, Berkeley, CA, USA*
[6] *The John Curtin School of Medical Research, Australian National University, Canberra, ACT, Australia*

Edited by:
Per Jesper Sjöström, University College London, UK

Reviewed by:
Attila Losonczy, Howard Hughes Medical Institute, USA
Ithai Rabinowitch, Medical Research Council Laboratory of Molecular Biology, UK
Dalton J. Surmeier, Northwestern University, USA

****Correspondence:***
Robert C. Froemke, Molecular Neurobiology Program, Departments of Otolaryngology, Physiology and Neuroscience, The Helen and Martin Kimmel Center for Biology and Medicine, Skirball Institute of Biomolecular Medicine, New York University School of Medicine, New York, NY 10016, USA.
e-mail: robert.froemke@med.nyu.edu

While it has been appreciated for decades that synapse location in the dendritic tree has a powerful influence on signal processing in neurons, the role of dendritic synapse location on the induction of long-term synaptic plasticity has only recently been explored. Here, we review recent work revealing how learning rules for spike-timing-dependent plasticity (STDP) in cortical neurons vary with the spatial location of synaptic input. A common principle appears to be that proximal synapses show conventional STDP, whereas distal inputs undergo plasticity according to novel learning rules. One crucial factor determining location-dependent STDP is the backpropagating action potential, which tends to decrease in amplitude and increase in width as it propagates into the dendritic tree of cortical neurons. We discuss additional location-dependent mechanisms as well as the functional implications of heterogeneous learning rules at different dendritic locations for the organization of synaptic inputs.

Keywords: cortex, dendrites, LTD, LTP, NMDA receptors, spikes, STDP, synaptic plasticity

INTRODUCTION

Cortical pyramidal neurons receive thousands of synaptic inputs distributed across an extensive dendritic tree. Rather than conducting synaptic events to the spike initiation zone unaltered, dendrites passively and actively shape the postsynaptic response to presynaptic input (Häusser and Mel, 2003; Stuart et al., 2008). Synaptic integration can be regulated by a number of dendritic phenomena, including cable filtering (Rall, 1964), activation and modulation of various ion channels (Migliore and Shepherd, 2002; Magee and Johnston, 2005; Nusser, 2009) and dendritic spike generation (Spruston, 2008). Because passive electrotonic propagation is generally weak, and active processes are often non-uniformly distributed throughout the dendritic arbor, one important determinant of the net strength of a given synapse is its dendritic location (Stuart and Spruston, 1998; Cash and Yuste, 1999; Magee and Cook, 2000; Segev and London, 2000; Häusser et al., 2001; Reyes, 2001; Tamás et al., 2002; Williams and Stuart, 2002).

Synaptic strength is not fixed, but can be altered by the pattern of neural activity (Buonomano and Merzenich, 1998; Feldman, 2009). In particular, repetitive pairing of pre- and postsynaptic action potentials (pre/post spike pairing) can induce persistent changes in synaptic strength depending on the temporal order and timing of pre/post pairing. Long-term potentiation (LTP) is induced at many glutamatergic synapses when presynaptic activity occurs just before postsynaptic spiking in the target cell (pre → post pairing). This timing can be viewed as causal, since the synaptic depolarization may contribute to eliciting the postsynaptic action potential. Conversely, long-term depression (LTD) is usually induced when the postsynaptic cell fires before the presynaptic input (post → pre pairing). These Hebbian forms of LTP and LTD are collectively known as spike-timing-dependent plasticity (STDP), because the sign and magnitude of changes in synaptic strength are dependent on the precise (millisecond) timing of pre/post spiking (Magee and Johnston, 1997; Markram et al., 1997; Bi and Poo, 1998; Debanne et al., 1998; Abbott and Nelson, 2000; Feldman, 2000; Song et al., 2000; Sjöström et al., 2001; Froemke and Dan, 2002; Kampa et al., 2006; Letzkus et al., 2006; Froemke et al., 2010).

Various forms of STDP have been observed in a variety of species, ranging from insects to humans. Despite the apparent generality of the STDP learning rule across synapses (Dan and Poo, 2006), there is considerable variability in the precise timing requirements for STDP induction, especially for LTD. Furthermore, several recent studies in cortical pyramidal neurons have revealed that the exact formulation of the temporal

window for spike-timing-dependent LTD depends on dendritic location (Froemke et al., 2005; Letzkus et al., 2006; Sjöström and Häusser, 2006).

Here we review the dendritic factors that influence the induction of cortical STDP and set the timing requirements for associative synaptic plasticity. These include passive dendritic properties, action potential backpropagation, NMDA receptor (NMDAR) activation, and active processes such as dendritic spikes. We then discuss experimental and theoretical work on the selective targeting of synaptic inputs to different dendritic locations. Other related topics such as plasticity of dendritic excitability, branch formation and spine growth (Magee and Johnston, 2005; Sjöström et al., 2008; Holtmaat and Svoboda, 2009) will not be covered here. We focus on experiments in cortical brain slices, which have revealed basic differences in the size and shape of the STDP window at proximal and distal dendritic synapses. Spatial gradients for STDP along dendritic trees may be important for the development and functional organization of cortical synapses, the structuring of synaptic integration and information processing within dendritic sub-regions, and defining the receptive field properties of cortical neurons.

LOCATION DEPENDENCE OF STDP: HEBBIAN AND ANTI-HEBBIAN LEARNING RULES

Dendritic geometry, ion channels, and receptor distributions interact to control the local voltage at a given synapse, which as we discuss below is a dominant factor in determining the magnitude of long-term synaptic modifications. As action potential backpropagation and postsynaptic processing of excitatory postsynaptic potentials (EPSPs) are both spatially regulated in dendrites of cortical neurons, it has been proposed that the sign and magnitude of STDP will depend on the dendritic location of synaptic input (Sourdet and Debanne, 1999).

Three experimental studies have recently provided evidence for location-dependent differences in STDP learning rules in neocortical pyramidal neurons (Froemke et al., 2005; Letzkus et al., 2006; Sjöström and Häusser, 2006). Together, these experiments have shown that synapses proximal to the cell body, where backpropagating action potentials are large and narrow, express conventional STDP in which pre → post spike pairing induces LTP (for relatively short inter-spike intervals of ~25 ms) and post → pre pairing leads to LTD (for inter-spike intervals of ~50 ms). At synapses more distal from the soma, however, the timing requirements for pre/post pairing shift such that the magnitude, and eventually the sign, of synaptic modifications during STDP at distal synapses is profoundly different from that found at proximal inputs (**Figure 1**).

Sjöström and Häusser (2006) and Letzkus et al. (2006) both observed a spatial gradient of STDP along the apical dendrites of layer 5 pyramidal neurons. For these experiments, EPSPs were evoked in postsynaptic layer 5 pyramidal neurons either by direct depolarization of a connected presynaptic layer 2/3 pyramidal neuron, or by focal stimulation of synaptic inputs at varying distances along the apical dendrite. Importantly, the rise time of the EPSP recorded at the soma was used as an indicator of the distance of synaptic inputs from the soma, allowing accurate determination of the dendritic location for a given synapse (Jack et al., 1971). For synapses close to the cell body (<100 μm), STDP induced by pre/post pairing was Hebbian: pre → post spike pairs induced LTP and post → pre pairing induced LTD (**Figures 1A,B**). But as dendritic distance increased, the amount of LTP induced by pre → post pairing gradually decreased to zero, and at more distal synaptic locations (>500 μm) pre → post pairing induced robust LTD. LTD at these distal synapses could be converted to LTP if postsynaptic action potentials were paired with dendritic depolarization (Sjöström and Häusser, 2006), which can boost action potential backpropagation (Larkum et al., 2001; Stuart and Häusser, 2001). Similarly, dendritic depolarization converting a single action potential to a high-frequency burst by generation of a dendritic calcium spike (Larkum et al., 1999b) could convert LTD to LTP (Letzkus et al., 2006). Consistent with a role of dendritic spikes in LTP induction, at distal synapses action potential bursts above the critical frequency for dendritic calcium spike generation (Larkum et al., 1999a) lead to LTP during post → pre pairing (Letzkus et al., 2006). A similar observation has been made for inputs onto basal dendrites of layer 5 pyramidal neurons (Kampa et al., 2006). This frequency dependence of STDP induction is reminiscent of earlier findings (Markram et al., 1997; Sjöström et al., 2001). The observation that post → pre pairing leads to LTD of proximal synapses, but can induce LTP at distal inputs when inputs were paired with high-frequency action potential bursts (**Figure 1B**), suggests a gradual shift of the timing requirements for STDP along the apical dendrite of layer 5 pyramidal neurons. Together with work in basal dendrites (Gordon et al., 2006; Kampa et al., 2006), these studies show that synapses located in the distal dendrites of layer 5 cortical pyramidal neurons express anti-Hebbian STDP timing rules, where LTD can be switched to LTP by boosting action potential backpropagation (Sjöström and Häusser, 2006), the generation of dendritic spikes (Kampa et al., 2006; Letzkus et al., 2006), or by pairing NMDA spikes with brain-derived neurotrophic factor (BDNF) application (Gordon et al., 2006).

Similarly, for lateral connections within layer 2/3 of developing visual cortex, the magnitude of STDP at more distal synapses (>100 μm from the soma) was found to be about half that of proximal synapses (<50 μm from the soma) (Froemke et al., 2005). In addition, the temporal window for spike-timing-dependent LTD of distal layer 2/3 synapses was much wider than that of proximal synapses (**Figure 1C**). As a result, during post → pre pairing between −50 and −100 ms LTD was induced at distal (**Figure 1C**, right) but not proximal inputs (**Figure 1C**, center).

BACKPROPAGATING ACTION POTENTIALS AND DENDRITIC EXCITABILITY

What factors govern the size and shape of the STDP time window at different dendritic sites? The amplitude and time course of the electrical events that cooperate to induce STDP – that is, EPSPs and postsynaptic action potentials – themselves depend on dendritic location. This implies that the local depolarization experienced by individual synapses during pre/post pairing will be affected not only by the temporal dynamics of pre- and postsynaptic spike trains, but also by the distance of synaptic inputs from the site of action potential initiation. Because the degree of postsynaptic depolarization is an important parameter controlling the induction of long-term synaptic plasticity (Zucker, 1999; Wespatat et al., 2004; Lisman and Spruston, 2005; Urakubo et al., 2008; Feldman, 2009), it is likely that the timing requirements for STDP will depend on the combined

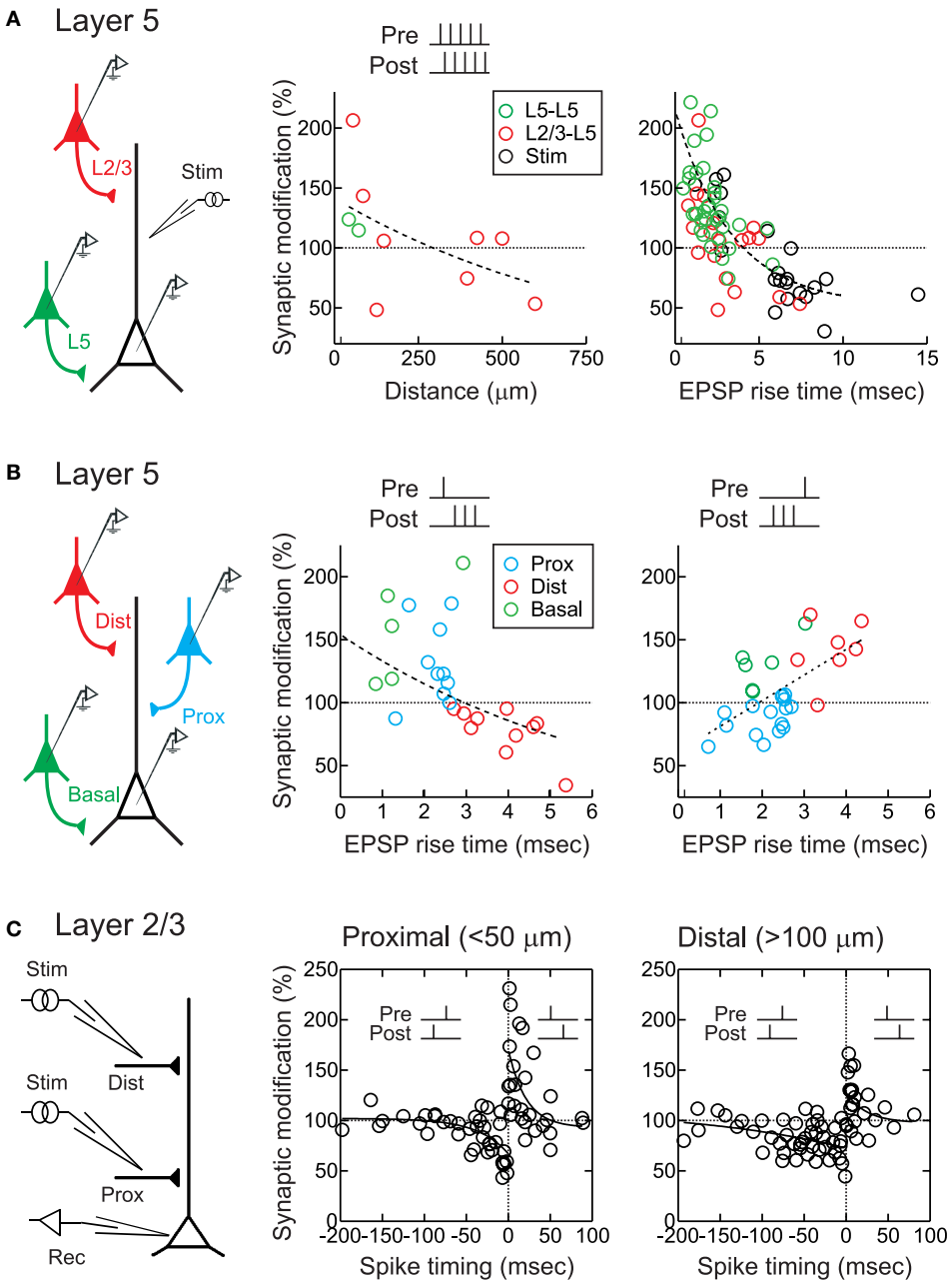

FIGURE 1 | STDP timing rules depend on dendritic synapse location. (A) STDP of layer 2/3 (red) and layer 5 (green) EPSPs in layer 5 pyramidal neurons. EPSPs were evoked during paired recordings or by extracellular stimulation ("stim", black). STDP was induced by repetitively pairing of five pre- and five postsynaptic action potentials/stimulations at +10 ms. Center, sign of synaptic modification was negatively correlated with distance of putative synaptic contact. Right, sign of synaptic modification was negatively correlated with EPSP rise time. From Sjöström and Häusser (2006). **(B)** STDP of proximal (blue) and distal (red) apical layer 2/3 inputs, and basal (green) layer 5 inputs, to layer 5 pyramidal neurons. Somatic EPSP rise time was used as a proxy for synaptic location, with fast EPSPs (<2.7 ms) indicating proximal EPSPs and slow rise times (> 2.7 ms) indicating distal EPSPs. STDP induction consisted of repeated pairings of single EPSPs with high-frequency postsynaptic bursts (200 Hz). EPSP rise time was negatively correlated with the sign and magnitude of the change in synaptic strength for pre → post pairings (middle), but positively correlated with the sign and magnitude of changes in synaptic strength for post → pre pairings (right), leading to a switch to anti-Hebbian STDP for more distal inputs. From Kampa et al. (2006) and Letzkus et al. (2006). **(C)** STDP of proximal (<50 μm) and distal (>100 μm) inputs onto apical dendrites of layer 2/3 visual cortical pyramidal neurons. Post → pre pairing at –50 to –100 ms induced LTD distally (right) but not proximally (middle). From Froemke et al. (2005).

voltage change at the synapse when pre/post spikes are paired at different time intervals (Sjöström et al., 2001; Froemke et al., 2005; Sjöström and Häusser, 2006). Thus the basic learning rules for STDP are likely to be determined in part by the biophysical factors within dendrites that regulate action potential backpropagation and local EPSP amplitude and kinetics.

After being initiated in or near the axon initial segment (Coombs et al., 1957; Fuortes et al., 1957; Palmer and Stuart, 2006; Meeks and Mennerick, 2007; Shu et al., 2007; Schmidt-Hieber et al., 2008), action potentials backpropagate into apical and basal dendrites of cortical pyramidal neurons (Stuart and Sakmann, 1994; Antic, 2003; Kampa and Stuart, 2006; Nevian et al., 2007). Usually, these backpropagating action potentials become smaller in amplitude and broader in width with increasing dendritic distance from the soma (**Figures 2A–D**). This occurs due to passive current spread as described by cable theory (Rall, 1964). Neuronal cell membranes are leaky, giving rise to rapid attenuation of electrical signals along dendrites (Stuart and Spruston, 1998; Williams and Mitchell, 2008). In cerebellar Purkinje cells, for example, somatic action potentials decrease in size by 80% or more within the first 100 μm (Stuart and Häusser, 1994).

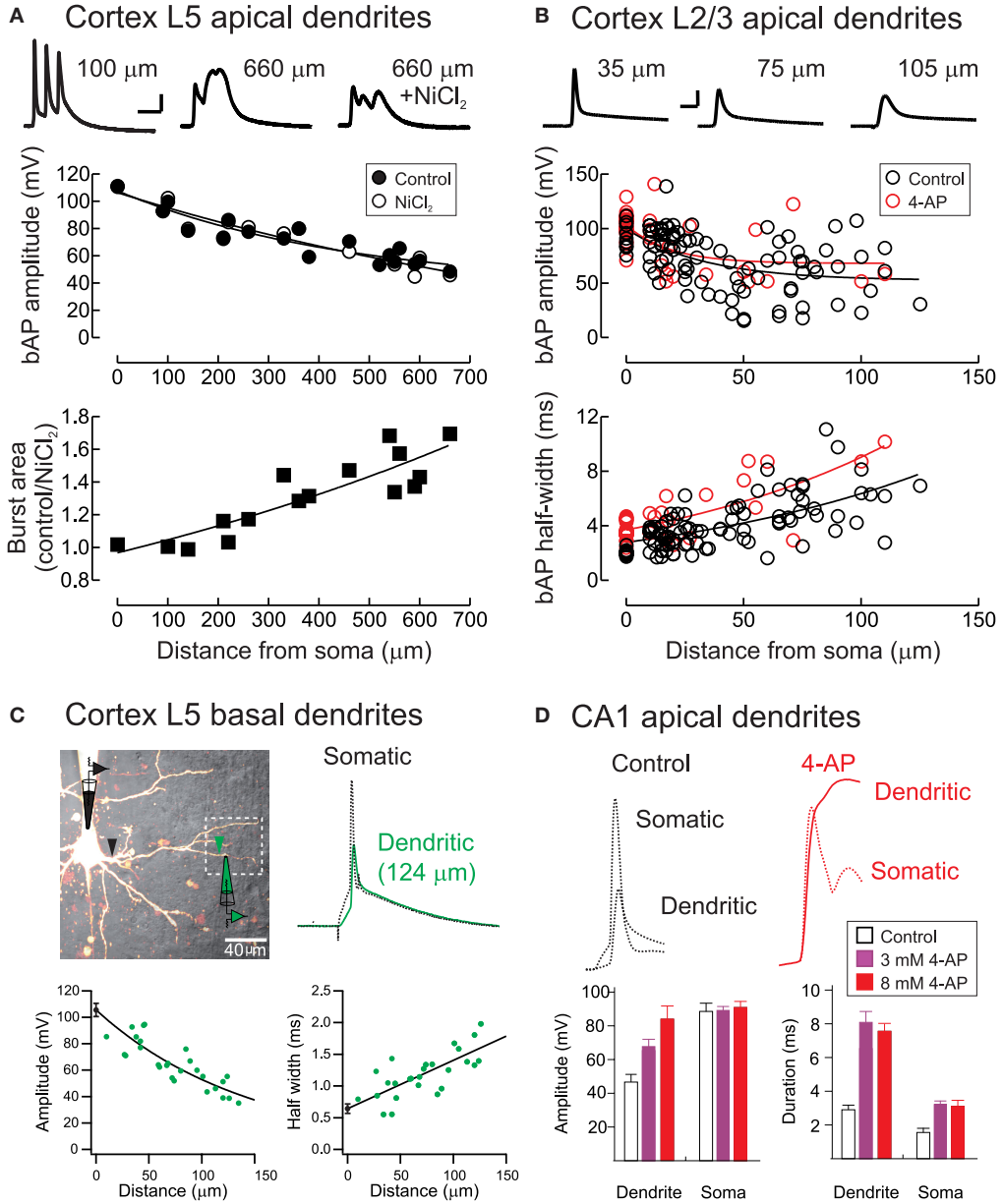

FIGURE 2 | Backpropagating action potentials in pyramidal neuron dendrites. (A) Top, Voltage waveforms during a high-frequency (200 Hz) action potential burst at proximal and distal apical dendritic locations in a layer 5 pyramidal neuron before and after block of voltage-activated calcium channels with $NiCl_2$ (0.1 mM, rat somatosensory cortex). Middle, the amplitude of single backpropagating action potentials (bAP) is unaffected by calcium channel block, whereas the area under action potential bursts is strongly Ca^{2+}-dependent (bottom). Scale bar: 10 ms, 20 mV. From Letzkus et al. (2006). **(B)** Backpropagation of single action potentials in layer 2/3 pyramidal cells in rat visual cortex. Red symbols indicate experiments performed with the A-type K^+ channel blocker 4-AP in the recording pipette. Scale bar, 5 ms, 40 mV. From Froemke et al. (2005). **(C)** Backpropagating action potentials in basal dendrites of layer 5 cortical pyramidal neurons. From Nevian et al. (2007). **(D)** Backpropagating action potentials in apical dendrites of hippocampal CA1 pyramidal neurons are enhanced in amplitude and duration by bath application of 4-AP. From Hoffman et al. (1997).

The dendrites of many central neurons, however, contain a variety of voltage-activated ion channels that support and regulate action potential backpropagation. As opposed to Purkinje cells, action potentials in neocortical and hippocampal pyramidal neurons decay in amplitude by less than 50% even several hundred μm from the cell body (Spruston et al., 1995; Stuart and Sakmann, 1994; Stuart and Spruston, 1998; Waters et al., 2003; Froemke et al., 2005). A relatively uniform distribution of dendritic Na^+ channels in many neuronal cell types boosts action potentials as they propagate into dendrites, enhancing action potential backpropagation, which can be further amplified when paired with appropriately timed EPSPs (Magee and Johnston, 1995; Stuart and Häusser, 2001; Migliore and Shepherd, 2002). Nevertheless, backpropagating action potentials can fail to invade the most distal dendrites (Stuart and Häusser, 2001; Golding et al., 2002).

In addition to voltage-gated sodium channels, which enhance backpropagation, several other dendritic conductances have been found to exert dampening effects on dendritic excitation. A-type (Kv4) channels are fast-acting and inactivating K^+ channels that counteract the depolarization produced by backpropagating action potentials. Blockade of dendritic A-type channels broadens dendritic EPSPs and backpropagating spikes (**Figures 2B,D**), suggesting that these channels help enforce spike-timing precision and reduce temporal summation of synaptic responses in dendrites (Hoffman et al., 1997; Froemke et al., 2006). Hyperpolarization-activated cyclic nucleotide-gated (HCN) channels can perform a similar normalizing function. Expressed at high levels in distal dendrites of hippocampal and cortical pyramidal neurons, HCN channels act to normalize both somatic EPSP time course and EPSP summation independent of the dendritic location of synaptic input (Magee, 2000; Williams and Stuart, 2000b). This effect depends on the total density of HCN channels, rather than their dendritic expression pattern (Angelo et al., 2007; Bullis et al., 2007).

Dendritic location profoundly impacts the amplitude and kinetics of synaptic responses as well as the characteristics of backpropagating action potentials. When measured in the dendrites close to the site of synaptic input, EPSPs evoked in distal dendrites are considerably larger (four-fold or more in amplitude) than EPSPs evoked more proximally (Magee and Cook, 2000; Williams and Stuart, 2002). For hippocampal CA1 pyramidal neurons, this scaling is due in part to a progressive increase in the number of AMPA receptors with dendritic distance from the soma (Smith et al., 2003). In contrast, synaptic conductance is relatively independent of dendritic location in layer 5 cortical pyramidal neurons (Williams and Stuart, 2002). For these cells, the smaller branch size of distal dendrites leads to a lower input capacitance, causing distal EPSPs to display larger amplitudes and faster kinetics than proximal inputs (Williams and Stuart, 2002; Nevian et al., 2007). In conjunction with the strong expression of HCN channels at distal sites, this leads to a brief temporal integration window for distal inputs (Williams and Stuart, 2002).

Given that distal inputs attenuate strongly on their way to the soma, additional mechanisms may be required for these events to influence axo-somatic synaptic integration and action potential generation. Dendritic spikes provide such a mechanism. Dendritic spikes are regenerative events which, depending on neuron type and dendritic location, can be mediated by voltage-gated Na^+ and Ca^{2+} channels or by NMDARs (Häusser and Mel, 2003; Gulledge et al., 2005; Spruston, 2008). They can be evoked by correlated synaptic input (Williams and Stuart, 2002; Gasparini et al., 2004; Losonczy and Magee, 2006), by bursts of action potentials above a critical frequency (**Figure 2A**; Larkum et al., 1999a; Williams and Stuart, 2000a), or by coincidence of a distal EPSP with a backpropagating action potential within a narrow time window (Larkum et al., 1999b). As they lead to significant dendritic depolarization they act as an anti-Hebbian mechanism for LTP induction at distal inputs in cortical pyramidal neurons (Golding et al., 2002). Dendritic spikes can occur in isolation (Schiller et al., 1997; Stuart et al., 1997), or can forward-propagate to the soma where they typically elicit a burst of action potentials (Larkum et al., 1999b; Williams and Stuart, 1999), impacting on somatic spike-timing (Gasparini et al., 2004). Both local and global dendritic spikes can influence synaptic plasticity expressed at different dendritic locations (Sjöström et al., 2008).

NMDA RECEPTOR ACTIVATION AND STDP

At cortical layer 2/3 and layer 5 synapses, STDP at all dendritic locations requires activation of NMDARs, as synaptic modifications are prevented by application of the selective NMDAR antagonist APV (Froemke et al., 2005; Kampa et al., 2006; Letzkus et al., 2006). Furthermore, pairing action potentials with EPSPs has been shown to increase NMDAR activation. Block of NMDAR-mediated EPSPs by the activity-dependent NMDAR antagonist MK-801 was significantly greater when NMDAR EPSPs were paired with high-frequency (200 Hz) action potential bursts compared to NMDAR EPSPs evoked on their own (**Figure 3A**; Kampa et al., 2006). This activation of NMDARs by action potential bursts had similar timing requirements as STDP (**Figure 3A**), suggesting an important role of backpropagating action potentials and action potential bursts in enhancing NMDAR activation during STDP induction.

In layer 2/3, while pre → post pairing also directly increased the amplitude of NMDAR EPSPs during pairing, NMDAR EPSPs were strongly suppressed during post → pre pairing (**Figure 3B**). The location dependence of the spike-timing window for action potential-induced alteration of NMDAR EPSPs was similar to the location dependence of the STDP timing window. Enhancement of NMDAR EPSPs during pre → post pairing was almost certainly due to removal of the classical Mg^{2+} block (Mayer et al., 1984; Nowak et al., 1984), while NMDAR EPSP suppression by post → pre pairing required postsynaptic Ca^{2+} influx, suggesting that Ca^{2+}-dependent NMDAR desensitization (Zorumski and Thio, 1992; Rosenmund et al., 1995; Tong et al., 1995; Kyrozis et al., 1996; Umemiya et al., 2001; Krupp et al., 2002) could be critical in setting the time window for LTD induction. EPSPs evoked by stimulation of layer 2/3 lateral connections in young visual cortex have strong NMDAR components even at hyperpolarized membrane potentials, apparently due to a relatively weak Mg^{2+} blockade (Kato and Yoshimura, 1993), similar to connections between layer 4 stellate cells (Fleidervish et al., 1998). This suggests that these connections might be highly dynamic and exquisitely sensitive to changes in pre- and postsynaptic activity patterns (Diamond et al., 1994; Das and Gilbert, 1995; Trachtenberg et al., 2000).

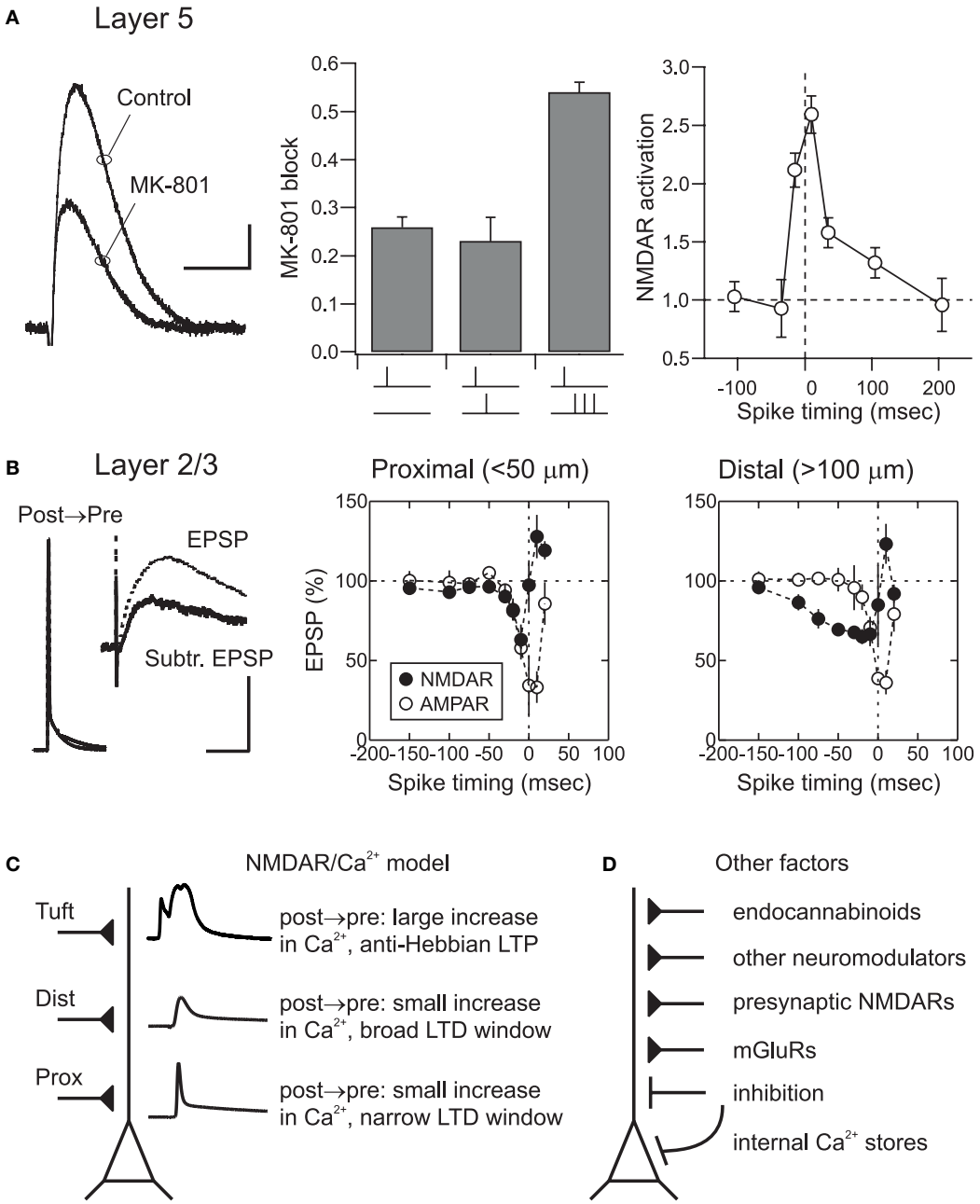

FIGURE 3 | Spatial determinants and other mechanisms of cortical STDP. **(A)** NMDAR activation during pairing of EPSPs and action potentials in layer 5 neurons. Degree of NMDAR activation was measured using MK-801, an open channel blocker. MK801 block was defined as: 1 – EPSP(MK801)/EPSP(control). The greater the extent of NMDAR activation, the more channels will be blocked; as a result, the NMDAR component will become smaller over time. Scale bar: 0.5 mV, 20 ms (left). Pairing a presynaptic stimulus with a high-frequency (200 Hz) burst of three action potentials caused significant more NMDAR activation (i.e., a larger reduction in EPSP amplitude in the presence of MK-801) than pairing with single action potentials (center). The timing requirements for NMDAR activation (right) closely matched the STDP learning rule in these neurons. see Kampa et al. (2006) for methodological details. **(B)** During post → pre pairing in layer 2/3 neurons, NMDAR EPSPs were suppressed by postsynaptic action potentials. Scale bar: 50 or 2 mV, 100 ms (left). The time window for NMDAR EPSP suppression (filled circles) matched the time window for STDP induction at both proximal (center) and distal (right) synaptic locations. AMPA receptor mediated EPSPs seemed to be shunted by action potentials at short pairing intervals, but were otherwise unaffected by pairing (open circles). From Froemke et al. (2005). **(C)** The NMDAR/Ca^{2+} model of STDP. In this model, Ca^{2+} influx through postsynaptic NMDARs determines the degree of long-term synaptic modification. Depolarization from backpropagating action potentials relieves Mg^{2+} blockade of NMDARs, allowing postsynaptic influx of Ca^{2+}. Lower levels of Ca^{2+} influx lead to LTD, whereas higher levels induce LTP. Conventional STDP is observed at proximal synapses. At more distal dendritic locations backpropagating action potentials are shorter and wider, increasing the time window of STDP. At the most distal dendritic locations, such as the apical tuft, action potentials interact locally with EPSPs to evoke dendritic Ca^{2+} spikes that induce anti-Hebbian LTP. **(D)** Other factors beyond Ca^{2+} influx through postsynaptic NMDARs also contribute to and control cortical STDP. These mechanisms may modulate postsynaptic excitability and spike generation, presynaptic release of neurotransmitter, or directly affect postsynaptic Ca^{2+} levels via release of Ca^{2+} from internal stores.

Analogously, Koester and Sakmann (1998) demonstrated that the precise timing of pre- and postsynaptic activity was directly related to the amplitude of Ca^{2+} signals in spines of layer 5 pyramidal cells. When the presynaptic EPSP was evoked first, Ca^{2+} signals in activated dendritic spines summed supralinearly, whereas when the postsynaptic cell fired first Ca^{2+} signals summed sublinearly.

These results support a causal relationship between modulation of NMDAR EPSPs and STDP induction in cortical pyramidal neurons. We therefore propose a model in which the extent of Ca^{2+} influx through NMDARs gated by the local depolarization due to backpropagating action potentials and dendritic spikes determines the sign and magnitude of plasticity (**Figure 3C**). While it has long been known that both NMDARs and postsynaptic Ca^{2+} influx are necessary for LTP and LTD induction at most central synapses (Malenka and Nicoll, 1999; Zucker, 1999), recent biophysical and biochemical models have quantitatively captured the dendritic location dependence of NMDAR activation and STDP. Simulations of the interactions between dendritic spikes and NMDAR kinetics recapitulated the progressive shift of the STDP learning rules with dendritic distance (Saudargiene et al., 2005; Letzkus et al., 2006), and could also account for anti-Hebbian LTP induced by short-interval post → pre pairing, depending on the rise time of the postsynaptic response (Saudargiene et al., 2004). Large-scale biochemical simulations of the mechanisms underlying long-term synaptic modification in layer 2/3 neurons revealed that the postsynaptic spike rapidly acts on NMDARs during post → pre pairing (Urakubo et al., 2008). This study revealed that, in addition to enzymatic action via calcineurin, it is likely that Ca^{2+}-bound calmodulin allosterically regulates layer 2/3 NMDARs to induce LTD. Taken together, these experimental and theoretical studies suggest that Ca^{2+} influx through NMDARs is a dominant factor in STDP induction. During pre → post pairing high levels of Ca^{2+} influx lead to LTP, whereas during post → pre pairing low levels of Ca^{2+} influx through a desensitized NMDA channel induces LTD.

OTHER POTENTIAL MECHANISMS FOR LOCATION-DEPENDENT STDP

In addition to backpropagating action potentials and postsynaptic NMDAR activation, a range of other mechanisms are known to be important for long-term synaptic plasticity in general and STDP in particular (**Figure 3D**). These factors include voltage-gated Ca^{2+} channels and Ca^{2+} spikes (Christie et al., 1997; Froemke et al., 2005; Kampa et al., 2006; Letzkus et al., 2006), metabotropic glutamate receptors (Nishiyama et al., 2000; Bender et al., 2006), endocannabinoid release (Sjöström et al., 2003; Sjöström and Häusser, 2006), BDNF signaling (Gordon et al., 2006), activation of other neuromodulators, G protein coupled receptors, and their downstream effectors (Lin et al., 2003; Froemke et al., 2007; Seol et al., 2007; Harvey et al., 2008), presynaptic NMDA autoreceptors (Sjöström et al., 2003; Corlew et al., 2007), Ca^{2+} release and/or sequestering by internal stores (Nishiyama et al., 2000) and disinhibition (Artola et al., 1990). Some of these systems are themselves expressed and regulated in a location-dependent manner, suggesting that processes and signaling mechanisms beyond direct activation and modulation of NMDARs is likely to control the local learning rules for synaptic modification at different inputs.

It remains unclear how these processes interact to ultimately control the induction of long-term synaptic modifications at cortical excitatory synapses. Some of these mechanisms can clearly influence dendritic excitability, such as adrenergic, cholinergic, or dopaminergic neuromodulation of K^+ channel kinetics and downstream effects on action potential backpropagation (Hoffman and Johnston, 1999). Changes in dendritic excitability have been shown to alter the size and shape of backpropagating action potentials and synaptic events (Frick et al., 2004), which in turn affects how these events are integrated to produce STDP. In addition, other mechanisms, including metabotropic glutamate receptor and voltage-gated Ca^{2+} channel activation, might more directly affect internal Ca^{2+} levels and thus STDP, as previously observed for induction of STDP in hippocampus (Nishiyama et al., 2000) and cortex (Bender et al., 2006). Finally, release of retrograde messengers or activation of presynaptic autoreceptors might control the amount or kinetics of transmitter release (Sjöström et al., 2003), regulating the degree of postsynaptic NMDAR activation or inducing long-term changes in presynaptic release. Given this mechanistic diversity, future studies are required to determine how these mechanisms affect STDP in a location-dependent manner.

Recruitment of inhibitory inputs may also differentially affect STDP induction at different dendritic locations, particularly since several interneuron sub-populations target specific subcellular compartments of pyramidal neurons (Markram et al., 2004). Perisomatic inhibition provided by basket cells serves to inhibit action potential firing (Cobb et al., 1995; Pouille and Scanziani, 2001), but would allow synaptic modifications induced by dendritic spikes to occur. Conversely, several distinct classes of interneurons target the dendrites of pyramidal neurons in neocortex (Markram et al., 2004), providing a rich repertoire for location-dependent modulation of dendritic synapses. Activation of ionotropic GABA receptors in cortical pyramidal neurons can be both inhibitory or excitatory (Gulledge and Stuart, 2003). This suggests that, depending on dendritic location and timing relative to excitatory input, GABAergic synapses can either enhance or suppress action potential firing and STDP induction. In contrast, activation of dendritic $GABA_B$ receptors strongly inhibits the generation of dendritic spikes in the apical tuft of layer 5 pyramidal neurons, but leaves action potential backpropagation largely intact (Pérez-Garci et al., 2006). This may selectively inhibit STDP at distal apical synapses, which require dendritic calcium spikes for STDP (Letzkus et al., 2006), while leaving STDP at proximal inputs unaffected.

While we know very little about the engagement of these various inhibitory circuits during information processing *in vivo*, a well-understood example is provided by the disynaptic loop between layer 5 pyramidal neurons and dendrite-targeting Martinotti interneurons. Sensory stimulation has recently been shown to elicit calcium spikes in the apical tuft of layer 5 pyramids *in vivo* (Murayama et al., 2009). Associated high-frequency action potential bursts in turn activate Martinotti interneurons (Silberberg and Markram, 2007; Murayama et al., 2009), which inhibit subsequent dendritic calcium electrogenesis in surrounding pyramidal cells. In effect, this suggests that STDP induction in tuft inputs to one set of pyramidal neurons may render the same synapses in the other layer 5 implastic for a brief time window.

Although forms of STDP have been observed at many synapses, pre/post spike pairing is just one of several protocols for induction of long-term synaptic modification. Pairing single pre/post spikes at low frequency, even with dozens of repetitions over minutes, sometimes fails to induce significant changes in synaptic strength, particularly at unitary connections between cortical pyramidal neurons (Sjöström et al., 2001; Kampa et al., 2006; Letzkus et al., 2006; Froemke et al., 2010). Even pairing 5 Hz bursts of somatically-triggered spikes can fail to induce LTP *in vitro* (Markram et al., 1997; Sjöström et al., 2001), and pre/post spike pairing may be insufficient for induction of long-term synaptic modifications *in vivo* (Froemke et al., 2007; Jacob et al., 2007). For synapses where the predominant mechanism of long-term modification involves Ca^{2+} influx through postsynaptic NMDARs (Zucker, 1999; Urakubo et al., 2008), the local voltage change at the synapse is more important than somatic depolarization and spike generation (Lisman and Spruston, 2005). Thus while somatic spikes sometimes fail to invade distal dendrites and inhibitory inputs may prevent postsynaptic NMDAR activation, other processes such as dendritic calcium spikes (Schiller et al., 1997; Larkum et al., 1999b) or neuromodulation (Lin et al., 2003; Froemke et al., 2007) may be engaged to enable long-term synaptic modifications in the absence of somatic action potentials. For example, Golding et al. (2002) have shown that in hippocampal CA1 pyramidal neurons LTP of distal inputs can occur independently of somatic action potential backpropagation, and instead requires dendritic calcium spikes. LTD in layer 5 cortical pyramidal neurons can be induced by pairing presynaptic stimulation with subthreshold depolarization (Sjöström et al., 2004), a finding reminiscent of earlier work showing that the magnitude of postsynaptic depolarization determines the sign and magnitude of synaptic plasticity (Artola et al., 1990; Feldman et al., 1999; Zucker, 1999; Wespatat et al., 2004).

Thus pre/post spike pairing is sufficient to induce synaptic modification at many synapses, but the precise timing requirements, temporal ordering, and number of spikes required can be highly synapse specific. Furthermore, the exact timing rules for STDP at a given synapse are likely to be regulated by a large number of spatial and temporal phenomena. In the end, local depolarization and postsynaptic Ca^{2+} influx are the key factors underlying synaptic plasticity, independent of whether backpropagating action potentials are required or not, in a manner resonant with the classical BCM model (Sjöström and Nelson, 2002; Izhikevich and Desai, 2003).

DENDRITIC ORGANIZATION OF SYNAPTIC INPUT

The recruitment of the different location-dependent plasticity mechanisms described above depends on the spatio-temporal activation pattern of synapses in the dendritic arbor. For this and other reasons, spatial organizing principles structuring input along the dendrites have recently received considerable attention. A landmark study by Petreanu et al. (2009) applied a novel technique to map the distribution of functional inputs to neocortical pyramidal neurons in barrel cortex. Using channelrhodopsin-2 to selectively activate various anatomical inputs (**Figure 4A**), they observed a hierarchical gradient of afferents on layer 3 pyramidal neurons, with bottom-up inputs impinging onto proximal dendritic locations and increasingly complex, more processed information arriving at progressively more distal sites (**Figure 4B**). A similar albeit more complex pattern was observed in layer 5B pyramidal neurons, where top-down inputs target both the basal dendritic domain and the apical tuft (**Figure 4C**). Since the rules of STDP induction depend on dendritic location, these input pathways are likely to display different timing requirements for potentiation and depression in response to postsynaptic firing. In response to uncorrelated firing, top-down inputs onto layer 3 neurons would be predicted to depress more than bottom-up synapses, possibly leading to an effective temporal sharpening of the top-down response (see below). In contrast, both bottom-up and top-down inputs to layer 5 pyramidal cells might be potentiated when activated after the initiation of a postsynaptic action potential, but only if top-down synapses are concomitantly active to transform the action potential into a burst by depolarizing the apical tuft (Larkum et al., 1999b).

In addition, dendritic compartmentalization also controls which input pathways can potentially interact locally, for example, at the level of individual dendritic branches. Spatially clustered and simultaneously active synaptic activity is required for initiation of dendritic spikes (Schiller et al., 1997; Williams and Stuart, 2002; Losonczy and Magee, 2006), which is important for induction of some forms of STDP (Kampa et al., 2007), as well as branch-specific plasticity of excitability (Losonczy et al., 2008). For most inputs onto layer 3 neurons, these local effects are likely to be confined within single afferent pathways, whereas in layer 5B neurons between-pathway interactions are also possible (**Figures 4B,C**; Petreanu et al., 2009).

Within a given pathway, it has been hypothesized that synapses of similar information content are further clustered (Larkum and Nevian, 2008). The first direct corroboration of this hypothesis was found in tectal neurons of *Xenopus* tadpoles (**Figures 4D–G**; Bollmann and Engert, 2009). Visual stimulation revealed that inputs were organized topographically, where axons of neighboring retinal ganglion cells were clustered into distinct input domains in the dendritic arbor of tectal neurons. In contrast, Jia et al. (2010) recently observed in mouse primary visual cortex that inputs onto layer 2/3 neurons with similar orientation preference are distributed onto different dendritic branches. Thus, it is at present unclear whether clustering of inputs with similar information content onto the same dendritic branch is an important organizing principle or not, and future research is clearly required. Nonetheless, the organization of dendritic afferents characterized so far makes it possible that both STDP and dendritic-spike-dependent plasticity mechanisms may be engaged *in vivo* in a region-specific manner (Kampa et al., 2007; Letzkus et al., 2007). While clustering of co-active inputs would favor dendritic spikes as a mechanism for plasticity induction during learning, dispersion of co-active synapses in the dendritic arbor would make dendritic spikes less likely, and thus would favor backpropagating action potentials as the primary mechanism for the induction of long-term synaptic modifications. Despite a growing knowledge on the learning rules and underlying biophysics important for induction of synaptic plasticity, we still know very little about the temporal engagement of afferents during normal brain function. This information will be vital for a more complete understanding of the plasticity mechanisms governing synaptic transmission, perceptual learning, and memory formation.

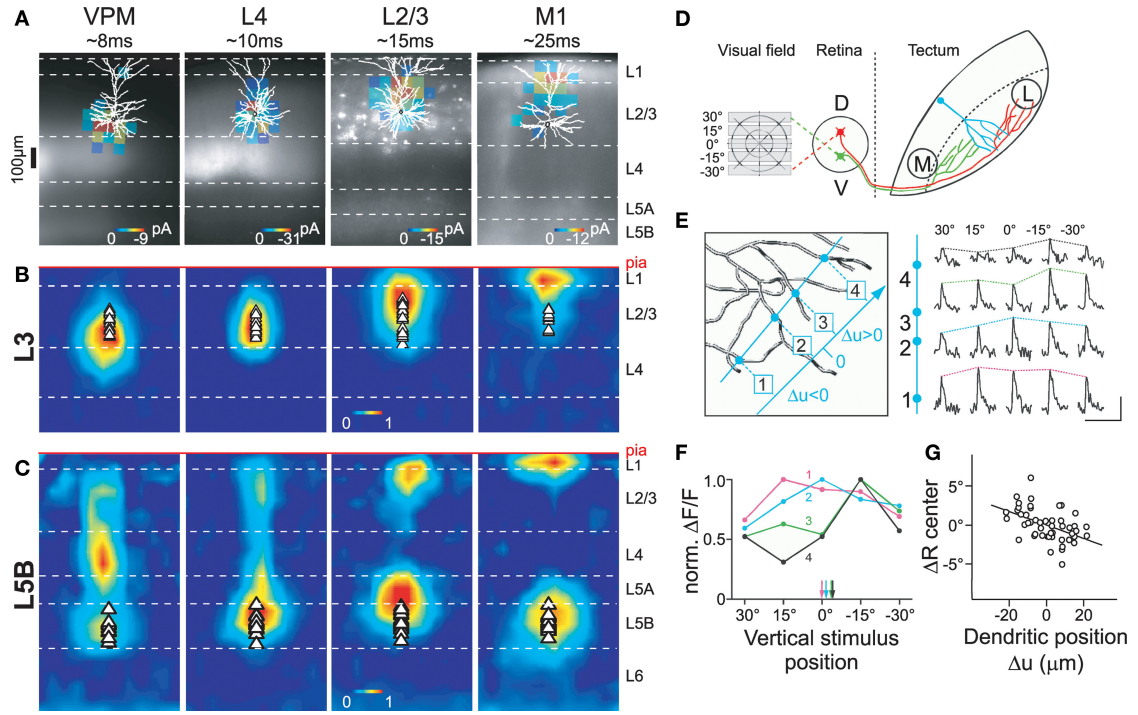

FIGURE 4 | Dendritic compartmentalization of synaptic input. (A) Subcellular channelrhodopsin-2 assisted circuit mapping (sCRACM) was used to map the dendritic location of excitatory inputs from the ventral posterior medial nucleus (VPM), barrel cortex layer 4 and layer 2/3, and primary whisker motor cortex (M1) on layer 3 **(A, B)** and layer 5B **(C)** neurons in barrel cortex (for details see Petreanu et al., 2009). Example maps superimposed on reconstructed morphologies and fluorescent images of ChR2-expression. **(B)** Average sCRACM-derived input map of layer 3 pyramidal neurons, displaying a hierarchical gradient of organization: bottom-up input (VPM) impinges onto the basal dendritic domain. Progressively more processed information arrives at progressively further apical locations. **(C)** Average input map of layer 5B pyramidal neurons corrected for dendritic attenuation of postsynaptic currents. Note that L2/3 and M1 inputs impinge onto both the basal dendrites and the apical tuft. Individual maps were aligned at the pia. Triangles indicate soma position. **(D)** Retinal input to dendrites of tectal neurons was elicited by presenting horizontal bars at different positions within the visual field of *Xenopus* tadpoles. **(E)** Line scans (blue) across 4 dendritic branches of one tectal neuron filled with the calcium-sensitive dye OGB-1 (left) reveal differential responses of the branches to the same stimulus position. Scale bar, 50% ΔF/F, 5 s. **(F)** Plotting normalized responses against stimulus position suggests branch-specific retinotopic input tuning. Arrows indicate centers of mass for each branch. **(G)** The mean subtracted center of mass (ΔR center) correlates with the relative position of a branch in the tectum. Reproduced with permission from (Petreanu et al., 2009) **(A–C)** and (Bollmann and Engert, 2009) **(D–G)**.

THEORETICAL CONSIDERATIONS FOR DEVELOPMENT AND INFORMATION PROCESSING

Synapses that exhibit STDP can perform a range of computations. These include sequence prediction (Abbott and Blum, 1996; Nowotny et al., 2003), memory storage (Roberts and Bell, 2002), principal component analysis (Oja, 1982; Abbott and Nelson, 2000), and temporal difference learning (Rao and Sejnowski, 2001). Simulations have shown that topographic maps and receptive field properties such as orientation tuning, ocular dominance, sound source localization, and velocity sensitivity can emerge when STDP is engaged as a developmental process (Gerstner et al., 1996; Song and Abbott, 2001; Tamosiunaite et al., 2007; Gandhi et al., 2008). Adult forms of plasticity, for example, stimulus-timing-dependent plasticity (Yao and Dan, 2001; Fu et al., 2002; Dahmen et al., 2008), recovery from retinal lesions (Young et al., 2007), and hippocampal phase procession (Mehta et al., 2002), have also been ascribed to forms of STDP.

In most of these theoretical studies, the STDP learning rule was assumed to be spatially and temporally homogeneous; that is, all synapses are assumed to have similar timing requirements for induction of LTP and LTD. Because experimental results demonstrate that STDP timing rules can depend on the dendritic location of synaptic inputs (**Figure 1**), and other studies document temporal modulation by spike bursts and high-frequency pre/post trains (Froemke et al., 2010), the assumption of uniformity for STDP time rules is probably only applicable for synapses located electrotonically close to the cell body and for pre- and postsynaptic spike trains at low frequencies (<10 Hz) that rarely contain bursts of two or more spikes. Furthermore, Goldberg et al. (2002) and Lisman and Spruston (2005) have raised several concerns about the importance of STDP as conventionally described, especially for synapses distal from the soma that have difficulty contributing to action potential generation in the absence of dendritic electrogenic mechanisms.

Spatial regulation of STDP helps alleviate some of these concerns. For example, synaptic weights in some neurons are scaled to normalize the effective strength of each input at the soma (Magee and Cook, 2000). As passive cable filtering of synaptic inputs would be expected to greatly reduce distal EPSP amplitudes, there may be mechanisms for adjusting synaptic efficacy, scaling the strength of synapses in proportion to their electrotonic distance from the spike initiation zone. Anti-Hebbian STDP is such a mechanism

(Goldberg et al., 2002; Letzkus et al., 2006; Sjöström and Häusser, 2006). As formalized by Rumsey and Abbott (2004), Hebbian STDP promotes proximal synapses and reduces the amplitude of distal synapses, because all else being equal, proximally-located inputs have a greater impact on somatic spike generation. However, if distal synapses express anti-Hebbian STDP, such that post → pre pairing induces LTP, then distal synapses will eventually be strengthened until some equilibrium point has been reached (**Figure 5A**).

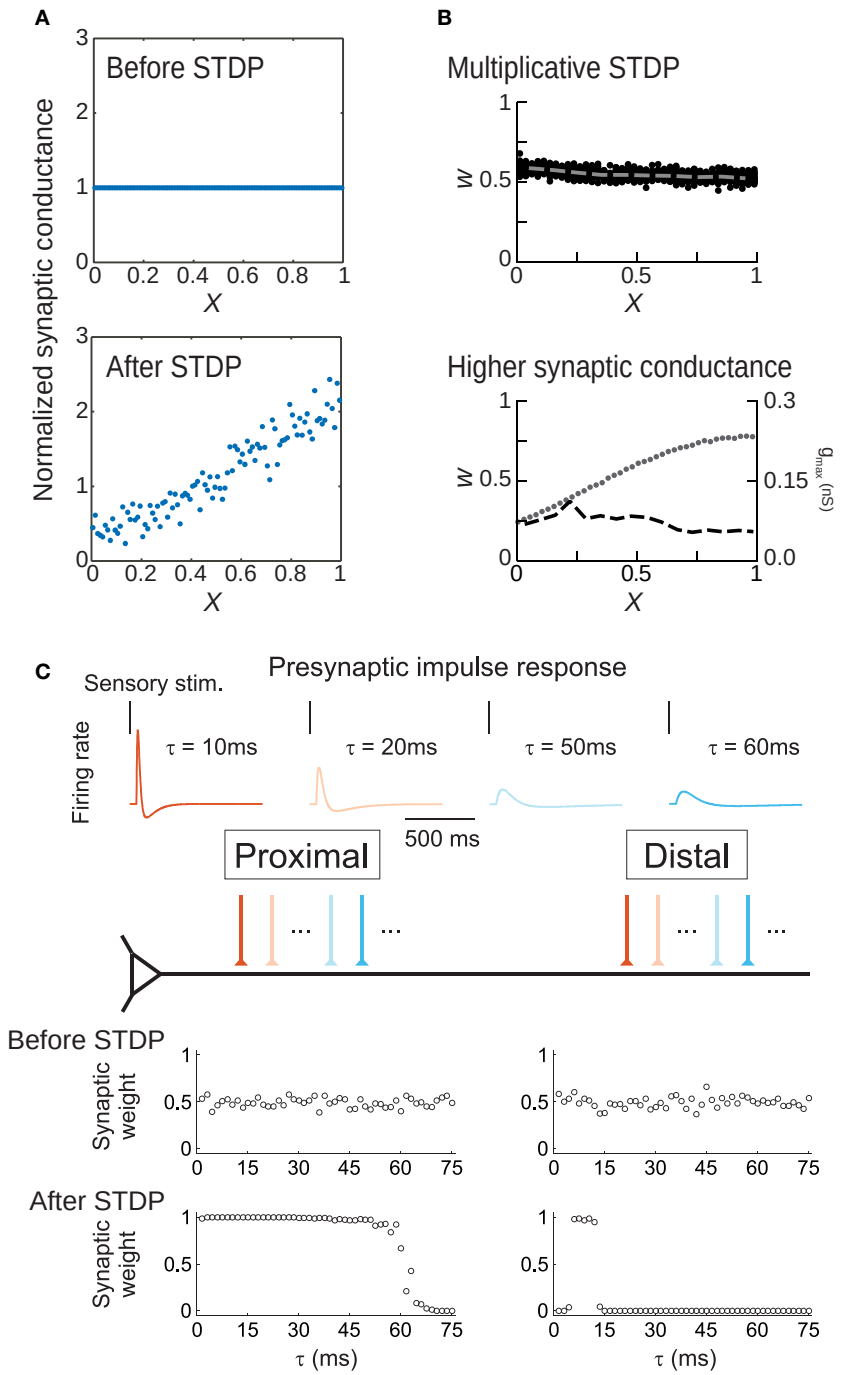

FIGURE 5 | Modeling location-dependent STDP. (A) Anti-Hebbian STDP scales synaptic strength as a function of electrotonic distance from the soma (*X*). Top, distribution of synaptic weights before training. Bottom, equilibrium synaptic strength after training. From Rumsey and Abbott (2004). **(B)** Uniform synaptic strength (*W*) can be achieved by multiplicative, weight-dependent STDP (top) or if distal synapses have larger maximally-possible peak conductances g_{max} (bottom). Dashed lines indicate average synaptic strengths; dots indicate g_{max}. From Gidon and Segev (2009). **(C)** In layer 2/3 neurons, location-dependent STDP selects for transient distal inputs. Top, example presynaptic responses to brief sensory stimuli. Warmer colors indicate more transient responses (τ < 15 ms). Bottom, synaptic inputs before and after induction of STDP. From Froemke et al. (2005).

In terms of synaptic organization, anti-Hebbian STDP provides a mechanism for retention of distal inputs, re-scaling synaptic strengths in proportion to electrotonic distance and preserving total excitatory drive. This can also be achieved with Hebbian STDP (Gidon and Segev, 2009) if formulated multiplicatively (**Figure 5B**, top) or if distal synapses have larger maximal peak conductances (**Figure 5B**, bottom), similar to reported experimental findings in CA1 hippocampal pyramidal cells (Magee and Cook, 2000).

Spatial gradients of STDP also increase the computational capacity of cortical pyramidal neurons. Previous simulations showed that LTD induced by post → pre spike pairs preferentially weakens synaptic inputs with long response latencies during competitive Hebbian synaptic modification (Song and Abbott, 2001). Dendritic regulation of STDP may therefore lead to differential selectivity of inputs along the apical dendrite. However, theoretical work from Mel and colleagues has demonstrated that additional computational power can only be harvested if synaptic inputs carrying different signals are clustered into distinct regions of the dendritic tree (Mel et al., 1998; Archie and Mel, 2000; Häusser and Mel, 2003). Thus, the location dependence of STDP not only demonstrates dendritic inhomogeneities in the properties governing activity-dependent synaptic modification, but also points to their potential role in the formation of branch-specific synaptic inputs; a feature that can greatly enrich the repertoire of dendritic information processing (Losonczy et al., 2008; Makara et al., 2009).

This idea was tested using a simple integrate-and-fire model neuron (**Figure 5C**), in which proximal and distal dendrites exhibited location-dependent STDP using presynaptic spike trains that were either transient and phasic or more prolonged and sustained, as observed *in vivo* (Baddeley et al., 1997). After training, inputs with relatively transient responses were strengthened and those with sustained responses were weakened at both distal and proximal locations. However, distal synapses were much more selective, retaining only those synaptic inputs that fired extremely transiently in response to sensory stimuli; these inputs must act synchronously to bring the postsynaptic cell to threshold, then quickly adapt so as to minimize the amount of depression caused by post → pre spiking in the postsynaptic cell. This is a direct consequence of the competitive advantage conferred to the proximal inputs over the distal inputs, by the difference in STDP. These simulations demonstrate that STDP may lead to functional differentiation of the capacity of distal and proximal dendrites to process signals with distinct temporal characteristics. Due to selection of more transient inputs, the distal dendrite may be specialized for processing the precise timing of sensory signals. These characteristics for distal inputs are precisely what have been found to be required for the initiation of distal dendritic Ca^{2+} spikes, which represent an effective way for distal inputs to influence neuronal output (Williams and Stuart, 2002). Moreover, variation in the statistical properties of inputs along the apical dendrite allows for topographic organization and coordination of receptive field properties such as temporal modulation sensitivity (Atencio and Schreiner, 2010).

CONCLUSION

There is a large literature on the dendritic factors that influence synaptic integration and action potential backpropagation in pyramidal neurons. These studies have demonstrated that action potentials and EPSPs are not the same size and shape in different regions of the dendritic tree, due to differences in dendritic geometry and passive properties, as well as differences in the dendritic distributions of neurotransmitter receptors, voltage-gated ion channels, Ca^{2+} buffers and stores, intracellular signaling molecules and mRNAs (Spruston, 2008; Stuart et al., 2008). Given the possible permutations of these factors, all of which may be crucial for long-term synaptic plasticity (Sanes and Lichtman, 1999), it is perhaps not surprising that STDP learning rules are different at different dendritic locations onto the same postsynaptic neuron, as previous hypothesized (Sourdet and Debanne, 1999).

In contrast to our more detailed understanding of dendritic integration, location dependence of STDP has to date only been investigated experimentally in a few studies (Froemke et al., 2005; Letzkus et al., 2006; Sjöström and Häusser, 2006). These data suggest that in general, proximal synapses undergo STDP according to conventional learning rules, while inputs onto distal dendrites display novel STDP induction requirements. A dominant factor shaping local learning rules is the decremental nature of action potential backpropagation (Stuart and Sakmann, 1994; Svoboda et al., 1999; Waters et al., 2003), causing distal synapses to experience a smaller local depolarization during STDP induction than proximal inputs. All forms of location-dependent STDP characterized so far employ NMDARs as coincidence detectors of synaptic activation and the backpropagating action potential (Froemke et al., 2005; Letzkus et al., 2006). However, STDP is known to depend on a variety of other signaling pathways, and future research will be needed to uncover their involvement in location-dependent STDP. Different input pathways have recently been shown to segregate onto distinct dendritic domains (Petreanu et al., 2009), suggesting that location-dependent forms of STDP may provide a mechanism for the regulation of dendritic inputs carrying different sensory signals.

REFERENCES

Abbott, L. F., and Blum, K. I. (1996). Functional significance of long-term potentiation for sequence learning and prediction. *Cereb. Cortex* 6, 406–416.

Abbott, L. F., and Nelson, S. B. (2000). Synaptic plasticity: taming the beast. *Nat. Neurosci.* 3, 1178–1183.

Angelo, K., London, M., Christensen, S. R., and Häusser, M. (2007). Local and global effects of Ih distribution in dendrites of mammalian neurons. *J. Neurosci.* 27, 8643–8653.

Antic, S. D. (2003). Action potentials in basal and oblique dendrites of rat neocortical neurons. *J. Physiol.* 550, 35–50.

Archie, K. A., and Mel, B. W. (2000). A model for intradendritic computation of binocular disparity. *Nat. Neurosci.* 3, 54–63.

Artola, A., Bröcher, S., and Singer, W. (1990). Different voltage-dependent thresholds for inducing long-term depression and long-term potentiation in slices of rat visual cortex. *Nature* 347, 69–72.

Atencio, C. A., and Schreiner, C. E. (2010). Laminar diversity of dynamic sound processing in cat primary auditory cortex. *J. Neurophysiol.* 103, 192–205.

Baddeley, R., Abbott, L. F., Booth, M. C., Sengpiel, F., Freeman, T., Wakeman, E. A., and Rolls, E. T. (1997). Responses of neurons in primary and inferior temporal visual cortices to natural scenes. *Proc. Biol. Sci.* 264, 1775–1783.

Bender, V. A., Bender, K. J., Brasier, D. J., and Feldman, D. E. (2006). Two coincidence detectors for spike timing-dependent plasticity in somatosensory cortex. *J. Neurosci.* 26, 4166–4177.

Bi, G.-Q., and Poo, M.-M. (1998). Synaptic modifications in cultured hippocampal neurons: dependence on spike timing, synaptic strength, and postsynaptic cell type. *J. Neurosci.* 18, 10464–10472.

Bollmann, J. H., and Engert, F. (2009). Subcellular topography of visually driven dendritic activity in the vertebrate visual system. *Neuron* 61, 895–905.

Bullis, J. B., Jones, T. D., and Poolos, N. P. (2007). Reversed somatodendritic Ih gradient in a class of rat hippocampal neurons with pyramidal morphology. *J. Physiol.* 579, 431–443.

Buonomano, D. V., and Merzenich, M. M. (1998). Cortical plasticity: from synapses to maps. *Annu. Rev. Neurosci.* 21, 149–186.

Cash, S., and Yuste, R. (1999). Linear summation of excitatory inputs by CA1 neurons. *Neuron* 22, 383–394.

Christie, B. R., Schexnayder, L. K., and Johnston, D. (1997). Contribution of voltage-gated Ca^{2+} channels to homosynaptic long-term depression in the CA1 region in vitro. *J. Neurophysiol.* 77, 1651–1655.

Cobb, S. R., Buhl, E. H., Halasy, K., Paulsen, O., and Somogyi, P. (1995). Synchronization of neuronal activity in hippocampus by individual GABAergic interneurons. *Nature* 378, 75–78.

Coombs, J. S., Curtis, D. R., and Eccles, J. C. (1957). The interpretation of spike potentials of motoneurones. *J. Physiol.* 139, 198–231.

Corlew, R., Wang, Y., Ghermazien, H., Erisir, A., and Philpot, B. D. (2007). Developmental switch in the contribution of presynaptic and postsynaptic NMDA receptors to long-term depression. *J. Neurosci.* 27, 9835–9845.

Dahmen, J. C., Hartley, D. E., and King, A. J. (2008). Stimulus-timing-dependent plasticity of cortical frequency processing. *J. Neurosci.* 28, 13629–13639.

Dan, Y., and Poo, M.-M. (2006). Spike timing-dependent plasticity: from synapse to perception. *Physiol. Rev.* 86, 1033–1048.

Das, A., and Gilbert, C. D. (1995). Long-range horizontal connections and their role in cortical reorganization revealed by optical recording of cat primary visual cortex. *Nature* 375, 780–784.

Debanne, D., Gahwiler, B. H., and Thompson, S. M. (1998). Long-term synaptic plasticity between pairs of individual CA3 pyramidal cells in rat hippocampal slice cultures. *J. Physiol.* 507, 237–247.

Diamond, M. E., Huang, W., and Ebner, F. F. (1994). Laminar comparison of somatosensory cortical plasticity. *Science* 265, 1885–1888.

Feldman, D. E. (2000). Timing-based LTP and LTD at vertical inputs to layer II/III pyramidal cells in rat barrel cortex. *Neuron* 27, 45–56.

Feldman, D. E. (2009). Synaptic mechanisms for plasticity in neocortex. *Annu. Rev. Neurosci.* 32, 33–55.

Feldman, D. E., Nicoll, R. A., and Malenka, R. C. (1999). Synaptic plasticity at thalamocortical synapses in developing rat somatosensory cortex: LTP, LTD, and silent synapses. *J. Neurobiol.* 41, 92–101.

Fleidervish, I. A., Binshtok, A. M., and Gutnick, M. J. (1998). Functionally distinct NMDA receptors mediate horizontal connectivity within layer 4 of mouse barrel cortex. *Neuron* 21, 1055–1065.

Frick, A., Magee, J., and Johnston, D. (2004). LTP is accompanied by an enhanced local excitability of pyramidal neuron dendrites. *Nat. Neurosci.* 7, 126–135.

Froemke, R. C., and Dan, Y. (2002). Spike-timing-dependent synaptic modification induced by natural spike trains. *Nature* 416, 433–438.

Froemke, R. C., Debanne, D., and Bi, G.-Q. (2010). Temporal modulation of spike-timing-dependent plasticity. *Front. Syn. Neurosci.* 2:19. doi:10.3389/fnsyn.2010.00019.

Froemke, R. C., Merzenich, M. M., and Schreiner, C. E. (2007). A synaptic memory trace for cortical receptive field plasticity. *Nature* 450, 425–429.

Froemke, R. C., Poo, M.-M., and Dan, Y. (2005). Spike-timing-dependent plasticity depends on dendritic location. *Nature* 434, 221–225.

Froemke, R. C., Tsay, I. A., Raad, M., Long, J. D., and Dan, Y. (2006). Contribution of individual spikes in burst-induced long-term synaptic modification. *J. Neurophysiol.* 95, 1620–1629.

Fu, Y.-X., Djupsund, K., Gao, H., Hayden, B., Shen, K., and Dan, Y. (2002). Temporal specificity in the cortical plasticity of visual space representation. *Science* 296, 1999–2003.

Fuortes, M. G., Frank, K., and Becker, M. C. (1957). Steps in the production of motoneuron spikes. *J. Gen. Physiol.* 40, 735–752.

Gandhi, S. P., Yanagawa, Y., and Stryker, M. P. (2008). Delayed plasticity of inhibitory neurons in developing visual cortex. *Proc. Natl. Acad. Sci. U.S.A.* 105, 16797–16802.

Gasparini, S., Migliore, M., and Magee, J. C. (2004). On the initiation and propagation of dendritic spikes in CA1 pyramidal neurons. *J. Neurosci.* 24, 11046–11056.

Gerstner, W., Kempter, R., van Hemmen, J. L., and Wagner, H. (1996). A neuronal learning rule for sub-millisecond temporal coding. *Nature* 383, 76–81.

Gidon, A., and Segev, I. (2009). Spike-timing-dependent synaptic plasticity and synaptic democracy in dendrites. *J. Neurophysiol.* 101, 3226–3234.

Goldberg, J., Holthoff, K., and Yuste, R. (2002). A problem with Hebb and local spikes. *Trends Neurosci.* 25, 433–435.

Golding, N. L., Staff, N. P., and Spruston, N. (2002). Dendritic spikes as a mechanism for cooperative long-term potentiation. *Nature* 418, 326–331.

Gordon, U., Polsky, A., and Schiller, J. (2006). Plasticity compartments in basal dendrites of neocortical pyramidal neurons. *J. Neurosci.* 26, 12717–12726.

Gulledge, A. T., Kampa, B. M., and Stuart, G. J. (2005). Synaptic integration in dendritic trees. *J. Neurobiol.* 64, 75–90.

Gulledge, A. T., and Stuart, G. J. (2003). Excitatory actions of GABA in the cortex. *Neuron* 37, 299–309.

Harvey, C. D., Yasuda, R., Zhong, H., and Svoboda, K. (2008). The spread of Ras activity triggered by activation of a single dendritic spine. *Science* 321, 136–140.

Häusser, M., Major, G., and Stuart, G. J. (2001). Differential shunting of EPSPs by action potentials. *Science* 291, 138–141.

Häusser, M., and Mel, B. (2003). Dendrites: bug or feature? *Curr. Opin. Neurobiol.* 13, 372–383.

Hoffman, D. A., and Johnston, D. (1999). Neuromodulation of dendritic action potentials. *J. Neurophysiol.* 81, 408–411.

Hoffman, D. A., Magee, J. C., Colbert, C. M., and Johnston, D. (1997). K^+ channel regulation of signal propagation in dendrites of hippocampal pyramidal neurons. *Nature* 387, 869–875.

Holtmaat, A., and Svoboda, K. (2009). Experience-dependent structural synaptic plasticity in the mammalian brain. *Nat. Rev. Neurosci.* 10, 647–658.

Izhikevich, E. M., and Desai, N. S. (2003). Relating STDP to BCM. *Neural. Comput.* 15, 1511–1523.

Jack, J. J., Miller, S., Porter, R., and Redman, S. J. (1971). The time course of minimal excitatory post-synaptic potentials evoked in spinal motoneurones by group Ia afferent fibres. *J. Physiol.* 215, 353–380.

Jacob, V., Brasier, D. J., Erchova, I., Feldman, D., and Shulz, D. E. (2007). Spike timing-dependent synaptic depression in the in vivo barrel cortex of the rat. *J. Neurosci.* 27, 1271–1284.

Jia, H., Rochefort, N. L., Chen, X., and Konnerth, A. (2010). Dendritic organization of sensory input to cortical neurons in vivo. *Nature* 464, 1307–1312.

Kampa, B. M., Letzkus, J. J., and Stuart, G. J. (2006). Requirement of dendritic calcium spikes for induction of spike-timing-dependent synaptic plasticity. *J. Physiol.* 574, 283–290.

Kampa, B. M., Letzkus, J. J., and Stuart, G. J. (2007). Dendritic mechanisms controlling spike-timing-dependent synaptic plasticity. *Trends Neurosci.* 30, 456–463.

Kampa, B. M., and Stuart, G. J. (2006). Calcium spikes in basal dendrites of layer 5 pyramidal neurons during action potential bursts. *J. Neurosci.* 26, 7424–7432.

Kato, N., and Yoshimura, H. (1993). Reduced Mg^{2+} block of N-methyl-D-aspartate receptor-mediated synaptic potentials in developing visual cortex. *Proc. Natl. Acad. Sci. U.S.A.* 90, 7114–7118.

Koester, H. J., and Sakmann, B. (1998). Calcium dynamics in single spines during coincident pre- and postsynaptic activity depend on relative timing of back-propagating action potentials and subthreshold excitatory postsynaptic potentials. *Proc. Natl. Acad. Sci. U.S.A.* 95, 9596–9601.

Krupp, J. J., Vissel, B., Thomas, C. G., Heinemann, S. F., and Westbrook, G. L. (2002). Calcineurin acts via the C-terminus of NR2A to modulate desensitization of NMDA receptors. *Neuropharmacology* 42, 593–602.

Kyrozis, A., Albuquerque, C., Gu, J., and MacDermott, A. B. (1996). Ca^{2+}-dependent inactivation of NMDA receptors: fast kinetics and high Ca^{2+} sensitivity in rat dorsal horn neurons. *J. Physiol.* 495, 449–463.

Larkum, M. E., Kaiser, K. M., and Sakmann, B. (1999a). Calcium electrogenesis in distal apical dendrites of layer 5 pyramidal cells at a critical frequency of back-propagating action potentials. *Proc. Natl. Acad. Sci. U.S.A.* 96, 14600–14604.

Larkum, M. E., Zhu, J. J., and Sakmann, B. (1999b). A new cellular mechanism for coupling inputs arriving at different cortical layers. *Nature* 398, 338–341.

Larkum, M. E., Zhu, J. J., and Sakmann, B. (2001). Dendritic mechanisms underlying the coupling of the dendritic with the axonal action potential initiation zone of adult rat layer 5 pyramidal neurons. *J. Physiol.* 533, 447–466.

Larkum, M. E., and Nevian, T. (2008). Synaptic clustering by dendritic signalling mechanisms. *Curr. Opin. Neurobiol.* 18, 321–331.

Letzkus, J. J., Kampa, B. M., and Stuart, G. J. (2006). Learning rules for spike timing-dependent plasticity depend on dendritic synapse location. *J. Neurosci.* 26, 10420–10429.

Letzkus, J. J., Kampa, B. M., and Stuart, G. J. (2007). Does spike timing-dependent synaptic plasticity underlie memory formation? *Clin. Exp. Pharmacol. Physiol.* 34, 1070–1076.

Lin, Y. W., Min, M. Y., Chiu, T. H., and Yang, H. W. (2003). Enhancement of associative long-term potentiation by activation of beta-adrenergic receptors at CA1 synapses in rat hippocampal slices. *J. Neurosci.* 23, 4173–4181.

Lisman, J., and Spruston, N. (2005). Postsynaptic depolarization requirements for LTP and LTD: a critique of spike-timing-dependent plasticity. *Nat. Neurosci.* 8, 839–841.

Losonczy, A., and Magee, J. C. (2006). Integrative properties of radial oblique dendrites in hippocampal CA1 pyramidal neurons. *Neuron* 50, 291–307.

Losonczy, A., Makara, J. K., and Magee, J. C. (2008). Compartmentalized dendritic plasticity and input feature storage in neurons. *Nature* 452, 436–441.

Magee, J. C. (2000). Dendritic integration of excitatory synaptic input. *Nat. Rev. Neurosci.* 1, 181–190.

Magee, J. C., and Cook, E. P. (2000). Somatic EPSP amplitude is independent of synapse location in hippocampal pyramidal neurons. *Nat. Neurosci.* 3, 895–903.

Magee, J. C., and Johnston, D. (1995). Synaptic activation of voltage-gated channels in the dendrites of hippocampal pyramidal neurons. *Science* 268, 301–304.

Magee, J.C., and Johnston, D. (1997). A synaptically controlled, associative signal for Hebbian plasticity in hippocampal neurons. *Science* 275, 209–213.

Magee, J. C., and Johnston, D. (2005). Plasticity of dendritic function. *Curr. Opin. Neurobiol.* 15, 334–342.

Makara, J. K., Losonczy, A., Wen, Q., and Magee, J. C. (2009). Experience-dependent compartmentalized dendritic plasticity in rat hippocampal CA1 pyramidal neurons. *Nat. Neurosci.* 12, 1485–1487.

Malenka, R. C., and Nicoll, R. A. (1999). Long-term potentiation- a decade of progress? *Science* 285, 1870–1874.

Markram, H., Lübke, J., Frotscher, M., and Sakmann, B. (1997). Regulation of synaptic efficacy by coincidence of postsynaptic APs and EPSPs. *Science* 275, 213–215.

Markram, H., Toledo-Rodriguez, M., Wang, Y., Gupta, A., Silberberg, G., and Wu, C. (2004). Interneurons of the neocortical inhibitory system. *Nat. Rev. Neurosci.* 5, 793–807.

Mayer, M. L., Westbrook, G. L., and Guthrie, P. B. (1984). Voltage-dependent block by Mg^{2+} of NMDA responses in spinal cord neurones. *Nature* 309, 261–263.

Meeks, J. P., and Mennerick, S. (2007). Action potential initiation and propagation in CA3 pyramidal axons. *J. Neurophysiol.* 97, 3460–3472.

Mehta, M. R., Lee, A. K., and Wilson, M. A. (2002). Role of experience and oscillations in transforming a rate code into a temporal code. *Nature* 417, 741–746.

Mel, B. W., Ruderman, D. L., and Archie, K. A. (1998). Translation-invariant orientation tuning in visual "complex" cells could derive from intradendritic computations. *J. Neurosci.* 18, 4325–4334.

Migliore, M., and Shepherd, G. M. (2002). Emerging rules for the distributions of active dendritic conductances. *Nat. Rev. Neurosci.* 3, 362–270.

Murayama, M., Pérez-Garci, E., Nevian, T., Bock, T., Senn, W., and Larkum, M. E. (2009). Dendritic encoding of sensory stimuli controlled by deep cortical interneurons. *Nature* 457, 1137–1141.

Nevian, T. Larkum, M. E., Polsky, A., and Schiller, J. (2007). Properties of basal dendrites of layer 5 pyramidal neurons: a direct patch-clamp recording study. *Nat. Neurosci.* 10, 206–214.

Nishiyama, M., Hong, K., Mikoshiba, K., Poo, M. M., and Kato, K. (2000). Calcium stores regulate the polarity and input specificity of synaptic modification. *Nature* 408, 584–588.

Nowak, L., Bregestovski, P., Ascher, P., Herbet, P., and Prochiantz, A. (1984). Magnesium gates glutamate-activated channels in mouse central neurones. *Nature* 307, 462–465.

Nowotny, T., Rabinovich, M. I., and Abarbanel, H. D. (2003). Spatial representation of temporal information through spike-timing-dependent plasticity. *Phys. Rev. E Stat. Nonlin. Soft Matter Phys.* 68, 011908.

Nusser, Z. (2009). Variability in the subcellular distribution of ion channels increases neuronal diversity. *Trends Neurosci.* 32, 267–274.

Oja, E. (1982). A simplified neuron model as a principal component analyzer. *J. Math. Biol.* 15, 267–273.

Palmer, L.M., and Stuart, G.J. (2006). Site of action potential initiation in layer 5 pyramidal neurons. *J. Neurosci.* 26, 1854–1863.

Pérez-Garci, E., Gassmann, M., Bettler, B., and Larkum, M. E. (2006). The GABAB1b isoform mediates long-lasting inhibition of dendritic Ca^{2+} spikes in layer 5 somatosensory pyramidal neurons. *Neuron* 50, 603–616.

Petreanu, L., Mao, T., Sternson, S. M., and Svoboda, K. (2009). The subcellular organization of neocortical excitatory connections. *Nature* 457, 1142–1145.

Pouille, F., and Scanziani, M. (2001). Enforcement of temporal fidelity in pyramidal cells by somatic feed-forward inhibition. *Science* 293, 1159–1163.

Rall, W. (1964). "Theoretical significance of dendritic trees for neuronal input-output relations," in *Neural Theory and Modeling*, ed R. F. Reiss (Palo Alto, CA: Stanford University Press), 73–97.

Rao, R. P. N., and Sejnowski, T. J. (2001). Spike-timing-dependent Hebbian plasticity as temporal difference learning. *Neural. Comput.* 13, 2221–2237.

Reyes, A. (2001). Influence of dendritic conductances on the input-output properties of neurons. *Annu. Rev. Neurosci.* 24, 653–675.

Roberts, P. D., and Bell, C. C. (2002). Spike timing dependent plasticity in biological systems. *Biol. Cybern.* 87, 392–403.

Rosenmund, C., Feltz, A., and Westbrook, G. L. (1995). Calcium-dependent inactivation of synaptic NMDA receptors in hippocampal neurons. *J. Neurophysiol.* 73, 427–430.

Rumsey, C. C., and Abbott, L. F. (2004). Equalization of synaptic efficacy by activity- and timing-dependent synaptic plasticity. *J. Neurophysiol.* 91, 2273–2280.

Sanes, J. R., and Lichtman, J. W. (1999). Can molecules explain long-term potentiation? *Nat. Neurosci.* 2, 597–604.

Saudargiene, A., Porr., B., and Wörgötter, F. (2004). How the shape of pre- and postsynaptic signals can influence STDP: a biophysical model. *Neural. Comput.* 16, 595–625.

Saudargiene, A., Porr., B., and Wörgötter, F. (2005). Local learning rules: predicted influence of dendritic location on synaptic modification in spike-timing-dependent plasticity. *Biol. Cybern.* 92, 128–138.

Schiller, J., Schiller, Y., Stuart, G., and Sakmann, B. (1997). Calcium action potentials restricted to distal apical dendrites of rat neocortical pyramidal neurons. *J. Physiol.* 505, 605–616.

Schmidt-Hieber, C., Jonas, P., and Bischofberger, J. (2008). Action potential initiation and propagation in hippocampal mossy fibre axons. *J. Physiol.* 586, 1849–1857.

Segev, I., and London, M. (2000). Untangling dendrites with quantitative models. *Science* 290, 744–750.

Seol, G. H., Ziburkus, J., Huang, S., Song, L., Kim, I. T., Takamiya, K., Huganir, R. L., Lee, H. -K., and Kirkwood, A. (2007). Neuromodulators control the polarity of spike-timing-dependent synaptic plasticity. *Neuron* 20, 919–929.

Shu, Y., Duque, A., Yu, Y., Haider, B., and McCormick, D. A. (2007). Properties of action-potential initiation in neocortical pyramidal cells: evidence from whole cell axon recordings. *J. Neurophysiol.* 97, 746–760.

Silberberg, G., and Markram, H. (2007). Disynaptic inhibition between neocortical pyramidal cells mediated by Martinotti cells. *Neuron* 53, 735–746.

Sjöström, P. J., and Häusser, M. (2006). A cooperative switch determines the sign of synaptic plasticity in distal dendrites of neocortical pyramidal neurons. *Neuron* 51, 227–238.

Sjöström, P. J., and Nelson, S. B. (2002). Spike timing, calcium signals, and synaptic plasticity. *Curr. Opin. Neurobiol.* 12, 305–314.

Sjöström, P. J., Rancz, E. A., Roth, A., and Häusser, M. (2008). Dendritic excitability and synaptic plasticity. *Physiol. Rev.* 88, 769–840.

Sjöström, P. J., Turrigiano, G. G., and Nelson, S. B. (2001). Rate, timing, and cooperativity jointly determine cortical synaptic plasticity. *Neuron* 32, 1149–1164.

Sjöström, P. J., Turrigiano, G. G., and Nelson, S. B. (2003). Neocortical LTD via coincident activation of presynaptic NMDA and cannabinoid receptors. *Neuron* 39, 641–654.

Sjöström, P. J., Turrigiano, G. G., and Nelson, S. B. (2004). Endocannabinoid-dependent neocortical layer-5 LTD in the absence of postsynaptic spiking. *J. Neurophysiol.* 92, 3338–3343.

Smith, M. A., Ellis-Davies, G. C. R., and Magee, J. C. (2003). Mechanism of the distance-dependent scaling of Schaffer collateral synapses in rat CA1 pyramidal neurons. *J. Physiol.* 548, 245–258.

Song, S., and Abbott, L. F. (2001). Column and map development and cortical re-mapping through spike timing-dependent synaptic plasticity. *Neuron* 32, 339–350.

Song, S., Miller, K. D., and Abbott, L. F. (2000). Competitive Hebbian learning through spike-timing-dependent synaptic plasticity. *Nat. Neurosci.* 3, 919–926.

Sourdet, V., and Debanne, D. (1999). The role of dendritic filtering in associative long-term synaptic plasticity. *Learn. Mem.* 6, 422–447.

Spruston, N. (2008). Pyramidal neurons: dendritic structure and synaptic integration. *Nat. Rev. Neurosci.* 9, 206–221.

Spruston, N., Schiller, Y., Stuart, G., and Sakmann, B. (1995). Activity-dependent action potential invasion and calcium influx into hippocampal CA1 dendrites. *Science* 268, 297–300.

Stuart, G. J., and Häusser, M. (1994). Initiation and spread of sodium action potentials in cerebellar Purkinje cells. *Neuron* 13, 703–712.

Stuart, G. J., and Häusser, M. (2001). Dendritic coincidence detection of EPSPs and action potentials. *Nat. Neurosci.* 4, 63–71.

Stuart, G. J., and Sakmann, B. (1994). Active propagation of somatic action potentials into neocortical pyramidal cell dendrites. *Nature* 367, 69–72.

Stuart, G., Schiller, J., and Sakmann, B. (1997). Action potential initiation and propagation in rat neocortical pyramidal neurons. *J. Physiol.* 505, 617–632.

Stuart, G. J., and Spruston, N. (1998). Determinants of voltage attenu-

ation in neocortical pyramidal neuron dendrites. *J. Neurosci.* 18, 3501–3510.

Stuart, G. J., Spruston, N., and Häusser, M. (2008). *Dendrites.* New York: Oxford University Press.

Svoboda, K., Helmchen, F., Denk, W., and Tank, D. W. (1999). Spread of dendritic excitation in layer 2/3 pyramidal neurons in rat barrel cortex in vivo. *Nat. Neurosci.* 2, 65–73.

Tamás, G., Szabadics, J., and Somogyi, P. (2002). Cell type- and subcellular position-dependent summation of unitary postsynaptic potentials in neocortical neurons. *J. Neurosci.* 22, 740–747.

Tamosiunaite, M., Porr, B., and Wörgötter, F. (2007). Developing velocity sensitivity in a model neuron by local synaptic plasticity. *Biol. Cybern.* 96, 507–518.

Tong, G., Shepherd, D., and Jahr, C. E. (1995). Synaptic desensitization of NMDA receptors by calcineurin. *Science* 267, 1510–1512.

Trachtenberg, J. T., Trepel, C., and Stryker, M. P. (2000). Rapid extragranular plasticity in the absence of thalamocortical plasticity in the developing primary visual cortex. *Science* 287, 2029–2032.

Umemiya, M., Chen, N., Raymond, L. A., and Murphy, T. H. (2001). A calcium-dependent feedback mechanism participates in shaping single NMDA miniature EPSCs. *J. Neurosci.* 21, 1–9.

Urakubo, H., Honda, M., Froemke, R. C., and Kuroda, S. (2008). Requirement of an allosteric kinetics of NMDA receptors for spike timing-dependent plasticity. *J. Neurosci.* 28, 3310–3323.

Waters, J., Larkum, M., Sakmann, B., and Helmchen, F. (2003). Supralinear Ca^{2+} influx into dendritic tufts of layer 2/3 neocortical pyramidal neurons in vitro and in vivo. *J. Neurosci.* 23, 8558–8567.

Wespatat, V., Tennigkeit, F., and Singer, W. (2004). Phase sensitivity of synaptic modifications in oscillating cells of rat visual cortex. *J. Neurosci.* 24, 9067–9075.

Williams, S. R., and Mitchell, S. J. (2008). Direct measurement of somatic voltage clamp errors in central neurons. *Nat. Neurosci.* 11, 790–798.

Williams, S. R., and Stuart, G. J. (1999). Mechanisms and consequences of action potential burst firing in rat neocortical pyramidal neurons. *J. Physiol.* 521, 467–482.

Williams, S. R., and Stuart, G. J. (2000a). Backpropagation of physiological spike trains in neocortical pyramidal neurons: implications for temporal coding in dendrites. *J. Neurosci.* 20, 8238–8246.

Williams, S. R., and Stuart, G. J. (2000b). Site independence of EPSP time course is mediated by dendritic Ih in neocortical pyramidal neurons. *J. Neurophysiol.* 83, 3177–3182.

Williams, S. R., and Stuart, G. J. (2002). Dependence of EPSP efficacy on synapse location in neocortical pyramidal neurons. *Science* 295, 1907–1910.

Yao, H., and Dan, Y. (2001). Stimulus timing-dependent plasticity in cortical processing of orientation. *Neuron* 32, 315–323.

Young, J. M., Waleszczyk, W. J., Wang, C., Calford, M. B., Dreher, B., and Obermayer, K. (2007). Cortical reorganization consistent with spike timing- but not correlation-dependent plasticity. *Nat. Neurosci.* 10, 887–895.

Zorumski, C. F., and Thio, L. L. (1992). Properties of vertebrate glutamate receptors: calcium mobilization and desensitization. *Prog. Neurobiol.* 39, 295–336.

Zucker, R. S. (1999). Calcium- and activity-dependent synaptic plasticity. *Curr. Opin. Neurobiol.* 9, 305–313.

Conflict of Interest Statement: The authors declare that the research was conducted in the absence of any commercial or financial relationships that could be construed as a potential conflict of interest.

Received: 02 February 2010; paper pending published: 23 February 2010; accepted: 27 June 2010; published online: 21 July 2010.
Citation: Froemke RC, Letzkus JJ, Kampa BM, Hang GB, Stuart GJ (2010) Dendritic synapse location and neocortical spike-timing-dependent plasticity. Front. Syn. Neurosci. ***2****:29. doi: 10.3389/fnsyn.2010.00029*

frontiers in
SYNAPTIC NEUROSCIENCE

REVIEW ARTICLE
published: 17 June 2010
doi: 10.3389/fnsyn.2010.00018

Presynaptic NMDA receptors and spike timing-dependent depression at cortical synapses

Antonio Rodríguez-Moreno[1,2]*, Abhishek Banerjee[1] and Ole Paulsen[1,3]*

[1] *Department of Physiology, Anatomy and Genetics, University of Oxford, Oxford, UK*
[2] *Department of Physiology, Anatomy and Cellular Biology, University Pablo de Olavide, Seville, Spain*
[3] *Department of Physiology, Development and Neuroscience, University of Cambridge, Cambridge, UK*

Edited by:
Per Jesper Sjöström, University College London, UK

Reviewed by:
Ian Duguid, The University of Edinburgh, UK
Mariano Casado, Ecole Normale Supérieure, France

****Correspondence:***
Antonio Rodríguez-Moreno, Department of Physiology, Anatomy and Cellular Biology, University Pablo de Olavide, Laboratory of Cellular Neuroscience and Plasticity, Ctra. de Utrera, Km. 141013, Seville, Spain.
e-mail: arodmor@upo.es;
Ole Paulsen, Department of Physiology, Development and Neuroscience, University of Cambridge, The Neuronal Oscillations Group, Physiological Laboratory, Downing Street, Cambridge CB2 3EG, UK.
e-mail: op210@cam.ac.uk

It has recently been discovered that some forms of timing-dependent long-term depression (t-LTD) require presynaptic *N*-methyl-D-aspartate (NMDA) receptors. In this review, we discuss the evidence for the presence of presynaptic NMDA receptors at cortical synapses and their possible role in the induction of t-LTD. Two basic models emerge for the induction of t-LTD at cortical synapses. In one model, coincident activation of presynaptic NMDA receptors and CB1 receptors mediates t-LTD. In a second model, CB1 receptors are not necessary, and the activation of presynaptic NMDA receptors alone appears to be sufficient for the induction of t-LTD.

Keywords: plasticity, STDP, t-LTD, NMDA, presynaptic mechanisms

SYNAPTIC PLASTICITY AND NMDA RECEPTORS

One of the most interesting properties of the brain is its ability to change in response to experience. This property has been termed plasticity and is involved in the reorganization of cortical maps during development, and in learning and memory processes in the adult animal (for review, see Malenka and Bear, 2004). Plasticity is assumed to be mediated primarily by synaptic changes. Synaptic plasticity can be short-term (lasting from milliseconds to several minutes) or long-term (lasting from hours to months; see Citri and Malenka, 2008 for review). The most extensively studied forms of synaptic plasticity are long-term potentiation (LTP) and long-term depression (LTD). Spike timing-dependent plasticity (STDP) is a Hebbian form of long-term plasticity (Caporale and Dan, 2008) and is a strong candidate for a synaptic plasticity mechanism involved in cortical development (Song and Abbott, 2001; Feldman and Brecht, 2005; Dan and Poo, 2006; Caporale and Dan, 2008). In STDP, the temporal order and relative timing of pre- and postsynaptic action potentials (spikes), with millisecond precision, determine the direction and magnitude of synaptic change. Thus, timing-dependent (t-) LTP occurs when a presynaptic spike is followed by a postsynaptic spike, whereas t-LTD is induced when this order is reversed (Markram et al., 1997; Bi and Poo, 1998; Debanne et al., 1998; for a detailed review of STDP, see Caporale and Dan, 2008). Both t-LTP and t-LTD depend on a specific type of ionotropic glutamate receptor, the *N*-methyl-D-aspartate (NMDA) receptor, for their induction (Bi and Poo, 1998; Debanne et al., 1998; Feldman, 2000; Sjöström et al., 2003).

The ionotropic family of glutamate receptors comprises α–amino-3-hydroxy-5-methyl-4-isoxazolepropionic acid (AMPA), kainate and NMDA receptors, which are widely distributed in the central nervous system (Dingledine et al., 1999). NMDA receptors are ligand-gated ion channels permeable to Ca^{2+}, Na^{+} and K^{+} ions. These receptors are hetero-tetramers composed of two essential GluN1 and two modulatory GluN2 subunits (using the subunit nomenclature recommended by the IUPHAR; Collingridge et al., 2009), which confer different functional, kinetic, pharmacological and signaling properties to the NMDA receptor (for review, see Cull-Candy et al., 2001). NMDA receptors participate in normal synaptic transmission, synaptic development and synaptic plasticity, and are involved in the pathogenesis of some neurological states and diseases including stroke, epilepsy, schizophrenia and neuropathic pain (Cull-Candy et al., 2001). These receptors have been localized in the postsynaptic membrane where they are activated by the co-agonists glutamate and glycine (or D-serine) and contribute to excitatory postsynaptic responses together with AMPA and kainate receptors. t-LTP depends on postsynaptic NMDA receptors acting as classical coincidence detectors where presynaptic spikes trigger the release of glutamate necessary to activate these receptors, and back-propagating action potentials produce postsynaptic depolarization which relieves the NMDA receptors of their voltage-dependent Mg^{2+} block leading to influx of Ca^{2+} ions. Surprisingly, in some cortical areas, postsynaptic loading of the NMDA receptor channel blocker MK-801 blocked t-LTP but

not t-LTD, suggesting that NMDA receptors involved in t-LTD are not postsynaptic. (Bender et al., 2006; Nevian and Sakmann, 2006; Corlew et al., 2007; see Corlew et al., 2008 for review). This finding raises the possibility that NMDA receptors involved in t-LTD might have a presynaptic location.

EVIDENCE FOR PRESYNAPTIC NMDA RECEPTORS

The existence of presynaptic NMDA receptors was first proposed following the finding that NMDA receptor agonists facilitated noradrenaline release in synaptosome preparations from the hippocampus (Pittaluga and Raiteri, 1990, 1992; Wang et al., 1992) and cerebral cortex (Fink et al., 1990; Wang et al., 1992), and dopamine release in the striatum (Johnson and Jeng, 1991; Krebs et al., 1991; Wang, 1991). Recently, more evidence has appeared for presynaptic NMDA receptors involved in dopamine release in synaptosomes and synaptoneurosomes in the striatum (Whittaker et al., 2008). Evidence for presynaptic NMDA receptors was also found at neuromuscular synapses from *Xenopus* in culture where NMDA enhances transmitter release (Fu et al., 1995). The existence of presynaptic NMDA receptors has also been supported by anatomical evidence. Anatomical support for presynaptic NMDA receptors has come from immuno-electron microscopy experiments which have identified NMDA receptor immunolabeling in presynaptic elements of the neocortex (Aoki et al., 1994; DeBiasi et al., 1996; Charton et al., 1999; Corlew et al., 2007), the hippocampus (Siegel et al., 1994; Charton et al., 1999; Jourdain et al., 2007), the spinal cord (Liu et al., 1994), the amygdala (Farb et al., 1995; Pickel et al., 2006) and the cerebellum (Petralia et al., 1994; Bidoret et al., 2009). Functionally, presynaptic NMDA receptors have been proposed to exist on both excitatory and inhibitory boutons, where they could modulate transmitter release. At cortical glutamatergic synapses they have generally been suggested to serve as facilitatory autoreceptors, reversibly enhancing glutamate release. A transient decrease of miniature excitatory postsynaptic current (mEPSC) frequency was seen following the application of the NMDA receptor antagonist D-AP5 when postsynaptic NMDA receptors were previously blocked by intracellular loading of MK-801 or by hyperpolarization. This was first demonstrated in the entorhinal cortex (Berretta and Jones, 1996; Woodhall et al., 2001) and subsequently in the visual cortex (Sjöström et al., 2003; Corlew et al., 2007; Li and Han, 2007; Li et al., 2008), somatosensory cortex (Bender et al., 2006; Brasier and Feldman, 2008) and hippocampus (Mameli et al., 2005; Jourdain et al., 2007; see Corlew et al., 2008 for review). Apart from the cerebral cortex, there is also evidence for physiologically active presynaptic NMDA receptors in the cerebellum (Glitsch and Marty, 1999; Casado et al., 2000; Duguid and Smart, 2004; Fiszman et al., 2005), amygdala (Humeau et al., 2003) and spinal cord (Liu et al., 1997; Bardoni et al., 2004). For broader reviews on the evidence for presynaptic glutamate receptors, see MacDermott et al. (1999), Engelman and MacDermott (2004) and Pinheiro and Mulle (2008).

Presynaptic NMDA receptors have been implicated in plasticity at both excitatory and inhibitory synapses, including heterosynaptic associative LTP at thalamic and cortical afferent synapses in the amygdala (Humeau et al., 2003), depolarization-induced potentiation (Duguid and Smart, 2004) and LTD (Casado et al., 2002) in the cerebellum, LTD at GABAergic synapses in the tadpole optic tectum (Lien et al., 2006) and t-LTD in different cortical areas as discussed by Duguid and Sjöström (2006) and Corlew et al. (2008).

While these putative functional NMDA receptors are generally assumed to be at axonal locations, the existence of presynaptic, axonal NMDA receptors has been challenged by the discovery that somatodendritic NMDA receptor activation can affect axonal Ca^{2+} levels through voltage-dependent calcium channel activation, at least in cerebellar stellate cells (Christie and Jahr, 2008). A further challenge has come from the apparent lack of direct effect of NMDA application on axonal Ca^{2+} levels and axon excitability in cortical layer (L) 5 pyramidal neurons (Christie and Jahr, 2009).

To summarize, experiments in synaptosomes are suggestive of NMDA receptors being present in presynaptic boutons; immuno-electron microscopy experiments are also consistent with axonal NMDA receptors since immunolabeling has been found in axons in different regions. In slices, the existence of axonal presynaptic NMDA receptors has been proposed based on the observation that the addition of an NMDA receptor antagonist affects spontaneous, miniature and evoked neurotransmitter release, even after intracellular blockade of postsynaptic NMDA receptors (see Corlew et al., 2008 for review). The recent experiments by Christie and Jahr (2008, 2009) question the interpretation of these results, suggesting that the observed effects could be mediated by NMDA receptors located in the somatodendritic compartment of the presynaptic neuron.

To unequivocally demonstrate the existence of functional presynaptic axonal NMDA receptors a combination of different approaches will be required (see Corlew et al., 2008 for review):

(1) Immunogold electron microscopy (Farb et al., 1995);
(2) Direct monitoring of presynaptic function by calcium imaging whilst adding agonists or antagonists at NMDA receptors (Shin and Linden, 2005);
(3) Direct electrophysiological recording from presynaptic boutons (Fiszman et al., 2005);
(4) Direct loading of NMDA receptor antagonists into the presynaptic neuron (Rodríguez-Moreno and Paulsen, 2008); and
(5) Compartment-specific interference with NMDA receptor function using molecular or genetic tools (Lynch, 2004; Safo and Regehr, 2005).

ROLE OF PRESYNAPTIC NMDA RECEPTORS IN SPIKE TIMING-DEPENDENT LTD

The first evidence for a role of presynaptic NMDA receptors in STDP came from experiments at L5-L5 synapses of visual cortex where an NMDA receptor-dependent presynaptic form of t-LTD was described (Sjöström et al., 2003). This t-LTD requires activation of postsynaptic group I mGluRs and postsynaptic Ca^{2+} elevation. Results indicate that this form of t-LTD is expressed as a reduction in the probability of neurotransmitter release, thus implicating a retrograde signal from the postsynaptic to the presynaptic compartment (Sjöström et al., 2003). This retrograde messenger has been suggested to be endocannabinoids, which mediate many forms of short-term (Wilson et al., 2001; Brown et al., 2004) and long-term plasticity (Chevaleyre et al., 2006). Thus, it has been proposed that

the coincidence detector for t-LTD at this synapse is presynaptic and involves both presynaptic NMDA receptors and cannabinoid receptor type 1 (CB1 receptors) (Sjöström et al., 2003) (**Figure 1**).

Direct evidence for presynaptic NMDA receptor involvement in t-LTD has recently been obtained at L4-L2/3 synapses of somatosensory cortex using dual whole-cell recordings of synaptically-connected L4 and L2/3 neurons by loading the NMDA receptor channel blocker MK-801 intracellularly via a patch pipette into pre- or postsynaptic neurons. Induction of t-LTD was unaffected by postsynaptic loading of MK-801 but completely blocked by presynaptic MK-801, indicating that t-LTD requires presynaptic, but not postsynaptic NMDA receptors (Rodríguez-Moreno and Paulsen, 2008).

The subunit composition of these presynaptic receptors has been analyzed (Banerjee et al., 2009). For this purpose, two GluN2C/D subunit-preferring NMDA receptor antagonists, PPDA and UBP141 were used. These compounds selectively blocked t-LTD at L4-L2/3 synapses with no effect on t-LTP at the same synapses, which was instead blocked by the GluN2A subunit-preferring antagonist NVP-AAM077. They also had no blocking effect on t-LTD at L2/3-L2/3 synapses, which was, however, blocked by a GluN2B subunit-selective antagonist (Ro 25-6981; Banerjee et al., 2009). Compounds currently available are not highly selective for GluN2C/D-containing NMDA receptors and, moreover, are competitive antagonists. Thus, the inhibition produced depends on the effective glutamate concentration (Neyton and Paoletti, 2006), precluding strong conclusions to be drawn. Nevertheless, the double dissociation found, and the fact that these GluN2C/D subunit-preferring antagonists did not block t-LTD at a different synapse, suggest that L4-L2/3 presynaptic NMDA receptors contain GluN2C/D subunits (Banerjee et al., 2009). When available, experiments with GluN2C/D non-competitive antagonists should confirm whether results are due to different subunit composition of the receptors at pre- and postsynaptic sites or to different kinetics of glutamate transients at different locations. The current lack of selective compounds that can distinguish between GluN2C and GluN2D subunits precludes an investigation into whether it is GluN2C or GluN2D that is the important subunit for the induction of t-LTD. The possible involvement of presynaptic GluN2C/D

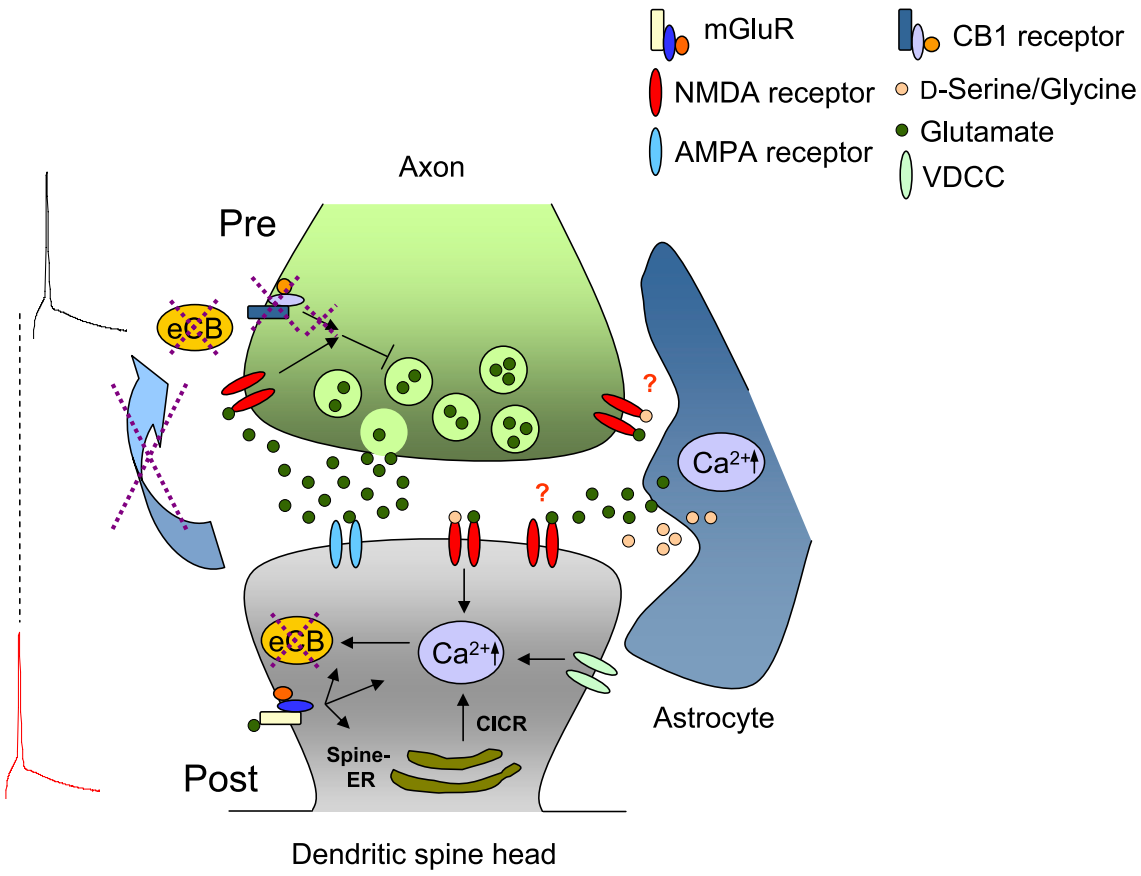

FIGURE 1 | Two models of presynaptic NMDA receptor-dependent t-LTD. **Model 1:** Presynaptic NMDA receptors and CB1 receptors drive t-LTD. In this model, during post-before-pre pairing, presynaptically released glutamate activates mGluRs and postsynaptic action potentials enhance Ca^{2+} influx. This would lead to endocannabinoid (eCB) synthesis. eCB diffuses retrogradely and binds to presynaptic CB1 receptors. Co-activation of presynaptic CB1 receptors and presynaptic NMDA receptors causes synaptic depression. In this model, presynaptic NMDA receptors are activated by glutamate release from the presynaptic terminal. Astrocytic release of gliotransmitters (glutamate as agonist and/or D-serine or glycine as co-agonist) may contribute to activating neuronal NMDA receptors. **Model 2:** In a second model, eCB-dependent retrograde signaling is not necessary for induction of t-LTD (dashed crosses), and activation of presynaptic NMDA receptors alone appears to be sufficient to drive presynaptic t-LTD. The source of transmitter activating presynaptic NMDA receptors is unknown.

subunits in t-LTD at layer 4-to-layer 2/3 synapses is particularly interesting because the deactivation time constant of GluN2C/D subunit-containing receptors is very slow (Momiyama et al., 1996; Brothwell et al., 2008; Wyllie, 2008). This might be relevant for the particularly broad time window for induction of t-LTD at this synapse (Feldman, 2000).

Several lines of evidence indicate that this form of t-LTD is presynaptic: (i) t-LTD is blocked when presynaptic NMDA receptors are blocked by internal MK-801 in recordings from pairs of synaptically-connected L4 and L2/3 cells (Rodríguez-Moreno and Paulsen, 2008), (ii) an increase in paired-pulse ratio is observed after a t-LTD protocol (Bender et al., 2006), and (iii) coefficient of variation (CV) analysis is consistent with presynaptic expression (Rodríguez-Moreno and Paulsen, 2008).

Although previous studies have implicated endocannabinoid signaling through CB1 receptors in this form of t-LTD at rat L4-L2/3 synapses (Bender et al., 2006), it was recently reported that t-LTD does not need CB1 receptor activation at the mouse L4-L2/3 synapse (Hardingham et al., 2008; Banerjee et al., 2009), suggesting a possible species and/or age difference. In contrast, CB1 receptors are necessary for induction of t-LTD at horizontal synapses (L2/3-L2/3), supporting the idea that different excitatory synapses onto the same postsynaptic neurons can have different requirements for the induction of synaptic plasticity (Banerjee et al., 2009).

It is clear from these results that endocannabinoids are not obligatory for all forms of timing-dependent synaptic depression. The results also suggest that at least two distinct forms of presynaptic NMDA receptor-dependent LTD can be dissociated, one dependent on endocannabinoid signaling and the GluN2B subunit (Sjöström et al., 2003; Banerjee et al., 2009) (**Figure 1**), and another, independent of endocannabinoids but dependent on presynaptic NMDA receptors containing GluN2C/D subunits (Rodríguez-Moreno and Paulsen, 2008; Banerjee et al., 2009) (**Figure 1**). Notably, both of these forms of t-LTD have in common a dependence on presynaptic NMDA receptors, suggesting that NMDA receptors mediate t-LTD while CB1 receptors may have a permissive role.

MECHANISM OF PRESYNAPTIC t-LTD

The results described above suggest that, at L4-L2/3 synapses, t-LTD is mediated by presynaptic NMDA receptors that contain GluN2C/D subunits. Since there is no evidence that other presynaptic receptors are implicated, we suggest that presynaptic NMDA receptors are effectively mediating this form of t-LTD. In this model, postsynaptic spikes allow the activation of presynaptic NMDA receptors when followed by a presynaptic spike. It is, however, unknown whether the depolarization requirement often observed for unblocking NMDA receptors is necessary for activation of presynaptic NMDA receptors, since GluN2C/D and GluN3A-containing NMDA receptors show less voltage sensitivity than other NMDA receptor types (Cull-Candy et al., 2001; Clarke and Johnson, 2006). The presence of NMDA receptors with low conductance and reduced susceptibility to Mg^{2+} block in the presynaptic layer 4 spiny stellate cells was reported earlier using transgenic mice (Binshtok et al., 2006). Another interesting aspect to consider is the relationship with frequency in the induction of this form of t-LTD. t-LTD has been observed in neocortical slices using different stimulation frequencies from 0.1 to 20 Hz, indicating that this form of plasticity can be elicited at low frequencies of stimulation (Feldman, 2000; Sjöström et al., 2001, 2003; Bender et al., 2006; Nevian and Sakmann, 2006; Rodríguez-Moreno and Paulsen, 2008; Banerjee et al., 2009). However, at 40 Hz and above, only t-LTP was observed, irrespective of the timing between pre- and postsynaptic action potentials (Sjöström et al., 2001). Timing-dependent LTD at L4-L2/3 synapses in synaptically-connected cells during paired recordings can be induced by pairing single presynaptic and postsynaptic action potentials at 0.2 Hz (Rodríguez-Moreno and Paulsen, 2008), constraining the possible mechanisms involved in this form of t-LTD.

The requirement of presynaptic NMDA receptors for t-LTD raises several interesting questions:

(i) What is the source of the transmitter that activates presynaptic NMDA receptors?
In principle, there are several possible different sources of transmitter mediating the activation of presynaptic NMDA receptors. Glutamate could be released by the presynaptic neuron and NMDA receptors activated as autoreceptors. Glutamate could also be released by the postsynaptic neuron, as retrograde release of glutamate has been suggested (Harkany et al., 2004). Glial cells have also been shown to release glutamate and modulate synaptic transmission and plasticity (see Perea et al., 2009 for review). Co-agonists at NMDA receptors, such as D-serine, are also released by astrocytes and have recently been shown to be involved in plasticity (Henneberger et al., 2010). Glutamate (and/or co-agonists at NMDA receptors) of glial origin could reach presynaptic NMDA receptors and activate them (Jourdain et al., 2007). Another possible source of transmitter could be the spillover from neighboring synapses. Spillover of transmitter appears less likely, however, since t-LTD can be induced at very low frequency in pairs of synaptically-connected cells, leaving the postsynaptic neuron and glial cells as the most likely sources. The exact source of transmitter that activates presynaptic NMDA receptors remains to be determined.

(ii) Is the activation of these presynaptic NMDA receptors tonic or phasic in nature?
Rodríguez-Moreno and Paulsen (2008) showed that the application of the NMDA receptor antagonist D-AP5 did not alter the EPSP slope at the L4-L2/3 synapse, suggesting that these receptors are not tonically active. Brasier and Feldman (2008) found that addition of D-AP5 caused a reduction of AMPA currents at the L4-L2/3 synapse, suggesting that, in principle, these receptors could be tonically activated, though these results were obtained in the presence of glutamate transporter blockers.

(iii) What is the role of the postsynaptic action potential in the pairing protocol?
Induction of t-LTD at this synapse requires pairing of postsynaptic action potentials with presynaptic activity. The exact role of the postsynaptic action potentials has not yet been determined. Previous experiments have shown that this form of LTD requires a rise in postsynaptic Ca^{2+}, as it is blocked by the presence of BAPTA in the postsynaptic cell (Bender et al., 2006; Nevian and Sakmann, 2006). The postsynaptic action potential could mediate Ca^{2+} entry through

voltage-dependent calcium channels and/or induce release of Ca^{2+} from internal stores. This implies that a Ca^{2+}–dependent signal from the postsynaptic neuron is most probably necessary, but the nature of this signal remains to be determined.

(iv) Why do t-LTP protocols not also produce LTD?
If a slow Ca^{2+}–dependent postsynaptic process is involved in the induction of t-LTD, one might expect that the postsynaptic condition for induction of t-LTD would also be satisfied during a pre-before-post paradigm. Why do t-LTP protocols not also induce t-LTD? Postsynaptic action potentials might trigger the release of a retrograde messenger that acts on the presynaptic element during the presynaptic action potential. Because the time window for post-before-pre pairing is relatively narrow, it would suggest that this retrograde signal has to act in a similarly short time window (~10 ms) to operate as a presynaptic coincidence signal. This time scale would appear to make postsynaptic enzyme-dependent mechanisms less likely candidates to provide the presynaptic coincidence signal during induction of t-LTD. There is clearly more work to be done before we understand the detailed mechanisms of induction of presynaptic NMDA receptor-dependent t-LTD.

CONCLUSION

In conclusion, spike timing-dependent LTD requires presynaptic NMDA receptors at some cortical synapses. Two basic models are emerging to explain the mechanism of these presynaptic forms of t-LTD. In one model, presynaptic NMDA receptors and CB1 receptors mediate t-LTD (Sjöström et al., 2003). A second model, suggests that presynaptic NMDA receptors mediate a form of t-LTD that is independent of CB1 receptor activation (Rodríguez-Moreno and Paulsen, 2008; Banerjee et al., 2009). Notably, both forms of t-LTD have in common a dependence of presynaptic NMDA receptors, suggesting that NMDA receptors, might be essential to mediate t-LTD, while CB1 receptors have a permissive role when involved.

ACKNOWLEDGMENTS

Antonio Rodríguez-Moreno was supported by a Marie Curie Intra-European Fellowship, by a Royal Society International Short Visit Grant and by a Network Grant from the McDonnell Network for Cognitive Neuroscience, University of Oxford. Abhishek Banerjee was supported by a Felix scholarship from the University of Oxford.

REFERENCES

Aoki, C., Venkatesam, C., Go, C. G., Mong, J. A., and Dawson, T. M. (1994). Cellular and subcellular localization of NMDA-R1subunit immunorreactivity in the visual cortex of adult and neonatal rats. *J. Neurosci.* 14, 5202–5222.

Banerjee, A., Meredith, R. M., Rodríguez-Moreno, A., Mierau, S. B., Auberson, Y. P., and Paulsen, O. (2009). Double dissociation of spike timing-dependent potentiation and depression by subunit-preferring NMDA receptor antagonists in mouse barrel cortex. *Cereb. Cortex* 19, 2959–2969.

Bardoni, R., Torsney, C., Tong, C.-T., Prandini, M., and MacDermott, A. B. (2004). Presynaptic NMDA receptors modulate glutamate release from primary sensory neurons in rat spinal cord dorsal horn. *J. Neurosci.* 24, 2774–2781.

Bender, V. A., Bender, K. J., Brasier, D. J., and Feldman, D. E. (2006). Two coincidence detectors for spike timing-dependent plasticity in somatosensory cortex. *J. Neurosci.* 16, 4166–4177.

Berretta, N., and Jones, R. S. (1996). Tonic facilitation of glutamate release by presynaptic N-methyl-D-aspartate autoreceptors in the entorhinal cortex. *Neuroscience* 75, 339–344.

Bi, G.-Q., and Poo, M.-M. (1998). Synaptic modifications in cultured hippocampal neurons: dependence of spike timing, synaptic strength, and postsynaptic cell type. *J. Neurosci.* 18, 10464–10472.

Bidoret, C., Ayon, A., Barbour, B., and Casado, M. (2009). Presynaptic NR2A-containing NMDA receptors implement a high-pass filter synaptic plasticity rule. *Proc. Natl. Acad. Sci. U.S.A.* 106, 14126–14131.

Binshtok, A. M., Fleidervish, I. A., Sprengel, R., and Gutnick, M. J. (2006). NMDA receptors in layer 4 spiny stellate cells of the mouse barrel cortex contain the NR2C subunit. *J. Neurosci.* 26, 708–715.

Brasier, D. J., and Feldman, D. E. (2008). Synapse-specific expression of functional presynaptic NMDA receptors in rat somatosensory cortex. *J. Neurosci.* 28, 2199–2211.

Brothwell, S. L., Barber, J. L., Monaghan, D. T., Jane, D. E., Gibb, A. J., and Jones, S. (2008). NR2B- and NR2D-containing synaptic NMDA receptors in developing rat substantia nigra pars compacta dopaminergic neurones. *J. Physiol.* 586, 739–750.

Brown, S. P., Safo, P. K., and Regehr, W. G. (2004). Endocannabinoids inhibit transmission at granule cell to Purkinje cell synapses by modulating three types of presynaptic calcium channels. *J. Neurosci.* 24, 5623–5631.

Caporale, N., and Dan, Y. (2008). Spike timing-dependent plasticity: A Hebbian learning rule. *Annu. Rev. Neurosci.* 31, 25–46.

Casado, M., and Dieudonne, S, Ascher, P. (2000). Presynaptic N-methyl-D-aspartate receptors at the parallel fiber-Purkinje cell synapse. *Proc. Natl. Acad. Sci. U.S.A.* 97, 11593–11597.

Casado, M., Isope, P., and Asher, P. (2002). Involvement of presynaptic N-methyl-D-aspartate receptors in cerebellar long-term depression. *Neuron* 33, 123–130.

Charton, J. P., Herkert, M., Becker, C. M., and Schroder, H. (1999). Cellular and subcellular localization of the 2B-subunit of the NMDA receptor in the adult rat telencephalon. *Brain Res.* 816, 609–617.

Chevaleyre, V., Takahashi, K. A., and Castillo, P. E. (2006). Endocannabinoid-mediated synaptic plasticity in the CNS. *Annu. Rev. Neurosci.* 29, 37–76.

Christie, J. M., and Jahr, C. E. (2008). Dendritic NMDA receptors activate axonal calcium channels. *Neuron* 60, 298–307.

Christie, J. M., and Jahr, C. E. (2009). Selective expression of ligand-gated ion channels in L5 pyramidal cell axons. *J. Neurosci.* 29, 11441–11450.

Citri, A., and Malenka, R. C. (2008). Synaptic plasticity: multiple forms, functions and mechanisms. *Neuropsychopharmacology* 33, 18–41.

Clarke, R. J., and Johnson, J. W. (2006). NMDA receptor NR2 subunit dependence of the slow component of magnesium unblock. *J. Neurosci.* 26, 5825–5834.

Collingridge, G. L., Olsen, R. W., Peters, J., and Spedding, M. (2009). A nomenclature for ligand-gated ion channels. *Neuropharmacology* 56, 2–5.

Corlew, R., Brasier, D. J., Feldman, D. E., and Philpot, B. D. (2008). Presynaptic NMDA receptors: newly appreciated roles in cortical synaptic function and plasticity. *Neuroscientist* 14, 609–625.

Corlew, R., Wang, Y., Ghermazien, H., Erisir, A., and Philpot, B. D. (2007). Developmental switch in the contribution of presynaptic and postsynaptic NMDA receptors to long-term depression. *J. Neurosci.* 27, 9835–9845.

Cull-Candy, S., Brickely, S., and Farrant, M. (2001). NMDA receptor subunits: diversity, development and disease. *Curr. Opin. Neurobiol.* 11, 327–335.

Dan, Y., and Poo, M. M. (2006). Spike timing-dependent plasticity: from synapse to perception. *Physiol. Rev.* 86, 1033–1048.

Debanne, D., Gahwiler, B. H., and Thompson, S. M. (1998). Long-term synaptic plasticity between pairs of individual CA3 pyramidal cells in rat hippocampal slice cultures. *J. Physiol.* 507, 237–247.

DeBiasi, S., Minnelli, A., Melone, M., and Conti, F. (1996). Presynaptic NMDA receptors in the neocortex are both auto- and heteroreceptors. *Neuroreport* 7, 2773–2776.

Dingledine, R., Borges, K., Bowie, D., and Traynelis, S. F. (1999). The glutamate receptor ion channels. *Pharmacol. Rev.* 51, 7–61.

Duguid, I. C., and Sjöström, P. J. (2006). Novel presynaptic mechanisms for coincidence detection in synaptic plasticity. *Curr. Opin. Neurobiol.* 16, 312–322.

Duguid, I. C., and Smart, T. G. (2004). Retrograde activation of presynaptic NMDA receptors enhances GABA release at cerebellar interneuron-Purkinje cell synapses. *Nat. Neurosci.* 7, 525–533.

Engelman, H. S., and MacDermott, A. B. (2004). Presynaptic ionotropic receptors and control of transmitter release. *Nat. Rev. Neurosci.* 5, 135–145.

Farb, C. R., Aoki, C., and Ledoux, J. E. (1995). Differential localization of NMDA and AMPA receptor subunits in the lateral and basal nuclei of the amygdala: a light and electron microscopic study. *J. Comp. Neurol.* 362, 86–108.

Feldman, D. E. (2000). Timing-based LTP and LTD at vertical inputs to layer II/III pyramidal cells in rat barrel cortex. *Neuron* 27, 45–56.

Feldman, D. E., and Brecht, M. (2005). Map plasticity in somatosensory cortex. *Science* 310, 810–815.

Fink, K., Bonisch, H., and Gothert, M. (1990). Presynaptic NMDA receptors stimulate noradrenaline release in the cerebral cortex. *Eur. J. Pharmacol.* 185, 115–117.

Fiszman, M. L., Barberis, A., Lu, C., Fu, Z., Erdelyi, F., Szabo, G., and Vicini, S. (2005). NMDA receptors increase the size of GABAergic terminals and enhance GABA release. *J. Neurosci.* 25, 2024–2031.

Fu, W., Liou, J., Lee, Y., and Liou, H. (1995). Potentiation of neurotransmitter release by activation of presynaptic glutamate receptors at developing neuromuscular synapses of Xenopus. *J. Physiol.* 489, 813–823.

Glitsch, M., and Marty, A. (1999). Presynaptic effects of NMDA in cerebellar Purkinje cells and interneurons. *J. Neurosci.* 19, 511–519.

Hardingham, N., Wright, N., Dachtler, J., and Fox, K. (2008). Sensory deprivation unmasks a PKA-dependent synaptic plasticity mechanism that operates in parallel with CaMKII. *Neuron* 60, 861–874.

Harkany, T., Holmgren, C., Härtig, W., Qureshi, T., Chaudhry, F. A., Storm-Mathisen, J., Dobszay, M. B., Berghuis, P., Schulte, G., Sousa, K. M., Fremeau, R. T. Jr., Edwards, R. H., Mackie, K., Ernfors, P., and Zilberter,Y. (2004). Endocannabinoid-independent retrograde signaling at inhibitory synapses in layer 2/3 of neocortex: involvement of vesicular glutamate transporter 3. *J. Neurosci.* 24, 4978–4988.

Henneberger, C., Papouin, T., Oliet, S. H., and Rusakov, D. A. (2010). Long-term potentiation depends on release of D-serine from astrocytes. *Nature* 463, 232–236.

Humeau, Y., Shaban, H., Bissiere, S., and Lüthi, A. (2003). Presynaptic induction of heterosynaptic associative plasticity in the mammalian brain. *Nature* 426, 841–845.

Johnson, K. M., and Jeng, Y. J. (1991). Pharmacological evidence for N-methyl-D-aspartate receptors on nigrostriatal dopaminergic terminals. *Can. J. Physiol. Pharmacol.* 69, 1416–1421.

Jourdain, P., Bergersen, L. H., Bhaukaurally, K., Bezzi, P., Santello, M., Domercq, M., Matute, C., Tonello, F., Gundersen, V., and Volterra, A. (2007). Glutamate exocytosis from astrocytes controls synaptic strength. *Nat. Neurosci.* 10, 331–339.

Krebs, M. O., Desce, J. M., Kemel, M. L., Gauchy, C., Godeheu, G., Cheramy, A., and Glowinski, J. (1991). Glutamatergic control of dopamine release in the rat striatum: evidence for presynaptic N-methyl-D-aspartate receptors on dopamine nerve terminals. *J. Neurochem.* 56, 81–85.

Li, Y. H., and Han, T. Z. (2007). Glycine binding sites of presynaptic NMDA receptors may tonically regulate glutamate release in the rat visual cortex. *J. Neurophysiol.* 97, 817–823.

Li, Y. H., Han, T. Z., and Meng, K. (2008). Tonic facilitation of glutamate release by glycine binding sites on presynaptic NR2B-containing NMDA autoreceptors in the rat visual cortex. *Neurosci. Lett.* 432, 212–216.

Lien, C. C., Mu, Y. Vargas-Caballero, M., and Poo, M. M. (2006). Visual stimuli-induced LTD of GABAergic synapses mediated by presynaptic NMDA receptors. *Nat. Neurosci.* 9, 372–380.

Liu, H., Mantyh, P. W., and Basbaum, A. I. (1997). NMDA-receptor regulation of substance P release from primary afferent nociceptors. *Nature* 386, 721–724.

Liu, H., Wang, H., Sheng, M., Jan, L. Y., Jan, Y. N., and Basbaum, A. I. (1994). Evidence for presynaptic N-methyl-D-aspartate autoreceptors in the spinal cord dorsal horn. *Proc. Natl. Acad. Sci. U.S.A.* 91, 8383–8387.

Lynch, M. A. (2004). Long-term potentiation and memory. *Physiol. Rev.* 84, 87–136.

MacDermott, A. B., Role, L. W., and Siegelbaum, S. A. (1999). Presynaptic ionotropic receptors and the control of transmitter release. *Annu. Rev. Neurosci.* 22, 443–485.

Malenka, R. C., and Bear, M. F. (2004). LTP and LTD: an embarrassment of riches. *Neuron* 44, 5–21.

Mameli, M., Carta, M., Partridge, L. D., and Valenzuela, C. F. (2005). Neurosteroid-induced plasticity of immature synapses via retrograde modulation of presynaptic NMDA receptors. *J. Neurosci.* 25, 2285–2294.

Markram, H., Lübke, J. Frotscher, M., and Sakmann, B. (1997). Regulation of synaptic efficacy by coincidence of postsynaptic APs and EPSPs. *Science* 275, 213–215.

Momiyama, A., Feldmeyer, D., and Cull-Candy, S. G. (1996). Identification of a native low-conductance NMDA channel with reduced sensitivity to Mg^{2+} in rat central neurones. *J. Physiol.* 494, 479–492.

Nevian, T., and Sakmann, B. (2006). Spine Ca^{2+} signaling in spike-timing-dependent plasticity. *J. Neurosci.* 43, 11001–11013.

Neyton, J., and Paoletti, P. (2006). Relating NMDA receptor function to receptor subunit composition: limitations of the pharmacological approach. *J. Neurosci.* 26,1331–1333.

Perea, G., Navarrete, M., and Araque, A. (2009). Tripartite synapses: astrocytes process and control synaptic information. *Trends Neurosci.* 32, 421–431.

Petralia, R. S., Wang, Y. X., and Wenthold, R. J. (1994). The NMDA receptor subunits NR2A and NR2B show histological and ultrastructural localization patterns similar to those of NR1. *J. Neurosci.* 14, 6102–6120.

Pickel, V. M., Colago, E. E., Mania, I., Molosh, A. I., and Rainnie, D. G. (2006). Dopamine D1 receptors co-distribute with N-methyl-D-aspartic acid type-1 subunits and modulate synaptically-evoked N-methyl-D-aspartic acid currents in basolateral amygdala. *Neuroscience* 142, 671–690.

Pinheiro, P. S., and Mulle, C. (2008). Presynaptic glutamate receptors: physiological functions and mechanisms of action. *Nat. Rev. Neurosci.* 9, 423–435.

Pittaluga, A., and Raiteri, M. (1990). Release-enhancing glycine-dependent presynaptic NMDA receptors exist on noradrenergic terminals of hippocampus. *Eur. J. Pharmacol.* 191, 231–234.

Pittaluga, A., and Raiteri, M. (1992). N-methyl-D-aspartic acid (NMDA) and non-NMDA receptors regulating hippocampal norepinephrine release. I. Location on axon terminals and pharmacological characterization. *J. Pharmacol. Exp. Ther.* 260, 232–237.

Rodríguez-Moreno, A., and Paulsen, O. (2008). Spike timing-dependent long-term depression requires presynaptic NMDA receptors. *Nat. Neurosci.* 11, 744–745.

Safo, P. K., and Regehr, W. G. (2005). Endocannabinoids control the induction of LTD. *Neuron* 48, 647–659.

Shin, J. H., and Linden, D. J. (2005). An NMDA receptor/nitric oxide cascade is involved in cerebellar LTD but is not localized to the parallel fiber terminal. *J. Neurophysiol.* 94, 4281–4289.

Siegel, S. J., Brose, N., Janssen, W. G., Gasic, G. P., Jahn, R., Heinemann, S. F., and Morrison, J. H. (1994). Regional, cellular, and ultrastructural distribution of N-methyl-D-aspartate receptor subunit 1 in monkey hippocampus. *Proc. Natl. Acad. Sci. U.S.A.* 91, 564–568.

Sjöström, P. J., Turrigiano, G. G., and Nelson, S. B. (2001). Rate, timing, and cooperativity jointly determine cortical synaptic plasticity. *Neuron* 32, 1149–1164.

Sjöström, P. J., Turrigiano, G. G., and Nelson, S. B. (2003). Neocortical LTD via coincident activation of presynaptic NMDA and cannabinoid receptors. *Neuron* 39, 641–654.

Song, S., and Abbott, L. F. (2001). Cortical development and remapping through spike timing-dependent plasticity. *Neuron* 39, 339–350.

Wang, J. K. T. (1991). Presynaptic NMDA receptors modulate dopamine release from striatal synaptosomes. *J. Neurochem.* 57, 819–822.

Wang, J. K. T., Andrews, H., and Thkral, V. (1992). Presynaptic NMDA receptors regulate noradrenaline release from isolated nerve terminals. *J. Neurochem.* 58, 204–211.

Whittaker, M. T., Gibbs, T. T., and Farb, D. H. (2008). Pregnenolone sulfate induces NMDA receptor dependent release of dopamine from synaptic terminals in the striatum. *J. Neurochem.* 107, 510–521.

Wilson, R. I., Kunos, G., and Nicoll, R. A. (2001). Presynaptic specificity of endocannabinoid signaling in the hippocampus. *Neuron* 31, 453–462.

Woodhall, G., Evans, D. I., Cunningham, M. O., and Jones, R. S. (2001). NR2B-containing NMDA autoreceptors at synapses on entorhinal cortical neurons. *J. Neurophysiol.* 86, 1644–1651.

Wyllie, D. J. (2008). 2B or 2B and 2D? - that is the question. *J. Physiol.* 586, 693.

Conflict of Interest Statement: The authors declare that the research was conducted in the absence of any commercial or financial relationships that could be construed as a potential conflict of interest.

Received: 12 February 2010; paper pending published: 05 March 2010; accepted: 24 May 2010; published online: 17 June 2010.

*Citation: Rodríguez-Moreno A, Banerjee A and Paulsen O (2010) Presynaptic NMDA receptors and spike timing-dependent long-term depression at cortical synapses. Front. Syn. Neurosci. **2**:18. doi: 10.3389/fnsyn.2010.00018*

frontiers in
SYNAPTIC NEUROSCIENCE

REVIEW ARTICLE
published: 25 October 2010
doi: 10.3389/fnsyn.2010.00146

Timing is not everything: neuromodulation opens the STDP gate

Verena Pawlak[1]*, Jeffery R. Wickens[2], Alfredo Kirkwood[3] and Jason N. D. Kerr[1]*

[1] *Network Imaging Group, Max Planck Institute for Biological Cybernetics, Tuebingen, Germany*
[2] *Neurobiology Research Unit, Okinawa Institute of Science and Technology, Okinawa, Japan*
[3] *Mind/Brain Institute and Department of Neurosciences, Johns Hopkins University, Baltimore, MD, USA*

Edited by:
Wulfram Gerstner, Ecole Polytechnique Fédérale de Lausanne, Switzerland

Reviewed by:
Markus Diesmann, RIKEN Brain Science Institute, Japan
Wulfram Gerstner, Ecole Polytechnique Fédérale de Lausanne, Switzerland
Henning Sprekeler , Ecole Polytechnique Fédérale de Lausanne, Switzerland
Nicolas Fremaux, Ecole Polytechnique Fédérale de Lausanne, Switzerland
Botond Szatmáry , Brain Corporation, USA

****Correspondence:***
Verena Pawlak and Jason N. D. Kerr, Network Imaging Group, Max Planck Institute for Biological Cybernetics, Spemannstrasse 41, 72076 Tuebingen, Germany.
e-mail: verena.pawlak@tuebingen.mpg.de; jason@tuebingen.mpg.de

Spike timing dependent plasticity (STDP) is a temporally specific extension of Hebbian associative plasticity that has tied together the timing of presynaptic inputs relative to the postsynaptic single spike. However, it is difficult to translate this mechanism to *in vivo* conditions where there is an abundance of presynaptic activity constantly impinging upon the dendritic tree as well as ongoing postsynaptic spiking activity that backpropagates along the dendrite. Theoretical studies have proposed that, in addition to this pre- and postsynaptic activity, a "third factor" would enable the association of specific inputs to specific outputs. Experimentally, the picture that is beginning to emerge, is that in addition to the precise timing of pre- and postsynaptic spikes, this third factor involves neuromodulators that have a distinctive influence on STDP rules. Specifically, neuromodulatory systems can influence STDP rules by acting via dopaminergic, noradrenergic, muscarinic, and nicotinic receptors. Neuromodulator actions can enable STDP induction or – by increasing or decreasing the threshold – can change the conditions for plasticity induction. Because some of the neuromodulators are also involved in reward, a link between STDP and reward-mediated learning is emerging. However, many outstanding questions concerning the relationship between neuromodulatory systems and STDP rules remain, that once solved, will help make the crucial link from timing-based synaptic plasticity rules to behaviorally based learning.

Keywords: reward, learning, dopamine, acetylcholine, noradrenaline, synaptic plasticity, calcium, behavior

INTRODUCTION

The first groundbreaking *in vitro* STDP studies seemed to paint a very clear picture: The near-coincidence of presynaptic input and postsynaptic spiking enables neurons to enhance or decrease their synaptic weights depending on the exact timing of these two events (Magee and Johnston, 1997; Markram et al., 1997; Bi and Poo, 1998; Debanne et al., 1998). This finding was a giant step forward in our view of synaptic plasticity rules: It tied together the idea that both *single spikes* and *their precise timing* matter; with the implication that neurons have a means to associate arriving inputs with the outgoing spikes and adapt the synaptic weights accordingly. It was therefore very intuitive to postulate STDP as a more temporally specific extension of Hebbian associative learning and experience driven plasticity (for definition, see below; and for modeling approaches see: Gerstner et al., 1993, 1996; Abbott and Blum, 1996; Blum and Abbott, 1996; Mehta et al., 2000).

However, for this idea to be relevant for behavioral learning as first formally proposed by Hebb (1949), it must hold true *in vivo*. This is where the STDP concept faces two conundrums, the first based on ongoing spiking activity, and the second based on the timing of spikes in relation to behavioral outcome.

Abbreviations: AP, action potential; EPSP, excitatory postsynaptic potential; ACh, acetylcholine; NA, noradrenaline; nAChR, nicotinic acetylcholine receptor; mAChR, muscarinic acetylcholine receptor; mGluR, metabotropic glutamate receptor; AC, adenylyl cyclase; PLC, phospholipase C; PKA, protein kinase A; t-LTP, timing-dependent LTP; t-LTD, timing-dependent LTD

(1) Unlike *in vitro*, *in vivo* there are continuous barrages of ongoing presynaptic activity impinging on the dendritic tree that can generate postsynaptic spikes (**Figures 1A,B**) (Wilson and Groves, 1981; Cowan et al., 1994; Wilson and Kawaguchi, 1996; Stern et al., 1997). These spikes backpropagate throughout the neuron (Waters et al., 2003; Waters and Helmchen, 2004), potentially interacting with the vast number of dendritically located synapses as these synapses continue to receive barrages of excitatory inputs (**Figure 1C$_2$**). Under these conditions, the implications of STDP rules on individual synapses would be that a synapse active just prior to a spike event will increase in efficacy, whereas a synapse that is active just after the spike, will decrease its efficacy. The question arises, whether the mere association of presynaptic input and postsynaptic spiking activity would be enough to alter synaptic efficacy, and whether individual synapses in turn continuously scale up and down as inputs and backpropagating spikes constantly interact? Moreover, do spontaneously occurring spikes (**Figure 1C$_2$**) and stimulus-evoked spikes (**Figure 1C$_3$**) equally change synaptic weights as they interact with presynaptic input (**Figure 1D**)? When a spike is fired, whether it is spontaneous or evoked, how are active synaptic inputs that are driven by a stimulus separated from those that are due to the ongoing activity? One possible solution to these selectivity problems was originally proposed in relation to reward mediated learning (Miller, 1981; Wickens, 1990). These theoretical studies proposed that, in addition

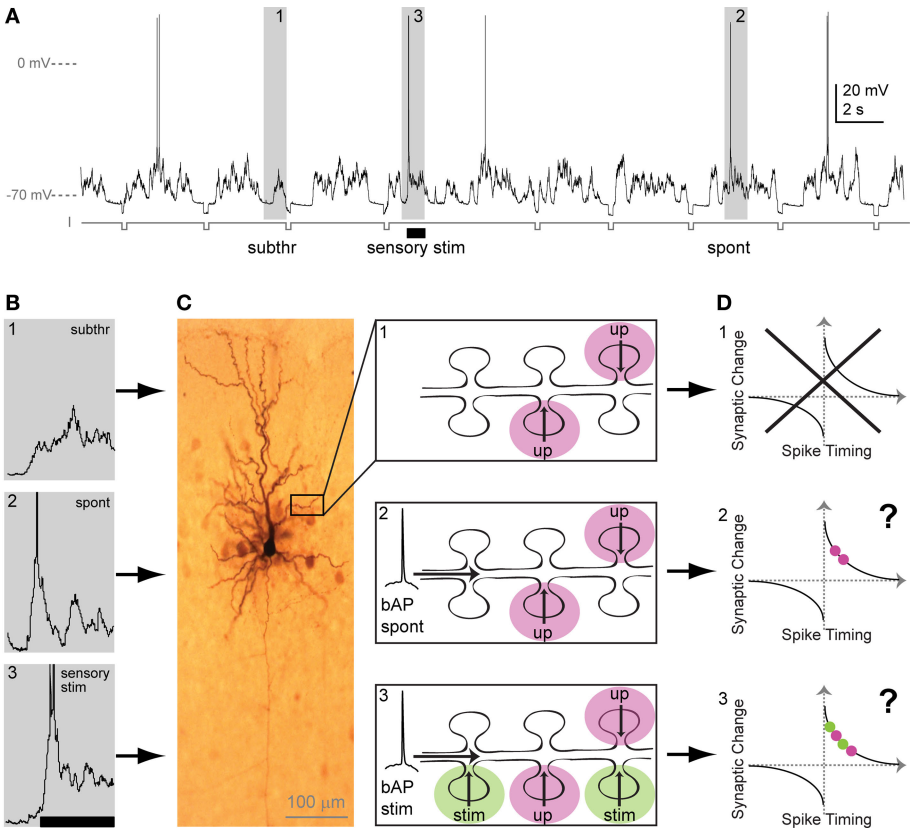

FIGURE 1 | Sub- and suprathreshold neuronal activity *in vivo* and putative consequences for STDP. (A) Whole-cell recording from a pyramidal neuron in primary sensory cortex *in vivo*. Membrane potential trace contains (1) upstates, generated by presynaptic input, with no APs (action potentials: subthreshold events; subthr), (2) upstates with spontaneous APs (spont), and (3) upstates with APs evoked by sensory stimulation (sensory stim, indicated by bar). Hyperpolarizing current steps (I) were applied to determine input resistance. **(B)** Examples of spontaneous and stimulus-evoked activity *in vivo*. Events marked 1–3 in A (gray boxes) are depicted here in higher magnification. APs are truncated. **(C)** Dendritic interactions of presynaptic inputs during both subthreshold upstates and suprathreshold upstates with a spontaneous or a stimulus-evoked backpropagating AP. Left: Biocytine-stained pyramidal neuron showing soma, dendritic and axonal arborization. Part of the dendrite is shown schematically in the three panels at the right: **(C_1)** During subthreshold events, upstate related synaptic input (up) arrives at dendritic spines. **(C_2)** Spontaneous backpropagating APs (bAP spont) putatively interact with upstate related synaptic input arriving at plasticity-relevant timings. **(C_3)** During sensory stimulation, stimulus-evoked backpropagating APs (bAP stim) can putatively interact with upstate related or with stimulus-evoked synaptic input (stim). **(D)** Putative changes in synaptic strength based on the timing of the AP with respect to incoming synaptic input (for both, upstate-related input [red] and/or stimulus-evoked input [green]). The question arises, if spontaneous bAPs as well as stimulus-evoked bAPs induce plasticity, when they interact with upstate related inputs (D_2 vs. D_3). In addition, the question arises, if both, stimulus-evoked and upstate-related input – when timed to coincide with bAPs – induce changes in synaptic strength **(D_3)**. Alternatively, in addition to timing, factors may exist that enable the spatial and temporal selection of activated synapses for plasticity.

to the associated pre- and postsynaptic activity, a "third factor" was available to the network that enabled both the temporal and the spatial selection of specific inputs. To apply this to the *in vivo* situation, raises several further questions: could a neuromodulator represent such a third factor for selecting specific active inputs to a neuron that is embedded in a continuously active network? Given that many repetitions of timed pre–post pairings are typically necessary for STDP induction, could a third factor modify the number of repetitions needed for plasticity induction? In addition to the third factor requirement, other possible solutions for plasticity induction *in vivo* have been proposed that are not covered in the present review (Gerstner et al., 1996; Kempter et al., 1999; Beggs, 2001; Seung, 2003; Xie and Seung, 2004).

(2) If spike timing dependent synaptic plasticity rules are the basis for the modification of behavior, and neuromodulatory systems are critical for this process, then a second conundrum of temporal credit assignment is faced. Both the behavioral signals and the behavioral outcome must be taken into account temporally. This likely also includes the activation of subcortical modulatory nuclei that can mediate for example alerting or rewarding signals to target structures (Schultz, 2000). How does such behavioral activation of a modulatory center influence the interaction of near-coincident pre- and postsynaptic activity with spatial and temporal specificity? Near-coincident pre- and postsynaptic spiking activity and neuromodulators most likely act on different timescales, ranging from tens of milliseconds for pre- and postsynaptic spikes to seconds or longer for some neuromodulators (for review see: Schultz, 2007). How will these

different temporal activation schemes work together during behavioral learning? This temporal credit assignment problem is not new in neuroscience, as for example in reward mediated learning the "distal-reward problem" has been recognized years ago: How can the reward relate to specific events that happened *earlier* in time than the reward (Hull, 1943; Blum and Abbott, 1996; Schultz, 1998, 2006; Sutton and Barto, 1998; Izhikevich, 2007; Vasilaki et al., 2009)? Specific subcortical "reward systems" have been implicated in such learning with the neuromodulator dopamine being the most characterized (for review see: Schultz, 2000, 2002).

Although the rules associated with STDP have started to be addressed *in vivo* (Meliza and Dan, 2006; Jacob et al., 2007), to date, all the data about the involvement of neuromodulators in STDP have come from *in vitro* studies. *In vitro*, the dopaminergic system, amongst a number of other neuromodulatory systems, has been found to influence timing-dependent plasticity (Bissiere et al., 2003; Couey et al., 2007; Seol et al., 2007; Lin et al., 2008; Pawlak and Kerr, 2008; Shen et al., 2008; Zhang et al., 2009). The following sections will present the existing *in vitro* experimental evidence concerning how neuromodulators are involved in timing-based plasticity. This review will be restricted to neuromodulator-actions on timing-dependent plasticity in the mammalian central nervous system. Furthermore, we concentrate on long-range neuromodulatory systems (that are thought to become activated by distinct behavioral states *in vivo*), although locally acting systems and retrograde messengers undoubtedly play an important role in STDP. Such locally acting systems important for STDP are for example endocannabinoids (Sjostrom et al., 2003; Bender et al., 2006; Nevian and Sakmann, 2006; Tzounopoulos et al., 2007), metabotropic glutamate receptors (mGluRs; Egger et al., 1999), and brain-derived neurotrophic factor (Mu and Poo, 2006; Sakata et al., 2009; Sivakumaran et al., 2009).

EXPERIMENTAL EVIDENCE FOR INVOLVEMENT OF NEUROMODULATORS IN STDP

Neuromodulators are involved in most forms of synaptic plasticity ranging from short-term plasticity (ms) (for review see: Lovinger, 2010) to long-term plasticity (hours) (Neuman and Harley, 1983; Frey et al., 1990; Huerta and Lisman, 1993; Thomas et al., 1996), to experience-dependent plasticity (Bear and Singer, 1986; Kilgard and Merzenich, 1998) as well as structural plasticity (Ingham et al., 1998; Day et al., 2006; Gerfen, 2006) (for definitions, see below). Although over the past few decades the role of neuromodulation in certain forms of synaptic plasticity that mainly used high frequency stimulation induction protocols has been well established, it is not clear how these results relate to STDP (for reviews see: Jay, 2003; Hasselmo, 2006; Sara, 2009; Wickens, 2009).

To identify common neuromodulatory rules across the existing STDP studies is potentially difficult as not all studies have used the same induction protocols. The induction protocols used range from pairing of single spikes with a single synaptic input (Lin et al., 2003; Couey et al., 2007; Pawlak and Kerr, 2008; Zhang et al., 2009), and spike bursts with a single synaptic input (Seol et al., 2007; Shen et al., 2008) to "theta" burst paradigms, in which multiple excitatory postsynaptic potentials (EPSPs) are interleaved with multiple spikes (Bissiere et al., 2003; Shen et al., 2008) (see also **Table 1**). The use of multiple spikes with multiple EPSPs during theta burst protocols, usually evoked at around 30–50 Hz, does not allow true timing to be investigated as the preceding spike is always temporally close to the following evoked EPSP (for more details see: Froemke et al., 2010) but this may, in some cell types, be closer to what occurs during behavior. Studies into such complex pairing protocols indicate that the complex EPSP–spike interactions affect downstream signaling cascades differently to seemingly more simple EPSP–single spike interactions (Wang et al., 2005; Froemke et al., 2006). Also, other alterations to STDP recording conditions, for example the presence of GABAergic transmission or pre–post repetition rate may change the STDP window (for further reading see: Wickens, 2009). This opens the possibility that neuromodulators can activate different second messenger pathways depending upon the STDP induction protocol and recording conditions that were used. The identification of common neuromodulatory rules is further complicated by the use of different tools to manipulate neuromodulatory systems amongst studies, for example application of receptor agonists, receptor antagonists, or of the neuromodulator itself, often with different application times.

Therefore, while we attempt to summarize neuromodulatory actions during timing-based plasticity in the following paragraph, one should be aware that differences in STDP induction protocols as well as method of neuromodulatory manipulation might impede finding common principles of neuromodulatory actions across studies.

PERMISSION TO CHANGE: NEUROMODULATORS AND STDP

Studies investigating the effect of neuromodulators on STDP have either used a fixed relative pre–post timing to induce timing-dependent long-term potentiation and depression (t-LTP or t-LTD) (Bissiere et al., 2003; Couey et al., 2007; Pawlak and Kerr, 2008; Shen et al., 2008), or used a whole range of pre–post stimulation timings to investigate the effects of neuromodulation on the STDP timing window shape (Lin et al., 2003; Seol et al., 2007; Zhang et al., 2009). As will be discussed in detail in the following section, the studies using a fixed pre–post timing have often identified neuromodulatory signaling as a requirement for STDP to occur.

Of the neuromodulators investigated, dopamine is the most widely studied and has been shown to influence timing-dependent plasticity across several brain regions. In amygdala, t-LTP was only induced by a protocol consisting of short bursts of afferent stimulation timed to action potential (AP) bursts, when either dopamine was applied or GABAergic inhibition was blocked (Bissiere et al., 2003). Here, dopamine acted by activating dopamine D2 receptors, thereby suppressing feedforward inhibition from local interneurons, which permitted t-LTP induction by burst-pairing. The effect of dopamine depended on intact GABAergic transmission, since no potentiation occurred when dopamine was applied during pairing when GABAergic transmission was blocked, suggesting that the pairing protocol triggers different processes depending on the absence or presence of synaptic inhibition (Bissiere et al., 2003). In dorsal striatum under $GABA_A$ block, timing-dependent LTP was induced when a single AP closely followed an EPSP, while timing-dependent LTD was induced when the order was reversed (Pawlak and Kerr, 2008). Here, blocking dopamine D1/D5 receptors prevented t-LTP as well as t-LTD (**Figures 2A,B**), while blocking dopamine D2 receptors altered the onset, but not the final peak change in plasticity.

Table 1 | Comparison of studies investigating the effect of neuromodulators on STDP.

Study	Brain region	Cell type investigated	Neuromodulator involved (via receptor subtype)	STDP induction protocol	Neuromodulator effect on STDP	Main method of neuromodulatory system manipulation	Mechanism mediating neuromodulator effect on STDP
Bissiere et al. (2003)	Lateral amygdala (mouse)	Projection neurons	Dopamine via D2 Rs	t-LTP: 3 EPSPs timed to 3 APs	Permitted t-LTP	Application of dopamine (100 μM) and receptor agonists	Suppression of feedforward inhibition
Pawlak and Kerr (2008)	Dorsal striatum (rat)	Spiny projection neurons (SPNs)	Dopamine via D1/D5 Rs	t-LTP: 1 EPSP – 1 AP; t-LTD: 1 AP – 1 EPSP	Permitted t-LTP and t-LTD	Application of dopamine receptor antagonists	?
Shen et al. (2008)	Dorsal striatum (mouse)	Spiny projection neurons	Dopamine via D1/D5 and D2 Rs	t-LTP: 3 EPSPs timed to 3 APs; t-LTD: 3 APs timed to 1 EPSP	Permitted t-LTP and t-LTD in specific SPN subgroups	Application of dopamine receptor antagonists	?
Couey et al. (2007)	Prefrontal cortex (mouse)	Layer 5 pyramidal neurons	Nicotine via nAChRs	t-LTP: 1 EPSP – 1 AP	Block of t-LTP; instead, induction of small amount of LTD (only 10 μM)	Application of nicotine (300 nM; 10 μM)	Increase in inhibition; note: stronger protocol (1 EPSP – 2 or 3 APs) still induces t-LTP in nicotine
Zhang et al. (2009)	Hippocampus (rat, dissociated culture)	Glutamatergic (presumably pyramidal) neurons	Dopamine via D1/D5 Rs	t-LTP: 1 pre-AP – 1 post-AP; t-LTD: 1 post-AP – 1 pre-AP	"Wider" range of spike timings induces t-LTP, less spike pairings required to induce t-LTP	Application of dopamine (20 μM)	?
Lin et al. (2003)	Hippocampus (rat)	CA1 pyramidal neurons	Noradrenaline via β-adrenergic Rs	t-LTP: 1 EPSP – 1 AP	"Wider" range of spike timings induces t-LTP	Application of agonists	Modulation of PKA or ERK/MAPK signaling??
Seol et al. (2007)	Visual cortex (rat)	Layer 2/3 pyramidal neurons	Acetylcholine via M1 muscarinic Rs; noradrenaline via β-adrenergic Rs	t-LTP: 1 EPSP timed to 4 APs; t-LTD: 4 APs timed to 1 EPSP	Cooperation between cholinergic and adrenergic systems allows for bidirectional STDP	Application of agonists	Promotion of AMPA receptor phosphorylation at sites implicated in plasticity expression

Rs, receptors; ERK, extracellular signal-regulated kinase; MAPK, mitogen-activated protein kinase; pre-AP, post-AP, connected pairs of neurons, in which an AP in the presynaptic neuron was timed with an AP in the postsynaptic neuron.

Hence, the activation of dopamine D1/D5 receptors allowed for two events, the presynaptic input and the postsynaptic spike that occurred on a timescale of a few tens of milliseconds, to induce a lasting change in synaptic efficiency. Because dopamine receptors were blocked throughout the experiment with specific antagonists, the issue still remains whether dopamine alone acts in the same way when applied during the induction period (see "Changes to the Shape of the STDP Window"). In the subpopulation of striatal principal neurons that do not express dopamine D1 receptors, other neuromodulatory receptor systems were required for STDP. Here, adenosine A2 receptors, which are coupled to the similar second messenger cascades as D1 receptors (Premont et al., 1977; Schwarzschild et al., 2006) had to be activated for t-LTP induction. Both, endocannabinoid CB1 receptor as well as dopamine D2 receptor activation was required for t-LTD induction (Shen et al., 2008). In contrast to the amygdala, in the striatum the effect of dopamine on STDP seems to operate independently of GABAergic transmission (Pawlak and Kerr, 2008; Shen et al., 2008).

Nicotine was shown to be involved in STDP by acting on nicotinic acetylcholine receptors (nAChRs) in prefrontal cortex (Couey et al., 2007). Here, nicotine application caused normally t-LTP-inducing pre–post pairings, consisting of EPSP and single APs to induce a small amount of t-LTD in layer 5 pyramidal neurons. As an underlying mechanism, nicotine was found to strongly increase inhibition of layer 5 pyramidal neurons. Accordingly, the blocking effect of nicotine on t-LTP was partly overcome when inhibition was also

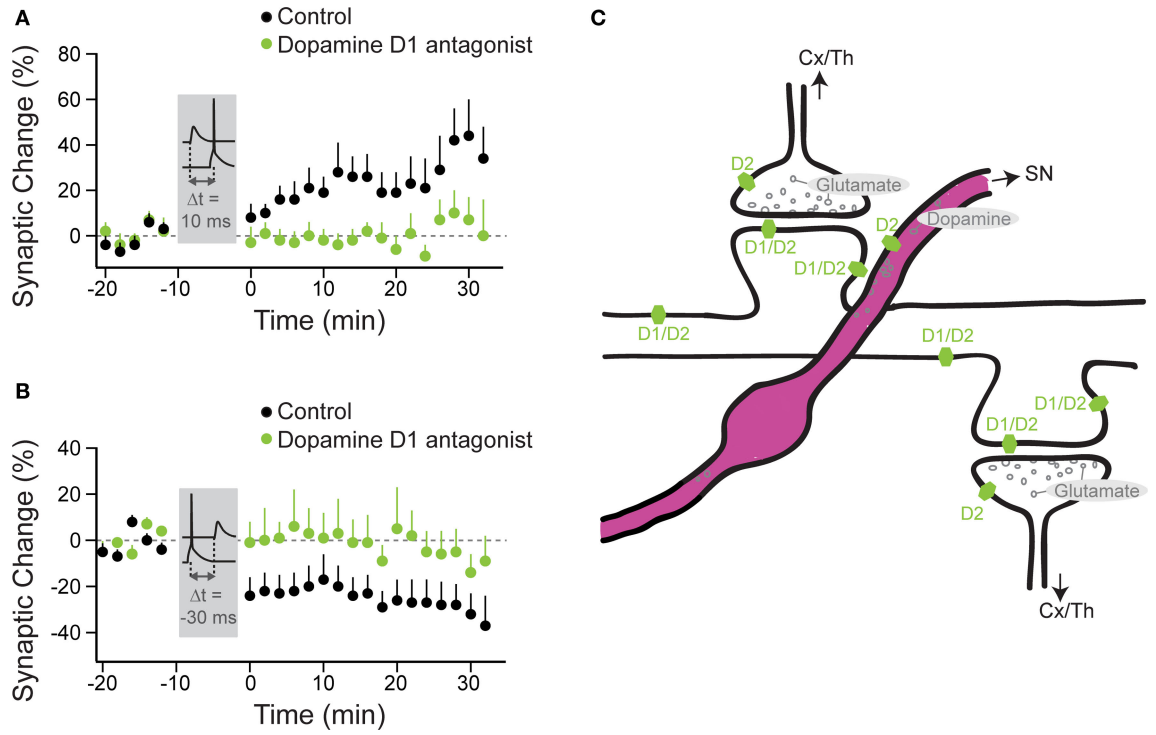

FIGURE 2 | Timing-dependent LTP and LTD are under the control of dopamine D1/D5 receptors in striatal principal neurons. Anatomy of neuromodulatory fibers and the respective receptors as exemplified for striatal dopamine. **(A)** t-LTP was induced under control conditions (black circles) with a STDP protocol, where the AP followed the EPSP by 10 ms (Δt = 10 ms). **(B)** t-LTD was induced under control conditions with a protocol, where the EPSP followed the AP by 30 ms (Δt = –30 ms). No plasticity was observed with these two protocols, when dopamine D1/D5 receptors were blocked (green circles). (**A,B** modified from: Pawlak and Kerr, 2008). **(C)** Excitatory (glutamatergic) synapses arising from the cortex (Cx) or the thalamus (Th) onto spines of a striatal principal neuron. Only some of these spines also receive innervation from nigrostriatal (SN) dopaminergic fibers. Dopamine receptors (D1 and D2 subgroups) are distributed across distinct pre- and postsynaptic sites. For simplicity, the dopaminergic receptors, which are located on several of the striatal interneuron classes, are omitted from this cartoon.

blocked or a stronger t-LTP-inducing stimulus, consisting of pairing EPSPs with AP bursts, was applied. Since calcium is thought to be a crucial second messenger in synaptic plasticity induced by using spike-timing or other plasticity inducing protocols (for reviews see: Artola and Singer, 1993; Malenka and Bear, 2004), and since pre–post timing protocols produce characteristic spatiotemporal calcium signals (Koester and Sakmann, 1998), Couey et al. (2007) also investigated dendritic calcium dynamics during AP–EPSP pairing. Under the influence of nicotine, calcium changes were reduced during a pairing protocol that normally induced t-LTP in control condition (single-AP pairings). In contrast, during a stronger t-LTP-inducing protocol (AP-burst pairings), changes in dendritic calcium were comparable between control groups and nicotine groups. Both, pre- and postsynaptic nAChRs, distributed across several classes of interneurons, were suggested as potential targets of nicotine when reversing prefrontal t-LTP into t-LTD (Couey et al., 2007).

Not only manipulations of nicotinergic signaling, but also manipulations of the balance between dopaminergic and adenosinergic signaling are capable of reversing the sign of plasticity (i.e., converting t-LTP into t-LTD or vice versa); when dopaminergic signaling via D2 receptors was blocked and adenosine signaling was "boosted" by application of adenosine A2 receptor agonists, t-LTP was reversed into t-LTD upon a pre–post timing protocol (Shen et al., 2008).

In summary, dopamine receptor activation is often a prerequisite for timing-dependent plasticity to occur, and nicotine's action is to increase the threshold for t-LTP induction. While the investigation of neuromodulatory influences using a few selective EPSP–AP timing protocols has led to important insights into specifically dopamine's and nicotine's actions during STDP, a more complete picture emerges when neuromodulatory influences are studied across the entire STDP window.

CHANGES TO THE SHAPE OF THE STDP WINDOW

In hippocampus, unlike in striatum and amygdala, dopamine receptor activation was not a critical requirement for STDP induction. Here, t-LTP was induced by a pre–post protocol in the presence of dopamine receptor blockers (Zhang et al., 2009). However, dopamine application resulted in a modest, albeit not significant, increase in the amount of t-LTP observed when single postsynaptic APs closely followed the presynaptic activation with a delay of 10 ms. The much more dramatic effect observed with dopamine application was a change in the shape of the STDP window, allowing for longer pre–post timing delays to increase synaptic efficiency (Zhang et al., 2009). This widening effect was attributed to dopamine D1/D5 receptor activation, and was estimated to expand the t-LTP window by at least 25 ms. Surprisingly, t-LTD, as normally induced by a post–pre protocol, was converted into t-LTP by dopamine

(**Figure 3A**). A similar broadening effect on the t-LTP window during the pairing of single APs with presynaptic activation was reported for the neuromodulator noradrenaline in hippocampal CA1 neurons (Lin et al., 2003). While the activation of β-adrenergic receptors widened the t-LTP window by about 15 ms, the overall amount of plasticity induced by the close pre–post pairings was not affected. Post–pre pairings were not tested. An unexpected similarity between both, β-adrenergic and dopaminergic actions on the "widening" of the t-LTP window is that the effect was expressed slowly, meaning that synaptic efficiency was unchanged directly after the pairing protocol and gradually started to increase from around 15 min post pairing protocol. The implications of window widening are that the activation of dopamine or noradrenaline receptors reduces the threshold for t-LTP induction by allowing for a wider range of pre–post timings to induce synaptic potentiation. The next question is whether the number of spikes needed to induce plasticity is altered with neuromodulation?

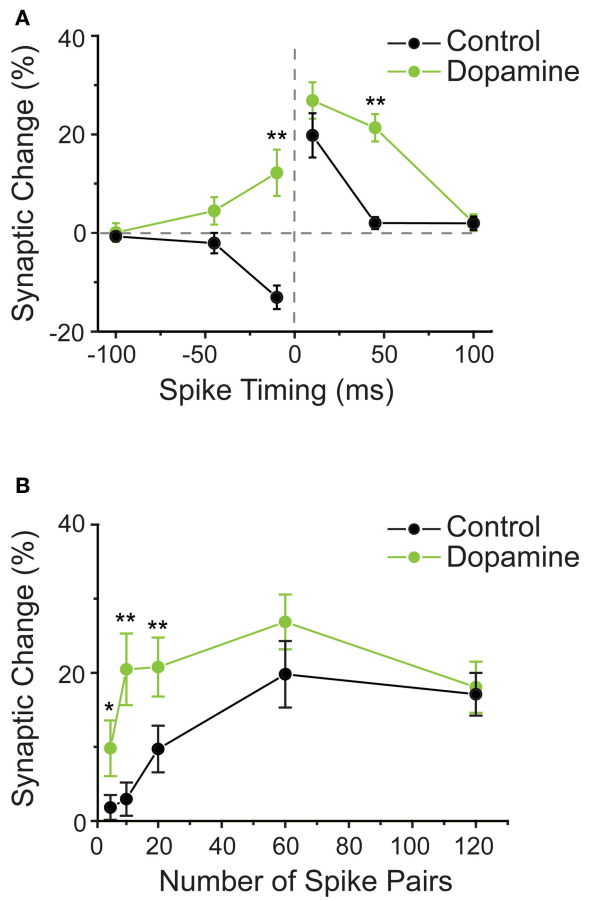

FIGURE 3 | (A) Dopamine changes the shape of the STDP window in hippocampal neurons. STDP window in control conditions (black circles) and when dopamine was present during the STDP induction protocol (green circles). On the "t-LTP side" of the window (positive pre–post timings), dopamine allowed for longer intervals between spike and synaptic activation to induce potentiation of synaptic strength. On the "t-LTD side" of the window (negative pre–post timings), dopamine enabled t-LTP induction with a protocol that induced t-LTD under control conditions. **(B)** Dopamine reduces the number of spike pairs required to induce t-LTP. In control conditions, about 60 repetitions of timed pre–post spike pairings were required to induce robust t-LTP. In presence of dopamine, already 5–10 such pairings were sufficient to induce significant t-LTP. (**A,B** modified from: Zhang et al., 2009).

CHANGES TO THE NUMBER OF TRIALS REQUIRED TO ACHIEVE PLASTICITY

In addition to having an effect on the shape of the STDP window, dopamine also affected the number of pre–post pairing episodes required to induce plasticity in hippocampal neurons (Zhang et al., 2009). Specifically, when dopamine D1/D5 receptors were activated, successful t-LTP induction required a strongly reduced number of timed pre–post pairings, namely instead of the typically required 60 pairing trials, less than 10 pairings were required (**Figure 3B**). Thus by decreasing the required number of spike pairings, dopamine decreases the threshold for t-LTP induction.

COOPERATION BETWEEN NEUROMODULATORS

As suggested by the anatomy of converging neuromodulatory fibers as well as direct physiological evidence, one neuromodulator often does not act in isolation, but several neuromodulatory systems interact (for example, see Bear and Singer, 1986; Zhou et al., 2001). In visual cortex layer 2/3 pyramidal neurons, pairing stimulation of layer 4 afferents with AP bursts did not result in plasticity, neither for pre–post protocols, nor for post–pre protocols (Seol et al., 2007; but compare Feldman, 2000; Froemke et al., 2005). For plasticity to occur, neuromodulatory receptors had to be activated during the pre–post timing protocols. Specifically under stimulation with β-adrenergic agonists, pre–post pairings, with timings between −50 and +50 ms, always induced t-LTP. Conversely, activation of M1 muscarinic receptors always resulted in t-LTD within the same range of timings. Finally, the "normal" standard STDP window displaying bidirectional plasticity, with causal pre–post timings leading to t-LTP and anticausal post–pre timings leading to t-LTD, was achieved with the combined application of β-adrenergic and M1 muscarinic agonists (**Figure 4**).

The activation of β-adrenergic and M1 muscarinic receptors resulted in temporary phosphorylation of distinct sites at AMPA receptors that have been suggested to be crucial for t-LTP and t-LTD, respectively. This led the authors to conclude that neuromodulators supply AMPA receptors with distinct "tags" that allow during certain pre–post spiking timings the induction of t-LTP and t-LTD, respectively. In summary, the activation of noradrenergic and muscarinic acetylcholine receptors (mAChRs) is required for STDP, and more specifically, only the concurrent activation of the two neuromodulatory systems is required to achieve a "standard" STDP window with a t-LTP and a t-LTD side.

CONCLUSION OF THIS SECTION

The observed neuromodulatory actions so far can be divided into two categories (see also **Table 1**): In the first category, neuromodulator receptor activation is necessary for plasticity (Bissiere et al., 2003; Seol et al., 2007; Pawlak and Kerr, 2008; Shen et al., 2008), thereby representing in addition to the precise timing of pre- and postsynaptic activity, a third factor essentially required for plasticity induction. Notably, in one study, two neuromodulators acted in concert to enable bidirectional STDP (Seol et al., 2007).

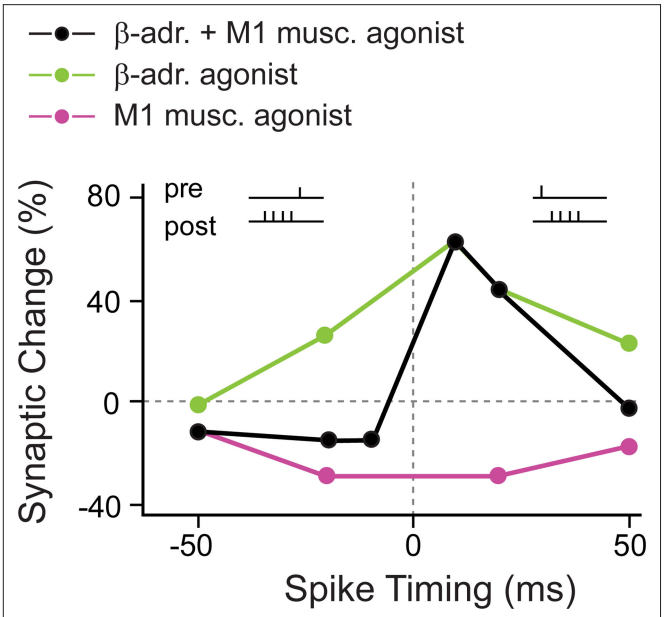

FIGURE 4 | Coapplication of β-adrenergic and M1 muscarinic agonists is required for "standard" bidirectional STDP in visual cortex. In the presence of a β-adrenergic agonist alone, close positive as well as negative pre–post timings induced t-LTP (green circles). When a M1 muscarinic agonist was present, close positive as well as negative pre–post timings induced t-LTD (red circles). Only the combined application of β-adrenergic and M1 muscarinic agonists resulted in the "standard" STDP window with close pre–post timings leading to t-LTP, and post–pre timings leading to t-LTD (black circles). (Modified from: Seol et al., 2007).

In the second category, the neuromodulator changes the conditions for plasticity by either increasing (Couey et al., 2007) or decreasing the threshold for plasticity induction (Lin et al., 2003; Zhang et al., 2009; but see also Bienenstock et al., 1982). An effect observed in studies from both categories is that specific manipulations of one or several neuromodulator systems, result in sign reversal of plasticity, meaning that a normally t-LTP-inducing stimulus induced t-LTD, or vice versa (Bissiere et al., 2003; Couey et al., 2007; Seol et al., 2007; Shen et al., 2008; Zhang et al., 2009). Although the mechanisms underlying such sign reversal are not clear, activity patterns that "boost" backpropagating APs in remote dendrites have been shown to "switch" t-LTD to t-LTP (Sjostrom and Hausser, 2006). Since some neuromodulators can exert a short-term effect on dendritic excitability and backpropagation (for review see: Waters et al., 2005), neuromodulators could also modulate backpropagating APs during STDP protocols, although this might not occur with all neuromodulators (Gulledge and Stuart, 2003).

The effect of neuromodulators on dendritic excitability is not restricted to short-term effects, since for example, the combination of mACh receptor activation with weak dendritic spikes in a distinct dendritic compartment resulted in a long-lasting excitability increase restricted to the involved dendritic compartment (Losonczy et al., 2008). This excitability increase transformed the weak dendritic spikes into strong dendritic spikes. Strong dendritic spikes have been implicated in drastic trial reduction to induce plasticity (Remy and Spruston, 2007). Such dendritic spikes are usually evoked with rather focused massive or convergent activity. Alternatively, a neuromodulator could reduce the trial number required for plasticity induction by making a dendritic compartment receptive for strong dendritic spike initiation (Losonczy et al., 2008).

From a temporal point of view, neuromodulators have been found to influence STDP on at least three timescales: on the scale of tens of milliseconds, neuromodulators influenced the interaction of pre- and postsynaptic spikes to induce plasticity; on the scale of seconds, neuromodulators influenced the number of repetitions of pre–post activity needed to evoke plasticity; and on the order of minutes, neuromodulators influenced the time course of plasticity.

DOES THE THIRD FACTOR HAVE A TIMING ISSUE, TOO?

The studies listed in Section "Experimental Evidence for Involvement of Neuromodulators in STDP" have either constantly manipulated neuromodulator receptors during the entire experimental period (Lin et al., 2003; Pawlak and Kerr, 2008; Shen et al., 2008) or only during the induction period (Bissiere et al., 2003; Couey et al., 2007; Seol et al., 2007; Zhang et al., 2009). An important question that is very difficult to address experimentally, is how the outcome, in terms of plasticity, depends on the exact point in time of activation of neuromodulator-receptors, relative to pre- and postsynaptic spiking?

Since neuromodulator release sites and the receptors for the neuromodulator are not necessarily located close together on either side of the synaptic cleft, as in the classical concept of a synapse, the time required for diffusion of the released molecules has to be taken into account (see also **Figure 2C**). The modulator molecules have first to be released, then "travel" and bind to the respective receptors and initiate some G-protein coupled signaling cascade, which is a very different scenario from fast glutamate transmission. The time course of neuromodulator action was traditionally thought to be slow (on the scale of minutes), but recent evidence suggests that the time course is on the order of a few seconds (for review see: Sarter et al., 2009). Despite this recent change in thinking the question still arises how do these different timescales of spikes (1–2 ms) and neuromodulation (seconds) fit together in a working mechanism?

Three possible scenarios can be devised of how such a mechanism could work. The first two are at the single neuron level involving an "eligibility trace", and the third is at the network level and relies on reverberating activity.

In the first scenario, the coordinated pre–post activity occurs before the neuromodulator release, as would be the case during unexpected reward. Here, spike and synaptic activation could leave a time decaying eligibility trace (Wang et al., 2000; Sarkisov and Wang, 2008) that subsequent neuromodulator receptor activation may then interact with to modulate plasticity.

In the second scenario, the neuromodulatory receptors are activated before the coordinated pre–post activity occurs, as would be expected during the learning of attention-based tasks. Here, the signaling mechanisms activated by neuromodulatory receptors themselves may create a slowly decaying eligibility trace, with which the coordinated pre–post activity can then interact with to modulate plasticity.

Experimental evidence for either scenario or the underlying molecular mechanisms is mostly lacking. However, the two presented scenarios resemble problems faced in the field of metaplasticity (Abraham, 2008) in which the concept of an eligibility trace has also been proposed. During metaplasticity, synapses will more easily undergo plasticity after a "priming" stimulus has changed the state of specific molecular signaling cascades; this change may for example "kick" plasticity-relevant enzymes into a more receptive state or it may result in enhanced phosphorylation of intracellular or extrasynaptic AMPARs that allows them to be inserted into postsynaptic membranes when an appropriate stimulus arrives (Sun et al., 2005; Abraham, 2008). For STDP, evidence for a similar gating mechanism in accordance with scenario two (neuromodulator receptor activation occurs first, followed by near-coincident pre–post spiking) was found by Seol and colleagues (see Sections "Experimental Evidence for Involvement of Neuromodulators in STDP and "Cellular and Molecular Targets of Neuromodulators During Timing-Dependent Plasticity"). When M1 muscarinic and β-adrenergic agonists were applied and washed out, a subsequent episode of timed pre–post pairings still initiated t-LTP or t-LTD, respectively. In addition, because neuromodulators have been shown to have a direct effect on glutamatergic receptor (AMPA and NMDA) location within the synapse and activated current efficacy (Seol et al., 2007; for review see: Cepeda and Levine, 2006), this is a possible mechanism that could create an eligibility trace to interact with subsequent pre–post pairing.

A third scenario how the three factors may interact *in vivo*, may be that the respective pre–post-activity patterns "reverberate" in the local circuit for some time (Hebb, 1949), and that such a memory trace can be transduced into a lasting modification if a third-factor success signal is present during the reverberation (Histed et al., 2009). A problem with such a mechanism is that the reverberating activity should not produce overt action, however if different circuits are involved, it is difficult to connect the success signal to the activity that did cause overt action.

HOW CAN NEUROMODULATORS INFLUENCE THE INTERACTION OF PRE- AND POSTSYNAPTIC SPIKES: ANATOMICAL AND PHYSIOLOGICAL CONSIDERATIONS

Increasing evidence for the critical involvement of neuromodulator systems in STDP raises the question of how the physical location of neuromodulator release sites relates to the pre- and postsynaptic complex, which is thought to be the locus of STDP induction. Typically, neuromodulatory centers are located quite distally from the brain regions they influence (see more in Section "Activation of Neuromodulatory Systems *In Vivo*"). In their distal target areas, generally only a subgroup of neuromodulatory fibers makes direct contact with dendritic spines that receive excitatory inputs (Freund et al., 1984; Groves et al., 1994; Smith et al., 1994), whereas other neuromodulatory fibers target dendritic shafts and somata or form varicosities that lack synaptic specializations (Seguela et al., 1989, 1990). Therefore the question arises if only this subset of directly targeted synapses is influenced by neuromodulators when pre- and postsynaptic spikes collide? This is unlikely, because the receptors for the respective neurotransmitters are widely distributed across pre- and postsynaptic sites of principal neurons and interneurons (Gerfen et al., 1990, 1995; Sesack et al., 1994; Bergson et al., 1995; Caille et al., 1996) (**Figure 2C**), and receptor density and location can change (Paspalas et al., 2006). A certain degree of spatial specificity of neuromodulator-actions is probably achieved during behavior, when phasic release events occur, which temporally increases the concentration of neuromodulator, locally (reviewed in: Arbuthnott and Wickens, 2007; Sarter et al., 2009, see below for definition of phasic release and also Section "Activation of Neuromodulatory Systems *In Vivo*"). Finally, both AMPA and NMDA receptors are located presynaptically on neuromodulatory release terminals, and the activation of these receptors by overspill from neighboring active glutamatergic synapses is thought to convey further spatial specificity to the neuromodulator signal (Roberts and Sharif, 1978; Desce et al., 1992, 1994; Jin and Fredholm, 1994). Because the actions of neuromodulators are through receptors, the specific receptor subtype involved in STDP has important implications for the interpretation of neuromodulatory actions at the single neuron level. Indeed, during STDP, neuromodulators acted through specific receptor subtypes (Bissiere et al., 2003; Lin et al., 2003; Seol et al., 2007; Pawlak and Kerr, 2008; Shen et al., 2008; Zhang et al., 2009). This is a complex issue as, for example for the neuromodulator dopamine, low concentrations are thought to activate dopamine D2-like receptors in their high-affinity state, whereas high concentrations are thought to activate dopamine D1-like receptors (Richfield et al., 1989). These two receptor-subgroups are differentially expressed across neuronal populations, and can activate opposing downstream target enzymes (Girault and Greengard, 2004). Hence, during phasic release, the heterogeneous structural arrangement of release sites, different receptors subtypes, and regulated degrading/reuptake mechanisms in combination with diffusional processes are likely to generate further spatiotemporal heterogeneity of the neuromodulator signal. In addition, there is strong evidence that local spines within a dendritic region are topographically organized functionally (Jia et al., 2010) and that activity-initiated signaling cascades within the postsynaptic spines and dendrites interact locally with other spines (Harvey and Svoboda, 2007). This implies that in addition to the spatial specificity of neuromodulator release, there is a postsynaptic organization that can potentially provide very spatially defined neuromodulator action without the need for individual fibers to innervate each and every postsynaptic spine. The implication for timing-dependent plasticity *in vivo* would be that the timing of neuromodulator release in relation to correlated pre- and postsynaptic activity can enable the spatiotemporal selection of specific synapses for plasticity.

CELLULAR AND MOLECULAR TARGETS OF NEUROMODULATORS DURING TIMING-DEPENDENT PLASTICITY

Only few studies so far have addressed the issue of the exact cellular and molecular targets of neuromodulators when they "gate" STDP. In general, their receptors are (often) coupled to G-proteins and hereby influence intracellular second messenger cascades; (for example dopamine D1 receptors are coupled directly to adenylyl cyclase (AC) and indirectly to protein kinase A (PKA) and protein phosphatase 1 (Hemmings et al., 1984), M1 muscarinic ACh receptors are coupled to phospholipase C (PLC), β-adrenergic receptors are coupled to PKA (exception: nicotinic ACh receptors

are ligand-gated channels). As a result, many different voltage-gated and calcium-dependent ion channels are influenced, which can affect membrane potential, neuronal spiking and excitatory transmission as well as inhibitory transmission (for review, see: Hasselmo, 1995; Nicola et al., 2000; Magee and Johnston, 2005; Sara, 2009). By their ability to affect dendritic ion channels, neuromodulators are certainly empowered to influence how the backpropagating AP will interact with incoming synaptic input during spike-timing paradigms (Hoffman and Johnston, 1999; Zhou et al., 2005; Sjostrom and Hausser, 2006; for review see: Tsubokawa, 2000), although specific studies investigating neuromodulatory influences on such interactions are required (but see: Couey et al., 2007).

Particularly in older animals, a preventing effect of inhibition on STDP has been described (Meredith et al., 2003). The influence that some neuromodulators have on inhibitory tone is certainly a means to affect STDP rules (D2, A2, mGluR5; Bissiere et al., 2003; Schwarzschild et al., 2006; Couey et al., 2007). However, several studies describe an effect of neuromodulators on STDP while inhibition is blocked, indicating at least one alternative mode of action of neuromodulators (Pawlak and Kerr, 2008; Shen et al., 2008).

Such an alternative mode of action is putatively an influence on the postsynaptic anchoring of glutamate receptors. For example, dopamine D1/D5 receptors and β-adrenergic receptors can increase surface expression of AMPA receptors (Chao et al., 2002; Sun et al., 2005; Oh et al., 2006) promoting synaptic insertion (for reviews see: Derkach et al., 2007; Lee and Huganir, 2008). The trafficking of AMPA receptors in and out of the synapse depends on phosphorylation of AMPA receptors at distinct sites (Lee et al., 2000, 2003; Boehm et al., 2006; He et al., 2009). In agreement with this, acetylcholine (coupled to PLC via M1 muscarinic receptors) and noradrenaline (coupled to AC via β-adrenergic receptors) gate phosphorylation at AMPA receptor sites implicated in t-LTP and t-LTD (Seol et al., 2007). In addition, β-adrenergic receptors were recently found to be anchored postsynaptically, forming a signaling complex with PKA and AMPA receptors (Joiner et al., 2010). Also, for dopamine, a complex interaction between D1 receptors and NMDA receptor channels has been reported (Cepeda et al., 1992; O'Donnell and Grace, 1994; Levine et al., 1996; Gao et al., 2001; Cepeda and Levine, 2006). Given that both dopamine and NMDA receptor activation were required for STDP (Pawlak and Kerr, 2008; Shen et al., 2008; Zhang et al., 2009), an interaction of these two receptor systems during the correlated pre- and postsynaptic spiking is possible.

Finally, it is worth considering the possibility that neuromodulators might also alter the dynamic balance of the phosphatases and kinases that control the induction of t-LTP and t-LTD (for review see: Lisman and McIntyre, 2001). For example, it is well established that PKA can reduce the activation of the phosphatases subserving LTD (Blitzer et al., 1998). This could be a plausible mechanism to account for the observation made in some studies that receptors coupled to AC, like D1 dopaminergic and β-adrenergic receptors, not only promote t-LTP but prevent t-LTD (Seol et al., 2007; Lin et al., 2008; Zhang et al., 2009).

In summary, the neuromodulatory systems can potentially affect STDP through a variety of mechanisms like changing the recruitment of inhibition at the network level, or changing excitability, kinase/phosphatase balance and priming AMPA receptor trafficking at the subcellular level. An important question that remains largely open is how those multiple actions are integrated in the different behavioral states defined by the neuromodulatory systems.

ACTIVATION OF NEUROMODULATORY SYSTEMS *IN VIVO*

If one attempts a synthesis of STDP and neuromodulation, the question arises at which points during behavior neuromodulatory nuclei become activated? Due to tonic background activity of these nuclei, their innervated areas experience a constant low tone of release resulting in neuromodulator concentrations in the low nanomolar range. Salient behavioral events serve to drastically increase and decrease the activity of the respective nuclei (see below). The exact spatiotemporal profile of neuromodulator concentrations achieved during behavior is mostly unknown. Perhaps the best studied neuromodulator in this respect is dopamine, and some information about dopamine's *in vivo* concentration is available (see below), whereas for noradrenaline and acetylcholine the concentration reached during behavior is not well studied.

DOPAMINE

Dopaminergic fibers arise from the ventral tegmental area and the substantia nigra. Dopaminergic neurons are activated by primary-rewarding stimuli: Unexpected rewards, but also the attentional and rewarding aspects of novel stimuli cause midbrain dopaminergic neurons to increase their firing rate (Ljungberg et al., 1992; Mirenowicz and Schultz, 1996). As a certain task is being learned, dopamine neurons shift their firing temporally toward the stimulus that indicates reward is to follow (Schultz et al., 1993). Hereby, the success-predicting stimulus has become rewarding. After a certain task has been learned, the primary-rewarding stimulus does not activate dopaminergic signals anymore; a dopaminergic signal is only initiated when a reward is unexpected or better than predicted. If a predicted reward is omitted, dopaminergic cells respond by decreasing their firing (Hollerman and Schultz, 1998). Together, this is consistent with theories of reinforcement learning stating that reinforcers only contribute to learning when they are not entirely predictable (Sutton and Barto, 1981). Recently, it has been found that a subpopulation of dopamine neurons also fire in response to aversive stimuli or associated cues (Joshua et al., 2008; Matsumoto and Hikosaka, 2009) suggesting that dopamine can code for multiple external events (Redgrave and Gurney, 2006).

The timescale of the phasic increase in firing rate of dopaminergic neurons is 50–110 ms (latency) and <200 ms (duration) with dopamine concentrations at target structures remaining elevated (150–400 nM) for up to 400 ms (Chergui et al., 1994; Dugast et al., 1994; Schultz, 2002). It is less clear how pauses in dopamine cell firing would affect local concentration levels, since the time course of clearance is relatively slow. However subtle changes in the degree of synchrony of firing have significant effects (Joshua et al., 2009).

NORADRENALINE

Noradrenaline neurons located in locus coeruleus seem to play a role in vigilance, since these neurons show low firing rates during drowsiness and slow-wave sleep, regular firing at quiet wakefulness, and burst-firing in response to arousing stimuli (Aston-Jones and Bloom, 1981). A large variety of arousing and attention-demanding

stimuli cause a response in these noradrenergic neurons, this also includes primary-rewarding stimuli and aversive stimuli (Foote et al., 1980; Rasmussen et al., 1986; Sara and Segal, 1991; Aston-Jones et al., 1994). In detail, this response consists of a very brief increase in AP firing (15–70 ms latency, 2–3 APs) followed by a longer suppression of AP firing (300–700 ms duration) (Berridge and Waterhouse, 2003). The noradrenergic response disappears with repeated stimulus presentations, but reappears when the stimulus is followed by reinforcement (Sara and Segal, 1991). In general, the noradrenaline signal is thought to be involved in sensory processing, decision-making, working memory, and memory formation (Cahill and McGaugh, 1996; Robbins and Roberts, 2007).

ACETYLCHOLINE

Cholinergic neurons in the basal forebrain nuclei are activated during arousal and attention (Paxinos, 2004; Sarter et al., 2005), they respond to unfamiliar stimuli (Wilson and Rolls, 1990), but also to unpredicted and predicted rewards (Richardson and DeLong, 1986, 1990). Also in striatum, tonically active striatal interneurons (TANs), which are cholinergic (Wilson et al., 1990; Zhou et al., 2002) respond to primary rewards and reward-predicting stimuli with a pause and sometimes a subsequent increase in firing (Aosaki et al., 1995; Apicella et al., 1997; Sardo et al., 2000; Zhou et al., 2002). The firing of TANs mainly encodes outcome delivery and omission at termination of the behavioral trial episode (Joshua et al., 2008). Within the cortex, acetylcholine has been suggested to enhance the response to sensory stimuli, and on more broad terms, to be important for attention and working memory (Hasselmo and Giocomo, 2006).

CONCLUSION OF THIS SECTION

This section shows that release of neuromodulators occurs in a wide range of behavioral situations. Hence, the combination of theoretical and experimental work suggests that neuromodulatory influence on STDP might be linked to an equally wide range of behavioral learning processes, namely fear-conditioning (Bissiere et al., 2003), rapid learning (Zhang et al., 2009), reward-based learning (Pawlak and Kerr, 2008; Zhang et al., 2009), cognitive performance (Couey et al., 2007), but also pathological states (Shen et al., 2008) (for modeling approaches see: Baras and Meir, 2007; Florian, 2007; Legenstein et al., 2008; Vasilaki et al., 2009; Fremaux et al., 2010; Potjans et al., 2010).

FUTURE DIRECTIONS

Our knowledge about STDP and its regulation by neuromodulators has substantially increased during the last years, although the overall number of published studies concerning this topic remains low. Current experimental evidence suggests that neuromodulators shape the interaction between presynaptic and postsynaptic spike activity across many brain areas, and the predominating effect of neuromodulators is to allow plasticity or to make plasticity induction easier. Although there is amassing data from many different brain regions, it needs to be clarified how universal this additional modulatory factor is in regulating STDP. In addition, many brain areas are targeted and influenced by not only one, but by several neuromodulators (Bear and Singer, 1986; Zhou et al., 2001; Wang et al., 2006; Sara, 2009), and accordingly, there is experimental evidence that several neuromodulatory systems can interact to influence STDP rules (Seol et al., 2007). How the interaction of multiple neuromodulator systems exactly occurs during STDP, and if this interaction is a universal principle across many brain areas, will be interesting targets for future studies. Perhaps the most important outstanding question regarding STDP and neuromodulation concerns the exact time, when neuromodulatory receptors need to be activated to exert an influence on synaptic efficacy during causal and anticausal pre- and postsynaptic spiking. Along these lines, it will be important to directly test whether neuromodulators are capable of spatial or temporal selection of specific synapses for plasticity (see Sections "How Can Neuromodulators Influence the Interaction of Pre- and Postsynaptic Spikes: Anatomical and Physiological Considerations" and "Conclusion").

Finally, not only will both experimentalists and theorists need to translate the effect of neuromodulators on STDP rules from *in vitro* to *in vivo* conditions (see: Meliza and Dan, 2006; Jacob et al., 2007), but also to the behaving animal. In addition, since it is almost certain that specific memories are stored across neuronal populations (Penfield, 1958, 1959), it will be important to see how STDP rules relate to neuronal populations in the behaving animal (Sawinski et al., 2009).

CONCLUSION

Spike timing dependent plasticity rules have been developed mainly on the basis of *in vitro* experimental data and have provided a temporally specific extension to the activity-based synaptic plasticity rules first proposed by Hebb (1949). However, when one tries to apply these rules to *in vivo* conditions and to the behaving animal, two conundrums arise: First, *in vivo*, a large amount of pre- and postsynaptic activity constantly arrives at the individual synapses. This raises the possibility that *in vivo*, synapses are constantly adapting their synaptic efficacy as pre- and postsynaptic spikes collide, which would be energetically inefficient for the involved neurons. An alternative possibility is that a "third factor" using a neuromodulator signal may represent a selection criteria that potentially allows presynaptic activity and postsynaptic spiking to be associated, both spatially and temporally. Thus, neuromodulators might enable the neuronal networks to select certain inputs and to make them eligible for changes in efficacy. To this end a large amount of indirect *in vitro* experimental evidence from many brain regions as well as theoretical evidence is being amassed that this may be the case, but a direct measurement of the third factor rule *in vivo* has yet to be achieved (for experimental evidence, see Section "Experimental Evidence for Involvement of Neuromodulators in STDP"; for modeling approaches see: Baras and Meir, 2007; Florian, 2007; Izhikevich, 2007; Legenstein et al., 2008; Vasilaki et al., 2009; Fremaux et al., 2010; Potjans et al., 2010).

Second, if one attempts to transfer the concepts of STDP to *in vivo* conditions, the obvious next questions are (a) if STDP rules are actually used for behaviorally based learning, and (b) how neuromodulation might be involved in this process. Neuromodulation alone is certainly an important factor involved in behavioral learning, as demonstrated by decades of research. If neuromodulation was instrumental in shaping STDP rules during behaviorally based learning, it would require fast time scale events like pre- and

postsynaptic spikes and the putatively "slowly acting" neuromodulators to interact. The existing *in vitro* studies are only starting to provide insights how this temporal interaction might work. And for the *in vivo* situation, this picture will be much more complex, as a variety of behavioral states will release different combinations of neuromodulators at different timings and at different concentrations, activating different target receptor subtypes.

Dopamine, to date, is the most investigated neuromodulator and represents an interesting case for neuromodulator-regulation of STDP, as it has both the effect of "broadening" the t-LTP window and of changing what would normally be t-LTD into t-LTP. With regards to reward-mediated learning, the implication of these experimental findings is that any spike occurring within a certain window either before or after the synaptic input will increase the synaptic efficacy, which implies that many different external events that occurred temporally around the rewarding event could be associated with the reward.

It is an open question how an animal succeeds in linking the specific neuronal activity involved in a behavior to the behavioral outcome. How neuromodulators released during different states such as attention, arousal and reward influence this linking process, is also unknown. To achieve a full understanding of the principles of how neuromodulation shapes STDP rules might represent a first step toward solving these important questions.

ACKNOWLEDGMENTS

Verena Pawlak and Jason N. D. Kerr were supported by the Max Planck Society. Alfredo Kirkwood was supported by NEI-R01-EY12124.

GLOSSARY

Neuromodulator: A substance that is released by a neuron and alters the function of other neurons – typically on a slower timescale than a neurotransmitter.

Experience-dependent plasticity: Changes in synaptic strength or structural plasticity that result from manipulations altering sensory experience (Hooks and Chen, 2007; Fox, 2009).

Structural plasticity: Formation or elimination of dendritic spines, axonal boutons, synaptic contacts. Also includes structural rearrangements on a larger scale like changes in axonal/ dendritic arbors (Lamprecht and LeDoux, 2004; Holtmaat and Svoboda, 2009).

Synaptic change/synaptic plasticity: A change in the strength of synaptic transmission, which can be measured in several ways, like for example a change in the postsynaptic potential or postsynaptic current. It can be expressed on the level of a single neuron or a population of neurons (Bliss and Collingridge, 1993; Luscher et al., 2000).

Phasic release: Increase in neurotransmitter release that is restricted temporally.

REFERENCES

Abbott, L. F., and Blum, K. I. (1996). Functional significance of long-term potentiation for sequence learning and prediction. *Cereb. Cortex* 6, 406–416.

Abraham, W. C. (2008). Metaplasticity: tuning synapses and networks for plasticity. *Nat. Rev. Neurosci.* 9, 387.

Aosaki, T., Kimura, M., and Graybiel, A. M. (1995). Temporal and spatial characteristics of tonically active neurons of the primate's striatum. *J. Neurophysiol.* 73, 1234–1252.

Apicella, P., Legallet, E., and Trouche, E. (1997). Responses of tonically discharging neurons in the monkey striatum to primary rewards delivered during different behavioral states. *Exp. Brain Res.* 116, 456–466.

Arbuthnott, G. W., and Wickens, J. (2007). Space, time and dopamine. *Trends Neurosci.* 30, 62–69.

Artola, A., and Singer, W. (1993). Long-term depression of excitatory synaptic transmission and its relationship to long-term potentiation. *Trends Neurosci.* 16, 480–487.

Aston-Jones, G., and Bloom, F. E. (1981). Activity of norepinephrine-containing locus coeruleus neurons in behaving rats anticipates fluctuations in the sleep-waking cycle. *J. Neurosci.* 1, 876–886.

Aston-Jones, G., Rajkowski, J., Kubiak, P., and Alexinsky, T. (1994). Locus coeruleus neurons in monkey are selectively activated by attended cues in a vigilance task. *J. Neurosci.* 14, 4467–4480.

Baras, D., and Meir, R. (2007). Reinforcement learning, spike-time-dependent plasticity, and the BCM rule. *Neural. Comput.* 19, 2245–2279.

Bear, M. F., and Singer, W. (1986). Modulation of visual cortical plasticity by acetylcholine and noradrenaline. *Nature* 320, 172–176.

Beggs, J. M. (2001). A statistical theory of long-term potentiation and depression. *Neural. Comput.* 13, 87–111.

Bender, V. A., Bender, K. J., Brasier, D. J., and Feldman, D. E. (2006). Two coincidence detectors for spike timing-dependent plasticity in somatosensory cortex. *J. Neurosci.* 26, 4166–4177.

Bergson, C., Mrzljak, L., Smiley, J. F., Pappy, M., Levenson, R., and Goldman-Rakic, P. S. (1995). Regional, cellular, and subcellular variations in the distribution of D1 and D5 dopamine receptors in primate brain. *J. Neurosci.* 15, 7821–7836.

Berridge, C. W., and Waterhouse, B. D. (2003). The locus coeruleus-noradrenergic system: modulation of behavioral state and state-dependent cognitive processes. *Brain Res. Brain Res. Rev.* 42, 33–84.

Bi, G. Q., and Poo, M. M. (1998). Synaptic modifications in cultured hippocampal neurons: dependence on spike timing, synaptic strength, and postsynaptic cell type. *J. Neurosci.* 18, 10464–10472.

Bienenstock, E. L., Cooper, L. N., and Munro, P. W. (1982). Theory for the development of neuron selectivity: orientation specificity and binocular interaction in visual cortex. *J. Neurosci.* 2, 32–48.

Bissiere, S., Humeau, Y., and Luthi, A. (2003). Dopamine gates LTP induction in lateral amygdala by suppressing feedforward inhibition. *Nat. Neurosci.* 6, 587–592.

Bliss, T. V., and Collingridge, G. L. (1993). A synaptic model of memory: long-term potentiation in the hippocampus. *Nature* 361, 31–39.

Blitzer, R. D., Connor, J. H., Brown, G. P., Wong, T., Shenolikar, S., Iyengar, R., and Landau, E. M. (1998). Gating of CaMKII by cAMP-regulated protein phosphatase activity during LTP. *Science* 280, 1940–1942.

Blum, K. I., and Abbott, L. F. (1996). A model of spatial map formation in the hippocampus of the rat. *Neural. Comput.* 8, 85–93.

Boehm, J., Kang, M. G., Johnson, R. C., Esteban, J., Huganir, R. L., and Malinow, R. (2006). Synaptic incorporation of AMPA receptors during LTP is controlled by a PKC phosphorylation site on GluR1. *Neuron* 51, 213–225.

Cahill, L., and McGaugh, J. L. (1996). Modulation of memory storage. *Curr. Opin. Neurobiol.* 6, 237–242.

Caille, I., Dumartin, B., and Bloch, B. (1996). Ultrastructural localization of D1 dopamine receptor immunoreactivity in rat striatonigral neurons and its relation with dopaminergic innervation. *Brain Res.* 730, 17–31.

Cepeda, C., and Levine, M. S. (2006). Where do you think you are going? The NMDA-D1 receptor trap. *Sci. STKE* 2006, pe20.

Cepeda, C., Radisavljevic, Z., Peacock, W., Levine, M. S., and Buchwald, N. A. (1992). Differential modulation by dopamine of responses evoked by excitatory amino acids in human cortex. *Synapse* 11, 330–341.

Chao, S. Z., Ariano, M. A., Peterson, D. A., and Wolf, M. E. (2002). D1 dopamine receptor stimulation increases GluR1 surface expression in nucleus accumbens neurons. *J. Neurochem.* 83, 704–712.

Chergui, K., Suaud-Chagny, M. F., and Gonon, F. (1994). Nonlinear relationship between impulse flow, dopamine release and dopamine elimination in the rat brain *in vivo*. *Neuroscience* 62, 641–645.

Couey, J. J., Meredith, R. M., Spijker, S., Poorthuis, R. B., Smit, A. B., Brussaard, A. B., and Mansvelder, H. D. (2007). Distributed network actions by nicotine increase the threshold for spike-timing-dependent plasticity in prefrontal cortex. *Neuron* 54, 73–87.

Cowan, R. L., Sesack, S. R., Van Bockstaele, E. J., Branchereau, P., Chain, J., and Pickel, V. M. (1994). Analysis of synaptic inputs and targets of physiologically characterized

neurons in rat frontal cortex: combined *in vivo* intracellular recording and immunolabeling. *Synapse* 17, 101–114.

Day, M., Wang, Z., Ding, J., An, X., Ingham, C. A., Shering, A. F., Wokosin, D., Ilijic, E., Sun, Z., Sampson, A. R., Mugnaini, E., Deutch, A. Y., Sesack, S. R., Arbuthnott, G. W., and Surmeier, D. J. (2006). Selective elimination of glutamatergic synapses on striatopallidal neurons in Parkinson disease models. *Nat. Neurosci.* 9, 251–259.

Debanne, D., Gahwiler, B. H., and Thompson, S. M. (1998). Long-term synaptic plasticity between pairs of individual CA3 pyramidal cells in rat hippocampal slice cultures. *J. Physiol.* 507(Pt 1), 237–247.

Derkach, V. A., Oh, M. C., Guire, E. S., and Soderling, T. R. (2007). Regulatory mechanisms of AMPA receptors in synaptic plasticity. *Nat. Rev. Neurosci.* 8, 101–113.

Desce, J. M., Godeheu, G., Galli, T., Artaud, F., Cheramy, A., and Glowinski, J. (1992). L-glutamate-evoked release of dopamine from synaptosomes of the rat striatum: involvement of AMPA and N-methyl-D-aspartate receptors. *Neuroscience* 47, 333–339.

Desce, J. M., Godeheu, G., Galli, T., Glowinski, J., and Cheramy, A. (1994). Opposite presynaptic regulations by glutamate through NMDA receptors of dopamine synthesis and release in rat striatal synaptosomes. *Brain Res.* 640, 205–214.

Dugast, C., Suaud-Chagny, M. F., and Gonon, F. (1994). Continuous *in vivo* monitoring of evoked dopamine release in the rat nucleus accumbens by amperometry. *Neuroscience* 62, 647–654.

Egger, V., Feldmeyer, D., and Sakmann, B. (1999). Coincidence detection and changes of synaptic efficacy in spiny stellate neurons in rat barrel cortex. *Nat. Neurosci.* 2, 1098–1105.

Feldman, D. E. (2000). Timing-based LTP and LTD at vertical inputs to layer II/III pyramidal cells in rat barrel cortex. *Neuron* 27, 45–56.

Florian, R. V. (2007). Reinforcement learning through modulation of spike-timing-dependent synaptic plasticity. *Neural. Comput.* 19, 1468–1502.

Foote, S. L., Aston-Jones, G., and Bloom, F. E. (1980). Impulse activity of locus coeruleus neurons in awake rats and monkeys is a function of sensory stimulation and arousal. *Proc. Natl. Acad. Sci. U.S.A.* 77, 3033–3037.

Fox, K. (2009). Experience-dependent plasticity mechanisms for neural rehabilitation in somatosensory cortex. *Philos. Trans. R. Soc. Lond., B, Biol. Sci.* 364, 369–381.

Fremaux, N., Sprekeler, H., and Gerstner, W. (2010). Functional requirements for reward-modulated spike-timing dependent plasticity. *J. Neurosci.* 30, 13326–13337.

Freund, T. F., Powell, J. F., and Smith, A. D. (1984). Tyrosine hydroxylase-immunoreactive boutons in synaptic contact with identified striatonigral neurons, with particular reference to dendritic spines. *Neuroscience* 13, 1189–1215.

Frey, U., Schroeder, H., and Matthies, H. (1990). Dopaminergic antagonists prevent long-term maintenance of posttetanic LTP in the CA1 region of rat hippocampal slices. *Brain Res.* 522, 69–75.

Froemke, R. C., Debanne, D., and Bi, G.-Q. (2010). Temporal modulation of spike-timing-dependent plasticity. *Front. Syn. Neurosci.* 2:12. doi: 10.3389/fnsyn.2010.00019.

Froemke, R. C., Poo, M. M., and Dan, Y. (2005). Spike-timing-dependent synaptic plasticity depends on dendritic location. *Nature* 434, 221–225.

Froemke, R. C., Tsay, I. A., Raad, M., Long, J. D., and Dan, Y. (2006). Contribution of individual spikes in burst-induced long-term synaptic modification. *J. Neurophysiol.* 95, 1620–1629.

Gao, W. J., Krimer, L. S., and Goldman-Rakic, P. S. (2001). Presynaptic regulation of recurrent excitation by D1 receptors in prefrontal circuits. *Proc. Natl. Acad. Sci. U.S.A.* 98, 295–300.

Gerfen, C. R. (2006). Indirect-pathway neurons lose their spines in Parkinson disease. *Nat. Neurosci.* 9, 157–158.

Gerfen, C. R., Engber, T. M., Mahan, L. C., Susel, Z., Chase, T. N., Monsma, F. J. Jr., and Sibley, D. R. (1990). D1 and D2 dopamine receptor-regulated gene expression of striatonigral and striatopallidal neurons. *Science* 250, 1429–1432.

Gerfen, C. R., Keefe, K. A., and Gauda, E. B. (1995). D1 and D2 dopamine receptor function in the striatum: coactivation of D1- and D2-dopamine receptors on separate populations of neurons results in potentiated immediate early gene response in D1-containing neurons. *J. Neurosci.* 15, 8167–8176.

Gerstner, W., Kempter, R., van Hemmen, J. L., and Wagner, H. (1996). A neuronal learning rule for sub-millisecond temporal coding. *Nature* 383, 76–81.

Gerstner, W., Ritz, R., and van Hemmen, J. L. (1993). Why spikes? Hebbian learning and retrieval of time-resolved excitation patterns. *Biol. Cybern.* 69, 503–515.

Girault, J. A., and Greengard, P. (2004). The neurobiology of dopamine signaling. *Arch. Neurol.* 61, 641–644.

Groves, P. M., Linder, J. C., and Young, S. J. (1994). 5-hydroxydopamine-labeled dopaminergic axons: three-dimensional reconstructions of axons, synapses and postsynaptic targets in rat neostriatum. *Neuroscience* 58, 593–604.

Gulledge, A. T., and Stuart, G. J. (2003). Action potential initiation and propagation in layer 5 pyramidal neurons of the rat prefrontal cortex: absence of dopamine modulation. *J. Neurosci.* 23, 11363–11372.

Harvey, C. D., and Svoboda, K. (2007). Locally dynamic synaptic learning rules in pyramidal neuron dendrites. *Nature* 450, 1195–1200.

Hasselmo, M. E. (1995). Neuromodulation and cortical function: modeling the physiological basis of behavior. *Behav. Brain Res.* 67, 1–27.

Hasselmo, M. E. (2006). The role of acetylcholine in learning and memory. *Curr. Opin. Neurobiol.* 16, 710–715.

Hasselmo, M. E., and Giocomo, L. M. (2006). Cholinergic modulation of cortical function. *J. Mol. Neurosci.* 30, 133–135.

He, K., Song, L., Cummings, L. W., Goldman, J., Huganir, R. L., and Lee, H. K. (2009). Stabilization of Ca^{2+}-permeable AMPA receptors at perisynaptic sites by GluR1-S845 phosphorylation. *Proc. Natl. Acad. Sci. U.S.A.* 106, 20033–20038.

Hebb, D. O. (1949). *The Organization of Behavior. A Neuropsychological Theory*. New York: John Wiley & Sons, Inc.

Hemmings, H. C. Jr., Greengard, P., Tung, H. Y., and Cohen, P. (1984). DARPP-32, a dopamine-regulated neuronal phosphoprotein, is a potent inhibitor of protein phosphatase-1. *Nature* 310, 503–505.

Histed, M. H., Pasupathy, A., and Miller, E. K. (2009). Learning substrates in the primate prefrontal cortex and striatum: sustained activity related to successful actions. *Neuron* 63, 244–253.

Hoffman, D. A., and Johnston, D. (1999). Neuromodulation of dendritic action potentials. *J. Neurophysiol.* 81, 408–411.

Hollerman, J. R., and Schultz, W. (1998). Dopamine neurons report an error in the temporal prediction of reward during learning. *Nat. Neurosci.* 1, 304–309.

Holtmaat, A., and Svoboda, K. (2009). Experience-dependent structural synaptic plasticity in the mammalian brain. *Nat. Rev. Neurosci.* 10, 647–658.

Hooks, B. M., and Chen, C. (2007). Critical periods in the visual system: changing views for a model of experience-dependent plasticity. *Neuron* 56, 312–326.

Huerta, P. T., and Lisman, J. E. (1993). Heightened synaptic plasticity of hippocampal CA1 neurons during a cholinergically induced rhythmic state. *Nature* 364, 723–725.

Hull, C. L. (1943). *Principles of Behavior*. New York: Appleton-Century.

Ingham, C. A., Hood, S. H., Taggart, P., and Arbuthnott, G. W. (1998). Plasticity of synapses in the rat neostriatum after unilateral lesion of the nigrostriatal dopaminergic pathway. *J. Neurosci.* 18, 4732–4743.

Izhikevich, E. M. (2007). Solving the distal reward problem through linkage of STDP and dopamine signaling. *Cereb. Cortex* 17, 2443–2452.

Jacob, V., Brasier, D. J., Erchova, I., Feldman, D., and Shulz, D. E. (2007). Spike timing-dependent synaptic depression in the *in vivo* barrel cortex of the rat. *J. Neurosci.* 27, 1271–1284.

Jay, T. M. (2003). Dopamine: a potential substrate for synaptic plasticity and memory mechanisms. *Prog. Neurobiol.* 69, 375–390.

Jia, H., Rochefort, N. L., Chen, X., and Konnerth, A. (2010). Dendritic organization of sensory input to cortical neurons *in vivo*. *Nature* 464, 1307–1312.

Jin, S., and Fredholm, B. B. (1994). Role of NMDA, AMPA and kainate receptors in mediating glutamate- and 4-AP-induced dopamine and acetylcholine release from rat striatal slices. *Neuropharmacology* 33, 1039–1048.

Joiner, M. L., Lise, M. F., Yuen, E. Y., Kam, A. Y., Zhang, M., Hall, D. D., Malik, Z. A., Qian, H., Chen, Y., Ulrich, J. D., Burette, A. C., Weinberg, R. J., Law, P. Y., El-Husseini, A., Yan, Z., and Hell, J. W. (2010). Assembly of a beta2-adrenergic receptor – GluR1 signalling complex for localized cAMP signalling. *EMBO J.* 29, 482–495.

Joshua, M., Adler, A., Mitelman, R., Vaadia, E., and Bergman, H. (2008). Midbrain dopaminergic neurons and striatal cholinergic interneurons encode the difference between reward and aversive events at different epochs of probabilistic classical conditioning trials. *J. Neurosci.* 28, 11673–11684.

Joshua, M., Adler, A., Prut, Y., Vaadia, E., Wickens, J. R., and Bergman, H. (2009). Synchronization of midbrain dopaminergic neurons is enhanced by rewarding events. *Neuron* 62, 695–704.

Kempter, R., Gerstner, W., and van Hemmen, J. L. (1999). Hebbian learning and spiking neurons. *Phys. Rev. E* 59, 4498.

Kilgard, M. P., and Merzenich, M. M. (1998). Cortical map reorganization enabled by nucleus basalis activity. *Science* 279, 1714–1718.

Koester, H. J., and Sakmann, B. (1998). Calcium dynamics in single spines during coincident pre- and postsynap-

tic activity depend on relative timing of back-propagating action potentials and subthreshold excitatory postsynaptic potentials. *Proc. Natl. Acad. Sci. U.S.A.* 95, 9596–9601.

Lamprecht, R., and LeDoux, J. (2004). Structural plasticity and memory. *Nat. Rev. Neurosci.* 5, 45–54.

Lee, H. K., Barbarosie, M., Kameyama, K., Bear, M. F., and Huganir, R. L. (2000). Regulation of distinct AMPA receptor phosphorylation sites during bidirectional synaptic plasticity. *Nature* 405, 955–959.

Lee, H. K., and Huganir, R. L. (2008). *AMPA Receptor Regulation and the Reversal of Synaptic Plasticity – LTP, LTD, Depotentiation, and Dedepression*, Vol. 4. San Diego: Elsevier Press.

Lee, H. K., Takamiya, K., Han, J. S., Man, H., Kim, C. H., Rumbaugh, G., Yu, S., Ding, L., He, C., Petralia, R. S., Wenthold, R. J., Gallagher, M., and Huganir, R. L. (2003). Phosphorylation of the AMPA receptor GluR1 subunit is required for synaptic plasticity and retention of spatial memory. *Cell* 112, 631–643.

Legenstein, R., Pecevski, D., and Maass, W. (2008). A learning theory for reward-modulated spike-timing-dependent plasticity with application to biofeedback. *PLoS Comput. Biol.* 4: e1000180. doi: 10.1371/journal.pcbi.1000180.

Levine, M. S., Li, Z., Cepeda, C., Cromwell, H. C., and Altemus, K. L. (1996). Neuromodulatory actions of dopamine on synaptically-evoked neostriatal responses in slices. *Synapse* 24, 65–78.

Lin, Y. W., Min, M. Y., Chiu, T. H., and Yang, H. W. (2003). Enhancement of associative long-term potentiation by activation of beta-adrenergic receptors at CA1 synapses in rat hippocampal slices. *J. Neurosci.* 23, 4173–4181.

Lin, Y. W., Yang, H. W., Min, M. Y., and Chiu, T. H. (2008). Inhibition of associative long-term depression by activation of beta-adrenergic receptors in rat hippocampal CA1 synapses. *J. Biomed. Sci.* 15, 123–131.

Lisman, J. E., and McIntyre, C. C. (2001). Synaptic plasticity: a molecular memory switch. *Curr. Biol.* 11, R788–R791.

Ljungberg, T., Apicella, P., and Schultz, W. (1992). Responses of monkey dopamine neurons during learning of behavioral reactions. *J. Neurophysiol.* 67, 145–163.

Losonczy, A., Makara, J. K., and Magee, J. C. (2008). Compartmentalized dendritic plasticity and input feature storage in neurons. *Nature* 452, 436–441.

Lovinger, D. M. (2010). Neurotransmitter roles in synaptic modulation, plasticity and learning in the dorsal striatum. *Neuropharmacology* 58, 951–961.

Luscher, C., Nicoll, R. A., Malenka, R. C., and Muller, D. (2000). Synaptic plasticity and dynamic modulation of the postsynaptic membrane. *Nat. Neurosci.* 3, 545–550.

Magee, J. C., and Johnston, D. (1997). A synaptically controlled, associative signal for Hebbian plasticity in hippocampal neurons. *Science* 275, 209–213.

Magee, J. C., and Johnston, D. (2005). Plasticity of dendritic function. *Curr. Opin. Neurobiol.* 15, 334–342.

Malenka, R. C., and Bear, M. F. (2004). LTP and LTD: an embarrassment of riches. *Neuron* 44, 5–21.

Markram, H., Lubke, J., Frotscher, M., and Sakmann, B. (1997). Regulation of synaptic efficacy by coincidence of postsynaptic APs and EPSPs. *Science* 275, 213–215.

Matsumoto, M., and Hikosaka, O. (2009). Two types of dopamine neuron distinctly convey positive and negative motivational signals. *Nature* 459, 837–841.

Mehta, M. R., Quirk, M. C., and Wilson, M. A. (2000). Experience-dependent asymmetric shape of hippocampal receptive fields. *Neuron* 25, 707–715.

Meliza, C. D., and Dan, Y. (2006). Receptive-field modification in rat visual cortex induced by paired visual stimulation and single-cell spiking. *Neuron* 49, 183–189.

Meredith, R. M., Floyer-Lea, A. M., and Paulsen, O. (2003). Maturation of long-term potentiation induction rules in rodent hippocampus: role of GABAergic inhibition. *J. Neurosci.* 23, 11142–11146.

Miller, R. (1981). *Meaning and Purpose in the Intact Brain*. Oxford: Oxford University Press.

Mirenowicz, J., and Schultz, W. (1996). Preferential activation of midbrain dopamine neurons by appetitive rather than aversive stimuli. *Nature* 379, 449–451.

Mu, Y., and Poo, M. M. (2006). Spike timing-dependent LTP/LTD mediates visual experience-dependent plasticity in a developing retinotectal system. *Neuron* 50, 115–125.

Neuman, R. S., and Harley, C. W. (1983). Long-lasting potentiation of the dentate gyrus population spike by norepinephrine. *Brain Res.* 273, 162–165.

Nevian, T., and Sakmann, B. (2006). Spine Ca^{2+} signaling in spike-timing-dependent plasticity. *J. Neurosci.* 26, 11001–11013.

Nicola, S. M., Surmeier, J., and Malenka, R. C. (2000). Dopaminergic modulation of neuronal excitability in the striatum and nucleus accumbens. *Annu. Rev. Neurosci.* 23, 185–215.

O'Donnell, P., and Grace, A. A. (1994). Tonic D2-mediated attenuation of cortical excitation in nucleus accumbens neurons recorded *in vitro*. *Brain Res.* 634, 105–112.

Oh, M. C., Derkach, V. A., Guire, E. S., and Soderling, T. R. (2006). Extrasynaptic membrane trafficking regulated by GluR1 serine 845 phosphorylation primes AMPA receptors for long-term potentiation. *J. Biol. Chem.* 281, 752–758.

Paspalas, C. D., Rakic, P., and Goldman-Rakic, P. S. (2006). Internalization of D2 dopamine receptors is clathrin-dependent and select to dendro-axonic appositions in primate prefrontal cortex. *Eur. J. Neurosci.* 24, 1395–1403.

Pawlak, V., and Kerr, J. N. (2008). Dopamine receptor activation is required for corticostriatal spike-timing-dependent plasticity. *J. Neurosci.* 28, 2435–2446.

Paxinos, G. (2004). *The Rat Nervous System*, 3rd Edn. London: Academic Press.

Penfield, W. (1958). Some mechanisms of consciousness discovered during electrical stimulation of the brain. *Proc. Natl. Acad. Sci. U.S.A.* 44, 51–66.

Penfield, W. (1959). The interpretive cortex; the stream of consciousness in the human brain can be electrically reactivated. *Science* 129, 1719–1725.

Potjans, W., Morrison, A., and Diesmann, M. (2010). Enabling functional neural circuit simulations with distributed computing of neuromodulated plasticity. *Front. Comput. Neurosci.* 4:141. doi: 10.3389/fncom.2010.00141

Premont, J., Perez, M., and Bockaert, J. (1977). Adenosine-sensitive adenylate cyclase in rat striatal homogenates and its relationship to dopamine- and Ca^{2+}-sensitive adenylate cyclases. *Mol. Pharmacol.* 13, 662–670.

Rasmussen, K., Morilak, D. A., and Jacobs, B. L. (1986). Single unit activity of locus coeruleus neurons in the freely moving cat. I. During naturalistic behaviors and in response to simple and complex stimuli. *Brain Res.* 371, 324–334.

Redgrave, P., and Gurney, K. (2006). The short-latency dopamine signal: a role in discovering novel actions? *Nat. Rev. Neurosci.* 7, 967–975.

Remy, S., and Spruston, N. (2007). Dendritic spikes induce single-burst long-term potentiation. *Proc. Natl. Acad. Sci. U.S.A.* 104, 17192–17197.

Richardson, R. T., and DeLong, M. R. (1986). Nucleus basalis of Meynert neuronal activity during a delayed response task in monkey. *Brain Res.* 399, 364–368.

Richardson, R. T., and DeLong, M. R. (1990). Context-dependent responses of primate nucleus basalis neurons in a go/no-go task. *J. Neurosci.* 10, 2528–2540.

Richfield, E. K., Penney, J. B., and Young, A. B. (1989). Anatomical and affinity state comparisons between dopamine D1 and D2 receptors in the rat central nervous system. *Neuroscience* 30, 767–777.

Robbins, T. W., and Roberts, A. C. (2007). Differential regulation of fronto-executive function by the monoamines and acetylcholine. *Cereb. Cortex* 17(Suppl. 1), i151–i160.

Roberts, P. J., and Sharif, N. A. (1978). Effects of l-glutamate and related amino acids upon the release of [3H] dopamine from rat striatal slices. *Brain Res.* 157, 391–395.

Sakata, K., Woo, N. H., Martinowich, K., Greene, J. S., Schloesser, R. J., Shen, L., and Lu, B. (2009). Critical role of promoter IV-driven BDNF transcription in GABAergic transmission and synaptic plasticity in the prefrontal cortex. *Proc. Natl. Acad. Sci. U.S.A.* 106, 5942–5947.

Sara, S. J. (2009). The locus coeruleus and noradrenergic modulation of cognition. *Nat. Rev. Neurosci.* 10, 211–223.

Sara, S. J., and Segal, M. (1991). Plasticity of sensory responses of locus coeruleus neurons in the behaving rat: implications for cognition. *Prog. Brain Res.* 88, 571–585.

Sardo, P., Ravel, S., Legallet, E., and Apicella, P. (2000). Influence of the predicted time of stimuli eliciting movements on responses of tonically active neurons in the monkey striatum. *Eur. J. Neurosci.* 12, 1801–1816.

Sarkisov, D. V., and Wang, S. S. (2008). Order-dependent coincidence detection in cerebellar Purkinje neurons at the inositol trisphosphate receptor. *J. Neurosci.* 28, 133–142.

Sarter, M., Hasselmo, M. E., Bruno, J. P., and Givens, B. (2005). Unraveling the attentional functions of cortical cholinergic inputs: interactions between signal-driven and cognitive modulation of signal detection. *Brain Res. Brain Res. Rev.* 48, 98–111.

Sarter, M., Parikh, V., and Howe, W. M. (2009). Phasic acetylcholine release and the volume transmission hypothesis: time to move on. *Nat. Rev. Neurosci.* 10, 383–390.

Sawinski, J., Wallace, D. J., Greenberg, D. S., Grossmann, S., Denk, W., and Kerr, J. N. (2009). Visually evoked activity in cortical cells imaged in freely moving animals. *Proc. Natl. Acad. Sci. U.S.A.* 106, 19557–19562.

Schultz, W. (1998). Predictive reward signal of dopamine neurons. *J. Neurophysiol.* 80, 1–27.

Schultz, W. (2000). Multiple reward signals in the brain. *Nat. Rev. Neurosci.* 1, 199–207.

Schultz, W. (2002). Getting formal with dopamine and reward. *Neuron* 36, 241–263.

Schultz, W. (2006). Behavioral theories and the neurophysiology of reward. *Annu. Rev. Psychol.* 57, 87–115.

Schultz, W. (2007). Multiple dopamine functions at different time courses. *Annu. Rev. Neurosci.* 30, 259–288.

Schultz, W., Apicella, P., and Ljungberg, T. (1993). Responses of monkey dopamine neurons to reward and conditioned stimuli during successive steps of learning a delayed response task. *J. Neurosci.* 13, 900–913.

Schwarzschild, M. A., Agnati, L., Fuxe, K., Chen, J. F., and Morelli, M. (2006). Targeting adenosine A2A receptors in Parkinson's disease. *Trends Neurosci.* 29, 647–654.

Seguela, P., Watkins, K. C., and Descarries, L. (1989). Ultrastructural relationships of serotonin axon terminals in the cerebral cortex of the adult rat. *J. Comp. Neurol.* 289, 129–142.

Seguela, P., Watkins, K. C., Geffard, M., and Descarries, L. (1990). Noradrenaline axon terminals in adult rat neocortex: an immunocytochemical analysis in serial thin sections. *Neuroscience* 35, 249–264.

Seol, G. H., Ziburkus, J., Huang, S., Song, L., Kim, I. T., Takamiya, K., Huganir, R. L., Lee, H. K., and Kirkwood, A. (2007). Neuromodulators control the polarity of spike-timing-dependent synaptic plasticity. *Neuron* 55, 919–929.

Sesack, S. R., Aoki, C., and Pickel, V. M. (1994). Ultrastructural localization of D2 receptor-like immunoreactivity in midbrain dopamine neurons and their striatal targets. *J. Neurosci.* 14, 88–106.

Seung, H. S. (2003). Learning in spiking neural networks by reinforcement of stochastic synaptic transmission. *Neuron* 40, 1063–1073.

Shen, W., Flajolet, M., Greengard, P., and Surmeier, D. J. (2008). Dichotomous dopaminergic control of striatal synaptic plasticity. *Science* 321, 848–851.

Sivakumaran, S., Mohajerani, M. H., and Cherubini, E. (2009). At immature mossy-fiber-CA3 synapses, correlated presynaptic and postsynaptic activity persistently enhances GABA release and network excitability via BDNF and cAMP-dependent PKA. *J. Neurosci.* 29, 2637–2647.

Sjostrom, P. J., and Hausser, M. (2006). A cooperative switch determines the sign of synaptic plasticity in distal dendrites of neocortical pyramidal neurons. *Neuron* 51, 227–238.

Sjostrom, P. J., Turrigiano, G. G., and Nelson, S. B. (2003). Neocortical LTD via coincident activation of presynaptic NMDA and cannabinoid receptors. *Neuron* 39, 641–654.

Smith, Y., Bennett, B. D., Bolam, J. P., Parent, A., and Sadikot, A. F. (1994). Synaptic relationships between dopaminergic afferents and cortical or thalamic input in the sensorimotor territory of the striatum in monkey. *J. Comp. Neurol.* 344, 1–19.

Stern, E. A., Kincaid, A. E., and Wilson, C. J. (1997). Spontaneous subthreshold membrane potential fluctuations and action potential variability of rat corticostriatal and striatal neurons *in vivo*. *J. Neurophysiol.* 77, 1697–1715.

Sun, X., Zhao, Y., and Wolf, M. E. (2005). Dopamine receptor stimulation modulates AMPA receptor synaptic insertion in prefrontal cortex neurons. *J. Neurosci.* 25, 7342–7351.

Sutton, R. S., and Barto, A. G. (1981). Toward a modern theory of adaptive networks: expectation and prediction. *Psychol. Rev.* 88, 135–170.

Sutton, R. S., and Barto, A. G. (1998). *Reinforcement Learning: An Introduction*. Cambridge, MA: MIT Press.

Thomas, M. J., Moody, T. D., Makhinson, M., and O'Dell, T. J. (1996). Activity-dependent beta-adrenergic modulation of low frequency stimulation induced LTP in the hippocampal CA1 region. *Neuron* 17, 475–482.

Tsubokawa, H. (2000). Control of Na+ spike backpropagation by intracellular signaling in the pyramidal neuron dendrites. *Mol. Neurobiol.* 22, 129–141.

Tzounopoulos, T., Rubio, M. E., Keen, J. E., and Trussell, L. O. (2007). Coactivation of pre- and postsynaptic signaling mechanisms determines cell-specific spike-timing-dependent plasticity. *Neuron* 54, 291–301.

Vasilaki, E., Fremaux, N., Urbanczik, R., Senn, W., and Gerstner, W. (2009). Spike-based reinforcement learning in continuous state and action space: when policy gradient methods fail. *PLoS Comput. Biol.* 5, e1000586. doi: 10.1371/journal.pcbi.1000586.

Wang, H. X., Gerkin, R. C., Nauen, D. W., and Bi, G. Q. (2005). Coactivation and timing-dependent integration of synaptic potentiation and depression. *Nat. Neurosci.* 8, 187–193.

Wang, S. S., Denk, W., and Hausser, M. (2000). Coincidence detection in single dendritic spines mediated by calcium release. *Nat. Neurosci.* 3, 1266–1273.

Wang, Z., Kai, L., Day, M., Ronesi, J., Yin, H. H., Ding, J., Tkatch, T., Lovinger, D. M., and Surmeier, D. J. (2006). Dopaminergic control of corticostriatal long-term synaptic depression in medium spiny neurons is mediated by cholinergic interneurons. *Neuron* 50, 443–452.

Waters, J., and Helmchen, F. (2004). Boosting of action potential backpropagation by neocortical network activity *in vivo*. *J. Neurosci.* 24, 11127–11136.

Waters, J., Larkum, M., Sakmann, B., and Helmchen, F. (2003). Supralinear Ca^{2+} influx into dendritic tufts of layer 2/3 neocortical pyramidal neurons *in vitro* and *in vivo*. *J. Neurosci.* 23, 8558–8567.

Waters, J., Schaefer, A., and Sakmann, B. (2005). Backpropagating action potentials in neurones: measurement, mechanisms and potential functions. *Prog. Biophys. Mol. Biol.* 87, 145–170.

Wickens, J. (1990). Striatal dopamine in motor activation and reward-mediated learning: steps towards a unifying model. *J. Neural Transm. Gen. Sect.* 80, 9–31.

Wickens, J. R. (2009). Synaptic plasticity in the basal ganglia. *Behav. Brain Res.* 199, 119–128.

Wilson, C. J., Chang, H. T., and Kitai, S. T. (1990). Firing patterns and synaptic potentials of identified giant aspiny interneurons in the rat neostriatum. *J. Neurosci.* 10, 508–519.

Wilson, C. J., and Groves, P. M. (1981). Spontaneous firing patterns of identified spiny neurons in the rat neostriatum. *Brain Res.* 220, 67–80.

Wilson, C. J., and Kawaguchi, Y. (1996). The origins of two-state spontaneous membrane potential fluctuations of neostriatal spiny neurons. *J. Neurosci.* 16, 2397–2410.

Wilson, F. A., and Rolls, E. T. (1990). Neuronal responses related to the novelty and familarity of visual stimuli in the substantia innominata, diagonal band of Broca and periventricular region of the primate basal forebrain. *Exp. Brain Res.* 80, 104–120.

Xie, X., and Seung, H. S. (2004). Learning in neural networks by reinforcement of irregular spiking. *Phys. Rev. E. Stat. Nonlin. Soft Matter Phys.* 69, 041909.

Zhang, J. C., Lau, P. M., and Bi, G. Q. (2009). Gain in sensitivity and loss in temporal contrast of STDP by dopaminergic modulation at hippocampal synapses. *Proc. Natl. Acad. Sci. U.S.A.* 106, 13028–13033.

Zhou, F. M., Liang, Y., and Dani, J. A. (2001). Endogenous nicotinic cholinergic activity regulates dopamine release in the striatum. *Nat. Neurosci.* 4, 1224–1229.

Zhou, F. M., Wilson, C. J., and Dani, J. A. (2002). Cholinergic interneuron characteristics and nicotinic properties in the striatum. *J. Neurobiol.* 53, 590–605.

Zhou, Y. D., Acker, C. D., Netoff, T. I., Sen, K., and White, J. A. (2005). Increasing Ca2+ transients by broadening postsynaptic action potentials enhances timing-dependent synaptic depression. *Proc. Natl. Acad. Sci. U.S.A.* 102, 19121–19125.

Conflict of Interest Statement: The authors declare that the research was conducted in the absence of any commercial or financial relationships that could be construed as a potential conflict of interest.

Received: 15 April 2010; accepted: 27 September 2010; published online: 25 October 2010.

Citation: Pawlak V, Wickens JR, Kirkwood A and Kerr JND (2010) Timing is not everything: neuromodulation opens the STDP gate. Front. Syn. Neurosci. ***2****:146. doi: 10.3389/fnsyn.2010.00146*

frontiers in
SYNAPTIC NEUROSCIENCE

REVIEW ARTICLE
published: 17 June 2010
doi: 10.3389/fnsyn.2010.00019

Temporal modulation of spike-timing-dependent plasticity

Robert C. Froemke[1]*, Dominique Debanne[2,3] and Guo-Qiang Bi[4,5]

[1] *Molecular Neurobiology Program, Departments of Otolaryngology and Physiology/Neuroscience, The Helen and Martin Kimmel Center for Biology and Medicine, Skirball Institute of Biomolecular Medicine, New York University School of Medicine, New York, NY, USA*
[2] *Institut National de la Santé et de la Recherche Médicale U641, Marseille, France*
[3] *Faculté de Médecine Nord, Université de la Méditerranée, Marseille, France*
[4] *Department of Neurobiology and Center for Neuroscience and Center for the Neural Basis of Cognition, University of Pittsburgh School of Medicine, Pittsburgh, PA, USA*
[5] *Hefei National Laboratory for Physical Sciences at the Microscale and School of Life Sciences, University of Science and Technology of China, Hefei, Anhui, China*

Edited by:
Per Jesper Sjöström, University College London, UK

Reviewed by:
Samuel S. H. Wang, Princeton University, USA
Kevin Bender, Oregon Health and Science University, USA
Per Jesper Sjöström, University College London, UK

****Correspondence:***
Robert C. Froemke, Molecular Neurobiology Program, Departments of Otolaryngology and Physiology/ Neuroscience, The Helen and Martin Kimmel Center for Biology and Medicine, Skirball Institute of Biomolecular Medicine, New York University School of Medicine, New York, NY 10016, USA.
e-mail: robert.froemke@med.nyu.edu

Spike-timing-dependent plasticity (STDP) has attracted considerable experimental and theoretical attention over the last decade. In the most basic formulation, STDP provides a fundamental unit – a spike pair – for quantifying the induction of long-term changes in synaptic strength. However, many factors, both pre- and postsynaptic, can affect synaptic transmission and integration, especially when multiple spikes are considered. Here we review the experimental evidence for multiple types of nonlinear temporal interactions in STDP, focusing on the contributions of individual spike pairs, overall spike rate, and precise spike timing for modification of cortical and hippocampal excitatory synapses. We discuss the underlying processes that determine the specific learning rules at different synapses, such as postsynaptic excitability and short-term depression. Finally, we describe the success of efforts toward building predictive, quantitative models of how complex and natural spike trains induce long-term synaptic modifications.

Keywords: cortex, hippocampus, LTD, LTP, model, spikes, STDP, synaptic plasticity

INTRODUCTION

Synaptic plasticity is essential for the organization and function of neural circuits. Long-term changes in synaptic strength have been described for many systems, ranging from the invertebrate neuromuscular junction to the mammalian hippocampus and neocortex (Malenka and Nicoll, 1999; Zucker, 1999). Correspondingly, it is believed that there are several important consequences of long-term synaptic modification depending on when and where synaptic modifications occur, including neural development (Katz and Shatz, 1996), cortical map formation, and reorganization (Cruikshank and Weinberger, 1996; Buonomano and Merzenich, 1998; Kilgard et al., 2002), alteration of receptive field properties (Fregnac and Shulz, 1999; Froemke et al., 2007), perceptual learning (Gilbert, 1998), behavioral conditioning (Schafe et al., 2001), and memory encoding and storage (Martin et al., 2000). It is therefore critical to understand the general rules by which synapses are changed in response to various patterns of neural activity.

Most types of long-term synaptic modification can be formulated in terms of Hebbian learning. The neurophysiological postulate of Hebb (1949) has exerted tremendous influence on the study of synaptic plasticity. Hebb's idea was that associative learning such as Pavlovian conditioning (Pavlov, 1927) could be represented in a neural circuit by changes in the patterns of synaptic connections, a concept that was inspired by the experimental findings of Lorente de Nó (1938). In particular, Hebb believed that persistent activation of a postsynaptic neuron by a presynaptic input should lead to a strengthening of the synapse between the two cells. This hypothesis for associative synaptic plasticity was later extended by Stent (1973), who suggested the converse idea for bidirectional synaptic modification – that persistent failure of a presynaptic input to activate the postsynaptic neuron should lead to weakening of that synapse.

In the years that followed, Hebb's postulate exerted a profound influence on theoretical and experimental neurophysiology. Spurred by the discovery of hippocampal long-term potentiation (LTP) by Bliss and Lømo (1973), along with other experimental reports of changes in cortical activity (Bindman et al., 1962), many different theoretical frameworks for long-term synaptic modification were proposed, such as the covariance model (Stanton and Sejnowski, 1989) or temporal difference learning (Sutton and Barto, 1998; Rao and Sejnowski, 2001).

One of the most successful paradigms for the study of long-term synaptic plasticity is the Bienenstock–Cooper–Munro (BCM) sliding threshold model (Bienenstock et al., 1982). In this scheme, the sign and degree of synaptic modification is a nonlinear function of postsynaptic spike rate. When the postsynaptic spike frequency is above a certain threshold (θ_m) LTP is induced, while long-term depression (LTD) is induced when the firing rate is below θ_m but greater than zero. The value of θ_m is not fixed, but varies so as to prevent runaway potentiation or depression to saturation. The BCM model was originally proposed as a method by which synaptic modifications could result in the development and plasticity

of ocular dominance and orientation tuning in cat and monkey visual cortex. Since its description, an abundance of experimental evidence for the BCM model has been obtained in many preparations, including the hippocampus and visual cortex (Kirkwood et al., 1993, 1995). Additionally, other properties of the postsynaptic cell beyond firing rate lead to biphasic functions reminiscent of the characteristic BCM curve, including presynaptic input rate, postsynaptic depolarization, inhibitory tonus, and internal calcium concentration ($[Ca^{2+}]_i$) (Artola et al., 1990; Hansel et al., 1997; Yang et al., 1999). The BCM model is Hebbian in that the requisite postsynaptic spiking presumably results from activation of a subset of presynaptic inputs. However, because the BCM model is a rate-based learning rule, it does not necessarily require the precise temporal ordering of pre- and postsynaptic activity. In particular, the BCM model predicts that for modest firing rates, LTD is induced even if the presynaptic cell routinely takes part in firing the postsynaptic cell.

Recently, Hebbian learning at the synaptic level has been recast in terms of correlated pre- and postsynaptic spiking, a formulation more consistent with Hebb's original thesis. Over the last few decades, some studies had found that the temporal order of pre- and postsynaptic activity was a crucial parameter for induction of both LTP and LTD (Baranyi and Fehér, 1981; Levy and Steward, 1983; Kelso et al., 1986; Gustafsson et al., 1987; Zador et al., 1990; Abbott and Blum, 1996; Sourdet and Debanne, 1999). Then in the 1990s, a number of groundbreaking papers showed that in a variety of preparations, repetitive stimulation with pairs of pre- and postsynaptic action potentials (pre/post pairs) led to induction of long-term synaptic plasticity. Importantly, the precise pre/post spike timing controlled both the sign and magnitude of synaptic modification (Debanne et al., 1994; Bell et al., 1997; Markram et al., 1997; Bi and Poo, 1998; Debanne et al., 1998; Zhang et al., 1998), and therefore this phenomenon was dubbed "spike-timing-dependent plasticity" (STDP) (Abbott and Nelson, 2000; Song et al., 2000).

Spike-timing-dependent plasticity has several properties that make it a useful protocol for investigating long-term synaptic plasticity. First, STDP is quantifiable. This allows for accurate predictions of synaptic plasticity spike for spike, enabling experiments to be designed that carefully measure the sign and degree of synaptic modification induced by complex patterns of neural activity (**Figure 1**). For this reason, STDP has rapidly become a popular choice for theoretical studies of synaptic plasticity in neural networks (Gerstner et al., 1996; Sejnowski, 1999; Senn et al., 1999; Abbott and Nelson, 2000; Gutig and Sompolinsky, 2006; Pfister and Gerstner, 2006; Morrison et al., 2008; Urakubo et al., 2008). Second, STDP is a robust phenomenon. The shape and size of the time window for induction of both LTP and LTD of excitatory synapses is remarkably conserved across different preparations (Abbott and Nelson, 2000; Dan and Poo, 2006), with a few notable exceptions (Bell et al., 1997; Egger et al., 1999; Letzkus et al., 2006; Sjöström and Häusser, 2006). Finally, STDP provides an intuitive cellular mechanism for associative learning and behavioral conditioning. The correlation between spike timing and the sign/magnitude of response modification is strikingly similar to that observed in classic conditioning experiments (Pavlov, 1927), albeit on a different time scale. STDP may also represent a basic neurophysiological correlate of the principle of causality (Berninger and Bi, 2002), responsible for *a priori* temporal organization of mental events, in the sense of Kant (1781). For these reasons, in the last 15 years there has been an explosion in the number of both experimental and theoretical studies of STDP, and in turn the unusually close collaboration between experiment and theory has been an important reason for the success of the STDP subfield.

In this review, we summarize the results of experiments on the timing requirements for STDP, focusing mainly on excitatory neocortical and hippocampal synapses in brain slices and culture. We detail the effects of temporal modulation during STDP induction, including variations in number of pre/post pairings, spike frequency, and precise spike timing. While other parameters such as dendritic location of synaptic inputs or local neuromodulatory status are also important, these variables are more fully described in other reviews in this issue (Froemke et al., 2007; Seol et al., 2007). The overall goal of these parametric experiments is a complete, predictive model of how complex patterns of pre- and postsynaptic activity modify synaptic strength. Such models will be required to support large-scale efforts to simulate brain circuitry (Markram, 2006; Izhikevich and Edelman, 2007), and to inform treatments for impairments of learning and memory in nervous system disorders (Merzenich et al., 1996; Tallal et al., 1996).

FIRST-ORDER STDP INDUCED WITH SPIKE PAIRS

Computationally, STDP is ideal as a synaptic learning rule, as it provides a basic discrete unit for long-term modification: the spike pair. Repetitive presentation of single pre- and postsynaptic spike pairs induces spike-timing-dependent LTP and LTD in hippocampus (Debanne et al., 1998; Bi and Poo, 1998; Nishiyama et al., 2000; Lin et al., 2003; Tsukada et al., 2005; **Figures 1 and 2A**), neocortex (Feldman, 2000; Sjöström et al., 2001; Froemke and Dan, 2002; Birtoli and Ulrich, 2004; Zilberter et al., 2009; **Figure 2B**), and other systems (Bell et al., 1997; Zhang et al., 1998; Pawlak and Kerr, 2008). In these studies, usually 50–100 pairs of spikes are evoked at low frequency (0.1–5 Hz) by focal extracellular stimulation and/or direct depolarizing current injection, where a critical parameter for determining synaptic modification is the time interval between the pre- and postsynaptic spikes.

At most glutamatergic synapses, LTP is induced when the presynaptic neuron fires before the postsynaptic neuron (pre→post pairing at positive time intervals), and LTD is induced if the postsynaptic cell fires before the presynaptic cell (post→pre pairing at negative time intervals), such that the degree of synaptic modification depends on the relative time between the two spikes or sets of spikes. Although there are many types of STDP learning rules (Abbott and Nelson 2000; Caporale and Dan 2008), the hallmark of excitatory STDP is a time window of approximately 0–20 ms for the induction of LTP and −1 to −100 ms for LTD, outside of which no synaptic modification occurs (**Figures 1 and 2**). Uncorrelated pre/post spiking at low firing rates generally leads to LTD because the integrated area under the spike timing window for depression is usually larger than that for potentiation. It is still unclear what cellular factors determine these timing requirements, especially the sharp transition point that occurs around time zero. There is evidence that, generally, the window for LTP is set by the activation kinetics of NMDA receptors (Kampa et al., 2004; Urakubo et al., 2008), but the LTD window seems to be more variable

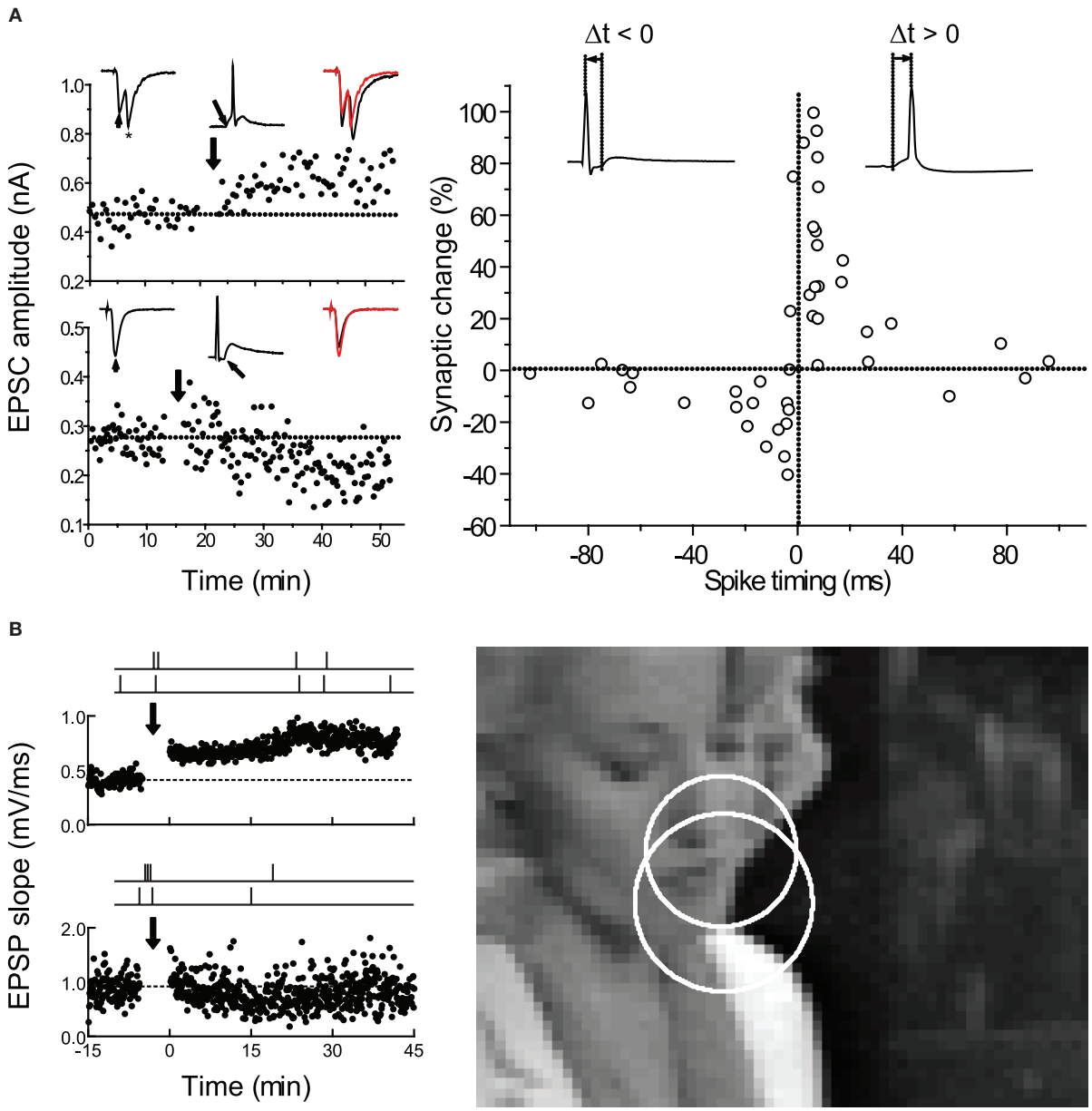

FIGURE 1 | Spike-timing-dependent plasticity can be used to predict how complex spike trains induce long-term changes in synaptic strength. (A) Timing requirements for STDP induction in excitatory neurons from low-density hippocampal cultures. Left, examples of LTP induced by pre→post pairing (top) and LTD induced by post→pre pairing (bottom) at short time intervals. Right, critical time window for synaptic modifications. Each circle represents one experiment. Curves, single exponential fits to the data. From Bi and Poo (1998, 2001). **(B)** How does the STDP learning rule for spike pairs need to be modified for predicting the effects of complex spike trains? Left, examples of LTP (top) and LTD (bottom) induced by natural spike train fragments in slices of young rat visual cortex. Right, scene from a movie used to obtain natural spike trains from the cat visual cortex *in vivo*. From Froemke and Dan (2002).

across different synapses, and may require such diverse processes as Ca^{2+}-dependent postsynaptic NMDA receptor suppression, presynaptic NMDA autoreceptor activation, endocannabinoid release, and metabotropic glutamate receptors, depending on cell type, strength of postsynaptic depolarization, pre/post spike rates, and location of synaptic input (Senn et al., 1999; Abarbanel et al., 2002; Franks and Sejnowski, 2002; Karmarkar and Buonomano, 2002; Shouval et al., 2002; Sjöström et al., 2003; Birtoli and Ulrich, 2004; Froemke et al., 2005; Bender et al., 2006; Corlew et al., 2007; Urakubo et al., 2008; Feldman, 2009). While a central mechanism for STDP is Ca^{2+} influx through voltage-gated Ca^{2+} channels and NMDA receptors (Koester and Sakmann, 1998; Johnston et al., 2003; Froemke et al., 2006; Nevian and Sakmann, 2006), other processes, including dendritic excitability (Letzkus et al., 2006; Sjöström and Häusser, 2006) and Ca^{2+} release from internal stores (Wang et al., 2000; Larkum et al., 2003), are also implicated in STDP induction at different synapses (Nishiyama et al., 2000; Froemke et al., 2010). It should be highlighted that

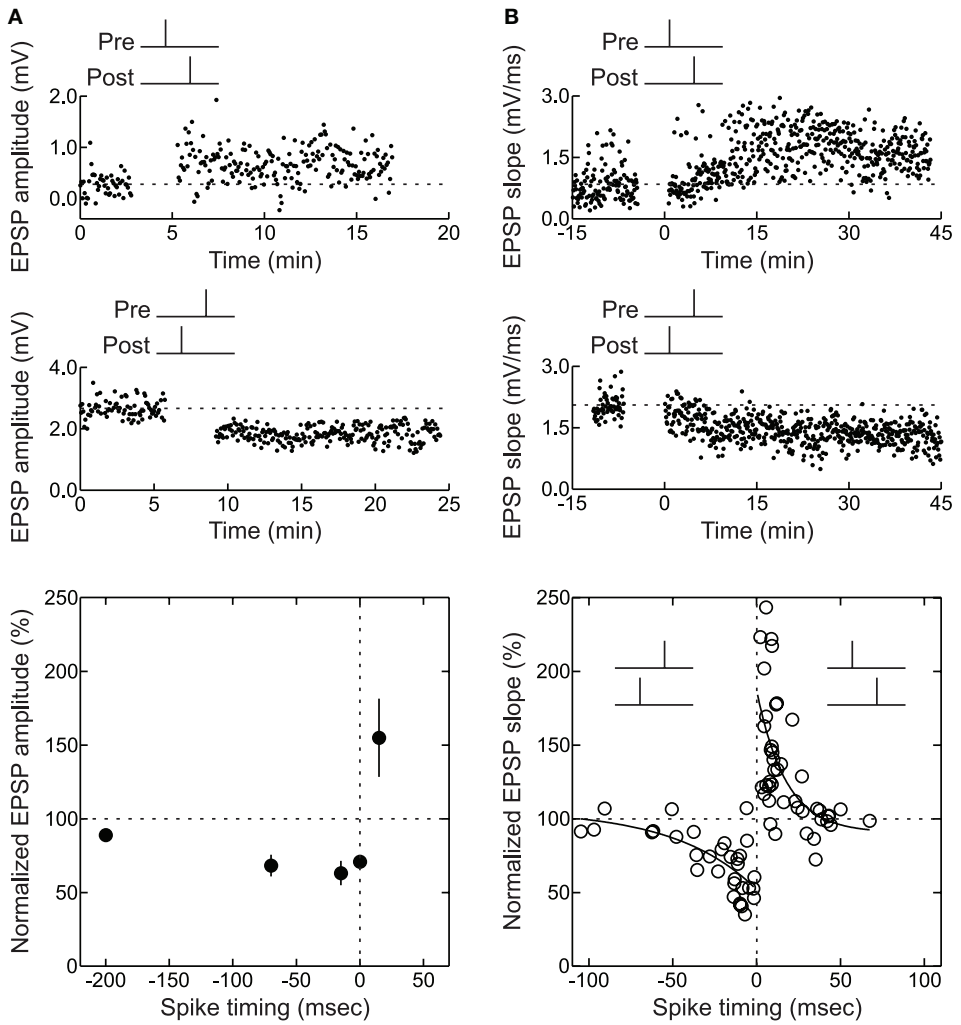

FIGURE 2 | Pre/post pairing induces STDP at hippocampal and neocortical synapses. (A) STDP induced at CA3-CA3 synapses in hippocampal slice cultures. Top, LTP induced by pre→post pairing (Δt = 15 ms). Center, LTD induced by post→pre spiking (Δt = -70 ms). Bottom, time window for pre/post pairing to induce synaptic modifications. From Debanne et al. (1998). **(B)** As in **A**, but for layer 2/3 connections in acute brain slices of young rat visual cortex. From Froemke and Dan (2002) and Froemke et al. (2006).

STDP induction seems to be somewhat sensitive to technical details, in terms of spike number, spike timing, spike frequency, and underlying mechanisms such as inhibitory regulation. This seems especially true for CA1 pyramidal cells in hippocampal slices, where it remains controversial what is minimally required for LTP and LTD (Pike et al., 1999; Nishiyama et al. 2000; Meredith et al., 2003; Wittenberg and Wang, 2006; Buchanan and Mellor, 2007; but see Campanac and Debanne, 2008).

This millisecond-scale time window for pre/post pairings to induce LTP or LTD forms the basis of the STDP learning rule for a given synaptic connection. To quantify the effect of pre/post pairing more precisely, both the pre→post and post→pre data can be fitted with single exponential functions: $\Delta w = Ae^{-|\Delta t|/\tau}$, where Δw is the percentage change in synaptic weight, Δt is the pre/post spike interval, and A and τ are two free parameters found by fitting the data, representing the scaling factor and time constant of the exponential function, respectively (Song et al., 2000; Bi and Poo, 2001; Froemke and Dan, 2002; **Figures 1 and 2**). Biologically, STDP is unlikely to be a true single exponential process, but these exponential fits are a convenient way to adequately formalize STDP using a low parameter model.

Here we refer to this formulation of STDP, in which only the intervals between each pre/post pairing are considered for determination of net synaptic modification, as the "history-independent" model. While sometimes found to be satisfactory when overall spike rates are relatively low (<10 Hz), in general the history-independent model provides poor estimates of the effects of more complex spike trains, even when one additional spike is added to a pre/post pair, i.e., using spike triplets instead of spike pairs to induce STDP (Pfister and Gerstner, 2006). Comparisons between the predicted and actual effects of spike trains on synaptic strength show that the predictions of the independent model are generally poor and

sometimes non-physiological (Sjöström et al., 2001; Froemke and Dan, 2002; Froemke et al., 2006; Butts et al., 2007). To better predict how arbitrary spike trains change synaptic strength in terms of spike pair contributions, there are three initial questions: (1) whether STDP requires the full number of 60–100 pre/post pairings repeated over several minutes for successful induction of LTP or LTD; (2) to what degree LTP and LTD saturate; and (3) how individual pairwise effects are combined or integrated to determine the net change in synaptic strength.

First we will consider how many pairing events are needed for STDP. The amount of LTP or LTD induced by repetitive spike pairing is usually measured 10+ minutes post-induction. However, for some cells, significant changes in synaptic strength can be observed to occur immediately after termination of spike pairing, while for other cells, synaptic modifications were delayed for several minutes. Across synapses, it seems that approximately one-third of synapses are changed immediately after pairing, one-third are changed with a delay of several minutes, and one-third show both immediate and delayed changes in synaptic strength (Magee and Johnston, 1997; Markram et al., 1997; Debanne et al., 1999; Sjöström et al., 2001; Hoffman et al., 2002; Froemke et al., 2006).

For those experiments in which LTP or LTD was rapidly induced, trial-by-trial examination of EPSPs during the spike pairing procedure might indicate how many pairings are needed to increase or decrease synaptic efficacy. For STDP of layer 2/3 lateral connections in slices of the young rat visual cortex, in which 60 pre/post pairs were presented at 0.2 Hz for 5 min (Froemke et al., 2006), there was a progressive increase in synaptic strength with repetitive pre→post spike pairing. About half of those pre→post experiments that could be analyzed showed a steady increase in EPSP size with continued spike pairing (**Figure 3A**), while other cells showed a pronounced, significant stepwise increase in synaptic strength at some point during the 5 min of spike pairing (**Figure 3B**). Remarkably, it appeared that as little as 1 min of conditioning (12 pairs) was sufficient to induce a modest but significant amount of potentiation (**Figure 3D**). The development of LTD induced with post→pre spike pairs, on the other hand, required more pairings than LTP. In general, while one minute of pre→post spike pairing induced significant LTP, LTD required 4 min of post→pre pairing to develop (**Figure 3C and D**). In general, induction of LTD requires more prolonged periods of activity than LTP (Dudek and Bear, 1992; Yang et al., 1999; Froemke et al., 2006; Wittenberg and Wang, 2006).

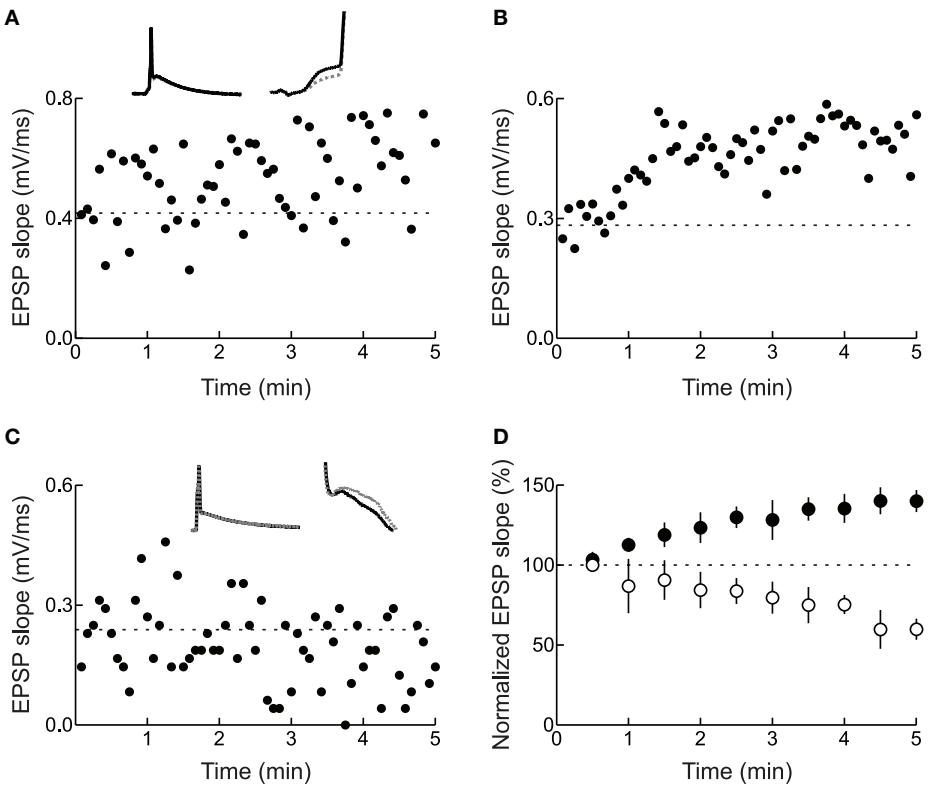

FIGURE 3 | Changes in synaptic strength during pre/post spike pairing. (A) Example of continual increase in initial slope during pre→post spike pairing with 60 pairs. This cell did not display a significant ($p < 0.05$) increase in slope from minute to minute. Dashed line, average initial slope during baseline period before conditioning. Left inset, average postsynaptic response during first six (gray dashed line) and last six (solid black line) pairings. Right inset, blow-up showing the increase in EPSP slope. **(B)** Example of a stepwise increase in initial slope induced by pre→post spike pairing. This cell showed a significant increase in initial slope from first to second minute of pairing. **(C)** Example of decrease in initial slope during post→pre spike pairing with 60 pairs. Dashed line, average initial slope of first six post→pre pairings. Left inset, average postsynaptic response during first six (gray dashed line) and last six (solid black line) pairings. Right inset, blow-up showing the decrease in EPSP slope. **(D)** Summary of conditioning period for cells that displayed significant changes in synaptic strength immediately after pre/post pairing. From Froemke et al. (2006).

The observation that some synapses were potentiated or depressed during or immediately after conditioning suggests that fewer than 60 pre/post spike pairs can induce long-term changes in synaptic strength. In the optic tectum of the tadpole *in vivo*, spike-timing-dependent LTP was maximal after 80–200 pairs, but 20 pre→post spike pairs induced a moderate amount of potentiation on average (Zhang et al., 1998). In cortex, a small number of pre/post pairs could induce either LTP or LTD, but LTP required fewer spike pairs (<15) than LTD (Froemke et al., 2006). Surprisingly, for those cells that expressed significant LTP, the magnitude of potentiation was independent of the number of pre/post pairings (**Figure 4**). One interpretation of these data is that the amount of LTP depends on the pre/post spike interval, while the probability of LTP induction depends on the number of spike pair repetitions. Such a scenario could imply certain co-operativity of LTP among multiple synaptic sites receiving the same inputs (Harvey and Svoboda, 2007). The magnitude of LTD, on the other hand, increased gradually with more post→pre pairs.

Alternatively, at individual pre- and postsynaptic loci, expression of LTP or LTD might be all-or-none, possibly down to the level of single glutamate receptors (Peterson et al., 1998; Lee et al., 2000; O'Connor et al., 2005; but see Tanaka et al., 2008 and Enoki et al., 2009). In this case, the magnitude of synaptic modification would be fixed at a given synapse, suggesting that both pre/post spike timing interval and the total number of pairings jointly determine the probability of induction. The time course of synaptic modification might still appear graded if enough separate inputs contribute to the overall synaptic response, with induction of synaptic plasticity staggered over multiple sites.

A third, non-mutually exclusive possibility is that synaptic strength is initially modified with a smaller number of spike pairs, but the duration of these changes depends on the total number of pairings. A larger number of spike pairings would then consolidate synaptic modifications and extend their duration. Without the occurrence of these additional events within some interval, synaptic modifications would not persist. For example, interleaving pre/post

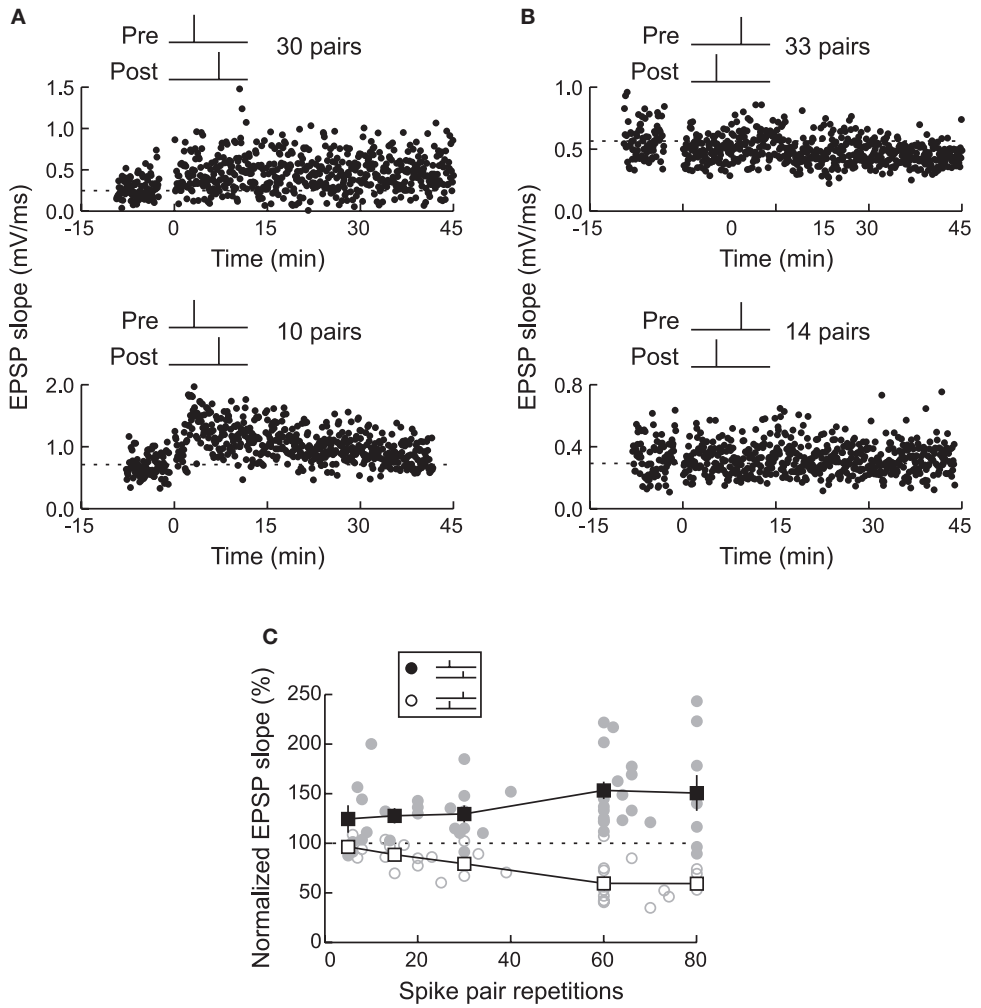

FIGURE 4 | Timing-dependent LTP requires fewer spike pairs than timing-dependent LTD. (A) LTP was induced by 30 pre→post spike pairs (top) or 10 pre→post pairs (bottom). **(B)** LTD was induced by 33 post→pre spike pairs (top), but not by 14 post→pre pairs (bottom). **(C)** The magnitude of LTP and LTD depended on the number of pre/post spike pairs. LTP required a smaller number of pairings (filled symbols) than LTD (open symbols). Each circle represents one experiment and squares represent summary data. From Froemke et al. (2006).

pairings with unpaired pre- or postsynaptic activation prevents induction of LTP (Bauer et al., 2001). In *Xenopus* optic tectum, synaptic modifications induced by spike pairing can be washed out or extinguished by subsequent short periods of random or spontaneous synaptic activity (Zhou et al., 2003). These findings indicate that there are cellular memory processes that integrate over longer time periods (Fusi et al., 2005), consolidating and extending the duration of changes in synaptic strength. The identities of such processes remain to be determined, although some molecular candidates are starting to be determined (Pagani et al., 2009).

Long-term potentiation and LTD are processes that saturate (Levy and Steward, 1979; Rioult-Pedotti et al., 2000; Scharfman and Sarvey, 1985). In most studies of STDP, synaptic weight can be increased up to 200–300% or decreased down to 50% of the original size (**Figures 2 and 4**), but physiological changes beyond these limits are rarely reported. The factors that control the maximum and minimum values of synaptic strength are still unknown, although limitations in receptor phosphorylation status (Lee et al., 2000), postsynaptic density size (Rasse et al., 2005), and vesicular release (Zucker and Regehr, 2002) may each contribute to saturation of synaptic modification. In phenomenological models, however, it is straightforward to implement saturation as a fixed bound on net synaptic modification. For example, the total amount of LTP induced by pre→post pairs and the total amount of LTD induced by post→pre pairs can be independently calculated, and set equal to the boundary values if greater/less than the saturation levels (Sjöström et al., 2001; Froemke et al., 2006). Boundary values are somewhat arbitrary, but it is reasonable to set the saturation points to be the empirically-measured mean amount of LTP and LTD induced by 60 pre/post pairs at short spike time intervals (approximately 100% increase for LTP and −50% decrease for LTD). Incorporating saturation is necessary to prevent STDP models from producing unrealistic predictions of synaptic modification.

How are the effects of individual pre/post pairs combined to determine the net change in synaptic strength? There are two main ways of integrating the contributions of single pre/post pairs, additively or multiplicatively. The additive model is the linear sum of individual pairwise contributions: $\Delta w = \sum_{i,j} \Delta w_{ij}$, and the multiplicative model is the product of spike pair effects: $1 + \Delta w = \prod_{i,j}(1 + \Delta w_{ij})$, where i and j represent individual spikes of the pre- and postsynaptic activity patterns, respectively. This is similar to the question about how a single pre/post pair might change synaptic strength- either by an incremental increase or decrease of a fixed magnitude, or in proportion to the current weight (van Rossum et al., 2000; Rubin et al., 2001). The additive model is often used in STDP simulations (Song et al., 2000; Hopfield and Brody, 2004; Knoblauch and Sommer, 2003) and overall provides lower-error predictions than the multiplicative model (Froemke et al., 2006). However, LTP and LTD are usually reported as a percentage change in synaptic efficacy, and there is evidence that the amount of synaptic modification depends on initial synaptic strength (Bi and Poo, 1998; Debanne et al., 1999; van Rossum et al., 2000; Sjöström et al., 2001), suggesting that the net effect of spike pairing may be multiplicative, especially for LTD. Regardless of the algorithm, both the additive and multiplicative independent models of STDP, including saturating LTP and LTD processes, still fail to provide good predictions of the effects of complex spike trains (having individual prediction errors of 40–50%). On average, predictions of the saturating independent model (Sjöström et al., 2001; Froemke and Dan, 2002; Froemke et al., 2006) are only weakly correlated with empirically-observed changes in synaptic strength (r: ~0.1–0.2).

FREQUENCY DEPENDENCE OF STDP

Although these studies show that STDP can result from repetitive pairing of single pre- and postsynaptic action potentials (Bell et al., 1997; Bi and Poo, 1998; Feldman, 2000; Sjöström et al., 2001; Froemke and Dan, 2002; Campanac and Debanne, 2008; Zilberter et al., 2009), in practice STDP is often induced by several iterations of pre- and postsynaptic spike bursts consisting of a small number of action potentials triggered at a high rate (Debanne et al., 1996; Magee and Johnston, 1997; Markram et al., 1997; Debanne et al., 1998; Boettiger and Doupe, 2001; Sjöström et al., 2001; Karmarkar et al., 2002; Watanabe et al., 2002; Tzounopoulos et al., 2004; Froemke et al., 2006; Nevian and Sakmann, 2006; Shen et al., 2008). Markram et al. (1997) originally used high-frequency pre/post spike bursts (10+ Hz) to induce LTP between pairs of layer five cortical pyramidal neurons, as spike burst pairing at lower frequency did not affect synaptic strength. This dependence of STDP on pre/post spike frequency demonstrates that the independent model, in which pairwise contributions are linearly summed or multiplied together, cannot entirely account for the effects of spike trains more complex than single pairs repeated at a low inter-pair interval (roughly <5 Hz). Therefore, there should be history-dependent processes that govern STDP learning rules beyond pre/post spike intervals. These forms of higher-order temporal modulation are the subject of the remainder of this review.

For unitary connections between pairs of neocortical pyramidal cells in brain slices, trains of five pre/post pairs induced LTD when the postsynaptic spike train led the presynaptic train, but only for intra-train spike rates below 40 Hz. At higher rates, the temporal precision seemed to break down, and LTP was induced regardless of the exact spike timing (Sjöström et al., 2001). At these connections LTP could not be induced with appropriately timed spike pairs unless the intra-train spike rate was at least 10–20 Hz (Markram et al., 1997; Sjöström et al., 2001). In an elegant study, Sjöström et al. (2001) showed that spike-timing-dependent LTP could be induced with low-frequency (0.1 Hz) repetition of single pre/post pairs, when extracellular stimulation was used to evoke EPSPs in the postsynaptic cell, rather than via direct stimulation of a single presynaptic neuron.

Most synapses show a similar breakdown of timing dependence and conversion from LTD to LTP when high-frequency trains are used to induce synaptic modification (**Figure 5**), although the number of spikes and frequency required for LTP vary between synapses (Sjöström et al., 2001; Froemke et al., 2006; Wittenberg and Wang, 2006). This rate-dependence and shift to LTP induction is reminiscent of the BCM model of synaptic plasticity, suggesting that these phenomena share a common set of underlying cellular mechanisms, e.g., Ca^{2+} influx through NMDA receptors (Zucker, 1999; Froemke et al., 2005; Feldman, 2009).

STDP INDUCED WITH SPIKE TRIPLETS AND QUADRUPLETS

To begin to predict the synaptic effects of complex spike trains, we have taken an incremental approach towards characterizing the history dependence of hippocampal and neocortical STDP. A

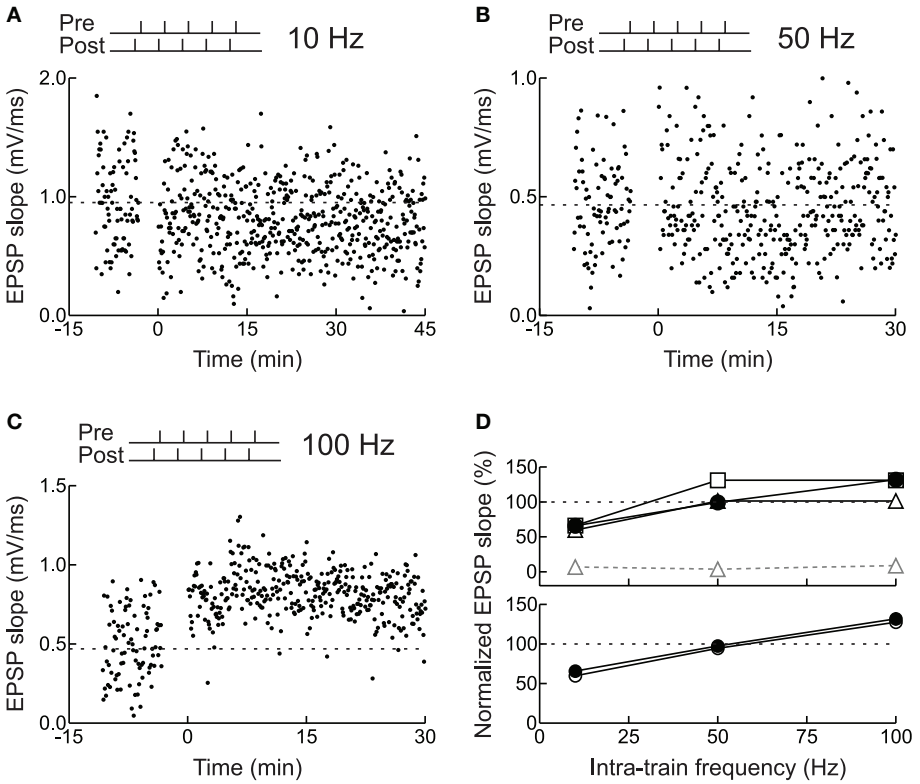

FIGURE 5 | Frequency dependence of STDP for layer 2/3 neurons in acute slices of young rat visual cortex. (A) Example of LTD induced by pairing pre- and postsynaptic spike bursts. Each burst consisted of five spikes with an intra-train frequency of 10 Hz (i.e., inter-spike interval of 100 ms). The postsynaptic train led the presynaptic train by 3 ms. **(B)** As in **(A)**, but no synaptic modification was induced when the intra-train frequency was 50 Hz. **(C)** As in **(A)**, but LTP was induced when the intra-train frequency was 100 Hz. **(D)** Actual and predicted synaptic modification after burst pairing. Filled symbols, experiments. Open symbols, model predictions: (top) gray triangles, multiplicative independent model without saturation; black triangles, multiplicative model with saturation; squares, additive model with saturation; (bottom) circles, additive suppression model with saturation. From Froemke et al. (2006).

straightforward way to study more complex spike trains is to systematically vary the parameters known to be important for induction of synaptic modification: the number, frequency, and precise timing of pre/post spikes presented during the induction protocol. In these experiments, we gradually increased the complexity of the pre/post spike pattern used to induce synaptic modification, starting by adding one additional spike – i.e., using spike triplets instead of spike pairs to induce long-term synaptic modification. From there, we have examined spike quadruplets and more complex burst patterns containing 6–12 action potentials at various inter-spike intervals (Debanne et al., 1994; Bi and Poo, 1998; Sourdet and Debanne, 1999; Froemke and Dan, 2002; Wang et al., 2005; Froemke et al., 2006). The goal of these parametric studies is the development of a phenomenological model, accounting for the rules and temporal modulation of STDP.

To determine the net change in synaptic strength by a given spike train, one possibility is that the effect of each pre/post spike pair is unaffected by the presence of other pre- and postsynaptic events. In this case, all pre/post pairs would be combined independently (either additively or multiplicatively), just by looking up each pre/post interval in the STDP time window (**Figures 1 and 2**). Alternatively, the presence of other spikes might somehow influence the contribution or eligibility of a given spike or spike pair for total synaptic modification.

We tested this hypothesis by using spike triplets instead of spike pairs for STDP induction. Although there are eight (2^3) basic ways to arrange three spikes among two neurons, two of these triplets are most informative for detecting history-dependent modulation of STDP: two presynaptic spikes flanking a single postsynaptic spike (pre→post→pre triplets) or two postsynaptic spikes flanking a presynaptic spike (post→pre→post triplets). In neurons from low-density hippocampal cultures, triplet experiments showed that post→pre→post triplets induced LTP, while pre→post→pre triplets led to no net change in synaptic strength (Bi and Poo, 1998; Bi and Wang, 2002; Wang et al., 2005; **Figure 6A**). This occurred even when the pre/post spike intervals were chosen to favor LTD, i.e., potentiation was dominant for these connections when the post→pre interval was shorter than the pre→post interval. Thus the effects of individual spike pairs in a triplet do not sum linearly – rather, LTP can cancel or "veto" previously induced LTD.

Almost the opposite effects were observed in layer 2/3 lateral connections of visual cortex. For these synapses, post→pre→post triplets induced LTD, while pre→post→pre triplets induced LTP, even when the time interval of the second pre/post pairing was considerably shorter than the first interval (Froemke and Dan, 2002; Froemke et al., 2006; **Figure 6B**). Therefore the presence of the first spike or spike pair somehow suppressed the efficacy or eligibility of the last

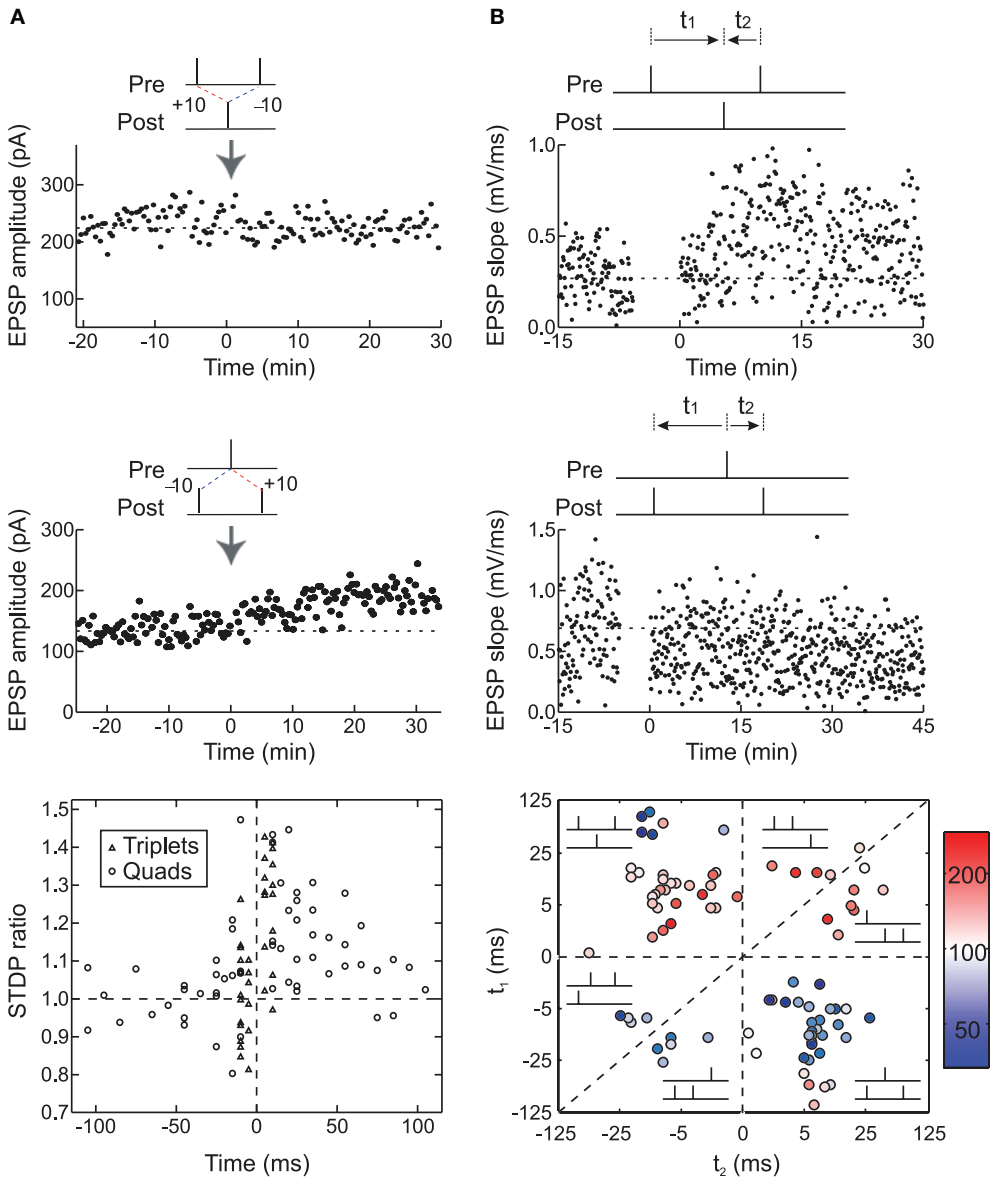

FIGURE 6 | Long-term synaptic modification induced by spike triplets. **(A)** In dissociated hippocampal cultured neurons, pre→post→pre triplets did not change synaptic strength (top) and post→pre→post triplets induced LTP (center). The time window for these temporal nonlinearities is ~70 ms; outside this interval, the effects of pre/post pairings were independent (bottom). From Wang et al. (2005). **(B)** In layer 2/3 visual cortical neurons in acute slices, pre→post→pre triplets induced LTP (top) and post→pre→post triplets induced LTD (center), demonstrating that the first spike pair is dominant in STDP, and the effect of the second spike pair is suppressed by the first. The time window for presynaptic suppression was found to be shorter than the duration of postsynaptic suppression (bottom). From Froemke and Dan (2002), and Froemke et al. (2006).

spike or spike pair to contribute to STDP. In other words, the effect of the first pair in the triplet was dominant for synaptic modification. These results are similar to the effects of pairing pre- and postsynaptic spike bursts in neurons of zebra finch forebrain – regardless of the timing of subsequent spikes, if a pre→post pair began the train, LTP was induced, but if the postsynaptic cell fires the first spike, LTD was induced (Boettiger and Doupe, 2001).

The nonlinear effects of spike triplets predicted the effects of spike quadruplets on STDP induction for both hippocampal and neocortical synapses. We used two kinds of quadruplets, pre→post→post→pre (type A: a pre→post pair followed at a short interval by a post→pre pair) and post→pre→pre→post (type B: a post→pre pair followed at a short interval by a pre→post pair). For hippocampal neurons, type A quadruplets did not affect synaptic strength (similar to pre→post→pre triplets), and type B quadruplets induced LTP (similar to post→pre→post triplets) (Wang et al., 2005). Conversely, for cortical neurons (Froemke and Dan, 2002), type A quadruplets induced LTP and type B quadruplets induced LTD, due to suppression of the effects of the latter spikes in the sequence, but only when the inter-pair interval (the post→post

interval for type A or the pre→pre interval for type B) was relatively short (approximately <100–200 ms). For longer inter-pair intervals, the effects of the two pairs summed linearly.

The effects of pre/post spike pairs are almost identical for hippocampal and neocortical neurons (**Figures 1 and 2**). Why then would spike triplets and quadruplets operate so differently for these two systems (**Figure 6**)? We hypothesize that there are distinct processes that govern the temporal modulation of STDP, controlling the eligibility of a given spike for contributing to synaptic modification under the pairwise STDP learning rule.

One set of important phenomena that could modulate the effectiveness of presynaptic spike trains for STDP are forms of short-term synaptic plasticity such as paired-pulse depression (PPD) or paired-pulse facilitation (PPF). When a presynaptic neuron fires twice within about 200 ms (5+ Hz), the amplitude of the second event is often facilitated (for PPF) or depressed (for PPD) relative to the size of the first event (Zucker and Regehr, 2002). These forms of short-term plasticity have the capability to influence the induction of long-term plasticity because NMDA receptor activation and consequently, the level of postsynaptic Ca^{2+} influx, depend on the amount of presynaptic transmitter release. In the limit, if a synapse shows strong PPD, such that the amount of transmitter released by the second presynaptic spike is essentially zero, then in terms of NMDA receptor activation and STDP, it is as if the second spike never occurred (i.e., pre→post→pre triplets would be equivalent to pre→post pairs). Conversely, if a synapse is strongly facilitating, evoking little to no EPSP from the first presynaptic spike but with EPSPs growing in size with subsequent spikes, the second presynaptic spike will be much more important than the first for determination of net synaptic modification (i.e., in this case a pre→post→pre triplet would be equivalent to a post→pre pair). Therefore, given that most synapses show some form of short-term plasticity (Zucker and Regehr, 2002), it would be surprising if the effect of spike triplets in STDP was just the linear sum of the pairwise contributions. By similar logic, temporal modulation of STDP may be different between synapses that facilitate and synapses that depress, at least for the effects of presynaptic spikes in a burst within the time scale of short-term plasticity.

In agreement with this idea, excitatory neocortical synapses usually exhibit PPD, especially during development (Reyes and Sakmann, 1999; Froemke et al., 2006), while PPF can often be observed at hippocampal synapses (Buonomano, 1999; Poncer and Malinow, 2001), although is not pronounced for cultured neurons (Wang et al., 2005). This fundamental difference in synaptic transmission might at least partially account for the dissimilar effects of spike triplets for STDP induction in these preparations. Under this hypothesis, pre→post→pre triplets at cortical synapses induce LTP due to suppression of the effect of the post→pre pair via presynaptic PPD. Conversely, in cultured hippocampal neurons, these triplets would not affect synaptic strength as the efficacy of the post→pre pair would also have a significant effect. Additional support for the role of short-term plasticity in temporal modulation of STDP comes from pharmacological experiments in visual cortical slices. Increasing PPD led to enhanced presynaptic suppression of STDP, while converting PPD into PPF removed presynaptic suppression, increasing the independence of these spikes and essentially linearizing the effects of presynaptic bursts for long-term synaptic modification (Froemke et al., 2006).

In a similar manner, postsynaptic spike bursts might modulate STDP induction through regulation of postsynaptic excitability or changes in presynaptic transmitter release. Both types of modulation have been found for hippocampal and neocortical synapses, implemented through a wide range of cellular mechanisms. Some of the best characterized activity-dependent regulators of postsynaptic excitability are K^+ channels (Debanne et al., 1997; Hoffman et al., 1997). In response to an initial increase in membrane potential, K^+ channel activation limits further depolarization, potentially weakening the impact of subsequent postsynaptic spikes for STDP induction. During high-frequency trains of postsynaptic spiking, action potentials can be observed to attenuate in size such that latter spikes in a burst are smaller than earlier spikes, which might impact gating of postsynaptic NMDA receptors and STDP induction (Tanaka et al., 1991; Froemke et al., 2006). Several groups have used pharmacological or genetic manipulation of A-type K^+ channels and SK channels in hippocampal and cortical neurons to show that these ion channels raise the threshold and enforce spike timing precision of STDP (Watanabe et al., 2002; Chen et al., 2006; Froemke et al., 2006; Lin et al., 2008). For visual cortical synapses, blockade of A-type channels widened the time window for timing-dependent LTD (Froemke et al., 2005), and removed postsynaptic suppression, such that post→pre→post triplets induced LTP instead of LTD (Froemke et al., 2006). This result, similar to the dominating effects of the LTP-inducing pair in post→pre→post triplets in hippocampal cultures, could indicate additional nonlinearity in downstream signal integration (Bi and Rubin, 2005; Wang et al. 2005).

At some synapses, prolonged postsynaptic depolarization leads to release of endocannabinoids, which act as retrograde messengers to decrease transmitter release and induce spike-timing-dependent LTD (Sjöström et al., 2003; Bender et al., 2006; Tzounopoulos et al., 2007). Furthermore, postsynaptic bursting by layer 5 neurons widens the time window for LTD induction (Sjöström et al., 2003), but postsynaptic depolarization in absence of spike firing is sufficient to induce LTD in those cells (Sjöström et al., 2004). At synapses onto layer 2/3 cells activated by focal extracellular stimulation near the apical dendrite, however, postsynaptic depolarization causes Ca^{2+}-dependent suppression of NMDA receptor activation. Potentially as a direct consequence of reduced Ca^{2+} flux through NMDA receptor channels, post→pre pairing induces LTD (Froemke et al., 2005; Urakubo et al., 2008). In both cases, the activity of the postsynaptic neuron seems to determine the timing requirements for LTD, suggesting that longer periods of postsynaptic spiking should prolong this temporal window. Indeed, this seems to be the case- for hippocampal neurons, the LTD time window is controlled by the exact number of spikes during a postsynaptic burst. When a single postsynaptic spike preceded presynaptic activation, LTD was induced only when the post→pre time interval was <200 ms. However, when a burst of four postsynaptic spikes was used instead, this interval was extended up to 800 ms, and a burst of ten spikes extended this window further, to 2000 ms (Debanne et al., 1994; Sourdet and Debanne, 1999). Together, these results suggest that it should be possible to build quantitative models that accurately predict, spike by spike, the net change in synaptic strength induced by a given spike train. The tight linkage between specific cellular mechanisms and aspects of STDP induction and temporal modulation further

suggests that biologically realistic simulations could eventually be used to predict how complex spike trains might induce enduring synaptic modifications.

PREDICTING THE EFFECTS OF COMPLEX SPIKE TRAINS

Complex spike trains with irregular patterns of spiking are not usually used as induction protocols for synaptic plasticity (Paulsen and Sejnowski, 2000). A seminal paper by Dobrunz and Stevens (1999) was the first study to use natural spike trains to induce long-term synaptic modification in slices of rat hippocampus. While that study demonstrated that repetitive presentation of natural spike train segments could lead to LTP, no attempt was made to predict or quantify the impact of individual spike trains on synaptic plasticity. Sjöström et al. (2001) then used random sequences of pre/post spike trains at various intra-train frequencies to induce synaptic modification. They used an additive model in which postsynaptic depolarization determined the amount of LTP, only nearest-neighbor spike pairs contributed to STDP, and spikes that participated in an LTP pairing could not participate in an LTD pairing (such that LTP effectively "wins out" over LTD). Their model captured the essential frequency dependence of STDP for cell pairs and predicted the net synaptic modification induced by random trains with high accuracy.

In slices of the mammalian lateral geniculate nucleus (LGN), stimulation of optic tract afferents onto thalamic neurons induced LTP or LTD depending on the time differences of pre- and postsynaptic spike bursts (Butts et al., 2007). Spike bursts consisted of 10–20 Hz trains for one second, simulating natural activity patterns that occur during spontaneous retinal waves. LTP was induced when the latency between bursts occurred within about 500 ms, regardless of the pre/post temporal ordering. The independent model of STDP failed to predict the extent of synaptic modification induced by burst pairing, but as in Sjöström et al. (2001), modifying STDP to consider only nearest-neighbor spikes and removing LTD significantly improved predictions of the model.

We wondered if a similar approach could be used more generally to account for the effect of sparse and irregular spike trains in layer 2/3 cortical connections. The aim of these experiments was to use STDP to quantitatively describe how the fine temporal structure within complex and naturalistic spike trains would influence the sign and magnitude of overall long-term synaptic modification, solely at the level of individual spikes. Specifically, we set out to construct an accretive, low-parameter phenomenological model that captured most of the variance in STDP induced by a wide range of different spiking patterns: spike pairs, triplets, quadruplets, low- and high-frequency bursts, and natural spike train fragments.

We started by extending the history-independent model of STDP to account for the effects of spike triplets. In this model (the "suppression" model), the contribution of a pre/post spike pair depends not only on the time interval between the two spikes (**Figure 2**), but also on the efficacy of each spike (Froemke and Dan, 2002). This spike efficacy is the eligibility of a spike to participate in synaptic modification, and acts to scale down the effect of a pre/post pair. Spike efficacy is defined as a coefficient between zero and one depending on the time from the preceding spike: it begins at one (full strength), but is suppressed to zero immediately after a spike, and recovers exponentially back to one. To predict the effects of spike train segments using the suppression model, each pre- and postsynaptic spike was assigned an efficacy, which depends only on the interval from the preceding spike in the same neuron: $\varepsilon_i = 1 - e^{-(t_i - t_{i-1})/\tau_s}$. Here, ε_i is the efficacy of the ith spike, t_i and t_{i-1}, are the timing of the ith and $(i-1)$th spike, respectively, and τ_s, is the time constant of single exponential recovery from suppression. Suppression time constants for the pre- and postsynaptic neurons, τ_s^{pre} and τ_s^{post}, were determined from the 2-1 and 1-2 triplet experiments (**Figure 6B**), chosen to minimize mean prediction error (|predicted effect − measured effect|). The contribution of each pre/post spike pair to synaptic modification was estimated as $\Delta w_{ij} = \varepsilon_i^{pre}\varepsilon_j^{post}F(\Delta t_{ij})$ (Δw_{ij}, synaptic modification due to the ith presynaptic spike and the jth postsynaptic spike; ε_i^{pre} and ε_j^{post}, efficacy of the two spikes, respectively; Δt_{ij}, the interval between the two spikes, $t_j^{post} - t_i^{pre}$). The function F represents the temporal window for STDP measured with isolated spike pairs, expressed as:

$$F(\Delta t) = \begin{cases} A_+ e^{-|\Delta t|/\tau_+} & \text{if } \Delta t > 0 \\ A_- e^{-|\Delta t|/\tau_-} & \text{if } \Delta t < 0 \end{cases}$$

(A, scaling factor; τ, time constant; +, LTP; −, LTD). The history-independent model is then a special case of the suppression model, where spike efficacies ε_i are always 1 for all i regardless of inter-spike interval.

Both the additive and multiplicative versions of the suppression model, without saturation, made significantly more accurate predictions than did the history-independent models of STDP induced by spike triplets, quadruplets, and fragments of natural spike trains initially recorded *in vivo* (Froemke and Dan, 2002). The suppression model prediction errors for individual cases were approximately 15–30%, compared to the larger errors of 30–50% produced by the history-independent model. These values are close to the individual error intrinsic to the single exponential fits to the pre/post spike pair experiments themselves (~15%), which can be considered the limit of predictive power for any model based on the pairwise STDP learning rule.

Thus, the original suppression model provided a good description of STDP induced by complex spike patterns encountered *in vivo* (Froemke and Dan, 2002). However, as this model was derived from spike pair and triplet experiments where temporal precision was a key parameter, it was not designed to account for the breakdown of STDP and rate-dependent conversion to LTP when high frequency bursts of five presynaptic and five postsynaptic spikes ("5–5" trains) were used for induction (Markram et al., 1997; Sjöström et al., 2001). Various reformulations of the original suppression model – with or without saturation of STDP, and assuming either additive or multiplicative combinations (open symbols in **Figure 5D**, top) – also failed to entirely account for the frequency dependence of STDP, although including saturating LTP and LTD into the suppression model greatly reduced prediction errors on high-frequency bursts (compare gray triangles with dashed line to triangles and squares with solid lines in **Figure 5D**, top). Therefore we tried to identify the processes that contribute to inter-spike suppression and frequency-dependent potentiation, and determine what additional factors or parameters beyond saturation were required for a more complete model (the "revised suppression" model of STDP).

We systematically varied the number of spikes between one and five in a high-frequency burst (100 Hz) of either the pre- or postsynaptic train, fixing the number of spikes in the other train to be one ("*x*-1" or "1-*x*" trains); in both cases the leading pre/post pair was post→pre (Froemke et al., 2006). We first examined the contribution of postsynaptic spiking. Using 1-5 trains for induction induced LTP; surprisingly, this effect was much more consistent with the history-independent model than with the suppression model. In general, there was a conversion from LTD to LTP as the number of postsynaptic spikes was increased over a range of one to five. The degree of potentiation and the gradual shift from LTD to LTP with an increasing number of postsynaptic spikes were strikingly similar to that observed in the 5-5 train experiments, strongly suggesting that the number and frequency of postsynaptic spikes, rather than presynaptic spikes, are main determinants of frequency-dependent STDP. This finding is consistent with earlier results from Gustafsson et al. (1987) and Debanne et al. (1994), showing that the number of postsynaptic spikes in a burst was correlated with the amount of LTP, and agree with work from Pike et al. (1999), in which postsynaptic but not presynaptic bursting was predominant for LTP induction. All of these experiments are reminiscent of the classic BCM model of long-term synaptic plasticity (Bienenstock et al., 1982), in which the level of postsynaptic activity is critical for determining the sign and magnitude of synaptic modification.

How might these results be reconciled with the original suppression model of STDP? One possibility is that a burst of postsynaptic spikes has certain synergy, and is qualitatively different from the individual component spikes within the burst. In this scheme, high-frequency postsynaptic bursting would tend to induce LTP whenever temporally correlated with presynaptic activity, irrespective of the exact spike timing. This is similar to the suggestion of Sjöström et al. (2001) for cortical layer 5 synapses, in which LTP is dominant over LTD when considering nearest-neighbor interactions. To test this hypothesis for layer 2/3 connections, we examined an alternate version of the 1-5 spike train, in which the single presynaptic spike has been moved towards the end of the train, occurring between the fourth and fifth postsynaptic spikes. Despite the high-frequency burst of five postsynaptic spikes, this protocol induced LTD (Froemke et al., 2006). Thus for layer 2/3 synapses in developing visual cortex, high-frequency bursts do not always induce LTP, and instead the sign and amount of synaptic modification still depends on the precise timing and arrangement of pre/post spikes.

In these experiments, there appeared to be a gradual relaxation of postsynaptic suppression, with the suppression model accounting for 1-2 trains (i.e., post→pre→post triplets) and the history-independent model accounting for 1-5 trains (i.e., post→pre→post→post→post→post bursts). Therefore, we altered the suppression model such that postsynaptic inter-spike suppression depended not only on the time from the previous postsynaptic spike, but also depended inversely on the degree of suppression of that spike. This can be formalized as: $\varepsilon_i = 1 - \varepsilon_{i-1} \times e^{-(t_i - t_{i-1})/\tau_s}$, where ε_i is the efficacy of the i^{th} postsynaptic spike (with the first postsynaptic spike having $\varepsilon_i = 1$). Incorporating this change made the suppression model behave as the history-independent model for 5-5 trains, suggesting that the revisions to the suppression model were not yet entirely complete.

We then examined the effect of presynaptic bursting. We found that *x*-1 trains, with a single postsynaptic spike and a variable number of presynaptic spikes, induced LTD in all cases. Given the high degree of short-term depression and the long time course of NMDA receptor activation at these synapses, it is perhaps not surprising that all *x*-1 spike trains produce approximately the same amount of depression. In other words, increasing the number of presynaptic spikes has little direct effect on the degree of synaptic modification induced by high-frequency spike trains. One interpretation of these results is that inter-spike suppression of presynaptic efficacy must also depend not only on the time to the previous spike, but also on the degree of suppression of this spike. Rather than depending inversely, presynaptic suppression may accumulate, in a manner reminiscent of short-term depression. We therefore corrected presynaptic efficacy to be: $\varepsilon_i = \Pi_{j=1}^{i}\left(1 - e^{-(t_i - t_{i-j})/\tau_s}\right)$, similar to the scheme used by Varela et al. (1997) for simulating neocortical short-term depression. In this scheme, the efficacy of each presynaptic spike depends on the time to all preceding spikes in the presynaptic burst. When this change was made to presynaptic suppression, the revised additive suppression model of STDP well-predicted the effects of high-frequency spike trains (**Figure 5D**, bottom).

Thus the suppression model was revised to account for the frequency-dependence of STDP by three modest corrections: one, a history-dependent relaxation of postsynaptic suppression; two, a history-dependent increase in presynaptic suppression; and three, incorporating physiological levels of saturation. Overall, the individual prediction error of the revised suppression model was approximately 10%, significantly better than each of the other models. For individual intra-train frequencies, the revised suppression model correctly predicted the gradual shift from LTD to LTP. Comparing mean amounts of synaptic modification induced at different intra-train spike rates, as in Sjöström et al. (2001), gave the following prediction errors: 10 Hz, 6.2%; 50 Hz, 2.8%; and 100 Hz, 4.2%. Additionally, the revised suppression model accounted for the results of the *x*-1 and 1-*x* experiments, quadruplets, and natural spike train fragments, resulting in a high correlation between predicted and empirically measured synaptic modification (*r*: ~0.6–0.8; **Figures 5D and 7**). The prediction errors of this model over all such complex spike trains (10–20% individual prediction errors) were comparable to the errors of the original suppression model tested only on the relatively sparse natural spike trains, and also comparable to the error inherent in the critical time window for spike pairs. It is difficult to improve the predictions of the models beyond errors of ~15% for individual experiments. This degree of error is also evident in the fits to the temporal window for pre/post spike pairs, and perhaps reflects heterogeneity among cells, e.g., an inherent bias toward LTP or LTD that may depend on how close the baseline synaptic strength is toward saturation.

Of course, the revised suppression model accounts only for the effects of complex spike trains in layer 2/3 cortical neurons. Given the difference in results between **Figures 6A and 6B**, this model cannot account *per se* for the effects of spike triplets and quadruplets in cultured hippocampal neurons. In particular, post→pre→post triplets increased synaptic strength by ~25–30% in cultured neurons (with either 5 or 10 ms inter-spike intervals) but decreased synaptic strength by about −20% in layer 2/3 of visual cortex, while pre→post→pre triplets did not affect synaptic strength in cultured

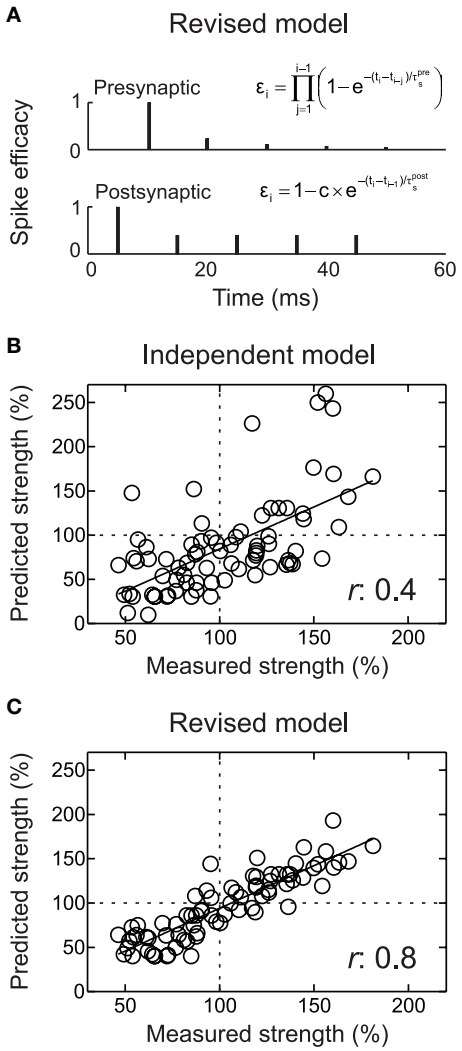

FIGURE 7 | The revised suppression model of STDP predicts the effects of complex and naturalistic spike trains. (A) Schematic of the revised suppression model. The height of each spike represents the efficacy of that event for contributing to STDP. **(B)** Comparison of predicted and measured effects of complex spike trains (quadruplets, high-frequency bursts, and natural spike train fragments) used to induce synaptic modification. Predicted values are from the additive history-independent model, with saturation of LTP and LTD and the number of pre/post spike pair repetitions taken into consideration. Each circle indicates one experiment. The linear correlation coefficient *r* between predicted and measured amount of STDP was 0.4. **(C)** As in **(B)**, but with using the predictions of the revised suppression model. The linear correlation coefficient was 0.8. From Froemke et al. (2006).

cells but enhanced EPSPs by ~25% in cortex (Froemke and Dan, 2002; Wang et al., 2005). However, short-term plasticity is but one way in which temporal modulation of STDP multi-spike interactions could be implemented in biological networks. For cultured hippocampal neurons, the nonlinear dynamics of biochemical activity (e.g., kinase and phosphatase metabolism) may be predominant over the contributions of other factors such as paired-pulse depression or facilitation (Rubin et al., 2005). Regardless, it may be possible to capture the effects of these interactions in a phenomenological framework like the suppression model of STDP, using the results of mechanistic experiments to inform the choice of variables and guide exploration through parameter space. We also note that the suppression model can recapitulate major features of STDP at other synapses with relatively straightforward changes- reducing presynaptic suppression mimics the effects of pre→post→pre triplets in cultured hippocampal neurons, while reducing postsynaptic suppression captures the lower-frequency shift to LTP with trains of pre- and postsynaptic spikes as observed for pairs of layer five pyramidal cells by Sjöström et al. (2001).

CONCLUSION

Determining the rules of long-term synaptic modification is crucial to understanding brain function and development, and several attempts have been made to build computational models of phenomena such as LTP and LTD. One of the most successful has been the BCM model, a rate-based approach developed in the 1980s toward understanding how synaptic modifications might underlie functional rearrangement of the cortex. However, work from many laboratories over the last 15 years has shown that the precise timing of spikes in the pre- and postsynaptic neurons is the critical determinant of long-term synaptic plasticity, likely due to the nonlinear dependence of NMDA receptor activation and postsynaptic Ca^{2+} influx on membrane potential. For several reasons, STDP has become a standard protocol for both experimental and theoretical investigation of learning and memory, and the STDP learning rule can be used to make accurate predictive models of the sign and magnitude of long-term synaptic modification induced by complex and naturalistic spike trains.

Collectively, these experiments are a proof-of-concept demonstration that STDP provides a basis for constructing such models. Here we have concentrated on characterizing history-dependent temporal nonlinearities that occur on relatively short timescales, from milliseconds to minutes. Forms of temporal modulation over longer periods, such as metaplasticity or homeostatic synaptic scaling, also play important roles in adjusting synaptic strength and organizing neural circuits (Abraham and Bear, 1996; Turrigiano and Nelson, 2000). Other types of modulation related to reinforcement schedule, arousal level, and motivational state (Cruikshank and Weinberger, 1996; Buonomano and Merzenich, 1998; Martin et al., 2000; Froemke et al., 2007; Zhang et al., 2009) will also eventually need to be quantified and incorporated into these models. The development of such hybrid phenomenological models incorporating mechanistic elements may be promising for providing better predictions of the effects of certain forms of experience on synaptic transmission. In the end, large-scale simulations of neural processing, with realistic forms of synaptic plasticity, learning, and memory, will be essential for the creation and optimization of behavioral programs, drugs, and devices for the treatment of neuropsychiatric disorders (Markram, 2006).

ACKNOWLEDGMENTS

The experiments on STDP of layer 2/3 cortical pyramidal cells were performed in the laboratory of Yang Dan. We are indebted to Beat Gähwiler and Scott Thompson for the help with experiments on STDP of CA3 pyramidal neurons. This work was supported by grants from the NEI, NIDCD, and the Howard Hughes Medical Institute (Robert C. Froemke); and grants from INSERM, CNRS, ANR and Région PACA (Dominique Debanne).

REFERENCES

Abarbanel, H. D. I., Huerta, R., and Rabinovich, M. I. (2002). Dynamical model of long-term synaptic plasticity. *Proc. Natl. Acad. Sci. U.S.A.* 99,10132–10137.

Abbott, L. F., and Blum, K. I. (1996). Functional significance of long-term potentiation for sequence learning and prediction. *Cereb. Cortex* 6, 406–416.

Abbott, L. F., and Nelson, S. B. (2000). Synaptic plasticity: taming the beast. *Nat. Neurosci.* 3, 1178–1183.

Abraham, W. C., and Bear, M. F. (1996). Metaplasticity: the plasticity of synaptic plasticity. *Trends Neurosci.* 19, 126–130.

Artola, A., Bröcher, S., and Singer, W. (1990). Different voltage-dependent thresholds for inducing long-term depression and long-term potentiation in slices of rat visual cortex. *Nature* 347, 69–72.

Baranyi, A., and Fehér, O. (1981). Synaptic facilitation requires paired activation of convergent pathways in the neocortex. *Nature* 290, 413–415.

Bauer, E. P., LeDoux, J. E., and Nader, K. (2001). Fear conditioning and LTP in the lateral amygdala are sensitive to the same stimulus contingencies. *Nat. Neurosci.* 4, 687–688.

Bell, C. C., Han, V. Z., Sugawara, Y., and Grant, K. (1997). Synaptic plasticity in a cerebellum-like structure depends on temporal order. *Nature* 387, 278–281.

Bender, V. A., Bender, K. J., Brasier, D. J., and Feldman, D. E. (2006). Two coincidence detectors for spike timing-dependent plasticity in somatosensory cortex. *J. Neurosci.* 26, 4166–4177.

Berninger, B., and Bi, G.-Q. (2002). Synaptic modification in neural circuits: a timely action. *Bioessays* 24, 212–222.

Bi, G.-Q., and Poo, M.-M. (1998). Synaptic modifications in cultured hippocampal neurons: dependence on spike timing, synaptic strength, and postsynaptic cell type. *J. Neurosci.* 18, 10464–10472.

Bi, G.-Q., and Poo, M.-M. (2001). Synaptic modification by correlated activity: Hebb's postulate revisited. *Annu. Rev. Neurosci.* 24, 139–166.

Bi, G.-Q., and Rubin, J. (2005). Timing in synaptic plasticity: from detection to integration. *Trends Neurosci.* 28, 222–228.

Bi, G.-Q., and Wang, H. X. (2002). Temporal asymmetry in spike timing-dependent synaptic plasticity. *Physiol. Behav.* 77, 551–555.

Bienenstock, E. L., Cooper, L. N., and Munro, P. W. (1982). Theory for the development of neuron selectivity: orientation specificity and binocular interaction in visual cortex. *J. Neurosci.* 2, 32–48.

Bindman, L. J., Lippold, O. C., and Redfearn, J. W. (1962). Long-lasting changes in the level of the electrical activity of the cerebral cortex produced by polarizing currents. *Nature* 196, 584–585.

Birtoli, B., and Ulrich, D. (2004). Firing mode-dependent synaptic plasticity in rat neocortical pyramidal neurons. *J. Neurosci.* 24, 4935–4940.

Bliss, T. V., and Lømo, T. (1973). Long-lasting potentiation of synaptic transmission in the dentate area of the anesthetized rabbit following stimulation of the perforant path. *J. Physiol.* 232, 331–356.

Boettiger, C. A., and Doupe, A. J. (2001). Developmentally restricted synaptic plasticity in a songbird nucleus required for song learning. *Neuron* 31, 809–818.

Buchanan, K. A., and Mellor, J. R. (2007). The development of synaptic plasticity induction rules and the requirement for postsynaptic spikes in rat hippocampal CA1 pyramidal neurones. *J. Physiol.* 585, 429–445.

Buonomano, D. V. (1999). Distinct functional types of associative long-term potentiation in neocortical and hippocampal pyramidal neurons. *J. Neurosci.* 19, 6748–6754.

Buonomano, D. V., and Merzenich, M. M. (1998). Cortical plasticity: from synapses to maps. *Annu. Rev. Neurosci.* 21, 149–186.

Butts, D. A., Kanold, P. O., and Shatz, C. J. (2007). A burst-based "Hebbian" learning rule at retinogeniculate synapses links retinal waves to activity-dependent refinement. *PLoS Biol.* 5, e61. doi:10.1371/journal.pbio.0050061.

Campanac, E. and Debanne, D. (2008) Spike timing-dependent plasticity: a learning rule for dendritic integration in rat CA1 pyramidal neurons. *J. Physiol.* 586, 779–793.

Caporale, N., and Dan, Y. (2008). Spike timing-dependent plasticity: a Hebbian learning rule. *Annu. Rev. Neurosci.* 31, 25–46.

Chen, X., Yuan, L. L., Zhao, C., Birnbaum, S. G., Frick, A., Jung, W. E., Schwarz, T. L., Sweatt, J. D., and Johnston, D. (2006). Deletion of Kv4.2 gene eliminates dendritic A-type current and enhances induction of long-term potentiation in hippocampal *CA1* pyramidal neurons. *J. Neurosci.* 26, 12143–12151.

Corlew, R., Wang, Y., Ghermazien, H., Erisir, A., and Philpot, B. D. (2007). Developmental switch in the contribution of presynaptic and postsynaptic NMDA receptors to long-term depression. *J. Neurosci.* 27, 9835–9845.

Cruikshank, S. J., and Weinberger, N. M. (1996). Evidence for the Hebbian hypothesis in experience-dependent physiological plasticity of neocortex: a critical review. *Brain Res. Brain Res. Rev.* 22, 191–228.

Dan, Y., and Poo, M. M. (2006). Spike timing-dependent plasticity: from synapse to perception. *Physiol. Rev.* 86, 1033–1048.

Debanne, D., Gähwiler, B. H., and Thompson, S. M. (1994). Asynchronous pre- and postsynaptic activity induces associative long-term depression in area CA1 of the rat hippocampus in vitro. *Proc. Natl. Acad. Sci. USA* 91, 1148–1152.

Debanne, D., Gähwiler, B. H., and Thompson, S. M. (1996). Cooperative interactions in the induction of long-term potentiation and depression of synaptic excitation between hippocampal CA3-CA1 cell pairs in vitro. *Proc. Natl. Acad. Sci. U.S.A.* 93, 11225–11230.

Debanne, D., Gähwiler, B. H., and Thompson, S. M. (1998). Long-term synaptic plasticity between pairs of individual CA3 pyramidal cells in rat hippocampal slice cultures. *J. Physiol.* 507, 237–247.

Debanne, D., Gähwiler, B. H., and Thomspon, S. M. (1999). Heterogeneity of synaptic plasticity at unitary CA3-CA1 and CA3-CA3 connections in rat hippocampal slice cultures. *J. Neurosci.* 19, 10664–10671.

Debanne, D., Guérineau, N. C., Gähwiler, B. H., and Thompson, S. M. (1997). Action-potential propagation gated by an axonal IA-like K+ conductance in hippocampus. *Nature* 389, 286–289.

Dobrunz, L. E., and Stevens, C. F. (1999). Response of hippocampal synapses to natural stimulation patterns. *Neuron* 22, 157–166.

Dudek, S. M., and Bear, M. F. (1992). Homosynaptic long-term depression in area CA1 of hippocampus and effects of N-methyl-D-aspartate receptor blockade. *Proc. Natl. Acad. Sci. U.S.A.* 89, 4363–4367.

Egger, V., Feldmeyer, D., and Sakmann, B. (1999). Coincidence detection and changes of synaptic efficacy in spiny stellate neurons in rat barrel cortex. *Nat. Neurosci.* 2, 1098–1105.

Enoki, R., Hu, Y. L., and Fine, A. (2009). Expression of long-term plasticity at individual synapses in hippocampus is graded, bidirectional, and mainly presynaptic: optical quantal analysis. *Neuron* 62, 242–253.

Feldman, D. E. (2000). Timing-based LTP and LTD at vertical inputs to layer II/III pyramidal cells in rat barrel cortex. *Neuron* 27, 45–56.

Feldman, D. E. (2009). Synaptic mechanisms for plasticity in neocortex. *Annu. Rev. Neurosci.* 32, 33–55.

Franks, K. M., and Sejnowski, T. J. (2002). Complexity of calcium signaling in synaptic spines. *Bioessays* 24, 1130–1144.

Fregnac, Y., and Shulz, D. E. (1999). Activity-dependent regulation of receptive field properties of cat area 17 by supervised Hebbian learning. *J. Neurobiol.* 41, 69–82.

Froemke, R. C., and Dan, Y. (2002). Spike-timing-dependent synaptic modification induced by natural spike trains. *Nature* 416, 433–438.

Froemke, R. C., Poo, M.-M., and Dan, Y. (2005). Spike-timing-dependent synaptic plasticity depends on dendritic location. *Nature* 434, 221–225.

Froemke, R. C., Merzenich, M. M., and Schreiner, C. E. (2007). A synaptic memory trace for cortical receptive field plasticity. *Nature* 450, 425–429.

Froemke, R. C., Tsay, I. A., Raad, M., Long, J. D., and Dan, Y. (2006). Contribution of individual spikes in burst-induced long-term synaptic modification. *J. Neurophysiol.* 95, 1620–1629.

Fusi, S., Drew, P. J., and Abbott, L. F. (2005). Cascade models of synaptically stored memories. *Neuron* 45, 599–611.

Gerstner, W., Kempter, R., van Hemmen, J. L., and Wagner, H. (1996). A neuronal learning rule for sub-millisecond temporal coding. *Nature* 383, 76–81.

Gilbert, C. D. (1998). Adult cortical dynamics. *Physiol. Rev.* 78, 467–485.

Gustafsson, B., Wigstrom, H., Abraham, W. C., and Huang, Y. Y. (1987). Long-term potentiation in the hippocampus using depolarizing current pulses as the conditioning stimulus to single volley synaptic potentials. *J. Neurosci.* 7, 774–780.

Gutig, R., and Sompolinsky, H. (2006). The tempotron: a neuron that learns spike timing-based decisions. *Nat. Neurosci.* 9, 420–428.

Hansel, C., Artola, A., and Singer, W. (1997). Relation between dendritic Ca2+ levels and the polarity of synaptic long-term modifications in rat visual cortex neurons. *Eur. J. Neurosci.* 9, 2309–2322.

Harvey, C. D., and Svoboda, K. (2007). Locally dynamic synaptic learning rules in pyramidal neuron dendrites. *Nature* 450, 1195–1200.

Hebb, D. O. (1949). *The Organization of Behavior*. New York, Wiley.

Hoffman, D. A., Magee, J. C., Colbert, C. M., and Johnston, D. (1997). K+ channel regulation of signal propagation in dendrites of hippocampal pyramidal neurons. *Nature* 387, 869–875.

Hoffman, D. A., Sprengel, R., and Sakmann, B. (2002). Molecular

dissection of hippocampal theta-burst pairing potentiation. *Proc. Natl. Acad. Sci. U.S.A.* 99, 7740–7745.

Hopfield, J. J., and Brody, C. D. (2004). Learning rules and network repair in spike-timing-based computation networks. *Proc. Natl. Acad. Sci. U.S.A.* 101, 337–342.

Izhikevich, E. M., and Edelman, G. M. (2007). Large-scale model of mammalian thalamocortical systems. *Proc. Natl. Acad. Sci. U.S.A.* 105, 3593–3598.

Johnston, D., Christie, B. R., Frick, A., Gray, R., Hoffman, D. A., Schexnayder, L. K., Watanabe, S., and Yuan, L. L. (2003). Active dendrites, potassium channels and synaptic plasticity. *Philos. Trans. R. Soc. Lond. B Biol. Sci.* 358, 667–674.

Kampa, B. M., Clements, J., Jonas, P., and Stuart, G. J. (2004). Kinetics of Mg2+ unblock of NMDA receptors: implications for spike-timing dependent plasticity. *J. Physiol.* 556, 337–345.

Kant, I. (1781). *Critique of Pure Reason*. New York, Prometheus.

Karmarkar, U. R., and Buonomano, D. V. (2002). A model of spike-timing-dependent plasticity: one or two coincidence detectors? *J. Neurophysiol.* 88, 507–513.

Karmarkar, U. R., Najarian, M. T., and Buonomano, D.V. (2002). Mechanisms and significance of spike-timing dependent plasticity. *Biol. Cybern.* 87, 373–382.

Katz, L. C., and Shatz, C. J. (1996). Synaptic activity and the construction of cortical circuits. *Science* 274, 1133–1138.

Kelso, S. R., Ganong, A. H., and Brown, T. H. (1986). Hebbian synapses in hippocampus. *Proc. Natl. Acad. Sci. U.S.A.* 83, 5326–5330.

Kilgard, M. P., Pandya, P. K., Engineer, N. D., and Moucha, R. (2002). Cortical network reorganization guided by sensory input features. *Biol. Cybern.* 87, 333–343.

Kirkwood, A., Dudek, S. M., Gold, J. T., Aizenman, C. D., and Bear, M. F. (1993). Common forms of synaptic plasticity in the hippocampus and neocortex in vitro. *Science* 260, 1518–1521.

Kirkwood, A., Lee, H.-K., and Bear, M. F. (1995). Co-regulation of long-term potentiation and experience-dependent synaptic plasticity in visual cortex by age and experience. *Nature* 375, 328–331.

Knoblauch, A., and Sommer, F. T. (2003). Synaptic plasticity, conduction delays, and inter-areal phase relations of spike activity in a model of reciprocally connected areas. *Neurocomputing* 52–54, 301–306.

Koester, H. J., and Sakmann, B. (1998). Calcium dynamics in single spines during coincident pre- and postsynaptic activity depend on relative timing of back-propagating action potentials and subthreshold excitatory postsynaptic potentials. *Proc. Natl. Acad. Sci. U.S.A.* 95, 9596–9601.

Larkum, M. E., Watanabe, S., Nakamura, T., Lasser-Ross, N., and Ross, W N. (2003). Synaptically activated Ca2+ waves in layer 2/3 and layer 5 rat neocortical pyramidal neurons. *J. Physiol.* 549, 471–488.

Lee, H.-K., Barbarosie, M., Kameyama, K., Bear, M. F., and Huganir, R. L. (2000). Regulation of distinct AMPA receptor phosphorylation sites during bidirectional synaptic plasticity. *Nature* 405, 955–959.

Letzkus, J. J., Kampa, B. M., and Stuart, G. J. (2006). Learning rules for spike timing-dependent plasticity depend on dendritic synapse location. *J. Neurosci.* 26, 10420–10429.

Levy, W. B., and Steward, O. (1979). Synapses as associative memory elements in the hippocampal formation. *Brain Res.* 175, 233–245.

Levy, W. B., and Steward, O. (1983). Temporal contiguity requirements for long-term associative potentiation/depression in the hippocampus. *Neuroscience* 8, 791–797.

Lin, M. T., Luján, R., Watanabe, M., Adelman, J. P., and Maylie, J. (2008). SK2 channel plasticity contributes to LTP at Schaffer collateral-CA1 synapses. *Nat. Neurosci.* 11, 170–177.

Lin, Y. W., Min, M. Y., Chiu, T. H., and Yang, H. W. (2003). Enhancement of associative long-term potentiation by activation of beta-adrenergic receptors at CA1 synapses in rat hippocampal slices. *J. Neurosci.* 23, 4173–4181.

Lorente de Nó, R. (1938). Synaptic stimulation of motoneurons as a local process. *J. Neurophysiol.* 1, 195–206.

Magee, J. C., and Johnston, D. (1997). A synaptically controlled, associative signal for Hebbian plasticity in hippocampal neurons. *Science* 275, 209–213.

Malenka, R. C., and Nicoll, R. A. (1999). Long-term potentiation – a decade of progress? *Science* 285, 1870–1874.

Markram, H. (2006). The blue brain project. *Nat. Rev. Neurosci.* 7, 153–160.

Markram, H., Lübke, J., Frotscher, M., and Sakmann, B. (1997). Regulation of synaptic efficacy by coincidence of postsynaptic APs and EPSPs. *Science* 275, 213–215.

Martin, S. J., Grimwood, P. D., and Morris, R. G. M. (2000). Synaptic plasticity and memory: an evaluation of the hypothesis. *Annu. Rev. Neurosci.* 23, 649–711.

Meredith, R. M., Floyer-Lea, A. M., and Paulsen, O. (2003). Maturation of long-term potentiation induction rules in rodent hippocampus: role of GABAergic inhibition. *J. Neurosci.* 23, 11142–11146.

Merzenich, M. M., Jenkins, W. M., Johnston, P., Schreiner, C., Miller, S. L., and Tallal, P. (1996). Temporal processing deficits of language-learning impaired children ameliorated by training. *Science* 271, 77–81.

Morrison, A., Diesmann, M., and Gerstner, W. (2008). Phenomenological models of synaptic plasticity based on spike timing. *Biol. Cybern.* 98, 459–478.

Nevian, T., and Sakmann, B. (2006). Spine Ca2+ signaling in spike-timing-dependent plasticity. *J. Neurosci.* 26, 11001–11013.

Nishiyama, M., Hong, K., Mikoshiba, K., Poo, M.-M., and Kato, K. (2000). Calcium stores regulate the polarity and input specificity of synaptic modification. *Nature* 408, 584–588.

O'Connor, D. H., Wittenberg, G. M., and Wang, S. S. (2005). Graded bidirectional synaptic plasticity is composed of switch-like unitary events. *Proc. Natl. Acad. Sci. U.S.A.* 102, 9679–9684.

Pagani, M. R., Oishi, K., Gelb, B. D., and Zhong, Y. (2009). The phosphatase SHP2 regulates the spacing effect for long-term memory induction. *Cell* 139, 186–198.

Paulsen, O., and Sejnowski, T. J. (2000). Natural patterns of activity and long-term synaptic plasticity. *Curr. Opin. Neurobiol.* 10, 172–179.

Pavlov, I. (1927). *Conditioned Reflexes*. New York, Dover.

Pawlak, V., and Kerr, J. N. D. (2008). Dopamine receptor activation is required for corticostriatal spike-timing-dependent plasticity. *J. Neurosci.* 28, 2435–2446.

Peterson, C. C., Malenka, R. C., Nicoll, R. A., and Hopfield, J. J. (1998). All-or-none potentiation at CA3-CA1 synapses. *Proc. Natl. Acad. Sci. U.S.A.* 95, 4732–4737.

Pfister, J.-P., and Gerstner, W. (2006). Triplets of spikes in a model of spike timing-dependent plasticity. *J. Neurosci.* 26, 9673–9682.

Pike, F. G., Meredith, R. M., Olding, A. W., and Paulsen, O. (1999). Postsynaptic bursting is essential for 'Hebbian' induction of associative long-term potentiation at excitatory synapses in rat hippocampus. *J. Physiol.* 518, 571–576.

Poncer, J. C., and Malinow, R. (2001). Postsynaptic conversion of silent synapses during LTP affects synaptic gain and transmission dynamics. *Nat. Neurosci.* 4, 989–996.

Rao, R. P. N., and Sejnowski, T. J. (2001). Spike-timing-dependent Hebbian plasticity as temporal difference learning. *Neural. Comput.* 13, 2221–2237.

Rasse, T. M., Fouquet, W., Schmid, A., Kittel, R. J., Mertel, S., Sigrist, C. B., Schmidt, M., Guzman, A., Merino, C., Qin, G., Quentin, C., Madeo, F. F., Heckmann, M., and Sigrist, S. J. (2005). Glutamate receptor dynamics organizing synapse formation in vivo. *Nat. Neurosci.* 8, 898–905.

Reyes, A., and Sakmann, B. (1999). Developmental switch in the short-term modification of unitary EPSPs evoked in layer 2/3 and layer 5 pyramidal neurons of rat neocortex. *J. Neurosci.* 19, 3827–3835.

Rioult-Pedotti, M.-S., Friedman, D., and Donoghue, J. P. (2000). Learning-induced LTP in neocortex. *Science* 290, 533–536.

Rubin, J., Lee, D. D., and Sompolinsky, H. (2001). Equilibrium properties of temporally asymmetric Hebbian plasticity. *Phys. Rev. Lett.* 86, 364–367.

Rubin, J. E., Gerkin, R. C., Bi, G.-Q., and Chow, C. C. (2005). Calcium time course as a signal for spike-timing-dependent plasticity. *J. Neurophysiol.* 93, 2600–2613.

Schafe, G. E., Nader, K., Blair, H. T., and LeDoux, J. E. (2001). Memory consolidation of Pavlovian fear conditioning: a cellular and molecular perspective. *Trends Neurosci.* 24, 540–546.

Scharfman, H. E., and Sarvey, J. M. (1985). Postsynaptic firing during repetitive stimulation is required for long-term potentiation in hippocampus. *Brain Res.* 331, 267–274.

Sejnowski, T. J. (1999). The book of Hebb. *Neuron* 24, 773–776.

Senn, W., Markram H., and Tsodyks, M. (1999). An algorithm for modifying neurotransmitter release probability based on pre- and postsynaptic spike timing. *Neural. Comput.* 13, 35–67.

Seol, G. H., Ziburkus, J., Huang, S., Song, L., Kim, I. T., Takamiya, K., Huganir, R. L., Lee, H. K., and Kirkwood, A. (2007). Neuromodulators control the polarity of spike-timing-dependent-synaptic plasticity. *Neuron* 55, 919–929.

Shen, W., Flajolet, M., Greengard, P., and Surmeier, D. J. (2008). Dichotomous dopaminergic control of striatal synaptic plasticity. *Science* 321, 848–851.

Shouval, H. Z., Bear, M. F., and Cooper, L. N. (2002). A unified model of NMDA receptor-dependent bidirectional synaptic plasticity. *Proc. Natl. Acad. Sci. U.S.A.* 99, 10831–10836.

Sjöström, P. J., and Häusser M. (2006). A cooperative switch determines the sign of synaptic plasticity in distal dendrites of neocortical pyramidal neurons. *Neuron* 51, 227–238.

Sjöström, P. J., Turrigiano, G. G., and Nelson S. B. (2001). Rate, timing, and cooperativity jointly determine cortical synaptic plasticity. *Neuron* 32, 1149–1164.

Sjöström, P. J., Turrigiano, G. G., and Nelson, S. B. (2003). Neocortical LTD via coincident activation of presynaptic NMDA and cannabinoid receptors. *Neuron* 39, 641–654.

Sjöström, P. J., Turrigiano, G. G., and Nelson, S. B. (2004). Endocannabinoid-dependent neocortical layer-5 LTD in the absence of postsynaptic spiking. *J. Neurophysiol.* 92, 3338–3343.

Song, S., Miller, K. D., and Abbott, L. F. (2000). Competitive Hebbian learning through spike-timing-dependent synaptic plasticity. *Nat. Neurosci.* 3, 919–926.

Sourdet, V., and Debanne, D. (1999). The role of dendritic filtering in associative long-term synaptic plasticity. *Learn. Mem.* 6, 422–447.

Stanton, P. K., and Sejnowski, T. J. (1989). Associative long-term depression in the hippocampus induced by Hebbian covariance. *Nature* 339, 215–218.

Stent, G. S. (1973). A physiological mechanism for Hebb's postulate of learning. *Proc. Natl. Acad. Sci. U.S.A.* 70, 997–1001.

Sutton, R. S., and Barto, A. G. (1998). *Reinforcement Learning: An Introduction*. Boston, The MIT Press.

Tallal, P., Miller, S. L., Bedi, G., Byma, G., Wang, X., Nagarajan, S. S., Schreiner, C., Jenkins, W. M., and Merzenich, M. M. (1996). Language comprehension in language-learning impaired children improved with acoustically modified speech. *Science* 271, 81–84.

Tanaka, E., Higashi, H., and Nishi, S. (1991). Membrane properties of guinea pig cingulate cortical neurons in vitro. *J. Neurophysiol.* 65, 808–821.

Tanaka, J.-I., Horiike, Y., Matsuzaki, M., Miyazaki, T., Ellis-Davies, G. C. R., and Kasai, H. (2008). Protein synthesis and neurotrophin-dependent structural plasticity of single dendritic spines. *Science* 319, 1683–1687.

Tsukada, M., Aihara, T., Kobayashi, Y., and Shimazaki, H. (2005). Spatial analysis of spike-timing-dependent LTP and LTD in the CA1 area of hippocampal slices using optical imaging. *Hippocampus* 15, 104–109.

Turrigiano, G. G., and Nelson, S. B. (2000). Hebb and homeostasis in neuronal plasticity. *Curr. Opin. Neurobiol.* 10, 358–364.

Tzounopoulos, T., Kim, Y., Oertel, D., and Trussell, L. O. (2004). Cell-specific, spike timing-dependent plasticities in the dorsal cochlear nucleus. *Nat. Neurosci.* 7, 719–725.

Tzounopoulos, T., Rubio, M. E., T., Keen, J. E., and Trussell, L. O. (2007). Coactivation of pre- and postsynaptic signaling mechanisms determines cell-specific spike-timing-dependent plasticity. *Neuron* 54, 291–301.

Urakubo, H., Honda, M., Froemke, R. C., and Kuroda, S. (2008). Requirement of an allosteric kinetics of NMDA receptors for spike timing-dependent plasticity. *J. Neurosci.* 28, 3310–3323.

van Rossum, M. C. W., Bi, G.-Q., and Turrigiano, G. G. (2000). Stable Hebbian learning from spike timing-dependent plasticity. *J. Neurosci.* 20, 8812–8821.

Varela, J. A., Sen, K., Gibson, J., Fost, J., Abbott, L. F., and Nelson, S. B. (1997). A quantitative description of short-term plasticity at excitatory synapses in layer 2/3 of rat primary visual cortex. *J. Neurosci.* 17, 7926–7940.

Wang, H.-X., Gerkin, R. C., Nauen, D. W., and Bi, G.-Q. (2005). Coactivation and timing-dependent integration of synaptic potentiation and depression. *Nat. Neurosci.* 8, 187–193.

Wang, S. S., Denk, W., and Häusser, M. (2000). Coincidence detection in single dendritic spines mediated by calcium release. *Nat. Neurosci.* 3, 1266–1273.

Watanabe, S., Hoffman, D. A., Migliore, M., and Johnston, D. (2002). Dendritic K+ channels contribute to spike-timing dependent long-term potentiation in hippocampal pyramidal neurons. *Proc. Natl. Acad. Sci. U.S.A.* 99, 8366–8371.

Wittenberg, G. M., and Wang, S. S. (2006). Malleability of spike-timing-dependent plasticity at the CA3-CA1 synapse. *J. Neurosci.* 26, 6610–6617.

Yang, S. N., Tang, Y. G., and Zucker, R. S. (1999). Selective induction of LTP and LTD by postsynaptic [Ca2+]i elevation. *J. Neurophysiol.* 81, 781–787.

Zador, A., Koch, C., and Brown, T. H. (1990). Biophysical model of a Hebbian synapse. *Proc. Natl. Acad. Sci. U.S.A.* 87, 6718–6722.

Zhang, J. C., Lau, P. M., and Bi, G.-Q. (2009). Gain in sensitivity and loss in temporal contrast of STDP by dopaminergic modulation at hippocampal synapses. *Proc. Natl. Acad. Sci. U.S.A.* 106, 13028–13033.

Zhang, L. I., Tao, H. W., Holt, C. E., Harris, W. A., and Poo, M. (1998). A critical window for cooperation and competition among developing retinotectal synapses. *Nature* 395, 37–44.

Zhou, Q., Tao, H. W., and Poo, M. M. (2003). Reversal and stabilization of synaptic modifications in a developing nervous system. *Science* 300, 1953–1957.

Zilberter, M., Holmgren, C., Shemer, I., Silberberg, G., Grillner, S., Harkany, T., and Zilberter, Y. (2009). Input specificity and dependence of spike timing-dependent plasticity on preceding postsynaptic activity at unitary connections between neocortical layer 2/3 pyramidal cells. *Cereb. Cortex* 19, 2308–2320.

Zucker, R. S. (1999). Calcium- and activity-dependent synaptic plasticity. *Curr. Opin. Neurobiol.* 9, 305–313.

Zucker, R. S., and Regehr, W. G. (2002). Short-term synaptic plasticity. *Annu. Rev. Physiol.* 64, 355–405.

Conflict-of-Interest Statement: The authors declare that the research was conducted in the absence of any commercial or financial relationships that could be construed as a potential conflict of interest.

Received: 01 February 2010; paper pending published: 30 April 2010; accepted: 27 May 2010; published online: 17 June 2010.

*Citation: Froemke RC, Debanne D and Bi G-Q (2010) Temporal modulation of spike-timing-dependent plasticity. Front. Syn. Neurosci. **2**:19. doi: 10.3389/fnsyn.2010.00019*

frontiers in
SYNAPTIC NEUROSCIENCE

REVIEW ARTICLE
published: 24 August 2010
doi: 10.3389/fnsyn.2010.00137

Spike-timing-dependent plasticity in the intact brain: counteracting spurious spike coincidences

Daniel E. Shulz* and Vincent Jacob†

Unité de Neurosciences, Information et Complexité, Centre National de la Recherche Scientifique, Gif sur Yvette, France

Edited by:
Henry Markram, Ecole Polytechnique Federale de Lausanne, Switzerland

Reviewed by:
Anita Luthi, UNIL-CHUV, Switzerland
Shigeru Kubota, Yamagata University, Japan

****Correspondence:***
Daniel E. Shulz, Unité de Neurosciences, Information et Complexité, UPR CNRS 3293, Centre National de la Recherche Scientifique, 1 Avenue de la Terrasse, 91198 Gif sur Yvette, France.
e-mail: shulz@unic.cnrs-gif.fr

†Present address:
Vincent Jacob, School of Biosciences, Cardiff University, Cardiff CF24 3AX, UK

A computationally rich algorithm of synaptic plasticity has been proposed based on the experimental observation that the sign and amplitude of the change in synaptic weight is dictated by the temporal order and temporal contiguity between pre- and postsynaptic activities. For more than a decade, this spike-timing-dependent plasticity (STDP) has been studied mainly in brain slices of different brain structures and cultured neurons. Although not yet compelling, evidences for the STDP rule in the intact brain, including primary sensory cortices, have been provided lastly. From insects to mammals, the presentation of precisely timed sensory inputs drives synaptic and functional plasticity in the intact central nervous system, with similar timing requirements than the *in vitro* defined STDP rule. The convergent evolution of this plasticity rule in species belonging to so distant phylogenic groups points to the efficiency of STDP, as a mechanism for modifying synaptic weights, as the basis of activity-dependent development, learning and memory. In spite of the ubiquity of STDP phenomena, a number of significant variations of the rule are observed in different structures, neuronal types and even synapses on the same neuron, as well as between *in vitro* and *in vivo* conditions. In addition, the state of the neuronal network, its ongoing activity and the activation of ascending neuromodulatory systems in different behavioral conditions have dramatic consequences on the expression of spike-timing-dependent synaptic plasticity, and should be further explored.

Keywords: Hebb, STDP, *in vivo*, ongoing activity, synaptic plasticity, learning

INTRODUCTION

Modification of the efficacy of synaptic transmission, or synaptic plasticity, is widely considered as the basis of activity-dependent neuronal development and learning (Feldman and Brecht, 2005). A well-characterized form of synaptic plasticity is the potentiation and depression of synaptic transmission occurring at many neuronal structures including primary sensory cortices (see, e.g., Frégnac and Shulz, 1999; Foeller and Feldman, 2004). Experimental approaches to unveil changes in the strength of connections between two neurons have extensively developed since the 1970ies, based on the theoretical ground proposed by Hebb (1949). In Chapter 4 (The first stages of perception: growth of the assembly) of his book "The organization of behavior," Hebb proposes that "repeated stimulation of specific receptors will lead slowly to the formation of an 'assembly' of association area cells which can act briefly as a closed system after stimulation has ceased." The formation of a neuronal assembly was proposed to be implemented by a decrease of "synaptic resistances" induced by the persistence of reverberating activity that is sustained ongoing activity after transient inputs. Locally, at the level of a synapse, a period of maintained temporal correlation between pre- and postsynaptic activity would lead to an increase in the efficacy of excitatory synaptic transmission.

Although Hebb's rule became a widely used algorithm in computational models of brain functioning, its straightforward application leads to instability of the system induced by the continuous growth of synaptic efficacies which in turn leads to a saturation of all the plastic elements of the network. This divergence of synaptic weights was solved by theoreticians by using various rules of normalization which require, in addition to Hebb's rule, depression of the gain of other competing synapses (Stent, 1973; von der Malsburg, 1973; Sejnowski, 1977a,b). For instance, a model of self-organization was proposed by von der Malsburg (1973) to account for the development of orientation selectivity in the visual cortex. Based on the Hebbian principle, the model introduces a normalization rule where the sum of the synaptic weights of afferent contacts on one neuron remains constant with time. This implies that local increase in synaptic weight is obtained in detriment of all other contacts that were inactive at the same time. This rule bears similarities with the rule proposed by Stent (1973) who assumed a selective decrease in the efficacy of synaptic transmission of afferent fibers which were inactive at the time when the postsynaptic neuron was discharging under the influence of other inputs.

The algorithms of synaptic plasticity introduced by Sejnowski (1977a,b) to model plasticity in the cerebellum, and later by Bienenstock et al. (1982) for the primary visual cortex, overcome the problem of the synaptic saturation without introducing an *ad hoc* normalization rule. They are based on an input/output covariance algorithm where the change in synaptic efficacy is proportional to the covariation of pre- and postsynaptic activities. This covariation corresponds to the product of the differences of the instantaneous pre- and postsynaptic activities from their respective mean values (averaged over a certain period of preceding time). Covariance-based algorithms predict that the same synapse can both increase and decrease its synaptic efficacy, thereby allowing the connectivity state of the network to evolve into non-trivial states, i.e., non-diverging stable points that attract the dynamics of

the system. Correlation-based algorithms of synaptic modification have been extensively studied experimentally *in vivo* in the developing visual cortex (Frégnac et al., 1988, 1992; Reiter and Stryker, 1988; Frégnac and Shulz, 1989; Bear et al., 1990; Debanne et al., 1998; McLean and Palmer, 1998), the adult visual cortex (Shulz and Frégnac, 1992) and the adult auditory cortex (Ahissar et al., 1992, 1998; Cruikshank and Weinberger, 1996).

Thus, most algorithms used to model synaptic plasticity in the developing or adult cortex include synaptic potentiation and depression rules. They can be mathematically described by a general equation where the modification of synaptic weight as a function of time is proportional to the product of a presynaptic and a postsynaptic term (review in Frégnac and Shulz, 1994, 1999). In these plasticity algorithms a precise temporal order between pre- and postsynaptic activation onsets is not required. Nonetheless, a temporal contiguity between the two events, that is a proximity in time of not more than several tens of milliseconds was required for synaptic potentiation in cortex both *in vivo* (Baranyi and Feher, 1981; Wigström and Gustafsson, 1985) and *in vitro* (Frégnac et al., 1994).

TEMPORAL CONTIGUITY AND ORDER MATTER: THE STDP RULE

More recently, a new form of Hebbian plasticity has been described in which tight temporal contiguity and order between presynaptic and postsynaptic activities determine the amplitude and the sign of the synaptic change respectively. On theoretical grounds, this plasticity rule called spike-timing-dependent plasticity (STDP) has been proposed to be a major, computationally powerful, mechanism for induction of synaptic plasticity *in vivo* (Gerstner et al., 1996; Abbott and Nelson, 2000; Song et al., 2000; van Rossum et al., 2000) and a biologically plausible information storage mechanism in the brain. As we will see later, experimental evidence *in vivo* for this is still scarce.

STDP has been readily observed *in vitro*. The induction of synaptic potentiation and depression depends, at least in the quiescent *in vitro* network, on the relative millisecond-scale timing of presynaptic and postsynaptic action potentials (Debanne et al., 1994, 1997; Bell et al., 1997; Markram et al., 1997; Bi and Poo, 1998; Nishiyama et al., 2000; Kobayashi and Poo, 2004; Wang et al., 2005; Fino et al., 2009). In pyramidal cells of layers 2–3 and 5 of sensory cortices, when an excitatory postsynaptic potential (EPSP) generated by the presynaptic action potential precedes by up to a few tens of milliseconds the postsynaptic action potential, potentiation of the synapse is induced. Conversely, depression of the synapse is observed when the EPSP follows the postsynaptic action potential by short (0–20 ms) or long (0–100 ms) intervals, depending on the synapse being studied (Feldman, 2000; Sjöström et al., 2001; Froemke and Dan, 2002; Sjöström and Nelson, 2002). This *in vitro* demonstrated STDP has been specifically proposed to be important for experience-dependent plasticity at layer 4 to layer 2/3 synapses *in vivo* (Feldman and Brecht, 2005). An anti-Hebbian form of STDP with similar temporal requirements but inverse order has been described in cerebellum-like structures with comparable cell types (Bell et al., 1997; Tzounopoulos et al., 2004) and in some corticostriatal connections (Fino et al., 2005). In the electrosensory lobe of the electric fish, this anti-Hebbian STDP has been proposed to suppress the afferent sensory consequences of an associated motor act, facilitating the detection of unexpected stimuli (review in Bell, 1989; Bell et al., 1999).

STDP IN THE INTACT BRAIN

Despite intensive studies in brain slices and cultured neurons showing that STDP is a robust phenomenon at many cortical synapses, much scarcer evidence is available about how STDP is induced by neuronal activity in the mammalian cortices *in vivo* (review in Dan and Poo, 2006; Caporale and Dan, 2008). Since the statistical properties of neuronal activity patterns differ between *in vitro* and *in vivo* recording conditions, it is crucial to determine if STDP exhibits similar induction requirements. An increasing number of studies are addressing this question, although only a few have directly observed STDP at the level of synaptic responses (see, e.g., Bell et al., 1997; Meliza and Dan, 2006; Cassenaer and Laurent, 2007; Jacob et al., 2007). One of the main difficulties in assessing STDP *in vivo* is that the induction protocols are not as uniform as *in vitro*, rendering the comparison between them hazardous.

The pioneering work of Levy and Steward (1983) defined for the first time the coactivity requirements for synaptic potentiation in the hippocampus of anesthetized rats. The associative induction of long-term potentiation did not require perfect synchronicity of convergent presynaptic elements but unexpectedly, Levy and Steward observed that the order of the potentiation trains of stimulation was crucial in defining the polarity, potentiation or depression, of the synaptic change. Based on this observation, Levy and Steward speculated that "a retrograde interaction between a process initiated within the main dendritic shaft and individual spines" was necessary and proposed a "retrograde electrical invasion of the spine structure" as an appealing possibility (see Stuart et al., 1997 for a review on action potential backpropagation into the dendrites).

STDP has been further shown *in vivo* at the single-cell level in the developing tectum of Xenopus tadpoles (Zhang et al., 1998). Evoked synaptic currents were recorded through whole-cell perforated patch electrodes while the contralateral retina was stimulated electrically at minimal stimulation intensity. By varying the time between the postsynaptic tectal action potential and the retinal input, Zhang and collaborators showed synaptic potentiation for inputs that repetitively arrived within 20 ms before the tectal spike and depression for inputs repetitively arriving within 20 ms after the tectal action potential. In the same preparation, visual inputs, instead of electrical stimulation, with particular time relationships with the postsynaptic action potential can induce long-term potentiation and depression compatible with STDP (Mu and Poo, 2006; see also Engert et al., 2002). The functional consequences of such changes in retinotectal connections have been studied by reverse correlation mapping at the level of the visual receptive field (Vislay-Meltzer et al., 2006). Positive or negative STDP protocols combining visual activation in ectopic areas of the visual field (i.e., outside the classical receptive field) and the postsynaptic current activation through the recording patch pipette were applied. These protocols were shown to sculpt receptive fields by enhancing or removing responses arising from the stimulation of conditioned sub-regions of the receptive field. (René et al. 2003) have shown similar changes in the receptive field structure

of primary visual cortex in cat, induced by a combined visual and intracellular stimulation protocol. Interestingly, the changes in receptive field structure could be dynamically reversed, although not completely, by 10 min of spiking activity induced by white noise visual stimulation (Vislay-Meltzer et al., 2006). This is reminiscent of the finding by Zhou et al. (2003) showing the reversibility of activity-dependent synaptic changes by a short period of spontaneous activity (mainly bursting activity) and points to the strong lability of plastic changes *in vivo* compared to the *in vitro* conditions (see below). The quiescent state of the network *in vitro* allows the maintenance of an induced synaptic change since no spurious pairings occur. However, if randomized pairings at time intervals encompassing both LTP and LTD windows are imposed *in vitro*, robust LTD is observed (Feldman, 2000). This results since the temporal window (i.e., the integral of the learning curve) of LTD is longer than that of LTP (Feldman, 2000; Froemke and Dan, 2002). Consequently, the lability of the changes observed *in vivo* could result from higher levels of ongoing activity associated to an asymmetric STDP rule. The asymmetry of the learning rule *in vivo* depends however on the studied system (compare Meliza and Dan, 2006 and Cassenaer and Laurent, 2007). In the somatosensory cortex *in vivo*, the learning rule seems more symmetric than *in vitro*. However, one cannot exclude that a smaller asymmetry of the plasticity rule combined to a high level of ongoing activity could have the same overall reversal effect. Since the STDP window looks narrower *in vivo* compared to *in vitro* (compare Feldman, 2000 with Jacob et al., 2007), an alternative scenario would be that the temporal windows for LTD and LTP were dynamically adjusted by the ongoing activity. Because the level of activity is higher *in vivo* than *in vitro*, the system would compensate for the spurious pre-post pairings by decreasing and rendering more symmetric the temporal windows for LTD and LTP. This alternative needs however experimental validation.

In the *in vivo* visual cortex, the occurrence of STDP has been indirectly studied by pairing sensory and/or electrical stimulations at time intervals compatible with the STDP rule (Schuett et al., 2001; Yao and Dan, 2001; Fu et al., 2002; Yao et al., 2004). The sensory stimulations increase the firing probability of neurons within a defined window of time, and thus the pairing of two stimuli favors the imposed spike-timing interactions. In most studies using sensory–sensory associations (see also Dahmen et al., 2008 for a similar study in A1), the modifications of the neuronal response properties are rather small, particularly at the single-cell level, but the temporal specificity and the sign of the resulting response modifications are in agreement with the direction of response modifications expected from an STDP scenario and support the idea that STDP could mediate experience-dependent modulation of receptive fields in the visual cortex *in vivo*. The protocol used by Schuett et al. (2001) included more than 25,000 pairings between a visual stimulus presented at 7 Hz during 3 h and an associated intracortical electrical stimulation. Although the changes in the intensity of the voltage sensitive dye signal and the expansion of the cortical area representing the paired visual orientation last for up to 18 h after pairing, that is, much more than shown in any other study, the number of pairings is a hundred times larger than the average number of pairings of other studies and thus precludes a reasonable comparison.

STDP has been directly observed *in vivo* at the level of synaptic responses in the visual cortex (Meliza and Dan, 2006). Whole-cell recordings in the rat primary visual cortex were used to pair visually induced depolarization with spiking of the recorded neuron induced by current injection. Depending on the order of the visual input and the postsynaptic action potential, potentiation or depression was observed. Here, but also as a general observation of synaptic modification *in vivo* (see, e.g., Jacob et al., 2007), the amplitude of the modifications is smaller and more variable than those observed in cortical slices (Froemke and Dan, 2002).

In the intact brain neurons are submitted to a strong bombardment of input activity that affects the temporal control of presynaptic activity during pairing and in turn, affects STDP induction. Thus, the question of STDP incidence in intact sensory cortices in mammals has still to be substantiated. In the *in vivo* somatosensory cortex of the rat, whisker deprivation results in cortical map modifications, which are concomitant with changes in the relative timing of thalamic and cortical action potentials within the STDP range (Allen et al., 2003; Celikel et al., 2004). This indicates that STDP could be involved in response modifications at the cellular level during experience-driven network reorganizations. However, evidence for STDP in the *in vivo* somatosensory cortex remains scarce. Indirect evidence for this comes from a combined electrical stimulation of somatosensory afferents and transcranial magnetic stimulation (TMS) of the somatosensory cortex in humans (Wolters et al., 2005, see also Wolters et al., 2003 for a similar study on the motor cortex). Evoked potentials induced by the TMS were either enhanced or depressed as a function of the order of the paired associative stimulation.

In the primary somatosensory cortex of anesthetized adult rats, backward pairings of spontaneous postsynaptic action potentials with subthreshold afferent excitation elicited by whisker deflections lead to depression of responses to the paired whisker with no significant changes to the unpaired whisker (Jacob et al., 2007). The experimental protocol was based on mechanical deflections of the whiskers only, and no electrical stimulation of the afferent pathway was used during the pairing (see **Figure 1A1**). Since the action potentials of the recorded neuron were not artificially triggered but spontaneously fired by the recorded neuron, it was impossible to program a whisker stimulation that systematically preceded the action potential. Consequently, only the depression side of the STDP curve was studied. Although still in agreement with the STDP rule, the effect was observed only for time intervals shorter than −17 ms(see an example in **Figure 1A2**), indicating that the range of synaptic delays that drive synaptic depression is narrower *in vivo* (see also Yao and Dan, 2001; Fu et al., 2002; Cassenaer and Laurent, 2007; Dahmen et al., 2008 for a similar observation) than *in vitro* (Feldman, 2000). The shortening of the STDP window seems to depend on the developmental stage of the animal, since short windows (<20 ms) were observed in the adult (Yao and Dan, 2001; Fu et al., 2002; Dahmen et al., 2008 and the extracellular backward pairings in Jacob et al., 2007, see **Figure 1A3**) whereas longer STDP windows (35–50 ms) were observed in younger (intracellular pairings in Jacob et al., 2007, see **Figure 1B3**) or developing (Meliza and Dan, 2006) animals. In the backward pairing (Jacob et al., 2007), the trains of whisker deflections were temporally irregular because the pairing was based on the spontaneously emitted action potentials

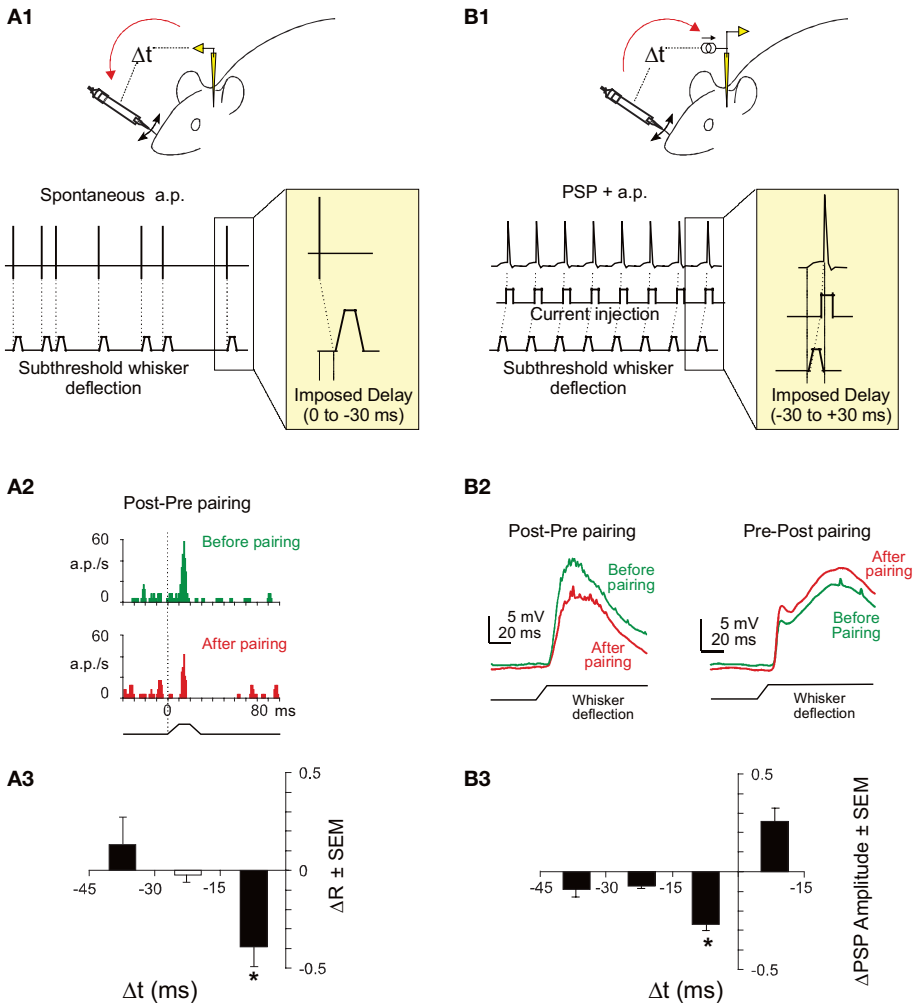

FIGURE 1 | STDP in the somatosensory cortex of the rat. (A1) Experimental protocol for backward pairing. During control and test (not shown) whisker deflection of the principal and one adjacent whiskers were presented in a pseudorandom sequence at 0.5 Hz. The input waveform for each deflection was a 10 ms rostrocaudal movement followed by a 10 ms plateau and a ramp back to the rest position. During pairing, a spontaneously emitted action potential triggered a subthreshold deflection of one whisker with a fixed delay (0, 10, 20, or 30 ms). One pairing period contained 400 associations between an action potential and a whisker deflection. **(A2)** Significant depression ($p < 0.05$) of response of a single neuron in the barrel cortex after a backward pairing (red histogram, After pairing) compared to control (green histogram, Before pairing). **(A3)** Specific depression for short delays of pairing. The mean response modification for the paired whisker (ΔR = after – before/after + before) is plotted against the delay of the pairing. The delay has been corrected to take into account the latency of the cortical response. The depression is significant (*t*-test, $^*p < 0.05$) only for pairings at a short-delay window (<17 ms). **(B1)** Experimental protocol for whole-cell induction of STDP *in vivo*. During control and test (not shown) whisker deflection of the principal and one adjacent whiskers were presented in alternation at 0.5 Hz. During pairing, whisker deflection was paired with current injection to elicit postsynaptic spikes at different delays (from –30 to +30 ms). **(B2)** Induction of spike-timing-dependent synaptic depression (left) or potentiation (right) in two representative neurons. Whisker deflection induced PSP (wPSP) were averaged over 50 trials during baseline (green line) and after pairing (red line). **(B3)** Learning rule for spike-timing-dependent synaptic depression in L2/3 *in vivo*. Mean pairing-induced changes in amplitude of the wPSP (ΔPSP = after – before/before) as a function of delay between postsynaptic spikes and wPSP onset. Adapted from Jacob et al. (2007).

of the recorded neuron. To assess the impact of such irregularities during pairing, several established models of integration of STDP (Song and Abbott, 2001; Froemke and Dan, 2002) were used to fit the experimental data. However, no satisfactory fitting was obtained (Jacob et al., 2007). To explore the potentiation side of the STDP curve *in vivo*, whole-cell patch recordings were needed (see **Figure 1B1**). Using this technique, a timing-dependent depression of responses specific for the paired whisker was observed but spike-timing-dependent potentiation was more sporadically induced (**Figures 1B2,B3**). Thus, spike-timing-dependent depression can be effectively induced *in vivo* and is therefore a plausible plasticity mechanism in the somatosensory cortex although a refinement of specific plasticity models is still necessary to fully account for the observed response and synaptic changes.

DIVERSITY OF STDP PROTOCOLS APPLIED IN THE INTACT BRAIN

As already mentioned, the different experimental protocols applied *in vivo* to induce STDP are rather heterogeneous in terms of the temporal frequency of the pairing and of the number of associations.

In addition, while some studies combined peripheral sensory stimulation with juxtacellular or intracellular current injection to control the postsynaptic spiking discharge, others used combined sensory-sensory stimulation at inter-stimulus intervals compatible with the STDP rule. A comparative analysis is presented in **Table 1** that shows a list of *in vivo* experiments with the corresponding characteristics of the pairings as well as the amplitude and duration of the induced effect. A peculiar correlation appears from such comparative study, which is the inverse link between the number of pairings (the Table is sorted from the highest to the lowest number of pairings) and the amplitude of the resulting modification in sensory responses [see column "Change (LTP or LTD)," expressed as percentage of baseline, in **Table 1**]. The inverse relation holds for response potentiations and depressions separately as well as for the cumulated effect (not shown in **Table 1**). The interpretation of this relationship is hazardous since there are noticeable experimental differences between the studies, including the age, the cortical area, the recording methods, the temporal frequency of pairings and more importantly, the induction protocols themselves (sensory versus electrical afferent activation). Many of the studies showing larger effects induced by a relatively small number of pairings include an intracellular control of the postsynaptic spiking activity whereas on the other hand many of the studies with a high number of pairings and relatively small plastic changes include sensory-sensory stimulation as a way of controlling the temporal correlation of pre and postsynaptic activities. Nonetheless, one plausible interpretation is that *in vivo* spontaneous activity generates spurious coincidences of both signs that dilute the effect of the pairing, and this effect accumulates with the number of pairings. Alternatively, homeostatic mechanisms with longer time scales than the STDP rule and saturation of synaptic modifications with several tens of associations (see Froemke et al., 2006) can regulate the expression of synaptic plasticity.

RATE DEPENDENCE OF STDP

Developmental synaptic plasticity based on covariance rules in sensory cortices depends on the firing rate of presynaptic neurons. At high firing rates, the synapse is potentiated whereas at low firing rates, the synapse is depressed (see review in Bear, 2003; Malenka and Bear, 2004). Conversely, within the framework of the STDP rule, potentiation or depression can be obtained by changing the relative timing between pre- and postsynaptic action potentials with no need for changes in the firing rates. The pairing protocol applied in the somatosensory cortex (Jacob et al., 2007) controls the temporal correlation between pre and postsynaptic spikes without inducing significant modifications of the firing rate of the neuron. Consequently, the induction of the observed functional plasticity is rate-independent although the level of plasticity itself can be modulated by the temporal frequency of the ongoing activity during pairing (see below). This is similar to the study by Ahissar et al. (1992, 1998) where an increase of the functional connectivity between two neurons was induced by increasing the temporal correlation of their activity using a backward pairing similar to the one applied in our study.

The temporal frequency of the pairing was shown to influence STDP (Sjöström et al., 2001): at low frequencies, depression dominates, whereas potentiation is induced at high frequencies. In the somatosensory cortex experiments (Jacob et al., 2007), the depression induced by short-delay pairings depended on the firing frequency during pairing. It should be noted that the pairing frequency in this protocol was dictated by the spontaneous activity of the recorded neuron and was not arbitrarily chosen by the experimenter. The vulnerable nature of the activity-dependent synaptic modifications *in vivo* could result from the effect of the ongoing activity irrespective of the sensory driven activity. Under this scenario, there should be a dependence of the level of synaptic plasticity on the ongoing activity. Indeed, the induced depression of response was maximal for intermediate spontaneous firing rates, with an optimal firing rate at 2.5 Hz (see **Figure 2**). Below one action potential per second, less depression was observed than for the intermediate firing frequencies. This decrease of the level of depression for very low frequency pairings has not been observed *in vitro*, and may result from the fact that at very low frequency of discharge the overall time of the pairing period (400 pairings in Jacob et al., 2007) is too long compared to the duration of the effect produced by each individual pair of action potentials. This result suggests that there is an optimal level of ongoing activity for the induction of STDP. Then, it can be proposed that *in vivo,* cortical structures with intermediate (a few action potentials per second) or sparser activities are more prone to show STDP.

IMPACT OF *IN VIVO* ACTIVITY PATTERNS ON STDP INDUCTION

STDP may be particularly useful in brain regions in which spike rates are low and information is conveyed in spike-timing information. The range of ongoing and evoked firing rate in awake animals differs in the different cortical areas. Extracellular recordings revealed firing rates between 10 and 25 Hz in the visual cortex (Kasamatsu and Adey, 1974; Livingstone and Hubel, 1981), less than 5 Hz in the auditory cortex (Edeline et al., 2001) and less than 1 Hz in the barrel subfield of the somatosensory cortex (Crochet and Petersen, 2006). Ongoing activity in the network affects postsynaptic membrane properties and can modulate the induction of plasticity and compromise the stability of the synaptic modifications. There are striking differences as well between sensory cortices in the ratio between phasic or tonic patterns of evoked firing.

Does STDP efficiency correlate with the sparseness of natural activity? In the retinotectal synapses of developing Xenopus, where STDP has been extensively demonstrated, the activity is sparser than in the cortex of mammals (the spontaneous firing rate is below 1 Hz, the evoked firing rate is between 1 and 2 Hz). In the Locust olfactory system, STDP has been induced in the synapses formed between the Kenyon cells of the mushroom body and cells located in the β-lobe (Cassenaer and Laurent, 2007). Here too, the activity of the Kenyon cells is extremely sparse: the average spontaneous firing rate is below 0.01 spikes per second and the activity evoked by odor presentation is still below 2 spikes per second (Perez-Orive et al., 2002; Jortner et al., 2007). Remarkably, long-term potentiation and depression can be induced in this system after only a few pairs of action potentials.

Different neuronal structures studied in awake animals show a range of activity patterns. Are the pairings used for inducing STDP likely to occur naturally? In other terms, is STDP plausible in a natural *in vivo* condition? In the hippocampus, a prominent activity

Table 1 | STDP experiments conducted in intact nervous systems (sorted by the number of pairings).

Species	Age	Structure	Protocol	Measured variable	Number of pairings	Pairing frequency (Hz)	Change (LTP) (% baseline)	Change (LTD) (% baseline)	Temporal window for LTP (ms)	Temporal window for LTD (ms)	Effect duration (min)	Reference
Cat	Juvenile	V1	V + ES	Intrinsic signal	>25,000	7	28	–24	ns	ns	840	Schuett et al. (2001)
Cat	Adult	V1	V + V	TC shift*	1600–4800	8	**	**	20	–20	10	Yao and Dan (2001)
Cat	Adult	V1	V + V	RF shift*	800	10	1.9	–1.7	10	–10	8	Fu et al. (2002)
Electric fish	Adult	Electrosensory lobe	sCD + IC	EPSPs	270–700	3–4	***	***	<–10	>+100	6	Bell et al. (1993)
Ferret	Adult	A1	A + A	BF shift*	600	7–9	1.7	–2.2	12	–12	6	Dahmen et al. (2008)
Rat	Adult	Hippocampus	ES + ES	EPSPs	600	5	12	–13.4	>15	<–15	>60	Dong et al. (2008)
Rat	Adult	S1	T + sAP	AP	400	3	ns	–33.6	ns	–17	5	Jacob et al. (2007)
Human	Adult	S1	ES + TMS	EP	180	0.1	12.5	–10	5	–20	>90	Wolters et al. (2005)
Xenopus	Embryo	Tectum	V + IC	CSC	100	0.33	30.4	–28.9	30	–40	>30	Mu and Poo (2006)
Rat	Juvenile	S1	T + IC	EPSPs	100	0.5	38.9	–16	>15	–33	12	Jacob et al. (2007)
Xenopus	Embryo	Tectum	ES + ES	EPSCs	100	1	42	–33	20	–30	>30	Zhang et al. (1998)
Xenopus	Embryo	Tectum	V + IC	CSC	90	0.3	24.8	–20.3	20	–25	>35	Vislay-Meltzer et al. (2006)
Human	Adult	M1	ES + TMS	EP	90	0.05	51	–25	10	–20	30	Wolters et al. (2003)
Xenopus	Embryo	Tectum	Moving V	CSC	60	0.2	48	ns	ns	ns	60	Engert et al. (2002)
Rat	Juvenile	V1	V + IC	EPSCs	30–40	0.33	16	–23.8	>30	<–50	60	Meliza and Dan (2006)
Locust	Adult	Mushroom body	O + IC	EPSPs	5–25	0.1	29.6	–33.9	30	–30	>4	Cassenaer and Laurent (2007)
Rat	Adult	Hippocampus	ES + ES****	LFP	8	0.1	47	–17	20	<–20	>5	Levy and Steward (1983)

A, auditory stimulus; AP, action potentials; BF, best frequency; CSC, Compound synaptic current; EP, Evoked potentials; EPSC, Excitatory postsynaptic currents; EPSP, Excitatory postsynaptic potentials; ES, Electrical afferent stimulation; IC, Intracellular current; LFP, Local field potential; Moving V, Moving oriented light bar; ns, not studied; O, Olfactory stimulus; RF, Receptive field; sAP, Spontaneous action potential; sCD, spontaneous corollary discharge; T, Tactile stimulus; TC, Tuning curve; TMS, Transcranial magnetic stimulation; V, Visual stimulus. Cumulated effect = LTP – LTD.

**No significant modifications of response amplitudes were observed. Thus, we considered here the percentage shift of the RF or BF. **The percentage change compared to baseline is not provided for the shift of the TC, ***the percentage change compared to baseline is not provided. ****Trains of 8 pulses at 400 Hz repeated eight times at 0.1 Hz.*

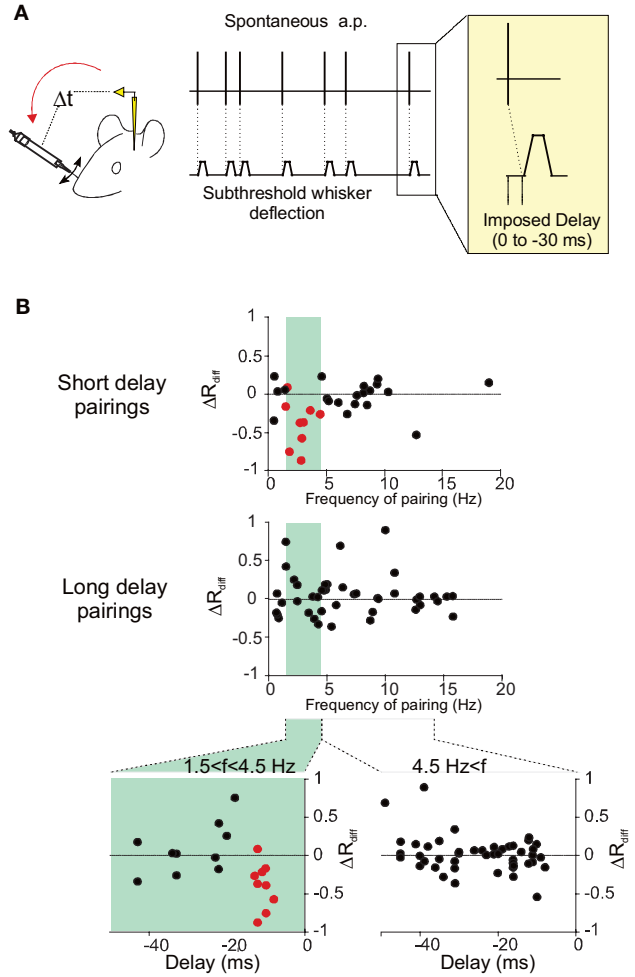

FIGURE 2 | Influence of the temporal frequency of pairing on STDP. **(A)** Experiments were performed in the barrel cortex of adult anesthetized rats (see Jacob et al., 2007 for further details). During pairing, a spontaneously emitted action potential triggers a subthreshold deflection of a whisker with a fixed delay (0, 10, 20, or 30 ms). One pairing period contains 400 associations between an action potential and a stimulation of the whisker. **(B)** The differential change in response (Δ*R*diff) defined as the difference between modifications of responses in the paired and the unpaired pathways, is plotted against the mean temporal frequency of the spontaneous action potential discharge during pairing, at short delays (upper plot, –17 < delay < –7 ms) and longer delays (middle plot, delay <–17 ms). A band-pass curve fitted to Δ*R*diff for the short-delay pairings (not shown) gives a preferred frequency for the induction of response depression of 2.57 Hz. In the lower two scatter plots, relative changes in response (Δ*R*diff) are plotted against the delay of the pairing computed as the imposed delay plus the latency between the stimulation and the arrival of the afferent volley to the cortex. The separation of the pairing population was based on the frequency during the pairing with frequencies between 1.5 and 4.5 Hz (left plot) leading to depression.

pattern is that of theta oscillations between 4 and 12 Hz (Buzsáki and Draguhn, 2004). The phase and frequency of the theta rhythm is under the fine control of at least two independent generators acting together (Kocsis et al., 1999). Recent intracellular recordings in hippocampus of freely moving rats confirmed that theta rhythms are present at the synaptic level (Lee et al., 2006, 2009). Single-cell activity includes a few action potentials per cycle constrained to a particular phase. However, the phase of action potentials in the cycle changes as a function of the position and the direction of the animal (O'Keefe and Recce, 1993). This observation suggests that the timing of the spikes conveys information and constitutes a potential basis for physiological STDP to occur. Similarly to the observation in the somatosensory cortex, STDP-like pairings in the CA1 field of the *in vivo* hippocampus by stimulation of the Schaffer pathway and of the contralateral commissural pathway, induced potentiation at 5 Hz but not at 1 or 10 Hz (Dong et al., 2008). It is likely that the occurrence and amplitude of plasticity is tuned by the frequency of the theta rhythm and the phase of the spikes in the theta cycle leads to a selection of the synapses being potentiated or depressed.

Different rhythms are present at the microscopic and macroscopic level also in the cortex (Steriade, 2001; Crochet and Petersen, 2006; Poulet and Petersen, 2008) and they might affect the induction of plasticity. Non-alert states have been associated with large oscillations at low frequency (1–5 Hz), which reveal a synchronized activity and are reminiscent of the up and down states observed in anesthetized animals. Sensory cortical neurons are highly sensitive to EEG state. Changes in the amplitude of the sensory responses, size of receptive fields, and rate of spontaneous firing are observed in the alert animal compared to the non-alert animal in the visual (Wörgötter et al., 1998; Eyding et al., 2003; Stoelzel et al., 2009), the auditory (Edeline et al., 2001) and the somatosensory (Chapin and Lin, 1984; de Kock and Sakmann, 2009) cortices. Interestingly, the spontaneous firing rate of thalamocortical neurons is lower and at the same time the rate of burst discharges is higher during synchronized non-alert states compared to alert desynchronized states (Stoelzel et al., 2009). These patterns of activity characteristic of the non-alert brain should have an impact in STDP induction since for example, cortical STDP induced *in vitro* at low frequency (Sjöström et al., 2001; Sjöström and Nelson, 2002; Froemke et al., 2006) and/or by bursts of action potentials (Birtoli and Ulrich, 2004; Froemke et al., 2006) favors synaptic depression, even if one has to keep in mind that these observations were made in layers 2–3 and 5, that is, in non-thalamo-recipient cortical layers.

Attention related modulatory signals can change the sparseness of activity in the cortex (Vinje and Gallant, 2002), increasing the temporal precision of the network activity regime (Frégnac et al., 2006), and rendering the system more prone to STDP induction. Cortical release of noradrenaline for example, produces a reduction of spontaneous and evoked activity in the visual cortex (Ego-Stengel et al., 2002). Through this powerful inhibitory action, the noradrenergic system might provide a reset signal (Dayan and Yu, 2006), broadcasted to the whole cortical mantle, leading to an optimized level of activity for the induction of STDP. Other neuromodulators can dynamically regulate timing-based plasticity rules by modifying the biophysical properties of dendrites and the efficacy of spike back propagation (Tsubokawa and Ross, 1997; Sandler and Ross, 1999). Action potentials back propagating into the dendritic tree critically determine the induction of STDP (Engelmann et al., 2008; Sjöström et al., 2008), and its amplitude can be modulated by the network state (Waters and Helmchen, 2004) and dendritic depolarization (Sjöström and Häusser, 2006), both known to be modulated in turn by ascending neuromodulatory signals. A recent comparative study

of corticostriatal plasticity in anesthetized and awake animals (Stoetzner et al., 2010) showed that the STDP plasticity rule depends critically on the behavioral state. Further *in vivo* experiments combining STDP induction protocols concomitant with the activation of neuromodulatory ascending systems (for slice and cell culture studies see Lin et al., 2003; Couey et al., 2007; Seol et al., 2007; Pawlak and Kerr, 2008; Zhang et al., 2009) are needed to explore how local rules of synaptic plasticity in general (Shulz et al., 2000, 2003; Ego-Stengel et al., 2001) and STDP in particular are regulated by global factors acting on several spatial (dendrites, neurons, network) and temporal (milliseconds to minutes) scales.

In conclusion, *in vivo* experimental evidence for STDP, although not yet compelling, has been recently provided in various species and neural structures. Significant variations of the rule (e.g., the temporal length of the STDP window) have been observed and some properties of the induced plasticity, like the duration of the effect, differ from those observed in *in vitro* preparations. Endogenous patterns of ongoing *in vivo* activity like oscillatory rhythms, burstiness and sparse neural activity might help to counteract the effect of spurious spike coincidences and reduce the vulnerability of plasticity *in vivo*. In addition, attention related neuromodulatory signals, through the regulation of activity patterns and/or the adaptation of the plasticity rule itself (i.e., metaplasticity, Abraham, 2008) might optimize the induction and expression of STDP in the intact brain.

ACKNOWLEDGMENTS

We thank Yves Frégnac and Kirsty Grant for helpful comments on the manuscript. This work was supported by the European Union under the FP6 program (FP6-015879, FACETS) and the FET Open program (FP7-243914, Brain-i-Net).

REFERENCES

Abbott, L. F., and Nelson, S. B. (2000). Synaptic plasticity: taming the beast. *Nat. Neurosci.* 3, 1178–1183.

Abraham, W. C. (2008). Metaplasticity: tuning synapses and networks for plasticity. *Nat. Rev. Neurosci.* 9, 387–399.

Ahissar, E., Abeles, M., Ahissar, M., Haidarliu, S., and Vaadia, E. (1998). Hebbian-like functional plasticity in the auditory cortex of the behaving monkey. *Neuropharmacology* 37, 633–655.

Ahissar, E., Vaadia, E., Ahissar, M., Bergman, H., Arieli, A., and Abeles, M. (1992). Dependence of cortical plasticity on correlated activity of single neurons and on behavioral context. *Science* 257, 1412–1415.

Allen, C. B., Celikel, T., and Feldman, D. E. (2003). Long-term depression induced by sensory deprivation during cortical map plasticity *in vivo*. *Nat. Neurosci.* 6, 291–299.

Baranyi, A., and Feher, O. (1981). Long-term facilitation of excitatory synaptic transmission in single motor cortical neurons produced by repetitive pairing of synaptic potentials and action potentials following intracellular stimulation. *Neurosci. Lett.* 23, 303–308.

Bear, M. F. (2003). Bidirectional synaptic plasticity: from theory to reality. *Philos. Trans. R. Soc. Lond., B, Biol. Sci.* 358, 649–655.

Bear, M. F., Kleinschmidt, A., Gu, Q. A., and Singer, W. (1990). Disruption of experience-dependent synaptic modifications in striate cortex by infusion of an NMDA receptor antagonist. *J. Neurosci.* 10, 909–925.

Bell, C. C. (1989). Sensory coding and corollary discharge effects in mormyrid electric fish. *J. Exp. Biol.* 146, 229–253.

Bell, C. C., Caputi, A., Grant, K., and Serrier, J. (1993). Storage of a sensory pattern by anti-Hebbian synaptic plasticity in an electric fish. *Proc. Natl. Acad. Sci. U.S.A.* 90, 4650–4654.

Bell, C. C., Han, V. Z., Sugawara, Y., and Grant, K. (1997). Synaptic plasticity in a cerebellum-like structure depends on temporal order. *Nature* 387, 278–281.

Bell, C. C., Han, V. Z., Sugawara, Y., and Grant, K. (1999). Synaptic plasticity in the mormyrid electrosensory lobe. *J. Exp. Biol.* 202, 1339–1347.

Bi, G. Q., and Poo, M. M. (1998). Synaptic modifications in cultured hippocampal neurons: dependence on spike timing, synaptic strength, and postsynaptic cell type. *J. Neurosci.* 18, 10464–10472.

Bienenstock, E., Cooper, L. N., and Munro, P. (1982). Theory for the development of neuron selectivity: orientation specificity and binocular interaction in visual cortex. *J. Neurosci.* 2, 32–48.

Birtoli, B., and Ulrich, D. (2004). Firing mode-dependent synaptic plasticity in rat neocortical pyramidal neurons. *J. Neurosci.* 24, 4935–4940.

Buzsáki, G., and Draguhn, A. (2004). Neuronal oscillations in cortical networks. *Science* 304, 1926–1929.

Caporale, N., and Dan, Y. (2008). Spike timing-dependent plasticity: a Hebbian learning rule. *Annu. Rev. Neurosci.* 31, 25–46.

Cassenaer, S., and Laurent, G. (2007). Hebbian STDP in mushroom bodies facilitates the synchronous flow of olfactory information in locusts. *Nature* 448, 709–713.

Celikel, T., Szostak, V. A., and Feldman, D. E. (2004). Modulation of spike timing by sensory deprivation during induction of cortical map plasticity. *Nat. Neurosci.* 7, 534–541.

Chapin, J. K., and Lin, C. S. (1984). Mapping the body representation in the SI cortex of anesthetized and awake rats. *J. Comp. Neurol.* 229, 199–213.

Couey, J. J., Meredith, R. M., Spijker, S., Poorthuis, R. B., Smit, A. B., Brussaard, A. B., and Mansvelder, H. D. (2007). Distributed network actions by nicotine increase the threshold for spike-timing-dependent plasticity in prefrontal cortex. *Neuron* 54, 73–87.

Crochet, S., and Petersen, C. C. (2006). Correlating whisker behavior with membrane potential in barrel cortex of awake mice. *Nat. Neurosci.* 9, 608–610.

Cruikshank, S. J., and Weinberger, N. M. (1996). Receptive field plasticity in adult auditory cortex induced by Hebbian covariance. *J. Neurosci.* 16, 861–875.

Dahmen, J. C., Hartley, D. E. H., and King, A. J. (2008). Stimulus-timing-dependent plasticity of cortical frequency representation. *J. Neurosci.* 28, 13629–13639.

Dan, Y., and Poo, M. M. (2006). Spike timing-dependent plasticity: from synapse to perception. *Physiol. Rev.* 86, 1033–1048.

Dayan, P., and Yu, A. J. (2006). Phasic norepinephrine: a neural interrupt signal for unexpected events. *Network* 17, 335–350.

de Kock, C. P., and Sakmann, B. (2009). Spiking in primary somatosensory cortex during natural whisking in awake head-restrained rats is cell-type specific. *Proc. Natl. Acad. Sci. U.S.A.* 106, 16446–16450.

Debanne, D., Gahwiler, B. H., and Thompson, S. M. (1994). Asynchronous presynaptic and postsynaptic activity induces associative long-term depression in area CA1 of the rat hippocampus in vitro. *Proc. Natl. Acad. Sci. U.S.A.* 91, 1148–1152.

Debanne, D., Gahwiler, B. H., and Thompson, S. M. (1997). Bidirectional associative plasticity of unitary CA3-CA1 EPSPs in the rat hippocampus in vitro. *J. Neurophysiol.* 77, 2851–2855.

Debanne, D., Shulz, D. E., and Frégnac, Y. (1998). Activity-dependent regulation of 'on' and 'off' responses in cat visual cortical receptive fields. *J. Physiol.* 15, 523–548.

Dong, Z., Han, H., Cao, J., Zhang, X., and Xu, L. (2008). Coincident activity of converging pathways enables simultaneous long-term potentiation and long-term depression in hippocampal CA1 network *in vivo*. *PLoS ONE* 3, e2848. doi: 10.1371/journal.pone.0002848.

Edeline, J. M., Dutrieux, G., Manunta, Y., and Hennevin, E. (2001). Diversity of receptive field changes in auditory cortex during natural sleep. *Eur. J. Neurosci.* 14, 1865–1880.

Ego-Stengel, V., Bringuier, V., and Shulz, D. E. (2002). Noradrenergic modulation of functional selectivity in the cat visual cortex: an *in vivo* extracellular and intracellular study. *Neuroscience* 111, 275–289.

Ego-Stengel, V., Shulz, D. E., Haidarliu, S., Sosnik, R., and Ahissar, E. (2001). Acethylcholine dependent induction and expression of functional plasticity in the barrel cortex of the adult rat. *J. Neurophysiol.* 86, 422–437.

Engelmann, J., van den Burg, E., Bacelo, J., de Ruijters, M., Kuwana, S., Sugawara, Y., and Grant, K. (2008). Dendritic backpropagation and synaptic plasticity in the mormyrid electrosensory lobe. *J. Physiol. (Paris)* 102, 233–245.

Engert, F., Tao, H. W., Zhang, L. I., and Poo, M. M. (2002). Moving visual stimuli rapidly induce direction sensitivity of developing tectal neurons. *Nature* 419, 470–475.

Eyding, D., Macklis, J. D., Neubacher, U., Funke, K., and Wörgötter, F. (2003). Selective elimination of corticogeniculate feedback abolishes the electroencephalogram dependence of primary visual cortical receptive fields

and reduces their spatial specificity. *J. Neurosci.* 23, 7021–7033.

Feldman, D. E. (2000). Timing-based LTP and LTD at vertical inputs to layer II/II pyramidal cells in rat barrel cortex. *Neuron* 27, 45–56.

Feldman, D. E., and Brecht, M. (2005). Map plasticity in somatosensory cortex. *Science* 310, 810–815.

Fino, E., Glowinski, J., and Venance, L. (2005). Bidirectional activity-dependent plasticity at corticostriatal synapses. *J. Neurosci.* 25, 11279–11287.

Fino, E., Paille, V., Deniau, J. M., and Venance, L. (2009). Asymmetric spike-timing dependent plasticity of striatal nitric oxide-synthase interneurons. *Neuroscience* 160, 744–754.

Foeller, E., and Feldman, D. E. (2004). Synaptic basis for developmental plasticity in somatosensory cortex. *Curr. Opin. Neurobiol.* 14, 89–95.

Frégnac, Y., Blatow, M., Changeux, J., DeFelipe, J., Markram, H., Lansner, A., Maass, W., McCormick, D., Michel, C., Monyer, H., Szathmary, E., and Yuste, R. (2006). "Ups and downs in the genesis of cortical computation," in *Microcircuits: The Interface between Neurons and Global Brain Function Microcircuits: Dahlem Workshop Report*, ed S. Grillner (Cambridge: The MIT Press), 397–437.

Frégnac, Y., Burke, J., Smith, D., and Friedlander, M. J. (1994). Temporal covariance of pre and postsynaptic activity regulates functional connectivity in the visual cortex. *J. Neurophysiol.* 71, 1403–1421.

Frégnac, Y., and Shulz, D. E. (1989). "Hebbian synapses in the visual cortex," in *Seeing Contour and Colour*, ed. K. K. Kulikowski (Oxford: Pergamon Press), 711–718.

Frégnac, Y., and Shulz, D. E. (1994). "Models of synaptic plasticity and cellular analogs of learning in the developing and adult vertebrate visual cortex," in *Advances in Neural and Behavioral Development*, eds V. Casagrande and P. Shinkman (New Jersey: Neural Ablex Publishers), 149–235.

Frégnac, Y., and Shulz, D. E. (1999). Activity-dependent regulation of receptive field properties of cat area 17 by supervised Hebbian learning. *J. Neurobiol.* 41, 69–82.

Frégnac, Y., Shulz, D. E., Thorpe, S., and Bienenstock, E. (1988). A cellular analogue of visual cortical plasticity. *Nature* 333, 367–370.

Frégnac, Y., Shulz, D. E., Thorpe, S., and Bienenstock, E. (1992). Cellular analogs of visual cortical epigenesis: I. Plasticity of orientation selectivity. *J. Neurosci.* 12, 1280–1300.

Froemke, R. C., and Dan, Y. (2002). Spike-timing-dependent synaptic modification induced by natural spike trains. *Nature* 416, 433–438.

Froemke, R. C., Tsay, I. A., Raad, M., Long, J. D., and Dan, Y. (2006). Contribution of individual spikes in burst-induced long-term synaptic modifications. *J. Neurophysiol.* 95, 1620–1629.

Fu, Y. X., Djupsund, K., Gao, H., Hayden, B., Shen, K., and Dan, Y. (2002). Temporal specificity in the cortical plasticity of visual space representation. *Science* 296, 1999–2003.

Gerstner, W., Kempter, R., van Hemmen, L., and Wagner, H. (1996). A neuronal learning rule for sub-millisecond temporal coding. *Nature* 383, 76–78.

Hebb, D. O. (1949). *The Organization of Behavior*. New-York: J. Wiley and Sons.

Jacob, V., Brasier, D. J., Erchova, I., Feldman, D., and Shulz, D. E. (2007). Spike timing-dependent synaptic depression in the *in vivo* barrel cortex of the rat. *J. Neurosci.* 27, 1271–1284.

Jortner, R. A., Farivar, S. S., and Laurent, G. (2007). A simple connectivity scheme for sparse coding in an olfactory system. *J. Neurosci.* 27, 1659–1669.

Kasamatsu, T., and Adey, W. R. (1974). Excitability changes in various types of visual cortical units in freely behaving cats. *Physiol. Behav.* 13, 101–112.

Kobayashi, K., and Poo, M. M. (2004). Spike train timing-dependent associative modification of hippocampal CA3 recurrent synapses by mossy fibers. *Neuron* 41, 445–454.

Kocsis, B., Bragin, A., and Buzsaki, G. (1999). Interdependence of multiple theta generators in the hippocampus: a partial coherence analysis. *J. Neurosci.* 19, 6200–6212.

Lee, A. K., Epsztein, J., and Brecht, M. (2009). Head-anchored whole-cell recordings in freely moving rats. *Nat. Protoc.* 4, 385–392.

Lee, A. K., Manns, I. D., Sakmann, B., and Brecht, M. (2006). Whole-cell recordings in freely moving rats. *Neuron* 51, 399–407.

Levy, W. B., and Steward, O. (1983). Temporal contiguity requirements for longterm associative potentiation/depression in the hippocampus. *Neuroscience* 8, 791–797.

Lin, Y. W., Min, M. Y., Chiu, T. H., and Yang, H. W. (2003). Enhancement of associative long-term potentiation by activation of beta-adrenergic receptors at CA1 synapses in rat hippocampal slices. *J. Neurosci.* 23, 4173–4181.

Livingstone, M. S., and Hubel, D. H. (1981). Effects of sleep and arousal on the processing of visual information in the cat. *Nature* 291, 554–561.

Malenka, R. C., and Bear, M. F. (2004). LTP and LTD: an embarrassment of riches. *Neuron* 44, 5–21.

Markram, H., Lubke, J., Frotscher, M., and Sakmann, B. (1997). Regulation of synaptic efficacy by coincidence of postsynaptic APs and EPSPs. *Science* 275, 213–215.

McLean, J., and Palmer, L. A. (1998). Plasticity of neuronal response properties in adult cat striate cortex. *Vis. Neurosci.* 15, 177–196.

Meliza, C. D., and Dan, Y. (2006). Receptive-field modification in rat visual cortex induced by paired visual stimulation and single-cell spiking. *Neuron* 49, 183–189.

Mu, Y., and Poo, M. M. (2006). Spike timing-dependent LTP/LTD mediates visual experience-dependent plasticity in a developing retinotectal system. *Neuron* 50, 115–125.

Nishiyama, M., Hong, K., Mikoshiba, K., Poo, M. M., and Kato, K. (2000). Calcium stores regulate the polarity and input specificity of synaptic modification. *Nature* 408, 584–588.

O'Keefe, J., and Recce, M. L. (1993). Phase relationship between hippocampal place units and the EEG theta rhythm. *Hippocampus* 3, 317–330.

Pawlak, V., and Kerr, J. N. (2008). Dopamine receptor activation is required for corticostriatal spike-timing-dependent plasticity. *J. Neurosci.* 28, 2435–2446.

Perez-Orive, J., Mazor, O., Turner, G. C., Cassenaer, S., Wilson, R. I., and Laurent, G. (2002). Oscillations and sparsening of odor representations in the mushroom body. *Science* 297, 359–365.

Poulet, J. F., and Petersen, C. C. (2008). Internal brain state regulates membrane potential synchrony in barrel cortex of behaving mice. *Nature* 454, 881–885.

Reiter, H. O., and Stryker, M. P. (1988). Neural plasticity without postsynaptic action potentials: less-active inputs become dominant when kitten visual cortical cells are pharmacologically inhibited. *Proc. Natl. Acad. Sci. U.S.A.* 85, 3623–3627.

René, A., Huguet, N., Pananceau, M., Grant, K., and Frégnac, Y. (2003). An *in vivo* generalisation of Hebbian plasticity rules in adult visual cortex to multiple pre-post synaptic activity correlations. *Soc. Neurosci. Abstr.* 29, 266.17.

Sandler, V. M., and Ross, W. N. (1999). Serotonin modulates spike backpropagation and associated [Ca2+]i changes in the apical dendrites of hippocampal CA1 pyramidal neurons. *J. Neurophysiol.* 81, 216–224.

Schuett, S., Bonhoeffer, T., and Hubener, M. (2001). Pairing-induced changes of orientation maps in cat visual cortex. *Neuron* 32, 325–337.

Sejnowski, T. J. (1977a). Storing covariance with non-linearly interacting neurons. *J. Math. Biol.* 4, 303–321.

Sejnowski, T. J. (1977b). Statistical constraints on synaptic plasticity. *J. Theor. Biol.* 69, 387–389.

Seol, G. H., Ziburkus, J., Huang, S., Song, L., Kim, I. T., Takamiya, K., Huganir, R. L., Lee, H. K., and Kirkwood, A. (2007). Neuromodulators control the polarity of spike-timing-dependent synaptic plasticity. *Neuron* 55, 919–929.

Shulz, D. E., Ego-Stengel, V., and Ahissar, E. (2003). Acetylcholine-dependent potentiation of temporal frequency representation in the barrel cortex does not depend on response magnitude during conditioning. *J. Physiol. Paris* 97, 431–439.

Shulz, D. E., and Frégnac, Y. (1992). Cellular analogs of visual cortical epigenesis: II. Plasticity of binocular integration. *J. Neurosci.* 12, 1301–1318.

Shulz, D. E., Sosnik, R., Ego, V., Haidarliu, S., and Ahissar, E. (2000). A neuronal analogue of state-dependent learning. *Nature* 403, 549–553.

Sjöström, P. J., and Häusser, M. (2006). A cooperative switch determines the sign of synaptic plasticity in distal dendrites of neocortical pyramidal neurons. *Neuron* 51, 227–238.

Sjöström, P. J., and Nelson, S. B. (2002). Spike timing, calcium signals and synaptic plasticity. *Curr. Opin. Neurobiol.* 12, 305–314.

Sjöström, P. J., Rancz, E. A., Roth, A., and Häusser, M. (2008). Dendritic excitability and synaptic plasticity. *Physiol. Rev.* 88, 769–840.

Sjöström, P. J., Turrigiano, G. G., and Nelson, S. B. (2001). Rate, timing, and cooperativity jointly determine cortical synaptic plasticity. *Neuron* 32, 1149–1164.

Song, S., and Abbott, L. F. (2001). Cortical development and remapping through spike timing-dependent plasticity. *Neuron* 32, 339–350.

Song, S., Miller, K. D., and Abbott, L. F. (2000). Competitive Hebbian learning through spike-timing-dependent synaptic plasticity. *Nat. Neurosci.* 3, 919–926.

Stent, G. (1973). A physiological mechanism for Hebb's postulate of learning. *Proc. Natl. Acad. Sci. U.S.A.* 70, 997–1001.

Steriade, M. (2001). Impact of network activities on neuronal properties in corticothalamic systems. *J. Neurophysiol.* 86, 1–39.

Stoelzel, C. R., Bereshpolova, Y., and Swadlow, H. A. (2009). Stability of thalamocortical synaptic transmission across awake brain states. *J. Neurosci.* 29, 6851–6859.

Stoetzner, C. R., Pettibone, J. R., and Berke, J. D. (2010). State-dependent plasticity of the corticostriatal pathway. *Neuroscience* 165, 1013–1018.

Stuart, G., Spruston, N., Sakmann, B., and Hausser, M. (1997). Action potential initiation and backpropagation in neurons of the mammalian CNS. *Trends Neurosci.* 20, 125–131.

Tsubokawa, H., and Ross, W. N. (1997). Muscarinic modulation of spike backpropagation in the apical dendrites of hippocampal CA1 pyramidal neurons. *J. Neurosci.* 17, 5782–5791.

Tzounopoulos, T., Kim, Y., Oertel, D., and Trussell, L. O. (2004). Cell-specific, spike timing-dependent plasticities in the dorsal cochlear nucleus. *Nat. Neurosci.* 7, 719–725.

van Rossum, M. C., Bi, G. Q., and Turrigiano, G. G. (2000). Stable Hebbian learning from spike timing-dependent plasticity. *J. Neurosci.* 20, 8812–8821.

Vinje, W. E., and Gallant, J. L. (2002). Natural stimulation of the nonclassical receptive field increases information transmission efficiency in V1. *J. Neurosci.* 22, 2904–2915.

Vislay-Meltzer, R. L., Kampff, A. R., and Engert, F. (2006). Spatiotemporal specificity of neuronal activity directs the modification of receptive fields in the developing retinotectal system. *Neuron* 50, 101–114.

von der Malsburg, C. (1973). Self-organization of orientation sensitive cells in the striate cortex. *Kybernetik* 14, 85–100.

Wang, H. X., Gerkin, R. C., Nauen, D. W., and Bi, G. Q. (2005). Coactivation and timing dependent integration of synaptic potentiation and depression. *Nat. Neurosci.* 8, 187–193.

Waters, J., and Helmchen, F. (2004). Boosting of action potential backpropagation by neocortical network activity *in vivo*. *J. Neurosci.* 24, 11127–11136.

Wigström, H., and Gustafsson, B. (1985). On long-lasting potentiation in the hippocampus: a proposed mechanism for its dependence on coincident pre- and postsynaptic activity. *Acta Physiol. Scand.* 123, 519–522.

Wolters, A., Sandbrink, F., Schlottmann, A., Kunesch, E., Stefan, K., Cohen, L. G., Benecke, R., and Classen, J. (2003). A temporally asymmetric Hebbian rule governing plasticity in the human motor cortex. *J. Neurophysiol.* 89, 2339–4523.

Wolters, A., Schmidt, A., Schramm, A., Zeller, D., Naumann, M., Kunesch, E., Benecke, R., Reiners, K., and Classen, J. (2005). Timing-dependent plasticity in human primary somatosensory cortex. *J. Physiol.* 565, 1039–1052.

Wörgötter, F., Suder, K., Zhao, Y., Kerscher, N., Eysel, U. T., and Funke, K. (1998). State-dependent receptive-field restructuring in the visual cortex. *Nature* 396, 165–168.

Yao, H., and Dan, Y. (2001). Stimulus timing-dependent plasticity in cortical processing of orientation. *Neuron* 32, 315–323.

Yao, H., Shen, Y., and Dan, Y. (2004). Intracortical mechanism of stimulus-timing dependent plasticity in visual cortical orientation tuning. *Proc. Natl. Acad. Sci. U.S.A.* 101, 5081–5086.

Zhang, J. C., Lau, P. M., and Bi, G. Q. (2009). Gain in sensitivity and loss in temporal contrast of STDP by dopaminergic modulation at hippocampal synapses. *Proc. Natl. Acad. Sci. U.S.A.* 106, 13028–13033.

Zhang, L. I., Tao, H. W., Holt, C. E., Harris, W. A., and Poo, M. (1998). A critical window for cooperation and competition among developing retinotectal synapses. *Nature* 395, 37–44.

Zhou, Q., Tao, H. W., and Poo, M. M. (2003). Reversal and stabilization of synaptic modifications in a developing visual system. *Science* 300, 1953–1957.

Conflict of Interest Statement: The authors declare that the research was conducted in the absence of any commercial or financial relationships that could be construed as a potential conflict of interest.

Received: 17 May 2010; paper pending published: 02 July 2010; accepted: 06 August 2010; published online: 24 August 2010.
*Citation: Shulz DE and Jacob V (2010) Spike-timing-dependent plasticity in the intact brain: counteracting spurious spike coincidences. Front. Syn. Neurosci. **2**:137. doi: 10.3389/fnsyn.2010.00137*

frontiers in
SYNAPTIC NEUROSCIENCE

REVIEW ARTICLE
published: 30 July 2010
doi: 10.3389/fnsyn.2010.00034

Plasticity resembling spike-timing dependent synaptic plasticity: the evidence in human cortex

Florian Müller-Dahlhaus[1], Ulf Ziemann[1]* and Joseph Classen[2]*

[1] *Department of Neurology, Johann Wolfgang Goethe University, Frankfurt/Main, Germany*
[2] *Department of Neurology, University of Leipzig, Leipzig, Germany*

Edited by:
Per Jesper Sjöström, University College London, UK

Reviewed by:
Huibert D. Mansvelder, VU University, Netherlands
Patricio T. Huerta, Weill Medical College of Cornell University, USA
Robert Chen, Toronto Western Hospital, Canada

****Correspondence:***
Ulf Ziemann, Department of Neurology, Goethe University Frankfurt, Schleusenweg 2-16, 60528 Frankfurt am Main, Germany; JosephClassen, Department of Neurology, University of Leipzig, Liebigstraße 20, 04103 Leipzig, Germany.
e-mail: u.ziemann@em.uni-frankfurt.de; joseph.classen@medizin.uni-leipzig.de

Spike-timing dependent plasticity (STDP) has been studied extensively in a variety of animal models during the past decade but whether it can be studied at the systems level of the human cortex has been a matter of debate. Only recently newly developed non-invasive brain stimulation techniques such as transcranial magnetic stimulation (TMS) have made it possible to induce and assess timing dependent plasticity in conscious human subjects. This review will present a critical synopsis of these experiments, which suggest that several of the principal characteristics and molecular mechanisms of TMS-induced plasticity correspond to those of STDP as studied at a cellular level. TMS combined with a second phasic stimulation modality can induce bidirectional long-lasting changes in the excitability of the stimulated cortex, whose polarity depends on the order of the associated stimulus-evoked events within a critical time window of tens of milliseconds. Pharmacological evidence suggests an NMDA receptor mediated form of synaptic plasticity. Studies in human motor cortex demonstrated that motor learning significantly modulates TMS-induced timing dependent plasticity, and, conversely, may be modulated bidirectionally by prior TMS-induced plasticity, providing circumstantial evidence that long-term potentiation-like mechanisms may be involved in motor learning. In summary, convergent evidence is being accumulated for the contention that it is now possible to induce STDP-like changes in the intact human central nervous system by means of TMS to study and interfere with synaptic plasticity in neural circuits in the context of behavior such as learning and memory.

Keywords: spike-timing dependent plasticity, long-term potentiation, long-term depression, paired associative stimulation, transcranial magnetic stimulation, human, cortex, translational neuroscience

INTRODUCTION

Spike-timing dependent plasticity (STDP) has been studied extensively in a variety of model systems, ranging from cultured neurons (Bi and Poo, 1998) and cortical slice preparations (Magee and Johnston, 1997; Markram et al., 1997) to intact animals (Zhang et al., 1998; Jacob et al., 2007), but whether or not timing dependent plasticity can be studied at the systems level of the human cortex has been a matter of debate. Human models, however, may contribute particularly relevant information as they may aid in translating knowledge about synaptic plasticity derived from animal studies into diagnostic or therapeutic progress for patients and inform further experimental animal studies.

Abbreviations: ACC, acceleration; APB, abductor pollicis brevis muscle; EEG, electroencephalography; GOT, grating orientation task; ISI, interstimulus interval; LTD, long-term depression; LTP, long-term potentiation; M1, primary motor cortex; MEP, motor-evoked potential; MN, median nerve; MN-SSEP, median nerve somatosensory-evoked cortical potential; MNS, median nerve stimulation; MP, motor practice; MRCP, movement-related cortical potential; MRI, magnetic resonance imaging; N20, component of the MN-SSEP (negative deflection ~20 ms after MNS); P14, component of the MN-SSEP (positive deflection ~14 ms after MNS); P25, component of the MN-SSEP (positive deflection ~25 ms after MNS); PAS, paired associative stimulation; PAS_{N20}, PAS with an ISI between MNS and TMS of the individual N20-latency of the MN-SSEP; PAS_{N20+2}, PAS with an ISI between MNS and TMS of the individual N20-latency of the MN-SSEP plus 2 ms; PAS_{N20-x}, PAS with an ISI between MNS and TMS of the individual N20-latency of the MN-SSEP minus x ms (x = 2.5, 5, 15); PAS_x, PAS with a fixed ISI between MNS and TMS of x ms (x = 10, 21.5, 25); PD, Parkinson's disease; pHFS, peripheral high frequency stimulation; S1, primary somatosensory cortex; STDP, spike-timing dependent plasticity; TMS, transcranial magnetic stimulation; UN, ulnar nerve.

Transcranial magnetic stimulation (TMS) is a painless non-invasive brain stimulation technique which allows for activation of the intact human cortex (Barker et al., 1985). Stimulation of the primary motor cortex (M1) activates pyramidal output neurons, most likely transsynaptically via a chain of interneurons (Amassian et al., 1987; Ziemann and Rothwell, 2000; Di Lazzaro et al., 2004; Di Lazzaro et al., 2008). Pyramidal neurons in the motor cortex or interneurons within the same microcolumn projecting onto them receive somatosensory input at short latency and with high topographical specificity via afferents from somatosensory cortex (Rosen and Asanuma, 1972; Caria et al., 1997). Thus, pairing of TMS of M1 conjointly with an afferent input to the motor cortex (such as somatosensory information by peripheral nerve stimulation) may result in convergent activation of neural elements in the motor cortex. Based on Hebb's theoretical framework of synaptic plasticity (Hebb, 1949), it was hypothesized that this form of associative stimulation may induce timing dependent plasticity at the systems level in conscious humans.

TIMING DEPENDENT BIDIRECTIONAL PLASTICITY IN HUMAN CORTEX INDUCED BY PAIRED ASSOCIATIVE STIMULATION

In the original experiments of paired associative stimulation (PAS) of the human cortex, PAS consists of electrical stimulation of the median nerve at the wrist (MNS) followed by TMS of the contralateral M1 (**Figures 1A–C**) (Stefan et al., 2000). Excitability of the corticospinal system is probed by TMS over the optimal scalp position for eliciting motor evoked potentials (MEPs) in a

resting intrinsic hand muscle (*M. abductor pollicis brevis*, APB) (**Figure 1D**). The interval between MNS and TMS was chosen to be 25 ms (PAS_{25}). The first component (N20) of the median nerve somatosensory-evoked potential (MN-SSEP) typically arrives in the primary somatosensory cortex (S1) at around 20 ms (**Figure 1D**) (Allison et al., 1991). Taking into account some additional milliseconds for the MNS signal to be relayed from S1 to M1, it is thought that the afferent signal evoked by MNS arrives in M1 nearly synchronously, or even shortly before transsynaptic excitation of corticospinal neurons by the TMS pulse. MNS intensity is set at three times the perceptual sensory threshold. This intensity is generally subthreshold for activation of corticospinal neurons in contralateral M1, as evidenced by the absence of long latency electromyographic reflex activity in the target muscle, which typically requires MNS intensities close to the motor threshold in addition to voluntary muscle activation (Deuschl et al., 1985; Deuschl and Lücking, 1990). In contrast, TMS intensity is adjusted to result in action potentials in corticospinal neurons as indicated by elicitation of MEPs of, on average, 1 mV peak-to-peak amplitude. Ninety pairs of MNS and TMS applied at a frequency of 0.05 Hz over 30 min significantly increase MEP amplitudes in the resting APB muscle (**Figure 1E**) (Stefan et al., 2000). This effect is critically dependent on the interval between MNS and TMS because an interstimulus interval (ISI) of only 10 ms (PAS_{10}) results in depression of MEPs (**Figure 1F**) (Wolters et al., 2003), while much longer ISIs of 100, 525, and 5000 ms have no effect (Stefan et al., 2000). These experiments demonstrate a temporally asymmetric Hebbian-like rule governing PAS-induced changes of excitability in the human motor cortex.

The physiological properties of this potentiation and depression of MEPs comprise inducibility within 30 min, duration of 30–60 min minimum, reversibility within 24 h and topographical specificity with respect to muscles with cortical representations not receiving dual and synchronous input from MNS and TMS (Stefan et al., 2000; Wolters et al., 2003). PAS most likely does not alter $GABA_A$ergic inhibition in motor cortex (Stefan et al., 2002), as indexed by short-latency paired-pulse TMS (Kujirai et al., 1993; Ziemann et al., 1996). Thus, timing dependent PAS effects are very likely not associated with $GABA_A$ergic disinhibition of the motor cortex. Experimental studies and modeling of PAS-induced changes in MEP amplitude as a function of the interstimulus interval between the associative stimuli revealed dependence on near-synchronicity of arrival of the two stimulus-induced events in M1, with a critical window in the order of tens of milliseconds and a relatively steep transition phase from depressant to facilitatory PAS effects (**Figure 2**) (Wolters et al., 2003, 2005). MEP amplitudes increase when suprathreshold TMS-induced activation of pyramidal neurons presumably follows subthreshold activation of these neural elements by MNS by a few milliseconds; reversing the sequence of these events decreases MEP size (Wolters et al., 2003). These findings are reminiscent of spike-timing dependent long-term potentiation (LTP) and long-term depression (LTD) windows for excitatory-to-excitatory connections as observed in animal experiments (Caporale and Dan, 2008).

Subsequent studies have modified the original LTP-like plasticity inducing PAS protocol (Stefan et al., 2000) by using a slightly shorter interval between MNS and TMS of 21.5 ms ($PAS_{21.5}$) (Weise et al., 2006) or by setting the interval to the individual N20 latency (PAS_{N20}) (Ziemann et al., 2004) or to N20 + 2 ms (PAS_{N20+2}) (Müller et al., 2007; Jung and Ziemann, 2009). All these protocols result in a significant and long-term increase of MEPs because the temporal order of events in motor cortex, i.e., arrival of the MNS input within a few milliseconds before or synchronously with the TMS pulse, is obeyed. A form of rapid-rate paired associative stimulation with a stimulation rate of 5 Hz induces timing dependent and long-lasting (up to 6 h) MEP increases within only 2 min providing evidence for rapid induction of PAS-induced LTP-like plasticity (Quartarone et al., 2006). The facilitatory PAS effect on MEPs has been shown to be dose-dependent, i.e., the magnitude and duration of MEP increases scale with the number of stimulus pairs (Nitsche et al., 2007). LTP-like PAS effects saturate at a level of around 160–170% of MEP baseline values (Wolters et al., 2003; Stefan et al., 2004; Nitsche et al., 2007).

The following lines of evidence suggest that the site of action of PAS-induced plasticity is at the level of the cortex: (i) PAS does not change the magnitude of F-waves, an index of spinal motor neuron excitability tested by median nerve stimulation, at the same time when MEP amplitudes were increased (Stefan et al., 2000). (ii) MEPs induced by electrical brainstem stimulation, which excites corticospinal axons directly at the level of the craniocervical junction, downstream of the cortex (Ugawa et al., 1991), remain unchanged after PAS (Stefan et al., 2000). (iii) The cortical silent period of electromyographic activity in the contracting APB muscle, a TMS measure of motor cortical inhibition (Inghilleri et al., 1993), is prolonged by PAS (Stefan et al., 2000) (discussed below in more detail). (iv) Epidural recordings of descending corticospinal activity evoked by TMS demonstrate PAS-induced changes of later descending volleys (Di Lazzaro et al., 2009a,b), which reflect the intracortical transsynaptic activation of pyramidal neurons by TMS (Ziemann and Rothwell, 2000; Di Lazzaro et al., 2004). (v) PAS-experiments targeting the primary somatosensory cortex (reviewed in more detail below) provided evidence for selective modulation of components of somatosensory evoked potentials known to be generated exclusively cortically in strictly confined cortical regions (Wolters et al., 2005; Litvak et al., 2007). (vi) Reversing the direction of the induced current in the brain, which likely leads to preferential activation of intracortical elements located in upper cortical layers with synaptic connection onto corticospinal neurons, allows to decrease the stimulus intensity to below the threshold for activation of corticospinal descending action potentials (Kujirai et al., 2006). (vii) Finally, PAS interferes in a highly specific manner with volitional preparatory cortical motor activity, as measured by changes in movement-related cortical potentials (MRCPs) in EEG recordings, affecting MRCPs only of those movements targeted by PAS (Lu et al., 2009).

Pharmacological studies showed that both PAS-induced timing dependent LTP- and LTD-like plasticity is dependent on *N*-methyl-D-aspartate (NMDA) receptor activation because the NMDA receptor antagonist dextromethorphan blocks both forms of plasticity (Stefan et al., 2002; Wolters et al., 2003). Moreover, PAS-induced LTD-like plasticity is blocked by the L-type voltage-gated calcium channel antagonist nimodipine (Wolters et al., 2003). These findings are in line with *in vitro* data indicating a role for NMDA receptors as coincidence detectors of pre- and postsynaptic activity during

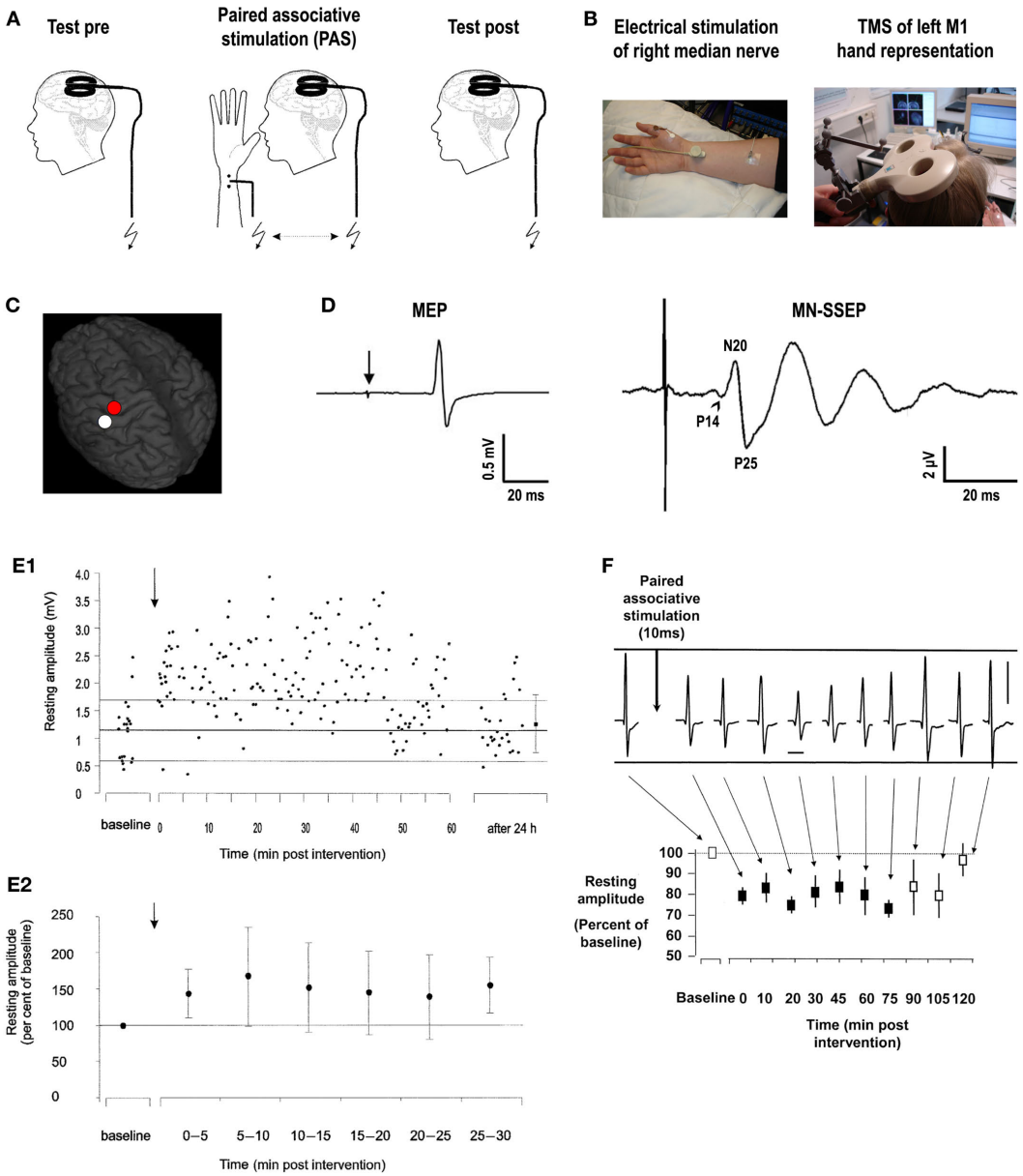

FIGURE 1 | Paired associative stimulation induces timing dependent plasticity in the human primary motor cortex. (A) Experimental design. Paired associative stimulation (PAS) consisted of electrical right median nerve stimulation (MNS) and transcranial magnetic stimulation (TMS) of the left primary motor cortex (M1) over the optimal site for eliciting motor evoked potentials (MEPs) in a muscle of the right hand (*M. abductor pollicis brevis*, APB). Ninety pairs of stimuli were applied with a constant interstimulus interval (ISI) at a frequency of 0.05 Hz. Corticospinal excitability was probed before and after PAS by MEP amplitude in the right APB elicited by single-pulse TMS (adapted from Figure 1, Stefan et al., 2000. Permission pending). **(B)** Experimental setup (see text for explanations). **(C)** Stimulation site of TMS superimposed on a 3-dimensional structural MRI (red dot over left precentral gyrus). The white dot over the left postcentral gyrus indicates the primary somatosensory cortex (S1) hand representation. **(D)** Illustrative examples of MEP in the target muscle (APB) elicited by single-pulse TMS over M1 (red dot in B) at rest (left; arrow, time of TMS pulse delivery) and median nerve somatosensory-evoked potential (MN-SSEP) recorded from scalp electrodes overlying S1 (white dot in **B**), respectively. P14, P14-potential (positive deflection ~14 ms after MNS, arrowhead); N20, N20-potential (negative deflection ~20 ms after MNS); P25, P25-potential (positive deflection ~25 ms after MNS). **(E)** PAS with an ISI of 25ms between MNS and TMS of M1 (PAS_{25}) induces long-lasting increases in MEPs. **(E1)** MEP amplitudes before and after PAS_{25} (arrow) from a representative subject at rest (resting amplitude, *y*-axis). The thick horizontal line indicates the mean resting MEP amplitude at baseline prior to PAS_{25}, and the thin lines indicate one standard deviation. Note persistence of increased excitability for 60 min and return to baseline 24 h after PAS_{25} (adapted from Figure 3B, Stefan et al., 2000. Permission pending). **(E2)** Time course of resting MEP amplitudes after PAS_{25} (arrow) normalized to baseline before PAS_{25}. Data are means from 11 subjects (±S.D.) and are binned to 5 min epochs after PAS_{25}. MEP amplitudes after PAS_{25} are significantly increased compared to baseline for each of the six epochs (adapted from Figure 3A, Stefan et al., 2000. Permission pending). **(F)** PAS with an ISI of 10 ms between MNS and TMS of M1 (PAS_{10}) induces long-lasting decreases in MEPs. Recordings from a representative subject (vertical bar, 1 mV; horizontal bar, 20 ms) and time course of mean MEP amplitudes at rest normalized to baseline before PAS_{10} (resting amplitude, *y*-axis) from 10 subjects (±S.E.M.) are shown. Filled squares indicate significant MEP amplitude decreases (adapted from Figure 3, Wolters et al., 2003. Permission pending).

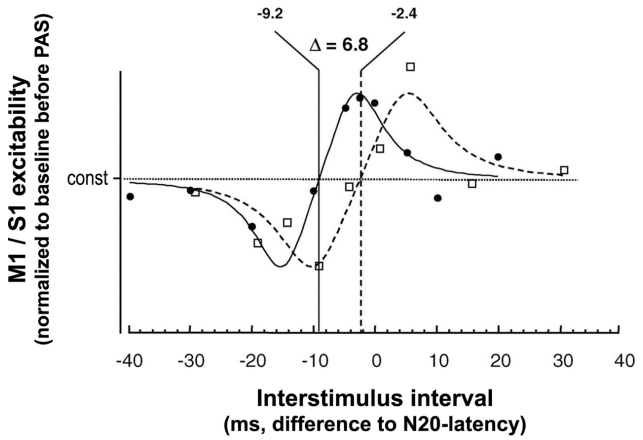

FIGURE 2 | Time window of PAS-induced timing dependent LTP- and LTD-like plasticity in human sensorimotor cortex. *X*-axis, interstimulus intervals (in ms) between MNS and TMS are given with respect to the individual N20-latency of the median nerve somatosensory-evoked potential (MN-SSEP). *Y*-axis, M1 and S1 excitability as determined by MEP amplitude and the P25 component of the MN-SSEP, respectively, normalized to baseline before PAS. Fitted data are scaled to their relative extremes. □, data from PAS of the primary motor cortex (M1), Wolters et al. (2003); •, data from PAS of the primary somatosensory cortex (S1), Wolters et al. (2005). In S1, LTD-like plasticity turns to LTP-like plasticity at an ISI 6.8 ms shorter than in M1 (modified from Figure 6 from Wolters et al., 2005. Permission pending). Continuous and dashed lines indicate modeling of the function relating the PAS-induced magnitude of the P25 and MEP amplitude change, respectively, to the interval between the stimulation modalities. Modeling was done using commercially available software (DataFit program, Version 8.0, Oakdale Engineering, Oakdale, PA, USA). The following function was found empirically $y = a + (x/b - c)/((x/b - c)^4 + d)$. *"const"* in the figure corresponds to "a" in the model. A similar function was found, if a was set to 1.

both spike-timing dependent LTD and LTP induction, while further mechanisms, likely involving Ca^{2+} influx through voltage-gated Ca^{2+} channels, additionally operate in spike-timing dependent LTD (Bi and Poo, 1998).

Further studies tested whether PAS induces timing dependent Hebbian-like associative plasticity in other cortical areas, such as S1. Here, PAS consisted of pairing MNS and TMS of S1 (**Figure 1C**). Excitability of the somatosensory cortex was probed by median nerve somatosensory-evoked cortical potentials (MN-SSEPs) (**Figure 1D**). These experiments demonstrated timing dependent bidirectional changes of the P25 cortical component of the MN-SSEP (Wolters et al., 2005), with associated behavioral changes in two-point discrimination thresholds (Litvak et al., 2007). Source modeling revealed that the changes in MN-SSEPs are best explained by synaptic modification of superficial layers 2/3 of Brodmann area 3b (Litvak et al., 2007). These findings are consistent with animal data showing that STDP can be induced at excitatory vertical inputs from layer 4 onto layer 2/3 pyramidal neurons in rat barrel cortex with behavioral relevance (Feldman, 2000). The N20 and P14 components of the MN-SSEP, which are thought to be generated in deeper cortical layers and subcortically in the thalamus, respectively, remain unchanged (Wolters et al., 2005). As for PAS of the motor system, PAS effects in the somatosensory cortex are rapidly inducible, long-lasting, yet reversible, topographically specific both for the peripheral and the transcranial stimulation, and confined to a narrow window of effective ISIs between MNS and TMS (Wolters et al., 2005; Litvak et al., 2007). Modeling the modulation of the P25 and MEP amplitude as a function of the ISI between MNS and TMS over S1 and M1, respectively, showed that the timing and widths of the time windows in which LTP- and LTD-like effects can be induced by PAS are quite similar in S1 and M1, with S1 leading M1 by ~7 ms (**Figure 2**) (Wolters et al., 2005). This delay of the turning point from LTD- to LTP-like plasticity by ~7 ms in S1 vs. M1 may be just sufficient for polysynaptic propagation of afferent somatosensory signals from S1 to M1 (Wolters et al., 2005) via relays in Brodmann areas 1 and 2 (Jones, 1986). In contrast, first evidence suggests that human hippocampal synapses change their efficacy in response to timed pre- and postsynaptic activity according to a significantly wider and left-shifted STDP rule in comparison to PAS-induced LTD- and LTP-like plasticity in human sensorimotor cortex (Testa-Silva et al., 2010). However, these findings cannot be directly compared to the PAS data reviewed above, as Testa-Silva and colleagues employed a different experimental approach (*ex vivo in vitro* vs. *in vivo*), a different plasticity induction protocol (electrical pairing vs. paired associative electrical peripheral nerve stimulation and TMS) and studied a different tissue substrate (allocortex from drug-resistant [i.e. with a history of drug therapy] epilepsy patients vs. neocortex in healthy human subjects).

In summary, these experiments provide convergent physiological and pharmacological evidence for the contention that PAS-induced timing dependent bidirectional changes of localized neural activity in the human sensorimotor cortex may represent STDP of synaptic efficacy or a closely related mechanism as studied at a cellular level. However, in the absence of invasive neuronal recordings any hypothesis about the precise nature or location of the cellular correlates of PAS-induced plasticity remains, to some extent, speculative. Specifically, a contribution of non-synaptic timing dependent modifications of intrinsic neuronal (Ganguly et al., 2000; Li et al., 2004) and/or local dendritic (Daoudal et al., 2002; Wang et al., 2003; Frick et al., 2004) excitability cannot be ruled out. Homeostatic plasticity such as homeostatic synaptic scaling (Nelson and Turrigiano, 2008) has been shown not only to globally adjust synaptic strength to chronic alterations in network activity (Turrigiano et al., 1998), but also to rapidly tune the efficacy of individual synapses (Pozo and Goda, 2010). Therefore, a full physiological explanation of PAS effects may also include activity-dependent (intrinsic and synaptic) homeostatic plasticity (Nelson and Turrigiano, 2008; Shah et al., 2010) in addition to synaptic STDP-like mechanisms. Further complexity in interpreting PAS effects at a cellular or even molecular level derives from the complex interactions between Hebbian and non-Hebbian forms of plasticity, the temporal and spatial aspects of which are just beginning to emerge (Nelson and Turrigiano, 2008). Finally, TMS-induced modifications of neural activity are coupled to alterations in cerebral hemodynamics (Allen et al., 2007). However, the experiments by Allen and coworkers indicated that TMS-induced changes in hemodynamics are secondary to changes in spontaneous or evoked neural activity, thus being compatible with the notion that PAS effects may be largely explained by terms of neural plasticity.

FUNCTIONAL SIGNIFICANCE: INVESTIGATIONS ON HUMAN CORTICAL PHYSIOLOGY

To keep synaptic weights in a physiological range and maintain overall neuronal and network activity, modifications of synaptic strength need to be carefully controlled. Metaplasticity refers to an activity-dependent mechanism which manifests as a change in the ability to induce subsequent synaptic plasticity (Abraham and Bear, 1996). PAS was used to induce timing dependent LTP-like plasticity (PAS_{N20+2}) in the primary motor cortex (M1) and study its regulation by prior activity in the stimulated neural pathway (Müller et al., 2007). In line with previous studies, this study showed that PAS_{N20+2} leads to a long-lasting increase in MEP amplitudes in the target muscle (APB) when applied to a naïve M1, but this LTP-like effect is occluded or even reversed to MEP depression when applied subsequent to a prior PAS_{N20+2} priming protocol (**Figure 3A**) (Müller et al., 2007). In contrast, priming PAS_{N20+2} by an LTD-like plasticity inducing PAS protocol (PAS_{N20-5}) leads to MEP facilitation similar to the naïve condition or when compared to priming with a control PAS protocol (PAS_{Ctrl}), which does not change MEP amplitude (**Figure 3A**). Control experiments ruled out that the suppressive interaction between two consecutive LTP-like plasticity inducing PAS_{N20+2} protocols is simply caused by a ceiling effect due to increased excitability of the stimulated cortex after the first PAS_{N20+2} intervention (**Figure 3A**). These findings suggest that homeostatic metaplasticity governs timing dependent PAS-induced plasticity in the human M1, most likely homosynaptically (Müller et al., 2007).

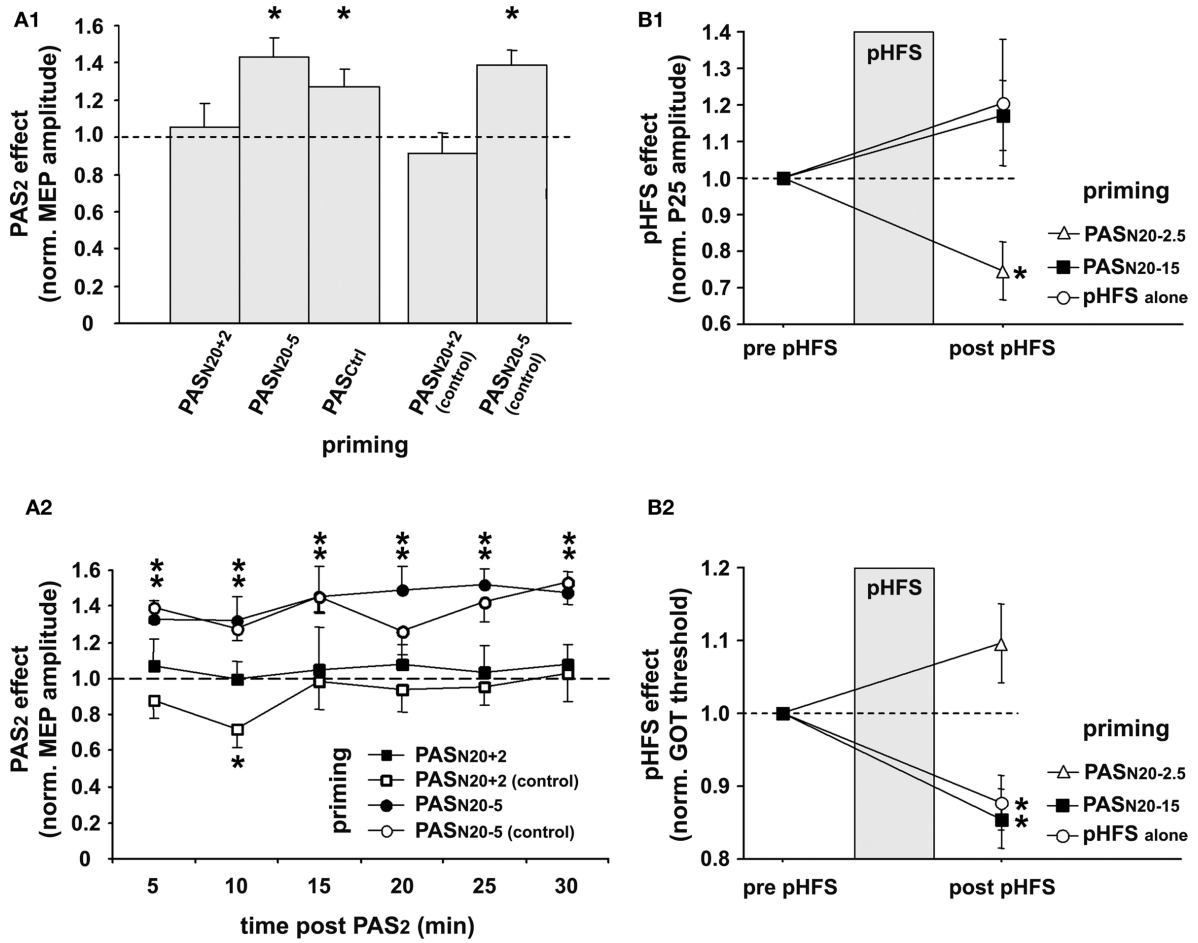

FIGURE 3 | Homeostatic metaplasticity governs timing dependent LTP-like plasticity in human primary motor (M1) and somatosensory (S1) cortex. **(A)** Homeostatic metaplasticity in M1. **(A1)** PAS was used to induce timing dependent LTP-like plasticity (PAS_{N20+2}), LTD-like plasticity (PAS_{N20-5}), or no change (PAS_{Ctrl}) in the naïve M1 (data not shown). A second PAS protocol (PAS_2) 30 min after the first PAS intervention (PAS_1) always consisted of PAS_{N20+2}. PAS_2 induced significant long-lasting MEP increases if primed by PAS_{N20-5} or PAS_{Ctrl}, but this effect was completely suppressed if primed by PAS_{N20+2}. $PAS_{N20+2\,(control)}$ and $PAS_{N20-5\,(control)}$ refer to control experiments, in which MEP amplitudes after priming with PAS_{N20+2} or PAS_{N20-5} were carefully re-adjusted to match those at baseline. The PAS_2 effects are shown as MEP amplitude after PAS_2 normalized to MEP amplitude after PAS_1 but before PAS_2. **(A2)** Time course over 30 min of PAS_2 effects primed by PAS_{N20+2} (filled squares), $PAS_{N20+2\,(control)}$ (open squares), PAS_{N20-5} (filled circles), or $PAS_{N20-5\,(control)}$ (open circles). Data are means ± S.E.M. of 11 subjects; asterisks indicate a significant difference to 1.0. **(B)** Homeostatic metaplasticity in S1. Changes in somatosensory cortical excitability (P25 amplitude of MN-SSEP, **(B1)**) and in tactile spatial discrimination (grating orientation task [GOT] threshold, **(B2)**) induced by peripheral high frequency stimulation (pHFS) of the median nerve alone (open circles), or by pHFS primed by $PAS_{N20-2.5}$ (open triangle) or PAS_{N20-15} (filled square). $PAS_{N20-2.5}$ and PAS_{N20-15} were shown to induce LTP- and LTD-like plasticity, respectively, in the naïve human S1 (cf. Figure 2, and Wolters et al., 2005). Data are mean ± S.E.M normalized to pre pHFS; asterisks indicate a significant difference to 1.0 (modified, with permission, from Figure 3, Müller et al., 2007, and Figure 5, Bliem et al., 2008).

Homeostatic mechanisms control PAS-induced plasticity in M1 even when priming involves an afferent input to the motor cortex such as the projection from dorsal premotor cortex to M1 (Pötter-Nerger et al., 2009). Due to the non-invasive nature of these studies the underlying cellular mechanisms remain unknown, but findings argue in favor of a global homeostatic integration of synaptic inputs within M1, consistent with homeostatic mechanisms formalized in the Bienenstock–Cooper–Munro theory of bidirectional synaptic plasticity (Bienenstock et al., 1982). Homeostatic metaplasticity and associated behavioral performance changes were also demonstrated in PAS experiments targeting the primary somatosensory cortex in humans (Bliem et al., 2008), indicating its generalizable occurrence in and across different regions of human cortex (**Figure 3B**).

Metaplasticity was also demonstrated in studies in which facilitatory or depressant PAS was applied after voluntary activation (**Figure 4**) (Ziemann et al., 2004; Stefan et al., 2006; Rosenkranz et al., 2007b). Repeated fastest possible thumb abduction movements or isometric thumb abductions result in learning, defined by an increase in the maximum peak acceleration of the practiced movement, or by an increase of successful force production, and occlude subsequent PAS-induced LTP-like plasticity, or even reverse it to LTD-like plasticity (**Figure 4A**), whereas subsequent PAS-induced LTD-like plasticity is either enhanced (**Figure 4B**) or remains unchanged (Ziemann et al., 2004; Stefan et al., 2006; Rosenkranz et al., 2007b). In contrast, interactions between motor learning and PAS-induced LTP-like plasticity are not observed, when PAS is applied with a delay of 6 h after motor learning, or if PAS is applied to the motor cortex ipsilateral to the training hand (Stefan et al., 2006).

Which aspect of motor training with the intention to acquire motor skill is relevant for the temporary suppression of PAS-induced timing dependent LTP-like plasticity or even its reversal to LTD-like plasticity? One hypothesis would be that voluntary activity *per se* without learning or skill acquisition is sufficient to act as an effective priming event. At least two arguments provide evidence against this notion to be the sole explanation for training-induced modulation of PAS effects (Ziemann et al., 2004; Stefan et al., 2006; Rosenkranz et al., 2007b): (i) When the same number of thumb abduction movements is performed slowly, this does not result in motor learning, and this form of motor practice does not alter subsequent PAS-induced plasticity (Ziemann et al., 2004). (ii) In another study (Rosenkranz et al., 2007b), subjects were instructed to optimize acceleration of fast thumb abduction movements during multiple training sessions performed over 5 days (Rosenkranz et al., 2007b). PAS was used to induce LTP-like plasticity, and excitability of M1 was tested by measuring input–output curves of MEPs. Task performance improved continuously over 5 days of training (Rosenkranz et al., 2007b). After practice on day 1, the PAS effect reversed from LTP-like to LTD-like plasticity in line with previous studies (Ziemann et al., 2004; Stefan et al., 2006). In contrast, on day 5 PAS-induced LTP-like plasticity was no longer influenced by the preceding motor practice but showed the same magnitude as at baseline before the first practice on day 1 despite a persistent practice-induced enhancement of the MEP input–output curve (Rosenkranz et al., 2007b). This differential modulation of timing dependent LTP-like plasticity by motor practice is consistent with the notion that not activity *per se*, but initial motor learning may trigger LTP of existing synaptic connections. Continued skill learning may induce synaptogenesis and motor cortical reorganization with susceptibility to LTP induction being fully restored (Rosenkranz et al., 2007b). These findings support the view that motor learning may be associated in its initial phase with LTP-like mechanisms in human M1.

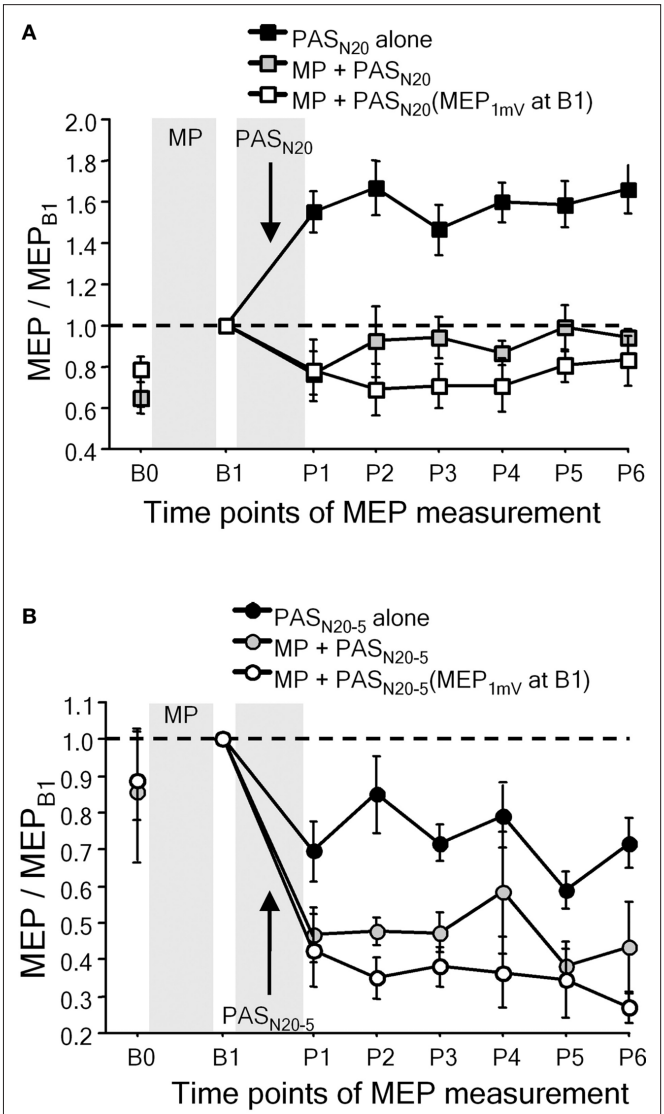

FIGURE 4 | Motor learning involves LTP-like mechanisms in human primary motor cortex. (A) Interactions between motor practice (MP) and timing dependent LTP-like plasticity induced by PAS$_{N20}$. The PAS$_{N20}$-induced long-lasting MEP increase (PAS$_{N20}$ alone, filled square) was completely suppressed by MP associated motor learning immediately prior to PAS (gray squares). White squares refer to a control experiment in which any increase in MEP amplitude induced by MP was adjusted for by a reduction in TMS intensity (reinstallation of baseline MEP amplitude (MEP$_{1mV}$) at time point B1) (adapted, with permission, from Figure 4, Ziemann et al., 2004). **(B)** Interactions between MP and timing dependent LTD-like plasticity induced by PAS$_{N20-5}$. Note that motor learning enhanced the lasting decrease in MEP amplitude induced by PAS$_{N20-5}$ alone (adapted, with permission, from Figure 5, Ziemann et al., 2004).

The magnitude of PAS-induced LTP-like plasticity is highly variable interindividually (Ridding and Ziemann, 2010) and PAS effects decrease significantly with age (Müller-Dahlhaus et al., 2008; Tecchio et al., 2008; Fathi et al., 2010). Likewise, professional musicians show a wider modification range of PAS-induced timing dependent plasticity than non-musicians, as demonstrated by a significantly enhanced increase and decrease of MEP amplitudes after PAS protocols to induce LTP- and LTD-like plasticity, respectively (Rosenkranz et al., 2007a). Similarly enhanced plasticity was noted in physically active individuals (Cirillo et al., 2009). The mechanisms of these findings are not clear, but interindividual differences in the expression level of key neural signals for synaptic plasticity, such as brain-derived neurotrophic factor (BDNF), which was shown to influence experience-dependent and PAS-induced motor cortical plasticity (Kleim et al., 2006; Cheeran et al., 2008), may, among others, account for the observed broad variation of timing dependent PAS effects between subjects. Moreover, LTP-like PAS effects were shown to be critically dependent on the subject's attention to the stimulation (Stefan et al., 2004). Direct evidence for a role of neuromodulators such as dopamine, norepinephrine, and acetylcholine in shaping associative plasticity in the human cortex comes from pharmacological studies (Ziemann et al., 2006; Kuo et al., 2007, 2008). Likewise, cortisol and $GABA_B$ergic input may suppress PAS-induced LTP-like plasticity (McDonnell et al., 2007; Sale et al., 2008). These findings are consistent with data from animal experiments showing that STDP is substantially regulated by neuromodulatory and inhibitory input (Caporale and Dan, 2008).

The cortical silent period of electromyographic activity in the contracting APB muscle, a TMS measure of motor cortical inhibition (Inghilleri et al., 1993), is prolonged by PAS (Stefan et al., 2000). PAS may also modulate other aspects of intracortical inhibition such as long-latency inhibition, which refers to the suppression of the MEP evoked by single-pulse TMS when conditioned by either peripheral afferent or magnetic cortical stimulation applied at long (>100 ms) intervals (Russmann et al., 2009). Recent studies utilizing associative stimulation of homologous areas of left and right human M1 demonstrated an interstimulus interval-specific increase of MEP in the conditioned M1 (Koganemaru et al., 2009; Rizzo et al., 2009a). This change in corticospinal excitability by cortico-cortical PAS is associated with a modulation in interhemispheric inhibition, the suppression of one primary motor cortex by the contralateral homologous M1 (Rizzo et al., 2009a). These studies indicate that PAS may influence inhibitory actions, but whether this occurs through an effect on synapses from inhibitory interneurons onto pyramidal cells or indirectly via modulation of excitatory connections, has not been established unequivocally. The studies by Rizzo et al. (2009a) and by Koganemaru et al. (2009) also suggest that timing dependency may govern plasticity between interconnected cortical areas. How this shapes functional and effective connectivity in health and disease is currently not known.

PATHOPHYSIOLOGY AND MODULATION OF SYNAPTIC PLASTICITY IN NEUROPSYCHIATRIC PATIENTS

Inducing timing dependent bidirectional plasticity in the human cortex by PAS offers the possibility to assess Hebbian-like associative plasticity on the systems level in patients with neuropsychiatric disorders. PAS-induced facilitation of corticospinal excitability is reduced or absent in a variety of neuropsychiatric disorders, consistent with observations of impaired synaptic plasticity in animal models of these disorders. In Parkinson's disease (PD), where degeneration of the nigrostriatal dopaminergic projection occurs, two studies showed that PAS with an interstimulus interval between MNS and TMS to induce LTP-like plasticity does not increase MEP amplitudes in the APB muscle of the more affected side in patients off medication (Morgante et al., 2006; Ueki et al., 2006) while another study reported stronger PAS-induced timing dependent LTP-like plasticity and loss of topographical specificity in PD patients off therapy in comparison to a control group (Bagnato et al., 2006). Reduced plasticity could be restored in a subgroup of patients by dopamine replacement therapy (Morgante et al., 2006; Ueki et al., 2006). Reduced plasticity was also found in two other disorders that have been linked with abnormal dopaminergic transmission: restless legs syndrome (Rizzo et al., 2009b) and schizophrenia (Frantseva et al., 2008). Qualitatively different observations were made in writer's cramp, a neurological disorder characterized by excessive and inappropriate muscular activation during writing. Both PAS-induced LTD- and LTP-like plasticity were enhanced in magnitude and duration in M1 (Quartarone et al., 2003; Weise et al., 2006) and S1 (Tamura et al., 2009). Moreover, in dystonic patients PAS may induce changes in MEP amplitudes in muscle representations of the functional surround of the representation receiving associative stimulation (Weise et al., 2006), suggesting a loss of the topographical specificity of PAS-induced timing dependent plasticity (**Figure 5**).

Plasticity mechanisms including activity-dependent rewiring and synaptic strengthening provide the physiological basis for long term functional recovery, for instance after stroke (Murphy and Corbett, 2009). Non-invasive brain stimulation techniques such as PAS may be applied to modulate cellular mechanisms of synaptic plasticity. In support of this notion, motor learning in healthy subjects can be bidirectionally modulated by prior PAS (**Figure 6**) (Jung and Ziemann, 2009). Motor learning, indexed by an increase in peak acceleration of the trained rapid thumb flexion movements, is enhanced by induction of timing dependent LTD-like plasticity (PAS_{N20-5}) 90 min prior to motor practice, but suppressed if primed by LTP-like plasticity inducing PAS_{N20+2} (**Figure 6B**) (Jung and Ziemann, 2009). These findings are in line with homeostatic metaplasticity rules regulating LTP-like processes such as motor learning in human M1 reviewed above (Ziemann et al., 2004; Stefan et al., 2006; Müller et al., 2007), and provide proof-of-principle that modulation of Hebbian-like associative plasticity by PAS may translate into behavioral performance gains. Additionally, the study by Jung and Ziemann (2009) reveals that motor learning immediately following PAS shows partly non-homeostatic interactions, i.e., motor learning is enhanced if primed by PAS_{N20+2} (although to a lesser extent than after PAS_{N20-5}) (**Figure 6A**) (Jung and Ziemann, 2009). This suggests that homeostatic metaplasticity is fully expressed only if there is a sufficient delay between priming protocol and the subsequent learning process. The underlying mechanisms of this non-homeostatic interaction can only be speculated upon. They include blockade of immediately subsequent LTD-like processes to prevent erasure of the just induced LTP-like plasticity

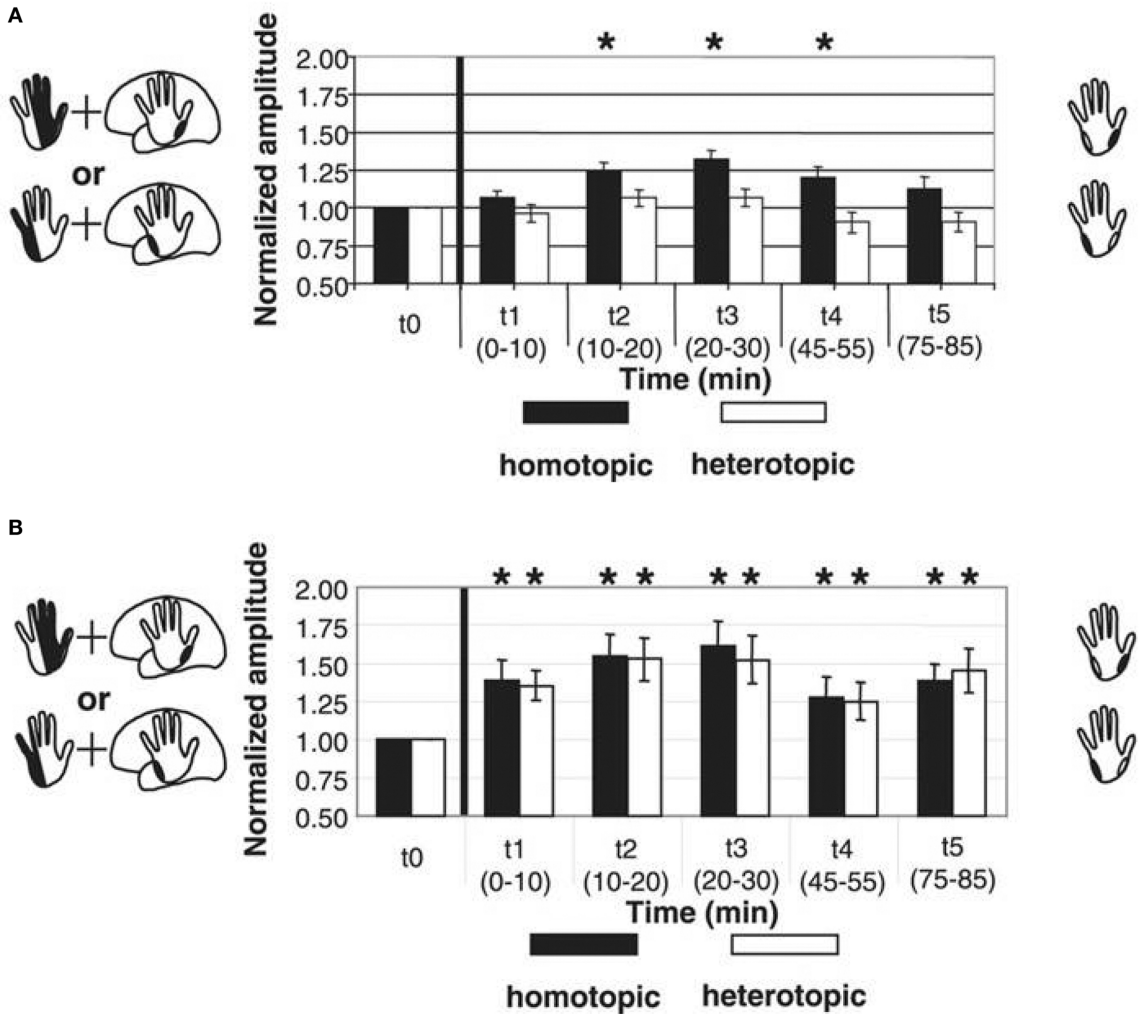

FIGURE 5 | Altered timing dependent LTP-like plasticity in human primary motor cortex (M1) in patients with writer's cramp. PAS consisted of either electrical median nerve (MN) stimulation combined with TMS over the M. abductor pollicis brevis (APB) M1 representation [upper left scheme in **(A)** and **(B)**] or ulnar nerve (UN) stimulation combined with TMS over the M. abductor digiti minimi (ADM) M1 representation [lower left scheme in **(A)** and **(B)**]. PAS-induced changes in MEP amplitude were assessed from both muscles, which served as a homotopic target (black in the right schemes) stimulated by PAS (APB in MN-PAS, ADM in UN-PAS) or heterotopic target not stimulated by PAS (APB in UN-PAS, ADM in MN-PAS). **(A)** In healthy controls, combined data from MN-PAS and UN-PAS with an ISI of 21.5 ms between electrical peripheral nerve and magnetic cortex stimulation ($PAS_{21.5}$) revealed MEP amplitude increases in homotopically stimulated muscle representations only (black bars) (adapted from Figure 2C, Weise et al., 2006. Permission pending). **(B)** In contrast, in patients with writer's cramp, following $PAS_{21.5}$ MEP amplitudes increased in both homotopically (black bars) and heterotopically (white bars) stimulated muscle representations. Asterisks indicate a significant difference from baseline (adapted from Figure 3C, Weise et al., 2006. Permission pending).

(cf. Peineau et al., 2007) and facilitation of learning if the priming LTP-like plasticity did not saturate the synaptic modification range (cf. Berger, 1984).

First evidence suggests that PAS can induce timing dependent plasticity in patients with chronic stroke, but whether this translates into behavioral performance gains is currently not known (Jayaram and Stinear, 2009). Several other important questions remain open: what is the best time window for priming interventions (e.g., PAS) to facilitate LTP-dependent processes such as motor learning? Which patients benefit most/at all, as these mechanisms may be altered in brain disease (Quartarone et al., 2005)? How do priming effects change during repeated interventional sessions (Rosenkranz et al., 2007b)? And what is the role of neuromodulatory pharmaceuticals in the framework of stimulation-induced timing dependent plasticity? Clearly, further studies are needed to address and clarify these issues. Only then plasticity-inducing non-invasive brain stimulation techniques such as PAS can be fully exploited to purposefully modulate motor, sensory and cognitive functions in humans.

SUMMARY

Paired associative stimulation (PAS) of the human sensorimotor cortex by electrical peripheral nerve and conjoint TMS may induce timing dependent bidirectional long-lasting excitability changes in

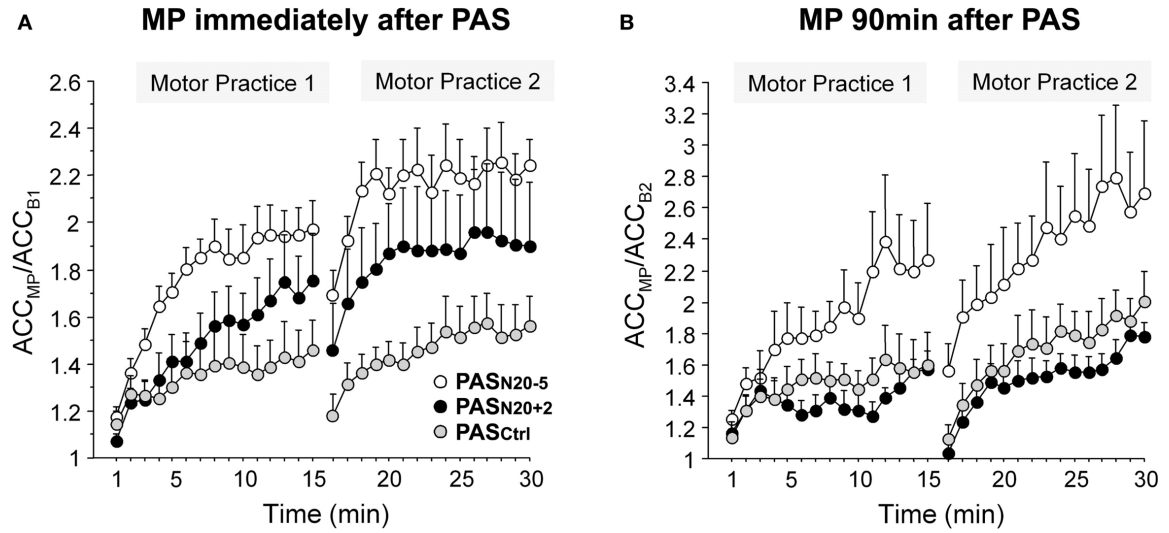

FIGURE 6 | Bidirectional modulation of motor learning in healthy subjects by prior PAS-induced timing dependent LTP- and LTD-like plasticity. Motor learning was indexed by an increase in peak acceleration (ACC) of the trained thumb flexion movement during two blocks of 15 min motor practice (MP) normalized to baseline peak ACC before MP. **(A)** MP immediately following PAS_{N20+2} (black circles) or PAS_{N20-5} (white circles) resulted in an enhancement of learning compared with priming by PAS_{Ctrl} (gray circles, control PAS condition without induction of LTP/LTD-like plasticity). **(B)** In contrast, MP 90 min after PAS_{N20-5} enhanced motor learning, whereas MP following PAS_{N20+2} showed a trend toward depression of learning with respect to the PAS_{Ctrl} condition. Note different scales of *y*-axes in **(A)** and **(B)**. Mean ± S.E.M. of nine subjects (adapted, with permission, from Figure 3 in Jung and Ziemann, 2009).

the stimulated cortex. Pharmacological and physiological evidence suggests that the after-effects of this non-invasive brain stimulation paradigm may be related to STDP. Thus, PAS may serve as an example of translation of studies on synaptic physiology on a cellular level to the systems physiology level of the human brain. PAS was extensively used to assess cortical plasticity in healthy human subjects and provided circumstantial evidence that motor learning involves LTP-like mechanisms, and that homeostatic metaplasticity regulates sensorimotor cortical plasticity. Moreover, PAS experiments may offer some new insight into the pathophysiology of a variety of neuropsychiatric diseases. PAS-induced modulation of synaptic plasticity in the context of behavior may be used purposefully in order to promote motor, sensory and cognitive performance in humans.

REFERENCES

Abraham, W. C., and Bear, M. F. (1996). Metaplasticity: the plasticity of synaptic plasticity. *Trends Neurosci.* 19, 126–130.

Allen, E. A., Pasley, B. N., Duong, T., and Freeman, R. D. (2007). Transcranial magnetic stimulation elicits coupled neural and hemodynamic consequences. *Science* 317, 1918–1921.

Allison, T., McCarthy, G., Wood, C. C., and Jones, S. J. (1991). Potentials evoked in human and monkey cerebral cortex by stimulation of the median nerve. A review of scalp and intracranial recordings. *Brain* 114(Pt 6), 2465–2503.

Amassian, V. E., Stewart, M., Quirk, G. J., and Rosenthal, J. L. (1987). Physiological basis of motor effects of a transient stimulus to cerebral cortex. *Neurosurgery* 20, 74–93.

Bagnato, S., Agostino, R., Modugno, N., Quartarone, A., and Berardelli, A. (2006). Plasticity of the motor cortex in Parkinson's disease patients on and off therapy. *Mov. Disord.* 21, 639–645.

Barker, A. T., Jalinous, R., and Freeston, I. L. (1985). Non-invasive magnetic stimulation of human motor cortex. *Lancet* 1, 1106–1107.

Berger, T. W. (1984). Long-term potentiation of hippocampal synaptic transmission affects rate of behavioral learning. *Science* 224, 627–630.

Bi, G. Q., and Poo, M. M. (1998). Synaptic modifications in cultured hippocampal neurons: dependence on spike timing, synaptic strength, and postsynaptic cell type. *J. Neurosci.* 18, 10464–10472.

Bienenstock, E. L., Cooper, L. N., and Munro, P. W. (1982). Theory for the development of neuron selectivity: orientation specificity and binocular interaction in visual cortex. *J. Neurosci.* 2, 32–48.

Bliem, B., Müller-Dahlhaus, J. F., Dinse, H. R., and Ziemann, U. (2008). Homeostatic metaplasticity in the human somatosensory cortex. *J. Cogn. Neurosci.* 20, 1517–1528.

Caporale, N., and Dan, Y. (2008). Spike timing-dependent plasticity: a Hebbian learning rule. *Annu. Rev. Neurosci.* 31, 25–46.

Caria, M. A., Kaneko, T., Kimura, A., and Asanuma, H. (1997). Functional organization of the projection from area 2 to area 4gamma in the cat. *J. Neurophysiol.* 77, 3107–3114.

Cheeran, B., Talelli, P., Mori, F., Koch, G., Suppa, A., Edwards, M., Houlden, H., Bhatia, K., Greenwood, R., and Rothwell, J. C. (2008). A common polymorphism in the brain-derived neurotrophic factor gene (BDNF) modulates human cortical plasticity and the response to rTMS. *J. Physiol.* 586, 5717–5725.

Cirillo, J., Lavender, A. P., Ridding, M. C., and Semmler, J. G. (2009). Motor cortex plasticity induced by paired associative stimulation is enhanced in physically active individuals. *J. Physiol.* 587, 5831–5842.

Daoudal, G., Hanada, Y., and Debanne, D. (2002). Bidirectional plasticity of excitatory postsynaptic potential (EPSP)-spike coupling in CA1 hippocampal pyramidal neurons. *Proc. Natl. Acad. Sci. U.S.A.* 99, 14512–14517.

Deuschl, G., and Lücking, C. H. (1990). Physiology and clinical applications of hand muscle reflexes. *Electroencephalogr. Clin. Neurophysiol. Suppl.* 41, 84–101.

Deuschl, G., Schenck, E., and Lücking, C. H. (1985). Long-latency responses in human thenar muscles mediated by fast conducting muscle and cutaneous afferents. *Neurosci. Lett.* 55, 361–366.

Di Lazzaro, V., Dileone, M., Pilato, F., Profice, P., Oliviero, A., Mazzone, P., Insola, A., Capone, F., Ranieri, F., and Tonali, P. A. (2009a). Associative motor cortex plasticity: direct evidence in humans. *Cereb. Cortex* 19, 2326–2330.

Di Lazzaro, V., Dileone, M., Profice, P., Pilato, F., Oliviero, A., Mazzone, P., Di Iorio, R., Capone, F., Ranieri, F., Florio, L., and Tonali, P. A. (2009b). LTD-like plasticity induced by paired associative stimulation: direct evidence in humans. *Exp. Brain Res.* 194, 661–664.

Di Lazzaro, V., Oliviero, A., Pilato, F., Saturno, E., Dileone, M., Mazzone, P., Insola, A., Tonali, P. A., and Rothwell, J. C. (2004). The physiological basis of transcranial motor cortex stimulation in conscious humans. *Clin. Neurophysiol.* 115, 255–266.

Di Lazzaro, V., Ziemann, U., and Lemon, R. N. (2008). State of the art: physiology of transcranial motor cortex stimulation. *Brain Stimul.* 1, 345–362.

Fathi, D., Ueki, Y., Mima, T., Koganemaru, S., Nagamine, T., Tawfik, A., and Fukuyama, H. (2010). Effects of aging on the human motor cortical plasticity studied by paired associative stimulation. *Clin. Neurophysiol.* 121, 90–93.

Feldman, D. E. (2000). Timing-based LTP and LTD at vertical inputs to layer II/III pyramidal cells in rat barrel cortex. *Neuron* 27, 45–56.

Frantseva, M. V., Fitzgerald, P. B., Chen, R., Moller, B., Daigle, M., and Daskalakis, Z. J. (2008). Evidence for impaired long-term potentiation in schizophrenia and its relationship to motor skill learning. *Cereb. Cortex* 18, 990–996.

Frick, A., Magee, J., and Johnston, D. (2004). LTP is accompanied by an enhanced local excitability of pyramidal neuron dendrites. *Nat. Neurosci.* 7, 126–135.

Ganguly, K., Kiss, L., and Poo, M. (2000). Enhancement of presynaptic neuronal excitability by correlated presynaptic and postsynaptic spiking. *Nat. Neurosci.* 3, 1018–1026.

Hebb, D. O. (1949). *The Organization of Behavior: A Neuropsychological Theory*. New York: Wiley.

Inghilleri, M., Berardelli, A., Cruccu, G., and Manfredi, M. (1993). Silent period evoked by transcranial stimulation of the human cortex and cervicomedullary junction. *J. Physiol.* 466, 521–534.

Jacob, V., Brasier, D. J., Erchova, I., Feldman, D., and Shulz, D. E. (2007). Spike timing-dependent synaptic depression in the in vivo barrel cortex of the rat. *J. Neurosci.* 27, 1271–1284.

Jayaram, G., and Stinear, J. W. (2009). The effects of transcranial stimulation on paretic lower limb motor excitability during walking. *J. Clin. Neurophysiol.* 26, 272–279.

Jones, E. G. (1986) "Connectivity of the primate sensory-motor cortex," in *Cerebral Cortex*, eds E. G. Jones and A. Peters (New York: Plenum Press), pp 113–183.

Jung, P., and Ziemann, U. (2009). Homeostatic and nonhomeostatic modulation of learning in human motor cortex. *J. Neurosci.* 29, 5597–5604.

Kleim, J. A., Chan, S., Pringle, E., Schallert, K., Procaccio, V., Jimenez, R., and Cramer, S. C. (2006). BDNF val66met polymorphism is associated with modified experience-dependent plasticity in human motor cortex. *Nat. Neurosci.* 9, 735–737.

Koganemaru, S., Mima, T., Nakatsuka, M., Ueki, Y., Fukuyama, H., and Domen, K. (2009). Human motor associative plasticity induced by paired bihemispheric stimulation. *J. Physiol.* 587, 4629–4644.

Kujirai, T., Caramia, M. D., Rothwell, J. C., Day, B. L., Thompson, P. D., Ferbert, A., Wroe, S., Asselman, P., and Marsden, C. D. (1993). Corticocortical inhibition in human motor cortex. *J. Physiol.* 471, 501–519.

Kujirai, K., Kujirai, T., Sinkjaer, T., and Rothwell, J. C. (2006). Associative plasticity in human motor cortex during voluntary muscle contraction. *J. Neurophysiol.* 96, 1337–1346.

Kuo, M. F., Grosch, J., Fregni, F., Paulus, W., and Nitsche, M. A. (2007). Focusing effect of acetylcholine on neuroplasticity in the human motor cortex. *J. Neurosci.* 27, 14442–14447.

Kuo, M. F., Paulus, W., and Nitsche, M. A. (2008). Boosting focally-induced brain plasticity by dopamine. *Cereb. Cortex* 18, 648–651.

Li, C. Y., Lu, J. T., Wu, C. P., Duan, S. M., and Poo, M. M. (2004). Bidirectional modification of presynaptic neuronal excitability accompanying spike timing-dependent synaptic plasticity. *Neuron* 41, 257–268.

Litvak, V., Zeller, D., Oostenveld, R., Maris, E., Cohen, A., Schramm, A., Gentner, R., Zaaroor, M., Pratt, H., and Classen, J. (2007). LTP-like changes induced by paired associative stimulation of the primary somatosensory cortex in humans: source analysis and associated changes in behaviour. *Eur. J. Neurosci.* 25, 2862–2874.

Lu, M. K., Bliem, B., Jung, P., Arai, N., Tsai, C. H., and Ziemann, U. (2009). Modulation of preparatory volitional motor cortical activity by paired associative transcranial magnetic stimulation. *Hum. Brain Mapp.* 30, 3645–3656.

Magee, J. C., and Johnston, D. (1997). A synaptically controlled, associative signal for Hebbian plasticity in hippocampal neurons. *Science* 275, 209–213.

Markram, H., Lubke, J., Frotscher, M., and Sakmann, B. (1997). Regulation of synaptic efficacy by coincidence of postsynaptic APs and EPSPs. *Science* 275, 213–215.

McDonnell, M. N., Orekhov, Y., and Ziemann, U. (2007). Suppression of LTP-like plasticity in human motor cortex by the GABA(B) receptor agonist baclofen. *Exp. Brain Res.* 180 181–186.

Morgante, F., Espay, A. J., Gunraj, C., Lang, A. E., and Chen, R. (2006). Motor cortex plasticity in Parkinson's disease and levodopa-induced dyskinesias. *Brain* 129, 1059–1069.

Müller, J. F., Orekhov, Y., Liu, Y., and Ziemann, U. (2007). Homeostatic plasticity in human motor cortex demonstrated by two consecutive sessions of paired associative stimulation. *Eur. J. Neurosci.* 25, 3461–3468.

Müller-Dahlhaus, J. F., Orekhov, Y., Liu, Y., and Ziemann, U. (2008). Interindividual variability and age-dependency of motor cortical plasticity induced by paired associative stimulation. *Exp. Brain Res.* 187, 467–475.

Murphy, T. H., and Corbett, D. (2009). Plasticity during stroke recovery: from synapse to behaviour. *Nat. Rev. Neurosci.* 10, 861–872.

Nelson, S. B., and Turrigiano, G. G. (2008). Strength through diversity. *Neuron* 60, 477–482.

Nitsche, M. A., Roth, A., Kuo, M. F., Fischer, A. K., Liebetanz, D., Lang, N., Tergau, F., and Paulus, W. (2007). Timing-dependent modulation of associative plasticity by general network excitability in the human motor cortex. *J. Neurosci.* 27, 3807–3812.

Peineau, S., Taghibiglou, C., Bradley, C., Wong, T. P., Liu, L., Lu, J., Lo, E., Wu, D., Saule, E., Bouschet, T., Matthews, P., Isaac, J. T., Bortolotto, Z. A., Wang, Y. T., and Collingridge, G. L. (2007). LTP inhibits LTD in the hippocampus via regulation of GSK3beta. *Neuron* 53, 703–717.

Pötter-Nerger, M., Fischer, S., Mastroeni, C., Groppa, S., Deuschl, G., Volkmann, J., Quartarone, A., Munchau, A., and Siebner, H. R. (2009). Inducing homeostatic-like plasticity in human motor cortex through converging corticocortical inputs. *J. Neurophysiol.* 102, 3180–3190.

Pozo, K., and Goda, Y. (2010). Unraveling mechanisms of homeostatic synaptic plasticity. *Neuron* 66, 337–351.

Quartarone, A., Bagnato, S., Rizzo, V., Siebner, H. R., Dattola, V., Scalfari, A., Morgante, F., Battaglia, F., Romano, M., and Girlanda, P. (2003). Abnormal associative plasticity of the human motor cortex in writer's cramp. *Brain* 126, 2586–2596.

Quartarone, A., Rizzo, V., Bagnato, S., Sant'angelo, A., Girlanda, P., and Roman Siebner, H. (2006). Rapid-rate paired associative stimulation of the median nerve and motor cortex can produce long-lasting changes in motor cortical excitability in humans. *J. Physiol.* 575, 657–670.

Quartarone, A., Rizzo, V., Bagnato, S., Morgante, F., Sant'Angelo, A., Romano, M., Crupi, D., Girlanda, P., Rothwell, J. C., and Siebner, H. R. (2005). Homeostatic-like plasticity of the primary motor hand area is impaired in focal hand dystonia. *Brain* 128, 1943–1950.

Ridding, M. C., and Ziemann, U. (2010). Determinants of the induction of cortical plasticity by non-invasive brain stimulation in healthy subjects. *J. Physiol.* 588, 2291–2304.

Rizzo, V., Siebner, H. S., Morgante, F., Mastroeni, C., Girlanda, P., and Quartarone, A. (2009a). Paired associative stimulation of left and right human motor cortex shapes interhemispheric motor inhibition based on a Hebbian mechanism. *Cereb. Cortex* 19, 907–915.

Rizzo, V., Arico, I., Mastroeni, C., Morgante, F., Liotta, G., Girlanda, P., Silvestri, R., and Quartarone, A. (2009b). Dopamine agonists restore cortical plasticity in patients with idiopathic restless legs syndrome. *Mov. Disord.* 24, 710–715.

Rosen, I., and Asanuma, H. (1972). Peripheral afferent inputs to the forelimb area of the monkey motor cortex: input–output relations. *Exp. Brain Res.* 14, 257–273.

Rosenkranz, K., Williamon, A., and Rothwell, J. C. (2007a). Motorcortical excitability and synaptic plasticity is enhanced in professional musicians. *J. Neurosci.* 27, 5200–5206.

Rosenkranz, K., Kacar, A., and Rothwell, J. C. (2007b). Differential modulation of motor cortical plasticity and excitability in early and late phases of human motor learning. *J. Neurosci.* 27, 12058–12066.

Russmann, H., Lamy, J. C., Shamim, E. A., Meunier, S., and Hallett, M. (2009). Associative plasticity in intracortical inhibitory circuits in human motor cortex. *Clin Neurophysiol* 120, 1204–1212.

Sale, M. V., Ridding, M. C., and Nordstrom, M. A. (2008). Cortisol inhibits neuroplasticity induction in human motor cortex. *J. Neurosci.* 28, 8285–8293.

Shah, M. M., Hammond, R. S., and Hoffman, D. A. (2010). Dendritic ion channel trafficking and plasticity. *Trends Neurosci.* 33, 307–316.

Stefan, K., Kunesch, E., Cohen, L. G., Benecke, R., and Classen, J. (2000). Induction of plasticity in the human motor cortex by paired associative stimulation. *Brain* 123 Pt 3, 572–584.

Stefan, K., Kunesch, E., Benecke, R., Cohen, L. G., and Classen, J. (2002). Mechanisms of enhancement of human motor cortex excitability induced by interventional paired

associative stimulation. *J. Physiol.* 543, 699–708.

Stefan, K., Wycislo, M., and Classen, J. (2004). Modulation of associative human motor cortical plasticity by attention. *J. Neurophysiol.* 92, 66–72.

Stefan, K., Wycislo, M., Gentner, R., Schramm, A., Naumann, M., Reiners, K., and Classen, J. (2006). Temporary occlusion of associative motor cortical plasticity by prior dynamic motor training. *Cereb. Cortex* 16, 376–385.

Tamura, Y., Ueki, Y., Lin, P., Vorbach, S., Mima, T., Kakigi, R., and Hallett, M. (2009). Disordered plasticity in the primary somatosensory cortex in focal hand dystonia. *Brain* 132, 749–755.

Tecchio, F., Zappasodi, F., Pasqualetti, P., De Gennaro, L., Pellicciari, M. C., Ercolani, M., Squitti, R., and Rossini, P. M. (2008). Age dependence of primary motor cortex plasticity induced by paired associative stimulation. *Clin Neurophysiol* 119, 675–682.

Testa-Silva, G., Verhoog, M. B., Goriounova, N. A., Loebel, A., Hjorth, J., Baayen, J. C., De Kock, C. P. J., and Mansvelder, H. D. (2010). Human synapses show a wide temporal window for spike-timing-dependent plasticity. *Front. Syn. Neurosci.* 2:12. doi: 10.3389/fnsyn.2010.00012.

Turrigiano, G. G., Leslie, K. R., Desai, N. S., Rutherford, L. C., and Nelson, S. B. (1998). Activity-dependent scaling of quantal amplitude in neocortical neurons. *Nature* 391, 892–896.

Ueki, Y., Mima, T., Kotb, M. A., Sawada, H., Saiki, H., Ikeda, A., Begum, T., Reza, F., Nagamine, T., and Fukuyama, H. (2006). Altered plasticity of the human motor cortex in Parkinson's disease. *Ann. Neurol.* 59, 60–71.

Ugawa, Y., Rothwell, J. C., Day, B. L., Thompson, P. D., and Marsden, C. D. (1991). Percutaneous electrical stimulation of corticospinal pathways at the level of the pyramidal decussation in humans. *Ann. Neurol.* 29, 418–427.

Wang, Z., Xu, N. L., Wu, C. P., Duan, S., and Poo, M. M. (2003). Bidirectional changes in spatial dendritic integration accompanying long-term synaptic modifications. *Neuron* 37, 463–472.

Weise, D., Schramm, A., Stefan, K., Wolters, A., Reiners, K., Naumann, M., and Classen, J. (2006). The two sides of associative plasticity in writer's cramp. *Brain* 129, 2709–2721.

Wolters, A., Sandbrink, F., Schlottmann, A., Kunesch, E., Stefan, K., Cohen, L. G., Benecke, R., and Classen, J. (2003). A temporally asymmetric Hebbian rule governing plasticity in the human motor cortex. *J. Neurophysiol.* 89, 2339–2345.

Wolters, A., Schmidt, A., Schramm, A., Zeller, D., Naumann, M., Kunesch, E., Benecke, R., Reiners, K., and Classen, J. (2005). Timing-dependent plasticity in human primary somatosensory cortex. *J. Physiol.* 565, 1039–1052.

Zhang, L. I., Tao, H. W., Holt, C. E., Harris, W. A., and Poo, M. (1998). A critical window for cooperation and competition among developing retinotectal synapses. *Nature* 395, 37–44.

Ziemann, U., Ilic, T. V., Pauli, C., Meintzschel, F., and Ruge, D. (2004). Learning modifies subsequent induction of long-term potentiation-like and long-term depression-like plasticity in human motor cortex. *J. Neurosci.* 24, 1666–1672.

Ziemann, U., Lonnecker, S., Steinhoff, B. J., and Paulus, W. (1996). Effects of antiepileptic drugs on motor cortex excitability in humans: a transcranial magnetic stimulation study. *Ann. Neurol.* 40, 367–378.

Ziemann, U., Meintzschel, F., Korchounov, A., and Ilic, T. V. (2006). Pharmacological modulation of plasticity in the human motor cortex. *Neurorehabil. Neural. Repair* 20, 243–251.

Ziemann, U., and Rothwell, J. C. (2000). I-waves in motor cortex. *J. Clin. Neurophysiol.* 17, 397–405.

Conflict of Interest Statement: The authors declare that the research was conducted in the absence of any commercial or financial relationships that could be construed as a potential conflict of interest.

Received: 02 February 2010; paper pending published: 19 February 2010; accepted: 11 July 2010; published online: 30 July 2010.

Citation: Müller-Dahlhaus F, Ziemann U and Classen J (2010) Plasticity resembling spike-timing dependent synaptic plasticity: the evidence in human cortex. Front. Syn. Neurosci. ***2****:34. doi: 10.3389/fnsyn.2010.00034*

frontiers in
SYNAPTIC NEUROSCIENCE

REVIEW ARTICLE
published: 10 June 2010
doi: 10.3389/fnsyn.2010.00007

In vivo spike-timing-dependent plasticity in the optic tectum of *Xenopus laevis*

Blake A. Richards[1], Carlos D. Aizenman[2] and Colin J. Akerman[1]*

[1] Department of Pharmacology, University of Oxford, Oxford, UK
[2] Department of Neuroscience, Brown University, Providence, RI, USA

Edited by:
Per Jesper Sjöström, University College London, UK

Reviewed by:
Melanie A. Woodin, University of Toronto, Canada
Edward S. Ruthazer, Montreal Neurological Institute, Canada;
Florian Engert, Harvard University, USA

***Correspondence:**
Colin J. Akerman, Department of Pharmacology, University of Oxford, Mansfield Road, Oxford, OX1 3QT, UK.
e-mail: colin.akerman@pharm.ox.ac.uk

Spike-timing-dependent plasticity (STDP) is found *in vivo* in a variety of systems and species, but the first demonstrations of *in vivo* STDP were carried out in the optic tectum of *Xenopus laevis* embryos. Since then, the optic tectum has served as an excellent experimental model for studying STDP in sensory systems, allowing researchers to probe the developmental consequences of this form of synaptic plasticity during early development. In this review, we will describe what is known about the role of STDP in shaping feed-forward and recurrent circuits in the optic tectum with a focus on the functional implications for vision. We will discuss both the similarities and differences between the optic tectum and mammalian sensory systems that are relevant to STDP. Finally, we will highlight the unique properties of the embryonic tectum that make it an important system for researchers who are interested in how STDP contributes to activity-dependent development of sensory computations.

Keywords: spike-timing-dependent plasticity, visual system, synaptic development, optic tectum, receptive field

INTRODUCTION

How do animals survive in ever-changing, complex environments? A critical feature is the brain's ability to exhibit lasting changes in neural circuits that enable flexible development, adaptation to changes in the environment, and storage of new information. The widespread consensus today is that these capabilities are mediated in part by long-term potentiation and depression (LTP/LTD) of synaptic efficacy (Martin et al., 2000), which are in turn driven by correlations in spiking activity (Bi and Poo, 2001). Uncovering the rules that determine how synapses change based on spiking activity was significantly advanced by the discovery that the temporal order of inputs to the hippocampus determines whether potentiation or depression is induced (Levy and Steward, 1983). A series of studies more than a decade later showed that synaptic plasticity in several systems depends on the specific timing of action potentials in presynaptic and postsynaptic cells (Markram et al., 1997; Debanne et al., 1998; Zhang et al., 1998; Sjöström et al., 2001; Tzounopoulos et al., 2004), a phenomena referred to as spike-timing-dependent plasticity (STDP). A full appreciation of how STDP is involved in development, adaptation, and information storage requires studies of STDP that are carried out *in vivo*. The first demonstration of *in vivo* STDP was performed in the embryonic optic tectum of the *Xenopus laevis* frog (Zhang et al., 1998). Since that initial study the optic tectum has continued to be a fruitful system for studying the roles played by STDP in the development and adaptation of sensory systems (Engert et al., 2002; Mu and Poo, 2006; Vislay-Meltzer et al., 2006; Pratt et al., 2008).

Research in the optic tectum has provided substantial insight into how STDP affects the function and organization of young, rapidly changing neural circuits *in vivo*. The evidence suggests that it plays a role in the development of fundamental properties of sensory circuits, such as receptive field (RF) architecture (Tao and Poo, 2005; Vislay-Meltzer et al., 2006; Dong et al., 2009), recurrent excitation (Pratt et al., 2008), and computations regarding motion in the visual environment (Engert et al., 2002; Mu and Poo, 2006). There remain many questions regarding STDP, for which the optic tectum remains an ideal experimental system for investigation. These include how the STDP rule changes during the development of distinct cellular morphologies and layers, the role of different neurotransmitters in shaping the effects of STDP, and how STDP operates on a population level. Understanding STDP's place in this circuit is likely to continue to provide important clues regarding the developmental role of this form of plasticity across neural systems.

Despite its importance in our current understanding of synaptic plasticity, some researchers may be less familiar with the optic tectum than with other model systems. Long before the identification of STDP, the optic tectum was one of the systems of choice for studying the role of activity in neural development. For many decades researchers have used its unique properties to investigate how activity shapes properties such as topographic maps and binocular circuits. Therefore, before focusing upon more recent research on STDP, this review will begin with a brief overview of the optic tectum, its development and key contributions this system has made to our understanding of activity-dependent mechanisms in development. A full discussion of the extensive research in these areas is obviously not possible here and we refer interested readers to the thorough reviews provided by others (Schmidt, 1985; Udin, 1985, 2007; Cline, 1991, 2003; Holt and Harris, 1993; Debski and Cline, 2002; Ruthazer and Cline, 2004). With this background in place, we will then review *in vivo* studies on STDP in the optic tectum, with the ultimate goal of linking this to the earlier work, thereby identifying future directions for STDP research that will be particularly tractable in this system.

BACKGROUND: THE OPTIC TECTUM AND ITS ACTIVITY-DEPENDENT DEVELOPMENT

The optic tectum is a layered, dorsal midbrain structure (**Figure 1A**), which is referred to as the superior colliculus in mammals (Butler and Hodos, 2005). Based on Golgi stain studies, the optic tectum of amphibians is typically described as having 9 layers, and 14 distinct cellular morphologies (**Figure 1B**) (Székely and Lázár, 1967, 1976; Lázár, 1973). Compared to many systems, the optic tectum exhibits a great deal of anatomical and functional conservation across the phylogenetic tree (Ingle, 1973a; Butler and Hodos, 2005). The common traits of the optic tectum of all species are (1) it receives direct projections from the contralateral retina in its superficial layers, (2) it receives projections from other sensory modalities in deeper layers, (3) it sends most of its outputs directly to motor systems in the brainstem and spinal cord but also projects reciprocally with itself, the telencephalon, and the diencephalon, (4) its inputs and outputs are organized into topographic maps that are matched across sensory modalities (Butler and Hodos, 2005). Functionally, the optic tectum is important for spatial orienting behaviors in many animals, and neurons in the adult optic tectum of every species studied are sensitive to sudden, sharp movements, or local brightness fluctuations in the visual field (Ingle, 1973a). The optic tectum has a particularly important role in amphibians, as ablation of this structure renders adult frogs completely unresponsive to moving stimuli, including both potential prey and predators (Ingle, 1973b). Thus, the optic tectum is central to amphibians' visual processing capabilities (Grüsser and Grüsser-Cornehls, 1976).

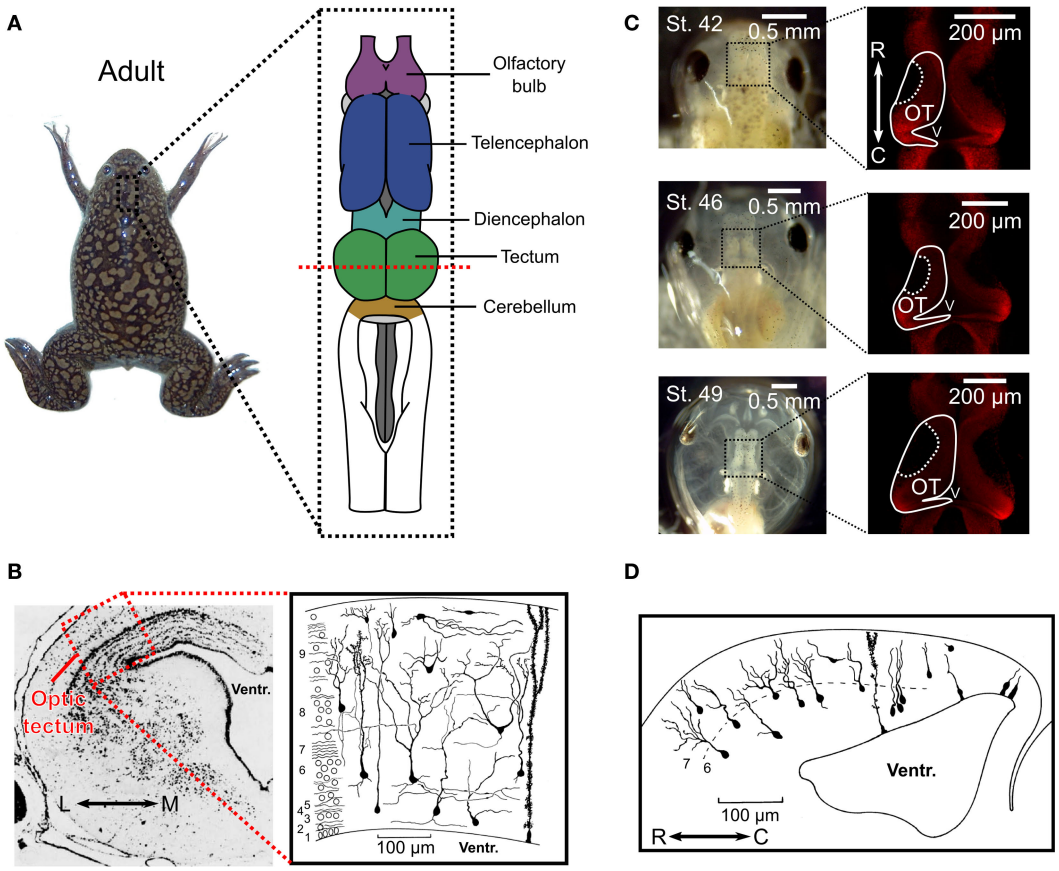

FIGURE 1 | Anatomy of the optic tectum in the adult *Xenopus laevis* and during tadpole development. (A) In the adult *Xenopus laevis* frog (photograph) the central nervous system (drawing) contains several distinct structures and the optic tectum is the roof of the large midbrain structure, situated caudally to the diencephalon and rostrally to the cerebellum. It is one of the largest dorsal structures in the *Xenopus* brain, along with the telencephalon and the olfactory bulb. **(B)** The layered structure of the adult optic tectum can be seen in the coronal section (left), which has been stained with cresyl-violet. The section is taken from the plane indicated by the red dashed line in **(A)**. As the drawing illustrates (right), there are several distinct cellular morphologies found within the optic tectum, which have been classified into 14 categories. The numbers at the side of the drawing indicate the 9 different layers of the tectum. **(C)** Photographs (left) of *Xenopus laevis* tadpoles taken dorsally at stages 42, 46, and 49 illustrate the changes that occur during the stages in which STDP is typically studied. During this time the optic tectum grows, as shown by confocal images of whole-mount brains with propidium iodide staining for cell nuclei. The images shown are in the horizontal plane and at a depth of 100 µm from the dorsal surface of the brain (right). Note the dark regions in the rostral–lateral optic tectum which are comprised mostly of neuropil. Neurogenesis takes place in the caudal–medial region surrounding the ventricle. **(D)** Due to the location of the neurogenerative zone there is a progression in the maturity and morphological complexity of cells in the optic tectum at these ages in the caudal–rostral axis, as shown by this camera lucida drawing of a sagittal slice from a stage 49 tadpole. Images in **(B)** and **(D)** are reproduced with permission from Lázár (1973) and Nikundiwe and Nieuwenhuys (1983).

In the frog species *X. laevis*, axons from retinal ganglion cells (RGCs) first innervate the embryonic optic tectum within 2–5 days post fertilization (d.p.f.), depending on the temperature of the environment, and tectal neurons become visually responsive in the following hours (Holt and Harris, 1983; Holt, 1984). These ages are usually referred to as stages 37–39 according to the common staging system used (Nieuwkoop and Faber, 1967). Most of the research on synaptic plasticity in the *Xenopus* optic tectum has been carried out over the course of the subsequent stages of development (40–48) (Zhang et al., 1998, 2000; Tao et al., 2001; Engert et al., 2002; Tao and Poo, 2005; Lien et al., 2006; Mu and Poo, 2006; Vislay-Meltzer et al., 2006; Liu et al., 2007; Pratt et al., 2008; Dong et al., 2009), during which the number of cells increases substantially (**Figure 1C**) and the cells themselves develop more complicated morphologies (**Figure 1D**) (Cline et al., 1996). These stages are intriguing because they provide a window into the very earliest moments of the impact of retinal activity and visual experience on this system. Interestingly, tectal growth occurs solely in a caudal-medial zone while the retina grows concentrically (Gaze et al., 1979) and the repercussion for the system is that connections must migrate as the retinotopic map constantly shifts (Cline, 1991). Thus, during the stages of development in which STDP is actively shaping the tectal circuit, the structure is undergoing substantial changes while also serving as a functional sensory system.

The receptors and intrinsic channels of neurons in the optic tectum are very similar to other neural systems. Analysis of the intrinsic properties of tectal neurons in early life shows they possess voltage-gated tetrodotoxin (TTX) sensitive Na^+ currents, transient and steady-state K^+ currents, and a steady-state Ca^{2+} current (Aizenman et al., 2003). Monosynaptic retinotectal projections are glutamatergic, activating both α-amino-3-hydroxy-5-methyl-4-isoxazole propionic acid (AMPA) and *N*-methyl D-aspartic acid (NMDA) receptors (Hickmott and Constantine-Paton, 1993). Projections within the optic tectum can be either glutamatergic, mediated via AMPA and NMDA receptors, or γ-amino-butyric-acid (GABA)-ergic, mediated by GABA-A receptors (Hickmott and Constantine-Paton, 1993). The AMPA receptors of the optic tectum are also known to include Ca^{2+}-permeable AMPA receptors (Aizenman et al., 2002). All of these signals are present in *X. laevis* at early stage of life following the initial formation of retinotectal synapses (Zhang et al., 1998, 2000; Aizenman et al., 2002, 2003; Akerman and Cline, 2006). On top of these basic signals, the optic tectum at later stages of development is known to receive modulatory cholinergic inputs from the nucleus isthmus (Gernert and Ewert, 1995; Edwards and Cline, 1999; Dudkin and Gruberg, 2003). At these stages the isthmus conveys signals from one tectal lobe to the other, thereby providing the circuit with binocular information (Udin and Fisher, 1985). In summary, the monosynaptic, polysynaptic, and modulatory input properties are very similar to those found in the superior colliculus of mammals (Isa, 2002).

As mentioned above, the inputs to the optic tectum arrive in a topographically ordered map so that particular anatomical regions of the tectum are sensitive to particular areas of sensory space (Gaze, 1958). Seminal early research showed that surgical rotation of the eye in frogs led to altered behaviors due to a corresponding rotation of the retinotopic map in the contralateral tectum (Sperry, 1944; Gaze, 1959), an effect which was not found to be sensitive to visual experience during formation of the projections (Jacobson, 1968). This suggested that the retinotopic map may be determined solely by activity independent chemical cues (Sperry, 1963), a hypothesis which received later support from work demonstrating the importance of various chemical gradients in the tectum for guiding RGC axon growth (Cheng et al., 1995; Drescher et al., 1995; Mann et al., 2002). However, the reality has turned out to be that both the establishment and maintenance of retinotopic maps in the tectum involve an interplay of chemical cues and activity (Cline, 1991, 2003; Debski and Cline, 2002).

Researchers discovered that the initial retinotopic projections are largely overlapping and sort out over time (Gaze et al., 1974; O'Rourke and Fraser, 1986). Evidence suggests that this process is activity-dependent, as TTX or the NMDA receptor antagonist 2-amino-5 -phosphonopentanoic acid (AP5) disrupt retinotectal refinement (Meyer, 1983; Schmidt and Edwards, 1983; Cline and Constantine-Paton, 1989). In addition, studies found that even a coarse retinotopic order in ipsilateral inputs, which arrive through an indirect route via the nucleus isthmus, is activity-dependent (Udin, 2007). Rotation of the ipsilateral eye produces an initially rotated ipsilateral retinotopic map, but with time the nucleus isthmus projections reorient themselves to match the contralateral inputs (Udin and Keating, 1981) in a process that requires visual experience (Keating and Feldman, 1975; Udin and Keating, 1981). The importance of activity has also been demonstrated through the use of surgically implanted third eyes onto frogs, which successfully innervate the optic tectum, but form segregated bands that are distinct from those of the native eye (Constantine-Paton and Law, 1978). This segregation is blocked both with TTX and NMDA receptor antagonists (Reh and Constantine-Paton, 1985; Cline et al., 1987). Studies suggest that these dynamic organizational properties in the tectum are mediated at least in part by activity-dependent growth and retraction of axonal and dendritic processes (Reh and Constantine-Paton, 1984; Cline and Constantine-Paton, 1990; O'Rourke et al., 1994; Rajan and Cline, 1998).

Early models put forward the idea that the strengthening or stabilization of mutually correlated inputs and weakening or retraction of uncorrelated inputs could help explain the observations of map remodeling within the retinotectal system (Changeux and Danchin, 1976; Willshaw and Von Der Malsburg, 1976; Whitelaw and Cowan, 1981). The necessity of visual experience, spiking activity, and NMDA receptor activation for organizing tectal inputs suggests that something akin to Hebbian LTP may be at work in the developing optic tectum (Cline, 1991; Ruthazer and Cline, 2004). Indeed, evidence from *in vivo* imaging suggests that NMDA receptors function as a correlation detecting mechanism for stabilizing or retracting connections (Ruthazer et al., 2003). It is possible that STDP itself interacts with these mechanisms, or even underpins some of them (Udin, 2007).

FIRST DEMONSTRATION OF STDP IN THE OPTIC TECTUM

The first demonstration of STDP *in vivo* was the seminal 1998 study by Zhang et al. (1998). The implications of this study were relevant to systems other than the optic tectum, but the fact that retinotectal map refinement is activity-dependent (Cline and Constantine-Paton, 1989), also made it directly relevant to the previous work that had been carried out in this system. The authors took advantage of the unrefined state of the retinotectal projections in embryonic

Xenopus. RGC axon arbors at stages 40–41 cover a substantial area of the tectum, such that a single tectal cell receives inputs from many different RGCs at many different positions across the retina. Zhang et al. (1998) used this feature to examine how inputs from two different RGCs might compete or co-operate in the induction of synaptic plasticity on the same tectal cell. Whole-cell perforated patch recordings of single tectal neurons were performed concurrently with loose-patch stimulation of two different RGCs that formed excitatory synaptic connections onto the tectal neuron (**Figure 2A**). Consistent with previous work on the mechanisms of LTP induction (Martin et al., 2000), Zhang et al. (1998) found that repetitive stimulation of a single RGC could induce potentiation of AMPA mediated excitatory postsynaptic currents (EPSCs), but only for the stimulated input and only if the tectal cell spiked and NMDA receptors were active. They also found that if the two inputs were activated simultaneously, and co-operated to induce spiking, they were both strengthened. The exciting discovery Zhang et al. (1998) made was that if the RGCs were repetitively stimulated at different times, the relative timing of the two inputs determined the effect on the synaptic connections. If the tectal cell spiked after the second input, both connections were strengthened, though the second connection was potentiated more than the first. In contrast, if the tectal cell spiked after the first input but before the second, the first connection was strengthened whereas the second was actually weakened. Zhang et al. (1998) performed a careful analysis of the relationship between the changes in synaptic strength and the timing of the RGC and tectal cell spikes, which revealed the now well-known asymmetric exponential relationship that characterizes STDP in a number of systems (**Figure 2B**) (Dan and Poo, 2004).

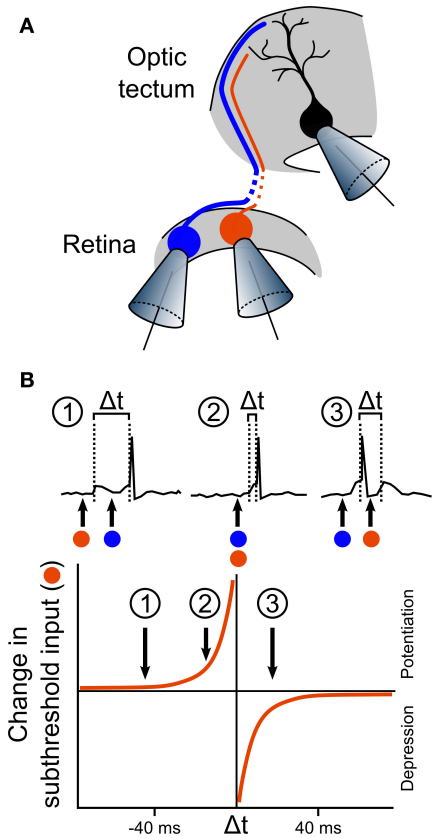

FIGURE 2 | First *in vivo* observation of STDP in the optic tectum. (A) The first *in vivo* demonstration of STDP was performed by Zhang et al. (1998) in an elegant experiment, illustrated here. Activity from a single tectal neuron was recorded using whole-cell perforated patch, while two different RGCs that form synaptic connections onto the tectal neuron were loose-patched, allowing stimulation for induction of LTP or LTD. In some of the recordings, one RGC produced suprathreshold responses (illustrated by the blue cell), whilst the other produced only subthreshold responses (illustrated by the orange cell). **(B)** Analysis of the effects of the timing of the inputs showed that the effect of stimulation on the subthreshold input depended on the timing of its excitatory postsynaptic potentials (EPSPs) relative to the tectal spike that was triggered by the suprathreshold input. If the subthreshold EPSP preceded the tectal spike by more than 20 ms, the input was relatively unaffected (inset 1). However, if the subthreshold EPSP occurred within the 20 ms before the suprathreshold EPSP, and therefore just before the tectal spike, the input was strongly potentiated (inset 2). In stark contrast, if the subthreshold EPSP occurred during the 20 ms immediately following the tectal cell spike, this input was depressed (inset 3). Examination of the effects of a range of timing differences led to an estimated curve for the STDP rule in retinotectal synapses.

The implications of these findings for development of the optic tectum were intriguing. Since spiking of tectal cells was required for changes in synaptic strength, it suggested that a sub-threshold input would either be co-operatively enhanced or competitively eliminated by a different, supra-threshold input, in a manner that critically depended on their relative timing. As such, early relationships in spike-timing between cells on the order of milliseconds are not inconsequential, and might be important determinants of the functional maturation of the system. This might be one of the mechanisms by which activity directs the development of topographic maps in the optic tectum – a possibility that has yet to be fully addressed. More broadly, another implication was that *in vivo* STDP could be one mechanism by which the environment exerts an instructive influence on the development of visual systems, as different statistics in the visual environment would produce different patterns of spike-timing. A later paper by the same authors demonstrated that visual inputs could also induce LTP in retinotectal connections (Zhang et al., 2000), an important demonstration if STDP were to actually enable an instructive role for the environment in optic tectum development. However, the exact functional consequences, and how the timing requirements of STDP might affect the emergence of computational properties of the neural circuits, remained to be established. Over the course of the decade following Zhang et al.'s (1998) study, this became one of the central themes of research on STDP in the *Xenopus* optic tectum.

STDP AND THE DEVELOPMENT OF DIRECTION SELECTIVITY

A comprehensive analysis of responses in the adult optic tectum of *X. laevis* has not been conducted, but it is known that in other frog species neurons in the adult optic tectum show a variety of response profiles, many of which exhibit direction selectivity – i.e., a bias in a cell's response to stimulus movement in a particular direction (Grüsser and Grüsser-Cornehls, 1976). How this property might emerge from visual experience was illustrated by Engert et al. (2002) in a study on instructive learning in *Xenopus* tadpoles of stages 42–45. They presented tadpoles with visual stimuli by focusing an image of an LCD screen onto their retinas. Repetitive presentation of a white bar moving across a dark background produced an increase in the synaptic currents tectal neurons received during presentation

of the bar (as measured by whole-cell perforated patch-clamp), but only for the direction that had been presented – other directions of movement showed no potentiation. Engert et al.'s data suggested that this was due to an asymmetric alteration of the tectal cells' excitatory RFs, such that those areas of the RF that were active early in the presentation of the bar were potentiated. Computational studies have suggested that asymmetric RF alterations of this sort could be produced by STDP (Mehta et al., 2000; Shon et al., 2004) and, given that the changes required postsynaptic spiking activity, it was proposed that the stimulus-driven learning observed in the tectum might be mediated by STDP (Engert et al., 2002).

Evidence supporting this postulate was provided in a later study by Mu and Poo (2006). After verifying the observations of Engert et al., the authors utilized a modified experimental protocol to demonstrate how STDP could produce the result. Rather than presenting a continuously moving bar, Mu and Poo presented the tadpoles with a bar in three different positions, flashed sequentially to mimic movement across the retina (**Figure 3A**). They then injected currents into the soma of the tectal cells to control when the cells spiked relative to the presentation of the three bars. As one would predict from the STDP rule previously observed in the optic tectum (Zhang et al., 1998), they found that there was a different effect on the excitatory RF depending on when the bar flash occurred relative to the tectal spikes: areas of the RF where bars had flashed before the spikes showed potentiated connections to the tectal cells, whereas areas where the bar had flashed after the spikes showed depressed connections. This supported the conclusion that asymmetric RF changes associated with exposure to a moving bar (Engert et al., 2002) could indeed be mediated by STDP. The study by Mu and Poo (2006) also highlighted candidate cellular mechanisms underlying STDP in the optic tectum. The asymmetric changes in excitatory RFs were altered both by inhibition of brain-derived neurotrophic factor (BDNF) signaling and nitric oxide (NO) synthase, but in different ways: inhibition of BDNF-trkB signaling eliminated the potentiation in the RFs, whereas inhibition of NO synthase eliminated the depression. This demonstrated a functional dissociation according to both the signaling mechanisms and the functional consequences of spike-timing-dependent potentiation and depression.

These studies (Zhang et al., 1998; Engert et al., 2002) provided some of the first *in vivo* experimental evidence that asymmetric RF alterations induced by STDP could produce direction selectivity, verifying predictions of computational models (**Figure 3B**) (Mehta et al., 2000; Rao and Sejnowski, 2001; Shon et al., 2004). It is interesting to note that more recent studies in mammalian primary visual cortex suggest that the development of direction selective neurons

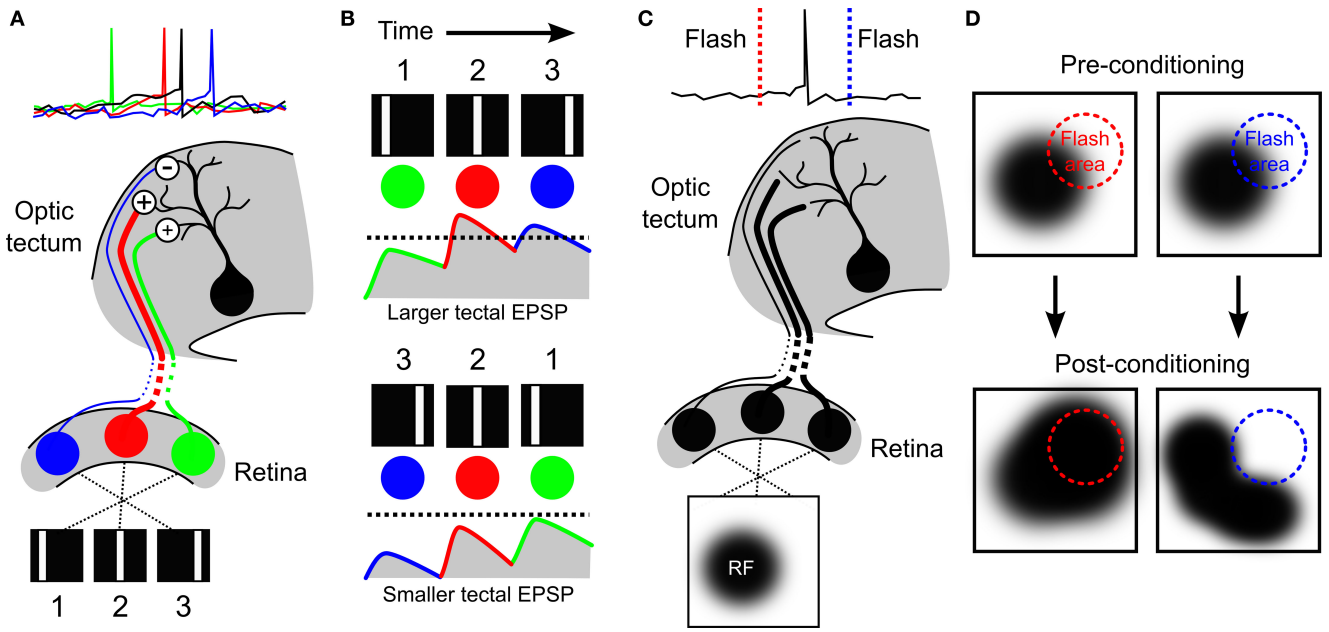

FIGURE 3 | Development of direction selectivity and RF structure via STDP in the optic tectum. (A) The principle of how STDP can induce direction selectivity in the optic tectum was demonstrated by Mu and Poo (2006), by mimicking movement across the retina with flashes of a white bar at three different locations in visual space. If the tectal cell (black) was forced to spike soon after the second flash, the RF of the cell was altered by STDP in an asymmetric manner that potentiated responses to the first and second bars (green and red cells), but depressed responses to the third bar (blue cell). **(B)** Asymmetric changes in a RF can produce direction selectivity due to the differences in temporal summation for one direction versus the other. If the strengthened inputs are activated first, they can summate with subsequent inputs to produce a high level of depolarization in postsynaptic tectal cells producing suprathreshold activity (top, dashed line indicates hypothetical spike threshold). In contrast, if the weaker inputs are stimulated first, they will have decayed by the time subsequent inputs arrive and so less temporal summation occurs and inputs remain subthreshold (bottom). **(C)** The strength of the connections onto a tectal neuron determines its RF profile, as illustrated here for a hypothetical cell. **(D)** Vislay-Meltzer et al. (2006) demonstrated that this RF profile could be altered by STDP to either move towards or away from a given region of space. If a flash occurred prior to a tectal cell's spikes (red line), the RF tended to shift toward that area. In contrast, if a flash occurred after a tectal cell's spikes (blue line) the RF tended to shift away from the area of the flash. Interestingly, they also observed that the RFs potentiated in areas outside of the area of the flash, as shown.

is very sensitive to the statistics of the early environment (Li et al., 2006, 2008), indicating that visually driven STDP may be a general mechanism for establishing direction selectivity.

STDP AND RF DEVELOPMENT IN THE OPTIC TECTUM

Early electrophysiology experiments examining multi-unit RFs in tadpoles suggested that RFs in young animals (before stage 47) are very large, but grow smaller over development (Gaze et al., 1974). This observation has been confirmed by more recent experiments using whole-cell voltage clamp recordings. Over stages 43–48, the visuotopic mapping of excitatory synaptic inputs to individual tectal cells reveal that their RF shrinks and becomes sharper with age, and that this process is NMDA receptor and GABA-A receptor dependent (Tao and Poo, 2005; Dong et al., 2009). This shrinking of the excitatory RF is coupled with increased spatial alignment between excitatory synaptic inputs, and GABAergic inhibitory synaptic inputs (Tao and Poo, 2005). These refinements appear to have behavioral implications, because even at these early stages of life RF refinement is required for the acquisition of a motion avoidance behavior in tadpoles (Dong et al., 2009).

What are the synaptic mechanisms behind such developmental refinements in RFs? One factor that would influence excitatory RF size is the distribution of synaptic inputs as constrained by the spatial extent of RGC axon arbors, relative to the size of the growing tectum (Sakaguchi and Murphey, 1985). However, this may not explain the requirement for NMDA and GABA-A receptor signaling in RF refinement. An alternative possibility is that RF refinement is directly related to STDP. In a 2006 study, Vislay-Meltzer et al. (2006) examined exactly how STDP affects the structure of excitatory RFs of tadpoles stage 41–45. In this study whole-cell perforated patch-clamp recordings were used to map excitatory RFs with a reverse-correlation technique. Then the cells experienced a training period during which a stimulus was repeatedly flashed in a restricted area of visual space whilst the experimenter controlled the spiking behavior of the tectal cell. After this the RF was remapped and the effects of the training period were examined. In accordance with an STDP rule in the optic tectum at these ages, they found that if the tectal cells spiked immediately after the flash, that area of the RF was potentiated, whereas if the cells spiked immediately before the flash, that area of the RF was depressed (**Figures 3C and 3D**). This demonstrated, importantly, that STDP could affect changes in the structure of RFs in a manner that depends upon both the spatiotemporal statistics of the sensory stimuli and the neural activity patterns.

In addition to the observation that STDP can shape tectal RF structure, the authors observed some very interesting changes that one might not have predicted. Not only did changes occur in those areas of the RF where the flashes had occurred, but also outside of these areas: in the case of either potentiation or depression in the trained region of the RF, the rest of the RF showed a net potentiation. Because this did not occur when the cells were clamped at hyperpolarized membrane potentials, it suggested that the effect was not due to plasticity occurring at synapses onto other cells. One explanation of these results is that the calcium signals that are important for STDP (Dan and Poo, 2004) might have spread to other areas of the cells' dendrites. This hypothesis is supported by the separate observation that immature tectal neurons show heterosynaptic plasticity effects mediated by calcium signals (Tao et al., 2001). However, this form of heterosynaptic spread of potentiation was induced with a theta-burst stimulation protocol and it is not known whether visually driven activity patterns could trigger heterosynaptic spread of potentiation. An alternative explanation is that potentiation also occurs within recurrent circuits of the tectum – at glutamatergic synapses from other tectal cells that converge onto the recorded neuron. At this point, this hypothesis cannot be fully assessed, as the interactions between STDP and recurrent circuitry in the optic tectum are only just beginning to be understood.

STDP AND DEVELOPMENT OF RECURRENT TECTAL CIRCUITS

The tectum is known to possess recurrent excitatory circuitry (Székely and Lázár, 1976; Hickmott and Constantine-Paton, 1993; Nakagawa et al., 1997). Recurrent connections can provide critical abilities for neural circuits, enabling persistent activity for a wider range of prediction and information storage capabilities (McCormick et al., 2003), as well as helping networks to maintain dynamics that increase general computational power (Bertschinger and Natschläger, 2004; Maass and Markram, 2004). Their contributions to the function of the optic tectum in amphibians are not fully known, but it is thought that they help to integrate information across modalities, and thereby aid in prey catching and predator avoidance behaviors (Grüsser and Grüsser-Cornehls, 1976). In mammals, recurrent excitation in the superior colliculus enables bursting activity that is important for direction of gaze-orienting movements (Sparks, 1986; Lee et al., 1997; Saito and Isa, 2003).

In a 2008 study, Pratt et al. (2008) examined the development of recurrent excitatory connections in the optic tectum of tadpoles between stages 44–49. First, they observed that in young animals (stages 44–46) stimulation of the optic nerve produced prolonged spiking, consistent with a recurrent excitation feed-back loop. Whole-cell recordings revealed excitatory synaptic currents that were not eliminated by physically isolating the tectum from other parts of the brain, suggesting that the prolonged tectal cell spiking was sustained by intratectal AMPA receptor mediated inputs. Interestingly, Pratt et al. (2008) observed that the temporal profiles of both the spike-trains and the excitatory currents were both significantly different in stage 49 animals, showing a tendency towards an increase in the early responses and a decrease in the later responses. Trial to trial spike time variability was also reduced in the older animals. This suggested that over these developmental stages the recurrent circuitry of the optic tectum is refined, such that the temporal processing of the retinal information is altered (**Figure 4A**).

Pratt et al. (2008) hypothesized that these changes may be mediated by STDP at intratectal synapses, such that when a presynaptic tectal cell tends to spike early synapses onto its postsynaptic partners would be strengthened by STDP, whilst tectal–tectal synapses where the presynaptic partner tends to spike late would be weakened. In this scenario STDP would reshape the circuit to favor synapses where the presynaptic partner gives rapid, reliable responses, thereby increasing the temporal precision of the recurrent excitation. As an initial assessment of this hypothesis they employed a training protocol of paired pulses to the optic nerve to mimic the hypothesized scenario. An initial pulse was used to stimulate the

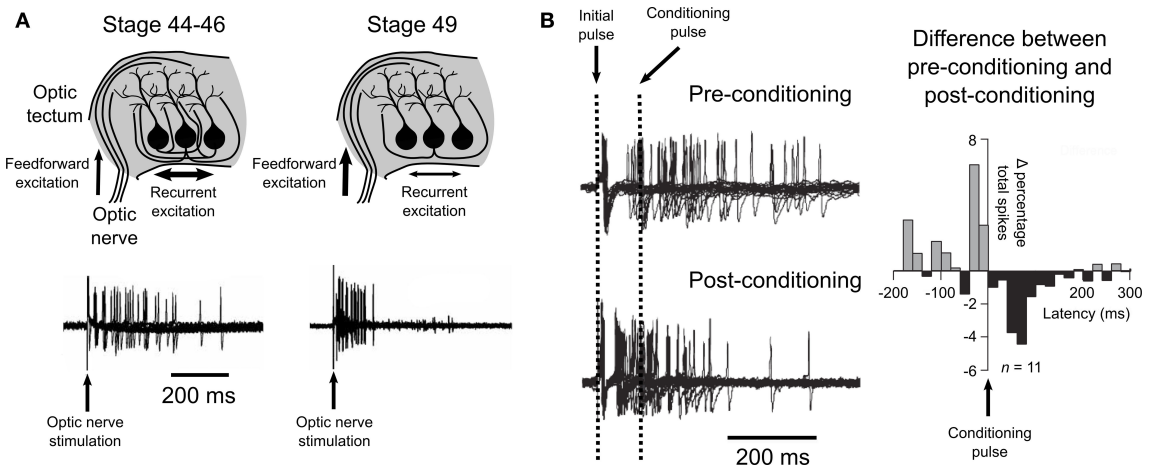

FIGURE 4 | Spike-timing-dependent plasticity and recurrent excitatory circuits in the optic tectum. (A) Pratt et al. (2008) observed evidence for a developmental refinement of the recurrent excitatory circuitry of the tectum between stages 44 and 49. Stimulation of the optic nerve at early stages (44–46) produced prolonged spiking activity, while stimulation at a later stage (49) produced an initial strong response that did not show prolonged activity, as illustrated by traces from loose-patch recordings shown here. **(B)** Training young tectum by delivering a timed "conditioning" pulse to the optic nerve induced a similar reshaping of spiking to that observed over development. Examination of the differences in the percentage of spikes that occurred before or after the conditioning pulse showed an effect that supported a role for STDP in this refinement of recurrent circuitry. Data are reproduced from Pratt et al. (2008).

recurrent excitation, while a second "conditioning" pulse was used to provoke STDP amongst tectal neurons. The authors predicted that any intratectal synapses where the presynaptic partner spiked before the conditioning pulse would show potentiation, whereas synapses where the presynaptic partner spiked after the conditioning pulse would depress. The post-conditioning temporal profiles of tectal spiking suggest that this is exactly what occurred (**Figure 4B**). In addition, the authors showed that this could take place *in vivo* via visual experience. Tadpoles raised in environments where paired flashes of light occurred at particular intervals showed temporal profiles of recurrent excitation that reflected the time between flashes. Taken together, this data suggests that *in vivo* STDP sculpts the intratectal recurrent excitatory drive in a manner that reflects the temporal properties of the animals' environments.

A question raised by Pratt et al.'s (2008) study is what is the functional purpose of this early reshaping of recurrent circuitry in the optic tectum? One possibility is that sharpening of the circuit is related to the spatial refinement of RFs in the system (Gaze et al., 1974; Tao and Poo, 2005), as much of the RF of tectal neurons may be mediated by the local circuit. Moreover, it seems possible that if the initial spatial RF requires refining, so too does the temporal RF. Alternatively, the increased precision may reflect a shift towards a neural code with greater temporal precision, which would require less integration time for accurate transmission of signals (VanRullen et al., 2005). Given the importance of the optic tectum for rapid detection of moving stimuli and orienting responses in frogs (Ingle, 1973b), it would be very interesting if one of the effects of STDP was to shift the circuit toward a "spike-timing code" that improved the rapidity with which the animals could respond to prey and predators. Equally, STDP in the recurrent circuits may be important for establishing proper multisensory integration within the tectum. Given the general importance of recurrent circuitry in many neural systems, the role and functional implications for STDP in shaping these connections deserves further investigation.

CHANGES IN STDP DURING DEVELOPMENT OF THE OPTIC TECTUM

The maturation of a circuit undoubtedly affects the rules for induction of synaptic plasticity. As we have seen, the optic tectum undergoes a number of dramatic changes in the days following innervation by RGC axons: retinotopic maps are readjusted and refined (Ruthazer and Cline, 2004), excitatory and inhibitory synaptic inputs are brought into spatial alignment (Tao and Poo, 2005), and recurrent circuitry is reshaped to favor greater precision in visual responses (Pratt et al., 2008). In addition to these adjustments at the systems-level, neurons in the optic tectum during this period are changing dramatically at a cellular-level. As the various distinct cellular morphologies emerge in the optic tectum (Lázár, 1973), the morphological complexity of tectal cells increases via a process that relies on both glutamatergic signaling and CaMKII (Rajan and Cline, 1998; Wu and Cline, 1998; Haas et al. 2006). Increased morphological complexity can alter synaptic plasticity by ensuring input specificity in LTP induction (Tao et al., 2001) and fundamental aspects of synaptic transmission are also altered during this period. The GABA-A receptor reversal potential in tectal neurons at early stages of life is depolarized relative to the resting membrane potential, which changes by stages 48–50 and has implications for NMDA receptor activation (Akerman and Cline, 2006). Moreover, the ratio of the strength of glutamatergic to GABAergic inputs is altered during this period. Tectal neurons shift from a GABAergically dominated regime to one exhibiting greater balance, and interestingly, this ratio determines the nature of visually driven plasticity of GABAergic synapses in the system (Liu et al., 2007). On top of all these changes, tectal neurons alter their sodium channel activity in a manner that tends to stabilize their input–output functions (Pratt and Aizenman, 2007). Taken together, it seems plausible that during development the induction rules for LTP and LTD may change from the original STDP rule observed at stages 40–41 by Zhang et al. (1998) (**Figure 2B**). This has been investigated by Tsui et al. (2010) in a study published in this issue.

Using a whole-cell perforated patch-clamp experimental preparation Tsui et al. (2010) investigated STDP at different stages of tectal development. In agreement with previous work on retinotectal STDP in wild-type animals stages 41–44 (Zhang et al., 1998; Mu and Poo, 2006; Vislay-Meltzer et al., 2006), they observed that pairing a RGC input with a tectal spike produced either LTP or LTD dependent on the timing of the input relative to that of the spike. However, they found that the same protocols did not produce LTP or LTD in wild-type animals of stages 46–48. Nonetheless, they did observe that repetitive low-frequency stimulation could produce LTD at these later stages. This data demonstrates that the induction mechanisms for plasticity change during tectal development in a manner that affects STDP.

One interpretation of this data is that there is a critical developmental window for STDP to shape the optic tectum in *Xenopus* that lasts only for a few days following innervation by the retina, after which STDP no longer plays a part in the modification of this circuit. However, it is possible that synaptic plasticity at these stages could still be "timing-dependent," i.e., sensitive to the precise timing of presynaptic and postsynaptic action potentials, but as the animals age there may be additional requirements for the induction of synaptic changes. For example, it could be that multiple synaptic inputs must be activated co-operatively for the necessary molecular signals to be triggered. Alternatively, signals from other neural systems may be required to enhance the incoming inputs, similar to the manner in which cholinergic signals from the nucleus isthmus can enhance axonal calcium transients in RGC inputs (Edwards and Cline, 1999; Dudkin and Gruberg, 2003). Another consideration must be that GABAergic inputs are more hyperpolarizing at these older stages of development (Akerman and Cline, 2006), and it is possible that under these conditions of more hyperpolarizing GABA, bursts of postsynaptic spikes become necessary to trigger synaptic plasticity, as has been reported in other systems (Meredith et al., 2003).

TOWARDS THE FUTURE OF STDP RESEARCH IN THE OPTIC TECTUM

There are many unresolved questions surrounding STDP, and the optic tectum of *X. laevis* is an ideal system in which to address many of them. Almost any issue related to STDP could be investigated in the optic tectum, from the molecular mechanisms underlying STDP to its long-term behavioral consequences. Here we will concentrate on questions for which this experimental system is particularly well placed to provide answers, due to its specific physiological, functional, and developmental properties.

One important issue for future investigation is how the development of dendritic morphology in early life affects STDP. Several studies have suggested that the rules governing STDP are very different depending upon the location of synapses on dendrites and the active properties of dendrites themselves (Kampa et al., 2007). Within the optic tectum, it is known that dendritic complexity affects the input specificity of LTP induction (Tao et al., 2001). The various distinct cellular morphologies of the optic tectum begin to emerge during the same stages where STDP is known to occur, such that by stage 49 most of the morphological traits of the adult can be seen in a subset of cells in the optic tectum (Lázár, 1973). These stages also provide a unique potential for studying this issue due to the caudal-medial mode of growth of the system (**Figure 2B**). Cells in the rostral part of the tectum are relatively more mature and show greater morphological complexity compared to those in the caudal part of the tectum (**Figure 1D**), thereby allowing researchers to examine cells of greatly different morphological class and maturity within the same animal (Rajan and Cline, 1998; Wu and Cline, 1998). Future work could examine how STDP induction at both retinotectal and intratectal synapses changes as a function of the morphological maturity of the cells. Equally, it will be important to establish how input specificity of plasticity is controlled during development, perhaps through changes in local intracellular signaling mechanisms or through visually driven neural–glia interactions in the tectum (Tao et al., 2001; Tremblay et al., 2009). It is also known that topographic mapping of retinal inputs is achieved at the level of individual dendrites of tectal cells (Bollmann and Engert, 2009). It would be interesting to investigate whether this subcellular mapping is achieved via STDP mechanisms.

One branch of STDP research that may prove critical for our understanding of the role of STDP in development is how developmental changes in GABAergic signaling impinge on this form of plasticity. GABAergic signals are known to modulate synaptic plasticity induction (Meredith et al., 2003), and evidence suggests they control a variety of activity-dependent plasticity mechanisms, possibly by modulating NMDA receptor transmission, controlling the statistics of spiking activity, or both (Akerman and Cline, 2007). Developmental shifts in GABAergic signals, such as changes in GABA-A receptor reversal potential, or alterations in inhibitory synaptic architecture and plasticity, may therefore have major ramifications for STDP induction. GABAergic transmission in the tectum has been shown to be important for the maturation of tectal dendritic arbors (Shen et al., 2009). Moreover, GABAergic inputs to tectal cells are plastic and are being actively reshaped by visual experience in a manner that is dependent on the developmental stage of the animal (Lien et al., 2006; Liu et al., 2007). Researchers can therefore use the optic tectum of *Xenopus* to address both how GABAergic signals may control STDP-mediated learning and how this might change over development.

Another area where STDP may be important is in the integration of multisensory information (Davison and Fregnac, 2006). The optic tectum is an obvious candidate for studying such questions due to its functional role in integrating cross-modal signals for initiating spatial orienting behaviors (Butler and Hodos, 2005). Indeed, studies have suggested that STDP could provide the superior colliculus with the ability to develop some of these capabilities (Huo et al., 2008; Yu et al., 2009). There is still much to learn about the development of multi-modal inputs in the optic tectum, but what is known is that axons from the hindbrain carrying information from mechanosensory neurons arrive in the optic tectum at the same time as retinal projections and converge on deeper layers of the tectum along more proximal dendritic processes than those that receive retinal inputs (Deeg et al., 2009; Hiramoto and Cline, 2009). Individual tectal neurons at these young ages receive glutamatergic inputs from both sensory modalities (Deeg et al., 2009; Hiramoto and Cline, 2009; Pratt and Aizenman, 2009) and show interesting developmental changes in their synaptic transmission properties (Deeg et al., 2009). Understanding how STDP might affect the integration of these different sensory modalities is yet to be examined.

Finally, we would also like to draw attention to a possible future role for the optic tectum in understanding STDP at a systems-level. A complete understanding of how STDP affects neural circuits will require studies of population wide activity at a single-cell, single-spike resolution. This presents a technical challenge, but one that might be best met with optical imaging techniques (Scanziani and Hausser, 2009). The optic tectum of animals like *X. laevis* or the zebrafish provide researchers the opportunity to measure activity across a large segment of an entire sensory circuit in a non-invasive manner (Niell and Smith, 2005). Researchers have already used this system to study binocular plasticity (Ramdya and Engert, 2008), and metaplasticity rules (Dunfield and Haas, 2009) across hundreds of cells simultaneously in the fully intact tectal circuit. As the temporal resolution of imaging techniques improves, this approach may prove invaluable to understanding STDP in a larger, circuit-wide context. Issues such as how STDP shapes topographic maps, adjusts circuits during periods of growth, or induces population coding of multisensory information are all questions that could be directly addressed in the optic tectum given the right imaging techniques.

CONCLUSION

The importance of the embryonic optic tectum for research into STDP is largely based on the interesting developmental questions that this system poses. But it is also based on the fact that it is possible to perform careful, well-controlled and physiologically relevant *in vivo* studies in the optic tectum. Of course, a complete picture of STDP will only emerge with research being carried out in many different systems. And to that end, researchers have investigated the possible roles of STDP in several other sensory systems *in vivo*, including the primary visual cortex of rodents (Meliza and Dan, 2006), cats, and humans (Yao and Dan, 2001), the olfactory bulb of locusts (Cassenaer and Laurent, 2007), the auditory cortex of ferrets (Dahmen et al., 2008), and the barrel cortex of rodents (Celikel et al., 2004). Together, these studies suggest that STDP is a component of sensory circuit plasticity in many different contexts and that it may represent an early evolutionary adaptation of neural systems. To really flesh out such a high-level, phylogenetic conception of this issue though, requires a comparative approach that examines both the molecular underpinnings and functional consequences of STDP in all the systems in which it is found. The optic tectum presents neuroscientists with an excellent model for this endeavor, due to the similarity of its function and connectivity across species (Ingle, 1973a; Butler and Hodos, 2005). And, continued investigations into the relationship between STDP and the development of the optic tectum have the potential to bring our understanding of this plasticity phenomenon in-line with the large body of scholarly work on activity-dependent development in the retinotectal circuit. As the first system in which STDP was demonstrated *in vivo*, and as one of the early favored systems for studying activity-dependent development, the optic tectum will continue to be an important model for STDP research.

ACKNOWLEDGMENTS

We would like to thank Leah Herrgen for assistance in preparing the figures and Ed Ruthazer for his helpful comments on the manuscript. The research leading to these results has received funding from the European Research Council under the European Community's Seventh Framework Program (FP7/2007-2013), ERC grant agreement No. 243273. This work was also supported by grants from the Biotechnology and Biological Sciences Research Council (BB/E0154761) and the Medical Research Council (G0601503). In addition, Colin J. Akerman was supported by a Fellowship from the Research Councils UK and British Pharmacological Society; Carlos D. Aizenman was supported by the National Eye Institute of the NIH, the NSF and the Klingenstein Fund; and Blake A. Richards was supported by a Welcome Trust Doctoral Fellowship and a Post-Graduate Scholarship from the Natural Sciences and Engineering Research Council of Canada.

REFERENCES

Aizenman, C. D., Akerman, C. J., Jensen, K. R., and Cline, H. T. (2003). Visually driven regulation of intrinsic neuronal excitability improves stimulus detection in vivo. *Neuron* 39, 831–842.

Aizenman, C. D., Muñoz-Elías, G., and Cline, H. T. (2002). Visually driven modulation of glutamatergic synaptic transmission is mediated by the regulation of intracellular polyamines. *Neuron* 34, 623–634.

Akerman, C. J., and Cline, H. T. (2006). Depolarizing GABAergic conductances regulate the balance of excitation to inhibition in the developing retinotectal circuit in vivo. *J. Neurosci.* 26, 5117–5130.

Akerman, C. J., and Cline, H. T. (2007). Refining the roles of GABAergic signaling during neural circuit formation. *Trends Neurosci.* 30, 382–389.

Bertschinger, N., and Natschläger, T. (2004). Real-time computation at the edge of chaos in recurrent neural networks. *Neural. Comput.* 16, 1413–1436.

Bi, G., and Poo, M. (2001). Synaptic modification by correlated activity: Hebb's postulate revisited. *Annu. Rev. Neurosci.* 24, 139–166.

Bollmann, J. H., and Engert, F. (2009). Subcellular topography of visually driven dendritic activity in the vertebrate visual system. *Neuron* 61, 895–905.

Butler, A., and Hodos, W. (2005). *Comparative Vertebrate Neuroanatomy: Evolution and Adaptation*. Hoboken, NJ: John Wiley and Sons.

Cassenaer, S., and Laurent, G. (2007). Hebbian STDP in mushroom bodies facilitates the synchronous flow of olfactory information in locusts. *Nature* 448, 709–713.

Celikel, T., Szostak, V. A., and Feldman, D. E. (2004). Modulation of spike timing by sensory deprivation during induction of cortical map plasticity. *Nat. Neurosci.* 7, 534–541.

Changeux, J., and Danchin, A. (1976). Selective stabilisation of developing synapses as a mechanism for the specification of neuronal networks. *Nature* 264, 705–712.

Cheng, H. J., Nakamoto, M., Bergemann, A. D., and Flanagan, J. G. (1995). Complementary gradients in expression and binding of ELF-1 and Mek4 in development of the topographic retinotectal projection map. *Cell* 82, 371–381.

Cline, H. T. (1991). Activity-dependent plasticity in the visual systems of frogs and fish. *Trends Neurosci.* 14, 104–111.

Cline, H. T. (2003). Sperry and Hebb: oil and vinegar? *Trends Neurosci.* 26, 655–661.

Cline, H. T., and Constantine-Paton, M. (1989). NMDA receptor antagonists disrupt the retinotectal topographic map. *Neuron* 3, 413–426.

Cline, H. T., and Constantine-Paton, M. (1990). NMDA receptor agonist and antagonists alter retinal ganglion cell arbor structure in the developing frog retinotectal projection. *J. Neurosci.* 10, 1197–1216.

Cline, H. T., Debski, E. A., and Constantine-Paton, M. (1987). *N*-methyl-D-aspartate receptor antagonist desegregates eye-specific stripes. *Proc. Natl. Acad. Sci. U.S.A.* 84, 4342–4345.

Cline, H. T., Wu, G., and Malinow, R. (1996) In vivo development of neuronal structure and function. *Cold Spring Harb. Symp. Quant. Biol.* 61, 95–104.

Constantine-Paton, M., and Law, M. I. (1978). Eye-specific termination bands in tecta of three-eyed frogs. *Science* 202, 639–641.

Dahmen, J. C., Hartley, D. E. H., and King, A. J. (2008). Stimulus-timing-dependent plasticity of cortical frequency representation. *J. Neurosci.* 28, 13629–13639.

Dan, Y., and Poo, M. (2004). Spike timing-dependent plasticity of neural circuits. *Neuron* 44, 23–30.

Davison, A. P., and Fregnac, Y. (2006). Learning cross-modal spatial transformations through spike

timing-dependent plasticity. *J. Neurosci.* 26, 5604–5615.

Debanne, D., Gohwiler, B. H., and Thompson, S. M. (1998). Long-term synaptic plasticity between pairs of individual CA3 pyramidal cells in rat hippocampal slice cultures. *J. Physiol. (Lond.)* 507, 237–247.

Debski, E. A., and Cline, H. T. (2002). Activity-dependent mapping in the retinotectal projection. *Curr. Opin. Neurobiol.* 12, 93–99.

Deeg, K. E., Sears, I. B., and Aizenman, C. D. (2009). Development of multisensory convergence in the *Xenopus* optic tectum. *J. Neurophysiol.* 102, 3392–3404.

Dong, W., Lee, R. H., Xu, H., Yang, S., Pratt, K. G., Cao, V., Song, Y. K., Nurmikko, A., and Aizenman, C. D. (2009). Visual avoidance in *Xenopus* tadpoles is correlated with the maturation of visual responses in the optic tectum. *J. Neurophysiol.* 101, 803–815.

Drescher, U., Kremoser, C., Handwerker, C., Löschinger, J., Noda, M., and Bonhoeffer, F. (1995). In vitro guidance of retinal ganglion cell axons by RAGS, a 25 kDa tectal protein related to ligands for Eph receptor tyrosine kinases. *Cell* 82, 359–370.

Dudkin, E. A., and Gruberg, E. R. (2003). Nucleus isthmi enhances calcium influx into optic nerve fiber terminals in *Rana pipiens*. *Brain Res.* 969, 44–52.

Dunfield, D., and Haas, K. (2009). Metaplasticity governs natural experience-driven plasticity of nascent embryonic brain circuits. *Neuron* 64, 240–250.

Edwards, J. A., and Cline, H. T. (1999). Light-induced calcium influx into retinal axons is regulated by presynaptic nicotinic acetylcholine receptor activity in vivo. *J. Neurophysiol.* 81, 895–907.

Engert, F., Tao, H. W., Zhang, L. I., and Poo, M. (2002). Moving visual stimuli rapidly induce direction sensitivity of developing tectal neurons. *Nature* 419, 470–475.

Gaze, R. M. (1958). The representation of the retina on the optic lobe of the frog. *Exp. Physiol.* 43, 209–214.

Gaze, R. M. (1959). Regeneration of the optic nerve in *Xenopus laevis*. *Exp. Physiol.* 44, 290–308.

Gaze, R. M., Keating, M. J., and Chung, S. H. (1974). The evolution of the retinotectal map during development in *Xenopus*. *Proc. R. Soc. Lond. B Biol. Sci.* 185, 301–330.

Gaze, R. M., Keating, M. J., Ostberg, A., and Chung, S. H. (1979). The relationship between retinal and tectal growth in larval *Xenopus*: implications for the development of the retino-tectal projection. *J. Embryol. Exp. Morphol.* 53, 103–143.

Gernert, M., and Ewert, J. (1995). Cholinergic, GABAergic, and dopaminergic influences on visually evoked field potentials in the superficial optic tectum of *Bufo marinus*. *Comp. Biochem. Physiol. A Physiol.* 112, 387–401.

Grüsser, O. J., and Grüsser-Cornehls, U. (1976). "Neurophysiology of the anuran visual system," in *Frog Neurobiology: A Handbook*. R. Llinás and W. Precht, eds (New York: Springer-Verlag), 297–385.

Haas, K., Li, J., and Cline, H. T. (2006). AMPA receptors regulate experience-dependent dendritic arbor growth in vivo. *Proc. Natl. Acad. Sci. U.S.A.* 103, 12127–12131.

Hickmott, P. W., and Constantine-Paton, M. (1993). The contributions of NMDA, non-NMDA, and GABA receptors to postsynaptic responses in neurons of the optic tectum. *J. Neurosci.* 13, 4339–4353.

Hiramoto, M., and Cline, H. T. (2009). Convergence of multisensory inputs in *Xenopus* tadpole tectum. *Dev. Neurobiol.* 69, 959–971.

Holt, C. E. (1984). Does timing of axon outgrowth influence initial retinotectal topography in *Xenopus*? *J. Neurosci.* 4, 1130–1152.

Holt, C. E., and Harris, W. A. (1993). Position, guidance, and mapping in the developing visual system. *J. Neurobiol.* 24, 1400–1422.

Holt, C. E., and Harris, W. A. (1983). Order in the initial retinotectal map in *Xenopus*: a new technique for labelling growing nerve fibres. *Nature* 301, 150–152.

Huo, J., Zhijun, Y., and Murray, A. (2008). "Modeling visual and auditory integration of barn owl superior colliculus with STDP," in *Proceedings of IEEE Conference on Cybernetics and Intelligent Systems* (Chengdu: IEEE), 1124–1128.

Ingle, D. (1973a). Evolutionary perspectives on the function of the optic tectum. *Brain Behav. Evol.* 8, 211–237.

Ingle, D. (1973b). Two visual systems in the frog. *Science* 181, 1053–1055.

Isa, T. (2002). Intrinsic processing in the mammalian superior colliculus. *Curr. Opin. Neurobiol.* 12, 668–677.

Jacobson, M. (1968). Development of neuronal specificity in retinal ganglion cells of *Xenopus*. *Dev. Biol.* 17, 202–218.

Kampa, B. M., Letzkus, J. J., and Stuart, G. J. (2007). Dendritic mechanisms controlling spike-timing-dependent synaptic plasticity. *Trends Neurosci.* 30, 456–463.

Keating, M. J., and Feldman, J. D. (1975). Visual deprivation and intertectal neuronal connexions in *Xenopus laevis*. *Proc. R. Soc. Lond. B Biol. Sci.* 191, 467–474.

Lázár, G. (1973). The development of the optic tectum in *Xenopus laevis*: a Golgi study. *J. Anat.* 116, 347.

Lee, P. H., Helms, M. C., Augustine, G. J., and Hall, W. C. (1997). Role of intrinsic synaptic circuitry in collicular sensorimotor integration. *Proc. R. Soc. Lond. B Biol. Sci.* 94, 13299–13304.

Levy, W. B., and Steward, O. (1983). Temporal contiguity requirements for long-term associative potentiation/depression in the hippocampus. *Neuroscience* 8, 791–797.

Lien, C., Mu, Y., Vargas-Caballero, M., and Poo, M. (2006). Visual stimuli-induced LTD of GABAergic synapses mediated by presynaptic NMDA receptors. *Nat. Neurosci.* 9, 372–380.

Li, Y., Fitzpatrick, D., and White, L. E. (2006). The development of direction selectivity in ferret visual cortex requires early visual experience. *Nat. Neurosci.* 9, 676–681.

Li, Y., Van Hooser, S. D., Mazurek, M., White, L. E., and Fitzpatrick, D. (2008). Experience with moving visual stimuli drives the early development of cortical direction selectivity. *Nature* 456, 952–956.

Liu, Y., Zhang, L. I., and Tao, H. W. (2007). Heterosynaptic scaling of developing GABAergic synapses: dependence on glutamatergic input and developmental stage. *J. Neurosci.* 27, 5301–5312.

Maass, W., and Markram, H. (2004). On the computational power of circuits of spiking neurons. *J. Comp. Syst. Sci.* 69, 593–616.

Mann, F., Ray, S., Harris, W. A., and Holt, C. E. (2002). Topographic mapping in dorsoventral axis of the *Xenopus* retinotectal system depends on signaling through ephrin-B ligands. *Neuron* 35, 461–473.

Markram, H., Lubke, J., Frotscher, M., and Sakmann, B. (1997). Regulation of synaptic efficacy by coincidence of postsynaptic APs and EPSPs. *Science* 275, 213–215.

Martin, S. J., Grimwood, P. D., and Morris, R. G. M. (2000). Synaptic plasticity and memory: an evaluation of the hypothesis. *Annu. Rev. Neurosci.* 23, 649–711.

McCormick, D. A., Shu, Y., Hasenstaub, A., Sanchez-Vives, M., Badoual, M., and Bal, T. (2003). Persistent cortical activity: mechanisms of generation and effects on neuronal excitability. *Cereb. Cortex* 13, 1219–1231.

Mehta, M. R., Quirk, M. C., and Wilson, M. A. (2000). Experience-dependent asymmetric shape of hippocampal receptive fields. *Neuron* 25, 707–715.

Meliza, C. D., and Dan, Y. (2006). Receptive-field modification in rat visual cortex induced by paired visual stimulation and single-cell spiking. *Neuron* 49, 183–189.

Meredith, R. M., Floyer-Lea, A. M., and Paulsen, O. (2003). Maturation of long-term potentiation induction rules in rodent hippocampus: role of GABAergic inhibition. *J. Neurosci.* 23, 11142–11146.

Meyer, R. L. (1983). Tetrodotoxin inhibits the formation of refined retinotopography in goldfish. *Dev. Brain Res.* 6, 293–298.

Mu, Y., and Poo, M. (2006). Spike timing-dependent LTP/LTD mediates visual experience-dependent plasticity in a developing retinotectal system. *Neuron* 50, 115–125.

Nakagawa, H., Miyazaki, H., and Matsumoto, N. (1997). Principal neuronal organization in the frog optic tectum revealed by a current source density analysis. *Vis. Neurosci.* 14, 263–275.

Niell, C. M., and Smith, S. J. (2005). Functional imaging reveals rapid development of visual response properties in the zebrafish tectum. *Neuron* 45, 941–951.

Nieuwkoop, P. D., and Faber, J. (1967). *Normal Table of Xenopus laevis (Daudin): A Systematical and Chronological Survey of the Development from the Fertilized Egg Till the End of Metamorphosis*. Amsterdam: North-Holland Publishing Co.

Nikundiwe, A. M. and Nieuwenhuys, R. (1983). The cell masses in the brainstem of African clawed frog Xenopus Laevis: a topographical and topological analysis. *J. Comp. Neurol.* 213, 199–219.

O'Rourke, N. A., Cline, H. T., and Fraser, S. E. (1994). Rapid remodeling of retinal arbors in the tectum with and without blockade of synaptic transmission. *Neuron* 12, 921–934.

O'Rourke, N. A., and Fraser, S. E. (1986). Dynamic aspects of retinotectal map formation revealed by a vital-dye fiber-tracing technique. *Dev. Biol.* 114, 265–276.

Pratt, K. G., and Aizenman, C. D. (2007). Homeostatic regulation of intrinsic excitability and synaptic transmission in a developing visual circuit. *J. Neurosci.* 27, 8268–8277.

Pratt, K. G., and Aizenman, C. D. (2009). Multisensory integration in mesencephalic trigeminal neurons in *Xenopus* tadpoles. *J. Neurophysiol.* 102, 399–412.

Pratt, K. G., Dong, W., and Aizenman, C. D. (2008). Development and spike timing-dependent plasticity of recurrent excitation in the *Xenopus* optic tectum. *Nat. Neurosci.* 11, 467–475.

Rajan, I., and Cline, H. T. (1998). Glutamate receptor activity is required for normal

development of tectal cell dendrites in vivo. *J. Neurosci.* 18, 7836–7846.

Ramdya, P., and Engert, F. (2008). Emergence of binocular functional properties in a monocular neural circuit. *Nat. Neurosci.* 11, 1083–1090.

Rao, R. P. N., and Sejnowski, T. J. (2001). "Predictive learning of temporal sequences in recurrent neocortical circuits," in *Novartis Foundation Symposia*, 208–229. Available at: http://www.scopus.com/inward/record.url?eid = 2-s2.0-0035235894&partnerID = 40.

Reh, T. A., and Constantine-Paton, M. (1984). Retinal ganglion cell terminals change their projection sites during larval development of *Rana pipiens*. *J. Neurosci.* 4, 442–457.

Reh, T. A., and Constantine-Paton, M. (1985). Eye-specific segregation requires neural activity in three-eyed *Rana pipiens*. *J. Neurosci.* 5, 1132–1143.

Ruthazer, E. S., Akerman, C. J., and Cline, H. T. (2003). Control of axon branch dynamics by correlated activity in vivo. *Science* 301, 66–70.

Ruthazer, E. S., and Cline, H. T. (2004). Insights into activity-dependent map formation from the retinotectal system: a middle-of-the-brain perspective. *J. Neurobiol.* 59, 134–146.

Saito, Y., and Isa, T. (2003). Local excitatory network and NMDA receptor activation generate a synchronous and bursting command from the superior colliculus. *J. Neurosci.* 23, 5854–5864.

Sakaguchi, D. S., and Murphey, R. K. (1985). Map formation in the developing *Xenopus* retinotectal system: an examination of ganglion cell terminal arborizations. *J. Neurosci.* 5, 3228–3245.

Scanziani, M., and Hausser, M. (2009). Electrophysiology in the age of light. *Nature* 461, 930–939.

Schmidt, J. T. (1985). Formation of retinotopic connections: Selective stabilization by an activity-dependent mechanism. *Cell. Mol. Neurobiol.* 5, 65–84.

Schmidt, J. T., and Edwards, D. L. (1983). Activity sharpens the map during the regeneration of the retinotectal projection in goldfish. *Brain Res.* 269, 29–39.

Shen, W., Da Silva, J. S., He, H., and Cline, H. T. (2009). Type A GABA-receptor-dependent synaptic transmission sculpts dendritic arbor structure in *Xenopus* tadpoles in vivo. *J. Neurosci.* 29, 5032–5043.

Shon, A. P., Rao, R. P. N., and Sejnowski, T. J. (2004). Motion detection and prediction through spike-timing dependent plasticity. *Network* 15, 179–198.

Sjöström, P. J., Turrigiano, G. G., and Nelson, S. B. (2001). Rate, timing, and cooperativity jointly determine cortical synaptic plasticity. *Neuron* 32, 1149–1164.

Sparks, D. L. (1986). Translation of sensory signals into commands for control of saccadic eye movements: role of primate superior colliculus. *Physiol. Rev.* 66, 118–171.

Sperry, R. W. (1944). Optic nerve regeneration with return of vision in anurans. *J. Neurophysiol.* 7, 57–69.

Sperry, R. W. (1963). Chemoaffinity in the orderly growth of nerve fiber patterns and connections. *Proc. Natl. Acad. Sci. U.S.A.* 50, 703–710.

Székely, G., and Lázár, G. (1967). Golgi studies on the optic center of the frog. *J. Hirnforsch.* 9, 329–344.

Székely, G., and Lázár, G. (1976). "Cellular and synaptic architecture of the optic tectum," in *Frog Neurobiology: a Handbook*, R. Llinás and W. Precht, eds. (Berlin: Springer-Verlag), 407–434.

Tao, H. W., and Poo, M. (2005). Activity-dependent matching of excitatory and inhibitory inputs during refinement of visual receptive fields. *Neuron* 45, 829–836.

Tao, H. W., Zhang, L. I., Engert, F., and Poo, M. (2001). Emergence of input specificity of LTP during development of retinotectal connections in vivo. *Neuron* 31, 569–580.

Tremblay, M., Fugère, V., Tsui, J., Schohl, A., Tavakoli, A., Travençolo, B. A., Costa, L. F., and Ruthazer, E. S. (2009). Regulation of radial glial motility by visual experience. *J. Neurosci.* 29, 14066–14076.

Tzounopoulos, T., Kim, Y., Oertel, D., and Trussell, L. O. (2004). Cell-specific, spike timing-dependent plasticities in the dorsal cochlear nucleus. *Nat. Neurosci.* 7, 719–725.

Udin, S. B. (1985). The role of visual experience in the formation of binocular projections in frogs. *Cell. Mol. Neurobiol.* 5, 85–102.

Udin, S. B. (2007). The instructive role of binocular vision in the *Xenopus* tectum. *Biol. Cybern.* 97, 493–503.

Udin, S. B., and Fisher, M. D. (1985). The development of the Nucleus Isthmi in *Xenopus laevis*. I. Cell genesis and the formation of connections with the tectum. *J. Comp. Neurol.* 232, 25–35.

Udin, S. B., and Keating, M. J. (1981). Plasticity in a central nervous pathway in *Xenopus*: anatomical changes in the isthmotectal projection after larval eye rotation. *J. Comp. Neurol.* 203, 575–594.

VanRullen, R., Guyonneau, R., and Thorpe, S. (2005). Spike times make sense. *Trends Neurosci.* 28, 1–4.

Vislay-Meltzer, R. L., Kampff, A. R., and Engert, F. (2006). Spatiotemporal specificity of neuronal activity directs the modification of receptive fields in the developing retinotectal system. *Neuron* 50, 101–114.

Whitelaw, V. A., and Cowan, J. D. (1981). Specificity and plasticity of retinotectal connections: a computational model. *J. Neurosci.* 1, 1369–1387.

Willshaw, D. J., and Von Der Malsburg, C. (1976). How patterned neural connections can be set up by self-organization. *Proc. R. Soc. Lond. B Biol. Sci.* 194, 431–445.

Wu, G., and Cline, H. T. (1998). Stabilization of dendritic arbor structure in vivo by CaMKII. *Science* 279, 222–226.

Yao, H., and Dan, Y. (2001). Stimulus timing-dependent plasticity in cortical processing of orientation. *Neuron* 32, 315–323.

Yu, L., Stein, B. E., and Rowland, B. A. (2009). Adult plasticity in multisensory neurons: short-term experience-dependent changes in the superior colliculus. *J. Neurosci.* 29, 15910–15922.

Zhang, L. I., Tao, H. W., Holt, C. E., Harris, W. A., and Poo, M. (1998). A critical window for cooperation and competition among developing retinotectal synapses. *Nature* 395, 37–44.

Zhang, L. I., Tao, H. W., and Poo, M. (2000). Visual input induces long-term potentiation of developing retinotectal synapses. *Nat. Neurosci.* 3, 708–715.

Conflict of Interest Statement: The authors declare that the research was conducted in the absence of any commercial or financial relationships that could be construed as a potential conflict of interest.

Received: 08 February 2010; paper pending published: 16 February 2010; accepted: 17 May 2010; published online: 10 June 2010.

*Citation: Richards BA, Aizenman CD and Akerman CJ (2010) In vivo spike-timing-dependent plasticity in the optic tectum of Xenopus laevis. Front. Syn. Neurosci. **2**:7. doi: 10.3389/fnsyn.2010.00007*

frontiers in
SYNAPTIC NEUROSCIENCE

REVIEW ARTICLE
published: 21 June 2010
doi: 10.3389/fnsyn.2010.00008

Spike-timing dependent plasticity in inhibitory circuits

Karri P. Lamsa[1]*, Dimitri M. Kullmann[2] and Melanie A. Woodin[3]

[1] *Department of Pharmacology, Oxford University, Oxford, UK*
[2] *Department of Clinical and Experimental Epilepsy, Institute of Neurology, University College London, London, UK*
[3] *Department of Cell and Systems Biology, University of Toronto, Canada*

Edited by:
Per Jesper Sjöström, University College London, UK

Reviewed by:
Julie Kauer, Brown University, USA
Yuri Zilberter, Institut de Neurobiologie de la MEDiterranée, France

****Correspondence:***
Karri P. Lamsa, Department of Pharmacology, Oxford University, Mansfield Road, Oxford OX1 3QT, UK.
e-mail: karri.lamsa@pharm.ox.ac.uk

Inhibitory circuits in the brain rely on GABA-releasing interneurons. For long, inhibitory circuits were considered weakly plastic in the face of patterns of neuronal activity that trigger long-term changes in the synapses between excitatory principal cells. Recent studies however have shown that GABAergic circuits undergo various forms of long-term plasticity. For the purpose of this review, we identify three major long-term plasticity expression sites. The first locus is the glutamatergic synapses that excite GABAergic inhibitory cells and drive their activity. Such synapses, on many but not all inhibitory interneurons, exhibit long-term potentiation (LTP) and depression (LTD). Second, GABAergic synapses themselves can undergo changes in GABA release probability or postsynaptic GABA receptors. The third site of plasticity is in the postsynaptic anion gradient of GABAergic synapses; coincident firing of GABAergic axons and postsynaptic neurons can cause a long-lasting change in the reversal potential of $GABA_A$ receptors mediating fast inhibitory postsynaptic potentials. We review the recent literature on these forms of plasticity by asking how they may be triggered by specific patterns of pre- and postsynaptic action potentials, although very few studies have directly examined spike-timing dependent plasticity (STDP) protocols in inhibitory circuits. Plasticity of interneuron recruitment and of GABAergic signaling provides for a rich flexibility in inhibition that may be central to many aspects of brain function. We do not consider plasticity at glutamatergic synapses on Purkinje cells and other GABAergic principal cells.

Keywords: interneuron, GABA, fast-spiking, oscillation, chloride, NKCC1, KCC2

PLASTICITY IN EXCITATORY AFFERENTS OF INHIBITORY CIRCUITS

Long-term potentiation (LTP) and depression (LTD) of glutamatergic synapses onto GABAergic interneurons has been discovered in several areas of the brain suggesting that plasticity in this locus is common in the CNS. Although these studies have concentrated heavily on the circuits of the hippocampal formation, there is evidence that similar plasticity takes place in the neocortex (Sarihi et al., 2008; Chen et al., 2009), as well as in striatum (Fino et al., 2008, 2009) and amygdala (Mahanty and Sah, 1998). In addition there are reports on analogous long-term plasticity in the spinal cord (Santos et al., 2009) and in sensory pathways (Tzounopoulos et al., 2004).

PLASTICITY IS SPECIFIC TO GABAergic INTERNEURON TYPE

One of the striking features of plasticity in this locus is that it can be highly specific to an interneuron type (Kullmann and Lamsa, 2007; Sarihi et al., 2008; Oren et al., 2009; Nissen et al., 2010). Subpopulations of unidentified interneurons may show LTP, LTD or no plasticity at all, for stimulation of the same afferent glutamatergic pathway (Buzsaki and Eidelberg, 1982; Lei and McBain, 2004; Lamsa et al., 2007a). Recent studies on identified interneurons in the hippocampus have revealed that these subpopulations are composed of anatomically distinct interneuron types. Plasticity has been shown to be consistent in individual anatomically identified GABAergic cell types (Alle et al., 2001; Oren et al., 2009; Nissen et al., 2010). More importantly, plastic properties can vary remarkably between two interneurons located in close proximity in the same hippocampal area, but showing different neurochemical marker expression or different axon distribution (Lamsa et al., 2007b; Nissen et al., 2010) (**Figure 1**). A specific pattern of pre- and postsynaptic activity that induces plasticity in one interneuron type can fail or elicit a different plastic change in another interneuron type located in the same layer (Lamsa et al., 2005, 2007b; Nissen et al., 2010).

These findings, that the interneuron plasticity is diverse and cell type-specific, have important impacts on the dynamics of the cortical networks. First, specific patterns of pre- and postsynaptic action potentials are capable of triggering plasticity in only a subpopulation of inhibitory cells (Lamsa et al., 2005, 2007b). Second, plasticity is likely to be induced in different brain states in distinct interneuron types. It has been shown that the activity of interneurons and their glutamatergic afferents is highly specific to a cell type during neuronal oscillations related to different behavioral states (Klausberger and Somogyi, 2008). It is therefore tempting to speculate that the distinct forms of LTP and LTD discovered in interneurons *in vitro* might underlie the use-dependent dynamics reported in selective parts of the inhibitory networks *in vivo* (Buzsaki and Eidelberg, 1982; Csicsvari et al., 1998; Yazaki-Sugiyama et al., 2009). Several important questions remain to be answered on plasticity in interneurons and one of the most intriguing is related to the

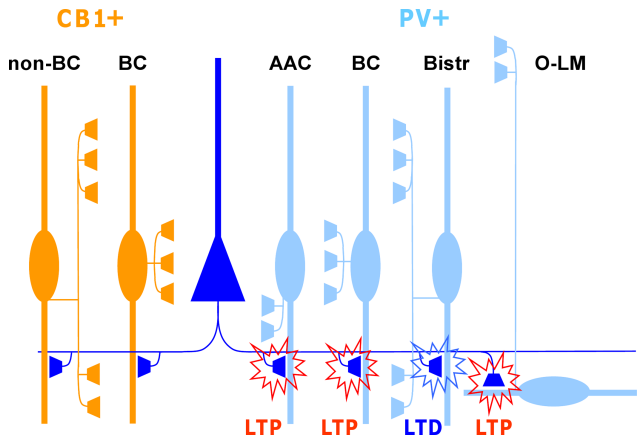

FIGURE 1 | Glutamatergic fiber plasticity on hippocampal CA1 interneurons is specific to a GABAergic cell type. Schematic illustrates cell type-specific plasticity in six anatomically identified interneuron types. Repetitive high-frequency (100 Hz tetanic or theta burst) stimulation of pyramidal cell axons induces target cell-specific plasticity in parvalbumin-expressing (PV+) interneuron types, whereas interneurons expressing cannabinoid receptor type 1 (CB1R+) but not PV, show no plasticity with these protocols. PV and CB1R are mutually exclusive neurochemical markers and cell types belonging to these two groups form very similar inhibitory circuits in the CA1. Detailed anatomical analyses reveal that glutamatergic synapses onto PV+ axo-axonic (AAC), basket cells (BC) and oriens-lacunosum moleculare (O-LM) interneurons show consistently LTP, whereas bistratified cells (Bistr) show predominantly LTD. In contrast, synapses onto BCs expressing CB1R or dendrite-targeting CB1R+ non-basket cells (non-BC) show no long-term plasticity at all (Lamsa et al., 2007b; Oren et al., 2009; Nissen et al., 2010).

physiological activity patterns that might generate cell type-specific plasticities *in vivo*. To answer this question it will be important to reveal spike-timing dependent plasticity (STDP) properties of common cortical interneuron types and their identified glutamatergic afferents (Klausberger and Somogyi, 2008).

Given that GABAergic interneuron diversity is rich in many areas of the brain and full identification of cells is often challenging, it is understandable that STDP has not yet been extensively studied among GABAergic interneuron types. Instead, in most of these studies relatively robust extracellular stimulation protocols have been used. However, the major purpose of these pioneering studies has been to investigate a capacity for synaptic plasticity in inhibitory interneurons in distinct areas (Buzsaki and Eidelberg, 1982; Perez et al., 2001; Lei and McBain, 2004; Lamsa et al., 2005, 2007b; Galvan et al., 2008). Unfortunately, interneurons in many of these studies have been pooled together on the basis of their electrophysiological properties. However, these parameters correlate quite weakly with anatomical, neurochemical and gene expression patterns that are commonly used to identify the hippocampal and neocortical interneuron types (Ascoli et al., 2008). Yet, some STDP studies have been made in GABAergic interneurons and these results also suggest that 'rules' underlying long-term plasticity may differ between distinct interneuron types. Significant differences in STDP were found between fast- and regularly-spiking interneuron populations in the neocortex (Lu et al., 2007). However, as mentioned above firing patterns do not reveal inhibitory circuit wiring patterns or molecular profiles of the cells, and therefore cell type-specific STDP properties still remain to be elucidated in the hippocampus and neocortex. Noteworthy, interneuron subpopulation-specific plasticity has also been demonstrated in striatal GABAergic interneurons. Glutamatergic afferents from somatosensory cortex to striatal nitric oxide-synthase (NOS)-expressing GABAergic interneurons show relatively consistent STDP properties (Fino et al., 2008, 2009). However, in many subcortical areas such as striatum the interneuron diversity is smaller than in the cortex (Freund and Buzsaki, 1996), which might explain homogeneity of striatal NOS-expressing GABAergic cells (Klausberger and Somogyi, 2008).

PLASTICITY MECHANISMS

The induction and expression mechanisms of LTP and LTD of glutamatergic excitation of interneurons have attracted considerable attention. The emerging evidence points to substantial heterogeneity, most likely reflecting the diversity of interneuron types mentioned above. LTP at glutamatergic synapses on many interneurons in the hippocampal formation and neocortex exhibits a 'Hebbian' induction rule; that is, it can be evoked by the conjunction of presynaptic action potentials and postsynaptic depolarization (Alle et al., 2001; Perez et al., 2001; Lamsa et al., 2005; Galvan et al., 2008; Sarihi et al., 2008). Hebbian plasticity may even occur in the human motor cortex (Russmann et al., 2009). However, different studies have applied distinct patterns of presynaptic stimulation (high-frequency tetanization, 'theta-burst' or low-frequency stimulation), and have either allowed the postsynaptic neurons to be depolarized by the activated synapses, or have imposed action potentials via the recording pipette. It is therefore difficult to compare among studies. Nevertheless, some striking differences are emerging, both between LTP in interneurons and in principal cells, and among different interneurons.

NMDA receptor-dependent LTP

'Hebbian' LTP in pyramidal neurons is generally explained by the involvement of NMDA receptors, which require both presynaptic glutamate release and postsynaptic depolarization for their activation, and which trigger postsynaptic Ca^{2+} influx and downstream activation of calcium/calmodulin-dependent kinase IIα (CaMKIIα). NMDA receptor-dependent LTP with very similar properties can be elicited at synapses made by Schaffer collaterals on a subset of interneurons in stratum radiatum of the rodent hippocampus (Lamsa et al., 2005). This phenomenon can be elicited by delivering postsynaptic depolarizing steps synchronously with low-frequency presynaptic stimulation, or by delivering a continuous postsynaptic depolarization to allow the presynaptic stimuli to evoke postsynaptic spiking. However, a pre- before post-protocol has not been explicitly tested. Although this shares many features with LTP in pyramidal neurons, including sensitivity to pharmacological blockers of CaMKIIα (Lamsa et al., 2007a), it exhibits one striking difference: LTP is intact in mice harboring a mutation that prevents autophosphorylation of CaMKIIα, which has a profound deficit in NMDA receptor-dependent LTP in pyramidal neurons (Giese et al., 1998). This is perhaps unsurprising, because CaMKIIα has not been detected in interneurons, so the result of the pharmacological intervention suggests the involvement of another member of the calcium/calmodulin-dependent kinase family.

Non-NMDA receptor-dependent LTP

At many other synapses on interneurons, pharmacological blockade of NMDA receptors fails to prevent LTP induction. Postsynaptic chelation of Ca^{2+} is however effective (Alle et al., 2001; Perez et al., 2001), implying a critical role for Ca^{2+}, which must enter the neuron from another source or be released from intracellular stores. Several studies have demonstrated an essential role for Ca^{2+}-permeable AMPA receptors (Mahanty and Sah, 1998; Lamsa et al., 2007b; Oren et al., 2009). A striking feature of such receptors, which are devoid of edited GluA2 subunits, is that they exhibit inward rectification, preferentially allowing Ca^{2+} influx at relatively negative potentials. Remarkably, LTP at synapses exhibiting strong inward rectification can be induced by pairing presynaptic action potentials with postsynaptic hyperpolarization. This phenomenon has been termed 'anti-Hebbian LTP' (Lamsa et al., 2007b; Oren et al., 2009; Nissen et al., 2010). It is most readily observed at synapses formed by axon collaterals of pyramidal neurons on interneurons in the feedback circuit in stratum oriens of the hippocampus, in particular (although not exclusively) in oriens lacunosum-moleculare (O-LM) cells, which have dendrites extending parallel to stratum pyramidale and an axon extending to stratum lacunosum-moleculare (McBain et al., 1994). Although STDP protocols have not been explored in detail, this form of LTP can be elicited by delivering presynaptic stimuli at the trough, but not at the peak, of a 5-Hz sinusoidal membrane potential oscillation delivered via the postsynaptic pipette.

An essential role for group I metabotropic glutamate receptors (mGluRs) has also been demonstrated in LTP (and LTD) induction in interneurons (Perez et al., 2001; Lapointe et al., 2004; Galvan et al., 2008; Gibson et al., 2008). Although many studies are difficult to compare because they have examined different brain regions, group I mGluR-dependent LTP has also been most extensively examined in O-LM cells. Indeed, these interneurons have abundant mGLuR1α, but also exhibit marked rectification of their synaptic AMPA receptors (Ferraguti et al., 2004; Oren et al., 2009). LTP at synapses made on O-LM cells by axon collaterals of local pyramidal neurons can be induced either with Hebbian or with anti-Hebbian protocols, and is sensitive to pharmacological blockade of either Ca^{2+}-permeable AMPA receptors or group I mGluRs (Perez et al., 2001; Oren et al., 2009). Although both group I mGluR subtypes (mGluR1 and mGluR5) are linked to Ca^{2+}, albeit via different cascades (Topolnik et al., 2005), how they interact with Ca^{2+} signaling triggered by AMPA receptor activation remains to be determined. LTP in stratum oriens interneurons can, furthermore, be facilitated by co-activation of nicotinic acetylcholine receptors (Jia et al., 2010).

An additional role for L-type Ca^{2+} channels in induction of NMDA receptor-independent LTP has been reported in interneurons in stratum lacunosum-moleculare, at synapses made by mossy fibers (Galvan et al., 2008). This phenomenon was elicited by high-frequency stimulation of presynaptic axons while allowing the postsynaptic neurons to fire. Here too, pharmacological dissection has revealed an essential role for mGluR1, blockade of which converted LTP into LTD. LTP however occurred at synapses with Ca^{2+}-impermeable AMPA receptors, and was blocked by postsynaptic Ca^{2+} chelation or interference with intracellular Ca^{2+} stores.

In subtle contrast to LTP at mossy fiber synapses on interneurons in stratum lacunosum-moleculare of the hippocampus, Sarihi et al. (2008) found that LTP in fast-spiking in layer II/III interneurons of the visual cortex, elicited by theta-burst stimulation, depended on mGluR5, but not mGluR1, and that L-type Ca^{2+} channels were not involved. Nevertheless, this form of LTP was again independent of NMDA receptors, but was prevented by chelating postsynaptic Ca^{2+}.

Unraveling how the different glutamate receptors and other sources of Ca^{2+} interact in LTP induction will require further work. Among possible factors influencing the outcome of different induction protocols is the method used to record from neurons: some studies resorted to perforated patch recordings to minimize disruption of the cytoplasm, but this approach renders voltage-clamping difficult, and prevents the routine introduction of markers for histological characterization (Kullmann and Lamsa, 2007). Furthermore, grouping together interneurons on the basis of their location or firing characteristics probably hides considerable diversity of subtypes (Klausberger and Somogyi, 2008).

Relatively little attention has thus far been given to the LTP expression mechanisms that maintain potentiation of synaptic transmission. NMDA receptor-dependent LTP in some interneurons appears not to be accompanied by changes in short-term plasticity (paired-pulse ratio), providing no evidence for an increase in presynaptic glutamate release probability (Lamsa et al., 2005). This phenomenon is therefore most simply explained by a postsynaptic insertion of AMPA receptors, much as has been reported for NMDA receptor-dependent LTP in pyramidal neurons. LTP dependent on group I mGluRs and Ca^{2+}-permeable AMPA receptors, on the other hand, has been shown at several synapses to be accompanied by changes in paired-pulse ratio, failure rates, trial-to-trial fluctuations, or sensitivity to use-dependent blockers of Ca^{2+}-permeable receptors (Perez et al., 2001; Oren et al., 2009). All of these observations point instead to an increase in presynaptic glutamate release (see also Alle et al., 2001; Galvan et al., 2008), implying the existence of a retrograde factor, the identity of which remains to be determined.

Another form of tetanic LTP at synapses on somatostatin-positive interneurons in the neocortex appears to be exclusively presynaptic, in that it does not depend on postsynaptic Ca^{2+} signaling (Chen et al., 2009). Instead, it depends on protein kinase A and therefore shares mechanisms in common with tetanus-induced mossy fiber LTP.

LTD

At several other synapses, LTD has been reported more robustly than LTP (Maccaferri et al., 1998; Laezza et al., 1999; Laezza and Dingledine, 2004). However, at least two forms of LTD have emerged. At synapses made by hippocampal mossy fibers equipped with calcium-impermeable AMPARs and NMDA receptors, high-frequency presynaptic stimulation leads to depression, which appears to share mechanisms with NMDA receptor-dependent LTD at glutamatergic synapses on pyramidal neurons (Lei and McBain, 2004). At other synapses equipped with rectifying AMPA receptors, similar stimuli trigger a form of LTD that is sensitive to postsynaptic Ca^{2+} chelation or blockade of group III mGluRs, and which appears to be expressed presynaptically. Synapses made

by hippocampal mossy fibers can express both forms of plasticity although it remains to be determined to what extent the identity of the postsynaptic neurons determine the outcome of the pairing protocol. Importantly, the somata of the mossy fiber-LTD expressing interneurons are located in a different layer (mainly strata lucidum and radiatum) than the mossy fiber-LTP interneurons reported by Galvan et al. (2008) (stratum lacunosum-moleculare) and described earlier in this review. Interestingly, synapses where mGluR-dependent LTD has been elicited can be rendered capable of subsequent potentiation with repeated rounds of high-frequency stimulation (Pelkey et al., 2005). This phenomenon has been related to internalization of mGluR7, which plays a key role in triggering the initial depression.

High-frequency stimulation of Schaffer collaterals has also been shown to induce a form of NMDA receptor-independent LTD at interneurons in stratum radiatum (McMahon and Kauer, 1997). This too appears to be expressed presynaptically, and depends on mGluR1 receptors (Gibson et al., 2008). Interestingly, the phenomenon is also sensitive to manipulation of TRPV1 receptors, suggesting that these channels may act as presynaptic receptors for a retrograde messenger.

STDP AT EXCITATORY SYNAPSES ON INTERNEURONS

STDP protocols have not been tested systematically at all the synapses where LTP or LTD can be elicited. However, the patterns that are beginning to emerge from published studies of STDP suggest that multiple mechanisms interact to determine the outcome of the pairing, and that the relative importance of these mechanisms differs extensively among synapses. In a study of layer 2/3 interneurons of the somatosensory cortex, low-frequency pairing delivered with various pre-post intervals exclusively yielded LTD in fast-spiking cells, which could be prevented by postsynaptic Ca^{2+} chelation or broad-spectrum blockade of mGluRs (Lu et al., 2007). However, in the dorsal cochlear nucleus, presynaptic spikes delivered 8 ms before postsynaptic depolarization led to NMDA receptor-dependent LTP in low-threshold-spiking interneurons (Tzounopoulos et al., 2004). This work has shown that the outcome of pairing presynaptic action potentials with postsynaptic depolarization depends both on the repetition rate and on the spike-EPSP interval. A protocol that generally yields LTP in principal cells (pre before post) appears to engage both presynaptic cannabinoid-dependent LTD and postsynaptic CaMKII-dependent LTP in 'cartwheel' interneurons. STDP in striatal NOS- positive interneurons is equally puzzling, with pairing leading to LTD for most intervals between the presynaptic spike and the postsynaptic depolarization, and LTP only elicited when the postsynaptic depolarization is delivered approximately 40 ms after the spike (Fino et al., 2009).

GLUTAMATERGIC AFFERENT PLASTICITY IN NETWORK FUNCTION

A key feature of the plasticity in this locus is that it allows afferent-specific modulation of the inhibitory circuit. This means that a potentiated excitatory pathway has an increased contribution to firing of the inhibitory cell and consequently to the disynaptic inhibition of the GABAergic neurons's target cells (Nissen et al., 2010). This is important because during cortical network oscillations, which provide spatiotemporal framework for information processing, synchronized cell assembly formation must be dynamic. Accordingly, the synaptic strengths between pyramidal cells and inhibitory interneurons must change in behaviorally relevant time scales (Csicsvari et al., 1998). Plasticity at glutamatergic afferents onto interneurons is a good candidate mechanism for maintaining the necessary flexibility in these connections during the formation or dissolution of cell assemblies.

In a recent study Yazaki-Sugiyame et al. (2009) demonstrated that inhibitory circuits of fast-spiking interneurons express robust use-dependent plasticity in the visual cortex by visual experience. By modeling a cortical circuit the authors conclude that the plasticity either locates in excitatory afferents onto PV+ inhibitory cells or in the GABAergic synapses made by these cells onto pyramidal cells. Interestingly, PV+ fast-spiking interneurons have recently been demonstrated to express robust LTP in the visual cortex and in the hippocampus (Lamsa et al., 2007b; Sarihi et al., 2008; Nissen et al., 2010).

LASTING PLASTICITY OF GABAergic SYNAPSES IS ROBUST AT EARLY DEVELOPMENTAL STAGES

Long-lasting potentiation or depression of inhibitory synapses has also been reported in many areas of the brain. However, unlike plasticity at glutamatergic synapses reviewed above, LTP in hippocampal GABAergic synapses is almost exclusively restricted to early developmental stages (Gaiarsa et al., 2002). Yet, GABAergic LTP can be induced also in mature hippocampal circuits by certain extracellular stimulation patterns (such as theta-burst high-frequency stimulation) but even in these cases LTP is smaller than in neonatal synapses (Patenaude et al., 2003, 2005). In neonatal hippocampus and in some areas of juvenile neocortex both LTP and LTD of GABAergic synapses are triggered by processes that depend on postsynaptic Ca^{2+} and involve either activation of NMDARs or voltage-gated calcium channels (VGCCs) (Holmgren and Zilberter, 2001; Haas et al., 2006). Interestingly, GABAergic LTP and LTD in neonatal hippocampus are expressed presynaptically (Caillard et al., 1999a,b; Gubellini et al., 2005) whereas LTD (and LTP) in mature hippocampus is postsynaptic (Stelzer et al., 1994; Lu et al., 2000; Patenaude et al., 2003; Maffei et al., 2006). In the visual cortex expression of LTP and LTD is also developmentally regulated (Maffei et al., 2006) and similar to hippocampus GABAergic LTP is less likely in mature animals (Komatsu, 1994). However, the expression site for the plasticity in the visual cortex is always postsynaptic, which suggests that the LTP is probably different from that described in the neonatal hippocampus. Induction of plasticity in GABAergic synapses with STDP protocols has been tested in a small number of studies only. In GABAergic synapses of juvenile rat entorhinal cortex, a pre-post-spiking sequence triggers LTP and a post-pre sequence elicits LTD. STDP plasticity of GABAergic synapses has also been demonstrated in GABAergic synapses in the *Xenopus* retino-tectal system during early development, where coincident pre- and post-activity leads to LTD (Lien et al., 2006). Interestingly in mature hippocampus STDP protocol induces mainly ionic shift plasticity, and changes in GABA release probability or postsynaptic receptor activity are negligible (Woodin et al., 2003).

In some GABAergic synapses a short or long-term suppression of GABA release can be triggered by postsynaptic activity without a specific requirement for presynaptic firing. Because many

of these plasticity forms such as cannabinoid receptor-mediated LTP characteristically affect transmission in a large number of local GABAergic synapses without recognizing presynaptic terminal activity history, they are not reviewed any further here. This type of GABAergic synapse modulation has been reviewed recently elsewhere (Nugent and Kauer, 2008; Heifets and Castillo, 2009; McBain and Kauer, 2009).

Altogether, plasticity at the site of GABAergic synapses provides a powerful modulation mechanism of neuronal networks in particular during the development of cortical circuits. However, more knowledge on the plasticity in this locus especially concerning STDP and GABAergic cell type-specificity would be needed to understand its role widely in the hippocampal and neocortical networks.

'IONIC SHIFT PLASTICITY' PROVIDES MODULATION OF GABAergic INHIBITION

GABAergic synapses are susceptible to a form of plasticity dependent upon alterations in ion gradients (Fiumelli and Woodin, 2007). Low-frequency STDP induction protocols cause long-term changes in the postsynaptic chloride (Cl^-) gradient. The Cl^- gradient predominantly determines the reversal potential for $GABA_A$ receptor-mediated transmission (E_{GABA-A}), which in turn is largely responsible for determining the strength of inhibition. At early developmental stages STDP induction at GABAergic synapses hyperpolarizes the reversal potential, which effectively strengthens inhibition (Balena and Woodin, 2008; Xu et al., 2008). In contrast, the same STDP induction protocol weakens inhibition in the mature CNS by depolarizing the reversal potential (Woodin et al., 2003; Fiumelli and Woodin, 2007; Ormond and Woodin, 2009). These bi-directional forms of GABAergic STDP are often referred to as 'ionic shift plasticity' (**Figure 2**).

MECHANISMS REGULATING THE $GABA_A$ REVERSAL POTENTIAL

Fast inhibitory GABAergic transmission in the mature CNS is largely mediated by $GABA_A$Rs. These are ionotropic receptors permeable to Cl^- and HCO_3^-, but due to differences in the permeabilities and reversal potentials of these two ions it is Cl^- that plays the most important role in determining the strength of GABAergic transmission under normal physiological conditions (Farrant and Kaila, 2007). The regulation of this gradient depends on the balance and function of the prominent neuronal Cl^- transporters: KCC2 and NKCC1. They are both members of the cation-chloride cotransporter gene family SLC12a1-9 (Payne et al., 2003; Mercado et al., 2004; Gamba, 2005). They are also both secondary active transporters that depend on ionic gradients established by the primary active transporter Na^+-K^+-ATPase; KCC2 derives energy from the K^+ gradient to transport Cl^- out of the cell, while NKCC1 derives energy for the Na^+ gradient to transport Cl^- inward.

During embryonic development and early postnatal life, NKCC1 is the dominantly expressed Cl^--cotransporter (Xu et al., 1994; Plotkin et al., 1997; Russell, 2000; Dzhala et al., 2005), and as a result neuronal Cl^- is high and GABAergic transmission causes postsynaptic depolarization that is sometimes excitatory (although E_{GABA-A} may also be affected by recording conditions, see Rheims et al., 2009). However during early postnatal development there is a significant increase in KCC2 expression that results in a hyperpolarizing shift in E_{GABA-A} below the resting membrane potential that produces synaptic inhibition (Rivera et al., 1999; Blaesse et al., 2009). This dynamic regulation of the sign of GABAergic transmission (excitatory vs. inhibitory) is also observed during neuronal injury, epilepsy, and neuropathic pain (van den Pol et al., 1996; Cohen et al., 2002; Rivera et al., 2002; Coull et al., 2005; Blaesse et al., 2009). In these pathophysiological cases KCC2 expression dramatically decreases, rending

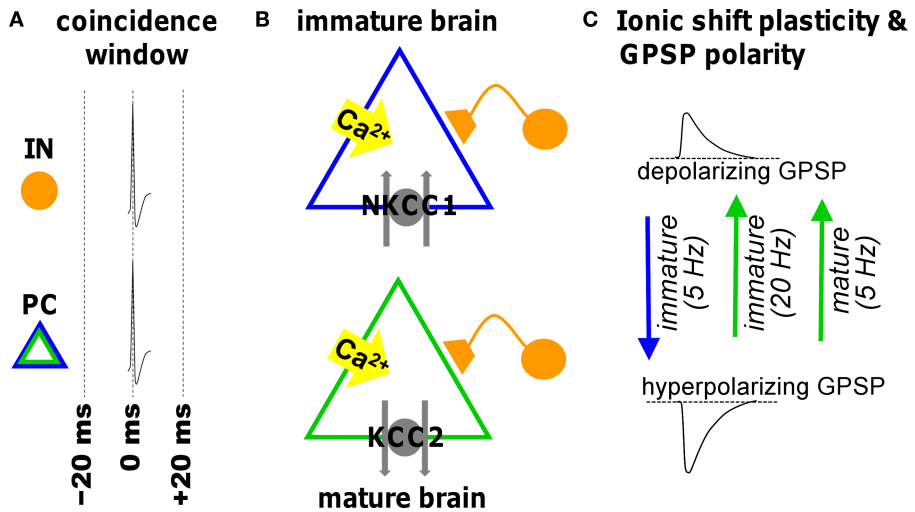

FIGURE 2 | Illustration of ionic shift plasticity in synaptically connected interneuron (IN) -principal cell (PC) pair in immature and mature brain. **(A)** Repetitive concurrent firing of the two cells inside the coincidence window activates a cascade that shifts the reversal potential of GABAergic PSPs (GPSP). **(B)** Spiking-associated calcium influx regulates cation-chloride cotransporter function altering neuronal Cl– transport. **(C)** The consequent shift in transmembrane chloride gradient shifts the reversal potential in either the positive or negative direction (indicated by arrows) depending on the developmental stage and the frequency. This can convert a depolarizing GPSP to a hyperpolarizing GPSP (and vice versa).

GABAergic transmission excitatory – in what has been proposed to be a recapitulation of developmental programs (Payne et al., 2003; Blaesse et al., 2009).

DEVELOPMENTALLY REGULATED IONIC SHIFT PLASTICITY

It is not just developmental and pathophysiological events that alter the electrochemical gradient for Cl^-. Physiologically normal patterns of neuronal activity such as those used during the induction of STDP can also shift the Cl^- gradient, resulting in changes in the strength of GABAergic transmission. Coincident pre- and postsynaptic activity within ±20 ms (at 5 Hz for 30 s) depolarizes E_{GABA-A} (with no corresponding change in conductance) (Woodin et al., 2003). Beyond ±50 ms GABAergic inhibition is weakened by a decrease in conductance (but no change in E_{GABA-A}). The result is a symmetrical spike timing window which leads to two initial observations: (1) GABAergic synapses are also sensitive to spike timing; and (2) the shape of the spike timing window differs from the asymmetrical window for glutamatergic synapses. This last point also implies that the pre-post order is not essential during GABAergic STDP induction, as it is during glutamatergic STDP. Rather during GABAergic STDP the essential requirement is correlated timing.

During the induction of GABAergic STDP postsynaptic Ca^{2+} influx through VGCCs leads to a decrease in the function of KCC2 (Woodin et al., 2003). This results in less outward Cl^- transport and thus a depolarization of E_{GABA-A} that weakens inhibition. This plasticity occurs in cultured hippocampal neurons (Woodin et al., 2003), and hippocampal slices prepared from juveniles and mature rats (Woodin et al., 2003; Ormond and Woodin, 2009). The central requirement for the induction of ionic shift plasticity appears to be an appropriate level of Ca^{2+} influx, and not the Ca^{2+} source. In hippocampal cultures and slices from juveniles, Ca^{2+} influx via VGCCs is sufficient (Woodin et al., 2003). However in slices from adults, Ca^{2+} influx through both VGCCs and NMDARs is required (Ormond and Woodin, 2009). In these experiments STDP was induced by paired stimulation of the Schaeffer collaterals and pyramidal neurons with both glutamatergic and GABAergic transmission intact. Thus in the adult there is cooperation between glutamatergic and GABAergic transmission; glutamate facilitates the opening of NMDARs, which is required for GABAergic STDP. Regardless of the source of Ca^{2+} influx, the mechanism appears to be a posttranslational modification of KCC2 (Acton et al., 2009; Ormond and Woodin, 2009). Ionic shift plasticity can also be induced by repetitive prolonged stimulation of the postsynaptic neuron (Fiumelli et al., 2005; Brumback and Staley, 2008). However there is discrepancy regarding the mechanism of this plasticity. In one scenario, the required Ca^{2+} influx occurs via release from internal stores, and results in a PKC-dependent regulation of KCC2 (Fiumelli et al., 2005). In the other scenario, the spiking resets the thermodynamic equilibrium for NKCC1 transport which indirectly lead to changes in neuronal Cl^- (Brumback and Staley, 2008).

During early postnatal life when NKCC1 is the dominantly expressed Cl^--transporter, the same STDP induction protocol that induces ionic shift plasticity in the mature CNS also modifies immature synapses (Balena and Woodin, 2008; Xu et al., 2008). The difference is that at immature synapses we see the direction of the plasticity reverse. Coincident pre- and postsynaptic activity at 5 Hz hyperpolarizes E_{GABA-A} through a regulation of NKCC1 which strengths inhibition. In the developing CNS ionic shift plasticity appears to be frequency dependent. Increasing the stimulation frequency above 20 Hz (while maintaining the spike timing interval) produces a $GABA_BR$ and CaMKII-dependent depolarization of E_{GABA-A}, likely due to GABA spillover that occurs at higher frequencies (Xu et al., 2008).

SYNAPSE-SPECIFICITY OF IONIC SHIFT PLASTICITY

One of the most prominent differences between ionic shift plasticity and glutamatergic plasticity onto interneurons is that while the latter is mainly homosynaptic, ionic shift plasticity has the potential to be heterosynaptic. Ionic shift plasticity produces a change in the Cl^- gradient at the activated synapse; because Cl^- is a diffusible ion we can expect this gradient change to also affect neighboring synapses within the same neuronal compartment. Moreover, given that GABAergic synapses terminate onto pyramidal cell dendritic shafts rather than spines, any postsynaptic change in the Cl^- concentration is unlikely to be restricted to the activated postsynaptic site. Because basket cell interneurons primarily target the principal cell perisomatic region, we would expect the shift in the Cl^- gradient to extend throughout the somatic compartment. However we would not necessarily expect the change in the Cl^- gradient to extend beyond the somatic compartment to dendrites or axon because it is known that pyramidal cells can maintain domain-specific intracellular Cl^- gradients (Szabadics et al., 2006; Khirug et al., 2008).

REGULATION OF INHIBITORY STRENGTH IN NEURONAL NETWORKS

What is the function of this ionic shift plasticity? Neuronal patterns of activity that induce glutamatergic STDP in the CA1 region of the hippocampus can also induce GABAergic STDP of interneurons onto pyramidal neurons (Ormond and Woodin, 2009). It has been demonstrated both computationally and experimentally that GABAergic STDP regulates pyramidal neuron spiking (Saraga et al., 2008) and produces a disinhibition-mediated LTP (Ormond and Woodin, 2009). This is perhaps not surprising given that GABAergic inhibition in the CA1 is known to regulate synaptic integration and spike timing (Pouille and Scanziani, 2001; Lamsa et al., 2005).

ACKNOWLEDGMENTS

Original work of the authors cited in this review has been supported by the Wellcome Trust, the UK Medical Research Council, the European Research Council, the Natural Sciences Research Council of Canada, and the DAAD German Academic Exchange Service.

REFERENCES

Acton, B. A., Mercado, A., Mount, D. B., and Woodin, M. A. (2009). *Activity-Dependent Modification of the K+/Cl– Cotransporter KCC2 in the Hippocampus*. Chicago, IL: Society for Neuroscience. Online.

Alle, H., Jonas, P., and Geiger, J. R. (2001). PTP and LTP at a hippocampal mossy fiber-interneuron synapse. *Proc. Natl. Acad. Sci. U.S.A.* 98, 14708–14713.

Ascoli, G. A., Alonso-Nanclares, L., Anderson, S. A., Barrionuevo, G., Benavides-Piccione, R., Burkhalter, A., Buzsaki, G., Cauli, B., Defelipe, J., Fairen, A., Feldmeyer, D., Fishell, G., Fregnac, Y., Freund, T. F., Gardner, D., Gardner, E. P., Goldberg, J. H., Helmstaedter, M., Hestrin, S., Karube, F., Kisvarday, Z. F., Lambolez, B., Lewis, D. A., Marin, O., Markram, H., Munoz, A., Packer, A., Petersen, C. C., Rockland, K. S., Rossier, J., Rudy, B., Somogyi, P., Staiger, J. F., Tamas, G., Thomson, A. M., Toledo-Rodriguez, M., Wang, Y., West, D. C., and Yuste, R. (2008).

Petilla terminology: nomenclature of features of GABAergic interneurons of the cerebral cortex. *Nat. Rev. Neurosci.* 9, 557–568.

Balena, T., and Woodin, M. A. (2008). Coincident pre- and postsynaptic activity downregulates NKCC1 to hyperpolarize E(Cl) during development. *Eur. J. Neurosci.* 27, 2402–2412.

Blaesse, P., Airaksinen, M. S., Rivera, C., and Kaila, K. (2009). Cation-chloride cotransporters and neuronal function. *Neuron* 61, 820–838.

Brumback, A. C., and Staley, K. J. (2008). Thermodynamic regulation of NKCC1-mediated Cl-cotransport underlies plasticity of GABA(A) signaling in neonatal neurons. *J. Neurosci.* 28, 1301–1312.

Buzsaki, G., and Eidelberg, E. (1982). Direct afferent excitation and long-term potentiation of hippocampal interneurons. *J. Neurophysiol.* 48, 597–607.

Caillard, O., Ben-Ari, Y., and Gaiarsa, J. L. (1999a). Mechanisms of induction and expression of long-term depression at GABAergic synapses in the neonatal rat hippocampus. *J. Neurosci.* 19, 7568–7577.

Caillard, O., Ben-Ari, Y., and Gaiarsa, J. L. (1999b). Long-term potentiation of GABAergic synaptic transmission in neonatal rat hippocampus. *J. Physiol. (Lond.)* 518(Pt 1), 109–119.

Chen, H. X., Jiang, M., Akakin, D., and Roper, S. N. (2009). Long-term potentiation of excitatory synapses on neocortical somatostatin-expressing interneurons. *J. Neurophysiol.* 102, 3251–3259.

Cohen, I., Navarro, V., Clemenceau, S., Baulac, M., and Miles, R. (2002). On the origin of interictal activity in human temporal lobe epilepsy in vitro. *Science* 298, 1418–1421.

Coull, J. A., Beggs, S., Boudreau, D., Boivin, D., Tsuda, M., Inoue, K., Gravel, C., Salter, M. W., and De Koninck, Y. (2005). BDNF from microglia causes the shift in neuronal anion gradient underlying neuropathic pain. *Nature* 438, 1017–1021.

Csicsvari, J., Hirase, H., Czurko, A., and Buzsaki, G. (1998). Reliability and state dependence of pyramidal cell-interneuron synapses in the hippocampus: an ensemble approach in the behaving rat. *Neuron* 21, 179–189.

Dzhala, V. I., Talos, D. M., Sdrulla, D. A., Brumback, A. C., Mathews, G. C., Benke, T. A., Delpire, E., Jensen, F. E., and Staley, K. J. (2005). NKCC1 transporter facilitates seizures in the developing brain. *Nat. Med.* 11, 1205–1213.

Farrant, M., and Kaila, K. (2007). The cellular, molecular and ionic basis of GABA(A) receptor signalling. *Prog. Brain Res.* 160, 59–87.

Ferraguti, F., Cobden, P., Pollard, M., Cope, D., Shigemoto, R., Watanabe, M., and Somogyi, P. (2004). Immunolocalization of metabotropic glutamate receptor 1alpha (mGluR1alpha) in distinct classes of interneuron in the CA1 region of the rat hippocampus. *Hippocampus* 14, 193–215.

Fino, E., Deniau, J. M., and Venance, L. (2008). Cell-specific spike-timing-dependent plasticity in GABAergic and cholinergic interneurons in corticostriatal rat brain slices. *J. Physiol. (Lond.)* 586, 265–282.

Fino, E., Paille, V., Deniau, J. M., and Venance, L. (2009). Asymmetric spike-timing dependent plasticity of striatal nitric oxide-synthase interneurons. *Neuroscience* 160, 744–754.

Fiumelli, H., Cancedda, L., and Poo, M. M. (2005). Modulation of GABAergic transmission by activity via postsynaptic Ca2+-dependent regulation of KCC2 function. *Neuron* 48, 773–786.

Fiumelli, H., and Woodin, M. A. (2007). Role of activity-dependent regulation of neuronal chloride homeostasis in development. *Curr. Opin. Neurobiol.* 17, 81–86.

Freund, T. F., and Buzsaki, G. (1996). Interneurons of the hippocampus. *Hippocampus* 6, 347–470.

Gaiarsa, J. L., Caillard, O., and Ben-Ari, Y. (2002). Long-term plasticity at GABAergic and glycinergic synapses: mechanisms and functional significance. *Trends Neurosci.* 25, 564–570.

Galvan, E. J., Calixto, E., and Barrionuevo, G. (2008). Bidirectional Hebbian plasticity at hippocampal mossy fiber synapses on CA3 interneurons. *J. Neurosci.* 28, 14042–14055.

Gamba, G. (2005). Molecular physiology and pathophysiology of electroneutral cation-chloride cotransporters. *Physiol. Rev.* 85, 423–493.

Gibson, H. E., Edwards, J. G., Page, R. S., Van Hook, M. J., and Kauer, J. A. (2008). TRPV1 channels mediate long-term depression at synapses on hippocampal interneurons. *Neuron* 57, 746–759.

Giese, K. P., Fedorov, N. B., Filipkowski, R. K., and Silva, A. J. (1998). Autophosphorylation at Thr286 of the alpha calcium-calmodulin kinase II in LTP and learning. *Science* 279, 870–873.

Gubellini, P., Ben-Ari, Y., and Gaiarsa, J. L. (2005). Endogenous neurotrophins are required for the induction of GABAergic long-term potentiation in the neonatal rat hippocampus. *J. Neurosci.* 25, 5796–5802.

Haas, J. S., Nowotny, T., and Abarbanel, H. D. (2006). Spike-timing-dependent plasticity of inhibitory synapses in the entorhinal cortex. *J. Neurophysiol.* 96, 3305–3313.

Heifets, B. D., and Castillo, P. E. (2009). Endocannabinoid signaling and long-term synaptic plasticity. *Annu. Rev. Physiol.* 71, 283–306.

Holmgren, C. D., and Zilberter, Y. (2001). Coincident spiking activity induces long-term changes in inhibition of neocortical pyramidal cells. *J. Neurosci.* 21, 8270–8277.

Jia, Y., Yamazaki, Y., Nakauchi, S., Ito, K., and Sumikawa, K. (2010). Nicotine facilitates long-term potentiation induction in oriens–lacunosum moleculare cells via Ca entry through non-alpha7 nicotinic acetylcholine receptors. *Eur. J. Neurosci.* 31, 463–476.

Khirug, S., Yamada, J., Afzalov, R., Voipio, J., Khiroug, L., and Kaila, K. (2008). GABAergic depolarization of the axon initial segment in cortical principal neurons is caused by the Na-K-2Cl cotransporter NKCC1. *J. Neurosci.* 28, 4635–4639.

Klausberger, T., and Somogyi, P. (2008). Neuronal diversity and temporal dynamics: the unity of hippocampal circuit operations. *Science* 321, 53–57.

Komatsu, Y. (1994). Age-dependent long-term potentiation of inhibitory synaptic transmission in rat visual cortex. *J. Neurosci.* 14, 6488–6499.

Kullmann, D. M., and Lamsa, K. P. (2007). Long-term synaptic plasticity in hippocampal interneurons. *Nat. Rev. Neurosci.* 8, 687–699.

Laezza, F., and Dingledine, R. (2004). Voltage-controlled plasticity at GluR2-deficient synapses onto hippocampal interneurons. *J. Neurophysiol.* 92, 3575–3581.

Laezza, F., Doherty, J. J., and Dingledine, R. (1999). Long-term depression in hippocampal interneurons: joint requirement for pre- and postsynaptic events. *Science* 285, 1411–1414.

Lamsa, K., Heeroma, J. H., and Kullmann, D. M. (2005). Hebbian LTP in feed-forward inhibitory interneurons and the temporal fidelity of input discrimination. *Nat. Neurosci.* 8, 916–924.

Lamsa, K., Irvine, E. E., Giese, K. P., and Kullmann, D. M. (2007a). NMDA receptor-dependent long-term potentiation in mouse hippocampal interneurons shows a unique dependence on Ca(2+)/calmodulin-dependent kinases. *J. Physiol. (Lond.)* 584, 885–894.

Lamsa, K. P., Heeroma, J. H., Somogyi, P., Rusakov, D. A., and Kullmann, D. M. (2007b). Anti-Hebbian long-term potentiation in the hippocampal feedback inhibitory circuit. *Science* 315, 1262–1266.

Lapointe, V., Morin, F., Ratte, S., Croce, A., Conquet, F., and Lacaille, J. C. (2004). Synapse-specific mGluR1-dependent long-term potentiation in interneurones regulates mouse hippocampal inhibition. *J. Physiol. (Lond.)* 555, 125–135.

Lei, S., and McBain, C. J. (2004). Two loci of expression for long-term depression at hippocampal mossy fiber-interneuron synapses. *J. Neurosci.* 24, 2112–2121.

Lien, C. C., Mu, Y., Vargas-Caballero, M., and Poo, M. M. (2006). Visual stimuli-induced LTD of GABAergic synapses mediated by presynaptic NMDA receptors. *Nat. Neurosci.* 9, 372–380.

Lu, J. T., Li, C. Y., Zhao, J. P., Poo, M. M., and Zhang, X. H. (2007). Spike-timing-dependent plasticity of neocortical excitatory synapses on inhibitory interneurons depends on target cell type. *J. Neurosci.* 27, 9711–9720.

Lu, Y. M., Mansuy, I. M., Kandel, E. R., and Roder, J. (2000). Calcineurin-mediated LTD of GABAergic inhibition underlies the increased excitability of CA1 neurons associated with LTP. *Neuron* 26, 197–205.

Maccaferri, G., Toth, K., and McBain, C. J. (1998). Target-specific expression of presynaptic mossy fiber plasticity. *Science* 279, 1368–1370.

Maffei, A., Nataraj, K., Nelson, S. B., and Turrigiano, G. G. (2006). Potentiation of cortical inhibition by visual deprivation. *Nature* 443, 81–84.

Mahanty, N. K., and Sah, P. (1998). Calcium-permeable AMPA receptors mediate long-term potentiation in interneurons in the amygdala. *Nature* 394, 683–687.

McBain, C. J., DiChiara, T. J., and Kauer, J. A. (1994). Activation of metabotropic glutamate receptors differentially affects two classes of hippocampal interneurons and potentiates excitatory synaptic transmission. *J. Neurosci.* 14, 4433–4445.

McBain, C. J., and Kauer, J. A. (2009). Presynaptic plasticity: targeted control of inhibitory networks. *Curr. Opin. Neurobiol.* 19, 254–262.

McMahon, L. L., and Kauer, J. A. (1997). Hippocampal interneurons express a novel form of synaptic plasticity. *Neuron* 18, 295–305.

Mercado, A., Mount, D. B., and Gamba, G. (2004). Electroneutral cation-chloride cotransporters in the central nervous system. *Neurochem. Res.* 29, 17–25.

Nissen, W., Szabo, A., Somogyi, J., Somogyi, P., and Lamsa, K. P. (2010). Cell type-specific long-term plasticity at glutamatergic synapses onto hippocampal interneurons expressing either parvalbumin or CB1

cannabinoid receptor. *J. Neurosci.* 30, 1337–1347.

Nugent, F. S., and Kauer, J. A. (2008). LTP of GABAergic synapses in the ventral tegmental area and beyond. *J. Physiol. (Lond.)* 586, 1487–1493.

Oren, I., Nissen, W., Kullmann, D. M., Somogyi, P., and Lamsa, K. P. (2009). Role of ionotropic glutamate receptors in long-term potentiation in rat hippocampal CA1 oriens-lacunosum moleculare interneurons. *J. Neurosci.* 29, 939–950.

Ormond, J., and Woodin, M. A. (2009). Disinhibition mediates a form of hippocampal long-term potentiation in area CA1. *PLoS ONE* 4, e7224. doi: 10.1371/journal.pone.0007224.

Patenaude, C., Chapman, C. A., Bertrand, S., Congar, P., and Lacaille, J. C. (2003). GABAB receptor- and metabotropic glutamate receptor-dependent cooperative long-term potentiation of rat hippocampal GABAA synaptic transmission. *J. Physiol. (Lond.)* 553, 155–167.

Patenaude, C., Massicotte, G., and Lacaille, J. C. (2005). Cell-type specific GABA synaptic transmission and activity-dependent plasticity in rat hippocampal stratum radiatum interneurons. *Eur. J. Neurosci.* 22, 179–188.

Payne, J. A., Rivera, C., Voipio, J., and Kaila, K. (2003). Cation-chloride co-transporters in neuronal communication, development and trauma. *Trends Neurosci.* 26, 199–206.

Pelkey, K. A., Lavezzari, G., Racca, C., Roche, K. W., and McBain, C. J. (2005). mGluR7 is a metaplastic switch controlling bidirectional plasticity of feedforward inhibition. *Neuron* 46, 89–102.

Perez, Y., Morin, F., and Lacaille, J. C. (2001). A hebbian form of long-term potentiation dependent on mGluR1a in hippocampal inhibitory interneurons. *Proc. Natl. Acad. Sci. U.S.A.* 98, 9401–9406.

Plotkin, M. D., Snyder, E. Y., Hebert, S. C., and Delpire, E. (1997). Expression of the Na-K-2Cl cotransporter is developmentally regulated in postnatal rat brains: a possible mechanism underlying GABA's excitatory role in immature brain. *J. Neurobiol.* 33, 781–795.

Pouille, F., and Scanziani, M. (2001). Enforcement of temporal fidelity in pyramidal cells by somatic feed-forward inhibition. *Science* 293, 1159–1163.

Rheims, S., Holmgren, C. D., Chazal, G., Mulder, J., Harkany, T., Zilberter, T., and Zilberter, Y. (2009). GABA action in immature neocortical neurons directly depends on the availability of ketone bodies. *J. Neurochem.* 110, 1330–1338.

Rivera, C., Li, H., Thomas-Crusells, J., Lahtinen, H., Viitanen, T., Nanobashvili, A., Kokaia, Z., Airaksinen, M. S., Voipio, J., Kaila, K., and Saarma, M. (2002). BDNF-induced TrkB activation down-regulates the K+-Cl– cotransporter KCC2 and impairs neuronal Cl– extrusion. *J. Cell Biol.* 159, 747–752.

Rivera, C., Voipio, J., Payne, J. A., Ruusuvuori, E., Lahtinen, H., Lamsa, K., Pirvola, U., Saarma, M., and Kaila, K. (1999). The K+/Cl– co-transporter KCC2 renders GABA hyperpolarizing during neuronal maturation. *Nature* 397, 251–255.

Russell, J. M. (2000). Sodium-potassium-chloride cotransport. *Physiol. Rev.* 80, 211–276.

Russmann, H., Lamy, J. C., Shamim, E. A., Meunier, S., and Hallett, M. (2009). Associative plasticity in intracortical inhibitory circuits in human motor cortex. *Clin. Neurophysiol* 120, 1204–1212.

Santos, S. F., Luz, L. L., Szucs, P., Lima, D., Derkach, V. A., and Safronov, B. V. (2009). Transmission efficacy and plasticity in glutamatergic synapses formed by excitatory interneurons of the substantia gelatinosa in the rat spinal cord. *PLoS ONE* 4, e8047. doi: 10.1371/journal.pone.0008047.

Saraga, F., Balena, T., Wolansky, T., Dickson, C. T., and Woodin, M. A. (2008). Inhibitory synaptic plasticity regulates pyramidal neuron spiking in the rodent hippocampus. *Neuroscience* 155, 64–75.

Sarihi, A., Jiang, B., Komaki, A., Sohya, K., Yanagawa, Y., and Tsumoto, T. (2008). Metabotropic glutamate receptor type 5-dependent long-term potentiation of excitatory synapses on fast-spiking GABAergic neurons in mouse visual cortex. *J. Neurosci.* 28, 1224–1235.

Stelzer, A., Simon, G., Kovacs, G., and Rai, R. (1994). Synaptic disinhibition during maintenance of long-term potentiation in the CA1 hippocampal subfield. *Proc. Natl. Acad. Sci. U.S.A.* 91, 3058–3062.

Szabadics, J., Varga, C., Molnar, G., Olah, S., Barzo, P., and Tamas, G. (2006). Excitatory effect of GABAergic axo-axonic cells in cortical microcircuits. *Science* 311, 233–235.

Topolnik, L., Congar, P., and Lacaille, J. C. (2005). Differential regulation of metabotropic glutamate receptor- and AMPA receptor-mediated dendritic Ca2+ signals by presynaptic and postsynaptic activity in hippocampal interneurons. *J. Neurosci.* 25, 990–1001.

Tzounopoulos, T., Kim, Y., Oertel, D., and Trussell, L. O. (2004). Cell-specific, spike timing-dependent plasticities in the dorsal cochlear nucleus. *Nat. Neurosci.* 7, 719–725.

van den Pol, A. N., Obrietan, K., and Chen, G. (1996). Excitatory actions of GABA after neuronal trauma. *J. Neurosci.* 16, 4283–4292.

Woodin, M. A., Ganguly, K., and Poo, M. M. (2003). Coincident pre- and postsynaptic activity modifies GABAergic synapses by postsynaptic changes in Cl– transporter activity. *Neuron* 39, 807–820.

Xu, C., Zhao, M. X., Poo, M. M., and Zhang, X. H. (2008). GABA(B) receptor activation mediates frequency-dependent plasticity of developing GABAergic synapses. *Nat. Neurosci.* 11, 1410–1418.

Xu, J. C., Lytle, C., Zhu, T. T., Payne, J. A., Benz, E., Jr., and Forbush, B., 3rd. (1994). Molecular cloning and functional expression of the bumetanide-sensitive Na-K-Cl cotransporter. *Proc. Natl. Acad. Sci. U.S.A.* 91, 2201–2205.

Yazaki-Sugiyama, Y., Kang, S., Cateau, H., Fukai, T., and Hensch, T. K. (2009). Bidirectional plasticity in fast-spiking GABA circuits by visual experience. *Nature* 462, 218–221.

Conflict of Interest Statement: The authors declare that the research was conducted in the absence of any commercial or financial relationships that could be construed as a potential conflict of interest.

Received: 31 January 2010; paper pending published: 15 February 2010; accepted: 17 May 2010; published online: 21 June 2010. Citation: Lamsa KP, Kullmann DM and Woodin MA (2010) Spike-timing dependent plasticity in inhibitory circuits. Front. Syn. Neurosci. 2:8. doi: 10.3389/fnsyn.2010.00008

frontiers in
COMPUTATIONAL NEUROSCIENCE

REVIEW ARTICLE
published: 31 December 2010
doi: 10.3389/fncom.2010.00156

Anti-Hebbian spike-timing-dependent plasticity and adaptive sensory processing

Patrick D. Roberts* and Todd K. Leen

Biomedical Engineering, Oregon Health and Science University, Portland, OR, USA

Edited by:
Wulfram Gerstner, Ecole Polytechnique Fédérale de Lausanne, Switzerland

Reviewed by:
Bruce A. Carlson, Washington University in St. Louis, USA
Jean-Pascal Pfister, Cambridge University, UK

****Correspondence:***
Patrick D. Roberts, Biomedical Engineering, Oregon Health and Science University, Portland, OR 97239, USA.
e-mail: robertpa@ohsu.edu

Adaptive sensory processing influences the central nervous system's interpretation of incoming sensory information. One of the functions of this adaptive sensory processing is to allow the nervous system to ignore predictable sensory information so that it may focus on important novel information needed to improve performance of specific tasks. The mechanism of spike-timing-dependent plasticity (STDP) has proven to be intriguing in this context because of its dual role in long-term memory and ongoing adaptation to maintain optimal tuning of neural responses. Some of the clearest links between STDP and adaptive sensory processing have come from *in vitro*, *in vivo*, and modeling studies of the electrosensory systems of weakly electric fish. Plasticity in these systems is anti-Hebbian, so that presynaptic inputs that repeatedly precede, and possibly could contribute to, a postsynaptic neuron's firing are weakened. The learning dynamics of anti-Hebbian STDP learning rules are stable if the timing relations obey strict constraints. The stability of these learning rules leads to clear predictions of how functional consequences can arise from the detailed structure of the plasticity. Here we review the connection between theoretical predictions and functional consequences of anti-Hebbian STDP, focusing on adaptive processing in the electrosensory system of weakly electric fish. After introducing electrosensory adaptive processing and the dynamics of anti-Hebbian STDP learning rules, we address issues of predictive sensory cancelation and novelty detection, descending control of plasticity, synaptic scaling, and optimal sensory tuning. We conclude with examples in other systems where these principles may apply.

Keyword: electrosensory, mormyrid, learning dynamics, stability, descending control, stochastic

Expectations and predictions are essential for efficient processing sensory information (Barlow, 1990). If expected sensory patterns are subtracted from sensory signals, then novel sensory patterns, important to the survival of an organism, are accentuated. Any novel stimulus that is persistently associated with other neural signals will eventually become predictable. Hence, sensory processing systems must continually adapt to changing sensory environmental conditions to take full advantage of such predictive coding strategies.

Because biological processes interact across different time scales in adaptive sensory systems, mathematical modeling is helpful to untangle multiple causes from their effects. This review discusses attempts that have been made to model adaptive sensory filters based on spike-timing-dependent plasticity (STDP). The model systems are found in electrosensory systems, but the principles discussed here are applicable to many sensory systems.

The two types of electrosensory systems that we will discuss in terms of modeling are the passive and active electrosensory system of weakly electric fish. We will focus on the initial processing structure in the electrosensory lateral line lobe (ELL) of mormyrid electric fish, where passive and active electrosensory information is conveyed and processed by separate sensory pathways. The basic functional structure of these two electrosensory pathways is the convergence of primary electrosensory input with a variety of sensory and motor signals that could serve to predict changes in the electrosensory input (**Figure 1**). Spike-timing-dependent synaptic plasticity at the synapse carrying predictive signals sculpts a negative image of predictable sensory input patterns from a background of sensorimotor activity. The summation of these negative images with the sensory input results in a cancelation of predictable features.

1 MORMYRID ELECTROSENSORY SYSTEM

Mormyrid electric fish have an electric organ in their tail that generates a weak electric field. A motor command causes the electric organ to discharge in pulses (Bennett, 1970; Hopkins, 1995), like the flexing of a muscle. By detecting distortions caused by external objects in the fish's own electric field, mormyrids can navigate through their environment without vision (Assad et al., 1999; Von der Emde, 1999). This active *electro*location system is similar to *echo*location in bats. The electric organ discharge (EOD) is also used for communication with conspecifics (Hopkins, 1988).

Mormyrids have three types of electroreceptors that serve three different functions (Bodznick and Montgomery, 2005; Kawasaki, 2005): active electrolocation, communication, and passive detection of external sources of electric fields, such as moving organisms. Behaviorally relevant stimuli associated with prey result in extremely small changes in the fish's self-generated field detected by receptors for active electrolocation and relatively weak fields caused by the prey's movement detected by receptors for passive electrolocation.

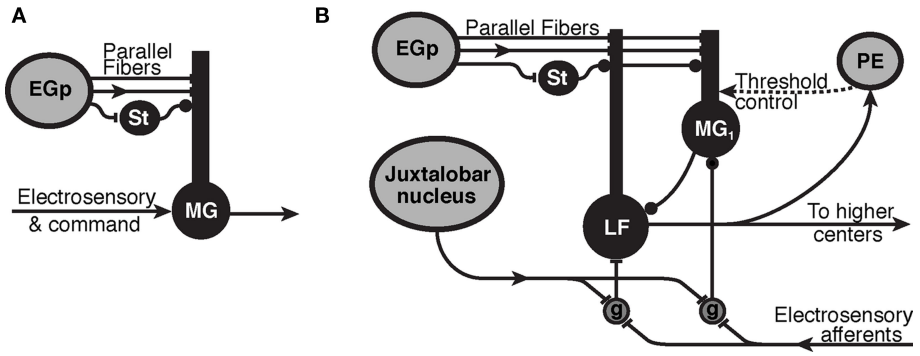

FIGURE 1 | Synaptic organization of cerebellum-like structures in mormyrid fish. **(A)** Simplified circuit of electrosensory lateral line lobe (ELL) used for modeling of the passive electrosensory system. Parallel fibers originate in the eminentia granularis posterior (EGp) and synapse onto the apical dendrites of medium ganglion (MG) cell with excitatory synapses (bar terminals) and inhibitory stellate cells (St) synapse in the same layer with inhibitory synapses (disk terminals). The parallel fibers carry a sequence of delayed inputs that convey the timing of the EOD command. The Purkinje-like MG cell cancels expected electrosensory signals with an STDP mechanism at the synapse from parallel fibers and stellate cells. Arrows represent the flow of information and mixed inputs. **(B)** ELL circuitry for the active electrosensory system. Mormyromast electroreceptors transform the field intensity at the skin into a spike latency code that is transformed into a spike burst duration code by deep granular cells (g) controlled by centrally generated corollary discharge input from the juxtalobar nucleus. The electrosensory signal is then transferred to the adaptive stage of electrosensory processing (type-1 medium ganglion (MG_1) and large fusiform (LF) cells), and the expected sensory responses are subtracted. Recurrent connections, modulated by higher centers (preeminential nucleus, PE), are hypothesized to control the threshold of back-propagating broad (dendritic) spikes in MG_1 cells.

In both the active and passive pathways, the challenge for the electrosensory system is to detect small behaviorally relevant signals in the midst of much larger signals resulting from the fish's own behavior. In the active system, moving the tail changes the position of the electric organ relative to the electroreceptors on the body surface and produces large changes in the electric field the receptors are exposed to. In the passive system, the fish's EOD swamps the receptors that need to detect weak, externally generated fields. In order to detect weak changes in signals, the fish integrates self-generated proprioceptive and timing information about where and when the EODs, information that could be used to process re-afferent signals. We will focus on the passive system first and the mechanism of canceling the EOD using timing information.

2 EXPECTATION CANCELATION IN PASSIVE ELECTROSENSORY SYSTEMS

The command to generate an EOD is sent to the electric organ, and results in a following sensory *re-afferent* signal (von Holst and Mittelstaedt, l950) from electroreceptors responding to the EOD signal that central neurons in the ELL. Simultaneously, information about the timing of the motor command is relayed to the ELL through another neural pathway as a corollary discharge signal.

The ELL is a laminar, cerebellum-like structure where electrosensory afferents enter from the deep layer. There is a layer of large cells in the ELL, called the ganglion layer, where the cells show strong adaptation to changing sensory images (Bell, 1982). We focus on one class of principal cells in this layer, the medium ganglion (MG) cells, because they receive the most parallel fiber synapses Meek and Grant (1994). MG cells have basal dendrites that receive the electrosensory afferent input and apical dendrites that reach into the molecular layer to receive a variety of synaptic inputs from parallel fibers (PF). The PF originate externally to the ELL, as granule cells that respond to the corollary discharge in the eminentia granularis posterior (EGp) nucleus, PF also drive inhibitory interneurons (stellate cells) that synapse onto MG cells (**Figure 1A**).

Recordings from the EGp nucleus containing granule cells suggest that the granule cells do not respond to the corollary discharge simultaneously, but their responses appear to be distributed sequentially during the time following the command signal (Bell et al., 1992; Sawtell, 2010). Following each EOD motor command, different granule cells fire at different latencies so that PF carry a distribution of spikes timed at different delays following each EOD. Because corollary discharge information on electric discharge timing arrives at MG cells through PF, a likely candidate for an adaptive mechanism would be the synapse between the PF and the apical dendrites of MG cells.

Medium ganglion cells respond to a depolarizing input with two types of spikes: a small narrow spike and a large, broad spike that is generated at a higher threshold than the narrow spike and mediates synaptic plasticity. Experimental evidence suggests that the small spike is axonal and the broad spike propagates into the dendrites (Grant et al., 1998). The dendritic spike would inform the parallel fiber synapses of strong depolarization caused by afferent sensory input to the basilar dendrites and mediates plasticity at the synapses from the PF to the MG cells.

Within each network shown in **Figure 1**, the main process is that principal cells are excited by a large set of inputs that carry contextual information. In addition, the principal MG cells are inhibited via inhibitory interneurons that respond to the same large set of inputs. The convergence of contextual information onto a Purkinje-like neuron suggests that associative plasticity at the synapses onto MG cells may provide the system a means of sorting the incoming information for sensory processing. In addition, the plasticity should be dependent on the timing of broad (dendritic) spikes in MG cells.

To test for spike-timing-dependent changes at the parallel fiber synapse onto MG cells, Bell et al. (1997d) used a slice preparation of the ELL to stimulate the PF and measure the resulting parallel

fiber-evoked excitatory postsynaptic potential (EPSP). In these experiments, changes in the size of the EPSPs were taken as a proxy for changes in the strength of excitatory parallel fiber synapses. The MG cell was depolarized to generate a broad spike at various delays from the parallel fiber stimulus. After repeatedly pairing a stimulation with a broad spike at a certain delay, the strength of the synapse was remeasured. Some delays increased the synaptic strength, while others decreased it. When all the changes were plotted as a function of the delays, it was found that the synapse was depressed if the broad spikes immediately followed the stimulation; otherwise the synaptic strength was enhanced. Furthermore, the depression was in a window of about the same duration, and coincident with, the EPSP evoked by PF.

The activity dependent changes do not appear to be limited to parallel fiber EPSPs. Some experiments showed spike-timing-dependent changes in parallel fiber-evoked, postsynaptic potentials, which were mostly inhibitory (IPSP; Bell et al., 1997c). The synapses where these changes take place are most likely from stellate cells in the molecular layer onto the MG cells. The precise characterization of the STDP learning rules led to theoretical investigations (Roberts, 2000b; Roberts and Bell, 2000, 2001) of the effects of STDP at both excitatory and inhibitory synapses to determine how the form of the STDP learning rule affects the function of adaptive sensory processing.

2.1 FORMAL MODEL OF THE MORMYRID PASSIVE ELECTROSENSORY SYSTEM

Several possible approaches present themselves to formalize the neuronal architecture of the ELL, such as conductance-based compartmental models that lead to complex dynamics described by a large set of differential equations. If the questions to be answered by modeling are about the precise spike dynamics of the principal cells in response to the inputs, a conductance-based model would be essential and will be demonstrated in Section 3.3.

However, we are presently interested in the adaptation of responses through many stimulation cycles, so that the details of individual spikes do not affect these dynamics. This leads to a modification, or a "coarse graining," of our model so that only those changes during time intervals greater than individual spikes will be represented. In this approach, only the spike times would be calculated, not the exact form of individual spikes. The different equations that result from this level of modeling emphasize changes in spike rates of the system, though the timing of individual spikes may be preserved. Although the equations are different in these approaches, there should be overlap in their results at certain time scales, if they are both to represent the actual dynamics of the system.

We now describe the analytical methods that have been used for investigating the adaptive responses of MG cell (Roberts, 2000b; Roberts and Bell, 2000, 2001). The MG cells have been modeled by a spike response model (Gerstner and van Hemmen, 1992) with no relative refractory period and two thresholds: a lower threshold for narrow spikes and a higher threshold for broad spikes which mediate plasticity.

There are two time scales in the model. The fast scale is limited to the duration of each EOD cycle on the scale of tens of milliseconds. The slow scale represents the adaptation of synaptic strengths due to synaptic plasticity lasting many EOD cycles and is on the scale of several minutes. These time scales are separated in the model into two components, fast and slow. The x-component is the time in milliseconds following the EOD, and the t-component represents the number of EOD cycles. These coordinates are typically used for representing electrophysiological data such as spike rasters showing changes in a spike response pattern during repeated presentation of a stimulus. In the present application, the x-component is discretized so that $x_n = n(\Delta x)$, with n an integer. The discretization in x_n is related to the times that the various delayed versions of the corollary discharge arrives at MG cells in the ELL. It is assumed that each presynaptic neuron n fires only once per cycle (i.e., at time x_n). Thus, the dynamical variables in the model are dependent on two temporal variables. For instance, the average membrane potential, denoted by $V(x_n, t)$, is a function of both x_n and t. The probability of a broad spike at time x_n in EOD cycle t is a sigmoidal function of the average membrane potential. With threshold θ, and noise parameter μ, the spike probability is given by the expression, $f(x_n,t) = (1 + exp[-\mu(V(x_n, t) - \theta)])^{-1}$. The instantaneous spike frequency is obtained by multiplying the spike probability by the maximum spike frequency.

The membrane potential, in the absence of noise, is the sum of all external inputs. The sensory image representing the re-afferent EOD signal is denoted by $V_{el}(x_n)$. This function is only dependent on x_n because it is held constant in t as the system adapts. The functional form of $V_{el}(x_n)$ represents the stereotyped response of sensory afferents to the EOD.

Excitatory synapses from PF are represented by the sum of a temporal series of weighted EPSP waveforms, $E(x_n)$. The weighting factors, $w(x_m, t)$, change in t as the system adapts due to a learning rule that depends on the relative timing of pre- and postsynaptic spikes (Gerstner et al., 1996; Abbott and Song, 1999; Kempter et al., 1999; Xie and Seung, 2000). The x-component in the argument of $w(x_m, t)$ labels the beginning of the EPSP. The contribution of PF to the MG cell's membrane potential at time x_n in EOD cycle t is

$$V_{pf}(x_n,t) = \sum_{m=1}^{N} w(x_m,t)E(x_n - x_m). \quad (1)$$

The fast time scale is discretized to the time of each synaptic input and N is the number of synaptic inputs so that the period of the EOD cycle is $N(\Delta x)$.

Likewise, inhibitory synapses from stellate cells are included in the model by subtracting a set of weighted IPSP waveforms, $V_{st}(x_n,t) = -\sum_{m=1}^{N} v(x_m,t)I(x_n - x_m)$. The IPSP waveform, $I(x_n)$, was derived from data collected in Dr. Bell's lab where postsynaptic potentials were recorded with and without the presence of bicuculline, a blocker of inhibitory synaptic currents (Grant et al., 1998). The difference yields the inhibitory contribution. The total membrane potential is the sum of the electrosensory input, the parallel fiber input, and the stellate input, $V(x_n, t) = V_{el}(x_n) + V_{pf}(x_n, t) + V_{st}(x_n, t)$.

The spike-timing-dependent learning rules are implemented by changing the synaptic weights with a function that is dependent on the timing of a postsynaptic broad spike, x_b (Roberts and Bell, 2000). The learning rules have two components: a non-associative part and an associative part (Bell et al., 1997d). The change in each excitatory synaptic weight per cycle is

$$\Delta w(x_n,t) = \alpha_w - \beta_w L_w(x_b - x_n). \quad (2)$$

The parameters α_w and β_w denote the non-associative and associative learning rates. The learning function, $L_w(x_b - x_n)$, is positive definite and has an area of unity. Similarly, the change in each inhibitory synaptic weight is,

$$\Delta v(x_n,t) = -\alpha_v + \beta_v L_v(x_b - x_n). \quad (3)$$

In the following calculations, the learning functions are set equal to their respective postsynaptic potential waveforms, $L_w(x_n) = E(x_n)$ and $L_v(x_n) = I(x_n)$.

The ensemble average weight change per EOD cycle calculated using the broad spike probability function, $f(x_p, t)$,

$$\langle \Delta w(x_n,t) \rangle = \alpha_w - \beta_w \sum_{p=1}^{N} L_w(x_p - x_n) f(x_p,t), \quad (4)$$

for excitatory synapses and similarly for the inhibitory synapses, but with the sign of the learning rates reversed. The system-level rate of adaptation is calculated by using the averaged changes in weights. The resultant equations were used to derive analytic results in the continuum approximation (Roberts, 1999; Roberts and Bell, 2000), and for numerical simulations (**Figure 2**). Both approaches have shown that the synaptic learning rule causes the system to adapt to cancel predictable inputs.

2.2 QUESTIONS ANSWERED BY THE FORMAL MODEL

When the learning rules in Eqs (2) and (3) are used in the model, the spike output of the MG cell approaches a fixed point at which the spike probability IS constant in x. The fixed point is at the constant broad spike probability

$$\hat{f} = \frac{\alpha_w + \alpha_v}{\beta_w + \beta_v}. \quad (5)$$

Although the spike probability is constant in t at the fixed point, the weights will be constant only if the learning rates of the excitatory synapses are equivalent to the learning rates of the inhibitory synapses. Otherwise, the weights will drift in such a way that the change in the excitatory input exactly balances the change in the inhibitory input. The drift rate is

$$\langle \Delta w(x_n,t) \rangle = \langle \Delta v(x_n,t) \rangle = \frac{\alpha_w \beta_v - \alpha_v \beta_w}{\beta_w + \beta_v}. \quad (6)$$

The result of this drift is that, in the generic case where the learning rates are not equal, the weights will saturate at their lowest or highest levels. This result is independent of whether the inhibitory inputs are correlated with the EOD cycle. When the inhibitory spikes from stellate cells were uncorrelated with respect to the EOD, then MG cell output reached an equilibrium level, but the inhibitory inputs did not help to cancel the re-afferent sensory image. In fact, if the learning rates of the inhibitory synapses were not set exactly to that of the excitatory synapse, then the synapses drifted to saturate at a level where sensory image cancelation was poor.

However, if the inhibitory spikes were correlated with respect to the EOD, then the system adapted better than without inhibitory inputs. Furthermore, the synaptic weight drift caused by a mismatch between the learning rates of the inhibitory and excitatory synapses would cause the system to save resources by reducing the synaptic input to the minimum that is necessary to cancel the re-afferent sensory image. These analyses suggest that the combination of stable STDP learning dynamics in both excitatory and inhibitory synapses can provide a mechanism for synaptic scaling (Turrigiano, 1999) that minimizes the global synaptic current into a neuron.

To test the stability of the image cancelation under perturbations of the learning rule for excitatory synapses, we analyzed the stability of the fixed point (Williams et al., 2003; Roberts et al., 2006). The negative image is stable only if the timing window for associative depression of excitatory synapses is close to the EPSP. In addition, stability could result if we relax the assumption that the learning function is positive definite to include associative potentiation. Some evidence of such associative potentiation has been observed *in vivo* (Bell et al., 1993) but the evidence has not been shown to be statistically significant *in vitro* (Bell et al., 1997d). All other forms of the STDP learning rule would destroy the function of adaptive mechanism by generating oscillations in the weights within each EOD cycle resulting in oscillating activity that would overwhelm any external stimuli.

In other analyses of the relationship between neural computation and the functional form of the learning rule, Toyoizumi et al. (2005) showed that a match between the learning function and the EPSP would maximize the mutual information. This principle of maximum information for non-predictable stimuli was found in ELL by Sawtell and Williams (2008) who demonstrated that the information about the position of an object was independent of the tail position after processing by ELL, but not in the primary afferents. In a different context, Pfister et al. (2006) showed that if

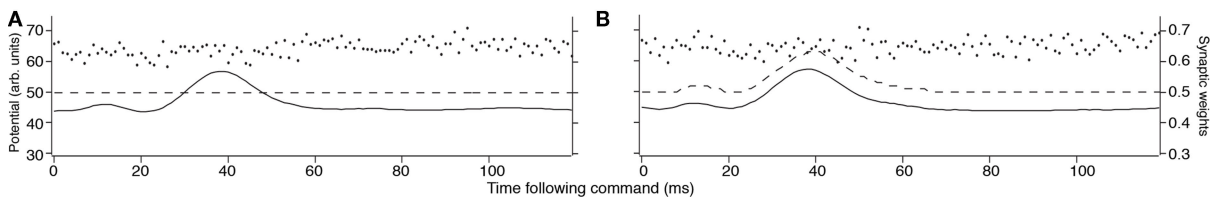

FIGURE 2 | Results of MG cell adaptation simulation. Membrane potential (solid line), dendritic spike threshold (dashed line), and synaptic weights (separate dots) for a model MG cell. **(A)** The idealized waveform represents the corollary discharge with the parallel fiber synaptic strengths, given a random initial weight distribution (arbitrary units where maximum weight = 1.0 and maximum potential V = 100). The horizontal location of the weights represents the delay following the EOD motor command where input begins, and the height represents the synaptic strength. **(B)** After adaptation, the spike-timing-dependent learning rule adjusted the synaptic weights. The synaptic weights for parallel fibers onto the model MG cell are depressed, resulting in a cancelation of the corollary discharge-evoked EPSP.

the postsynaptic neuron is constrained to fire at a constant rate, then the time constant of the learning function has to be matched to the postsynaptic potential for precise timing.

2.3 CHARACTERIZATION OF SYNAPTIC WEIGHT DISTRIBUTIONS

Rate-dependent learning models involve, by definition, averaging over many spike events (either in time, or across a statistical ensemble). Consequently random fluctuations between events are naturally averaged out. In such models, synaptic dynamics are naturally described by *deterministic differential equations*.

The discovery that synaptic changes are mediated by processes sensitive to the relative timing between *individual* pre- and postsynaptic events voided traditional models based on spike *rates*. The random variation in the broad spike timing relative to the PSP (c.f. the broad spike probability from Section 2.1) and the experimentally observed variability in synaptic change even at constant timing, suggest that in contrast to rate-dependent models, the dynamics in our system are more appropriately described by stochastic dynamics.

In our models, the random fluctuations in the weight changes Δw and Δv arise from fluctuations in the postsynaptic broad spike time x_b in Eqs (2) and (3). These fluctuations enter the model through the broad spike probability function $f(x_b)$[1]. In other researchers' models, fluctuations enter learning models from other sources. For example, van Rossum et al. (2000) model the Hebbian learning rule observed by Bi and Mu-Ming Poo (1998) in hippocampal neurons by a learning rule that has exponential dependence on the relative timing between presynaptic and postsynaptic events, and has *additive noise* whose variance is proportional to the synaptic weight.

Regardless of the source of the fluctuations, the time evolution of synaptic weights under STDP is conveniently treated by *stochastic dynamics*. A large class of learning rules, including our models of STDP in the mormyrid ELL and the model that van Rossum et al. (2000) apply to hippocampal neuron, follow a Markov process described by a suitable master equation. Several other authors have modeled STDP by such Markov processes. Authors usually replace the master equation (see below) that describes these processes with a pseudo-approximation – the Fokker–Planck equation (FPE) – obtained by truncating to second order an expansion in powers of the synaptic jumps. As cited above, van Rosum et al. use FPE to model the equilibrium distribution of synaptic weights in the STDP learning rule discovered by Bi and Poo. Their analytic equilibrium distribution agrees well with Monte Carlo simulations, and provides qualitative agreement with experimental quantal amplitude distributions observed in a pyramidal. Cateau and Fukai (2003) use a numerically integrated FPE to determine the equilibrium distribution of synaptic strengths under learning rules similar to those observed in rat hippocampus CA1 neurons. Kepecs et al. (2002) use the FPE to analytically calculate equilibrium distributions arising from learning rules with STDP, and to confirm that Monte Carlo simulations have reached equilibrium. Masuda and Aihara (2004) use the FPE to analyze synaptic competition and the formation of functional clusters. Their theoretical equilibrium distributions match Monte Carlo simulations well. Finally, Burkitt et al. (2004) use the FPE to predict equilibrium synaptic distributions, and compare their analytic results with histograms from Monte Carlo simulations of the learning rules they study. Hence, there is wide agreement that the dynamics of STDP are appropriately treated by stochastic dynamics, in many cases well-described by a Markov process[2]. We note however that *average* ensemble behavior, which can be illuminated by deterministic dynamics, is certainly of interest. For example, Saudargiene et al. (2004) developed a biophysical model of asymmetric STDP learning from a differential Hebbian learning rule in a deterministic framework.

In this description, the synaptic weights $w(x_n, t)$ (respectively $v(x_n, t)$) are random variables with density function $P_w(w(x_n), t)$ (respectively $P_v(v(x_n), t)$). The dynamics of these densities, together with inputs to the circuitry and the response functions of the cells, determine the functional properties of the network. In particular, the stable negative image equilibria of the network correspond to fixed points of the average weight changes; that is, $\langle \Delta w(x_n) \rangle = 0$ in Eq. (4) (and similarly $\langle \Delta v(x_n) \rangle = 0$). (Equation (5) expresses the equilibrium in terms of the broad spike probability.) A consequence of the random fluctuations in the learning rule is that the negative image will be imprecise. The equilibrium density $P_w(w(x_n), t \to \infty)$ for the weights will have, in general, non-zero variance. Hence individual weight values at equilibrium will differ from the average value $<w(x_n)>$ corresponding to the negative image given by Roberts and Bell (2000). This variability, captured by the covariance of w, leads to imprecision in the cancelation of the re-afferent signal.

This is a familiar situation in engineering adaptive filter theory and statistical estimation by stochastic approximation algorithms (a.k.a. on-line learning in the machine learning; Haykin, 2002). In the language of adaptive filter theory, one of the ELL's tasks is to estimate parameters (the synaptic weights from the PF onto the MG cells) so that the network filters out the re-afferent signal. However, the weight-adjustment procedure is noisy, and hence we get noisy estimates of the optimal weights[3].

2.3.1 Mathematical formulation of the synaptic distribution

The Master Equation for learning under the Markov process in Eq. (2) reads

$$P(w, t+1) = \int d\Delta \, \rho_{\Delta|w-\Delta} P(w-\Delta, t), \tag{7}$$

where $P(w, t)$ is the probability density for the weight w at trial t, and $\rho(\Delta \mid w)$ is the probability density of taking a step of size Δ in one EOD cycle, starting from point w (see for example Gardiner, 1985).

[1]Our deterministic learning rule is an idealization of the original data shown by Bell et al. (1997d). Those data show that for given fixed time difference the presynaptic event and the broad spike, there is significant variability (noise) about the mean synaptic change. Hence, even at the level of individual learning events, there is randomness in the mormyrid ELL system.

[2]We are *not* here advocating the use of the FPE to treat these systems since the non-linear Fokker–Planck equation can generate misleading results. We have constructed and applied rigorous perturbation methods in place of the FPE and will make those available in future work. The point here is that stochastic dynamics is an appropriate tool to describe the evolution of synaptic weights under learning rules described by STDP, particularly as in our case where the fluctuations around the weight equilibrium have consequences for the sensory functioning of the circuitry.

[3]The fluctuations about the optimal weights arise here because of noise in the learning rule. This is distinct from the usual variance in statistical estimates owing to sample size restrictions.

The step probability $\rho(\Delta \mid w)$ is governed by the learning rule Eq. (2). The full development was fleshed out by us in Williams et al. (2004) with the resulting master equation

$$P(w,t+1)=\left[1-\frac{1}{T}\int_0^T dx\, f(x,w-\alpha)\right]P(w-\alpha,t) + \frac{1}{T}\int_0^T dx\, f\left(x,w-[\alpha+L_w(x)]\right)P(w-[\alpha+L_w(x)],t), \tag{8}$$

where α is the non-associative learning rate, $L_w(x)$ is the learning function that represents the spike timing dependence, and T is the period of the EOD cycle.

Master equations such as this are, for the most part, intractable. A common approach in computational neuroscience is to substitute a more tractable non-linear FPE for the full master equation as discussed above (van Rossum et al., 2000; Kepecs et al., 2002; Cateau and Fukai, 2003; Burkitt et al., 2004; Masuda and Aihara, 2004). This has met with success, but we advise more care than wholesale adoption of the FPE. The conditions under which the discrete random walk can be properly described by a non-linear FPE are quite narrow as discussed by van Kampen (1992). The required conditions are nearly universally overlooked by practitioners in computational neuroscience.

In our work, we have adopted the random walk in Eq. (8) directly, and approximate a solution by replacing the broad spike firing probability $f(x)$ is with its *linear* approximation. This approximation is equivalent to assuming that the tails of the equilibrium synaptic weight density $P(w, t \to \infty)$ do not penetrate significantly into the non-linear parts of sigmoidal-shaped density f. We verified that for the physiologically relevant parameter range this assumption is valid.

Our analysis (Williams et al., 2004) includes expressions for the first four moments of the equilibrium synaptic weight density for a model consisting of a single synapse. For the more interesting case of multiple synapses, we give a recurrence relation for the equilibrium moments, and solve the recurrence for the equilibrium mean and covariance function

$$\mathrm{cov}(x,y) \equiv \left(w(x) - < w(x) >\right)\left(w(y) - < w(y) >\right).$$

As discussed in Section 2.3 above, the equilibrium covariance affects the precision of the negative image; its contribution to the variance of the true negative image around the optimum is

$$var\left(V_{pf}(x)\right) = \sum_{y,z} E(x-y)cov(y,z)E(x-z). \tag{9}$$

Theoretical prediction of the weight variance for physiologically relevant model parameters, and Monte Carlo simulations confirming the analytic predictions were developed fully in Williams et al. (2004). The results confirm that the error of the negative image estimation is within the tolerance of the sensory image cancelation function for a large number of PF found in cerebellum-like structures.

3 MODIFICATION OF STDP DYNAMICS IN ACTIVE ELECTROLOCATION

3.1 ACTIVE ELECTROLOCATION SYSTEM IN MORMYRIDS

The active electrosensory system is an elaboration of the passive electrosensory system discussed in the previous section, and has additional sources of corollary discharge inputs that refine sensory processing. In addition to the corollary discharge in PF, the active system has deep layer inputs that appear to be necessary for reading out latency coded information about the strength of the electric field. In the passive system, the corollary discharge conveyed by PFs exhibit anti-Hebbian plasticity to eliminate electrosensory responses caused by the EOD. The significance of this plasticity is less clear in the active system, which is designed to specifically process re-afferent signals. One possibility is that plasticity implements a simple gain control so that plastic electric organ corollary discharge inputs serve to control the level of response to maintain best sensitivity. Another possibility is a similar function as in the passive system, to eliminate the effects of predictable signals from the sensory image. However, sensory cancelation algorithm must be more subtle in the active system because it must preserve details in the image related to distortions of the electric field. To clarify the differences in function between the passive and active systems, we introduce further physiological details that appear in the active system.

Specialized *mormyromast* electroreceptors sense the self-generated field and its distortions. Afferent fibers from this type of electroreceptors responds to the fish's own EOD with a small number of spikes that encode the strength of the electric field in the latency of the first spike following the EOD. These responses are conveyed to the cortex of the ELL where the fibers terminate in the mormyromast zone (Bell, 1990).

With each EOD, the ELL cortex is affected not only by inputs from the periphery but also by electric organ corollary discharge signals that originate centrally. These corollary discharge signals are time-locked with the EOD motor command, which elicits the EOD (Zipser and Bennet, 1976). The corollary discharge signals arise from various central structures, one of which is the *juxtalobar nucleus* (JLN), which provides a short, fixed latency timing signal to the deeper layers of the ELL (**Figure 1B**). A second such structure is the EGp, which gives rise to the PF of ELL (**Figure 1**). EGp receives corollary discharge signals at various delays to about 80 ms (Bell et al., 1992).

A clear example of the mechanisms of central control of sensory processing is present in the deeper layers of the region of ELL dedicated to activation electrolocation, where a centrally originating corollary discharge signal from the JLN provides the timing signal (Mohr et al., 2003a) for the decoding of afferent latency as a measure of stimulus intensity. Mormyromast afferents respond to the EOD with a single spike (or short burst). The strength of electrosensory stimuli is encoded as the latency to the leading spike (Bell, 1990; Sawtell and Williams, 2008). The JLN fibers converge onto granular cells that also receive primary afferent inputs. The granular cells act as a coincidence detector that measure the time difference between corollary discharge and the arrival of the mormyromast afferent spike (Meek and Grant, 1994).

Electrosensory processing in the mormyrid is highly specialized for discriminating precise timing of mormyromast afferent signals. Behavioral studies reveal that the fish can discriminate afferent timing changes of less than 100 μs (Hall et al., 1995). In addition, timing is remarkably well-preserved in the pathway from the EOD motor command to the corollary discharge signal in the ELL. Although this signal traverses five synaptic junctions, the signal maintains a variability of less than 50 μs (Bell and Emde, 1995).

As we focus on adaptive processing in the active system, we are first confronted by a serious discrepancy; the output of MG cells should be constant throughout the EOD cycle as in passive system, but MG cells respond with a burst to each EOD command. There are two reasons why this would be functionally expected. First, the active system is designed to detect small changes in the re-afferent signal, not eliminate it like the passive system, so some modulation of the MG cell response should be expected. Secondly, MG cells are interneurons that inhibit efferent cells (**Figure 1B**), so their activity does not represent the final output of the ELL. However, the dynamical stability of the learning rule contradicts the observation of the MG cell spike bursts in the active system. This contradiction suggested that another mechanism is at play to control how the dynamics of STDP regulate electrosensory processing.

3.2 DENDRITIC SPIKE THRESHOLD CONTROL TO REGULATE SYNAPTIC PLASTICITY

In the passive circuit of the ELL, the principal cells respond to the combined external electrical signals with a constant output spike rate that is modulated by *novel* sensory patterns. However, if the principal cells in the active circuit responded with a constant output spike rate, then no information about distortions of the fish's own field could be used to identify external objects. To avoid cancelation of critical information, the learning dynamics are altered by controlling the threshold of back-propagating spikes in the principal cells (Mohr et al., 2003b; Sawtell et al., 2007). This mechanism allows for the neurons of the ELL to respond with a burst of spikes to every command in spite of the dynamics of the STDP learning rule. In addition, this mechanism of controlling the learning dynamics allows control of adaptation in the initial sensory processing stage by higher centers.

Recent studies by Sawtell et al. (2007) suggest that centrally generated signals actively control the threshold of dendritic spikes following the EOD motor command and, thus, control synaptic plasticity and adaptive sensory processing in the ELL. We wish to resolve the apparently paradoxical empirical observation that MG cells are inhibited in the part of the cell where dendritic spikes are initiated, while they are excited in another part of the cell where axon spikes are initiated.

We have constructed a morphologically accurate model of a MG cell that we have used to test the hypotheses that inhibitory synaptic inputs to the apical dendrites that are time-locked to the corollary discharge increase the threshold of dendritic spikes while excitatory inputs simultaneously excite axon spikes. Our simulation demonstrates that inhibitory synaptic current in the dendrites shunt depolarizing currents and modulate the propagation of dendritic spikes during an EPSP that increases the rate of axon spikes.

Our analytic model of the region of ELL that is used for active electrolocation showed that an increase of the dendritic spike threshold relative to the axon spike threshold during the EOD is necessary to reproduce the qualitative features of the MG cell response to the mormyromast burst (Roberts, 2000a; Roberts and Bell, 2003). This prediction was confirmed by Mohr et al. (2003b) in experimental observations of a pause in dendritic spike activity during the command response (**Figure 3B**).

Subsequent experiments showed that the threshold for generating a dendritic spike threshold increases during the corollary discharge response of MG cells (Mohr et al., 2003a). This increase is sufficient to explain the response of MG cells to the corollary discharge. In our simulation, we inserted the predicted increase in the dendritic spike threshold during the corollary discharge into our numerical model neurons (**Figure 3A**). The simulation showed that the corollary discharge-driven EPSP is still present. This modification of the dendritic spike threshold causes the system to be globally stable under the STDP learning rule (Roberts et al., 2006), consistent with the experimentally demonstrated corollary discharge-driven EPSP.

3.3 MG CELL MODEL: MORPHOLOGY AND CURRENTS

To evaluate how descending inputs could modify the dendritic spike threshold, and thereby control STDP we developed a conductance-based model of an MG cell. An MG cell of mormyrid ELL, that was classified as an MG_2, broad spiking cell, was traced (Engelmann et al., 2008) and converted to the format of the NEURON simulation package (Hines and Carnevale, 1997). The original tracing by adding axonal compartments to generate axonal, narrow spikes, and a passive hillock to reduce the size of the narrow spikes as measured at the some, to match the known electrophysiology (Bell et al., 1997b,d).

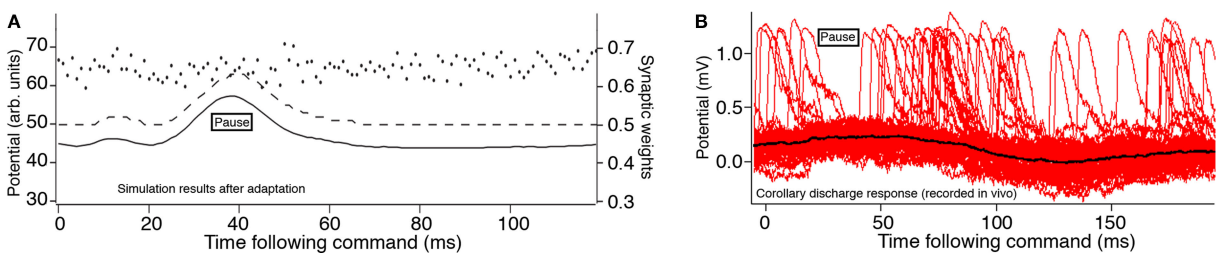

FIGURE 3 | Effects of an increased dendritic spike threshold. Membrane potential (solid line), dendritic spike threshold (dashed line), and synaptic weights (separate dots) for a model MG cells. **(A)** The modified model in which the dendritic spike threshold increases during the time course of the juxtalobar nucleus evoked EPSP, allowing this waveform to persist in the presence of parallel fiber synaptic plasticity (arbitrary units where maximum weight = 1.0 and maximum potential $V = 100$). **(B)** Intracellular recordings by Mohr et al. (2003a) showing several sweeps triggered to the EOD motor command with many broad (dendritic) spikes. There is a pause in broad spikes during the corollary discharge response, even though the average membrane potential (black) increases.

Each of the 276 compartments of the model neuron obeyed the membrane current balance equation of the Hodgkin–Huxley formalism (Hodgkin and Huxley, l952). The membrane potential, V, was computed by numerically integrating the equation for each compartment:

$$C\frac{dV}{dt} = \sum_a g_a(V - E_a) + I_{ex} \tag{10}$$

where C is the membrane capacitance, g_a is the ionic conductance of an a-type ion channel, and E_a is the reversal potential of an a-type ion channel. The sum is over all types of ion conductances in the model, and I_{ex} represents an externally applied current.

The voltage-sensitive membrane conductances were calculated using activation (x_a) and inactivation (y_a) variables:

$$g_a = \bar{g}_a x_a^{n_a} y_a^{m_a}, \text{ and } \frac{dx_a}{dt} = \frac{1}{\tau_{x_a}}\left(x_a^{\infty} - x_a\right), \tag{11}$$

where $\bar{g}_a$ is the maximum ionic conductance, and n_a is the power of the activation variable. The asymptote (x_a^{∞}) and decay (τ_{x_a}) constants are functionally related to the first-order rate constants α_{x_a} and β_{x_a} by $x_a^{\infty} = \alpha_{x_a}/(\alpha_{x_a} + \beta_{x_a})$ and $\tau_{x_a} = 1/(\alpha_{x_a} + \beta_{x_a})$. The inactivation variables obey a similar first-order equation. The rate constants are themselves dependent on the membrane potential, V, through empirically derived relations for each channel type.

Although it is likely that a reduced model with fewer compartments (Rall, 1964) would exhibit similar behavior, we wish to show that a morphologically accurate MG cell could regulate the broad (dendritic) spike threshold without silencing the narrow (axonal) spikes. In addition, the detailed model allows us to identify the precise location of the dendritic spike initiation zone and supports the hypothesis that inputs to the deep molecular layer regulate dendritic spikes *in vivo*.

3.4 MG CELL DENDRITIC SPIKE SIMULATION

In vitro experiments showed that dendritic spikes are dependent on sodium ion channels (Bell et al., 1997b). The simplest choice of conductance types to generate spikes is a fast, inactivating sodium current, I_{Na-f}, and a delayed rectifier potassium current, I_{K-V}. In addition, a leak current, I_l, was added to each compartment of the model neuron with a reversal potential of $E_l = -70$ mV.

To yield a model with a broad spike threshold that was higher than the axonal spike threshold required a I_{Na-f} density that was sparser in the dendrites than in the axon. A broadening of the dendritic spikes required a reduced ratio of I_{K-V} density to I_{Na-f} density. In a previous MG model, we used active currents that were based on the classical Hodgkin–Huxley kinetics of the squid axon. We found it difficult to replicate the physiological broadness of dendritic spikes, though the depolarization of the dendritic tree would sum to yield a broad spike in the soma. Since we knew that recordings in the dendritic branches were also broad (Mohr et al., 2003a,b), we sought to improve the dendritic spike representation in the present model. Since MG cells are Purkinje neurons, we used the kinetics of I_{Na-f} and I_{K-V} from Purkinje cells (DeSchutter and Bower, 1994). In our new simulations, the resulting broad spikes were robustly as broad as the physiologically observed broad spikes in dendrites of MG cells.

To simulate dendritic and axonal spikes, we applied parameter settings in the MG model neuron from **Table 1**. The soma and dendrites were initialized with passive properties: $\bar{g}_l = 0.0003(\text{S/cm}^2)$ and $E_l = -70$ mV. I_{Na-f} and I_{K-V} conductances were added to the axon to generate independent axon spikes. The result of a 50 ms, 0.5 nA pulse is shown in **Figure 4**, where the red trace is the voltage at the distal end of the axon, the blue trace is the voltage at the distal end of one of the dendrites, and the black trace is the voltage in the soma. The resultant dendritic spike propagates from the soma outward.

This simulation suggests that the properties of the two spike types arise from the morphology and membrane conductance densities in different segments of the model neuron. We next investigate how inhibitory synaptic inputs increase the threshold of dendritic spikes. The difference between the axon and broad dendritic spike thresholds will be controlled by the density of I_{Na-f} and I_{K-V} currents in the soma. The dependence of the axon-to-dendritic spike

Table 1 | Maximum current densities, $\bar{g}_a$ (S/cm²), for active membrane currents of MG cell by morphological region. The proximal compartments of the axon (axon_p) are the spike initiation zone and have a higher I_{Na-f} density than the distal axon compartments (axon_d). The dendritic spikes of the apical dendrites are initiated in compartments in the ventral molecular layer (VML), and propagate into apical dendritic compartments in the dorsal molecular layer (DML). The basilar dendrites are passive in this model.

Channel(I_a)	Soma	Hillock	Axon_p	Axon_d	DML	VML	Basilar
I_{Na-f}	0.0	0.0	4.0	0.1	0.5	0.2	0
I_{K-V}	0.0	0.0	0.2	0.03	0.2	0.05	0
I_l	0.0003	0.0	0.0003	0.0003	0.0003	0.0003	0.0003

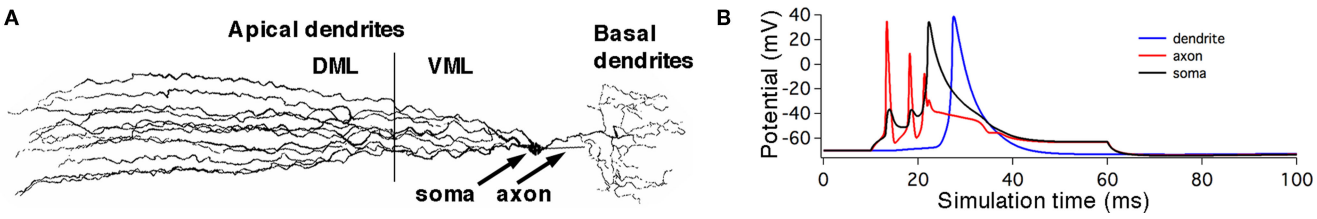

FIGURE 4 | Conductance-based compartmental model of a MG cell. **(A)** Morphology of MG cell model. Synaptic inputs were applied to both the dorsal molecular layer (DML) dendrites and the ventral molecular layer (VML) regions of the apical dendrites, but the broad spike regulating synaptic current was applied only to the VML. The basal dendrites received electrosensory inputs representing inputs from deep layers of the ELL. **(B)** Simulated small and broad spikes from three different compartments, soma (black trace), axon (red), and tip of a dendrite (blue). Current pulse at soma, 0.05 nA for 50 ms.

threshold ratio on the conductance properties of the soma suggests that membrane currents, which we have not yet tested, alter that ratio. A gap in narrow spikes followed the initiation of each broad spike because of inactivation of I_{Na-f} in the axonal compartments, as noted in recent physiological observations (Sawtell et al., 2007).

3.5 THRESHOLD CONTROL OF BROAD SPIKES BY INHIBITORY SYNAPTIC CURRENTS

We simulated the effects of background parallel fiber activity and stellate cell activity by assigning AMPA and $GABA_A$ synaptic currents with random latencies on each of the apical dendritic segments. The maximum $GABA_A$ currents were adjusted to recover the original spike thresholds and responses to current injections so that the background inputs were balanced between excitation and inhibition.

These inputs were divided into ventral (VML) and dorsal (DML) molecular layer regions. The maximum $GABA_A$ current was increased until the broad spike, generated by a 0.5-pA current step, was blocked. The VML inhibitory inputs were over twice as effective as the DML inputs at blocking the broad spike. The maximum inhibitory synaptic currents for broad spike blockage are $(\bar{g}_{VML} = 0.05, \bar{g}_{DML} = 0.03)$ and $(\bar{g}_{VML} = 0.03, \bar{g}_{DML} = 0.12)$, where $\bar{g} = 0.03$ was used as the balanced background $GABA_A$ current.

Electric organ discharge corollary discharge inputs from the JLN excite MG cells via the basilar dendrites. These timing inputs were modeled by injecting bursts of 1 ms current pulses (0.05 nA) into each segment of the basilar dendrites to simulate electrical synapses. The burst durations at each dendritic segment were randomized uniformly from one to six spikes per burst, with 5 ms inter-spike interval. The initial spike latency was also randomized from 10 to 30 ms. During each simulation run, the latencies of inputs and burst durations at each segment was randomized. This initial randomization simulated synaptic and spike propagation failures in the inputs, and yielded a Monte Carlo simulation of the response of MG cells to the EOD command.

To compare Monte Carlo samples of responses given randomized synaptic latencies, we simulated command-evoked parallel fiber inputs by adding an α-function distribution of latencies of excitatory AMPA synapses to the simulation ($\bar{g}_{pf} = 0.001$, PF-onset = $\alpha(\tau = 20$ ms)). The results of five trials is shown in the **Figure 5A** as overlays of membrane voltages. The latencies of the broad spikes are near the crest of the parallel fiber inputs distribution as would be expected if there were no broad spike gap.

Command-driven GABA synaptic inputs were added to the model to determine whether the broad spike activity could be controlled independently of the narrow spikes. In **Figure 5B**, a narrow, normal distribution of GABA input latencies were applied in the VML dendritic sections ($\bar{g}_{st} = 0.1$, PF-onset = Normal (20 ms ± 10)). The GABA inputs resulted in delays of most of the broad spikes until late in the cycle.

The main finding here is that we could suppress dendritic spikes in the model without silencing the narrow spikes, even though the distance between the spike generation zones is merely across the soma. The mechanism is a shunting of the Na currents in the VML-dendrites (see **Figure 5A**) so that the dendritic (broad) spike cannot propagate into the dendrites. Detailed inspection of the dendritic spike initiation reveals that the initiation zone is less than 50 μm from the soma, in a single dendritic branch, and then the depolarization spreads to other branches as it propagates up the dendritic tree.

4 FUNCTIONAL CONSEQUENCES OF ANTI-HEBBIAN STDP IN OTHER SYSTEMS

The principle of predictable image cancelation is found in other electrosensory systems, both passive and active (Bell et al., 1997a), such as the octavolateral nucleus of sharks and rays (Montgomery and Bodznick, 1994; Bodznick et al., 1999) and the gymnotid ELL (Bastian, 1995). In sharks and rays, the electroreceptors are affected by a current flow between the gills and the rest of the fish's body. This current flow is modulated by gill movement. Gill movement, therefore, affects the electrosensory system. The effects

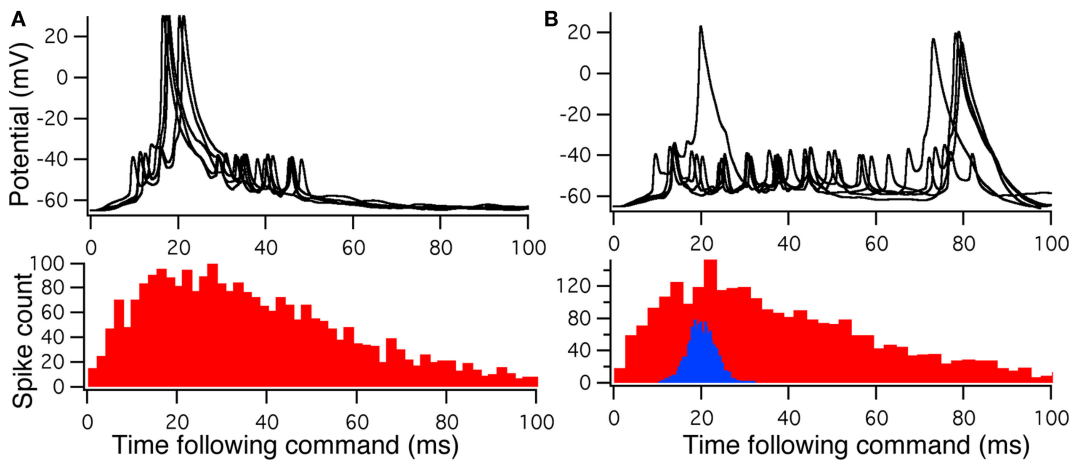

FIGURE 5 | Monte Carlo samples of responses to the electric organ discharge command. (A) Only background inhibition in VML dendritic sections yields broad spikes centered near the beginning of the command-evoked burst of spikes (top panel). The distribution of command-driven (non-background) parallel fiber latencies is shown in the histogram (bottom panel). **(B)** Inhibitory GABA synaptic inputs are injected in the VML dendritic segments with a latencies normally distributed (blue histogram in bottom panel). The broad spikes are nearly eliminated during the burst, but the narrow spikes are not strongly affected by the inhibition.

of movements on the electrosensory signal appear to be filtered out by neurons in a primary sensory structure similar to ELL. Principal neurons of ascending efferent neurons, do not modulate their spike output in response to gill movements. Thus, although the primary afferents are modulated by the gill movements, other inputs to the structure (Conley and Bodznick, 1994; Bodznick et al., 1999) are used to eliminate this predictable modulation of the electrosensory pattern caused by gill movements.

The final requirement for this system to operate as an adaptive filter is for the gain control of inputs that carry information about gill movements to be sensitive to changes in the electrosensory signals. If the synaptic learning rule is anti-Hebbian, then the synapses should reduce in strength during persistent correlated firing. Also, in order to decorrelate the parallel fiber inputs relative to the sensory inputs, a mechanism must be present for increasing the synaptic strength. Such bi-directional plasticity has been observed (Bodznick et al., 1999) by directly stimulating the inputs if followed by a reduction in the responses to electrosensory signal that have paired with the stimulation.

Nelson and Paulin (1995) developed a formal model of the elasmobranch electrosensory system to support this conceptual model. Given biologically realistic afferent currents, the model was used to test whether the synaptically driven adaptive processes would be sufficient to flatten the response of the electrosensory neurons during the respiratory cycle. The functional results is that the effects of gill movements on the electrosensory signal is eliminated so that the fish becomes more sensitive to external sources of electrical signals. Numerical simulations determined that the cancelation of predictable afferent patterns was possible only if the synaptic learning rule were anti-Hebbian.

Similar studies have been carried out in gymnotid fish (Bastian, 1995). These weakly electric fish have an active electrosensory system that has been shown to adjust the gain of the responses of principal cells in ELL to movements of the tail. Proprioceptive information is used to cancel the predicted changes in the electrosensory response caused by the fish's own movements. Anti-Hebbian plasticity has been observed in the gymnotid ELL, but it is not clear whether underlying mechanism of sensory adaptation is an STDP learning rule similar to the one found in mormyrid fish.

Another feature of the gymnotid ELL is that descending feedback is an active part of electrosensory processing (Bastian and Bratton, 1990; Bratton and Bastian, 1990), and that dendritic spikes may be controlled by these descending inputs. The functional similarities with the mormyrid ELL are striking in spite of anatomical differences (Bell et al., 1997a), and suggest that the mechanism of descending control of STDP plasticity may be a general principle in sensory processing.

The dorsal cochlear nucleus (DCN) is one of the two initial sites of auditory processing in the mammalian brainstem and is another cerebellum-like structure similar to the above electrosensory systems. Along with receiving primary auditory inputs, the DCN receives additional ascending and descending auditory and non-auditory inputs. This convergence of information may be important for utilizing synaptic plasticity to alter auditory responses to predictable stimuli. The function of the DCN from the standpoint of its similarity to the cerebellum and cerebellar-like structures suggests that anti-Hebbian synaptic plasticity functions to cancel out the neural activity derived from self-generated movements (Roberts and Portfors, 2008) as in ELL. A similar form of STDP has been shown in the DCN of mouse (Tzounopoulos et al., 2004) suggesting that similar adaptive mechanisms may exist in both structures.

The stability of the learning dynamics associated with the anti-Hebbian learning rule discussed here provides a compelling basis for interpreting the functional consequences of STDP in sensory processing. Some of the principles presented here, such as control of STDP by regulating dendritic spike thresholds, are likely to be general principles found other parts of the nervous system besides early sensory processing.

ACKNOWLEDGMENTS

We wish to thank Jacob Engelmann for providing the medium ganglion tracing. This work was supported in part by the National Science Foundation under Grant No. CRCNS IIS-0827722 and IIS-0812687.

REFERENCES

Abbott, L. F., and Song, S. (1999). "Temporally asymmetric Hebbian learning, spike timing and neuronal response variability," in *Advances in Neural Information Processing Systems 11*, eds M. Kearns, S. A. Solla, and D. Cohn (Cambridge: MIT Press), 69–75.

Assad, C., Rasnow, B., and Stoddard, P. (1999). Electric organ discharges and electric images during electrolocation. *J. Exp. Biol.* 202, 1185.

Barlow, H. (1990). Conditions for versatile learning, Helmholtz's unconscious inference, and the task of perception. *Vision Res.* 30, 1561–1571.

Bastian, J. (1995). Pyramidal-cell plasticity in weakly electric fish: a mechanism for attenuating responses to reafferent electrosensory inputs. *J. Comp. Physiol. A* 176, 63–73.

Bastian, J., and Bratton, B. (1990). Descending control of electroreception. I. Properties of nucleus praeeminentialis neurons projecting indirectly to the electrosensory lateral line lobe. *J. Neurosci.* 10, 1226.

Bell, C. C. (1982). Properties of a modifiable efference copy in an electric fish. *J. Neurophysiol.* 47, 1043–1056.

Bell, C. C. (1990). Mormyromast electroreceptor organs and their afferent fibers in mormyrid fish. II. Intraaxonal recordings show initial stages of central processing. *J. Neurophysiol.* 63, 303–318.

Bell, C. C., Bodznick, D., Montgomery, J., and Bastian, J. (1997a). The generation and subtraction of sensory expectations within cerebellum-like structures. *Brain Behav. Evol.* 50(Suppl. 1), 17–31.

Bell, C. C., Caputi, A., and Grant, K. (1997b). Physiology and plasticity of morphologically identified cells in the mormyrid electrosensory lobe. *J. Neurosci.* 17, 6409–6423.

Bell, C. C., Han, V., Sugawara, Y., and Grant, K. (1997c). Direction of change in synaptic efficacy following pairing depends on the temporal relation of presynaptic input and postsynaptic spike during pairing. *Soc. Neurosci. Abstr.* 23, 1840.

Bell, C. C., Han, V., Sugawara, Y., and Grant, K. (1997d). Synaptic plasticity in a cerebellum-like structure depends on temporal order. *Nature* 387, 278–281.

Bell, C. C., Caputi, A., Grant, K., and Serrier, J. (1993). Storage of a sensory pattern by anti-Hebbian synaptic plasticity in an electric fish. *Proc. Natl. Acad. Sci. U.S.A.* 90, 4650–4654.

Bell, C. C., and Emde, G. v. (1995). Electric organ corollary discharge pathways in mormyrid fish. II. The medial juxtalobar nucleus. *J. Comp. Physiol. A* 177, 463–479.

Bell, C. C., Grant, K., and Serrier, J. (1992). Sensory processing and corollary discharge effects in the mormyromast regions of the mormyrid electrosensory lobe: I. Field potentials and cellular activity in associated structures. *J. Neurophysiol.* 68, 843–858.

Bennett, M. (1970). Comparative physiology: electric organs. *Annu. Rev. Physiol.* 32, 471.

Bi, Q., and Poo, M.-M. (1998). Precise spike timing determines the direction and extent of synaptic modifications in cultured hippocampal neurons. *J. Neurosci.* 18, 10464–10472.

Bodznick, D., and Montgomery, J. C. (2005). "The physiology of low-frequency electrosensory systems," in *Electroreception. Vol. 21 of Springer Handbook of Auditory Research*, eds R.

R. Fay, A. N. Popper, T. H. Bullock, C. D. Hopkins, A. N. Popper, and R. R. Fay (New York: Springer), 132–153.

Bodznick, D., Montgomery, J. C., and Carey, M. (1999). Adaptive mechanisms in the elasmobranch hindbrain. *J. Exp. Biol.* 202, 1357–1364.

Bratton, B., and Bastian, J. (1990). Descending control of electroreception. II. Properties of nucleus praeeminentialis neurons projecting directly to the electrosensory lateral line lobe. *J. Neurosci.* 10, 1241.

Burkitt, A., Meffin, H., and Grayden, D. (2004). Spike-timing-dependent plasticity: the relationship to rate-based learning for models with weight dynamics determined by a stable fixed point. *Neural Comput.* 16, 885–940.

Cateau, H., and Fukai, T. (2003). A stochastic method to predict the consequence of arbitrary forms of spike-timing-dependent plasticity. *Neural Comput.* 15, 597–620.

Conley, R. A., and Bodznick, D. (1994). The cerebellar dorsal granular ridge in an elasmobranch has proprioceptive and electroreceptive representations and projects homotopically to the medullary electrosensory nucleus. *J. Comp. Physiol. A* 174, 707–721.

DeSchutter, E., and Bower, J. M. (1994). Simulated responses of cerebellar Purkinje cells are independent of the dendritic location of granule cell synaptic inputs. *Proc. Natl. Acad. Sci. U.S.A.* 91, 4736–4740.

Engelmann, J., van den Burg, E., Bacelo, J., de Ruijters, M., Kuwana, S., Sugawara, Y., and Grant, K. (2008). Dendritic backpropagation and synaptic plasticity in the mormyrid electrosensory lobe. *J. Physiol. (Paris)* 102, 233–245.

Gardiner, C. (1985). *Handbook of Stochastic Methods*. Berlin: Springer.

Gerstner, W., Kempter, R., van Hemmen, J. L., and Wagner, H. (1996). A neuronal learning rule for sub-millisecond temporal coding. *Nature* 383, 76–78.

Gerstner, W., and van Hemmen, J. L. (1992). Associative memory in a network of 'spiking' neurons. *Network* 3, 139–164.

Grant, K., Sugawara, Y., Gomes, L., Han, V., and Bell, C. C. (1998). The mormyrid electrosensory lobe in vitro: physiology and pharmacology of cells and circuits. *J. Neurosci.* 18, 6009–6025.

Hall, C., Bell, C. C., and Zelick, R. (1995). Behavioral evidence of a latency code for stimulus intensity in mormyrid electric fish. *J. Comp. Physiol. A* 177, 29–39.

Haykin, S. (2002). *Adaptive Filter Theory*. Upper Saddle River, NJ: Prentice Hall.

Hines, M., and Carnevale, T. (1997). The neuron simulation environment. *Neural Comput.* 9, 1179–1209.

Hodgkin, A. L., and Huxley, A. F. (1952). A quantitative description of membrane current and its application to conduction and excitation in nerve. *J. Physiol. (Lond.)* 108, 37–77.

Hopkins, C. (1988). Neuroethology of electric communication. *Annu. Rev. Neurosci.* 11, 497–535.

Hopkins, C. (1995). Convergent designs for electrogenesis and electroreception. *Curr. Opin. Neurobiol.* 5, 769–777.

Kawasaki, M. (2005). "Physiology of tuberous electrosensory systems," in *Electroreception. Vol. 21 of Springer Handbook of Auditory Research*, eds R. R. Fay, A. N. Popper, T. H. Bullock, C. D. Hopkins, A. N. Popper, R. R. Fay (New York: Springer), 154–194.

Kempter, R., Gerstner, W., and van Hemmen, J. L. (1999). Hebbian learning and spiking neurons. *Phys. Rev. E* 59, 4498–4514.

Kepecs, A., van Rossum, M., Song, S., and Tegner, J. (2002). Spike-timing-dependent plasticity: common themes and divergent vistas. *Biol. Cybern.* 87, 446–458.

Masuda, N., and Aihara, K. (2004). Self-organizing dual coding based on spike-time-dependent plasticity. *Neural Comput.* 16, 627–663.

Meek, J., and Grant, K. (1994). The role of motor command feedback in electrosensory processing. *Eur. J. Morphol.* 32, 225–234.

Mohr, C., Roberts, P. D., and Bell, C. C. (2003a). Cells of the mormyrid electrosensory lobe: II. Responses to input from central sources. *J. Neurophysiol.* 90, 1211–1223.

Mohr, C., Roberts, P. D., and Bell, C. C. (2003b). Cells of the mormyrid electrosensory lobe: I. Responses to the electric organ corollary discharge and to electrosensory stimuli. *J. Neurophysiol.* 90, 1193–1210.

Montgomery, J. C., and Bodznick, D. (1994). An adaptive filter that cancels self-induced noise in the electrosensory and lateral line mechanosensory systems of fish. *Neurosci. Lett.* 174, 145–148.

Nelson, M. E., and Paulin, M. G. (1995). Neural simulations of adaptive reafference suppression in the elasmobranch electrosensory system. *J. Comp. Physiol. A* 177, 723–736.

Pfister, J., Toyoizumi, T., Barber, D., and Gerstner, W. (2006). Optimal spike-timing-dependent plasticity for precise action potential firing in supervised learning. *Neural Comput.* 18, 1318–1348.

Rall, W. (1964). "Theoretical significance of dendritic trees for neuronal input–output relations," in *Neural Theory and Modeling*, ed. R. Reiss (Stanford: Stanford University Press), 73–97.

Roberts, P. D. (1999). Computational consequences of temporally asymmetric learning rules: I. Differential Hebbian learning. *J. Comput. Neurosci.* 7, 235–246.

Roberts, P. D. (2000a). Electrosensory response mechanisms in mormyrid electric fish. *Neurocomputing* 32–33, 243–248.

Roberts, P. D. (2000b). Modeling inhibitory plasticity in the electrosensory system of mormyrid electric fish. *J. Neurophysiol.* 84, 2035–2047.

Roberts, P. D., and Bell, C. C. (2000). Computational consequences of temporally asymmetric learning rules: II. Sensory image cancellation. *J. Comput. Neurosci.* 9, 67–83.

Roberts, P. D., and Bell, C. C. (2001). Mutual inhibition increases adaptation rate in an electrosensory system. *Neurocomputing* 38–40, 845–850.

Roberts, P. D., and Bell, C. C. (2003). Active control of spike-timing dependent synaptic plasticity in an electrosensory system. *J. Physiol. (Paris)* 96, 445–449.

Roberts, P. D., Lafferriere, G., Sawtell, N., Williams, A., and Bell, C. C. (2006). Dynamic regulation of spike-timing dependent plasticity in electrosensory processing. *Neurocomputing* 69, 1195–1198.

Roberts, P., and Portfors, C. (2008). Design principles of sensory processing in cerebellum-like structures. *Biol. Cybern.* 98, 491–507.

Saudargiene, A., Porr, B., and Wörgötter, F. (2004). How the shape of pre- and postsynaptic signals can influence STDP: a biophysical model. *Neural Comput.* 16, 595–625.

Sawtell, N. (2010). Multimodal integration in granule cells as a basis for associative plasticity and sensory prediction in a cerebellum-like circuit. *Neuron* 66, 573–584.

Sawtell, N., and Williams, A. (2008). Transformations of electrosensory encoding associated with an adaptive filter. *J. Neurosci.* 28, 1598.

Sawtell, N. B., Williams, A., and Bell, C. C. (2007). Central control of dendritic spikes shapes the responses of Purkinje-like cells through spike timing-dependent synaptic plasticity. *J. Neurosci.* 27, 1552–1565.

Toyoizumi, T., Pfister, J. P., Aihara, K., and Gerstner, W. (2005). Generalized Bienenstock–Cooper–Munro rule for spiking neurons that maximizes information transmission. *Proc. Natl. Acad. Sci. U.S.A.* 102, 5239–5244.

Turrigiano, G. G. (1999). Homeostatic plasticity in neuronal networks: the more things change, the more they stay the same. *Trends Neurosci.* 22, 221–227.

Tzounopoulos, T., Kim, Y., Oertel, D., and Trussell, L. O. (2004). Cell-specific, spike timing-dependent plasticities in the dorsal cochlear nucleus. *Nat. Neurosci.* 7, 719–725.

van Kampen, N. (1992). *Stochastic Processes in Physics and Chemistry*. Amsterdam: NH PL.

van Rossum, M. C. W., Bi, G. Q., and Turrigiano, G. G. (2000). Stable Hebbian learning from spike timing-dependent plasticity. *J. Neurosci.* 20, 8812–8821.

Von der Emde, G. (1999). Active electrolocation of objects in weakly electric fish. *J. Exp. Biol.* 202, 1205.

von Holst, E., and Mittelstaedt, H. (1950). Das Reafferenzprinzip. *Naturwissenschaften* 37, 464–476.

Williams, A., Leen, T. K., and Roberts, P. D. (2004). Random walks for spike-timing dependent plasticity. *Phys. Rev. E* 70, 021916.

Williams, A., Roberts, P. D., and Leen, T. K. (2003). Stability of negative-image equilibria in spike-timing-dependent plasticity. *Phys. Rev. E* 68, 021923.

Xie, X.-H., and Seung, H. S. (2000). "Spike-based learning rules and stabilization of persistent neural activity," in *Advances in Neural Information Processing Systems 12*, eds S. A. Solla, T. K. Leen, and K.-R. Muller (Cambridge: MIT Press), 164–170.

Zipser, B., and Bennet, M. V. L. (1976). Interaction of electrosensory and electromotor signals in lateral line lobe of a mormyrid fish. *J. Neurophysiol.* 39, 713–721.

Conflict of Interest Statement: The authors declare that the research was conducted in the absence of any commercial or financial relationships that could be construed as a potential conflict of interest.

Received: 21 February 2010; accepted: 15 December 2010; published online: 31 December 2010.

Citation: Roberts PD and Leen TK (2010) Anti-Hebbian spike-timing-dependent plasticity and adaptive sensory processing. Front. Comput. Neurosci. ***4****:156. doi: 10.3389/fncom.2010.00156*

frontiers in
SYNAPTIC NEUROSCIENCE

REVIEW ARTICLE
published: 10 June 2010
doi: 10.3389/fnsyn.2010.00006

Spike-timing dependent plasticity in the striatum

Elodie Fino[1,2,3]* and Laurent Venance[1,2]*

[1] *Dynamics and Pathophysiology of Neuronal Networks (Institut National de la Santé et de la Recherche Médicale Unité Mixte de Recherche en Santé 667), Center for Interdisciplinary Research in Biology, Collège de France, Paris, France*
[2] *Université Pierre et Marie Curie, Paris, France*
[3] *Department of Biological Science, Columbia University, New York, NY, USA*

Edited by:
Per Jesper Sjöström, University College London, UK

Reviewed by:
Antonio Pisani, Università di Roma "Tor Vergata," Italy
David M. Lovinger, National Institutes of Health, USA

****Correspondence:***
Laurent Venance, Dynamics and Pathophysiology of Neuronal Networks (Institut National de la Santé et de la Recherche Médicale Unité Mixte de Recherche en Santé 667), College de France, 11 Place Marcelin Berthelot, 75005 Paris, France.
e-mail: laurent.venance@college-de-france.fr;
Elodie Fino, Department of Biological Science, Columbia University, 1212 Amsterdam Avenue, 1002 Fairchild building, New York, NY 10027, USA.
e-mail: ef2308@columbia.edu

The striatum is the major input nucleus of basal ganglia, an ensemble of interconnected subcortical nuclei associated with fundamental processes of action-selection and procedural learning and memory. The striatum receives afferents from the cerebral cortex and the thalamus. In turn, it relays the integrated information towards the basal ganglia output nuclei through which it operates a selected activation of behavioral effectors. The striatal output neurons, the GABAergic medium-sized spiny neurons (MSNs), are in charge of the detection and integration of behaviorally relevant information. This property confers to the striatum the ability to extract relevant information from the background noise and select cognitive-motor sequences adapted to environmental stimuli. As long-term synaptic efficacy changes are believed to underlie learning and memory, the corticostriatal long-term plasticity provides a fundamental mechanism for the function of the basal ganglia in procedural learning. Here, we reviewed the different forms of spike-timing dependent plasticity (STDP) occurring at corticostriatal synapses. Most of the studies have focused on MSNs and their ability to develop long-term plasticity. Nevertheless, the striatal interneurons (the fast-spiking GABAergic, NO-synthase and cholinergic interneurons) also receive monosynaptic afferents from the cortex and tightly regulated corticostriatal information processing. Therefore, it is important to take into account the variety of striatal neurons to fully understand the ability of striatum to develop long-term plasticity. Corticostriatal STDP with various spike-timing dependence have been observed depending on the neuronal sub-populations and experimental conditions. This complexity highlights the extraordinary potentiality in term of plasticity of the corticostriatal pathway.

Keywords: spike-timing dependent plasticity, corticostriatal, striatum, GABAergic interneurons, cholinergic interneurons, LTP, LTD, basal ganglia

BASAL GANGLIA AND THEIR MAIN INPUT PATHWAY: THE CORTICOSTRIATAL PATHWAY

Basal ganglia are involved in the learning and memory of cognitive and motor sequences related to environmental stimuli (Graybiel et al., 1994; Packard and Knowlton, 2002; Graybiel, 2005; Yin and Knowlton, 2006). Learning and memory are believed to be underlie by long-term synaptic efficacy changes (Bliss and Collingridge, 1993; Martin and Morris, 2002; Lynch, 2004; Malenka and Bear, 2004). Accordingly, the long-term plasticity at different key pathways within the basal ganglia, provides a basic mechanism for the function of basal ganglia in procedural learning and memory (Yin et al., 2009). As the main input structure of the basal ganglia (**Figure 1**), the striatum is regarded as a major site of memory formation for sensorimotor and cognitive associations, indicating the importance of the occurrence of different forms of plasticity at corticostriatal synapses (Calabresi et al., 1996; Mahon et al., 2004; Costa, 2007; Kreitzer and Malenka, 2008; Di Filippo et al., 2009). In addition, corticostriatal plasticity is severely altered in several pathologies affecting basal ganglia (Kreitzer and Malenka, 2008; Calabresi et al., 2009). Therefore, it is essential to understand in which conditions of cortical and striatal activity, long-term plasticity occurs at corticostriatal synapses. It is now well established that the temporal relationship of activity in pre- and post-synaptic neurons is determinant for the induction of activity-dependent long-term plasticity, a process named spike-timing dependent plasticity (STDP) described from insects to mammalian brain structures (Sjöström and Nelson, 2002; Bi and Rubin, 2005; Dan and Poo, 2006; Caporale and Dan, 2008). In this review, we will focus on STDP experiments recently reported at the corticostriatal synapses as a Hebbian synaptic learning rule.

Basal ganglia are composed of six nuclei: two input nuclei, the striatum and the subthalamic nucleus (STN), two output nuclei, the substantia nigra *pars reticulata* (SNr) and the internal segment of the globus pallidus (GPi), one relay nucleus, the external segment of the globus pallidus (GPe) and one dopaminergic neuromodulatory nucleus, the substantia nigra *pars compacta* (SNc) (**Figure 1**). The striatum is the main input nucleus of basal ganglia and receives massive convergent glutamatergic inputs from the cerebral cortex and the thalamus. In turn, the striatum relays the integrated cortical information towards the two basal ganglia output nuclei (SNr and GPi), through two anatomo-functional pathways: the direct pathway (cortico-striato-nigral) and the indirect pathway (cortico-striato-pallido-nigral) (**Figure 1**). In the motor control, the direct and indirect pathways exert opposite influence, respectively, inhibitory and excitatory on basal output nuclei. Therefore, the activation of the direct pathway would initiate or facilitate the movement while the activation of the indirect pathway would constitute a brake. The neuromodulation of different basal ganglia

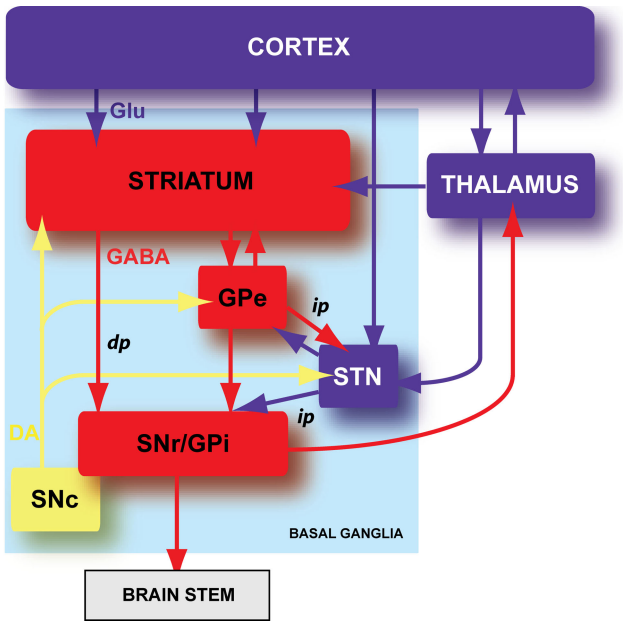

FIGURE 1 | Schematic organization of the basal ganglia. Basal ganglia are an ensemble of tightly interconnected sub-cortical nuclei. In blue are represented the glutamatergic (Glu) structures, in red the GABAergic (GABA) nuclei and in yellow the dopaminergic (DA) nucleus. GPe: external part of the globus pallidus; GPi: internal part of the globus pallidus; SNr: substantia nigra pars reticulata; SNc: substantia nigra pars compacta; dp: direct pathway; ip: indirect pathway.

nuclei by SNc dopaminergic neurons plays a central role since the dopamine brings a motivational side of the cortical information integration in the basal ganglia (Redgrave and Gurney, 2006; Costa, 2007; Schultz, 2007).

Most models of basal ganglia emphasize the importance of the corticostriatal connection. However, the glutamatergic neurons from intralaminar thalamus also innervate the striatum (Groenewegen and Berendse, 1994; Smith et al., 2004). Corticostriatal and thalamostriatal synapses on MSNs appear to be nearly equal in number (Smith et al., 2004), but display different functional characteristics (Smeal et al., 2007; Ding et al., 2008). Because of the lack of experimental data targeting the thalamostriatal long-term plasticity, we will focus on the corticostriatal pathway in this review.

A MARKED ANATOMO-FUNCTIONAL HETEROGENEITY UNDER THE STRIATAL SURFACE

The striatum displays numerous heterogeneities based, not only on its anatomo-functional organization (striosome versus matrix compartments, and somatosensory/motor/prefrontal projection areas), but also on a cellular diversity (Graybiel, 1990; Groenewegen et al., 1990; Deniau and Thierry, 1997). The striatum is composed for a vast majority (95% in rodents and 80% in primates) of striatal output neurons, the medium-sized spiny neurons (MSNs). Among MSNs, different populations can be distinguished based on their specific expression of receptors, channels, peptides or modes of communication (Graybiel, 1990; Gerfen, 1992; Nicola et al., 2000; Venance et al., 2004; Vandecasteele et al., 2007). In addition, the striatum also comprises GABAergic and cholinergic interneurons, which tightly regulate MSN excitability and consequently, the corticostriatal information processing. Therefore, the striatum is a highly complex structure and the link between such complexity and the different modes of synaptic plasticity needs to be characterized.

THE STRIATAL OUTPUT NEURONS: THE MEDIUM-SIZED SPINY NEURONS

Medium-sized spiny neurons are in charge of the detection and integration of behaviorally relevant information. MSNs, *in vivo* as well as *in vitro*, are characterized by their low level of spontaneous activity that can be explained by non-linear electrical membrane properties due to a set of voltage-gated potassium and sodium currents (Nisenbaum et al., 1994; Nisenbaum and Wilson, 1995). These non-linear membrane properties allow an efficient filtering of the small and uncorrelated synaptic events. Consequently, MSNs, quiescent at rest, need strong and correlated cortical inputs to discharge (Calabresi et al., 1987; Nisenbaum and Wilson, 1995). Therefore, MSNs act as coincidence detectors of cortical activity and have the ability to extract relevant information from the background noise. Among MSNs, different sub-populations can be distinguished based on receptors or peptides specific expression. Specifically, MSNs expressing mainly either dopaminergic type-1 (D1) or type-2 (D2) receptors project through, respectively, the direct or the indirect pathway (**Figure 1**). Such heterogeneity is the most studied at the moment thank to the use of D1-EGFP and D2-EGFP mice that constitute a useful tool to distinguish between MSNs belonging to the direct or indirect pathways (Surmeier et al., 2007; Valjent et al., 2009). However, if MSNs appear to be segregated in mice (D2-GFP staining being restricted to the indirect pathway; Matamales et al., 2009), it exists in rats and primates a significant population (respectively, 30 and 80%) of MSNs that project to both direct and indirect pathways (Kawaguchi et al., 1990; Wu et al., 2000; Levesque and Parent, 2005).

THE GABAergic INTERNEURONS

Three classes of striatal GABAergic interneurons can be distinguished (1) the parvalbumin positive cells (fast-spiking interneurons) (Kawaguchi, 1993), (2) the calretinin positive cells (Figueredo-Cardenas et al., 1996) (their electrophysiological features remain to be determined) (Tepper and Bolam, 2004) and (3) the neuronal nitric oxide synthase (nNOS) interneurons (persistent and low-threshold spiking cells, PLTS) (Kawaguchi, 1993). Fast-spiking GABAergic interneurons exert a powerful inhibitory weight (**Figure 2A**) since they can delay or prevent the emission of an action potential in MSNs (Kita, 1996; Plenz and Kitai, 1998; Koos and Tepper, 1999). These interneurons preferentially contact MSNs on the soma (Kita et al., 1990; Bennett and Bolam, 1994), which reinforces the inhibitory shunt. Because they also receive cortical inputs (Bennett and Bolam, 1994; Ramanathan et al., 2002; Mallet et al., 2005), fast-spiking interneurons could provide a feed-forward mechanism increasing the selectivity of MSN responsiveness to cortical inputs and the funneling of the corticostriatal information processing. Compared to fast-spiking interneurons, nNOS interneurons contact MSN mainly on the neck of the spines and display a lower number of synapses (Kubota and Kawaguchi, 2000). Anatomical and functional existence of synapses between cortical glutamatergic afferents and striatal nNOS interneurons has been reported (Vuillet et al., 1989; Fino et al.,

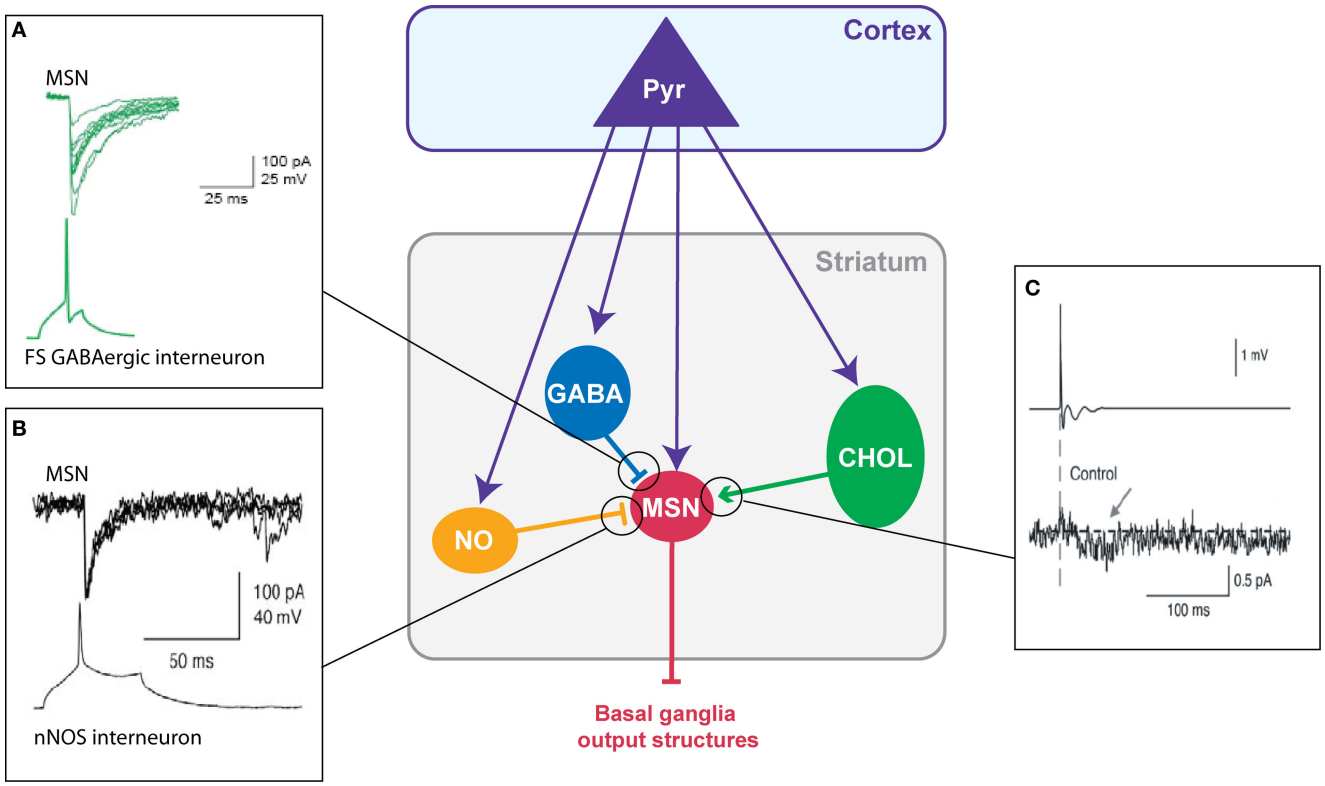

FIGURE 2 | Chemical transmission between striatal neurons. (A) Fast-spiking GABAergic interneurons have a strong inhibitory weight on MSNs: an action potential in the interneuron evokes an IPSC in the MSN (Adapted from Tepper et al., 2004). **(B)** Dual patch-clamp recording illustrating the inhibitory action of nNOS interneurons on MSNs (Adapted from Tepper and Bolam, 2004) **(C)** Illustration of the excitatory effect of cholinergic interneurons on MSNs: an extracellularly evoked action potential in a cholinergic interneuron evokes an EPSC in the MSNs (Adapted from Lin et al., 2004).

2009b). In addition to NOS, nNOS interneurons express the synthetic enzyme for GABA (Vuillet et al., 1990; Kawaguchi, 1993; Figueredo-Cardenas et al., 1996; Kubota and Kawaguchi, 2000) and have been characterized functionally as GABAergic cells that efficiently inhibit MSNs (**Figure 2B**) (Koos and Tepper, 1999; Tepper and Bolam, 2004). They also exert an inhibitory influence on MSNs via NO release (Sardo et al., 2002; West and Grace, 2004). NO modulates the MSN synaptic plasticity since the blockade of NO synthesis or the application of NO precludes or promotes, respectively, the induction of a long-term depression (LTD) after a high-frequency stimulation (HFS) (Calabresi et al., 1999; Sergeeva et al., 2007).

THE CHOLINERGIC INTERNEURONS

Cholinergic interneurons receive cortical inputs (Thomas et al., 2000; Reynolds and Wickens, 2004; Fino et al., 2008) and regulate the excitability of MSNs. Cholinergic cells fire tonically *in vivo* and provide a synchronized signal throughout the striatal network in response to sensory cues predictive of reward (Aosaki et al., 1994; Kimura et al., 2003; Morris et al., 2004; Apicella, 2007). Indeed, dopamine controls the discharge activity of cholinergic cells. Cholinergic interneurons modulate MSNs activity through various muscarinic receptors (Bennett and Bolam, 1994). MSNs of the direct and indirect pathways bear distinct patterns of muscarinic receptor expression. MSNs of the direct pathway express both muscarinic type-1, M1, (excitatory) and type-4, M4, (inhibitory) receptors and MSNs of the indirect pathway express M1 receptors (Acquas and DiChiara, 2002). Therefore, a same change in the cortical synaptic weight of cholinergic interneurons should result in opposite effects in the two sub-populations of MSNs. Nevertheless, muscarinic agonists (acetylcholine or muscarine) have mainly an excitatory effect on the MSNs by increasing their activity (Perez-Rosello et al., 2005) or the EPSC amplitude (Lin et al., 2004; Pakhotin and Bracci, 2007) due to M1 receptor activation (**Figure 2C**). In addition, acetylcholine acts on nicotinic receptors mainly located within the striatum on dopaminergic terminals (Clarke and Pert, 1985; Exley and Cragg, 2008). Finally, cholinergic interneurons also strongly influence the corticostriatal HFS-induced plasticity on MSNs since they favor the induction of a long-term potentiation (LTP) (Centonze et al., 2003; Surmeier et al., 2007) via the activation of muscarinic receptors whereas nicotinic receptor activation contributes to the induction of LTD (Partridge et al., 2002).

Therefore, besides MSNs, it is primordial to take into account the synaptic plasticity at striatal interneurons since they are directly connected to the cerebral cortex and control striatal microcircuits as well as corticostriatal information processing.

SPIKE-TIMING DEPENDENT PLASTICITY IN STRIATAL OUTPUT NEURONS

Corticostriatal plasticity has been extensively studied with classical conditioning protocols using low (1 Hz), medium (10 Hz) or high-frequency stimulation (100 Hz) (Mahon et al., 2004; Kreitzer

and Malenka, 2008; Di Filippo et al., 2009). HFS of striatal afferents applied within the striatum or the corpus callosum leads to LTD at MSN synapses (Calabresi et al., 1992a), but to LTP when the electrical stimulation was performed within the cortex (Fino et al., 2005). HFS-induced LTD relies on group-1 metabotropic glutamate receptors, dopamine D2 receptors, voltage-sensitive calcium channels and CB1 receptor activation (Di Filippo et al., 2009; Kreitzer and Malenka, 2008). Corticostriatal LTP was induced by cortical HFS (Fino et al., 2005), while the removal of extracellular magnesium was requested to observe a LTP when stimulation were performed into the striatum or the corpus callosum (Calabresi et al., 1992a,b). HFS-induced LTP requires NMDA receptor activation (Di Filippo et al., 2009; Kreitzer and Malenka, 2008).

STDP is based on the quasi-coincidence between pre- and post-synaptic activity within several milliseconds time scale. Despite numerous studies addressing the corticostriatal plasticity, to this day STDP at the corticostriatal synapses onto MSNs has been explored in only three different studies (Fino et al., 2005; Pawlak and Kerr, 2008; Shen et al., 2008). STDP was reported to be a very efficient phenomenon occurring at corticostriatal synapses since it occurred in roughly 80% of the cells (Fino et al., 2005; Pawlak and Kerr, 2008). Depending on the experimental conditions, different spike-timing dependences have been reported. Using a classical STDP protocol (100 paired stimulations at 1 Hz) without pharmacological manipulation, a "reversed" time-dependence is observed (Fino et al., 2005), compared to those described so far in other mammalian brain structures (Markram et al., 1997; Dan and Poo, 2004, 2006). Indeed, post-pre pairings induced STDP-LTP (t-LTP) and pre-post pairings induced STDP-LTD (t-LTD) in MSNs (Fino et al., 2005) (**Figure 3A**). Conversely, paired stimulations at 0.1 Hz with blockade of $GABA_A$ transmission, was found to evoke a t-LTD after post-pre pairings and a t-LTP following pre-post pairings (Pawlak and Kerr, 2008) (**Figure 3B**). Recently, another study using theta-burst protocol associated to a blockade of $GABA_A$ transmission reported a lack of STDP at D1 receptor expressing MSNs after post-pre pairings (Shen et al., 2008). Therefore, the striatal anatomo-functional heterogeneity could be revealed with specific experimental conditions, highlighting the fantastic complexity of the striatum. Depending on the experimental conditions, different receptors and intracellular pathways appear to underlie the MSN STDP. Indeed, t-LTP and t-LTD induced by a 0.1 Hz pairings relied on one coincidence detector, the NMDA receptor, associated with D1 receptor activation (Pawlak and Kerr, 2008). A different picture is obtained with the t-LTP and t-LTD induced by 1 Hz pairings, since they are mediated by independent signaling mechanisms, each one controlled by distinct coincidence detectors. Namely, t-LTP relies on the NMDA receptor, while t-LTD requires distinct coincident detectors: the phospholipase Cβ (PLCβ), the inositol-triphosphate receptor (IP_3R)-gated calcium stores and the diacylglycerol lipase α (DGLα) (Fino et al., 2010). PLCβ activation is controlled by group-I metabotropic glutamate receptors, type-1 muscarinic receptors and voltage-sensitive calcium channels activities. The activation of PLCβ, IP_3Rs and DGLα leads to robust retrograde endocannabinoid signaling mediated by 2-arachidonoyl-glycerol and cannabinoid CB1 receptors (Fino et al., 2010). Similarly, in the theta-burst based STDP, t-LTP is NMDA receptor and D1 receptor activation dependent whereas t-LTD is dependent on mGluRs, endocannabinoids and dopaminergic D2 receptor activation (Shen et al., 2008). The signaling pathways involved in corticostriatal STDP appear to be similar to those requires for HFS- or LFS-induced corticostriatal plasticity. These observations suggest that the corticostriatal pathway is a highly responsive system, in which different signaling cascades are involved, depending on the corticostriatal paired activity.

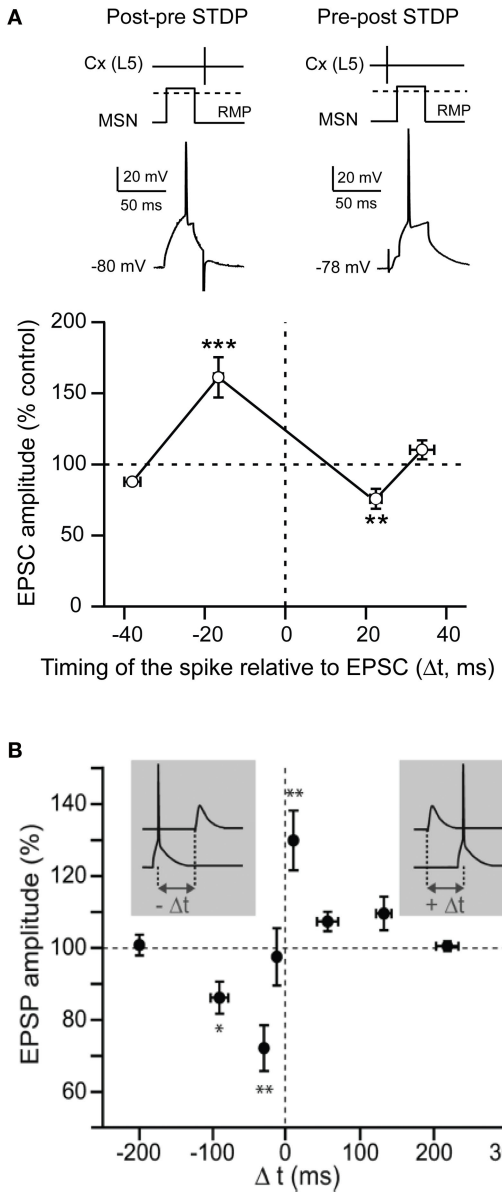

FIGURE 3 | Spike-timing dependent plasticity in MSNs. (A) STDP evoked potent bidirectional plasticity at corticostriatal synapses: post-pre pairings (100 paired stimulations at 1 Hz, in native condition) and pre-post pairings induced, respectively, t-LTP and t-LTD (Adapted from Fino et al., 2005). **(B)** STDP (60 paired stimulations at 0.1 Hz, in picrotoxine condition): post-pre and pre-post pairings induced, respectively, a t-LTD and a t-LTP (Adapted from Pawlak and Kerr, 2008). In conclusion, although the spike-timing dependence appears to be highly dependent on the experimental conditions, it highlights the wide potentiality of the corticostriatal plasticity.

The differences between these studies, instead of being presenting as conflicting, should be seen as many promising leads to decipher the extraordinary complexity of the striatum and its potentiality to display various corticostriatal plasticity. The first important observation is that different experimental conditions and different STDP protocols can lead to long-term plasticity. In any cases, discrepancies between the results could be explained by various experimental conditions. First, the different species used (mice versus rats) may matter, especially when analyzing the direct and indirect pathways. Second, the location of the electrical stimulation of the "presynaptic" element is performed either in the layer 5 of the somatosensory cortex (Fino et al., 2005), or in the corpus callosum (Pawlak and Kerr, 2008), or directly within the striatum at the MSN dendrites (Shen et al., 2008). In addition, the STDP protocols are different since they consist in the emission of a single action potential in the post-synaptic MSNs (Fino et al., 2005; Pawlak and Kerr, 2008) or a burst of action potentials (Shen et al., 2008). The frequency of the pairing varies between 0.1 Hz (Pawlak and Kerr, 2008), 1 Hz (Fino et al., 2005) and 5 Hz (Shen et al., 2008). Finally, and most importantly, the "classical" time-dependence of corticostriatal STDP has been observed while the GABAergic transmission was blocked (Pawlak and Kerr, 2008; Shen et al., 2008) and the "reversed" STDP without any blockade of GABAergic circuits (Fino et al., 2005). The GABAergic microcircuits, including GABAergic interneurons and MSN collaterals, play a crucial role in the local interactions in the striatum (Koos and Tepper, 1999; Tepper et al., 2004; Venance et al., 2004). Therefore, it remains necessary to evaluate the contribution of GABAergic circuits in the corticostriatal spike-timing dependence.

STDP IN STRIATAL INTERNEURONS

Attention has been merely focused on corticostriatal long-term plasticity in MSNs, the striatal output neurons. Nevertheless, as previously mentioned, striatal interneurons regulate MSN excitability and are contacted monosynaptically by glutamatergic afferents from the cortex; consequently, they are expected to play a determinant role in the corticostriatal information processing. Despite their role, the induction of long-term plasticity onto striatal interneurons has been barely addressed. It has been reported that HFS in the corpus callosum induced a LTP in cholinergic interneurons (Suzuki et al., 2001; Bonsi et al., 2004). More recently, it as been shown that the three types of striatal interneurons, cholinergic, fast-spiking GABAergic and nNOS interneurons, were able to develop long-term plasticity following STDP pairings (100 paired stimulations at 1 Hz, in native conditions) (**Figure 4**) (Fino et al., 2008, 2009b). Fast-spiking GABAergic interneurons display a STDP with a spike-timing dependence similar to those described in the cerebral cortex or in the hippocampus. Indeed, post-pre pairings induced t-LTD and pre-post pairings induced t-LTP in GABAergic interneurons (**Figure 4A**). t-LTP as well as t-LTD were dependent of the activation of NMDA receptors (Fino et al., 2008). Concerning cholinergic interneurons, we observed a partially reversed STDP: post-pre pairings induced t-LTP as well as t-LTD (with a majority of t-LTP) whereas pre-post pairings induced exclusively t-LTD (**Figure4B**). Interestingly, the state of excitability of cholinergic interneurons is correlated to the induction of either a t-LTD or a t-LTP after post-pre pairings (Fino et al., 2008). Pharmacological

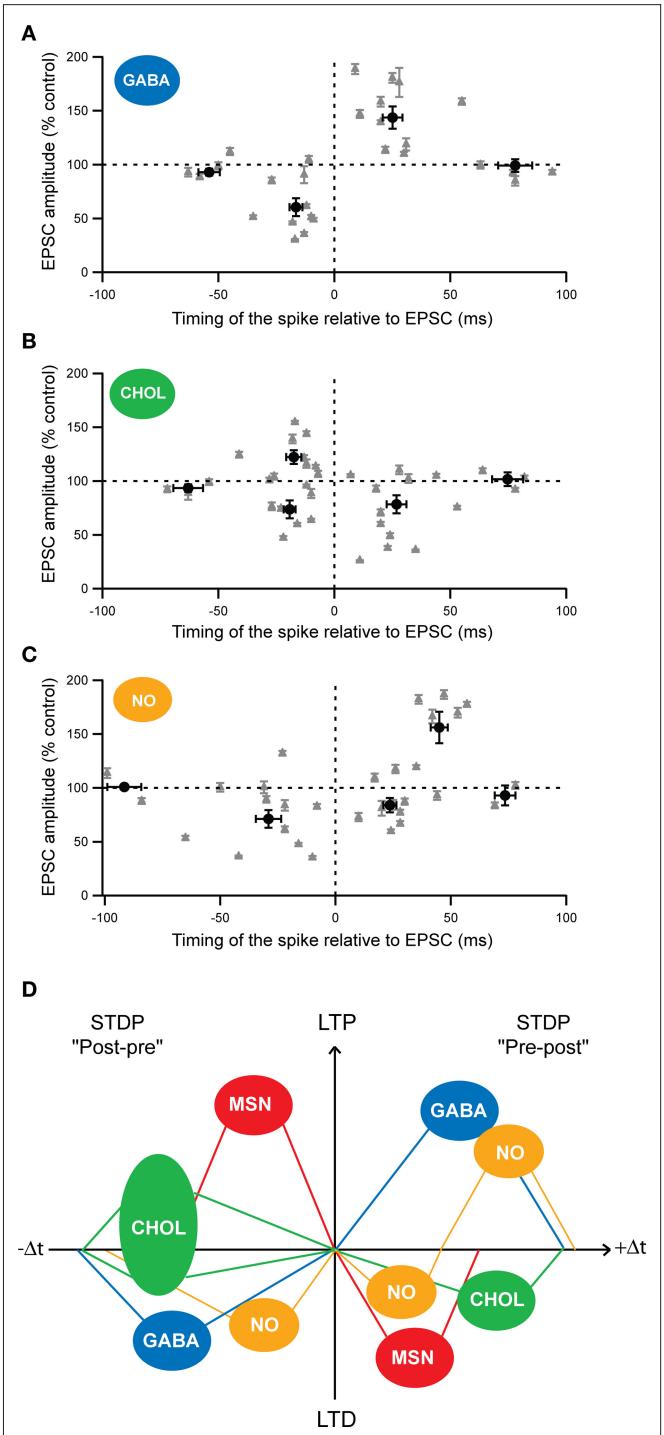

FIGURE 4 | Cell-specificity of the STDP among MSNs and striatal interneurons. (A–C) Spike-timing dependence of the STDP for the different striatal interneurons: **(A)** fast-spiking GABAergic interneurons (GABA), **(B)** cholinergic interneurons (CHOL) and **(C)** nNOS interneurons (NO). Each recorded neuron is represented by a gray triangle and the averages (±SEM) of the synaptic efficacy changes 1 hour after the STDP paired protocol are indicated by the black dots. **(D)** Schematic representation of the cell-specificity of the spike-timing dependence of STDP developed by the different striatal neurons after post-pre (left) or pre-post (right) pairings (100 paired stimulations at 1 Hz). (Adapted from Fino et al., 2005, 2008, 2009b).

experiments have indicated that t-LTP was NMDA receptor activation dependent whereas t-LTD was dependent of the activation of group-1 glutamate metabotropic receptors (mGluR) (Fino et al., 2008). Concerning the nNOS interneurons, STDP was atypical since it displayed an asymmetric time-dependence: t-LTD was induced by post-pre ($-65 < \Delta t < 0$ ms) but also by "early" pre-post sequences ($0 < \Delta t < +30$ ms), whereas t-LTP was exclusively induced by "late" pre-post sequences ($+30 < \Delta t < +65$ ms) (**Figure 4C**) (Fino et al., 2009b). This constitutes the first example of a STDP with such a form of asymmetric plasticity (t-LTD) spanning over negative and positive Δt and followed by the other form of synaptic efficacy changes (t-LTP). Concerning the nNOS interneurons, the signaling pathways underlying the STDP remain to be characterized.

These results reveal the existence of a marked cell-specificity of the spike-timing dependence (**Figure 4D**) and of the signaling cascades among striatal neuronal populations. Such cell-specificity of STDP has also been observed in the cochlear nucleus where the principal cells and the glycinergic interneurons display different STDP time-dependence (Tzounopoulos et al., 2004) and in the cortex, with different time-dependence of pyramidal cells and layer 4 spiny stellate cells (Markram et al., 1997; Egger et al., 1999).

CONSEQUENCES OF THE STRIATAL STDP CELL-SPECIFICITY

The common feature within all the different striatal neuronal subtypes is that STDP can be induced at a very high occurrence in MSNs (90%), fast-spiking GABAergic (95%), cholinergic (86%) and nNOS interneurons (90%) (Fino et al., 2005, 2008, 2009b; Pawlak and Kerr, 2008).

Among striatal neurons, the temporal window in which STDP is induced, displays a marked cell-specificity. Indeed, it is narrower for MSNs ($-30 < \Delta t < +30$ ms) than for fast-spiking GABAergic ($-40 < \Delta t < +60$ ms), cholinergic ($-50 < \Delta t < +60$ ms) and nNOS ($-65 < \Delta t < +65$ ms) interneurons (Fino et al., 2005, 2008, 2009b). The temporal window for STDP induction is larger for the different striatal interneurons than MSNs. Functionally, this means that, for $\Delta t < -30$ ms and for $\Delta t > +30$ ms, the synapses onto interneurons are still subject to long-term plasticity whereas the synaptic efficacy changes at the MSNs themselves become unaffected. In addition, interneurons are recruited by cortical afferents slightly before the MSNs (Mallet et al., 2005; Fino et al., 2008), meaning that they are able to influence directly the cortical information integration by the MSNs. These different aspects highlight the impact of the interneurons on the control of the striatal output.

Considering the cell-specificity of the STDP together with the local interactions between striatal interneurons and MSNs, we propose a simplified scheme of the impact of the interplay of the different STDP on the striatal output (**Figure 5**). It should be noted that this scheme is based on data obtained in the same experimental conditions: the horizontal brain slices without affecting the GABAergic transmission with identical STDP protocol (100 paired stimulations at 1 Hz). A post-pre pairing induces a t-LTP in MSN, a t-LTD in GABAergic and nNOS interneurons and both forms of plasticity in cholinergic interneurons (with a majority of t-LTP) (**Figures 4D and 5A**). Conversely, after a pre-post pairing, MSNs and cholinergic interneurons develop a t-LTD while GABAergic and nNOS interneurons display a strictly opposite STDP orientation, a t-LTP (**Figures 4D and 5B**). The question is: how this cell-specificity of STDP acts to influence the striatal output? To answer this question, we need to consider the local interactions between the striatal interneurons and MSNs. As previously described in this review, local interactions between interneurons and MSNs are

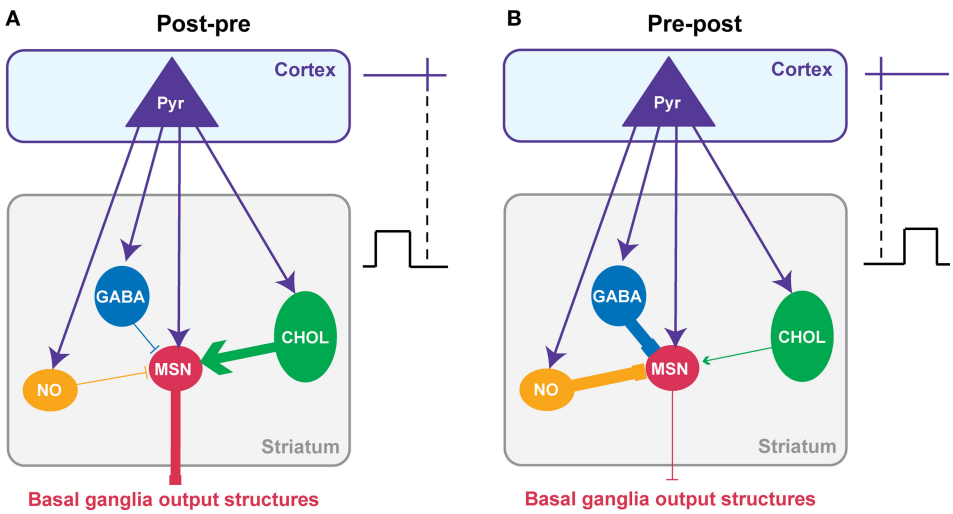

FIGURE 5 | Putative functional consequences of corticostriatal STDP cell-specificity on the striatal output. A simplified model of the interplay of the STDP occurring at the different striatal neuron populations taking into account the main synaptic interactions between striatal interneurons and MSNs. The effects of the combined STDP on the striatal output were considered after post-pre **(A)** or pre-post pairings **(B)**. **(A)** Post-pre pairings induced a depression of the GABAergic inhibition from interneurons while reinforcing the synaptic efficacy of MSNs and cholinergic interneurons. Consequently, it is expected that the synaptic weight of the striatal output would be increased. **(B)** Conversely, pre-post pairings lead to a potentiation of the GABAergic inhibition exerts by interneurons on MSNs while synaptic weight of MSNs and cholinergic interneurons decreases. Consequently, it is expected that the striatal output would be decreased. In conclusion, it appears that striatal STDP occurring at the different striatal neuronal population would act synergistically to increase or decrease the striatal output.

characterized as following: GABAergic and nNOS interneurons have a strong inhibitory weight on MSNs and we will consider here the excitatory effect of cholinergic interneurons (**Figure 2**).

For a post-pre corticostriatal paired activity, the effect of the potentiation of the MSN synaptic efficacy would then be reinforced by the decreased inhibitory weight of GABAergic and nNOS interneurons. In addition, the excitatory effect of cholinergic interneurons would be increased by the induction of t-LTP at their level. Therefore, all these synaptic efficacy changes would work in synergy to increase the striatal output (**Figure 5A**). Conversely, after pre-post pairings, the corticostriatal transmission is depressed for MSNs, and this would be accentuated by the increase of the inhibition from GABAergic and nNOS interneurons and the decrease of excitatory effect of cholinergic interneurons (**Figure 5B**). In conclusion, the STDP of striatal interneurons and MSNs would act together to either increase or depress the striatal output.

Of course this scheme is quite simple and do not consider all the fine regulation and the specificity of STDP within the striatum. Indeed, it only considers the excitatory effect of cholinergic interneurons onto MSNs via M1 receptors, although an inhibitory effect mediated by M4 receptors has been also reported (Acquas and DiChiara, 2002). In addition, even though post-pre sequences induced a majority of t-LTP at cholinergic interneurons, they also induced t-LTD; the occurrence of t-LTP or t-LTD was dependent on the excitability of the cells (Fino et al., 2008). We should also consider that nNOS interneurons displayed a specific STDP time-dependence since for pre-post sequences they develop t-LTD for short Δt and t-LTP for longer Δt (Fino et al., 2009b). Finally, we will need to consider the strong effect of local modulation within the striatum like the dopaminergic afferents from the SNc for example (Nicola et al., 2000; Costa, 2007). Nevertheless, this scheme helps to understand how all these STDP interact synergistically. These results show that it is very important to consider the striatal neuronal heterogeneity to understand properly the integration of the cortical information by the striatum and its transmission toward the basal ganglia output structures.

SUBTHRESHOLD EVENTS ACT AS HEBBIAN SIGNAL FOR CORTICOSTRIATAL LONG-TERM PLASTICITY: THE SUBTHRESHOLD-DEPOLARIZATION DEPENDENT PLASTICITY

In the current conception of activity-dependent plasticity, as highlighted by STDP, the action potential constitutes the physiologically pertinent coding event determinant for the induction of long-term synaptic plasticity. However, neuronal activity does not lead systematically to an action potential but also, in many cases, to subthreshold events. Accordingly, experimental data suggested that the back-propagating action potential would not be the only post-synaptic depolarizing event necessary for the induction of long-term synaptic plasticity. In the hippocampus, a low-frequency stimulation at 1 Hz induced exclusively LTD whatever the amplitude of post-synaptic depolarization (subthreshold EPSP *versus* action potential) (Staubli and Ji, 1996); the amplitude of post-synaptic depolarization only influencing the LTD magnitude. Changes of holding membrane potential for relatively long duration (1 min; Artola et al., 1990 and 250 ms; Sjöström et al., 2004) paired with theta burst or action potential, respectively, induced either LTP (Artola et al., 1990) or LTD (Sjöström et al., 2004).

Due to MSN electrophysiological properties (Calabresi et al., 1987; Nisenbaum and Wilson, 1995), cortical inputs do not systematically trigger an action potential but a wide range of post-synaptic depolarizations, which mostly remain subthreshold (Wilson, 1995; Stern et al., 1997, 1998; Mahon et al., 2006) (**Figure 6A**). Therefore, considering the role of striatum in sensorimotor and cognitive learning, the implication of subthreshold signals in long-term coding at MSN corticostriatal synapses would be determinant. Moreover, a subthreshold depolarization back-propagates very efficiently in the dendritic tree of the MSNs and modulates the activity of voltage-sensitive calcium channels (Carter et al., 2007). Subthreshold depolarization in MSNs, paired with a quasi-coincident cortical activity, are able to induce long-term synaptic plasticity, named "subthreshold-depolarization dependent plasticity" (SDDP with "sd" coding for subthreshold depolarization) (Fino et al., 2009a) (**Figures 6B,C**). The induction protocol was similar than the one for corticostriatal STDP: same duration of depolarization (30 ms), same stimulation frequency but with the post-synaptic depolarization remaining subthreshold. Pre-post pairings (subthreshold depolarization evoked just after a cortical stimulation) induce mainly sd-LTD and post-pre pairings (subthreshold depolarization evoked just before a cortical stimulation) induce either sd-LTP or sd-LTD. The occurrence of sd-LTP and sd-LTD was dependent on the level of MSN excitability. Comparison of corticostriatal SDDP and STDP indicates that a post-synaptic subthreshold depolarization is sufficient to induce bidirectional long-term plasticity while a post-synaptic action potential appears to be determinant in the strict orientation of the plasticity and the precision of the time window (Fino et al., 2009a) (**Figure 6C**). The same receptors are involved in the induction of corticostriatal STDP and SDDP since sd-LTD is dependent of CB1-receptor activation and sd-LTP requires the activation of NMDA receptors. Such similar pharmacology indicates that subthreshold events are very efficiently transmitted throughout the dendritic tree in MSNs since, in coincidence with a presynaptic activation, they are able to activate NMDA receptors or to induce a release of endocannabinoids similarly to a back-propagating action potential.

SDDP demonstrates that MSNs have the capability to fully take into account post-synaptic subthreshold signals paired with cortical activity and, depending on the timing between these activities and on neuronal excitability, to generate robust sd-LTD or sd-LTP. SDDP could have multiple consequences for corticostriatal transmission. Thus, change in the corticostriatal transmission efficacy induced by SDDP is expected to shift the threshold of MSN coincidence detection and firing. Indeed, LTP induced by theta burst in the hippocampus has been shown to facilitate the coincidence detection (Xu et al., 2006). In MSNs, SDDP should therefore induce a temporal shift of the spike timing and consequently modify the occurrence and magnitude of a subsequent STDP. Such impact of SDDP on STDP is reinforced by the fact that STDP is highly temporally restricted and the temporal position of the action potential has a determinant weight on the induced long-term plasticity orientation and magnitude. In conclusion, SDDP extends considerably the capabilities of neuronal long-term coding, beyond the action potential, making the neuron a genuine analogue element.

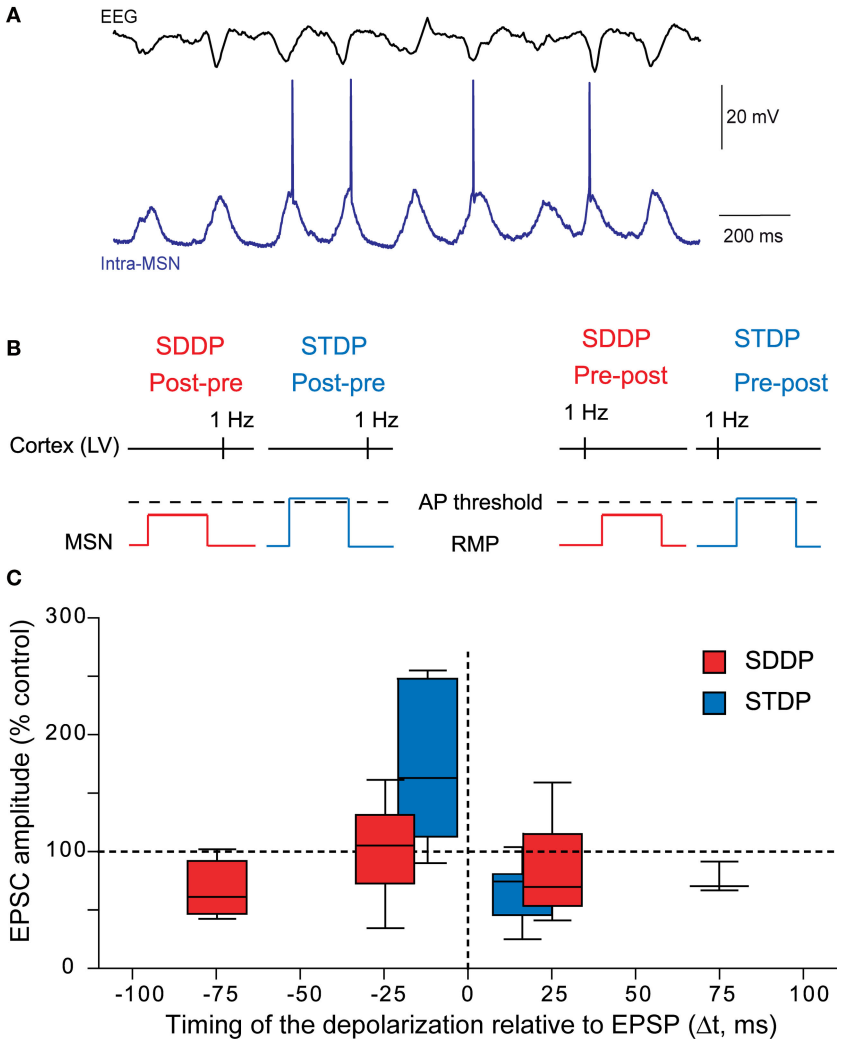

FIGURE 6 | Beyond the action potential, the subthreshold-depolarization dependent plasticity. (A) *In vivo* simultaneous recordings of the EEG of the cortical activity and the intracellular recording of one MSN. Synchronous cortical activity triggers action potentials in the MSN but also leads to subthreshold events (Adapted from Mahon et al., 2001). **(B)** Schematic representations of post-pre and pre-post SDDP and STDP protocols (the two protocols differ by the presence or not of a post-synaptic action potential). **(C)** Comparison of the occurrence, orientation, magnitude and temporal extent of SDDP and STDP. Long-term synaptic efficacy changes evoked by SDDP and STDP protocols illustrated with Box and Whiskers plots. When compared to SDDP, STDP changes were strictly orientated. SDDP changes were inducible in wider time windows than STDP (±110 vs. ±30 ms). (Adapted from Fino et al., 2009a).

CONCLUSION

The characterization of the different forms of non-synaptic and synaptic plasticity at the corticostriatal pathway constitutes a step toward the goal of understanding the cortico-basal ganglia information processing and the cellular basis of procedural learning. Nevertheless, to fully understand the modality of striatal plasticity and therefore the strength of the coincidence detection operated by MSNs, it will be determinant to consider the heterogeneity of the striatal compartments, the effects of neuromodulators (dopamine, serotonine, acetylcholine) and fully integrate the diversity of the neuronal sub-populations. In addition, although the corticostriatal pathway constitutes the main input pathway of the basal ganglia responsible for the selection of behaviorally pertinent information, it will be necessary to explore the synaptic plasticity occurring at the basal ganglia nuclei located downstream of the striatum to have the full picture of the successive plasticities all along cortico-basal ganglia information processing. Namely, STDP should be also investigated at relay (GPe) or output (SNr and GPi) nuclei (**Figure 1**). Lastly, it remains to investigate *in vivo* the genuine impact of the corticostriatal STDP on the selection of cortical and thalamic activity. *In vivo* investigation of the effect of corticostriatal STDP during natural behaviors will indeed constitute a key step in understanding the cellular and synaptic mechanisms underlying procedural learning and memory in the basal ganglia.

ACKNOWLEDGMENTS

This work was supported by the INSERM and Collège de France.

REFERENCES

Acquas, E., and DiChiara, G. (2002). Dopamine-Acetylcholine interactions. *Handb. Exp. Pharmacol.* 154, 85–115.

Aosaki, T., Graybiel, A. M., and Kimura, M. (1994). Effect of the nigrostriatal dopamine system on acquired neural responses in the striatum of behaving monkeys. *Science* 265, 412–415.

Apicella, P. (2007). Leading tonically active neurons of the striatum from reward detection to context recognition. *Trends Neurosci.* 30, 299–306.

Artola, A., Brocher, S., and Singer, W. (1990). Different voltage-dependent thresholds for inducing long-term depression and long-term potentiation in slices of rat visual cortex. *Nature* 347, 69–72.

Bennett, B. D., and Bolam, J. P. (1994). Synaptic input and output of parvalbumin-immunoreactive neurons in the neostriatum of the rat. *Neuroscience* 62, 707–719.

Bi, G. Q., and Rubin, J. (2005). Timing in synaptic plasticity: from detection to integration. *Trends Neurosci.* 28, 222–228.

Bliss, T. V., and Collingridge, G. L. (1993). A synaptic model of memory: long-term potentiation in the hippocampus. *Nature* 361, 31–39.

Bonsi, P., De Persis, C., Calabresi, P., Bernardi, G., and Pisani, A. (2004). Coordinate high-frequency pattern of stimulation and calcium levels control the induction of LTP in striatal cholinergic interneurons. *Learn. Mem.* 11, 755–760.

Calabresi, P., Gubellini, P., Centonze, D., Sancesario, G., Morello, M., Giorgi, M., Pisani, A., and Bernardi, G. (1999). A critical role of the nitric oxide/cGMP pathway in corticostriatal long-term depression. *J. Neurosci.* 19, 2489–2499.

Calabresi, P., Maj, R., Pisani, A., Mercuri, N. B., and Bernardi, G. (1992a). Long-term synaptic depression in the striatum: physiological and pharmacological characterization. *J. Neurosci.* 12, 4224–4233.

Calabresi, P., Pisani, A., Mercuri, N. B., and Bernardi, G. (1992b). Long-term potentiation in the striatum is unmasked by removing the voltage-dependent magnesium block of NMDA receptor channels. *Eur. J. Neurosci.* 4, 929–935.

Calabresi, P., Mercuri, N. B., and Di Filippo, M. (2009). Synaptic plasticity, dopamine and Parkinson's disease: one step ahead. *Brain* 132, 285–287.

Calabresi, P., Misgeld, U., and Dodt, H. U. (1987). Intrinsic membrane properties of neostriatal neurons can account for their low level of spontaneous activity. *Neuroscience* 20, 293–303.

Calabresi, P., Pisani, A., Mercuri, N. B., and Bernardi, G. (1996). The corticostriatal projection: from synaptic plasticity to dysfunctions of the basal ganglia. *Trends Neurosci.* 19, 19–24.

Caporale, N., and Dan, Y. (2008). Spike timing-dependent plasticity: a Hebbian learning rule. *Annu. Rev. Neurosci.* 31, 25–46.

Carter, A. G., Soler-Llavina, G. J., and Sabatini, B. L. (2007). Timing and location of synaptic inputs determine modes of subthreshold integration in striatal medium spiny neurons. *J. Neurosci.* 27, 8967–8977.

Centonze, D., Gubellini, P., Pisani, A., Bernardi, G., and Calabresi, P. (2003). Dopamine, acetylcholine and nitric oxide systems interact to induce corticostriatal synaptic plasticity. *Rev. Neurosci.* 14, 207–216.

Clarke, P. B., and Pert, A. (1985). Autoradiographic evidence for nicotine receptors on nigrostriatal and mesolimbic dopaminergic neurons. *Brain Res.* 348, 355–358.

Costa, R. M. (2007). Plastic corticostriatal circuits for action learning: what's dopamine got to do with it? *Ann. N. Y. Acad. Sci.* 1104, 172–191.

Dan, Y., and Poo, M. M. (2004). Spike timing-dependent plasticity of neural circuits. *Neuron* 44, 23–30.

Dan, Y., and Poo, M. M. (2006). Spike timing-dependent plasticity: from synapse to perception. *Physiol. Rev.* 86, 1033–1048.

Deniau, J. M., and Thierry, A. M. (1997). Anatomical segregation of information processing in the rat substantia nigra pars reticulata. *Adv. Neurol.* 74, 83–96.

Di Filippo, M., Picconi, B., Tantucci, M., Ghiglieri, V., Bagetta, V., Sgobio, C., Tozzi, A., Parnetti, L., and Calabresi, P. (2009). Short-term and long-term plasticity at corticostriatal synapses: implications for learning and memory. *Behav. Brain Res.* 199, 108–118.

Ding, J., Peterson, J. D., and Surmeier, D. J. (2008). Corticostriatal and thalamostriatal synapses have distinctive properties. *J. Neurosci.* 28, 6483–6492.

Egger, V., Feldmeyer, D., and Sakmann, B. (1999). Coincidence detection and changes of synaptic efficacy in spiny stellate neurons in rat barrel cortex. *Nat. Neurosci.* 2, 1098–1105.

Exley, R., and Cragg, S. J. (2008). Presynaptic nicotinic receptors: a dynamic and diverse cholinergic filter of striatal dopamine neurotransmission. *Br. J. Pharmacol.* 153(Suppl. 1), S283–S297.

Figueredo-Cardenas, G., Medina, L., and Reiner, A. (1996). Calretinin is largely localized to a unique population of striatal interneurons in rats. *Brain Res.* 709, 145–150.

Fino, E., Deniau, J. M., and Venance, L. (2008). Cell-specific spike-timing-dependent plasticity in GABAergic and cholinergic interneurons in corticostriatal rat brain slices. *J. Physiol. (Lond.)* 586, 265–282.

Fino, E., Deniau, J. M., and Venance, L. (2009a). Brief subthreshold events can act as Hebbian signals for long-term plasticity. *PLoS ONE* 4, e6557. doi:10.1371/journal.pone.0006557.

Fino, E., Paille, V., Deniau, J. M., and Venance, L. (2009b). Asymmetric spike-timing dependent plasticity of striatal nitric oxide-synthase interneurons. *Neuroscience* 160, 744–754.

Fino, E., Glowinski, J., and Venance, L. (2005). Bidirectional activity-dependent plasticity at corticostriatal synapses. *J. Neurosci.* 25, 11279–11287.

Fino, E., Paille, V., Cui, Y., Morera-Herreras, T., Deniau, J., and Venance, L. (2010). Distinct coincidence detectors govern the corticostriatal sipke timing dependent plasticity. *J. Physiol. (Lond.)*. (in press).

Gerfen, C. R. (1992). The neostriatal mosaic: multiple levels of compartmental organization in the basal ganglia. *Annu. Rev. Neurosci.* 15, 285–320.

Graybiel, A. M. (1990). Neurotransmitters and neuromodulators in the basal ganglia. *Trends Neurosci.* 13, 244–254.

Graybiel, A. M. (2005). The basal ganglia: learning new tricks and loving it. *Curr. Opin. Neurobiol.* 15, 638–644.

Graybiel, A. M., Aosaki, T., Flaherty, A. W., and Kimura, M. (1994). The basal ganglia and adaptive motor control. *Science* 265, 1826–1831.

Groenewegen, H. J., and Berendse, H. W. (1994). The specificity of the 'non-specific' midline and intralaminar thalamic nuclei. *Trends Neurosci.* 17, 52–57.

Groenewegen, H. J., Berendse, H. W., Wolters, J. G., and Lohman, A. H. (1990). The anatomical relationship of the prefrontal cortex with the striatopallidal system, the thalamus and the amygdala: evidence for a parallel organization. *Prog. Brain Res.* 85, 95–116; discussion 116–118.

Kawaguchi, Y. (1993). Physiological, morphological, and histochemical characterization of three classes of interneurons in rat neostriatum. *J. Neurosci.* 13, 4908–4923.

Kawaguchi, Y., Wilson, C. J., and Emson, P. C. (1990). Projection subtypes of rat neostriatal matrix cells revealed by intracellular injection of biocytin. *J. Neurosci.* 10, 3421–3438.

Kimura, M., Yamada, H., and Matsumoto, N. (2003). Tonically active neurons in the striatum encode motivational contexts of action. *Brain Dev.* 25(Suppl. 1), S20–S23.

Kita, H. (1996). Glutamatergic and GABAergic postsynaptic responses of striatal spiny neurons to intrastriatal and cortical stimulation recorded in slice preparations. *Neuroscience* 70, 925–940.

Kita, H., Kosaka, T., and Heizmann, C. W. (1990). Parvalbumin-immunoreactive neurons in the rat neostriatum: a light and electron microscopic study. *Brain Res.* 536, 1–15.

Koos, T., and Tepper, J. M. (1999). Inhibitory control of neostriatal projection neurons by GABAergic interneurons. *Nat. Neurosci.* 2, 467–472.

Kreitzer, A. C., and Malenka, R. C. (2008). Striatal plasticity and basal ganglia circuit function. *Neuron* 60, 543–554.

Kubota, Y., and Kawaguchi, Y. (2000). Dependence of GABAergic synaptic areas on the interneuron type and target size. *J. Neurosci.* 20, 375–386.

Levesque, M., and Parent, A. (2005). The striatofugal fiber system in primates: a reevaluation of its organization based on single-axon tracing studies. *Proc. Natl. Acad. Sci. U.S.A.* 102, 11888–11893.

Lin, J. Y., Chung, K. K., de Castro, D., Funk, G. D., and Lipski, J. (2004). Effects of muscarinic acetylcholine receptor activation on membrane currents and intracellular messengers in medium spiny neurones of the rat striatum. *Eur. J. Neurosci.* 20, 1219–1230.

Lynch, M. A. (2004). Long-term potentiation and memory. *Physiol. Rev.* 84, 87–136.

Mahon, S., Deniau, J. M., and Charpier, S. (2001). Relationship between EEG potentials and intracellular activity of striatal and cortico-striatal neurons: an in vivo study under different anesthetics. *Cereb. Cortex* 11, 360–373.

Mahon, S., Deniau, J. M., and Charpier, S. (2004). Corticostriatal plasticity: life after the depression. *Trends Neurosci.* 27, 460–467.

Mahon, S., Vautrelle, N., Pezard, L., Slaght, S. J., Deniau, J. M., Chouvet, G., and Charpier, S. (2006). Distinct patterns of striatal medium spiny neuron activity during the natural sleep-wake cycle. *J. Neurosci.* 26, 12587–12595.

Malenka, R. C., and Bear, M. F. (2004). LTP and LTD: an embarrassment of riches. *Neuron* 44, 5–21.

Mallet, N., Le Moine, C., Charpier, S., and Gonon, F. (2005). Feedforward inhibition of projection neurons by fast-spiking GABA interneurons in the rat striatum in vivo. *J. Neurosci.* 25, 3857–3869.

Markram, H., Lubke, J., Frotscher, M., and Sakmann, B. (1997). Regulation of synaptic efficacy by coincidence of postsynaptic APs and EPSPs. *Science* 275, 213–215.

Martin, S. J., and Morris, R. G. (2002). New life in an old idea: the synaptic plasticity and memory hypothesis revisited. *Hippocampus* 12, 609–636.

Matamales, M., Bertran-Gonzalez, J., Salomon, L., Degos, B., Deniau, J. M., Valjent, E., Herve, D., and Girault, J. A. (2009). Striatal medium-sized spiny neurons: identification by nuclear staining and study of neuronal subpopulations in BAC transgenic mice. *PLoS ONE* 4, e4770. doi:10.1371/journal.pone.0004770.

Morris, G., Arkadir, D., Nevet, A., Vaadia, E., and Bergman, H. (2004). Coincident but distinct messages of midbrain dopamine and striatal tonically active neurons. *Neuron* 43, 133–143.

Nicola, S. M., Surmeier, J., and Malenka, R. C. (2000). Dopaminergic modulation of neuronal excitability in the striatum and nucleus accumbens. *Annu. Rev. Neurosci.* 23, 185–215.

Nisenbaum, E. S., and Wilson, C. J. (1995). Potassium currents responsible for inward and outward rectification in rat neostriatal spiny projection neurons. *J. Neurosci.* 15, 4449–4463.

Nisenbaum, E. S., Xu, Z. C., and Wilson, C. J. (1994). Contribution of a slowly inactivating potassium current to the transition to firing of neostriatal spiny projection neurons. *J. Neurophysiol.* 71, 1174–1189.

Packard, M. G., and Knowlton, B. J. (2002). Learning and memory functions of the Basal Ganglia. *Annu. Rev. Neurosci.* 25, 563–593.

Pakhotin, P., and Bracci, E. (2007). Cholinergic interneurons control the excitatory input to the striatum. *J. Neurosci.* 27, 391–400.

Partridge, J. G., Apparsundaram, S., Gerhardt, G. A., Ronesi, J., and Lovinger, D. M. (2002). Nicotinic acetylcholine receptors interact with dopamine in induction of striatal long-term depression. *J. Neurosci.* 22, 2541–2549.

Pawlak, V., and Kerr, J. N. (2008). Dopamine receptor activation is required for corticostriatal spike-timing-dependent plasticity. *J. Neurosci.* 28, 2435–2446.

Perez-Rosello, T., Figueroa, A., Salgado, H., Vilchis, C., Tecuapetla, F., Guzman, J. N., Galarraga, E., and Bargas, J. (2005). Cholinergic control of firing pattern and neurotransmission in rat neostriatal projection neurons: role of CaV2.1 and CaV2.2 Ca2+ channels. *J. Neurophysiol.* 93, 2507–2519.

Plenz, D., and Kitai, S. T. (1998). Up and down states in striatal medium spiny neurons simultaneously recorded with spontaneous activity in fast-spiking interneurons studied in cortex-striatum-substantia nigra organotypic cultures. *J. Neurosci.* 18, 266–283.

Ramanathan, S., Hanley, J. J., Deniau, J. M., and Bolam, J. P. (2002). Synaptic convergence of motor and somatosensory cortical afferents onto GABAergic interneurons in the rat striatum. *J. Neurosci.* 22, 8158–8169.

Redgrave, P., and Gurney, K. (2006). The short-latency dopamine signal: a role in discovering novel actions? *Nat. Rev. Neurosci.* 7, 967–975.

Reynolds, J. N., and Wickens, J. R. (2004). The corticostriatal input to giant aspiny interneurons in the rat: a candidate pathway for synchronising the response to reward-related cues. *Brain Res.* 1011, 115–128.

Sardo, P., Ferraro, G., Di Giovanni, G., Galati, S., and La Grutta, V. (2002). Inhibition of nitric oxide synthase influences the activity of striatal neurons in the rat. *Neurosci. Lett.* 325, 179–182.

Schultz, W. (2007). Behavioral dopamine signals. *Trends Neurosci.* 30, 203–210.

Sergeeva, O. A., Doreulee, N., Chepkova, A. N., Kazmierczak, T., and Haas, H. L. (2007). Long-term depression of cortico-striatal synaptic transmission by DHPG depends on endocannabinoid release and nitric oxide synthesis. *Eur. J. Neurosci.* 26, 1889–1894.

Shen, W., Flajolet, M., Greengard, P., and Surmeier, D. J. (2008). Dichotomous dopaminergic control of striatal synaptic plasticity. *Science* 321, 848–851.

Sjöström, P. J., and Nelson, S. B. (2002). Spike timing, calcium signals and synaptic plasticity. *Curr. Opin. Neurobiol.* 12, 305–314.

Sjöström, P. J., Turrigiano, G. G., and Nelson, S. B. (2004). Endocannabinoid-dependent neocortical layer-5 LTD in the absence of postsynaptic spiking. *J. Neurophysiol.* 92, 3338–3343.

Smeal, R. M., Gaspar, R. C., Keefe, K. A., and Wilcox, K. S. (2007). A rat brain slice preparation for characterizing both thalamostriatal and corticostriatal afferents. *J. Neurosci. Methods* 159, 224–235.

Smith, Y., Raju, D. V., Pare, J. F., and Sidibe, M. (2004). The thalamostriatal system: a highly specific network of the basal ganglia circuitry. *Trends Neurosci.* 27, 520–527.

Staubli, U. V., and Ji, Z. X. (1996). The induction of homo- vs. heterosynaptic LTD in area CA1 of hippocampal slices from adult rats. *Brain Res.* 714, 169–176.

Stern, E. A., Jaeger, D., and Wilson, C. J. (1998). Membrane potential synchrony of simultaneously recorded striatal spiny neurons in vivo. *Nature* 394, 475–478.

Stern, E. A., Kincaid, A. E., and Wilson, C. J. (1997). Spontaneous subthreshold membrane potential fluctuations and action potential variability of rat corticostriatal and striatal neurons in vivo. *J. Neurophysiol.* 77, 1697–1715.

Surmeier, D. J., Ding, J., Day, M., Wang, Z., and Shen, W. (2007). D1 and D2 dopamine-receptor modulation of striatal glutamatergic signaling in striatal medium spiny neurons. *Trends Neurosci.* 30, 228–235.

Suzuki, T., Miura, M., Nishimura, K., and Aosaki, T. (2001). Dopamine-dependent synaptic plasticity in the striatal cholinergic interneurons. *J. Neurosci.* 21, 6492–6501.

Tepper, J. M., and Bolam, J. P. (2004). Functional diversity and specificity of neostriatal interneurons. *Curr. Opin. Neurobiol.* 14, 685–692.

Tepper, J. M., Koos, T., and Wilson, C. J. (2004). GABAergic microcircuits in the neostriatum. *Trends Neurosci.* 27, 662–669.

Thomas, T. M., Smith, Y., Levey, A. I., and Hersch, S. M. (2000). Cortical inputs to m2-immunoreactive striatal interneurons in rat and monkey. *Synapse* 37, 252–261.

Tzounopoulos, T., Kim, Y., Oertel, D., and Trussell, L. O. (2004). Cell-specific, spike timing-dependent plasticities in the dorsal cochlear nucleus. *Nat. Neurosci.* 7, 719–725.

Valjent, E., Bertran-Gonzalez, J., Herve, D., Fisone, G., and Girault, J. A. (2009). Looking BAC at striatal signaling: cell-specific analysis in new transgenic mice. *Trends Neurosci.* 32, 538–547.

Vandecasteele, M., Deniau, J. M., Glowinski, J., and Venance, L. (2007). Electrical synapses in basal ganglia. *Rev. Neurosci.* 18, 15–35.

Venance, L., Glowinski, J., and Giaume, C. (2004). Electrical and chemical transmission between striatal GABAergic output neurones in rat brain slices. *J. Physiol. (Lond.)* 559, 215–230.

Vuillet, J., Kerkerian, L., Kachidian, P., Bosler, O., and Nieoullon, A. (1989). Ultrastructural correlates of functional relationships between nigral dopaminergic or cortical afferent fibers and neuropeptide Y-containing neurons in the rat striatum. *Neurosci. Lett.* 100, 99–104.

Vuillet, J., Kerkerian-Le Goff, L., Kachidian, P., Dusticier, G., Bosler, O., and Nieoullon, A. (1990). Striatal NPY-containing neurons receive GABAergic afferents and may also contain GABA: an electron microscopic study in the rat. *Eur. J. Neurosci.* 2, 672–681.

West, A. R., and Grace, A. A. (2004). The nitric oxide-guanylyl cyclase signaling pathway modulates membrane activity States and electrophysiological properties of striatal medium spiny neurons recorded in vivo. *J. Neurosci.* 24, 1924–1935.

Wilson, C. J. (1995). "The contribution of cortical neurons to the firing pattern of striatal spiny neurons," in *Models of Information Processing in the Basal Ganglia*, eds J. C. Houk, J. L. Davies, and D. G. Beiser (Cambridge, MIT Press), 29–50.

Wu, Y., Richard, S., and Parent, A. (2000). The organization of the striatal output system: a single-cell juxtacellular labeling study in the rat. *Neurosci. Res.* 38, 49–62.

Xu, N. L., Ye, C. Q., Poo, M. M., and Zhang, X. H. (2006). Coincidence detection of synaptic inputs is facilitated at the distal dendrites after long-term potentiation induction. *J. Neurosci.* 26, 3002–3009.

Yin, H. H., and Knowlton, B. J. (2006). The role of the basal ganglia in habit formation. *Nat. Rev. Neurosci.* 7, 464–476.

Yin, H. H., Mulcare, S. P., Hilario, M. R., Clouse, E., Holloway, T., Davis, M. I., Hansson, A. C., Lovinger, D. M., and Costa, R. M. (2009). Dynamic reorganization of striatal circuits during the acquisition and consolidation of a skill. *Nat. Neurosci.* 12, 333–341.

Conflict of Interest Statement: The authors declare that the research was conducted in the absence of any commercial or financial relationship that could be construed as a potential conflict of interest.

Received: 08 February 2010; paper pending published: 14 March 2010; accepted: 17 May 2010; published online: 10 June 2010.

*Citation: Fino E and Venance L (2010) Spike-timing dependent plasticity in the striatum. Front. Syn. Neurosci. **2**:6. doi: 10.3389/fnsyn.2010.00006*

frontiers in
SYNAPTIC NEUROSCIENCE

REVIEW ARTICLE
published: 09 June 2010
doi: 10.3389/fnsyn.2010.00009

STDP in the developing sensory neocortex

Rylan S. Larsen[1], Deepti Rao[1], Paul B. Manis[1,2,3,4]* and Benjamin D. Philpot[1,3,4,5]*

[1] *Department of Cell and Molecular Physiology, The University of North Carolina at Chapel Hill, Chapel Hill, NC, USA*
[2] *Department of Otolaryngology/Head and Neck Surgery, The University of North Carolina at Chapel Hill, Chapel Hill, NC, USA*
[3] *Curriculum in Neurobiology, The University of North Carolina at Chapel Hill, Chapel Hill, NC, USA*
[4] *UNC Neuroscience Center, The University of North Carolina at Chapel Hill, Chapel Hill, NC, USA*
[5] *Neurodevelopmental Disorders Research Center, The University of North Carolina at Chapel Hill, Chapel Hill, NC, USA*

Edited by:
Per Jesper Sjöström, University College London, UK

Reviewed by:
Ole Paulsen, University of Oxford, UK
Vincent Jacob, Cardiff University, UK

****Correspondence:***
Benjamin D. Philpot, University of North Carolina, Campus Box 7545, 115 Mason Farm Road, Chapel Hill, NC 27599-7545, USA.
e-mail: bphilpot@med.unc.edu
Paul B. Manis, University of North Carolina, G127 Physician's Office Building, Campus Box 7070, 170 Manning Drive, Chapel Hill, NC 27599-7070, USA.
e-mail: pmanis@med.unc.edu

Spike timing-dependent plasticity (STDP) has been proposed as a mechanism for optimizing the tuning of neurons to sensory inputs, a process that underlies the formation of receptive field properties and associative memories. The properties of STDP must adjust during development to enable neurons to optimally tune their selectivity for environmental stimuli, but these changes are poorly understood. Here we review the properties of STDP and how these may change during development in primary sensory cortical layers 2/3 and 4, initial sites for intracortical processing. We provide a primer discussing postnatal developmental changes in synaptic proteins and neuromodulators that are thought to influence STDP induction and expression. We propose that STDP is shaped by, but also modifies, synapses to produce refinements in neuronal responses to sensory inputs.

Keywords: spike timing-dependent plasticity, presynaptic NMDA receptor, endocannabinoid, visual cortex, auditory cortex, somatosensory cortex, neuromodulation

INTRODUCTION

A fundamental property of the brain is its ability to change in response to sensory stimuli. These adaptations to changes in either the sensory environment or sensory receptor function provide a substrate for the memory of sensory experiences and perceptual learning. A long-term goal of neuroscience research has been to determine the molecular mechanisms that underlie the formation of cortical responses to environmental stimuli. Changes in synaptic strength have been modeled *in vitro* using low- or high-frequency stimulation to produce long-term depression (LTD) and long-term potentiation (LTP), respectively (Bliss and Lomo, 1973; Dudek and Bear, 1992). While frequency-dependent plasticity has provided a wonderful tool to study the mechanism for the strengthening and weakening of cortical synapses during early stages of development, frequency-dependent plasticity is not sufficient to explain many modifications in synaptic strength that result from changes in sensory experience. Manipulations that produce synaptic plasticity *in vivo* are not always associated with significant changes in firing rates, and changes in firing rates that induce plasticity *in vitro* do not always produce plasticity when occurring naturally *in vivo* (Carandini and Ferster, 2000; Celikel et al., 2004; Fox and Wong, 2005). The discovery that the precise temporal precision of spiking between pre- and postsynaptic neurons in the hippocampus can dictate whether a synapse is strengthened or weakened raised great excitement, as this timing-dependent plasticity mechanism could readily account for changes observed *in vivo* that were not readily explained by frequency-dependent forms of plasticity (Levy and Steward, 1983; Magee and Johnston, 1997).

Since the initial discoveries of spike timing-dependent plasticity (STDP) (Levy and Steward, 1983; Bell et al., 1997; Magee and Johnston, 1997; Markram et al., 1997; Bi and Poo, 1998; Debanne et al., 1998), it has been proposed as a mechanism by which receptive field maps and sensory selectivity can be formed and modified *in vivo* (Song and Abbott, 2001; Clopath et al., 2010). STDP has been observed in sensory cortices just following birth, and is also thought to provide a mechanism for modifying synaptic strength in adulthood (Fu et al., 2002; Banerjee et al., 2009; Pellicciari et al., 2009). Although synaptic plasticity can occur throughout life, the induction and expression mechanisms of both frequency-dependent plasticity and STDP are believed to change over development. For example, adult plasticity in response to sensory deprivation is believed to result primarily from the potentiation of spared (sensory-driven) inputs and not by depression of the lost (sensory-independent) inputs (Glazewski and Fox, 1996). Similarly, both frequency- and spike timing-dependent LTD (tLTD) are difficult to induce following postnatal day 30 (P30) in rodents (Dudek and Bear, 1993; Fox, 2002; Corlew et al., 2007; Banerjee et al., 2009). This suggests that while the ability to strengthen and weaken sensory synapses remains throughout life, changes in synaptic proteins that occur throughout development may influence how plasticity is induced or expressed. Herein, we describe mechanisms by which STDP can be shaped through development via the expression of synaptic proteins in the cortices of the somatosensory, visual, and auditory systems (**Table 1**). Although STDP has been observed in many neocortical layers (Egger et al., 1999; Sjostrom et al., 2003; Kampa and Stuart, 2006; Letzkus et al., 2006), for simplicity we focus on the synaptic connection between cortical layer (L) 4 and

TABLE 1 | Excitatory STDP in sensory neocortices.

Author	Area	Species	Pathway	Method	Age	*In vivo / in vitro*	tLTP Δt (ms)	tLTD Δt (ms)	NMDARs	Pre-NMDARs	Postsynaptic Ca^{2+}	mGluRs	Ca^{2+} Stores	Endo-cannabinoid	Other
Karmarkar, 2002	A1	Rat	L2/3-L2/3	whole-cell, extra. stim.	P12-18	*in vitro*	10	-40							
Dahmen, 2008	A1	Ferret	?	single units	adult	*in vivo*	8 to 12	-12 to -8							
Jacob, 2007	S1	Rat	L2/3, L5, L6	single units, whole-cell	P27-32, adult (single units)	*in vivo*		-17 to -7							
Frey, 2009	S1	Mouse	L2/3-L2/3	whole-cell, extra. stim.	P39-100	*in vitro*	10		tLTP		tLTP				GluR1 NR
Feldman, 2000	S1	Rat	L4-L2/3	whole-cell, extra. stim.	P18-31	*in vitro*	3 to 15	-50 to 0	tLTP, tLTD						
Banerjee, 2009	S1	Mouse	L4-L2/3, L2/3-L2/3	whole-cell, extra. stim.	P6-8, P11-15, P19-25, P25-42	*in vitro*	10	-15 to -10	tLTP L4-L2/3 (NR2A)	tLTD L4-L2/3 (NR2C/D) L2/3-L2/3 (NR2B)				tLTD - (L2/3-L2/3, NR at L4-L2/3)	
Hardingham, 2008	S1	Mouse	L4- L2/3	whole-cell, extra. stim.	P28-42	*in vitro, in vivo*	10	-50						NR	
Rodriguez-Moreno, 2008	S1	Mouse	L4-L2/3	paired, extra. stim.	P9-14	*in vitro*	10	-15	tLTP (post)	tLTD					
Bender, 2006	S1	Rat	L4-L2/3	whole-cell, extra. stim.	P16-23	*in vitro*	5	-25	tLTP (post)	tLTD	tLTP, tLTD- (T- & L-type)	tLTD - (mGluR5)	tLTD- IP_3R , CICR NR	tLTD - (2-AG & CB1Rs)	
Egger, 1999	S1	Rat	L4-L4	paired	P12-14	*in vitro*		<25	NR		tLTP	tLTP - (group 2)			
Nevian, 2006	S1	Rat	L2/3-L2/3	whole-cell, focal stim.	P13-15	*in vitro*	10	-50 to -10	tLTP	tLTD	tLTP, tLTD - (T-type)	tLTD - (group 1), tLTP - NR	tLTD - IP_3R NR	tLTD - CB1Rs	tLTD - PLC
Letzkus, 2006	S1	Rat	L2/3-L5	paired	P21-42	*in vitro*	-10 (distal) 10 (proximal)	-10 (proximal) 10 (distal)	tLTP, tLTD (distal)		tLTP - (T- or R-type)				
Kampa, 2006	S1	Rat	L5-L5	paired, extra. stim.	P21-28	*in vitro*	10 (3 APs) -15 (3 APs)	-40 (3 APs)	tLTP		tLTP - (T- or R-type)				
Yao, 2001	V1	Cat Human	?	single units	adult	*in vivo*	~0 to ~45	~-20 to ~-5							
Seol, 2007	V1	Mouse	L4-L2/3	whole-cell, extra. stim.	P21-28	*in vitro*	no tLTP *	no tLTD *							
Sjöström, 2003	V1	Rat	L5-L5	paired	P12-21	*in vitro*		-10 and -25		tLTD NR2B	tLTD			tLTD- CB1Rs	
Zilberter, 2009	V1	Rat	L2/3-L2/3	paired	P14-21	*in vitro*	3 to 5 (10 APs)	2 to 10 (1 AP) -12 to -5 ms (10 APs)	tLTP, tLTD - NR		tLTD, tLTP - (L-type)	tLTD - (group 1/2)		tLTP or tLTD - NR	
Corlew, 2007	V1	Mouse	L4-L2/3	whole-cell, extra. stim.	P13-17, P23-30	*In vitro*		-25 to -5	tLTD (P23-30, post)	tLTD (P13-17)					
Markam, 1997	V1	Rat	L5-L5	paired	P14-16	*in vitro*	-10	5 to 10	tLTP						
Froemke, 2005	V1	Rat	L2/3	whole-cell, focal stim.	P14-28	*in vitro*	0 to 30	-100 to 0 (distal) -50 to 0 (proximal)**	tLTD		tLTD - (L-type)				tLTD - calcineurin
Froemke, 2002	V1	Rat	L2/3-L2/3	whole-cell, extra. stim.	P14-35	*in vitro*	0 to 20	-50 to 0 (proximal)							
Froemke, 2006	V1	Rat	L2/3	whole-cell, focal stim.	P10-35	*in vitro*	-15 to -2	2 to 15	tLTP, tLTD		tLTP, tLTD - (L-type)				
Wespatat, 2004	V1	Rat	L2/3-L2/3	whole-cell, extra. stim.	P13, P18-33	*in vitro*	9 to 10 γ peak pairing ***	-13, -5 γ peak pairing	tLTP ***		tLTD				
Urakubo, 2008	V1	Rat	L2/3	whole-cell, focal stim.	P14-28	*in vitro*		-10	tLTD (post)						
Schuett, 2001	V1	Cat	L2/3, L4, L5	single units, extra. stim.	P56-77	*in vivo*	~18	~11							
Sjöström, 2001	V1	Rat	L5-L5	paired	P12-21	*in vitro*	10 (10 Hz)	-10 (0.1 to 20 Hz)	tLTP, tLTD						
Sjöström, 2006	V1	Rat	L5-L5 L5-L2/3	paired, extra. stim.	P21-28	*in vitro*	10 (L5-L5)	10 (L5-L2/3)						LTD (distal) w/o spiking	
Meliza, 2006	V1	Rat	?	whole-cell	P16-21	*in vivo*	1 to 50	-65 to -1			tLTP, tLTD				
Fu, 2002	V1	Cat Human	?	single units	adult	*in vivo*	8 (Cat) 20 (Human)	-8 (Cat) -20 (Human)							

Abbrevations: **Post**=Postsynaptic, **NR**=Not Required, **VGCC**=voltage-gated calcium channnels, **CICR**=calcium-induced calcium release, **2-AG**= 2-arachidonyl glycerol, **extra.**=extracellular, **stim.**=stimulation, **paired**=paired whole-cell recordings, **γ**=gamma oscillation, **proximal**=proximal dendrite, **distal**=distal dendrite.

* β-adrenergic agonist induces tLTP. Muscarinic receptor M1 agonist induces tLTD, at - and + pairing intervals.

** Blockade of voltage-gated potassium channels broadened tLTD window of proximal dendrites up to ~ -100ms

*** Only in the presence of cholinergic agonists at P21-33.

L2/3 neurons and between L2/3 neurons. These synapses represent the major site of intracortical processing for inputs arriving from the thalamic relays. In addition, STDP in L2/3 synapses has been observed throughout development, is relatively well characterized *in vitro*, and occurs in response to sensory deprivation (Diamond et al., 1994; Drew and Feldman, 2009). We also consider the contribution of neuromodulation to the expression and development of cortical STDP. Although we emphasize changes in synaptic proteins between excitatory cortical connections that may influence STDP expression, considerable evidence demonstrates that STDP exists at inhibitory connections (Holmgren and Zilberter, 2001; Haas et al., 2006) and that there are considerable changes in inhibitory circuitry during development (Yazaki-Sugiyama et al., 2009) that are likely to be shaped by STDP.

STDP IN SOMATOSENSORY CORTEX

Spike timing-dependent plasticity in rodent primary somatosensory cortex (S1) has been proposed to underlie refinement of receptive fields in response to changes in whisker stimulation (Fox and Wong, 2005; Feldman, 2009). In support of this idea, whisker trimming during early life alters the firing sequence of L4–L2/3 synaptic connections *in vivo* to produce timing patterns known to weaken synapses *in vitro*, and this change in the temporal precision of spiking precedes the degradation of L2/3 receptive field maps (Feldman, 2000; Celikel et al., 2004). Response depression can also be produced *in vivo* by pairing natural spike trains with coincident whisker deflection to mimic the timing requirements for inducing tLTD *in vitro* (Jacob et al., 2007). Such findings suggest that STDP is likely to occur naturally during receptive field refinements through development and even into adulthood (Clark et al., 1988). Below, we discuss the molecular mechanisms underlying STDP and how they may be regulated to produce and tune STDP in developing S1.

tLTP IN S1

In general, the induction of timing-dependent LTP (tLTP) in cortical areas requires glutamate binding of NMDA receptors (NMDARs) coincident with arrival of a backpropagating action potential (BAP) into the postsynaptic dendrite (Magee and Johnston, 1997; Froemke et al., 2005; Letzkus et al., 2006). The pairing of glutamate binding with the BAP causes the removal of Mg^{2+} from NMDARs and produces a supralinear summation of calcium entering through NMDARs and voltage-gated calcium channels (VGCCs) (Koester and Sakmann, 1998; Kampa and Stuart, 2006; Nevian and Sakmann, 2006). Despite the importance of both VGCCs and NMDAR activation for tLTP induction, postsynaptic NMDARs are believed to act as the sole coincidence detector for tLTP within the neocortex (Froemke et al., 2005, 2006; Rodriguez-Moreno and Paulsen, 2008).

S1 pyramidal cells maintain the ability to express tLTP into adulthood, and many of the induction parameters appear to be similar throughout life. For example, the timing requirements for tLTP induction are largely unchanged across development, as pre–post pairings with positive intervals of ~10 ms readily induce tLTP from P6–P100 (Feldman, 2000; Bender et al., 2006; Rodriguez-Moreno and Paulsen, 2008; Banerjee et al., 2009). The requirement for postsynaptic NMDAR activation is also maintained across development, because intracortical tLTP is blocked by the NMDAR antagonist APV in S1 in both younger (<P20) and older (>P35) rodents (Rodriguez-Moreno and Paulsen, 2008; Banerjee et al., 2009; Frey et al., 2009). The induction of tLTP between S1 L4–L2/3 synapses requires postsynaptic NMDARs, because selectively loading the postsynaptic recording pipette with the NMDAR antagonist MK-801 is sufficient to abolish tLTP (Bender et al., 2006; Rodriguez-Moreno and Paulsen, 2008). In addition to having many similar induction requirements across development, the magnitude of tLTP expression also does not correlate with age in rats across the P18–P32 developmental period (Feldman, 2000).

While many aspects of tLTP induction are similar throughout life, there are also likely to be important developmental differences. Because postsynaptic NMDARs are thought to be the sole coincidence detector for tLTP, developmental changes in NMDAR functions may by one important modulator of the properties of tLTP induction. In the neocortex, postsynaptic NMDARs undergo a developmental switch from primarily NR2B-containing to NR2A-containing receptors. In rodent S1, this switch to predominately NR2A-containing receptors occurs ~P9 in L2/3 pyramidal cells (Flint et al., 1997; Liu et al., 2004). As would be predicted based on this expression pattern in S1, NR2A-, but not NR2B-containing, receptors are required for tLTP induction at L4–L2/3 synapses in P11–P15 mice (Banerjee et al., 2009). The contribution of NR2B to tLTP induction has not been studied at young ages (<P6), thus it is not yet clear how the developmental switch from NR2B to NR2A influences tLTP induction. There are currently two ideas as to how an increased NR2A/NR2B ratio would affect tLTP, with one prediction suggesting that a higher ratio would compress the tLTP timing window (Shouval et al., 2002) and the other suggesting that it will make tLTP less likely to be induced (Gerkin et al., 2007). Both predictions suggest that a shift in the NR2A/NR2B ratio would adjust the balance between tLTD and tLTP. Thus, further studies are warranted to determine how changes in S1 postsynaptic NMDAR composition and downstream signaling cascades at different ages influence the expression, magnitude, and timing requirements of tLTP.

tLTD

While postsynaptic NMDARs act as a coincidence detector for tLTP, they have not been shown to act as the coincidence detector for tLTD between L4 and L2/3 synapses. Instead, the near-simultaneous activation of postsynaptic mGluRs coincident with both postsynaptic depolarization and activation of VGCCs is thought to constitute a separate coincidence detector for tLTD (Karmarkar and Buonomano, 2002; Bender et al., 2006). In this model, tLTD is induced when postsynaptic group 1 mGluRs (likely mGluR5) are activated with T- or L-type VGCCs to increase PLC activity (Bender et al., 2006; Nevian and Sakmann, 2006). Activation of PLC leads to generation of inositol 1,4,5-triphosphate (IP_3) and intracellular release of calcium from IP_3-mediated internal stores (Bender et al., 2006; Nevian and Sakmann, 2006). This calcium, along with the calcium released from VGCCs, combines to trigger release of the endocannabinoid 2-arachidonyl glycerol (2-AG) from the postsynaptic neuron (Bender et al., 2006). Activation of presynaptic CB1 receptors and presynaptic NMDARs results in lasting reductions in release probability from the presynaptic neuron, although the time course and pathways by which this occurs remains to be determined.

This type of LTD can become manifest with post-before-pre action potential pairings occurring with intervals up to 50 ms (Feldman, 2000; Bender et al., 2006; Nevian and Sakmann, 2006), which is much longer than the 10–20 ms pre-before-post timing window required for tLTP induction. It should be noted that tLTD in the visual cortex can also be induced in a manner thought to rely on postsynaptic NMDARs as the coincidence detector (Froemke et al., 2005; Urakubo et al., 2008), and a similar mechanism is likely to occur in S1. Exactly how these two forms of tLTD cooperate or are segregated is not clear, and it is possible that development influences tLTD in a location or spike-dependent manner.

While tLTP is thought to be inducible throughout life, a dramatic reduction in the ability to induce tLTD *in vitro* between L4 and L2/3 synapses in rodent S1 occurs by P25 (Banerjee et al., 2009). This decrease in tLTD magnitude is reminiscent of the developmental loss of frequency-dependent LTD in CA1 of the hippocampus (Dudek and Bear, 1993) and to the loss of LTP at S1 thalamocortical synapses (Crair and Malenka, 1995). A developmental reduction in tLTD magnitude has also been observed in L4–L2/3 synapses in primary visual cortex, and this loss is curiously dependent on inhibition (Corlew et al., 2007). This suggests that a developmental increase in inhibition might limit tLTD induction, perhaps through shunting inhibition, but this hypothesis has yet to be rigorously tested. Since standard experimental protocols do not reliably induce tLTD in mature neocortex, it is possible that the requirements for tLTD induction are different, and will require increasing the number or adjusting the timing of the pairings. In support of this idea, a very narrow window for inducing tLTD has been observed in adult rats *in vivo* (Jacob et al., 2007).

Before P25 in rodents, it is remarkable that the magnitude of tLTD is similar at all ages tested (P6–P32; Feldman, 2000; Banerjee et al., 2009, despite large changes in many of the proteins involved in tLTD induction. Among these proteins, mGluRs and their downstream effectors are developmentally upregulated before P15. The requirement for group 1 mGluRs for tLTD at L2/3 synapses has been shown at P13–P23, when mGluR expression begins to plateau (Bender et al., 2006; Nevian and Sakmann, 2006). In S1, mGluR5 expression is uniform in all layers by P16 and remains constant at these levels through adulthood (Blue et al., 1997). Similarly, the expression of group 1 mGluR's downstream effector, PLC, reaches stable expression in S1 by P14 (Hannan et al., 1998). The early developmental upregulation of mGluR5 and PLC expression do not seem to influence the magnitude or induction of tLTD, because mice aged P6–P8 show tLTD with a similar magnitude to mice at P11–P25 (Banerjee et al., 2009). This suggests that mGluRs do not developmentally gate tLTD induction, but may influence tLTD in other ways. It is clear that mGluRs and their downstream effectors play an important role in S1 development because the genetic deletion of mGluR5 or PLC causes barrels to form improperly (Hannan et al., 2001), yet whether this is a direct consequence of altered tLTD remains unknown.

Synaptic proteins involved in tLTD induction have also been suggested to be segregated based on synapse. For example, the requirement both for endocannabinoid signaling and specific preNMDAR subunits differs by synaptic pathway. In mice, CB1Rs are not required for tLTD between L4 and L2/3 synapses at either P11–P15 or P28–P42 but are required between L2/3 and L2/3 synapses at P11–P15 (Hardingham et al., 2008; Banerjee et al., 2009). In contrast, CB1Rs and postsynaptic endocannabinoid synthesis are required for tLTD induction between L4 and L2/3 rat neurons at P16–P23 (Bender et al., 2006). These differences may reflect laminar and species-specific differences in the activation of CB1Rs or their downstream signaling. The expression of CB1Rs reaches stable adult levels by P16 in rats and CB1R function is required during this period for barrel receptive field formation (Bodor et al., 2005; Deshmukh et al., 2007). Chronically blocking CB1Rs with the *in vivo* administration of the antagonist AM251 between P13 and P16 disrupts whisker tuning and results in the loss of experience-dependent plasticity in L2/3 rat S1 (Li et al., 2009). This demonstrates the importance of CB1R signaling in rats at a time when tLTD is readily inducible both *in vivo* and *in vitro* by CB1R activation, suggesting that there may be a causal relationship between tLTD induction and receptive field tuning in S1.

In a similar fashion to the segregation of endocannabinoid signaling across cortical layers, there are differing layer-dependent requirements for presynaptic NMDAR subunits. Moderately selective NR2C/D antagonists, but not NR2B or NR2A antagonists, block the induction of tLTD between L4 and L2/3 S1 synapses (Banerjee et al., 2009). In contrast, L2/3–L2/3 synapses show a requirement for NR2B-containing receptors, but not NR2C/D (Banerjee et al., 2009). The segregation of presynaptic NMDAR subunits may permit differential modulation of tLTD depending on the synaptic pathway, which is consistent with previous findings that the induction requirements and timing windows of STDP depend on dendritic location (Froemke et al., 2005; Letzkus et al., 2006). The mechanisms by which STDP are induced appear diverse and synapse-specific. Due to the wide variety of synaptic mechanisms for induction, tLTD may be developmentally regulated in a unique way at each synapse. Studies that compare the pathway-specific tLTD mechanisms could determine the exact requirements for tLTD induction at each S1 synapse. The existing evidence suggests that the molecular mechanisms of tLTD are not universal across synapses within sensory cortices.

STDP IN VISUAL CORTEX

The importance of coordinated activity in the developing visual cortex was first demonstrated in groundbreaking experiments by Hubel and Wiesel (1965) where binocular receptive fields were converted to monocular receptive fields by changing the synchrony of visual inputs in kittens with artificial strabismus. STDP within the visual cortex likely follows constraints unique to the environmental stimuli it receives, allowing this form of plasticity to modulate synaptic connectivity in a manner that is different from S1. Like plasticity in S1, STDP in V1 is a relevant mechanism for synaptic strengthening and weakening. Indeed, pairing action potentials with precisely timed visual stimuli induces STDP *in vivo* (Meliza and Dan, 2006). In further support of the idea that STDP can shape visual processing, manipulating the temporal order of spiking in V1 neurons is sufficient to change orientation preferences and receptive fields *in vivo,* and these modifications can occur in a bidirectional manner similar to STDP timing rules observed *in vitro* (Schuett et al., 2001). For example, when visual stimuli of a particular orientation are paired with electrical stimulation of a neuron, the orientation preference of that neuron shifts toward that of the given

stimuli (Schuett et al., 2001). Reversing the pairing order (so that the neuron fires before the visual stimuli) weakens the orientation preference away from the given orientation in a tLTD-like manner. Additionally, the pairing of visual stimuli at two orientations shifts the orientation preference of V1 neurons depending on the temporal order of the pairings and can be predicted based on the temporal windows of STDP induced *in vitro* (Yao and Dan, 2001). The ability to modify visual responses via STDP learning rules exists through adulthood, as the pairing of visual stimuli can rapidly modify receptive fields and orientation preferences in adult cats (Yao and Dan, 2001; Fu et al., 2002). Lastly, STDP learning rules have been shown to be sufficient to segregate sensory inputs onto specific dendritic branches, underscoring how STDP may be essential for shaping cortical connectivity (Froemke et al., 2005). Overall these observations suggest that STDP provides a powerful mechanism by which visual cortical circuitry can be modeled and by which neurons can rapidly adapt to an ever-changing visual environment throughout life. Many synaptic proteins implicated in STDP induction or expression are developmentally regulated between P10 and P35 in rodents, overlapping with periods of receptive field development and the visual cortical critical period (Hensch, 2005; Smith and Trachtenberg, 2007). The regulation of these synaptic proteins may therefore favor the development and stability of visual circuits through adulthood by modulating STDP.

A surprising observation, which we will discuss below, is that the mechanisms of STDP appear largely similar between S1 and V1. The most pronounced differences in STDP between these regions are due to a developmental delay in V1 development compared to S1 development, and this delay is likely due to a delay in sensory-driven activity in V1.

tLTP

Similar to tLTP observed in the somatosensory cortex, tLTP in V1 is believed to rely on the interaction of BAPs with calcium influx through postsynaptic NMDARs and L-type VGCCs (Froemke et al., 2005, 2006). NMDARs are required for tLTP induction between P12 and P35 at both L5 and L2/3 V1 synapses (Markram et al., 1997; Froemke et al., 2006; Zilberter et al., 2009). Unlike S1, the exact postsynaptic NMDAR subunits required for tLTP have not been investigated. Postsynaptic NMDARs in V1 show a developmental shift from NR2B to NR2A at a period later in development (~P25) as compared to other cortical areas (de Marchena et al., 2008). This suggests that a greater proportion of NR2B-containing receptors may participate in tLTP induction before P25 in the visual cortex compared to somatosensory cortex, although it has been reported that the NR2B antagonist ifenprodil does not have a major impact on the NMDA:AMPA ratio in L5 neurons of P14–P15 rats (Sjostrom et al., 2003). How the switch in NMDAR subunits during the visual critical period influences STDP induction and expression is not known, but it may involve temporal changes in NMDAR glutamate binding (Laurie and Seeburg, 1994), magnesium sensitivity (Clarke and Johnson, 2006), or allosteric interactions (Urakubo et al., 2008) that could alter dendritic calcium and shape the temporal window for inducing STDP (Shouval et al., 2002).

Surprisingly little is known about how the properties of tLTP adjust over development in the visual cortex, but some assumptions can be made based on known tLTP mechanisms. In addition to the aforementioned changes in NMDAR subunit expression, there are other developmental changes in tLTP-related proteins that can affect tLTP induction across the length of the dendrite. The magnitude of tLTP in L2/3 pyramidal neurons varies with location of the stimulated inputs, such that stimulation of synapses on the proximal dendrite produce a larger magnitude of tLTP than stimulation of synapses on more distal dendrites (Froemke et al., 2005). This effect probably depends on the attenuation of the BAP along the extent of the dendrite (Magee and Johnston, 1997; Froemke et al., 2005; Sjostrom and Hausser, 2006), which would be predicted to affect the supralinear potentiation of calcium that has been observed with tLTP induction (Nevian and Sakmann, 2006). Such an interpretation is consistent with studies in the somatosensory cortex showing that voltage-gated sodium channel dependent action potentials, in turn activate VGCCs (Kampa and Stuart, 2006; Komai et al., 2006). Consequently, any developmental changes in the magnitude or localization of dendritic sodium or calcium channels would be expected to alter the timing requirements and magnitude of tLTP, perhaps by changing the resulting calcium transient. Developmental changes in other dendritic proteins that can affect the shape or size of the BAP, such as A-type potassium channels (Hoffman et al., 1997; Froemke et al., 2005), would likewise be expected to alter tLTP induction and expression.

tLTD

Like tLTP, NMDAR activation is required for the induction of tLTD. Unlike tLTP, there appears to be both a presynaptic and a postsynaptic contribution of NMDARs. The relative contribution of pre- and postsynaptic NMDARs may vary by age and pathway. Initial studies using bath-applied APV to globally block NMDARs led to the assumption that the NMDARs relevant to tLTD were exclusively postsynaptic (Markram et al., 1997; Feldman, 2000). Later studies in ~P14–P18 rodents found that tLTD could still be induced when postsynaptic (but not presynaptic) NMDARs were blocked (Sjostrom et al., 2003; Corlew et al., 2007). This form of tLTD appeared to have a dual requirement for presynaptic NMDAR and CB1R activation, similar to what has been described for S1 (Sjostrom et al., 2003; Bender et al., 2006; Rodriguez-Moreno and Paulsen, 2008), although whether preNMDARs are acting on a rapid or slow time scale has been debated (Sjostrom et al., 2003; Bender et al., 2006).

While some studies have shown that tLTD at L5–L5 and L4–L2/3 synapses requires presynaptic NMDAR activation (Sjostrom et al., 2003; Corlew et al., 2007), others have shown that tLTD is fully blocked by postsynaptic inhibition of NMDARs in L2/3 V1 neurons (Froemke et al., 2005; Urakubo et al., 2008). This apparent discrepancy might be explained by age-related modifications in the mechanisms of tLTD. Presynaptic NMDARs, which are required for tLTD during early life, are sharply downregulated between P16 and P27 (Corlew et al., 2007). Remarkably, this anatomical reduction in presynaptic NMDARs coincides with the loss of presynaptically expressed tLTD between L4 and L2/3 synapses, which occurs around 3 weeks of age, suggesting that there may be a causal relationship between the two events. In support of this idea, studies showing a requirement for presynaptic NMDARs in tLTD have been performed in P14–P18 rodents, while those that support a postsynaptic requirement for NMDARs have been performed in

rodents including ages >P21. The form of tLTD involving postsynaptic NMDARs requires activation of the phosphatase calcineurin (Froemke et al., 2005; Urakubo et al., 2008), but it is not known if this is a requirement in younger rodents (**Figure 1**).

In addition to developmental changes in the contribution of presynaptic NMDARs to tLTD, there are also likely to be differences in the role that inhibition plays in tLTD. A developmental loss of tLTD at L4–L2/3 synapses is evident in V1 by ~P23 (Corlew et al., 2007), similar to that observed in S1 by ~P25 (Banerjee et al., 2009). However, the induction of tLTD can be restored in older mice by performing the post-before-pre pairing protocol in the presence of $GABA_A$ receptor antagonists (Corlew et al., 2007). When inhibition is blocked at these older ages, tLTD requires *post*synaptic NMDARs instead of *pre*synaptic NMDARs. This suggests development may shape the mechanism by which tLTD is induced from one that is predominately presynaptic to one that is predominately postsynaptic. It is interesting that tLTD that relies on postsynaptic NMDAR activation in older animals is smaller in magnitude than that induced at younger ages, suggesting development may also subtly affect tLTD magnitude in V1 (Corlew et al., 2007). As the loss of presynaptically expressed tLTD coincides with a period of rapid inhibitory development (Hensch, 2005), it suggests that inhibition may influence the mechanisms underlying tLTD. An unresolved issue is whether tLTD requires one or two coincidence detectors. While inhibition is one factor that influences tLTD induction mechanisms, others such as dendritic location (Froemke et al., 2005) and dendritic calcium buffering (Kampa and Stuart, 2006; Nevian and Sakmann, 2006) may also influence how tLTD is induced.

STDP IN AUDITORY CORTEX

Sounds in the acoustic environment have complex temporal structures that overlap in time, space, and frequency content. Cortical lesion studies demonstrate the importance of the auditory cortex in the perception of time-varying sounds across a large range of time scales (Whitfield, 1980). As in visual cortex, coordinated activity may play a role in plasticity in auditory cortex. Raising rats in a noisy environment devoid of structured spectral and temporal cues delays the refinement of the tonotopic map in primary auditory cortex (A1), and this can be reversed by experience in an acoustic environment with tonal structure (Chang and Merzenich, 2003). Neurons in A1 can fire with millisecond precision to the fine temporal structure of acoustic stimuli (for example, Eggermont, 2007), and it was recently shown that millisecond differences in neural activity in A1 can be exploited to guide decisions (Yang et al., 2008). Given the robust plasticity, importance of temporal features in sound identification and discrimination, and the precision of spiking timing in A1 (Recanzone et al., 1993; Kudoh and Shibuki, 1994; Bao et al., 2004), it is natural to wonder whether A1 has unique timing rules for STDP. Although surprisingly few studies of STDP have been performed in A1, the studies to date suggest that the properties of STDP in A1 are fundamentally similar to those observed in other sensory cortices.

Spike timing-dependent plasticity-like rules have been observed in a variety of species (Gerstner et al., 1996) throughout the auditory pathway, including brainstem (Tzounopoulos et al., 2004) and cortical areas (Schnupp et al., 2006). STDP in the dorsal cochlear nucleus appears to follow Hebbian and anti-Hebbian patterns in a cell-specific manner (Tzounopoulos et al., 2004). In contrast, STDP

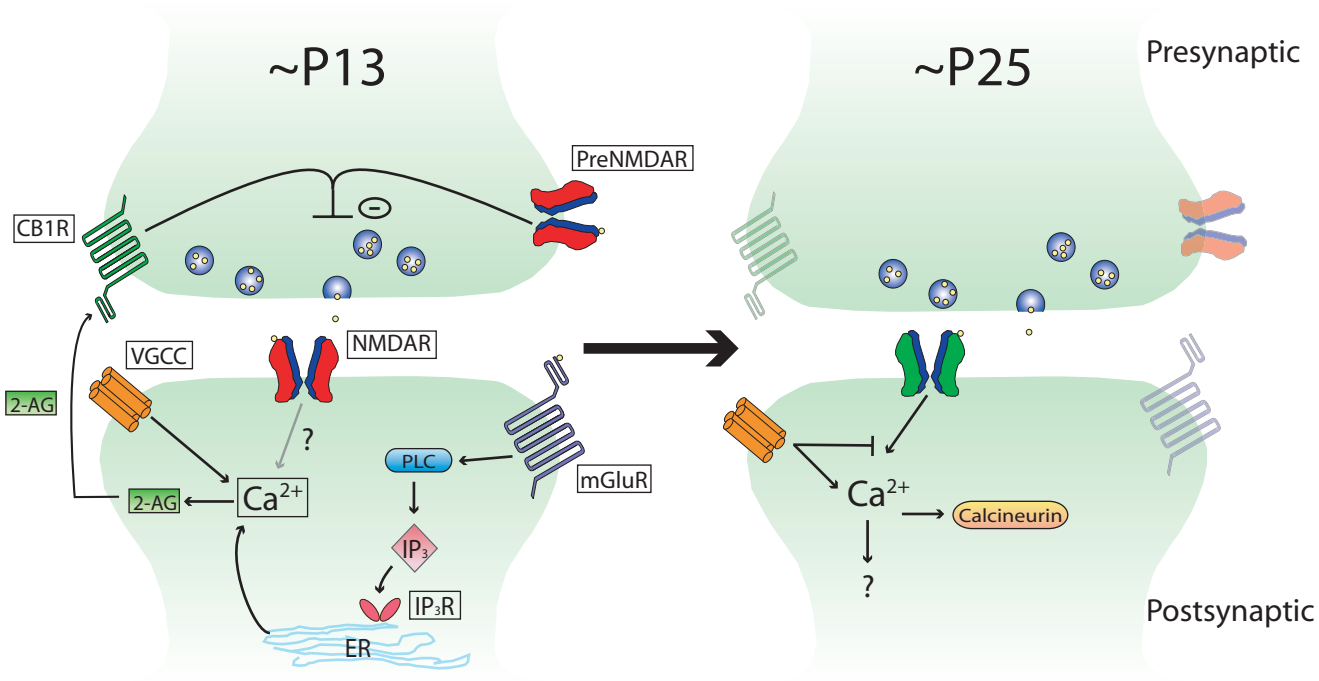

FIGURE 1 | Schematic depicting developmental changes in known tLTD induction mechanisms at L4–L2/3 synapses in rodent sensory neocortex. Note that the mechanisms are very similar between the different sensory areas, and that this scheme could apply to primary visual cortex as well as primary somatosensory cortex (see text for details).

in the auditory cortex, at least at some synapses onto pyramidal cells, appears to follow a traditional Hebbian rule. In P12–P18 rat auditory cortical slices, repetitive pairing of pre-before-post spiking activity at 10 ms intervals produces tLTP and post-before-pre intervals at 40 ms produces tLTD at L2/3–L2/3 synapses (Karmarkar and Buonomano, 2002). Although the entire STDP window in A1 was not investigated in this study, the results are consistent with findings at similar synapses in P10–P35 rat V1 (Froemke et al., 2006) and in P13–P15 rat S1 (Nevian and Sakmann, 2006). These data suggest that, at least *in vitro*, STDP rules between L2/3 neurons appear roughly similar in all sensory cortices.

In vivo studies also support a role for STDP in A1. In anesthetized and awake adult ferrets, repetitive and asynchronous pairings of pure tones of different frequencies produce shifts in the frequency selectivity of neurons recorded extracellularly (Dahmen et al., 2008), and the temporal specificity of these shifts is similar to that observed *in vitro*. In this study, a non-preferred tone frequency was paired with a preferred tone frequency with an 8- to 12-ms time delay between the two tones. When the non-preferred tone was presented before the preferred tone, there was a shift in the neuronal best frequency toward the non-preferred tone frequency. Conversely, when the non-preferred tone frequency was played after the preferred tone frequency, then the neuronal best frequency shifted away from the non-preferred tone. The duration of STDP in A1 observed *in vivo* is similar to that reported in visual receptive fields of V1 in anesthetized cats (Yao and Dan, 2001) and for STDP in whisker-evoked responses of barrel cortex in rats (Jacob et al., 2007). Interestingly, in A1, the shifts in cortical frequency tuning are restricted to cortical L2/3 and L4 (Dahmen et al., 2008). These observations highlight that the temporal relationships among the components of acoustic stimuli on a millisecond scale to influence auditory processing and suggest that STDP is a relevant mechanism for plasticity in the auditory cortex.

To date, little is known about the mechanistic pathway or developmental modifications of STDP in A1. As STDP displays components of frequency-dependent LTP and LTD, it is rational to speculate that it may use the same mechanisms known to underlie associative LTP and LTD (Malenka and Bear, 2004). Indeed, many of the mechanisms for frequency-dependent plasticity in S1 and V1 are similar to those demonstrated for STDP, it is reasonable to assume that the same may be true for A1. In A1, frequency-dependent LTP and LTD have been demonstrated at thalamocortical synapses and at excitatory intracortical synapses (Kudoh and Shibuki, 1994, 1996, 1997; Bandrowski et al., 2001). The induction of frequency-dependent LTP is regulated by age and experience (Speechley et al., 2007), suggesting that the same may be true for tLTP. Frequency-dependent LTP of thalamocortical synapses requires activation of NMDARs (Kudoh and Shibuki, 1994, 1996), while LTD at the same synapse requires activation of mGluRs receptors and protein kinase C (Bandrowski et al., 2001). It might be expected in A1 that tLTD requires mGluR activation and activation of a PKC pathway, while tLTP may involve the classic postsynaptic NMDAR pathway. While such a finding would be consistent with tLTP and tLTD mechanisms in V1 and S1, there is not yet experimental evidence that this is true.

NEUROMODULATION OF STDP IN SENSORY CORTICES

Neuromodulators alter receptive field plasticity in sensory cortices by expanding the cellular representation of sensory stimuli (Weinberger, 2003). Examples thought to engage neuromodulators include the observations that (1) classical conditioning using whisker stimuli expands the representation of trained whiskers in S1 (Siucinska and Kossut, 2004), (2) perceptual training on visual stimulus orientation discrimination tasks alters V1 tuning for the trained feature (Fu et al., 2002), and (3) activation of cholinergic or dopaminergic inputs during tonal stimuli increases A1 responses to the tone frequency (Bakin and Weinberger, 1996; Bao et al., 2001; Weinberger et al., 2006). At the cellular level, neuromodulators have both facilitating and depressing effects on cortical activity that depend on the type of neuromodulators and the pattern of neuromodulator receptors expressed in sensory cortices (Spehlmann, 1971).

The effects of neuromodulators on receptive field plasticity appear to depend on the engagement of STDP-like mechanisms. The properties of STDP can be powerfully adjusted by neuromodulators, which can control the polarity, magnitude, or even the ability to induce STDP through development. In the absence of neuromodulators, tLTD and tLTP can be induced in L2/3–L2/3 synapses in developing V1 by temporally pairing EPSPs to β or γ oscillations produced by injected sinusoidal currents, such that EPSPs synchronous with hyperpolarizing and depolarizing membrane potentials produced tLTD and tLTP, respectively (Wespatat et al., 2004). This form of tLTP is impaired in V1 slices from older rats (>P21), but it can be rescued when pairings are made while muscarinic receptors are activated (Wespatat et al., 2004). Similarly, both tLTP and tLTD are impaired at L4–L2/3 synapses in older rat V1, but both tLTD and tLTP can be recovered when AP–EPSP pairings are made in the presence of M1 muscarinic or β-adrenergic receptor activation, respectively (Seol et al., 2007). These results demonstrate that neuromodulators gate STDP in the adult brain. In addition to their role as permissive gatekeepers for STDP induction, neuromodulators are also likely to control the polarity and temporal requirements for inducing STDP plasticity in sensory cortices, as such roles for neuromodulators have been observed in other areas of the brain. For example, in L2/3–L5 synapses in prefrontal cortex, nicotine application converts tLTP to tLTD (Couey et al., 2007). In hippocampal CA1, a β-adrenergic receptor agonist broadens the tLTP window from 3–10 to 15 ms without affecting tLTP magnitude (Lin et al., 2003). Also at hippocampal synapses, dopamine agonists not only extends the tLTP window from 20 ms to at least 45 ms but, also converts tLTD to tLTP (Zhang et al., 2009). Thus, neuromodulators can adjust multiple aspects of STDP induction, and the precise effects of neuromodulators on STDP induction likely depend on the neuromodulator, receptor types, synaptic pathway, and age.

How might neuromodulators alter the properties of STDP? Although there are many targets of neuromodulators, the common denominator for most of these mechanisms is that they ultimately influence local calcium levels associated with AP–EPSP pairings. There are several mechanisms by which neuromodulators bring about their effects on calcium levels. First, neuromodulators can activate kinases and phosphatases that regulate the kinetics and availability of dendritic ion channels, such as transient (I_A) and Ca^{2+}-activated K^+ channels (Watanabe et al., 2002). Such modula-

tion brings about profound changes in the width and amplitude of BAPs, ultimately influencing dendritic calcium (Magee and Johnston, 1997; Froemke et al., 2006). For example, β-adrenergic and muscarinic receptor agonists enhance spike backpropagating efficacy by phosphorylating protein kinase A and protein kinase C that result in reduction of I_A channel availability (Tsubokawa and Ross, 1997; Hoffman and Johnston, 1998, 1999). Such changes in I_A might contribute to the observations that M1 muscarinic receptors promote tLTD induction through a PLC-dependent pathway, while β-adrenergic receptor activation promotes tLTP through the adenylate cyclase cascade (Seol et al., 2007). Second, neuromodulators can target IP_3 receptors and activate calcium-induced-calcium-release from intracellular stores, thereby influencing polarity and input-specificity of STDP (Nishiyama et al., 2000). Third, neuromodulators can facilitate NMDAR currents (Brocher et al., 1992; Kirkwood et al., 1999) and presumably directly regulate STDP induction. Although it has not yet been investigated, developmental changes in neuromodulator influences are also likely to affect the timing rules for inducing STDP in sensory cortices and could play a role in defining critical periods. In support of this possibility, the expression of certain neuromodulator receptor families, such as alpha 7 nicotinic receptors and 5HT receptors, exhibit dramatic regulation around the critical period for receptive field plasticity in sensory cortices (Broide et al., 1995, 1996; Aramakis and Metherate, 1998; Basura et al., 2008).

CONCLUSION

The studies discussed here support the argument that STDP is a key mechanism used in sensory processing in somatosensory, visual, and auditory cortices, both for the establishment of circuits during development, and for the storage and processing of sensory information later in life. At a cellular level, STDP is shaped by, but also modifies, specific synapses to produce refinements in neuronal responses to sensory stimuli. While we have emphasized the role of synaptic proteins in shaping STDP, very little is known about how these changes influence the exact characteristics of induction, expression, and timing of STDP. As STDP depends not just on timing, but on spike patterning (Sjostrom et al., 2001; Froemke and Dan, 2002; Nelson et al., 2002; Froemke et al., 2006), dendritic location (Froemke et al., 2005; Letzkus et al., 2006; Sjostrom and Hausser, 2006), and previous neuronal activity (Zilberter et al., 2009), the roles of specific synaptic proteins in regulating STDP are likely both state- and context-dependent. These changes likely coincide with developmental changes in inhibition and neuromodulation that also shape how STDP learning rules are applied to sensory information (Kirkwood et al., 1999; Meredith et al., 2003). Therefore, STDP refines sensory inputs in a manner that is dependent on the developmental context while providing feedback that further changes cortical structure and function.

It is clear that there are large gaps in our knowledge regarding STDP in sensory cortices as well. For example, STDP timing windows, as measured experimentally, are quite noisy, which may reflect either the basal state of synapses prior to the experimental measurement, or the specific selection of synaptic pathways during recording. This variability makes it difficult to discern whether the timing windows are truly different between sensory areas or within different local circuit pathways, as might be predicted from the different temporal dynamics of the incoming sensory information versus the temporal dynamics of local and long-distance intracortical pathways. This biological variability is confounded by inevitable discrepancies in experimental approaches. Second, the reversibility of STDP in sensory cortex has not been investigated. In one of the first investigations of STDP (Bell et al., 1997) in the electrosensory lobe of mormyrid fish, STDP could be induced rapidly and was readily reversed within minutes with appropriate pairing patterns. Reversibility of timing-dependent plasticity has also been observed in the xenopus retinotectal system (Zhou et al., 2003). Is STDP in sensory cortex similarly reversible? Such rapid and reversible plasticity would seem to have clear utility in sensory processing, independent of a role in establishing longer sensory memory or shaping response maps. Third, the role of STDP in the inhibitory network is far from understood. Developmental changes in inhibition help drive the establishment of cortical circuits, and may involve STDP (Kanold and Shatz, 2006). Within established cortical networks, both inhibition and excitation exhibit plasticity (Froemke et al., 2007; Lu et al., 2007; Galindo-Leon et al., 2009), but it is not known whether this *in vivo* plasticity is spike-timing based or not. Given the critical role of inhibition in shaping response maps and spike timing, the role of STDP at inhibitory synapses merits greater investigation. Fourth, the role of STDP in the development and establishment of sensory response maps, while an attractive hypothesis supported by computational studies (Song and Abbott, 2001) and consistent with the available data, has not yet been unequivocally tested. To clarify the role of STDP, rate-based versus timing-based plasticity mechanisms must be disentagled to identify their respective roles in receptive field plasticity *in vivo*. Experimental approaches that allow manipulation of spike trains with millisecond precision *in vivo* are just emerging (Boyden et al., 2005; Chow et al., 2010; Gunaydin et al., 2010). These technologies can be leveraged in cleverly-designed experiments and carefully-posed questions to answer the major issues outstanding in the field of STDP.

ACKNOWLEDGMENTS

We wish to thank Thorfinn Riday for assistance with the making of the figure and table, and Dr. Serena Dudek and Dr. Rob Froemke for helpful discussions. Our work was funded by the National Science Foundation grant # 0822969 and the National Eye Institute R01EY018323 (BDP), and NIDCD grant R01DC000425 (PBM).

REFERENCES

Aramakis, V. B., and Metherate, R. (1998). Nicotine selectively enhances NMDA receptor-mediated synaptic transmission during postnatal development in sensory neocortex. *J. Neurosci.* 18, 8485–8495.

Bakin, J. S., and Weinberger, N. M. (1996). Induction of a physiological memory in the cerebral cortex by stimulation of the nucleus basalis. *Proc. Natl. Acad. Sci. U.S.A.* 93, 11219–11224.

Bandrowski, A. E., Ashe, J. H., and Crawford, C. A. (2001). Tetanic stimulation and metabotropic glutamate receptor agonists modify synaptic responses and protein kinase activity in rat auditory cortex. *Brain Res.* 894, 218–232.

Banerjee, A., Meredith, R. M., Rodriguez-Moreno, A., Mierau, S. B., Auberson, Y. P., and Paulsen, O. (2009). Double dissociation of spike timing-dependent potentiation and depression by subunit-preferring NMDA receptor

antagonists in mouse barrel cortex. *Cereb. Cortex* 19, 2959–2969.

Bao, S., Chan, V. T., and Merzenich, M. M. (2001). Cortical remodelling induced by activity of ventral tegmental dopamine neurons. *Nature* 412, 79–83.

Bao, S., Chang, E. F., Woods, J., and Merzenich, M. M. (2004). Temporal plasticity in the primary auditory cortex induced by operant perceptual learning. *Nat. Neurosci.* 7, 974–981.

Basura, G. J., Abbas, A. I., O'Donohue, H., Lauder, J. M., Roth, B. L., Walker, P. D., and Manis, P. B. (2008). Ontogeny of serotonin and serotonin2A receptors in rat auditory cortex. *Hear. Res.* 244, 45–50.

Bell, C. C., Han, V. Z., Sugawara, Y., and Grant, K. (1997). Synaptic plasticity in a cerebellum-like structure depends on temporal order. *Nature* 387, 278–281.

Bender, V. A., Bender, K. J., Brasier, D. J., and Feldman, D. E. (2006). Two coincidence detectors for spike timing-dependent plasticity in somatosensory cortex. *J. Neurosci.* 26, 4166–4177.

Bi, G. Q., and Poo, M. M. (1998). Synaptic modifications in cultured hippocampal neurons: dependence on spike timing, synaptic strength, and postsynaptic cell type. *J. Neurosci.* 18, 10464–10472.

Bliss, T. V., and Lomo, T. (1973). Long-lasting potentiation of synaptic transmission in the dentate area of the anaesthetized rabbit following stimulation of the perforant path. *J. Physiol. (Lond.)* 232, 331–356.

Blue, M. E., Martin, L. J., Brennan, E. M., and Johnston, M. V. (1997). Ontogeny of non-NMDA glutamate receptors in rat barrel field cortex: I. Metabotropic receptors. *J. Comp. Neurol.* 386, 16–28.

Bodor, A. L., Katona, I., Nyiri, G., Mackie, K., Ledent, C., Hajos, N., and Freund, T. F. (2005). Endocannabinoid signaling in rat somatosensory cortex: laminar differences and involvement of specific interneuron types. *J. Neurosci.* 25, 6845–6856.

Boyden, E. S., Zhang, F., Bamberg, E., Nagel, G., and Deisseroth, K. (2005). Millisecond-timescale, genetically targeted optical control of neural activity. *Nat. Neurosci.* 8, 1263–1268.

Brocher, S., Artola, A., and Singer, W. (1992). Agonists of cholinergic and noradrenergic receptors facilitate synergistically the induction of long-term potentiation in slices of rat visual cortex. *Brain Res.* 573, 27–36.

Broide, R. S., O'Connor, L. T., Smith, M. A., Smith, J. A., and Leslie, F. M. (1995). Developmental expression of alpha 7 neuronal nicotinic receptor messenger RNA in rat sensory cortex and thalamus. *Neuroscience* 67, 83–94.

Broide, R. S., Robertson, R. T., and Leslie, F. M. (1996). Regulation of alpha7 nicotinic acetylcholine receptors in the developing rat somatosensory cortex by thalamocortical afferents. *J. Neurosci.* 16, 2956–2971.

Carandini, M., and Ferster, D. (2000). Membrane potential and firing rate in cat primary visual cortex. *J. Neurosci.* 20, 470–484.

Celikel, T., Szostak, V. A., and Feldman, D. E. (2004). Modulation of spike timing by sensory deprivation during induction of cortical map plasticity. *Nat. Neurosci.* 7, 534–541.

Chang, E. F., and Merzenich, M. M. (2003).Environmental noise retards auditory cortical development. *Science* 18, 498–502.

Chow, B. Y., Han, X., Dobry, A. S., Qian, X., Chuong, A. S., Li, M., Henninger, M. A., Belfort, G. M., Lin, Y., Monahan, P. E., and Boyden, E. S. (2010). High-performance genetically targetable optical neural silencing by light-driven proton pumps. *Nature* 463, 98–102.

Clark, S. A., Allard, T., Jenkins, W. M., and Merzenich, M. M. (1988). Receptive fields in the body-surface map in adult cortex defined by temporally correlated inputs. *Nature* 332, 444–445.

Clarke, R. J., and Johnson, J. W. (2006). NMDA receptor NR2 subunit dependence of the slow component of magnesium unblock. *J. Neurosci.* 26, 5825–5834.

Clopath, C., Busing, L., Vasilaki, E., and Gerstner, W. (2010). Connectivity reflects coding: a model of voltage-based STDP with homeostasis. *Nat. Neurosci.* 13, 344–352.

Corlew, R., Wang, Y., Ghermazien, H., Erisir, A., and Philpot, B. D. (2007). Developmental switch in the contribution of presynaptic and postsynaptic NMDA receptors to long-term depression. *J. Neurosci.* 27, 9835–9845.

Couey, J. J., Meredith, R. M., Spijker, S., Poorthuis, R. B., Smit, A. B., Brussaard, A. B., and Mansvelder, H. D. (2007). Distributed network actions by nicotine increase the threshold for spike-timing-dependent plasticity in prefrontal cortex. *Neuron* 54, 73–87.

Crair, M. C., and Malenka, R. C. (1995). A critical period for long-term potentiation at thalamocortical synapses. *Nature* 375, 325–328.

Dahmen, J. C., Hartley, D. E., and King, A. J. (2008). Stimulus-timing-dependent plasticity of cortical frequency representation. *J. Neurosci.* 28, 13629–13639.

de Marchena, J., Roberts, A. C., Middlebrooks, P. G., Valakh, V., Yashiro, K., Wilfley, L. R., and Philpot, B. D. (2008). NMDA receptor antagonists reveal age-dependent differences in the properties of visual cortical plasticity. *J. Neurophysiol.* 100, 1936–1948.

Debanne, D., Gahwiler, B. H., and Thompson, S. M. (1998). Long-term synaptic plasticity between pairs of individual CA3 pyramidal cells in rat hippocampal slice cultures. *J. Physiol. (Lond.)* 507 (Pt 1), 237–247.

Deshmukh, S., Onozuka, K., Bender, K. J., Bender, V. A., Lutz, B., Mackie, K., and Feldman, D. E. (2007). Postnatal development of cannabinoid receptor type 1 expression in rodent somatosensory cortex. *Neuroscience* 145, 279–287.

Diamond, M. E., Huang, W., and Ebner, F. F. (1994). Laminar comparison of somatosensory cortical plasticity. *Science* 265, 1885–1888.

Drew, P. J., and Feldman, D. E. (2009). Intrinsic signal imaging of deprivation-induced contraction of whisker representations in rat somatosensory cortex. *Cereb. Cortex* 19, 331–348.

Dudek, S. M., and Bear, M. F. (1992). Homosynaptic long-term depression in area CA1 of hippocampus and effects of *N*-methyl-D-aspartate receptor blockade. *Proc. Natl. Acad. Sci. U.S.A.* 89, 4363–4367.

Dudek, S. M., and Bear, M. F. (1993). Bidirectional long-term modification of synaptic effectiveness in the adult and immature hippocampus. *J. Neurosci.* 13, 2910–2918.

Egger, V., Feldmeyer, D., and Sakmann, B. (1999). Coincidence detection and changes of synaptic efficacy in spiny stellate neurons in rat barrel cortex. *Nat. Neurosci.* 2, 1098–1105.

Eggermont, J. J. (2007). Correlated neural activity as the driving force for functional changes in auditory cortex. *Hear Res.* 229, 69–80.

Feldman, D. E. (2000). Timing-based LTP and LTD at vertical inputs to layer II/III pyramidal cells in rat barrel cortex. *Neuron* 27, 45–56.

Feldman, D. E. (2009). Synaptic mechanisms for plasticity in neocortex. *Annu. Rev. Neurosci.* 32, 33–55.

Flint, A. C., Maisch, U. S., Weishaupt, J. H., Kriegstein, A. R., and Monyer, H. (1997). NR2A subunit expression shortens NMDA receptor synaptic currents in developing neocortex. *J. Neurosci.* 17, 2469–2476.

Fox, K. (2002). Anatomical pathways and molecular mechanisms for plasticity in the barrel cortex. *Neuroscience* 111, 799–814.

Fox, K., and Wong, R. O. (2005). A comparison of experience-dependent plasticity in the visual and somatosensory systems. *Neuron* 48, 465–477.

Frey, M. C., Sprengel, R., and Nevian, T. (2009). Activity pattern-dependent long-term potentiation in neocortex and hippocampus of GluA1 (GluR-A) subunit-deficient mice. *J. Neurosci.* 29, 5587–5596.

Froemke, R. C., and Dan, Y. (2002). Spike-timing-dependent synaptic modification induced by natural spike trains. *Nature* 416, 433–438.

Froemke, R. C., Merzenich, M. M., and Schreiner, C. E. (2007). A synaptic memory trace for cortical receptive field plasticity. *Nature* 450, 425–429.

Froemke, R. C., Poo, M. M., and Dan, Y. (2005). Spike-timing-dependent synaptic plasticity depends on dendritic location. *Nature* 434, 221–225.

Froemke, R. C., Tsay, I. A., Raad, M., Long, J. D., and Dan, Y. (2006). Contribution of individual spikes in burst-induced long-term synaptic modification. *J. Neurophysiol.* 95, 1620–1629.

Fu, Y. X., Djupsund, K., Gao, H., Hayden, B., Shen, K., and Dan, Y. (2002). Temporal specificity in the cortical plasticity of visual space representation. *Science* 296, 1999–2003.

Galindo-Leon, E. E., Lin, F. G., and Liu, R. C. (2009). Inhibitory plasticity in a lateral band improves cortical detection of natural vocalizations. *Neuron* 62, 705–716.

Gerkin, R. C., Lau, P. M., Nauen, D. W., Wang, Y. T., and Bi, G. Q. (2007). Modular competition driven by NMDA receptor subtypes in spike-timing-dependent plasticity. *J. Neurophysiol.* 97, 2851–2862.

Gerstner, W., Kempter, R., van Hemmen, J. L., and Wagner, H. (1996). A neuronal learning rule for sub-millisecond temporal coding. *Nature* 383, 76–81.

Glazewski, S., and Fox, K. (1996). Time course of experience-dependent synaptic potentiation and depression in barrel cortex of adolescent rats. *J. Neurophysiol.* 75, 1714–1729.

Gunaydin, L. A., Yizhar, O., Berndt, A., Sohal, V. S., Deisseroth, K., and Hegemann, P. (2010). Ultrafast optogenetic control. *Nat. Neurosci.* 13, 387–392.

Haas, J. S., Nowotny, T., and Abarbanel, H. D. (2006). Spike-timing-dependent plasticity of inhibitory synapses in the entorhinal cortex. *J. Neurophysiol.* 96, 3305–3313.

Hannan, A. J., Blakemore, C., Katsnelson, A., Vitalis, T., Huber, K. M., Bear, M., Roder, J., Kim, D., Shin, H. S., and Kind, P. C. (2001). PLC-beta1, activated via mGluRs, mediates activity-dependent differentiation in cerebral cortex. *Nat. Neurosci.* 4, 282–288.

Hannan, A. J., Kind, P. C., and Blakemore, C. (1998). Phospholipase C-beta1 expression correlates with neuronal differentiation and synaptic plas-

ticity in rat somatosensory cortex. *Neuropharmacology* 37, 593–605.

Hardingham, N., Wright, N., Dachtler, J., and Fox, K. (2008). Sensory deprivation unmasks a PKA-dependent synaptic plasticity mechanism that operates in parallel with CaMKII. *Neuron* 60, 861–874.

Hensch, T. K. (2005). Critical period plasticity in local cortical circuits. *Nat. Rev. Neurosci.* 6, 877–888.

Hoffman, D. A., and Johnston, D. (1998). Downregulation of transient K+ channels in dendrites of hippocampal CA1 pyramidal neurons by activation of PKA and PKC. *J. Neurosci.* 18, 3521–3528.

Hoffman, D. A., and Johnston, D. (1999). Neuromodulation of dendritic action potentials. *J. Neurophysiol.* 81, 408–411.

Hoffman, D. A., Magee, J. C., Colbert, C. M., and Johnston, D. (1997). K+ channel regulation of signal propagation in dendrites of hippocampal pyramidal neurons. *Nature* 387, 869–875.

Holmgren, C. D., and Zilberter, Y. (2001). Coincident spiking activity induces long-term changes in inhibition of neocortical pyramidal cells. *J. Neurosci.* 21, 8270–8277.

Hubel, D. H., and Wiesel, T. N. (1965). Binocular interaction in striate cortex of kittens reared with artificial squint. *J. Neurophysiol.* 28, 1041–1059.

Jacob, V., Brasier, D. J., Erchova, I., Feldman, D., and Shulz, D. E. (2007). Spike timing-dependent synaptic depression in the in vivo barrel cortex of the rat. *J. Neurosci.* 27, 1271–1284.

Kampa, B. M., and Stuart, G. J. (2006). Calcium spikes in basal dendrites of layer 5 pyramidal neurons during action potential bursts. *J. Neurosci.* 26, 7424–7432.

Kanold, P. O., and Shatz, C. J. (2006). Subplate neurons regulate maturation of cortical inhibition and outcome of ocular dominance plasticity. *Neuron* 51, 627–638.

Karmarkar, U. R., and Buonomano, D. V. (2002). A model of spike-timing dependent plasticity: one or two coincidence detectors? *J. Neurophysiol.* 88, 507–513.

Kirkwood, A., Rozas, C., Kirkwood, J., Perez, F., and Bear, M. F. (1999). Modulation of long-term synaptic depression in visual cortex by acetylcholine and norepinephrine. *J. Neurosci.* 19, 1599–1609.

Koester, H. J., and Sakmann, B. (1998). Calcium dynamics in single spines during coincident pre- and postsynaptic activity depend on relative timing of back-propagating action potentials and subthreshold excitatory postsynaptic potentials. *Proc. Natl. Acad. Sci. U.S.A.* 95, 9596–9601.

Komai, S., Licznerski, P., Cetin, A., Waters, J., Denk, W., Brecht, M., and Osten, P. (2006). Postsynaptic excitability is necessary for strengthening of cortical sensory responses during experience-dependent development. *Nat. Neurosci.* 9, 1125–1133.

Kudoh, M., and Shibuki, K. (1994). Long-term potentiation in the auditory cortex of adult rats. *Neurosci. Lett.* 171, 21–23.

Kudoh, M., and Shibuki, K. (1996). Long-term potentiation of supragranular pyramidal outputs in the rat auditory cortex. *Exp. Brain Res.* 110, 21–27.

Kudoh, M., and Shibuki, K. (1997). Importance of polysynaptic inputs and horizontal connectivity in the generation of tetanus-induced long-term potentiation in the rat auditory cortex. *J. Neurosci.* 17, 9458–9465.

Laurie, D. J., and Seeburg, P. H. (1994). Ligand affinities at recombinant *N*-methyl-D-aspartate receptors depend on subunit composition. *Eur. J. Pharmacol.* 268, 335–345.

Letzkus, J. J., Kampa, B. M., and Stuart, G. J. (2006). Learning rules for spike timing-dependent plasticity depend on dendritic synapse location. *J. Neurosci.* 26, 10420–10429.

Levy, W. B., and Steward, O. (1983). Temporal contiguity requirements for long-term associative potentiation/depression in the hippocampus. *Neuroscience* 8, 791–797.

Li, L., Bender, K. J., Drew, P. J., Jadhav, S. P., Sylwestrak, E., and Feldman, D. E. (2009). Endocannabinoid signaling is required for development and critical period plasticity of the whisker map in somatosensory cortex. *Neuron* 64, 537–549.

Lin, Y. W., Min, M. Y., Chiu, T. H., and Yang, H. W. (2003). Enhancement of associative long-term potentiation by activation of beta-adrenergic receptors at CA1 synapses in rat hippocampal slices. *J. Neurosci.* 23, 4173–4181.

Liu, X. B., Murray, K. D., and Jones, E. G. (2004). Switching of NMDA receptor 2A and 2B subunits at thalamic and cortical synapses during early postnatal development. *J. Neurosci.* 24, 8885–8895.

Lu, J. T., Li, C. Y., Zhao, J. P., Poo, M. M., and Zhang, X. H. (2007). Spike-timing-dependent plasticity of neocortical excitatory synapses on inhibitory interneurons depends on target cell type. *J. Neurosci.* 27, 9711–9720.

Magee, J. C., and Johnston, D. (1997). A synaptically controlled, associative signal for Hebbian plasticity in hippocampal neurons. *Science* 275, 209–213.

Malenka, R. C., and Bear, M. F. (2004). LTP and LTD: an embarrassment of riches. *Neuron* 44, 5–21.

Markram, H., Lubke, J., Frotscher, M., and Sakmann, B. (1997). Regulation of synaptic efficacy by coincidence of postsynaptic APs and EPSPs. *Science* 275, 213–215.

Meliza, C. D., and Dan, Y. (2006). Receptive-field modification in rat visual cortex induced by paired visual stimulation and single-cell spiking. *Neuron* 49, 183–189.

Meredith, R. M., Floyer-Lea, A. M., and Paulsen, O. (2003). Maturation of long-term potentiation induction rules in rodent hippocampus: role of GABAergic inhibition. *J. Neurosci.* 23, 11142–11146.

Nelson, S. B., Sjostrom, P. J., and Turrigiano, G. G. (2002). Rate and timing in cortical synaptic plasticity. *Philos. Trans. R. Soc. Lond., B, Biol. Sci.* 357, 1851–1857.

Nevian, T., and Sakmann, B. (2006). Spine Ca2+ signaling in spike-timing-dependent plasticity. *J. Neurosci.* 26, 11001–11013.

Nishiyama, M., Hong, K., Mikoshiba, K., Poo, M. M., and Kato, K. (2000). Calcium stores regulate the polarity and input specificity of synaptic modification. *Nature* 408, 584–588.

Pellicciari, M. C., Miniussi, C., Rossini, P. M., and De Gennaro, L. (2009). Increased cortical plasticity in the elderly: changes in the somatosensory cortex after paired associative stimulation. *Neuroscience* 163, 266–276.

Recanzone, G. H., Schreiner, C. E., and Merzenich, M. M. (1993). Plasticity in the frequency representation of primary auditory cortex following discrimination training in adult owl monkeys. *J. Neurosci.* 13, 87–103.

Rodriguez-Moreno, A., and Paulsen, O. (2008). Spike timing-dependent long-term depression requires presynaptic NMDA receptors. *Nat. Neurosci.* 11, 744–745.

Schnupp, J. W., Hall, T. M., Kokelaar, R. F., and Ahmed, B. (2006). Plasticity of temporal pattern codes for vocalization stimuli in primary auditory cortex. *J. Neurosci.* 26, 4785–4795.

Schuett, S., Bonhoeffer, T., and Hubener, M. (2001). Pairing-induced changes of orientation maps in cat visual cortex. *Neuron* 32, 325–337.

Seol, G. H., Ziburkus, J., Huang, S., Song, L., Kim, I. T., Takamiya, K., Huganir, R. L., Lee, H. K., and Kirkwood, A. (2007). Neuromodulators control the polarity of spike-timing-dependent synaptic plasticity. *Neuron* 55, 919–929.

Shouval, H. Z., Bear, M. F., and Cooper, L. N. (2002). A unified model of NMDA receptor-dependent bidirectional synaptic plasticity. *Proc. Natl. Acad. Sci. U.S.A.* 99, 10831–10836.

Siucinska, E., and Kossut, M. (2004). Experience-dependent changes in cortical whisker representation in the adult mouse: a 2-deoxyglucose study. *Neuroscience* 127, 961–971.

Sjostrom, P. J., and Hausser, M. (2006). A cooperative switch determines the sign of synaptic plasticity in distal dendrites of neocortical pyramidal neurons. *Neuron* 51, 227–238.

Sjostrom, P. J., Turrigiano, G. G., and Nelson, S. B. (2001). Rate, timing, and cooperativity jointly determine cortical synaptic plasticity. *Neuron* 32, 1149–1164.

Sjostrom, P. J., Turrigiano, G. G., and Nelson, S. B. (2003). Neocortical LTD via coincident activation of presynaptic NMDA and cannabinoid receptors. *Neuron* 39, 641–654.

Smith, S. L., and Trachtenberg, J. T. (2007). Experience-dependent binocular competition in the visual cortex begins at eye opening. *Nat. Neurosci.* 10, 370–375.

Song, S., and Abbott, L. F. (2001). Cortical development and remapping through spike timing-dependent plasticity. *Neuron* 32, 339–350.

Speechley, W. J., Hogsden, J. L., and Dringenberg, H. C. (2007). Continuous white noise exposure during and after auditory critical period differentially alters bidirectional thalamocortical plasticity in rat auditory cortex in vivo. *Eur. J. Neurosci.* 26, 2576–2584.

Spehlmann, R. (1971). Acetylcholine and the synaptic transmission of non-specific impulses to the visual cortex. *Brain* 94, 139–150.

Tsubokawa, H., and Ross, W. N. (1997). Muscarinic modulation of spike back-propagation in the apical dendrites of hippocampal CA1 pyramidal neurons. *J. Neurosci.* 17, 5782–5791.

Tzounopoulos, T., Kim, Y., Oertel, D., and Trussell, L. O. (2004). Cell-specific, spike timing-dependent plasticities in the dorsal cochlear nucleus. *Nat. Neurosci.* 7, 719–725.

Urakubo, H., Honda, M., Froemke, R. C., and Kuroda, S. (2008). Requirement of an allosteric kinetics of NMDA receptors for spike timing-dependent plasticity. *J. Neurosci.* 28, 3310–3323.

Watanabe, S., Hoffman, D. A., Migliore, M., and Johnston, D. (2002). Dendritic K+ channels contribute to spike-timing dependent long-term potentiation in hippocampal pyramidal neurons. *Proc. Natl. Acad. Sci. U.S.A.* 99, 8366–8371.

Weinberger, N. M. (2003). The nucleus basalis and memory codes: auditory cortical plasticity and the induction of

specific, associative behavioral memory. *Neurobiol. Learn. Mem.* 80, 268–284.

Weinberger, N. M., Miasnikov, A. A., and Chen, J. C. (2006). The level of cholinergic nucleus basalis activation controls the specificity of auditory associative memory. *Neurobiol. Learn. Mem.* 86, 270–285.

Wespatat, V., Tennigkeit, F., and Singer, W. (2004). Phase sensitivity of synaptic modifications in oscillating cells of rat visual cortex. *J. Neurosci.* 24, 9067–9075.

Whitfield, I. C. (1980). Auditory cortex and the pitch of complex tones. *J. Acoust. Soc. Am.* 67, 644–647.

Yang, Y., DeWeese, M. R., Otazu, G. H., and Zador, A. M. (2008). Millisecond-scale differences in neural activity in auditory cortex can drive decisions. *Nat. Neurosci.* 11, 1262–1263.

Yao, H., and Dan, Y. (2001). Stimulus timing-dependent plasticity in cortical processing of orientation. *Neuron* 32, 315–323.

Yazaki-Sugiyama, Y., Kang, S., Cateau, H., Fukai, T., and Hensch, T. K. (2009). Bidirectional plasticity in fast-spiking GABA circuits by visual experience. *Nature* 462, 218–221.

Zhang, J. C., Lau, P. M., and Bi, G. Q. (2009). Gain in sensitivity and loss in temporal contrast of STDP by dopaminergic modulation at hippocampal synapses. *Proc. Natl. Acad. Sci. U.S.A.* 106, 13028–13033.

Zhou, Q., Tao, H. W., and Poo, M. M. (2003). Reversal and stabilization of synaptic modifications in a developing visual system. *Science* 300, 1953–1957.

Zilberter, M., Holmgren, C., Shemer, I., Silberberg, G., Grillner, S., Harkany, T., and Zilberter, Y. (2009). Input specificity and dependence of spike timing-dependent plasticity on preceding postsynaptic activity at unitary connections between neocortical layer 2/3 pyramidal cells. *Cereb. Cortex* 19, 2308–2320.

Conflict of Interest Statement: The authors declare the absence of any commercial or financial relationships that could be construed as a potential conflict of interest.

Received: 12 February 2010; paper pending published: 01 March 2010; accepted: 17 May 2010; published online: 09 June 2010.
Citation: Larsen RS, Rao D, Manis PB and Philpot BD (2010) STDP in the developing sensory neocortex. Front. Syn. Neurosci. ***2****:9. doi: 10.3389/fnsyn.2010.00009*

frontiers in
SYNAPTIC NEUROSCIENCE

REVIEW ARTICLE
published: 07 June 2010
doi: 10.3389/fnsyn.2010.00005

Homeostatic plasticity and STDP: keeping a neuron's cool in a fluctuating world

Alanna J. Watt*[1] *and Niraj S. Desai*[2]*

[1] *Wolfson Institute for Biomedical Research, University College London, London, UK*
[2] *The Neurosciences Institute, San Diego, CA, USA*

Edited by:
Henry Markram, Ecole Polytechnique Federale de Lausanne, Switzerland

Reviewed by:
Gina Turrigiano, Brandeis University, USA

****Correspondence:***
Niraj S. Desai, The Neurosciences Institute, 10640 John Jay Hopkins Drive, San Diego, CA 92121, USA. e-mail: desai@nsi.edu

Spike-timing-dependent plasticity (STDP) offers a powerful means of forming and modifying neural circuits. Experimental and theoretical studies have demonstrated its potential usefulness for functions as varied as cortical map development, sharpening of sensory receptive fields, working memory, and associative learning. Even so, it is unlikely that STDP works alone. Unless changes in synaptic strength are coordinated across multiple synapses and with other neuronal properties, it is difficult to maintain the stability and functionality of neural circuits. Moreover, there are certain features of early postnatal development (e.g., rapid changes in sensory input) that threaten neural circuit stability in ways that STDP may not be well placed to counter. These considerations have led researchers to investigate additional types of plasticity, complementary to STDP, that may serve to constrain synaptic weights and/or neuronal firing. These are collectively known as "homeostatic plasticity" and include schemes that control the total synaptic strength of a neuron, that modulate its intrinsic excitability as a function of average activity, or that make the ability of synapses to undergo Hebbian modification depend upon their history of use. In this article, we will review the experimental evidence for homeostatic forms of plasticity and consider how they might interact with STDP during development, and learning and memory.

Keywords: homeostatic plasticity, synaptic scaling, intrinsic plasticity, STDP, BCM, LTP, LTD, stability

INTRODUCTION

The typical academic's day involves many long hours at one's desk, reading the literature and writing articles. Picture yourself in London in January: it is cold, gray, and wet. Engrossed in reading, sitting at your desk for hours without exercise, you get chilled in your drafty office. What do you do? Simple: pull on a sweater, which you handily keep hanging on the back of your office door. But 20 min later, you realize that the sweater isn't enough; you're still cold. Again, no problem: just turn up the office radiator, and take a quick coffee break. Now you can work on, happy and comfortable. However, a few hours later, your office feels stuffy and warm, and you're getting sleepy. Now what? Easy: you pull off your sweater, and once again comfortable, keep reading, hardly having noticed the interruption. What we've described above is a familiar experience, whether you live in London or Boston: you respond to the fluctuations in temperature in your surroundings.

Although important for brain function, maintenance of body temperature is not the type of homeostasis we will review in this article. The homeostatic plasticity mechanisms we will review concern a neuron's activity, its synaptic drive, and its spiking output. This is a relatively young field, and evidence for these homeostatic plasticity mechanisms in the central nervous system (CNS) has been in the literature for just over a decade. Thus, many details of these mechanisms are still being elucidated.

What is the brain regulating with homeostatic plasticity mechanisms? There is now quite good evidence that homeostatic plasticity mechanisms regulate a neuron's output – its firing rate – in such a way to keep it relatively stable. Why does the brain need such mechanisms? There are many changes the brain can undergo – for instance, Hebbian plasticity mechanisms and developmentally associated plasticity – that can alter a neuron's input dramatically, pushing its output into an unstable regime. Homeostatic plasticity mechanisms counter things like this with the net result being a neuron whose activity is maintained in an optimal range.

To illustrate, take spike-timing-dependent plasticity (STDP). This is an attractive learning rule that seems to capture the essence of Donald Hebb's postulate about the cellular basis of learning, namely that "cells that fire together wire together" (Hebb, 1949; Caporale and Dan, 2008). Though it appears that many forms of STDP exist at different synapse types (Abbott and Nelson, 2000; Caporale and Dan, 2008), in the archetypical form of STDP, spikes occurring in the presynaptic cell a few milliseconds before those in the postsynaptic cell trigger long-term potentiation (LTP), whereas the opposite temporal order results in long-term depression (LTD) (Markram et al., 1997; Bi and Poo, 1998; Debanne et al., 1998; Zhang et al., 1998). Encompassing both synaptic strengthening and synaptic weakening mechanisms, STDP may appear sufficient for neuronal stability, for instance, if that could be achieved through balanced and opposite changes in synaptic strength of different inputs. Although there may be cases when STDP can promote stability (discussed in Section "Balanced STDP"), there are also clear cases when it is insufficient. For instance, at high frequencies, STDP favors LTP regardless of precise spike timing (Sjostrom et al., 2001; Froemke et al., 2006). A regime in which LTP is favored would lack stability and move neurons out of their ideal functional regime (Tsodyks, 2002). To illustrate, picture two neurons that experience correlated pre- and

postsynaptic firing at high frequencies, leading to LTP of the synaptic connection between them. Strengthening their synaptic connection will make it even more likely that they will experience correlated pre- and postsynaptic firing in the future, which would lead to yet more LTP. As the strength of the connection increases, the postsynaptic cell's firing rate will slowly increase, since it is being driven more and more by this input. This will cause other presynaptic partners, whose activity has hitherto been uncorrelated with the postsynaptic cell's activity, to become correlated with postsynaptic firing. This means that they will also undergo LTP, and their synapses will be strengthened as well. The postsynaptic cell's firing will rapidly and dramatically increase, eventually rendering the neuron unable to transmit meaningful information, but allowing it to potentiate all its synapses, a positive feedback loop that is termed "runaway potentiation" (**Figure 1A**). And the effect would spread: increasing firing rates would cause a cascade of runaway potentiation to travel from neuron to neuron, shifting the entire network's activity into an unstable regime and possibly into pathology. And yet for the vast majority of healthy people, our brains never experience such extreme activity regimes, but keep their activity well within an optimal range. How do our brains achieve this feat?

When you feel cold, a range of homeostatic adaptations can occur: you may get "goose bumps," shiver, or change your behavior or environment. In a similar vein, there are multiple forms of homeostatic plasticity that can work to stabilize a neuron's output. We will discuss the major ones in this review, including synaptic scaling, homeostatic intrinsic plasticity, and metaplasticity, as well as stability mechanisms that are intrinsic to STDP. These different homeostatic mechanisms will intersect with Hebbian plasticity differently, and thus may have profoundly different effects on a neuron's subsequent action within a circuit.

SYNAPTIC SCALING

One adaptive mechanism possessed by many neurons to promote stability is synaptic scaling. Synaptic scaling appears to be a particularly parsimonious cellular stability mechanism. It directly regulates the strength of synapses – the same synapses that, undergoing synaptic plasticity like STDP, are likely to be among the sources of destabilization of a neuron's firing rate. With scaling, a neuron can keep its synapses within some optimal size range, which might be energetically advantageous. Synaptic scaling has been widely observed in the brain: including in cortical (Turrigiano et al., 1998; Watt et al., 2000), hippocampal (Lissin et al., 1998; Burrone et al., 2002; Thiagarajan et al., 2005), and spinal neurons (O'Brien et al., 1998), with the result that synaptic scaling is one of the best-studied homeostatic plasticity mechanisms to date.

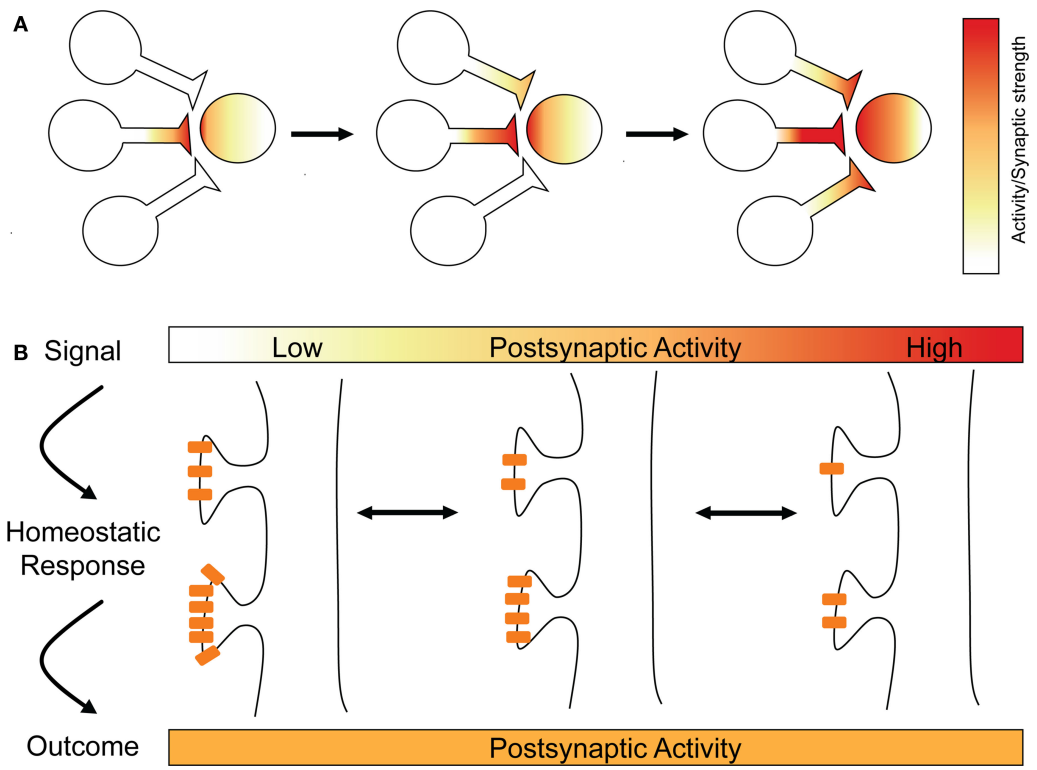

FIGURE 1 | Runaway LTP and synaptic scaling. (A) Hebbian plasticity mechanisms can be unstable, as illustrated here with runaway potentiation. One synapse undergoes LTP (left), making it more likely that it will drive the postsynaptic cell, leading to more LTP (middle). As the postsynaptic cell's firing increases, other synapses can now undergo LTP (right) that would not otherwise, leading to runaway potentiation and the loss of the postsynaptic neuron's capacity to store information in its synaptic weights. **(B)**. Long-term changes in postsynaptic activity is the signal for synaptic scaling, which acts homeostatically to bring the postsynaptic cell's activity back to its optimal range. Synaptic scaling is illustrated by multiplicative changes in AMPA receptor content at synapses.

BASIC EXPERIMENTAL EVIDENCE

Synaptic scaling generally occurs on a much slower timescale than Hebbian plasticity mechanisms like STDP: from hours to days (Ibata et al., 2008). Much of the work to date on synaptic scaling has utilized primary cultured neurons as a model system: dissociated neurons from a mixed population of excitatory and inhibitory neurons in culture form synapses and develop spontaneous activity. Since these networks are grown on culture dishes, global activity levels can be easily modulated pharmacologically; additionally, it is straightforward to measure synaptic strengths either electrophysiologically or immunocytochemically in real time.

When global activity levels are lowered with either antagonists of excitatory synaptic transmission or tetrodotoxin (TTX), which blocks spiking activity, neurons scale their excitatory synapses up in strength (O'Brien et al., 1998; Turrigiano et al., 1998; Watt et al., 2000; Thiagarajan et al., 2005; Shepherd et al., 2006). This scaling takes the form of larger currents in response to spontaneous and/or evoked vesicle release (**Figure 1B**). It is an adaptive response, meaning that its effect should lead the neuron to move its firing rate back to its functional regime, although neurons will not be able to compensate for the complete block of firing due to TTX. Synaptic scaling occurs gradually over hours to days (Turrigiano et al., 1998), but can be observed as early as 4 h after activity is blocked (Ibata et al., 2008). Synergistic, homeostatic changes at inhibitory synapses have also been observed (Kilman et al., 2002; Maffei et al., 2004, 2006; Swanwick et al., 2006); however, this will focus on excitatory synapses.

As is true of temperature homeostasis, synaptic scaling is bidirectional, and neurons can respond to lowered neuronal activity as well as enhanced neuronal activity by altering the strength of their synapses. When inhibition mediated by the $GABA_A$ receptor is blocked in cultured neurons with drugs like bicuculline, this causes about a three-fold increase in the firing rates of excitatory neurons (Turrigiano et al., 1998). However, when this blockade is maintained for long time periods of 24–48 h, neurons slowly and progressively scale the strength of their synapses down, moving the firing rates of individual neurons back into their optimal range (**Figure 1B**) (Lissin et al., 1998; Turrigiano et al., 1998). Similar effects on a neuron's synapses are observed in spinal cultures when inhibition mediated by glycinergic neurons is blocked with strychnine (O'Brien et al., 1998).

One major difference between synaptic scaling and Hebbian forms of synaptic plasticity is that, in most experiments, the changes underlying synaptic scaling appear to occur across the entire population of a neuron's synapses (Turrigiano et al., 1998; Harms and Craig, 2005; Thiagarajan et al., 2005; Ibata et al., 2008), rather than, as is normally true of LTP for instance, only a small fraction of a neuron's inputs (Engert and Bonhoeffer, 1999). In this case, synaptic weights are scaled multiplicatively, which means that the relative differences in strength between any two inputs will be maintained (**Figure 1B**). Functionally, this is important, since our current best understanding of processes like learning and memory in the brain suggest that memories are encoded in the relative differences in strength between inputs (Malenka and Nicoll, 1999; Neves et al., 2008).

However, some studies suggest that it is also possible for scaling-like processes to occur at a more local level, perhaps even at individual synapses (Sutton et al., 2006; Branco et al., 2008; Hou et al., 2008). Two points remain uncertain. First, there is the question of whether these local forms of scaling are the same as the global form that has typically been called "synaptic scaling." In certain respects, the experiments supporting local scaling are difficult to reconcile with those supporting global scaling (e.g., compare Hou et al., 2008, to Ehlers et al., 2007). And local scaling may be mediated by different physical mechanisms, sensitive to spontaneous rather than spike-evoked vesicle release (Sutton and Schuman, 2009). Second, it is not clear how local scaling coexists with Hebbian plasticity. The concern is that local scaling might counteract learning by erasing the relative differences in synaptic strength previously produced by LTP and LTD. A possible answer to this concern was offered by Rabinowitch and Segev (2008). Noting that neighboring synapses on a single dendritic branch are not electrically isolated from each other, they argued that signals triggering homeostatic scaling at any one synapse would also affect synapses in close proximity. Multiplicative scaling would then still pertain, but the functional unit would be the dendritic compartment rather than the whole neuron. Rabinowitch and Segev further argued that local scaling of this type offers two distinct advantages: it prevents any one dendritic branch from dominating over the others and it allows for the selection of spatial patterns of inputs that are particularly efficacious in controlling neuronal output.

Although the culture preparation has proven to be ideally suited to characterizing synaptic scaling mechanisms, it is nonetheless somewhat removed from the intact animal. However, there is good evidence that synaptic scaling occurs *in vivo* (Desai et al., 2002; Maffei et al., 2004; Goel and Lee, 2007). In these studies, neurons of rodent visual cortex were deprived of normal activity for hours or days by either eyelid suture or intraocular TTX injection. Subsequent *ex vivo* recordings revealed that these manipulations produced homeostatic synaptic adaptations resulting in enhanced excitability in neurons of layers 2/3 and 4.

DETECTING ACTIVITY

What is being regulated? Is it the firing rate of individual neurons, the levels of synaptic activation, or some property of the network as a whole? In principle all of these are possible – because the design of most of the experiments has not allowed for a clean separation of cellular, synaptic, and network parameters – but the first (or something closely related) seems most likely. Burrone and colleagues were able to address this question elegantly, by overexpressing a potassium channel (Kir2.1) to lower activity in a small fraction of neurons in a culture dish (Burrone and Murthy, 2003). They found that synaptic inputs onto a neuron were scaled up when the neuron's firing rate was reduced, and that this synaptic scaling brought its firing rate back to near control levels. This result provided strong evidence that homeostatic synaptic scaling occurs at the level of individual neurons, and suggests that the strength of input that a neuron receives is titrated to keep its output stable. This study illustrates the complexity of homeostatic mechanisms, since changes in postsynaptic activity were precisely balanced by presynaptic changes in synaptic release dynamics. Furthermore, these changes happened only once synapses had been already established, and in fact opposite effects were observed when activity levels were reduced in younger cultures, when synapses were

still forming. This is consistent with a recurring trend in the field of homeostatic plasticity: different mechanisms exist at different developmental stages.

What is the signal for synaptic scaling? Burrone's work shows that a neuron's own firing rate seems to be the key signal regulated, but what aspect of it is most important? Firing rate can be integrated over different time periods, for instance, and may look different in different parts of the neuron: its axon versus its dendrites, for instance. Furthermore, how a neuron reads this out, how it measures its own firing rate remains poorly understood. One recent study addressed the question of where activity is measured in a cell. By microperfusing TTX either onto a neuron's soma or onto its primary apical dendrite, Ibata et al. (2008) demonstrated that somatic action potentials are required for synaptic scaling, and that blocking action potentials locally in the dendrite does not cause detectable alterations in synaptic strengths, either within the activity-blocked region or on dendritic regions outside of it. However, a study by Branco et al. (2008) shows that presynaptic release probability can be homeostatically controlled by depolarization of the local dendritic branch. How can we account for these apparently conflicting results? Perhaps synaptic scaling expressed through pre- and postsynaptic mechanisms are triggered by different signals that have different loci of origin.

One of the usual suspects when considering activity signals is internal calcium, an ion whose concentration is tightly regulated in neurons, and is known to play a critical role in many cellular processes. Indeed, Ibata et al. (2008) found that blocking somatic calcium transients had an effect on synaptic strengths similar to that of spiking activity. Furthermore, they found that activity deprivation caused decreased expression of the nuclear Ca^{2+}-calmodulin-dependent kinase CaMKIV, and that this likely had its effect through protein transcription. Thiagarajan et al. (2005) have also found that homeostatic synaptic alterations are linked to reductions in calcium entry in the postsynaptic cell.

This would appear to make good intuitive sense: a neuron somehow integrates its calcium levels as a read-out for activity, leading to alterations in gene expression in the soma that is then directed to synapses. In this way, the same signal – however, with different location and integrated over a different timescale – could be responsible for both Hebbian synaptic plasticity (Amici et al., 2009) and synaptic scaling (Ibata et al., 2008). However elegant and satisfying this may be from a design perspective, it is probably an incomplete picture of synaptic plasticity. As is often the case in biological systems, the truth is somewhat more complicated. Indeed, there may be multiple signaling mechanisms involved in signaling in homeostatic plasticity. In particular, there is evidence that a number of molecules that are released into the extracellular space can affect scaling and may well mediate it in some cases (Rutherford et al., 1998; Stellwagen and Malenka, 2006; Aoto et al., 2008). These molecules can diffuse over distances spanning small numbers of neurons.

Perhaps the most surprising result of this sort in recent years was made by Stellwagen and Malenka (2006), when they showed that a soluble released factor, a molecule called tumor necrosis factor alpha (TNFα) was required for synaptic scaling. What made this finding so surprising was that TNFα was released from glial cells rather than neurons. In hindsight, this finding makes sense: glial cells are abundant in the CNS, are intimately related to neurons, and have mechanisms in place to measure a neuron's activity levels (Haydon, 2001). These experiments were performed in cultured neurons that are grown on beds of glial cells, a typical procedure for culturing neurons (Smith, 1998). However, it will be interesting to determine if in the intact neuron, it is a particular class of glial cells – perhaps one that preferentially associates with neuronal soma – that is responsible for mediating this signal for synaptic scaling. This work also suggests that in diseases that affect glial cells, pathogenesis may arise through feedback to synapses via this synaptic scaling mechanism (McCoy and Tansey, 2008).

Brain-derived neurotrophic factor (BDNF) is another soluble factor implicated in synaptic scaling (Rutherford et al., 1998). BDNF is produced in excitatory pyramidal neurons, and its expression and release depend on neuronal activity (Poo, 2001). Since soluble release factors participate in synaptic scaling, the relative physical locations of neurons and glia will partly determine whether neurons respond only to their own activity or also that of their neighbors. If a neuron is isolated and receives signals via BDNF in a mostly autocrine fashion, it is likely to respond to its own activity exclusively. Yet if the glial cells that insulated it from its neighbors were perturbed, it may begin to respond to more widespread changes in activity. Similarly, if glial cells sense a neuron's activity levels and signal back to it by releasing TNFα, then the precise location and spread of those glial cells will be critical in determining just what activity is being sensed. Interestingly, BDNF is also implicated in LTP, where it is thought to be required for expression of the late, protein-dependent phase of LTP (Minichiello, 2009), or alternatively, synaptic tagging (Lu et al., 2008). How can a molecule be involved in two opposing processes: Hebbian and homeostatic plasticity? It could be that differences in release location or volume of BDNF determine whether homeostatic or Hebbian mechanisms are engaged. An alternative explanation is that BDNF is permissive for both processes, while other signals determine the type of plasticity expressed.

The usefulness of a cell autonomous signal, such as calcium, seems clear: it provides a straightforward means of implementing single-cell homeostasis (LeMasson et al., 1993). But why should there be cell non-autonomous (diffusable) signals as well? One idea is that they help to implement network-level homeostasis (Maffei and Fontanini, 2009). Single neurons obviously do not operate in isolation but as members of neural circuits. While it is possible, in principle, to maintain stable circuit behavior even without a coordinating signal between neurons (Renart et al., 2003), in practice, coordination might make for more robust regulation. Evidence that this is so comes from studies of the effects of sensory deprivation in visual cortex (Desai et al., 2002; Maffei et al., 2004; Maffei and Turrigiano, 2008). Rather than a simple upregulation of excitatory synapses, deprivation triggers a number of different homeostatic responses, which vary depending upon cortical layer, developmental age, cell identity, and the specific deprivation protocol employed. It has not actually been established that these responses are coordinated – much less what the coordinating signals are – but it is difficult picture how this system would work otherwise.

EXPRESSION MECHANISMS

How are synapses altered during synaptic scaling? This has been one of the most well studied aspects of synaptic scaling to date, and has been reviewed elsewhere extensively (Turrigiano, 2008). Here we will limit ourselves to aspects of the question that intersect most directly with Hebbian plasticity.

Several groups have found evidence for postsynaptic changes in the densities of both AMPA receptors (Lissin et al., 1998; O'Brien et al., 1998; Turrigiano et al., 1998; Wierenga et al., 2005; Shepherd et al., 2006; Stellwagen and Malenka, 2006) and NMDA receptors (Rao and Craig, 1997; Watt et al., 2000; Mu et al., 2003). While there is broad agreement that AMPA receptor numbers are regulated, there are conflicting reports about the subunit composition of the affected receptors. Some researchers have observed changes in GluR2-containing receptors (O'Brien et al., 1998; Cingolani et al., 2008), others in GluR1-containing receptors (Ju et al., 2004; Thiagarajan et al., 2005), and still others in both (Wierenga et al., 2005).

AMPA and NMDA appear to be proportionally regulated by activity in cortical neurons (Watt et al., 2000). While we might expect that processes like LTP and LTD, which appear to affect AMPA receptors preferentially, would degrade this relationship (Lisman, 2003), this is apparently not always the case. Watt et al. (2004) demonstrated that, at neocortical synapses, LTP of AMPA currents, whether induced chemically or by an STDP protocol, is followed by LTP of NMDA currents on a slower timescale (hours versus minutes). Most importantly, the late NMDA potentiation is done in such a way that the original NMDA-to-AMPA ratio is regained (Watt et al., 2004). This highlights the importance of timescale in our understanding of how mechanisms like Hebbian and homeostatic plasticity interact.

In addition to postsynaptic changes, homeostatic presynaptic changes have also been observed (Murthy et al., 2001; Burrone et al., 2002; De Gois et al., 2005; Erickson et al., 2006; Wierenga et al., 2006; Branco et al., 2008). Some of the differences in expression location may reflect developmental differences: Wierenga and colleagues showed that in neurons in culture for less than 3 weeks, synaptic scaling is expressed purely postsynaptically, whereas in older cultures, both pre- and postsynaptic alterations contribute (Wierenga et al., 2006). This suggests that neurons may possess several different mechanisms for synaptic scaling, and that the precise expression mechanism utilized will depend on several factors, including developmental stage.

You may be forgiven if you are experiencing a sense of déjà vu at this moment; research into the expression mechanisms of synaptic scaling have interesting parallels with the LTP and LTD fields (Lisman, 2003; Duguid and Sjostrom, 2006), both in the "pre- versus postsynaptic" debate, and in the apparent resolution of this debate, that neurons may use either or both loci. Furthermore, many of the players in both the LTP and synaptic scaling fields are the same: calcium acts as the signal that is ultimately expressed as a change in AMPA receptors at synapses. Indeed, these are not the only similarities. Several other intracellular signaling molecules have been implicated in synaptic scaling that also may play a role in LTP or LTD, such as Arc (Rial Verde et al., 2006; Shepherd et al., 2006), polo-like kinase 2 (Plk2) and CDK5 (Seeburg et al., 2008), and CaMKIV (Ibata et al., 2008). Additionally, trans-synaptic signaling molecules like β3 Integrin (Cingolani et al., 2008) and MHC1 (Goddard et al., 2007) have been implicated in mediating synaptic scaling. How these signaling mechanisms interact remains to be determined.

HOMEOSTATIC INTRINSIC PLASTICITY

The intrinsic electrical properties of neurons are determined largely by their expression of voltage- and calcium-gated ion channels. The diversity of these channels in mammalian central neurons is staggering: no fewer than 36 separate genes are required to account for the principal subunits of the potassium channels alone (Vacher et al., 2008). How the brain actually uses this diversity is among the most puzzling questions in neuroscience. It is made especially challenging by the fact that a neuron's complement of ion channels is not simply dictated by a set of genetic instructions, nor is it hard-wired during early childhood. Rather, like its synapses, a neuron's intrinsic electrical properties evolve throughout life, often under the influence of activity-dependent plasticity (Zhang and Linden, 2003; Frick and Johnston, 2005). Indeed, many of the same experimental protocols used to study synaptic plasticity (including STDP) also produce intrinsic plasticity.

BASIC EXPERIMENTAL EVIDENCE

The most straightforward way for changes in intrinsic properties to help neurons and circuits maintain appropriate levels of electrical activity is through overall shifts in cellular excitability. In particular, the gain and/or threshold of individual neurons might be adjusted to match whatever average synaptic input they receive. Consider an idealized *f–I* curve (**Figure 2A**), which relates a neuron's output (firing rate) to its input (synaptic current). If the average input is too low, the neuron will hardly ever fire, because of the spike threshold; if it is too high, the firing rate will saturate, because there is some physical limit on how fast a neuron can fire. Between the two extremes is a sensitive region, in which the neuron's output really does reflect its input. A robust strategy for firing rate stability, when there are large or long-lasting fluctuations in average input, is to shift the position or slope of the *f–I* curve so that the sensitive region always corresponds well with the distribution of inputs. In this way, the neuron's dynamic range can be preserved.

This is a simple idea that nevertheless appears to hold (roughly) in a wide variety of real systems. Experimental evidence for the general strategy has been found in neocortex, hippocampus, striatum, and brainstem; in pyramidal neurons and interneurons; in mammalian brains and invertebrate brains; using tissue from juvenile animals and adult animals; after activity manipulation in cell cultures, slice cultures, and the intact brain (Turrigiano et al., 1994; Desai et al., 1999a,b; Aizenman et al., 2003; Nelson et al., 2003; Aptowicz et al., 2004; Gibson et al., 2006; Karmarkar and Buonomano, 2006; van Welie et al., 2006b; Echegoyen et al., 2007; Pratt and Aizenman, 2007; Bartley et al., 2008; Maffei and Turrigiano, 2008; Azdad et al., 2009; Breton and Stuart, 2009; Mohapatra et al., 2009; Wilhelm et al., 2009; O'Leary et al., 2010). A typical experiment is that of Karmarkar and Buonomano (2006), who examined the intrinsic excitability of CA1 pyramidal neurons in organotypic slice cultures. This preparation, like other culture systems, exhibits pronounced spontaneous spiking activity even in the absence of external stimuli. The activity is driven by the cultures' dense excitatory and inhibitory

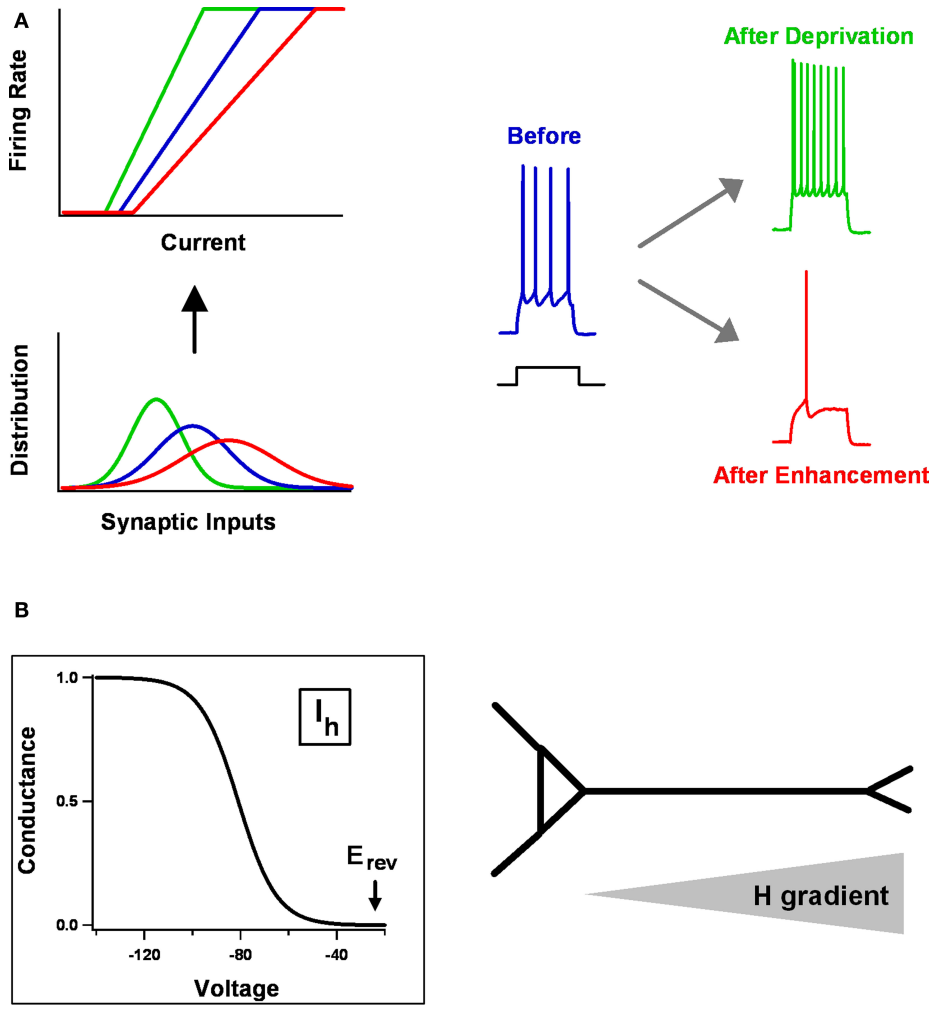

FIGURE 2 | Homeostatic intrinsic plasticity. (A) A general way of adapting a neuron's intrinsic excitability in response to changes in the mean or variance of synaptic inputs is by adjusting the gain (slope) or threshold (x-intercept) of its *f–I* curve. At top-left are stylized *f–I* curves, relating input current to output firing rate. These are matched to the three synaptic input distributions shown below. Experimentally what one observes is at right. After prolonged activity deprivation, neurons become hyper-excitable – for example, they fire more strongly in response to a given current step. After activity enhancement, they become hypo-excitable. **(B)** Distinctive properties of I_h make it interact with synaptic changes wrought by STDP. I_h activates in response to hyperpolarization, is partially active at resting potentials (≈ –60 mV), and its E_{rev} sits at the base of the activation curve, making it a stabilizing force. In pyramidal neurons, HCN channels are expressed mostly in apical dendrites, with a density that increases as one moves distally.

connectivity. Karmarkar and Buonomano (2006) were therefore able, by applying pharmacological blockers of either inhibition or excitation, to drive average spontaneous firing rates up or down for a period of days. At the end of this period, they assayed the excitability of individual neurons by measuring the number of spikes fired in response to current injections of different amplitudes, and used the measurements to construct *f–I* curves. What they found was similar to the idealized case (**Figure 2A**). Chronically reducing firing rates tilted the *f–I* curve up and to the left, whereas increasing them tilted it down and to the right. The changes in intrinsic excitability were accomplished without grossly deforming firing properties: individual spike waveforms were unaltered, as were the neurons' electrophysiological identities (i.e., regular spiking neurons did not become fast spiking or rhythmically bursting). Instead, what was tuned by the activity manipulations was sensitivity: neurons responded to low (or high) activity conditions by becoming more (or less) sensitive to whatever input they received, as one would want for homeostatic regulation.

What is being regulated? Or more precisely, what signal controls whether neuronal excitability is increased or decreased? As is true of synaptic scaling, the answer appears to be calcium influx due to spike firing and depolarization (LeMasson et al., 1993). For mammalian central neurons, the argument rests on the observations that activity-dependent shifts in excitability can be produced by directly depolarizing neurons with externally-applied potassium (van Welie et al., 2004; O'Leary et al., 2010) or with puffs of glutamate (van Welie et al., 2004) and that homeostatic intrinsic plasticity can be prevented by blocking voltage-dependent calcium channels, other sources of calcium, and downstream calcium-related pathways (Fan et al., 2005; Frick and Johnston, 2005; Wu et al., 2008; O'Leary et al.,

2010). Intracellular calcium levels track average firing rates quite well under physiological conditions. Using them as an "activity signal" would make for a robust regulatory mechanism, because each neuron could self-regulate. It would also allow for some kind of coordination between homeostatic intrinsic plasticity and both Hebbian and homeostatic forms of synaptic plasticity, as all would depend (somehow) on shared calcium signals. However, as is also true of synaptic scaling, there may be separate extracellular signaling pathways. In particular, manipulating BDNF levels and receptor activation affects the induction of intrinsic plasticity in culture (Desai et al., 1999a). Whether BDNF actually mediates network-level homeostasis under physiological conditions is not known.

While the similarity of results obtained in different preparations and under different experimental conditions is remarkable, there are important differences. One is in the timescale of effects. In some cases, intrinsic excitability alters in response to activity only after hours or days have passed (Desai et al., 1999b; Aptowicz et al., 2004; Gibson et al., 2006). In others, homeostatic regulation of excitability is apparent after only minutes (Nelson et al., 2003; Misonou et al., 2004; Fan et al., 2005; van Welie et al., 2006a). The reason for the variability is uncertain. Part of it may simply be a consequence of differences in experimental techniques and methodology, but part of it probably reflects real differences in the underlying physiology. The experiments showing slow intrinsic plasticity were designed mainly to explore how neurons and neural circuits might respond to the stability challenges posed by postnatal development, which is an inherently slow process. On the other hand, the experiments showing fast intrinsic plasticity were motivated more by the need to counter the destabilizing effects of Hebbian plasticity and of temporary fluctuations in synaptic input. In fact, several actually employed standard LTP protocols in order to demonstrate homeostatic regulation of intrinsic excitability (Fan et al., 2005; Brager and Johnston, 2007; Campanac et al., 2008).

The other major difference between the various experimental results is in the specific ion channels regulated by homeostatic processes. In mammalian systems alone, depending on the activity manipulation employed and the type of neurons studied, the channels carrying one or more of the following currents might be altered: transient sodium, sustained potassium, M-type potassium, long-lasting calcium, hyperpolarization-activated cyclic nucleotide (HCN), and leak (Desai et al., 1999b; van Welie et al., 2004; Fan et al., 2005; Gibson et al., 2006; Trasande and Ramirez, 2007; Wu et al., 2008; Breton and Stuart, 2009). Moreover, activity manipulation affects not only channel density, but also localization and gating characteristics. Consequently, while the idealized regulation of **Figure 2A** (a simple shift of the *f–I* curve) is often true, the effects of homeostatic intrinsic plasticity can be quite complicated. In some cases, intrinsic plasticity involves not simply changes in gain or threshold but changes in spike frequency adaptation, afterpotentials, synaptic integration, local dendritic excitability, temporal firing patterns, and resonance characteristics (van Welie et al., 2004; Frick and Johnston, 2005; Trasande and Ramirez, 2007; Johnston and Narayanan, 2008). This diversity can be both good and bad, if the goal is neuronal and network stability. Some systems make excellent use of it. One of these is the crustacean stomatogastric ganglion (STG), a small circuit in which neurons have well-defined roles and stereotyped firing behavior (Marder and Bucher, 2007). Maintaining particular firing patterns (e.g., bursting or rhythmic activity) is crucial to circuit function; and the STG exhibits a broad range of homeostatic responses to perturbations that alter firing characteristics, adjusting inward and outward conductances in a coordinated way so as to restore function. But in other systems the diverse intrinsic changes can produce pathological states. Sensory deprivation of rat barrel cortex, by whisker trimming, downregulates HCN channel density in the dendrites of layer 5 pyramidal neurons (Breton and Stuart, 2009). This makes the dendrites more excitable, but it also increases the proportion of neurons that discharge strong bursts of action potentials. This might leave the system vulnerable to epileptic instability (Poolos, 2005). Indeed, such untoward effects of homeostatic plasticity have been hypothesized to contribute not only to epilepsy but to neuropsychiatric disorders (Ramocki and Zoghbi, 2008).

RELATION TO SYNAPTIC SCALING

The experimental protocols used to induce homeostatic intrinsic plasticity have (with some exceptions) been identical to those used to induce synaptic scaling: chronic activity manipulation of cultured neurons and networks, sensory deprivation of cortex, pharmacological silencing of spiking activity in hippocampus. Even so, the relationship between the two types of homeostatic plasticity remains unclear. Why do they both exist? Are they expressed under the same circumstances? How do they work together? The answers to these questions are required if we are truly to understand how homeostatic regulation operates in real networks (Maffei and Fontanini, 2009).

An attractive idea is that synaptic scaling and homeostatic intrinsic plasticity operate in parallel as redundant regulatory mechanisms. Redundancy seems to be a ubiquitous design principle of biological systems (Tononi et al., 1999). Along these lines, a notable result is that of Maffei and Turrigiano (2008). They studied the effects on the rodent monocular visual cortex of two forms of sensory deprivation: lid suture and intraocular injection of the sodium channel blocker TTX. Both disrupt normal visually-evoked drive to cortex, but whereas intraocular TTX eliminates all retinal activity, lid suture allows for the spontaneous firing of retinal ganglion cells. Maffei and Turrigiano found that layer 2/3 pyramidal neurons exhibited homeostatic responses to both types of deprivation, but that the nature of the responses differed. After lid suture, the intrinsic excitability of individual cells was upregulated; after intraocular TTX, the upregulation was instead that of excitatory synapses. Spontaneous retinal firing after lid suture is known to drive robust LTD in visual cortex (Rittenhouse et al., 1999). One explanation for the difference between intraocular TTX and lid suture is that, while synaptic scaling was able to produce a sufficient homeostatic response to the former, it was unable to overcome the strong LTD produced by the latter. Instead, a redundant homeostatic mechanism, intrinsic plasticity, was recruited.

Another attractive idea is that synaptic scaling and homeostatic intrinsic plasticity may be active at different developmental stages and may be engaged in a definite temporal order (Karmarkar and Buonomano, 2006; Echegoyen et al., 2007). Returning to the Karmarkar and Buonomano (2006) experiments described above: using the same recordings with which they examined plasticity of intrinsic excitability, they also examined plasticity of inhibition. They found that both were expressed in immature cultures, with changes

in intrinsic excitability always appearing first, followed some time later by changes in inhibition. However, in mature cultures, only intrinsic plasticity was expressed. To the extent that development of organotypic slices seems to mimic that of hippocampus *in vivo* (De Simoni et al., 2003), this raises the possibility that intrinsic plasticity is the dominant homeostatic process of the adult brain. This notion is also hinted at by the work of Echegoyen et al. (2007) who subjected hippocampal networks *in vivo* to activity deprivation by sustained release of TTX via implanted polymer strips. These experiments showed that homeostatic intrinsic plasticity was robust in both juvenile and adult animals, but that effects on synaptic currents varied over development in ways that might not necessarily promote homeostasis. It may be that, in some cases, relying on homeostatic intrinsic plasticity is preferable to relying on synaptic scaling so as not to interfere with synaptically-stored information.

Perhaps the most attractive idea of all is that synaptic scaling and homeostatic intrinsic plasticity act synergistically. The term "homeostatic regulation" is a rather general one that can mean different things in different contexts. It can encompass tasks as distinct as controlling the firing rates of individual neurons or the activity of large networks, preserving uniform synaptic weight distributions (or at least ones in which weights do not cluster at extremes), and ensuring that the dynamic range of response properties matches that of inputs. Neither synaptic scaling nor homeostatic intrinsic plasticity, as complicated and flexible as they may be, seems well positioned to do all of these things by themselves. Lazar et al. (2009) explored this idea in a thought-provoking computational model. They endowed a recurrent neural network with three forms of plasticity – STDP, synaptic normalization (similar to scaling), and homeostatic intrinsic plasticity – and investigated its ability to learn spatio-temporal patterns in its inputs. Not only did the network outperform comparable, optimally tuned static networks, but both types of homeostatic plasticity were necessary to maintain healthy dynamics. Without synaptic normalization, the network exhibited seizure-like bursts of activity, even when driven by random inputs. Without intrinsic plasticity, many neurons in the network fired at aberrantly high rates, while others fell silent. Only when both were included was the network able to make efficient use of its resources.

INTERACTION WITH STDP

STDP is sensitive to several features of cellular excitability, including resting potential, firing frequency, and action potential backpropagation (reviewed by Sjostrom et al., 2008). We expect then that, rather than simply acting in parallel with synaptic plasticity, homeostatic intrinsic plasticity should be able to affect the induction of STDP itself. When a neuron's average activity is low, increasing intrinsic excitability (by whatever means) should make subsequent synaptic potentiation more likely. Conversely, when average activity is high, decreasing intrinsic excitability should instead make subsequent synaptic depression more likely. This plasticity of plasticity, which has been termed "metaplasticity," represents a way for plasticity of intrinsic properties to affect (indirectly) synaptic ones and a distinct method of homeostatic adaptation (Abraham, 2008). The idea has been treated most formally in the context of the Bienenstock, Cooper, and Munro (BCM) model of synaptic plasticity, which we discuss in the next section.

One class of the ion channels regulated by homeostatic plasticity, the HCN channels that carry the H current, display unique biophysical properties that make them especially suited to modulating STDP (**Figure 2B**) (Atkinson and Williams, 2009; Biel et al., 2009). Unlike "normal" voltage-gated channels, HCN channels are activated by membrane hyperpolarization rather than depolarization, with a reversal potential that sits near the base of the activation curve. They do not display voltage-dependent inactivation, and they are partially open at typical resting potentials. In both hippocampal CA1 and neocortical layer 5 pyramidal neurons, HCN channels are highly expressed along the apical dendrite, with a channel density that gets progressively greater with distance from the soma. Together, these properties endow HCN channels with several important physiological roles (Narayanan and Johnston, 2008; Atkinson and Williams, 2009; Biel et al., 2009): they help determine resting potential and input resistance, shape the time course of synaptic potentials and how they summate, and control the spread of synaptic potentials along the dendritic tree.

All of these roles suggest ways in which plasticity of the H current might affect STDP and vice versa (Kampa et al., 2007; Shin and Chetkovich, 2007; Campanac and Debanne, 2008; Sjostrom et al., 2008). For the case of homeostatic regulation, most are as yet unexplored. However, there has been relevant work using traditional rate-based LTP and LTD protocols in hippocampal CA1 neurons. Fan et al. (2005) found that theta-burst pairing of Schaffer collateral inputs and postsynaptic firing not only resulted in robust LTP but also produced a general decrease in cellular excitability, which like LTP itself depended on NMDA activation and downstream calcium pathways. Brager and Johnston (2007) complemented this finding by showing that LTD evoked by low-frequency pairing was instead accompanied by a general increase in cellular excitability. In both cases, the intrinsic plasticity was mediated by up- or downregulation of the H current and the attendant effects on input resistance. At first glance, these two results might seem to contradict experiments showing that LTP (or LTD) evoked by STDP produces a localized increase (or decrease) in excitability (Campanac and Debanne, 2008). However, the discrepancy might be resolved by the observation that the magnitude of LTP controls whether the H current is up- or downregulated (Campanac et al., 2008). Strong LTP results in upregulation, weak LTP in downregulation. In other words, homeostatic intrinsic plasticity may only kick in when synapses are near saturation, which is when one would expect homeostatic regulation to be most necessary (Roth-Alpermann et al., 2006).

METAPLASTICITY AND THE BCM MODEL OF SYNAPTIC PLASTICITY

Most studies of homeostatic plasticity, whether synaptic or intrinsic, have treated its actions as essentially independent of those of Hebbian plasticity. That is, the general picture has been one of homeostatic plasticity operating in parallel with LTP and LTD, complementing them, but mediated by distinct biophysical mechanisms and operating without any specific coordination. But, as we have noted, this dichotomy between the two types of plasticity is not strictly necessary. Indeed, one might argue that, from the standpoint of network function, the most stable kind of homeostatic regulation is one that is embedded in the rules of Hebbian

plasticity itself. One way of doing this is by making the capacity of synapses to undergo Hebbian modification depend upon their history of use or upon the history of neuronal activity, an idea called metaplasticity (Abraham, 2008). The most influential attempt to understand plasticity in this way was made by BCM nearly 30 years ago (Bienenstock et al., 1982).

BCM RULE

In the BCM formulation, individual excitatory synapses can undergo both potentiation and depression (**Figure 3A**). Whether a synapse is strengthened or weakened by presynaptic activity depends upon whether postsynaptic activity is above or below a threshold. Synaptic input that drives postsynaptic firing to high levels results in an increase in synaptic strength, whereas input that produces only low levels of postsynaptic firing results in a decrease. The threshold firing rate – the crossover point between LTP and LTD – is itself a slow function of postsynaptic activity, moving so as to make LTP more likely when average activity is low and less likely when it is high. This sliding of the threshold can stabilize synaptic dynamics, if its dependence on activity is chosen appropriately. For example, a simple implementation of the BCM rule is:

$$\tau \frac{dw}{dt} = r_{\text{pre}} r_{\text{post}} \left(r_{\text{post}} - \theta_{\text{th}} \right),$$

where w is the synaptic weight, τ is a time constant (a characteristic time for Hebbian modification), r_{pre} and r_{post} are the presynaptic and postsynaptic firing rates, and Θ_{th} is the threshold. The condition for stability is that Θ_{th} grows faster than linearly with a running average of postsynaptic firing rate. The average is taken on a timescale slower than that of fluctuations in activity patterns but faster than that of changes in synaptic weight distribution. Other formulations of the BCM idea, with somewhat different properties, have also been proposed (Artola and Singer, 1993; Law and Cooper, 1994; Toyoizumi et al., 2005).

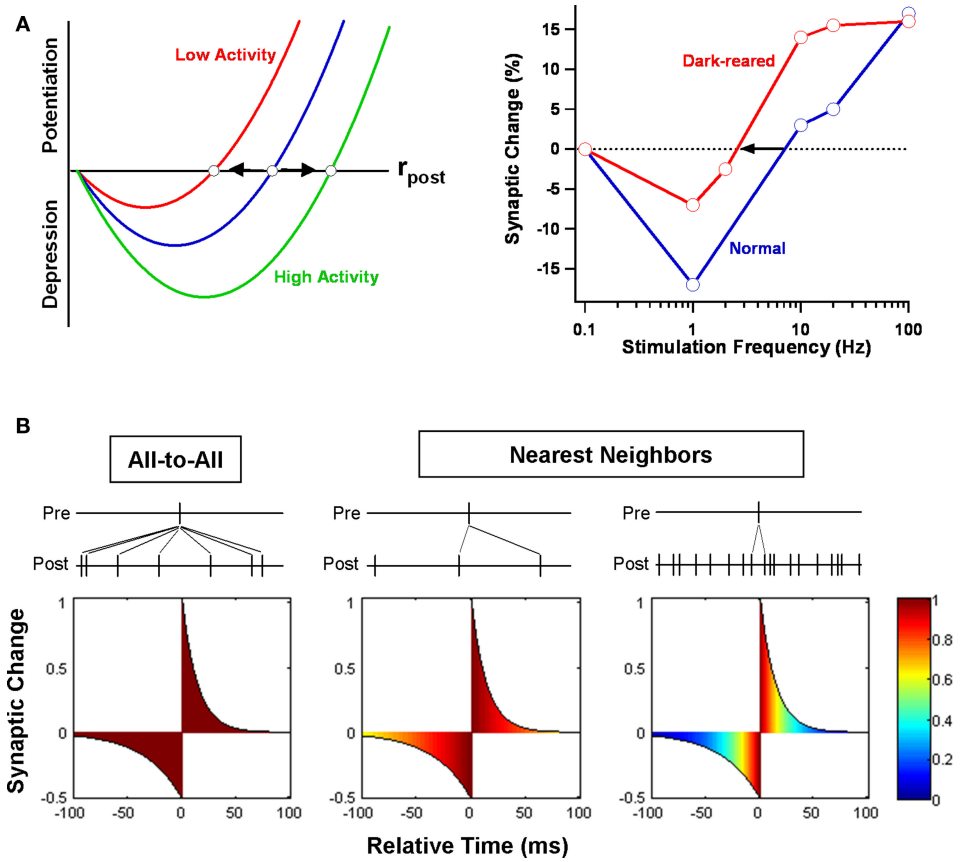

FIGURE 3 | BCM model. (A) A standard implementation of the BCM rule is shown at left. Plasticity is a quadratic function of postsynaptic firing rate r_{post}. When r_{post} is below a specified threshold, presynaptic firing induces LTD; when above, LTP. Prolonged periods of low or high activity slide the position of the threshold bidirectionally. An experimental demonstration of the rule at rat visual cortical synapses is illustrated at right (Kirkwood et al., 1996). The threshold stimulation frequency separating LTD and LTP shifted left after several days of dark rearing. **(B)** Whether the BCM model and STDP are compatible depends on the STDP update rule employed (Izhikevich and Desai, 2003). If neurons are only weakly correlated, assuming that all combinations of pre- and postsynaptic spikes (all-to-all) contribute to plasticity means that the distribution of relative times will be uniform, as illustrated in the leftmost figure. (The color scale indicates the (normalized) fraction of contributing spike pairs for each relative time.) The integral of the STDP learning window is negative and only depression results in the all-to-all case. On the other hand, if only nearest-neighbor pairs contribute to plasticity, its sign depends on r_{post}. For low rates, the distribution of times is still mostly uniform, but for high rates, the distribution peaks near the origin. In the first case, net depression results, but in the second case, net potentiation results. Between the two rates sits a BCM-like threshold.

Numerous experimental tests of the BCM model have been conducted over the years – and it has stood up to them very well (Bear, 2003). Using rate-based protocols for induction of long-term plasticity, several different groups have confirmed the validity of key features of the BCM rule to synapses in both neocortex and hippocampus (Dudek and Bear, 1992; Kirkwood et al., 1996; Wang and Wagner, 1999; Abraham et al., 2001; Roth-Alpermann et al., 2006; Xu et al., 2009a). Most importantly, they have demonstrated the existence of a threshold Θ_{th} that moves based on prior activity. To cite one example, when 2 days of dark rearing is used to decrease activity in rodent visual cortex, the threshold shifts so that LTP becomes easier to induce and LTD harder (Kirkwood et al., 1996; Philpot et al., 2001). More precisely, the minimum stimulation frequency necessary to produce LTP (at synapses connecting layer 4 to layer 2/3) is reduced, as is the amount of LTD produced by the smallest effective frequency (**Figure 3A**). Brief re-exposure to light rapidly reverses the shift in the modification threshold, indicating that the effect is bidirectional. To cite another example, when granule cells of the dentate gyrus in awake rats are activated by strong stimulation of the medial perforant path, it becomes more difficult to potentiate synapses from the neighboring (but separate) lateral perforant path (Abraham et al., 2001). Moreover, a similar effect can be obtained by directly activating granule cells via antidromic stimulation of their mossy fiber axons. This is an important finding because it shows that sliding of the threshold is a postsynaptic, cell-wide property and not restricted to the synapses previously activated. It is also worth pointing out that, in just these two examples, the timescale of threshold modification varies between days, in the first case, to minutes, in the second.

MAPPING STDP ONTO BCM

Since its introduction, the BCM rule has been widely used to model brain processes related to learning and experience-dependent development (Bear, 2003; Cooper et al., 2004; Abraham, 2008). Given its success, there has been considerable interest in understanding the relationship between BCM and STDP (Izhikevich and Desai, 2003; Burkitt et al., 2004; Pfister and Gerstner, 2006; Benuskova and Abraham, 2007). This is an aspect of a broader interest in understanding how traditional rate-based protocols for LTP and LTD are related to the newer timing-based protocols. If STDP rules can be mapped onto the BCM rule, the thinking goes, not only can a large body of experimental work be unified within a single conceptual framework, but network models based on STDP will inherit the useful competitive and stability properties that models based on BCM exhibit (Clopath et al., 2010). Efforts to combine STDP and BCM have typically fallen into one of two categories: phenomenology (reviewed by Morrison et al., 2008) or biophysics (Shouval et al., 2002; Yeung et al., 2004; Rubin et al., 2005).

The phenomenological efforts have sometimes adopted the strategy of beginning with a simple STDP rule and asking under what conditions it results in BCM-like plasticity. One builds up BCM from STDP by making the (not uncontested) assumption that spike timing is more fundamental to plasticity than spike rate (Lisman and Spruston, 2005). The simplest of these efforts is instructive, even if its applicability is limited (Izhikevich and Desai, 2003). Say that a neuron receives a large number of independent Poisson inputs and that each synapse evolves according to the rules of STDP. Is the end-result compatible with the BCM rule? The answer depends on how STDP is implemented (**Figure 3B**). Under a standard implementation (Song et al., 2000), for each presynaptic spike, one sums the contributions from all preceding and all succeeding postsynaptic spikes. But if we do this, the distribution of relative times will be nearly flat. We end up sampling the whole STDP curve uniformly, and the net effect on synaptic weight is simply proportional to its integral. At most neocortical synapses, this is negative (Feldman, 2000), resulting in net depression regardless of postsynaptic firing rate. However, if we instead restrict STDP to nearest-neighbor pairs (Sjostrom et al., 2001), then, for high firing rates, relative times will mostly be short. We effectively sample the STDP curve only near the origin. The LTP maximum is larger than the LTD minimum, and we get potentiation. For low firing rates, longer relative times will also be common, so we sample more of the tails of the STDP curve. The LTD part decays more slowly than the LTP part, and we get depression. By varying the postsynaptic firing rate, we can obtain a function that mimics the BCM rule, with the threshold expressed in terms of the STDP parameters. One might then mimic sliding of the threshold by varying the parameters (Benuskova and Abraham, 2007).

Simple pair-based STDP rules, even if complemented with additional constraints, are not able to capture much of the phenomenology of STDP (Morrison et al., 2008). They do not, for example, account for the results of experiments in which the repetition frequency of pairs of spikes was varied or those in which spikes were paired, not singly, but in triplets or quadruplets. For this reason, more elaborate phenomenological models have been proposed, including ones that incorporate interactions between more than two spikes, postulate a hidden variable modulating efficacy, or allow synapses to exist in multiple states (Appleby and Elliott, 2005; Froemke et al., 2006; Pfister and Gerstner, 2006). A notable result is that of Clopath and colleagues (Clopath et al., 2010). In their model, synaptic changes elicited by presynaptic spikes depended not on postsynaptic spikes as such, but on postsynaptic membrane potential. Homeostasis was implemented by making the amount of LTD depend on a slow average of membrane potential. This approach not only accounted for much of the empirical STDP data, but allowed, in the case of Poisson inputs, for a good mapping to the BCM rule.

At the other end of the spectrum from phenomenology lies biophysics: perhaps more fundamental but also more difficult. The starting point for any biophysical description of plasticity is calcium (Castellani et al., 2001; Karmarkar and Buonomano, 2002; Shouval et al., 2002; Yeung et al., 2004; Rubin et al., 2005). The general approach models calcium influx and dynamics (e.g., buffering mechanisms), and relates these to variables known to affect synaptic transmission (e.g., activation of calcium-dependent enzymes). This approach is challenging for a couple of reasons: the biophysical workings of these processes are not fully understood, necessitating an element of phenomenology in every case; and there is evidence that the induction and the expression of synaptic plasticity have multiple loci, presynaptic as well as postsynaptic (Duguid and Sjostrom, 2006; Corlew et al., 2008). Even so, the work to date has been intriguing. For example, Shouval and colleagues built a

model of plasticity that used calcium currents mediated by NMDA receptors as an associative signal (Shouval et al., 2002; Yeung et al., 2004). The resulting model neuron was both sensitive to temporal correlations in spike trains, as one expects from STDP, and able to respond selectively to a set of input rate patterns, as one expects from BCM. Stability was provided by a slow, homeostatic regulation of NMDA receptor levels. This seems compatible with the effects of synaptic scaling on NMDA conductance (Watt et al., 2000), but it is a bit difficult to reconcile with evidence that NMDA and AMPA currents are coregulated by LTP (Watt et al., 2004). We consider this issue next.

WHAT SHIFTS THE BCM THRESHOLD?

The feature of the BCM rule that enables homeostatic regulation is the fact that the threshold between potentiation and depression shifts as a function of average postsynaptic activity. What might cause such a shift? Several answers to this question have been offered (Abraham, 2008).

The most compelling evidence involves activity-dependent regulation of NMDA receptor subunit composition (Cho et al., 2009; McCoy et al., 2009). NMDA receptors are heteromers consisting of two obligatory NR1 subunits and two regulatory subunits, usually a combination of NR2A and NR2B (Yashiro and Philpot, 2008). Early in life, NR2B levels are much higher than NR2A levels. However, as the brain matures, the ratio of NR2A to NR2B increases dramatically, as does the ratio of NMDA receptors containing NR2A to those containing NR2B. This increased NR2A/NR2B ratio has multiple effects on synaptic transmission and plasticity, because NR2B-containing receptors have slower channel kinetics and produce longer-lasting EPSPs; allow more calcium influx per EPSP; are more mobile; and interact more strongly with proteins important in the induction of LTP. For the BCM model, the important point is that the NR2A/NR2B ratio is sensitive to both sensory experience and activity-dependent plasticity. The leftward shift in the LTP/LTD threshold after dark rearing, described above, is accompanied by a decrease in the ratio; the rightward return after re-exposure to light is, conversely, accompanied by an increase (Quinlan et al., 1999; Philpot et al., 2001, 2003). A causal relationship between changes in the ratio and sliding of the threshold is indicated by experiments on mutant mice in which the NR2A subunit was knocked out; these mice failed to show a threshold shift after dark rearing (Philpot et al., 2007). Furthermore, activity-dependent regulation of the NR2A/NR2B ratio is not limited to developmental timescales: at Schaffer collateral synapses onto CA1 pyramidal neurons, the ratio can be moved up or down by priming stimulations, with corresponding effects on LTP and LTD, after only minutes (Xu et al., 2009b).

Might synaptic scaling of NMDA conductances (see Synaptic Scaling) contribute to sliding of the BCM threshold? It probably does. While both LTP and LTD require calcium influx through NMDA receptors, LTP is somewhat more sensitive to postsynaptic calcium than LTD, and in the developing neocortex LTD depends upon presynaptic rather than postsynaptic NMDA receptors (Sjostrom et al., 2003; Bender et al., 2006; Corlew et al., 2007). As a result, postsynaptic NMDA scaling might shift the balance between LTP and LTD, in a manner compatible with the BCM rule. However, NMDA scaling is unlikely to be the initial cause of threshold modification. NMDA and AMPA current amplitudes are coregulated by synaptic scaling in neocortical cultures, with no evidence that NMDA scaling precedes or triggers AMPA scaling (Watt et al., 2000). In fact, LTP of AMPA currents, whether induced pharmacologically or by STDP, is followed on a slower timescale by a corresponding increase in NMDA currents (Watt et al., 2004), which is the opposite of what the BCM model would suggest. Moreover, NMDA scaling does not affect the decay time constant of NMDA currents, as one would expect if the NR2A/NR2B ratio were being altered and as is observed in visual cortex after dark rearing (Watt et al., 2000; Philpot et al., 2001).

There are at least two other ways in which synaptic scaling and homeostatic intrinsic plasticity might affect the BCM threshold. These are in addition to and more direct than their general effects on average postsynaptic firing rate. One way is by regulating dendritic excitability. By this we mean such things as backpropagation of action potentials, generation of calcium bursts and dendritic spikes, and compartmentalization of the dendritic tree. All are believed to affect the induction of STDP at excitatory synapses (Kampa et al., 2007; Sjostrom et al., 2008), and all will be affected by the synaptic and intrinsic changes described in the previous two sections. The other way is simply by regulating average membrane conductance. Conductance is important to STDP because of its effect on EPSP kinetics (Fuenzalida et al., 2007). Intrinsic plasticity changes conductance more or less directly. Synaptic scaling does so through its effects on synaptic background activity, which is a ubiquitous feature of the brains of behaving animals and which, in pyramidal neurons, can increase average membrane conductance by as much as a factor of five (Destexhe et al., 2003). Crucially, postsynaptic conductance preferentially affects the LTP part of STDP; even high levels of conductance have only a minimal effect on timing-dependent LTD (Delgado et al., 2009). This asymmetry suggests that modulating conductance is an effective method of moving the threshold between LTP and LTD.

BALANCED STDP

In the introduction, we noted that one motivation for studies of homeostatic plasticity is the concern that Hebbian networks are potentially unstable because of positive feedback loops. The concern is especially great when plasticity is based only on presynaptic–postsynaptic correlations. But for STDP at synapses that also express short-term plasticity, there may be ways, in some circumstances, to address this concern that do not require separate regulatory mechanisms. Here we describe two of them.

REDISTRIBUTION OF SYNAPTIC EFFICACY

Most experimental studies of STDP have quantified synaptic strength by measuring the postsynaptic response to a single presynaptic action potential or a single presynaptic stimulation. This is a useful metric because of its simplicity, but it neglects an important fact: neurons in the brains of behaving animals do not fire action potentials in isolation but as part of complex, irregular spike trains. Even among neocortical pyramidal cells, interspike intervals can be as short as 10 ms. This is easily short enough to engage non-Hebbian forms of short-term synaptic plasticity, including synaptic depression and facilitation, which can profoundly alter response properties (Zucker and Regehr, 2002).

In a landmark paper, Markram and Tsodyks (1996) demonstrated how the interaction between short- and long-term plasticity might result in changes in the content, rather than the gain, of neural signals. Using intracellular recordings, they examined synapses between individual layer 5 pyramidal cells from juvenile rats. These synapses exhibited considerable frequency-dependent synaptic depression, which is likely mediated by depletion of the pool of readily releasable vesicles at each synaptic site. Inducing LTP with paired burst activity increased EPSP amplitude in response to single presynaptic spikes. However, it did not alter the steady-state response to moderate- and high-frequency (>10 Hz) spike trains (**Figure 4A**). Markram and Tsodyks argued that the LTP had been expressed presynaptically, as an increase in the probability of vesicle release. When the presynaptic neuron fired a train of spikes, this simply depleted the readily releasable pool more quickly, as reflected in an increased (post-pairing) rate of frequency-dependent depression, but it did not affect the size of the pool or any postsynaptic properties. In other words, LTP "redistributed" efficacy to the first spikes in the train, while having a minimal effect on the last ones. Describing quite what this means for a complex spike train, which might include a broad distribution of interspike intervals, is difficult, but it certainly suggests a useful means of imposing stability (Carpenter and Milenova, 2002). As rates increase, synapses become more depressed; the level at which they settle is unchanged by LTP.

How general a means of stabilization is this "redistribution of synaptic efficacy" phenomenon? The complementary effect (reduced short-term depression) has been observed after timing-dependent LTD in layer 5 neocortex (Sjostrom et al., 2003), and both effects have been observed at hippocampal CA1 synapses following certain protocols for LTP and LTD (Yasui et al., 2005). However, at some synapses, STDP appears to be mediated by postsynaptic changes in addition to, or instead of, presynaptic ones (Hardingham et al., 2007; Feldman, 2009). And many synapses either do not exhibit strong frequency-dependent depression or do so only early in development (Reyes and Sakmann, 1999; Zucker and Regehr, 2002). For these synapses, some other means of containing runaway potentiation, such as those we have described, would seem to be necessary.

LTP VERSUS LTD

In principle, purely Hebbian forms of plasticity might be able, by themselves, to regulate total synaptic drive, if the effects of LTP can be countered by those of LTD (and vice versa). This requires a rather delicate balance, which is difficult to maintain for rate-based plasticity. But STDP's dependence on precise spike timing might allow for such a balance to be established and maintained.

In particular, this might happen if the STDP learning window is biased toward depression – that is, if the area over the LTD part of the curve is larger than the area under the LTP part (Feldman, 2000; Sjostrom et al., 2001). The basic argument is simple and intuitive (Abbott and Nelson, 2000). Imagine that a neuron receives excessively large synaptic input, which causes it to fire excessively fast. Each presynaptic spike will have only a weak effect on postsynaptic firing and is as likely to be preceded by postsynaptic spikes as it is to be followed by them. Both LTP and LTD will be induced as a result. If we assume that all spike pairings contribute to synaptic change (i.e., not just nearest neighbors), then the net effect will be depression of all synapses, because LTD dominates over LTP. As synapses get weaker, the firing rate will drop, until the only postsynaptic spikes are driven by chance clustering in the timing of presynaptic spikes. The synapses from these presynaptic neurons will grow stronger, because now their spikes will, on average, precede the postsynaptic ones. The end-result is a stable postsynaptic firing rate and a synaptic weight distribution in which some synapses are very strong and the others are very weak (assuming an additive STDP update rule; **Figure 4B**) (Song et al., 2000).

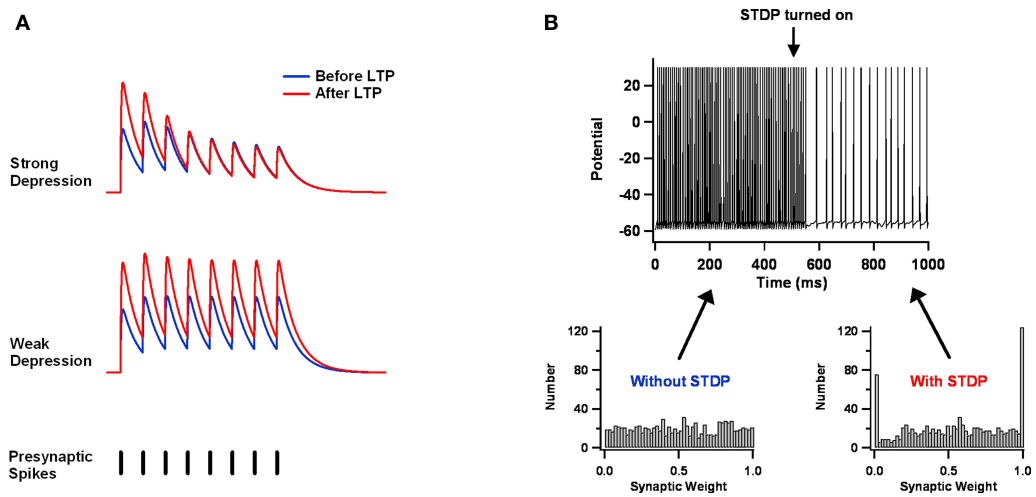

FIGURE 4 | Balanced STDP. (A) Synaptic depression might balance STDP. At strongly depressing synapses, presynaptically expressed STDP increases the amplitude of the first potential in response to a train of presynaptic stimuli, but not the steady-state response. Weakly depressing synapses lack this normalization mechanism. The illustrations are derived from the phenomenological model of Tsodyks and Markram (1997). **(B)** LTD might balance LTP. A leaky integrate and fire neuron receives a large number of excitatory and inhibitory Poisson inputs. Initially, the excitatory weight distribution is static and nearly uniform, and it results in aberrantly fast and regular firing. But once STDP is turned on, firing slows and becomes irregular. Excitatory weights move toward the two extremes. Parameters used here are similar to those of Song et al. (2000).

As appealing as this argument is, simulation-based and analytical studies indicate that the approach has significant limitations (Song et al., 2000; van Rossum et al., 2000; Kempter et al., 2001; Rubin, 2001; Gutig et al., 2003; Morrison et al., 2007; Billings and van Rossum, 2009). Even for the simplified case of a single postsynaptic neuron receiving Poisson inputs, the final result depends quite a lot on the particular STDP implementation employed. Among the choices that matter: whether one adopts additive, multiplicative, or mixed update rules; how one treats multi-spike interactions; and whether one imposes hard bounds on the growth and decay of individual synapses. These choices determine the shape of the steady-state weight distribution, whether there is competition between synapses, and how stable synaptic weights are. Furthermore, some of the final results, like the bimodal weight distribution just described, contradict experimental data (Turrigiano et al., 1998; Song et al., 2005). Balancing LTP versus LTD should be useful for homeostasis, but present evidence suggests it is best complemented by additional mechanisms, such as lateral inhibition (Billings and van Rossum, 2009) or synaptic scaling (van Rossum et al., 2000).

WORKING TOGETHER

We have in this paper described multiple mechanisms for homeostatic regulation of firing rates. The list has been extensive while not being exhaustive. For example, we did not discuss anti-STDP (Rumsey and Abbott, 2006) or heterosynaptic LTP and LTD (Royer and Pare, 2003; Chistiakova and Volgushev, 2009), which are somewhat separate from STDP proper. An obvious question is: why are there so many mechanisms? The answer probably arises from a combination of things: (1) Somewhat different needs have been grouped together under the label of "homeostasis," namely preventing runaway potentiation due to Hebbian synaptic change, and maintaining dynamic range during periods of intense synaptogenesis and neural growth. (2) The stability challenges faced by the nervous system differ between brain areas and at different developmental ages, perhaps necessitating different responses. (3) In complicated neural circuits, homeostatic regulation might require multiple processes acting on different timescales and in different ways. Given the complexity, what we most need now are investigations in which multiple forms of plasticity, both homeostatic and Hebbian, interact in defined systems. This is challenging but several studies of this sort have been done. To end this paper, we highlight a particularly illuminating one.

The rodent visual cortex is unusual in that one of its zones is strictly monocular, while the binocular cells in the other zone are interspersed and not segregated into patches based on eye preference. Mrsic-Flogel et al. (2007) exploited this organization to disentangle the effects of competition from those of activity deprivation. Using calcium imaging of individual cells, they quantified changes in response properties after short (2 days) and long (≥4 days) periods of monocular deprivation (MD). As expected, short MD durations decreased deprived-eye responses and long MD durations increased open-eye responses. But surprisingly, the longer MD durations also strengthened deprived-eye responses in neurons devoid of open-eye input; and binocular deprivation strengthened (not weakened) responsiveness to both eyes. Most strikingly, the bidirectional response adjustments in binocular cells after MD effectively preserved the net visual drive for each neuron. The most likely explanation for these results is that two distinct forces were at work: a Hebbian process (e.g., LTD of excitatory synapses) that weakened deprived-eye responses in binocular cells, and a non-Hebbian process that strengthened all responses. The first implemented competition between afferents from the two eyes; the second implemented homeostatic regulation in response to deprivation. Furthermore, the preservation of net visual drive suggests the two acted in complementary ways.

Thus, just as you have multiple mechanisms enabling you to cope with variations in temperature, ranging from the Sahara to the Arctic, a neuron is equipped with a range of different, and sometimes overlapping, homeostatic mechanisms that allow it to "maintain its cool" with its output, over a wide range of different input "environments".

ACKNOWLEDGMENTS

The authors' work is supported by a Royal Society Dorothy Hodgkin Fellowship (Alanna J. Watt), and by the Neurosciences Research Foundation and the G. Harold and Leila Y. Mathers Charitable Foundation (Niraj S. Desai).

REFERENCES

Abbott, L. F., and Nelson, S. B. (2000). Synaptic plasticity: taming the beast. *Nat. Neurosci.* 3(Suppl.), 1178–1183.

Abraham, W. C. (2008). Metaplasticity: tuning synapses and networks for plasticity. *Nat. Rev. Neurosci.* 9, 387.

Abraham, W. C., Mason-Parker, S. E., Bear, M. F., Webb, S., and Tate, W. P. (2001). Heterosynaptic metaplasticity in the hippocampus in vivo: a BCM-like modifiable threshold for LTP. *Proc. Natl. Acad. Sci. U.S.A.* 98, 10924–10929.

Aizenman, C. D., Akerman, C. J., Jensen, K. R., and Cline, H. T. (2003). Visually driven regulation of intrinsic neuronal excitability improves stimulus detection in vivo. *Neuron* 39, 831–842.

Amici, M., Doherty, A., Jo, J., Jane, D., Cho, K., Collingridge, G., and Dargan, S. (2009). Neuronal calcium sensors and synaptic plasticity. *Biochem. Soc. Trans.* 37, 1359–1363.

Aoto, J., Nam, C. I., Poon, M. M., Ting, P., and Chen, L. (2008). Synaptic signaling by all-trans retinoic acid in homeostatic synaptic plasticity. *Neuron* 60, 308–320.

Appleby, P. A., and Elliott, T. (2005). Synaptic and temporal ensemble interpretation of spike-timing-dependent plasticity. *Neural Comput.* 17, 2316–2336.

Aptowicz, C. O., Kunkler, P. E., and Kraig, R. P. (2004). Homeostatic plasticity in hippocampal slice cultures involves changes in voltage-gated Na+ channel expression. *Brain Res.* 998, 155–163.

Artola, A., and Singer, W. (1993). Long-term depression of excitatory synaptic transmission and its relationship to long-term potentiation. *Trends Neurosci.* 16, 480–487.

Atkinson, S. E., and Williams, S. R. (2009). Postnatal development of dendritic synaptic integration in rat neocortical pyramidal neurons. *J. Neurophysiol.* 102, 735–751.

Azdad, K., Chavez, M., Don Bischop, P., Wetzelaer, P., Marescau, B., De Deyn, P. P., Gall, D., and Schiffmann, S. N. (2009). Homeostatic plasticity of striatal neurons intrinsic excitability following dopamine depletion. *PLoS ONE* 4, e6908. doi: 10.1371/journal.pone.0006908.

Bartley, A. F., Huang, Z. J., Huber, K. M., and Gibson, J. R. (2008). Differential activity-dependent, homeostatic plasticity of two neocortical inhibitory circuits. *J. Neurophysiol.* 100, 1983–1994.

Bear, M. F. (2003). Bidirectional synaptic plasticity: from theory to reality. *Philos. Trans. R. Soc. Lond., B, Biol. Sci.* 358, 649–655.

Bender, V. A., Bender, K. J., Brasier, D. J., and Feldman, D. E. (2006). Two coincidence detectors for spike timing-dependent plasticity in somatosensory cortex. *J. Neurosci.* 26, 4166–4177.

Benuskova, L., and Abraham, W. C. (2007). STDP rule endowed with the BCM sliding threshold accounts for hippocampal heterosynaptic plasticity. *J. Comput. Neurosci.* 22, 129–133.

Bi, G. Q., and Poo, M. M. (1998). Synaptic modifications in cultured hippocampal neurons: dependence on spike timing, synaptic strength, and postsynaptic cell type. *J. Neurosci.* 18, 10464–10472.

Biel, M., Wahl-Schott, C., Michalakis, S., and Zong, X. (2009). Hyperpolarization-activated cation channels: from genes to function. *Physiol. Rev.* 89, 847–885.

Bienenstock, E. L., Cooper, L. N., and Munro, P. W. (1982). Theory for the development of neuron selectivity: orientation specificity and binocular interaction in visual cortex. *J. Neurosci.* 2, 32–48.

Billings, G., and van Rossum, M. C. (2009). Memory retention and spike-timing-dependent plasticity. *J. Neurophysiol.* 101, 2775–2788.

Brager, D. H., and Johnston, D. (2007). Plasticity of intrinsic excitability during long-term depression is mediated through mGluR-dependent changes in I(h) in hippocampal CA1 pyramidal neurons. *J. Neurosci.* 27, 13926–13937.

Branco, T., Staras, K., Darcy, K. J., and Goda, Y. (2008). Local dendritic activity sets release probability at hippocampal synapses. *Neuron* 59, 475–485.

Breton, J. D., and Stuart, G. J. (2009). Loss of sensory input increases the intrinsic excitability of layer 5 pyramidal neurons in rat barrel cortex. *J. Physiol.* 587, 5107–5119.

Burkitt, A. N., Meffin, H., and Grayden, D. B. (2004). Spike-timing-dependent plasticity: the relationship to rate-based learning for models with weight dynamics determined by a stable fixed point. *Neural Comput.* 16, 885–940.

Burrone, J., and Murthy, V. N. (2003). Synaptic gain control and homeostasis. *Curr. Opin. Neurobiol.* 13, 560–567.

Burrone, J., O'Byrne, M., and Murthy, V. N. (2002). Multiple forms of synaptic plasticity triggered by selective suppression of activity in individual neurons. *Nature* 420, 414–418.

Campanac, E., Daoudal, G., Ankri, N., and Debanne, D. (2008). Downregulation of dendritic I(h) in CA1 pyramidal neurons after LTP. *J. Neurosci.* 28, 8635–8643.

Campanac, E., and Debanne, D. (2008). Spike timing-dependent plasticity: a learning rule for dendritic integration in rat CA1 pyramidal neurons. *J. Physiol.* 586, 779–793.

Caporale, N., and Dan, Y. (2008). Spike timing-dependent plasticity: a Hebbian learning rule. *Annu. Rev. Neurosci.* 31, 25–46.

Carpenter, G. A., and Milenova, B. L. (2002). Redistribution of synaptic efficacy supports stable pattern learning in neural networks. *Neural Comput.* 14, 873–888.

Castellani, G. C., Quinlan, E. M., Cooper, L. N., and Shouval, H. Z. (2001). A biophysical model of bidirectional synaptic plasticity: dependence on AMPA and NMDA receptors. *Proc. Natl. Acad. Sci. U.S.A.* 98, 12772–12777.

Chistiakova, M., and Volgushev, M. (2009). Heterosynaptic plasticity in the neocortex. *Exp. Brain Res.* 199, 377–390.

Cho, K. K., Khibnik, L., Philpot, B. D., and Bear, M. F. (2009). The ratio of NR2A/B NMDA receptor subunits determines the qualities of ocular dominance plasticity in visual cortex. *Proc. Natl. Acad. Sci. U.S.A.* 106, 5377–5382.

Cingolani, L. A., Thalhammer, A., Yu, L. M., Catalano, M., Ramos, T., Colicos, M. A., and Goda, Y. (2008). Activity-dependent regulation of synaptic AMPA receptor composition and abundance by beta3 integrins. *Neuron* 58, 749–762.

Clopath, C., Busing, L., Vasilaki, E., and Gerstner, W. (2010). Connectivity reflects coding: a model of voltage-based STDP with homeostasis. *Nat. Neurosci.* 13, 344–352.

Cooper, L. N., Intrator, N., Blais, B. S., and Shouval, H. Z. (2004). *Theory of Cortical Plasticity*. River Edge, NJ: World Scientific.

Corlew, R., Brasier, D. J., Feldman, D. E., and Philpot, B. D. (2008). Presynaptic NMDA receptors: newly appreciated roles in cortical synaptic function and plasticity. *Neuroscientist* 14, 609–625.

Corlew, R., Wang, Y., Ghermazien, H., Erisir, A., and Philpot, B. D. (2007). Developmental switch in the contribution of presynaptic and postsynaptic NMDA receptors to long-term depression. *J. Neurosci.* 27, 9835–9845.

Debanne, D., Gahwiler, B. H., and Thompson, S. M. (1998). Long-term synaptic plasticity between pairs of individual CA3 pyramidal cells in rat hippocampal slice cultures. *J. Physiol.* 507, 237–247.

De Gois, S., Schafer, M. K., Defamie, N., Chen, C., Ricci, A., Weihe, E., Varoqui, H., and Erickson, J. D. (2005). Homeostatic scaling of vesicular glutamate and GABA transporter expression in rat neocortical circuits. *J. Neurosci.* 25, 7121–7133.

Delgado, J. Y., Gomez, J. F., and Desai, N. S. (2009). In vivo-like conductance levels control the induction of spike-timing dependent plasticity. *Soc. Neurosci. Abstr.* 35, 41.8.

Desai, N. S., Cudmore, R. H., Nelson, S. B., and Turrigiano, G. G. (2002). Critical periods for experience-dependent synaptic scaling in visual cortex. *Nat. Neurosci.* 5, 783–789.

Desai, N. S., Rutherford, L. C., and Turrigiano, G. G. (1999a). BDNF regulates the intrinsic excitability of cortical neurons. *Learn. Mem.* 6, 284–291.

Desai, N. S., Rutherford, L. C., and Turrigiano, G. G. (1999b). Plasticity in the intrinsic excitability of cortical pyramidal neurons. *Nat. Neurosci.* 2, 515–520.

De Simoni, A., Griesinger, C. B., and Edwards, F. A. (2003). Development of rat CA1 neurones in acute versus organotypic slices: role of experience in synaptic morphology and activity. *J. Physiol.* 550, 135–147.

Destexhe, A., Rudolph, M., and Pare, D. (2003). The high-conductance state of neocortical neurons in vivo. *Nat. Rev. Neurosci.* 4, 739–751.

Dudek, S. M., and Bear, M. F. (1992). Homosynaptic long-term depression in area CA1 of hippocampus and effects of *N*-methyl-D-aspartate receptor blockade. *Proc. Natl. Acad. Sci. U.S.A.* 89, 4363–4367.

Duguid, I., and Sjostrom, P. J. (2006). Novel presynaptic mechanisms for coincidence detection in synaptic plasticity. *Curr. Opin. Neurobiol.* 16, 312–322.

Echegoyen, J., Neu, A., Graber, K. D., and Soltesz, I. (2007). Homeostatic plasticity studied using in vivo hippocampal activity-blockade: synaptic scaling, intrinsic plasticity and age-dependence. *PLoS ONE* 2, e700. doi: 10.1371/journal.pone.0000700.

Ehlers, M. D., Heine, M., Groc, L., Lee, M. C., and Choquet, D. (2007). Diffusional trapping of GluR1 AMPA receptors by input-specific synaptic activity. *Neuron* 54, 447–460.

Engert, F., and Bonhoeffer, T. (1999). Dendritic spine changes associated with hippocampal long-term synaptic plasticity. *Nature* 399, 66–70.

Erickson, J. D., De Gois, S., Varoqui, H., Schafer, M. K., and Weihe, E. (2006). Activity-dependent regulation of vesicular glutamate and GABA transporters: a means to scale quantal size. *Neurochem. Int.* 48, 643–649.

Fan, Y., Fricker, D., Brager, D. H., Chen, X., Lu, H. C., Chitwood, R. A., and Johnston, D. (2005). Activity-dependent decrease of excitability in rat hippocampal neurons through increases in I(h). *Nat. Neurosci.* 8, 1542–1551.

Feldman, D. E. (2000). Inhibition and plasticity. *Nat. Neurosci.* 3, 303–304.

Feldman, D. E. (2009). Synaptic mechanisms for plasticity in neocortex. *Annu. Rev. Neurosci.* 32, 33–55.

Frick, A., and Johnston, D. (2005). Plasticity of dendritic excitability. *J. Neurobiol.* 64, 100–115.

Froemke, R. C., Tsay, I. A., Raad, M., Long, J. D., and Dan, Y. (2006). Contribution of individual spikes in burst-induced long-term synaptic modification. *J. Neurophysiol.* 95, 1620–1629.

Fuenzalida, M., Fernandez de Sevilla, D., and Buno, W. (2007). Changes of the EPSP waveform regulate the temporal window for spike-timing-dependent plasticity. *J. Neurosci.* 27, 11940–11948.

Gibson, J. R., Bartley, A. F., and Huber, K. M. (2006). Role for the subthreshold currents ILeak and IH in the homeostatic control of excitability in neocortical somatostatin-positive inhibitory neurons. *J. Neurophysiol.* 96, 420–432.

Goddard, C. A., Butts, D. A., and Shatz, C. J. (2007). Regulation of CNS synapses by neuronal MHC class I. *Proc. Natl. Acad. Sci. U.S.A.* 104, 6828–6833.

Goel, A., and Lee, H. K. (2007). Persistence of experience-induced homeostatic synaptic plasticity through adulthood in superficial layers of mouse visual cortex. *J. Neurosci.* 27, 6692–6700.

Gutig, R., Aharonov, R., Rotter, S., and Sompolinsky, H. (2003). Learning input correlations through nonlinear temporally asymmetric Hebbian plasticity. *J. Neurosci.* 23, 3697–3714.

Hardingham, N. R., Hardingham, G. E., Fox, K. D., and Jack, J. J. (2007). Presynaptic efficacy directs normalization of synaptic strength in layer 2/3 rat neocortex after paired activity. *J. Neurophysiol.* 97, 2965–2975.

Harms, K. J., and Craig, A. M. (2005). Synapse composition and organization following chronic activity blockade in cultured hippocampal neurons. *J. Comp. Neurol.* 490, 72–84.

Haydon, P. G. (2001). GLIA: listening and talking to the synapse. *Nat. Rev. Neurosci.* 2, 185–193.

Hebb, D. O. (1949). *The Organization of Behavior: A Neuropsychological Theory*. New York, NY: John Wiley and Sons.

Hou, Q., Zhang, D., Jarzylo, L., Huganir, R. L., and Man, H. Y. (2008). Homeostatic regulation of AMPA receptor expression at single hippocampal synapses. *Proc. Natl. Acad. Sci. U.S.A.* 105, 775–780.

Ibata, K., Sun, Q., and Turrigiano, G. G. (2008). Rapid synaptic scaling induced by changes in postsynaptic firing. *Neuron* 57, 819–826.

Izhikevich, E. M., and Desai, N. S. (2003). Relating STDP to BCM. *Neural Comput.* 15, 1511–1523.

Johnston, D., and Narayanan, R. (2008). Active dendrites: colorful wings of the mysterious butterflies. *Trends Neurosci.* 31, 309–316.

Ju, W., Morishita, W., Tsui, J., Gaietta, G., Deerinck, T. J., Adams, S. R., Garner, C. C., Tsien, R. Y., Ellisman, M. H., and Malenka, R. C. (2004). Activity-dependent regulation of dendritic synthesis and trafficking of AMPA receptors. *Nat. Neurosci.* 7, 244–253.

Kampa, B. M., Letzkus, J. J., and Stuart, G. J. (2007). Dendritic mechanisms controlling spike-timing-dependent synaptic plasticity. *Trends Neurosci.* 30, 456–463.

Karmarkar, U. R., and Buonomano, D. V. (2002). A model of spike-timing dependent plasticity: one or two coincidence detectors? *J. Neurophysiol.* 88, 507–513.

Karmarkar, U. R., and Buonomano, D. V. (2006). Different forms of homeostatic plasticity are engaged with distinct temporal profiles. *Eur. J. Neurosci.* 23, 1575–1584.

Kempter, R., Gerstner, W., and van Hemmen, J. L. (2001). Intrinsic stabilization of output rates by spike-based Hebbian learning. *Neural Comput.* 13, 2709–2741.

Kilman, V., van Rossum, M. C., and Turrigiano, G. G. (2002). Activity deprivation reduces miniature IPSC amplitude by decreasing the number of postsynaptic GABA(A) receptors clustered at neocortical synapses. *J. Neurosci.* 22, 1328–1337.

Kirkwood, A., Rioult, M. C., and Bear, M. F. (1996). Experience-dependent modification of synaptic plasticity in visual cortex. *Nature* 381, 526–528.

Law, C. C., and Cooper, L. N. (1994). Formation of receptive fields in realistic visual environments according to the Bienenstock, Cooper, and Munro (BCM) theory. *Proc. Natl. Acad. Sci. U.S.A.* 91, 7797–7801.

Lazar, A., Pipa, G., and Triesch, J. (2009). SORN: a self-organizing recurrent neural network. *Front. Comput. Neurosci.* 3:23. doi: 10.3389/neuro.10.023.2009.

LeMasson, G., Marder, E., and Abbott, L. F. (1993). Activity-dependent regulation of conductances in model neurons. *Science* 259, 1915–1917.

Lisman, J. (2003). Long-term potentiation: outstanding questions and attempted synthesis. *Philos. Trans. R. Soc. Lond., B, Biol. Sci.* 358, 829–842.

Lisman, J., and Spruston, N. (2005). Postsynaptic depolarization requirements for LTP and LTD: a critique of spike timing-dependent plasticity. *Nat. Neurosci.* 8, 839–841.

Lissin, D. V., Gomperts, S. N., Carroll, R. C., Christine, C. W., Kalman, D., Kitamura, M., Hardy, S., Nicoll, R. A., Malenka, R. C., and von Zastrow, M. (1998). Activity differentially regulates the surface expression of synaptic AMPA and NMDA glutamate receptors. *Proc. Natl. Acad. Sci. U.S.A.* 95, 7097–7102.

Lu, Y., Christian, K., and Lu, B. (2008). BDNF: a key regulator for protein synthesis-dependent LTP and long-term memory? *Neurobiol. Learn. Mem.* 89, 312–323.

Maffei, A., and Fontanini, A. (2009). Network homeostasis: a matter of coordination. *Curr. Opin. Neurobiol.* 19, 168–173.

Maffei, A., Nataraj, K., Nelson, S. B., and Turrigiano, G. G. (2006). Potentiation of cortical inhibition by visual deprivation. *Nature* 443, 81–84.

Maffei, A., Nelson, S. B., and Turrigiano, G. G. (2004). Selective reconfiguration of layer 4 visual cortical circuitry by visual deprivation. *Nat. Neurosci.* 7, 1353–1359.

Maffei, A., and Turrigiano, G. G. (2008). Multiple modes of network homeostasis in visual cortical layer 2/3. *J. Neurosci.* 28, 4377–4384.

Malenka, R. C., and Nicoll, R. A. (1999). Long-term potentiation – a decade of progress? *Science* 285, 1870–1874.

Marder, E., and Bucher, D. (2007). Understanding circuit dynamics using the stomatogastric nervous system of lobsters and crabs. *Annu. Rev. Physiol.* 69, 291–316.

Markram, H., Lubke, J., Frotscher, M., and Sakmann, B. (1997). Regulation of synaptic efficacy by coincidence of postsynaptic APs and EPSPs. *Science* 275, 213–215.

Markram, H., and Tsodyks, M. (1996). Redistribution of synaptic efficacy between neocortical pyramidal neurons. *Nature* 382, 807–810.

McCoy, M. K., and Tansey, M. G. (2008). TNF signaling inhibition in the CNS: implications for normal brain function and neurodegenerative disease. *J. Neuroinflammation* 5, 45.

McCoy, P. A., Huang, H. S., and Philpot, B. D. (2009). Advances in understanding visual cortex plasticity. *Curr. Opin. Neurobiol.* 19, 298–304.

Minichiello, L. (2009). TrkB signalling pathways in LTP and learning. *Nat. Rev. Neurosci.* 10, 850–860.

Misonou, H., Mohapatra, D. P., Park, E. W., Leung, V., Zhen, D., Misonou, K., Anderson, A. E., and Trimmer, J. S. (2004). Regulation of ion channel localization and phosphorylation by neuronal activity. *Nat. Neurosci.* 7, 711–718.

Mohapatra, D. P., Misonou, H., Pan, S. J., Held, J. E., Surmeier, D. J., and Trimmer, J. S. (2009). Regulation of intrinsic excitability in hippocampal neurons by activity-dependent modulation of the KV2.1 potassium channel. *Channels (Austin)* 3, 46–56.

Morrison, A., Aertsen, A., and Diesmann, M. (2007). Spike-timing-dependent plasticity in balanced random networks. *Neural Comput.* 19, 1437–1467.

Morrison, A., Diesmann, M., and Gerstner, W. (2008). Phenomenological models of synaptic plasticity based on spike timing. *Biol. Cybern.* 98, 459–478.

Mrsic-Flogel, T. D., Hofer, S. B., Ohki, K., Reid, R. C., Bonhoeffer, T., and Hubener, M. (2007). Homeostatic regulation of eye-specific responses in visual cortex during ocular dominance plasticity. *Neuron* 54, 961–972.

Mu, Y., Otsuka, T., Horton, A. C., Scott, D. B., and Ehlers, M. D. (2003). Activity-dependent mRNA splicing controls ER export and synaptic delivery of NMDA receptors. *Neuron* 40, 581–594.

Murthy, V. N., Schikorski, T., Stevens, C. F., and Zhu, Y. (2001). Inactivity produces increases in neurotransmitter release and synapse size. *Neuron* 32, 673–682.

Narayanan, R., and Johnston, D. (2008). The h channel mediates location dependence and plasticity of intrinsic phase response in rat hippocampal neurons. *J. Neurosci.* 28, 5846–5860.

Nelson, A. B., Krispel, C. M., Sekirnjak, C., and du Lac, S. (2003). Long-lasting increases in intrinsic excitability triggered by inhibition. *Neuron* 40, 609–620.

Neves, G., Cooke, S. F., and Bliss, T. V. (2008). Synaptic plasticity, memory and the hippocampus: a neural network approach to causality. *Nat. Rev. Neurosci.* 9, 65–75.

O'Brien, R. J., Kamboj, S., Ehlers, M. D., Rosen, K. R., Fischbach, G. D., and Huganir, R. L. (1998). Activity-dependent modulation of synaptic AMPA receptor accumulation. *Neuron* 21, 1067–1078.

O'Leary, T., van Rossum, M. C., and Wyllie, D. J. (2010). Homeostasis of intrinsic excitability in hippocampal neurones: dynamics and mechanism of the response to chronic depolarization. *J. Physiol.* 588, 157–170.

Pfister, J. P., and Gerstner, W. (2006). Triplets of spikes in a model of spike timing-dependent plasticity. *J. Neurosci.* 26, 9673–9682.

Philpot, B. D., Cho, K. K., and Bear, M. F. (2007). Obligatory role of NR2A for metaplasticity in visual cortex. *Neuron* 53, 495–502.

Philpot, B. D., Espinosa, J. S., and Bear, M. F. (2003). Evidence for altered NMDA receptor function as a basis for metaplasticity in visual cortex. *J. Neurosci.* 23, 5583–5588.

Philpot, B. D., Sekhar, A. K., Shouval, H. Z., and Bear, M. F. (2001). Visual experience and deprivation bidirectionally modify the composition and function of NMDA receptors in visual cortex. *Neuron* 29, 157–169.

Poo, M. M. (2001). Neurotrophins as synaptic modulators. *Nat. Rev. Neurosci.* 2, 24–32.

Poolos, N. P. (2005). The h-channel: a potential channelopathy in epilepsy? *Epilepsy Behav.* 7, 51–56.

Pratt, K. G., and Aizenman, C. D. (2007). Homeostatic regulation of intrinsic excitability and synaptic transmission in a developing visual circuit. *J. Neurosci.* 27, 8268–8277.

Quinlan, E. M., Philpot, B. D., Huganir, R. L., and Bear, M. F. (1999). Rapid, experience-dependent expression of synaptic NMDA receptors in visual cortex in vivo. *Nat. Neurosci.* 2, 352–357.

Rabinowitch, I., and Segev, I. (2008). Two opposing plasticity mechanisms pulling a single synapse. *Trends Neurosci.* 31, 377–383.

Ramocki, M. B., and Zoghbi, H. Y. (2008). Failure of neuronal homeostasis results in common neuropsychiatric phenotypes. *Nature* 455, 912–918.

Rao, A., and Craig, A. M. (1997). Activity regulates the synaptic localization of the NMDA receptor in hippocampal neurons. *Neuron* 19, 801–812.

Renart, A., Song, P., and Wang, X. J. (2003). Robust spatial working memory through homeostatic synaptic scaling in heterogeneous cortical networks. *Neuron* 38, 473–485.

Reyes, A., and Sakmann, B. (1999). Developmental switch in the short-term modification of unitary EPSPs evoked in layer 2/3 and layer 5 pyramidal neurons of rat neocortex. *J. Neurosci.* 19, 3827–3835.

Rial Verde, E. M., Lee-Osbourne, J., Worley, P. F., Malinow, R., and Cline, H. T. (2006). Increased expression of the immediate-early gene arc/arg3.1 reduces AMPA receptor-mediated synaptic transmission. *Neuron* 52, 461–474.

Rittenhouse, C. D., Shouval, H. Z., Paradiso, M. A., and Bear, M. F. (1999). Monocular deprivation induces homosynaptic long-term depression in visual cortex. *Nature* 397, 347–350.

Roth-Alpermann, C., Morris, R. G., Korte, M., and Bonhoeffer, T. (2006). Homeostatic shutdown of long-term potentiation in the adult hippocampus. *Proc. Natl. Acad. Sci. U.S.A.* 103, 11039–11044.

Royer, S., and Pare, D. (2003). Conservation of total synaptic weight through bal-

anced synaptic depression and potentiation. *Nature* 422, 518–522.
Rubin, J. E. (2001). Steady states in an iterative model for multiplicative spike-timing-dependent plasticity. *Network* 12, 131–140.
Rubin, J. E., Gerkin, R. C., Bi, G. Q., and Chow, C. C. (2005). Calcium time course as a signal for spike-timing-dependent plasticity. *J. Neurophysiol.* 93, 2600–2613.
Rumsey, C. C., and Abbott, L. F. (2006). Synaptic democracy in active dendrites. *J. Neurophysiol.* 96, 2307–2318.
Rutherford, L. C., Nelson, S. B., and Turrigiano, G. G. (1998). BDNF has opposite effects on the quantal amplitude of pyramidal neuron and interneuron excitatory synapses. *Neuron* 21, 521–530.
Seeburg, D. P., Feliu-Mojer, M., Gaiottino, J., Pak, D. T., and Sheng, M. (2008). Critical role of CDK5 and Polo-like kinase 2 in homeostatic synaptic plasticity during elevated activity. *Neuron* 58, 571–583.
Shepherd, J. D., Rumbaugh, G., Wu, J., Chowdhury, S., Plath, N., Kuhl, D., Huganir, R. L., and Worley, P. F. (2006). Arc/Arg3.1 mediates homeostatic synaptic scaling of AMPA receptors. *Neuron* 52, 475–484.
Shin, M., and Chetkovich, D. M. (2007). Activity-dependent regulation of h channel distribution in hippocampal CA1 pyramidal neurons. *J. Biol. Chem.* 282, 33168–33180.
Shouval, H. Z., Bear, M. F., and Cooper, L. N. (2002). A unified model of NMDA receptor-dependent bidirectional synaptic plasticity. *Proc. Natl. Acad. Sci. U.S.A.* 99, 10831–10836.
Sjostrom, P. J., Rancz, E. A., Roth, A., and Hausser, M. (2008). Dendritic excitability and synaptic plasticity. *Physiol. Rev.* 88, 769–840.
Sjostrom, P. J., Turrigiano, G. G., and Nelson, S. B. (2001). Rate, timing, and cooperativity jointly determine cortical synaptic plasticity. *Neuron* 32, 1149–1164.
Sjostrom, P. J., Turrigiano, G. G., and Nelson, S. B. (2003). Neocortical LTD via coincident activation of presynaptic NMDA and cannabinoid receptors. *Neuron* 39, 641–654.
Smith, S. J. (1998). Glia help synapses form and function. *Curr. Biol.* 8, R158–R160.
Song, S., Miller, K. D., and Abbott, L. F. (2000). Competitive Hebbian learning through spike-timing-dependent synaptic plasticity. *Nat. Neurosci.* 3, 919–926.
Song, S., Sjostrom, P. J., Reigl, M., Nelson, S., and Chklovskii, D. B. (2005). Highly nonrandom features of synaptic connectivity in local cortical circuits. *PLoS Biol.* 3, e68. doi: 10.1371/journal.pbio.0030068.
Stellwagen, D., and Malenka, R. C. (2006). Synaptic scaling mediated by glial TNF-alpha. *Nature* 440, 1054–1059.
Sutton, M. A., Ito, H. T., Cressy, P., Kempf, C., Woo, J. C., and Schuman, E. M. (2006). Miniature neurotransmission stabilizes synaptic function via tonic suppression of local dendritic protein synthesis. *Cell* 125, 785–799.
Sutton, M. A., and Schuman, E. M. (2009). Partitioning the synaptic landscape: distinct microdomains for spontaneous and spike-triggered neurotransmission. *Sci. Signal.* 2, pe19.
Swanwick, C. C., Murthy, N. R., and Kapur, J. (2006). Activity-dependent scaling of GABAergic synapse strength is regulated by brain-derived neurotrophic factor. *Mol. Cell. Neurosci.* 31, 481–492.
Thiagarajan, T. C., Lindskog, M., and Tsien, R. W. (2005). Adaptation to synaptic inactivity in hippocampal neurons. *Neuron* 47, 725–737.
Tononi, G., Sporns, O., and Edelman, G. M. (1999). Measures of degeneracy and redundancy in biological networks. *Proc. Natl. Acad. Sci. U.S.A.* 96, 3257–3262.
Toyoizumi, T., Pfister, J. P., Aihara, K., and Gerstner, W. (2005). Generalized Bienenstock–Cooper–Munro rule for spiking neurons that maximizes information transmission. *Proc. Natl. Acad. Sci. U.S.A.* 102, 5239–5244.
Trasande, C. A., and Ramirez, J. M. (2007). Activity deprivation leads to seizures in hippocampal slice cultures: is epilepsy the consequence of homeostatic plasticity? *J. Clin. Neurophysiol.* 24, 154–164.
Tsodyks, M. (2002). Spike-timing-dependent synaptic plasticity – the long road towards understanding neuronal mechanisms of learning and memory. *Trends Neurosci.* 25, 599–600.
Tsodyks, M. V., and Markram, H. (1997). The neural code between neocortical pyramidal neurons depends on neurotransmitter release probability. *Proc. Natl. Acad. Sci. U.S.A.* 94, 719–723.
Turrigiano, G., Abbott, L. F., and Marder, E. (1994). Activity-dependent changes in the intrinsic properties of cultured neurons. *Science* 264, 974–977.
Turrigiano, G. G. (2008). The self-tuning neuron: synaptic scaling of excitatory synapses. *Cell* 135, 422–435.
Turrigiano, G. G., Leslie, K. R., Desai, N. S., Rutherford, L. C., and Nelson, S. B. (1998). Activity-dependent scaling of quantal amplitude in neocortical neurons. *Nature* 391, 892–896.
Vacher, H., Mohapatra, D. P., and Trimmer, J. S. (2008). Localization and targeting of voltage-dependent ion channels in mammalian central neurons. *Physiol. Rev.* 88, 1407–1447.
van Rossum, M. C., Bi, G. Q., and Turrigiano, G. G. (2000). Stable Hebbian learning from spike timing-dependent plasticity. *J. Neurosci.* 20, 8812–8821.
van Welie, I., Remme, M. W., van Hooft, J. A., and Wadman, W. J. (2006a). Different levels of Ih determine distinct temporal integration in bursting and regular-spiking neurons in rat subiculum. *J. Physiol.* 576, 203–214.
van Welie, I., van Hooft, J. A., and Wadman, W. J. (2006b). Background activity regulates excitability of rat hippocampal CA1 pyramidal neurons by adaptation of a K+ conductance. *J. Neurophysiol.* 95, 2007–2012.
van Welie, I., van Hooft, J. A., and Wadman, W. J. (2004). Homeostatic scaling of neuronal excitability by synaptic modulation of somatic hyperpolarization-activated Ih channels. *Proc. Natl. Acad. Sci. U.S.A.* 101, 5123–5128.
Wang, H., and Wagner, J. J. (1999). Priming-induced shift in synaptic plasticity in the rat hippocampus. *J. Neurophysiol.* 82, 2024–2028.
Watt, A. J., Sjostrom, P. J., Hausser, M., Nelson, S. B., and Turrigiano, G. G. (2004). A proportional but slower NMDA potentiation follows AMPA potentiation in LTP. *Nat. Neurosci.* 7, 518–524.
Watt, A. J., van Rossum, M. C., MacLeod, K. M., Nelson, S. B., and Turrigiano, G. G. (2000). Activity coregulates quantal AMPA and NMDA currents at neocortical synapses. *Neuron* 26, 659–670.
Wierenga, C. J., Ibata, K., and Turrigiano, G. G. (2005). Postsynaptic expression of homeostatic plasticity at neocortical synapses. *J. Neurosci.* 25, 2895–2905.
Wierenga, C. J., Walsh, M. F., and Turrigiano, G. G. (2006). Temporal regulation of the expression locus of homeostatic plasticity. *J. Neurophysiol.* 96, 2127–2133.
Wilhelm, J. C., Rich, M. M., and Wenner, P. (2009). Compensatory changes in cellular excitability, not synaptic scaling, contribute to homeostatic recovery of embryonic network activity. *Proc. Natl. Acad. Sci. U.S.A.* 106, 6760–6765.
Wu, W. W., Chan, C. S., Surmeier, D. J., and Disterhoft, J. F. (2008). Coupling of L-type Ca^{2+} channels to KV7/KCNQ channels creates a novel, activity-dependent, homeostatic intrinsic plasticity. *J. Neurophysiol.* 100, 1897–1908.
Xu, T. X., Sotnikova, T. D., Liang, C., Zhang, J., Jung, J. U., Spealman, R. D., Gainetdinov, R. R., and Yao, W. D. (2009a). Hyperdopaminergic tone erodes prefrontal long-term potential via a D2 receptor-operated protein phosphatase gate. *J. Neurosci.* 29, 14086–14099.
Xu, Z., Chen, R. Q., Gu, Q. H., Yan, J. Z., Wang, S. H., Liu, S. Y., and Lu, W. (2009b). Metaplastic regulation of long-term potentiation/long-term depression threshold by activity-dependent changes of NR2A/NR2B ratio. *J. Neurosci.* 29, 8764–8773.
Yashiro, K., and Philpot, B. D. (2008). Regulation of NMDA receptor subunit expression and its implications for LTD, LTP, and metaplasticity. *Neuropharmacology* 55, 1081–1094.
Yasui, T., Fujisawa, S., Tsukamoto, M., Matsuki, N., and Ikegaya, Y. (2005). Dynamic synapses as archives of synaptic history: state-dependent redistribution of synaptic efficacy in the rat hippocampal CA1. *J. Physiol.* 566, 143–160.
Yeung, L. C., Shouval, H. Z., Blais, B. S., and Cooper, L. N. (2004). Synaptic homeostasis and input selectivity follow from a calcium-dependent plasticity model. *Proc. Natl. Acad. Sci. U.S.A.* 101, 14943–14948.
Zhang, L. I., Tao, H. W., Holt, C. E., Harris, W. A., and Poo, M. (1998). A critical window for cooperation and competition among developing retinotectal synapses. *Nature* 395, 37–44.
Zhang, W., and Linden, D. J. (2003). The other side of the engram: experience-driven changes in neuronal intrinsic excitability. *Nat. Rev. Neurosci.* 4, 885–900.
Zucker, R. S., and Regehr, W. G. (2002). Short-term synaptic plasticity. *Annu. Rev. Physiol.* 64, 355–405.

Conflict of Interest Statement: The authors declare that the research was conducted in the absence of any commercial or financial relationships that could be construed as a potential conflict of interest.

Received: 18 February 2010; paper pending published: 23 April 2010; accepted: 17 May 2010; published online: 07 June 2010.
Citation: Watt AJ and Desai NS (2010) Homeostatic plasticity and STDP: keeping a neuron's cool in a fluctuating world. Front. Syn. Neurosci. ***2****:5. doi: 10.3389/fnsyn.2010.00005*

frontiers in
SYNAPTIC NEUROSCIENCE

REVIEW ARTICLE
published: 18 June 2010
doi: 10.3389/fnsyn.2010.00021

Spike-timing dependent plasticity beyond synapse – pre- and post-synaptic plasticity of intrinsic neuronal excitability

Dominique Debanne[1,2]* and Mu-Ming Poo[3]

[1] *Institut National de la Santé et de la Recherche Médicale Unité 641, Marseille, France*
[2] *Faculté de Médecine secteur nord, Université de la Méditerranée, Marseille, France*
[3] *Department of Molecular and Cell Biology, Division of Neurobiology, University of California, Berkeley, CA, USA*

Edited by:
Henry Markram, Ecole Polytechnique Federale de Lausanne, Switzerland

Reviewed by:
Eve Marder, Brandeis University, USA;
Henry Markram, Ecole Polytechnique Federale de Lausanne, Switzerland

****Correspondence:***
Dominique Debanne, Institut National de la Santé et de la Recherche Médicale Unité 641, Faculté de Médecine secteur nord, Boulevard Pierre, Dramard 13344, Marseille, France.
e-mail: dominique.debanne@univmed.fr

Long-lasting plasticity of synaptic transmission is classically thought to be the cellular substrate for information storage in the brain. Recent data indicate however that it is not the whole story and persistent changes in the intrinsic neuronal excitability have been shown to occur in parallel to the induction of long-term synaptic modifications. This form of plasticity depends on the regulation of voltage-gated ion channels. Here we review the experimental evidence for plasticity of neuronal excitability induced at pre- or postsynaptic sites when long-term plasticity of synaptic transmission is induced with Spike-Timing Dependent Plasticity (STDP) protocols. We describe the induction and expression mechanisms of the induced changes in excitability. Finally, the functional synergy between synaptic and non-synaptic plasticity and their spatial extent are discussed.

Keywords: hippocampus, cortex, LTP, LTD, ion channel, plasticity, STDP

INTRODUCTION

Long-lasting plasticity of synaptic transmission was for years considered as the favorite mechanism to account for information storage in the brain. Bidirectional long-term synaptic plasticity is indeed computationally appealing, principally because of synapse-specific changes among a large array of inputs. However, this is not the whole story and many additional electrophysiological components of neurons may undergo use-dependent long-term plasticity (Kim and Linden, 2007). Besides electrical synapses and glutamate transporters, voltage-gated ion channels occupy a key position in the persistent filtering of the neuronal message (Sjöström et al., 2008).

PLASTICITY OF INTRINSIC NEURONAL EXCITABILITY: A CELLULAR MECHANISM OF LEARNING AND MEMORY

The postulate that modification in intrinsic excitability could underlie the formation of functional neuronal assemblies and may thus contribute to a specific memory trace has its origin in invertebrate neural systems. The first evidence for intrinsic plasticity came from the pioneering work of Alkon who showed that phototaxic learning in the marine mollusk *Hermissenda crassicornis* involved the reduction of voltage-gated A-type and Ca^{2+}-activated K^+ currents in a photoreceptor (Alkon, 1984). Several forms of learning in *Aplysia* (sensitization and operant conditioning) were also found to be associated with persistent changed in neuronal excitability (Scholz and Byrne, 1987; reviewed in Mozzachiodi and Byrne, 2010). Interest in plasticity of intrinsic excitability of mammalian neurons was for a long-time occluded by the challenge of dissecting the mechanisms underlying long-term synaptic potentiation (LTP) and depression (LTD). A new interest in the study of intrinsic plasticity in mammalian brain has flourished only during the 1990s. The search for cellular excitability correlates of learning and memory in the mammalian brain has focused on neurons that are specifically active during learning. Eyeblink conditioning in the cat or the rabbit is well documented in this respect since neurons from active circuits during the conditioning exhibit *in vitro* an excitability that is significantly elevated (Disterhoft et al., 1986; Aou et al., 1992; Schreurs et al., 1997; Matthews et al., 2008). In several cases, the after-hyperpolarization (AHP) current was found to be depressed. Other forms of learning such as spatial or olfactory learning involve the regulation of neuronal excitability (Saar et al., 1998; Oh et al., 2003). These observations therefore suggest that the memory trace could not only be supported by selective changes in synaptic strength but that modifications in neuronal excitability might also contribute to the cellular substrate of the memory trace in the brain. This conclusion must be however qualified since in hippocampal and cortical neurons, increased neuronal excitability is no longer detectable 8 days after eyeblink conditioning, although learning is still established (Moyer et al., 1996). These *in vivo* studies, therefore suggest that synaptic or propagated activity during the induction phase may determine the induction of intrinsic plasticity. However, several key questions regarding the induction and expression mechanisms of intrinsic plasticity cannot be satisfactorily addressed at a cellular and molecular scale in the *in vivo* preparation and the use of *in vitro* assays must be envisaged to accurately control synaptic activity, membrane potential as well as pharmacologically isolated membrane currents.

In central cortical neurons, excitatory postsynaptic potentials (EPSPs) measured at the axon hillock result from a tight interplay between synaptic and intrinsic voltage-gated conductances that either amplify or attenuate excitatory synaptic potentials (review in Spruston, 2008). Any modifications in this fragile equilibrium may in turn facilitate or diminish the probability that a given

synaptic input triggers an action potential. Thus, regulation of ion channel activity represents a powerful means to control the principal neuronal output. For instance, tetanic stimulation of glutamatergic synaptic inputs not only induces LTP in hippocampal neurons but also persistently facilitates the generation of a postsynaptic action potential by the EPSP (Bliss et al., 1973; Andersen et al., 1980), a phenomenon known as EPSP-Spike potentiation. Notably, this form of plasticity is also observed in the presence of blockers of synaptic inhibition and is bidirectional (reviewed in Daoudal and Debanne, 2003). Induction of LTD with low frequency stimulation of the Schaffer collateral-CA1 neuron input is associated with a long-lasting decrease in EPSP-Spike coupling (Daoudal et al., 2002). The three major classes of glutamate receptors (i.e., *N*-methyl-D-aspartate (NMDAR), metabotropic glutamate (mGluR) and kainate (KR) receptors) play a central role in the induction of long-lasting plasticity of intrinsic neuronal excitability. Synaptic activation of NMDAR induces a wide range of pre- and postsynaptic plasticities of neuronal excitability in hippocampal, neocortical and cerebellar neurons (Aizenman and Linden, 2000; Armano et al., 2000; Ganguly et al., 2000; Wang et al., 2003; Li et al., 2004; Fan et al., 2005; Kim et al., 2007; Campanac et al., 2008; Losonczy et al., 2008). And many different voltage-gated sodium, potassium and cationic currents are targeted by the stimulation NMDAR. Activation of mGluR also produces many forms of short- and long-term regulation of intrinsic excitability in hippocampal and neocortical and modulate calcium-activated potassium, voltage-gated sodium, and hyperpolarization-activated cationic channels (Ireland and Abraham, 2002; Sourdet et al., 2003; Carlier et al., 2006; Brager and Johnston, 2007). Synaptic activation of KR induces long-term increase in hippocampal neuron excitability that is mediated by a reduction of the slow calcium-activated potassium current I_{sAHP} (Melyan et al., 2004; Ruiz et al., 2005).

Activation of glutamate receptors is not the only means to induce long-term plasticity of intrinsic excitability in central neurons. Postsynaptic spiking may also induce persistent increases in neuronal excitability of cerebellar and cortical neurons *in vitro* and *in vivo* (Aizenman and Linden, 2000; Egorov et al., 2002; Nelson et al., 2003; Cudmore and Turrigiano, 2004; Paz et al., 2009). In most of these cases, the cellular conditioning consists of repeated postsynaptic bursting induced by direct injection of depolarizing current in the neuron that produce a postsynaptic elevation in Ca^{2+} concentration, and the subsequent activation of protein kinases and the regulation of voltage-gated ion channels.

SPIKE-TIMING DEPENDENT PLASTICITY

Spike-timing dependent plasticity (STDP) has originally been defined for excitatory synaptic transmission in hippocampal and neocortical circuits (Levy and Steward, 1983; Gustafsson et al., 1987; Debanne et al., 1994, 1996, 1998; Markram et al., 1997; Bi and Poo, 1998; Feldman, 2000; Sjöström et al., 2001; reviewed in Abbott and Nelson, 2000; Dan and Poo, 2006). Synaptic efficacy is persistently and bi-directionally altered depending on the temporal interaction between afferent synaptic activity (EPSP) and postsynaptic spiking (the action potential). In most excitatory synapses positively correlated pre- and postsynaptic activity (EPSP before action potential) leads to synaptic reinforcement whereas negative correlation (action potential before EPSP) induces LTD. Thus, as initially postulated by Hebb (1949), synapses that repeatedly contribute to the postsynaptic discharge are reinforced whereas synapses that repeatedly fails to participate to the neuronal activity are depressed (Stent, 1973). Since the early 1990's, this rule has been verified in a large number of glutamatergic synapses impinging on glutamate neurons (Gustafsson et al., 1987; Debanne et al., 1994, 1996, 1998; Markram et al., 1997; Bi and Poo, 1998; Tzounopoulos et al., 2004; but see Egger et al., 1999). However, when the postsynaptic neuron is inhibitory this rule is generally inverted (Bell et al., 1997; Wang et al., 2000; Tzounopoulos et al., 2004; Fino et al., 2005; but see Pawlak and Kerr, 2008). A major consequence of STDP is that synaptic inputs compete for postsynaptic spike-timing and short-latency inputs win over long-latency synapses (Song et al., 2000). STDP is also observed in many different *in vivo* preparations in which synaptic activity can be monitored in response to electrical or sensory stimulation (Zhang et al., 1998; Jacob et al., 2007). It may account for activity-dependent plasticity of orientation maps in the cat striate cortex (Schuett et al., 2001), sensory adaptation (Yao and Dan, 2001) or shaping of hippocampal place-fields in the rat (Mehta et al., 2000). STDP rules have also been verified in the human brain with peripheral and transcranial stimulation (Wolters et al., 2003). However, when functional plasticity is monitored *in vivo*, it is virtually impossible to precisely identify the neuronal substrate and the underlying mechanisms of the observed changes. They may, indeed, equally result from modification of either synaptic strength or intrinsic excitability, or both. Therefore, it is of great importance to know whether protocols based on temporal interactions also produce long-lasting modifications of neuronal excitability in hippocampal and cortical neurons, and the spatial and temporal extent of these modifications.

PRESYNAPTIC CHANGES IN NEURONAL EXCITABILITY AND STDP

Changes in neuronal excitability associated with synaptic plasticity induced by STDP protocols have first been identified at the presynaptic side. Using paired-recordings from synaptically coupled hippocampal neurons, Ganguly et al. (2000) found that correlated pre- and postsynaptic spiking not only induces LTP of synaptic transmission but also increases the excitability of the presynaptic neuron. This presynaptic plasticity of neuronal excitability is rapidly expressed (<2 min) and is long-lasting (>30 min). Its induction requires activation of NMDA receptors (NMDAR), postsynaptic Ca^{2+} elevation and activation of protein kinases C (PKC). The expression mechanisms have been studied at the soma of the presynaptic neuron and involve a shift in the activation curve of the Na^{+} current towards hyperpolarizing values that may account for the lower spike threshold (Ganguly et al., 2000). In addition, the sodium current exhibits an improved recovery from inactivation following correlated pre- and postsynaptic activity.

Mirror effects have been observed presynaptically when LTD is induced by negative correlation in hippocampal and neocortical pyramidal neurons (Li et al., 2004). The excitability of the presynaptic cell is persistently reduced following induction of LTD. This plasticity requires postsynaptic calcium elevation and

presynaptic PKA- and PKC-dependent modification of slow-activating K^+ channels. The reduction in excitability is reversible if LTP is induced with positive correlation (Li et al., 2004). It is important to note here that these presynaptic changes in excitability were also observed in pairs of L4 spiny neurons from brain slices, suggesting that this form of intrinsic plasticity might also be present *in vivo*.

The functional consequences of long-lasting plasticity of presynaptic excitability might be of great importance for the dynamics of the neural circuits. For instance, the presynaptic increase in neuronal excitability following correlated spiking activity may facilitate the induction of bursting-like behavior and will enhance the reliability of signal transmission by creating privileged activity pathways in the brain. In addition, enhancement of presynaptic neuronal excitability may affect the plasticity of upstream synapses made onto the presynaptic cell by facilitating the initiation of back-propagated action potentials (Tao et al., 2000). Indeed, retrograde spread of LTP and LTD from developing retinotectal synapses to upstream synapses made by bipolar cells on retinal ganglion cells in the retina has been observed *in vivo*, through cytoplasmic retrograde signaling with the order of minutes after the induction of LTP/LTD (Du et al., 2009). Presynaptic modifications of neuronal excitability and efficacy of upstream synapses may be attributed to the actions of common retrograde signals and serve synergistic functions in neuronal circuit plasticity.

POSTSYNAPTIC CHANGES IN NEURONAL EXCITABILITY AND STDP

Neuronal excitability is also affected on the postsynaptic side when long-term synaptic plasticity is induced with STDP protocols. At least two neuronal functions, namely EPSP summation and EPSP-spike coupling, are modulated after the induction of spike-timing dependent LTP/LTD, through changes in postsynaptic voltage-gated channels.

In hippocampal CA1 pyramidal neurons, summation of EPSPs is determined by voltage-gated conductances that amplify or attenuate synaptic potentials. The property of EPSP summation in these neurons is strongly modulated following induction of LTP or LTD (Wang et al., 2003; Xu et al., 2006). A gain in EPSP summation is consistently observed when LTP is induced with positively correlated activity whereas a loss of summation is associated with LTD induced by negative correlation. The activity-dependent increase in EPSP summation requires activation of NMDA receptors, PKC and Ca^{2+}/calmodulin-dependent protein kinase II (CaMKII), but is independent of $GABA_A$ receptor-mediated inhibition (Wang et al., 2003). Interestingly, blockers of hyperpolarization-activated cationic (h) channels prevent the facilitation in EPSP summation, suggesting that the facilitation results from the down-regulation of h-channel activity in the dendrites.

EPSP-spike coupling is also profoundly affected in CA1 pyramidal neurons when long-term synaptic plasticity is induced with STDP protocols (Campanac and Debanne, 2008). Positive correlation between pre- and postsynaptic activity not only induces LTP but also facilitates EPSP-spike coupling. Conversely, LTD induced by negative correlation is associated with EPSP-spike depression. Both EPSP-spike potentiation and depression require activation of NMDA receptors but are independent of $GABA_A$ receptor dependent inhibition (Campanac and Debanne, 2008). The amplitude-slope relation of the EPSP was facilitated after LTP but depressed after LTD, indicating that mechanisms of EPSP amplification are regulated (see also Wang et al., 2003). Most importantly, the regulation of h-channel activity may constitute a major mechanism of expression. Apparent input resistance measured in the cell body is increased following induction of LTP induced by correlated activity or by high frequency stimulation (Campanac et al., 2008). This change is more pronounced when apical dendrites are recorded. In addition, the local decrease of the dendritic h-conductance with the use of dynamic-clamp techniques mimics EPSP-spike potentiation (Campanac et al., 2008). However, the regulation of A-type K^+ current in the dendrite (Frick et al., 2004; Kim et al., 2007) or the fast transient Na^+ current in the cell body (Xu et al., 2005) induced by positive correlation between synaptic activity and postsynaptic spiking may also facilitate EPSP-spike coupling in CA1 pyramidal neurons.

SPATIAL AND TEMPORAL SELECTIVITY OF STDP-INDUCED INTRINSIC PLASTICITY

SPATIAL SELECTIVITY

The storage of information through the regulation of synaptic strength in models of memory is particularly attractive because of the property of input specificity. Given the large number of synapses per neuron (>10000) and the huge number of neurons found in the brain (10^{11}), a memory storage system that uses input-specific changes in synaptic transmission has a potentially enormous storage capacity. Although chemical synapses represent the major functional interface between neurons, following dendritic integration neuronal information is conveyed by action potentials. Thus, the activity-dependent regulation of ion channels located near the spike generation zone (the axon initial segment or the cell body) would change the throughput of all synapses that the neuron receives (Daoudal and Debanne, 2003; Zhang and Linden, 2003; Mozzachiodi and Byrne, 2010), possibly leading to a loss in the information stored at specific synapses. In this case, the specificity might be observed at the cellular level. Such global changes in neuronal excitability have been observed following brief episodes of synaptic (Aizenman and Linden, 2000; Sourdet et al., 2003) or spiking activity (Cudmore and Turrigiano, 2004; Paz et al., 2009) and in the presynaptic neuron when LTP or LTD is induced in hippocampal cells with spike-timing dependent protocols (Ganguly et al., 2000; Li et al., 2004). In these studies, neuronal excitability was assessed only in the cell body. Whether and to what extent intrinsic excitability changes in axonal and dendritic membranes remains unclear. Global changes have also been reported on the postsynaptic side when LTP is induced with correlated activity in CA1 pyramidal neurons (Xu et al., 2005). However, several lines of evidence indicate that postsynaptic changes in intrinsic excitability induced by spike-timing dependent protocols are restricted to a localized region of the dendrites. Enhanced EPSP summation associated with synaptic potentiation is dependent on the position of the synaptic inputs (Wang et al., 2003). A-type K^+ channels are regulated in the dendrites of CA1 pyramidal neurons after induction of LTP (Frick et al., 2004). Potentiation and depression of dendritic integration observed in parallel with induction of spike-timing dependent

synaptic plasticity are input specific (Campanac and Debanne, 2008). Finally, dendritic h-channel activity is locally reduced following induction of LTP (Campanac et al., 2008). Thus, intrinsic excitability changes associated with STDP-related protocols are localized in the dendrites of CA1 pyramidal neurons and may thus preserve the input specificity property for high-capacity information storage.

TEMPORAL SELECTIVITY

The temporal windows for synaptic potentiation and depression induced by correlated activity are generally not wider than a few tens of millisecond (Markram et al., 1997; Bi and Poo, 1998; Debanne et al., 1998; Feldman, 2000). They are usually precisely defined (at the millisecond scale) and depend on both the number of postsynaptic spikes (Debanne et al., 1994; Sourdet and Debanne, 1999) and dendritic location of the synaptic input (Froemke et al., 2005). Similar plasticity windows are observed for intrinsic plasticity. Presynaptic changes in neuronal excitability follow precisely the STDP rule (Li et al., 2004). At the postsynaptic side, EPSP-spike plasticity also obeys the STDP learning rule (Campanac and Debanne, 2008). In these two examples, no changes in excitability at the pre- or postsynaptic side are observed out of the LTP and LTD time windows (i.e., for long positive or long negative intervals), suggesting common induction mechanisms for plasticity in synaptic efficacy and intrinsic excitability.

FUNCTIONAL SYNERGY BETWEEN SYNAPTIC AND INTRINSIC PLASTICITY INDUCED BY STDP

A functional synergy has been demonstrated for synaptic and intrinsic plasticity in central neurons at the pre- and postsynaptic side. LTP is generally associated with an increase in neuronal excitability (Armano et al., 2000; Ganguly et al., 2000; Daoudal et al., 2002; Wang et al., 2003; Xu et al., 2005; Campanac and Debanne, 2008; Campanac et al., 2008) whereas synaptic depression is usually accompanied by a reduced intrinsic excitability (Daoudal et al., 2002; Wang et al., 2003; Campanac and Debanne, 2008). Thus, plasticity in intrinsic excitability cannot be simply considered as an additional level of plasticity that makes understanding brain storage mechanisms more complex but rather, it can be incorporated into a general framework in which synaptic and intrinsic plasticity interact coherently (Daoudal and Debanne, 2003). This functional synergy insures significant changes in the neuronal output when synaptic plasticity is induced.

Functional synergy between synaptic and intrinsic plasticities might, however, be broken if the magnitude of synaptic plasticity is excessive and comes out of the physiological range (Debanne et al., 2003). This form of compensatory plasticity has been first studied theoretically in multi-compartment model of CA1 pyramidal neurons where intrinsic plasticity restored optimal firing range after synaptic potentiation (Siegel et al., 1994). In biological CA1 pyramidal neurons, synaptic potentiation of very large amplitude (~300% of the control EPSP) is accompanied by a *decrease* in excitability of CA1 pyramidal neurons (Fan et al., 2005). Conversely, nearly maximal synaptic depression (~50%) is associated with an *increase* in excitability (Brager and Johnston, 2007). Both changes globally affect neuronal excitability, involve the regulation of h-channel activity, and are aimed to stabilize the overall neuronal activity by preventing excessive synaptic excitation. Therefore, these regulations are homeostatic in nature and compensate for excessive increases or decreases in synaptic excitation (Turrigiano and Nelson, 2004).

CONCLUDING REMARKS

Temporal interactions of pre- and postsynaptic spiking in neural circuits bidirectionally regulate not only synaptic strength but also intrinsic excitability of pyramidal cells at both pre- and postsynaptic sides. At the postsynaptic side this plasticity is largely localized within the dendrites – involving the regulation of A-type K^+ and h-type cationic channels – and respects the input specificity of synaptic modifications, thus preserving high capacity of information storage. However, intrinsic plasticity is probably not synapse specific but rather may alter the excitability of dendritic branches over a few tens of micrometers (Losonczy et al., 2008). Additional experimental investigations will be necessary to precisely determine the spatial extent of intrinsic plasticity in branched neurons.

Synaptic activation of glutamate receptors is critical in the induction of long-term plasticity of intrinsic excitability in central neurons but one cannot exclude the contribution of other factors. Indeed, in most of the experiments reported so far (except the studies of Li et al., 2004; Losonczy et al., 2008), intrinsic plasticity is induced by stimulation of a large bundle of glutamatergic inputs and one cannot exclude stimulation of neuromodulators containing varicosities. In fact, neuromodulators are potent regulators of back-propagating action potentials (Hoffman and Johnston, 1999), ion channel activity (Cantrell and Catterall, 2001) and spike-timing dependent synaptic plasticity (Lin et al., 2003; Seol et al., 2007; Zhang et al., 2009). There are good reasons to believe that neuromodulators may also modulate induction of spike-timing dependent intrinsic plasticity. In addition, the gliotransmitter D-serine that is thought to be released by astrocytes upon neuronal stimulation (Mothet et al., 2005; review in Hamilton and Attwell, 2010) play a critical role in the induction of long-term synaptic plasticity (Henneberger et al., 2010). One cannot exclude that such new actors in interneuronal signaling may also play a major role in the induction of spike-timing dependent intrinsic plasticity.

Plasticity of intrinsic excitability is synergistic to synaptic plasticity in modulating neuronal output, thus enhancing the functional significance of synaptic modifications. However, compensatory mechanisms acting both at intrinsic and synaptic currents concur to maintain neuronal activity within physiological bounds (Siegel et al., 1994; Rumsay and Abbott, 2004; Rabinowitch and Segev, 2006). The synergy between synaptic and intrinsic plasticity might be broken outside this physiological range (Fan et al., 2005; Campanac et al., 2008). While learning rules for STDP of synaptic efficacy and intrinsic excitability are coordinated in pyramidal neurons, additional work is still needed to define the corresponding properties in GABAergic interneurons (Kullmann and Lamsa, 2007).

ACKNOWLEDGMENTS

This work is supported by CNRS, INSERM, ANR (Excion 2006 to Dominique Debanne), Région PACA (APO 2009 Plexin to Dominique Debanne), USNIH (NS36999 to Mu-Ming Poo).

REFERENCES

Abbott, L. F., and Nelson, S. B. (2000). Synaptic plasticity: taming the beast. *Nat. Neurosci.* 3, 1178–1183.

Aizenman, C., and Linden, D. J. (2000). Rapid, synaptically driven increases in the intrinsic excitability of cerebellar deep nuclear neurons. *Nat. Neurosci.* 3, 109–111.

Alkon, D. L. (1984). Calcium-mediated reduction of ionic currents: a biophysical memory trace. *Science* 226, 1037–1045.

Andersen, P., Sundberg, S. H., Sveen, O., Swann, J. W., and Wigström, H. (1980). Possible mechanisms for long-lasting potentiation of synaptic transmission in hippocampal slices from guinea-pigs. *J. Physiol.* 302, 463–482.

Aou, S., Woody, C. D., and Birt, D. (1992). Increases in excitability of neurons of the motor cortex of cats after rapid acquisition of eye blink conditioning. *J. Neurosci.* 12, 560–569.

Armano, S., Rossi, P., Taglietti, V., and D'Angelo, E. (2000). Long-term potentiation of intrinsic excitability at the mossy fiber-granule cell synapse of rat cerebellum. *J. Neurosci.* 20, 5208–5216.

Bell, C., Han, V. Z., Sugawara, Y., and Grant, K. (1997). Synaptic plasticity in a cerebellum-like structure depends on temporal order. *Nature* 387, 278–281.

Bi, G. Q., and Poo, M. M. (1998). Synaptic modifications in cultured hippocampal neurons: dependence on spike timing, synaptic strength, and postsynaptic cell type. *J. Neurosci.* 18, 10484–10472.

Bliss, T. V. P., Lømo, T., and Gardner-Medvin, A. R. (1973). "Synaptic plasticity in the hippocampal formation," in *Macromolecules and Behaviour*, eds G. B. Ansell and P. B. Bradley (London: MacMillan), 193–203.

Brager, D. H., and Johnston, D. (2007). Plasticity of intrinsic excitability during long-term depression is mediated through mGluR-dependent changes in Ih in hippocampal CA1 pyramidal neurons. *J. Neurosci.* 27, 13926–13937.

Campanac, E., Daoudal, G., Ankri, N., and Debanne, D. (2008). Down-regulation of dendritic Ih in CA1 pyramidal neurons after LTP. *J. Neurosci.* 28, 8635–8643.

Campanac, E., and Debanne, D. (2008). Spike timing-dependent plasticity: a learning rule for dendritic integration in rat CA1 pyramidal neurons. *J. Physiol.* 586, 779–793.

Cantrell, A. R., and Catterall, W. A. (2001). Neuromodulation of Na^+ channels: an unexpected form of cellular plasticity. *Nat. Rev. Neurosci.* 2, 397–407.

Carlier, E., Sourdet, V., Boudkkazi, S., Déglise, P., Ankri, N., Fronzaroli-Molinieres, L., and Debanne, D. (2006). Metabotropic glutamate receptor subtype 1 regulates sodium currents in rat neocortical pyramidal neurons. *J. Physiol.* 577, 141–154.

Cudmore, R. H., and Turrigiano, G. G. (2004). Long-term potentiation of intrinsic excitability in LV visual cortical neurons. *J. Neurophysiol.* 92, 341–348.

Dan, Y., and Poo, M. M. (2006). Spike timing-dependent plasticity: from synapse to perception. *Physiol. Rev.* 86, 1033–1048.

Daoudal, G., and Debanne, D. (2003). Long-term plasticity of intrinsic excitability: learning rules and mechanisms. *Learn. Mem.* 10, 456–465.

Daoudal, G., Hanada, Y., and Debanne, D. (2002). Bidirectional plasticity of excitatory postsynaptic potential (EPSP)-spike coupling in CA1 hippocampal pyramidal neurons. *Proc. Natl. Acad. Sci. U.S.A.* 99, 14512–14517.

Debanne, D., Daoudal, G., Sourdet, V., and Russier, M. (2003). Brain plasticity and ion channels. *J. Physiol. Paris* 97, 403–414.

Debanne, D., Gähwiler, B. H., and Thompson, S. M. (1994). Asynchronous pre- and postsynaptic activity induces associative long-term depression in area CA1 of the rat hippocampus in vitro. *Proc. Natl. Acad. Sci. U.S.A.* 91, 1148–1152.

Debanne, D., Gähwiler, B. H., and Thompson, S. M. (1996). Cooperative interactions in the induction of long-term potentation and depression of synaptic excitation between hippocampal CA3-CA1 cell pairs in vitro. *Proc. Natl. Acad. Sci. U.S.A.* 93, 11225–11230.

Debanne, D., Gähwiler, B. H., and Thompson, S. M. (1998). Long-term synaptic plasticity between pairs of individual CA3 pyramidal cells in rat hippocampal slice cultures. *J. Physiol.* 507, 237–247.

Disterhoft, J. F., Coulter, D. A., and Alkon, D. L. (1986). Conditioning-specific membrane changes of rabbit hippocampal neurons measured in vitro. *Proc. Natl. Acad. Sci. U.S.A.* 83, 2733–2737.

Du, J. L., Wei, H. P., Wang, Z. R., Wong, S. T., and Poo, M. M. (2009). Long-range retrograde spread of LTP and LTD from optic tectum to retina. *Proc. Natl. Acad. Sci. U.S.A.* 106, 1889–1896.

Egger, V., Feldmeyer, D., and Sakmann, B. (1999). Coincidence detection and changes of synaptic efficacy in spiny stellate neurons in rat barrel cortex. *Nat. Neurosci.* 2, 1098–1105.

Egorov, A. V., Hamam, B. N., Fransén, E., Hasselmo, M. E., and Alonso, A. A. (2002). Graded persistent activity in entorhinal cortex neurons. *Nature* 420, 173–178.

Fan, Y., Fricker, D., Brager, D. H., Chen, X., Lu, H. C., Chitwood, R. A., and Johnston, D. (2005). Activity-dependent decrease of excitability in rat hippocampal neurons through increases in Ih. *Nat. Neurosci.* 8, 1542–1551.

Feldman, D. E. (2000). Timing-based LTP and LTD at vertical inputs to layer II/III pyramidal cells in rat barrel cortex. *Neuron* 27, 45–56.

Fino, E., Glowinski, J., and Venance, L. (2005). Bidirectional activity-dependent plasticity at corticostriatal synapses. *J. Neurosci.* 25, 11279–11287.

Frick, A., Magee, J., and Johnston, D. (2004). LTP is accompanied by an enhanced local excitability of pyramidal neuron dendrites. *Nat. Neurosci.* 7, 126–135.

Froemke, R. C., Poo, M. M., and Dan, Y. (2005). Spike-timing-dependent synaptic plasticity depends on dendritic location. *Nature* 434, 221–225.

Ganguly, K., Kiss, L., and Poo, M. M. (2000). Enhancement of presynaptic neuronal excitability by correlated presynaptic and postsynaptic spiking. *Nat. Neurosci.* 3, 1018–1026.

Gustafsson, B., Wigström, H., Abraham, W. C., and Huang, Y. Y. (1987). Long-term potentiation in the hippocampus using depolarizing current pulses as the conditioning stimulus to single volley synaptic potentials. *J. Neurosci.* 7, 774–780.

Hamilton, N. B., and Attwell, D. (2010). Do astrocytes really exocytose neurotransmitters? *Nat. Rev. Neurosci.* 11, 227–238.

Hebb, D. O. (1949). *The Organization of Behaviour*. New York, NY: Wiley.

Henneberger, C., Papouin, T., Oliet, S. H., and Rusakov, D. A. (2010). Long-term potentiation depends on release of D-serine from astrocytes. *Nature* 463, 232–236.

Hoffman, D. A., and Johnston, D. (1999). Neuromodulation of dendritic action potentials. *J. Neurophysiol.* 81, 408–441.

Ireland, D. R., and Abraham, W. C. (2002). Group I mGluRs increase excitability of hippocampal CA1 pyramidal neurons by a PLC-independent mechanism. *J. Neurophysiol.* 88, 107–116.

Jacob, V., Brasier, D. J., Erchova, I., Feldman, D., and Shulz, D. E. (2007). Spike timing-dependent synaptic depression in the in vivo barrel cortex of the rat. *J. Neurosci.* 27, 1271–1284.

Kim, J., Jung, S. C., Clemens, A. M., Petralia, R. S., and Hoffman, D. A. (2007). Regulation of dendritic excitability by activity-dependent trafficking of the A-type K+ channel subunit Kv4.2 in hippocampal neurons. *Neuron* 54, 933–947.

Kim, S. J., and Linden, D. J. (2007). Ubiquitous plasticity and memory storage. *Neuron* 56, 582–592.

Kullmann, D. M., and Lamsa, K. P. (2007). Long-term synaptic plasticity in hippocampal interneurons. *Nat. Rev. Neurosci.* 8, 687–699.

Levy, W. B., and Steward, O. (1983). Temporal contiguity requirements for long-term associative potentiation/depression in the hippocampus. *Neuroscience* 8, 791–797.

Li, C. Y., Lu, J. T., Wu, C. P., Duan, S. M., and Poo, M. M. (2004). Bidirectional modification of presynaptic neuronal excitability accompanying spike timing-dependent synaptic plasticity. *Neuron* 41, 257–268.

Lin, Y. W., Min, M. Y., Chiu, T. H., and Yang, H. W. (2003). Enhancement of associative long-term potentiation by activation of β-adrenergic receptors at CA1 synapses in rat hippocampal slices. *J. Neurosci.* 23, 4173–4181.

Losonczy, A., Makara, J. K., and Magee, J. C. (2008). Compartmentalized dendritic plasticity and input feature storage in neurons. *Nature* 452, 436–441.

Markram, H., Lübke, J., Frotscher, M., and Sakmann, B. (1997). Regulation of synaptic efficacy by coincidence of postsynaptic APs and EPSPs. *Science* 275, 213–215.

Matthews, E. A., Weible, A. P., Shah, S., and Disterhoft, J. F. (2008). The BK-mediated fAHP is modulated by learning a hippocampus-dependent task. *Proc. Natl. Acad. Sci. U.S.A.* 105, 15154–15159.

Mehta, M. R., Quirk, M. C., and Wilson, M. A. (2000). Experience-dependent asymmetric shape of hippocampal receptive fields. *Neuron* 25, 707–715.

Melyan, Z., Lancaster, B., and Wheal, H. V. (2004). Metabotropic regulation of intrinsic excitability by synaptic activation of kainate receptors. *J. Neurosci.* 24, 4530–4534.

Mothet, J. P., Pollegioni, L., Ouanounou, G., Martineau, M., Fossier, P., and Baux, G. (2005). Glutamate receptor activation triggers a calcium-dependent and SNARE protein-dependent release of the gliotransmitter D-serine. *Proc. Natl. Acad. Sci. U.S.A.* 102, 5606–5611.

Moyer, J. R., Thompson, L. T., and Disterhoft, J. F. (1996). Trace eyeblink conditioning increases CA1 excitability in a transient and learning-specific manner. *J. Neurosci.* 16, 5536–5546.

Mozzachiodi, R., and Byrne, J. H. (2010). More than synaptic plasticity: role of nonsynaptic plasticity in learning and memory. *Trends Neurosci.* 33, 17–26.

Nelson, A. B., Krispel C. M., Sekimjak, C., and du Lac, S. (2003). Long-lasting

increases in intrinsic excitability triggered by inhibition. *Neuron* 40, 609–620.

Oh, M. M., Kuo, A. G., Wu, W. W., Sametsky, E. A., and Disterhoft, J. F. (2003). Watermaze learning enhances excitability of CA1 pyramidal neurons. *J. Neurophysiol.* 90, 2171–2179.

Pawlak, V., and Kerr J. N. D. (2008). Dopamine receptor activation is required for corticostriatal spike-timing-dependent plasticity. *J. Neurosci.* 28, 2435–2446.

Paz, J. T., Mahon, S., Tiret, P., Genet, S., Delord, B., and Charpier, S. (2009). Multiple forms of activity-dependent intrinsic plasticity in layer V cortical neurones *in vivo*. *J. Physiol.* 587, 3189–3205.

Rabinowitch, I., and Segev, I. (2006). The endurance and selectivity of spatial patterns of long-term potentiation/depression in dendrites under homeostatic synaptic plasticity. *J. Neurosci.* 26, 13474–13484.

Ruiz, A., Sachdhanandam, S., Utvik, J. K., Coussen, F., and Mulle, C. (2005). Distinct subunits in heteromeric kainite receptors mediate ionotropic and metabotropic function at hippocampal mossy fiber synapses. *J. Neurosci.* 25, 11710–11718.

Rumsay C. C., and Abbott L. F. (2004). Equalization of synaptic efficacy by activity- and timing-dependent synaptic plasticity. *J. Neurophysiol.* 91, 2273–2280.

Saar, D., Grossman, Y., and Barkai, E. (1998). Reduced after-hyperpolarization in rat piriform cortex pyramidal neurons is associated with increased learning capability during operant conditioning. *Eur. J. Neurosci.* 10, 1518–1523.

Scholz, K. P., and Byrne, J. H. (1987). Long-term sensitization in Aplysia: biophysical correlates in tail sensory neurons. *Science* 235, 685–687.

Schreurs, B. G., Tomsic, D., Gusev, P. A., and Alkon, D. L. (1997). Dendritic excitability microzones and occluded long-term depression after classical conditioning of the rabbit's nictitating membrane response. *J. Neurophysiol.* 77, 86–92.

Schuett, S., Bonhoeffer, T., and Hübener M. (2001). Pairing-induced changes of orientation maps in cat visual cortex. *Neuron* 32, 325–337.

Seol, G. H., Ziburkus, J., Huang, S. Y., Song, L., Kim, I. T., Takamiya, K., Huganir, R. L., Lee, H. K., and Kirkwood, A. (2007). Neuromodulators control the polarity of spike-timing-dependent synaptic plasticity. *Neuron* 55, 919–929.

Siegel, M., Marder, E., and Abbott, L. F. (1994). Activity-dependent current distribution in model neurons. *Proc. Natl. Acad. Sci. U.S.A.* 91, 11308–11312.

Sjöström, P. J., Rancz, E. A., Roth, A., and Häusser, M. (2008). Dendritic excitability and synaptic plasticity. *Physiol. Rev.* 88, 768–840.

Sjöström, P. J., Turrigiano, G. G., and Nelson, S. B. (2001). Rate, timing, and cooperativity jointly determine cortical synaptic plasticity. *Neuron* 32, 1149–1164.

Song, S., Miller, K. D., and Abbott, L. F. (2000). Competitive Hebbian learning through spike-timing-dependent synaptic plasticity. *Nat. Neurosci.* 3, 919–926.

Sourdet, V., and Debanne, D. (1999). The role of dendritic filtering in associative long-term synaptic plasticity. *Learn. Mem.* 6, 422–447.

Sourdet, V., Russier, M., Daoudal, G., Ankri, N., and Debanne, D. (2003). Long-term enhancement of neuronal excitability and temporal fidelity mediated by metabotropic glutamate receptor subtype 5. *J. Neurosci.* 23, 10238–10248.

Spruston, N. (2008). Pyramidal neurons: dendritic structure and synaptic integration. *Nat. Rev. Neurosci.* 9, 206–221.

Stent, G. S. (1973). A physiological mechanism for Hebb's postulate of learning. *Proc. Natl. Acad. Sci. U.S.A.* 70, 997–1001.

Tao, H., Zhang, L. I., Bi, G. Q., and Poo, M. M. (2000). Selective presynaptic propagation of long-term potentiation in defined neural networks. *J. Neurosci.* 20, 3233–3243.

Turrigiano, G. G., and Nelson, S. B. (2004). Homeostatic plasticity in the developing nervous system. *Nat. Rev. Neurosci.* 5, 97–107.

Tzounopoulos, T., Kim, Y., Oertel, D., and Trussell, L. O. (2004). Cell-specific, spike timing-dependent plasticities in the dorsal cochlear nucleus. *Nat. Neurosci.* 7, 719–725.

Wang, S. S. H., Denk, W., and Häusser, M. (2000). Coincidence detection in single dendritic spines mediated by calcium release. *Nat. Neurosci.* 3, 1266–1273.

Wang, Z., Xu, N. I., Wu, C. P., Duan, S., and Poo, M. M. (2003). Bidirectional changes in spatial dendritic integration accompanying long-term synaptic modifications. *Neuron* 37, 463–472.

Wolters, A., Sandbrink, F., Schlottmann, A., Kunesch, E., Stefan, K., Cohen, L. G., Benecke, R., and Classen, J. (2003). A temporally asymmetric Hebbian rule governing plasticity in the human motor cortex. *J. Neurophysiol.* 89, 2339–2345.

Xu, J., Kang, N., Jiang, L., Nedergaard, M., and Kang, J. (2005). Activity-dependent long-term potentiation of intrinsic excitability in hippocampal CA1 pyramidal neurons. *J. Neurosci.* 25, 1750–1760.

Xu, N. L., Ye, C. Q., Poo, M. M., and Zhang, X. H. (2006). Coincidence detection of synaptic inputs is facilitated at the distal dendrites after long-term potentiation induction. *J. Neurosci.* 26, 3002–3009.

Yao, H., and Dan, Y. (2001). Stimulus timing-dependent plasticity in cortical processing of orientation. *Neuron* 32, 315–323.

Zhang, J. C., Lau, P. M., and Bi, G. Q. (2009). Gain in sensitivity and loss in temporal contrast of STDP by dopaminergic modulation at hippocampal synapses. *Proc. Natl. Acad. Sci. U.S.A.* 106, 13028–13033.

Zhang, L. I., Tao, H. W., Holt, C. E., Harris, W. A., and Poo, M. M. (1998). A critical window for cooperation and competition among developing retinotectal synapses. *Nature* 395, 37–44.

Zhang, W., and Linden, D. J. (2003). The other side of the engram: experience-driven changes in neuronal intrinsic excitability. *Nat. Rev. Neurosci.* 4, 885–900.

Conflict of Interest Statement: The authors declare that the research was conducted in the absence of any commercial or financial relationships that could be construed as a potential conflict of interest.

Received: 29 January 2010; paper pending published: 16 February 2010; accepted: 30 May 2010; published online: 18 June 2010.

Citation: Debanne D and Poo M-M (2010) Spike-timing dependent plasticity beyond synapse – pre- and post-synaptic plasticity of intrinsic neuronal excitability. Front. Syn. Neurosci. 2:21. doi: 10.3389/fnsyn.2010.00021

frontiers in
SYNAPTIC NEUROSCIENCE

REVIEW ARTICLE
published: 19 July 2010
doi: 10.3389/fnsyn.2010.00030

The applicability of spike time dependent plasticity to development

Daniel A. Butts[1]* and Patrick O. Kanold[1,2]*

[1] *Department of Biology and Program in Neuroscience and Cognitive Science, University of Maryland, College Park, MD, USA*
[2] *Institute for Systems Research, University of Maryland, College Park, MD, USA*

Edited by:
Per Jesper Sjöström, University College London, UK

Reviewed by:
Marla B. Feller, University of California, USA
Carlos D. Aizenman, Brown University, USA
David Stellwagen, McGill University, Canada

****Correspondence:***
Daniel A. Butts and Patrick O. Kanold, Department of Biology, University of Maryland, 1118 Biosciences Research Building, College Park, MD 20742, USA. e-mail: dab@umd.edu and pkanold@umd.edu

Spike time dependent plasticity (STDP) has been observed in both developing and adult animals. Theoretical studies suggest that it implicitly leads to both competition and homeostasis in addition to correlation-based plasticity, making it a good candidate to explain developmental refinement and plasticity in a number of systems. However, it has only been observed to play a clear role in development in a small number of cases. Because the fast time scales necessary to elicit STDP, it would likely be inefficient in governing synaptic modifications in the absence of fast correlations in neural activity. In contrast, later stages of development often depend on sensory inputs that can drive activity on much faster time scales, suggesting a role in STDP in many sensory systems after opening of the eyes and ear canals. Correlations on fast time scales can be also be present earlier in developing microcircuits, such as those produced by specific transient "teacher" circuits in the cerebral cortex. By reviewing examples of each case, we suggest that STDP is not a universal rule, but rather might be masked or phased in, depending on the information available to instruct refinement in different developing circuits. Thus, this review describes selected cases where STDP has been studied in developmental contexts, and uses these examples to suggest a more general framework for understanding where it could be playing a role in development.

Keywords: cortex, thalamus, timescale, burst, subplate, teacher, microcircuit

INTRODUCTION

Spike time dependent plasticity (STDP) was initially reported in both developing and adult animals (Bell et al., 1997; Magee and Johnston, 1997; Markram et al., 1997; Zhang et al., 1998; Feldman, 2000). As a result, STDP has always been thought to have a role in development: reflecting a more general conception that rules of synaptic plasticity, or "learning rules", may be conserved across developing and adult brains, as well as across different brain areas.

The prospect of STDP functioning during development is captivating for experimentalists and theorists alike, because it offers opportunities to connect *in vivo* neural activity to observable system-level organization of neural connections. Making this connection in a developing system is facilitated by the presence of observable organizing principles in these systems that describe the establishment of connections, such as the refinement of retinal ganglion cells (RGC) axons into eye specific layers/regions in the lateral geniculate nucleus (LGN) and superior colliculus (SC) as well as formation and plasticity of ocular dominance columns in the visual cortex (Katz and Shatz, 1996; Crair, 1999; Sur and Rubenstein, 2005). In contrast, the patterns of connectivity established during adult functions such as learning and memory do not have easily observable system-level organizational patterns associated with them, and as a result, in these contexts it is much more difficult to gauge the effects of STDP (or other learning rules).

A second reason the prospect of STDP acting during development is so compelling is the nature of STDP itself, compared with other types of synaptic plasticity. Realistic spike trains are generally composed of complex temporal patterns, and these "natural" patterns of activity do not fit into the categories of tetanic stimulation, theta burst, pairing, and other simplified experimental contexts that synaptic learning rules are usually studied with. The basis of STDP on the timing of single spikes potentially provides a formula for taking an arbitrary set of pre- and postsynaptic activity and predicting what the effect of such activity patterns on the synaptic efficacy will be. Furthermore, because of its close apposition of windows for potentiation and depression, as described below, several theoretical studies have shown that STDP implicitly introduces both competition and homeostatic regulation between the inputs to a given neuron (Song et al., 2000; Tegner and Kepecs, 2002; Izhikevich and Desai, 2003; Watt and Desai, 2010), potentially explaining what have been traditionally thought of as separate aspects of developmental plasticity.

Thus, STDP studies during development present the possibility of understanding the role of synaptic plasticity *in vivo*, whereby known activity patterns might be combined with known changes in connectivity and arrive at a known outcome. However, though appealing, STDP may be only one form of synaptic plasticity that governs development. As we describe in this review, STDP fits more broadly into the category of Hebbian plasticity (Caporale and Dan, 2008), but with the additional requirement for relationships of neural activity between presynaptic afferents and postsynaptic targets on the order of 10 ms. As a result, for STDP to yield consistent results at a given synapse, neuronal activity must contain information at these "fast" time scales. Likewise, the tight temporal correlation requirement limits the applicability of STDP in cases where there is no such tight pairing between pre- and postsynaptic activity. As a result, below, we describe

where STDP likely does not work (the developing retinogeniculate synapse), where it likely does (the developing somatosensory cortical microcircuit), and where it could (early visual cortical development). By bringing together these disparate studies, both experimental and theoretical, in multiple brain areas, we hope to focus investigations from a simple study of mechanisms independent of what might be accessed in an animals' development, to mechanisms that are likely to play a role in particular developmental contexts.

"HEBBIAN" DEVELOPMENT AND STDP

Based on developmental studies in which either sensory experience or neuronal activity was modulated, activity-dependent development is generally thought to be governed by Hebbian plasticity: "cells that fire together wire together" (Katz and Shatz, 1996). This principle was originally postulated to explain learning in the guise of classical conditioning (Hebb, 1949), and reflects the idea that the brain is attempting to internalize the causal nature of the world in connections between individual neurons. Such a principle also offers a compelling explanation for many aspects of observed development. In particular, during stages of development thought to be driven by activity, many axonal arbors – in particular those that project from one brain area or cortical layer to another (and thus are observably distinct) – become refined from initially more diffuse projections (**Figure 1A**). Given that these diffuse projections are coarsely organized (most likely by molecular cues; Sur and Rubenstein, 2005), any local presynaptic activity patterns will lead to the largest correlations in activity between a given presynaptic neuron and postsynaptic neurons at the center of its axonal arbor. As a result, Hebbian principles predict the strengthening of the appropriate connections in such contexts, and thus have been postulated to govern developmental refinement throughout.

Because of its requirement for correlation between pre- and postsynaptic neurons, STDP is considered a "Hebbian" learning rule as well (Caporale and Dan, 2008). However, its sensitivity to fast time scales and strict temporal order between inputs and targets also seems to be at odds with looser causality described above. Namely, if presynaptic afferents onto the postsynaptic neuron are weak and diffuse – as is often the case earlier in development – there will only be very subtle correlations over the short time scales required for STDP-based potentiation. Even in the case where pre- and postsynaptic firing rates are correlated, there will still be many spike pairs falling into the window for depression (**Figure 1B**). As a result, depending on the relative strength of induced potentiation versus depression, this could be very inefficient at strengthening the correct synapses, or even counterproductive (Lu et al., 2006).

However, while STDP is clearly inefficient in this context, its sensitivity to strict temporal order leads to effects that are consistent with other aspects of developmental refinement. In particular, simple Hebbian learning rules are not sufficient to explain developmental refinement alone, without further rules governing synaptic strength. For example, the overall amount of synaptic input to a given neuron is thought to be regulated, such that a given neuron maintains a relatively constant amount of activity over time. *Homeostatic regulation* is presumably present at all times but is likely to be particularly important during development, when synaptic remodeling typically does not preserve the total number of inputs (Chen and Regehr, 2000; Turrigiano and Nelson, 2000, 2004; Chandrasekaran et al., 2007; Goel and Lee, 2007). *Synaptic competition*, whereby the strengthening of one input is balanced by the weakening of other inputs is also postulated to be important for refinement and plasticity during development. For example, closure of one eye during the critical period of visual development will often increase the number of inputs into the cortex representing the open eye, at the expense of the inputs representing the closed eye (Wiesel and Hubel, 1963).

In a series of theoretical studies, STDP has been shown to implicitly result in synaptic competition and homeostatic regulation of postsynaptic firing (Song et al., 2000), and thus could explicitly

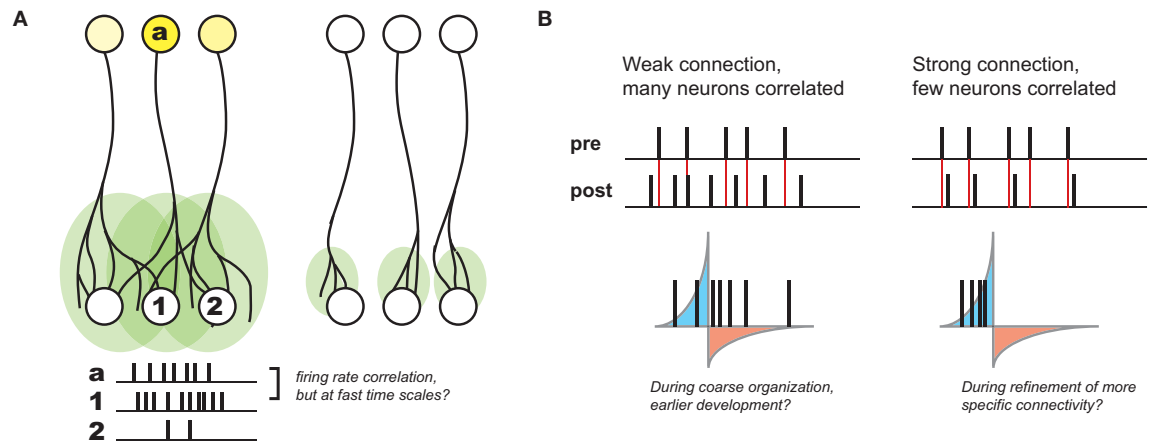

FIGURE 1 | Development of coarse patterning of CNS connections. **(A)** Projections between different brain regions often are initially larger and diffuse (*left*), but refine over time in an activity dependent manner (*right*). Because of initial organization of this map, local activity patterns generally drive the highest postsynaptic firing in the center of a given afferent (a) projection (compare activity of neuron #1 with #2). As a result, Hebbian principles generally can explain this refinement. **(B)**. However, without a strong connection between pre- and postsynaptic neurons, STDP might be quite inefficient at supporting such Hebbian development, such as earlier in development when connections are weak and diffuse (*left*). When connections become stronger, the relationship between pre- and postsynaptic activity might develop much more precise correlations, when presynaptic spikes have a larger role in driving postsynaptic activity (*right*).

explain synaptic refinement in a handful of developmental contexts (Song and Abbott, 2001). These elements arise because the balance of potentiation and depression is skewed in favor of depression for uncorrelated inputs. What this means is that as one input gets stronger, it will have an increased probability of driving a postsynaptic spike. Because these postsynaptic spikes follow the presynaptic spike that preceded it – as well as those correlated with this input – it will further strengthen these correlated inputs. At the same time, inputs that are uncorrelated will on average be depressed, and thus potentiation of correlated inputs implicitly occurs at the expense of uncorrelated inputs: resulting in competition. Furthermore, this competition for the timing of the postsynaptic spike will also result in a form of homeostatic regulation of postsynaptic activity. For example, if the amount of input activity to a postsynaptic neuron increases, there will initially be more postsynaptic spikes, leading to more weakening overall given the overall predominance of depression over potentiation postulated above. This implicitly acts to down-regulate the total amount of input into the neuron. Likewise, when there are fewer postsynaptic spikes, there will be less depression overall, making it easier for a given input to become potentiated through weaker correlations with postsynaptic activity. This implicit homeostasis of STDP is likely only one aspect of overall homeostatic regulation of neurons, as discussed in more detail in an accompanying review in this issue (Watt and Desai, 2010).

Thus, from a theoretical perspective, STDP is an excellent candidate to explain many elements of synaptic plasticity during development. Yet, at the same time, in many developmental systems, STDP is not appropriately tuned to the time scales of their observed neural activity, and thus would be inefficient in many contexts, if not completely ineffective. With this background, we will thus discuss several examples of observed developmental plasticity, and its relationship to STDP.

A LIMITED ROLE FOR STDP AT THE DEVELOPING RETINOGENICULATE SYNAPSE

The developing retinogeniculate system provides an example where the neural activity itself is not structured to take advantage of the temporal sensitivity of STDP, and thus serves as a counter-example to the universal applicability of STDP. Before eye opening, spontaneous correlated activity sweeps across the developing retina, called "retinal waves" (Meister et al., 1991; Feller et al., 1996). Such retinal wave activity has been implicated in coarse system-level organizational refinement in the visual pathway, including eye-segregation and retinotopic refinement in the LGN (Katz and Shatz, 1996; Penn et al., 1998; Grubb et al., 2003; Pfeiffenberger et al., 2006), SC (Simon et al., 1992; Shah and Crair, 2008), and retinotopic refinement in the visual cortex (Cang et al., 2005).

Changes in efficacy of retinogeniculate synapses can be induced by tetanic stimulation (Mooney et al., 1993; Ziburkus et al., 2009), showing that this synapse can be plastic, albeit in the context of an unphysiological stimulation paradigm (**Figure 2A**, *top*). However, these studies did not make clear how plasticity would evince in the context of the well-studied activity patterns present in the RG system during this period, and it was tempting to imagine that development at the retinogeniculate synapse might also be governed by STDP, as has been observed at the corresponding retinotectal synapse of *Xenopus* (Zhang et al., 1998). However, it was unclear if such a learning rule could take advantage of the activity present in the retina at this time: retinal waves themselves consist of RGC bursts over a second or more, travel over small domains of the retina over the course of several seconds (Feller et al., 1997), and result in bursts in the LGN that also can last for a second or more (Mooney et al., 1996). Because of the slow speed of wave propagation, the information content of this activity has very little information available at fast (<20 ms) time scales, with the bulk present at time scales of 500 ms or more (Butts and Rokhsar, 2001). Thus, both the activity and coarse refinement thought to be driven by this activity reflect the situation described in **Figure 1**, where STDP based on millisecond time scales would be very inefficient at driving developmental refinement.

As a result, synaptic plasticity was measured using physiological 1-s bursts of with different latencies (**Figure 2B**), revealing a broad temporal window for potentiation surrounded by weak depression windows (**Figure 2C**). This defines burst-time dependent plasticity (BTDP; Butts et al., 2007a), in which the amount of synaptic plasticity depends on the latency differences between pre- and postsynaptic bursts. Subsequently, BTDP has also been observed in the developing SC (Shah and Crair, 2008). The induction protocol of BTDP offered the ability to test for an underlying spike-based learning rule using activity patterns like those seen *in vivo*. A collection of spike-time latencies could be measured for each pair of pre- and postsynaptic bursts, and correlating the observed plasticity induced by the burst pairing with the histogram of spike latencies led to two main conclusions about a spike-based learning rule. First, as predicted above, the observed amounts of potentiation can only be explained if the depressive window of STDP is neglected. Second, the burst-rule, with a time scale of 1 s, can actually be predicted by a spike-coincidence rule on time scales ~50 ms (**Figure 2D**), provided there is no sensitivity to temporal order.

It is important to note that while such results might seem to suggest that STDP does not explain the observed plasticity at the retinogeniculate synapse, they are in fact consistent with the detailed "interaction rules" for STDP discovered using more complicated spike trains in other preparations (Sjostrom et al., 2001; Froemke et al., 2006). In cases where multiple spike pairs are involved, the resulting plasticity is consistent with ignoring the spike pairs that predict depression, in favor of those predicting potentiation. In the context of more complex spike trains, this implies that the strict order of spike pairs might be less important, and that STDP could resemble a more conventional Hebbian rule.

In this way, one might imagine that differences in neural activity driving different developmental programs might select for different types of Hebbian plasticity. Though it is not known whether STDP functions at the LGN synapse in isolated-spike contexts, the existence of spike-interaction rules that make the synaptic plasticity more appropriate for the longer time scales of spike trains with multiple spikes raises the possibility that STDP might be part of a broader continuum of Hebbian plasticity that acts during development, and its function either actively adjusts through, for example, neuromodulation (Seol et al., 2007), or passively adjusts through explicit interaction rules (Sjostrom et al., 2001; Froemke et al., 2006) to efficiently drive developmental plasticity in each context.

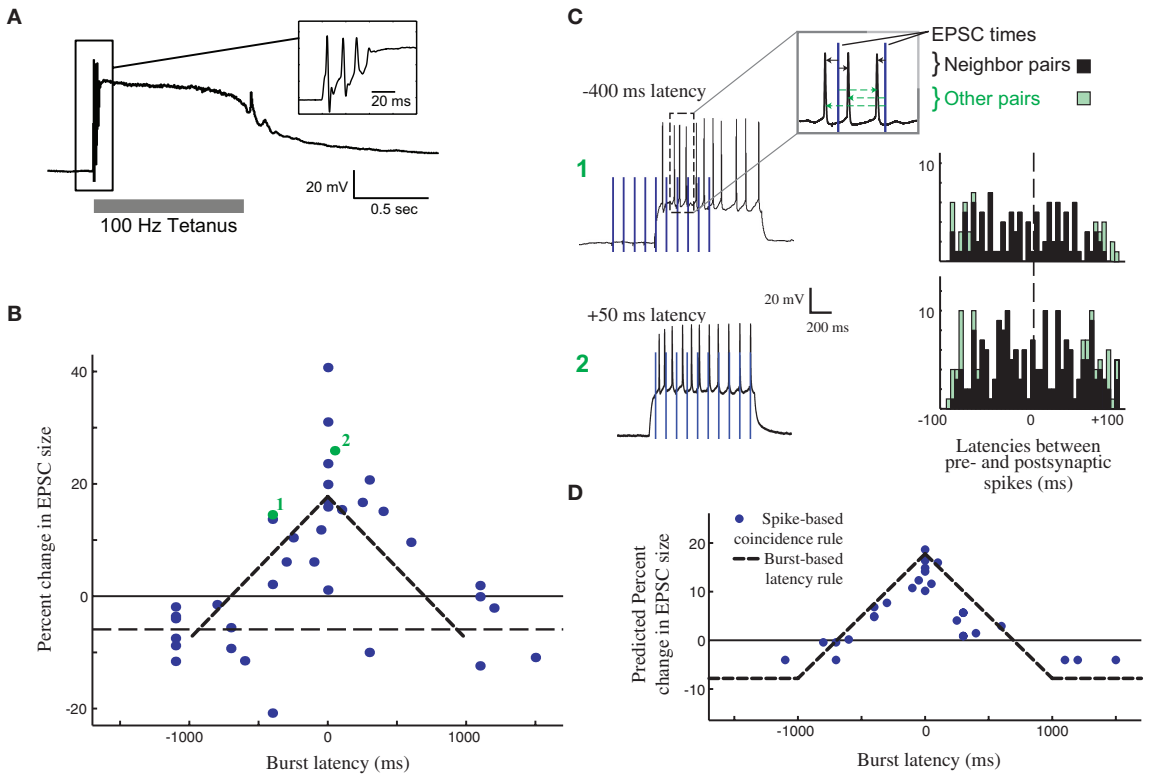

FIGURE 2 | Burst time dependent – but not spike time dependent – learning rule at the developing retinogeniculate synapse. (A) The effect of tetanic stimulation on the voltage of postsynaptic LGN neuron, resulting in an unphysiological state, especially in comparison to experiments that approximate in activity *in vivo* **(C)**. **(B)** The burst time dependent learning rule, demonstrating a tent-shape peaked at 0 latency, and decreasing to slight depression after 1 s on either side. Each *dot* shows an individual measurement in the percent change in peak postsynaptic current before and after burst stimulation. **(C)** The timing of all pairs of pre- and postsynaptic spikes during the burst-based protocol can be tabulated (*right*) in order to test whether the observed effects can be attributed to some form of STDP. Two example bursts with two different latencies are shown (*left*), leading to the observed plasticity reported in (**B**, #1, and #2). **(D)** The predicted learning rule using a single-spike based coincidence detector, which explains the burst-based rule much better than STDP. All panels are reproduced from Butts et al. (2007a).

A ROLE FOR STDP IN CORTICAL MICROCIRCUIT PLASTICITY

The inefficiency of "isolated-spike" STDP in the canonical example of development depicted in **Figure 1** does not necessarily apply to other aspects of activity dependent development. In other contexts, correlations between neural activity between afferents and postsynaptic targets can be quite tight – especially when the activity is driven by sensory stimulation, or more generally in the case of microcircuits driven by common input. In these situations, the Hebbian principles thought to govern coarse development at coarse time scales might likewise be applied at finer scales through STDP, and a more conventional Hebbian learning rule such as BTDP described would not be able to take advantage of information at finer time scales that distinguishes one input from another.

One of the most established examples of STDP playing a clear role in development is sensory driven map plasticity at excitatory layer 4 (L4) to layer 2/3 (L2/3) synapses in the barrel cortex during the critical period (Foeller and Feldman, 2004). Over this period of development, deprivation of sensory stimulation to a set of whiskers induces rapid map plasticity such that L2/3 neurons in the corresponding barrels begin responding to adjacent non-deprived barrels, resulting from weakening of the deprived barrel inputs and strengthening of non-deprived barrel inputs (Foeller and Feldman, 2004).

A model for how STDP leads to barrel map plasticity in L2/3 relies on the relative latencies between direct feed-forward input from L4 and horizontal connections between L2/3 neurons in different barrels (**Figure 3**). Initially, L2/3 neurons are driven by L4 neurons of the same barrel (*left*), but after deprivation, the L2/3 neurons in the deprived barrel can still be driven through horizontal connections from other barrels, coordinated by sensory activity that can correlate inputs of multiple barrels. The ability of horizontal connections to drive L2/3 activity directly will lead to short latencies between these horizontal connections consistent with STDP-mediated strengthening. In the meantime, the direct input from L4 is only spontaneously active, which cannot reliably drive postsynaptic responses. Because synaptic input that is uncorrelated with postsynaptic firing leads to net depression (Feldman, 2000) – presumably because of a larger window for depression than strengthening – the direct L4 to L2/3 connection in the deprived barrel will weaken.

This model of STDP-mediated plasticity is validated by two further observations. First, *in vivo* studies demonstrate that neural activity in the barrels is largely composed of few spikes (Higley and Contreras, 2006; Vijayan et al., 2010), and the relative latencies between the involved neurons in behaviorally relevant conditions

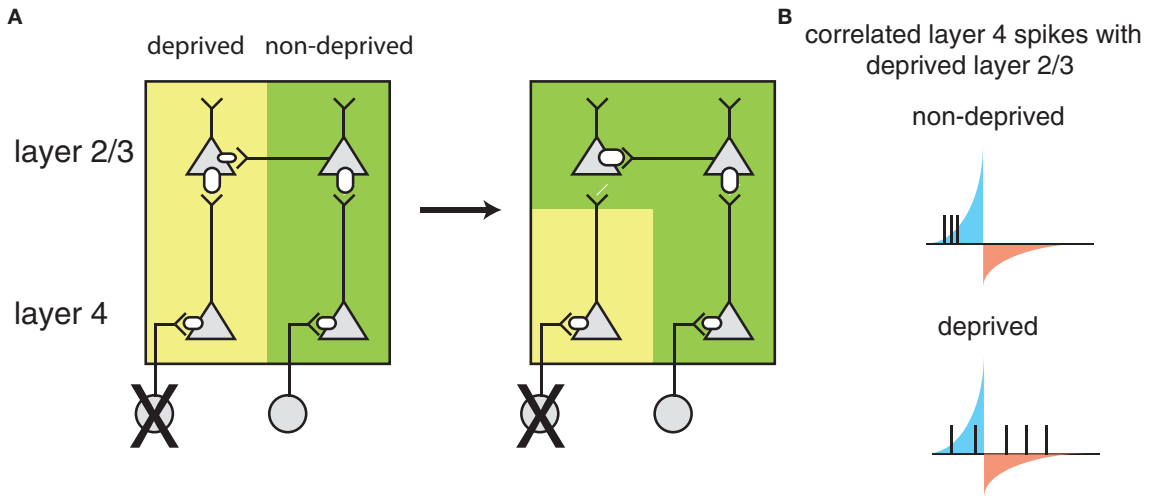

FIGURE 3 | Barrel cortex plasticity. (A) Local circuit changes in barrel cortex following whisker deprivation. Shown are layer 4 (L4) and layer 2/3 (L2/3) cells and their excitatory synaptic connections. The size of the receptors indicates the strength of the synapse. *Yellow shading* indicates cells driven by the deprived barrel and *green shading* indicates cells driven by the non-deprived barrel. Reducing sensory input to one barrel by whisker deprivation (deprived) (*left*) results in weakening of L4 to L2/3 synapses and strengthening of horizontal connections in L2/3 originating from a non-deprived barrel (*right*) such that L2/3 in the deprived region of barrel cortex will respond strongly to the stimulation of a non-deprived whisker. **(B)** L2/3 neurons in deprived barrel cortex show correlated activity with L4 neurons in the non-deprived region of barrel cortex leading to strengthening of horizontal connections. Correlations with the deprived L4 are weak as the deprived whisker provides little sensory input. The potentiating and weakening windows of STDP rule are indicated in blue and red shading.

is on the fast time scales of STDP (Armstrong-James et al., 1992; Allen et al., 2003). Second, a causal relationship between deprivation *in vivo* and effects on observed STDP in the relevant barrel *in vitro* has been observed (Feldman, 2000; Allen et al., 2003; Foeller and Feldman, 2004; Jacob et al., 2007), suggesting a direct role of STDP in barrel map plasticity.

STDP AND THE FRAMEWORK OF "TEACHER CIRCUITS"

The circuits involved in barrel cortex plasticity described above fit into a general framework called a *teacher circuit* (Song and Abbott, 2001; Friedel and van Hemmen, 2008), where a weak "nascent" input that it is not able to drive the postsynaptic "student" neuron alone, is paired with a stronger "teacher" input or inputs (**Figure 4**, *left*). Analogous to the classical conditioning paradigm of Hebbian plasticity, if the teacher input is paired within a certain time window with the nascent input and can drive precisely timed postsynaptic spikes, the spikes will fall into the potentiating window of STDP and the nascent inputs become strengthened, i.e., the student learns the input. Once the nascent input is able to drive postsynaptic spikes on its own, it will induce further self-potentiation. Additionally, if it more efficiently drives postsynaptic activity, it will occur ahead of the teacher input, placing teacher spikes in the depression window of STDP and result in weakening of the teacher input. As a result, the teacher will withdraw as the student learns other inputs, with the more efficient connections taking over.

The process is reversed in the context of deprivation, such as whisker removal (described above). Under deprivation conditions – because the learned input no longer drives postsynaptic spikes – the teacher again begins to dominate the firing of the student and re-potentiate. As a result, spontaneous firing from the learned inputs will now more often fall into larger depression windows and weaken (**Figure 4B**).

A key requirement for this teacher circuit to work is that the timing of teacher-evoked postsynaptic spikes must be closely correlated with the inputs to be learned, such that their spikes fall within the potentiating window of the STDP rule. In the scenario of the barrel cortex described above, the timing relationships are due to coactivation of neighboring barrels while whisking. Because the teacher pathway involves an additional synapse that sensory input must traverse, teacher-evoked spikes in the student neurons will always occur after direct L4 inputs. Such a scenario might also be present in the case of monocular deprivation (MD) in the visual cortex (Song and Abbott, 2001), and may underlie observation of initial remapping in L2/3 followed by L4 in visual deprivation experiments at later ages (Trachtenberg et al., 2000).

Thus, in this microcircuit, precisely timed sensory-evoked activity can travel through two different pathways, and STDP serves to establish connectivity that most efficiently represents the causation. In this instance, horizontal connections are able to take over in the case of deprivation, and allow the cortex to process sensory stimuli even without direct input. As described below, when deprivation ends, the same STDP rules will reestablish the previous connectivity, flexibly supporting cortical processing of sensory stimuli.

HYPOTHESIZED ROLE OF STDP IN VISUAL CORTICAL DEVELOPMENT

For reasons explored above, STDP has not been observed or probed in most developmental systems. However, the framework above sets a foundation for understanding more generally where STDP might play a part in guiding development. For example, similar circuit topologies are also present in early development. The formation of feed-forward connections between the thalamus and the cortex is thought to be mediated by a distinct class of cells: subplate neurons, which form one of the first functional cortical circuits (Kanold,

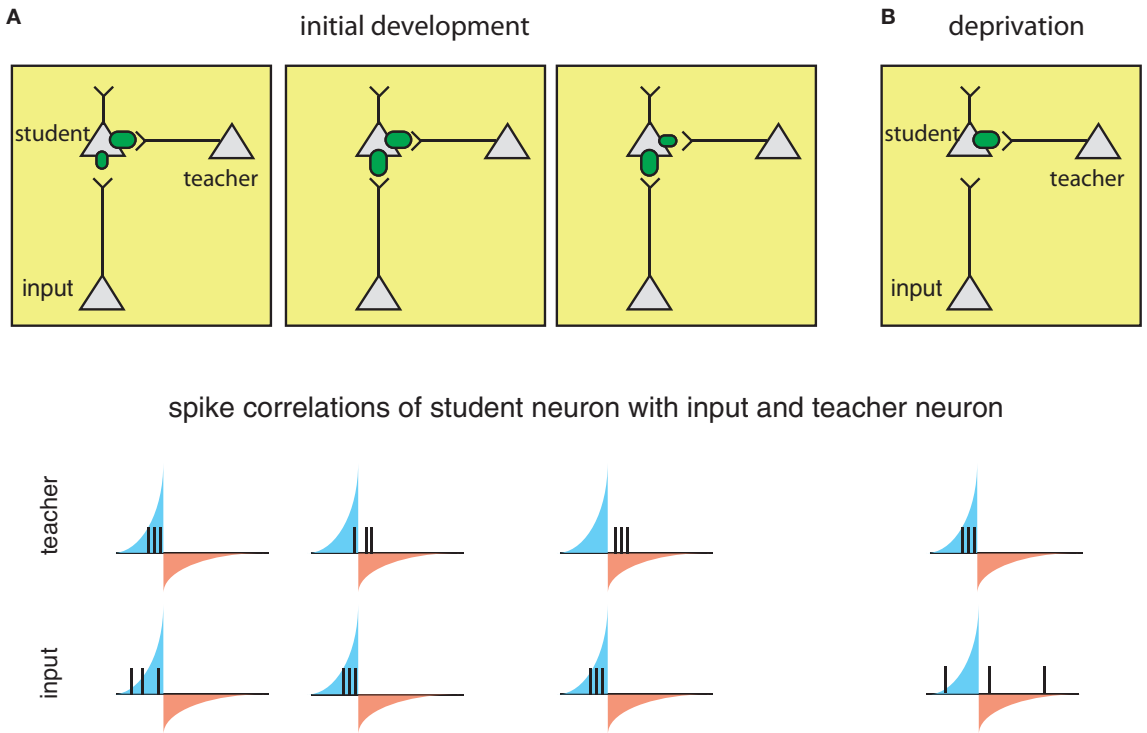

FIGURE 4 | The framework of the "teacher circuit." (A) The teacher circuit consists of a student neuron with two inputs: the teacher (*inside box*) and nascent inputs to be learned (*inside box*). *Left*: Initially, the teacher has a strong connection (*top*), and its activity is paired with a weaker input, leading to spikes from both inputs falling in the potentiation window of STDP (*bottom*). The potentiating and weakening windows of STDP rule are indicated in blue and red shading. *Middle*: The pairing of the teacher and nascent input strengthens the nascent input (*top*), but also results in some teacher spikes in the LTD window (*bottom*), resulting in eventual weakening of the teacher. *Right*: With the nascent input "learned", teacher spikes fall completely in the weakening window (*bottom*), reinforcing a weak teacher input and strong learned input. **(B)** During deprivation, the learned input can no longer drive postsynaptic firing, and learned input becomes uncorrelated with postsynaptic spikes (*bottom*), and the teacher begins to drive student firing again and strengthens.

2009; Zhao et al., 2009). Subplate neurons excite L4 neurons and themselves receive inputs from thalamic axons before these axons reach L4 (Shatz and Luskin, 1986; Kanold, 2009; Zhao et al., 2009) (**Figure 5A**). Thus subplate neurons provide a strong feed-forward projection of thalamic inputs to L4 before thalamic inputs to L4 strengthen. Furthermore, removal of subplate neurons prevents the maturation of connections between the LGN and visual cortex, and the emergence of ocular dominance columns in visual cortex (Ghosh and Shatz, 1992; Kanold et al., 2003; Kanold and Shatz, 2006). However, why the cortex would need a transiently expressed circuit to guide thalamocortical connectivity, and how the specific connectivity and activity of subplate neurons plays a role in this development, is currently not well understood (Kanold and Luhmann, 2010).

The structure of the circuit formed by the subplate and thalamocortical afferents, and L4 neurons is not unlike the teacher circuit described above. Subplate neurons at early ages have a high input resistance, allowing them to spike with minimal latency (Zhao et al., 2009). In addition to the rapid firing onset, subplate neurons at young ages fire only few spikes to sustained inputs, thus marking the onset of a stimulus. Thus, subplate neurons potentially can convert neuronal bursts that are prevalent in the early stages of the visual pathway due to retinal waves (Meister et al., 1991; Feller et al., 1996) into sparse spike trains allowing the analysis with STDP. Furthermore, subplate activity is likely able to drive spiking activity in L4, because L4 neurons at relevant ages also have high input resistances (Zhao et al., 2009).

As a result, it has been suggested that STDP might govern circuit maturation in an analogous way to the teacher circuit described above (Kanold and Shatz, 2006). In this case subplate neurons play the role of the teacher, with a strong input onto L4 neurons (the students), and the nascent inputs are the thalamocortical afferents (**Figure 5A**). Because subplate neurons are driven by thalamic activity, subplate mediated depolarization of L4 cells occurs after direct thalamocortical input to L4, meaning that presynaptic thalamic input will fall into the potentiation window of STDP (**Figure 5A**). In the meantime, the strong subplate input is slightly delayed due to the disynaptic pathway from the thalamus. Thus, the initially strong subplate inputs will lead to the strengthening of thalamic inputs, which would replace the subplate as the main driving input to the cortex through the framework discussed above.

This framework can also explain the effects of the subplate ablation (Ghosh and Shatz, 1992; Kanold et al., 2003; Kanold and Shatz, 2006) (**Figure 5B**). Without the subplate present, thalamic activity would no longer drive L4 neurons with the appropriate time scales to fall into the potentiation window of STDP, analogously to the deprived barrel inputs described above. If activity levels in both eyes are equal, inputs representing both eyes are weakened equally over

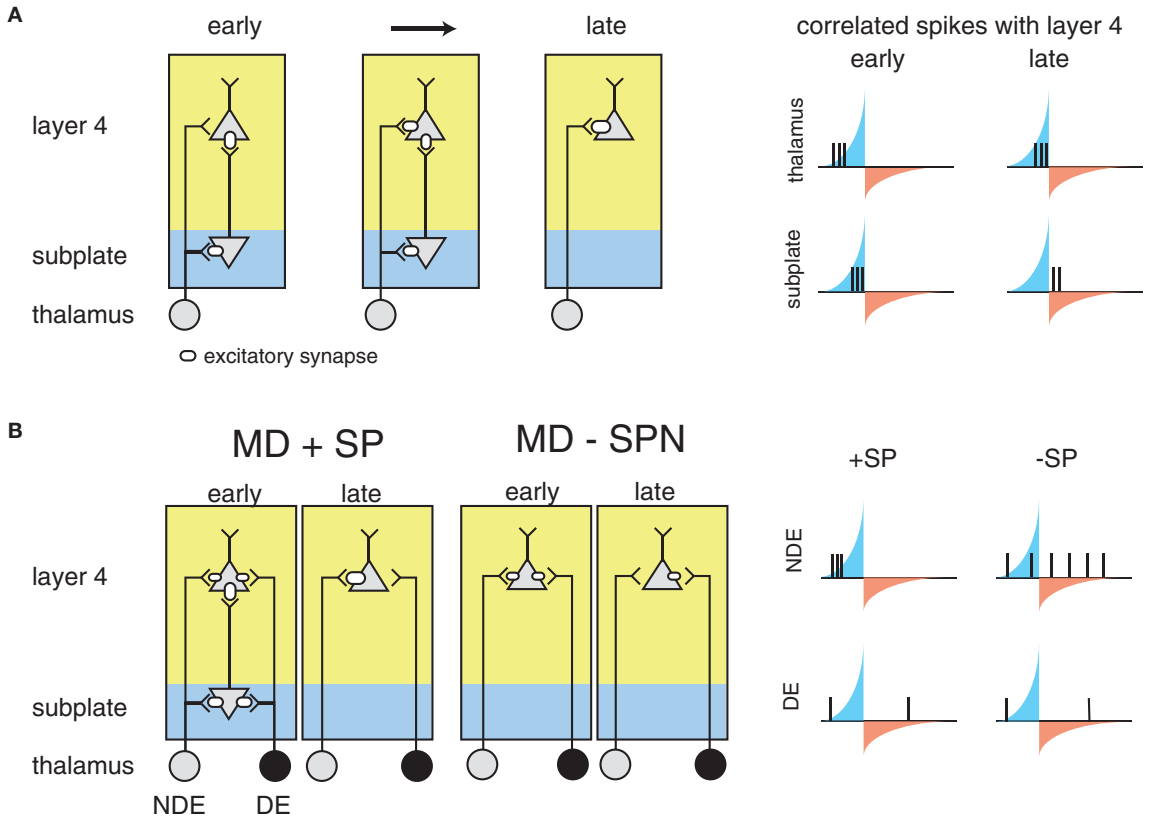

FIGURE 5 | The influence of subplate on thalamocortical microcircuit development and plasticity. Diagramed are subplate neurons and the connections of thalamic neurons with subplate neurons and layer 4 neurons. The strength of the excitatory synaptic connections is indicated by the size of the receptor. **(A)** Changing subplate circuits (*left*) from early to late in development when subplate neurons die. Blue shading indicates the subplate while yellow indicates the cortical plate. Spike correlations between layer 4 and its inputs from subplate and thalamus at these developmental stages are plotted at *right*. The STDP rule is superimposed illustrating the changing correlations over development. The potentiating and weakening windows of STDP rule are indicated in *blue* and *red shading*. **(B)** Effects of subplate neurons on the outcome of monocular deprivation (MD) on ocular dominance. *Left panels* show strengthening of the non-deprived eye (NDE) inputs and weakening of deprived eye (DE) inputs when subplate is present. *Right panels* show weakening of the NDE inputs and retention of DE inputs when subplate is absent, leading to paradoxical ocular dominance plasticity. Spike correlation at *right* show that layer 4 activity is uncorrelated with thalamic activity when subplate is removed, leading to selective weakening of NDE.

time and no refinement of ocular dominance would be observed (Kanold and Shatz, 2006) matching observations from physiological experiments (Kanold et al., 2003). In contrast, if activity levels in both eyes are unequal, for example during MD thalamic axons representing the open eye would have a larger amount of uncorrelated activity with L4 neurons than axons representing the closed eye (Kanold and Shatz, 2006) (**Figure 5B**). Thus, over time the projections representing the open eye would disappear while projections representing the closed eye would be retained, paralleling experimental observations (Kanold and Shatz, 2006).

One key property of the subplate circuit discussed above is its transient existence, which is consistent with it no longer being useful once the students have "learned" the correct thalamocortical inputs. One other transient aspect of the developing cortical circuit is the existence of depolarizing GABAergic circuits (Ben-Ari, 2002). Such circuits may also act as "teachers" during early development, and – just as the subplate disappearance removes feed-forward excitatory drive – the switch of GABA signaling from depolarizing to hyperpolarizing might occur after the relevant developmental phase.

In conclusion, STDP provides an elegant explanation of multiple aspects of the development of the cortical microcircuit, driven by a combination of spontaneous and sensory-evoked activity though the stages of cortical development. Because of the feed-forward nature of the involved microcircuit, relevant information about the desired presynaptic targets are contained in the fast time scales of STDP, and the difference between potentiation and depression is determined by the difference between monosynaptic versus disynaptic connections. In such a situation, it is clear how STDP could play a direct role in development.

RELEVANCE OF STDP IN DIFFERENT STAGES OF DEVELOPMENT

The primary difference between retinal-wave-driven development of the retinogeniculate system and microcircuit development in the cortex is the time scale of the information contained in activity in these different systems. Information that can instruct the coarse system-level organization of retinogeniculate development is contained in the seconds-long time scales of retinal wave propa-

gation (Butts and Rokhsar, 2001). In contrast, the development of cortical microcircuitry may predominantly rely on differences in timing between latencies of monosynaptic versus disynaptic connections. Though arising through different mechanisms, such fast time scales are also typical of visually driven activity of thalamocortical afferents, due to the precise response properties of LGN neurons during natural visual stimulation (Butts et al., 2007b).

As a result, STDP may also be relevant when activity in the visual system is visually evoked, rather than spontaneously generated. In fact, one of the first places that STDP was observed was the developing retinotectal system of *Xenopus* (Zhang et al., 1998), which is visually responsive throughout development. As reviewed in a companion article (Richards et al., 2010), such a rule can be exploited to train retinotectal cells to become motion selective using visual input (Engert et al., 2002), drive receptive field refinement through pair of visual activity and stimulation (Vislay-Meltzer et al., 2006), or alter the temporal responses of tectal cells by recruiting recurrent circuits (Pratt et al., 2008). Similar studies have demonstrated STDP-like effects in later stages of development and adult. For example, temporally pairing related auditory or visual stimuli with each other over fast time scales can elicit in changes in the stimulus tuning of cortical neurons, and these changes depended on temporal order and follow the general temporal STDP shape (Yao and Dan, 2001; Dahmen et al., 2008). Further evidence for STDP in driving synaptic remodeling in adult comes from studies of shifts in receptive fields following retinal lesions (Young et al., 2007). In these cases the activity present in the system contains information at fast time scales, and the observed shifts are consistent with the strict temporal ordering of the STDP rule.

Thus, over the course of development, the formation of the functional circuitry involves formation, refinement, and plasticity of connections on vastly different spatial scales, from the development of topographic projections between areas (e.g., between retina and LGN) to development of specific microcircuits between nearby neurons, for example in the cerebral cortex. The development of connections on different spatial scales occurs at different times and involves different activity patterns. While spontaneous activity patterns drive early coarse refinement, sensory-evoked activity drives later fine scale development.

Given that STDP extracts information at fast time scales, the canonical form of STDP, with close apposition of windows for potentiation and depression, might operate at stages in development that are dominated by sensory inputs after opening of the eyes and ear canals. At earlier stages of development when activity is still spontaneously generated, development that relies on STDP (such as cortical microcircuit development) might use teacher circuits such as those formed by subplate neurons, which can transform long lasting spontaneous waves in precisely timed spike signals. Or, as suggested above in the case of the retinogeniculate system, the same underlying mechanisms that result in STDP might be active in a different form, more appropriate for the time scales relevant for instructing development.

CONCLUSION

Spike time dependent plasticity likely supports the development and plasticity of several neuronal circuits, explaining a variety of elements that must be present for refinement of neuronal connectivity. For a full understanding of circuit plasticity one needs to take into account both the synaptic learning rule, the activity patters present, and the timescales of their information content. As a result, STDP is likely to play a role in the development of circuits where information is present at fast timescales (<20 ms) or where specific teacher circuits aid the development of fast temporal correlation, as is done by the feed-forward connections formed by subplate neurons. However, STDP is unlikely to play a role in development in systems where high spike rates are present or where information is only present at longer time scales, such as the developing retinogeniculate system.

ACKNOWLEDGMENT

Patrick O. Kanold is supported by NIH R01DC009607.

REFERENCES

Allen, C. B., Celikel, T., and Feldman, D. E. (2003). Long-term depression induced by sensory deprivation during cortical map plasticity in vivo. *Nat. Neurosci.* 6, 291–299.

Armstrong-James, M., Fox, K., and Das-Gupta, A. (1992). Flow of excitation within rat barrel cortex on striking a single vibrissa. *J. Neurophysiol.* 68, 1345–1358.

Bell, C. C., Han, V. Z., Sugawara, Y., and Grant, K. (1997). Synaptic plasticity in a cerebellum-like structure depends on temporal order. *Nature* 387, 278–281.

Ben-Ari, Y. (2002). Excitatory actions of gaba during development: the nature of the nurture. *Nat. Rev. Neurosci.* 3, 728–739.

Butts, D. A., Kanold, P. O., and Shatz, C. J. (2007a). A burst-based "Hebbian" learning rule at retinogeniculate synapses links retinal waves to activity-dependent refinement. *PLoS Biol.* 5, e61. doi:10.1371/journal.pbio.0050061.

Butts, D. A., Weng, C., Jin, J., Yeh, C. I., Lesica, N. A., Alonso, J. M., and Stanley, G. B. (2007b). Temporal precision in the neural code and the timescales of natural vision. *Nature* 449, 92–95.

Butts, D. A., and Rokhsar, D. S. (2001). The information content of spontaneous retinal waves. *J. Neurosci.* 21, 961–973.

Cang, J., Renteria, R. C., Kaneko, M., Liu, X., Copenhagen, D. R., and Stryker, M. P. (2005). Development of precise maps in visual cortex requires patterned spontaneous activity in the retina. *Neuron* 48, 797–809.

Caporale, N., and Dan, Y. (2008). Spike timing-dependent plasticity: a Hebbian learning rule. *Annu. Rev. Neurosci.* 31, 25–46.

Chandrasekaran, A. R., Shah, R. D., and Crair, M. C. (2007). Developmental homeostasis of mouse retinocollicular synapses. *J. Neurosci.* 27, 1746–1755.

Chen, C., and Regehr, W. G. (2000). Developmental remodeling of the retinogeniculate synapse. *Neuron* 28, 955–966.

Crair, M. C. (1999). Neuronal activity during development: permissive or instructive? *Curr. Opin. Neurobiol.* 9, 88–93.

Dahmen, J. C., Hartley, D. E., and King, A. J. (2008). Stimulus-timing-dependent plasticity of cortical frequency representation. *J. Neurosci.* 28, 13629–13639.

Engert, F., Tao, H. W., Zhang, L. I., and Poo, M. M. (2002). Moving visual stimuli rapidly induce direction sensitivity of developing tectal neurons. *Nature* 419, 470–475.

Feldman, D. E. (2000). Timing-based LTP and LTD at vertical inputs to layer II/III pyramidal cells in rat barrel cortex. *Neuron* 27, 45–56.

Feller, M. B., Butts, D. A., Aaron, H. L., Rokhsar, D. S., and Shatz, C. J. (1997). Dynamic processes shape spatiotemporal properties of retinal waves. *Neuron* 19, 293–306.

Feller, M. B., Wellis, D. P., Stellwagen, D., Werblin, F. S., and Shatz, C. J. (1996). Requirement for cholinergic synaptic transmission in the propagation of spontaneous retinal waves. *Science* 272, 1182–1187.

Foeller, E., and Feldman, D. E. (2004). Synaptic basis for developmental plasticity in somatosensory cortex. *Curr. Opin. Neurobiol.* 14, 89–95.

Friedel, P., and van Hemmen, J. L. (2008). Inhibition, not excitation, is the key to multimodal sensory integration. *Biol. Cybern.* 98, 597–618.

Froemke, R. C., Tsay, I. A., Raad, M., Long, J. D., and Dan, Y. (2006). Contribution of individual spikes in burst-induced long-term synaptic modification. *J. Neurophysiol.* 95, 1620–1629.

Ghosh, A., and Shatz, C. J. (1992). Involvement of subplate neurons in the formation of ocular dominance columns. *Science* 255, 1441–1443.

Goel, A., and Lee, H. K. (2007). Persistence of experience-induced homeostatic synaptic plasticity through adulthood in superficial layers of mouse visual cortex. *J. Neurosci.* 27, 6692–6700.

Grubb, M. S., Rossi, F. M., Changeux, J. P., and Thompson, I. D. (2003). Abnormal functional organization in the dorsal lateral geniculate nucleus of mice lacking the beta 2 subunit of the nicotinic acetylcholine receptor. *Neuron* 40, 1161–1172.

Hebb, D. (1949). *The Organization of Behavior*. New York: Wiley.

Higley, M. J., and Contreras, D. (2006). Balanced excitation and inhibition determine spike timing during frequency adaptation. *J. Neurosci.* 26, 448–457.

Izhikevich, E. M., and Desai, N. S. (2003). Relating STDP to BCM. *Neural. Comput.* 15, 1511–1523.

Jacob, V., Brasier, D. J., Erchova, I., Feldman, D., and Shulz, D. E. (2007). Spike timing-dependent synaptic depression in the in vivo barrel cortex of the rat. *J. Neurosci.* 27, 1271–1284.

Kanold, P. O. (2009). Subplate neurons: crucial regulators of cortical development and plasticity. *Front. Neuroanat.* 3:16. doi:10.3389/neuro.05.016.2009.

Kanold, P. O., Kara, P., Reid, R. C., and Shatz, C. J. (2003). Role of subplate neurons in functional maturation of visual cortical columns. *Science* 301, 521–525.

Kanold, P. O., and Luhmann, H. J. (2010). The subplate and early cortical circuits. *Annu. Rev. Neurosci.* 33, 23–48.

Kanold, P. O., and Shatz, C. J. (2006). Subplate neurons regulate maturation of cortical inhibition and outcome of ocular dominance plasticity. *Neuron* 51, 627–638.

Katz, L. C., and Shatz, C. J. (1996). Synaptic activity and the construction of cortical circuits. *Science* 274, 1133–1138.

Lu, H. C., Butts, D. A., Kaeser, P. S., She, W. C., Janz, R., and Crair, M. C. (2006). Role of efficient neurotransmitter release in barrel map development. *J. Neurosci.* 26, 2692–2703.

Magee, J. C., and Johnston, D. (1997). A synaptically controlled, associative signal for Hebbian plasticity in hippocampal neurons. *Science* 275, 209–213.

Markram, H., Lubke, J., Frotscher, M., and Sakmann, B. (1997). Regulation of synaptic efficacy by coincidence of postsynaptic APs and EPSPs. *Science* 275, 213–215.

Meister, M., Wong, R. O., Baylor, D. A., and Shatz, C. J. (1991). Synchronous bursts of action potentials in ganglion cells of the developing mammalian retina. *Science* 252, 939–943.

Mooney, R., Madison, D. V., and Shatz, C. J. (1993). Enhancement of transmission at the developing retinogeniculate synapse. *Neuron* 10, 815–825.

Mooney, R., Penn, A. A., Gallego, R., and Shatz, C. J. (1996). Thalamic relay of spontaneous retinal activity prior to vision. *Neuron* 17, 863–874.

Penn, A. A., Riquelme, P. A., Feller, M. B., and Shatz, C. J. (1998). Competition in retinogeniculate patterning driven by spontaneous activity. *Science* 279, 2108–2112.

Pfeiffenberger, C., Yamada, J., and Feldheim, D. A. (2006). Ephrin-As and patterned retinal activity act together in the development of topographic maps in the primary visual system. *J. Neurosci.* 26, 12873–12884.

Pratt, K. G., Dong, W., and Aizenman, C. D. (2008). Development and spike timing-dependent plasticity of recurrent excitation in the *Xenopus* optic tectum. *Nat. Neurosci.* 11, 467–475.

Richards, B. A., Aizenman, C. D., and Akerman, C. J. (2010). *In vivo* spike-timing-dependent plasticity in the optic tectum of *Xenopus laevis*. *Front. Syn. Neurosci.* 2:7. doi:10.3389/fnsyn.2010.00007.

Seol, G. H., Ziburkus, J., Huang, S., Song, L., Kim, I. T., Takamiya, K., Huganir, R. L., Lee, H. K., and Kirkwood, A. (2007). Neuromodulators control the polarity of spike-timing-dependent synaptic plasticity. *Neuron* 55, 919–929.

Shah, R. D., and Crair, M. C. (2008). Retinocollicular synapse maturation and plasticity are regulated by correlated retinal waves. *J. Neurosci.* 28, 292–303.

Shatz, C. J., and Luskin, M. B. (1986). The relationship between the geniculocortical afferents and their cortical target cells during development of the cat's primary visual cortex. *J. Neurosci.* 6, 3655–3668.

Simon, D. K., Prusky, G. T., O'Leary, D. D., and Constantine-Paton, M. (1992). *N*-methyl-D-aspartate receptor antagonists disrupt the formation of a mammalian neural map. *Proc. Natl. Acad. Sci. U.S.A.* 89, 10593–10597.

Sjostrom, P. J., Turrigiano, G. G., and Nelson, S. B. (2001). Rate, timing, and cooperativity jointly determine cortical synaptic plasticity. *Neuron* 32, 1149–1164.

Song, S., and Abbott, L. F. (2001). Cortical development and remapping through spike timing-dependent plasticity. *Neuron* 32, 339–350.

Song, S., Miller, K. D., and Abbott, L. F. (2000). Competitive Hebbian learning through spike-timing-dependent synaptic plasticity. *Nat. Neurosci.* 3, 919–926.

Sur, M., and Rubenstein, J. L. (2005). Patterning and plasticity of the cerebral cortex. *Science* 310, 805–810.

Tegner, J., and Kepecs, A. (2002). Sliding threshold correlational learning rule follows from spike-timing dependent plasticity. In *Society for Neuroscience Annual Meeting*, 32, 152.115 (Abstract).

Trachtenberg, J. T., Trepel, C., and Stryker, M. P. (2000). Rapid extragranular plasticity in the absence of thalamocortical plasticity in the developing primary visual cortex. *Science* 287, 2029–2032.

Turrigiano, G. G., and Nelson, S. B. (2000). Hebb and homeostasis in neuronal plasticity. *Curr. Opin. Neurobiol.* 10, 358–364.

Turrigiano, G. G., and Nelson, S. B. (2004). Homeostatic plasticity in the developing nervous system. *Nat. Rev. Neurosci.* 5, 97–107.

Vijayan, S., Hale, G. J., Moore, C. I., Brown, E. N., and Wilson, M. A. (2010). Activity in the barrel cortex during active behavior and sleep. *J Neurophysiol.* 103, 2074–2084.

Vislay-Meltzer, R. L., Kampff, A. R., and Engert, F. (2006). Spatiotemporal specificity of neuronal activity directs the modification of receptive fields in the developing retinotectal system. *Neuron* 50, 101–114.

Watt, J., and Desai, N. (2010). Homeostatic plasticity and STDP: keeping a neuron's cool in a fluctuating world. *Front. Syn. Neurosci.* 2, 1–16. doi:10.3389/fnsyn.2010.00005.

Wiesel, T. N., and Hubel, D. H. (1963). Single-cell responses in striate cortex of kittens deprived of vision in one eye. *J. Neurophysiol.* 26, 1003–1017.

Yao, H., and Dan, Y. (2001). Stimulus timing-dependent plasticity in cortical processing of orientation. *Neuron* 32, 315–323.

Young, J. M., Waleszczyk, W. J., Wang, C., Calford, M. B., Dreher, B., and Obermayer, K. (2007). Cortical reorganization consistent with spike timing-but not correlation-dependent plasticity. *Nat. Neurosci.* 10, 887–895.

Zhang, L. I., Tao, H. W., Holt, C. E., Harris, W. A., and Poo, M. (1998). A critical window for cooperation and competition among developing retinotectal synapses. *Nature* 395, 37–44.

Zhao, C., Kao, J. P., and Kanold, P. O. (2009). Functional excitatory microcircuits in neonatal cortex connect thalamus and layer 4. *J. Neurosci.* 29, 15479–15488.

Ziburkus, J., Dilger, E. K., Lo, F. S., and Guido, W. (2009). LTD and LTP at the developing retinogeniculate synapse. *J. Neurophysiol.* 102, 3082–3090.

Conflict of Interest Statement: The authors declare that the research was conducted in the absence of any commercial or financial relationships that could be construed as a potential conflict of interest.

Received: 22 February 2010; paper pending published: 10 March 2010; accepted: 27 June 2010; published online: 19 July 2010. Citation: Butts DA and Kanold PO (2010) The applicability of spike time dependent plasticity to development. Front. Syn. Neurosci. ***2****:30. doi: 10.3389/fnsyn.2010.00030*

frontiers in
COMPUTATIONAL NEUROSCIENCE

REVIEW ARTICLE
published: 10 September 2010
doi: 10.3389/fncom.2010.00023

STDP in recurrent neuronal networks

Matthieu Gilson[1,2,3]*, Anthony Burkitt[1,3] and J. Leo van Hemmen[4]

[1] *The Bionic Ear Institute, Melbourne, VIC, Australia*
[2] *NICTA Victoria Research Lab, The University of Melbourne, Melbourne, VIC, Australia*
[3] *Department of Electrical and Electronic Engineering, The University of Melbourne, Melbourne, VIC, Australia*
[4] *Physik Department T35 and BCCN-Munich, Technische Universität München, Garching bei München, Germany*

Edited by:
Wulfram Gerstner, Ecole Polytechnique Fédérale de Lausanne, Switzerland

Reviewed by:
Christian Leibold, Ludwig Maximilians University, Germany
Guillaume Hennequin, Brain-Mind Institute, Switzerland

***Correspondence:**
Matthieu Gilson, Lab for Neural Circuit Theory, Riken Brain Science Institute, Hirosawa 2-1, Wako-shi, Saitama 351-0198, Japan.
e-mail: gilsonm@unimelb.edu.au

Recent results about spike-timing-dependent plasticity (STDP) in recurrently connected neurons are reviewed, with a focus on the relationship between the weight dynamics and the emergence of network structure. In particular, the evolution of synaptic weights in the two cases of incoming connections for a single neuron and recurrent connections are compared and contrasted. A theoretical framework is used that is based upon Poisson neurons with a temporally inhomogeneous firing rate and the asymptotic distribution of weights generated by the learning dynamics. Different network configurations examined in recent studies are discussed and an overview of the current understanding of STDP in recurrently connected neuronal networks is presented.

Keywords: recurrent neuronal network, network structure, STDP, spike-time correlations, self-organization / unsupervised learning

INTRODUCTION

Ten years after spike-timing-dependent plasticity (STDP) appeared (Gerstner et al., 1996; Markram et al., 1997), a profusion of publications have investigated its physiological basis and functional implications, both on experimental and theoretical grounds (for reviews, see Dan and Poo, 2006; Caporale and Dan, 2008; Morrison et al., 2008). STDP has led to a re-evaluation by the research community about Hebbian learning (Hebb, 1949), in the sense of focusing on causality between input and output spike trains, as an underlying mechanism for memory. Following preliminary studies that suggested the concept of STDP (Levy and Steward, 1983; Gerstner et al., 1993), the model initially proposed by Gerstner et al. (1996) and first observed by Markram et al. (1997) based on a pair of pre- and postsynaptic spikes has been extended to incorporate additional physiological mechanisms and account for more recent experimental data. This includes, for example, biophysical models based on calcium channels (Hartley et al., 2006; Graupner and Brunel, 2007; Zou and Destexhe, 2007) and more elaborate experimental stimulation protocols such as triplets of spikes (Sjöström et al., 2001; Froemke and Dan, 2002; Froemke et al., 2006; Pfister and Gerstner, 2006; Appleby and Elliott, 2007). In order to investigate the functional implications of STDP, previous mathematical studies (Kempter et al., 1999; van Rossum et al., 2000; Gütig et al., 2003) have used simpler phenomenological models to relate the learning dynamics to the learning parameters and input stimulation. However, a lack of theoretical results even for the original pairwise STDP with *recurrently* connected neurons persisted until recently, mainly because of the difficulty of incorporating the effect of feedback loops in the learning dynamics. The present paper reviews recent results about the weight dynamics induced by STDP in recurrent network architectures with a focus on the emergence of network structure. Note that we constrain STDP to excitatory glutamatergic synapses, although there is some experimental evidence for a similar property for inhibitory GABAergic connections (Woodin et al., 2003; Tzounopoulos et al., 2004).

Due to its temporal resolution, STDP can lead to input selectivity based on spiking information at the scale of milliseconds, namely spike-time correlations (Gerstner et al., 1996; Kempter et al., 1999). To achieve this, STDP can regulate the output firing rate in a regime that is neither quiescent nor saturated by means of enforcing stability upon the mean incoming synaptic weight and in this way establishing a homeostatic equilibrium (Kempter et al., 2001). In addition, a proper weight specialization requires STDP to generate competition between individual weights (Kempter et al., 1999; van Rossum et al., 2000; Gütig et al., 2003). In the case of several similar input pathways, a desirable outcome is that the weight selection corresponds to a splitting between (but not within) the functional input pools, hence performing symmetry breaking of an initially homogeneous weight distribution that reflects the synaptic input structure (Kempter et al., 1999; Song and Abbott, 2001; Gütig et al., 2003; Meffin et al., 2006).

In this review, we examine how the concepts described above extend from a single neuron (or feed-forward architecture) to recurrent networks, focusing on how the corresponding weight dynamics differs in both cases. The learning dynamics causes synaptic weights to be either potentiated or depressed. Accordingly, STDP can lead to the evolution of different network structures that depend on both the correlation structure of the external inputs and the activity of the network In particular, we relate our recent body of analytical work shortcite (Gilson et al., 2009a–c, 2010) to other studies with a view to illustrating how theory applies to the corresponding network configurations.

MODELS

In the present paper, we use a model of STDP that contains two key features: the dependence upon relative timing for pairs of spikes via a temporally asymmetric learning window W (Gerstner et al.,

1996; Markram et al., 1997; Kempter et al., 1999), as illustrated in **Figure 1**, and upon the current strength of the synaptic weight (Bi and Poo, 1998; van Rossum et al., 2000; Gütig et al., 2003; Morrison et al., 2007; Gilson et al., 2010). In this review we will therefore consider the STDP learning window as a function of two variables: $W(J_{ij}, u)$. The spike-time difference u in **Figure 1B** corresponds to the times when the effect of the presynaptic and the postsynaptic spike reaches the synapse, which involves the axonal and back-propagation delays, respectively d_{ij}^{ax} and d_{ij}^{b}, in **Figure 1A**. Although the present theoretical framework is suited to account for individual STDP properties for distinct synapses (Froemke et al., 2005), we only consider a single function W for all synapses in the present paper for the purpose of clarity. We note that the continuity of the curve for W in **Figure 1B** does not play any significant role in the following analysis.

In addition to the learning window function W, a number of studies (Kempter et al., 1999; Gilson et al., 2009a) have included rate-based terms w^{in} and w^{out}, namely modifications of the weights for each pre- and postsynaptic spike (Sejnowski, 1977; Bienenstock et al., 1982). This choice leads to a general form of synaptic plasticity (van Hemmen, 2001; Gerstner and Kistler, 2002) that incorporates changes for both single spikes and pairs of spikes. The choice of the Poisson neuron model with temporally inhomogeneous firing rate and with a linear input–output function for the firing rates makes it possible to incorporate such rate-based terms in order to obtain homeostasis (Turrigiano, 2008).

In order to study the evolution of plastic weights in a given network configuration, it is necessary to define the stimulating inputs. For pairwise STDP, spiking information is conveyed in the firing rates and cross-correlograms, and Poisson-like spiking is often used to reproduce the variability observed in experiments (Gerstner et al., 1996; Kempter et al., 1999; Song et al., 2000; Gütig et al., 2003). Spike coordination or rate covariation can be combined to generate correlated spike trains (Staude et al., 2008). The present review will focus on narrowly correlated inputs (almost synchronous) that are partitioned in pools; in this configuration, correlated inputs belong to a common pathway (e.g., monocular visual processing). We will also discuss more elaborate input correlation structures that use narrow spike-time correlations (Krumin and Shoham, 2009; Macke et al., 2009), oscillatory inputs (Marinaro et al., 2007), and spike patterns (Masquelier et al., 2008). Our series of papers has also made minimal assumptions about the network topology, namely mainly considering recurrent connectivity to be homogeneous. The starting situation consists in unorganized (input and/or recurrent) weights that are randomly distributed around a given value.

Once the input and network configuration is fixed, it is necessary to evaluate the spiking activity in the network in order to predict the evolution of the weights. The Poisson neuron model has proven to be quite a valuable tool (Kempter et al., 1999; Gütig et al., 2003; Burkitt et al., 2007; Gilson et al., 2009a,d), although recent progress has been made toward a similar framework for integrate-and-fire neurons (Moreno-Bote et al., 2008). In the Poisson neuron model, the output firing mechanism for a given neuron i is approximated by an *in*homogeneous Poisson process with rate function or intensity $\lambda_i(t)$ that evolves over time according to the presynaptic activity received by the neuron:

$$\lambda_i(t) = \lambda_0 + \sum_{j,n} J_{ij}\left(t_j^n\right)\epsilon\left[t - t_j^n - \left(d_{ij}^{\mathrm{den}} + d_{ij}^{\mathrm{ax}}\right)\right], \tag{1}$$

where t_j^n, $1 \leq n$, are the spike times for neuron j, and λ_0 describes background excitation/inhibition from synapses that are not considered in detail. The kernel function ϵ describes the time course of the postsynaptic response (chosen identical for all synapses here), such as an alpha function. We also discriminate between axonal and dendritic components for the conduction delay, cf. **Figure 1A**. Although only coarsely approximating real neuronal firing mechanisms, this model transmits input spike-time correlations and leads to a tractable mathematical formulation of the input–output correlogram, which allows the analytical description of the evolution of the plastic weights.

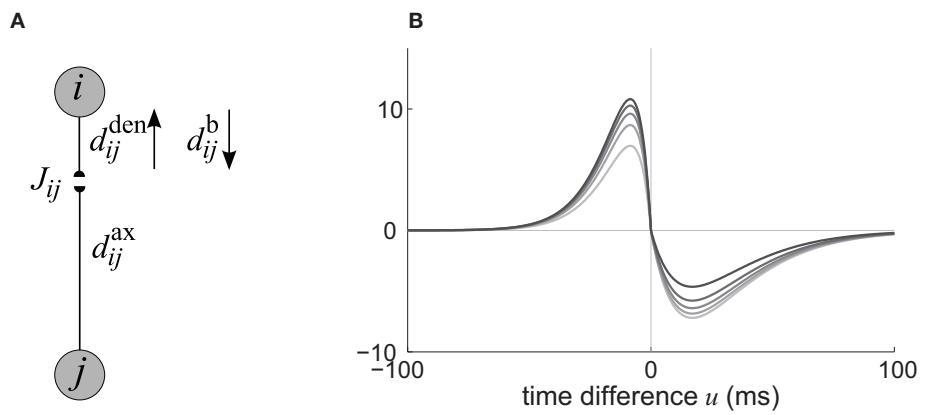

FIGURE 1 | (A) Schematic representation of a synapse from the source neuron j to the target neuron i. The synaptic weight is J_{ij} and axonal delay d_{ij}^{ax}; d_{ij}^{den} accounts for the conduction of the postsynaptic response along the dendritic tree toward the soma while the d_{ij}^{b} accounts for the back-propagation of action potential to the synapse. Here d_{ij}^{den} and d_{ij}^{b} are distinguished, but they can be considered to be equal if the conduction along the dendrite in both directions is passive. **(B)** Examples of STDP learning window function; the vertical scale (dimensionless) indicates the change of synaptic strength arising from the occurrence of a pair of pre- and postsynaptic spikes with time difference u. The darker curves correspond to stronger values for the current weight, indicating the effect of weight dependence.

ANALYSIS OF SYNAPTIC WEIGHT DYNAMICS

Before starting we quickly explain what STDP means and how Poisson neurons function in the present context. Then we focus on the asymptotics of an analytic description for the development of synaptic strengths by means of a set of coupled differential equations and introduce the notion of "almost-additive" STDP. In so doing we will also see how a population of recursively connected neurons influences the synaptic development in the population as a whole so that one gets a "grouping" of the synapses on the neurons. Input by itself and input in conjunction with or, more interestingly, versus recurrence play an important role in this game. Finally, we will see how the *form* of the learning window influences the neuron-to-input and neuron-to-neuron spike-time correlations. This is a preparation of the next section where we will analyze emerging network structures and their functional implications.

SPIKE-TIMING-DEPENDENT PLASTICITY

The barn owl (*Tyto alba*) is able to determine the prey direction in the dark by measuring interaural time differences (ITDs) with an azimuthal accuracy of 1–2° corresponding to a temporal precision of a few microseconds, a process of binaural sound localization. The first place in the brain where binaural signals are combined to ITDs is the laminar nucleus. A temporal precision as low as a few microseconds was hailed by Konishi (1993) as a paradox – and rightly so since at a first sight it contradicts the slowness of the neuronal "hardware," viz., membrane time constants of the order of 200 μs. In addition, transmission delays from the ears to laminar nucleus scatter between 2 and 3 ms (Carr and Konishi, 1990) and are thus in an interval that greatly exceeds the period of the relevant oscillations (100–500 μs). The key to the solution (Gerstner et al., 1996) is a Hebbian learning process that tunes the hardware so that only synapses and, hence, axonal connections with the right timing survive. Genetic coding is implausible because 3 weeks after hatching, when the head is full-grown, the young barn owl cannot perform azimuthal sound localization. Three weeks later it can. So what happens in between? The solution to the paradox involves a careful study of how synapses develop during ontogeny (Gerstner et al., 1996; Kempter et al., 1999). The inputs provided by many synapses decide what a neuron does but, once it has fired, the neuron determines whether each of the synaptic efficacies will increase or decrease, a process governed by the synaptic learning window, a notion that will be introduced shortly. Each of the terms below in Eq. 2 has a neurobiological origin. The process they describe is what we call *infinitesimal learning* in that synaptic increments and decrements are small. Consequently it takes quite a while before the organism has built up a "noticeable" effect. Though processes that happen in the long term are not fully understood yet, their effect is well described by Eq. 2.

For the sake of definiteness we are going to study waxing and waning of synaptic strengths associated with a *single* neuron *i*; cf. **Figure 2A**. Here we ignore the weight dependence to focus on the temporal aspect and thus use $W(\cdot,u)$ as the STDP learning window function. The $1 \le j \le N$ synapses provide their input at times t_j^n, where n is a label denoting the sequential spikes. The firing times of the neuron are denoted by t_i^m, it being understood that m is a label like n. Given the firing times, the change $\Delta J_{ij}(t) := J_{ij}(t) - J_{ij}(t-T)$ of the weight of synapse $j \to i$ (synaptic strength) during a learning session of duration T and ending at time t is governed by several factors,

$$\Delta J_{ij}(t) = \eta \left[\sum_{t-T \le t_j^n \le t} w^{\text{in}} + \sum_{t-T \le t_i^m \le t} w^{\text{out}} + \sum_{t-T \le t_j^n, t_i^m \le t} W(\cdot, t_j^n - t_i^m) \right]. \quad (2)$$

Here the firing times t_i^m of the postsynaptic neuron may, and in general will, depend on J_{ij}. We now focus on the individual terms. The prefactor $0 < \eta \ll 1$ reminds us explicitly of learning being slow on a neuronal time scale. This condition is usually referred to as the "adiabatic hypothesis." It holds in numerous

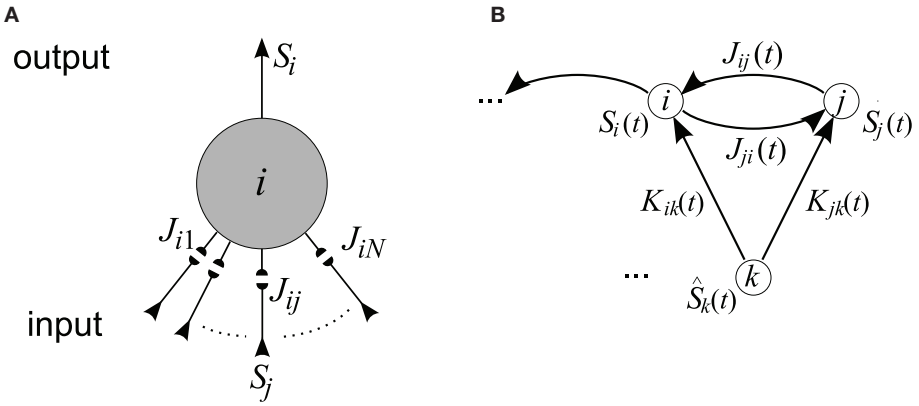

FIGURE 2 | (A) Single neuron. Spike-timing-dependent plasticity (STDP) refers to the development of synaptic weights J_{ij} (small filled circles, $1 \le j \le N$) of a single neuron (large circle) in dependence upon the arrival times of presynaptic spikes (input) and firing times of the postsynaptic neuron (output). Here the neuron receives input spike trains denoted by S_j and produces output spikes denoted by S_i. The collective interaction of *all* the input spikes determines the firing times of the postsynaptic neuron they are all sitting on and in this way the input spike times at *different* synapses influence the latter's waxing and waning. **(B)** Recurrently connected network. Schematic representation of two neurons *i* and *j* stimulated by one external input *k* with spike train $\hat{S}_k$. Input and recurrent weights are denoted by *K* and *J*, respectively.

biological situations and has been a mainstay of computational neuroscience ever since. It may also play a beneficial role in an applied context. If it is does not hold, a numerical implementation of the learning rule (Eq. 2) is straightforward, but an analytical treatment is not.

Each incoming spike and each action potential of the postsynaptic neuron change the synaptic efficacy by ηw^{in} and ηw^{out}, respectively. The last term in Eq. 2 represents the *learning window* $W(\cdot,u)$, which indicates the synaptic change in dependence upon the time difference $u = t_j^n - t_i^m$ between an incoming spike t_j^n and an outgoing spike t_i^m. When the former precedes the latter, we have $u < 0 \Leftrightarrow t_j^n < t_i^m$, and the result is $W(\cdot,u) > 0$, implying potentiation. This seems reasonable since NMDA receptors, which are important for long-term potentiation (LTP), need a strongly positive membrane voltage to become "accessible" by loosing the Mg^{2+} ions that block their "gate." A postsynaptic action potential induces a fast retrograde "spike" doing exactly this (Stuart et al., 1997). Because the presynaptic spike arrived slightly earlier, neurotransmitter is waiting to obtain access, which is allowed after the Mg^{2+} ions are gone. The result is Ca^{2+} influx. On the other hand, if the incoming spike comes "too late," then $u > 0$ and $W(\cdot,u) < 0$, implying depression – in agreement with a general rule in politics, discovered two decades ago: "Those who come too late shall be punished." In neurobiological terms, there is no neurotransmitter waiting to be admitted.

POISSON NEURONS

Since Poisson neurons (Kempter et al., 1999; van Hemmen, 2001) are cardinal to obtaining analytically exact solutions and at the same time effortlessly reflect uncertainty in response to input stimuli, which we then interpret as "stochastic," we first quickly discuss what "inhomogeneous Poisson" is all about.

A general Poisson process with intensity $\lambda_i(t)$ is defined by three properties:

(i) the probability of finding a spike between t and $t + \Delta t$ is $\lambda_i(t)\Delta t$,
(ii) the probability of finding two or more spikes there is $o(\Delta t)$,
(iii) the process has independent increments, i.e., events in disjoint intervals are independent.

In a neuronal context it is fair to call property (ii) a mathematical realization of a neuron's refractory behavior. Property (iii) makes it all exactly soluble (cf. van Hemmen, 2001, App. B). When the "membrane potential" $\lambda_i(t)$ in Eq. 1 is high/low, the probability of getting a spike is high/low too. For those who like an explicit nonlinearity better, the *clipped* Poisson neuron with

$$\lambda_i^{\text{clipped}} = \lambda_i(t)\Theta\left[\lambda_i(t) - \vartheta_1\right], \tag{3}$$

where ϑ_1 is a given threshold and Θ is the Heaviside step function [$\Theta(t) = 0$ for $t < 0$ and $\Theta(t) = 1$ for $t \geq 0$], is a suitable substitute that also allows an exact disentanglement (Kistler and van Hemmen, 2000). For $\lambda_i(t) \equiv \lambda_0$ where λ_0 is a constant we regain the classical Poisson process. The information content of the single number λ_0 is rather restricted and so is that of a spike sequence generated by a classical Poisson process. If, on the other hand, $\lambda_i(t)$ is a periodic function with high maxima, steep slopes, and low ($\approx$0) minima, then we get a pronounced periodic-like but not exactly periodic response. The latter property is convenient to simulate, e.g., neuronal response to periodic input.

DYNAMICAL SYSTEM AND ASYMPTOTIC SOLUTION

We now turn to general pre- and postsynaptic spike trains, with no reference to a neuronal model or a specific input structure. The only assumption here is that the learning is sufficiently slow so that averaging over the spike trains can be performed (van Hemmen, 2001); note that significant weight evolution over tens of minutes still satisfies this requirement. For pairwise (possibly weight-dependent) STDP, the evolution of the mean weight averaged over all trajectories (drift of the stochastic process) results in a learning-dynamics equation of the general form

$$\dot{J}_{ij} = f\left(J_{ij};\nu_j,\nu_i\right) + g\left(J_{ij};C_{ij},d_{ij}^{\text{ax}} - d_{ij}^{\text{b}}\right), \tag{4}$$

where the dependence of the variables upon time has been omitted. In Eq. 4 the spiking information conveyed by the spike trains $S_i(t)$ and $S_j(t)$ for neurons i and j, respectively, is contained in the firing rates

$$\nu_i(t) := \frac{1}{T}\int_{t-T}^{t} \langle S_i(t')\rangle \mathrm{d}t' \tag{5}$$

and the spike-time covariance coefficient

$$\begin{aligned} C_{ij}(t,u) := {} & \frac{1}{T}\int_{t-T}^{t} \langle S_i(t')S_j(t'+u)\rangle \mathrm{d}t' \\ & - \frac{1}{T}\int_{t-T}^{t} \langle S_i(t')\rangle \mathrm{d}t' \frac{1}{T}\int_{t-T}^{t} \langle S_j(t''+u)\rangle \mathrm{d}t''. \end{aligned} \tag{6}$$

This separation of time scales (involving the averaging duration T) is dictated by the STDP learning window W (cf. **Figure 1**): typically, phenomena "faster" than 10 Hz (i.e., 100 ms) will be captured by W as spike effects through C_{ij}, such as oscillatory activity (Marinaro et al., 2007) and spike patterns (Masquelier et al., 2008). The formulation in Eq. 6 is slightly more general than that used by Gerstner and Kistler (2002) and Gilson et al. (2009a); it can account for covariation of underlying rate functions (Sprekeler et al., 2007) as well as (stochastic) spike coordination (Kempter et al., 1999; Gütig et al., 2003; see also Staude et al., 2008). Finally, we note that the averaging $\langle\ldots\rangle$ in Eqs 5 and 6 comes for free as the "learning time" T is so large and the temporal correlations in naturally generated stochastic processes in Eq. 2 have so small a range that we can apply a law of large numbers (van Hemmen, 2001, App. A) so as to end up with the averages as indicated. That is, we need not explicitly average as it all comes, so to speak, for free.

For a given network configuration, predicting the evolution of the weight distribution requires the evaluation of the neuronal variables involved in Eq. 4 as functions of the parameters for the stimulating inputs. For all network neurons, the output spike trains are constrained by the neuron model and input spike trains: the key to the analysis is the derivation of self-consistency equations that describe this relationship for the firing rates and spike-time correlations. In particular, recurrent connectivity implies nonlinearity in the network input–output function for the neuronal firing rates. The interplay between the spiking activity and network

connectivity, where the latter is modified by plasticity on a slower time scale, is crucial to understanding the effect of STDP. A network of Poisson neurons with input weights K and recurrent weights J as in **Figure 2B** leads to the following system of matrix equations (Gilson et al., 2009a,d):

$$\nu = [1 - J]^{-1}[\lambda_0 \mathbf{e} + K\hat{\nu}], \tag{7}$$

$$F(\cdot,u) = [1 - J]^{-1} K \hat{C}^{\psi}(u),$$

$$C(\cdot,u) = [1 - J]^{-1} K \hat{C}^{\zeta}(u) K^{\mathrm{T}} [1 - J]^{-1\mathrm{T}}$$

The vector of neuronal firing rates ν is expressed in terms of the input firing rates $\hat{\nu}$ and the weight matrices K and J. Vector $\mathbf{e}$ has all element equal to ones and the superscript $\mathbf{T}$ denotes the transposition. Matrices C and F respectively contain the neuron-to-neuron and neuron-to-input spike-time covariances, cf. Eq. 6. Only their dependence upon u is considered here and they are expressed in terms of the input-to-input covariance matrix $\hat{C}$ convolved with the following functions (indicated by the superscript):

$$\psi(u) \simeq \epsilon\left(-u + d_{ij}^{\mathrm{ax}} + d_{ij}^{\mathrm{den}}\right), \tag{8}$$

$$\zeta(u) \simeq \int \epsilon(u + r)\epsilon(r)\,\mathrm{d}r,$$

where ϵ is the postsynaptic response kernel for the Poisson neuron; cf. Eq. 1. The dependence upon time t has been omitted, as the time-averaged firing rates and spike-time covariances practically only vary at the same pace as the plastic weights. In this framework, the effect of the recurrence is taken into account in the inverse of the matrix $1 - J$ in Eq. 7. For the rates ν and the neuron-to-input covariances F, this leads to a linear feedback, whereas the dependence is quadratic-like for the neuron-to-neuron covariances C. These equations allow the analysis of the learning equation (Eq. 4) for recurrent weights J, as well as an equivalent expression for input weights K with the neuron-to-input spike-time covariance F in place of C.

For both a single neuron and recurrently connected network, the learning equation (Eq. 4) can lead to a double dynamics that operates upon the incoming synaptic weights for each neuron (Kempter et al., 1999; Gilson et al., 2009a,d, 2010):

- a partial (homeostatic) equilibrium that stabilizes the mean incoming weight, and hence the output firing rate, through the constraint $f(J_{ij};\nu_j,\nu_i) \simeq 0$ for each neuron i;
- competition between individual weights based on the spike-time covariances embedded in $g(J_{ij};C_{ij},d_{ij}^{\mathrm{ax}} - d_{ij}^{\mathrm{b}})$, which can result in splitting the weight distribution.

Note that this discrimination between rate and spike effects is valid irrespective of the neuron model. The following analysis, which is based on the Poisson neuron model, can be extended to more elaborate models, such as the integrate-and-fire neuron when it is in a (roughly) linear input-output regime.

Several features have been used to ensure a stable and realizable homeostatic equilibrium. That is, the mean incoming weight J_{av} for each neuron has a stable fixed point between the bounds $[J_{\min}, J_{\max}]$. This is important so as to ensure proper weight specialization in that, if the fixed point is not realizable (outside the bounds) or unstable, all weights will tend to cluster at one of the bounds and no effective selection is then possible, as is illustrated by **Figure 3A**. On the other hand, in **Figure 3B** splitting of the weights occurs on each side of the stable value for the mean weight (thick black line). If rate-based terms can be added to obtain a polynomial form of f (Kempter et al., 1999; Gilson et al., 2009a,d), weight dependence can also be chosen to bring stability (Gütig et al., 2003; Gilson et al., 2010), as is illustrated in **Figure 3**. Such features preserve the local character of the plasticity rule and homeostasis is then a consequence of local plasticity (Kempter et al., 2001). In contrast, additional mechanisms such as synaptic scaling (or normalization) can be enforced to constrain the mean incoming weight (van Rossum et al., 2000). In any case, only if $f(J_{ij};\nu_j,\nu_i) \simeq 0$ for all synapses $j \to i$ is the weight specialization determined by the spike-time covariance. Otherwise, firing rates are likely to take part in the weight competition and the dichotomy between rate and spike effects may not be effective.

Lack of proper homeostatic stability can lead to dramatic changes in the spiking activity when slightly modifying some parameters in simulations, such as an "explosive" behavior where the neuron saturates at a very high firing rate (Song et al., 2000). Non-linear activation mechanisms (e.g., sigmoidal rate function, integrate-and-fire) may play a role in the weight dynamics and possibly affect the correlograms. In particular, stable homeostatic equilibrium can

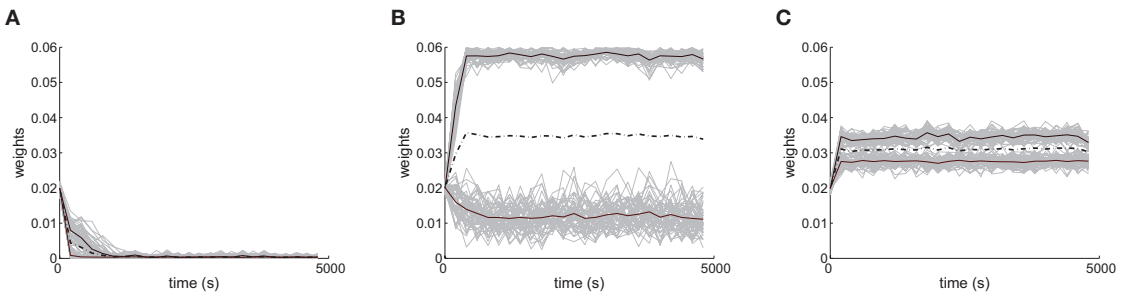

FIGURE 3 | Evolution of synaptic weights. In each plot individual weights are represented (gray traces) as well as their overall mean J_{av} (thick solid black line) and the two means over each input pool (thick dashed and dashed-dotted black lines). In the simulations, one pool had spike-time correlation while the other had none while $w^{\mathrm{in}} = w^{\mathrm{in}} = 0$. **(A)** Case of non-realizable (but stable) fixed point $J_{av}^{*} < 0$. **(B)** Stability of the mean incoming weight ($0 = J_{\min} < J_{\mathrm{av}}^{*} < J_{\max} = 0.06$) and competition between individual weights when using almost-additive STDP. **(C)** Similar plot to **(B)** with medium weight dependence, which implies weaker competition.

be obtained without use of rate-based terms w^{in} and w^{out} for additive STDP through integrate-and-fire neurons (this is not possible with Poisson neuron), but the range of adequate learning parameters, in particular the value of $\widetilde{W}$, was found to be smaller (Song et al., 2000) than when using rate-based plasticity terms (Kempter et al., 1999; Gilson et al., 2009a).

After the homeostatic equilibrium has been reached, spike-time correlations become the dominating term in the learning-dynamics equation (Eq. 4) and hence determine the subsequent weight specialization. The rule of thumb for the weight splitting after reaching the homeostatic equilibrium is that synapses $j \to i$ with larger coefficients $g(J_{ij} \simeq J^*_{\text{av}}; C_{ij}, d^{\text{ax}}_{ij} - d^{\text{b}}_{ij})$ will be potentiated at the expense of the others. The function g involves the convolution of the correlogram C_{ij}, such as those in **Figures 4B,C**, with the STDP function W

$$g\left(J_{ij}; C_{ij}, \Delta d_{ij}\right) = \int_{-\infty}^{+\infty} W\left(J_{ij}, u + \Delta d_{ij}\right) C_{ij}(t,u)\,\mathrm{d}u. \tag{9}$$

This implies that the STDP learning function W is shifted by the difference between the axonal and the dendritic back-propagation delays Δd_{ij} in Eq. 4,

$$\Delta d_{ij} := d^{\text{ax}}_{ij} - d^{\text{b}}_{ij}. \tag{10}$$

Hence a purely dendritic delay implies $\Delta d_{ij} < 0$, which is equivalent to shifting the STDP learning window function (solid line) in **Figure 4D** to the right (dashed line), i.e., toward more potentiation. Conversely, a purely axonal delay shifts the curve to the left (dashed-dotted line) and thus toward more depression since $\Delta d_{ij} < 0$. A previous analysis of this effect (Gilson et al., 2010) assumed $d^{\text{den}}_{ij} = d^{\text{b}}_{ij}$ but the conclusions can be straightforwardly adapted to the more general case; the respective roles played by the delays in determining the spike-time correlations and learning dynamics is highlighted below.

The weight dependence ensuing from STDP modulates the weight specialization. This can lead to either a unimodal or bimodal distribution at the end of the learning epoch (van Rossum et al., 2000; Gütig et al., 2003; Gilson et al., 2010); see **Figures 3C,B**, respectively. We will refer to *almost-additive STDP* in the case where the weight-dependence is small, i.e., small values of the $\mu > 0$ parameter of Gütig et al. (2003). Almost-additive STDP can generate effective weight competition including partial stability whenever the weight dependence leads to more depression and/or less potentiation for higher values of the current weight and the homeostatic equilibrium (Gilson et al., 2010). In general, stronger weight dependence implies more stability for both the mean incoming weight and individual weights, whereas competition is more effective for almost-additive STDP.

INPUT VERSUS RECURRENT CONNECTIONS

An interesting example illustrates the difference in the weight dynamics when stepping from a single neuron to a recurrently connected network. We consider neurons that are excited by external synaptic inputs with narrow spike-time correlations (i.e., almost-synchronous spiking), as illustrated in **Figure 4A**. We also assume homogeneous input and recurrent connectivity, which can

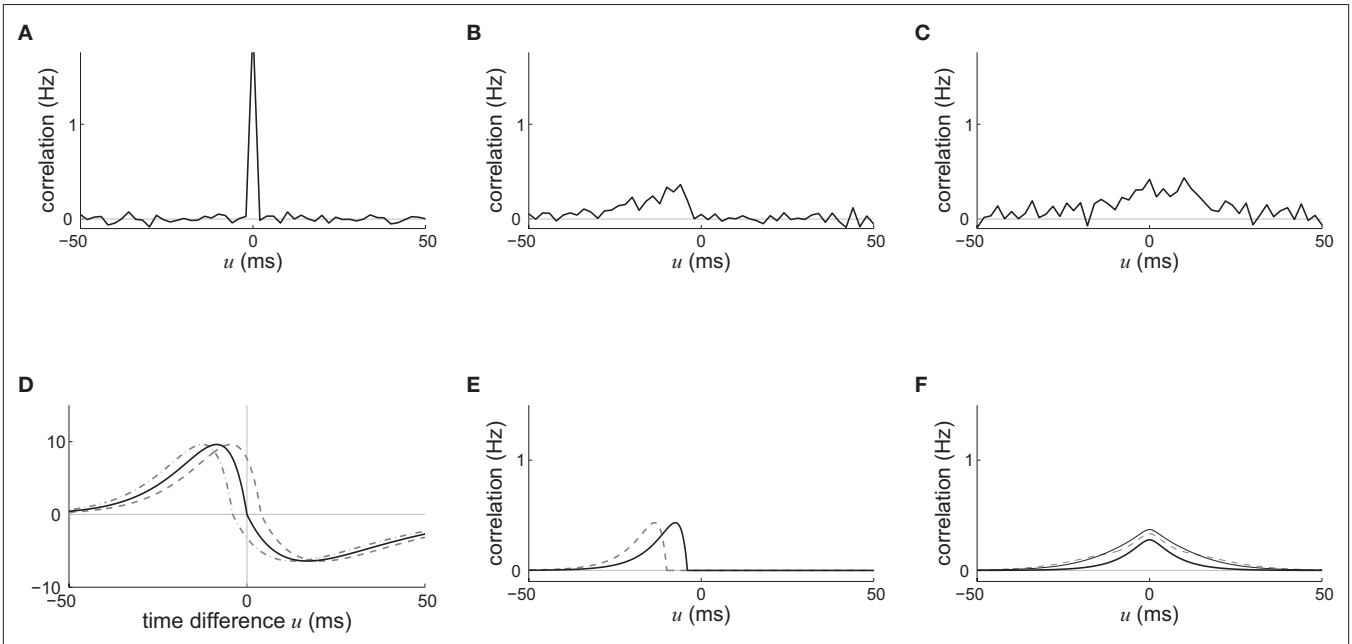

FIGURE 4 | Spike-time correlograms between (A) two inputs, **(B)** an input and a neuron, and **(C)** two neurons. These three plots correspond to Eq. 6 for randomly chosen pairs of inputs/neurons in a network of 100 neurons excited by 100 inputs (30% probability of connection; no learning was applied) and simulated over 1000 s with the sum of delays $d^{\text{ax}}_{ij} + d^{\text{den}}_{ij} = 4$ ms; the time bin is 2 ms. **(D)** Learning window function $W(J^*_{\text{av}}, u)$ with no delay (solid line, $\Delta d_{ij} = 0$ ms), purely dendritic delay $d^{\text{b}}_{ij} = 4$ ms (dashed line, $\Delta d_{ij} = -4$ ms) and purely axonal delay $d^{\text{ax}}_{ij} = 4$ ms (dashed-dotted line, $\Delta d_{ij} = 4$ ms). **(E,F)** Theoretical curves of ψ and ζ corresponding to approximation at the first order of the correlograms in **(B,C)**, respectively, with short (4 ms, solid lines) and large (10 ms, dashed lines) values for $d^{\text{ax}}_{ij} + d^{\text{den}}_{ij}$; cf. Eq. 8. The two curves (for 4 and 10 ms) are superimposed for ζ and the thin lines represent the corresponding predictions when incorporating a further order in the recurrent connectivity. The agreement with the spreading and amplitude of the curves in **(B,C)**, which correspond to 4 ms, is only qualitative.

be partial. We compare the effect of STDP for an input connection from an external input to a given network neuron on the one hand, and a recurrent connection between two neurons on the other hand. In so doing we recall that a positive (resp. negative) value for the convolution in Eq. 9 implies potentiation (depression) of the more correlated input pathways (Gilson et al., 2009a) and outgoing recurrent connections for more correlated neuronal groups (Gilson et al., 2009d). Typical correlograms are illustrated in **Figures 4B,C** for input and recurrent connections, respectively. For the input connection the distribution is clearly non-symmetrical, whereas it is roughly symmetrical for recurrently connected neurons (in a homogeneous network). The shifted STDP curve W in **Figure 4D** depends on the delays d_{ij}^{ax} and d_{ij}^{b}, which we assumed to be of the same order as d_{ij}^{den}. The correlograms in **Figures 4B,C** can be evaluated with first-order approximations by the following functions ψ and ζ in Eq. 8, respectively. In **Figure 4E**, the theoretical correlogram ψ that corresponds to **Figure 4B** is shifted to the left by the sum of the delays $d_{ij}^{\mathrm{ax}} + d_{ij}^{\mathrm{den}}$; it follows that the curve always overlaps with the potentiation side of W, irrespective of the axonal/dendritic ratio (assuming d_{ij}^{den} and d_{ij}^{b} to be of the same order). However, for the recurrent connection in **Figure 4F**, the delays affect only higher-order approximations of the correlogram ζ in Eq. 8, namely by increasing the spread of the distribution (thin lines); the distribution of ϕ remains symmetrical and similar to the simulated distribution in **Figure 4C**, while the convolution with W can give a positive or negative value, depending upon the shift of W.

The effect of the delay difference Δd_{ij} upon the dynamical evolution of the input and recurrent weights induced by STDP becomes clearer in **Figure 5**, where the dashed and dashed-dotted curves represent the convolutions in Eq. 9 for the two corresponding correlograms plotted as a function of Δd_{ij}. For an input connection (dashed curve), delays do not qualitatively change the specialization scheme for input plastic connections, viz., the sign of the dashed curve in the range of Δd_{ij} considered (between −4 and 4 ms here). Delays, however, are found to crucially determine the sign of the dashed-dotted curve for recurrent weights (dashed-dotted curve) around $\Delta d_{ij} = 0$: a predominantly dendritic component ($\Delta d_{ij} \lll 0$) favors strengthening of feedback connections for synchronous neurons. On the other hand, predominantly axonal delays ($\Delta d_{ij} \ggg 0$) lead to decorrelation, viz., weakening of self-feedback connections. Note that these conclusions apply to *positively* correlated input spike trains.

The shape of W around 0 is also important to determine the sign of the convolution in Eq. 9: stronger potentiation than depression strengthens self-feedback for correlated groups of neurons and thus favors synchrony, as illustrated in **Figures 5A,B**. In general this effect is more pronounced when using a non-continuous W function since the discrepancies around $u = 0$ are larger; see **Figures 5C,D**. In conclusion, a suitable typical choice for W involves a longer time constant for depression but higher amplitude for potentiation, which is in agreement with previous experimental results (Bi and Poo, 1998).

Another difference between plasticity for input and recurrent connections lies in stability issues for the spiking activity: ("soft" or "hard") bounds on the weights must be chosen such that recurrent feedback does not become too strong (in particular, at the homeostatic equilibrium). Otherwise, potentiation of synapses may lead to an "explosive" spiking behavior, where all neurons saturate at a high firing rate (Morrison et al., 2007).

EXTENSION OF RESULTS TO MORE ELABORATE STDP RULES

The analysis presented above does not depend on precise quantitative values, but rather the conclusions depend on qualitative properties, namely the signs of functions within some range. The methods are also valid for non-strictly pairwise STDP. For restrictions on the spike interactions that contribute to STDP (Sjöström et al., 2001; Izhikevich and Desai, 2003; Burkitt et al., 2004), an effective correlogram can be evaluated to be convolved with the STDP window function W. When the interaction restrictions do not modify the global shape of the correlograms, the predicted trends for the weight specialization should still hold and the effect of parameters such as dendritic/axonal delays should be similar for more elaborate STDP rules.

In other words, only non-linearities that would significantly change the qualitative properties of the correlograms in **Figure 4** are important; for example, those that alter their (non-)symmetrical character. It has been shown that the rate-based contribution for STDP can be significantly affected by the restriction scheme (Izhikevich and Desai, 2003; Burkitt et al., 2004); STDP can then exhibit a BCM-like behavior (Bienenstock et al., 1982) with respect to the input firing rate and lead to depression below a given threshold and potentiation above that threshold.

Further work is necessary to understand the implications of interaction restrictions for an arbitrary correlation structure. More biophysically accurate plasticity rules that exhibit a STDP profile for spike pairs (Graupner and Brunel, 2007; Zou and Destexhe, 2007) are also expected to exhibit qualitatively similar behavior when stimulated by spike trains with pairwise spike-time correlations. The rule proposed by Appleby and Elliott (2006) is an exception where higher-order correlations are necessary to obtain competition. Other synaptic plasticity rules involving a temporal learning window, such as "burst-time-dependent plasticity" that corresponds to the longer time scale of a second (Butts et al., 2007), can be analyzed using the same framework and similar dynamical ingredients are expected to participate to the weight evolution (stabilization and competition).

EMERGENCE OF NETWORK STRUCTURE AND FUNCTIONAL IMPLICATIONS

Finally, we illustrate how the interplay between STDP, connectivity topology, and input correlation *structure* can lead to the emergence of synaptic structure in a recurrently connected network. First we describe how the weight dynamics presented above can shape synaptic pathways using the simple example of narrowly (or delta) correlated inputs. Second we extend the analysis to more elaborate input structures, such as oscillatory spiking activity. We also discuss the link between these results and the resulting processing of spiking information performed by trained neurons and networks.

ORGANIZING SYNAPTIC PATHWAYS

We start by focusing on a specific configuration of the external stimulating inputs, viz., two pools of external inputs that can have within-pool, but no between-pool spike-time correlations; see **Figure 6** where filled bottom circles indicate input pools with narrowly distributed spike-time correlations, in a similar fashion to **Figure 3**. Each pool represents a functional pathway and the spiking information is mainly contained in the spike-time correlations between pairs of neurons. This scheme has been used in many studies to examine input selectivity, such as how a neuron

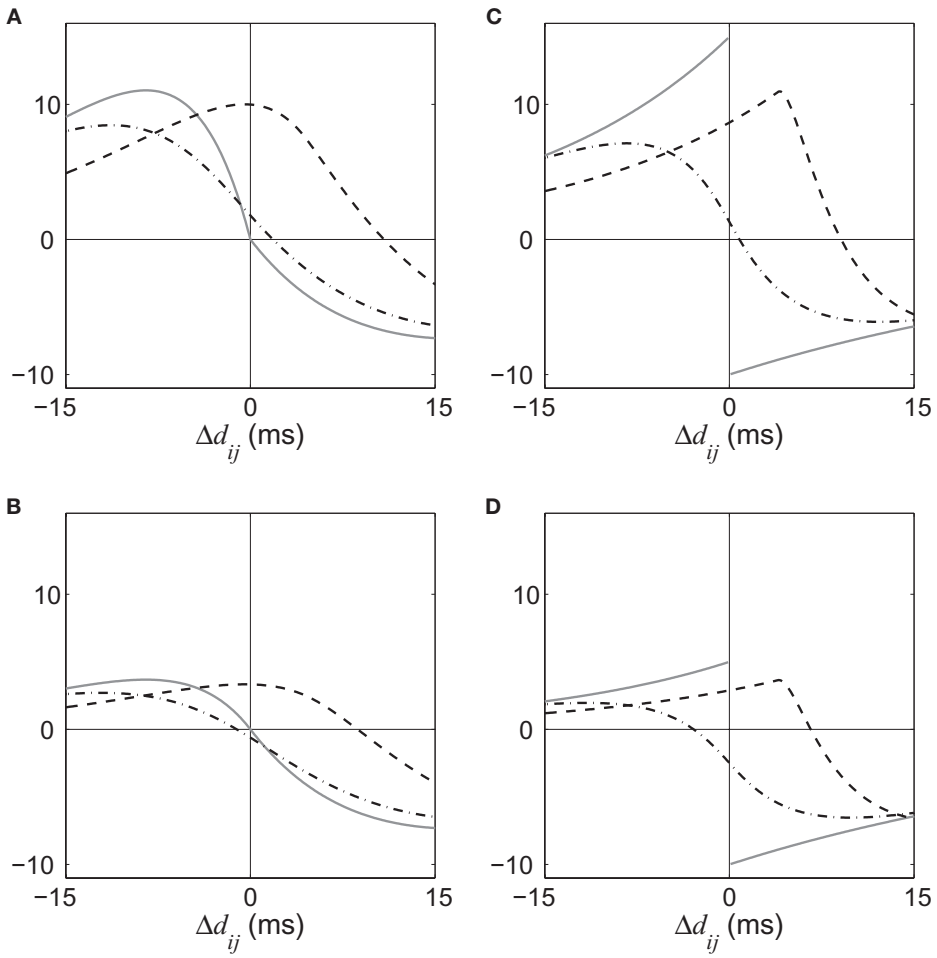

FIGURE 5 | Four illustrative plots of the STDP learning window W (gray solid line) and its convolutions in Eq. 9: $W*\psi$ for input connections (dashed line) and $W*\zeta$ for recurrent connections (dashed-dotted line). The theoretical spike-time correlograms ψ and ζ in Eq. 8 can be found in **Figures 4E,F**, respectively. The sign of the function resulting from the convolution for the argument Δd_{ij} predicts the weight evolution. The curves correspond to delays such that $d_{ij}^{ax} + d_{ij}^{den} = 4$ ms and the effect of Δd_{ij} can be read on the horizontal axis (technically, it should be read $-4 \leq \Delta d_{ij} \leq 4$). Comparison between an STDP learning window $W(J_{av}^*, u)$ that induces **(A)** more potentiation than depression for small values of u and **(B)** the converse situation. We note that the integral is negative in both cases, which means more overall depression (for uncorrelated inputs), which is required for stability. **(C,D)** Similar plots to **(A,B)** with a discontinuous curve W in $u = 0$.

can become sensitive to only a portion of its stimulating inputs, hence specializing to a given pathway (Kempter et al., 1999; Song and Abbott, 2001; Gütig et al., 2003).

For a single neuron, input pathways with a narrow spike-time correlation distribution are potentiated by Hebbian STDP (Kempter et al., 1999; Song et al., 2000), as explained in Section "Input Versus Recurrent Connections." This conclusion still holds when we train input connections for recurrently connected neurons, as illustrated in **Figure 6A**. When the spike-time correlations have a broader distribution, their widths matter and the more peaked pool is selected (Kistler and van Hemmen, 2000).

When two input pathways have similar correlation strengths, additive-like STDP induces sufficient competition to lead to a winner-take-all situation where only one pool is selected (Song and Abbott, 2001; Gütig et al., 2003). When using STDP without the rate-based terms w^{in} and w^{out}, a stricter condition on the weight dependence has been found to ensure a similar behavior (Meffin et al., 2006). Then two STDP modes can be distinguished depending on the strength of weight dependence: Either the competition is sufficiently strong to induce a splitting of the weight distribution (additive-like STDP) or the asymptotic weight remains unimodal (Gütig et al., 2003).

The limit between the above two classes of behavior also depends on the strength of the input correlation, so there exists a parameter range for which proper weight specialization only occurs when there is spiking information in the sense of spike-time correlations for two or more input pools (Meffin et al., 2006; Gilson et al., 2010). During this symmetry breaking of initially homogeneous input connections, recurrent connections may play a role (irrespective of their plasticity) so that recurrently connected neurons with excitatory synapses tend to specialize preferably to the same input pathway (Gilson et al., 2009b); this effect is more pronounced for stronger recurrent connections. In **Figure 6B**, only one of the two input correlated pools is selected (with 50% probability in the case of two pools). This group specialization is important to

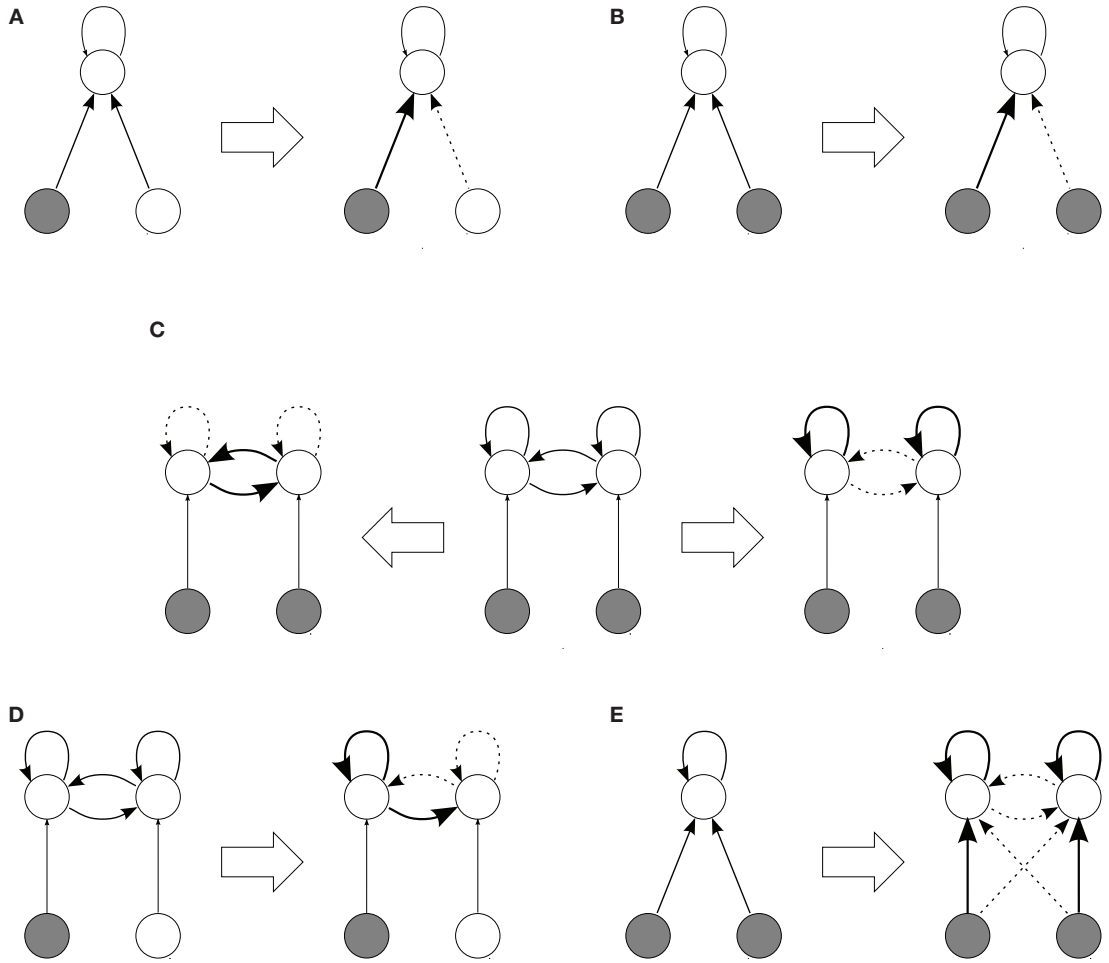

FIGURE 6 | Self-organization scheme in a network (top circles) stimulated by two correlated pools of external inputs (bottom circles). The diagrams represent the connectivity before and after learning (indicated by the block arrows, ⇒ and ⇐). For initial configurations, thin arrows represent fixed connections while thick arrows denote plastic connections. After learning, very thick (resp. dashed) arrows indicate potentiated (depressed) weights. In case **(C)** two different network topologies that can emerge are represented, depending on the particular learning and neuronal parameters. A mathematical analysis of the weight dynamics for configurations in **(A)**, **(B)**, **(C,D)**, and **(E)** can be found in Gilson et al. (2009a), Gilson et al. (2009b), Gilson et al. (2009d), and Gilson et al. (2010), respectively.

obtain consistent input selectivity within areas with strong local feedback, and not "salt-and-pepper" organization where neurons would become selective independently of each other.

Specialization within a network with recurrent connections requires that neurons receive different inputs in terms of firing rates and correlations (Gilson et al., 2009d), which can be obtained after the emergence of input selectivity. As mentioned above, different learning parameters can lead to a strengthening or weakening of feedback within neuronal groups when they receive correlated input. This phenomenon is illustrated in **Figure 6C** by the right and left arrows (⇒ and ⇐) that correspond to **Figures 5A,B**, respectively. In other words, for recurrent delays, a prominent dendritic component favors emergence of strongly connected neuronal groups, whereas a prominent axonal component leads to the converse evolution. Likewise, parameters corresponding to strengthening feedback lead to dominance by the group that receives stronger correlated input than the "other" neurons, which results in the emergence of a feed-forward pathway in an initially homogeneous recurrent network, as illustrated in **Figure 6D**.

The above conclusions describe conditions on the parameters for which the results presented by Song and Abbott (2001) are valid: the rewiring of recurrent connections corresponded to favoring groups that receive more correlated inputs; cf. **Figures 6C(⇒),D**. In a more realistic network with different populations of neurons, such as one with excitatory and inhibitory connections (Morrison et al., 2007) but with different delay components for distinct sets of connections (e.g., dendritic for short-range connections and axonal for medium-range ones), a combination of synchronization and decorrelation between neurons, depending on their spatial location, may well be obtained.

When input and recurrent connections are both plastic, it is possible to arrive at input selectivity as well as specialization of recurrent connections as described above (Gilson et al., 2010). This requires weight-dependent STDP in order to stabilize the mean weights for both input and recurrent connections, and relates to the fact that all incoming plastic weights compete with each other, irrespectively of their input or recurrent nature, and firing

rates may play a role here too. For additive STDP the learning dynamics causes the sets of input and recurrent weights to diverge from each other (Gilson et al., 2010). Splitting of weight distributions, however, is impaired for medium weight dependence (Gütig et al., 2003; Gilson et al., 2010). There is thus a trade-off between stability and competition to obtain proper weight specialization in the sense of separating input weights into distinct groups. In **Figure 6E**, the input structure consisting of the two pools lead the network neurons to organize into two groups in a similar manner to **Figure 6B**, each specialized to only one pool; in addition, the recurrent connections within each neuronal group are strengthened at the expense of the between-group connections, cf. **Figure 6C** (⇒). An interesting point here is that such self-organization does not require a prerequisite network topology since STDP alone can cause neurons to separate into two groups and preserve the consistency of the two input pathways. By this we mean that the information of both input pathways is represented by the synaptic structure after learning and processed by the two resulting neuronal groups.

All typical weight evolution scenarios described in this section hold when applying STDP to homogeneous initial weights. The initial weight distribution can also be of importance, at least for additive-like STDP (Gilson et al., 2009a,c); it was observed in numerical simulation that even weak weight dependence can lead to palimpsest behavior, where previous weight specialization is forgotten after some duration of stimulation using uncorrelated inputs (Gilson et al., 2010).

EXTERNAL STIMULATION USING OSCILLATORY AND "PACEMAKER" ACTIVITY

We now consider two types of stimulating input that have been widely used in conjunction with STDP in recurrent networks, viz., pacemaker-like and oscillatory activity. One reason for their success is that these global periodic phenomena (applied on a whole network, not locally) constrain the spike-time correlograms and, consequently, a global trend for the weight evolution can be sketched. For two neurons chosen arbitrarily in a network with homogeneous and partial connectivity, the stimulating signals we just described induce strong neuron-to-neuron correlation with peaks corresponding to the frequency, as illustrated in **Figure 7**. We can thus predict the synaptic-weight evolution using the convolution of the STDP learning window W and an idealization of such correlograms, in a similar fashion to **Figure 5**, since the periodicity overpowers other correlation effects in the recurrent network, even for medium coupling between them.

For a global "pacemaker" activity with a low frequency (below the time scale of STDP, say, 10 Hz), the effect of delays is similar to the exposition in Section "Input Versus Recurrent Connections" in that purely dendritic delays lead to an increase of within-group connections (Morrison et al., 2007) whereas purely axonal delays can cause STDP to decouple neurons during population bursts (Lubenov and Siapas, 2008). Comparison between the situations where input/output spike trains are uncorrelated and time-locked (i.e., highly correlated) shows that STDP can behave as a BCM rule (Bienenstock et al., 1982) for a single neuron (Standage et al., 2007). Frequency may play a similar role for oscillations, although this does not appear to have been studied in detail. When the intrinsic properties of neurons subject to oscillations determine a specific phase response that tend to desynchronize these neurons (e.g., positive phase-response curve), a network with axonal delays can become partitioned into groups that have no self-feedback, but connections between some of them (Câteau et al., 2008); cf. **Figure 6C**(⇐).

In an all-to-all connected network of heterogeneous oscillators, STDP tends to break coupling between neurons, which can result in asymmetry in the sense of the emergence of feed-forward pathways (Karbowski and Ermentrout, 2002; Masuda and Kori, 2007), in a similar fashion to **Figure 6D**. When this happens, the neuron with highest frequency may end up driving of the rest of the population of oscillators at its own frequency (Takahashi et al., 2009). The propensity of STDP for such time locking is supported by a study of Nowotny et al. (2003b) using a real neuron and a simulated plastic synapse, which showed that STDP can compensate intrinsic neuronal mechanisms to enable synchronization with a stimulating pacemaker. UP and DOWN states of network spiking activity consist in depolarization and hyperpolarization, respectively, for a large portion of the neurons; they can be related to two levels of correlation at the scale of the network. A recurrently connected network with spontaneous UP and DOWN states can organize in a

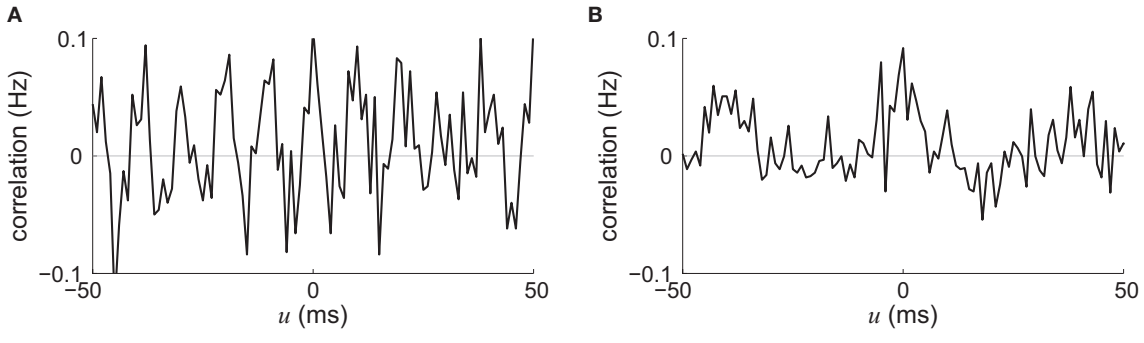

FIGURE 7 | Spike-time cross-correlograms $C_{ij}(\cdot,u)$ for 2 out of 100 recurrently connected neurons with 30% probability that receive (A) oscillatory stimulation at 100 Hz and **(B)** pacemaker-like activity (regular pulse train at 25 Hz). Both input and recurrent delays were chosen equal to 4 ± 1 ms (uniformly distributed in the interval [3,5] ms).

more a feed-forward structure (Kang et al., 2008). Interestingly, the synaptic structure that emerged preserved the transitions between the two states.

EMERGING SYNCHRONIZATION BETWEEN RECURRENT NEURONS

Synchronous firing activity has been discussed as a basis of neuronal information, although a comprehensive understanding of such a mechanism is yet to be elucidated. Since STDP is by essence sensitive to temporal coordination in spike trains, its study is an important aspect of such correlation-based neuronal coding. As evidence of its synchronizing properties, STDP has been demonstrated to shape spike-time correlograms both for a single neuron (Song et al., 2000) and within a recurrent network (Morrison et al., 2007), in contrast to other (non-temporally asymmetric) versions of Hebbian learning (Amit and Brunel, 1997). In a population of synapses with varying properties, STDP can perform delay selection (Gerstner et al., 1996; Kempter et al., 2001; Leibold et al., 2002; Senn, 2002). Here we review recent results on the implications at different topological and temporal scales.

At the mesoscopic scale in a recurrent network, the weight specialization as described in **Figure 6C** can be related to the increase or decrease of synchronization when the recurrent delays $d_{ij}^{\mathrm{ax}} + d_{ij}^{\mathrm{den}}$ are small. Depending on the learning parameters, neurons that receive synchronously correlated input tend to reinforce or eliminate their coupling, which then determines the probability of firing at almost coincident times. In this way a number of studies (cited below) have aimed at understanding how the spiking activity of recurrently connected neurons can be constrained by synaptic plasticity. An increase in synchrony arises from the strengthening of within-group recurrent connections when receiving correlated input (Gilson et al., 2009d), cf. **Figure 6C**($\Rightarrow$). Typical connectivity matrices before and after a learning epoch are represented in **Figures 8A,B**, respectively. The corresponding spike-time correlograms in the absence of external stimulation (i.e., intrinsic to the recurrent connectivity) show stronger "coincident" firing within a range of several times the postsynaptic response (here tens of milliseconds) for two neurons that do not have direct connections but belong to the same group, as illustrated in **Figure 8C**. Likewise, when the network receives external stimulation from two correlated input pools as in **Figure 6C**, the neuronal spike-time correlation is higher for stronger recurrent connections, see **Figure 8D**. This can also be related to a reduction in the variability of the neural response for a single neuron due to STDP, as analyzed using information theory techniques (Bohte and Mozer, 2007). Global synchrony has been obtained by repeatedly stimulating recurrently connected neurons with given spike trains, which resulted in the network behaving as a pacemaker. This evolution of network structure is also related to the concept of synfire chains, where neuronal groups successively activate one another within a feed-forward architecture (Hosaka et al., 2008); see **Figures 8E,F** for an illustrative example with three groups. Similarly, the repeating stimulation of a group of neurons can lead to a synfire chain structure in an initially homogeneous recurrent network provided the divergent growth of outgoing connections due to potentiation by STDP is prevented from taking over the whole network (Jun and Jin, 2007). In contrast, a population of neurons can become decorrelated through synchronous stimulation, as happens when the neurons involved in the burst are not the same for each burst. Then no causal (feed-forward) network structure emerges since synchronization does not involve a growing population of neurons (Lubenov and Siapas, 2008); cf. **Figure 6C**($\Leftarrow$) for different neuronal subgroups of the network at each burst time. In agreement with the theory in Section "Input Versus Recurrent Connections," the time constants of the STDP learning window can also determine whether the network is constrained to synchronized (e.g., successive firing of several groups) or asynchronous activity (Kitano et al., 2002).

In the case of inhomogeneous delays in a recurrent network, STDP can lead to distributed synchronization over time for neuronal groups at the microscopic scale (Izhikevich, 2006). This concept has been coined as polychronization and consists of neuronal groups whose firing is time locked in accordance to the synaptic delays of the connections between these neurons. In a network, such functional groups of, say, tens of neurons then fire sequences of spikes; note that a neuron can take part in several groups and the synaptic connections for a given group may be cyclic or not. A group is tagged as active when a large portion (e.g., 50%) of its members fires with the corresponding timing. Such self-organization can occur even without external stimulation, but then one crucial feature in obtaining stable functional groups that persist over time is the degree of coupling between individual neurons. Such spike-time precision can also be obtained in parallel to oscillatory spiking activity at the scale of a population of neurons, hence providing two different levels of synchrony (Shen et al., 2008).

INPUT REPRESENTATION AND APPLICATIONS

The same dynamical ingredients highlighted above have been used to train single neurons and networks for classification and/or detection tasks, many of which involved more elaborate input spike trains than the pools of narrowly correlated spikes considered above (although most of these studies where done using numerical simulations). We briefly review some of these studies as an illustration of applications for the theoretical framework presented above.

Note that learning based on the covariance between firing rates has been used to extract most significant features (in the sense of a principal component analysis) within input stimuli (Sejnowski, 1977; Oja, 1982). In the case of STDP, such features mainly relate to spike-time correlations (van Rossum and Turrigiano, 2001; Gilson et al., 2009a,d). When input spike trains have reliable spike times down to the scale of a millisecond, they convey temporal information that can be picked up by a suitable temporal plasticity rule (Delorme et al., 2001). It has been demonstrated that STDP can train a single neuron to detect a given spike pattern with no specific structure once the pattern is repeatedly presented among noisy spike trains that have similar firing rates (Masquelier et al., 2008). This propensity of STDP to capture spiking information and generate proper input selectivity can explain the storage of sequences of spikes and their retrieval using cues (namely the start of the sequences) using a network with (all-to-all) plastic recurrent connections (Nowotny et al., 2003a). Similarly, patterns relying on oscillatory spiking activity have also been successfully learnt in a recurrent network of oscillatory neurons (Marinaro et al., 2007). STDP can also be used for

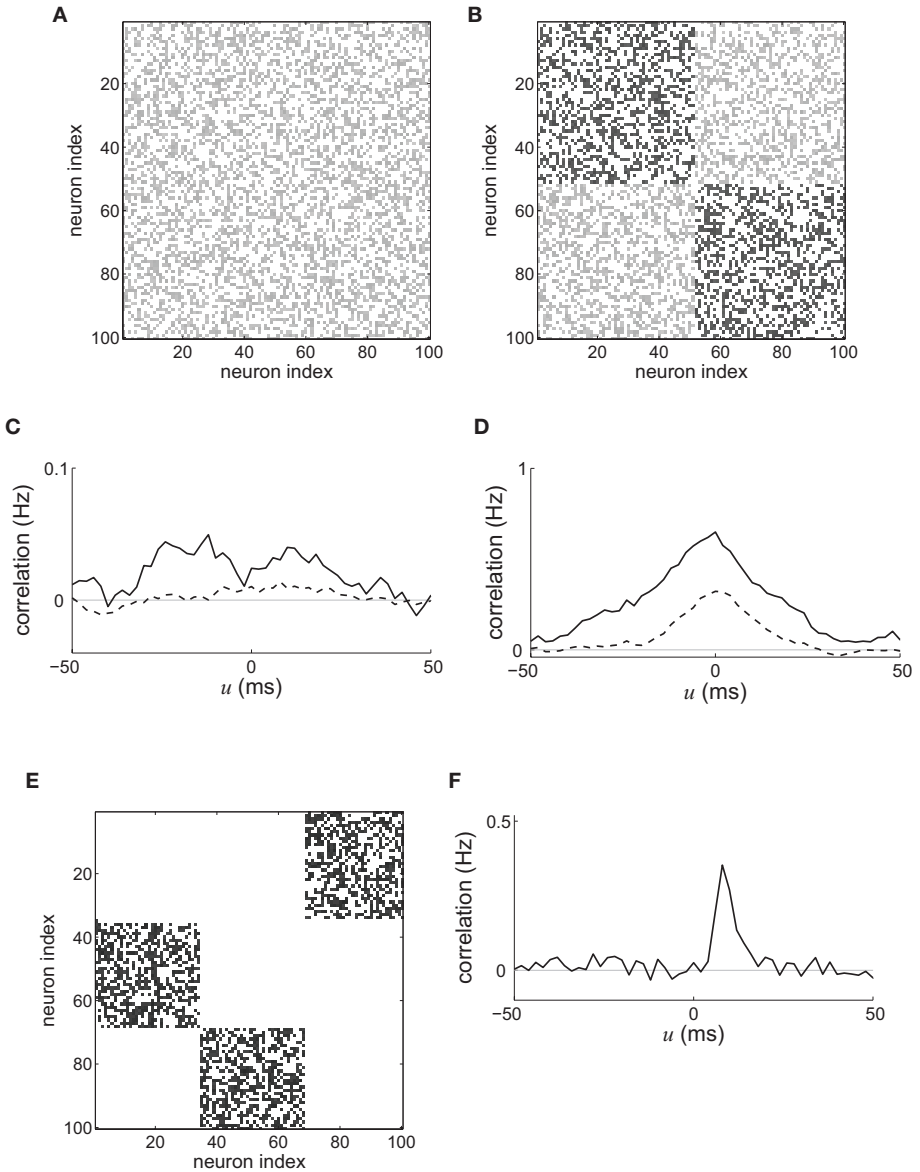

FIGURE 8 | Typical connectivity matrices for recurrent connections (A) before and **(B)** after a learning epoch during which the weight specialization due to STDP corresponds to Figure 6C(⇒). Darker pixels indicate stronger weights. **(C)** Resulting spike-time correlograms for two neurons within the same emerged group in the recurrently connected network that only receives spontaneous (homogeneous) excitation before (dashed curve) and after (solid curve) the above mentioned weight specialization. These neurons do not have direct synaptic connections between each other. **(D)** Similar to **(C)** with external stimulation from two delta-correlated pools similar to **Figure 6C**. **(E)** Connectivity matrix corresponding to three groups forming a feed-forward loop. **(F)** Spike-time correlogram (averaged over several neurons) between two successively connected groups when the first group receives correlated external stimulation.

phase coding in networks with oscillatory activity (Lengyel et al., 2005; Masquelier et al., 2009). Such theoretical studies are further steps toward a better understanding of recent experimental findings with neurons in the auditory pathway known to experience STDP: these neurons can change their spectrum responses after receiving stimulation using combinations of their preferred/non-preferred frequencies (Dahmen et al., 2008).

Self-organizing neural maps provide an interesting example of how networks can build a representation of many input stimuli, though they need not always rely on neuronal characteristics (Kohonen, 1982). STDP has been shown capable of generating such a topological unsupervised organization in a recurrent neuronal network with spatial extension; for example, to detect ITDs (Leibold et al., 2002) and to reproduce an orientation map similar to that observed in the visual cortex (Wenisch et al., 2005). Training lateral (internal recurrent) connections crucially determines the shape of orientation fields in such maps (Bartsch and van Hemmen, 2001). When several sensory neuronal maps have been established, STDP can further learn mappings between these maps (Davison and Frégnac, 2006; Friedel and van Hemmen, 2008), in this way performing multimodal integration of sensory stimuli.

Another abstract concept to learn and detect general spiking signals has appeared recently, which does not rely on an emerging topological organization. For instance, in the liquid-state machine a recurrently connected network behaves as a reservoir that performs many arbitrary operations on the inputs, which allows simple supervised training to discriminate between different classes of input (Maass et al., 2002). Recent studies have shown that STDP applied on the recurrent network can boost the performance of the detection by such a system, by tuning the operations performed by the reservoir, which can be seen as a projection of the input signals onto a large-dimensional space (Henry et al., 2007; Carnell, 2009; Lazar et al., 2009). The resulting information encoding is then distributed, but hidden, in the learned synaptic structure, which can be analyzed in the spiking activity at a fine time scale, e.g., by polychronized groups (Paugam-Moisy et al., 2008). Altogether, STDP is capable of organizing a recurrent neuronal network to exhibit specific spiking activity depending on the presentation of input stimuli, as illustrated in **Figure 9**.

Finally, a number of studies focused on linking STDP to more abstract schemes of processing neuronal (spiking) information. A plasticity rule with probabilistic change for the weights has been found to modulate the speed of learning/forgetting (Fusi, 2002). A similar concept of non-deterministic modification in the weight strength for STDP proved to be fruitful in terms of capturing multi-correlation between input and output spike trains (Appleby and Elliott, 2007). STDP has also been demonstrated to be capable of training a single neuron to perform a broad range of operations for input–output mapping on the spike trains (Legenstein et al., 2005). Recently, STDP has been used to perform an independent component analysis on input signals that mimic retinal influx (Clopath et al., 2010). Using information theory, STDP has been related to optimality in supervised and unsupervised learning (Toyoizumi et al., 2005, 2007; Pfister et al., 2006; Bohte and Mozer, 2007). These contributions are important steps toward a global picture of the functional implications of STDP at a higher level of abstraction.

CONCLUSION

Spike-timing-dependent plasticity has led to a re-evaluation of our understanding of Hebbian learning, in particular by discriminating between rate-based and spike-based contributions to synaptic plasticity for which temporal causality plays a crucial role. The resulting learning dynamics appears richer than what can be obtained by rate-based plasticity rules, in the sense that STDP alone can generate a mixture of stability and competition on different time scales. For neurons communicate through spikes and not rates, a procedure such as STDP is quite natural, whereas rates are an afterthought.

In a recurrently connected neuronal network, the weight evolution is determined by an interplay between the STDP parameters, neuronal properties, input correlation structure and network topology. The functional implications of the resulting organization, which can be unsupervised or supervised, have been the subject of intense research recently. For both single neurons and recurrent networks, it has been demonstrated how STDP can generate a network structure that accurately reflects the synaptic input representation for a broad range of stimuli, which can lead to neuronal sensory maps or implicit representation in networks. In particular, the study of the emerging (pairwise or higher-order) correlation structure has started to uncover some interesting properties of trained networks that are hypothesized to play an important role in information encoding schemes.

It is not yet clear, however, what underlying algorithm on the stimuli signals is performed through the weight dynamics, and how STDP encodes the input structure into the synaptic weight. This research may establish links between physiological learning mechanisms and the more abstract domain of machine learning, hence expanding our understanding of the functional role of synaptic plasticity in the brain.

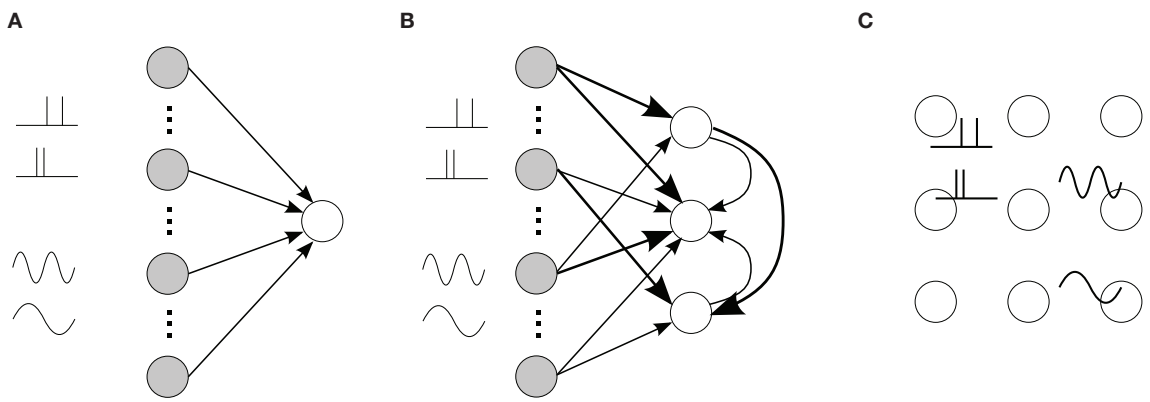

FIGURE 9 | (A) Single neuron (open circle) excited by external input neurons (filled circles) that correspond to specific spike-time correlation structure, such as oscillatory activity and spike patterns. The four thumbnail sketches on the LHS of the plot represent two different types of input correlation structure: inputs containing a repeated spike patterns (top two thumbnails) and inputs with an oscillating firing rate (bottom two thumbnails). **(B)** Strengthening of some input and recurrent connections (thick arrows) for several such neurons. **(C)** Resulting specialization of some areas (neighbor neurons) in the network to some of the presented stimuli (thumbnails), which implies differentiated topological spiking activity depending on the presented stimulus. External inputs are not represented in **(C)**.

ACKNOWLEDGMENTS

Matthieu Gilson was funded by scholarships from the University of Melbourne and NICTA. J. Leo van Hemmen is partially supported by the BCCN–Munich. Funding is acknowledged from the Australian Research Council (ARC Discovery Projects #DP0771815 and #DP1096699). The Bionic Ear Institute acknowledges the support it receives from the Victorian Government through its Operational Infrastructure Support Program.

REFERENCES

Amit, D. J., and Brunel, N. (1997). Dynamics of a recurrent network of spiking neurons before and following learning. *Netw. Comput. Neural Syst.* 8, 373–404.

Appleby, P. A., and Elliott, T. (2006). Stable competitive dynamics emerge from multispike interactions in a stochastic model of spike-timing-dependent plasticity. *Neural Comput.* 18, 2414–2464.

Appleby, P. A., and Elliott, T. (2007). Multispike interactions in a stochastic model of spike-timing-dependent plasticity. *Neural Comput.* 19, 1362–1399.

Bartsch, A. P., and van Hemmen, J. L. (2001). Combined Hebbian development of geniculocortical and lateral connectivity in a model of primary visual cortex. *Biol. Cybern.* 84, 41–55.

Bi, G. Q., and Poo, M. M. (1998). Synaptic modifications in cultured hippocampal neurons: dependence on spike timing, synaptic strength, and postsynaptic cell type. *J. Neurosci.* 18, 10464–10472.

Bienenstock, E. L., Cooper, L. N., and Munro, P. W. (1982). Theory for the development of neuron selectivity – orientation specificity and binocular interaction in visual-cortex. *J. Neurosci.* 2, 32–48.

Bohte, S. M., and Mozer, M. C. (2007). Reducing the variability of neural responses: a computational theory of spike-timing-dependent plasticity. *Neural Comput.* 19, 371–403.

Burkitt, A. N., Gilson, M., and van Hemmen, J. L. (2007). Spike-timing-dependent plasticity for neurons with recurrent connections. *Biol. Cybern.* 96, 533–546.

Burkitt, A. N., Meffin, H., and Grayden, D. B. (2004). Spike-timing-dependent plasticity: the relationship to rate-based learning for models with weight dynamics determined by a stable fixed point. *Neural Comput.* 16, 885–940.

Butts, D. A., Kanold, P. O., and Shatz, C. J. (2007). A burst-based "Hebbian" learning rule at retinogeniculate synapses links retinal waves to activity-dependent refinement. *PLoS Biol.* 5, e61. doi:10.1371/journal.pbio.0050061.

Caporale, N., and Dan, Y. (2008). Spike timing-dependent plasticity: a Hebbian learning rule. *Annu. Rev. Neurosci.* 31, 25–46.

Carnell, A. (2009). An analysis of the use of Hebbian and anti-Hebbian spike time dependent plasticity learning functions within the context of recurrent spiking neural networks. *Neurocomputing* 72, 685–692.

Carr, C. E., and Konishi, M. (1990). A circuit for detection of interaural time differences in the brain-stem of the barn owl. *J. Neurosci.* 10, 3227–3246.

Câteau, H., Kitano, K., and Fukai, T. (2008). Interplay between a phase response curve and spike-timing-dependent plasticity leading to wireless clustering. *Phys. Rev. E* 77, 051909.

Clopath, C., Büsing, L., Vasilaki, E., and Gerstner, W. (2010). Connectivity reflects coding: a model of voltage-based STDP with homeostasis. *Nat. Neurosci.* 13, 344–352.

Dahmen, J. C., Hartley, D. E., and King, A. J. (2008). Stimulus-timing-dependent plasticity of cortical frequency representation. *J. Neurosci.* 28, 13629–13639.

Dan, Y., and Poo, M. M. (2006). Spike timing-dependent plasticity: from synapse to perception. *Physiol. Rev.* 86, 1033–1048.

Davison, A. P., and Frégnac, Y. (2006). Learning cross-modal spatial transformations through spike timing-dependent plasticity. *J. Neurosci.* 26, 5604–5615.

Delorme, A., Perrinet, L., and Thorpe, S. J. (2001). Networks of integrate-and-fire neurons using rank order coding B: spike timing dependent plasticity and emergence of orientation selectivity. *Neurocomputing* 38, 539–545.

Friedel, P., and van Hemmen, J. L. (2008). Inhibition, not excitation, is the key to multimodal sensory integration. *Biol. Cybern.* 98, 597–618.

Froemke, R. C., and Dan, Y. (2002). Spike-timing-dependent synaptic modification induced by natural spike trains. *Nature* 416, 433–438.

Froemke, R. C., Poo, M. M., and Dan, Y. (2005). Spike-timing-dependent synaptic plasticity depends on dendritic location. *Nature* 434, 221–225.

Froemke, R. C., Tsay, I. A., Raad, M., Long, J. D., and Dan, Y. (2006). Contribution of individual spikes in burst-induced long-term synaptic modification. *J. Neurophysiol.* 95, 1620–1629.

Fusi, S. (2002). Hebbian spike-driven synaptic plasticity for learning patterns of mean firing rates. *Biol. Cybern.* 87, 459–470.

Gerstner, W., Kempter, R., van Hemmen, J. L., and Wagner, H. (1996). A neuronal learning rule for sub-millisecond temporal coding. *Nature* 383, 76–78.

Gerstner, W., and Kistler, W. M. (2002). Mathematical formulations of Hebbian learning. *Biol. Cybern.* 87, 404–415.

Gerstner, W., Ritz, R., and van Hemmen, J. L. (1993). Why spikes? Hebbian learning and retrieval of time-resolved excitation patterns. *Biol. Cybern.* 69, 503–515.

Gilson, M., Burkitt, A. N., Grayden, D. B., Thomas, D. A., and van Hemmen, J. L. (2009a). Emergence of network structure due to spike-timing-dependent plasticity in recurrent neuronal networks. I: input selectivity – strengthening correlated input pathways. *Biol. Cybern.* 101, 81–102.

Gilson, M., Burkitt, A. N., Grayden, D. B., Thomas, D. A., and van Hemmen, J. L. (2009b). Emergence of network structure due to spike-timing-dependent plasticity in recurrent neuronal networks. II: input selectivity – symmetry breaking. *Biol. Cybern.* 101, 103–114.

Gilson, M., Burkitt, A. N., Grayden, D. B., Thomas, D. A., and van Hemmen, J. L. (2009c). Emergence of network structure due to spike-timing-dependent plasticity in recurrent neuronal networks. III: partially connected neurons driven by spontaneous activity. *Biol. Cybern.* 101, 411–426.

Gilson, M., Burkitt, A. N., Grayden, D. B., Thomas, D. A., and van Hemmen, J. L. (2009d). Emergence of network structure due to spike-timing-dependent plasticity in recurrent neuronal networks. IV: structuring synaptic pathways among recurrent connections. *Biol. Cybern.* 101, 427–444.

Gilson, M., Burkitt, A. N., Grayden, D. B., Thomas, D. A., and van Hemmen, J. L. (2010). Emergence of network structure due to spike-timing-dependent plasticity in recurrent neuronal networks. V: self-organization schemes and weight dependence. *Biol. Cybern* (accepted).

Graupner, M., and Brunel, N. (2007). STDP in a bistable synapse model based on CaMKII and associated signaling pathways. *PLoS Comput. Biol.* 3, 2299–2323. doi:10.1371/journal.pcbi.0030221.

Gütig, R., Aharonov, R., Rotter, S., and Sompolinsky, H. (2003). Learning input correlations through nonlinear temporally asymmetric Hebbian plasticity. *J. Neurosci.* 23, 3697–3714.

Hartley, M., Taylor, N., and Taylor, J. (2006). Understanding spike-time-dependent plasticity: a biologically motivated computational model. *Neurocomputing* 69, 2005–2016.

Hebb, D. O. (1949). *The Organization of Behavior: A Neuropsychological Theory.* New York, NY, Wiley.

Henry, F., Dauce, E., and Soula, H. (2007). Temporal pattern identification using spike-timing dependent plasticity. *Neurocomputing* 70, 2009–2016.

Hosaka, R., Araki, O., and Ikeguchi, T. (2008). STDP provides the substrate for igniting synfire chains by spatiotemporal input patterns. *Neural Comput.* 20, 415–435.

Izhikevich, E. M. (2006). Polychronization: computation with spikes. *Neural Comput.* 18, 245–282.

Izhikevich, E. M., and Desai, N. S. (2003). Relating STDP to BCM. *Neural Comput.* 15, 1511–1523.

Jun, J. K., and Jin, D. Z. (2007). Development of neural circuitry for precise temporal sequences through spontaneous activity, axon remodeling, and synaptic plasticity. *PLoS ONE* 2, e723. doi:10.1371/journal.pone.0000723.

Kang, S., Isomura, Y., Takekawa, T., Câteau, H., and Fukai, T. (2008). Multineuronal dynamics in rat neocortex and hippocampus during natural sleep. *Neurosci. Res.* 61, S189–S189.

Karbowski, J., and Ermentrout, G. B. (2002). Synchrony arising from a balanced synaptic plasticity in a network of heterogeneous neural oscillators. *Phys. Rev. E* 65, 031902.

Kempter, R., Gerstner, W., and van Hemmen, J. L. (1999). Hebbian learning and spiking neurons. *Phys. Rev. E* 59, 4498–4514.

Kempter, R., Gerstner, W., and van Hemmen, J. L. (2001). Intrinsic stabilization of output rates by spike-based Hebbian learning. *Neural Comput.* 13, 2709–2741.

Kistler, W. M., and van Hemmen, J. L. (2000). Modeling synaptic plasticity in conjunction with the timing of pre- and postsynaptic action potentials. *Neural Comput.* 12, 385–405.

Kitano, K., Câteau, H., and Fukai, T. (2002). Self-organization of memory activity through spike-timing-dependent plasticity. *Neuroreport* 13, 795–798.

Kohonen, T. (1982). Self-organized formation of topologically correct feature maps. *Biol. Cybern.* 43, 59–69.

Konishi, M. (1993). Listening with two ears. *Sci. Am.* 268, 66–73.

Krumin, M., and Shoham, S. (2009). Generation of spike trains with controlled auto- and cross-correlation functions. *Neural Comput.* 21, 1642–1664.

Lazar, A., Pipa, G., and Triesch, J. (2009). SORN: a self-organizing recurrent neural network. *Front. Comput. Neurosci.* 3:23. doi:10.3389/neuro.10.023.2009.

Legenstein, R., Naeger, C., and Maass, W. (2005). What can a neuron learn with spike-timing-dependent plasticity? *Neural Comput.* 17, 2337–2382.

Leibold, C., Kempter, R., and van Hemmen, J. L. (2002). How spiking neurons give rise to a temporal-feature map: from synaptic plasticity to axonal selection. *Phys. Rev. E* 65, 051915.

Lengyel, M., Kwag, J., Paulsen, O., and Dayan, P. (2005). Matching storage and recall: hippocampal spike timing-dependent plasticity and phase response curves. *Nat. Neurosci.* 8, 1677–1683.

Levy, W. B., and Steward, O. (1983). Temporal contiguity requirements for long-term associative potentiation depression in the hippocampus. *Neuroscience* 8, 791–797.

Lubenov, E. V., and Siapas, A. G. (2008). Decoupling through synchrony in neuronal circuits with propagation delays. *Neuron* 58, 118–131.

Maass, W., Natschlager, T., and Markram, H. (2002). Real-time computing without stable states: a new framework for neural computation based on perturbations. *Neural Comput.* 14, 2531–2560.

Macke, J. H., Berens, P., Ecker, A. S. Tolias, A. S., and Bethge, M. (2009). Generating spike trains with specified correlation coefficients. *Neural Comput.* 21, 397–423.

Marinaro, M., Scarpetta, S., and Yoshioka, M. (2007). Learning of oscillatory correlated patterns in a cortical network by a STDP-based learning rule. *Math. Biosci.* 207, 322–335.

Markram, H., Lübke, J., Frotscher, M., and Sakmann B. (1997). Regulation of synaptic efficacy by coincidence of postsynaptic APs and EPSPs. *Science* 275, 213–215.

Masquelier, T., Guyonneau, R., and Thorpe, S. J. (2008). Spike timing dependent plasticity finds the start of repeating patterns in continuous spike trains. *PLoS ONE* 3, e1377. doi:10.1371/journal.pone.0001377.

Masquelier, T., Hugues, E., Deco, G., and Thorpe, S. J. (2009). Oscillations, phase-of-firing coding, and spike-timing-dependent plasticity: an efficient learning scheme. *J. Neurosci.* 29, 13484–13493.

Masuda, N., and Kori, H. (2007). Formation of feedforward networks and frequency synchrony by spike-timing-dependent plasticity. *J. Comput. Neurosci.* 22, 327–345.

Meffin, H., Besson, J., Burkitt, A. N., and Grayden, D. B. (2006). Learning the structure of correlated synaptic subgroups using stable and competitive spike-timing-dependent plasticity. *Phys. Rev. E* 73, 041911.

Moreno-Bote, R., Renart, A., and Parga, N. (2008). Theory of input spike auto- and cross-correlations and their effect on the response of spiking neurons. *Neural Comput.* 20, 1651–1705.

Morrison, A., Aertsen, A., and Diesmann, M. (2007). Spike-timing-dependent plasticity in balanced random networks. *Neural Comput.* 19, 1437–1467.

Morrison, A., Diesmann, M., and Gerstner, W. (2008). Phenomenological models of synaptic plasticity based on spike timing. *Biol. Cybern.* 98, 459–478.

Nowotny, T., Rabinovich, M. I., and Abarbanel, H. D. I. (2003a). Spatial representation of temporal information through spike-timing-dependent plasticity. *Phys. Rev. E* 68, 011908.

Nowotny, T., Zhigulin, V. P., Selverston, A. I., Abarbanel, H. D. I., and Rabinovich, M. I. (2003b). Enhancement of synchronization in a hybrid neural circuit by spike-timing dependent plasticity. *J. Neurosci.* 23, 9776–9785.

Oja, E. (1982). A simplified neuron model as a principal component analyzer. *J. Math. Biol.* 15, 267–273.

Paugam-Moisy, H., Martinez, R., and Bengio, S. (2008). Delay learning and polychronization for reservoir computing. *Neurocomputing* 71, 1143–1158.

Pfister, J.-P., and Gerstner, W. (2006). Triplets of spikes in a model of spike timing-dependent plasticity. *J. Neurosci.* 26, 9673–9682.

Pfister, J.-P., Toyoizumi, T., Barber, D., and Gerstner, W. (2006). Optimal spike-timing-dependent plasticity for precise action potential firing in supervised learning. *Neural Comput.* 18, 1318–1348.

Sejnowski, T. J. (1977). Storing covariance with nonlinearly interacting neurons. *J. Math. Biol.* 4, 303–321.

Senn, W. (2002). Beyond spike timing: the role of nonlinear plasticity and unreliable synapses. *Biol. Cybern.* 87, 344–355.

Shen, X., Lin, X. B., and De Wilde, P. (2008). Oscillations and spiking pairs: behavior of a neuronal model with STDP learning. *Neural Comput.* 20, 2037–2069.

Sjöström, P. J., Turrigiano, G. G., and Nelson, S. B. (2001). Rate, timing, and cooperativity jointly determine cortical synaptic plasticity. *Neuron* 32, 1149–1164.

Song, S., and Abbott, L. F. (2001). Cortical development and remapping through spike timing-dependent plasticity. *Neuron* 32, 339–350.

Song, S., Miller, K. D., and Abbott, L. F. (2000). Competitive Hebbian learning through spike-timing-dependent synaptic plasticity. *Nat. Neurosci.* 3, 919–926.

Sprekeler, H., Michaelis, C., and Wiskott, L. (2007). Slowness: an objective for spike-timing-dependent plasticity? *PLoS Comput. Biol.* 3, 1136–1148. doi:10.1371/journal.pcbi.0030112.

Standage, D., Jalil, S., and Trappenberg, T. (2007). Computational consequences of experimentally derived spike-time and weight dependent plasticity rules. *Biol. Cybern.* 96, 615–623.

Staude, B., Rotter, S., and Grun, S. (2008). Can spike coordination be differentiated from rate covariation? *Neural Comput.* 20, 1973–1999.

Stuart, G., Spruston, N., Sakmann, B., and Häusser, M. (1997). Action potential initiation and backpropagation in neurons of the mammalian CNS. *Trends Neurosci.* 20, 125–131.

Takahashi, Y. K., Kori, H., and Masuda, N. (2009). Self-organization of feedforward structure and entrainment in excitatory neural networks with spike-timing-dependent plasticity. *Phys. Rev. E* 79, 051904.

Toyoizumi, T., Pfister, J.-P., Aihara, K., and Gerstner, W. (2005). Generalized Bienenstock–Cooper–Munro rule for spiking neurons that maximizes information transmission. *Proc. Natl. Acad. Sci. U.S.A.* 102, 5239–5244.

Toyoizumi, T., Pfister, J.-P., Aihara, K., and Gerstner, W. (2007). Optimality model of unsupervised spike-timing-dependent plasticity: synaptic memory and weight distribution. *Neural Comput.* 19, 639–671.

Turrigiano, G. G. (2008). The self-tuning neuron: synaptic scaling of excitatory synapses. *Cell* 135, 422–435.

Tzounopoulos, T., Kim, Y., Oertel, D., and Trussell, L. O. (2004). Cell-specific, spike timing-dependent plasticities in the dorsal cochlear nucleus. *Nat. Neurosci.* 7, 719–725.

van Hemmen, J. L. (2001). "Theory of synaptic plasticity (Chapter 18)," in *Handbook of Biological Physics*, Vol. 4, *Neuro-informatics and Neural Modelling*, eds F Moss and S Gielen (Amsterdam: Elsevier), 771–823.

van Rossum, M. C. W., Bi, G. Q., and Turrigiano, G. G. (2000). Stable Hebbian learning from spike timing-dependent plasticity. *J. Neurosci.* 20, 8812–8821.

van Rossum, M. C. W., and Turrigiano, G. G. (2001). Correlation based learning from spike timing dependent plasticity. *Neurocomputing* 38, 409–415.

Wenisch, O. G., Noll, J., and van Hemmen, J. L. (2005). Spontaneously emerging direction selectivity maps in visual cortex through STDP. *Biol. Cybern.* 93, 239–247.

Woodin, M. A., Ganguly, K., and Poo, M. M. (2003). Coincident pre- and postsynaptic activity modifies GABAergic synapses by postsynaptic changes in Cl^- transporter activity. *Neuron* 39, 807–820.

Zou, Q., and Destexhe, A. (2007). Kinetic models of spike-timing dependent plasticity and their functional consequences in detecting correlations. *Biol. Cybern.* 97, 81–97.

Conflict of Interest Statement: The authors declare that the research was conducted in the absence of any commercial or financial relationships that could be construed as a potential conflict of interest.

Received: 01 March 2010; paper pending published: 18 May 2010; accepted: 28 June 2010; published online: 10 September 2010.

Citation: Gilson M, Burkitt A and van Hemmen JL (2010) STDP in recurrent neuronal networks. Front. Comput. Neurosci. ***4****:23. doi: 10.3389/fncom.2010.00023*

frontiers in
SYNAPTIC NEUROSCIENCE

REVIEW ARTICLE
published: 10 June 2010
doi: 10.3389/fnsyn.2010.00010

STDP and mental retardation: dysregulation of dendritic excitability in Fragile X syndrome

Rhiannon M. Meredith* and Huibert D. Mansvelder

Department of Integrative Neurophysiology, Center for Neurogenomics and Cognitive Research, Neuroscience Campus Amsterdam, VU University, Amsterdam, Netherlands

Edited by:
Per Jesper Sjöström, University College London, UK

Reviewed by:
Niraj S. Desai, The Neurosciences Institute, USA
Gül Dölen, Massachusetts Institute of Technology, USA

****Correspondence:***
Rhiannon M. Meredith, Department of Integrative Neurophysiology, Center for Neurogenomics and Cognitive Research, Neuroscience Campus Amsterdam, VU University, De Boelelaan 1085, 1081 HV Amsterdam, Netherlands.
e-mail: rhiannon.meredith@cncr.vu.nl

Development of cognitive function requires the formation and refinement of synaptic networks of neurons in the brain. Morphological abnormalities of synaptic spines occur throughout the brain in a wide variety of syndromic and non-syndromic disorders of mental retardation (MR). In both neurons from human post-mortem tissue and mouse models of retardation, the changes observed in synaptic spine and dendritic morphology can be subtle, in the range of 10–20% alterations for spine protrusion length and density. Functionally, synapses in hippocampus and cortex show deficits in long-term potentiation (LTP) and long-term depression (LTD) in an array of neurodevelopmental disorders including Down's, Angelman, Fragile X and Rett syndrome. Recent studies have shown that in principle the machinery for synaptic plasticity is in place in these synapses, but that significant alterations in spike-timing-dependent plasticity (STDP) induction rules exist in cortical synaptic pathways of Fragile X MR syndrome. In this model, the threshold for inducing timing-dependent long-term potentiation (tLTP) is increased in these synapses. Increased postsynaptic activity can overcome this threshold and induce normal levels of tLTP. In this review, we bring together recent studies investigating STDP in neurodevelopmental learning disorders using Fragile X syndrome as a model and we argue that alterations in dendritic excitability underlie deficits seen in STDP. Known and candidate dendritic mechanisms that may underlie the plasticity deficits are discussed. Studying STDP in monogenic MR syndromes with clear deficits in information processing at the cognitive level also provides the field with an opportunity to make direct links between cognition and processing rules at the synapse during development.

Keywords: STDP, mental retardation, Fragile X syndrome, LTP, dendritic excitability, calcium, spine, dendrite

INTRODUCTION: MENTAL RETARDATION, SYNAPSE PATHOLOGY AND PLASTICITY

The formation and refinement of synaptic connections in the brain is crucial for development of cognitive function. Changing synaptic strength is widely believed to be a cellular mechanism underlying storage of information in the brain (Martin et al., 2000). Mental retardation (MR) is characterized by deficits in learning and memory with significantly low IQ levels (<70) and often accompanied by impaired social communication and autistic traits. Over the last decade, traditional methods for studying synaptic plasticity in mouse models for MR syndromes have revealed alterations in long-term potentiation (LTP) and long-term depression (LTD) using tetanic stimulation protocols or chemical induction methods. Deficits in LTP using these paradigms are reported in hippocampal and cortical synapses in an array of syndromes including Down's (Siarey et al., 1997), Angelman (Jiang et al., 1998; Weeber et al., 2003), Fragile X (Li et al., 2002) and Rett syndrome (Asaka et al., 2006; Moretti et al., 2006). A number of impairments in intracellular signaling pathways are implicated in these differing forms of retardation, which often have co-morbidity for autistic traits and epilepsy. However, this variety of signaling deficits all lead to changes in synaptic plasticity and show abnormalities in dendrite and synaptic structures in the brain.

SYNAPSE AND DENDRITE STRUCTURAL ABNORMALITIES

There are many signaling pathways implicated in the underlying causes of MR but the majority have direct interactions with Rho, Rac and Ras small GTPases (Ramakers, 2002; Newey et al., 2005). These proteins are all key regulators of the actin and microtubule cytoskeleton and affect both the structure and function of dendrites and synapses. A morphological characteristic common to many different forms of syndromic and non-syndromic MR is an altered filopodia-to-spine ratio and abnormal distribution of dendritic protrusions in both humans and mouse models for MR (Ramakers, 2002). The majority of excitatory synapses in the brain are made on to these dendritic protrusions. Over the course of normal development, long, thin filopodia commonly found in immature networks are replaced in later stages by shorter, more stubby spines (Harris, 1999). Spine abnormalities in MR are seen in many different brain regions and during both early and late stages of postnatal development (Purpura, 1974). For example, in the Fmr1-KO mouse model of Fragile X syndrome, more immature filopodial protrusions are observed along with an increased protrusion density along the dendrite (Irwin et al., 2000) and are seen from the end of the first postnatal week (Nimchinsky et al., 2001). In Rett syndrome, differing spine distribution patterns are reported in mouse models but the overall consensus is

of a decrease in spine density at symptomatic stages, in line with findings in human post-mortem tissue and methyl CpG binding protein 2 (MeCP2) knockdown in cell cultures (Chapleau et al., 2009). Manipulation of expression levels of Rho and Rac GTPases in cultured neurons also leads to clear changes in spine morphology. Expression of a constitutively active form of Rac in mice leads to increased spine density and reduction in spine size (Luo et al., 1996; Tashiro et al., 2000). In contrast, expression of constitutively active Rho led to dramatic decreases in spine density, reduction in spine length and in some cases an absence of spines on pyramidal neurons (Tashiro et al., 2000).

Abnormalities of dendrite morphology in the brain are also a feature common to many different forms of MR (Kaufmann and Moser, 2000; Nadif Kasri and Van Aelst, 2008). The distribution of dendritic branching patterns shows abnormalities in cortical neurons in genetic forms of MR, such as Rett and Fragile X syndromes, (Kaufmann and Moser, 2000; Galvez et al., 2003; Restivo et al., 2005). Dendritic morphology is significantly altered following alteration of Rac and Rho expression levels, with Rac and Cdc42 increasing the growth and branching of neurites whereas Rho may act to negatively regulate dendritic growth (Threadgill et al., 1997; Negishi and Katoh, 2005). Thus, Rac and Rho both play a role in spine and dendrite morphology, with Rac promoting protrusion and branch growth and Rho having a regulatory role in dendrite and spine formation and maintenance. In the Fmr1-KO mouse model, Fragile X Mental Retardation Protein (FMRP) interacts directly with two cytoplastic proteins located in synaptosome extracts, CYFIP1/2 (Schenck et al., 2001), with CYFIP1 interacting with Rac1 small Rho GTPase (Kobayashi et al., 1998). Mutations in regulators and effectors of Rho GTPases have been associated with MR (Nadif Kasri and Van Aelst, 2008). Thus, effects upon spine dysmorphogenesis single gene MR disorders are likely to arise via effects mediated by interactions with pathways such as Rho and Rac signaling cascades.

The direct influence of spine morphology on spike-timing-dependent plasticity (STDP) has not been widely studied, although the effects of spine shape upon biochemical and electrical compartmentalization of synaptic input and AP backpropagation are beginning to be understood (see later section on 'Dendritic Excitability'). Geometry of the postsynaptic spine is correlated with functional AMPA receptor expression, with thin long-necked protrusions showing little or no sensitivity to synaptic glutamate and thicker spines of greater volume showing large glutamate-induced synaptic currents (Matsuzaki et al., 2001). Thus the greater proportion of longer protrusions reported in Fragile X syndrome, particularly in early cortical development (Nimchinsky et al., 2001) may account for a higher proportion of silent synapses observed in sensory cortex (Harlow et al., 2010). Changes in dendritic spines and dendritic branching underlying MR syndromes can be small, in the region of 10–20% in cortex and hippocampus. These small structural changes cause only modest or no significant effects on the somatic-recordings of overall baseline measures of quantal synaptic function in MR models (Jiang et al., 1998; Braun and Segal, 2000; Desai et al., 2006; Pfeiffer and Huber, 2007; Best et al., 2008). However, these structural changes and the intracellular signaling mediated across the synaptic junctions have significant effects upon the synaptic plasticity in cortical and hippocampal circuits. In the Fmr1-KO mouse, an impairment in Ras-dependent trafficking of AMPA receptor subunits underlies a decrease in the level of LTP following a pairing protocol in cultured slices (Hu et al., 2008). By enhancing Ras signaling directly or via manipulation of the PI3K-PKB pathway, the deficits in paired LTP could be overcome, thus demonstrating a direct signaling cascade link between factors affecting both spine morphology and synapse plasticity.

STDP IN MOUSE MODELS FOR INHERITED MENTAL RETARDATION

Activity-dependent alterations in synapse strength are key factors in refining neural circuits and learning based on experience. Compromised synaptic plasticity is likely to contribute to deficits underlying cognitive impairments in many MR syndromes. In the last decades, it has become clear that synapse strength can be modified depending on the millisecond timing of action potential firing with the sign of synaptic plasticity depending on the spike order of presynaptic and postsynaptic neurons (Levy and Steward, 1983; Gustafsson et al., 1987; Bell et al., 1997; Magee and Johnston, 1997; Markram et al., 1997). By varying the timing and order of pre- and postsynaptic spiking, it was found that critical time windows exist for synaptic modification on the order of tens of milliseconds (Bi and Poo, 1998, 2001). Recently, it was found that induction rules for timing-dependent LTP (tLTP) and LTD (tLTD) are different in two mouse models for the X-linked syndromes of Rett and Fragile X. These syndromes, although caused by different distinct mutations on the X chromosome, have an overlap of phenotypic features such as MR and co-morbidity of autistic traits and epilepsy in some cases.

POSTSYNAPTIC THRESHOLD FOR STDP

Spike-timing-dependent plasticity protocols with timing-dependent stimulation of pre- and postsynaptic activity using single postsynaptic action potentials were tested in the Fmr1-KO mouse, a model for Fragile X syndrome (Bakker et al., 1994). Fragile X syndrome, resulting from mutations in the Fmr1 gene on the X chromosome (Jin and Warren, 2000), is accompanied by significantly reduced or absent levels of FMRP which plays a key role in regulation of mRNA translation at or near dendritic spines (Weiler et al., 1997; Zalfa et al., 2003). In sensory and prefrontal cortex, there is a deficit in tLTP in sensory and prefrontal cortex from 2- to 3-week-old Fmr1-KO mice (Desai et al., 2006; Meredith et al., 2007). A similar deficit in tLTP was also observed in prefrontal cortex of older Fmr1-KO mice (Meredith et al., 2007). In hippocampal cultures and slices, a timing-dependent pairing protocol also showed a reduction in LTP in Fmr1-KO mice (Hu et al., 2008). Thus in both hippocampal and cortical tissue, timing-dependent stimulation with single postsynaptic action potentials revealed tLTP deficits in the Fmr1-KO mouse.

Absence of LTP could imply that the cellular machinery to support plasticity is not present in the dendrites and spines. Fragile X Mental Retardation Protein acts as a local regulator of mRNA translation and affects a number of cytoskeletal and synaptic proteins, many of which could have deleterious effects on plasticity. However, it was possible to overcome the deficits in tLTP by enhancement of postsynaptic activity or intracellular signaling factors. In 2-week-old cortex, increasing the level of postsynaptic stimulation from single

action potentials to postsynaptic bursting activity *in vitro* rescued the tLTP deficit in Fmr1-KO mice (Meredith et al., 2007). Boosting postsynaptic activity via environmental enrichment stimulation for 2 months prior to recording also improved tLTP in old prefrontal cortex of Fmr1-KO mice (Meredith et al., 2007). Thus at both developmental ages, increased postsynaptic stimulation in STDP paradigms was able to demonstrate that cortical synapses in Fmr1-KO mice could potentiate but that stronger activity was necessary to rescue the synaptic plasticity impairment. Furthermore, the mechanisms capable of supporting potentiation are still present in the synapse but require a higher threshold for activation (see **Figure 1**). These findings echo data using traditional synaptic plasticity paradigms in Fmr1-KO mice: no significant differences in field LTP were reported initially in the Fmr1-KO mouse model following tetanic stimulation in hippocampus (Godfraind et al., 1996; Paradee et al., 1999; Li et al., 2002). However, reduced LTP induction was later observed with weak but not strong theta-burst stimulation in hippocampus (Lauterborn et al., 2007), suggesting that use of strong stimulation to induce LTP can mask some of the subtle changes in plasticity and overcome 'threshold' limitations that may be present in more physiological stimulation patterns in the retardation syndrome.

The idea of a higher threshold for induction of plasticity is not unique to Fragile X syndrome and is emerging as a common factor from data in other mouse models. In the UBE3A-KO mouse model for Angelman syndrome, a similar higher threshold level for induction of plasticity using tetanic and theta-burst stimulation paradigms is observed in neocortex and in hippocampus (Jiang et al., 1998; Weeber et al., 2003; Yashiro et al., 2009). Deficits in the Ts65Dn mouse model for Down's syndrome observed with theta-burst stimulation can also be overcome with stronger tetanic paradigms or by unblocking inhibition (Kleschevnikov et al., 2004; Costa and Grybko, 2005). A modifiable threshold level to describe the balance of potentiation and depression in synapses is described in the Bienenstock, Cooper, Munro (BCM) model (Bienenstock et al., 1982). Here, the threshold for modification is a non-linear function of postsynaptic activity in the synapses with low activity levels leading to depression and higher rates leading to potentiation. The application of this theory to STDP protocols is not straightforward but has been applied to experimental data using triplet spiking rules and a burst-firing paradigm with differing postsynaptic activity levels (Sjostrom et al., 2001; Morrison et al., 2008). In Fmr1-KO mouse model, no evidence exists for a shift in BCM threshold at

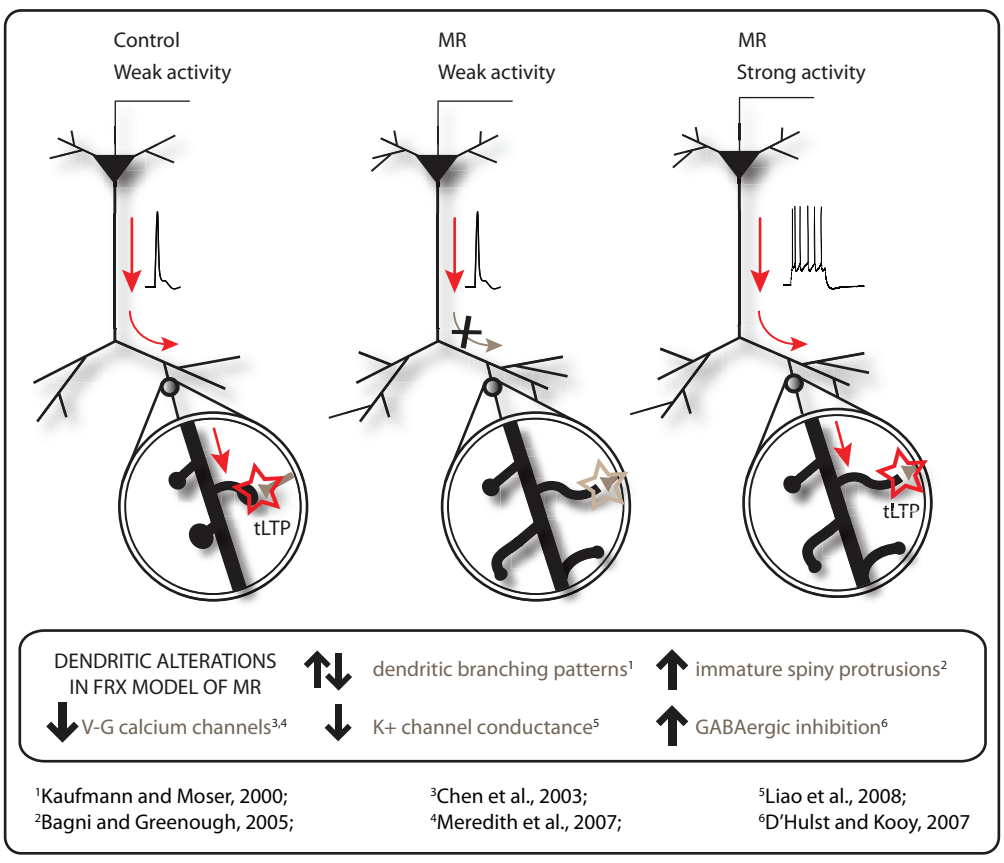

FIGURE 1 | Modulation of dendritic excitability in mental retardation (MR). tLTP can be induced in pyramidal neurons with single backpropagating APs during a timing-dependent paradigm in control cortex but not in that from a mouse model for Fragile X syndrome. Instead, the postsynaptic threshold for tLTP is shifted in Fragile X MR synapses, requiring a burst of postsynaptic APs during the STDP protocol to induce synaptic potentiation (data from Meredith et al., 2007). Abnormalities of dendritic branching patterns and spiny protrusion density and maturity are observed in many forms of MR. A number of candidate mechanisms including down-regulation of calcium channels, increased GABAergic inhibition and alteration of K^+ conductance affecting function of dendrites and spines may underlie this tLTP deficit to reduce the dendritic excitability in the brain in MR syndromes.

layer 2/3 cortical synapses, with tLTD and tLTP resulting from low and high respective frequency of postsynaptic bursts during pairing in a manner similar to WT synapses (Supplementary data in Meredith et al., 2007).

Despite significant effects upon tLTP, timing-dependent synaptic depression (tLTD) appears normal in both sensory and prefrontal cortex of Fmr1-KO mice mouse (Desai et al., 2006; Meredith et al., 2007). The reasons for this lack of change in cortical synaptic depression in the Fmr1-KO mouse model are not currently known. In hippocampus and cerebellum, plasticity mechanisms for chemically-induced mGluR-mediated synaptic depression in the Fmr1-KO mouse reveal an enhanced LTD (Huber et al., 2002; Koekkoek et al., 2005). These findings led to the theory of altered signaling via group 1 mGluRs in Fragile X syndrome (Bear et al., 2004). tLTD protocols can be considered distinct from mGluR-dependent forms of synaptic depression, relying on presynaptic rather than postsynaptic NMDA receptors for induction (Rodriguez-Moreno and Paulsen, 2008; Banerjee et al., 2009) and not being heavily-dependent upon protein synthesis. Further investigations into these distinct synaptic depression mechanisms in cortex, hippocampus and cerebellum may provide mechanisms to explain the absence of effects upon tLTD in the Fmr1-KO mouse to-date.

NEURODEVELOPMENTAL ONSET OF PLASTICITY

Many forms of autism and MR are classified as neurodevelopmental cognitive disorders with noticeable onset of phenotypic symptoms and immature dendritic spine morphology occurring during early postnatal stages (Zoghbi, 2003). Rett syndrome is a neurodevelopmental disorder typified by autistic behaviors, movement impairments and MR and caused by mutations in the X-linked MECP2 gene, which acts to regulation transcription (Nan et al., 1997; Amir et al., 1999). A MECP2-null mouse model was created that develops symptoms reminiscent of Rett syndrome with a delayed phenotypic onset similar to the human condition (Chen et al., 2001; Guy et al., 2001). Early onset of spine pathologies in MR raises the question of whether abnormalities are causal for changes in synaptic plasticity for example, or arise as a consequence of changes in synaptic processing (Fiala et al., 2002). The MECP2 mouse model gives the possibility to investigate the relationship between plasticity, synapse morphology and behavioral abnormalities.

At pre-symptomatic stages of two postnatal weeks old, MECP2 mutant mice show no alterations in tLTP paradigms with single postsynaptic action potentials in layer 5 of sensory cortex. At 4 weeks old, when onset of symptoms first occurs in MECP2 null mice, tLTP is also unimpaired, despite decreases in synaptic connectivity, weakened excitatory synapse strength and alteration in excitatory/inhibitory balance (Dani et al., 2005; Dani and Nelson, 2009). Impairments in LTP, induced with tetanic or theta-burst stimulation, are only seen in older symptomatic mice in both hippocampus and cortex (Asaka et al., 2006; Moretti et al., 2006). This suggests that deficits in synaptic plasticity seen after the onset of behavioral abnormalities, occur as a consequence of baseline synaptic function and connectivity impairments (Guy et al., 2007). Thus, alterations in mechanisms that underlie functional processing and integration of signaling in both dendrites and spines are likely candidates for a role in MR pathophysiology regulating STDP.

DENDRITIC MECHANISMS AFFECTING LOCAL MEMBRANE EXCITABILITY

Dendritic excitability plays a key role in understanding the mechanisms of timing-dependent synaptic plasticity in the brain. Structural alterations, as documented in MR syndromes, will have profound effects upon distribution of ion channels in dendritic membranes and resultant effects on active and passive processing properties of signaling in the dendrites. During tLTP paradigms, backpropagation of a single action potential depolarizes the dendritic membrane, opening voltage-gated calcium channels on both the dendritic shaft (Callaway and Ross, 1995) and spines (Koester and Sakmann, 1998). The action potential does not always propagate throughout the entire dendritic tree and can follow a distant-dependent profile with lack of signal at distal dendritic regions (Jaffe et al., 1992). The degree of backpropagation into the dendrites depends critically upon dendritic morphology, including dendritic diameter and branching patterns (Vetter et al., 2001). Failure of signal propagation can also occur after dendritic branching points (Spruston et al., 1995). In Fragile X syndrome, alterations in basal dendritic branching patterns have been observed in both visual and somatosensory cortex of adult Fmr1-KO mice on a C57BL/6 background (Galvez et al., 2003; Restivo et al., 2005). Dendritic excitability may also be affected via alterations in axonal arborization patterns, with more spatially diffuse aborization seen during a restricted developmental period in superficial barrel cortex layers of the Fmr1-KO mouse (Bureau et al., 2008).

In modeling studies, the role of spine morphology on dendritic excitability and AP backpropagation is shown to be influential, where the inactivation threshold of sodium channels along the dendrite and potentially in the spines can regulate signal failure in the distal dendritic regions (Tsay and Yuste, 2002). In proximal dendrites of cortical layer 5 pyramidal neurons, AP backpropagation reliably transmitted to large spines without loss of voltage (Palmer and Stuart, 2009). However, the propagation into spines on smaller, more distal dendrites or into the filopodial protrusions with differing spine neck diameters and resistance more commonly seen along dendrites in MR syndromes, could well differ. Thus, alterations in dendritic morphology and cytoskeleton in retardation syndromes are likely to affect the efficacy of backpropagation into the dendritic tree and have consequences upon integrative signaling processes in dendritic compartments.

CALCIUM TRANSIENT FAILURES

Induction of LTP of excitatory synapses is critically dependent on increases in postsynaptic calcium signaling during both tetanic induction or STDP stimulation paradigms (Lynch et al., 1983; Nevian and Sakmann, 2006). In pyramidal neurons of prefrontal cortex from Fmr1-KO mice, action potential-mediated calcium transients in both dendrites and postsynaptic spines were more prone to failures than those in control neurons (Meredith et al., 2007). Active properties of dendrites are strongly shaped by the density, localization and properties of voltage-gated calcium channels distributed in the membrane (Magee and Johnston, 2005). Dendrites and spines express a variety of different voltage-gated calcium channels, localized to specific regions of the dendritic tree and spine location on the dendrite (Magee and Johnston, 1995; Bloodgood and Sabatini, 2007). In Fmr1-KO neurons in prefrontal

cortex, calcium transients were less sensitive to L-type calcium channel antagonists, that could explain the decrease in calcium transients in these dendritic protrusions (Meredith et al., 2007). L-type calcium channel protein levels were also found to be down-regulated in frontal cortex in these KO mice (Chen et al., 2003). L-type calcium channels are found in both dendrites and spines and contribute to both resting calcium levels (Magee et al., 1996), excitability of the dendrite in the hippocampus (Moyer et al., 1992) and coupling of postsynaptic calcium influx activity to gene transcription (Murphy et al., 1991). Blocking L-type calcium channels in prefrontal cortex of wild-type mice prevents tLTP (Meredith et al., 2007). Thus, alterations in L-type channels in dendritic spines are one indicator of an impairment in activity-coupled plasticity mechanisms mediated via calcium transients in neuronal dendrites in Fragile X syndrome.

K^+ CHANNELS AND DENDRITE EXCITABILITY

Dendritic excitability is also modulated by alterations in the distribution and modulatory state of sodium and potassium channels in the dendritic membrane. Modeling studies demonstrate severe attenuation of the spread of backpropagation via subtle alterations in the distribution and density of sodium and potassium channels along the dendrite (Golding et al., 2001). In the peripheral nervous system, such 'channelopathies' affect dendritic excitability and mediate severe neuromuscular and cell signaling disorders. In temporal lobe epilepsy, a channelopathy involving A-type potassium channels directly modulates dendritic excitability via transcriptional and post-translational mechanisms (Bernard et al., 2004). The prevalence of epilepsy increases greatly with severe intellectual disability in many forms of MR. In both human and mouse forms of Fragile X syndrome, an increased incidence of epileptic activity is reported (Musumeci et al., 1999; Chen and Toth, 2001). It is not currently known whether significant alterations in ion channel distributions occur in dendrites in models of MR.

Levels of protein expression of specific potassium channels revealed significant up-regulation in subunits of the G-protein coupled inwardly-rectifying K^+ channel in hippocampus and frontal cortex of the Ts65Dn mouse model for Down's syndrome (Chie et al., 2006). Proteomics analysis of cortical synaptosomes from Fmr1-KO mice revealed a down-regulation in a set of proteins governing membrane excitability, including a large conductance, calcium-activated BK potassium channel subunit, Kcnma1α (Liao et al., 2008). BK ion channels are activated by membrane depolarization and increases in intracellular calcium concentration, resulting in hyperpolarization and decreased local dendritic excitability (Faber and Sah, 2003).

It is interesting to speculate that the increased threshold for tLTP in dendrites of Fmr1-KO neurons point towards regional dendritic impairments in excitability that are coupled to an interplay between local calcium transients, voltage-activated ion channels and synaptic stimulation. In prefrontal cortex, tLTP is blocked by application of the group 1 mGluR antagonist MPEP (Meredith et al., 2007) but the mechanisms governing this blockade are not known. The perisynaptic location of group 1 mGluRs (Baude et al., 1993) make them ideally placed postsynaptically to regulate dendritic channels governing excitability. Stimulation of group 1 mGluRs on hippocampal dendrites causes depolarization and firing of CA1 pyramidal cells, mediated by both voltage-gated calcium channels and inhibition of differing potassium currents (Anwyl, 1999). Although no changes in group 1 mGluR5 protein expression alone are found in Fmr1-KO mice, the alteration in linkage with postsynaptic density proteins such as Homer family may have resultant effects on other dendritically-located postsynaptic ion channels to mediate an alteration in excitability (Giuffrida et al., 2005).

INHIBITORY DENDRITIC TONE

In addition to alterations in voltage-activated ion channels, another key player affecting synaptic plasticity is the role of GABAergic inhibition. In many different forms of MR, there are abnormalities in the balance of excitation to inhibition in the brain (Kleschevnikov et al., 2004; Dani et al., 2005; Gibson et al., 2008). GABAergic inhibition has significant effects on synaptic plasticity. Blocking GABAergic inhibition via GABA-A receptors reveals tLTP in mature hippocampal neurons (Meredith et al., 2003; Campanac and Debanne, 2008) and also rescues LTP induction in a mouse model for Down's syndrome (Kleschevnikov et al., 2004). At the dendritic level, interneurons target highly specific compartments of dendrites of pyramidal neurons (Klausberger and Somogyi, 2008). Alterations in inhibitory tone in dendritic branches would have significant impact upon integration and plasticity at sites away from the cell soma. Backpropagation of an AP along the apical dendrite is under inhibitory regulation, suggesting that attenuation or even failure of signaling could be due to increased inhibitory tone (Tsubokawa and Ross, 1996; Meredith and Groen, 2010). It is not known whether inhibitory mechanisms in dendrites are altered in MR. In Fragile X syndrome, decreased expression of mRNA and protein levels of a number of GABA-A subunits are reported in the Fmr1-KO mouse (El Idrissi et al., 2005; D'Hulst et al., 2006). Furthermore, GABAergic inhibition at the network level is altered, as seen by prolonged epileptoform activity and altered connectivity in both hippocampus and cortex (Chuang et al., 2005; Gibson et al., 2008). The disinhibition leading to epileptogenesis in the Fmr1-KO model is sensitive to excitation via group 1 metabotropic receptors, since the antagonist MPEP suppresses epileptiform discharges in hippocampus (Chuang et al., 2005). Group 1 mGluRs are also present on inhibitory interneurons (Lopez-Bendito et al., 2002). Their direct activation may also regulate dendritic excitability of pyramidal neurons via alterations in inhibitory tone upon dendritic compartments. Dissection of the alterations in GABAergic inhibition, the role of specific interneurons involved and their activation patterns may elucidate many of the impairments in synaptic plasticity and network processing observed in the Fragile X retardation model. This delicate balance of inhibition in the brain may be an important feature common to many neurodevelopmental cognitive disorders (Rubenstein and Merzenich, 2003).

SUMMARY

In summary, this review highlights timing-based cortical plasticity in the Fragile X syndrome model of MR and proposes that alterations in dendritic excitability underlie deficits seen in STDP. Subtle alterations in dendritic and spine morphology can have dramatic effects on efficacy of calcium signaling throughout the dendritic tree, with downstream consequences on calcium-activated

intracellular signaling cascades. In Fragile X syndrome, FMRP interacts directly with many other proteins playing key roles in synapse morphology and plasticity, including Rho GTPase family members and excitatory mGluRs. Morphological abnormalities can also alter the distribution of ion channels, in particular K^+ conductances that play a critical role in dendritic excitability. Finally, the alteration in inhibition/excitation balance observed from measurements at neuronal soma is likely to arise from significant imbalances in dendritic compartments and as a consequence, alter local dendritic depolarization necessary for STDP. Further investigation into these local dendritic mechanisms will give new insight into the deficits in dendrites and spiny protrusions that mediate deficits in these cognitive disorders.

ACKNOWLEDGMENTS

Related research in the department is funded by FRAXA Research Organisation, Fondation Jérôme Lejeune, Nederlandse Organisatie voor Wetenschappelijk Onderzoek (NWO) to HDM and RMM.

REFERENCES

Amir, R. E., Van den Veyver, I. B., Wan, M., Tran, C. Q., Francke, U., and Zoghbi, H. Y. (1999). Rett syndrome is caused by mutations in X-linked MECP2, encoding methyl-CpG-binding protein 2. *Nat. Genet.* 23, 185–188.

Anwyl, R. (1999). Metabotropic glutamate receptors: electrophysiological properties and role in plasticity. *Brain Res. Brain Res. Rev.* 29, 83–120.

Asaka, Y., Jugloff, D. G., Zhang, L., Eubanks, J. H., and Fitzsimonds, R. M. (2006). Hippocampal synaptic plasticity is impaired in the Mecp2-null mouse model of Rett syndrome. *Neurobiol. Dis.* 21, 217–227.

Bagni, C., and Greenough, W. T. (2005). From mRNP trafficking to spine dysmorphogenesis: the roots of fragile X syndrome. *Nat. Rev. Neurosci.* 6, 376–387.

Bakker, E. C., Verheij, C., Willemsen, R., van der Helm, R., Oerlemans, F., Vermey, M., Bygraved, A., Hoogeveen, A. T., Oostra, B. A., Reyniers, E., De Boule, K., D'Hooge, R., Cras, P., van Velzen, D., Nagels, G., Martin, J. J., De Deyn, P. P., Darby, J. K., Willems, P. J. (1994). Fmr1 knockout mice: a model to study fragile X mental retardation. The Dutch-Belgian Fragile X Consortium. *Cell* 78, 23–33.

Banerjee, A., Meredith, R. M., Rodriguez-Moreno, A., Mierau, S. B., Auberson, Y. P., and Paulsen, O. (2009). Double dissociation of spike timing-dependent potentiation and depression by subunit-preferring NMDA receptor antagonists in mouse barrel cortex. *Cereb. Cortex* 19, 2959–2969.

Baude, A., Nusser, Z., Roberts, J. D., Mulvihill, E., McIlhinney, R. A., and Somogyi, P. (1993). The metabotropic glutamate receptor (mGluR1 alpha) is concentrated at perisynaptic membrane of neuronal subpopulations as detected by immunogold reaction. *Neuron* 11, 771–787.

Bear, M. F., Huber, K. M., and Warren, S. T. (2004). The mGluR theory of fragile X mental retardation. *Trends Neurosci.* 27, 370–377.

Bell, C. C., Han, V. Z., Sugawara, Y., and Grant, K. (1997). Synaptic plasticity in a cerebellum-like structure depends on temporal order. *Nature* 387, 278–281.

Bernard, C., Anderson, A., Becker, A., Poolos, N. P., Beck, H., and Johnston, D. (2004). Acquired dendritic channelopathy in temporal lobe epilepsy. *Science* 305, 532–535.

Best, T. K., Cho-Clark, M., Siarey, R. J., and Galdzicki, Z. (2008). Speeding of miniature excitatory post-synaptic currents in Ts65Dn cultured hippocampal neurons. *Neurosci. Lett.* 438, 356–361.

Bi, G., and Poo, M. (2001). Synaptic modification by correlated activity: Hebb's postulate revisited. *Annu. Rev. Neurosci.* 24, 139–166.

Bi, G. Q., and Poo, M. M. (1998). Synaptic modifications in cultured hippocampal neurons: dependence on spike timing, synaptic strength, and postsynaptic cell type. *J. Neurosci.* 18, 10464–10472.

Bienenstock, E. L., Cooper, L. N., and Munro, P. W. (1982). Theory for the development of neuron selectivity: orientation specificity and binocular interaction in visual cortex. *J. Neurosci.* 2, 32–48.

Bloodgood, B. L., and Sabatini, B. L. (2007). Ca(2+) signaling in dendritic spines. *Curr. Opin. Neurobiol.* 17, 345–351.

Braun, K., and Segal, M. (2000). FMRP involvement in formation of synapses among cultured hippocampal neurons. *Cereb. Cortex* 10, 1045–1052.

Bureau, I., Shepherd, G. M., and Svoboda, K. (2008). Circuit and plasticity defects in the developing somatosensory cortex of FMR1 knock-out mice. *J. Neurosci.* 28, 5178–5188.

Callaway, J. C., and Ross, W. N. (1995). Frequency-dependent propagation of sodium action potentials in dendrites of hippocampal CA1 pyramidal neurons. *J. Neurophysiol.* 74, 1395–1403.

Campanac, E., and Debanne, D. (2008). Spike timing-dependent plasticity: a learning rule for dendritic integration in rat CA1 pyramidal neurons. *J. Physiol. (Lond.)* 586, 779–793.

Chapleau, C. A., Calfa, G. D., Lane, M. C., Albertson, A. J., Larimore, J. L., Kudo, S., Armstrong, D. L., Percy, A. K., and Pozzo-Miller, L. (2009). Dendritic spine pathologies in hippocampal pyramidal neurons from Rett syndrome brain and after expression of Rett-associated MECP2 mutations. *Neurobiol. Dis.* 35, 219–233.

Chen, L., and Toth, M. (2001). Fragile X mice develop sensory hyperreactivity to auditory stimuli. *Neuroscience* 103, 1043–1050.

Chen, L., Yun, S. W., Seto, J., Liu, W., and Toth, M. (2003). The fragile X mental retardation protein binds and regulates a novel class of mRNAs containing U rich target sequences. *Neuroscience* 120, 1005–1017.

Chen, R. Z., Akbarian, S., Tudor, M., and Jaenisch, R. (2001). Deficiency of methyl-CpG binding protein-2 in CNS neurons results in a Rett-like phenotype in mice. *Nat. Genet.* 27, 327–331.

Chie, H., David, M. J., Jassir, W., Rosemary, C. B., Tyler, K. B., Richard, J. S., and Zygmunt, G. (2006). Abnormal expression of the G-protein-activated inwardly rectifying potassium channel 2 (GIRK2) in hippocampus, frontal cortex, and substantia nigra of Ts65Dn mouse: a model of Down syndrome. *J. Comp. Neurol.* 494, 815–833.

Chuang, S. C., Zhao, W., Bauchwitz, R., Yan, Q., Bianchi, R., and Wong, R. K. (2005). Prolonged epileptiform discharges induced by altered group I metabotropic glutamate receptor-mediated synaptic responses in hippocampal slices of a fragile X mouse model. *J. Neurosci.* 25, 8048–8055.

Costa, A. C., and Grybko, M. J. (2005). Deficits in hippocampal CA1 LTP induced by TBS but not HFS in the Ts65Dn mouse: a model of Down syndrome. *Neurosci. Lett.* 382, 317–322.

D'Hulst, C., De Geest, N., Reeve, S. P., Van Dam, D., De Deyn, P. P., Hassan, B. A., and Kooy, R. F. (2006). Decreased expression of the GABA(A) receptor in fragile X syndrome. *Brain Res.* 1121, 238–245.

D'Hulst, C., and Kooy, R. F. (2007). The GABAA receptor: a novel target for treatment of fragile X? *Trends in Neurosci.* 30:425-431.

Dani, V. S., Chang, Q., Maffei, A., Turrigiano, G. G., Jaenisch, R., and Nelson, S. B. (2005). Reduced cortical activity due to a shift in the balance between excitation and inhibition in a mouse model of Rett syndrome. *Proc. Natl. Acad. Sci. U.S.A.* 102, 12560–12565.

Dani, V. S., and Nelson, S. B. (2009). Intact long-term potentiation but reduced connectivity between neocortical layer 5 pyramidal neurons in a mouse model of Rett syndrome. *J. Neurosci.* 29, 11263–11270.

Desai, N. S., Casimiro, T. M., Gruber, S. M., and Vanderklish, P. W. (2006). Early postnatal plasticity in neocortex of Fmr1 knockout mice. *J. Neurophysiol.* 96, 1734–1745.

El Idrissi, A., Ding, X. H., Scalia, J., Trenkner, E., Brown, W. T., and Dobkin, C. (2005). Decreased GABA(A) receptor expression in the seizure-prone fragile X mouse. *Neurosci. Lett.* 377, 141–146.

Faber, E. S. L., and Sah, P. (2003). Calcium-activated potassium channels: multiple contributions to neuronal function. *Neuroscientist.* 9, 181–194.

Fiala, J. C., Spacek, J., and Harris, K. M. (2002). Dendritic spine pathology: cause or consequence of neurological disorders? *Brain Res. Brain Res. Rev.* 39, 29–54.

Galvez, R., Gopal, A. R., and Greenough, W. T. (2003). Somatosensory cortical barrel dendritic abnormalities in a mouse model of the fragile X mental retardation syndrome. *Brain Res.* 971, 83–89.

Gibson, J. R., Bartley, A. F., Hays, S. A., and Huber, K. M. (2008). Imbalance of neocortical excitation and inhibition and altered UP states reflect network hyperexcitability in the mouse model of fragile X syndrome. *J. Neurophysiol.* 100, 2615–2626.

Giuffrida, R., Musumeci, S., D'Antoni, S., Bonaccorso, C. M., Giuffrida-Stella, A. M., Oostra, B. A., and Catania, M. V. (2005). A reduced number of metabotropic glutamate subtype 5 receptors are associated with constitutive homer proteins in a mouse model of fragile X syndrome. *J. Neurosci.* 25, 8908–8916. doi: 10.1523/JNEUROSCI.0932-05.2005.

Godfraind, J. M., Reyniers, E., De Boulle, K., D'Hooge, R., De Deyn, P. P., Bakker, C. E., Oostra, B. A., Kooy, R. F., and

Willems, P. J. (1996). Long-term potentiation in the hippocampus of fragile X knockout mice. *Am. J. Med. Genet.* 64, 246–251.

Golding, N. L., Kath, W. L., and Spruston, N. (2001). Dichotomy of action-potential backpropagation in CA1 pyramidal neuron dendrites. *J. Neurophysiol.* 86, 2998–3010.

Gustafsson, B., Wigstrom, H., Abraham, W. C., and Huang, Y. Y. (1987). Long-term potentiation in the hippocampus using depolarizing current pulses as the conditioning stimulus to single volley synaptic potentials. *J. Neurosci.* 7, 774–780.

Guy, J., Gan, J., Selfridge, J., Cobb, S., and Bird, A. (2007). Reversal of neurological defects in a mouse model of Rett syndrome. *Science* 315, 1143–1147. doi: 10.1126/science.1138389.

Guy, J., Hendrich, B., Holmes, M., Martin, J. E., and Bird, A. (2001). A mouse Mecp2-null mutation causes neurological symptoms that mimic Rett syndrome. *Nat. Genet.* 27, 322–326.

Harlow, E. G., Till, S. M., Russell, T. A., Wijetunge, L. S., Kind, P., and Contractor, A. (2010). Critical period plasticity is disrupted in the barrel cortex of FMR1 knockout mice. *Neuron* 65, 385–398.

Harris, K. M. (1999). Structure, development, and plasticity of dendritic spines. *Curr. Opin. Neurobiol.* 9, 343–348.

Hu, H., Qin, Y., Bochorishvili, G., Zhu, Y., van Aelst, L., and Zhu, J. J. (2008). Ras signaling mechanisms underlying impaired GluR1-dependent plasticity associated with fragile X syndrome. *J. Neurosci.* 28, 7847–7862.

Huber, K. M., Gallagher, S. M., Warren, S. T., and Bear, M. F. (2002). Altered synaptic plasticity in a mouse model of fragile X mental retardation. *Proc. Natl. Acad. Sci. U.S.A.* 99, 7746–7750.

Irwin, S. A., Galvez, R., and Greenough, W. T. (2000). Dendritic spine structural anomalies in fragile-X mental retardation syndrome. *Cereb. Cortex* 10, 1038–1044.

Jaffe, D. B., Johnston, D., Lasser-Ross, N., Lisman, J. E., Miyakawa, H., and Ross, W. N. (1992). The spread of Na+ spikes determines the pattern of dendritic Ca2+ entry into hippocampal neurons. *Nature* 357, 244–246.

Jiang, Y. H., Armstrong, D., Albrecht, U., Atkins, C. M., Noebels, J. L., Eichele, G., Sweatt, J. D., and Beaudet, A. L. (1998). Mutation of the Angelman ubiquitin ligase in mice causes increased cytoplasmic p53 and deficits of contextual learning and long-term potentiation. *Neuron* 21, 799–811.

Jin, P., and Warren, S. T. (2000). Understanding the molecular basis of fragile X syndrome. *Hum. Mol. Genet.* 9, 901–908.

Kaufmann, W. E., and Moser, H. W. (2000). Dendritic anomalies in disorders associated with mental retardation. *Cereb. Cortex* 10, 981–991.

Klausberger, T., and Somogyi, P. (2008). Neuronal diversity and temporal dynamics: the unity of hippocampal circuit operations. *Science* 321, 53–57.

Kleschevnikov, A. M., Belichenko, P. V., Villar, A. J., Epstein, C. J., Malenka, R. C., and Mobley, W. C. (2004). Hippocampal long-term potentiation suppressed by increased inhibition in the Ts65Dn mouse, a genetic model of down syndrome. *J. Neurosci.* 24, 8153–8160.

Kobayashi, K., Kuroda, S., Fukata, M., Nakamura, T., Nagase, T., Nomura, N., Matsuura, Y., Yoshida-Kubomura, N., Iwamatsu, A., and Kaibuchi, K. (1998). p140Sra-1 (specifically Rac1-associated protein) is a novel specific target for Rac1 small GTPase. *J. Biol. Chem.* 273, 291–295.

Koekkoek, S. K., Yamaguchi, K., Milojkovic, B. A., Dortland, B. R., Ruigrok, T. J., Maex, R., De Graaf, W., Smit, A. E., VanderWerf, F., Bakker, C. E., Willemsen, R., Ikeda, T., Kakizawa, S., Onodera, K., Nelson, D. L., Mientjes, E., Joosten, M., De Schutter, E., Oostra, B. A., Ito, M., De Zeeuw, C. I. (2005). Deletion of FMR1 in Purkinje cells enhances parallel fiber LTD, enlarges spines, and attenuates cerebellar eyelid conditioning in Fragile X syndrome. *Neuron* 47, 339–352.

Koester, H. J., and Sakmann, B. (1998). Calcium dynamics in single spines during coincident pre- and postsynaptic activity depend on relative timing of back-propagating action potentials and subthreshold excitatory postsynaptic potentials. *Proc. Natl. Acad. Sci. U.S.A.* 95, 9596–9601.

Lauterborn, J. C., Rex, C. S., Kramar, E., Chen, L. Y., Pandyarajan, V., Lynch, G., and Gall, C. M. (2007). Brain-derived neurotrophic factor rescues synaptic plasticity in a mouse model of fragile x syndrome. *J. Neurosci.* 27, 10685–10694.

Levy, W. B., and Steward, O. (1983). Temporal contiguity requirements for long-term associative potentiation/depression in the hippocampus. *Neuroscience* 8, 791–797.

Li, J., Pelletier, M. R., Perez Velazquez, J. L., and Carlen, P. L. (2002). Reduced cortical synaptic plasticity and GluR1 expression associated with fragile X mental retardation protein deficiency. *Mol. Cell. Neurosci.* 19, 138–151.

Liao, L., Park, S. K., Xu, T., Vanderklish, P., and Yates, J. R., 3rd. (2008). Quantitative proteomic analysis of primary neurons reveals diverse changes in synaptic protein content in fmr1 knockout mice. *Proc. Natl. Acad. Sci. U.S.A.* 105, 15281–15286.

Lopez-Bendito, G., Shigemoto, R., Fairen, A., and Lujan, R. (2002). Differential distribution of group I metabotropic glutamate receptors during rat cortical development. *Cereb. Cortex* 12, 625–638.

Luo, L., Hensch, T. K., Ackerman, L., Barbel, S., Jan, L. Y., and Jan, Y. N. (1996). Differential effects of the Rac GTPase on Purkinje cell axons and dendritic trunks and spines. *Nature* 379, 837–840.

Lynch, G., Larson, J., Kelso, S., Barrionuevo, G., and Schottler, F. (1983). Intracellular injections of EGTA block induction of hippocampal long-term potentiation. *Nature* 305, 719–721.

Magee, J. C., Avery, R. B., Christie, B. R., and Johnston, D. (1996). Dihydropyridine-sensitive, voltage-gated Ca2+ channels contribute to the resting intracellular Ca2+ concentration of hippocampal CA1 pyramidal neurons. *J. Neurophysiol.* 76, 3460–3470.

Magee, J. C., and Johnston, D. (1995). Characterization of single voltage-gated Na+ and Ca2+ channels in apical dendrites of rat CA1 pyramidal neurons. *J. Physiol. (Lond.)* 487, 67–90.

Magee, J. C., and Johnston, D. (1997). A synaptically controlled, associative signal for Hebbian plasticity in hippocampal neurons. *Science* 275, 209–213.

Magee, J. C., and Johnston, D. (2005). Plasticity of dendritic function. *Curr. Opin. Neurobiol.* 15, 334–342.

Markram, H., Lubke, J., Frotscher, M., and Sakmann, B. (1997). Regulation of synaptic efficacy by coincidence of postsynaptic APs and EPSPs. *Science* 275, 213–215.

Martin, S. J., Grimwood, P. D., and Morris, R. G. M. (2000). Synaptic plasticity and memory: an evaluation of the hypothesis. *Annu. Rev. Neurosci.* 23, 649–711.

Matsuzaki, M., Ellis-Davies, G. C., Nemoto, T., Miyashita, Y., Iino, M., and Kasai, H. (2001). Dendritic spine geometry is critical for AMPA receptor expression in hippocampal CA1 pyramidal neurons. *Nat. Neurosci.* 4, 1086–1092.

Meredith, R. M., Floyer-Lea, A. M., and Paulsen, O. (2003). Maturation of long-term potentiation induction rules in rodent hippocampus: role of GABAergic inhibition. *J. Neurosci.* 23, 11142–11146.

Meredith, R. M., and Groen, M. R. (2010). Inhibition of action potential backpropagation during postnatal development of the hippocampus. *J. Neurophysiol.* 103, 2313.

Meredith, R. M., Holmgren, C. D., Weidum, M., Burnashev, N., and Mansvelder, H. D. (2007). Increased threshold for spike-timing-dependent plasticity is caused by unreliable calcium signaling in mice lacking fragile X gene FMR1. *Neuron* 54, 627–638.

Moretti, P., Levenson, J. M., Battaglia, F., Atkinson, R., Teague, R., Antalffy, B., Armstrong, D., Arancio, O., Sweatt, J. D., and Zoghbi, H. Y. (2006). Learning and memory and synaptic plasticity are impaired in a mouse model of Rett syndrome. *J. Neurosci.* 26, 319–327.

Morrison, A., Diesmann, M., and Gerstner, W. (2008). Phenomenological models of synaptic plasticity based on spike timing. *Biol. Cybern.* 98, 459–478.

Moyer, J. R., Jr., Thompson, L. T., Black, J. P., and Disterhoft, J. F. (1992). Nimodipine increases excitability of rabbit CA1 pyramidal neurons in an age- and concentration-dependent manner. *J. Neurophysiol.* 68, 2100–2109.

Murphy, T. H., Worley, P. F., and Baraban, J. M. (1991). L-type voltage-sensitive calcium channels mediate synaptic activation of immediate early genes. *Neuron* 7, 625–635.

Musumeci, S. A., Hagerman, R. J., Ferri, R., Bosco, P., Dalla Bernardina, B., Tassinari, C. A., De Sarro, G. B., and Elia, M. (1999). Epilepsy and EEG findings in males with fragile X syndrome. *Epilepsia* 40, 1092–1099.

Nadif Kasri, N., and Van Aelst, L. (2008). Rho-linked genes and neurological disorders. *Pflugers Arch.* 455, 787–797.

Nan, X., Campoy, F. J., and Bird, A. (1997). MeCP2 is a transcriptional repressor with abundant binding sites in genomic chromatin. *Cell* 88, 471–481.

Negishi, M., and Katoh, H. (2005). Rho family GTPases and dendrite plasticity. *Neuroscientist.* 11, 187–191.

Nevian, T., and Sakmann, B. (2006). Spine Ca2+ signaling in spike-timing-dependent plasticity. *J. Neurosci.* 26, 11001–11013.

Newey, S. E., Velamoor, V., Govek, E. E., and Van Aelst, L. (2005). Rho GTPases, dendritic structure, and mental retardation. *J. Neurobiol.* 64, 58–74.

Nimchinsky, E. A., Oberlander, A. M., and Svoboda, K. (2001). Abnormal development of dendritic spines in FMR1 knock-out mice. *J. Neurosci.* 21, 5139–5146.

Palmer, L. M., and Stuart, G. J. (2009). Membrane potential changes in dendritic spines during action potentials and synaptic input. *J. Neurosci.* 29, 6897–6903.

Paradee, W., Melikian, H. E., Rasmussen, D. L., Kenneson, A., Conn, P. J., and Warren, S. T. (1999). Fragile X mouse: strain effects of knockout phenotype and evidence suggesting deficient amygdala function. *Neuroscience* 94, 185–192.

Pfeiffer, B. E., and Huber, K. M. (2007). Fragile X mental retardation protein induces synapse loss through acute postsynaptic translational regulation. *J. Neurosci.* 27, 3120–3130. doi: 10.1523/JNEUROSCI.0054-07.2007.

Purpura, D. P. (1974). Dendritic spine "dysgenesis" and mental retardation. *Science* 186, 1126–1128.

Ramakers, G. J. (2002). Rho proteins, mental retardation and the cellular basis of cognition. *Trends Neurosci.* 25, 191–199.

Restivo, L., Ferrari, F., Passino, E., Sgobio, C., Bock, J., Oostra, B. A., Bagni, C., and Ammassari-Teule, M. (2005). Enriched environment promotes behavioral and morphological recovery in a mouse model for the fragile X syndrome. *Proc. Natl. Acad. Sci. U.S.A.* 102, 11557–11562.

Rodriguez-Moreno, A., and Paulsen, O. (2008). Spike timing-dependent long-term depression requires presynaptic NMDA receptors. *Nat. Neurosci.* 11, 744–745.

Rubenstein, J. L., and Merzenich, M. M. (2003). Model of autism: increased ratio of excitation/inhibition in key neural systems. *Genes Brain Behav.* 2, 255–267.

Schenck, A., Bardoni, B., Moro, A., Bagni, C., and Mandel, J.-L. (2001). A highly conserved protein family interacting with the fragile X mental retardation protein (FMRP) and displaying selective interactions with FMRP-related proteins FXR1P and FXR2P. *Proc. Natl. Acad. Sci. U.S.A.* 98, 8844–8849.

Siarey, R. J., Stoll, J., Rapoport, S. I., and Galdzicki, Z. (1997). Altered long-term potentiation in the young and old Ts65Dn mouse, a model for Down syndrome. *Neuropharmacology* 36, 1549–1554.

Sjostrom, P. J., Turrigiano, G. G., and Nelson, S. B. (2001). Rate, timing, and cooperativity jointly determine cortical synaptic plasticity. *Neuron* 32, 1149–1164.

Spruston, N., Schiller, Y., Stuart, G., and Sakmann, B. (1995). Activity-dependent action potential invasion and calcium influx into hippocampal CA1 dendrites. *Science* 268, 297–300.

Tashiro, A., Minden, A., and Yuste, R. (2000). Regulation of dendritic spine morphology by the Rho family of small GTPases: antagonistic roles of Rac and Rho. *Cereb. Cortex* 10, 927–938.

Threadgill, R., Bobb, K., and Ghosh, A. (1997). Regulation of dendritic growth and remodeling by Rho, Rac, and Cdc42. *Neuron* 19, 625–634.

Tsay, D., and Yuste, R. (2002). Role of dendritic spines in action potential backpropagation: a numerical simulation study. *J. Neurophysiol.* 88, 2834–2845.

Tsubokawa, H., and Ross, W. N. (1996). IPSPs modulate spike backpropagation and associated $[Ca^{2+}]i$ changes in the dendrites of hippocampal CA1 pyramidal neurons. *J. Neurophysiol.* 76, 2896–2906.

Vetter, P., Roth, A., and Hausser, M. (2001). Propagation of action potentials in dendrites depends on dendritic morphology. *J. Neurophysiol.* 85, 926–937.

Weeber, E. J., Jiang, Y.-H., Elgersma, Y., Varga, A. W., Carrasquillo, Y., Brown, S. E., Christian, J. M., Mirnikjoo, B., Silva, A., Beaudet, A. L., and Sweatt, J. D. (2003). Derangements of hippocampal calcium/calmodulin-dependent protein kinase II in a mouse model for Angelman mental retardation syndrome. *J. Neurosci.* 23, 2634–2644.

Weiler, I. J., Irwin, S. A., Klintsova, A. Y., Spencer, C. M., Brazelton, A. D., Miyashiro, K., Comery, T. A., Patel, B., Eberwine, J., and Greenough, W. T. (1997). Fragile X mental retardation protein is translated near synapses in response to neurotransmitter activation. *Proc. Natl. Acad. Sci. U.S.A.* 94, 5395–5400.

Yashiro, K., Riday, T. T., Condon, K. H., Roberts, A. C., Bernardo, D. R., Prakash, R., Weinberg, R. J., Ehlers, M. D., and Philpot, B. D. (2009). Ube3a is required for experience-dependent maturation of the neocortex. *Nat. Neurosci.* 12, 777–783.

Zalfa, F., Giorgi, M., Primerano, B., Moro, A., Di Penta, A., Reis, S., Oostra, B., and Bagni, C. (2003). The fragile X syndrome protein FMRP associates with BC1 RNA and regulates the translation of specific mRNAs at synapses. *Cell* 112, 317–327.

Zoghbi, H. Y. (2003). Postnatal neurodevelopmental disorders: meeting at the synapse? *Science* 302, 826–830.

Conflict of Interest Statement: The authors declare that the research was conducted in the absence of any commercial or financial relationships that could be construed as a potential conflict of interest.

Received: 01 February 2010; paper pending published: 20 February 2010; accepted: 17 May 2010; published online: 10 June 2010. Citation: Meredith RM and Mansvelder HD (2010) STDP and mental retardation: dysregulation of dendritic excitability in Fragile X syndrome. Front. Syn. Neurosci. ***2****:10. doi: 10.3389/fnsyn.2010.00010*

frontiers in
SYNAPTIC NEUROSCIENCE

ORIGINAL RESEARCH ARTICLE
published: 21 July 2010
doi: 10.3389/fnsyn.2010.00025

Voltage and spike timing interact in STDP – a unified model

Claudia Clopath*[1,2] *and* ***Wulfram Gerstner*[1]**

[1] *Laboratory of Computational Neuroscience, Brain-Mind Institute, Ecole Polytechnique Fédérale de Lausanne, Lausanne, Switzerland*
[2] *Laboratory of Neurophysics and Physiology, Unite Mixte de Recherche 8119, Centre National de la Recherche Scientifique, Université Paris Descartes, Paris, France*

Edited by:
Per Jesper Sjöström, University College London, UK

Reviewed by:
Björn Kampa, Swiss Federal Institute of Technology Zurich, Switzerland
Robert C. Froemke, New York University School of Medicine, USA
Sen Song, Massachusetts Institute of Technology, USA
Larry F. Abbott, Columbia University, USA
Walter Senn, University of Bern, Switzerland

****Correspondence:***
Claudia Clopath, Laboratory of Neurophysics and Physiology, Unite Mixte de Recherche 8119, Centre National de la Recherche Scientifique, Université Paris Descartes, 45 Rue des Saints Pères, 75270 Paris Cedex 06, France.
e-mail: claudia.clopath@parisdescartes.fr

A phenomenological model of synaptic plasticity is able to account for a large body of experimental data on spike-timing-dependent plasticity (STDP). The basic ingredient of the model is the correlation of presynaptic spike arrival with postsynaptic voltage. The local membrane voltage is used twice: a first term accounts for the instantaneous voltage and the second one for a low-pass filtered voltage trace. Spike-timing effects emerge as a special case. We hypothesize that the voltage dependence can explain differential effects of STDP in dendrites, since the amplitude and time course of backpropagating action potentials or dendritic spikes influences the plasticity results in the model. The dendritic effects are simulated by variable choices of voltage time course at the site of the synapse, i.e., without an explicit model of the spatial structure of the neuron.

Keywords: synaptic plasticity, computational neuroscience, STDP, LTP, LTD, voltage, model, frequency

INTRODUCTION

Spike-timing-dependent plasticity (STDP; Bell et al., 1997; Markram et al., 1997; Bi and Poo, 1998; Sjöström et al., 2001) is induced for most synapses by stimulating pairs of pre- and postsynaptic spikes. For synapses between cortical or hippocampal pyramidal neurons, a presynaptic spike a few milliseconds before a postsynaptic one typically leads to long-term potentiation (LTP) whereas the reverse timing leads to depression (Markram et al., 1997; Bi and Poo, 1998; Sjöström et al., 2001), but other preparations exhibit a wide range of other dependencies upon spike timing (Bell et al., 1997; Debanne et al., 1998; Abbott and Nelson, 2000). Classical models of STDP (Gerstner et al., 1996; Kempter et al., 1999; Roberts, 1999; Song et al., 2000) take the dependence upon the time difference between pre- and postsynaptic spikes explicitly into account by a learning window or STDP function with two phases, one for potentiation and another one for depression (for a review see Gerstner and van Hemmen, 1992; Morrison et al., 2008). However, the dependence upon the timing of a *pair* of spikes visualized in the STDP function is only one of many aspects of plasticity. First, in standard pairing experiments, pairings are repeated several times. The final outcome of experiments depends non-linearly on the number of pairings and, for a fixed number of pairings, on the repetition frequency (Markram et al., 1997; Senn et al., 2001; Sjöström et al., 2001). Second, a symmetric triplet of spikes in a post-pre-post configuration has the exact same two pairs as a symmetric pre-post-pre triplet. Hence, any pair-dependent STDP function predicts the same outcome for both protocols whereas experiments show significant differences (Wang et al., 2005). In particular, pre-post-pre with the same timing difference leads to insignificant changes, whereas post-pre-post induces a strong potentiation of synapses in hippocampal cultures (Wang et al., 2005). Quite generally, triplet and quadruplet dependencies measured in various experiments (Froemke and Dan, 2002; Wang et al., 2005) cannot be explained by standard STDP models. Third, the STDP function derived from standard experiments with pairs of spikes (Markram et al., 1997; Bi and Poo, 1998; Sjöström et al., 2001) does not explain the dependence of plasticity upon the timing of bursts of several postsynaptic spikes (Kampa et al., 2006; Nevian and Sakmann, 2006). Fourth, the outcome of synaptic plasticity depends on the dendritic location of the synapse (Froemke et al., 2005; Kampa et al., 2006; Letzkus et al., 2006; Sjöström and Häusser, 2006). Finally, plasticity can also be induced in the absence of postsynaptic firing, e.g., in voltage-clamp experiments (Kelso et al., 1986; Artola et al., 1990; Ngezahayo et al., 2000). None of these aspects is taken into account in classical phenomenological STDP models (Gerstner et al., 1996; Kempter et al., 1999; Roberts, 1999; Song et al., 2000). Modifications of the classical STDP models including weight-dependence (Kistler and van Hemmen, 2000; van Rossum et al., 2000; Rubin et al., 2001) or alternative summation schemes (Izhikevich, 2003), introduction of frequency dependence (Froemke and Dan, 2002) or some voltage dependence (Brader et al., 2007) resolve at most one or two of the above issues, but not all of them.

The basic shortcoming of the family of classical phenomenological STDP models is an inappropriate focus on a single *pair* of pre- and postsynaptic spikes. There are a couple of promising phenomenological STDP models that go beyond the pair

interaction, most notably the model of Senn and colleagues (Senn et al., 1997, 2001; Senn, 2002). This model exploits basic interactions of spike triplets, such as pre-post-post or post-pre-pre (for reviews see Gerstner and Kistler, 2002; Senn, 2002). Because of these non-linearities, it is able to account not only for the timing dependence of experimental STDP, but also for the frequency dependence of STDP and some triplet effects (Senn, 2002). Similar in spirit is the model of Pfister and Gerstner (2006). In this model depression is induced by post-pre pairs, while LTP requires at least a triplet of spikes, e.g., pre-post-post or post-pre-post. The frequency dependence of STDP (Markram et al., 1997; Sjöström et al., 2001) then follows directly from the assumptions (Pfister and Gerstner, 2006). However, neither the model of Senn et al. nor that of Pfister and Gerstner can be applied outside the realm of spike-triggered plasticity. In particular, no voltage dependence is included in these models. Effects of dendritic location are also out of the scope of these two models. Another category of models offers biophysical mechanisms of plasticity (Lisman and Zhabotinsky, 2001; Shouval et al., 2002; Miller et al., 2005; Rubin et al., 2005; Graupner and Brunel, 2007). Most of these are, however, not usually tested on more elaborate plasticity protocols.

In this paper, we aim at a unified explanation of all of the above experimental results with one single model, proposed previously (Clopath et al., 2008, 2010). The model is a minimal one in the sense that it should be complex enough to reproduce, at least qualitatively, the data mentioned above but still with a restricted number of parameters; and a phenomenological one in the sense that it is composed of abstract variables that are not directly linked to identified biophysical quantities. This approach enables the research to be generic, i.e., it presents a framework in which one can reason about synaptic plasticity experiments even when the biophysical pathways are unknown. Note that the framework could be the same, even if the biophysical implementation in terms of molecules differs from one type of synapse to the next. For example, synaptic depression in STDP experiments seems to depend crucially on calcium concentration in hippocampus (Bi and Poo, 2001), but also on retrograde messenger like endocannabinoid in visual cortex (Sjöström et al., 2003, 2004). The drawback of the phenomenological model is that the biophysical nature of synaptic plasticity cannot be addressed in this paper. In particular, we do not consider pharmacological data. Moreover the model only focuses on the induction of synaptic plasticity but not on its maintenance. It has to be combined with a model of consolidation (Clopath et al., 2008; Barrett et al., 2009) to arrive at a more complete description of synaptic plasticity across different time scales.

Even though we put some focus on a phenomenological explanation of experimental plasticity results in dendrites we did not want to implement our plasticity model in a detailed biophysical neuron model with multiple compartments and ion channels. While modeling backpropagating action potentials and dendritic spikes in biophysical models is possible (Achard and De Schutter, 2006; Druckmann et al., 2007), it is a project in its own right. Instead of explicitly modeling the dendritic effects we shortcut the argument and impose a putative time course of the voltage at the site of the synapse. The exact time course could have been the result of a more detailed model (which we did not do) or could come from experimental measurements. Whenever such experiments were available we took that data into account.

MATERIALS AND METHODS

MODEL OF SYNAPTIC PLASTICITY

The plasticity model we are exploring in this paper is described in Clopath et al. (2010). It depends on the presynaptic spike time and on the (momentary or filtered) time course of the postsynaptic membrane potential. Depression and potentiation are modeled as two independent mechanisms and lead to a downregulation or upregulation of the synaptic weight w characterizing the strength of the connection from a presynaptic neuron to the postsynaptic neuron under consideration. For biophysical reasons we impose that the weight always stays between 0 and a maximal value $w_{\max}$.

The synapse is depressed if a presynaptic spike occurs when the neuron is depolarized for some time. We can formalize this idea mathematically defining a presynaptic spike train as a series of delta pulses $X(t) = \Sigma_i \delta(t - t_i)$ where t_i are the spike times. The postsynaptic membrane potential u is low-pass filtered with a time constant τ_-

$$\tau_- \frac{d}{dt}\bar{u}_-(t) = -\bar{u}_-(t) + u(t).$$

Depression is induced at the moment of presynaptic spike arrival if the postsynaptic trace $\bar{u}_-$ is above a threshold θ_-. This typically happens if there was a postsynaptic spike some time before the presynaptic spike, leading to spike-timing dependence; if synaptic input at other synapses induced some compound EPSP and hence a depolarization at the site of the active synapse, leading to associativity of depression; if any source of depolarizing current input is given in an experiment. Mathematically, the change of the synapse is described by the differential equation

$$\frac{d}{dt}w^- = -A_{\mathrm{LTD}} X(t) \left[\bar{u}_-(t) - \theta_-\right]_+ \quad \text{if } w > 0, \tag{1}$$

where A_{LTD} is an amplitude (see **Figure 1A**). The notation $[x]_+$ equals x if x is positive and is 0 otherwise. Downregulation of the synapse stops if w hits 0.

Potentiation of the synapse occurs if the following three conditions are met simultaneously: (i) The momentary postsynaptic voltage u is above a threshold θ_+ which is around the firing threshold of the neuron, in particular $\theta_+ > \theta_-$. (ii) The low-pass filtered voltage $\bar{u}_+$ is above θ_-. (iii) A presynaptic spike occurred a few milliseconds earlier and has left a "trace" $\bar{x}$ at the site of the synapse. The trace could represent the amount of glutamate bound at the postsynaptic receptor; or the percentage of NMDA receptors in an upregulated state or something similar.

The weight change during potentiation can be written as

$$\frac{d}{dt}w^+ = +A_{\mathrm{LTP}} \bar{x}(t) \left[u(t) - \theta_+\right]_+ \left[\bar{u}_+(t) - \theta_-\right]_+ \quad \text{if } w < w_{\max}, \tag{2}$$

where $\bar{u}_+$ is a similar to $\bar{u}_-$ but with a filter time constant τ_+ instead of τ_- and $\bar{x}$ is a low-pass filter of the presynaptic spike train with time constant τ_x (see **Figure 1B**)

$$\tau_x \frac{d}{dt}\bar{x}(t) = -\bar{x}(t) + X(t).$$

Note that the postsynaptic variable enters twice. First, we need a spike to overcome the threshold θ_+ and second, the *filtered* membrane must be depolarized *before* the spike. This depolarization could

be due to earlier action potentials which have left a depolarizing spike after-potential which explains the relevance of post-pre-post or pre-post-post triplets of spikes (see **Figure 1B**); or to sustained input at other synapses, leading to associativity of LTP.

The total synaptic change is the contribution of depression and potentiation:

$$\frac{d}{dt}w = -A_{\mathrm{LTD}}X(t)\left[\bar{u}_{-}(t)-\theta_{-}\right]_{+} + A_{\mathrm{LTP}}\bar{x}(t)\left[u(t)-\theta_{+}\right]_{+}\left[\bar{u}_{+}(t)-\theta_{-}\right]_{+}, \quad (3)$$

where the differential equation is applied within the hard bounds $0 < w < w_{\max}$. The initial weight is put to $w = 1$ (arbitrary units) and the maximal weight to $w_{\max} = 1.6$ (**Figure 2**), corresponding to a maximal weight increase by 60%, consistent with the experiments of Markram and colleagues (Markram et al., 1997; Senn et al., 2001). The free parameters of the plasticity models that need to be fitted to experiments are the two amplitudes A_{LTD} and A_{LTP} as well as the three time constants τ_x, τ_+, and τ_-. Finally the thresholds θ_+ and θ_- can vary but for most of the experiments they are set to the firing threshold and the resting potential respectively.

NEURON MODEL

Since the voltage is a key quantity in our plasticity model, an appropriate neuron model is needed. Since the plasticity model is a phenomenological one, we opted also for a phenomenological neuron model. We took the Adaptive Exponential Integrate-and-Fire (AdEx) model (Brette and Gerstner, 2005) described by

$$C\frac{d}{dt}u = -g_L\left(u-E_L\right)+g_L\Delta_T\exp\left(\frac{u-V_T}{\Delta_T}\right)-w_{\mathrm{ad}}+z+I,$$

where C is the membrane capacitance, g_L the leak conductance, E_L the resting potential and I the stimulating current. The exponential term describes the rapid activation of the sodium channel, V_T is the threshold above which the dynamics is driven by this exponential and Δ_T controls the rise in the upswing of the action potential. Integration is stopped if the u reaches 100 mV above rest which corresponds to the peak of the action potential. At this time, the voltage is reset to $V_{T_{\mathrm{rest}}}$. An adaptation variable w_{ad} (acting as a hyperpolarizing current) increases by an amount of b after each spike. Moreover adaptation is also coupled to the voltage. The adaptation dynamics is written as

$$\tau_{w_{\mathrm{ad}}}\frac{d}{dt}w_{\mathrm{ad}} = a\left(u-E_L\right)-w_{\mathrm{ad}},$$

where a is responsible for a subthreshold adaptation and $\tau_{w_{\mathrm{ad}}}$ is a time constant. In an extension to the AdEx model we added an additional current z responsible for a depolarizing spike afterpotential which is set to a value I_{sp} at each spike, decaying otherwise with a time constant τ_z

$$\tau_z\frac{d}{dt}z = -z.$$

The z variable can be seen as a simplified description of a slowly inactivating sodium current such as the I_{NaP} (Magistretti and Alonsoa, 1999). Finally the threshold is adaptive as in Badel et al. (2008). At every spike the threshold jumps to $V_{T_{\max}}$ and decays to $V_{T_{\mathrm{rest}}}$ otherwise with a time constant τ_{V_T}

$$\tau_{V_T}\frac{d}{dt}V_T = -\left(V_T - V_{T_{\mathrm{rest}}}\right).$$

The neuron model has a number of variables listed above. For plasticity experiments considered here, it is crucial to have a spike after depolarization in order to have a trace of the spike lasting for about 50 ms, as explained in Clopath et al. (2010). It is therefore necessary to have an adaptive threshold, to prevent the neuron from spiking during this after spike phase. The exponential term and the adaption variable are not important for the results here but are part of the neuron model to make it more accurate, as shown in Clopath et al. (2007), Badel et al. (2008), and Naud et al. (2008). All the parameters are taken from Clopath et al. (2010) and are shown in **Table 1**.

PARAMETERS

The free parameters of the plasticity model are fitted to the different experiments described above (Markram et al., 1997; Sjöström et al., 2001; Froemke and Dan, 2002; Wang et al., 2005; Kampa et al., 2006) (**Table 2**). The thresholds are fixed to the resting potential and the firing threshold for all the experiments except the ones of Froemke and Dan (2002) and Kampa et al. (2006). The error, defined as the difference between the experimental and the theoretical value squared, is minimized. For **Figures 5 and 6**, the STDP learning window is only characterized by two experimental data points. We thus gave those points five times more weight than the others in the

Table 1 | Parameters of the neuron model.

Parameters	Value
C – membrane capacitance	281 pF
g_L – leak conductance	30 nS
E_L – resting potential	–70.6 mV
Δ_T – slope factor	2 mV
$V_{T_{\mathrm{rest}}}$ – threshold potential at rest	–50.4 mV
$\tau_{w_{\mathrm{ad}}}$ – adaptation time constant	144 ms
a – subthreshold adaptation	4 nS
b – spike triggered adaptation	0.805 pA
I_{sp} – spike current after a spike	400 pA
τ_z – spike current time constant	40 ms
τ_{V_T} – threshold potential time constant	50 ms
$V_{T_{\max}}$ – threshold potential after a spike	–30.4 mV

Table 2 | Parameters of the plasticity model fitted to different experiments.

Experiment	θ_- (mV)	θ_+ (mV)	A_{LTD} (1/mV)	A_{LTP} (1/mV^2)	τ_x (ms)	τ_- (ms)	τ_+ (ms)
Figure 2	–70.6	–45.3	**21e^{-5}**	**65e^{-6}**	**13.3**	**13.8**	**58.7**
Figure 3	–70.6	–45.3	**14e^{-5}**	**12e^{-5}**	**15**	**10**	**7**
Figure 4	–70.6	**–65**	**48e^{-5}**	**6e^{-5}**	**11**	**95**	**5**
Figure 5	**–71.3**	**–62.7**	**27e^{-5}**	**12e^{-5}**	**9.6**	**10.5**	**200**
Figure 6	–70.6	–45.3	**16e^{-5}**	**10e^{-5}**	**46**	**23**	**2.6**

The bold numbers represent the variables that were fitted.

computation of the error. Note that the experimental values were taken from the figures of the different experimental papers (since we did not have the raw data) and thus the data points redrawn on the figures of the present paper are not precise.

RESULTS

As explained in Section "Materials and Methods," our model of voltage based plasticity (Clopath et al., 2008, 2010) requires a minimal membrane voltage $\bar{u}_- > \theta_-$ at the site of the synapse in order to allow synaptic depression; and a momentary voltage larger than the firing threshold $u > \theta_+$ to allow potentiation to occur. The combination of potentiation and depression leads, in voltage clamp experiments, to a voltage dependence shown in **Figure 1C** which is reminiscent of that found in earlier studies on voltage dependence of synaptic plasticity (Kelso et al., 1986; Artola et al., 1990; Ngezahayo et al., 2000). In a simulated STDP experiment, a single post-pre spike pairing leads to LTD if the time difference is short enough, but no plasticity is induced if the timing difference is too big or if the time is inversed (**Figures 1A,B**). However, a triplet of spikes in post-pre-post configuration can induce a small amount of LTP, since the following three conditions are met: the first postsynaptic spike induces a trace in the average voltage $\bar{u}_+ > \theta_-$; the presynaptic spike leaves a trace $\bar{x} > 0$ at the site of the synapse; and the momentary voltage during the second postsynaptic action potential is sufficiently high to surpass the second threshold $u(t) > \theta_+$ (see **Figure 1B**). In our previous papers (Clopath et al., 2008, 2010), the model has already been shown to be in qualitative agreement with the voltage clamp experiment that is the basis of the Artola–Bröcher–Singer (ABS) plasticity rule (Artola et al., 1990), to yield a plausible dependence upon presynaptic frequency (Dudek and Bear, 1992), an STDP learning window (Markram et al., 1997), a burst-timing-dependent learning window (Nevian and Sakmann, 2006) as well as a tight relation between spike timing and voltage during manipulations of somatic voltage by current injection (Sjöström et al., 2001). In this paper, the model will be tested against several other classical experimental data on synaptic plasticity. Note that experimental data on STDP in different preparations and experimental conditions is now so rich, that the list of tests that can be carried out and presented in a single paper cannot be exhaustive. The result section is organized in three parts. We first turn to the data from the classical 1997 STDP paper of Markram et al. (1997) and some follow-up experiments (Senn et al., 2001). We then address a couple of more recent studies that explored plasticity in dendrites. We emphasize that dendrites are not modeled explicitly. Rather, we consider plasticity as a local event at the site of the synapse. Since the essential ingredient of our voltage based plasticity model is the time course of the voltage, it is sufficient to model the local voltage at the site of the synapse. In the final part, we focus on STDP experiments using slightly different protocols, for example extracellular stimulation, leading to a large compound EPSP in the postsynaptic neuron or hippocampal cultures which have slightly different dynamics than acute cortical slices.

STDP IS SENSITIVE TO FREQUENCY

As early as in 1997, Markram et al. (1997) showed that the amount of plasticity resulting in pre-post pairing does not only depend on the lag between the pre- and postsynaptic spike but also on the frequency at which these pairings are repeated. By injecting short current pulses into two pyramidal cells, five pairs of pre- and postsynaptic spikes with a lag of 2 ms are elicited at different frequencies and repeated 10 times every 4 s. The data (Markram et al., 1997) show no change of synaptic weight at low frequency pairing whereas LTP is induced at high frequency. Pair-based STDP rules (Gerstner et al., 1996; Kempter et al., 1999; Song et al., 2000), where a pre-post pair leads to LTP and a post-pre pair leads to LTD, cannot account for this frequency dependency. Indeed, independent of the specific choice of parameters, pre-post pairings at low frequency will result in LTP with standard pair-based STDP models (**Figure 2B**, dashed lines); moreover raising the repetition frequency of the pre-post pairings induces a weak post-pre interaction which decreases the potentiation in the pair-based models, whereas LTP increases in the experiments. This picture changes completely with our model (**Figure 2B**). The reason is that our model needs a post-pre-post triplet to induce potentiation. At low pairing frequencies such triplets are quasi inexistent since the interval between two postsynaptic action potentials is too long whereas higher frequencies induce the triplet interaction necessary for LTP (see **Figures 1 and 2B**).

In the modeling literature, the frequency dependence is also studied in an alternative scenario where both the pre- and postsynaptic neuron fire stochastically with Poisson distributed interspike intervals. In our simulations, the presynaptic neuron fires at 10 Hz and the postsynaptic one fires at a fixed frequency different from one simulation experiment to the next. If plasticity is plotted as a function of the firing rate of the postsynaptic neuron (across repeated epochs of 1 s), both LTD and LTP are exhibited: low firing rates lead to LTD whereas high rates induce LTP (**Figure 2C**). This result is to be contrasted with the frequency dependence found in the *same* model with identical parameters in an experiment simulating repeated pre-post pairings as in **Figure 2B**. These results show that timing dependence and frequency dependence of synaptic plasticity interact. For the same firing frequency of, say 10 Hz, of pre- and postsynaptic neuron, systematic timing of action potentials in the causal order of "pre before post" leads to strong LTP, whereas random timing of the same number of action potentials leads to significant LTD. The frequency dependence in **Figure 2C** is similar to the one of the well known Bienenstock–Cooper–Munro (BCM) model (Bienenstock et al., 1982). A standard pair-based rule, where all the pairs are considered, is linear with respect to the frequency. For a typical case where the integral of the STDP learning window is negative, the weight change decreased linearly with frequency. However, a pair-based rule where only the nearest pair is considered results in a non-linear frequency dependence, if an appropriate set of parameters is chosen (see Izhikevich and Desai, 2003) (**Figure 2C**, dashed red line). The qualitative frequency dependence of the pair-based nearest-neighbor rule for the Poisson input is similar to, but much weaker than the one in our model (**Figure 2**, inset). For pairing experiments (**Figure 2B**), the models are qualitatively different.

A further question explored by Senn et al. (2001) was how many pairings were needed to induce potentiation. Pre- and postsynaptic spike trains of 20 Hz were paired with a postsynaptic spike delay of 2 ms, repeated 10 times every 4 s. The number of spikes in the paired trains was varied from 2 up to 20 in the experiment, and

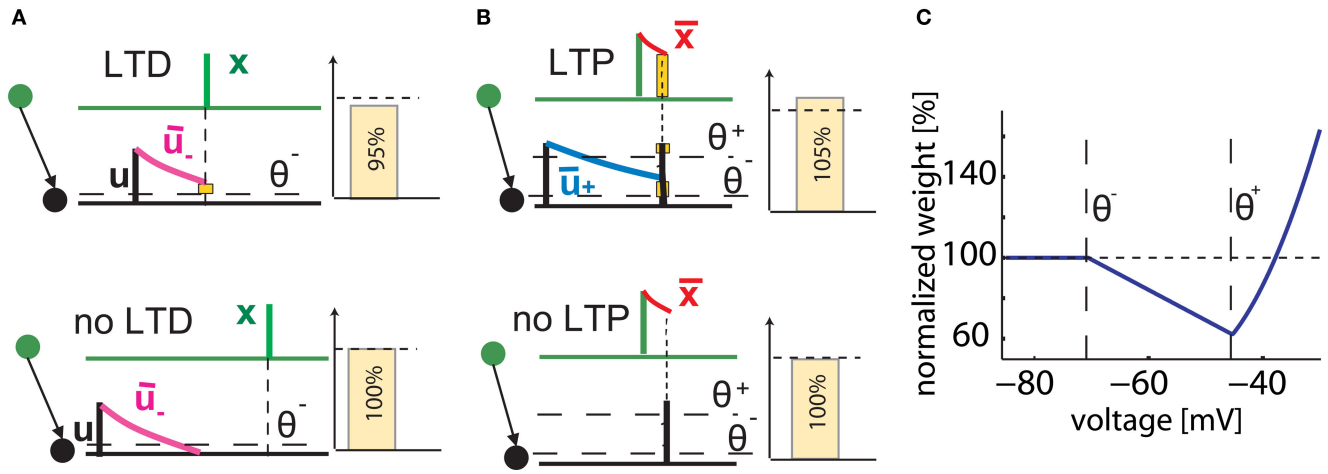

FIGURE 1 | Schematics of the model. (A) LTD occurs at the time of a presynaptic spike (green) if the low-pass filtered voltage trace $\bar{u}_-$ (magenta) is above θ_- (dashed line). The amount of LTD is proportional to the size of the yellow box. If the timing difference between post- and presynaptic spikes is too big, no LTD is induced (bottom). **(B)** LTP requires three factors: a momentary voltage u (black) above θ_+ (dashed line), the trace $\bar{x}$ (red) left from a previous presynaptic spike above 0, and the trace $\bar{u}_+$ (blue) of the low-pass filtered voltage above θ_- (dashed line). The three conditions are met at the moment of the second postsynaptic spike in a post-pre-post triplet (top panel), but not after a single pre-post pair (bottom). The amount of plasticity is proportional to the multiplication of the yellow boxes. **(C)** Presynaptic stimulation under voltage clamp conditions shows the relevance of the threshold θ_- for onset of LTD and θ_+ for the onset of the LTP contribution. LTP becomes dominant if the voltage is 10 mV or more above θ_+.

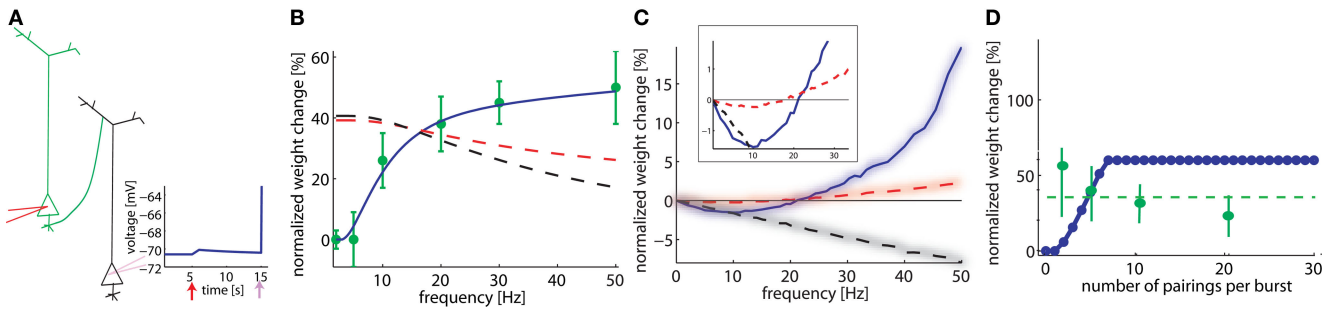

FIGURE 2 | Model depends on spike frequency. (A). Schematics of STDP experiment. Injection of a current pulse in the presynaptic neuron at $t = 5$ ms leads to an EPSP which is followed $t = 15$ ms by an action potential triggered by a current pulse into the postsynaptic neuron. **(B)** If pre-post pairings at lags of 2 ms are repeated, the total amount of weight change (vertical) depends on the repetition frequency (horizontal axis). Model in blue, data redrawn from Markram et al. (1997) in green. A standard pair-based STDP model cannot account for the frequency, whatever the summation scheme (black dashed line: all pairs contribute; red dashed line: only pairs between the nearest spikes contribute to plasticity). **(C)** The frequency dependence is different, if both pre- and postsynaptic spikes are generated by a Poisson process (box: zoom). **(D)** The total amount of plasticity depends on the number of pre-post pairings at 2 ms lag. At least two pairs at 20 Hz are necessary. With our set of parameters, saturation at the maximal weight occurs for around seven pairings (model is blue, data redrawn from Senn et al. (2001) in green; in experiments, saturation is maybe already reached after two pairings, dashed green line).

between 0 and 30 in our model. Isolated pre-post pairings showed no effects in the experiment (as can be seen from the LTP results at low frequency in **Figure 2B**), whereas pairings with two and more pre-post gave an effect (Senn et al., 2001). In our model, isolated pairings give no effect (because the triplet term is not activated), whereas two or more repetitions at 20 Hz induce LTP. In contrast to the results of Senn et al. more spikes lead in our model to a linear increase before plasticity enters into saturation (**Figure 2D**). This could be due to the fact that the sliding threshold for the LTD to LTP transition (Bienenstock et al., 1982; Clopath et al., 2010) is not taken into account in this simulation. Since each plasticity induction protocol lasts more than 40 s, it is possible that the first pairing leads to LTP but with time the threshold slides so that later parings result in LTD. The net effect would give less LTP. Note the large error bars in the statistics of the experiments presented in Senn et al. (2001), which make the results consistent with a horizontal fit (dashed green line) or with a decrease with the number of pairings.

BEYOND THE POINT NEURON: WHAT COUNTS IS THE VOLTAGE AT THE SYNAPSE

The plasticity model depends directly on the postsynaptic voltage at the synapse; depending on the location of the synapse along the dendrite, the time course of the voltage is expected to be different. A change in the time course of the modeled voltage during plasticity experiments enables us to explore the

effects that the failure of a backpropagating action potential or the form of dendritic spikes could have on the outcome of plasticity experiments.

The role of backpropagating action potentials

In the protocol from Sjöström and Häusser (2006), five pre-post pairs of spikes at 50 Hz are induced 15 times every 10 s. The lag between the first pre- and the first postsynaptic spike is 10 ms. Data of Sjöström and Häusser (2006) show that such a high-frequency pairing leads to LTP in basal dendrites, but to LTD in apical dendrites. A potential explanation is that LTP does not occur in distal dendrites, if there is a failure of the backpropagating action potential to reach the synapse. In agreement with this interpretation, LTP can be rescued in the apical dendrites if, in addition to the pairing, a depolarizing current in the dendrite is injected, boosting the backpropagating action potential (Sjöström and Häusser, 2006).

In a simulation of the high-frequency pairing experiment in our model of synaptic plasticity, we consider two different situations. In both cases, a current pulse is injected in the neuron model, but two different pulse amplitudes are studied. In the first case, the current pulse is sufficient to elicit a postsynaptic spike (**Figure 3A**, left). We find that presence of the postsynaptic spikes resulted in LTP (**Figure 3B**, left). We assume that the spike in the basal dendrite has 80% of the amplitude of a somatic spike. This scenario corresponds to the situation in the basal dendrites (where the action potential is damped); but also to the apical dendrites with depolarizing current, under the assumption that the depolarizing current is sufficient to allow transmission of the backpropagating action potential.

In the second case, the pulse amplitude of the injected current is reduced so that it provokes a subthreshold response only (**Figure 3A**, right). We imagine that this corresponds to the situation that is seen by a synapse located distantly on the apical dendrite. Because of the large electrotonic distance, it will not feel the somatic action potential, but only voltage deflection of small amplitude. In our model, this scenario leads to LTD at the synapse, as in the apical dendrites (**Figure 3B**, right).

We note that the actual value of LTP in proximal synapses, predicted by the model, is slightly higher than that measured in experiments. However, the data (Sjöström and Häusser, 2006) show that

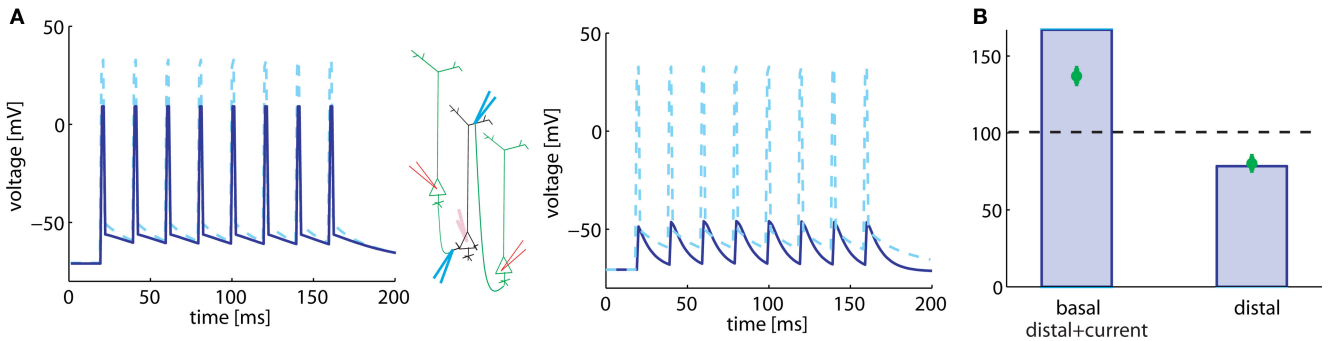

FIGURE 3 | Plasticity results depend on voltage trajectory. (A) Eight 50 Hz pre-post pairings are induced by injection of somatic current pulses (center, schematic). We model the voltage time course at synapses located on the soma (dashed) and basal (solid) dendrite by the sequence of action potentials, shown on the left. The voltage time course at synapses located distally on apical dendrites is modeled as subthreshold response (right, solid line). **(B)** 50 Hz pre-post pairing leads to LTP (left column) when postsynaptic response consists of spikes as in the basal dendrite (or if the presence of backpropagating action potentials) and to LTD when the postsynaptic response stays subthreshold (right column). Green, data redrawn from Sjöström and Häusser (2006); blue, simulations.

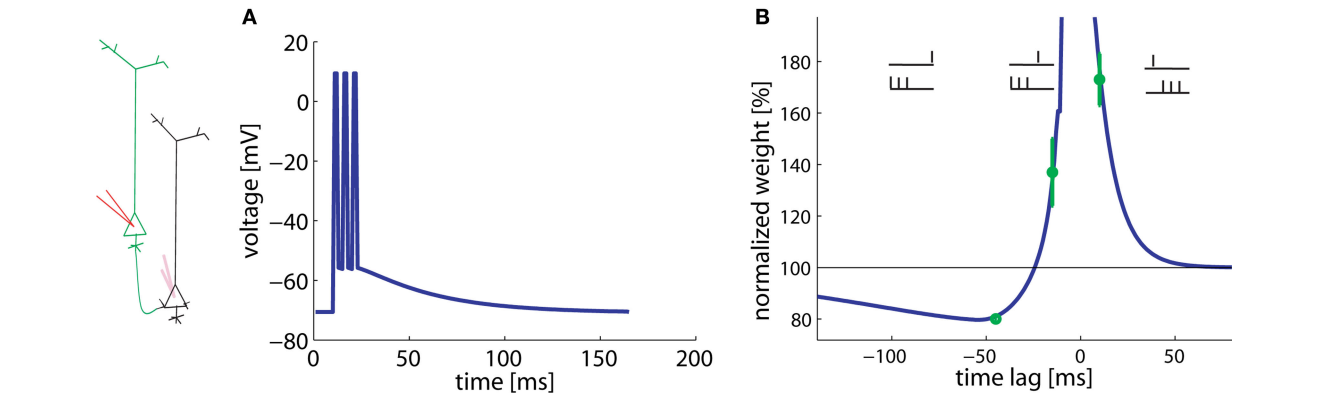

FIGURE 4 | Burst-timing-dependent learning window. A postsynaptic burst of three spikes is paired with a presynaptic spike. **(A)** Assumed voltage waveform at the basal dendrite. **(B)** The total weight change plotted as a function of the time between the presynaptic spike and the start of the postsynaptic burst varies. Data redrawn from Kampa et al. (2006) in green, simulations in blue.

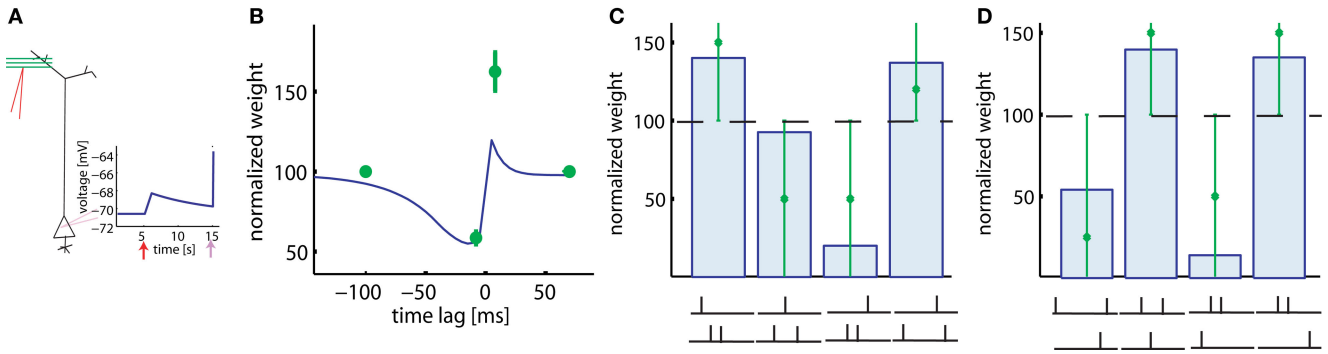

FIGURE 5 | Results with extracellular stimulation. (A) Extracellular stimulation of presynaptic fibers followed 10 ms later by postsynaptic stimulation is described by a compound EPSP of 2.5 mV and the upswing of an action potential (schematic). **(B)** 60 repetitions of pre-post pairs lead to LTP despite a repetition frequency of only 0.2 Hz. The amount of LTP in our model (blue line) is smaller than in the corresponding experiment (green). The reverse firing leads to LTD. **(C)** Triplets consisting of two post- and one presynaptic spikes in various configurations (see drawing) are repeated at low frequencies. Presynaptic stimulation is extracellular. Line and bars: simulations, green: data redrawn from Froemke and Dan (2002). **(D)** Same, but triplets consisting of two pre- and one postsynaptic spike. The big error bars in **(C,D)** indicate that data are very noisy and thus it is only relevant whether triplets induce LTP or LTD in each configurations.

the connections closest to the soma undergo a synaptic change of about 150–200%, whereas those further away show less potentiation. The experiential data in **Figure 3A** corresponds to an average over all "proximal" synapses.

The role of bursts in basal dendrites

Experiments of Kampa et al. (2006) studied the pairing of a presynaptic spike with a burst of three postsynaptic spikes at 200 Hz. Hence the total duration of a burst was 10 ms. The time between the presynaptic spike and the postsynaptic burst varies. Pairs of presynaptic spike and postsynaptic burst (three spikes, intra burst frequency of 200 Hz) were repeated 60 times every 10 s.

In agreement with the experimental results, a presynaptic spike followed 10 ms later by the start of the postsynaptic burst results in LTP whereas a postsynaptic burst followed 45 ms later by a presynaptic spike gives LTD (**Figure 4**). Hence pre-before-burst yields LTP whereas burst-before-pre yields LTD, as expected. Experiments have shown that bursts, and hence dendritic calcium spikes, are important for the induction of plasticity (Kampa et al., 2006). This aspect is modeled here by the non-linear term for potentiation. The plasticity changes for −45 and +10 ms are found to be a stable result of our model over a broad range of parameters.

Surprisingly, however, burst-before-pre gives LTP in the experiments, if the burst starts 15 ms before the presynaptic spike. Our model shows that this effect can be explained under the assumption of a low LTP threshold (θ_+) in the basal dendrites. The optimal value is about 10 mV above rest (see **Table 2**). Since the spikes have a long depolarizing spike after-potential (Nevian et al., 2007) (**Figure 4A**), a low LTP threshold allows, for a timing difference burst-before-pre of 15 ms, an overlap between presynaptic and postsynaptic events. Thus, a low threshold corresponds to a shift in the horizontal position of the transition from LTP to LTD in the burst-timing learning window.

PLASTICITY IN DIFFERENT PREPARATIONS

In the previous sections, we focused on data obtained from experiments with multiple patch electrodes. In this last section, we explore plasticity data coming from different preparations.

Extracellular stimulation

In experiments of Froemke and Dan (2002), pairs and triplets of spikes are repeated 60 times at 0.2 Hz. The main difference to the pairing experiments of Markram et al. (1997) is that current injection into the presynaptic neuron is replaced by extracellular stimulation of axonal fibers projecting onto the postsynaptic neuron (**Figure 5A**). Since presynaptic stimulation in these experiments (Froemke and Dan, 2002) is extracellular and most likely triggers activity in many presynaptic fibers, we adjust the postsynaptic response to the presynaptic activity to an amplitude of 2.5 mV, corresponding to the estimated size of compound EPSP. The real compound EPSP amplitude at the site of the synapse might be even bigger (Palmer and Stuart, 2009), but this seems to be a reasonable estimate. If the time lag between the presynaptic spike arrival and postsynaptic firing is changed, the model generates a STDP function of the standard form, albeit with an amplitude slightly lower than that measured in experimental results (**Figure 5B**). In contrast to the results of Markram et al. (1997), LTP occurs in the pre-post configuration in our model despite the fact that the repetition frequency is only 0.2 Hz. The difference is due to the fact that extracellular stimulation leads to a significant depolarization of the postsynaptic membrane because of the large compound EPSP. This depolarization is followed in the pre-post configuration a few milliseconds later by a postsynaptic spike. Activation of the synapse, sustained depolarization before the spike, and momentary spiking are exactly the three requirements in the model to evoke LTP. The amount of potentiation in the learning window is however smaller in the model than in the experiment with this choice of EPSP amplitude; a larger amplitude yields similar results. Note that the voltage threshold θ_+ for LTP induction found by parameters optimization is about 11 mV above resting potential (see **Table 2**).

We use the same plasticity model also for the triplet experiments conducted by Froemke and Dan (2002). Triplets of one pre- and two postsynaptic spikes are induced in four different configurations: (a) pre-5ms-post-5ms-post, (b) post-5ms-pre-10ms-post, (c) post-5ms-post-5ms-pre, and (d) post-25ms-pre-5ms-post. Similarly, triplets of two pre- and one

postsynaptic spikes can have one of four possible timings: (a) pre-30ms-post-10ms-pre, (b) pre-3ms-post-10ms-pre, (c) post-5ms-pre-20ms-pre, and (d) pre-7ms-pre-3ms-post. All the eight data points can be explained qualitatively by the model (**Figures 5C,D**).

Pairs, triplets, and quadruplets elicited in culture hippocampal cells

In hippocampal culture, Wang et al. (2005) studied a large range of pair, triplet, and quadruplet experiments. All stimuli (pairs, triplets, or quadruplets) are repeated 60 times at 1 Hz. Since neuronal and synaptic parameters in a culture can be somewhat different, we assumed a relatively large EPSP amplitude of 7.5 mV. With such a large EPSP we find, in analogy to the results in **Figure 5**, a standard STDP learning window for pairing experiments at 1 Hz (**Figure 6B**), however with a smaller amplitude compared to that of the experiment.

Our model enables us to account qualitatively for seven out of eight results with triplet stimulation. Triplets in the experiments of **Figure 6** are designed so that the pair interactions (pre-post or post-pre) in the pre-post-pre triplet are identical to those in the post-pre-post triplet (**Figure 6C**, blue and red schematic traces). Hence a pure pair-based STDP rule would predict the same result. However, in our triplet model the effective contribution of LTP is different in the two configurations (**Figure 6C**). Moreover, the model also enables us to explain the quadruplet experiments that used the following configurations: pre-5ms-post-T-post-5ms-pre or post-5ms-pre-T-pre-5ms-post, where T varies (**Figure 6D**). The only point in **Figure 6C** which is badly fitted is the one in the paradigm with pre-5ms-post-15ms-pre. We wondered whether the quality of the fit would increase if we included short-term plasticity into the model framework. The reason is that our plasticity model predicts too much depression, but depression would be decreased if the EPSP caused by the second presynaptic spike has a smaller amplitude than the first one. It is not clear what type of short-term plasticity is expressed hippocampal culture synapses, but, if the synapses are depressing, the scenario (5, −15) is improved without altering the qualitative behavior of the other scenarios (data not shown).

DISCUSSION

The model presented in this paper can explain a number of synaptic plasticity experiments. It covers the presynaptic frequency dependency (Dudek and Bear, 1992), voltage-clamp experiment (ABS rule) (Artola et al., 1990), spike-timing and pairing frequency dependency (Markram et al., 1997; Sjöström et al., 2001), tight relation between voltage and spike timing (Sjöström et al., 2001), and burst-timing-dependent plasticity (Nevian and Sakmann, 2006), as shown previously (Clopath et al., 2008, 2010). In addition, the model was tested here successfully on some subtle protocols that showed an influence of the cell morphology on plasticity results (Kampa et al., 2006; Sjöström and Häusser, 2006). Our interpretation is that the morphology enters only indirectly and only as much as it leads to a change of the voltage trajectory at the site of the synapse, compared to the voltage at the soma. Accounting for presence or absence of backpropagating action potentials or dendritic location by an appropriate choice of the local voltage time course was found to be sufficient to describe the experiments considered. For example, the difference between plasticity at the basal and at the apical dendrite (failure of backpropagating action potential) can be explained only by the voltage difference. We think that this model is thus a good compromise between complexity and performance. Indeed, more detailed descriptions as provided by biophysical models (Lisman and Zhabotinsky, 2001; Shouval et al., 2002; Miller et al., 2005; Rubin et al., 2005; Graupner and Brunel, 2007) have a price to pay since they have many parameters to be tuned and cannot be treated analytically.

Some experimental results look at first sight contradictory, e.g., low frequency pairing leads to LTP in Froemke and Dan (2002) and no weight change in Sjöström et al. (2001). However, our mathematical model reconciles these two data, taking into account the

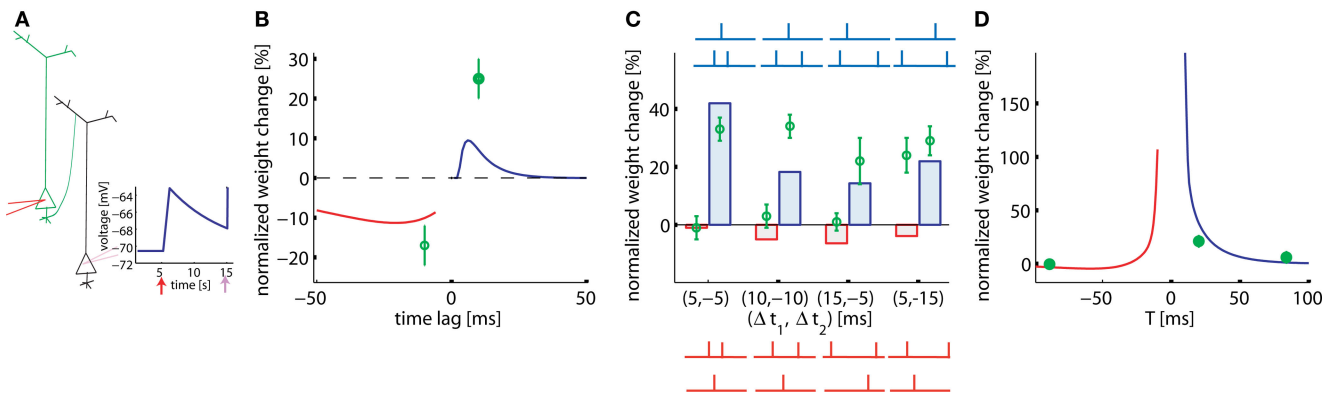

FIGURE 6 | Pairs, triplets, and quadruplets of spikes in cultured hippocampal neurons. (A) Intracellular presynaptic stimulation results in a model EPSP of 7.5 mV (schematic). **(B)** STDP function in the pair-experiment. **(C)** Triplet experiments. $\Delta t_{1,2}$ in the post-pre-post configuration is the time between the single pre- and the two postsynaptic spikes (blue histogram bars and schematics) or, in the pre-post-pre experiment the time between the single post- and the two presynaptic spikes (red histogram bars and schematics). The four different post-pre-post triplets are: (a) post-5ms-pre-5ms-post, (b) post-10ms-pre-10ms-post, (c) post-5ms-pre-15ms-post, and (d) post-15ms-pre-5ms-post. The four different pre-post-pre triplets are: (a) pre-5ms-post-5ms-pre, (b) pre-10ms-post-10ms-pre, (c) pre-15ms-post-5ms-pre, and (d) pre-5ms-post-15ms-pre. Lines and bars: simulations. Green circles: data redrawn from Wang et al. (2005). **(D)** Quadruplet experiment (see main text).

different preparations. Indeed, the STDP learning window from Froemke and Dan (2002) is obtained with extracellular stimulation, which results in a large compound EPSP. This large compound EPSP allows the model to fulfill the three conditions for LTP.

The fitted parameters differ for the various experiments, up to an order of magnitude. This is however not surprising since the preparations and the synapse types are different. For example, τ_x is three times bigger in hippocampal slices (fitted from data of Wang et al., 2005) than in visual cortex (fitted from Sjöström et al., 2001). Would that mean that the dynamics of, say glutamate binding, is slower in hippocampal slices? We think a lot more experimental data are needed before such conclusions should be drawn.

What are the limitations of our model compared to the other plasticity models? First, standard STDP models (Gerstner et al., 1996; Song et al., 2000) cannot account for frequency dependency since they only consider pair interactions of spikes: pre-post for potentiation and post-pre for depression. The original model of Froemke (Froemke and Dan, 2002) did not catch the frequency dependency either, as explained in Froemke et al. (2006). This frequency dependency can be described by non-linear spiking models such as the model of Senn et al. (2001) or the one of Pfister and Gerstner as Pfister and Gerstner (2006) but, by construction, these earlier spike-based models (where action potentials are treated as momentary events) cannot deal with voltage clamp experiment and any other form of plasticity depending on the dendritic structure. Note that the model of Senn et al. (2001) can be interpreted either as a phenomenological model like ours (i.e., formal mathematical quantities that are upregulated and downregulated during spike events) or as a first step toward a biophysical model (where the formal variables are identified with the up- or downregulation of NMDA receptors and second messengers; Senn et al., 2001). Some classical biophysical models depend on (i) the voltage (Abarbanel et al., 2002; Brader et al., 2007), (ii) the calcium/calmodulin-dependent protein kinase II (CaMKII) phosphorylation and bistability (Lisman, 1985, 1989; Lisman and Zhabotinsky, 2001; Miller et al., 2005; Graupner and Brunel, 2007), (iii) the calcium concentration (Abarbanel et al., 2002; Karmarkar and Buonomano, 2002; Karmarkar et al., 2002; Shouval et al., 2002; Rubin et al., 2005), glutamate binding, AMPA receptors (Saudargiene et al., 2003), NMDA receptors (Senn et al., 2001) etc. Maybe the closest in spirit to our model is the Shouval model (Shouval et al., 2002) that also covers the frequency dependency and voltage-clamp experiments. However, this model predicts depression for pre-post pairs at medium to long lags for which only some evidence exists (Nishiyama et al., 2000; Wittenberg and Wang, 2006). Moreover, it was never compared to dendritic synaptic plasticity.

Most of the models described above show their power only qualitatively. In order to compare plasticity models quantitatively, it would be important to have common benchmarks, possibly with some raw experimental data online, and design a score measure. Such a synaptic plasticity challenge could be constructed in analogy to the competition "Quantitative Single-Neuron Modeling" (Gerstner and Naud, 2009) proposed by the International Neuroinformatics Coordinating Facility (INCF). The first step is to use as benchmarks the already published data. However, the perfect type of data would be a consistent set of experiments (same synapse type, same preparation, many repetitions) that describes each synaptic plasticity feature, i.e., frequency, spike timing, complex spike patterns, voltage control (ideally at the synapse location), and intracellular stimulation of several presynaptic neurons connecting the same postsynaptic cell with synapses at different dendritic locations. Since the neurons are highly non-linear (Larkum et al., 2009), it is important to study the precise voltage time course at the postsynaptic site as well as the dynamics of some biophysical quantities related to plasticity mechanism, e.g., calcium. What are the aspects of plasticity that need to be explored next? Apart from the functional implication of synaptic plasticity in networks that is understudied, the relation between early-long-term, late-long-term and short-term plasticity needs to be understood. Is the molecular machinery for consolidation present during standard STDP protocol (e.g., plasticity related proteins)? What is the role of neuromodulators? Are the synapse binary, do they have a few states or are they continuous? The molecular details of plasticity are not well modeled by the theoreticians except for a few promising models (Lisman and Zhabotinsky, 2001; Miller et al., 2005; Rubin et al., 2005; Graupner and Brunel, 2007). Biophysical questions have to be addressed for all major synapse types. Hopefully the structure of the model is constant across synapses, so that just the parameters vary due to different molecular roles, which would enable us theoreticians to develop consistent modeling framework but it is not clear that single model is sufficient to account for different synapse types.

An obvious extension of the work presented in this paper would be to associate the plasticity model with a detailed biophysical neuron model with multiple compartments that would automatically generate, for arbitrary stimuli, the appropriate voltage time course at the site of the synapse. This implies that active dendrites must be considered so as to allow the backpropagation of somatic action potentials as well as intrinsic dendritic spikes under appropriate stimulation. Finally, our model cannot grasp sensitivity upon synaptic strength, for example shown by Bi and Poo (1998), but in principle we can make the amplitudes for depression and potentiation dependent directly on the synaptic weight. The exact shape of this function can be inspired by previous studies (van Rossum et al., 2000; Gütig et al., 2003; Morrison et al., 2007). Additional work in that direction is planned. The list of STDP experiments is long and we did not try to fit all the available experimental data. Here we have shown that a diverse set of experiments from different labs can be explained by our model. However, we think that our model cannot provide an explanation of the following results. Letzkus et al. (2006) show that a presynaptic spike followed by a postsynaptic burst induces LTP in proximal synapses whereas reverse timing leads to depression, which is in agreement with our model. However, in distal synapses, the results are opposite: a presynaptic spike before a postsynaptic burst induces LTD and post before pre results in potentiation. These results are *a priori* not reproducible by our model. Maybe the neuron non-linear dynamics would allow to reconcile our model with these data, but in order to tackle this problem a more detailed neuron model is necessary. Second, the study of Wittenberg and Wang (2006) shows that a pre- and a postsynaptic spike pairing induces only LTD. Moreover, potentiation is expressed after only tens of presynaptic spike with postsynaptic burst pairing whereas depression can only be measured after hundreds of pairings. This dependency is not captured by our model; an additional long time constant would help to describe this phenomenon.

ACKNOWLEDGMENTS

Claudia Clopath has been supported by the Swiss National Science Foundation (grant to Wulfram Gerstner) and by the Agence Nationale de la Recherche grant ANR-08-SYSC-005.

REFERENCES

Abarbanel, H., Huerta, R., and Rabinovich, M. (2002). Dynamical model of long-term synaptic plasticity. *Proc. Natl. Acad. Sci. U.S.A.* 59, 10137–10143.

Abbott, L. F., and Nelson, S. B. (2000). Synaptic plasticity – taming the beast. *Nat. Neurosci.* 3, 1178–1183.

Achard, P., and De Schutter, E. (2006). Complex parameter landscape for a complex neuron model. *PLoS Comput. Biol.* 2, e94. doi:10.1371/journal.pcbi.0020094.

Artola, A., Bröcher, S., and Singer, W. (1990). Different voltage dependent thresholds for inducing long-term depression and long-term potentiation in slices of rat visual cortex. *Nature* 347, 69–72.

Badel, L., Lefort, S., Brette, R., Petersen, C., Gerstner, W., and Richardson, M. (2008). Dynamic i-v curves are reliable predictors of naturalistic pyramidal-neuron voltage traces. *J. Neurophysiol.* 99, 656–666.

Barrett, A., Billings, G., Morris, R., and van Rossum, M. (2009). State based model of long-term potentiation and synaptic tagging and capture. *PLoS Comput. Biol.* 5, e1000259. doi:10.1371/journal.pcbi.1000259.

Bell, C., Han, V., Sugawara, Y., and Grant, K. (1997). Synaptic plasticity in a cerebellum-like structure depends on temporal order. *Nature* 387, 278–281.

Bi, G., and Poo, M. (1998). Synaptic modifications in cultured hippocampal neurons: dependence on spike timing, synaptic strength, and postsynaptic cell type. *J. Neurosci.* 18, 10464–10472.

Bi, G., and Poo, M. (2001). Synaptic modification of correlated activity: Hebb's postulate revisited. *Annu. Rev. Neurosci.* 24, 139–166.

Bienenstock, E., Cooper, L., and Munro, P. (1982). Theory of the development of neuron selectivity: orientation specificity and binocular interaction in visual cortex. *J. Neurosci.* 2, 32–48.

Brader, J., Senn, W., and Fusi, S. (2007). Learning real-world stimuli in a neural network with spike-driven synaptic dynamics. *Neural Comput.* 19, 2881–2912.

Brette, R., and Gerstner, W. (2005). Adaptive exponential integrate-and-fire model as an effective description of neuronal activity. *J. Neurophysiol.* 94, 3637–3642.

Clopath, C., Büsing, L., Vasilaki, E., and Gerstner, W. (2010). Connectivity reflects coding: a model of voltage-based spike-timing-dependent-plasticity with homeostasis. *Nat. Neurosci.* 13, 344–352.

Clopath, C., Jolivet, R., Rauch, A., Luescher, H.-R., and Gerstner, W. (2007). Predicting neuronal activity with simple models of the threshold type: adaptive exponential integrate-and-fire model with two compartments. *Neurocomputing* 70, 1668–1673.

Clopath, C., Ziegler, L., Vasilaki, E., Büsing, L., and Gerstner, W. (2008). Tag-trigger-consolidation: a model of early and late long-term-potentiation and depression. *PLoS Comput. Biol.* 4, e1000248. doi:10.1371/journal.pcbi.1000248. http://dx.doi.org/10.1371%2Fjournal.pcbi.1000248.

Debanne, D., Gähwiler, B., and Thompson, S. (1998). Long-term synaptic plasticity between pairs of individual CA3 pyramidal cells in rat hippocampal slice cultures. *J. Physiol.* 507, 237–247.

Druckmann, S., Bannitt, Y., Gidon, A. A., Schuermann, F., and Segev, I. (2007). A novel multiple objective optimization framework for constraining conductance-based neuron models by experimental data. *Front. Neurosci.* 1, 7–18. doi:10.3389/neuro.01.1.1.001.2007.

Dudek, S. M., and Bear, M. F. (1992). Homosynaptic long-term depression in area ca1 of hippocampus and effects of *N*-methyl-D-aspartate receptor blockade. *Proc. Natl. Acad. Sci. U.S.A.* 89, 4363–4367.

Froemke, R., and Dan, Y. (2002). Spike-timing dependent plasticity induced by natural spike trains. *Nature* 416, 433–438.

Froemke, R. C., Poo, M.-M., and Dan, Y. (2005). Spike-timing-dependent synaptic plasticity depends on dendritic location. *Nature* 434, 221–225.

Froemke, R. C., Tsay, I., Raad, M., Long, J., and Dan, Y. (2006). Contribution of individual spikes in burst-induced long-term synaptic modification. *J. Neurophysiol.* 95, 1620–1629.

Gerstner, W., Kempter, R., van Hemmen, J., and Wagner, H. (1996). A neuronal learning rule for sub-millisecond temporal coding. *Nature* 383, 76–78.

Gerstner, W., and Kistler, W. (2002). *Spiking Neuron Models*. New York: Cambridge University Press.

Gerstner, W., and Naud, R. (2009). How good are neuron models? *Science* 326, 379–380.

Gerstner, W., and van Hemmen, J. L. (1992). Universality in neural networks: the importance of the mean firing rate. *Biol. Cybern.* 67, 195–205.

Graupner, M., and Brunel, N. (2007). STDP in a bistable synapse model based on CaMKII and associated signaling pathways. *PLOS Comput. Biol.* 3, e221. doi:10.1371/journal.pcbi.0030221.

Gütig, R., Aharonov, S., Rotter, S., and Sompolinsky, H. (2003). Learning input correlations through nonlinear temporally asymmetric Hebbian plasticity. *J. Neurosci.* 23, 3697–3714.

Izhikevich, E. (2003). Simple model of spiking neurons. *IEEE Trans. Neural Netw.* 14, 1569–1572.

Izhikevich, E., and Desai, N. (2003). Relating STDP to BCM. *Neural Comput.* 15, 1511–1523.

Kampa, B., Letzkus, J., and Stuart, G. (2006). Requirement of dendritic calcium spikes for induction of spike-timing-dependent synaptic plasticity. *J. Physiol. (Lond.)* 574, 283–290.

Karmarkar, U., and Buonomano, D. (2002). A model of spike-timing dependent plasticity: one or two coincidence detectors. *J. Neurophysiol.* 88, 507–513.

Karmarkar, U., Najarian, M., and Buonomano, D. (2002). Mechanisms and significance of spike-timing dependent plasticity. *Biol. Cybern.* 87, 373–382.

Kelso, S. R., Ganong, A. H., and Brown, T. H. (1986). Hebbian synapses in hippocampus. *Proc. Natl. Acad. Sci. U.S.A.* 83, 5326–5330.

Kempter, R., Gerstner, W., and van Hemmen, J. L. (1999). Hebbian learning and spiking neurons. *Phys. Rev. E* 59, 4498–4514.

Kistler, W. M., and van Hemmen, J. L. (2000). Modeling synaptic plasticity in conjunction with the timing of pre- and postsynaptic potentials. *Neural Comput.* 12, 385–405.

Larkum, M., Nevian, T., Sandler, M., Polsky, A., and Schiller, J. (2009). Synaptic integration in tuft dendrites of layer 5 pyramidal neurons: a new unifying principle. *Science* 325, 756–760.

Letzkus, J., Kampa, B., and Stuart, G. (2006). Learning rules for spike timing-dependent plasticity depend on dendritic synapse location. *J. Neurosci.* 26, 10420–10429. http://www.jneurosci.org/cgi/content/abstract/26/41/104%20.

Lisman, J. (1985). A mechanism for memory storage insensitive to molecular turnover: a bistable autophosphorylating kinase. *Proc. Natl. Acad. Sci. U.S.A.* 82, 3055–3057.

Lisman, J. (1989). A mechanism for Hebb and anti-Hebb processes underlying learning and memory. *Proc. Natl. Acad. Sci. U.S.A.* 86, 9574–9578.

Lisman, J., and Zhabotinsky, A. (2001). A model of synaptic memory: A CaMKII/PP1 switch that potentiates transmission by organizing an AMPA receptor anchoring assembly. *Neuron* 31, 191–201.

Magistretti, J., and Alonsoa, A. (1999). Biophysical properties and slow voltage-dependent inactivation of a sustained sodium current in entorhinal cortex layer-ii principal neurons. a whole-cell and single-channel study. *J. Gen. Physiol.* 114, 4491–509.

Markram, H., Lübke, J., Frotscher, M., and Sakmann, B. (1997). Regulation of synaptic efficacy by coincidence of postsynaptic APs and EPSPs. *Science* 275, 213–215.

Miller, P., Zhabotinsky, A., Lisman, J., and Wang, X. (2005). The stability of a stochastic CaMKII switch: dependence on the number of enzyme molecules and protein turnover. *PLoS Biol.* 3, e107. doi:10.1371/journal.pbio.0030107.

Morrison, A., Aertsen, A., and Diesmann, M. (2007). Spike-timing dependent plasticity in balanced random networks. *Neural Comput.* 19, 1437–1467.

Morrison, A., Diesmann, M., and Gerstner, W. (2008). Phenomenological models of synaptic plasticity based on spike timing. *Biol. Cybern.* 98, 459–478.

Naud, R., Marcille, N., Clopath, C., and Gerstner, W. (2008). Firing patterns in the adaptive exponential integrate-and-fire model. *Biol. Cybern.* 99, 335–347.

Nevian, T., Larkum, M., Polsky, A., and Schiller, J. (2007). Properties of basal dendrites of layer 5 pyramidal neurons: a direct patch-clamp recording study. *Nat. Neurosci.* 10, 206–214.

Nevian, T., and Sakmann, B. (2006). Spine Ca^{2+} signaling in spike-timing-dependent plasticity. *J. Neurosci.* 26, 11001–11013. http://www.jneurosci.org/cgi/content/abstract/26/43/110%01.

Ngezahayo, A., Schachner, M., and Artola, A. (2000). Synaptic activation modulates the induction of bidirectional synaptic changes in adult mouse hippocampus. *J. Neurosci.* 20, 2451–2458.

Nishiyama, M., Hong, K., Miskoshiba, K., Poo, M., and Kato, K. (2000). Calcium stores regulate the polarity and input specificity of synaptic modification. *Nature* 408, 584–588.

Palmer, L., and Stuart, G. (2009). Membrane potential changes in dendritic spines during action potentials and synaptic input. *J. Neurosci.* 29, 6897–6903.

Pfister, J.-P., and Gerstner, W. (2006). Triplets of spikes in a model of spike timing-dependent plasticity. *J. Neurosci.* 26, 9673–9682.

Roberts, P. (1999). Computational consequences of temporally asymmetric learning rules: I. Differential Hebbian learning. *J. Comput. Neurosci.* 7, 235–246.

Rubin, J., Gerkin, R., Bi, G.-Q., and Chow, C. (2005). Calcium time course as a signal for spike-timing-dependent plasticity. *J. Neurophysiol.* 93, 2600–2613.

Rubin, J., Lee, D. D., and Sompolinsky, H. (2001). Equilibrium properties of temporally asymmetric Hebbian plasticity. *Phys. Rev. Lett.* 86, 364–367.

Saudargiene, A., Porr, B., and Wörgötter, F. (2003). How the shape of pre- and postsynaptic signals can influence STDP: a biophysical model. *Neural Comput.* 16, 595–626.

Senn, W. (2002). Beyond spike timing: the role of non-linear plasticity and unreliable synapses. *Biol. Cybern.* 87, 344–355.

Senn, W., Tsodyks, M., and Markram, H. (1997). "An algorithm for synaptic modification based on exact timing of pre-and postsynaptic action potentials," in *Artificial Neural Networks – ICANN'97. Lecture Notes in Computer Science*, Vol. 1327, eds W. Gerstner, A. Germond, M. Hasler, and J.-D. Nicoud (Berlin: Springer), 121–126.

Senn, W., Tsodyks, M., and Markram, H. (2001). An algorithm for modifying neurotransmitter release probability based on pre- and postsynaptic spike timing. *Neural Comput.* 13, 35–67.

Shouval, H. Z., Bear, M. F., and Cooper, L. N. (2002). A unified model of NMDA receptor dependent bidirectional synaptic plasticity. *Proc. Natl. Acad. Sci. U.S.A.* 99, 10831–10836.

Sjöström, P., and Häusser, M. (2006). A cooperative switch determines the sign of synaptic plasticity in distal dendrites of neocortical pyramidal neurons. *Neuron* 51, 227–238.

Sjöström, P., Turrigiano, G., and Nelson, S. (2001). Rate, timing, and cooperativity jointly determine cortical synaptic plasticity. *Neuron* 32, 1149–1164.

Sjöström, P., Turrigiano, G., and Nelson, S. (2003). Neocortical LTD via coincident activation of presynaptic NMDA and cannabinoid receptors. *Neuron* 39, 641–654.

Sjöström, P., Turrigiano, G., and Nelson, S. (2004). Endocannabinoid-dependent neocortical layer-5 LTD in the absence of postsynaptic spiking. *J. Neurophysiol.* 92, 3338–3343.

Song, S., Miller, K., and Abbott, L. (2000). Competitive Hebbian learning through spike-time-dependent synaptic plasticity. *Nat. Neurosci.* 3, 919–926.

van Rossum, M. C. W., Bi, G. Q., and Turrigiano, G. G. (2000). Stable Hebbian learning from spike timing-dependent plasticity. *J. Neurosci.* 20, 8812–8821.

Wang, H.-X., Gerkin, R., Nauen, D., and Wang, G.-Q. (2005). Coactivation and timing-dependent integration of synaptic potentiation and depression. *Nat. Neurosci.* 8, 187–193.

Wittenberg, G. M., and Wang, S. S.-H. (2006). Malleability of spike-timing dependent plasticity at the CA3–CA1 synapse. *J. Neurosci.* 26, 6610–6617.

Conflict of Interest Statement: The authors declare that the research was conducted in the absence of any commercial or financial relationships that could be construed as a potential conflict of interest.

Received: 01 February 2010; paper pending published: 20 February 2010; accepted: 07 June 2010; published online: 21 July 2010.

*Citation: Clopath C and Gerstner W (2010) Voltage and spike timing interact in STDP – a unified model. Front. Syn. Neurosci. **2**:25. doi: 10.3389/fnsyn.2010.00025*

frontiers in
SYNAPTIC NEUROSCIENCE

ORIGINAL RESEARCH ARTICLE
published: 03 September 2010
doi: 10.3389/fnsyn.2010.00033

Rate and pulse based plasticity governed by local synaptic state variables

Christian G. Mayr* and Johannes Partzsch

Endowed Chair of Highly Parallel VLSI Systems and Neural Microelectronics, Institute of Circuits and Systems, Faculty of Electrical Engineering and Information Science, University of Technology Dresden, Dresden, Sachsen, Germany

Edited by:
Per Jesper Sjöström, University College London, UK

Reviewed by:
Sen Song, Massachusetts Institute of Technology, USA
Claudia Clopath, Ecole Polytechnique Fédérale de Lausanne, Switzerland

****Correspondence:***
Christian G. Mayr, Endowed Chair of Highly Parallel VLSI Systems and Neural Microelectronics, Institute of Circuits and Systems, Faculty of Electrical Engineering and Information Technology, University of Technology Dresden, 01062 Dresden, Germany.
e-mail: mayr@iee.et.tu-dresden.de

Classically, action-potential-based learning paradigms such as the Bienenstock–Cooper–Munroe (BCM) rule for pulse rates or spike timing-dependent plasticity for pulse pairings have been experimentally demonstrated to evoke long-lasting synaptic weight changes (i.e., plasticity). However, several recent experiments have shown that plasticity also depends on the local dynamics at the synapse, such as membrane voltage, Calcium time course and level, or dendritic spikes. In this paper, we introduce a formulation of the BCM rule which is based on the instantaneous postsynaptic membrane potential as well as the transmission profile of the presynaptic spike. While this rule incorporates only simple local voltage- and current dynamics and is thus neither directly rate nor timing based, it can replicate a range of experiments, such as various rate and spike pairing protocols, combinations of the two, as well as voltage-dependent plasticity. A detailed comparison of current plasticity models with respect to this range of experiments also demonstrates the efficacy of the new plasticity rule. All experiments can be replicated with a limited set of parameters, avoiding the overfitting problem of more involved plasticity rules.

Keywords: voltage-based BCM, BCM/STDP synthesis, local state plasticity, neuron dynamics based plasticity

INTRODUCTION

One of the major research areas of neurobiology is long-term learning (i.e., plasticity) of synapses in neural tissue (Koch, 1999; Lisman and Spruston, 2005; Pfister and Gerstner, 2006; Morrison et al., 2008). Synapses are the contact points between neurons, where information from the sending neuron arrives at the so-called presynaptic side and is transmitted via the synapse as a postsynaptic current (PSC) pulse to the receiving neuron. The concept of plasticity is used to describe the phenomenon that certain types of pre- and postsynaptic stimuli can have long-lasting effects on the efficacy of this transmission (Bienenstock et al., 1982; Dudek and Bear, 1992; Morrison et al., 2008), i.e., the size of the PSC, ranging from days up to a year. These phenomena are called long-term depression (LTD) for diminished synaptic responses and long-term potentiation (LTP) for enhanced responses. Depending on the induction protocol, spike rates (Dudek and Bear, 1992; Mayford et al., 1995; Wang and Wagner, 1999; Abraham et al., 2001) or different spike patterns (Markram et al., 1997; Bi and Poo, 1998; Sjöström et al., 2001; Froemke and Dan, 2002) have been found to elicit changes in synaptic weight. Various models have tried to incorporate the principal experimental findings, e.g., in implementations of the classical rate-based Bienenstock–Cooper–Munroe (BCM) rule (Bienenstock et al., 1982; Shouval et al., 2002; Kurashige and Sakai, 2006) or the newer spike timing-dependent plasticity (STDP) rule (Badoual et al., 2006; Morrison et al., 2008). Since both rules describe phenomena which have been shown to coexist at the same synapse, several models try to achieve a synthesis of both rules (Senn, 2002; Izhikevich and Desai, 2003; Pfister and Gerstner, 2006; Benuskova and Abraham, 2007).

However, these models usually represent only a statistical average of synaptic responses, as the relevant experiments exhibit a large spread in experimental data (Dudek and Bear, 1992; Bi and Poo, 1998; Froemke and Dan, 2002). This statistical spread may be explained by the fact that relevant local plasticity variables are only unreliably influenced by action potentials (Lisman and Spruston, 2005). Consequently, some experiments seem to indicate that LTP and LTD can be more reliably induced qualitatively as well as quantitatively (i.e., with less variability in the direction and amount of weight change) if local variables are directly influenced, e.g., by evoking dendritic spikes (Holthoff et al., 2006) or by setting the membrane potential artificially (Artola et al., 1990; Ngezahayo et al., 2000; Sjöström et al., 2001). Thus, we hypothesize that the governing variables of plasticity are based on the local environment of the synapse such as the local depolarization or Ca^{2+} levels (Aihara et al., 2007).

Motivated by these findings, several models have tried to incorporate a dependence of plasticity on the Ca^{2+} concentration or the membrane potential. However, most of the Ca^{2+} based models, while able to reproduce BCM-type plasticity, result in unrealistic STDP curves (Shouval et al., 2002; Kurashige and Sakai, 2006; Shah et al., 2006). In addition, the reproduction of higher-order spike interaction effects such as spike triplets (Froemke and Dan, 2002) are either not attempted by the authors or produce results only partially consistent with experimental data (Shah et al., 2006). As well, due to their biophysical motivation, these models tend to be very complex and thus computationally expensive and difficult to analyze mathematically.

Models incorporating the membrane potential have mostly been influenced by computational aspects (Saudargiene et al., 2004; Toyoizumi et al., 2005; Pfister et al., 2006; Baras and Meir,

2007). Pfister et al. (2006) and Saudargiene et al. (2004) have tried to link the learning capability of a neuron to its inherent temporal dynamics and to its structure. STDP-type plasticity is derived for both models, while BCM behavior is not explicitly shown. In the context of reward based learning (Baras and Meir, 2007) and optimal information transmission (Toyoizumi et al., 2005), two further authors show BCM-like behavior based on the timing of pre- and postsynaptic spikes and the membrane potential, but their actual weight change curve in STDP terms is unclear. In general, as the above authors were mainly interested in computational aspects, there was no effort to show the generalization capability of their models by explicitly reproducing experimental protocols. As in the case of the Ca^{2+} based plasticity, the model description is on average very complex, with multiple different time traces/equations interacting with each other. One notable exception is the model described in Clopath et al. (2008a, 2010), where an STDP rule is extended by voltage thresholds and a dependence on the membrane potential to reproduce several experimental findings in the areas of rate-, pulse-, and voltage-based plasticity.

As can be seen from the above, there are various models which can reproduce/explain individual facets of the experimental data, and also some more general models linking two of the three major groups of plasticity phenomena (i.e., voltage, rate, spike timing), but there is only a very limited number of efforts which would link all three.

In the following, we will fully develop a model introduced in an earlier paper (Partzsch et al., 2008) which tries to achieve such a synthesis. In contrast to the extended STDP of Clopath et al. (2010), we start out with the original formulation of the BCM rule, but interpret its state variables for pre- and postsynaptic activity as synaptic current respectively membrane potential and its threshold as membrane resting potential, arriving at a plasticity dependent on local synaptical dynamics, which we call local correlation plasticity (LCP). In Section "Plasticity Model Review," we list a number of experimental benchmarks, followed by a classification scheme for current plasticity models. Based on this framework, we give an overview of plasticity models (see Model Comparison), which serves as a database against which we can compare our models. In Section "Local Correlation Plasticity," we introduce the LCP variant of Partzsch et al. (2008), which uses a simple spike response model (SRM) for its postsynaptic dynamics. In Section "Neuron Dynamics: Leaky Integrate-and-Fire" we introduce a leaky integrate-and-fire (LIAF) neuron which augments LCP with more realistic postsynaptic dynamics. Following, we relate the (biophysical) parameters of the SRM neuron to the (phenomenological) parameters from STDP experiments (see Analysis Results). Also, we show the relationship between the sliding threshold of the original BCM and the parameters inherent in our LCP rule. In Section "Simulation Results," we give simulation results for various kinds of experimental stimulation protocols, subsequently discussing the limits of LCP using the SRM neuron model as evident from the simulations. Section "LCP with LIAF Neuron" shows results on how LCP with the LIAF neuron model resolves the discrepancies of the previous section. Also, the extension enables our model to reproduce several more experimental results. Finally, repercussions and limits of our model as well as further research directions such as the incorporation of a more realistic neuron model are discussed in Section "Discussion."

MATERIALS AND METHODS

PLASTICITY MODEL REVIEW

Benchmark experiments

In order to enable a qualified comparison of the LCP rule with current state-of-the-art, we have gathered a listing of BCM- and STDP-related biological experiments, describing different facets of LTP and LTD induction. The experiment summary in **Table 1** includes the pulse induction protocol necessary for replicating the experiment with a plasticity model, as well as the experimental conditions as derived from the papers or related literature. The experimental conditions are mainly given to judge how similar the setup is for different protocols, i.e., should a plasticity model be able to replicate several experiments using the same parameter set, or is a change in model parameters justified by the change in experimental setup. For example, differences in the age of the experimental animal significantly affect plasticity (Disterhoft and Oh, 2006; Lante et al., 2006), which justifies using different parameter sets, while differences in preparation (i.e., slice or dissociated) may or may not change neuron behavior (Du and Bradley, 1996; Taubenfeld et al., 2002).

Starting point for the above listing is conventional STDP (Bi and Poo, 1998), i.e., the plasticity or change in PSC amplitude evoked by several repetitions of single presynaptic-postsynaptic spike pairings (at various positive and negative time differences) at a low repetition frequency. In related experiments, Sjöström et al. (2001) have also tested the frequency dependence of plasticity for pre-post and post-pre pairings. They found an increasing potentiation effect in both cases, leading to a transition from overall depression to potentiation in the post-pre case at approx. 30 Hz (cf. **Figure 10**). Froemke and Dan (2002) have shown that spike pairings do not sum linearly, for example that spike triplets in post-pre-post order cannot be treated as separate pairings post-pre and pre-post when computing the cumulative weight change. Wang et al. (2005) also carried out triplet experiments, which show somewhat differing behavior. The major difference seems to occur for post-pre-post triplets with low time differences, where Wang et al. (2005) observe postsynaptic facilitation for the second postsynaptic pulse, resulting in amplified LTP, contrary to the postsynaptic depression seen in Froemke and Dan (2002) for the same triplets (cf. circles in the lower right quadrant of **Figures 7A,B**). This difference between the enhancing and depressing effect for these particular triplets seems to be fundamental, i.e., models which accommodate one effect cannot replicate the other. Thus, we classify a model as compatible with experimental triplet results if it can emulate one of the two results. A further common spiking protocol is the quadruplet protocol, consisting of a post-pre and a pre-post pair with equal time difference Δt that are separated by a short time interval T. Wang et al. (2005) have performed a series of such experiments, using $\Delta t = 5$ ms. Subsets of the above protocols (conventional STDP, STDP and rate, triplets, and quadruplets) are commonly used in the verification of newly introduced plasticity rules (Froemke and Dan, 2002; Senn, 2002; Pfister and Gerstner, 2006; Shah et al., 2006).

The experiments in Froemke et al. (2006) examine plasticity with respect to bursts and individual spike timing. The experiment documented in Figure 2 of Froemke et al. (2006) uses short bursts of 5 spikes at different burst frequencies and individual pre-post-spike timing of 6 ms. This is very similar to the experiment in **Figure 8A** in Sjöström et al. (2001), (frequency-dependent

Table 1 | Listing of plasticity experiments, the numbers and keywords assigned in bold font to the single experiments are used for later reference in the text.

Short description and reference	Experimental characteristics	Presynaptic protocol	Postsynaptic protocol
(1) Conventional **STDP** (Bi and Poo, 1998)	Glutamatergic synapses onto cultured disassociated rat hippocampal neurons, embryonic rat	Sub-threshold EPSC evoked via a 100 mV 1 ms depolarization step at 1 Hz, 60 repetitions	AP evoked by current pulse 2 nA 2 ms, same timing protocol as presyn., Δt to presyn. spikes: sweep –90…+90 ms
(2) Frequency-dependent STDP, Figure 8A of Sjöström et al. (2001)	Slices of visual cortex, synapses in apical dendrites in thick tufted L5 neurons 12–21 day Long-Evans rats	Extracellular stimulation, 50 single pairings at 0.1 Hz repetition, pairings at 10, 20, 40, 50 Hz: in groups of 5, with 15 repetitions at 0.1 Hz	Single AP by 0.8–1.5 nA 5 ms current injection, Δt to presyn. spikes: ±10 ms
(3) Triplet pulse patterns (Froemke and Dan, 2002)	Slices of visual cortex, glutamatergic synapses onto L2/3 pyramidal neurons, 2–5 week Sprague-Dawley rats	60–80 triplets at 0.2 Hz, 5–150 μA 0.1–1 ms single pulse extracellular stimulation	AP evoked by 1 nA 2–3 ms postsyn. current injection, triplets with one or two presyn pulses, Δt's of triplet spikes wrt each other: sweep –100…+100 ms
(4) Quadruplet pulse patterns (Wang et al., 2005)	Glutamatergic monosynaptic connections between cultured disassociated rat hippocampal neurons, embryonic rat	60 spike patterns at 1 Hz, Δt in measurements: the interval between the two innermost spikes of the quadruplet (either pre or post) plus 5 ms	Pairs of postsynaptic spikes centered around presyn. spikes in pre-post-post-pre and post-pre-pre-post order, 5 ms time difference in each pre-post and post-pre pair
(5) Presynaptic **burst** patterns, Figure 4 of Froemke et al. (2006)	Slices of visual cortex L2/3 pyramidal cells, 10–35 day Sprague-Dawley rats	5–150 μA 0.1–1 ms extracellular stimulation, 2–5 EPSPs at 100 Hz, 30–40 repetitions at 0.2 Hz	0.5–2.5 nA, 1.5–5 ms current injection, single AP $\Delta t \leq 6$ ms before/after presyn. burst
(6) Standard rate (Dudek and Bear, 1992)	Slices of hippocampal area CA1, Schaffer collateral fibers onto pyramidal cells, adult male albino rats	Presynaptic tetanus, 900 pulses, single repetition, pulse frequencies 1–50 Hz, excited with 10–30 μA, 0.2 ms current injection	No control/recording of postsynaptic cell activity mentioned, Three assumptions tested: (1) uncorrelated 10 Hz Poisson, (2) postsyn. APs evoked by EPSCs in LIAF neuron with 5% threshold noise, (3) no postsyn. APs, only sub-threshold EPSC influence
(7) Correlated rate, Figure 8D of Sjöström et al. (2001)	Same as for "STDP and frequency" above	75 single pairings at 0.14 Hz, pairings at 20, 35, 50 Hz in groups of 5, with 15 repetitions at 0.1 Hz	Δt to presyn. spikes as uniform distribution in the interval [–10… +10 ms]
(8) Voltage control (Artola et al., 1990), additional similar experiments in Ngezahayo et al. (2000)	Slices of adult rat visual cortex, L2/3 regular spiking neurons	Extracellular stimulation 50 Hz tetanus, five 2 s pulse trains spaced at 10 s intervals, four times EPSC test intensity	Intracellular current injection to target membrane voltage

STDP), so we did not include this experiment in our table. We also did not include the experiment of **Figure 3** in Froemke et al. (2006), since weight saturation or dependence on initial weight is a very active topic and few assured facts exist (Kepecs et al., 2002; Standage and Trappenberg, 2007; Zou and Destexhe, 2007). We did include the post-pre-burst and pre-burst-post pairing protocol of **Figure 4** in Froemke et al. (2006) as a testcase, since this protocol can very likely not be replicated even with models that take triplet effects into account (Froemke et al., 2006). Figures 6A,B of Froemke et al. (2006) show that there is no significant difference between conventional post-pre-post triplets and post-burst-pre-post, i.e., triplet models should be able to express this behavior, therefore we also did not include this protocol. The crossover from LTD to LTP for the post-pre-post-burst stimulation protocol of Figures 6C,D, although not replicated by the model of Froemke and Dan (2002), can be reproduced by conventional nearest-neighbor STDP and also by LCP with SRM (see **Figure 9**). Since this protocol seems not to represent a major challenge to plasticity models, we also did not include it.

The behavior of synapses with respect to pulse rates is usually characterized by the BCM formulation (Bienenstock et al., 1982). That is, a low postsynaptic rate produces LTD, with an increase in frequency corresponding to a gradual reduction of LTD. Above a certain threshold, LTP is produced, which increases with postsynaptic rate. The presynaptic rate scales this behavior. The postsynaptic frequency threshold separating LTD and LTP is variable, i.e., it changes its value dependent on past activity at the synapse (Wang and Wagner, 1999).

A synthetic version of a rate protocol is usually employed for confirming compatibility with the BCM paradigm (Senn, 2002; Izhikevich and Desai, 2003; Toyoizumi et al., 2005; Baras and Meir, 2007), neglecting a detailed replication of experimental BCM-type results, although some authors employ more realistic stimulation protocols for their models (Shouval et al., 2002; Benuskova and Abraham, 2007). In contrast to that, two experimental rate protocols are included in **Table 1** to ensure accuracy of the LCP rule with respect to actual experiments. The first pulse rate experiment uses a presynaptically applied high frequency tetanus, while the postsynaptic side seems not to have been controlled (Dudek and Bear, 1992). Since there is no data about the postsynaptic side, we use three different settings to cover a wide range of possible postsynaptic activity: the first assumption is that of a silent, non-spiking slice preparation, i.e., neither the presynaptic tetanus nor background activity does result in firing of the neuron, the membrane potential is only depolarized in the sub-threshold regime due to the presynaptic currents. The second setting assumes that the firing of the neuron is completely driven by unspecific background activity, modeled by a 10 Hz Poisson process. In contrast, the third setting neglects the background activity and assumes that the presynaptic tetanus drives the postsynaptic firing, modeled by an LIAF neuron with threshold noise (Gerstner and Kistler, 2002), which is described in detail in Section "Neuron Dynamics: Leaky Integrate-and-Fire." This assumption results in strongly correlated pre- and postsynaptic firing, similar to the postsynaptic reconstructions of Beggs (2001) and Standage et al. (2007). The first and third assumptions are also very similar to the postsynaptic reconstruction of experiment (6) carried out in Shouval et al. (2002) (see also the supplementary material of Shouval et al., 2002).

In an alternative approach to classical tetanus rate protocols, Sjöström et al. (2001) use pre-post-spike pairings with random time difference and vary the pairing frequency. They draw the time differences from a uniform distribution with mean 0 and extension ±10 ms (For details, see also Mayr et al., 2010b) and apply 15 bursts consisting of 5 pairings for each frequency. While the frequency-dependent STDP experiments of Sjöström et al. (2001) have received a lot of attention, this experiment has been largely overlooked, despite the fact that it exhibits BCM behavior even for a rate-independent distribution of post- versus presynaptic spikes. This is in contrast to the usual assumption of frequency-varying pre- and postsynaptic Poisson spike trains (Senn, 2002; Izhikevich and Desai, 2003; Appleby and Elliot, 2005; Pfister and Gerstner, 2006; Lu et al., 2007), with probability distribution of the time difference between pre- and post-synaptic spike dependent on rate. Thus, the influential BCM-STDP modification of Izhikevich and Desai (2003) as well as other models (Pfister and Gerstner, 2006) which require this change in pre-post probability distribution to exhibit BCM behavior, are not able to reproduce this experiment (Standage and Trappenberg, 2007; Mayr et al., 2010b). For STDP, this failure can be easily explained, as it is due to the fact that the Sjoestroem rate protocol "samples" the conventional STDP curves always at the same short time distance from the origin, where LTP dominates for experimentally derived parameter sets (Froemke and Dan, 2002), thus never exhibiting LTD behavior (see **Figure 6A**).

Experiments featuring voltage-controlled plasticity (Artola et al., 1990; Ngezahayo et al., 2000; Sjöström et al., 2001) seem to provide a direct way to synaptical plasticity, but have so far only been used in very few papers (Sjöström et al., 2001; Abarbanel et al., 2002; Clopath et al., 2010), mainly because most models do not include a mechanism for direct voltage control of plasticity (see **Table 3**).

Model classification

Plasticity models can be classified according to their motivation as computational, biophysical and phenomenological (see **Figure 1**). Computational models try to replicate some information processing task attributed to neural networks, they usually make no or little *a priori* assumptions about their plasticity rule, but instead try to implicitly develop a form of plasticity optimized for a given task (Toyoizumi et al., 2005; Pfister et al., 2006; Baras and Meir, 2007). Biophysical models, in contrast, include a variety of detailed neural molecular and ion channel dynamics, deducing from those dynamics the form of plasticity most likely carried out at the particular synapse (Senn, 2002; Shouval et al., 2002; Shah et al., 2006). Phenomenological models try to qualitatively and quantitatively replicate experimental findings. For example, the triplet model of Pfister and Gerstner (2006) is validated with respect to experiments (2)–(4) of **Table 1**. There is no sharp division between the above categories, i.e., a computational model can incorporate biophysical aspects, e.g., the computational derivation could result in an optimal plasticity form dependent on the PSC dynamics, ion channel characteristics or the membrane time constant (Saudargiene et al., 2004; Pfister et al., 2006). Of course, there is also no sharp division between phenomenological and biophysical models, e.g., the plasticity model of Froemke et al. (2006) incorporates a form of short term synaptic plasticity simply to fit experimental data, which however is very similar to a biophysical model for synaptical neurotransmitter release by Markram et al. (1998), Mayr et al. (2009). Phenomenological models are also often investigated with respect to their computational properties (Abbott and Nelson, 2000; Zou and Destexhe, 2007). **Figure 1** takes this into account by providing not only classification with respect to a single motivation, but also to the continuum in between, e.g., a classification of $1 \rightarrow 3$ denotes a model with a mainly computational motivation, but also some biophysical aspects.

Plasticity models can also be classified with respect to the mechanisms incorporated in them. **Figure 2** contains a systematization of the mechanisms postulated in long-term plasticity. To enable a classification of the three types of model groups described earlier, some generalization is obviously needed, since usually only the biophysical models provide explicit statements about the underlying mechanisms, while other models state their mechanisms only implicitly and may also assume mechanisms inconsistent with biological evidence. Thus, this mechanism listing is neither comprehensive nor biophysically accurate. It simply resembles the most common denominator of effects found in various plasticity models, enabling a taxonomy of the whole model range expressed in **Table 3** in Section "Model Comparison."

On the presynaptic side, the most common mechanism included in models is a simple "time of event" of the presynaptic spike arriving at the synapse, denoted as "presynaptic action potential" in

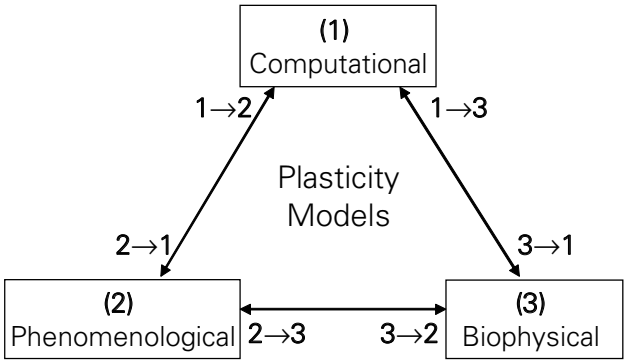

FIGURE 1 | Common motivations for plasticity models. The numbers denote affiliation of a model with respect to the three basic motivations, i.e., a model classified as 2 → 1 would be mostly phenomenologically based, but with some computational features. This classification is employed for the taxonomy of the models in **Table 3.**

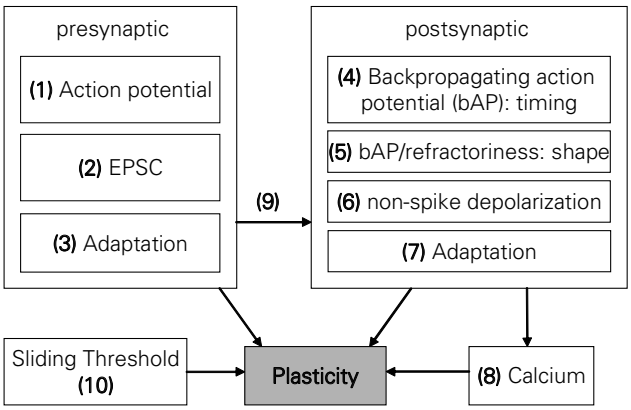

FIGURE 2 | Overview of mechanisms commonly included in plasticity models. The numbers are used in the taxonomy of the models in **Table 3**. A standard STDP (Song et al., 2000; Froemke et al., 2006) that computes the change in plasticity directly from the relative timing of pre- and postsynaptic spikes would be denoted by (1, 4). Some kind of presynaptic influence on the postsynaptic side (e.g., if a PSC raises the postsynaptic potential) is denoted by 9, a metaplastic sliding threshold by 10, etc.

Figure 2. The next level of detail in presynaptic mechanisms of plasticity may be the explicit modeling of an EPSC or some derivation of it, with the waveform of the EPSC having influence on the shape of the plasticity function (Abarbanel et al., 2002; Shouval et al., 2002; Saudargiene et al., 2004). Another commonly included mechanism is presynaptic adaptation, i.e., some form of short term plasticity which governs how presynaptic spikes occurring in close temporal proximity to each other interact in their respective plastic influence on the synapse (Sjöström et al., 2001; Froemke et al., 2006; Shah et al., 2006; Lu et al., 2007; Zou and Destexhe, 2007).

On the postsynaptic side, the counterpart to the presynaptic spike arrival would be the backpropagating action potential (bAP), which according to most common STDP models signals the timing of an action potential at the soma back to the synapse. Thus, the complete classification of a simple STDP model (Song et al., 2000) would be "1, 4" which symbolizes the "relative-time-of-event" nature of STDP, i.e., the weight change is only driven by the pre- and postsynaptic timing difference. Complimentary to plasticity driven by the shape of the EPSC, there are also models which incorporate the exact shape of the bAP or the postsynaptic membrane characteristics (e.g., refractoriness) in computing their plasticity (Abarbanel et al., 2002; Shouval et al., 2002; Saudargiene et al., 2004; Badoual et al., 2006; Pfister et al., 2006; Shah et al., 2006). A model classified with non-spike depolarization would mean there is an explicit voltage driven mechanism on the postsynaptic side, i.e., the membrane voltage is not just assumed to convey the timing or shape of a bAP, but can in itself be altered (hyper- or depolarized with respect to the resting potential) to affect plasticity (Abarbanel et al., 2002; Clopath et al., 2010). Postsynaptic adaptation is also part of some models, mostly based on the decreased excitability of a neuron immediately after its action potential (Badoual et al., 2006; Froemke et al., 2006; Shah et al., 2006). However, there are also models which assume increased excitability (Pfister and Gerstner, 2006). Partially or wholly Ca^{2+}-based models, such as (Shouval et al., 2002; Kurashige and Sakai, 2006; Shah et al., 2006) would be denoted by "Calcium" in **Figure 2**.

Metaplasticity can occur at various different organizational levels from synapse to network and express itself in various parameters of the involved neurons (Abraham, 2008). However, all models reviewed in this paper which touch on the subject of metaplasticity do so only in terms of the sliding threshold property separating LTD and LTP on a postsynaptic frequency scale, as introduced in the original BCM formulation (Bienenstock et al., 1982). Three major possible mechanisms for this sliding threshold can be discerned, i.e., direct influence on the plasticity parameters (Izhikevich and Desai, 2003; Benuskova and Abraham, 2007), a sliding adjustment of one of the postsynaptic state variables (Abarbanel et al., 2002), or a frequency threshold as a function of the mean Ca^{2+} elevation (Kurashige and Sakai, 2006). For **Table 3**, we classify a model as "10," i.e., containing a sliding threshold, if this model either just derives a sliding threshold based on its original parameters (Izhikevich and Desai, 2003) or if it in addition contains an explicit mechanism adjusting this sliding threshold (Benuskova and Abraham, 2007).

LOCAL CORRELATION PLASTICITY AND CORRESPONDING PRE- AND POSTSYNAPTIC DYNAMICS

Local correlation plasticity

A variety of experiments have shown the marked influence of membrane voltage on synaptic plasticity (Artola et al., 1990; Ngezahayo et al., 2000; Sjöström et al., 2001). On the other hand, spike timings as used in STDP protocols (Bi and Poo, 1998; Froemke and Dan, 2002) have to be detected locally by a synapse to trigger changes in its transmission properties. For this detection mechanism at the postsynaptic site, the membrane potential is a readily available candidate variable. One could assume that the membrane potential becomes progressively higher close to an postsynaptic AP, whereas after an AP it rises out of its hyperpolarization with an exponential curve (Koch, 1999). Thus, a read-out of the postsynaptic membrane potential at presynaptic spikes would lead to an STDP-like rule in this case (Brader et al., 2007).

Plasticity being bound to the co-occurrence of presynaptic and postsynaptic activity is also reminiscent of the BCM rule (Bienenstock et al., 1982), a well-established, rate-based learning paradigm with great experimental evidence (Dudek and Bear, 1992; Mayford et al., 1995; Wang and Wagner, 1999). In this rule, a presynaptic activity variable $d(t)$ is multiplied with a shifted postsynaptic activity variable $c(t)$ to define the change of synapse weight m:

$$\frac{\mathrm{d}m}{\mathrm{d}t} = \phi\left(c(t) - \Theta_M\right) \cdot \mathrm{d}(t), \tag{1}$$

where Θ_M is an activity threshold and $\phi(.)$ represents a continuous non-linear function that changes sign at zero. The above formulation is somewhat reminiscent of the weight derivation in Abarbanel et al. (2002), where a product of pre- and postsynaptic activity results in the overall weight change. However, apart from the differing expression for pre- and postsynaptic activity, the model of Abarbanel et al. (2002) derives its weight as a competition between both activities, whereas the above equation simply describes the combined actions of both pre- and postsynaptic state variables.

From our point of view, the postsynaptic activity $c(t)$ is the membrane potential and the threshold Θ_M is a voltage threshold. This recasting is partially inspired by earlier work of our research group on a membrane voltage-based plasticity rule for PCNN image processing, which takes on a similar form (Schreiter et al., 2002). As well, a voltage threshold for separating LTD and LTP induction is supported by the results reported in Artola et al. (1990), Fusi et al. (2000), and Ngezahayo et al. (2000). Formulating BCM using spike time-dependent instead of purely rate-dependent components is also beneficial in terms of its resultant computational capability (Toyoizumi et al., 2005).

The presynaptic activity $d(t)$ still needs to be defined in our framework. Because the plasticity mechanism needs to have direct access to the membrane potential, it can only work at the postsynaptic site; thus, also the presynaptic read-out has to occur there. Under this assumption, a candidate read-out variable is the conductance change of postsynaptic ion channels that is triggered by presynaptic neurotransmitters, released in reaction to presynaptic spikes. With this conductance change, the complete LCP rule reads as follows:

$$\frac{\mathrm{d}w}{\mathrm{d}t} = B \cdot \left(u(t) - \Theta_u\right) \cdot g(t). \tag{2}$$

In this equation, $w(t)$ is the weight of the synapse, $g(t)$ is the conductance of presynaptically activated channels, $u(t)$ is the membrane potential and Θ_u is the threshold between potentiation and depression. Besides the recasting of the pre- and postsynaptic variables, the main difference between the original BCM formulation and Eq. 2 is that the non-linear function $\phi()$ relating postsynaptic activity to plasticity is replaced by a linear scaling with a proportionality constant B. However, as we show later, this linear dependence of plasticity on voltage translates to a non-linear dependence on the postsynaptic rate which is compatible with the original BCM intentions.

We assume that the postsynaptic membrane potential eliminates the block of NMDA receptors, subsequently releasing Ca^{2+} and plastically changing the synaptic weight (Senn, 2002; Shouval et al., 2002). Thus, B should be defined in units of $1/(As)$, which has the effect of "canceling" the Ca^{2+} charge unit, allowing us to arrive at a dimensionless synaptical weight as required for comparison with most of the experimental results (Bi and Poo, 1998; Sjöström et al., 2001; Froemke and Dan, 2002). The postsynaptic expression $B \cdot (u(t) - \Theta_u)$ thus results in units Ω/s, which could be interpreted as the opening/closing speed of the Ca^{2+} channel (i.e., its resistance change), consequently linking LTP/LTD of our expression with the rate of Ca^{2+} release (Aihara et al., 2007).

The behavior of the LCP rule crucially depends on the models for the neuron and the synaptic conductance. In the following two sections, we introduce simple models for both which are suited for analyzing the principal rule characteristics as well as for quantitatively deriving the weight changes in response to experimental protocols. In Section "Neuron Dynamics: Leaky Integrate-and-Fire," we extend the neuron model to a more realistic LIAF formulation.

Synapse dynamics

For the synaptic conductance $g(t)$, we use an exponential decay function in response to each presynaptic spike, which is a simplification of the synapse model described in Gerstner and Kistler (2002):

$$g(t) = \hat{G} \cdot \mathrm{e}^{-\frac{t - t_j^{\mathrm{pre}}}{\tau_g}}, t_j^{\mathrm{pre}} \le t < t_{j+1}^{\mathrm{pre}}, \tag{3}$$

where τ_g is the time constant of the decay and $\hat{G}$ is the amplitude of the response. Setting the presynaptic conductance to its maximum $\hat{G}$ at the beginning of each presynaptic pulse effectively makes the learning carried out in the LCP rule history-independent. In standard STDP terminology, this would be equivalent to a presynaptic nearest-neighbor interaction (Morrison et al., 2008).

This can be extended to a presynaptic all-to-all interaction via the integration of all presynaptic spikes in the current weight dynamics. Mathematically, this amounts to replacing the constant conductance $\hat{G}$ by a spike-varying conductance G_j as follows:

$$G_j = g\left(t_j^{\mathrm{pre}} - \varepsilon\right) + \hat{G} \tag{4}$$

Thus, the conductance amplitude immediately before the current presynaptic spike is contained in the new amplitude, conserving the spiking history at the synapse, leading to presynaptic all-to-all interaction (Morrison et al., 2008).

Neuron dynamics: spike response model

For the membrane potential, we choose a spike response neuron model (Gerstner and Kistler, 2002), consisting of a Dirac function for the action potential and an exponential decay function for the hyperpolarization after firing:

$$u(t) = U_{\mathrm{p},n} \cdot \delta\left(t - t_n^{\mathrm{post}}\right) + U_{\mathrm{refr}} \cdot \mathrm{e}^{-\frac{t - t_n^{\mathrm{post}}}{\tau_{\mathrm{refr}}}}, \quad t_n^{\mathrm{post}} \le t < t_{n+1}^{\mathrm{post}} \tag{5}$$

Thereby, t_n^{post} denotes the n-th postsynaptic spike, $U_{\mathrm{p},n}$ is the area under the pulse curve and $U_{\mathrm{refr}} < 0$ and τ_{refr} are the amplitude and time constant of hyperpolarization. Note that $u(t)$ reflects deviations of the membrane potential from its equilibrium; a resting potential could be added when adjusting the voltage threshold Θ_u accordingly.

Additionally to the hyperpolarization of the membrane potential, we added an attenuation of the spike amplitude during refractoriness to model the decreased excitability during this period (Shah et al., 2006) and the frequency-dependent attenuation of both amplitude and duration found in Froemke et al. (2006) and Tanaka et al. (1991). Therefore, we used a simple formulation that weights the amplitude of the n-th postsynaptic spike with the amount of membrane hyperpolarization directly before the spike:

$$U_{\mathrm{p},n} = U_{\mathrm{p}} \cdot \left(1 - \alpha_{\mathrm{att}} \frac{u\left(t_n^{\mathrm{post}} - \varepsilon\right)}{U_{\mathrm{refr}}}\right) \quad \text{if} \quad u\left(t_n^{\mathrm{post}} - \varepsilon\right) < 0, \tag{6}$$

where U_{p} is a fixed parameter that determines the maximum amplitude of the postsynaptic pulse. Please note that in contrast to the similar postsynaptic attenuation of Froemke et al. (2006), we did not introduce a new time constant for this saturation effect. This addition has significant influence on the rule behavior in triplet experiments, as we will show in Section "Simulation Results."

The biophysical motivation for this influence of the postsynaptic attenuation on plasticity is somewhat speculative. Shah et al. (2006) contain some references to the attenuation of BPAPs from which they derive a modeling argument for including this attenuation effect in plasticity. However, we have only found one reference (Froemke et al., 2006), where both postsynaptic adaptation and its influence on plasticity is shown. In **Figure 7** of Froemke et al. (2006), it is shown that when chemically blocking postsynaptic attenuation in plasticity experiments which involve several postsynaptic spikes, the resulting plasticity at the synapse is actually replicated better by naïve STDP than by their attenuation model. For the unaltered preparation, the opposite is shown, i.e., their attenuation model captures the data significantly better than STDP without attenuation. So at least for the preparation of Froemke et al. (2006), a postsynaptic attenuation is proven which has the proposed influence on plasticity, i.e., for closely following postsynaptic spikes, the effect of later spikes on the overall plastic change at the synapse diminishes. **Figure 9** in Section "Simulation Results" shows the correspondence of the attenuation of Eq. 6 with the experimental data of Figure 7B of Froemke et al. (2006).

Neuron dynamics: leaky integrate-and-fire

In the previous section, we have introduced a simple neuron for the LCP rule. Thereby, we have neglected important ingredients of neuronal signal transmission. In the following, we therefore extend the neuron model, incorporating the influence of a presynaptic spike on the postsynaptic membrane potential. This influence can be determined by the current flow through the cell membrane that is triggered by presynaptic neurotransmitter release. The current can be modeled similar to Eq. 2 as:

$$I_{\mathrm{syn}}(t) = \left(E_{\mathrm{syn}} - u(t)\right) \cdot g(t), \tag{7}$$

where E_{syn} is the reversal potential of that channel, which is approx. 70 mV above resting potential for excitatory synapses (Gerstner and Kistler, 2002). The conductance $g(t)$ is defined as in Eq. 3. Because we are only interested in sub-threshold variations of the membrane potential, we use the approximation $E_{\mathrm{syn}} \gg u(t)$, so that the time course of $I_{\mathrm{syn}}(t)$ is only determined by $g(t)$.

To calculate the influence of the synaptic current on the membrane potential, we use a LIAF neuron, which is defined by the differential equation:

$$C \cdot \frac{\mathrm{d}u}{\mathrm{d}t} = -\frac{u}{R} + I_{\mathrm{syn}}(t), \tag{8}$$

where C and R are the capacitance and resistance of the membrane that together result in the membrane time constant $\tau_{\mathrm{refr}} = C \cdot R$, which was already used in the SRM neuron model in Eq. 5. As for the learning rule in Eq. 2, we assume a resting potential of 0 V. We then have to solve the following differential equation:

$$\tau_{\mathrm{refr}} \frac{\mathrm{d}u}{\mathrm{d}t} + u = R \cdot \hat{G} \cdot E_{\mathrm{syn}} \cdot \mathrm{e}^{-\frac{t}{\tau_g}}, \tag{9}$$

whereby we assume, without loss of generality, that the presynaptic pulse occurs at $t = 0$. Furthermore, we only regard the case $\tau_{\mathrm{refr}} \neq \tau_g$, which is justified by the parameter sets in use (cf. **Table 4**).

We suppose that the solution has the form:

$$u(t) = C_1 \cdot \mathrm{e}^{-\frac{t}{\tau_g}} + C_2 \cdot \mathrm{e}^{-\frac{t}{\tau_{\mathrm{refr}}}}, \tag{10}$$

with constants C_1 and C_2. Calculating these constants results in the solution:

$$u(t) = u(0)\mathrm{e}^{-\frac{t}{\tau_{\mathrm{refr}}}} + \frac{R\hat{G}E_{\mathrm{syn}}}{1 - \frac{\tau_{\mathrm{refr}}}{\tau_g}}\left(\mathrm{e}^{-\frac{t}{\tau_g}} - \mathrm{e}^{-\frac{t}{\tau_{\mathrm{refr}}}}\right). \tag{11}$$

We want to dimension the unknown amplitude $R\hat{G}E_{\mathrm{syn}}$ by the amplitude of the postsynaptic potential U_{PSP} that results from a presynaptically triggered current injection at postsynaptic rest ($u(0) = 0$). Calculating this maximum from the necessary condition $\mathrm{d}u/\mathrm{d}t = 0$ results in:

$$U_{\mathrm{PSP}} = R\hat{G}E_{\mathrm{syn}} \cdot \left(\frac{\tau_{\mathrm{refr}}}{\tau_g}\right)^{\frac{\tau_{\mathrm{refr}}}{\tau_g - \tau_{\mathrm{refr}}}} \tag{12}$$

The final explicit formulation for $u(t)$ then is:

$$u(t) = u(0)\mathrm{e}^{-\frac{t}{\tau_{refr}}} + U_{\mathrm{PSP}} \cdot W \cdot \left(\mathrm{e}^{-\frac{t}{\tau_g}} - \mathrm{e}^{-\frac{t}{\tau_{\mathrm{refr}}}}\right)$$

$$\text{with} \quad W = \frac{\left(\frac{\tau_{\mathrm{refr}}}{\tau_g}\right)^{\frac{\tau_{\mathrm{refr}}}{\tau_{\mathrm{refr}} - \tau_g}}}{1 - \frac{\tau_{\mathrm{refr}}}{\tau_g}}. \tag{13}$$

We will use these equations for the simulations with PSP amplitude.

The remainder of the neuron behavior is the same as for the SRM model: at a postsynaptic spike time, a Dirac pulse with area U_{p} is generated. Afterwards, the membrane potential u is reset to

the refractory amplitude U_{refr} from where it evolves according to Eq. 13. In the case of no presynaptic activity, this results in an identical time course compared to the SRM model.

In the standard configuration, the LIAF neuron does only generate postsynaptic spikes at the times defined by the experimental protocol. As an exception, for the correlated activity setting in the Dudek and Bear (1992) protocol (cf. Benchmark Experiments), the LIAF neuron may pulse on its own. Thereby, a spike is emitted if the membrane potential exceeds a noisy threshold Θ_{fire} (Gerstner and Kistler, 2002). The value of Θ_{fire} is changed at each presynaptic spike, drawing it from a Gaussian distribution with mean $2 \cdot U_{PSP}$ and standard deviation 5% of the mean.

Summary of LCP versions

As stated in the Section "Introduction," two versions of the LCP learning rule will be analyzed in Section "LCP with SRM Neuron" respectively Section "LCP with LIAF Neuron." Both versions use the LCP rule as defined in Eq. 2, the PSC of Eq. 3 and the attenuation of postsynaptic action potentials in Eq. 6. The main difference between both versions is the type of neuron used to construct the postsynaptic membrane voltage profile $u(t)$, i.e., the SRM of Section "Neuron Dynamics: Spike Response Model" or the LIAF of Section "Neuron Dynamics: Leaky Integrate-and Fire":

- The first version of the LCP rule, referred to as *LCP with SRM*, employs the definition of the membrane potential in Eq. 5.
- The second version of the LCP rule, referred to as *LCP with LIAF*, employs the definition of the membrane potential of Eq. 13 and the corresponding U_{PSP} of Eq. 12. The all-to-all presynaptic PSC interaction of Eq. 4 is also part of this version of the rule.

The fit of both versions of the LCP rule to the experimental data in Sections "LCP with SRM Neuron" and "LCP with LIAF Neuron" was estimated using the normalized mean-square error E defined in Pfister and Gerstner (2006). In summary, the analysis of the two versions of the LCP rule uses the symbols given in **Table 2**.

Table 2 | Listing of symbols used in the analysis of LCP with SRM in Section "LCP with SRM Neuron" and LCP with LIAF in Section "LCP with LIAF Neuron."

$u(t)$	Neuron membrane voltage
$g(t)$	Synaptic conductance
U_{refr}	Amplitude of the hyperpolarization
U_p	Area under the pulse curve, i.e., the size of the action potential
τ_{refr}	Membrane time constant (also governs hyperpolarization curve)
$\hat{G}$	Maximum synaptic conductance
τ_g	Time constant of synaptic conductance
Θ_u	Voltage threshold of the LCP rule
α_{att}	Attenuation of postsynaptic action potentials
B	Proportionality constant relating synaptic dynamics in the LCP formulation to the synaptic weight change
U_{PSP}	Amplitude of the postsynaptic potential resulting from a single presynaptic pulse
τ_{all}	Inverse combination of τ_{refr} and τ_g, introduced for convenience in Eq. 15
E	Normalized mean-square error of model with respect to experimental data
A_+, A_-, τ_+, τ_-	Standard STDP parameters (Song et al., 2000)
λ	Pulse rate

RESULTS

MODEL COMPARISON

Table 3 gives a comparison of a broad selection of plasticity models. Emphasis is laid on reproduction of biological experiments and generalization capability. In this context, the number of parameters in a model is included in **Table 3** to identify which models make parsimonious use of parameters in fitting experiments. Possible overfitting problems can thus be identified (Wei, 1975) and a rough comparison of computational effort in simulating a given model is possible. The performance of the models with respect to the experiments is classified with symbols "f," "h," "fc," "hc," "u," "n," and "?," with their meaning given in the caption of **Table 3**. The comparison is started with the standard exponential formulation of STDP (Song et al., 2000), since STDP experiments (1) are replicated by most of the models in the table and can thus serve as a basis for the assessment of those models. Also, STDP should serve as Occams razor for more elaborate models, i.e., whether those models are able to replicate more phenomena than STDP. The detailed discussion of all reviewed models is given in the Appendix.

To complete **Table 3**, an assessment of both LCP with SRM and LCP with LIAF is given, with detailed treatment of both model versions deferred to Section "LCP with SRM Neuron" and Section "LCP with LIAF Neuron." LCP with SRM is able to reproduce basic STDP (1) behavior (**Figure 4**). The LTD half of frequency-dependent STDP (2) is reproduced (**Figure 10B**), but the LTP half lacks the weight increase for high frequencies. Experiments (3, 4, 7) are reproduced (**Figures 7C, 8A, and 6B**, respectively), but the parameter settings across the experiments are slightly inconsistent. LCP with SRM cannot reproduce the standard rate experiment (6) satisfactorily for any of the assumptions regarding the activity on the postsynaptic side. With respect to burst (5) plasticity, LCP with SRM basically behaves as conventional STDP (**Figure 14A**), not able to show the plasticity behavior found in this experiment. Both versions of the LCP rule can replicate the LTD/LTP threshold in the voltage control experiment (8) (**Figure 12C**), but not the lower bound of the LTD window, so a "h" classification is given. LCP with LIAF is able to reproduce almost all experiments (see **Table 4** and Figures in LCP with LIAF Neuron). The exceptions are bursts (5), where either the pre-burst-post or the post-pre-burst case can be reproduced (**Figures 14B,C**), and the limit just discussed for experiment (8). In the next section, detailed results on LCP with SRM and the reasoning corresponding to the above assessment will be given.

LCP WITH SRM NEURON

Analysis results

Figure 3 shows the principal operation of LCP with the SRM neuron. Unlike spike-based learning rules, there is a continuous update of the synapse weight whenever the membrane potential deviates from the voltage threshold Θ_u during presynaptic activity.

Table 3 | Comparison of models for LTP and LTD.

Short description and reference	Parameters	Experimental protocols								Classification in	
		(1)	(2)	(3)	(4)	(5)	(6)	(7)	(8)	Figure 1	Figure 2
Song et al. (2000): conventional nearest-neighbor exponential STDP (Pfister and Gerstner, 2006)	2 TC, 2SF	f	n	h	n	n	n	n	n	2	1, 4, 10
Froemke et al. (2006): standard STDP model, with added pre and post suppression of spike efficacy. The efficacy of the pre spike is dependent on all the preceding spikes, while the post-spike depends only on the last preceding one (The model is an extension of Froemke and Dan, 2002)	Conventional STDP: 2 TC, 2 SF; suppression: 2 TC pre and post suppression, 1 SF post suppression	fc	h	fc	fc	f	n	n	n	2 → 3	1, 3, 4, 7
Pfister and Gerstner (2006): reduced triplet model: standard STDP model, with amplitude of LTP dependent on additional post spike trace	Conventional STDP: 2 TC, 2 SF, additional spike trace: 1 TC, 1 SF	f	f	f	f	u	n	f	n	2	1, 4, 7, 10
Benuskova and Abraham (2007): scaling constants of conventional STDP exponential functions are metaplastically changed according to mean over post-spike train	Conventional STDP: 2 TC, 2 SF; post mean for scaling: 1 TC, 1 SF	fc	u	hc	u	u	?	u	n	2	1, 3, 10
Senn (2002): STDP modeling of neurotransmitter discharge probability, based on pre- and postsynaptic traces sampled at corresponding pulses, pre and post adaptation through secondary messengers	Receptors: 1 TC, 3 SF, secondary messengers: 1 TC, 2 SF, discharge prob.: 1 TC, 2 SF	f	h	f	fc	fc	fc	fc	?	3 → 1	1, 2, 3, 4, 7, 10
Abarbanel et al. (2002): two ODEs describing pre neurotransmitter release and post voltage, disturbance functions representing pre and post action potentials. Weight derivation as a mixture of temporal competition and cooperation between processes	Pre- and post-ODEs: 2 TC, 2 SF (reduces to 1 SF for size (AP_{pre}) = size (AP_{post}), weight combination: 2 SF	f	h	hc	u	u	?	?	hc	2 → 3	1, 4, 5, 6, 10
Badoual et al. (2006): biophysical model of realistic compartmental neuron and kinetic equations for separate LTP and LTD	LTP kinetics: 2 TC, LTD: 4 TC, AMPA/NMDA receptors: 2 TC, 3 SF, Calcium pump: 1 SF, 1 TC, ca. 20 TC/SF neuron model	f	f	h	u	?	?	?	?	3 → 2	2, 3, 5, 6, 7, 8, 9
Badoual et al. (2006): original suppression model of Froemke and Dan (2002) plus additional weight bounds	Conventional STDP: 2 TC; suppression: 2 TC pre and post suppression, weight scaling/bounds: 2 SF	f	n	f	f	f	u	u	n	2	1, 3, 4, 7

(Continued)

Table 3 | ***Continued***

Short description and reference	Parameters	Experimental protocols								Classification in	
		(1)	(2)	(3)	(4)	(5)	(6)	(7)	(8)	Figure 1	Figure 2
Lu et al. (2007): pulse transition governed model, three states: pre event, post event, resting. Transitions incorporate short term adaptation	Transitions: 2 TC, weight computation: 3 SF	f	?	f	f	fc	hc	?	n	2	1, 3, 4, 7, 10
Pfister et al. (2006): STDP curve based on neuron/PSC characteristics derived from supervised pattern classification task	STDP: 2 TC, 2SF; constraint: 1 SF	f	u	hc	u	u	u	u	n	1	2, 5
Shah et al. (2006): calcium based model with formulations of bAP and EPSP influence on Calcium dynamics, additional pre and post attenuation, weight dependent on Calcium amplitude and slope (The model is an extension of Shouval et al., 2002)	Ω: 5 SF; η/τ: 2 TC, 2 SF; Calcium: 1 TC; pre and post attenuation 2 SF, 2 TC	h	f	f	?	fc	f	fc	fc	3	1, 2, 3, 4, 5, 7, 8
Clopath et al. (2010): triplet model of Pfister and Gerstner (2006) with additional voltage thresholds	LTD: 1TC, 2SF; LTP: 2TC, 2 SF; after-potential: 1 SF, 1 TC	f	f	fc	fc	?	fc	fc	f	2	1, 4, 6, 7, 10
Sjöström et al. (2001): LTP behavior as a sigmoidal dependence on (measured) residual depolarization, LTD as single scaling, post nearest-neighbor interaction	LTP sigmoid: 3SF, 1TC, LTD: 1 SF, 1 TC, Frequency dependence of LTP: 2 SF	fc	f	hc	fc	fc	fc	f	hc	2 → 3	1, 4, 6, 7
Fusi et al. (2000): LTP and LTD probability dependent on post membrane potential at pre spike, probability governs transition of two-state synapse	8 SF, 4 TC	f	f	hc	u	u	fc	fc	hc	1	1, 5, 6, 10
This paper, LCP with SRM: exponential decay for PSC; post membrane potential: spike response model; weight change: integral of the product of pre and post side; Voltage threshold for LTP/LTD, refractoriness-based attenuation of post pulses	1 TC PSC; 1 TC, 2 SF post-spike response; 1 SF attenuation	f	h	f	f	n	n	f	h	2 → 3	2, 5, 6, 7, 10
This paper, LCP with LIAF: PSC as above; post side leaky integrate-and-fire neuron, PSC charges post neuron; attenuation and plasticity as above	same as above, one additional SF for U_{PSP}	f	f	f	f	h	f	f	h	2 → 3	2, 5, 6, 7, 9, 10

The numbers for the experimental protocols denote the experiments as listed in **Table 1**.
The evaluation of the models with respect to biological experiments employs the following symbols: "f" this experiment has been fully reproduced in literature using the respective model, "h" reproduction of one half of the experiment shown, "fc" has not been shown to work, but will likely be fully compatible based on the performance of similar models; "hc" has not been shown to work, but at least one half of the experiment will likely be compatible based on the performance of similar models; "u" we speculate that it is unlikely that this experiment can be reproduced with the model (for discussion, see Appendix); "n" it is shown in literature that this experiment can not be reproduced with the model; "?" there is no data/investigation to relate the model to this particular biological experiment. The last two categories provide a classification with respect to the mechanisms and model types shown in **Figures 1 and 2**.
TC, time constant; SF, scaling factor; pre, presynaptic; post, postsynaptic.

Table 4 | Parameters used for experiment reproduction. Normalized errors (*E*) are given for all experiments for which data points with standard errors were available. If several Figure numbers are given in a row, the corresponding normalized error is calculated over all experiments in the Figures for the parameter set in the row (which may deviate from the parameter set used in the Figures).

Parameter set (units)	U_p (mVms)	U_{refr} (mV)	$B\hat{G}$; (mVms)$^{-1}$	A_+	A_-	$\tau_g = \tau_+$ (ms)	$\tau_{refr} = \tau_-$ (ms)	Θ_u (mV)	α_{att}	pre	U_{PSP} (mV)	Figures	*E*
LCP WITH SRM													
Froemke 1[a]	151	–5	1.68×10^{-4}	1.7×10^{-2}	8.7×10^{-3}	14.8	33.8	0	0.8	NN	–	4, 5, 6 ,7	–
Wang	151	–5	8.4×10^{-5}	8.4×10^{-3}	4.3×10^{-3}	14.8	33.8	0.5	0	NN	–	4	0.92
												7	10.4
												8	5.6
												4, 7, 8	7.8
Sjöström	162	–5	7.2×10^{-5}	4.2×10^{-3}	7.4×10^{-3}	29.6	67.6	0	0	NN	–	6	3.2
												10	6.8
												6, 10	5.8
Froemke 2[b]	151	–5	1.1×10^{-4}	1.1×10^{-2}	5.8×10^{-3}	13.5	42.8	0	0	NN	–	9, 14	–
LCP WITH LIAF													
Dudek	162	–5	4.8×10^{-6}	2.8×10^{-4}	4.9×10^{-4}	29.6	67.6	2.0	0	NN	1.5	11	1.5
Wang	151	–5	8.4×10^{-5}	8.4×10^{-3}	4.3×10^{-3}	14.8	33.8	0.5	0	AA	0	12	1.9
												4, 7, 12	6.5
Sjöström	162	–5	7.2×10^{-5}	4.2×10^{-3}	7.4×10^{-3}	29.6	67.6	3.0	0.8	AA	4.5	13B	6.3
												13C	2.9
												13B, 13C	3.9
Ngezahayo	151	–5	4.2×10^{-5}	1.7×10^{-2}	8.7×10^{-3}	14.8	33.8	50	0.8	AA	0	12C	177

The values for the STDP parameters A_+ and A_- correspond to the values fitted in the corresponding literature to the overall plasticity change divided by the number of pairings.

[a]*The parameter set Froemke 1 is based on the STDP parameters of Froemke and Dan (2002); see also discussion at* ***Figure 3****.*

[b]*The parameter set Froemke 2 is based on the STDP parameters of Froemke et al. (2006); see also discussion at* ***Figure 3****.*

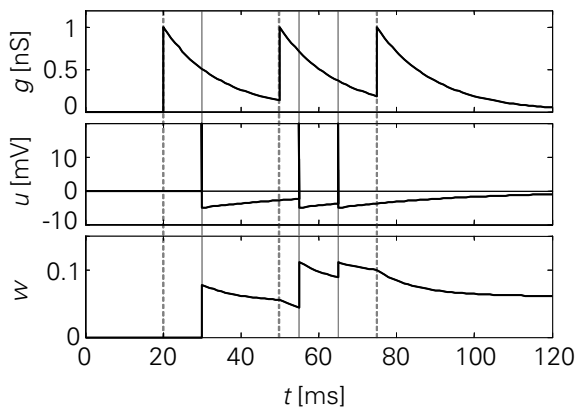

FIGURE 3 | Progression of the conductance *g*, the membrane potential *u* and the synapse weight *w* for a sample spike pattern. Units were chosen to be in a biologically realistic range: $\hat{G}$ = 1nS, B = 1/(1 *pC*). The remainder of the neuron and synapse parameters were taken from the Froemke 1 parameter set listed in **Table 4**.

For the SRM neuron model, there is a single mechanism each for LTP and LTD: LTP is triggered at each postsynaptic spike. Due to the idealized pulse shape, the conductance variable $g(t)$ is sampled at each postsynaptic spike time. Integrating Eq. 2 expresses this in the formula:

$$\Delta w_{\text{pot}}(t_n^{\text{post}}) = \int_{t_n^{\text{post}}-\varepsilon}^{t_n^{\text{post}}+\varepsilon} B \cdot g(t) \cdot U_{\text{p}} \delta(t - t_n^{\text{post}}) \mathrm{d}t = B \cdot U_{\text{p}} \cdot g\left(t_n^{\text{post}}\right). \quad (14)$$

This mechanism is equivalent to an iterative implementation of LTP in pair-based STDP models (Pfister and Gerstner, 2006). LTD, on the other hand, is mediated by continuous integration of the presynaptic conductance in the refractoriness period after a postsynaptic spike. Thus, the LTD mechanism always acts if pre- and postsynaptic spikes occur in close temporal proximity. Additionally, LTD is active if the voltage threshold is above resting potential, i.e., $\Theta_u > 0$. In the interval (t_0, t_1) between two consecutive spikes, the resulting LTD weight change can be calculated based on Eq. 2 from the starting values $g(t_0)$ and $u(t_0)$:

$$\begin{aligned}
\Delta w_{\text{dep}}(t_0, t_1) &= \int_{t_0}^{t_1} B \cdot g(t) \cdot \left(u(t) - \Theta_u\right) \mathrm{d}t \\
&= \int_{t_0}^{t_1} B \cdot g\left(t_0\right) \mathrm{e}^{-\frac{t-t_0}{\tau_g}} \cdot \left(u\left(t_0\right) \mathrm{e}^{-\frac{t-t_0}{\tau_{\text{refr}}}} - \Theta_u\right) \mathrm{d}t \\
&= B g(t_0) u(t_0) \tau_{\text{all}} \cdot \left(1 - \mathrm{e}^{-\frac{t_1-t_0}{\tau_{\text{all}}}}\right) \\
&\quad - B \Theta_u g(t_0) \tau_g \cdot \left(1 - \mathrm{e}^{-\frac{t_1-t_0}{\tau_g}}\right)
\end{aligned}$$

$$\text{with} \quad \tau_{\text{all}} = \frac{1}{\frac{1}{\tau_g} + \frac{1}{\tau_{\text{refr}}}}. \quad (15)$$

In the final weight change, potentiation may override this depression if there is presynaptic activity at a postsynaptic spike, i.e., if a presynaptic spike occurs shortly before a postsynaptic spike. This

directly leads to the temporal asymmetry seen in pair-based STDP rules. We show this by calculating the weight change induced by a spike pairing with time difference $\Delta t = t^{\text{post}} - t^{\text{pre}}$. For a pre-post pairing, the weight is at first potentiated by the postsynaptic spike and then depressed due to refractoriness. The amount of potentiation can be calculated from Eq. 14, with the conductance at the postsynaptic spike being equal to $g(t^{\text{post}}) = \hat{G}\mathrm{e}^{-(t^{\text{post}}-t^{\text{pre}})/\tau_g}$. The amount of depression that accumulates up to a time $t > t^{\text{post}}$ is determined by Eq. 15, with the depression starting at $t_0 = t^{\text{post}}$ and ending at $t_1 = t$, so that $g(t_0) = g(t^{\text{post}})$ as above and $u(t_0) = U_{\text{refr}}$. Combining the potentiation and depression parts results in:

$$\begin{aligned}\Delta w(\Delta t \geq 0) = B\hat{G}\left(U_{\text{p}} + U_{\text{refr}}\tau_{\text{all}} - \Theta_u\tau_g\right)\mathrm{e}^{-\frac{|\Delta t|}{\tau_g}} \\ -B\hat{G}U_{\text{refr}}\tau_{\text{all}}\cdot\mathrm{e}^{-\frac{t-t^{\text{pre}}}{\tau_g}}\cdot\mathrm{e}^{-\frac{t-t^{\text{post}}}{\tau_{\text{refr}}}} \\ +B\hat{G}\Theta_u\tau_g\cdot\mathrm{e}^{-\frac{t-t^{\text{pre}}}{\tau_g}}, \quad t > t^{\text{post}}.\end{aligned} \tag{16}$$

In contrast, for a post-pre pairing no potentiation occurs at all, because there is yet no presynaptic activity present at the postsynaptic spike. For the same reason, depression starts to act only from the presynaptic spike onward, i.e., $t_0 = t^{\text{pre}}$. Thus, the starting values are $g(t_0) = \hat{G}$ and $u(t_0) = U_{\text{refr}}\,\mathrm{e}^{-(t^{\text{pre}}-t^{\text{post}})/\tau_{\text{refr}}}$ Again from Eq. 15, the resulting weight change calculates as:

$$\begin{aligned}\Delta w(\Delta t < 0) = B\hat{G}U_{\text{refr}}\tau_{\text{all}}\cdot\mathrm{e}^{-\frac{|\Delta t|}{\tau_{\text{refr}}}} \\ -B\hat{G}U_{\text{refr}}\tau_{\text{all}}\cdot\mathrm{e}^{-\frac{t-t^{\text{pre}}}{\tau_g}}\cdot\mathrm{e}^{-\frac{t-t^{\text{post}}}{\tau_{\text{refr}}}} \\ +B\hat{G}\Theta_u\tau_{\text{g}}\cdot\mathrm{e}^{-\frac{t-t^{\text{pre}}}{\tau_g}} - B\hat{G}\Theta_u\tau_{\text{g}}, \quad t > t^{\text{pre}}.\end{aligned} \tag{17}$$

Using Eqs. 16 and 17, our LCP with SRM can be directly mapped to pair-based (nearest-neighbor) STDP rules (Morrison et al., 2008). Thereby, we set $\Theta_u = 0$. Then, a spike pairing with time difference $\Delta t = t^{\text{post}} - t^{\text{pre}}$ results in the time-continuous weight change function:

$$\Delta w(t) = \Delta w_\infty - B\hat{G}U_{\text{refr}}\tau_{\text{all}}\cdot\mathrm{e}^{-\frac{t-t^{\text{pre}}}{\tau_g}}\cdot\mathrm{e}^{-\frac{t-t^{\text{post}}}{\tau_{\text{refr}}}} \quad \text{with}$$

$$\Delta w_\infty = \begin{cases} B\hat{G}U_{\text{refr}}\tau_{\text{all}}\cdot\mathrm{e}^{-\frac{|\Delta t|}{\tau_{\text{refr}}}} & : \quad \Delta t < 0 \\ B\hat{G}\left(U_{\text{p}} + U_{\text{refr}}\tau_{\text{all}}\right)\mathrm{e}^{-\frac{|\Delta t|}{\tau_g}} & : \quad \Delta t \geq 0 \end{cases} \tag{18}$$

As denoted, the solution of the integral can be split into a time-invariant term Δw_∞ that depends on the order of the spike pairing, and an additional time-dependent term that diminishes for $t \to \infty$. For the low pairing frequency used in standard STDP experiments (Bi and Poo, 1998; Froemke and Dan, 2002), the resulting weight change is well approximated by the term Δw_∞. This term equals the exponential time window of pair-based STDP, as is shown in **Figure 4**.

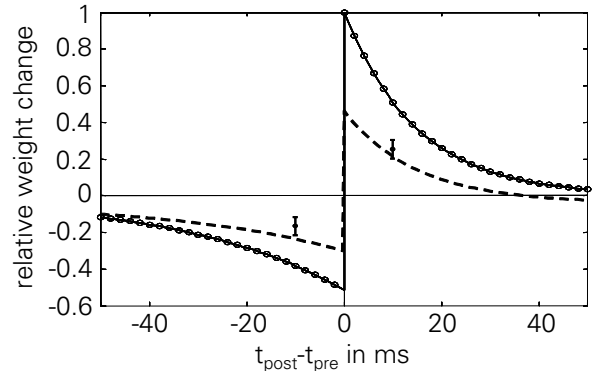

FIGURE 4 | Normalized STDP window of LCP with SRM: analytical value Δw_∞ (solid line) and simulation results (circles, 60 pairings at 1 Hz, protocol of Bi and Poo, 1998; Froemke and Dan, 2002). STDP parameters are taken from Froemke and Dan (2002) and corrected by the number of repetitions, cf. Froemke 1 parameter set in **Table 4**. Error bars are measurements from Wang et al. (2005), as extracted by Pfister and Gerstner (2006); dashed line: simulation results for Wang parameter set, used to account for the smaller weight changes found throughout the experiments in Wang et al. (2005), as stated there. Normalized error in this case: $E = 0.92$.

From this correspondence, the parameters of LCP with SRM can be directly derived from the parameters of the exponential STDP time window:

$$U_{\text{refr}} = \frac{1}{B\hat{G}}\cdot A_-\cdot\left(\frac{1}{\tau_g} + \frac{1}{\tau_{\text{refr}}}\right) \qquad \tau_{\text{refr}} = \tau_-$$

$$U_{\text{p}} = \frac{1}{B\hat{G}}\cdot\left(A_+ - A_-\right) \qquad \tau_g = \tau_- \tag{19}$$

In these correspondences, the parameters $A_-(<0)$, τ_- and A_+, τ_+ denote the amplitude and time constant of LTD and LTP, respectively (Song et al., 2000). To arrive at biologically realistic membrane voltage values, we calculate the amplification factor $B\hat{G}$ such that the refractory amplitude U_{refr} equals −5 mV (Koch, 1999).

It is important to note that the parameters of LCP with SRM, being strongly linked to biophysical parameters, take on biologically realistic values when they are derived from measured STDP parameters. The conductance time constant τ_g equals the STDP time constant for LTP, which is in the order of 20 ms, a value compatible with NMDA synapse conductance changes (Gerstner and Kistler, 2002; Badoual et al., 2006). In contrast to (Pfister et al., 2006), this time constant is chosen different from τ_{mem}, since those characteristics are not necessarily correlated (Koch, 1999; Senn, 2002). The STDP time constant for LTD equals the membrane time constant τ_{refr}, which was found to be in the order of 10–40 ms (Koch, 1999). As can be derived from Eq. 19, the STDP parameters A_+, τ_+ and A_-, τ_- set the relation between U_{p} and U_{refr}. For our assumption, $U_{\text{refr}} = -5$ mV, the STDP parameters of Froemke and Dan (2002) result in $U_{\text{p}} = 151$ μVs (cf. Froemke 1 parameter set in **Table 4**), corresponding to a rectangular pulse of length 2 ms and height 75 mV, which are reasonable values for an action potential (Koch, 1999).

The increase in LTD with the amplitude of the refractoriness, U_{refr}, as evident from Eq. 18, is in direct contrast with Pfister et al. (2006), where LTD increases with a decrease in refractoriness. The

motivation given in Pfister et al. (2006) is that an additional refractoriness has to be introduced through the learning rule to block a presynaptic spike which is not sufficiently suppressed by the refractoriness. In contrast, the LTD mechanism of LCP with SRM could be interpreted as enhancing the effectiveness of the presynaptic pulse, i.e., a given presynaptic PSC is not allowed to simply spend itself against the refractoriness as in Pfister et al. (2006), which would be wasteful from an information- and energy-conserving point of view.

Besides the temporal asymmetry seen in STDP, the LCP rule also exhibits a close similarity to the BCM model in its formulation, as was discussed in Section "Local Correlation Plasticity." It is therefore interesting to check whether LCP with SRM can be mapped to the original BCM rule as well. Especially, relating the voltage threshold Θ_u in the LCP rule to the frequency threshold Θ_M in the BCM rule could open BCM arguments on rate-based metaplasticity (Abraham et al., 2001) to our rule, as well as providing a possible link to voltage-based expressions of metaplasticity (Ngezahayo et al., 2000). For deriving such a relationship, we use an analysis similar to that in Izhikevich and Desai (2003). We start out with the general derivation for the weight change of a single pair of spikes as done above, and again assume low pairing frequency, so omit the terms dependent on t. But in contrast to the STDP derivation, we treat Θ_u as non-zero parameter. The resulting expression for LTP is as follows:

$$\Delta w(\Delta t) = B\hat{G}\left(U_{\mathrm{p}} + U_{\mathrm{refr}}\tau_{\mathrm{all}} - \Theta_u\tau_g\right)\mathrm{e}^{-\frac{|\Delta t|}{\tau_g}} \tag{20}$$

and for LTD:

$$\Delta w(\Delta t) = B\hat{G}U_{\mathrm{refr}}\tau_{\mathrm{all}}\cdot \mathrm{e}^{-\frac{|\Delta t|}{\tau_{\mathrm{refr}}}} - B\hat{G}\Theta_u\tau_g \tag{21}$$

Assuming a Poisson process for postsynaptic spike times, the expected weight change $\Delta w(\lambda)$ for a single presynaptic spike and a postsynaptic firing rate λ can be explicitly derived. This is done by integrating the product of the weight change as a function of time Δt and the Poisson probability density $p(\Delta t) = \lambda \cdot \exp(-\lambda \cdot \Delta t)$ separately for LTP and LTD. Adding both integrals results in the overall weight change (Izhikevich and Desai, 2003):

$$\begin{aligned}\Delta w(\lambda) = &\int_0^{\infty} B\hat{G}\left(U_{\mathrm{p}} + U_{\mathrm{refr}}\tau_{\mathrm{all}} - \Theta_u\tau_g\right)\mathrm{e}^{-\frac{\Delta t}{\tau_g}}\cdot\lambda\mathrm{e}^{-\lambda\Delta t}\,\mathrm{d}\Delta t \\ &+ \int_{-\infty}^{0} B\hat{G}\left(U_{\mathrm{refr}}\tau_{\mathrm{all}}\,\mathrm{e}^{\frac{\Delta t}{\tau_{\mathrm{refr}}}} - \Theta_u\tau_g\right)\cdot\lambda\mathrm{e}^{\lambda\Delta t}\,\mathrm{d}\Delta t\end{aligned} \tag{22}$$

Carrying out this integration results in the following expression:

$$\begin{aligned}\Delta w(\lambda) = &\lambda B\hat{G}\left(\frac{U_{\mathrm{p}} + U_{\mathrm{refr}}\tau_{\mathrm{all}}}{\frac{1}{\tau_g}+\lambda} + \frac{U_{\mathrm{refr}}\tau_{\mathrm{all}}}{\frac{1}{\tau_{\mathrm{refr}}}+\lambda}\right) \\ &-B\hat{G}\Theta_u\tau_g\left(\frac{\lambda}{\frac{1}{\tau_g}+\lambda}+1\right)\end{aligned} \tag{23}$$

The first part of the above expression is basically the same STDP-BCM translation as in Izhikevich and Desai (2003), with the standard STDP parameters substituted as in Eq. 19. The second expression causes the entire weight change curve to shift upwards or downwards, dependent on Θ_u, while the additional dependence on λ can be neglected for a small λ, only causing an increase in the slope of the curve for a high λ ($>1/\tau_g$), thus letting the curve crossover from LTD to LTP slightly earlier. Consequently, as is evident from Eq. 23 and the curves in **Figure 5A**, the voltage threshold for plasticity introduced in the LCP rule can be related to the sliding frequency threshold found in the context of rate-based induction protocols (Mayford et al., 1995; Wang and Wagner, 1999; Abraham et al., 2001). Ngezahayo et al. (2000) show that such a voltage threshold separating LTP and LTD exists and that it can be metaplastically adjusted. This adjustment changes the ratio and crossover point between LTD and LTP in a fashion qualitatively compatible with the original formulation for the sliding frequency threshold (Bienenstock et al., 1982; Ngezahayo et al., 2000). An interesting observation in **Figure 5A** is that for low frequencies, contrary to most BCM formulations that assume no plasticity change, the plasticity can exhibit an offset toward either LTD or LTP, depending on the voltage threshold. This kind of voltage offset is very similar to the results reported in

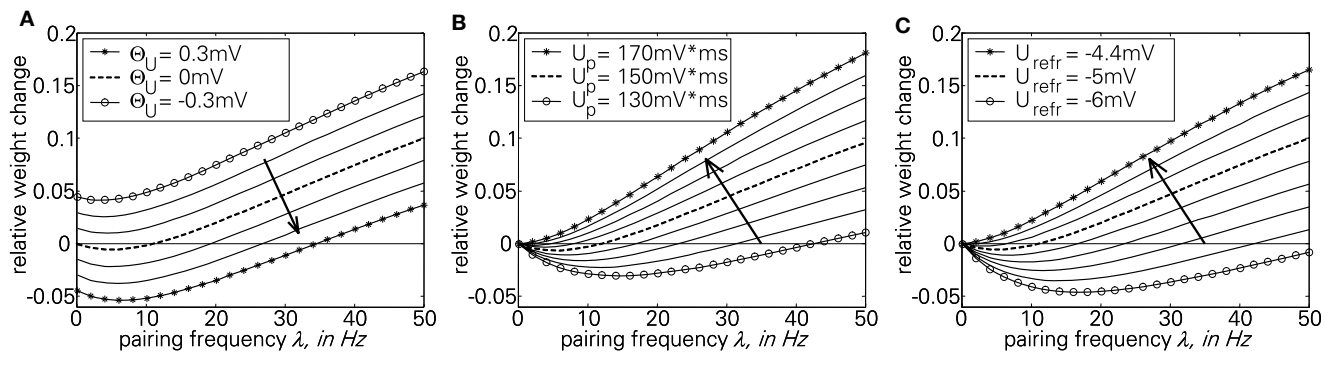

FIGURE 5 | Plot of the analytical BCM expression of Eq. 23 for sweeps of different variables. The standard parameter set (Froemke 1 in **Table 4**: Θ_u = 0 mV, U_{p} = 151 mV·ms, U_{refr} = –5 mV) is always denoted by the broken line. **(A)** sweep of Θ_u; **(B)** sweep of U_{p}; **(C)** sweep of U_{refr}.

Sjöström et al. (2001), where a depolarization causes an offset toward LTP at low frequencies, while a hyperpolarization results in enhanced LTD at low frequencies. Also, similar to the theory of Beggs (2001), **Figure 5A** shows that a vertical shift of the plasticity curve via a voltage offset results in a horizontal shift of the frequency threshold.

In contrast to Θ_u, a sweep of the two amplitude parameters U_p and U_{refr} affects only the second threshold from LTD to LTP, while the plasticity for low frequencies remains unchanged (**Figures 5B,C**). Both have a very similar effect of lowering/raising this frequency threshold while changing the overall shape of the curve from a "U" shape to an almost linear characteristic.

Simulation results

In a first test related to the BCM discussion of the previous section, we use the correlated rate protocol (7) to verify that LCP with SRM follows the simplifications of Eq. 23. Since the experiments of Sjöström et al. (2001) employ a different cell preparation and produce, e.g., zero potentiation for a standard pre-post pairing protocol in contrast to the strong LTP of conventional STDP experiments (Bi and Poo, 1998; Froemke and Dan, 2002), a parameter set different from the one of Froemke and Dan (2002) is used in **Figures 6 and 10**. This parameter set has been chosen to approximate the STDP window of Sjöström et al. (2001), see also the motivation in **Figure 13**.

Figure 6 shows the corresponding weight changes for a standard STDP model (A) and LCP with SRM (B). The STDP model exhibits only a slight dependence on the pairing frequency, producing either LTP or LTD throughout the frequency range, dependent on the parameter set. This is in contradiction to the experimental results of Sjöström et al. (2001) that show depression below approx. 35 Hz and potentiation for frequencies above only (cf. error bars in **Figure 6**). In contrast, LCP with SRM is qualitatively compatible with the experimental data, exhibiting a transition from LTD to LTP at approx. 25 Hz. However, attenuation of postsynaptic action potentials would add a source of depression at higher frequencies that prevents a transition to LTP. Thus, this addition is not compatible with the experimental protocol.

We further tested LCP with SRM for spike triplet experiments (3). Therefore, we used the STDP parameters given in Froemke and Dan (2002) to compare to their triplet measurements. **Figure 7** shows the original data points (A) together with predicted weight changes for LCP with SRM (B and C) as well as for a standard pair-based STDP rule (D). LCP with SRM (B) and STDP (D) show almost the same behavior, which is also in good agreement with the measurements. Only for the post-pre-post triplet (lower right quarter), qualitative differences are visible: whereas the models predict potentiation for small time differences t_1 and t_2, the measurements show depression. Introducing the attenuation of closely following postsynaptic spikes ($\alpha_{att} = 0.8$), the amount of potentiation is significantly reduced in

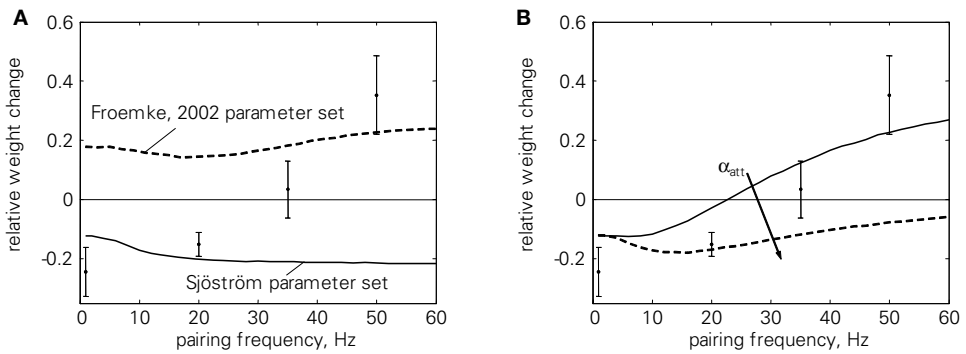

FIGURE 6 | Correlated rate protocol (7); (A) standard nearest-neighbor STDP; (B) LCP with SRM without and with attenuation ($\alpha_{att} = 0$, $\alpha_{att} = 0.8$), using Sjöström parameter set (see Table 4). Error without attenuation: $E = 3.2$. Error bars denote experimental data by Sjöström et al. (2001).

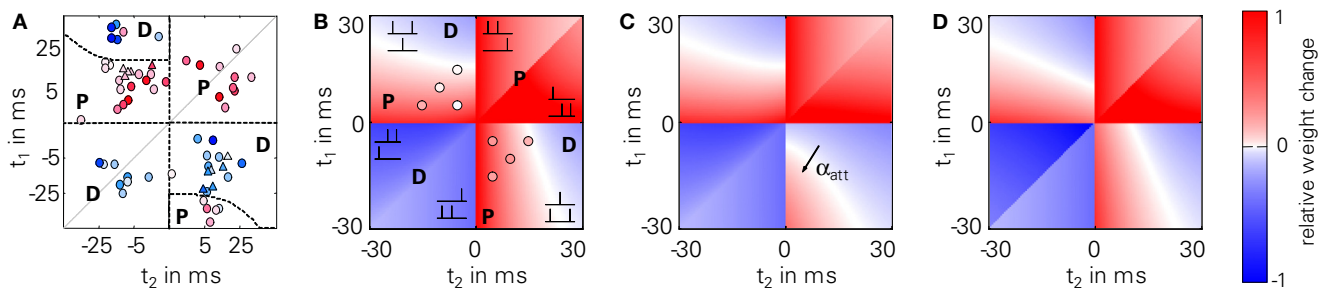

FIGURE 7 | Triplet protocol (3). Upper left part: 2 presynaptic, 1 postsynaptic spike; lower right part: 1 presynaptic, 2 postsynaptic spikes; **(A)** experimental data of Froemke and Dan (2002); **(B)** LCP with SRM, using parameters from Froemke and Dan (2002), as listed in **Table 4** (Froemke 1 parameter set); circles: data by Wang et al. (2005) (error to Wang data for LCP with SRM and Wang parameter set: $E = 10.2$); **(C)** LCP with SRM with postsynaptic attenuation ($\alpha_{att} = 0.8$); **(D)** standard STDP rule with same parameters, for comparison (error to Wang data with Wang parameter set: $E = 12.9$).

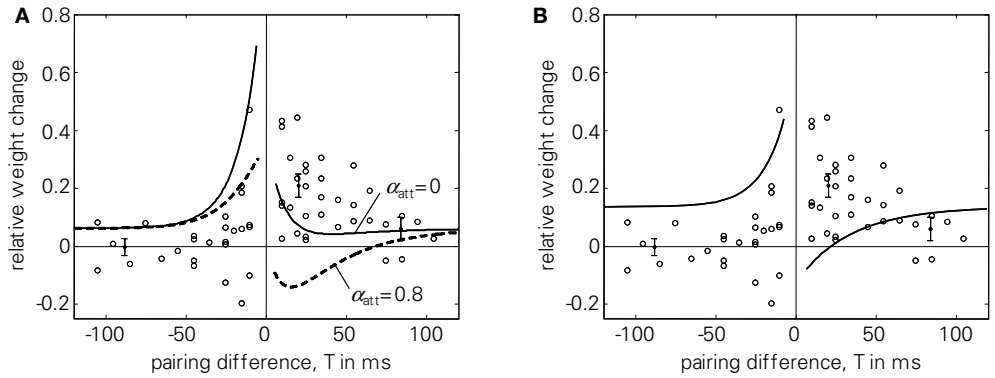

FIGURE 8 | Quadruplet protocol (4). Single data points in the diagrams extracted from Wang et al. (2005), points with error measures as given in Pfister and Gerstner (2006), based also on Wang et al. (2005). **(A)** LCP with SRM with (dashed) and without (solid) postsynaptic attenuation, Wang parameter set (see **Table 4**); E = 5.6 without attenuation; **(B)** standard STDP rule with same parameter set, E = 17.8.

this case, so that depression dominates as in the measurements, see **Figure 7C**. Thus, even LCP with SRM can fully reproduce these triplet experiments, contrasting, e.g., the more extensive models by Badoual et al. (2006). If postsynaptic attenuation is switched off, our model is also somewhat compatible with the triplet experiments of Wang et al. (2005) (cf. circles in **Figure 7B**), slightly outperforming standard STDP (cf. error measures in **Figure 7**). As discussed in Section "Benchmark Experiments," a full compatibility for both triplet results cannot be achieved in a single model due to the fundamental difference in experimental behavior.

Regarding the quadruplet protocol of Wang et al. (2005), pair-based STDP rules fail to reproduce the experimental results, see (Pfister and Gerstner, 2006) and **Figure 8B**. In contrast, LCP with SRM can reproduce the dependency of weight change on the time interval T, see **Figure 8A**. To account for the reduced potentiation for big time differences T compared to standard STDP, we used an increased voltage threshold in the Wang parameter set (Θ_u = 0.5 mV, cf. **Table 4**). Like for the triplet experiments, LCP with SRM can not reproduce the Wang data if attenuation of postsynaptic spikes is activated, as is shown in **Figure 8A**.

These observations casts doubt on the validity of the postsynaptic attenuation in Eq. 6. To show the necessity of the attenuation at least in the scope of the experiments of Froemke and Dan (2002) and Froemke et al. (2006), **Figure 9** replicates the experiment of Figure 7B in Froemke et al. (2006), where postsynaptic attenuation and its influence on plasticity is explicitly tested. As is shown, LCP with SRM replicates both the standard experiment and the one with suppressed attenuation satisfactorily for the corresponding settings of α_{att}. The LCP rule produces somewhat too much potentiation for 4 and 5 postsynaptic APs, which could be due to the fact that the synapses in the preparation of Froemke et al. (2006) seem to exhibit a hard weight bound at about 60% potentiation, i.e., any hypothetical further weight increase is checked by the saturation of the weights. As stated earlier, such a saturation is not included in the LCP model.

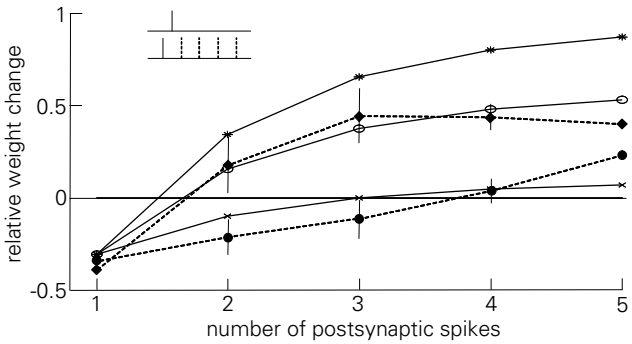

FIGURE 9 | Plasticity curves for the post-pre-post-burst protocol of Figure 7B of Froemke et al. (2006), change in EPSP for the standard experiment (dashed line, filled circles) and with suppressed postsynaptic attenuation (dashed line, diamonds), including error bars This experiment for LCP with SRM (parameters taken from Froemke et al., 2006), compare (Froemke 2 parameter set in **Table 4**) and activated attenuation (crosses, α_{att} = 0.8) or deactivated attenuation (stars, α_{att} = 0); For comparison: standard STDP (empty circles), same parameters as LCP with SRM.

Limits of LCP with SRM

In the previous section, we have shown that LCP with SRM can reproduce a variety of experimental protocols, but only with conflicting settings for the attenuation of postsynaptic spikes: whereas this attenuation is necessary for replicating the data by Froemke and Dan (2002) for the triplet protocol (3), it leads to incompatible results in the quadruplet protocol (4) and the correlated rate protocol (7).

As a further limitation, LCP with SRM has some difficulties in reproducing frequency-dependent STDP (2), even without postsynaptic attenuation, cf. **Figure 10B**. Still, it is compatible with the experimental data at least qualitatively, in contrast to standard STDP, cf. **Figure 10A**. However, LCP with SRM fails to account for the increasing potentiation for pre-post pairings.

LCP WITH LIAF NEURON

In the following, we want to investigate whether the second LCP version of Section "Summary of LCP Versions," i.e., extending LCP with the LIAF neuron of Section "Neuron Dynamics: Leaky Integrate-and-Fire," can overcome the current limits of LCP as evident from Section "Limits of LCP with SRM." Therefore, we

test LCP with LIAF on a variety of experimental protocols. We start with results for the standard rate protocol (6) to illustrate the effects of the extensions.

In the LCP rule, a weight change can only occur if presynaptic activity coincides with the postsynaptic membrane potential u deviating from the voltage threshold Θ_u. Furthermore, the direction of the weight change is directly related to the sign of the deviation $(u-\Theta_u)$. In protocols with only presynaptic stimulation, a transition from depression to potentiation is thus impossible if the presynaptic activity has no influence on the postsynaptic membrane potential, as in LCP with SRM. As a consequence, LCP with SRM, like standard STDP rules, can not account for the standard rate (6) results without making strong assumptions on postsynaptic firing, like postsynaptic firing rate being proportional to presynaptic firing rate (Izhikevich and Desai, 2003), or even single-spike correlations (Beggs, 2001; Standage and Trappenberg, 2007). This is documented in **Figure 11C**.

In contrast, the postsynaptic potential added by the LIAF neuron depolarizes the membrane voltage with increasing presynaptic stimulation frequency, so that the membrane voltage can cross the voltage threshold Θ_u, leading to potentiation even in the absence of postsynaptic spikes. As **Figure 11A** shows, this leads to a transition from weight depression to potentiation, which is what Dudek and Bear (1992) found experimentally. The point of transition from depression to potentiation is dependent on the STDP time constants. To account for the relatively low transition frequency in the data by Dudek and Bear (1992), we therefore used the Sjöström parameter set as reference, because it has longer time constants. Even though the induction protocol in Dudek and Bear (1992) was much stronger than for spike-based experiments (900 pulses compared to, e.g., 60 pairings), the resulting weight changes of both are in the same order of magnitude. To account for this difference, we divided the weight change amplitudes by a factor of 900/60 = 15.

Besides the non-spiking postsynaptic side investigated above, we also tested the uncorrelated and correlated spiking settings as discussed in Section "Benchmark Experiments" by triggering postsynaptic spikes and membrane potential resets at the given times, while keeping the influence of presynaptic spikes on the membrane

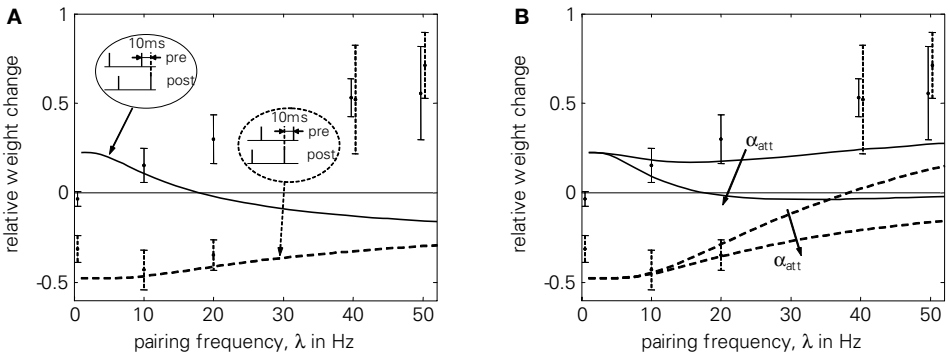

FIGURE 10 | Frequency-dependent STDP (2); error bars denote measurement data of Sjöström et al. (2001). Dashed curves and error bars: post-pre pairings, solid lines and error bars: pre-post pairings. Error bars at 40 and 50 Hz were slightly moved apart to make them distinguishable. **(A)** standard STDP [the upper curve (pre-post pairings) is also shown qualitatively in Standage et al. (2007)], **(B)** LCP with SRM neuron for $\alpha_{att} = 0$ and $\alpha_{att} = 0.8$. Sjöström parameter set as listed in **Table 4.** Normalized error without attenuation: $E = 6.8$.

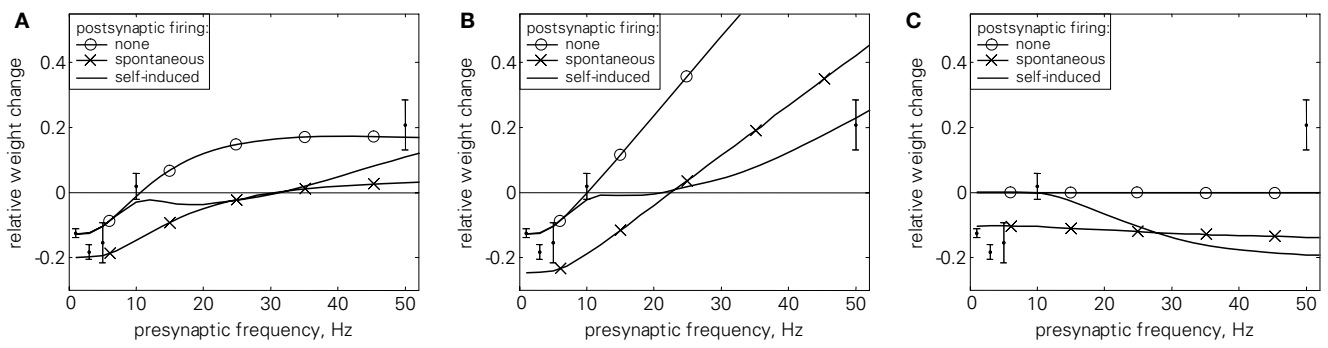

FIGURE 11 | Standard rate protocol (6). Error bars denote measurement data by Dudek and Bear (1992). **(A)** LCP with LIAF for different postsynaptic spike settings, nearest-neighbor mode; Dudek parameter set (cf. text and **Table 4**); errors for the postsynaptic settings: none: $E = 1.5$, spontaneous: $E = 10.7$, self-induced: $E = 2.0$. **(B)** Same as **(A)**, but with all-to-all interaction and postsynaptic attenuation ($\alpha_{att} = 0.8$); **(C)** nearest-neighbor STDP model with same parameters for comparison.

via postsynaptic potentials. Both protocols result in additional depression because of the resetting and hyperpolarization of the membrane potential. However, the initial results are not changed qualitatively. As an aside, the depression introduced by uncorrelated spiking is almost frequency-independent (cf. **Figure 11A**), and can be compensated, e.g., by increasing the PSP (error for U_{PSP} = 2.5 mV: E = 1.9, not shown).

Introducing presynaptic all-to-all interaction cancels the LTP saturation in nearest-neighbor mode, as **Figure 11B** shows. This is caused by the accumulation in the presynaptic activity $g(t)$, which counterbalances the increased leakage at higher membrane potentials, leading to a linear dependence of potentiation and presynaptic frequency in a broad range for uncorrelated and no postsynaptic spiking. As a consequence, weight change amplitudes would have to be reduced to at least partly account for the experimental results. As an exception, correlated firing still results in significant depression at higher frequencies, leading to compatible results with the parameter set in use (E = 1.6).

As **Figure 11C** shows, pair-based STDP consistently fails to account for the experimental results, irrespective of the postsynaptic spike setting.

For the quadruplet protocol (4), the LCP rule also benefits from the additions of the LIAF model. As **Figure 12A** shows, using all-to-all presynaptic interaction results in higher LTP for small positive pairing differences T, which is more compatible with the experimental data. Furthermore, in this case, the depression effect due to postsynaptic attenuation can be compensated by introducing PSPs, as is evident from **Figure 12B**.

Local correlation plasticity with SRM failed to reproduce the correlated rate experiment (7) when postsynaptic spikes were attenuated. Using the postsynaptic potential and the presynaptic all-to-all interaction counterbalances the negative attenuation effect, as is shown in **Figure 13B**. The postsynaptic potential leads to increased potentiation already for small frequencies. Therefore, we had to increase Θ_u to make the overall response negative. At high frequencies, the all-to-all interaction leads to increased postsynaptic potentials, which in turn flattens out the hyperpolarization after postsynaptic spikes and thus compensates for the attenuated spike amplitudes in this regime. Due to the postsynaptic potential the LTP part of the STDP modification window is distorted, as **Figure 13A** shows. By coincidence, this additional depression was also measured in Figure 2D of Sjöström et al. (2001).

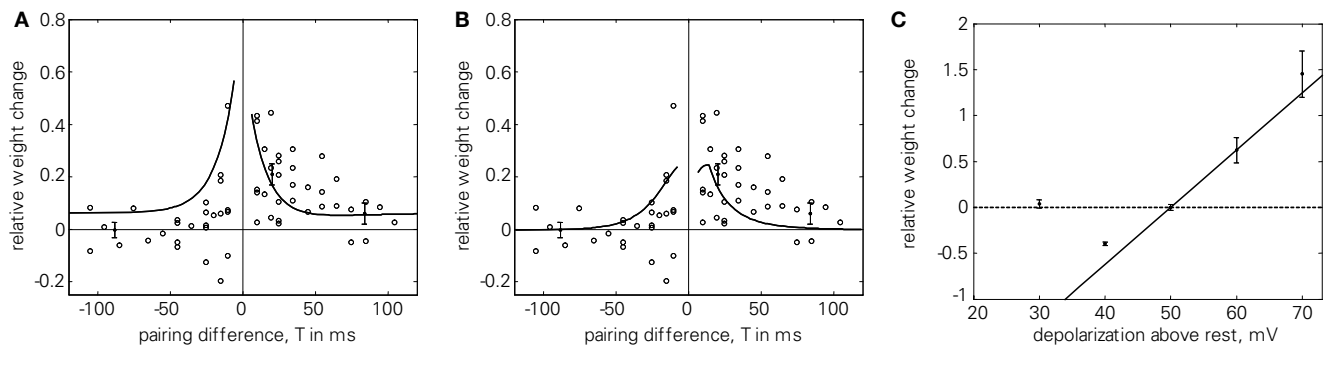

FIGURE 12 | (A, B); Quadruplet protocol (4) using LCP with LIAF: **(A)** same parameters as in **Figure 8B**, but all-to-all interaction (Wang parameter set in **Table 4**), E = 1.9; **(B)** all-to-all interaction, with attenuation (α_{att} = 0.8), which is compensated by PSP influence: $U_{PSP} = \Theta_u$ = 2 mV; E = 1.2. **(C)** Voltage control experiment (8). Error bars denote data for unconditioned synapse by Ngezahayo et al. (2000). Froemke 1 STDP parameters with downscaled weight amplitudes were used, and the voltage threshold was shifted according to the experimental data (see Ngezahayo parameter set in **Table 4**). Normalized error: E = 177.

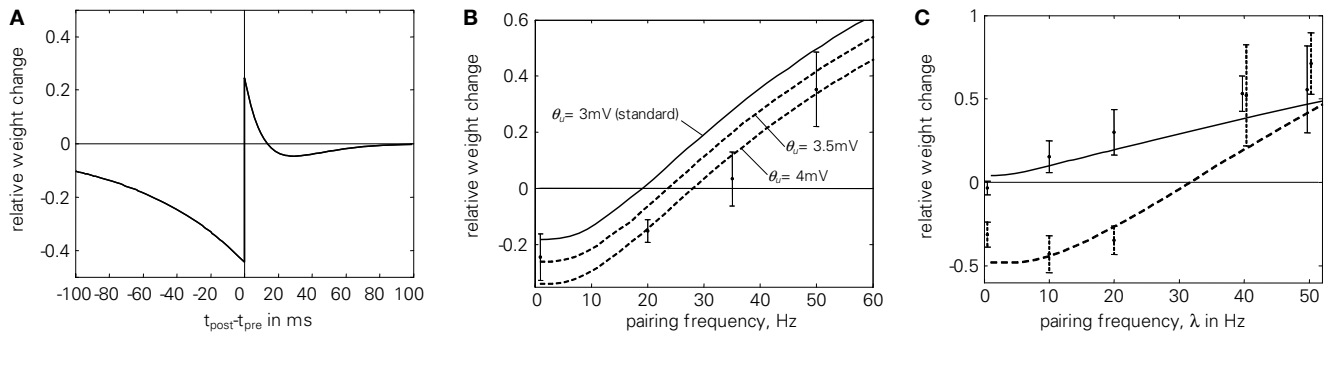

FIGURE 13 | Experiments of Sjöström et al. (2001) using LCP with LIAF and Sjöström parameter set (cf. Table 4). **(A)** resulting STDP window; **(B)** correlated rate protocol (7), E = 6.3; **(C)** Frequency-dependent STDP (2), E = 1.6. Total error: E = 2.9.

As can be seen when comparing the analytical expression of **Figure 5A** and the simulation of **Figure 13B**, the qualitative plasticity behavior caused by a $\Theta_u \neq 0$ corresponds to the analytical derivation, but the absolute value of Θ_u necessary to effect a certain behavioral change differs. This is due to the fact that Θ_u works mainly as an offset to the exponential refractoriness, which is assumed to extend to infinity in the analytical derivation. Thus, the overall area of the refractoriness and consequently the effect of Θ_u is larger in the analytical expression compared to the simulation, where the refractoriness is cut off with the next pulse. Correspondingly, Θ_u has to have higher absolute values in the simulation to achieve the same kind of effect.

The increased potentiation due to accumulated presynaptic conductance (all-to-all interaction) and its influence on membrane voltage via postsynaptic potentials also leads to more potentiation at high frequencies in the frequency-dependent STDP experiment (2), despite attenuation of postsynaptic spikes, cf. **Figure 13C**. Consequently, LCP with LIAF leads to steadily increasing LTP with pairing frequency for both pre-post and post-pre pairings, which is more consistent with the experimental data than LCP with SRM (see **Figure 10B**).

Figure 12C investigates the behavior of LCP with LIAF with respect to the voltage control experiment (8). Since the LCP rule contains only a single voltage threshold, whereas the experimental results in Artola et al. (1990) and Ngezahayo et al. (2000) suggest two thresholds, only the crossover from LTD to LTP is replicated, not the diminishing LTD below a certain membrane voltage.

However, if we rather take the LCP voltage threshold as a parameter and interpret the postsynaptic voltage clamp as activity level (i.e., equivalent to the time-averaged postsynaptic frequency, see also the discussion in Ngezahayo et al., 2000), some similarity can still be observed to the plasticity reported in Ngezahayo et al. (2000). As seen in **Figure 5A**, a decrease in Θ_u shifts the lower (i.e., LTD) threshold to higher frequencies, while at the same time transferring the LTP threshold to lower frequencies. So the curve for a depressed synapse in Ngezahayo et al. (2000) with an almost flat part followed by a single threshold for LTP could be approximately reproduced by a low Θ_u, while a high positive Θ_u acts to widen the LTD portion of the plasticity curve in both directions, similar to the potentiated synapse of Ngezahayo et al. (2000).

We further tested LCP with LIAF with the presynaptic burst protocol (5). Experimental results showed a decreasing amount of potentiation if more presynaptic spikes were added to a pre-burst-post pairing. In contrast, for post-pre-burst pairings, the number of presynaptic spikes did not influence the amount of depression. A standard STDP model can not reproduce these findings, as is shown in **Figure 14A**. In nearest-neighbor mode, potentiation for pre-burst-post stays constant regardless of the number of presynaptic spikes, whereas in all-to-all mode, potentiation even increases, because more pre-post pairings are taken into account. For the post-pre-burst case, depression increases with the number of presynaptic spikes, since more post-pre pairings exist.

Figures 14B,C shows that LCP with LIAF has similar problems in reproducing the experimental results. Without extensions, LCP with LIAF behaves essentially like standard STDP. Because the protocol employs only one postsynaptic spike, behavioral differences due to the resetting of the postsynaptic membrane potential do not appear; also, attenuation of postsynaptic spikes is effectless. All other parameters affect both pre-post and post-pre pairings in the same direction. Increasing the voltage threshold Θ_u adds depression that increases with the number of presynaptic spikes, because the (constant) negative voltage difference $(u - \Theta_u)$ is integrated over a longer time, multiplied with more presynaptic activity. Postsynaptic potentials counterbalance this effect, because they raise the membrane potential. Replacing nearest-neighbor with all-to-all interaction strengthens the influence of postsynaptic potentials and otherwise amplifies the weight change with increased number of presynaptic spikes, because presynaptic activity is accumulating. Incorporating all these effects, either pre-post or post-pre behavior can be reproduced, but not both with the same parameter set. Like for the standard STDP rule, the difference between the weight changes for the pre-post and the post-pre case increases in both versions of the LCP rule, but it decreases in the experimental results.

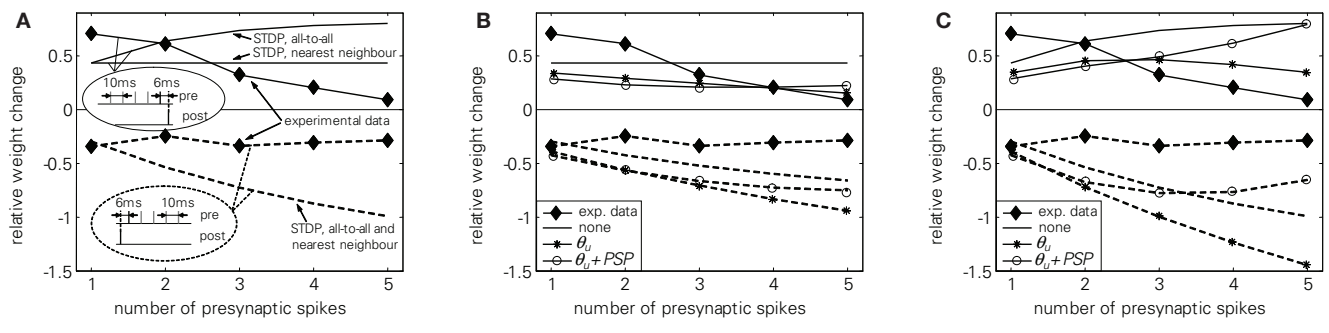

FIGURE 14 | Presynaptic burst pairing protocol (5), full lines: pre-burst-post case, experiments and reproduction, dashed lines post-pre-burst case, experiments and reproduction. (A) standard STDP, **(B)** LCP with LIAF with nearest-neighbor interaction, **(C)** LCP with LIAF with all-to-all interaction. For the Θ_u curve in **(B)** and **(C)**, we set Θ_u = 1 mV; for the Θ_u + PSP curve, we set Θ_u = 2 mV and U_{PSP} = 1 mV; for the "none" curve, we set Θ_u = 0 mV and U_{PSP} = 0 mV. STDP parameters taken from Froemke et al. (2006) (cf. Froemke 2 parameter set, see also discussion at **Figure 3** for LCP with SRM in **Table 4**, additional LCP with LIAF parameters (interaction mode, U_{PSP}) as stated in the last sentences).

DISCUSSION

From the experiments described in Artola et al. (1990), Holthoff et al. (2006), Kampa et al. (2007), Lisman and Spruston (2005), Ngezahayo et al. (2000), and Sjöström et al. (2008), it can be postulated that a significant ingredient of synaptic plasticity are localized, voltage driven processes. We have taken this hypothesis one step further, creating a plasticity rule where the complete synaptic plasticity is dependent on the postsynaptic membrane potential. Is this supported by the mechanisms underlying the generation of synaptic plasticity? According to (Aihara et al., 2007; Sjöström et al., 2008), a slow inactivation of the Calcium channels following a medium Calcium elevation is necessary for LTD, whereas a fast Calcium spike produces LTP. According to the time constants and voltage dependencies shown on page 217 of Koch (1999), a membrane potential below resting (<−65 mV) produces this slow inactivation. If a PSC arrives during the refractoriness period, it would lead to a temporary increase in membrane potential (while staying below resting potential), thus producing this medium Calcium activation followed by a prolonged inactivation. This mechanism is replicated in the LCP rule by the convolution of the PSC with the membrane potential during the refractoriness period. However, if the membrane potential is above rest when the PSC arrives, the shorter time constant governing this operating region of the membrane voltage (see Figure 9.3 of Koch, 1999) produces a sharp increase and subsequent decay in Calcium levels as a response to the PSC, thus forming LTP (Aihara et al., 2007). In our LCP rule, the membrane potential is above rest for a postsynaptic action potential and (for LCP with LIAF) for PSC-caused sub-threshold elevations of the membrane. When this depolarized membrane potential is convolved with a coincident PSC, the rule produces LTP.

The LCP rule is thus driven by the underlying short term dynamics of the neuron and synapse. The mechanisms producing LTP and LTD are similar to (Saudargiene et al., 2004; Shah et al., 2006), with the weight determined by a convolution of pre- and postsynaptic waveforms. Introducing a voltage dependence for such a rule, however, does not necessarily result in a plasticity function dependent on voltage. For example, in Saudargiene et al. (2004), the voltage dependence is cancelled out by the symmetric scaling of both the LTP and LTD part of the STDP curve. Similarly, the model of Saudargiene et al. (2004) indicates that a voltage-dependent threshold does not necessarily translate in a BCM-like frequency threshold. In contrast, we show in Eq. 23 for LCP with SRM a direct relation between the sliding frequency threshold as defined in the BCM rule and the membrane potential threshold of Eq. 2. Also, we show the direct plasticity-voltage dependence as defined in Eq. 2 for the experiment in **Figure 12C**, albeit only with the LTP/LTD threshold emulated.

The LCP rule, while simple in itself, can replicate complex behavior by incorporating a realistic synaptic/dendritic environment. For example, the inclusion of the AP attenuation (**Figure 7**) or the addition of the PSC influence on the postsynaptic membrane potential (see LCP with LIAF Neuron) resulted in a clear improvement in the ability of the model to replicate experimental findings. These examples show that the LCP rule is very amenable to combinations with further presynaptic or postsynaptic adaption mechanisms (Farajidavar et al., 2008). For example, we expect that a presynaptic adaptation such as the one described in Markram et al. (1998) would resolve the discrepancy of the LCP rule with respect to presynaptic bursts (5). This would be similar to what Froemke et al. (2006) achieved when making their revised suppression model dependent on all presynaptic pulses.

Of course, when including additional effects in a plasticity model, there is always the risk of simply fitting the model to specific experimental data. For example, while the state-machine model of Lu et al. (2007) might actually capture some underlying biophysical mechanisms, the fact that its parameters have to be fitted individually for each experiment argues against this. Another example would be the model of Clopath et al. (2010), which extends the original triplet model of Pfister and Gerstner (2006) with two voltage thresholds to replicate the data of Artola et al. (1990) and Ngezahayo et al. (2000). While this extension works well, the model produces significantly shorter time constants than the original triplet model after being fitted for experimental data. Thus, an additional longer time constant seems to have been introduced through the depolarizing after-potential of the neuron so that the plasticity model would replicate realistic STDP time windows.

In this context, we argue that the inclusion of the postsynaptic adaptation in both versions of the LCP rule is not simply a fit to experiments. Rather, it is in broad agreement with actual experimental evidence and mechanisms. For example, similar to our implementation, this adaptation chiefly alters the size (amplitude and duration) of the postsynaptic action potential (Tanaka et al., 1991; Froemke et al., 2006), and the adaptation has the postulated effect on plasticity (Froemke et al., 2006). Also, the time constant is compatible (Shah et al., 2006). The deflection of the postsynaptic membrane voltage due to the charge represented by the PSC (as included in LCP with LIAF) can, of course, also be motivated from experimental evidence (Artola et al., 1990; Koch, 1999). The veracity of including presynaptic adaptation similar to (Markram et al., 1998) in models of plasticity is proven experimentally in Froemke et al. (2006). We did not include a mechanism for weight dependency in the LCP rule, i.e., all weight changes that are sufficiently separated in time sum linearly. This is because the experimental evidence and computational effect of weight-dependent plasticity is still a matter of controversy (Standage and Trappenberg, 2007; Morrison et al., 2008). Furthermore, the weight change would depend on the initial weight, a parameter that is unknown in most experimental setups. In the LCP rule, a weight dependence would most naturally be included in the conductance $g(t)$, leading to equal weight dependence for LTP and LTD.

Regarding the actual weight computation in the LCP rule, a continuously generated synaptic weight based on local state variables seems more in line with the also continuously operating biological processes at the synapse than the assumption of purely discrete, spike timing-driven events as in STDP-type models. For example, a single exponential relating spike time to weight change in classical STDP rules seems an artificial simplification when compared to the spread of results for actual experiments (Bi and Poo, 1998). Other plasticity rules take a fundamentally stochastic approach to modeling synaptic plasticity (Elliott, 2008), which also replicates the variation seen in classical STDP experiments. However, those rules cannot reconcile the stochastic nature of spike timing experiments with the more deterministic behavior for voltage

control (Ngezahayo et al., 2000; Sjöström et al., 2001) or dendritic spike experiments (Holthoff et al., 2006; Kampa et al., 2007). In the LCP rule, deterministic or stochastic deflections of the membrane voltage could account for a significant proportion of the statistical spread (see the sweeps in **Figures 5A and 13B**). Even for controlled postsynaptic conditions in plasticity experiments, such as APs induced by current pulses or even for a voltage clamp of the soma, the local dendritic membrane potential is subject to stochastic variation (Artola et al., 1990) and thus to these possible influences on plasticity.

To further a general model comparison, a detailed discussion of a broad selection of plasticity models is included in the Appendix, with a summarized comparison derived from this discussion given in **Table 3**. The discussion also includes estimated or proven performance of a model against a fixed set of eight experiments described in **Table 1**. In the original publications corresponding to each model, these are only verified against an arbitrary sample set of experimental data (usually significantly smaller than the listing provided in **Table 1**), making a performance comparison of the models very difficult. In contrast, we attempt to describe a "set union" of experiments which incorporates significantly differing aspects of spike-, rate-, and voltage-based plasticity, requiring a model to contain mechanisms that replicate these differing aspects. Single mechanisms can then be extracted from **Table 3** which exhibit both good experiment reproduction and are common to several models. These mechanisms may in turn hint at some underlying biophysical process.

For example, based on the comparison, a case can be made for plasticity influenced by an exponential form of postsynaptic adaptation (Badoual et al., 2006; Froemke et al., 2006; Pfister and Gerstner, 2006; Shah et al., 2006), which is included in the LCP rule. LCP also exhibits plasticity dependent on waveforms of local state variables (Shouval et al., 2002; Saudargiene et al., 2004; Badoual et al., 2006; Shah et al., 2006). As suggested by computational analysis (Pfister et al., 2006), the LTP time constant of the LCP rule is equivalent to the PSC time constant, while LTD is based on the membrane time constant. Voltage control is realized in the form of a threshold applied to the postsynaptic membrane potential similar to the models of Clopath et al. (2010), Fusi et al. (2000), and Sjöström et al. (2001). Reproduction of rate behavior (Dudek and Bear, 1992) in the LCP rule is assured by applying an event-based form of the pre- and postsynaptic activity to a BCM-like rule as in Toyoizumi et al. (2005). Spike timing is inherent in the LCP rule in the form of starting points of PSCs, APs and the refractoriness period similar to (Abarbanel et al., 2002; Badoual et al., 2006), but not explicitly modeled as discrete events such as in Froemke et al. (2006), Izhikevich and Desai (2003), and Pfister and Gerstner (2006). Compared to kinetic or state transition models (Abarbanel et al., 2002; Senn, 2002; Lu et al., 2007), which generate a waveform based on kinetic mechanisms and then compute the resultant weight change based on this waveform, the LCP rule omits this step, taking the (idealized) waveform directly as input. The actual weight generation in the LCP rule based on these waveforms is somewhat similar to trace-based versions of spike timing-driven plasticity rules (Senn, 2002; Badoual et al., 2006). However, the traces are not merely sampled at the respective opposite event (presynaptic trace for postsynaptic event and vice versa), rather they are convolved and integrated across time. This convolution with a time-continuous presynaptic waveform is also the main difference to the model of Fusi et al. (2000).

Overall, the LCP rule provides a very compact implementation of the above mechanisms. As seen in **Table 3**, both LCP with SRM and LCP with LIAF combine a very general experiment reproduction ability with one of the lowest parameter counts. Legitimately, the LCP rule could even be interpreted as containing only the voltage threshold and one weight scaling constant as in Eq. 2, since all the behavior shown in this paper can be replicated with a reasonable model for the synaptic current and neuron, which are already contained in most simulations or hardware realizations (Indiveri et al., 2006; Schemmel et al., 2007). Our LCP rule would then be reduced to Eq. 2, while the time functions of PSC and postsynaptic membrane potential are taken from other parts of the system. The downside of such an approach would be the reduction in flexibility of the learning rule, making it very dependent on the details of the postsynaptic modeling. However, it significantly reduces the computational effort involved in implementing this rule in hardware or software compared to other STDP/BCM formulations (Mayr et al., 2010a).

The parameters of the LCP rule may also be metaplastically adjusted in a fashion similar to **Figure 5** to replicate metaplasticity mechanisms experimentally observed *in vivo* (Lebel et al., 2001; Zelcer et al., 2006). For example, reduced post-spike after-hyperpolarization (AHP) seems to be related to enhanced learning in experimental animals (Disterhoft and Oh, 2006; Zelcer et al., 2006). In the LCP rule, this would correspond to reduced spike attenuation or reduced refractoriness and thus a predisposition toward LTP (see **Figure 5C**). However, after the training is concluded, not only is the AHP again reduced to a relaxed state (Disterhoft and Oh, 2006), thus balancing LTD and LTP, there is also an overshoot toward enhanced LTD which can be observed in experimental animals (Lebel et al., 2001). Thus, a second effect such as an increase of Θ_u in the LCP rule might follow this reduced AHP and outlast it once the AHP has again assumed a naive state. Do the corresponding time constants support this course of events? From Lebel et al. (2001) and Zelcer et al. (2006), the time constant for changes in AHP can be inferred as approximately 1 day. If we assume Θ_u to be changed by voltage-based metaplasticity similar to (Ngezahayo et al., 2000), there seems to be a contradiction, since this metaplasticity is induced more rapidly than the AHP change and would probably also decay long before the respective AHP change, not outlast it. However, this may not represent the true time constant inherent in this form of metaplasticity. We have already established a link between the voltage and frequency thresholds (see Eq. 23), so in this context, we may assume the voltage-based (Ngezahayo et al., 2000) and rate-based (Wang and Wagner, 1999; Abraham et al., 2001) metaplastic effects to be caused by a similar mechanism. Both can be established very rapidly by strong stimuli (Wang and Wagner, 1999; Ngezahayo et al., 2000). This is similar to the one-shot plasticity induction of Holthoff et al. (2006), which does, however, not represent the actual time course of plasticity induction *in vivo* (Lisman and Spruston, 2005). In the same vain, the actual time constant of the metaplastic LTD/LTP threshold could rather be inferred from its relaxation time, i.e., the time it takes to return to a naive state, which is about ten days (Abraham et al., 2001). This would support the view above, i.e., that the AHP

reduction is first activated by a learning task, followed by a slower metaplastic or homeostatic change in the LTD/LTP threshold, which outlasts it after the training is over. In the LCP rule, these AHP changes could be emulated through the adjustment of the extension τ_{refr} and depth U_{refr} of the refractoriness. At the same time, a second slower process would adjust Θ_u (see **Figure 5**) to account for the change in LTP/LTD threshold.

Thus, at the price of two additional metaplasticity time constants and the corresponding equations providing long-term adjustments of τ_{refr} and Θ_u, the LCP rule could be extended to provide a holistic yet parsimonious method for exploring the so far little model-accessible field of metaplasticity, while at the same time retaining the ability to replicate a wide range of conventional experimental plasticity data as shown in this manuscript.

APPENDIX

REVIEW OF PLASTICITY MODELS

In the following, each paragraph is devoted to a short discussion of a current plasticity model, which, together with the classification of plasticity mechanisms of **Figure 2** and the motivational classification of **Figure 1**, form the basis for the model comparison in **Table 3**. Where possible, Figure and manuscript references for a given model and experiment are detailed in the text.

Conventional STDP

(Song et al., 2000; Izhikevich and Desai, 2003): Since the conventional exponential formulation of STDP has originally been proposed to reproduce STDP (1) of **Table 1**, this experiment poses no problem (Figure 1E in Froemke and Dan, 2002), receiving classification "f" in **Table 3**. Experiments (2)–(5) rely mainly on some type of short time adaptation, which is not included in basic STDP. The unsatisfactory behavior of conventional STDP with respect to experiments (2), (4), (5) is shown in **Figures 10A, 8B, and 14A**, thus receiving "*n*." Triplets (3) are partially reproduced by STDP (**Figure 7D**), the short time adaptation being only necessary for one quadrant, thus STDP is classified as "h" with respect to this experiment. Conventional STDP is not able to reproduce standard rate (6) (**Figure 11C**). STDP is able to reproduce BCM behavior for a non-stochastic presynaptic rate sweep as in experiment (6), if the postsynaptic spike is assumed to occur exactly in the middle between two presynaptic spikes (Standage et al., 2007). However, since this would assume a very specific rate-dependent pre-post latency which is likely incompatible with actual neuron behavior, we do not take this reproduction into account in **Table 1**. Also, this STDP protocol is not able to reproduce correlated rate (7), as argued in Section "Benchmark Experiments" (see also **Figure 6A**).

However, the performance of STDP with respect to the rate experiments (6) and (7) is said to depend on the exact implementation of the spike interaction (Izhikevich and Desai, 2003). The STDP modification of Izhikevich and Desai (2003) employs a nearest-neighbor protocol that is centered on the postsynaptic side, i.e., a presynaptic pulse is combined with the immediately preceding and subsequent postsynaptic pulses. It is claimed that this modification makes conventional STDP compatible with BCM. However, at least for the assumption of a fixed postsynaptic Poisson spiking, the presynaptic rate sweep of standard rate (6) has no discernible influence on the plasticity curve (Figure 3 in Mayr et al., 2010b), producing a flat line that can be altered only through the postsynaptic side. This is of course somewhat due to the postsynaptic stimulus assumption, since the STDP protocol of Izhikevich and Desai (2003) is centered around a postsynaptic sweep, not a fixed rate. However, Standage et al. (2007) have shown that STDP cannot reproduce BCM behavior for several other possible postsynaptic reconstructions of Dudek and Bear (1992) even when the protocol of Izhikevich and Desai (2003) is applied.

Also, the spike protocol assumption of Izhikevich and Desai (2003) is somewhat artificial, since conventional rate experiments are stimulated with a changing rate on the presynaptic side, not a fixed one. Even with changing presynaptic rate, this experimental protocol is very unlikely to lead to a postsynaptic rate that experiences a frequency sweep, but has single spikes totally uncorrelated to the presynaptic spike times, as is assumed for the postsynaptic Poisson sweep in that publication. A more natural assumption would be a strong correlation between presynaptic and postsynaptic rate, with a weak correlation between individual pre- and postsynaptic spike times, as expressed in the stimulation protocol of correlated rate (7). In the context of this experiment, the STDP modification of Izhikevich and Desai (2003) is unable to reproduce experimental results (Figure 2 in Mayr et al., 2010b). Again, the STDP curve is sampled on either side of the postsynaptic pulse, leading to LTP behavior for realistic STDP parameters (i.e., with LTP dominating LTD at short time intervals). Since there is no real difference in simulation results, the more widely used STDP protocol of Morrison et al. (2008) (nearest-neighbor) is employed for STDP simulations. Voltage Control (8) necessitates a mechanism relating voltage to plasticity, which is not included in STDP.

Froemke et al. (2006)

The revised suppression model of Froemke et al. (2006) is an extension of the conventional, pair-based STDP formulation. The spike efficacies A_+ and A_- of STDP are governed by time-averaged versions of the pre- and post-spike train, where short inter-spike-intervals (ISI) have a depressing effect, i.e., the influence of the corresponding pre-post-spike pair on overall plasticity is diminished. The revised suppression model is an extension of the original suppression model (Froemke and Dan, 2002), where A_+ and A_- scale with the complete history of the presynaptic spike train rather than just the last ISI. Standard STDP behavior is not explicitly shown for the revised suppression model, but can very likely be reproduced since both the original and revised suppression model reduce to STDP for low pairing frequencies. An experiment similar to frequency-dependent STDP (2) of **Table 1** is shown to be valid for the model, but this experiment only covers negative pairing time differences. The reproduction of the behavior in experiment (2) for positive time differences (pre-post pairings), is not possible (**Figure 15**). There is very high LTP at low pairing frequencies, not the zero weight potentiation found in Sjöström et al. (2001), caused by the essentially STDP nature of the model at these frequencies. For an increase in pairing frequency, the LTP decreases steeply to the amplitude difference between LTP and LTD bounds (the horizontal line between 15 and 70 Hz), since a very large amount of LTP is still being generated by the pre-post pairings, but there is an increase in postsynaptic relative to presynaptic efficacy suppression, due to the differing time constants. The effect of the later

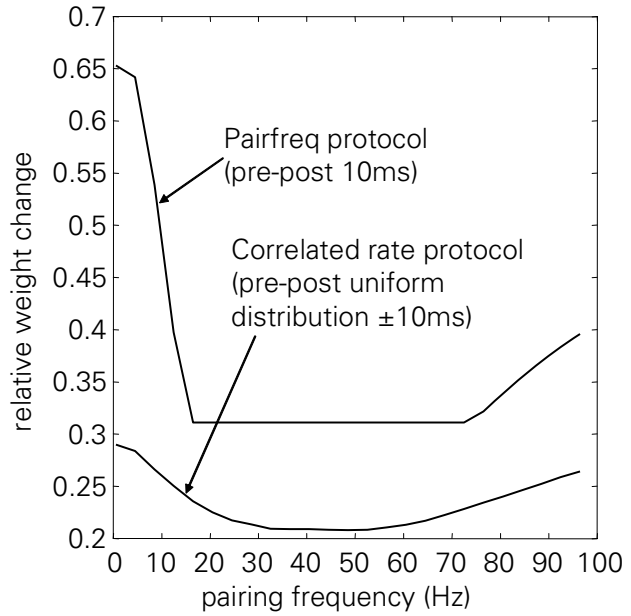

FIGURE 15 | Reproduction of frequency-dependent STDP (pre-post pairings) and of the correlated rate protocol for the revised suppression model of Froemke et al. (2006), parameters from Froemke et al. (2006).

postsynaptic spikes diminishes, causing a large increase in LTD. For frequencies above 70 Hz, the presynaptic spikes in each burst are also suppressed, so that the equivalent protocol would reduce to conventional one-pairing STDP (all spikes after the first spike in each burst are suppressed), leading to enhanced LTP. Turning off the weight bounds of Froemke et al. (2006) completes the curve now obscured by the horizontal line, but results in no qualitative difference.

The original suppression model is able to reproduce triplet (3) behavior (Figure 3B in Froemke and Dan, 2002). However, triplet behavior for the revised model discussed here has only been shown for the limited number of cases which overlap with the burst experiments of Froemke et al. (2006). It is somewhat likely that the revised suppression model is also compatible with the other triplet experiments, since the newly introduced dependence on all presynaptic pulses reduces to the immediately preceding one for low triplet repetition frequencies. However, it is not clear what consequence the postsynaptic scaling and the significantly longer postsynaptic efficacy time constant have especially in the post-pre-post case. The reproduction of quadruplet (4) behavior is not shown, but is also likely since quadruplets are replicated with the original suppression model (Figure 3C in Froemke and Dan, 2002) and also because of the similarities between (Froemke et al., 2006) and the model of Pfister and Gerstner (2006). The revised suppression model is of course able to reproduce burst (5) plasticity (Figures 4B,D in Froemke et al., 2006), since it is built on the basis of those experiments.

As derived analytically by (Izhikevich and Desai, 2003), the original suppression model of Froemke and Dan (2002) is not able to reproduce BCM-like behavior for Poisson spike trains. This is also evident from the simulations documented in Figure 3 of Froemke et al. (2006), where the original suppression model fails to cross from LTD to LTP with rising burst frequency. However, the same diagram shows BCM-like behavior for the revised suppression model. Thus, the nearest-neighbor protocol of Izhikevich and Desai (2003) is not the only way to make STDP compatible with protocols showing BCM-like behavior, the presynaptic all-to-all suppression of spike efficacy in the revised suppression model (Froemke et al., 2006) can evidently serve the same purpose.

However, the model is still incompatible both with the standard rate experiment (6) for all postsynaptic settings (Figure 3 in Mayr et al., 2010b) and with correlated rate (7). Replicating the correlated rate experiment in the revised suppression model with the parameter set of Froemke et al. (2006) leads only to LTP behavior, with 30% weight increase for low pairing frequencies (**Figure 15**). As argued above for STDP in connection with this experimental protocol, this is caused by the sampling/summation of the asymmetric STDP LTP/LTD amplitudes. The overall curve progression to higher pairing frequencies is caused by similar effects as cited above for the pre-post frequency-dependent STDP protocol, with a decrease in LTP and subsequent increase at very high pairing frequencies. However, the amplitude is reduced due to the averaging/scaling effect of having both post-pre and pre-post pairings at varying time differences. There is no mechanism for voltage control (8) included in the model.

Pfister and Gerstner (2006)

The model of Pfister and Gerstner (2006) is another extension of the conventional, pair-based STDP formulation. Additional to the presynaptic and postsynaptic pulse traces used in iterative implementations of standard STDP (Morrison et al., 2008), secondary presynaptic and postsynaptic trace variables with separate time constants are introduced. These new traces modulate the weight change: at a postsynaptic spike, the weight is increased dependent on the first presynaptic trace like in standard STDP, but the amplitude of the LTP weight change is increased with the second postsynaptic trace. Likewise, the LTD amplitude is modulated by the second presynaptic trace. Thus, these new traces introduce a form of adaptation to the presynaptic and postsynaptic side. However, in contrast to the model of Froemke et al. (2006), previous spiking activity increases LTD and LTP amplitude. Pfister and Gerstner (2006) show that the second presynaptic trace in their model can be neglected without significantly impairing reproduction of experimental results, reducing the model to 3 time constants and 3 scaling factors. We therefore use this simplified model in our comparison. Standard STDP (1) (Figure 3 in Pfister and Gerstner, 2006) and quadruplet (4) (Figure 5B in Pfister and Gerstner, 2006) protocols pose no problem to the model. Furthermore, the model can well reproduce frequency-dependent STDP (2) (Figure 5A in Pfister and Gerstner, 2006). Regarding experiment (3), the model of Pfister and Gerstner (2006) is built to replicate the triplets of Wang et al. (2005) (Figures 5C,D in Pfister and Gerstner, 2006), not the ones of Froemke and Dan (2002). The presynaptic burst pairing protocol (5) can very likely not be accounted for by the reduced Pfister and Gerstner (2006) model, because it does not incorporate presynaptic adaptation and thus performs like STDP. Even the full model is likely to be not compatible with the experimental results, because for the pre-burst-post protocol, its presynaptic adaption is not included in the weight change and for the post-pre-burst protocol, presynaptic adaptation leads to increased LTD, conflicting with the measurements. The authors show an analytical relationship to BCM behavior

for their rule for presynaptic and postsynaptic Poisson spike trains. However, this derivation cannot be generalized to experimental protocols as discussed in Section "Benchmark Experiments," e.g., standard rate (6) is not reproduced (Figure 3 in Mayr et al., 2010b). In the nearest-neighbor version, the reduced model is compatible with correlated rate (7) (Figure 2B in Mayr et al., 2010b). Voltage control experiments (8) can not be reproduced by the model, because it does not include a dependency on membrane potential.

Benuskova and Abraham (2007)

The STDP modification described in Benuskova and Abraham (2007) aims to provide a level of metaplasticity to the standard STDP formulation. The positive and negative weight scaling factors are adjusted by dividing respectively multiplying with the mean of the postsynaptic pulse activity across a 60 s time window. The expression used for the sliding mean is somewhat problematic in the context of the BCM formulation of Izhikevich and Desai (2003). Benuskova and Abraham (2007) state that their Θ_M translates in a sliding of the frequency threshold ϑ computed in Izhikevich and Desai (2003). However, when computing the original ϑ of Izhikevich and Desai (2003) as a function of the weight scaling "threshold" Θ_M for the STDP parameters used in Benuskova and Abraham (2007), only a very narrow useful range of Θ_M can be found where the resulting ϑ forms a valid threshold. This range starts at $\Theta_M = \sqrt{-A_+/\tau_- \cdot \tau_+/A_-} = 0.63$, where ϑ crosses to positive values, and $\Theta_M = \sqrt{-A_+/A_-} = 1.41$, where ϑ has a pole, i.e., the threshold jumps to infinity. In reality, this range is even smaller, since ϑ leaves the range of useful frequency values at about $\Theta_M = 1.2$. At Θ_M values above the pole, ϑ is negative, reaching $\vartheta_{inf} = -1/\tau_+$ when Θ_M goes to infinity. Since this dynamic range for Θ_M is quite narrow, a Θ_M that according to Eq. 10 of Benuskova and Abraham (2007) varies almost linearly with the pulse frequency (i.e., exhibits the same dynamic range) is not compatible with the declared goal of the authors of providing ϑ of Izhikevich and Desai (2003) with a valid metaplastic variation ability. The scaling constant α given in Benuskova and Abraham (2007) would also result in $\Theta_M \gg 1.41$ and thus in a negative frequency threshold. As to the experiment reproduction, the model of Benuskova and Abraham (2007) can probably show the conventional STDP (1) behavior it is originally derived from, although the metaplasticity time constant (60 s) is longer than the usual pairing separation distance in experiments (10 s), which might result in a change in the shape of the STDP curves during the course of the experiment. The assessment for experiments (2)–(5) and (7) is as stated above for conventional STDP, the metaplasticity time constant is too large to significantly affect the models' behavior with respect to these experiments. Although a protocol similar to (Dudek and Bear, 1992) is employed in eliciting heterosynaptic metaplasticity, standard rate (6) behavior is not demonstrated, i.e., no frequency sweep is carried out (Figure 1 in Benuskova and Abraham, 2007). Also, the link between the sliding threshold and the postsynaptic membrane potential is not clear, so the derivation cannot be used to extend STDP to voltage control (8).

Senn (2002)

This paper models the discharge probability P_{dis} of a synapse for each incoming pulse as being modified in a plastic way, equivalent to the synaptic strength/weight in other plasticity mechanisms. A set of receptors N is introduced that can make transitions from a recovered state N_{rec} either into an upregulating state N_{up} triggered by a presynaptic spike, or into a downregulating state triggered by a postsynaptic spike N_{dn}. Two secondary messengers S_{up} and S_{dn} are used to generate a time-averaged version of these receptor states. For generation of LTP, the running mean of the presynaptic activity as stored in its corresponding secondary messenger is weighted with a threshold and then read out when a postsynaptic pulse occurs, which upregulates P_{dis}. The opposite mechanism (presynaptic spike samples mean of postsynaptic activity) is active for the downregulation (LTD). This is similar to a trace-based version of STDP (Morrison et al., 2008), with additional pre- and postsynaptic adaptation through the secondary messengers. For low frequency pairings as in the conventional STDP (1) protocol, very little overall plasticity is produced (Figure 6A in Senn et al., 2001). For higher pairing frequencies, the curve shape diverges significantly from the conventional exponential STDP assumption, but still seems a good reproduction (Figure 6B in Senn et al., 2001). With regard to frequency-dependent STDP (2), only the pre-post pairing sweep is reproduced (Figure 1B in Senn, 2002). Due to the threshold property of the model, post-pre pairings start at zero potentiation for low frequencies, not at significant LTD as seen in the experimental data. Triplets (3) are reproduced by the model (Figure 2A in Senn, 2002). Quadruplet (4) reproduction is somewhat likely, since there exists both pre- and postsynaptic attenuation in the model, but has not been shown. Burst (5) is expected to be compatible with the model, since presynaptic adaptation/depression is part of the model and since at least an increasing number of pairings shows decreasing LTP (Figure 5A in Senn et al., 2001). An experiment similar to standard rate (6) is shown to be compatible with the model (Figure 1D in Senn, 2002). Correlated rate (7) can likely be reproduced, since at least the pre-post case of frequency-dependent STDP is compatible with the model. As to voltage control (8), there are two separate thresholds for LTP and LTD included in the model, but their mapping to voltage remains unclear.

Abarbanel et al. (2002)

This model is based on kinetic equations, i.e., first order differential equations which govern the transition between two states of a system. The processes represented by the differential equations are presynaptic neurotransmitter release P(t) and postsynaptic activity D(t), with disturbance functions that represent pre- and postsynaptic action potentials. Both processes are cross-wise added to derive the weight in a mixture of competition and cooperation, i.e., both are needed for a weight change, but the relative timing of events in P(t) and D(t) determines the sign of the weight change. Pre- and postsynaptic competition respectively cooperation as a source for LTP and LTD has also been shown experimentally (Tzounopoulos et al., 2007). Based on the fact that the kinetic equations for dirac-like disturbance functions can be solved as exponential functions scaled with the dirac area, expressions for STDP-like single-spike pairings as well as random spike trains are derived. Based on the STDP (1) plasticity replication shown in these analyses (Figure 1 in Abarbanel et al., 2002), a parameter fit to STDP is carried out which is used for simulating other spike protocols. Frequency-dependent STDP (2) is replicated qualitatively (Figure 2 in Abarbanel et al., 2002, with LTP/LTD behavior at low pairing frequency, the difference between both curves decreases with increasing frequency, the LTP

curve increases, the LTD curve crosses over to LTP). However, there are significant differences in the quantitative reproduction, e.g., relative to the LTP value of both curves for 50 Hz, both start out at almost zero weight change, i.e., the LTD behavior of the low frequency pairings and the initial difference between both curves is almost insignificant. As evident from this experiment, the model offers pre- and postsynaptic superposition, i.e., the effects of subsequent pulses overlap. However, no pre- or postsynaptic adaptation is included where earlier pulses influence subsequent ones. Thus, Triplets (3), which rely on postsynaptic adaptation, can probably be reproduced by the model only in an STDP-fashion. Likewise, bursts (5) rely on presynaptic adaptation, and quadruplets (4) on pre- and postsynaptic adaptation, which likely make them incompatible with the model of Abarbanel et al. (2002). As to standard (6) and correlated (7) rate, although BCM-like behavior could be inferred from the reproduction of experiment (2), a standard pre- and postsynaptic Poisson sweep produces only LTP (Figure 3 in Abarbanel et al., 2002). If the clamped postsynaptic behavior in Figure 5 of Abarbanel et al. (2002) is taken to represent membrane voltage, the model of Abarbanel et al. (2002) seems to provide at least an LTD/LTP threshold, so voltage control (8) can probably be partially replicated.

Badoual et al. (2006)

In this model, biophysically realistic formulations for a compartmental neuron and an AMPA/NMDA synapse are given, and a two-state kinetic plasticity process is assumed, with separate artificial LTP and LTD "enzymes." The behavior of the model is similar to other kinetic models (Abarbanel et al., 2002; Lu et al., 2007; Zou and Destexhe, 2007), producing a conventional STDP (1) curve with a soft crossover from LTP to LTD at small time differences between pre- and postsynaptic pulses (Figure 6 in Badoual et al., 2006). The plasticity derivation is similar to (Saudargiene et al., 2004), i.e., since the weight update is a function of the underlying waveforms (e.g., Calcium), the STDP weight change curve is a function of the waveform characteristics (time constants, amplitudes). Similar to STDP, the biophysical model partially reproduces triplet (3) behavior (Figure 11C in Badoual et al., 2006, compare also **Figure 7D**). Frequency-dependent STDP (2) is reproduced by this model, albeit with significantly lower LTD/LTP threshold frequency (Figure 7A in Badoual et al., 2006). Quadruplets (4) are not tested for the model, but its performance is probably similar to STDP, based on the triplet results. The performance with respect to the experiments (5), (6), and (7) involving rate changes is unknown, since the model on the one hand performs very similar to STDP for some experiments, but also incorporates rate effects which enable it to reproduce experiment (2). With regard to voltage control (8), there exist possibly voltage-dependent state variables (e.g., Ca^{2+} concentration), but it is not clear if those state variables can be influenced by a voltage signal in a way that would produce behavior compatible with experiment (8).

In a second modeling approach, the authors carry out a simplification of their biophysical model, essentially reducing it to conventional STDP, then add pre- and postsynaptic efficacy traces (for current and preceding spike). Basically, this results in a copy of the original suppression model of Froemke and Dan (2002), with added soft weight bounds, but as stated in Badoual et al. (2006), these bounds do not affect its basic behavior. STDP behavior (1) is replicated (Figure 4B in Badoual et al., 2006), while frequency-dependent STDP (2), cannot be replicated (Figure 7B in Badoual et al., 2006). Triplets (3) are naturally fully compatible with the model (Figure 11D in Badoual et al., 2006, also Figure 2A in Froemke and Dan, 2002). Quadruplets and presynaptic bursts (5) are fully replicated (Figure 3C in Froemke and Dan (2002) respectively Figures 4B,D in Froemke et al., 2006). The performance with respect to the rate experiments (6) and (7) is very likely similar to the model of Froemke et al. (2006) without weight bounds, which would still leave the model incapable of replicating the experiment (Figures 2 and 3 in Mayr et al., 2010b). A voltage threshold/dependence (8) is not included in the model. A slightly different version of this model is introduced in Zou and Destexhe (2007), with the soft weight bounds and the pre- and postsynaptic efficacy traces directly coupled with the kinetic model. Since this only introduces the same spike efficacies as the original suppression model (Froemke and Dan, 2002) onto a basically STDP curve shape, the results with regard to experiments (1) through (8) should be the same as those discussed for the simplified model of Badoual et al. (2006).

Lu et al. (2007)

This paper presents a finite state model with a resting, a pre and a post state governed by the local actions at the synapse. Transitions between states are caused by a change from a pre- to a postsynaptic pulse (and vice versa), as well as between two consecutive pre- or postsynaptic pulses. This is somewhat similar to the transitions between states in a kinetic model. Each transition starts a decaying and an increasing exponential trace with different time constants, with the amplitude of the exponential trace read-out at the time difference between the pulses defining the transition (pre-pre, pre-post, post-pre, post-post). Both traces are multiplied to form a weight change rate. The weight change rates for all transitions are then non-linearly weighted in a weight-saturation (soft bound) scheme and added to arrive at the overall weight change. A drawback of this model is that it employs the same time constants and scaling factors for pre- and postsynaptic adaptation as for the pre-post and post-pre weight derivation function. Consequently, while the model is able to replicate a range of experimental results, a new parameter set (with values differing by a factor of 10) is required for each new experiment, even though all experimental data is derived from very similar synapses (same preparation, brain region, animal, etc.), and should therefore be reproducible with a single parameter set. Experiments (1), (3), and (4) are replicated (Figure 2 in Lu et al., 2007; Table 1 in Lu et al., 2007; Figure 3 in Lu et al., 2007, respectively). The error fit for quadruplets (4) results in a different, but still faithful approximation curve compared to the usual assumption in Hartley et al. (2006) and Pfister and Gerstner (2006). With regard to any of the experiments involving rate changes, an analytical expression similar to (Appleby and Elliot, 2005) for a pre- and postsynaptic Poisson sweep is developed, which shows typical BCM behavior. However, the derivation of Appleby and Elliot (2005) relies on rate-dependent changes in the distribution of the pre-post time difference, which would make this derivation (and possibly the entire rule) incompatible with correlated rate (7). The model may be able to reproduce standard rate (6) at least for some postsynaptic reconstructions, since this experiment is more in line with the Poisson sweep of the mathematical derivation in Appleby and Elliot (2005) and Lu et al. (2007). Since it is not proven whether the model is compatible with experiments involving a fixed pre-post

distribution in combination with a frequency sweep, the reproduction of frequency-dependent STDP (2) is also unclear. Bursts (5) are probably compatible since they involve a presynaptic adaptation also required for the conventional triplet experiment (compare burst reproduction with original triplet model in Figures 4B,D in Froemke et al., 2006). Regarding experiment (8), there is no mechanism for voltage control; the model is purely spike timing governed.

Pfister et al. (2006)

A learning rule is derived which lets a postsynaptic neuron fire at precise moments in time relative to some presynaptic input. The presynaptic input is modeled similar to the PSC of Eq. 3, but with a second exponential producing an additional rise time. The neuron is also similar to Section "Neuron Dynamics: Spike Response Model," i.e., a simple spike response model as in Eq. 5, but without the action potential and with escape noise added to the firing threshold. Based on this neuron and a supervised learning paradigm, the neuron has to learn to spike relative to presynaptic single spikes, a spike ensemble and a spike pattern (repeated spikes by the same neuron relative, combined over a population). Constraints are used in the form of a penalty for spiking at undesired times, or a mean target firing rate, or in restricting the learning rule to temporal locality. Extracting the equivalent STDP window from the learning rule, the LTP for pre-post pairings is always governed by the time constant of the presynaptic pulse, reflecting the charging of the membrane capacitance by the EPSP. LTD for post-pre pairings results from the learning rule only if constraints are used. In most cases, the LTD side reflects the refractoriness characteristics of the spike response model (time constant and amplitude). Thus, STDP behavior (1) is shown (Figure 3B in Pfister et al., 2006). Since no adaptation or general second order effects are integrated in the model and its plasticity curve reflects STDP, the performance with respect to the other experiments is expected to be very similar to conventional STDP (Song et al., 2000). The reproduction of the rate experiments (6, 7) is probably similar to (Baras and Meir, 2007), i.e., such supervised optimized learning rules can replicate BCM in a fashion similar to (Izhikevich and Desai, 2003), with its attendant shortcomings as discussed for STDP. Computational learning rules based on neuron characteristics such as refractoriness can be made more broadly compatible with BCM terminology by incorporating additional rate-dependent state variables (Toyoizumi et al., 2005). However, the model of Pfister et al. (2006) lacks these higher-order dependencies. Computational models can also be extended toward biophysically realistic formulations. For example, Saudargiene et al. (2004) introduce a biology-driven plasticity function that develops the computational capability of detecting correlations between input and output signals in an unsupervised scenario. Similar to (Pfister et al., 2006), the LTP part of the STDP window is based on the shape of the EPSP. However, the LTD for the post-pre case is dependent on bAP, not on refractoriness characteristics. Different forms of STDP are accounted for by modifying those curve shapes or the interaction between the pre- and postsynaptic side. Interestingly, the model of Saudargiene et al. (2004), in contrast to (Pfister et al., 2006), includes a voltage dependence. However, this results only in a correlated scaling of both LTP and LTD, so that the resulting overall plasticity is unchanged. Thus, neither the model of Pfister et al. (2006) nor (Saudargiene et al., 2004) can replicate the voltage control (8) experiment.

Shah et al. (2006)

This model employs a biophysical formulation of the bAP as well as an exponential decay modeling of the EPSP to compute the postsynaptic membrane potential, which in turn governs a biophysical formulation of the resultant Calcium dynamics. The Calcium time course is then entered into two separate functions, η and Ω, driven by its temporal dynamics and its amplitude. Both functions are multiplicatively combined to form the overall weight change. This basic model, introduced in Shouval et al. (2002), is extended in Shah et al. (2006) to include attenuation of EPSPs similar to (Tsodyks and Markram, 1997). Also, to achieve a better fit to the triplet experiments, this attenuation is extended to the bAPs with a motivation parallel to the model of Froemke and Dan (2002). Most of the parameters of the biophysical model are not based on numerical fits to the plasticity experiments and thus do not represent degrees of freedom of the model, consequently not being listed in **Table 3**. Degrees of freedom with regard to resultant plasticity are represented by all parameters of η and Ω, the Calcium equation, and both attenuations. The presynaptic attenuation is initially supplied with biophysically motivated parameters, but then modified using an unrealistic pre- time constant and magnitude to achieve a better experimental fit. With regard to STDP (1), Calcium based rules usually are able to reproduce the LTD side of STDP (1), but also partially produce LTD for positive spike time differences (Figure 3C in Shouval et al., 2002). There exist attempts at deriving a more realistic STDP curve by changing the relation between Calcium dynamics and change in weight (Kurashige and Sakai, 2006), which are, however, much removed from a quantitatively realistic Ca^{2+}-weight dependence (Aihara et al., 2007). Even those heavily modified Ca^{2+} dependencies result in STDP curves with unrealistic LTD/LTP ratio and time constants/curves not supported by experimental data (Bi and Poo, 1998; Froemke and Dan, 2002). Although shown only indirectly (Figure 4B in Shouval et al., 2002), the model should be able to replicate frequency-dependent STDP (2). Triplets (3) are reproduced (Figure 4 in Shah et al., 2006). No data exists with regard to quadruplets (4). Since the model incorporates both pre- and postsynaptic attenuation and exhibits triplet behavior, burst (5) plasticity should be compatible. Standard rate (6) is reproduced by the model (Figure 3B in Shouval et al., 2002). Since both this and experiment (2) are compatible with the model, correlated rate (7) should also pose no problem. The model contains an explicit modeling of the membrane voltage and uses this voltage, e.g., when computing the NMDA receptor current. Based on this and the voltage sweep of Figure 5 in Shouval et al. (2002), a compatibility with voltage control (8) is assigned in **Table 3**. However, since both (Shah et al., 2006) and (Shouval et al., 2002) are missing the equations for BPAP summation and overall membrane voltage computation, the compatibility with voltage control (8) cannot be completely ascertained. A notable exception to the unrealistic STDP curves produced by Ca^{2+} based models is the model of Hartley et al. (2006), where a Ca^{2+} based model uses two separate mechanisms for LTP and LTD, essentially combining a kinetic and a Calcium model, which exhibits a realistic STDP (1) curve, reproduces triplets (3), and somewhat reproduces quadruplets (4). Its main drawback is its large parameter space (ca. 20), similar to other biophysically realistic models, which either makes it unreliable in fitting specific plasticity data or would require a large database of differently styled experiments to be accurately determined.

Clopath et al. (2010)

The model introduced in Clopath et al. (2008a) and Clopath et al. (2010) combines the spike-based methodology of STDP with voltage-based mechanisms. For LTD, a trace of the postsynaptic membrane potential is used as indicator of postsynaptic activity (pulses). This trace is sampled at presynaptic pulses, similar to an iterative implementation of STDP (Morrison et al., 2008). However, if the trace has a value lower than a threshold Θ_-, no LTD is induced. For LTP, a trace of presynaptic pulses is integrated during postsynaptic spiking. Thereby, the spike is detected by a second threshold Θ_+. With this mechanism, the sampling of presynaptic activity as in STDP is combined with a LTP voltage threshold compatible with experimental results (Ngezahayo et al., 2000). These two thresholds are similar to those in the model of Senn (2002). Additionally, the presynaptic trace is weighted with a second trace of the membrane potential, introducing a postsynaptic adaptation mechanism. With its direct and temporally filtered influence of the postsynaptic activity on plasticity, the model also has some similarities to the model of Toyoizumi et al. (2005). The model relies on the adaptive exponential integrate-and-fire (AdEx) neuron, extended by a depolarizing spike after-potential, for generating the membrane voltage curves necessary for calculating the weight change. In Clopath et al. (2010), this after-potential has a longer time constant than that of the voltage traces. Thus, it dominates their behavior and is essential for, e.g., the LTD part of STDP (1) and the frequency dependence of STDP (2). We therefore included its scaling and time constant in the list of learning parameters. In contrast, the parameters of the AdEx neuron are not based on plasticity experiments, so we did not include them.

STDP results (1) are reproduced (Figure 2A in Clopath et al., 2010). For purely spike-based protocols, the model of Clopath et al. (2010) essentially maps to the reduced triplet rule of Pfister and Gerstner (2006). Thus, results of triplet (3) and quadruplet experiments (4) are expected to be reproducible with the model, as also stated in the discussion in Clopath et al. (2010). A postsynaptic burst protocol is shown (Figure 3 in Clopath et al., 2010), but as with the reduced triplet rule, doubts can be raised with respect to the performance in a presynaptic burst experiment (5). As the performance cannot be estimated with any confidence, the model of Clopath et al. (2010) receives "?" for experiment (5). A similar induction protocol to the standard rate protocol (6) is shown in Figure 1F of Clopath et al. (2008b). Thus the model can likely reproduce the protocol, although significant differences between both induction protocols in the pulse patterns and number of stimulated synapses do not validate a classification "f." In extension of the original model of Pfister and Gerstner (2006), the model may even be compatible with a non-spiking postsynaptic side for experiment (6) if the influence of the presynaptic pulses on the neuron is assumed to increase the postsynaptic membrane potential. As the model is able to reproduce both experiment (2) and a version of standard rate (6), correlated rate should also be compatible (7). With its two voltage thresholds, the model can well reproduce voltage control experiments (8) (Figure 1H in Clopath et al., 2010).

Sjöström et al. (2001)

This model derives LTP behavior as a sigmoidal dependence on the measurement of the residual depolarization just before a postsynaptic spike. In addition, the amount of LTP is linearly dependent on the interval between the last two postsynaptic spikes (similar to Froemke and Dan, 2002). LTP is produced only if the presynaptic spike occurs within a certain time window prior to the postsynaptic one. LTD is obtained as the mean amount of LTD produced by a set of experiments, which is awarded to a spike pairing occurring within a certain time window. The discussion in the following centers on Model 3, which has a postsynaptic-centered nearest-neighbor interaction similar to (Izhikevich and Desai, 2003), with the modifications that a postsynaptic spike that participated in an LTP interaction cannot also partake in an LTD pairing.

Interestingly, this model is also one of the few possessing a direct membrane voltage dependence, emulating experiments which feature forms of voltage control (Figures 5 and 6 in Sjöström et al., 2001). Thus, it might be usable to reproduce experiment (8) if coupled with some kind of neuron/depolarization model. However, since it lacks those features at the moment, instead deriving one measured parameter (plasticity) based on another measured parameter (depolarization), it cannot be employed in stand-alone simulations of plasticity. Since the behavior of the depolarization during the experimental protocols not carried out in Sjöström et al. (2001) is unclear, the following assessment of the rule is very speculative. The rule is probably able to reproduce STDP (1) in a fashion similar to the experimental results of Figure 2D in Sjöström et al., 2001. As the membrane voltage rises before an AP, the LTP-depolarization dependence should result in a pseudo-exponential time-plasticity relation for the LTP half. The LTD side of the STDP window is assumed as a single weight scaling if the post-pre interaction happens within the LTD time window. The reproduction of triplets (3) should be about as well as conventional STDP. However, the contribution of the interaction rule contained in Model 3 is not clear, since this modification causes an exception for pre-post-pre interactions, whereas the crucial case (where triplets differ from what would be expected based on an STDP rule) is in the post-pre-post interaction case. Frequency-dependent STDP (2) (Figure 8A in Sjöström et al., 2001) and correlated rate (7) (Figure 8D in Sjöström et al., 2001) have been shown to be compatible with the model. Since other BCM characteristics are reproduced well, the model should be able to reproduce standard rate (6) (Due to the depolarization dependence, this experiment may even be reproduced for the postsynaptic non-spiking sub-threshold assumption). Quadruplet (4) plasticity should be compatible, since the plasticity this model aims to describe is similar to the one reported in Wang et al. (2005). With regard to bursts (5), the LTP behavior of the pre-before-post case should be replicated, but post-before-pre will probably also result in LTP due to its high overall frequency, whereas the original data of Froemke et al. (2006) indicates LTD behavior. Some of that difference is probably due to the differing cortical areas of the preparations (see **Table 1**), i.e., this could be remedied by a different parameter set.

Fusi et al. (2000)

This model is motivated by computational considerations. It tries to balance weight change due to learning with the conflicting requirement of protecting learned weights. The synapse itself can only assume two distinct states, potentiated or depressed, but the transition probability can be finely tuned, which lets strong/persistent stimuli (e.g., repeated spike correlations) effect a rapid change of the synapse state, whereas random fluctuations are suppressed. A trace is started at each presynaptic spike, with the sign of the trace dependent on the thresholded postsynaptic membrane potential

during the spike. For, e.g., a potentiated synapse and a membrane potential below the threshold (which should cause an increased probability for LTD), the trace draws the synapse state away from potentiation, constituting a learning process. At the same time, a weight-preserving leakage draws the synapse back to its original value. Only if several of the learning traces occur in close temporal proximity will the synapse cross over the weight-preserving threshold into the opposite state. In the form of "stop learning," a metaplastic homeostasis mechanism is also contained in the model. A postsynaptic long-term pulse average is computed, and a synapse is only potentiated if this average is sufficiently low, while it is depressed only if this activity average is high. In Brader et al. (2007), an investigation regarding experimental compatibility is carried out for the model, where the weight is expressed in terms of the probability of a transition from potentiated to depressed synapse (LTD probability) and vice versa (LTP probability). STDP (1) is shown (Figure 8D in Brader et al., 2007), but seems to require a higher pairing frequency (12 Hz) than in experimental protocols. Frequency-dependent STDP (2) is also shown (Figures 8A,B in Brader et al., 2007). However, due to the stop learning, LTP diminishes to zero for high frequencies. Triplets (3) and quadruplets (4) require postsynaptic adaptation, which is not part of the model. The triplet behavior in the first three quadrants should be equivalent to STDP models, while for the post-pre-post quadrant, the rule of Fusi et al. (2000) only "sees" the first post-pre pairing, so that there is only the LTD half of a conventional STDP curve extending along the t_1 axis (cf. **Figure 7**), while t_2 has no influence. Bursts (6) require presynaptic adaption, which is also not contained in the model. For the post-pre-burst case, every pre pulse would sample the low post potential after the spike, resulting in an LTD curve similar to conventional STDP. For the pre-burst-post case, the pre pulses would sample an increasing membrane potential, resulting in progressively higher LTP, also similar to STDP (see **Figure 14A**). Standard rate (6) (Figure 5 in Fusi et al., 2000) and correlated rate (7) should be compatible, since this rule seems rate- rather than spike-dependent in a BCM context (compare Figures 5 in Brader et al., 2007). With regard to voltage control (8), the general behavior of the rule is compatible, a voltage threshold is applied separating LTD and LTP, but the second threshold is missing.

ACKNOWLEDGMENTS

We would thank R. Schueffny for his contributions to the initial version of the LCP rule and many constructive comments. We are also grateful to W. Gerstner for fruitful discussions on plasticity. P. Sjöström has been very helpful in explaining his experimental protocols and the details of his plasticity model. We would also thank P. Sjöström and A. Artola for providing us with their experimental data. A. Heittmann and U. Ramacher have provided the initial inspiration for the PCNN research of our group. Many thanks also go to the two reviewers for their helpful comments on this manuscript. This work is supported by funding under the Sixth Framework Programme of the European Union under the grant no. 15879 (FACETS). In addition, J. Partzsch is supported by a graduate scholarship of the Konrad-Adenauer-Stiftung.

REFERENCES

Abarbanel, H., Huerta, R., and Rabinovich, M. (2002). Dynamical model of long-term synaptic plasticity. *Proc. Natl. Acad. Sci. U.S.A.* 99, 10132–10137.

Abbott, L., and Nelson, S. (2000). Synaptic plasticity: taming the beast. *Nat. Neurosci.* 3, 1178–1183.

Abraham, W. (2008). Metaplasticity: tuning synapses and networks for plasticity. *Nat. Rev. Neurosci.* 9, 387–399.

Abraham, W., Mason-Parker, S., Bear, M., Webb, S., and Tate, W. (2001). Heterosynaptic metaplasticity in the hippocampus in vivo: a BCM-like modifiable threshold for LTP. *Proc. Natl. Acad. Sci. U.S.A.* 98, 10924–10929.

Aihara, T., Abiru, Y., Yamazaki, Y., Watanabe, H., Fukushima, Y., and Tsukada, M. (2007). The relation between spike-timing dependent plasticity and Ca_ dynamics in the hippocampal CA1 network. *Neuroscience* 145, 80–87.

Appleby, P. A., and Elliot, T. (2005). Synaptic and temporal ensemble interpretation of spike-timing-dependent plasticity. *Neural Comput.* 17, 2316–2336.

Artola, A., Bröcher, S., and Singer, W. (1990). Different voltage-dependent thresholds for inducing long-term depression and long-term potentiation in slices of rat visual cortex. *Nature* 347, 69–72.

Badoual, M., Zou, Q., Davison, A., Rudolph, M., Bal, T., Fregnac, Y., and Destexhe, A. (2006). Biophysical and phenomenological models of multiple spike interactions in spike-timing dependent plasticity. *Int. J. Neural Syst.* 16, 79–97.

Baras, D., and Meir, R. (2007). Reinforcement learning, spike-time-dependent plasticity, and the BCM rule. *Neural Comput.* 19, 2245–2279.

Beggs, J. (2001). A statistical theory of long-term potentiation and depression. *Neural Comput.* 13, 87–111.

Benuskova, L., and Abraham, W. (2007). STDP rule endowed with the BCM sliding threshold accounts for hippocampal heterosynaptic plasticity. *J. Comput. Neurosci.* 22, 129–133.

Bi, G. Q., and Poo, M. M. (1998). Synaptic modifications in cultured hippocampal neurons: dependence on spike timing, synaptic strength, and postsynaptic cell type. *J. Neurosci.* 18, 10464–10472.

Bienenstock, E., Cooper, L., and Munro, P. (1982). Theory for the development of neuron selectivity: orientation specificity and binocular interaction in visual cortex. *J. Neurosci.* 2, 32–48.

Brader, J., Senn, W., and Fusi, S. (2007). Learning real-world stimuli in a neural network with spike-driven synaptic dynamics. *Neural Comput.* 19, 2881–2912.

Clopath, C., Buesing, L., Vasilaki, E., and Gerstner, W. (2008a). "A unified voltage-based model for STDP, LTP and LTD," in *Computational and Systems Neuroscience COSYNE08*, poster presentation.

Clopath, C., Ziegler, L., Vasilaki, E., Büsing, L., and Gerstner, W. (2008b). Tag-trigger-consolidation: a model of early and late long-term-potentiation and depression. *PLoS Comput. Biol.* 4, e1000248. doi:10.1371/journal.pcbi.1000248.

Clopath, C., Büsing, L., Vasilaki, E., and Gerstner, W. (2010). Connectivity reflects coding: a model of voltage-based STDP with homeostasis. *Nat. Neurosci.* 13, 344–352.

Disterhoft, J., and Oh, M. (2006). Learning, aging and intrinsic neuronal plasticity. *Trends Neurosci.* 29, 587–598.

Du, J., and Bradley, R. (1996). Electrophysiological and morphological properties of neurons acutely isolated from the rostral gustatory zone of the rat nucleus of the solitary tract. *Chem. Senses* 21, 729–737.

Dudek, S., and Bear, M. (1992). Homosynaptic long-term depression in area CAl of hippocampus and effects of N-methyl-D-aspartate receptor blockade. *Proc. Natl. Acad. Sci. U.S.A.* 89, 4363–4367.

Elliott, T. (2008). Temporal dynamics of rate-based synaptic plasticity rules in a stochastic model of spike-timing-dependent plasticity. *Neural Comput.* 20, 2253–2307.

Farajidavar, A., Saeb, S., and Behbehani, K. (2008). Incorporating synaptic-time-dependent plasticity and dynamic synapse into a computational model of wind-up. *Neural Netw.* 21, 241–249.

Froemke, R., and Dan, Y. (2002). Spike-timing-dependent synaptic modification induced by natural spike trains. *Nature* 416, 433–438.

Froemke, R., Tsay, I., Raad, M., Long, J., and Dan, Y. (2006). Contribution of individual spikes in burst-induced long-term synaptic modification. *J. Neurophysiol.* 95, 1620–1629.

Fusi, S., Annunziato, M., Badoni, D., Salamon, A., and Amit, D. (2000). Spike-driven synaptic plasticity: theory, simulation, VLSI implementation. *Neural Comput.* 12, 2227–2258.

Gerstner, W., and Kistler, W. (2002). *Spiking Neuron Models: Single Neurons, Populations, Plasticity*. Cambridge: Cambridge University Press.

Hartley, M., Taylor, N., and Taylor, J. (2006). Understanding spike-time-dependent

plasticity: a biologically motivated computational model. *Neurocomputing* 69, 2005–2016.

Holthoff, K., Kovalchuk, Y., and Konnerth, A. (2006). Dendritic spikes and activity-dependent synaptic plasticity. *Cell Tissue Res.* 326, 369–377.

Indiveri, G., Chicca, E., and Douglas, R. (2006). A VLSI array of low-power spiking neurons and bistable synapses with spike-timing dependent plasticity. *IEEE Trans. Neural Netw.* 17, 211–221.

Izhikevich, E., and Desai, N. (2003). Relating STDP to BCM. *Neural Comput.* 15, 1511–1523.

Kampa, B., Letzkus, J., and Stuart, G. (2007). Dendritic mechanisms controlling spike-timing-dependent synaptic plasticity. *Trends Neurosci.* 30, 456–463.

Kepecs, A., van Rossum, M., Song, S., and Tegner, J. (2002). spike-timing-dependent plasticity: common themes and divergent vistas. *Biol. Cybern.* 87, 446–458.

Koch, C. (1999). *Biophysics of Computation. Information Processing in Single Neurons* (Computational Neuroscience). New York: Oxford University Press.

Kurashige, H., and Sakai, Y. (2006). "BCM-type synaptic plasticity model using a linear summation of calcium elevations as a sliding threshold," in *Proceedings of the 15th International Conference on Advances in Neural Information Processing – 2006, Lecture Notes in Computer Science*, Vol. 4232, Hong Kong, 19–29.

Lante, F., Cavalier, M., Cohen-Solal, C., Guiramand, J., and Vignes, M. (2006). Developmental switch from LTD to LTP in low frequency-induced plasticity. *Hippocampus* 16, 981–989.

Lebel, D., Grossman, Y., and Barkai, E. (2001). Olfactory learning modifies predisposition for long-term potentation and long-term depression induction in the rat piriform (olfactory) cortex. *Cereb. Cortex* 11, 485–489.

Lisman, J., and Spruston, N. (2005). Postsynaptic depolarization requirements for LTP and LTD: a critique of spike timing dependent plasticity. *Nat. Neurosci.* 8, 839–841.

Lu, B., Yamada, W., and Berger, T. (2007). "Asymmetric synaptic plasticity based on arbitrary pre- and postsynaptic timing spikes using finite state model," in *Proceedings of International Joint Conference on Neural Networks IJCNN07*, Orlando, FL, 841–846.

Markram, H., Lübke, J., Frotscher, M., and Sakmann, B. (1997). Regulation of synaptic efficacy by coincidence of postsynaptic APs and EPSPs. *Science* 275, 213–215.

Markram, H., Wang, Y., and Tsodyks, M. (1998). differential signaling via the same axon of neocortical pyramidal neurons. *Proc. Natl. Acad. Sci. U.S.A.* 95, 5323–5328.

Mayford, M., Wang, J., Kandel, E., and O'Dell, T. (1995). CaMKII regulates the frequency-response function of hippocampal synapses for the production of both L TD and L TP. *Cell* 81, 891–904.

Mayr, C., Noack, M., Partzsch, J., and Schüffny, R. (2010a). "Replicating experimental spike and rate based neural learning in CMOS," in *IEEE International Symposium on Circuits and Systems (ISCAS)*, Paris, 105–108.

Mayr, C., Partzsch, J., and Schüffny, R. (2010b). "A critique of BCM behavior verification for STDP-type plasticity models," in *European Symposium on Artificial Neural Networks, Computational Intelligence and Machine Learning, ESANN*, Bruges, 369–374.

Mayr, C., Partzsch, J., and Schüffny, R. (2009). On the relation between bursts and dynamic synapse properties: a modulation-based ansatz. *Comput. Intell. Neurosci.* 2009, article ID 658474, 13 pages.

Morrison, A., Diesmann, M., and Gerstner, W. (2008). Phenomenological models of synaptic plasticity based on spike timing. *Biol. Cybern.* 98, 459–478.

Ngezahayo, A., Schachner, M., and Artola, A. (2000). Synaptic activity modulates the induction of bidirectional synaptic changes in adult mouse hippocampus. *J. Neurosci.* 20, 2451–2458.

Partzsch, J., Mayr, C., and Schüffny, R. (2008). "BCM and membrane potential: alternative ways to timing dependent plasticity," in *Proceedings of 15th International Conference on Neural Information Processing - 2008*, *Lecture Notes in Computer Science*, Vol. 5506, 137–144.

Pfister, J. P., and Gerstner, W. (2006). Triplets of spikes in a model of spike timing-dependent plasticity. *J. Neurosci.* 26, 9673–9682.

Pfister, J. P., Toyoizumi, T., Barber, D., and Gerstner, W. (2006). Optimal spike-timing dependent plasticity for precise action potential firing in supervised learning. *Neural Comput.* 18, 1309–1339.

Saudargiene, A., Porr, B., and Wörgötter, F. (2004). How the shape of pre- and postsynaptic signals can influence STDP: a biophysical model. *Neural Comput.* 16, 595–625.

Schemmel, J., Brüderle, D., Meier, K., and Ostendorf, B. (2007). "Modeling synaptic plasticity within networks of highly accelerated I&F neurons," in *Proceedings of the 2007 IEEE International Symposium on Circuits and Systems*, New Orleans, 3367–3370.

Schreiter, J., Ramacher, U., Heittmann, A., Matolin, D., and Schüffny, R. (2002). "Analog implementation for networks of integrate-and-fire neurons with adaptive local connectivity," in *Proceedings of the 2002 12th IEEE Workshop on Neural Networks for Signal Processing*, Martigny, 657–666.

Senn, W. (2002). Beyond spike timing: the role of nonlinear plasticity and unreliable synapses. *Biol. Cybern.* 87, 344–355.

Senn, W., Markram, H., and Tsodyks, M. (2001). An algorithm for modifying neurotransmitter release probability based on pre- and postsynaptic spike timing. *Neural Comput.* 13, 35–67.

Shah, N., Yeung, L., Cooper, L., Cai, Y., and Shouval, H. (2006). A biophysical basis for the inter-spike interaction of spike-timing-dependent plasticity. *Biol. Cybern.* 95, 113–121.

Shouval, H., Bear, M., and Cooper, L. (2002). a unified model of NMDA receptor-dependent bidirectional synaptic plasticity. *Proc. Natl. Acad. Sci. U.S.A.* 99, 10831–10836.

Sjöström, P., Rancz, E., Roth, A., and Häusser, M. (2008). Dendritic excitability and synaptic plasticity. *Physiol. Rev.* 88, 769–840.

Sjöström, P., Turrigiano, G., and Nelson, S. (2001). Rate, timing, and cooperativity jointly determine cortical synaptic plasticity. *Neuron* 32, 1149–1164.

Song, S., Miller, K., and Abbott, L. (2000). Competitive hebbian learning through spike-timing-dependent synaptic plasticity. *Nat. Neurosci.* 3(9):919–926.

Standage, D., Jalil, S., and Trappenberg, T. (2007). Computational consequences of experimentally derived spike-time and weight dependent plasticity rules. *Biol. Cybern.* 96, 615–623.

Standage, D., and Trappenberg, T. (2007). "The trouble with weight-dependent STDP," in *Proceedings of International Joint Conference on Neural Networks IJCNN07*, Orlando, FL, 1348–1353.

Tanaka, E., Higashi, H., and Nishi, S. (1991). Membrane properties of guinea pig cingulate cortical neurons in vitro. *J. Neurophysiol.* 65, 808–821.

Taubenfeld, S., Stevens, K., Pollonini, G., Ruggiero, J., and Alberini, C. (2002). Profound molecular changes following hippocampal slice preparation: loss of AMPA receptor subunits and uncoupled mRNA/protein expression. *J. Neurochem.* 81, 1348–1360.

Toyoizumi, T., Pfister, J. P., Aihara, K., and Gerstner, W. (2005). Generalized bienenstock-cooper-munroe rule for spiking neurons that maximizes information transmission. *Proc. Natl. Acad. Sci. U.S.A.* 102, 5239–5244.

Tsodyks, M., and Markram, H. (1997). The neural code between neocortical pyramidal neurons depends on neurotransmitter release probability. *Proc. Natl. Acad. Sci. U.S.A.* 94, 719–723.

Tzounopoulos, T., Rubio, M., Keen, J., and Trussell, L. (2007). Coactivation of pre- and postsynaptic signaling mechanisms determines cell-specific spike-timing-dependent plasticity. *Neuron* 54, 291–301.

Wang, H., and Wagner, J. J. (1999). Priming-induced shift in synaptic plasticity in the rat hippocampus. *J. Neurophysiol.* 82, 2024–2028.

Wang, H. X., Gerkin, R., Nauen, D., and Bi, G. Q. (2005). Coactivation and timing-dependent integration of synaptic potentiation and depression. *Nat. Neurosci.* 8, 187–193.

Wei, J. (1975). Least square fitting of an elephant. *Chemtech* 5, 128–129.

Zelcer, I., Cohen, H., Richter-Levin, G., Lebiosn, T., Grossberger, T., and Barkai, E. (2006). A cellular correlate of learning-induced metaplasticity in the hippocampus. *Cereb. Cortex* 16, 460–468.

Zou, Q., and Destexhe, A. (2007). Kinetic models of spike-timing dependent plasticity and their functional consequences in detecting correlations. *Biol. Cybern.* 97, 81–97.

Conflict of Interest Statement: The authors declare that the research was conducted in the absence of any commercial or financial relationships that could be construed as a potential conflict of interest.

Received: 31 January 2010; paper pending published: 17 February 2010; accepted: 08 July 2010; published online: 03 September 2010. Citation: Mayr CG and Partzsch J (2010) Rate and pulse based plasticity governed by local synaptic state variables. Front. Syn. Neurosci. 2:33. doi: 10.3389/fnsyn.2010.00033

frontiers in
SYNAPTIC NEUROSCIENCE

ORIGINAL RESEARCH ARTICLE
published: 23 August 2010
doi: 10.3389/fnsyn.2010.00032

Storage of phase-coded patterns via STDP in fully-connected and sparse network: a study of the network capacity

Silvia Scarpetta[1,2]*, Antonio de Candia[2,3,4] and Ferdinando Giacco[1,2]

[1] *Dipartimento di Fisica "E.R.Caianiello," Università di Salerno, Fisciano, Italy*
[2] *INFN, Sezione di Napoli e Gruppo Coll. di Salerno, Naples, Italy*
[3] *Dipartimento di Scienze Fisiche, Università di Napoli Federico II, Naples, Italy*
[4] *CNR-SPIN, Unità di Napoli, Naples, Italy*

Edited by:
Wulfram Gerstner, Ecole Polytechnique Fédérale de Lausanne, Switzerland

Reviewed by:
Mate Lengyel, University of Cambridge, UK
Marc Timme, Max-Planck-Institute for Dynamics and Self-Organization, Germany

***Correspondence:**
Silvia Scarpetta, Dipartimento di Fisica "E.R. Caianiello," Università di Salerno, via Ponte Don Melillo, Fisciano, Italy.
e-mail: silvia@sa.infn.it

We study the storage and retrieval of phase-coded patterns as stable dynamical attractors in recurrent neural networks, for both an analog and a integrate and fire spiking model. The synaptic strength is determined by a learning rule based on spike-time-dependent plasticity, with an asymmetric time window depending on the relative timing between pre and postsynaptic activity. We store multiple patterns and study the network capacity. For the analog model, we find that the network capacity scales linearly with the network size, and that both capacity and the oscillation frequency of the retrieval state depend on the asymmetry of the learning time window. In addition to fully connected networks, we study sparse networks, where each neuron is connected only to a small number $z \ll N$ of other neurons. Connections can be short range, between neighboring neurons placed on a regular lattice, or long range, between randomly chosen pairs of neurons. We find that a small fraction of long range connections is able to amplify the capacity of the network. This imply that a small-world-network topology is optimal, as a compromise between the cost of long range connections and the capacity increase. Also in the spiking integrate and fire model the crucial result of storing and retrieval of multiple phase-coded patterns is observed. The capacity of the fully-connected spiking network is investigated, together with the relation between oscillation frequency of retrieval state and window asymmetry.

Keywords: phase-coding, associative memory, storage capacity, replay, STDP

Recent advances in brain research have generated renewed awareness and appreciation that the brain operates as a complex non-linear dynamic system, and synchronous and phase-locked oscillations may play a crucial role in information processing, such as feature grouping, saliency enhancing (Singer, 1999; Fries, 2005; Fries et al., 2007) and phase-dependent coding of objects in short-term memory (Siegel et al., 2009). Many results led to the conjecture that synchronized and phase-locked oscillatory neural activity play a fundamental role in perception, memory, and sensory computation (Buzsaki and Draguhn, 2004; Gelperin, 2006; Düzel et al., 2010).

There is increasing evidence that information encoding may depend on the temporal dynamics between neurons, namely, the specific phase alignment of spikes relative to rhythmic activity across the neuronal population (as reflected in the local field potential, or LFP) (O'Keefe and Recce, 1993; König et al., 1995; Laurent, 2002; Mehta et al., 2002; Kayser et al., 2009; Siegel et al., 2009). Indeed phase-dependent coding, that exploits the precise temporal relations between the discharges of neurons, may be an effective strategy to encode information (Singer, 1999; Scarpetta et al., 2002a; Scarpetta et al., 2002b; Yoshioka et al., 2007; Latham and Lengyel, 2008; Kayser et al., 2009; Siegel et al., 2009). Data from rodents indicate that spatial information may be encoded at specific phases of ongoing population theta oscillations in the hippocampus (O'Keefe and Recce, 1993), and that spike sequences can be replayed at a different time scale (Diba and Buzsaki, 2007), while data from monkeys (Siegel et al., 2009) show that phase coding may be a more general coding scheme.

The existence of a periodic spatio-temporal pattern of precisely timed spikes, as attractor of neural dynamics, has been investigated in different recurrent neural models (Gerstner et al., 1993; Borisyuk and Hoppensteadt, 1999; Jin, 2002; Lengyel et al., 2005b; Memmesheimer and Timme, 2006a,b). In Jin (2002) it was shown that periodic spike sequences are attractors of the dynamics, and the stronger the global inhibition of the network, the faster the rate of convergence to a periodic pattern. In Memmesheimer and Timme (2006a,b) the problem of finding the set of all networks that exhibit a predefinite periodic precisely timed pattern was studied.

Here we study how a spike timing dependent plasticity (STDP) learning rule can encode many different periodic patterns in a recurrent network, in such a way that a pattern can be retrieved initializing the network in a state similar to it, or inducing a short train of spikes extracted from the pattern.

In our model, information about an item is encoded in the specific phases of firing, and each item corresponds to a different pattern of phases among units. Multiple items can be memorized in the synaptic connections, and the intrinsic network dynamics recall the specific phases of firing when a partial cue is presented.

Each item with specific phases of firing corresponds to specific relative timings between neurons. Therefore it seems that phase coding may be well suited to facilitate long-term storage of items by means of STDP (Markram et al., 1997; Bi and Poo, 1998, 2001).

Indeed experimental findings on STDP further underlined the importance of precise temporal relationships of the dynamics, by showing that long-term changes in synaptic strengths depend on the precise relative timing of pre and postsynaptic spikes (Magee and Johnston, 1997; Markram et al., 1997; Bi and Poo, 1998, 2001; Debanne et al., 1998; Feldman, 2000).

The computational role and functional implications of STDP have been explored from many points of view (see for example Gerstner et al., 1996; Kempter et al., 1999; Song et al., 2000; Rao and Sejnowski, 2001; Abarbanel et al., 2002; Lengyel et al., 2005b; Drew and Abbott, 2006; Wittenberg and Wang, 2006; Masquelier et al., 2009 and papers of this special issue). STDP has also been supposed to play a role in the hippocampus theta phase precession phenomenon (Mehta et al., 2002; Scarpetta and Marinaro, 2005; Lengyel et al., 2005a; Florian and Muresan, 2006), even though other explanations has also been proposed for this phenomena (see Leibold et al., 2008; Thurley et al., 2008 and references therein). Here we analyze the role of a learning rule based on STDP in storing multiple phase-coded memories as attractor states of the neural dynamics, and the ability of the network to selectively retrieve a stored memory, when a partial cue is presented. The framework of storing and retrieval of memories as attractors of the dynamics is widely accepted, and recently received experimental support, such as in the work of Wills et al. (2005), which gives strong experimental evidence for the expression of rate-coded attractor states in the hippocampus.

Another characteristic of the neural network, crucial to its functioning, is its topology, that is the average number of neurons connected to a neuron, the average length of the shortest path connecting two neurons, etc. In the last decade, there has been a growing interest in the study of the topological structure of the brain network (Sporns and Zwi, 2004; Sporns et al., 2004; Bullmore and Sporns, 2009). This interest has been stimulated by the simultaneous development of the science of complex networks, that studies how the behavior of complex systems (such as societies, computer networks, brains, etc.) is shaped by the way their constituent elements are connected.

A network may have the property that the degree distribution, i.e. the probability that a randomly chosen node is connected to k other nodes, has a slow power law decay. Networks having this property are called "scale-free". Barabási and Albert (1999) demonstrated that this property can originate from a process in which each node is added preferentially to nodes that already have high degree. Scale-free properties have been found in functional network topology using functional magnetic resonance in human brain (Eguìluz et al., 2005), and have been investigated in some models in relation with scale-free avalanche brain activity and criticality (Pellegrini et al., 2007; de Arcangelis and Herrmann, 2010).

Another important class of complex networks is the so called "small world" networks (Watts and Strogatz, 1998). They combine two important properties. The first is an high level of clustering, that is an high probability of direct connection between two nodes, given that they are both connected to a third node. This property usually occurs in networks where the nodes are connected preferentially to the nearest nodes, in a physical (for example three-dimensional) space. The second property is the shortness of paths connecting any two nodes, characteristic of random networks. Therefore, a measure of the small-worldness of a network is given by a high ratio of the clustering coefficient to the path length.

There is increasing evidence that the connections of neurons in many areas of the nervous system have a small world structure (Hellwig, 2000; Sporns and Zwi, 2004; Sporns et al., 2004; Yu et al., 2008; Bullmore and Sporns, 2009; Pajevic and Plenz, 2009). Up to now, the only nervous system to have been comprehensively mapped at a cellular level is the one of *Caenorhabditis elegans* (White et al., 1986; Achacoso and Yamamoto, 1991), and it has been found that is has indeed a small world structure. The same property was found for the correlation network of neurons in the visual cortex of the cat (Yu et al., 2008).

In this paper we focus on the ability of STDP to memorize multiple phase-coded items, in both fully connected and sparse networks, with varying degree of small-worldness, in a way that each phase-coded item is an attractor of the network.

Partial presentation of the pattern, i.e. short externally induced spike sequences, with phases similar to the ones of the stored phase pattern, induces the network to retrieve selectively the stored item, as far as the number of stored items is not larger then the network capacity. If the network retrieves one of the stored items, the neural population spontaneously fires with the specific phase alignments of that pattern, until external input does not change the state of the network.

We find that the proposed learning rule is really able to store multiple phase-coded patterns, and we study the network capacity, i.e. how many phase-coded items can be stored and retrieved in the network as a function of the parameters of the network and the learning rule.

In Section 1 we describe the learning rule and the analog model used. In Section 2 we study the case of an analog fully connected network, that is a network in which each neuron is connected to any other neuron. In Section 3 we study instead the case of an analog sparse network, where each neuron is connected to a finite number of other neurons, with a varying degree of small-worldness. In Section 4 we study the case of a fully connected spiking integrate and fire (IF) model, and finally the summary and discussion is in Section 5.

THE MODEL

We consider a network of N neurons, with $N(N-1)$ possible (directed) connections J_{ij}. The synaptic connections J_{ij}, during the learning mode when patterns to be stored are presented, are subject to plasticity and change their efficacy according to a learning rule inspired to the STDP. In STDP (Magee and Johnston, 1997; Markram et al., 1997; Bi and Poo, 1998, 2001; Debanne et al., 1998; Feldman, 2000) synaptic strength increases or decreases whether the presynaptic spike precedes or follows the postsynaptic one by few milliseconds, with a degree of change that depends on the delay between pre and postsynaptic spikes, through a temporally asymmetric learning window. We indicate with $x_i(t)$ the activity, or firing rate, of ith neuron at time t. It means that the firing probability of unit i in the interval $(t, t+\Delta t)$ is proportional to $x_i(t)\Delta t$ in the limit $\Delta t \to 0$. According to the learning rule we use in this work, already introduced in (Scarpetta et al.,

2001, 2002a; Yoshioka et al., 2007), the change in the connection J_{ij} occurring in the time interval $[-T, 0]$ can be formulated as follows:

$$\delta J_{ij} \propto \int_{-T}^{0} \partial t \int_{-T}^{0} \partial t' x_i(t) A(t-t') x_j(t') \quad (1)$$

where $x_j(t)$ is the activity of the presynaptic neuron, and $x_i(t)$ the activity of the postsynaptic one. The learning window $A(\tau)$ is the measure of the strength of synaptic change when there is a time delay τ between pre and postsynaptic activity. To model the experimental results of STDP, the learning window $A(\tau)$ should be an asymmetric function of τ, mainly positive (LTP) for $\tau > 0$ and mainly negative (LTD) for $\tau < 0$. The shape of $A(\tau)$ strongly affects J_{ij} and the dynamics of the networks, as discussed in the following. An example of the learning window used here is shown in **Figure 1**.

Writing Eq. (1), implicitly we have assumed that the effects of separate spike pairs due to STDP sum linearly. However note that non-linear effects have been observed when both pre and postsynaptic neurons fire simultaneously at more then 40 Hz (Sjostrom et al., 2001; Froemke and Dan, 2002), therefore our model holds only in the case of lower firing rates, and in cases where linear summation is a good approximation.

We consider periodic patterns of activity that are periodic patterns, in which the information is encoded in the relative phases, that is in the relative timing of the maximum firing rate of a neuron. Therefore, we define the pattern to be stored by

$$x_i^{\mu}(t) = \frac{1}{2}\left[1 + \cos(\omega_{\mu} t - \phi_i^{\mu})\right], \quad (2)$$

where phases ϕ_i^{μ} are randomly chosen from a uniform distribution in $[0,2\pi)$, and $\omega_{\mu}/2\pi$ is the frequency of oscillation of the neurons (see **Figure 2A**). Each pattern μ is therefore defined by its frequency $\omega_{\mu}/2\pi$, and by the specific phases ϕ_i^{μ} of the neurons $i = 1,..,N$.

In the limit of large T, when the network is forced in the state given by Eq. (2), using Eq. (1), the change in the synaptic strength will be given by

$$\delta J_{ij} = \eta |\tilde{A}(\omega_{\mu})| \cos\left[\phi_i^{\mu} - \phi_j^{\mu} - \varphi(\omega_{\mu})\right] + 2\eta\tilde{A}(0) \quad (3)$$

where $\tilde{A}(\omega)$ is the Fourier transform of the kernel, defined by

$$\tilde{A}(\omega) = \int_{-\infty}^{\infty} A(\tau) e^{i\omega\tau} d\tau,$$

and $\varphi(\omega) = \arg[\tilde{A}(\omega)]$ is the phase of the Fourier transform. The factor η depends on the learning rate and on the total learning time T (Scarpetta et al., 2002a, 2008).

When we store multiple patterns $\mu = 1,2,\ldots,P$, the learned weights are the sum of the contributions from individual patterns. After learning P patterns, each with frequency $\omega_{\mu}/2\pi$ and phase-shift ϕ_i^{μ}, we get the connections

$$J_{ij} = \eta \sum_{\mu=1}^{P} |\tilde{A}(\omega_{\mu})| \cos\left[\phi_i^{\mu} - \phi_j^{\mu} - \varphi(\omega_{\mu})\right] + 2\eta P\tilde{A}(0). \quad (4)$$

In this paper we choose $\tilde{A}(0) = \int_{-\infty}^{\infty} A(\tau) d\tau = 0$, which gives a balance between potentiation and inhibition. Notably, the condition $\tilde{A}(0) = 0$ also holds when using the learning window of **Figure 1**. In the present study, we choose to store patterns all with the same ω_{μ}, and to ease the notation we define $\varphi^* = \varphi(\omega_{\mu})$.

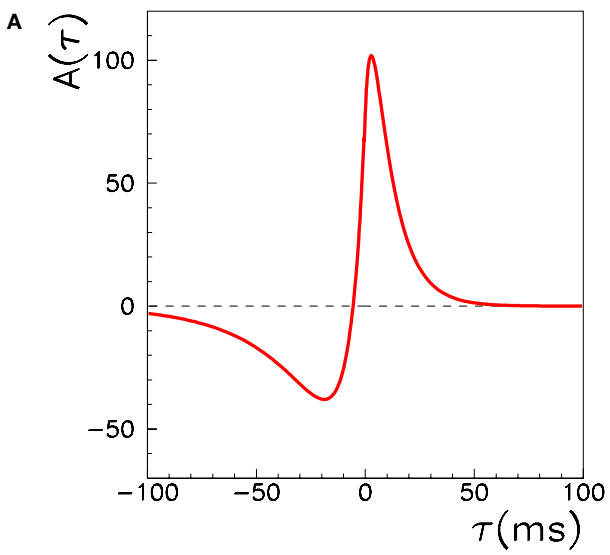

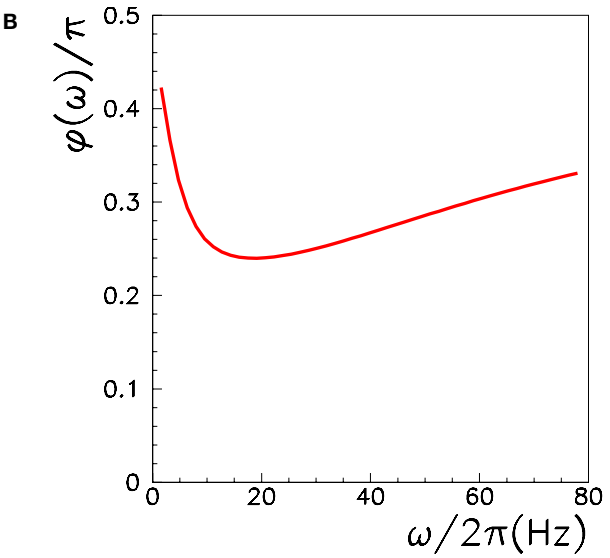

FIGURE 1 | (A) The learning window $A(\tau)$ used in the learning rule in Eq. (1) to model STDP. The window is the one introduced and motivated by Abarbanel et al. (2002), $A(\tau) = a_p e^{-\tau/T_p} - a_D e^{-\eta\tau/T_p}$ if $\tau > 0$, $A(\tau) = a_p e^{\eta\tau/T_D} - a_D e^{\tau/T_D}$ if $\tau < 0$, with the same parameters used in Abarbanel et al. (2002) to fit the experimental data of Bi and Poo (1998), $a_p = \gamma[1/T_p + \eta/T_D]^{-1}$, $a_D = \gamma[\eta/T_p + 1/T_D]^{-1}$, with $T_p = 10.2$ ms, $T_D = 28.6$ ms, $\eta = 4$, $\gamma = 42$. Notably, this function satisfies the condition $\int_{-\infty}^{\infty} A(\tau) d\tau = 0$, i.e. $\tilde{A}(0) = 0$. **(B)** The phase of the Fourier transform of $A(\tau)$ as a function of the frequency.

In the retrieval mode, the connections are fixed to the values given in Eq. (4). In the analog model, the dynamic equations for unit x_i are given by

$$\tau_m \dot{x}_i = -\dot{x}_i + F[h_i(t)] \tag{5}$$

where the transfer function $F(h)$ denotes the input–output relationship of neurons, $h_i(t) = \Sigma_j J_{ij} x_j(t)$ is the local field acting on neuron i, τ_m is the time constant of neuron i (for simplicity, τ_m has the same value for all neurons), and J_{ij} is the connection after the learning procedure given in Eq. (4). Spontaneous activity dynamics of the coupled non-linear system is therefore determined by the function $F(h)$ and by the coupling matrix J_{ij}. We take the function $F(h)$ to be equal to the Heaviside function $\Theta(h)$. Note that in this case the learning factor η is immaterial.

During the retrieval mode, the network selectively replays one of the stored phase-coded patterns, depending on the initial conditions. It means that if we force the network, for $t < 0$, with an input which resembles one of the phase-coded patterns, and then we switch off the input at times $t > 0$, the network spontaneously gives sustained oscillatory activity with the relative phases of the retrieved pattern, while the frequency can be different (see **Figure 2**). For the analog model (5), where the state of the network is represented by the rates $x_i(t)$, the same can be achieved if we simply initialize the rates at $t = 0$ with values $x_i^\mu(0)$ corresponding to one of the phase-coded patterns, or also to a partially corrupted version of it. Analytical calculations (Yoshioka et al., 2007; Scarpetta et al., 2008) show that the output frequency of oscillation is given by

$$\bar{\omega}/2\pi = \tan(\varphi^*)/2\pi\tau_m,$$

and this is confirmed by numerical simulations of Eq. (5) with connections given by Eq. (4).

As an example, the learning window in **Figure 1**, when the frequency of the stored pattern is $\omega_\mu/2\pi = 20$ Hz, gives $\varphi^* = 0.24\pi$, and an output frequency of oscillation $\bar{\omega}/2\pi = 15$ Hz (with $\tau_m = 10$ ms). Numerical simulations of the network with $\varphi^* = 0.24\pi$, $N = 3000$ fully connected neurons and $P = 30$ stored patterns, are shown in **Figure 2B**. In **Figure 2C** the case $\varphi^* = 0.45\pi$ is shown. Here, the output frequency is much higher, while the oscillations of the firing rates with respect to the mean value 1/2 is much smaller.

In the following sections, we analyze the behavior when multiple patterns are stored and we study the network capacity as a function of learning window parameters and as a function of connectivity topology.

CAPACITY OF THE FULLY CONNECTED NETWORK

In this section we study the network capacity, in the case of fully connected network, where all the $N(N-1)$ connections are subject to the learning process given by Eq. (4).

During the retrieval mode, the spontaneous dynamics of the network selectively replay one of the stored phase-coded patterns, depending on initial condition, so that, when retrieval is successful, the spontaneous activity of the network is an oscillating pattern of activity with phase of firing equal to the stored phases ϕ_i^μ (while the frequency of oscillation is governed by the time scale of single neuron and by the parameter φ^* of learning window). Similarity between the network activity during retrieval mode and the stored phase-coded pattern is measured by the overlap $|m^\mu|$, *introduced in* (Scarpetta et al., 2002a) and studied in (Yoshioka et al., 2007),

$$|m^\mu(t)| = \left| \frac{1}{N} \sum_{j=1,\ldots,N} x_j(t) e^{i\phi_j^\mu} \right| \tag{6}$$

If the activity $x_i(t)$ is equal to the pattern $x_i^\mu(t)$ in Eq. (2), then the overlap is equal to 1/4 (perfect retrieval), while it is $\sim 1/\sqrt{N}$ when the phases of firing have nothing to do with the stored phases. Numerically we study the capacity of the network, $\alpha_c = P_{max}/N$, where N is the number of neurons and P_{max} is the maximum number of items that can be stored and retrieved successfully.

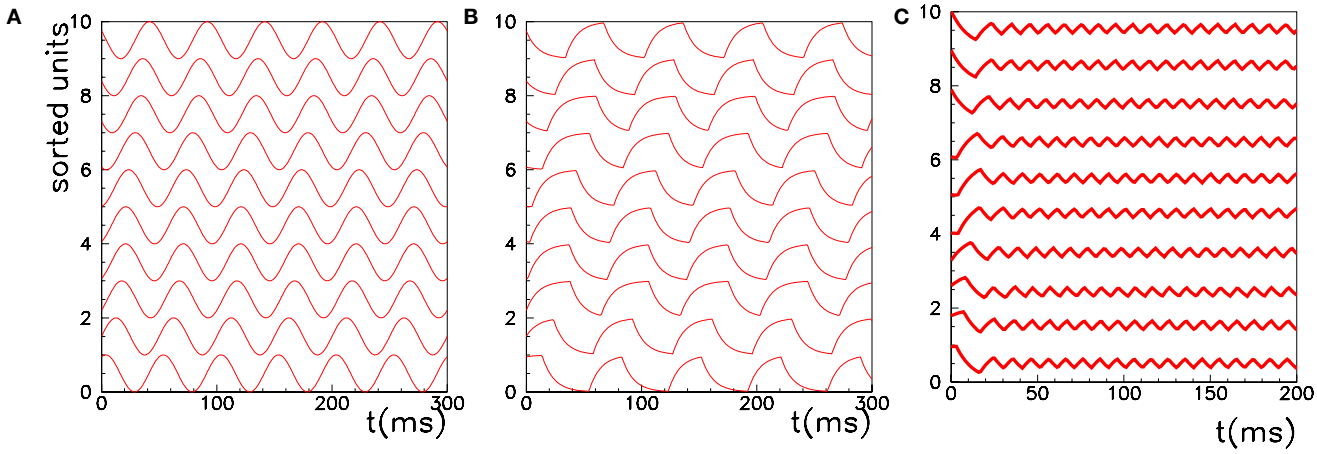

FIGURE 2 | The activity of 10 randomly chosen neurons in a network of $N = 3000$ fully connected analog neurons, with $P = 30$ stored patterns. The learning rule is given by Eq. (4) with $\varphi^* = 0.24\pi$. Neurons are sorted by increasing phase ϕ_i^1 of the first pattern, and shifted correspondingly on the vertical axis. **(A)** The first stored pattern, that is the activity of the network given by Eq. (2) used to encode the pattern in the learning mode, with frequency $\omega_\mu/2\pi = 20$ Hz. **(B)** The self-sustained dynamics of the network, when the initial condition is given by the first pattern $x_i^1(0)$. The retrieved pattern has the same phase relationships of the encoded one. In this case the overlap is $|m^1| = 0.22$, and the output frequency is in agreement with the analytical value $\tan(\varphi^*)/2\pi\tau_m = 15$ Hz. **(C)** Same as in **(B)**, but with $\varphi^* = 0.45\pi$. Output frequency is in agreement with the analytical value $\tan(\varphi^*)/2\pi\tau_m = 100$ Hz.

We extract P different random patterns, choosing phases ϕ_j^μ randomly from a uniform distribution in $[0, 2\pi)$. Then we define the connections J_{ij} with the rule Eq. (4). The values of the firing rates are initialized at time $t = 0$ at the value given by Eq. (2) with $t = 0$ and $\mu = 1$ of the first pattern, the dynamics in Eq. (5) is simulated, and the overlap Eq. (6) with $\mu = 1$ is evaluated. If the absolute value $|m^\mu(t)|$ tends to a constant greater than 0.1 at long times, then we consider that the pattern has been encoded and replayed well by the network. The maximum value of P at which the network is able to replay the pattern is the capacity of the network. We have verified that a small noise in the initialization do not change the results. A systematic study of the robustness of the dynamical basins of attraction from the noise in the initialization has not been carried out yet.

Here we study the dependence of the network capacity on the learning rule parameter φ^*. The parameter φ^* depends on the learning window shape, and on the frequency of oscillation $\omega_\mu/2\pi$ of the pattern presented during the learning process. In **Figure 3** we plot the capacity as a function of $0 < \varphi^* < \pi/2$ for a fully connected network with $N = 3000$ and $N = 6000$, considering P_{max} the maximum number of patterns such that the retrieved patterns have overlaps $|m^\mu| > 0.1$. The capacity is approximately constant with the network size, showing that the maximum number of patterns P_{max} scales linearly with the number of neurons.

We see that capacity strongly depends on the shape of learning window through parameter φ^*. The limit of φ^* equal to zero corresponds to output frequency $\bar{\omega}/2\pi$ equal to zero, and therefore to the limit of static output. We see that the capacity of the oscillating network is larger then the static limit for a large range of frequencies. When φ^* approaches $\pi/2$, then the output frequency $\bar{\omega}/2\pi = \tan(\varphi^*)/2\pi\tau_m$ tends to infinity, and capacity decreases. The best performance is given at intermediate values of φ^*. Therefore, since φ^* depends on the degree of time asymmetry of the learning window, we see that there is a range of time asymmetry of the learning window which provides good capacity, while both the case of perfectly symmetric learning window $\varphi^* = 0$, and the case of perfectly anti-symmetric learning window $\varphi^* = \pi/2$, give worse capacity performances. Interestingly, the learning window in **Figure 1** gives intermediate values of φ^* for a large interval of frequencies ω_μ.

Note that the decrease in the capacity of the network when the phase φ^* approaches $\pi/2$ is essentially due to the fact that the oscillations of the firing rates with respect to the mean value 1/2 become small in this regime. When the firing rates tend to a constant, the overlap defined by Eq. (6) goes to zero.

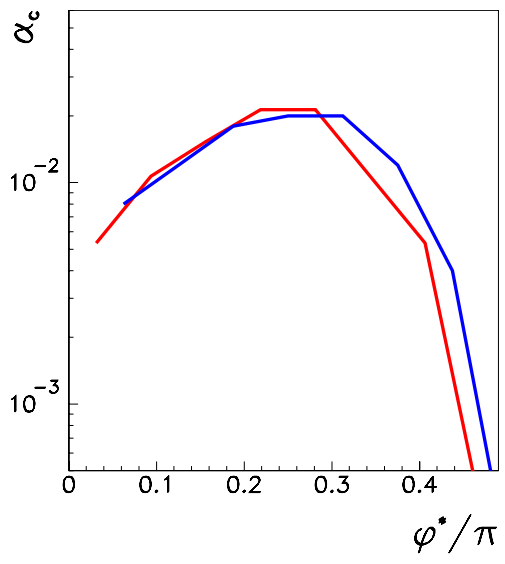

FIGURE 3 | Maximum capacity $\alpha_c = P_{max}/N$ of a network of $N = 3000$ (red) and $N = 6000$ (blue) fully connected analog neurons, as a function of the learning window asymmetry φ^*. The limit $\varphi^* = 0$ corresponds to a symmetric learning window (J_{ij}=J_{ji}) that is to output frequency $\bar{\omega}/2\pi$ that tends to zero. The limit $\varphi^* = \pi/2$ corresponds instead to a perfectly anti-symmetric learning window, and output frequency $\bar{\omega}/2\pi = \infty$. The intermediate value $\varphi^* \simeq 0.25\pi$ gives the best performance of the network.

CAPACITY OF THE SPARSE NETWORK

In this section we study the capacity of the network described through Eq. (5) in the case of sparse connectivity, where only a fraction of the connections are subject to the learning rule given by Eq. (4), while all the others are set to zero. The role of connectivity's topology is also investigated. We start from a network in which neurons are put on the vertices of a two- or three-dimensional lattice; each neuron is connected only to neurons within a given distance (in units of lattice spacings) and we call z the number of connections of a single neuron. For each neuron, we then "rewire" a finite fraction γ of its connections, deleting the existing short-range connections and creating, in place of them, long range connections to randomly chosen neurons.

We consider a three-dimensional network with 24^3 neurons, and a two-dimensional one with 118^2 neurons. In **Figure 4A** we plot the maximum capacity $\alpha_c = P_{max}/N$ as a function of the connectivity z/N for three different values of γ, for the three-dimensional case. The value $\gamma = 0$ (red curve) corresponds to the pure short-range network, in which all connections are between neurons within a given distance on the three-dimensional lattice, $\gamma = 1$ (blue curve) corresponds to the random network, where the three-dimensional topology is completely lost, and $\gamma = 0.3$ to an intermediate case, where 30% of the connections are long range, and the others are short range.

Considering that the capacity of the fully connected network ($z/N = 1$) is $\alpha_c \simeq 0.02$, we see that the random network with $z/N \simeq 0.1$ already has ~40% of the capacity of the fully connected network. This means the capacity does not scale linearly with the density of connections, and when the density of connections grows there is a sort of saturation effect, due to the presence of partially redundant connections.

Then, we look at the dependence of the capacity from the fraction of short range and long range connections for $z/N \simeq 0.11$. In **Figure 4B**, we see that the capacity gain, with respect to the short-range network, given by 30% long range connections ($\gamma = 0.3$), is about 80% the one of the fully random network ($\gamma = 1$). Therefore, the presence of a small number of long range connections is able to amplify the capacity of the network. This is shown in **Figure 4B**, where the capacity as a function of γ for $z/N = 0.11$ is plotted (red curve). Note that the above effect is not so important in smaller networks, for example with $N = 18^3$ neurons, where the capacity of the short-range network

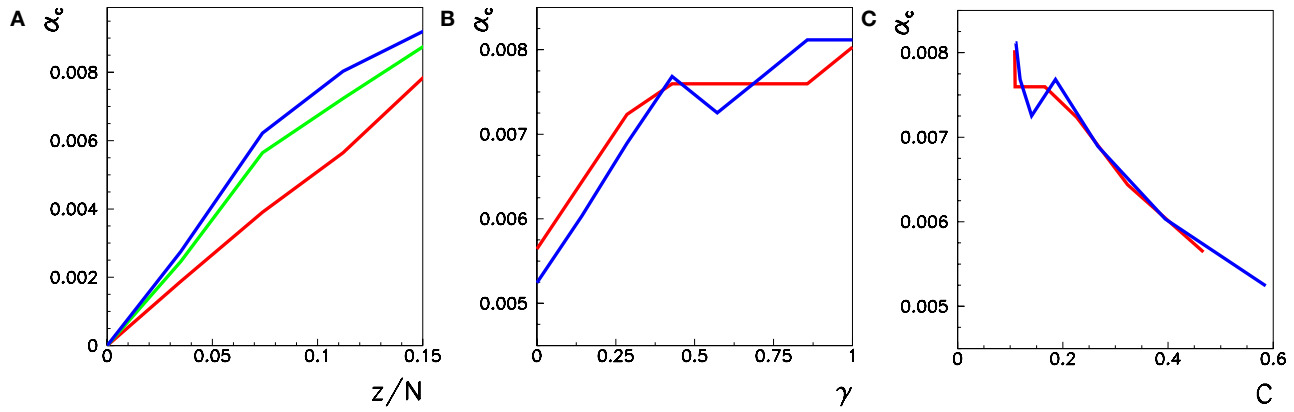

FIGURE 4 | (A) Maximum capacity $\alpha_c = P_{max}/N$ for a network with 24^3 analog neurons, with z connections per neuron, with φ^* fixed to its optimal value 0.24π. The red curve corresponds to $\gamma = 0$, that is to a network with only short-range connections. The green one to $\gamma = 0.3$, and the blue one to $\gamma = 1$, that is to a random network where the finite dimensional topology is completely lost. **(B)** Maximum capacity $\alpha_c = P_{max}/N$, for the same values of N and φ^* and for connectivity $z/N = 0.11$, as a function of γ, for the 24^3 lattice (red) and for a two dimensional 118^2 lattice (blue). **(C)** Same data as in **(B)**, but as a function of the clustering coefficient C.

is nearer to that of a random network. Therefore, it seems plausible that, for very large networks, the amplifying effect of a small fraction of long range connections will be even stronger.

It is reasonable to suppose that the fraction of long range connections, in real networks, is determined by a trade-off between the increase of capacity given by long range connections, and their higher wiring cost. A large amplifying effect of long range connections on the capacity, together with a large wiring cost with respect to short range ones, will result in the optimal topology of the network being small-world like, with a small fraction of long range connections, as observed in many areas of the brain, from *C. elegans* (White et al., 1986; Achacoso and Yamamoto, 1991) to the visual cortex of the cat (Yu et al., 2008).

The experiments on a two-dimensional lattice with 118^2 neurons do not show any qualitative differences with respect to the three-dimensional case. In **Figure 4B** we plot the capacity of the two-dimensional network (blue curve) as a function of γ, along with the capacity of the three-dimensional one (red curve).

The **Figure 4C** shows the same data of **Figure 4B**, but as a function of the clustering coefficient C, defined as the probability that two sites, neighbors of a given site, are neighbors themselves. As reported in **Figure 4C**, once fixed the number of connections per neuron z, the lower the clustering coefficient, the higher the capacity of the network. This is reasonable, because a high clustering coefficient means that connections will be partially redundant, as already observed in the case of the dependence on the connectivity z/N.

Note that the mean path length λ, for the considered value of $z/N = 0.11$, is a decreasing function of γ from $\gamma = 0$ up to $\gamma = 0.01$, and then remains practically constant for higher values of γ. This means that the ratio between C and λ, that is the small-worldness of the network, has a maximum about $\gamma = 0.01$. The capacity therefore is not an increasing function of the small-worldness. Only when the wiring cost of the connections is taken in account, the optimal topology turns out to be one with a small fraction of long range connections. Note also that for more realistic values of z/N, much lower than $z/N = 0.11$, the maximum of the small-worldness shifts to higher values of γ.

INTEGRATE AND FIRE MODEL

The previous results refer to network dynamics described in Eq. (5), that is simple enough to admit analytical predictions for dynamics when the connectivity is given by Eq. (4). The simple model defined by Eq. (5) has state variables $x_i(t)$, representing instantaneous firing rate or probability of firing, and it has only one time scale τ_m, which is the time constant of a single unit, allowing us to focus on the effect of the learning window shape and connectivity structure. However, we expect that, while details of dynamics may depend on the model of single unit, the crucial results of storing and recall of phase-coded patterns can be seen also in a spiking model. Therefore we simulate a leaky integrate and fire (IF) spiking model. We use a simple spike response model formulation (SRM) (Gerstner and Kistler, 2002; Gerstner et al., 1993) of the leaky integrate and fire model. While integrate and fire models are usually defined in terms of differential equations, the SRM expresses the membrane potential at time t as an integral over the past (Gerstner and Kistler, 2002). This allows us to use an event-driven programming and makes the numerical simulations faster than in the differential equation formulation.

Each presynaptic spike j, with arrival time t_j, is supposed to add to the membrane potential a postsynaptic potential of the form $J_{ij} \in (t-t_j)$, where

$$\in (t-t_j) = K\left[\exp\left(-\frac{t-t_j}{\tau_m}\right) - \exp\left(-\frac{t-t_j}{\tau_s}\right)\right]\Theta(t-t_j) \qquad (7)$$

where τ_m is the membrane time constant (here 10 ms), τ_s is the synapse time constant (here 5 ms), $\Theta(t)$ is the Heaviside step function, and K is a multiplicative constant chosen so that the maximum value of the kernel is 1. The sign of the synaptic connection J_{ij} set the sign of the postsynaptic potential change. The synaptic signals received by neuron i, after time t_i of the last spike of neuron i, are added to find the total postsynaptic potential

$$h_i(t) = \sum_{j/t_j > t_i} J_{ij} \in (t-t_j) \qquad (8)$$

When the postsynaptic potential of neuron i reaches the threshold T, a postsynaptic spike is scheduled, and postsynaptic potential is set to the resting value zero. We simulate this simple model with J_{ij} taken from the learning rule given by Eq. (4), with P patterns in a network of N units. The learning rule Eq. (4) comes out of the learning process given by Eq. (1), when a sequence of spikes is learned, and spikes are generated in such a way that the probability that unit i has a spike in the interval $(t, t + \Delta t)$ is proportional to $x_i^{\mu}(t)\Delta t$ in the limit $\Delta t \to 0$, with the rate $x_i^{\mu}(t)$ given by Eq. (2). The J_{ij} are measured in units such that $\eta\tilde{A}(\omega_{\mu}) = 1$.

After the learning process, to recall one of the encoded patterns, we give an initial signal made up of $M < N$ spikes, taken from the stored pattern μ, and we check that after this short signal the spontaneous dynamics of the network gives sustained activity with spikes aligned to the phases ϕ_i^{μ} of pattern μ (**Figure 5**).

We also investigate the role of the threshold T. As shown in **Figure 5**, when the threshold T is lower a burst of activity takes place within each cycle, with phases aligned with the pattern. Therefore the same phase-coded pattern is retrieved, but with a different number of spikes per cycle. This open the possibility to have a coding scheme in which the phases encode pattern's informations, and rate in each cycle represents the strength and saliency of the retrieval or it may encode another variable. The recall of the same phase-coded pattern with different number of spikes per cycle, shown in **Figure 5**, accords well with recent observation of Huxter et al. (2003) in hippocampal place cells, showing occurrence of the same phases with different rates. They show that the phase of firing and firing rate are dissociable and can represent two independent variables, e.g. the animals location within the place field and its speed of movement through the field. Note that a change of T in our model may correspond to a change in the value of physical threshold, or to a change in the value of the parameter $\eta\tilde{A}(\omega_{\mu})$ appearing in the synaptic connections J_{ij}.

The role of parameter φ^* in connections J_{ij} in Eq. (4) is that of changing the output frequency of collective oscillation during retrieval. Here, as well as in the analog model of Eq. (5), lower values

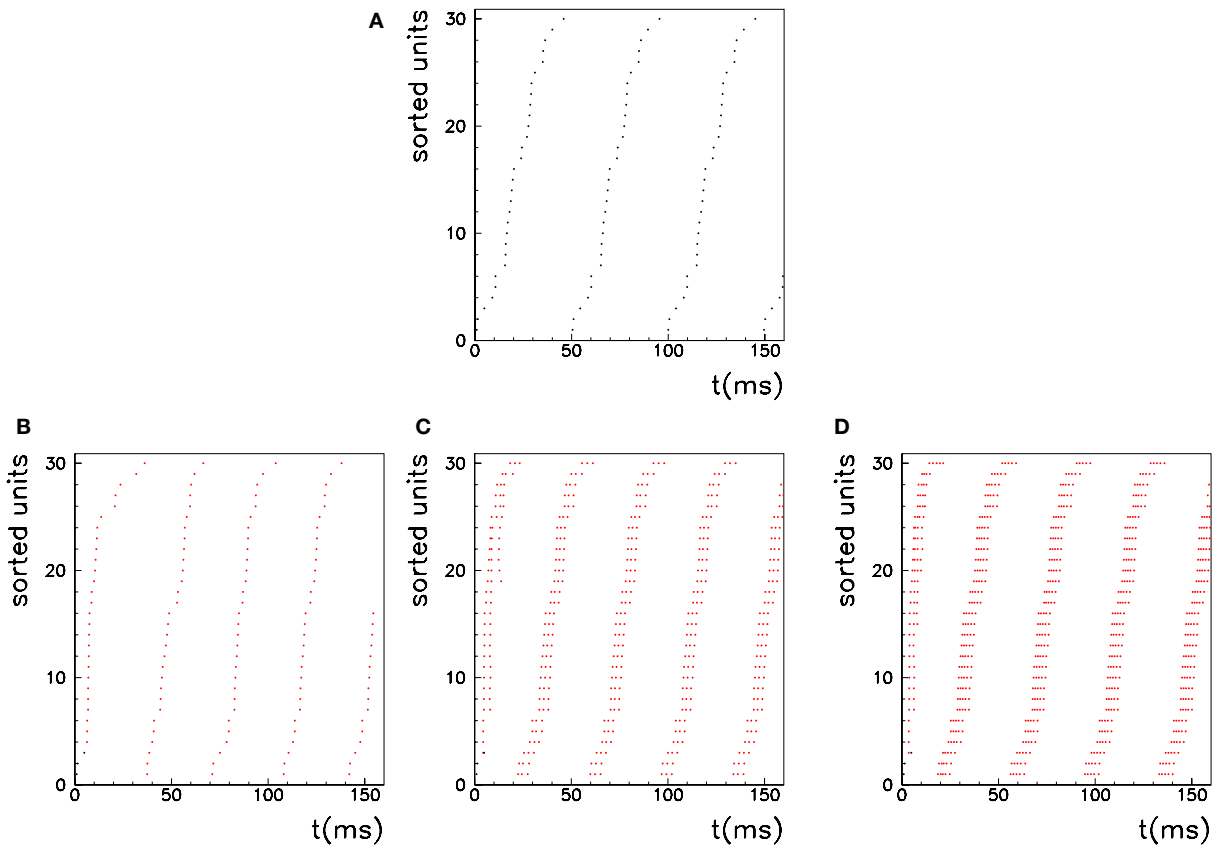

FIGURE 5 | Recall of a pattern by the spiking IF model, with $N = 1000$ neurons and $\varphi^* = 0.24\pi$. One pattern ($P = 1$) defined by the phases ϕ_i^{μ} is stored in the network with the rule given by Eq. (4). Then a short train of $M = 150$ spikes, at times $t_i = \phi_i^{\mu} / \omega_{\mu}$ with $\omega_{\mu}/2\pi = 20$ Hz, is induced on the neurons that have the M lowest phases ϕ_i^{μ}. This short train triggers the replay of the pattern by the network. Depending on the value of T, the phase-coded pattern is replayed with a different number of spikes per cycle. Note that changing T in our model may correspond to a change in the value of physical threshold or in the value of the parameter $\eta\tilde{A}(\omega_{\mu})$ appearing in the synaptic connections J_{ij} learning rule. **(A)** Thirty neurons of the network are randomly chosen and sorted by the value of the phase ϕ_i^{μ}. Then the phases of the encoded pattern are shown, plotting on the x axis the times $(\phi_i^{\mu} + 2\pi n) / \omega_{\mu}$, and on the y axis the label of the neuron. **(B)** The replayed pattern with threshold $T = 85$ is shown, plotting on the x axis the times of the spikes, and on the y axis the label of the spiking neuron. Black dots represent externally induced spikes, while red dots represent spikes generated by the intrinsic dynamics of the network. **(C)** The replayed pattern with threshold $T = 50$. **(D)** The replayed pattern with threshold $T = 35$.

of φ^* correspond to lower frequencies, even though in the spiking model both time constants of the single neuron (τ_m and τ_s) play a role to set output frequency. Therefore, the simple formula that holds for the output frequency of the analog model is not valid in the spiking model. Output activity during recall, for $\varphi^* = 0.24\pi$, is shown in **Figure 5**, while output activity when $\varphi^* = 0.4\pi$ has a higher frequency, as shown in **Figure 6**. Selective recall of two of the stored patterns are shown in **Figure 6** when $P = 5$ patterns are stored, and $\varphi^* = 0.4\pi$.

To estimate the network capacity of the spiking model, we did numerical simulations of the IF network in Eqs. (7) and (8), with $N = 3000$ neurons, and connections J_{ij} given by Eq. (4), with different number of patterns P. We give an initial short train of $M = 300$ spikes chosen at times $t_i = \phi_i^\mu / \omega_\mu$ from pattern $\mu = 1$. To check if the initial train triggers the replay of pattern $\mu = 1$ at large times, we measure the overlap $m^\mu(t)$ between the spontaneous dynamics of the network and the phases of pattern $\mu = 1$. In analogy with Eq. (6), the overlap $m^\mu(t)$ is defined as

$$| m^\mu(t) = \left| \frac{1}{N} \sum_{j=1,\ldots,N} e^{-i2\pi t_j^*/T^*} e^{i\phi_j^\mu} \right|, \qquad (9)$$

where t_j^* is the spike timing of neuron j during the spontaneous dynamics, and T^* is an estimation of the period of the collective spontaneous dynamics. The overlap in Eq. (9) is equal to 1 when the phase-coded pattern is perfectly retrieved (even though on a different time scale), and is of order $\simeq 1/\sqrt{N}$ when the phases of spikes have nothing to do with the stored phases of pattern μ. We consider a successful recall each time the overlap (averaged over 50 runs) is larger then 0.7. The capacity of the fully connected spiking network as a function of φ^* is shown in **Figure 7**, for threshold $T = 200$ and $N = 3000$.

While in the analog model the output frequency tends to infinity when $\varphi^* \to \pi/2$, in the spiking model output frequency increases but not diverge at $\pi/2$, as shown in **Figure 7B**. As in the analog model, the capacity decreases as soon as φ^* is near or larger then $\pi/2$. With parameters used in **Figure 7**, we see that, for φ^* larger then 0.55π, the stimulation spikes are not able to initiate the recall of the pattern and the network is silent, unless we choose a lower threshold. This behavior is similar to a small oscillation obtained in the analog model at $\varphi^* \to \pi/2$.

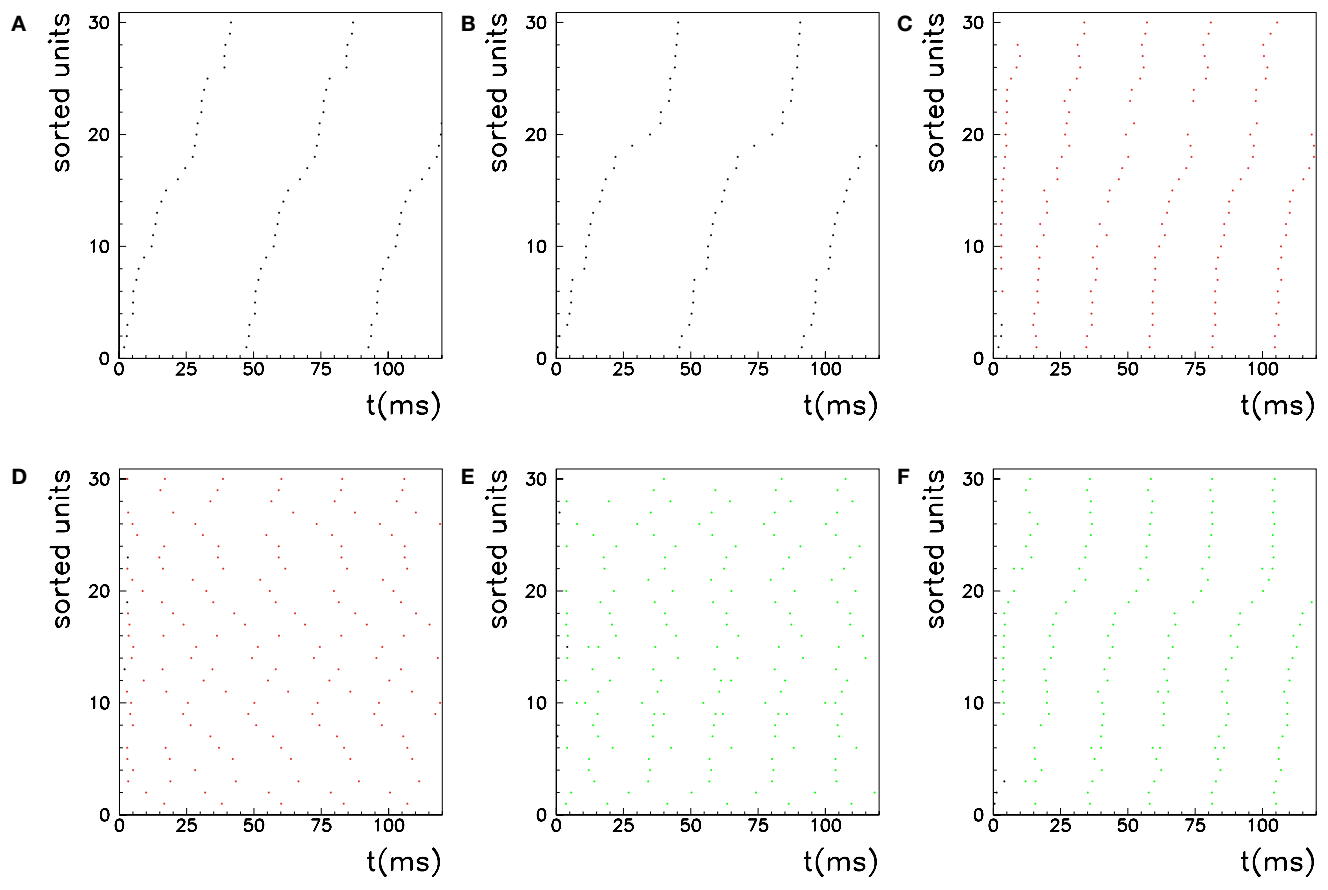

FIGURE 6 | Example of selective retrieval of different patterns, in a network with $N = 1000$ IF neurons and $P = 5$ stored patterns. Here we choose the asymmetry parameter to be $\varphi^* = -0.4\pi$. Thirty neurons are chosen randomly, and then sorted by the value of ϕ_i^1 in **(A–C)**, and sorted by the value of ϕ_i^2 in **(D–F)**. In **(A)** and **(D)** we show the phases of the first two stored patterns, plotting the times $(\phi_i^\mu + 2\pi n)/\omega_\mu$ respectively for $\mu = 1$ and $\mu = 2$. In **(B)** and **(E)** we show the generated dynamics when a short train of $M = 100$ spikes corresponding to the $\mu = 1$ pattern is induced on the network, while in **(C)** and **(F)** the dynamics when the $\mu = 2$ pattern is instead triggered. The network dynamics selectively replay the stored pattern, depending on the partial cue stimulation. Note that, because the parameter φ^* here is greater than in **Figure 5**, the frequency of the retrieved pattern here is greater.

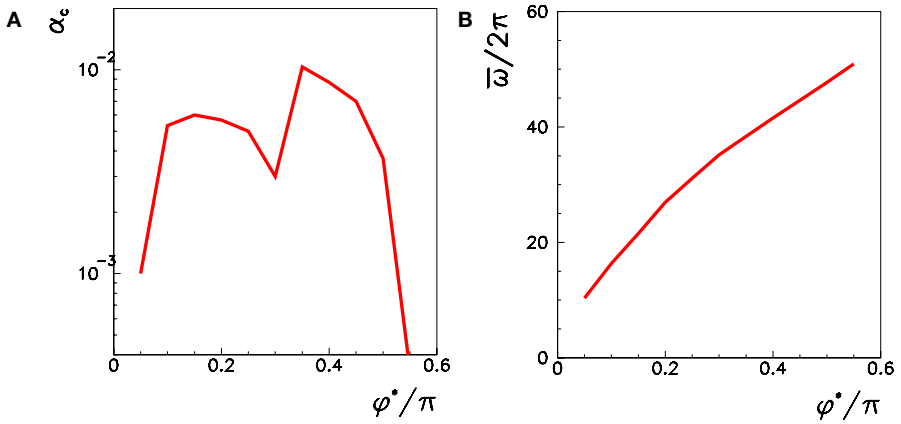

FIGURE 7 | (A) Maximum capacity $\alpha_c = P_{max}/N$ of a network of $N = 3000$ fully connected spiking IF neurons, as a function of the learning window asymmetry φ^*. The spontaneous dynamics induced by a short train of $M = 300$ spikes with $\omega_\mu = 20$ Hz and phases given by encoded pattern $\mu = 1$ is considered, with threshold set to $T = 200$. **(B)** The output frequency of the replay, as a function of φ^*, when $P = 1$, $T = 200$, $N = 3000$.

A systematic study of the dependence of the storage capacity on the threshold T, on the number M of spikes used to trigger the recall, and on time constants τ_m and τ_s still has to be done. Future work will also consider the case in which patterns to be learned are not defined through the rate x_i^μ in Eq. (2), but are defined as sequences of spikes whose timing is exactly given by $(\phi_i^\mu + 2\pi n)/\omega_m u$. We expect for this case a higher storage capacity.

SUMMARY AND DISCUSSION

In this paper we studied the storage and recall of patterns in which information is encoded in the phase-based timing of firing relative to the cycle. We analyze the ability of the learning rule given by Eq. (4) to memorize multiple phase-coded patterns, such that the spontaneous dynamics of the network, defined by Eq. (5), selectively gives sustained activity which matches one of the stored phase-coded patterns, depending on the initialization of the network. It means that if one of the stored items is presented as input to the network at time $t < 0$, and it is switched off at time $t \geq 0$, the spontaneous activity of the network at $t > 0$ gives sustained activity whose phases alignments match those presented before. It is not trivial that the network performed retrieval competently, as analog associative memory is hard (Treves, 1990).

We compute the storage capacity of phase-coded patterns in the analog model, finding a linear scaling of number of patterns with network size, with maximal capacity $\alpha_c \simeq 0.02$ for the fully connected network. Our model cannot be easily compared to classical models such as Hopfield's, since the dynamical phases-coded patterns are strongly different from the classical static rate-coded patterns. Whereas the capacity of rate-coded networks has been well understood, that of spiking or phase-coded networks is not yet well understood. We are not aware of previous work who measures the storage capacity of phase-coded patterns, except of the phase-coded patterns in a spin model by Yoshioka (2009), whose capacity is in quantitative agreement with our analog model results. However, the scaling of capacity with connectivity displays properties similar to those of classical models. For strong dilution ($z \ll N$), the capacity P_{max}, that is the maximum number of patterns encodable in the network, is proportional to z rather than to N. On the other hand, for weak dilution (z of the order of N), P_{max} is proportional to the number of neurons N.

Our results on the IF spiking model show that there is a qualitative agreement between the analog and the spiking model ability to store multiple phase-coded patterns and recall them selectively.

We also study the storage capacity of the analog model for different degrees of sparseness and small-worldness of the connections. We put neurons on the vertices of a two- or three-dimensional lattice, and connect each neuron to neurons that are nearer than some distance in units of lattice spacings. Then a fraction γ of these connections are rewired, deleting the short-range connection and creating a long range connection to a random neuron. The existing connections are then defined by the learning rule Eq. (4), while other connections are set to zero.

Changing the proportion γ between short-range and long-range connections, we go from a two- or three-dimensional network with only nearest-neighbors connections ($\gamma = 0$) to a random network ($\gamma = 1$). Small but finite values of γ give a "small world" topology, similar to that found in many areas of nervous system. We see that, for system size $N = 24^3$, the capacity of a random network with only 10% connectivity already has about 40% the capacity of the fully connected network, showing that there is a saturation effect when the density of connections grows above 10%.

Looking at the dependence on the fraction of short range and long range connections, we see that at $z/N = 0.11$ the capacity gain with respect to the short range network, given by 30% long range connections, already is about 80% the gain given by the full random network. This last factor is likely to increase for larger system sizes, because the larger the system, the more different are long range connections with respect to short-range ones. This is interesting considering that a long-range connection clearly have a higher cost then a short-range one, and implies that a small-world network topology is optimal, as a compromise between the cost of long range connections and the capacity increase.

These results have been found for the analog model in Eq. (5). However, this is not a really spiking model, since only "firing activity" or "probability of spiking" is evaluated. Therefore we perform numerical simulation of a IF model with spike response kernels, to show that while details of dynamics may depend on the model of single unit, the crucial results of ability to store and recall of phase-coded memories can be seen also in a spiking model. Indeed numerical simulations of the spiking model in Eq. (7) shows competent storage and recall of phase-coded memories. A pattern of spikes with the stored phases, i.e. with the phase-based timing of spikes relative to the cycle, is activated by the intrinsic dynamics of the network when a partial cue of the stored pattern (few spikes at proper timings) is presented for a short time. **Figure 6** shows that the network is able to store multiple phase-coded memories and selectively replay one of them depending from the partial cue that is presented. Changing the parameter φ^* of the learning rule changes the period of the cycle during recall dynamics, while changing the value of T changes the number of spikes per cycle, without changing the phase pattern. So the same phase-coded pattern can be recalled with one spike per cycle or with a short burst per cycle. This agrees well with recent observations, like occurrence of phase precession with very low as well as high firing rate (Huxter et al., 2003). The number of spikes per cycle is a sort of strength or saliency of recall. This leaves open the possibility that variations in number of spikes per cycle might convey additional information about other variables not coded in the phase pattern, as suggested in (Huxter et al., 2003; Huhn et al., 2005; Wu and Yamaguchi, 2010) for place cells, or may convey information about the saliency of retrieved pattern (Lengyel and Dayan, 2007).

In our treatment, we distinguish a learning mode, in which connections are plastic and activity is clamped to the phase-coded pattern to be stored in the synaptic connections J_{ij}, from a recall mode, in which connection strengths do not change. Of course, this distinction is somewhat artificial; real neural dynamics may not be separated so clearly into such distinct modes. Nevertheless, data on cholinergic neuromodulatory effects (Hasselmo, 1993, 1999) in cortical structures suggesting that high levels of acetylcholine selectively suppress intrinsic but not afferent fiber transmission and enhance long-term plasticity, seems to provide a possible neurophysiological mechanism for this distinction in two operational modes.

Another point is given by the physical constraints on the sign of synaptic connections J_{ij}, that for a given presynaptic unit j, are all positive when presynaptic unit j is excitatory, and all negative when presynaptic unit j is inhibitory, a condition not respected by our learning formula Eq. (4) so far. As a remedy, one may add an initial background weight J_0 to each connection, independent of i and j, such that $J_{ij} + J_0 > 0$ for all i and j, to make all the units excitatory and plastic connections positive, and then one has to add a global inhibition equal to $-J_0$ times the mean field $y = \Sigma_j x_j$ to save equilibrium between excitation and inhibition. In such a way, we have a network of N excitatory units, with positive couplings, and a global inhibition,

$$\tau_m \dot{x}_i = -x_i + F\left[\sum_j (J_{ij} + J_0)x_j(t) - J_0 y\right] \tag{10}$$

that is mathematically equivalent to Eq. (5) when $y = \Sigma_j x_j$, and numerically also gives the same results when $y = N/2$.

Considering the IF model of section "Integrate and fire model", also in this case we can consider a network of all excitatory neurons, with plastic positive connections given by $J_{ij} + J_0$ with J_0 constant such that $J_{ij} + J_0 > 0$, and then add a proper inhibitory term to save the equilibrium between excitation and inhibition. In this way, the postsynaptic potential of neuron i, after time t_i of its last spike, is given by

$$h_i(t) = \sum_{j/t_j > t_i} (J_{ij} + J_0)\in(t - t_j) - J_0 \sum_{j/t_j > t_i} \in (t - t_j). \tag{11}$$

The inhibitory term $-J_0 \sum_{j/t_j > t_i} \in (t - t_j)$ can be realized in different ways, for example imaging that for each excitatory unit j, there is a fast inhibitory interneuron j, that emits a spike each time its excitatory unit does, and is connected with all the other excitatory neurons with constant weight connections J_0.

The task of storing and recalling phase-coded memories has been also investigated in (Lengyel et al., 2005b) in the framework of probabilistic inference. While we study the effects of couplings given by Eq. (4) in the network model Eq. (5), and in a network of IF neurons given by Eq. (7), the paper (Lengyel et al., 2005b) studies this problem from a normative theory of autoassociative memory, in which variable x_i of neuron i represents the neuron i spike timing with respect to a reference point of an ongoing field potential, and the interaction $H(x_i, x_j)$ among units is mediated by the derivative of the synaptic plasticity rule used to store memories. In (Lengyel et al., 2005b), the case of limited connectivity is studied, showing how recall performance depends to the degree of connectivity when connections are cut randomly. Here we show that performance also depends from the topology of the connectivity, and capacity depends not only from the number of connections but also from the fraction of long range versus short-range connections.

The role of STDP in learning and detecting spatio-temporal patterns has been studied recently in (Masquelier et al., 2009). They show that a repeating spatio-temporal spike pattern, hidden in equally dense distracter spike trains, can be robustly detected by a set of "listening" neurons equipped with STDP. When a spatio-temporal pattern repeats periodically, it can be considered a periodic phase-coded pattern. While in Masquelier et al. (2009) the detection of the pattern is investigated when it is the input of the "listening" neurons, in our paper we investigate the associative memory property, which makes the pattern imprinted in the connectivity of the population an attractor of the dynamics. When a partial cue of the pattern μ is presented (or in the analog case the network is initialized with $x_i^\mu(0)$), then the original stored pattern is replayed. Differently from Masquelier et al. (2009), here the pattern μ is imprinted in the neural population, in such a way that exactly the same encoded phase-coded pattern is replayed during persistent spontaneous activity. This associative memory behavior, that replay the stored sequence, can be a method for recognize an item, by activating the same memorized pattern in response of a similar input, or may be also a way to transfer the memorized item to another area of the brain (such as for memory consolidation during sleep).

Our results shows that in the spiking model a critical role is played by the threshold T: changing the threshold one goes from a silent state to a spontaneously active phase-coded pattern with one spike per cycle, and then to the same phase-coded pattern with

many spikes per cycle (bursting). Therefore, a possible conjecture is that when we observe the replay of a periodic spatio-temporal pattern, then if one is able to change the threshold of spiking of the neurons, one can observe the same phase pattern but with more or less spikes per cycle.

In future we will also investigate the capacity when patterns with different frequencies are encoded in the same network. In this paper we compute the capacity when encoded patterns have all the same frequency, however it would be interesting to see how the network work with different frequencies. Preliminary results on the analog model (Scarpetta et al., 2008) show that it's possible to store two different frequencies in a manner that both are stable if a relationship holds between the two frequencies and the shape of the learning window. We plan to investigate this both in the analog and in the spiking model.

Concerning the shape of learning kernel $A(\tau)$, in our model the values of the connections J_{ij} depend on the kernel shape only through the time integral of the kernel, and the Fourier transform of the kernel at the frequency of the encoded pattern. As shown in our previous paper (Yoshioka et al., 2007), best results are obtained when the time integral of the kernel is equal to zero $\int_{-\infty}^{\infty} A(\tau)d\tau = \tilde{A}(0) = 0$. This choice will assure the global balance between excitation and inhibition. Hence in the present paper we choose to set this value to zero, and varied only the phase φ^* of the Fourier transform. The case of a purely symmetric kernel corresponds to $\varphi^* = 0$, while a purely anti-symmetric (causal) one corresponds to $\varphi^* = \pi/2$. We find that intermediate values $0 < \varphi^* < \pi/2$ work better then values $\pi/2 < \varphi^* < \pi$, for which the network is not able to replay patterns competently. We study here positive values of φ^*, i.e. a causal kernel (potentiation for pre–post, and depotentiation for post–pre), however an anti-causal kernel would give a negative value of φ^*, and a negative frequency of replay, that is the pattern would be replayed in time reversed order (Scarpetta et al., 2008).

For what concerns the variety of shapes of the learning window observed in the brain, it has to be considered that they may accomplish different needs, such as maximize storage capacity, or set the time scale of replay, which in our model depends on the kernel shape. Notably, in our model we observe a good storage capacity for values of phase φ^* which correspond to a large interval of frequency of oscillation during replay, and therefore there is good storage capacity also for values of φ^* which correspond to a compressed-in-time replay of phase pattern on very short time scale. Future work will investigate the relation between this framework and the time-compressed replay of spatial experience in rat. It has been indeed observed that during pauses in exploration and during sleep, ensembles of place cells in the rat hippocampus and cortex re-express firing sequences corresponding to past spatial experience (Lee and Wilson, 2002; Foster and Wilson, 2006; David et al., 2007; Diba and Buzsaki, 2007; Hasselmo, 2008; Davidson et al., 2009). Such time-compressed hippocampal replay of behavioral sequences co-occurs with ripple events: high-frequency oscillations that are associated with increased hippocampal–cortical communication. It's intriguing the hypothesis that sequence replay during ripple is the recall of one of the multiple stored phase-coded memories, a replay that occur on a fast time scale (high $\bar{\omega}$), triggered by a short sequence of spike.

REFERENCES

Abarbanel, H., Huerta, R., and Rabinovich, M. I. (2002) Dynamical model of long-term synaptic plasticity. *Proc. Natl. Acad. Sci.* 99, 10132–10137.

Achacoso, T. B., and Yamamoto, W. S. (1991). *AY's Neuroanatomy of C. elegans for Computation*. Boca Raton: CRC Press.

Barabási, A. L., and Albert, R. (1999). Emergence of scaling in random networks. *Science* 286, 509–512.

Bi, G. Q., and Poo, M. M. (1998). Precise spike timing determines the direction and extent of synaptic modifications in cultured hippocampal neurons. *J. Neurosci.* 18, 10464–10472.

Bi, G. Q., and Poo, M. M. (2001). Synaptic modification by correlated activity: Hebb's postulate revisited. *Ann. Rev. Neurosci.* 24, 139–166.

Borisyuk, R. M., and Hoppensteadt, F. C. (1999). Oscillatory models of the hippocampus: a study of spatio-temporal patterns of neural activity. *Biol. Cybern.* 81, 359–371.

Bullmore, E., and Sporns, O. (2009). Complex brain networks: graph theoretical analysis of structural and functional systems. *Nat. Rev. Neurosci.* 10, 186–198.

Buzsaki, G., and Draguhn, A. (2004). Neuronal oscillations in cortical networks. *Science* 304, 1926–1929.

David, R. E., Masami, T., and McNaughton, B. L. (2007). Sequences in prefrontal cortex during sleep fast-forward playback of recent memory. *Science* 318, 1147–1150.

Davidson, T. J., Kloosterman, F., and Wilson, M. A. (2009). Hippocampal replay of extended experience. *Neuron* 63, 497–507.

de Arcangelis, L., and Herrmann, H. J. (2010). Learning as a phenomenon occurring in a critical state. *PNAS* 107, 3977–3981.

Debanne, D., Gahwiler, B. H., and Thompson, S. M. (1998). Long-term synaptic plasticity between pairs of individual CA3 pyramidal cells in rat hippocampal slice cultures. *J. Physiol.* 507, 237–247.

Diba, K., and Buzsaki, G. (2007). Forward and reverse hippocampal place-cell sequences during ripples. *Nat. Neurosci.* 10, 1241–1242.

Drew, P. J., and Abbott, L. F. (2006). Extending the effects of spike-timing-dependent plasticity to behavioral timescales. *Proc. Natl. Acad. Sci.* 103, 8876–8881.

Eguìluz, V. M., Chialvo, D. R., Cecchi, G. A., Baliki, M., and Apkarian, A. V. (2005). Scale-free brain functional networks. *Phys. Rev. Lett.* 94, 018102.

Düzel, E., Penny, W. D., and Burgess, N. (2010). Brain oscillations and memory. *Curr. Opin. Neurobiol.* 20, 143–149.

Feldman, D. E. (2000). Timing-based LTP and LTD and vertical inputs to layer II/III pyramidal cells in rat barrel cortex. *Neuron* 27, 45–56.

Florian, R. V., and Muresan, R. C. (2006). Phase precession and recession with STDP and anti-STDP. *Lect. Notes Comp. Sci.* 4131, 718–727.

Foster, D. J., and Wilson, M. A. (2006). Reverse replay of behavioral sequences in hippocampal place cells during the awake state. *Nature* 440, 680–683.

Fries, N. (2005). A mechanism for cognitive dynamics: neuronal communication through neuronal coherence. *Trend Cogn. Sci.* 9, 474–480.

Fries, N., Nikoli¢ D., and Singer, W. (2007). The gamma cycle. *Trends Neurosci.* 30, 309–316.

Froemke, R. C., and Dan, Y. (2002). Spike-timing-dependent synaptic modification induced by natural spike trains. *Nature* 416, 433–438.

Gelperin, A. (2006). Olfactory computations and network oscillation. *J. Neurosci.* 26, 1663–1668.

Gerstner, W., and Kistler, W. (2002). *Spiking Neuron Models: Single Neurons, Populations, Plasticity*. New York, NY: Cambridge University Press.

Gerstner, W., Kempter, R., van Hemmen, L., and Wagner, H. (1996). A neuronal learning rule for sub-millisecond temporal coding. *Nature* 383, 76–78.

Gerstner, W., Ritz, R., and van Hemmen, J. L. (1993). Why spikes? Hebbian learning and retrieval of time-resolved excitation patterns. *Biol. Cybern.* 69, 503–515.

Hasselmo, M. E. (1993). Acetylcholine and learning in a cortical associative memory. *Neural Comput.* 5, 32–44.

Hasselmo, M. E. (1999). Neuromodulation: acetylcholine and memory consolidation. *Trends Cogn. Sci.* 3, 351.

Hasselmo, M. E. (2008). Temporally structured replay of neural activity in a model of entorhinal cortex, hippocampus and postsubiculum. *Eur. J. Neurosci.* 28, 1301–1315.

Hellwig, B. (2000). A quantitative analysis of the local connectivity between pyramidal neurons in layers 2/3 of the rat visual cortex. *Biol. Cybern.* 82, 111–121.

Huhn, Z., Orbán, G., Érdi, P., and Lengyel, M. (2005) Theta oscillation-coupled dendritic spiking integrates inputs on a long time scale. *Hippocampus* 15, 950–962.

Huxter, J., Burgess, N., and O'Keefe, J. (2003). Independent rate and temporal

coding in hippocampal pyramidal cells. *Nature* 425, 828–832.

Jin, D. Z. (2002). Fast convergence of spike sequences to periodic patterns in recurrent networks. *Phys. Rev. Lett.* 89, 208102.

Kayser, C., Montemurro, M. A., Logothetis, N. K., and Panzeri, S. (2009). Spike-phase coding boosts and stabilizes information carried by spatial and temporal spike patterns. *Neuron* 61, 597–608.

Kempter, R., Gerstner, W., and van Hemmen, L. (1999). Hebbian learning and spiking neurons. *Phys. Rev. E* 59, 4498–4514.

König, P., Engel, A. K., Roelfsema, P. R., and Singer, W. (1995). How precise is neuronal synchronization? *Neural Comput.* 7, 469–485.

Latham, P. E., and Lengyel, M. (2008). Phase coding: spikes get a boost from local fields. *Curr. Biol.* 18, R349–R351.

Laurent, G. (2002). Olfactory network dynamics and the coding of multidimensional signals. *Nat. Rev. Neurosci.* 3, 884–895.

Lee, A. K., and Wilson, M. A. (2002). Memory of sequential experience in the hippocampus during slow wave sleep. *Neuron* 36, 1183–1194.

Leibold, C., Gundlfinger, A., Schmidt, R., Thurley, K., Schmitz, D., and Kempter, R. (2008). Temporal compression mediated by short-term synaptic plasticity. *Proc. Natl. Acad. Sci. U.S.A.* 105, 11, 4417–4422.

Lengyel, M., and Dayan, P. (2007). "Uncertainty, phase and oscillatory hippocampal recall," in *Advances in Neural Information Processing Systems 19* eds D. Schölkopf et al. (Cambridge, MA: MIT Press), 833–840.

Lengyel, M., Huhn, Z., and Érdi, P. (2005a). Computational theories on the function of theta oscillations. *Biol. Cybern.* 92, 393–408.

Lengyel, M., Kwag, J., Paulsen, O., and Dayan, P. (2005b). Matching storage and recall: hippocampal spike timing-dependent plasticity and phase response curves. *Nat. Neurosci.* 8, 1677–1683.

Magee, J. C., and Johnston, D. (1997). A synaptically controlled associative signal for Hebbian plasticity in hippocampal neurons. *Science* 275, 209–212.

Markram, H., Lubke, J., Frotscher, M., and Sakmann, B. (1997). Regulation of synaptic efficacy by coincidence of postsynaptic APs and EPSPs. *Science*, 275, 213–215.

Masquelier, T., Guyonneau, R., and Thorpe, S. J. (2009). Competitive STDP-based spike pattern learning. *Neural Comput.* 21, 1259–1276.

Mehta, M. R., Lee, A. K., and Wilson, M. A. (2002). Role of experience and oscillations in transforming a rate code into a temporal code. *Nature* 417, 741–746.

Memmesheimer, R.-M., and Timme, M. (2006a). Designing the dynamics of spiking neural networks. *Phys. Rev. Lett.* 97, 188101.

Memmesheimer, R.-M., and Timme, M. (2006b). Designing complex networks. *Physica D* 224, 182–201.

O'Keefe, J., and Recce, M. L. (1993). Phase relationship between hippocampal place units and the EEG theta rhythm. *Hippocampus* 3, 317–330.

Pajevic, S., and Plenz, D. (2009). Efficient network reconstruction from dynamical cascades identifies small-world topology of neuronal avalanches. *PLoS Comput. Biol.* 5, e1000271. doi:10.1371/journal.pcbi.1000271.

Pellegrini, G. L., de Arcangelis, L., Herrmann, H. J., and Perrone-Capano, C. (2007) Activity-dependent neural network model on scale-free networks *Phys. Rev. E.* 76, 016107.

Rao, R. P., and Sejnowski, T. J. (2001). Spike-timing-dependent Hebbian plasticity as temporal difference learning. *Neural Comput.* 13, 2221–2237.

Scarpetta, S., and Marinaro, M. (2005). A learning rule for place fields in a cortical model: theta phase precession as a network effect. *Hippocampus* 15, 979–989.

Scarpetta, S., Yoshioka, M., and Marinaro, M. (2008). Encoding and replay of dynamic attractors with multiple frequencies. *Lect. Notes Comp. Sci.* 5286, 38–61.

Scarpetta, S., Zhaoping, L., and Hertz, J. (2001). "Spike-timing-dependent learning for oscillatory networks, in *NIPS*, Vol. 13, eds T. Leen, T. Dietterich and V. Tresp (Cambridge, MA: MIT Press), 152–165.

Scarpetta, S., Zhaoping, L., and Hertz, J. (2002a). Hebbian imprinting and retrieval in oscillatory neural networks. *Neural Comput.* 14, 2371–2396.

Scarpetta, S., Zhaoping, L., and Hertz, J. (2002b). "Learning in an oscillatory cortical model," in *Scaling and Disordered Systems*, eds F. Family, M. Daoud, H. Herrmann and E. H. Stanley (Singapore: World Scientific Publishing), 292.

Siegel, M., Warden, M. R., and Miller, E. K. (2009). Phase-dependent neuronal coding of objects in short-term memory. *PNAS* 106, 21341–21346.

Singer, W. (1999). Neuronal synchrony: a versatile code for the definition of relations. *Neuron* 24, 49–65.

Sjostrom, P. J., Turrigiano, G., and Nelson, S. B. (2001). Rate, timing, and cooperativity jointly determine cortical synaptic plasticity. *Neuron* 32, 1149–1164.

Song, S., Miller, K. D., and Abbott, L. F. (2000). Competitive Hebbian learning through spike-timing-dependent synaptic plasticity. *Nat. Neurosci.* 3, 919–926.

Sporns, O., Chialvo, D., Kaiser, M., and Hilgetag, C. C. (2004). Organization, development and function of complex brain networks. *Trends Cogn. Sci.* 8, 418–425.

Sporns, O., and Zwi, J. D. (2004). The small world of the cerebral cortex. *Neuroinformatics* 2, 145–162.

Thurley, K., Leibold, C., Gundlfinger, A., Schmitz, D., and Kempter, R. (2008). Phase precession through synaptic facilitation. *Neural Comput.* 20, 1285–1324.

Treves, A. (1990). Graded-response neurons and information encodings in autoassociative memories. *Phys. Rev. A* 42, 2418.

Watts, D. J., and Strogatz, S. H. (1998). Collective dynamics of "small-world" networks. *Nature* 393, 440–442.

White, J. G., Southgate, E., Thomson, J. N., and Brenner, S. (1986). The structure of the nervous system of the nematode Caenorhabditis elegans. *Philos. Trans. R. Soc. Lond. B Biol. Sci.* 314, 1–340.

Wills, T., Lever, C., Cacucci, F., Burgess, N., and O'Keefe, J. (2005). Attractor dynamics in the hippocampal representation of the local environment. *Science* 308, 873–876.

Wittenberg, G. M., and Wang, S.-H. (2006). Malleability of spike-timing-dependent plasticity at the CA3-CA1 synapse. *J. Neurosci.* 26, 6610–6617.

Wu, Z., and Yamaguchi, Y. (2010). Independence of the unimodal tuning of firing rate from theta phase precession in hippocampal place cells. *Biol. Cybern.* 102, 95–107.

Yoshioka, M. (2009). Learning of spatio-temporal patterns in ising-spin neural networks: analysis of storage capacity by path integral methods. *Phys. Rev. Lett.* 102, 158102.

Yoshioka, M., Scarpetta, S., and Marinaro, M. (2007). Spatiotemporal learning in analog neural networks using spike-timing-dependent synaptic plasticity. *Phys. Rev. E* 75, 051917.

Yu, S., Huang, D., Singer, W., and Nikolić, D. (2008). A small world of neuronal synchrony. *Cerebral Cortex* 18, 2891–2901.

Conflict of Interest Statement: The authors declare that the research was conducted in the absence of any commercial or financial relationships that could be construed as a potential conflict of interest.

Received: 31 January 2010; paper pending published: 26 February 2010; accepted: 28 June 2010; published online: 23 August 2010.

*Citation: Scarpetta S, de Candia A and Giacco F (2010) Storage of phase-coded patterns via STDP in fully-connected and sparse network: a study of the network capacity. Front. Syn. Neurosci. **2**:32. doi: 10.3389/fnsyn.2010.00032*

frontiers in
SYNAPTIC NEUROSCIENCE

ORIGINAL RESEARCH ARTICLE
published: 21 July 2010
doi: 10.3389/fnsyn.2010.00031

A Ca^{2+}-based computational model for NMDA receptor-dependent synaptic plasticity at individual post-synaptic spines in the hippocampus

Owen J. L. Rackham[1], Krasimira Tsaneva-Atanasova[2], Ayalvadi Ganesh[3] and Jack R. Mellor[4]*

[1] *Department of Engineering Mathematics, Bristol Centre for Complexity Sciences, University of Bristol, University Walk, Bristol, UK*
[2] *Department of Engineering Mathematics, Bristol Centre for Applied Nonlinear Mathematics, University of Bristol, University Walk, Bristol, UK*
[3] *Department of Mathematics, Bristol Centre for Complexity Sciences, University of Bristol, University Walk, Bristol, UK*
[4] *Department of Anatomy, Medical Research Council Centre for Synaptic Plasticity, University of Bristol, University Walk, Bristol, UK*

Edited by:
Per Jesper Sjöström, University College London, UK

Reviewed by:
Harel Z. Shouval, University of Texas Medical School at Houston, USA
Thomas G. Oertner, Friedrich Miescher Institute for Biomedical Research, Switzerland

****Correspondence:***
Jack R. Mellor, Department of Anatomy, Medical Research Council Centre for Synaptic Plasticity, University of Bristol, University Walk, Bristol, UK. e-mail: jack.mellor@bristol.ac.uk

Associative synaptic plasticity is synapse specific and requires coincident activity in pre-synaptic and post-synaptic neurons to activate NMDA receptors (NMDARs). The resultant Ca^{2+} influx is the critical trigger for the induction of synaptic plasticity. Given its centrality for the induction of synaptic plasticity, a model for NMDAR activation incorporating the timing of pre-synaptic glutamate release and post-synaptic depolarization by back-propagating action potentials could potentially predict the pre- and post-synaptic spike patterns required to induce synaptic plasticity. We have developed such a model by incorporating currently available data on the timecourse and amplitude of the post-synaptic membrane potential within individual spines. We couple this with data on the kinetics of synaptic NMDARs and then use the model to predict the continuous spine $[Ca^{2+}]$ in response to regular or irregular pre- and post-synaptic spike patterns. We then incorporate experimental data from synaptic plasticity induction protocols by regular activity patterns to couple the predicted local peak $[Ca^{2+}]$ to changes in synaptic strength. We find that our model accurately describes $[Ca^{2+}]$ in dendritic spines resulting from NMDAR activation during pre-synaptic and post-synaptic activity when compared to previous experimental observations. The model also replicates the experimentally determined plasticity outcome of regular and irregular spike patterns when applied to a single synapse. This model could therefore be used to predict the induction of synaptic plasticity under a variety of experimental conditions and spike patterns.

Keywords: synaptic plasticity, hippocampus, dendritic spines, NMDA receptor, spike timing-dependent plasticity

INTRODUCTION

Hebbian synaptic plasticity is the cellular and molecular correlate of associative learning in the brain. During presentation of information that needs to be retained for future use, specific synapses are subjected to activity patterns that induce a long-term change in synaptic strength. For Hebbian synaptic plasticity at Schaffer collateral synapses in the hippocampus, these patterns require coincident activity in pre- and post-synaptic neurons to activate NMDA receptors (NMDARs) present on the membrane of the post-synaptic dendritic spine. The resulting Ca^{2+} influx through NMDARs is the critical trigger for induction of synapse specific plasticity (Lisman, 1989).

Classically, high frequency synaptic stimulation induces long-term potentiation (LTP) whereas low frequency stimulation induces long-term depression (LTD) suggesting that brief high concentrations of Ca^{2+} in the post-synaptic spine induce LTP whereas prolonged lower concentrations of Ca^{2+} induce LTD (Bear et al., 1987; Hansel et al., 1996). This hypothesis is supported by measurements of Ca^{2+} concentration during plasticity induction (Hansel et al., 1997; Cho et al., 2001; Cormier et al., 2001; Ismailov et al., 2004; Gall et al., 2005) and by plasticity induction protocols designed to vary Ca^{2+} influx through NMDARs by fixing the post-synaptic membrane potential during low frequency synaptic stimulation (Isaac et al., 1995; Daw et al., 2000).

Spike timing-dependent plasticity (STDP) is a form of Hebbian synaptic plasticity that incorporates a temporal specificity to coincident pre- and post-synaptic activity. In the hippocampus, STDP was originally thought to be induced by single pairs of pre- and post-synaptic action potentials such that if the pre-synaptic action potential occurs before the post-synaptic action potential LTP is induced whereas if the order of action potentials is reversed then LTD is induced (Bi and Poo, 1998; Debanne et al., 1998; Nishiyama et al., 2000; Campanac and Debanne, 2008; Kwag and Paulsen, 2009). Other data have proposed this model should include a requirement for bursts of post-synaptic action potentials for the induction of LTP although LTD may be induced by single pairs (Pike et al., 1999; Wittenberg and Wang, 2006; Buchanan and Mellor, 2007) reviewed in (Buchanan and Mellor, 2010). This is a divergence from the situation at cortical synapses where single pairs of action potentials can induce both LTP and LTD (Sjostrom et al., 2001; Sjostrom and Nelson, 2002; Froemke et al., 2006, but see Nevian and Sakmann, 2006).

Since Ca^{2+} influx through NMDARs is pivotal for LTP and LTD, this suggests the induction of synaptic plasticity can be predicted by NMDAR opening kinetics in response to pre-synaptic glutamate release and post-synaptic depolarization. This approach has been adopted for the modeling of post-synaptic calcium dynamics in response to synaptic stimulation or back-propagating action potentials (Franks et al., 2002; Grunditz et al., 2008; Keller et al., 2008) and to STDP induction protocols (Shouval et al., 2002; Rubin et al., 2005; Graupner and Brunel, 2007; Helias et al., 2008; Urakubo et al., 2008; Castellani et al., 2009). However, these STDP models are limited by the experimental data used to determine their parameters and, in addition, ought to accurately predict the plasticity outcomes of a variety of induction protocols. Recent advances in dendritic spine imaging provide data on spine depolarization and Ca^{2+} concentrations in response to pre- and post-synaptic action potentials (Sabatini et al., 2002; Nevian and Sakmann, 2006; Bloodgood and Sabatini, 2007; Canepari et al., 2007; Palmer and Stuart, 2009) that potentially greatly increase the accuracy of such models of plasticity induction.

We have developed a computational model of synaptic plasticity induction based on one originally described by Shouval et al. Our model incorporates the latest experimental data on dendritic spine depolarization and Ca^{2+} dynamics. We also test the predictive power of our model on many plasticity induction protocols by calculating continuous Ca^{2+} concentrations during long induction periods. We find that our model accurately predicts the experimental data tested and we hypothesize that it can thus be used to search for instances of synaptic plasticity induction during continuous activity at Hebbian synapses in the hippocampus.

MATERIALS AND METHODS

We use a physiologically plausible model based on intracellular Ca^{2+} dynamics caused by NMDAR activation during the induction of synaptic plasticity to predict the plasticity outcome of any set of pre- and post-synaptic activity patterns that occur at the Schaffer collateral synapse in the hippocampus. Since we are interested in studying experimental spike trains we modify a model originally proposed by Shouval et al. (2002) to allow us to carry out such analysis. We make a number of critical modifications to analyze the Ca^{2+} dynamics in individual dendritic spines during long periods of irregular spiking activity. This is illustrated using short epochs of overlapping hippocampal place cell activity (**Figure 1**) (Isaac et al., 2009).

Essential components of the experimental spike trains for the activation of NMDARs and therefore the induction of synaptic plasticity are (i) the pre-synaptic release of glutamate that dictates the binding of glutamate to the NMDARs and (ii) the post-synaptic membrane potential that determines the relative blockade of NMDARs by Mg^{2+}. For the purposes of this model, we have assumed the two events that determine the post-synaptic membrane potential within an individual dendritic spine are excitatory post-synaptic potentials (EPSPs) and back-propagating action potentials (BPAPs). We start by modeling the BPAPs as follows:

$$\mathrm{BPAP}(t) = \sum_{t_i^{\mathrm{post}} < t} V_{\max}^{\mathrm{bs}} \left(I_{\mathrm{f}}^{\mathrm{bs}} \exp\left(\frac{-(t - t_i^{\mathrm{post}})}{\tau_{\mathrm{f}}^{\mathrm{bs}}} \right), + I_{\mathrm{s}}^{\mathrm{bs}} \exp\left(\frac{-(t - t_i^{\mathrm{post}})}{\tau_{\mathrm{s}}^{\mathrm{bs}}} \right) \right) \quad (1)$$

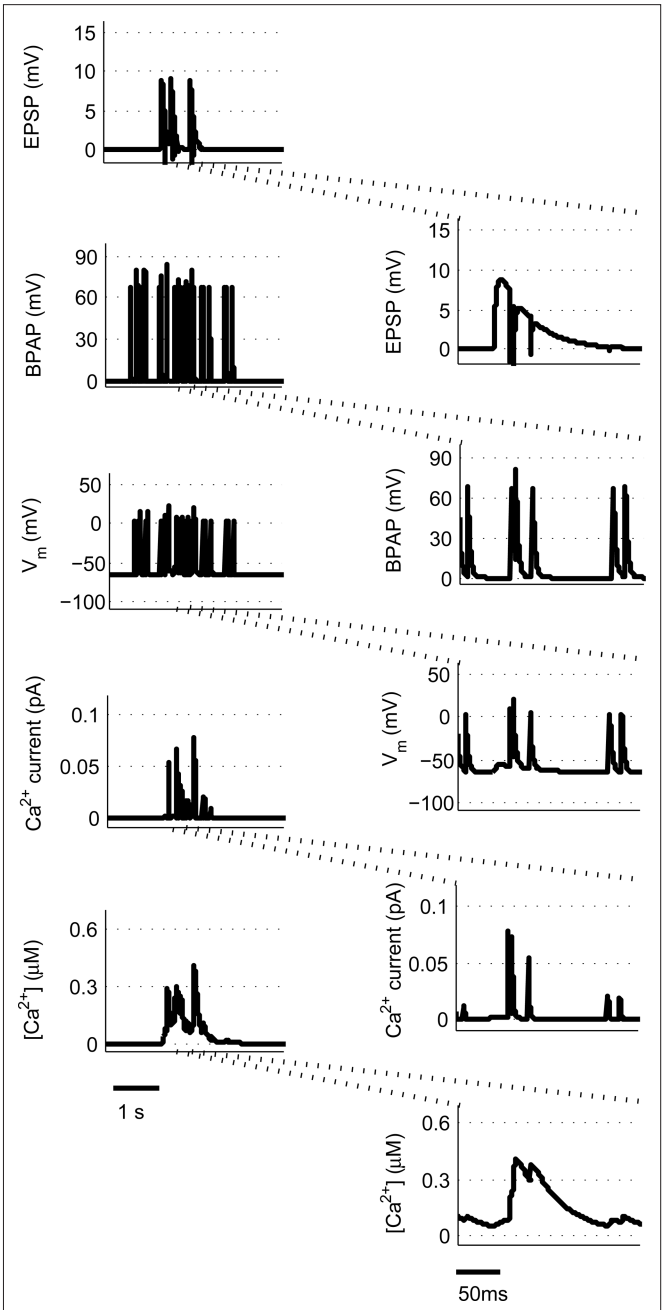

FIGURE 1 | Calculating $[Ca^{2+}]$ in dendritic spines during continuous pre- and post-synaptic activity. The model initially calculates the membrane potential during continuous activity by summating the membrane potential changes due to EPSPs and BPAPs from a resting membrane potential of –65 mV. The Ca^{2+} current passing through synaptic NMDARs is then calculated from the membrane potential and glutamate binding kinetics. Finally spine $[Ca^{2+}]$ is calculated from Ca^{2+} buffering and diffusion kinetics. Left hand panels show the post-synaptic responses to an epoch of place cell activity spanning 3500 ms. Right hand panels show a 200 ms excerpt from this epoch.

where $V_{\max}^{\mathrm{bs}}$ is the maximum depolarization due to the BPAP, $I_{\mathrm{f}}^{\mathrm{bs}}$, and $I_{\mathrm{s}}^{\mathrm{bs}}$ are the relative magnitudes of the fast and slow components of the BPAP, respectively, that sum to one, and the integration time step δ is 0.1 ms. Due to the slower (and much smaller) after-depolarizing

potential, if two spikes happen near enough to each other that the first spike is still decaying, the effect of the BPAPs is additive. Since we are modeling the BPAP at the spine V_{max}^{bs} is set at 67 mV in line with experimental data measuring membrane potential in spines with voltage-sensitive dyes (Canepari et al., 2007; Palmer and Stuart, 2009). This is smaller than the maximum BPAP amplitude found at the soma used by Shouval et al. An example of the modeled BPAP during place cell activity can be seen in **Figure 1**.

The equation that governs the behavior of AMPAR-mediated EPSPs in the model is similar to (1) having a slow and a fast exponential component:

$$\mathrm{EPSP}_{\mathrm{AMPA}}(t) = N_a \sum_{t_i^{pre}<t} \left(\exp\left(\frac{-(t-t_i^{pre})}{\tau_s^{ep}}\right) + \exp\left(\frac{-(t-t_i^{pre})}{\tau_f^{ep}}\right)\right)\frac{(V_m - V_{r1})}{V_{rest}}, \quad (2)$$

where the parameter N_a reflects the maximum effect that a single AMPAR-mediated EPSP can have. The value of N_a can vary depending on the number of synapses activated. Activation of a single synapse results in a membrane depolarization in the spine of approximately 10 mV (Palmer and Stuart, 2009). Again this deviates from the value of 1 mV recorded at the soma and used by Shouval et al. Assuming that the maximum depolarization that a single EPSP can generate is 10 mV we define N_a in the following way:

$$\mathrm{EPSP}_{\mathrm{AMPA}}(t) = \left[\exp\left(\frac{-t}{\tau_f^{ep}}\right) + \exp\left(\frac{-t}{\tau_s^{ep}}\right)\right]\frac{(V_m - V_{r1})}{V_{rest}} \Rightarrow$$

$$\frac{d\mathrm{EPSP}_{\mathrm{AMPA}}(t)}{dt} = \left[-\frac{1}{\tau_f^{ep}}\exp\left(\frac{-t}{\tau_f^{ep}}\right) - \frac{1}{\tau_s^{ep}}\exp\left(\frac{-t}{\tau_s^{ep}}\right)\right]\frac{(V_m - V_{r1})}{V_{rest}}$$

$$= 0 \Rightarrow$$

$$t = -\left(\frac{\tau_f^{ep}\tau_s^{ep}(\log\tau_s^{ep} + \log\tau_f^{ep})}{\tau_f^{ep} + \tau_s^{ep}}\right) \Rightarrow$$

$$\max(t) = 0.0128 \Rightarrow \mathrm{EPSP}(\max(t)) = 0.6968 \Rightarrow$$

$$N_a = \frac{10}{0.6968}.$$

$\mathrm{EPSP}_{\mathrm{AMPA}}$ also depends on the membrane potential, V_m. This dependence is represented by the term $(V_m - V_{r1})/V_{rest}$ where V_{r1} is the reversal potential for AMPARs (0 mV) and V_{rest} is the resting membrane potential (−65 mV).

The equation that governs the behavior of NMDA-mediated EPSPs in the model has the following form:

$$\mathrm{EPSP}_{\mathrm{NMDA}}(t) = N_n \sum_{t_i^{pre}<t} \left(I_f \Theta(t_i)\exp\left(\frac{-(t-t_i)}{\tau_f}\right) + I_s \Theta(t_i)\exp\left(\frac{-(t-t_i)}{\tau_s}\right)\right) B(V_m)\frac{(V_m - V_{r1})}{V_{rest}}, \quad (3)$$

where the parameter N_n reflects the maximum effect of the NMDAR-mediated component of the EPSP. This is calculated in a similar fashion to N_a for $\mathrm{EPSP}_{\mathrm{AMPA}}$ using a value of 5 mV for the NMDAR-mediated EPSP at −65 mV in the absence of Mg^{2+} measured by dendritic recordings (Fernandez de Sevilla et al., 2007).

$$\mathrm{EPSP}_{\mathrm{NMDA}}(t) = \left[I_f \exp\left(\frac{-t}{\tau_f^{ep}}\right) + I_s \exp\left(\frac{-t}{\tau_s^{ep}}\right)\right]\frac{(V_m - V_{r1})}{V_{rest}} \Rightarrow$$

$$\frac{d\mathrm{EPSP}_{\mathrm{NMDA}}(t)}{dt} = \left[-I_f \frac{1}{\tau_f^{ep}}\exp\left(\frac{-t}{\tau_f^{ep}}\right) - I_s \frac{1}{\tau_s^{ep}}\exp\left(\frac{-t}{\tau_s^{ep}}\right)\right]\frac{(V_m - V_{r1})}{V_{rest}}$$

$$= 0 \Rightarrow$$

$$\max(t) = 0.0924 \Rightarrow \mathrm{EPSP}(\max(t)) = 0.0812 \Rightarrow$$

$$N_n = \frac{5}{0.0812}.$$

I_f and I_s are the relative magnitudes of the fast and slow component of the NMDAR current as a result of glutamate binding, respectively, that sum to one, and Θ is the Heaviside (unit) step function. The voltage dependence of the current that takes into account Mg^{2+} block of the receptor (Jahr and Stevens, 1990) is represented by the term $B(V_m)(V_m - V_{r1})/V_{rest}$, where $(V_m - V_{r1})$ is the driving force determined by the reversal potential, V_{r1} (0 mV), and

$$B(V_m) = \frac{1}{1 + \exp(-K_M V_m)([\mathrm{Mg}]/3.57)}.$$

We then calculate the spine membrane potential as the summation of BPAP and $\mathrm{EPSP}_{\mathrm{AMPA}}$ and $\mathrm{EPSP}_{\mathrm{NMDA}}$:

$$V_m(t) = V_{rest} + \mathrm{BPAP}(t) + \mathrm{EPSP}_{\mathrm{AMPA}}(t) + \mathrm{EPSP}_{\mathrm{NMDA}}(t), \quad (4)$$

where V_{rest} is set at −65 mV unless otherwise stated. An example of the predicted spine voltage can be seen for a sample epoch of overlapping place cell activity in **Figure 1**.

Since NMDARs provide the major source of Ca^{2+} influx into post-synaptic dendritic spines (Bloodgood and Sabatini, 2007), we incorporate in our model the Ca^{2+} current through NMDAR that takes the following form (Shouval et al., 2002):

$$I_{\mathrm{NMDA}}(t) = \sum_{t_i^{pre}<t} P_0 G_{\mathrm{NMDA}} \left(I_f \Theta(t_i)\exp\left(\frac{-(t-t_i)}{\tau_f}\right) + I_s \Theta(t_i)\exp\left(\frac{-(t-t_i)}{\tau_s}\right)\right) B(V_m)(V_m - V_{r2}), \quad (5)$$

This is similar to Eq. 3 except for the terms P_0 and G_{NMDA} that represent the open channel probability and NMDAR Ca^{2+} conductance respectively and V_{r2} is the reversal potential for calcium (130 mV).

Next, the rate of change of the $[Ca^{2+}]$ inside the post-synaptic spine is governed by:

$$\frac{d[Ca^{2+}]}{dt} = \alpha I_{\mathrm{NMDA}} - \frac{[Ca^{2+}]}{\tau_{Ca}}, \quad (6)$$

where α is a factor that converts current to flux and τ_{Ca} is the calcium passive decay time constant. An example of the Ca^{2+} current flow through NMDARs and the resulting predicted $[Ca^{2+}]$ in the spine can be seen in **Figure 1**.

Finally, we assume that spine $[Ca^{2+}]$ is the trigger for synaptic strength change. For the purposes of our study the continuous model for synaptic strength used in Shouval et al. is modified to act as a Ca^{2+}-gated function based on local peaks in $[Ca^{2+}]$ as follows:

$$\forall [Ca^{2+}]' = 0 \wedge [Ca^{2+}]'' < 0 : W_{j+1} = \begin{cases} W_j + \frac{1}{W_j}\left(\eta[Ca_j^{2+}]\right)\left(\Omega[Ca_j^{2+}]\right), & \left(\Omega[Ca_j^{2+}]\right) > 0 \\ W_j\left[1 + \left(\eta[Ca_j^{2+}]\right)\left(\Omega[Ca_j^{2+}]\right)\right], & \left(\Omega[Ca_j^{2+}]\right) \leq 0 \end{cases} \quad (7)$$

where

$$\Omega[Ca_j^{2+}] = \frac{\exp(\beta_2(Ca_j^{2+} - \alpha_2))}{1 + \exp(\beta_2(Ca_j^{2+} - \alpha_2))} - 0.25\frac{\exp(\beta_1(Ca_j^{2+} - \alpha_1))}{1 + \exp(\beta_1(Ca_j^{2+} - \alpha_1))},$$

$$\eta[Ca_j^{2+}] = \frac{1}{f(Ca_j^{2+})}, \quad f(Ca_j^{2+}) = \frac{P_1}{P_2 + (Ca_j^{2+})^{P_3}} + P_4.$$

The critical target for Ca^{2+} influx through NMDARs is the enzyme CAMKII. Due to its ability to autophosphorylate, the activation of this molecule can be long lived and the level is determined by local peak $[Ca^{2+}]$. Thus, synaptic weight change is determined at local peak $[Ca^{2+}]$ (Miller et al., 2005; Graupner and Brunel, 2007; Helias et al., 2008; Urakubo et al., 2008; Castellani et al., 2009). Since there is no noise associated with our model, these peaks are measured instantaneously without smoothing. Experimentally, increases in synaptic weight tend towards saturation as synaptic weight increases. In addition, decreases require synaptic weight to always be >0. These constraints explain the form of Eq. 7.

Numerical integration was performed using forward Euler method implemented in MATLAB.

The parameter values used in the simulations are given for completeness in **Table 1**.

Table 1 | Parameter values of the synaptic model.

Parameter	Value	Parameter	Value
I_f^{bs}	0.75	α_1	0.3
τ_f^{bs}	3 ms	α_2	0.45
τ_s^{bs}	25 ms	β_1	80
τ_f^{ep}	5 ms	β_2	80
τ_s^{ep}	50 ms	P_1	100 ms
I_f	0.5	P_2	0.02 ms
τ_f	50 ms	P_3	4
τ_s	200 ms	P_4	1000 ms
τ_{Ca}	50 ms	P_0	0.5
V_{max}^{bs}	67 mV	G_{NMDA}	0.002 μM/ms mV
V_{rest}	–65 mV	K_M	0.092 mV^{-1}
V_{r1}	0 mV	N_a	14.35 mV
V_{r2}	130 mV	N_n	61.58 mV

RESULTS

Our starting point for developing a model for the induction of synaptic plasticity was to incorporate the most recent and accurate measurements of voltage changes within dendritic spines using data from measurements of voltage-dependent dyes (Canepari et al., 2007; Palmer and Stuart, 2009). We model the membrane potential at the spine rather than the soma because this is the site of the NMDARs critical for the induction of synaptic plasticity. This shifts the determination of membrane depolarization away from BPAPs and towards EPSPs since the former attenuate as they pass along the dendrite and the latter are now measured at their site of origin. This is a departure from previous models that used values for BPAPs and EPSPs recorded at the soma (Shouval et al., 2002). With this change, our model predicts that an EPSP resulting from the activation of a single synapse is sufficient to cause a significant Ca^{2+} influx through NMDARs (**Figure 2A**) in line with experimentally observed data (Bloodgood and Sabatini, 2007; Canepari et al., 2007; Sobczyk and Svoboda, 2007). The pairing of a BPAP with a single EPSP with a time delay of 10 ms produces 3–4 times the Ca^{2+} influx (**Figure 2A**) that again agrees qualitatively with experimentally observed data (Bloodgood and Sabatini, 2007). For comparison we changed the maximal EPSP and BPAP amplitudes to those known to occur at the soma (~1 and ~100 mV respectively). With these parameters, a single EPSP produces limited Ca^{2+} influx whereas pairing an EPSP with a BPAP produces a large Ca^{2+} influx (**Figure 2B**).

Having validated our model for the observed Ca^{2+} influx at dendritic spines we next asked the question if the model could replicate experimental data for the induction of synaptic plasticity using a variety of protocols. We have restricted our model to comparisons with experimental data from the Schaffer collateral synapse of the hippocampus and not considered other synapses in other brain regions.

SPIKE TIMING-DEPENDENT PLASTICITY WITH PAIRS OF PRE- AND POST-SYNAPTIC SPIKES

To model STDP with pairs of pre- and post-synaptic spikes we initially assumed single synaptic activation and varied Δt between –20 and + 100 ms at intervals of 0.1 ms measuring the peak $[Ca^{2+}]$ at each value of Δt (**Figure 3A**). $[Ca^{2+}]$ rose from its baseline of 72 nM (the peak $[Ca^{2+}]$ attained for a single EPSP in isolation) to a peak of 230 nM at $\Delta t \approx 10$ ms (**Figure 3B**). Experiments such as these have been shown to generate no significant synaptic plasticity (Buchanan and Mellor, 2007) whereas those using larger amplitude EPSPs have been shown to generate LTD (Wittenberg and Wang, 2006). We estimated the activation of multiple synapses at the same time would increase the depolarization within a single dendritic spine during an EPSP from 10 to 20 mV based on experimental predictions (Palmer and Stuart, 2009). Thus we have estimated that the activation of other spines will contribute an additional 10 mV of depolarization within an activated spine above and beyond the experimentally determined 10 mV for activation of a single synapse. This doubling of the EPSP amplitude resulted in an increase in peak $[Ca^{2+}]$ at all values of Δt with a peak of 279 nM occurring at $\Delta t \approx 10$ ms (**Figure 3C**).

It has also been shown that the frequency of spike pairing is important for the induction of plasticity such that at higher frequencies (>5–10 Hz) LTP can be induced (Wittenberg and Wang, 2006; Buchanan and Mellor, 2007). We varied the frequency of spike pairings in our model for 10 mV EPSPs over a range of frequencies from 1 to 100 Hz (**Figure 3D**). Summation of Ca^{2+} transients was found to occur at frequencies greater than ~5 Hz indicating that increasing the frequency will shift the STDP protocol towards larger $[Ca^{2+}]$ and therefore LTP in line with the experimental data.

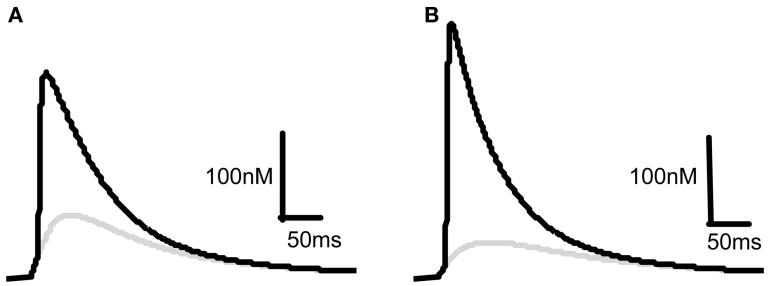

FIGURE 2 | Comparison of predicted [Ca^{2+}] dynamics in dendritic spines and in the soma. [Ca^{2+}] profiles in response to a 10 mV EPSP at the spine **(A)** or a 1 mV EPSP at the soma **(B)** on their own (gray) or in combination with a BPAP (black) of amplitude 60 mV at the spine **(A)** or 100 mV at the soma **(B)**. The delay between EPSP and BPAP initiation is 10 ms.

SPIKE TIMING-DEPENDENT PLASTICITY WITH TRIPLETS OF SPIKES

Post-synaptic burst firing has been shown to be important for the induction of LTP at Schaffer collateral synapses in the hippocampus where burst firing in this instance refers to any number of spikes greater than one (Pike et al., 1999; Wittenberg and Wang, 2006; Buchanan and Mellor, 2007). We tested this on our model using triplets of spikes composed of one pre-synaptic spike and two post-synaptic spikes where Δt is the time between the pre-synaptic spike and the first post-synaptic spike and Δs is the delay between the two post-synaptic spikes (**Figure 4A**). We first used 10 mV EPSPs with a constant Δs of 10 ms and varied Δt between −20 and +100 ms. This produced a peak [Ca^{2+}] of 420 nM at $\Delta t = 4$ ms which increased to a peak [Ca^{2+}] of 475 nM when 20 mV EPSPs were used (**Figure 4B**) confirming that spike triplets produce higher peak [Ca^{2+}] than spike pairs and therefore are more likely to induce LTP.

We next varied Δs whilst maintaining Δt constant at 10 ms for both 10 and 20 mV EPSPs revealing a decrease in peak [Ca^{2+}] as Δs increases (**Figure 4C**). Finally, we varied the frequency of triplets for 10 mV EPSPs over a range of frequencies from 1 to 100 Hz whilst keeping Δt and Δs constant at 10 ms each (**Figure 4D**). Summation of Ca^{2+} transients was found to occur at frequencies greater than ~4 Hz.

THETA BURST PLASTICITY

We now moved away from STDP to look at other common synaptic plasticity induction protocols. The theta burst protocol was developed to mimic the activity patterns believed to occur at hippocampal synapses during learning and consists of bursts of four or five spikes at 100 Hz with an interburst interval of 200 ms. These can either be applied to the pre- and post-synaptic neuron coincidentally (Frick et al., 2004) or to just the pre-synaptic neuron (Larson et al., 1986). The latter then leads to post-synaptic spikes through EPSP summation if the initial EPSP amplitude is sufficiently large (Buchanan and Mellor, 2007). We used our model to mimic coincident theta burst activity in pre- and post-synaptic neurons using 10 mV EPSPs and found that this type of synaptic stimulation produces very large peak [Ca^{2+}] within dendritic spines (**Figure 5**) indicating that this protocol is very efficient at producing LTP in agreement with experimental data. Experimental data also shows when theta burst stimulation is given to only the pre-synaptic neuron without initiating action potentials then no plasticity is induced (Buchanan and Mellor, 2007). When we used theta burst stimulation with five stimuli to only the pre-synaptic input, the model predicted peak [Ca^{2+}] within the spine to be 325 nM (**Figure 5**) and with four stimuli 250 nM. The value for four stimuli is more physiologically relevant since the probability of neurotransmitter release at any one Schaffer collateral synapse is considerably less than 1. Therefore it is highly unlikely that an experimental theta burst will ever generate five EPSPs at an individual synapse.

PAIRING POST-SYNAPTIC DEPOLARIZATION WITH PRE-SYNAPTIC STIMULATION

Other common synaptic plasticity induction protocols have dispensed with the need for post-synaptic spikes altogether and use voltage clamp to depolarize the post-synaptic membrane and allow NMDAR activation. This technique neatly demonstrates the bidirectional nature of NMDAR-dependent plasticity since depolarization to moderate levels (−40 mV) produces LTD whereas higher depolarization (0 mV) produces LTP (Isaac et al., 1995; Daw et al., 2000). We tested this with our model by clamping the membrane potential (V_m) at either −40 or 0 mV (**Figure 6**). Peak [Ca^{2+}] in response to EPSPs were 336 nM and 2.43 μM respectively, which when compared to peak [Ca^{2+}] produced by other protocols would be expected to induce LTD and LTP respectively in agreement with experimental data.

THE CA^{2+} HYPOTHESIS CAN EXPLAIN PREVIOUS EXPERIMENTAL DATA

The Ca^{2+} hypothesis states that brief high concentrations of Ca^{2+} in the post-synaptic spine induce LTP whereas prolonged lower concentrations of Ca^{2+} induce LTD (Bear et al., 1987; Hansel et al., 1996). This is expressed graphically in **Figure 7**. Points are indicated representing the predicted [Ca^{2+}] from our model for specific plasticity inducing protocols. STDP with single pairs of BPAPs and small EPSPs do not induce plasticity (Buchanan and Mellor, 2007) but when large EPSPs are used LTD is induced (Wittenberg and Wang, 2006) and STDP with triplets of single EPSPs and bursts of BPAPs produces LTP (Pike et al., 1999; Wittenberg and Wang, 2006; Buchanan and Mellor, 2007). When the post-synaptic membrane potential is set at −40 mV during pre-synaptic stimulation LTD is induced (Daw et al., 2000) whereas at 0 mV LTP is induced (Isaac et al., 1996). Theta burst pairing also induces LTP (Frick et al.,

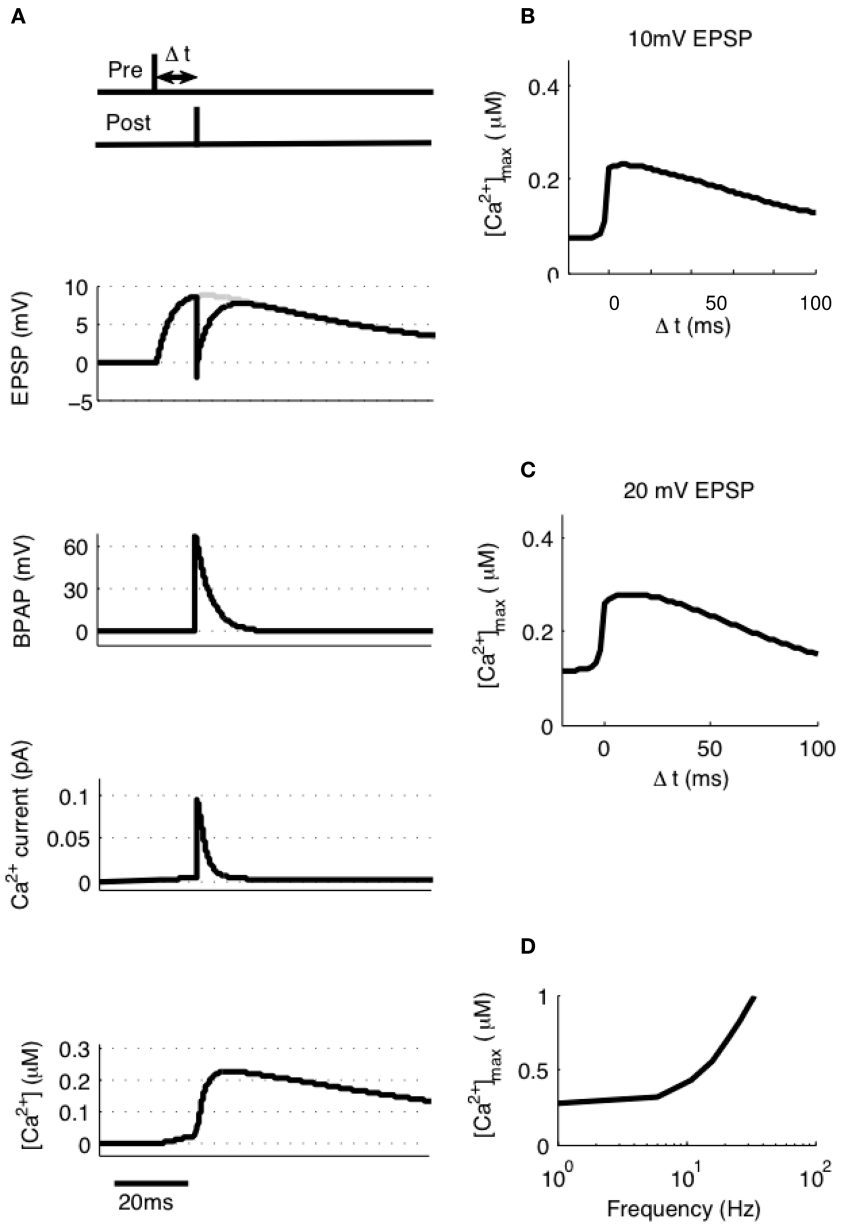

FIGURE 3 | [Ca²⁺] dynamics in response to paired pre- and post-synaptic spikes. (A) The model calculates [Ca^{2+}] within a spine from the membrane potential resulting from a pair of pre- and post-synaptic spikes. Gray line shows EPSP in the absence of BPAP. Varying Δt shows that $[Ca^{2+}]_{max}$ is greatest when $0 \leq \Delta t \leq 30$ ms for 10 mV **(B)** or 20 mV **(C)** EPSPs. **(D)** The frequency of spike pairings given at $\Delta t = 10$ ms determines $[Ca^{2+}]_{max}$.

2004; Buchanan and Mellor, 2007) whereas theta burst to only pre-synaptic inputs does not (Buchanan and Mellor, 2007). In this instance the absolute [Ca^{2+}] values predicted by the model are not as important as the relative magnitudes between plasticity induction protocols. However, it is interesting to note that the absolute [Ca^{2+}] values predicted by the model broadly agree with those measured experimentally for the induction of synaptic plasticity at Schaffer collateral synapses on CA1 pyramidal neurons (Cormier et al., 2001). Thus the predictions from our model support the Ca^{2+} hypothesis for synaptic plasticity induction.

INDUCTION OF SYNAPTIC PLASTICITY BY HIPPOCAMPAL PLACE CELL FIRING PATTERNS

One of the main purposes for developing a model that is capable of continuously monitoring [Ca^{2+}] in spines and therefore predicts changes in synaptic strength is to scan long periods of neuronal activity for epochs that would be expected to induce plasticity without having to directly measure synaptic strength. To test if the model could perform this task we used data from experiments where long sections of hippocampal place cell activity were replayed into single hippocampal synapses to test the plasticity outcome (Isaac et al., 2009).

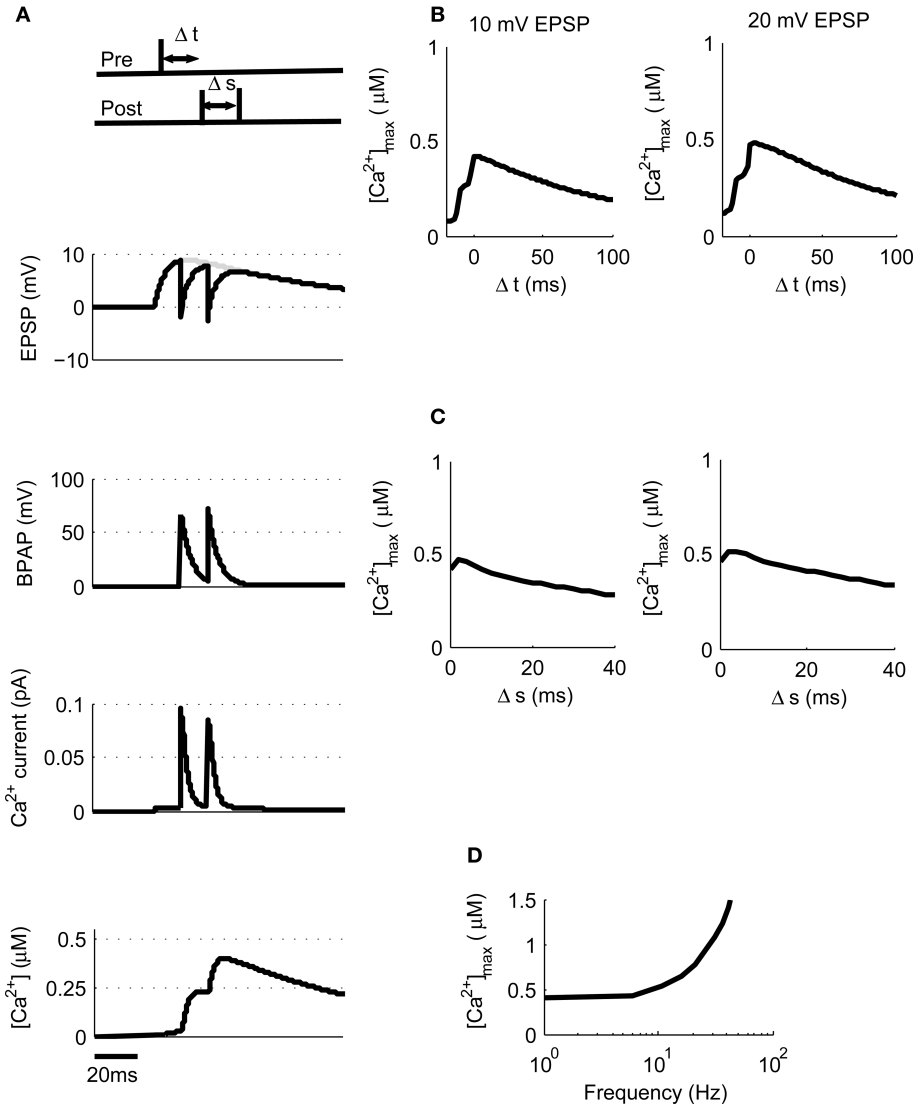

FIGURE 4 | [Ca^{2+}] dynamics in response to triplets of one pre- and two post-synaptic spikes. (A) The model calculates [Ca^{2+}] within a spine from the membrane potential resulting from a triplet of pre- and post-synaptic spikes. Gray line shows EPSP in the absence of BPAP. **(B)**. Varying Δt shows that $[Ca^{2+}]_{max}$ is greatest when $0 \leq \Delta t \leq 30$ ms for 10 or 20 mV EPSPs for $\Delta s = 10$ ms. **(C)** Varying Δs shows that $[Ca^{2+}]_{max}$ decreases as Δs increases for 10 or 20 mV EPSPs and $\Delta t = 10$ ms. **(D)** The frequency of spike pairings given at $\Delta t = 10$ ms and $\Delta s = 10$ ms determines $[Ca^{2+}]_{max}$.

We first took an ~16-min period of activity from a pair of place cells (1_A and 1_B) that had overlapping place fields and therefore would be expected to fire at approximately the same time (Isaac et al., 2009). During the ~16-min period short coincident bursts of activity could be seen in the two place cells that the model predicted would produce large [Ca^{2+}] sufficient to induce LTP (**Figures 1 and 8**). This LTP was initiated in the first few minutes of activity and eventually reached a plateau.

We tested a set of four further pairs of place cells (2_A and 2_B, 2_C and 2_D, 3_A and 3_B, 4_A and 4_B) with overlapping place fields but with strikingly different spiking characteristics [for a full description of the place cell spike pattern characteristics and plasticity outcomes see Isaac et al. (2009)] and found in each case the model predicted robust LTP induction in agreement with the experimental data (**Figures 9A–D**). We also tested two further pairs of place cells with non-overlapping or adjacent place fields (1_A and 1_C, 2_E and 2_D) and found the model predicted only a small LTD for the non-overlapping pair and a small LTP for the adjacent pair (**Figures 9E–F**).

Our original experimental data also tested a pair of place cells that had an asymmetric cross-correlation such that cell 1_A preferentially fired just before cell 1_B. Because classical STDP rules state that the temporal order of pre- and post-synaptic spikes controls the direction of synaptic plasticity (Bi and Poo, 1998; Song et al., 2000), the existence of this asymmetry suggested that when cell 1_A was pre-synaptic and cell 1_B post-synaptic then LTP would be induced but if the cells were reversed then LTD would be induced.

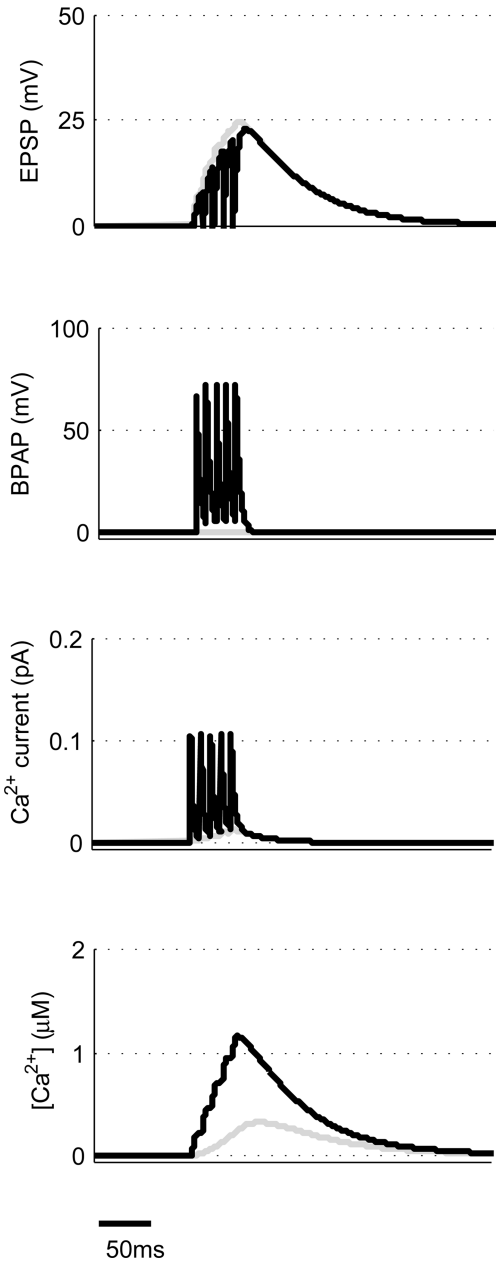

FIGURE 5 | Theta burst pairing produces large spine [Ca²⁺]. The model calculates [Ca²⁺] within a spine from the membrane potential resulting from coincident theta burst stimulation of pre- and post-synaptic neurons (black) or only pre-synaptic neuron (gray).

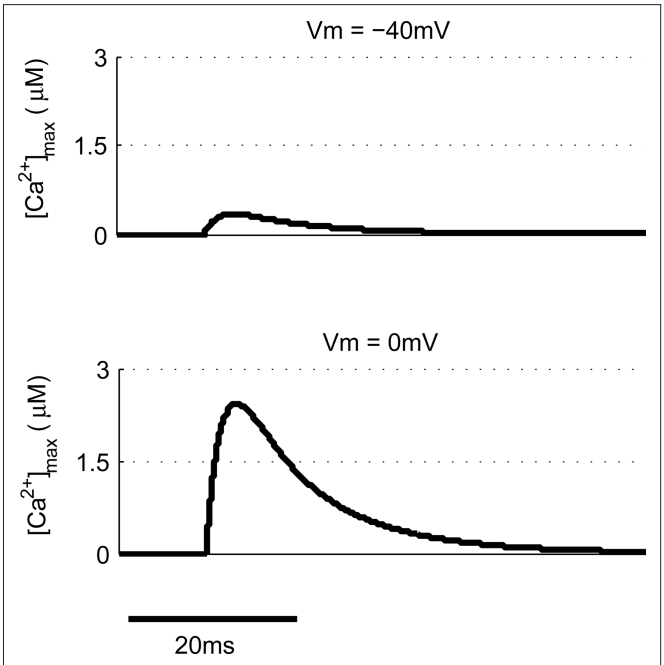

FIGURE 6 | Post-synaptic voltage clamp paired with pre-synaptic stimulation determines spine [Ca²⁺]. The model predicts that voltage clamp of the post-synaptic membrane potential at –40 mV produces a much smaller spine [Ca²⁺] than 0 mV when paired with a single pre-synaptic stimulation.

However, when we reversed the place cell firing patterns such that cell 1_B was pre-synaptic and cell 1_A post-synaptic the model predicted LTP (**Figure 10A**) that corroborates the experimental results and closely reproduces the experimentally determined timecourse of LTP development (Isaac et al., 2009). We also manipulated the spike patterns in cell 1_B to remove all spikes that occurred less than 100 ms after a spike in cell 1_A leaving only spikes that occurred before any spike in cell 1_A. Classical STDP rules would again predict that if cell 1_A was pre-synaptic and the modified cell 1_B was post-synaptic then LTD would be induced but the model predicted only marginal LTD (**Figure 10B**) in line with the experimental data (Isaac et al., 2009).

Finally we have compared the experimentally determined plasticity outcome from nine pairs of place cells with the outcome predicted by our model. We find that the correlation between the predicted and observed values is significant (**Figure 10C**, $r^2 = 0.58$, $P < 0.05$ by linear regression) and therefore conclude that the model successfully predicts the induction of synaptic plasticity by irregular activity patterns.

DISCUSSION

The model described in this study incorporates two important components of Ca^{2+} dynamics in dendritic spines that are necessary for the induction of synaptic plasticity. Firstly, our model is capable of analyzing Ca^{2+} influx and concentration continuously and therefore it can determine the plasticity outcome of multiple synaptic events that occur *in vivo* in an irregular pattern. Secondly, $[Ca^{2+}]$ is modeled at the synapse in dendritic spines rather than at the soma. This is important since the critical Ca^{2+} signal for the induction of synaptic plasticity occurs at the spine. It also changes the relative importance of EPSP vs BPAP depolarization which has major implications for the predicted induction of STDP. This approach is validated by comparison of the predicted vs observed Ca^{2+} transients in response to either a single EPSP or coupled with a BPAP (**Figure 2**) (Bloodgood and Sabatini, 2007).

The absolute values for $[Ca^{2+}]$ within the dendrite required for the induction of synaptic plasticity have been estimated as 150–500 nM for LTD and >500 nM for LTP (Cormier et al., 2001). However, other researchers have estimated $[Ca^{2+}]$ within a spine

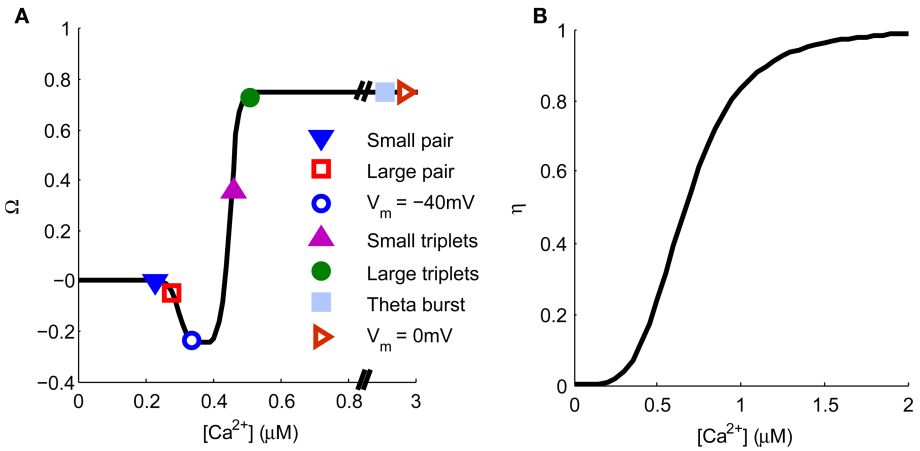

FIGURE 7 | Spine [Ca^{2+}] determines the direction and magnitude of synaptic weight change. (A). The Ω–function describes the relationship between peak spine [Ca^{2+}] and synaptic weight change. Symbols represent the peak [Ca^{2+}] produced by a single application of the plasticity induction protocols shown in **Figures 3–6** and indicate the resulting predicted synaptic weight change. **(B)** The η-function describes the learning rate for synaptic weight change as a function of peak spine [Ca^{2+}].

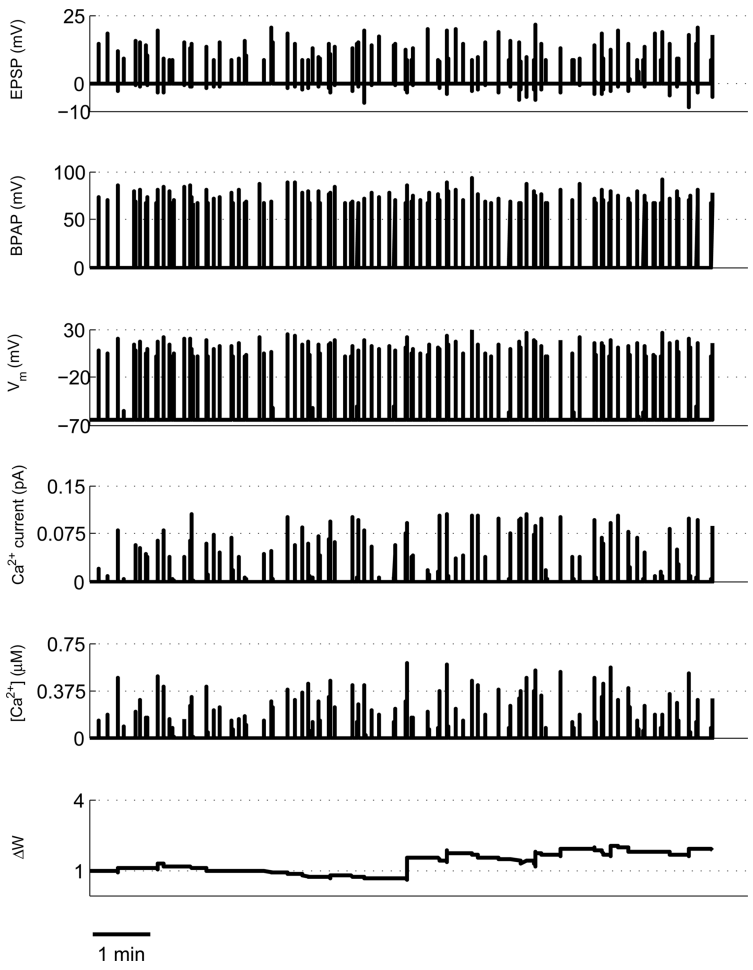

FIGURE 8 | Example of predicted synaptic weight change during overlapping place cell activity. The model calculates spine [Ca^{2+}] during a ~16-min period of activity from two place cells (1_A and 1_B) with overlapping place fields. The synaptic weight change is then calculated from the peak spine [Ca^{2+}] and shows a robust, rapidly developing potentiation.

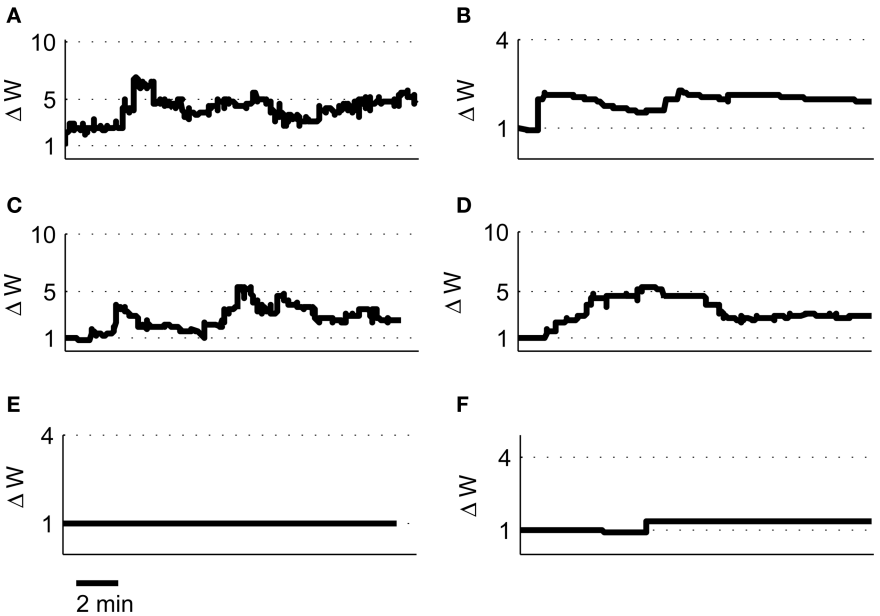

FIGURE 9 | Predicted synaptic weight changes for overlapping and non-overlapping place cell activity. Calculated synaptic weight changes for four pairs of overlapping place cells 2_A, 2_B **(A)**, 2_C, 2_D **(B)**, 3_A, 3_B **(C)**, and 4_A, 4_B **(D)** as well as one pair of non-overlapping place cells 1_A, 1_C **(E)** and one pair of adjacent place cells 2_E, 2_D **(F)**.

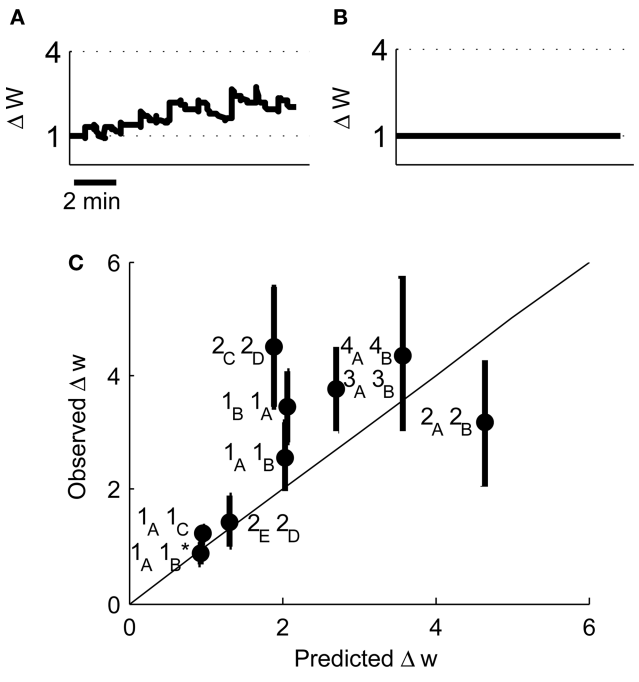

FIGURE 10 | Predicted synaptic weight changes for place cell activity with specific spike patterns. Calculated synaptic weight changes for a pair of overlapping place cells with an asymmetric cross-correlation 1_B, 1_A **(A)** and a pair of place cells where all spike intervals with positive Δt less than 100 ms have been removed 1_A, 1_B **(B)**. **(C)** A comparison between the induced plasticity predicted by the model and the observed plasticity from experimental data (Isaac et al., 2009).

in response to a single EPSP at 700 nM and a much higher 12 μM during pairing of post-synaptic depolarization with synaptic stimulation (Sabatini et al., 2002). This discrepancy could be explained in a number of ways. The $[Ca^{2+}]$ in a dendritic spine in response to synaptic stimulation could be considerably higher than in the dendritic shaft because of the diffusion barrier created by the spine neck. In addition, accurate absolute values for $[Ca^{2+}]$ measured by fluorescent Ca^{2+} indicators are difficult to achieve and therefore most studies are restricted to ratiometric measurements of transient $[Ca^{2+}]$ increases. For the purposes of synaptic plasticity this is sufficient since the increase in $[Ca^{2+}]$ triggers induction. Here, we have calculated the $[Ca^{2+}]$ based on a number of assumptions for channel conductance and Ca^{2+} diffusion. More importantly, we have modeled the relative $[Ca^{2+}]$ increases caused by various induction protocols and used these to define the graph in **Figure 7** that predicts the plasticity outcome.

Inhibitory synaptic transmission has a major role regulating the induction of synaptic plasticity in the hippocampus. The transient depression of inhibition induced by activation of pre-synaptic cannabinoid or $GABA_B$ receptors facilitates the induction of LTP (Davies et al., 1991; Chevaleyre and Castillo, 2004). This modulation of synaptic plasticity is not included in our current model but incorporation of the hyperpolarizing effects of GABAergic transmission would be an important future improvement and might, for example, contribute to the frequency dependence of STDP induction.

NMDARs are not the only sources of Ca^{2+} within dendritic spines but are certainly the most important for the induction of synaptic plasticity. A role has also been demonstrated for Ca^{2+} stores present in the endoplasmic reticulum in dendrites and spines (linked to Ca^{2+} influx through NMDARs or mGluRs) and also voltage-dependent

calcium channels present on the membrane of dendritic spines that generate local dendritic Ca^{2+} spikes (Golding et al., 2002; Remy and Spruston, 2007) and can contribute to some forms of LTD (Nevian and Sakmann, 2006). The contribution of non-NMDAR-mediated Ca^{2+} increases to synaptic plasticity induction is specifically omitted from our model but would be a useful future addition. There are also potential alternative mechanisms for the induction of synaptic plasticity that do not involve Ca^{2+} such as mGluRs (Moult et al., 2006) or muscarinic acetylcholine receptors (Dickinson et al., 2009) that are also specifically omitted from our model. Future experimental data may, however, require their addition.

There is a wealth of data on the spiking requirements for plasticity at various synapses in the cortex (Dan and Poo, 2006). However, these requirements have been shown to be somewhat different to those found in the hippocampus perhaps due to variations in dendritic architecture and NMDAR subunit expression and therefore we have restricted our model specifically to the Schaffer collateral synapse in the hippocampus. Even within the hippocampus there is some controversy surrounding the precise spiking requirements for STDP (Buchanan and Mellor, 2010) for example whether single pairs of spikes at low frequency can induce LTP (Bi and Poo, 1998; Debanne et al., 1998; Nishiyama et al., 2000; Wittenberg and Wang, 2006; Buchanan and Mellor, 2007; Campanac and Debanne, 2008; Kwag and Paulsen, 2009). These discrepancies can potentially be explained by variations in experimental conditions [For example, size of EPSPs, age of animals, frequency of stimulus presentation, presence of inhibitory inputs, etc. discussed in Buchanan and Mellor (2010)]. To reduce these discrepancies our model is based on data from acute hippocampal slices but future modifications could enable it to accurately replicate data from all systems including cortical synapses if one assumes that the general mechanism for the induction of synaptic plasticity is similar for all synapses that have NMDAR-dependent synaptic plasticity.

Our experimental data has revealed a critical role for muscarinic acetylcholine receptors in facilitating LTP induced by place cell firing patterns (Isaac et al., 2009). In the absence of muscarinic receptor activation no plasticity is induced but in the presence of a muscarinic agonist we obtain the results described above. This suggests that muscarinic receptor activation is permissive for the induction of synaptic plasticity under conditions where single synapses are activated and EPSP amplitude is small. A similar role has also been suggested for other G-protein coupled receptors such as mGluRs (Bashir et al., 1993) and β-adrenoreceptors (Seol et al., 2007). The observation that muscarinic receptor activation is not required when multiple synapses are activated and EPSP amplitude is large also demonstrates the critical role that multiple synaptic activation plays in the induction of synaptic plasticity. The model described in this study does not currently include a role for G-protein-mediated modulation of synaptic plasticity and this is an important consideration for future modifications and improvements. For example, it would be potentially possible to incorporate a negative feedback on Ca^{2+} influx under normal conditions that is inhibited by activation of G-protein coupled receptors or overridden by larger EPSPs.

Technical considerations make the visualization or recording of single synapses during behavior extremely difficult. This makes determination of the events that induce synaptic plasticity in the hippocampus almost impossible. These limitations could be circumvented by using the model described in this study to predict the plasticity outcome at a single synapse for any pattern of pre- and post-synaptic activity. Potentially, this will enable the determination of when synaptic plasticity is induced during behavior by examining the spike patterns of pairs of cells recorded during a memory task. This represents an exciting future application for this model.

ACKNOWLEDGMENTS

Jack R. Mellor is supported by the Wellcome Trust and by the European Union ENI-NET. The Bristol Centre for Complexity Sciences is funded by the EPSRC, UK (EP/E501214/1) which supports OJLR and AG.

REFERENCES

Bashir, Z. I., Bortolotto, Z. A., Davies, C. H., Berretta, N., Irving, A. J., Seal, A. J., Henley, J. M., Jane, D. E., Watkins, J. C., and Collingridge, G. L. (1993). Induction of LTP in the hippocampus needs synaptic activation of glutamate metabotropic receptors. *Nature* 363, 347–350.

Bear, M. F., Cooper, L. N., and Ebner, F. F. (1987). A physiological-basis for a theory of synapse modification. *Science* 237, 42–48.

Bi, G. Q., and Poo, M. M. (1998). Synaptic modifications in cultured hippocampal neurons: Dependence on spike timing, synaptic strength, and postsynaptic cell type. *J. Neurosci.* 18, 10464–10472.

Bloodgood, B. L., and Sabatini, B. L. (2007). Nonlinear regulation of unitary synaptic signals by CaV(2.3) voltage-sensitive calcium channels located in dendritic spines. *Neuron* 53, 249–260.

Buchanan, K. A., and Mellor, J. R. (2007). The development of synaptic plasticity induction rules and the requirement for postsynaptic spikes in rat hippocampal CA1 pyramidal neurones. *J. Physiol.* 585, 429–445.

Buchanan, K. A., and Mellor, J. R. (2010). The activity requirements for spike timing-dependent plasticity in the hippocampus. *Front. Synaptic Neurosci.* 2, 1–5.

Campanac, E., and Debanne, D. (2008). Spike timing-dependent plasticity: a learning rule for dendritic integration in rat CA1 pyramidal neurons. *J. Physiol.* 586, 779–793.

Canepari, M., Djurisic, M., and Zecevic, D. (2007). Dendritic signals from rat hippocampal CA1 pyramidal neurons during coincident pre- and post-synaptic activity: a combined voltage- and calcium-imaging study. *J. Physiol.* 580, 463–484.

Castellani, G. C., Bazzani, A., and Cooper, L. N. (2009). Toward a microscopic model of bidirectional synaptic plasticity. *Proc. Natl. Acad. Sci. U.S.A.* 106, 14091–14095.

Chevaleyre, V., and Castillo, P. E. (2004). Endocannabinoid-mediated metaplasticity in the hippocampus. *Neuron* 43, 871–881.

Cho, K., Aggleton, J. P., Brown, M. W., and Bashir, Z. I. (2001). An experimental test of the role of postsynaptic calcium levels in determining synaptic strength using perirhinal cortex of rat. *J. Physiol.* 532, 459–466.

Cormier, R. J., Greenwood, A. C., and Connor, J. A. (2001). Bidirectional synaptic plasticity correlated with the magnitude of dendritic calcium transients above a threshold. *J. Neurophysiol.* 85, 399–406.

Dan, Y., and Poo, M. M. (2006). Spike timing-dependent plasticity: From synapse to perception. *Physiol. Rev.* 86, 1033–1048.

Davies, C. H., Starkey, S. J., Pozza, M. F., and Collingridge, G. L. (1991). GABA autoreceptors regulate the induction of LTP. *Nature* 349, 609–611.

Daw, M. I., Chittajallu, R., Bortolotto, Z. A., Dev, K. K., Duprat, F., Henley, J. M., Collingridge, G. L., and Isaac, J. T. R. (2000). PDZ proteins interacting with C-terminal GluR2/3 are involved in a PKC-dependent regulation of AMPA receptors at hippocampal synapses. *Neuron* 28, 873–886.

Debanne, D., Gahwiler, B. H., and Thompson, S. M. (1998). Long-term synaptic plasticity between pairs of individual CA3 pyramidal cells in rat hippocampal slice cultures. *J. Physiol.* 507, 237–247.

Dickinson, B. A., Jo, J., Seok, H., Son, G. H., Whitcomb, D. J., Davies, C. H., Sheng, M., Collingridge, G. L., and Cho, K. (2009). A novel mechanism of hippocampal LTD involving muscarinic receptor-triggered interactions between AMPARs, GRIP and liprin-alpha. *Mol. Brain* 2, 18.

Fernandez de Sevilla, D., Fuenzalida, M., Porto Pazos, A. B., and Buno, W. (2007). Selective shunting of the NMDA EPSP component by the slow afterhyperpolarization in rat CA1

pyramidal neurons. *J. Neurophysiol.* 97, 3242–3255.

Franks, K. M., Bartol, T. M. Jr., and Sejnowski, T. J. (2002). A Monte Carlo model reveals independent signaling at central glutamatergic synapses. *Biophys. J.* 83, 2333–2348.

Frick, A., Magee, J., and Johnston, D. (2004). LTP is accompanied by an enhanced local excitability of pyramidal neuron dendrites. *Nat. Neurosci.* 7, 126–135.

Froemke, R. C., Tsay, I. A., Raad, M., Long, J. D., and Dan, Y. (2006). Contribution of individual spikes in burst-induced long-term synaptic modification. *J. Neurophysiol.* 95, 1620–1629.

Gall, D., Prestori, F., Sola, E., D'Errico, A., Roussel, C., Forti, L., Rossi, P., and D'Angelo, E. (2005). Intracellular calcium regulation by burst discharge determines bidirectional long-term synaptic plasticity at the cerebellum input stage. *J. Neurosci.* 25, 4813–4822.

Golding, N. L., Staff, N. P., and Spruston, N. (2002). Dendritic spikes as a mechanism for cooperative long-term potentiation. *Nature* 418, 326–331.

Graupner, M., and Brunel, N. (2007). STDP in a bistable synapse model based on CaMKII and associated signaling pathways. *PLoS Comput. Biol.* 3, 2299–2323.

Grunditz, A., Holbro, N., Tian, L., Zuo, Y., and Oertner, T. G. (2008). Spine neck plasticity controls postsynaptic calcium signals through electrical compartmentalization. *J. Neurosci.* 28, 13457–13466.

Hansel, C., Artola, A., and Singer, W. (1996). Different threshold levels of postsynaptic $[Ca^{2+}]i$ have to be reached to induce LTP and LTD in neocortical pyramidal cells. *J. Physiol. Paris* 90, 317–319.

Hansel, C., Artola, A., and Singer, W. (1997). Relation between dendritic Ca^{2+} levels and the polarity of synaptic long-term modifications in rat visual cortex neurons. *Eur. J. Neurosci.* 9, 2309–2322.

Helias, M., Rotter, S., Gewaltig, M. O., and Diesmann, M. (2008). Structural plasticity controlled by calcium based correlation detection. *Front. Comput. Neurosci.* 2, 1–21.

Isaac, J. T., Buchanan, K. A., Muller, R. U., and Mellor, J. R. (2009). Hippocampal place cell firing patterns can induce long-term synaptic plasticity in vitro. *J. Neurosci.* 29, 6840–6850.

Isaac, J. T., Hjelmstad, G. O., Nicoll, R. A., and Malenka, R. C. (1996). Long-term potentiation at single fiber inputs to hippocampal CA1 pyramidal cells. *Proc. Natl. Acad. Sci. U.S.A.* 93, 8710–8715.

Isaac, J. T., Nicoll, R. A., and Malenka, R. C. (1995). Evidence for silent synapses: implications for the expression of LTP. *Neuron* 15, 427–434.

Ismailov, I., Kalikulov, D., Inoue, T., and Friedlander, M. J. (2004). The kinetic profile of intracellular calcium predicts long-term potentiation and long-term depression. *J. Neurosci.* 24, 9847–9861.

Jahr, C. E., and Stevens, C. F. (1990). A quantitative description of NMDA receptor-channel kinetic behavior. *J. Neurosci.* 10, 1830–1837.

Keller, D. X., Franks, K. M., Bartol, T. M. Jr., and Sejnowski, T. J. (2008). Calmodulin activation by calcium transients in the postsynaptic density of dendritic spines. *PLoS One* 3, e2045.

Kwag, J., and Paulsen, O. (2009). The timing of external input controls the sign of plasticity at local synapses. *Nat. Neurosci.* 12, 1219–1221.

Larson, J., Wong, D., and Lynch, G. (1986). Patterned stimulation at the theta-frequency is optimal for the induction of hippocampal long-term potentiation. *Brain Res.* 368, 347–350.

Lisman, J. (1989). A mechanism for the Hebb and the anti-Hebb processes underlying learning and memory. *Proc. Natl. Acad. Sci. U.S.A.* 86, 9574–9578.

Miller, P., Zhabotinsky, A. M., Lisman, J. E., and Wang, X. J. (2005). The stability of a stochastic CaMKII switch: dependence on the number of enzyme molecules and protein turnover. *PLoS Biol.* 3, e107. doi:10.1371/journal.pbio.0030107.

Moult, P. R., Gladding, C. M., Sanderson, T. M., Fitzjohn, S. M., Bashir, Z. I., Molnar, E., and Collingridge, G. L. (2006). Tyrosine phosphatases regulate AMPA receptor trafficking during metabotropic glutamate receptor-mediated long-term depression. *J. Neurosci.* 26, 2544–2554.

Nevian, T., and Sakmann, B. (2006). Spine Ca^{2+} signaling in spike-timing-dependent plasticity. *J. Neurosci.* 26, 11001–11013.

Nishiyama, M., Hong, K., Mikoshiba, K., Poo, M., and Kato, K. (2000). Calcium stores regulate the polarity and input specificity of synaptic modification. *Nature* 408, 584–588.

Palmer, L. M., and Stuart, G. J. (2009). Membrane potential changes in dendritic spines during action potentials and synaptic input. *J. Neurosci.* 29, 6897–6903.

Pike, F. G., Meredith, R. M., Olding, A. W. A., and Paulsen, O. (1999). Postsynaptic bursting is essential for 'Hebbian' induction of associative long-term potentiation at excitatory synapses in rat hippocampus. *J. Physiol.* 518, 571–576.

Remy, S., and Spruston, N. (2007). Dendritic spikes induce single-burst long-term potentiation. *Proc. Natl. Acad. Sci. U.S.A.* 104, 17192–17197.

Rubin, J. E., Gerkin, R. C., Bi, G. Q., and Chow, C. C. (2005). Calcium time course as a signal for spike-timing-dependent plasticity. *J. Neurophysiol.* 93, 2600–2613.

Sabatini, B. L., Oertner, T. G., and Svoboda, K. (2002). The life cycle of Ca^{2+} ions in dendritic spines. *Neuron* 33, 439–452.

Seol, G. H., Ziburkus, J., Huang, S., Song, L., Kim, I. T., Takamiya, K., Huganir, R. L., Lee, H. K., and Kirkwood, A. (2007). Neuromodulators control the polarity of spike-timing-dependent synaptic plasticity. *Neuron* 55, 919–929.

Shouval, H. Z., Bear, M. F., and Cooper, L. N. (2002). A unified model of NMDA receptor-dependent bidirectional synaptic plasticity. *Proc. Natl. Acad. Sci. U.S.A.* 99, 10831–10836.

Sjostrom, P. J., and Nelson, S. B. (2002). Spike timing, calcium signals and synaptic plasticity. *Curr. Opin. Neurobiol.* 12, 305–314.

Sjostrom, P. J., Turrigiano, G. G., and Nelson, S. B. (2001). Rate, timing, and cooperativity jointly determine cortical synaptic plasticity. *Neuron* 32, 1149–1164.

Sobczyk, A., and Svoboda, K. (2007). Activity-dependent plasticity of the NMDA-receptor fractional Ca^{2+} current. *Neuron* 53, 17–24.

Song, S., Miller, K. D., and Abbott, L. F. (2000). Competitive Hebbian learning through spike-timing-dependent synaptic plasticity. *Nat. Neurosci.* 3, 919–926.

Urakubo, H., Honda, M., Froemke, R. C., and Kuroda, S. (2008). Requirement of an allosteric kinetics of NMDA receptors for spike timing-dependent plasticity. *J. Neurosci.* 28, 3310–3323.

Wittenberg, G. M., and Wang, S. S. H. (2006). Malleability of spike-timing-dependent plasticity at the CA3-CA1 synapse. *J. Neurosci.* 26, 6610–6617.

Conflict of Interest Statement: The authors declare that the research was conducted in the absence of any commercial or financial relationships that could be construed as a potential conflict of interest.

Received: 21 January 2010; paper pending published: 22 February 2010; accepted: 27 June 2010; published online: 21 July 2010.

Citation: Rackham OJL, Tsaneva-Atanasova K, Ganesh A and Mellor JR (2010) A Ca^{2+}-based computational model for NMDA receptor-dependent synaptic plasticity at individual post-synaptic spines in the hippocampus. Front. Syn. Neurosci. 2:31. doi: 10.3389/fnsyn.2010.00031

frontiers in
COMPUTATIONAL NEUROSCIENCE

ORIGINAL RESEARCH ARTICLE
published: 23 November 2010
doi: 10.3389/fncom.2010.00141

Enabling functional neural circuit simulations with distributed computing of neuromodulated plasticity

Wiebke Potjans[1,2,3]*, Abigail Morrison[2,3,4] and Markus Diesmann[2,4,5]

[1] *Institute of Neuroscience and Medicine (INM-6), Computational and Systems Neuroscience, Research Center Jülich, Jülich, Germany*
[2] *RIKEN Brain Science Institute, Wako City, Saitama, Japan*
[3] *Functional Neural Circuits Group, Faculty of Biology, Albert-Ludwigs-University of Freiburg, Freiburg, Germany*
[4] *Bernstein Center Freiburg, Albert-Ludwigs-University of Freiburg, Freiburg, Germany*
[5] *RIKEN Computational Science Research Program, Wako City, Saitama, Japan*

Edited by:
Per Jesper Sjöström, University College London, UK

Reviewed by:
Alfonso Renart, Rutgers University, USA
Andrew P. Davison, CNRS, France
Wulfram Gerstner, Ecole Polytechnique Fédérale de Lausanne, Switzerland

Correspondence:
Wiebke Potjans, Research Center Jülich, Institute of Neuroscience and Medicine (INM-6), 52425 Jülich, Germany.
e-mail: w.potjans@fz-juelich.de

A major puzzle in the field of computational neuroscience is how to relate system-level learning in higher organisms to synaptic plasticity. Recently, plasticity rules depending not only on pre- and post-synaptic activity but also on a third, non-local neuromodulatory signal have emerged as key candidates to bridge the gap between the macroscopic and the microscopic level of learning. Crucial insights into this topic are expected to be gained from simulations of neural systems, as these allow the simultaneous study of the multiple spatial and temporal scales that are involved in the problem. In particular, synaptic plasticity can be studied during the whole learning process, i.e., on a time scale of minutes to hours and across multiple brain areas. Implementing neuromodulated plasticity in large-scale network simulations where the neuromodulatory signal is dynamically generated by the network itself is challenging, because the network structure is commonly defined purely by the connectivity graph without explicit reference to the embedding of the nodes in physical space. Furthermore, the simulation of networks with realistic connectivity entails the use of distributed computing. A neuromodulated synapse must therefore be informed in an efficient way about the neuromodulatory signal, which is typically generated by a population of neurons located on different machines than either the pre- or post-synaptic neuron. Here, we develop a general framework to solve the problem of implementing neuromodulated plasticity in a time-driven distributed simulation, without reference to a particular implementation language, neuromodulator, or neuromodulated plasticity mechanism. We implement our framework in the simulator NEST and demonstrate excellent scaling up to 1024 processors for simulations of a recurrent network incorporating neuromodulated spike-timing dependent plasticity.

Keywords: synaptic plasticity, neuromodulator, computational neuroscience, modeling, large-scale simulations, integrate-and-fire neurons, distributed computing, spiking networks

1 INTRODUCTION

It is generally assumed that mammalian learning is implemented by changes in synaptic efficacy, as it is the case in simpler organisms (see e.g., Antonov et al., 2003). Historically, attempts to provide a theoretical explanation of learning have mainly been influenced by Hebb's postulate (Hebb, 1949) that the sequential activation of two neurons strengthens the synapse connecting them. Thus, theoretical "Hebbian" plasticity rules depend on the pre- and post-synaptic activity and sometimes also on the weight itself. Although these rules have been shown to solve some interesting problems (Gerstner et al., 1996; Song et al., 2000; Song and Abbott, 2001) it is not clear that such "two factor" rules can be the mechanism that enables animals to learn complicated tasks, such as those to find sparse rewards in complex environments.

However, experiments have shown that in some preparations, synaptic plasticity depends not only on the activity of the pre- and post-synaptic neurons but also on the presence of neuromodulators such as acetylcholine, norepinephrine, serotonin, and dopamine. Neuromodulators are released from neurons that are primarily located in the brainstem and basal forebrain, but that innervate many brain areas through long range connections (for a review see Cooper et al., 2002). The functional consequences of the long-range neuromodulatory projections are very diverse and depend strongly on the specific neuromodulator, the target area and the neuromodulatory concentration. For example, the release of acetylcholine from the basal forebrain into the cortex is involved in the control of attention (Hasselmo and McGaughy, 2004; Herrero et al., 2008; Deco and Thiele, 2009), and noradrenaline, mainly originating from the locus coeruleus, is released throughout the central nervous system facilitating the processing of relevant, or salient, information (Berridge and Waterhouse, 2003). One neuromodulatory function which has evoked high interest in the experimental as well as the theoretical neuroscience communities is reward learning on the basis of dopamine released in the striatum from midbrain areas (Schultz et al., 1997; Reynolds et al., 2001).

An influential hypothesis on the mechanism of neuromodulation is that neuromodulators can be released extrasynaptically from en passant boutons on neuromodulatory axons and modulate the plasticity of synapses that are remote from release sites, a concept known as volume transmission (Agnati et al., 1995;

Zoli and Agnati, 1996). This is illustrated in **Figure 1**. For an illustration of en passant boutons on a neuromodulatory axon and a schematic representation of the main sources of volume transmission signals, see Moreau et al. (2010) and Zoli et al. (1999), respectively. This hypothesis implies a temporal rather than a spatial selectivity for neuromodulatory action (Arbuthnott and Wickens, 2007). Pawlak et al. (2010) in this special issue review the recent experimental *in vitro* findings concerning the effects of neuromodulators released from long-range neuromodulatory systems on STDP. Despite the large range of time scales and the variety of mechanisms by which the neuromodulators influence STDP, the review finds that the effects can be divided into two categories. In the first category, the neuromodulator is essentially required for the induction of STDP. In the second category, the neuromodulator alters the threshold for the plasticity induction. The review argues that the neuromodulatory influence is the crucial mechanism linking synaptic plasticity to behaviorally based learning, especially when learning depends on a reward signal. This hypothesis is further supported by a number of spiking neuronal network models that can learn a reward related task, due to the incorporation of three-factor synaptic plasticity rules (Seung, 2003; Xie and Seung, 2004; Baras and Meir, 2007; Florian, 2007; Izhikevich, 2007; Legenstein et al., 2008; Potjans et al., 2009b; Vasilaki et al., 2009).

These spiking neuronal network models of reward learning are typically formulated in a general way before being tested in concrete tasks. The generation of the neuromodulatory signal, or third factor, is determined by the task to be solved. Three categories can be identified for the generation of the neuromodulatory signal: either the signal is injected into the spiking network by an external controller, or it is determined by a mixture of an external supervisor and the spiking activity of the network or it is generated purely internally. The categories can be further discriminated with respect to the points in time leading to discontinuous changes in the value of the signal. An update can be triggered by an external event (such as an external stimulus), by the generation of a spike or it can be driven in discrete time steps. The neuromodulatory signal is either represented as a discrete variable that has a non-zero value only at the points in time that an update is triggered, or it is represented as a continuous variable between discontinuous updates. The three categories and their sub-categories are illustrated in **Figure 2**.

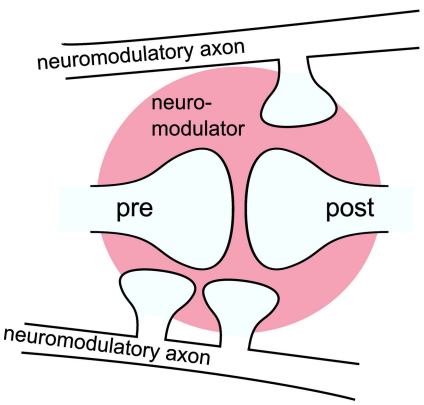

FIGURE 1 | Volume transmission: a neuromodulator is released from en passant boutons on neuromodulatory axons and modulates the plasticity of synapses remote from the release sites as a "third factor." The modulatory signal is a composition of the neuromodulator released by multiple boutons in a certain area (three are shown). For simplicity the figure shows only one modulated synapse. However, commonly the signal is assumed to affect multiple synapses within a certain volume (pink area).

In the first category (**Figure 2A**), the plasticity modulating signal does not depend on the spiking activity of the network at all. The signal is updated in an event-driven fashion triggered by external events, such as entering a reward-related state in a navigation task or the occurrence of a reward predicting stimulus in classical conditioning tasks. Both discrete-time (Potjans et al., 2009b; Vasilaki et al., 2009) and continuous-time (task two in Izhikevich, 2007) representations of the neuromodulatory signal have been investigated.

In the second category (**Figure 2B**), the generation of the plasticity modulating signal requires the presence of an all-knowing external supervisor. The signal depends on the interplay between information provided externally and internally. Signal updates are triggered by the occurrence of an external event (task three in Izhikevich, 2007) or the emission of a spike of a specific output neuron within the network (XOR task in Florian, 2007; Seung, 2003; Xie and Seung, 2004); alternatively, the signal is generated in discrete time steps (Baras and Meir, 2007, target firing learning model in Florian, 2007). In the event-driven model proposed by Izhikevich (2007) to solve an instrumental conditioning task, the signal is modeled as a continuous variable where the timing and magnitude of updates are determined externally. Whether the update is actually carried out by the synapses is contingent on an internal condition (i.e., a comparison of firing rates in two pools) meeting an externally imposed criterion (i.e., the desired ordering of the firing rates). In the models proposed by Seung (2003), Xie and Seung (2004), and Florian (2007) to solve a XOR task, updates are triggered by the spikes of an output neuron; the magnitudes of the updates are determined by an external supervisor that evaluates the response of the output neuron to the spiking activity of an input layer representing different combinations of 0 and 1. For an input of [0,1] or [1,0], every spike of the output neuron results in a positive value for the neuromodulatory signal, whereas a negative value is generated for each input spike in response to an input of [0,0] or [1,1]. Between spikes of the output neuron, the value of the neuromodulatory signal is zero.

Other models in the second category assume that the signal is updated in discrete-time steps in $n{\cdot}\Delta T$, where n is an integer; ΔT can be a small step size or the duration of a certain episode. This is illustrated in the middle row of **Figure 2B**. Here the values of the signal are determined as a function of the spiking activity in comparison to a desired activity which is provided by an external supervisor. The signal can either take continuous values, as in the model proposed by Baras and Meir (2007) to solve a path learning task and the target firing-rate learning model proposed by Florian (2007) or discrete values at specific times, as in an alternative variant of the target firing-rate learning model proposed by Florian (2007) and the XOR learning model proposed by Baras and Meir (2007).

The first two categories demonstrate the importance of three-factor rules in solving reward related tasks of different complexity, ranging from XOR to navigation tasks. However, in order to

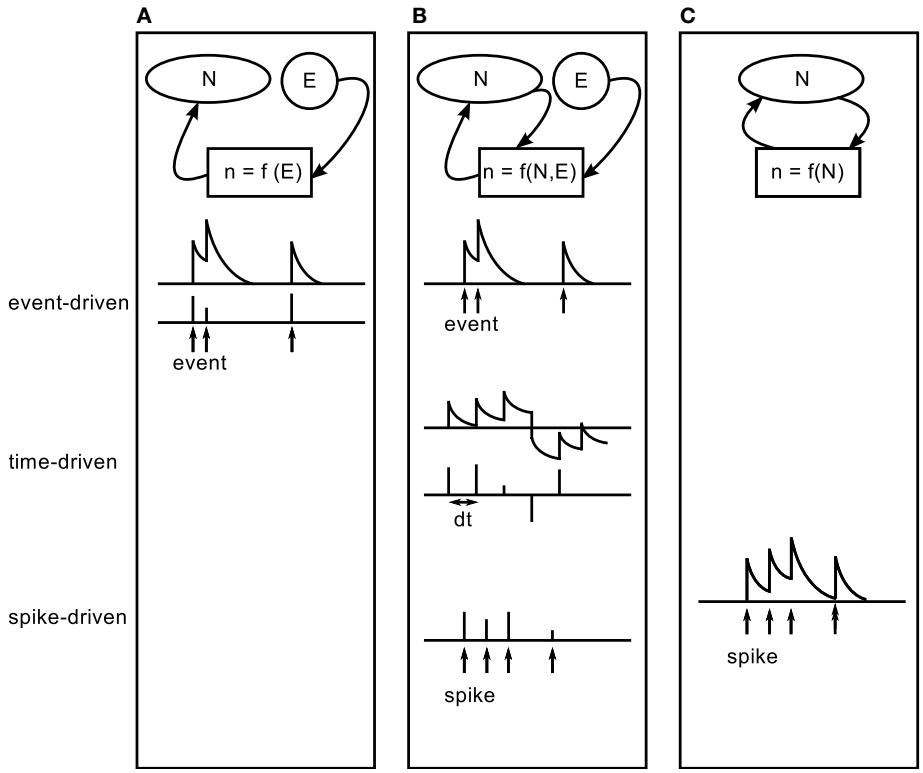

FIGURE 2 | Characterization of existing modeling studies with respect to the generation process of a plasticity modulating signal. From left to right: interplay between external (E) and internal (N) information in the generation process of the modulatory signal (n). **(A)** The signal is generated purely externally (task two in Izhikevich, 2007; Potjans et al., 2009b; Vasilaki et al., 2009). **(B)** The signal combines information from an external supervisor and internal information (Seung, 2003; Xie and Seung, 2004; Baras and Meir, 2007; Florian, 2007; Izhikevich, 2007, task three). **(C)** The signal is generated purely internally (task four in Izhikevich, 2007; Legenstein et al., 2008). From top to bottom: timing of discontinuous updates to the signal. Top: updates are triggered by external events, indicated by arrows (event-driven). Middle: updates occur in discrete time steps dt (time-driven). Bottom: updates triggered by the arrival of neuromodulatory spikes, indicated by arrows (spike-driven). Upper and lower rows show a signal that takes continuous values between updates, or discrete values at the times of updates, respectively.

understand how different brain areas interact to produce cognitive functions these models are not sufficient. This problem requires the consideration of functionally closed loop models, where the neuromodulatory signal is generated by the network itself (**Figure 2C**). So far, only two studies have investigated such models. In both the model proposed by Izhikevich (2007), which learns a shift in dopamine response from an unconditional stimulus to a reward-predicting conditional stimulus, and that proposed by Legenstein et al. (2008) which learns a biofeedback task, each spike of a specific population of neurons leads to an update of a continuous-time variable.

The simulation of models in this third category and the spike-based models of the second category is beset by considerable technical challenges. Spike-driven updates are intrinsically more troublesome than updates driven by external events or occurring in regular intervals, as they do not entail a natural interruption point for the simulation at which signal information can be calculated and conveyed to the relevant synapses. This difficulty is compounded in the context of models where different brain regions interact, as the neuromodulatory signal is not only likely to be composed of the activity of a population of neurons, but also affecting synapses between entirely different populations. A final hurdle comes with model size. The spiking network models implementing three-factor synaptic plasticity rules discussed above consist only of a small (of the order of 10 to 10^2) (Seung, 2003; Xie and Seung, 2004; Baras and Meir, 2007; Florian, 2007; Potjans et al., 2009b; Vasilaki et al., 2009) to moderate (of the order of 10^3) number of neurons (Izhikevich, 2007; Legenstein et al., 2008). However, to simultaneously achieve cortical levels of connectivity (10%) and number of inputs (10^4) (Braitenberg and Schüz, 1998), a minimal network size of 10^5 neurons is required. Similarly, to investigate brain-scale circuits involving the interaction of multiple brain areas, large-scale networks are likely to be necessary. Consequently, distributed computing techniques are required. Indeed, even the systematic study of smaller networks demand such techniques as learning often takes place on a very long time scale compared to the time scale of synaptic plasticity. The requirement for distributed computing adds to the complexity of the problem of implementing neuromodulated plasticity via volume transmission. The challenge can be stated as follows: how can a synapse, which is typically only accessed through its pre-synaptic neuron, be efficiently informed about a neuromodulatory signal generated by a population of neurons that are generally located on machines different than those of either the pre- or the postsynaptic neuron. Whereas efficient

methods exist to integrate the dynamics of large-scale models by distributed computing (Hammarlund and Ekeberg, 1998; Harris et al., 2003; Morrison et al., 2005), so far no solution for the efficient implementation of neuromodulated plasticity in spiking neuronal networks has been presented. Studies of network models in which the neuromodulatory signal is internally generated have not provided any technical details (Izhikevich, 2007; Legenstein et al., 2008), thus the models cannot be reproduced or extended by the wider modeling community.

To address this gap and thus open up this fascinating area of research, we present a framework for the implementation of neuromodulated plasticity in time-driven simulators operating in a distributed environment. The framework is general, in that it is suitable for all manner of simulations rather than one specific network model or task. Moreover, we do not focus on a specific implementation language, neuromodulator or neuromodulated plasticity mechanism and rely on only a few assumptions about the infrastructure of the underlying simulator. In the framework the plasticity modulating signal is generated by a user-defined population of neurons contained within the network. The neuromodulatory signal influences all synapses located in a user-defined specific volume, modeling the effect of volume transmission (see **Figure 1**). Our framework yields excellent scaling for recurrent networks incorporating neuromodulated STDP in its excitatory to excitatory connections. In order to analyze the efficiency of the framework implementation accurately, we develop a general technique to decompose the total run time into the portion consumed by communication between machines and the portion consumed by computation. This separation enables us to distinguish the saturation in run time caused by communication overhead from any potential saturation caused by a sub-optimal algorithm design. This technique can be applied to arbitrary network simulations und will thus aid the future development and analysis of extensions to distributed simulation tools.

A general scheme for the distributed simulation of neural networks is summarized in section 2.1 to clarify terminology and make explicit the assumptions made about the simulator infrastructure. In section 3.1 we present an efficient way to implement neuromodulated plasticity in this distributed simulation environment. To illustrate the technique, in section 3.2 we compare the run times of recurrent networks (10^4 and 10^5 neurons) incorporating neuromodulated spike-timing dependent plasticity (Izhikevich, 2007) to those of networks incorporating the corresponding "two factor" spike-timing dependent plasticity.

The conceptual and algorithmic work described here is a module in our long-term collaborative project to provide the technology for neural systems simulations (Gewaltig and Diesmann, 2007). Preliminary results have been already presented in abstract form (Potjans et al., 2009a).

2 MATERIALS AND METHODS

2.1 DISTRIBUTED NEURAL NETWORK SIMULATION

To clarify the terminology used in the rest of the manuscript and define the requirements a simulator must fulfill in order to incorporate our framework for neuromodulated plasticity, in the following we briefly describe a general purpose time-driven simulation scheme for distributed computation. For a more thorough and illustrated description, see Morrison et al. (2005). Variants of this scheme underlie the majority of simulators that are designed for simulating networks of point neurons, for example NEST (Gewaltig and Diesmann, 2007), C2 (Ananthanarayanan and Modha, 2007) and PCSIM (Pecevski et al., 2009), see Brette et al. (2007) for a review.

2.1.1 Network representation

Our fundamental assumption is that a neural network can be represented as a directed graph, consisting of nodes and the connections between them. The class of nodes comprises spiking neurons (either single- or few-compartment models) and devices, which are used to stimulate or record from neurons. A connection enables information to be sent from a sending node to a receiving node. The definition of a connection typically includes at least a weight and a delay. The weight determines the strength of a signal and the delay how long it takes for the signal to travel from the sending to the receiving node. The simplest synapse model delivers a fixed connection weight to the post-synaptic node. If the connection is intended to be plastic, the connection definition must also include a mechanism that defines the weight dynamics. "Two factor" rules, such as spike-timing dependent plasticity, can be implemented if the post-synaptic node maintains a history of its relevant state variables (e.g., as described in Morrison et al., 2007).

Each neuron is represented on exactly one of the m machines running the simulation, and synapses are distributed such that they are represented on the same machine as their post-synaptic target. Distributing the axon of a sending node in this way has a considerable advantage in communication costs compared to distributing dendrites (Morrison et al., 2005). In contrast to the neurons, each device is represented on every machine and only interacts with the local neurons. This reduces the communication load, as measured data or stimulation signals do not have to be transferred between machines. The cost of this approach is that m data files are generated for each recording device.

2.1.2 Simulation dynamics

Time-driven network update. The network is evaluated on an evenly spaced time grid $t_i = i \cdot \Delta t$. At each grid point the network is in a well defined state S_i. The time interval Δt between two updates can be maximized by setting it to the minimal propagation delay $d_{\min}$ of the network. This is the largest permissible temporal desynchronization between any two nodes in the network (see Lamport, 1978; Morrison et al., 2005; Plesser et al., 2007). Note that the computation resolution for the neuron models can be much finer than the resolution of the global scheduling algorithm, for example neurons can advance their dynamics with a time step $h = 0.1$ ms even if the global algorithm advances in communication intervals of $\Delta t = 1$ ms. Alternatively, neuron model implementations can be defined within this framework that advance their dynamics in an event-driven fashion, i.e., from one incoming spike to the next (Morrison et al., 2007; Hanuschkin et al., 2010).

During a network update from one time step to the next, i.e., the interval $(t_{i-1}, t_i]$, a global state transfer function $U(S_i)$ propagates the network from one state S_i to the next S_{i+1}. As a result of this, each neuron may generate one or more spike events which are communicated to the other machines at the end of the update interval

at t_i. Before the start of the next network update, i.e., the interval $(t_i, t_{i+1}]$, the communicated events are delivered to their targets. This is described in greater detail below. In the following, we will refer to Δt as the communication interval. To implement our framework for neuromodulated plasticity, we therefore assume that the update cycle of the underlying simulator in a distributed environment can be expressed as the following algorithm:

```
1: T ← 0
2: while T < T_stop do
3:     parallel on all machines do
4:        deliver events received at last
            communication to targets
5:        call U(s_T )
6:     end parallel
7:     communicate new events between machines
8:     increment network time: T ← T + Δt
9: end while
```

Event delivery. A neuron's spike events must be delivered to its target nodes with a propagation delay determined by the connecting synapse. After the communication of events that takes place after each Δt interval, the simulation algorithm activates the outgoing synapses of the neurons that spiked during the previous interval. The sequence diagram for a simple synapse model is shown in **Figure 3A**. The synapse generates an event of weight w and delay d. The delay is determined by subtracting the lag between spike generation and communication from the propagation delay associated with the synapse: for a spike generated at s_{pre} and communicated at t_i with a total synaptic propagation delay d_{syn}, the remaining delay d is equal to $d_{\text{syn}} - (t_i - s_{\text{pre}})$. The event is sent to the synapse's target node, which writes the event to its incoming event buffer such that it becomes visible to the update dynamics of the target neuron at the correct time step, $s_{\text{pre}} + d_{\text{syn}}$. A description of the ordering of buffer reading and writing operations to ensure that events are integrated correctly can be found in Morrison and Diesmann (2008). For the purposes of this manuscript, we assume that a simulator delivers events as described above, i.e., spikes have propagation delays, are communicated between machines at regular intervals and are buffered at the target neuron until they are due to be incorporated in the neuronal dynamics.

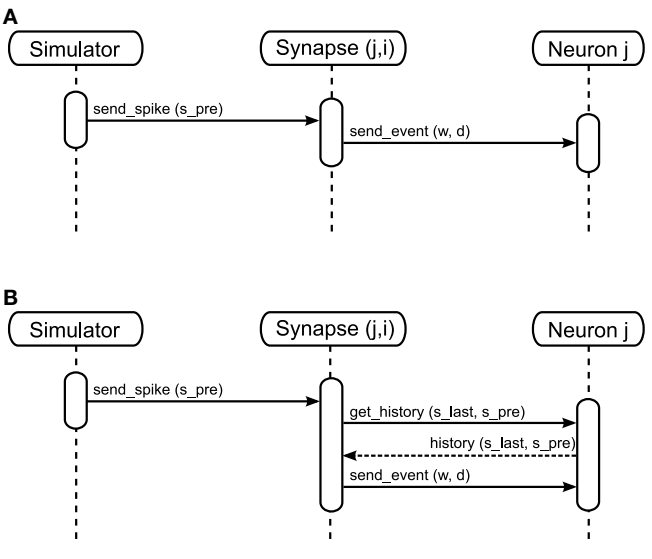

FIGURE 3 | Sequence diagram for static (A) and STDP (B) synapses. The object Synapse (*j,i*) denotes a synapse from source neuron *i* to target neuron *j*; neuron *i* emits a spike at time s_{pre}.

Synapse update. In contrast to neurons, incoming events are rare for individual synapses at realistic firing rates. Therefore, to develop our framework we make the assumption that a simulator uses the more efficient strategy of updating synapses in an event-driven fashion only on the arrival of a pre-synaptic spike rather than in a time-driven fashion as neurons are. This is possible for the class of synaptic models that only depend on local factors such as the current weight of the synapse, the time since the last update and state information available from the post-synaptic neuron (Morrison et al., 2008). This class includes synaptic depression (Thomson and Deuchars, 1994), synaptic redistribution (Markram and Tsodyks, 1996) and spike-timing dependent plasticity (STDP) (Markram et al., 1997; Bi and Poo, 1998, 2001).

As we measure performance on the example of STDP with a neuromodulatory third factor (see section 3.2) it is worth discussing the infrastructure for calculating STDP updates triggered only on the arrival of pre-synaptic spikes in somewhat more detail. See **Figure 3B** for the sequence diagram for the activation of an STDP synapse; the corresponding pseudo-code is given in Morrison et al. (2007). All post-synaptic variables, such as the post-synaptic spike times and the low-pass filtered post-synaptic rate, are stored at the post-synaptic neuron. On the arrival of a pre-synaptic spike, the synapse requests these variables from the post-synaptic neuron for the period between the last and the current pre-synaptic spike (`get_history(s_last,s_pre)`). Based on this information the synapse can integrate its weight dynamics from one spike time to the next. The post-synaptic variables only have to be stored until they have been processed by every incoming synapse. After the weight has been updated an event is sent to the post-synaptic neuron as in the case of the simple synapse model discussed in section 2.1.2 and illustrated in **Figure 3A**.

2.2 BENCHMARK NETWORK MODELS

To investigate the performance of our proposed framework, we measure the simulation times of recurrent networks incorporating neuromodulated spike-timing dependent plasticity at their excitatory–excitatory connections whilst systematically varying the number of processors used. The STDP model uses an all-to-all spike pairing scheme and is based on the model proposed by Izhikevich (2007):

$$\dot{w} = c(n-b)$$

$$\dot{c} = -\frac{c}{\tau_c} + \text{STDP}(\Delta t)\delta(t - s_{\text{pre/post}})C_1$$

$$\dot{n} = -\frac{n}{\tau_n} + \frac{\delta(t-s_n)}{\tau_n}C_2,$$

where c is an eligibility trace, n the neuromodulator concentration, $s_{\text{pre/post}}$ the time of a pre- or post-synaptic spike, s_n the time of a neuromodulatory spike, and C_1 and C_2 are constant coefficients.

$\delta(t)$ is the Dirac delta function; τ_c and τ_n are the time constants of the eligibility trace and the neuromodulator concentration, respectively. Unlike the networks investigated by Izhikevich (2007), the neuromodulator concentration is always present, so we subtract a baseline b from the neuromodulator concentration. STDP(Δt) is the window function of additive STDP:

$$\mathrm{STDP}(\Delta t) = \begin{cases} A_+ e^{-|\Delta t|/\tau_+} & \text{if } \Delta t > 0 \\ A_- e^{-|\Delta t|/\tau_-} & \text{if } \Delta t \le 0 \end{cases},$$

where $\Delta t = s_{\mathrm{post}} - s_{\mathrm{pre}}$ is the temporal difference between a post-synaptic and a pre-synaptic spike, A_+ and A_- are the amplitudes of the weight change and τ_+ and τ_- are time constants. As a control, we also measure the simulation times of networks in which the neuromodulated STDP is exchanged for STDP without neuromodulation according to the model of Song and Abbott (2001), i.e., $\dot{w} = \mathrm{STDP}(\Delta t)\delta(t - s_{\mathrm{pre/post}})$. In the neuromodulated and the unmodulated networks the synaptic weights are bounded between 0 and a maximal synaptic weight $w_{\max}$.

We investigate the performance for networks of two different sizes: 1.125×10^4 and 1.125×10^5, referred to in the rest of the manuscript as the 10^4 and 10^5 networks, respectively. Both networks consist of 80% excitatory and 20% inhibitory current based integrate-and-fire neurons. In the subthreshold range the membrane potential V is determined by the following dynamics:

$$\frac{dV}{dt} = -\frac{1}{\tau_m} V + \frac{1}{C_m} I(t),$$

where τ_m is the membrane time constant, C_m the membrane capacity and $I(t)$ the input current to the neuron, which is the sum of any external currents and the synaptic currents. The synaptic current I_{syn} due to an incoming spike is represented by an exponential function:

$$I_{\mathrm{syn}}(t) = w e^{-t/\tau_{\mathrm{syn}}},$$

where w is the weight of the corresponding synapse and τ_{syn} the rise time. If the membrane potential passes the threshold V_{th} a spike is emitted and the neuron is clamped to the reset potential V_{reset} for the duration of the refractory period τ_{ref}.

The excitatory–excitatory connections are plastic, as described above; all other connections are static. All neurons receive additional Poissonian background noise. The network firing rate due to the Poissonian background noise of both networks is approximately 10 Hz in the asynchronous irregular regime. We arbitrarily choose the first N_{nm} excitatory neurons to be the neuromodulator releasing neurons. A tabular description of the benchmark network models and a specification of the parameters used can be found in **Tables 1 and 2** of Appendix.

The simulations are carried out using the simulation tool NEST (Gewaltig and Diesmann, 2007) with a computation time step of 0.1 ms and a communication interval equal to the minimal propagation delay $d_{\min}$. The simulations of the 10^4 neuron networks are performed on a cluster of SUN X86 consisting of 23 compute nodes equipped with two AMD Opteron 2834 quad core processors with 2.7 GHz clock speed running Ubuntu Linux. The nodes are connected via InfiniBand (24 ports InfiniBand switch, Voltaire ISR9024D-M); the MPI implementation is OpenMPI 1.3.1. The simulations for the 10^5 neuron networks are performed on a Bluegene/P (JUGENE[1]).

3 RESULTS

3.1 IMPLEMENTING NEUROMODULATED PLASTICITY IN A DISTRIBUTED ENVIRONMENT

In this section we present a novel and general framework to implement neuromodulated plasticity efficiently for a distributed time-driven simulator as described in section 2.1. The neuromodulator concentration available in a certain volume is the superposition of the neuromodulator concentration released by a population of neurons projecting into the same volume. We assume, in agreement with experimental findings (e.g., Garris et al., 1994; Montague et al., 2004), that each spike of the neuromodulator releasing neurons contributes to the extracellular neuromodulator concentration and thus the concentration can be given as a function of spike times.

3.1.1 A distributed volume transmitter

The major challenge is to provide an efficient mechanism to inform a set of synapses about a non-local neuromodulatory signal in a manner that respects the temporal ordering of spikes and signal changes, without making the assumption that the neurons generating the signal are identical with the modulated synapses' pre- or post-synaptic neurons or even that they are represented on the same machines as the pre- or post-synaptic neurons. Our solution is to introduce a new category of node, which we will refer to as a "volume transmitter." The volume transmitter collects all spikes from a neuromodulator releasing population of neurons and transmits the spikes to a user-specified subset of synapses (see **Figure 4A**). As the subset of synapses is typically distributed over all machines, we define the volume transmitter to be duplicated on each machine. It provides the spikes to the synapses local to its machine, in common with the "device" category of nodes (see section 2.1.1). However, as the population of neurons releasing the neuromodulator into a given volume is also typically distributed over all machines, the volume transmitter must receive spikes from a globally defined population, in common with the "neuron" category of nodes. The volume transmitter, therefore, represents a third category of nodes, duplicated on each machine and transmitting information locally like a device, but receiving events from all machines like a neuron. The distribution of the volume transmitter, the transmission of the spikes to the local synapses and the global collection of the spikes from the neuromodulator releasing neurons are depicted for an example network distributed over two machines in **Figure 4B**.

Note that the dynamics of the neuromodulator concentration is calculated by the synapses rather than the volume transmitter. This enables the same framework to be used for a variety of neuromodulatory dynamics as long as they depend only on the spike history. Moreover, the association of a volume transmitter with a specific population of neuromodulator releasing neurons and a specific subset of synapses allows multiple volume transmitters to be defined in the same network model. Thus a network model can represent multiple projection volumes and multiple neuromodulatory interactions.

[1]http://www.fz-juelich.de/jsc/jugene/

3.1.2 Managing the spike history

In order to calculate its weight update, a neuromodulated synapse must have access to all the spikes from the neuromodulator releasing neuron population that occurred since the last pre-synaptic spike. This is similar to the requirement of an STDP synapse, which needs access to the post-synaptic spike history since the last pre-synaptic spike (see section 2.1.2). For STDP, this requirement can be met if the post-synaptic neuron stores its spike times (Morrison et al., 2007). To prevent a continual growth in memory requirements as a simulation progresses, the spike times are discarded once all incoming synapses have accessed them. This is an inappropriate strategy for managing the neuromodulatory spikes, as they are typically generated by a population of neurons and so have a substantially higher total rate than the pre-synaptic spike rate. Having a large number of spikes in the history entails proportionally higher computational costs for the algorithm that determines which spikes can be discarded. We propose a novel alternative approach: in addition to delivering a spike history "on demand" when a pre-synaptic spike arrives (**Figure 5A**), the volume transmitter also delivers

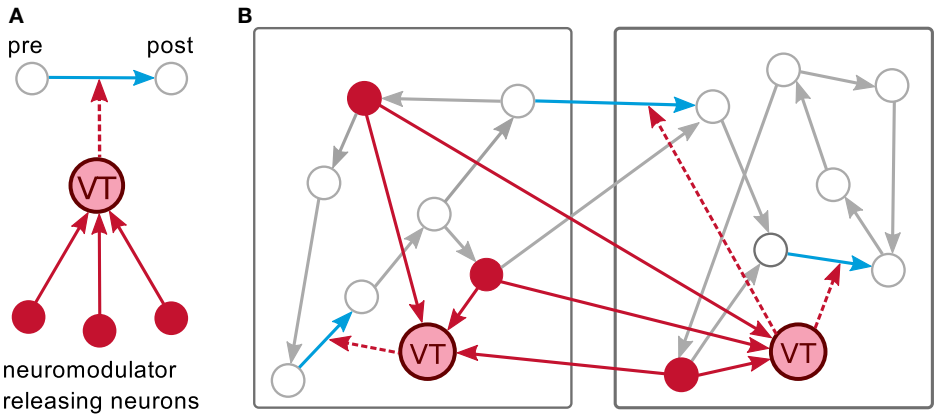

FIGURE 4 | A distributed volume transmitter object. (A) The volume transmitter (VT) collects all spikes from the neurons releasing the neuromodulator into a given volume and delivers them to any associated synapses. **(B)** An example network is distributed over two machines. The volume transmitter (VT) is duplicated on each machine. It collects globally the spikes of the neuromodulator releasing neurons (red) and delivers them locally to the neuromodulated synapses (blue).

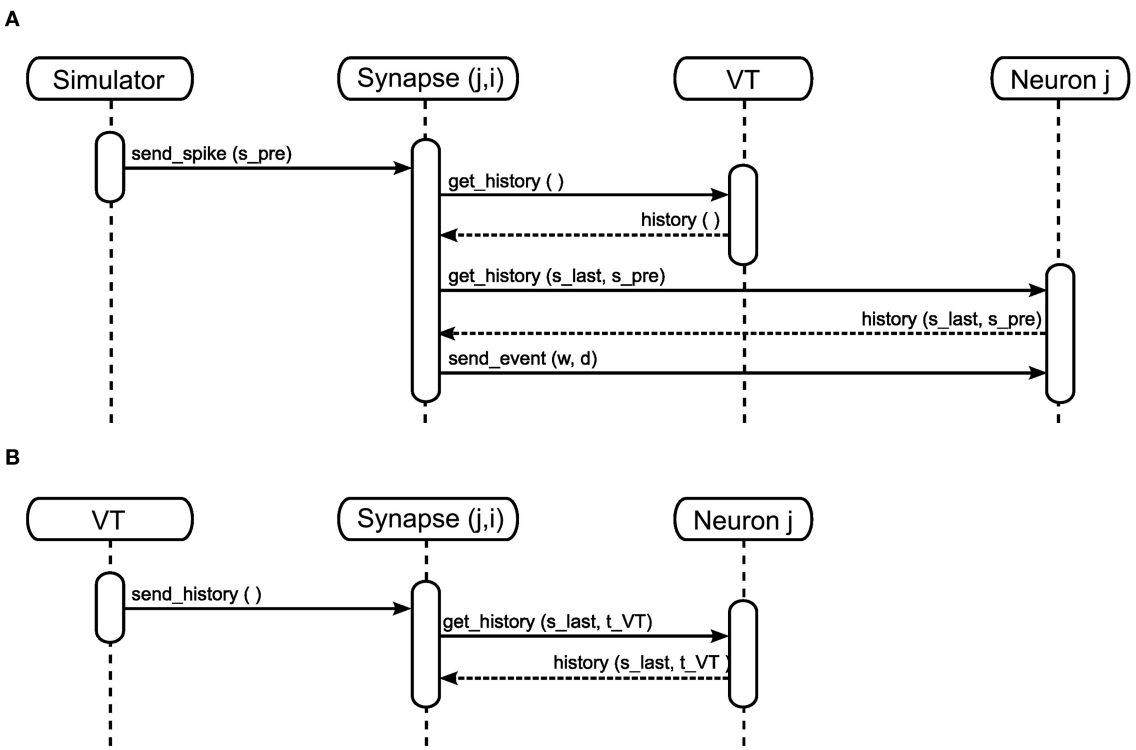

FIGURE 5 | Sequence diagram for neuromodulated synapses in the event-driven (A) and the time-driven (B) mode.

its spike history to all associated synapses at regular intervals (**Figure 5B**). Not only does this combination of an event- and time-driven approach allows us to dispense with an algorithm to discard spikes from the history, it also has the major advantage of enabling the spike history to be stored in a static data structure, rather than a computationally more expensive dynamic data structure.

Let us first consider the collection and storing of the spikes of the neuromodulator releasing neurons (**Figure 4**). A suitable structure to store the spikes is a traditional ring buffer which stores data in a contiguous series of segments as shown in **Figure 6**, where each segment of the buffer corresponds to one integration time step h (see also Morrison et al., 2005; Morrison and Diesmann, 2006). However, unlike the standard usage of a ring buffer in neuronal network simulations, where only one object reads from it and exactly one read operation from one segment is carried out in each time step, in this situation multiple objects depend on the data and read operations are carried out at unpredictable times and require information from a range of segments at once. Consequently, a new approach to writing to and reading from a ring buffer is necessary, as we describe in the following.

When a neuromodulator releasing neuron n emits a spike at time s_n, a certain propagation delay d_n is required for the spike to arrive at the projection volume, as illustrated in **Figure 6A**. Following the description in section 2.1.2, events are communicated after each communication interval of length Δt. Assuming s_n is in the interval $(t_{i-1}, t_i]$ where $t_i = i\Delta t$, the neuromodulatory spike event is communicated between machines at time t_i along with all the other spike events generated in that interval (see Morrison and Diesmann, 2006 for an in depth discussion of the interval borders). Neuromodulatory spike events generated in that interval are delivered to the volume transmitter and sorted into the ring buffer according to their propagation delays. Assigning the "front" of the ring buffer the index 0, for a spike emitted at s_n with a delay d_n, the counter at position $(s_n + d_n - t_i)/h - 1$ is incremented. This is depicted in the left side of **Figure 6B**. Setting the ring buffer size to $d_{\max}/h$, where $d_{\max}$ is the maximal propagation delay, allows the correct order of spikes to be maintained for all possible configurations of spike generation time, communication time, and propagation delay. The communication interval Δt can be set to any integer multiple of h up to $d_{\min}$, the minimum synaptic propagation delay. A communication interval of $\Delta t = h$, where events are communicated in every time step, is the most obvious, naive approach and is probably implemented in at least the first version of almost all simulators. As mentioned in section 2.1.2, a choice of $\Delta t = d_{\min}$ is the largest possible communication interval that still maintains the correct ordering of events. Maximizing Δt has two advantages: it reduces the communication overhead (see Morrison et al., 2005), and each neuron can perform $d_{\min}/h$ integration time steps as an uninterrupted sequence, improving the cache efficacy considerably (Plesser et al., 2007).

As a result of the sorting, right before the event delivery phase at time t_{i+1}, the counters for positions in the range $[0, \Delta t/h - 1]$ give the total number of neuromodulatory spikes that are due to arrive at the synapses in each time step from $t_i + h$ to t_{i+1}. Counters at positions greater than $\Delta t/h$ do not necessarily contain the total number of spikes for their respective time steps, as these positions

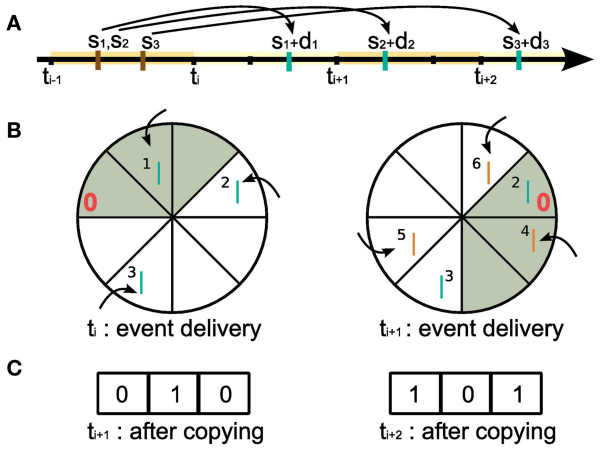

FIGURE 6 | Writing to and reading from the ring buffer of the volume transmitter for event communication in intervals of Δt. In this example, $\Delta t = 3h$, where h is the computation time step. **(A)** Short black bars indicate the grid h imposes on the temporal axis. At time step $t_i = i\Delta t$ all spikes generated by the neuromodulator releasing neurons in the time interval $(t_{i-1}, t_i]$ are delivered to the volume transmitter (here: the spike times s_1, s_2, s_3 (brown bars) with propagation delays d_1, d_2, d_3). Blue bars indicate the arrival of the spikes in the projection volume. **(B)** Ring buffer. Left: at time t_i during event delivery. The neuromodulatory spikes generated in $(t_{i-1}, t_i]$ (blue bars, labeled by the event id for illustration only) increment the counters at the positions $(s_x + d_x - t_i)/h - 1$ for $x = [1,2,3]$ from the "front" of the ring buffer (indicated by the red 0). At the end of the event delivery phase, the first $\Delta t/h$ elements (gray) contain the neuromodulatory spikes due to arrive in the projection volume during $(t_i, t_{i+1}]$. Right: at t_{i+1} during event delivery. The 'front' of the buffer has been rotated $\Delta t/h$ segments clockwise with respect to the buffer at time t_i. Neuromodulatory spikes generated in the time interval $(t_i, t_{i+1}]$ by the neuromodulator releasing neurons (generation times not shown) are written to the buffer (orange bars), the first $\Delta t/h$ elements (gray) contain the neuromodulatory spikes due to arrive in the projection volume during $(t_{i+1}, t_{i+2}]$. **(C)** The spike history buffer. Left: at t_{i+1} before the event delivery phase the contents of the top $\Delta t/h$ elements of the ring buffer at t_i (gray) are copied to the spike history buffer and the counters are reset. Right: at t_{i+2} before the event delivery phase the contents of the top $\Delta t/h$ elements of the ring buffer at t_{i+1} are copied to the spike history buffer and the counters are reset.

could still receive events at later event delivery phases. At this point, the volume transmitter copies the contents of the ring buffer in the range $[0, \Delta t/h - 1]$ to a separate spike history buffer of length $\Delta t/h$, see **Figure 6C**. It then resets those counters to zero and rotates the 'front' of the ring buffer by $\Delta t/h$ segments as shown in the right side of **Figure 6B**. Thus the spike history buffer contains all the neuromodulatory spikes that are due to arrive in the projected volume in the interval $(t_i, t_{i+1}]$, and the ring buffer is prepared to receive the events communicated at time t_{i+1}.

We now turn to the delivery of the neuromodulatory spikes to the synapses. Let us assume that a synapse associated with a given volume transmitter has received and processed all the neuromodulatory spikes with arrival times up to and including t_i. Therefore the last update time of the synapse s_{last} is equal to the last neuromodulatory spike time $\leq t_i$. At time t_{i+1} the machines exchange all events generated in the interval $(t_i, t_{i+1}]$. If the synapse's pre-synaptic neuron emits a spike at time s_{pre} within this interval, all neuromodulatory spikes with $t_i < (s_n + d_n) < s_{\text{pre}}$ still need to be taken into account to calculate the weight dynamics of the synapse up to s_{pre}. Conversely,

neuromodulatory spikes that have already been generated and communicated between machines, but are due to arrive at the projection volume after s_{pre}, i.e., $(s_n + d_n) \geq s_{pre}$, should not be taken into account. When the synapse is activated during the event delivery phase at t_{i+1}, it therefore requests the spike history buffer from the volume transmitter, which contains those neuromodulatory spikes for which $(s_n + d_n)$ is in the range $(t_i, t_{i+1}]$, as described above. Depending on its dynamics, it may also need additional information from the post-synaptic neuron; this is illustrated for the case of dopamine-modulated STDP (Izhikevich, 2007) in **Figure 5A**, where the post-synaptic spikes between s_{last} and s_{pre} must also be requested. At the end of its weight update, the synapse emits an event of the appropriate weight and delay to its post-synaptic target, and sets its variable s_{last} to the value of s_{pre}.

Directly after the event delivery phase at t_{i+1}, the volume transmitter sends its spike history buffer to every associated synapse (see **Figure 5B**: `send_history()`). This triggers a weight update for every synapse in which the synapse's last update time s_{last} is earlier than the latest spike in the spike history buffer, s_{VT}. In the dopamine-modulated STDP synapse shown in **Figure 5B**, calculating the weight update involves requesting all post-synaptic spikes between s_{last} and s_{VT}. After calculating the weight update, the synapse sets its variable s_{last} to the value of s_{VT}. Thus at the event delivery phase at time t_{i+2}, each synapse associated with the volume transmitter has received and processed all neuromodulatory spikes with arrival times up to and including t_{i+1}.

In the above we have described how the synapse can be informed of the spikes necessary for calculating its weight updates without requiring dynamic memory structures or an algorithm to discard spikes that are no longer necessary. The key insight is that event-driven requests for the volume transmitter's spike history triggered by the arrival of pre-synaptic spikes can be complemented by delivering the spike history at regular intervals in a time-driven fashion. This combined approach does not entail any additional computational costs for the synapse. It must process every neuromodulatory spike, so it makes no difference when the processing takes place, as long as all the information required to calculate a weight update is available when an event is generated. On a global level there are additional costs, as accessing every synapse every Δt interval involves more operations than accessing synapses only on the arrival of pre-synaptic spikes. However, these additional costs can be reduced by transferring the neuromodulatory spikes not in intervals of Δt, but in intervals of $n \cdot \Delta t$, where n is an integer. We leave n as a parameter that can be chosen by the user; the consequences of the choice of transfer interval are discussed in section 3.2.3. The only alterations that need to be made to the above description to accommodate this improvement is that the spike history buffer must be correspondingly longer (i.e., $n \cdot \Delta t/h$), and spikes must be copied from the ring buffer to the correct section of it.

3.1.3 Establishing a neuromodulated connection

The interaction between the volume transmitter and the synapses requires a bidirectional link. This link from synapse to volume transmitter can be realized by passing the volume transmitter as a parameter when a neuromodulated synapse is defined. The synapse stores a pointer to the volume transmitter and passes its own pointer to the volume transmitter, which maintains a list of associated synapse pointers. For the simulation tool NEST (Gewaltig and Diesmann, 2007) this can be expressed as follows:

```
1 neuron1=nest.Create("iaf_neuron")
2 neuron2=nest.Create("iaf_neuron")
3 vt=nest.Create("volume_transmitter")
4 nest.SetDefaults("neuromodulated_
    synapse",{"vt": vt[0]})
5 nest.Connect(neuron1, neuron2,
    model="neuromodulated_synapse")
```

Here we are using NEST's interface to the Python[2] programming language PyNEST (Eppler et al., 2009). The population of neurons releasing the neuromodulator are connected to the volume transmitter with standard synaptic connections specifying the propagation delays. For example, in NEST:

```
6 nest.ConvergentConnect(neuromodulator_neurons,
   vt, delay=d, model="static_synapse")
```

These operations can be performed in either order.

3.2 PERFORMANCE

To investigate the efficiency and scalability of our framework, we simulated networks of 10^4 and 10^5 neurons incorporating STDP with and without neuromodulation at their excitatory–excitatory synapses as a function of the number of processors used (see section 2.2). The results are illustrated in **Figure 7**. **Figure 7A** shows the simulation times for one biological second of the 10^4 neuron network and **Figure 7B** shows the corresponding speed-up curves, i.e., how much faster a simulation runs with m machines than with 1 machine (Wilkinson and Allen, 2004). When neuromodulatory spikes are transferred in intervals of $\Delta t = d_{min}$, a supralinear scaling can be observed up to 32 machines, beyond which the scaling is approximately linear. Simulation times are on average 17 times slower than those for the corresponding network incorporating unmodulated STDP. If neuromodulatory spikes are transmitted less often, in intervals of $70 \cdot d_{min}$, the reduced number of operations results in a supralinear scaling up to 184 machines. As the number of machines grows, the disparity in simulation times between the neuromodulated and unmodulated networks decreases. The supralinear scaling in all simulations of the 10^4 neuron network is due to cache effects.

Figures 7C and D show the simulation times for one biological second of the 10^5 neuron network and the corresponding speed-up curves. The neuromodulated network (transfer interval: $100 \cdot d_{min}$) and the unmodulated control network both scale approximately linearly up to 1024 machines. On average the neuromodulated network is 3.2 times slower than the unmodulated network.

These results demonstrate that the framework scales well, up to at least 184 or 1024 machines, depending on the network size. However, they also raise a number of questions. Firstly, in **Figures 7A and B** we observe that the unmodulated network shows a supralinear scaling up to 64 processors, but then the simulation time saturates at 0.65 s. This suggests that an increase in communication overhead is masking the decrease in computation time. How do the scaling properties of the neuromodulated and unmodulated networks compare if the communication overhead is factored out? Secondly, the neuromodulated network simulations take longer

[2]http://www.python.org

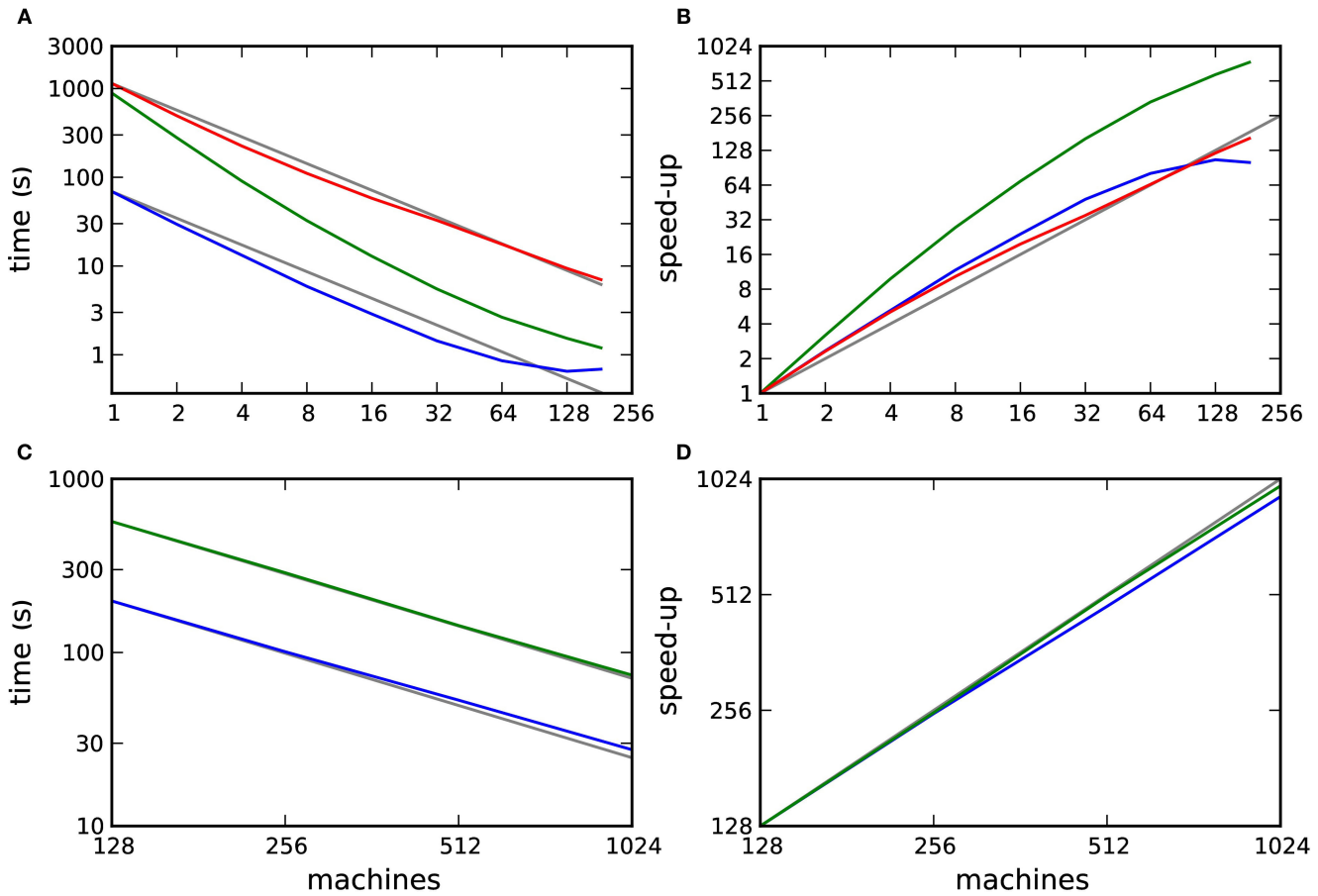

FIGURE 7 | Performance of simulations of networks incorporating STDP with and without neuromodulation. (A) Time to simulate 1 biological second of the 10^4 neuron network as a function of the number of machines in double logarithmic representation. Neuromodulated STDP with transference of neuromodulatory spikes from the volume transmitter in intervals of d_{min} (red), $70 \cdot d_{min}$ (green), unmodulated STDP (blue). **(B)** Speed-up factor for the simulation times shown in **(A)**. **(C)** Time to simulate 1 biological second of the 10^5 neuron network as a function of the number of machines in double logarithmic representation. Neuromodulated STDP with transference of neuromodulatory spikes from the volume transmitter in intervals of $100 \cdot d_{min}$ (green), unmodulated STDP (blue). **(D)** Speed-up factor for the simulation times shown in **(C)**. Gray lines indicate linear predictions.

than the unmodulated network simulations. Is this due to the overhead of the volume transmitter infrastructure or due to the increased complexity of the neuromodulated STDP update rule? Finally, faster simulation times are observed when the transfer interval of the volume transmitter is increased. What is the relationship between the performance and the choice of transfer interval? We address these questions in the following three sections.

3.2.1 Saturation due to communication overhead

Let us assume that the simulation time $T_{sim}(m)$ for m machines is composed of two components: the computing time $T_c(m)$ required to perform the parallel simulation operations such as calculating the neuronal and synaptic dynamics, and the communication time $T_{ex}(m)$ required to exchange events between machines:

$$T_{sim}(m) = T_c(m) + T_{ex}(m)$$

The communication time $T_{ex}(m)$ is a characteristic of the computing architecture used for simulation and typically depends on the number of communicated bytes. As described in section 2.1.2 communication buffers containing spike entries are communicated between machines in time steps of d_{min}. The number of spikes that each machine sends can be approximated as $(N/m)\lambda d_{min}$, where N is the total number of neurons, m the number of machines and λ the average firing rate. If the spikes of successive time steps of length h are separated in the communication buffers by markers, the total number of bytes in each communication buffer is:

$$b(m) = \frac{N}{m}\lambda d_{min} b_{spike} + \frac{d_{min}}{h} b_{marker}$$

where b_{spike} is the number of bytes to represent the global identifier of a neuron and b_{marker} is the number of bytes taken up by a marker. In our implementation in NEST, $b_{spike} = b_{marker} = 8$. For a given network simulation we can calculate $b(m)$ and thus the communication time as:

$$T_{ex}(m) = \frac{T}{d_{min}} T_{Ex}^1\left(m, b(m)\right)$$

where $T^1_{Ex}(m,b)$ is the time taken to perform one exchange between m machines of b bytes per machine and T is the biological time simulated. The single exchange time $T^1_{Ex}(m,b)$ can be determined empirically by measuring the time taken for n calls of the exchange routine for a packet of size b and dividing the total time by n. We measured the single exchange time $T^1_{Ex}(m,b)$ on our X86 computing cluster by averaging over 1000 function calls exchanging packets of sizes determined by the 10^4 neuron network simulation (see section 2.2). **Figure 8A** shows the total communication time T_{ex} as a function of the number of machines for the 10^4 neuron network simulation. The communication time increases with the number of machines in proportion to $m\ln(m)$, which is to be expected for the algorithm underlying the `MPI_Allgather()` routine from the MPI library[3] used in our implementation. **Figure 8B** shows the communication time as a percentage of the total simulation time T_{sim}. The proportion of the simulation time taken up by data exchange increases rapidly with the number of machines. This representation underlines the fact that the communication overhead plays a proportionally bigger role for computationally less expensive applications: the proportion of the total time consumed by data exchange increases more quickly for the unmodulated network simulation than for the neuromodulated cases, rising to more than 40% for the unmodulated network at 184 machines and to 25 and 5% for the neuromodulated networks with transfer intervals of $70\cdot d_{min}$ and d_{min} respectively.

To obtain the pure computation time $T_c(m)$, we substract the communication time $T_{ex}(m)$ from the total run time $T_{sim}(m)$. The result is shown in **Figure 9A** and the corresponding speed-up curves in **Figure 9B**.

The effect on the scaling of the neuromodulated network simulations is small. However, the saturation of simulation time for the unmodulated network observed in **Figures 7A and B** is no longer visible, demonstrating that the saturation was due to communication overhead rather than suboptimal simulation algorithms. All network simulations exhibit linear scaling or better up to 184 machines.

[3]http://www.open-mpi.org/

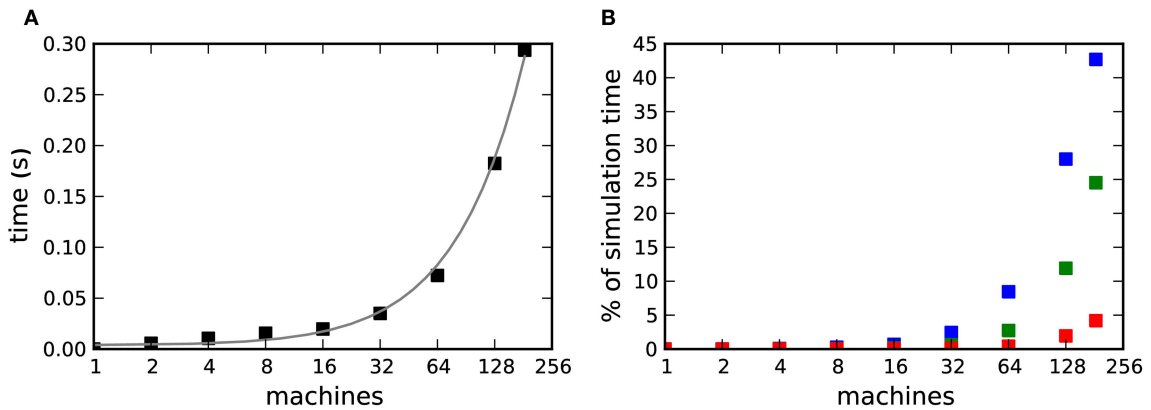

FIGURE 8 | Communication overhead in a distributed simulation of the 10^4 neuron network. (A) Time required for all necessary data exchanges for a simulation of one biological second as a function of the number of machines. The gray curve is a fit of $m\cdot\ln(m)$ to the data. **(B)** Communication time as a percentage of the total simulation time as a function of the number of machines. Neuromodulated STDP with transference of neuromodulatory spikes from the volume transmitter in intervals of d_{min} (red), $70\cdot d_{min}$ (green), unmodulated STDP (blue).

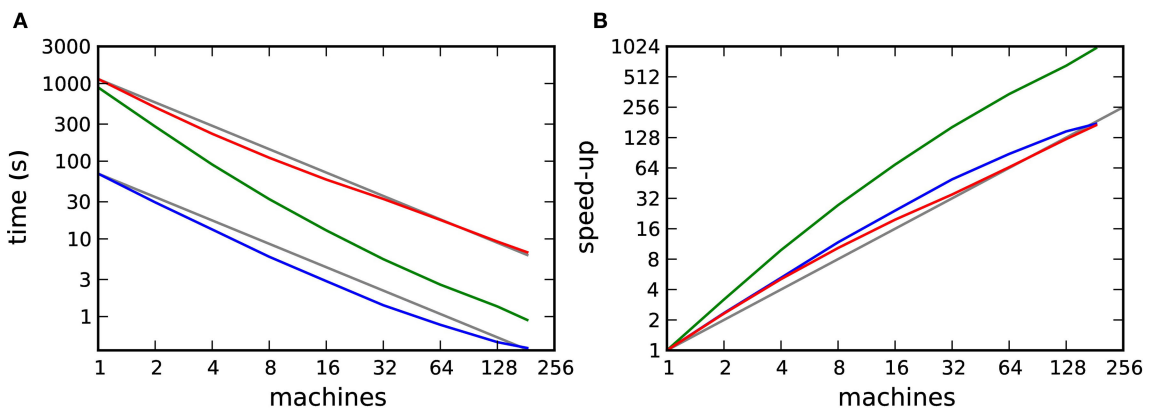

FIGURE 9 | Computation time for a distributed simulation of one biological second of the 10^4 neuron network. (A) Computation time as a function of number of machines in double logarithmic representation. Neuromodulated STDP with transference of neuromodulatory spikes from the volume transmitter in intervals of d_{min} (red), $70\cdot d_{min}$ (green), unmodulated STDP (blue). **(B)** Speed-up factor for the simulation times shown in **(A)**. Gray lines indicate linear predictions.

3.2.2 Dependence of performance on the neuromodulatory firing rate

Figures 7 and 9 show that the simulation times for the neuromodulated network simulations are much longer than for the unmodulated network simulations. This could be due to the computational cost of the volume transmitter overhead, or to the increased complexity of the neuromodulated STDP update rule, which depends not only on the pre- and post-synaptic rate but also on the rate of the population of neuromodulator releasing neurons (see section 2.2). For the curves shown in **Figures 7 and 9**, the size of the neuromodulator releasing population N_{nm} was set to 50, resulting in a neuromodulatory firing rate of ≈500 Hz.

Figure 10 shows the dependence of the simulation time for the 10^4 neuron network on 184 processors as a function of the firing rate of the neuromodulatory population. The different firing rates are realized by varying the number of neuromodulator releasing neuron N_{nm} from 0 to 60 in steps of 5. Note that the network activity is not affected by the choice of N_{nm} on the time scale of one second, so the pre- and post-synaptic firing rates are constant for all values of N_{nm}. A linear increase of simulation time with neuromodulatory firing rate can be observed, with a greater slope for a transfer interval of d_{min} than for $70{\cdot}d_{min}$. For a neuromodulatory spike rate of 0 Hz, the simulation times for the neuromodulated networks are only slightly larger than for the unmodulated network. These results demonstrate that the large disparity in simulation times observed between the neuromodulated and unmodulated simulations is not due to overheads related to the volume transmitter infrastructure but to the increased computational complexity of the neuromodulated STDP update rule. As a further test, we carried out an experiment for a neuromodulatory firing rate of 500 Hz in which the volume transmitter infrastructure transfers the neuromodulatory spikes to the synapse, but the synapse performs the unmodulated STDP update rule, i.e., the synapse ignores the transferred spikes. In this case the simulation times are reduced to those of the unmodulated STDP control case (data not shown).

These results confirm the decision to store the neuromodulatory spikes in a fixed-size buffer and ensure all spikes are taken into consideration by regular updates of the associated synapses.

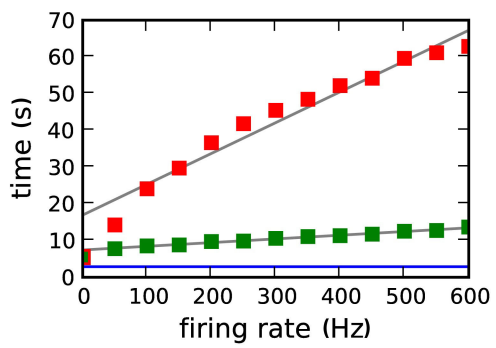

FIGURE 10 | Simulation time for one biological second of the 10^4 neuron network for 184 machines as a function of the neuromodulatory firing rate. Neuromodulated STDP with transference of neuromodulatory spikes from the volume transmitter in intervals of d_{min} (red squares), $70{\cdot}d_{min}$ (green squares). The blue line indicates the simulation time for the unmodulated network; the gray lines are linear fits to the data.

The alternative approach, to store spikes in a dynamically sized buffer and update synapses only on demand, requires the use of an algorithm to discard spikes that have already been processed. The complexity of such an algorithm is linear in the number of spikes in the buffer, therefore such a scheme would entail proportionally higher costs with increased neuromodulatory spike rate, whereas the cost for our framework is approximately constant.

3.2.3 Dependence of performance on the transfer interval

Figures 7 and 10 show that faster simulation times are achieved with a transfer time of $70{\cdot}d_{min}$ than with a transfer time of d_{min} for all numbers of machines and all neuromodulatory rates. This is unsurprising, as the longer transfer time entails proportionally fewer transfer operations: the number of transfer operations is given by $T/(n{\cdot}d_{min})$, where T is the biological time simulated. However, a longer transfer time also requires a larger data structure to hold all the buffered spikes. As increasing the memory used by an application will generally decrease its speed, optimizing performance may require a trade-off to be found between reducing the number of operations and limiting the memory requirements.

To obtain the dependence of the simulation time on the transfer time, we carried out simulations of the 10^4 neuron network whilst varying the parameter n, where $n{\cdot}d_{min}$ is the transfer interval for communicating spikes in a time-driven fashion from the volume transmitter to the synapses (see section 3.1.2). The results are shown in **Figure 11A**. By plotting the simulation time as a function of $1/n$ in **Figure 11B**, we can see that the simulation time is indeed proportional to $1/n$ for $n>2$. For smaller values of n the neuromodulator spike buffers are sometimes empty, in which case the transfer operation is omitted, leading to a faster simulation time than the linear prediction. These results demonstrate that increasing the memory requirements of the volume transmitter does not result in a decrease in performance, so in practice a large value of n should be selected.

DISCUSSION

Neuromodulated plasticity has recently become a hot topic in computational as well as experimental neuroscience. There is evidence for neuromodulator involvement in many cognitive functions, such as attention or reward learning (Reynolds et al., 2001; Hasselmo and McGaughy, 2004). On the cellular level it has been shown that long-range neuromodulatory systems strongly influence the induction of spike-timing dependent plasticity (see Pawlak et al., 2010 in this special issue). Neuromodulated plasticity is a strong candidate for a mechanism that links synaptic plasticity to system level learning (Seung, 2003; Xie and Seung, 2004; Baras and Meir, 2007; Florian, 2007; Izhikevich, 2007; Legenstein et al., 2008; Potjans et al., 2009b, 2010; Vasilaki et al., 2009; Pawlak et al., 2010, this special issue). However, so far in most spiking neural networks models implementing neuromodulated synaptic plasticity, the signal is injected externally into the network rather than being generated by the network itself (but see Izhikevich, 2007 and Legenstein et al., 2008). Furthermore, technical details about the implementation of neuromodulated plasticity in spiking neural networks have not been provided. Due to this lack models cannot be easily reproduced or extended by the wider modeling community.

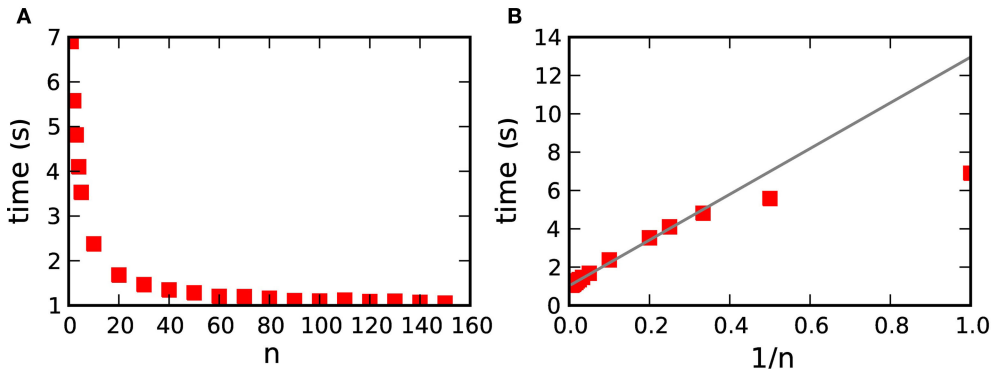

FIGURE 11 | Simulation time for one biological second of the 10^4 neuron network for 184 machines with respect to *n*, where $n \cdot d_{min}$ is the transfer interval of the volume transmitter. (A) Simulation time as a function of *n*. **(B)** Simulation time as a function of $1/n$. The gray line shows the linear fit for $n>2$.

Here, we present for the first time a general framework for the efficient implementation of neuromodulated plasticity in time-driven distributed simulations where the neuromodulatory signal is generated within the network. The presented framework paves the way for the investigation of a wide range of neural circuits which generate and exploit a neuromodulatory signal to carry out cognitive functions, such as dopamine-driven learning and noradrenaline-mediated stress response. The framework is general in the sense that it does not rely on a particular implementation language, neuromodulator, or neuromodulated plasticity and makes few and easily fulfilled assumptions about the data structures and algorithms of the underlying simulation tool. The main difficulty in the implementation of neuromodulated plasticity in distributed simulations is how to inform the neuromodulated synapses efficiently about the non-local neuromodulatory signal, which is typically generated by a population of neurons on different machines than either the pre- or the post-synaptic neuron. We solved this problem by introducing a new object called "volume transmitter," which represents the neuromodulatory signal available in a certain volume by globally collecting all the spikes from neurons in a specified neuromodulator releasing population and transferring the spikes to a user-specified subset of local synapses. We propose a hybrid algorithm for the transfer of spikes from the volume transmitter to the neuromodulated synapses. In addition to the delivery triggered by every pre-synaptic spike, the neuromodulatory spike history is delivered in discrete time intervals of $n \cdot \Delta t$, where n is an integer and Δt the communication interval of the network. This has three advantages over a purely event-based transfer: first, the neuromodulatory spikes can be stored in a static data structure; second, no additional algorithm is required to determine which spikes can be cleared from the history; and third, the memory requirements are known and fixed regardless of the network activity. The technology is fully implemented and available in NEST including an example and can be controlled through the application interface to the Python programming language (Eppler et al., 2009).

Our results show that simulation time is proportional to $1/n$ for $n>2$; this is due to the decrease in the number of operations performed. As no deterioration in performance can be observed for large n as a result of the larger memory structure, in practice a large n should be selected. For a suitably large choice of n, our framework exhibits supralinear scaling up to 184 machines on simulations of a balanced random network of 10^4 neurons incorporating neuromodulated STDP in its excitatory to excitatory connections. Further, linear scaling can be observed up to 1024 machines on simulations of a network containing 10^5 neurons with a biologically realistic number of inputs to each neuron (10^4) and connectivity (10%), corresponding to 1 mm^3 of mammalian cortex. The scaling properties of the neuromodulated network simulations are comparable to, or better than, that of an unmodulated network simulation. Additionally, our framework does not incur any additional costs with increased firing rate of the neuromodulatory neuron population other than those necessarily imposed by the complexity of the neuromodulated synaptic update rules. Although our motivation was to provide a framework capable of meeting the demands of very large distributed neuronal network simulations, it can be used without adaptation for the serial simulation of smaller-scale networks in which the neuromodulatory signal is generated within the network.

In the context of analyzing the benchmark simulations we developed a technique to determine what proportion of the run time of a simulation is taken up by communication between machines. This generally applicable technique enables a developer of distributed software to distinguish a saturation due to communication overheads from one due to a suboptimally implemented algorithm.

Although our hybrid communication strategy was developed in the context of the particular challenges of neuromodulated plasticity, it could well enable a more efficient formulation of algorithms to model unmodulated plasticity such as STDP. Combining event-driven weight updates triggered by pre-synaptic spikes with time-driven updates at regular intervals would permit also the post-synaptic spike history to be stored in a static data structure and remove the need for an algorithm to discard spikes that are no longer relevant. However, as one spike history structure is required for each post-synaptic neuron (rather than one for an entire neuromodulatory population), the memory requirements of the simulation will depend more strongly on the choice of transfer interval. In future work, we will investigate the trade-off between reducing the number of transfer operations and increasing the memory requirements.

We have formulated the neuromodulator dynamics as a dynamics on a graph where the interaction is mediated by point events. This integrates well into the representation of spiking neuronal networks

used for large-scale simulation. In addition we have decided to place the dynamics of the neuromodulatory signal at the site of the individual synapse. An alternative approach would be to low-pass filter the neuromodulatory spikes on each machine and then exchange and add the filtered signals between machines. As the global signal is mostly likely to be slow, this exchange could perhaps be performed less often than the communication of spikes in intervals of Δt. However, this alternative approach has several disadvantages with respect to our proposal. First, whereas the alternative proposal would require additional communication to exchange the filtered signals among machines, our framework causes no additional communication costs, as spikes have to be exchanged anyway in the distributed framework. Therefore, an approximate solution is unlikely to be more efficient. Second, our approach has the advantage that neuromodulated synaptic dynamics where changes of the synaptic state depend on the instantaneous value of the neuromodulator level can be implemented exactly. Therefore, even in the case that an approximate solution is more efficient for a particular application, it would be useful to have the exact implementation at hand for a verification of the results. Third, in our proposal the same framework can be used for a variety of different neuromodulators with different neuromodulatory dynamics, assuming the neuromodulator level can be calculated solely on the basis of the spike train of the releasing population. However, this generality comes at a price. The time course of a neuromodulator, which is probably essentially identical within a certain volume of cortex, is recomputed in every synapse, resulting in redundant operations. Moreover, we assumed that each spike of the neuromodulator releasing population contributes the same amount to the neuromodulator concentration. If necessary, these disadvantages can be remedied in the context of a specific scientific question by developing more specialized versions of the volume transmitter that calculate the dynamics of the neuromodulator under investigation and then deliver the results of this calculation to the synapses.

Our solution is based on the assumption that it is sufficiently accurate to represent the times of the neuromodulatory spikes on the grid defined by the computation step size. The framework can be modified to process "off-grid" spike times, but at the cost of maintaining dynamic data structures in the volume transmitter which would result in a deterioration of performance. A further limitation of our framework is that it has no capacity to represent spatial variations in neuromodulator concentration within the population of synapses such as diffusion processes. Recently, a simulation tool has been presented which considers diffusion processes by explicitly modeling the extracellular space (Zubler and Douglas, 2009).

As our solution enables networks to be simulated that generate their own modulatory signals, it paves the way for the investigation of closed-loop functional models. We already successfully applied our framework to a model that implements temporal-difference learning based on dopamine modulated plasticity to solve a navigation problem (Potjans et al., 2009c). Even though the network investigated here was comparatively small (order of 10^3 neurons), systematic investigation of it required distributed computing; although the plasticity process occurs on a time scale of tens of milliseconds, the learning process on the network level takes place on a time scale of minutes to hours. The user has full flexibility to assign the volume transmitter to specific groups of neuromodulator releasing neurons and neuromodulated synapses, thus allowing the simulation of multiple volumes with different neuromodulator concentrations or multiple neuromodulators with different dynamics in the same network. Our results suggest that the framework will scale up to much larger networks than those investigated here. This will enable the investigation of "brain-scale" networks modeling circuits made up of several brain areas. One possible application is to investigate the role of neuromodulators such as acetylcholine in the cortex simultaneously with its generation process, which takes place in subcortical areas. It is our hope that our novel technology will make it easy for computational neuroscientists to study sophisticated models with interesting system-level behavior based on neuromodulated plasticity.

ACKNOWLEDGMENTS

We are most grateful to Hans Ekkehard Plesser for language legality consultation. We also thank the editor and the reviewers for the constructive interaction which helped us to considerably improve the integration of our work into the special issue. Partially funded by DIP F1.2, BMBF Grant 01GQ0420 to the Bernstein Center for Computational Neuroscience Freiburg, EU Grant 15879 (FACETS), the Junior Professor Program of Baden-Württemberg, "The Next-Generation Integrated Simulation of Living Matter" project, part of the Development and Use of the Next-Generation Supercomputer Project of the Ministry of Education, Culture, Sports, Science and Technology (MEXT) of Japan and the Helmholtz Alliance on Systems Biology. Access to supercomputing facility through JUGENE-Grant JINB33.

REFERENCES

Agnati, L., Zoli, M., Strömberg, I., and Fuxe, K. (1995). Intercellular communication in the brain: wiring versus volume transmission. *Neuroscience* 69, 711–726.

Ananthanarayanan, R., and Modha, D. S. (2007). "Anatomy of a cortical simulator," in *Supercomputing 2007: Proceedings of the ACM/IEEE SC2007 Conference on High Performance Networking and Computing* (New York, NY: Association for Computing Machinery).

Antonov, I., Antonova, I., Kandel, E. R., and Hawkins, R. D. (2003). Activity-dependent presynaptic facilitation and hebbian LTP are both required and interact during classical conditioning in aplysia. *Neuron* 37, 135–147.

Arbuthnott, G., and Wickens, J. (2007). Space, time and dopamine. *Trends Neuroscience* 30, 62–69.

Baras, D., and Meir, R. (2007). Reinforcement learning, spike-time-dependent plasticity, and the BCM rule. *Neural Comput.* 19, 2245–2279.

Berridge, C. W., and Waterhouse, B. D. (2003). The locus coeruleus-noradrenergic system: modulation of behavioral state and state-dependent cognitive processes. *Brain Res. Brain Res. Rev.* 42, 33–84.

Bi, G., and Poo, M. (2001). Synaptic modification by correlated activity: Hebb's postulate revisited. *Annu. Rev. Neurosci.* 24, 139–66.

Bi, G.-Q., and Poo, M.-M. (1998). Synaptic modifications in cultured hippocampal neurons: dependence on spike timing, synaptic strength, and postsynaptic cell type. *J. Neurosci.* 18, 10464–10472.

Braitenberg, V., and Schüz, A. (1998). *Cortex: Statistics and Geometry of Neuronal Connectivity*, 2nd Edn. Berlin: Springer-Verlag.

Brette, R., Rudolph, M., Carnevale, T., Hines, M., Beeman, D., Bower, J. M., Diesmann, M., Morrison, A., Goodman, P. H., Harris, F. C. Jr., Zirpe, M., Natschläger, T., Pecevski, D., Ermentrout, B., Djurfeldt, M., Lansner, A., Rochel, O., Vieville, T., Muller, E., Davison, A. P., El Boustani, S., and Destexhe, A. (2007). Simulation of networks of spiking neurons: a review of tools and strategies. *J. Comput. Neurosci.* 23, 349–398.

Cooper, J., Bloom, F., and Roth, R. (2002). *The Biochemical Basis of Neuropharmacology*. New York, Oxford: Oxford University Press.

Deco, G., and Thiele, A. (2009). Attention: oscillations and neuropharmacology. *Eur. J. Neurosci.* 30, 347–354.

Eppler, J. M., Helias, M., Muller, E., Diesmann, M., and Gewaltig, M. (2009). PyNEST: a convenient interface to the NEST simulator. *Front. Neuroinformatics* 2, 12.

Florian, R. V. (2007). Reinforcement learning through modulation of spike-timing-dependent synaptic plasticity. *Neural Comput.* 19, 1468–1502.

Garris, P. A., Ciolkowski, E. L., Pastore, P., and Wightman, R. M. (1994). Efflux of dopamine from the synaptic cleft in the nucleus accumbens of the rat brain. *J. Neurosci.* 14, 6084–6093.

Gerstner, W., Kempter, R., van Hemmen, J. L., and Wagner, H. (1996). A neuronal learning rule for sub-millisecond temporal coding. *Nature 383*, 76–78.

Gewaltig, M.-O., and Diesmann, M. (2007). NEST (Neural Simulation Tool). *Scholarpedia J.* 2, 1430.

Hammarlund, P., and Ekeberg, O. (1998). Large neural network simulations on multiple hardware platforms. *J. Comput. Neurosci.* 5, 443–459.

Hanuschkin, A., Kunkel, S., Helias, M., Morrison, A., and Diesmann, M. (2010). A general and efficient method for incorporating precise spike times in globally time-driven simulations. *Front. Neuroinform.* 4:133. doi: 10.3389/fninf.2010.00113.

Harris, J., Baurick, J., Frye, J., King, J., Ballew, M., Goodman, P., and Drewes, R. (2003). A novel parallel hardware and software solution for a large-scale biologically realistic cortical simulation. *Technical Report*, University of Nevada, Reno, NV.

Hasselmo, M., and McGaughy, J. (2004). High acetylcholine levels set circuit dynamics for attention and encoding and low acetylcholine levels set dynamics for consolidation. *Prog. Brain Res.* 145, 207–231.

Hebb, D. O. (1949). *The Organization of Behavior: A Neuropsychological Theory*. New York: John Wiley and Sons.

Herrero, J. L., Roberts, M. J., Delicato, L. S., Gieselmann, M. A., Dayan, P., and Thiele, A. (2008). Acetylcholine contributes through muscarinic receptors to attentional modulation in v1. *Nature* 454, 1110–1113.

Izhikevich, E. M. (2007). Solving the distal reward problem through linkage of STDP and dopamine signaling. *Cereb. Cortex* 17, 2443–2452.

Lamport, L. (1978). Time, clocks, and the ordering of events in a distributed system. *Commun. ACM* 21, 558–565.

Legenstein, R., Pecevski, D., and Maass, W. (2008). A learning theory for reward-modulated spike-timing-dependent plasticity with application to biofeedback. *PLoS Comput. Biol.* 4, e1000180. doi: 10.1371/journal.pcbi.1000180.

Markram, H., Lübke, J., Frotscher, M., and Sakmann, B. (1997). Regulation of synaptic efficacy by coincidence of postsynaptic APs and EPSPs. *Science* 275, 213–215.

Markram, H., and Tsodyks, M. (1996). Redistribution of synaptic efficacy between neocortical pyramidal neurons. *Nature* 382, 807–810.

Montague, P. R., McClure, S. M., Baldwin, P., Phillips, P. E., Budygin, E. A., Stuber, G. D., Kilpatrick, M. R., and Wightman, R. M. (2004). Dynamic gain control of dopamine delivery in freely moving animals. *J. Neurosci.* 24, 1754–1759.

Moreau, A., Amar, M., Le Roux, N., Morel, N., and Fossier, P. (2010). Serotoninergic fine-tuning of the excitation–inhibition balance in rat visual cortical networks. *Cereb. Cortex* 20, 456–467.

Morrison, A., Aertsen, A., and Diesmann, M. (2007). Spike-timing dependent plasticity in balanced random networks. *Neural Comput.* 19, 1437–1467.

Morrison, A., and Diesmann, M. (2006). "Maintaining causality in discrete time neuronal network simulations," in *Proceedings of the Potsdam Supercomputer School 2005, Germany*.

Morrison, A., and Diesmann, M. (2008). "Maintaining causality in discrete time neuronal network simulations," in *Lectures in Supercomputational Neuroscience: Dynamics in Complex Brain Networks, Understanding Complex Systems*, eds P. Beim Graben, C. Zhou, M. Thiel, and J. Kurths (Springer, Verlag: Berlin Heidelberg), 267–278.

Morrison, A., Diesmann, M., and Gerstner, W. (2008). Phenomenological models of synaptic plasticity based on spike-timing. *Biol. Cybern. 98*, 459–478.

Morrison, A., Mehring, C., Geisel, T., Aertsen, A., and Diesmann, M. (2005). Advancing the boundaries of high connectivity network simulation with distributed computing. *Neural Comput.* 17, 1776–1801.

Morrison, A., Straube, S., Plesser, H. E., and Diesmann, M. (2007). Exact subthreshold integration with continuous spike times in discrete time neural network simulations. *Neural Comput.* 19, 47–79.

Nordlie, E., Gewaltig, M.-O., and Plesser, H. E. (2009). Towards reproducible descriptions of neuronal network models. *PLoS Comput. Biol. 5*, e1000456. doi: 10.1371/journal.pcbi.1000456.

Pawlak, V., Wickens, J. R., Kirkwood, A., and Kerr, J. N. D. (2010). Timing is not everything: neuromodulation opens the STDP gate. *Front. Syn. Neurosci.* 2:146. doi: 10.3389/fnsyn.2010.00146.

Pecevski, D., Natschläger, T., and Schuch, K. (2009). PCSIM: a parallel simulation environment for neural circuits fully integrated with python. *Front. Neuroinformatics* 3:11. doi: 10.3389/neuro.11.011.2009.

Plesser, H. E., Eppler, J. M., Morrison, A., Diesmann, M., and Gewaltig, M.-O. (2007). "Efficient parallel simulation of large-scale neuronal networks on clusters of multiprocessor computers," in *Euro-Par 2007: Parallel Processing, volume 4641 of Lecture Notes in Computer Science*, eds A.-M. Kermarrec, L. Bougé, and T. Priol (Berlin: Springer-Verlag), 672–681.

Potjans, W., Morrison, A., and Diesmann, M. (2009a). Implementing neuromodulated plasticity in distributed simulations. *Front. Neuroinformatics* Conference Abstract: 2nd INCF Congress of Neuroinformatics. doi: 10.3389/conf.neuro.11.2009.08.043.

Potjans, W., Morrison, A., and Diesmann, M. (2009b). A spiking neural network model of an actor-critic learning agent. *Neural Comput.* 21, 301–339.

Potjans, W., Morrison, A., and Diesmann, M. (2009c). A spiking temporal-difference learning model based on dopamine-modulated plasticity. *BMC Neurosci.* 10(Supp 1), 140.

Reynolds, J. N. J., Hyland, B. I., and Wickens, J. R. (2001). A cellular mechanism of reward-related learning. *Nature* 413, 67–70.

Schultz, W., Dayan, P., and Montague, P. R. (1997). A neural substrate of prediction and reward. *Science* 275, 1593–1599.

Seung, H. S. (2003). Learning spiking neural networks by reinforcement of stochastic synaptic transmission. *Neuron* 40, 1063–1073.

Song, S., and Abbott, L. F. (2001). Cortical development and remapping through spike timing-dependent plasticity. *Neuron* 32, 339–350.

Song, S., Miller, K. D., and Abbott, L. F. (2000). Competitive Hebbian learning through spike-timing-dependent synaptic plasticity. *Nat. Neurosci.* 3, 919–926.

Thomson, A. M., and Deuchars, J. (1994). Temporal and spatial properties of local circuits in neocortex. *Trends Neurosci.* 17, 119–126.

Vasilaki, E., Frémaux, N., Urbanczik, R., Senn, W., and Gerstner, W. (2009). Spike-based reinforcement learning in continuous state and action space: When policy gradient methods fail. *PLoS Comput. Biol.* 5, e1000586. doi: 10.1371/journal.pcbi.1000586.

Wilkinson, B., and Allen, M. (2004). *Parallel Programming: Techniques and Applications Using Networked Workstations and Parallel Computers* (2 ed.). Prentice Hall.

Xie, X., and Seung, H. S. (2004). Learning in neural networks by reinforcement of irregular spiking. *Phys. Rev. E* 69, 41909.

Zoli, M., and Agnati, L. F. (1996). Wiring and volume transmission in the central nervous system: The concept of closed and open synapses. *Prog. Neurobiol.* 49, 363–380.

Zoli, M., Jansson, A., Syková, E., Agnati, L. F., and Fuxe, K. (1999). Volume transmission in the cns and its relevance for neuropsychopharmacology. *Trends Pharmacol. Sci.* 20, 142–150.

Zubler, F., and Douglas, R. (2009). A framework for modeling the growth and development of neurons and networks. *Front. Comput. Neurosci.* 3:25. doi: 10.3389/neuro.10.025.2009.

Conflict of Interest Statement: The authors declare that the research was conducted in the absence of any commercial or financial relationships that could be construed as a potential conflict of interest.

Received: 01 February 2010; accepted: 15 September 2010; published online: 23 November 2010.

*Citation: Potjans W, Morrison A and Diesmann M (2010) Enabling functional neural circuit simulations with distributed computing of neuromodulated plasticity. Front. Comput. Neurosci. **4**:141. doi: 10.3389/fncom.2010.00141*

APPENDIX

BENCHMARK MODEL DESCRIPTION AND SPECIFICATION

Table 1 | Tabular description of benchmark network model after Nordlie et al. (2009).

A: MODEL SUMMARY

Populations	Three: excitatory (E), inhibitory (I), neuromodulator releasing neurons (M) ($\subset$ excitatory population)
Connectivity	Random convergent connections
Neuron model	Leaky integrate-and-fire, fixed voltage threshold, fixed absolute refractory time (voltage clamp), exponential synaptic current inputs
Plasticity	Additive STDP/neuromodulated additive STDP in all excitatory to excitatory connections
Input	Independent fixed-rate Poisson spike trains to all neurons
Measurements	Simulation time

B: POPULATIONS

Name	Elements	Size
E	laf neuron	$N_E = 4N_I$
I	laf neuron	N_I
M	laf neuron	N_{nm}

C: CONNECTIVITY

Name	Source	Target	Pattern
EE	E	E	Random convergent $C_E \to 1$, variable weight, delay d
IE	E	I	Random convergent $C_E \to 1$, weight w_E, delay d
EI	I	E	Random convergent $C_I \to 1$, weight $-gw_E$, delay d
II	I	I	Random convergent $C_I \to 1$, weight $-gw_E$, delay d

D: NEURON AND SYNAPSE MODEL

Name	laf neuron
Type	Leaky integrate-and-fire, exponential shaped synaptic current input
Subthreshold dynamics	$\frac{dV}{dt} = -\frac{1}{\tau_m}V + \frac{1}{C_m}I(t)$ if $t > t^* + \tau_{ref}$ $V(t) = V_{reset}$ otherwise $I_{syn}(t) = w\,e^{-t/\tau_{syn}}$
Spiking	If $V(t-) < V_{th} \wedge V(t+) \geq V_{th}$ 1. Set $t^* = t$ 2. Emit spike with time stamp t^*

E: PLASTICITY

Type	Source	Target	Weight dynamics
Additive STDP	E	E	$\dot{w} = \mathrm{STDP}(\Delta t)\delta(t - s_{pre/post})$ $\mathrm{STDP}(\Delta t) = \begin{cases} A_+ e^{-\lvert\Delta t\rvert/\tau_+} & \text{if } \Delta t > 0 \\ A_- e^{-\lvert\Delta t\rvert/\tau_-} & \text{if } \Delta t \leq 0 \end{cases}$
Neuromodulated additive STDP	E	E	$\dot{w} = c(n - b)$ $\dot{c} = -\frac{c}{\tau_c} + \mathrm{STDP}(\Delta t)\delta(t - s_{pre/post})C_1$ $\dot{n} = -\frac{n}{\tau_n} + \frac{\delta(t - s_n)}{\tau_n}C_2$

F: INPUT

Type	Description
Poisson generators	Independent for each neuron, rate ν_{ext}, weight w_{ext}

G: Measurements

Time to complete simulation, not including network construction time

Table 2 | Specification of default parameters used in the 10^4 and 10^5 benchmark networks. Table labeling refers to the model description in **Table 1.**

Name	Value (10^4)	Value (10^5)	Description
B: POPULATION			
N_E	9000	90000	Number of excitatory neurons
N_I	2250	22500	Number of inhibitory neurons
N_{nm}	50	50	Number of neuromodulator releasing neurons
C: CONNECTIVITY			
C_E	900	9000	Number of excitatory inputs per neuron
C_I	225	2250	Number of inhibitory inputs per neuron
w_E	175 pA	45.61 pA	Synaptic weights E → I
g	17	5	Relative inhibitory strength
d	1.5 ms	1.5 ms	Synaptic delay
D: NEURON MODEL			
τ_m	10 ms	10 ms	Membrane time constant
C_m	250 pF	250 pF	Membrane capacity
V_{reset}	0 mV	0 mV	Reset potential
τ_{ref}	0.5 ms	0.5 ms	Absolute refractory period
τ_{syn}	0.33 ms	0.33 ms	Rise time of postsynaptic current
V_{th}	20 mV	20 mV	Fixed firing threshold
E: PLASTICITY			
$w_{initial}$	175 pA	45.61 pA	Initial synaptic weights for plastic synapses (E → E)
w_{max}	350 pA	91.22 pA	Maximal synaptic weights for plastic synapses
A_+	0.005 pA	0.005 pA	Amplitude of weight change due to facilitation
A_-	$1.05 \cdot A_+$	$1.05 \cdot A_+$	Amplitude of the weight change due to depression
τ_+	20 ms	20 ms	Time constant of facilitation
τ_-	20 ms	20 ms	Time constant of depression
b	0.5 μM	0.5 μM	Neuromodulatory baseline concentration
τ_c	1000 ms	1000 ms	Time constant of eligibility trace
C_1	$1 (1/s^2 \mu M)$	$1 (1/s^2 \mu M)$	Constant coefficient
τ_n	200 ms	200 ms	Time constant of neuromodulator concentration
C_2	1 μM	1 μM	Constant coefficients
F: INPUT			
w_{ext}	175 pA	45.61 pA	Synaptic weight of external connections
ν_{ext}	27 kHz	46 kHz	External Poisson rate

frontiers in
COMPUTATIONAL NEUROSCIENCE

ORIGINAL RESEARCH ARTICLE
published: 30 July 2010
doi: 10.3389/fncom.2010.00022

STDP in oscillatory recurrent networks: theoretical conditions for desynchronization and applications to deep brain stimulation

Jean-Pascal Pfister[1]* and Peter A. Tass[2,3]

[1] *Computational and Biological Learning Lab, Department of Engineering, University of Cambridge, Cambridge, UK*
[2] *Institute for Neuroscience and Medicine – Neuromodulation, Research Centre Jülich, Jülich, Germany*
[3] *Department of Stereotaxic and Functional Neurosurgery, University of Cologne, Cologne, Germany*

Edited by:
Wulfram Gerstner, Ecole Polytechnique Fédérale de Lausanne, Switzerland

Reviewed by:
Markus Diesmann, RIKEN Brain Science Institute, Japan
Wulfram Gerstner, Ecole Polytechnique Fédérale de Lausanne, Switzerland

****Correspondence:***
Jean-Pascal Pfister, Computational and Biological Learning Lab, Engineering Department, University of Cambridge, Trumpington Street, CB2 1PZ Cambridge, UK.
e-mail: jean-pascal.pfister@eng.cam.ac.uk

Highly synchronized neural networks can be the source of various pathologies such as Parkinson's disease or essential tremor. Therefore, it is crucial to better understand the dynamics of such networks and the conditions under which a high level of synchronization can be observed. One of the key factors that influences the level of synchronization is the type of learning rule that governs synaptic plasticity. Most of the existing work on synchronization in recurrent networks with synaptic plasticity are based on numerical simulations and there is a clear lack of a theoretical framework for studying the effects of various synaptic plasticity rules. In this paper we derive analytically the conditions for spike-timing dependent plasticity (STDP) to lead a network into a synchronized or a desynchronized state. We also show that under appropriate conditions bistability occurs in recurrent networks governed by STDP. Indeed, a pathological regime with strong connections and therefore strong synchronized activity, as well as a physiological regime with weaker connections and lower levels of synchronization are found to coexist. Furthermore, we show that with appropriate stimulation, the network dynamics can be pushed to the low synchronization stable state. This type of therapeutical stimulation is very different from the existing high-frequency stimulation for deep brain stimulation since once the stimulation is stopped the network stays in the low synchronization regime.

Keywords: STDP, recurrent networks, desynchronization, anti-kindling, synaptic plasticity, bistability, deep brain stimulation

INTRODUCTION

High level of synchrony in neural tissue can be the cause of several diseases. For example, Parkinson's disease is characterized by high level of neuronal synchrony in the thalamus and in the basal ganglia. In opposition, the same neural tissues in healthy conditions have been shown to fire in an asynchronous way (Nini et al., 1995). The Parkinsonian resting tremor (3–6 Hz) is not only related to the subcortical oscillations (Pare et al., 1990), but has been recently shown to be driven by those oscillations (Smirnov et al., 2008; Tass et al., 2010). In addition, the extent of akinesia and rigidity is closely related to synchronized neuronal activity in the beta band (8–30 Hz) (Kuhn et al., 2006).

A standard treatment for patients with Parkinson's disease is to chronically implant an electrode typically in the sub-thalamic nucleus (STN) and perform a high-frequency (>100 Hz) deep brain stimulation (HF-DBS) (Benabid et al., 1991, 2009). Although HF-DBS delivered to the STN is able to reduce tremor, akinesia, and rigidity, this type of stimulation, which was found empirically, does not cure the cause of the tremor. It merely silences the targeted neurons during the stimulation but as soon as the stimulation is turned off, the tremor restarts instantaneously, whereas akinesia and rigidity revert back within minutes to half an hour (Temperli et al., 2003).

Recently, other types of stimulation (Tass, 1999, 2003; Tass and Majtanik, 2006; Hauptmann and Tass, 2007, 2009; Tass and Hauptmann, 2007) have been proposed which are not designed to 'silence' the neurons during the stimulation but rather reshape the network architecture in a way that long-lasting desynchronizing effects occur which outlast the offset of stimulation. This approach relies on two properties or requirements of the neural tissue. First, the network dynamics must elicit bistability such that both the synchronized and the desynchronized state are stable (see **Figure 1A**). Second, there must exist a stimulation that (momentarily) destroys the stability of the synchronous state such that the network is driven into the desynchronized stable state (see **Figure 1B**).

Unfortunately, most of the work that follows this idea of therapeutical stimulation is based on numerical simulations (Tass and Majtanik, 2006; Hauptmann and Tass, 2007, 2009; Tass and Hauptmann, 2007) and only very little has been done analytically (Maistrenko et al., 2007) in order to understand what are the crucial parameters that lead to the two above requirements. Here we consider a recurrent network model that is sufficiently simple to be treated analytically but still captures the desired properties.

Concretely, we consider in this paper a network dynamics that acts on two different time scales. On a short-time scale, neurons integrate the inputs from neighboring neurons and fire periodically. On a longer time scale, synapses can change their strength and hence influence the overall level of synchrony. In principle the above mentioned requirement on bistability can be present in either the neuronal dynamics (short-time scale) or the synaptic dynamics (longer time scale). Since we are aiming for long-lasting effects, we focus on the bistability in the synaptic dynamics. More precisely, we consider a synaptic plasticity learning rule that depends on the precise timing of the action

of the pre- and postsynaptic neurons. This form of plasticity called spike-timing dependent plasticity (STDP) (Gerstner et al., 1996b; Markram et al., 1997; Bi and Poo, 1998) enhances synapses for which the presynaptic spike precedes the postsynaptic one and decreases the synaptic strength when the timing is reversed (see **Figure 3A**).

Regarding the stimulation itself, several candidates have been proposed. For example, it has been shown that a patterned, multi-site and timed-delayed stimulation termed as coordinated reset (CR) stimulation (Tass, 2003) which forces sub-populations to fire in a precise sequence generates transiently a nearly uniform phase distribution. In fact, long-lasting desynchronizing effects of CR stimulation have been verified in rat hippocampal slice rendered epileptic by magnesium withdrawal (Tass et al., 2009).

In the present study, we do not focus on a precise stimulation but rather assume that there exists a stimulation that desynchronizes transiently a given population. Furthermore a given stimulation rarely affects the whole population which fires in a pathological way but only part of it. So we consider two populations. An input population which is affected by the stimulation (see **Figure 2A**) and a recurrent population with plastic synapses which is driven by the input population.

In order to calculate the expected weight change in the recurrent network, we need to get an expression for the spiking covariance of this recurrent population. This technical step has been achieved by Hawkes (1971) and used by Gilson et al. (2009a,b) in the context of recurrent network with STDP. The present study extends the work of Gilson et al. (2009b) to the case of oscillatory inputs and highlights the conditions for which the network elicits bistability.

MATERIALS AND METHODS

NEURONAL DYNAMICS

Let us consider an input population consisting of M neurons and a recurrent population containing N neurons (see **Figure 2A**). Let $x(t) = (x_1(t),\ldots,x_M(t))$ denote the input spike trains at time t with $x_j(t) = \sum_{t_j^{\text{pre}}} \delta(t - t_j^{\text{pre}})$ being the Dirac delta spike train of the j^{th} input neuron. Let $x^t = \{x(s), 0 \le s < t\}$ describe the whole input spike pattern from 0 to t. Similarly, let $y(t) = (y_1(t),\ldots,y_N(t))$ denote the spike trains of the recurrent (or output) population, i.e., $y_i(t) = \sum_{t_i^{\text{post}}} \delta(t - t_i^{\text{post}})$ denotes the Dirac delta spike train of the i^{th} neuron in the recurrent population at time t. $y^t = \{y(s), 0 \le s < t\}$ represents the output spike train from 0 to t.

Let us assume that the input spike trains $x(t)$ have instantaneous firing rates $\rho(t) = (\rho_1(t),\ldots,\rho_M(t)) = \langle x(t)\rangle_{x(t)}$ which are assumed to be periodic (i.e., $\rho(t) = \rho(t + T)$, see **Figure 2B**) and a spatio-temporal covariance matrix $\Delta C(\tau)$ given by

$$\Delta C(\tau) = \frac{1}{T}\int_0^T \left\langle x(t)x^T(t-\tau)\right\rangle_{x(t),x(t-\tau)} dt - \bar{\rho}\bar{\rho}^T \qquad (1)$$

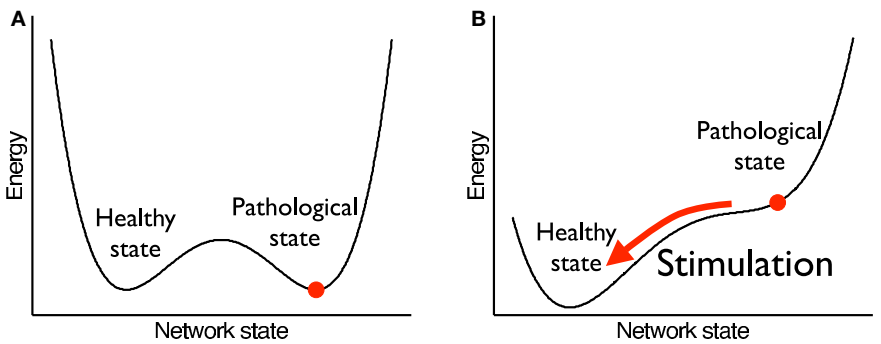

FIGURE 1 | Bistability for therapeutical stimulation. (A) Before stimulation, both the pathological state (strong weights, high neuronal synchrony) and the healthy state (weak weights, low neuronal synchrony) are stable, i.e., they are local minima of an abstract energy function. **(B)** During stimulation, the pathological state becomes unstable and the network is driven towards the healthy state. After stimulation has stopped, the network stays in the healthy state.

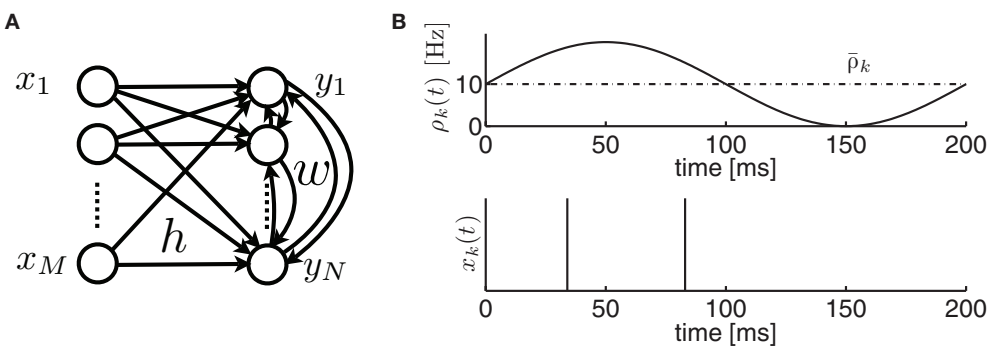

FIGURE 2 | (A) Network architecture. **(B)** The input spike train $x_k(t)$ (*bottom*) of neuron k has an instantaneous firing rate $\rho_k(t)$ (*top*) which is oscillating around an averaged firing rate $\bar{\rho}_k$.

where $\bar{\rho} = T^{-1}\int_0^T \rho(t)dt$ is the mean firing rate averaged over one period T. Note that the input covariance matrix $\Delta C(\tau)$ has an atomic discontinuity at $\tau = 0$, i.e., $\Delta C(0) = \mathrm{diag}(\bar{\rho})\delta(0)$. Let $u(t) = (u_1(t),\ldots,u_N(t))$ denote the membrane potential of all the neurons in the recurrent population (see the Spike-Response Model in Gerstner and Kistler, 2002):

$$u(t) = hx^{\epsilon}(t) + wy^{\epsilon}(t) \tag{2}$$

where the superscript ϵ denotes a convolution[1] with the EPSP kernel $\epsilon(s)$, i.e., $x^{\epsilon}(t) = \int_0^\infty \epsilon(s)x(t-s)ds$ and $y^{\epsilon}(t) = \int_0^\infty \epsilon(s)y(t-s)ds$. Without loss of generality, we will assume that the EPSP kernel is such that $\int_0^\infty \epsilon(s)ds = 1$. More precisely, we take $\epsilon(s) = (\tau - \tau_s)^{-1}(\exp(-s/\tau) - \exp(-s/\tau_s))\Theta(s)$, where $\Theta(s)$ is the Heaviside step function. The $N \times M$ matrix h denotes the weight matrix between the input and the recurrent population. w is a $N \times N$ matrix denoting the recurrent weights (see **Figure 2A**).

In this model, output spikes are generated stochastically, i.e., the higher the membrane potential the more likely a spike will be emitted. Formally a spike is generated in neuron i at time t with an instantaneous probability density $g(u_i(t)) = \langle y_i(t)\rangle_{y_i(t)|x^t,y^t}$ given by

$$g(u_i(t)) \simeq g(\bar{u}_i) + g'(\bar{u}_i)(u_i(t) - \bar{u}_i) \tag{3}$$

where $g'(\bar{u}_i) = dg(u)/du\,|_{u=\bar{u}_i}$ with $\bar{u}_i = T^{-1}\int_0^T \langle u_i(t)\rangle_{x^t,y^t}dt$ denoting the expected membrane potential of neuron i averaged over a period T, and $\bar{u} = (\bar{u}_1,\ldots,\bar{u}_N)$ its vectorial representation. The expected output firing rates $\nu(t) = \langle y(t)\rangle_{y(t)} = \langle\langle y(t)\rangle_{y(t)|x^t,y^t}\rangle_{x^t,y^t}$ at time t is therefore given by

$$\nu(t) = g(\bar{u}) + D'\left(h\rho^{\epsilon}(t) + w\nu^{\epsilon}(t) - \bar{u}\right) \tag{4}$$

where $D' = \mathrm{diag}(g'(\bar{u}))$. Note that from Eq. 2, the averaged expected membrane potential $\bar{u}$ can be expressed as $\bar{u} = h\bar{\rho} + w\bar{\nu}$, where $\bar{\nu} = T^{-1}\int_0^T \nu(t)dt = g(\bar{u})$ is the averaged output firing rate. Combining those two expressions, we get a self-consistent equation for the averaged output firing rate $\bar{\nu}$:

$$\bar{\nu} = g\left(h\bar{\rho} + w\bar{\nu}\right) \tag{5}$$

Note that if the transfer function $g(u)$ is linear, i.e., $g(u) = u$, we have $\bar{\nu} = (\mathbb{1} - w)^{-1}h\bar{\rho}$. Let $\Delta\nu(t) = \nu(t) - \bar{\nu}$ denote the amplitude of the oscillation in the recurrent population:

$$\Delta\nu(t) = D'\left(h\Delta\rho^{\epsilon}(t) + w\Delta\nu^{\epsilon}(t)\right) \tag{6}$$

where $\Delta\rho(t) = \rho(t) - \bar{\rho}$ denotes the amplitude of the input oscillation and $\Delta\rho^{\epsilon}(t) = \int_0^\infty \epsilon(s)\rho(t-s)ds$. Since $\Delta\nu(t)$ appears on the l.h.s of Eq. 6 and in a convolved form on the r.h.s, we can Fourier transform this equation in order to express explicitly the amplitude $\Delta\tilde{\nu}$ of the oscillation in the recurrent population as a function of the angular frequency ω:

$$\Delta\tilde{\nu}(\omega) = \left(\mathbb{1} - \tilde{J}(\omega)\right)^{-1}\tilde{K}(\omega)\Delta\tilde{\rho}(\omega) \tag{7}$$

where $\mathbb{1}$ denotes the $N \times N$ identity matrix, $\tilde{J}(\omega) = \tilde{\epsilon}(\omega)D'w$, $\tilde{K}(\omega) = \tilde{\epsilon}(\omega)D'h$. The tilde symbol ($\tilde{}$) denotes the Fourier transform, i.e., $\Delta\tilde{\nu}(\omega) = \int_{-\infty}^{\infty}\exp(-i\omega t)\Delta\nu(t)dt$. The recurrent population is said to be highly synchronous if $\Delta\tilde{\nu}(\omega_0)$ is large where $\omega_0 = 2\pi/T$. It is well known that coupled Kuramoto oscillators do synchronize if the coupling exceeds a certain threshold (Kuramoto, 1984)[2]. Here, because we do not consider phase oscillators (such as the Kuramoto oscillators) as neuronal models, this result does not apply directly. However, as we can see in Eq. 7 the stronger the recurrent weights w, the bigger the amplitude of the output oscillation $\Delta\tilde{\nu}(\omega_0)$. Let $\Delta Q(\tau)$ be the spiking covariance matrix of the recurrent population:

$$\Delta Q(\tau) = \frac{1}{T}\int_0^T \left\langle y(t)y^T(t-\tau)\right\rangle_{y(t),y(t-\tau)} dt - \bar{\nu}\bar{\nu}^T \tag{8}$$

Note that $\Delta Q(\tau)$ contains an atomic discontinuity at $\tau = 0$, i.e., $\Delta Q(0) = D\delta(0)$ with $D = \mathrm{diag}(\bar{\nu})$. As can be seen in "Spiking Covariance Matrices" in Appendix, it is easier to calculate this covariance matrix in the frequency domain, i.e., $\Delta\tilde{Q}(\omega) = \int_{-\infty}^{\infty}\exp(-i\omega t)\Delta Q(t)dt$ rather than in the time domain. So the Fourier transform of this output covariance matrix yields

$$\Delta\tilde{Q}(\omega) = \left(\mathbb{1} - \tilde{J}(\omega)\right)^{-1}\left\{\tilde{K}(\omega)\Delta\tilde{C}(\omega)\tilde{K}^T(-\omega) + D\right\}\left(\mathbb{1} - \tilde{J}^T(-\omega)\right)^{-1} \tag{9}$$

where $\Delta\tilde{C}(\omega) = \int_{-\infty}^{\infty}\exp(-i\omega t)\Delta C(t)dt$ denotes the Fourier transform of the input covariance matrix.

SYNAPTIC DYNAMICS

In the previous section, we assumed that all the weights were constant in order to calculate the output covariance matrix. Let us now allow the recurrent weights w to change very slowly (w.r.t. the neuronal dynamics) and keep the input weights h fixed. Because of this separation of time scales, we can still use the results derived so far.

In the same spirit as Kempter et al. (1999), Gerstner and Kistler (2002), Gilson et al. (2009b), we can express the weight change as a Volterra expansion of both the pre- and postsynaptic spike trains. If we keep terms up to second order we get for all $i \neq j$:

$$\begin{aligned}\dot{w}_{ij} = {} & a^{\mathrm{pre}}\left(w_{ij}\right)y_j(t) + a^{\mathrm{post}}\left(w_{ij}\right)y_i(t) \\ & + y_i(t)\int_0^\infty W\left(s, w_{ij}\right)y_j(t-s)ds + y_j(t)\int_0^\infty W\left(-s, w_{ij}\right)y_i(t-s)ds\end{aligned} \tag{10}$$

Since we do not allow for self-coupling, we will set $\dot{w}_{ii} = 0$. $a^{\mathrm{pre}}(w)$ (and $a^{\mathrm{post}}(w)$) denote the weight change induced by a single presynaptic (resp. postsynaptic) spike. $W(s,w)$ denotes the STDP learning window (see **Figure 3A**) and $\widetilde{W}(\omega,w)$ its Fourier transform (see **Figure 3B**):

[1] Each component of $x^{\epsilon}(t)$ is convoluted with $\epsilon(s)$, i.e., $x_k^{\epsilon}(t) = \int_0^\infty \epsilon(s)x_k(t-s)ds$, $k = 1,\ldots,M$.

[2] Other types of coupled oscillators have the property that strong coupling may destroy synchronization under particular conditions, e.g., in a population of identical diffusively coupled Rössler oscillators (Heagy et al., 1995) or in a system of two coupled chaotic non-invertible maps (Maistrenko et al., 1998). However, such models do not apply to the pathophysiology considered here. Furthermore, these models do not contain STDP, and it remains to be shown whether such phenomena persist in the presence of STDP.

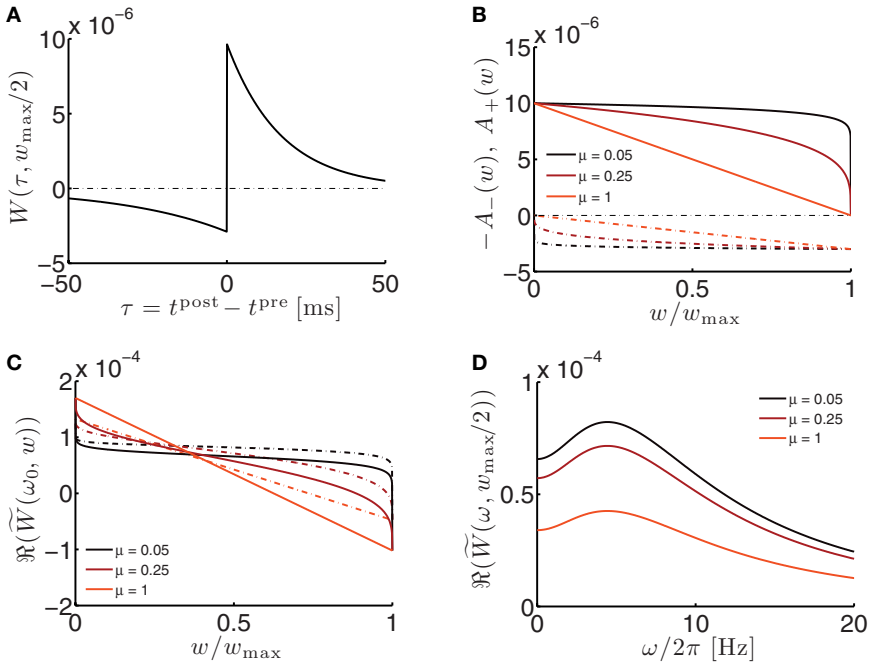

FIGURE 3 | Properties of the STP learning window. (A) STDP learning window evaluated at $w = w_{\max}/2$. $A_+^0 = 1 \cdot 10^{-5}$, $A_-^0 = 0.3 \cdot 10^{-5}$, $\tau_+ = 17$ ms, $\tau_- = 34$ ms. **(B)** LTP factor $A_+(w)$ (*solid lines*) and LTD factor $A_-(w)$ (*dot-dashed lines*) as a function of the weight. See Eqs 12 and 13. **(C)** Real part of the Fourier transformed learning window (*solid lines*) as a function of the weight w at the angular frequency $\omega_0 = 2\pi/T$, with $T = 200$ ms. *Dot-dashed lines*: integral of the learning window $\widetilde{W}(w) = \Re(\widetilde{W}(0, w))$ as a function of the weight w. **(D)** Real part of the Fourier transformed learning window as a function of the oscillation frequency $f = \omega/2\pi$.

$$W(t,w) = \begin{cases} A_+(w)\mathrm{e}^{-t/\tau_+} & \text{if } t > 0 \\ 0 & \text{if } t = 0 \\ -A_-(w)\mathrm{e}^{t/\tau_-} & \text{if } t < 0 \end{cases} \Rightarrow \tilde{W}(\omega,w) = \frac{A_+(w)\tau_+}{1+i\omega\tau_+} - \frac{A_-(w)\tau_-}{1-i\omega\tau_-} \tag{11}$$

Consistently with the modeling literature on STDP (van Rossum et al., 2000; Gütig et al., 2003; Morrison et al., 2007, 2008) both the potentiation factor A_+ and the depression factor $A_-(w)$ are assumed to depend on the weight. Here, the precise dependence on the weights corresponds to the one used by Gütig et al. (2003):

$$A_+(w) = A_+^0\left(w/w_{\max} - 1\right)^{\mu} \tag{12}$$

$$A_-(w) = A_-^0\left(w/w_{\max}\right)^{\mu} \tag{13}$$

where the parameter $\mu \in [0,1]$ controls the dependence upon the weight. If $\mu \to 0$, the rule is additive and therefore independent on the weight w. Conversely, if $\mu \to 1$, the rule becomes multiplicative. Unless specified otherwise, we set $\mu = 0.05$. In addition to this learning rule, hard bounds for the weights ($0 \le w_{ij} \le w_{\max}$, $\forall i \ne j$) are required if the factors $a^{\mathrm{pre}}(w)$ and $a^{\mathrm{post}}(w)$ are independent of the weights (which we will assume here) or if they do not contain implicit soft bounds. Because of the separation of time scales assumption, we can replace the recurrent weights by their expected value averaged over one period T, i.e., $w(t) \leftarrow T^{-1}\int_{t-T}^{t}\langle w(s)\rangle_{y^s}\,ds$ and get:

$$\dot{w}_{ij} \simeq a^{\mathrm{pre}}\left(w_{ij}\right)\bar{\nu}_j + a^{\mathrm{post}}\left(w_{ij}\right)\bar{\nu}_i + \overline{W}\left(w_{ij}\right)\bar{\nu}_i\bar{\nu}_j + \int_{-\infty}^{\infty} W\left(s,w_{ij}\right)\Delta Q_{ij}(s)\,ds \tag{14}$$

where $\overline{W}(w_{ij}) = \int_{-\infty}^{\infty} W(s,w_{ij})\,ds$ denotes the area under the STDP curve for a given weight w_{ij}. Since it is easier to express this covariance matrix in the frequency domain we can rewrite Eq. 14 (in matrix form) as[3]:

$$\dot{w} = \phi\left\{a^{\mathrm{pre}}(w)\circ\left(\mathbf{1}\bar{\nu}^T\right) + a^{\mathrm{post}}(w)\circ\left(\bar{\nu}\mathbf{1}^T\right) + \overline{W}(w)\circ\bar{\nu}\,\bar{\nu}^T + \frac{1}{2\pi}\int_{-\infty}^{\infty}\tilde{W}(-\omega,w)\circ\Delta\tilde{Q}(\omega)\,d\omega\right\} \tag{15}$$

where $\Delta\tilde{Q}(\omega)$ is given by Eq. 9 and the '$\circ$' operator denotes the pointwise matrix multiplication (also known as the Hadamard product). The operator ϕ sets to zero the diagonal elements and keep the off-diagonal elements unchanged. This implements the fact that we are not allowing autapses. $\mathbf{1} = (1,\ldots,1)$ is a vector containing N ones.

SINUSOIDAL INPUTS

Let us now assume that the input population is exciting the recurrent population with independent Poisson spike trains of sinusoidal intensity $\rho(t) = \bar{\rho} + \Delta\rho_0\sin(\omega_0 t)$ where $\omega_0 = 2\pi/T$ is the angular frequency. Because of the independence assumption, the input correlation matrix yields

[3]The last term in Eq. 15 is obtained by defining $A_{ij}(t) = \int_{-\infty}^{\infty} W(s-t,w_{ij})\Delta Q_{ij}(s)\,ds$, then taking the Fourier transform $\tilde{A}_{ij}(\omega) = \widetilde{W}(-\omega,w_{ij})\Delta\tilde{Q}_{ij}(\omega)$ and finally taking the inverse Fourier transform $A_{ij}(t) = (2\pi)^{-1}\int_{\infty}^{\infty}\exp(i\omega t)\tilde{A}_{ij}(\omega)\,d\omega$ and evaluate it at $t = 0$.

$$\Delta C(\tau) = \frac{1}{2}\cos(\omega_0 \tau)\Delta\rho_0 \Delta\rho_0^T + \mathrm{diag}(\bar{\rho})\delta(\tau) \tag{16}$$

and its Fourier transform yields

$$\Delta\tilde{C}(\omega) = \frac{\pi}{2}\left(\delta(\omega-\omega_0)+\delta(\omega+\omega_0)\right)\Delta\rho_0\Delta\rho_0^T + \mathrm{diag}(\bar{\rho}) \tag{17}$$

By using this expression of the input correlation, we get an explicit expression for the output covariance matrix $\Delta\tilde{Q}(\omega)$ (see Eq. 9) which can be approximated as:

$$\Delta\tilde{Q}(\omega) \simeq \frac{\pi}{2}\Delta\tilde{\nu}(\omega)\Delta\tilde{\nu}(-\omega)^T\left\{\delta(\omega-\omega_0)+\delta(\omega+\omega_0)\right\} \tag{18}$$

with $\Delta\tilde{\nu}(\omega) = (\mathbb{1}-\tilde{J}(\omega))^{-1}\tilde{K}(\omega)\Delta\rho_0$; see Eq. 7. This approximation is valid in the limit of large networks ($M \gg 1$, $N \gg 1$) where the terms involving diagonal matrices can be neglected. Indeed the term which depends on $\mathrm{diag}(\bar{\rho})$ scales as M^{-1} and the term which depends on $D = \mathrm{diag}(\bar{\nu})$ scales as N^{-1} if the output firing rate $\bar{\nu}$ is kept constant. For a detailed discussion, see Kempter et al. (1999), Gilson et al. (2009b). By inserting Eq. 18 into Eq. 15, we get:

$$\dot{w} \simeq \phi\left\{a^{\mathrm{pre}}\mathbf{1}\bar{\nu}^T + a^{\mathrm{post}}\bar{\nu}\mathbf{1}^T + \overline{W}(w)\bar{\nu}\,\bar{\nu}^T + \frac{1}{2}\Re\left(\tilde{W}(-\omega_0, w)\circ\Delta\tilde{\nu}(\omega_0)\Delta\tilde{\nu}^T(-\omega_0)\right)\right\} \tag{19}$$

where $\Re(x)$ takes the real part of x. Here, we assumed that both a^{pre} and a^{post} are independent of the recurrent weights w. Furthermore, if $g(u) = u$, then the diagonal matrix $D' = \mathbb{1}$ (which is present in $\tilde{J}$ and $\tilde{K}$) is independent of the recurrent weights w.

RESULTS

So far, we derived analytically the neuronal dynamics of a recurrent population that is stimulated by an oscillatory input. Furthermore we calculated the synaptic dynamics of such a recurrent network when synapses are governed by STDP. This rich synaptic dynamics has several interesting properties that are relevant for therapeutical stimulation and that we describe below.

Firstly, under some conditions that will be detailed below, the synaptic dynamics can elicit bistability (see **Figures 4A,B**). Concretely, if synapses are initialized above a critical value w^*, they will grow and reach the upper bound $w_{\max}$. Conversely, if they are initialized below w^*, they will decrease down to their minimal value. As a consequence, because the amplitudes of the oscillations

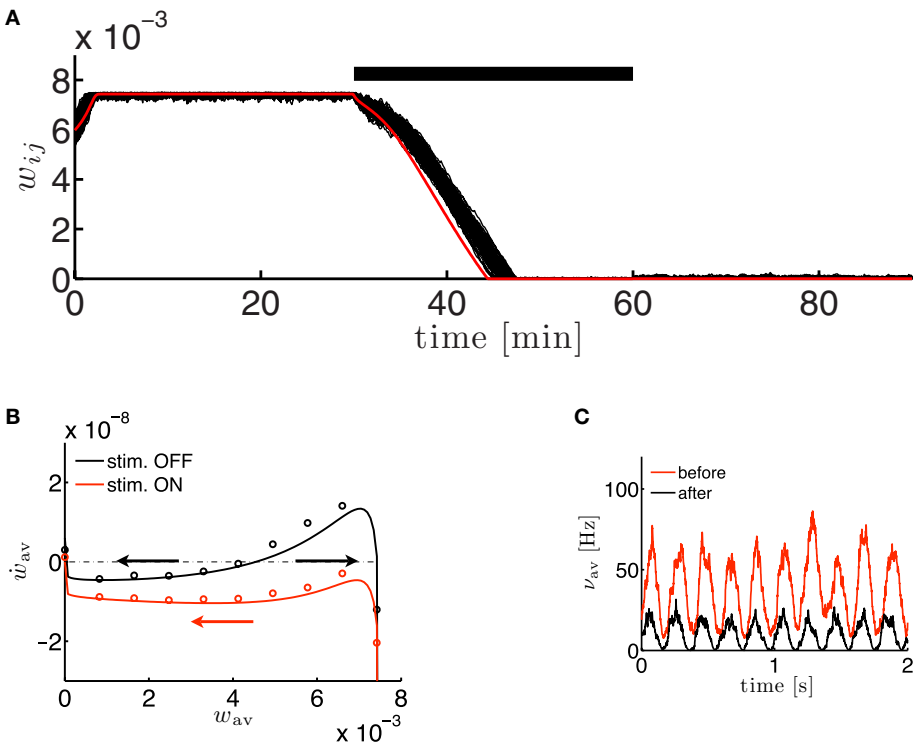

FIGURE 4 | The bistability of the recurrent network with STDP can be exploited for therapeutical stimulation. (A) Evolution of the recurrent weights w_{ij} as a function of time for $M = N = 100$. *Black lines*: individual weights in a numerical simulation. *Red line*: Evolution of the averaged recurrent weight $w_{\mathrm{av}} = N^{-2}\sum_{ij} w_{ij}$ obtained analytically (see Eq. 20) *Thick black line*: extent of stimulation. **(B)** Phase plane analysis of the averaged weight w_{av}. In the presence of a stimulation that annihilates the oscillations in the input (*red*: stim. ON, $\Delta\rho_0 = 0$ Hz) the averaged recurrent weight tends towards the lower bound $w_{\min} = 0$. In the absence of the stimulation (*black*: stim. OFF, $\Delta\sigma_0 = 10$ Hz), w increases up to the upper bound if it is bigger than a critical value $w^* \simeq 4.5\cdot10^{-3}$. *Black and red lines*: analytical result, *black and red circles*: numerical simulation. **(C)** Evolution of the averaged output firing rate $\nu_{\mathrm{av}}(t) = N^{-1}\sum_j \nu_j(t)$ before (*red*) and after (*black*) stimulation. The parameters are: $\tau = 10$ ms, $\tau_s = 0$ ms, $a^{\mathrm{pre}} = 0$, $a^{\mathrm{post}} = -1.7\cdot10^{-6}$, $h = 1/N$, $\bar{\rho} = 10$ Hz. Parameters of the learning window same as in **Figure 3**.

in the recurrent population depend on the strength of the recurrent weights (see Eqs 7 and 22), then this bistability at the level of the weights implies a similar bistability at the level of the oscillation amplitude of the recurrent population (see **Figure 4C**).

Secondly, the presence of the desynchronizing stimulation, which is modeled by setting the amplitude of the oscillatory input $\Delta\rho_0$ to 0, removes the bistability and pushes all the weights to their minimal value (see **Figures 4A,B**). Once the stimulation is removed the recurrent weights stay at their minimum value because it is a fixed point of the dynamics.

HOMOGENEOUS CASE

Because the analysis of the non-linear dynamical system given by Eq. 19 can be challenging, let us consider the dynamics of the averaged recurrent weight $w_{av} = N^{-2}\sum_{i,j} w_{ij}$ in the homogeneous case.

More precisely, we assume here that all the mean input firing rates $\bar{\rho}_j$ are close to their averaged value $\bar{\rho}_{av} = M^{-1}\sum_j \bar{\rho}_j$, and that the input weights h_{ij} are close to their averaged value $h_{av} = (MN)^{-1}\sum_{ij} h_{ij}$. If we further assume that the initial values of the recurrent weights $w_{ij}(0)$ are close to w_{av}, then, as long as the individual weights do not diverge too much, the dynamics of the averaged recurrent weight $\dot{w}_{av} = F(w_{av})$ can be approximated as[4]:

$$\dot{w}_{av} \simeq \left(a^{pre} + a^{post}\right)\bar{\nu}_{av} + \overline{W}\left(w_{av}\right)\bar{\nu}_{av}^2 + \frac{1}{2}\Re\left(\widetilde{W}\left(\omega_0, w_{av}\right)\right)\left|\Delta\tilde{\nu}_{av}\left(\omega_0\right)\right|^2 \quad (20)$$

If the transfer function is linear, i.e., $g(u) = u$, the averaged output firing rate $\bar{\nu}_{av} = N^{-1}\sum_j \bar{\nu}_j$ and the oscillation amplitude of the recurrent population $\Delta\tilde{\nu}_{av}$ can be approximated as:

$$\bar{\nu}_{av} \simeq \left(1 - Nw_{av}\right)^{-1} Mh_{av}\bar{\rho}_{av} \quad (21)$$

$$\Delta\tilde{\nu}_{av} \simeq \left(1 - N\tilde{\epsilon}\left(\omega_0\right)w_{av}\right)^{-1}\tilde{\epsilon}\left(\omega_0\right)Mh_{av}\Delta\rho_{av} \quad (22)$$

with $\Delta\rho_{av} = M^{-1}\sum_j \Delta\rho_{0j}$ The dynamics of the averaged recurrent weight w_{av} given by Eq. 20 is remarkably consistent with numerical simulations performed with spiking neurons (see **Figures 4A,B**).

[4]Note that from the definition of the Fourier transform we have $\Re\left(\widetilde{W}(-\omega_0, w_{av})\right) = \Re\left(\widetilde{W}(\omega_0, w_{av})\right)$.

The small discrepancy between the numerics and analytics can be attributed to two factors. First, Eq. 20 assumes the limit of large networks, i.e., $N, M \to \infty$ whereas in the numerical simulations, we used $N = M = 100$. Secondly, Eq. 20 is valid in the limit of small recurrent weights, i.e., $w_{av} \ll 1/N$ (here we used $Nw_{max} = 0.75$). As we can see on **Figure 4B**, the smaller averaged weights w_{av}, the better the correspondence between the numerical simulation and the analytical calculations. Even, for large recurrent weights ($w_{av} \simeq w_{max}$), the discrepancy between numerics and analytics is remarkably small.

CONDITIONS FOR BISTABILITY

So far, we discussed a scenario in which the stimulation effectively acted as a therapeutical stimulation because it shifted the network state from the highly synchronous (and therefore pathological) state to the low synchronous state. In order to have this property, the network must satisfy two conditions:

- C1. Bistability condition. In the absence of stimulation, the network must elicit bistability such that both the synchronized and the desynchronized state are stable. Formally this gives

$$\exists w_{av}^* \in \left[0, w_{max}\right] \text{ such that } F\left(w_{av}^*\right) = 0 \text{ and } F'\left(w_{av}^*\right) > 0 \quad (C1)$$

- C2. Desynchronizing stimulation condition. In the presence of a desynchronizing stimulation, the highly synchronous state looses its stability and the network is driven to the low synchronous state. This can be expressed as:

$$F\left(w_{av}\right) < 0 \quad \forall w_{av} \in [0, w_{max}] \quad \text{with} \quad \Delta\rho_{av} = 0 \quad (C2)$$

In order to keep the discussion reasonably simple, let us make several assumptions. First, let us consider the near-additive learning rule i.e., $\mu \simeq 0$. Indeed in the case of a multiplicative learning rule (i.e., $\mu \gg 0$), the potentiation factor $A_+(w)$ and the depressing factor $A_-(w)$ have a strong stabilization effect and therefore no bistability can be expected; see **Figure 5A** with $\mu = 0.5$. This is consistent with the findings of Gütig et al. (2003) who showed that there is a symmetry breaking in feedforward networks with weight-dependent STDP for μ bigger than a critical value.

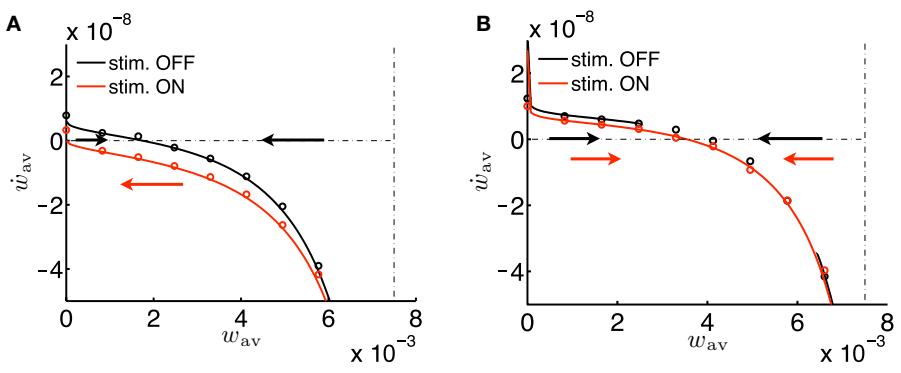

FIGURE 5 | Conditions for the absence of bistability. (A) Phase plane analysis similar to the one in **Figure 4B**, but for $\mu = 0.5$. There is no bistability because the weight-dependent factors $A_-(w)$ and $A_+(w)$ play here a dominant role. **(B)** Same as in **Figure 4B**, but with an overall negative learning window, i.e., all parameters identical except $A_-^0 = 0.7 \cdot 10^{-5}$ and $a^{post} = 0.1 \cdot 10^{-5}$.

With this additivity assumption and the linear transfer function assumption ($g(u) = u$), the averaged recurrent weight dynamics can be simply expressed from Eq. 20 combined with Eqs 21 and 22:

$$\dot{w}_{av} \simeq \frac{\alpha_1}{1-Nw_{av}} + \frac{\alpha_2}{\left(1-Nw_{av}\right)^2} + \frac{\alpha_3}{\left|1-\tilde{\epsilon}\left(\omega_0\right)Nw_{av}\right|^2} \tag{23}$$

where $\alpha_1 = (a^{pre} + a^{post})Mh_{av}\bar{\rho}_{av}$, $\alpha_2 = \overline{W}M^2h_{av}^2\bar{\rho}_{av}^2$ and $\alpha_3 = |\tilde{\epsilon}(\omega_0)|^2 M^2h_{av}^2\Delta\rho_{av}^2\Re(\widetilde{W}(\omega_0))/2$ are constant and do not depend on the averaged recurrent weight w_{av}.

Another greatly simplifying assumption is to consider the low oscillatory frequency regime, i.e., $\omega_0\tau \ll 1$ which gives $\tilde{\epsilon}(\omega_0) \simeq 1$.

Bistability condition C1

With these assumptions, the fixed point w_{av}^* expressed in the bistability condition C1 yields

$$w_{av}^* \simeq \frac{1}{N}\left(1+\frac{\alpha_2+\alpha_3}{\alpha_1}\right) \tag{24}$$

Because this fixed point has to be between 0 and w_{max}, we have $-1 < (\alpha_2+\alpha_3)/\alpha_1 < Nw_{max} - 1$, or equivalently

$$-1 < \left(\overline{W} + \frac{1}{2}\Re\left(\widetilde{W}\left(\omega_0\right)\right)\frac{\Delta\rho_{av}^2}{\bar{\rho}_{av}^2}\right)\frac{Mh_{av}\bar{\rho}_{av}}{a^{pre}+a^{post}} < Nw_{max} - 1 \tag{25}$$

If we push the low-frequency assumption further such that $\omega_0\tau_+ \ll 1$ and $\omega_0\tau_- \ll 1$, we have $\overline{W} \simeq \Re(\widetilde{W}(\omega_0))$ (see **Figure 3C**). In this case, Eq. 25 yields a simple necessary condition: $a^{pre} + a^{post}$ and the integral of the learning window $\overline{W}$ must be of opposite sign:

$$\mathrm{sgn}\left(a^{pre}+a^{post}\right) = -\mathrm{sgn}\left(\overline{W}\right) \tag{26}$$

Finally, the fact that the fixed point w_{av}^* must be unstable (see condition C1), we have $F'(w_{av}^*) > 0$ which gives $\alpha_1 < 0$. By using the expression of w_{av}^* given in Eq. 24 we have $\alpha_2 + \alpha_3 > 0$ and therefore with Eq. 26, we get:

$$\overline{W} > 0 \quad \text{and} \quad a^{pre} + a^{post} < 0 \tag{27}$$

which is consistent with the parameters used in **Figures 3 and 4**. Note that in **Figure 5B**, we violated this condition and as a consequence the bistability property is lost.

Desynchronization stimulation condition C2

In the presence of the desynchronization stimulation (i.e., $\Delta\rho_{av} = 0$), the condition C2 implies that $\alpha_1(1 - Nw_{av}) + \alpha_2 < 0$. Because $\alpha_1 < 0$ (see Eq. 27), this condition is satisfied for all w_{av} if $\alpha_1(1 - Nw_{max}) + \alpha_2 < 0$. By introducing the values for α_1 and α_2, we get:

$$a^{pre} + a^{post} < -\overline{W}\frac{Mh_{av}\rho_{av}}{1-Nw_{max}} \tag{28}$$

By combining the conditions C1 and C2, α_1 has to obey

$$-\frac{\alpha_2+\alpha_3}{1-Nw_{max}} < \alpha_1 < \min\left(-\frac{\alpha_2}{1-Nw_{max}}, -\left(\alpha_2+\alpha_3\right)\right) \tag{29}$$

In summary, in order to satisfy both conditions C1 and C2, the learning rule must be nearly additive ($\mu \simeq 0$), the learning window must be overall positive ($\overline{W} > 0$) and the sum of the coefficients tuning the effect of single spikes (a^{pre} and a^{post}) must be negative with upper and lower bounds set by Eq. 29.

Note that the bistability conditions derived above are valid for the averaged recurrent weight and do not apply for the individual weights of the recurrent population. As a consequence, this bistability condition does not necessarily imply a bimodal weight distribution. Indeed, if we consider the same set-up as in **Figure 4**, but draw the initial weights from a uniform distribution, between 0 and w_{max}, then all the weights will eventually settle into a unimodal distribution, around $w = 0$ (data not shown).

A bimodal weight distribution has been shown to occur in recurrent networks with additive STDP learning rule (Gilson et al., 2009b) favoring neurons that receive correlated inputs. For the sake of simplicity we considered in the simulations identical (and uncorrelated) inputs but the recurrent weight dynamics described by Eq. 15 remains valid for any type of inputs.

DISCUSSION

In this paper, we developed a model of a recurrent network with plastic synapses that is sufficiently simple to be treated analytically but that still yields the desired properties. In particular, we showed that when (a) the STDP learning rule is near additive and (b) the learning window is overall positive and (c) the terms in the learning rule involving single spikes ($a^{pre} + a^{post}$) have a depressing effect (within some bounds), then a desynchronizing stimulation favors long-term depression in the recurrent synapses and therefore drives the network from a highly synchronous state to a desynchronous state. In this way, our study confirms previously performed simulation studies (Tass and Majtanik, 2006; Hauptmann and Tass, 2007, 2009; Tass and Hauptmann, 2007) and, in particular, contributes to a theoretically sound foundation for the development of desynchronizing and, especially, anti-kindling brain stimulation techniques.

The concept of anti-kindling, i.e., of an unlearning of pathological synchrony and connectivity by desynchronizing stimulation, has been introduced by Tass and Majtanik (2006). For this, STDP was incorporated into a generic network of phase oscillators, and both kindling and anti-kindling processes were studied numerically. To approach a more microscopic level of description, a network of bursting neurons has been introduced as a simple model for an oscillatory population in the STN (Tass and Hauptmann, 2006, 2007; Hauptmann and Tass, 2007). With this model different aspects of kindling and anti-kindling processes have been studied numerically, such as the effect of inhibition vs. excitation (Hauptmann and Tass, 2007), the impact of weak and particularly short stimuli (Tass and Hauptmann, 2006), post-stimulus transients and cumulative stimulation effects (Hauptmann and Tass, 2009) as well as the differential effects of different sorts of desynchronizing stimulation protocols (Tass and Hauptmann, 2009). These questions are highly relevant for the clinical application of desynchronizing stimulation to the therapy of diseases with abnormal synchrony, e.g., Parkinson's disease. In forthcoming studies, more microscopic models will be studied. However, apart from this type of numerical simulation analysis, we aim at establishing a thorough, analytical framework

for the anti-kindling concept. As a first step into that direction, we presented here an analytical analysis of a simple network model which we validated by numerical analysis.

Different types of neurons and, hence, different target areas in the brain may be associated with different types of STDP learning rules. Accordingly, brain stimulation approaches might be optimized with respect to a particular type of STDP learning rule in order to achieve superior therapeutic effects.

This work is not the first one to treat STDP in oscillatory recurrent network. Karbowski and Ermentrout (2002) consider neurons as formal phase oscillators and therefore do not consider spiking neurons as such. Furthermore Karbowski and Ermentrout (2002) consider a learning window with identical potentiation and depression time constants which limits the potential output of the study. Maistrenko et al. (2007) describe as well neurons as phase oscillators, but they allow potentiation and depression time constants to be different. Interestingly they find multistability depending on those time constants and on the weight upper bound. Morrison et al. (2007) consider a STDP learning rule with multiplicative depression and power-law dependence for potentiation and showed numerically that this STDP rule decouples synchronous inputs from the rest of the network.

Our present model can be seen as an extension of the work of Gilson et al. (2009a,b) in several aspects. First, and most importantly, we consider here oscillatory input whereas Gilson et al. (2009b) assume stationary inputs. In this way we are able to discuss the conditions on the learning parameters to get a bistable regime with high and low synchrony. Secondly, our approach does not require to calculate the inverse Fourier transform of the spiking covariance matrix. In this way we do not need to make the (unrealistic) assumption that the EPSP time constant is much smaller than potentiation time constant in the learning window. Finally, we consider a larger class of neuronal model since we do not restrict ourself to linear neurons, but consider instead (locally linearized) non-linear neurons.

There are several ways in which we can extend the present model. It is known that propagation delays play an important role in the neuronal synchrony (Gerstner et al., 1996a; Cassenaer and Laurent, 2007; Lubenov and Siapas, 2008). Our framework can be easily extended to incorporate those propagation delays. A systematic analysis of the influence of those delays is out of the scope of the current study but would be definitely relevant. According to the arguments of Lubenov and Siapas (2008), one could expect that the bigger the synaptic delays, the stronger the effective amount of depression. This can potentially change the stability of highly synchronous states.

Another way to extend the current model is to consider learning rules that depend on high order statistics of the pre- and postsynaptic neuron. For example, it is known that a triplet learning rule which considers 1 pre- and 2 postsynaptic spikes (Pfister and Gerstner, 2006a,b; Clopath et al., 2010) is more realistic in terms a reproducing experimental data than the pair-based STDP considered here. Another extension would be to consider second order terms in the Taylor expansion of the transfer function. Both of those extensions would require a substantial amount of work since the results of Hawkes (1971) could not be used anymore.

APPENDIX
SPIKING COVARIANCE MATRICES

INPUT–OUTPUT COVARIANCE MATRIX

In order to express the output spiking covariance matrix ΔQ as a function of the input spiking covariance matrix ΔC, we need first to define the input–output covariance matrix ΔP:

$$\Delta P(\tau) = \frac{1}{T}\int_0^T \left\langle y(t)x^T(t-\tau)\right\rangle_{y(t),x(t-\tau)} dt - \overline{\nu}\overline{\rho}^T \tag{30}$$

By rewriting the average $\langle\cdot\rangle_{y(t),x(t-\tau)}$ involved here and by using Eqs 1, 2, and 3, the input–output covariance matrix can be expressed in a self-consistent way as:

$$\begin{aligned}\Delta P(\tau) &= \frac{1}{T}\int_0^T \left\langle \left\langle y(t)\right\rangle_{y(t)|x^t,y^t,x(t-\tau)} x^T(t-\tau)\right\rangle_{x^t,y^t,x(t-\tau)} dt - \overline{\nu}\overline{\rho}^T \\ &= \frac{1}{T}\int_0^T \left\langle \left(\overline{\nu} + D'(hx^\epsilon(t) + wy^\epsilon(t) - \overline{u})\right)x^T(t-\tau)\right\rangle_{x^t,y^t,x(t-\tau)} dt \\ &= D'h\Delta C^\epsilon(\tau) + D'w\Delta P^\epsilon(\tau)\end{aligned} \tag{31}$$

where $D' = \mathrm{diag}(g'(\bar{u}))$ is a diagonal matrix with $D'_{ii} = g'(\bar{u}_i)$. Here the ϵ superscript denotes as before the convolution with $\epsilon(s)$, i.e., $\Delta C^\epsilon(\tau) = \int_\infty^\infty \epsilon(s)\Delta C(\tau - s)ds$ and $\Delta P^\epsilon(s) = \int_\infty^\infty \epsilon(s)\Delta P(\tau - s)ds$. In order to get an explicit expression of this input–output covariance matrix, we can Fourier transform Eq. 31 and therefore turn the convolution into a product in the angular frequency domain ω:

$$\Delta\tilde{P}(\omega) = (\mathbb{1} - \tilde{J}(\omega))^{-1}\tilde{K}(\omega)\Delta\tilde{C}(\omega) \tag{32}$$

where $\mathbb{1}$ denotes the $N \times N$ identity matrix, $\tilde{J}(\omega) = \tilde{\epsilon}(\omega)D'w$, $\tilde{K}(\omega) = \tilde{\epsilon}(\omega)D'h$. As before the tilde symbol ($\tilde{}$) denotes the Fourier transform, i.e., $\Delta\tilde{C}(\omega) = \int_{-\infty}^{\infty} \exp(-i\omega t)\Delta C(t)dt$.

OUTPUT COVARIANCE MATRIX

We recall here for convenience the definition of the output covariance matrix (see Eq. 8):

$$\Delta Q(\tau) = \frac{1}{T}\int_0^T \left\langle y(t)y^T(t-\tau)\right\rangle_{y(t),y(t-\tau)} dt - \overline{\nu}\,\overline{\nu}^T \tag{33}$$

For $\tau \geq 0$, we have:

$$\begin{aligned}\Delta Q(\tau) &= \frac{1}{T}\int_0^T \left\langle \left\langle y(t)\right\rangle_{y(t)|x^t,y^t} y^T(t-\tau)\right\rangle_{x^t,y^t} dt - \overline{\nu}\,\overline{\nu}^T + D\delta(\tau) \\ &= \frac{1}{T}\int_0^T \left\langle \left(\overline{\nu} + D'\left(hx^\epsilon(t) + wy^\epsilon(t) - \overline{u}\right)\right)y^T(t-\tau)\right\rangle_{x^t,y^t} dt \\ &\quad - \overline{\nu}\,\overline{\nu}^T + D\delta(\tau) \\ &= D'h\Delta P^{\epsilon T}(-\tau) + D'w\Delta Q^\epsilon(\tau) + D\delta(\tau)\end{aligned} \tag{34}$$

with $D = \mathrm{diag}(g(\bar{u}))$. Since the above identity is only valid for $\tau \geq 0$, we can not simply Fourier transform this expression and extract the output covariance matrix in frequency domain. We will use here the same method as proposed by Hawkes (1971). Let $B(\tau)$ be a supplementary matrix defined as:

$$B(\tau) = D'\left(h\Delta P^{\epsilon T}(-\tau) + w\Delta Q^\epsilon(\tau)\right) + D\delta(\tau) - \Delta Q(\tau) \tag{35}$$

Because this supplementary matrix is defined $\forall\tau$, we can Fourier transform it and express the output covariance matrix in frequency domain:

$$\Delta\tilde{Q}(\omega) = (\mathbb{1} - \tilde{J}(\omega))^{-1}\left(\tilde{K}(\omega)\Delta\tilde{P}^T(-\omega) + D - \tilde{B}(\omega)\right) \tag{36}$$

From the definition of the output covariance matrix $\Delta Q(\tau)$ in Eq. 33, we have $\Delta Q(-\tau) = \Delta Q^T(\tau)$ and hence $\Delta\tilde{Q}(-\omega) = \Delta\tilde{Q}^T(\omega)$. By using this property and the fact that $(\mathbb{1}-\tilde{J}(-\omega))^{-1}\tilde{K}(-\omega)\Delta\tilde{P}^T(\omega) = \Delta\tilde{P}(-\omega)\tilde{K}^T(\omega)(\mathbb{1}-\tilde{J}^T(\omega))^{-1}$, we have

$$(\mathbb{1} - \tilde{J}(-\omega))^{-1}(D - \tilde{B}(-\omega)) = \left(D - \tilde{B}^T(\omega)\right)\left(\mathbb{1} + \tilde{J}^T(\omega)\right)^{-1} \tag{37}$$

or, equivalently

$$\tilde{B}(-\omega)\left(\mathbb{1} - \tilde{J}^T(\omega)\right) + D\tilde{J}^T(\omega) = (\mathbb{1} - \tilde{J}(-\omega))\tilde{B}^T(\omega) + \tilde{J}(-\omega)D \tag{38}$$

In order to express $\tilde{B}(\omega)$, Hawkes (1971) used a regularity argument which goes as follows. Let us assume $\epsilon(t)$ and $|B(t)|$ are bounded as follows:

$$\epsilon(t) < \epsilon_0 \exp(-\eta t)$$

$$|B(t)| < B_0 \exp(\eta t) \tag{39}$$

We can show that both $\tilde{\epsilon}(\omega)$ (and hence $\tilde{J}(\omega)$) is regular for $\Im(\omega) < \eta$ and $\tilde{B}(\omega)$ is regular for $\Im(\omega) > -\eta$. Let $H(\omega)$ be defined as the l.h.s. of Eq. 38 for $\Im(\omega) < \eta$ and the r.h.s of Eq. 38 when $\Im(\omega) > -\eta$. In this way $H(\omega)$ is regular everywhere and since we have $H(\omega) \to 0$ when $|\omega| \to \infty$, we know from Liouville's theorem that $H(\omega) = 0$. In particular, from the r.h.s of Eq. 38, we can express the supplementary matrix as:

$$\tilde{B}(\omega) = -D\tilde{J}^T(-\omega)(\mathbb{1} - \tilde{J}(-\omega))^{-1} \tag{40}$$

If we insert this expression back into Eq. 36, we get:

$$\Delta\tilde{Q}(\omega) = (\mathbb{1} - \tilde{J}(\omega))^{-1}\left\{\tilde{K}(\omega)\Delta\tilde{C}(\omega)\tilde{K}^T(-\omega) + D\right\}\left(\mathbb{1} - \tilde{J}^T(-\omega)\right)^{-1} \tag{41}$$

ACKNOWLEDGMENTS

We thank Oleksandr Popovych for fruitful discussions. Jean-Pascal Pfister has been supported by the Wellcome Trust.

REFERENCES

Benabid, A., Chabardes, S., Mitrofanis, J., and Pollak, P. (2009). Deep brain stimulation of the subthalamic nucleus for the treatment of Parkinson's disease. *Lancet Neurol.* 8, 67–81.

Benabid, A., Pollak, P., Gervason, C., Hoffmann, D., Gao, D., Hommel, M., Perret, J., and De Rougemont, J. (1991). Long-term suppression of tremor by chronic stimulation of the ventral intermediate thalamic nucleus. *Lancet* 337, 403.

Bi, G., and Poo, M. (1998). Synaptic modifications in cultured hippocampal neurons: dependence on spike timing, synaptic strength, and postsynaptic cell type. *J. Neurosci.* 18, 10464–10472.

Cassenaer, S., and Laurent, G. (2007). Hebbian STDP in mushroom bodies facilitates the synchronous flow of olfactory information in locusts. *Nature* 448, 709–713.

Clopath, C., Büsing, L., Vasilaki, E., and Gerstner, W. (2010). Connectivity reflects coding: a model of voltage-based STDP with homeostasis. *Nat. Neurosci.* 13, 344–352.

Gerstner, W., Kempter, R., van Hemmen, J., and Wagner, H. (1996a). A neuronal learning rule for sub-millisecond temporal coding. *Nature* 383, 76–78.

Gerstner, W., and Kistler, W. K. (2002). *Spiking Neuron Models*. Cambridge UK: Cambridge University Press.

Gerstner, W., van Hemmen, J. L., and Cowan, J. D. (1996b). What matters in neuronal locking. *Neural. Comput.* 8, 1653–1676.

Gilson, M., Burkitt, A., Grayden, D., Thomas, D., and van Hemmen, J. (2009a). Emergence of network structure due to spike-timing-dependent plasticity in recurrent neuronal networks iii: partially connected neurons driven by spontaneous activity. *Biol. Cybern.* 101, 411–426.

Gilson, M., Burkitt, A., Grayden, D., Thomas, D., and van Hemmen, J. (2009b). Emergence of network structure due to spike-timing-dependent plasticity in recurrent neuronal networks iv: structuring synaptic pathways among recurrent connections. *Biol. Cybern.* 101, 427–444.

Gütig, R., Aharonov, R., Rotter, S., and Sompolinsky, H. (2003). Learning input correlations through non-linear temporally asymmetric hebbian plasticity. *J. Neurosci.* 23, 3697–3714.

Hauptmann, C., and Tass, P. A. (2007). Therapeutic rewiring by means of desynchronizing brain stimulation. *Biosystems* 89, 173–181.

Hauptmann, C., and Tass, P. A. (2009). Cumulative and after-effects of short and weak coordinated reset stimulation: a modeling study. *J. Neural Eng.* 6, 016004.

Hawkes, A. G. (1971). Spectra of some self-exciting and mutually exciting processes. *Biometrika* 58, 83–90.

Heagy, J., Pecora, L., and Carroll, T. (1995). Short wavelength bifurcations and size instabilities in coupled oscillator systems. *Phys. Rev. Lett.* 74, 4185–4188.

Karbowski, J., and Ermentrout, G. (2002). Synchrony arising from a balanced synaptic plasticity in a network of heterogeneous neural oscillators. *Phys. Rev. E* 65, 31902.

Kempter, R., Gerstner, W., and van Hemmen, J. L. (1999). Hebbian learning and spiking neurons. *Phys. Rev. E* 59, 4498–4514.

Kuhn, A., Kupsch, A., Schneider, G., and Brown, P. (2006). Reduction in subthalamic 8–35 Hz oscillatory activity correlates with clinical improvement in Parkinson's disease. *Eur. J. Neurosci.* 23, 1956.

Kuramoto, Y. (1984). *Chemical Oscillations, Waves, and Turbulence*. Berlin, Heidelberg, New York: Springer, 68–77.

Lubenov, E., and Siapas, A. (2008). Decoupling through synchrony in neuronal circuits with propagation delays. *Neuron* 58, 118–131.

Maistrenko, Y., Maistrenko, V., Popovich, A., and Mosekilde, E. (1998). Transverse instability and riddled basins in a system of two coupled logistic maps. *Phys. Rev. E* 57, 2713–2724.

Maistrenko, Y. L., Lysyansky, B., Hauptmann, C., Burylko, O., and Tass, P. A. (2007). Multistability in the kuramoto model with synaptic plasticity. *Phys. Rev. E* 75, 66207.

Markram, H., Lübke, J., Frotscher, M., and Sakmann, B. (1997). Regulation of synaptic efficacy by coincidence of postysnaptic AP and EPSP. *Science* 275, 213–215.

Morrison, A., Aertsen, A., and Diesmann, M. (2007). Spike-timing dependent plasticity in balanced random networks. *Neural. Comput.* 19, 1437–1467.

Morrison, A., Diesmann, M., and Gerstner, W. (2008). Phenomenological models of synaptic plasticity based on spike timing. *Biol. Cybern.* 98, 459–478.

Nini, A., Feingold, A., Slovin, H., and Bergman, H. (1995). Neurons in the globus pallidus do not show correlated activity in the normal monkey, but phase-locked oscillations appear in the MPTP model of Parkinsonism. *J. Neurophysiol.* 74, 1800.

Pare, D., Curro'Dossi, R., and Steriade, M. (1990). Neuronal basis of the Parkinsonian resting tremor: a hypothesis and its implications for treatment. *Neuroscience* 35, 217–226.

Pfister, J.-P., and Gerstner, W. (2006a). "Beyond pair-based STDP: a phenomenological rule for spike triplet and frequency effects," in *Advances in Neural Information Processing Systems 18*, eds Y. Weiss, B. Schölkopf, and J. Platt (Cambridge: MIT Press), 1083–1090.

Pfister, J.-P., and Gerstner, W. (2006b). Triplets of spikes in a model of spike timing-dependent plasticity. *J. Neurosci.* 26, 9673–9682.

Smirnov, D., Barnikol, U., Barnikol, T., Bezruchko, B. P., Hauptmann, C., Bührle, C., Maarouf, M., Sturm, V., Freund, H. J., and Tass, P. A. (2008). The generation of Parkinsonian tremor as revealed by directional coupling analysis. *Europhys. Lett.* 83, 20003.

Tass, P. A. (1999). *Phase Resetting in Medicine and Biology: Stochastic Modelling and Data Analysis*. Berlin: Springer.

Tass, P. A. (2003). A model of desynchronizing deep brain stimulation with a demand-controlled coordinated reset of neural subpopulations. *Biol. Cybern.* 89, 81–88.

Tass, P. A., and Hauptmann, C. (2006). Long-term anti-kindling effects induced by short-term, weak desynchronizing stimulation. *Nonlinear Phenomena Complex Syst.* 9, 298.

Tass, P. A., and Hauptmann, C. (2007). Therapeutic modulation of synaptic connectivity with desynchronizing brain stimulation. *Int. J. Psychophysiol.* 64, 53–61.

Tass, P. A., and Hauptmann, C. (2009). Anti-kindling achieved by stimulation targeting slow synaptic dynamics. *Restor. Neurol. Neurosci.* 27, 589–609.

Tass, P. A., and Majtanik, M. (2006). Long-term anti-kindling effects of desynchronizing brain stimulation: a theoretical study. *Biol. Cybern.* 94, 58–66.

Tass, P. A., Silchenko, A. N., Hauptmann, C., Barnikol, U. B., and Speckmann, E. J. (2009). Long-lasting desynchronization in rat hippocampal slice induced by coordinated reset stimulation. *Phys. Rev. E* 80, 11902.

Tass, P. A., Smirnov, D., Karavaev, A., Barnikol, U., Barnikol, T., Adamchic, I., Hauptmann, C., Pawelcyzk, N., Maarouf, M., Sturm, V., Freund, H., and Bezruchko, B. (2010). The causal relationship between subcortical local field potential oscillations and Parkinsonian resting tremor. *J. Neural Eng.* 7, 1–16.

Temperli, P., Ghika, J., Villemure, J., Burkhard, P., Bogousslavsky, J., and Vingerhoets, F. (2003). How do Parkinsonian signs return after discontinuation of subthalamic DBS? *Neurology* 60, 78.

van Rossum, M. C. W., Bi, G. Q., and Turrigiano, G. G. (2000). Stable Hebbian learning from spike timing-dependent plasticity. *J. Neurosci.* 20, 8812–8821.

Conflict of Interest Statement: The authors declare that the research was conducted in the absence of any commercial or financial relationships that could be construed as a potential conflict of interest.

Received: 02 February 2010; paper pending published: 25 March 2010; accepted: 18 June 2010; published online: 30 July 2010. Citation: Pfister J-P and Tass PA (2010) STDP in oscillatory recurrent networks: theoretical conditions for desynchronization and applications to deep brain stimulation. Front. Comput. Neurosci. ***4****:22. doi: 10.3389/fncom.2010.00022*

frontiers in
COMPUTATIONAL NEUROSCIENCE

ORIGINAL RESEARCH ARTICLE
published: 15 October 2010
doi: 10.3389/fncom.2010.00142

Spike-timing dependent plasticity and the cognitive map

Daniel Bush[1,2]*, Andrew Philippides[2], Phil Husbands[2] and Michael O'Shea[2]

[1] Department of Physics and Astronomy, University of California Los Angeles, Los Angeles, CA, USA
[2] Centre for Computational Neuroscience and Robotics, University of Sussex, Brighton, UK

Edited by:
Per Jesper Sjöström, University College London, UK

Reviewed by:
Niraj S. Desai, The Neurosciences Institute, USA
Jack Mellor, Bristol University, UK

***Correspondence:**
Daniel Bush, Department of Physics and Astronomy, University of California Los Angeles, Knudsen Hall 5-170, 475 Portola Plaza, Los Angeles, CA 90095, USA.
e-mail: drdanielbush@gmail.com

Since the discovery of place cells – single pyramidal neurons that encode spatial location – it has been hypothesized that the hippocampus may act as a cognitive map of known environments. This putative function has been extensively modeled using auto-associative networks, which utilize rate-coded synaptic plasticity rules in order to generate strong bi-directional connections between concurrently active place cells that encode for neighboring place fields. However, empirical studies using hippocampal cultures have demonstrated that the magnitude and direction of changes in synaptic strength can also be dictated by the relative timing of pre- and post-synaptic firing according to a spike-timing dependent plasticity (STDP) rule. Furthermore, electrophysiology studies have identified persistent "theta-coded" temporal correlations in place cell activity *in vivo*, characterized by phase precession of firing as the corresponding place field is traversed. It is not yet clear if STDP and theta-coded neural dynamics are compatible with cognitive map theory and previous rate-coded models of spatial learning in the hippocampus. Here, we demonstrate that an STDP rule based on empirical data obtained from the hippocampus can mediate rate-coded Hebbian learning when pre- and post-synaptic activity is stochastic and has no persistent sequence bias. We subsequently demonstrate that a spiking recurrent neural network that utilizes this STDP rule, alongside theta-coded neural activity, allows the rapid development of a cognitive map during directed or random exploration of an environment of overlapping place fields. Hence, we establish that STDP and phase precession are compatible with rate-coded models of cognitive map development.

Keywords: STDP, hippocampus, spatial memory, synaptic plasticity, auto-associative network, phase precession, navigation

INTRODUCTION

The hippocampus and surrounding medial temporal lobe are implicated in declarative memory function in humans and other mammals (Morris, 2007). It has been demonstrated that the firing rate of place cells within the hippocampus encodes for spatial location in the corresponding place field within an environment (O'Keefe and Dostrovsky, 1971; O'Keefe, 2007). It has therefore been suggested that the hippocampus may act as a cognitive map of known locations (O'Keefe and Nadel, 1978; Muller et al., 1991). Behavioral experiments supporting this hypothesis demonstrate that the hippocampus is required for efficient navigation and spatial learning in novel environments (Morris et al., 1982; McNaughton et al., 2006; Morris, 2007).

At the cellular level, processes of learning and memory are believed to be mediated by synaptic plasticity (Hebb, 1949; Martin et al., 2000; Neves et al., 2008). Hippocampal mnemonic function has most frequently been modeled using auto-associative networks – recurrent neural architectures that implement a Hebbian learning rule (Marr, 1971; Hopfield, 1982; Burgess, 2007; Rolls, 2008). The biological correlate of these models is generally taken as the CA3 region of the hippocampus, which exhibits extensive recurrent connectivity and wherein synaptic plasticity can be easily and reliably induced (Rolls and Kesner, 2006; Rolls, 2007).

Initially, empirical studies of activity dependent changes in synaptic strength utilized tetanic stimulation protocols to induce long-term potentiation (LTP) with high frequency stimulation and long-term depression (LTD) with low frequency stimulation (Bliss and Lomo, 1973; Bienenstock et al., 1982; Dudek and Bear, 1992; Malenka and Bear, 2004). Consequently, in models of spatial learning, rate-coded synaptic plasticity rules have been implemented to produce connection weights between place cells that correlate with the relative distance between the corresponding place fields (Muller et al., 1991; Burgess et al., 1994; Burgess, 2007). This approach is supported by evidence for the potentiation of synaptic connections between place cells during exploration of a novel environment (Isaac et al., 2009).

Subsequent research using cultures of hippocampal neurons has demonstrated that bi-directional changes in synaptic strength can also be induced by temporal correlations in low frequency stimulation according to a spike-timing dependent plasticity (STDP) rule (Bi and Poo, 1998; Debanne et al., 1998; Wang et al., 2005). Concurrently, persistent temporal correlations in place cell activity, characterized by the phase precession phenomenon, have been observed during spatial exploration (O'Keefe and Recce, 1993; O'Keefe, 2007; Huxter et al., 2008). Furthermore, the selective elimination of causal temporal correlations in place cell activity prevents the potentiation of interconnecting synapses (Isaac et al., 2009). These findings suggest that rate-based models may not be adequate to replicate the dynamics of hippocampal spatial learning.

Although STDP, combined with the temporally coded patterns of neural activity observed in hippocampus, is ideally suited for route or sequence learning, it has been suggested that the inherent asymmetry of this plasticity rule may not allow the development

of strong bi-directional connections between place cells that are required by cognitive map theory (Skaggs et al., 1996; Song and Abbott, 2001; Wagatsuma and Yamaguchi, 2007; but see Mongillo et al., 2005; Samura and Hattori, 2005). Computational modeling has also demonstrated that STDP can provide a putative homeostatic function by reducing synaptic currents in response to an increase in input firing rate, and thus provide global stability for local Hebbian learning rules (Song et al., 2000; Song and Abbott, 2001). However, these emergent dynamics directly contradict empirical observations and computational models of rate-coded synaptic plasticity (Bush et al., 2010a).

Here, we present a spiking recurrent neural network model with theta-coded neural dynamics and an STDP rule based on empirical data obtained from the hippocampus *in vitro*. We demonstrate that this form of STDP is compatible with rate-coded Hebbian learning, producing strong bi-directional connections between neurons that fire stochastically at an elevated rate with no persistent sequence bias. We subsequently demonstrate that this network model can produce a cognitive map of arbitrary one- and two-dimensional environments during shuttle runs and random exploration respectively, such that the magnitude of bi-directional connections between place cells correlates with the relative distance between corresponding place fields. The asymmetry of the plasticity rule dictates that the strength of synaptic connections between place cells are also biased by the frequency and direction in which the corresponding place fields are traversed during exploration. This indicates that STDP can mediate both rate- and temporally coded learning, corresponding to cognitive map formation during open field exploration and sequence learning during route navigation, respectively. However, our results also demonstrate that this form of STDP does not generate any inherent synaptic competition, and some additional mechanism is therefore required to guarantee the long-term stability of network operation.

MATERIALS AND METHODS

NEURAL DYNAMICS

The neural network consists of N_p simulated place cells that are fully recurrently connected except for self-connections. Simulated place cells operate according to the Izhikevich (2004) spiking model, which dynamically calculates the membrane potential (v) and a membrane recovery variable (u) based on the values of four dimensionless constants (a–d) and a dimensionless current input (I) according to Eq. 1. The values used to replicate firing of a standard excitatory neuron are ($a = 0.02$, $b = 0.2$, $c = -65$, $d = 6$). Under these conditions, simulated neurons fire single spikes at low levels of stimulation, but produce complex spike bursts that are representative of hippocampal pyramidal cells (i.e., several action potentials at a spontaneous rate of ~150 Hz) at higher levels of stimulation (Ranck, 1973; Izhikevich, 2004; O'Keefe, 2007).

$$v' = 0.04v^2 + 5v + 140 - u + I$$
$$u' = a(bv - u)$$
$$\text{if } v \geq 30 \text{ then } \begin{cases} v \rightarrow c \\ u \rightarrow u + d \end{cases}$$

Equation 1: The Izhikevich (2004) spiking model.

Each simulated neuron has a randomly chosen axonal delay in the range (1 ms:5 ms), this being realistic of the CA3 region (Miles, 1990). Previous research has indicated that the scale of axonal delays can have a significant effect on the quantitative, but not qualitative, nature of synaptic dynamics produced by STDP (Bush et al., 2010b). However, it is important to note that the delay between the firing of an action potential and its arrival at post-synaptic targets is unlikely to be uniform for a single neuron *in vivo*.

THE PLASTICITY MODEL

Mathematically, with $s = t_{post} - t_{pre}$ being the time difference between pre- and post-synaptic spiking, the change in the weight of a synapse (Δw) according to a standard implementation of additive STDP can be calculated using Eq. 2. The parameters A_+ and A_- correspond to the maximum possible change in the synaptic weight per spike pair, while τ_+ and τ_- denote the time constants of exponential decay for potentiation and depression increments respectively. In accordance with experimental observations, coincident pre- and post-synaptic firing elicits maximal depression (Debanne et al., 1998). A nearest-neighbor spike pairing scheme – which dictates that values of $P_\pm \rightarrow A_\pm$ upon afferent or efferent firing – is employed. In all simulations, hard limits are placed on the achievable strength of synapses, such that synaptic weights are maintained continuously in the range ($0{:}w_{max}$).

Empirical data obtained from the hippocampus suggests that $A_+ > A_-$ and $\tau_+ < \tau_-$ (Bi and Poo, 1998; Debanne et al., 1998; Wang et al., 2005). Accordingly, we employ values of ($A_+ = 0.015$; $A_- = -0.012$; $\tau_+ = 20$ ms; $\tau_- = 50$ ms). Experimental observations in cultures of hippocampal neurons also suggest a non-linear integration of potentiation and depression processes at short temporal offsets (Wang et al., 2005; Pfister and Gerstner, 2006). We therefore utilize an additional potentiation term to replicate this data. Whenever a synaptic connection is depressed, the absolute magnitude of weight decrease is recorded as a parameter P_{++} which subsequently decays with a time constant of $\tau_{++} = 20$ ms. The value of P_{++} is then used to supplement any subsequent potentiation of the same synaptic connection (after time $s_{++} = t_{\Delta w+} - t_{\Delta w-}$). While this method differs from that employed in the computational model of Pfister and Gerstner (2006), it corresponds to the parameters A_3^+ and τ_x utilized in that study.

It is important to note that the STDP rule utilized here, like the majority of previous computational models, is based primarily on data obtained from cultures of hippocampal pyramidal neurons (Bi and Poo, 1998; Debanne et al., 1998; Wang et al., 2005). More recent empirical studies utilizing acute slices have delineated a more complex relationship between temporal correlations in neural activity and subsequent changes in synaptic strength: primarily, that multiple post-synaptic spikes are required to induce LTP using low frequency temporal correlations (Pike et al., 1999; Meredith et al., 2003; Wittenberg and Wang, 2006; Buchanan and Mellor, 2007; but see Kwag and Paulsen, 2009; Buchanan and Mellor, 2010). In order to retain computational efficiency, we do not aim to explicitly model these findings, but appraise the properties of our STDP rule in light of that data at all relevant junctures.

$$\Delta w_+ = F(s) = P_+ + P_{++} \qquad \text{for } s > 0$$
$$\Delta w_- = F(s) = P_- \qquad \text{for } s \le 0$$
$$P_+ = A_+\left(1-\frac{1}{\tau_+}\right)^{S}$$
$$P_- = A_-\left(1-\frac{1}{\tau_-}\right)^{-S}$$
$$P_{++} = \Delta w_-\left(1-\frac{1}{\tau_{++}}\right)^{-S_{++}}$$

Equation 2: The spike-timing dependent plasticity rule.

SIMULATION DETAILS

Our initial aim is to characterize the emergent synaptic dynamics produced by the STDP rule described above when neural activity corresponds to a variety of standard stimulation protocols used experimentally to induce LTP and LTD (Bi and Poo, 1998; Wang et al., 2005; Wittenberg and Wang, 2006). Firstly, we examine changes in the strength of bi-directional connections between $N_p = 2$ simulated neurons when pairs and triplets of pre- and post-synaptic spikes are delivered at low frequency (1 Hz) for a period of 60 s. These include single pre- and post-synaptic spikes with a temporal offset of 10 ms; a single action potential and a complex burst of two to three spikes with ~5 ms inter-spike intervals (ISI) offset by 10 ms; and a single action potential with two spikes of differing temporal correlations at various temporal offsets (**Figure 1**).

Secondly, we examine emergent synaptic dynamics in a small, fully recurrently connected network (excluding self-connections) of $N_p = 100$ simulated neurons when neural activity corresponds to previous rate-coded auto-associative network models (Marr, 1971; Hopfield, 1982; Burgess, 2007; Rolls, 2008). A subset of simulated place cells (10%) fire stochastically at an elevated "foreground" rate ($r_{fore} \approx 20$ Hz) while the remainder fire stochastically at a low "background" rate ($r_{back} \approx 0.1$ Hz, these values being realistic of CA3) (Frerking et al., 2005). This activity is generated using external excitatory input drawn from a random, uniform distribution in the range $(0{:}I_{max})$, with $I_{max} = 12$ for foreground neurons and $I_{max} = 4.5$ for background neurons. An examination of the resultant neural dynamics confirms that this form of input produces a Gaussian distribution of ISI (data not shown). In each of these simulations, all synaptic connections in the network are initialized with a weight of $w_{ij} = 0.3$ unless specified otherwise.

In further simulations, theta-coded neural dynamics are dictated by a phenomenological phase precession model (O'Keefe and Recce, 1993; O'Keefe, 2007; Huxter et al., 2008). A variable θ, which oscillates sinsuoidally in the range (0:1) at a rate of 8 Hz, is used to represent theoretical theta frequency oscillations in the local field potential (LFP) that dominate the hippocampal EEG during stereotyped learning behavior (Buzsaki, 2006; O'Keefe, 2007). Inhibitory input to each simulated neuron at each millisecond time step is drawn randomly from a Gaussian distribution with mean $I_{inh} = -15(1 - \theta)$ and standard deviation $\sigma_{inh} = 2$. Neural noise at a rate of ~0.1 Hz (this being realistic of CA3) is generated in the network by the constant application of excitatory current drawn from a uniform random distribution in the range $(0{:}I_{noise})$ where $I_{noise} = 0.8$ in all simulations (Frerking et al., 2005). The interplay between afferent inhibitory and excitatory currents means that the majority of firing due to neural noise tends to occur around the peak of the LFP, as defined by the value of θ.

External stimulation of place cells is subsequently provided within different, discrete theta phase windows depending on hypothetical location within (or outside of) the corresponding place field (**Figure 2**). Circular place fields of 80 cm diameter are divided into eight equally sized sections of 10 cm, and theta oscillations in the LFP (as defined by the value of θ) are similarly divided into "phase windows" of $\pi/4$ between $\pi/8$ and $15\pi/8$. External input, randomly sampled from a normal distribution with mean $I_{ext} = 0$ and standard deviation $\sigma_{ext} = 30$, is subsequently applied to simulated place cells for the duration of a theta phase window if the hypothetical position lies within the corresponding place field section. This generates a mean in-field firing rate of ~15 Hz, with active place cells tending to fire stochastic bursts at the peak of the LFP (as defined by the value of θ) and single spikes on the ascending and descending slope, in accordance with empirical data (O'Keefe

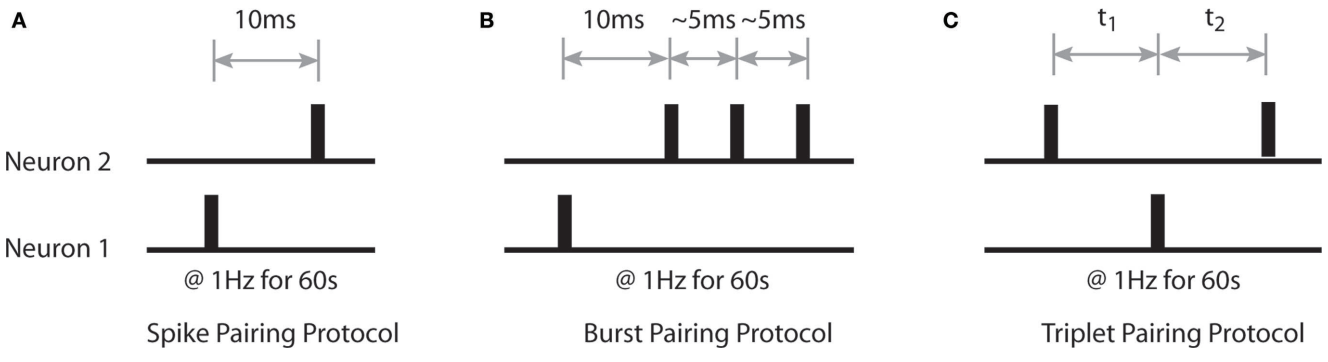

FIGURE 1 | Details of sample spike trains used to characterize the properties of the STDP rule. (A) The spike pairing protocol, in which single action potentials with a temporal offset of 10 ms are generated at a rate of 1 Hz for 60 s. **(B)** The burst pairing protocol, in which a single action potential and a complex spike burst of several spikes with ~5 ms ISI are generated with a temporal offset of 10 ms at a frequency of 1 Hz for 60 s. **(C)** The triplet pairing protocol, in which a single action potential in one simulated neuron is paired with two action potentials of different temporal correlations and differing temporal offsets in the second simulated neuron at a rate of 1 Hz for 60 s.

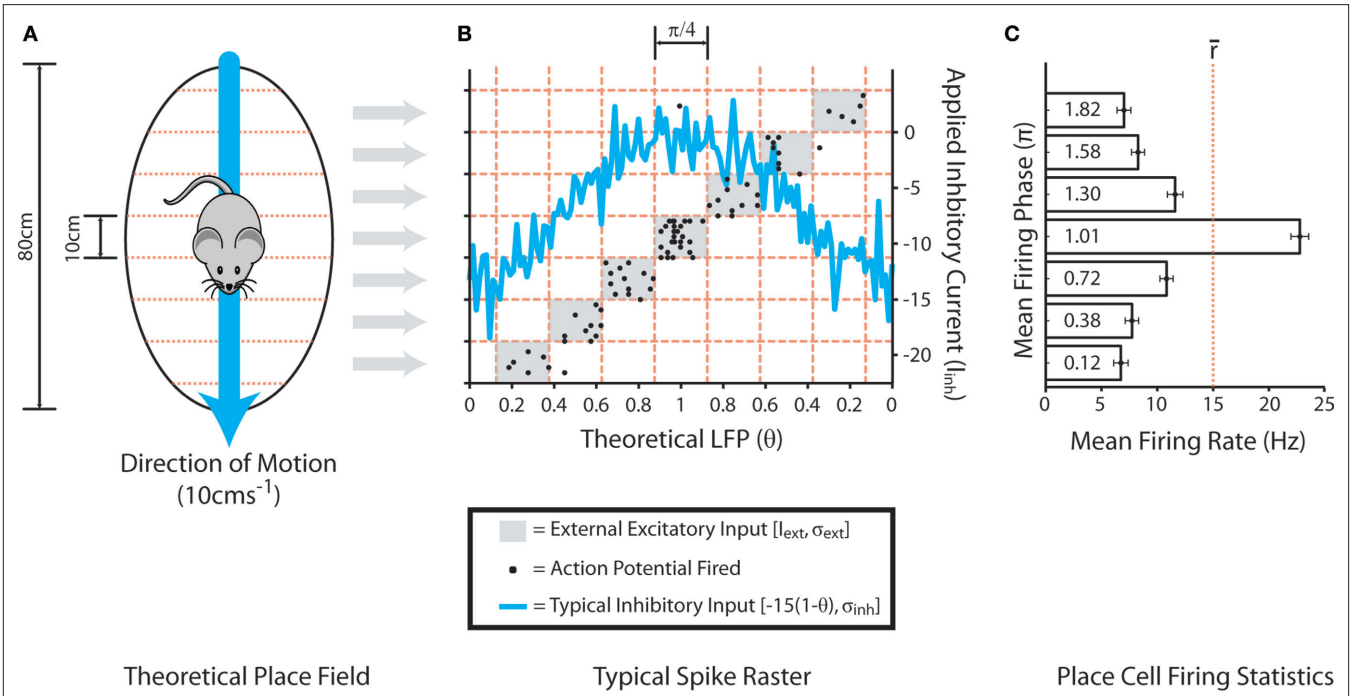

FIGURE 2 | Mechanism of the phenomenological phase precession model. **(A)** Theoretical circular place fields of 80 cm diameter, divided into discrete segments of 10 cm width, are traversed at a constant speed of 10 cms^{-1}. **(B)** Each place cell continually receives external inhibitory input drawn from a normal distribution with mean $I_{inh} = -15(1 - \theta)$ and standard deviation $\sigma_{inh} = 2$, where θ is a dynamic variable representing the hypothetical LFP which oscillates sinusoidally in the range (0:1) at a rate of 8 Hz throughout all simulations. The blue line illustrates a typical example of this applied inhibitory current over a single theta cycle. Each place cell also receives continual excitatory input drawn from a random uniform distribution in the range (0:I_{noise}) to generate low frequency stochastic neural noise. In order to replicate the gross features of phase precession observed in the hippocampus, each putative theta cycle is divided into eight equally sized phase windows of $\pi/4$, and theoretical position within a place field dictates the theta phase window during which the corresponding place cell receives external input drawn from a normal distribution with mean $I_{ext} = 0$ and standard deviation $\sigma_{ext} = 30$. The light gray windows illustrate the theta phase window during which this excitatory current is applied, as determined by position within the corresponding place field segment shown in **(A)**. Black points illustrate a typical spike raster from a simulated place cell as the place field for which it encodes is traversed. **(C)** The mean phase of firing and mean firing rate of simulated place cells when theoretical position lies within each different segment of the corresponding place field.

and Recce, 1993; Huxter et al., 2008). It is important to note that the phenomenological phase precession mechanism utilized here, wherein the phase of place cell firing is dictated by the timing of external excitatory input, contrasts with previous computational models which suggest that phase precession may itself be the result of cell assemblies produced by STDP (Jensen and Lisman, 1996; de Almeida et al., 2007). However, there is considerable debate regarding the mechanisms by which theta-coded neural dynamics are produced *in vivo*, and modeling studies suggest that phase precession in CA3 may largely be inherited from upstream circuits (Baker and Olds, 2007; Maurer and McNaughton, 2007).

Using this phenomenological phase precession model, we first examine changes in the strength of bi-directional connections between $N_p = 2$ simulated neurons when neural activity corresponds to that observed in hippocampal place cells encoding for overlapping place fields. One simulated place cell consistently fires a complex spike burst (two to three action potentials with ~5 ms ISI) at the peak of theta (as defined by the value of θ) while the second neuron fires stochastically within a different theta phase window for each set of 10 s simulations performed.

Having established the synaptic dynamics produced by our STDP rule with various sample spike trains, we then examine a fully recurrently connected network of $N_p = 490$ simulated neurons with theta-coded neural dynamics that correspond to various spatial exploration strategies within a hypothetical square arena. The arena consists of a grid of 49 evenly distributed place fields, each encoded for by 10 place cells, that are offset by 10 cm and traversed by a hypothetical agent at a constant speed of 10 cm s^{-1}. In the first set of "shuttle run" simulations, a randomly selected one-dimensional route of 10 place fields in length is traversed 10 times in alternating directions. Next, in "random exploration" simulations, initial position within the arena is randomly selected, the subsequent direction of movement is chosen randomly at the beginning of each second of simulated time, and thus the agent traverses the arena in an undirected manner for a total period of 490 s. In both cases, these parameter values dictate that there are generally seven different simultaneously active ensembles of 10 place cells, each encoding for a different place field and therefore firing within a different theta phase window. After each 1 s of simulated time, the mean phase of firing in each place cell ensemble recedes to an earlier theta phase window as the hypothetical agent advances to the next place field segment. In each of these simulations, all synaptic connections in the network are initialized with a weight of $w_{ij} = 0.01$ unless specified otherwise.

Experimental data suggests that identical stimulation protocols can induce a differing degree and magnitude of synaptic plasticity within the hippocampus depending on their timing relative to

ongoing theta oscillations – potentiation generally being incurred at the peak of the LFP, while depression (or depotentiation) is incurred at the trough (Hyman et al., 2003). This is most likely a result of the transient changes in membrane depolarization that proceed over the course of a theta cycle. Here, we perform simulations both with and without plasticity modulation. When dynamic plasticity modulation is implemented, all synaptic weight changes dictated by the STDP rule are scaled by the instantaneous value of θ according to Eq. 3.

Fifty independent simulations are performed for each set of experiments described above, and the Mann–Whitney *U*-test is used to assess the significance of differences in resultant synaptic weight distributions.

$$\Delta w_{+} = \theta\left(P_{+} + P_{++}\right)$$
$$\Delta w_{-} = (1-\theta)P_{-}$$

Equation 3: Details of the dynamic synaptic plasticity modulation mechanism.

RESULTS

THE STDP RULE

In order to appraise the accuracy with which our phenomenological plasticity rule can replicate empirical data obtained from the hippocampus, we first examine the emergent synaptic dynamics generated when neural activity corresponds to several different stimulation protocols commonly used to induce LTP and LTD. Initially, we employ two different spike pairing protocols in which either single pre- and post-synaptic spikes or a single spike and complex burst are paired at short temporal offsets (**Figures 1A,B**). This generates asymmetric connections that correspond to the "causal" input correlation, with synaptic weights being driven toward either the upper or lower bounds (**Figure 3A**). These results concur with empirical data obtained using similar stimulation protocols in cultures of hippocampal pyramidal neurons (Bi and Poo, 1998; Debanne et al., 1998; Wang et al., 2005). However, studies using acute hippocampal slices suggest that multiple post-synaptic spikes are required to generate potentiation (Pike et al., 1999; Meredith et al., 2003; Wittenberg and Wang, 2006; Buchanan and Mellor, 2007). Our STDP rule does not replicate this data – although it is important to note that potentiation is more rapid, and thus a greater mean synaptic weight is achieved over the 60 s stimulation period, when the post-synaptic neuron fires multiple spikes.

Secondly, we employ triplets of pre- and post-synaptic spikes at various temporal offsets (**Figure 1C**). Under these conditions, the non-linear integration of depression and potentiation processes dictated by the P_{++} term generate more complex emergent synaptic dynamics that depend explicitly on the order of spike pairings. When the temporal offset of each spike pairing is equal, then the synaptic connection that experiences a potentiating ("causal") spike pairing after a depressing spike pairing is significantly potentiated (**Figure 3B**). Conversely, spike pairings in the opposite order (potentiation then depression) generate a much less significant increase in synaptic weight. In the majority of cases – particularly for post–pre–post spike triplets, the magnitude of synaptic changes produced in these simulations approximates that observed in hippocampal cultures when identical stimulation protocols are employed (Wang et al., 2005; Pfister and Gerstner, 2006).

However, asymmetry in the profile of the STDP window employed in this study (i.e., $A_{+} > A_{-}$ and $\tau_{+} < \tau_{-}$) dictates that the potentiation and subsequent depression increments produced by pre–post–pre triplets are not equal and do not directly negate. Hence, mild LTP is generated by pre–post–pre triplets with equal temporal offsets (i.e., $t_1 = t_2$) and mild LTD is induced when a potentiating spike pairing with a longer temporal offset precedes a depressing increment with a shorter temporal offset (i.e., w_{21} when $t_1 > t_2$). This is in contrast to empirical data, where no significant weight change is observed in either case (Wang et al., 2005; Pfister and Gerstner, 2006). Furthermore, the magnitude of potentiation incurred when a depressing spike pairing with a shorter offset precedes a potentiating increment with a longer temporal offset is much less significant than that observed experimentally. This is surprising, considering the fact that the profile of the STDP window employed in this study is also based directly on empirical data from hippocampal cultures (Bi and Poo, 1998).

Thirdly, we demonstrate that this form of STDP can mediate rate-coded Hebbian learning, in accordance with empirical data regarding observations of LTP induced by tetanic stimulation protocols (Bliss and Lomo, 1973; Malenka and Bear, 2004). When stochastic neural activity at high ("foreground") and low ("background") firing rates is generated in distinct groups of neurons within a small, fully recurrently connected network, those synaptic connections with elevated pre- and post-synaptic firing rate are rapidly, selectively and significantly potentiated (**Figures 3C,D**). Synaptic connections with solely elevated post-synaptic firing rate undergo modest but continual potentiation, while those with solely elevated pre-synaptic firing rate are significantly depressed. This indicates that the STDP rule reduces the weight of connections that have a negative (i.e., "non-causal") rate correlation. Finally, the strength of synapses with background pre- and post-synaptic firing rate does not change significantly. This is in contrast to the robust LTD usually observed following prolonged low frequency stimulation, and most likely due to the small number of temporally proximate spike pairings that occur at these connections (Dudek and Bear, 1992; Buchanan and Mellor, 2010).

However, over very long periods of simulated time (~20,000 s or more) the mean weight of all pre-synaptic connections of neurons firing at an elevated rate saturate at a similarly high value (~$0.8w_{max}$, data not shown). This indicates that the STDP rule utilized here fails to generate competition between synaptic inputs to a single neuron. This absence of hetero-synaptic competition, and subsequent issues with global network stability, is a common feature of previous rate-coded Hebbian plasticity rules, and require the inclusion of some additional mechanism to ensure stable long-term operation (Desai, 2004).

Finally, we examine the synaptic dynamics generated when neural activity approximates the theta-coded temporal activity correlations observed in place cells encoding for overlapping place fields within the hippocampus (O'Keefe and Recce, 1993; O'Keefe, 2007; Huxter et al., 2008). We consider two bi-directionally connected place cells that fire stochastically at differing mean phase of a putative theta cycle (**Figure 4A**). Our results demonstrate that asymmetric connections of varying strength are generated when a persistent temporal correlation in pre- and post-synaptic activity exists, while strong bi-directional

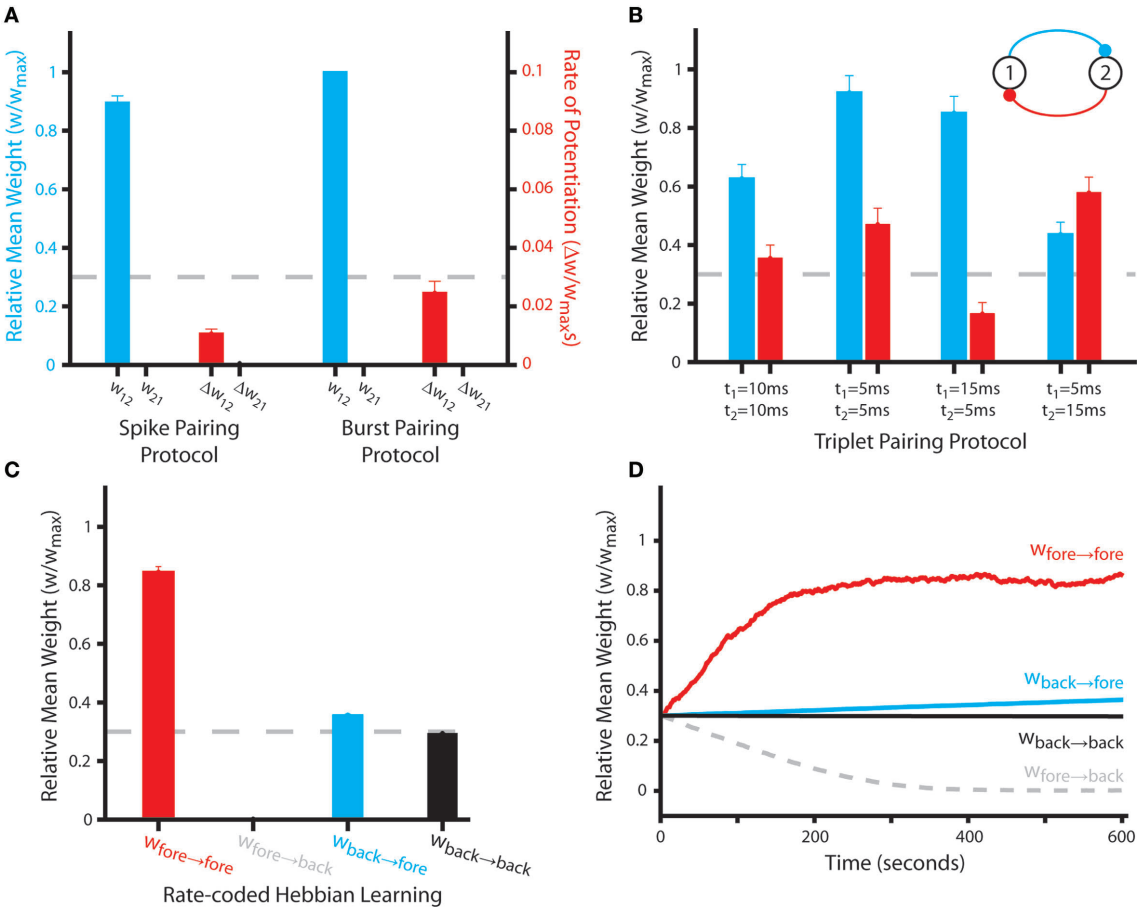

FIGURE 3 | Synaptic weight dynamics produced by the STDP rule with sample rate- and temporally coded spike trains. (A) The final mean weight (w_{ij}) and rate of weight change per spike pairing (Δw_{ij}) at bi-directional synaptic connections between $N_p = 2$ simulated neurons over 50 independent simulations in which single action potentials with an offset of 10 ms are incurred at a rate of 1 Hz for 60 s (the spike pairing protocol, **Figure 1A**); or a single action potential and complex spike burst with an offset of 10 ms are incurred at a rate of 1 Hz for 60 s (the burst pairing protocol, **Figure 1B**). The dashed line indicates the initial synaptic weight value of $w_{ij} = 0.3$. **(B)** The final mean weight of bi-directional synaptic connections between $N_p = 2$ simulated neurons over 50 independent simulations in which triplets of pre- and post-synaptic spikes with differing temporal offsets are incurred at a rate of 1 Hz for 60 s (**Figure 1C**). The dashed line indicates the initial synaptic weight value of $w_{ij} = 0.3$. **(C)** The final mean weight of synaptic connections between $N_p = 490$ simulated neurons over 50 independent "rate-coded Hebbian learning" simulations, in which a subset (10%) fire stochastically at an elevated "foreground" mean rate ($r_{fore} \approx 20$ Hz) while the remainder fire stochastically at a lower "background" mean rate ($r_{back} \approx 0.1$ Hz) for a period of 10 s. Synaptic connections are grouped according to whether pre- and post-synaptic neurons fire at a foreground or background rate. Those between neurons with elevated pre- and post-synaptic firing rate are selectively and significantly potentiated, while those with solely elevated pre-synaptic firing rate are selectively and significantly depressed (Mann–Whitney *U*-test, $p < 0.01$). The dashed line indicates the initial synaptic weight value of $w_{ij} = 0.3$. **(D)** Synaptic weight dynamics in a typical rate-coded Hebbian learning simulation, illustrating the rapid potentiation of connections between neurons firing stochastically at an elevated rate.

connections are generated when pre- and post-synaptic activity is stochastic but approximately synchronous with no persistent sequence bias (**Figures 4B,C**). The presence of strong bi-directional connections in these simulations is again indicative of a lack of synaptic competition generated by this form of STDP. When dynamic plasticity modulation is implemented, the mean weight of bi-directional connections between neurons firing synchronous, stochastic spike bursts at the peak of theta is significantly greater. Furthermore, the mean weight of asymmetric connections generated when the pre-synaptic neuron fires a complex burst and the post-synaptic neuron fires fewer spikes (i.e., when there is a negative rate correlation) are significantly lower. It is also important to note that previous research has delineated a significant correlation between the magnitude of bi-directional connections between simultaneously active simulated neurons and the scale of recurrent axonal delays between those neurons (Bush et al., 2010b).

In summary, these results demonstrate that the phenomenological plasticity rule utilized here can approximate the primary characteristics of synaptic plasticity data obtained *in vitro* using either rate or temporally coded stimulation protocols. The STDP model can generate both asymmetric and bi-directional connectivity patterns, according to long-term correlations in neural activity, and thus mediate both hetero-associative and auto-associative learning in recurrently connected networks (Bush et al., 2010b). However, these emergent properties come at the cost of the inherent synaptic competition observed in previous computational models of STDP (Song et al., 2000; Song and Abbott, 2001; Bush et al., 2010a). It is

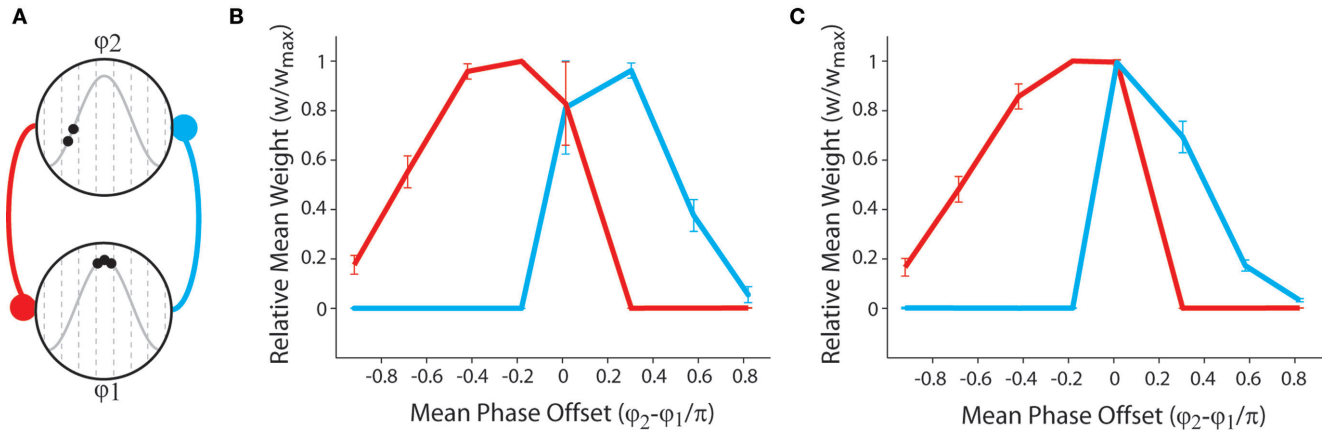

FIGURE 4 | Synaptic weight dynamics produced by the STDP rule with theta-coded spike trains that are representative of activity observed in place cells encoding for overlapping place fields within the hippocampus. **(A)** Illustration of neural dynamics in these simulations: in a network of $N_p = 2$ simulated neurons, one neuron consistently fires stochastic complex spike bursts at the peak of an 8 Hz inhibitory theta oscillation ($\varphi_1 \approx \pi$), while the other fires stochastic bursts or single spikes within another theta phase window (φ_2, see **Figure 2**) which differs for each set of 50 independent simulations, of length 10 s, that are performed. **(B)** The mean and standard deviation of final synaptic weights for each value of φ_2 with no plasticity modulation. Strong asymmetric connections are generated when there is a persistent temporal correlation in neural activity (i.e., $\varphi_2 - \varphi_1 \neq 0$), while strong bi-directional connections are generated when neural activity is stochastic but approximately synchronous (i.e., $\varphi_2 - \varphi_1 \approx 0$). Furthermore, the strength of asymmetric connections is lower when pre-synaptic firing rate is higher than post-synaptic firing rate (i.e., when $\varphi_2 - \varphi_1 > 0$) in accordance with the results described in **Figure 3C**. **(C)** The mean and standard deviation of final synaptic weights for each value of φ_2 with dynamic plasticity modulation. Note that the strength of bi-directional connections formed when there is no persistent sequence bias in pre- and post-synaptic activity (i.e., $\varphi_1 - \varphi_2 \approx 0$) is greater, and the strength of asymmetric connections generated when pre-synaptic firing rate exceeds post-synaptic firing rate (i.e., $\varphi_2 - \varphi_1 > 0$) is lower when dynamic plasticity modulation is implemented.

important to note that the qualitative nature of these findings do not depend explicitly upon the use of a triplet-based STDP rule (i.e., one which incorporate a P_{++} term), but can also be achieved by a pair-based STDP rule if certain constraints are placed on the profile of the STDP window and spike pair interactions, although the latter cannot replicate empirical data obtained with triplets of pre- and post-synaptic action potentials delivered at low frequencies (Bush et al., 2010a,b).

SHUTTLE RUN SIMULATIONS

Having established that the emergent synaptic dynamics produced by this form of STDP concur broadly with empirical data, we next implement the plasticity rule within an abstract spiking recurrent neural network model of hippocampal spatial learning. In these simulations, neural dynamics correspond hypothetically to those observed in hippocampal pyramidal neurons during spatial exploration, with theta-coded activity patterns created in simulated place cells by the phenomenological phase precession model (O'Keefe and Recce, 1993; O'Keefe, 2007; Huxter et al., 2008). We consider different navigation strategies in a square arena of equidistant place fields, each of which is encoded for by an ensemble of place cells.

Initially, neural activity corresponds hypothetically to repeated shuttle runs along a one-dimensional route of overlapping place fields. Subsequently, interconnected place cells encoding for neighboring place fields exhibit temporal correlations in firing activity with repeatedly alternating direction but approximately equal ISIs. It has been suggested that the asymmetric nature of the STDP learning window dictates that purely asymmetric connections will develop under these conditions (Skaggs et al., 1996; Wagatsuma and Yamaguchi, 2007; Song and Abbott, 2001; but see Mongillo et al., 2005; Samura and Hattori, 2005). For the purposes of cognitive map theory, however, it is essential that strong bi-directional connections which reflect the relative location of corresponding place fields in the environment and the long-term history of navigation through this one-dimensional environment are generated (Muller et al., 1991; Burgess et al., 1994; Burgess, 2007).

Our results demonstrate that, following 10 shuttle runs along the route, the mean weight of hetero-associative connections between place cells encoding for each place field and those up to three steps in either direction on the learned route are selectively and significantly potentiated (**Figures 5A,B**). Strong bi-directional connections also develop between place cells that encode for the same location. When no dynamic plasticity modulation is implemented, these auto-associative connections are weaker than hetero-associative connections between place cells encoding for adjacent place fields. These results correspond closely with the synaptic dynamics observed at connections between hippocampal neurons with overlapping place fields *in vivo* (Figure 5G in Isaac et al., 2009).

An examination of the synaptic dynamics generated in these simulations demonstrates that, although the mean weight of hetero-associative connections remains significantly higher than that of other synaptic weights in the network, those against the direction of motion are significantly depressed during a single traversal of the route (**Figures 5C,D**). The relative magnitude of hetero-associative connections corresponding to opposing directions of traversal therefore fluctuate continually during these shuttle runs. Hence, the resultant "cognitive map" of the learned route is biased in the direction that the environment was most recently explored. This implies that, if a sequence of place fields is repeatedly traversed in a single direction, then hetero-associative connections between

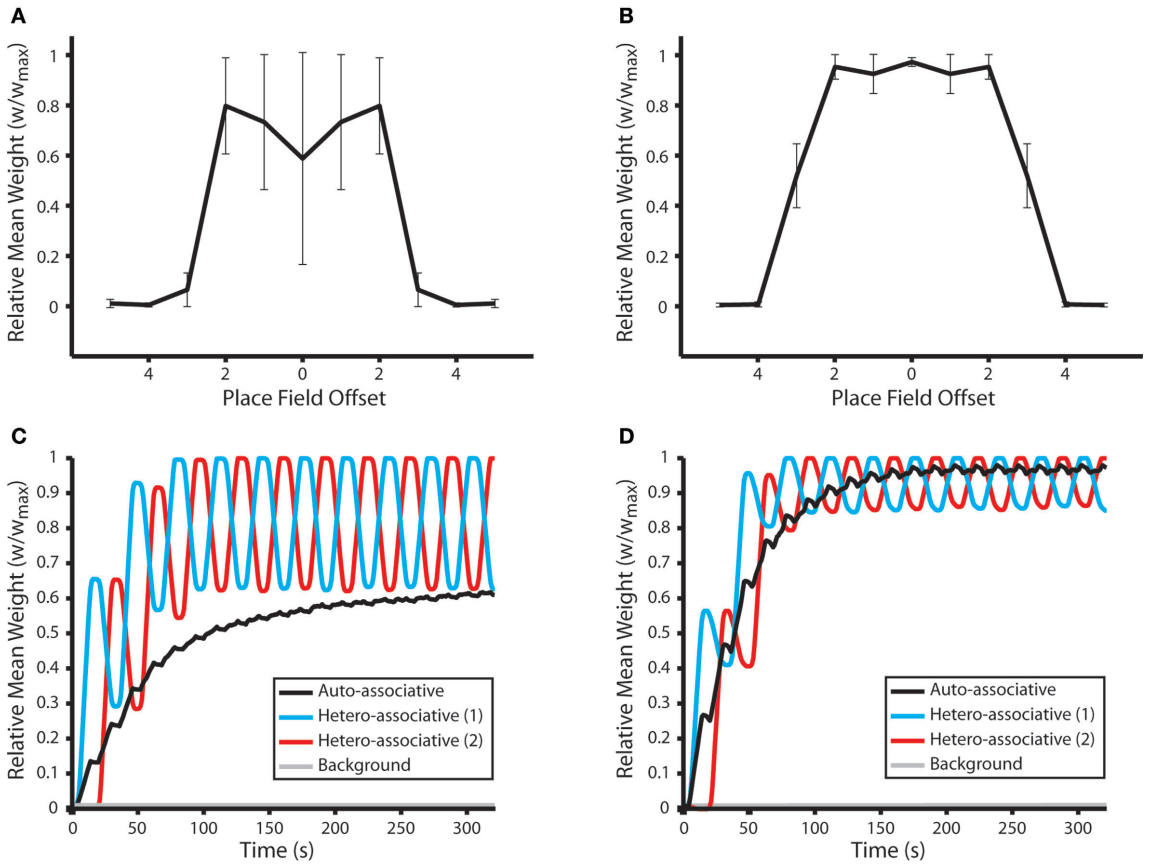

FIGURE 5 | Synaptic weight dynamics during repeated shuttle runs along a route of overlapping place fields. (A) The mean and standard deviation of final synaptic weights following 50 independent simulations of a network consisting of $N_P = 490$ simulated neurons. Neural activity corresponds to 10 shuttle runs along a one-dimensional route of 10 place fields, each of which is encoded by the activity of 10 randomly selected place cells. Synaptic weights evolve to reflect the relative distance between corresponding place fields, in accordance with cognitive map theory, with connections between neurons that encode for the same place field or two neighboring place fields being selectively and significantly potentiated (Mann–Whitney *U*-test, $p < 0.01$). Data illustrated here for simulations with no plasticity modulation. **(B)** Mean and standard deviation of final synaptic weights following 50 independent shuttle run simulations, as described for **(A)**, when dynamic plasticity modulation is implemented. Note that synaptic connections between a greater number of adjoining place fields are selectively and significantly potentiated in this case, and the magnitude of auto- and hetero-associative connections is also greater than that observed in the absence of plasticity modulation. **(C)** Synaptic dynamics during a typical shuttle run simulation in the absence of plasticity modulation. The mean weight of connections between place cells encoding for each place field on the one-dimensional route and those encoding for the same place field (auto-associative); the neighboring place fields in opposing directions along the route (hetero-associative); and all place fields that are not part of the route (background) are illustrated. Auto- and hetero-associative connections are rapidly, selectively and significantly potentiated, while the mean weight of background connections does not change significantly. **(D)** Synaptic dynamics during a typical shuttle run simulation in the presence of dynamic plasticity modulation, as described for **(C)**.

the corresponding place cells will become purely asymmetric, as synapses against the direction of motion undergo sustained depression (Bush et al., 2010b).

RANDOM EXPLORATION SIMULATIONS

Next, we examine the emergent synaptic dynamics produced during random exploration of a two-dimensional arena of place fields, each of which is encoded by an ensemble of place cells that exhibit theta-coded neural dynamics. Our results demonstrate that, following approximately 8 min of random exploration, a putative cognitive map of the environment is encoded in recurrent connections such that the relative distance between place fields for which pre- and post-synaptic place cells encode correlates with the magnitude of interconnecting synaptic weights (**Figures 6A,B**). Strong, bi-directional (auto-associative) connections again develop between place cells that encode for the same location, although these are weaker than hetero-associative connections between place cells that encode for neighboring locations in the environment when no plasticity modulation is implemented. Hetero-associative connections are also more rapidly potentiated (**Figure 6C**), although this depends on the corresponding place fields being traversed in the necessary order, while auto-associative connections are strengthened whenever a place field is entered. An examination of sample "cognitive maps" for single place fields illustrates that uniform, omnidirectional connections between place cells are not created in all locations (**Figure 6D**). Hence, while the overall/mean connectivity pattern of the network is characterized by strong bi-directional connections between place cells encoding for proximate place fields

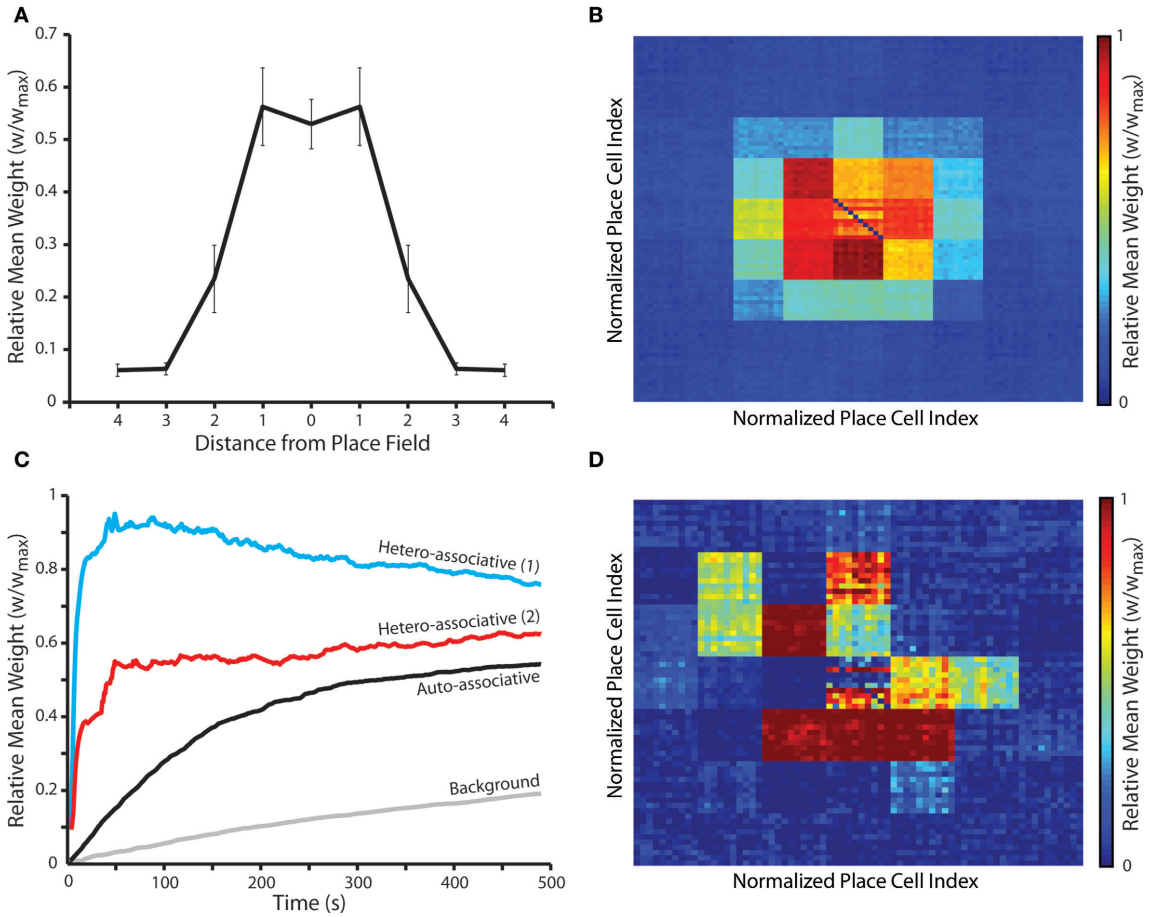

FIGURE 6 | Synaptic weight dynamics during random exploration of a square arena populated by multiple overlapping place fields. (A) The mean and standard deviation of final synaptic weights following 50 independent simulations of a network consisting of $N_p = 490$ simulated neurons, where neural activity corresponds to the random exploration of a square environment of 49 place fields, each of which is encoded by the activity of 10 randomly selected place cells, for a total of 490 s. Synaptic weights evolve to reflect the relative distance between corresponding place fields, in accordance with cognitive map theory, with connections between neurons that encode for the same place field, or the two neighboring place fields, being selectively and significantly potentiated (Mann–Whitney *U*-test, $p < 0.01$). Data illustrated here for simulations with no plasticity modulation. **(B)** The mean weight of post-synaptic connections between place cells encoding for each place field and all other place cells in the network, re-arranged to correspond with the structure of the square arena. There is no significant difference between this data and that for pre-synaptic connection weights (data not shown). **(C)** Synaptic dynamics during a typical random exploration simulation in the absence of plasticity modulation. The mean weight of connections between place cells encoding for each place field on the route taken and those encoding for the same place field (auto-associative); place fields that are one and two steps in any direction (hetero-associative 1 and 2 respectively); and all place fields that are not part of the route (background) are illustrated. Auto- and hetero-associative connections are rapidly, selectively and significantly potentiated, while background connections undergo modest but sustained potentiation. **(D)** The mean weight of post-synaptic connections between a single randomly selected place field in a typical simulation and all other place cells in the network, re-arranged to correspond with the structure of the square arena. This illustrates how the cognitive map formed for a single place field is biased by the trajectories taken through that place field during random exploration. Again, there is no significant difference between this data and that for pre-synaptic connection weights (data not shown).

in the environment, local connectivity patterns tend to reflect the specific trajectories taken through that place field during random exploration. It seems likely that this effect would disappear over longer periods, as all possible trajectories through each place field are explored.

It is important to note that "background" connections in the network – i.e., synapses between place cells encoding for place fields that do not overlap – undergo modest but sustained potentiation throughout these simulations (**Figure 6C**). This is again indicative of the lack of synaptic competition generated by this form of STDP. Over prolonged periods of operation, the increase in background synaptic weights eventually destabilizes network operation by generating runaway recurrent excitation. The length of time for which the network maintains stable operation is inversely correlated with the background firing rate, as higher background firing rates generate a more rapid potentiation of background connections due to the increased frequency of spike pairings (data not shown). However, the inclusion of any additional mechanism that generates hetero-synaptic competition between all synaptic inputs of a single neuron can ameliorate this issue (Desai, 2004). For example, a small, global, uniform weight decay term eliminates the potentiation of background

connections without any significant effect on the generation of auto- and hetero-associative connections between place cells encoding for overlapping place fields, and thereby stabilizes long-term network operation (data not shown).

Finally, we examine the emergent synaptic dynamics generated when neural activity corresponds to the repeated traversal of a one-dimensional route through the environment of place fields in a single direction, following the random exploration simulations described above. While the overall shape of the synaptic weight matrix changes very little (**Figures 6A and 7A**), the strength of connections between place cells encoding for those place fields that lie on the learned route are significantly altered. For example, **Figure 7B** illustrates how the cognitive map formed for a single place field (that illustrated in **Figure 6D**) changes when a route of seven place fields that horizontally transects that place field is subsequently traversed 10 times. Strong asymmetric connections are formed between place cells encoding for place fields that are successively activated, while those connections against the direction of motion are fully depressed.

These novel hetero-associative connections are embedded within the previously learned map, which reflects routes taken through that place field during the initial random exploration, without any significant effect on previously learned associations that do not form part of the newly learned route. Hence, the hetero-associative connections formed by place cells encoding for each place field represent the relative distance between place fields and the relative frequency with which those place fields have been sequentially traversed. These results also indicate that STDP and theta-coded neural dynamics allow rapid sequence learning, via the formation of asymmetrically connected place cell assemblies, in accordance with previous models of route learning in recurrent networks (Skaggs et al., 1996; Wagatsuma and Yamaguchi, 2007; Bush et al., 2010b).

DISCUSSION

We have presented a phenomenological STDP rule that approximates empirical synaptic plasticity data obtained using both rate and temporal stimulation protocols, and can thus generate both bi-directional and asymmetric connections in response to persistently synchronous or sequential correlations in pre- and post-synaptic activity respectively. We have subsequently demonstrated that a spiking recurrent neural network model which utilizes this STDP rule alongside theta-coded neural dynamics can mediate the development of a cognitive map during shuttle runs along a one-dimensional track or open field exploration within a two-dimensional environment, such that the geometric distance between place fields is encoded by the magnitude of bi-directional synaptic connections between place cells. This demonstrates that temporally asymmetric synaptic plasticity and phase precession are compatible with previous computational models of rate-coded cognitive map formation. Furthermore, it allows the integration of those rate-coded auto-associative network models with temporally coded, hetero-associative, spiking neural network models of route and sequence learning, and thus provides them with a firmer basis in modern neurobiology.

However, the STDP rule described here also exhibits several theoretical and functional weaknesses. Firstly, it fails to replicate recent experimental data obtained from acute hippocampal slices that suggest a requirement for multiple post-synaptic spikes to induce LTP with low frequency temporally correlated stimulation (Pike et al., 1999; Meredith et al., 2003; Wittenberg and Wang, 2006;

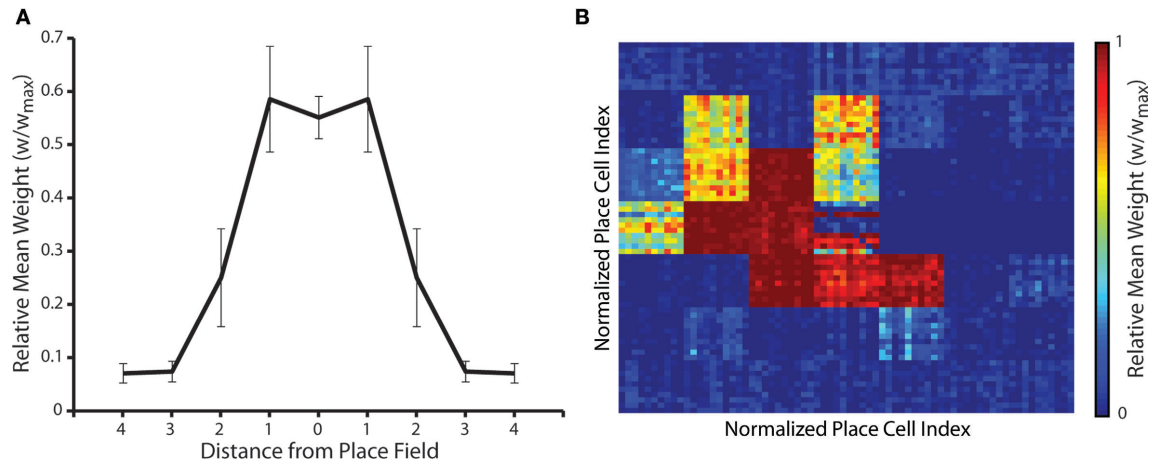

FIGURE 7 | Change in synaptic weights when a one-dimensional route is repeatedly traversed in a single direction following random exploration. **(A)** Mean and standard deviation of synaptic weights after an arbitrary one-dimensional route of seven place fields in length is traversed 10 times following the formation of a putative cognitive map. The only significant difference between this data and that observed prior to the traversal of the one-dimensional route (as illustrated in **Figure 6A**) is that the standard deviation of synaptic weights between place cells encoding for a place field and those encoding for the two neighboring place fields has increased (Mann–Whitney *U*-test, $p < 0.01$). **(B)** Changes in the cognitive map for the single randomly selected place field illustrated in **Figure 6D** following the repeated traversal of a linear route that transects the place field from right to left. Strong post-synaptic connections between place cells encoding for the central place field and those encoding for successive place fields on the route have been formed, while post-synaptic connections between place cells encoding for the central place field and those encoding for place fields against the direction of motion have been fully depressed. Conversely, the strength of connections between place cells encoding for the central place field and those encoding for all other place fields in the arena that do not form part of the newly learned route have not changed significantly (Mann–Whitney *U*-test, $p < 0.01$).

Buchanan and Mellor, 2007, 2010), although it is important to note that empirical findings often disagree and other studies have demonstrated robust potentiation using single spike pairs in similar preparations (Kwag and Paulsen, 2009). These differences can be attributed to the multiple factors (such as membrane depolarization, the state of network inhibition, developmental stage and neuromodulatory tone) that influence post-synaptic calcium influx, which is generally recognized as the critical trigger for synaptic plasticity (Buchanan and Mellor, 2010). Furthermore, the vast majority of empirical plasticity data is obtained at the CA3-CA1 synapse, while significant differences may exist at recurrent CA3 connections. Place cells are known to receive rhythmic inhibitory input during spatial exploration, and be significantly depolarized when the corresponding place field is traversed (which concurs with the experimental procedure employed in Kwag and Paulsen, 2009), while cholinergic tone is vastly increased during stereotype learning behavior (Harvey et al., 2009; Isaac et al., 2009). Each of these factors could contribute to the induction of LTP with less intensive stimulation protocols. A wider range of experimental data might be approximated by incorporating a more explicit consideration of intra-cellular calcium dynamics, NMDA receptor kinetics and/or the backpropagation of action potentials in the dendritic tree.

Secondly, it has been empirically demonstrated that reversing the temporal order of action potentials in pairs of place cells that exhibit asymmetric spike timing cross-correlations does not prevent the induction of LTP at the interconnecting synapse, casting doubt on the existence of STDP *in vivo* (Isaac et al., 2009). However, it is important to note that place cells in that study exhibited only weak sequence bias in pre- and post-synaptic spike timing, while each firing at an elevated rate – circumstances that would likely generate significant bi-directional potentiation using the STDP rule presented here (**Figures 3B,C**). Furthermore, in the same study, the selective elimination of all spike pairings with a positive temporal correlation of <100 ms prevented the induction of LTP, which suggests some requirement for temporal asymmetry to generate potentiation.

Finally, our STDP rule fails to induce any competition between the inputs of a single neuron. Some additional mechanism – such as synaptic scaling, weight decay or metaplasticity – is therefore required to ensure the long-term stability of network operation, particularly at higher background firing rates (Desai, 2004). For example, the inclusion of a slow, global weight decay term ameliorates the potentiation of background connections and thus maintains stable long-term network operation without affecting the generation of auto- and hetero-associative connections between place cells encoding for overlapping place fields (data not shown). It is important to note that this propensity for potentiation is a feature of all STDP rules that can mediate rate-coded Hebbian learning (Bush et al., 2010a,b). This might be considered a significant functional weakness and failure to replicate bi-directional changes in synaptic strength. However, it is important to note that no significant depression of synaptic connections between hippocampal place cells is observed during spatial exploration (Isaac et al., 2009). In fact, there is a convincing similarity between the data presented here and that recorded at synaptic connections between place cells whose place field have varying degrees of overlap *in vivo* (i.e., **Figure 5A** in this manuscript and Figure 5G in Isaac et al., 2009). It has also been demonstrated that synaptic connections throughout the cortex undergo net potentiation during waking, and are subsequently depressed during sleep (Vyazovskiy et al., 2008). It may be that the rapid formation of novel associations in the hippocampus is achieved at the cost of a slower but continual positive drift in background synaptic weights.

Although the neural network presented here is not intended to address the function of CA3 directly, it can also be appraised in terms of more general auto- and hetero-associative models of spatial learning. One significant omission, which therefore represents a critical direction for future research, is an examination of recall dynamics mediated by recurrent excitation, whereby external stimulation following learning generates pattern completion in encoded static or sequential activity patterns. Although we have previously demonstrated this ability following the learning of single, isolated auto- and hetero-associative activity patterns (Bush et al., 2010b), the overlap of encoded associations required by cognitive mapping generates the undirected and unrestricted spread of recurrent excitation throughout the entire network (Molter et al., 2007). Conversely, to be of any functional use, recall activity within network models of spatial learning needs to be biased by goal-directed excitatory or inhibitory input (Burgess, 2007). It seems feasible that inhibitory plasticity during spatial learning could contribute to disambiguating overlapping encoded sequences during subsequent reactivation via putative winner-take-all dynamics. This highlights a need for the inclusion of feedback inhibition in future extensions of this model, which might also dynamically regulate the firing rate of background neurons, reducing the potentiation of redundant synaptic connections and thus contributing to the long-term stability of network operation.

Finally, it is unclear to what extent rate-coded models of cognitive map formation can explain the involvement of the hippocampus in spatial learning and navigation. There is no evidence for fixed point attractor dynamics in CA3, and it remains to be seen if models of cognitive mapping can be reconciled with the transient, temporally coded cell assembly dynamics that characterize hippocampal activity during exploration (Harris, 2005). Furthermore, it is generally accepted that the role of the hippocampus in declarative memory is time-limited, and recent experimental evidence demonstrates that the neocortex is involved in spatial learning and memory consolidation from a very early stage (Leon et al., 2010). In accordance with standard "two stage" models of declarative memory processing, it seems likely that a global cognitive map would ultimately be stored in the neocortex, while recent routes or environments – "episodes" encoded in a single trial – are stored for a limited period in the hippocampus for rapid integration with this "semantic" spatial knowledge (McClelland et al., 1995). The exact contribution of the hippocampus and neocortex to spatial memory and goal-directed navigation remains to be elucidated.

ACKNOWLEDGMENTS

The authors would like to thank Jesper Sjostrom, Bart Baddeley, the anonymous referees and members of the CCNR for useful discussions during the preparation of this manuscript. This work was supported by Wellcome VIP funding and the EPSRC grant EP/H024638/1.

REFERENCES

Baker, J. L., and Olds, J. L. (2007). Theta phase precession emerges from a hybrid computational model of a CA3 place cell. *Cogn. Neurodyn.* 1, 237–248.

Bi, G. Q., and Poo, M. M. (1998). Synaptic modifications in cultured hippocampal neurons: dependence on spike timing, synaptic strength, and postsynaptic cell type. *J. Neurosci.* 18, 10464–10472.

Bienenstock, E. L., Cooper, L. N., and Munro, P. W. (1982). Theory for the development of neuron selectivity: orientation specificity and binocular interaction in visual cortex. *J. Neurosci.* 2, 32–48.

Bliss, T. V., and Lomo, T. (1973). Long-lasting potentiation of synaptic transmission in the dentate area of the anaesthetized rabbit following stimulation of the perforant path. *J. Physiol.* 232, 331–356.

Buchanan, K. A., and Mellor, J. R. (2007). The development of synaptic plasticity induction rules and the requirement for postsynaptic spikes in rat hippocampal CA1 pyramidal neurones. *J. Physiol.* 585, 429–445.

Buchanan, K. A., and Mellor, J. R. (2010). The activity requirements for spike timing-dependent plasticity in the hippocampus. *Front. Syn. Neurosci.* 2:11. doi: 10.3389/fnsyn.2010.00011.

Burgess, N. (2007). "Computational models of the spatial and mnemonic functions of the hippocampus," in *The Hippocampus Book*, eds P. Andersen, R. Morris, D. Amaral, T. Bliss, and J. O'Keefe (Oxford: Oxford University Press), 715–749.

Burgess, N., Recce, M., and O'Keefe, J. (1994). A model of hippocampal function. *Neural Netw.* 7, 1065–1081.

Bush, D., Philippides, A., Husbands, P., and O'Shea, M. (2010a). Reconciling the STDP and BCM models of synaptic plasticity in a spiking recurrent neural network. *Neural Comput.* 22, 1–27.

Bush, D., Philippides, A., Husbands, P., and O'Shea, M. (2010b). Dual coding with STDP in a spiking recurrent neural network model of the hippocampus. *PLoS Comput. Biol.* 6, e1000839. doi: 10.1371/journal.pcbi.1000839.

Buzsaki, G. (2006). *Rhythms of the Brain*. Oxford: Oxford University Press.

de Almeida, L., Idiart, M., and Lisman, J. E. (2007). Memory retrieval time and memory capacity of the CA3 network: role of gamma frequency oscillations. *Learn. Mem.* 14, 795–806.

Debanne, D., Gahwiler, B. H., and Thompson, S. M. (1998). Long-term synaptic plasticity between pairs of individual CA3 pyramidal cells in rat hippocampal slice cultures. *J. Physiol.* 507, 237–247.

Desai, N. S. (2004). Homeostatic plasticity in the CNS: synaptic and intrinsic forms. *J. Physiol. (Paris)* 97, 391–402.

Dudek, S. M., and Bear, M. F. (1992). Homosynaptic long-term depression in area CA1 of hippocampus and effects of N-methyl-D-aspartate receptor blockade. *Proc. Natl. Acad. Sci. U.S.A.* 89, 4363–4367.

Frerking, M., Schulte, J., Wiebe, S. P., and Stäubli, U. (2005). Spike timing in CA3 pyramidal cells during behavior: implications for synaptic transmission. *J. Neurophysiol.* 94, 1528–1540.

Harris, K. D. (2005). Neural signatures of cell assembly organization. *Nat. Rev. Neurosci.* 6, 399–407.

Harvey, C. D., Collman, F., Dombeck, D. A., and Tank, D. W. (2009). Intracellular dynamics of hippocampal place cells during virtual navigation. *Nature* 461, 941–946.

Hebb, D. O. (1949). *Organisation of Behaviour*. New York: Wiley.

Hopfield, J. J. (1982). Neural networks and physical systems with emergent collective computational abilities. *Proc. Natl. Acad. Sci. U.S.A.* 79, 2554–2558.

Huxter, J. R., Senior, T. J., Allen, K., and Csicsvari, J. (2008). Theta phase-specific codes for two-dimensional position, trajectory and heading in the hippocampus. *Nat. Neurosci.* 11, 587–594.

Hyman, J. M., Wyble, B. P., Goyal, V., Rossi, C. A., and Hasselmo, M. E. (2003). Stimulation in hippocampal region CA1 in behaving rats yields LTP when delivered to the peak of theta and LTD when delivered to the trough. *J. Neurosci.* 23, 11725–11731.

Isaac, J. T. R., Buchanan, K. A., Muller, R. U., and Mellor, J. R. (2009). Hippocampal place cell firing patterns can induce long-term synaptic plasticity in vitro. *J. Neurosci.* 29, 6840–6850.

Izhikevich, E. M. (2004). Which model to use for cortical spiking neurons? *IEEE Trans. Neural Netw.* 15, 1063–1070.

Jensen, O., and Lisman, J. E. (1996). Novel lists of 7 ± 2 known items can be reliably stored in an oscillatory short-term memory network: interaction with long-term memory *Learn. Mem.* 3, 257–263.

Kwag, J., and Paulsen, O. (2009). The timing of external input controls the sign of plasticity at local synapses. *Nat. Neurosci.* 12, 1219–1221.

Leon, W. C., Bruno, M. A., Allard, S., Nader, K., and Cuello, A. C. (2010). Engagement of the PFC in consolidation and recall of recent spatial memory. *Learn. Mem.* 17, 297–305.

Malenka, R. C., and Bear, M. F. (2004). LTP and LTD: an embarrassment of riches. *Neuron* 44, 5–21.

Marr, D. (1971). Simple memory: a theory for archicortex. *Philos. Trans. R. Soc. Lond., B, Biol. Sci.* 262, 23–81.

Martin, S. J., Greenwood, P. D., and Morris, R. G. (2000). Synaptic plasticity and memory: an evaluation of the hypothesis. *Annu. Rev. Neurosci.* 23, 649–711.

Maurer, A. P., and McNaughton, B. L. (2007). Network and intrinsic cellular mechanisms underlying theta phase precession of hippocampal neurons. *Trends Neurosci.* 7, 325–333.

McClelland, J. L., McNaughton, B. L., and O'Reilly, R. C. (1995). Why there are complementary learning systems in the hippocampus and cortex: insights from the successes and failures of connectionist models of learning and memory. *Psychol. Rev.* 102, 419–457.

McNaughton, B. L., Battaglia, F. P., Jensen, O., Moser, E. I., and Moser, M.-B. (2006). Path integration and the neural basis of the 'cognitive map'. *Nat. Rev. Neurosci.* 7, 663–678.

Meredith, R. M., Floyer-Lea, A. M., and Paulsen, O. (2003). Maturation of long-term potentiation induction rules in rodent hippocampus: role of GABAergic inhibition. *J. Neurosci.* 23, 11142–11146.

Miles, R. (1990). Synaptic excitation of inhibitory cells by single CA3 pyramidal cells of the guinea pig in vitro. *J. Physiol.* 428, 61–77.

Molter, C., Sato, N., and Yamaguchi, Y. (2007). Reactivation of behavioural activity during sharp waves: a computational model for two stage hippocampal dynamics. *Hippocampus* 17, 201–209.

Mongillo, G., Curti, E., Romani, S., and Amit, D. J. (2005). Learning in realistic networks of spiking neurons and spike-driven plastic synapses. *Eur. J. Neurosci.* 21, 3143–3160.

Morris, R. (2007). "Theories of hippocampal function," in *The Hippocampus Book*, eds P. Andersen, R. Morris, D. Amaral, T. Bliss, and J. O'Keefe (Oxford: Oxford University Press), 581–713.

Morris, R. G., Garrud, P., Rawlins, J. N., and O'Keefe, J. (1982). Place navigation impaired in rats with hippocampal lesions. *Nature* 297, 681–683.

Muller, R. U., Kubie, J. L., and Saypoff, R. (1991). The hippocampus as a cognitive graph (abridged version). *Hippocampus* 1, 243–246.

Neves, G., Cooke, S. F., and Bliss, T. V. P. (2008). Synaptic plasticity, memory and the hippocampus: a neural network approach to causality. *Nat. Rev. Neurosci.* 9, 65–75.

O'Keefe, J. (2007). "Hippocampal neurophysiology in the behaving animal," in *The Hippocampus Book*, eds P. Andersen, R. Morris, D. Amaral, T. Bliss, and J. O'Keefe (Oxford: Oxford University Press), 475–548.

O'Keefe, J., and Dostrovsky, J. (1971). The hippocampus as a spatial map. Preliminary evidence from unit activity in the freely-moving rat. *Brain Res.* 34, 171–175.

O'Keefe, J., and Nadel, L. (1978). *The Hippocampus as a Cognitive Map*. Oxford: Oxford University Press.

O'Keefe, J., and Recce, M. L. (1993). Phase relationship between hippocampal place units and the EEG theta rhythm. *Hippocampus* 3, 317–330.

Pfister, J.-P., and Gerstner, W. (2006). Triplets of spikes in a model of spike timing-dependent plasticity. *J. Neurosci.* 26, 9673–9682.

Pike, F. G., Meredith, R. M., Olding, A. W. A., and Paulsen, O. (1999). Postsynaptic bursting is essential for 'Hebbian' induction of associative long-term potentiation at excitatory synapses in rat hippocampus. *J. Physiol.* 518, 571–576.

Ranck, J. B. (1973). Studies on single neurons in dorsal hippocampal formation and septum in unrestrained rats. I: Behavioural correlates and firing repertoires. *Exp. Neurol.* 41, 461–531.

Rolls, E. T. (2007). An attractor network in the hippocampus: theory and neurophysiology. *Learn. Mem.* 14, 714–731.

Rolls, E. T. (2008). *Memory, Attention and Decision Making*. Oxford: Oxford University Press.

Rolls, E. T., and Kesner, R. P. (2006). A computational theory of hippocampal function, and empirical tests of the theory. *Prog. Neurobiol.* 79, 1–48.

Samura, T., and Hattori, M. (2005). Hippocampal memory modification induced by pattern completion and spike-timing dependent synaptic plasticity. *Int. J. Neural Syst.* 15, 13–22.

Skaggs, W. E., McNaughton, B. L., Wilson, M. A., and Barnes, C. A. (1996). Theta phase precession in hippocampal neuronal populations and the compression of temporal sequences. *Hippocampus* 6, 149–172.

Song, S., and Abbott, L. F. (2001). Cortical development and remapping through spike timing-dependent plasticity. *Neuron* 32, 339–350.

Song, S., Miller, K. D., and Abbott, L. F. (2000). Competitive Hebbian learn-

ing through spike-timing-dependent synaptic plasticity. *Nat. Neurosci.* 3, 919–926.

Vyazovskiy, V. V., Cirelli, C., Pfister-Genskow, M., Faraguna, U., and Tononi, G. (2008). Molecular and electrophysiological evidence for net synaptic potentiation in wake and depression in sleep. *Nat. Neurosci.* 11, 200–208.

Wagatsuma, H., and Yamaguchi, Y. (2007). Neural dynamics of the cognitive map in the hippocampus. *Cogn. Neurodyn.* 1, 119–141.

Wang, H. X., Gerkin, R. C., Nauen, D. W., and Bi, G.-Q. (2005). Coactivation and timing-dependent integration of synaptic potentiation and depression. *Nat. Neurosci.* 8, 187–193.

Wittenberg, G. M., and Wang, S.-S. H. (2006). Malleability of spike-timing-dependent plasticity at the CA3-CA1 synapse. *J. Neurosci.* 26, 6610–6617.

Conflict of Interest Statement: The authors declare that the research was conducted in the absence of any commercial or financial relationships that could be construed as a potential conflict of interest.

Received: 17 February 2010; accepted: 24 September 2010; published: 15 October 2010.

Citation: Bush D, Philippides A, Husbands P and O'Shea M (2010) Spike-timing dependent plasticity and the cognitive map. Front. Comput. Neurosci. ***4****:142. doi: 10.3389/fncom.2010.00142*

frontiers in
COMPUTATIONAL NEUROSCIENCE

ORIGINAL RESEARCH ARTICLE
published: 03 December 2010
doi: 10.3389/fncom.2010.00143

STDP in adaptive neurons gives close-to-optimal information transmission

Guillaume Hennequin[1]*, Wulfram Gerstner[1] and Jean-Pascal Pfister[2]

[1] *School of Computer and Communication Sciences, Brain-Mind Institute, Ecole Polytechnique Fédérale de Lausanne, Lausanne, Switzerland*
[2] *Department of Engineering, University of Cambridge, Cambridge, UK*

Edited by:
Per Jesper Sjöström, University College London, UK

Reviewed by:
Walter Senn, University of Bern, Switzerland
Rasmus S. Petersen, University of Manchester, UK
Abigail Morrison, Albert-Ludwig University Freiburg, Germany

****Correspondence:***
Guillaume Hennequin, Laboratory of Computational Neuroscience, Ecole Polytechnique Fédérale de Lausanne, Station 15, CH-1015 Lausanne, Switzerland.
e-mail: guillaume.hennequin@epfl.ch

Spike-frequency adaptation is known to enhance the transmission of information in sensory spiking neurons by rescaling the dynamic range for input processing, matching it to the temporal statistics of the sensory stimulus. Achieving maximal information transmission has also been recently postulated as a role for spike-timing-dependent plasticity (STDP). However, the link between optimal plasticity and STDP in cortex remains loose, as does the relationship between STDP and adaptation processes. We investigate how STDP, as described by recent minimal models derived from experimental data, influences the quality of information transmission in an adapting neuron. We show that a phenomenological model based on triplets of spikes yields almost the same information rate as an optimal model specially designed to this end. In contrast, the standard pair-based model of STDP does not improve information transmission as much. This result holds not only for additive STDP with hard weight bounds, known to produce bimodal distributions of synaptic weights, but also for weight-dependent STDP in the context of unimodal but skewed weight distributions. We analyze the similarities between the triplet model and the optimal learning rule, and find that the triplet effect is an important feature of the optimal model when the neuron is adaptive. If STDP is optimized for information transmission, it must take into account the dynamical properties of the postsynaptic cell, which might explain the target-cell specificity of STDP. In particular, it accounts for the differences found *in vitro* between STDP at excitatory synapses onto principal cells and those onto fast-spiking interneurons.

Keywords: STDP, plasticity, spike-frequency adaptation, information theory, optimality

INTRODUCTION

The experimental discovery of spike-timing-dependent plasticity (STDP) in the mid-nineties (Bell et al., 1997; Magee and Johnston, 1997; Markram et al., 1997; Bi and Poo, 1998; Zhang et al., 1998) led to two questions, in particular. The first is: what is the simplest way of describing this complex phenomenon? This question has been answered in a couple of minimal models (phenomenological approach) whereby long-term potentiation (LTP) and long-term depression (LTD) are reduced to the behavior of a small number of variables (Gerstner et al., 1996; Kempter et al., 1999; Song et al., 2000; van Rossum et al., 2000; Rubin et al., 2001; Gerstner and Kistler, 2002a; Froemke et al., 2006; Pfister and Gerstner, 2006; Clopath et al., 2010; see Morrison et al., 2008 for a review). Because they are inspired by *in vitro* plasticity experiments, the state variables usually depend solely on what is experimentally controlled, i.e., on spike times and possibly on the postsynaptic membrane potential. They are computationally cheap enough to be used in large-scale simulations (Morrison et al., 2007; Izhikevich and Edelman, 2008). The second question has to do with the functional role of STDP: what is STDP good for? The minimal models mentioned above can address this question only indirectly, by solving the dynamical equation of synaptic plasticity for input with given stationary properties (Kempter et al., 1999; van Rossum et al., 2000; Rubin et al., 2001). An alternative approach is to postulate a role for synaptic plasticity, and formulate it in the mathematical framework of optimization ("top-down approach"). Thus, in artificial neural networks, Hebbian-like learning rules were shown to arise from unsupervised learning paradigms such as principal components analysis (Oja, 1982, 1989), independent components analysis (ICA; Intrator and Cooper, 1992; Bell and Sejnowski, 1995; Clopath et al., 2008), maximization of mutual information (MI; Linsker, 1989), sparse coding (Olshausen and Field, 1996; Smith and Lewicki, 2006), and predictive coding (Rao and Ballard, 1999). In spiking neurons, local STDP-like learning rules were obtained from optimization criteria such as maximization of information transmission (Chechik, 2003; Toyoizumi et al., 2005, 2007), information bottleneck (Klampfl et al., 2009), maximization of the neuron's sensitivity to the input (Bell and Parra, 2005), reduction of the conditional entropy (Bohte and Mozer, 2007), slow-feature analysis (Sprekeler et al., 2007), and maximization of the expected reward (Xie and Seung, 2004; Pfister et al., 2006; Florian, 2007; Sprekeler et al., 2009).

The functional consequences of STDP have mainly been investigated in simple integrate-and-fire neurons, where the range of temporal dependencies in the postsynaptic spike train spans no more than the membrane time constant. Few studies have addressed the question of the synergy between STDP and more complex dynamical properties on different timescales. In Seung (2003), more complex dynamics were introduced not at the cell level, but through short-term plasticity of the synapses. The postsynaptic neuron was then able to become selective to temporal order in the input. Another elegant approach to this question was taken in Lengyel et al. (2005) in a model of hippocampal autoassociative memory. Memories were

encoded in the phase of firing of a population of neurons relative to an ongoing theta oscillation. Under the assumption that memories are stored using a classical form of STDP, they derived the form of the postsynaptic dynamics that would optimally achieve their recall. This turned out to match what they recorded *in vitro*, suggesting that STDP might optimally interact with the dynamical properties of the postsynaptic cell in this memory storage task.

More generally, optimality models are ideally suited to study plasticity and dynamics together. Indeed, optimal learning rules contain an explicit reference to the dynamical properties of the postsynaptic cell, by means of the transfer function that maps input to output values. This function usually appears in the formulation of a gradient ascent on the objective function. In this article, we exploit this in order to relate STDP to spike-frequency adaptation (SFA), an important feature of the dynamics of a number of cell types found in cortex. Recent phenomenological models of STDP have emphasized the importance of the interaction between postsynaptic spikes in the LTP process (Senn et al., 2001; Pfister and Gerstner, 2006; Clopath et al., 2010). In these models, the amount of LTP obtained from a pre-before-post spike pair increases with the number of postsynaptic spikes fired in the recent past, which we call the "triplet effect" (combination of one pre-spike and at least two post-spikes). The timescale of this post–post interaction was fitted to *in vitro* STDP experiments, and found to be very close to that of adaptation (100–150 ms).

We reason that STDP may be ideally tuned to SFA of the postsynaptic cell. We specifically study this idea within the framework of optimal information transmission (infomax) between input and output spike trains. We compare the performance of a learning rule derived from the infomax principle in Toyoizumi et al. (2005), to that of the triplet model developed in Pfister and Gerstner (2006). We also compare them to the standard pair-based learning window used in most STDP papers. Performance is measured in terms of information theoretic quantities. We find that the triplet learning rule yields a better performance than pair-STDP on a spatio-temporal receptive field formation task, and that this advantage crucially depends on the presence of postsynaptic SFA. This reflects a synergy between the triplet effect and adaptation. The reasons for this optimality are further studied by showing that the optimal model features a similar triplet effect when the postsynaptic neuron adapts. We also show that both the optimal and triplet learning rules increase the variability of the postsynaptic spike trains, and enlarge the frequency band in which signals are transmitted, extending it toward lower frequencies (1–5 Hz). Finally, we exploit the optimal model to predict the form of the STDP mechanism for two different target cell types. The results qualitatively agree with the *in vitro* data reported for excitatory synapses onto principal cells and those onto fast-spiking (FS) inhibitory interneurons. In the model, the learning windows are different because the intrinsic dynamical properties of the two postsynaptic cell types are different. This might be the functional reason for the target-cell specificity of STDP.

MATERIALS AND METHODS

NEURON MODEL

We simulate a single stochastic point neuron (Gerstner and Kistler, 2002b) and a small portion of its incoming synapses ($N = 1$ for the simulation of *in vitro* experiments, $N = 100$ in the rest of the paper). Each postsynaptic potential (PSP) adds up linearly to form the total modeled synaptic drive

$$u(t) = \sum_{j=1}^{N} w_j \varepsilon_j(t) \tag{1}$$

with

$$\varepsilon_j(t) = \int_0^t x_j(t') \exp\left(-\frac{t-t'}{\tau_m}\right) dt' \tag{2}$$

where $x_j(t) = \Sigma_{t_j^f} \delta(t - t_j^f)$ denotes the j^{th} input spike train, and w_j (mV) are the synaptic weights. The effect of thousands of other synapses is not modeled explicitly, but treated as background noise. The firing activity of the neuron is entirely described by an instantaneous firing density

$$\rho(t) = g[u(t)]M(t) \tag{3}$$

where

$$g[u] = g_0 + r_0 \log\left[1 + \exp\left(\beta\left(u - u_T\right)\right)\right] \tag{4}$$

is the gain function, drawn in **Figure 1A**. Refractoriness and SFA both modulate the instantaneous firing rate via

$$M(t) = \exp\left[-\left(g_R(t) + g_A(t)\right)\right] \tag{5}$$

The variables g_R and g_A evolve according to

$$\frac{dg_R}{dt} = -\frac{g_R(t)}{\tau_R} + q_R y(t) \quad \text{and} \quad \frac{dg_A}{dt} = -\frac{g_A(t)}{\tau_A} + q_A y(t) \tag{6}$$

where $y(t) = \Sigma_{t_{\text{post}}^f} \delta(t - t_{\text{post}}^f)$ is the postsynaptic spike train and $0 < \tau_R \ll \tau_A$ are the time constants of refractoriness and adaptation respectively. The firing rate thus becomes a compressive function of the average gain, as shown in **Figure 1B**. The response of the neuron to a step in input firing rate is depicted in **Figure 1C**.

For the simulation of *in vitro* STDP experiments, only one synapse is investigated. The potential u is thus given a baseline u_b (to which the PSP of the single synapse will add) such that $g(u_b)$ yields a spontaneous firing rate of 7.5 Hz (**Figure 1B**).

In some of our simulations, postsynaptic SFA is switched off ($q_A = 0$). In order to preserve the same average firing rate given the same synaptic weights, r_0 is rescaled accordingly (**Figures 1A,B**, dashed lines).

In the simulation of **Figure 8**, we add a third variable g_B in the after-spike kernel M in order to model a FS inhibitory interneuron. This variable jumps down ($q_B < 0$) following every postsynaptic spike, and decays exponentially with time constant τ_B (with $\tau_R \ll \tau_B < \tau_A$).

All simulations were written in Objective Caml and run on a standard desktop computer operated by Linux. We used simple Euler integration of all differential equations, with 1 ms time resolution (0.1 ms for the simulation of *in vitro* experiments). All parameters are listed in **Table 1** together with their values.

PRESYNAPTIC FIRING STATISTICS

To analyze the evolution of information transmission under different plasticity learning rules, we consider $N = 100$ periodic input spike of 5 s duration generated once and for all (see below). This "frozen noise" is then replayed continuously, feeding the postsynaptic neuron for as long as is necessary (e.g., for learning, or for MI estimation).

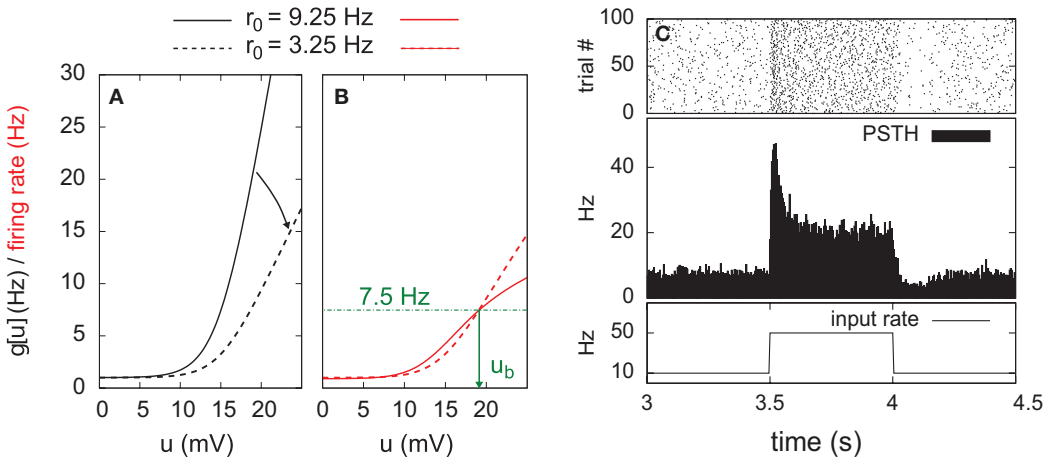

FIGURE 1 | Stochastic neuron model. (A) The gain function $g(u)$ (Eq. 4, solid line here) shows the momentary rate of a non-refractory neuron as a function of the membrane potential u. **(B)** The mean rate $\langle g[u(t)]M(t)\rangle$ of a neuron with refractoriness and adaptation is lower (solid red line). The baseline potential u_b used in the simulation is defined as the membrane potential that yields a spontaneous firing rate of 7.5 Hz (green arrow and dashed line). In some simulations, we need to switch off adaptation, but we want the same holding potential u_b to evoke the same 7.5 Hz output firing rate. The slope r_0 of the gain function is therefore rescaled (**A**, dashed curve) so that the frequency curves in the adaptation and no-adaptation cases (**B**, solid and dashed red curves) cross at $u = u_b$. **(C)** Example response property of an adaptive neuron. A single neuron receives synaptic inputs from 100 Poisson spike trains with a time-varying rate. The experiment is repeated 1000 times independently. Bottom: the input rate jumps from 10 to 50 Hz, stays there for half a second and returns back to 10 Hz (bottom). Middle: Peri-stimulus time histogram (PSTH, 4 ms bin). Top: example spike trains (first 100 trials).

Table 1 | Baseline values of all parameters defined in the text.

Neuron model		Optimal rule		Triplet rule		Pair rule		Weight bounds	
τ_m	20 ms	η_o	0.04	η_3	1.0	η_2	1.0	w_{min}	0 mV
g_0	1 Hz **(35)**	τ_C	20 ms	τ_+	16.8 ms	τ_+	16.8 ms	w_{max}	4 mV
r_0	9.25 Hz *(3.25)*	τ_g	10 s	τ_-	33.7 ms	τ_-	33.7 ms	a	9
β	0.5 mV^{-1}	γ	1 **(0)**	τ_y	114 ms				
u_T	15 mV	g_{targ}	*ad hoc*	$\tilde{A}_2^-$	2.8×10^{-3}	$\tilde{A}_2^-$	2.8×10^{-3}		
τ_R	2 ms	λ	0.0094	A_3^+	6.5×10^{-3}	A_2^+	5.6×10^{-3}		
τ_A	150 ms			ρ_{targ}	*ad hoc*	ρ_{targ}	*ad hoc*		
q_R	100			τ_ρ	10 s	τ_ρ	10 s		
q_A	1 *(0)*								

Some parameters were set to different values when the neuron was non-adapting (italic numbers). Similarly, some parameters were different for the simulations of in vitro experiment (bold faces).

To generate the time-varying rates of the N processes underlying this frozen noise, we first draw point events at a constant Poisson rate of 10 Hz, and then smooth them with a Gaussian kernel of width 150 ms. Rates are further multiplicatively normalized so that each presynaptic neuron fires an average of 10 spikes per second. We emphasize that this process describes the statistics of the inputs *across different learning experiments*. When we mention "independent trials," we mean a set of experiments which have their own independent realizations of those input spike trains. However, in one learning experiment, a single such set of N input spike trains is chosen and replayed continuously as input to the postsynaptic neuron. The input is therefore deterministic and periodic. When the periodic input is generated, some neurons can happen to fire at some point during those 5 s within a few milliseconds of each other, and by virtue of the periodicity, these synchronous firing events will repeat in each period, giving rise to strong spatio-temporal correlations in the inputs. We are interested in seeing how different learning rules can exploit this correlational structure to improve the information carried by the postsynaptic activity about those presynaptic spike trains. We now describe what we mean by information transmission under this specific stimulation scenario.

INFORMATION THEORETIC MEASUREMENTS

The neuron can be seen as a noisy communication channel in which multidimensional signals are compressed and distorted before being transmitted to subsequent receivers. The goodness of a communication channel is traditionally measured by Shannon's MI between the input and output variables, where the input is chosen randomly from some "alphabet" or vocabulary of symbols.

Here, the input is deterministic and periodic (**Figure 2A**). We therefore define the quality of information transmission by the reduction of uncertainty about the phase of the current input if we observe a certain output spike train at an unknown time. In discrete time (with time bin $\Delta = 1$ ms), there are only $N_\phi = 5000$ possible phases since the input has a period of 5 s. Therefore, the maximum number of bits that the noisy postsynaptic neuron can transmit is $\log_2(N_\phi) \simeq 12.3$ bits. We further assume that an observer of the output neuron can only see "words" corresponding to spike trains of finite duration $T = K\Delta$. We assume $T = 1$ s for most of the paper, which corresponds to $K = 1000$ time bins. This choice is justified below.

The discretized output spike trains of size K (binary vectors), called $\mathbf{Y^K}$, can be observed at random times and play the role of the output variable. The input random variable is the phase ϕ of the input. The quality of information transmission is quantified by the MI, i.e., the difference between the total response entropy $H(\mathbf{Y^K}) = \left\langle \log_2 P(\mathbf{Y^K}) \right\rangle_{\mathbf{Y^K}}$ and the noise entropy $H\left(\mathbf{Y^K} \mid \phi\right) = \left\langle \left\langle \log_2 P(\mathbf{Y^K} \mid \phi) \right\rangle_{\mathbf{Y^K}\mid\phi} \right\rangle_\phi$. Here $\langle\cdot\rangle$ denotes the ensemble average. In order to compute these entropies, we need to be able to estimate the probability of occurrence of any sample word Y^K, knowing and not knowing the phase. To do so, a large amount of data is first generated. The noisy neuron is fed continuously for a large number of periods $N_p = 100$ with a single periodic set of input spike trains and a fixed set of synaptic weights. The output spikes are recorded with $\Delta = 1$ ms precision. From this very long output spike train, we randomly pick words of length K and gather them in a set $\mathcal{S}$. We take $|\mathcal{S}| = 1000$. This is our sample data.

In general, estimating the probability of a random binary vector of size K is very difficult if K is large. Luckily, we have a statistical model for how spike trains are generated (Eq. 3), which considerably reduces the amount of data needed to produce a good estimate. Specifically, if the refractory state of the neuron $[g_R(t), g_A(t)]$ is known at time t (initial conditions), then the probability $1 - \exp(-\rho_k\Delta) \simeq \rho_k\Delta$ of the postsynaptic neuron spiking is also known for each of the K time bins following t (Eqs 3–5). The neuron model gives us the probability that a word Y^K occurred at time t – not necessarily the time at which the word was actually picked – (Toyoizumi et al., 2005):

$$P\left(Y^K \mid t, g_R(t), g_A(t)\right) = \exp\left[\sum_{k=1}^{K} Y_k^K \log\left(\rho_k\Delta\right) + \left(1 - Y_k^K\right)\log\left(1-\rho_k\Delta\right)\right] \quad (7)$$

where $\rho_k = \rho(t + k\Delta)$ and Y_k^K is one if there is a spike in the word at position k, and 0 otherwise. To compute the conditional probability of occurrence of a word Y^K knowing the phase ϕ, we have to further average Eq. 7:

$$P(Y^K \mid \phi) = \left\langle P(Y^K \mid t) \right\rangle_{t \text{ with } \Phi(t)=\phi} \quad (8)$$

where $\Phi(t) = 1 + (t \bmod N_\phi)$ denotes the phase at time t. Averaging over multiple times with same phase also averages over the initial conditions $[g_R(t), g_A(t)]$, so that they do not appear in Eq. 8. The average in Eq. 8 is estimated using a set of 10 randomly chosen times t_i with $\Phi(t_i) = \phi$.

The full probability of observing a word Y^K is given by $P(Y^K) = 1/N_\phi \, \Sigma_{\phi=1}^{N_\phi} P(Y^K \mid \phi)$ where $P(Y^K \mid \phi)$ is computed as described above. Owing to the knowledge of the model that underlies spike generation, and to this huge averaging over all the possible phases, the obtained $P(Y^K)$ is a very good estimate of the true density. We can then take a Monte-Carlo approach to estimate the entropies, using the set $\mathcal{S}$ of randomly picked words: $H(\mathbf{Y^K}) = -\Sigma_{Y^K} P(Y^K)\log_2 P(Y^K)$ can be estimated by

$$\hat{H}(\mathbf{Y^K}) = -\frac{1}{|\mathcal{S}|}\sum_{Y^K \in \mathcal{S}} \log_2 P\left(Y^K\right) \quad (9)$$

and $H\left(\mathbf{Y^K} \mid \phi\right) = -\sum_\phi P(\phi) \sum_{Y^K} P\left(Y^K\right) \frac{P\left(Y^K \mid \phi\right)}{P\left(Y^K\right)} \log_2 P\left(Y^K \mid \phi\right)$ is estimated using

$$\hat{H}\left(\mathbf{Y^K} \mid \phi\right) = -\frac{1}{N_\phi}\sum_{\phi=1}^{N_\phi} \frac{1}{|\mathcal{S}|} \sum_{Y^K \in \mathcal{S}} \frac{P\left(Y^K \mid \phi\right)}{P\left(Y^K\right)} \log_2 P\left(Y^K \mid \phi\right) \quad (10)$$

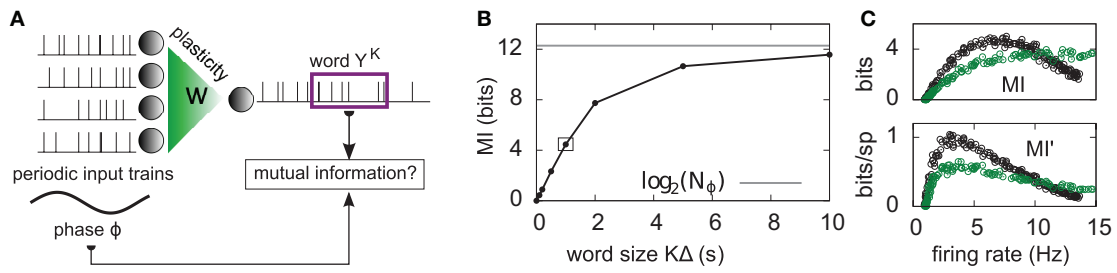

FIGURE 2 | Information transmission through a noisy postsynaptic neuron. **(A)** Schematic representation of the feed-forward network. Five-second input spike trains repeat continuously in time (periodic input) and drive a noisy and possibly adapting output neuron via plastic synapses. It is assumed that an observer of the output spike train has access to portions Y^K of it, called "words," of duration $T = K\Delta$. The observer does not have access to a clock, and therefore has a flat prior expectation over possible phases before observing a word. The goodness of the system, given a set of synaptic weights **w**, is measured by the reduction of uncertainty about the phase, gained from the observation of an output word Y^K (mutual information, see text). **(B)** For a random set of synaptic weights (20 weights at 4 mV, the rest at 0), the mutual information (MI) is reported as a function of the output word size $K\Delta$. Asymptotically, the MI converges to the theoretical limit given by $\log_2(N_\phi)$ (12.3 bits. In the rest of this study, 1-s output words are considered (square). **(C)** Mutual information (MI, top) and information per spike (MI', bottom) as a function of the average firing rate. Black: with SFA. Green: without SFA. Each dot is obtained by setting a fraction of randomly chosen synaptic efficacies to the upper bound (4 mV) and the rest to 0. The higher the fraction of non-zero weights, the higher the firing rate. The information per spike is a relevant quantity because spike generation costs energy.

The MI estimate is the difference of these two entropies, and is expressed in bits. In **Figure 2C**, we introduce the information per spike MI' (bits/spike), obtained by dividing the MI by the expected number of spikes in a window of duration $K\Delta$. **Figure 2B** shows that the MI approaches its upper bound $\log_2(N_\phi)$ as the word size increases. The word size considered here (1 s) is large enough to capture the effects of SFA while being small enough not to saturate the bound.

Although we constrain the postsynaptic firing rate to lie around a fixed value ρ_{targ} (see homeostasis in the next section), the rate will always jitter. Even a small jitter of less than 0.5 Hz (which we have in the present case) makes it impossible to directly compare entropies across learning rules. Indeed, while the MI depends only weakly on small deviations of the firing rate around ρ_{targ}, the response and noise entropies have much larger (co-) variations. In order to compare the entropies across learning rules, we need to know what the entropy would have been if the rate was exactly ρ_{targ} instead of $\rho_{\text{targ}} + \varepsilon$. We therefore compute the entropy [$H(\mathbf{Y}^K)$ or $H(\mathbf{Y}^K|\phi)$] for different firing rates in the vicinity of ρ_{targ}. These firing rates are achieved by slightly rescaling the synaptic weights, i.e., $w_{ij} \leftarrow \kappa w_{ij}$ where κ takes several values around 1. We then fit a linear model $H = a\rho + b$, and evaluate H at ρ_{targ}.

The computation of the conditional probabilities $P(Y^K|\phi)$ was accelerated on an ATI Radeon (HD 4850) graphics processing unit (GPU), which was 130 times faster than a decent CPU implementation.

LEARNING RULES

Optimal learning rule

The optimal learning rule aims at maximizing information transmission under some metabolic constraints ("infomax" principle). Toyoizumi et al. (2005, 2007) showed that this can be achieved by means of a stochastic gradient ascent on the following objective function

$$\mathbb{L} = \mathbb{I} - \gamma\mathbb{D} - \lambda\Psi \tag{11}$$

whereby the mutual information $\mathbb{I}$ between input and output spike trains competes with a homeostatic constraint on the mean firing rate $\mathbb{D}$ and a metabolic penalty Ψ for strong weights that are often active. The first constraint is formulated as $\mathbb{D} = \text{KL}\left[P(\mathbf{Y}^K), \tilde{P}(\mathbf{Y}^K)\right]$ where KL denotes the Kullback–Leibler (KL) divergence. P denotes the true probability distribution of output spike trains produced by the stochastic neuron model, while $\tilde{P}$ assumes a similar model in which the gain $g(t)$ is kept constant at a target gain g_{targ}. Minimizing the divergence between P and $\tilde{P}$ therefore means driving the average gain close to g_{targ}, thus implementing firing rate homeostasis. The second constraint reads $\Psi = \Sigma_j w_j \langle n_j \rangle_{\mathbf{X}_K}$, whereby the cost for synapse j is proportional to its weight w_j and to the average number n_j of presynaptic spikes relayed during the K time bins under consideration. The Lagrange multipliers γ and λ set the relative importance of the three objectives.

Performing gradient ascent on $\mathbb{L}$ yields the following online learning rule (Toyoizumi et al., 2005, 2007):

$$\frac{dw_j}{dt} = \eta_o\left[C_j(t)B_{\text{post}}(t) - \lambda x_j(t)\right] \tag{12}$$

where

$$C_j(t) = \int_0^t dt' \exp\left(-\frac{t-t'}{\tau_C}\right)\varepsilon_j(t')\frac{g'[u(t')]}{g[u(t')]}\left[y(t') - g[u(t')]M(t')\right] \tag{13}$$

and

$$B_{\text{post}}(t) = y(t)\log\left[\frac{g[u(t)]}{\overline{g}}\left(\frac{g_{\text{targ}}}{\overline{g}}\right)^\gamma\right] - M(t)\left[g[u(t)] - \overline{g} + \gamma\left(g_{\text{targ}} - \overline{g}\right)\right] \tag{14}$$

η_o is a small learning rate. The first term C_j is Hebbian in the sense that it reflects the correlations between the input and output spike trains. B_{post} is purely postsynaptic: it compares the instantaneous gain g to its average $\overline{g}$ (information term), as well as the average gain to its target value g_{targ} (homeostasis). The average $\overline{g}$ is estimated online by a low pass filter of g with time constant τ_g. The time course of these quantities is shown in **Figure 3A** for example spike trains of 1 s duration, for $\gamma = 0$.

Because of the competition between the three objectives in Eq. 11, the homeostatic constraint does not yield the exact desired gain g_{targ}. In practice, we set the value of g_{targ} empirically, such that the actual mean firing rate approaches the desired value.

Finally, we use τ_C, η_o, and λ as three free parameters to fit the results of *in vitro* STDP pairing experiments (**Figure 8**). τ_C is set empirically equal to the membrane time constant $\tau_m = 20$ ms, while η_o and λ are determined through a least-squares fit of the experimental data. The learning rate η_o can be rescaled arbitrarily. In the simulations of receptive-field development (**Figures 4–6**), λ is set to 0 so as not to perturb unnecessarily the prime objective of maximizing information transmission. It is also possible to remove the homeostasis constraint ($\gamma = 0$) in the presence of SFA. As can be seen in **Figure 2C**, the MI has a maximum at 7.5 Hz when the neuron adapts, so that firing rate control comes for free in the information maximization objective. We therefore set $\gamma = 0$ when the neuron adapts, and $\gamma = 1$ when is does not. In fact, the homeostasis constraint only slightly impairs the infomax objective: we have checked that the MI reached after learning (**Figures 4 and 5**) does not vary by more than 0.1 bit when γ takes values as large as 20.

Triplet-based learning rule

We use the minimal model developed in Pfister and Gerstner (2006) with "all-to-all" spike interactions. Presynaptic spikes at synapse j leave a trace r_j (**Figure 3B**) which jumps by 1 after each spike and otherwise decays exponentially with time constant τ_+. Similarly, the postsynaptic spikes leave two traces, o_1 and o_2, which jump by 1 after each postsynaptic spike and decay exponentially with time constants τ_- and τ_y respectively:

$$\frac{dr_j}{dt} = -\frac{r_j}{\tau_+} + x_j(t) \qquad \frac{do_1}{dt} = -\frac{o_1}{\tau_-} + y(t) \qquad \frac{do_2}{dt} = -\frac{o_2}{\tau_y} + y(t) \tag{15}$$

where $x_j(t)$ and $y(t)$ are sums of δ-functions at each firing time as introduced above. The synaptic weight w_j undergoes LTD proportionally to o_1 after each presynaptic spike, and LTP proportionally to $r_j o_2$ following each postsynaptic spike:

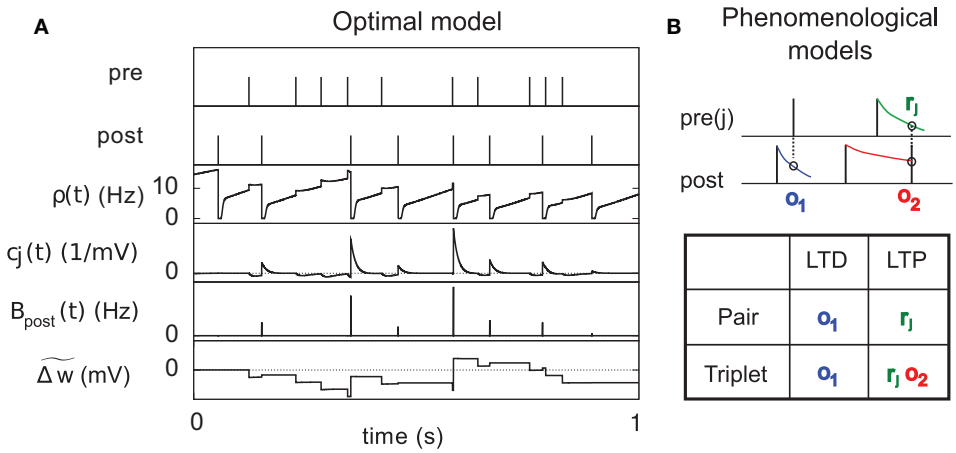

FIGURE 3 | Description of the three learning rules. (A) Time course of the variables involved in the optimal model. $\widetilde{\Delta w}$ denotes the cumulative weight change. **(B)** Schematic representation of the phenomenological models of STDP used in this paper. Each presynaptic spike yields LTD proportionally to o_1 (blue trace) in both models (pair and triplet). In the pair model, postsynaptic spikes evoke LTP proportionally to r_j (green trace), while in the triplet model r_j is combined with an additional postsynaptic trace o_2 (red).

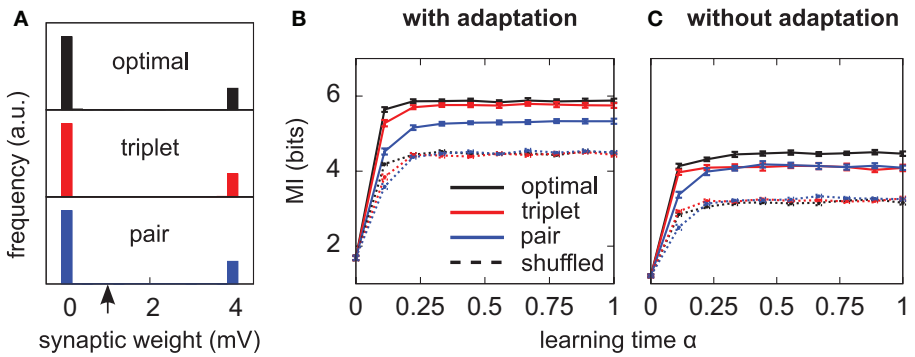

FIGURE 4 | Triplets are better than pairs when the neuron adapts. **(A)** Distributions of synaptic efficacies obtained after learning. The weights were all initialized at 1 mV before learning (black arrow). When SFA is switched off, the very same bimodal distributions emerge (not shown). **(B)** Evolution of the MI along learning time. Learning time is arbitrarily indexed from $0 < \alpha < 1$. The dashed curves represent the MI when the weights taken from the momentary distribution at time α are shuffled. Each point is obtained from averaging the MI over 10 different shuffled versions of the synaptic weights. Error bars denote standard error of the mean (SEM) over 10 independent learning episodes with different input spike trains. **(C)** Same as in **(B)**, but SFA is switched off. The *y*-scale is the same as in **(B)**. Parameters for those simulations were $\lambda = 0$, $\gamma = 0$ with SFA, and $\gamma = 1$ without SFA. Other parameters took the values given in **Table 1**.

$$\frac{dw_j}{dt} = \eta_3 \left[A_3^+ r_j(t) o_2(t-\varepsilon) y(t) - A_2^- o_1(t) x_j(t) \right] \tag{16}$$

where η_3 denotes the learning rate. Note that o_2 is taken just before its update. Under the assumption that pre- and postsynaptic spike trains are independent Poisson processes with rates ρ_x and ρ_y respectively, the average weight change was shown in Pfister and Gerstner (2006) to be proportional to

$$\langle \Delta w \rangle \propto \rho_x \rho_y \left(\rho_y - \frac{\tau_- A_2^-}{\tau_+ \tau_y A_3^+} \right) \tag{17}$$

The rule is thus structurally similar to a Bienenstock–Cooper–Munro (BCM) learning rule (Bienenstock et al., 1982) since it is linear in the presynaptic firing rates and non-linear in the postsynaptic rate. It is possible to roughly stabilize the postsynaptic firing rate at a target value ρ_{targ}, by having A_2^- slide in an activity-dependent manner:

$$A_2^-(t) = \tilde{A}_2^- \frac{\bar{\rho}^3(t)}{\rho_{targ}^3} \tag{18}$$

where $\tilde{A}_2^-$ is a starting value and $\bar{\rho}$ is an average of the instantaneous firing rate on the timescale of seconds or minutes (time constant τ_ρ). Finally, A_3^+ is set to make ρ_{targ} an initial fixed point of the dynamics in Eq. 17:

$$A_3^+ = \frac{\tau_- \tilde{A}_2^-}{\rho_{targ} \tau_+ \tau_y} \tag{19}$$

The postsynaptic rate should therefore roughly remain equal to its starting value ρ_{targ}. In practice, the Poisson assumption is not valid because of adaptation and refractoriness, and independence becomes violated as learning operates. This causes the postsynaptic firing rate to deviate and stabilize slightly away from the target ρ_{targ}. We therefore always set ρ_{targ} empirically so that the firing rate stabilizes to the true desired target.

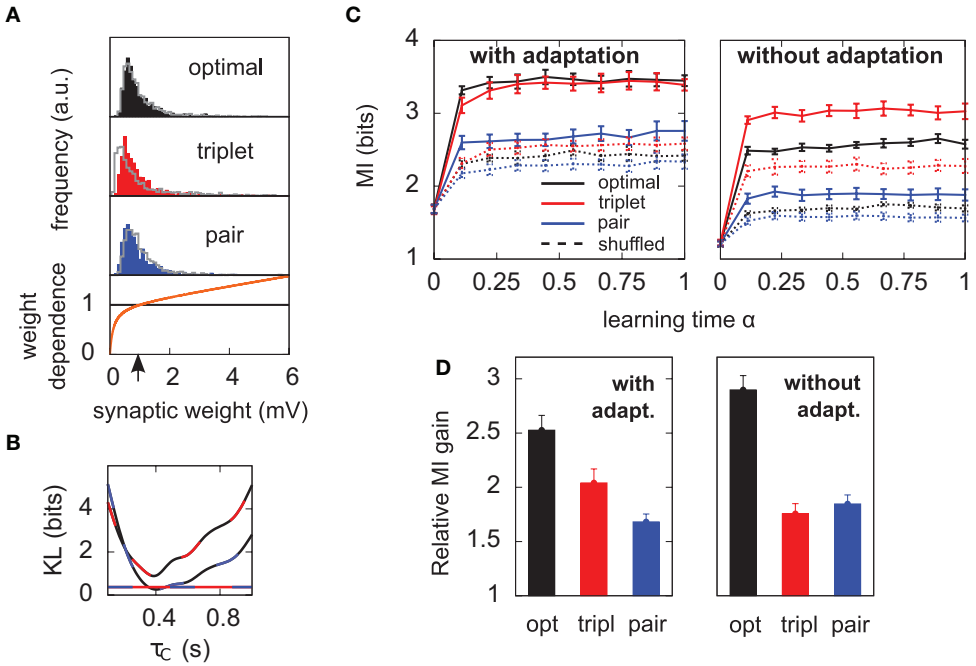

FIGURE 5 | Results hold for "soft-bounded" STDP. The experiments of **Figure 4** are repeated with soft-bounds on the synaptic weights (see Materials and Methods). **(A)** Bottom: LTP is weight-independent (black line), whereas the amount of LTD required by each learning rule ($\Delta w < 0$) is modulated by a growing function of the momentary weight value (orange curve). The LTP and LTD curves cross at $w_0 = 1$ mV, which is also the initial value of the weights in our simulations. Top: this form of weight dependence produces unimodal but skewed distributions of synaptic weights after learning, for all three learning rules. The learning paradigm is the same as in **Figure 4**. Gray lines denote the weight distributions when adaptation is switched off. Note that histograms are computed by binning all weight values from all learning experiments, but the distributions look similar on individual experiments. In these simulations $\lambda = 0$, $a = 9$, and $\tau_c = 0.4$ s. **(B)** The parameter τ_c of the optimal learning rule has been chosen such that the weight distribution after learning stays as close as possible to that of the pair and triplet models. $\tau_c = 0.4$ s minimizes the KL divergences between the distribution obtained from the optimal model and those from the pair (black-blue) and triplet (black-red) learning rules. The distance is then nearly as small as the triplet-pair distance (red-blue). **(C)** MI along learning time in this weight-dependent STDP scenario (cf. **Figures 4B,C**). **(D)** Normalized information gain (see text for definition).

Pair-based learning rule

We use a pair-based STDP rule structurally similar to the triplet rule described by Eq. 16 (**Figure 3B**). The mechanism for LTD is identical, but LTP does not take into account previous postsynaptic firing:

$$\frac{dw_j}{dt} = \eta_2 \left[A_2^+ r_j(t) y(t) - A_2^- o_1(t) x_j(t) \right] \tag{20}$$

where η_2 is the learning rate. A_2^- also slides in an activity-dependent manner according to Eq. 18, to help stabilizing the output firing rate at a target ρ_{targ}. A_2^+ is set such that LTD initially balances LTP, i.e.,

$$A_2^+ = \frac{\tilde{A}_2^- \tau_-}{\tau_+} \tag{21}$$

Comparing learning rules in a fair way requires making sure that their learning rates are equivalent. Since the two rules share the same LTD mechanism, we can simply take the same value for $\tilde{A}_2^-$ as well as $\eta_2 = \eta_3$. Since LTD is dynamically regulated to balance LTP on average in both rules, this ensures that they also share the same LTP rate.

Weight bounds

In order to prevent the weights from becoming negative or from growing too large, we set hard bounds on the synaptic efficacies for all three learning rules, when not stated otherwise. That is, if the learning rule requires a weight change Δw_j, w_j is set to

$$w_j \leftarrow \min\left[w_{\max}, \max\left(0, w_j + \Delta w_j\right) \right] \tag{22}$$

This type of bounds, in which the weight change is independent of the initial synaptic weight itself, is known to yield bimodal distributions of synaptic efficacies. In the simulation of **Figure 5**, we also consider the following soft bounds to extend the validity of our results to unimodal distributions of weights:

$$\text{if } \Delta w_j \geq 0 \quad \text{then} \quad w_j \leftarrow w_j + \Delta w_j$$

$$\text{if } \Delta w_j < 0 \quad \text{then} \quad w_j \leftarrow w_j + \left[1 - \frac{1}{1 + a\dfrac{w_j}{w_0}} + \left(\frac{1}{1+a} \right) \frac{w_j}{w_0} \right] \Delta w_j \tag{23}$$

where a is a free parameter and $w_0 = 1$ mV is the value at which synaptic weights are initialized at the beginning of all learning experiments. This choice of soft-bounds is further motivated in Section "Results." The shapes of the LTP and LTD weight-dependent factors are drawn in **Figure 5A**, for $a = 9$. Note that the LTD and LTP factors cross at w_0, which ensures that the balance between LTP and LTD set by Eqs 19 and 21 is initially preserved.

When the soft-bounds are used, the parameter τ_c of the optimal model is adjusted so that the weight distribution obtained with the optimal rule best matches the weight distributions of the

pair and triplet rules. This parameter indeed has an impact on the spread of the weight distribution: the optimal model knows about the generative model that underlies postsynaptic spike generation, and therefore takes optimally the noise into account, as long as τ_C spans no more than the width of the postsynaptic autocorrelation Toyoizumi et al. (2005). If τ_C is equal to this width (about 20 ms), some weights can grow very large (>50 mV), which results in non-realistic weight distributions. Increasing τ_C imposes more detrimental noise such that all weights are kept within reasonable bounds. In order to constrain τ_C in a non-arbitrary way, we ran the learning experiment for several values of τ_C and computed the KL divergences between weight distributions (optimal-triplet, optimal-pair). τ_C is chosen to minimize these, as shown in **Figure 5B**.

SIMULATION OF *IN VITRO* EXPERIMENTS

To obtain the predictions of the optimal model on standard *in vitro* STDP experiments, we compute the weight change of a single synapse ($N = 1$) according to Eq. 12. The effect of the remaining thousands of synapses is concentrated in a large background noise, obtained by adding a $u_b = 19$ mV baseline to the voltage. The gain becomes $g_b = g(u_b) \simeq (\ 21.45$ Hz, which in combination with adaptation and refractoriness would yield a spontaneous firing rate of about 7.5 Hz (see **Figure 1**). Spontaneous firing is artificially blocked, however. Instead, the neuron is forced to fire at precise times as described below.

The standard pairing protocol is made of a series of pre–post spike pairs, the spikes within the same pair being separated by $\Delta s = t_{\text{post}} - t_{\text{pre}}$. Pairs are repeated with some frequency f. The average $\bar{g}$ is taken fixed and equal to g_b, considering that STDP is optimal for *in vivo* conditions such that $\bar{g}$ should not adapt to the statistics of *in vitro* conditions. The homeostasis is turned off ($\gamma = 0$) in order to consider only the effects of the infomax principle.

RESULTS

We study information transmission through a neuron modeled as a noisy communication channel. It receives input spike trains from a hundred plastic excitatory synapses, and stochastically generates output spikes according to an instantaneous firing rate modulated by presynaptic activities. Importantly, the firing rate is also modulated by the neuron's own firing history, in a way that captures the SFA mechanism found in a large number of cortical cell types. We investigate the ability of three different learning rules to enhance information transmission in this framework. The first learning rule is the standard pair-based STDP model, whereby every single pre-before-post (resp. post-before-pre) spike pair yields LTP (resp. LTD) according to a standard double exponential asymmetric window (Bi and Poo, 1998; Song et al., 2000). The second one was developed in Pfister and Gerstner (2006) and is based on triplets of spikes. LTD is obtained similarly to the pair rule, whereas LTP is obtained from pairing a presynaptic spike with two postsynaptic spikes. The third learning rule (Toyoizumi et al., 2005) is derived from the infomax principle, under some metabolic constraints.

TRIPLET-STDP IS BETTER THAN PAIR-STDP WHEN THE NEURON ADAPTS

We assess and compare the performance of each learning rule on a simple spatio-temporal receptive field development task, with $N = 100$ presynaptic neurons converging onto a single postsynaptic cell (**Figure 2A**).

For each presynaptic neuron, a 5-s input spike train is generated once and for all (see Materials and Methods). All presynaptic spike trains are then replayed continuously 5,000 times. All synapses undergo STDP according to one of the three learning rules. Synaptic weights are all initially set to 1 mV, which yields an initial output firing rate of about 7.5 Hz. We set the target firing rate ρ_{targ} of each learning rule such that the output firing rate stays very close to 7.5 Hz. To gather enough statistics, the whole experiment is repeated 10 times independently, each time with different input patterns. All results are therefore reported as mean and standard error of the mean (SEM) over the 10 trials.

All three learning rules developed very similar bimodal distributions of synaptic efficacies (**Figure 4A**), irrespective of the presence or absence of SFA. This is a well known consequence of additive STDP with hard bounds imposed on the synaptic weights (Kempter et al., 1999; Song et al., 2000). The firing rate stabilizes at 7.5 Hz as desired, for all plasticity rules (not shown). In **Figure 4B**, we show the evolution of the MI (solid lines) as a function of learning time. It is computed as described in Section "Materials and Methods," from the postsynaptic activity gathered during 100 periods (500 s). Since we are interested in quantifying the ability of different learning rules to enhance information transmission, we look at the information gain [defined as $\text{MI}(\alpha = 1) - \text{MI}(\alpha = 0)$] rather than the absolute value of the MI after learning. The triplet model reaches 98% of the "optimal" information gain while the pair model reaches 86% of it. Note that we call "optimal" what comes from the optimality model, but it is not necessarily the optimum in the space of solutions, because (i) a stochastic gradient ascent may not always lead to the global maximum, (ii) Toyoizumi et al.'s (2005) optimal learning rule involves a couple of approximations that may result in a sub-optimal algorithm, and (iii) their learning rule does not specifically optimize information transmission for our periodic input scenario, but rather in a more general setting where input spike trains are drawn continuously from a fixed distribution (stationarity).

It is instructive to compare how much information is lost for each learning rule when the synaptic weights are shuffled. Shuffling means that the distribution stays exactly the same, while the detailed assignment of each w_j is randomized. The dashed lines in **Figure 4B** depict the MI under these shuffling conditions. Each point is obtained from averaging the MI over 10 different shuffled versions of the weights. The optimal and triplet model lose respectively 33 and 32% of their information gains, while the pair model loses only 23%. This means that the optimal and triplet learning rules make a better choice in terms of the detailed assignment of each synaptic weight. For the pair learning rule, a larger part of the information gain is a mere side-effect of the weight distribution becoming bimodal. As an aside, we observe that the MI is the same (4.5 bits) in the "shuffled" condition for all three learning rules. This is an indication that we can trust our information comparisons. The result is also compatible with the value found by randomly setting 20 weights to the maximum value and the others to 0 (**Figure 2B**, square mark).

How is adaptation involved in this increased channel capacity? In **Figure 2C**, the MI is plotted as a function of the postsynaptic firing rate, for an adaptive (black dots) and a non-adaptive (gray dots) neuron, irrespective of synaptic plasticity. Each point in the figure is obtained by setting randomly a given fraction χ of synaptic

weights to the upper bound (4 mV), and the rest to 0 mV. The weight distribution stays bimodal, which leaves the neuron in a high information transmission state. χ is varied in order to cover a wide range of firing rates. We see that adaptation enhances information transmission at low firing rates (<10 Hz). The MI has a maximum at 7.5 Hz when the neuron is adapting (black circles). If adaptation is removed, the peak broadens and shifts to about 15 Hz (green circles). If the energetic cost of firing spikes is also taken into account, the best performance is achieved at 3 Hz, whether adaptation is enabled or not. This is illustrated in **Figure 2C** (lower plot) where the information per spike is reported as a function of the firing rate.

Is adaptation beneficial in a general sense only, or does it differentially affect the three learning rules? To answer this question, we have the neuron learn again from the beginning, SFA being switched off. The temporal evolution of the MI for each learning rule is shown in **Figure 4C**. Overall, the MI is lower when the neuron does not adapt (compare **Figure 4B** and **Figure 4C**), which is in agreement with the previous paragraph and **Figure 2C**. Importantly, the triplet model loses its advantage over the pair model when adaptation is removed (compared red and blue lines in **Figure 4C**). This suggests a specific interaction between synaptic plasticity and the intrinsic postsynaptic dynamics in the optimal and triplet models. This is further investigated in later sections.

Finally, the main results of **Figure 4** also hold when the distribution of weights remains unimodal. To achieve unimodal distributions with STDP, the hypothesis of hard-bounded synaptic efficacies must be relaxed. We implemented a form of weight-dependence of the weight change, such that LTP stays independent of the synaptic efficacy, while stronger synapses are depressed more strongly (see Materials and Methods). The weight-dependent factor for LTD had traditionally been modeled as being directly proportional to w_j (e.g., van Rossum et al., 2000), which provides a good fit to the data obtained from cultured hippocampal neurons by Bi and Poo (1998). Morrison et al. (2007) proposed an alternative fit of the same data with a different form of weight-dependence of LTP. Here we use a further alternative (see Materials and Methods, and **Figure 5A**). We require that the multiplicative factors for LTP and LTD exactly match at $w_j = w_0 = 1$ mV, where initial weights are set in our simulations. Further, we found it necessary that the slope of the LTD modulation around w_0 be less than 1. Indeed, our neuron model is very noisy, such that reproducible pre–post pairs that need to be reinforced actually occur among a sea of random pre–post and post–pre pairs. If LTD too rapidly overcomes LTP above w_0, there is no chance for the correlated pre–post spikes to evoke sustainable LTP. The slope must be small enough for correlations to be picked up. This motivates our choice of weight dependence for LTD as depicted in **Figure 5A**. The weight distributions for all three learning rules stay indeed unimodal, but highly positively skewed, such that the neuron can really "learn" by giving some relevant synapses large weights (tails of the distributions in **Figure 5A**). Note that the obtained weight distributions resemble those recorded by Sjöström et al. (2001) (see e.g., Figure 3C in their paper).

The evolution of the MI along learning time is reported in **Figure 5C**. Overall, MI values are lower than those of **Figure 4B**. Unimodal distributions of synaptic efficacies are less informative than purely bimodal distributions, reflecting the lower degree of specialization to input features. Such distributions may however be advantageous in a memory storage task where old memories which are not recalled often need to be erased to store new ones. In this scenario, strong weights which become irrelevant can quickly be sent back from the tail to the main weight pool around 1 mV. For a detailed study of the impact of the weight-dependence on memory retention, see Billings and van Rossum (2009).

We see that it is difficult to directly compare absolute values of the MI in **Figure 5C**, since the "shuffled" MIs (dashed lines) do not converge to the same value. This is because some weight distributions are more skewed than others (compare red and blue distributions in **Figure 5A**). In the present study, we are more interested in knowing how good plasticity rules are at selecting individual weights for up- or down-regulation, on the basis of the input structure. We would like our performance measure to be free of the actual weight distribution, which is mainly shaped by the weight-dependence of Eq. 23. We therefore compare the normalized information gain, i.e., $[\mathrm{MI}(\alpha = 1) - \mathrm{MI}(\alpha = 0)] / [\mathrm{MI}_{\mathrm{sh}}(\alpha = 1) - \mathrm{MI}(\alpha = 0)]$, where $\mathrm{MI}_{\mathrm{sh}}$ denotes the MI for shuffled weights. The result is shown in **Figure 5D**: the triplet is again better than the pair model, provided the postsynaptic neuron adapts.

Our simulations show that when SFA modulates the postsynaptic firing rate, the triplet model yields a better gain in information transmission than pair-STDP does. When adaptation is removed, this advantage vanishes. There must be a specific interaction between triplet-STDP and adaptation that we now seek to unravel.

TRIPLET-STDP INCREASES THE RESPONSE ENTROPY WHEN THE NEURON ADAPTS

Information transmission improves if the neuron learns to produce more diverse spike trains [$H(\mathbf{Y}^{\mathbf{K}})$ increases], and if the neuron becomes more reliable [$H(\mathbf{Y}^{\mathbf{K}}|\phi)$ decreases] In **Figure 6A** we perform a differential analysis of both entropies, on the same data as presented in **Figure 4** (i.e., for hard-bounded STDP). Whether the postsynaptic neuron adapts (top) or not (bottom), the noise entropy (right) is drastically reduced, and the triplet learning rule does so better than the pair model (compare red and blue). The differential impact of adaptation on the two models can only be seen in the behavior of the response entropy $H(\mathbf{Y}^{\mathbf{K}})$ (left). When the postsynaptic neuron adapts, triplet- and optimal STDP both increase the response entropy, while it decreases with the pair model. This behavior is reflected in the interspike-interval (ISI) distributions, shown in **Figure 6B**. With adaptation, the optimal and triplet rules produce distributions that are close to an exponential (which would be a straight line in the logarithmic y-scale). In contrast, the ISI distribution obtained from pair-STDP stays almost flat for ISIs between 25 and 120 ms. Without adaptation, the optimal and triplet models further sparsifies the ISI distribution which then becomes sparser than an exponential, reducing the response entropy.

Qualitative similarities between the optimal and triplet models can also be found in the power spectrum of the peri-stimulus time histogram (PSTH). The PSTHs are plotted in **Figure 6C** over a full 5-s period, and their average power spectra are displayed in **Figure 6D**. The PSTH is almost flat prior to learning, reflecting the absence of feature selection in the input. Learning in all three learning rules creates sharp peaks in the PSTH, which illustrates the drop

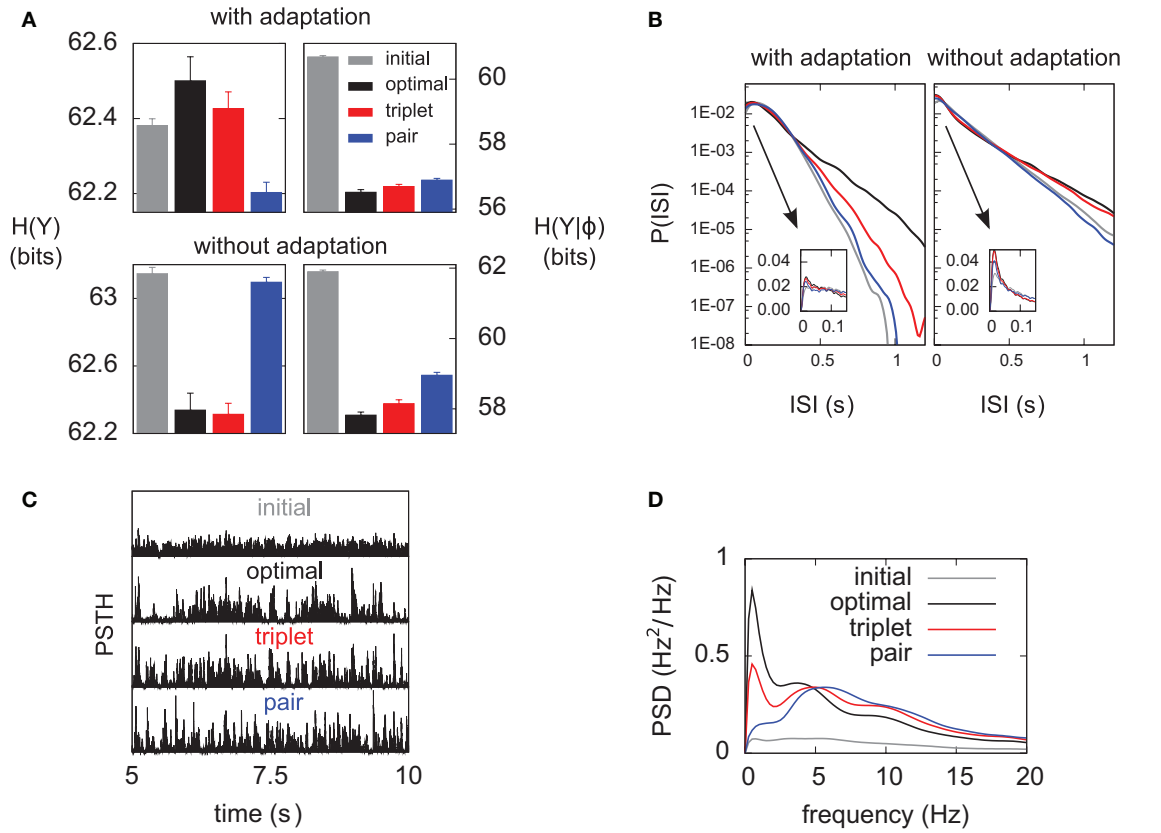

FIGURE 6 | Differential analysis of the entropies. The learning experiments are the same as in **Figure 4**, using hard-bounds on the synaptic weights. **(A)** Response entropy (left) and noise entropy (right) with (top) and without (bottom) postsynaptic SFA. Entropies are calculated at the end of the learning process, except for the gray boxes which denote the entropies prior to learning. **(B)** Interspike-interval distributions with (left) and without (right) SFA, after learning (except gray line, before learning). The main plots have a logarithmic *y*-scale, whereas the insets have a linear one. **(C)** Peri-stimulus time histograms (PSTHs) prior to learning (top) and after learning for each learning rule, over a full 5-s period. All plots share the same *y*-scale. **(D)** Power spectra of the PSTHs shown in **(C)**, averaged over the 10 independent learning experiments.

in noise entropy seen in **Figure 6A** (right). The pair learning rule produces PSTHs with almost no power at low frequencies (below 5 Hz). In contrast, these low frequencies are strongly boosted by the optimal and triplet models. This is however not specific to SFA being on or off (not shown). We give an intuitive account for this in Section "Discussion."

This section has shed light on qualitative similarities in the way the optimal and triplet learning rules enhance information transmission in an adaptive neuron. We now seek to understand the reason why taking account of triplets of spikes would be close-to-optimal in the presence of postsynaptic SFA.

THE OPTIMAL MODEL EXHIBITS A TRIPLET EFFECT

How similar is the optimal model to the triplet learning rule? In essence, the optimal model is a stochastic gradient learning rule, which updates the synaptic weights at every time step depending on the recent input–output correlations and the current relevance of the postsynaptic state. In contrast to this, phenomenological models require changing the synaptic efficacy upon spike occurrence only. It is difficult to compress what happens between spikes in the optimal model down to a single weight change at spike times. However we know that the dependence of LTP on previous postsynaptic firing is a hallmark of the triplet rule, and is absent in the pair rule. We therefore investigate the behavior of the optimal learning rule on post–pre–post triplets of spikes, and find a clear triplet effect (**Figure 7**).

We consider an isolated post–pre–post triplet of spikes, in this order (**Figure 7A**). Isolated means that the last pre- and postsynaptic spikes occurred a very long time before this triplet. Let t^1_{post}, t_{pre}, and t^2_{post} denote the spike times. The pre–post interval is kept constant equal to $\Delta s = t^2_{\text{post}} - t_{\text{pre}} = 15$ ms. We vary the length of the post–post interval $\Delta p = t^2_{\text{post}} - t^1_{\text{post}}$ from 16 to 500 ms. The resulting weight change is depicted in **Figure 7B**. For comparison, the triplet model would produce – by construction – a decaying exponential with time constant τ_y. In the optimal model, potentiation decreases as the post–post interval increases. Two times constants show up in this decay, which reflect that of refractoriness (2 ms) and adaptation (150 ms). The same curve is drawn for two other adaptation time constants (see red and blue curves). When adaptation is removed, the triplet effect vanishes (dashed curve). It should be noted that the isolated pre–post pair itself (i.e., large post–post interval) results in a baseline amount of LTP, which is not the case in the triplet model. **Figure 7A** shows how this effect arises mechanistically. Three different triplets

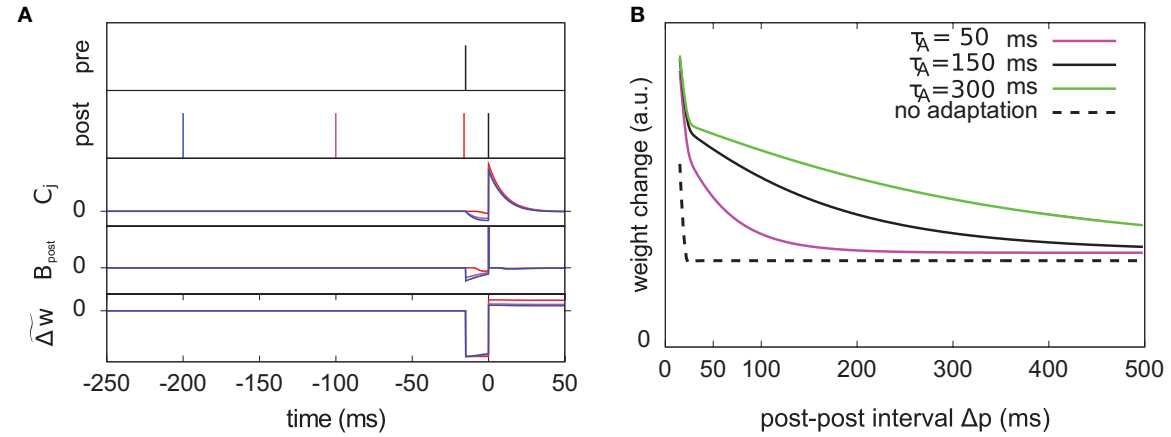

FIGURE 7 | The optimal model incorporates a triplet effect when the postsynaptic neuron adapts. (A) A pre–post pair (Δs = 15 ms interval, black lines in the first two rows) is preceded by another postsynaptic spike. The post–post interval Δp is made either 16 (red line), 100 (purple), and 200 ms (blue). The time course of C_j, B_{post}, and the cumulative weight change $\widetilde{\Delta w}$ are plotted in the bottom rows. **(B)** Total weight change (optimal model) as a function of the post–post interval, for various adaptation time constants, and without adaptation (dashed line).

are shown, with the pre–post pair being fixed, and the post–post interval being either 16, 100, or 200 ms (red, purple, and blue respectively).

To further highlight the similarity between the optimal learning rule and the triplet model, we now derive an analytical expression for the optimal weight change that follows a post–pre–post triplet of spikes. Let us observe that the final cumulated weight change evoked by the triplet is dominated by the jump that occurs just following the second postsynaptic spike (**Figure 7A**) – except for the negative jump of size λ that follows the presynaptic spike arrival, but this is a constant. Our analysis therefore concentrates on the values of $C_j(t^2_{\text{post}})$ and $B_{\text{post}}(t^2_{\text{post}})$. Let us denote by $\varepsilon_j = \exp(-\Delta s/\tau_m)$ the value of the unitary synaptic PSP at time t^2_{post}. Around the baseline potential u_b = 19 mV, the gain function is approximately linear (cf. **Figure 1A**), i.e., $g(u_b + w_j\varepsilon_j) \simeq g_b + g'_b w_j \varepsilon_j$ where $g_b = g(u_b)$ and $g'_b = dg/du|_{u_b}$ are constants. From Eq. 14, we read $B_{\text{post}}(t^2_{\text{post}}) = \log[1+(g'_b w_j \varepsilon_j / g_b)]\delta(0)$, which is approximately equal to

$$B_{\text{post}}\left(t^2_{\text{post}}\right) \simeq \frac{g'_b}{g_b} w_j \varepsilon_j \delta(0) \tag{24}$$

assuming the contribution of $w_j\varepsilon_j$ is small compared to the baseline gain g_b. The term proportional to M in Eq. 14 is negligible compared to the δ-function. From Eq. 13, we see that

$$C_j\left(t^2_{\text{post}}\right) = \frac{\varepsilon_j g'_b}{g_b + g'_b w_j \varepsilon_j} + C_j\left(t^2_{\text{post}} - \varepsilon\right) \tag{25}$$

The total weight change following the second postsynaptic spike is therefore

$$\Delta w_j\left(t^2_{\text{post}}\right) \simeq \left(\frac{g'_b}{g_b}\right)^2 w_j \varepsilon_j^2 + \frac{g'_b}{g_b} w_j \varepsilon_j C_j\left(t^2_{\text{post}} - \varepsilon\right) \tag{26}$$

where

$$C_j\left(t^2_{\text{post}} - \varepsilon\right) = -\int_{t_{\text{pre}}}^{t^2_{\text{post}}-\varepsilon} \exp\left(-\frac{t^2_{\text{post}} - t}{\tau_C}\right) \exp\left(-\frac{t - t_{\text{pre}}}{\tau_m}\right) g'_b M(t) dt \tag{27}$$

Since we have taken $\tau_C = \tau_m$, the first two exponentials collapse into ε_j. To carry out the integration, let us further simplify the adaptation model into $M(t) = 1 - \exp(-(t - t^1_{\text{post}})/\tau_A)$, assuming that $t_{\text{pre}} - t^1_{\text{post}} > 2$ ms so that the refractoriness has already vanished at the time of the presynaptic spike, while adaptation remains. It is also assumed that the triplet is isolated, so that we can neglect the cumulative effect of adaptation. Eq. 27 becomes

$$C_j\left(t^2_{\text{post}} - \varepsilon\right) = -g'_b \varepsilon_j \left[\Delta s + \tau_A \exp\left(-\frac{\Delta p}{\tau_A}\right)\left(1 - \exp\left(\frac{\Delta s}{\tau_a}\right)\right)\right] \tag{28}$$

If $\Delta s \ll \tau_A$, the last term into square brackets is approximately $\Delta s/\tau_A$. If not, ε_j becomes so small that the whole r.h.s of Eq. 26 vanishes. To sum up, the total weight change following the second postsynaptic spike is given by

$$\Delta w_j\left(t^2_{\text{post}}\right) = \frac{g'^2_b}{g_b} w_j \varepsilon_j^2 \left(\frac{1}{g_b} - \Delta s\right) + \frac{g'^2_b}{g_b} \Delta s w_j \varepsilon_j^2 \exp\left(-\frac{\Delta p}{\tau_A}\right) \tag{29}$$

The first term on the r.h.s of Eq. 29 is a pair term, i.e., a weight change that depends only on the pre–post interval Δs. We note that it is proportional to ε_j^2, meaning that the time constant of the causal part of the STDP learning window is half the membrane time constant. The second term exactly matches the triplet model, when $\tau_A = \tau_y$ and $\tau_+ = \tau_m/2$. Indeed, the triplet model would yield the following weight change:

$$\Delta w_j^{\text{triplet}}\left(t^2_{\text{post}}\right) \simeq A_3^+ \varepsilon_j \exp\left(-\frac{\Delta p}{\tau_y}\right) \tag{30}$$

From this we conclude that the triplet effect, which primarily arose from phenomenological minimal modeling of experimental data, also emerges from an optimal learning rule when the postsynaptic neuron adapts. To understand in more intuitive terms how the triplet mechanism relates to optimal information transmission, let us consider the case where the postsynaptic neuron is fully deterministic. If so, the noise entropy is null, so that maximizing

information transfer means producing output spike trains with maximum entropy. If the mean firing rate ρ_{targ} is a further constraint, output spike trains should be Poisson processes, which as a by-product would produce exponentially distributed ISIs. If the neuron is endowed with refractory and adapting mechanisms, there is a natural tendency for short ISIs to appear rarely. Therefore, plasticity has to fight against adaptation and refractoriness to bind more and more stimulus features to short ISIs. The triplet effect is precisely what is needed to achieve this: if a presynaptic spike is found to be responsible for a short ISI, it should be reinforced more than if the ISI was longer. This issue is further developed in Section "Discussion."

OPTIMAL STDP IS TARGET-CELL SPECIFIC

The results of the previous sections suggest that STDP may optimally interact with adaptation to enhance the channel capacity. In principle, if STDP is optimized for information transmission, it cannot ignore the intrinsic dynamics of the postsynaptic cell which influences the mapping between input and output spikes. The cortex is known to exhibit a rich diversity of cell types, with the corresponding range of intrinsic dynamics, and in parallel, STDP is target-cell specific (Tzounopoulos et al., 2004; Lu et al., 2007). Within the optimality framework, we should therefore be able to predict this target-cell specificity of STDP by investigating the predictions of the optimal model in the context of *in vitro* pairing experiments. Predictions should be made for different types of postsynaptic neurons, and be compared to experimental data. The optimal learning rule was shown in Toyoizumi et al. (2007) to share some features with STDP. We here extend this work to a couple of additional features including the frequency dependence. We also apply it to another type of postsynaptic cell, an inhibitory FS interneuron, for which *in vitro* data exist.

Only one synapse is investigated, with unit weight $w_0 = 1$ mV before the start of the experiment. Sixty pre–post pairs with given interspike time Δs are repeated in time with frequency f. The subsequent weight change given by Eq. 12 is reported as a function of both parameters (**Figures 8A,B**).

The optimal model features asymmetric timing windows at 1, 20, and 50 Hz pairing frequencies (**Figure 8A**). At 1 and 20 Hz, pre-before-post yields LTP and post-before-pre leads to LTD. At 50 Hz the whole curve is shifted upwards, resulting in LTP on both sides. The model qualitatively agrees with the experimental data reported in Sjöström et al. (2001), redrawn for comparison (**Figure 8A**, circles).

The frequency dependence experimentally found in Markram et al. (1997) and Sjöström et al. (2001) is also qualitatively reproduced (**Figure 8B**). Post–pre pairing ($\Delta s = -10$ ms, green curve) switches from LTD at low frequency to LTP at higher frequencies, which is consistent with the timing windows in **Figure 8A**. For pre–post pairing ($\Delta s = +10$ ms, blue curve), LTP also increases with the pairing frequency. We also found that when SFA was removed, it was impossible to have a good fit for both the time window and the frequency dependence (not shown).

To further elucidate the link between optimal STDP and the after-spike kernel ($g_R + g_A$ in Eq. 5), we ask whether plasticity at excitatory synapses onto FS interneurons can be accounted for in the same principled manner. In general, the intrinsic dynamics of inhibitory interneurons are very different from that of principal cells in cortex. STDP at synapses onto those cells is also different from STDP at excitatory-to-excitatory synapses (Tzounopoulos et al., 2004; Lu et al., 2007). The dynamics of FS cells are well modeled using a kernel which is shown in **Figure 8D** (Mensi et al., 2010). We augment the after-spike kernel with an additional variable g_B governed by

$$\frac{dg_B}{dt} = -\frac{g_B}{\tau_B} + q_B Y(t) \tag{31}$$

Parameters were set to $\tau_B = 30$ ms, $\tau_A = 150$ ms, $q_B = -9$, and $q_A = 4$. The resulting kernel (i.e., $g_R + g_A + g_B$ – **Figure 8D**, blue kernel) exhibits after-spike refractoriness followed by a short facilitating period before adaptation takes over (note that the kernel is suppressive, meaning that positive values correspond to suppression of activity while negative values mean facilitation). Since interneurons do not project over long distances to other areas, the infomax objective function might not appear as well justified. Instead, let us consider the simple microcircuit shown in **Figure 8D**. A first principal cell (PC) makes an excitatory synapse onto a second PC, and we assume the infomax principle is at work. The first PC inhibits the second PC via a FS interneuron. How, intuitively, should the PC-to-FS synapse change so that the FS cell also contributes to the overall information maximization between the two PCs? In a very crude understanding of the infomax principle, if a pre-before-post pair of spikes is evoked at the PC–PC synapse (see spike trains in **Figure 8D**), the probability of having this pair again should be increased. If a similar pre-before-post pair is simultaneously evoked at the PC–FS synapse, then decreasing its weight will make it less likely that the FS spike again after the first PC. This in turn makes it more likely that the first PC–PC pair of spike will occur again. Therefore, PC–FS synapses should undergo some sort of anti-Hebbian learning. In fact, we found information minimization (i.e., the optimal model with opposite learning rate) to yield a good match between the simulated STDP time window (**Figure 8C**) and that found in Lu et al. (2007), which also exhibits LTD on both sides with some LTP at large intervals (see orange dots, superimposed). The post-before-pre part of the window can be understood intuitively: when a presynaptic spike arrives a few milliseconds after a postsynaptic spike, it falls in the period where postsynaptic firing is facilitated ($q_B < 0$). Therefore, it still has some influence on the subsequent postsynaptic activity. In order to avoid later causal pre–post events, the weight should be decreased. We see that the optimal STDP window depends on the after-spike kernel that describes the dynamical properties of the postsynaptic cell: q_B directly modulates the post–pre part of the window (see dashed curve in **Figure 8C**).

Together, these results suggest that if STDP is considered as arising from an optimality principle, it naturally interacts with the dynamics of the postsynaptic cell. This might underlie the target-cell specificity of STDP (Tzounopoulos et al., 2004; Lu et al., 2007).

DISCUSSION

Experiments (Markram et al., 1997; Sjöström et al., 2001; Froemke et al., 2006) as well as phenomenological models of STDP (Senn et al., 2001; Froemke et al., 2006; Pfister and

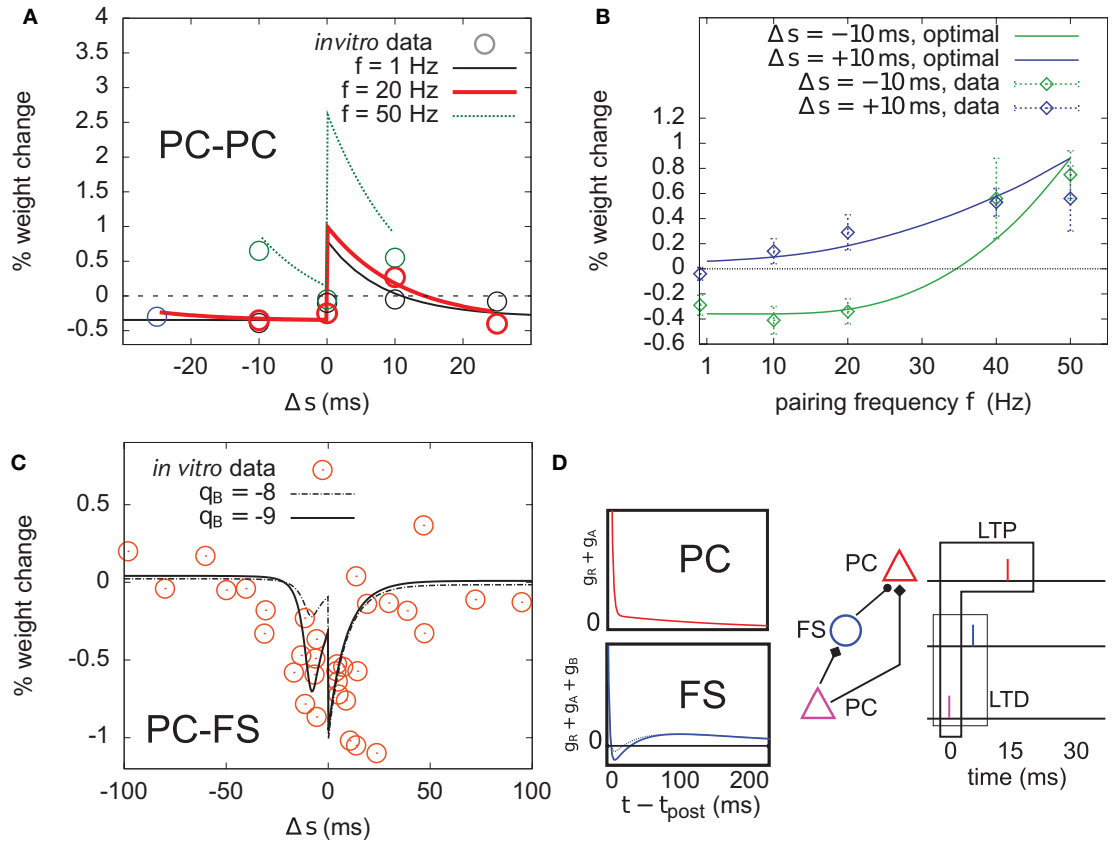

FIGURE 8 | Optimal plasticity shares features with target-cell specific STDP. (A) The optimal model applied on 60 pre–post pairs repeating at 1 (black line), 20 (red thick), and 50 Hz (green) yields STDP learning windows that qualitatively match those recorded in Sjöström et al. (2001). For comparison, the *in vitro* data has been redrawn with permission. **(B)** LTP dominates when the pairing frequency is increased. The optimal frequency window is plotted for post-before-pre (–10 ms, solid green curve) and pre-before-post pairs (+10 ms, solid blue) repeated with frequency f (x-axis). Points and error bars are the experimental data, redrawn from Sjöström et al. (2001) with permission. **(C)** Learning window that minimizes information transmission at an excitatory synapse onto a fast-spiking (FS) inhibitory interneuron. The procedure is the same as in **(A)**. The spike-triggered adaptation kernel was updated to better match that of a FS cell (see **D**). Dots are redrawn from Lu et al. (2007). **(D)** Left: after-spike kernels of firing rate suppression for the principal excitatory cell (red, same as the one we used throughout the article, see Materials and Methods) and the fast-spiking interneuron (blue). The latter was modeled by adding a third variable $q_B < 0$ with time constant $\tau_B = 30$ ms to the initial kernel. Solid blue line: $q_B = -9$. Dashed blue line: $q_B = -8$. Right: schematic of a feed-forward inhibition microcircuit. A first principal cell (PC) makes an excitatory connection to another PC. It also inhibits it indirectly through a FS interneuron. The example spike trains illustrate the benefit of having LTD for pre-before-post pairing at the PC–FS synapse (see text).

Gerstner, 2006; Clopath et al., 2010) point to the fact that LTP is not accurately described by independent contributions from neighboring postsynaptic spikes. In order to reproduce the results of recent STDP experiments, at least two postsynaptic spikes must interact in the LTP process. We have shown that this key feature ("triplet effect" in Pfister and Gerstner, 2006; Clopath et al., 2010; and similarly in Senn et al., 2001) happens to be optimal for an adapting neuron to learn to maximize information transmission. We have compared the performance of an optimal model (Toyoizumi et al., 2005) to that of two minimal STDP models. One of them incorporated the triplet effect (Pfister and Gerstner, 2006), while the second one did not (standard pair-based learning rule; Gerstner et al., 1996; Kempter et al., 1999; Song et al., 2000). The triplet-based model performs very close to the optimal one, and this advantage over pair-STDP disappears when SFA is removed from the intrinsic dynamics of the postsynaptic cell.

Our results are not restricted to additive STDP in which the amount of weight change is independent of the weight itself. It also holds when the amount of LTD increases with the efficacy of the synapse, a form which better reflects experimental observations (Bi and Poo, 1998; Sjöström et al., 2001). In the model introduced here, the amount of LTD is modulated by a sub-linear function of the synaptic weight. The deviation from linearity is set by a single parameter $a > 0$, with the purely multiplicative dependence of van Rossum et al. (2000) being recovered when $a = 0$. Since we modeled only a fraction of the total input synapses, we assumed a certain level of noise in the postsynaptic cell to account for the activity of the remaining synapses, thereby staying consistent with the framework of information theory in which communication channels are generally considered noisy. Because of this noise level, we found a large a was required for the weight distribution to become positively skewed as reported by Sjöström et al. (2001) (cortex layer V). For both the pair and triplet learning rules, the noisier the postsynaptic

neuron, the weaker the LTD weight-dependence (i.e., the larger a) must be to keep a significant spread of the weight distribution. This means that other (possibly simpler) forms of weight dependence for LTD would work equally well, provided the noise level is adjusted accordingly. For example, in a nearly deterministic neuron, input–output correlations are strong enough for the weight-distribution to spread even when LTD depends linearly on the synaptic weight ($a = 0$, not shown).

In the original papers where the optimal and triplet rule were first described, it was pointed out that both rules could be mapped onto the BCM learning rule (Bienenstock et al., 1982). Both learning rules are quadratic in the postsynaptic activity. In turn, the link between the BCM rule and ICA has also already been researched (Intrator and Cooper, 1992; Blais et al., 1998; Clopath et al., 2010), as has the relationship between the infomax principle and ICA (Bell and Sejnowski, 1995). It therefore does not come as a surprise that the triplet model performs close to the infomax optimal learning rule. What is novel is the link to adaptation and spike after-potential.

We have also shown that when the optimal or triplet plasticity models are at work, the postsynaptic neuron learns to transmit information in a wider frequency band (**Figure 6D**): both rules evoke postsynaptic responses that have substantial power below 5 Hz, in contrast to the pair-based STDP rule. This is intuitively understood from the triplet effect combined with adaptation. Let us imagine STDP starts creating a peak in the PSTH so that we have, with high probability, a first postsynaptic spike at time t_0. If a presynaptic spike at time $t_0 + (\Delta/2)$ is followed by a further postsynaptic spike at time $t_0 + \Delta$ (Δ on the order of 10 ms), the triplet effect reinforces the connection from this presynaptic unit. In turn, it will create another peak at time $t_0 + \Delta$, and this process can continue. Peaks thus extend and become broader, until adaptation becomes strong enough to prevent further immediate firing. The next series of peaks will then be delayed by a few hundred milliseconds. Broadening of peak widths and ISIs together introduce more power at lower frequencies in the PSTH.

One should bear in mind that neurons process incoming signals in order to convey them to other receivers. Although the information content of the output spike train really is an important quantity with respect to information processing, the way it can be decoded by downstream neurons should also be taken into account. Some "words" in the output spike train may be more suited for subsequent transmission than others. It has been suggested (Lisman, 1997) that since cortical synapses are intrinsically unreliable, isolated incoming spikes cannot be received properly, whereas bursts of action potentials evoke a reliable response in the receiving neuron. There is a lot of evidence for burst firing in many sensory systems (see Krahe and Gabbiani, 2004 for a review). As shown in **Figure 6**, the optimal and triplet STDP models tend to sparsify the distribution of ISIs, meaning that the neuron learns to respond vigorously (very short ISIs) to a larger number of features in the input stream, while remaining silent for longer portions of the stimulus. The neuron thus overcomes the effects of adaptation, which in baseline conditions (before learning) gives the ISI distribution a broad peak and a Gaussian-like drop-off. Our results therefore suggest that reliable occurrence of short ISIs can arise from STDP in adaptive neurons that are not intrinsic bursters. This is in line with Eyherabide et al. (2008), which recently provided evidence for high information transmission through burst activity in an insect auditory system (*Locusta migratoria*). The recorded neurons encoded almost half of the total transmitted information in bursts, and this was also shown not to require intrinsic burst dynamics.

Since our results rely on the outcome of a couple of numerical experiments, one might be concerned about the validity of the findings outside the range of parameter values we have used. There are for example a couple of free parameters in the neuron model. It is obviously difficult to browse the full high-dimensional parameter space and search for regions where the results would break down. We therefore tried to constrain our neuron parameters in a sensible manner. For example, the parameters of the SFA mechanism (q_A and τ_A) were chosen such that the response properties to a step in input firing rate would look plausible (**Figure 1C**). The noise parameter r_0 and the threshold value u_T were chosen so as to achieve an output rate of 7.5 Hz when all synaptic weights are at 1 mV. We acknowledge, though, that r_0 could be made arbitrarily large (reducing the amount of noise) since u_T can compensate for it. In the limit of very low noise, information transmission cannot be improved by increasing the neuron's reliability anymore, since the noise entropy would already be minimal. We have shown however that a substantial part of the information gain found in the optimal and triplet models are due to an increased response entropy. This qualitative similarity, together with the structural similarities highlighted in **Figures 7 and 8**, lead us to believe that our results would still hold in the deterministic limit, and for noise levels in between. The optimal plasticity rule becoming ill-defined in this limit, we did not investigate this further.

To what extent can we extrapolate our results to the optimality of synaptic plasticity in the real brain? It obviously depends on the amount of trust one can put into this triplet model. Phenomenological models of STDP are usually constructed based on the results of *in vitro* experiments. They end up reproducing the quantitative outcome of only a few pre–post pairing schemes which are far from spanning the full complexity of real spike trains. To what extent can these models be trusted in more natural situations? From a machine learning perspective, a minimal model is likely to generalize better than a more detailed model, because its small number of free parameters might prevent it from overfitting the experimental data at the expense of its interpolation/extrapolation power. In this study, we have put the emphasis on an extrapolation of recent minimal models (Pfister and Gerstner, 2006; Clopath et al., 2010): the amount of LTP obtained from a pre-before-post pair increases with the recent postsynaptic firing frequency. By construction, the models account for the frequency dependence of the classical pairing experiment (they are fitted on this, among other things). However, they are seriously challenged by a more detailed study of spike interactions at L2/3 pyramidal cells (Froemke et al., 2006). There, it was explicitly shown that (n-posts)–pre–post bursts yield an amount of LTD which grows with n, the number of postsynaptic spikes in the burst preceding the pair. In contrast, post–pre–post triplets in hippocampal slices lead to LTP in a way that is consistent with the triplet model (Wang et al., 2005). The results of our study should therefore be interpreted bearing in mind the variability in experimental results. The recurrent *in vitro* versus *in vivo* debate should also be considered: synaptic

plasticity depends on a lot of biochemical parameters for which the slice conditions do not faithfully reflect the normal operating mode of the brain.

A second controversy lies in our optimality model itself. While efficient coding of presynaptic spike trains may seem a reasonable goal to achieve at, say, thalamocortical synapses in sensory cortices, many other objectives could well be considered when it comes to other brain areas. Some examples are optimal decision making through risk balancing, reinforcement learning via reward maximization, or optimal memory storage and recall in autoassociative memories. It will be interesting to see more STDP learning rules in functionally different areas and how these relate to optimality principles.

Finally, while we investigated information transmission through a single postsynaptic cell, it remains to be elucidated how local information maximization in large recurrent networks of spiking neurons translates into a better information flow through the network.

ACKNOWLEDGMENTS

This work was partially supported by the European Union Framework 7 ICT Project 215910 (BIOTACT, www.biotact.org). Jean-Pascal Pfister was supported by the Wellcome Trust. We thank Dr. Eilif Muller for having motivated the use of graphics cards (GPU) to compute the MI.

REFERENCES

Bell, A. J., and Parra, L. C. (2005). "Maximising sensitivity in a spiking network," in *Advances in Neural Information Processing Systems*, Vol. 17, eds L. K. Saul, Y. Weiss, and L. Bottou (Cambridge, MA: MIT Press), 121–128.

Bell, A. J., and Sejnowski, T. J. (1995). An information maximization approach to blind separation and blind deconvolution. *Neural Comput.* 7, 1129–1159.

Bell, C. C., V., H., Sugawara, Y., and Grant, K. (1997). Synaptic plasticity in a cerebellum-like structure depends on temporal order. *Nature* 387, 278–281.

Bi, G. Q., and Poo, M. M. (1998). Synaptic modifications in cultured hippocampal neurons: dependence on spike timing, synaptic strength, and postsynaptic cell type. *J. Neurosci.* 18, 10464–10472.

Bienenstock, E. L., Cooper, L. N., and Munro, P. W. (1982). Theory for the development of neuron selectivity: orientation specificity and binocular interaction in visual cortex. *J. Neurosci.* 2, 32–48.

Billings, G., and van Rossum, M. C. W. (2009). Memory retention and spike-timing dependent plasticity. *J. Neurophysiol.* 101, 2775–2788.

Blais, B. S., Intrator, N., Shouval, H., and Cooper, L. N. (1998). Receptive field formation in natural scene environments: comparison of single-cell learning rules. *Neural Comput.* 10, 1797–1813.

Bohte, S. M., and Mozer, M. C. (2007). Reducing the variability of neural responses: a computational theory of spike-timing-dependent plasticity. *Neural Comput.* 19, 371–403.

Chechik, G. (2003). Spike timing-dependent plasticity and relevant mutual information maximization. *Neural Comput.* 15, 1481–1510.

Clopath, C., Büsing, L., Vasilaki, E., and Gerstner, W. (2010). Connectivity reflects coding: a model of voltage-based STDP with homeostasis. *Nat. Neurosci.* 13, 344–352.

Clopath, C., Longtin, A., and Gerstner, W. (2008). "An online Hebbian learning rule that performs independent component analysis," in *Advances in Neural Information Processing Systems*, Vol. 20, eds J. Platt, D. Koller, Y. Singer, and S. Roweis (Cambridge, MA: MIT Press), 321–328.

Eyherabide, H. G., Rokem, A., Herz, A. V. M., and I., S. (2008). Burst firing is a neural code in an insect auditory system. *Front. Comput. Neurosci.* 2, 1–17. doi: 10.3389/neuro.10.003.2008.

Florian, R. V. (2007). Reinforcement learning through modulation of spike timing-dependent synaptic plasticity. *Neural Comput.* 19, 1468–1502.

Froemke, R. C., Tsay, I., Raad, M., Long, J., and Dan, Y. (2006). Contribution of individual spikes in burst-induced long-term synaptic modification. *J. Neurophysiol.* 95, 1620–1629.

Gerstner, W., Kempter, R., van Hemmen, J., and Wagner, H. (1996). A neuronal learning rule for sub-millisecond temporal coding. *Nature* 383, 76–78.

Gerstner, W., and Kistler, W. K. (2002a). Mathematical formulations of Hebbian learning. *Biol. Cybern.* 87, 404–415.

Gerstner, W., and Kistler, W. (2002b). *Spiking Neuron Models*. New York: Cambridge University Press.

Intrator, N., and Cooper, L. (1992). Objective function formulation of the BCM theory of visual cortical plasticity – statistical connections, stability conditions. *Neural Netw.* 5, 3–17.

Izhikevich, E., and Edelman, G. M. (2008). Large-scale model of mammalian thalamocortical systems. *Proc. Natl. Acad. Sci. U.S.A.* 105, 3593–3598.

Kempter, R., Gerstner, W., and van Hemmen, J. L. (1999). Hebbian learning and spiking neurons. *Phys. Rev. E* 59, 4498–4514.

Klampfl, S., Legenstein, R., and Maass, W. (2009). Spiking neurons can learn to solve information bottleneck problems and to extract independent components. *Neural Comput.* 21, 911–959.

Krahe, R., and Gabbiani, F. (2004). Burst firing in sensory systems. *Nat. Rev. Neurosci.* 5, 13–23.

Lengyel, M., Kwag, J., Paulsen, O., and Dayan, P. (2005). Matching storage and recall: hippocampal spike timing-dependent plasticity and phase response curves. *Nat. Neurosci.* 8, 1677–1683.

Linsker, R. (1989). How to generate ordered maps by maximizing the mutual information between input and output signals. *Neural Comput.* 1, 402–411.

Lisman, J. (1997). Bursts as a unit of neural information: making unreliable synapses reliable. *Trends Neurosci.* 20, 38–43.

Lu, J., Li, C., Zhao, J.-P., Poo, M., and Zhang, X. (2007). Spike-timing-dependent plasticity of neocortical excitatory synapses on inhibitory interneurons depends on target cell type. *J. Neurosci.* 27, 9711–9720.

Magee, J. C., and Johnston, D. (1997). A synaptically controlled associative signal for Hebbian plasticity in hippocampal neurons. *Science* 275, 209–213.

Mensi, S., Naud, R., Avermann, M., Peterson, C., and Gerstner, W. (2010). Complexity and performance in simple neuron models. *Front. Neurosci.* doi: 10.3389/conf. fnins.2010.03.00064.

Markram, H., Lübke, J., Frotscher, M., and Sakmann, B. (1997). Regulation of synaptic efficacy by coincidence of postsynaptic AP and EPSPs. *Science* 275, 213–215.

Morrison, A., Aertsen, A., and Diesmann, M. (2007). Spike-timing dependent plasticity in balanced random networks. *Neural Comput.* 19, 1437–1467.

Morrison, A., Diesmann, M., and Gerstner, W. (2008). Phenomenological models of synaptic plasticity based on spike timing. *Biol. Cybern.* 98, 459–478.

Oja, E. (1982). A simplified neuron model as a principal component analyzer. *J. Math. Biol.* 15, 267–273.

Oja, E. (1989). Neural networks, principal components, and subspaces. *Int. J. Neural Syst.* 1, 61–68.

Olshausen, B. A., and Field, D. J. (1996). Emergence of simple-cell receptive field properties by learning a sparse code for natural images. *Nature* 381, 607–609.

Pfister, J.-P., and Gerstner, W. (2006). Triplets of spikes in a model of spike timing-dependent plasticity. *J. Neurosci.* 26, 9673–9682.

Pfister, J.-P., Toyoizumi, T., Barber, D., and Gerstner, W. (2006). Optimal spike-timing dependent plasticity for precise action potential firing in supervised learning. *Neural Comput.* 18, 1309–1339.

Rao, R. P., and Ballard, D. H. (1999). Predictive coding in the visual cortex: a functional interpretation of some extra-classical receptive-field effects. *Nat. Neurosci.* 2, 79–87.

Rubin, J., Lee, D. D., and Sompolinsky, H. (2001). Equilibrium properties of temporally asymmetric Hebbian plasticity. *Phys. Rev. Lett.* 86, 364–367.

Senn, W., Tsodyks, M., and Markram, H. (2001). An algorithm for modifying neurotransmitter release probability based on pre- and postsynaptic spike timing. *Neural Comput.* 13, 35–67.

Seung, H. S. (2003). Learning in spiking neural networks by reinforcement of stochastic synaptic transmission. *Neuron* 40, 1063–1073.

Sjöström, P., Turrigiano, G., and Nelson, S. (2001). Rate, timing, and cooperativity jointly determine cortical synaptic plasticity. *Neuron* 32, 1149–1164.

Smith, E. C., and Lewicki, M. S. (2006). Efficient auditory coding. *Nature* 439, 978–982.

Song, S., Miller, K. D., and Abbott, L. F. (2000). Competitive Hebbian learning through spike-time-dependent synaptic plasticity. *Nat. Neurosci.* 3, 919–926.

Sprekeler, H., Hennequin, G., and Gerstner, W. (2009). "Code-specific policy gradient rules for spiking neurons," in *Advances in Neural Information Processing Systems*, Vol. 22, eds Y. Bengio, D. Schuurmans, J. Lafferty, C. K. I. Williams, and A. Culotta (Cambridge, MA: MIT Press), 1741–1749.

Sprekeler, H., Michaelis, C., and Wiskott, L. (2007). Slowness: an objective for spike-timing-dependent plasticity? *PLoS Comput. Biol.* 3, e112. doi: 10.1371/journal.pcbi.0030112.

Toyoizumi, T., Pfister, J.-P., Aihara, K., and Gerstner, W. (2005). Generalized Bienenstock–Cooper–Munro rule for spiking neurons that maximizes information transmission. *Proc. Natl. Acad. Sci. U.S.A.* 102, 5239–5244.

Toyoizumi, T., Pfister, J.-P., Aihara, K., and Gerstner, W. (2007). Optimality model of unsupervised spike-timing-dependent plasticity: synaptic memory and weight distribution. *Neural Comput.* 19, 639.

Tzounopoulos, T., Kim, Y., Oertel, D., and Trussell, L. (2004). Cell-specific, spike timing-dependent plasticity in the dorsal cochlear nucleus. *Nat. Neurosci.* 7, 719–725.

van Rossum, M. C. W., Bi, G. Q., and Turrigiano, G. G. (2000). Stable Hebbian learning from spike timing-dependent plasticity. *J. Neurosci.* 20, 8812–8821.

Wang, H.-X., Gerkin, R. C., Nauen, D. W., and Wang, G.-Q. (2005). Coactivation and timing-dependent integration of synaptic potentiation and depression. *Nat. Neurosci.* 8, 187–193.

Xie, X., and Seung, H. S. (2004). Learning in neural networks by reinforcement of irregular spiking. *Phys. Rev. E* 69, 041909.

Zhang, L. I., Tao, H. W., Holt, C. E., Harris, W. A., and Poo, M. M. (1998). A critical window for cooperation and competition among developing retinotectal synapses. *Nature* 395, 37–44.

Conflict of Interest Statement: The authors declare that the research was conducted in the absence of any commercial or financial relationships that could be construed as a potential conflict of interest.

Received: 19 February 2010; accepted: 28 September 2010; published online: 03 December 2010.

*Citation: Hennequin G, Gerstner W and Pfister J-P (2010) STDP in adaptive neurons gives close-to-optimal information transmission. Front. Comput. Neurosci. **4**:143. doi: 10.3389/fncom.2010.00143*

frontiers in
COMPUTATIONAL NEUROSCIENCE

ORIGINAL RESEARCH ARTICLE
published: 27 October 2010
doi: 10.3389/fncom.2010.00134

Closed-form treatment of the interactions between neuronal activity and timing-dependent plasticity in networks of linear neurons

***Christoph Kolodziejski*[1,2,3]*, *Christian Tetzlaff*[1,2,3] *and Florentin Wörgötter*[1,2]**

[1] *Bernstein Center for Computational Neuroscience, Göttingen, Germany*
[2] *Department for Computational Neuroscience, III. Physikalisches Institut - Biophysik, Georg-August-University Göttingen, Göttingen, Germany*
[3] *Network Dynamics Group, Max-Planck-Institute for Dynamics and Self-Organization, Göttingen, Germany*

Edited by:
Wulfram Gerstner, Ecole Polytechnique Fédérale de Lausanne, Switzerland

Reviewed by:
Anthony Burkitt, University of Melbourne, Australia
Jean-Pascal Pfister, University of Cambridge, UK

***Correspondence:**
Christoph Kolodziejski, Network Dynamics Group, Max Planck Institute for Dynamics and Self-Organization, Göttingen, Germany.
e-mail: kolo@bccn-goettingen.de

Network activity and network connectivity mutually influence each other. Especially for fast processes, like spike-timing-dependent plasticity (STDP), which depends on the interaction of few (two) signals, the question arises how these interactions are continuously altering the behavior and structure of the network. To address this question a time-continuous treatment of plasticity is required. However, this is – even in simple recurrent network structures – currently not possible. Thus, here we develop for a linear differential Hebbian learning system a method by which we can analytically investigate the dynamics and stability of the connections in recurrent networks. We use noisy periodic external input signals, which through the recurrent connections lead to complex actual ongoing inputs and observe that large stable ranges emerge in these networks without boundaries or weight-normalization. Somewhat counter-intuitively, we find that about 40% of these cases are obtained with a long-term potentiation-dominated STDP curve. Noise can reduce stability in some cases, but generally this does not occur. Instead stable domains are often enlarged. This study is a first step toward a better understanding of the ongoing interactions between activity and plasticity in recurrent networks using STDP. The results suggest that stability of (sub-)networks should generically be present also in larger structures.

Keywords: spike-timing-dependent plasticity, differential Hebbian plasticity, recurrent networks, stability analysis, asymmetric STDP, long-term potentiation, long-term depression

INTRODUCTION

At the network level recent theoretical advances have made it possible to analytically calculate the activity patterns for certain types of simplified neuron models as long as one keeps the synaptic connectivity fixed (Memmesheimer and Timme, 2006a,b). Concerning plasticity, the situation is reversed. When fixing the activity pattern or rather, when considering long-term activity averages, it is for many plasticity rules possible to calculate the overall development of synaptic weights. Older results exist which provide specific solutions for estimating synaptic strengths in certain types of networks and learning rules, all of which however need to constrain structure or dynamics of the system in different ways (Hopfield, 1982; Miller and MacKay, 1994; Roberts, 2000; van Rossum et al., 2000; Kempter et al., 2001; Burkitt et al., 2007; Kolodziejski et al., 2008) and many of them do not resemble spike-timing-dependent plasticity (STDP, Magee and Johnston, 1997; Markram et al., 1997). Concerning STDP, in large networks one finds that over longer times the distribution of synaptic efficiencies usually develops into either an unimodal (van Rossum et al., 2000; Gütig et al., 2003) or a bimodal (Song et al., 2000; Izhikevich et al., 2004) shape. These results mainly rely on simulations (Song et al., 2000; van Rossum et al., 2000) or mean-field approximations (van Rossum et al., 2000; Gütig et al., 2003). Additionally, in order to keep the weights beyond a given value, soft (van Rossum et al., 2000; Morrison et al., 2007) or hard (Song et al., 2000; Izhikevich et al., 2004; Burkitt et al., 2007; Lubenov and Siapas, 2008; Gilson et al., 2009; Clopath et al., 2010) boundaries have to be introduced.

All these observations pose a problem, because STDP can generically lead to the situation that *individual* pre- and post-synaptic spike pairs influence the synaptic strength of their connection and thereby in a recurrent way immediately also the activity in the network. The question arises, thus, whether such fast synaptic changes would carry any functional significance or whether they will be averaged out by the ongoing network activity? At the moment this issue is left open because resolving it would require measuring or calculating the step-by-step changes of synaptic connectivity together with their activity for a large number of neurons and ideally for every spike pair.

Experimentally this is at the moment still impossible and so far there are also no theoretical tools available (apart from simulations) to address the issue of ongoing mutual interactions between activity and plasticity in networks. For this, analytical methods would be particularly helpful with which it would be possible to predict the dynamics of synaptic connections under STDP.

As discussed above, this is typically investigated with mean-field methods (van Rossum et al., 2000; Gütig et al., 2003) that have average values in their focus. However, here we would like to examine the fine temporal dynamics of each weight as, fundamentally, the

concept of STDP needs to rely on temporally local (pulse–pulse) interactions. Thus, in the current study we will start addressing the issue of temporal locality by providing a general analytical framework for calculating plasticity in a time-continuous way in networks with an arbitrary number of synapses using Hebbian plasticity rules. These are, for example, plain Hebbian or differential Hebbian learning, where the latter is known to have properties similar to STDP (Roberts, 1999; Wörgötter and Porr, 2004).

Naturally, the complexity of the solution is high and, while it could be used to investigate the interplay of activity and plasticity in any network topology, we will here first look at three, still rather simple, cases of recurrent networks, which have been chosen because they could be considered as fundamental network building blocks. This allows us to arrive at several interesting observations which may be the starting point for the investigation of more complex topologies of which we will give a brief example at the end.

For example, we find that in the investigated simple recurrent networks many fixed points exist where synapses stabilize in spite of the recurrently arriving inputs and that boundaries (soft or hard) are not required. More intriguing, this can lead to the situation that such a network can better stabilize when there is an asymmetric STDP curve in which the long-term potentiation (LTP) part dominates.

We will address these topics by organizing the paper in the following way. In Section "Materials and Methods" we define the system we are going to solve analytically, depict the three different network structures the analytical solution is applied to and also describe the specifics of the recurrent connections. In Section "Results" we provide the analytical solution of our general Hebbian system and also verify several useful approximations. Next we use our solution to calculate all configurations in the investigated network structures that lead to non-divergent weights. Here, we describe the results under different conditions, i.e., with/out noise and with an asymmetric STDP rule. Finally, in Section "Discussion", we put the results to a broader context. Detailed calculations can be found in Section "Appendix".

MATERIALS AND METHODS

STDP-LIKE PLASTICITY RULE

The general one-neuron system used as the basis of this study consists of N synapses with strength ω_i that receive input from neurons i with continuous values x_i. Each input produces an excitatory post-synaptic potential (EPSP) which is modeled by filter functions h_i (see **Figure 1A** for an example). The output of the neuron is, thus:

$$v(t) = \sum_{i=1}^{N} (x_i * h_i)(t) \cdot \omega_i(t) \tag{1}$$

where $(\xi * \eta)(t) = \int_0^\infty \xi(\tau)\eta(t-\tau)d\tau$ describes a convolution.

Synapses change according to a generally formalized Hebbian plasticity rule

$$\dot{\omega}_i(t) := \frac{d\omega_i(t)}{dt} = \mu F[x_i * h_i](t) G[v](t) \tag{2}$$

where μ (set to 0.01 throughout the article) is the plasticity rate and $F[\xi]$ and $G[\xi]$ are linear functionals. However, although the analytical solution that we will present later on holds for the generally formalized plasticity rule (Eq. 2), we will only consider $F = 1$ (where 1 is the identity) and $G = d/dt$. This is called differential Hebbian learning (Kosco, 1986; Klopf, 1988) and allows for the learning of temporal sequences of input events (Porr and Wörgötter, 2003). It resembles STDP (Roberts, 1999; Wörgötter and Porr, 2004). Another important setting for F and G is conventional Hebbian learning with $F = G = 1$.

To avoid that weight changes will follow spurious random correlations one generally assumes that learning is a slow process, where inputs change much faster than weights, with $d\omega_i/\omega_i \ll d(x_i * h_i)/x_i * h_i$, $\mu \to 0$. In spite of this separation of time scales, such a simplification makes it still possible to investigate the dynamics of each weight separately. The separation simplifies Eq. 2 and we neglect all temporal derivatives of ω_i on the right hand side which leads to $\dot{\omega}_i(t) = \mu F[x_i * h_i](t) \Sigma_{j=1}^{N} \omega_j(t) G[x_j * h_j](t)$ where we used $G[\Sigma_j \xi_j] = \Sigma_j G[\xi_j]$ as $G[\xi]$ is linear.

If we take ω_i as the i-th component of a vector $\boldsymbol{\omega}$, we write its most general form

$$\dot{\boldsymbol{\omega}}(t) = \mu A(t)\boldsymbol{\omega}(t), \tag{3}$$

with $A_{ij}(t) = F[x_i * h_i](t) G[x_j * h_j](t)$ or in matrix form $\boldsymbol{A}(t) = F[\boldsymbol{x} * \boldsymbol{h}](t) \cdot \overline{G[\boldsymbol{x} * \boldsymbol{h}]}(t)$ where $\overline{\boldsymbol{\xi}}$ denotes the transposition of matrix $\boldsymbol{\xi}$. In the results section we will show that following closed-form solution is possible

$$\boldsymbol{\omega}(t) = \mathfrak{B}(t)\boldsymbol{\omega}(t_0), \tag{4}$$

however, $\mathfrak{B}(t)$ as such is quite complex. Nevertheless, we will also show that for our quasi-static assumption $\mu \to 0$ the approximation $\mathfrak{B}(t) = \boldsymbol{I} + \mu \int_{t_0}^{t} \boldsymbol{A}(\tau) d\tau$, where $\boldsymbol{I}$ is the identity matrix, is arguable.

Relation to spike-timing-dependent plasticity

In order to show that $F = 1$ and $G = d/dt$ resembles STDP we use a simplified version of the system, namely a system with $N = 2$ (see **Figure 1C**), however, where only one of the synapses is plastic (ω_1); the other stays fixed ($\omega_2 = 1$). In order to get the correct STDP protocol, we now present two pulses to this system, one at $t = 0$ to the input connected with the plastic synapse, hence a pre-synaptic spike, and another at $t = T$ to the other input. As we are using a linear model and as the corresponding weight ω_2 is set to a fixed value of 1, a pulse at the input is also a pulse at the output, hence creating the *pendant* of a post-synaptic spike. The equivalence of relating differential Hebbian plasticity with STDP arises essentially from this and its implications are discussed in detail in Saudargiene et al. (2004) and Tamosiunaite et al. (2007). Recently also Clopath et al. (2010) related voltage-based Hebbian learning to STDP.

For such a network structure, it is possible to analytically calculate the shape of the STDP curve. We start with Eq. 3 where we focus on the first entry of $\boldsymbol{\omega}(t)$: $\omega_1(t)$. The second synapse stays fixed: $\omega_2(t) = \omega_2$.

$$\dot{\omega}_1(t) = \mu \cdot (x_1 * h_1)(t) \frac{d}{dt}(x_1 * h_1)(t) \cdot \omega_1(t) + \mu \cdot (x_1 * h_1)(t) \frac{d}{dt}(x_2 * h_2)(t) \cdot \omega_2 \tag{5}$$

First, we calculate the influence of a single pulse on the weight ω_1. To this end we set $x_2(t) = 0$ for all t and $x_1(t) = \delta(t)$ which is a spike at $t = 0$. It simplifies the convolution to a temporal shift in the filter function h: $h(t - t_i) = \int_0^\infty \delta(t - t_i - \tau)h(\tau)d\tau$. This leaves us with a first order differential equation with following solution:

$$\omega_1^s(t) = \omega_1^s(t_0)\exp\left(\frac{1}{2}\mu h_1^2(t)\right)$$
$$\Rightarrow \Delta\omega_1^s(t) = \omega_1^s(t) - \omega_1^s(t_0) = \omega_1^s(t_0)\left(\exp\left(\frac{1}{2}\mu h_1^2(t)\right) - 1\right) \quad (6)$$

Filters usually have the property that they decay to 0 after a while which turns the exponential function into 1 and results in no weight change. Thus, a single pulse or a rate produced by a single input does not have any influence on the weight when not combined with another pulse. For these pulse–pulse correlations we have to set the other input to have a pulse at $t = T$: $x_2(t) = \delta(t - T)$. If we use a simplification (with all the details in Kolodziejski et al., 2008) the result of the differential Eq. 5 for very long times writes

$$\Delta\omega = \lim_{t\to\infty}\Delta\omega_1(t) \approx \underbrace{\lim_{t\to\infty}\Delta\omega_1^s(t)}_{=0} + \mu\omega_2\int_0^\infty h(\tau)\dot{h}(\tau - T)d\tau$$
$$= \omega_2 \mathrm{sign}(T)\frac{\beta - \alpha}{2(\alpha + \beta)\sigma}h(|T|) \quad (7)$$

where we used here and throughout the manuscript

$$h(t) = \frac{1}{\sigma}\left(e^{-\alpha t} - e^{-\beta t}\right)\Theta(t), \quad (8)$$

Hence, different values of the pulse timing T lead to different $\Delta\omega$ values, which, when plotted in **Figure 1B** against T, resemble a fully symmetrical STDP curve (for more details see Porr and Wörgötter, 2003; Saudargiene et al., 2004; Tamosiunaite et al., 2007; Kolodziejski et al., 2008). The shape and symmetry of the STDP curve depends purely on the filters' shape, thus on the post-synaptic potentials' (PSPs) shapes (see **Figure 1A**). Thus, with different filters h for x_1 and for x_2 one could get either LTP or long-term depression (LTD)-dominated curves (see Figure 2c in Porr and Wörgötter, 2003).

We used $h(t)$ with parameters $\alpha = 0.009$, $\beta = 0.0099$, and $\sigma = 0.029$. The maximum of $h(t)$ is at $t_{max} = (\log(\beta) - \log(\alpha))/(\beta - \alpha)$. The width of the STDP curve measured at biological synapses is usually about $T = \pm 50$ ms (Bi and Poo, 1998; Caporale and Dan, 2008). Thus, as our filter ceases to 10^{-4} at around $t \approx 1000$, we define 1000 time steps as 50 ms (which corresponds to $\alpha = 0.18$ ms^{-1} and $\beta = 0.198$ ms^{-1}) to which we will refer throughout the text.

Not only the shape of the STDP curve is determined by the filter function (Eq. 8) but also the shape of the pulses. As our model is linear, each pulse could be thought of as a weighted delta function (pseudo spike) convoluted with the filter function.

NETWORK STRUCTURES AND INPUTS

Although our method would allow investigating general network structures, we will concentrate on only three very simple, but fundamental ones.

The first structure consists of a single neuron with two plastic synapses (see **Figure 1D**). Although quite simple, the analytical solution of this feed-forward structure demonstrates the power of the method developed in this paper. The next structure is a small network with two neurons and only one plastic synapse (see **Figure 2A**). This network structure is equivalent to just one neuron with a plastic recurrent connection of total delay d. This is due to our assumption of linearity. The last structure we consider is a network with three neurons and two plastic synapses (see **Figure 2C**). Here the equivalence is to a single neuron with two plastic recurrent connections. Note, these two structures could be considered as part of a larger recurrent network, where – after some intermittent stages – activity arrives back at its origin (with unchanging synapses in between). Hence, recurrent structure like those could be seen as simple network building blocks and in the end we shortly discuss larger network structures (i.e., a ring of neurons) that have similar stability properties as those building blocks.

For the input we will use input spike distributions with first moment P (expectation value) that comes in three different conditions. The firing will be without any noise and thus, periodic, with Gaussian noise using a mean value of P and a standard deviation of $\sigma = 5$ ms and, additionally, we will also apply a purely Poisson distributed firing with rate P (hence no periodic input).

As our model is linear, it can not as such produce spikes on its own. However, we could at any point introduce a threshold so that each time a pulse exceeds this threshold a spike would travel along the axon to the next neuron via its synapses. In our first order approximation we do not need this threshold, however, we could apply it afterward.

INPUT PULSE TIMING AND AMPLITUDE

The external input to the system is a sequence of δ-function spikes, which are being transformed into PSPs by convolving the normalized filter function h with the input sequence. As the model is linear, outputs are graded pulses, which result from the weighted linear summation of all inputs at the soma of the neuron (Eq. 1). As we do not use spike thresholds, these outputs directly provide the recurrent part of the input to the system.

We need to calculate the complete input time function, notable the timing and amplitude of all pulses that enter a neuron. We investigate recurrent systems with an external input of periodicity P with delays d_i, $i = 1,\ldots,R$ (in this study we only consider $R = 1$ and 2 but the analysis holds for $R \in \mathbb{N}$). To get a better intuition for recurrences in networks like those described above (**Figures 2A,C**) we can compare each recurrence to a modulo operation. We find all pulse timings pt by iterating the map $pt_{c+1} = \mathrm{mod}\,(pt_c + d_i, P)$ until $pt_{c+1=N_s} = pt_0$. The total number of relevant pulse times $N_s = P/\gcd(P, d_1, \ldots, d_R)$ depends on the greatest common divisor (gcd) of P and all R delays d_i. For instance, all relevant pulse times for $P = 75$ and $d = 60$ are $pt_c = \{0, 60, 45, 30, 15\}$. This gives us the timings of the pulses. In order to calculate the amplitude $\mathbf{\Gamma}$ of each pulse of a system with R recurrent connections, we need to go further and solve this linear system of equations: $\mathbf{\Gamma} = (\boldsymbol{I} - \mathbf{\Lambda})^{-1}\boldsymbol{\lambda}$ where $\mathbf{\Lambda}$ is a matrix that handles the delayed recurrences and $\boldsymbol{\lambda}$ the external input; $\boldsymbol{I}$ is the identity matrix. The details of the derivation are provided in Section "Pulse Timings and Amplitude" in the Appendix. Having calculated the pulse amplitudes we are now able to calculate the weight change.

RESULTS

ANALYTICAL SOLUTION OF WEIGHT DYNAMICS

Here we are going to develop a closed-form for the matrix $\mathfrak{B}(t)$ which governs the temporal development (Eq. 4) of the weights $\boldsymbol{\omega}(t)$ according to Eq. 3. This solution is not trivial as the matrix $\boldsymbol{A}(t)$ is also a function of time. This problem is often found in quantum mechanics and the main problem is that matrices usually do not commute. A solution exists, however, it includes an infinite series, called the Magnus series (see Magnus, 1954 for more details), with

$$\boldsymbol{\omega}(t) = \exp \boldsymbol{\Omega}(t) \cdot \boldsymbol{\omega}(t_0) \tag{9}$$

where $\boldsymbol{\omega}(t_0)$ are the synaptic strengths at time t_0, hence before plasticity, and $\boldsymbol{\Omega}(t)$ is the solution of following equation

$$\dot{\boldsymbol{\Omega}}(t) = \left\{ \mu \boldsymbol{A}(t), \frac{\boldsymbol{\Omega}(t)}{1-\exp(-\boldsymbol{\Omega}(t))} \right\} = \sum_{n=0}^{\infty} \beta_n \left\{ \boldsymbol{A}, \boldsymbol{\Omega}^n \right\}. \tag{10}$$

Here the braces $\left\{\eta, \xi^n\right\} = [\cdots[[\eta,\xi],\xi]\cdots\xi]$ are nested commutators $[\eta,\xi] = \eta\xi - \xi\eta$ and β_n are the coefficients of the Taylor expansion of $\boldsymbol{\Omega}/(1-\exp(-\boldsymbol{\Omega}))$ around $\boldsymbol{\Omega} = 0$. Equation 10 is solved through integration by iteration to the Magnus series:

$$\begin{aligned} \boldsymbol{\Omega}(t) = {} & \mu \mathfrak{A}(t) + \frac{\mu^2}{2} \int_0^t [\boldsymbol{A}(\tau), \mathfrak{A}(\tau)]\, d\tau \\ & + \frac{\mu^3}{4} \int_0^t \left[\boldsymbol{A}(\tau), \int_0^\tau [\boldsymbol{A}(\sigma), \mathfrak{A}(\sigma)] d\sigma \right] d\tau \\ & + \frac{\mu^3}{12} \int_0^t \left[[\boldsymbol{A}(t), \mathfrak{A}(\tau)], \mathfrak{A}(\tau) \right] d\tau + o(\mu^4) \end{aligned} \tag{11}$$

with $\mathfrak{A}(t) = \int_0^t \boldsymbol{A}(\tau) d\tau$. Thus, Eq. 9 combined with Eq. 11, gives us analytically the time development of all weights connected to a neuron under Hebbian plasticity in the limit of small plasticity rates μ. With this we are able to calculate without simulations in principle directly the synaptic strengths of N synapses given N different pulse trains. This property will be useful to analytically calculate the fixed-point values of the weights of our small network structures.

Approximations for the analytical solution

Before we apply the solution to our network structures, we transform it into a computable form and provide error estimates. As the commutators in the infinite series in Eq. 11 are generally non-zero we truncate the series and neglect iterations above degree (k). We write the truncated solution as $\mathfrak{B}_{E,(k)}(t) = \exp \boldsymbol{\Omega}_{(k)}(t)$. For two synapses this is solved directly later on, most often, however this needs to be calculated by expanding the exponential function. We denote this approximation, where we neglect terms of both the exponential as well as the Magnus series greater than of order (k), with an S instead of an E, i.e., $S,(k)$, thus $\mathfrak{B}_{S,(k)}(t) = (\boldsymbol{I} + \Sigma_{p=2,q=1}^{p\cdot q \le k} 1/q \cdot (\boldsymbol{\Omega}_{(p)}(t))^q)$. Notice that in the limit $k \to \infty$ the approximation transforms into the general solution (Eq. 9). This solution is computable for arbitrary input patterns.

Now, as we know the complete analytical solution of Eq. 3, we investigate approximations and their errors in order to judge their usefulness for further considerations. To estimate the approximation errors we can use δ functions as inputs to the system. Furthermore, we assume that all $h_i = h$ are equal. The pulses are again modeled as δ functions $\delta(t - t_i)$ for times t_i which simplifies the convolution to a temporal shift in the filter function $h: h(t - t_i) = \int_0^\infty \delta(t - t_i - \tau) h(\tau) d\tau$. This leads for elements of $\boldsymbol{A}(t)$ to $A_{ij}(t) = F[h](t - t_i) G[h](t - t_j)$ where t_i and t_j are the pulse timings of neuron x_i and x_j respectively. We will use the filter shown in **Figure 1A**, given by Eq. 8.

The different approximation errors are exemplified in **Figure 1E**. For this we are using a single pulse pair at two synapses (see **Figure 1C**) for which we calculate the final synaptic strength $\tilde{\boldsymbol{\omega}} = \lim_{\tau\to\infty} \boldsymbol{\omega}(\tau)$ (Eq. 9). This has been performed for differential Hebbian learning, but we remark that the error is identical for Hebbian learning. For this setup, weight changes are computed in three ways: without any approximations, yielding $\tilde{\boldsymbol{\omega}}$ (Eqs. 9 and 11); using the truncated solution only, yielding $\tilde{\boldsymbol{\omega}}_{E,(k)}$; and using the truncated solution while also expanding the exponential function, yielding $\tilde{\boldsymbol{\omega}}_{S,(k)}$. Thus, we use $\tilde{\boldsymbol{\omega}}$ and compare it to approximations $\tilde{\boldsymbol{\omega}}_{\cdot,(k)}$, calculating the error as: $\Delta_{\cdot,(k)} = \left| \tilde{\boldsymbol{\omega}}_{\cdot,(k)} - \tilde{\boldsymbol{\omega}} \right|$. This is plotted in **Figure 1E** for different approximations against the plasticity rate μ on a log-log scale where we set the maximal value of the input filter h to 1. As approximations $E,(k)$ and $S,(k)$ become very similar for $k > 2$, only four curves are shown. We observe that the behavior of the difference-error $\Delta_{\cdot,(k)}$ follows the order of the approximation used. The error for the linear expansion approximation $S,(k = 2)$ is slightly higher than that from its corresponding truncation approximation $E,(k = 2)$. However, using a plasticity rate of $\mu = 0.001$ already results in a difference-error value of 10^{-8} compared to 10^{-2} when using the same value for μ and the maximum of h. Therefore, one can in most applications use even the simplest possible linear approximation $S,(k = 2)$ to calculate the change in synaptic strength.

As this calculation has been based on two pulses at two synapses only, we need to ask how the error develops when using N synapses and complex pulse trains. For this we first consider pulse trains, which are grouped "vertically" into groups with each input firing at most once. Filters of pulses within a group will overlap but we assume that grouping is possible such that adjacent groups are spaced with a temporal distance sufficient to prevent overlap between filter responses of temporally adjacent groups. Thus we calculate $\boldsymbol{\omega}$ in the same way as above leading to: $\tilde{\mathfrak{B}}_{\cdot,(k)} = \lim_{\tau\to\infty} \mathfrak{B}_{\cdot,(k)}(\tau)$. When using such a temporal tiling, $\tilde{\mathfrak{B}}_{\cdot,(k)}$ depends only on the pulse timing matrix $\boldsymbol{T}$ with elements $T_{ij} = t_j - t_i$. Then, we get the synaptic strength after M groups by calculating the product over all groups m to $\boldsymbol{\omega}_{M,\cdot,(k)} = \Pi_{m=1}^{M} \tilde{\mathfrak{B}}_{\cdot,(k)}(\boldsymbol{T}_m) \cdot \boldsymbol{\omega}(t_0)$.

This solution is easy to compute. Because a product of matrices results in a summation of matrix elements, the error does not increase exponentially but only linearly in M. Because of this it follows that even after 10000 pulses the error is still of an order of only 10^{-4} given the example above (see **Figure 1E**).

Finally we estimate how the error behaves when filters overlap. This mainly happens during bursts of pulses with temporarily high spiking frequencies, which are, in general, rare events. However, using the solution which assumes independent temporal intervals instead of the time-continuous calculation (Eq. 4), only includes

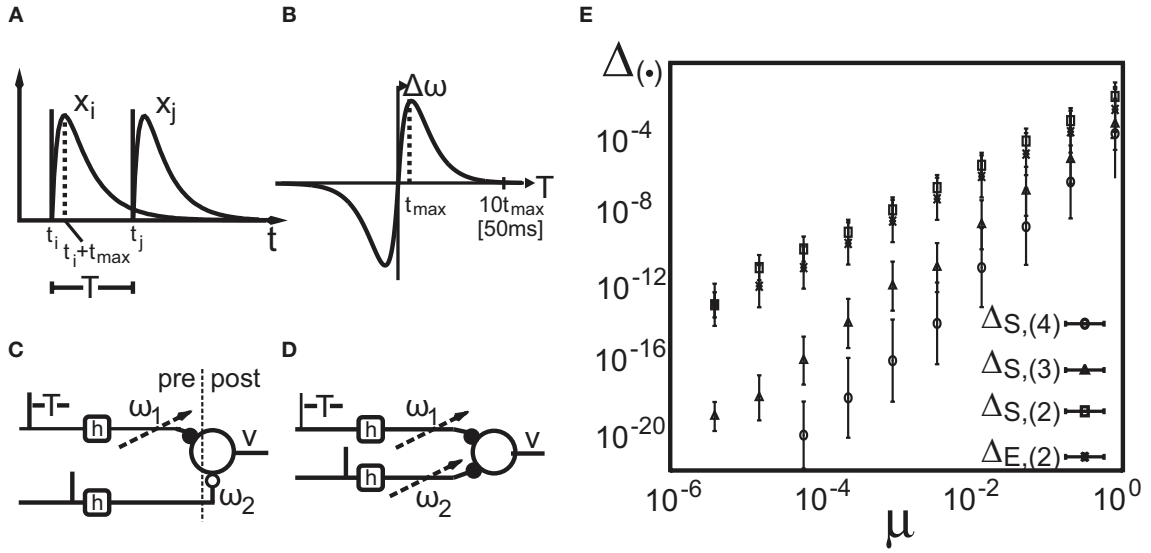

FIGURE 1 | Setup (A–D) and verification (E) of the approximation of Eq. 4. **(A)** Two pulses x_i and x_j at times t_i and t_j respectively are convolved with filter h. **(B)** Depending on the time difference T, differential Hebbian plasticity leads to a STDP-like weight change curve $\Delta\omega$ (Porr and Wörgötter, 2003; Kolodziejski et al., 2008). The maximum is at $t_{max} = (\log(\beta) - \log(\alpha))/(\beta - \alpha)$. **(C)** A simple network with only a single plastic synapse with which the relation of differential Hebbian plasticity to spike-timing-dependent plasticity is shown. **(D)** The used feed-forward network with two plastic synapses. **(E)** Here we show the degree of consistency between our general solution and the proposed approximations. To this end we plot the difference $\Delta_{,(k)} = |\tilde{\boldsymbol{\omega}}_{,(k)} - \tilde{\boldsymbol{\omega}}|$ (see Approximations for the Analytical Solution) between the approximation and the exact solution of Eq. 3 for one input pulse pair against the plasticity rate μ on a log-log scale. Here, a filter function h with $\alpha = 0.1$, $\beta = 0.2$, $\sigma = 0.25$, and $\max_t h(t) = 1$ is used (Eq. 8). The temporal difference $T = t_i - t_j$ between the two input pulses was varied over the length of the used filter functions (here between 1 and 100 steps) and error bars representing the standard deviation are given.

an additional error of order $k = 2$ due to the linearity of the filter functions h. The error after matrix multiplication results in the square of the lowest term of the Magnus series (Eq. 11).

Thus, the easily computable group decomposition $\tilde{\mathfrak{B}}_{,(k)}$ will yield accurate enough results even for long, non-bursting pulse trains.

FIXED-POINT ANALYSIS

Now we are able to calculate the temporal development of the weight dynamics in our networks. Most interesting are those developments that eventually lead to a stable, thus non-diverging, weight dynamics. Here, we develop the equations with which configurations of parameters (i.e., periodicity and delays of the recurrences) can be identified that lead to stable weights.

As mentioned, some of those (P, d_i) configurations converge to stable weight configurations, others do not. In order to reveal whether a configuration is stable, hence whether the plastic weights do not diverge, the nullclines ($\dot{\boldsymbol{\omega}} = 0$) need to have stable crossing points in the open region $]-1, +1[^R$ with R being the number of recurrent connections (±1 would lead to diverging activity since a constant input is added periodically for a theoretically infinite number of times). A crossing point outside this interval is never stable because of the recurrent connections involved [$\omega(n+1) = \xi\omega(n)$ with $\xi > 1$ always diverges].

For the calculations we place all input pulses on a discrete grid, but calculate correlations by continuous analytical integration. Hence, the weight change in the discretized version of Eq. 4 is $\boldsymbol{\omega}(n) = \mathfrak{B}(n,m)\cdot\boldsymbol{\omega}(m)$ where $\mathfrak{B}(n,m)$ denotes $\mathfrak{B}(t)$ with lower and upper boundaries m and n respectively. Weights are (periodically or asymptotically) stable if they take the same value after a certain number of periods P: $\boldsymbol{\omega}(n) = \boldsymbol{\omega}(n + \xi\cdot P)$ for $\xi \geq 1$ and n large enough. Here in this study we concentrate on the analytical solution for $\xi = 1$.

Therefore, in order to calculate those fixed-point weights, the following system of equations needs to be solved:

$$\left(\hat{\mathfrak{B}} - I\right)\cdot\boldsymbol{\omega}(n) = 0 \tag{12}$$

with n large enough so that the weights have already converged. $\hat{\mathfrak{B}} = \mathfrak{B}(n+P,n)$ is defined to include all relevant pulse correlations; it is, thus, similar to $\tilde{\mathfrak{B}}$. The roots of this system represent the fixed-points which are stable if all eigenvalues of $\hat{\mathfrak{B}}$ are negative.

In the next step we will use the $E,(k = 2)$ simplification for $\hat{\mathfrak{B}}$ which is $\boldsymbol{I} + \mu\int_U \boldsymbol{A}(\tau)d\tau$ with U being an interval that includes all relevant correlations. A detailed definition is given in Section "Fixed-Point Analysis" in the Appendix. With this we will arrive at an analytical solution of the weight dynamics of the recurrent structures. If we include this simplification into Eq. 12 we get

$$\int_U \boldsymbol{A}(\tau)d\tau\cdot\boldsymbol{\omega}(n) = 0. \tag{13}$$

Now we have to write down matrix $\boldsymbol{A}$ to get its integral. With R recurrences and a single input, $\boldsymbol{A}$ is of dimension $R + 1$. The first R rows and columns describe the in- and outputs to the plastic synapses and the last row and the last column the in- and output to the constant input synapse. We define its input as K, which is a sum of δ functions always at the beginning of each period. The inputs to the plastic synapses are given by the pulse amplitudes $\boldsymbol{\Gamma}$ (Eq. A.2), however, delayed by different delay times d_i. Putting everything together, we have to solve following integral:

$$\int_U \boldsymbol{A}(\tau)d\tau = \int_U \left(\begin{array}{ccc|c} \ddots & \vdots & \iddots & \vdots \\ \cdots & (x_i * h)(\tau)\frac{d}{d\tau}(x_j * h)(\tau) & \cdots & (x_i * h)(\tau)\frac{d}{d\tau}(K * h)(\tau) \\ \iddots & \vdots & \ddots & \vdots \\ \hline \cdots & (K * h)(\tau)\frac{d}{d\tau}(x_j * h)(\tau) & \cdots & (K * h)(\tau)\frac{d}{d\tau}(K * h)(\tau) \end{array}\right) d\tau = \int_U \left(\begin{array}{ccc|c} \ddots & \vdots & \iddots & \vdots \\ \cdots & a_{i,j}(\tau) & \cdots & q_i(\tau) \\ \iddots & \vdots & \ddots & \vdots \\ \hline \cdots & p_j(\tau) & \cdots & b(\tau) \end{array}\right) d\tau \tag{14}$$

We skip the detailed calculations (including the definition for $\bar{s}$) here, given in Section "Fixed-Point Analysis" in the Appendix, and directly write the result where only correlations in the interval U have been considered and the pulse amplitudes $\boldsymbol{\Gamma}$ (Eq. A.2) were applied:

$$\begin{aligned} \int_U a_{i,j}(\tau)d\tau &= \sum_{m=-\bar{s}}^{\bar{s}} \sum_{k=1}^{P} \sum_{l=1}^{P} \Gamma_k \cdot \Gamma_l \cdot \Delta\omega\left(l-k+d_j-d_i+mP\right) \\ \int_U q_i(\tau)d\tau &= \sum_{m=-\bar{s}}^{\bar{s}} \sum_{k=1}^{P} \Gamma_k \cdot \Delta\omega\left(-k-d_i+mP\right) \\ \int_U p_j(\tau)d\tau &= \sum_{m=-\bar{s}}^{\bar{s}} \sum_{k=1}^{P} \Gamma_k \cdot \Delta\omega\left(k+d_j+mP\right) \\ \int_U b(\tau)d\tau &= \sum_{m=-\bar{s}}^{\bar{s}} \Delta\omega(mP). \end{aligned} \tag{15}$$

Obviously, the number of fixed points is not restricted to one and there exist many configuration with more than one fixed-point. However, we will show below that if a configuration is stable, than it does not matter how many fixed points in the interval]−1, 1[exist.

Here we would like to stress again that we are not interested in average quantities (no mean-field approach) but in the fine temporal dynamics of each single weight and additionally that a non-diverging weight is also a necessary condition for a non-diverging overall activity as we do not use any kind of boundaries.

Now, we have all tools ready to analyze the network structures (**Figures 1C and 2A,C**) starting without additional noise, thereafter with noise and finally by also considering asymmetrical STDP rules.

ANALYSIS OF THE NETWORK STRUCTURES WITHOUT NOISE

First, we will investigate the structures, which we introduced in the beginning of this study, in the absence of noise. The feed-forward structure always displays oscillation of weights and activity whereas the recurrent structures show more complex behavior. Depending on the network parameters, the weights either diverge, converge to a fixed-point or oscillate.

Feed-forward single neuron model

Here we look in more detail at symmetrical differential Hebbian plasticity with two plastic synapses (see **Figure 1D**) where the simplification $E,(k = 2)$ is analytically fully solvable. We have also based the error analysis provided in **Figure 1E** on these calculations. For the approximation $E,(k = 2)$ the matrix results in

$$\mathfrak{B}_{E,(2)}(t) = \exp\left[\begin{pmatrix} 0 & \mu\nu_{T,-1}(t) \\ \mu\nu_{T,+1}(t) & 0 \end{pmatrix}\right] \tag{16}$$

where $\nu_{T,-1}(t) = \int_0^t h(\tau)\cdot dh(\tau - T)/d\tau \cdot d\tau$ and $\nu_{T,+1}(t) = \int_0^t h(\tau - T)\cdot dh(\tau)/d\tau \cdot d\tau$. Here we use two input neurons ($N = 2$), which receive inputs at $t = 0$ and T, respectively. Overall, this results in following solution for the weight after a pulse pair ($\tilde{\mathfrak{B}}_{E,(2)} = \lim_{\tau\to\infty} \mathfrak{B}_{E,(2)}(\tau)$) with the calculations provided in Section "Feed-Forward Structure" in the Appendix (special solution for $\rho = 1$)

$$\tilde{\mathfrak{B}}_{E,(2)} = \begin{pmatrix} \cos\left(\mu\tilde{\nu}_T\right) & \sin\left(\mu\tilde{\nu}_T\right) \\ -\sin\left(\mu\tilde{\nu}_T\right) & \cos\left(\mu\tilde{\nu}_T\right) \end{pmatrix}. \tag{17}$$

Having found the analytical solution we now determine dynamics of the temporal development by calculating the eigenvalues λ_i of $\tilde{\mathfrak{B}}_{E,(2)} - \boldsymbol{I}$ which are:

$$\lambda_1 = \exp\left(i\mu\tilde{\nu}_T\right) - 1 \qquad \lambda_2 = \exp\left(-i\mu\tilde{\nu}_T\right) - 1. \tag{18}$$

This shows clearly that the weights oscillate around 0 and that the oscillations of the weights are damped if the real parts of the eigenvalues λ_i are smaller than 0. This constraint holds for almost all T values as $\Re\left(\lambda_i\right) = \cos\left(\mu\tilde{\nu}_T\right) - 1 = 0$ is only true for a multiple of the number 2π. However, $0 \le \mu\tilde{\nu}_T < \pi$ holds since we assume μ to be small. Furthermore, $\mu\tilde{\nu}_T = 0$ is trivial and does not lead to any weight change at all. Hence, the weights will continuously shrink to 0.

Recurrent networks

Next, we investigate the stability of the two neuron model with a single recurrence (see **Figure 2A**) for which we need the previously provided solution for Eq. 13. In small panels to the right of **Figure 2B** we show three different temporal developments of the plastic weight. The top panel depicts a divergent weight (P = 100 ms and d = 85 ms), the middle panel a convergent weight development (P = 100 ms and d = 60 ms) and the bottom panel an oscillating weight (P = 59 ms and d = 94 ms). In the main panel of **Figure 2B** the weight values of all configurations for $0 < P < 100$ ms and $0 < d < 100$ ms (which is 0–2.0 times the characteristic STDP length of 50 ms) are plotted. In case of convergence the final weight is depicted, however, if the weight diverges, no point is plotted at all (white regions). For oscillating weights we plot the mean value.

Figure 2B reveals that if (P, d) is stable, then (nP, nd) with $n \ge 1$ is also stable (lines through origin). However, weights will not be the same for (P, d) and (nP, nd). The stability statement only holds for configurations in which the weight has not reached a value whose absolute value is ≥1. This immediately leads to divergence and is the reason why the lines through the origin not always start at the origin.

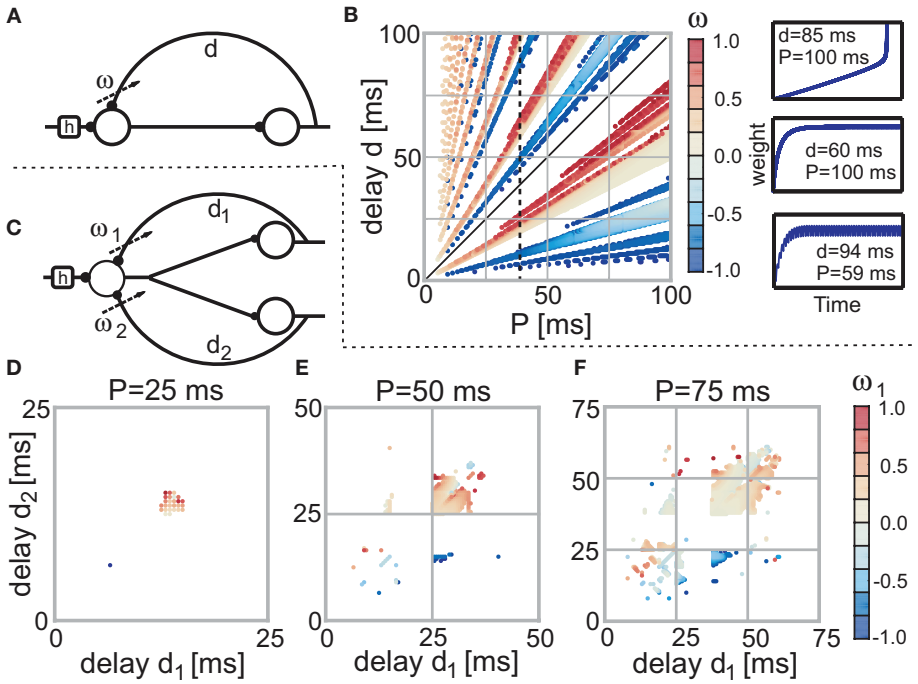

FIGURE 2 | Stable fixed points of the single (A) and double (C) recurrence networks without noise. **(B)** The color code indicates the actual weight values of each fixed-point dependent on the parameter *P* and *d* (delay) of the network. Parameter configurations which lead to divergent weights are not shown (i.e., are white). The three panels on the right side of **(B)** exemplify the three possible temporal weight developments (from top to bottom: divergent, convergent, and oscillating). **(D–F)** Dependent on two delays d_1 and d_2 the stable fixed points for the three neuron structure **(C)** are shown. Each panel uses a different *P* value (**D**: 25 ms; **E**: 50 ms; **F**: 75 ms). Note that we only need to plot one of the two weights as the other weight is just a reflection in the diagonal; the diagonal as such represents the single recurrence weights (half of the value).

Additionally, **Figure 2B** shows that excitatory and inhibitory regions always alternate and that the two regions for $d < P$ (below diagonal) are almost of the same size as the many regions for $d > P$ (above diagonal). Furthermore, if the first delayed pulse is closer to its input pulse (i.e., $d < P/2$), than the final weight is inhibitory. By contrast, if the first delayed pulse is closer to the consecutive input pulse (i.e., $P/2 < d < P$), than the final weight is excitatory. In the excitatory case, the pulse at the plastic synapse is followed by another pulse. This resembles a causal relationship which should lead to a weight growth. The opposite is true for the inhibitory case.

We also conducted a perturbation analysis in which we perturbed the weight for each configuration with increasing amplitude until the weight could not converge back to its fixed point. It turns out that the crucial measure for stability is whether the absolute value of the sum of the fixed-point value and the perturbation amplitude exceeds 1. This is true for almost all configurations with stable weights which is why we do not need to plot the results of the perturbation analysis.

Another property of the system is that the final weights are identical for $(P, d + nP)$ configurations for all $n \geq 1$ (see **Figure 2B**, in particular the black dashed line at $P = 40$ ms). Thus, if the weight for e.g., $P = 40$ ms and $d = 25$ ms converges to ω, so does the weight for $P = 40$ ms and $d = 65$ ms. We use this property to simplify the convergence plots of the network structure with three neurons or two quasi recurrences (**Figures 2D–F**) and only depict fixed points for delay values *up to* the periodicity *P*. We show the fixed points for three different values of *P*: 0.5, 1.0, and 1.5 times the characteristic STDP time window (we leave out the 2.0 times as we do not get anything novel at higher periodicity values according to **Figure 2B**).

Starting with $P = 25$ ms (**Figure 2D**) it is apparent that only a few inhibitory connections evolved (only about 10%). However, when moving to higher *P* values (**Figures 2E,F**), more and more inhibitory connections show up. If we had plotted (not shown) the ratio of excitatory connections, we would find that at about $P = 100$ ms the ratio of excitatory connections reaches 0.5 and for all smaller values the ratio is always >0.5, thus more excitatory connections develop. We note that all properties mentioned in this paragraph remain essentially the same, when adding noise to the input.

Figures 2E,F reveal that the main regions (upper-right, middle) move to higher (d_1, d_2) configurations and enlarge at the same time. In addition, new regions originate at smaller (d_1, d_2) configurations.

The total number of fixed points N_0 scaled by the number of the possible configurations, of which there are P^2, also grows with increasing periodicity (see **Figure 3**, black dots). In the next section we will compare the number of fixed points to two different noisy input protocols.

ANALYSIS OF THE NETWORK STRUCTURES WITH NOISE

Above we used deterministic timing at the input to our system. As this is not realistic, we will now use two different types of noise. The first one is Gaussian jitter around the given periodicity value

P with a standard deviation of 5 ms. The second one is Poisson firing with rate P. Due to the stochastic nature of the signals, analytical results cannot be obtained anymore and we have to rely on simulations.

Feed-forward structure

The general behavior of the feed-forward structure does not change in the presence of either noise. Although the oscillations are not "perfect" anymore, weights are still oscillating and eventually they decay to 0.

Recurrent structures

For the recurrent structures the situation is different as noise is able to change an initially unstable configuration to now exhibit a convergent weight development and vice versa. In **Figure 4** we show the stability of the weights for different configurations. Here, red stands for highly stable weights (i.e., all trials lead to convergence) and blue for rarely stable ones (i.e., only a few trials lead to convergence). Stability in between where half of the trials lead to convergence is very rare, so we included those configurations to the rarely stable ones. In order to compare the noise results with those for no noise, we include the no noise stable regions in gray in **Figure 4**. Additionally, the color of each configuration that is stable both with and without noise is lighter (i.e., light red and light blue). We do not plot the actual final weight values as those are not largely different from the no noise ones.

For the two neuron structure, a few of the branches in **Figures 4A,B** completely disappeared, others moved slightly. The two main branches for $d < T$ (below diagonal) remain highly stable, however, only in the "core". The more diffuse, non-compact regions, i.e., regions with detached stable configurations become either completely unstable or at least rarely stable. Noise affects the input periodicity, thus configurations that are stable for a large range of different P values survive when noise has been added. By contrast, configurations within non-compact regions are always deflected toward unstable configurations, thus, compromising or even losing their stability. However, in a few trials they still happen to survive which leads to the regions with many rarely stable configurations.

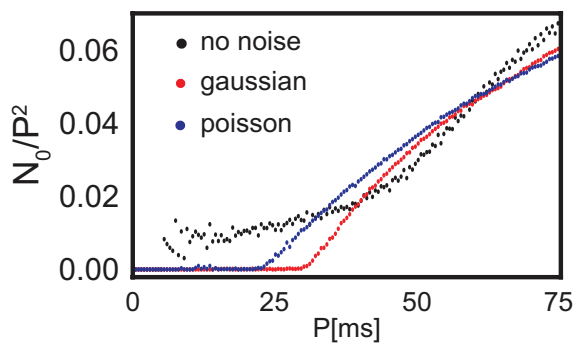

FIGURE 3 | Number of configurations N_0 that lead to stable weights multiplied with the probability that such a configuration leads to stability (see Figure 4) with respect to the periodicity P. Additionally, N_0 is normalized by the maximum possible configurations (P^2) and we plot the results without noise (black), with Poisson distributed firing with rate P (blue) and Gaussian distributed periodicity with mean P and a variance of 5 ms (red).

It is clearly visible that the number of stable configurations for the structure with a single recurrence substantially decreases. This is, however, not the case for the double recurrence structure. There, the number of stable configurations increases (see red border in **Figures 4G,H**) because of the compact structure. However, this effect starts above $P = 30$ ms which is revealed by **Figure 3**. In this figure we plot the number of stable (non-divergent) configurations N_0 normalized by the maximum possible configurations (P^2) against the periodicity P. Only between about 30 and 60 ms noise increases the number of stable configurations by about 20%. Above 60 ms the smaller non-compact areas that lose stability dominate over the border areas that gained stability. Above a certain periodicity the smaller areas become large enough so that noise becomes advantageous again and border regions become stable. Therefore, the effect that noise slightly increases stability reoccurs periodically. **Figure 3** also shows clearly that Poisson statistics leads to slightly more stable configurations than adding Gaussian noise. Most important, however, is the fact that noise does not deteriorate the system, i.e., the number of stable configurations stays almost unchanged.

Similar to the feed-forward structure, weights sometimes change from positive to negative values (or vice versa), hence they switch from being excitatory to being inhibitory which is not known from biology. However, this could be easily solved if we exchange our linear synapse with two non-linear synapses (one that is linear in the positive regime and 0 elsewhere and the other vice versa), so that such a push–pull mechanism covers the full linear range. This is the conventional way of addressing this issue (Pollen and Ronner, 1982; Ferster, 1988; Palmer et al., 1991; Heeger, 1993; Wörgötter et al., 1998). Note, however, in general we found that without noise switching is rather rare in our recurrent structures anyways. Even with additional noise weights tend to switch only if the final weight is close to 0.

ANALYSIS OF THE NETWORK STRUCTURES WITH ASYMMETRIC STDP RULES

In biological systems, the STDP curve is not symmetrical (Bi and Poo, 1998; Caporale and Dan, 2008). In order to achieve an asymmetric differential Hebbian plasticity curve, we leave the positive part which describes the strengthening of the weight (LTP) as it is and shrink or stretch the negative part which describes the weakening (LTD). This is done by multiplying negative weight changes with a factor ρ.

Feed-forward structure

For the feed-forward structure we calculated the temporal development analytically (see Section "Feed-Forward Structure" in the Appendix) and find that the general behavior is not changed by the asymmetry. This becomes visible from the eigenvalues of the system:

$$\lambda_1 = \exp\left(i\mu\tilde{\nu}_T\sqrt{\rho}\right) - 1 \qquad \lambda_2 = \exp\left(-i\mu\tilde{\nu}_T\sqrt{\rho}\right) - 1. \tag{19}$$

Both oscillation and damping still exist, however, damping constant and frequency of the oscillation is scaled by the asymmetry ρ.

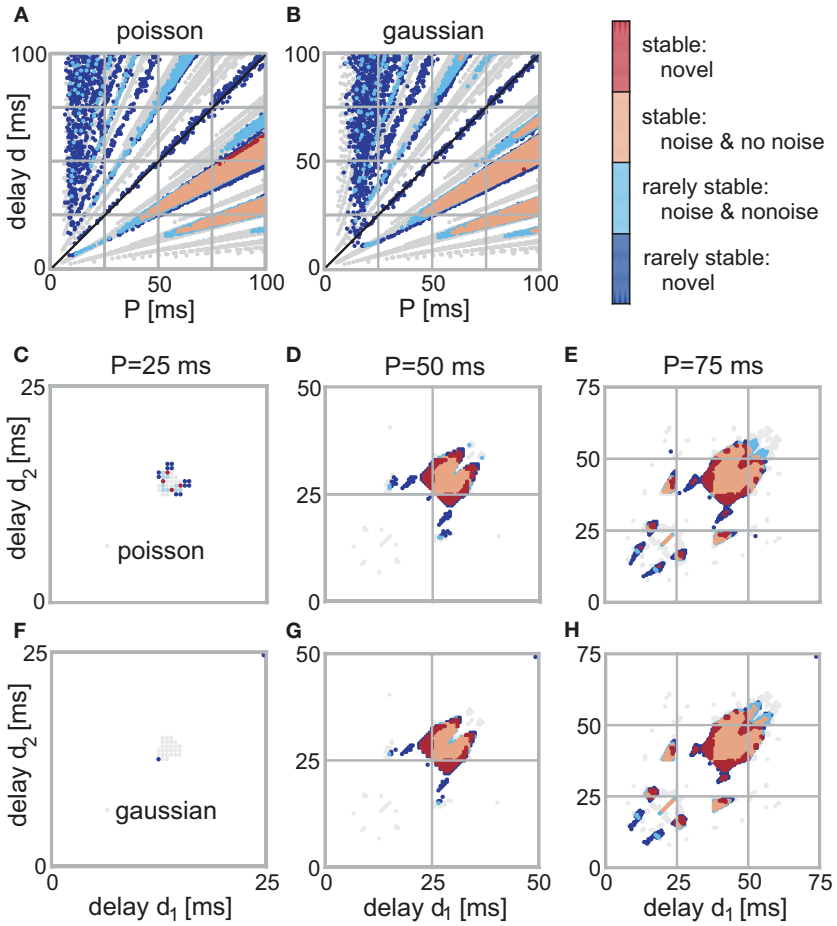

FIGURE 4 | Stable fixed-points of the single (A,B) and double (C–H) recurrence network with noise. The color code indicates the stability of each point. (Light)red is for points which are stable at each trial (out of 10 simulations) and (light)blue for rarely stable points. In gray are the no noise fixed points; light colors indicate that a point is stable with and without noise. **(A,B)** Those panels show the weight stability where the firing was distributed following Poisson statistics **(A)** using P as rate. **(B)** Shows the results with Gaussian noise with a mean P and a variance 5 ms. **(C–H)** Three neuron structure; the left column depicts the converged weights for $P = 25$ ms, the middle for $P = 50$ ms, and the right for $P = 75$ ms. **(C–E)** Poisson distributed firing with rate P, **(F–H)** Gaussian distributed periodicity with mean P and a variance of 5 ms.

Recurrent structures

Now we come to the recurrent structures. Here, similar to the introduction of noise, the situation is different. With an additional asymmetry the number of stable configurations changes. In the following, we depict the number of stable configuration achieved with a certain asymmetry $\rho = 2^a$ (logarithmic representation) by N_a. Thus, the number of stable configuration for the symmetric STDP curve is still N_0. Then, to better compare the different results, we normalize N_a to the symmetric number N_0 plotting N_a/N_0 in **Figure 5**. It is worthwhile to note that the total (not the relative) number of stable configurations without noise is reduced for any value of a for the single recurrence structure and stays almost unchanged for the double recurrence structure (see **Figure 3**).

First, we look in more detail at the single recurrence structure (**Figure 5A**). We plot the normalized number N_a/N_0 of stable configurations up to a periodicity of $P = 50$ ms. The respective N_0 values can be found in the caption of **Figure 5**. The no noise results have a peak for positive and for negative asymmetries, thus an asymmetric STDP curve yields more stable configurations than a symmetric one. Here, a dominant LTP part is advantageous over a dominant LTD part. This situation changes when we introduce noise. An STDP curve with a dominant LTD part results now in more stable configurations than a LTP-dominant STDP curve. However, almost all asymmetric STDP curves lead to many more stable configurations as compared to a symmetric STDP curve. Here we note again that making the input spiking obeying the Poisson statistics is advantageous over adding Gaussian noise (if comparing absolute numbers).

Next, we consider the double recurrence structure (**Figure 5B**) where the number of stable configurations were also counted up to $P = 50$ ms. Here, the no noise result looks more similar to the results with noise; two peaks, one for an LTP-dominant and one for an LTD-dominant STDP curve, are visible. However, adding noise to the system again changes the relative heights of the peaks: the STDP curve with more LTD becomes advantageous over the STDP curve with more LTP. Similar to the single

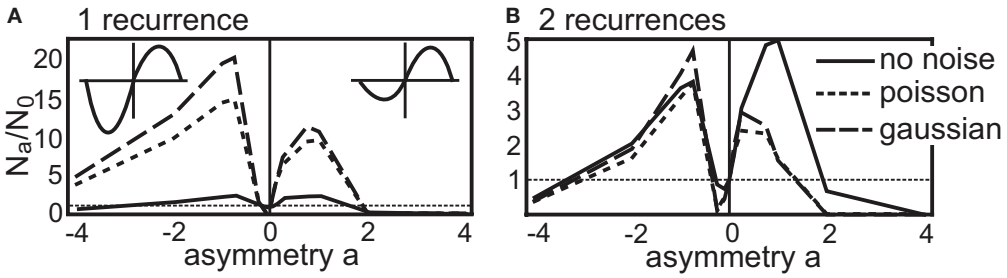

FIGURE 5 | Number of stable configurations N_a with respect to the asymmetry a of the STDP curve normalized by the number of stable configurations without asymmetry N_0. The part that leads to a reduction in synaptic efficiency (LTD-side) is scaled by 2^a. **(A)** This panel shows the number of stable configurations of the single recurrence and **(B)** for the double recurrence structure both up to a periodicity of $P = 50$ ms. The results that were obtained without noise are depicted by the solid line, the results with Gaussian noise by the dash-dotted line and the results with Poisson statistics by the dotted line. The N_0 values for no noise, Gaussian and Poisson are 737, 73, 105 for the single recurrence network and for the double recurrence network they are 6464, 5693, 7435.

recurrence structure, there are more stable configurations when using Poisson noise, however, with Gaussian noise the boost in stability for asymmetrical as compared to the symmetrical STDP curve is larger. If we compare the number of stable configurations between LTP-dominant and LTD-dominant STDP curves we find that without noise about 55.0% LTP-dominant configurations of the total number of configurations exists. With Gaussian noise this ratio decreases to 41.7% and with Poisson statistics to 44.0%.

The dynamics of the structures examined here (and the reasoning should extend to all possible structures) would allow only for diverging weights if we set $a \to \pm\infty$. As this would correspond to an STDP curve with pure LTP or LTD respectively, the dynamics pushes the weight only in one direction (either positive or negative) which leads to no fixed point (see Eqs. 14 and 15). This is also indicated in **Figure 5** where the number of configurations leading to convergence is severely reduced even for $a = \pm 4$.

DISCUSSION

Real neurons often display rich, non-stationary, firing patterns by which all synaptic weights will be affected. The so far existing solutions which describe Hebbian learning, on the other hand, constrain the temporal dynamics of the system or limit plasticity to a subset of synapses. With the solution presented here we can calculate weight changes for the first time without these restrictions. This is a valuable step forward in our understanding of synaptic dynamics of general Hebbian plasticity as well as of STDP (which is a special case of the general Hebbian plasticity rule) in different networks. Specifically, we have presented the time-continuous solution for the synaptic change of general Hebbian plasticity (Eqs 9 and 11), its approximation for general spiking or continuous inputs as well as a specific solution for non-bursting pulse trains. Of practical importance is the fact that the error of the computable approximations remains small even for long pulse trains.

We think that there is in general no intuitive access, which would allow us to understand the temporal development of activity and plasticity in networks with recurrent connections. Even small structures driven by periodic activity, such as the ones investigated here, display unexpected and counterintuitive behavior. The systems investigated are linear and summation takes place at the level of PSPs, which are here modeled by ways of the filter function h. This way closed-form solutions can be found. Spiking could be introduced by ways of a threshold. Introducing such a threshold essentially leads to the reduction of activity (eliminating all small linearly summed signals) but the general recurrence is not altered.

The first network investigated was a simple feed-forward structure (see **Figure 1C**) which displays oscillating weights which decay to 0. This observation is interesting and not expected as this network and its inputs represent a fully symmetrical situation. Hence, oscillation should occur, one would think, but without damping. Asymmetrical STDP curves do not alter this observation, because the asymmetry of the STDP curve only affects the frequency of the weight oscillation.

The focus of the current study, however, was to investigate recurrent network structures without averaging the activity. The two small recurrent networks studied here can be seen as fundamental network building blocks. This is due to the fact that the direct recurrent connections used here could also be replaced by a network, the output of which providing the recurrent signals. This seems to be similar to Roberts (2004), Burkitt et al. (2007), and Gilson et al. (2009), however, in those studies only average activities are considered. Roberts (2004) does not treat plasticity, Burkitt et al. (2007) and Gilson et al. (2009) do not have self-connections, and Roberts (2004) and Burkitt et al. (2007) do not have delays included. Without delays, self-connections would be cumbersome to implement in a general way (i.e., for different delays a different number of neurons need to be interposed). However, Burkitt et al. (2007) and also Gilson et al. (2009) could easily extend their models to include self-connections.

As a side remark, almost all of the above mentioned studies only consider pair-wise STDP correlations although a method for three-pair couplings exists (Pfister and Gerstner, 2006). By contrast, differential Hebbian plasticity treats multi-correlations naturally.

In the much cited study of Bi and Poo (1998) a clear asymmetry is visible in the STDP curve (Figure 7 of Bi and Poo, 1998): the part which describes the strengthening of synaptic efficiency, LTP, is more pronounced than the LTD part. In general, asymmetrical

STDP curves are found in many studies (see Caporale and Dan, 2008 for a review) where sometimes the situation is reversed (LTD more pronounced than LTP). Many theoretical studies of large-scale network development use STDP curves with stronger LTD part, because in many cases it has been found that otherwise weights will diverge (Song et al., 2000; Izhikevich et al., 2004). The current study, on the other hand, suggests that collective divergent behavior could also be prevented by more specific network designs. Here we were able to show that stability without boundaries is possible. We observe that – at least in those small linear networks – many fixed points exist for different types of STDP curves. Notably there are almost always more fixed points for asymmetrical as compared to the symmetrical STDP curve. Furthermore, the notion that an LTD dominance would be beneficial for stability does not seem to be unequivocally correct. Even in the presence of noise large numbers of fixed points are found when using LTP-dominated STDP curves.

The studies of Izhikevich et al. (2004), Burkitt et al. (2007), Morrison et al. (2007), Lubenov and Siapas (2008), Gilson et al. (2009), and Clopath et al. (2010) have considered fully as well as randomly connected networks with external drive, where they need to apply soft or even hard boundaries to stabilize weights. By contrast here we have looked at small recurrent networks without averaging and without boundaries. Thus, these approaches cannot be directly compared. Our results, however, appear promising. It may well be that networks with specific topologies can be constructed (or generated by self-organization), where stability exists using STDP for a large number of input patters without boundaries or weight-normalization.

Additionally, there exists a Hebbian rule that is not using boundaries either. It has been shown that the so called BCM rule (Bienenstock et al., 1982) is a rate description-based rule which is analogous to the STDP rule (Izhikevich and Desai, 2003; Pfister and Gerstner, 2006). However, to get weights stabilized, BCM is using an additional variable that pushes the weights so that the output activity is close to a set value. This rule, besides that it relies on a rate model, uses the activity to limit the weights in an indirect way, similar to other homeostasis mechanisms (Turrigiano and Nelson, 2004). Thus, it is possible that the BCM rule among others makes the weights diverge or rather diffuse which, nevertheless, would lead to a state with a finite and stable mean activity. Such a behavior does not emerge in our model as a single diverging weight will eventually reach infinity resulting in an infinite activity. Besides, our focus here is on the fine temporal dynamics of the weights.

Furthermore, we observe that noise has an influence on the recurrent structures (see **Figures 2A,C**). For some input periodicities P the number of stable configurations decreases, for other settings it grows. Growth is found especially for the double-recurrent structure. A reduced number of stable configurations is mainly visible in areas with many initially stable *isolated* points from where such a point can be easily "nudged out" to an unstable domain by noise. Such a nudging effect, however, is also the reason why the number of stable configurations can increase. Our results show that stable regions either enlarge at their boundaries or within dense but not fully covered areas. Here initially unstable data points are "nudged in" to adjacent stable regions. The difference between Gaussian and Poisson statistic is small, however, we found that Poisson statistics, thus the statistics most often used to describe neuronal spiking (Bair et al., 1994; Shadlen and Newsome, 1998; Dayan and Abbott, 2001), yields more stability. More importantly, noise does not deteriorate but even improves the system. The benefits of noise for neuronal signal processing has been discussed in several other studies (Fellous et al., 2003; Deco and Romo, 2008). The fact that synaptic stability benefits from noise, especially in the more complex double-recurrent structures, adds to this discussion. In our networks noise helps to reach out to nearby stable regions to exploit their stability.

The temporal development of multi-synapse systems and the conditions of stability are still not well understood. Some convergence conditions have been found (see for example Hopfield, 1982; Miller and MacKay, 1994; Roberts, 2000; van Rossum et al., 2000; Kempter et al., 2001; Burkitt et al., 2007; Kolodziejski et al., 2008), however, in general the synaptic strengths of such networks will diverge or oscillate. This is undesired, because network stability is important for the formation of, e.g., stable memories or receptive fields. Using the time-continuous solution for linear Hebbian plasticity described here serves therefore as a starting point to better understand mechanisms, structures and conditions for which stable network configurations will emerge. The rich dynamics, which govern many closed-loop adaptive, network based physical systems can, thus, now be better understood and predicted, which might have substantial future influence for the guided design of network controlled systems.

An important next step to improve our understanding of the interaction of plasticity and activity is to increase the complexity of the investigated network structures. Raising the number of recurrences is straightforward as we have already presented a general method to solve such networks. It will be more challenging to include plastic synapses at more than one neuron. **Figure 6A** shows as a small outlook such a possible network structure where we used $N = 5$ "building blocks" (see **Figure 2C**) each receiving constant periodic input (i.e., pulses), activity from itself (self-connection) and from the previous neuron (ring-connection). In this example we set all delays to the same value ($d_i = d$ and $d_{is} = d$) and the input has periodicity P (see **Figures 6C,D**). Each neuron i receives its first input spike at time $t = (i - 1) \cdot P/N$. Both the self-connection and the ring-connection are eligible to changes and **Figures 6C,D** show that, similar to our fundamental building blocks (see **Figures 1D and 2A,C**), configurations which lead to converging weights exist. The temporal development depicted in **Figure 6B** exemplifies the typical behavior found in those networks: due to its symmetry all self-connections and all ring-connections converge each to practically the same weight value. Many possible network topologies could visioned using those or similar building blocks. Hence, investigating those structures in more detail goes beyond the scope of this paper.

Also more complex input protocols must be investigated. The current study suggest that dynamically stable recurrent substructures can exist within larger networks. Similar results exist for the generation of stable activity patterns in (non-plastic) networks (Memmesheimer and Timme, 2006a,b). These studies may allow us to gradually approach a better understanding of dynamically

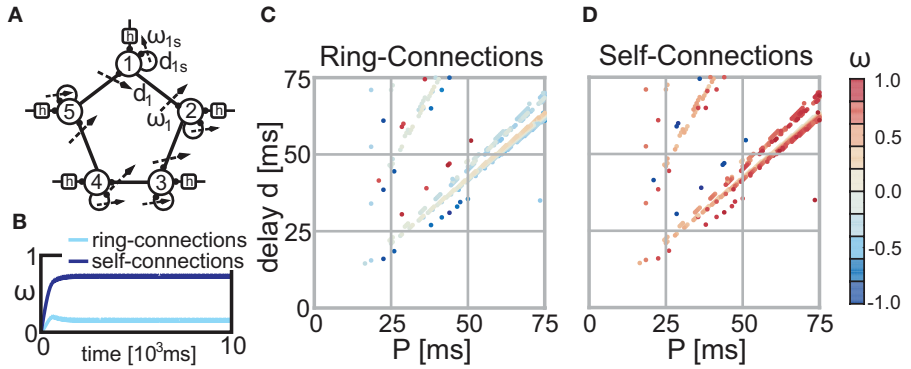

FIGURE 6 | Stable fixed points of the ring structure (A) without noise. **(B)** This panel exemplifies the temporal weight development for configuration $P = 70$ ms and $d = 58$ ms. All self-connections follow practically the same temporal development and this is also true for all ring-connections. **(C,D)** The color code indicates the actual weight values of the fixed-points of the self-connections **(C)** and the ring-connections **(D)** dependent on the parameter P and d (delay) of the network. Parameter configurations which lead to divergent weights are not shown (i.e., are white).

changing modular networks going beyond the currently still dominating unifying approaches, which mostly only consider feed-forward structures or randomly connected networks with average activities. This will require intensive studies but we hope that the current contribution can provide useful analytical tools and first insights into these very difficult problems.

ACKNOWLEDGMENT

We wish to thank M. Timme and R.-M. Memmesheimer for fruitful discussions and the German Ministry for Education and Research (BMBF) via the Bernstein Center for Computational Neuroscience (BCCN) Göttingen under Grant No. 01GQ1005A and 01GQ1005B as well as the Max Planck Society for financial support.

REFERENCES

Bair, W., Koch, C., Newsome, W., and Britten, K. (1994). Power spectrum analysis of bursting cells in area MT in the behaving monkey. *J. Neurosci.* 74, 2870–2892.

Bi, G., and Poo, M. (1998). Synaptic modifications in cultured hippocampal neurons: dependence on spike timing, synaptic strength, and postsynaptic cell type. *J. Neurosci.* 18, 10464–10472.

Bienenstock, E., Cooper, L. N., and Munro, P. (1982). Theory for the development of neuron selectivity: orientation specificity and binocular interaction in visual cortex. *J. Neurosci.* 2, 23–48.

Burkitt, A. N., Gilson, M., and van Hemmen, J. L. (2007). Spike-timing-dependent plasticity for neurons with recurrent connections. *Biol. Cybern.* 96, 533–546.

Caporale, N., and Dan, Y. (2008). Spike-timing-dependent plasticity: a Hebbian learning rule. *Annu. Rev. Neurosci.* 31, 25–46.

Clopath, C., Büsing, L., Vasilaki, E., and Gerstner, W. (2010). Connectivity reflects coding: a model of voltage-based STDP with homeostasis. *Nat. Neurosci.* 13, 344–352.

Dayan, P., and Abbott, L. F. (2001). *Theoretical Neuroscience*. Cambridge, MA: MIT Press.

Deco, G., and Romo, R. (2008). The role of fluctuations in perception. *Trends Neurosci.* 31, 591–598.

Fellous, J., Rudolph, M., Destexhe, A., and Sejnowski, T. (2003). Synaptic background noise controls the input/output characteristics of single cells in an in vitro model of in vivo activity. *Neuroscience* 122, 811–829.

Ferster, D. (1988). Spatially opponent excitation and inhibition in simple cells of the cat visual cortex. *J. Neurosci.* 8, 1172–1180.

Gilson, M., Burkitt, A. N., Grayden, D. B., Thomas, D. A., and van Hemmen, J. L. (2009). Emergence of network structure due to spike-timing-dependent plasticity in recurrent neuronal networks iv. *Biol. Cybern.* 101, 427–444.

Gütig, R., Aharonov, R., Rotter, S., and Sompolinsky, H. (2003). Learning input correlations through non-linear temporally asymmetric Hebbian plasticity. *J. Neurosci.* 23, 3697–3714.

Heeger, D. J. (1993). Modeling simple-cell direction selectivity with normalized, half-squared, linear operators. *J. Neurophysiol.* 70, 1885–1898.

Hopfield, J. J. (1982). Neural networks and physical systems with emergent collective computational properties. *Proc. Natl. Acad. Sci. U.S.A.* 79, 2554–2558.

Izhikevich, E. M., and Desai, N. S. (2003). Relating STDP to BCM. *Neural Comput.* 15, 1511–1523.

Izhikevich, E. M., Gally, J. A., and Edelman, G. M. (2004). Spike-timing dynamics of neuronal groups. *Cereb. Cortex* 14, 933–944.

Kempter, R., Gerstner, W., and van Hemmen, J. L. (2001). Intrinsic stabilization of output rates by spike-based Hebbian learning. *Neural. Comput.* 13, 2709–2741.

Klopf, A. H. (1988). A neuronal model of classical conditioning. *Psychobiology* 16, 85–123.

Kolodziejski, C., Porr, B., and Wörgötter, F. (2008). Mathematical properties of neuronal TD-rules and differential Hebbian learning: a comparison. *Biol. Cybern.* 98, 259–272.

Kosco, B. (1986). "Differential Hebbian learning," in *Neural Networks for Computing: AIP Conference Proceedings*, Vol. 151, ed. J. S. Denker (New York: American Institute of Physics), 277–282.

Lubenov, E. V., and Siapas, A. G. (2008). Decoupling through synchrony in neuronal circuits with propagation delays. *Neuron* 58, 118–131.

Magee, J. C., and Johnston, D. (1997). A synaptically controlled, associative signal for Hebbian plasticity in hippocampal neurons. *Science* 275, 209–213.

Magnus, W. (1954). On the exponential solution of differential equations for a linear operator. *Commun. Pure Appl. Math.* VII, 649–673.

Markram, H., Lübke, J., Frotscher, M., and Sakmann, B. (1997). Regulation of synaptic efficacy by coincidence of postsynaptic APs and EPSPs. *Science* 275, 213–215.

Memmesheimer, R.-M., and Timme, M. (2006a). Designing complex networks. *Physica D* 224, 182–201.

Memmesheimer, R.-M., and Timme, M. (2006b). Designing the dynamics of spiking neural networks. *Phys. Rev. Lett.* 97, 188101.

Miller, K. D., and MacKay, D. J. C. (1994). The role of constraints in Hebbian learning. *Neural Comput.* 6, 100–126.

Morrison, A., Aertsen, A., and Aertsen, A. (2007). Spike-timing-dependent plasticity in balanced random networks. *Neural. Comput.* 19, 1437–1467.

Palmer, L., Jones, J., and Stepnowski, R. (1991). "Striate receptive fields as linear filters: characterization in two dimensions of space," in *The Neural Basis of Visual Function. Vision and Visual Dysfunction*, Vol. 4, ed. A. G. Leventhal (Boca Raton: CRC Press), 246–265.

Pfister, J.-P., and Gerstner, W. (2006). Triplets of spikes in a model of spike timing-dependent plasticity. *J. Neurosci.* 26, 9673–9682.

Pollen, D. A., and Ronner, S. F. (1982). Spatial computation performed by simple and complex cells in the visual cortex of the cat. *Vision Res.* 22, 101–118.

Porr, B., and Wörgötter, F. (2003). Isotropic sequence order learning. *Neural Comput.* 15, 831–864.

Roberts, P. D. (1999). Computational consequences of temporally asymmetric learning rules: I. Differential Hebbian learning. *J. Comput. Neurosci.* 7, 235–246.

Roberts, P. D. (2004). Recurrent biological neuronal networks: the weak and noisy limit. *Phys. Rev. E* 69, 031910.

Roberts, P. D. (2000). Dynamics of temporal learning rules. *Phys. Rev. E* 62, 4077–4082.

Saudargiene, A., Porr, B., and Wörgötter, F. (2004). How the shape of pre- and postsynaptic signals can influence STDP: a biophysical model. *Neural Comput.* 16, 595–626.

Shadlen, M. N., and Newsome, W. T. (1998). The variable discharge of cortical neurons: implications for connectivity, computation, and information coding. *J. Neurosci.* 18, 3870–3896.

Song, S., Miller, K., and Abbott, L. (2000). Competitive Hebbian learning through spike-timing-dependent synaptic plasticity. *Nat. Neurosci.* 3, 919–926.

Tamosiunaite, M., Porr, B., and Wörgötter, F. (2007). Self-influencing synaptic plasticity: recurrent changes of synaptic weights can lead to specific functional properties. *J. Comput. Neurosci.* 23, 113–127.

Turrigiano, G. G., and Nelson, S. B. (2004). Homeostatic plasticity in the developing nervous system. *Nat. Rev. Neurosci.* 5, 97–107.

van Rossum, M. C. W., Bi, G. Q., and Turrigiano, G. G. (2000). Stable Hebbian learning from spike timing-dependent plasticity. *J. Neurosci.* 20, 8812–8821.

Wörgötter, F., Nelle, E., Li, B., Wang, L., and Diao, Y. (1998). A possible basic cortical microcircuit called "cascaded inhibition." results from cortical network models and recording experiments from striate simple cells. *Exp. Brain Res.* 122, 318–332.

Wörgötter, F., and Porr, B. (2004). Temporal sequence learning, prediction, and control – a review of different models and their relation to biological mechanisms. *Neural Comput.* 17, 245–319.

Conflict of Interest Statement: The authors declare that the research was conducted in the absence of any commercial or financial relationships that could be construed as a potential conflict of interest.

Received: 23 February 2010; paper pending published: 13 April 2010; accepted: 23 August 2010; published online: 27 October 2010.

*Citation: Kolodziejski C, Tetzlaff C and Wörgötter F (2010) Closed-form treatment of the interactions between neuronal activity and timing-dependent plasticity in networks of linear neurons. Front. Comput. Neurosci. **4**:134. doi: 10.3389/fncom.2010.00134*

APPENDIX

PULSE TIMINGS AND AMPLITUDE

In the main text we only calculated the timings of the pulses. In order to determine the amplitude of each pulse of a system with R recurrent connections, we need to go further and solve a linear system of equations. Doing this we need to assume that the weights eventually converge, therefore being constant.

In more detail, in each period of length P there are at most P pulses, each having different amplitude. Within each period each pulse gets multiplied by certain weights (which we assume to be constant) and is then delayed. Additionally, the input provides the neuron with another pulse of amplitude 1. Hence, if we write the pulse amplitudes in a vector $\mathbf{\Gamma}$ and put the multiplicative factors (i.e., the weights) into a matrix $\mathbf{\Lambda}$ always at the delayed position, we find the pulse amplitude $\mathbf{\Gamma}$ of the next period according to

$$\mathbf{\Gamma}^{(k+P)} = \mathbf{\Lambda}\mathbf{\Gamma}^{(k)} + \boldsymbol{\lambda} \tag{A.1}$$

with $\boldsymbol{\lambda} = (1,0,\ldots,0)^T$. Additionally, we set $\Lambda_{n,m=m_i} = \omega_i$ and $\Lambda_{n,m\neq m_i} = 0$ where $m_i = \mathrm{mod}\,(n - d_i, P)$. Since Eq. A.1 is linear, the amplitudes of the pulses will converge to a certain amplitude $\mathbf{\Gamma} = \lim_{k\to\infty} \mathbf{\Gamma}^{(k)}$ and we get

$$\mathbf{\Gamma} = (\boldsymbol{I} - \mathbf{\Lambda})^{-1}\boldsymbol{\lambda}. \tag{A.2}$$

The solution results in equations that involve high polynomial terms and are, thus, complicated to simplify. An example for the pulse timings with $P = 10, d_1 = 4$ and $d_2 = 6$ (here in arbitrary units) can be found below:

$$\mathbf{\Lambda} = \begin{pmatrix} 0 & 0 & 0 & 0 & \omega_2 & 0 & \omega_1 & 0 & 0 & 0 \\ 0 & 0 & 0 & 0 & 0 & \omega_2 & 0 & \omega_1 & 0 & 0 \\ 0 & 0 & 0 & 0 & 0 & 0 & \omega_2 & 0 & \omega_1 & 0 \\ 0 & 0 & 0 & 0 & 0 & 0 & 0 & \omega_2 & 0 & \omega_1 \\ \omega_1 & 0 & 0 & 0 & 0 & 0 & 0 & \mathbf{0} & \omega_2 & 0 \\ 0 & \omega_1 & 0 & 0 & 0 & 0 & 0 & 0 & 0 & \omega_2 \\ \omega_2 & 0 & \omega_1 & 0 & 0 & 0 & 0 & 0 & 0 & 0 \\ 0 & \omega_2 & 0 & \omega_1 & 0 & 0 & 0 & 0 & 0 & 0 \\ 0 & 0 & \omega_2 & 0 & \omega_1 & 0 & 0 & 0 & 0 & 0 \\ 0 & 0 & 0 & \omega_2 & \mathbf{0} & \omega_1 & 0 & 0 & 0 & 0 \end{pmatrix}; \quad \mathbf{\Gamma} = \begin{pmatrix} -1 + \omega_1\omega_2(3 - \omega_1\omega_2) \\ 0 \\ -\omega_1^3 - \omega_1^2 + \omega_1\omega_2^3 \\ 0 \\ -\omega_1 + 2\omega_1^2\omega_2 - \omega_2^4 \\ 0 \\ -\omega_1^4 - \omega_2 + 2\omega_1\omega_2^2 \\ 0 \\ -\omega_1^2 + \omega_1^3\omega_2 - \omega_2^3 \\ 0 \end{pmatrix} \tag{A.3}$$

where U is defined to be a meaningful range. It is, however, simpler to restrict the pulse timings to a meaningful range S (defined later) to arrive at a comprehensive description of the equations. In this case, the integral needs to range from 0 to ∞ and we have to start with all possible pulses for the input in this range.

The input $K(t) = \Sigma_{n=s}^{\infty}\delta(t - nP)$ (concerning s see below) to the constant synapse is a sum of δ functions always at the beginning of a period. As already mentioned in the main part, the δ function $\delta(t - t_i)$ for pulse time t_i simplifies the convolution to a temporal shift in the filter function h: $\int_0^{\infty}\delta(t - t_i - \tau)h(\tau)d\tau = h(t - t_i)$. Further on, the inputs x_i to the plastic synapses are given by the pulse amplitudes $\mathbf{\Gamma}$, however, delayed by different delay times d_i. Thus, we have to exchange the inputs x_i with the full representation of all pulses of the whole temporal development from time $s \cdot P$ (at which the pulse amplitudes $\mathbf{\Gamma}$ already converged) to infinity: $x_i = \Sigma_{n=s}^{\infty}\Sigma_{k=1}^{P}\Gamma_k \cdot \delta(\tau - nP - d_i - k)$. At the same time we simplify all the δ functions of the input.

$$\begin{aligned} a_{i,j}(\tau) &= \sum_{n=s}^{\infty}\sum_{k=1}^{P}\Gamma_k \cdot h\left(\tau - nP - d_i - k\right) \\ &\quad \times \sum_{m=s}^{\infty}\sum_{l=1}^{P}\Gamma_l \cdot \frac{d}{d\tau}h\left(\tau - mP - d_j - l\right) \\ q_i(\tau) &= \sum_{n=s}^{\infty}\sum_{k=1}^{P}\Gamma_k \cdot h\left(\tau - nP - d_i - k\right) \cdot \sum_{m=s}^{\infty}\frac{d}{d\tau}h(\tau - mP) \\ p_j(\tau) &= \sum_{n=s}^{\infty}h(\tau - nP) \cdot \sum_{m=s}^{\infty}\sum_{k=1}^{P}\Gamma_k \cdot \frac{d}{d\tau}h\left(\tau - mP - d_j - k\right) \\ b(\tau) &= \sum_{n=s}^{\infty}h(\tau - nP) \cdot \sum_{m=s}^{\infty}\frac{d}{d\tau}h(\tau - mP) \end{aligned}$$

Next, we neglect all terms but one on the pre-synaptic site (index n) as spiking is repetitive anyways. Additionally, we reduce the range of the sum from infinity to a meaningful range S that is determined by the time window W of the STDP curve under consideration (e.g., 50 ms in the main part): $S = [-\bar{s}, \bar{s}]$ with $\bar{s} = W / P\rceil$ where $\xi\rceil$ is the ceiling function.

FIXED-POINT ANALYSIS

In order to get the fixed points, we start with Eq. 14

$$\int_U \boldsymbol{A}(\tau)d\tau = \int_U \left(\begin{array}{ccc|c} \ddots & \vdots & \iddots & \vdots \\ \cdots & (x_i * h)(\tau)\frac{d}{d\tau}(x_j * h)(\tau) & \cdots & (x_i * h)(\tau)\frac{d}{d\tau}(K * h)(\tau) \\ \iddots & \vdots & \ddots & \vdots \\ \hline \cdots & (K * h)(\tau)\frac{d}{d\tau}(x_j * h)(\tau) & \cdots & (K * h)(\tau)\frac{d}{d\tau}(K * h)(\tau) \end{array}\right) d\tau = \int_U \left(\begin{array}{ccc|c} \ddots & \vdots & \iddots & \vdots \\ \cdots & a_{i,j}(\tau) & \cdots & q_i(\tau) \\ \iddots & \vdots & \ddots & \vdots \\ \hline \cdots & p_j(\tau) & \cdots & b(\tau) \end{array}\right) d\tau \tag{B.1}$$

$$
\begin{aligned}
a_{i,j}(\tau) &= \sum_{m=-\bar{s}}^{\bar{s}} \sum_{k=1}^{P} \sum_{l=1}^{P} \Gamma_k \cdot \Gamma_l \cdot h\left(\tau - k - d_i\right) \cdot \frac{d}{d\tau} h\left(\tau - mP - l - d_j\right) \\
q_i(\tau) &= \sum_{m=-\bar{s}}^{\bar{s}} \sum_{k=1}^{P} \Gamma_k \cdot h\left(\tau - k - d_i\right) \cdot \frac{d}{d\tau} h(\tau - mP) \\
p_j(\tau) &= \sum_{m=-\bar{s}}^{\bar{s}} \sum_{k=1}^{P} \Gamma_k \cdot h(\tau) \cdot \frac{d}{d\tau} h\left(\tau - mP - k - d_j\right) \\
b(\tau) &= \sum_{m=-\bar{s}}^{\bar{s}} h(\tau) \cdot \frac{d}{d\tau} h(\tau - mP)
\end{aligned}
$$

and solve the integral

$$
\begin{aligned}
\int_0^\infty a_{i,j}(\tau)d\tau &= \sum_{m=-\bar{s}}^{\bar{s}} \sum_{k=1}^{P} \sum_{l=1}^{P} \Gamma_k \cdot \Gamma_l \cdot \Delta\omega\left(l - k + d_j - d_i + mP\right) \\
\int_0^\infty q_i(\tau)d\tau &= \sum_{m=-\bar{s}}^{\bar{s}} \sum_{k=1}^{P} \Gamma_k \cdot \Delta\omega\left(-k - d_i + mP\right) \\
\int_0^\infty p_j(\tau)d\tau &= \sum_{m=-\bar{s}}^{\bar{s}} \sum_{k=1}^{P} \Gamma_k \cdot \Delta\omega\left(k + d_j + mP\right) \\
\int_0^\infty b(\tau)d\tau &= \sum_{m=-\bar{s}}^{\bar{s}} \Delta\omega(mP)
\end{aligned}
\tag{B.2}
$$

where we replaced $\int_0^\infty h(\tau + T) \cdot dh(\tau)/d\tau \cdot d\tau$ with the weight change function $\Delta\omega(T)$ representing STDP. The final step is to find all roots of the R top-most rows of matrix (see Eq. 14) which lead to a negative Jacobi matrix at this point. Those are the stable fixed-points.

FEED-FORWARD STRUCTURE

As we use the $E,(k = 2)$ approximation, we truncate the Magnus series after the first term and additionally assume that the negative changes (since we can set $T > 0$ without loss of generality, only $h(\tau - T) \cdot dh(\tau)/d\tau$ yields negative changes) are scaled by ρ which resembles the asymmetric STDP curve. The first term writes then

$$
\begin{aligned}
\mathfrak{A}(t) &= \int_0^t \begin{pmatrix} h(\tau) \cdot \frac{d}{d\tau} h(\tau) & h(\tau) \cdot \frac{d}{d\tau} h(\tau - T) \\ \rho \cdot h(\tau - T) \cdot \frac{d}{d\tau} h(\tau) & h(\tau - T) \cdot \frac{d}{d\tau} h(\tau - T) \end{pmatrix} d\tau \\
&= \begin{pmatrix} \frac{1}{2} h^2(t) & \nu_{T,-1}(t) \\ \rho \cdot \nu_{T,+1}(t) & \frac{1}{2} h^2(t - T) \end{pmatrix}
\end{aligned}
\tag{C.1}
$$

where the two inputs receive a pulse at $t = 0$ and at $t = T$ respectively. The functions $\nu_{T,\pm 1}(t)$ have an analytical solution which is

$$
\begin{aligned}
\nu_{T,\eta}(t) = \frac{\Theta(t - T)\Theta(t)}{2(\alpha + \beta)\sigma^2} &\left(\eta \,\mathrm{sign}\,(T)\sigma(\alpha - \beta)h(|T|) - 2e^{-t(\alpha+\beta)}\right) \\
&\left(\alpha e^{\alpha T} + \beta e^{\beta T}\right) + (\alpha + \beta)\left(e^{-\alpha(2t-T)} + e^{-\beta(2t-T)}\right)
\end{aligned}
\tag{C.2}
$$

In the limit of t to infinity matrix $\mathfrak{A}(t)$ changes into $\tilde{\mathfrak{A}}$ and so do the secondary diagonal elements

$$
\tilde{\nu}_{T,\eta}(t) = \lim_{t \to \infty} \nu_{T,\eta}(t) = \eta \,\mathrm{sign}\,(T) \frac{\alpha - \beta}{2(\alpha + \beta)\sigma} h(|T|). \tag{C.3}
$$

and the diagonal elements vanish to 0 as $\lim_{t \to \infty} h(t) = 0$ and $h(0) = 0$. Furthermore, we find that $\tilde{\nu}_T = \tilde{\nu}_{T,+1} = -\tilde{\nu}_{T,-1}$, for the considered filter function $\tilde{\nu}_T$ is positive definite as α is smaller than β. Therefore $\tilde{\mathfrak{A}}$ results in

$$
\tilde{\mathfrak{A}} = \lim_{t \to \infty} \mathfrak{A}(t) = \begin{pmatrix} 0 & \tilde{\nu}_T \\ -\rho \cdot \tilde{\nu}_T & 0 \end{pmatrix} = \nu_T \begin{pmatrix} 0 & 1 \\ -\rho & 0 \end{pmatrix}. \tag{C.4}
$$

As the square is $\tilde{\mathfrak{A}}^2 = -\tilde{\nu}_T^2 \rho \boldsymbol{I}$, we get for an error of order $E,(k = 2)$:

$$
\begin{aligned}
\tilde{\mathfrak{B}}_{E,(2)} &= \exp \mu \tilde{\mathfrak{A}} = \sum_{n=0}^{\infty} \frac{1}{n!} (\mu \tilde{\mathfrak{A}})^n \\
&= \sum_{n=0}^{\infty} \frac{(-1)^n}{(2n)!} \left(\mu \tilde{\nu}_T \sqrt{\rho}\right)^{2n} \boldsymbol{I} + \sum_{n=0}^{\infty} \frac{(-1)^n}{(2n+1)!} \left(\mu \tilde{\nu}_T \sqrt{\rho}\right)^{2n+1} \boldsymbol{J} \\
&= \cos\left(\mu \tilde{\nu}_T \sqrt{\rho}\right) \boldsymbol{I} + \sin\left(\mu \tilde{\nu}_T \sqrt{\rho}\right) \boldsymbol{J} \\
&= \begin{pmatrix} \cos\left(\mu \tilde{\nu}_T \sqrt{\rho}\right) & \frac{1}{\sqrt{\rho}} \sin\left(\mu \tilde{\nu}_T \sqrt{\rho}\right) \\ -\sqrt{\rho} \sin\left(\mu \tilde{\nu}_T \sqrt{\rho}\right) & \cos\left(\mu \tilde{\nu}_T \sqrt{\rho}\right) \end{pmatrix}
\end{aligned}
\tag{C.5}
$$

where

$$
\boldsymbol{J} = \begin{pmatrix} 0 & \frac{1}{\sqrt{\rho}} \\ -\sqrt{\rho} & 0 \end{pmatrix}.
$$

This solution was used to calculate the difference $\Delta_{\cdot,(k)}$ for different values of T in **Figure 1E**.

frontiers in
COMPUTATIONAL NEUROSCIENCE

ORIGINAL RESEARCH ARTICLE
published: 03 August 2010
doi: 10.3389/fncom.2010.00018

A spiking neural network model of the medial superior olive using spike timing dependent plasticity for sound localization

Brendan Glackin, Julie A. Wall, Thomas M. McGinnity*, Liam P. Maguire and Liam J. McDaid

Intelligent Systems Research Centre, Magee Campus, University of Ulster, Derry, Northern Ireland, UK

Edited by:
Henry Markram, Ecole Polytechnique Federale de Lausanne, Switzerland

Reviewed by:
Silvia Scarpetta, University of Salerno, Italy
Claudia Clopath, Ecole Polytechnique Federale de Lausanne, Switzerland

****Correspondence:***
Thomas M. McGinnity, Intelligent Systems Research Centre, Magee Campus, University of Ulster, Derry, Northern Ireland BT48 7JL, UK.
e-mail: tm.mcginnity@ulster.ac.uk

Sound localization can be defined as the ability to identify the position of an input sound source and is considered a powerful aspect of mammalian perception. For low frequency sounds, i.e., in the range 270 Hz–1.5 KHz, the mammalian auditory pathway achieves this by extracting the Interaural Time Difference between sound signals being received by the left and right ear. This processing is performed in a region of the brain known as the Medial Superior Olive (MSO). This paper presents a Spiking Neural Network (SNN) based model of the MSO. The network model is trained using the Spike Timing Dependent Plasticity learning rule using experimentally observed Head Related Transfer Function data in an adult domestic cat. The results presented demonstrate how the proposed SNN model is able to perform sound localization with an accuracy of 91.82% when an error tolerance of ±10° is used. For angular resolutions down to 2.5°, it will be demonstrated how software based simulations of the model incur significant computation times. The paper thus also addresses preliminary implementation on a Field Programmable Gate Array based hardware platform to accelerate system performance.

Keywords: sound localisation, MSO, SNN, STDP

INTRODUCTION

One of the key functions the ears and auditory pathways perform is that of sound localization, defined as the ability to determine from where a sound signal is generated, in relation to the position of the human head. Sound localization is considered a powerful aspect of mammalian perception, allowing an awareness of the environment and permitting mammals to locate prey, potential mates and predators (McAlpine and Grothe, 2003). In humans, sound localization depends on binaural cues which are extracted from the sound signal at each ear and compared to each other to determine from which direction the sound is traveling. The two binaural cues which play the most dominant role in sound localization are called the Interaural Time Difference (ITD), processed in the Medial Superior Olive (MSO) of the auditory system and the Interaural Intensity Difference (IID), processed in the Lateral Superior Olive (LSO). The ITD can be defined as the small difference in arrival times between a sound signal reaching each individual ear. Low frequency sound waves in the range 270 Hz–1.5 KHz have a wavelength that is greater than the diameter of the head; therefore each ear receives the sound wave at a different point in time. From this time difference, the brain can therefore calculate the angle of the originating sound source in relation to the orientation of the head (Carr, 1993; Grothe, 2003). At frequencies greater than 1.5 KHz the wavelength of the sound is similar to or smaller than the diameter of the human head, the time delay between the sound arriving at the two ears cannot be distinguished and so IID is used for localization. The combination of ITD and IID is better known as the "duplex theory of sound localization" and was first devised by Thompson and Rayleigh around the late 19th and early 20th century (Rayleigh, 1875–1876, 1907; Thompson, 1882).

An illustration of the mammalian auditory pathways involved in sound localization can be found in **Figure 1**. ITD processing involves the cochlea, Auditory Nerve (AN), Cochlear Nucleus (CN) and MSO. Whilst the LSO covers the wider frequency band of 1.5–20 KHz, the human MSO is calculated to be the largest of the nuclei in the Superior Olivary Complex (SOC) containing in the region of 10,000–11,000 cells (Moore, 2000) and is considered as the dominant nucleus for sound localization in humans (Kulesza, 2007). MSO cells receive excitatory innervation from both ears, and their main functionality is to work as coincidence detectors to identify the ITD and thus the azimuth sound source angle (Hancock and Delgutte, 2004). The ITDs in continuous and periodic sounds produce interaural phase differences, i.e., differences in the phase of the sound wave that approaches each ear. The fibers of the auditory nerve which respond best to low frequencies produce spike trains which are time locked to the signals' sine curve, meaning the intervals between spikes is at the period of the curve or a multiple of that period. This occurs at both the signal onset and the ongoing signal and is important in sound localization for extracting the ITD from the sound arriving at each ear (Smith et al., 1998; Grothe, 2003; Ryugo and Parks, 2003; Joris and Yin, 2007). The stimuli at each ear which differ in phase, cause the auditory nerve fibers to produce spike trains which also exhibit a phase difference. The MSO combines the sound from the two ears; the ipsilateral inputs come directly while the contralateral inputs pass through a graded series of delays. For a sound source at a particular angle to the direction the listener is facing, an optimal delay will allow the ipsilateral and contralateral inputs to arrive coincidentally at the neuron or group of neurons, thus causing the neuron to fire. MSO neurons are organized spatially as a place map of location, i.e., a group of

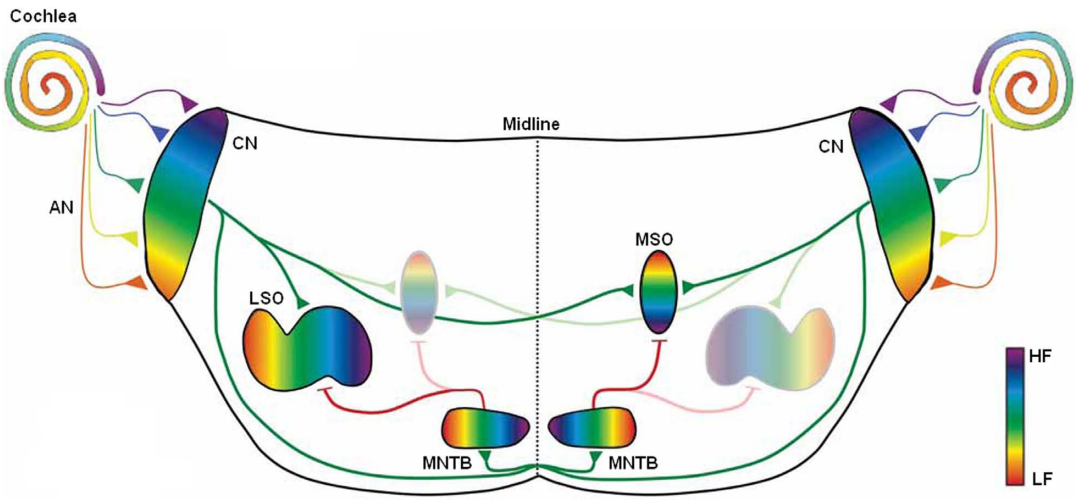

FIGURE 1 | Spatial organization by frequency occurring in elements of the auditory system which achieve sound localization from Kandler et al. (2009).

neurons are allocated for each particular angle on the horizontal plane (Grothe, 2003; Shi and Horiuchi, 2004). At a higher level these subgroups are subsequently also organized into frequency selective clusters as indicated in **Figure 1** from Low Frequency (LF) to High Frequency (HF) regions (Kandler, 2009).

This paper presents a Spiking Neural Network (SNN) model for sound localization. A model of the MSO based on a graded delay structure is presented which is used to perform sound localization using a biologically plausible training mechanism in the form of the Spike Timing Dependent Plasticity (STDP) learning rule (Bell et al., 1997; Markram et al., 1997; Bi and Poo, 1998; Zhang et al., 1998; Song et al., 2000). Acoustical input data, generated from an adult domestic cat is used for training and testing purposes (Tollin, 2004, 2008; Tollin et al., 2008; Tollin and Koka, 2009). Section "Models of Sound Localization" of this paper contains a review of models for sound localization previously reported in the research literature. In Section "SNN Model of the MSO", an overview of the proposed MSO model is provided including details on the SNN architecture, neuron model and training mechanism employed. Experimental results are presented in Section "Results" including a comparison between software and hardware based implementation approaches, subsequently followed by a discussion on the most significant findings of the research in Section "Discussion". Finally, the conclusions and a summary of future work are presented in Section "Conclusions and Future Work".

MODELS OF SOUND LOCALIZATION

The first computational model to demonstrate how ITD in mammals is used to determine the angle of origin of a sound signal was developed by Jeffress (1948). This model involved time or phase-locked inputs, facilitated via a set of delay lines, to vary the axonal path lengths arriving at the neuron and an array of coincidence detector neurons which only fire when presented with simultaneous inputs from both ears (Carr, 1993; Grothe, 2003; McAlpine and Grothe, 2003). The fundamental importance of Jeffress' model and why it has become the prevailing model of binaural sound localization is its ability to depict auditory space with a neural representation in the form of a topological map. A graphical representation of the Jeffress model is shown in **Figure 2**.

Up to the 1980s this simplistic model remained hypothetical until evidence was found which showed that the nucleus laminaris of the barn owl (homologous to the MSO in mammals) works in a similar manner (Carr and Konishi, 1990; Carr, 1993; Konishi, 2000; Burger and Rubel, 2008). However, the occurrence, structure and function of this simple delay line model in the MSO of mammals has been debated at length. Studies of the cat MSO have found evidence for differing axon lengths from the contralateral ear to the MSO where the shortest axons innervate the rostral MSO cells and the longer axons innervate caudal MSO cells, thus indicating agreement with the Jeffress model (Smith et al., 1993; Beckius et al., 1999). However, both studies also show that each axon only innervates a small portion of the MSO, unlike in the nucleus laminaris of the bird in which the entire nucleus is innervated. Less studies have been carried out on the anatomical and physiological structure and function of the mammalian MSO in comparison to the avian nucleus laminaris to determine conclusively whether the Jeffress model is an appropriate representation.

A number of computational models utilizing various mathematical techniques for sound localization have been reported in the literature (Huang et al., 1999; Handzel and Krishnaprasad, 2002; Nakashima et al., 2003; Willert et al., 2006; Keyrouz and Diepold, 2008, Li et al., 2009; Murray et al., 2009). In attempting to develop more biologically inspired approaches, a number of researchers have also proposed ANN based models (Palmieri et al., 1991; Backman and Karjalainen, 1993; Datum et al., 1996; Abdel Alim and Farag, 2000; Chung et al., 2000; Hao et al., 2007; Keyrouz and Diepold, 2008). As with their computational counterparts, it has been demonstrated that such networks can be used to localize sound sources. The neuron models used in such networks however, are highly abstracted from their biological counterparts. Inspired by neurophysiological studies on the functionalities of specific

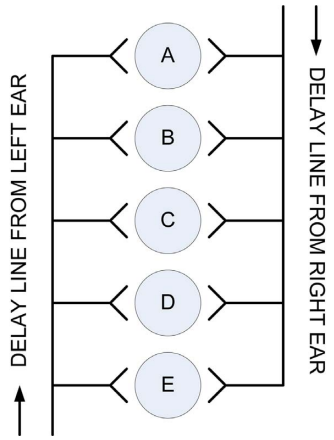

FIGURE 2 | The Jeffress model of ITD based binaural hearing (Jeffress, 1948).

auditory neurons, a number of researchers have therefore sought to create SNN models for sound localization more closely aligned with the biological principles of auditory processing.

The first such example was proposed in 1996 by Gerstner and colleagues (Gerstner et al., 1996; Kempter et al., 1996), where Integrate-and-Fire (I&F) neurons were used to model the high precision temporal processing of the barn owl auditory pathway. Before learning, the model of the nucleus magnocellularis neuron is converged upon by many auditory input fibers with varying delays. The input to the system is a periodically modulated signal from which input spikes are generated via a stochastic process. An unsupervised Hebbian learning rule is subsequently used to strengthen the synaptic connections which enable the neuron to generate a periodic phase-locked output whilst those that are deemed unnecessary are removed. Thus, the neuron is effectively tuned to emit spiking behavior when a particular input frequency signal is applied. Whilst this technique was initially used on monaural inputs, the model was subsequently expanded to enable the ITD for binaural inputs to be determined. In this model, the neuron is stimulated simultaneously by an input signal as well as a fixed ITD time shifted signal where an unsupervised Hebbian learning rule is again used to select the optimal synaptic connections which enable a phase-locked spike output to be produced. After learning, this neuron is subsequently tuned to respond to this particular ITD for the given input frequency used during training. The authors subsequently propose that a series of these neurons may be used, each tuned to a particular interaural delay, where the overall ITD is estimated from the neural firing pattern by a population vector decoding scheme. Using this method it was estimated that approximately 100 neurons could be used to estimate the ITD with a temporal precision of 5 μs, i.e., the temporal precision of the barn owl auditory system. This work presented an efficient method for determining the ITD and was the first example of a model which accomplished this using spiking neurons. Subsequent research in this field has sought to build on this initial work through the development of models incorporating additional aspects of the auditory processing pathway which can be used to estimate azimuthal angles for sound sources across appropriate frequency ranges.

In a related approach but targeting lower latency responses, Smith (2001) employed the use of depressing synapses to detect the onsets in a phase-locked sound signal. It was observed that these onsets could be used to measure the ITDs and thus perform sound source localization. As opposed to the stochastic process used in Gerstner et al. (1996), the input audio signal was converted into a spike train by passing it through a cochlear filter, half-wave rectifier and a logistic spike generation function. Digitized sound signals were played in the presence of a model head with two microphones positioned in each ear canal. The signals covered an angular range from −70° to 30° with a resolution of 10°, at frequencies ranging from 220 Hz–3.25 KHz. This method has shown that ITDs can successfully be estimated using the approach described whilst higher accuracy was observed for lower angles at higher sound frequencies. A SNN based extensively on the Jeffress sound localization model has also been developed by Schauer et al. (2000) for implementation in a custom Very Large Scale Integration (VLSI) device. A digital delay line with AND gates was used to capture the inherent principles of the Jeffress model in an efficient manner for a hardware based implementation. Input data was recorded in an open environment with results indicating that the model was proficient at localizing single sound sources for 65 azimuthal angles. In 2007, BiSoLaNN was developed with functionality based on the ITD auditory cue (Voutsas and Adamy, 2007). The network can be described as a cross-correlation model of spiking neurons with multiple delay lines and both inhibitory and excitatory connections. Also developed was a model of the cochlea, inner hair cells and coincidence neurons. The system was subsequently tested on pure-tone sound signals between 120 Hz–1.24 KHz, which were recorded in an anechoic chamber using the Darmstadt robotic head. The localization accuracy of these frequencies was found to be 59% where it was noted that signals originating from the front of the head were localized with a higher degree of accuracy than those which originated from the two sides. In the same year, Poulsen and Moore (2007) demonstrated how SNNs could be combined with an evolutionary learning algorithm to facilitate sound localization. This work involved a simulation in a 2-dimensional environment wherein multiple agents possess an SNN which controls their movements based on binaural acoustical inputs. The evolutionary learning algorithm is employed to evolve the connectivity and weights between neurons which were based on the Spike Response Model (SRM) (Gerstner and Kistler, 2002). The evolutionary training algorithm involved updating an agents' fitness score, i.e., increasing it if they moved closer to the sound source and decreasing it if they moved further away. After training, most agents were able to localize single sound sources, however a notable degradation in performance was observed when multiple sound sources were tested. Research on SNNs for sound localization has also led to the development of an auditory processing system to provide live sound source positions utilizing both ITD and IID to localize a broadband sound (Liu et al., 2008a). The input to the system is determined by passing the sound from two microphones through a Gamma-tone filter-bank. This process splits it into a number of frequency channels which are then encoded as phase-locking spikes. These spikes then take two routes, through the ITD and IID pathways. The ITD pathway consists of a Leaky Integrate-and-Fire (LIF) neuron which produces spikes relating to

the time difference between the two inputs whilst the IID pathway uses a logarithmic ratio which computes the intensity difference and produces a spike based on this value. The network was tested on an artificial sound source covering a sweep from −90° to 90° with a relatively coarse resolution step of 30° between input locations. In the experiments conducted it was again observed that the highest localization accuracy was observed when the sound source was directly in front of the target, i.e., at the 0° position. The overall localization efficiency was determined to be 80%, which increased to 90% when a subset of input angles was used, i.e., $-45° \leq \theta \leq 45°$. Further work by the same authors has involved replacing the logarithmic ratio mathematics for the IID pathway with a neuron model (Liu et al., 2008b). Experiments were performed on the network using artificial sound and real tones again with the same set of angles as before. Similar results of 80% occurred for the artificial sound across all angles whilst a localization accuracy of 95% was observed for the angles $-45° \leq \theta \leq 45°$. Testing on a real sound gave 65% accuracy across all angles. In 2009, this work was again extended through the incorporation of a model of the inferior colliculus into the network where successful localization of white noise, speech and pure-tone inputs was again observed (Liu et al., 2009).

It is evident that a growing trend is emerging in the research literature towards forming a deeper understanding of how sound localization is performed in biological systems. In terms of sound localization, many researchers have based their work on the Jeffress model which, despite its relative simplicity, is generally regarded as being an appropriate representation of the MSO in mammals. Limited progress has been made however, on the development of a Jeffress inspired architecture using spiking neurons. This paper therefore, aims to address these issues by creating a Jeffress based model for the MSO using spiking neurons which is inspired by the biology of the auditory pathways to emulate the way in which mammals can localize sounds. Whilst the approaches discussed in this section have all used either simulated input data or Head Related Transfer Function (HRTF) data generated from a theoretical model of the human head, this work seeks to use real biologically observed data as input to the system. Furthermore, the network is trained to perform sound localization by means of a biologically plausible training mechanism observed in the biological brain in the form of the STDP learning rule. Whilst alternative SNN based models have typically used a resolution of $\theta \geq 10°$, an additional aim of this work is to determine the impact on localization accuracy when this input resolution is significantly increased, i.e., for $\theta \geq 2.5°$. Finally, this paper also considers that the eventual deployment environment for this model is likely to require a mobile solution such as on a robotic based platform, where powerful desktop processing is simply not available. Hence, the paper will also examine the implications and considerations for adopting a hardware based implementation strategy for the proposed model.

SNN MODEL OF THE MSO

In this section, details on the MSO model developed for performing sound localization are presented. This model is an extension of work previously presented by Wall et al. (2007, 2008). The model description commences with a high level overview of the network topology which includes a discussion on the method used to generate input data for the system. This is followed by descriptions of the spiking neuron model and the STDP learning rule used in the implementation.

NETWORK ARCHITECTURE

The complete network architecture for the MSO model is shown in **Figure 3** and consists of a series of layers:

- Input Layer
- Cochlea Model Layer
- Bushy Cell Neurons
- Graded Delay Structure
- Output Layer

The input layer directly corresponds to the ipsilateral and contralateral ear inputs in the mammalian auditory system. As previously discussed, rather than utilize purely simulated data or HRTF generated from models of the human head, this research sought to process biologically realistic input data. To accommodate this, acoustical data generated from the adult domestic cat was supplied by Dr. Daniel J. Tollin (Tollin, 2004, 2008; Tollin et al., 2008; Tollin and Koka, 2009). This data consists of a set of HRTFs for a series of sound wave frequencies for both the left and right ears at a specific azimuthal angle. HRTF data designates the filtering of a sound before it reaches the cochlea after the diffraction and reflection properties of the head, pinna and torso have affected it. The complete data set includes ipsilateral and contralateral sample pairs for 36 different azimuthal angles (−180° to 170° in steps of 10°) at 148 distinct sound frequencies (600 Hz–30 kHz in steps of 200 Hz). As previously discussed, this research is primarily interested in developing a model of the MSO, hence the frequency range of particular interest in this regard was from 600 Hz–1.6 KHz, i.e., the upper frequency bound for which the ITD can be used for sound localization. It has also been stated however, that a further goal of this work is to ascertain the impact of increasing the azimuthal angle resolution during the training and testing phases. To facilitate this, interpolation of the input dataset was used to provide the required resolution. A 3D surface plot of the acoustical data for the left and right inputs is shown in **Figure 4**.

As indicated in **Figure 3**, the next layer in the network is the cochlea, with two instantiations of the model receiving inputs from the ipsilateral and contralateral inputs in a manner which is consistent with the mammalian auditory processing pathway. The cochlea model in this work was developed by Zilany and Bruce (2006, 2007). It is based on empirical observations in the cat and as such, is highly appropriate for post-processing the aforementioned HRTF data, which was also generated from an adult cat (Tollin and Koka, 2009). Each cochlea takes the frequency and the HRTF of a sound at a particular angle as input and produces a spike train based on and relating to that input. The input to the cochlea model initially passes through a middle-ear filter and then through three parallel filter paths; a wideband filter which depicts the filtering properties of the basilar membrane, a chirping filter which is similar to the wideband filter but does not include properties from the Outer Hair Cells (OHC), and a control path filter which models the effects of the OHC functionality. The outputs of the wideband and chirping filters then pass through models of Inner Hair Cells (IHC), after which the two outputs are summed and then low-pass filtered to

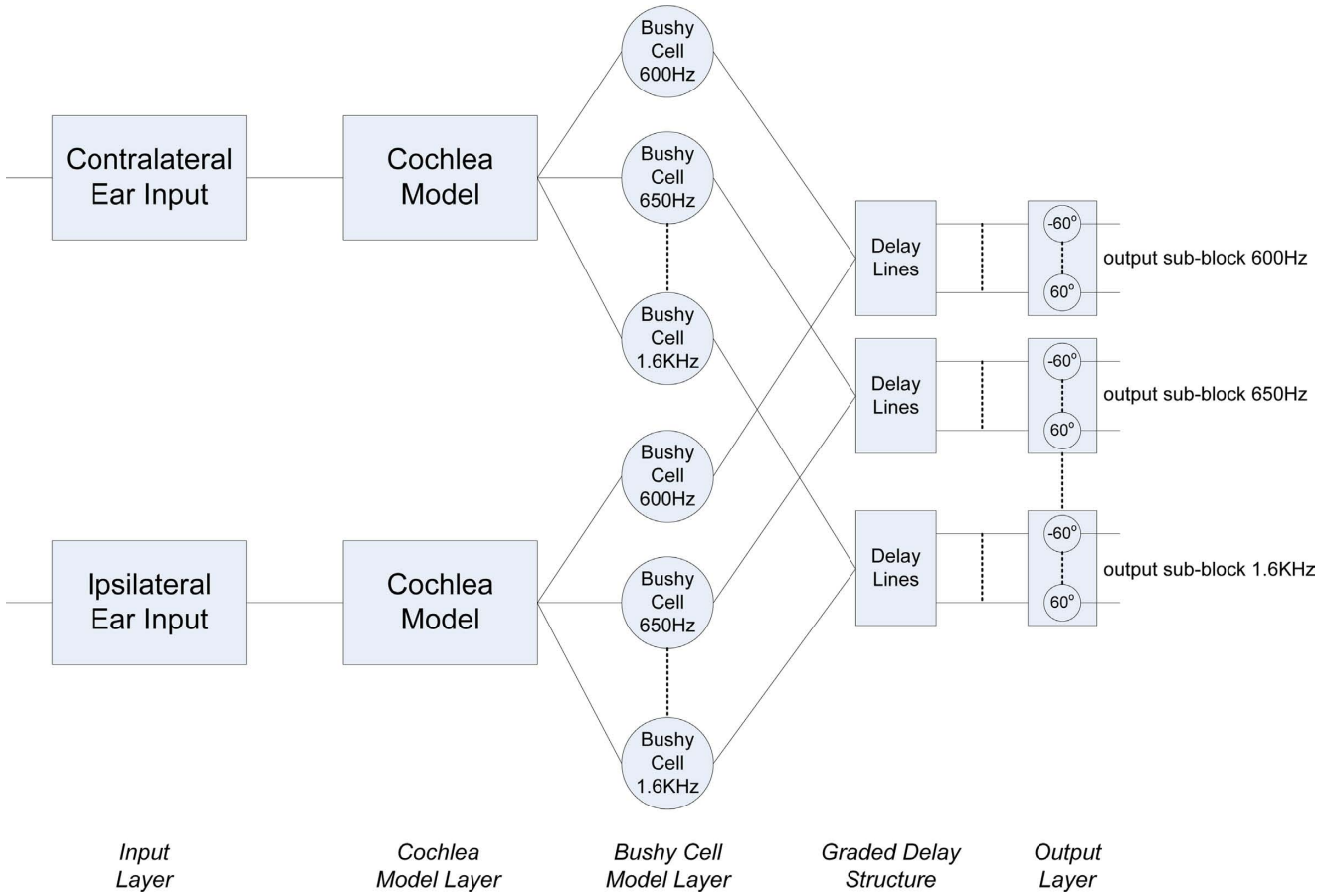

FIGURE 3 | An overview of the proposed MSO model for sound localization.

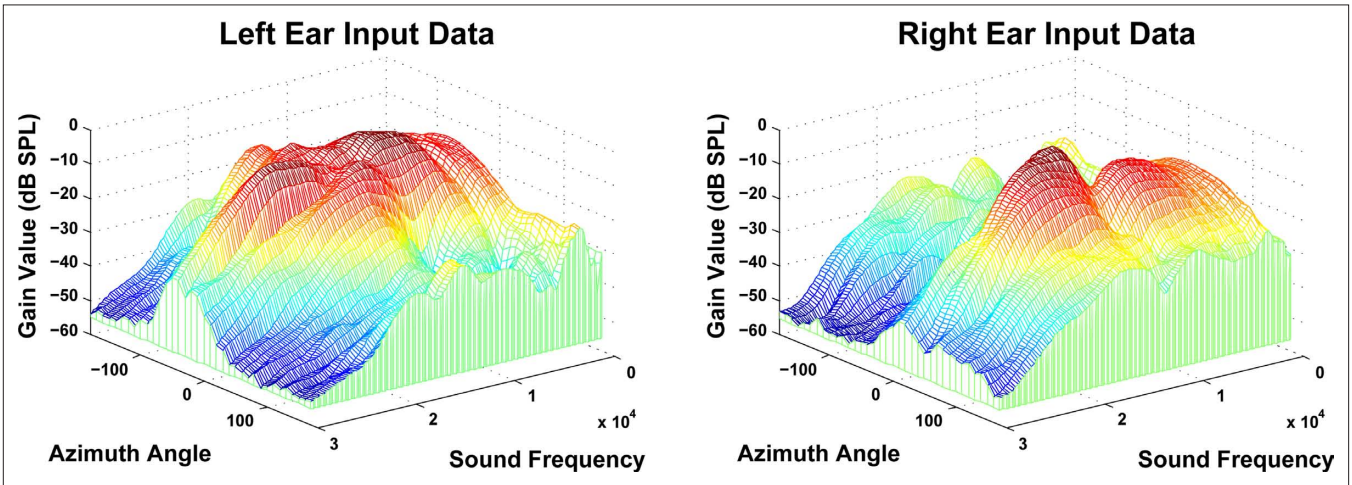

FIGURE 4 | 3-D mesh surface plot of the acoustical input data.

produce the IHC receptor potential. This potential causes activity at a synapse model and ultimately spikes are generated through an inhomogeneous Poisson encoding process. As the spike trains generated by the cochlea model are encoded by a Poisson process, when the same data point is passed through the cochlea multiple times the spike train frequencies generated will not be identical but will be distributed around a mean frequency. Spike train frequencies generated are usually within ±30 Hz of that mean frequency,

but in some cases spike trains will be generated with a frequency which is far removed from that mean frequency; these spike trains do not naturally lend themselves to being successfully classified. Thus, in the experiments conducted as part of this research, the training and testing phases were repeated several times to reduce the possibility of such anomalies distorting the results. The output of the cochlea model is characterized by bursts of spikes which are phase locked to the original sound frequency as shown in **Figure 5**. As indicated in **Figure 3**, a series of frequency selective outputs are emitted from the cochlea model (e.g., 600, 650 Hz etc.). This relates back to the auditory system presented in **Figure 1**, which indicates the presence of frequency selective clusters or regions in the biological MSO.

The next step in the auditory processing pathway is to process this bursting spiking activity via the bushy cell neuron layer. Knowledge of the role of bushy cells in biology remains somewhat limited but it is known that the main function of these cells in the auditory processing pathway is to maintain the phase-locked signal and to minimize the impact of noise. It is thought that bushy cells do not have a one-to-one response to auditory nerve input at low frequencies, but that a number of inputs occurring in a short space of time are required to cause the bushy cell to respond (Yin, 2002). These cells were used in the proposed network as a form of coincidence detector to convert the phase-locked bursting activity of the cochlea model to the single spike instances, as shown in **Figure 6**. This processing was implemented using a LIF neuron (see Appendix) where the phase-locked single spike output in place of a burst of spikes was achieved through selection of an appropriate neuron threshold and refractory period. The parameters are fixed for each bushy cell in the network, i.e., the same parameters are used for each sound frequency with which the network was trained and tested.

Inspired by the Jeffress model for sound localization (Jeffress, 1948), the authors propose that the multiple delay structure employed in the network model is a viable representation of the graded series of delays found in the biological MSO. In the mammalian auditory pathway, the stimuli at each ear which differ in phase, cause the auditory nerve fibers to produce spike trains which also exhibit a phase difference. The MSO combines these spike trains from each ear; the ipsilateral inputs are delivered directly while the contralateral inputs pass through a series of graded delays. For a sound source at a particular angle to the listener, only one particular delay will allow the ipsilateral and contralateral inputs to match, i.e., the original out-of-synch phase-locked spike trains come into phase. The network topology shown in **Figure 7** demonstrates a method for accomplishing this functionality using spiking neurons. The neuron model used in this instance was the conductance based Integrate-and-Fire (I&F) model proposed by Destexhe (1997). This model was selected as it provides comparable behavior to more complex neuron models such as Hodgkin-Huxley (HH) (Hodgkin and Huxley, 1952) but with considerably less computational demands. Further details of the neuron model equations and parameters can be found in an Appendix.

As shown in the **Figure 7**, the output of each bushy cell neuron is fully connected to the output layer, where each output neuron represents a distinct azimuthal angle. It can also be seen that the output neuron layer is organized into two groups, one for sound sources originating to the left of the head ($-60° \leq \theta \leq 0°$) and the other for angles to the right of the head ($0° < \theta \leq 60°$). As the delay structures are fully connected to the output layer, each output neuron receives a series of delayed spikes for each single spike emitted by the corresponding bushy cell. In the proposed network model, these connections are facilitated via STDP synapses. In addition

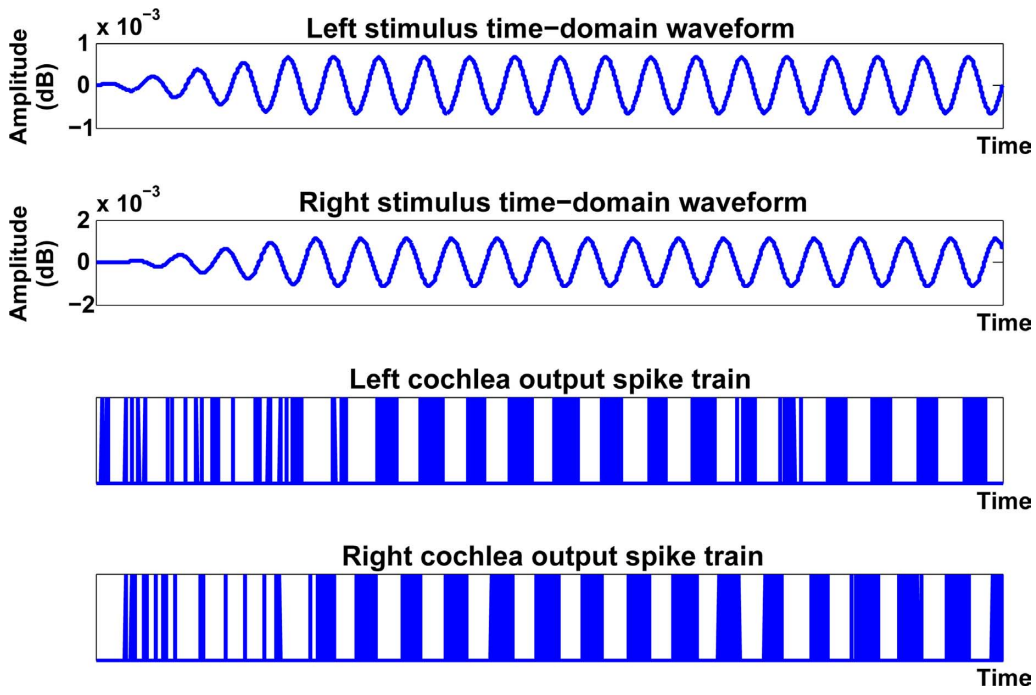

FIGURE 5 | Plot showing sample output data from the cochlea model.

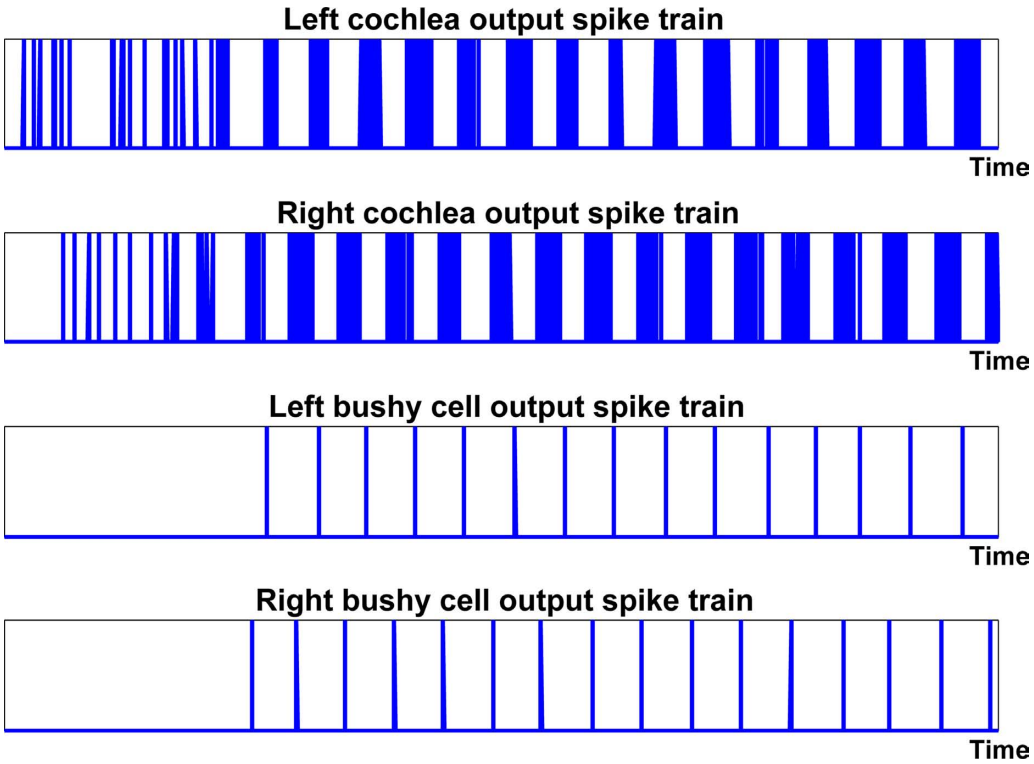

FIGURE 6 | Plot showing sample output data from the bushy cell neuron.

to these plastic synapses, each output neuron is also connected directly to the opposite bushy cell neuron using a fixed synapse, i.e., all left neurons ($-60° \leq \theta \leq 0°$) receive direct input from the right bushy cell neuron and vise versa. Thus, when spikes from the direct and delayed inputs to the neuron coincide and the strength of the synaptic connection is of a sufficient value, an output spike or action potential is generated.

During the training phase for the network, a teaching signal in the form of a spike train is supplied to indicate which of the output neurons should be displaying spiking activity. Based on the principles first proposed by Deneve et al. (2001) the training method adopted has previously been used by the authors to facilitate co-ordinate transformation using SNNs (Wu et al., 2005, 2008). As indicated in **Figure 7**, each output neuron is connected to a delay line source via the training layers (contralateral and ipsilateral) where the dashed line is used to indicate a non-permanent connection. For example, if during the training process the data being supplied to the model is for a sound source located at −55°, enabling the corresponding training neuron will provide a connection between the delay line and the target output neuron. As the synaptic strength of these training layer connections are of a sufficiently high level, a single input spike will ensure that an action potential is generated for the target neuron. By nature of the STDP learning rule, any preceding input spikes to this neuron via the delay lines will result in an increase in synaptic weight for that connection. Subsequently, when the training phase is complete and the network is supplied with just the ipsilateral and contralateral input data, the corresponding output neuron representing the source azimuth angle should display spiking behavior.

The length of each delay indicated in **Figure 7** was determined using a simple formula devised by Lord Rayleigh (Abdel Alim and Farag, 2000). He considered a sound wave traveling at the speed of sound, $c = 343$ m/s, which makes contact with a spherical head of radius r from a direction at an angle θ. The sound arrives at the first ear and then has to travel the extra distance of $r\theta + r\sin\theta$ to reach the other ear as indicated in **Figure 8**. Dividing that distance by the speed of sound gives the simple formula:

$$\mathrm{ITD} = \frac{r}{c}(\theta + \sin\theta) \tag{1}$$

It should be noted that this formula determines the ITD based on the assumption that the head is spherical or round. In consideration, it was decided to investigate the research of Nordlund (1962) where a series of experiments were conducted to measure the interaural time differences using a model of a true standard head. A plot of the ITD values as a function of azimuth angle for those calculated by Rayleighâ™ formula against those measured in Nordlundâ™ experiments is presented in **Figure 9**. It can be seen from this figure that the estimated ITDs provide an acceptable approximation with an average error of 0.0457 ms being observed across the full range of angles from 0° to 180°.

SPIKE TIMING DEPENDENT PLASTICITY

Spike Timing Dependent Plasticity is a form of Hebbian learning that can be used to modulate synaptic weights due to temporal correlations between pre- and post-synaptic neurons. The STDP rule

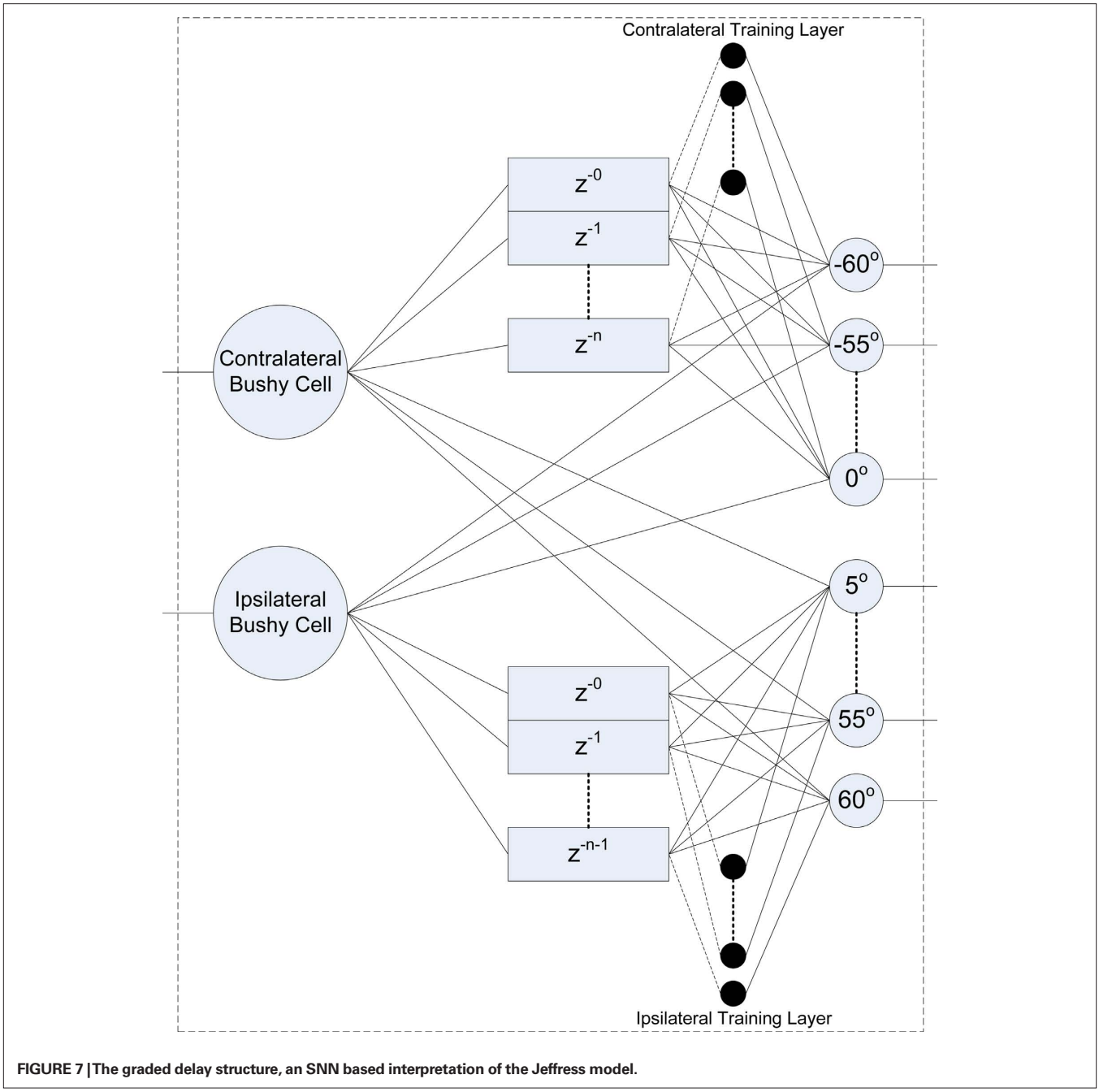

FIGURE 7 | The graded delay structure, an SNN based interpretation of the Jeffress model.

essentially validates Hebbs postulate dating back to 1949 (Hebb, 1949), but adds a mechanism to replicate the impact temporal information has on synaptic modifications. The first experiments that precisely measured this biological effect were presented in 1997 by Markram et al. (1997) with subsequent experimental observations being reported soon after Bell et al. (1997), Bi and Poo (1998), and Zhang et al. (1998). Examples of STDP in large scale SNNs have been reported for both software (Izhikevich et al., 2004; Hosaka et al., 2008; Masquelier et al., 2009) and hardware (Indiveri et al., 2006; Yang and Murray, 2006; Schemmel et al., 2007; Arena et al., 2009) based implementations whilst application domains of STDP have included handwritten digit recognition (Nessler et al., 2009), pattern analysis (Natschläger and Ruf, 1999) co-ordinate transformation (Wu et al., 2008) and robotic control (Northmore, 2004; Alnajjar and Murase, 2008).

The STDP learning rule is used in the proposed model to regulate the synaptic weights between the delay lines and the output neuron layer. The underlying premise of STDP is that each synapse in a SNN is characterized by a weight or peak conductance, q (the peak value of the synaptic conductance following a single pre-synaptic action potential), that is constrained to lie between 0 and a maximum value q_{max}. Every pair of pre- and post-synaptic spikes can potentially modify the value of q, and the changes due to each spike pair are continually summed to determine how q changes

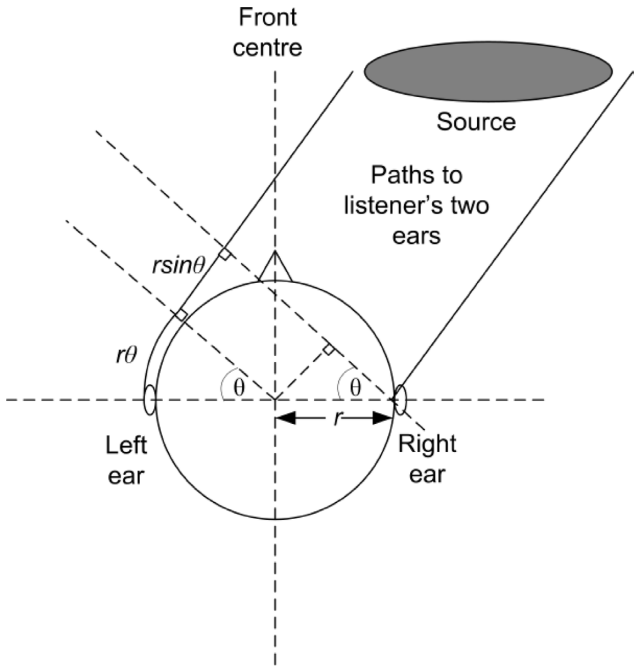

FIGURE 8 | Diagrammatic view of Rayleigh's simple formula for determining the ITD, adapted from Rumsey (2001).

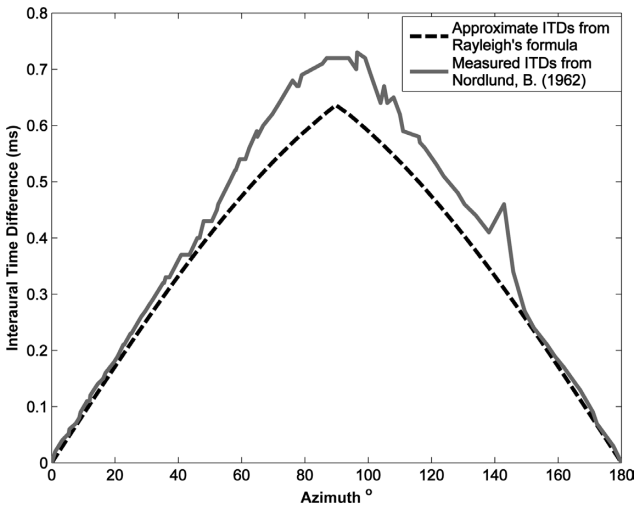

FIGURE 9 | Interaural time difference as a function of azimuth, comparing the approximate ITD values determined by Rayleigh's formula and those experimentally measured by Nordlund (1962).

over time. As stated in Song and Abbott (2001), a pre-synaptic spike occurring at time t_{pre} and a post-synaptic spike at time t_{post} modify the corresponding synaptic conductance by $q \rightarrow q + q_{max} \cdot F(\Delta t)$ where $\Delta t = t_{post} - t_{pre}$ and $F(\Delta t)$ is defined by:

$$F(\Delta t) = \begin{cases} A_+ \cdot e^{\frac{\Delta t}{\tau_+}} & \text{if } \Delta t \geq 0 \\ -A_- \cdot e^{\frac{\Delta t}{\tau_-}} & \text{if } \Delta t < 0 \end{cases} \quad (2)$$

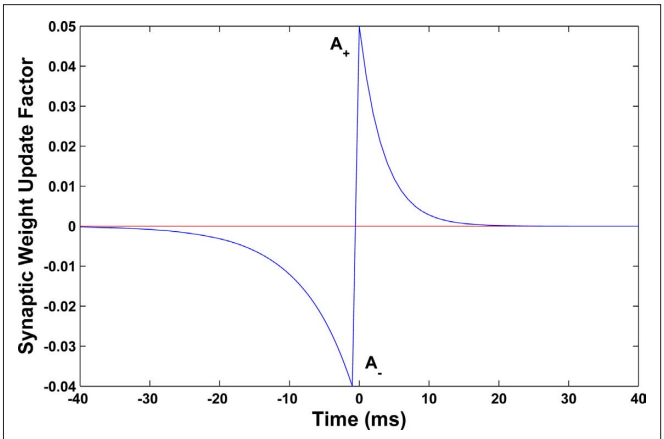

FIGURE 10 | STDP modification function used to determine the change in synaptic weight.

The time constants τ_+ and τ_- determine the range of the plasticity window and A_+ and A_- determine the maximum amount of synaptic modification in each case. The plasticity window for the MSO model implementation is presented in **Figure 10** where the STDP parameter set used was ($A_+ = 0.05$, $A_- = 0.04$, $\tau_+ = 4$, $\tau_- = 8$). Whilst the temporal window for plasticity has been found to vary in different parts of the brain (Bi and Poo, 1998; Abarbanel et al., 2002; Dan and Poo, 2006), the chosen parameter set was selected based on observations by Tzounopoulos et al. (2004) which indicate that the precise timing requirements for coincident detection of pre- and post-synaptic spike events in the auditory processing pathway have resulted in plasticity windows that are shorter when compared to other mammalian synapses exhibiting STDP. This assumption is based on observations of STDP in the auditory processing pathway of mice where no synaptic plasticity updates were detected when the interval between pre and post events was longer than 20 ms (Tzounopoulos et al., 2004).

The chosen implementation method is based on the Song and Abbott approach (Song et al., 2000; Song and Abbott, 2001). To enable on-line calculation of weight updates, the STDP potentiation and depression values for each synapse are determined in a similar manner to how the excitatory and inhibitory conductances are calculated. Each pre-synaptic spike causes the STDP potentiation $a_+(t)$ to increase by an amount A_+ followed by an exponential decay in the form:

$$\frac{da_+(t)}{dt} = \frac{-1}{\tau_+} a_+(t) \quad (3)$$

In a similar manner, each post-synaptic spike causes the STDP depression $a_-(t)$ to increase by an amount A_- followed by the exponential decay:

$$\frac{da_-(t)}{dt} = \frac{-1}{\tau_-} a_-(t) \quad (4)$$

Using the forward Euler integration scheme, these equations can be solved respectively as:

$$a_+(t) = a_+(t-1) + \left(\frac{-1}{\tau_+} a_+(t-1) \right) dt \quad (5)$$

$$a\_(t) = a\_(t-1) + \left(\frac{-1}{\tau\_} a\_(t-1)\right) dt \quad (6)$$

Whilst these equations are used to determine STDP potentiation and depression values, the next stage is to determine the actual changes in synaptic conductance. To achieve this, the synaptic weight is increased when a post-synaptic spike event occurs where the updated weight value is calculated as:

$$q = q + a_{+}(t) \cdot q_{\max} \quad (7)$$

In a similar manner, the synaptic weight is decreased when a pre-synaptic spike event occurs where the update is calculated as:

$$q = q - a\_(t) \cdot q_{\max} \quad (8)$$

RESULTS

This section will discuss the results obtained when the model described in the previous section was implemented in software. Preliminary hardware results will also be presented which will indicate the potential acceleration performance that can be achieved. The cochlea model supplied by Zilany and Bruce (2006, 2007) was developed to integrate with the Matlab environment, hence the input, cochlea and bushy cell neuron layers were simulated using this tool. This Matlab model, created as outputs, a spike event list for each bushy cell neuron in the network using an Address Event Representation (AER) scheme. This data could subsequently be processed by a software or hardware based implementation of the delay layer and output layer of the MSO model.

SOFTWARE IMPLEMENTATION

As the number of neurons and STDP synapses were expected to grow to a considerable size, particularly at the finer azimuth angular resolutions being targeted, it was decided to use a compiled language (C++) to reduce computation times. A user interface to control simulations was developed using the wxWidgets Graphical User Interface (GUI) library. Training and testing data were prepared by sweeping across the angular range of sound source signals ($-60° \leq \theta \leq 60°$). The training stimulus was supplied first where the input stimulus for each angle was applied for the equivalent of 10-s real time. After the weights had stabilized, this procedure was subsequently repeated using test data to determine how well the network was able to perform sound localization.

In the first experiment, an angular resolution of $\theta = 5°$ was used where the input frequency of the sound source was also increased incrementally from 600 Hz to 1.6 KHz in steps of 50 Hz. The overall network topology to accommodate this involved 21 frequency selective clusters each containing 25 output neurons, thus giving a total of 525 neurons in the network. As indicated in **Figure 7**, within each cluster, the left output neurons ($n = 13$) were fully connected to the graded delays emanating from the left bushy cell neuron and the right neurons ($n - 1 = 12$) were connected in the same manner to the graded delays from the right bushy cell neuron. Thus, with 313 STDP synaptic connections in each cluster ($13^2 + 12^2$), the total number of STDP synapses in the network was 6,573.

The classification accuracy of the network was evaluated using two metrics. As the spiking activity of the output layer can be distributed across multiple neurons simultaneously, the number of spikes occurring within both ±5° and ±10° of the target azimuth angle were determined and used to create an overall classification accuracy for these tolerance values. Due to the Poisson based nature of the spike data emanating from the cochlea model, the training and testing procedures were repeated four times to calculate mean values. A plot of the classification accuracies across the frequency range used in the experiments is shown in **Figure 11**. Overall, an average classification accuracy of 70.63% was obtained for the ±5° tolerance whilst this increased to 90.65% for the ±10° tolerance. As can be seen in the diagram, the network reports high accuracies above 90% for angles in the frequency range 600 Hz–1.25 KHz with a slight degradation being observed for higher frequencies. It should be noted however that this is consistent with the research literature which signifies the MSO as being the dominant nucleus in performing sound localization at lower frequencies whilst the LSO is used for higher frequencies. A plot illustrating the spiking activity of the output layer when an 1 KHz input signal is rotated from −60° to 60° is shown in **Figure 12** whilst the weight distribution for the STDP synapses after training is complete, is shown in **Figure 13** where each output neuron indicates a specific azimuth angle.

To further evaluate the impact of azimuth angle resolution on classification accuracy, the above experiment was repeated this time using a step size of 2.5°. This resulted in an overall increase in neuron density from 525 to 1,029 and an increase in the number of STDP synapses from 6,573 to 25,221. Once again the classification accuracies were determined for ±5° and ±10° and the results obtained are plotted in **Figure 14**. It can be seen from this figure that a higher classification accuracy is obtained when compared to the results for the 5° angular resolution. In this case an average classification accuracy of 78.64% was observed for a tolerance of ±5° whilst this increased to 91.82% for the ±10° tolerance.

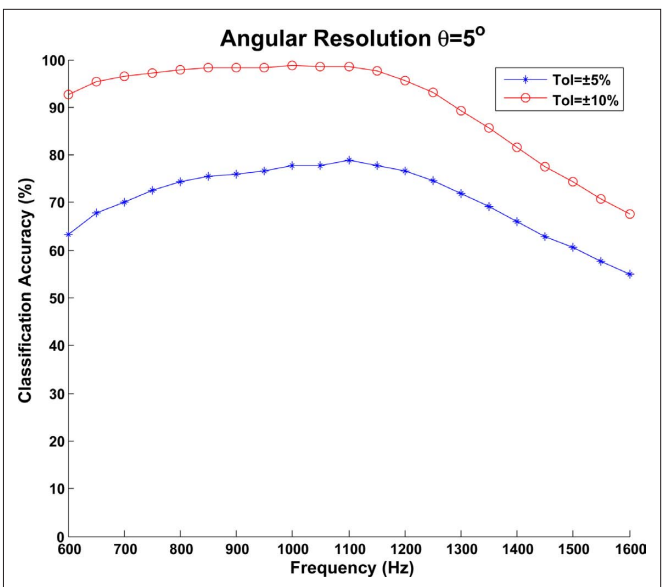

FIGURE 11 | Classification accuracy of the MSO model when an angular resolution of θ = 5° was used. An input frequency sweep from 600 Hz to 1.6 KHz was performed in 50-Hz steps and data is shown for both ±5° and ±10° tolerances.

HARDWARE IMPLEMENTATION

To investigate potential acceleration performance and to acknowledge the possibility of a future deployment in an embedded systems platform, a hardware based implementation of the MSO model on Field Programmable Gate Array (FPGA) hardware has also been targeted. Previous work by the authors has demonstrated the suitability of such reconfigurable devices for replicating the natural plasticity of SNNs (Glackin et al., 2009a,b) and an approach for facilitating large scale implementation of SNNs with STDP has been reported in Maguire et al. (2007). The implementation utilizes Time Division Multiplexing (TDM) to facilitate large scale network topologies whilst minimizing the logic requirements. Whilst this approach facilitates much larger networks than what would be achievable using a fully parallel implementation approach, it is important to carefully consider the speed/area trade-off and the impact this has on computational performance. If resource sharing is over utilized for instance with just one single node performing TDM control, the processing becomes almost serial in nature and no significant benefit can be obtained from the hardware implementation. Thus, for improved performance, it is necessary to maintain a level of parallelism. A degree of on-chip parallelism can be exploited by attaching a number of independent memory banks to the FPGA to allow independent TDM controllers to operate concurrently. Further parallel processing can also be achieved if a multi-FPGA platform is targeted. Thus, the proposed reconfigurable architecture is presented in **Figure 15**, illustrating a series of SNN routers, each connected to four SNN nodes with a communication interface to a local microprocessor host.

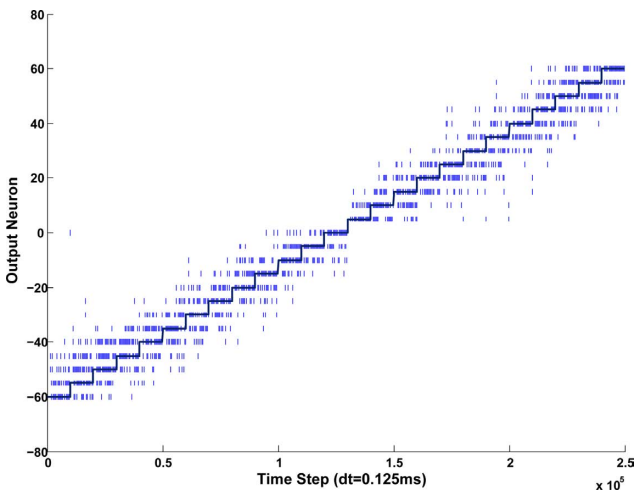

FIGURE 12 | To illustrate typical output behavior of the model, a 1 KHz input signal was rotated from –60° to +60° and the spiking activity was recorded. These spikes are indicated as the vertical lines in the plot. The target or desired output is indicated by the stepped solid line.

In this configuration, a single SNN router attached to four SNN nodes is referred to as an SNN cluster. The SNN router within each cluster provides local communication of spike events between nodes and also supports the propagation of user data throughout the architecture. This provides an effective method of communicating data between large numbers of neurons without consuming significant on-chip routing resources. The neuron and synapse computations pertaining to an SNN network are subsequently mapped to each of the SNN nodes on the architecture providing a method of parallelizing the network. The proposed approach uses the SNN router and nodes to provide both temporal and spatial parallelism, allowing a balance between the level of speed-up and the complexity of inter-neuron routing. Moreover, it provides a configurable infrastructure whereby a number of SNN clusters can be added to allow the system to scale in performance with area.

To validate the hardware implementation approach, the SNN node processor has been developed using the VHDL language to compute a sub-cluster within the MSO model. Whilst the long term goal of this work is to fully implement the complete MSO model in hardware, to date a behavioral simulation of the SNN node processor has been completed using the ModelSim tool to perform functional verification of the design. In this instance the angular resolution used was 2.5°, hence a total of 49 neurons

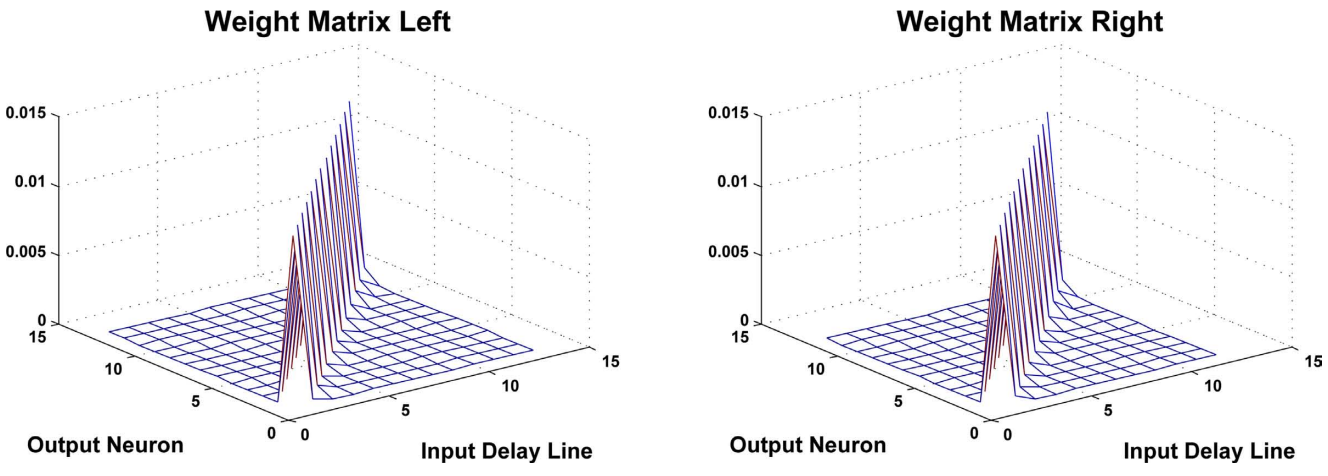

FIGURE 13 | To indicate typical weight distributions between delay lines and output layer neurons, this figure plots the values of the left (contralateral) and right (ipsilateral) STDP weight matrices after training has been performed. The matrices shown are from the 1-KHz cluster of the network.

and 1,201 STDP synapses have been validated to perform in the desired manner. Deploying an individual *snn_node* for each frequency sub-cluster will allow the network to scale to the same dimensions as used in the software model, i.e., 1,029 neurons and 25,221 STDP synapses. The logic requirements for an individual *snn_node* implementation, as reported by the Xilinx ISE design tools, are reported in **Table 1**. In this instance, the target device was the Xilinx XC4VLX160 which has been previously used by the authors for implementing SNNs (Glackin et al. (2009a,b). In terms of performance, a timing constraint of 150 MHz was placed on the primary system clock and a place and route of the design performed to ensure no timing errors were reported. As such it can be deduced that for a 10-s real time simulation with STDP training enabled, the computation time for the FPGA hardware is 4.11 s. When compared to an averaged software execution time of 27.6 s which was obtained from running the same simulation on a workstation with a dual core 2.2-GHz AMD Processor, it can be seen that a speed-up factor of ×6.7 was observed. The main strength of the hardware implementation strategy however is that multiple nodes can be deployed in parallel such that while software execution times will scale linearly depending on the number of frequency selective clusters, the FPGA execution time will remain the same. Thus, it is evident that the hardware based implementation reported offers significant acceleration potential.

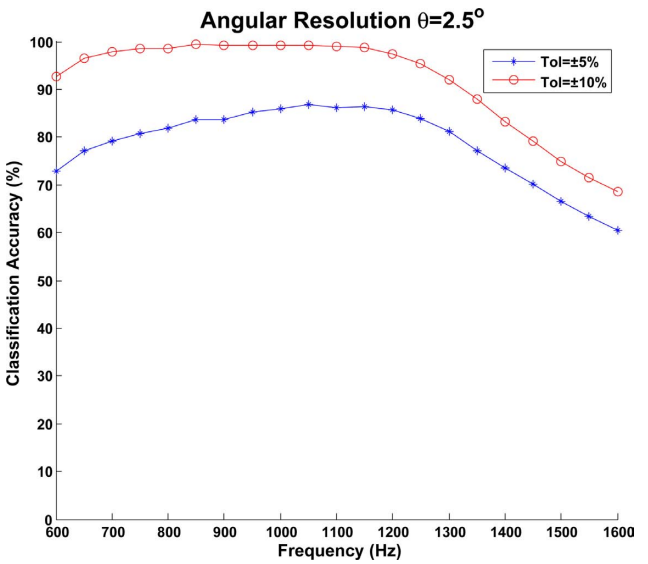

FIGURE 14 | Classification accuracy of the MSO model when an angular resolution of θ = 2.5° was used. Again, an input frequency sweep from 600 Hz to 1.6 KHz was performed in 50-Hz steps and data is shown for both ±5° and ±10° tolerances.

DISCUSSION

Section "Results" has presented results obtained from an implementation of an SNN based model of the MSO for performing sound localization. In attempting to evaluate these results however, it is difficult to make direct comparisons with those presented by other researchers in this field. This is due to the many different methods that are used for sound localization modeling, such as: the implementation approach which can range from purely computational to biologically inspired; the type of data from pure tones to HRTF measurements, and whether this data is simulated or experimentally derived; the resolution of angles being localized; the range of sound frequencies tested by the model; and the use of a learning algorithm to train the models. This information has been summarized for the various SNN based approaches reported in the literature and is presented in **Table 2**.

Table 1 | Device usage statistics (XC4VLX160).

Resource	Usage	Percentage (%)
Slices	1,011 out of 67,584	1
RAMB16s	23 out of 288	7
DSP48s	2 out of 96	2

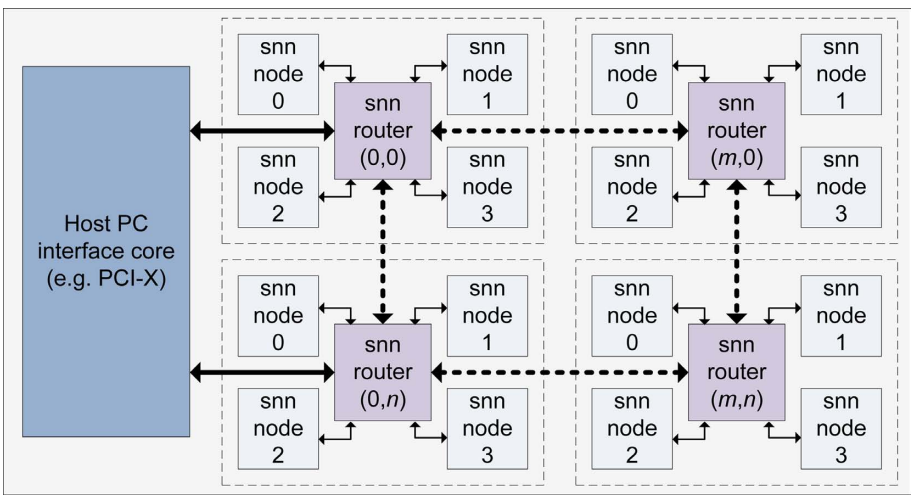

FIGURE 15 | Reconfigurable hardware architecture containing multiple parallel SNN processing nodes.

Table 2 | Comparison of SNN models for sound localization as reported in the research literature, the results of the work presented in this paper are indicated in the final row.

Input data	Spike encoding	Freq. range	Angular sweep	Angular resolution	Training method	Localization accuracy	Ref.
Pure tone	Stochastic	2000 to 5000 Hz	N/A	N/A	Unsupervised Hebbian	N/A	Gerstner et al. (1996)
Digital short tone pulse	Probabilistic	200 to 3250 Hz	–70° to + 30°	10°	Fixed structure	N/A	Smith (2001)
Analog signal	Cochlea + IHC model	100 to 2500 Hz	± 90°	N/A	Competitive learning	N/A	Schauer et al. (2000)
Pure tone	Zero-crossing method	120 to 1240 Hz	± 105°	30°	Evolutionary algorithm	59%	Voutsas and Adamy (2007)
Pulse signals	N/A	N/A	N/A	N/A	Evolutionary algorithm	N/A	Poulsen and Moore (2007)
Broad-band + Pure tone	Cochlea + IHC model	500 to 2000 Hz	± 90°	10°	Winner-take all with weighted mean	80%	Liu et al. (2008b)
Measured HRTF	Auditory periphery model	600 to 1600 Hz	± 60°	2.5°	Supervised STDP	91.82%	–

Analysis of this table indicates a number of ways in which the work described in this paper offers advancements over the current state of the art. Whilst the early work of Gerstner et al. (1996) provided the first Jeffress inspired SNN model for sound localization, it can be seen from the table that the underlying hypothesis was not validated through experimental results to indicate how the model actually performed across relevant frequency ranges for various azimuth angles. Furthermore, the manner in which the sound source signal was converted into spike train inputs was based on a stochastic process as opposed to using biologically realistic data. In contrast, the work of Schauer et al. (2000) and Liu et al. (2008a,b) have attempted to more closely replicate the auditory processing pathway through the integration of both cochlea and IHC models. The presented work has adopted a similar approach, using a cochlea model based on empirical observations in the cat (Zilany and Bruce, 2006, 2007), but has further extended this to use experimentally measured real-world HRTF data obtained from an adult cat (Tollin and Koka, 2009). Hence, the approach described constitutes the most biologically plausible representation of the mammalian auditory processing pathway for sound localization currently reported in the literature.

The work presented has also described the incorporation of the biologically plausible STDP learning rule for network training. Whilst the nature of the teaching signal used means that the overall training approach can be considered supervised, for a task such as sound localization, some form of instruction is required to enable the model to map a particular ITD to the relevant azimuthal angle. Whilst an unsupervised Hebbian learning rule was used in Gerstner et al. (1996) to automatically determine delay line connections, each neuron was trained on an individual basis where no method was described for mapping ITDs to actual angles of sound source location. In the absence of multi-modal sensory information such as visual or tactile data to complete the required feedback loop, the authors suggest that the supervised STDP method described provides an adequate intermediate solution to this problem.

In accordance with the research literature, it has been shown that the spiking neuron model is able to localize lower sound frequencies in a more efficient manner than higher frequencies. This work also sought to investigate the impact of azimuth angular resolution on localization performance. From the results presented in the previous section it can be seen that a notable improvement in accuracy was observed, particularly for the 5° tolerance where an increase from 70.63 to 78.64% was observed. If a 10° tolerance is considered this figure increases to 91.82% when averaged over the complete frequency band. From **Table 2** it can be seen that this figure compares very favorably with alternative SNN models for sound localization. Whilst a localization accuracy of 80% was reported in Liu et al. (2008b), the angular resolution of 30° was considerably lower than that used in the presented work.

The hardware implementation results, whilst preliminary, indicate the significant potential of this approach. With a ×6.7 speed-up factor observed for one processing node, increasing the scale of the hardware implementation such that each SNN processor node is responsible for an individual frequency cluster would lead to an overall acceleration of almost ×150 if the full network topology of 21 frequency clusters used for the software implementation was adopted. Whilst a software computation time of approximately 580 s is required to perform a 10-s real time simulation of this full network, the same computation can be performed on FPGA hardware in just over 4 s, thus ensuring real time performance can be maintained. As has been shown in **Table 1**, only a very small percentage of the FPGA device resources available have been utilized. Furthermore, the on-chip memory usage reported (RAMB16s) can be considered inflated here as the memory interface has been designed to accommodate future increases in resolution. If the angular resolution is increased to 1° and the network model extended to support a full 360° sweep of input angles, the total number of neurons required would be 7,539 whilst the number of STDP synapses would increase to 1,353,261. At this resolution, the model could be considered as approaching the biological scale

as the human MSO, which is believed to contain in the region of 10,000–11,000 neurons (Moore, 2000). In terms of network data storage, this would require approximately 2.8 MB of system memory. Given that there is a total of 192 MB of external memory available on the target hardware platform it is evident that there is significant scope to accommodate this size of network and also to extend the model by incorporating additional components of the auditory processing pathway such as the LSO which is estimated to contain a further 2,500–4,000 neurons (Moore, 2000).

CONCLUSIONS AND FUTURE WORK

This paper has presented a Jeffress inspired spiking based model of the MSO for sound localization. It has been shown that, when presented with biologically observed data from the adult cat, the model has been able to successfully localize the sound source. The model presented is heavily inspired by the mammalian auditory processing pathway, where the ITD was utilized to extract the azimuth angle for sounds in the frequency range of 600 Hz–1.6 KHz. A biologically plausible training mechanism in the form of the STDP rule was used to regulate the synaptic connection weights in the network and thus facilitate the desired behavior.

This paper has also evaluated the impact of increasing the angular resolution on classification performance. Here it was observed that a notable improvement was achieved when the resolution was increased from 10° to 5°. At this resolution, a classification accuracy of almost 92% was obtained from the network when an error tolerance of ±10° was allowed. It has also been shown however that this increase in resolution also results in an increase in network density from 525 to 1,029 neurons and from 6,573 to 25,221 STDP synapses. To mitigate the increased software execution times this incurs, a hardware based implementation of the model has also been proposed. It has been shown that significant acceleration performance is achievable when an FPGA based implementation platform is targeted.

In terms of future work the authors intend to investigate further refinement of the angular resolution and to extend the network architecture to localize sounds from all angles rather than the current subset of $-60° \le \theta \le 60°$. The current single node FPGA implementation will also be extended to accommodate this extended MSO model before eventually combining it with a model of the LSO to provide a complete model for sound localization across all frequency ranges. The long term goal of this work is to create a biologically realistic model of the mammalian auditory processing pathway.

APPENDIX – NEURON MODELS

BUSHY CELL: LIF NEURON MODEL

The spiking neuron model used to implement the bushy cell neurons was the Leaky Integrate-and-Fire (LIF) (Gerstner and Kistler, 2002). The LIF model can be implemented using the following equation:

$$\tau_m \frac{dv}{dt} = -v(t) + R_{\text{in}} I_{\text{syn}}(t) \tag{9}$$

where τ_m refers to the membrane time constant of the neuron, v is the membrane potential and R_{in} is the membrane resistance driven by a synaptic current $I_{\text{syn}}(t)$. The implementation parameters used can be found in **Table 3**.

MSO: CONDUCTANCE BASED I&F NEURON MODEL

For the MSO implementation, the conductance based I&F neuron model used consists of a first order differential equation where the neuron membrane potential, v, is related to the membrane currents in the form:

$$c_m \frac{dv(t)}{dt} = g_l(E_l - v(t)) + \sum_j \frac{q^j g_s^j(t)}{A}\left(E_s^j - v(t)\right) \tag{10}$$

A description of the terms used can be found in **Table 4**. For a given synapse j, an action potential event at the pre-synaptic neuron at time t_{ap} triggers a synaptic release event at time $t_{\text{ap}} + t^j_{\text{delay}}$, causing a discontinuous increase in the synaptic conductance

$$g_s^j\left(t_{\text{ap}} + t^j_{\text{delay}} + dt\right) = g_s^j\left(t_{\text{ap}} + t^j_{\text{delay}}\right) + q_s^j \tag{11}$$

otherwise $g_s^j(t)$ is governed by

$$\frac{dg_s^j(t)}{dt} = \frac{-1}{\tau_s^j} g_s^j(t) \tag{12}$$

where q_s^j refers to the weight or peak conductance of the synapse. The forward Euler integration scheme with a time step of $dt = 0.125$ ms can be used to solve the conductance based I&F model equations. Using this method, Eq. 10 is re-expressed as:

$$v(t+dt) = v(t) + \frac{1}{c}\left(\left(g_l\left(E_l - v(t)\right) + \sum_j \frac{q^j g_s^j(t)}{A}\left(E_s^j - v(t)\right)\right)\right)dt \tag{13}$$

and differential equation (3) becomes,

Table 3 | LIF neuron model parameters.

Param	Value	Description
v_{th}	0.5 mV	Threshold voltage
τ_{ref}	8 ms	Refractory period
τ_m	4 ms	Membrane time constant

Table 4 | Conductance based I&F neuron model parameters.

Param	Common	Excitatory	Inhibitory	Description
c_m	8 nF/mm^2	–	–	Membrane capacitance
E_l	–70 mV	–	–	Membrane reversal potential
v_{th}	–56 mV	–	–	Threshold voltage
V_{reset}	–70 mV	–	–	Reset voltage
τ_{ref}	6.5 ms	–	–	Refractory period
t^j_{delay}	0.5 ms	–	–	Propagation delay
g_l	1 μS	–	–	Membrane leak conductance
A	–	0.03125 mm^2	0.015625 mm^2	Membrane surface area
E_s^j	–	0 mV	–75 mV	Reverse potential of synapse
τ_s^j	–	1 ms	4 ms	Synapse decay time

$$g_s^j(t+dt) = g_s^j(t) + \left(\frac{-1}{\tau_s^j} g_s^j(t)\right) dt \quad (14)$$

As previously discussed, an aspect of this research is to consider an eventual hardware based implementation of the network model. Hence, when selecting the neuron model parameters, a number of considerations were taken into account, For example, multiplicand and divisor parameters (e.g., A, τ_s^j) were chosen as powers of 2 such that they could be implemented using binary shift operators thus minimizing the amount of required by a full multiplier or divider. A description of the various parameters and the values used for the software and hardware implementations reported in this paper can be found in **Table 4**.

ACKNOWLEDGMENTS

Our thanks go to Dr. D. J. Tollin at the University of Colorado Medical School for providing us with the HRTF data and recommending which auditory periphery models to use. Dr. Glackin is supported under the CoEIS grant from the Integrated Development Fund.

REFERENCES

Abarbanel, H. D. I., Huerta, R., and Rabinovich, M. I. (2002). Dynamical model of long-term synaptic plasticity. *Proc. Natl. Acad. Sci. U.S.A.* 99, 10132–10137.

Abdel Alim, O., and Farag, H. (2000). "Modeling non-individualized binaural sound localization in the horizontal plane using artificial neural networks," in *Proceedings of the IEEE-INNS-ENNS International Joint Conference on Neural Networks (IJCNN)*, Vol. 3. Como, 642–647.

Alnajjar, F., and Murase, K. (2008). A simple aplysia-like spiking neural network to generate adaptive behavior in autonomous robots. *Adapt. Behav.* 16, 306–324.

Arena, P., Fortuna, L., Frasca, M., and Patane, L. (2009). Learning anticipation via spiking networks: application to navigation control. *IEEE Trans. Neural Netw.* 20, 202–216.

Backman, J., and Karjalainen, M. (1993). "Modelling of human directional and spatial hearing using neural networks," in *1993 IEEE International Conference on Acoustics, Speech, and Signal Processing, 1993. ICASSP-93*, Vol. 1, Minneapolis.

Beckius, G. E., Batra, R., and Oliver, D. L. (1999). Axons from anteroventral cochlear nucleus that terminate in medial superior olive of cat: observations related to delay lines. *J. Neurosci.* 19, 3146–3161.

Bell, C. C., Han, V. Z., Sugawara, Y., and Grant, K. (1997). Synaptic plasticity in a cerebellum-like structure depends on temporal order. *Nature* 387, 278–281.

Bi, G., and Poo, M. (1998). Synaptic modifications in cultured hippocampal neurons: dependence on spike timing, synaptic strength, and postsynaptic cell type. *J. Neurosci.* 18, 10464–10472.

Burger, R., and Rubel, E. (2008). "Encoding of interaural timing for binaural hearing" in *The Senses: A Comprehensive Reference*, Vol. 3, A. I. Basbaum, M. C. Bushnell, D. V. Smith, G. K. Beauchamp, S. J. Firestein, P. Dallos, D. Oertel, R. H. Masland, T. Albright, J. H. Kaas, and E. P. Gardner (San Diego: Academic Press), 613–630.

Carr, C. E. (1993). Delay line models of sound localization in the barn owl. *Am. Zool.* 33, 79–85.

Carr, C. E., and Konishi, M. (1990). A circuit for detection of interaural time differences in the brain stem of the barn owl. *J. Neurosci.* 10, 3227–3246.

Chung, W., Carlile, S., and Leong, P. (2000). A performance adequate computational model for auditory localization. *J. Acoust. Soc. Am.* 107, 432.

Dan, Y., and Poo, M. (2006). Spike timing-dependent plasticity: from synapse to perception. *Physiol. Rev.* 86, 1033–1048.

Datum, M. S., Palmieri, F., and Moiseff, A. (1996). An artificial neural network for sound localization using binaural cues. *J. Acoust. Soc. Am.* 100, 372–383.

Deneve, S., Latham, P. E., and Pouget, A. (2001). Efficient computation and cue integration with noisy population codes. *Nat. Neurosci.* 4, 826–831.

Destexhe, A. (1997). Conductance-based integrate-and-fire models. *Neural. Comput.* 9, 503–514.

Gerstner, W., Kempter, R., Van Hemmen, J., and Wagner, H. (1996). A neuronal learning rule for sub-millisecond temporal coding. *Nature* 383, 76–78.

Gerstner, W., and Kistler, W. (2002). *Spiking Neuron Models: Single Neurons, Populations, Plasticity*. Cambridge: Cambridge University Press.

Glackin, B., Harkin, J., McGinnity, T., and Maguire, L. (2009a). "A hardware accelerated simulation environment for spiking neural networks," in *Proceedings of 5th International Workshop on Applied Reconfigurable Computing (ARC'09), Vol. 5453 of Lecture Notes in Computer Science*, Prague, 336–341.

Glackin, B., Harkin, J., McGinnity, T., Maguire, L., and Wu, Q. (2009b). "Emulating spiking neural networks for edge detection on FPGA hardware," in *Proceedings of International Conference on Field Programmable Logic and Applications FPL 2009*, Karlsruhe, 670–673.

Grothe, B. (2003). New roles for synaptic inhibition in sound localization. *Nat. Rev. Neurosci.* 4, 540–550.

Hancock, K., and Delgutte, B. (2004). A physiologically based model of interaural time difference discrimination. *J. Neurosci.* 24, 7110–7117.

Handzel, A., and Krishnaprasad, P. (2002). Biomimetic sound-source localization. *IEEE Sens. J.* 2, 607–616.

Hao, M., Lin, Z., Hongmei, H., and Zhenyang, W. (2007). "A novel sound localization method based on head related transfer function," in *8th International Conference on Electronic Measurement and Instruments*, ICEMI, Xian, 4–428.

Hebb, D. O. (1949). *The Organization of Behavior*. New York: John Wiley.

Hodgkin, A., and Huxley, A. (1952). A quantitative description of membrane current and its application to conduction and excitation in nerve. *J. Physiol.* 117, 500–544.

Hosaka, R., Araki, O., and Ikeguchi, T. (2008). STDP provides the substrate for igniting synfire chains by spatiotemporal input patterns. *Neural. Comput.* 20, 415–435.

Huang, J., Supaongprapa, T., Terakura, I., Wang, F., Ohnishi, N., and Sugie, N. (1999). A model-based sound localization system and its application to robot navigation. *Rob. Auton. Syst.* 27, 199–209.

Indiveri, G., Chicca, E., and Douglas, R. (2006). A VLSI array of low-power spiking neurons and bistable synapses with spike-timing dependent plasticity. *IEEE Trans. Neural Netw.* 17, 211–221.

Izhikevich, E. M., Gally, J. A., and Edelman, G. M. (2004). Spike-timing dynamics of neuronal groups. *Cereb. Cortex* 14, 933–944.

Jeffress, L. A. (1948). A place theory of sound localization. *J. Comp. Physiol. Psychol.* 41, 35–39.

Joris, P., and Yin, T. C. T. (2007). A matter of time: internal delays in binaural processing. *Trends Neurosci.* 30, 70–78.

Kempter, R., Gerstner, W., van Hemmen, J. L., and Wagner, H. (1996). Temporal coding in the submillisecond range: model of barn owl auditory pathway. Adv. Neural Inf. Process Syst. 8, 124–130.

Kempter, R., Gerstner, W., van Hemmen, J. L., and Wagner, H. (1996). Temporal coding in the submillisecond range: model of barn owl auditory pathway. *Adv. Neural Inf. Process Syst.* 8, 124–130.

Keyrouz, F., and Diepold, K. (2008). A novel biologically inspired neural network solution for robotic 3D sound source sensing. *Soft Comput. Fusion Found. Methodologies Appl.* 12, 721–729.

Konishi, M. (2000). Study of sound localization by owls and its relevance to humans. *Comp. Biochem. Physiol. A* 126, 459–469.

Kulesza, R. (2007). Cytoarchitecture of the human superior olivary complex: medial and lateral superior olive. *Hear. Res.* 225, 80–90.

Li, H., Lu, J., Huang, J., and Yoshiara, T. (2009). "Spatial localization of multiple sound sources in a reverberant environment," in *International Computer Symposium (ICS), 2008 ICS*, Tamshui.

Liu, J., Erwin, H., Wermter, S., and Elsaid, M. (2008a). "A biologically inspired spiking neural network for sound localisation by the inferior colliculus," in *Proceedings of the 18th International Conference on Artificial Neural Networks*, Part II (Nice: Springer), 396–405.

Liu, J., Erwin, H., and Wermter, S. (2008b). "Mobile robot broadband sound localisation using a biologically inspired spiking neural network," in *IEEE/RSJ International Conference on Intelligent Robots and Systems, IROS*, Heidelberg, 2191–2196.

Liu, J., Perez-Gonzalez, D., Rees, A., Erwin, H., and Wermter, S. (2009). "Multiple sound source localisation in reverberant environments inspired by the auditory midbrain," in *19th International Conference on Artificial Neural Networks (ICANN'09), Vol. 5768 of Lecture Notes in Computer Science* (Heidelberg: Springer), 208–217.

Maguire, L. P., McGinnity, T. M., Glackin, B., Ghani, A., Belatreche, A., and Harkin, J. (2007). Challenges

for large-scale implementations of spiking neural networks on FPGAs. *Neurocomputing* 71, 13–29.

Markram, H., Lübke, J., Frotscher, M., and Sakmann, B. (1997). Regulation of synaptic efficacy by coincidence of postsynaptic APs and EPSPs. *Science* 275, 213–215.

Masquelier, T., Hugues, E., Deco, G., and Thorpe, S. J. (2009). Oscillations, phase-of-firing coding, and spike timing-dependent plasticity: an efficient learning scheme. *J. Neurosci.* 29, 13484–13493.

McAlpine, D., and Grothe, B. (2003). Sound localization and delay lines – do mammals fit the model? *Trends Neurosci.* 26, 347–350.

Moore, J. K. (2000). Organization of the human superior olivary complex. *Microsc. Res. Tech.* 51, 403–412.

Murray, J. C., Erwin, H. R., and Wermter, S. (2009). Robotic sound-source localisation architecture using cross-correlation and recurrent neural networks. *Neural. Netw.* 22, 173–189.

Nakashima, H., Chisaki, Y., Usagawa, T., and Ebata, M. (2003). Frequency domain binaural model based on interaural phase and level differences. *Acoust. Sci. Technol.* 24, 172–178.

Natschläger, T., and Ruf, B. (1999). Pattern analysis with spiking neurons using delay coding. *Neurocomputing* 26–27, 463–469.

Nessler, B., Pfeiffer, M., and Maass, W. (2009). "STDP enables spiking neurons to detect hidden causes of their inputs," in *Advances in Neural Information Processing Systems (NIPS'09)* (Cambridge MA: MIT Press), 1357–1365.

Nordlund, B. (1962). Physical factors in angular localization. *Acta Otolaryngol.* 54, 75–93.

Northmore, D. P. M. (2004). A network of spiking neurons develops sensorimotor mechanisms while guiding behavior. *Neurocomputing* 58–60, 1057–1063.

Palmieri, F., Datum, M., Shah, A., and Moiseff, A. (1991). Sound localization with a neural network trained with the multiple extended Kalman algorithm. *International Joint Conference on Neural Networks, IJCNN,* Vol. 1. Seattle.

Poulsen, T. M., and Moore, R. K. (2007). "Sound localization through evolutionary learning applied to spiking neural networks," in *IEEE Symposium on Foundations of Computational Intelligence, FOCI*, Honolulu, 350–356

Rayleigh, L. (1875–1876). On our perception of the direction of a source of sound. J. R. Musical Assoc. 2nd Sess., 75–84.

Rayleigh, L. (1907). On our perception of sound direction. *Philos. Mag.* 13, 214–232.

Rumsey, F. (2001). Spatial Audio. Oxford: Focal Press.

Ryugo, D. K., and Parks, T. N. (2003). Primary innervation of the avian and mammalian cochlear nucleus. *Brain Res. Bull.* 60, 435–456.

Schauer, C., Zahn, T., Paschke, P., and Gross, H. M. (2000). "Binaural sound localization in an artificial neural network," in *Proceedings of the IEEE International Conference on Acoustics, Speech, and Signal Processing, ICASSP*, Vol. 2, Istanbul.

Schemmel, J., Bruderle, D., Meier, K., and Ostendorf, B. (2007). "Modeling synaptic plasticity within networks of highly accelerated I&F neurons," in *IEEE International Symposium on Circuits and Systems (ISCAS'07)*, New Orleans, 3367–3370.

Shi, R. Z., and Horiuchi, T. K. (2004). "A VLSI model of the bat lateral superior olive for azimuthal echolocation," in *Proceedings of the International Symposium on Circuits and Systems, ISCAS*, Vol. 4, Vancouver.

Smith, L. S. (2001). Using depressing synapses for phase locked auditory onset detection. *Lect. Notes Comput. Sci.* 2130, 1103–1108.

Smith, P. H., Joris, P. X., and Yin, T. C. (1993). Projections of physiologically characterized spherical bushy cell axons from the cochlear nucleus of the cat: evidence for delay lines to the medial superior olive. *J. Comp. Neurol.* 331, 245–260.

Smith, P. H., Joris, P. X., and Yin, T. C. T. (1998). Anatomy and physiology of principal cells of the medial nucleus of the trapezoid body (MNTB) of the cat. *J. Neurophysiol.* 79, 3127–3142.

Song, S., and Abbott, L. (2001). Cortical development and remapping through spike timing-dependent plasticity. *Neuron* 32, 339–350.

Song, S., Miller, K., and Abbott, L. (2000). Competitive Hebbian learning through spike-timing-dependent synaptic plasticity. *Nat. Neurosci.* 3, 919–926.

Thompson, S. (1882). On the function of the two ears in the perception of space. *Philos. Mag.* 13, 406–416.

Tollin, D. J. (2004). The development of the acoustical cues to sound localization in cats. *Assoc. Res. Otol.* 27, 161.

Tollin, D. J. (2008). "Encoding of interaural level differences for sound localization," in The Senses: A Comprehensive Reference Vol. 3, (San Diego: Academic Press), 631–654.

Tollin, D., and Koka, K. (2009). Postnatal development of sound pressure transformations by the head and pinnae of the cat: monaural characteristics. *J. Acoust. Soc. Am.* 125, 980.

Tollin, D., Koka, K., and Tsai, J. (2008). Interaural level difference discrimination thresholds for single neurons in the lateral superior olive. *J. Neurosci.* 28, 4848.

Tzounopoulos, T., Kim, Y., Oertel, D., and Trussell, L. O. (2004). Cell-specific, spike timing-dependent plasticities in the dorsal cochlear nucleus. *Nat. Neurosci.* 7, 719–725.

Voutsas, K., and Adamy, J. (2007). A biologically inspired spiking neural network for sound source lateralization. *IEEE Trans. Neural. Netw.* 18, 1785–1799.

Wall, J., McDaid, L., Maguire, L., and McGinnity, T. (2008). "Spiking neuron models of the medial and lateral superior olive for sound localisation," in *IEEE International Joint Conference on Neural Networks (IJCNN'08)*, Hong Kong, 2641–2647.

Wall, J. A., McDaid, L. J., Maguire, L. P., and McGinnity, T. M. (2007). "A spiking neural network implementation of sound localisation," in *Proceedings of the IET Irish Signals and Systems*, Derry, pp. 19–23.

Willert, V., Eggert, J., Adamy, J., Stahl, R., and Korner, E. (2006). A probabilistic model for binaural sound localization. *IEEE Trans. Syst. Man Cybern. B Cybern.* 36, 982.

Wu, Q., McGinnity, T., Maguire, L., Belatreche, A., and Glackin, B. (2005). Adaptive co-ordinate transformation based on spike timing-dependent plasticity learning paradigm. *Adv. Nat. Comput.* 3610, 420–428.

Wu, Q., McGinnity, T., Maguire, L., Belatreche, A., and Glackin, B. (2008). 2d co-ordinate transformation based on a spike timing-dependent plasticity learning mechanism. *Neural. Netw.* 21, 1318–1327.

Yang, Z., and Murray, A. F. (2006). An artificial early visual model adopting spike-timing-dependent plasticity. *Neurocomputing* 69, 1904–1911.

Yin, T. C. T. (2002). "Neural mechanisms of encoding binaural localization cues in the auditory brainstem," in *Integrative Functions in the Mammalian Auditory Pathway*, eds D. Oertel, R. R. Fay, and A. N. Popper (New York: Springer-Verlag), 99–159.

Zhang, L. I., Tao, H. W., Holt, C. E., Harris, W. A., and Poo, M. (1998). A critical window for cooperation and competition among developing retinotectal synapses. *Nature* 395, 37–44.

Zilany, M. S. A., and Bruce, I. C. (2006). Modeling auditory-nerve responses for high sound pressure levels in the normal and impaired auditory periphery. *J. Acoust. Soc. Am.* 120, 1446.

Zilany, M. S. A., and Bruce, I. C. (2007). Representation of the vowel/ɛ/in normal and impaired auditory nerve fibers: model predictions of responses in cats. *J. Acoust. Soc. Am.* 122, 402.

Conflict of Interest Statement: The authors declare that the research was conducted in the absence of any commercial or financial relationships that could be construed as a potential conflict of interest.

Received: 22 February 2010; paper pending published: 20 March 2010; accepted: 04 June 2010; published online: 03 August 2010.
Citation: Glackin B, Wall JA, McGinnity TM, Maguire LP and McDaid LJ (2010) A spiking neural network model of the medial superior olive using spike timing dependent plasticity for sound localization. Front. Comput. Neurosci. ***4****:18. doi: 10.3389/fncom.2010.00018*

frontiers in
COMPUTATIONAL NEUROSCIENCE

ORIGINAL RESEARCH ARTICLE
published: 28 December 2010
doi: 10.3389/fncom.2010.00157

Decorrelation of odor representations via spike timing-dependent plasticity

Christiane Linster*[1,2] *and Thomas A. Cleland*[1,3]

[1] *Computational Physiology Laboratory, Cornell University, Ithaca, NY, USA*
[2] *Department of Neurobiology and Behavior, Cornell University, Ithaca, NY, USA*
[3] *Department of Psychology, Cornell University, Ithaca, NY, USA*

Edited by:
Wulfram Gerstner, Ecole Polytechnique Fédérale de Lausanne, Switzerland

Reviewed by:
Guillaume Hennequin, Ecole Polytechnique Fédérale de Lausanne, Switzerland

***Correspondence:**
Thomas A. Cleland, Department of Psychology, Cornell University, Ithaca, NY 14853, USA.
e-mail: thomas.cleland@cornell.edu

The non-topographical representation of odor quality space differentiates early olfactory representations from those in other sensory systems. Decorrelation among olfactory representations with respect to physical odorant similarities has been proposed to rely upon local feed-forward inhibitory circuits in the glomerular layer that decorrelate odor representations with respect to the intrinsically high-dimensional space of ligand–receptor potency relationships. A second stage of decorrelation is likely to be mediated by the circuitry of the olfactory bulb external plexiform layer. Computations in this layer, or in the analogous interneuronal network of the insect antennal lobe, are dependent on fast network oscillations that regulate the timing of mitral cell and projection neuron (MC/PN) action potentials; this suggests a largely spike timing-dependent metric for representing odor information, here proposed to be a precedence code. We first illustrate how the rate coding metric of the glomerular layer can be transformed into a spike precedence code in MC/PNs. We then show how this mechanism of representation, combined with spike timing-dependent plasticity at MC/PN output synapses, can progressively decorrelate high-dimensional, non-topographical odor representations in third-layer olfactory neurons. Reducing MC/PN oscillations abolishes the spike precedence code and blocks this progressive decorrelation, demonstrating the learning network's selectivity for these sparsely synchronized MC/PN spikes even in the presence of temporally disorganized background activity. Finally, we apply this model to odor representations derived from calcium imaging in the honeybee antennal lobe, and show how odor learning progressively decorrelates odor representations, and how the abolition of PN oscillations impairs odor discrimination.

Keywords: olfaction, gamma oscillations, sparse synchronization, STDP, olfactory bulb, antennal lobe, odor learning, conditioning

INTRODUCTION

As neural representations of sensory stimuli progress from peripheral sensors into the central nervous system, they are transformed not only in terms of feature selectivity but also in terms of the underlying spike encoding metric. Specifically, whereas neurons embedded in primary sensory organs appear to represent information largely by "rate coding" – a simple metric in which the instantaneous spike rate of a cell represents its level of activation, and the timecourse of activity follows that of the stimulus – higher-order sensory neurons can transform this information into more sophisticated metrics, with evoked action potentials typically sparser in terms of total activity and more tightly regulated in time (*temporal precision*; Panzeri et al., 2009). In particular, the coordinated regulation of action potential timing within and among regions of the brain is associated with fast oscillations in the local field potential (LFP) that exhibit frequencies of 15–100 Hz (i.e., in the beta and gamma bands). Fast LFP oscillations are observed in visual cortex (Gray and Singer, 1989; Nase et al., 2003), in the olfactory systems of vertebrates (Buonviso et al., 2003; Neville and Haberly, 2003; Lagier et al., 2004; David et al., 2009) and insects (Laurent and Davidowitz, 1994; Stopfer et al., 1997; Cassenaer and Laurent, 2007), as well as broadly across associational areas including hippocampus and isocortex (Sirota et al., 2008; Hajos and Paulsen, 2009). In the honeybee olfactory system, the disruption of coordinated oscillations in the antennal lobe (AL) reduces sensory acuity and broadens generalization among similar odors (Stopfer et al., 1997). In the analogous mammalian olfactory bulb (OB), the enhancement of oscillations has been associated with increased perceptual acuity (Nusser et al., 2001; Beshel et al., 2007; Kay et al., 2009); moreover, olfactory acuity is impaired by reducing inhibitory synaptic strengths in the recurrent circuit from which gamma oscillations are generated, and enhanced by the potentiation of this inhibition (Abraham et al., 2010). That is, in this system, and perhaps generally, spike timing regulation appears not to replace but to supplement and modify the specificity of the underlying identity code, in which chemosensory information is represented by the identities of the ensemble of spiking projection neurons (reviewed by Laurent, 1999) – or, more precisely, by the pattern of relative levels of activation across the ensemble (Cleland et al., 2007).

There are multiple metrics by which information can be represented via the regulation of spike timing (Hopfield, 1995; Masquelier et al., 2009; Panzeri et al., 2009). One of the biophysically simplest of these utilizes *precedence coding*, a term that reflects both the *latency code* and *phase code* described by Panzeri et al. (2009). In precedence coding, information about the level of neuronal activation is converted into relative spike latency, such that neurons that are more

strongly activated generate correspondingly shorter-latency spikes – i.e., a given spike's precedence with respect to the ensemble of its peers signals the relative strength or importance of its signal. Prerequisite to such a code, however, is a common time reference among all neurons participating in the representation. This reference can originate from a single, common external event such as an experimental stimulus presentation or active sampling behavior – in tetrapod olfaction, the latter corresponds to a sniff (Schaefer and Margrie, 2007; Wachowiak et al., 2009), whereas in arthropods antennal flicking appears to serve a similar purpose (Koehl et al., 2001). Alternatively, or additionally, the time reference can be a shared internal clock such as is indicated by the presence of fast LFP oscillations (Fries et al., 2007); indeed, oscillatory coherence within and among cortical structures has been clearly associated with sensory activation and selective attention to stimuli (Kay and Freeman, 1998; Martin et al., 2007; Uhlhaas et al., 2009; Ardid et al., 2010). In this context, precedence codes reflect the phase precedence of each neuron's spiking with respect to the periodically distributed collective activity of its peers, as can be estimated by measuring the LFP oscillation.

Direct evidence for the functional importance of precedence codes in fast oscillations is rare but accumulating. The relative phase lead of evoked spikes in primary visual cortex neurons corresponds to the strengths of their excitatory drives (reviewed in Fries et al., 2007) and can be exploited to create sparse representations when paired with a spike timing-dependent plasticity rule, as proposed by Thorpe and colleagues (Guyonneau et al., 2005; Masquelier et al., 2009). In an odor-activated subset of mitral cells in the rodent OB, spikes are sharply phase-constrained with respect to underlying gamma oscillations, and the phase of spiking in a given cell can persist across multiple gamma cycles (David et al., 2009). While there is no direct evidence regarding whether or not the spike timing-sensitivity of second-order olfactory principal neurons reflects such a precedence code, theoretical work based on OB slice recordings does suggest that spike precedence in activated mitral cells, coordinated in time by an input-induced phase reset in their subthreshold oscillations, will directly reflect their presynaptic activation levels (Desmaisons et al., 1999; Rubin and Cleland, 2006). We here outline a model framework in which odor representations embedded in OB/AL spike precedence codes can be read and appropriately interpreted by spike timing-dependent computations that systematically modify synaptic weights and construct sparse representations in the next neuronal layer.

The model is predicated on the common architectural principles of complex olfactory systems in vertebrates and arthropods, as illustrated in **Figure 1A**. Briefly, a population of odor-selective primary olfactory sensory neurons (OSNs) in the sensory periphery responds to odorant stimuli, the axons of these OSNs project to the OB/AL and segregate therein into discrete glomeruli on the basis of their chemoreceptive fields; i.e., each glomerulus directly inherits the chemoreceptive field of its constituent OSNs. Second-order principal neurons (e.g., mitral cells, projection neurons) are excited by OSN activity, though their spiking output is substantially shaped by intrinsic inhibitory interneurons, resulting in the decorrelation of different odor representations and the phase-constraining of MC/PN spiking with respect to a periodic beta/gamma-band clock. While several factors, both intrinsic and learned, contribute to the regulation of olfactory decorrelation in the OB (reviewed in Cleland et al. 2009; Mandairon and Linster, 2009), we here focus specifically on the regulation of MC/PN spiking activity by intrabulbar oscillatory dynamics and how odor representations based upon spike precedence coding could be utilized by postbulbar computations.

MATERIALS AND METHODS

NETWORK ARCHITECTURE

The model architecture is depicted in **Figure 1A**. To minimize free parameters and facilitate systematic analysis, we used simplified neuron models and a reduced version of the OB/AL network. A total of 100 glomeruli, including associated OSNs and mitral cells (MCs; or, equivalently, insect projection neurons, PNs) were simulated and arranged for display in a two-dimensional 10×10 array (spatial location in this array had no influence on computations). Simulated odorants each activated characteristic, arbitrary subgroups of model OSNs to differing degrees. Specifically, each model OSN exhibited a normally distributed receptive field with a ligand–receptor potency value for each odorant drawn randomly from this distribution. The statistical distribution of OSN receptive fields was random with respect to location across the 10×10 array. Glomerular-layer computations were not explicitly simulated; as this circuitry is thought to perform initial decorrelation operations and limit the range of absolute activity levels among MC/PNs (Linster et al., 2005; Cleland, 2010), its effect can be approximated by appropriately limiting the range of model odorant stimuli presented to the model. Model MC/PNs received direct synaptic excitation from the OSN population associated with a given glomerulus (modeled in aggregate) as well as periodic feedforward inhibition from a non-spiking interneuron representing a population of interconnected inhibitory interneurons (e.g., vertebrate granule cells or insect homoLN interneurons). (The network mechanisms responsible for generating fast oscillations in the OB and AL are contested, and it is not the goal of the present model to explore their relative merits). The single interneuron implemented herein (GC/hLN) received excitatory input from all OSNs and fed inhibition back onto itself as well as delivering inhibition onto all MC/PNs. This connectivity resembles that described in the insect AL, in which oscillatory activity is thought to be generated by a network of inhibitory local interneurons (MacLeod and Laurent, 1996; Stopfer et al., 1997); in the olfactory bulb, fast oscillations also depend on inhibitory synaptic interactions, although granule cells receive their afferent activation indirectly (via mitral cells). This autoinhibitory feedback loop generated stimulus-evoked gamma-band oscillations in the GC/hLN interneuron that also phase-constrained the spike timing of MC/PNs via periodic inhibition (**Figure 1B**). MC/PNs in turn projected excitatory, plastic synapses onto a second 10×10 layer of principal neurons representing higher processing centers such as piriform cortical pyramidal cells (PCs) or insect mushroom body Kenyon cells. The projection matrix between MC/PNs and PCs was sparse (5% connectivity), uniformly distributed, and randomized (Linster et al., 2007, 2009), and generated sparse, distributed, and plastic patterns of odor-responsive activity in PNs after conditioning (**Figure 1C**), as has been observed in rodent piriform cortex (Johnson et al., 2000; Illig and Haberly, 2003; Roesch et al., 2007; Poo and Isaacson, 2009; Stettler and Axel, 2009). Synaptic connections and parameter values are presented in **Table 1**.

MODEL NEURON EQUATIONS

All neurons were represented as single compartments; each compartment was characterized by a membrane time constant that can be regarded as the mean product of the membrane capacitance and the membrane input resistance. Consequently, the evolution of the membrane voltage over time is described by a first order differential equation:

$$\tau \frac{dv(t)}{dt} + v(t) = I_{ext}(t), \quad (1)$$

where τ is the charging time constant of the neuron and $I_{ext}(t)$ is the total input at time t.

MC/PN and PC neurons produced discrete spikes of unit amplitude for output, computed according to the instantaneous spiking probability, a continuous, bounded function of the membrane potential with a threshold θ_{min} and a saturation value θ_{max}. The instantaneous spiking probability $P(x = 1)$ was 0 below the threshold, varied linearly between the threshold and saturation and was 1.0 above saturation. Membrane potential was reset to rest after each spike.

$$\begin{aligned} &P(x=1) = 0 \text{ if } v(t) \le \theta_{min} \\ &P(x=1) = (v(t) - \theta_{min})/(\theta_{max} - \theta_{min}) \text{ if } \theta_{min} < v(t) < \theta_{max} \\ &P(x=1) = 1 \text{ if } v(t) \ge \theta_{max} \end{aligned} \quad (2)$$

The inhibitory interneuron was a non-spiking interneuron with a continuous output variable. The interneuron output was calculated according to the same continuous, bounded function of the membrane potential:

$$\begin{aligned} &x(t) = 0 \text{ if } v(t) \le \theta_{min} \\ &x(t) = (v(t) - \theta_{min})/(\theta_{max} - \theta_{min}) \text{ if } \theta_{min} < v(t) < \theta_{max} \\ &x(t) = 1 \text{ if } v(t) \ge \theta_{max} \end{aligned} \quad (3)$$

The input to a postsynaptic neuron i from a particular presynaptic neuron j at time t was computed as a function of the synaptic strength w_{ij}, the conductance change $g(t)$ due to a presynaptic output event x_j (either a unitary event representing an action potential or an analog value in the case of the inhibitory interneuron), and the difference between the Nernst potential $E_{N,ij}$ of the associated synaptic channel and the current membrane potential v_i of the postsynaptic neuron:

$$I_{i,ext}(t) = \sum_j W_{ij} \sum_{tj<t} g(t - t_j)\left[E_{N,ij} - V_i(t)\right] \quad (4)$$

The time course of g was described by a double exponential function:

$$g(t - t_j) = g_{max} \frac{\tau_1 \tau_2}{\tau_1 - \tau_2}\left(e^{-(t-t_j)/\tau_1} - e^{-(t-t_j)/\tau_2}\right) \quad (5)$$

DECORRELATION CALCULATIONS

To calculate the overlap between representations and thereby measure the effectiveness of decorrelation, 80 simulations, each using a new pair of randomly determined odorants, were run for each of two conditions: a normal oscillatory condition and a condition in which oscillations were suppressed so as to eliminate MC/PN precedence coding. Odor representations at each level of the network were represented by 100-element activity vectors in which each element represented the average output activity of the corresponding MC/PN or PC pyramidal neuron over the course of a 500-ms stimulation. The overlaps between the representations of each odor stimulus pair by the MC/PN and PC ensembles were calculated as the normalized dot product between the corresponding 100-element activity vectors O_1 and O_2:

$$\text{Overlap}_{O_1,O_2} = \frac{\sum_{i=1}^{N} O_{1i} O_{2i}}{||O_1|| ||O_2||} \quad (6)$$

where O_{1i},O_{2i} are the elements of the activity vectors O_1 and O_2, respectively, and $||O_1||$, $||O_2||$ are the norms of vectors O_1 and O_2. Activity vectors were computed from the numbers of spikes evoked in each neuron during the time of stimulus application.

STDP LEARNING RULE

The strengths of synaptic inputs from MC/PNs to PCs were each set to a baseline value w_{PC} when the network was created. During the odor conditioning phase, the strengths of these synapses were altered according to a spike timing-dependent plasticity (STDP) learning rule (**Figure 1D**). The degree of synaptic modification depends on the relative timing between pre- and post-synaptic action potentials, according to a function $F(\Delta t)$ of the time Δt between the presynaptic (MC/PN) and postsynaptic (PC) spikes, such that:

$$F(\Delta t) = \begin{cases} A_+ \exp(\Delta t/\tau_+) & \text{if } \Delta t < 0 \\ A_- \exp(-\Delta t/\tau_-) & \text{if } \Delta t > 0 \end{cases} \quad (7)$$

That is, when a presynaptic spike precedes the postsynaptic spike, the associated synapse becomes strengthened in a manner that depends on the time delay between the two spikes. Similarly, when the presynaptic spike follows the postsynaptic spike, the synapse is weakened (**Figure 1D**). Synaptic strength changes depend on all spike combinations within the time constant of the rule, not only nearest neighbors. The conditioning phases were short enough so that reinforced weights did not grow excessively large. Since synapses undergoing reinforcement were excitatory, synaptic weights were not allowed to decrease below 0.

When constructing each network, all parameters were chosen from a randomized uniform distribution of ±10% around the mean values listed in **Table 1**. Cellular resting potentials were set to 0 mV and ionic Nernst potentials were adjusted accordingly. The associative learning rule time constants τ_+ and τ_- were the same for all model neurons (**Table 1**; **Figure 1D**). Two conditions were simulated: (a) a condition in which the inhibitory interneuron generated a stable, fast network oscillation due to inhibitory feedback in the GC/hLN interneuron and (b) a condition in which this feedback inhibition was reduced such that stable oscillations did not occur. The net inhibition delivered onto the MC/PN population was also reduced in the latter condition so as to maintain similar overall firing rates in these neurons in response to olfactory input (**Figure 1E**).

RESULTS

STDP RULE RESPONDS TO PRECEDENCE CODES

The STDP rule is inherently sensitive to spike timing, and its temporal stringency can be arbitrarily adjusted by altering the values of τ_+ and τ_- (Eq. 7; **Figure 1D**). Moreover, its asymmetry around the time of the postsynaptic spike suggests a proclivity for "edge enhancement" akin to the ubiquitous Mexican-hat decorrelation function but operating with respect to a spike timing-based metric. That is, incoming spike times preceding the postsynaptic spike constitute the central peak of the receptive field and are consequently strengthened, and spike times immediately following the postsynaptic spike – i.e., immediately adjacent to the edge of the representation – constitute the "inhibitory surround" and are specifically weakened.

As proof of concept, we modeled a postsynaptic neuron receiving incoming spikes from 10 presynaptic neurons; these 10 neurons were differentially activated so as to each evoke a spike at a different time. Initially, the synaptic integration properties of the postsynaptic neuron were set such that the first six spikes arriving within a 10 ms window would evoke a postsynaptic action potential (**Figure 1D**, left); hence, the corresponding six synapses were strengthened (*blue*) and the remaining four weakened (*red*) by the STDP rule. After a period of conditioning, the potentiated synapses evoked a postsynaptic spike after only five of the presynaptic neurons had fired, because fewer of these strengthened inputs were required to evoke that spike. The neuron firing sixth consequently had its synaptic weight dramatically weakened – even though it had been the strongest synapse up until that point – and thereafter became excluded from the relevant presynaptic representation (i.e., it effectively lost the capacity to influence the activity of the postsynaptic neuron). This progressive sharpening, and the concomitant functional "pruning" of synapses, proceeded in response to continued conditioning

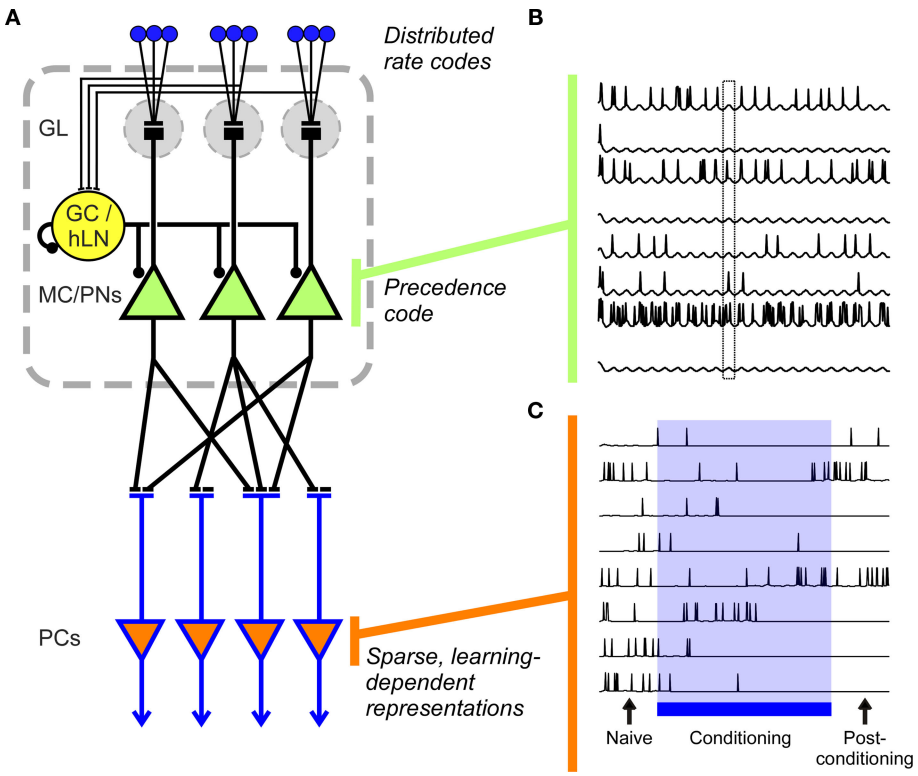

FIGURE 1 | Precedence coding in a model of vertebrate olfactory bulb/insect antennal lobe (OB/AL). (A) Model architecture. In the model, OSNs, each expressing a specific distribution of sensitivities to simulated odorants, project to principal neurons: mitral cells (MCs) in the OB or projection neurons (PNs) in the AL. A single local interneuron (GC/hLN), corresponding to a population of local inhibitory neurons (granule cells in the OB, homoLNs in the AL), also receives excitatory input from the OSNs. (In the OB, the corresponding excitation of deep-layer interneurons is indirect, whereas in the AL these interneurons are directly activated by OSNs). MC/PN neurons project to principal neurons in the next layer, corresponding to insect mushroom bodies or vertebrate piriform cortex (PC) with a sparse but uniform probability. The MC/PN synapses onto PC neurons are plastic according to the STDP learning rule. GL, glomerular layer; MC/PNs, mitral cells/projection neurons; PCs, piriform pyramidal neurons/mushroom body Kenyon cells. **(B)** MC/PN spiking patterns are shaped by global oscillatory dynamics. Periodic inhibitory input from the local interneuron phase-constrains spikes from odor-activated MC/PNs such that a precedence code is established in which the most strongly activated cells tend to spike early in the oscillation period (phase lead). Traces from eight differentially activated MC/PNs are depicted. The *box outline* highlights the difference in spike phase among three different activated neurons. **(C)** PC neurons respond broadly to odors before conditioning and generate a sparse and robust representation after conditioning. Initial uniform (5%) connectivity (*Naïve*) results in relatively weak and broadly distributed odor responses in PC neurons. During the conditioning phase (*Conditioning*), the distribution of synaptic weights between MC/PNs and PC is progressively adjusted via the STDP learning rule, eventually yielding a sparse, robust distribution of odor responses across the PC population (*Post-conditioning*). Note that during the conditioning process, individual PC odor responses may evolve non-monotonically; some PCs may at first be suppressed by learning but then become part of the durably activated ensemble (e.g., second trace), whereas others may initially be potentiated in their responses but in the end be excluded from the odor-specific ensemble (e.g., sixth trace).

(continued)

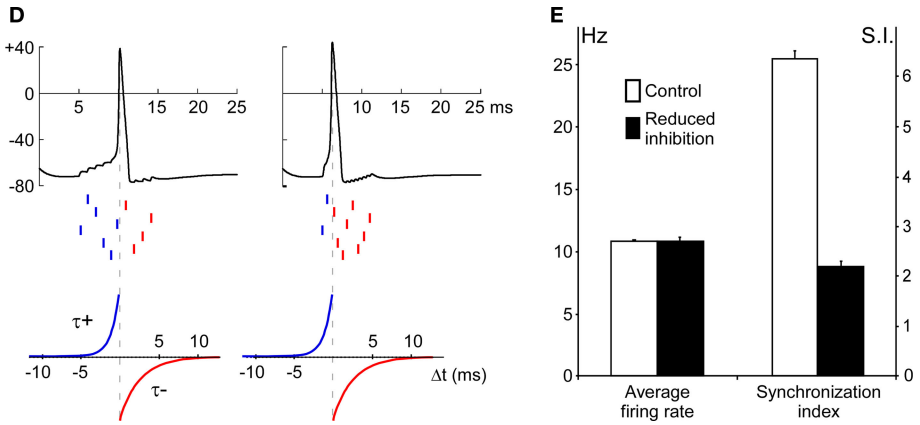

FIGURE 1 | Precedence coding in a model of vertebrate olfactory bulb/insect antennal lobe (OB/AL). (D) Mechanism underlying decorrelation of precedence-coded neural representations via the STDP learning rule. Left: Ten presynaptic MC/PN neurons deliver spikes (*middle raster marks*) to a postsynaptic PC neuron (*top trace*) within a ~10 ms phase window. Here, the PC neuron accumulates inputs and fires an action potential after the sixth presynaptic spike. According to the STDP learning rule (*bottom*; Song et al., 2000), the synapses from the presynaptic neurons associated with the first six spikes should be potentiated (*blue*), with the synapse associated with the sixth spike being the most strongly potentiated and the synapse associated with the first spike being relatively weakly potentiated if at all. The synapses associated with the four latest spikes are all weakened (*red*; corresponding to the negative region of the STDP rule in the bottom panel). This potentiation of the first six synapses will lead to the progressively earlier evocation of the postsynaptic PC spike; i.e., once the first five potentiated synaptic inputs suffice to evoke the postsynaptic spike, the synapse from the sixth-firing neuron will be powerfully weakened – even though it had previously been the most strongly potentiated – and eventually that MC/PN neuron will be excluded from the effective presynaptic ensemble. *Right panel.* Higher odorant concentrations evoke higher-power oscillations and more tightly phase-constrained presynaptic action potentials (discussed in Cleland and Linster, 2002); these tightly synchronized spikes integrate more effectively in postsynaptic neurons such that spikes from fewer neurons are required to evoke a postsynaptic action potential, all else being equal. This has the intrinsic effect of increasing the rate of synaptic learning; i.e., the rate at which the postsynaptic spike time phase-advances to exclude increasing numbers of MC/PNs from the effective presynaptic representation (i.e., the set of MC/PN cells with synaptic weights sufficient to affect the activity of the postsynaptic neuron). Interestingly, this effect of stimulus intensity on learned representations is in accord with classical learning theory (discussed in Cleland et al., 2009). Dotted vertical lines represent the spike time for purposes of the STDP rule. Ordinates in the top panels represent membrane potential in millivolts. **(E)** Average spike rate (Hz) and synchronization among MC/PN neurons during control and reduced-inhibition conditions. The synchronization index was calculated as the number of pairs of spikes occurring within 1 ms of each other divided by the total number of spikes (Linster and Cleland, 2001).

until an asymptotically minimal effective ensemble was reached. Interestingly, spike series that are more tightly constrained in time, such as are associated with higher-concentration odorant stimuli evoking higher-power oscillations (Cleland and Linster, 2002), intrinsically generate sharper representations by this metric. That is, all else being equal, they are able to evoke postsynaptic spikes with fewer presynaptic spikes so as to more rapidly exclude neurons from the presynaptic representation, essentially increasing the rate of conditioning (**Figure 1D**, right). Notably, olfactory psychophysical experiments in mice have shown that presenting higher-concentration odorants both increases the rate of conditioning and generates sharper odor representations, as this model predicts (Cleland et al., 2009).

NAÏVE ODOR RESPONSES IN MODEL PC ARE BROAD AND POORLY SELECTIVE

We then constructed a larger-scale network model of the vertebrate olfactory bulb/insect antennal lobe (OB/AL) to measure the capacity of this STDP implementation to progressively sharpen odor representations in the PC layer, and specifically to measure the selectivity of this conditioning mechanism for spike precedence-based representations in MC/PNs even in the presence of temporally uncoordinated background spiking. First, we measured the capacity of the STDP learning rule to extract precedence codes from the MC/PN cell layer in order to create representations in the PC layer. Broad, complex odorant stimuli were designed to activate a large proportion of OSNs in order to better visualize the progression of olfactory decorrelation in the model (**Figure 2A**, OSNs). The action potentials of MC/PNs that responded to odor stimulation with increased firing rates were strongly phase-modulated by the underlying fast oscillations. While the OB circuitry explicitly implementing glomerular-layer decorrelation (Cleland and Sethupathy, 2006; Cleland et al., 2007) was omitted for simplicity, this intrinsic inhibition nevertheless generated a modest decorrelation (**Figure 2A**, MC/PNs). The matrix of projections from MC/PNs to PCs was sparse (5% of possible connections, randomly determined) and initially comprised only weak synaptic interactions; consequently, PCs initially responded weakly, and relatively broadly, to odorant stimulation (**Figure 2A**, PC, *naive*). Specifically, whereas OSNs responded with varying degrees of activation to an average of 69 ± 2% of randomly chosen complex odorants, MC/PNs responded to 24 ± 2% and PCs initially responded to 30 ± 5% of these odorants.

CONDITIONED ODOR RESPONSES IN MODEL PC ARE SPARSE AND SELECTIVE

Olfactory conditioning was simulated by presenting an odorant to the model for an epoch of 20–30 cycles of the underlying gamma oscillation, corresponding to a stimulus presentation of 500–750 ms in rodents or 1000–1500 ms in locusts or bees (due

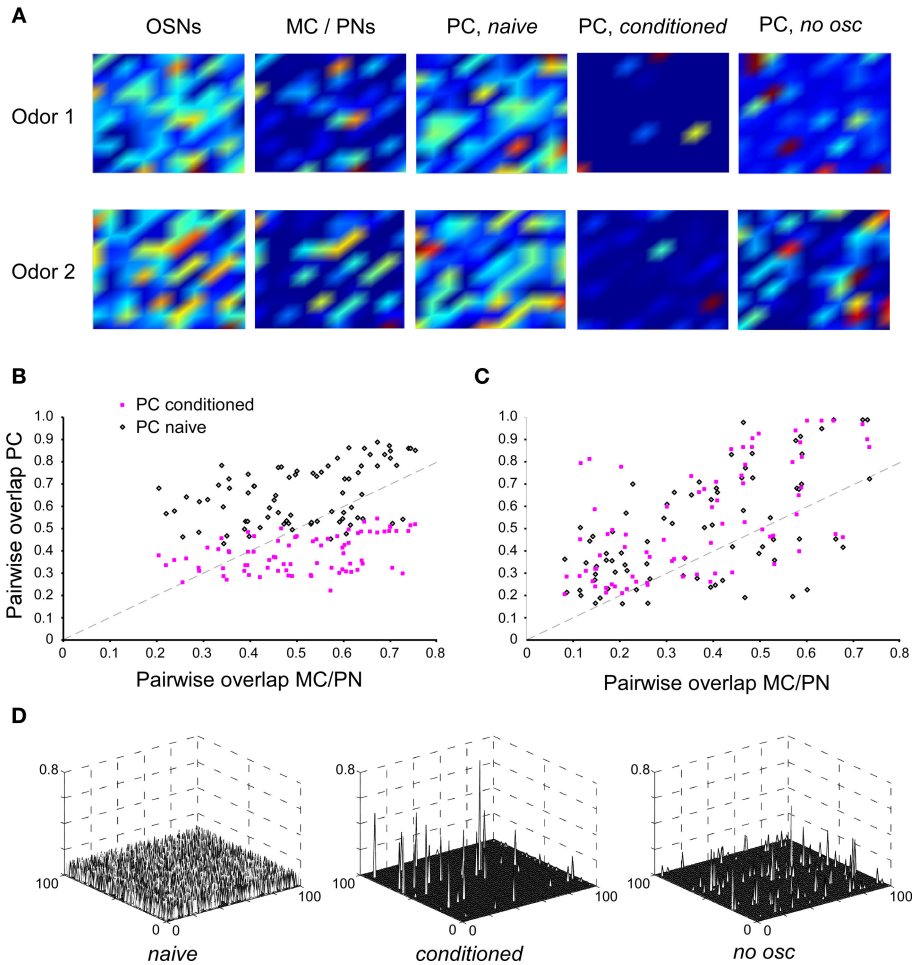

FIGURE 2 | Effects of single odor learning in PC and its dependence on MC/PN precedence coding. (A) Color–contour plots of odor-evoked activity patterns in each layer of the model. The neurons in each layer are displayed in a 10×10 matrix, with warmer colors indicating higher activation levels. Plots were smoothed using Matlab's built-in interpolation function. Two random odors, Odor 1 and Odor 2, were chosen for this example. First, each odor was presented for 20 gamma cycle periods (with the STDP learning rule disabled) and the resulting activity levels (total number of spikes in each neuron during the stimulus application) were measured and averaged. In the OSN layer, both odorants evoked relatively diffuse, overlapping patterns of activity; a slightly less diffuse pattern was observed in the MC/PN layer. In the naïve PC layer, odor activity was again highly broad and diffuse. The network was then conditioned by presenting Odor 1 for 20 gamma cycle periods with the STDP rule turned on. Subsequently, both odorants were presented again for 20 cycles with the learning rule disabled and the evoked activity measured. After conditioning, the PC network responded sparsely to the two odorants with highly decorrelated, non-overlapping patterns (PC, *conditioned*). The same procedure was then followed using a network in which oscillations were reduced substantially by interrupting the inhibitory feedback loop, thus disrupting the spike precedence code. Post-conditioning activation patterns in the PC in the absence of MC/PN oscillations were substantially more diffuse and overlapping (PC, *no osc*). **(B)** Effect of conditioning on pairwise overlap between odorants in the PC with MC/PN oscillations intact. Eighty random pairs of odorants were chosen; in each case the network was conditioned using one odorant of the pair. The graph depicts the degree of overlap between PC response patterns as a function of the overlap in MC/PN response patterns before (black open diamonds) and after (pink solid squares) conditioning. The dotted line indicates the diagonal. **(C)** Effect of conditioning on pairwise overlap between odorants in the PC with reduced oscillations in the MC/PN layer. Eighty random pairs of odorants were chosen; in each case the network was conditioned using one odorant of the pair. The graph depicts the degree of overlap between PC response patterns as a function of the overlap in MC/PN response patterns before (black open diamonds) and after (pink solid squares) conditioning. The dotted line indicates the diagonal. In the absence of MC/PN oscillations, the PC representation is not systematically decorrelated with respect to the MC/PN representation, either before or after conditioning. **(D)** Synaptic weight matrices from all MC/PN neurons to all PC neurons (100x100) in the naïve state, after normal conditioning (*conditioned*), and after conditioning in the absence of MC/PN oscillations (*no osc*).

to the slower oscillations exhibited by these insects). Comparable levels of learning also could be obtained using fewer cycles with a greater learning rate, or vice versa; the important criterion is that conditioning must persist for enough gamma cycles to enable extraction of the precedence code by the STDP learning rule. Importantly, after conditioning, the average number of complex odorants to which individual PC cells responded decreased ~3-fold, to 11 ± 3%, rendering cortical odor representations significantly sparser than those mediated by earlier layers. To measure the effect of this conditioning on the degree of overlap between odor representations, the following procedure was followed. First, a "naive" network was constructed with parameters chosen around the values

Table 1| Mean parameters for network simulations.

NEURONS				
Olfactory sensory neurons (OSN)	$\tau = 5.0$ ms	$\theta_{min} = 0.0$	$\theta_{max} = 1.0$	
Local interneuron (HomoLN)	$\tau = 5.0$ ms	$\theta_{min} = 0.0$	$\theta_{max} = 4.0$	
Mitral cells/projection neurons (MC/PN)	$\tau = 2.0$ ms	$\theta_{min} = -1.0$	$\theta_{max} = 20.0$	
Cortical/MB neurons (PC)	$\tau = 5.0$ ms	$\theta_{min} = 0.0$	$\theta_{max} = 10.0$	
SYNAPSES				
Afferent, OSN to MC/PN	$g_{max} = 1.0$; $w_{MC,OSN} = 0.14$	$E_N = 70$	$\tau_1 = 1.0$	$\tau_2 = 2.0$
Afferent, OSN to HomoLN	$g_{max} = 1.0$; $w_{hLN,OSN} = 0.015$	$E_N = 70$	$\tau_1 = 1.0$	$\tau_2 = 2.0$
HomoLN inhibitory feedback	$g_{max} = 1.0$; $w_{hLN-hLN} = 0.5$ (*normal*) or 0.1 (*reduced oscillations*)	$E_N = -10$	$\tau_1 = 4.0$	$\tau_2 = 8.0$
HomoLN to MC/PN	$g_{max} = 1.0$; $w_{MC,hLN} = 0.2$ (*normal*) or 0.05 (*reduced oscillations*)	$E_N = -10$	$\tau_1 = 4.0$	$\tau_2 = 8.0$
MC/PN to PC (*initial value*)	$g_{max} = 1.0$; $w_{PC,MC} = 0.003$	$E_N = 70$	$\tau_1 = 1.0$	$\tau_2 = 2.0$
STDP LEARNING RULE				
MC/PN to PC synapse	$\tau+ = 5$ ms	$\tau- = 5$ ms	$A+ = 0.6$	$A- = -0.4$

A new network was created for each simulation; for each such network, all parameter values were determined randomly from a uniform distribution (±10%) around these mean values. The instantaneous spiking probability for each cell type is a continuous, bounded function of the membrane potential with a threshold θ_{min} and a saturation value θ_{max}. Omega values (w_{ij}) designate synaptic weights, and values of E_N designate synaptic reversal potentials. τ designates the membrane time constant, τ_1 and τ_2 the synaptic time constants, and $\tau+$ and $\tau-$ the time constants of the STDP associative learning rule. A+ and A– determine the STDP learning rates.

detailed in **Table 1** (see Materials and Methods), and randomized pairs of complex odor presentations were simulated. The overlap between the representations of these odorant pairs at the OSN level ranged from 40 to 93% with a mean overlap of 74 ± 0.8%, replicating typical experimental data for pairs of structurally related odorants (Meister and Bonhoeffer, 2001; Stettler and Axel, 2009). This overlap was reduced at the level of MC/PN spiking outputs, ranging from 20 to 82% with an average overlap of 50 ± 1.8%. In the naïve PC network, the overlap between pairs of odor representations *increased*, ranging from 43 to 88% with an average overlap of 65 ± 1.5% owing to the weak and randomly distributed initial connections between MC/PNs and PCs.

Next, one of the odorants in the pair was presented for a conditioning epoch, after which both odorants were again presented to the newly conditioned network and overlaps between the two representations in the PC layer were recalculated (**Figure 2A**, PC, *conditioned*). After conditioning, overlaps between pairs of representations ranged from 22 to 55% with an average of 39 ± 1.0%, reasonably replicating the overlap between the representations of structurally similar odorant pairs observed in piriform cortex (Stettler and Axel, 2009). The difference between the overlaps in naïve and post-conditioning odorant representations was highly significant (paired samples *t*-test; $p < 0.01$; **Figure 2B**).

PRECEDENCE CODE IS REQUIRED FOR DECORRELATION VIA STDP

As illustrated in **Figure 1D**, the STDP synaptic learning rule requires both sufficiently dense presynaptic spiking input to evoke postsynaptic action potentials and a common singular or periodic time reference that can disambiguate leading from lagging spikes, e.g., by binning them into a phase-constrained window with respect to the underlying gamma oscillation. Hence, in the present model, if the presynaptic neurons were not phase-constrained by gamma oscillations then they would not generate a coherent, readable precedence code; consequently, the STDP rule then should be unable to extract the information necessary to decorrelate odor representations in the PC layer. We tested this hypothesis by reducing the oscillatory drive onto the MC/PN neurons to a tonic inhibition, while ensuring that the overall firing rate of these neurons was not dramatically changed, thereby replicating the experimental protocol of Stopfer et al. (1997). This was achieved by reducing GABAergic inhibition in the model to 25% of its original value, reducing the feedback autoinhibition of the inhibitory interneuron and decreasing its oscillatory power while simultaneously weakening its inhibition of MC/PN neurons to maintain their average firing rates. While the average firing rates of MC/PN neurons did not change (*t*-test; $p > 0.05$; **Figure 1E**, left), the pairwise synchronization between MC/PN neurons was significantly reduced (*t*-test; $p < 0.01$; **Figure 1E**, right). Whereas postsynaptic spikes were still evoked in PC neurons, and the STDP learning rule still modified synaptic strengths and cortical representations accordingly, learning in this layer was weak and highly disorganized as a result of the loss of spike precedence information (**Figure 2A**, PC, *no osc*). Specifically, in the absence of the oscillation-driven phasing of MC/PN action potentials, measured overlaps between pairs of representations in the MC/PN layer ranged from 8 to 59% with an average overlap of 33 ± 1.9% (a somewhat lower value than in the oscillatory condition owing to the adjustments needed to maintain common MC/PN spike rates). Measured overlaps in the naïve PC layer (before conditioning) under these conditions ranged from 16 to 98% with an average overlap of 46 ± 2.6%, an increase in overlap comparable to that occurring under oscillatory conditions. However, after conditioning, in the absence of the oscillation-driven phasing of action potentials, measured overlaps increased still further, ranging from 21 to 94% with an average overlap of 53 ± 2.6% (**Figure 2C**). Pairwise synaptic weight matrices after conditioning reveal STDP-dependent plasticity in both the *conditioned* and *no osc* cases, compared to the naïve state (**Figure 2D**); however, in the absence of a coherent precedence code, STDP-dependent learning in the PC layer was disorganized, and consequently increased, rather than reduced, the similarities among different odor representations (**Figure 2C**). The decorrelation of odor representations by

post-bulbar STDP-based learning consequently depends on, and is selective for, spike precedence coding based on the metric proposed to exist in MC/PNs.

DECORRELATION OF HONEYBEE ANTENNAL LOBE ODOR REPRESENTATIONS

To further test the olfactory decorrelation mechanism described above, we adjusted the model to incorporate natural odor-evoked glomerular input patterns obtained from calcium imaging of the honeybee AL (Sachse and Galizia, 2003; Linster et al., 2005). The number of glomeruli in the model was reduced to 30, corresponding to the number for which calcium imaging data in response to stimulation with a homologous odor series of straight-chain aliphatic alcohols could be obtained (Sachse and Galizia, 2003). To adjust for this smaller network size, the projection matrix density from MC/PN to PC neurons was increased so that each MC/PN targeted 10% of PC neurons. The local interneuron in the model directly corresponds in the honeybee AL to a morphologically distinct class of local interneurons termed homoLNs (Fonta et al., 1993), which receive excitatory input from all glomeruli and inhibit all PNs in a homogeneous manner. Consistent with the present model architecture, oscillatory dynamics and phase-locking in the AL are dependent on homoLN inhibitory feedback connections, and disappear when these connections are blocked, whereas other inhibitory circuits in the honeybee and locust AL are spared (MacLeod and Laurent, 1996; Stopfer et al., 1997).

The patterns of OSN sensitivity to different odorants were directly derived from published glomerular calcium-imaging data in honeybees (Sachse and Galizia, 2003; courtesy of G. Galizia). Specifically, the model was stimulated with inputs corresponding to the patterned glomerular responses evoked by 1-hexanol, 1-heptanol, 1-octanol, and 1-nonanol (**Figure 3A**), and generated MC/PN and naïve PC network representations as described above. To simulate the proboscis extension training used in honeybee conditioning studies (Bhagavan and Smith, 1997; Laska et al., 1999; Guerrieri et al., 2005), the model was then stimulated for 20 oscillatory cycles with the glomerular hexanol pattern while synaptic plasticity between MC/PNs and PC neurons was active (Linster and Cleland, 2001; Cleland and Linster, 2002). After conditioning, the network was again stimulated with patterned glomerular inputs corresponding to each of the four odorants and the pairwise overlaps between responses to hexanol and responses to the other three odorants in the cortical layer were calculated. This phase corresponded to extinction trials during which the behavioral responses to the conditioned odor (hexanol) and novel test odors (heptanol, octanol, nonanol) are tested (Bhagavan and Smith, 1997; Laska et al., 1999; Guerrieri et al., 2005). The relative response magnitude to conditioned and test odors is a measure of odor discrimination. We performed this conditioning study twice: first with fast oscillations intact and then again with reduced feedback inhibition to the homoLN such that oscillations were abolished and MC/PN spike times were desynchronized on this timescale.

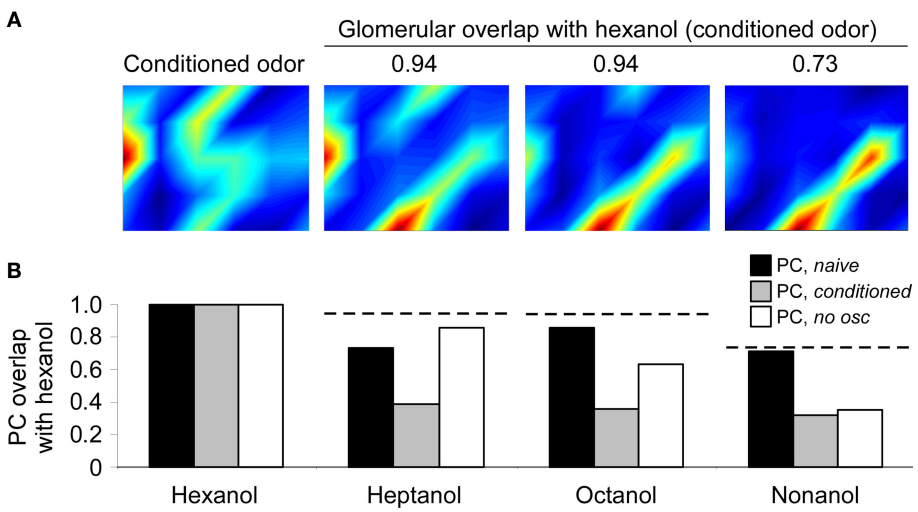

FIGURE 3 | Progressive decorrelation of odor representations via learning in the honeybee olfactory system. (A) Glomerular input patterns evoked by the odorants hexanol, heptanol, octanol, and nonanol as measured by calcium imaging of the honeybee antennal lobe (AL; Sachse and Galizia, 2003). The activation levels of the 30 glomeruli modeled are depicted in a 6×5 array that does not correspond to the anatomical arrangement of glomeruli on the AL. The degree of overlap (normalized dot product) between the glomerular-layer representations of hexanol and each of the other odors are indicated above the corresponding activation patterns. **(B)** Effects on odor representations by conditioning the network with hexanol. Overlaps between the representations of hexanol (the conditioned odor) and each of the other three test odors (heptanol, octanol, and nonanol) in PC neurons were calculated before (*PC, naive*) and after conditioning with hexanol (*PC, conditioned*). Overlaps were also calculated after conditioning using a network in which AL oscillations were substantially reduced as described above (*PC, no osc*). Because real odor input data were used to drive the model, each stimulus was presented only once (hence no error bars). Conditioning in the presence of oscillations sharply reduced the overlap between hexanol and each of the three test odorants. In the absence of oscillations, only the most dissimilar test odorant – nonanol – was decorrelated to the same extent. This indicates that spike timing-dependent decorrelation primarily affects highly similar odorants, as has been demonstrated behaviorally in honeybees (Stopfer et al., 1997). For purposes of comparison, dotted horizontal lines depict the degree of overlap with hexanol measured in the glomerular layer (as listed in **A**).

Odor-evoked representations in the naïve PC network were broad, and overlapped with the representations of similar odorants to roughly the same extent as in the glomerular layer (**Figure 3B**). After conditioning with hexanol, the pairwise overlaps between hexanol and each other test odor were strongly reduced (decorrelated) in the PC representation. This decorrelation replicates the pattern observed when honeybees' responses to structurally and perceptually similar odorants are measured after conditioning to sucrose rewards in the proboscis extension paradigm (Bhagavan and Smith, 1997; Laska et al., 1999; Guerrieri et al., 2005). In contrast, when oscillations and spike synchronization in the OB/AL were impaired, the overlaps between hexanol and highly similar odorants (heptanol, octanol) were substantially larger, exhibiting relatively little decorrelation with respect to the naïve representations. In contrast, the overlap between hexanol and the least-similar test odorant (nonanol) was reduced in the conditioned PC with or without the presence of oscillations, suggesting that the lower initial overlap between these odorants enabled sufficient decorrelation of these patterns even in the absence of oscillations. This similarity-dependent profile of responses is consistent with behavioral observations in honeybees demonstrating that abolishing oscillations in the AL during odor conditioning impairs bees' and moths' capacity to discriminate between highly similar, but not moderately similar or dissimilar, odorants (Stopfer et al., 1997; Mwilaria et al., 2008; see also Linster and Cleland, 2001; Cleland and Linster, 2002).

DISCUSSION

Second-order sensory neurons in the vertebrate and insect olfactory systems exhibit spiking activity that is phase-locked to underlying LFP oscillations, indicating a transformation in odor representations to a spike timing-based metric. Among candidate metrics for odor representation at this level, a simple spike precedence code, initiated by active sampling and maintained by intrinsic oscillations within the OB/AL network, is suggested. Whereas the first stage of post-sampling processing of odor representations appears to decorrelate odor representations with respect to their physical similarities via the selective silencing of moderately activated MC/PNs (reviewed in Cleland, 2010), the second stage model depicted herein further decorrelates odor representations not by silencing additional MC/PNs, but via the selective and progressive reduction of these neurons' capacity to influence the activity of specific post-synaptic PC neurons, resulting in a progressively sharper and more durable odor representation in this third-order neuronal population. This selectivity for correlated, precedent spikes also enables the PC to disregard the disorganized background spiking of MC/PNs that are neither substantially activated nor inhibited by odorants. Interestingly, it also could explain the observed psychophysical phenomenon in which increased odorant concentrations improve the rate and selectivity of odor learning (Yue et al., 2004; Wei et al., 2006; Cleland et al., 2009). Note that the proposed mechanism is not the only means by which representations could be decorrelated at this synapse: modulation of firing threshold or a sparsening of inputs by creating a sparser connectivity matrix would also achieve a basic decorrelation of all patterns. However, neither would exploit the spike dynamics observed in MC/PN neurons or decorrelate specific representations of interest from all others.

How well is this model of mitral cell precedence coding supported by electrophysiological and behavioral data? Mitral cells exhibit substantial background activity, particularly in awake animals (Rinberg et al., 2006); responses to odor stimulation evoke a range of qualitatively different initial responses from no effect, to inhibition (a common effect) to relatively fast excitation (Hamilton and Kauer, 1989; Wellis et al., 1989). A substantial fraction of odor-activated mitral cells exhibit phase-locked spiking (Kashiwadani et al., 1999; Buonviso et al., 2003; Lagier et al., 2004); in anesthetized, freely breathing (~2 Hz) rats, it has been estimated that 31% of mitral cells that are not silenced by a given odor presentation respond with gamma phase-locked spiking (David et al., 2009). Moreover, in studies mapping mitral cells' chemoreceptive fields, the "best" odorants that map to the central peak of a given cell's receptive field tend to evoke spikes at substantially shorter latencies than do odorants to which that cell is less well tuned (Wellis et al., 1989; Mori et al., 1999; Kaluza and Breer, 2000; Fletcher and Wilson, 2003; Stopfer et al., 2003; Friedrich et al., 2004), thereby creating the substrate for a precedence code based on odor quality tuning. While most of these studies measured spike latency on the respiratory (theta-band) timescale, there also is evidence for spike phasing with respect to fast oscillations (David et al., 2009). In the insect olfactory system, there is no direct evidence that PN spike phase is modulated by a cell's level of activation, although the transformation of temporal synchronization patterns into sparse spatial representations has been experimentally described (Perez-Orive et al., 2002).

Spike latency codes for odor quality representation have been proposed in a number of theoretical studies, though to different ends (Fort and Rospars, 1992; Hopfield, 1996; White et al., 1998; Schaefer et al., 2006). We here show how such a precedence code among second-order olfactory neurons could be read out and further processed using STDP to create sparse, plastic cortical representations comparable to those demonstrated experimentally (Roesch et al., 2007). The simulations presented here correspond to behavioral studies showing that, in a perceptual learning paradigm, repeated exposure to one or two odorants increases the perceptual contrast between these odorants and novel test odorants (Mandairon et al., 2006; **Figure 2** in the present manuscript). These effects of perceptual learning persist for less than 2 weeks; within this time window, repeated exposure to a new odorant can modify the perceptual changes due to a previous exposure. As we here make no provision for associating particular odors with reward or other contingencies, the simulations presented here do not address the larger question of long-term olfactory learning, by which a sparse functional projection matrix between bulb and cortex is formed and modified in response to a complex, slowly changing odor environment.

ACKNOWLEDGMENTS

We thank Giovanni Galizia for the use of calcium imaging data gathered in his laboratory. This work was supported by grants R03DC007725, R01DC009948, and R01DC008702 from the National Institute on Deafness and Communication Disorders (NIDCD).

REFERENCES

Abraham, N. M., Egger, V., Shimshek, D. R., Renden, R., Fukunaga, I., Sprengel, R., Seeburg, P. H., Klugmann, M., Margrie, T. W., Schaefer, A. T., and Kuner, T. (2010). Synaptic inhibition in the olfactory bulb accelerates odor discrimination in mice. *Neuron* 65, 399–411.

Ardid, S., Wang, X. J., Gomez-Cabrero, D., and Compte, A. (2010). Reconciling coherent oscillation with modulation of irregular spiking activity in selective attention: gamma-range synchronization between sensory and executive cortical areas. *J. Neurosci.* 30, 2856–2870.

Beshel, J., Kopell, N., and Kay, L. M. (2007). Olfactory bulb gamma oscillations are enhanced with task demands. *J. Neurosci.* 27, 8358–8365.

Bhagavan, S., and Smith, B. H. (1997). Olfactory conditioning in the honey bee, *Apis mellifera*: effects of odor intensity. *Physiol. Behav.* 61, 107–117.

Buonviso, N., Amat, C., Litaudon, P., Roux, S., Royet, J. P., Farget, V., and Sicard, G. (2003). Rhythm sequence through the olfactory bulb layers during the time window of a respiratory cycle. *Eur. J. Neurosci.* 17, 1811–1819.

Cassenaer, S., and Laurent, G. (2007). Hebbian STDP in mushroom bodies facilitates the synchronous flow of olfactory information in locusts. *Nature* 448, 709–713.

Cleland, T. A. (2010). Early transformations in odor representation. *Trends Neurosci.* 33, 130–139.

Cleland, T. A., Johnson, B. A., Leon, M., and Linster, C. (2007). Relational representation in the olfactory system. *Proc. Natl. Acad. Sci. U.S.A.* 104, 1953–1958.

Cleland, T. A., and Linster, C. (2002). How synchronization properties among second-order sensory neurons can mediate stimulus salience. *Behav. Neurosci.* 116, 212–221.

Cleland, T. A., Narla, V. A., and Boudadi, K. (2009). Multiple learning parameters differentially regulate olfactory generalization. *Behav. Neurosci.* 123, 26–35.

Cleland, T. A., and Sethupathy, P. (2006). Non-topographical contrast enhancement in the olfactory bulb. *BMC Neurosci.* 7, 7. doi: 10.1186/1471-2202-7-7.

David, F. O., Hugues, E., Cenier, T., Fourcaud-Trocme, N., and Buonviso, N. (2009). Specific entrainment of mitral cells during gamma oscillation in the rat olfactory bulb. *PLoS Comput. Biol.* 5, e1000551. doi: 10.1371/journal.pcbi.1000551.

Desmaisons, D., Vincent, J. D., and Lledo, P. M. (1999). Control of action potential timing by intrinsic subthreshold oscillations in olfactory bulb output neurons. *J. Neurosci.* 19, 10727–10737.

Fletcher, M. L., and Wilson, D. A. (2003). Olfactory bulb mitral-tufted cell plasticity: odorant-specific tuning reflects previous odorant exposure. *J. Neurosci.* 23, 6946–6955.

Fonta, C., Sun, X., and Masson, C. (1993). Morphology and spatial distribution of bee antennal lobe interneurons responsive to odours. *Chem. Senses* 18, 101–119.

Fort, J. C., and Rospars, J. P. (1992). Modelling of the qualitative discrimination of odours in the first two layers of olfactory system by Jutten and Herault algorithm. *CR Acad. Sci. III* 315, 331–336.

Friedrich, R. W., Habermann, C. J., and Laurent, G. (2004). Multiplexing using synchrony in the zebrafish olfactory bulb. *Nat. Neurosci.* 7, 862–871.

Fries, P., Nikolic, D., and Singer, W. (2007). The gamma cycle. *Trends Neurosci.* 30, 309–316.

Gray, C. M., and Singer, W. (1989). Stimulus-specific neuronal oscillations in orientation columns of cat visual cortex. *Proc. Natl. Acad. Sci. U.S.A.* 86, 1698–1702.

Guerrieri, F., Schubert, M., Sandoz, J. C., and Giurfa, M. (2005). Perceptual and neural olfactory similarity in honeybees. *PLoS Biol.* 3, e60. doi: 10.1371/journal.pbio.0030060.

Guyonneau, R., VanRullen, R., and Thorpe, S. J. (2005). Neurons tune to the earliest spikes through STDP. *Neural Comput.* 17, 859–879.

Hajos, N., and Paulsen, O. (2009). Network mechanisms of gamma oscillations in the CA3 region of the hippocampus. *Neural Netw.* 22, 1113–1119.

Hamilton, K. A., and Kauer, J. S. (1989). Patterns of intracellular potentials in salamander mitral/tufted cells in response to odor stimulation. *J. Neurophysiol.* 62, 609–625.

Hopfield, J. J. (1995). Pattern recognition computation using action potential timing for stimulus representation. *Nature* 376, 33–36.

Hopfield, J. J. (1996). Transforming neural computations and representing time. *Proc. Natl. Acad. Sci U.S.A.* 93, 15440–15444.

Illig, K. R., and Haberly, L. B. (2003). Odor-evoked activity is spatially distributed in piriform cortex. *J. Comp. Neurol.* 457, 361–373.

Johnson, D. M., Illig, K. R., Behan, M., and Haberly, L. B. (2000). New features of connectivity in piriform cortex visualized by intracellular injection of pyramidal cells suggest that "primary" olfactory cortex functions like "association" cortex in other sensory systems. *J. Neurosci.* 20, 6974–6982.

Kaluza, J. F., and Breer, H. (2000). Responsiveness of olfactory neurons to distinct aliphatic aldehydes. *J. Exp. Biol.* 203, 927–933.

Kashiwadani, H., Sasaki, Y. F., Uchida, N., and Mori, K. (1999). Synchronized oscillatory discharges of mitral/tufted cells with different molecular receptive ranges in the rabbit olfactory bulb. *J. Neurophysiol.* 82, 1786–1792.

Kay, L. M., Beshel, J., Brea, J., Martin, C., Rojas-Libano, D., and Kopell, N. (2009). Olfactory oscillations: the what, how and what for. *Trends Neurosci.* 32, 207–214.

Kay, L. M., and Freeman, W. J. (1998). Bidirectional processing in the olfactory-limbic axis during olfactory behavior. *Behav. Neurosci.* 112, 541–553.

Koehl, M. A., Koseff, J. R., Crimaldi, J. P., McCay, M. G., Cooper, T., Wiley, M. B., and Moore, P. A. (2001). Lobster sniffing: antennule design and hydrodynamic filtering of information in an odor plume. *Science* 294, 1948–1951.

Lagier, S., Carleton, A., and Lledo, P. M. (2004). Interplay between local GABAergic interneurons and relay neurons generates gamma oscillations in the rat olfactory bulb. *J. Neurosci.* 24, 4382–4392.

Laska, M., Galizia, C. G., Giurfa, M., and Menzel, R. (1999). Olfactory discrimination ability and odor structure-activity relationships in honeybees. *Chem. Senses* 24, 429–438.

Laurent, G. (1999). A systems perspective on early olfactory coding. *Science* 286, 723–728.

Laurent, G., and Davidowitz, H. (1994). Encoding of olfactory information with oscillating neural assemblies. *Science* 265, 1872–1875.

Linster, C., and Cleland, T. A. (2001). How spike synchronization among olfactory neurons can contribute to sensory discrimination. *J. Comput. Neurosci.* 10, 187–193.

Linster, C., Henry, L., Kadohisa, M., and Wilson, D. A. (2007). Synaptic adaptation and odor-background segmentation. *Neurobiol. Learn Mem.* 87, 352–360.

Linster, C., Menon, A. V., Singh, C. Y., and Wilson, D. A. (2009). Odor-specific habituation arises from interaction of afferent synaptic adaptation and intrinsic synaptic potentiation in olfactory cortex. *Learn Mem.* 16, 452–459.

Linster, C., Sachse, S., and Galizia, C. G. (2005). Computational modeling suggests that response properties rather than spatial position determine connectivity between olfactory glomeruli. *J. Neurophysiol.* 93, 3410–3417.

MacLeod, K., and Laurent, G. (1996). Distinct mechanisms for synchronization and temporal patterning of odor-encoding neural assemblies. *Science* 274, 976–979.

Mandairon, N., and Linster, C. (2009). Odor perception and olfactory bulb plasticity in adult mammals. *J. Neurophysiol.* 101, 2204–2209.

Mandairon, N., Stack, C., Kiselycznyk, C., and Linster, C. (2006). Enrichment to odors improves olfactory discrimination in adult rats. *Behav. Neurosci.* 120, 173–179.

Martin, C., Beshel, J., and Kay, L. M. (2007). An olfacto-hippocampal network is dynamically involved in odor-discrimination learning. *J. Neurophysiol.* 98, 2196–2205.

Masquelier, T., Hugues, E., Deco, G., and Thorpe, S. J. (2009). Oscillations, phase-of-firing coding, and spike timing-dependent plasticity: an efficient learning scheme. *J. Neurosci.* 29, 13484–13493.

Meister, M., and Bonhoeffer, T. (2001). Tuning and topography in an odor map on the rat olfactory bulb. *J. Neurosci.* 21, 1351–1360.

Mori, K., Nagao, H., and Yoshihara, Y. (1999). The olfactory bulb: coding and processing of odor molecule information. *Science* 286, 711–715.

Mwilaria, E. K., Ghatak, C., and Daly, K. C. (2008). Disruption of GABAA in the insect antennal lobe generally increases odor detection and discrimination thresholds. *Chem. Senses* 33, 267–281.

Nase, G., Singer, W., Monyer, H., and Engel, A. K. (2003). Features of neuronal synchrony in mouse visual cortex. *J. Neurophysiol.* 90, 1115–1123.

Neville, K. R., and Haberly, L. B. (2003). Beta and gamma oscillations in the olfactory system of the urethane-anesthetized rat. *J. Neurophysiol.* 90, 3921–3930.

Nusser, Z., Kay, L. M., Laurent, G., Homanics, G. E., and Mody, I. (2001). Disruption of GABA(A) receptors on GABAergic interneurons leads to increased oscillatory power in the olfactory bulb network. *J. Neurophysiol.* 86, 2823–2833.

Panzeri, S., Brunel, N., Logothetis, N. K., and Kayser, C. (2009). Sensory neural codes using multiplexed temporal scales. *Trends Neurosci.* 33, 111–120.

Perez-Orive, J., Mazor, O., Turner, G. C., Cassenaer, S., Wilson, R. I., and Laurent, G. (2002). Oscillations and sparsening of odor representations in the mushroom body. *Science* 297, 359–365.

Poo, C., and Isaacson, J. S. (2009). Odor representations in olfactory cortex: "sparse" coding, global inhibition, and oscillations. *Neuron* 62, 850–861.

Rinberg, D., Koulakov, A., and Gelperin, A. (2006). Sparse odor coding in awake behaving mice. *J. Neurosci.* 26, 8857–8865.

Roesch, M. R., Stalnaker, T. A., and Schoenbaum, G. (2007). Associative encoding in anterior piriform cortex versus orbitofrontal cortex during odor discrimination and reversal learning. *Cereb. Cortex* 17, 643–652.

Rubin, D. B., and Cleland, T. A. (2006). Dynamical mechanisms of odor processing in olfactory bulb mitral cells. *J. Neurophysiol.* 96, 555–568.

Sachse, S., and Galizia, C. G. (2003). The coding of odour-intensity in the honeybee antennal lobe: local computation optimizes odour representation. *Eur. J. Neurosci.* 18, 2119–2132.

Schaefer, A. T., Angelo, K., Spors, H., and Margrie, T. W. (2006). Neuronal oscillations enhance stimulus discrimination by ensuring action potential precision. *PLoS Biol.* 4, e163. doi: 10.1371/journal.pbio.0040163.

Schaefer, A. T., and Margrie, T. W. (2007). Spatiotemporal representations in the olfactory system. *Trends Neurosci.* 30, 92–100.

Sirota, A., Montgomery, S., Fujisawa, S., Isomura, Y., Zugaro, M., and Buzsaki, G. (2008). Entrainment of neocortical neurons and gamma oscillations by the hippocampal theta rhythm. *Neuron* 60, 683–697.

Song, S., Miller, K. D., and Abbott, L. F. (2000). Competitive Hebbian learning through spike-timing-dependent synaptic plasticity. *Nat. Neurosci.* 3, 919–926.

Stettler, D. D., and Axel, R. (2009). Representations of odor in the piriform cortex. *Neuron* 63, 854–864.

Stopfer, M., Bhagavan, S., Smith, B. H., and Laurent, G. (1997). Impaired odour discrimination on desynchronization of odour-encoding neural assemblies. *Nature* 390, 70–74.

Stopfer, M., Jayaraman, V., and Laurent, G. (2003). Intensity versus identity coding in an olfactory system. *Neuron* 39, 991–1004.

Uhlhaas, P. J., Pipa, G., Lima, B., Melloni, L., Neuenschwander, S., Nikolic, D., and Singer, W. (2009). Neural synchrony in cortical networks: history, concept and current status. *Front Integr. Neurosci.* 3: 17. doi: 10.3389/neuro.07.017.2009.

Wachowiak, M., Wesson, D. W., Pirez, N., Verhagen, J. V., and Carey, R. M. (2009). Low-level mechanisms for processing odor information in the behaving animal. *Ann. N.Y. Acad. Sci.* 1170, 286–292.

Wei, C. J., Linster, C., and Cleland, T. A. (2006). Dopamine D(2) receptor activation modulates perceived odor intensity. *Behav. Neurosci.* 120, 393–400.

Wellis, D. P., Scott, J. W., and Harrison, T. A. (1989). Discrimination among odorants by single neurons of the rat olfactory bulb. *J. Neurophysiol.* 61, 1161–1177.

White, J., Dickinson, T. A., Walt, D. R., and Kauer, J. S. (1998). An olfactory neuronal network for vapor recognition in an artificial nose. *Biol. Cybern.* 78, 245–251.

Yue, E. L., Cleland, T. A., Pavlis, M., and Linster, C. (2004). Opposing effects of D1 and D2 receptor activation on odor discrimination learning. *Behav. Neurosci.* 118, 184–190.

Conflict of Interest Statement: The authors declare that the research was conducted in the absence of any commercial or financial relationships that could be construed as a potential conflict of interest.

Received: 03 March 2010; accepted: 15 December 2010; published online: 28 December 2010.

*Citation: Linster C and Cleland TA (2010) Decorrelation of odor representations via spike timing-dependent plasticity. Front. Comput. Neurosci. **4**:157. doi: 10.3389/fncom.2010.00157*

frontiers in
COMPUTATIONAL NEUROSCIENCE

ORIGINAL RESEARCH ARTICLE
published: 14 July 2010
doi: 10.3389/fncom.2010.00021

Spike timing-dependent plasticity as the origin of the formation of clustered synaptic efficacy engrams

Nicolangelo Libero Iannella[1,2,3]*, Thomas Launey[1] and Shigeru Tanaka[4]

[1] *Launey Research Unit for Molecular Neurocybernetics, RIKEN Brain Science Institute, Wako-shi, Saitama, Japan*
[2] *School of Electrical and Electronic Engineering, The University of Adelaide, Adelaide, SA, Australia*
[3] *Theoretical and Experimental Neurobiology Unit, Okinawa Institute of Science and Technology, Kunigami, Okinawa, Japan*
[4] *Department of Information and Communications Engineering, The University of Electro-Communications, Chofu-shi, Japan*

Edited by:
Wulfram Gerstner, Ecole Polytechnique Fédérale de Lausanne, Switzerland

Reviewed by:
Claudia Clopath, Ecole Polytechnique Fédérale de Lausanne, Switzerland
Robert Legenstein, Graz University of Technology, Austria

****Correspondence:***
Nicolangelo Libero Iannella, Launey Research Unit for Molecular Neurocybernetics, RIKEN Brain Science Institute, 2-1 Hirosawa, Wako-shi, Saitama 351-0198, Japan.
e-mail: nicolang@brain.riken.jp

Synapse location, dendritic active properties and synaptic plasticity are all known to play some role in shaping the different input streams impinging onto a neuron. It remains unclear however, how the magnitude and spatial distribution of synaptic efficacies emerge from this interplay. Here, we investigate this interplay using a biophysically detailed neuron model of a reconstructed layer 2/3 pyramidal cell and spike timing-dependent plasticity (STDP). Specifically, we focus on the issue of how the efficacy of synapses contributed by different input streams are spatially represented in dendrites after STDP learning. We construct a simple feed forward network where a detailed model neuron receives synaptic inputs independently from multiple yet equally sized groups of afferent fibers with correlated activity, mimicking the spike activity from different neuronal populations encoding, for example, different sensory modalities. Interestingly, ensuing STDP learning, we observe that for all afferent groups, STDP leads to synaptic efficacies arranged into spatially segregated clusters effectively partitioning the dendritic tree. These segregated clusters possess a characteristic global organization in space, where they form a tessellation in which each group dominates mutually exclusive regions of the dendrite. Put simply, the dendritic imprint from different input streams left after STDP learning effectively forms what we term a "dendritic efficacy mosaic." Furthermore, we show how variations of the inputs and STDP rule affect such an organization. Our model suggests that STDP may be an important mechanism for creating a clustered plasticity engram, which shapes how different input streams are spatially represented in dendrite.

Keywords: STDP, dendrite, spatial patterning, mutual information index, dendritic efficacy mosaic

INTRODUCTION

In all the cortical brain areas studied so far, neurons can modify their input/output characteristics, usually via activity-dependent modification of synaptic efficacies of the afferent axons targeting their dendrites. Experiments have shown that the pattern of synaptic inputs can trigger either long-term potentiation (LTP, Bliss and Collingridge, 1993) or long-term depression (LTD, Kirkwood and Bear, 1994) at stimulated synapses. The discovery of spike timing-dependent plasticity (STDP, Markram et al., 1997a; Bi and Poo, 1998; Debanne et al., 1998; Zhang et al., 1998) illustrated that temporal specificity and timing information plays an important role, typically characterized by a temporally asymmetric window for synaptic change, where the temporal order of pre- and postsynaptic firing determines whether a synapse is potentiated or depressed. However, for a neuron with spatial extent, not only is timing important, but also biophysical properties and the strengths and spatial arrangement of synaptic inputs across the dendrite, as these will dictate neuronal firing properties.

Whether the mechanisms underlying synaptic change also leads to the emergence of some preferred form of spatial organization of synaptic inputs across the dendrite, still requires further elucidation. Converging groups of afferent fibers form synapses which may be strong in some localized regions of the dendrite but weak or absent elsewhere. Whether such a functionally clustered spatial organization of synaptic efficacy patterning may emerge as a result of synaptic plasticity is a question that is still being actively pursued.

Notably, why would clustering be a desirable emergent property? Firstly, previous studies have illustrated non-linear summation between nearby synchronous (or near-synchronous) synaptic inputs (Koch et al., 1983; Tuckwell, 1986; Polsky et al., 2004), allowing for easier spike generation in regions with clustered inputs. Other studies have shown that altering the spatial configuration of inputs changes firing properties (Mel, 1993; Poirazi et al., 2003; Iannella et al., 2004), while correlated activity can alter the integrative properties of neurons (Destexhe and Paré, 1999; Rudolph and Destexhe, 2003). Such clusters may provide part of the scaffolding underlying the emergence of functional dendritic compartments, subregions where activity tends to be correlated and where local signal integration permits some state-dependent non-linear computation to take place, but simultaneously different to what is happening in other compartments (Polsky et al., 2004; Gasparini and Magee, 2006; Rabinowitch and Segev, 2006a,b).

Importantly, various studies have indicated that plasticity may lead to arrange afferent fiber contacts into spatial clusters. Three-eyed frog experiments have shown that synapses contributed by

eye-specific afferent form spatially segregated but interdigitated series of clusters across the dendrite (Katz and Constantine-Paton, 1988). In some cases, the axons are actually restricted to specific parts of the dendritic arborization as in the hippocampus, both *in vivo* (CA3 to CA1 connections) and in culture (Glanzman et al., 1991; Kavalali et al., 1999; Cove et al., 2006). For the neocortex, however, the rule seems to be scattered afferents (Hellwig et al., 1994; Hellwig, 2000; Anderson et al., 2002; Stepanyants et al., 2002, 2008; Binzegger et al., 2004). Little can be inferred, however, regarding functional consequences, since the presence of a synapse does not indicate strength (Somogyi et al., 1998; Megías et al., 2001; Thomson et al., 2002; Binzegger et al., 2004; Kalisman et al., 2005) and efficacies are heterogeneous (Cotrell et al., 2001; Frick et al., 2001), but see Magee and Cook (2000). Recent experiments support the clustered plasticity model (Govindarajan et al., 2006) having illustrated that LTP not only gives rise to cooperativity and coordinated regulation between nearby synapses (Harvey and Svoboda, 2007; Harvey et al., 2008), but also leads to the selection of inputs promoting spatiotemporal coincidence and thus promotes the creation of hotspots of functional synapses (De Roo et al., 2008). Taken together, these investigations suggest that the efficacy of synapses contributed by different afferent groups display a functionally clustered spatial arrangement.

Understanding how synaptic plasticity controls the strengths and spatial organization of synapses across dendrites is experimentally challenging since simultaneously tracking the formation, changes and elimination of sets of synapses remains extremely difficult. Instead, simulation provides a viable means to gain important insights. One may ask whether STDP in a compartmental model neuron can lead to some spatially heterogeneous distribution of synaptic strength akin to what has been predicted by the clustered plasticity model. For neurons receiving stimulation from several different input streams, such as layer 4 stellate cells in the visual cortex, could such a model provide insights into how plasticity maps the information contained in the activity originating from multiple input streams onto the dendrites, and whether the emergence of spatially segregated synaptic clusters form a substrate for such a mapping, such as those seen in ocular dominance formation. Our previous study is the only investigation so far to have shown that the emergence of such a spatial organization is feasible (Iannella and Tanaka, 2006). This model only incorporated sodium and delayed rectifier k_{dr} potassium channels, lacking many other ion channels known to exist in real pyramidal cells (Stafstrom et al., 1985; Schwindt et al., 1988; Lorenzon and Foehring, 1995; Hille, 2001; Larkum et al., 2001). Our previous study, however, did not address the role of STDP in the emergence of such a spatial organization in a biophysically realistic model nor did it examine the alteration of spatial organization when multiple groups are considered. Here we investigate how STDP, admitting different degrees of competition, shapes the spatial organization of synaptic efficacies originating from multiple groups and factors which affect this organization. We show that when a neuron is stimulated by multiple independent groups of afferent fibers, spatially segregated efficacy clusters can emerge via STDP, forming a dendritic efficacy mosaic. Collectively, our results suggest that spike timing may play an important role in the mapping of information contained in multiple input streams onto dendrites.

MATERIALS AND METHODS

ASSESSING THE DEGREE OF SEGREGATION BETWEEN MULTIPLE SPATIAL PATTERNS

The first systematic analysis of spatial segregation was conducted by Duncan and Duncan (1955) who introduced the spatial dissimilarity index (SDI). This index has historically been the measure of choice. However, measuring the segregation between two patterns has limited real world applications, which typically require measuring segregation between multiple spatial patterns. Since the 1980s, there have been many advances in measuring the segregation between multiple patterns along with the development of comprehensive methods and criteria with which measurements are evaluated (James and Taeuber, 1985; Massey and Denton, 1988; Reardon and Firebaugh, 2002). Recent studies have shown that the M-index, a segregation measure based upon mutual information was first proposed by Theil (1971), satisfies more quality criteria than previous measures (Frankel and Volij, 2005, 2009; Mora and Ruiz-Castillo, 2009). The M-index will be used herein to assess the degree of spatial segregation between different streams of inputs. Before we present the expression for this segregation index, we will introduce the following set of notation, subscripts j denotes dendritic location and m indexes the particular afferent group:

$W_{\cdot j} = \sum_m W_{mj}$ total synaptic efficiency at dendritic location j.
$W_{m\cdot} = \sum_j W_{mj}$ total of group m's synaptic efficacies.
$W_{\text{tot}} = \sum_{m,j} W_{mj}$ total synaptic efficacy contributed by all groups.
$\pi_m = W_{m\cdot}/W_{\text{tot}}$ proportion of group m synaptic weights.
$\pi_{jm} = W_{mj}/W_{\cdot j}$ proportion of group m synaptic weights at j.

The mutual information M-index is defined as

$$M = \sum_j \frac{W_{\cdot j}}{W_{tot}} \sum_m \pi_{jm} \ln\left(\frac{\pi_{jm}}{\pi_m}\right). \quad (1)$$

This index can be interpreted as a likelihood-ratio measure between variables respectively indexing dendritic location j and group membership.

THE NEOCORTICAL LAYER 2/3 PYRAMIDAL CELL MODEL

A biophysically detailed compartmental model of a reconstructed layer 2/3 pyramidal neuron receiving randomly timed excitatory and inhibitory synaptic inputs across the dendrite, was simulated using the NEURON simulation package (Hines and Carnevale, 2001). The model consisted of 119 sections with 294 segments in the dendrite. The model also included a simplified myelinated axon, similar to those used previously (Mainen et al., 1995; Iannella and Tanaka, 2006), consisting of a hillock, initial segment, five nodes and five myelin internodes, respectively. The parameters and channel types used in the simplified axon were similar to those used by others (Mainen et al., 1995; Iannella and Tanaka, 2006). A variety of synaptic receptors, voltage- and calcium-dependent ion channels experimentally found in layer 2/3 pyramidal cells were incorporated into the model. These included four types of synaptic currents; AMPA, $GABA_A$, $GABA_B$, and calcium permeable NMDA and various voltage-dependent currents such as, a passive leak (I_{leak}), a fast sodium (I_{Na}) and delayed rectifier potassium ($I_{K_{dr}}$), a transient A-type potassium current (I_A), a hyperpolarization activated potassium (I_h), a muscarinic potassium (I_M), a low voltage activated T-type calcium

(I_T), high voltage activated N- and L-type calcium current (I_N) and (I_{HVA}), three types of Ca^{2+}-dependent potassium channels: (I_C), medium AHP (I_{mAHP}); and slow AHP (I_{sAHP}) currents. These active channels were included throughout the axon, soma, and dendrites with densities and distributions based upon available experimental data mostly from the rat, or those used in previous studies. Passive properties used for the dendrite were similar to previous studies (Mainen et al., 1995; Iannella et al., 2004; Iannella and Tanaka, 2006): the membrane capacitance in the dendrite was $C_m = 0.9$ μF/cm^2, the resting potential was −80 mV and the internal resistivity R_a was 200 Ωm. The effect of dendritic spines was included by correcting both the membrane capacitance and leak by a scaling factor.

The descriptions of the ionic currents used in the simulations were the same or similar to those used in previous modeling studies (Rhodes and Gray, 1994; Mainen et al., 1995; Rhodes and Llinás, 2001; Traub et al., 2003; Iannella et al., 2004; Iannella and Tanaka, 2006) and are given in the Supplementary Materials.

Stimulation was provided by a group of 250 inhibitory afferent fibers and typically four equally sized groups of 250 correlated excitatory afferents, unless stated otherwise. Inhibitory and excitatory afferents are not correlated with each other. Furthermore, we ascertain that any afferent from one excitatory group was not correlated with any afferent from the other excitatory group. Each fiber, either excitatory or inhibitory, forms five synaptic contacts in the model, as suggested by current anatomical data (Thomson et al., 1994, 2002; Markram et al., 1997b; Feldmeyer et al., 2002).

Simulations proceeded by initially connecting each excitatory afferent fiber to five randomly selected locations across the dendrite. Similarly, each inhibitory afferent also formed five synapses at random locations throughout the initial segment, hillock, soma, and dendrite. All synapses were activated at random times. The activity of inhibitory fibers were modeled by temporally homogeneous Poisson processes with a mean frequency of 10 Hz. The activity of excitatory afferents were modeled by a previously published realization of correlated Poisson processes where the ensemble activity of a group of fibers contains higher order statistics (Kuhn et al., 2003). The higher order interactions are mediated by synchronized activity involving only subsets of afferents belonging to a single group. The mean firing rates of all excitatory afferents used in the simulations was typically 40 Hz, with a within group correlation coefficient of C = 0.05, except where otherwise stated. A typical simulation took 500 s of simulated time, unless stated otherwise.

STDP LEARNING RULES

Two different STDP rules were used to change only the weights of AMPA conductances $W_j(t) \in [0,1]$, (NMDA, $GABA_A$, and $GABA_B$ conductances were not altered). The first rule is a previously described non-linear STDP rule (Gütig et al., 2003), while the remaining two are non-linear generalizations of two previously published multispike interaction based STDP rules. For clarity, we will simply call these the Gütig and Froemke STDP rules, respectively. These rules are given below.

Gütig Rule: Pair based non-linear STDP

$$\Delta w_j = \begin{cases} A_+ \left(1 - w_j\right)^{\mu} \exp\left(-|\Delta t|/\tau_+\right) & \text{if } \Delta t > 0 \\ -A_- w_j^{\mu} \exp\left(-|\Delta t|/\tau_-\right) & \text{if } \Delta t \le 0 \end{cases},$$

where $\Delta t = t^{post} - t^{pre}$ denotes the timing difference between pre- and postsynaptic events. A_+ and A_- are positive constants scaling the magnitude of individual weight changes, and τ_+ and τ_- are time constants determining the size of the temporal learning window in which potentiation and depression occurs. The presynaptic event t^{pre} denotes the arrival time of presynaptic input to some specific dendritic location, while the postsynaptic event t^{post} typically denotes the time when a local dendritic spike was generated. When Δt is positive, synaptic efficacy is potentiated, and depressed otherwise; where individual changes in synaptic efficacy W_j are also weight dependent. This weight dependence has the form of a power law where the exponent μ is a positive constant. The case when μ = 0 corresponds to the additive STDP rule, where changes in synaptic efficacy are independent of W_j; while μ = 1 corresponds to the multiplicative STDP rule, where such changes are linearly dependent on the weight. For intermediate values of μ the weight dependence is non-linear. The parameters used for the non-linear STDP learning rule were $A_+ = 0.0025$, $A_- = 0.001125$, $\tau_+ = 13.5$ ms and $\tau_- = 34.5$ ms, in agreement with previous experiments (Froemke and Dan, 2002). Postsynaptic events were detected when the local membrane potential surpasses a pre-specified threshold θ = −20 mV.

Froemke Rule: Quadruplet spike interaction based non-linear STDP

$$\Delta w_j = \begin{cases} \varepsilon^{pre}\varepsilon^{post} A_+ \left(1 - w_j\right)^{\mu} \exp\left(-|\Delta t|/\tau_+\right) & \text{if } \Delta t > 0 \\ -\varepsilon^{pre}\varepsilon^{post} A_- w_j^{\mu} \exp\left(-|\Delta t|/\tau_-\right) & \text{if } \Delta t \le 0 \end{cases},$$

where $\Delta t = t^{post} - t^{pre}$ is the temporal difference between pre and postsynaptic spikes, $A_+ = 0.025$, $A_- = 0.01125$, $\varepsilon^{\chi} = 1 - \exp(-(t_i^{\chi} - t_{i-1}^{\chi})/\tau_s^{\chi})$ $\chi = \{pre, post\}$ denotes the pre-/postsynaptic suppression factor, t_i^{χ} and t_{i-1}^{χ} are the event times of the i^{th} and $(i-1)^{th}$ pre-/postsynaptic spikes, and $\tau_s^{\chi} = \{28, 88\}$ ms denotes the pre-/postsynaptic suppression time constants, respectively.

MEASURES OF FUNCTIONAL SPATIAL ASSOCIATION

Developing methods for measuring how related two different entities are in space has lead to the emergence of a relatively new field, called *Spatial Analysis*. This field has already lead to novel yet widely used analytical and computational techniques, and whose objective sets out to provide robust methods for measuring the spatial association between events, is currently under active development. It is often assumed that entities which are close to each other share more features in common than those entities which are distant. Spatial dependencies between entities can arise via either correlation, causality or interaction, and formal measures often rely on calculating the spatial autocorrelation. Historically, Moran's I index (Moran, 1950) is a widely used global measure of spatial association which assesses the correlation or similarities amongst the attributes of neighboring observations in a spatial pattern. Moran's I index is a tool which measures the spatial autocorrelation of a pattern and evaluates whether the pattern is clustered, dispersed or random in space. This index is best interpreted as a weighted correlation coefficient used to detect departures from spatial randomness (Moran, 1950). It is defined as

$$I = \frac{N \sum_i \sum_i \vartheta_{ij} \left(W_i^G - \overline{W}^G\right)\left(W_j^G - \overline{W}^G\right)}{\left(\sum_i \sum_i \vartheta_{ij}\right) \sum_k \left(W_k^G - \overline{W}^G\right)^2},$$

where N is the total number of dendritic locations j, ϑ_{ij} is a spatial weight matrix of proximity where the simplest case is that of nearest neighbor (1 if location i is the neighbor of location j and 0 otherwise), W_j^G is the total synaptic weight of group G at dendritic location j, and $\overline{W}^G$ is the mean synaptic weight of a single group G. Calculated values range from −1 to 1, whose positive (negative) values indicate positive (negative) spatial autocorrelation, and where each extreme indicates either perfect dispersion or perfect correlation, respectively.

Alternatively, another index which has been used for assessing spatial autocorrelation is the Geary C index (Geary, 1954). Despite being inversely related, the Geary C index is not the inverse of Moran's I index. Furthermore, while Moran's I index is a global measure of spatial functional association, the Geary C index is sensitive to local autocorrelations and can be regarded as local indicator of functional association. The Geary C index is defined as follows,

$$C = \frac{(N-1)\sum_i \sum_j \vartheta_{ij}\left(W_i^G - W_j^G\right)^2}{\left(\sum_I \sum_J \vartheta_{ij}\right)\sum_k \left(W_k^G - \overline{W}^G\right)^2},$$

where the meanings of the symbols N, ϑ_{ij}, W^G, and $\overline{W}^G$ are the same as those defined for Moran's I index. Calculated values range between 0 and 2, where numbers smaller or larger than one indicate positive or negative autocorrelation, respectively. Note that a Geary C index of 1 means that there is no spatial autocorrelation present.

RESULTS

VALIDATION OF A DETAILED MODEL OF A LAYER 2/3 PYRAMIDAL CELL

Biophysically detailed models typically try to embrace the full complexity of real cells, by incorporating as much of the morphology and known biophysical details as is feasibly possible, so that the model can replicate as much of the behavior of the cell under consideration. To investigate the emergence of spatially heterogeneous patterns of synaptic strengths in dendrites, a biophysically detailed model is required since STDP depends locally on the postsynaptic depolarization and calcium, thus the description and distribution of voltage-dependent conductances should be accurate. Note however, that the adopted STDP rule (see Materials and Methods) used in this paper does not have an explicit calcium dependence.

In constructing our biophysical model of a layer 2/3 pyramidal cell, detailed in the appendix, emphasis was placed on reproducing a variety of dendritic responses, including the frequency dependence of dendritic spike generation and distance-dependent calcium accumulation, similar to those seen in recent experiments (Kampa et al., 2006; Larkum et al., 2007). **Figure 1** summaries model responses to a variety of experimental stimulus protocols. First, a short train of six simulated current pulses was injected into the soma to produce six somatic action potentials (APs). **Figure 1A** illustrates the dendritic voltage responses from six different locations in the dendrite to the somatically injected pulses delivered at a frequencies of 130 and 200 Hz, respectively. Dendritic spikes are clearly present but do not occur at every location in the dendritic tree. The position of dendritic responses are color-coded for clarity. Dendritic spike generation is caused by electrogenesis occurring at various locations and at different critical frequencies in the dendrite. **Figure 1B** indicates how the peak dendritic voltage amplitude varies non-linearly as a function of input pulse frequency for two different color-coded dendritic locations (as indicated in **Figure 1A**). One begins to see the generation of dendritic spikes in the model at a critical frequency of 130 Hz. This is in excellent agreement with recent experimental data from layer 2/3 pyramidal cells indicating that a critical frequency of 128 Hz is required for dendritic spike generation (Larkum et al., 2007). **Figure 1C** shows the corresponding peak calcium concentration as a function of frequency for the same color-coded locations (see **Figure 1A**). **Figure 1D** depicts the normalized peak calcium transient amplitudes (dF/F_{peak}) during trains of six APs at increasing input frequencies for proximal and distal positions as indicated in **Figure 1A**. For increasing input frequencies, these trains lead to similar increases in calcium at proximal dendritic locations, however peak calcium transients (dF/F_{peak}) at distal dendritic locations, were significantly larger during AP trains at and above the critical frequency for triggering a dendritic spike when compared with trains evoked at 100 Hz. This behavior is in agreement with recent experimental observations (Kampa et al., 2006). **Figure 1E** shows the normalized ratio of peak calcium transients evoked by three somatic APs relative to one AP at different distances from the soma along the indicated path and depicts a non-linear distance-dependent increase similar to the one observed experimentally (Kampa et al., 2006). Finally, **Figure 1F** shows how pairing a dendritic injection of EPSP-shaped current with a back-propagating action potential (BPAP) gives rise to a facilitatory effect where the threshold for dendritic spike generation was reduced by 25%, when a somatic spike was evoked by a brief current pulse 10 ms before dendritic current injection. The magnitude of this effect is again in excellent agreement with experimental observations from layer 2/3 pyramidal cells (compare to Figure 6C in Larkum et al., 2007).

THE DENDRITIC EFFICACY MOSAIC AND FUNCTIONAL CONSEQUENCES

Prior to applying any learning rule, a decision needs to be made regarding how the model neuron is to be simulated. Past studies have investigated the temporal evolution and outcome of STDP in models where stimulation is primarily driven by two neural populations (Gerstner et al., 1996; Song et al., 2000; Song and Abbott, 2001; Gütig et al., 2003). More recently, multispike interactions have also been explored (Froemke and Dan, 2002; Izhikevich and Desai, 2003; Burkitt and Grayden, 2004; Appleby and Elliott, 2005, 2006, 2007; Pfister and Gerstner, 2006). In order to better understand the impact of plasticity and spike timing in cortical circuits, recent studies have focused on network-level simulations and the outcome of stimulations driven by the activity of multiple afferent groups, mimicking different neuronal populations that may, for example, encode different sensory modalities (Meffin et al., 2004; Wenisch et al., 2005; Burkitt et al., 2007; Masquelier and Thorpe, 2007; Gilson et al., 2009a,b,c,d; Masquelier et al., 2009). Here, we will adopt this multiple stream approach and compare the outcome of both spike-pair and multispike interaction based STDP. Stimulation to our spatially extended model neuron is provided by multiple equally sized groups of afferent fibers where the spike activity within a single group was correlated, but was independent of the activity in other groups. This stimulation paradigm is similar

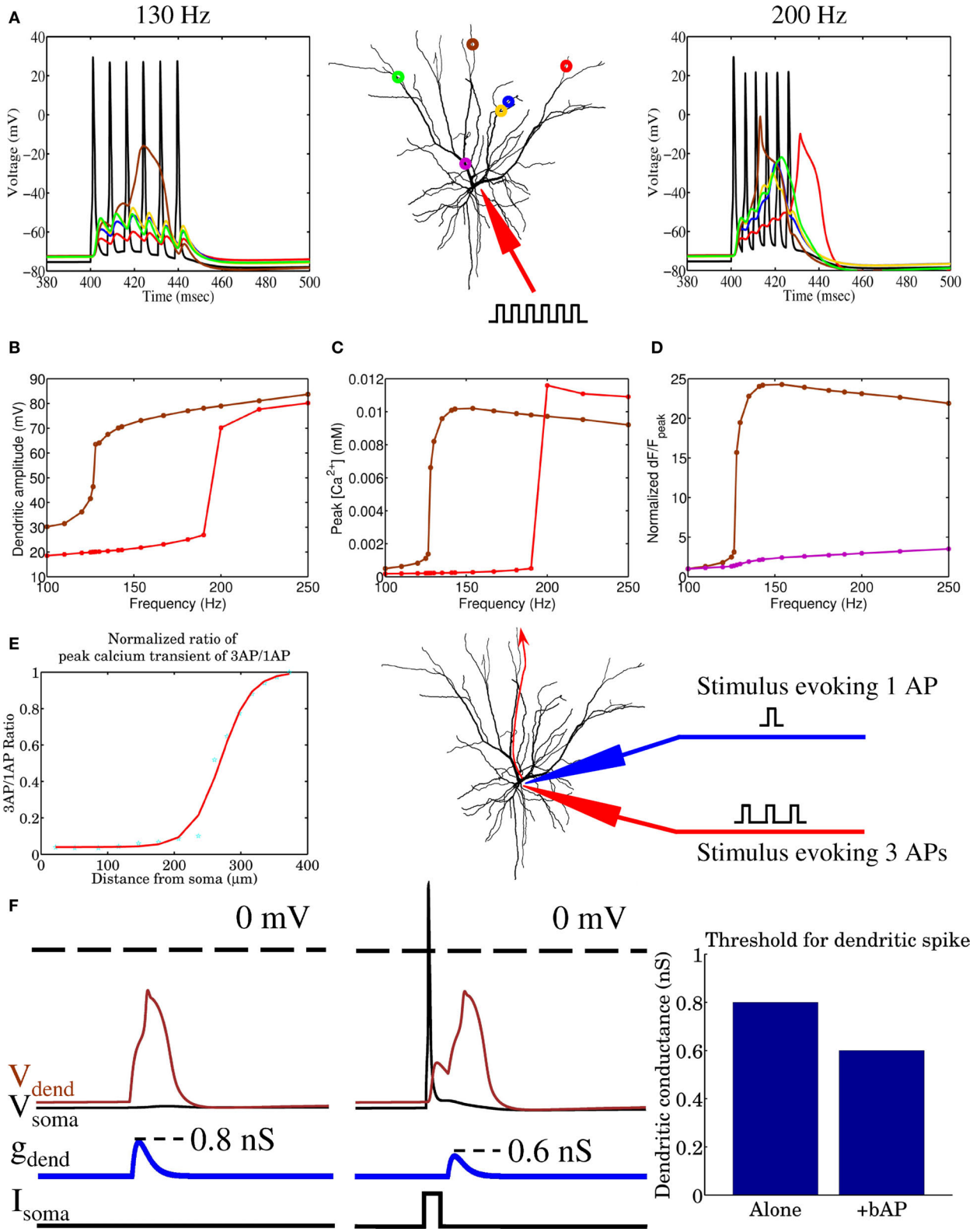

FIGURE 1 | The biophysical model of a layer 2/3 pyramidal cell is shown to reproduce several experimentally observed properties, (A,B) including frequency dependent dendritic spike generation, a non-linear distance-dependent increase in **(C)** peak calcium and **(D,E)** the normalized ratio of peak calcium transients, and **(F)** a 25% reduction in the threshold for generating dendritic spikes when somatically generated spikes precede dendritic current injection by 10 ms.

to previous STDP studies (Gerstner et al., 1996; Song et al., 2000; Gütig et al., 2003) where STDP leads to the activity-dependent formation of heterogeneous spatiotemporal patterns of synaptic efficacy. Similar to our previous study (Iannella and Tanaka, 2006), when the biophysical model receives inputs from multiple independent groups of afferent fibers with correlated activity, STDP, in conjunction with strong competition between synapses, leads to synaptic efficacies being arranged into spatially segregated clusters which effectively forms a partitioning of the dendritic tree. The resulting dendritic imprint effectively forms a tessellated spatial pattern of synaptic strength across the dendrite, as seen in **Figure 2**, which we will simply call a *dendritic efficacy mosaic* hereafter. When stimulating with four groups, **Figure 2** shows the spatial organization of synaptic efficacies, before and after STDP, for each respective group. These plots display the relative dominance of a single groups compared to the total, defined as the ratio between the total efficacy by a single group and total efficacy of all groups for each location on the dendrite. **Figure 2B** shows the corresponding dendritic efficacy mosaic by color-coding the strongest group at each dendritic location after STDP. Before analyzing how synaptic competition affects such a dendritic partitioning, it is instructive to observe how voltage responses have changed before and after STDP. **Figures 3A,B** provides an example of the voltage response to stimulation from a single group of afferents, taken from the soma before and after STDP learning. Note that before STDP (**Figure 3A**), the somatic voltage trace contains no clear APs and is depolarized to an unusually high level. After STDP however, spikes are readily observed and the mean baseline depolarization is about −60 mV. These somatic spikes occurred since STDP led to an overall reduction in the total synaptic currents being generated throughout the neuron. The high level of depolarization observed in **Figure 3A** is simply attributed to the synaptic weight for the AMPA conductance initialized to $w_j(t) = 0.5$. Starting from a lower initialization does not disrupt the emergence of either spatially segregated clusters or the dendritic mosaic (data not shown). The main difference is a reduction in the firing rate of the pyramidal cell after STDP. **Figures S1A,B** in the Supplementary Materials is one such example where the weights were initialized to $w_j(t) = 0.1$; before STDP the somatic membrane recording shows that many spikes are present, but after STDP there are clearly fewer APs present. **Figures 3C–F** shows the voltage traces from two different (color-coded) dendritic locations (blue and green as shown in **Figure 3**) when stimulation is provided by a single afferent group before and after STDP. Note the presence of dendritic spikes in both **Figures 3D,F**, which have emerged, where STDP has led to clear changes to both somatic and dendritic voltage responses.

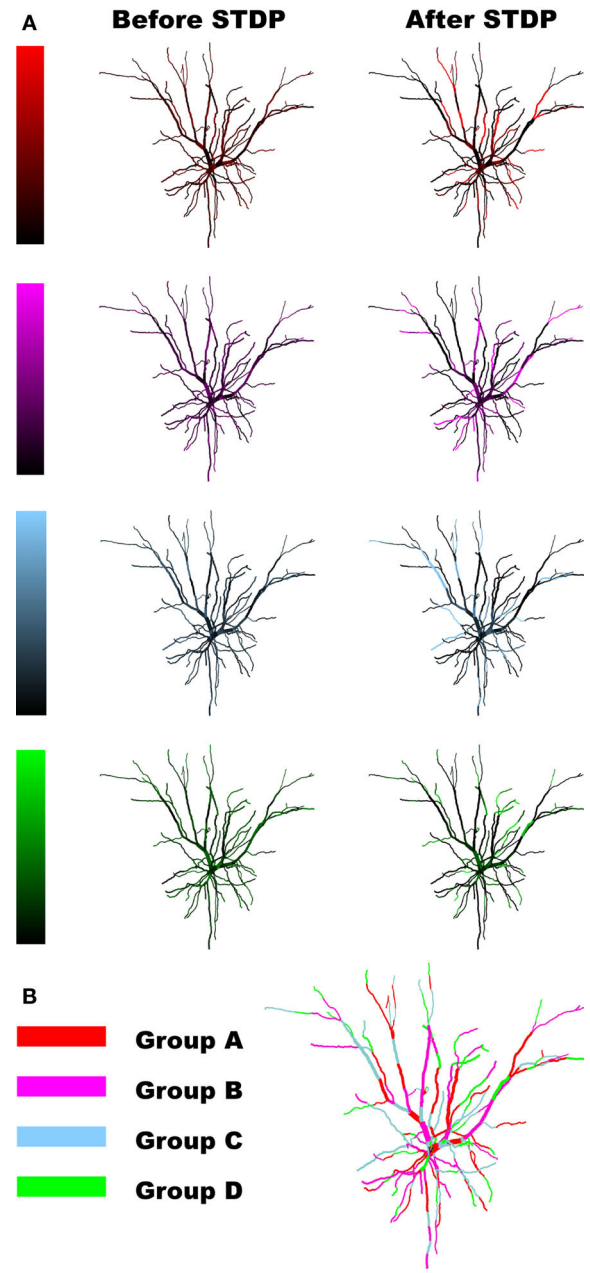

FIGURE 2 | (A) STDP learning changes the initial spatial organization of synaptic strength and leads to emergence of regions dominated by a single group of afferent fibers. **(B)** After STDP learning the four competing groups form spatially segregated efficacy clusters. Here only the winning group is color-coded at each dendritic location.

FORMATION OF THE DENDRITIC EFFICACY MOSAIC DEPENDS ON COMPETITION

The formation of spatial patterns displaying a clustered spatial organization typically emerge by competing for some limited resource (Murray, 2003). In the case of our biophysical neuron model, the processes by which STDP leads to the emergence of a dendritic efficacy mosaic was implemented using Gütig's non-linear rule (see Materials and Methods for details), where synapses compete both spatially and temporally to control the timing of somatic and/or dendritic spike generation. Therefore it is important to determine how and under what conditions such an efficacy mosaic emerges. A key feature of Gütig's rule is the presence of the exponent μ. This parameter controls the weight dependence of the rule and thus the degree of competition, since for $\mu = 0$ the rule corresponds to the original additive STDP used by Abbott and Song (Song et al., 2000) and exhibits strong competition (Song et al., 2000; Song and Abbott, 2001); while for $\mu = 1$ recovers the multiplicative STDP rule, a rule known to display stable yet weak competition between synapses (van Rossum

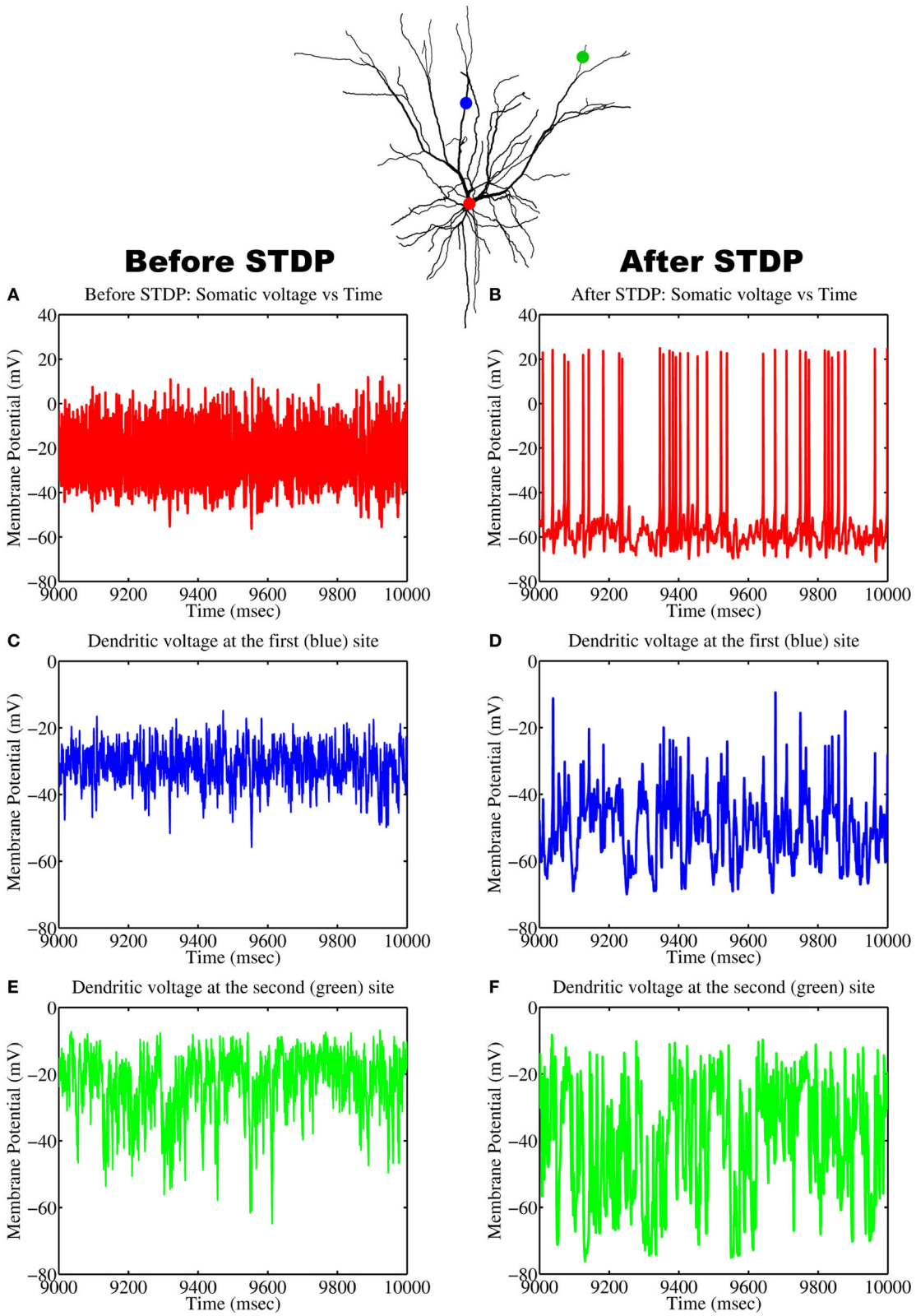

FIGURE 3 | Changes to the voltage responses recorded at the soma and two different locations on the dendrite before and after STDP to stimulation from a single group of afferent fibers. Recording positions have been color-coded: **(A,B)** soma (red), **(C,D)** first dendritic position (blue), and **(E,F)** the second location (green).

et al., 2000). For intermediate values of μ the weight dependence is non-linear. We can now assess how the formation of such a dendritic efficacy mosaic is affected by changing the degree of synaptic competition, through the parameter μ of the STDP rule (Gütig et al., 2003). **Figure 4** illustrates how the M-index, which quantifies the degree of spatial segregation between the spatial arrangements of synaptic strengths, contributed by four independent groups of correlated afferent fibers, changes as a function of the exponent μ. Note that the index is high for small μ, indicating that efficacy clusters are spatially segregated while for $\mu > 0.25$ this segregation is poor. Spatial segregation occurs for small μ since STDP implementing strong competition between synapses, along with an active membrane, is seen to implement a winner-take-all self-organization process in space, where a single group can dominate some dendritic regions at the expense of others, while surrendering the remainder of the dendrite.

THE EFFECT OF FREQUENCY ON SPATIALLY SEGREGATED CLUSTERS

The frequency of input spikes has previously been shown to influence the outcome of STDP via changes to the final distribution of synaptic weights (Song et al., 2000). For the case of spatially extended excitable neurons stimulated by various independent groups of fibers with correlated activity, we examine the impact of altering input frequency on the degree of spatial segregation and overall spatial organization. For the case when non-linear STDP admits strong competition, one expectation is that spatial segregation should be adversely affected for low frequencies when compared to higher input frequencies, primarily due to a reduction in the amount of potentiation; while for the weak competition case, there should be little change between the initial and final spatial distributions of synaptic efficacies across the dendritic tree, irrespective of the mean frequency of input spike activity. **Figure 5** shows how the M-index changes as a function of mean input frequency when non-linear STDP admits both strong and weak competition. In the case of strong competition, for $A_- = 0.001125$ and frequencies less than 20 Hz, the small values for the M-index indicates that spatial segregation and hence the degree of spatial partitioning between the efficacies contributed by all four afferent groups is poor. As mean afferent input frequencies are increased, the magnitude of the M-index, which measures the degree of spatial segregation, increases. For frequencies higher than 30 Hz, spatial segregation is good (indicated by the high M-index values) where maximal spatial segregation between efficacy patterns occurring for a mean input frequency of 35 Hz. In contrast, when synaptic competition is weak, the magnitude of the M-index remains low even when the mean frequencies of afferent inputs to the dendrite is increased. For the $A_- = 0.001125$ case, high mean input frequencies of 30 Hz or more are needed to produce a high degree of spatial partitioning. This suggests that bursts may have a role to play, however for comparison, simply increasing A_- by 10% to $A_- = 0.0012375$ leads to higher M-index values over the range of selected mean input frequencies. Importantly for this specific case, we observe that a mean input frequency of 20 Hz is sufficient for a dendritic mosaic to emerge. Note that the selected values for A_- were chosen so that the ratio A_-/A_+ lies within the experimentally observed range for this ratio (Froemke and Dan, 2002).

We have observed that the mean input frequency of afferent fibers alters the M-index, however, what are the consequences of these frequency effects on the response properties of the model neuron? **Figure 6** shows how the firing rate of the pyramidal cell changes as a function of mean input frequency. Interestingly, the firing rate displays a dip, initially decreasing from 51.1 to 31.1 Hz for a mean input rate of 20 Hz and then rising almost linearly to

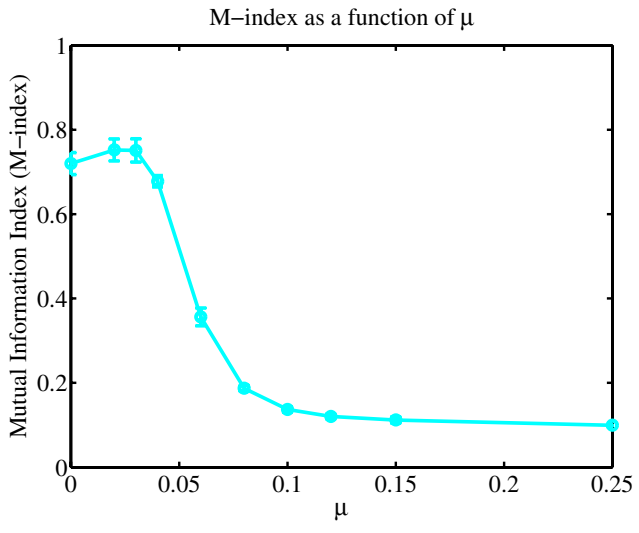

FIGURE 4 | A plot of the M-index as a function of μ. Notice the high value of the M-index occurs when the non-linear STDP rule admits strong competition, but its value is small when synaptic competition is weak.

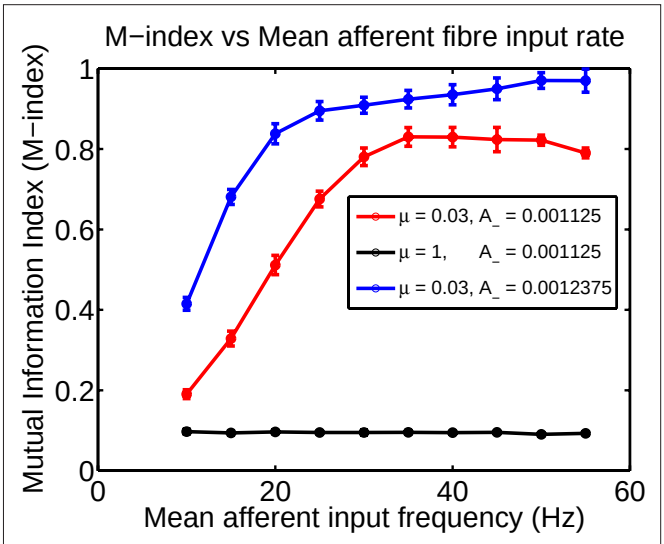

FIGURE 5 | Plot of the M-index as a function of the mean frequency of input afferent fiber activity for two different values of μ; μ = 0.03 (representing strong competition) and μ = 1 for weak competition between synapses. When synaptic competition is strong, for frequencies less than 20 Hz, the indices indicate that the degree of spatial segregation and the degree of partitioning is poor but improves as input frequency is increased. Computation times for the μ = 0.03 and μ = 1 were 4000 and 500 s of simulated time, respectively.

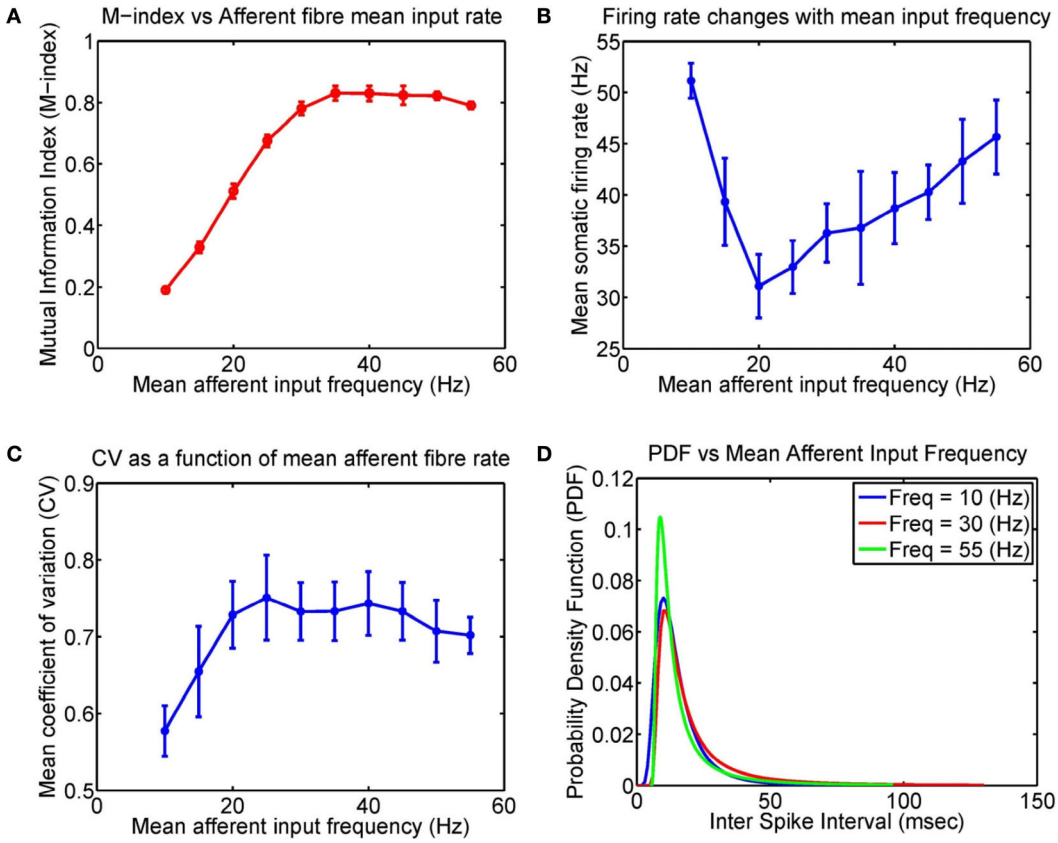

FIGURE 6 | Input frequency affects the firing properties of the model layer 2/3 pyramidal cell after STDP learning. Here four groups of excitatory fibers and one group of inhibitory fibers were active. **(A)** Plot of the M-index as a function of the afferent fiber mean input frequency for μ = 0.03 (repeated from **Figure 5**, after 4000 s). **(B)** The corresponding changes to the somatic firing rates, **(C)**, Coefficient of variation (CV), and **(D)** Probability density function (PDF) as a function of mean input frequency of afferent inputs, respectively. Note that the initial decrease in the firing rate may be attributed to several factors including sodium inactivation and the non-trivial effects of noise in neuron models (see Figure 1A of Gutkin et al., 2009).

45.7 Hz for higher (mean) input rates. There are likely to be any number of contributing reasons for such non-linear behavior, including a reduction in firing rate via sodium inactivation and the non-trivial effects of noise in Hodgkin–Huxley based neuron models (Gutkin et al., 2009). Although the non-linear behavior of the somatic firing rate initially falls and then rises, we want to stress that the monotonous increase of the M-index suggests that what happens in the dendrite is more important than the activity in the soma, which is critical for STDP models based upon BPAPs. Also displayed are the corresponding changes to the probability density function (PDF), and the coefficient of variation (CV) as a function of mean input frequency. Raw interspike interval histograms are presented in **Figure S2** in Supplementary Materials.

EMERGENCE OF SPATIALLY SEGREGATED CLUSTERS VIA MULTISPIKE STDP RULES

So far spatially segregated efficacy clusters have emerged through spike-pair based STDP rules, however, previous STDP experiments have shown that changes to synaptic efficacy depends upon several factors including multiple spike interactions (Froemke and Dan, 2002; Froemke et al., 2006) and the frequency of presynaptic inputs (Sjöström et al., 2001). Pair based STDP rules are inadequate for reproducing observed changes in synaptic efficacy induced by either varying the frequency of presynaptic inputs or when triplets or more spikes are used in experimental protocols. STDP rules based upon multiple spike interactions, such as a recent rule based upon triplets of spikes (Pfister and Gerstner, 2006), are important to explain both the changes in efficacy when driven by multiple spike based stimulation and frequency effects observed during classical pairing protocol experiments (Sjöström et al., 2001). We next examine the impact of such type of rule (Froemke rule – see Materials and Methods) on the final spatial organization of synaptic efficacies after the learning process.

Figure 7 illustrates how varying the degree of synaptic competition affects the M-index. There are clear differences between spike-pair (**Figure 4**) and multispike interaction (**Figure 7**) based rules for small values of μ. By comparing **Figures 4 and 7**, we observe that the M-index was larger for STDP based upon multispike interactions (Froemke rule) rather than spike-pair based rules (Gütig rule). Explaining why these differences occur for small values of μ is difficult because a theoretical framework for studying changes in synaptic efficacy in realistic neuron models, as used here, is still lacking.

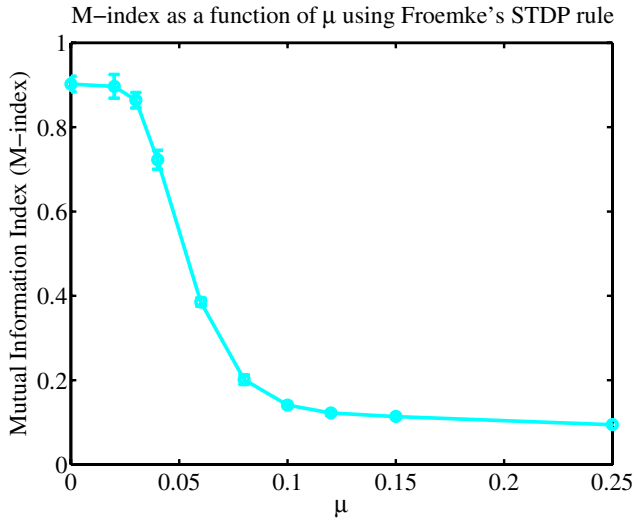

FIGURE 7 | Spatially segregated efficacy clusters can emerge from multispike based STDP rules. To quantify how competition influences the final spatial organization of synaptic weights, again the M-index are displayed as a function of μ.

ROBUSTNESS OF DENDRITIC EFFICACY MOSAIC AND SPATIALLY SEGREGATED CLUSTERS

So far, we have seen that four independent groups of correlated afferent fibers each gives rise to spatially segregated synaptic efficacy clusters. Being contributed by each respective afferent group, these segregated clusters possess a unique global organization in space, where they form a tessellation or a mosaic which partitions the dendritic tree whereby each group dominates mutually exclusive regions of the dendrite. This leads to the question of how robust is this type of spatial patterning when the number of groups is increased. This indirectly permits one to explore the spatial scale for information storage and representation that is preferred after STDP. In particular, recent studies have emphasized that information may be stored over several nearby synapses, rather than at a single synapse (Govindarajan et al., 2006; Harvey and Svoboda, 2007; De Roo et al., 2008; Harvey et al., 2008; Larkum and Nevian, 2008; Yoshihara et al., 2009). Since information storage over several nearby synapses is indeed the main mode of information storage, one would expect that only a finite number of independent afferent groups, less than the number of synapses, can be represented throughout the dendrite. The key questions are therefore, how input representation as efficacy clusters changes and, more importantly, whether the degree of functional association between synapses degrades as the number of groups increases.

Functional association between synapses from a single group of afferent fibers is created on the postsynaptic side by STDP, resulting in local and stable potentiation of a group of synapses receiving correlated activity. Stability results because the group of synapses mutually re-enforce each other (association), where they all become more resistant to spurious changes of synaptic weight triggered random events, permitting them to maintain their function. Put simply, function is improved by the fact that they are locally associated, leading to a more robust system. In order to quantify the association between synapses, we have adopted two indices extensively used in spatial analysis. Both Moran's I and Geary C indices were adopted as these (as previously stated in Section "Materials and Methods") are essentially measures of spatial autocorrelation, widely used for testing the presence of spatial dependencies.

To sample more finely the effect of increasing the number of groups but keeping the total number of axons close to 1000, we selected groups so that the integer number of axons per group multiplied by the number of groups was 1000 ± 1. **Figure 8A** illustrates how the M-index changes as a function of increasing number of independent afferent fiber groups. Significantly, **Figure 8B** depicts both the Moran's and Geary C indices, being respective global and local indicators of functional association, showing that there is a decrease in the degree of functional clustering when the number of groups increases. Note that there is a clear reduction in the rate of loss of functional clustering, where both indices are respectively expected to eventually asymptote to some finite non-zero values, keeping some degree of functional clustering between neighboring synapses. This suggests that only a finite number of afferent groups are represented in a manner where nearby synapses are functionally related and a high degree of spatial segregation can be maintained.

DISCUSSION

SYNAPTIC COMPETITION AND STDP JOINTLY REGULATE CLUSTERED EFFICACY ENGRAM FORMATION

In this current study, we have extended our original study (Iannella and Tanaka, 2006) by further investigating the issue of forming clustered synaptic efficacy engrams within the dendritic tree via STDP, subject to multiple input streams. A biophysical model, whose channel types and distributions are based upon available experimental findings, was used suggesting that the phenomena may exist *in vivo*. Specifically, when stimulation to the model was provided by four groups of correlated afferent fibers with no inter-group correlation, STDP allowed each respective group to dominate mutually exclusive regions of the dendrite, resulting in the emergence of spatially segregated clusters. These emergent clusters possess a unique spatial organization where they form a tessellated pattern which effectively partitions the dendritic tree, a patterning which we have termed a dendritic mosaic. This organization was stable in both space and time.

Significantly, we further showed that this spatial organization was robust to variations in the type of STDP (either spike-pair or multispike interaction based) rule used in the simulations. The emergence of the dendritic mosaic was prevented only when the number of independent input streams exceeded a critical value.

FUNCTIONAL CONSEQUENCES OF CLUSTERED SYNAPTIC EFFICACY ENGRAMS

The presence of a clustered spatial organization of synaptic efficacy within the dendrite can play important functional roles. One immediate consequence is clear; for inputs originating from a single group of afferents, activating potentiated synapses within efficacy clusters will favorably take part in neuronal firing. Specifically, activating such synapses will typically result in a larger dendritic depolarization when compared to the activation of synapses distributed diffusely in the dendritic tree, therefore making a bigger contribution toward spike generation. Previous experimental and

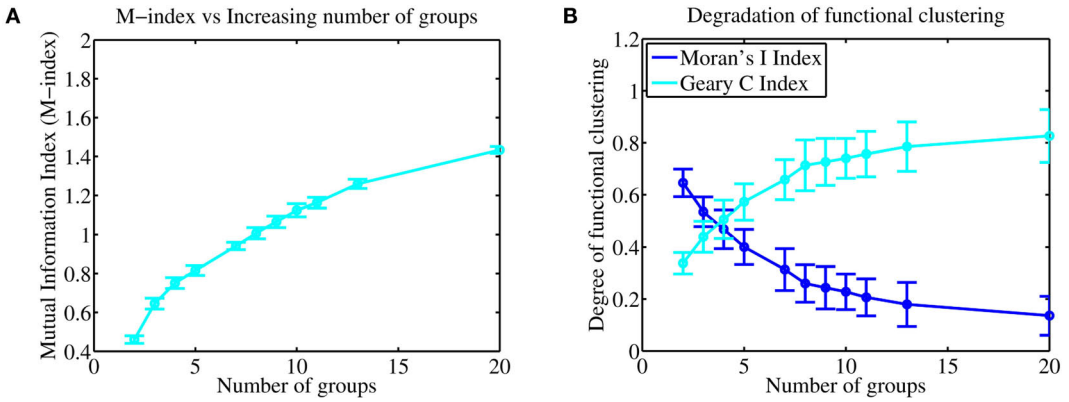

FIGURE 8 | (A) Increasing the number of independent afferent fiber groups leads to an increase in the M-index indicating that there may be an increase in the degree of spatial segregation. **(B)** Interestingly, both the Moran and Geary indices show that there is a loss in the degree of functional clustering and association between nearby synapses, however, the rate of loss slows and is eventually seen to reduce to 0 where both indices are expected to asymptote to finite values, suggesting that functional clustering, both globally and locally between neighboring synapses persists. This suggests that smallest spatial scale for information storage (and representation) in the dendrite is likely to be distributed over several nearby synapses.

theoretical studies support this, having shown that near synchronous activation of nearby synapses within a dendritic branch can lead to supralinear summation of their synaptic inputs. However, only linear summation was observed when synapses were activated on different dendritic branches (Poirazi et al., 2003; Gasparini et al., 2004; Polsky et al., 2004; Gasparini and Magee, 2006; Losonczy and Magee, 2006).

LOCAL VS GLOBAL POSTSYNAPTIC TIMING INFORMATION: THE CASE FOR DENDRITIC SPIKES

In classical STDP models, synaptic weights are modified according to the timing difference between presynaptic input t^{pre} and a postsynaptic spike t^{post}. Such studies assume a somatic spike can reliably back propagate to all regions of the dendritic tree, where this BPAP "tells" synapses about when the neuron fired a spike. In real pyramidal cells, however, spike generation is not restricted to the soma/axon initial segment region, but can be generated almost anywhere in the dendrite. This raises an important question as what signal conveys postsynaptic timing information and whether it should be local or global in nature. There is now mounting evidence from numerous experiments showing that the BPAP is an unreliable global signal since its known that it cannot fully invade the entire dendrite (Larkum et al., 2001; Stuart and Häusser, 2001). The extent of back-propagation varies depending upon various influences including potassium channel activation (Kampa and Stuart, 2006), synaptic background activity (Paré et al., 1998; Mickus et al., 1999), and inhibitory inputs (Larkum et al., 1999). Importantly, experimental studies have shown that synaptic efficacy can change without the need of a BPAP. Specifically, these studies illustrated that generating a local dendritic spike, by spatially clustered and near synchronous synaptic inputs, can lead to changes in synaptic strength (Schiller et al., 2000; Golding et al., 2002; Holthoff et al., 2004). For models, assuming that local dendritic spikes carry postsynaptic timing information are detected locally at each synapse is true, then the results of this paper and our previous work (Iannella and Tanaka, 2006) suggest that spatially segregated clusters emerge as a consequence.

It is now pertinent to ask what would happen if only the BPAP was used to convey postsynaptic timing information? A single theoretical study using a reconstructed CA1 pyramidal cell has shown that by assuming somatic spikes in two different models of dendritic excitability, one with a high capacity and the other with a low capacity to generate dendritic spikes, stimulated by a single group of afferents led to a large portion of highly potentiated synapses (Rumsey and Abbott, 2006). For the low capacity model potentiated synapses were typically located closer to the soma than depressed synapses (see Figure 10 in Rumsey and Abbott, 2006). Now if one considers the case when stimulation is provided by multiple groups of afferents, the results of Rumsey and Abbott (2004) seems to indicate that most synapses close to the soma, irrespective of the contributing group, would be potentiated, suggesting that the dendritic mosaic would not emerge.

Allowing the synapse to detect spikes locally has the advantage that different dendritic regions will have different sequences of postsynaptic times, and these different times essentially provides a "seed or scaffold" for clusters to emerge. This can be simply understood by the following intuitive example. When an afferent group begins to dominate some dendritic location(s) then the strength of its contributed synapses to neighboring locations are also like to be strengthened since dendritic spike generation at locations where the group dominates will also strongly depolarize adjacent locations. Synaptic inputs to these adjacent locations are likely to generate dendritic spikes and this eventually strengthens some of the synapses contributed by the dominant group, while weakening those of other groups, leading to the formation of a cluster.

Although the current STDP model provides useful insights into cluster formation, it is inadequate for understanding the biophysical mechanisms responsible such processes. Given that calcium signaling is known to be an important factor, not only for STDP (Nevian and Sakmann, 2006), but also for synaptic plasticity in general (Bliss and Lomo, 1973; Bienenstock et al., 1982; Brown et al., 1988; Dudek and Bear, 1992; Hille, 2001), we would argue that a biophysical model of STDP, based upon calcium and known (and/or yet to be discovered) biochemical signaling cascades is required

(see Larkum and Nevian, 2008 for an excellent review). This model may provide useful insights for understanding the basis of synaptic plasticity and potential biophysical mechanisms, such as synaptic cross-talk, underlying cluster formation. Such a study, including the development of such a new calcium based model of STDP, is currently being pursued and whose results will be presented in a future publication.

RELATIONSHIP TO PREVIOUS MODELS

Standard theoretical STDP studies are typically conducted using simplified point or single compartment models having mainly focused on computational approaches toward the evolution of synaptic weights or the development of selective functional properties (Song et al., 2000; Song and Abbott, 2001; Gütig et al., 2003). Such investigations have provided useful insights into the role of spike timing in neuronal circuit formation or the emergence of some functional property.

However, to investigate how plasticity and active dendritic properties influences synaptic strength, the use of an elaborated compartmental model with active dendrites is gaining popularity (Rumsey and Abbott, 2004, 2006; Rabinowitch and Segev, 2006a,b). To date, few studies have addressed the formation of spatial patterns of synaptic efficacies. The model presented here improves upon our previous model (Iannella and Tanaka, 2006). This previous study provided some indication that STDP may be an important mechanism involved in the development of spatially segregated efficacy clusters. Significantly, the model presented here is fundamentally different to the previous one since it not only includes several types of postsynaptic receptors, but also various voltage- and calcium-dependent ion channels, with their densities and distributions based upon data from the rat neocortex. Such biophysical detail was previously not included. The model response to high frequency stimulation patterns is now in good agreement with experimental findings.

The model presented here addresses a potentially important role for STDP in the development of spatially patterned functional synaptic inputs across the dendritic arbor. Previous models have proposed different plasticity mechanisms underlying the emergence of distance-dependent scaling in synaptic strength associated with location independent synapses (Rumsey and Abbott, 2004, 2006). In other studies, different homoeostatic plasticity mechanisms (Rabinowitch and Segev, 2006a,b) were used to examine the emergence of functional compartments within the dendrite. The current model complements these earlier studies by employing a biophysically realistic model neuron to not only illustrate a connection between the degree of clustering in the resulting arrangement of synaptic efficacies and the level of competition associated with STDP, but also the robustness of this emergent mode of spatial organization.

PREDICTIONS OF THE MODEL

Our biophysical model predicts that competition between synapses in both space and time underlies the emerging spatial arrangement of functional synaptic inputs. For neurons innervated by independent groups of afferent fibers with correlated activity, strong spatiotemporal competition may be essential for developing a dendritic efficacy mosaic, as observed in ocular dominance patterns (Katz and Constantine-Paton, 1988). Our biophysical model supports this hypothesis but shows that the segregation appears only when spatiotemporal competition was strong. When competition was weak, the dendritic efficacy mosaic fails to emerge. In this case both clustering and spatial segregation was severely degraded.

Our model also predicts that the spatial organization of synaptic efficacies along the dendrite *is not random*, but ordered, despite being heterogeneously distributed (Cotrell et al., 2001; Frick et al., 2001). It may reflect the nature and occurrence of correlations embedded in the spiking activity originating from different afferent groups. Support for this comes from previous studies illustrating supralinear summation of near synchronous inputs between neighboring synapses (Gasparini et al., 2004; Polsky et al., 2004; Gasparini and Magee, 2006; Losonczy and Magee, 2006); and coupling this form of electrical cooperativity with STDP then leads to the selective potentiation of those correlated inputs which led to dendritic spike generation. However, the most compelling supporting evidence comes from two recent studies by Harvey and Svoboda (2007) and De Roo et al. (2008). Harvey and Svoboda illustrated that inducing LTP at a synapse with suprathreshold stimuli, reduces the threshold of LTP induction in neighboring synapses on the same dendritic branch, allowing such synapses to be potentiated using subthreshold stimuli. This cooperativity between groups of nearby synapses (within a dendritic neighborhood) clearly leads to their coordinated regulation (Harvey and Svoboda, 2007). While the second study by De Roo et al. (2008) showed that LTP leads to the selection of inputs promoting spatiotemporal coincidence, thus promoting the creation of hotspots of functional synapses Indicating that any information or features embedded within a stimulus, such as correlations, are likely to be stored across several neighboring synapses forming a clustered engram. Using natural stimulation *in vivo* (such as visual), combined with recent advances in optical imaging of dendritic voltage using either organic dyes (Bradley et al., 2009) or red-shifted genetically encoded voltage sensitive proteins (Perron et al., 2009) *in vivo* would enable to directly test the presence of a dendritic efficacy mosaic.

LIMITATIONS OF THE MODEL

The present model was designed to test the hypothesis that STDP could serve as a mechanism involved in the formation of synaptic efficacy clusters within the dendritic tree. Despite the biophysical detail of the current neuron model, no effort was made to embed the neuron into a realistic network. The current study only considered a simple feed forward network structure, where the biophysically detailed model received feed forward inputs from neurons modeled as simple stochastic processes. Non-linear membrane dynamics and more appropriate model representations of these constituent neurons should be considered in future models.

An important issue is to elucidate both the molecular mechanisms and the role of calcium influx underlying the induction of STDP (as well as other forms of synaptic plasticity). Current STDP learning rules possess no dependence on calcium or any other molecular factors, and are exclusively parameterized by the precise timing of presynaptic inputs and postsynaptic spike generation (Zhang et al., 1998; Froemke and Dan, 2002; Froemke et al., 2005, 2006; Pfister and Gerstner, 2006). Experiments have shown that the induction of synaptic plasticity, including STDP, relies

upon calcium entry into the cytoplasm of the neuron typically through NMDA receptors, voltage-dependent calcium channels and/or *IP*3-gated calcium release from the endoplasmic reticulum (ER). A key question here is how calcium influx via NMDA receptor activation leads to either potentiation or depression. Also experimentally verified is the consistency of LTP and LTD induction in synapses with the BCM theory of synaptic plasticity (Bienenstock et al., 1982; Dudek and Bear, 1992; Kirkwood et al., 1996; Philpot et al., 2001a,b, 2007).

Another limitation of the model is that other forms of plasticity, such as structural plasticity, were not considered. Previous experiments have shown that synaptic plasticity and learning are associated with changes to cortical/dendritic structure. One example is that the alteration of synapse morphology depends upon changing the structure of cytoskeletal filaments (Matus, 2000) through actin polymerization (Fischer et al., 1998; Dunaevsky et al., 1999) and another is the involvement of adhesion molecules in the formation of new synapses (Benson et al., 2000). Theoretical studies have also investigated the impact of structural plasticity on the memory capacity of information storage (Poirazi et al., 2001; Stepanyants et al., 2002). Here however, incorporating the biophysical details of structural plasticity, through the creation, modification and removal of synapses/spines via activity-dependent remodeling of afferent connectivity onto the dendrite was not included due to the extra complexity and computational load this would have imposed.

Ideally one should test the role of STDP (as well as other forms of plasticity) in a network composed of entirely biophysically realistic spatial model neurons specifically aimed at simulating some cortical region, like the primary visual cortex, the area corresponding to the early stage of signal processing of visual information, incorporating details of both cell type and spatial morphology of such constituent neurons. The complexity and computational resources required to conduct such simulations are enormous, only possible on the most powerful supercomputers. Despite this current obstacle, intermediate levels of model representation should be considered and are currently under investigation.

We believe that the current study provides useful insights toward understanding how the interplay between synapse location, active dendritic properties and synaptic plasticity shapes the strengths and spatial arrangements of synapses. Our study suggests that "clustering" may be the favored outcome of synaptic plasticity. More importantly, this model proposes that STDP, driven by timing differences between synaptic inputs and dendritic spike generation, may be an important mechanism contributing to the efficacy and spatial arrangements of synapses within the dendrite.

ACKNOWLEDGMENTS

The authors would like to thank the support of RIKEN BSI and the Advanced Center for Computing and Communication for their technical assistance.

SUPPLEMENTARY MATERIAL

The Supplementary Material for this article can be found online at http://www.frontiersin.org/neuroscience/frontiersincomputationalneuroscience/paper/10.3389/fncom.2010.00021/

REFERENCES

Anderson, J. C., Binzegger, T., Douglas, R. J., and Martin, K. A. C. (2002). Chance or design? Some specific considerations concerning synaptic boutons in cat visual cortex. *J. Neurocytol.* 31, 211–229.

Appleby, P. A., and Elliott, T. (2005). Synaptic and temporal ensemble interpretation of spike-timing-dependent plasticity. *Neural Comput.* 17, 2316–2336.

Appleby, P. A., and Elliott, T. (2006). Stable competitive dynamics emerge from multispike interactions in a stochastic model of spike-timing-dependent plasticity, *Neural Comput.* 18, 2414–2464.

Appleby, P. A., and Elliott, T. (2007). Multispike interactions in a stochastic model of spike-timing-dependent plasticity. *Neural Comput.* 19, 1362–1399.

Benson, D., Schnapp, L., Shapiro, L., and Huntley, G. (2000). Making memories stick: cell-adhesion molecules in synaptic plasticity. *Trends Cell Biol.* 10, 473–482.

Bi, G.-Q., and Poo, M.-M. (1998). Synaptic modifications in cultured hippocampal neurons: dependence on spike timing, synaptic strength, and postsynaptic cell type. *J. Neurosci.* 18, 10464–10472.

Bienenstock, E. L., Cooper, L. N., and Munro, P. W. (1982). Theory for the development of neuron selectivity: orientation specificity and binocular interaction in visual cortex. *J. Neurosci.* 2, 32–48.

Binzegger, T., Douglas, R. J., and Martin, K. A. C. (2004). A quantitative map of the circuit of cat primary visual cortex. *J. Neurosci.* 24, 8441–8453.

Bliss, T. V., and Lomo, T. (1973). Long-lasting potentiation of synaptic transmission in the dentate area of the anaesthetized rabbit following stimulation of the perforant path. *J. Physiol.* 232, 331–356.

Bliss, T. V. P., and Collingridge, G. L. (1993). A synaptic model of memory: long-term potentiation in the hippocampus. *Nature* 361, 31–39.

Bradley, J., Luo, R., Otis, T. S., and DiGregorio, D. A. (2009). Submillisecond optical reporting of membrane potential in situ using a neuronal tracer dye. *J. Neurosci.* 29, 9197–9209.

Brown, T. H., Chapman, P. F., Kairiss, E. W., and Keenan, C. L. (1988). Long-term synaptic potentiation. *Science* 242, 724.

Burkitt, A. N., Gilson, M., and Leo van Hemmen, J. (2007). Spike-timing-dependent plasticity for neurons with recurrent connections. *Biol. Cybern.* 96, 533–546.

Burkitt, A. N., and Grayden, D. B. (2004). Spike-timing-dependent plasticity: the relationship to rate-based learning for models with weight dynamics determined by a stable fixed point. *Neural Comput.* 16, 885–940.

Cotrell, J. R., Dubé, G. R., Egles, C., and Liu, G. (2001). Distribution, density, and clustering of functional glutamate receptors before and after synaptogenesis in hippocampal neurons. *J. Neurophysiol.* 84, 1573–1587.

Cove, J., Blinder, P., Abi-Jaoude, E., Lafrenière-Roula, M., Devroye, L., and Baranes, D. (2006). Growth of neurites toward neurite–neurite contact sites increases synaptic clustering and secretion and is regulated by synaptic activity. *Cereb. Cortex* 16, 83–92.

Debanne, D., Gähwiler, B. H., and Thompson, S. M. (1998). Long-term synaptic plasticity between pairs of individual CA3 pyramidal cells in rat hippocampal slice cultures. *J. Physiol.* 507, 237–247.

De Roo, M., Klauser, P., and Muller, D. (2008). LTP promotes a selective long-term stabilization and clustering of dendritic spines. *PLoS Biol.* 6, e219. doi: 10.1371/journal.pbio.0060219.

Destexhe, A., and Paré, D. (1999). Impact of network activity on the integrative properties of neocortical pyramidal neurons *in vivo*. *J. Neurophysiol.* 81, 1531–1547.

Dudek, S. M., and Bear, M. F. (1992). Homosynaptic long-term depression in area CA1 of hippocampus and the effects of N-methyl-D-aspartate receptor blockade. *Proc. Natl. Acad. Sci. U.S.A.* 89, 4363–4367.

Dunaevsky, A., Tashiro, A., Majewska, A., Mason, C., and Yuste, R. (1999). Developmental regulation of spine motility in the mammalian central nervous system. *Proc. Natl. Acad. Sci. U.S.A.* 96, 13438–13443.

Duncan, O., and Duncan, B. (1955). A methodological analysis of segregation indexes. *Am. Sociol. Rev.* 20, 210–217.

Feldmeyer, D., Lubke, J., Silver, R. A., and Sakmann, B. (2002). Synaptic connections between layer 4 spiny neurone-layer 2/3 pyramidal cell pairs in juvenile rat barrel cortex: physiology and anatomy of interlaminar signalling within a cortical column. *J. Physiol.* 538(Pt 3), 803–822.

Fischer, M., Kaech, S., Knutti, D., and Matus, A. (1998). Rapid actin-based plasticity in dendritic spines. *Neuron* 20, 847–854.

Frankel, D., and Volij, O. (2005). *Scale Invariant Measures of Segregation*. Econ. Theory and Game Theory, 18.

Frankel, D., and Volij, O. (2009). *Measuring School Segregation*, Technical Report. Mimeo.

Frick, A., Zieglgänsberger, W., and Dodt, H.-U. (2001). Glutamate receptors form hot spots on apical dendrites of neocortical pyramidal neurons. *J. Neurophysiol.* 86, 1412–1421.

Froemke, R. C., and Dan, Y. (2002). Spike-timing dependent synaptic modification induced by natural spike trains. *Nature* 416, 433–438.

Froemke, R. C., Poo, M.-M., and Dan, Y. (2005). Spike-timing-dependent synaptic plasticity depends on dendritic location. *Nature* 434, 221–225.

Froemke, R. C., Tsay, I. A., Raad, M., Long, J. D., and Dan, Y. (2006). Contribution of individual spikes in burst-induced long-term synaptic modification. *J. Neurophysiol.* 95, 1620–1629.

Gasparini, S., and Magee, J. C. (2006). State-dependent dendritic computation in hippocampal CA1 pyramidal neurons. *J. Neurosci.* 26, 2088–2100.

Gasparini, S., Migliore, M., and Magee, J. C. (2004). On the initiation and propagation of dendritic spikes in CA1 pyramidal neurons. *J. Neurosci.* 24, 11046–11056.

Geary, R. C. (1954). The contiguity ratio and statistical mapping. *Inc. Stat.* 5, 115–145.

Gerstner, W., Kempter, R., Leo van Hemmen, J., and Wagner, H. (1996). A neuronal learning rule for sub-millisecond temporal coding. *Nature* 383, 76–78.

Gilson, M., Burkitt, A., Grayden, D., Thomas, D., and van Hemmen, J. (2009a). Emergence of network structure due to spike-timing-dependent plasticity in recurrent neuronal networks. I. Input selectivity–strengthening correlated input pathways. *Biol. Cybern.* 101, 81–102.

Gilson, M., Burkitt, A., Grayden, D., Thomas, D., and van Hemmen, J. (2009b). Emergence of network structure due to spike-timing-dependent plasticity in recurrent neuronal networks. II. Input selectivity–symmetry breaking. *Biol. Cybern.* 101, 103–114.

Gilson, M., Burkitt, A., Grayden, D., Thomas, D., and van Hemmen, J. (2009c). Emergence of network structure due to spike-timing-dependent plasticity in recurrent neuronal networks. III: Partially connected neurons driven by spontaneous activity. *Biol. Cybern.* 101, 411–426.

Gilson, M., Burkitt, A. N., Grayden, D. B., Thomas, D. A., and van Hemmen, J. L. (2009d). Emergence of network structure due to spike-timing-dependent plasticity in recurrent neuronal networks IV: structuring synaptic pathways among recurrent connections. *Biol. Cybern.* 101, 427–444.

Glanzman, D. L., Kandel, E. R., and Schacher, S. (1991). Target-dependent morphological segregation of Aplysia sensory outgrowth in vitro. *Neuron* 7, 903–913.

Golding, N. L., Staff, N. P., and Spruston, N. (2002). Dendritic spikes as a mechanism for cooperative long-term potentiation. *Nature* 418, 326–331.

Govindarajan, A., Kelleher, R., and Tonegawa, S. (2006). A clustered plasticity model of long-term memory engrams. *Nat. Rev. Neurosci.* 7, 575–583.

Gütig, R., Aharonov, R., Rotter, S., and Sompolinsky, H. (2003). Learning input correlations through nonlinear temporally asymmetric Hebbian plasticity. *J. Neurosci.* 23, 3697–3714.

Gutkin, B., Jost, J., and Tuckwell, H. (2009). Inhibition of rhythmic neural spiking by noise: the occurrence of a minimum in activity with increasing noise. *Naturwissenschaften* 96, 1091–1097.

Harvey, C. D., and Svoboda, K. (2007). Locally dynamic synaptic learning rules in pyramidal neuron dendrites. *Nature* 450, 1195–1202.

Harvey, C. D., Yasuda, R., Zhong, H., and Svoboda, K. (2008). The spread of Ras activity triggered by activation of a single dendritic spine. *Science* 321, 136–140.

Hellwig, B. (2000). A quantitative analysis of the local connectivity between pyramidal neurons in layers 2/3 of the rat visual cortex. *Biol. Cybern.* 82, 111–121.

Hellwig, B., Schuez, A., and Aertsen, A. (1994). Synapses on axon collaterals of pyramidal cells are spaced at random intervals: a Golgi study in the mouse cerebral cortex. *Biol. Cybern.* 71, 1–12.

Hille, B. (2001). *Ionic Channels of Excitable Membranes*, 3rd Edn. Sunderland, MA: Sinauer.

Hines, M. L., and Carnevale, N. T. (2001). NEURON: a tool for neuroscientists. *Neuroscientist* 7, 123–135.

Holthoff, K., Kovalchuk, Y., Yuste, R., and Konnerth, A. (2004). Single-shock LTD by local dendritic spikes. *J. Physiol.* 560, 27–36.

Iannella, N., and Tanaka, S. (2006). Synaptic efficacy cluster formation across the dendrite via STDP. *Neurosci. Lett.* 403, 24–29.

Iannella, N., Tuckwell, H., and Tanaka, S. (2004). Firing properties of a stochastic PDE model of a rat sensory cortex layer 2/3 pyramidal cell. *Math. Biosci.* 188, 117–132.

Izhikevich, E. M., and Desai, N. S. (2003). Relating stdp to bcm. *Neural Comput.* 15, 1511–1523.

James, D. R., and Taeuber, K. E. (1985). Measures of segregation. *Sociol. Methodol.* 15, 1–32.

Kalisman, N., Silberberg, G., and Markram, H. (2005). The neocortical microcircuit as a tabula rasa. *Proc. Natl. Acad. Sci. U.S.A.* 102, 880–885.

Kampa, B. M., Letzkus, J. J., and Stuart, G. J. (2006). Requirement of dendritic calcium spikes for induction of spike-timing-dependent synaptic plasticity. *J. Physiol.* 574(Pt 1) 283–290.

Kampa, B. M., and Stuart, G. J. (2006). Calcium spikes in basal dendrites of layer 5 pyramidal neurons during action potential bursts. *J. Neurosci.* 26, 7424–7432.

Katz, L. C., and Constantine-Paton, M. (1988). Relationships between segregated afferents and postsynaptic neurons in the optic tectum of three-eyed frogs. *J. Neurosci.* 8, 3160–3180.

Kavalali, E. T., Klingauf, J., and Tsien, R. W. (1999). Activity dependent regulation of synaptic clustering in a hippocampal culture system. *Proc. Natl. Acad. Sci. U.S.A.* 96, 12893–12900.

Kirkwood, A., and Bear, M. F. (1994). Homosynaptic long-term depression in the visual cortex. *J. Neurosci.* 14, 3404–3412.

Kirkwood, A., Rioult, M. C., and Bear, M. F. (1996). Experience-dependent modification of synaptic plasticity in visual cortex. *Nature* 381, 526–528.

Koch, C., Poggio, T., and Torre, V. (1983). Nonlinear interactions in a dendritic tree: localization, timing and role in information processing. *Proc. Natl. Acad. Sci. U.S.A.* 80, 2799–2802.

Kuhn, A., Aertsen, A., and Rotter, S. (2003). Higher-order statistics of input ensembles and the response of simple model neurons. *Neural Comput.* 15, 67–101.

Larkum, M. E., Kaiser, K. M. M., and Sakmann, B. (1999). Calcium electrogenesis in distal apical dendrites of layer 5 pyramidal cells at a critical frequency of back-propagating action potentials. *Proc. Natl. Acad. Sci. U.S.A.* 96, 14600–14604.

Larkum, M. E., Kaiser, K. M. M., and Sakmann, B. (2001). Dendritic mechanisms underlying the coupling of the dendritic with the axonal action potential initiation zone of adult layer 5 pyramidal neurons. *J. Physiol.* 533, 447–466.

Larkum, M. E., and Nevian, T. (2008). Synaptic clustering by dendritic signalling mechanisms. *Curr. Opin. Neurobiol.* 18, 321–331.

Larkum, M. E., Waters, J., Sakmann, B., and Helmchen, F. (2007). Dendritic spikes in apical dendrites of neocortical layer 2/3 pyramidal neurons. *J. Neurosci.* 27, 8999–9008.

Lorenzon, N. M., and Foehring, R. C. (1995). Characterization of pharmacologically identified voltage-gated calcium channel currents in acutely isolated rat neocortical neurons. I. Adult neurons. *J. Neurophysiol.* 73, 1430–1442.

Losonczy, A., and Magee, J. C. (2006). Integrative properties of radial oblique dendrites in hippocampal CA1 pyramidal neurons. *Neuron* 50, 291–307.

Magee, J. C., and Cook, E. P. (2000). Somatic EPSP amplitude is independent of synapse location in hippocampal pyramidal neurons. *Nat. Neurosci.* 3, 895–903.

Mainen, Z. F., Joerges, J., Huguenard, J. R., and Sejnowski, T. J. (1995). A model of spike initiation in neocortical pyramidal cells. *Neuron* 15, 1427–1439.

Markram, H., Lübke, J., Frotscher, M., and Sakmann, B. (1997a). Regulation of synaptic efficacy by coincidence of postsynaptic AP and EPSP. *Science* 275, 213–215.

Markram, H., Lubke, J., Frotscher, M., Roth, A., and Sakmann, B. (1997b). Physiology and anatomy of synaptic connections between thick tufted pyramidal neurones in the developing rat neocortex. *J. Physiol.* 500(Pt 2), 409–440.

Masquelier, T., Guyonneau, R., and Thorpe, S. J. (2009). Competitive STDP-based spike pattern learning. *Neural Comput.* 21, 1259–1276.

Masquelier, T., and Thorpe, S. J. (2007). Unsupervised learning of visual features through spike timing dependent plasticity. *PLoS Comput. Biol.* 3, 0247–0257. doi: 10.1371/journal.pcbi.0030031.

Massey, D. S., and Denton, N. A. (1988). The dimensions of residential segregation. *Soc. Forces* 67, 281–315.

Matus, A. (2000). Actin-based plasticity in dendritic spines. *Science* 290, 754–758.

Meffin, H., Besson, J., Burkitt, A. N., and Grayden, D. B. (2004). Learning the structure of correlated synaptic subgroups using stable and competitive spike-timing-dependent plasticity. *Neural Comput.* 16, 885–940.

Megías, M., Emri, Z. S., Freund, T. F., and Gulyás, I. A. (2001). Total number and distribution of inhibitory and excitatory synapses on hippocampal CA1 pyramidal cells. *Neuroscience* 102, 527–540.

Mel, B. W. (1993). Synaptic integration in an excitable dendritic tree. *J. Neurophysiol.* 70, 1086–1101.

Mickus, T., Jung, H.-Y., and Spruston, N. (1999). Properties of slow, cumulative sodium channel inactivation in rat hippocampal CA1 pyramidal cells. *Biophys. J.* 76, 846–860.

Mora, R., and Ruiz-Castillo, J. (2009). "The invariance properties of the Mutual Information Index of multigroup segregation," in *Occupational and Residential Segregation*, Vol. 17, eds Y. Flückiger, S. F. Reardon, and J. Silber (London: Emerald), 33–54.

Moran, P. A. P. (1950). Notes on continuous stochastic phenomena. *Biometrika* 37, 17–23.

Murray, J. (2003). *Mathematical Biology*, Vols I and II. New York: Springer Verlag.

Nevian, T., and Sakmann, B. (2006). Spine Ca^{2+} signaling in spike-timing-dependent plasticity. *J. Neurosci.* 26, 11001–11013.

Paré, D., Shink, E., Gaudreau, H., Destexhe, A., and Lang, E. J. (1998). Impact of spontaneous synaptic activity on the resting properties of cat neocortical pyramidal neurons *in vivo*. *J. Neurophysiol.* 79, 1450–1460.

Perron, A., Mutoh, H., Launey, T., and Knöpfel, T. (2009). Red-shifted voltage-sensitive fluorescent proteins. *Chem. Biol.* 16, 1268–1277.

Pfister, J.-P., and Gerstner, W. (2006). Triplets of spikes in a model of spike timing-dependent plasticity. *J. Neurosci.* 26, 9673–9682.

Philpot, B. D., Cho, K. K. A., and Bear, M. F. (2007). Obligatory role of NR2A for metaplasticity in visual cortex. *Neuron* 53, 495–502.

Philpot, B. D., Sekhar, A. K., Shouval, H. Z., Bear, M. F., and Cooper, L. N. (2001a). Visual experience and deprivation bidirectionally modify the composition and function of NMDA receptors in visual cortex. *Neuron* 29, 157–169.

Philpot, B. D., Espinosa, J. S., and Bear, M. F. (2001b). Evidence for altered NMDA receptor function as a basis for metaplasticity in visual cortex. *J. Neurosci.* 23, 5583–5588.

Poirazi, P., Brannon, T., and Mel, B. W. (2001). Impact of active dendrites and structural plasticity on the memory capacity of neural tissue. *Neuron* 29, 779–796.

Poirazi, P., Brannon, T., and Mel, B. W. (2003). Arithmetic of subthreshold synaptic summation in a model CA1 pyramidal cell. *Neuron* 37, 977–987.

Polsky, A., Mel, B. W., and Schiller, J. (2004). Computational subunits in thin dendrites of pyramidal cells. *Nat. Neurosci.* 7, 621–627.

Rabinowitch, I., and Segev, I. (2006a). The interplay between homeostatic synaptic plasticity and functional dendritic compartments. *J. Neurophysiol.* 96, 276–283.

Rabinowitch, I., and Segev, I. (2006b). The endurance and selectivity of spatial patterns of long-term potentiation/depression in dendrites under homeostatic synaptic plasticity. *J. Neurosci.* 26, 13474–13484.

Reardon, S. F., and Firebaugh, G. (2002). Measures of multigroup segregation. *Sociol. Methodol.* 32, 33–67.

Rhodes, P. A., and Gray, C. M. (1994). Simulations of intrinsically bursting neocortical pyramidal neurons. *Neural Comput.* 6, 1086–1110.

Rhodes, P. A., and Llinás, R. R. (2001). Apical tuft input efficacy in layer 5 pyramidal cells from rat visual cortex. *J. Physiol.* 6, 1086–1110.

Rudolph, M., and Destexhe, A. (2003). A fast-conducting stochastic integrative mode for neocortical neurons *in vivo*. *J. Neurosci.* 23, 2466–2476.

Rumsey, C. C., and Abbott, L. F. (2004). Equalization of synaptic efficacy by activity and timing-dependent synaptic plasticity. *J. Neurophysiol.* 91, 2273–2280.

Rumsey, C. C., and Abbott, L. F. (2006). Synaptic democracy in active dendrites. *J. Neurophysiol.* 96, 2307–2318.

Schiller, J., Major, G., Koester, H. J., and Schiller, Y. (2000). NMDA spikes in basal dendrites of cortical pyramidal cells. *Nature* 404, 285–289.

Schwindt, P. C., Spain, W. J., Foehring, R. C., Stafstrom, C. E., Chubb, W. E., and Crill, M. C. (1988). Multiple potassium conductances and their functions in neurons from cat sensorimotor cortex in vitro. *J. Neurophysiol.* 59, 424–449.

Sjöström, P. J., Turrigiano, G. G., and Nelson, S. B. (2001). Rate, timing, and cooperativity jointly determine cortical synaptic plasticity. *Neuron* 32, 1149–1164.

Somogyi, P., Tamás, G., Lujan, R., and Buhl, E. H. (1998). Salient features of synaptic organisation in the cerebral cortex. *Brain Res. Rev.* 26, 113–135.

Song, S., and Abbott, L. F. (2001). Cortical development and remapping through spike timing-dependent plasticity. *Neuron* 32, 339–350.

Song, S., Miller, K. D., and Abbott, L. F. (2000). Competitive Hebbian learning through spike-timing-dependent synaptic plasticity. *Nat. Neurosci.* 3, 919–926.

Stafstrom, C. E., Schwindt, P. C., Chubb, M. C., and Crill, W. E. (1985). Properties of persistent sodium conductance and calcium conductance of layer v neurons from cat sensorimotor cortex in vitro. *J. Neurophys.* 53, 153–170.

Stepanyants, A., Hirsch, J. A., Martinez, L. M., Kisvarday, Z. F., Ferecsko, A. S., and Chklovskii, D. B. (2008). Local potential connectivity in cat primary visual cortex. *Cereb. Cortex* 18, 13–28.

Stepanyants, A., Hof, P. R., and Chklovskii, D. B. (2002). Geometry and structural plasticity of synaptic connectivity. *Neuron* 34, 275–288.

Stuart, G. J., and Häusser, M. (2001). Dendritic coincidence detection of EPSPs and action potentials. *Nat. Neurosci.* 4, 63–71.

Theil, H. (1971). *Principles of Econometrics*. New York: Wiley.

Thomson, A. M., Deuchars, J., and West, D. C. (1994). Relationships between morphology and physiology of pyramid–pyramid single axon connections in rat neocortex *in vitro*. *J. Physiol.* 478(Pt 3), 423–435.

Thomson, A. M., West, D. C., Wang, Y., and Bannister, A. P. (2002). Synaptic connections and small circuits involving excitatory and inhibitory neurons in layers 2–5 of adult rat and cat neocortex: triple intracellular recordings and biocytin labelling *in vitro*. *Cereb. Cortex* 12, 936–953.

Traub, R. D., Buhl, E. H., Gloveli, T., and Whittington, M. A. (2003). Fast rhythmic bursting can be induced in a layer 2/3 cortical neurons by enhancing persistent Na^+ conductance or by blocking BK channels. *J. Neurophysiol.* 89, 909–921.

Tuckwell, H. C. (1986). On shunting inhibition. *Biol. Cybern.* 86, 83–90.

van Rossum, M. C. W., Bi, G.-Q., and Turrigiano, G. G. (2000). Stable Hebbian learning from spike timing-dependent plasticity. *J. Neurosci.* 20, 8812–8821.

Wenisch, O. G., Noll, J., and Leo van Hemmen, J. (2005). Spontaneously emerging direction selectivity maps in the visual cortex through STDP. *Biol. Cybern.* 93, 239–247.

Yoshihara, Y., De Roo, M., and Muller, D. (2009). Dendritic spine formation and stabilization, *Curr. Opin. Neurobiol.* 19, 146–153.

Zhang, L. I., Tao, H. W., Holt, C. E., Harris, W. A., and Poo, M.-M. (1998). A critical window for cooperation and competition among developing retinotectal synapses. *Nature* 395, 37–44.

Conflict of Interest Statement: The authors declare that the research was conducted in the absence of any commercial or financial relationships that could be construed as a potential conflict of interest.

Received: 08 March 2010; Paper pending published: 01 April 2010; Accepted: 14 June 2010; published online: 14 July 2010.

*Citation: Iannella NL, Launey T and Tanaka S (2010) Spike timing-dependent plasticity as the origin of the formation of clustered synaptic efficacy engrams. Front. Comput. Neurosci. **4**:21. doi: 10.3389/fncom.2010.00021*

frontiers in
COMPUTATIONAL NEUROSCIENCE

ORIGINAL RESEARCH ARTICLE
published: 14 February 2011
doi: 10.3389/fncom.2010.00160

Limits to the development of feed-forward structures in large recurrent neuronal networks

Susanne Kunkel[1,2], Markus Diesmann[3,4,5] and Abigail Morrison[1,2,3]*

[1] *Functional Neural Circuits Group, Faculty of Biology, Albert-Ludwig University of Freiburg, Germany*
[2] *Bernstein Center Freiburg, Albert-Ludwig University of Freiburg, Germany*
[3] *RIKEN Brain Science Institute, Wako, Japan*
[4] *Institute of Neuroscience and Medicine (INM-6), Computational and Systems Neuroscience, Research Center Jülich, Germany*
[5] *RIKEN Computational Science Research Program, Wako, Japan*

Edited by:
Per Jesper Sjöström, University College London, UK

Reviewed by:
Brent Doiron, University of Pittsburgh, USA
Sean L. Hill, Ecole Polytechnique Fédérale de Lausanne, Switzerland
Tim P. Vogels, Ecole Polytechnique Fédérale de Lausanne, Switzerland

***Correspondence:**
Abigail Morrison, Bernstein Center Freiburg, Hansastrasse 9a, 79104 Freiburg im Breisgau, Germany.
e-mail: morrison@bcf.uni-freiburg.de

Spike-timing dependent plasticity (STDP) has traditionally been of great interest to theoreticians, as it seems to provide an answer to the question of how the brain can develop functional structure in response to repeated stimuli. However, despite this high level of interest, convincing demonstrations of this capacity in large, initially random networks have not been forthcoming. Such demonstrations as there are typically rely on constraining the problem artificially. Techniques include employing additional pruning mechanisms or STDP rules that enhance symmetry breaking, simulating networks with low connectivity that magnify competition between synapses, or combinations of the above. In this paper, we first review modeling choices that carry particularly high risks of producing non-generalizable results in the context of STDP in recurrent networks. We then develop a theory for the development of feed-forward structure in random networks and conclude that an unstable fixed point in the dynamics prevents the stable propagation of structure in recurrent networks with weight-dependent STDP. We demonstrate that the key predictions of the theory hold in large-scale simulations. The theory provides insight into the reasons why such development does not take place in unconstrained systems and enables us to identify biologically motivated candidate adaptations to the balanced random network model that might enable it.

Keywords: spike-timing dependent plasticity, feed-forward structure, random recurrent network

1 INTRODUCTION

For several decades now it has been commonly assumed that functional structures in the brain develop by strengthening synapses between neurons that fire in a correlated fashion (Hebb, 1949). In particular, feed-forward structures in which neural activity is propagated as a wave from one pool to the next (Abeles, 1991) would seem to be favored by a synaptic plasticity dynamics which strengthens causally correlated connections and weakens acausally correlated connections. This key property of spike-timing dependent plasticity (STDP) was postulated theoretically (Gerstner et al., 1993) before it was observed experimentally on the timescale of 10 ms (Markram and Sakmann, 1995; Markram et al., 1997; Bi and Poo, 1998), although strengthening of causal correlations on the timescale of 100 ms had already been found (Gustafsson et al., 1987).

Such feed-forward structures, also known as synfire chains or braids, have been postulated to underlie experimentally observed precise spike-timing, for example in mammalian cortex (Eckhorn et al., 1988; Gray and Singer, 1989; Abeles et al., 1993; Prut et al., 1998; Ikegaya et al., 2004; Pulvermüller and Shtyrov, 2009) or songbird HVC (Hahnloser et al., 2002; Kozhevnikov and Fee, 2007). The propagation of waves of activity along synfire chains has been shown to be stable under quite general conditions (Diesmann et al., 1999; Gewaltig et al., 2001). Apart from being a natural candidate for the representation of serial activities, such as the sequential activation of muscles to generate a movement, Bienenstock (1995) conjectured that all cortical computation is carried out by the action and interaction of such structures. It has since been shown that co-ordinated activity between synfire chains can realize the phenomenon of compositionality (Hayon et al., 2004).

Given the great degree of interest in feed-forward structures, the experimentally confirmed existence of a plasticity rule that is apparently predestined to generate them, and the growing availability of both tools suitable for large-scale neuronal network simulations (e.g., Morrison et al., 2005; Migliore et al., 2006; Gewaltig and Diesmann, 2007; Pecevski et al., 2009) and the high-performance computers on which to run them, it seems curious that there have been no truly convincing studies demonstrating their development.

It is in the nature of numerical studies that they use simplified models and therefore run the risk of generating artifacts, i.e., behavior that does not occur if a simplified model is replaced with a more realistic one. When investigating STDP in recurrent networks, there are at least two commonly chosen model simplifications that run a high risk of yielding such non-generalizable behavior. So far, all reports of structure development in a recurrent network have been based on network models which represent only a small fraction of the number of synaptic inputs a neuron typically receives (Hertz and Prügel-Bennet, 1996; Levy et al., 2001; Izhikevich et al., 2004; Iglesias et al., 2005; Doursat and Bienenstock, 2006; Jun and Jin, 2007; Masuda and Kori, 2007; Hosaka et al., 2008; Liu and Buonomano, 2009; Fiete et al., 2010). This is a serious issue, as STDP is driven by correlation between pre- and post-synaptic neurons. Scaling down

the network size and increasing the strength of individual synapses increases the correlation between pre- and post-synaptic neurons. This leads to a strong competition effect between the inputs which can result in a very small number of inputs driving the post-synaptic neuron in a non-biological winner-takes-all manner. This is particularly so if, as for the majority of previous studies, an additive model for STDP is assumed, which has a strong symmetry breaking tendency leading to a bimodal distribution of synaptic strengths (Song et al., 2000). However, even very early experimental findings on STDP revealed that the strength of potentiation and depression is dependent on the initial strength of the synapse (Bi and Poo, 1998, but see also Debanne et al., 1996, 1999; Montgomery et al., 2001; Wang et al., 2005). Theoretical studies have revealed that even quite a small dependence on the weight leads to a qualitatively different behavior and a unimodal distribution of synaptic strengths (van Rossum et al., 2000; Rubin et al., 2001; Gütig et al., 2003; see also Morrison et al., 2008) which is more similar to the distributions observed experimentally (Turrigiano et al., 1998; Sjöström et al., 2001; Song et al., 2005). Moreover, weight-dependent "soft-bounded" rules can be more plausibly generated with a kinetic modeling approach than an additive "hard-bounded" rule (Zou and Destexhe, 2007). It is therefore not clear, and should not be assumed, that behavior observed in networks with low numbers of synapses per neuron and/or additive STDP are representative for networks with biologically realistic numbers of synapses and weight-dependent STDP. Indeed, a network exhibiting cortical connectivity levels and using a model for STDP with weight dependence fitted to experimental findings did not develop structure either spontaneously or as a result of repeated synchronous stimuli to a subset of neurons (Morrison et al., 2007).

One reason for this may have been that a critical additional mechanism is required. Many of the above mentioned studies include homeostatic regulating mechanisms such as normalization of weights on the axon and dendrite (Doursat and Bienenstock, 2006; Fiete et al., 2010), pre-synaptic activity dependent weight dynamics to maintain a given post-synaptic rate (Liu and Buonomano, 2009) or axonal pruning of weak synapses once a certain number of very strong synapses have been created (Jun and Jin, 2007). Additionally, STDP has been supplemented with plasticity dynamics on other time scales: Izhikevich et al. (2004) employ both short-term plasticity and slow long-term potentiation, whereas Jun and Jin (2007) implement slow long-term depression and a reversible activation and silencing of synapses. Clearly, some of these mechanisms are more biologically plausible than others and it may well turn out that one or more of them is necessary for the development of structure in networks with realistic connectivity.

In this article, we develop a theory for the recruitment into a structure of neurons in a recurrent network in response to repeated external synchronous input. We show that recruitment is characterized by an unstable fixed point that cannot be stabilized by simply introducing pre- or post-synaptic homeostatic mechanisms such as those proposed in previous studies (Doursat and Bienenstock, 2006; Fiete et al., 2010). We demonstrate that the key predictions of the theory can be reproduced by a large-scale neuronal network model. Finally, we consider what biologically plausible adaptations to the network model could allow the stable propagation of feed-forward structure.

2 MATERIALS AND METHODS

2.1 NETWORK MODEL

Our network model is based on the balanced random network model of Brunel (2000), see **Figure 1A**. The neurons are 80% excitatory and 20% inhibitory and randomly connected; excitatory–excitatory connections are subject to weight-dependent STDP, all other connections are static. The network activity is presumed to be in the asynchronous irregular regime with an average firing rate of ν_r.

A subset E_{stim} of the excitatory population receives feed-forward input from each element of an external group of size N_{SIP}; these connections are also subject to STDP. Each neuron in the external group spikes independently as a Poisson process of rate ν_a and synchronously with the rest of the group as a Poisson process of rate ν_s, thus implementing a single interaction process (SIP, see Kuhn et al., 2003). The total rate of a neuron in the external group is the same as the network firing rate, i.e., $\nu_a + \nu_s = \nu_r$. All neurons in the network receive additional excitatory independent Poisson spike trains; the neurons in the externally stimulated group receive Poisson spike trains at a slightly reduced rate to compensate for their additional external stimulus.

Due to the random connectivity, the number of connections neurons receive from E_{stim} is binomially distributed. For a given connectivity threshold C_{hc}, a high-connectivity group E_{hc} can be located within the excitatory population (not including E_{stim}). Each neuron in E_{hc} receives at least C_{hc} connections from E_{stim}, whereas all other excitatory neurons receive fewer than C_{hc} connections from E_{stim}. This is illustrated in **Figure 1B**. In general, N_{SIP}, N_{stim}, and C_{hc} can all be chosen independently. For a given binomial distribution of connections from E_{stim}, the choice of N_{stim} and C_{hc} completely determines N_{hc}, the number of neurons in the high-connectivity group E_{hc}. As we are investigating the development of feed-forward structures in this article, we are interested in the case that successive groups have similar sizes. We therefore link the independent variables such that $C_{hc} = N_{SIP}$ and require $N_{hc} \approx N_{stim}$. In other words, for a given value of N_{SIP}, we select the size of the externally stimulated population N_{stim} such that the binomial distribution of connections results in $N_{hc} \approx N_{stim}$ neurons that receive at least N_{SIP} connections from E_{stim} and all other excitatory neurons in the network receive fewer than N_{SIP} connections from E_{stim}.

2.2 FIXED POINT ANALYSIS OF STRUCTURAL DEVELOPMENT

If pre- and post-synaptic spike trains are stochastic, the weight updates of a synapse can be described as a random walk. Using Fokker–Planck mean field theory, the drift of the random walk corresponds to the average rate of change of synaptic strength. The drift can be calculated as a function of the correlation of the pre- and post-synaptic spike trains. Assuming stationarity, the raw cross-correlation function of the pre-synaptic spike train $\rho_j = \sum_{t_j^f} \delta(t - t_j^f)$ and the post-synaptic spike train $\rho_i = \sum_{t_i^f} \delta(t - t_i^f)$ with mean firing rates of $\nu_{i/j} = \langle \rho_{i/j} \rangle$ is given by:

$$\Gamma_{ji}(\Delta t) = \langle \rho_j(t) \rho_i(t + \Delta t) \rangle_t$$

This results in the following expression for the mean synaptic drift:

$$\dot{w} = -F_-(w) \int_{-\infty}^{0} d\Delta t K_-(\Delta t) \Gamma_{ji}(\Delta t) + F_+(w) \int_{0}^{\infty} d\Delta t K_+(\Delta t) \Gamma_{ji}(\Delta t) \quad (1)$$

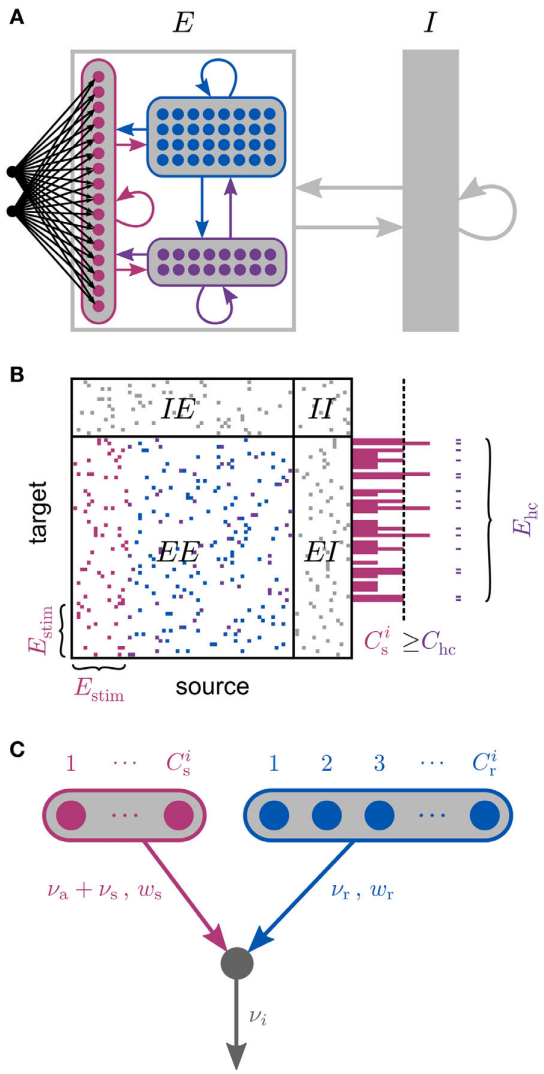

FIGURE 1 | Network and single neuron model. (A) Balanced recurrent network model based on Brunel (2000). A subset of the excitatory population (E_{stim}, pink disks) receives feed-forward input from each member of an external group of size N_{SIP} (black disks). The external group fires synchronously with rate ν_s and asynchronously with rate ν_a. The externally stimulated population E_{stim} makes recurrent connections to the rest of the excitatory population. N_{hc} neurons receive a number of connections from E_{stim} above a given threshold C_{hc} (high-connectivity group, purple disks) whereas all other neurons receive fewer connections from E_{stim} (blue disks). All neurons also receive external excitatory Poisson input (not shown). **(B)** Determination of the high-connectivity group from the connectivity matrix (shown here in diluted form). The subdivisions of the connectivity matrix indicate the source and target populations, e.g., *EI* contains the connections from the inhibitory population *I* to the excitatory population *E*. The entries in row *i* of the connectivity matrix indicate the sources of the synaptic inputs of neuron *i* according to the color scheme in **(A)**. The histogram gives the number of connections C_s^i each neuron receives from E_{stim}. If neuron *i* receives a number of connections from E_{stim} greater than or equal to the arbitrary threshold C_{hc} (vertical dashed line) it is considered a member of the high-connectivity group E_{hc}. **(C)** Simplified input structure of a neuron in a recurrent network: the post-synaptic neuron *i* (gray disk) receives input from C_s^i neurons from E_{stim} (pink disks) that fire asynchronously with rate ν_a and synchronously with rate ν_s and from C_r^i neurons selected from the rest of the network (blue disks) that fire asynchronously with rate ν_r. The mean synaptic weights from these populations are w_s and w_r, respectively.

where $F_{\pm}(w)$ describe the weight-dependent potentiation/depression of a synapse due to a single spike pair and $K_{\pm}(\Delta t) = \exp(-|\Delta t|/\tau_{\pm})$ is the window function of STDP. A more thorough derivation of (1) can be found in Kempter et al. (1999) and Kistler and van Hemmen (2000; but see also Kempter et al., 2001; Rubin et al., 2001; Gütig et al., 2003; Morrison et al., 2008; Gilson et al., 2009a).

To investigate the fixed point behavior of STDP in the context of a large recurrent network in which structure development is being induced by synchronous stimulation of a subset of neurons, we make the following assumptions, abstracted from the network model displayed in **Figure 1A**. Each neuron *i* receives C_s^i excitatory connections from neurons selected from the subset of neurons E_{stim} receiving synchronous stimulation and C_r^i connections from neurons selected from the rest of the network. Synchronous spikes from the stimulated subset occur irregularly and are governed by a Poisson process with a rate of ν_s. Each neuron in the stimulated subset also fires independently as a Poisson process with rate ν_a; the composite activity for a neuron from the stimulated subset is therefore a Poisson process with rate $\nu_a + \nu_s$. The activity of a neuron in the rest of the network can be described as a Poisson process with rate ν_r. The input structure of an excitatory neuron in the recurrent network is illustrated in **Figure 1C**. We further assume that the post-synaptic spike rate is generated by an inhomogeneous Poisson process $\nu_i(u_i) = [\gamma u_i - \nu_0]_+$ with scaling factor γ, threshold ν_0 and membrane potential u_i, where $[\cdot]_+$ denotes a piecewise linear function that is defined as 0 for negative values, i.e., $[x]_+ = (x + |x|)/2$. In the following, we will assume the function is positive and omit the square brackets. The membrane potential is given by $u_i(t) = \sum_j w_{ij} \epsilon(t - t_j^f)$ where w_{ij} is the weight of the synapse between neuron *j* and neuron *i*, and $\epsilon(t)$ describes the time course of the response of the membrane potential to the arrival of an excitatory event, i.e., $w_{ij}\epsilon(t)$ is the post-synaptic potential. Finally, we assume that the dynamics of the system is sufficiently well captured by considering the changes to the mean values of the synapses between the two input populations and the output neuron, $w_r = (\sum_j^{C_r^i} w_{ij})/C_r^i$ and $w_s = (\sum_j^{C_s^i} w_{ij})/C_s^i$. The expected rate of the output neuron is therefore:

$$\nu_i = -\nu_0 + \gamma \nu_r C_r^i \bar{\epsilon} w_r + \gamma (\nu_a + \nu_s) C_s^i \bar{\epsilon} w_s \tag{2}$$

where $w_x \bar{\epsilon} = w_x \int_0^\infty \epsilon(s)\, ds$ is the total area under the respective post-synaptic potential. The conditional firing rate after a spike at t_j^f from a neuron in the unstimulated input population is:

$$\nu_i(t) = -\nu_0 + \gamma \nu_r C_r^i \bar{\epsilon} w_r + \gamma (\nu_a + \nu_s) C_s^i \bar{\epsilon} w_s + \gamma w_r \epsilon(t - t_j^f) \tag{3}$$

Similarly, the conditional firing rate after a spike at t_j^f from a neuron in the population receiving synchronous stimulus is:

$$\nu_i(t) = -\nu_0 + \gamma \nu_r C_r^i \bar{\epsilon} w_r + \gamma (\nu_a + \nu_s) C_s^i \bar{\epsilon} w_s + \gamma \frac{\nu_a + C_s^i \nu_s}{\nu_a + \nu_s} w_s \epsilon(t - t_j^f) \tag{4}$$

Inserting these pre- and post-synaptic spike trains into the expression for the synaptic drift given in (1) results in a coupled system of differential equations for the evolution of the mean weights:

$$\dot{w}_r = \nu_r\left[-F_-(w_r)\tau_- + F_+(w_r)\tau_+\right]\left(-\nu_0 + \gamma\nu_r C_r^i \bar{\epsilon} w_r + \gamma(\nu_a+\nu_s)C_s^i\bar{\epsilon}w_s\right) + F_+(w_r)\nu_r\gamma w_r\bar{K} \quad (5)$$

$$\dot{w}_s = (\nu_a+\nu_s)\left[-F_-(w_s)\tau_- + F_+(w_s)\tau_+\right]\left(-\nu_0 + \gamma\nu_r C_r^i \bar{\epsilon} w_r + \gamma(\nu_a+\nu_s)C_s^i\bar{\epsilon}w_s\right) + F_+(w_s)(\nu_a+C_s^i\nu_s)\gamma w_s\bar{K} \quad (6)$$

where $\bar{K} = \int K_+(s)\,\epsilon(s)\,ds$. The nullclines for w_r and w_s can be found by setting the left hand side of these equations to zero and solving for w_r and w_s respectively. The crossing points of the nullclines (if any) represent the fixed points of the system and can be found numerically.

To do this, appropriate values must be determined for the model parameters. For the numerical simulations in this study (see Section 2.3) we use a current-based integrate-and-fire neuron model with α-shaped post-synaptic currents, i.e., the dynamics of the membrane potential is given by:

$$\dot{V} = -\frac{V}{\tau_m} + \frac{I}{C} \quad (7)$$

where τ_m is the time constant of the membrane potential, C is the membrane capacitance and I is the input current. The time course of a post-synaptic current with peak amplitude w is given by:

$$I(t) = w\cdot\frac{e}{\tau_\alpha}te^{-t/\tau_\alpha} \quad (8)$$

We can therefore calculate the time course of the post-synaptic potential as:

$$\epsilon(t) = \frac{e}{C\tau_\alpha}\left(\frac{e^{-t/\tau_m}-e^{-t/\tau_\alpha}}{(1/\tau_\alpha-1/\tau_m)^2} - \frac{te^{-t/\tau_\alpha}}{(1/\tau_\alpha-1/\tau_m)}\right) \quad (9)$$

and determine the model parameters.

$$\bar{\epsilon} = \int_0^\infty \epsilon(s)ds = \frac{e\tau_m\tau_\alpha}{C} \quad (10)$$

and

$$\bar{K} = \int K_+(s)\epsilon(s)\,ds = \frac{e\tau_m\tau_\alpha\tau_+^3}{C(\tau_m+\tau_+)(\tau_\alpha+\tau_+)^2} \quad (11)$$

in terms of the parameters of the integrate-and-fire neuron model and the STDP update rule.

2.3 NUMERICAL SIMULATIONS

We perform numerical simulations of the network model described in Section 2.1. Our realization of the abstract model consists of 80,000 leaky integrate-and-fire neurons with α-shaped post-synaptic currents. The neurons are 80% excitatory and 20% inhibitory, each receiving 3840 excitatory and 960 inhibitory recurrent connections. Excitatory–excitatory connections are drawn from an initial normal distribution and are subject to weight-dependent power-law STDP (Morrison et al., 2007; Standage et al., 2007).

Each neuron except the externally stimulated group E_{stim} receives an additional independent Poisson spike train equivalent to 1200 excitatory inputs each spiking at ν_x. When no external synchronous stimulation is provided ($N_{stim} = 0$), a choice for the rate of the independent Poisson input to each neuron of ν_x = 14 Hz results in network activity in the asynchronous irregular regime (Brunel, 2000) with an average firing rate of ν_r and a unimodal distribution of the plastic recurrent weights with mean 38.6 pA and SD 3 pA (data not shown). In the absence of homeostasis, ν_r = 9.6 Hz; in the presence of weight normalizing pre-synaptic homeostasis applied every 3 s, ν_r = 9.5 Hz; in the presence of pre- and post-synaptic homeostasis applied alternately every 1.5 s, ν_r = 9.2 Hz.

When external synchronous stimulation is provided ($N_{stim} > 0$), each neuron in E_{stim} receives additional external stimulus at a total rate of ν_r from each of the N_{SIP} neurons in the external group E_{SIP}. Consequently, the total rate of the independent Poisson spike trains received by neurons in E_{stim} is reduced to $1200\cdot\nu_x - N_{SIP}\,\nu_r$ to compensate for the additional external stimulus. We draw the initial weights of the recurrent plastic synapses in the stimulated network from a normal distribution with the same mean and SD as the equilibrium weight distribution of the unstimulated network. The initial weights of the connections from the external group E_{SIP} to the stimulated group E_{stim} are set to the mean of the equilibrium weight distribution of the unstimulated network.

During an initial equilibration period of 100 s the external group E_{SIP} generates independent Poisson spike trains at rate $\nu_a = \nu_r$ with no synchronous events, i.e., ν_s = 0 Hz. After this period, the external group E_{SIP} provides partially synchronous stimulus to the stimulated group E_{stim} with a synchronous rate of ν_s = 3 Hz and an asynchronous rate of $\nu_a = \nu_r - \nu_s$.

We perform simulations with different values for the size N_{SIP} of the external group. The threshold C_{hc} for membership of the high-connectivity group E_{hc} is set equal to N_{SIP}. For each value of N_{SIP}, we examine the connectivity of the network to determine empirically the value of N_{stim} that results in a high-connectivity group of approximately equal size, i.e., $N_{hc} \approx N_{stim}$.

Following the standards suggested by Nordlie et al. (2009), the network model details are provided in tabular form in **Table 1**. **Table 2** contains the values for the parameters used in the network simulations.

The network simulations were carried out with a computation time step of 0.1 ms on the Stallo Linux cluster (Notur, UiT) and the JUGENE BlueGene/P supercomputer using the simulation software NEST (Gewaltig and Diesmann, 2007) at revision 8611. Simulation scripts are available from the authors on request.

2.4 DATA ANALYSIS

Spike times are recorded from the stimulated group, the high-connectivity group, and from 500 neurons randomly chosen from the excitatory population (random group). The times of the synchronous spikes of the external group are also recorded. Weights of all outgoing connections were recorded in intervals of 3 s from the external group, the stimulated group, the high-connectivity group and the random group.

The development of the mean weights shown in **Figure 5** is determined from the outgoing weights of the external group and the weights of the connections from the stimulated group to the

Table 1 | Tabular description of network model after Nordlie et al. (2009).

A: MODEL SUMMARY			
Populations	Three: excitatory, inhibitory, SIP external input		
Connectivity	Random convergent connections and feed-forward connections from the SIP external input to the stimulated group		
Neuron model	Leaky integrate-and-fire, fixed voltage threshold, fixed absolute refractory time (voltage clamp), α-currents		
Synaptic plasticity	Spike-timing dependent plasticity at the EE recurrent connections and feed-forward connections		
Input	Independent fixed-rate Poisson spike trains to all neurons		
Measurements	Spike activity, synaptic weights		
B: POPULATIONS			
Name	**Elements**	**Size**	
E	Iaf neuron	$N_E = 4N_I$	
I	Iaf neuron	N_I	
E_{stim}	Iaf neuron	first N_{stim} taken from E	
E_{SIP}	Parrot neuron	N_{SIP}	
C: CONNECTIVITY			
Name	**Source**	**Target**	**Pattern**
EE	E	E	Random convergent, $C_E \to 1$, weight variable, delay d
IE	E	I	Random convergent, $C_E \to 1$, weight J, delay d
EI	I	E	Random convergent, $C_I \to 1$, weight $-gJ$, delay d
II	I	I	Random convergent, $C_I \to 1$, weight $-gJ$, delay d
FF	E_{SIP}	E_{stim}	Convergent, $N_{SIP} \to 1$, weight variable, delay d
D: NEURON MODELS			
Name	Iaf neuron		
Type	Leaky integrate-and-fire, α-current input		
Subthreshold dynamics	if $(t > t^* + t_{ref})$ $\dot{V} = -\frac{V}{\tau_m} + \frac{I(t)}{C_m}$ else $V(t) = V_{reset}$ $I_\alpha(t) = w \frac{e}{\tau_\alpha} t\, e^{-t/\tau_\alpha}$		
Spiking	If $V(t-) < \Theta$ and $V(t+) \geq \Theta$ 1. Set $t^* = t$ 2. Emit spike with time stamp t^*		
Name	Parrot neuron		
Type	Repeater for creating a superposition of spike trains from multiple sources		
Spiking	Spikes whenever it receives a spike		
E: SYNAPSE MODEL			
Name	Power-law STDP (Morrison et al., 2007)		
Type	Weight-dependent STDP with a power-law update rule for potentiation and a multiplicative update rule for depression		
Spike pairing scheme	All-to-all (for nomenclature see Morrison et al., 2008)		
Pair-based update rule	$\Delta w_+ = F_+(w) e^{-\lvert\Delta t\rvert/\tau_+}$ if $\Delta t > 0$ $\Delta w_- = F_-(w) e^{-\lvert\Delta t\rvert/\tau_-}$ else Δt : temporal difference between post- and pre-synaptic spikes, synaptic delay considered to be 50% axonal		
Weight dependence	$F_+(w) = \lambda w_0^{1-\mu} w^\mu$, $F_-(w) = \lambda \alpha w$		
F: INPUT			
Type	**Target**	**Description**	
Poisson generator	I and E except E_{stim}	Independent for each neuron, rate $\nu_x \cdot C_x$, weight J	
Poisson generator	E_{stim}	Independent for each neuron, rate $\nu_x \cdot C_x - N_{SIP} \cdot \nu_r$, weight J	
Poisson generator	E_{SIP}	Identical for each neuron, rate ν_s, weight 1	
Poisson generator	E_{SIP}	Independent for each neuron, rate ν_a, weight 1	
G: MEASUREMENTS			
Spikes and outgoing synaptic weights (recorded every 3 s) from E_{SIP}, E_{stim}, high-connectivity group E_{hc}, and 500 randomly selected excitatory neurons			

high-connectivity group. The weight distributions in **Figures 6D,H** are histograms (bin size 1 pA) of the weights of the connections between the specific neuronal groups recorded at 25 min.

To create the histograms in **Figures 6A,C,E,G** we record the number of spikes in each group in each 1 ms time bin within the 10 ms directly after a synchronous event over a period of 10 s and

Table 2 | Simulation parameters.

Name	Value	Description
POPULATIONS		
N_E	64,000	Size of excitatory population E
N_I	16,000	Size of inhibitory population I
N_{stim}	Varied	Size of externally stimulated excitatory sub-population E_{stim}
N_{SIP}	Varied	Size of external group E_{SIP}
CONNECTIVITY		
C_E	3840	Number of incoming connections from E
C_I	960	Number of incoming connections from I
g	5	Scales weight of inhibitory connections with respect to J
J	38.5 pA	Weight of static excitatory connections
d	1.5 ms	Synaptic transmission delay
NEURON MODEL		
τ_m	10 ms	Membrane time constant
C_m	250 pF	Membrane capacitance
Θ	20 mV	Fixed firing threshold
V_0	0 mV	Resting potential
V_{reset}	V_0	Reset potential
τ_{ref}	0.5 ms	Absolute refractory period
τ_α	0.3258 ms	Rise time of PSC
μ_V	5.7 mV	Mean value of initial normal distribution of membrane potentials
σ_V	7.2 mV	SD of initial normal distribution of membrane potentials
SYNAPSE MODEL		
τ_+	15 ms	Time constant of potentiation window
τ_-	30 ms	Time constant of depression window
λ	0.1	Learning rate
μ	0.4	Weight-dependence parameter of potentiation
α	0.057	Asymmetry parameter
w_0	1 pA	Normalization parameter
μ_w	38.58 pA	Mean value of initial normal distribution of synaptic weights
σ_w	3 pA	SD of initial normal distribution of synaptic weights
INPUT		
C_x	1200	Number of external inputs
ν_x	14 Hz	External rate
ν_r	9.6 Hz	Total firing rate of E_{SIP}
ν_s	3 Hz	Rate of synchronous spike trains from E_{SIP}
ν_a	ν_r–ν_s	Rate of asynchronous spike trains from E_{SIP}

normalize by the number of neurons and the number of synchronous input events. **Figures 6B,F and 7A–D** show the development of the peri-stimulus spiking activity of the specific neuronal groups, which is the number of spikes within the 10 ms before (control) and within the 10 ms after each synchronous input event. Data is normalized with respect to the number of neurons in a group and the number of synchronous input events within successive periods of 10 s.

The scatter plots in **Figure 7E** are generated by recording the time-to-first-spike following each synchronous event in a 1 min period for all excitatory neurons in the network. Each marker in the plot shows the mean and SD of the response times for a specific neuron; the color of the markers indicates the likelihood of the neuron to respond to a synchronous stimulus within 10 ms.

3 RESULTS

3.1 FIXED POINT ANALYSIS OF WEIGHT DYNAMICS

To investigate the dynamics of STDP in a recurrent network undergoing synchronous stimulation, we select the update rule proposed by van Rossum et al. (2000), which is additive for potentiation ($F_+(w) = \lambda$) and multiplicative for depression ($F_-(w) = \alpha\lambda w$). This rule is a good fit to the experimental data on the dependence of the magnitude of synaptic strength change on the initial synaptic strength (Bi and Poo, 1998). Furthermore, this choice has the advantage that the rule exhibits the same qualitative behavior as other weight-dependent rules (see Morrison et al., 2008), yet is more tractable than many other weight-dependent rules such as the partially multiplicative model proposed by Gütig et al. (2003) or the power-law formulation (Morrison et al., 2007; Standage et al., 2007).

Inserting $F_\pm(w)$ into the equation system for the synaptic drifts given in (5) and (6) and setting the left hand sides to zero results in the following quadratic expressions for the nullclines of w_r and w_s:

$$0 = w_r^2 - \left[\frac{\alpha\tau_-\nu_0 + \tau_+\gamma\nu_r C_r^i\bar{\epsilon} + \gamma\bar{K}}{\alpha\tau_-\gamma\nu_r C_r^i\bar{\epsilon}} - \frac{(\nu_a+\nu_s)C_s^i w_s}{\nu_r C_r^i}\right] w_r + \frac{\tau_+\nu_0}{\alpha\tau_-\gamma\nu_r C_r^i\bar{\epsilon}} - \frac{\tau_+(\nu_a+\nu_s)C_s^i w_s}{\alpha\tau_-\nu_r C_r^i} \quad (12)$$

$$0 = w_s^2 - \left[\frac{\alpha\tau_-\nu_0 + \tau_+\gamma(\nu_a+\nu_s)C_s^i\bar{\epsilon} + \left(\frac{\nu_a + C_s^i\nu_s}{\nu_a+\nu_s}\right)\gamma\bar{K}}{\alpha\tau_-\gamma(\nu_a+\nu_s)C_s^i\bar{\epsilon}} - \frac{\nu_r C_r^i w_r}{(\nu_a+\nu_s)C_s^i}\right] w_s + \frac{\tau_+\nu_0}{\alpha\tau_-\gamma(\nu_a+\nu_s)C_s^i\bar{\epsilon}} - \frac{\tau_+\nu_r C_r^i w_r}{\alpha\tau_-(\nu_a+\nu_s)C_s^i} \quad (13)$$

The nullclines can be determined analytically; the crossing of the nullclines can be found numerically. To this end we assume input to the neuron analogous to that received by a neuron in the recurrent network simulation described in Section 2.3. The rate of the asynchronous background population is $\nu_r = 9.6$ Hz, and the asynchronous and synchronous rates of the SIP input are $\nu_a = 6.6$ Hz and $\nu_s = 3$ Hz. The total number of incoming recurrent excitatory synapses is $C = C_r^i + C_s^i = 3840$. We set STDP parameters $\alpha = 0.0132$ pA^{-1}, $\lambda = 0.03$ pA, $\tau_+ = 15$ ms and $\tau_- = 30$ ms and neuronal parameters $\gamma = 3.66 \times 10^3(Vs)^{-1}$ and $\nu_0 = 176.1$ Hz. In the absence of synchronous stimulation ($C_s^i = 0$), this choice of synaptic and neuronal parameters results in a self-consistent output rate $\nu_i = \nu_r$ and a stable fixed point $w_r^* = 38.6$ pA, thus reproducing the corresponding values of the unstimulated network simulation. The parameters $\bar{\epsilon}$ and $\bar{K}$ are calculated from the neuronal and STDP parameters as described in Section 2.2. The nullclines for $C_s^i = 80$

are illustrated in **Figure 2A**. Note that as $C_s^i \ll C_r^i$, the nullcline for w_s is much more sensitive to the value of w_r than vice versa. The value of $\dot{w}_s$ is negative for values of w_s above the w_s-nullcline and positive for values of w_s below it. Similarly, $\dot{w}_r$ is positive for values of w_r to the left of the w_r-nullcline and negative for values to the right of it. Consequently, the fixed point indicated by the intersection of the nullclines is a stable attractor. **Figure 2B** shows the location of the fixed point as a function of the number of synchronous inputs C_s^i. Again, w_s is the more sensitive variable.

We can now exploit our knowledge of the network connectivity to determine the distribution of C_s^i and thus the distribution of fixed points. Each neuron receives C_E connections drawn randomly from the N_E excitatory neurons in the network, so the number of connections drawn from the E_{stim} population receiving synchronous stimulus is distributed binomially; the number of trials is C_E and the probability of success in an individual trial is $p = N_{stim}/N_E$, where N_{stim} is the number of neurons in E_{stim}. Multiplying the probability of drawing C_s connections $P_p(C_s, C_E)$ with the number of excitatory neurons N_E gives the expected number of neurons in the network that have C_s connections from E_{stim}. Let us now consider an idealized network model in which the number of neurons with C_s connections from E_{stim} is indeed $\lfloor N_E \cdot P_p(C_s, C_E) \rfloor$ and assign each neuron a connectivity rank R^i, where $R^j < R^k$ entails $C_s^j \geq C_s^k$. **Figure 3A** shows the equilibrium average strength of the synapses from the stimulated neurons w_s^* as a function of the size of the stimulated group N_{stim} and the connectivity rank of the post-synaptic neuron in the idealized network. Only the neurons with the highest connectivity are displayed ($R^i \leq 1000$), as these are the neurons that will most

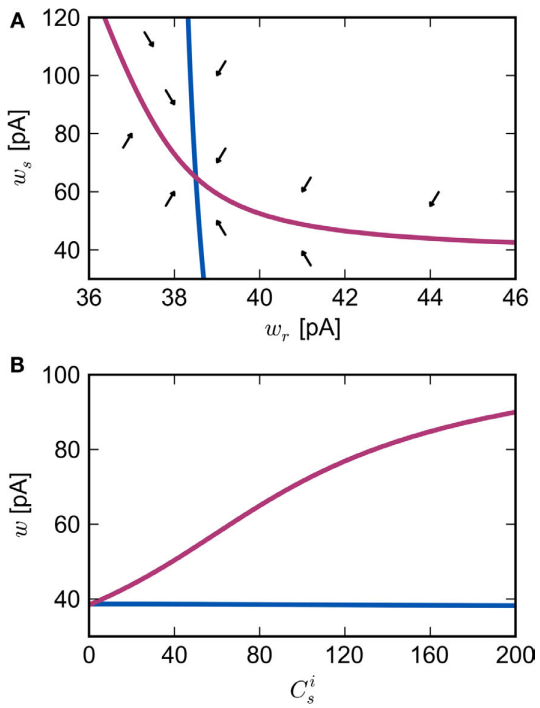

FIGURE 2 | Fixed point of the synaptic drift equations. (A) Nullcline for w_s as a function of w_r (red curve) and for w_r as a function of w_s (blue curve) for $C_s^i = 80$. The crossing point of the nullclines determines the fixed point (w_r^*, w_s^*) of the coupled equations. Arrows show the sign of the derivatives of w_r and w_s; arrows pointing up (down) indicate $\dot{w}_s > 0$ ($\dot{w}_s < 0$), arrows pointing right (left) indicate $\dot{w}_r > 0$ ($\dot{w}_r < 0$), for the values of w_r and w_s at the base of the arrows. **(B)** Location of fixed point (w_r^*; blue, w_s^*; red) as a function of the number of synchronous inputs C_s^i.

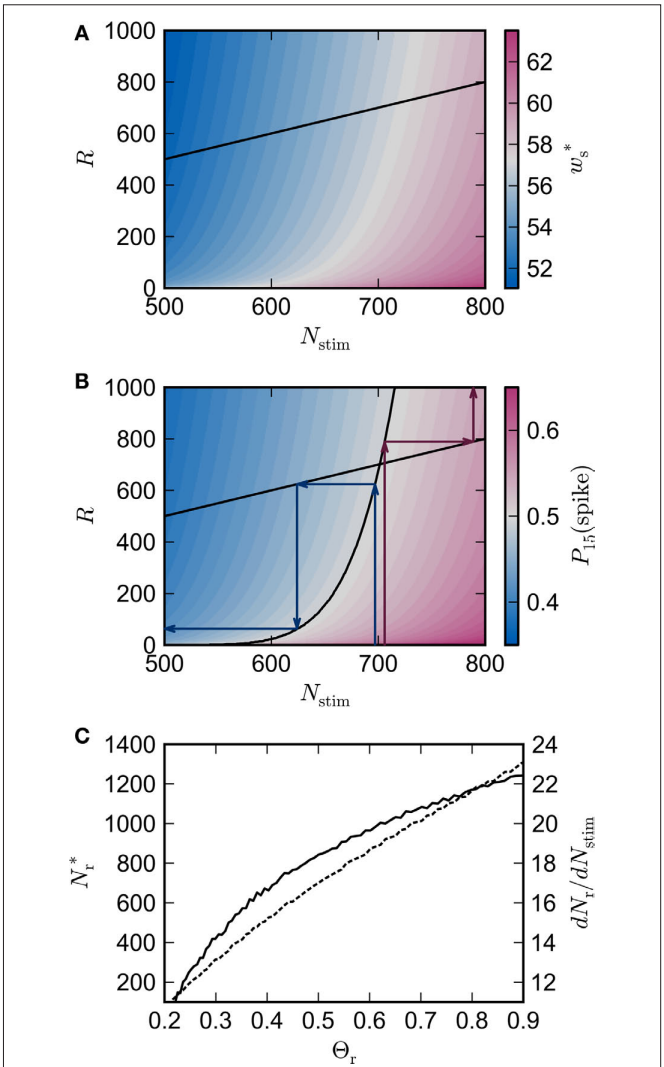

FIGURE 3 | Distribution of fixed points and likelihood of responding to synchronous stimulus. (A) Average strength of synapse from the stimulated group w_s^* as a function of the size of the stimulated group (horizontal axis) and the connectivity rank of the post-synaptic neuron (vertical axis). The black line indicates the group of highest connectivity equal in size to the stimulated group ($R = N_{stim}$). **(B)** Expected number of spikes emitted by the post-synaptic neuron in the 15 ms following a synchronous spike in the stimulated group; axes and black line as in **(A)**; the black curve indicates the number of neurons which respond to a synchronous event with a spike with probability greater than or equal to the recruitment threshold $\Theta_r = 0.5$. The black line and curve represent a return map for the development of feed-forward structure in a network with an unstable fixed point at $N_{stim} = 701$. The blue arrows show two iterations of the return map for an initial stimulated population of size $N_{stim} = 697$; the pink arrows show one iteration for $N_{stim} = 706$. **(C)** Location and nature of the fixed point as functions of the recruitment threshold Θ_r. Dashed curve: fixed point N_r^*, solid curve: slope of the tangent to the N_r (N_{stim}) curve at N_r^*.

easily be recruited into a structure. However, **Figure 3A** suggests that this is unlikely to occur, as w_s^* increases slowly with decreasing R, i.e., neurons which receive similar numbers of connections from the stimulated group will tend to develop similar synaptic strengths. Consequently, there will be no development of clearly defined groups that respond in a qualitatively different fashion to a synchronous event in the stimulated group. The increase of w_s^* with increasing N_{stim} is more rapid; small variations in the size of a synchronously firing group can have a large effect on the outgoing weight distribution.

This insight can be further clarified by calculating the number of spikes a post-synaptic neuron is expected to produce within a given time t after a synchronous event in the stimulated input group. This can be found by integrating the conditional firing rate:

$$\begin{aligned}\left\langle n_{sp}\right\rangle_0^t &= \int_0^t \nu_i(t')dt' = \nu_i t + \gamma C_s^i w_s \int_0^t \epsilon(t')dt' \\ &= \left[-\nu_0 + \gamma\nu_r C_r^i \bar{\epsilon} w_r + \gamma(\nu_a+\nu_s)C_s^i\bar{\epsilon}w_s\right]t \\ &\quad + \gamma C_s^i w_s \frac{e}{C\tau_\alpha}\int_0^t \frac{e^{-t'/\tau_m}-e^{-t'/\tau_\alpha}}{(1/\tau_\alpha - 1/\tau_m)^2} - \frac{t'e - t'/\tau_\alpha}{(1/\tau_\alpha - 1/\tau_m)}dt' \\ &= \left[-\nu_0 + \gamma\nu_r C_r^i \bar{\epsilon} w_r + \gamma(\nu_a+\nu_s)C_s^i\bar{\epsilon}w_s\right]t \\ &\quad + \gamma C_s^i w_s \frac{e}{C\tau_\alpha}\left[\frac{\tau_\alpha\left(e^{-t/\tau_\alpha}-1\right)-\tau_m\left(e^{-t/\tau_m}-1\right)}{(1/\tau_\alpha - 1/\tau_m)^2}\right. \\ &\quad \left. + \frac{\left(\tau_\alpha t + \tau_\alpha^2\right)e^{-t/\tau_\alpha} - \tau_\alpha^2}{(1/\tau_\alpha - 1/\tau_m)}\right]\end{aligned} \tag{14}$$

Figure 3B shows the number of spikes expected within 15 ms after a synchronous event for every fixed point calculated in **Figure 3A**. To determine the development of functional structure, we introduce a recruitment threshold Θ_r. All neurons that have a probability of responding to a synchronous event in E_{stim} of at least Θ_r are considered to have been recruited into the structure, neurons for which P_{15} (spike) $< \Theta_r$ are considered to be outside the structure. The black curve indicates the number of neurons recruited N_r as a function of the size of the stimulated group N_{stim} for an arbitrary choice of recruitment threshold $\Theta_r = 0.5$, i.e., for a choice of N_{stim}, the height of the black curve gives the number of neurons that are recruited by this stimulus such that each neuron has at least a 50% probability of firing immediately after a synchronous event in E_{stim}.

The black diagonal line indicates a connectivity rank equal to the size of the stimulated group, i.e., the N_{stim} neurons in the network that receive the most input from the synchronously stimulated group. The two lines represent an approximation of a return map for groups of synchronously firing neurons: the curve indicates $N_r(N_{stim})$ and the diagonal indicates N_{stim}, therefore their intersection reveals the fixed point at which the number of neurons recruited is equal to the number of neurons stimulated, $N_r^* = N_{stim}$. If the fixed point were stable, the N_r^* recruited neurons would recruit another group of N_r^* neurons, which would in turn recruit another such group, thus stably propagating structure through the network. However, the fixed point is unstable, since the slope of the $N_r(N_{stim})$ curve is positive at the intersection. If N_{stim} is initially below the crossing point, the number of neurons recruited is smaller than N_{stim}. These neurons will in turn recruit even fewer neurons, and so the structure will decay to nothing within a few iterations. Conversely, if the number of stimulated neurons is larger than the crossing point, the number of neurons recruited will be greater than N_{stim}. These neurons will in turn recruit an even greater number of neurons, until the entire network is recruited within a few iterations. This is illustrated by the map iterations shown as arrows in **Figure 3B**. Note that the iterations are approximative, as the composition of pre- and post-synaptic rates is in general not constant over iterations.

Figure 3C shows the dependence of the fixed point on the choice of the recruitment threshold Θ_r. As the requirement on the reliability of spiking following a synchronous event increases, the fixed point shifts to greater values of N_{stim}. The slope of the tangent of the $N_r(N_{stim})$ curve is positive across the whole range of Θ_r, demonstrating that the fixed point is always unstable.

The main factors influencing the shape of **Figure 3** are the random wiring of the network and the smooth change of the fixed point of the weight distribution (w_r^*, w_s^*) with increasing number of synchronous connections (**Figure 2B**). The number of connections a neuron receives from a given group is binomially distributed. This causes a "fan-out" structure – if we can find a group of neurons which receives at least k inputs from a synchronously active group, we can also find an even larger group which receives slightly fewer than k connections. Due to the smooth change of the fixed point of the weight distribution with k, the equilibrium weight distribution and thus the equilibrium response to a synchronous event of a neuron receiving $k-1$ or $k-2$ synchronous connections is very similar to the equilibrium distribution and response of a neuron receiving k connections.

It is therefore worthwhile to determine to what extent the smooth shift of the weight distribution shown in **Figure 2B** is robust to parameter changes. **Figure 4A** shows the development of fixed points as a function of the number of synchronous connections for four different scenarios. In the top left panel we consider the case of lower input rates: $\nu_r = 5$ Hz, $\nu_a = 3.5$ Hz and $\nu_s = 1.5$ Hz, corresponding to a lower recurrent network rate and a lower synchronous stimulus rate. We set $\nu_0 = 190$ Hz and $\gamma = 7.02 \times 10^3\,(\mathrm{Vs})^{-1}$, which corresponds to a reduced external Poisson rate and results in a self-consistent rate $\nu_i = \nu_r$ when there is no synchronous stimulus ($C_s^i = 0$). The top right panel reproduces the standard input scenario ($\nu_r = 9.6$ Hz, $\nu_0 = 175$ Hz) except the rate of synchronous events is a greater proportion of the total rate of the synchronous population: $\nu_a = 2.6$ Hz and $\nu_s = 7$ Hz. The bottom left panel reproduces the standard input scenario ($\nu_r = 9.6$ Hz, $\nu_a = 6.6$ Hz, $\nu_s = 3$ Hz, $\nu_0 = 175$ Hz) for the multiplicative STDP model introduced by Rubin et al. (2001): $F_+(w) = \lambda(W_{max} - w)$ and $F_-(w) = \alpha\lambda w$. The synaptic parameters are chosen as for the additive/multiplicative model of van Rossum et al. (2000) investigated above, but with $\alpha = 2.13$ and $W_{max} = 200$ pA. Finally, the bottom right panel shows the results for the standard input scenario in combination with the power-law STDP developed in Morrison et al. (2007) and investigated numerically in Section 3.2: $F_+(w) = \lambda w_0^{1-\mu} w^\mu$ and $F_-(w) = \lambda\alpha w$. Synaptic parameters are set as above, but with $\alpha = 0.057$, $w_0 = 1$ pA and $\mu = 0.4$. In this example, the nullclines cannot be calculated analytically. For both the alternative STDP models investigated, the deviating parameters are chosen to give the same results

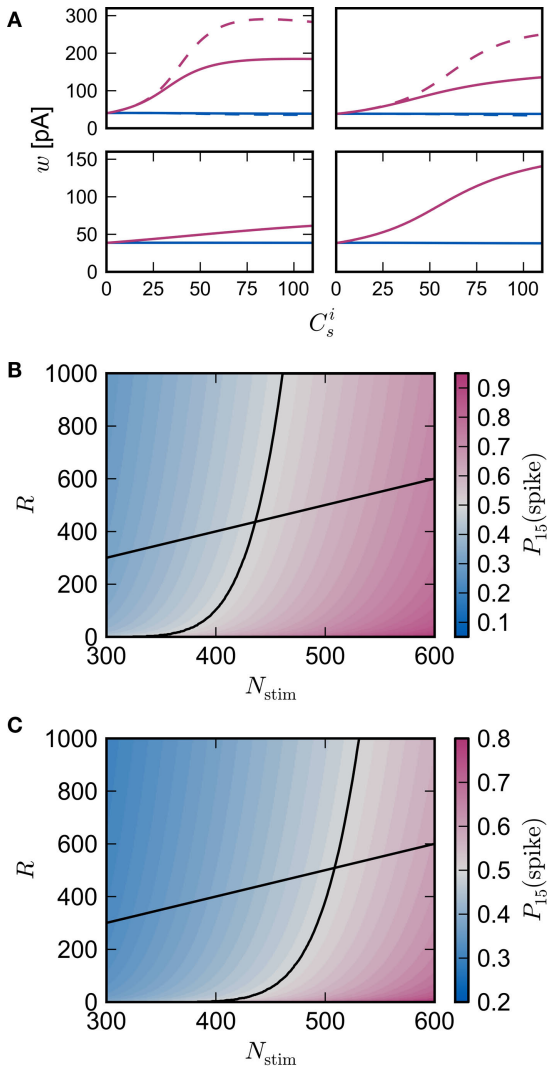

FIGURE 4 | Robustness of results with respect to input rate, STDP model and post-synaptic homeostasis. (A) Location of fixed point (w_r^*; blue, w_s^*; red) as a function of the number of synchronous inputs C_s^i for different scenarios, see text for details. Top left: low recurrent and external rates (solid curves) with additional homeostatic regulation of the post-synaptic rate (dashed curves). Top right: high synchronous rate (solid curves) with additional homeostatic regulation of the incoming synaptic weights of the post-synaptic neuron. Bottom left: standard input rates and multiplicative STDP model. Bottom right: standard input rates and power-law STDP model. **(B)** Expected number of spikes emitted by the post-synaptic neuron in the 15 ms following a synchronous spike in the stimulated group in the low rate scenario; axes and black curves as in **Figure 3**. **(C)** As in **(B)** for the standard input rate scenario with the power-law STDP model.

for the standard input scenario with no synchronous input ($C_s^i = 0$) as the additive/multiplicative model of van Rossum et al. (2000) investigated above: a self-consistent rate ($\nu_i = \nu_r$) and a stable fixed point $w_r^* = 38.6$ pA.

It has previously been suggested that homeostatic regulatory mechanisms are crucial for the development of structure (Doursat and Bienenstock, 2006; Liu and Buonomano, 2009; Fiete et al., 2010). The equation system for the synaptic drifts given in (5) and (6) can easily be extended to incorporate post-synaptic homeostatic mechanisms. A term $-\lambda_\nu(\nu_i - \nu_h)$ acts to increase the synaptic weights if the rate of the post-synaptic neuron is less than a desired rate ν_h and to decrease them if the post-synaptic rate exceeds ν_h. A natural choice for ν_h is the self-consistent rate of the unstimulated network, ν_r. Similarly, a homeostatic mechanism to conserve the sum of a neuron's incoming synaptic weights can be modeled by an additional term $-\lambda_w(w_r C_r^i/C + w_s C_s^i/C - w_h)$, where $C = C_r^i + C_s^i$ is the total number of incoming synapses and w_h is a desired mean synaptic weight. A natural choice for w_h is the fixed point of the one-dimensional system in the case that the neuron receives no synchronous input ($C_s^i = 0$). For both models of post-synaptic homeostasis, the expressions for the nullclines of w_r and w_s given in (12) and (13) acquire additional contributions to the linear and constant coefficients but maintain their quadratic form. In **Figure 4A**, the development of the fixed point assuming post-synaptic rate homeostasis is shown for the low rate scenario with $\lambda_\nu = 3 \times 10^{-4}$ pA. Similarly, the fixed point development assuming post-synaptic weight homeostasis is shown for the high synchronous rate scenario with $\lambda_w = 5 \times 10^{-6}\ s^{-1}$. In both cases, the presence of post-synaptic homeostasis causes a greater separation to develop between the mean weights of the unsynchronized inputs and the synchronized inputs.

In all scenarios, a smooth shift of the fixed point of the weight distribution (w_r^*, w_s^*) with increasing number of synchronous connections can be observed. When combined with the assumption of random connectivity, all scenarios result in a qualitatively similar return map to that shown in **Figure 3** with an unstable fixed point. This is demonstrated in **Figures 4B,C** with a recruitment threshold of $\Theta_r = 0.5$ for the low rate scenario (without homeostasis) and the power-law STDP scenario, respectively. As the theoretical model is developed from the point of view of the post-synaptic neuron, it is not easily extensible to account for pre-synaptic homeostatic mechanisms such as the normalization of outgoing weights. However, due to the similarity in behavior between neurons with similar numbers of synchronous inputs, implementing a pre-synaptic mechanism to regulate the total strength of outgoing synapses will not result in symmetry breaking for some specific value of C_s^i. These results lead us to conclude that stable development of structure as a response to synchronous stimulation cannot occur in randomly connected networks incorporating weight-dependent STDP without additional network, cellular or sub-cellular assumptions.

3.2 SIMULATION RESULTS

To check the predictions of the theoretical model we simulate a large-scale neuronal network with biologically realistic numbers of incoming synapses per neuron and weight-dependent STDP, see Section 2.3 for details. An excitatory sub-population of the network E_{stim} of size N_{stim} is stimulated by an external group E_{SIP} of size N_{SIP} in which the neurons fire mostly independently but with synchronous events at 3 Hz. **Figure 5** shows the development of the mean synaptic weight between the external synchronous group and the stimulated group (top panel) and between the stimulated group and the high-connectivity group (bottom panel) for different sizes of the external group N_{SIP}. The size of the stimulated group N_{stim} is chosen such that a high-connectivity group E_{hc} can be found of similar size ($N_{hc} \approx N_{stim}$) where each neuron in the high-connectivity

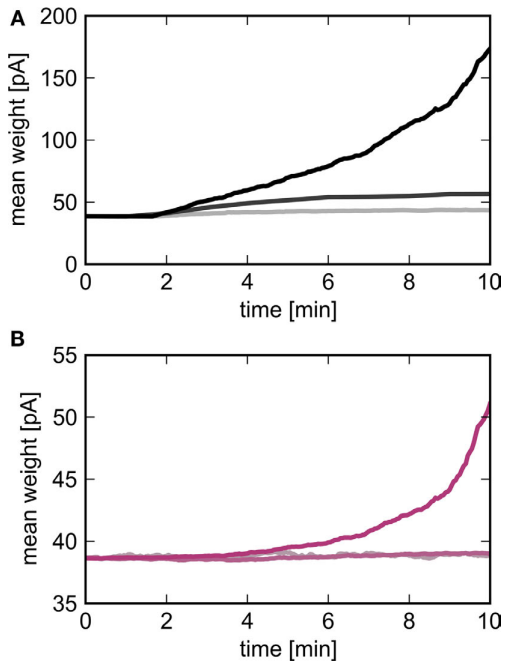

FIGURE 5 | Evolution of the mean synaptic weights as a function of the size of the external group N_{SIP}. Light to dark curves correspond to N_{SIP} = 10, 20, 30 resulting in a size for the stimulated group N_{stim} = 46, 164, 295 respectively. **(A)** Mean weight of synapses between the external group E_{SIP} and the stimulated group E_{stim} as a function of time. **(B)** Mean weight of synapses between the stimulated group and the high-connectivity group receiving at least N_{SIP} connections from it (N_{hc} = 44, 158, 291).

group receives at least N_{SIP} connections from the stimulated group whereas all other excitatory neurons in the network receive fewer than N_{SIP} connections from the stimulated group. For low values of N_{SIP}, the mean synaptic weight between E_{SIP} and E_{stim} saturates within 10 min. As predicted by the theoretical model derived above, the downstream effect is much weaker; little change can be seen in the mean synaptic weight between E_{stim} and E_{hc}, even though each neuron in the E_{hc} receives at least as many inputs from E_{stim} as each neuron in E_{stim} receives from E_{SIP}. For higher values of N_{SIP}, the network is still evolving at 10 min, but the substantially greater effect on the mean synaptic weights between E_{SIP} and E_{stim}, and between E_{stim} and E_{hc} can be clearly seen.

The rapid change in network behavior as the number of synchronous inputs increases can be seen in **Figure 6**, see Section 2.4 for the data analysis details. In the upper panel, N_{SIP} = 20 and N_{stim} = 164. Each neuron in the stimulated group E_{stim} receives input from each of the 20 neurons in the external stimulating group E_{SIP}. Each neuron in the corresponding high-connectivity group E_{hc} of a similar size (N_{hc} = 158) receives at least 20 synaptic inputs from E_{stim}. All other excitatory neurons in the network receive 19 or fewer synaptic inputs from E_{stim} and on average 10. The probability that neurons in the stimulated group fire in response (i.e., within 10 ms) to a synchronous stimulation event increases slightly in the first 10 min and then saturates. The probability that neurons in E_{hc} fire in response to a synchronous stimulation event mediated by E_{stim} remains at base level (i.e., determined by the network firing rate of ≈10 Hz) throughout the simulation. The weight distributions between all groups are very similar (see **Figure 6D**).

In the lower panel, N_{SIP} = 25, N_{stim} = 228 and N_{hc} = 228. Each neuron in E_{hc} receives 25 or more synaptic inputs from E_{stim}, whereas all other excitatory neurons in the network receive 24 or fewer inputs from E_{stim} and on average 14. The probability that neurons in E_{stim} fire in response to a synchronous stimulation event increases steadily over the course of the simulation until almost all neurons are firing in response to every synchronous event. The probability that neurons in E_{hc} fire in response to a synchronous stimulation event, mediated by E_{stim}, remains at approximately base level for the first 20 min. Between 20 and 25 min, the probability of response increases sharply. However, the probability that neurons randomly selected from the rest of the network fire in response to a synchronous stimulation event also increases sharply during this period. This is reflected in the weight distributions. The middle panel of **Figure 6H** shows the distribution of incoming synaptic weights to the high-connectivity group E_{hc}. The mean of the distribution of weights between E_{stim} and E_{hc} shifts to a higher value than that between randomly selected neurons and E_{hc}, as seen in **Figure 2B**. However, the same is true to a lesser extent for the distributions of the incoming weights to the random group (bottom panel of **Figure 6H**). Note that the mean of the distribution of the incoming synaptic weights to the stimulated group from the rest of the network has shifted to a lower value (top panel of **Figure 6H**) due to the acausal correlation between activity in the network and activity in the stimulated group. If the synapses from E_{SIP} to E_{stim} are clipped to an upper bound, this drift eventually leads to a decoupling of the stimulated group, as was reported in Morrison et al. (2007). However, the insight that STDP reduces the strength of recurrent connections was originally described by Abbott and Nelson (2000), and more recently proved for polysynaptic loops of arbitrary length by Kozloski and Cecchi (2010).

Between 27 and 28 min the increasing response of the network to synchronous events causes it to enter a pathological state in which some neurons are firing very rapidly all the time and some are almost silent. The theoretical model developed in Section 3.1 does not predict the occurrence or the characteristics of the pathological state, as it does not take into account the interactions between neurons in the network, only the interactions between a synchronously firing group and its post-synaptic targets.

To test the conclusion that the introduction of homeostatic mechanisms do not alter the nature of the fixed point, we repeat the above experiments with pre-synaptic homeostasis. Every 3 s the outgoing synapses of every excitatory neuron in the recurrent network are adjusted by a multiplicative factor such that the total sum of its plastic synapses is reset. Similarly to the results obtained without homeostasis, synchronous stimulation from a group of N_{SIP} = 20 external neurons is neither enough to produce a reliable response of the stimulated group (N_{stim} = 164) nor any substantial changes in the high-connectivity group (N_{hc} = 158), whereas a slightly stronger stimulus (N_{SIP} = 25, N_{stim} = 228, N_{hc} = 228) causes a network to enter a pathological state (see **Figures 7A,B**). The transition occurs much later, at around 90 min rather than 28 min in the absence of homeostasis, demonstrating the stabilizing effect of the weight normalization. Unlike the results shown in

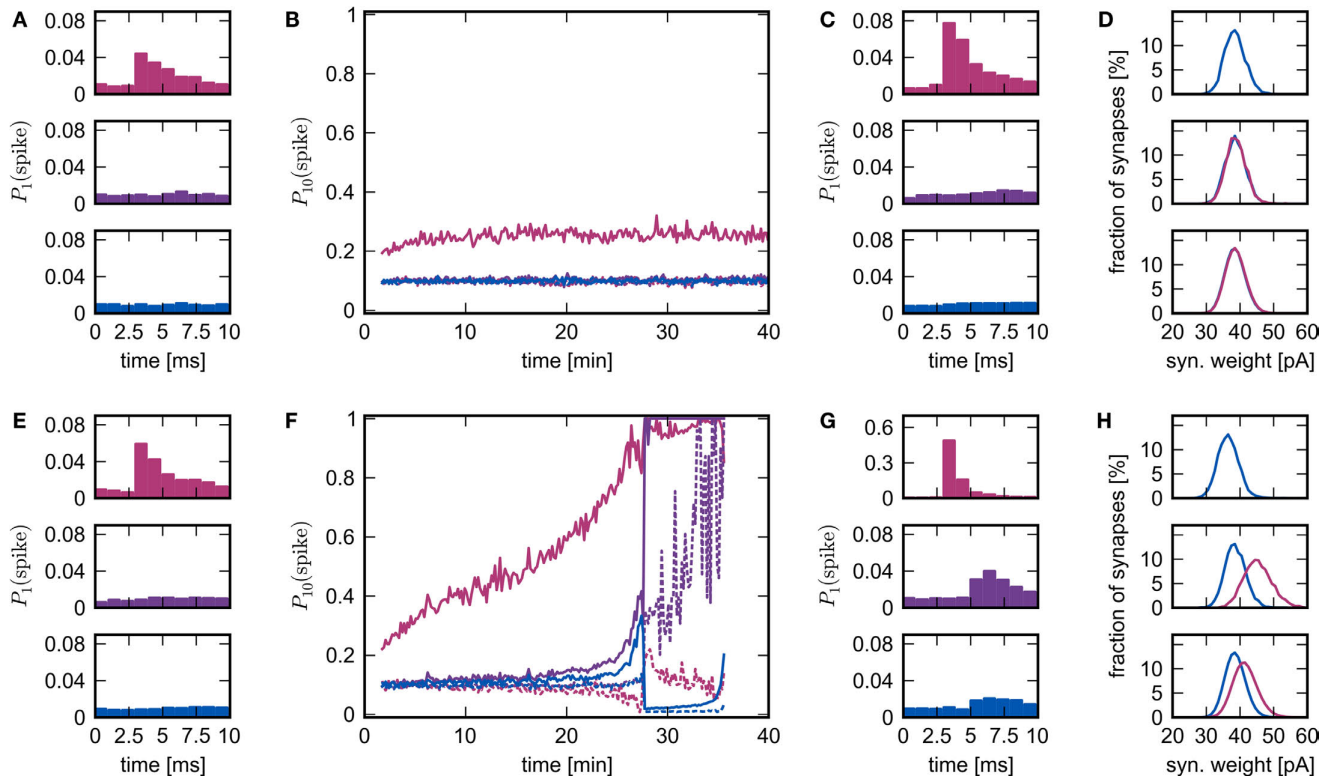

FIGURE 6 | Evolution of network response to synchronous stimulus. **(A)** Probability of emitting a spike after a synchronous event in the first 10 s of stimulation for the stimulated group (top), the high-connectivity group (middle) and the random group (bottom) for $N_{SIP} = 20$ and $N_{stim} = 164$. **(B)** Evolution of the probability of emitting a spike in the 10 ms immediately before (dashed lines) or immediately after a synchronous event (solid lines) in successive 10 s periods. Colors as in **(A)**. **(C)** As in **(A)** but for the 10 s period following 25 min of simulation. **(D)** Distribution of incoming synaptic weights at 25 min for the stimulated group (top) from the random group (blue), the synaptic weight distribution from the external group (mean 56.9 pA) is not shown; for the high-connectivity group (middle) from the random group (blue) and the stimulated group (pink); for the random group (bottom) from the random group (blue) and the stimulated group (pink). **(E–H)**: As for **(A–D)** but for $N_{SIP} = 25$ and $N_{stim} = 228$. The synaptic weight distribution from the external group to the stimulated group (mean 161.4 pA) is not shown in the top panel of **(H)**.

Figure 6F for pure STDP, as soon as the stimulated group reflects the stimulus with sufficient reliability, a clear difference between the response likelihood of the high-connectivity group and the network as a whole can be observed. The high response likelihood of the high-connectivity group breaks down rapidly when the network starts responding more strongly to the synchronous stimulation at around 60 min. This is another example of the decoupling of a synchronously active group from its embedding network as described above and in Morrison et al. (2007). As the response to the synchronous stimulus of the network generally lags behind the response in the high-connectivity group, acausal correlations are generated in the incoming synapses of the high-connectivity group. As the synaptic weights decrease, so does the mean membrane potential, thus diminishing the response of the neurons to the synchronous stimulus events. The stimulated group E_{stim} does not decouple in this fashion because the increasing strength of the connections from the external input can compensate for the loss of input from the recurrent network.

Figures 7C,D show the development of the response likelihood when post-synaptic homeostasis is also applied, such that the total strength of incoming and outgoing synapses are normalized alternately every 1.5 s. The network behavior is much more stable. The network remains in a stable asynchronous irregular activity regime even when an external group of size $N_{SIP} = 50$ stimulates a group of $N_{stim} = 584$ excitatory neurons (**Figure 7C**). However, the response probability of the high-connectivity group ($N_{hc} = 576$) saturates at a lower level than the maximum response likelihood reached in **Figure 7B** with purely pre-synaptic homeostasis. Although increasing N_{SIP} increases the number of neurons in E_{stim} available to drive a potential high-connectivity group E_{hc}, it also increases the size of E_{hc}. In the presence of pre-synaptic homeostasis, this reduces the mean strength of the connections between E_{stim} and E_{hc}.

Synchronous stimulation from an external group of size $N_{SIP} = 75$ drives the network into a pathological state despite the homeostasis as can be seen in **Figure 7D**. The interaction between the homeostasis and the strong stimulus sets up an oscillatory behavior in which the network repeatedly enters a pathological state but is reset by the application of homeostasis. Between pathological interludes, all neurons have a high probability of responding to a synchronous stimulus. The absence of clearly defined neuronal groups can be seen in **Figure 7E**. In the left panel, the network with STDP, pre- and post-synaptic homeostasis shows little response to synchronous

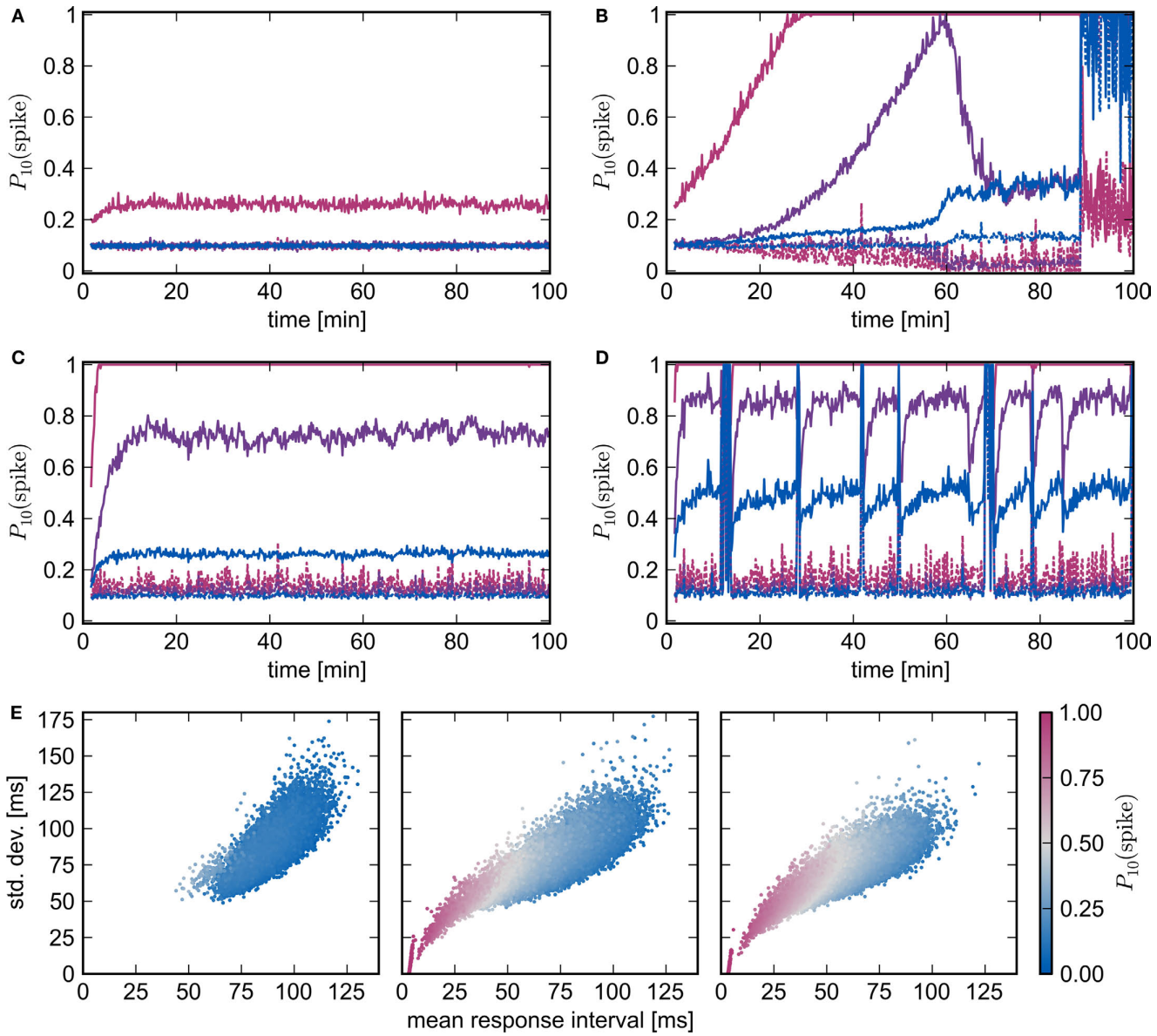

FIGURE 7 | Spike-timing dependent plasticity and homeostasis. **(A,B)** Evolution of network response to synchronous stimulus where STDP synapses in the recurrent network are subject to weight normalizing pre-synaptic homeostasis for $N_{SIP} = 20$, $N_{stim} = 164$, $N_{hc} = 158$ and $N_{SIP} = 25$, $N_{stim} = 228$, $N_{hc} = 228$, respectively. Probability of emitting a spike in the 10 ms immediately before (dashed lines) or immediately after a synchronous event (solid lines) in successive 10 s periods for the stimulated group (pink), the high-connectivity group (purple) and the random group (blue). **(C,D)** As in **(A,B)** but for pre- and post-synaptic homeostasis; $N_{SIP} = 50$, $N_{stim} = 584$, $N_{hc} = 576$ and $N_{SIP} = 75$, $N_{stim} = 961$, $N_{hc} = 963$, respectively. **(E)** Response latency and reliability for a network with STDP, pre- and post-synaptic homeostasis. Mean and SD of the response interval for each excitatory neuron to each synchronous event in the 26th minute (left, middle) or 21st minute (right). Marker color indicates the likelihood of the neuron to fire within 10 ms of a synchronous event. From left to right the panels correspond to $N_{SIP} = 20$, 50, 75 and $N_{stim} = 164$, 584, 961.

stimulation by a small group of $N_{SIP} = 20$ external neurons: the average latency is approximately the inter-spike interval of the network background rate. The middle and the left panel correspond to **Figures 7C,D**, i.e., synchronous stimulation by much larger external groups of $N_{SIP} = 50$ and $N_{SIP} = 75$ neurons, respectively. The neurons of the stimulated group ($N_{stim} = 584$ and $N_{stim} = 961$) can be seen to have separated themselves and respond quickly and reliably to the synchronous stimulus. The mean response latency shifts to an earlier value and the mean SD of the latency is reduced, demonstrating that the network as a whole responds earlier and more reliably to the stronger stimulus. Those neurons that respond earliest also have the lowest SD and are thus most likely to respond within 10 ms of a synchronous stimulus. However, there is no separation of a second group from the mass. We therefore conclude that no development of feed-forward structure can be observed, even in the presence of pre- and post-synaptic homeostasis and strong synchronous stimulus.

4 DISCUSSION

We have developed a simple model using a mean field approach and a linear neuron model to investigate the propagation of feed-forward structure in plastic recurrent networks. The key prediction of the model is that the number of neurons recruited by a repeated synchronous stimulus protocol is subject to an unstable fixed point. A synchronously firing group of neurons of a size below that of the fixed point recruits a smaller group, leading to a failure of the structure to propagate, whereas a synchronously firing group of a size above that of the fixed point recruits a larger group, causing the whole network to be recruited. In other words, a repeated synchronous stimulus is always either not enough or too much. We demonstrated by simulation that a large-scale network behaves as predicted by the mean field theory.

The existence of the unstable fixed point is robust. Employing a different weight-dependent STDP model, altering the input rates or introducing homeostatic mechanisms, e.g., regulating incoming synapses so as to maintain the total synaptic strength or post-synaptic rate, only influences the dynamics quantitatively. The unstable fixed point can be shifted to a larger or smaller group size, but it cannot be turned into a stable fixed point. The instability arises through the combination of a binomial distribution of connections from a given synchronously active group with the smooth change of the stable fixed point in the synaptic weight distribution as a function of the number of synchronous connections. Thus, any change to the model assumptions which does not produce a qualitative change in at least one of these factors will produce similar results, e.g., distributing the conduction delays or defining the conduction delay to be largely axonal, although such adaptations of the network model may well suppress or alter the pathological state the network enters when the amount of stimulation is too high (see Lubenov and Siapas, 2008). As an example, we demonstrated that the introduction of pre- and post-synaptic homeostatic mechanisms that maintain the total strength of outgoing and incoming recurrent synapses makes the network more stable, but does not enable the development of feed-forward structures.

Stable propagation of feed-forward structure is only possible if one or more of our assumptions are false. Other simulation studies have previously reported structure development (Hertz and Prügel-Bennet, 1996; Levy et al., 2001; Izhikevich et al., 2004; Doursat and Bienenstock, 2006; Jun and Jin, 2007; Masuda and Kori, 2007; Hosaka et al., 2008; Liu and Buonomano, 2009; Fiete et al., 2010). However, it is our contention that the risk of non-generalizable results is high when studying networks that are small, have few incoming synapses per neuron, or assume STDP rules that are independent of the synaptic weight. Each neuron in our network model receives a biologically realistic number of inputs (6000) and the network exhibits a biologically realistic degree of sparseness (connection probability of 0.06), while our model of STDP reproduces the experimentally found weight dependence of the amount of potentiation and depression a synapse undergoes (Bi and Poo, 1998; Morrison et al., 2007). We therefore suggest that the previously reported development of structure be considered artifactual until a greater degree of validation can be obtained. In our view, a weak proof of principle would be the demonstration of bounded structural growth in a network model with at least as great a degree of biological realism as in our study with respect to connectivity and plasticity, with additional assumptions that at least do not contradict experimental findings. A stronger, more convincing, proof would be provided by such a network model in which the additional assumptions are experimentally motivated.

Given that the brain does develop stable signal pathways, there is every reason to expect that a network model can be developed that fulfills these criteria for a strong proof of principle. One indication that the model we have investigated is overly simplified is that the combination of network structure, neuronal dynamics and plasticity leads to a symmetrical distribution of synaptic weights, rather than the skewed distribution observed experimentally (Sjöström et al., 2001). Therefore, a promising candidate adaptation that might result in a stable fixed point and thus stable propagation of feed-forward structure is the initial connectivity of the network. Here, we assume a random graph; however, the cortical network consists of several layers with layer-specific connectivity and exhibits long range patchy connections (Lewis et al., 2002; Schüz and Braitenberg, 2002; Thomson and Bannister, 2003; Binzegger et al., 2004). A more realistic graph structure might eliminate the "fan-out" tendency that underlies the instability of the fixed point. Such adaptations may also entail the use of a more complex neuron model than assumed here. Kumar et al. (2008) demonstrated that the regime enabling stable propagation activity in a feed-forward sub-network embedded in a locally connected random network is much greater for a conductance-based neuron model than previously found for a current-based model (Mehring et al., 2003). Moreover, a more sophisticated neuron model, particularly with respect to the dendritic integration of inputs, might exhibit greater symmetry breaking properties.

Another candidate is the formulation of the STDP rule. Although we have shown that our results are robust to the choice of update rule, we have only considered extremely simplified models of STDP exclusively at excitatory–excitatory synapses; the role of plasticity at inhibitory synapses is neglected. We addressed models in which the STDP window is fitted by two exponential functions, which is easy to analyze but may be too simplistic. Further, we have so far only considered rules based on pairs of spikes. Pfister and Gerstner (2006) introduced a rule based on triplets of spikes which accounts for experimental findings on the dependence of the weight change on the frequency of the pairing protocols (Sjöström et al., 2001). The triplet model has been shown to map to the BCM rule (Bienenstock et al., 1982) and to give near-optimal information transmission when combined with spike-frequency adaptation in the post-synaptic neuron (Hennequin et al., 2010). The triplet interaction could well also prove to be important for the development of structure. Moreover, recent experimental findings reveal that neuromodulation can influence STDP. Seol et al. (2007) showed that the polarity of the STDP window depends on the activation of receptors sensitive to cholinergic and adrenergic activity. A recent study by Kozloski and Cecchi (2010) demonstrated that polysynaptic loops eliminated by standard STDP can be restored by such a reversed rule. This finding suggests that the interaction of causal and anti-causal windows may indeed result in the kind of symmetry breaking that would enable groups of neurons to develop a qualitatively different response to a given synchronous stimulus. Neuromodulation can also be essential either for inducing STDP or for altering the threshold for induction, see Pawlak et al. (2010) in this special issue for a

review. Finally, our theoretical approach does not take into account interactions of STDP with other forms of plasticity except postsynaptic homeostasis. Although no development of feed-forward structure occurs in our homeostatically regulated network models, the presence of homeostasis certainly has a strong stabilizing effect on the network dynamics. Therefore, homeostasis may be a crucial element that enables network dynamics to be maintained during stimulus-driven development of structure. Short-term plasticity is another feature overlooked in the current study. The interaction of STDP with depression and facilitation could result in different network dynamics that would be more favorable to symmetry breaking, as could the incorporation of tagging processes to stabilize the developed structures (Frey and Morris, 1997; Reymann and Frey, 2007; Clopath et al., 2008). We therefore conclude that the development and investigation of more sophisticated models of STDP that interact with other forms of plasticity on different time scales would be a useful future extension of this research.

A third area in which the model presented here could be adapted is the stimulus protocol. Here, we investigated whether structure can develop from the seed of a single correlated group. Several forms of synaptic pathway organization have been identified and mathematically analyzed for recurrent networks under the assumption that they receive input from more than one pool of correlated inputs (e.g., Gilson et al., 2009b,c; see Gilson et al., 2010 for a thorough review). However, the majority of the findings assume STDP that is independent of the synaptic weight or only very weakly dependent. Moreover, only small networks are considered in which each neuron receives external correlated input. It will therefore be interesting to discover how these results scale up to the large, sparsely connected networks with weight-dependent plasticity considered in this article.

These candidate adaptations are not intended to be exhaustive. There are many ways in which the theoretical approach and network model presented here could be improved and supplemented. However, we hope that the suggestions above can serve to stimulate research to reveal the necessary and sufficient conditions for the development of structure in the mammalian brain.

ACKNOWLEDGMENTS

Partially funded by DIP F1.2, BMBF Grant 01GQ0420 to BCCN Freiburg, EU Grant 15879 (FACETS), EU Grant 269921 (BrainScaleS), Helmholtz Alliance on Systems Biology (Germany), Next-Generation Supercomputer Project of MEXT (Japan), Neurex, and the Junior Professor Program of Baden-Württemberg. High-performance computing facilities were made available through the Norwegian Metacenter for Computational Science (Notur) and JUGENE Grant JINB33 at the Research Center Jülich. We gratefully acknowledge T. Potjans for his help in determining appropriate connectivity levels for our network model and S. Jahnke for his comments on an earlier version of the manuscript.

REFERENCES

Abbott, L. F., and Nelson, S. B. (2000). Synaptic plasticity: taming the beast. *Nat. Neurosci.* 3(Suppl.), 1178–1183.

Abeles, M. (1991). *Corticonics: Neural Circuits of the Cerebral Cortex*, 1st Edn. Cambridge: Cambridge University Press.

Abeles, M., Bergman, H., Margalit, E., and Vaadia, E. (1993). Spatiotemporal firing patterns in the frontal cortex of behaving monkeys. *J. Neurophysiol.* 70, 1629–1638.

Bi, G.-Q., and Poo, M.-M. (1998). Synaptic modifications in cultured hippocampal neurons: dependence on spike timing, synaptic strength, and postsynaptic cell type. *J. Neurosci.* 18, 10464–10472.

Bienenstock, E. (1995). A model of neocortex. *Network* 6, 179–224.

Bienenstock, E. L., Cooper, L. N., and Munro, P. W. (1982). Theory for the development of neuron selectivity: orientation specificity and binocular interaction in visual cortex. *J. Neurosci.* 2, 32–48.

Binzegger, T., Douglas, R. J., and Martin, K. A. C. (2004). A quantitative map of the circuit of cat primary visual cortex. *J. Neurosci.* 39, 8441–8453.

Brunel, N. (2000). Dynamics of sparsely connected networks of excitatory and inhibitory spiking neurons. *J. Comput. Neurosci.* 8, 183–208.

Clopath, C., Ziegler, L., Vasilaki, E., Büsing, L., and Gerstner, W. (2008). Tag-trigger-consolidation: a model of early and late long-term-potentiation and depression. *PLoS Comput. Biol.* 4, e1000248. doi: 10.1371/journal.pcbi.1000248

Debanne, D., Gähwiler, B. H., and Thompson, S. M. (1996). Cooperative interactions in the induction of long-term potentiation and depression of synaptic excitation between hippocampal CA3-CA1 cell pairs in vitro. *Proc. Natl. Acad. Sci. U.S.A.* 93, 11225–11230.

Debanne, D., Gähwiler, B. H., and Thompson, S. M. (1999). Heterogeneity of synaptic plasticity at unitary CA1-CA3 and CA3-CA3 connections in rat hippocampal slice cultures. *J. Neurosci.* 19, 10664–10671.

Diesmann, M., Gewaltig, M.-O., and Aertsen, A. (1999). Stable propagation of synchronous spiking in cortical neural networks. *Nature* 402, 529–533.

Doursat, R., and Bienenstock, E. (2006). "Neocortical self-structuration as a basis for learning," in *5th International Conference on Development and Learning (ICDL 2006)*, Indiana University, Bloomington, IN.

Eckhorn, R., Bauer, R., Jordan, W., Brosch, M., Kruse, W., Munk, M., and Reitböck, H. J. (1988). Coherent oscillations: a mechanism of feature linking in the visual cortex? *Biol. Cybern.* 60, 121–130.

Fiete, I. R., Senn, W., Wang, C. Z. H., and Hahnloser, R. H. R. (2010). Spike-time-dependent plasticity and heterosynaptic competition organize networks to produce long scale-free sequences of neural activity. *Neuron* 65, 563–576.

Frey, U., and Morris, R. (1997). Synaptic tagging and long-term potentiation. *Nature* 385, 533–536.

Gerstner, W., Ritz, R., and van Hemmen, J. (1993). Why spikes? Hebbian learning and retrieval of time-resolved excitation patterns. *Biol. Cybern.* 69, 503–515.

Gewaltig, M.-O., and Diesmann, M. (2007). NEST (Neural Simulation Tool). *Scholarpedia* 2, 1430.

Gewaltig, M.-O., Diesmann, M., and Aertsen, A. (2001). Propagation of cortical synfire activity: survival probability in single trials and stability in the mean. *Neural Netw.* 657–673.

Gilson, M., Burkitt, A. N., Grayden, D. B., Thomas, D. A., and van Hemmen, J. L. (2009a). Emergence of network structure due to spike-timing-dependent plasticity in recurrent neuronal networks. I. Input selectivity – strengthening correlated input pathways. *Biol. Cybern.* 101, 81–102.

Gilson, M., Burkitt, A. N., Grayden, D. B., Thomas, D. A., and van Hemmen, J. L. (2009b). Emergence of network structure due to spike-timing-dependent plasticity in recurrent neuronal networks. II. Input selectivity – symmetry breaking. *Biol. Cybern.* 101, 103–114.

Gilson, M., Burkitt, A. N., Grayden, D. B., Thomas, D. A., and van Hemmen, J. L. (2009c). Emergence of network structure due to spike-timing-dependent plasticity in recurrent neuronal networks IV. *Structuring synaptic pathways among recurrent connections. Biol. Cybern.* 101, 427–444.

Gilson, M., Burkitt, A. N., and van Hemmen, J. L. (2010). STDP in recurrent neuronal networks. *Front. Comput. Neurosci.* 4:23. doi: 10.3389/fncom.2010.00023

Gray, C. M., and Singer, W. (1989). Stimulus-specific neuronal oscillations in orientation columns of cat visual cortex. *Proc. Natl. Acad. Sci. U.S.A.* 86, 1698–1702.

Gustafsson, B., Wigstrom, H., Abraham, W. C., and Huang, Y.-Y. (1987). Long-term potentiation in the hippocampus using depolarizing current pulses as the conditioning stimulus to single volley synaptic potentials. *J. Neurosci.* 7, 774–780.

Gütig, R., Aharonov, R., Rotter, S., and Sompolinsky, H. (2003). Learning input correlations through nonlinear temporally asymmetric Hebbian plasticity. *J. Neurosci.* 23, 3697–3714.

Hahnloser, R. H., Kozhevnikov, A. A., and Fee, M. S. (2002). An ultra-sparse code underlies the generation of neural sequences in a songbird. *Nature* 419, 65–70.

Hayon, G., Abeles, M., and Lehmann, D. (2004). Modeling compositionality by dynamic binding of synfire chains. *J. Comput. Neurosci.* 17, 179–201.

Hebb, D. O. (1949). *The Organization of Behavior: A Neuropsychological Theory*. New York: John Wiley and Sons.

Hennequin, G., Gerstner, W., and Pfister, J.-P. (2010). STDP in adaptive neurons gives close-to-optimal information transmission. *Front. Comput. Neurosci.* 4:143. doi: 10.3389/fncom.2010.00143

Hertz, J., and Prügel-Bennet, A. (1996). Learning synfire-chains by self-organization. *Network* 7, 357–363.

Hosaka, R., Araki, O., and Ikeguchi, T. (2008). STDP provides the substrate for igniting synfire chains by spatiotemporal input patterns. *Neural Comput.* 20, 415–435.

Iglesias, J., Eriksson, J., Grize, F., Tomassini, M., and Villa, A. (2005). Dynamics of pruning in simulated large-scale spiking neural networks. *Biosystems* 79, 11–20.

Ikegaya, Y., Aaron, G., Cossart, R., Aronov, D., Lampl, I., Ferster, D., and Yuste, R. (2004). Synfire chains and cortical songs: temporal modules of cortical activity. *Science* 5670, 559–564.

Izhikevich, E. M., Gally, J. A., and Edelman, G. M. (2004). Spike-timing dynamics of neuronal groups. *Cereb. Cortex* 14, 933–944.

Jun, J. K., and Jin, D. Z. (2007). Development of neural circuitry for precise temporal sequences through spontaneous activity, axon remodeling, and synaptic plasticity. *PLoS ONE* 2, e723. doi: 10.1371/journal.pone.0000723

Kempter, R., Gerstner, W., and van Hemmen, J. L. (1999). Hebbian learning and spiking neurons. *Phys. Rev. E* 59, 4498–4514.

Kempter, R., Gerstner, W., and van Hemmen, J. L. (2001). Intrinsic stabilization of output rates by spike-based Hebbian learning. *Neural Comput.* 12, 2709–2742.

Kistler, W. M., and van Hemmen, J. L. (2000). Modeling synaptic plasticity in conjunction with the timing of pre- and postsynaptic action potentials. *Neural Comput.* 12, 385–405.

Kozhevnikov, A., and Fee, M. S. (2007). Singing-related activity of identified HVC neurons in the zebra finch. *J. Neurophysiol.* 97, 4271–4283.

Kozloski, J., and Cecchi, G. A. (2010). A theory of loop formation and elimination by spike timing-dependent plasticity. *Front. Neural Circuits* 4:7. doi: 10.3389/fncir.2010.00007

Kuhn, A., Aertsen, A., and Rotter, S. (2003). Higher-order statistics of input ensembles and the response of simple model neurons. *Neural Comput.* 1, 67–101.

Kumar, A., Rotter, S., and Aertsen, A. (2008). Conditions for propagating synchronous spiking and asynchronous firing rates in a cortical network model. *J. Neurosci.* 28, 5268–5280.

Levy, N., Horn, D., Meilijson, I., and Ruppin, E. (2001). Distributed synchrony in a cell assembly of spiking neurons. *Neural Netw.* 14, 815–824.

Lewis, D., Melchitzky, D., and Burgos, G.-G. (2002). Specificity in the functional architecture of primate prefontal cortex. *J. Neurocytol.* 31, 265–276.

Liu, J. K., and Buonomano, D. V. (2009). Embedding multiple trajectories in simulated recurrent neural networks in a self-organizing manner. *J. Neurosci.* 29, 13172–13181.

Lubenov, E. V., and Siapas, A. G. (2008). Decoupling through synchrony in neuronal circuits with propagation delays. *Neuron* 58, 118–131.

Markram, H., Lübke, J., Frotscher, M., and Sakmann, B. (1997). Regulation of synaptic efficacy by coincidence of postsynaptic APs and EPSPs. *Science* 275, 213–215.

Markram, H., and Sakmann, B. (1995). Action potentials propagating back into dendrites trigger changes in efficacy of single-axon synapses between layer V pyramidal neurons. *Soc. Neurosci. Abstr.* 21, 2007.

Masuda, N., and Kori, H. (2007). Formation of feedforward networks and frequency synchrony by spike-timing-dependent plasticity. *J. Comput. Neurosci.* 22, 327–345.

Mehring, C., Hehl, U., Kubo, M., Diesmann, M., and Aertsen, A. (2003). Activity dynamics and propagation of synchronous spiking in locally connected random networks. *Biol. Cybern.* 88, 395–408.

Migliore, M., Cannia, C., Lytton, W. W., Markram, H., and Hines, M. (2006). Parallel network simulations with neuron. *J. Comput. Neurosci.* 21, 119–223.

Montgomery, J., Pavlidis, P., and Madison, D. (2001). Pair recordings reveal all-silent synaptic connections and the postsynaptic expression of long-term potentiation. *Neuron* 29, 691–701.

Morrison, A., Aertsen, A., and Diesmann, M. (2007). Spike-timing dependent plasticity in balanced random networks. *Neural Comput.* 19, 1437–1467.

Morrison, A., Diesmann, M., and Gerstner, W. (2008). Phenomenological models of synaptic plasticity based on spike-timing. *Biol. Cybern.* 98, 459–478.

Morrison, A., Mehring, C., Geisel, T., Aertsen, A., and Diesmann, M. (2005). Advancing the boundaries of high connectivity network simulation with distributed computing. *Neural Comput.* 17, 1776–1801.

Nordlie, E., Plesser, H. E., and Gewaltig, M.-O. (2009). Towards reproducible descriptions of neuronal network models. *PLoS Comput. Biol.* 5, e1000456. doi: 10.1371/journal.pcbi.1000456

Pawlak, V., Wickens, J. R., Kirkwood, A., and Kerr, J. N. D. (2010). Timing is not everything: neuromodulation opens the STDP gate. *Front. Syn. Neurosci.* 2:146. doi: 10.3389/fnsyn.2010.00146

Pecevski, D., Natschläger, T., and Schuch, K. (2009). PCSIM: a parallel simulation environment for neural circuits fully integrated with python. *Front. Neuroinform.* 3:11. doi: 10.3389/neuro.11.011.2009

Pfister, J.-P., and Gerstner, W. (2006). Triplets of spikes in a model of spike timing-dependent plasticity. *J. Neurosci.* 26, 9673–9682.

Prut, Y., Vaadia, E., Bergman, H., Haalman, I., Hamutal, S., and Abeles, M. (1998). Spatiotemporal structure of cortical activity: Properties and behavioral relevance. *J. Neurophysiol.* 79, 2857–2874.

Pulvermüller, F., and Shtyrov, Y. (2009). Spatiotemporal signatures of large-scale synfire chains for speech processing as revealed by MEG. *Cereb. Cortex* 19, 79–88.

Reymann, K. G., and Frey, J. U. (2007). The late maintenance of hippocampal LTP: Requirements, phases, "synaptic tagging," "late-associativity" and implications. *Neuropharmacology* 52, 24–40.

Rubin, J., Lee, D., and Sompolinsky, H. (2001). Equilibrium properties of temporally asymmetric Hebbian plasticity. *Phys. Rev. Lett.* 86, 364–367.

Schüz, A., and Braitenberg, V. (2002). "The human cortical white matter: quantitative aspects of cortico-cortical long-range connectivity," in *Cortical Areas: Unity and Diversity*, Chapter 16, eds A. Schüz and R. Miller (London: Taylor and Francis), 377–385.

Seol, G., Ziburkus, J., Huang, S., Song, L., Kim, I., Takamiya, K., Huganir, R., Lee, H.-K., and Kirkwood, A. (2007). Neuromodulators control the polarity of spike-timing-dependent plasticity. *Neuron* 55, 919–929.

Sjöström, P., Turrigiano, G., and Nelson, S. (2001). Rate, timing, and cooperativity jointly determine cortical synaptic plasticity. *Neuron* 32, 1149–1164.

Song, S., Miller, K. D., and Abbott, L. F. (2000). Competitive Hebbian learning through spike-timing-dependent synaptic plasticity. *Nat. Neurosci.* 3, 919–926.

Song, S., Sjöström, P. J., Reigl, M., Nelson, S., and Chklovskii, D. B. (2005). Highly nonrandom features of synaptic connectivity in local cortical circuits. *PLoS Biol.* 3, e350. doi: 10.1371/journal.pbio.0030350

Standage, D., Jalil, S., and Trappenberg, T. (2007). Computational consequences of experimentally derived spike-time and weight dependent plasticity rules. *Biol. Cybern.* 96, 615–623.

Thomson, A. M., and Bannister, P. (2003). Interlaminar connections in the neocortex. *Cereb. Cortex* 13, 5–14.

Turrigiano, G. G., Leslie, K. R., Desai, N. S., Rutherford, L. C., and Nelson, S. B. (1998). Activity-dependent scaling of quantal amplitude in neocortical neurons. *Nature* 391, 892–896.

van Rossum, M. C. W., Bi, G.-Q., and Turrigiano, G. G. (2000). Stable Hebbian learning from spike timing-dependent plasticity. *J. Neurosci.* 20, 8812–8821.

Wang, H.-X., Gerkin, R. C., Nauen, D. W., and Bi, G.-Q. (2005). Coactivation and timing-dependent integration of synaptic potentiation and depression. *Nat. Neurosci.* 8, 187–193.

Zou, Q., and Destexhe, A. (2007). Kinetic models of spike-timing dependent plasticity and their functional consequences in detecting correlations. *Biol. Cybern.* 97, 81–97.

Conflict of Interest Statement: The authors declare that the research was conducted in the absence of any commercial or financial relationships that could be construed as a potential conflict of interest.

Received: 15 March 2010; accepted: 25 December 2010; published online: 14 February 2011.

*Citation: Kunkel S, Diesmann M and Morrison A (2011) Limits to the development of feed-forward structures in large recurrent neuronal networks. Front. Comput. Neurosci. **4**:160. doi: 10.3389/fncom.2010.00160*

frontiers in
SYNAPTIC NEUROSCIENCE

ORIGINAL RESEARCH ARTICLE
published: 02 July 2010
doi: 10.3389/fnsyn.2010.00012

Human synapses show a wide temporal window for spike-timing-dependent plasticity

Guilherme Testa-Silva[1†], Matthijs B. Verhoog[1†], Natalia A. Goriounova[1†], Alex Loebel[2], J. J. Johannes Hjorth[1], Johannes C. Baayen[3], Christiaan P. J. de Kock[1] and Huibert D. Mansvelder[1]*

[1] *Department of Integrative Neurophysiology, Center for Neurogenomics and Cognitive Research, VU University, Amsterdam, Netherlands*
[2] *Division of Neurobiology, Department of Biology II, Ludwig-Maximillians University Munich, Munich, Germany*
[3] *Department of Neurosurgery, VU University Medical Center, Neuroscience Campus Amsterdam, Amsterdam, Netherlands*

Edited by:
Per Jesper Sjöström, University College London, UK

Reviewed by:
Yang Dan, University of California, Berkeley, USA
Johannes J. Letzkus, Friedrich Miescher Institute for Biomedical Research, Switzerland
Laurent Venance, Collège de France, France

***Correspondence:**
Huibert D. Mansvelder, Neuroscience Campus Amsterdam, Center for Neurogenomics and Cognitive Research, De Boelelaan 1085, 1081 HV Amsterdam, Netherlands.
e-mail: huibert.mansvelder@cncr.vu.nl

†*Guilherme Testa Silva, Matthijs B. Verhoog, and Natalia A. Goriounova have contributed equally to this work.*

Throughout our lifetime, activity-dependent changes in neuronal connection strength enable the brain to refine neural circuits and learn based on experience. Synapses can bi-directionally alter strength and the magnitude and sign depend on the millisecond timing of presynaptic and postsynaptic action potential firing. Recent findings on laboratory animals have shown that neurons can show a variety of temporal windows for spike-timing-dependent plasticity (STDP). It is unknown what synaptic learning rules exist in human synapses and whether similar temporal windows for STDP at synapses hold true for the human brain. Here, we directly tested in human slices cut from hippocampal tissue removed for surgical treatment of deeper brain structures in drug-resistant epilepsy patients, whether adult human synapses can change strength in response to millisecond timing of pre- and postsynaptic firing. We find that adult human hippocampal synapses can alter synapse strength in response to timed pre- and postsynaptic activity. In contrast to rodent hippocampal synapses, the sign of plasticity does not sharply switch around 0-ms timing. Instead, both positive timing intervals, in which presynaptic firing preceded the postsynaptic action potential, and negative timing intervals, in which postsynaptic firing preceded presynaptic activity down to –80 ms, increase synapse strength (tLTP). Negative timing intervals between –80 to –130 ms induce a lasting reduction of synapse strength (tLTD). Thus, similar to rodent synapses, adult human synapses can show spike-timing-dependent changes in strength. The timing rules of STDP in human hippocampus, however, seem to differ from rodent hippocampus, and suggest a less strict interpretation of Hebb's predictions.

Keywords: human, synapse, hippocampus, neocortex, synaptic plasticity, spike-timing-dependent plasticity, Hebbian plasticity

INTRODUCTION

One of the central questions in neuroscience is how memories are formed and stored in the human brain. From a large number of studies on laboratory animals it is known that learning and memory are most likely mediated by activity-dependent neuronal circuit modifications resulting from synaptic plasticity (Bliss and Lomo, 1973; Cooke and Bliss, 2006; Whitlock et al., 2006; Letzkus et al., 2007). The ability to shape neuronal connections in an activity-dependent manner enables the brain to functionally refine neural circuits in response to sensory experience and adapt to changing environments (for review see Caporale and Dan, 2008). In line with predictions made by Hebb (1949), synapse strength can be modified depending on the millisecond timing of action potential firing and the sign of synaptic plasticity depends on the spike order of presynaptic and postsynaptic neurons (Levy and Steward, 1983; Gustafsson et al., 1987; Bell et al., 1997; Magee and Johnston, 1997; Markram et al., 1997). By varying the timing and order of pre- and postsynaptic spiking, it was found that critical time windows exist for synaptic modification on the order of tens of milliseconds (Bi and Poo, 1998, 2001). In recent years, it has become clear that diversity exists of temporal windows for spike-timing-dependent plasticity (STDP) depending on parameters such as brain area and neuron type (Froemke et al., 2005; Wittenberg and Wang, 2006; Meredith et al., 2007; Caporale and Dan, 2008). However, it is unknown what synaptic learning rules exist in human synapses and whether similar temporal windows for STDP at synapses hold true for the human brain.

There are few studies on synaptic LTP and LTD in humans. With field potential recordings from hippocampal and neocortical tissue excised from human patients it was shown that high frequency stimulation (100 Hz) induces LTP in human synapses (Chen et al., 1996; Beck et al., 2000). Blocking NMDA receptors with APV prevents LTP induction, indicating that plasticity of human synapses shares molecular mechanisms with animal models. Low frequency stimulation (1 Hz) resulted in LTD (Chen et al., 1996), showing that the strength of human synapses can be regulated bi-directionally. Indirect evidence suggests that coincident millisecond timing of activity is likely to govern synaptic changes in humans as well (Stefan et al., 2000; Wolters et al., 2003). Pairing transcranial magnetic stimulation (TMS) of motor cortex with peripheral nerve stimulation *in vivo* can alter motor-evoked potentials in muscles, and precise timing determines the sign of this plasticity (Wolters

et al., 2003, 2005). Timed TMS of motor cortex and peripheral stimulation may induce synaptic plasticity in cortical circuits, but a direct demonstration thereof is lacking. In this study, we set out to directly test whether human synapses can alter strength in response to millisecond timing of pre- and postsynaptic firing. In addition, we explored the temporal window for STDP at these synapses. We find that in contrast to rodent hippocampus, adult human hippocampal synapses show a wide temporal window for STDP.

MATERIALS AND METHODS

HUMAN HIPPOCAMPAL SLICE PREPARATION

All procedures on human tissue were performed with the approval of the Medical Ethical Committee of the VU University Medical Center and in accordance with Dutch license procedures and the declaration of Helsinki. Human slices were cut from hippocampal tissue that had to be removed for the surgical treatment of deeper brain structures for epilepsy with written informed consent of the patients (aged 20–66 years) prior to surgery. Anesthesia was induced with intravenous fentanyl 1–3 μg/kg and a bolus dose of propofol (2–10 mg/kg) and was maintained with remyfentanyl 250 μg/kg/min and propofol 4–12 mg/kg.

After resection, the hippocampal tissue was placed within 30 s in ice-cold artificial cerebrospinal fluid (ACSF) slicing solution which contained in (mM): 110 choline chloride, 26 $NaHCO_3$, 10 D-glucose, 11.6 sodium ascorbate, 7 $MgCl_2$, 3.1 sodium pyruvate, 2.5 KCl, 1.25 NaH_2PO_4, and 0.5 $CaCl_2$ –300 mOsm. (Bureau et al., 2006) and transported to the neurophysiology laboratory, which is located within 200 m distance from the operating room. The transition time between resection of the tissue and the start of preparing slices was less than 15 min.

Hippocampal slices (300 μm) were prepared in ice-cold slicing solution, and were then transferred to holding chambers in which they were stored for 30 min at 34°C and for 30 min at room temperature before recording in ACSF which contained (in mM): NaCl 125; KCl 3; NaH_2PO_4 1.25; $MgSO_4$ 2; $CaCl_2$ 2; $NaHCO_3$ 26; glucose 10, bubbled with carbogen gas (95% O_2/5% CO_2).

ELECTROPHYSIOLOGY

Hippocampal slices were visualized using either infrared differential interference contrast (IR-DIC) microscopy or Hoffman modulation contrast. After the whole cell configuration was established, membrane potential responses to steps of current injection were used to classify each cell electrophysiologically. Cells were loaded with biocytin through the recording pipette for *post hoc* identification. All experiments were performed at 32–35°C. Although the hippocampal tissue was resected from the brains of epilepsy patients, none of the neurons recorded from showed spontaneous epileptiform spiking activity. Resting membrane potentials were in line with previous reports on recordings from human neurons (-64±5 mV for Pyramidal and -65±7 mV for Non-pyramidal cells). All experiments were performed in the absence of blockers of GABAergic synaptic transmission.

Recordings were made using Multiclamp 700A/B amplifiers (Axon Instruments, CA, USA) sampling at intervals of 50 or 100 μs, digitized by the pClamp software (Axon) or custom written scripts in Igor Pro, and later analyzed off-line using custom written Matlab scripts (Mathworks). Whole cell current injection and extracellular stimulation (both timing and levels) were controlled with a Master-8 stimulator (A.M.P.I., Jerusalem, Israel) triggered by the data acquisition software. Patch pipettes (3–5 MΩ) were pulled from standard-wall borosilicate capillaries and filled with intracellular solutions containing (in mM): K-gluconate 140; KCl 1; HEPES 10; K-phosphocreatine 4; ATP-Mg 4; GTP 0.4, pH 7.2–7.3, pH adjusted to 7.3 with KOH; 280–290 mOsm. 0.5 mg/ml Biocytin.

Table 1 | Summary table of action potential properties.

	Pyramidals ($n = 9$)	Non-pyramidals ($n = 7$)
First AP amplitude (mV)	113.8 ± 8.0	114.5 ± 2.3
Second AP amplitude (mV)	115.7 ± 4.8	111.9 ± 1.6
First AP upstroke (mV/ms)	231.3 ± 38.4	147.0 ± 14.2
Second AP upstroke (mV/ms)	207.3 ± 28	119.1 ± 10.7
First AP downstroke (mV/ms)	99.2 ± 8.3	103.3 ± 2.7
Second AP downstroke (mV/ms)	74.3 ± 16.5	83.3 ± 2.4
First AP half-width (ms)	1.1 ± 0.2	1.03 ± 0.04
Second AP half-width (ms)	1.3 ± 0.1	1.23 ± 0.03
Max ADP avg (mV)	11.3 ± 0.6	12.6 ± 0.4 ($n = 1$)
Tau ADP avg (ms)	16.6 ± 1.2 ($n = 7$)	20.3 ± 2.3 ($n = 1$)

Data presented as mean (absolute values) ± S.E.M.

Post hoc visualization and neuron identification using biocytin labeling was performed as described previously (Horikawa and Armstrong, 1988; de Kock et al., 2007). Image-stacks were created using a 20× air objective using Surveyor software (Objective Imaging Ltd., Stow cum Quy, Cambridge UK available from Chromaphor, Bottrop, Germany) and ImageJ. Pyramidal and non-pyramidal neurons were classified based on morphological and electrophysiological criteria. Pyramidal neurons typically had an input resistance below 100 MΩ; non-pyramidal neurons typically had an input resistance above 100 MΩ (**Tables 2 and 3**).

SPIKE-TIMING-DEPENDENT PLASTICITY

Excitatory postsynaptic potential (EPSPs) were evoked every 7 s using an extracellular stimulation electrode positioned at approximately 100–150 μm along the cell's somatodendritic axis (**Figures 1A,B**). The slope of the initial 2 ms of the EPSP was analyzed to ensure that the data reflected only the monosynaptic component of each experiment (Froemke et al., 2005; Couey et al., 2007). Synaptic gain was measured as the percent change in EPSP slope when comparing the average in the period 20–30 min postconditioning to the average baseline EPSP slope. During the induction protocol spike-timings were measured from the onset of the evoked EPSP to the peak of the postsynaptic AP. Mean baseline EPSP slopes were averaged from at least 30 sweeps (with amplitudes in the range of 6–7.5 mV). During the conditioning period pre-postsynaptic stimulus pairing was repeated 40–50 times, with a 7 s (0.14 Hz) interval between each pairing. Two distinct conditioning protocols were used, two spikes with 10-ms interval (tested in 17 cells) and single spike (tested in two cells). During experiments, cell input resistance was monitored throughout by applying a −10 to −100 pA, 200–500 ms hyperpolarizing pulse at the end of each sweep, additional determination of input resistance was done by extracting an I–V curve from each cell, in the beginning of the experiment, after pairing and at the

Table 2 | Summary table of EPSP kinetic changes in response to tLTP paradigm (two action potential pairing).

	Pyramidals ($n = 7$)		Non-pyramidals ($n = 6$)	
	Pre-pairing	**Post-pairing**	**Pre-pairing**	**Post-pairing**
Slope (mV/ms)	1.97 ± 0.23	3.24 ± 0.48 (64%)	2.79 ± 0.49	4.08 ± 1.31 (46%)
Amplitude (mV)	6.24 ± 0.62	10.05 ± 1.29 (61%)	7.51 ± 1.21	10.49 ± 2.49 (40%)
Half-width (ms)	34 ± 4	26 ± 4 (–24%)	24 ± 2	23 ± 3 (–4%)
Decay time constant (ms)	38 ± 5	29 ± 4 (–24%)	36 ± 3	31 ± 4 (–14%)
Onset (ms)	1.64 ± 0.14	1.67 ± 0.22 (2%)	1.59 ± 0.14	1.60 ± 0.14 (1%)
Input resistance (MΩ)	55 ± 13	57 ± 13 (4%)	139 ± 6	154 ± 9 (10%)

Data presented as mean ± S.E.M. and percent change between parenthesis.

Table 3 | Summary table of EPSP kinetic changes in response to tLTD paradigm (two action potential pairing).

	Pyramidals ($n = 3$)		Non-pyramidal ($n = 1$)	
	Pre-pairing	**Post-pairing**	**Pre-pairing**	**Post-pairing**
Slope (mV/ms)	2.22 ± 1.10	1.37 ± 1.06 (–38%)	1.73 ± 0.51	1.05 ± 0.43 (–39%)
Amplitude (mV)	6.47 ± 2.89	3.64 ± 2.57 (–44%)	6.76 ± 1.51	2.83 ± 1.05 (–58%)
Half-width (ms)	20 ± 2	12 ± 4 (–40%)	30 ± 3	20 ± 7 (–33%)
Decay time constant (ms)	25 ± 3	15 ± 5 (–40%)	34 ± 3	27 ± 11 (–20%)
Onset (ms)	1.76 ± 0.46	1.29 ± 0.38 (–27%)	1.99 ± 0.09	1.63 ± 0.10 (18%)
Input resistance (MΩ)	41 ± 12	43 ± 13 (4%)	155 ± 3	141 ± 7 (–9%)

Data presented as mean ± S.E.M. and percent change between parenthesis. For non-pyramidal cell, data presented as mean ± S.D. and percent change between parenthesis.

end of the recording. Experiments were not included in the analysis if the cell input resistance varied by more than ± 30% during the experiment, which was the case for 13 out of 32 recordings. The *t*-test and the Mann–Whitney *U* test were used to assess significance on changes in slope for each experiment. Data are given as mean ± SEM, with $p < 0.05$ as minimum for statistical significance. Experiments lasted 20–70 min and where interrupted if the conditions of the patch degenerated or if the cell displayed repeated spiking after potentiation or failures after depression. When recording lasted less than 30 min (two of 19 recordings included in analysis), the average of baseline was compared to the average of all points in the post-pairing period.

The amplitude of the ADP component of the voltage response was measured from its maxima. The time constant of the decay of the ADP response back to the resting potential, τ_{decay}, was estimated from the fitting to a single exponential, that is,

$$v(t) = \boldsymbol{A} \cdot \exp\left(-\frac{t}{\tau_{decay}}\right) \quad (1)$$

where "*A*" is a dummy scaling factor.

RESULTS

Spike-timing-dependent modifications of synapse strength have been found in brains of laboratory animals (Levy and Steward, 1983; Gustafsson et al., 1987; Bell et al., 1997; Magee and Johnston, 1997; Markram et al., 1997, for review see Caporale and Dan, 2008), but it has not been tested directly whether adult human synapses can change strength as a result of the precise timing of pre- and postsynaptic spiking activity. To test this, we made whole-cell recordings from pyramidal neurons and non-pyramidal cells of adult human hippocampus (20–66 years of age) and stimulated glutamatergic inputs by extracellular stimulation (**Figure 1**). During whole-cell recordings, neurons were labeled with biocytin for *post hoc* morphological identification. Hippocampal pyramidal neurons and non-pyramidal cells had distinct characteristic morphologies (**Figure 1**). As described for pyramidal neurons and non-pyramidal cells in human association cortex (Foehring et al., 1991), hippocampal pyramidal neurons, and non-pyramidal cells also showed distinct basic electrophysiological properties (**Tables 1–3**; **Figure 1**).

Passive and active cell properties measured in human hippocampal cells were in some aspects comparable to values obtained from rodent cells (Staff et al., 2000; Mercer et al., 2007; Routh et al., 2009). For example pyramidal cell input resistance in rat is 65.6 ± 4.4 MΩ, in mouse (C57BL/6) is 65.4 ± 1.7 MΩ, while in human pyramidals it tends to be slightly lower: 49.1 ± 8.7 MΩ. Input resistance of wide arbor basket cells in rat CA2 is 111.8 ± 36.7 MΩ, while in human, non-pyramidal cells we found a slightly higher average input resistance of 141.7 ± 6MΩ. Pyramidal cell AP amplitude agree well with reported values for rat pyramidal cells (humans: 113.8 ± 8.0 mV; rat: 112.0 ± 9.0 mV). Human cells however, have slower rate of rise compared with CA1 rat pyramidal cells. Rat: 381 ± 18 mV/ms and human: 231.3 ± 38.4 mV/ms, but similar

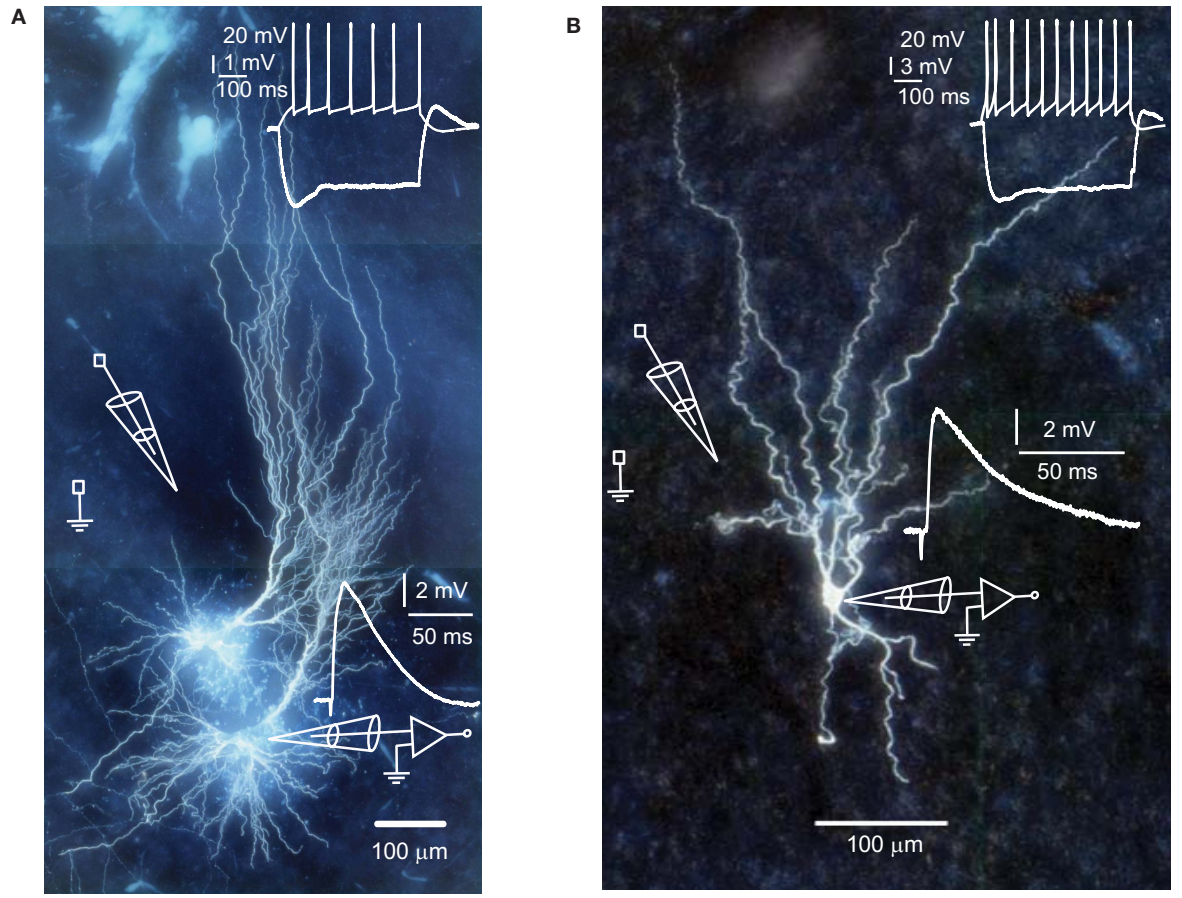

FIGURE 1 | Human hippocampal pyramidal (A) and non-pyramidal neuron (B). Top insets show membrane potential changes in response to step current injections. Different scale bars apply to the hyperpolarizing and depolarizing step. Bottom insets show EPSPs in response to extracellular stimulation.

half-width, rat: 0.93 ± 0.03 ms and human 1.1 ± 0.2 ms, which may indicate possible differences in voltage-gated sodium channel dynamics.

In rodent hippocampus, glutamatergic inputs to pyramidal neurons potentiate when the temporal order of action potential firing is such that spiking of presynaptic fibers is followed by postsynaptic firing (Bi and Poo, 1998; Meredith et al., 2003). The temporal window in which the postsynaptic neuron must spike is ~20 ms after the presynaptic stimulus for spike-timing-dependent potentiation (tLTP) to occur (Bi and Poo, 1998). To test whether human hippocampal synapses increase strength in response to spike-timing within this positive timing window of 20 ms, we paired presynaptic stimulation with postsynaptic firing with a positive interval of 10 ms (**Figure 2**). Since it was reported that in rodent hippocampus the effectiveness of tLTP induction diminishes with age (Meredith et al., 2003), we induced two postsynaptic action potentials (10-ms interval) with each presynaptic stimulus to optimize tLTP induction. After recording 4–5 min of baseline EPSPs, repeated pairing of EPSPs with postsynaptic action potentials (**Figure 2A**; 40–50 times at 0.14 Hz) resulted in a lasting increase of both EPSP amplitude (from 5.47 ± 1.17 mV at baseline to 9.39 ± 1.90 mV after pairing, an increase of 72%) and slope (from 2.21 ± 0.39 mV/ms at baseline to 3.25 ± 0.79 mV/ms after pairing, an increase of 65%, *t*-test $p < 0.0001$; **Figures 2C,D**). During the entire recording, other basic electrophysiological parameters such as resting membrane potential and input resistance did not change significantly (**Figure 2B**; see Section "Materials and Methods"). Pairing pre- and postsynaptic activity at positive intervals (5–10 ms) resulted in tLTP in both pyramidal neurons (96%, $n = 3$) as well as non-pyramidal cells (21%, $n = 4$; **Figure 6**, **Table 2**). These results show that excitatory human synapses can show potentiation in response to millisecond timing of pre- and postsynaptic activity.

Reversing the order of presynaptic and postsynaptic action potential firing such that the postsynaptic neuron fires before the presynaptic stimulation induces synaptic depression in rodent hippocampal synapses (Bi and Poo, 1998; Nishiyama et al., 2000; Wittenberg and Wang, 2006). The temporal window for spike-timing synaptic depression (tLTD) in these synapses is around 20 ms. To test whether adult human hippocampal synapses show tLTD in response to negative timing intervals, postsynaptic action potentials were induced 10–80 ms before the presynaptic stimulus during pairing (**Figure 3**). In contrast to rodent hippocampal synapses, these intervals induced a robust increase in EPSP amplitude and slope (**Figures 3C,D**). At −35 ms interval, the EPSP amplitude increased from 5.22 ± 1.13 to 9.44 ± 1.13 mV after pairing (an increase of 80%) and the slope from 1.57 ± 0.31 mV/ms at baseline

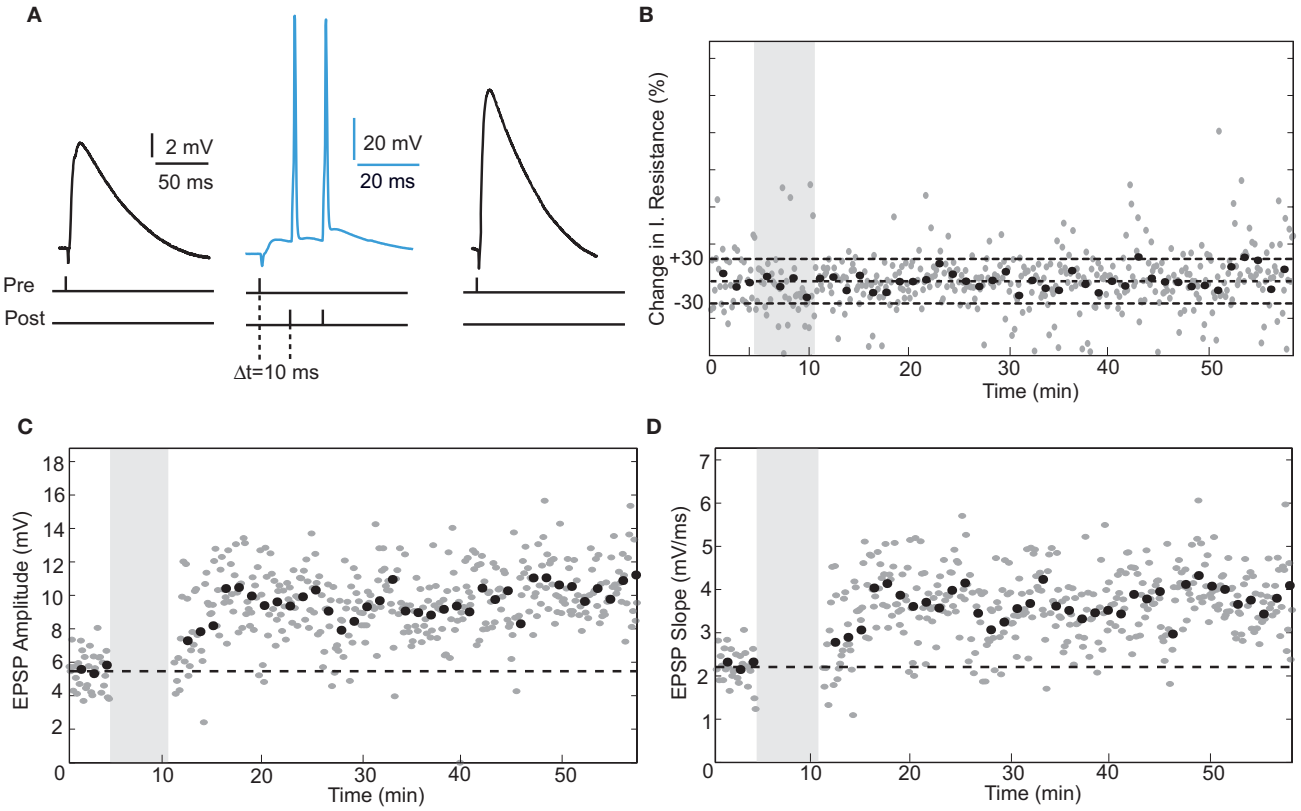

FIGURE 2 | STDP at human excitatory synapses in a hippocampal pyramidal neuron. (A) Schematic representation of the experiment shown in **(B–D)** with example EPSP and action potential traces. **(B)** Input resistance calculated from the membrane potential response to a small negative current step delivered through the recording electrode after each EPSP. Grey area indicates the pairing period. **(C,D)** EPSP amplitude and slope recorded from a hippocampal pyramidal neuron. Same recording as in **(B)**.

to 2.85 ± 0.34 mV/ms after pairing (an increase of 81%, *t*-test $p < 0.0001$ **Figures 3C,D**). On average, in pyramidal neurons in which post- before presynaptic timing was applied, synapse strength increased by 58% ($n = 4$). In non-pyramidal cells, a negative time interval of −10 ms induced a 116% change in EPSP slope and a negative time interval of −20 ms induced a 10% increase in slope (**Figure 6**). These results indicate that in contrast to rodent hippocampal synapses, adult human hippocampal synapses show tLTP at negative timing intervals up to −80 ms. The temporal window for tLTP induction covers intervals between −80 and +10 ms.

Action potentials in human pyramidal neurons showed a prominent after-depolarization (ADP; **Figures 3A and 4A**; **Table 1**), possibly reflecting dendritic action potential propagation (Larkum et al., 2001). Dendritic action potential propagation is crucial for tLTP induction (Kampa et al., 2006, 2007; Couey et al., 2007; Fuenzalida et al., 2010). In the recordings with negative timing interval pairings between −10 and −80 ms, EPSPs coincided with the downward slope of the ADP (**Figure 3A**), which may have contributed to induction of tLTP. To test whether tLTD would be induced when the EPSP would occur after the membrane potential had returned to baseline, we increased the negative timing interval (**Figure 4**). When postsynaptic firing was followed by an EPSP after 130 ms, the membrane potential had returned to baseline at the time of presynaptic stimulation (**Figure 4A**). At this interval, the EPSP amplitude and slope indeed showed a sustained reduction (**Figures 4C,D**). Both in pyramidal neurons and non-pyramidal cells negative timing intervals between −80 and −130 ms induced tLTD. On average, the EPSPs slope was reduced by −55% ($n = 3$) in pyramidal neurons. In one non-pyramidal cell, negative timing of −110 ms also resulted in a reduction of EPSP slope of −31% (**Figure 6**, **Table 2**). These findings show that in contrast to rodent hippocampal synapses, the sign of plasticity does not sharply switch around 0 ms timing in human hippocampal synapses. It switches around −80 ms.

During maturation of the rodent hippocampus, the effectiveness of postsynaptic spikes to induce tLTP diminishes. Pairing EPSPs with single action potentials fails to induce tLTP at ages beyond 20 days, while pairing EPSPs with a pair of action potentials suffices to induce tLTP at these ages (Meredith et al., 2003). To test whether single spikes paired with EPSPs would induce tLTP in adult human synapses, we applied a timed presynaptic stimulus with a single postsynaptic spike (**Figure 5**). When the action potential was followed by an EPSP after 75 ms in a pyramidal neuron, the EPSP slope showed a small but significant increase from 1.34 ± 0.27 mV/ms to 1.48 ± 0.36 mV/ms after pairing (an increase of 10%, *t*-test $p < 0.05$, **Figure 5D**). In a non-pyramidal neuron, when the EPSP was followed by a single postsynaptic

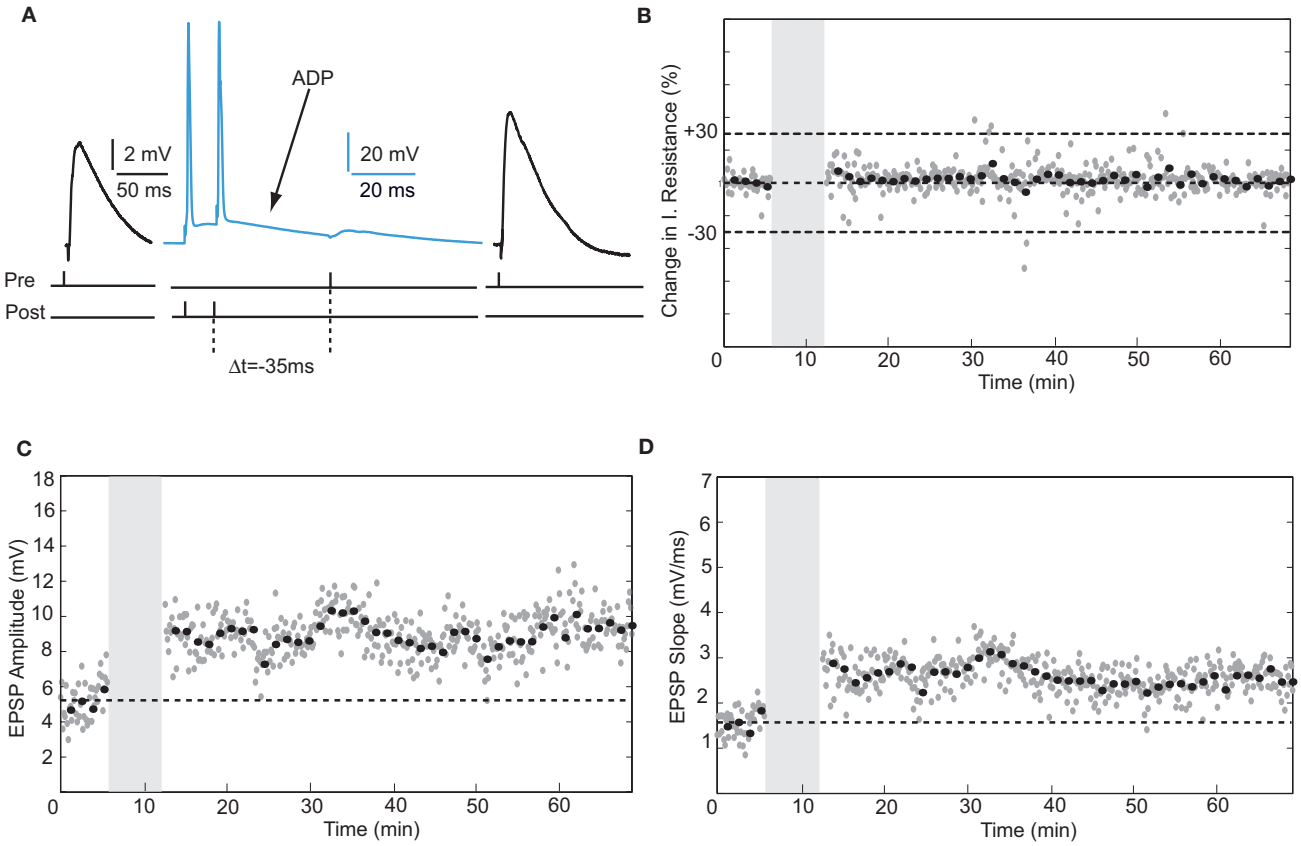

FIGURE 3 | Negative timing intervals at which the postsynaptic neuron fired an action potential before the presynaptic stimulus resulted in tLTP. **(A)** Example EPSPs before and after pairing postsynaptic action potential firing and presynaptic stimulation. **(B)** Input resistance during the entire recording in **(C)** and **(D)**. **(C,D)** EPSP amplitude and slope recorded from a hippocampal pyramidal neuron.

action potential after 5 ms, the slope increased by 69%, *t*-test $p < 0.0001$. These data may suggest that excitatory synapses in human hippocampus can change strength in response to single postsynaptic action potential pairing. However, given the low number of observations on this induction protocol a firm conclusion on this issue awaits further testing.

In rodents and other species, the size and shape of the time windows in which positive and negative synaptic weight changes occur vary for different brain regions (Bi and Poo, 2001; Caporale and Dan, 2008). Excitatory synapses in the human hippocampus showed a wide temporal window for STDP (**Figure 6**). Pairing intervals between −80 and +10 ms induced robust increases in synaptic weight, showing that tLTP was induced at positive and negative timing intervals. Negative timing intervals between −130 and −80 ms induced substantial tLTD. Our findings show that both for excitatory synapses on pyramidal neurons as well as on non-pyramidal neurons, synapse strength could be altered bi-directionally by spike-timing.

DISCUSSION

In this study, we directly tested in whole-cell recordings from human hippocampal neurons whether human synapses can alter strength in response to millisecond timing of pre- and postsynaptic activity and what timing rules determine the sign of plasticity. Our main findings are: (1) Adult human hippocampal synapses can alter synapse strength in response to pairing EPSPs with postsynaptic burst activity and possibly also with single postsynaptic action potentials. (2) In contrast to rodent hippocampal synapses, the sign of plasticity does not sharply switch around 0 ms timing. Instead, both positive timing intervals, in which presynaptic firing preceded the postsynaptic action potential up to 20 ms, and negative timing intervals, in which postsynaptic firing preceded presynaptic activity down to −80 ms, induce tLTP. (3) Negative timing intervals between −80 to −130 ms induce tLTD.

In rodent hippocampus, the rules for induction of STDP change over development (Meredith et al., 2003). A developmental shift occurs in the effectiveness of a single-spike pairing protocol at inducing tLTP. In young hippocampus, repeated pairing of presynaptic activity with a single postsynaptic action potential suffices to induce tLTP, whereas in older rodents a postsynaptic burst of action potentials is necessary to induce synaptic strengthening (Meredith et al., 2003). Blocking GABAergic inhibition with bicuculline rescued the effectiveness of single-spike pairing in inducing tLTP in older animals, which suggests that rules for STDP are affected by a developmental maturation of GABAergic inhibition in the rodent hippocampus (Meredith et al., 2003). In pyramidal neurons, somatic action

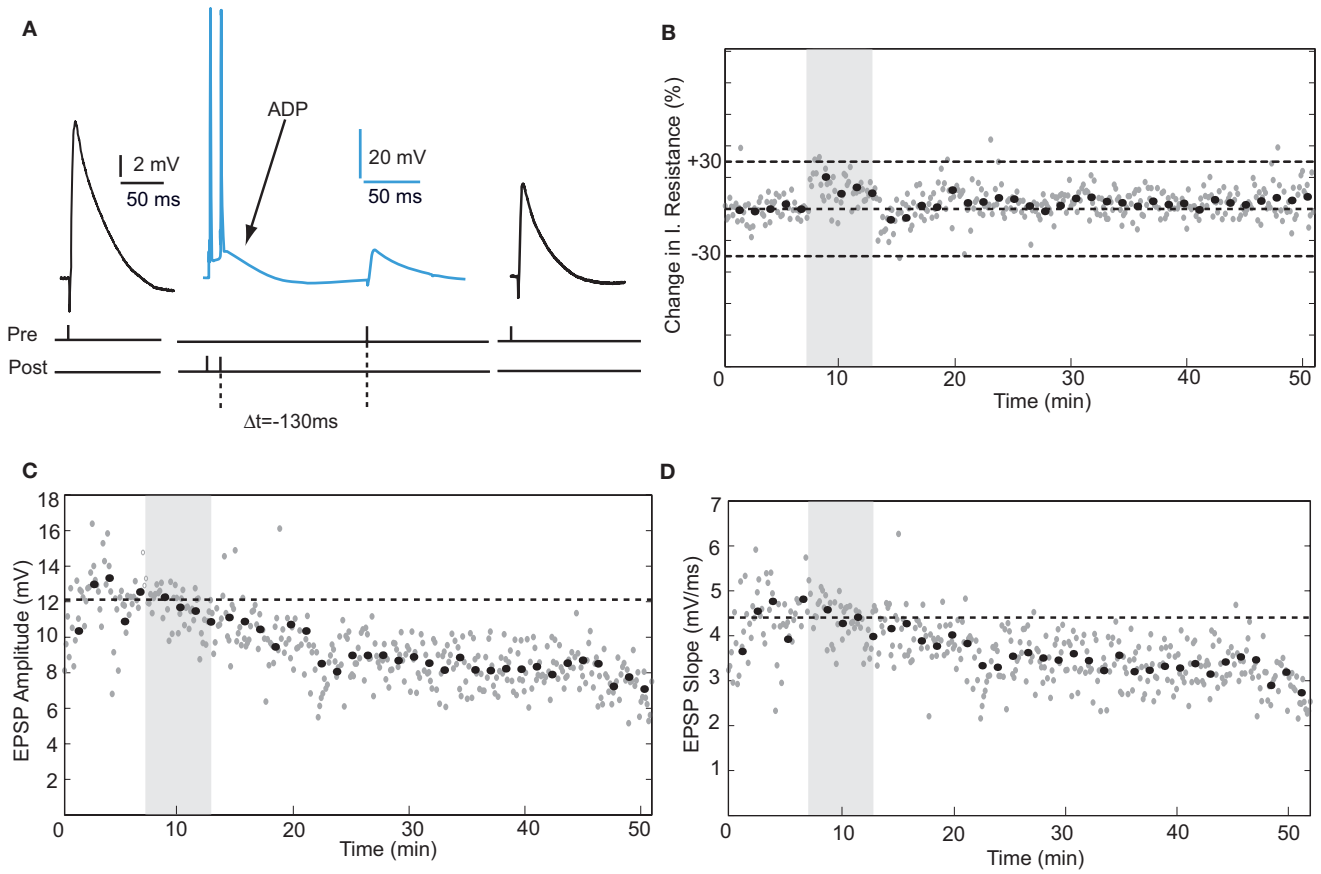

FIGURE 4 | tLTD is induced at negative timing intervals between −80 and −130 ms. (A) Schematic representation of the experiment with example traces. **(B)** Input resistance during the entire recording period. **(C,D)** Example of EPSP amplitude and slope recorded from a hippocampal pyramidal neuron. Same recording as in **(B)**.

potentials back-propagate deep into the dendritic tree and activate voltage-gated calcium channels in proximal and distal parts of dendrites, inducing substantial amounts of calcium influx in dendrites and dendritic spines that can trigger synaptic strength changes (Yuste and Denk, 1995; Magee and Johnston, 1997; Stuart et al., 1997; Koester and Sakmann, 1998). Dendritic back-propagation of action potentials is under GABAergic inhibitory control (Tsubokawa and Ross, 1996). Coincident activation of GABAergic inputs reduces dendritic action potential amplitude and dendritic calcium signals associated with the action potential, which may explain the loss of effectiveness of single-spike pairing in inducing tLTP in older rodent hippocampus. In adult human hippocampus of 20- to 66-years old, repeated pairing of presynaptic activity with a single postsynaptic action potential did induce tLTP. This may suggest that differences may exist between human and rodent adult hippocampal dendrites either in the effectiveness of action potential propagation or in the effectiveness of postsynaptic calcium to trigger the molecular machinery for synapse strengthening. Despite the absence of epileptiform activity, brain slices used in our study were removed from brains of epileptic patients, where GABA might have a depolarizing effect (Dzhala and Staley, 2003; Rheims et al., 2008). It is valid to consider the influence that GABAergic input, potentially recruited via extracellular stimulation, might have on the time window for STDP induction.

The size and shape of the temporal STDP windows in which positive and negative synapse strength changes can vary for different brain regions (Caporale and Dan, 2008). In rodent hippocampus, the window for synaptic modification is restricted to about 40 ms (Bi and Poo, 1998; Debanne et al., 1998; Nishiyama et al., 2000; Wittenberg and Wang, 2006) and a sharp switch of the direction of synaptic change exists at 0-ms timing interval. In adult human hippocampus we did not observe a sharp change of sign of plasticity; positive as well as negative timing intervals induce tLTP. Increases in synapse strength at negative timing intervals have been observed at excitatory synapses onto GABAergic Purkinje-like neurons in electric fish (Bell et al., 1997). Negative timing intervals up to −50 ms resulted in tLTP. Increases in synapse strength in response to negative timing intervals have also been observed in excitatory synapses at distal dendritic locations in neocortex. In neocortex, the shape of the temporal STDP windows depends on dendritic location of synapses (Froemke et al., 2005). In layer 5 pyramidal neurons, proximal and distal synapses exhibit a progressive distance-dependent shift in the timing requirements of the induction of tLTP and tLTD (Letzkus et al., 2006). Distal synapses potentiate when the EPSP arrives after the onset of an AP, in contrast to the timing requirements of proximal synapses at the same dendrites. Most likely during pairing at −10 ms, distal

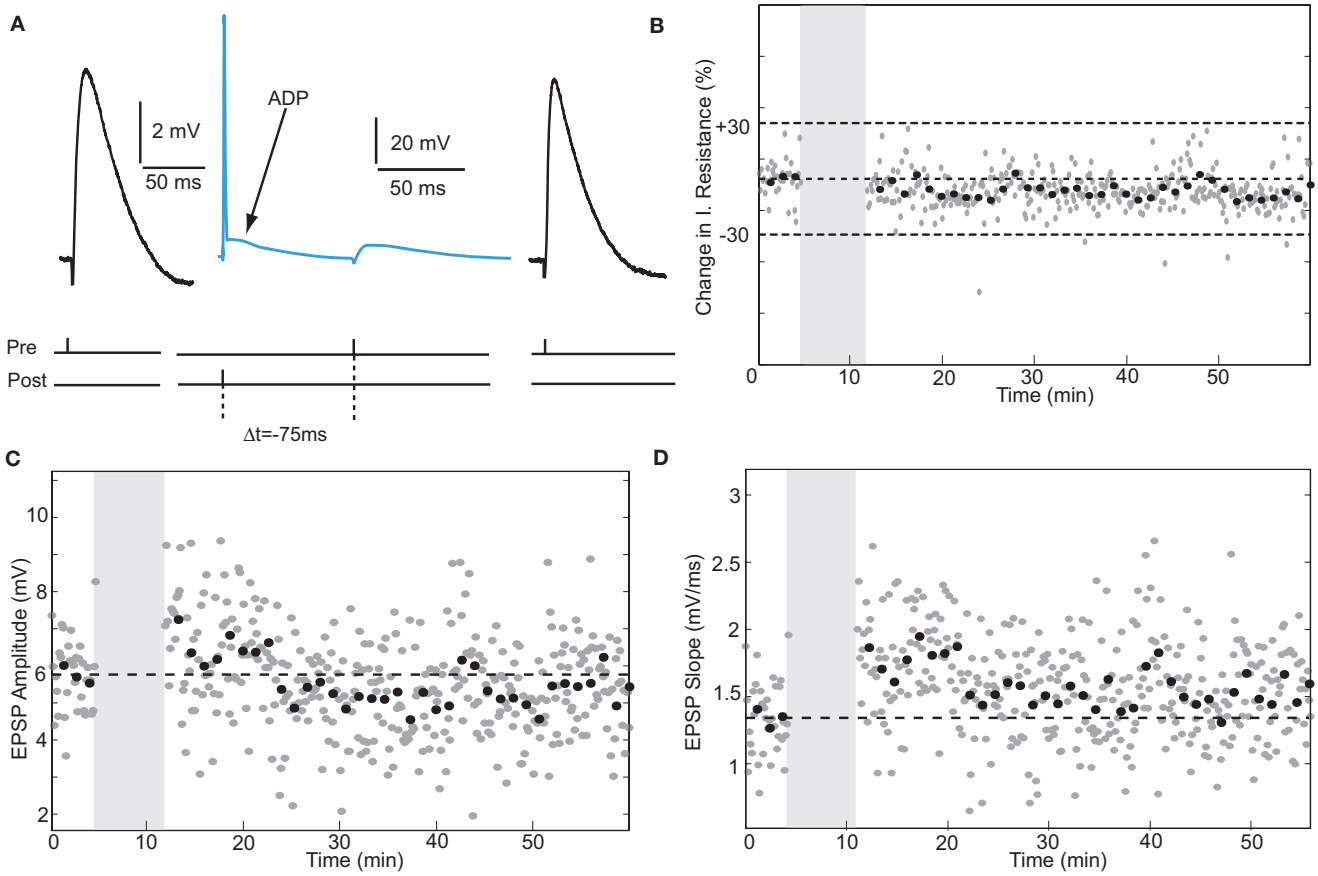

FIGURE 5 | Single postsynaptic action potentials paired with EPSPs induce STDP in adult human hippocampal neurons. (A) Schematic representation of the experiment with example traces. **(B)** Input resistance during the entire recording period. **(C,D)** Single-spike pairing did not alter EPSP amplitude, but induced a small but significant change in slope.

EPSPs coincide with dendritic calcium dynamics induced by the backpropagating action potential (Letzkus et al., 2006; Cornelisse et al., 2007). To prevent variability in the amount of synaptic gain due to spatial dependence of the stimulation site (Sjöström and Häusser, 2006), distance between the recording and stimulation electrodes was carefully controlled in the present study, as described in the Section "Materials and methods". Here, we observed that in human hippocampal synapses a wide window for tLTP exists. Possibly timing delays due to propagation of action potentials in extensive dendritic trees could play a role in determining the timing windows. Alternatively, species differences in synapse dynamics may explain wide STDP temporal window in human synapses.

Whether similar mechanisms as for rat neocortical distal synapses underlie tLTP induction at negative timing intervals in human hippocampal synapses is not clear. Human hippocampal pyramidal neurons did show a prominent ADP, which may result from dendritic action potential propagation. At negative timing intervals between 0 and −80 ms, the EPSP coincided with the falling flank of the ADP, possibly indicating that the EPSP coincided with calcium dynamics induced by the dendritic action potential. Similar mechanisms as in distal neocortical layer 5 synapses may extend the tLTP window to negative timing intervals in human synapses. However, important differences also exist. In contrast to the human synapses, for both synapses on Purkinje-like neurons and rat neocortical distal synapses there was a sharp switch of the sign of plasticity at 0-ms timing interval. Uncovering the mechanisms underlying the tLTP window in human synapses requires further experimental testing.

In rodent hippocampus, the capacity for synaptic depression in synapses declines with age (Dudek and Bear, 1993; Bear and Abraham, 1996). In mouse somatosensory cortex, tLTD induced by a negative timing order in which the postsynaptic neuron fires before the EPSP disappears with age (Banerjee et al., 2009). At ages up to postnatal day 25, negative timing intervals of −10 to −15 ms elicited robust tLTD. At ages beyond 25 days, these timing intervals did not change synaptic strength at all. In adult human hippocampus we find that negative timing intervals between −130 and −80 ms elicit robust tLTD. What the mechanisms are can explain the observation that the timing window lies around −100 ms is currently not known. However, at these intervals, the ADP that follows the action potential has subsided back to baseline by the time the EPSP occurs, which may indicate that at this time the EPSP does not coincide with dendritic calcium dynamics. Our findings do show that human synapses can change bi-directionally depending on spike-timing.

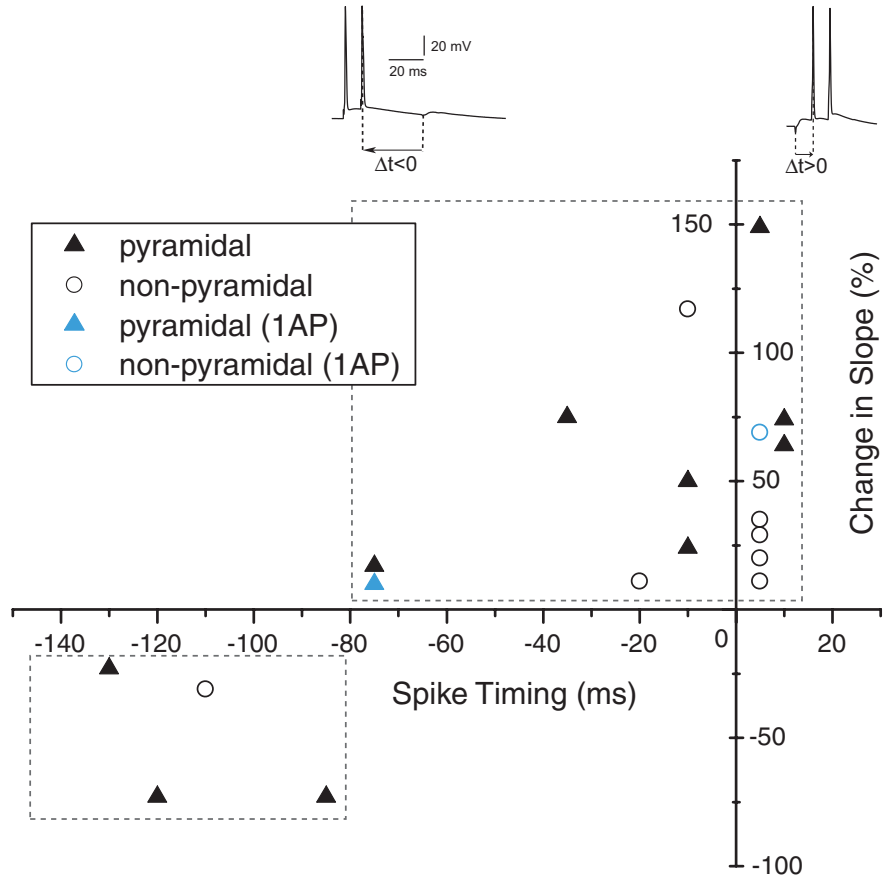

FIGURE 6 | Spike timing window for STDP in human hippocampal synapses.

Do Hebb's predictions hold for human synapses (Hebb, 1949)? He proposed that neurons that fire together, also wire together. With the finding that the sign of plasticity depends on the order of presynaptic and postsynaptic firing (Bell et al., 1997; Magee and Johnston, 1997; Markram et al., 1997) it has been emphasized that temporal specificity is a central feature of Hebb's postulate (Bi and Poo, 2001). Indeed, in rodent hippocampus with a temporal window of 20 ms for tLTP (Bi and Poo, 1998; Debanne et al., 1998; Nishiyama et al., 2000; Wittenberg and Wang, 2006), neurons that fire together will only wire together if pre- and postsynaptic spike timing is tightly correlated. In human synapses it seems that the timing that is necessary to wire together is less strict. The neurons we recorded from showed tLTP in a wide temporal window of about 100 ms. This may be an underestimation since we did not test intervals outside −130 and +10 ms in this study. Different timing windows have been found in different brain areas (Caporale and Dan, 2008). Asymmetric anti-Hebbian STDP, or the depression of an EPSP that occurs if a presynaptic spike follows an increase in the probability of a postsynaptic spike during pairing and reverses into potentiation if the pairing order is reversed (Roberts and Bell, 2002; Zilberter et al., 2009), has been observed in a cell-specific manner in the dorsal cochlear nucleus of the rodent brainstem (Tzounopoulos et al., 2004). The mechanistic basis for a wide temporal window in human hippocampus is at this point not clear, but dendritic calcium dynamics induced by dendritic action potential backpropagation may be involved. If this is the case, and EPSPs coinciding with dendritic calcium dynamics induced by dendritic firing can induce tLTP, then a less strict interpretation of Hebb's theory still applies to human synapses. A wider temporal window for strengthening of synapses in the human brain may allow for the association of larger variety of events with less emphasis on the temporal order. In conclusion, we find that the temporal window for STDP in adult human hippocampal synapses differs from rodent hippocampus, but that the core principles of spike-timing-dependent plasticity apply also to human synapses.

ACKNOWLEDGMENTS

We thank Hans Lodder and Brendan Lodder for excellent technical assistance, Dr. Rhiannon Meredith and Dr. Diana Rotaru for discussions, Dr. Philip de Witt Hamer for assistance with human brain tissue handling, and Prof. Menno Witter and Prof. Tamás Freund for advice on hippocampal and neuronal anatomy. Funding for this work was provided by grants from NWO (917.76.360), Neuroscience Campus Amsterdam, VU University board (Stg VU-ERC) and Neurobsik to Huibert D. Mansvelder.

REFERENCES

Banerjee, A., Meredith, R. M., Rodriguez-Moreno, A., Mierau, S. B., Auberson, Y. P., and Paulsen, O. (2009). Double dissociation of spike timing-dependent potentiation and depression by subunit-preferring NMDA receptor antagonists in mouse barrel cortex. *Cereb. Cortex* 19, 2959–2969.

Bear, M. F., and Abraham, W. C. (1996). Long-term depression in hippocampus. *Annu. Rev. Neurosci.* 19, 437–462.

Beck, H., Goussakov, I. V., Lie, A., Helmstaedter, C., and Elger, C. E. (2000). Synaptic plasticity in the human dentate gyrus. *J. Neurosci.* 20, 7080–7086.

Bell, C. C., Han, V. Z., Sugawara, Y., and Grant, K. (1997). Synaptic plasticity in a cerebellum-like structure depends on temporal order. *Nature* 387, 278–281.

Bi, G., and Poo, M. (2001). Synaptic modification by correlated activity: Hebb's postulate revisited. *Annu. Rev. Neurosci.* 24, 139–166.

Bi, G. Q., and Poo, M. M. (1998). Synaptic modifications in cultured hippocampal neurons: dependence on spike timing, synaptic strength, and postsynaptic cell type. *J. Neurosci.* 18, 10464–10472.

Bliss, T. V., and Lomo, T. (1973). Long-lasting potentiation of synaptic transmission in the dentate area of the anaesthetized rabbit following stimulation of the perforant path. *J. Physiol. (Lond.)* 232, 331–356.

Bureau, I., von Saint Paul, F., and Svoboda, K. (2006). Interdigitated paralemniscal and lemniscal pathways in the mouse barrel cortex. *PLoS Biol.* 4:e382. doi:10.1371/journal.pbio.0040382.

Caporale, N., and Dan, Y. (2008). Spike timing-dependent plasticity: a Hebbian learning rule. *Annu. Rev. Neurosci.* 31, 25–46.

Chen, W. R., Lee, S., Kato, K., Spencer, D. D., Shepherd, G. M., and Williamson, A. (1996). Long-term modifications of synaptic efficacy in the human inferior and middle temporal cortex. *Proc. Natl. Acad. Sci. USA* 93, 8011–8015.

Cooke, S. F., and Bliss, T. V. P. (2006). Plasticity in the human central nervous system. *Brain* 129, 1659–1673.

Cornelisse, L. N., van Elburg, R. A., Meredith, R. M., Yuste, R., and Mansvelder, H. D. (2007). High speed two-photon imaging of calcium dynamics in dendritic spines: consequences for spine calcium kinetics and buffer capacity. *PLoS One* 2:e1073 doi:10.1371/journal.pone.0001073.

Couey, J. J., Meredith, R. M., Spijker, S., Poorthuis, R., Smit, A. B., Brussaard, A. B., and Mansvelder, H. D. (2007). Distributed network actions by nicotine increase the threshold for spike-timing-dependent plasticity in prefrontal cortex. *Neuron* 54, 73–87.

de Kock, C. P., Bruno, R. M., Spors, H., and Sakmann, B. (2007). Layer- and cell-type-specific suprathreshold stimulus representation in rat primary somatosensory cortex. *J. Physiol. (Lond.)* 581, 139–154.

Debanne, D., Gahwiler, B. H., and Thompson, S. M. (1998). Long-term synaptic plasticity between pairs of individual CA3 pyramidal cells in rat hippocampal slice cultures. *J. Physiol. (Lond.)* 507(Pt 1), 237–247.

Dudek, S. M., and Bear, M. F. (1993). Bidirectional long-term modification of synaptic effectiveness in the adult and immature hippocampus. *J. Neurosci.* 13, 2910–2918.

Dzhala, V. I., and Staley, K. J. (2003). Excitatory actions of endogenously released GABA contribute to initiation of ictal epileptiform activity in the developing hippocampus. *J. Neurosci.* 23, 1840–1846.

Foehring, R. C., Lorenzon, N. M., Herron, P., and Wilson, C. J. (1991). Correlation of physiologically and morphologically identified neuronal types in human association cortex *in vitro*. *J. Neurophysiol.* 66, 1825–1837.

Froemke, R. C., Poo, M. M., and Dan, Y. (2005). Spike-timing-dependent synaptic plasticity depends on dendritic location. *Nature* 434, 221–225.

Fuenzalida, M., Fernandez de Sevilla, D., Couve, A., and Buno, W. (2010). Role of AMPA and NMDA receptors and back-propagating action potentials in spike timing-dependent plasticity. *J. Neurophysiol.* 103, 47–54.

Gustafsson, B., Wigstrom, H., Abraham, W. C., and Huang, Y. Y. (1987). Long-term potentiation in the hippocampus using depolarizing current pulses as the conditioning stimulus to single volley synaptic potentials. *J. Neurosci.* 7, 774–780.

Hebb, D. (1949). *The Organization of Behavior*. New York: John Wiley.

Horikawa, K., and Armstrong, W. E. (1988). A versatile means of intracellular labeling: injection of biocytin and its detection with avidin conjugates. *J. Neurosci. Methods* 25, 1–11.

Kampa, B. M., Letzkus, J. J., and Stuart, G. J. (2006). Requirement of dendritic calcium spikes for induction of spike-timing-dependent synaptic plasticity. *J. Physiol. (Lond.)* 574, 283–290.

Kampa, B. M., Letzkus, J. J., and Stuart, G. J. (2007). Dendritic mechanisms controlling spike-timing-dependent synaptic plasticity. *Trends Neurosci.* 30, 456–463.

Koester, H. J., and Sakmann, B. (1998). Calcium dynamics in single spines during coincident pre- and postsynaptic activity depend on relative timing of back-propagating action potentials and subthreshold excitatory postsynaptic potentials. *Proc. Natl. Acad. Sci. USA* 95, 9596–9601.

Larkum, M. E., Zhu, J. J., and Sakmann, B. (2001). Dendritic mechanisms underlying the coupling of the dendritic with the axonal action potential initiation zone of adult rat layer 5 pyramidal neurons. *J. Physiol.* 533, 447–466.

Letzkus, J. J., Kampa, B. M., and Stuart, G. J. (2006). Learning rules for spike timing-dependent plasticity depend on dendritic synapse location. *J. Neurosci.* 26, 10420–10429.

Letzkus, J. J., Kampa, B. M., and Stuart, G. J. (2007). Does spike timing-dependent synaptic plasticity underlie memory formation? *Clin. Exp. Pharmacol. Physiol.* 34, 1070–1076.

Levy, W. B., and Steward, O. (1983). Temporal contiguity requirements for long-term associative potentiation/depression in the hippocampus. *Neuroscience* 8, 791–797.

Magee, J. C., and Johnston, D. (1997). A synaptically controlled, associative signal for Hebbian plasticity in hippocampal neurons. *Science* 275, 209–213.

Markram, H., Lubke, J., Frotscher, M., and Sakmann, B. (1997). Regulation of synaptic efficacy by coincidence of postsynaptic APs and EPSPs. *Science* 275, 213–215.

Mercer, A., Trigg, H. L., and Thomson, A. M. (2007). Characterization of neurons in the CA2 subfield of the adult rat hippocampus. *J. Neurosci.* 27, 7329–7338.

Meredith, R. M., Floyer-Lea, A. M., and Paulsen, O. (2003). Maturation of long-term potentiation induction rules in rodent hippocampus: role of GABAergic inhibition. *J. Neurosci.* 23, 11142–11146.

Meredith, R. M., Holmgren, C. D., Weidum, M., Burnashev, N., and Mansvelder, H. D. (2007). Increased threshold for spike-timing-dependent plasticity is caused by unreliable calcium signaling in mice lacking fragile X gene FMR1. *Neuron* 54, 627–638.

Nishiyama, M., Hong, K., Mikoshiba, K., Poo, M.-M., and Kato, K. (2000). Calcium stores regulate the polarity and input specificity of synaptic modification. *Nature* 408, 584–588.

Rheims, S., Represa, A., Ben-Ari, Y., and Zilberter, Y. (2008). Layer-specific generation and propagation of seizures in slices of developing neocortex: role of excitatory GABAergic synapses. *J. Neurophysiol.* 100, 620–628.

Roberts, P. D., and Bell, C. C. (2002). Spike timing dependent synaptic plasticity in biological systems. *Biol. Cybern.* 87, 392–403.

Routh, B. N., Johnston, D., Harris, K., and Chitwood, R. A. (2009). Anatomical and electrophysiological comparison of CA1 pyramidal neurons of the rat and mouse. *J. Neurophysiol.* 102, 2288–2302.

Sjöström, P. J., Häusser, M. (2006). A cooperative switch determines the sign of synaptic plasticity in distal dendrites of neocortical pyramidal neurons. *Neuron* 51, 227–238.

Staff, N. P., Jung, H. Y., Thiagarajan, T., Yao, M., and Spruston, N. (2000). Resting and active properties of pyramidal neurons in subiculum and CA1 of rat hippocampus. *J. Neurophysiol.* 84, 2398–2408.

Stefan, K., Kunesch, E., Cohen, L. G., Benecke, R., and Classen, J. (2000). Induction of plasticity in the human motor cortex by paired associative stimulation. *Brain* 123, 572–584.

Stuart, G., Spruston, N., Sakmann, B., and Hausser, M. (1997). Action potential initiation and backpropagation in neurons of the mammalian CNS. *Trends Neurosci.* 20, 125–131.

Tsubokawa, H., and Ross, W. N. (1996). IPSPs modulate spike backpropagation and associated [Ca^{2+}]i changes in the dendrites of hippocampal CA1 pyramidal neurons. *J. Neurophysiol.* 76, 2896–2906.

Tzounopoulos, T., Kim, Y., Oertel, D., and Trussell, L. O. (2004). Cell-specific, spike timing-dependent plasticities in the dorsal cochlear nucleus. *Nat. Neurosci.* 7, 719–725.

Whitlock, J. R., Heynen, A. J., Shuler, M. G., and Bear, M. F. (2006). Learning induces long-term potentiation in the hippocampus. *Science* 313, 1093–1097.

Wittenberg, G. M., and Wang, S. S. (2006). Malleability of spike-timing-dependent plasticity at the CA3-CA1 synapse. *J. Neurosci.* 26, 6610–6617.

Wolters, A., Sandbrink, F., Schlottmann, A., Kunesch, E., Stefan, K., Cohen, L. G., Benecke, R., and Classen, J. (2003). A temporally asymmetric Hebbian rule governing plasticity in the human motor cortex. *J. Neurophysiol.* 89, 2339–2345.

Wolters, A., Schmidt, A., Schramm, A., Zeller, D., Naumann, M., Kunesch, E., Benecke, R., Reiners, K., and Classen, J. (2005). Timing-dependent plasticity in human primary somatosensory cortex. *J. Physiol. (Lond.)* 565, 1039–1052.

Yuste, R., and Denk, W. (1995). Dendritic spines as basic functional units of neuronal integration. *Nature* 375, 682–684.

Zilberter, M., Holmgren, C., Shemer, I., Silberberg, G., Grillner, S., Harkany, T., and Zilberter, Y. (2009). Input specificity and dependence of spike timing-dependent plasticity on preceding postsynaptic activity at unitary connections between neocortical layer 2/3 pyramidal cells. *Cereb. Cortex* 19, 2308–2320.

Conflict of Interest Statement: The authors declare that the research was conducted in the absence of any commercial or financial relationships that could be construed as a potential conflict of interest.

Received: 01 February 2010; paper pending published: 16 February 2010; accepted: 17 May 2010; published online: 02 July 2010. Citation: Testa-Silva G, Verhoog MB, Goriounova NA, Loebel A, Hjorth JJJ, Baayen JC, de Kock CPJ and Mansvelder HD (2010) Human synapses show a wide temporal window for spike-timing-dependent plasticity. Front. Syn. Neurosci. ***2****:12. doi: 10.3389/fnsyn.2010.00012*

frontiers in
SYNAPTIC NEUROSCIENCE

ORIGINAL RESEARCH ARTICLE
published: 11 June 2010
doi: 10.3389/fnsyn.2010.00013

A developmental sensitive period for spike timing-dependent plasticity in the retinotectal projection

Jennifer Tsui, Neil Schwartz and Edward S. Ruthazer*

Montreal Neurological Institute, McGill University, Montreal, QC, Canada

Edited by:
Per Jesper Sjöström, University College London, UK

Reviewed by:
Hollis Cline, The Scripps Research Institute, USA
Mu-Ming Poo, University of California at Berkeley, USA
Susan B. Udin, State University of New York, Buffalo, USA

***Correspondence:**
Edward S. Ruthazer, Montreal Neurological Institute, McGill University, 3801 University Street, Montreal, QC, H3A 2B4, Canada.
e-mail: edward.ruthazer@mcgill.ca

The retinotectal projection in *Xenopus laevis* has been shown to exhibit correlation-based refinement of both anatomical and functional connectivity during development. Spike timing-dependent plasticity (STDP) is an appealing experimental model for correlation-based synaptic plasticity because, in contrast to plasticity induction paradigms using tetanic stimulation or sustained postsynaptic depolarization, its induction protocol more closely resembles natural physiological activity. In Xenopus tadpoles, where anatomical remodeling has been reported throughout much of the life of the animal, *in vivo* retinotectal STDP has only been examined under a limited set of experimental conditions. Using perforated-patch recordings of retina-evoked EPSCs in tectal neurons, we confirmed that repeatedly driving a retinotectal EPSP 5–10 ms prior to inducing an action potential in the postsynaptic cell, reliably produced timing-dependent long-term potentiation (t-LTP) of the retinotectal synapse in young wild type tadpoles (stages 41–44). At these stages, retinotectal timing-dependent long-term depression (t-LTD) also could be induced by evoking an EPSP to arrive 5–10 ms after an action potential in the tectal cell. However, retinotectal STDP using this standard protocol was limited to a developmental sensitive period, as we were unable to induce t-LTP or t-LTD after stage 44. Surprisingly, this STDP protocol also failed to induce reliable STDP in albino tadpoles at the early ages when it was effective in wild type pigmented animals. Nonetheless, low-frequency flashes to the eye produced a robust NMDA receptor-dependent retinotectal LTD in stage 47 albino tadpoles, demonstrating that the retinotectal synapse can nonetheless be modified in these animals using different plasticity paradigms.

Keywords: synaptic plasticity, retinotectal, albino, visual system, *N*-methyl-*d*-aspartate receptor, *Xenopus laevis*, development

INTRODUCTION

Patterned neural activity and early sensory experience profoundly impact the development of organized circuit connectivity and can dramatically modify receptive field properties in the developing nervous system (Katz and Shatz, 1996; Holtmaat and Svoboda, 2009). The developing visual system has served as a model system in which to investigate the influences of sensory experience on circuit formation (Ruthazer and Cline, 2004; Huberman et al., 2008). In particular, the retinotectal projection in *Xenopus laevis* tadpoles has been a powerful platform for these studies, as it is possible to carry out both time-lapse imaging of structural development and electrophysiological measurements of synaptic physiology and receptive field structure on single neurons in the intact animal.

Computational models of activity-dependent map formation have traditionally employed a learning rule in which synapses between two neurons are strengthened in proportion to the degree of correlation in their firing (Abbott and Nelson, 2000). Such learning rules are sometimes referred to as "Hebbian", in recognition of the Canadian psychologist Donald O. Hebb, who first formally proposed that when one neuron "repeatedly or persistently takes part in firing" another neuron, its connection to that cell should be strengthened (Hebb, 1949). While many Hebbian models simplify this concept to reflect correlation in the firing rates of two cells, Hebb's original formulation specifically considered temporal causality.

Spike timing-dependent plasticity (STDP) is an experimentally observed form of Hebbian synaptic plasticity in which the precise order of firing of the pre- and postsynaptic partners determines the direction of changes in synaptic efficacy. STDP not only constitutes a plasticity mechanism that satisfies Hebb's requirement for temporal causality by strengthening those synapses at which the presynaptic cell fires just prior to its postsynaptic partner, but also includes a convenient mechanism for weakening synapses in the case when the postsynaptic cell fires first. It has been described in various forms in many circuits (Levy and Steward, 1983; Bell et al., 1997; Magee and Johnston, 1997; Markram et al., 1997; Feldman, 2000; Sjostrom et al., 2001), and was demonstrated *in vivo* in the Xenopus retinotectal system by Zhang et al. (1998). These seminal retinotectal experiments have been followed up by an impressive series of studies demonstrating the ability of STDP to modify various receptive field properties in the immature visual system, including direction selectivity and receptive field shape (Tao et al., 2001; Zhou et al., 2003; Vislay-Meltzer et al., 2005; Mu and Poo, 2006).

In principle, STDP could also provide an elegant potential mechanism for mediating the activity-dependent refinement and maintenance of topographic organization in the retinotectal circuit, a process in which patterned neural activity and *N*-methyl-D-aspartate receptors (NMDARs) as correlation detectors have been directly implicated (Cline and Constantine-Paton, 1989; Ruthazer

et al., 2003; Dong et al., 2009). Retinotectal map development in Xenopus is a protracted process that continues even after metamorphosis (Gaze et al., 1974). On the other hand, Xenopus retinotectal STDP experiments to date have focused almost exclusively on the initial period of innervation from developmental stages 40–45, a period during which time retinotectal axons are largely overlapping within the tectal neuropil and the emerging retinotopic map is barely detectable anatomically (Sakaguchi and Murphey, 1985; O'Rourke and Fraser, 1990). It had been unknown, however, whether the same STDP mechanisms could also drive retinotectal input modification at later stages, perhaps participating in the activity-dependent refinement and maintenance of the retinotopic map. In the present study, we confirm previous findings that correlated firing of pre- and postsynaptic neurons within a narrow spike-timing window leads to robust timing-dependent long-term potentiation (t-LTP) and depression (t-LTD) in early stage tadpoles, but find that after stage 44 the same STDP protocols no longer caused long-lasting changes in synaptic efficacy. On the other hand, we demonstrate a protocol for retinotectal plasticity induction using patterned visual stimulation that is effective in older tadpoles, arguing for distinct activity-dependent plasticity mechanisms participating at different stages of Xenopus retinotectal development.

MATERIAL AND METHODS

IN VIVO ELECTROPHYSIOLOGY PREPARATION

Wild type and albino *X. laevis* tadpoles staged 41–47 according to criteria from Nieuwkoop and Faber (1956) were anesthetized in modified Barth's solution (MBS-H) containing 0.02% MS222 (Sigma) for dissection. For retinal loose patch stimulation experiments, the lens was removed from one eye to expose the retina. The skin on the head was cut and the brain was opened along the midline for recording in the contralateral tectal lobe. For recording, the tadpole was fixed to a Sylgard insert in the recording chamber with insect pins. The tadpole was constantly perfused with fresh external solution, and all experiments were performed at the room temperature. Movement of red blood cells could be observed in healthy animals in the vessels of the tectum and was monitored throughout the experiment.

STDP EXPERIMENTS

Whole-cell perforated-patch recording was performed as previously described (Zhang et al., 1998). The external solution was composed of (in mM): NaCl, 115; KCl, 2; HEPES, 10; $CaCl_2$, 3; $MgCl_2$, 1.5; glucose, 10; glycine, 0.005 (pH 7.3). To paralyze the tadpole, the external solution also contained 2.5 mM tubocurare (Sigma). Borosilicate glass micropipettes (Warner), with a resistance in the range of 4–7 MΩ were briefly dipped in internal solution, and then back-filled with amphotericin B (250 μg/ml, Calbiochem) containing internal solution. The internal solution contained (in mM): K-gluconate, 110 KCl, 10; NaCl, 5; $MgCl_2$, 1.5; EGTA, 0.5; HEPES, 20; ATP, 2; GTP, 0.3 (pH 7.3). 4–7 MΩ patch pipettes were also used for extracellular retinal stimulation except that they were filled with external solution. Cells in the rostral tectum were targeted for recording. Test pulses were applied every 30 s in voltage clamp. Measurements of monosynaptically driven EPSCs were made using response latency to define the input. In a single case (t-LTP at stage 47) two consistently separable inputs onto a single cell were both included for analysis. STDP was induced by switching to current clamp mode and pairing retinal stimulation with postsynaptic current injection to produce an action potential in the tectal cell at the time intervals indicated. These pairings were repeated 100 times at 1 Hz. Recordings were acquired with a patch clamp amplifier (Axopatch 200B; Axon Instruments) and Clampex software (Axon Instruments). Input resistance (0.5–1 GΩ) and series resistance (30–70 MΩ) were monitored continuously during recordings. Data were accepted for analysis only if the series resistance remained relatively constant (<20% change) throughout the experiment. Cells were held at a constant potential of −60 mV (except during spike pairing). Liquid junction potential was not corrected.

VISUALLY INDUCED LTD EXPERIMENTS

Stage 47 albino tadpoles were immobilized while anesthetized 0.02% MS222 (Sigma) in MBS-H. A custom built harp was placed over the tadpole and the preparation was fixed in place in the recording chamber with 3% low-melting point agarose and insect pins (Sigma). A window over the brain was then opened in the set agarose. The chamber was then flooded with external solution (in mM): 135 NaCl, 2 KCl, 10 HEPES, 10 glucose, $3CaCl_2$, 1.5 $MgCl_2$, pH 7.3, osm: 255–260. The skin was then split along the midline of the brain and the overlying pia mater carefully removed with a broken patch pipette to gain access to the tectal cells. A custom bent bipolar electrode (FHC) was then inserted into the optic chiasm. After allowing the preparation to stabilize for 20 min, tectal cells were patched in the whole cell configuration using borosilicate glass pipettes with resistances of 4–9 MΩ. Access resistance (typically 50 MΩ) was monitored throughout the experiment and cells that changed by more than 20% were excluded. The internal solution consisted of 120 K-gluconate, 5 NaCl, 1.5 MgCl, 20 HEPES, 1 EGTA, 2 ATP, 0.3 GTP (in mM). For monitoring-evoked currents, cells were clamped at −70 mV. Cells were discarded if evoked events had latencies that varied with stimulus intensity, if the event did not occur within 5 ms of the stimulus, or if more than two failures were observed during the baseline. After a 6 min baseline (test stimulus every 30 s), the recording was switched to current clamp ($I = 0$; average resting potential −67.4 mV). The animal was then stimulated with a 4×3 array of green LEDs placed approximately 12 cm from the eye contralateral to the recording pipette for 15 min, with each of the four rows of LEDs illuminating for 1 s in sequence followed by 1 s of darkness (1 Hz transitions within a 0.2 Hz cycle). Cells exhibited consistent subthreshold response to the LEDs but did not spike consistently in response to the stimulus. After the 15 min stimulation period, EPSCs were again monitored at −70 mV in voltage clamp. For NMDA receptor blockade, CPP (40 μm) (Tocris) was bath applied 1 min after obtaining the whole cell configuration.

DATA ANALYSIS

Data were analyzed using ClampFit software (Molecular Devices). Statistics were performed with SPSS software. Plasticity was assessed using a one-sample *t*-test on EPSC peak amplitudes averaged from 20 to 30 min after induction, normalized to the baseline amplitudes collected during the 10 minutes immediately before

induction. Differences across experimental groups were analyzed for significance using Student's *t*-test for two groups and ANOVA with Bonferroni *post hoc* analyses for multiple groups.

EXPERIMENTAL ANIMALS

Experiments were approved by the Montreal Neurological Institute Animal Research Committee and performed in accordance with guidelines of the Canadian Council on Animal Care.

RESULTS

STDP INDUCTION IN THE XENOPUS TADPOLE

We sought to determine whether retinotectal STDP mechanisms that have been implicated in early retinotectal plasticity and receptive field modifications continue to be expressed at later stages as the anatomical retinotectal map gradually emerges and tectal neuronal receptive fields refine (O'Rourke and Fraser, 1990; Tao and Poo, 2005). *In vivo* perforated-patch voltage clamp recordings were made to monitor the strength of retinal ganglion cell (RGC) synaptic inputs over time (**Figure 1A**; Zhang et al., 1998). Extracellular stimulation using a loose patch electrode positioned in the contralateral eye evoked a monosynaptic inward current with an onset latency of about 5 ms in tectal cells clamped at −60 mV to block NMDARs (**Figure 1B**). The amplitude of this evoked excitatory postsynaptic current (EPSC) was monitored every 30 s to measure changes in retinotectal synaptic efficacy.

For the induction of STDP, recordings were temporarily switched to current clamp mode to permit the firing of an action potential in response to depolarizing current injection through the recording pipette. One of three standard induction protocols was applied: (1) for t-LTP, retinal stimulation was timed to evoke an EPSP 5–10 ms prior to the induction of an action potential in the tectal neuron (**Figure 1C**), (2) for t-LTD the EPSP was timed to arrive 5–10 ms after the action potential (**Figure 1D**), and (3) a negative control protocol in which the interval between the action potential and the EPSP is outside the window to induce synaptic plasticity (+100 ms interval, **Figure 1E**). Intervals of 5–10 ms were chosen because these timing differences produced large changes in synaptic efficacy in previous reports (Zhang et al., 1998). Pairings were repeated 100 times at 1 Hz.

RETINOTECTAL STDP IN WILD TYPE TADPOLES IS LIMITED TO EARLY DEVELOPMENT

As illustrated in the example from a stage 43 tadpole, the pre/post pairing protocol produced a robust retinotectal t-LTP in young, stage 41–44 wild type tadpoles (**Figure 2A**) consistent with previous reports (Zhang et al., 1998). This protocol for induction of t-LTP was highly

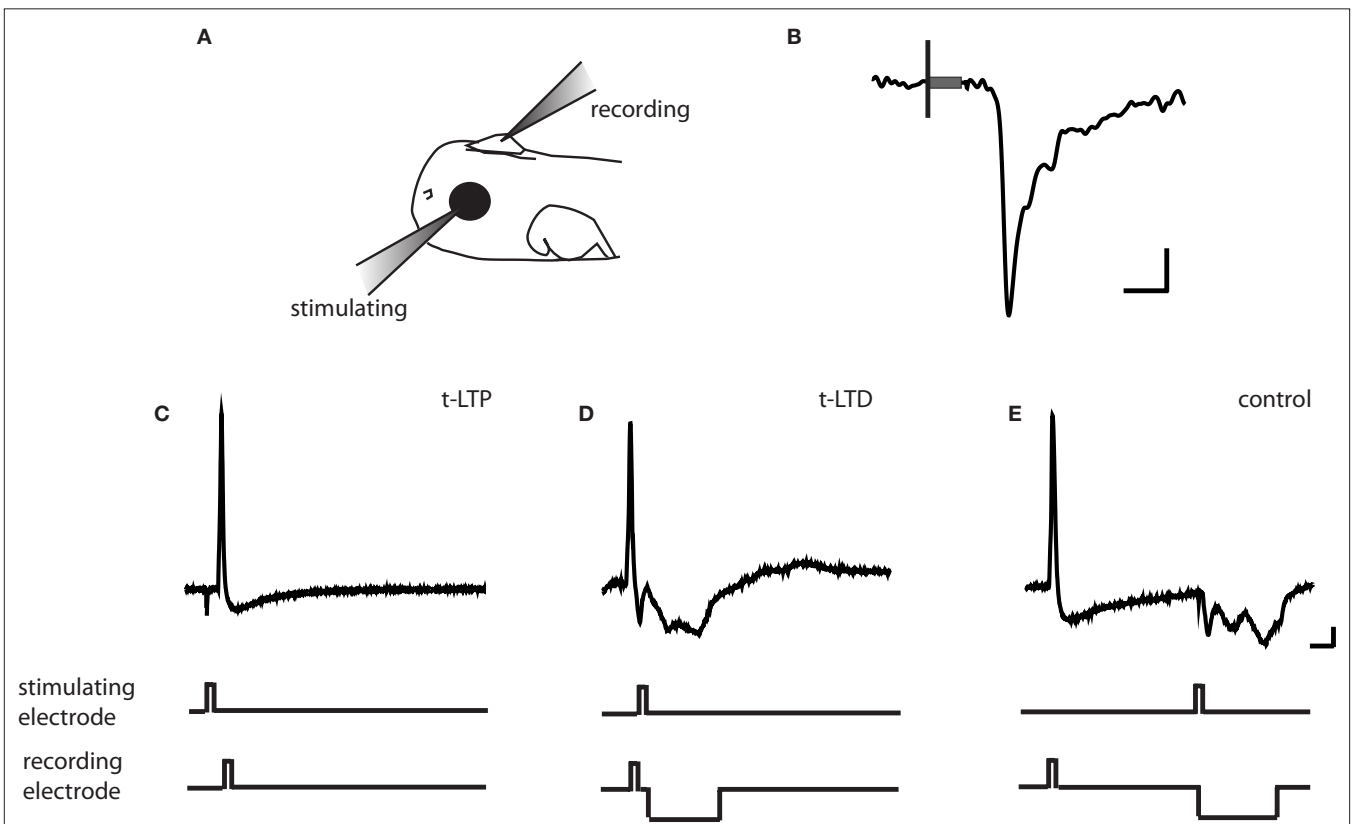

FIGURE 1 | Protocols for inducing STDP. (A) Schematic of *in vivo* recording set-up. **(B)** Representative tectal response to retinal stimulation. Scale bar is 5pA and 5 ms. Black line indicates beginning of 100-ms stimulus and gray box indicates stimulus artifact. **(C)** t-LTP protocol. A 2 ms 0.17–0.2 pA current pulse was injected in the post-synaptic tectal cell to evoke an action potential 5–10 ms following the onset of the EPSC. **(D)** t-LTD protocol. The stimulating electrode in the retina was timed to evoke an EPSC 5–10 ms after an action potential in the tectal neuron. **(E)** In the control conditioning protocol, this timing window was lengthened to 100 ms, outside the described window for plasticity at this synapse (Zhang et al., 1998). A 20–60 ms hyperpolarizing current pulse was timed to prevent action potential firing due to the retinal EPSC. Traces are from cells held at –40 to –50 mV in current clamp. Scale bar is 10 mV and 20 ms.

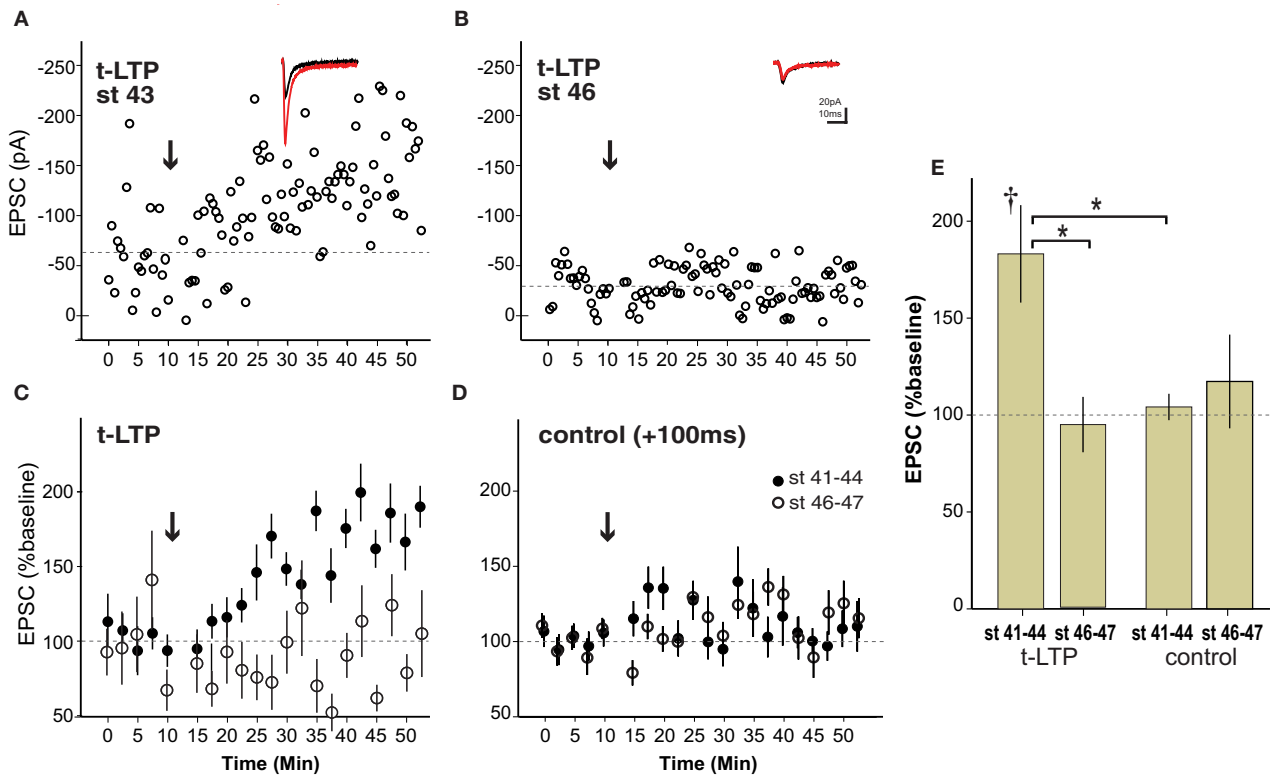

FIGURE 2 | Spike timing-dependent LTP is limited to a sensitive period ending around stage 45 in wild type tadpoles. (A) Experiment in a stage 43 tadpole in with t-LTP was induced (arrow) using a 5–10 ms preàpost pairing interval. Inset shows averaged EPSC before (black) and 20–30 min after (red) t-LTP induction. **(B)** Example from stage 46 animal lacking t-LTP. **(C)** Averages of t-LTP induction experiments in stage 41–44 (filled circles, $n = 4$) and stage 46–47 (open circles, $n = 4$) tadpoles. **(D)** Control (100-ms interval) pairing did not induce reliable STDP at any age (stage 41–44, $n = 7$; stage 46–47, $n = 5$). **(E)** Graph summarizing t-LTP experiments by age. †$p < 0.05$ one-sample *t*-test (0–10 vs. 30–40 min), *$p < 0.05$ ANOVA with Bonferroni post-test.

reliable, leading to a significant increase in EPSC amplitude by 20 min after induction (183 ± 25% baseline, $p < 0.05$) in four out of four cases (**Figure 2C**). In contrast, the same induction protocol failed to produce a potentiation (94 ± 14% baseline, $n = 4$, $p > 0.05$) in animals after stage 45 (**Figures 2B,C**). The control pairing protocol (+100-ms interval) did not cause a significant change in EPSC amplitude at any age tested (108 ± 10% baseline, $n = 12$, $p > 0.05$), confirming that the potentiation before stage 45 was indeed a consequence of the spike timing interval rather than a non-specific synaptic run-up following repeated stimulation in the younger animals (**Figures 2D,E**). This result demonstrates that t-LTP in wild type tadpoles is restricted to a developmental sensitive period that ends around stage 45.

The mechanisms underlying t-LTP and t-LTD have been shown to be separable in some systems (Bender et al., 2006). We therefore examined whether retinotectal t-LTD was also restricted to a developmental period similar to that for t-LTP. **Figure 3A** shows the induction of t-LTD in a stage 41 tadpole, during the sensitive period. On the other hand at stage 45 t-LTD could not be induced using the same protocol (**Figure 3B**). Overall, the t-LTD induction protocol produced a significant reduction of EPSC amplitude in stage 41–44 wild type tadpoles (65 ± 11% baseline, $n = 7$, $p < 0.05$; **Figure 3C**). The same protocol in older tadpoles did not reliably produce t-LTD, but instead led to a small, non-significant increase in EPSC amplitude (123 ± 12% baseline, $n = 6$, $p > 0.05$). Thus, retinotectal t-LTD also exhibits an age-dependence with tadpoles younger than stage 45 responding differently from older animals (stage 41–44 vs. stage 45–47, $p < 0.01$; **Figure 3D**). **Figure 4** presents a scatter plot of all the STDP experiments by age. While it is not possible from this dataset to precisely define an exact point when the STDP sensitive period ends it is clear that the efficacy of the standard spike-timing protocols to induce reliable synaptic changes falls off substantially around stage 45 in wild type tadpoles.

ALBINO TADPOLES DO NOT EXHIBIT ROBUST CLASSIC RETINOTECTAL STDP

The albino *X. laevis* tadpole is a useful experimental model for *in vivo* imaging due to the relative ease with which the brain can be visualized in the intact animal. In order to be able to more directly relate retinotectal imaging data from the literature to synaptic plasticity studies, we examined STDP in albino tadpoles (**Figure 5**). Surprisingly, neither t-LTP (97 ± 28% baseline, $n = 4$) nor t-LTD (96 ± 7% baseline, $n = 4$) could be reliably induced in albino tadpoles during the STDP sensitive period defined from wild type animals.

VISUAL STIMULATION PROTOCOL CAN INDUCE RETINOTECTAL LTD IN STAGE 47 ALBINO TADPOLES

Previous experiments in albino tadpoles in which signaling through Ca/calmodulin kinase 2 (Wu et al., 1996), AMPAR trafficking (Haas et al., 2006) or calcineurin (Schwartz et al., 2009)

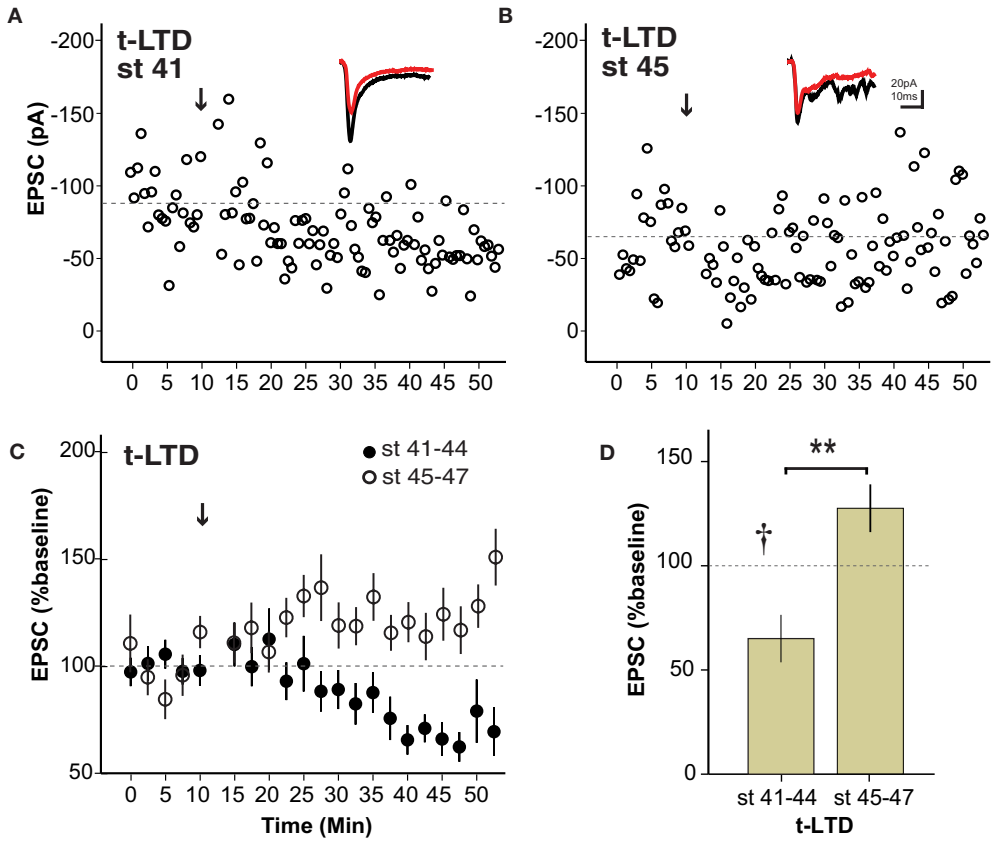

FIGURE 3 | The sensitive period for spike timing-dependent LTD is similar to that for t-LTP. (A) Experiment from a stage 41 tadpole in which t-LTD was induced (arrow) using the 5–10 ms postàpre protocol. **(B)** The same pairing protocol failed to induce synaptic depression in a stage 45 tadpole. Insets show sample traces as in **Figure 1. (C)** Average of all t-LTD experiments grouped by developmental stage. **(D)** Graph summarizing t-LTD experiments by developmental stage. $n = 7$ stage 41–44, $n = 6$ stage 45–47, †$p < 0.05$ one-sample *t*-test (0–10 vs. 30–40 min), **$p < 0.01$ Student's *t*-test.

was genetically disrupted suggest that they are likely to possess the necessary signaling machinery to exhibit some forms of retinotectal synaptic plasticity. Furthermore, Dunfield and Haas (2009) have shown that repeated presentation of visual stimuli can induce a long-lasting change in the amplitude of calcium signals measured at tectal cell somata in stage 50 albino tadpoles. The limitation of such measurements is that they cannot distinguish between retinotectal synaptic plasticity and changes in the intrinsic excitability or local connectivity of the tectal neurons or retinal neurons themselves. We therefore examined the effects of repeated visual stimulation on retinotectal synaptic efficacy in albino tadpoles by placing a bipolar stimulating electrode in the optic chiasm to evoke test pulses in RGC afferent axons. Plasticity was induced by sequentially flashing an array of LEDs in front of the eye contralateral to the recording pipette at low frequency for 15 min (see Section "Methods"). This low-frequency visual stimulation protocol resulted in a dramatic LTD of the retinotectal EPSC amplitude (59 ± 10% baseline, $n = 9$) in stage 47 albino tadpoles (**Figures 6A,C**). This LTD was significantly attenuated (85 ± 6% baseline, $n = 4, p < 0.001$) in the presence of the NMDAR antagonist CPP (**Figures 6 B,C**). These results demonstrate that the Xenopus retinotectal synapse can exhibit robust LTD in response to natural sensory stimulation in older albino animals despite the fact that neither albino nor late stage tadpoles appeared to exhibit STDP when tested using standard induction protocols.

DISCUSSION

Our study confirmed previous reports that repeated pairing of pre- and postsynaptic neuronal firing using a 5–10 ms EPSP-to-spike interval is highly effective at driving retinotectal t-LTP and t-LTD in the developing Xenopus visual system. We found that STDP induced by this classic protocol is restricted to the period of early retinotectal development ending around stage 45 in wild type tadpoles. Surprisingly, unlike wild type pigmented animals, albino tadpoles did not exhibit reliable STDP even during the sensitive period. Stage 47 albino tadpoles nonetheless did show a profound retinotectal LTD in response to repeated low-frequency visual stimulation, suggesting that diverse mechanisms can participate in retinotectal circuit plasticity.

SENSITIVE PERIODS IN CIRCUIT DEVELOPMENT

Sensitive periods for developmental plasticity in many different brain areas have been described, including for ocular dominance shifts in primary visual cortex (Wiesel, 1982; Hensch, 2005), eye

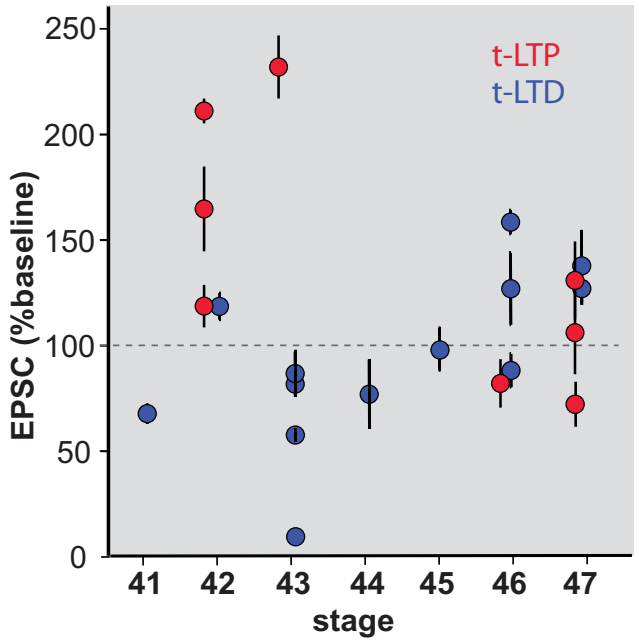

FIGURE 4 | Scatterplot showing STDP efficacy as a function of developmental stage. Mean EPSC amplitude measured at 20–30 min after induction, normalized to baseline amplitude during the 10 min immediately prior to induction.

specific segregation in the lateral geniculate nucleus (Huberman et al., 2008), thalamocortical LTP and LTD (Inan and Crair, 2007), and map plasticity in supragranular layers of cortex (Kirkwood et al., 1995; Li et al., 2009). While at first glance it may seem that any loss of potential for plasticity imposes undesirable limits on a developing circuit, it is likely that the development of fully functional circuits requires that the susceptibility of some inputs, especially primary inputs, to undergo plastic changes be restricted to permit the progressive refinement of others. For example, the relatively early stabilization of thalamic inputs to layer 4 of cortex may be necessary to provide the precise timing of firing in layer 4 that later drives STDP in the projection to layer 2/3 (Celikel et al., 2004). The mapping of auditory space onto the visuotopic map in the optic tectum in barn owls is another example where restricted plasticity in the visual inputs facilitates appropriate modifications of the coordinated auditory inputs (Knudsen, 2002). Similarly, in the Xenopus optic tectum STDP of recurrent excitation, which helps sculpt the temporal properties of the tectal response (Pratt et al., 2008), and multimodal integration in which other sensory modalities are mapped onto the retinotopic representation (Deeg et al., 2009; Hiramoto and Cline, 2009) are both likely to benefit from reduced plasticity in the primary sensory inputs from the retina. Interestingly, STDP of recurrent excitation in the tectum has been observed at stages 47–48, meaning that distinct populations of synapses onto the same cells can exhibit different potential to undergo this form of plasticity.

Tectal growth, shifting of retinal terminals across the developing tectum and accompanying receptive field changes proceed long after the period when STDP can no longer be induced (Fraser, 1983; Sakaguchi and Murphey, 1985). Our finding that specific patterns of visual stimulation were still capable of driving retinotectal synaptic changes at a later stage of development raises the possibility that other plasticity mechanisms than STDP may be involved in refining tectal cell responses in older animals. STDP may be the mechanism best suited for implementing temporally precise interactions in the immature visual system while other mechanisms are more efficient at later stages. For example, STDP has been shown to be input specific from the youngest stages at which it has been examined in Xenopus, whereas induction of LTP by theta-burst stimulation (TBS) lacks tight input specificity in very immature tectal neurons, but becomes input specific at roughly the same stage that STDP can no longer be induced (Tao et al., 2001). Thus retinotectal STDP might serve as a transient means to refine the initial projection until it becomes mature enough to take full advantage of other mechanisms.

MECHANISTIC CONSIDERATIONS

Several potentially relevant developmental changes occur in tectal neurons around stage 45 that could underlie the loss of STDP. One important developmental shift that occurs around this stage, but continues much later, is the KCC2-mediated conversion of the chloride reversal potential (E_{Cl}) from depolarizing to hyperpolarizing (Akerman and Cline, 2006). However, we do not believe that this change can fully explain our observations. First of all, despite the evidence that the gradual shift in E_{Cl} is already under way, its reported value as late as stage 47 is still fairly depolarizing relative to the typical resting membrane potential of a tectal cell. Secondly, the retinotectal projection is exclusively glutamatergic and the vast majority of polysynaptic activation does not occur until after the STDP pairing period. Finally, we found that adding picrotoxin to the bath did not impact our ability to induce STDP (data not shown).

Another important event is that the lateral spread of stimulus-evoked calcium influx within tectal neuron dendrites becomes spatially restricted around this time, possibly reflecting a change in the calcium buffering capacity of the cell (Tao et al., 2001). It has been proposed that STDP may depend in part on a non-linear summation of calcium elevation induced by the EPSP and the back-propagating action potential (Nevian and Sakmann, 2004). Thus, the development increase in the calcium buffering capacity of tectal neurons could potentially impact their ability to undergo STDP.

OTHER PLASTICITY INDUCTION PROTOCOLS

This is the first report of a sensitive period for retintotectal plasticity in Xenopus to our knowledge. However in the regenerating retinotectal system of goldfish, it has been reported that the period of greatest susceptibility to LTP, induced by 0.1 Hz supramaximal stimulation of the optic nerve, corresponds to a period from 20 to 40 days post-nerve-crush, when RGC inputs are still actively in the process of reestablishing contacts (Schmidt, 1990). One limitation of our current experimental design is that in order to test STDP at a range of developmental stages, we were forced to focus on just three spike-timing intervals, + 100 ms post→pre, 5–10 ms pre→post and 5–10 ms post→pre. It is conceivable, for example, that beyond the ages defined as the sensitive period in our experiments a shorter timing interval might have produced reliable plasticity.

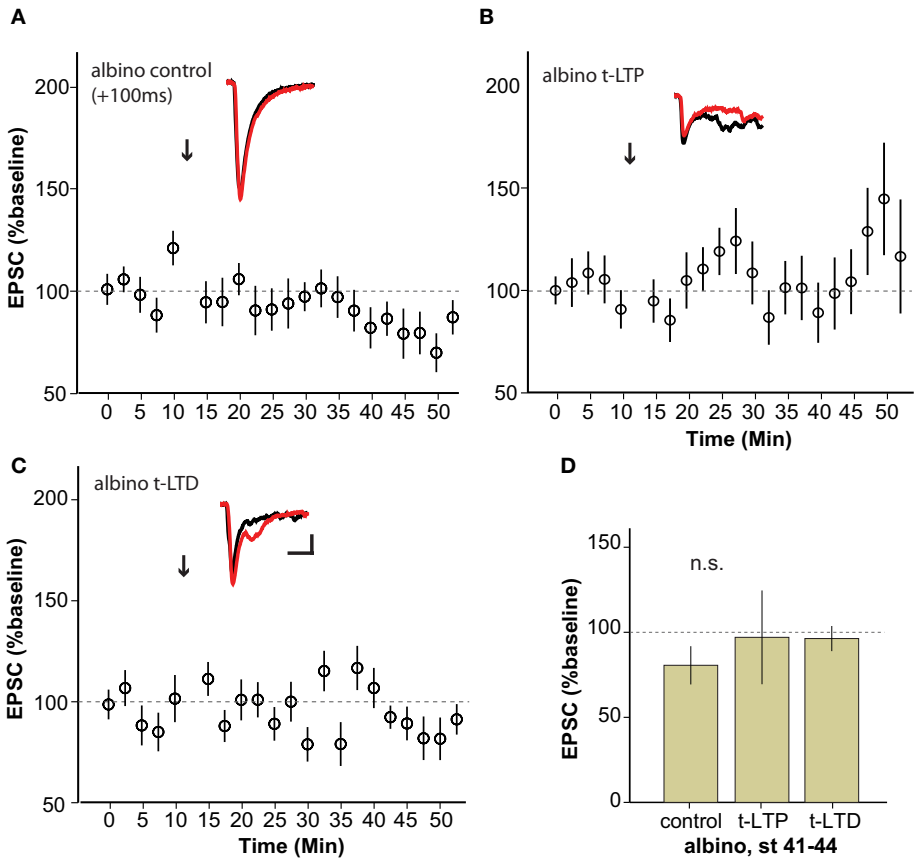

FIGURE 5 | Albino Xenopus tadpoles do not exhibit reliable STDP during the sensitive period. (A–C) Average of experiments to induce t-LTP ($n = 4$) **(B)** and t-LTD ($n = 4$) **(C)** using the protocols that succeeded in wild type animals, applied to stage 41–44 albino tadpoles. No STDP was reliably generated using the classic STDP protocol in albinos.

It remains unclear whether STDP and other synaptic plasticity induction protocols act through common biochemical pathways within tectal cells or depend on different signaling cascades. Tectal neurons are morphologically quite small and their high input resistances (0.5–1 GΩ) render them are electrotonically compact, making it unlikely that the loss of STDP in older animals was simply due to a failure of action potential back-propagation. Inhibition was not blocked in these experiments, raising the possibility of local dendritic shunting in older animals as a possible mechanism by which STDP might be lost with age (Corlew et al., 2007). However, in pilot experiments performed with picrotoxin in the bath, we were also unable to induce STDP in older tadpoles (data not shown) – these were discontinued, however, as excessive recurrent activity in picrotoxin interfered with accurate measurement of evoked EPSC amplitudes.

Although retinotectal STDP could not be induced after stage 45, repeated visual stimulation was able to induce a robust NMDAR-dependent LTD at stage 47. Other groups have previously demonstrated retinotectal plasticity induced using slightly different visual stimulation protocols at younger (Zhang et al., 2000) and older (Dunfield and Haas, 2009) stages. What properties of visually induced plasticity might be permissive for effecting synaptic changes in older animals when classic STDP protocols fail? Unlike the STDP protocol in which only a small handful of inputs are activated during conditioning, visual induction of plasticity involves the coherent excitation of a large number of RGCs. In this case, for example, there may be sufficient convergent afferent drive to overcome a developmental change in calcium buffering of the neuron or whatever critical change may have led to the loss of STDP.

LACK OF STDP IN ALBINO TADPOLES

We found that STDP was not reliably induced in albino tadpoles during the wild type sensitive period. While it is possible that albino animals may simply have a delayed sensitive period, this would not be consistent with the fact that morphological and basic electrophysiological properties of RGCs and tectal neurons are overall indistinguishable between wild type and albino tadpoles of the same ages. The differences in STDP sensitivity between wild type and albino tadpoles can perhaps be explained by genetic differences between animals. Albinos of many species including humans, in which the tyrosinase gene is disrupted, are known to have abnormalities in the anatomy and physiology of their visual systems (Diykov et al., 2008; Herrera and Garcia-Frigola, 2008), however the Xenopus mutation does not involve this gene (MacMillan, 1979). Xenopus mutants exhibit periodic albinism, in

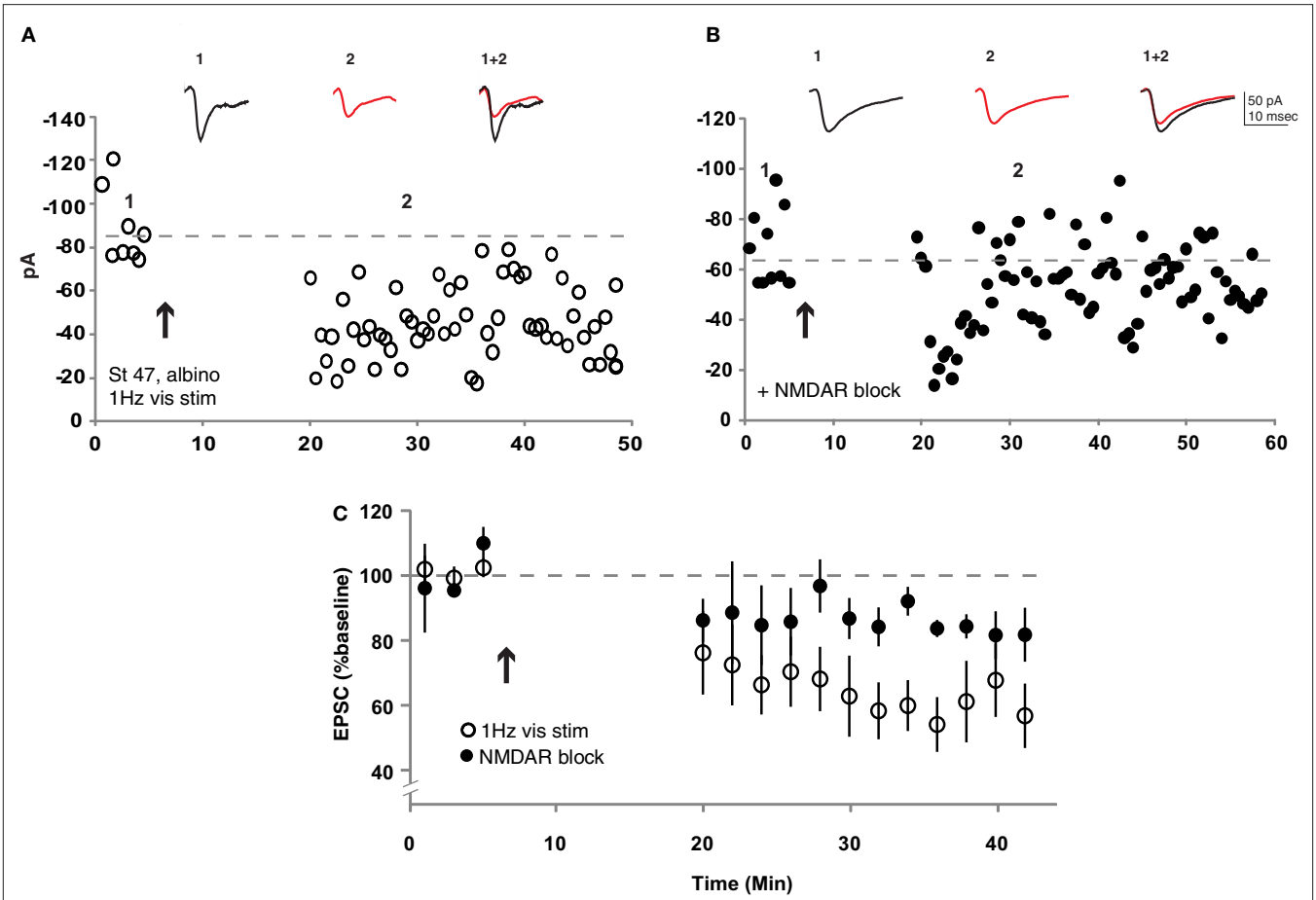

FIGURE 6 | Repeated low-frequency visual stimulation induced LTD in albino stage 47 tadpoles. (A) Repeatedly flashing an array of LEDs at 1 Hz for 15 min induced retinotectal synaptic depression. **(B)** This visual stimulation-induced LTD was largely blocked in the presence of CPP (40 mM). **(C)** Average of all experiments with (filled circles, $n = 4$) and without (open circles, $n = 9$) NMDARs pharmacologically blocked. $p < 0.001$ Student's *t*-test.

which melanophore production occurs but is delayed and reduced. However, as the specific genes involved in the Xenopus albino mutation are not known, there could potentially be a subtle change in signaling or synaptic function that would alter the response to the STDP protocol.

Alternatively, differences in past sensory experience between albino and wild type tadpoles may account for their differential sensitivities. Although laboratory strains of albino tadpoles do not entirely lack melanophores, a striking feature of albino tadpoles is the extremely sparse pigmentation around their eyes, which in wild type animals is dark enough to completely block light from entering the retina except through the lens. This difference in normal visual input could potentially drive meta-plasticity such that albinos, which would have generally less well-structured activation of their photoreceptors may somehow lose sensitivity to precisely timed input. Dark-rearing of wild type and albino tadpoles to eliminate differences in visual experience might be informative in this case, but could be confounded by additional changes in the susceptibility of the visual system to undergo synaptic plasticity. A better experiment would be to take advantage of the ability to transplant tissues in tadpole embryos by examining STDP in wild type animals in which an eye primodium from an albino embryo had been transplanted to produce a chimera with a wild type tectum innervated by a faintly pigmented albino eye.

FUTURE DIRECTIONS

Given that retinotectal map remodeling occurs over an extended time beyond the STDP sensitive period, the specific contribution of STDP to retinotectal function and map refinement remains unclear. Does this relatively brief period of early plasticity provide a foundation upon which later tectal development occurs? It may be possible to exploit the differences between wild type and albino animals to determine electrophysiologically and anatomically whether their retinotopic organization differs immediately following the critical period and then several weeks afterwards when alternative plasticity mechanisms have had a chance to act in both. Ultimately, t-LTP and t-LTD protocols are merely idealized experimental assays that at best approximate natural sensory stimuli encountered during normal development. Testing retinotectal connectivity changes in response to presentation of natural scenes (Froemke and Dan, 2002) that closely mimic what tadpoles might see in the wild might provide the best understanding of how activity-dependent plasticity truly contributes to the development of visual processing.

ACKNOWLEDGMENTS

The authors thank Dr. Carlos Aizenman for assistance in setting up the initial recordings. This work was supported by grants to Edward S. Ruthazer from the March of Dimes, EJLB Foundation, the Canadian Institutes of Health Research, and by fellowships from the following agencies: MNI Jeanne-Timmins-Costello (Jennifer Tsui), Fonds de la recherche en santé Québec (Jennifer Tsui), and IPN Jeanne-Timmins-Costello (Neil Schwartz), Scottish Rite Charitable Foundation (Neil Schwartz).

REFERENCES

Abbott, L. F., and Nelson, S. B. (2000). Synaptic plasticity: taming the beast. *Nat. Neurosci.* 3, 1178–1183.

Akerman C. J., and Cline H. T. (2006). Depolarizing GABAergic conductances regulate the balance of excitation to inhibition in the developing retinotectal circuit *in vivo*. *J. Neurosci.* 26, 5117–5130.

Bell, C. C., Han, V. Z., Sugawara, Y., and Grant, K. (1997). Synaptic plasticity in a cerebellum-like structure depends on temporal order. *Nature* 387, 278–281.

Bender, V. A., Bender, K. J., Brasier, D. J., and Feldman, D. E. (2006). Two coincidence detectors for spike timing-dependent plasticity in somatosensory cortex. *J. Neurosci.* 6, 4166–4177.

Celikel, T. Stostak, V. A., and Feldman, D. E. (2004). Modulation of spike timing by sensory deprivation during induction of cortical map plasticity. *Nat. Neurosci.* 7, 534–541.

Cline, H. T., and Constantine-Paton, M. (1989). NMDA receptor antagonists disrupt the retinotectal topographic map. *Neuron* 3, 413–426.

Corlew, R., Wang, Y. Ghermazien, H., Erisir, A., and Philpot, B. D. (2007). Developmental switch in the contribution of presynaptic and postsynaptic NMDA receptors to long-term depression. *J. Neurosci.* 27, 9835–9845.

Deeg, K. E., Sears, I. B., and Aizenman, C. D. (2009). Development of multisensory convergence in the Xenopus optic tectum. *J. Neurophysiol.* 102, 3392–3404.

Dong W., Lee, R. H., Xu, H., Yang, S., Pratt, K. G., Cao, V., Song, Y. K., Nurmikko, A., and Aizenman CD. (2009). Visual avoidance in Xenopus tadpoles is correlated with the maturation of visual responses in the optic tectum. *J. Neurophysiol.* 101, 803–815.

Diykov, D. Turchinovich, A. Zoidl, G., and Hofmann, K. P. (2008). Elevated intracellular chloride level in albino visual cortex neurons is mediated by Na-K-Cl co-transporter. *BMC Neurosci.* 9, 57.

Dunfield, D., and Haas, K. (2009). Metaplasticity governs natural experience-driven plasticity of nascent embryonic brain circuits. *Neuron* 64, 240–250.

Feldman, D. E. (2000). Timing-based LTP and LTD at vertical inputs to layer II/III pyramidal cells in rat barrel cortex. *Neuron* 27, 45–56.

Fraser, S. E. (1983). Fiber optic mapping of the Xenopus visual system: shift in the retinotectal projection during development. *Dev. Biol.* 95, 505–511.

Froemke, R. C., and Dan, Y. (2002). Spike-timing-dependent synaptic modification induced by natural spike trains. *Nature* 416, 433–438.

Gaze, R. M., Keating, M. J., and Chung, S. H. (1974). The evolution of the retinotectal map during development in Xenopus. *Proc. R. Soc. Lond. B Biol. Sci.* 185, 301–330.

Haas, K. Li, J., and Cline, H. T. (2006). AMPA receptors regulate experience-dependent dendritic arbor growth *in vivo*. *Proc. Natl. Acad. Sci. USA* 103, 12127–12131.

Hebb, D. O. (1949). *The Organization of Behavior: A Neuropsychological Theory*. New York: Wiley.

Hensch, T. K. (2005). Critical period plasticity in local cortical circuits. *Nat. Rev. Neurosci.* 6, 877–888.

Herrera, E., and Garcia-Frigola, C. (2008). Genetics and the development of the optic chiasm. *Front. Biosci.* 13, 1646–1653.

Hiramoto, M., and Cline, H. T. (2009). Convergence of multisensory inputs in Xenopus tadpole tectum. *Dev. Neurobiol.* 69, 959–971.

Holtmaat, A., and Svoboda, K. (2009). Experience-dependent structural synaptic plasticity in the mammalian brain. *Nat. Rev. Neurosci.* 10, 647–658.

Huberman, A. D., Feller, M. B., and Chapman, B. (2008). Mechanisms underlying development of visual maps and receptive fields. *Annu. Rev. Neurosci.* 31, 479–509.

Inan, M., and Crair, M. C. (2007). Development of cortical maps: perspectives from the barrel cortex. *Neuroscientist* 13, 49–61.

Katz, L. C., and Shatz, C. J. (1996). Synaptic activity and the construction of cortical circuits. *Science* 274, 1133–1138.

Kirkwood, A., Lee H. K., and Bear, M. F. (1995). Co-regulation of long-term potentiation and experience-dependent synaptic plasticity in visual cortex by age and experience. *Nature* 375, 328–331.

Knudsen, E. I. (2002). Instructed learning in the auditory localization pathway of the barn owl. *Nature* 417, 322–328.

Levy, W. B., and Steward, O. (1983). Temporal contiguity requirements for long-term associative potentiation/depression in the hippocampus. *Neuroscience* 8, 791–797.

Li, L., Bender, K. J., Drew, P. J., Jadhav, S. P., Sylwestrak, E., and Feldman, D. E. (2009). Endocannabinoid signaling is required for development and critical period plasticity of the whisker map in somatosensory cortex. *Neuron* 64, 537–549.

MacMillan, G. J. (1979). An analysis of pigment cell development in the periodic albino mutant of Xenopus. *J. Embryol. Exp. Morphol.* 52, 165–170.

Magee, J. C., and Johnston, D. (1997). A synaptically controlled, associative signal for Hebbian plasticity in hippocampal neurons. *Science* 275, 209–213.

Markram, H. Lübke, J., Frotscher, M., and Sakman, B. (1997). Regulation of synaptic efficacy by coincidence of postsynaptic APs and EPSPs. *Science* 275, 213–215.

Mu, Y., and Poo, M. M. (2006). Spike timing-dependent LTP/LTD mediates visual experience-dependent plasticity in a developing retinotectal system. *Neuron* 50, 115–125.

Nevian T., and Sakmann, B. (2004). Single spine Ca^{2+} signals evoked by coincident EPSPs and backpropagating action potentials in spiny stellate cells of layer 4 in the juvenile rat somatosensory barrel cortex. *J. Neurosci.* 24, 1689–1699.

Nieuwkoop, P. D., and Faber, J. (1956). *Normal Table of Xenopus laevis (Daudin): A Systematical and Chronological Survey of the Development from the Fertilized Egg till the End of Metamorphosis.* Amsterdam: North-Holland Pub. Co.

O'Rourke, N. A., and Fraser, S. E. (1990). Dynamic changes in optic fiber terminal arbors lead to retinotopic map formation: an *in vivo* confocal microscopic study. *Neuron* 5, 159–171.

Pratt, K. G., Dong, W., and Aizenman, C. D. (2008). Development and spike timing-dependent plasticity of recurrent excitation in the Xenopus optic tectum. *Nat. Neurosci.* 11, 467–475.

Ruthazer, E. S., Akerman, C. J., and Cline, H. T. (2003). Control of axon branch dynamics by correlated activity *in vivo*. *Science* 301, 66–70.

Ruthazer, E. S., and Cline, H. T. (2004). Insights into activity-dependent map formation from the retinotectal system: a middle-of-the-brain perspective. *J. Neurobiol.* 59, 134–146.

Sakaguchi, D. S., and Murphey, R. K. (1985). Map formation in the developing Xenopus retinotectal system: an examination of ganglion cell terminal arborizations. *J. Neurosci.* 5, 3228–3245.

Schmidt, J. T. (1990). Long-term potentiation and activity-dependent retinotopic sharpening in the regenerating retinotectal projection of goldfish: common sensitive period and sensitivity to NMDA blockers. *J. Neurosci.* 10, 233–246.

Schwartz, N., Schohl, A., and Ruthazer, E. S. (2009). Neural activity regulates synaptic properties and dendritic structure *in vivo* through calcineurin/NFAT signaling. *Neuron* 62, 655–669.

Sjostrom, P. J., Turrigiano, G. G., and Nelson, S. B. (2001). Rate, timing, and cooperativity jointly determine cortical synaptic plasticity. *Neuron* 32, 1149–1164.

Tao, H. W., and Poo, M.-M. (2005). Activity-dependent matching of excitatory and inhibitory inputs during refinement of visual receptive fields. *Neuron* 45, 829–836.

Tao, H. Z., Zhang, L. I., Engert, F., and Poo, M. (2001). Emergence of input specificity of ltp during development of retinotectal connections *in vivo*. *Neuron* 31, 569–580.

Vislay-Meltzer, R. L., Kampff, A. R., and Engert, F. (2005). Spatiotemporal specificity of neuronal activity directs the modification of receptive fields in the developing retinotectal system. *Neuron* 50, 101–114.

Wiesel, T. (1982). Postnatal development of the visual cortex and the influence of environment. *Nature* 299, 583–591.

Wu, G., Malinow, R., and Cline, H. T. (1996). Maturation of a central glutamatergic synapse. *Science* 274, 972–976.

Zhang, L. I., Tao, H. W., Holt, C. E., Harris, W. A., and Poo, M. M. (1998). A critical window for cooperation and competition among developing retinotectal synapses. *Nature* 395, 37–44.

Zhang, L. I., Tao, H. W., and Poo, M. (2000). Visual input induces long-term potentiation of developing retinotectal synapses. *Nat. Neurosci.* 3, 708–715.

Zhou, Q., Tao, H. W., and Poo, M. M. (2003) Reversal and stabilization of synaptic modifications in a developing visual system. *Science* 300, 1953–1957.

Conflict of Interest Statement: The authors declare that the research was conducted in the absence of any commercial or financial relationships that could be construed as a potential conflict of interest.

Received: 01 February 2010; paper pending published: 01 March 2010; accepted: 17 May 2010; published online: 11 June 2010.
Citation: Tsui J, Schwartz N and Ruthazer ES (2010) A developmental sensitive period for spike timing-dependent plasticity in the retinotectal projection. Front. Syn. Neurosci. ***2****:13. doi: 10.3389/fnsyn.2010.00013*

frontiers in
SYNAPTIC NEUROSCIENCE

ORIGINAL RESEARCH ARTICLE
published: 28 June 2010
doi: 10.3389/fnsyn.2010.00016

GABAergic synaptic transmission regulates calcium influx during spike-timing dependent plasticity

Trevor Balena, Brooke A. Acton and Melanie A. Woodin*

Department of Cell and Systems Biology, University of Toronto, Toronto, ON, Canada

Edited by:
Per Jesper Sjöström, University College London, UK

Reviewed by:
David M. Lovinger, National Institutes of Health, USA
Laura Cancedda, Istituto Italiano di Tecnologia, Italy

***Correspondence:**
Melanie A. Woodin, Department of Cell and Systems Biology, University of Toronto, 25 Harbord Street, Toronto, ON M5S 3G5, Canada.
e-mail: m.woodin@utoronto.ca

Coincident pre- and postsynaptic activity of hippocampal neurons alters the strength of gamma-aminobutyric acid ($GABA_A$)-mediated inhibition through a Ca^{2+}-dependent regulation of cation-chloride cotransporters. This long-term synaptic modulation is termed GABAergic spike-timing dependent plasticity (STDP). In the present study, we examined whether the properties of the GABAergic synapses themselves modulate the required postsynaptic Ca^{2+} influx during GABAergic STDP induction. To do this we first identified GABAergic synapses between cultured hippocampal neurons based on their relatively long decay time constants and their reversal potentials which lay close to the resting membrane potential. GABAergic STDP was then induced by coincidentally (±1 ms) firing the pre- and postsynaptic neurons at 5 Hz for 30 s, while postsynaptic Ca^{2+} was imaged with the Ca^{2+}-sensitive fluorescent dye Fluo4-AM. In all cases, the induction of GABAergic STDP increased postsynaptic Ca^{2+} above resting levels. We further found that the magnitude of this increase correlated with the amplitude and polarity of the GABAergic postsynaptic current (GPSC); hyperpolarizing GPSCs reduced the Ca^{2+} influx in comparison to both depolarizing GPSCs, and postsynaptic neurons spiked alone. This relationship was influenced by both the driving force for Cl^- and $GABA_A$ conductance (which had positive correlations with the Ca^{2+} influx). The spike-timing order during STDP induction did not influence the correlation between GPSC amplitude and Ca^{2+} influx, which is likely accounted for by the symmetrical GABAergic STDP window.

Keywords: calcium, chloride, spike-timing dependent plasticity, inhibitory synaptic transmission, hippocampus, KCC2, NKCC1, cation-chloride cotransporter

INTRODUCTION

GABAergic synaptic transmission can be either excitatory or inhibitory at different stages of nervous system development (Kaila, 1994; Blaesse et al., 2009), or during various pathological states (Kahle et al., 2008). The polarity of GABAergic transmission (hyperpolarizing versus depolarizing) depends on the intracellular concentration of Cl^- ($[Cl^-]_i$); this is because the $GABA_A$ receptor is a Cl^--permeable ion channel (Kaila, 1994). The $[Cl^-]_i$ is largely determined by the cation-chloride cotransporters expressed in the neuronal membrane: NKCC1 accumulates Cl^- into the neuron (Yamada et al., 2004; Dzhala et al., 2005), while KCC2 transports it out (Rivera et al., 1999). When neuronal Cl^- is relatively high due to the dominant expression of NKCC1 during early development, the reversal potential for GABA ($E_{GABA} \approx E_{Cl}$) is depolarized with respect to the resting membrane potential and so GABAergic transmission is depolarizing and sometimes excitatory. In contrast, when neuronal Cl^- is low due to the expression of KCC2 in the mature nervous system, E_{Cl} is hyperpolarized with respect to the resting membrane potential making GABAergic transmission inhibitory.

Recent studies have demonstrated that NKCC1 and KCC2 transporter function is not only regulated by their developmental program, but can also be regulated by neuronal activity (Fiumelli and Woodin, 2007; Blaesse et al., 2009). Coincident pre- and postsynaptic activity at GABAergic synapses results in GABAergic STDP (Woodin et al., 2003; Fiumelli and Woodin, 2007; Balena and Woodin, 2008; Saraga et al., 2008; Xu et al., 2008; Ormond and Woodin, 2009). Early in development, coincident pre- and postsynaptic activity strengthens inhibition through a Ca^{2+}-dependent regulation of NKCC1, which hyperpolarizes E_{Cl} (Balena and Woodin, 2008). The same pattern of neuronal activity also modifies GABAergic transmission in the mature nervous system through a Ca^{2+}-dependent decrease in KCC2 activity, which depolarizes E_{Cl} (Woodin et al., 2003). The spike-timing window for mature GABAergic inhibition has been characterized as symmetrical. Both positive and negative spike-timing intervals (within 15 ms; ±15 ms) decrease the strength of inhibition due to E_{Cl} depolarization (as described above). Non-coincident activity (±50 ms) also reduces inhibition, but through a decrease in conductance (Woodin et al., 2003).

During GABAergic STDP the Ca^{2+} influx occurs via voltage-gated Ca^{2+} channels (VGCCs) (Woodin et al., 2003) opened by the back-propagating action potential. When glutamatergic transmission occurs simultaneously with GABAergic STDP induction in hippocampal slices, Ca^{2+} can also influx via NMDARs (Ormond and Woodin, 2009). Because the opening of VGCCs and NMDARs are voltage-dependent, we hypothesize that GABAergic transmission, which regulates the postsynaptic membrane potential, will regulate the opening of these Ca^{2+} channel proteins. In turn, this would regulate the Ca^{2+} influx during GABAergic STDP. It is important to understand how GABAergic synapses regulate Ca^{2+} influx, because the magnitude of this influx can determine the outcome of plasticity induction (Kano, 1994; Bi and Poo, 1998; Nishiyama et al., 2000; Dan and Poo, 2006).

We examined Ca^{2+} dynamics during STDP induction in hippocampal neurons which have formed either depolarizing or hyperpolarizing GABAergic synapses. Using perforated patch-clamp recordings (with gramicidin) and imaging postsynaptic Ca^{2+} (using Fluo4), we investigated how the polarity and strength of GABAergic transmission regulates Ca^{2+} influx. We further analyzed this relationship by examining several aspects of GABAergic transmission, including $GABA_A$ conductance, E_{Cl}, and Cl^- driving force. We found that $GABA_A$-mediated transmission regulates Ca^{2+} influx during the induction of STDP, with the strength of the synapse significantly altering the magnitude of the postsynaptic Ca^{2+} influx in a linear fashion.

MATERIALS AND METHODS

HIPPOCAMPAL CULTURES

Low-density cultures of dissociated embryonic rat hippocampal neurons were prepared as previously described (Balena and Woodin, 2008). In brief, embryonic day 18 (E18) pregnant Sprague-Dawley rats were briefly exposed to carbon dioxide and cervically dislocated in accordance with guidelines from the University of Toronto Animal Care Committee and the Canadian Council on Animal Care. Hippocampi were then removed and treated with trypsin for 15 min at 37°C, followed by gentle trituration. The dissociated cells were plated at a density of 50,000 cells/mL on poly-L-lysine coated 25 mm glass coverslips (in 35 mm Petri dishes). Cells were plated in Neurobasal medium (Invitrogen, Carlsbad, California, USA), supplemented with 2% B-27 (Invitrogen, Carlsbad, California, USA). Twenty-four hours after plating, half of the medium was replaced with the original plating medium containing 20 mM KCl. Forty-eight hours after plating, and every 3 days following, one third of the medium was replaced with DMEM (Invitrogen, Carlsbad, California, USA) supplemented with 10% heat-inactivated fetal bovine serum (Invitrogen, Carlsbad, California, USA), 10% Ham's F12 with L-glutamine (Invitrogen, Carlsbad, California, USA), 1% penicillin-streptomycin (Sigma-Adrich, Oakville, Ontario, Canada), 10 mM KCl and 15 mM HEPES. Both glia and neurons were present under these culture conditions. Cells were recorded from after 8–13 days in culture.

ELECTROPHYSIOLOGY

Whole-cell perforated patch recordings using gramicidin (50 μg/mL; Sigma-Adrich, Oakville, Ontario, Canada) were performed on pairs of synaptically connected cultured hippocampal neurons. The recording pipettes were made from glass capillaries (World Precision Instruments Inc., Sarasota, Florida, USA), with a resistance of 4–10 MΩ. The pipettes were filled with an internal solution containing 150 mM KCl, 10 mM HEPES, and gramicidin, pH 7.4, osmolarity = 300 mOsmol. The cultures were continuously perfused (approximately 1 mL/min) with extracellular recording solution containing (in mM): 150 NaCl, 3 KCl, 3 $CaCl_2 \cdot 2H_2O$, 2 $MgCl_2 \cdot 6H_2O$, 10 HEPES, 5 Glucose, pH 7.4, osmolarity = 307–315 mOsmol. Recordings were performed with a MultiClamp 700B (Molecular Devices Inc., Sunnyvale, California, USA) patch-clamp amplifier. Signals were filtered at 5 kHz using amplifier circuitry. Data was acquired and analyzed using Clampfit 9 (Molecular Devices Inc., Sunnyvale, California, USA). Recordings started after the series resistance had dropped below 30 MΩ. For assaying synaptic connectivity, each neuron was stimulated at a low frequency (0.05 Hz) by a 1 ms step depolarization from −70 to +20 mV in voltage-clamp mode. GPSCs were distinguishable from excitatory postsynaptic currents (EPSCs) by longer decay times. Upon occasion we did detect autaptic GABAergic synapses in our cultures, however we did not examine these synapses in the present study. During the STDP induction protocol both neurons were switched to current-clamp mode and injected with current (minimal stimulation, 2 ms) both pre- and postsynaptically to generate an action potential in each cell at a frequency of 5 Hz for 30 s. The interval between spike induction was ±5 ms, which resulted in a spike-timing interval of ±1 ms between onset of the GABAergic postsynaptic potential (GPSP) and the postsynaptic action potential. This protocol resulted in 150 pairs of pre- and postsynaptic action potentials. All recordings were performed at room temperature (25°C).

The resting membrane potential was determined in current-clamp mode in the absence of current injection or synaptic activity. E_{Cl} was determined by varying the holding potential of the postsynaptic cell in 10 mV increments and measuring the resulting GPSC amplitude; each set of current-voltage (I–V) measurements was repeated after a 5-min interval. A linear regression of both sets of GPSC amplitude measurements was then used to calculate the voltage dependence of GPSCs. The intercept of this line with the abscissa was taken as E_{Cl}. The slope of the same line was taken as GPSC conductance. The difference between the resting membrane potential and E_{Cl} was taken as the driving force.

$GABA_A$ receptors are permeable to both HCO_3^- and Cl^- (~0.2–0.4 ratio; Kaila, 1994). Due to the relatively positive HCO_3^- equilibrium potential (~−10 mV), which is set by mechanisms that control intracellular pH regulation (Kaila and Voipio, 1987), HCO_3^- mediates an inward, depolarizing current (Kaila and Voipio, 1987; Kaila et al., 1993; Gulledge and Stuart, 2003). However, our experiments were performed in bicarbonate-free solution buffered with HEPES, and thus $GABA_A$ receptor activation was solely mediating a Cl^- current. For this reason we report E_{Cl} and not E_{GABA}.

FLUORESCENCE IMAGING

To assess the effect of STDP induction on postsynaptic Ca^{2+} influx the hippocampal neurons were loaded with the membrane-permeable fluorescent Ca^{2+} indicator Fluo4-AM (Invitrogen; Carlsbad, CA, USA) for 30 min at 37°C, 5% CO_2. The Fluo4 was dissolved in dimethyl sulfoxide (DMSO) and 20% pluronic acid to a stock concentration of 1 mM and then diluted to 1 μM in our extracellular recording solution. Following dye-loading the cells were thoroughly washed with extracellular recording solution. Cells were then transferred to the recording chamber of an inverted microscope (Olympus IX71) equipped with an Olympus 0.6 NA × 40 objective. Fluo4 was excited at 488 nm through a monochromator (Photon Technology International (Canada) Inc., London, ON), controlled by the ImageMaster software (Photon Technology International (Canada) Inc., London, ON). Fluorescence emission of labeled cells at 510 nm was detected with a 16-bit CCD camera (Cascade 650, Photometrics, Roper Scientific, Tuscon, AZ, USA). Images of 653 × 492 pixels were accumulated at 500–1000 ms intervals.

FLUORESCENCE ANALYSIS

Analysis of the fluorescence signals was performed off-line on the image sequences as they were originally acquired. Analysis was performed on regions of interest (ROIs) that encompassed

approximately 80% of the soma (which ranged from 10–50 μM in diameter). Fluorescence was plotted against time to yield a graph of the fluorescence changes over the STDP induction period. F_0 was taken to be the fluorescence from the last image before induction began. F_{peak} was taken to be the maximum fluorescence level reached over the course of the induction. F_{30} was taken to be the fluorescence from the final image during the induction period. ΔF_{30} was calculated as the percentage difference between F_0 and F_{30}; ΔF_{peak} was calculated as the percentage difference between F_0 and F_{peak}. The area under the graph was normalized to F_0 to provide F_{area}. We determined that photobleaching did not impact our Ca^{2+} analysis. This determination was made by comparing the fluorescence of quiescent cells during the first and last 5 s of a 30-s image acquisition and finding no significant difference in fluorescence ($p = 0.06$). Thus, we did not alter the image analysis further to account for photobleaching.

STATISTICAL ANALYSIS

All data are presented as mean ± SEM. Linear regression analysis was used to obtain correlation coefficients and corresponding *p*-values. One-way ANOVA was used to compare the F_{area} values of depolarizing and hyperpolarizing synapses to those of neurons fired alone (post only). Paired *t*-tests were used to compare E_{Cl} and resting membrane potential values when those values were obtained from the same neurons. All other statistical analysis used unpaired *t*-tests. All statistical analysis was performed using SigmaStat 2.03.

RESULTS

CHARACTERIZATION AND LOCALIZATION OF GABAergic SYNAPSES

In order to examine Ca^{2+} influx during STDP induction, we first had to locate synaptically connected neurons and characterize the synapse between them. We did this using dual perforated patch-clamp recordings from pairs of hippocampal neurons cultured at a low density. Hippocampal cultures were prepared from E18 rats and recorded from after 8–13 days in culture; they contained glia, pyramidal neurons and GABAergic interneurons. Synaptic connections were identified by stimulating one neuron and monitoring for the presence of postsynaptic currents in the other. After we located a synapse, our first indication that it was GABAergic came from the relatively long time course of the GPSC in voltage-clamp mode (35.50 ± 3.37 ms for GPSCs, as opposed to 5.76 ± 0.64 ms for glutamatergic currents; Balena and Woodin, 2008). If the synapse had a time course consistent with GABAergic currents we then determined the E_{Cl} by constructing an I–V curve; the intersection of the curve with the *x*-axis was taken to be E_{Cl} (**Figures 1A,B**). Because the extracellular recording solution was free of HCO_3^-, $E_{Cl} \approx E_{GABA}$. Based on the relation of E_{Cl} to resting membrane potential, we characterized GABAergic synapses as either: (1) depolarizing, when E_{Cl} was more positive than the resting membrane potential (**Figure 1A**); or (2) hyperpolarizing, when E_{Cl} was more negative than the resting membrane potential (**Figure 1B**). Depolarizing GABAergic synapses had an average E_{Cl} of −58.33 ± 2.63 mV, which was significantly different from the resting membrane potential of those neurons (−70.33 ± 1.17 mV; $n = 12$; paired *t*-test $p < 0.001$; **Figure 1C**). In all cases E_{Cl} was hyperpolarizing with respect to action potential threshold, and thus depolarizing synapses were not excitatory. Hyperpolarizing synapses had an average E_{Cl} of −75.87 ± 1.74 mV, which was significantly different from

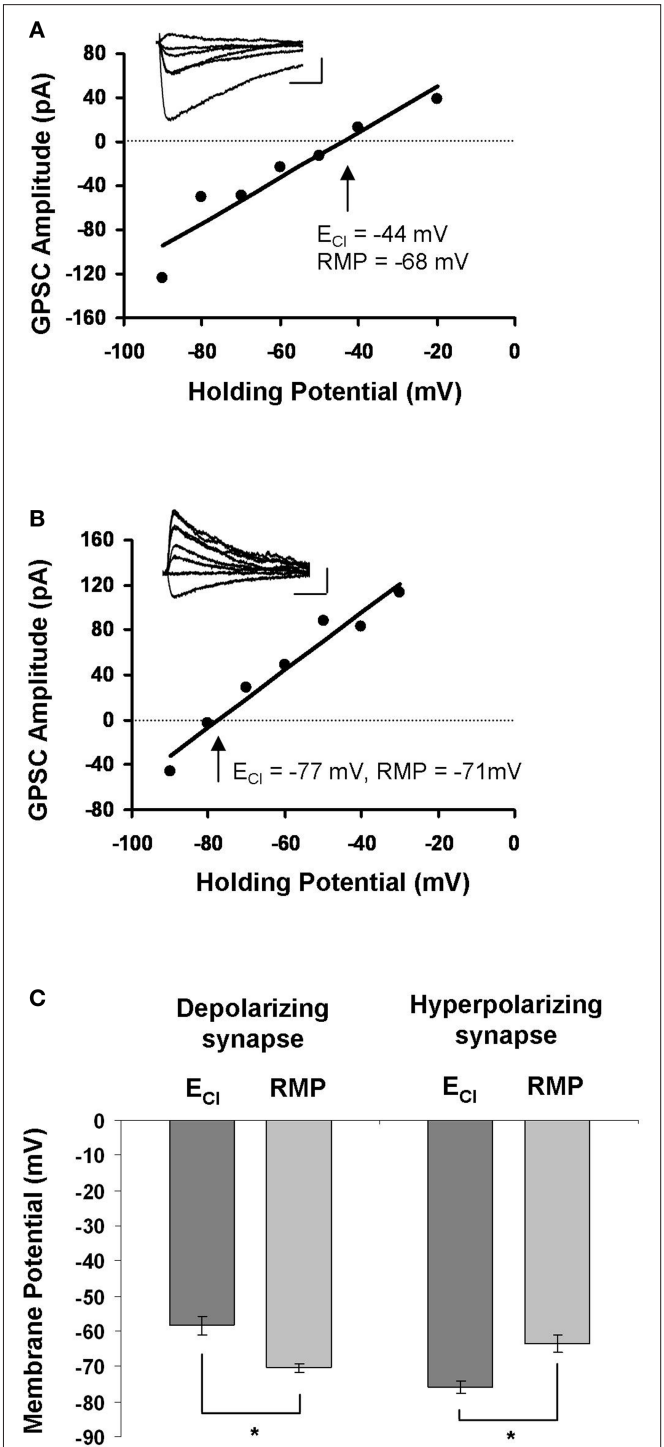

FIGURE 1 | Characterization of GABAergic synapses. (A) Example of an I–V curve from a depolarizing GABAergic synapse. The postsynaptic membrane potential was stepped in 10 mV increments while stimulating GABAergic synapses to generate the I–V curve. The holding potential at which the GPSC amplitude was 0 mV (dashed line) was taken as E_{Cl}. *Inset:* sample traces of GPSCs recorded during the construction of the I–V curve. Legend: 20 ms, 45 mV. **(B)** Example of an I–V curve from a hyperpolarizing GABAergic synapse. Characterized as in **(A)**. Legend: 20 ms, 45 mV. **(C)** The average ± SEM for E_{Cl} and resting membrane potential (RMP) at depolarizing and hyperpolarizing synapses. *indicates statistical significance.

their resting membrane potential values (−63.40 ± 2.44 mV; $n = 10$; paired t-test $p < 0.001$; **Figure 1C**). There was a significant difference between the E_{Cl} values ($p < 0.001$) and resting membrane potential values ($p = 0.014$) of depolarizing and hyperpolarizing synapses. The slope of each I–V curve provided the $GABA_A$ conductance of that synapse. Depolarizing GABAergic synapses had a conductance of 1.85 ± 0.34 pS ($n = 12$), and hyperpolarizing synapses had a conductance of 1.74 ± 0.35 pS ($n = 10$); there was no significant difference between the conductances of the two populations ($p = 0.824$).

SIMULTANEOUS STDP INDUCTION AND IMAGING OF CA^{2+} DYNAMICS

Following characterization of the GABAergic synapse we examined the Ca^{2+} dynamics during the induction of STDP. To do this, we loaded neurons with the Ca^{2+}-sensitive cell permeant fluorescent dye Fluo4-AM (**Figures 2A,B**). A sequence of fluorescence images was then acquired at 1–2 Hz during STDP induction. GABAergic STDP was induced in current-clamp mode; both the pre- and postsynaptic neurons were induced to fire action potentials (using minimal stimulation) at a frequency of 5 Hz for 30 s. The interval between spike induction was ±5 ms, which resulted in a spike-timing interval of ±1 ms between onset of the GPSP and the postsynaptic action potential. This yielded a graph representing the changes in Fluo4 fluorescence (as a measure of Ca^{2+}) over time (**Figure 2C**). This data was normalized to the baseline fluorescence level and expressed as a percentage increase. We analyzed three measures of the change in fluorescence during STDP induction: (1) ΔF_{30} (%), the change in fluorescence from F_0 to F_{30}; (2) ΔF_{peak} (%), the change in fluorescence from F_0 to F_{peak}; and (3) F_{area}, the area

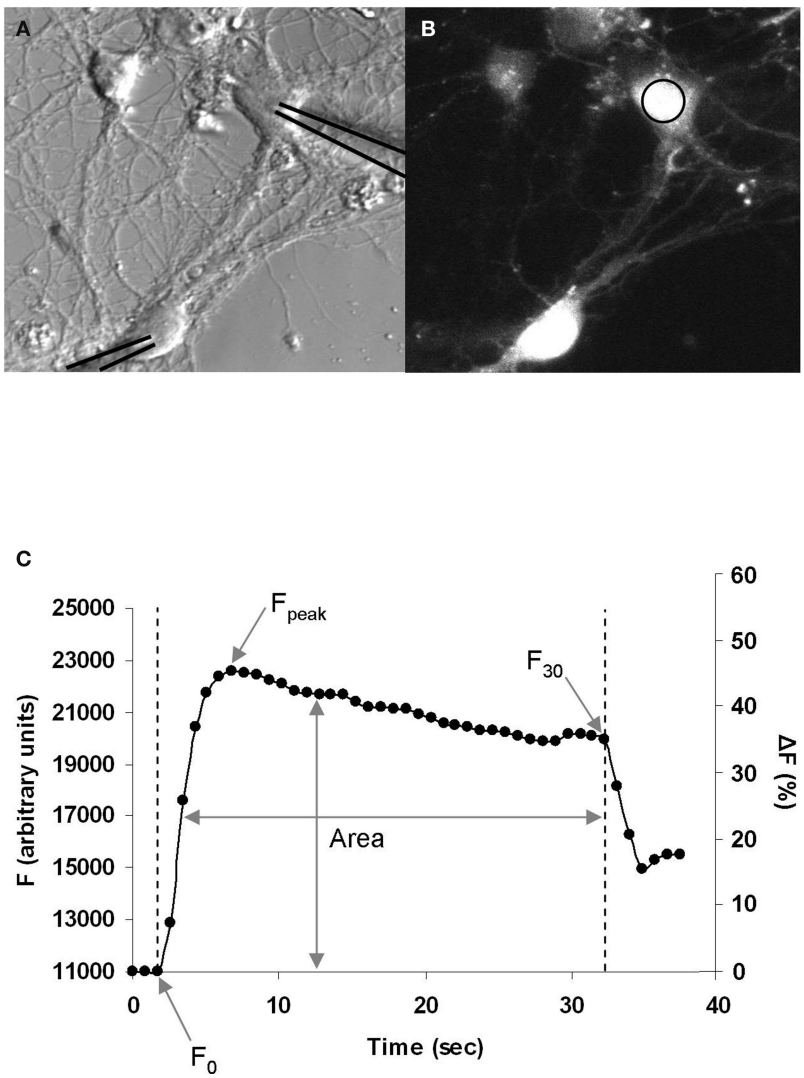

FIGURE 2 | Postsynaptic Ca^{2+} imaging during GABAergic STDP induction. **(A)** Bright field image of neurons during recording. The recording pipettes have been overlaid with black lines to clearly indicate the neurons being recorded. **(B)** Fluo4-AM fluorescence image of the same neurons as in **(A)**, measuring changes in Ca^{2+} during STDP induction. Ca^{2+} was measured in the area of interest on the soma (circle). **(C)** Example graph of the increase in Fluo4 fluorescence during induction, which begins at F_0 with the onset of stimulation, peaks at F_{peak}, and ends at F_{30} after 30 s of stimulation. The area of under the curve over this time period was used to calculate F_{area}, which normalizes the area to F_0. *Left axis:* arbitrary fluorescence units. *Right axis:* the same graph expressed as a percentage increase from baseline.

under the curve normalized to F_0. Increasing the image acquisition frequency to 100–200 ms intervals did not significantly change the ΔF_{peak} for depolarizing GABAergic synapses ($p = 0.898$), indicating that the standard acquisition rate was sufficient to resolve the peak of the Ca^{2+} fluorescence. We chose to exclusively examine the Ca^{2+} influx at the soma of the postsynaptic neurons for two reasons. First, the majority of GABAergic neurons innervate the proximal dendrites and soma of postsynaptic neurons (Cobb et al., 1995; Freund and Buzsaki, 1996; Di Cristo et al., 2004; Huang, 2006). Second, we recently demonstrated that GABAergic STDP is induced by feed-forward interneurons which target the soma of pyramidal neurons in the CA1 region of the hippocampus (Ormond and Woodin, 2009).

GPSC POLARITY DETERMINES THE MAGNITUDE OF CA^{2+} INFLUX DURING STDP INDUCTION

Ca^{2+} influx is required for GABAergic STDP (Woodin et al., 2003), but whether or not the dynamics of the influx depend on the properties of the synapse had not yet been determined. After recording from a population of neurons that included both depolarizing and hyperpolarizing GPSCs and imaging their Ca^{2+} dynamics, we examined the relationship between GPSC amplitude and Ca^{2+} influx during STDP induction. GPSC amplitude correlated strongly with Ca^{2+} influx (F_{area}); the linear regression analysis yielded similarly high r-squared value regardless of the spike-timing order [pre/post r-squared = 0.66 ($p = 0.002$), post/pre r-squared = 0.65 ($p = 0.003$), all synapses r-squared = 0.65 ($p < 0.001$); **Figure 3A**]. GPSC amplitude also correlated strongly with other measure of Ca^{2+} influx, ΔF_{30} [pre/post r-squared = 0.65 ($p = 0.002$), post/pre r-squared = 0.60 ($p = 0.005$), all synapses r-squared = 0.62 ($p < 0.001$)] and ΔF_{peak} [pre/post r-squared = 0.62 ($p = 0.004$), post/pre r-squared = 0.63 ($p = 0.004$), all synapses r-squared = 0.62 ($p < 0.001$)]. Thus, regardless of the fluorescence measure examined, there was a strong relationship between Ca^{2+} influx and the nature of the GABAergic synapse; depolarizing synapses correlated with large increases in Ca^{2+}, while hyperpolarizing synapses correlated with smaller increases.

The correlation between Ca^{2+} influx and GPSC amplitude was further quantified by comparing the fluorescence increase during STDP induction between all depolarizing synapses ($E_{Cl} = -58.33 \pm 2.63$ mV; $n = 12$), all hyperpolarizing synapses ($E_{Cl} = -75.87 \pm 1.74$ mV; $n = 10$), and neurons with no synapses (which we call "post only"; $n = 11$). The post only neurons were also stimulated at 5 Hz for 30 s. There were significant differences between the Ca^{2+} influx at depolarizing and hyperpolarizing synapses regardless of the measure analyzed (F_{area} $p = 0.004$; F_{peak} $p = 0.005$; F_{30} $p = 0.004$; **Figure 3B**). Ca^{2+} influx at hyperpolarizing synapses were also significantly different from the influx at post only neurons that fired in the absence of a synapse when F_{area} and F_{30} were analyzed ($p = 0.04$ and $p = 0.048$, respectively); however when F_{peak} was analyzed there was not a significant difference between hyperpolarizing synapses and post only neurons ($p = 0.06$). Thus, we can conclude that depolarizing neurons let in the same amount of Ca^{2+} during STDP induction as the postsynaptic neurons spiking alone (independent of a synapse). However, when the GPSC becomes hyperpolarizing it has a strong ability to decrease the Ca^{2+} influx.

At glutamatergic synapses the order of spiking (pre/post versus post/pre) during STDP induction determines the polarity of the plasticity (LTP versus LTD, respectively; Bi and Poo, 1998). However, at GABAergic synapses the order of spiking during induction does not determine the nature of plasticity (as evidenced by the symmetrical spike-timing window Woodin et al., 2003). We thus hypothesized that Ca^{2+} influx during STDP induction should be independent of the spike-timing order. We found no significant difference in Ca^{2+} influx (F_{area}) between synapses induced with positive or negative spike-timing intervals; this was true for both depolarizing ($p = 0.96$) and hyperpolarizing synapses ($p = 0.77$; **Figure 3C**). We also found no significant difference between the time taken for the Ca^{2+} influx to reach its maximum between pre/post and post/pre synapses ($p = 0.968$).

GABAergic SYNAPSE PROPERTIES DETERMINE CA^{2+} DYNAMICS DURING STDP INDUCTION

The Ca^{2+} influx during STDP induction was affected by GPSC amplitude. GPSC amplitude is determined by both E_{Cl} and $GABA_A$ conductance (Kaila, 1994); thus we asked which of these properties was the most influential in regulating postsynaptic Ca^{2+}. We found that the linear regression of E_{Cl} versus Ca^{2+} influx (F_{area}) yielded low r-squared values [0.31 ($p = 0.078$) for pre/post synapses, 0.25 ($p = 0.114$) for post/pre synapses, and 0.26 ($p = 0.015$) for all synapses] (**Figure 4A**). Low r-squared values indicate that the trend line does not accurately predict the relationship between E_{Cl} and Ca^{2+} influx. Thus, the difference between the slopes of the trend lines for pre/post and post/pre synapses does not necessarily indicate that the spike-timing order influences the Ca^{2+} influx. E_{Cl} also did not correlate strongly with ΔF_{30} [pre/post r-squared = 0.26 ($p = 0.114$), post/pre r-squared = 0.27 ($p = 0.104$), all synapses r-squared = 0.26 ($p = 0.017$)] or ΔF_{peak} [pre/post r-squared = 0.29 ($p = 0.086$), post/pre r-squared = 0.25 ($p = 0.119$), all synapses r-squared = 0.26 ($p = 0.016$)].

Perhaps a more useful measure when considering the Cl^- gradient is the driving force for Cl^-, which is the difference between the membrane potential and E_{Cl}. We found that the driving force correlated more strongly with Ca^{2+} influx (F_{area}) than did E_{Cl} alone, with r-squared values of 0.39 ($p = 0.041$) for pre/post synapses, 0.31 ($p = 0.076$) for post/pre synapses, and 0.34 ($p = 0.004$) for all synapses (**Figure 4B**). Other measures of Ca^{2+} influx, ΔF_{30} [pre/post r-squared = 0.42 ($p = 0.032$), post/pre r-squared = 0.33 ($p = 0.063$), all synapses r-squared = 0.37 ($p = 0.003$)] and ΔF_{peak} [pre/post r-squared = 0.35 ($p = 0.055$), post/pre r-squared = 0.33 ($p = 0.066$), all synapses r-squared = 0.33 ($p = 0.005$)], provided similar results as F_{area}.

$GABA_A$ conductance was found to correlate with F_{area} to a higher degree than did E_{Cl} or driving force, with r-squared values of 0.57 ($p = 0.007$) for pre/post synapses, 0.68 ($p = 0.002$) for post/pre synapses, and 0.62 ($p < 0.001$) for all synapses (**Figure 4C**). Conductance also correlated well with ΔF_{30} [pre/post r-squared = 0.52 ($p = 0.013$), post/pre r-squared = 0.62 ($p = 0.004$), all synapses r-squared = 0.56 ($p < 0.001$)] and ΔF_{peak} [pre/post r-squared = 0.52 ($p = 0.012$), post/pre r-squared = 0.66 ($p = 0.003$, all synapses r-squared = 0.58($p < 0.001$)].

DISCUSSION

At GABAergic synapses, the induction of STDP requires an increase in postsynaptic Ca^{2+} (Woodin et al., 2003; Xu et al., 2008; Ormond and Woodin, 2009). Depending on the stage of nervous system

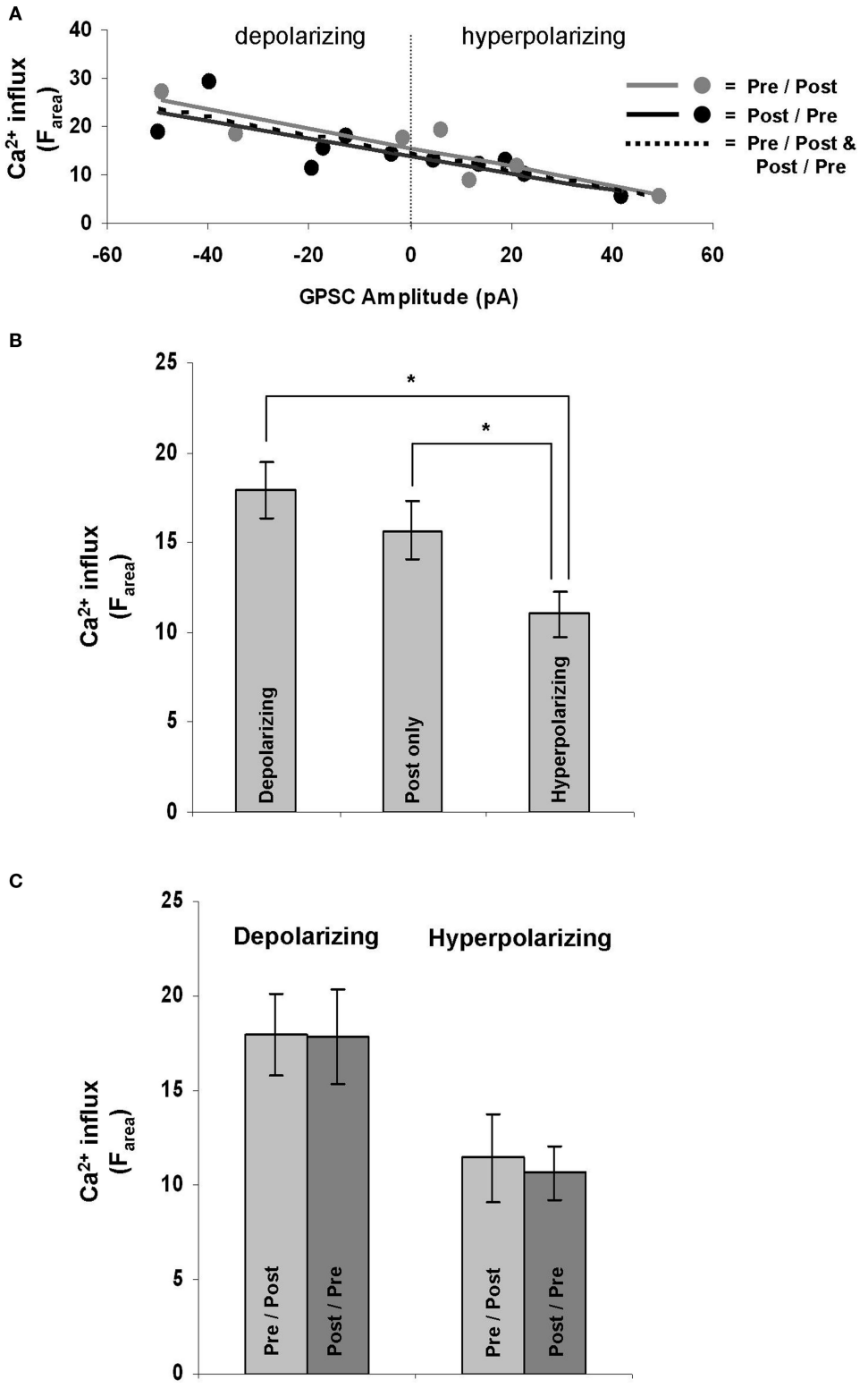

FIGURE 3 | GPSC amplitude affects postsynaptic Ca^{2+} dynamics during STDP induction. (A) GPSC amplitude strongly correlates with Ca^{2+} influx regardless of the order of spike-timing. **(B)** Depolarizing synapses result in a significantly larger Ca^{2+} influx during STDP induction than do hyperpolarizing synapses ($p = 0.004$). Hyperpolarizing synapses also result in a significantly lower Ca^{2+} influx than the firing of a neuron alone (post only; $p = 0.045$). **(C)** There was no significant difference in Ca^{2+} influx when STDP was induced in post/pre or pre/post orders at depolarizing ($p = 0.96$) and hyperpolarizing synapses ($p = 0.77$).

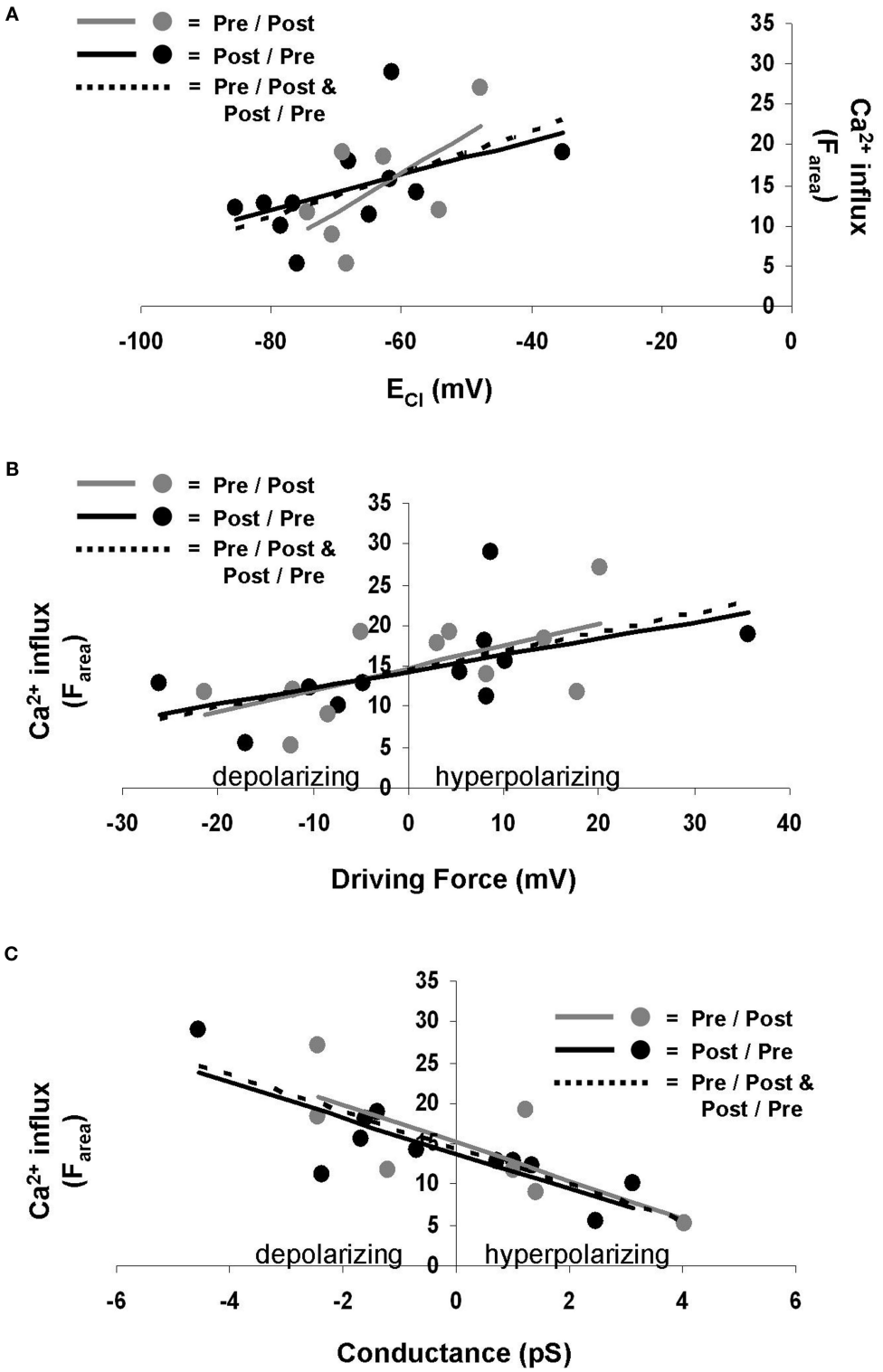

FIGURE 4 | E_{Cl}, driving force, and $GABA_A$ conductance influence Ca^{2+} influx during STDP induction. (A) E_{Cl} does not correlate well with Ca^{2+} influx. Gray points and solid gray line represent pre/post synapses. Black points and solid black line indicate post/pre synapses. Dotted line indicates all synapses combined. **(B)** Driving force correlates better with Ca^{2+} influx. Gray points and solid gray line represent pre/post synapses. Black points and solid black line indicate post/pre synapses. Dotted line indicates all synapses combined. **(C)** $GABA_A$ conductance also correlates well with Ca^{2+} influx. Gray points and solid gray line represent pre/post synapses. Black points and solid black line indicate post/pre synapses. Dotted line indicates all synapses combined.

development GABAergic synapses can be either depolarizing or hyperpolarizing, which led us to hypothesize that the nature of GABAergic transmission regulates the magnitude of the Ca^{2+} influx. Our present results found this hypothesis to be true; depolarizing GABAergic synapses characteristic of immature neuronal circuits produced larger Ca^{2+} influxes during STDP induction than hyperpolarizing GABAergic synapses, which are more commonly found in the mature central nervous system. Our analysis further revealed that this relationship between GABAergic synapses and Ca^{2+} influx can be accounted for by the two main properties of GABAergic synapses (the driving force for Cl^- and the $GABA_A$ receptor conductance) but did not depend on the order of spike timing.

It is already well known that synaptic transmission contributes to the postsynaptic Ca^{2+} influx during glutamatergic STDP induction (Markram et al., 1997; Bi and Poo, 1998, 2001; Debanne et al., 1998; Zhang et al., 1998). At these excitatory synapses, Ca^{2+} influx occurs primarily via VGCCs opened by the back-propagating action potential, and via NMDARs opened by the coincident occurrence of the back-propagating action potential and postsynaptic glutamate binding. How can our understanding of the Ca^{2+} influx during glutamatergic STDP induction be related to GABAergic STDP? It depends on the polarity of the GABAergic synapse. When E_{Cl} sits below the resting membrane potential the GPSC will hyperpolarize the postsynaptic membrane during STDP induction, resulting in a smaller Ca^{2+} influx than if that same postsynaptic neuron was spiking alone (at 5 Hz for 30 s, in the absence of synaptic transmission). This smaller Ca^{2+} influx presumably results from hyperpolarizing GPSCs decreases the opening of VGCCs (which are activated by action potential firing during STDP induction). However, at depolarizing GABAergic synapses, the Ca^{2+} influx during STDP induction for both positive and negative spike-timing intervals does not differ significantly from when the postsynaptic neuron spikes alone. This indicates that the additional depolarization is insufficient to open more VGCCs, either because the majority of available VGCCs have already been opened by the action potential, or because the magnitude of depolarization is not sufficient to open VGCCs.

We already know that the required Ca^{2+} influx during GABAergic STDP occurs partly through L-type VGCCs (Woodin et al., 2003; Ormond and Woodin, 2009). However, this cannot be the only source of Ca^{2+} influx because when GABAergic synapses are blocked or absent (post only) the same spiking pattern which also opens VGCCs fails to induce plasticity. This indicates that there are either additional sources of Ca^{2+} influx required for STDP, or that a component of the GABAergic signaling combines with the L-type Ca^{2+} influx to induce plasticity. We have preliminary evidence for the involvement of T-type VGCCs during hyperpolarizing GABAergic STDP (Balena and Woodin, 2009); these channels require membrane hyperpolarization to be removed from their inactive state but also require subsequent membrane depolarization to become activated (Magee et al., 1995; Perez-Reyes and Lory, 2006). Thus during hyperpolarizing GABAergic transmission we believe that the Ca^{2+} influx occurs both through L-type VGCCs (which have a reduced opening compared to post only) and through T-type VGCCs.

The strength of GABAergic synapses depends upon both the conductance of the channel and on the driving force for ions flowing through the channel. Because we recorded in a HCO_3^--free medium, $E_{GABA} \approx E_{Cl}$; thus the driving force through the $GABA_A$ receptors was largely determined by E_{Cl}. We found that neither the channel conductance nor the Cl^- driving force alone could predict the relationship between GPSC amplitude and Ca^{2+} influx. This indicates that it is the combination of these properties of GABAergic transmission that is important in regulating Ca^{2+} influx during STDP induction.

At glutamatergic synapses, positive and negative spike-timing intervals lead to long-term potentiation and depression, respectively, resulting in an asymmetric spike-timing window (Markram et al., 1997; Bi and Poo, 1998, 2001; Debanne et al., 1998; Zhang et al., 1998). In contrast, the spike-timing window for GABAergic synapses is symmetric, with coincident activity (within ±15 ms) resulting in decreased inhibition, independent of the spike-timing order (Woodin et al., 2003). This likely accounts for the non-significant differences in Ca^{2+}-influx between positive and negative spike-timing intervals. However, the present study only examined spike-timing intervals of <5 ms; whether the results are similar for intervals >5 ms remains to be determined.

We identified a significant difference in the resting membrane potentials between depolarizing and hyperpolarizing synapses. This difference may result from our ability to identify GABAergic synapses where E_{Cl} sits close to the resting membrane potential; if $E_{Cl} \approx$ resting membrane potential there would be no driving force for Cl^- and thus we did not characterize a synapse electrophysiologically. This may have biased our selection of synapses for those with larger driving forces; depolarizing synapses would be more likely to be found onto neurons with relatively hyperpolarized resting membrane potentials, and hyperpolarizing synapses would be common onto neurons with relatively depolarized resting membrane potentials.

Following acute neuronal trauma (van den Pol et al., 1996; Toyoda et al., 2003), oxygen-glucose deprivation (Galeffi et al., 2004), and seizure activity (Galanopoulou, 2007), there is a depolarization of E_{Cl} which renders GABAergic transmission depolarizing (Fiumelli and Woodin, 2007; Kahle et al., 2008). Based on our present results, this switch in the polarity of GABAergic transmission increases the amount of Ca^{2+} influx during subsequent neuronal activity. In fact, the magnitude of the E_{Cl} depolarization following neuronal insults is so large it often renders GABAergic transmission excitatory (Kahle et al., 2008), which should produce even larger Ca^{2+} influxes than those observed in the present study. This may be particularly relevant given that the large Ca^{2+} influxes resulting from neuronal injury contribute to cell death (Bano and Nicotera, 2007).

Taken together, a model emerges where postsynaptic Ca^{2+} influx is required for STDP induction at GABAergic synapses, and where the magnitude of this influx is regulated by the GABAergic transmission itself. Further work will be need to elucidate both how the Ca^{2+} influx in turn regulates E_{Cl}, and how the Ca^{2+} influx is regulated when GABAergic and glutamatergic STDP are induced simultaneously.

ACKNOWLEDGMENTS

This work was supported by a Natural Sciences and Engineering Research Council of Canada (NSERC) Discover Grant to Melanie A Woodin, and a NSERC Fellowship to Trevor Balena.

REFERENCES

Balena, T., and Woodin, M. A. (2008). Coincident pre- and postsynaptic activity downregulates NKCC1 to hyperpolarize E(Cl) during development. *Eur. J. Neurosci.* 27, 2402–2412.

Balena, T., and Woodin, M. A. (2009). "Calcium dynamics underlying the induction of inhibitory synaptic plasticity," in *Proceedings of the Society for Neuroscience Annual Meeting* (Chicago, Illinois), 41.16.

Bano, D., and Nicotera, P. (2007). Ca2+ signals and neuronal death in brain ischemia. *Stroke* 38, 674–676.

Bi, G., and Poo, M., 2001. Synaptic modification by correlated activity: Hebb's postulate revisited. *Annu Rev Neurosci.* 24, 139–166.

Bi, G. Q., and Poo, M. M. (1998). Synaptic modifications in cultured hippocampal neurons: dependence on spike timing, synaptic strength, and postsynaptic cell type. *J. Neurosci.* 18, 10464–10472.

Blaesse, P., Airaksinen, M. S., Rivera, C., and Kaila, K. (2009). Cation-chloride cotransporters and neuronal function. *Neuron* 61, 820–838.

Cobb, S. R., Buhl, E. H., Halasy, K., Paulsen, O., and Somogyi, P. (1995). Synchronization of neuronal activity in hippocampus by individual GABAergic interneurons. *Nature* 378, 75–78.

Dan, Y., and Poo, M. M. (2006). Spike timing-dependent plasticity: from synapse to perception. *Physiol. Rev.* 86, 1033–1048.

Debanne, D., Gahwiler, B. H., and Thompson, S. M. (1998). Long-term synaptic plasticity between pairs of individual CA3 pyramidal cells in rat hippocampal slice cultures. *J. Physiol. (Lond.)* 507(Pt 1), 237–247.

Di Cristo, G., Wu, C., Chattopadhyaya, B., Ango, F., Knott, G., Welker, E., Svoboda, K., and Huang, Z. J. (2004). Subcellular domain-restricted GABAergic innervation in primary visual cortex in the absence of sensory and thalamic inputs. *Nat. Neurosci.* 7, 1184–1186.

Dzhala, V. I., Talos, D. M., Sdrulla, D. A., Brumback, A. C., Mathews, G. C., Benke, T. A., Delpire, E., Jensen, F. E., and Staley, K. J. (2005). NKCC1 transporter facilitates seizures in the developing brain. *Nat. Med.* 11, 1205–1213.

Fiumelli, H., and Woodin, M. A. (2007). Role of activity-dependent regulation of neuronal chloride homeostasis in development. *Curr. Opin. Neurobiol.* 17, 81–86.

Freund, T. F., and Buzsaki, G. (1996). Interneurons of the hippocampus. *Hippocampus* 6, 347–470.

Galanopoulou, A. S. (2007). Developmental patterns in the regulation of chloride homeostasis and GABA(A) receptor signaling by seizures. *Epilepsia* 48(Suppl. 5), 14–18.

Galeffi, F., Sah, R., Pond, B. B., George, A., and Schwartz-Bloom, R. D. (2004). Changes in intracellular chloride after oxygen-glucose deprivation of the adult hippocampal slice: effect of diazepam. *J. Neurosci.* 24, 4478–4488.

Gulledge, A. T., and Stuart, G. J. (2003). Excitatory actions of GABA in the cortex. *Neuron* 37, 299–309.

Huang, Z. J. (2006). Subcellular organization of GABAergic synapses: role of ankyrins and L1 cell adhesion molecules. *Nat. Neurosci.* 9, 163–166.

Kahle, K. T., Staley, K. J., Nahed, B. V., Gamba, G., Hebert, S. C., Lifton, R. P., and Mount, D. B. (2008). Roles of the cation-chloride cotransporters in neurological disease. *Nat. Clin. Pract. Neurol.* 4, 490–503.

Kaila, K. (1994). Ionic basis of GABAA receptor channel function in the nervous system. *Prog. Neurobiol.* 42, 489–537.

Kaila, K., and Voipio, J. (1987). Postsynaptic fall in intracellular pH induced by GABA-activated bicarbonate conductance. *Nature* 330, 163–165.

Kaila, K., Voipio, J., Paalasmaa, P., Pasternack, M., and Deisz, R. A. (1993). The role of bicarbonate in GABAA receptor-mediated IPSPs of rat neocortical neurones. *J. Physiol.* 464, 273–289.

Kano, M. (1994). Calcium-induced long-lasting potentiation of GABAergic currents in cerebellar Purkinje cells. *Jpn. J. Physiol.* 44(Suppl. 2), S131–S136.

Magee, J. C., Christofi, G., Miyakawa, H., Christie, B., Lasser-Ross, N., and Johnston, D. (1995). Subthreshold synaptic activation of voltage-gated Ca2+ channels mediates a localized Ca2+ influx into the dendrites of hippocampal pyramidal neurons. *J. Neurophysiol.* 74, 1335–1342.

Markram, H., Lubke, J., Frotscher, M., and Sakmann, B. (1997). Regulation of synaptic efficacy by coincidence of postsynaptic APs and EPSPs. *Science* 275, 213–215.

Nishiyama, M., Hong, K., Mikoshiba, K., Poo, M. M., and Kato, K. (2000). Calcium stores regulate the polarity and input specificity of synaptic modification. *Nature* 408, 584–588.

Ormond, J., and Woodin, M. A. (2009). Disinhibition mediates a form of hippocampal long-term potentiation in area CA1. *PLoS ONE* 4, e7224. doi:10.1371/journal.pone.0007224.

Perez-Reyes, E., and Lory, P. (2006). Molecular biology of T-type calcium channels. *CNS Neurol. Disord. Drug Targets* 5, 605–609.

Rivera, C., Voipio, J., Payne, J. A., Ruusuvuori, E., Lahtinen, H., Lamsa, K., Pirvola, U., Saarma, M., and Kaila, K. (1999). The K+/Cl- co-transporter KCC2 renders GABA hyperpolarizing during neuronal maturation. *Nature* 397, 251–255.

Saraga, F., Balena, T., Wolansky, T., Dickson, C. T., and Woodin, M. A. (2008). Inhibitory synaptic plasticity regulates pyramidal neuron spiking in the rodent hippocampus. *Neuroscience* 155, 64–75.

Toyoda, H., Ohno, K., Yamada, J., Ikeda, M., Okabe, A., Sato, K., Hashimoto, K., and Fukuda, A. (2003). Induction of NMDA and GABAA receptor-mediated Ca2+ oscillations with KCC2 mRNA downregulation in injured facial motoneurons. *J. Neurophysiol.* 89, 1353–1362.

van den Pol, A. N., Obrietan, K., and Chen, G. (1996). Excitatory actions of GABA after neuronal trauma. *J. Neurosci.* 16, 4283–4292.

Woodin, M. A., Ganguly, K., and Poo, M. M. (2003). Coincident pre- and postsynaptic activity modifies GABAergic synapses by postsynaptic changes in Cl- transporter activity. *Neuron* 39, 807–820.

Xu, C., Zhao, M. X., Poo, M. M., and Zhang, X. H. (2008). GABA(B) receptor activation mediates frequency-dependent plasticity of developing GABAergic synapses. *Nat. Neurosci.* 11, 1410–1418.

Yamada, J., Okabe, A., Toyoda, H., Kilb, W., Luhmann, H. J., and Fukuda, A. (2004). Cl- uptake promoting depolarizing GABA actions in immature rat neocortical neurones is mediated by NKCC1. *J. Physiol.* 557, 829–841.

Zhang, L. I., Tao, H. W., Holt, C. E., Harris, W. A., and Poo, M. (1998). A critical window for cooperation and competition among developing retinotectal synapses. *Nature* 395, 37–44.

Conflict of Interest Statement: The authors declare that the research was conducted in the absence of any commercial or financial relationships that could be construed as a potential conflict of interest.

Received: 04 February 2010; paper pending published: 22 February 2010; accepted: 20 May 2010; published online: 28 June 2010.

Citation: Balena T, Acton BA and Woodin MA (2010) GABAergic synaptic transmission regulates calcium influx during spike-timing dependent plasticity. Front. Syn. Neurosci. ***2****:16. doi: 10.3389/fnsyn.2010.00016*

frontiers in
SYNAPTIC NEUROSCIENCE

ORIGINAL RESEARCH ARTICLE
published: 23 June 2010
doi: 10.3389/fnsyn.2010.00022

GABAergic activities control spike timing- and frequency-dependent long-term depression at hippocampal excitatory synapses

Makoto Nishiyama[1]*, Kazunobu Togashi[1], Takeshi Aihara[2] and Kyonsoo Hong[1]*

[1] *Department of Biochemistry, New York University School of Medicine, New York, NY, USA*
[2] *Department of Information-Communication Engineering, Tamagawa University, Tokyo, Japan*

Edited by:
Henry Markram, Ecole Polytechnique Federale de Lausanne, Switzerland

Reviewed by:
Takao Hench, Harvard University, USA;
Shigeru Kubota, Yamagata University, Japan
Yoshiyuki Kubota, National Institute for Physiological Sciences, Japan

****Correspondence:***
Makoto Nishiyama, Department of Biochemistry, New York University School of Medicine, New York, NY, 10016, USA.
e-mail: nishim01@nyumc.org;
Kyonsoo Hong, Department of Biochemistry, New York University School of Medicine, New York, NY, 10016, USA.
e-mail: hongk02@nyumc.org

GABAergic interneuronal network activities in the hippocampus control a variety of neural functions, including learning and memory, by regulating θ and γ oscillations. How these GABAergic activities at pre- and postsynaptic sites of hippocampal CA1 pyramidal cells differentially contribute to synaptic function and plasticity during their repetitive pre- and postsynaptic spiking at θ and γ oscillations is largely unknown. We show here that activities mediated by postsynaptic $GABA_A$Rs and presynaptic $GABA_B$Rs determine, respectively, the spike timing- and frequency-dependence of activity-induced synaptic modifications at Schaffer collateral-CA1 excitatory synapses. We demonstrate that both feedforward and feedback $GABA_A$R-mediated inhibition in the postsynaptic cell controls the spike timing-dependent long-term depression of excitatory inputs ("*e*-LTD") at the θ frequency. We also show that feedback postsynaptic inhibition specifically causes *e*-LTD of inputs that induce small postsynaptic currents (<70 pA) with LTP-timing, thus enforcing the requirement of cooperativity for induction of long-term potentiation at excitatory inputs ("*e*-LTP"). Furthermore, under spike-timing protocols that induce *e*-LTP and *e*-LTD at excitatory synapses, we observed parallel induction of LTP and LTD at inhibitory inputs ("*i*-LTP" and "*i*-LTD") to the same postsynaptic cells. Finally, we show that presynaptic $GABA_B$R-mediated inhibition plays a major role in the induction of frequency-dependent *e*-LTD at α and β frequencies. These observations demonstrate the critical influence of GABAergic interneuronal network activities in regulating the spike timing- and frequency-dependences of long-term synaptic modifications in the hippocampus.

Keywords: STDP, CA1, GABA, spike timing, frequency, hippocampal oscillation

INTRODUCTION

GABAergic interneuronal network activities regulate a variety of neural functions, such as modulation of activity-dependent synaptic plasticity (Meredith et al., 2003), i.e., long-term potentiation (LTP) and depression (LTD), and serve as a driving force for the hippocampal θ and γ oscillations important for processing learning and memory (Buzsáki, 2002; Csicsvari et al., 2003; Lisman et al., 2005). GABA functions as a major inhibitory neurotransmitter at both excitatory (glutamatergic) and inhibitory (GABAergic) neurons in the central nervous system by activating $GABA_A$ receptors ($GABA_A$Rs) and $GABA_B$ receptors ($GABA_B$Rs) in both pre- and postsynaptic cells (Connors et al., 1988; Davies and Collingridge, 1996). However, the inhibitory function of GABA on postsynaptic $GABA_A$Rs depends on the state of the Cl^- ion reversal potential relative to the resting membrane potential (Staley et al., 1995). For example, in the hippocampus, GABAergic inhibition induced by stimuli at the α/β (low, 10 Hz) frequency shifts to excitation when stimuli occur at the γ (high, 40 Hz) frequency as a consequence of intracellular Cl^- ion ($[Cl^-]_i$) accumulation in postsynaptic CA1 pyramidal cells (Staley et al., 1995; Bracci et al., 2001). In addition, GABA inhibition through presynaptic $GABA_B$Rs, which are linked to G-protein-coupled inwardly rectifying K^+ channels (GIRK), imposes different frequency dependencies at excitatory and inhibitory presynaptic terminals that are effective, respectively, above the α/β frequency (Ohliger-Frerking et al., 2003) and near the θ frequency (Davies and Collingridge, 1996).

In hippocampal neural networks, different populations of GABAergic interneurons (Maccaferri et al., 2000; Klausberger and Somogyi, 2008) contribute to postsynaptic feedforward (FF) and feedback (FB) inhibition at CA1 pyramidal cells (Pouille and Scanziani, 2001, 2004) and to presynaptic inhibition at excitatory and inhibitory presynaptic terminals to CA1 pyramidal cells. However, it is unknown how these distinct GABA actions affect excitatory synaptic gains, either differentially or synergistically. Depending on the precise timing of pre- and postsynaptic neuronal spikes, repetitive spiking reliably induces either LTP or LTD, collectively known as spike-timing-dependent plasticity (STDP), in hippocampal neurons in culture (Bi and Poo, 1998; Debanne et al., 1998), in hippocampal or cortical neurons in slices (Markram et al., 1997; Feldman, 2000; Nishiyama et al., 2000; Sjöström et al., 2001; Froemke and Dan, 2002; Woodin et al., 2003), and in neurons of the tectum *in vivo* (Zhang et al., 1998). Previously, we showed that at hippocampal Schaffer collateral (SC)-CA1 pyramidal cell excitatory synapses, STDP induced by stimuli at 5 Hz (θ frequency) is composed of two distinct LTD time intervals (−LTD: −28 to −16 ms and +LTD: +15 to +20 ms) that flank an LTP time interval (−2 to

+15 ms) (Nishiyama et al., 2000). Interestingly, this LTP/LTD time interval cycle is completed within 25 ms at 40 Hz (γ frequency), similar to the time course of the γ oscillation *in vivo* (Csicsvari et al., 2003), which hippocampal GABAergic interneuronal networks are believed to regulate (Whittington et al., 1995; Bartos et al., 2007; Cardin et al., 2008; Sohal et al., 2008). Also, repetitive stimuli at SC inputs persistently alter synaptic efficacy at GABAergic inputs to CA1 pyramidal cells (Woodin et al., 2003; Chevaleyre and Castillo, 2004; Lamsa et al., 2005; Gibson et al., 2008). We, therefore, monitored synaptic efficacy at CA1 pyramidal cells to investigate how these dynamic patterns of GABAergic interneuronal inputs regulate spike timing- and frequency-dependent STDP at excitatory synapses (*e*-STDP).

MATERIALS AND METHODS

HIPPOCAMPAL SLICE PREPARATION

Hippocampal slices were prepared by a standard procedure (Nishiyama et al., 2000). Male Sprague-Dawley rats (26- to 35-day old) were anaesthetized and decapitated. Right hippocampi were dissected rapidly and placed in a gassed (95% O_2–5% CO_2) extracellular solution containing (in mM) 124 NaCl, 3 KCl, 2.6 $CaCl_2$, 1.3 $MgSO_4$, 1.25 NaH_2PO_4, 22 $NaHCO_3$ and 10 D-glucose at 10°C. Transverse slices of 500-μm thickness were cut with a rotor tissue slicer (Dosaka, DTY7700) and maintained at room temperature (23–26°C) in an incubation chamber for at least 2 h. For experiments, individual slices were transferred to a submersion recording chamber and perfused continuously with extracellular solution (4.0~4.5 ml/min) at room temperature. Experiments using a K^+-based internal recording solution (see below) were performed at 30–33°C. To prevent epileptiform activity, the CA3 region was removed in experiments that used GABA and muscarinic receptor antagonists.

WHOLE-CELL RECORDING

Whole-cell recordings were made in the CA1 cell body layer with the "blind" patch clamp method, using an Axopatch 200B amplifier (Axon Inst.). Test stimuli were applied at 0.05 Hz and alternated between two non-overlapping SC inputs using bipolar electrodes (MCE-100, RMI) under voltage-clamp (V_c = −80 mV) [except when inhibitory postsynaptic currents (IPSCs) were measured] to evoke excitatory postsynaptic currents (EPSCs). Both stimulating electrodes were positioned at the *stratum radiatum* at least 500 μm distant from the recording electrode to avoid stimulation of monosynaptic (direct) inhibitory inputs. The non-overlap of the two inputs was confirmed by applying alternate paired-pulse test stimuli (at 50-ms intervals) to demonstrate the absence of cross facilitation between the two inputs. Constant current pulses (amplitude, 6–14 μA; duration, 300 μs) evoked EPSCs with amplitudes of 100–200 pA. These current intensities were at least three fold smaller than the stimulation currents that evoke population spikes. Following a stable recording period of about 12 (K^+-based internal recording solution) or 15 (Cs^+-based internal recording solution) min, the recording was switched to current clamp and a train of stimuli at a frequency of 5 Hz was delivered to one of the two inputs for either 20 s (K^+-based) or 16 s (Cs^+-based). Each presynaptic stimulus was paired with the injection of a spike-form (K^+-based: 2 nA for 2 ms at the peak, I_{max}) or square (Cs^+-based: 2 nA for 2 ms) depolarizing current pulse into the postsynaptic neuron to initiate spiking at various time intervals. The spike-form depolarizing currents (t in ms): $I_{max}\cdot 10\cdot t$, $0 \le t < 0.1$; I_{max}, $0.1 \le t < 2.1$; $I_{max}\cdot[(1-(0.8/1.5)\cdot(t-2.1)]$, $2.1 \le t < 3.6$; $I_{max}\cdot[0.2-(0.12/2)\cdot(t-3.6)]$, $3.6 \le t < 5.6$; $I_{max}\cdot 0.08\cdot[1-(1/2.5)\cdot(t-5.6)]$, $5.6 \le t < 8.1$ were designed to reduce the jitter of postsynaptic spikes but not to affect the spike decay time. Depolarization-induced suppression of inhibition (DSI) was induced by changing V_c from −80 to 0 mV for 2–3 s, followed by the application of the spike-timing protocol (at 5-, 12- and 25-Hz for 16, 6.7 and 3.2 s, respectively) for various time intervals after 5–10 s. A voltage-step of +90 mV from the holding potential (at −80 mV) was applied for 40 ms every 60 s to visualize feedforward (FF)-IPSCs during the concurrent monitoring of EPSC/FF-IPSC. A 40-ms voltage-step was chosen to avoid the induction of DSI (estimated to be less than 1% according to Lenz and Alger, 1999) but was long enough to detect peak currents of disynaptic FF-IPSCs. During this voltage-step, EPSC was masked because the commanding potential (i.e., +10 mV) was approximately equivalent to the EPSC reversal potential. The identity of FF-IPSC was confirmed as a result of its abolition by bath-applied gabazine (10–100 μM) and kynurenic acid (5 mM). Data were filtered at 2 kHz and digitized at 10 kHz. Patch electrodes were pulled from borosilicate glass (1.2-mm O.D.) and had a resistance of 3.5~6 MΩ. Pipettes were filled with a solution containing (in mM): 120 K-gluconate, 10 $KMeSO_3$, 10 KCl, 0.075 BAPTA, 20 HEPES, 4 Mg-ATP, 2 Na2-ATP, pH adjusted to 7.35 with KOH. For experiments that required sustained postsynaptic depolarization, a Cs^+-based internal solution was used that contained (in mM): 130 cesium methanesulphonate ($CsMeSO_3$), 10 tetraethylammonium (TEA) chloride (Cl^-), 0.25 1,2-bis(2-aminophenoxy)ethane-N,N,N',N'-tetraacetic acid (BAPTA), 10 N-[1-hydroxyethyl]-piperazine-N'-[2-ethanesulphonic acid] (HEPES), 2 Mg-ATP, 2 Na_2-ATP, pH adjusted to 7.35 with CsOH,. The series resistance (typically 10–14 MΩ) was compensated 50–80% and was monitored throughout the experiment using a −5 mV step command. Cells that showed an unstable series resistance (>20% changes after the spike-timing protocol) were not used. To monitor monosynaptic IPSCs, 40 μM CNQX and 50 μM D(−)-2-amino-5-phosphonovaleric acid (AP5) were present in the extracellular solution and CsCl instead of $CsMeSO_3$ was used intracellularly while the cells were held at −70 mV. Drugs (bicuculline, kynurenic acid, gabazine, CNQX, AP5 and phaclofen) were purchased from either RBI or Tocris. CGP35348 was a generous gift from Novartis.

RESULTS

SINGLE, PRE- AND POSTSYNAPTIC SPIKING AT THE θ FREQUENCY RECRUITS BOTH FEEDFORWARD AND FEEDBACK POSTSYNAPTIC $GABA_A$R-MEDIATED INHIBITION

We performed whole-cell recordings at CA1 pyramidal cells in hippocampal slices (**Figure 1A**) in which the GABAergic networks are well defined (**Figure 1B**) (Maccaferri et al., 2000; Pouille and Scanziani, 2001, 2004; Klausberger and Somogyi, 2008). We stimulated SC inputs in the *stratum radiatum* at 100–150 μm away from the *stratum pyramidale* (SP, somatic layer) to evoke both EPSCs and FF-IPSCs in 500 μm thick slices. We used a $CsMeSO_3$-based (Cs^+-based) internal solution, which blocks GIRKs, to isolate the effects of postsynaptic $GABA_A$R-mediated inhibition from those of postsynaptic $GABA_B$R-mediated inhibition. In this

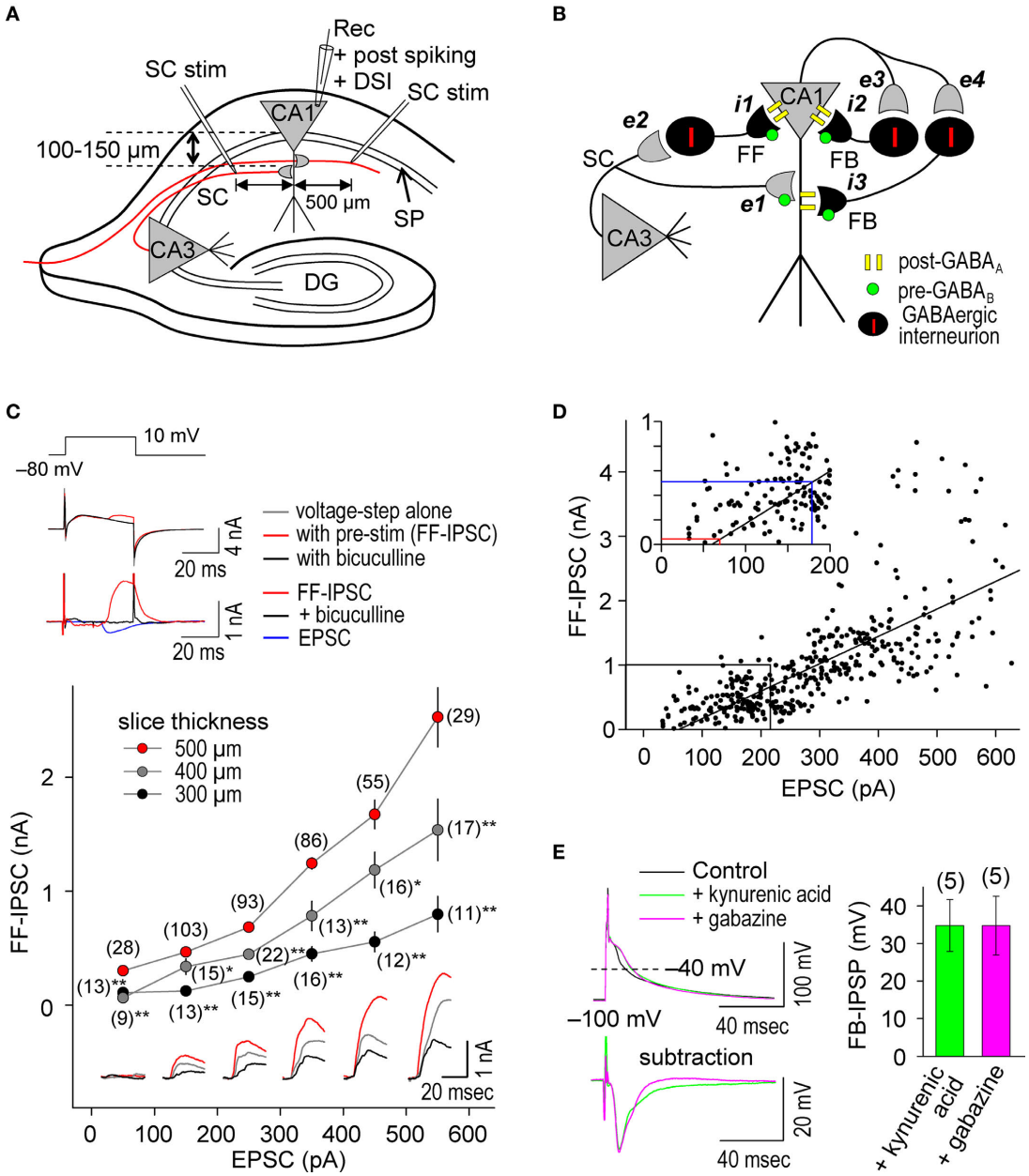

FIGURE 1 | Repetitive, single pre- and postsynaptic spiking recruits both FF and FB postsynaptic GABA$_A$R-mediated inhibition in hippocampal CA1 pyramidal cells. (A) Experimental paradigm depicting the positions of stimulating and recording electrodes. Whole-cell recordings were made in the CA1 cell body and the test stimuli were applied at the *stratum radiatum* at least 500 µm distant from the recording electrode. **(B)** Schematic diagram of neuronal networks involved in the induction of STDP in CA1 pyramidal cells. Locations of excitatory (*e*) and inhibitory (*i*) inputs and GABA receptors are indicated. **(C)** Procedure for concurrent measurement of EPSCs and FF-IPSCs (top) and summary of their amplitudes (bottom). FF-IPSC is detected (top middle) with the use of voltage-steps (top upper) and presynaptic stimulation (pre-stim). The magnitude of FF-IPSC (top lower, black) is calculated by subtracting the voltage-step alone (top middle, black) from the pre-stimulation value (top middle, blue). The voltage-step at +10 mV was applied for 40 ms to prevent the induction of DSI (less than 1%; Lenz and Alger, 1999). The FF-IPSC was confirmed by GABA$_A$ blockade with bicuculline (20 µM, top middle and lower, red). The ratio of FF-IPSCs to EPSCs increased as the slice thickness increased. Data represent the mean EPSC/FF-IPSC (±sem). Traces: FF-IPSC in 500-µm (red), 400-µm (gray) and 300-µm (black) thick slices. The (number) indicates the total number of trials. Significant differences from corresponding data in 500-µm thick slices are indicated ("*" $p < 0.05$ and "**" $p < 0.01$; Mann–Whitney U test). **(D)** The amplitude of FF-IPSC is proportional to the EPSC amplitude. When the EPSC level is <70 pA, there is no FF-IPSC (see red line in inset). The EPSC amplitude normally used in this study is indicated (blue line in inset). **(E)** Prominent FB postsynaptic GABA$_A$R-mediated inhibition is recruited by repetitive 5-Hz postsynaptic spiking in CA1 pyramidal cells. Postsynaptic spiking was induced by depolarizing current injections (6 nA, 2 ms, 20 pulses at 5 Hz) while postsynaptic CA1 pyramidal cells were held at –100 mV in a current-clamp configuration using a Cs^+-based internal recording solution. The top left panel shows the postsynaptic membrane potentials monitored when FB postsynaptic GABA$_A$R-mediated inhibition was blocked by either kynurenic acid (5 mM) or gabazine (10 µM). The control, in which GABA$_A$R was not blocked, showed a feedback inhibition-inclusive membrane potential. Subtraction analysis (bottom left) revealed a membrane potential resulting from FB postsynaptic GABA$_A$R-mediated inhibition. Average FB-IPSP (right).

configuration, we found that substantially more GABAergic inputs relative to glutamatergic inputs were retained than in thinner (300 and 400 μm) slices (**Figure 1C**); the FF-IPSC amplitude was 1045 ± 44 pA when the EPSC amplitude was 301 ± 8 pA (±sem, $n = 408$; differences between commanding and reversal potentials were ca. 90 mV for both FF-IPSCs and EPSCs) (Megias et al., 2001). Consistent with the idea that monosynaptic EPSCs and disynaptic FF-IPSCs normally share the same population of SC inputs in our experimental paradigm, the magnitudes of both EPSCs and FF-IPSCs changed in positive correlation with the magnitudes of presynaptic stimuli at SC inputs (**Figures 1C,D**). Weak, superlinearly- increased FF-IPSC amplitudes, greater than those of EPSCs, were observed when strong stimuli were applied to SC inputs (i.e., EPSC amplitudes >300 pA; **Figure 1D**, bottom). This superlinearity, the mechanism for which is unknown, may help to facilitate the failure of LTP induction at strong inputs, which has been demonstrated in cultured hippocampal neurons (Bi and Poo, 1998) and is believed to maintain gain levels of the entire network activity (van Rossum et al., 2000). It is noteworthy that as presynaptic stimulation was decreased, FF-IPSCs disappeared at a level at which EPSCs of ~70 pA remained (see **Figure 1D** inset), indicating that *e*-STDP can be examined in the absence of functional FF-IPSCs to individually-recorded pyramidal cells.

To ascertain whether FB postsynaptic $GABA_A$R-mediated inhibition occurred during the θ frequency (5 Hz) spike-timing protocol, we injected postsynaptic spike-inducing depolarizing currents (6 nA for 2 ms) through the whole-cell recording electrodes for 20 pulses (at 5 Hz) in the absence of presynaptic stimuli. The recorded cell was held at −100 mV under the current clamp to avoid sustained depolarization after spikes in the absence of K^+ channel function. Feedback postsynaptic $GABA_A$R-mediated membrane hyperpolarization was measured as differential potentials in which the spike afterpotential (averaged between the 15th and 20th spikes) in the presence of either gabazine (10–100 μM), a $GABA_A$R antagonist, or kynurenic acid (5 mM), a glutamate receptor antagonist (to eliminate disynaptic responses), was subtracted from that in the absence of antagonists (**Figure 1E**). We observed a FB postsynaptic $GABA_A$R-mediated hyperpolarizing effect of ca. −34 mV when cell membrane potentials were at ca. −40 mV, demonstrating the occurrence of functional FB postsynaptic $GABA_A$R-mediated inhibition. Thus, our experimental paradigm is a unique method to investigate differential GABAergic effects (e.g., pre- vs. postsynaptic, $GABA_A$R- vs. $GABA_B$R-mediated and FF vs. FB) on the induction of *e*-STDP.

e-STDP INDUCED AT THE θ FREQUENCY IS INDEPENDENT OF POSTSYNAPTIC $GABA_B$R-MEDIATED INHIBITION

Blocking postsynaptic K^+ channel activity, including that linked to $GABA_B$R function, may also affect the spike-timing dependence of *e*-STDP. We, therefore, examined the timing-dependent feature of *e*-STDP using a K-gluconate-based (control) internal solution in the recording pipette. We applied SC stimulation that evoked EPSCs of amplitude >70 pA to ensure the presence of functional FF-IPSCs (**Figure 1D**). When presynaptic stimuli at SC-CA1 synapses were paired with postsynaptic spike-inducing depolarizing currents with a time interval of +5 ms at 5 Hz for 20 s, we observed input-specific *e*-LTP (**Figure 2A**), which was comparable to that induced by a 16-s spike-timing protocol (at positive time interval) in the Cs^+-based internal solution (**Figure 2A**). That a comparable LTP was induced is likely attributable to the fact that activated postsynaptic sites were close enough to the soma to receive back-propagating action potentials due to the absence of prominent A-type K^+ channel activity (Hoffman et al., 1997). These conditions permit repetitive, single pre- and postsynaptic spiking to induce *e*-LTP (Nishiyama et al., 2000).

We also compared the postsynaptic spike wave forms during the LTP-timing protocol in the Cs^+-based internal solution with those in the K^+-base internal solution (**Figure 2B**). In the Cs^+-based internal solution, the spikes evoked by the postsynaptic depolarizing currents were ca. 50% broader (half-maximal width of 3.1 ± 0.3 ms, $n = 18$) than in the K^+-based solution. However, this spike width is noticeably smaller than that reported previously in thinner (300 μm) slices (Wittenberg and Wang, 2006). Moreover, membrane potential changes recorded in the postsynaptic cell during the LTP-timing protocol were stably maintained, even when the Cs^+-based internal solution was used, in 500-μm thick slices (**Figure 2C**). In contrast, a strong depolarization was observed when we applied the same spike-timing protocol in thinner (i.e., 300-μm thick) slices or slices (500-μm thick) treated with 20 μM bicuculline, which eliminated postsynaptic $GABA_A$R-mediated inhibition (**Figure 2C**). Collectively, the observations of relatively small spike width and stable postsynaptic membrane potential in the Cs^+-based internal solution support the presence of prominent postsynaptic $GABA_A$R-mediated inhibition that accelerated spike after-repolarization.

We systematically examined the spike-timing dependence of *e*-STDP at the θ frequency. As shown in **Figure 2D**, we observed two distinct time windows for the induction of *e*-LTD, −31 to −18 ms (–LTD) and +18 to +34 ms (+LTD), that flanked single time intervals of +3 to +9 ms for the induction of *e*-LTP. Moreover, the induction of *e*-LTD for both negative and positive time intervals at activated synapses was associated with heterosynaptic *e*-LTD at non-activated synapses. Although a broader time window for +LTD (20 ms duration) was observed in the K^+-based internal solution, the timing dependence of this *e*-STDP was similar to that in the Cs^+-based internal solution (in the absence of postsynaptic $GABA_B$R-mediated inhibition, **Figure 2D**; modified from Nishiyama et al., 2000 by the addition of new data points). This suggests that postsynaptic $GABA_B$R-mediated inhibition-linked GIRKs and other K^+ channel activities, including that of A-type K^+ channels, are not essential determinants of the spike-timing dependence of *e*-STDP induced at the θ frequency.

POSTSYNAPTIC $GABA_A$R-MEDIATED INHIBITION CONTROLS THE SPIKE-TIMING DEPENDENCE OF *e*-LTD

The induction of STDP depends on the pattern of postsynaptic Ca^{2+} elevation (Magee and Johnston, 1997; Nishiyama et al., 2000; Sjöström and Nelson, 2002; Dan and Poo, 2006; Nevian and Sakmann, 2006; Caporale and Dan, 2008), which results from interactions between dendritic back-propagating action potentials and excitatory postsynaptic potentials (EPSPs) (Koester and Sakmann, 1998; Schiller et al., 1998; Stuart and Häusser, 2001). Since dendritic action potentials are regulated by FF and FB postsynaptic $GABA_A$R-mediated inhibition (Buzsáki et al., 1996; Tsubokawa and

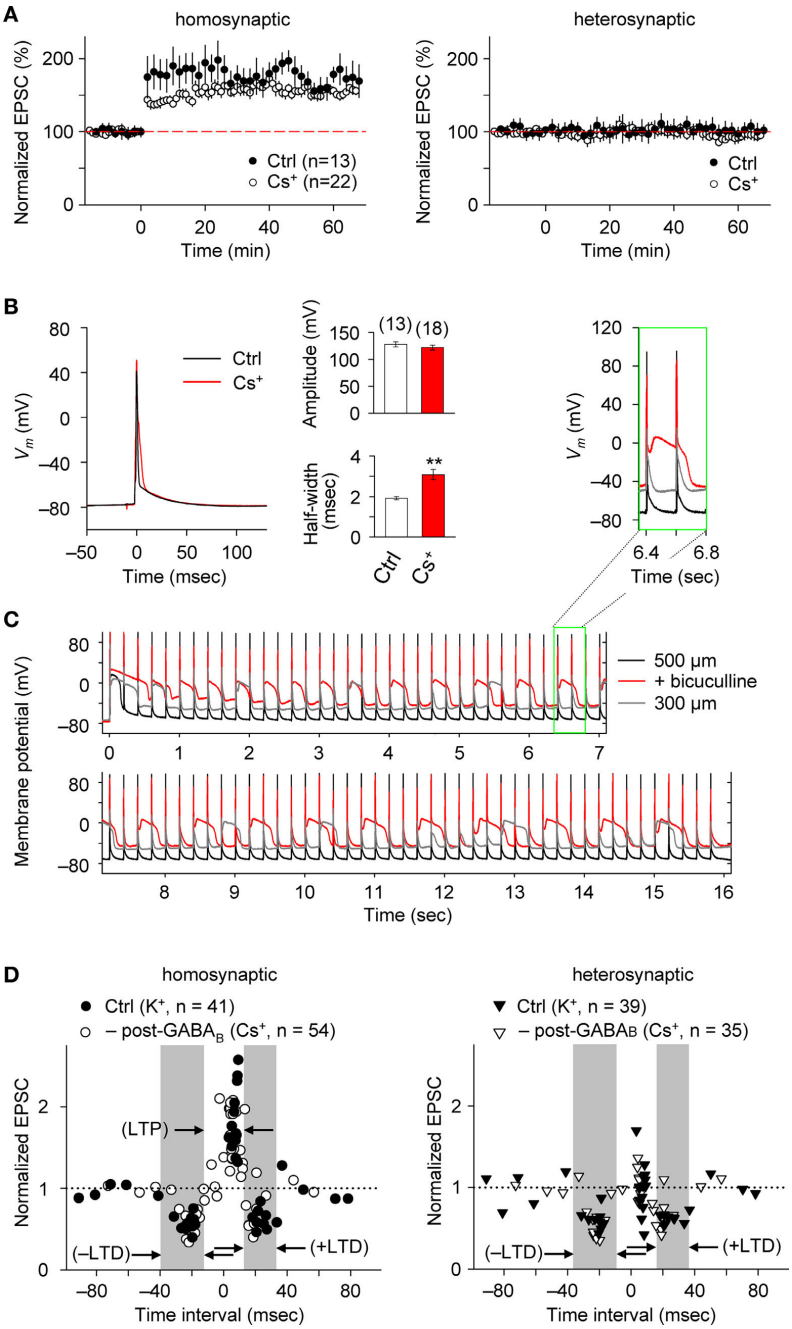

FIGURE 2 | *e*-STDP is induced at the θ frequency independently of postsynaptic $GABA_B$R function at SC-CA1 synapses. (A) Time course of changes in EPSC amplitudes induced by the LTP-timing protocol in homosynaptic, activated inputs (left) and heterosynaptic, non-activated inputs (right). Input-specific *e*-LTP was observed in K^+-based (control, Ctrl) and Cs^+-based internal recording solution. Data represent the normalized mean EPSC (±sem). **(B)** Action potentials recorded at the soma with the LTP time intervals in the presence or absence of K^+ channel activities. Membrane potential (*Vm*) changes in either K^+-based (black) or Cs^+-based (red) internal solution (left). The average spike amplitude (right upper) and the half maximum width (right lower) were not as significantly different between the two experimental conditions as reported previously (Wittenberg and Wang, 2006). This may be due to extensive postsynaptic $GABA_A$R-mediated inhibition in our preparation. Significant difference from the control is indicated ("**" $p < 0.01$; Mann–Whitney U test). **(C)** Membrane potentials (*Vm*) controlled by $GABA_A$R-mediated inhibition. Stable *Vm* was observed in 500-µm (black), but not in 300-µm (gray) thick hippocampal slices in which elimination of postsynaptic $GABA_A$R-mediated inhibition by bicuculline (20 µM) treatment caused depolarization (red). Inset: twice magnified view. **(D)** Summary of normalized EPSC changes in homosynaptic (left) and heterosynaptic (right) inputs. A similar timing dependence of *e*-STDP was observed in both K^+-based (Ctrl) and Cs^+-based (–post-$GABA_B$; without postsynaptic $GABA_B$R-mediated inhibition) internal solution. *e*-LTD at both negative and positive time intervals propagated to heterosynaptic, non-activated synapses (right). Gray areas indicate *e*-LTD time intervals in the K^+-based internal solution. Data recorded in the Cs^+-based internal solution is adapted from (Nishiyama et al., 2000).

Ross, 1996; Pouille and Scanziani, 2001), we examined whether postsynaptic $GABA_A$R-mediated inhibition affects the spike-timing dependence of *e*-STDP induced at the θ frequency. We first investigated the impact of postsynaptic $GABA_A$R-mediated inhibition on the induction of *e*-LTD (–LTD; **Figure 2D**), in the K^+-based internal solution as a control. To eliminate postsynaptic $GABA_A$R-mediated inhibition, gabazine (5 μM), a $GABA_A$R antagonist (Pouille and Scanziani, 2004), was administrated in the bath a few minutes before the spike-timing protocol and remained throughout the *e*-LTD induction protocol. As shown in **Figure 3A**, *e*-LTD was abolished in the presence of gabazine, demonstrating that $GABA_A$R activity is required for the induction of *e*-LTD. To confirm that postsynaptic $GABA_A$R-mediated membrane hyperpolarization was responsible for the *e*-LTD induction, the recorded cells were held at –85 mV (in current clamp) while postsynaptic $GABA_A$R-mediated inhibition was blocked by bath-applied gabazine. The reversal potential of $GABA_A$R was –73.8 ± 3.1 mV ($n = 4$), when the Cs^+-based internal solution was used. Application of hyperpolarizing currents to the recorded cells restored the induction of *e*-LTD, which, unlike in the control, was expressed immediately after the spike-timing

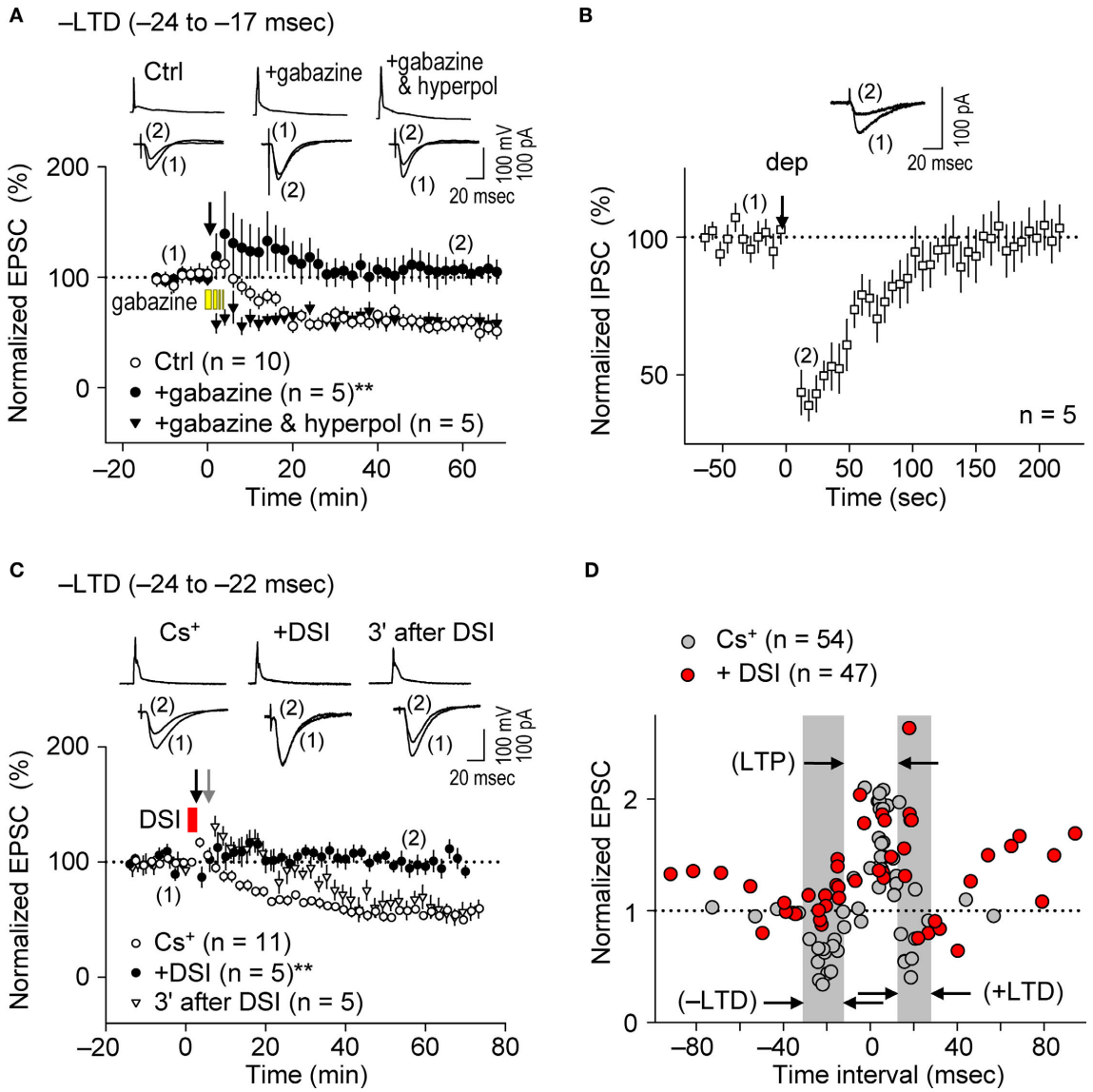

FIGURE 3 | Postsynaptic $GABA_A$R-mediated inhibition controls the spike-timing dependence of *e*-LTD at the θ frequency. (A) Bath application of gabazine (5 μM, yellow bars) abolished *e*-LTD (time intervals: –24 to –17 ms), whereas hyperpolarization (hyperpol) of postsynaptic cells restored *e*-LTD. **(B)** Brief postsynaptic depolarization (arrow; dep, 3 s) induced DSI at SC inputs. **(C)** DSI (red bar) induction immediately preceding the spike-timing protocol (black arrow) abolished *e*-LTD (time intervals: –24 to –22 ms), whereas DSI applied 3 min before (gray arrow) had no effect on the *e*-LTD. Data represent normalized mean EPSCs/IPSCs (±sem). Sample traces of membrane potentials during the spike-timing protocol (top, in **A,C**) and of IPSCs (in **B**)/EPSCs (bottom, in **A,C**) before (1) and after (2) the induction protocols. Significant differences from corresponding controls are indicated ("**" $p < 0.01$; Mann–Whitney U test). **(D)** Summary of time windows for *e*-STDP in the presence (filled red circle) and absence (filled gray circle) of DSI. Gray areas show LTD time intervals in the absence of DSI.

protocol (**Figure 3A**). The slow onset of *e*-LTD in the presence of $GABA_A$R function may be due to robustly enhanced FF-IPSCs immediately after the spike-timing protocol (see **Figure 5C**), the FF-IPSC component of which is expected to be 14.5 ± 0.8% of the EPSC amplitude ($n = 4$) before the induction protocol.

The bath application of gabazine would eliminate total $GABA_A$R function in hippocampal networks. Therefore, to test the effects of postsynaptic $GABA_A$R-mediated inhibition specifically on the recorded cells, we applied the method of depolarization-induced suppression of inhibition (DSI, Lenz and Alger, 1999) by clamping the recorded cell at 0 mV using the Cs^+-based internal solution. Since stimulation at the *stratum oriens/alveus* has been used to demonstrate DSI (Lenz and Alger, 1999), we examined the effects of DSI on IPSCs evoked by stimuli at the *stratum radiatum*. Application of a 2–3 s depolarization (from −70 to 0 mV) to the recorded postsynaptic CA1 pyramidal cell induced DSI (43 ± 6% of the control, $n = 5$) for about 2 min (**Figure 3B**), similarly as previously reported (Lenz and Alger, 1999). In this particular experiment, we applied ca. two to three fold stronger stimuli (amplitude, 20–40 μA; duration, 300 μs) to evoke monosynaptic IPSCs of ca. 70 pA. When the DSI procedure was applied 5–10 s before the application of the spike-timing protocol at the θ frequency, induction of *e*-LTD within the time interval of −24 to −22 ms (–LTD) was eliminated (**Figure 3C**). In contrast, when the DSI procedure was applied 3 min before the same spike-timing protocol, by which time FF-IPSCs should have recovered to normal levels from the DSI (**Figure 3B**), the induction of *e*-LTD was successfully restored to control levels (**Figure 3C**). The postsynaptic Ca^{2+} increase caused by the DSI procedure, which is known to last for only a few seconds (Isokawa and Alger, 2006), is unlikely to have overlapped with that subsequently induced by the spike-timing protocol (applied 5–10 s later).

The effects of DSI on *e*-STDP induced at various time intervals (from −92 to +94 ms) were also examined. As shown in **Figure 3D**, the DSI did not affect significantly the magnitude of *e*-LTP induced by the LTP-timing protocol (time interval at +5 ms). In contrast, DSI not only eliminated *e*-LTD induction at both the –LTD and +LTD time intervals, but induced the most robust *e*-LTP at the original +LTD time intervals (**Figure 3D**). This might be due to the induction of higher NMDA receptor-mediated currents that coincided with postsynaptic spikes (Vargas-Caballero and Robinson, 2004). Moreover, reduction of postsynaptic $GABA_A$R-mediated inhibition to approximately one half by the DSI resulted in two effects on the STDP time window for *e*-LTP induction: First, the original window of −2 to +15 ms was expanded to −15 to +20 ms, and second, additional LTP time windows appeared at −100 to −55 ms and at +45 to +100 ms (**Figure 3D**). This temporal feature of *e*-LTP induction may be consistent with the idea that DSI biases the STDP learning rule toward LTP. In the presence of DSI, we observed two distinct time windows (−55 to −15 ms and +20 to +45 ms) in which no *e*-LTP could be induced. The absence of *e*-LTP at −55 to −15 ms may have been due to the overlapping slow component of spike afterhyperpolarization, which was sensitive to blockade of inositol 1,4,5-trisphosphate receptors (unpublished data). The current study, however, cannot explain the absence of *e*-LTP (and slight *e*-LTD) at the intervals of +20 to +45 ms. Taken together, these results demonstrate the essential role of postsynaptic $GABA_A$R-mediated inhibition as a critical determinant for the timing dependence of the *e*-STDP induction protocol at the θ frequency.

FEEDBACK POSTSYNAPTIC $GABA_A$R-MEDIATED INHIBITION CAUSES *e*-LTD TO ENFORCE COOPERATIVE *e*-LTP

As demonstrated above, prominent FB postsynaptic $GABA_A$R-mediated inhibition was induced by 5-Hz postsynaptic spiking (**Figure 1E**), whereas FF postsynaptic $GABA_A$R-mediated inhibition was diminished as the intensity of presynaptic stimulation at SC inputs was reduced to a level that induced EPSCs of amplitudes <70 pA (red line in **Figure 1D** inset). We, therefore, examined the effect of FB inhibition on *e*-STDP in the absence of functional FF inhibition by stimulating a smaller population of SC inputs that evoked small EPSCs (<70 pA), using the Cs^+-based recording solution. Unexpectedly, we found that the LTP-timing protocol (spiking intervals of +4 to +6 ms) induced *e*-LTD instead of *e*-LTP (**Figures 4A,B**), consistent with the requirement of cooperativity among multiple, coincident inputs for the induction of *e*-LTP (Bliss and Collingridge, 1993). Moreover, when FB postsynaptic $GABA_A$R-mediated inhibition was suppressed by DSI, this *e*-LTD became a robust *e*-LTP, similar to that induced at inputs of amplitudes >70 pA (**Figures 4A,B**). Associative *e*-LTP can be induced at a single SC input to CA1 pyramidal cells by the pairing protocol (postsynaptic depolarization to 0 mV with presynaptic stimuli of 200 pulses at 1 Hz) in the absence of $GABA_A$R-mediated inhibition (Petersen et al., 1998). These results, therefore, suggest that FB postsynaptic $GABA_A$R-mediated inhibition not only prevents *e*-LTP induction at LTP time intervals (i.e., enforcing the requirement of cooperativity), but also causes the induction of *e*-LTD (i.e., gating for the induction of *e*-LTD). Similar *e*-LTD induction with the LTP-timing protocol has been reported in layer V cortical neurons at inputs from layer II/III neurons with stimuli at 50 Hz (Sjöström and Häusser, 2006). This *e*-LTD induction by a high-frequency (>50 Hz) protocol may be attributable to the difference of the threshold frequency of the spiking required to evoke FB postsynaptic $GABA_A$R-mediated inhibition in these cortical neurons (Silberberg and Markram, 2007). Thus, this gating function of *e*-LTD by FB inhibition may be a universal rule for *e*-STDP. In contrast, *e*-LTD induction at the negative time intervals (–LTD) did not show this cooperative requirement (**Figures 4C,D**). An EPSC amplitude of 70 pA normally represents the co-activation of 10–20 synapses, as estimated from the average mini-EPSC amplitude of 3–5 pA (Kato et al., 1994), which may be capable of generating local dendritic Ca^{2+} spikes (Schiller et al., 2000). Therefore, intricate dendritic processing (e.g., integration or competition) of information according to the learning rule based on local spiking and that based on the back-propagating action potential (Jarsky et al., 2005; Rumsey and Abbott, 2006) may occur during the spike-timing protocol at the θ frequency.

PARALLEL INDUCTION OF *e*-LTP/*i*-LTP AND *e*-LTD/*i*-LTD OCCURS AT θ FREQUENCY STIMULATION

It is widely accepted that during the induction of *e*-LTP at SC-CA1 inputs by tetanic stimulation, inhibitory inputs undergo LTD (*i*-LTD, McMahon and Kauer, 1997; Chevaleyre and Castillo, 2003; Gibson et al., 2008), which is mediated by endocannabinoid signaling (Chevaleyre and Castillo, 2003). Conversely, repetitive

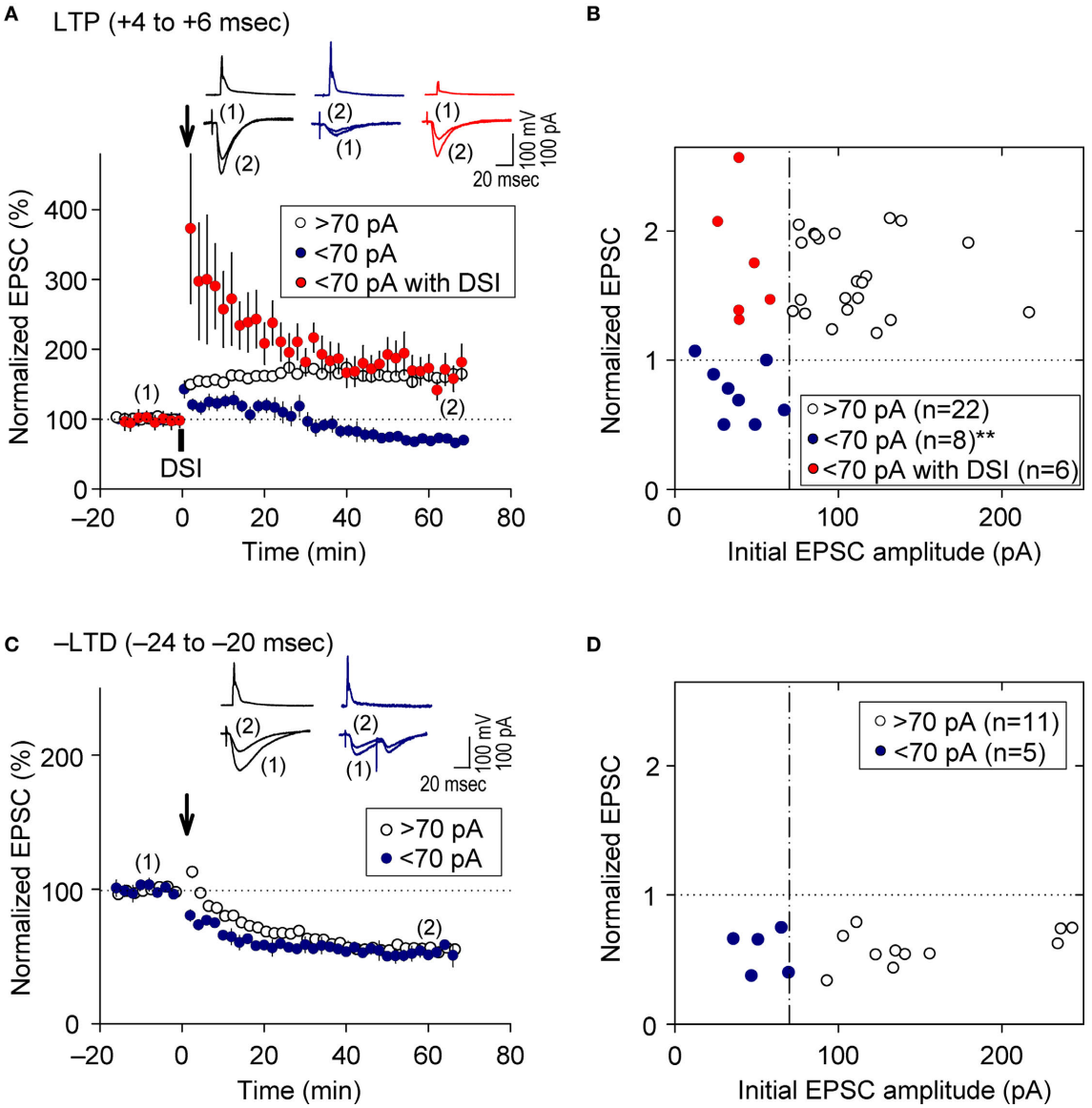

FIGURE 4 | Feedback postsynaptic $GABA_AR$-mediated inhibition causes *e*-LTD that enforces the requirement of cooperative *e*-LTP. (A,B) *e*-LTD is induced by the LTP-timing protocol when the initial EPSC amplitudes are <70 pA. DSI converts this *e*-LTD to *e*-LTP to the same extent as that induced normally at EPSC inputs of amplitude >70 pA. **(C,D)** *e*-LTD is induced to a similar extent independent of the initial EPSC amplitudes. Significant difference from corresponding controls is indicated ("**" $p < 0.01$; Mann–Whitney U test).

presynaptic stimulation, even at relatively low frequency (10 Hz), induces endocannabinoid-mediated *i*-LTD that facilitates *e*-LTP induction at neighboring synapses (Chevaleyre and Castillo, 2004). Furthermore, the DSI procedure facilitates LTP induction known as endocannabinoid-mediated disinhibition, which requires 50-Hz tetanic stimulation with small numbers of pulses at excitatory synapses (Carlson et al., 2002). We, therefore, examined *i*-STDP induction following application of the θ frequency spike-timing protocol at excitatory synapses. We concurrently measured EPSCs and FF-IPSCs from the same CA1 pyramidal cells at spiking time intervals for both LTP (+4 to +6 ms) and –LTD (–24 to –20 ms). Stimuli of the same intensity were applied to the same SC inputs to evoke both EPSCs and FF-IPSCs while 40-ms voltage-steps from –80 to +10 mV (the EPSC reversal potential) were applied to the recorded neurons to monitor FF-IPSCs. This allowed the stable recording of both EPSCs and FF-IPSCs for more than 90 min (**Figure 5A**). Surprisingly, we found that EPSCs and FF-IPSCs underwent parallel potentiation and depression of similar magnitudes following paired stimulation with spiking intervals that induced *e*-LTP (**Figure 5B**) and *e*-LTD (**Figure 5C**), although FF-IPSCs showed extensive short-term potentiation, regardless of the timing of the induction protocol. These results suggest that endocannabinoid-mediated *i*-LTD (Chevaleyre and Castillo, 2004) did not occur following the induction of *e*-LTP

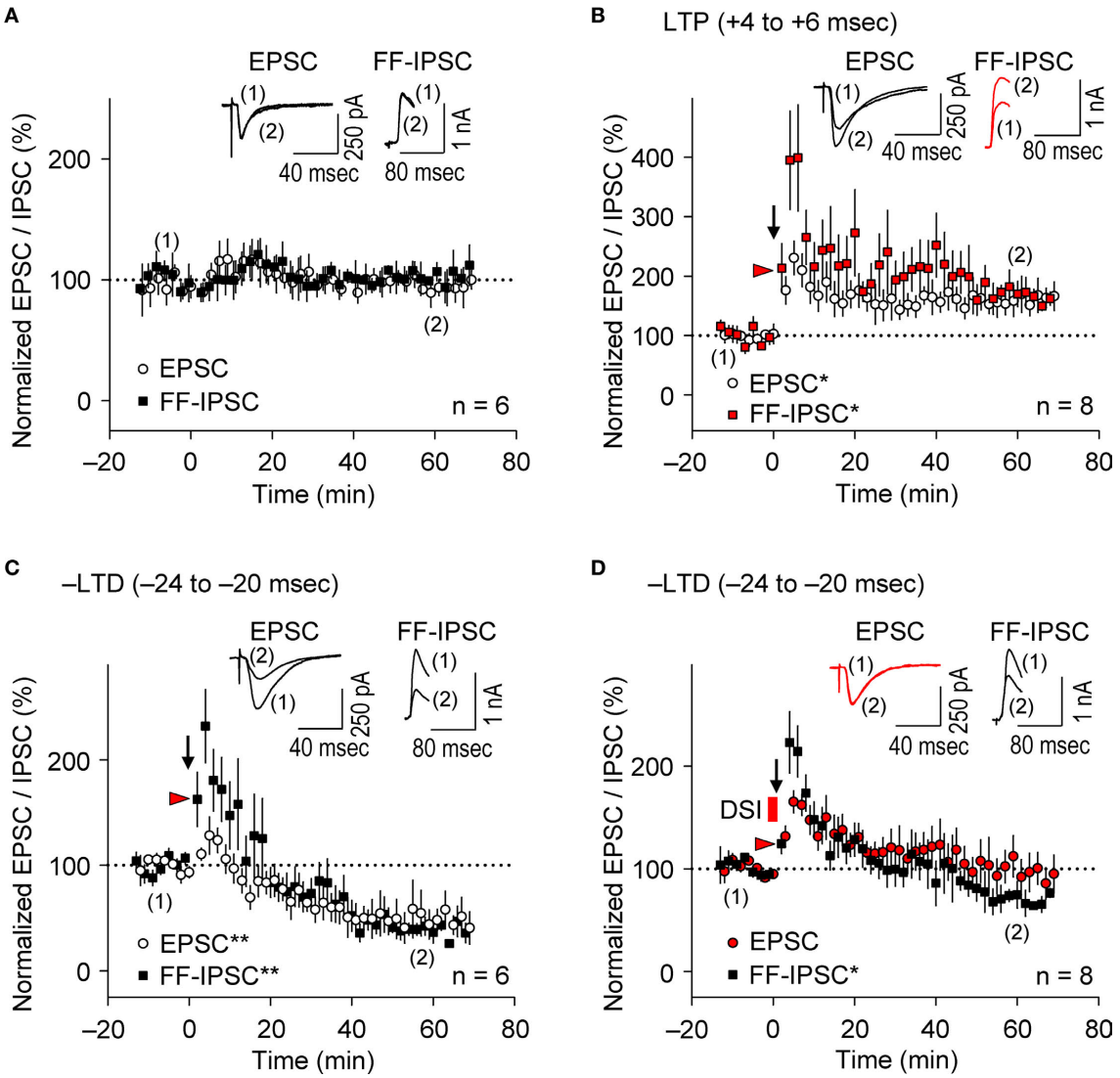

FIGURE 5 | Parallel induction of *e*-LTP/*i*-LTP and *e*-LTD/*i*-LTD occurs under prominent postsynaptic $GABA_A$R-mediated inhibition. (A) Normalized EPSC/FF-IPSC amplitudes (%) without the spike-timing protocol. No changes in either EPSCs or FF-IPSCs were observed during the time course of the experiments. **(B,C)** EPSCs and FF-IPSCs were both potentiated at the LTP time intervals **(B)**, and depressed at the –LTD time intervals **(C)**. **(D)** DSI abolished LTD of EPSC, but not of FF-IPSC at the –LTD time intervals. Data represent normalized mean EPSCs/FF-IPSCs (±sem). Sample traces of EPSCs/FF-IPSCs (in **B–D**) before (1) and after (2) the induction protocols. Significant differences from corresponding controls are indicated ("*" $p < 0.05$ and "**" $p < 0.01$; Mann–Whitney U test).

in our preparations (**Figure 5B**). Moreover, we found that DSI preceding the LTD-timing protocol abolished only *e*-LTD, not *i*-LTD (**Figure 5D**), demonstrating that the effects of the DSI were specific. Importantly, the magnitude of FF-IPSC immediately after the spike-timing protocol, regardless of the presence of DSI, was significantly greater than that of the basal FF-IPSC (indicated by red arrowheads, **Figure 5B–D**), suggesting the occurrence of prominent postsynaptic $GABA_A$R-mediated inhibition during the spike-timing protocol at the θ frequency. This indicates that endocannabinoid-mediated disinhibition, i.e., passive modulation (Carlson et al., 2002), was also unlikely to have occurred. Thus, these results support the idea that postsynaptic $GABA_A$R-mediated inhibition actively controls the timing dependence of *e*-LTD at the θ frequency.

PRESYNAPTIC $GABA_B$R-MEDIATED INHIBITION CAUSES FREQUENCY-DEPENDENT *e*-LTD

Presynaptic glutamate release, which determines the EPSC amplitude, would be reduced if the frequency of presynaptic spiking were to increase (Ohliger-Frerking et al., 2003) as a result of activation of G-protein coupled receptors (GPCRs) at presynaptic terminals (Wu and Saggau, 1997). Because $GABA_B$Rs are the major GPCRs at glutamatergic presynaptic terminals (Wu and Saggau, 1997), we tested whether presynaptic $GABA_B$R-mediated inhibition could also cause *e*-LTD as the frequency of the spike-timing protocol increased. Application of the LTP-timing protocol (time intervals at the +4 to +6 ms), which normally induced *e*-LTP at the θ frequency (**Figure 6A**, top), had no significant effect on synaptic efficacy at 12 Hz (α frequency, for 6.7 s; 91.4 ± 10.6%, $n = 6$, in the Cs^+-based

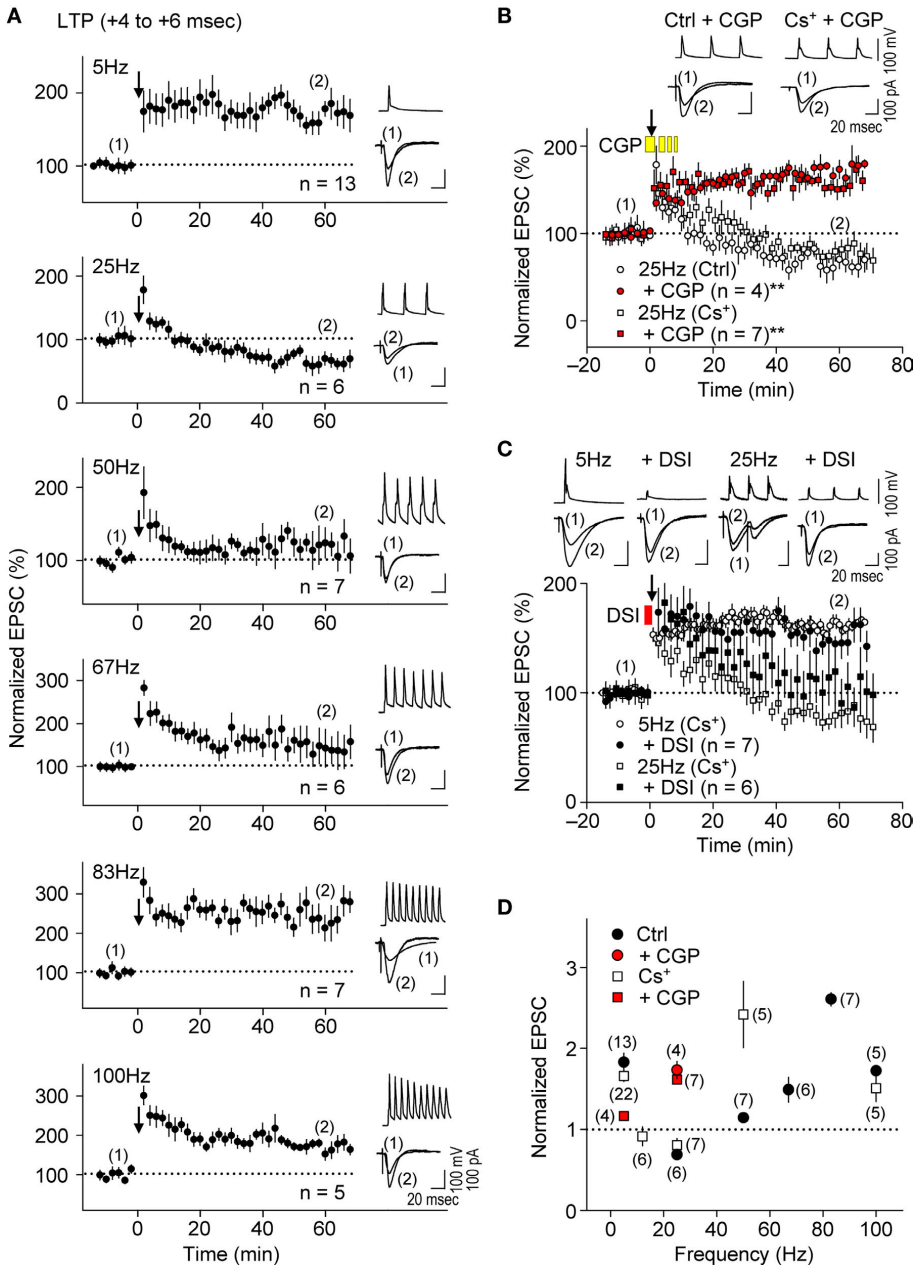

FIGURE 6 | Presynaptic $GABA_BR$-mediated inhibition causes frequency-dependent *e*-LTD at α/β frequencies. (A,D) Summary of frequency-dependent changes in synaptic efficacy induced by the spike-timing protocol for LTP-timing (+4 to +6 ms). Frequency-dependent effects (between 5 Hz and 100 Hz) in either the K^+- or Cs^+-based internal recording solution. Frequency-dependent *e*-LTD is induced at the same magnitude at 25 Hz and *e*-LTP is robust at the γ frequency in both recording solutions. **(B)** Bath application of CGP 35348 (1 mM, yellow bars) abolished *e*-LTD at 25 Hz, and instead induced *e*-LTP in both K^+- and the Cs^+-based internal recording solutions. **(C)** DSI failed to restore *e*-LTP induction at 25 Hz and had no significant effect on *e*-LTP at 5 Hz. Data represent normalized mean EPSCs (±sem). Membrane potentials during the spike-timing protocol (upper traces) and EPSCs (lower traces) before (1) and after (2) the induction protocols (in **A–C**). Scales: 100 pA (or 100 mV), 20 ms. Significant differences from corresponding controls are indicated ("**" $p < 0.01$; Mann–Whitney U test).

internal solution; see **Figure 6D**). A further increase in the frequency of paired stimulation to 25 Hz (β frequency) resulted in *e*-LTD, not *e*-LTP, in both K^+- and Cs^+-based solutions. Furthermore, the most robust *e*-LTP was observed (substantially greater than that induced by the LTP-timing protocol at 5 and 100 Hz) when the frequency of the LTP-timing protocol reached the γ frequency (50–80 Hz) in both the K^+- and Cs^+-based internal solutions. However, the optimal frequency for induction of the maximal *e*-LTP in the Cs^+-based internal solution (50 Hz) appears to be lower than that in the K^+-based internal solution (83 Hz). This may have resulted from the slower kinetics of EPSPs in the Cs^+-based internal solution, which allows overlap with the preceding EPSPs to cause a postsynaptic depolarization, even at a lower frequency. It is noteworthy that during LTP induction at the γ frequency the postsynaptic $GABA_AR$

function should be excitatory (Staley et al., 1995; Taira et al., 1997; Bracci et al., 2001), thereby likely enhancing the magnitude of *e*-LTP. These results support the idea that the induction of *e*-LTD also depends on the frequency of the spike-timing protocol, which is independent of postsynaptic K^+ channel function.

We examined further the effect of presynaptic $GABA_BR$-mediated inhibition on the frequency-dependent induction of *e*-LTD by applying the $GABA_BR$ antagonist CGP35348 (1 mM, Davies and Collingridge, 1996) in the bath during the spike-timing protocol. This treatment abolished *e*-LTD induction at 25 Hz and resulted in a substantial *e*-LTP instead, in both K^+- and Cs^+-based solutions (**Figures 6B,D**), suggesting that $GABA_BR$ function is required for the induction of this frequency-dependent *e*-LTD. Interestingly, CGP35348 suppressed *e*-LTP induction at 5 Hz, the frequency at which presynaptic $GABA_BR$ is most prominent at inhibitory inputs (**Figure 6D**, Davies and Collingridge, 1993), suggesting that postsynaptic $GABA_AR$ function is enhanced as a consequence of this treatment. Bath application of phaclofen, another $GABA_BR$ antagonist, at the concentration (100 μM) that blocks presynaptic $GABA_BR$-mediated inhibition at excitatory (Hasselmo and Fehlau, 2001) but not at inhibitory (Davies and Collingridge, 1993) inputs during the spike-timing protocol, similarly converted the *e*-LTD to robust *e*-LTP at 25 Hz (178.0 ± 17.4%, $n = 4$). Thus, presynaptic $GABA_BR$-mediated inhibition at excitatory synapses is likely responsible for the frequency-dependent expression of *e*-LTD. Consistent with the idea that presynaptic $GABA_BR$-mediated inhibition, but not postsynaptic $GABA_AR$-mediated inhibition, may be a major inducer of frequency-dependent *e*-LTD, DSI affected *e*-LTD at 25 Hz only partially, while it had no significant effect on *e*-LTP induction at 5 Hz (**Figure 6C**). This partial effect could be due to a reduction of GABA release by DSI (Lenz and Alger, 1999), which would also reduce presynaptic $GABA_BR$-mediated inhibition. Taken together, these results suggest that presynaptic $GABA_BR$-mediated inhibition controls the frequency dependence of *e*-LTD at α/β frequencies and accounts for the expression of *e*-LTP at θ and γ frequencies.

DISCUSSION

We demonstrated that GABAergic interneuronal network activities control the spike timing- and frequency-dependent induction of the *e*-LTD (at –LTD and +LTD time intervals) that delineates the expression of *e*-LTP in hippocampal CA1 pyramidal cells (see **Figure 7A**). The timing dependence of *e*-LTD induced by the θ frequency spike-timing protocol is regulated by both FF and FB postsynaptic $GABA_AR$-mediated inhibition. Feedback postsynaptic $GABA_AR$-mediated inhibition enforces the cooperative induction of *e*-LTP by causing *e*-LTD from a small population of the SC inputs during the LTP-timing. In contrast, the frequency-dependent expression of *e*-LTD at α/β frequencies is regulated predominantly by presynaptic $GABA_BR$-mediated inhibition. This *e*-LTD then segregates the expression of *e*-LTP into θ (timing-dependent) and γ (timing-independent) frequencies. The induction of similar magnitudes of *e*- and *i*-STDP in hippocampal SC-CA1 networks further demonstrates a novel mechanism by which GABAergic inhibition actively causes the induction of *e*-LTD.

Previously, the timing dependence of *e*-STDP was extensively studied using a low-frequency (<2 Hz) spike-timing induction protocol in various systems (Bi and Poo, 1998; Debanne et al., 1998; Zhang et al., 1998; Feldman, 2000; Froemke and Dan, 2002; Nevian and Sakmann, 2006). These studies led to the formulation of the asymmetric STDP learning rule: pre-before-post (causal order) results in *e*-LTP and post-before-pre (anti-causal order) results in *e*-LTD at the negative time intervals. The asymmetric STDP learning rule, which is compatible with Hebbian synaptic plasticity (Bliss and Collingridge, 1993) has been applied to explain bidirectional neuronal functions. In contrast, stimulation at the θ frequency (5 Hz), as in our previous (Nishiyama et al., 2000) and current studies and those of others (Wittenberg and Wang, 2006), results in the induction of a second *e*-LTD time window at positive time intervals. Also, a low-frequency (<2 Hz) spike-timing protocol induces a relatively broad *e*-LTD time window (>50 ms) at negative time intervals, whereas θ frequency induction of the STDP protocol induces relatively narrow *e*-LTD time windows (~20 ms) at both –LTD and +LTD. Although the mechanisms of the appearance of narrow windows and an additional +LTD stimulated by the θ frequency are not understood, we found that while –LTD is fully sensitive to postsynaptic $GABA_AR$-mediated inhibition, +LTD is only partially sensitive (Wittenberg and Wang, 2006), suggesting the involvement of unidentified mechanisms other than postsynaptic $GABA_AR$-mediated inhibition and mechanisms related to spike afterhyperpolarization that suppress postsynaptic Ca^{2+} increase. Interestingly, computational analyses predict the stable presence of +LTD if the number of postsynaptic NMDARs increases (Shouval and Kalantzis, 2005). In support of this idea, recent electron microscopy study using the freeze-fracture replica method (Shinohara et al., 2008) demonstrated a much greater number of NMDARs at the spines of CA1 pyramidal cells compared to that reported previously (Racca et al., 2000). The greater number of NMDARs may be attributable to the persistent presence of +LTD induced by the θ frequency spike-timing protocol. Alternatively, it is also plausible that in addition to the different frequency dependency of FB IPSC recruitment in cortical neurons (Silberberg and Markram, 2007), cortical neurons may be innately endowed with an asymmetric, not a symmetric, STDP learning rule by these low-frequency stimuli.

In the current study, we applied DSI to investigate the timing dependence of *e*-STDP. Surprisingly, the DSI procedure caused drastic effects on the induction of *e*-STDP, even though a relatively minor population of interneurons (Glickfeld and Scanziani, 2006) are expected to be sensitive to it. Endocannabinoid receptor CB1R-expressing basket cells apparently receive inputs from both CA3 (the SC) and CA1 (the recurrent) pyramidal cells (Glickfeld and Scanziani, 2006). Therefore, these CB1R-expressing interneurons are highly likely to be involved in the determination of the timing dependence and the requirement for cooperative *e*-STDP by inducing both FF and FB postsynaptic $GABA_AR$-mediated inhibition to the CA1 pyramidal cells during the spike-timing protocol. It has been demonstrated that burst postsynaptic spiking is required for *e*-LTP induction by θ frequency stimuli at SC-CA1 synapses (Thomas et al., 1998; Pike et al., 1999; Meredith et al., 2003; Wittenberg and Wang, 2006). In this case, the burst spiking, which is known to silence A-type K^+ channel activity in distal dendrites (Hoffman et al., 1997), likely facilitates the back-propagation of action potentials during the induction protocol. In our protocol, however, repetitive single (no burst) postsynaptic spiking is sufficient to induce *e*-LTP (Nishiyama et al., 2000), suggesting that the activated synapses are distant from functional A-type channels (Hoffman et al., 1997).

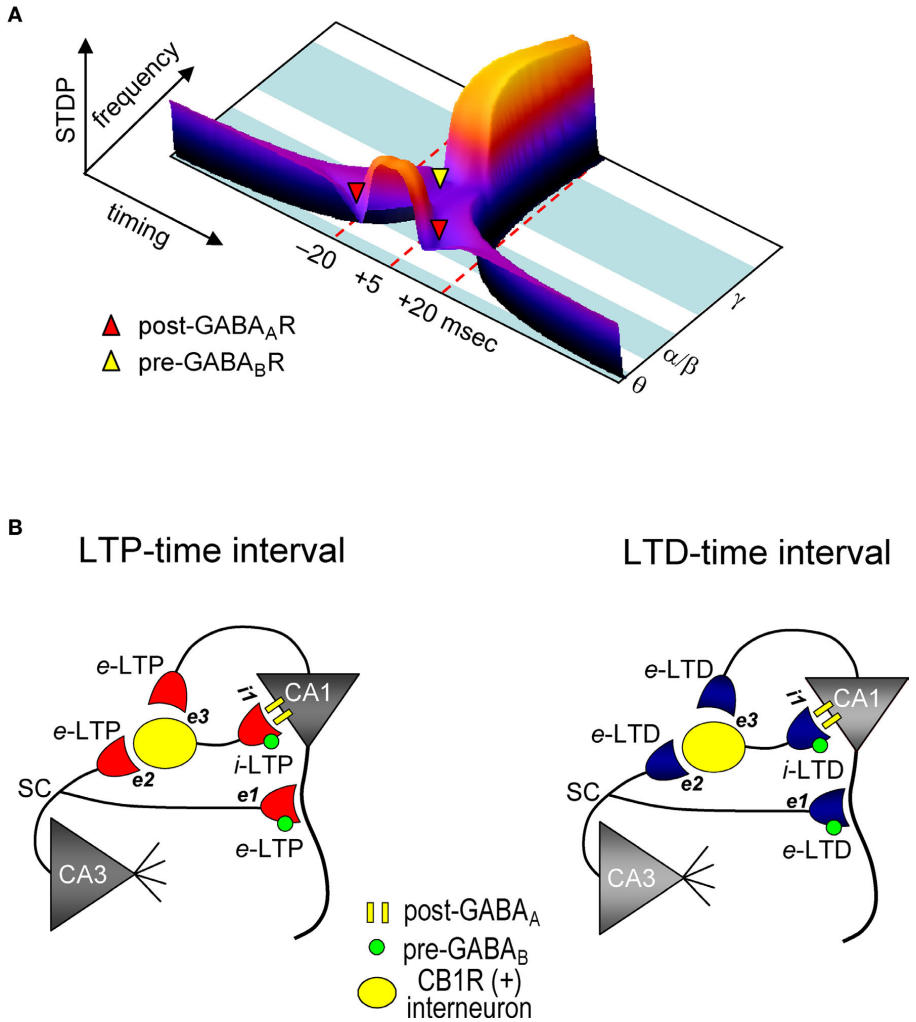

FIGURE 7 | Model for STDP controlled by GABA functions in the CA1 network. (A) Both spike timing- and frequency-dependence of *e*-STDP and differential GABA function that gates *e*-LTD. **(B)** Parallel induction of *e*-LTP/*i*-LTP and *e*-LTD/*i*-LTD. Upon application of the LTP- (left) or LTD-timing (right) protocol at 5 Hz, all excitatory synapses undergo, respectively, either *e*-LTP or *e*-LTD. *e*-LTP or *e*-LTD in the CB1R-expressing interneuron (both at inputs *e2* and *e3*) propagates passively to input *i-1*, respectively, as either *i*-LTP or *i*-LTD.

We also found that the magnitudes of FF postsynaptic $GABA_A$R-mediated inhibition in thin slices (300–400 μm) were significantly smaller than in thick (500 μm) slices. Moreover, we observed FB postsynaptic $GABA_A$R-mediated inhibition during θ frequency postsynaptic spiking, which is unlikely to occur during the application of a low-frequency (<2 Hz) spike-timing protocol (Silberberg and Markram, 2007). Therefore, the molecular mechanisms underlying the induction of *e*-LTD through postsynaptic $GABA_A$R-mediated inhibition stimulated at the θ frequency likely differ from those of low-frequency stimulation-induced STDP (Bi and Poo, 1998; Feldman, 2000; Normann et al., 2000; Froemke and Dan, 2002). In support of this idea, the activity of mGluRs, rather than VDCCs, is required for *e*-LTD induction in our preparations (Nishiyama et al., 2000). We also compared the postsynaptic spike wave forms during the LTP-timing protocol in a Cs^+-based internal solution with those in a K^+-base internal solution and found a broadened spike width in the Cs^+-based internal solution. However, it appears that postsynaptic spikes broadened by Cs^+ do not contribute significantly to the features of *e*-STDP. This may also be consistent with the idea that Ca^{2+} entry through VDCCs is not essential for the induction of *e*-LTP (Bi and Poo, 1998) and *e*-LTD (Nishiyama et al., 2000). Our experimental paradigm is, thus, a unique procedure for the investigation of GABAergic activities during STDP. It has been shown that local dendritic spikes, without back-propagating action potentials, cause the induction of *e*-LTP (Golding et al., 2002). This type of synaptic plasticity is prominent at synaptic inputs of distal dendrites, where A-type channels prohibit invasion of single back-propagating action potentials (Hoffman et al., 1997). Our study, however, reveals the existence of bidirectional synaptic plasticity at proximal synaptic inputs that relies on the timing of single back-propagating action potentials. Depending on the location (i.e., proximal or distal dendrites) of activated synapses, different types of induction mechanisms, therefore, may be required to determine bidirectional synaptic plasticity.

Using weak SC input stimuli, we demonstrated that FB postsynaptic $GABA_A$R-mediated inhibition enforces the cooperative requirement for LTP induction (i.e., EPSC amplitude of >70 pA). However, we cannot exclude the following possibilities: The DSI procedure may diminish the postsynaptic $GABA_A$R-mediated actions by one half, including tonic inhibition (Mody and Pearce, 2004). Thus, the actual EPSC amplitude during the LTP-timing protocol (i.e., EPSP amplitude) may become greater than 70 pA as a result of the diminished shunting effect. Since, in our preparation, the EPSP amplitude is below 1 mV when the EPSC amplitude is smaller than 70 pA, it is not possible to accurately assess changes in EPSP amplitudes during the spike-timing protocol if they increased above the amplitude equivalent to EPSCs of 70 pA. We did not observe noticeable differences in the EPSP amplitudes in the presence of DSI compared to the control (data not shown). Moreover, the DSI permits induction of robust LTP, even at inputs with initial EPSC amplitudes of less than 40 pA (see **Figure 4B**). Therefore, DSI is unlikely to have caused increases of the actual EPSP during the spike-timing protocol. We demonstrated the absence of functional FF-IPSCs when the EPSC amplitude was less than 70 pA with the use of single stimuli at SC inputs. However, in response to sequential stimuli, such as during the spike-timing protocol, FF-IPSCs may become manifest due to sequential pulse facilitation, particularly in interneurons that receive both SC and recurrent inputs. Even if a potential contamination from FF-IPSCs occurs, it is likely negligible compared to the prominent FB-IPSCs (an IPSP amplitude of ca. –34 mV, which is equivalent to an IPSC amplitude of ca. 800 to 900 pA). Therefore, our conclusion that FB postsynaptic $GABA_A$R-mediated inhibition enforces the cooperative requirement for LTP induction would not be affected significantly.

We showed that FF-IPSCs undergo *i*-LTP and *i*-LTD, which are associated, respectively, with *e*-LTP and *e*-LTD induced by the θ frequency spike-timing protocol at SC-CA1 excitatory synapses. Two distinct mechanisms, passive and active induction, that cause synaptic efficacy changes in excitatory inputs to interneurons have been demonstrated. Both *e*-LTP and *e*-LTD propagate passively to FB interneurons (Maccaferri and McBain, 1995, 1996). Interneurons also express *e*-LTP directly (Kullmann and Lamsa, 2007) at the SC input (Lamsa et al., 2005) and at the input from CA1 pyramidal cells (Lamsa et al., 2007). Interestingly, *e*-LTP at the SC-FF interneuron synapses propagates to the inhibitory input to CA1 pyramidal cells (Lamsa et al., 2005). The parallel induction of *e*-LTP/*i*-LTP and *e*-LTD/*i*-LTD that we observed may, therefore, depend on both the passive and active mechanisms of induction of inhibitory synaptic plasticity (**Figure 7B**). Since CB1R-expressing basket cells (Glickfeld and Scanziani, 2006) receive inputs from both CA3 and from the recorded CA1 pyramidal cells, the magnitudes of which are each sufficient to spike these interneurons, both *e*-LTP and *e*-LTD can be induced. These excitatory inputs to interneurons may follow a similar STDP learning rule for excitatory inputs to recorded CA1 pyramidal cells. During the LTP-timing protocol, the disynaptic inputs from CA3 and CA1 should be the LTP-timing for one another (i.e., time intervals of ~0 ms). Conversely, during the LTD-timing protocol, these inputs become either the +LTD or –LTD time intervals for one another, because the time difference between two inputs to an interneuron is approximately 20 ms, which is the LTD time interval. Therefore, upon application of the spike-timing protocol, excitatory inputs to both CA1 recording cells and interneurons undergo *e*-STDP with the same polarity. Then, either *e*-LTP or *e*-LTD in interneurons propagates passively to inputs to CA1 recording cells to become, respectively, either *i*-LTP or *i*-LTD. Thus, the parallel induction of *e*- and *i*-LTP may help to maintain the temporal resolution of excitatory synaptic integration and the generation of an action potential in excitatory LTP-expressing CA1 pyramidal cells (Pouille and Scanziani, 2001; Lamsa et al., 2005).

We also showed that the frequency dependence of *e*-LTD at α/β frequencies, which likely delineates the expression of *e*-LTP at the θ and γ frequencies, requires presynaptic $GABA_B$R-mediated inhibition. This is consistent with the optimal frequencies required for induction of presynaptic $GABA_B$R-mediated inhibition, which are maximal at the θ and above the α/β frequencies for inhibitory and excitatory presynaptic terminals, respectively (Davies and Collingridge, 1996; Ohliger-Frerking et al., 2003). In addition to the appearance of *e*-LTD at α/β frequencies, we observed that the magnitude of *e*-LTP begins to decrease if the frequency of the spike-timing protocol increases above the γ frequency (i.e., at 100 Hz). Although the molecular mechanisms underlying the reduction of *e*-LTP at a high frequency requires further investigation, its non-linearity apparently violates Ca^{2+} theory for synaptic plasticity. Despite this, our study demonstrates that *e*-STDP in CA1 pyramidal cells is likely self-limited by the neural network function. It has been reported that postsynaptic $GABA_B$Rs inactivate VDCCs independent of GIRK activity (Perez-Garci et al., 2006). However, since *e*-LTD at the θ frequency appears to be independent of VDCC activity (Nishiyama et al., 2000), postsynaptic $GABA_B$Rs may not be involved in *e*-LTD induction. The potential contribution of postsynaptic $GABA_B$R-mediated inhibition to frequency-dependent *e*-LTD at the α/β frequencies requires further investigation.

Taken together, our study demonstrates the mechanism by which GABAergic inhibitory activities cause *e*-LTD at time intervals of ±20 ms (at the θ frequency) or at α/β frequencies to control the timing- and frequency-dependent features of *e*-STDP; *e*-LTP/*e*-LTD switches within the γ cycle (Nishiyama et al., 2000) and *e*-LTP appears at the θ and γ frequencies. Therefore, the GABAergic interneuronal network activities that regulate STDP may similarly govern hippocampal oscillations *in vivo* (Buzsáki, 2002; Csicsvari et al., 2003; Lisman et al., 2005). Interestingly, the parallel induction of STDP demonstrated in this study, in which *e*-LTP likely depolarizes dendrites when *i*-LTP hyperpolarizes the soma, is consistent with the *in vivo* hippocampal θ oscillation that yields a phase-shift, a current sink at the dendrite and a current source at the soma resulting from GABAergic and cholinergic activities (Kamondi et al., 1998; Buzsáki, 2002). Future studies will determine whether the underlying mechanisms of GABAergic interneuronal network activities that govern STDP also apply to θ and γ oscillations.

ACKNOWLEDGMENTS

This work was supported by the CRCNS program NSF/NIH (MH068027), the Whitehall Foundation Inc. and the Brain Science Foundation. We thank Drs. M. M. Poo, D. Debanne, H. Eichenbaum, B. H. Gaehwiler, J. E. Lisman, N. Spruston and H. Sei for discussion and comments; W. Jelinek and N. Cowen for critical comments on the manuscript; K. Kato for technical support.

REFERENCES

Bartos, M., Vida, I., and Jonas, P. (2007). Synaptic mechanisms of synchronized gamma oscillations in inhibitory interneuron networks. *Nat. Rev. Neurosci.* 8, 45–56.

Bi, G.-q., and Poo, M.-m. (1998). Synaptic modifications in cultured hippocampal neurons: dependence on spike timing, synaptic strength, and postsynaptic cell type. *J. Neurosci.* 18, 10464–10472.

Bliss, T. V., and Collingridge, G. L. (1993). A synaptic model of memory: long-term potentiation in the hippocampus. *Nature* 361, 31–39.

Bracci, E., Vreugdenhil, M., Hack, S. P., and Jefferys, J. G. R. (2001). Dynamic modulation of excitation and inhibition during stimulation at gamma and beta frequencies in the CA1 hippocampal region. *J. Neurophysiol.* 85, 2412–2422.

Buzsáki, G. (2002). Theta oscillations in the hippocampus. *Neuron* 33, 325–340.

Buzsáki, G., Penttonen, M., Nádasdy, Z., and Bragin, A. (1996). Pattern and inhibition-dependent invasion of pyramidal cell dendrites by fast spikes in the hippocampus *in vivo*. *Proc. Natl. Acad. Sci. U.S.A.* 93, 9921–9925.

Caporale, N., and Dan, Y. (2008). Spike timing-dependent plasticity: a Hebbian learning rule. *Annu. Rev. Neurosci.* 31, 25–46.

Cardin, J. A., Carlén, M., Meletis, K., Knoblich, U., Zhang, F., Deisseroth, K., Tsai, L. H., and Moore, C. I. (2008). Driving fast-spiking cells induces gamma rhythm and controls sensory responses. *Nature* 459, 663–667.

Carlson, G., Wang, Y., and Alger, B. (2002). Endocannabinoids facilitate the induction of LTP in the hippocampus. *Nat. Neurosci.* 5, 723–724.

Chevaleyre, V., and Castillo, P. (2003). Heterosynaptic LTD of hippocampal GABAergic synapses: a novel role of endocannabinoids in regulating excitability. *Neuron* 38, 461–472.

Chevaleyre, V., and Castillo, P. (2004). Endocannabinoid-mediated metaplasticity in the hippocampus. *Neuron* 43, 871–881.

Connors, B. W., Malenka, R. C., and Silva, L. R. (1988). Two inhibitory postsynaptic potentials, and $GABA_A$ and $GABA_B$ receptor-mediated responses in neocortex of rat and cat. *J. Physiol.* 406, 443–468.

Csicsvari, J., Jamieson, B., Wise, K., and Buzsáki, G. (2003). Mechanisms of gamma oscillations in the hippocampus of the behaving rat. *Neuron* 37, 311–322.

Dan, Y., and Poo, M.-M. (2006). Spike timing-dependent plasticity: from synapse to perception. *Physiol. Rev.* 86, 1033–1048.

Davies, C. H., and Collingridge, G. L. (1993). The physiological regulation of synaptic inhibition by $GABA_B$ autoreceptors in rat hippocampus. *J. Physiol.* 472, 245–265.

Davies, C. H., and Collingridge, G. L. (1996). Regulation of EPSPs by the synaptic activation of $GABA_B$ autoreceptors in rat hippocampus. *J. Physiol.* 496, 451–470.

Debanne, D., Gahwiler, B. H., and Thompson, S. M. (1998). Long-term synaptic plasticity between pairs of individual CA3 pyramidal cells in rat hippocampal slice cultures. *J. Physiol.* 507, 237–247.

Feldman, D. (2000). Timing-based LTP and LTD at vertical inputs to layer II/III pyramidal cells in rat barrel cortex. *Neuron* 27, 45–56.

Froemke, R., and Dan, Y. (2002). Spike-timing-dependent synaptic modification induced by natural spike trains. *Nature* 416, 433–438.

Gibson, H. E., Edwards, J. G., Page, R. S., Van Hook, M. J., and Kauer, J. A. (2008). TRPV1 channels mediate long-term depression at synapses on hippocampal interneurons. *Neuron* 57, 746–759.

Glickfeld, L. L., and Scanziani, M. (2006). Distinct timing in the activity of cannabinoid-sensitive and cannabinoid-insensitive basket cells. *Nat. Neurosci.* 9, 807–815.

Golding, N., Staff, N., and Spruston, N. (2002). Dendritic spikes as a mechanism for cooperative long-term potentiation. *Nature* 418, 326–331.

Hasselmo, M. E., and Fehlau, B. P. (2001). Differences in time course of ACh and GABA modulation of excitatory synaptic potentials in slices of rat hippocampus. *J. Neurophysiol.* 86, 1792–1802.

Hoffman, D., Magee, J., Colbert, C., and Johnston, D. (1997). K^+ channel regulation of signal propagation in dendrites of hippocampal pyramidal neurons. *Nature* 387, 869–875.

Isokawa, M., and Alger, B. E. (2006). Ryanodine receptor regulates endogenous cannabinoid mobilization in the hippocampus. *J. Neurophysiol.* 95, 3001–3011.

Jarsky, T., Roxin, A., Kath, W. L., and Spruston, N. (2005). Conditional dendritic spike propagation following distal synaptic activation of hippocampal CA1 pyramidal neurons. *Nat. Neurosci.* 8, 1667–1676.

Kamondi, A., Acsady, L., Wang, X., and Buzsáki, G. (1998). Theta oscillations in somata and dendrites of hippocampal pyramidal cells *in vivo*: activity-dependent phase-precession of action potentials. *Hippocampus* 8, 244–261.

Kato, K., Clark, G. D., Bazan, N. G., and Zorumski, C. F. (1994). Platelet-activating factor as a potential retrograde messenger in CA1 hippocampal long-term potentiation. *Nature* 367, 175–179.

Klausberger, T., and Somogyi, P. (2008). Neuronal diversity and temporal dynamics: the unity of hippocampal circuit operations. *Science* 321, 53–57.

Koester, H. J., and Sakmann, B. (1998). Calcium dynamics in single spines during coincident pre- and postsynaptic activity depend on relative timing of back-propagating action potentials and subthreshold excitatory postsynaptic potentials. *Proc. Natl. Acad. Sci. U.S.A.* 95, 9596–9601.

Kullmann, D. M., and Lamsa, K. P. (2007). Long-term synaptic plasticity in hippocampal interneurons. *Nat. Rev. Neurosci.* 8, 687–699.

Lamsa, K., Heeroma, J., and Kullmann, D. (2005). Hebbian LTP in feed-forward inhibitory interneurons and the temporal fidelity of input discrimination. *Nat. Neurosci.* 8, 916–924.

Lamsa, K. P., Heeroma, J. H., Somogyi, P., Rusakov, D. A., and Kullmann, D. M. (2007). Anti-Hebbian long-term potentiation in the hippocampal feedback inhibitory circuit. *Science* 315, 1262–1266.

Lenz, R. A., and Alger, B. (1999). Calcium dependence of depolarization-induced suppression of inhibition in rat hippocampal CA1 pyramidal neurons. *J. Physiol.* 521, 147–157.

Lisman, J., Talamini, L., and Raffone, A. (2005). Recall of memory sequences by interaction of the dentate and CA3: a revised model of the phase precession. *Neural. Netw.* 18, 1191–1201.

Maccaferri, G., David, J., Roberts, B., Szucs, P., Cottingham, C. A., and Somogyi, P. (2000). Cell surface domain specific postsynaptic currents evoked by identified GABAergic neurones in rat hippocampus *in vitro*. *J. Physiol.* 524, 91–116.

Maccaferri, G., and McBain, C. J. (1995). Passive propagation of LTD to stratum oriens-alveus inhibitory neurons modulates the temporoammonic input to the hippocampal CA1 region. *Neuron* 15, 137–145.

Maccaferri, G., and McBain, C. J. (1996). Long-term potentiation in distinct subtypes of hippocampal nonpyramidal neurons. *J. Neurosci.* 16, 5334–5343.

Magee, J. C., and Johnston, D. (1997). A synaptically controlled, associative signal for Hebbian plasticity in hippocampal neurons. *Science* 275, 209–213.

Markram, H., Lübke, J., Frotscher, M., and Sakmann, B. (1997). Regulation of synaptic efficacy by coincidence of postsynaptic APs and EPSPs. *Science* 275, 213–215.

McMahon, L. L., and Kauer, J. A. (1997). Hippocampal interneurons express a novel form of synaptic plasticity. *Neuron* 18, 295–305.

Megias, M., Emri, Z., Freund, T., and Gulyas, A. (2001). Total number and distribution of inhibitory and excitatory synapses on hippocampal CA1 pyramidal cells. *Neuroscience* 102, 527–540.

Meredith, R. M., Floyer-Lea, A. M., and Paulsen, O. (2003). Maturation of long-term potentiation induction rules in rodent hippocampus: role of GABAergic inhibition. *J. Neurosci.* 23, 11142–11146.

Mody, I., and Pearce, R. A. (2004). Diversity of inhibitory neurotransmission through $GABA_A$ receptors. *Trends Neurosci.* 27, 569–575.

Nevian, T., and Sakmann, B. (2006). Spine $Ca2^+$ signaling in spike-timing-dependent plasticity. *J. Neurosci.* 26, 11001–11013.

Nishiyama, M., Hong, K., Mikoshiba, K., Poo, M., and Kato, K. (2000). Calcium stores regulate the polarity and input specificity of synaptic modification. *Nature* 408, 584–588.

Normann, C., Peckys, D., Schulze, C. H., Walden, J., Jonas, P., and Bischofberger, J. (2000). Associative long-term depression in the hippocampus is dependent on postsynaptic N-type $Ca2^+$ channels. *J. Neurosci.* 20, 8290–8297.

Ohliger-Frerking, P., Wiebe, S. P., Stäubli, U., and Frerking, M. (2003). $GABA_B$ receptor-mediated presynaptic inhibition has history-dependent effects on synaptic transmission during physiologically relevant spike trains. *J. Neurosci.* 23, 4809–4814.

Perez-Garci, E., Gassmann, M., Bettler, B., and Larkum, M. (2006). The $GABA_B1b$ isoform mediates long-lasting inhibition of dendritic $Ca2^+$ spikes in layer 5 somatosensory pyramidal neurons. *Neuron* 50, 603–616.

Petersen, C. C., Malenka, R. C., Nicoll, R. A., and Hopfield, J. J. (1998). All-or-none potentiation at CA3-CA1 synapses. *Proc. Natl. Acad. Sci. U.S.A.* 95, 4732–4737.

Pike, F. G., Meredith, R. M., Olding, A. W., and Paulsen, O. (1999). Rapid report: postsynaptic bursting is essential for 'Hebbian' induction of associative long-term potentiation at excitatory synapses in rat hippocampus. *J. Physiol.* 518, 571–576.

Pouille, F., and Scanziani, M. (2001). Enforcement of temporal fidelity in pyramidal cells by somatic

feed-forward Inhibition. *Science* 293, 1159–1163.

Pouille, F., and Scanziani, M. (2004). Routing of spike series by dynamic circuits in the hippocampus. *Nature* 429, 717–723.

Racca, C., Stephenson, F. A., Streit, P., Roberts, J. D., and Somogyi, P. (2000). NMDA receptor content of synapses in stratum radiatum of the hippocampal CA1 area. *J. Neurosci.* 20, 2512–2522.

Rumsey, C. C., and Abbott, L. F. (2006). Synaptic democracy in active dendrites. *J. Neurophysiol.* 96, 2307–2318.

Schiller, J., Major, G., Koester, H. J., and Schiller, Y. (2000). NMDA spikes in basal dendrites of cortical pyramidal neurons. *Nature* 404, 285–289.

Schiller, J., Schiller, Y., and Clapham, D. (1998). NMDA receptors amplify calcium influx into dendritic spines during associative pre- and post-synaptic activation. *Nat. Neurosci.* 1, 114–118.

Shinohara, Y., Hirase, H., Watanabe, M., Itakura, M., Takahashi, M., and Shigemoto, R. (2008). Left-right asymmetry of the hippocampal synapses with differential subunit allocation of glutamate receptors. *Proc. Natl. Acad. Sci. U.S.A.* 105, 19498–19503.

Shouval, H. Z., and Kalantzis, G. (2005). Stochastic properties of synaptic transmission affect the shape of spike time-dependent plasticity curves. *J. Neurophysiol.* 93, 1069–1073.

Silberberg, G., and Markram, H. (2007). Disynaptic inhibition between neocortical pyramidal cells mediated by Martinotti cells. *Neuron* 53, 735–746.

Sjöström, P., and Nelson, S. (2002). Spike timing, calcium signals and synaptic plasticity. *Curr. Opin. Neurobiol.* 12, 305–314.

Sjöström, P., Turrigiano, G., and Nelson, S. (2001). Rate, timing, and cooperativity jointly determine cortical synaptic plasticity. *Neuron* 32, 1149–1164.

Sjöström, P. J., and Häusser, M. (2006). A cooperative switch determines the sign of synaptic plasticity in distal dendrites of neocortical pyramidal neurons. *Neuron* 51, 227–238.

Sohal, V. S., Zhang, F., Yizhar, O., and Deisseroth, K. (2008). Parvalbumin neurons and gamma rhythms enhance cortical circuit performance. *Nature* 459, 698–702.

Staley, K., Soldo, B., and Proctor, W. (1995). Ionic mechanisms of neuronal excitation by inhibitory $GABA_A$ receptors. *Science* 269, 977–981.

Stuart, G., and Häusser, M. (2001). Dendritic coincidence detection of EPSPs and action potentials. *Nat. Neurosci.* 4, 63–71.

Taira, T., Lamsa, K., and Kaila, K. (1997). Posttetanic excitation mediated by $GABA_A$ receptors in rat CA1 pyramidal neurons. *J. Neurophysiol.* 77, 2213–2218.

Thomas, M. J., Watabe, A. M., Moody, T. D., Makhinson, M., and O'Dell, T. J. (1998). Postsynaptic complex spike bursting enables the induction of LTP by theta frequency synaptic stimulation. *J. Neurosci.* 18, 7118–7126.

Tsubokawa, H., and Ross, W. N. (1996). IPSPs modulate spike backpropagation and associated [Ca2$^+$]i changes in the dendrites of hippocampal CA1 pyramidal neurons. *J. Neurophysiol.* 76, 2896–2906.

van Rossum, M. C., Bi, G. Q., and Turrigiano, G. G. (2000). Stable Hebbian learning from spike timing-dependent plasticity. *J. Neurosci.* 20, 8812–8821.

Vargas-Caballero, M., and Robinson, H. P. (2004). Fast and slow voltage-dependent dynamics of magnesium block in the NMDA receptor: the asymmetric trapping block model. *J. Neurosci.* 24, 6171–6180.

Whittington, M., Traub, R., and Jefferys, J. (1995). Synchronized oscillations in interneuron networks driven by metabotropic glutamate receptor activation. *Nature* 373, 612–615.

Wittenberg, G. M., and Wang, S. S.-H. (2006). Malleability of spike-timing-dependent plasticity at the CA3-CA1 synapse. *J. Neurosci.* 26, 6610–6617.

Woodin, M., Ganguly, K., and Poo, M. (2003). Coincident pre- and postsynaptic activity modifies GABAergic synapses by postsynaptic changes in Cl- transporter activity. *Neuron* 39, 807–820.

Wu, L., and Saggau, P. (1997). Presynaptic inhibition of elicited neurotransmitter release. *Trends Neurosci.* 20, 204–212.

Zhang, L., Tao, H., Holt, C., Harris, W., and Poo, M. (1998). A critical window for cooperation and competition among developing retinotectal synapses. *Nature* 395, 37–44.

Conflict of Interest Statement: The authors declare that the research was conducted in the absence of any commercial or financial relationships that could be construed as a potential conflict of interest.

Received: 12 March 2010; paper pending published: 23 April 2010; accepted: 30 May 2010; published online: 23 June 2010.

*Citation: Nishiyama M, Togashi K, Aihara T and Hong K (2010) GABAergic activities control spike timing- and frequency-dependent long-term depression at hippocampal excitatory synapses. Front. Syn. Neurosci. **2**:22. doi: 10.3389/fnsyn.2010.00022*

frontiers in
COMPUTATIONAL NEUROSCIENCE

ORIGINAL RESEARCH ARTICLE
published: 13 January 2011
doi: 10.3389/fncom.2010.00158

Calcium messenger heterogeneity: a possible signal for spike-timing-dependent plasticity

Stefan Mihalas*

Department of Neuroscience, Zanvyl Krieger Mind/Brain Institute, Johns Hopkins University, Baltimore, MD, USA

Edited by:
Per Jesper Sjöström, University College London, UK

Reviewed by:
Harel Z. Shouval, University of Texas Medical School at Houston, USA
Guo-Qiang Bi, University of Pittsburgh, USA
Terrence J. Sejnowski, The Salk Institute for Biological Studies, USA

***Correspondence:**
Stefan Mihalas, Department of Neuroscience, Zanvyl Krieger Mind/Brain Institute, Johns Hopkins University, Baltimore, MD 21218, USA.
e-mail: mihalas@jhu.edu

Calcium concentrations as well as time courses have been used to model the signaling cascades leading to changes in the strength of synaptic connections. Previous models consider the dendritic spines as uniform compartments regarding calcium signaling. However, calcium concentrations can vary drastically on distances much smaller than typical spine sizes, and downstream targets of calcium signals are often found exactly in these calcium nanodomains. Even though most downstream targets are activated by calcium via calmodulin, which is a diffusive molecule, the capacity of calmodulin to bind to its targets even when it is not fully loaded with calcium allows its downstream cascade to be highly local. In this study, a model is proposed which uses the heterogeneity of calcium concentrations as a signal for spike-timing-dependent plasticity (STDP). The model is minimalistic and includes three sources of calcium in spines: NMDA receptors (NMDARs), voltage gated calcium channels (VGCCs) and IP3 receptors (IP3Rs). It is based on the biochemical cascades and assumption of spatial locations of four calcium-dependent enzymes: calcium/calmodulin-dependent protein kinase II located near NMDARs, calcineurin located near VGCCs, cyclic nucleotide phosphodiesterase (PDE) located near IP3Rs or NMDARs and adenylyl cyclase, located between VDCCs and NMDARs. To quantify the changes in synaptic weights the model also includes a simple description of AMPA receptor insertion in the membrane and docking to the postsynaptic density. Two parameters of the model are tuned such that weight changes produced by either pre or postsynaptic firing alone are minimal. The model reproduces the typical shape of STDP for spike doublets. If PDE is located near IP3Rs, the behavior for spike triplets is consistent with that observed in hippocampal cell culture; if near NMDAR, the behavior is similar to that observed in cortical L2/3 slices.

Keywords: STDP, calmodulin, LTP, microdomain, LTD, nanodomain, calcium, CaMKII

INTRODUCTION

In recent years several distinct classes of models have been proposed, which, in varying degrees of detail, map the rise in calcium concentration in a dendritic spine to the long-term potentiation (LTP) or depression (LTD) of the synaptic strength. One class of such models considers the calcium concentration resulting from a stimulation protocol as the main determinant of the future changes in plasticity: high calcium elevations lead to LTP, moderate calcium elevations lead to LTD and small calcium elevations produce no changes, which is generally referred as the "differential threshold hypothesis" (Lisman, 1989; Artola and Singer, 1993). This basic principle has both biochemical and physiological foundations. Calcium/calmodulin-dependent protein kinase II (CaMKII), which has been implicated in the expression of LTP (Glazewski et al., 1996; Frankland et al., 2001), can autophosphorylate, a process which maintains its kinase activity even in the absence of calcium (Bennett et al., 1983). Autophosphorylation is assumed to require one active CaMKII subunit neighboring a non-phosphorylated subunit with calmodulin bound to it. Thus, the most simplistic model of CaMKII activation assumes an initial step which is dependent on the square of the concentration of calcium-loaded calmodulin. At the same time, the activation of protein phosphatase 2B (calcineurin, CaN), besides some high affinity calcium binding sites, requires the binding of one calcium-loaded calmodulin. The most simplistic model for CaN activation is to consider its activity being proportional to the concentration of calcium-loaded calmodulin. Associating the kinase activity to LTP (making it quadratic in calmodulin activation) and phosphatase activity to LTD (making it linear in calmodulin activation), it is possible to build a very simple model of synaptic plasticity. While the core of the model is very simple, extensive modeling work has shown that it is possible for simulations of the biochemical signals within postsynaptic spines to reproduce these results (Bhalla, 2002; Hayer and Bhalla, 2005; Graupner and Brunel, 2007). In addition to the induction, these models have the property of including a bistable switch at the biochemical level. While experimental evidence of CaMKII autophosphorylation in the presence of protein phosphatase 1 (PP1) failed to observe bistability (Bradshaw et al., 2003), it can be included in the model at protein translation level (Aslam et al., 2009).

Traditional induction protocols: high and low frequency afferent stimulation, as well as more direct manipulations of calcium concentrations in postsynaptic spines (Yang et al., 1999; Cho et al., 2001; Cormier et al., 2001) support the "differential threshold hypothesis." However, in typical spike-timing-dependent plasticity (STDP) induction (Markram et al., 1997; Bi and Poo, 1998), such a model would predict a second depression window at a long pre–post time interval. The model can be rescued by considering that pre stimulation alone does not produce calcium concentrations lower

than those needed for LTD, but rather resides in the narrow band of calcium concentration between the induction of LTD and that of LTP, and that a post–pre at short time intervals produces smaller calcium input (Urakubo et al., 2008). This model can also qualitatively reproduce the spike triplet protocols measured in cortex (Froemke and Dan, 2002). A very high diversity of rules for synaptic plasticity can be observed in diverse systems (Nelson and Turrigiano, 2008). In hippocampal cell cultures a different triplet rule has been observed (Wang et al., 2005), in which symmetric pre–post–pre triplets at short time interval (5 and 10 ms) produce little synaptic change, while symmetric post–pre–post triplets at the same intervals produce robust LTP. This triplet structure was explained by considering the temporal structure of the calcium transient as the main signal for STDP (Rubin et al., 2005). Without being tuned for, this triplet structure is qualitatively reproduced in the model presented in this study. In addition, both theoretical (Karmarkar and Buonomano, 2002) and experimental (Sjostrom et al., 2003) work point toward an additional coincidence detector for the pre–post tLTD window. Experimental observations point toward a presynaptic mechanism, however in these experiments (Sjostrom et al., 2003) the presynaptic neuron fires multiple times in a short interval, which allows autocrine NMDA activation. In protocols in which this is absent, how can such a coincidence detector be implemented?

A minimalistic model is proposed which uses the assumption that different enzymes in the biochemical pathways localize to different calcium sources. This general principle is supported by multiple experiments which show problems in plasticity caused by interference with scaffold proteins and the general observation that the diversity of the forms of synaptic plasticity, while caused by a small number of second messengers, is surpassed by the diversity in scaffolds (Jordan et al., 2004). A potential problem with such a model is that, while calcium gradients are very sharp (Naraghi and Neher, 1997), most of the calcium-dependent enzymes are activated by calmodulin, which is soluble. Simulations of calcium dynamics in dendritic spines with simple geometries show the diffusion coefficient of calmodulin as having a strong influence on the local calmodulin signaling (Naoki et al., 2005). Using the calmodulin diffusion constant measured *in vivo* (Luby-Phelps et al., 1995), simulations show large differences between the nanodomain and spine-wide calmodulin activations. More detailed simulations also show a very different probability for a calmodulin to become fully calcium loaded if it is located in the postsynaptic density (PSD) or randomly in the spine (Keller et al., 2008). In addition, calmodulin with less than four calcium bound can bind to CaMKII (Shifman et al., 2006), and possibly, via a similar mechanism, to other targets. This influences the calcium transient dependence of CaMKII (Mihalas, 2009; Pepke et al., 2010), but also has drastic implication over the distance from a calcium source which produces activation of CaMKII (Mihalas, 2009). This distance is smaller than the typical size of a spine, such that it is reasonable to assume subspine size domains in signaling.

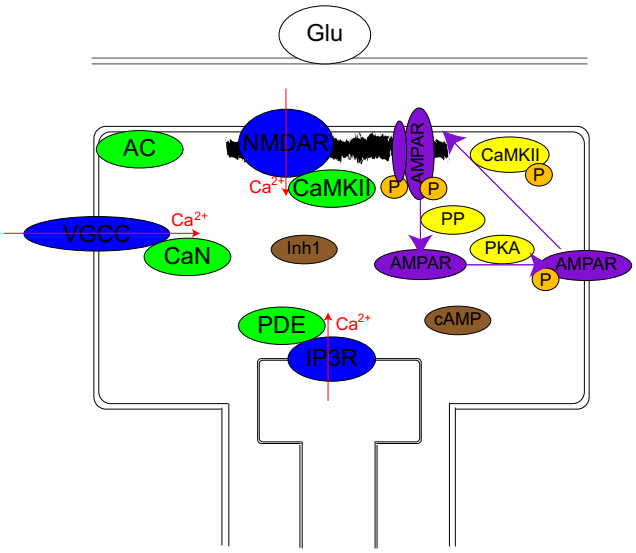

FIGURE 1 | Schematic representation of the model. Calcium channels (blue ovals) are differentially activated by different stimulation protocols: The firing of the postsynaptic neuron activates mainly VGCCs, the firing of the presynaptic neuron via mGlus mainly activates IP3Rs, and to a lesser extent NMDARs and VGCCs while a pre–post activation results in large activation of all sources. The essential assumption of the model consists of localization of calcium-dependent enzymes (green ovals) near these calcium sources: CaMKII near NMDAR, CaN near VGCC, PDE near IP3R, and AC in between VGCC and NMDAR. Their transient (10 ms) calcium-dependent activation is assumed to remain localized. Either directly or via less localized intermediaries (Inh1 and cAMP: brown ovals), these produce changes over intermediate time scales in several enzyme activations (CaMKII, PKA, and several PPs: yellow ovals). These intermediate time scale changes produce long-term changes in the synaptic weight via phosphorylation or dephosphorylation of AMPAR and PSD targets which lead to insertion and stabilization of AMPAR in PSD or destabilization and endocytosis of AMPAR respectively.

MODEL

CALCIUM ENTRY

Three calcium sources are considered in the model: NMDARs, VGCCs, and calcium release from internal stores via IP3-dependent channels (**Figure 1**). Since at the next step of the signaling cascade activation parameters are unknown, the relative timing of opening of the calcium channels and not their relative strength are important. Thus the magnitude of each current is normalized, and the parameters in future sections are relative to the magnitude of the calcium current. For a quantitative description of the model, see the Section "Appendix."

Voltage gated calcium channels provide a short calcium current following depolarization. A model for L-type VGCC identical to previous simulation work was used (Urakubo et al., 2008). Both APs and EPSPs are assumed to be biexponential with a rise time of 0.5 ms, a decay time of 5 ms and maximum amplitudes of 60 and 10 mV respectively. APs and EPSPs are assumed to be linearly additive. The calcium current through VGCCs is mainly a result of backpropagating action potentials in the dendritic tree following postsynaptic neuron firing. To a smaller extent they respond to EPSPs caused by presynaptic neuron firings. The normalized calcium currents under different stimulation protocols are presented in **Figure 2**.

Calcium release from internal stores via IP3-dependent channels (IP3R) is initiated by activation of mGluRs. Since there are many unknown parameters in the cascade resulting in calcium release, the calcium current is considered to be the convolution

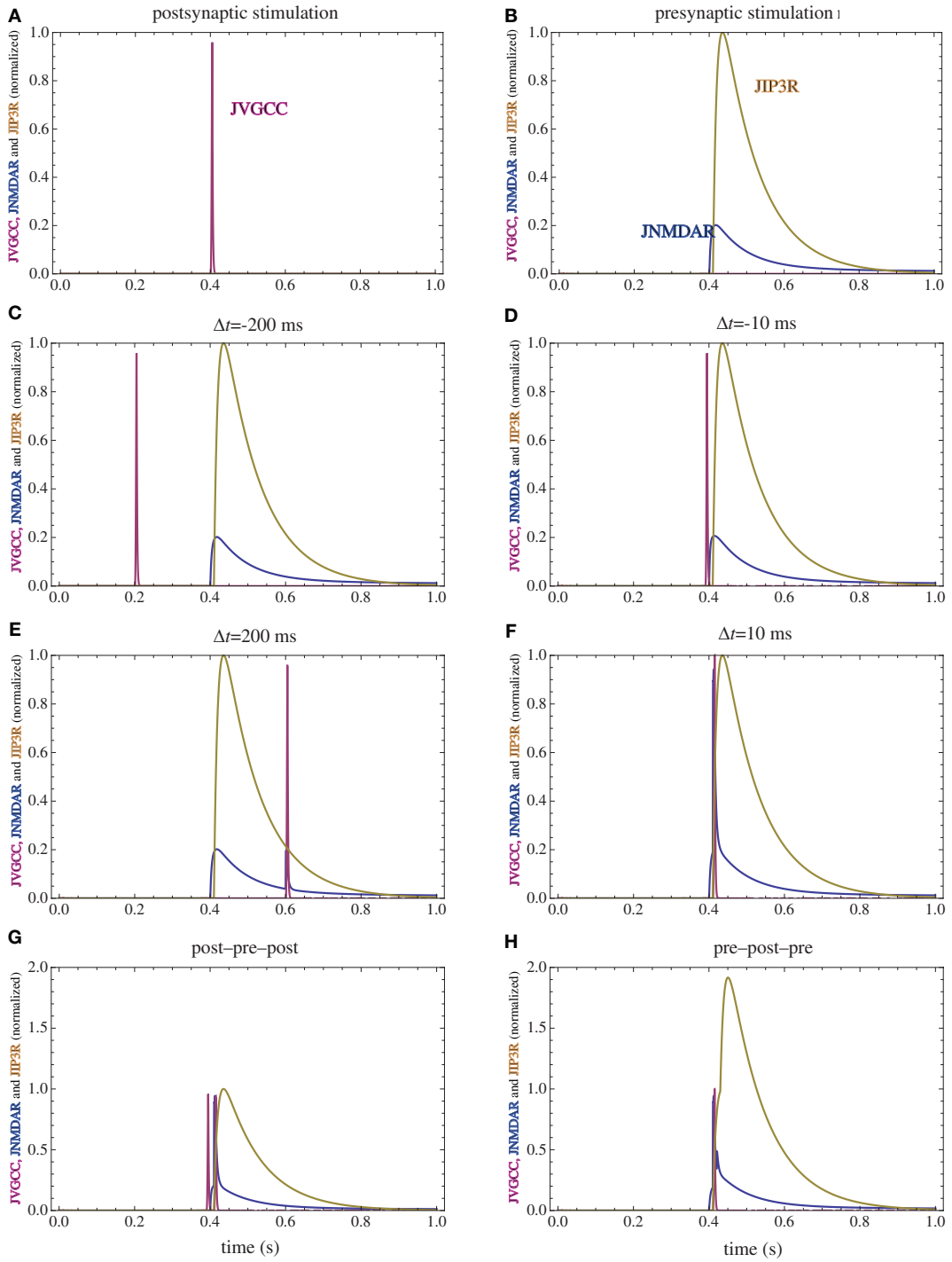

FIGURE 2 | Calcium currents through NMDAR, VGCC, and IP3R following several stimulation paradigms. (A) Postsynaptic firing alone. **(B)** Presynaptic firing alone. **(C,D)** Post–pre at different time intervals. **(E,F)** Pre–post at different time intervals. **(G)** Post–pre–post symmetric triplet with 10 ms between each spike. **(H)** Pre–post–pre symmetric triplet with 10 ms between each spike. The currents for each channel type are normalized to the maximum current which can be observed for that channel type in the doublet simulations consisting of one spike for the pre and postsynaptic neuron.

between glutamate concentration and a convolution kernel which is a biexponential delayed by 10 ms with a 10-ms rise time and a 100-ms decay time. For mGluR activation, glutamate diffusion is practically instantaneous and can be approximated by a delta function. To test the influence of the timing of the IP3R activation, all stimulations protocols were simulated in a model with a considerably slower (99 ms) rise time of the mGluR activation. The normalized calcium currents for the modified model are presented

in **Figure 8**. With a corresponding change in the affinity for the calcium-dependent enzymes assumed to be in the vicinity of the IP3R, while keeping all the other parameters in the model to be identical, the simulated changes in synaptic weights are only modestly modified (**Figure 9**).

NMDARs provide a small and prolonged calcium current if the presynaptic neuron fires alone (pre), and a larger and shorter current in addition to the previous one if the postsynaptic neuron fires following presynaptic neuron activation (pre–post). Even though the model does not strongly depend on the minute details of the NMDAR current, since parameters are available a relatively detailed model of NMDAR is used. The parameters for the NMDAR activation are obtained from Lester and Jahr (1992), with magnesium block obtained from Jahr and Stevens (1990). Glutamate diffusion in the cleft is analytically solved using the approximations that the cleft is narrow compared to its length, glutamate has a point release and its reuptake mechanism is linear. Median values of previous, more detailed simulations were used (Franks et al., 2002).

CALCIUM-DEPENDENT ENZYME ACTIVATION

After entering the postsynaptic spine, calcium ions are very quickly bound to buffers and are extruded. Calcium concentration differs vastly between the mouth of the channel and points hundreds of nanometers away (Naraghi and Neher, 1997). Calmodulin, as a diffusible calcium binding protein shows a less steep gradient. However, the fact that calmodulin with less than four calcium bound can bind to some target enzymes like CaMKII (Shifman et al., 2006), has a large influence on the spatial extent around the channel in which CaMKII can be activated. Calmodulin binding to its target before being fully calcium loaded is immobilized, forcing its subsequent activation to be dependent on the calcium concentration on that particular position rather than the average calcium concentration in its vicinity. For typical spine morphologies it can be estimated that the range of CaMKII half-activation is a few tens on nanometers surrounding an NMDAR (Mihalas, 2009). An enzyme bound near the mouth of a channel is also primarily activated by calcium coming though that type of channel. In order to focus exclusively on the effects caused calcium heterogeneity, the effects of global calcium concentration changes in the spine are neglected. The activation of calcium-dependent enzymes is considered to be dependent exclusively on the calcium current through the channel type near which they are located.

In this study, crosstalk between the different sources of calcium is neglected. This approximation allows a drastic reduction in the complexity of the model as the activation of each enzyme is considered dependent only on the calcium current from one source. While clustering of the same type of calcium channels certainly helps this approximation, it is not required. It is possible to consider a functional calcium domain near the mouth of VGCCs which consists of several spatially disjoined regions.

Calcium/calmodulin-dependent protein kinase II is enriched in the PSD (Kennedy, 2000), thus it is considered to be mainly activated by calcium influx though postsynaptic NMDARs.

Protein phosphatase 2B (CaN) is assumed to be, under physiological conditions, primarily activated by calcium coming through VGCCs. While proteomic studies have found small quantities of CaN in the PSD (Jordan et al., 2004), it is possible that small quantities of other protein aggregates are found in PSD fractions.

Adenylyl cyclase (AC) is assumed to have a mixed distribution and is partially activated by calcium coming either from NMDAR or VDCC. This assumption is consistent with a membrane-bound enzyme which can diffuse in the membrane and temporarily bind to other proteinaceous structures.

Cyclic AMP phosphodiesterase (PDE) is assumed to mainly be activated by signals related to the firing of the presynaptic neuron. This can be realized by localization of PDE near sources of calcium coming from internal stores as a result of mGluR activation. While a significant fraction of dendritic spines do not have endoplasmic reticulum protruding into the spine (Harris and Stevens, 1989), it is possible that either a dendritic calcium source is used, or that PDE localizes near NMDARs. Recent studies observed an enrichment of inactive protein kinase A in dendrites with an active removal from the spines (Zhong et al., 2009). A colocalization with PKA could help PDE in inhibiting cAMP downstream signaling. Three sets of simulations are performed: two sets assuming the PDE is localized in the vicinity of IP3Rs, and one set assuming PDE is localized in the vicinity of NMDARs.

The calcium unbinding rate from the low affinity sites of calmodulin is very fast (>1/ms). While calmodulin binding to target proteins slows down this unbinding (Olwin and Storm, 1985; Pepke et al., 2010), it is still faster than the NMDA and IP3 calcium transients, which will thus be determining the inactivation of the calcium-dependent enzymes.

PROLONGED ENZYME ACTIVATION

Following calcium entry through either NMDARs or VGCCs, AC is transiently activated (**Figure 3**), which results in a rise in cAMP concentration (**Figure 4**). This rise is also transient, and the basal rate of consumption/diffusion is important in determining the length of the tLTD window and is chosen to be 0.1/s. The cAMP transient can be decreased or shortened by activation of PDE by IP3R. Long-term PKA activation is assumed to be proportional to the integral of cAMP concentration. The ratio of PDE and AC enzyme activities is a key parameter of the model. It was tuned such that the presynaptic activation alone produces little PKA activation.

Following calcium entry through VGCCs, CaN is transiently activated (**Figure 5**). This leads to dephosphorylation of Inhibitor 1, and subsequent activation of PP1. Activation of PKA leads to phosphorylation of Inh1 and subsequent inactivation of PP1. The long-term PP1 activity is assumed to be proportional to the integral of CaN activity minus PKA activation, if this difference is positive and zero otherwise. The ratio between PKA and CaN activities is another crucial parameter in the model, and it was tuned such that the postsynaptic activation alone produces equal PKA and CaN activation (**Figure 6**).

Following calcium entry though NMDARs, CaMKII is transiently activated. A fraction of this activation can be transformed in long-term activity via autophosphorylation. The long-term CaMKII activity is assumed to be proportional to the integral of the square of the instantaneous calcium-dependent activity.

While the calcium-dependent enzyme activation which happens on time scales of tens of milliseconds is assumed to be localized, at least some of the downstream targets (Inh1, cAMP) are assumed to be present at similar concentrations in all the spine subcompartments.

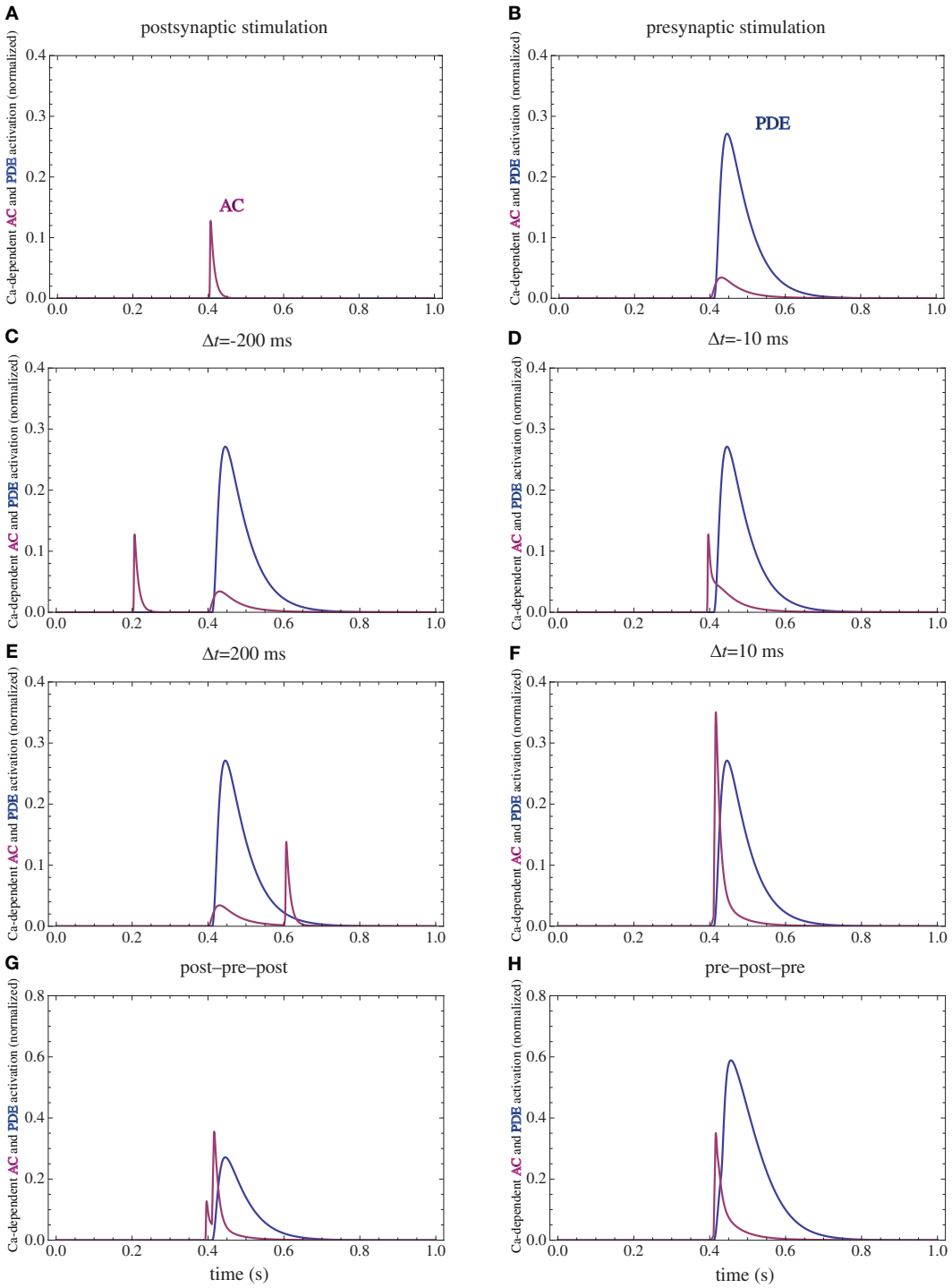

FIGURE 3 | PDE and AC activations. (A) Postsynaptic firing alone. **(B)** Presynaptic firing alone. **(C,D)** Post–pre at different time intervals. **(E,F)** Pre–post at different time intervals. **(G)** Post–pre–post symmetric triplet with 10 ms between each spike. **(H)** Pre–post–pre symmetric triplet with 10 ms between each spike. The activation of each enzyme is normalized to their respective maximal activation under saturating calcium.

CHANGES IN SYNAPTIC WEIGHT

AMPAR trafficking, membrane insertion, binding to the PSD and extrusion are key elements in the expression of long-term changes in synaptic plasticity (Song and Huganir, 2002). Activation of PKA leads to GluR1 phosphorylation at Ser845 and its membrane insertion (Esteban et al., 2003). Subsequently (Yang et al., 2008), CaMKII phosphorylation of multiple postsynaptic targets as well as Ser831 stabilize AMPAR in the PSD. The concentration

of the intermediate step: the perisynaptic AMPAR is assumed to be relatively small. Thus, the rate of AMPAR insertion and stabilization is proportional to the product of PKA and CaMKII activities.

Dephosphorylation of PSD proteins can interfere with AMPAR stability in the PSD, and dephosphorylation of Ser845 could prevent recently endocytosed AMPARs to be reinserted in the membrane. Multiple phosphatases can contribute to these dephosphorylation steps. Since some of the targets are in the PSD, PP1 activity is used as a proxy for this average protein phosphatase (PP) activity. Besides the role of CaMKII in LTP, it is assumed to have a divisive influence on LTD as well. This can be caused by its presence in large quantities in PSD providing competitive inhibition, or by rephosphorylating targets in the intermediate steps on endocytosis. Two models for AMPAR extrusion are used. In the first, the rate of AMPAR extrusion is assumed to be proportional to PP activity (**Figures 7, 9, 10, E and F**). In the second, it is proportional to PP activity and divided by a constant plus CaMKII long-term activity (**Figures 7, 9, 10, G and H**). The value of this constant was chosen to be the mean CaMKII long-term activity during a sampling of STDP protocols. The influence of CaMKII on LTD does not affect STDP for spike doublets, and plays a small role in the ability of the model to reproduce the STDP for spike triplets observed in cultured hippocampal neurons (Wang et al., 2005).

The final change in the synaptic weight is assumed to be the sum of LTP and LTD activities.

RESULTS

POSTSYNAPTIC FIRING

The firing of the postsynaptic neuron leads to calcium currents through VGCCs (**Figure 2A**) and activation of AC (**Figure 3A**) and CaN (**Figure 5A**). AC leads to activation of PKA (**Figure 6B**). The ratio between CaN and PKA activities was tuned such that postsynaptic firing alone produces equal CaN and PKA activation resulting in no PP1 activation (**Figure 6D**). This leads to no change in weight caused by the LTD mechanism (**Figure 7D**). Since CaMKII is not activated (**Figure 6F**), no change in synaptic weight is caused by the LTP mechanism (**Figure 7B**).

PRESYNAPTIC FIRING

The firing of the presynaptic neuron alone activates to a low extent the NMDARs and IP3Rs. While the peak current through an NMDAR is small if the membrane is not depolarized, due to the slow dynamics of the channel the total current can not be neglected (**Figure 2B**). Given the assumption of enzyme localizations, presynaptic firing leads to transient AC, PDE (**Figure 3B**), and CaMKII (**Figure 5B**) activations, all to a small extent. The ratio of AC and PDE activity was tuned to cancel out (**Figure 4B**) and to lead to little PKA activation (**Figure 6B**). Without activation of PKA, the change in synaptic weight caused by LTP mechanisms is zero (**Figure 7B**). Presynaptic firing leads to little CaN (**Figure 5B**) activation, which, via PP1 leads to no change in synaptic weight caused by LTD mechanisms (**Figure 7D**).

LONG DELAYS

If pre and postsynaptic neurons fire at intervals longer than the transient enzyme activations (e.g., 200 ms, **Figures 2–5 C,E**), due to the linear characteristics of long-term enzyme activations, the total changes will be additive and zero in this case (**Figure 7**).

POST–PRE

The firing of the postsynaptic neuron leads to activation of CaN and AC. The transient activation of CaN is unaffected by the firing in quick succession of the presynaptic neuron (**Figure 5D**). The transient rise in cAMP is however truncated by the activation of PDE by the presynaptic neuron (**Figure 4D**). The closer the presynaptic neuron fires after the postsynaptic one, the shorter the cAMP transient is. This leads to a reduced PKA activation (**Figure 6A**) compared to the firing of the postsynaptic neuron alone (**Figure 6B**) and an imbalance between CaN and PKA which leads to activation of the LTD pathway (**Figure 7C**). Since little CaMKII activity is obtained, the LTP pathway is not activated in this case (**Figure 7A**). This mechanism is also consistent with experiments in which CaN was inhibited (Wang et al., 2005) producing no significant change in synaptic weight.

PRE–POST

The firing of the postsynaptic neuron quickly following the presynaptic one leads to opening of all calcium sources and massive currents through NMDAR (**Figure 2F**). These currents lead to high CaMKII (**Figure 5F**) and AC (**Figure 3F**) activation. At the same time, the superposition between the PDE activation and AC activation (**Figure 3F**) leads to efficient consumption of cAMP (**Figure 4F**). One free parameter in the model, the ratio of how well NMDAR and VGCC activate AC can shift the pre–post activation of PKA, but it has a small impact on the presynaptic firing only. The pre–post LTP window which results from this activation (**Figure 7A**) is roughly half the glutamate unbinding halftime from NMDAR due to the requirement that two CaMKII subunits to be active to produce an autophosphorylation event. In addition, adjusting the exact position of AC relative to NMDAR and VGCC can also influence this window. In this model, the rise in AC activation due to the large NMDARs current is larger than the PDE activation, leading to zero PP1 activation and zero weight change due to LTD mechanisms (**Figure 7C**). This result is consistent with biochemical manipulations in which CaMKII was inhibited (Wang et al., 2005), however no significant change in synaptic weigh is observed.

POST–PRE–POST

The post–pre–post symmetric triplet with 10 ms between each spike produces weight changes similar to the pre–post doublet (Wang et al., 2005). CaN (**Figure 5G**) and AC (**Figure 3G**) are increased, but they roughly cancel each other (though not perfectly). This results in a large LTP (similar to the best doublet) and a small LTD (**Figures 7B,D**). While the net effect is LTP (**Figure 7H**), both pathways are activated. This is qualitatively consistent with experimental results which show that inhibition of CaMKII produces LTD and inhibition of CaN produces LTP in this protocol (Wang et al., 2005).

PRE–POST–PRE

The symmetric pre–post–pre triplet with 10 ms between each spike produces an increased PDE activity (**Figure 3H**), which strongly reduces PKA activity (**Figure 6B**). The CaMKII activation is high, comparable to pre–post doublet (**Figure 6H**). The reduced PKA activity leads to a small activation of LTP (**Figure 7B**). If it is assumed to inhibit LTD, the high activation of CaMKII results in a small activation of the LTD pathway (**Figure 7H**). Their values

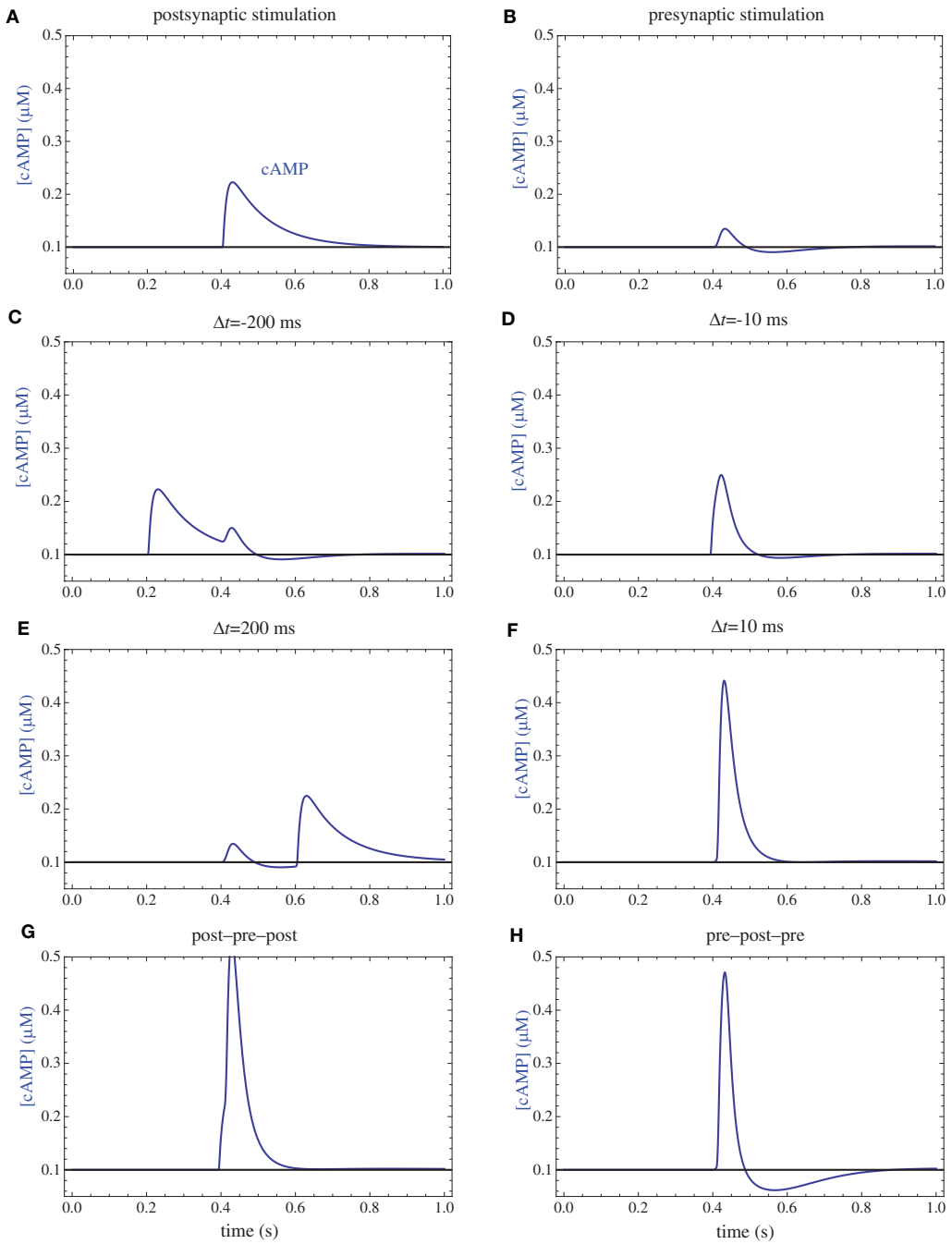

FIGURE 4 | cAMP concentrations. (A) Postsynaptic firing alone. **(B)** Presynaptic firing alone. **(C,D)** Post–pre at different time intervals. **(E,F)** Pre–post at different time intervals. **(G)** Post–pre–post symmetric triplet with 10 ms between each spike. **(H)** Pre–post–pre symmetric triplet with 10 ms between each spike.

are similar, and the net synaptic weight change is small (**Figure 7H**). This result is consistent with experimental observations in which CaMKII inactivation produces an LTD window and CaN inactivation produces LTP in this case (Wang et al., 2005).

MODEL VARIATIONS

Three sets of simulations were performed, which differ primarily in the quantitative aspects of PDE activation. In the first set of simulations, which was presented until now, the calcium current through IP3R has a fast rise time. This is possible considering the below micrometer distances second messengers need to travel in a spine.

In a second set of simulations the rise time for the calcium current through IP3R is increased by a factor of 10 (**Figure 8**), leading to a time scale similar to those observed in dendrites (Nakamura et al., 1999). The only other parameter which was changed in the second model is the on rate of the PDE for calcium which was decreased by a factor of square root of 10 (the square root was used

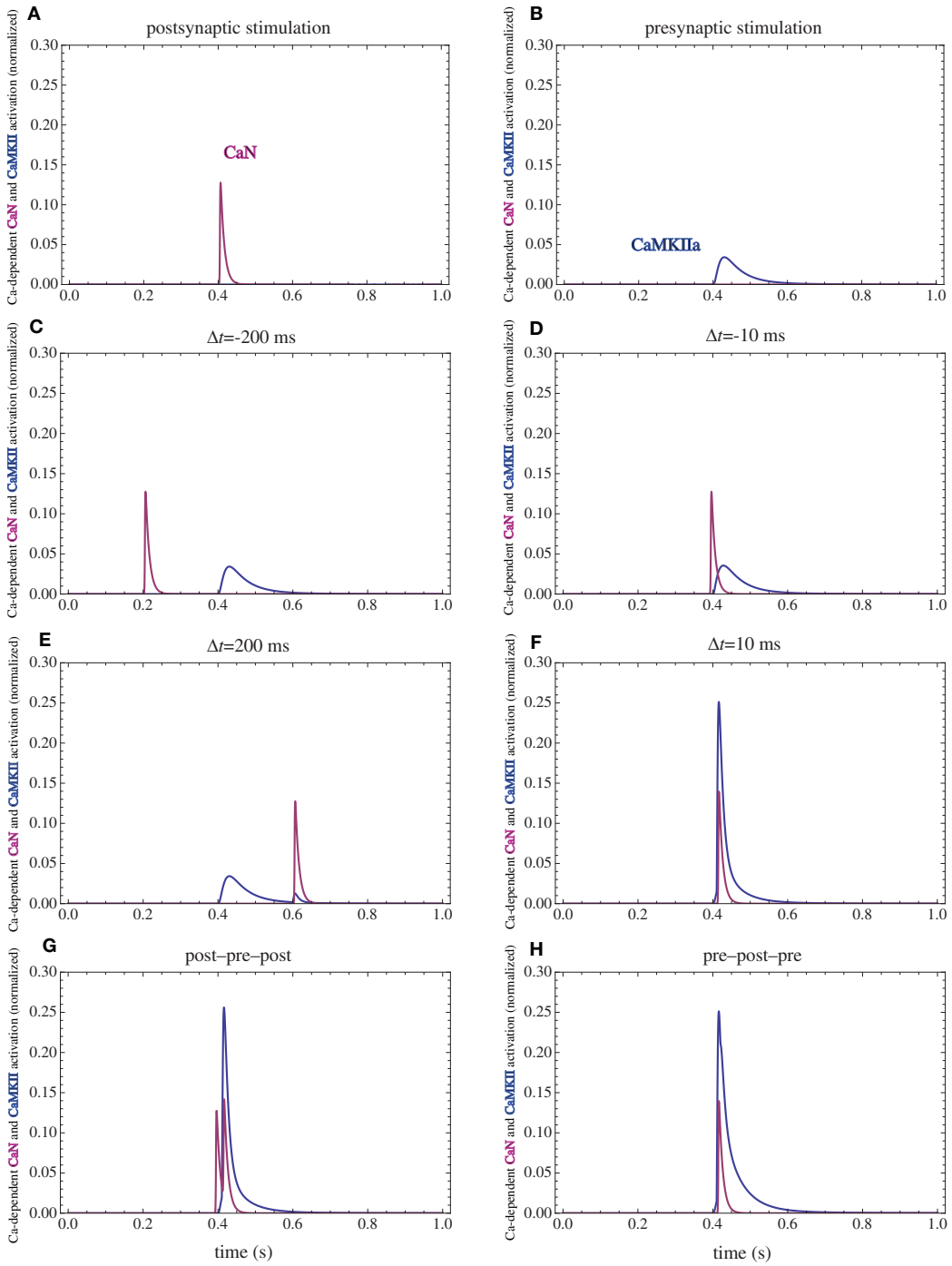

FIGURE 5 | Calcium-dependent activation of CaMKII and CaN. (A) Postsynaptic firing alone. **(B)** Presynaptic firing alone. **(C,D)** Post–pre at different time intervals. **(E,F)** Pre–post at different time intervals. **(G)** Post–pre–post symmetric triplet with 10 ms between each spike. **(H)** Pre–post–pre symmetric triplet with 10 ms between each spike. The activation of each enzyme is normalized to their respective maximal activation under saturating calcium.

since the hill coefficient for the calcium-dependent activation of enzymes was assumed to be 2). This change maintains the desired null change for the weight following a presynaptic stimulus only. Together, these modifications qualitatively reproduce the observed weight changes (**Figure 9 E,F**), but for a simpler LTD model.

A third set of simulations are performed for spines which lack internal calcium stores. In the model, PDE needs to be activated by a source mainly determined by presynaptic firing. This can theoretically be achieved by relying on a dendritic calcium source, however, under this condition, the shape of STDP for spike

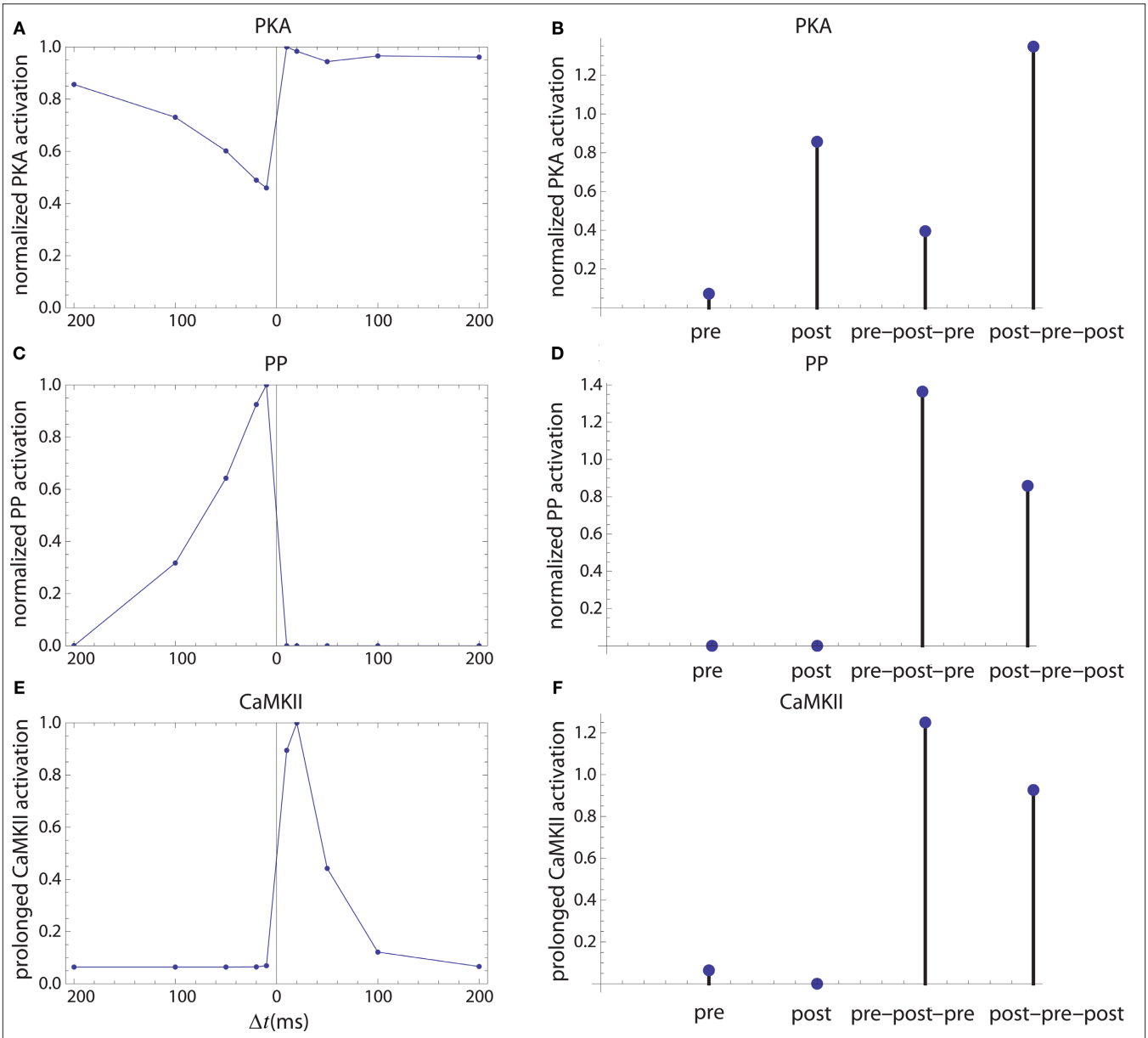

FIGURE 6 | Long-term enzyme activations. Activation of PKA **(A,B)**, PP1 [**(C,D)** which is considered as a proxy for average protein phosphatase activity in PSD] and calcium-independent activation of CaMKII **(E,F)**. The first column corresponds to activation by pre–post doublets and the second column corresponds to activations caused by pre, post spiking alone, and by symmetric 10 ms time interval spike triplets.

doublets could not be obtained by this simple model. An alternative is to consider that PDE is localized in the vicinity of NMDARs. While the NMDAR currents are very small in the absence of a backpropagating action potential, this trickle of calcium is sufficient to create a marker for the presynaptic firing (**Figure 10**). As in all the simulations, the on rate of PDE was tuned such that the presynaptic activation alone produces only minimal changes in synaptic weights. In these simulations, the shape of STDP produced by spike doublets is maintained, however qualitative changes are observed in the behavior of STDP caused by triplets (**Figures 10E,F**). Unlike the STDP caused by triplets observed in cultured hippocampal neurons (Wang et al., 2005), the symmetric pre–post–pre triplet is potent at inducing LTP, while the symmetric post–pre–post produces LTD. However, such a triplet behavior is consistent with those measured in L2/3 in visual cortical slices (Froemke and Dan, 2002).

DISCUSSIONS

This study provides a very different paradigm of modeling biochemical networks, in which affinities and kinetics of different enzymes come secondary to their location. This can possibly allow robust and diverse signaling pathways based on a small number of second messengers. From an evolutionary perspective this type of signaling shifts the complexity from fine tuning the kinetics of

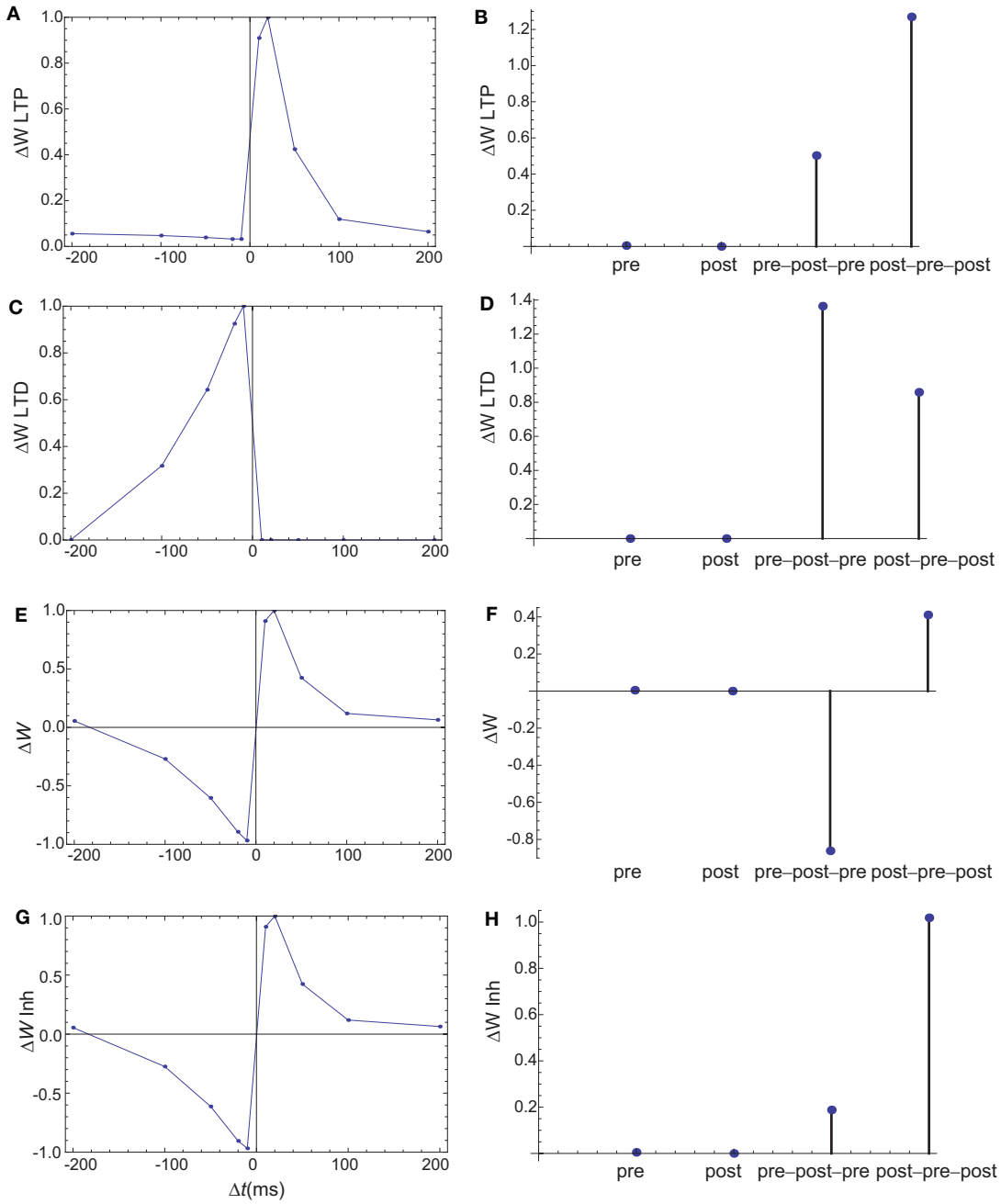

FIGURE 7 | Changes in synaptic weights (E,F) caused by LTP **(A,B)** and LTD **(C,D)** pathways. **(G,H)** The changes in synaptic weights if the LTD pathway is inhibited by CaMKII. Columns as in **Figure 6**. The weight changes for single spike and spike doublets are qualitatively similar to those in cultured hippocampal neurons: antisymmetric STDP for spike doublets with a slightly longer window for depression and infinitesimal changes for pre and postsynaptic stimulation alone. If the LTD pathway is inhibited by CaMKII, the results for spike triplets are also similar to those observed in cultured hippocampal neurons: small changes for symmetric 10 ms pre–post–pre triplet, and strong potentiation for symmetric 10 ms post–pre–post triplet.

different enzymes to produce diverse behaviors, to the production of novel scaffolds. The sheer diversity of existing scaffolds makes such a mechanism at least plausible.

The model can explain the apparently opposite behaviors observed for spike triplets in L2/3 visual cortical slices and hippocampal cell cultures by keeping all the parameters of the model the same and simply assuming a different localization for PDE: In the vicinity of IP3R for hippocampal cell cultures, and near the mouth of the NMDAR for cortical slices. It should be noted that, since the on rate for all calcium-dependent enzymes is described in term of calcium currents, it will be strongly affected by the exact position of the enzyme with respect to the

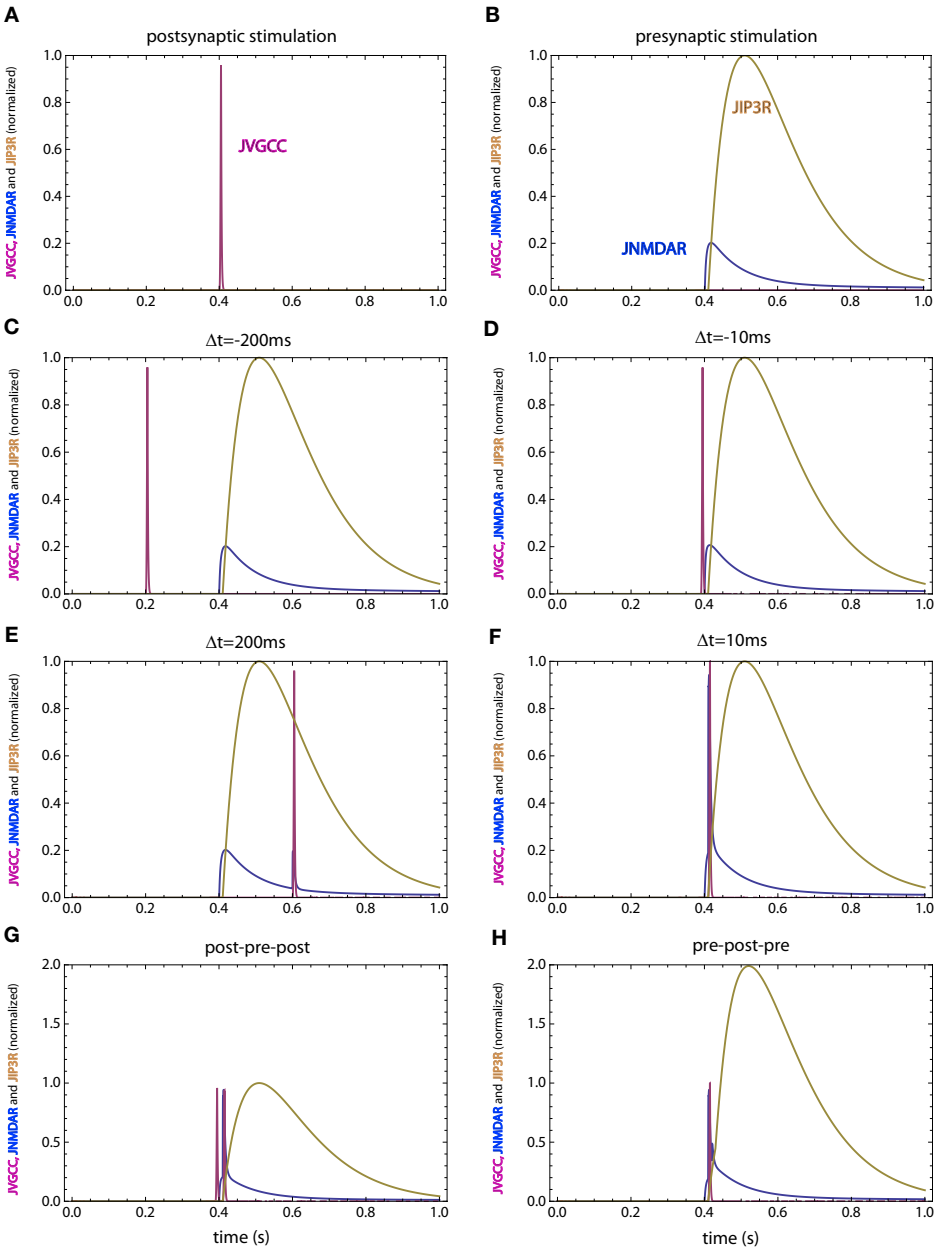

FIGURE 8 | Calcium currents through NMDAR, VGCC and IP3R for the second set of simulations in which the IP3R has a slower rise time. (A) Postsynaptic firing alone. **(B)** Presynaptic firing alone. **(C,D)** Post–pre at different time intervals. **(E,F)** Pre–post at different time intervals. **(G)** Post–pre–post symmetric triplet with 10 ms between each spike. **(H)** Pre–post–pre symmetric triplet with 10 ms between each spike. The NMDAR and VGCC currents are the same as those in **Figure 2**.

mouth of the channel: A higher on rate for locations closer to the mouth. The localization of PDE which best reproduces the spike triplets for the two preparations seems reasonable, since cell cultures have typically stronger synapses than slices, which often correlates with larger spines, which are more likely to have a spine apparatus.

This study relies on the assumption that calcium concentrations and downstream cascades have strong spatial heterogeneities on scales smaller than the size of a spine. In previous simulations of calcium transients during STDP protocols, which involve strong calcium currents persisting only a few milliseconds, such a heterogeneity is observed (Keller et al., 2008; Mihalas, 2009). In earlier simulations (Holmes, 1990) a relatively uniform calcium concentration is observed at the end of the stimulation protocol simulating a 200-Hz tetanic stimulation. While these studies used different simulation methods, one key difference is in the stimulation protocol. In the former studies, simulating STDP, large calcium currents persist for 10 ms or less, while in the simulation of the tetanic stimulation large calcium currents persist for 40–100 ms. Even in the simulations of tetanic stimulation, calcium

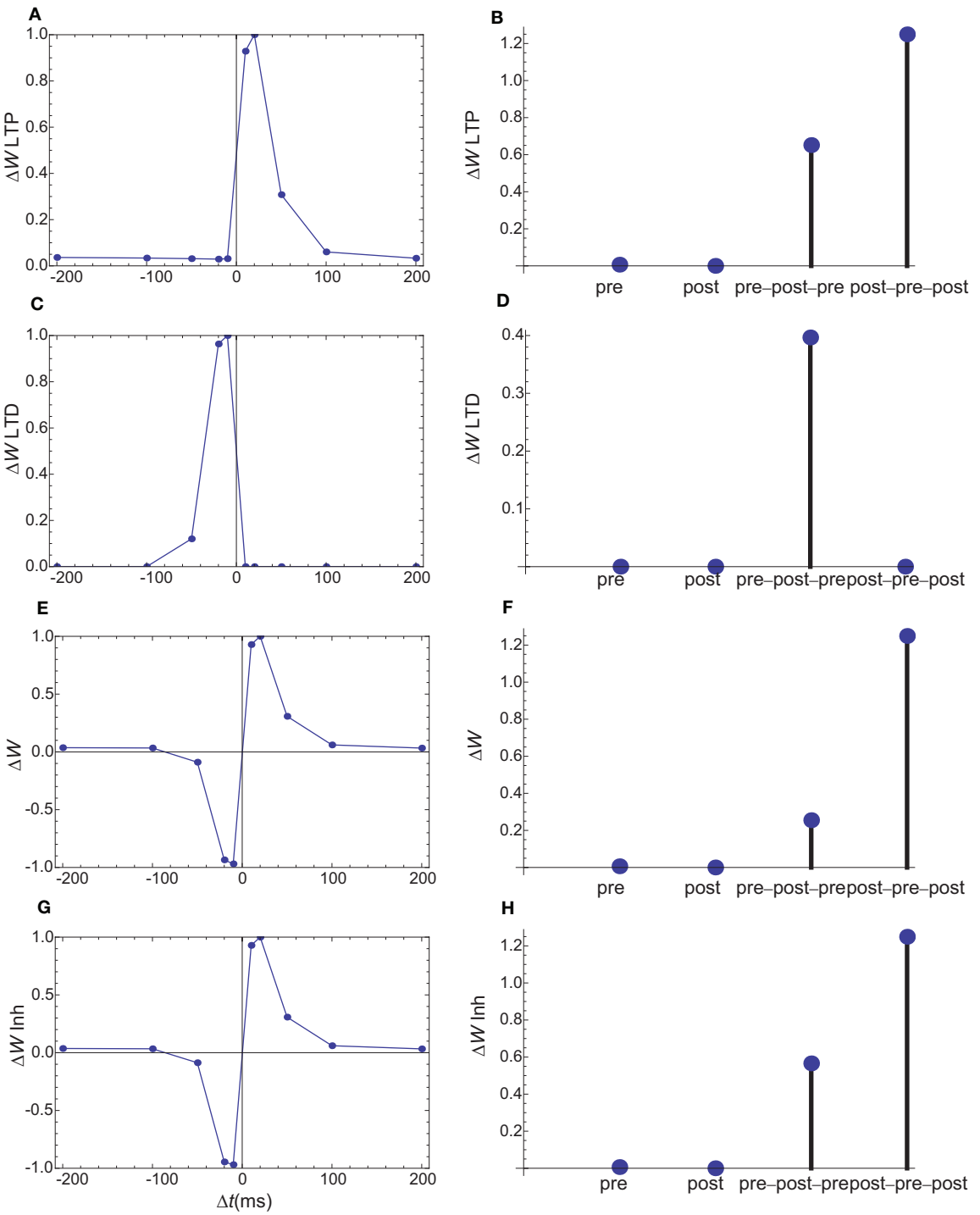

FIGURE 9 | Changes in synaptic weights (E,F) caused by LTP **(A,B)** and LTD **(C,D)** pathways for the second set of simulations, in which the IP3R current has a slower rise time. Columns as in **Figure 6**. **(G,H)** The changes in synaptic weights if the LTD pathway is inhibited by CaMKII. As in the first simulation set, the weight changes for single spike and spike doublets are similar to those observed. However, for the slower IP3R current the observed triplet behavior is obtained without an inhibition of the LTD pathway by CaMKII.

concentrations in a PSD-like compartment and near the base of the spine are very different for the first 30–50 ms, depending on the spine geometry.

Numerous additional gates can be added to the model. If activation of PKC by mGluR is included in the requirement for LTD, if PKC localized near either NMDARs or IP3Rs, the dynamic of the model is

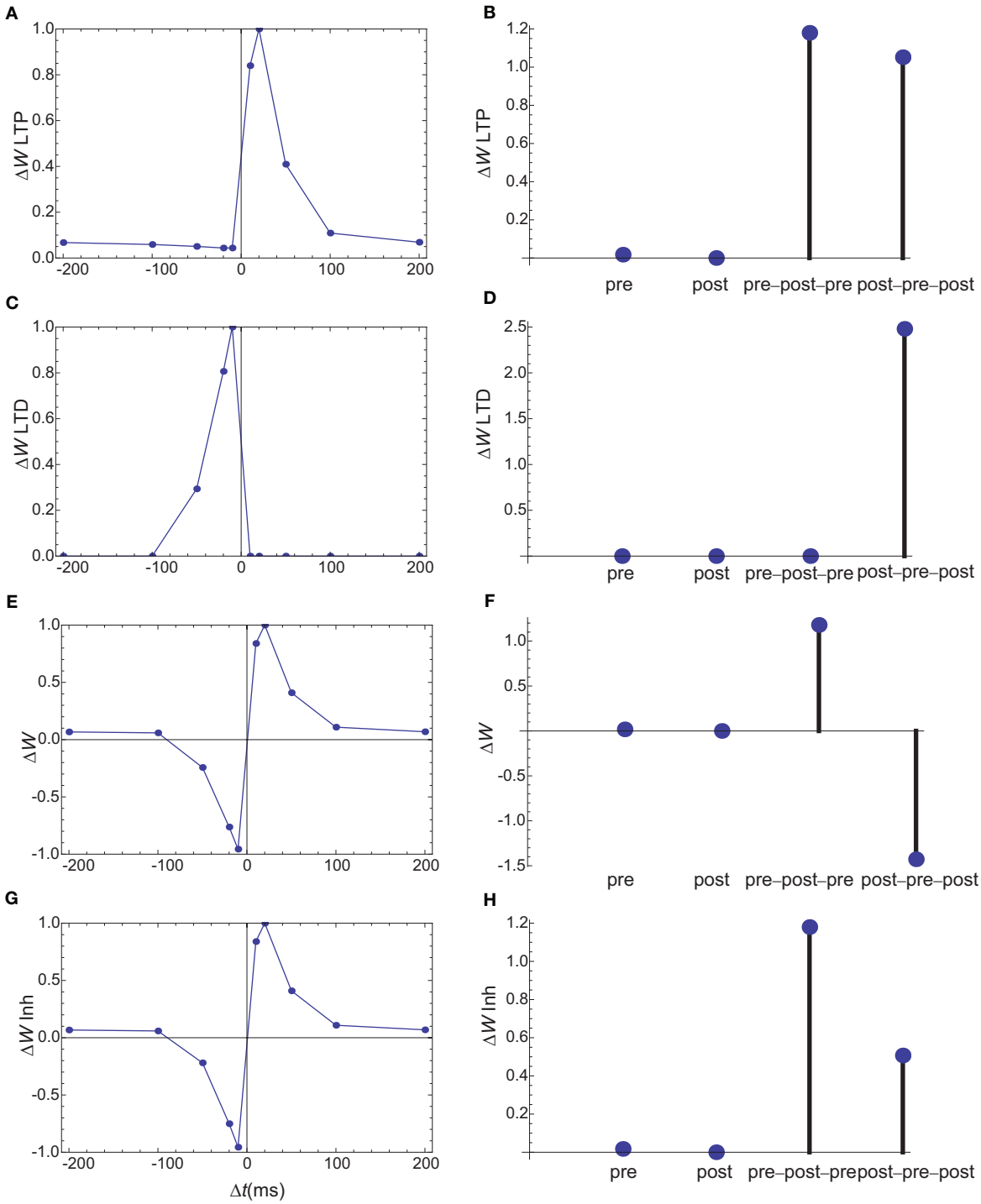

FIGURE 10 | Changes in synaptic weights (E,F) caused by LTP **(A,B)** and LTD **(C,D)** pathways for a third set of simulations, in which PDE is assumed to localize in the vicinity of NMDARs. Columns as in **Figure 6**. **(G,H)** The changes in synaptic weights if the LTD pathway is inhibited by CaMKII. The results for spike doublets are qualitatively similar to those obtained if PDE is assumed to localize near IP3Rs, however the results for spike triplets are qualitatively different. In the absence of inhibition of LTD by CaMKII, the 10-ms symmetric pre–post–pre triplet lead to potentiation, while the post–pre–post triplet leads to inhibition.

left practically unchanged. This is possibly supported by experimental observations showing that phosphorylation of Ser880 of GluR2 by PKC interferes with its anchoring in PSD. While qualitative aspects of the influence of neuromodulators (Seol et al., 2007) can be reproduced by the presented model, their exact effect on the STDP window might require additional gates or further tuning of the model's parameters.

Some previous experimental results could be reinterpreted in the light of a spatial model. Introducing different levels of the calcium buffer EGTA reduces the average calcium concentration in spines (Cho et al., 2001). However it does so in a heterogeneous manner: the larger the distance to the calcium source, the bigger the effect. Increasing EGTA concentration results in smaller and smaller domains which are left unaffected. Thus their result: increasing EGTA concentrations first affects LTP and subsequently LTD can be interpreted that a key enzyme in the LTP pathway is located further away from the calcium sources than those in the LTD pathway. In the case of the model proposed this enzyme is AC, which is located between NMDARs and VGCCs.

The exact location of different enzymes proposed in this model is oversimplified and highly speculative. The space of possible spatial distributions of the entire biochemical network is very large, and other distributions could as well fit multiple experimental observations. Therefore this study should mainly be seen as an incentive for experimental studies of relative localizations for multiple steps of the biochemical networks. Considering that calcium/calmodulin-dependent enzymes are mainly activated by the calcium source in the vicinity of which they are anchored is also an oversimplification. A full description of the interactions between calcium sources at different distances with different dynamics is computationally complex. A simulation environment which performs these computations and has the spatial precision required to characterize calcium nanodomains near the mouth of calcium channels is MCell (Stiles et al., 2001). It has been used to describe calcium dynamics (Franks et al., 2002) and calmodulin activation (Keller et al., 2008) in dendritic spines. It is an excellent simulation environment for future detailed models of synaptic plasticity, but it is currently limited by the knowledge of the parameters describing the direct and scaffold-mediated interactions in the biochemical cascades as well as knowledge of typical spatial distributions of different molecules.

ACKNOWLEDGMENT

NIH grant NEI R01EY016281 to E. Niebur.

REFERENCES

Artola, A., and Singer, W. (1993). Long-term depression of excitatory synaptic transmission and its relationship to long-term potentiation. *Trends Neurosci.* 16, 480–487.

Aslam, N., Kubota, Y., Wells, D., and Shouval, H. Z. (2009). Translational switch for long-term maintenance of synaptic plasticity. *Mol. Syst. Biol.* 5, 284.

Bennett, M. K., Erondu, N. E., and Kennedy, M. B. (1983). Purification and characterization of a calmodulin-dependent protein kinase that is highly concentrated in brain. *J. Biol. Chem.* 258, 12735–12744.

Bhalla, U. S. (2002). Biochemical signaling networks decode temporal patterns of synaptic input. *J. Comput. Neurosci.* 13, 49–62.

Bi, G. Q., and Poo, M. M. (1998). Synaptic modifications in cultured hippocampal neurons: dependence on spike timing, synaptic strength, and postsynaptic cell type. *J. Neurosci.* 18, 10464–10472.

Bradshaw, J. M., Kubota, Y., Meyer, T., and Schulman, H. (2003). An ultrasensitive Ca^{2+}/calmodulin-dependent protein kinase II-protein phosphatase 1 switch facilitates specificity in postsynaptic calcium signaling. *Proc. Natl. Acad. Sci. U.S.A.* 100, 10512–10517.

Cho, K., Aggleton, J. P., Brown, M. W., and Bashir, Z. I. (2001). An experimental test of the role of postsynaptic calcium levels in determining synaptic strength using perirhinal cortex of rat. *J. Physiol.* 532, 459–466.

Cormier, R. J., Greenwood, A. C., and Connor, J. A. (2001). Bidirectional synaptic plasticity correlated with the magnitude of dendritic calcium transients above a threshold. *J. Neurophysiol.* 85, 399–406.

Esteban, J. A., Shi, S. H., Wilson, C., Nuriya, M., Huganir, R. L., and Malinow, R. (2003). PKA phosphorylation of AMPA receptor subunits controls synaptic trafficking underlying plasticity. *Nat. Neurosci.* 6, 136–143.

Frankland, P. W., O'Brien, C., Ohno, M., Kirkwood, A., and Silva, A. J. (2001). Alpha-CaMKII-dependent plasticity in the cortex is required for permanent memory. *Nature* 411, 309–313.

Franks, K. M., Bartol, T. M. Jr., and Sejnowski, T. J. (2002). A Monte Carlo model reveals independent signaling at central glutamatergic synapses. *Biophys. J.* 83, 2333–2348.

Froemke, R. C., and Dan, Y. (2002). Spike-timing-dependent synaptic modification induced by natural spike trains. *Nature* 416, 433–438.

Glazewski, S., Chen, C. M., Silva, A., and Fox, K. (1996). Requirement for alpha-CaMKII in experience-dependent plasticity of the barrel cortex. *Science* 272, 421–423.

Graupner, M., and Brunel, N. (2007). STDP in a bistable synapse model based on CaMKII and associated signaling pathways. *PLoS Comput. Biol.* 3, e221. doi: 10.1371/journal.pcbi.0030221

Harris, K. M., and Stevens, J. K. (1989). Dendritic spines of CA 1 pyramidal cells in the rat hippocampus: serial electron microscopy with reference to their biophysical characteristics. *J. Neurosci.* 9, 2982–2997.

Hayer, A., and Bhalla, U. S. (2005). Molecular switches at the synapse emerge from receptor and kinase traffic. *PLoS Comput. Biol.* 1, 137–154. doi: 10.1371/journal.pcbi.0010020

Holmes, W. R. (1990). Is the function of dendritic spines to concentrate calcium? *Brain Res.* 519, 338–342.

Jahr, C. E., and Stevens, C. F. (1990). Voltage dependence of NMDA-activated macroscopic conductances predicted by single-channel kinetics. *J. Neurosci.* 10, 3178–3182.

Jordan, B. A., Fernholz, B. D., Boussac, M., Xu, C., Grigorean, G., Ziff, E. B., and Neubert, T. A. (2004). Identification and verification of novel rodent postsynaptic density proteins. *Mol. Cell Proteomics* 3, 857–871.

Karmarkar, U. R., and Buonomano, D. V. (2002). A model of spike-timing dependent plasticity: one or two coincidence detectors? *J. Neurophysiol.* 88, 507–513.

Keller, D. X., Franks, K. M., Bartol, T. M. Jr., and Sejnowski, T. J. (2008). Calmodulin activation by calcium transients in the postsynaptic density of dendritic spines. *PLoS ONE* 3, e2045. doi: 10.1371/journal.pone.0002045

Kennedy, M. B. (2000). Signal-processing machines at the postsynaptic density. *Science* 290, 750–754.

Lester, R. A., and Jahr, C. E. (1992). NMDA channel behavior depends on agonist affinity. *J. Neurosci.* 12, 635–643.

Lisman, J. (1989). A mechanism for the Hebb and the anti-Hebb processes underlying learning and memory. *Proc. Natl. Acad. Sci. U.S.A.* 86, 9574–9578.

Luby-Phelps, K., Hori, M., Phelps, J. M., and Won, D. (1995). Ca(2+)-regulated dynamic compartmentalization of calmodulin in living smooth muscle cells. *J. Biol. Chem.* 270, 21532–21538.

Markram, H., Lubke, J., Frotscher, M., and Sakmann, B. (1997). Regulation of synaptic efficacy by coincidence of postsynaptic APs and EPSPs. *Science* 275, 213–215.

Mihalas, S. (2009). *How Local are Calcium Messenger Cascades in Postsynaptic Spines?* SfN Program Number 135.12.

Nakamura, T., Barbara, J. G., Nakamura, K., and Ross, W. N. (1999). Synergistic release of Ca2+ from IP3-sensitive stores evoked by synaptic activation of mGluRs paired with backpropagating action potentials. *Neuron* 24, 727–737.

Naoki, H., Sakumura, Y., and Ishii, S. (2005). Local signaling with molecular diffusion as a decoder of Ca2+ signals in synaptic plasticity. *Mol. Syst. Biol.* 1, 2005.0027.

Naraghi, M., and Neher, E. (1997). Linearized buffered Ca2+ diffusion in microdomains and its implications for calculation of [Ca2+] at the mouth of a calcium channel. *J. Neurosci.* 17, 6961–6973.

Nelson, S. B., and Turrigiano, G. G. (2008). Strength through diversity. *Neuron* 60, 477–482.

Olwin, B. B., and Storm, D. R. (1985). Calcium binding to complexes of calmodulin and calmodulin binding proteins. *Biochemistry* 24, 8081–8086.

Pepke, S., Kinzer-Ursem, T., Mihalas, S., and Kennedy, M. B. (2010). A dynamic model of interactions of Ca2+, calmodulin, and catalytic subunits of Ca2+/calmodulin-dependent protein kinase II. *PLoS Comput. Biol.* 6, e1000675. doi: 10.1371/journal.pcbi.1000675

Rubin, J. E., Gerkin, R. C., Bi, G. Q., and Chow, C. C. (2005). Calcium time course as a signal for spike-timing-dependent plasticity. *J. Neurophysiol.* 93, 2600–2613.

Seol, G. H., Ziburkus, J., Huang, S., Song, L., Kim, I. T., Takamiya, K., Huganir, R. L., Lee, H. K., and Kirkwood, A. (2007). Neuromodulators control the polarity of spike-timing-dependent synaptic plasticity. *Neuron* 55, 919–929.

Shifman, J. M., Choi, M. H., Mihalas, S., Mayo, S. L., and Kennedy, M. B. (2006). Ca^{2+}/calmodulin-dependent protein kinase II (CaMKII) is activated by calmodulin with two bound calciums. *Proc. Natl. Acad. Sci. U.S.A.* 103, 13968–13973.

Sjostrom, P. J., Turrigiano, G. G., and Nelson, S. B. (2003). Neocortical LTD via coincident activation of presynaptic NMDA and cannabinoid receptors. *Neuron* 39, 641–654.

Song, I., and Huganir, R. L. (2002). Regulation of AMPA receptors during synaptic plasticity. *Trends Neurosci.* 25, 578–588.

Stiles, J. S., Bartol T. M. Jr., Salpeter, M. M., Salpeter, E. E., and Sejnowski, T. J. (2001). *Synaptic Variability: New Insights from Reconstructions and Monte Carlo Simulations with MCell.* Baltimore, MD: Johns Hopkins University Press.

Urakubo, H., Honda, M., Froemke, R. C., and Kuroda, S. (2008). Requirement of an allosteric kinetics of NMDA receptors for spike timing-dependent plasticity. *J. Neurosci.* 28, 3310–3323.

Wang, H. X., Gerkin, R. C., Nauen, D. W., and Bi, G. Q. (2005). Coactivation and timing-dependent integration of synaptic potentiation and depression. *Nat. Neurosci.* 8, 187–193.

Yang, S. N., Tang, Y. G., and Zucker, R. S. (1999). Selective induction of LTP and LTD by postsynaptic [Ca2+]i elevation. *J. Neurophysiol.* 81, 781–787.

Yang, Y., Wang, X. B., Frerking, M., and Zhou, Q. (2008). Delivery of AMPA receptors to perisynaptic sites precedes the full expression of long-term potentiation. *Proc. Natl. Acad. Sci. U.S.A.* 105, 11388–11393.

Zhong, H., Sia, G. M., Sato, T. R., Gray, N. W., Mao, T., Khuchua, Z., Huganir, R. L., and Svoboda, K. (2009). Subcellular dynamics of type II PKA in neurons. *Neuron* 62, 363–374.

Conflict of Interest Statement: The author declares that the research was conducted in the absence of any commercial or financial relationships that could be construed as a potential conflict of interest.

Received: 16 February 2010; accepted: 22 December 2010; published online: 13 January 2011.

Citation: Mihalas S (2011) Calcium messenger heterogeneity: a possible signal for spike-timing-dependent plasticity. Front. Comput. Neurosci. ***4****:158. doi: 10.3389/fncom.2010.00158*

APPENDIX

CALCIUM ENTRY

The time dependence of backpropagating action potentials is assumed to be

$$V_{\mathrm{AP1}}(t,t_0) = H(t-t_0)\times V_{\mathrm{AP0}}\times\left(\mathrm{e}^{-\frac{t-t0}{\tau_{\mathrm{APd}}}} - \mathrm{e}^{-\frac{t-t0}{\tau_{\mathrm{APr}}}}\right) \quad (1)$$

where:

$H(x)$ represents the Heaviside step function which is 0 if $x \le 0$ and 1 if $x > 0$

$\tau_{\mathrm{APd}} = 5\ \mathrm{ms}$

$\tau_{\mathrm{APr}} = 0.5\ \mathrm{ms}$

V_{AP0} = 86.1 mV which corresponds to a maximal depolarization of 60 mV.

Excitatory postsynaptic potential are assumed to follow AMPAR dynamics

$$V_{\mathrm{EPSP1}}(t,t_0) = H(t-t_0)\times V_{\mathrm{EPSP0}}\times\left(\mathrm{e}^{-\frac{t-t0}{\tau_{\mathrm{EPSPd}}}} - \mathrm{e}^{-\frac{t-t0}{\tau_{\mathrm{EPSPr}}}}\right) \quad (2)$$

where:

$\tau_{\mathrm{EPSPd}} = 5\,\mathrm{ms}$

$\tau_{\mathrm{EPSPr}} = 0.5\,\mathrm{ms}$

V_{EPSP0} = 14.35 mV which corresponds to a maximal depolarization of 10 mV.

Membrane potential

$$V_{\mathrm{m}}(t) = V_{\mathrm{rest}} + \sum_i V_{\mathrm{EPSP1}}\left(t,t_{\mathrm{prei}}\right) + \sum_j V_{\mathrm{AP1}}\left(t,t_{\mathrm{postj}}\right) \quad (3)$$

where:

$V_{\mathrm{rest}} = -70\,\mathrm{mV}$

Glutamate diffusion

$$\mathrm{Glu}(t) = \mathrm{Glu}_T \sum_i D2\delta(t,t_i,r,D)\times\exp\left(-(t-t_t)/\tau_{\mathrm{Glu}}\right) \quad (4)$$

where:

τ_{Glu} = 1.8 ms can be obtained by considering the concentration of glutamate reuptake molecules to be 0.1 mM

Glu_T was estimated considering 3000 glutamate molecules released in a cleft 15 nm wide and

$$D2\delta(t,t_0,r,D) = H(t-t_0)\frac{1}{4\pi D\times(t-t_0)}\times\exp\left(-\frac{r^2}{4\times D\times(t-t_0)}\right) \quad (5)$$

where:

D = 0.3 μm²/ms is the glutamate diffusion constant

r = 0.1 μm is the average distance for release site to receptors for a circular PSD of 0.3 μm diameter

A five state model was used for NMDAR with two independent glutamate binding sites with the transition rates:

Ro = 0.0465/ms opening rate

Rc = 0.0916/ms closing rate

Rd = 0.0084/ms desensitization rate

Rr = 0.0018/ms resensitization rate

Ru = 0.0047/ms unbinding rate of glutamate

Rb = 5/(mM*ms) glutamate binding rate

The opening of NMDAR under different stimulation protocols is computed numerically in Mathematica, obtaining the time dependence of the open state: NMDAO(t).

Magnesium-dependent blocking of NMDARs:

$$B[V] = 1/\left(1+\exp(-0.062\times V)\times[\mathrm{Mg}]/3.57\right) \quad (6)$$

where:

[Mg] = 1.5 mM

Calcium current through NMDARs:

$$\mathrm{JNMDA}(t) = \mathrm{JN}\times\mathrm{NMDAO}(t)\times\mathrm{B}(Vm(t)) \times\frac{Vm(t)}{VF2}\times\frac{\exp(-Vm(t)/VF2)}{(1-\exp(-Vm(t)/VF2))} \quad (7)$$

where:

$VF2 = RT/2F$ = 13.2 mV

JN is a normalization constant chosen such that the maximal calcium current through NMDARs in a pre–post experiment is 1.

Calcium current though L-type VGCCs:

$$\mathrm{JVGCC}(t) = -\mathrm{JV}\times m(t)^3\times h(t)\times\frac{V_m(t)}{1-\exp(V_m(t)/VF2)} \quad (8)$$

where the time dependence of the gates m and h is numerically solved from:

$$m'(t) = 1/3.6\times\left(1/\left(1+\exp\left(-(Vm(t)+37)\right)\right)-m(t)\right) \quad (9)$$

$$h'(t) = 1/29\times\left(1/\left(1+\exp\left((Vm(t)+41)/0.5\right)\right)-h(t)\right) \quad (10)$$

JV is a normalization constant chosen such that the maximal calcium current through VGCCs in a pre–post experiment is 1.

Activation of mGluRs:

$$\mathrm{mGluR1}(t,t_0+\tau_{\mathrm{mGluR}}) = H(t-t_0)\times\mathrm{mGluR0}\times\left(\mathrm{e}^{-\frac{t-t0}{\tau_{\mathrm{mGluRd}}}} - \mathrm{e}^{-\frac{t-t0}{\tau_{\mathrm{mGluRr}}}}\right) \quad (11)$$

where:

$\tau_{\mathrm{mGluRd}} = 100\ \mathrm{ms}$

$\tau_{\mathrm{mGluR}} = 10\ \mathrm{ms}$

$\tau_{\mathrm{mGluRr}} = 10\ \mathrm{ms}$

mGluR0 = 1.435 which corresponds to a maximal depolarization of 1.

To quantify the influence of the time scale of the calcium current through the IP3R, an second set of simulations was performed using $\tau_{\mathrm{mGluRr}} = 99$ ms (with a corresponding change in mGluR0 = 270 such that the maximal activation is 1) which produces a considerably slower calcium input.

$$\mathrm{mGluR}(t) = \sum_i \mathrm{mGluR1}\left(t, t_{\mathrm{prei}}\right) \tag{12}$$

Calcium currents through IP3-dependent channels are assumed to be proportional to mGluR activation.

TRANSIENT ENZYME ACTIVATION

Calcium-dependent enzymes are assumed to be activated only by the type of calcium channel in the vicinity of which they are localized. They have a transient activation as the off rates of calcium from the lower affinity binding sites of calmodulin is very rapid.

$$\begin{aligned}\mathrm{PDE}'(t) = {} & \mathrm{kon}_{\mathrm{PDE}} \times \left(\mathrm{PDE}t - \mathrm{PDE}(t)\right) \times \mathrm{JIP3}(t)^n \\ & - \mathrm{koff}_{\mathrm{PDE}} \times \mathrm{PDE}(t)\end{aligned} \tag{13}$$

$$\begin{aligned}\mathrm{AC}'(t) = {} & \mathrm{kon}_{\mathrm{AC}} \times \left(\mathrm{AC}t - \mathrm{AC}(t)\right) \\ & \times \left(\mathrm{JVGCC}(t)^n + r_{\mathrm{N}} \times \mathrm{JNMDA}(t)^n\right) - \mathrm{koff}_{\mathrm{AC}} \times \mathrm{AC}(t)\end{aligned} \tag{14}$$

$$\begin{aligned}\mathrm{CaN}'(t) = {} & \mathrm{kon}_{\mathrm{CaN}} \times \left(\mathrm{CaN}t - \mathrm{CaN}(t)\right) \times \mathrm{JVGCC}(t)^n \\ & - \mathrm{koff}_{\mathrm{CaN}} \times \mathrm{CaN}(t)\end{aligned} \tag{15}$$

$$\begin{aligned}\mathrm{KIIa}'(t) = {} & \mathrm{kon}_{\mathrm{KII}} \times \left(\mathrm{KIIt} - \mathrm{KIIa}(t)\right) \times \mathrm{JNMDA}(t)^n \\ & - \mathrm{koff}_{\mathrm{KII}} \times \mathrm{KIIa}(t)\end{aligned} \tag{16}$$

$$\begin{aligned}\mathrm{cAMP}'(t) = {} & \mathrm{kAC} \times \mathrm{AC}(t) - \mathrm{kPDE} \times \mathrm{PDE}(t) \times \mathrm{cAMP}(t) \\ & + \mathrm{k}_{\mathrm{cAMPp}} - \mathrm{k}_{\mathrm{cAMPd}} \times \mathrm{cAMP}(t)\end{aligned} \tag{17}$$

All the total enzyme concentrations are normalized. Calmodulin has two calcium binding sites of relatively high affinity and slow kinetics, and two calcium binding sites of low affinity and fast kinetics. Assuming that calmodulin with two calcium bound can temporarily bind to a target, thus immobilizing it, and assuming the requirement of calcium-loaded calmodulin for full enzyme activation, n is considered to be 2. The constants koff correspond to the first unbinding of calcium from the calmodulin–enzyme complex. It is taken to be 100/s, corresponding to typical time scale for the calcium ions in spines, however the value is not critical to the model as long as it is faster than the calcium currents through NMDA and IP3 channels. If saturation is not reached, the on rates are scaling parameters in the model, and have identical effects to higher enzyme activities. They are chosen to be 100/s for all enzymes except PDE, where an on rate of 40/s was used due to the slower calcium transients released from internal stores. The on rate for PDE is one of the two tuned parameters in the model. The on rates are measured in units of s^{-1}, as the calcium currents are normalized.

For the second set of simulations, in which the calcium current through the IP3R is slowed by a factor of 10, the on rate for PDE was chosen to be 12.65/s, a decrease by a $\sqrt{10}$ from the first set of simulations. This choice maintains the constraint that presynaptic stimulation alone has only modest effects on the synaptic weight.

The third set of simulations does not include internal calcium stores, and PDE is assumed to be localized in the vicinity of the NMDAR, and the on rate of PDE for calcium is retuned. A value of 800/s fits the constraint that presynaptic stimulation alone has only modest effects on the synaptic weight, and does reproduce the typical shape of the STDP caused by spike doublets.

For cAMP, the rate of basal decay $k_{\mathrm{cAMPd}} = 10$/s is a critical parameter. If the inactivation of AC is faster, it is the primary determinant of the length of LTD window in STDP. The basal cAMP production rate is constrained by the resting cAMP concentration which is assumed to be 100 nM. Adenylyl cyclase activity (kAC) is a scaling parameter and chosen to be100/s. PDE activity (kPDE) and the ratio of how well NMDARs activate AC relative to VGCCs are together constrained by the requirement that presynaptic stimulation alone produces little synaptic weight change. The value for kPDE was chosen to be 100/s and r_{N} was chosen to be 1.

PROLONGED ENZYME ACTIVATION

The total changes in enzymes which maintain their activity for periods of time significantly longer than the calcium transients are estimated as the integral of production minus consumption during the transient period.

PKA activation is assumed to be proportional to the integral of the cAMP transient relative to its resting concentration. In all simulations, following any of the stimulations protocols studied, the change in PKA activation was positive.

$$\Delta\mathrm{PKA} \propto \int \left(\mathrm{cAMP}(t) - \mathrm{cAMPr}\right) dt \tag{18}$$

This activation (Eq. 18) can be obtained from the mass action law assuming linear activation on cAMP

$$\mathrm{PKA}'(t) = k_{\mathrm{actPKA}} \times \mathrm{cAMP}(t) - \mathrm{k}_{\mathrm{metPKA}} \times \mathrm{PKA}(t)$$

under the assumption that during the stimulation the instantaneous PKA concentration [PKA(t)] changes only little from its basal one ($\mathrm{PKAr} = k_{\mathrm{actPKA}} \times \mathrm{cAMPr}/k_{\mathrm{metPKA}}$). The activation constant k_{actPKA} becomes a normalization constant, as only relative activation levels are discussed.

Prolonged phosphatase activity, for which PP1 is considered to be the main contributor, is assumed to be proportional to the rectified difference between total CaN and PKA activations.

$$\Delta\mathrm{PP1} \propto \left\lfloor \int \mathrm{CaN}(t)dt - k_{\mathrm{PKA}} \times \Delta\mathrm{PKA} \right\rfloor_+ \tag{19}$$

$\lfloor \cdot \rfloor_+$ represents rectification. The value of kPKA = 0.1 is an important parameter in the model and was tuned such that postsynaptic neuron firing alone does not produce a change in synaptic weight. The equation for the prolonged phosphatase activity (Eq. 19) can be obtained by assuming a very high affinity of phosphorylated Inhibitor 1 for PP1 (which results in $\mathrm{PP1}(t) \approx \left\lfloor \mathrm{PP1}_{\mathrm{T}} - \mathrm{Inh1}_{\mathrm{T}}^{\mathrm{P}}(t) \right\rfloor_+$), an initial total concentration of phosphorylated Inhibitor 1,

$\mathrm{Inh1}_{\mathrm{T}}^{\mathrm{P}}(0)$, equal to the total PP1 concentration $\mathrm{PP1}_{\mathrm{T}}$ (which results in $\mathrm{PP1}(t) \approx \left\lfloor -\left(\mathrm{Inh1}_{\mathrm{T}}^{\mathrm{P}}(t) - \mathrm{Inh1}_{\mathrm{T}}^{\mathrm{P}}(0)\right)\right\rfloor_{+}$) and a dynamic of $\mathrm{Inh1}_{\mathrm{T}}^{\mathrm{P}}(t)$ which leaves both the unphosphorylated Inhibitor 1 as well as the total phosphorylated Inhibitor 1 at values not hugely different from the resting ones (which results in $\mathrm{Inh1}_{\mathrm{T}}^{\mathrm{P}}(t_{\mathrm{end}}) - \mathrm{Inh1}_{\mathrm{T}}^{\mathrm{P}}(0) = \mathrm{k}_{\mathrm{PKA}} \times \Delta\mathrm{PKA} - \int \mathrm{CaN}(t)\,dt$).

Calcium-independent activation of CaMKII is assumed to be the integral of the square of the instantaneous calcium dependent activity.

$$\Delta\mathrm{CaMKIIp} \propto \int \mathrm{KIIa}(t)^2\,dt \tag{20}$$

The equation for the prolonged CaMKII activation (Eq. 20) can be obtained from the dynamical equation

$$\mathrm{CaMKIIp}'(t) = \mathrm{k}_{\mathrm{actKII}} \times \mathrm{KIIa}(t)^2 + k_{\mathrm{actKIIrest}} - k_{\mathrm{metKII}} \times \mathrm{CaMKIIp}(t)$$

under the assumptions that two neighboring CaMKII subunits in a holoenzyme need to be active for the phosphorylation to happen, that the phosphorylation fraction is very low, and it does not change drastically from the resting value, which is stationary ($\mathrm{CaMKIIp}(0) = k_{\mathrm{actKIIrest}}/k_{\mathrm{metKII}}$).

SYNAPTIC WEIGHT CHANGES

The changes in synaptic weight due to LTP and LTD are assumed to be independent and additive.

The change in synaptic weight caused by LTP is assumed to be the result of two phosphorylation events, one produced by PKA and the other by CaMKII.

$$\Delta\mathrm{W}_{\mathrm{LTP}} \propto \Delta\mathrm{PKA} \times \Delta\mathrm{CaMKIIp} \tag{21}$$

Two models are used for LTD. In the first, the change in weight caused by LTD is assumed to be the result of a dephosphorylation event produced by PP1.

$$\Delta\mathrm{W}_{\mathrm{LTD}} \propto \Delta\mathrm{PP1} \tag{22}$$

In the second model the dephosphorylation event produced by PP1 is assumed to be inhibited by CaMKII in a divisive manner. The value of I_{CaMKIIp} was chosen as the mean CaMKII activation in spike doublets STDP protocols with the samplings presented in **Figures 6 and 7**.

$$\Delta\mathrm{W}_{\mathrm{LTD}} \propto \Delta\mathrm{PP1} \times \frac{1}{1 + \Delta\mathrm{CaMKIIp}/\mathrm{I}_{\mathrm{CaMKIIp}}} \tag{23}$$

In each model, both the LTP and LTD components are normalized to the maximal value obtained in a spike doublet STDP protocol. The combined change in synaptic weight is obtained by summing the normalized LTP and LTD components.

frontiers in
SYNAPTIC NEUROSCIENCE

ORIGINAL RESEARCH ARTICLE
published: 02 July 2010
doi: 10.3389/fnsyn.2010.00023

Cortico-striatal spike-timing dependent plasticity after activation of subcortical pathways

Jan M. Schulz[1]*, Peter Redgrave[2] and John N. J. Reynolds[1]

[1] *Department of Anatomy and Structural Biology, School of Medical Sciences, University of Otago, Dunedin, New Zealand*
[2] *Department of Psychology, University of Sheffield, Western Bank, Sheffield, UK*

Edited by:
Henry Markram, Ecole Polytechnique Federale de Lausanne, Switzerland

Reviewed by:
Guo-Qiang Bi, University of Pittsburgh, USA
Henry Markram, Ecole Polytechnique Federale de Lausanne, Switzerland

***Correspondence:**
Jan M. Schulz, Department of Anatomy and Structural Biology, University of Otago, P.O. Box 913, Dunedin 9054, New Zealand.
e-mail: jan.schulz@anatomy.otago.ac.nz

Cortico-striatal spike-timing dependent plasticity (STDP) is modulated by dopamine *in vitro*. The present study investigated STDP *in vivo* using alternative procedures for modulating dopaminergic inputs. Postsynaptic potentials (PSP) were evoked in intracellularly recorded spiny neurons by electrical stimulation of the contralateral motor cortex. PSPs often consisted of up to three distinct components, likely representing distinct cortico-striatal pathways. After baseline recording, bicuculline (BIC) was ejected into the superior colliculus (SC) to disinhibit visual pathways to the dopamine cells and striatum. Repetitive cortical stimulation (~60; 0.2 Hz) was then paired with postsynaptic spike discharge induced by an intracellular current pulse, with each pairing followed 250 ms later by a light flash to the contralateral eye ($n = 13$). Changes in PSPs, measured as the maximal slope normalized to 5-min pre, ranged from potentiation (~120%) to depression (~80%). The determining factor was the relative timing between PSP components and spike: PSP components coinciding or closely following the spike tended towards potentiation, whereas PSP components preceding the spike were depressed. Importantly, STDP was only seen in experiments with successful BIC-mediated disinhibition ($n = 10$). Cortico-striatal high-frequency stimulation (50 pulses at 100 Hz) followed 100 ms later by a light flash did not induce more robust synaptic plasticity ($n = 9$). However, an elevated post-light spike rate correlated with depression across plasticity protocols ($R^2 = 0.55$, $p = 0.009$, $n = 11$ active neurons). These results confirm that the direction of cortico-striatal plasticity is determined by the timing of pre- and postsynaptic activity and that synaptic modification is dependent on the activation of additional subcortical inputs.

Keywords: STDP, striatum, superior colliculus, spiny projection neuron, HFS, *in vivo*, intracellular, dopamine

INTRODUCTION

The striatum, the main input nucleus of the basal ganglia, receives sensorimotor, cognitive, and motivational information from almost all cortical areas (McGeorge and Faull, 1989) and several thalamic nuclei (Erro et al., 2002). In addition, evaluative inputs from dopaminergic neurons in the substantia nigra pars compacta (Redgrave et al., 2008; Wickens et al., 2007a) and glutamatergic neurons in the thalamic intralaminar nuclei (Minamimoto et al., 2005; Schulz et al., 2009) signal the saliency of ongoing sensory events to broad areas of the striatum. The convergence of these different sets of inputs places the striatum in an ideal position for learning guided by experience. Based on anatomy and physiology, it is likely that the underlying mechanisms are dopamine-dependent (Wickens et al., 2007a,b). Thus, synaptic plasticity in the striatum is strongly modulated by dopamine (Wickens et al., 1996; Reynolds and Wickens, 2000; Kerr and Wickens, 2001; Pawlak and Kerr, 2008; Shen et al., 2008). Furthermore, the stimulation of the substantia nigra in intracranial self-stimulating experiments is behaviorally reinforcing and the same stimulation parameters induce robust potentiation of cortico-striatal synapses (Reynolds et al., 2001). These observations indicate that dopamine is a critical ingredient for modulating cortico-striatal neurotransmission.

A major problem in investigating the functional role of dopamine signals for synaptic plasticity is that it has been technically challenging to manipulate its levels in a physiological meaningful way. In the present study, therefore, we deployed procedures that have been shown previously to evoke the release of dopamine by more natural means (Coizet et al., 2003; Comoli et al., 2003; Dommett et al., 2005). In urethane anesthetized rats, disinhibition of the superior colliculus (SC) by a local injection of the $GABA_A$ antagonist bicuculline (BIC) enables visual-evoked activation of dopaminergic neurons. Thus, a visual event can activate dopaminergic neurons via a subcortical pathway from retinal ganglion cells through the SC. In parallel, a tecto-thalamo-striatal pathway mediates excitatory inputs that rapidly depolarize spiny projection neurons (SPN), the principal neurons of the striatum, in response to the same sensory event (Schulz et al., 2009). Therefore, for the first time it was possible to control these subcortical inputs to the striatum using a physiological stimulus during intracellular recordings from SPNs.

This study investigated how visual-evoked inputs from tecto-striatal pathways affected the outcome of conventional plasticity protocols on the cortico-striatal synapse. The visual stimulus was delivered at a short, physiological meaningful delay as suggested by theoretical work (Izhikevich, 2007) and our previous experience (Reynolds et al., 2001). First, we measured cortico-striatal

synaptic efficacy after cortico-striatal high-frequency stimulation (HFS) paired with visual stimulation. Previously, we reported that HFS induced synaptic depression *in vivo* that could be blocked or reversed by concomitant electrical stimulation of dopaminergic neurons (Reynolds and Wickens, 2000). In this study, we tested the effects of a more physiological activation of afferent networks. Next, a spike-timing dependent plasticity (STDP) protocol involving pairing of single pre- and postsynaptic spikes in the cortico-striatal pathway was tested in combination with visual activation. Although STDP has been demonstrated at the cortico-striatal synapse *in vitro*, there is controversy as to whether a pre-post pairing protocol induces depression or potentiation (Fino et al., 2005; Pawlak and Kerr, 2008). The present study aimed at clarifying this issue in an intact *in vivo* model.

MATERIALS AND METHODS

EXPERIMENTAL PREPARATION

Every effort was made to minimize the pain and discomfort of the experimental animals used in this study, in accordance with approvals granted by the University of Otago Animal Ethics Committee. Hundred and forty male Long-Evans rats (230–410 g) were anesthetized with urethane (1.4–1.9 g/kg i.p.; Biolab Ltd., Auckland, New Zealand), supplemented with additional urethane (0.2 g/kg) one to two-hourly, as required. The core temperature was maintained at 36°C by a homoeothermic blanket. All wounds and pressure points were infiltrated with a long-acting local anesthetic (bupivacaine, 0.5%). The head was fixed in a stereotaxic frame and surgery was performed as previously described (Schulz et al., 2009). Briefly, a hole was drilled above the left SC, around 6.5 mm posterior bregma (AP −6.5) and 1.4 mm mediolateral from the midline (ML +1.4), to accept a pipette pulled from pre-calibrated glass capillaries (volume 5 µl, diameter 1.0 mm; Modulohm I/S, Denmark) and filled with BIC (0.01% in saline; Sigma). The BIC ejection pipette was lowered 4.1 mm from brain surface into the SC deep layers and secured in place with dental cement. To document the restoration of visual sensitivity enabled by BIC (Coizet et al., 2003; Dommett et al., 2005), the local field potential (LFP) was routinely recorded in the SC deep layers through an attached recording electrode. Above the right motor cortex, a hole was drilled around AP +2.0/ML −1.8 to accept concentric electrodes (NEX-100, Rhodes, USA). Stimulating electrodes were secured in place at a depth of 1.8 to 2 mm. A craniotomy from AP −2.0 to +2.5 and ML +0.5 to +4.0 was made to provide access to the left medial striatum.

INTRACELLULAR RECORDINGS

Intracellular records were made using micropipettes pulled from 3.0-mm diameter glass (Harvard Apparatus, UK) and filled with 1 M K-acetate (45 to 95-MΩ resistance), in some cases containing 2% biocytin. The micropipette was advanced through the striatum from initial penetrations between AP −0.1 to +1.6 and ML +2.6 to +4.0, until a stable recording was obtained from a putative SPN. These coordinates were chosen to maximize the chance that recorded neurons would receive direct innervation from the contralateral motor cortex that was stimulated (Wilson, 1987; McGeorge and Faull, 1989). All electrophysiologically identified SPNs exhibited: (i) fluctuations of >7 mV in amplitude between a hyperpolarized Down state and a depolarized Up state (Wilson and Kawaguchi, 1996), (ii) a Down state membrane potential more negative than −70 mV, and (iii) a slow ramp-like depolarization in response to a just suprathreshold current pulse (see **Figure 1**), as typical for these neurons (Nisenbaum and Wilson, 1995; Mahon et al., 2000; Reynolds and Wickens, 2000). Current-voltage relations were obtained by injecting hyperpolarizing and depolarizing current pulses through the micropipette during the neuron's Down state, using an Axoclamp-2B amplifier (Axon Instruments Inc., Union City, CA, USA) configured in current-clamp mode. Input resistance was determined from the slope of a regression line fitted to four membrane potentials produced by a series of subthreshold current pulses (−0.2, 0, +0.2, +0.4 nA).

STIMULATION OF AFFERENT PATHWAYS

Biphasic rectangular stimulus pulses of 100 to 200-µs duration were applied to the contralateral motor cortex to evoke cortico-striatal postsynaptic potentials (PSPs) in SPNs. Stimulus intensity (<1 mA) and width were chosen to produce a PSP of 5 to 10 mV in amplitude. Except for group 3 (see below), test stimuli were applied during a recorded neuron's Down state. Up to Down state transitions were detected using a locally-constructed threshold discriminator (Reynolds and Wickens, 2003). Detected transitions were used to trigger data acquisition and cortical stimulation after a 25-ms delay. All waveform data were digitized at 10 kHz by a Digidata 1322A (Axon Instruments Inc.), displayed using pClamp 10 software (Axon Instruments Inc.) and stored to disk. The baseline recording consisted of at least 50 responses to test stimuli at 0.1 Hz (group 1 and 2) or 0.2 Hz (group 3 and 4) recorded over 15 min ($n = 68$ neurons recorded over 2 years). Following baseline recording, BIC (200–300 nl) was ejected into the SC at a rate of ~200 nl/min. Striatal membrane potential activity was recorded directly after the BIC ejection, before cortical stimulation was paired repetitively with a light stimulus (1500 mcd, 10-ms duration) from a white LED positioned <3 cm directly in front of the animal's right eye. After the plasticity protocol, single pulse stimulation was resumed (0.1 or 0.2 Hz).

PLASTICITY PROTOCOLS

Four different pairing protocols were used (**Figure 2**). In experiments involving HFS, stimulation was always triggered at Down state membrane potentials. Because of BIC-induced loss of EEG slow-wave activity (Schulz et al., 2009), the inter-HFS train intervals without data acquisition varied from 10 to 60 s. Therefore, the period of the plasticity protocol (of ~5 min) is not included in the time-resolved membrane potential distribution in **Figure 3**.

Group 1: HFS + spikes then light

High-frequency stimulation (six trains of 50 pulses at 100 Hz) of the cortex was paired with a just suprathreshold depolarizing current pulse (0.5 to 0.9 nA, 570 ms). Each train was followed by a light stimulus at a delay of 100 ms after the cessation of the HFS.

Group 2: HFS then light + spikes

During the HFS protocol (six trains of 50 pulses at 100 Hz), the suprathreshold current step (0.5 to 0.9 nA, 570 ms) was shifted to 90 ms after the light flash to ensure action potential discharge during the visual-evoked inputs.

Group 3: single stimulus then light

Single cortical stimulations were paired with light flashes at a delay of 250 ms (113 to 173 pulses, 0.2 Hz). To aid occasional spike discharge in response to the stimulation, constant positive current was applied in two experiments. In contrast to all other groups, test stimuli before and after the plasticity protocol were applied at a fixed interval of 5-s independent of the neuron's membrane potential.

Group 4: pre-post pairing then light

Single cortical stimulations (60 to 108 pulses, 0.2 Hz) were paired with a short intracellular current step (0.8 to 2 nA, 5 to 10 ms) at a delay of 5 to 10 ms, ideally inducing one action potential, and followed by a light flash at 250 ms.

In three pre-post pairing experiments, BIC was ejected outside the SC ($n = 1$) or not ejected at all ($n = 2$). These experiments were excluded from group 4 ($n = 10$) and were used as a control for BIC-mediated visual responsiveness of subcortical visual pathways. In all other experiments, LFP recordings from the SC confirmed visual activation post BIC.

HISTOLOGY

In all experiments except for one rejected from group 4, tips of BIC ejection pipettes were verified to be within the SC using light microscopy of unstained sections or sections stained with cresyl violet (0.1%). During recordings of at least 40 min, neurons were passively filled with biocytin. Vibratome sections (50 μm) containing biocytin-filled neurons were processed using standard histological procedures (Horikawa and Armstrong, 1988) and labeled cells were identified by fluorescent microscopy.

DATA ANALYSIS

Data was analyzed offline using MATLAB 7.1 with Signal Processing 6.4 and Statistics 5.1 Toolboxes. Axon binary files were imported into MATLAB using a function written by John Bender (http://www.mathworks.de/matlabcentral/fileexchange/).

Assessment of membrane potential fluctuations

The membrane potential of all neurons at each time point was corrected offline by the estimated tip potential present at the time of recording. The distribution of the membrane potentials was assessed by all-amplitude histograms of intracellular recording over single trials of 5 to 10-s duration. In order to visualize changes in membrane potential fluctuations over time, histograms of successive trials were concatenated and plotted as color-coded distributions over time, where each bin on the *x*-axis represents intervals, depending on trial length, of either 5 or 10 s and the *y*-axis displays the membrane potential values. In **Figures 3–5**, the time on the *x*-axis is approximate because of gaps in the recording. To quantify stability of membrane potential fluctuations across experiments, we evaluated the last minute of the baseline and the first minute of the second 5-min period after the end of the pairing protocol. This second time point was chosen because it was close to the time of maximal change in PSP slopes and the EEG slow-wave activity had completely recovered to baseline levels in all experiments. Recordings were rejected if there was progressive deterioration of the membrane potential fluctuations or the current-voltage relation between blocks of ~30 stimulus trials.

Assessment of changes in synaptic transmission

Independent of stimulation modus, only episodes with an initial membrane potential below a defined threshold close to the modal Down state membrane potential were accepted for analysis. The threshold was set at the membrane potential one third of the way between the 10th and 90th percentiles of the membrane potentials for each trial. Additionally, the membrane potential was required to have returned to below this threshold within 150 ms after stimulus to ensure that the evoked PSP was not contaminated by a spontaneous Up state. Membrane potential-dependent effects on included PSP amplitudes were small (**Figure 1C**, compare the lower two averages, all contributing single trials fell below the threshold). This was confirmed by initial results using a more stringent criterion (1/5 of the way between the 10th and 90th percentiles of the membrane potentials; data not shown) that remained qualitatively unchanged.

The strength of synaptic transmission was measured as the *PSP slope*. A linear fit to the PSP was calculated for a window of 1-ms length sliding over the whole ascending phase of the PSP and the maximal value was recorded. This way, the non-NMDA-mediated component of the early depolarization caused by directly activated synapses was measured (Herrling, 1984, 1985; Jiang and North, 1991).

The time difference between stimulation and the center of the 1 ms-long linear fit of the maximum slope was measured as the *slope latency*. If the distribution of slope latencies contained more than one peak clearly separated from others by troughs, individual peaks were used to define discernable *PSP components* separated by times of adjoining troughs (**Figure 1D**). Each PSP component was examined separately for the whole experiment. A potentially confounding factor was that later PSP components could be influenced by the depolarization caused by preceding PSP components. Linear regression analysis of the 5 min baseline period showed that there was no significant interaction in 13 out of 17 PSP component pairs (data not shown). In only one of the other four cases, both PSP components were significantly altered after the pairing protocol ($p < 0.05$; Wilcoxon rank sum test). Except for this case, PSP components were treated as independent measurements.

Statistical evaluation

To test for changes induced in individual experiments, PSP slope values measured during the first 10 min after the end of the plasticity protocol were compared to baseline values (5 min before plasticity protocol start) using a Wilcoxon rank sum test. For group analysis, means of PSP slopes recorded over 5-min periods were normalized to baseline. Differences from baseline were tested for significant deviation from zero using a two-tailed student's *t*-test. To test for a timing dependent effect, PSP components were grouped in 3 ms-wide bins to include sufficient data points for statistical evaluation. With this or any smaller bin width, the relationship described by a polynomial fit (see below) was maintained in the binned means. For inter-group comparisons, a two-tailed student's *t*-test for comparison between two samples was used. The significance level was set to $p = 0.05$. Unless noted, all data presented consists of mean ± SEM.

Assessment of postsynaptic spike pattern during pairing protocol

The *percentage of trials with spikes* was calculated from the ratio of trials including at least one spike during the 30-ms time window following the cortico-striatal stimulus and the total number of trials of the pairing protocol. The *percentage of trials with doublets* was calculated accordingly from the ratio of trials including at least two spikes. The *latency to spike* was defined as the time difference between the time of the stimulus onset and the peak of the first spike.

The *post-light spike rate* was defined as the mean spike number within a 1-s window following the light flash, thus, capturing all spikes elicited during the relatively long visual-evoked Up states (Schulz et al., 2009).

Regression models

The data of potentially correlated parameters were fitted by a linear least-square fit to test for a significant interaction. To compensate for the spread of post-light spike rates over several orders of magnitude (from 0.1 to >20 Hz), these values were log-transformed before the linear regression analysis. To visualize the complex nature of spike-timing dependent plastic changes in PSP components, a 5th order polynomial was fitted to the data. This relationship could not be tested statistically because of the limited data set. The binned means at −3 and 3 ms were close to the maximum and the minimum of the polynomial fit at about −2.5 and 2.5 ms, respectively, delimiting the linear portion of the polynomial fit. The values included in the binned means at −3, 0 and 3 ms (i.e. −4.5 to 4.5 ms) were tested for a significant linear correlation. Using narrower windows, e.g. −3 to 3 ms, yielded R^2 values similar to those shown in **Figure 6B**, demonstrating that the result of the fit was not an accidental outcome of the chosen window width. In all other cases, no indications for a non-linear relationship between parameters were apparent from visual inspection of scatter plots.

RESULTS

All striatal neurons included in this study (stable for >35 min; $n = 27$) were identified as SPNs by established electrophysiological criteria (Wilson and Kawaguchi, 1996; Mahon et al., 2000; Reynolds and Wickens, 2000), and verified in four experiments by morphology (**Figure 1**). Stimulation of the contralateral motor cortex elicited cortico-striatal PSPs, the amplitude of which was dependent

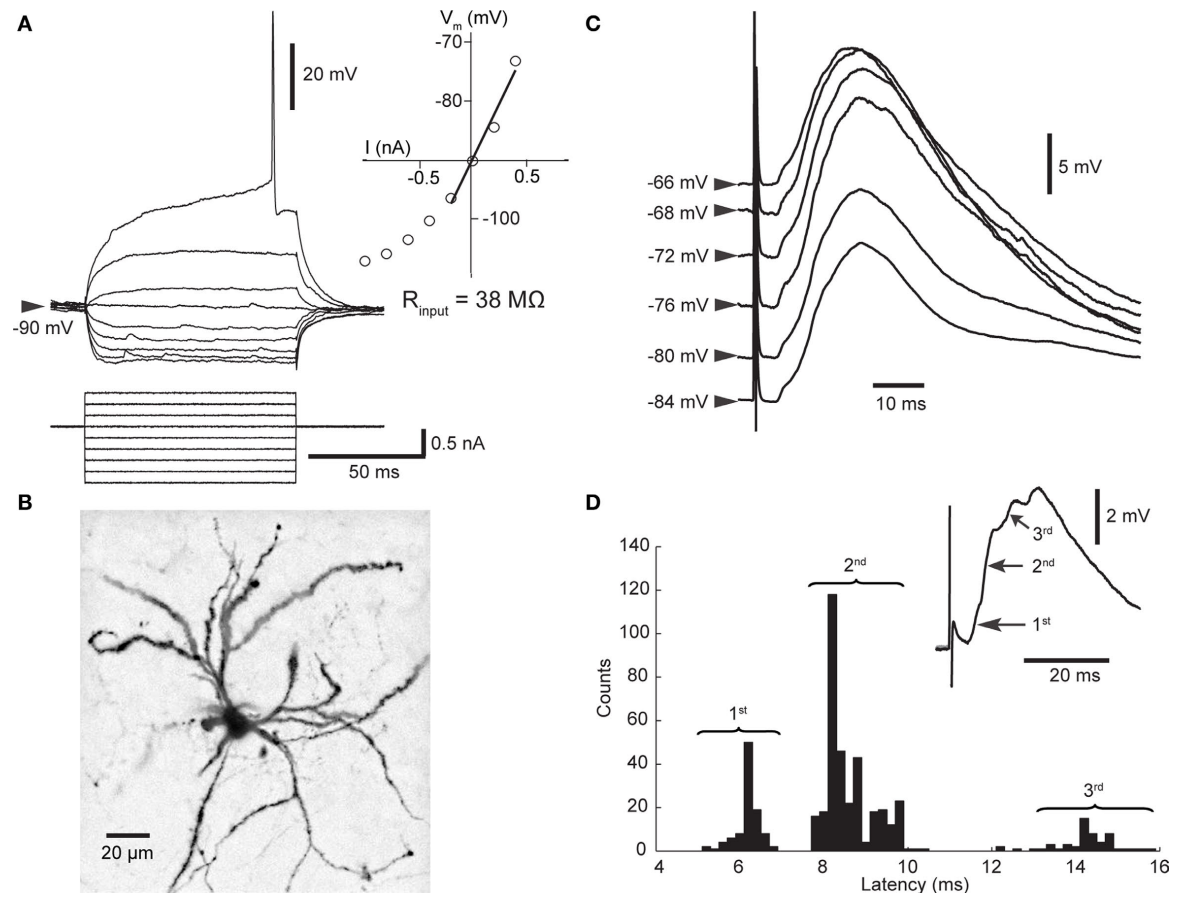

FIGURE 1 | Properties of SPNs and cortico-striatal PSPs. (A) Membrane potential response to linear current steps. The inset shows the current–voltage relationship; the input resistance was derived from the slope of the regression line. **(B)** Biocytin-filled SPN. The dendrites are densely studded with spines. **(C)** Dependence of PSP (mean of 5–63 trials) on membrane potential. All PSPs recorded over 15 min were sorted according to initial membrane potential and then averaged. Note the decreased amplitude when cortical stimulation was applied at depolarized membrane potentials. **(D)** PSPs consisted of several components. Distribution of latencies to maximum slope shows that latencies scattered around three distinct values representing PSP components as indicated in the mean PSP (inset).

on the neuron's membrane potential (**Figure 1C**). Besides the voltage-dependent contribution of NMDA receptor-mediated currents (Ding et al., 2008; Pomata et al., 2008), voltage-dependent potassium conductances responsible for outward rectification likely contributed to this observation (Nisenbaum and Wilson, 1995). Note that the maximum potential of the evoked PSP changed little when evoked at depolarized membrane potentials (**Figure 1C**); therefore, changes in the amplitude of evoked PSPs do not necessarily represent synaptic plastic changes. Two strategies were used to minimize the influence of voltage sensitive conductance changes on the measurement of synaptic strength. Firstly, analysis of PSPs was restricted to those evoked during the SPN's more hyperpolarized Down state. Secondly, the maximum slope of the PSP rather than the amplitude was measured. Interestingly, the distribution of slope latencies exhibited two or three maxima in the majority of experiments (**Figure 1D**). Individual maxima represented different components of the PSP, probably mediated by distinct pathways. This observation was of particular interest in experiments investigating STDP.

EFFECTS OF BIC-MEDIATED DISINHIBITION

Disinhibition of subcortical visual pathways by local ejection of BIC into the SC caused a transient disruption of the Down to Up state membrane potential transitions typically observed in SPNs, as previously described (Schulz et al., 2009). Time-resolved membrane potential recordings, however, demonstrate that changes in PSP slopes we report here were not caused by shifts in the SPN's membrane potential activity (see **Figures 3–5**, panels labeled 'a'). As apparent in **Table 1**, all SPNs returned to Down state-Up state fluctuations comparable to baseline after the pairing protocol. Critically, the Down state membrane potential remained unchanged ($p > 0.1$, paired *t*-test, $n = 27$ neurons).

EFFECTS OF VISUAL-EVOKED INPUTS IN COMBINATION WITH CORTICAL HFS

During BIC-mediated disinhibition of subcortical visual pathways, cortical HFS was repetitively paired with a light flash to the contralateral eye. As the HFS was not sufficient to reliably induce postsynaptic spike discharge (**Figure 2B**), an intracellular current step was applied simultaneously to ensure spike discharge (**Figure 2A**). This protocol did not induce any changes in cortico-striatal synaptic strength during the first 10-min post ($p > 0.2$ for all five neurons; Wilcoxon rank sum test; **Figure 3A**). For the group, the normalized PSP slopes increased to 109.2 ± 7.6% at 10-min post, although this elevation was not significantly different from baseline ($p = 0.29$; *t*-test, $n = 5$, $t = 1.21$).

A previous study induced strong and lasting potentiation in the cortico-striatal pathway when a suprathreshold current step was applied simultaneously to HFS of the substantia nigra pars compacta (Reynolds et al., 2001). To test the requirement of spike discharge during the phasic dopamine signal for synaptic potentiation, the same current step was applied delayed to the HFS, shortly after the light flash (**Figure 2B**). However, the presence of an increased post-light spike rate resulted in a significant depression during the first 10 min post in two SPNs ($p < 0.05$; Wilcoxon rank sum test; **Figure 3B**), and a near-significant depression ($p = 0.061$) in a third. For the group, the normalized PSP slopes decreased to 82.7 ± 2.4% at 5 min and 88.4 ± 5.9% at 10 min post before returning to baseline values. In comparison with the previous HFS protocol, it was revealed that spike firing induced by a current step during the period of time at which the visual response was present significantly reduced PSP slopes at 5 min ($p = 0.014$; *t*-test, $n1 = 5$, $n2 = 4$, $t = 3.25$; **Figure 6A**).

These results suggest that our HFS protocol was unable to induce significant potentiation of the cortico-striatal pathway even when consistently followed by visual-evoked subcortical inputs. This may have resulted from a restricted number of pairings (nominally 6) with the visual-evoked inputs. Thus, we next tested a protocol involving repetitive pairing of single cortical stimuli with light flashes.

EFFECTS OF VISUAL-EVOKED INPUTS AND SINGLE CORTICAL STIMULI

The effect of the repetitive pairing of single cortical stimulations (~120; 0.2 Hz) followed 250 ms later by a light flash to the contralateral eye was tested in five SPNs. The number of spikes elicited during the protocol varied greatly between neurons, as evidenced from the percentage of trials with spikes (**Table 2**). The pairing protocol induced significant synaptic depression in three SPNs

Table 1 | Properties of SPNs before and after the plasticity protocols.

Cellular properties		HFS + spikes then light ($n = 5$)	HFS then light + spikes ($n = 4$)	Single stimulus then light ($n = 5; 3$)	Pre-post then light ($n = 10; 9$)	No BIC ($n = 3; 2$)
Down state potential (mV)	pre	–88.2 ± 5.1	–85.1 ± 7.0	–87.7 ± 4.6	–87.8 ± 2.9	–85.1 ± 7.7
	post	–88.7 ± 6.9	–83.2 ± 7.7	–84.5 ± 6.0	–88.3 ± 3.6	–81.2 ± 5.1
Up state potential (mV)	pre	–76.6 ± 5.5	–73.2 ± 9.6	–70.1 ± 7.7	–73.6 ± 4.4	–67.1 ± 6.4
	post	–78.5 ± 6.6	–72.5 ± 10.1	–71.6 ± 5.3	–77.2 ± 3.0	–67.8 ± 4.6
Difference (mV)	pre	11.6 ± 4.0	12.0 ± 3.8	17.6 ± 6.3	14.2 ± 4.4	18.0 ± 3.7
	post	10.2 ± 3.3	10.7 ± 4.4	12.9 ± 2.6	11.0 ± 3.1	13.4 ± 0.5
Input resistance (MΩ)	pre	39.3 ± 20.6	39.9 ± 19.6	42.7 ± 13.0	31.1 ± 7.5	36.2 ± 19.7
	post	39.9 ± 28.4	53.9 ± 32.4	35.7 ± 11.6	27.8 ± 3.6	55.8 ± 41.3
Rheobase current (nA)	pre	0.99 ± 0.26	0.86 ± 0.19	0.93 ± 0.51	1.04 ± 0.22	0.94 ± 0.30
	post	1.50 ± 0.36	1.37 ± 0.35	1.60 ± 0.00	1.41 ± 0.36	0.86 ± 0.35

Total numbers of neurons are indicated for each group. When intracellular current responses could not be recorded in all neurons post protocol, the number of experiments included is represented by the second n value. Data are mean ± S.D. across neurons.

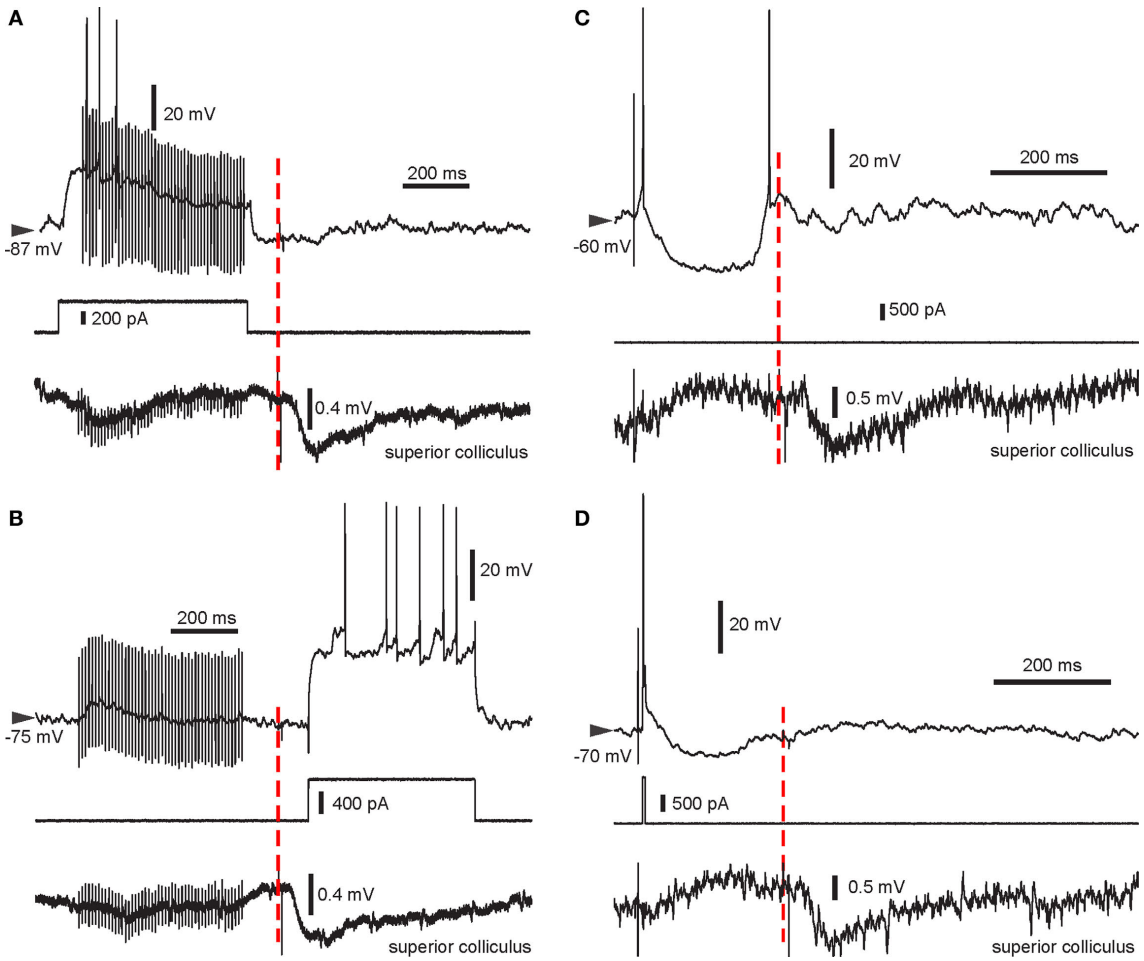

FIGURE 2 | Example traces from all four pairing protocols used. Intracellular recording (top trace), intracellular current injection (middle) and LFP recorded in the SC (bottom) are shown. The start of the light flash is indicated by the red dashed line. Note the negative deflection in the LFP recording indicating the VEP enabled by BIC. **(A)** HFS + spikes then light. **(B)** HFS then light + spikes. Note the absence of spikes during the HFS in this recording. **(C)** Single stimulus then light. In this trial, the SPN elicited a spike following cortical stimulation and rebound activation after the stimulus-induced cortical disfacilitation. **(D)** Pre-post pairing then light, with a single spike elicited using a short current pulse.

($p < 0.05$; Wilcoxon rank sum test), even when the percentage of trials with spikes was increased by constant current injection. However, one SPN showed a tendency towards increased PSP slopes (08812*n*2). In this case, the pairing protocol involved a much higher percentage of trials with spikes than in all other experiments (61.9%). To determine whether a high percentage of trials with spikes would favor the induction of potentiation, a further set of experiments was conducted with spikes consistently induced by a short current pulse.

EFFECTS OF VISUAL-EVOKED INPUTS AND PRE-POST SPIKE PAIRING

In 13 experiments, a short current pulse (5 to 10 ms, +0.8 to +2 nA) was applied during the pairing protocol at a latency of 5–10 ms after the cortico-striatal stimulus. This regularly resulted in trials with spikes in 90.9 ± 14.3% of pairing trials (mean ± SD; range: 49.1–100%). The mean latency across experiments to the evoked spike ranged from 8 to 15 ms after cortical stimulation. In three experiments without BIC ejection into the SC, no significant change of the PSP slope could be detected ($p > 0.1$; Wilcoxon rank sum test). In experiments involving BIC-mediated disinhibition of the SC ($n = 10$), significant changes in the PSP slope were induced in four experiments ($p < 0.05$; Wilcoxon rank sum test), with two showing significant increases and two showing a decrease despite the similarity of the applied pairing protocol. In three of these cases (shown in **Figures 4 and 5**), the change in PSP slope appeared relatively stable and persisted for >20 min.

FACTORS CONTRIBUTING TO VARIABLE PLASTICITY OUTCOME

A number of factors were evaluated to determine if they contributed to the variability in plasticity results between SPNs. In regression analyses, the normalized PSP slope at 10–20 min post was not correlated to stimulus strength, initial PSP slope at baseline, VEP amplitude recorded from the SC, or number of pairings during the plasticity-inducing protocol (all: $p > 0.1$, $n = 10$). This suggested that variation of experimental parameters was an unlikely explanation.

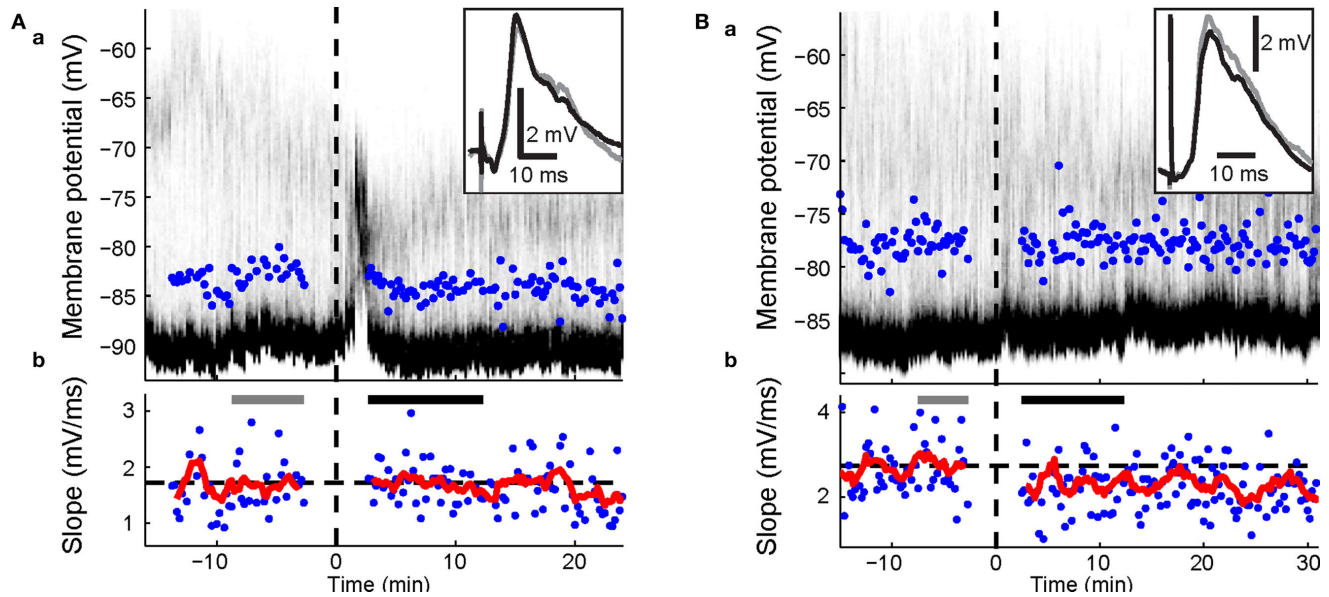

FIGURE 3 | Effects of visual-evoked inputs in combination with cortico-striatal HFS. Panels a, time-resolved membrane potential distribution. Gray-scale indicates the probability for the neuron to be at respective membrane potential (*y*-axis); black depicts a high probability, white a low probability. Time on the *x*-axis is given in relation to BIC ejection (dotted line at 0). Maximum amplitude of PSPs are indicated. Panels b, maximal slopes of PSP. Dashed line indicates mean PSP slopes at baseline. Running average of 9 consecutive values is indicated (red trace). PSP traces (top right inset in a) are mean PSPs recorded in the time indicated by the gray and black bars, respectively. **(A)** Representative example of cortico-striatal HFS with current-evoked spike discharge followed by light. No significant changes were induced. **(B)** HFS followed by light with current-evoked spike discharge induced depression ($p = 0.002$; Wilcoxon rank sum test).

Table 2 | Summary of results from pairing single cortical stimuli followed by light.

		Individual experiments				
		08701*n*1	**09811*n*1**	**08604*n*2**	**09721*n*1**	**08812*n*2**
PSP slope (mV/ms)	pre	2.20 ± 0.10	2.43 ± 0.06	2.27 ± 0.11	2.39 ± 0.08	2.48 ± 0.10
	post	1.76 ± 0.05	1.97 ± 0.05	1.96 ± 0.05	2.26 ± 0.06	2.68 ± 0.10
Percentage of baseline		(80.0%)	(81.1%)	(86.3%)	(94.6%)	(108%)
p-value		<0.001	<0.001	0.010	0.231	0.097
Current (nA)		–	–	+0.1	+0.4	–
Nº pairings		120	121	116	173	113
Trials with spikes (%)		0	25.6	31.9	13.9	61.9
Trials with doublets (%)		0	0	0	0	7.1
Post-light spike rate (Hz)		0	0.74	3.49	0.37	1.02

p-values are from Wilcoxon rank sum tests of single trial data with approximately 30 trials per period.

Postsynaptic spiking

Number and timing of postsynaptic spikes were examined for effects on the plasticity outcome. There was no significant correlation between normalized PSP slope at 10 to 20-min post and the percentage of trials with spikes or the mean spike latency ($p > 0.1$, $n = 10$). The short current pulse (5–10 ms) occasionally induced multiple spikes (3.0–63.3% of trials; $n = 5$ neurons) and postsynaptic high-frequency spike bursts may have been more efficient for inducing potentiation than single spikes (Pike et al., 1999; Kampa et al., 2006). However, no significant correlation between plasticity outcome and percentage of trials with doublets could be found ($p > 0.1$, $n = 10$). Therefore, there appeared to be no statistically significant influence on the PSP slope at 10–20 min, from the number of postsynaptic spikes following the cortical stimulation.

Results from the HFS experiments suggested that an elevated spike rate during the visual-evoked inputs could potentially bias the plasticity outcome towards depression. Three SPNs in the pre-post pairing group fired spikes during the second following light in at least some trials. One SPN exhibited a particularly high post-light spike rate of 4.55 Hz (**Figure 4A**). Ten to twenty minutes of post pairing protocol, this neuron exhibited a significant decrease of the PSP slope from 1.40 ± 0.09 to 1.05 ± 0.05 mV/ms (75% of baseline; $p < 0.001$; Wilcoxon rank sum test, $n1 = 40$, $n2 = 55$,

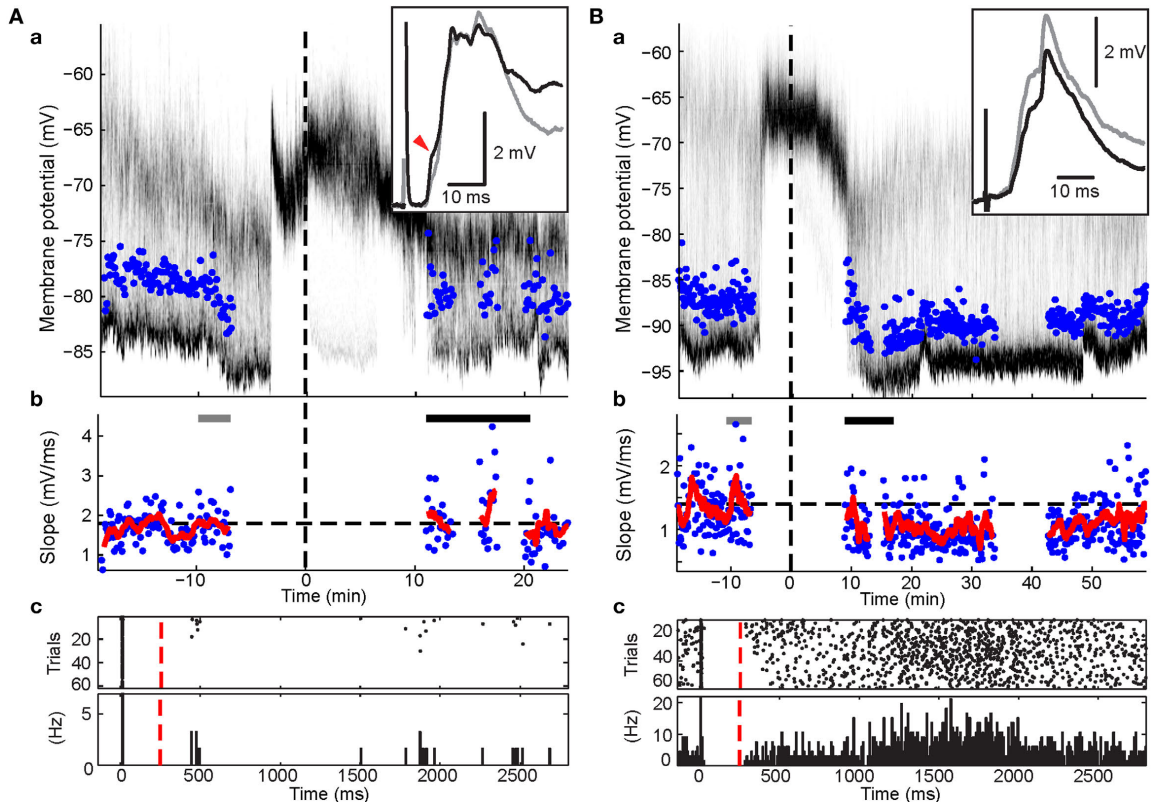

FIGURE 4 | Effects of post-light spike rate on cortico-striatal plasticity in experiments involving pre-post pairing. Format for panels a and b is the same as in **Figure 3**. Panels c, raster plot and peri-stimulus time histogram of spikes during the pairing protocol. Cortical stimulus was applied at 0, the intracellular current pulse at approximately 10 ms, and light at 250 ms (red dashed line). **(A)** Example recording showing depression ($p < 0.001$; Wilcoxon rank sum test). Note the high spike rate post light. **(B)** Example recording showing selective increases in a PSP component (red arrow head; $p < 0.05$; Wilcoxon rank sum test) without a significant change of the overall PSP slope.

rank sum = 2407.5). In contrast, synaptic potentiation of either a single PSP component (**Figure 4B**) or the whole PSP (**Figure 5A**) was found in the other two cases after the pairing protocol when the post-light spike rate was 0.1 and 0.13 Hz, respectively. Across experimental groups, increasing log-transformed post-light spike rates were highly correlated with decreased normalized PSP slopes following the pairing protocol ($R^2 = 0.55$, $p = 0.009$, $n = 11$ active neurons, $F = 11.04$; **Figure 6D**). These observations supported the hypothesis that post-light spike rates modulated the plasticity outcome and provided an explanation for the depression in one pre-post pairing experiment.

Presynaptic factors

The observation that PSPs regularly consisted of up to three distinct components suggested that evoked presynaptic spikes reached the postsynaptic striatal SPN via multiple axon projection trajectories, potentially involving several mono- and di-synaptic pathways (Wilson, 1986, 1987; Reiner et al., 2003; Lei et al., 2004). If pathways were affected differently by the plasticity protocol, then the relative contribution of individual pathways to the evoked PSP would have determined the plasticity outcome. Therefore, all identified PSP components were analyzed individually. There were no indications for a relationship between latencies and normalized PSP slope at 10–20 min (**Figure 6Bb**) and 20–30 min post (data not shown). Thus, a pathway-specific effect was an unlikely explanation of the observed variability in plasticity outcomes.

Interaction between pre- and postsynaptic activation

An alternative explanation was that the precise timing between pre- and postsynaptic spikes influenced the plasticity outcomes (**Figure 5**). To test this hypothesis, normalized slopes of PSP components were plotted against the time difference between PSP component latency and the first postsynaptic spike (**Figure 6Bc**). Latencies of individual PSP components were expected to follow closely the timing of the presynaptic spike at the synapses that caused the inputs. Therefore, PSP component latencies represented a more meaningful reference time than the time of the electrical stimulus to the contralateral cortex. This analysis revealed that PSP components with a latency equal to or up to 4.5 ms slower than the mean latency to spike (i.e. negative time-to-spike points in **Figure 6Bc**, plotted as 3 ms bins at −3 ms and 0 ms in **Figure 6Bd**) always showed a tendency to increase after the pairing protocol. At 10 to 20 min after the protocol, PSP components within 1.5 ms either side of spike latency (plotted at 0 ms in **Figure 6Bd**) were significantly potentiated (115.2 ± 3.9%; $p = 0.011$; *t*-test, $n = 6$, $t = 3.93$). In contrast, PSP components preceding the spike (i.e. positive time-to-spike

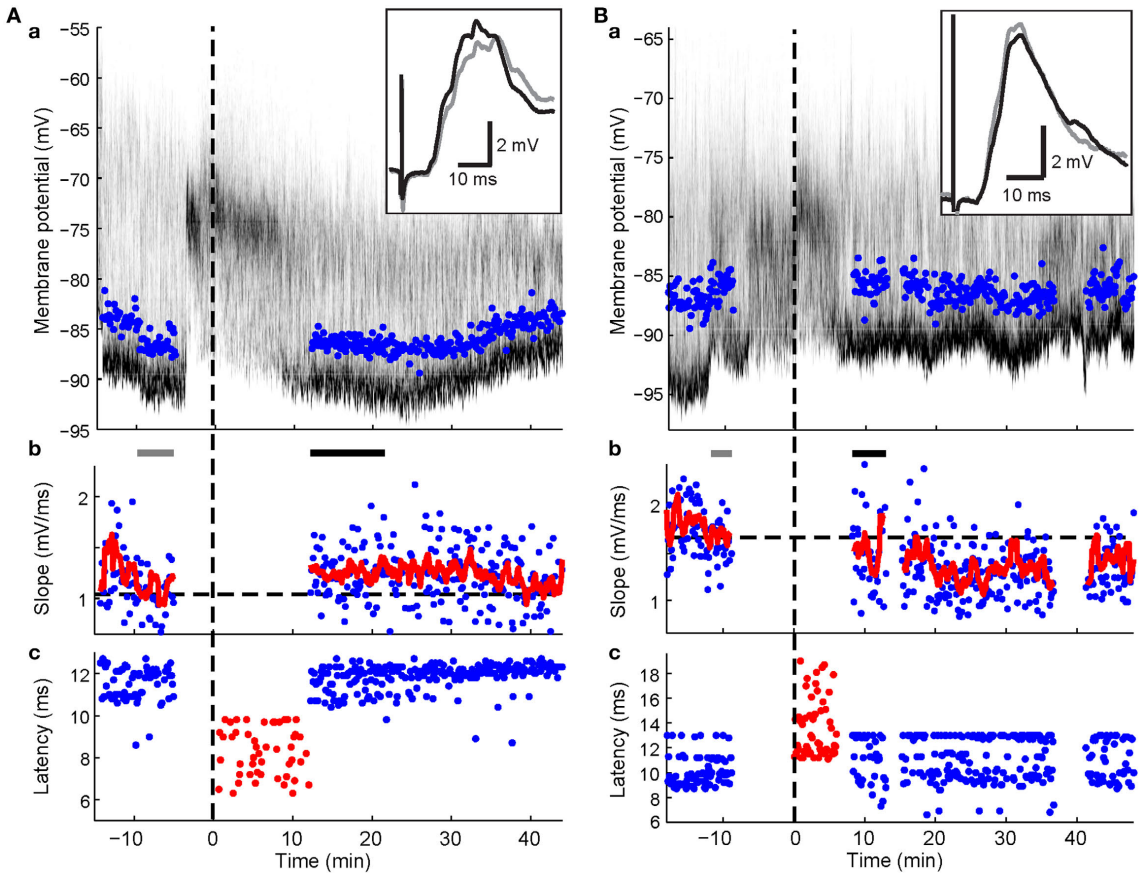

FIGURE 5 | Spike-timing-dependent increases and decreases in cortico-striatal synaptic efficacy. Format for panels a and b is the same as in **Figure 3**. Panels c, latencies of maximal slope measurements (blue dots) and spike times during the plasticity protocol (red dots). **(A)** Example recording showing potentiation ($p < 0.001$; Wilcoxon rank sum test) after pairing PSPs with a postsynaptic spike elicited by somatic current injection. Note spike latencies were relatively early compared to maximal slope latencies. **(B)** Example recording showing depression ($p = 0.038$; Wilcoxon rank sum test) after pairing with current-evoked spikes following the maximal PSP slope. Note the relative higher frequency of later latency components after the protocol.

points in **Figure 6Bc**) showed a higher variability but a tendency towards depression. At 20–30 min post, PSP components between 1.5 and 4.5 ms before the spike (plotted at +3 ms in **Figure 6Bd**) were significantly decreased (86.5 ± 4.5%; $p = 0.024$; *t*-test, $n = 7$, $t = -3.0$). Thus, at 10–20 min after the protocol, synaptic potentiation appeared to be favored for most PSP components, however, over the ensuing 10-min period, a more balanced picture of potentiation of components following the spike but depression of components prior to the spike emerged (**Figure 6Bc**). Spike-timing and induced synaptic changes of PSP components between −4.5 and 4.5 ms to spike latency were significantly negatively correlated for both time points following the protocol ($p < 0.05$, $n = 16$ PSP components; **Figure 6Bd**). However, in the absence of BIC-mediated disinhibition of the SC, PSP components remained largely unchanged and were not subject to STDP (**Figure 6C**).

In summary, the precise temporal relationship between individual PSP components and the evoked spike appeared to be the determining factor for the direction of the induced plasticity and thus accounted for a large proportion of the variability between experiments involving BIC-mediated disinhibition of subcortical visual pathways.

DISCUSSION

The aim of the present investigation was to test the effect of a more physiological procedure for evoking dopamine release into the striatum (Dommett et al., 2005) on the outcome of established synaptic plasticity protocols at the cortico-striatal synapse. The results showed that HFS protocols did not induce significant potentiation under these conditions. Consistent pre-post pairing induced significant changes in at least one PSP component in every experiment that involved disinhibition of the SC. However, the direction of change exhibited a high variability. This was attributed to the relative timing between pre- and postsynaptic spikes on a scale of a few milliseconds. The discussion will focus on this unexpected outcome and its implications for synaptic plasticity *in vivo*.

CORTICO-STRIATAL STDP

The direction of change induced by pre-post pairing depended on the relative timing of the PSP component relative to the spike. The phenomenon of STDP at the cortico-striatal synapse has been described in previous *in vitro* studies (Fino et al., 2005; Pawlak and Kerr, 2008). However, the characteristics of the underlying temporal rule remains controversial. Thus, Fino et al. (2005) found that repeti-

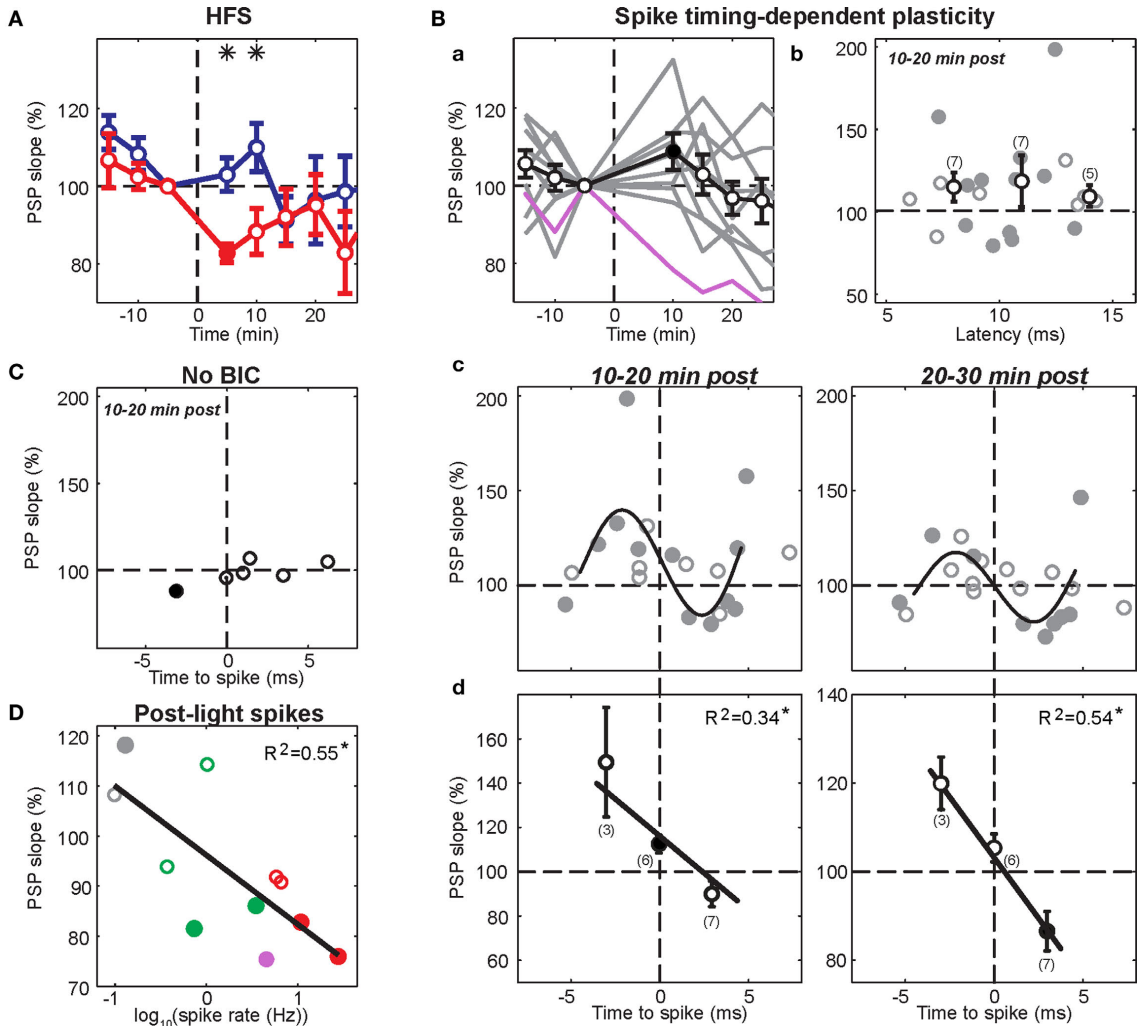

FIGURE 6 | Summary of cortico-striatal plasticity after visual activation of subcortical pathways. In all panels, significant changes from baseline are indicated by filled circles. **(A)** Effects of HFS on normalized PSP slope. Current-evoked spike discharge during visual inputs (red, $n = 4$) resulted in depression (asterisks; $p < 0.05$, *t*-test) when compared to current-evoked spike discharge during HFS (blue, $n = 5$). **(B)** Panel a, pre-post pairing resulted in variable outcomes across experiments (gray traces). One SPN (purple; same as **Figure 4A**) was excluded because of a high post-light spike rate. Panels b–d, analysis of individual PSP components. Means (black) of binned data (3-ms bins; number of included points in brackets) indicate that changes did not depend on latency (**B**, panel b) but on relative timing to evoked spike (**B**, panel d). Although the true relationship between spike-timing and synaptic change was complex (approximated by a 5th order polynomial fit in **B**, panel c), there was a significant linear correlation for spike-timing values between –4.5 and 4.5 ms ($p < 0.05$, $n = 16$; **B**, panel d). **(C)** PSP components remained largely unchanged in experiments without BIC-mediated disinhibition of the SC ($n = 3$). **(D)** Significant effect of post-light spike rate on normalized PSP slope 10–20 min post across experimental groups ($p = 0.009$). Color-code is the same as in **(A–C)**; green represents pairing of visual and single cortical stimuli without a postsynaptic current step.

tive pre-post pairing induced depression, while post-pre pairing induced potentiation. This is the reverse of results by Pawlak and Kerr (2008) and the established rule for most intracortical excitatory synapses (Markram et al., 1997; Sjostrom et al., 2001; Froemke and Dan, 2002). Protocols used by the two groups exhibit two potentially important differences: Fino et al. (2005) stimulated the cortex at 1 Hz during the pairing protocol; in contrast, Pawlak and Kerr (2008) maintained the stimulation frequency at 0.1 Hz throughout the experiment; however, their experiments were performed in the presence of the $GABA_A$ receptor antagonist picrotoxin. In the present study, we used a pairing protocol (60 pairings at 0.2 Hz) very similar to the one used by Pawlak and Kerr (2008). On the other hand, the SPNs were recorded *in vivo* where all GABAergic inhibition was completely intact. Using this approach, we found synaptic changes of similar magnitude (±20%) to those observed by Pawlak and Kerr (2008) during the first 20 min after the end of the pairing protocol. However, in most experiments synaptic modifications followed a much more stringent timing rule *in vivo* and affected only single components rather than the whole PSP. Note that the experiments were designed to induce potentiation by near coincident pre-and postsynaptic activation. Yet, synaptic inputs preceding the spike by about 3 ms were depressed. In contrast, PSP components exactly coinciding with or closely following the postsynaptic spike by about 3 ms were potentiated (an impressive example is shown in **Figure**

5A). Components of the PSP outside of this narrow time window remained on average unaffected by the protocol. Thus, STDP *in vivo* appears to require a relative temporal order that is closer to the rules proposed by Fino et al. (2005), albeit on a contracted time scale. We will next consider how *in vivo* background activity and synaptic inhibition may have contributed to these observations.

STDP *IN VIVO*

To our knowledge, this is the first study using electrical stimulus-evoked PSPs for an STDP protocol in a vertebrate *in vivo*. Previous *in vivo* studies on STDP used sensory evoked PSPs with much more complex pre- and postsynaptic activation patterns and were performed in young or developing neural systems (Meliza and Dan, 2006; Mu and Poo, 2006; Jacob et al., 2007). Most relevant to the current study, Jacob et al. (2007) restricted whisker-evoked PSPs to subthreshold amplitudes and paired them with 1–2 current-evoked spikes. Under these conditions, pre-post pairing induced a significant increase in amplitude but not in slope in most neurons (Jacob et al., 2007), indicating that non-synaptic mechanisms like dendritic plasticity may have contributed (Campanac and Debanne, 2008). However, when significant increases or decreases in slopes were induced by pre-post and post-pre pairing, respectively, the effects were of a magnitude (±20%) similar to the present study (Jacob et al., 2007). Further support for a reduced efficacy of STDP *in vivo* comes from *in vitro* studies employing the dynamic clamp technique (Delgado and Desai, 2008, 2009) in order to simulate the high-conductance state of neurons *in vivo* (Destexhe et al., 2003). Under these conditions, windows for efficient modulation of synaptic transmission strength were greatly reduced to less than 10 ms and the magnitude of induced changes was also reduced to levels comparable with the present study. Interestingly, β-adrenergic receptor activation could increase the induced potentiation (Delgado and Desai, 2009). These results show striking parallels to the present study: STDP does not appear to be a very effective mechanism under more physiological conditions, unless an additional neuromodulatory signal boosts its effect.

Mechanistically, less effective STDP under *in vivo* conditions could be explained by attenuated back-propagation of spikes. However, calcium transients evoked by spike invasion of dendrites appear to be a pre-requisite for STDP (Kampa et al., 2006). Potassium conductances in particular have been shown to significantly attenuate back-propagation of spikes (Hoffman et al., 1997). The prominent potassium conductances during the Up state in SPNs (Nisenbaum and Wilson, 1995) likely impede action potential back-propagation (Day et al., 2008). Accordingly, spontaneous action potentials in SPNs in organotypic cultures elicit the largest calcium transient in dendrites when they are evoked early in the Up state (Kerr and Plenz, 2004).

GABA inputs can also impair spike back-propagation (Tsubokawa and Ross, 1996; Xiong and Chen, 2002). In the present study, spike back-propagation was most likely subject to inhibitory modulation. The striatum is a structure that consists almost exclusively of inhibitory GABAergic neurons, most prominently of SPNs that have extensive local axon arborizations on neighboring SPNs (Wilson and Groves, 1980). In the same animal, cortical stimulation at parameters that elicited large-amplitude PSPs in one SPN often failed to induce a sizeable PSP in another SPN only a few hundred microns away (data not shown). This suggests that some striatal neurons close to the neuron recorded from were likely to be more strongly activated, including occasional spike discharge. These coincident inhibitory inputs would have hampered effective spike back-propagation (Tsubokawa and Ross, 1996; Xiong and Chen, 2002) and therefore the induction of potentiation. This could potentially explain the curious observation that PSP components preceding a spike by more than 2 ms were regularly depressed: the same PSP component could already have caused a spike in neighboring cells and the evoked inhibitory inputs onto the recorded neuron prevented an effective invasion of the dendrites by the spike. Two distinct signaling mechanisms underlying potentiation and depression after an STDP protocol have recently been described for the cortico-striatal synapse (Venance et al., 2009). Using the close timing of pre- and postsynaptic activation in the present study, we likely activated both mechanisms simultaneously. Then, simultaneous inhibitory inputs may have selectively hampered the NMDA-dependent mechanism for the induction of potentiation by locally clamping the membrane potential below the depolarization required for the removal of the magnesium block. It is intriguing that the study by Fino et al. (2005) that originally described depression induced by pre-post pairing was performed in the absence of GABA antagonists. However, a reversed STDP window has also been described for Purkinje-like GABAergic neurons (Bell et al., 1997). Similarly, cortical and other GABAergic interneurons exhibit at least partially reversed STDP windows (Tzounopoulos et al., 2004; Lu et al., 2007). Further work is therefore needed to clarify the specific contributions of cell-intrinsic versus competitive inhibitory mechanisms in regulating the STDP window at the cortico-striatal synapse.

EFFECTS OF CORTICO-STRIATAL HFS

High-frequency stimulation protocols have been widely applied in striatal preparations and regularly result in synaptic depression rather than potentiation (Calabresi et al., 2007; Surmeier et al., 2007). However, simultaneously increased levels of dopamine prevent depression and promote potentiation *in vitro* and *in vivo* (Wickens et al., 1996; Reynolds and Wickens, 2000). Accordingly, the results from group 1 (HFS + spikes then light) are very similar to results from a group of SPNs in a previous *in vivo* study that received contralateral HFS plus intracellular current and simultaneous low-frequency stimulation of the substantia nigra pars compacta (Reynolds and Wickens, 2000). This would indicate that dopamine is able to block depression even if it is released shortly after the HFS. It is important to note, however, that the HFS protocol was apparently not sufficient to induce stronger potentiation than the STDP protocol. It is possible that the number of pairings of cortico-striatal inputs with the visual stimulus was insufficient. Visual-evoked dopamine release is expected to be much smaller than if the substantia nigra was stimulated directly at high frequency. In previous *in vivo* studies using the same design of six 500-ms stimulation trains, robust potentiation was only induced if stimulation to the substantia nigra pars compacta was applied at high frequency, but not if it was applied at low frequency (Reynolds and Wickens, 2000; Reynolds et al., 2001). This suggests that a particularly large dopamine transient during each pairing is necessary to induce potentiation if the pairing number is low.

IMPACT OF POSTSYNAPTIC SPIKING AFTER THE LIGHT FLASH

Interestingly, SPNs that were driven to a high spike rate after the light flash showed a strong tendency towards depression of the preceding cortico-striatal inputs across experimental groups. Assuming this reflects a functionally meaningful mechanism, synaptic plasticity rules in the striatum would appear to prevent potentiation of synaptic weights at SPNs if they are also activated at the time of a different set of inputs. This mechanism could promote segregation of movements, cues and outcome representations by SPNs during learning (Barnes et al., 2005).

In conclusion, the present study has demonstrated that synaptic plasticity can, in principle, be induced using visual-evoked subcortical inputs, very likely including dopamine. However, potentiation could only be induced in a subset of single-spike pairing experiments involving many repetitions. In contrast to common expectations, post-pre pairing on a millisecond-timescale promoted potentiation, whereas pre-post pairing promoted depression. Additional *in vivo* studies are required to test the effectiveness of STDP and its regulation by neuromodulators in other brain areas in order to validate our present models of brain computations.

ACKNOWLEDGMENTS

This work was supported by the Marsden Fund of the Royal Society of New Zealand (John N. J. Reynolds), and Wellcome Trust grant WT080943 (Peter Redgrave). Jan M. Schulz received a University of Otago Postgraduate Scholarship.

REFERENCES

Barnes, T. D., Kubota, Y., Hu, D., Jin, D. Z. Z., and Graybiel, A. M. (2005). Activity of striatal neurons reflects dynamic encoding and recoding of procedural memories. *Nature* 437, 1158–1161.

Bell, C. C., Han, V. Z., Sugawara, Y., and Grant, K. (1997). Synaptic plasticity in a cerebellum-like structure depends on temporal order. *Nature* 387, 278–281.

Calabresi, P., Picconi, B., Tozzi, A., and Di Filippo, M. (2007). Dopamine-mediated regulation of corticostriatal synaptic plasticity. *Trends Neurosci.* 30, 211–219.

Campanac, E., and Debanne, D. (2008). Spike timing-dependent plasticity: a learning rule for dendritic integration in rat CA1 pyramidal neurons. *J. Physiol. (Lond.)* 586, 779–793.

Coizet, V., Comoli, E., Westby, G. W. M., and Redgrave, P. (2003). Phasic activation of substantia nigra and the ventral tegmental area by chemical stimulation of the superior colliculus: an electrophysiological investigation in the rat. *Eur. J. Neurosci.* 17, 28–40.

Comoli, E., Coizet, V., Boyes, J., Bolam, J. P., Canteras, N. S., Quirk, R. H., Overton, P. G., and Redgrave, P. (2003). A direct projection from superior colliculus to substantia nigra for detecting salient visual events. *Nat. Neurosci.* 6, 974–980.

Day, M., Wokosin, D., Plotkin, J. L., Tian, X. Y., and Surmeier, D. J. (2008). Differential excitability and modulation of striatal medium spiny neuron dendrites. *J. Neurosci.* 28, 11603–11614.

Delgado, J. Y., and Desai, N. S. (2008). *In vivo*-like conductances limit spike-timing dependent plasticity. *Abstr. - Soc. Neurosci.* 39, 40.43.

Delgado, J. Y., and Desai, N. S. (2009). *In vivo*-like conductance levels control the induction of spike-timing dependent plasticity. *Abstr. - Soc. Neurosci* 40, 41.48.

Destexhe, A., Rudolph, M., and Pare, D. (2003). The high-conductance state of neocortical neurons *in vivo*. *Nat. Rev. Neurosci.* 4, 739–751.

Ding, J., Peterson, J. D., and Surmeier, D. J. (2008). Corticostriatal and thalamostriatal synapses have distinctive properties. *J. Neurosci.* 28, 6483–6492.

Dommett, E., Coizet, V., Blaha, C. D., Martindale, J., Lefebvre, V., Walton, N., Mayhew, J. E., Overton, P. G., and Redgrave, P. (2005). How visual stimuli activate dopaminergic neurons at short latency. *Science* 307, 1476–1479.

Erro, M. E., Lanciego, J. L., and Gimenez-Amaya, J. M. (2002). Re-examination of the thalamostriatal projections in the rat with retrograde tracers. *Neurosci. Res.* 42, 45–55.

Fino, E., Glowinski, J., and Venance, L. (2005). Bidirectional activity-dependent plasticity at corticostriatal synapses. *J. Neurosci.* 25, 11279–11287.

Froemke, R. C., and Dan, Y. (2002). Spike-timing-dependent synaptic modification induced by natural spike trains. *Nature* 416, 433–438.

Herrling, P. L. (1984). Evidence that the cortically evoked EPSP in cat caudate neurons is mediated by non-NMDA excitatory amino-acid receptors. *J. Physiol. (Lond.)* 353, P98–P98.

Herrling, P. L. (1985). Pharmacology of the corticocaudate excitatory postsynaptic potential in the cat: evidence for its mediation by quisqualate- or kainate-receptors. *Neuroscience* 14, 417–426.

Hoffman, D. A., Magee, J. C., Colbert, C. M., and Johnston, D. (1997). K^+ channel regulation of signal propagation in dendrites of hippocampal pyramidal neurons. *Nature* 387, 869–875.

Horikawa, K., and Armstrong, W. E. (1988). A versatile means of intracellular labeling: Injection of biocytin and its detection with avidin conjugates. *J. Neurosci. Methods* 25, 1–11.

Izhikevich, E. M. (2007). Solving the distal reward problem through linkage of STDP and dopamine signaling. *Cereb. Cortex* 17, 2443–2452.

Jacob, V., Brasier, D. J., Erchova, I., Feldman, D., and Shulz, D. E. (2007). Spike timing-dependent synaptic depression in the *in vivo* barrel cortex of the rat. *J. Neurosci.* 27, 1271–1284.

Jiang, Z. G., and North, R. A. (1991). Membrane properties and synaptic responses of rat striatal neurones *in vitro*. *J. Physiol.* 443, 533–553.

Kampa, B. M., Letzkus, J. J., and Stuart, G. J. (2006). Requirement of dendritic calcium spikes for induction of spike-timing-dependent synaptic plasticity. *J. Physiol. (Lond.)* 574, 283–290.

Kerr, J. N., and Plenz, D. (2004). Action potential timing determines dendritic calcium during striatal up-states. *J. Neurosci.* 24, 877–885.

Kerr, J. N., and Wickens, J. R. (2001). Dopamine D1/D5 receptor activation is required for long-term potentiation in the rat neostriatum *in vitro*. *J. Neurophysiol.* 85, 117–124.

Lei, W. L., Jiao, Y., Del Mar, N., and Reiner, A. (2004). Evidence for differential cortical input to direct pathway versus indirect pathway striatal projection neurons in rats. *J. Neurosci.* 24, 8289–8299.

Lu, J. T., Li, C. Y., Zhao, J. P., Poo, M. M., and Zhang, X. H. (2007). Spike-timing-dependent plasticity of neocortical excitatory synapses on inhibitory interneurons depends on target cell type. *J. Neurosci.* 27, 9711–9720.

Mahon, S., Delord, B., Deniau, J. M., and Charpier, S. (2000). Intrinsic properties of rat striatal output neurones and time-dependent facilitation of cortical inputs *in vivo*. *J. Physiol.* 527(Pt 2), 345–354.

Markram, H., Lubke, J., Frotscher, M., and Sakmann, B. (1997). Regulation of synaptic efficacy by coincidence of postsynaptic APs and EPSPs. *Science* 275, 213–215.

McGeorge, A. J., and Faull, R. L. (1989). The organization of the projection from the cerebral cortex to the striatum in the rat. *Neuroscience* 29, 503–537.

Meliza, C. D., and Dan, Y. (2006). Receptive-field modification in rat visual cortex induced by paired visual stimulation and single-cell spiking. *Neuron* 49, 183–189.

Minamimoto, T., Hori, Y., and Kimura, M. (2005). Complementary process to response bias in the centromedian nucleus of the thalamus. *Science* 308, 1798–1801.

Mu, Y., and Poo, M. M. (2006). Spike timing-dependent LTP/LTD mediates visual experience-dependent plasticity in a developing retinotectal system. *Neuron* 50, 115–125.

Nisenbaum, E. S., and Wilson, C. J. (1995). Potassium currents responsible for inward and outward rectification in rat neostriatal spiny projection neurons. *J. Neurosci.* 15, 4449–4463.

Pawlak, V., and Kerr, J. N. D. (2008). Dopamine receptor activation is required for corticostriatal spike-timing-dependent plasticity. *J. Neurosci.* 28, 2435–2446.

Pike, F. G., Meredith, R. M., Olding, A. W. A., and Paulsen, O. (1999). Postsynaptic bursting is essential for 'Hebbian' induction of associative long-term potentiation at excitatory synapses in rat hippocampus. *J. Physiol. (Lond.)* 518, 571–576.

Pomata, P. E., Belluscio, M. A., Riquelme, L. A., and Murer, M. G. (2008). NMDA receptor gating of information flow through the striatum *in vivo*. *J. Neurosci.* 28, 13384–13389.

Redgrave, P., Gurney, K., and Reynolds, J. (2008). What is reinforced by phasic dopamine signals? *Brain Res. Rev.* 58, 322–339.

Reiner, A., Jiao, Y., Del Mar, N., Laverghetta, A. V., and Lei, W. L. (2003). Differential morphology of pyramidal tract-type and intratelencephalically projecting-type corticostriatal neurons and their intrastriatal terminals in rats. *J. Comp. Neurol.* 457, 420–440.

Reynolds, J. N. J., Hyland, B. I., and Wickens, J. R. (2001). A cellular

mechanism of reward-related learning. *Nature* 413, 67–70.

Reynolds, J. N. J., and Wickens, J. R. (2000). Substantia nigra dopamine regulates synaptic plasticity and membrane potential fluctuations in the rat neostriatum, *in vivo*. *Neuroscience* 99, 199–203.

Reynolds, J. N. J., and Wickens, J. R. (2003). A state-dependent trigger for electrophysiological recording at predetermined membrane potentials. *J. Neurosci. Methods* 131, 111–119.

Schulz, J. M., Redgrave, P., Mehring, C., Aertsen, A., Clements, K. M., Wickens, J. R., and Reynolds, J. N. J. (2009). Short-latency activation of striatal spiny neurons via subcortical visual pathways. *J. Neurosci.* 29, 6336–6347.

Shen, W. X., Flajolet, M., Greengard, P., and Surmeier, D. J. (2008). Dichotomous dopaminergic control of striatal synaptic plasticity. *Science* 321, 848–851.

Sjostrom, P. J., Turrigiano, G. G., and Nelson, S. B. (2001). Rate, timing, and cooperativity jointly determine cortical synaptic plasticity. *Neuron* 32, 1149–1164.

Surmeier, D. J., Ding, J., Day, M., Wang, Z. F., and Shen, W. X. (2007). D1 and D2 dopamine-receptor modulation of striatal glutamatergic signaling in striatal medium spiny neurons. *Trends Neurosci.* 30, 228–235.

Tsubokawa, H., and Ross, W. N. (1996). IPSPs modulate spike backpropagation and associated $[Ca^{2+}]i$ changes in the dendrites of hippocampal CA1 pyramidal neurons. *J. Neurophysiol.* 76, 2896–2906.

Tzounopoulos, T., Kim, Y., Oertel, D., and Trussell, L. O. (2004). Cell-specific, spike timing-dependent plasticities in the dorsal cochlear nucleus. *Nat. Neurosci.* 7, 719–725.

Venance, L., Paille, V., Cui, Y., Morera-Herreras, T., Deniau, J.-M., and Fino, E. (2009). Two coincidence detectors are required for the corticostriatal spike timing-dependent plasticity. *Abstr. - Soc. Neurosci.* 40, 41.42.

Wickens, J. R., Begg, A. J., and Arbuthnott, G. W. (1996). Dopamine reverses the depression of rat corticostriatal synapses which normally follows high-frequency stimulation of cortex *in vitro*. *Neuroscience* 70, 1–5.

Wickens, J. R., Budd, C. S., Hyland, B. I., and Arbuthnott, G. W. (2007a). Striatal contributions to reward and decision making – Making sense of regional variations in a reiterated processing matrix. *Ann. N. Y. Acad. Sci.* 1104, 192–212.

Wickens, J. R., Horvitz, J. C., Costa, R. M., and Killcross, S. (2007b). Dopaminergic mechanisms in actions and habits. *J. Neurosci.* 27, 8181–8183.

Wilson, C. J. (1986). Postsynaptic potentials evoked in spiny neostriatal projection neurons by stimulation of ipsilateral and contralateral neocortex. *Brain Res.* 367, 201–213.

Wilson, C. J. (1987). Morphology and synaptic connections of crossed corticostriatal neurons in the rat. *J. Comp. Neurol.* 263, 567–580.

Wilson, C. J., and Groves, P. M. (1980). Fine structure and synaptic connections of the common spiny neuron of the rat neostriatum: a study employing intracellular inject of horseradish peroxidase. *J. Comp. Neurol.* 194, 599–615.

Wilson, C. J., and Kawaguchi, Y. (1996). The origins of two-state spontaneous membrane potential fluctuations of neostriatal spiny neurons. *J. Neurosci.* 16, 2397–2410.

Xiong, W. H., and Chen, W. R. (2002). Dynamic gating of spike propagation in the mitral cell lateral dendrites. *Neuron* 34, 115–126.

Conflict of Interest Statement: The authors declare that research was conducted in the absence of any commercial or financial relationships that could be construed as a potential conflict of interest.

Received: 14 February 2010; paper pending published: 23 April 2010; accepted: 31 May 2010; published online: 02 July 2010.

Citation: Schulz JM, Redgrave P and Reynolds JNJ (2010) Cortico-striatal spike-timing dependent plasticity after activation of subcortical pathways. Front. Syn. Neurosci. ***2****:23. doi: 10.3389/fnsyn.2010.00023*

frontiers in
SYNAPTIC NEUROSCIENCE

ORIGINAL RESEARCH ARTICLE
published: 14 June 2010
doi: 10.3389/fnsyn.2010.00017

Information carried by population spike times in the whisker sensory cortex can be decoded without knowledge of stimulus time

Stefano Panzeri*[1]* and *Mathew E. Diamond*[2,3]

[1] *Robotics, Brain and Cognitive Sciences Department, Italian Institute of Technology, Genova, Italy*
[2] *Cognitive Neuroscience Sector, International School for Advanced Studies, Trieste, Italy*
[3] *Italian Institute of Technology- SISSA Unit, Trieste, Italy*

Edited by:
Per Jesper Sjöström, University College London, UK

Reviewed by:
Guglielmo Foffani, Hospital Nacional de Parapléjicos, Spain; Drexel University, USA
Miguel Maravall, Universidad Miguel Hernández, Spain
Demetris Soteropoulos, Newcastle University, UK

***Correspondence:**
Stefano Panzeri, Department of Robotics, Brain and Cognitive Sciences, Italian Institute of Technology, Via Morego 30, 16163 Genova, Italy.
e-mail: stefano.panzeri@iit.it
Mathew E. Diamond, Cognitive Neuroscience Sector, International School for Advanced Studies (SISSA), Via Beirut, 9 34014 Trieste, Italy.
e-mail: diamond@sissa.it

Computational analyses have revealed that precisely timed spikes emitted by somatosensory cortical neuronal populations encode basic stimulus features in the rat's whisker sensory system. Efficient spike time based decoding schemes both for the spatial location of a stimulus and for the kinetic features of complex whisker movements have been defined. To date, these decoding schemes have been based upon spike times referenced to an external temporal frame – the time of the stimulus itself. Such schemes are limited by the requirement of precise knowledge of the stimulus time signal, and it is not clear whether stimulus times are known to rats making sensory judgments. Here, we first review studies of the information obtained from spike timing referenced to the stimulus time. Then we explore new methods for extracting spike train information independently of any external temporal reference frame. These proposed methods are based on the detection of stimulus-dependent differences in the firing time within a neuronal population. We apply them to a data set using single-whisker stimulation in anesthetized rats and find that stimulus site can be decoded based on the millisecond-range relative differences in spike times even without knowledge of stimulus time. If spike counts alone are measured over tens or hundreds of milliseconds rather than milliseconds, such decoders are much less effective. These results suggest that decoding schemes based on millisecond-precise spike times are likely to subserve robust and information-rich transmission of information in the somatosensory system.

Keywords: information theory, somatosensation, neural coding, decoding, spike patterns, population coding

INTRODUCTION

Explorations of sensory processing are founded on the model that, if two sensory stimuli can be discriminated, their associated neural representations must be in some way distinct (for reviews see e.g., Petersen et al., 2002a; Quian Quiroga and Panzeri, 2009; Panzeri et al., 2010). A fundamental challenge, then, is to discover the essential differences in the neural representations of two perceptually discriminable stimuli.

Behaving rats can perform whisker-mediated texture discriminations between tactile stimuli in as little as 100 ms between first touch and choice action, as shown by Figure 4 in von Heimendahl et al. (2007). Thus, the signal supporting their decision must reside in spike trains of some tens or at most a few hundred milliseconds (Diamond et al., 2008). Well before any recordings are collected during the course of active sensory discriminations, it is crucial to delineate candidate coding mechanisms under more controlled conditions so that the data obtained from the behaving animal can be interpreted profitably. Although there are many cases where neural activity collected in the absence of any quantitative hypothesis has proven uninterpretable (Prigg et al., 2002), the notion somehow survives that the search for potential coding mechanisms should not be undertaken except from the perspective of documented sensory capacities (Stuttgen, 2010). In contrast, our view is that the starting point is to ask what signals neuronal populations are capable of carrying, and by what principles. In this way, models and assumptions can be ruled out or reinforced in parallel with the collection of new data sets.

Information theory has proved to be a profitable way to evaluate the salient differences between the neural representations of sensory events and the potential mechanisms by which neurons convey signals about stimuli. In rat whisker cortex, information theoretic studies have highlighted the potentially important role of spike times in encoding sensory information: the knowledge of the timing of spikes with millisecond precision adds large amounts of information that cannot be gained by counting the spikes over tens or hundreds of millisecond (Panzeri et al., 2001; Petersen et al., 2001; Arabzadeh et al., 2006). When stimuli are presented to anesthetized animals, the experimenter, of course, knows the stimulus timing. As a result, most spike timing based codes that have been proposed rely on stimulus time knowledge. For example, in rat whisker cortex the short latency of neural responses carries almost all the information that neurons transmit about stimulus location, yet the latency is calculated with respect to a known stimulus onset time (Panzeri et al., 2001, 2003b; Petersen et al., 2001, 2002a,b).

Latency codes are the simplest and most prominent case of information encoding by spike times measured with an external temporal reference, and they offer a number of significant computational

advantages. First-spike coding is metabolically efficient, and is the fastest possible way to encode information (no neural message can be faster than a first-spike-time). Van Rullen and Thorpe (2001) have argued that first-spike coding is the only way information can be encoded compatible with the speed of processing in the visual system. Latency coding is also a convenient way to represent analog variables in a format ready for further computation (Hopfield, 1995). However, a potential problem arises if latencies are measured with respect to the stimulus onset. Since the brain, unlike the experimenter, does not have direct access to the time of stimulus onset, it is uncertain whether this timing could be used. Indeed, we have investigated the issue of the robustness of spike timing codes during naturalistic whisker deflections (Arabzadeh et al., 2006). We found that in cortex the information in spike times of single neurons or of small populations was largely lost if the decoder had imprecise knowledge of the stimulus time (Arabzadeh et al., 2006).

Encoding of information by latency has been reported not only in the rat whisker system but also in other different sensory modalities (e.g., Gawne et al., 1996; Furukawa et al., 2000; Muller et al., 2001; Reich et al., 2001; Foffani et al., 2004, 2008, 2009; Chechik et al., 2006). The consistent finding that latency coding is informative at the cortical level raises the question of whether, and how, information in precise spike times of cortical neurons can be read out by other brain areas even without independent knowledge of the stimulus time.

The problem of decoding the information in precise spike times could be solved if the sensory input were generated in response to an active motor command, in which case the time of the command could constitute an estimate of stimulus time. For example, rats sweep their vibrissae toward objects of interest (Kleinfeld et al., 2006) and they may be able to register incoming spike trains with respect to their own whisker protraction with a resolution of some tens of milliseconds (Kleinfeld et al., 2006; Diamond et al., 2008). However, it seems unlikely that motor "efference copy" possesses the necessary temporal resolution to align first-spike times with ms precision (von Heimendahl et al., 2007). Still, even if motor commands do not constitute a ms-precise clock, they may serve as a "window of expectation", and within such windows the brain may use spike timing relative to an internal reference frame to extract a representation of the stimulus (Hopfield, 1995; Van Rullen and Thorpe, 2001; Brody and Hopfield, 2003; Johansson and Birznieks, 2004; Kayser et al., 2009; Panzeri et al., 2010). Timing relative to an internal reference frame could be defined either from spike times within a single neuron's train, or as relative timing between multiple neurons. The feasibility of this "relative timing" population code has been demonstrated on simulated networks (Van Rullen and Thorpe, 2001) and at the peripheral level (Johansson and Birznieks, 2004; Gollisch and Meister, 2008; Saal et al., 2009).

In this article, we investigate the feasibility of decoding fine-scale relative spike timing information in cortex by considering somatosensory cortical recordings in response to instantaneous whisker deflections. We are particularly interested in testing whether decoders based upon relative spike times can operate robustly even in the presence of spontaneous activity (which complicates the estimates of response latencies of individual neurons), and in understanding whether they can provide information beyond what can be extracted by counting spikes over coarser time scales. The information that we attempt to extract from the spike trains is the identity of the deflected whisker. Knowing which whisker has contacted an object is thought to be part of the process of object localization, in which rats have excellent capacities (Diamond et al., 1999, 2008; Harris et al., 1999; Mehta et al., 2007; Knutsen and Ahissar, 2009).

The article is organized as follows. After reviewing concepts and results from information theory showing the role of spike timing in encoding whisker information, we present methods for stimulus decoding in the absence of externally added knowledge of the stimulus time course. We apply these methods, as a feasibility test, to data from anesthetized rats. We show that stimulus site can be decoded from millisecond-precise population spike times without absolute stimulus time knowledge.

INFORMATION THEORETIC ANALYSIS

The information that a single neuron or a neuronal population response conveys about the stimulus can be quantified by Shannon's Mutual Information formula (Cover and Thomas, 1991), abbreviated hereafter as Information:

$$I(S;\mathbf{R}) = \sum_{r,s} P(s)P(\mathbf{r}\,|\,s)\log_2 \frac{P(\mathbf{r}\,|\,s)}{P(\mathbf{r})} \quad (1)$$

where $P(s)$ is the probability of presentation of stimulus s, $P(\mathbf{r}\,|\,s)$ is the probability of observing response $\mathbf{r}$ given presentation of stimulus s, and $P(\mathbf{r})$ is the probability of observing response $\mathbf{r}$ across all trials to any stimulus. This equation quantifies the maximal reduction of uncertainty (i.e., the gain in information) about the stimuli obtained from a single-trial observation of a neuronal response (averaged over all stimuli and responses). Information is measured in bits (1 bits corresponds to a reduction of uncertainty by a factor of two), and is an upper bound on the amount of knowledge about stimuli that can be extracted by any decoding algorithm operating on neural responses. By evaluating the information carried by different ways of defining and quantifying the response $\mathbf{r}$, we can evaluate the capacity of different candidate neural codes.

The computation of information requires the estimation of the stimulus-conditional response probabilities. These probabilities are not known a priori and must be measured experimentally from a finite number of trials. The estimated probabilities suffer from finite sampling errors, which induce a systematic error (bias) in estimates of the information (Panzeri et al., 2007). In this article, unless otherwise stated we used the following procedure to correct for the bias when computing information from real data. First, to facilitate the sampling of its probability, we considered responses $\mathbf{r}$ which are discrete in nature or which are binned into some discrete set of possible responses. Although the discretization facilitates the sampling of neural response probabilities, the information measures still suffer from limited sampling bias. We thus used a quadratic extrapolation procedure (Strong et al., 1998) to estimate and subtract the bias of each information quantity.

Information theory has been shown to be a useful tool to validate or exclude potential information-carrying mechanisms, such as firing rate, temporal firing patterns of single-neurons, and firing synergies among multiple neurons (Theunissen and Miller, 1995; Nirenberg and Latham, 1998; Borst and Theunissen, 1999;

Victor, 2000, 2006; Nirenberg et al., 2001; Panzeri and Schultz, 2001; Golledge et al., 2003; Panzeri et al., 2003a; Schneidman et al., 2003; Foffani et al., 2004; Schnupp et al., 2006; Nelken and Chechik, 2007; Scaglione et al., 2008; Montani et al., 2009; Petersen et al., 2009; Quian Quiroga and Panzeri, 2009).

THE DATA SET

Before presenting the information analysis, we briefly illustrate and describe the dataset of single neuron recordings from the somatosensory cortex of rats that we will use for all the analyses in this article. These data were originally published in Lebedev et al. (2000). In the following, we provide an overview of the experimental conditions.

Adult male Wistar rats weighing approximately 350 g were used. Anesthesia was induced by urethane (1.5 g/kg of body weight). The subject was placed in a stereotaxic apparatus and left somatosensory cortex was exposed by a craniotomy. Anesthesia was held at a depth characterized by a bursting rate and local field potential frequency of 0.5–8 Hz (Erchova et al., 2002). An array of six tungsten microelectrodes with 300 ± 50 μm separation between adjacent electrode tips was advanced into the cortical barrel field. Neurons in barrel-column D2 and surrounding D-row barrel-columns were sampled. Neuronal activity was amplified and band-pass filtered in the range 300–7,500 Hz. Action potentials were digitized at 25 kHz and stored on a PC.

All whiskers were trimmed to a 3-mm length. Individual whiskers were deflected by piezoelectric wafer positioned just below the whisker shaft, 2 mm from the skin. The stimulus was an up-down step function of 80-μm amplitude and 100 ms duration delivered once per second 50 times for each vibrissa. The stimulated vibrissae were C1-3, D1-3, E1-3, gamma, and delta. Single-unit action potentials were discriminated using a template-matching algorithm written in MATLAB (Mathworks, Inc, Natwick, MA, USA). Classified action potentials were time-stamped with 0.1 ms resolution.

INFORMATION CARRIED BY SPIKE TIMING MEASURED ALIGNED TO AN EXTERNAL REFERENCE FRAME

To introduce the concept of extracting information from neural responses using knowledge of the stimulus time, we review the previously reported results (Panzeri et al., 2001) concerning the stimulus location information carried by spike counts and spike times of single neurons recorded in barrel D2.

This analysis was based on a post-stimulus time window 0–T, where T was varied parametrically in the range 5–40 ms in steps of 5 ms. To evaluate spike count information, the "response" **r** on each trial was simply the number of spikes occurring in the time window 0–T. To evaluate spike timing information, the window 0–T was broken into bins of size Δt, where Δt is the temporal precision at which spike times are considered. Different values of Δt (from 20 to 2.5 ms) were used. The overall contribution of temporal encoding was then quantified as the difference between the spike timing and the spike count information. The resulting information calculation corresponds to the amount of knowledge available to an observer that can read spike times with a resolution of Δt. Since in both the spike count and the spike timing analysis the post-stimulus window and the presence and timing of spikes were measured with respect to the stimulus time, the implicit assumption of this analysis is that the downstream system reading information has precise knowledge of the stimulus onset time.

Given that typical spike counts for barrel cortical neurons are low, in this particular dataset we could compute the mutual information reliably using the so-called series expansion method (Panzeri and Schultz, 2001), which provides a data-robust information evaluation. Using this formalism and the associated sampling bias corrections (Panzeri and Schultz, 2001), we addressed whether spike timing was important for the coding of the location of the stimulated whisker. Further, we asked what were the most important components of the code.

The time course of information (averaged over a population of 106 cells recorded in barrel D2) is shown in **Figure 1A**. Early in the response (0–10 ms post-stimulus onset), the spike count provided almost as much information (90% on average) as spike times measured with precision $\Delta t = 5$ ms. Later, however, there was a significant advantage for the timing code: at 40 ms, spike times sampled at precision $\Delta t = 5$ ms provided 55% more information than did total spike counts.

What is the temporal resolution of the readout necessary to extract the entire quantity of information? To answer this question, we varied the width Δt of the time bins in the range 2.5–20 ms. We found that the transmitted information increased steadily with decreasing Δt, with more than 50% additional information transmitted using precision $\Delta t = 2.5$ ms compared to $\Delta t = 20$ ms (Panzeri et al., 2001). This suggests spike times carry their information using a temporal precision of a few milliseconds.

Further, we asked what were the most important components of the code. We used the series expansion formalism (Panzeri and Schultz, 2001) to separate the contribution of stimulus modulation of the time-dependent firing rates from the contribution of correlations between spike times. At 40 ms post-stimulus onset, firing rate modulations conveyed 83% of the total information (**Figure 1B**). The contribution to information of correlations between the spike times was smaller (17%) (Panzeri et al., 2001).

To understand whether response latency played a special part in the spike timing code, we compared the information transmitted using all spikes after whisker deflection on each trial to that using only the first spike after whisker deflection. The result (**Figure 1B**) was that 83% of the total information in the spike train for 0–40 ms was available in the time of the first spike alone. Moreover, for each time step in the 0–40 ms interval, the first spike accounted for essentially all of the information in firing rate modulation (**Figure 1B**). Hence, the only information bearing part of the time-varying firing rate modulations was the response onset.

The conclusion is that individual rat somatosensory cortical neurons encode stimulus location largely by differences in time-varying firing rate, and that the response latency measured with millisecond resolution is the key symbol in this code. This encouraged us to look for a decoding mechanism based upon the relative spike latency of different neurons, the goal of the current work.

INFORMATION CARRIED BY SPIKE TIMING MEASURED WITHOUT AN EXTERNAL REFERENCE FRAME

We address the problem of decoding without stimulus time knowledge by considering the single-whisker deflection data reviewed in previous sections. This dataset is particularly interesting for our

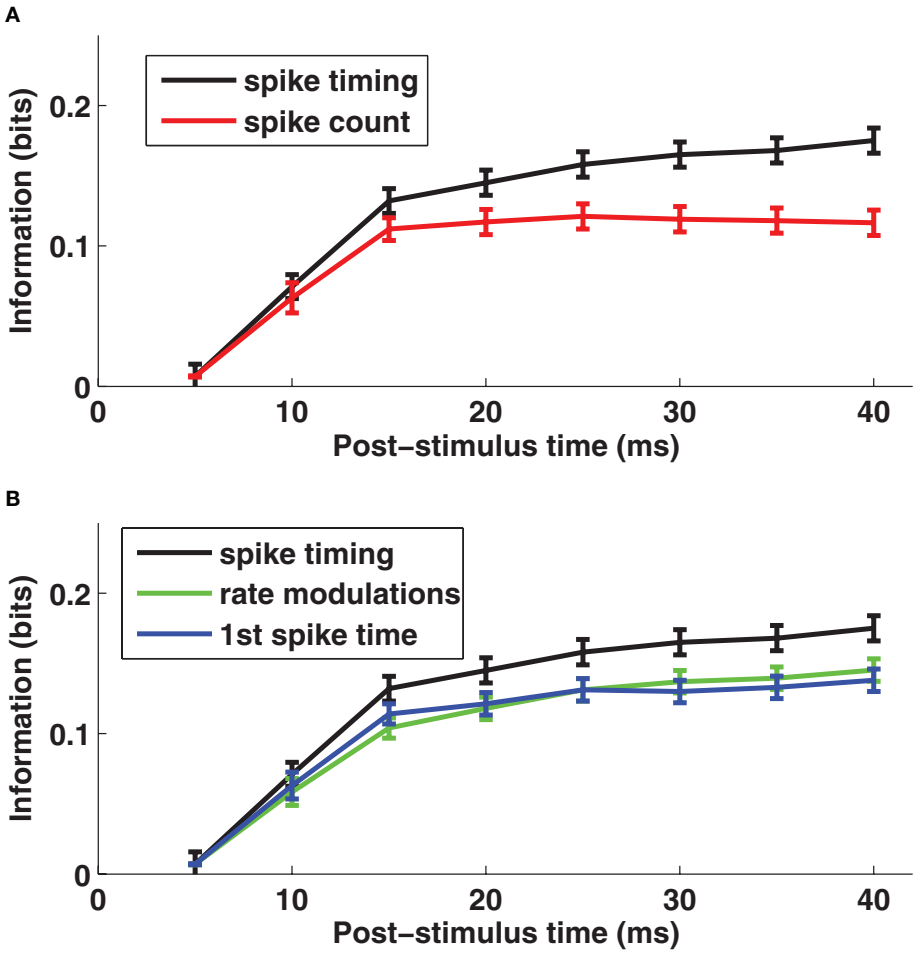

FIGURE 1 | The encoding of stimulus location by single neuron spike times with knowledge of external clock. (A) The post-stimulus time course of the information about stimulus site available from two different neural codes provided the decoder knows stimulus time. Results are plotted as average (±SEM) across cells of the mutual information functions. The black line denotes the spike timing information obtained when sampling spikes with temporal resolution Δt = 5 ms, and the red line denotes the spike count information. **(B)** The post-stimulus time course of the total information carried by spike times (black line) obtained when sampling spikes with temporal resolution Δt = 5 ms, compared to the information carried by the time-varying firing rate (green line) and to the information computed using only the timing of the first spike on each trial (blue line), both obtained with the same resolution Δt = 5 ms. Results are plotted as average (±SEM) across all recorded cells. Figure modified from results presented in Panzeri et al. (2001).

purpose because the population carried, at both the single neuron and the neuronal-pairs level, essentially all information about stimulus location in the timing of the first spike emitted post-stimulus deflection (Panzeri et al., 2001; Petersen et al., 2001). Therefore it is particularly important to understand if the information content of these spike times can be decoded without a precise knowledge of the stimulus time.

COLUMNAR POPULATION LATENCIES AND COLUMNAR POPULATION SPIKE COUNTS IN RESPONSE TO SINGLE-WHISKER DEFLECTION

Let us start by examining population activity in a *single trial*. **Figure 2A** shows the responses of 100 non-simultaneously recorded neurons in column D2 to one deflection of whisker D2 at time $t = 0$. The neurons are treated as if recorded simultaneously – the effect of non-simultaneity of recordings will be addressed later by simulations. Approximately 10 ms after stimulus onset, there was a sharp increase in firing rate which led many neurons to fire nearly simultaneously (gray area in **Figure 2A**). By 50 ms after stimulus onset, activity had almost returned to baseline level (**Figure 2A**). Responses of these neurons to deflection of a different whisker (D1) are shown in panel 2B, where spikes were now more distributed in time. **Figures 2C,D** shows the summed activity of column D2 units in response to deflection of whiskers D1 and D2. The response to the topographically matching whisker was stronger, had shorter latency and was more uniformly timed across the population.

Let us now consider how a downstream observer may decode such population activity. As shown in **Figure 1**, the information carried by single neurons was only a fraction of a bit and thus was not high enough to support reliable stimulus discrimination; therefore, if the whole rat can localize tactile stimuli, decoding must be done at the population level. We have previously shown that pooling of neurons located within the same column (i.e., summing their population activity) does not lead to any loss of

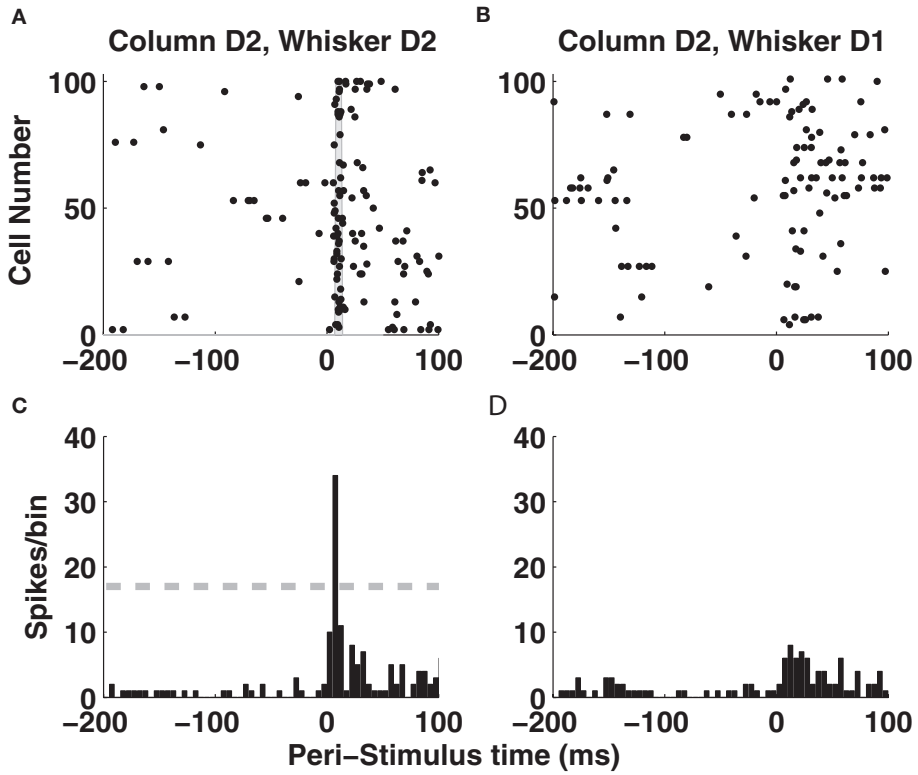

FIGURE 2 | Single-trial responses of a barrel column to whisker deflection. **(A)** Raster plots of the spike times emitted in a single example trial by 100 neurons recorded non-simultaneously in barrel-column D2 around the time of deflection of the principal whisker D2. The gray area denotes the time window around 10 ms when many neurons synchronously fire their first post-stimulus spike. **(B)** Raster plots of the spike times emitted in a single example trial by 100 neurons recorded non-simultaneously recorded in barrel-column D2 around the time of deflection of the whisker D1. **(C)** The time course (sampled in 5-ms bins) of the summed activity of the whole population of D2 neurons around the time of deflection of D2 whisker in the same trial plotted in **(A)**. The dashed horizontal line plots the threshold used to detect a "columnar synchronous response" (CSR) event. **(D)** The time course of the summed activity of the whole population of D2 neurons around the time of deflection of D1 whisker in the same trial plotted in **(B)**.

information about whisker identity (Panzeri et al., 2003b); we will therefore consider in the following the summed population activity within a column.

It is tempting to reason that, without accurate knowledge of stimulus time it would be more efficient to count spikes over relatively large time windows, because coarse measures may be more robust to stimulus time uncertainty. To evaluate this hypothesis, we investigated how decoding accuracy using the summed spike count of the columnar population over long response windows depends on the knowledge of the stimulus time. A decoder based on columnar population spike counts exploits the fact that more spikes are emitted in response to the stimulation of the principal whisker than to any other whisker, both in the anesthetized (Petersen et al., 2002a) and awake, behaving brain (von Heimendahl et al., 2007). **Figure 3A** (left part) shows a scatterplot of the summed spike counts of 100 cells in barrel D2 on each trial in a 0–50 ms post-stimulus window. In this window, high spike counts correspond to stimulation of principal whisker D2 and low spike counts correspond to stimulation of the non-principal whisker D1. The distribution of counts is well separated and only two trials out of 96 would be confusable. However, since spike counts are stimulus-modulated only briefly following the stimulation, this excellent discriminability can be achieved only if the decoder knows *when* to count the spikes. Suppose the decoder is uncertain about stimulus time, and therefore erroneously counts spikes comprising non-stimulus-driven activity, for example in the –500 to +50 peri-stimulus time. In this case, the population spike counts cannot be correctly decoded in most trials (**Figure 3A**, right part). The conclusion, perhaps counterintuitive, is that integrating columnar spike counts over long windows is not an effective way to make the neural code robust to errors in the estimation of the stimulus time. In this data set, population spike counts can only be decoded with some knowledge of the stimulus time.

An alternative hypothesis is that registering the time course of population response with high temporal precision can actually make the code more robust to the stimulus time errors. **Figures 2A,B** shows that the first spikes emitted by the 100 neurons in barrel D2 after stimulation of their principal whisker are much more precisely timed than second spikes or than spikes emitted in response to a non-principal whisker. This suggests that we can indeed use the precisely aligned response latencies of individual neurons to define a "columnar synchronous response" (CSR) event characterized by the firing of at least a certain fraction f of neurons within a short interval of Δt ms (see illustration in **Figure 2C**). The fraction f of neurons firing and the width of the time window Δt are free parameters. In this article, we use $f = 0.17$ and $\Delta t = 5$ ms

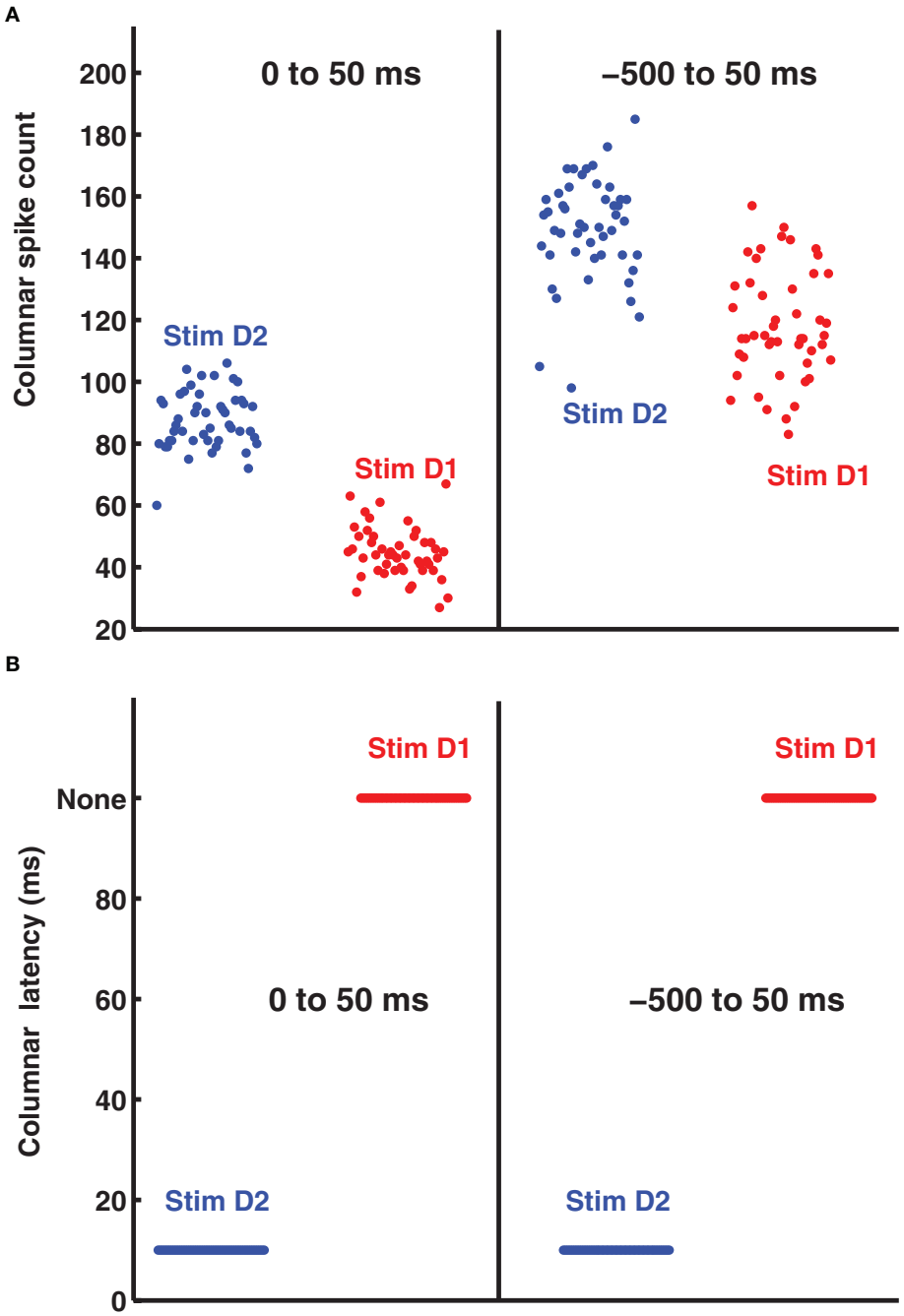

FIGURE 3 | The distribution of single trial D2-columnar spike counts and of columnar latencies. (A) Reports the scatter plot of the single-trial summed spike count of a population of 100 neurons in barrel D2 over all the trials available to deflection of whisker D2 (blue dots) and whisker D1 (red dots). The left and right part of (A) report respectively the spike counts obtained in the 0 to 50 ms and –500 to 50 ms peri-stimulus window respectively. **(B)** Shows the scatter plot of the timing of columnar latency (defined as the timing of single-trial synchronous columnar response events) of a population of 100 neurons in barrel D2 over all trials to deflection of whisker D2 (blue dots) and whisker D1 (red dots). The left and right part of (B) show, respectively, the results obtained in the 0 to 50 ms and –500 to 50 ms peri-stimulus window.

(as in **Figure 2C**), because we found empirically that these values were optimal. We systematically searched for CSR events by moving a sliding window of size $\Delta t = 5$ throughout the peri-stimulus time. The event occurred only in the window [10–15] ms after deflection of the principal whisker, and never during spontaneous activity or after stimulation of a non-principal whisker. This result is exemplified in one selected trial in **Figures 2C,D** but (as shown in **Figure 3B**), it holds for all trials. Thus, detecting

spike synchrony at fine temporal precision leads to 100%-correct detection of the stimulation of the principal whisker D2. In stark contrast to the spike count code, CSR detection was not degraded by the inclusion of spontaneous activity periods due to incorrect stimulus onset knowledge, because no CSR ever occurred during spontaneous activity (**Figures 2D and 3B**). In addition, since the response onset always happened 10–15 ms after deflection of the principal whisker (**Figure 3B**), CSR can specify the stimulus timing with a few milliseconds of precision, as well as the identity of the stimulus. A similar mechanism has been proposed for detection of the high-speed whisker jumps that occur during texture palpation (Jadhav et al., 2009). Of course, the mechanism works if a decoder can perform a CSR detection operation such as that done by a post-synaptic neuron with an integration time constant of a few milliseconds and a fixed threshold for firing (Ayling, 2008; Stuttgen and Schwarz, 2010).

INFORMATION CONTENT OF POPULATION LATENCIES AND COUNTS IN A SINGLE COLUMN

The above analysis suggests that detecting the population response leads to a more reliable and robust decoding of stimulus identity as opposed to simply counting all the spikes in the population over long time windows. We studied in more detail how the performance of the two candidate decoding schemes depends on both the size of the columnar population and on the amount of uncertainty about the stimulus time.

We considered a population of n sequentially recorded neurons in column D2, and varied n parametrically from 1 to 100. We computed how much information the population encoded about whether whisker D1 or D2 was stimulated. Perfect discrimination corresponds to 1 bit of information. We assumed that the decoder has only imprecise knowledge about when whisker deflection will occur and, as a consequence, processes both periods of spontaneous activity preceding the stimulus as well as the stimulus-evoked response. We mimicked this by quantifying the columnar population responses from a time X before the stimulus time to a post-stimulus time $T = 50$ ms. Larger values of X correspond to higher uncertainty about the stimulus application time. The parameter X was varied between −500 ms and 0 ms (i.e., exact knowledge of stimulus time). There are other ways to model uncertainty about stimulus time when the events are presented continuously and the purpose is to select between potential stimulus features rather than select between evoked and spontaneous activity (e.g., Arabzadeh et al., 2006). For detection of the onset of a stimulus, the method used here has two advantages. First, spontaneous activity is one of the greatest problems for measuring latency, and so its inclusion is a stringent and relevant test for the robustness of latency codes. Second, it is a simple but reasonable way to model a coarse "window of stimulus expectation" that may for example accompany the motor commands initiating active whisking.

For any choice of X, we considered the information carried by two types of neural codes, the columnar spike count and the columnar latency code, as described next. For the columnar spike count we quantified the response $\boldsymbol{r}$ (Eq. 1) as the total number of spikes emitted within the window by all neurons in the population (as in the example of **Figures 2 and 3**). To compute the information encoded by the columnar latency, we detected CSR events (as explained above and illustrated in **Figure 2C**); we called the time at which the first CSR event was detected in a certain barrel in a given trial the "columnar latency" and we used it as the variable **r** in Eq. 1.

We first considered the case in which the stimulus time is known precisely ($X = 0$ ms). The corresponding dependence of information on the population size is plotted in **Figure 4A**. With a single cell ($n = 1$), the columnar latency reduces to the first-spike latency, and the columnar population spike count matches the single cell spike count. Consequently, the information values for columnar latency and columnar count equal those previously reported (Panzeri et al., 2001) for single neuron first-spike latency and single neuron spike count (0.15 bits and 0.10 bits respectively). The information available in both columnar counts and columnar latencies increased steeply with the population size n (**Figure 4A**). When considering $n = 100$ cells, 1 bit of information (corresponding in this case to 100% correct discrimination) was available from columnar latencies and 0.89 bits were available from columnar counts. Thus, when stimulus time is known precisely the information available in columnar latency is higher than that available from counts over a large range of population size, but the information gain by columnar latency is moderate.

The situation was different when there was stimulus time uncertainty of 500 ms (i.e. $X = -500$ ms; **Figure 4D**). For small population sizes there was essentially no advantage in columnar latencies over counts. For single cells ($n = 1$), the information available in latencies (0.1 bits) was similar to that available in counts (0.09 bits). This is because for small population sizes the columnar latency reduces to a single neuron first-spike latency code, and the latter is difficult to extract without knowledge of the stimulus time. However, as the population size increased, the information available in population latencies increased much more steeply than the information available in population counts. This is because the population latency, but not the spike count code, became robustly separable from the pre-stimulus activity. For $n = 100$ cells, perfect stimulus discriminability (1 bit) was achieved by the population latency code, but a much poorer discriminability (0.30 bits) was achieved by the spike count.

Intermediate values of stimulus time uncertainty ($X = -100$ and −200 ms, **Figures 4B,C**) led to an intermediate increase of the information advantage of using population latencies rather than counts. For populations larger than 10 neurons, the larger the error in stimulus time knowledge, the larger was the information advantage of a columnar latency code. An information of 0.6 bits could be extracted from the columnar latency code with as few as 25 cells even in total absence of stimulus time knowledge. Once the uncertainty in the stimulus time exceeded 200 ms, extracting the same 0.6 bits from the spike count code could not be achieved for any population size.

In the above analysis, varying the parameter X affected both the amount of uncertainty about the stimulus time and (in the case of spike counts) the duration of the integration time window. To check that window variation did not confound our estimate of the effect of stimulus time ignorance, we repeated the same analysis as in **Figure 4** but using a different parameterization of stimulus time uncertainty. Now we used sliding windows of equal

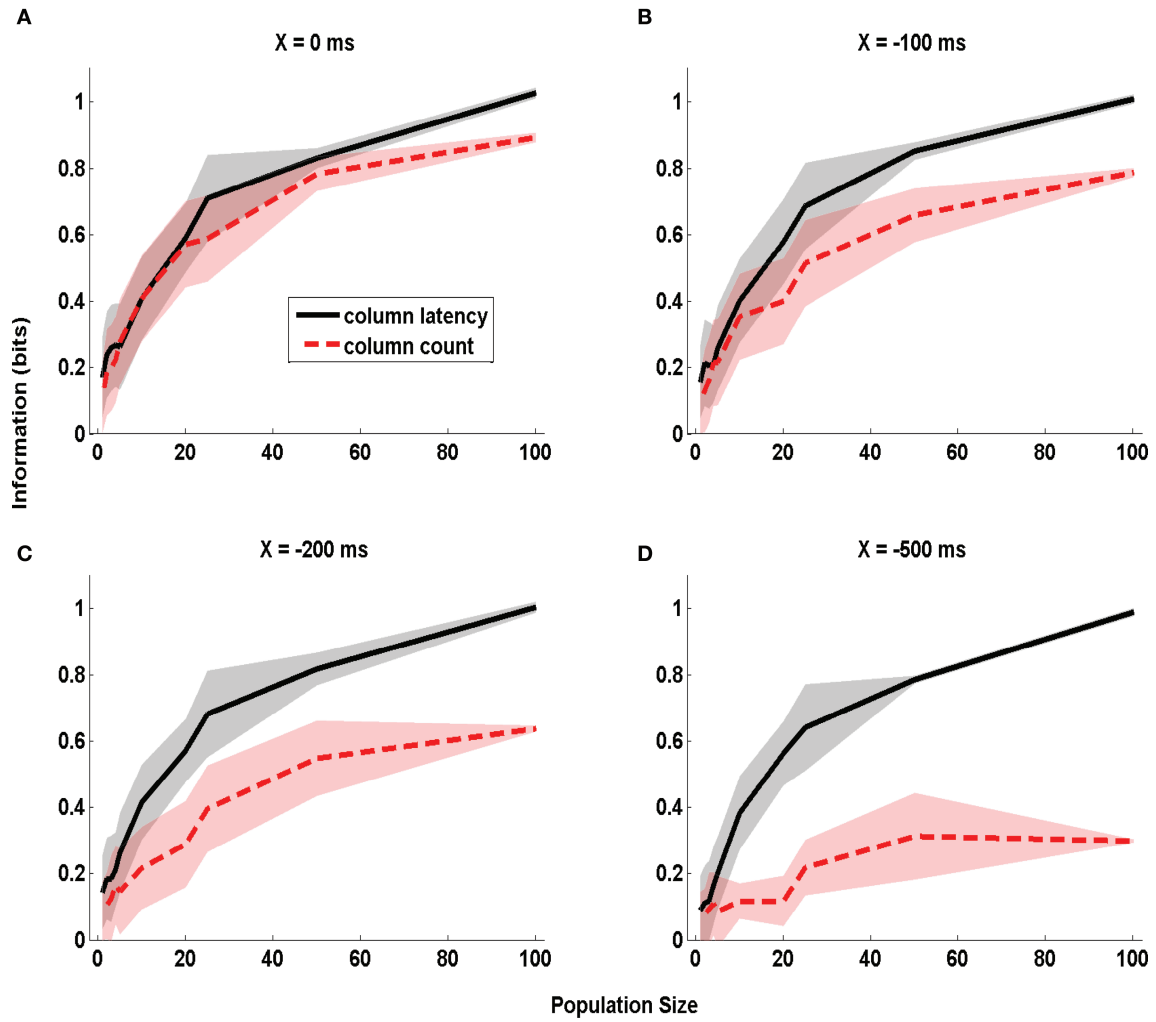

FIGURE 4 | The dependence of information obtained by decoding the activity of one column on stimulus time uncertainty *X*. The information about whether whisker D1 or D2 was deflected, obtained by the summed counts (red line) or the latency of synchronous population activity (black line) of a population of neurons located in a single column (barrel D2). The information is computed in a time window starting *X* ms before stimulus onset and extending to 50 ms post-stimulus, and is plotted as a function of the size of the population of D2 neurons considered. **(A–D)** Report information values which were obtained when using respectively the values 0, –100, –200, and –500 ms for the parameter *X* quantifying the uncertainty about the stimulus time. Results are plotted as average (±SD; colored area) across all analyzed subgroups of cells with the specified population size.

duration (50 ms), but parametrized stimulus time uncertainty by varying the time step Y by which this sliding window was shifted with respect to the correct stimulus onset. The information was, as above, relative to stimulus site D1 or D2. The dependence of extracted information on Y is reported in **Figure 5**. It is clear that the information in the columnar latency was more robust to errors in the stimulus time than the information in the columnar spike counts, even when using such parametrization of the uncertainty of stimulus time.

In sum, decoding strategies based on the synchronized columnar population latency have multiple advantages with respect to decoding by integrating spike counts over longer windows: columnar latency decoding (1) conveys more information per cell and requires fewer cells for reliable discrimination, and (2) is more robust to uncertainty about stimulus time.

DECODING THE RESPONSES OF POPULATIONS OF NEURONS IN MULTIPLE BARRELS

Next we consider the more complex problem of decoding the activity of multiple columns to identify stimulus site from among several candidate whiskers.

We took the activity of 100 non-simultaneously recorded neurons per column from three different barrel-columns (D1, D2, and D3) in response to stimulation of whisker D1, D2, D3 or another whisker, E1, non-principal to any of the considered columns. We again considered an uncertainty *X* in the knowledge of the stimulus time, and again evaluated different decoding schemes based on relative latency and spike counts respectively.

Quantification of information from the populations in three columns is much more difficult than a single column: the response ***r*** of the three-column population is a three dimensional array, and the

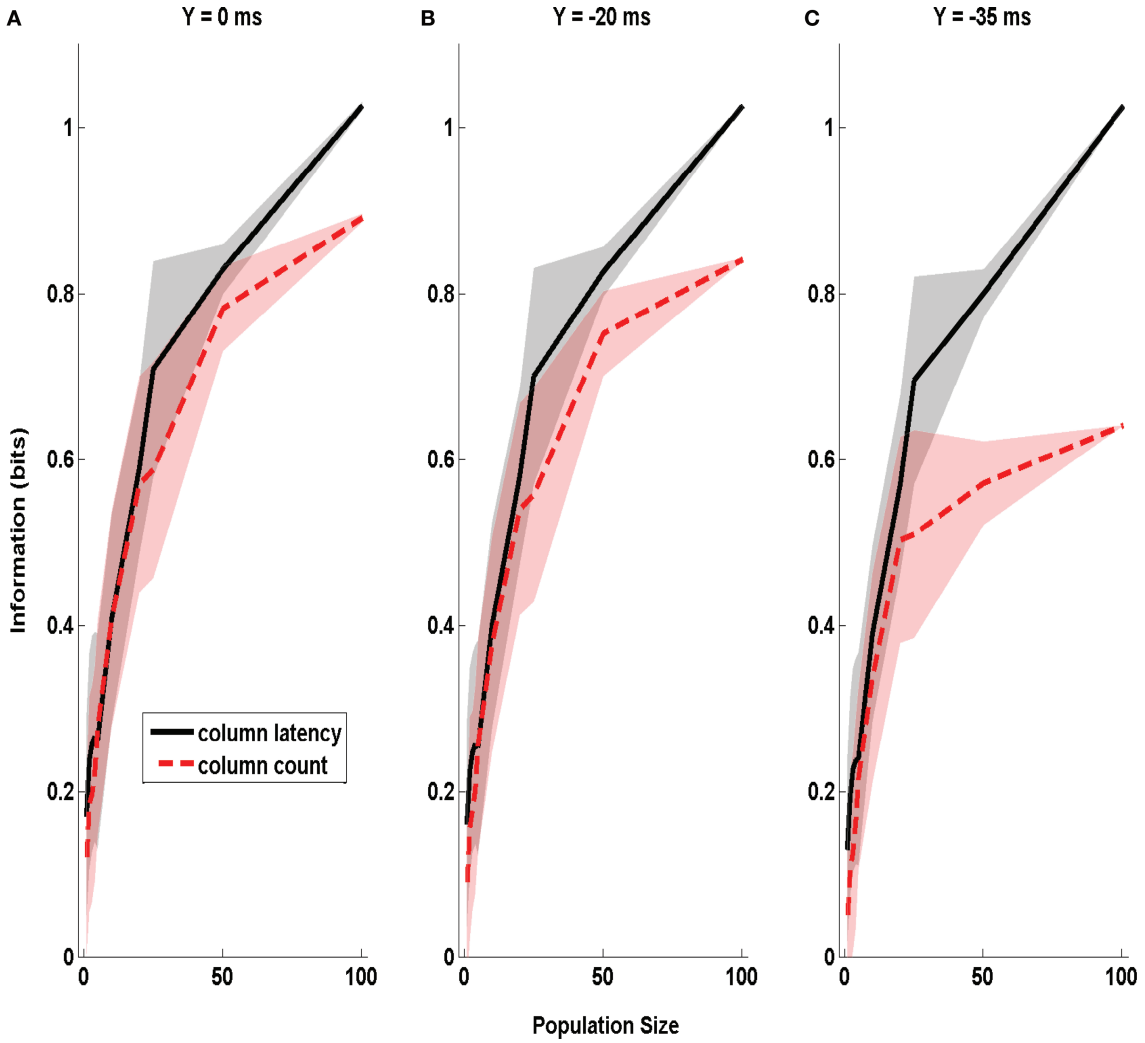

FIGURE 5 | The dependence of Information obtained by decoding the activity of one column on stimulus time uncertainty *Y*. The information about whether whisker D1 or D2 was deflected, obtained by the summed counts (red line) or the latency of synchronous population activity (black line) of a population of neurons located in a single column (barrel D2). The information is computed in a time window of duration 50 ms starting Y ms before stimulus onset, and is plotted as a function of the size of the population of D2 neurons considered. **(A–C)** Report information values which were obtained when using respectively the values 0, –20, and –35 ms for the parameter *Y* quantifying the uncertainty about the stimulus time. Results are plotted as average (±SD; colored area) across all analyzed subgroups of cells with the specified population size.

number of trials per stimulus available is not sufficient to sample in enough detail the full multivariate stimulus-response probabilities. For this reason, we computed the information available in the activity of the three columns by using an intermediate stimulus reconstruction step. Stimulus reconstruction can be operationally defined as a rule leading to the prediction of which stimulus or behavior elicited a neuronal response in a single trial. It can be mathematically defined as a function $g(\mathbf{r})$ operating on the population response in any given trial and giving a prediction $s^P(\mathbf{r})$ of the stimulus that elicited the observed neural population response in that trial:

$$s^P(\mathbf{r}) = g(\mathbf{r}). \tag{2}$$

The information extracted through the stimulus reconstruction scheme can be quantified as follows (Quian Quiroga and Panzeri, 2009):

$$I(S;S^P) = \sum_{s,s^P} P(s)Q(s^P \mid s)\log_2 \frac{Q(s^P \mid s)}{Q(s^P)} \tag{3}$$

where in the above $Q(s^P) = \Sigma_s P(s)Q(s^P \mid s)$, and $Q(s^P \mid s)$ is the "confusion matrix." Its values in a given row s and column s^P of a confusion matrix represent the (normalized) number of times that a presentation of stimulus s is predicted by the decoder to be stimulus s^P:

$$Q(s^P \mid s) = \sum_{\mathbf{r}} \delta(s^P, g(\mathbf{r}))P(\mathbf{r} \mid s) \tag{4}$$

where δ is a Kronecker Delta. The decoded information $I(S;S^P)$ quantifies the total information gained when predicting the stimulus using a specific algorithm, and takes into account both the

fraction of correct decoding and the spread of the decoding errors. Information theoretic inequalities ensure that $I(S;S^P) \leq I(S;\mathbf{R})$. The reason $I(S;S^P)$ can sometimes be strictly less than $I(S;\mathbf{R})$ is that $I(S;S^P)$ refers to a specific algorithm, whereas $I(S;\mathbf{R})$ bounds the performance of all possible algorithms operating on the response r.

We computed the information $I(S;S^P)$ gained with three different decoding schemes, each corresponding to a different choice of coding scheme (i.e., a different quantification of the population response $\boldsymbol{r}$) and of stimulus reconstruction function g in Eq. 2, as described next.

The first decoding scheme was the one based on the relative population latency of each column (in the following termed "columnar latency difference decoder"). This decoding was implemented as follows. In each trial we detected, independently in each column, the presence and timing of synchronous columnar response (CSR, as described earlier) events, exactly as described in the previous section. Then, in each trial, we decoded the stimulus by the following rule: if at least one barrel-column exhibited a CSR event, we decoded the stimulus site as being principal to the column firing the first event (note that this implies that the relative, rather than the absolute timing of each column is used for decoding). If no synchronous columnar population event was detected in the trial from any of the columns, we decoded the stimulus in that trial as whisker E1 (the only one not principal to any of the considered columns). It is important to note that the relative population latency coding scheme is a genuine form of population temporal encoding, and cannot be reduced to a simple spike count code in a short time window: events are defined separately for a population in each column, and information is computed from the relative timing of such events. In fact, when we considered fewer than $n = 100$ neurons in each barrel, there were several trials in which CSR events occur in more than one barrel (6% and 21% of trials on average for $n = 50$ and $n = 25$ respectively), and in this case the decoded whisker is the one principal to the barrel in which the first CSR event was evoked.

The second decoder was recruitment order. This algorithm considers the relative order in which each neuron within the population (rather than the pooled columnar activity) fires its first spike (Van Rullen and Thorpe, 2001; Johansson and Birznieks, 2004; Saal et al., 2009). We tested the performance of the recruitment order decoding with a procedure very close to that of (Johansson and Birznieks, 2004). In each trial, the first-spike latency of each neuron was measured as the time between the beginning of the sampling window and the appearance of the first spike. For each stimulated whisker, we constructed a template of the recruitment order of the neurons in response to the stimulus by sorting the neurons according to their mean rank over a set of training trials. We then used the remaining set of "test" trials to compute how well the recruitment order could predict the stimulus. For each test trial, the population response was defined as the rank order of first-spike latencies of each neuron. We then denoted the most likely whisker S^P as that with the highest Spearman rank correlation to the population response of the current test trial. Two different procedures of cross-validation were employed: random division into 10 training and 38 test trials, and the leave-one-out procedure. The procedures gave equivalent results. It is important to note that the rank order coding scheme is also a genuine form of population temporal encoding.

The third decoder was the "columnar spike count decoder", which operated on the summed spike count within each column. The population response $\boldsymbol{r}$ was a three dimensional array whose components correspond to the total spike count in columns D1, D2, and D3, respectively, and it was discretized into five equispaced classes independently in each column (the number of classes was set to five because we found empirically that this parameter choice maximized the performance of this decoder). From the training data, we computed the empirical posterior probability of joint columnar $P(s \mid \mathbf{r})$ and then decoded the most likely stimulus, i.e., $s^P(\mathbf{r}) = \arg\max_s P(s \mid \mathbf{r})$. Cross-validation was performed as described above.

Results of the three coding schemes are reported in **Figure 6** for different values of the stimulus time error X (from −500 to 0 ms) and for three different population sizes ($n = 25$, 50, and 100 cells per column). It is apparent that the first scheme, the columnar latency difference decoder, was the most informative and was also most robust to the stimulus time ignorance, for all population sizes considered. For example, when considering 100 cells per column (**Figure 6A**), the columnar latency difference decoder yielded 100% accurate stimulus reconstructions (2 bits of information) whatever the stimulus time uncertainty X. Rank order decoding also performed well when the stimulus time was known precisely ($X = 0$), but was much less robust to the inclusion of periods of spontaneous activity. This is because the longer the spontaneous activity period, the higher the chance that the rank of individual neurons will be random. The columnar pooling operation removes this noise in the activation order at the single neuron level (because stimulus-evoked peaks are narrower and stronger than spontaneous peaks). Consistent with the results of **Figures 2 and 3**, the spike count decoder performed well when the stimulus time was known, but it performed poorly when periods of spontaneous activity were incorporated.

The criticism can be raised that our calculations do not take into account the effects of correlated noise, because they are based on a pseudo-simultaneous response arrays constructed by collecting together responses of non-simultaneously recorded neurons. Correlated noise may amplify the variability of the time course of the population activity (Mazurek and Shadlen, 2002), and by canceling such correlations our method may eliminate any strong and narrow spontaneous activity peaks in the pooled population – in effect, simulated populations may reduce "false positives" compared to real populations that contain correlated noise. To test for this, we used the procedure of Mikula and Niebur (2003) to generate correlated spike trains that matched exactly the true population-averaged PSTH of the neurons (sampled with 1-ms bins) and the true pair-wise Pearson cross-correlation value of neurons within the same column (the latter collected from a dataset of 52 D2–D2 neuronal pairs simultaneously recorded in the same conditions with a small array of electrodes, see Petersen et al., 2001) in each 1-ms-wide peri-stimulus time bin. When the simulated population of 100 cells per column with realistic correlation values was tested, performance of the columnar latency difference decoder as a function of X was unchanged ($P > 0.3$, one way ANOVA). To further check the robustness of the decoder to increased values of correlation, we increased correlations by a factor of four with respect to those present in real data. The columnar decoder then

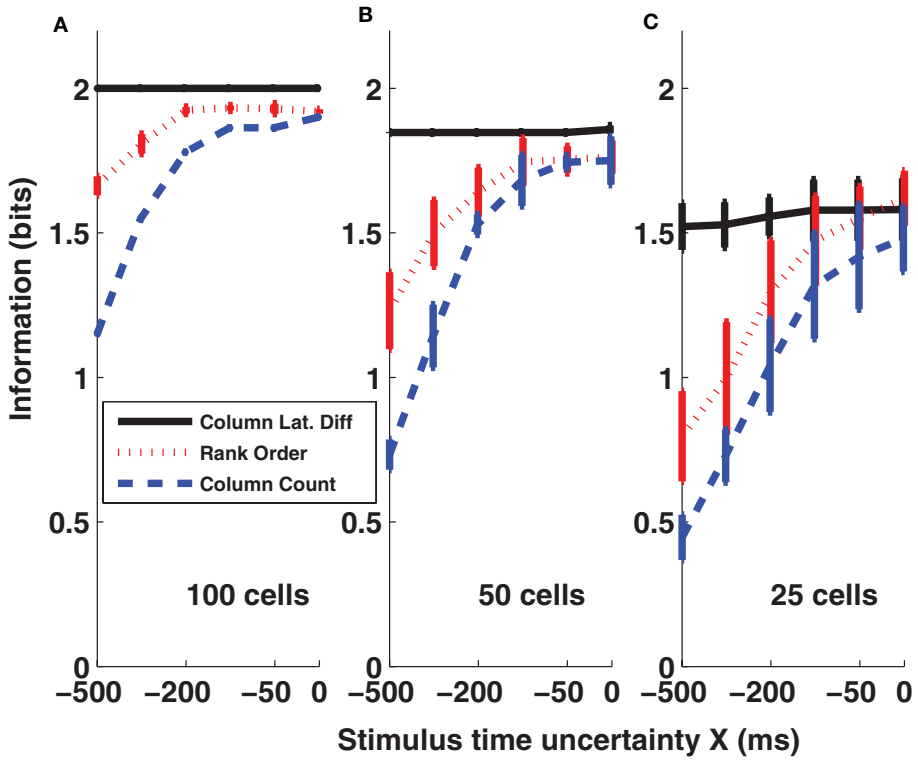

FIGURE 6 | Information obtained by decoding the activity of three columns (barrels D1, D2, and D3). The amounts of information (Eq. 3) decoded by the columnar latency (black line), the rank order (red line) and the columnar count (blue line) decoders respectively are plotted as a function of the parameter *X* which quantifies the uncertainty about the stimulus time. **(A–C)** Plot the results obtained when using populations of 100, 50, and 25 cells in each column respectively. Results are plotted as average (±SD) across all analyzed subgroups of cells with the specified population size.

showed only a very small decrease in the decoding performance (less than 0.1 bits for each value of X compared to those reported in **Figure 6A** when using 100 cells per barrel; results not shown, but see Ayling, 2008 for more details). For other studies of the effect of correlated activity on the robustness of relative-timing decoders, we refer the reader to (Chase and Young, 2007; Gollisch and Meister, 2008).

DISCUSSION AND CONCLUSIONS

The temporal precision at which neural responses carry information has been systematically investigated over the last 20 years in several sensory structures. Substantial evidence (recently reviewed in Panzeri et al., 2010) shows that the timing of spikes with millisecond precision carries much more information than that carried by spike counts over windows of tens or hundreds of milliseconds. However, the observation that information is carried by neural codes at a high temporal precision does not guarantee that the nervous system makes use of such codes. One of the most compelling criticisms is that temporally precise signals may not be decodable unless the downstream population has access to an equally precise external reference frame. The results presented here suggest that a precise external reference frame is not always necessary: spike timing-based decoders can work well without knowledge of the stimulus time in some conditions. Moreover, our results corroborate previous reports (Soteropoulos and Baker, 2009; Stuttgen and Schwarz, 2010) that the time course of neural population activity can be used to estimate the timing of stimulus application. We also found that, contrarily to simple intuition, relative timing codes are less degraded than spike count codes by inaccuracies in stimulus time knowledge.

Another caveat regarding spike timing coding is that in large populations there may be enough information available in spike counts to make the extra spike timing information unneeded; a ceiling effect. Our results show that, while this may be the case when the stimulus time is known with precision, in the harder task of decoding the stimulus without stimulus time knowledge, spike time mechanisms outperform those based on spike counts, and especially so as population size grows. With stimulus time uncertainty, even large populations of neurons could not be perfectly decoded by spike counts (see **Figures 4 and 6**), implying that population signals never reach a ceiling if decoded inefficiently. This suggests that previous small-population reports of encoding information by spike timing may actually underestimate (rather than overestimate) the importance of spike timing at the population level.

The results in this article were obtained considering only the encoding of simple stimuli (single-whiskers deflected in a binary manner – on/off) and need to be extended to stimulus time-free decoding of dynamic stimulus features of naturalistic complexity. There is reason to expect that the information-carrying advantage of relative timing codes over spike count codes may be even more advantageous for such stimuli. Naturalistic stimuli often consist of complex sequences of features – in the whisker system, such features

include position, velocity, absolute speed, acceleration (Arabzadeh et al., 2005; Hipp et al., 2006; Lottem and Azouz, 2008). By reverse correlation methods, it has been shown that neurons in the sensory pathway act as "filters" for different features: they fire with varying probability and latency according to the strength of some set of features in some preceding moment (Petersen et al., 2008). Because neurons respond to multiple features and because the features often occur in close temporal proximity or even in temporal superposition, single-neuron decoding will always be ambiguous. To decode the sequence of features and their magnitude, a highly efficient readout of the population would be based upon the relative latencies of neurons with heightened sensitivity to specific features. For example, the firing of "high-acceleration neurons" a few milliseconds before "high-speed neurons" would signal a change in whisker direction followed by a high-speed jump. Target neurons receiving combined inputs could achieve this sort of decoding. Timing comparisons would be done not between whole columns (the condition for stimulus localization) but between sets of neurons within or across columns with varying feature selectivity.

The stimulus time-free decoding algorithms of response latencies which was presented in this study relies on the concept that there are classes of neurons activated with similar latencies by the stimulus feature to be decoded. This assumption is conceivable when considering primary cortical sensory areas, in which first-spike latency codes have been consistently reported. It however remains to be understood whether such conditions extend to higher order cortical systems where neurons can show both increases and decreases in response to a sensory stimulus or a behavioral event, or even whether constant sensory feedback in the awake behaving animal may disrupt the conditions for detection of synchronous activation of a neural population.

An important question for theoretical research is how a downstream system could learn to be selective to the "first wave" of spikes in each column that forms the basis of the stimulus-time free coding scheme. Recently, Thorpe and colleagues (Masquelier et al., 2008, 2009) proposed that spike time-dependent plasticity (STDP) (Markram et al., 1997; Bi and Poo, 2001; Jacob et al., 2007) may provide the appropriate synaptic mechanism for learning such first spike codes: a certain "downstream" post-synaptic neuron will fire at random during the wave of first spikes at the beginning of the learning phase. When this happens, STDP reinforces the connections with all the afferents that take part in the first wave of spikes, thereby increasing the probability of the downstream neurons firing again in response to the first wave of spikes.

In general, to determine the extent to which spike time codes are used in the nervous system, it is important to establish links between the temporal precision of neural codes and behavior. The current evidence is vigorously debated (Luna et al., 2005; Engineer et al., 2008; Yang et al., 2008; Jacobs et al., 2009; Gerdjikov et al., 2010). While the data presented here do not speak directly to this issue, it is interesting to note that a mechanism similar to our was used by Stuttgen and Schwarz (2010), who demonstrated that the distribution of occurrence of such events across trials in different stimulus discrimination conditions is significantly correlated with the animal's behavioral performance. Whisker kinetic features also seem to be encoded by CSR-like firing (Jadhav et al., 2009). Future developments of the clock-free method will therefore focus on decoding complex stimuli (Maravall et al., 2007; Petersen et al., 2008) and stimuli experienced by awake, behaving rats, such as those reported in von Heimendahl et al. (2007).

In conclusion, our results demonstrate that the precise timing of spikes emitted shortly after stimulus presentation forms the basis for an information-rich code, which is robust to the stimulus time problem at the population level. Moreover, the time course of population responses can be used by the nervous system to provide information not only about the stimulus identity but also about the stimulus time itself.

ACKNOWLEDGMENTS

We thank the referees for thoughtful and detailed critiques which significantly improved the revised version of the manuscript. We thank C. Kayser, R.S. Petersen, and G. Notaro for useful discussions, and M.A. Ayling for contributing to the implementation of the rank order decoding algorithm. This research was supported by the BMI project of the Italian Institute of Technology and by the San Paolo Foundation, the Human Frontier Science Program (contract RG0041/2009-C), the European Community (contract BIOTACT-21590), and the Ministry of Economic Development.

REFERENCES

Arabzadeh, E., Panzeri, S., and Diamond, M. E. (2006). Deciphering the spike train of a sensory neuron: counts and temporal patterns in the rat whisker pathway. *J. Neurosci.* 26, 9216–9226.

Arabzadeh, E., Zorzin, E., and Diamond, M. E. (2005). Neuronal encoding of texture in the whisker sensory pathway. *PLoS Biol.* 3:e17. doi:10.1371/journal.pbio.0030017.

Ayling, M. (2008). *A computational analysis of the functional role of GABAergic synaptic transmission in striatal medium spiny neurons*. Ph.D. thesis, Faculty of Life Sciences, University of Manchester, Manchester.

Bi, G., and Poo, M. (2001). Synaptic modification by correlated activity: Hebb's postulate revisited. *Annu. Rev. Neurosci.* 24, 139–166.

Borst, A., and Theunissen, F. E. (1999). Information theory and neural coding. *Nat. Neurosci.* 2, 947–957.

Brody, C. D., and Hopfield, J. J. (2003). Simple networks for spike-timing-based computation, with application to olfactory processing. *Neuron* 37, 843–852.

Chase, S. M., and Young, E. D. (2007). First-spike latency information in single neurons increases when referenced to population onset. *Proc. Natl. Acad. Sci. U.S.A.* 104, 5175–5180.

Chechik, G., Anderson, M. J., Bar-Yosef, O., Young, E. D., Tishby, N., and Nelken, I. (2006). Reduction of information redundancy in the ascending auditory pathway. *Neuron* 51, 359–368.

Cover, T. M., and Thomas, J. A. (1991). *Elements of Information Theory*. New York: John Wiley & Sons, Inc.

Diamond, M. E., Petersen, R. S., and Harris, J. A. (1999). Learning through maps: functional significance of topographic organization in primary sensory cortex. *J. Neurobiol.* 41, 64–68.

Diamond, M. E., von Heimendahl, M., Knutsen, P. M., Kleinfeld, D., and Ahissar, E. (2008). 'Where' and 'what' in the whisker sensorimotor system. *Nat. Rev. Neurosci.* 9, 601–612.

Engineer, C. T., Perez, C. A., Chen, Y. H., Carraway, R. S., Reed, A. C., Shetake, J. A., Jakkamsetti, V., Chang, K. Q., and Kilgard, M. P. (2008). Cortical activity patterns predict speech discrimination ability. *Nat. Neurosci.* 11, 603–608.

Erchova, I. A., Lebedev, M. A., and Diamond, M. E. (2002). Somatosensory cortical neuronal population activity across states of anaesthesia. *Eur. J. Neurosci.* 15, 744–752.

Foffani, G., Chapin, J. K., and Moxon, K. A. (2008). Computational role of large receptive fields in the primary somatosensory cortex. *J. Neurophysiol.* 100, 268–280.

Foffani, G., Morales-Botello, M. L., and Aguilar, J. (2009). Spike timing, spike

count, and temporal information for the discrimination of tactile stimuli in the rat ventrobasal complex. *J. Neurosci.* 29, 5964–5973.

Foffani, G., Tutunculer, B., and Moxon, K. A. (2004). Role of spike timing in the forelimb somatosensory cortex of the rat. *J. Neurosci.* 24, 7266–7271.

Furukawa, S., Xu, L., and Middlebrooks, J. C. (2000). Coding of sound-source location by ensembles of cortical neurons. *J. Neurosci.* 20, 1216–1228.

Gawne, T. J., Kjaer, T. W., and Richmond, B. J. (1996). Latency: another potential code for feature binding in striate cortex. *J. Neurophysiol.* 76, 1356–1360.

Gerdjikov, T. V., Bergner, C. G., Stuttgen, M. C., Wiblingen, C., and Schwarz, C. (2010). Discrimination of vibrotactile stimuli in the rat whisker system: behavior and neurometrics. *Neuron* 65, 530–540.

Golledge, H. D., Panzeri, S., Zheng, F., Pola, G., Scannell, J. W., Giannikopoulos, D. V., Mason, R. J., Tovee, M. J., and Young, M. P. (2003). Correlations, feature-binding and population coding in primary visual cortex. *Neuroreport* 14, 1045–1050.

Gollisch, T., and Meister, M. (2008). Rapid neural coding in the retina with relative spike latencies. *Science* 319, 1108–1111.

Harris, J. A., Petersen, R. S., and Diamond, M. E. (1999). Distribution of tactile learning and its neural basis. *Proc. Natl. Acad. Sci. U.S.A.* 96, 7587–7591.

Hipp, J., Arabzadeh, E., Zorzin, E., Conradt, J., Kayser, C., Diamond, M. E., and Konig, P. (2006). Texture signals in whisker vibrations. *J. Neurophysiol.* 95, 1792–1799.

Hopfield, J. J. (1995). Pattern recognition computation using action potential timing for stimulus representation. *Nature* 376, 33–36.

Jacob, V., Brasier, D. J., Erchova, I., Feldman, D., and Shulz, D. E. (2007). Spike timing-dependent synaptic depression in the in vivo barrel cortex of the rat. *J. Neurosci.* 27, 1271–1284.

Jacobs, A. L., Fridman, G., Douglas, R. M., Alam, N. M., Latham, P. E., Prusky, G. T., and Nirenberg, S. (2009). Ruling out and ruling in neural codes. *Proc. Natl. Acad. Sci. U.S.A.* 106, 5936–5941.

Jadhav, S. P., Wolfe, J., and Feldman, D. E. (2009). Sparse temporal coding of elementary tactile features during active whisker sensation. *Nat. Neurosci.* 12, 792–800.

Johansson, R. S., and Birznieks, I. (2004). First spikes in ensembles of human tactile afferents code complex spatial fingertip events. *Nat. Neurosci.* 7, 170–177.

Kayser, C., Montemurro, M. A., Logothetis, N., and Panzeri, S. (2009). Spike-phase coding boosts and stabilizes the information carried by spatial and temporal spike patterns. *Neuron* 61, 597–608.

Kleinfeld, D., Ahissar, E., and Diamond, M. E. (2006). Active sensation: insights from the rodent vibrissa sensorimotor system. *Curr. Opin. Neurobiol.* 16, 435–444.

Knutsen, P. M., and Ahissar, E. (2009). Orthogonal coding of object location. *Trends Neurosci.* 32, 101–109.

Lebedev, M. A., Mirabella, G., Erchova, I., and Diamond, M. E. (2000). Experience-dependent plasticity of rat barrel cortex: redistribution of activity across barrel-columns. *Cereb. Cortex* 10, 23–31.

Lottem, E., and Azouz, R. (2008). Dynamic translation of surface coarseness into whisker vibrations. *J. Neurophysiol.* 100, 2852–2865.

Luna, R., Hernandez, A., Brody, C. D., and Romo, R. (2005). Neural codes for perceptual discrimination in primary somatosensory cortex. *Nat. Neurosci.* 8, 1210–1219.

Maravall, M., Petersen, R. S., Fairhall, A. L., Arabzadeh, E., and Diamond, M. E. (2007). Shifts in coding properties and maintenance of information transmission during adaptation in barrel cortex. *PLoS Biol.* 5:e19. doi:10.1371/journal.pbio.0050019.

Markram, H., Lubke, J., Frotscher, M., and Sakmann, B. (1997). Regulation of synaptic efficacy by coincidence of postsynaptic APs and EPSPs. *Science* 275, 213–215.

Masquelier, T., Guyonneau, R., and Thorpe, S. J. (2008). Spike timing dependent plasticity finds the start of repeating patterns in continuous spike trains. *PLoS ONE* 3:e1377. doi:10.1371/journal.pone.0001377.

Masquelier, T., Hugues, E., Deco, G., and Thorpe, S. J. (2009). Oscillations, phase-of-firing coding, and spike timing-dependent plasticity: an efficient learning scheme. *J. Neurosci.* 29, 13484–13493.

Mazurek, M. E., and Shadlen, M. N. (2002). Limits to the temporal fidelity of cortical spike rate signals. *Nat. Neurosci.* 5, 463–471.

Mehta, S. B., Whitmer, D., Figueroa, R., Williams, B. A., and Kleinfeld, D. (2007). Active spatial perception in the vibrissa scanning sensorimotor system. *PLoS Biol.* 5:e15. doi:10.1371/journal.pbio.0050015.

Mikula, S., and Niebur, E. (2003). The effects of input rate and synchrony on a coincidence detector: analytical solution. *Neural. Comput.* 15, 539–547.

Montani, F., Ince, R. A., Senatore, R., Arabzadeh, E., Diamond, M. E., and Panzeri, S. (2009). The impact of high-order interactions on the rate of synchronous discharge and information transmission in somatosensory cortex. *Philos. Trans. A Math. Phys. Eng. Sci.* 367, 3297–3310.

Muller, J. R., Metha, A. B., Krauskopf, J., and Lennie, P. (2001). Information conveyed by onset transients in responses of striate cortical neurons. *J. Neurosci.* 21, 6978–6990.

Nelken, I., and Chechik, G. (2007). Information theory in auditory research. *Hear. Res.* 229, 94–105.

Nirenberg, S., Carcieri, S. M., Jacobs, A. L., and Latham, P. E. (2001). Retinal ganglion cells act largely as independent encoders. *Nature* 411, 698–701.

Nirenberg, S., and Latham, P. E. (1998). Population coding in the retina. *Curr. Opin. Neurobiol.* 8, 488–493.

Panzeri, S., Brunel, N., Logothetis, N. K., and Kayser, C. (2010). Sensory neural codes using multiplexed temporal scales. *Trends Neurosci.* 33, 111–120.

Panzeri, S., Petersen, R. S., Schultz, S. R., Lebedev, M., and Diamond, M. E. (2001). The role of spike timing in the coding of stimulus location in rat somatosensory cortex. *Neuron* 29, 769–777.

Panzeri, S., Petroni, F., Petersen, R. S., and Diamond, M. E. (2003b). Decoding neuronal population activity in rat somatosensory cortex: role of columnar organization. *Cereb. Cortex* 13, 45–52.

Panzeri, S., Pola, G., and Petersen, R. S. (2003a). Coding of sensory signals by neuronal populations: the role of correlated activity. *Neuroscientist.* 9, 175–180.

Panzeri, S., and Schultz, S. R. (2001). A unified approach to the study of temporal, correlational, and rate coding. *Neural. Comput.* 13, 1311–1349.

Panzeri, S., Senatore, R., Montemurro, M. A., and Petersen, R. S. (2007). Correcting for the sampling bias problem in spike train information measures. *J. Neurophysiol.* 98, 1064–1072.

Petersen, R. S., Brambilla, M., Bale, M. R., Alenda, A., Panzeri, S., Montemurro, M. A., and Maravall, M. (2008). Diverse and temporally precise kinetic feature selectivity in the VPm thalamic nucleus. *Neuron* 60, 890–903.

Petersen, R. S., Panzeri, S., and Diamond, M. E. (2001). Population coding of stimulus location in rat somatosensory cortex. *Neuron* 32, 503–514.

Petersen, R. S., Panzeri, S., and Diamond, M. E. (2002a). Population coding in somatosensory cortex. *Curr. Opin. Neurobiol.* 12, 441–447.

Petersen, R. S., Panzeri, S., and Diamond, M. E. (2002b). The role of individual spikes and spike patterns in population coding of stimulus location in rat somatosensory cortex. *BioSystems* 67, 187–193.

Petersen, R. S., Panzeri, S., and Maravall, M. (2009). Neural coding and contextual influences in the whisker system. *Biol. Cybern.* 100, 427–446.

Prigg, T., Goldreich, D., Carvell, G. E., and Simons, D. J. (2002). Texture discrimination and unit recordings in the rat whisker/barrel system. *Physiol. Behav.* 77, 671–675.

Quian Quiroga, R., and Panzeri, S. (2009). Extracting information from neuronal populations: information theory and decoding approaches. *Nat. Rev. Neurosci.* 10, 173–185.

Reich, D. S., Mechler, F., and Victor, J. D. (2001). Temporal coding of contrast in primary visual cortex: when, what, and why. *J. Neurophysiol.* 85, 1039–1050.

Saal, H. P., Vijayakumar, S., and Johansson, R. S. (2009). Information about complex fingertip parameters in individual human tactile afferent neurons. *J. Neurosci.* 29, 8022–8031.

Scaglione, A., Foffani, G., Scannella, G., Cerutti, S., and Moxon, K. A. (2008). Mutual information expansion for studying the role of correlations in population codes: how important are autocorrelations? *Neural Comput.* 20, 2662–2695.

Schneidman, E., Bialek, W., and Berry, M. J. II. (2003). Synergy, redundancy, and independence in population codes. *J. Neurosci.* 23, 11539–11553.

Schnupp, J. W., Hall, T. M., Kokelaar, R. F., and Ahmed, B. (2006). Plasticity of temporal pattern codes for vocalization stimuli in primary auditory cortex. *J. Neurosci.* 26, 4785–4795.

Soteropoulos, D. S., and Baker, S. N. (2009). Quantifying neural coding of event timing. *J. Neurophysiol.* 101, 402–417.

Strong, S. P., Koberle, R., de Ruyter van Steveninck, R. R., and Bialek, W. (1998). Entropy and information in neuroal spike trains. *Phys. Rev. Lett.* 80, 197–200.

Stuttgen, M. C. (2010). Toward behavioral benchmarks for whisker-related sensory processing. *J. Neurosci.* 30, 4827–4829.

Stuttgen, M. C., and Schwarz, C. (2010). Integration of vibrotactile signals for whisker-related perception in rats is governed by short time constants: comparison of neurometric and

psychometric detection performance. *J. Neurosci.* 30, 2060–2069.
Theunissen, F., and Miller, J. P. (1995). Temporal encoding in nervous systems: a rigorous definition. *J. Comput. Neurosci.* 2, 149–162.
Van Rullen, R., and Thorpe, S. J. (2001). Rate coding versus temporal order coding: what the retinal ganglion cells tell the visual cortex. *Neural. Comput.* 13, 1255–1283.
Victor, J. D. (2000). How the brain uses time to represent and process visual information(1). *Brain Res.* 886, 33–46.
Victor, J. D. (2006). Approaches to information-theoretic analysis of neural activity. *Biol. Theory* 1, 302–316.
von Heimendahl, M., Itskov, P. M., Arabzadeh, E., and Diamond, M. E. (2007). Neuronal activity in rat barrel cortex underlying texture discrimination. *PLoS Biol.* 5:e305. doi:10.1371/journal.pbio.0050305.
Yang, Y., DeWeese, M. R., Otazu, G. H., and Zador, A. M. (2008). Millisecond-scale differences in neural activity in auditory cortex can drive decisions. *Nat. Neurosci.* 11, 1262–1263.

Conflict of Interest Statement: The authors declare that the research was conducted in the absence of any commercial or financial relationships that could be construed as a potential conflict of interest.

Received: 27 February 2010; paper pending published: 14 March 2010; accepted: 21 May 2010; published online: 14 June 2010.

Citation: Panzeri1 S and Diamond ME (2010) Information carried by population spike times in the whisker sensory cortex can be decoded without knowledge of stimulus time. Front. Syn. Neurosci. ***2****:17. doi: 10.3389/fnsyn.2010.00017*